TRANSLATIONAL ADVANCES IN ALZHEIMER'S, PARKINSON'S, AND OTHER NEURODEGENERATIVE DEMENTIAS

EDITED BY: Jiehui Jiang, Kuangyu Shi, Fangyu Peng, Chih-Yu Hsu and Woon-Man Kung

PUBLISHED IN: Frontiers in Aging Neuroscience and Frontiers in Neuroscience

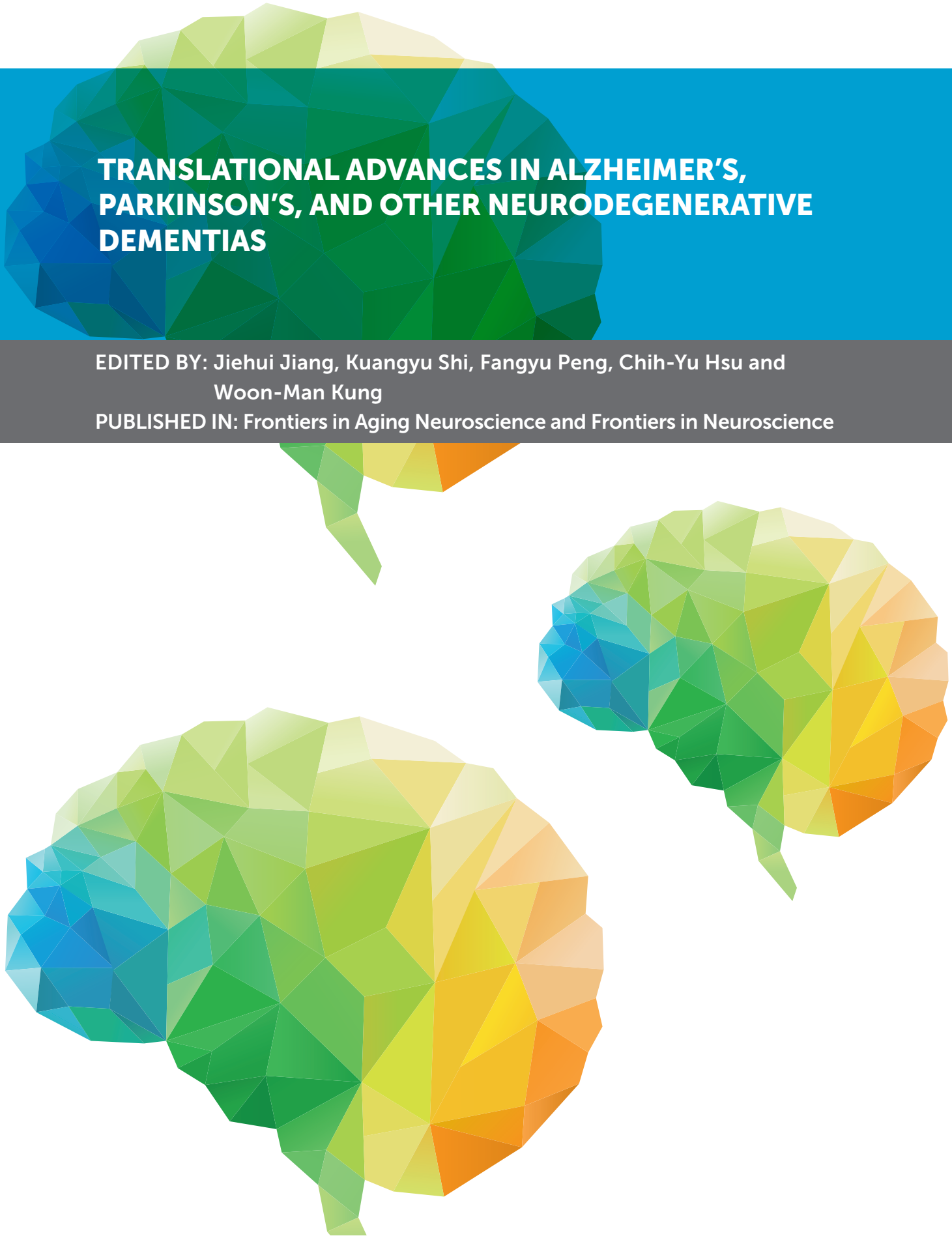

frontiers Research Topics

frontiers

ISSN 1664-8714
ISBN 978-2-88976-371-9
DOI 10.3389/978-2-88976-371-9

About Frontiers

Frontiers is more than just an open-access publisher of scholarly articles: it is a pioneering approach to the world of academia, radically improving the way scholarly research is managed. The grand vision of Frontiers is a world where all people have an equal opportunity to seek, share and generate knowledge. Frontiers provides immediate and permanent online open access to all its publications, but this alone is not enough to realize our grand goals.

Frontiers Journal Series

The Frontiers Journal Series is a multi-tier and interdisciplinary set of open-access, online journals, promising a paradigm shift from the current review, selection and dissemination processes in academic publishing. All Frontiers journals are driven by researchers for researchers; therefore, they constitute a service to the scholarly community. At the same time, the Frontiers Journal Series operates on a revolutionary invention, the tiered publishing system, initially addressing specific communities of scholars, and gradually climbing up to broader public understanding, thus serving the interests of the lay society, too.

Dedication to Quality

Each Frontiers article is a landmark of the highest quality, thanks to genuinely collaborative interactions between authors and review editors, who include some of the world's best academicians. Research must be certified by peers before entering a stream of knowledge that may eventually reach the public - and shape society; therefore, Frontiers only applies the most rigorous and unbiased reviews.
Frontiers revolutionizes research publishing by freely delivering the most outstanding research, evaluated with no bias from both the academic and social point of view. By applying the most advanced information technologies, Frontiers is catapulting scholarly publishing into a new generation.

What are Frontiers Research Topics?

Frontiers Research Topics are very popular trademarks of the Frontiers Journals Series: they are collections of at least ten articles, all centered on a particular subject. With their unique mix of varied contributions from Original Research to Review Articles, Frontiers Research Topics unify the most influential researchers, the latest key findings and historical advances in a hot research area! Find out more on how to host your own Frontiers Research Topic or contribute to one as an author by contacting the Frontiers Editorial Office: frontiersin.org/about/contact

TRANSLATIONAL ADVANCES IN ALZHEIMER'S, PARKINSON'S, AND OTHER NEURODEGENERATIVE DEMENTIAS

Topic Editors:
Jiehui Jiang, Shanghai University, China
Kuangyu Shi, University of Bern, Switzerland
Fangyu Peng, University of Texas Southwestern Medical Center, United States
Chih-Yu Hsu, Fujian University of Technology, China
Woon-Man Kung, Chinese Culture University, Taiwan

Citation: Jiang, J., Shi, K., Peng, F., Hsu, C.-Y., Kung, W.-M., eds. (2022). Translational Advances in Alzheimer's, Parkinson's, and Other Neurodegenerative Dementias. Lausanne: Frontiers Media SA. doi: 10.3389/978-2-88976-371-9

Table of Contents

frontiers in Aging Neuroscience

EDITORIAL
published: 17 March 2022
doi: 10.3389/fnagi.2022.858467

Editorial: Translational Advances in Alzheimer's, Parkinson's, and Other Neurodegenerative Dementias

Jiehui Jiang[1†], *Kuangyu Shi*[2,3†], *Fangyu Peng*[4†], *Chih-Yu Hsu*[5†] *and Woon-Man Kung*[6*†]

[1] School of Life Science, Institute of Biomedical Engineering, Shanghai University, Shanghai, China, [2] Department of Nuclear Medicine, Inselspital, Bern University Hospital, University of Bern, Bern, Switzerland, [3] Department of Informatics, Technical University of Munich, Munich, Germany, [4] Department of Radiology, The University of Texas Southwestern Medical Center, Dallas, TX, United States, [5] Fujian Provincial Key Laboratory of Big Data Mining and Applications, School of Computer Science and Mathematics, Fujian University of Technology, Fuzhou, China, [6] Division of Neurosurgery, Department of Surgery, Taipei Tzu Chi Hospital, Buddhist Tzu Chi Medical Foundation, New Taipei City, Taiwan

Keywords: Alzheimer's disease, Parkinson's disease, dementia, neurodegenerative disorders, big data mining, imaging methods, bioinformatic applications

OPEN ACCESS

Edited and reviewed by:
Allison B. Reiss,
New York University, United States

***Correspondence:**
Woon-Man Kung
nskungwm@yahoo.com.tw

†ORCID:
Jiehui Jiang
orcid.org/0000-0003-4948-3683
Kuangyu Shi
orcid.org/0000-0002-8714-3084
Fangyu Peng
orcid.org/0000-0002-3142-3845
Chih-Yu Hsu
orcid.org/0000-0003-1074-8170
Woon-Man Kung
orcid.org/0000-0001-8311-2902

Specialty section:
This article was submitted to Alzheimer's Disease and Related Dementias, a section of the journal Frontiers in Aging Neuroscience

Received: *20 January 2022*
Accepted: *07 February 2022*
Published: *17 March 2022*

Citation:
Jiang J, Shi K, Peng F, Hsu C-Y and Kung W-M (2022) Editorial: Translational Advances in Alzheimer's, Parkinson's, and Other Neurodegenerative Dementias. Front. Aging Neurosci. 14:858467. doi: 10.3389/fnagi.2022.858467

Editorial on the Research Topic

Editorial: Translational Advances in Alzheimer's, Parkinson's, and Other Neurodegenerative Dementias

The increase in number of people suffering from neurodegenerative dementia (ND), such as Alzheimer's disease (AD) and Parkinson's disease (PD), has placed a huge burden on society. Precise detection of ND in an early phase is still challenging in daily clinical practice (Tisher and Salardini, 2019). There is a continuous escalation in effort from more researchers to investigate molecular mechanism of ND pathophysiology and develop new biomarkers for diagnosis and treatment of ND, as reflected by significant numbers of articles contained in this Research Topic.

In addition to metabolic changes such as altered glucose metabolism, alterations of amyloid-beta and tau protein are biomarkers associated with pathology of AD, whereas alpha-synuclein is proven to be related to PD and other NDs (Congdon and Sigurdsson, 2018; Rocha et al., 2018; Butterfield and Halliwell, 2019; Pinheiro and Faustino, 2019). Molecular imaging techniques using radiotracers like 2-deoxy-2-[^{18}F]fluoroglucose (^{18}F-FDG), 4-[(E)-2-(6-{2-[2-(2-(^{18}F)fluoroethoxy)ethoxy]ethoxy}pyridin-3-yl)ethen-1-yl]-N-methylaniline (^{18}F-AV45), and 7-(6-(^{18}F)fluoropyridin-3-yl)-5H-pyrido[4,3-b]indole (^{18}F-AV1451) have been widely used in research and diagnostic imaging of ND. Development of bioinformatics analysis and artificial intelligence methods has significantly facilitated advances in research of ND. Nowadays, researchers are facing difficulties in choosing the best method in order to conduct research in a comprehensible fashion with estimates of accuracy and reproducibility.

Taking this into consideration, the present Research Topic on *"Translational Advances in Alzheimer's, Parkinson's, and Other Neurodegenerative Dementias"* by Frontiers in Aging Neuroscience made a contribution with updates and different perspectives on this important theme to contain over 69 papers. These updates focus on exploring reliable biomarkers and prediction indexes for the progression of ND from multidisciplinary perspectives. In addition, researches in development of novel therapies were also included.

Based on univariate and multivariate analyses, Wei et al. found that the apolipoprotein E (APOE) e4 allele might affect the relationship between serum lipid levels and cognitive impairment. In addition, Hu, Li, Zhao, et al. provided evidence that the combination of telmisartan and rosuvastatin might be an effective prevention and/or treatment strategy for cognitive impairment

and dementia, especially in hypertensive patients with the APOE e4 allele. Kuang et al. demonstrated that the e4 genotype leads to distinct default mode network (DMN) functional alterations in early phases of AD using persistent homology approach. Lin investigated whether CDGSH iron-sulfur domain 2 ($CISD_2$) gene attenuation had an influence on anti-inflammatory effects and M1-M2 polarization in microglia. This study promised a potential therapeutic target for ND.

For clinical diagnosis of AD, Jiao et al. focused on plasma biomarkers which are less expensive and invasive than those necessitating a spinal fluid sample. The results of their study showed that the multifactor model of plasma amyloid-beta 42 and total-tau in combination with Montreal Cognitive Assessment (MoCA) could be a viable model separate health and AD subjects in clinical practice. Gao et al. characterized the relationship between plasma amyloid-beta levels and cognitive decline in 1,240 cognitively normal participants. The relationship between plasma amyloid-beta 40 and cognitive decline was an inverted-U shape in a cognitively normal population. None of relationship between plasma amyloid-beta 42, amyloid-beta 42/40, and cognitive decline was found during a 2-year follow-up. Lin et al. enrolled cognitively normal amyloid-beta-positive participants from 2 cohort studies, all types of resilience to cerebrospinal fluid (CSF) amyloid-beta could predict longitudinal cognitive decline.

Identification of novel molecular biomarkers for diagnosis and treatment of AD is urgently demanded. Based on bioinformatics analysis, Yu et al. identified 16 hub genes correlated to the neuropathological stage and 35 potential biomarkers for the diagnosis of AD. Yuen et al. demonstrated a systematic workflow for evidence synthesis of transcriptomic studies using both meta-analysis and bioinformatics methods to identify potential pathogenic factors. The results showed that reduced amyloid-beta clearance in AD pathogenesis was associated with genes encoding Fyn and EGFR, which were key receptors in amyloid-beta downstream signaling. Robin et al. comprehensively profiled phenotypic features over time in one commercially-available induced Pluripotent Stem Cell (iPSC)-derived human neuron cell line. This study provided a tool to investigate neurodegenerative and other central nervous system (CNS) diseases. Deng et al. applied multivariate model to estimate the association between leukocyte telomere length (LTL) and cognitive performance. Their results suggested that LTL might be a biomarker of cognitive aging.

Kong et al. explored the links between diabetes and AD by studying the advanced glycation end products (AGEs) and the receptors for AGEs (RAGE). The results of their study suggested that patients with diabetes were at a higher risk of developing AD. They further reviewed the interaction between RAGE and amyloid-beta as well as tau, which highlighted the potential of RAGE to be used as an effective target for AD diagnosis and treatment. Ho et al. explored type 2 diabetes mellitus (T2DM) pathogenesis in the amyloidogenic evolvability. A better understanding of the role of T2DM in amyloidogenic evolvability might reveal new targets for therapeutic intervention in AD patients who are comorbid with T2DM.

Using magnetic resonance (MR) imaging, Li et al. found that T2DM could give rise to the white matter atrophy of several brain regions, including left posterior cingulate, precuneus, insula, and right rostral middle frontal gyrus. In addition, they investigated the white matter structural network disruption in T2DM patients with MCI. Chen et al. developed MR glucose chemical exchange saturation transfer (glucoCEST) imaging in a rat model of AD. The findings from their study showed that this method could explore the occurrence and progress of diabetes-related AD or dementia.

Based on live-cell imaging combined with behavioral tests, Feng et al. explored the role and underlying mechanism of calcium-sensing receptor (CaSR) in cognitive deficits in AD mice. Their study might provide novel insights on the potential of CaSR as a therapeutic target for AD. Wu et al. examined whether steroid receptor coactivator 1 (SRC-1) is involved in pathogenesis of AD. Tyagi et al. reviewed the role of cyclooxygenases (COX) and mammalian/mechanistic target of rapamycin (mTOR) and potential therapeutic approaches targeting COX-2 and mTOR in AD and cancer.

Bjorkli et al. reviewed the preclinical and clinical investigations of commonly used biomarkers in animal models of AD and AD patients respectively. They also provided recommendations for standardization of procedures in sample collection to enhance the translational validity of preclinical study using AD animal models.

TDP-43 is a protein related to amyotrophic lateral sclerosis (ALS) and many cases of tau-negative frontotemporal lobar degeneration. Zhang, Chen, et al. reviewed the researches about TDP-43 and its relationship with limbic-predominant age-related TDP-43 encephalopathy (LATE).

In an effort to develop neurodegenerative disease model at cellular level, Zhang, Xie, et al. reported prospects of 2 kinds of reprogramming technologies for neurodegenerative diseases: (1) convert adult somatic cells to iPSCs and (2) directly reprogramming adult somatic cells to induced Neurons (iN).

Jang et al. provided updates on current progress in stem cell-derived dopaminergic neuron transplantation as a therapeutic alternative for PD. Yang, Zhang, et al. aimed to uncover the metabolic pathways across anatomical regions in the brain of PD and levodopa-induced dyskinesia (LID). Based on principal component analysis (PCA) and multivariate general linear model, the midbrain and right cortex were identified as the primary regions of metabolic abnormalities in PD and LID rats. In addition, PD and LID rats exhibited lower levels of synaptophysin (SYP). All results provided key insights for developing targeted therapies in PD. Harsanyiova et al. discussed the relationship between gastrointestinal tract and the pathology or treatment of PD symptoms.

Bao et al. surveyed the various positron emission tomography (PET) radiotracers available for AD imaging and discussed their clinical applications especially in terms of early detection and cognitive relevance. Based on [^{18}F]-APN-1607 PET tracer, Lu et al. detected tau deposition in AD and reported that individual tauopathy is correlated with impaired cerebral glucose metabolism and cognitive function. Using combined PET and MR imaging, Kim et al. investigated the effect of conductive

hearing loss in an AD mouse model. The findings from their study indicated that even partial hearing loss could aggravate memory impairment in AD.

^{11}C-PE2I is a PET radiotracer targeting neuronal dopamine transporters (DaT). Ivanidze et al. investigated neurovascular unit (NVU) integrity by using arterial spin labeling (ASL) MR imaging and correlated the findings of NVU integrity with striatal DaT density from ^{11}C-PE2I PET imaging. This exploratory research could serve as a foundation for further development of combined NVU and striatal DaT density as early disease biomarkers and potential new therapeutic targets. Based on ^{11}C-CFT and ^{18}F-FDG PET imaging data, Fei et al. studied the relevancy between UPDRS motor scores and PDQ39 mobility sub-scores.

Based on partial volume-coil ^{31}P MR spectroscopy of parieto-occipital lobes with 7-Tesla MR imaging, Das et al. accurately quantified high-energy phosphate and membrane phospholipid metabolites in amnestic MCI (aMCI). Furthermore, they have also found that brain energy metabolism and membrane phospholipid indexes were related to cognitive performance in domains of executive function (EF), memory, attention, and visuospatial skills using aMCI.

Liu, Jiang, et al. explored functional and structural properties of abnormal brain networks associated with PD. The authors showed that both the expressions of metabolic and structural patterns in PD patients were significantly higher than healthy controls, and verified their results in connectome analysis, which provided new information for elucidating the neuropathological mechanisms of PD. Shu et al. developed an integrative nomogram based on white matter radiomics biomarkers and nonmotor symptoms for the identification of early-stage PD.

Tsai et al. explored the skull score (SS) distribution of tremor patients, and correlated the SS with image feature from customized skull density ratio (cSDR). This study provided useful information for clinical study of MR-guided focused ultrasound thalamotomy. Chiu, Tzeng, et al. found that the patients with tremor and vascular cognitive impairment (VCI) had high possibility of mixed pathology of PD and Lewy body disease (LBD).

Ye et al. investigated the volumetric changes in thalamus and hypothalamus in ALS. The results from their study revealed no significant difference of the volume in thalamus and hypothalamus between ALS patients of normal frontotemporal function and healthy controls.

Yu et al. identified the brain function activity differences between MCI patients with depression and MCI patients without depression using resting state MR imaging measurements. This study provided useful information for a better understanding of the relationship between depressive symptoms and memory deficits. Xing et al. explored the alterations in intra- and inter-network functional connectivity of multiple networks in presbycusis patients, suggesting that functional network connectivity can be used to predict potential cognitive impairment in their early stage.

Wan et al. compared the changes in subcortical nuclei in older adults with cognitive frailty (CF) and studied their relationship with cognitive decline and physical frailty. Their results showed significant volume reductions in five subcortical nuclei, including the bilateral thalami, left caudate, right pallidum, and accumbens area in older adults with CF. Lee et al. used surface-based analysis to evaluate subcortical structural characteristics and its relationship with early onset Alzheimer's disease (EOAD) and late-onset Alzheimer's disease (LOAD). The results from their study demonstrated that EOAD and LOAD might have different courses of pathomechanism.

Qiao et al. examined the neural substrates and mechanisms that generate memory deficits, seizures, and neuropsychiatric abnormalities in encephalitis with leucine-rich, glioma-inactivated 1 (LGI_1) antibodies. The results showed that neural disorder and behavioral deficits of anti-LGI_1 encephalitis might be associated with extensive changes in brain connectivity and microstructure.

Bruchhage et al. performed machine learning to assess the contribution of volume fraction myelin and gray matter volume. They proposed a refined model of cerebellar contribution to early AD development. The results from their study showed higher anterior cerebellar contribution to MCI and higher posterior cerebellar contribution to mild/moderate stages of AD for each tissue property. Ma et al. proposed a generative adversarial network (GAN) framework to distinguish brain images of human subjects of normal brain aging from those of human subjects with AD and frontotemporal dementia (FTD). The results from their study showed an accuracy of 88.28% in distinguishing human subjects of normal brain aging from those of human subjects with AD and FTD based on GAN framework derived from brain image.

Hu, Li, Zhang, et al. found that periodontitis was associated with learning and memory impairment, probably induced by neuroinflammation via activating the toll-like receptor 4/Nuclear factor kappa B signaling pathway. Ding et al. aimed to evaluate the value of odors in olfactory identification (OI) test and other known risk factors for predicting incident dementia. The results from their study suggested that peppermint smell capability might be one of the useful indicators for predicting dementia. Nie et al. assessed the differences of eye movement parameters between healthy elderly individuals and patients with MCI. They found that cognitive deficits and eye movement indexes were correlated, which could be further explored as early markers for MCI.

The paper by Yang, Huang, et al. proposed a neuroimaging approach to identify MCI using a deep learning method and functional near-infrared spectroscopy (fNIRS). Their results indicated that fNIRS imaging approach based on temporal feature maps as a promising diagnostic method for early detection of MCI and clinicians might use it as a tool for evaluation of MCI.

Tseng et al. used multivariate time-series electrocardiogram (ECG) analysis to diagnose cardiovascular diseases. They investigated various ECG features and found some associations between features of ECG and medical records (e.g. smokers, obesity, and hypertension).

Chiu, Hung, et al. studied the relationship between freezing of speech (FOS) and dementia with Lewy bodies (DLB). They

designed a freezing of speech single questionnaire (FOSSQ) and compared the association factors of FOS in non-demented participants, patients with AD, vascular dementia (VaD), and DLB. The results of their study supported validity of the FOSSQ for discriminating DLB from individuals with non-demented or other forms of dementia. Similarly, Wang, Hung, et al. designed a novel questionnaire for visuospatial dysfunction (VSD) in DLB.

To distinguish stable MCI (MCIs) from converting MCI (MCIc), Gupta et al. proposed different neuroimaging modalities combined with APOE genotype to form a multimodal system for discrimination of AD to increase the classification accuracy.

In order to determine whether a MCI patient is at high risk of progressing to AD, Lin et al. developed an extreme learning machine (ELM)-based grading method to predict MCI-to-AD conversion. The method was validated by Alzheimer's Disease Neuroimaging Initiative (ADNI) cohort, with an accuracy of 84.7% in prediction of MCI progression to AD within 3 years.

Wang, Wei, et al. conducted a systematic review and meta-analysis to assess the available preclinical evidence and possible mechanisms of baicalein for animal models of PD. Li et al. investigated the efficacy and safety of 3 Erinacine A-enriched Hericium erinaceus mycelia (EAHE) capsules for the treatment of patients with mild AD. The study lasted for 49 weeks and the results showed that EAHE was well-tolerated without significant side effects. Flavonoid containing natural products, Myricetin (MYR) and Dihydromyricetin (DMY) are abundant in fruits and vegetables. Liu, Guo, et al. reviewed the benefits of MYR and DMY in AD patients at molecular level, including effects on amyloid-beta protein imbalance, neuroinflammation, dyshomeostasis of metal ions, autophagy disorder, and oxidative stress.

The early intervention for MCI could decrease the rate of conversion from MCI to AD. Lai et al. compared and ranked 9 treatment methods for MCI in AD based on meta-analysis. They pointed out that music therapy might be the best treatment for MCI followed by acupuncture, among the nine treatment methods included for their meta-analysis. Similar to those non-pharmacological interventions, Pei et al. proposed a neurofeedback training based on mismatch negativity to regulate sensory ability and memory.

Stuckenschneider et al. investigated the effects of a 12-month structured exercise program on the progression of 183 amnestic MCI patients. No significant improvement of cognitive performance was found based on the results from their study. In another study based on event-related measurement of auditory memory, Laptinskaya et al. found no improvements of cognitive performance in a 10-week unimodal cognitive or physical training and an active lifestyle for older adults at risk for dementia. In the narrative review by Meng et al., patients with AD who presented with long-term exercise interventions appeared to have improved blood flow, increased hippocampal volume, and improved neurogenesis. These results indicated that exercise intervention might be an important moderator to prevent long term disease progression.

Kumar et al. reviewed and discussed nano-enabled drug delivery systems and their current and potential applications for the treatment of various NDs, including AD and PD, in studies to overcome the limits of blood-brain barrier (BBB). Huang et al. developed a medical red light treatment (RLT) device to treat older adults with mild to moderate AD. They planned a study protocol to verify the safety and efficacy for a 24 weeks period. On the other hand, Zhu et al. found that there was more efficacy via tele-health interventions in lowering depression for careers of dementia patients based on meta-analysis.

Deep brain stimulation (DBS) is widely used in the field of mental and neurological diseases. Luo et al. reviewed the therapeutic effect of DBS in AD, and analyzed its stimulation parameters and potential mechanism of action. Tan et al. used a convolutional neural network (CNN) to classify handwritten digits and letters and applied dropout at different stages to simulate DBS effects on engrams. The results of their study showed that dropout of engram nodes might be a possible mechanism by which neuromodulation techniques could disrupt or enhance memory. Hwang et al. pointed out the applications of phase amplitude coupling-based phase-dependent DBS technique in PD, which aimed to deliver timed stimulation pulses to a specific phase precisely to modulate pathological network activities and behavior in real time.

Tang et al. investigated the effect of electroacupuncture (EA) on cognitive impairment and the role of c-Jun N-terminal kinase (JNK) signaling pathway in AD model mice. The results of their study showed that EA could reverse cognitive deficits and substantially lower the burden of amyloid precursor protein. In another study, Hongna et al. demonstrated the improvements of locomotor function by promoting autophagy flux and inhibiting necroptosis in rats with spinal cord injury treated with Jia-Ji electro-acupuncture.

In summary, large number of articles collected in this Research Topic reflected recent advances in mechanistic study of pathophysiology of AD and PD, development of biomarkers and molecular imaging techniques for diagnosis and treatment of AD and PD. We hope that publications of this Research Topic will not only report recent advances in ND research, but also facilitate translation of new discovery to development of new diagnostic tests and therapeutic agents for early diagnosis and treatment of ND, including AD and PD.

AUTHOR CONTRIBUTIONS

JJ and KS wrote the draft. FP copyedited for the language. C-YH and W-MK reviewed and revised the manuscript. All authors listed have made a substantial, direct, and intellectual contribution to the work and approved it for publication.

REFERENCES

Butterfield, D. A., and Halliwell, B. (2019). Oxidative stress, dysfunctional glucose metabolism and Alzheimer disease. *Nat Rev Neurosci*. 20, 148–160. doi: 10.1038/s41583-019-0132-6

Congdon, E. E., and Sigurdsson, E. M. (2018). Tau-targeting therapies for Alzheimer disease. *Nat Rev Neurol*. 14, 399–415. doi: 10.1038/s41582-018-0013-z

Pinheiro, L., and Faustino, C. (2019). Therapeutic strategies targeting amyloid-beta in Alzheimer's disease. *Curr Alzheimer Res*. 16, 418–452. doi: 10.2174/1567205016666190321163438

Rocha, E. M., De Miranda, B., and Sanders, L. H. (2018). Alpha-synuclein: pathology, mitochondrial dysfunction and neuroinflammation in Parkinson's disease. *Neurobiol Dis*. 109, 249–257. doi: 10.1016/j.nbd.2017.04.004

Tisher, A., and Salardini, A. (2019). A comprehensive update on treatment of dementia. *Semin Neurol*. 39, 167–178. doi: 10.1055/s-0039-1683408

Conflict of Interest: The authors declare that the research was conducted in the absence of any commercial or financial relationships that could be construed as a potential conflict of interest.

frontiers in Neuroscience

ORIGINAL RESEARCH
published: 17 December 2019
doi: 10.3389/fnins.2019.01333

Depression Affects Intrinsic Brain Activity in Patients With Mild Cognitive Impairment

Yang Yu[1], Ziqi Li[2], Yajie Lin[1], Jie Yu[1], Guoping Peng[1], Kan Zhang[1], Xize Jia[3,4] and Benyan Luo[1]**

[1] Department of Neurology, First Affiliated Hospital, School of Medicine, Zhejiang University, Hangzhou, China, [2] School of Information and Electronics Technology, Jiamusi University, Jiamusi, China, [3] Center for Cognition and Brain Disorders, Institutes of Psychological Sciences, Hangzhou Normal University, Hangzhou, China, [4] Zhejiang Key Laboratory for Research in Assessment of Cognitive Impairments, Hangzhou, China

Numerous observational studies have shown that depressive symptoms are common in individuals with mild cognitive impairment (MCI) who have a higher rate of progress to dementia. However, it is still uncertain whether there are any differences between MCI patients with and without depression symptom in their brain function activities. Here we have identified the brain function activity differences in two groups of MCI patients (with depression or without depression) using the resting state MRI (rsfMRI) measurements. 76 right-handed MCI subjects have been recruited in this study, including 27 MCI patients with depression symptom (MCID), 49 MCI patients without depression symptom (MCIND). Analyses based on 7 rsfMRI measurements, including four static measurements (ALFF, fALFF, PerAF, and ReHo) and three dynamic measurements (dALFF, dfALFF, and dReHo) have been used to explore the temporal variability of intrinsic brain activity. No significant differences in ALFF and dALFF between the two group were found. In the MCID group, fALFF decreased in temporal gyrus, frontal gyrus, inferior occipital gyrus, middle frontal gyrus and cerebellum, but increased in cuneus, calcarine, lingual; while PerAF increased in left parahippocampus. The differences of ReHo in the two groups was only found in cerebellum. Compared to MCIND group, dfALFF in MCID decreased in cuneus, occipital gyrus and calcarine, while dReHo in MCID increased in bilateral temporal gyrus, frontal gyrus, superior parietal gyrus, inferior parietal gyrus and precuneus. Our results may provide a better understanding in the relationship between the depressive symptoms and memory deficits.

Keywords: Alzheimer's disease, aging, cognition, depression, brain function

OPEN ACCESS

Edited by:
Jiehui Jiang,
Shanghai University, China

Reviewed by:
Zaixu Cui,
University of Pennsylvania, United States
Drozdstoy Stoyanov Stoyanov, Plovdiv Medical University, Bulgaria

****Correspondence:***
Benyan Luo
luobenyan@zju.edu.cn
Xize Jia
jiaxize@foxmail.com

Specialty section:
This article was submitted to Neurodegeneration, a section of the journal Frontiers in Neuroscience

Received: *01 October 2019*
Accepted: *27 November 2019*
Published: *17 December 2019*

Citation:
Yu Y, Li Z, Lin Y, Yu J, Peng G, Zhang K, Jia X and Luo B (2019) Depression Affects Intrinsic Brain Activity in Patients With Mild Cognitive Impairment. Front. Neurosci. 13:1333. doi: 10.3389/fnins.2019.01333

INTRODUCTION

Mild cognitive impairment (MCI) is the clinical status of an individual with memory impairment who had memory defect but is otherwise functioning properly and does not meet clinical diagnosis criteria for dementia (Petersen et al., 1999, 2001). Cognitive deficits can be a single symptom, they also coexist with other non-cognitive features, of all the non-cognitive features, the prevalence of depression is the highest (Chi et al., 2015). Further, evidence suggests that MCI patients combined with depression symptoms (MCID) progress more rapidly from MCI to Alzheimer's disease (AD)

along the neurodegenerative spectrum, with a reported prevalence of 32% (Gao et al., 2013; Chi et al., 2015; Ismail et al., 2017). Thus, for early diagnosis and treatment purposes, an appropriate screening strategy to define the probable risk factors in those cognitive impaired individuals is meaningful (Ismail et al., 2017).

In recent years, based on the development of neuroimaging technology, magnetic resonance imaging, as a tool for detecting brain structure and function has been provided. Blood oxygenation level-dependent (BOLD) resting-state functional MRI (rsfMRI), has attracted enormous research interest in studying the neural mechanisms of cognitive dysfunction in individuals with psychiatric disorders (Biswal, 2012). Various rsfMRI measures such as functional connectivity (FC) (Biswal et al., 1995), amplitude of low-frequency fluctuation (ALFF) (Zang et al., 2007) fractional ALFF (fALFF) (Zou et al., 2008), percent amplitude of fluctuation (PerAF) (Jia et al., 2017, 2019) regional homogeneity (ReHo) (Zang et al., 2004) and degree centrality (DC) (Zuo et al., 2012) have been used to describe the intrinsic brain activity (IBA). IBA involves dynamic neural and metabolic activities, it is activity and plays a pivotal role in brain function (Dai and He, 2014; Raichle, 2015). These methods have been widely used to evaluate the IBA of neurological disorders or neuropsychiatric disorders, such as AD, depression, and MCI (Yao et al., 2009; Zhang et al., 2012; Guo et al., 2016; Wee et al., 2016; Li et al., 2017; Stoyanov et al., 2017; Zhang et al., 2017; Kandilarova et al., 2018; Yang et al., 2018; Liu et al., 2019). Furthermore, evidence indicated that once brain got an internal or external stimuli, it could respond by dynamic integration or adjustment over multiple time scales (Hutchison et al., 2013; Bassett and Sporns, 2017; Yan et al., 2017). However, the aforementioned measures are static, which ignoring the characteristics of dynamic changes of IBA over time, they assumed that during the entire rsfMRI scan, the BOLD signal is stationary (Liao et al., 2014, 2015). Compared with the static rsfMRI measures, the dynamic sliding window approaches are effective for capturing the dynamic characteristics of regional brain activity over different times which could be used to examine abnormal brain function (Yan et al., 2017; Tang et al., 2018). These evidence all indicated that rsfMRI is a proper approach to compare the differences between MCID and MCIND.

Studies have identified regions in MCI compared with the NC, with a decreased or increased ALFF/fALFF/ReHo (Han et al., 2011; Zhang et al., 2012; Dai and He, 2014; Li et al., 2017; Liu et al., 2018, 2019; Yang et al., 2018). Previous study found that changes from ALFF/fALFF measurements of IBA may be worthwhile to characterize the early and gradual changes in physiological alterations throughout AD progression (Yang et al., 2018). Moreover, in MCID group the FC density values were higher in the left MTG than those in the MCI without depression patients (MCIND) (Liu et al., 2018). Another study found that abnormal ALFF values in MCID group could serve as markers to effectively differentiate MCID from MCI patients (Li et al., 2017). As for ReHo, it can be used to classify the depression subtypes and MCI, also changes in ReHo could be a biomarker for the pathophysiology and therapeutic response of depression (Guo et al., 2013; Liu et al., 2019). Previously, by combining dynamic FC with static FC, some studies found that the diagnostic accuracy for MCI could be significantly improved (Wee et al., 2016; Zhang et al., 2017). So far, no study explored the dynamic characteristics of local brain activity indexes in MCID patients.

We employed 7 resting state measurements, including four static measurements (ALFF, fALFF, PerAF, and ReHo) and three dynamic measurements (dALFF, dfALFF, and dReHo) to investigate the temporal variability of voxel-wise brain activity. These combinations were designed to explore the variability of IBA and to enhance our understanding of brain function by recognizing specific pathophysiological features and further deepen our understanding of cognitive behavior. We assumed that MCID patients would exhibit abnormal spontaneous brain activity compared with those MCIND. These would enhance understanding of the relationship between depressive symptoms and memory deficits.

MATERIALS AND METHODS

Participants

The study was endorsed by the Research Ethics Review Board of the First Affiliated Hospital of Medical School of Zhejiang University (FAHZU). A total of 76 right-handed MCI subjects were recruited in the study, including 27 patients combined with depression symptoms (MCID), 49 MCI without depression patients (MCIND). All MCI patients were recruited at the clinic of the Department of Neurology, FAHZU. Diagnoses of MCI were made by experienced neurologists according to Petersen's criteria (Petersen, 2004). Depressive symptoms were identified by qualified psychiatrists according to the Diagnostic and Statistical Manual of Mental Disorders, fifth edition (DSM-V) and the Geriatric Depression Scale (GDS) (Yesavage et al., 1982; Chau et al., 2006) [we also recruited 50 right-handed normal controls, who were matched for age and gender from the local communities (**Supplementary Methods** in **Supplementary Material**)].

The diagnosis of MCID and MCIND both fulfilled the published MCI diagnostic criteria (Petersen, 2004). The inclusion criteria for the MCID group included an acute episode of mild depression with DSM-V for the diagnosis of depression symptom who were first suffered from MCI and the 30-item GDS was > 10 scores (Yesavage et al., 1982; Chau et al., 2006). The MCIND subjects were excluded if they had been diagnosed with major depression, recurrent depression, or other psychiatric disorders as described in DSM-V.

Imaging Data Acquisition

MRI data were obtained using a 3.0 Tesla GE Discovery MR750 scanner (HD, General Electric Healthcare, Waukesha, WI, United States). 3D T1-weighted structural images were acquired using the following parameters: 128 slices, TR of 8,100 ms, TE of 3.1 ms, slice thickness of 1 mm, FA of 8°, matrix size of 256×256, FOV of 256×256 mm^2. Functional images were acquired using the following parameters: 43 contiguous axial slices, repetition time (TR) of 2,000 ms, echo time (TE) of 30 ms, slice thickness of 3.2 mm, flip angle (FA) of 90°, matrix size of 64×64, field of view (FOV) of 200×200 mm^2, total scan time of 8'00". During the

rsfMRI scan, the patients were given no task but were instructed to simply rest with eyes closed.

rsfMRI Preprocessing

The rsfMRI data were processed using SPM12[1] and RESTplus (Jia et al., 2019)[2]. The first 10 time points were discarded as adaptation of the participant to the scanner noise. The data preprocessing steps included slice timing, realignment, and spatial normalization. First, an individual T1-weighted image was co-registered to the mean functional image and then the T1-weighted image was segmented into gray matter (GM), white matter (WM) signal, and cerebrospinal fluid (CSF) signal. The EPI images were spatially normalized to the Montreal Neurological Institute (MNI) space and voxel size was resampled to 3 mm × 3 mm × 3 mm using the normalization parameters estimated during segmentation. Smoothing was performed with a 6 mm full width - half maximum (FWHM) Gaussian kernel. After removing the linear trend, we regressed out of covariates, which consisted of Friston-24 head motion parameters (Friston et al., 1996; Yan et al., 2013), WM signal, and CSF signal. The time courses were filtered by a (0.01–0.08 Hz) band to reduce high-frequency noise and low-frequency drifts.

Static ALFF, Fractional ALFF (fALFF), Percent Amplitude of Fluctuation (PerAF) and Regional Homogeneity (ReHo) Calculation

We performed ALFF, fALFF, PerAF and ReHo analysis for each scan. The calculation of ALFF was based on fast Fourier transform (FFT). Using FFT, each time course was converted to the frequency domain. Then, the square root of the power spectrum at each frequency was averaged across the filtered band (0.01–0.08 Hz). The ALFF of each voxel was then normalized by the global mean of the ALFF values (mALFF) for standardization. For each given voxel, mALFF reflected the degree of its raw ALFF value relative to the average ALFF value of the whole brain (Zang et al., 2007). Then we calculated fALFF by obtaining the ratio of the power spectrum of low frequency (0.01–0.08 Hz) to that of the entire frequency range. Then, the resulting spatial fALFF maps were then divided with each voxel divided by the whole-brain fALFF mean (mfALFF), providing mfALFF spatial maps (Zou et al., 2008). PerAF designated the percentage amplitude of BOLD fluctuation relative to the mean BOLD signal intensity of a given time series (Jia et al., 2017) with RESTplus (Jia et al., 2019). PerAF is standardized at the single voxel level, the resulting spatial PerAF maps were then normalized with each voxel divided by the global mean PerAF (mPerAF). Both PerAF and mPerAF can be used for group-level statistical analysis, here we used mPerAF for further statistical analyses (Jia et al., 2019; Yu et al., 2019). For ReHo, the Kendall's coefficient of concordance (KCC) of the time course of every 27 nearest neighboring voxels was calculated (Zang et al., 2004). To reduce the influence of individual variations in the KCC value, ReHo map normalizations were performed by dividing the KCC among each voxel by the averaged KCC of the whole brain.

Dynamic ALFF, fALFF and ReHo Calculation

Dynamic parameters were performed using Temporal Dynamic Analysis (TDA) toolkits based on DPABI (Yan et al., 2016) Sliding window-based analysis, which is sensitive in detecting time-dependent variations, was applied to examine three dynamic measurements (dALFF, dfALFF or dReHo) variability over the whole brain (Hindriks et al., 2016; Liu et al., 2017; Yan et al., 2017; Yip et al., 2017; Tang et al., 2018; Vergara et al., 2019).

In the sliding window analysis, a temporal window of certain size and shape is chosen, and ALFF, fALFF and ReHo within that window are calculated. Theoretically, the window size should be designed feasibly. It should be small enough to monitor potentially transient signals, and yet large enough to describe the lowest frequencies of interest in the signals (Sakoglu et al., 2010). Previous studies of sliding window connectivity have applied a sliding window length from to 10 to 180 s (Thompson et al., 2013; Gonzalez-Castillo et al., 2015; Chen et al., 2018). Here we applied a sliding window length of 32 TR (64 s) and a shifting step size of two TR (4 s) (Chen et al., 2018). The remaining 230 time points after removing the first 10 time points for each individual were segmented into 100 windows in total. In each sliding window, ALFF, fALFF and ReHo were calculated. After calculating ALFF of all voxel in time windows, each participant will get several window-based ALFF maps (similar as fALFF and ReHo). Then, we computed the mean and standard deviation of each voxel in all window-based ALFF maps for each subject and further got the corresponding coefficient of variation (CV) which was acquired by dividing the standard deviation by the mean. To better measure the dynamic variation of regional brain activity between different individuals, we used CV as dALFF (similar as dfALFF), which represented the temporal variability of absolute energy consumption in low-frequency regional brain activity (Tang et al., 2018).

Statistical Analyses

Scales Analysis

To examine the between-group differences in the seven measurements, two-sample *t*-test was held between the MCID and MCIND groups using DPABI (Yan et al., 2016). The figure was drawn by both DPABI and BrainNet Viewer (Xia et al., 2013; Yan et al., 2016). To reduce the effect of confounding variables in the statistical analysis, we performed two-sample *t*-tests with the mean relative displacements of age, sex, and education as covariance. Multiple comparison correction was performed based on Gaussian random field theory (GRF, voxel-wise $p < 0.05$, cluster-wise $p < 0.05$, two-tailed).

Correlation Analysis

With the peak voxels of abnormal regions as spherical centers, spherical ROIs were constructed around these abnormal regions (with a 6 mm radius). To assess the relationship between the behavioral scores (include MMSE, MoCA and GDS scores) and

[1] http://www.fil.ion.ucl.ac.uk/spm

[2] http://www.restfmri.net/forum/

metrics in these abnormal regions, we used Partial correlation analysis that controlled for age, sex and education by SPSS software (version 20.0; IBM, Chicago, IL, United States). Statistical significance was defined as $p < 0.05$. To control for false positives from multiple comparisons, we used the false discovery rate (FDR) correction in which the *p*-values were multiplied by the number of comparisons.

RESULTS

Neuropsychological Results

Demographic and clinical characteristics of 76 patients with MCI, 49 MCIND (19 men; mean age, 65.88 ± 9.762 years) and 27 MCID (11 men; mean age, 63.44 ± 10.58 years) are listed in **Table 1**. No significant differences were found ($p > 0.05$) in gender, age, education level, and MMSE, MoCA scores between the MCID group and MCIND group. Detailed demographics and the psychological characteristics of the two groups are shown in **Table 1**.

Alterations of Region IBA Changes Between MCID and MCIND

The Comparison of ALFF

There were no significant differences in ALFF between the MCID group and MCIND group.

The Comparison of fALFF

As shown in the **Figure 1**, for fALFF, MCID decreased in inferior temporal gyrus (ITG), middle temporal gyrus (MTG), middle frontal gyrus, inferior occipital gyrus, and cerebellum, but increased in cuneus, calcarine, lingual. The significant differences in fALFF between the two groups are shown in **Table 2** and **Figure 1A**.

The Comparison of PerAF

We found that in MCID group, PerAF increased in left parahippocampus gyrus and temporal gyrus. The significant differences in PerAF between the MCID and MCIND group are shown in **Table 2** and **Figure 1B**.

TABLE 1 | Demographic and neuropsychological data.

	MCIND (*n* = 49)	MCID (*n* = 27)	*p*
Age (y, mean ± SD)	65.88 ± 9.762	63.44 ± 10.58	0.2766^{t}
Gender (M/F)	19/30	11/16	0.053^{χ}
Education (y, mean ± SD)	9.8 ± 3.563	9.444 ± 3.105	0.5412^{t}
MMSE (mean of all points ± SD)	25.43 ± 3.506	25.04 ± 4.052	0.6492^{t}
MoCA (mean of all points ± SD)	19.92 ± 3.416	19.78 ± 4.917	0.8166^{t}
GDS (mean of all points ± SD)	5.66 ± 2.847	15.44 ± 4.635	$<0.0001^{t}$

MCID, mild cognitive impairment with the symptom of depression; MCIND, non-depressed mild cognitive impairment; MMSE, Mini Mental State Examination; MoCA, Montreal Cognitive Assessment; GDS, Geriatric Depression Scale; SD, standard deviation. χ, the p-value was obtained by the chi-square test; t, The p-value was obtained by the two-sample t-test.

The Comparison of ReHo

Using ReHo, there were only a small amount of group differences between MCID and MCIND group in cerebellum. More details were shown in the **Table 2** and **Figure 1C**.

The Comparison of dALFF

There were no significant differences in dALFF between the MCID group and MCIND group.

The Comparison of dfALFF

As shown in the **Figure 1**, for dALFF, compared to MCIND group, MCID group showed decreased dALFF in the bilateral cuneus, middle occipital gyrus, right superior occipital gyrus and calcarine. The significant differences in dfALFF between the MCID group and MCIND group are shown in **Table 2** and **Figure 1D**.

The Comparison of dReHo

Using dReHo, compared to MCIND group, MCID group exhibited obvious increase in bilateral MTG, ITG, superior temporal gyrus (STG), superior parietal lobule, inferior parietal gyrus (IPG), precuneus, superior frontal gyrus (SFG), middle frontal gyrus (MFG), opercular part of inferior frontal gyrus (IFG) and right cerebellum. More details were shown in the **Table 2** and **Figure 1E**.

Correlational Analysis

There was no significant correlation between clinical behavioral scores and any rsfMRI metrics.

DISCUSSION

Most previous studies have focused on the depression-related or MCI-related brain functional changes. However, the brain function in MCI patients combined with depression is still uncertain. In the current study, we observed alterations in IBA during the resting state in 7 resting state parameters, including four static measurements and three dynamic characteristics in MCID and MCIND patients. We found several brain regions especially in frontal gyrus, temporal gyrus and parahippocampus gyrus, showed significant differences in fALFF, PerAF, ReHo, dfALFF and dReHo between the MCID and MCIND groups. These findings may develop a better understanding of the relationship between depressive symptoms and memory deficits.

As we supposed, the differences of abnormal spontaneous brain activity between MCID and MCIND patients could be distinguished by rsfMRI. We found significant differences between MCID and MCIND group in frontal gyrus [included superior frontal gyrus (SFG), middle frontal gyrus (MFG) and inferior frontal gyrus (IFG)], temporal gyrus (included MTG, ITG and STG), hippocampus, parahippocampus gyrus, IPG and cuneus. The robustness of the results was tested to prove the regions we found was stability and repeatability (**Supplementary Figures S2**, **S3**). In the studies pretend to explore the neural mechanism about MCI, AD or depression, these regions also have been mentioned (Langenecker et al., 2007;

TABLE 2 | Brain regions with significantly differences rsfMRI values in the MCID group compared with the MCIND group.

Measurements	Brain regions	MNI coordinates			Voxles	*T*-value
		x	y	z		
fALFF	Cerebellum Posterior Lobe	−15	−54	−57	339	−3.9226
	Middle Temporal Gyrus_L	−57	−57	0	241	−3.8508
	Precuneus_R	24	−48	3	459	4.3631
	Middle Frontal Gyrus_R	36	57	18	230	−3.6827
PerAF	Parahippocampus_L	−24	−30	−18	287	4.2358
ReHo	Left Cerebellum	−9	−60	−48	571	−4.2962
	Opercular part of inferior frontal gyrus_R	48	21	33	93	4.019
	Superior Frontal Gyrus_R	3	42	36	79	3.3601
	Inferior Parietal Lobule_R	42	−54	48	176	3.7523
dfALFF	Middle Occipital Gyrus, Cuneus, Calcarine, right Superior occipital gyrus	18	−81	21	218	−4.1399
dReHo	Left Cerebellum Posterior Lobe	−36	−63	−39	92	4.4288
	Middle Temporal Gyrus, Inferior Temporal Gyrus	−54	−45	−12	87	4.2681
	Medial Frontal Gyrus, Superior Frontal Gyrus	15	69	3	175	3.501
	Superior Temporal Gyrus, Middle Temporal Gyrus	63	−39	6	84	3.7049
	Middle Frontal Gyrus, opercular part of inferior frontal gyrus, Right Cerebrum	48	21	33	93	4.019
	Medial Frontal Gyrus, Superior Frontal Gyrus	3	42	36	79	3.3601
	Inferior Parietal Lobule, Superior Parietal Lobule, Precuneus	42	−54	48	176	3.7523
	Middle Temporal Gyrus_L	−57	−57	0	241	−3.8508
	Precuneus_R	24	−48	3	459	4.3631
	Middle Frontal Gyrus_R	36	57	18	230	−3.6827

Alexopoulos et al., 2008; Yao et al., 2009; Lee et al., 2012; Xie et al., 2012; Zhang et al., 2012; Rizio and Dennis, 2014; Guo et al., 2016; Stoyanov et al., 2017; Kandilarova et al., 2018; Yang et al., 2018; Kandilarova et al., 2019). These brain regions may be the proof of a possible shared pathophysiology in both depression and MCI (Yao et al., 2009; Zhang et al., 2012). Other studies found that depressive symptoms in AD had biochemical manifestations similar to depression, suggesting that they might share a common pathway at the biochemical level, this phenomenon may be same in those MCI (Langenecker et al., 2007; Alexopoulos et al., 2008; Lee et al., 2012; Xie et al., 2012; Taylor et al., 2013; Rizio and Dennis, 2014). In studies focused on brain structure found that depression may cause structural changes in frontal and temporal regions (Koolschijn et al., 2009; Kandilarova et al., 2019). These findings suggested that a circuit may be involved in the frontal cortex is associated with the functional neuroanatomy of depression (Langenecker et al., 2007; Yang et al., 2016).

Meanwhile, regions we found the IBA changes mostly related to default mode network (DMN) and executive control network (ECN). Executive functions are control mechanisms that adjust aspects of emotion and cognition, and disruption to these processes is related to worse clinical prognosis of depression (Morimoto et al., 2015). According to previous neuroimaging studies, the DMN s linked to self-referential thought, and the episodic memory retrieval and scene construction (Lei et al., 2013). It is supported by results from previous studies about late-life depression (LLD). LLD usually has a hyperactive DMN (increased rumination, defected cognition) and a hypoactive ECN (low cognitive control associated with emotional response), which may reflect clinical features of depressive symptoms (Aizenstein et al., 2014; Karim et al., 2017).

Above all the parameters we estimated, we didn't find significant differences in ALFF or dALFF. It has been pointed out that the ALFF could be influenced by the physiological noise irrelevant to brain activity, and dALFF has a temporal variability related to specific topographic (Zou et al., 2008; Liao et al., 2019). As for fALFF, it could effectively suppress the physiological noise, but is not as stable as ALFF in gray matter regions (Zou et al., 2008; Zuo et al., 2010). We firstly used PerAF to estimate IBA of MCID patients, in parahippocampus, MCID had an increased PerAF. Previous study by using both ALFF and PerAF found that the ALFF was similar to PerAF, but PerAF was better than ALFF in inter-scanner reliability (Zhao et al., 2018). Although it is still unclear what causes the difference between those parameters and the potential physiological significance might be, with the limitation of each parameters, it is still necessary to take into consideration all these metrics (Zuo et al., 2010). We found ReHo only decreased in cerebellum, while another study found that MCID patients showed significantly higher coherence ReHo (cReHo) than MCIND patients in the left Heschl's gyrus and thalamus, lower cReHo in the left postcentral gyrus (Liu et al., 2019). These differences may be influenced by different calculation of ReHo. Also, the recruit criteria of MCID group could be another factor. Depression is a highly heterogeneous disease, and there are no clear gold biomarkers for diagnosis (Ismail et al., 2017). In addition, the diagnose of depression syndrome is based on clinical symptoms and a rating scale, which is inevitably subjective. Further, evidence suggests that evaluating depressive symptoms comprehensively

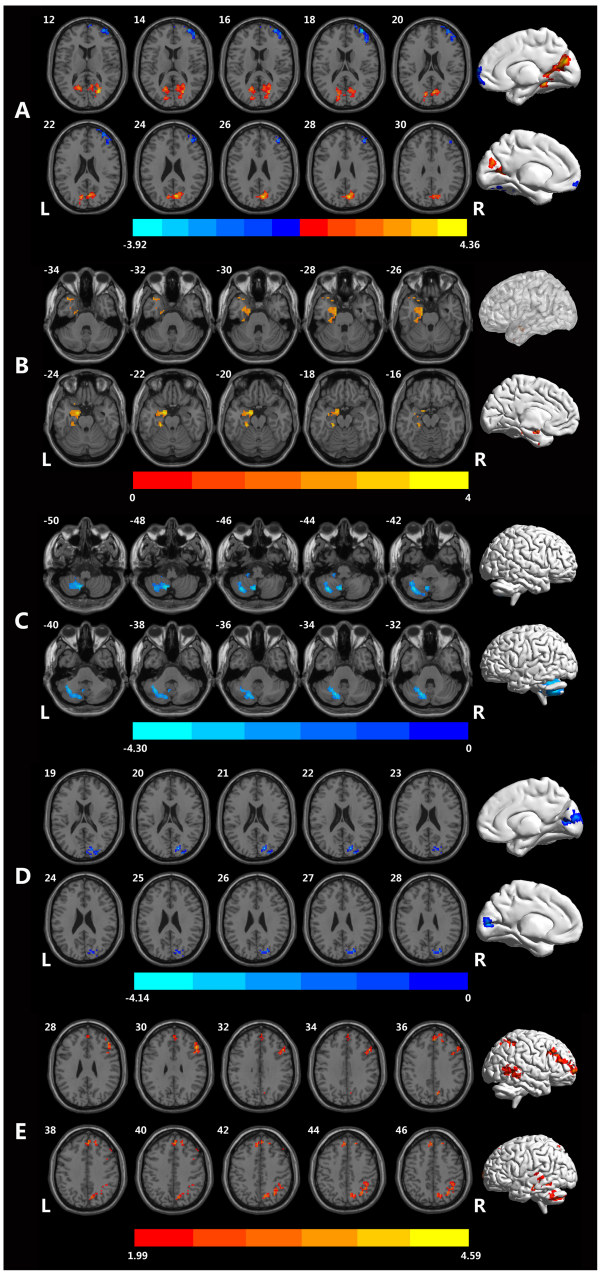

FIGURE 1 | Brain regions showing different rsfMRI values between the MCID and MCIND groups. **(A)** Brain regions with significant differences in fALFF between the MCID group and MCIND group. **(B)** Brain regions with significant differences in PerAF between the MCID group and MCIND group. **(C)** Brain regions with significant differences in ReHo between the MCID group and MCIND. **(D)** Brain regions with significant differences in dfALFF between the MCID group and MCIND group. **(E)** Brain regions with significant differences in dReHo between the MCID group and MCIND group (after GRF correction; voxel-wise $p < 0.05$, cluster-wise $p < 0.05$, two-tailed). The color bar indicates the *T*-value.

and accurately in those with neurocognitive disorders is difficult because of atypical symptoms in elders, and the interaction between depression and cognitive impairment in older adults makes it further complicated (Ting et al., 2010; Ismail et al., 2017). In our study, we selected the GDS to evaluate depressive symptoms in MCI, while other studies have used different scales, such as HAMD and the NPI (Liu et al., 2019).

Interestingly, we found that the results of dynamic measures differ from the static measures, this had also been found in other studies of diseases (Sourty et al., 2016; Cordova-Palomera et al., 2017). We found that fALFF in MCID decreased in temporal gyrus (ITG, MTG), MFG and inferior occipital gyrus, but increased in cuneus, calcarine, lingual, while in d fALFF, we found an increase in the cuneus, middle occipital gyrus. Also, the ReHo doesn't change in line with dReHo. As for dReHo, compared to MCIND group, MCID group exhibited an obvious increase in temporal gyrus (MTG, ITG, STG), frontal gyrus (MFG, SFG, IFG) and right cerebellum. However, using ReHo, we only found differences in cerebellum. Sourty et al. (2016) implied that some brain function alterations in Lewy body dementia can be detected utilizing dynamic FC but not static FC by sliding-window analysis (Sourty et al., 2016). The concept of dynamic neuroimage characteristics may provide a proper way to summarize changes in spatial patterns over time and to track differences in disease (Calhoun et al., 2014).

This study had several potential limitations. Firstly, this is a cross-sectional study, we did not investigate the conversion of MCID/MCIND to AD. These two sub-types of MCI patients may have different disease progress into AD. We will focus on not only the different clinical symptoms and their different brain areas, but also the potential different follow up consequences for MCID and MCIND patients. Secondly, it remains unclear that the mechanism of the differences and abnormalities in the patients of MCID and MCIND. In further studies, we would like to combine the rsfMRI, structural MRI and other biophysical data simultaneously with a larger sample and would reveal structural and biological substrates underlying these functional deficits in MCI and MCID patients.

CONCLUSION

In summary, we have investigated the IBA of MCID and MCIND using rsfMRI technique. We have found some obvious difference in the IBA between MCID and MCIND in the regions such as frontal gyrus (included SFG, MFG and IFG), temporal gyrus (included MTG, ITG and STG), parietal gyrus (superior parietal gyrus, IPG), occipital gyrus, parahippocampus gyrus and cuneus. The rsfMRI study suggests that the abnormal IBA pattern of the whole-brain functional activity may serve as an early biomarker for the detection of cognitive deficits and emotional problems in MCI patients.

AUTHOR CONTRIBUTIONS

YY analyzed the data and wrote the manuscript. ZL analyzed the data. YL, JY, GP, and KZ evaluated

the subjects and collected the data. XJ and BL designed the experiment and monitored the quality of the experiment.

FUNDING

This study was funded by grants from the Science and Technology Program of Zhejiang Province (2017C03011), the National Key Research and Development Program of China (2016YFC1306402).

SUPPLEMENTARY MATERIAL

The Supplementary Material for this article can be found online at: https://www.frontiersin.org/articles/10.3389/fnins.2019.01333/full#supplementary-material

REFERENCES

Aizenstein, H. J., Khalaf, A., Walker, S. E., and Andreescu, C. (2014). Magnetic resonance imaging predictors of treatment response in late-life depression. *J. Geriatr. Psychiatry Neurol.* 27, 24–32. doi: 10.1177/0891988713516541

Alexopoulos, G. S., Gunning-Dixon, F. M., Latoussakis, V., Kanellopoulos, D., and Murphy, C. F. (2008). Anterior cingulate dysfunction in geriatric depression. *Int. J. Geriatr. Psychiatry* 23, 347–355. doi: 10.1002/gps.1939

Bassett, D. S., and Sporns, O. (2017). Network neuroscience. *Nat. Neurosci.* 20, 353–364. doi: 10.1038/nn.4502

Biswal, B., Yetkin, F. Z., Haughton, V. M., and Hyde, J. S. (1995). Functional connectivity in the motor cortex of resting human brain using echo-planar MRI. *Magn. Reson. Med.* 34, 537–541. doi: 10.1002/mrm.1910340409

Biswal, B. B. (2012). Resting state fMRI: a personal history. *Neuroimage* 62, 938–944. doi: 10.1016/j.neuroimage.2012.01.090

Calhoun, V. D., Miller, R., Pearlson, G., and Adali, T. (2014). The chronnectome: time-varying connectivity networks as the next frontier in fMRI data discovery. *Neuron* 84, 262–274. doi: 10.1016/j.neuron.2014.10.015

Chau, J., Martin, C. R., Thompson, D. R., Chang, A. M., and Woo, J. (2006). Factor structure of the Chinese version of the geriatric depression scale. *Psychol. Health Med.* 11, 48–59. doi: 10.1080/13548500500093688

Chen, J., Sun, D., Shi, Y., Jin, W., Wang, Y., Xi, Q., et al. (2018). Dynamic alterations in spontaneous neural activity in multiple brain networks in subacute stroke patients: a resting-state fMRI study. *Front. Neurosci.* 12:994. doi: 10.3389/fnins.2018.00994

Chi, S., Wang, C., Jiang, T., Zhu, X.-C., Yu, J.-T., and Tan, L. (2015). The prevalence of depression in Alzheimer’s disease: a systematic review and meta-analysis. *Curr. Alzheimer Res.* 12, 189–198. doi: 10.2174/1567205012666150204124310

Cordova-Palomera, A., Kaufmann, T., Persson, K., Alnaes, D., Doan, N. T., Moberget, T., et al. (2017). Disrupted global metastability and static and dynamic brain connectivity across individuals in the Alzheimer's disease continuum. *Sci. Rep.* 7:40268. doi: 10.1038/srep40268

Dai, Z., and He, Y. (2014). Disrupted structural and functional brain connectomes in mild cognitive impairment and Alzheimer's disease. *Neurosci. Bull.* 30, 217–232. doi: 10.1007/s12264-013-1421-1420

Esterman, M., Tamber-Rosenau, B. J., Chiu, Y. C., and Yantis, S. (2010). Avoiding non-independence in fMRI data analysis: leave one subject out. *Neuroimage* 50, 572–576. doi: 10.1016/j.neuroimage.2009.10.092

Friston, K. J., Williams, S., Howard, R., Frackowiak, R. S., and Turner, R. (1996). Movement-related effects in fMRI time-series. *Magn. Reson. Med.* 35, 346–355. doi: 10.1002/mrm.1910350312

Gao, Y., Huang, C., Zhao, K., Ma, L., Qiu, X., Zhang, L., et al. (2013). Depression as a risk factor for dementia and mild cognitive impairment: a meta-analysis of longitudinal studies. *Int. J. Geriatr. Psychiatry* 28, 441–449. doi: 10.1002/gps.3845

Gonzalez-Castillo, J., Hoy, C. W., Handwerker, D. A., Robinson, M. E., Buchanan, L. C., Saad, Z. S., et al. (2015). Tracking ongoing cognition in individuals using brief, whole-brain functional connectivity patterns. *Proc. Natl. Acad. Sci. U.S.A.* 112, 8762–8767. doi: 10.1073/pnas.1501242112

Guo, W., Liu, F., Liu, J., Yu, L., Zhang, Z., Zhang, J., et al. (2013). Is there a cerebellar compensatory effort in first-episode, treatment-naive major depressive disorder at rest? *Prog. Neuropsychopharmacol. Biol. Psychiatry* 46, 13–18. doi: 10.1016/j.pnpbp.2013.06.009

Guo, Z., Liu, X., Hou, H., Wei, F., Liu, J., and Chen, X. (2016). Abnormal degree centrality in Alzheimer's disease patients with depression: a resting-state functional magnetic resonance imaging study. *Exp. Gerontol.* 79, 61–66. doi: 10.1016/j.exger.2016.03.017

Han, Y., Wang, J., Zhao, Z., Min, B., Lu, J., Li, K., et al. (2011). Frequency-dependent changes in the amplitude of low-frequency fluctuations in amnestic mild cognitive impairment: a resting-state fMRI study. *Neuroimage* 55, 287–295. doi: 10.1016/j.neuroimage.2010.11.059

Hindriks, R., Adhikari, M. H., Murayama, Y., Ganzetti, M., Mantini, D., Logothetis, N. K., et al. (2016). Corrigendum to "Can sliding-window correlations reveal dynamic functional connectivity in resting-state fMRI?" [NeuroImage 127 (2016) 242-256]. *Neuroimage* 132:115. doi: 10.1016/j.neuroimage.2016.02.007

Hutchison, R. M., Womelsdorf, T., Allen, E. A., Bandettini, P. A., Calhoun, V. D., Corbetta, M., et al. (2013). Dynamic functional connectivity: promise, issues, and interpretations. *Neuroimage* 80, 360–378. doi: 10.1016/j.neuroimage.2013.05.079

Ismail, Z., Elbayoumi, H., Fischer, C. E., Hogan, D. B., Millikin, C. P., Schweizer, T., et al. (2017). Prevalence of depression in patients with mild cognitive impairment: a systematic review and meta-analysis. *JAMA Psychiatry* 74, 58–67. doi: 10.1001/jamapsychiatry.2016.3162

Jia, X.-Z., Ji, G.-J., Liao, W., Lv, Y.-T., Wang, J., Wang, Z., et al. (2017). Percent amplitude of fluctuation: a simple measure for resting-state fMRI signal at single voxel level. *bioRxiv* [Preprint]. doi: 10.1101/214098

Jia, X.-Z., Wang, J., Sun, H.-Y., Zhang, H., Liao, W., Wang, Z., et al. (2019). RESTplus: an improved toolkit for resting-state functional magnetic resonance imaging data processing. *Sci. Bull.* 64, 953–954. doi: 10.1016/j.scib.2019.05.008

Kandilarova, S., Stoyanov, D., Kostianev, S., and Specht, K. (2018). Altered resting state effective connectivity of anterior insula in depression. *Front. Psychiatry* 9:83. doi: 10.3389/fpsyt.2018.00083

Kandilarova, S., Stoyanov, D., Sirakov, N., Maes, M., and Specht, K. (2019). Reduced grey matter volume in frontal and temporal areas in depression: contributions from voxel-based morphometry study. *Acta Neuropsychiatr.* 31, 252–257. doi: 10.1017/neu.2019.20

Karim, H. T., Andreescu, C., Tudorascu, D., Smagula, S. F., Butters, M. A., Karp, J. F., et al. (2017). Intrinsic functional connectivity in late-life depression: trajectories over the course of pharmacotherapy in remitters and non-remitters. *Mol. Psychiatry* 22, 450–457. doi: 10.1038/mp.2016.55

Koolschijn, P. C., van Haren, N. E., Lensvelt-Mulders, G. J., Hulshoff Pol, H. E., and Kahn, R. S. (2009). Brain volume abnormalities in major depressive disorder: a meta-analysis of magnetic resonance imaging studies. *Hum. Brain Mapp.* 30, 3719–3735. doi: 10.1002/hbm.20801

Langenecker, S. A., Kennedy, S. E., Guidotti, L. M., Briceno, E. M., Own, L. S., Hooven, T., et al. (2007). Frontal and limbic activation during inhibitory control predicts treatment response in major depressive disorder. *Biol. Psychiatry* 62, 1272–1280. doi: 10.1016/j.biopsych.2007.02.019

Lee, G. J., Lu, P. H., Hua, X., Lee, S., Wu, S., Nguyen, K., et al. (2012). Depressive symptoms in mild cognitive impairment predict greater atrophy in Alzheimer's disease-related regions. *Biol. Psychiatry* 71, 814–821. doi: 10.1016/j.biopsych.2011.12.024

Lei, X., Zhao, Z., and Chen, H. (2013). Extraversion is encoded by scale-free dynamics of default mode network. *Neuroimage* 74, 52–57. doi: 10.1016/j.neuroimage.2013.02.020

Li, H. J., Xu, Y., Zhang, K. R., Hoptman, M. J., and Zuo, X. N. (2015). Homotopic connectivity in drug-naive, first-episode, early-onset schizophrenia. *J. Child Psychol. Psychiatry* 56, 432–443. doi: 10.1111/jcpp.12307

Li, R., Li, Y., An, D., Gong, Q., Zhou, D., and Chen, H. (2015). Altered regional activity and inter-regional functional connectivity in psychogenic non-epileptic seizures. *Sci. Rep.* 5:11635. doi: 10.1038/srep11635

Li, Y., Jing, B., Liu, H., Li, Y., Gao, X., Li, Y., et al. (2017). Frequency-dependent changes in the amplitude of low-frequency fluctuations in mild cognitive impairment with mild depression. *J. Alzheimers Dis.* 58, 1175–1187. doi: 10.3233/JAD-161282

Liao, W., Chen, H., Li, J., Ji, G. J., Wu, G. R., Long, Z., et al. (2019). Endless fluctuations: temporal dynamics of the amplitude of low frequency fluctuations. *IEEE Trans. Med. Imaging* 38, 2523–2532. doi: 10.1109/TMI.2019.2904555

Liao, W., Wu, G. R., Xu, Q., Ji, G. J., Zhang, Z., Zang, Y. F., et al. (2014). DynamicBC: a MATLAB toolbox for dynamic brain connectome analysis. *Brain Connect.* 4, 780–790. doi: 10.1089/brain.2014.0253

Liao, X., Yuan, L., Zhao, T., Dai, Z., Shu, N., Xia, M., et al. (2015). Spontaneous functional network dynamics and associated structural substrates in the human brain. *Front. Hum. Neurosci.* 9:478. doi: 10.3389/fnhum.2015.00478

Liu, F., Wang, Y., Li, M., Wang, W., Li, R., Zhang, Z., et al. (2017). Dynamic functional network connectivity in idiopathic generalized epilepsy with generalized tonic-clonic seizure. *Hum. Brain Mapp.* 38, 957–973. doi: 10.1002/hbm.23430

Liu, X., Chen, J., Shen, B., Wang, G., Li, J., Hou, H., et al. (2018). Altered intrinsic coupling between functional connectivity density and amplitude of low-frequency fluctuation in mild cognitive impairment with depressive symptoms. *Neural Plast.* 2018:1672708. doi: 10.1155/2018/1672708

Liu, X., Tu, Y., Zang, Y., Wu, A., Guo, Z., and He, J. (2019). Disrupted regional spontaneous neural activity in mild cognitive impairment patients with depressive symptoms: a resting-state fMRI study. *Neural Plast.* 2019:2981764. doi: 10.1155/2019/2981764

Morimoto, S. S., Kanellopoulos, D., Manning, K. J., and Alexopoulos, G. S. (2015). Diagnosis and treatment of depression and cognitive impairment in late life. *Ann. N. Y. Acad. Sci.* 1345, 36–46. doi: 10.1111/nyas.12669

Petersen, R. C. (2004). Mild cognitive impairment as a diagnostic entity. *J. Intern. Med.* 256, 183–194. doi: 10.1111/j.1365-2796.2004.01388.x

Petersen, R. C., Smith, G. E., Waring, S. C., Ivnik, R. J., Tangalos, E. G., and Kokmen, E. (1999). Mild cognitive impairment: clinical characterization and outcome. *Arch. Neurol.* 56, 303–308. doi: 10.1001/archneur.56.3.303

Petersen, R. C., Stevens, J. C., Ganguli, M., Tangalos, E. G., Cummings, J. L., and DeKosky, S. T. (2001). Practice parameter: early detection of dementia: mild cognitive impairment (an evidence-based review). report of the quality standards subcommittee of the american academy of neurology. *Neurology* 56, 1133–1142. doi: 10.1212/wnl.56.9.1133

Raichle, M. E. (2015). The restless brain: how intrinsic activity organizes brain function. *Philos. Trans. R. Soc. Lond. B Biol. Sci.* 370:1668. doi: 10.1098/rstb.2014.0172

Rizio, A. A., and Dennis, N. A. (2014). The cognitive control of memory: age differences in the neural correlates of successful remembering and intentional forgetting. *PLoS One* 9:e87010. doi: 10.1371/journal.pone.0087010

Sakoglu, U., Pearlson, G. D., Kiehl, K. A., Wang, Y. M., Michael, A. M., and Calhoun, V. D. (2010). A method for evaluating dynamic functional network connectivity and task-modulation: application to schizophrenia. *MAGMA* 23, 351–366. doi: 10.1007/s10334-010-0197-198

Sourty, M., Thoraval, L., Roquet, D., Armspach, J. P., Foucher, J., and Blanc, F. (2016). Identifying dynamic functional connectivity changes in dementia with lewy bodies based on product hidden markov models. *Front. Comput. Neurosci.* 10:60. doi: 10.3389/fncom.2016.00060

Stoyanov, D., Kandilarova, S., and Borgwardt, S. (2017). Translational functional neuroimaging in the explanation of depression. *Balkan Med. J.* 34, 493–503. doi: 10.4274/balkanmedj.2017.1160

Tang, C., Wei, Y., Zhao, J., and Nie, J. (2018). "The dynamic measurements of regional brain activity for resting-state fMRI: d-ALFF, d-fALFF and d-ReHo," in *Proceedings of the International Conference on Medical Image Computing and Computer-Assisted Intervention*. MICCAI: Shenzhen.

Taylor, W. D., Aizenstein, H. J., and Alexopoulos, G. S. (2013). The vascular depression hypothesis: mechanisms linking vascular disease with depression. *Mol. Psychiatry* 18, 963–974. doi: 10.1038/mp.2013.20

Thompson, G. J., Magnuson, M. E., Merritt, M. D., Schwarb, H., Pan, W. J., McKinley, A., et al. (2013). Short-time windows of correlation between large-scale functional brain networks predict vigilance intraindividually and interindividually. *Hum. Brain Mapp.* 34, 3280–3298. doi: 10.1002/hbm.22140

Ting, C., Rajji, T. K., Ismail, Z., Tang-Wai, D. F., Apanasiewicz, N., Miranda, D., et al. (2010). Differentiating the cognitive profile of schizophrenia from that of Alzheimer disease and depression in late life. *PLoS One* 5:e10151. doi: 10.1371/journal.pone.0010151

Vergara, V. M., Abrol, A., and Calhoun, V. D. (2019). An average sliding window correlation method for dynamic functional connectivity. *Hum. Brain Mapp.* 40, 2089–2103. doi: 10.1002/hbm.24509

Wee, C. Y., Yang, S., Yap, P. T., Shen, D., and Alzheimer's Disease Neuroimaging Initiative (2016). Sparse temporally dynamic resting-state functional connectivity networks for early MCI identification. *Brain Imaging Behav.* 10, 342–356. doi: 10.1007/s11682-015-9408-2

Xia, M., Wang, J., and He, Y. (2013). BrainNet Viewer: a network visualization tool for human brain connectomics. *PLoS One* 8:e68910. doi: 10.1371/journal.pone.0068910

Xie, C., Li, W., Chen, G., Douglas Ward, B., Franczak, M. B., Jones, J. L., et al. (2012). The co-existence of geriatric depression and amnestic mild cognitive impairment detrimentally affect gray matter volumes: voxel-based morphometry study. *Behav. Brain Res.* 235, 244–250. doi: 10.1016/j.bbr.2012.08.007

Yan, C. G., Cheung, B., Kelly, C., Colcombe, S., Craddock, R. C., Di Martino, A., et al. (2013). A comprehensive assessment of regional variation in the impact of head micromovements on functional connectomics. *Neuroimage* 76, 183–201. doi: 10.1016/j.neuroimage.2013.03.004

Yan, C. G., Wang, X. D., Zuo, X. N., and Zang, Y. F. (2016). DPABI: data processing & analysis for (resting-state) brain imaging. *Neuroinformatics* 14, 339–351. doi: 10.1007/s12021-016-9299-9294

Yan, C.-G., Yang, Z., Colcombe, S. J., Zuo, X.-N., and Milham, M. P. (2017). Concordance among indices of intrinsic brain function: insights from inter-individual variation and temporal dynamics. *Sci. Bull.* 62, 1572–1584. doi: 10.1016/j.scib.2017.09.015

Yang, L., Yan, Y., Wang, Y., Hu, X., Lu, J., Chan, P., et al. (2018). Gradual disturbances of the amplitude of low-frequency fluctuations (ALFF) and fractional ALFF in Alzheimer spectrum. *Front. Neurosci.* 12:975. doi: 10.3389/fnins.2018.00975

Yang, W., Chen, Q., Liu, P., Cheng, H., Cui, Q., Wei, D., et al. (2016). Abnormal brain activation during directed forgetting of negative memory in depressed patients. *J. Affect. Disord.* 190, 880–888. doi: 10.1016/j.jad.2015.05.034

Yao, Z., Wang, L., Lu, Q., Liu, H., and Teng, G. (2009). Regional homogeneity in depression and its relationship with separate depressive symptom clusters: a resting-state fMRI study. *J. Affect. Disord.* 115, 430–438. doi: 10.1016/j.jad.2008.10.013

Yesavage, J. A., Brink, T. L., Rose, T. L., Lum, O., Huang, V., Adey, M., et al. (1982). Development and validation of a geriatric depression screening scale: a preliminary report. *J. Psychiatr. Res.* 17, 37–49. doi: 10.1016/0022-3956(82)90033-4

Yip, E., Yun, J., Wachowicz, K., Gabos, Z., Rathee, S., and Fallone, B. G. (2017). Sliding window prior data assisted compressed sensing for MRI tracking of lung tumors. *Med. Phys.* 44, 84–98. doi: 10.1002/mp.12027

Yu, Y., Chen, L., Wang, Q., Hu, L., Ding, Q., Jia, X., et al. (2019). Altered amplitude of low-frequency fluctuations in inactive patients with nonneuropsychiatric systemic lupus erythematosus. *Neural Plast.* 2019, 1–10. doi: 10.1155/2019/9408612

Zang, Y., Jiang, T., Lu, Y., He, Y., and Tian, L. (2004). Regional homogeneity approach to fMRI data analysis. *Neuroimage* 22, 394–400. doi: 10.1016/j.neuroimage.2003.12.030

Zang, Y. F., He, Y., Zhu, C. Z., Cao, Q. J., Sui, M. Q., Liang, M., et al. (2007). Altered baseline brain activity in children with ADHD revealed by resting-state functional MRI. *Brain Dev.* 29, 83–91. doi: 10.1016/j.braindev.2006.07.002

Zhang, Y., Zhang, H., Chen, X., Lee, S. W., and Shen, D. (2017). Hybrid high-order functional connectivity networks using resting-state functional MRI for mild cognitive impairment diagnosis. *Sci. Rep.* 7:6530. doi: 10.1038/s41598-017-06509-6500

Zhang, Z., Liu, Y., Jiang, T., Zhou, B., An, N., Dai, H., et al. (2012). Altered spontaneous activity in Alzheimer's disease and mild cognitive impairment revealed by Regional Homogeneity. *Neuroimage* 59, 1429–1440. doi: 10.1016/j.neuroimage.2011.08.049

Zhao, N., Yuan, L. X., Jia, X. Z., Zhou, X. F., Deng, X. P., He, H. J., et al. (2018). Intra- and inter-scanner reliability of voxel-wise whole-brain analytic metrics for resting state fMRI. *Front. Neuroinform.* 12:54. doi: 10.3389/fninf.2018.00054

Zou, Q. H., Zhu, C. Z., Yang, Y., Zuo, X. N., Long, X. Y., Cao, Q. J., et al. (2008). An improved approach to detection of amplitude of low-frequency fluctuation (ALFF) for resting-state fMRI: fractional ALFF. *J. Neurosci. Methods* 172, 137–141. doi: 10.1016/j.jneumeth.2008.04.012

Zuo, X. N., Di Martino, A., Kelly, C., Shehzad, Z. E., Gee, D. G., Klein, D. F., et al. (2010). The oscillating brain: complex and reliable. *Neuroimage* 49, 1432–1445. doi: 10.1016/j.neuroimage.2009.09.037

Zuo, X. N., Ehmke, R., Mennes, M., Imperati, D., Castellanos, F. X., Sporns, O., et al. (2012). Network centrality in the human functional connectome. *Cereb. Cortex* 22, 1862–1875. doi: 10.1093/cercor/bhr269

Conflict of Interest: The authors declare that the research was conducted in the absence of any commercial or financial relationships that could be construed as a potential conflict of interest.

frontiers in Aging Neuroscience

MINI REVIEW
published: 14 January 2020
doi: 10.3389/fnagi.2019.00376

TDP-43 and Limbic-Predominant Age-Related TDP-43 Encephalopathy

Lumi Zhang[1], *Yi Chen*[1], *Min Liu*[1,2], *Yunyun Wang*[1,3] *and Guoping Peng*[1]*

[1]*Department of Neurology, First Affiliated Hospital, Zhejiang University School of Medicine, Hangzhou, China,* [2]*Department of Neurology, Zhejiang University ShuLan International Hospital, Hangzhou, China,* [3]*Department of Neurology, Shengzhou People's Hospital, Shengzhou, China*

Through a number of an extensive autopsy, biomarker, and genomics studies, researchers have recently defined a novel type of dementia known as limbic-predominant age-related TDP-43 encephalopathy (LATE). LATE is perhaps best characterized by the presence of hyperphosphorylated TDP-43, which plays multi-functional roles through interactions with DNA and RNA, leading to significant alterations in the transcription and translation of particular genes. As individuals of advanced age represent a rapidly growing demographic group globally, there is a steadily increasing rate of LATE incidence that has to date received insufficient recognition despite its serious implications for public health. TDP-43 is the common pathology of various age-related dementia, therefore, it may be a potential and promising therapeutic target for such diseases. In the present review, we discuss the pathways regulating TDP-43 expression, metabolism, and disease activity in order to better understand the link between TDP-43 proteinopathy and LATE at the genetic, pathological, and clinical levels.

Keywords: TDP-43, neuropathology, Alzheimer's disease, neurodegeneration, hippocampal sclerosis, dementia

OPEN ACCESS

Edited by:
Jiehui Jiang,
Shanghai University, China

Reviewed by:
Lei Yu,
Thomas Jefferson University, United States
Peter T. Nelson,
University of Kentucky, United States

***Correspondence:**
Guoping Peng
guopingpeng@zju.edu.cn

Received: *19 November 2019*
Accepted: *23 December 2019*
Published: *14 January 2020*

Citation:
Zhang L, Chen Y, Liu M, Wang Y and Peng G (2020) TDP-43 and Limbic-Predominant Age-Related TDP-43 Encephalopathy. Front. Aging Neurosci. 11:376. doi: 10.3389/fnagi.2019.00376

INTRODUCTION

TDP-43 is a protein first discovered in 2006 to be present within the ubiquitinated inclusions that are a hallmark of amyotrophic lateral sclerosis (ALS) and in many cases of Tau-negative frontotemporal lobar degeneration (FTLD-TDP; Neumann et al., 2006; Cairns et al., 2007). More recent studies have shown that phosphorylated TDP-43 is similarly present in the brain of individuals over 80 years-old that have not been diagnosed with FTLD or ALS, but who often exhibit sights of Alzheimer's disease (AD) or hippocampal sclerosis (Amador-Ortiz et al., 2007a,b). These rates of TDP-43 proteinopathy as well as associated hippocampal sclerosis and amnestic dementia have been found to increase at more advanced ages, whereas severe AD cases become less common as individuals attain such advanced age (Nelson et al., 2019).

Abbreviations: LATE, limbic-predominant age-related TDP-43 encephalopathy; LATE-NC, LATE- neuropathological change; ALS, amyotrophic lateral sclerosis; FTLD-TDP, frontotemporal lobar degeneration with TDP-43 proteinopathy; FTLD, frontotemporal lobar degeneration; FTD, frontotemporal dementia; AD, Alzheimer's disease; ADNC, AD neuropathologic changes; HpScl, Hippocampal sclerosis; Aβ, amyloid-β; NFTs, Nerve Fiber Tangles; TARDBP, TAR DNA binding protein; GRN, granulin; APOE, apolipoprotein E; TMEM106B, transmembrane protein 106B; ABCC9, ATP-binding cassette sub-family member 9; VCP, valosin-containing protein; RRMs, RNA recognition motifs; AMPA, alpha-amino-3-hydroxy-5-methyl-4-isoxazolepropionate; CSF, cerebrospinal fluid; UTR, untranslated region.

At present, therapeutic efforts have failed to achieve satisfactory outcomes for treating AD, and given its apparent differences from AD, limbic-predominant age-related TDP-43 encephalopathy (LATE) has recently been defined as a unique clinical entity. This new disease classification highlights the importance of thoroughly exploring the role of TDP-43 in the context of age-related dementia development in general, and in the context of LATE specifically. However, as LATE remains a relatively new concept, much of the surrounding literature pertaining to AD or hippocampal sclerosis may inadvertently refer in whole or in part to cases of LATE, thereby complicating interpretations.

THE TDP-43 PROTEIN

TDP-43 is a protein that is 414 amino acids long and 43 kDa in size encoded by the *TARDBP* gene which includes nuclear localization and nuclear export signals, RNA recognition motifs (RRMs) and C-terminal domain (Diaper et al., 2013). The TDP-43 N-terminal domain is important as a regulator of monomer folding and homodimerizing (Zhang et al., 2013). In contrast, the C-terminal domain functions to control gene expression and nucleic acid binding, allowing it to modulate RNA turnover and alternative splicing (Buratti and Baralle, 2010; Lee et al., 2011). Normally, TDP-43 is found primarily in the nucleus of cells, with only 5–20% of TDP-43 being cytoplasmic (Woo et al., 2017), and this imbalance is thought to be autoregulated by negative feedback signaling mediated by nuclear TDP-43 (Polymenidou et al., 2011).

In the context of diseases such as ALS or FTLD, TDP-43 can become cleaved, hyperphosphorylated, and ubiquitinylated such that it aggregates and forms large inclusions within the cytoplasm of cells such as neurons and glia (Neumann et al., 2006). Normally, cellular stress-mediated TDP-43 aggregates are degraded following ubiquitinylation by the caspase-3-mediated proteasome, or through autophagic processes into fragments of 25 or 35 kDa (Chang et al., 2016). However, in pathological contexts this TDP-43 degradation is impaired thereby leading to increased aggregation of 25 and 35-kDa fragments that cannot be eliminated from cells (Huang et al., 2014).

As 25 kDa TDP-43 fragments accumulate, this drives the formation of cytoplasmic aggregates at the expense of normal nuclear localization (Chang et al., 2016). These 25 kDa TDP aggregates have been linked with cognitive deficits (Caccamo et al., 2012), whereas the 35 kDa fragments have been linked to behavioral deficits (Medina et al., 2014). Mutations in TARDBP have been shown to result in inflammation-mediated deregulation of TDP-43 homeostasis which through increased interleukin (IL)-6 levels that in turn drive the formation of aggregates and the progressive deterioration of motor neurons (Swarup et al., 2011; Diaper et al., 2013). TDP-43 expression levels have also been linked to the expression and activity of particular synaptic proteins including synapsin-I and alpha-amino-3-hydroxy-5-methyl-4-isoxazolepropionate (AMPA) receptor subunits (Gulino et al., 2015). As such, when TDP-43 becomes dysregulated, this can result in a cascade of altered signaling events that mediate impaired synaptic transmission, progressive neuronal deterioration, and motor defects (Diaper et al., 2013).

TDP-43 RELATED PROTEINOPATHY

Pathological conditions associated with TDP-43 aggregates include: aggregate inclusions within the cytoplasm of neurons and glial cells, pathological swelling or dystrophy of axonal, rounded neuropil grains, diffuse cytoplasmic TDP-43 staining with a lack of normal nuclear TDP-43 staining indicative of pre-inclusions, and in rare cases the presence of TDP-43 inclusions within the nuclei of neurons (Geser et al., 2010). TDP-43-linked neurodegeneration are divided into four categories according to the lesion patterns: perivascular, focal, sub-pial/sub-ependymal, and diffuse in the deep brain parenchyma (Geser et al., 2010).

Various neurodegenerative diseases have been shown to exhibit signs of TDP-43 aggregates, including, dementia with Lewy bodies (Higashi et al., 2007), argyrophilic grain disease (Fujishiro et al., 2009) and corticobasal degeneration (Uryu et al., 2008). Individuals with perivascular TDP-43 pathology also frequently exhibit significant cardiovascular symptoms such as hypertension and cerebral microinfarcts (Geser et al., 2010), with certain chronic vascular disease having the potential to drive the phosphorylation and misfolding of TDP-43. The most prominent and well-understood forms of TDP-43 proteinopathy are FTLD, ALS, and AD.

FTLD is a form of pre-senile dementia that impacts between 0.01 and 0.03% of individuals between 45 and 65 years of age (Bennion Callister and Pickering-Brown, 2014), leading to progressive deterioration of the frontal and anterior temporal brain lobes, finally causing frontotemporal dementia (FTD). The two primary hallmarks of FTLD at the pathological level include hyperphosphorylated tau protein and TDP-43 aggregate inclusions (Neumann et al., 2006).

ALS is a progressive disease best characterized by the gradual and progressive degeneration of motor neuron function, with males and females having respective lifetime ALS rates of 1/350 and 1/500 (Salameh et al., 2015). The presence of altered TDP-43 has been recognized as a hallmark of ALS. As with FTLD, many studies have explored the mechanisms whereby TDP-43 influences ALS pathogenesis, but at present these studies have been inconclusive and have yielded inconsistent results, suggesting more work is needed to establish the therapeutic value of targeting TDP-43 in this disease.

AD is the best-known and most prevalent form of dementia affecting individuals of advanced age. Extracellular amyloid-β (Aβ) plaque deposition, hyperphosphorylated tau aggregates that form within neurons to generate nerve fiber tangles (NFTs) are hallmarks of AD. Recent work has shown that phosphorylated TDP-43 is also evident within the brains of those with AD (Amador-Ortiz et al., 2007a,b).

In certain cases, TDP-43 aggregation and associated pathology may be a secondary consequence of some upstream neurodegenerative, developmental, or stress-induced influence (Nelson et al., 2016). Much as is the case for tau aggregates, however, once these TDP-43 aggregates form, that can significantly and adversely impact normal protein homeostasis

and gene expression to increase the risk of a wide range of diseases, thereby facilitating their development and progression (Nelson et al., 2016).

Therefore, TDP-43 proteinopathy is a promiscuous misfoldingopathy and can overlap with each other in many aspects, so it's necessary to differentiate them for better clinical diagnosis (Nelson et al., 2010). The main differences are risk genes, pathological proteins and types, clinical syndromes, as well as biomarkers. As granulin (GRN), apolipoprotein E (APOE), TMEM106B and many other risk genes present in more than one TDP-43 proteinopathy, it would be a prosperous finding if there are risk genes that specific to a particular subtype. Previous reports found that ALS and FTLD patients had higher TDP-43 levels in cerebrospinal fluid (CSF; Steinacker et al., 2008), despite not so convinced currently, increased TDP-43 in CSF may be related to the involvement of lesions near the ventricle or a sign of disease severity. Other methods like magnetic resonance imaging (MRI) and FDG-PET has been used to aid diagnosis in TDP-43 proteinopathy. As studies indicate that neurodegenerative diseases are related with specific intrinsic functional connectivity networks that varied among individuals, functional MRI studies may help to explain which groups are susceptible to certain diseases based on brain connectivity (Franzmeier et al., 2018).

THE ASSOCIATION BETWEEN LATE AND TDP-43

LATE has been classified as a form of TDP-43 proteinopathy that impacts adults of advanced age regardless of whether or not they exhibit hippocampal sclerosis; LATE neuropathological change (LATE-NC) is characterized by mislocalized and phosphorylated TDP-43 that mainly affects limbic structures (Nelson et al., 2019). According to the anatomical distribution of TDP-43, the simplified staging includes the amygdala (stage 1); hippocampus (stage 2); middle frontal gyrus (stage 3; Nag et al., 2018). An updated staging scheme suggests amygdala (stage 1); entorhinal cortex and subiculum (stage 2); dentate gyrus of the hippocampus and occipitotemporal cortex (stage 3); insular cortex, ventral striatum, basal forebrain and inferior temporal cortex (stage 4); substantia nigra, inferior olive and midbrain tectum (stage 5); basal ganglia and middle frontal cortex (stage 6; Josephs et al., 2016). From a clinical perspective, LATE is very similar to AD with patients exhibiting progressive memory loss (Nelson et al., 2019). One study described AD with different neuropathologic subtypes (typical, limbic-predominant, and hippocampal sparing; Murray et al., 2011), and another study suggested the association between pTau and pTDP-43 is important in the limbic-predominant subtype (Latimer et al., 2019). However, compared with AD, LATE most commonly affects individuals of very advanced age and many cases with "end-stage" AD neuropathologic changes (ADNC) disease actually lack TDP-43 proteinopathy (Nelson et al., 2019). The current definition of LATE-NC includes cases without ADNC and the subtypes of AD brought by Murray et al. (2011) may refer in part to cases of LATE. Despite this, TDP-43 can comorbid amyloid-β and various tau pathologies in the context of LATE-NC. Studies have shown that Aβ deposition can increase TDP-43 phosphorylation and cytoplasmic localization, whereas Aβ clearance prevents TDP-43 propagation (Herman et al., 2011). TDP-43 and Aβ can oligomerize to seed the amyloid oligomerization (Fang et al., 2014). TDP-43 inclusions have also been detected within neurons exhibiting NFTs that are distinct from tau-based NFTs, suggesting that TDP-43 can mediate NFT formation either alone or through tau interactions (Amador-Ortiz et al., 2007b). Further studies are needed to explore the relationships and interactions between TDP-43, Aβ, and tau in order to determine whether these interactions can be targeted to mediate therapeutic treatment of AD and LATE.

LATE-NC shows feature reminiscent of FTLD-TDP Type A often related to HS, TMEM and GRN genetic risk factors, and it's necessary to discuss the overlap and differences between these two pathologies. As for differences, LATE-NC was more common in the elderly, associated with more marked neuronal and synaptic loss and with greater reactive gliosis, as well as more corpora amylacea and less cortical atrophy (Amador-Ortiz et al., 2007a). Previous studies found the fragments in LATE and FTLD-TDP TypeA were of no difference (Hasegawa et al., 2008). However, a recent study found that different band patterns of the C-terminal fragments can varied among diseases (Hasegawa et al., 2011).

THE GENETIC RELATIONSHIP BETWEEN LATE AND TDP-43

Five risk alleles have been identified to be associated with LATE (Nelson et al., 2019). Both GRN and TMEM106B have been found to be linked to the risk of hippocampal sclerosis and TDP-43 proteinopathy in the context of FTLD (Baker et al., 2006; Boeve et al., 2006; Van Deerlin et al., 2010). Therefore FTLD and LATE may show one common pathologic pathway. The key to this pathway is reduced progranulin levels. Progranulin expression plays a modulatory role in tissue damage within the central nervous system (CNS) to suppress excessive immunity-based microglial activation and protecting neurons from reactive oxygen species and proinflammatory cytokines (Sun and Eriksen, 2011). Both GRN and TMEM106B variations can result in reduced progranulin levels, the former through creating null alleles while the latter function in the presence of GRN mutations (Finch et al., 2011; Murray et al., 2014; Nelson et al., 2015). In addition, there are pieces of evidence that TDP-43 can regulate the stability of the GRN mRNA through interacting with its 3'-untranslated region (UTR), thereby regulating progranulin levels (Fontana et al., 2015). The reduced progranulin level has direct neurotrophic and inflammatory response-modulating functions and higher susceptibility for stress, which is found to play a role in TDP-43 processing and increase the vulnerability of specific CA1 neuron populations (Zhang et al., 2007; Hokkanen et al., 2019). When GRN is depleted, this leads to enhanced caspase-3 activation, which may serve as an initiating event mediating TDP-43 cleavage and associated TDP-43 pathology (Guo et al., 2010).

Beyond these key risk genes, other genes such as TARDBP, valosin-containing protein (VCP), and C9ORF72 have been found to be associated with TDP-43 proteinopathy (Pesiridis et al., 2009; Mackenzie et al., 2011; Wilson et al., 2013). However, what if any relationship these genes may have with LATE remains to be determined.

THE PATHOLOGICAL RELATIONSHIP BETWEEN LATE AND TDP-43

Previous study has described two types of TDP-43 distribution: limbic and diffuse (Amador-Ortiz et al., 2007b). One research found that a 10-year increase in age was associated with a 1.8-fold increase in the odds of limbic-type relative to being TDP-43 negative (Josephs et al., 2014b). Therefore, limbic group corresponds most closely to the stage I–III (Josephs et al., 2016), i.e., typical LATE. From stages I to III, besides the severity of amygdala TDP-43 immunoreactivity increased across the stages, only the hippocampus and entorhinal cortex volumes progressively declined with increasing stage (Josephs et al., 2014a). Hippocampal sclerosis (HpScl) in LATE cases, is frequently asymmetric, progressing along a rostral-caudal gradient compared with HpScl in AD (Nelson et al., 2019). Perhaps, the interaction of TDP-43 and tau could change and aggravate the HpScl in AD. In stage B2 and B3 of NFTs, hippocampal TDP-43 is associated with more rapid atrophy of this region, while a link between higher NFT stage and more rapid hippocampal atrophy was detected for TDP-43 stages of 0 and 1 (Josephs et al., 2017). However, as many other factors can cause HpScl and above half LATE cases without HpScl, it is hard to definitely tell that TDP-43 accelerate HpScl in LATE, more studies are needed to make clear relationships among TDP-43, HpScl and LATE.

TDP-43 pathological findings can also include the presence of abnormal TDP-43 fibrillary inclusions in astrocytes, potentially suggesting that the blood-brain barrier may be compromised in affected individuals (Lin et al., 2009). Meanwhile, TDP-43 inclusion-sensitive neurons have also been found in the limbic lobe (Amador-Ortiz et al., 2007b).

THE CLINICAL ASSOCIATION BETWEEN LATE AND TDP-43

Both hippocampal sclerosis and TDP-43-associated pathology are increasingly recognized to adversely impact cognition (Dutra et al., 2015), with these two conditions acting in an additive manner to impair cognitive function (Josephs et al., 2014b). As mentioned before, LATE is associated with progressive memory deficits (Nelson et al., 2019), and recent work suggests that TDP-43 pathology must progress to stage 2 prior to these AD-like dementia symptoms being evident (James et al., 2016).

Increased TDP-43 inclusion levels have been linked to decreased global cognition and faster cognitive decline in a linear manner (Wilson et al., 2013). Combined hippocampal sclerosis and TDP-43 pathology have been linked to impairment of global cognition and episodic and semantic memory, while TDP-43 pathology in the absence of hippocampal sclerosis has been linked only to poorer episodic memory (Lin et al., 2009; Wilson et al., 2013; Nag et al., 2015). Hippocampal sclerosis on its own has been linked to semantic memory deficits (Wilson et al., 2013). One study suggested that subjects with both AD and TDP-43 proteinopathy were more likely to exhibit symptoms of agitation and aggression (Sennik et al., 2017). These results clearly demonstrate that TDP-43 pathology plays a major role in the loss of cognitive function in those of a more advanced age. Moreover, the specific locations of TDP-43 aggregate formation likely impact the associated clinical symptoms. TDP-43 pathology is most frequently evident in the medial temporal lobe, potentially accounting for its clear link with the loss of episodic memory (Wilson et al., 2013). Other studies have also found TDP-43 deposition in the ventral striatum and basal forebrain is linked to poorer performance on memory, language, and executive tests (Josephs et al., 2016).

In all, the symptoms associated with TDP-43-linked pathology depend on the nature of the pathology and the brain regions wherein these aggregates manifest. As such, further studies of the stages and mechanistic basis for TDP-43 progression in the context of pathological and clinical progression are warranted.

CONCLUDING REMARKS AND FUTURE PROSPECTS

There is increasing recognition of the prevalence and importance of TDP-43-associated neurodegenerative disease in individuals of advanced age. While many of the studies on this topic to date have demonstrated TDP-43 are associated with various diseases, it is unclear for the most part whether this pathology is causative, promote and/or enhance disease, or instead is a consequence of otherwise related pathophysiology. Although the mechanism is not that clear, Methylene blue and dimebon have been found to inhibit aggregation of TDP-43 in cellular models (Arai et al., 2010) and the former has also been shown to inhibit AD-like Aβ and tau aggregation *in vitro* (Wischik et al., 1996; Taniguchi et al., 2005). Future research should focus on several aspects in order to better understand the TDP-43 and LATE, then to find a potential therapeutic target. There are many ways to be explored, such as the common pathway of the formation of dementia-related protein; the synergy and interaction among Aβ, tau, TDP-43 as well as other related pathological protein; the real role of progranulin in LATE and the mechanism of Methylene blue and dimebon therapy in LATE. In addition, more research is needed to clearly classify the relationship of TDP-43 pathological features with TDP-43 involved regions as well as corresponding clinical syndromes. It is of importance to address the following questions: why pathological change can also present in part of normal individuals? Is it a prediction of people who will develop age-related dementia? As the 35 kDa fragment of TDP-43 caused motor deficits, can LATE cases show motor syndromes in end-stage? No matter TDP-43 is a cause or an effect, what is the upstream or downstream target of TDP-43? Additional elucidation of the role of TDP-43 in ALS and FTLD may shine further light on its role in LATE as well. It is also important that further studies fully

explore clinical neuropathological correlations that may guide the diagnosis and treatment of individuals suffering from age-related dementia.

AUTHOR CONTRIBUTIONS

GP and LZ conceived and designed the project. LZ and YC wrote the manuscript with inputs from other authors. ML and YW helped to revise the manuscript. All authors reviewed and edited the manuscript and approved the final version of the manuscript.

FUNDING

This work was supported by the National Key Technology R&D Program of China (No. 2016YFC1306402, 2019YFC0118203) and the Science and Technology Program of Zhejiang Province (2017C03011), respectively.

ACKNOWLEDGMENTS

We thank Dr. Eric, Ph.D., from the USA for editing a draft of this manuscript.

REFERENCES

Amador-Ortiz, C., Ahmed, Z., Zehr, C., and Dickson, D. W. (2007a). Hippocampal sclerosis dementia differs from hippocampal sclerosis in frontal lobe degeneration. *Acta Neuropathol.* 113, 245–252. doi: 10.1007/s00401-006-0183-4

Amador-Ortiz, C., Lin, W. L., Ahmed, Z., Personett, D., Davies, P., Duara, R., et al. (2007b). TDP-43 immunoreactivity in hippocampal sclerosis and Alzheimer's disease. *Ann. Neurol.* 61, 435–445. doi: 10.1002/ana.21154

Arai, T., Hasegawa, M., Nonoka, T., Kametani, F., Yamashita, M., Hosokawa, M., et al. (2010). Phosphorylated and cleaved TDP-43 in ALS, FTLD and other neurodegenerative disorders and in cellular models of TDP-43 proteinopathy. *Neuropathology* 30, 170–181. doi: 10.1111/j.1440-1789.2009.01089.x

Baker, M., Mackenzie, I. R., Pickering-Brown, S. M., Gass, J., Rademakers, R., Lindholm, C., et al. (2006). Mutations in progranulin cause tau-negative frontotemporal dementia linked to chromosome 17. *Nature* 442, 916–919. doi: 10.1038/nature05016

Bennion Callister, J., and Pickering-Brown, S. M. (2014). Pathogenesis/genetics of frontotemporal dementia and how it relates to ALS. *Exp. Neurol.* 262, 84–90. doi: 10.1016/j.expneurol.2014.06.001

Boeve, B. F., Baker, M., Dickson, D. W., Parisi, J. E., Giannini, C., Josephs, K. A., et al. (2006). Frontotemporal dementia and parkinsonism associated with the IVS1 + 1G-4A mutation in progranulin: a clinicopathologic study. *Brain* 129, 3103–3114. doi: 10.1093/brain/awl268

Buratti, E., and Baralle, F. E. (2010). The multiple roles of TDP-43 in pre-mRNA processing and gene expression regulation. *RNA Biol.* 7, 420–429. doi: 10.4161/rna.7.4.12205

Caccamo, A., Majumder, S., and Oddo, S. (2012). Cognitive decline typical of frontotemporal lobar degeneration in transgenic mice expressing the 25-kDa C-terminal fragment of TDP-43. *Am. J. Pathol.* 180, 293–302. doi: 10.1016/j.ajpath.2011.09.022

Cairns, N. J., Bigio, E. H., Mackenzie, I. R., Neumann, M., Lee, V. M., Hatanpaa, K. J., et al. (2007). Neuropathologic diagnostic and nosologic criteria for frontotemporal lobar degeneration: consensus of the consortium for frontotemporal lobar degeneration. *Acta Neuropathol.* 114, 5–22. doi: 10.1007/s00401-007-0237-2

Chang, X. L., Tan, M. S., Tan, L., and Yu, J. T. (2016). The role of TDP-43 in Alzheimer's disease. *Mol. Neurobiol.* 53, 3349–3359. doi: 10.1007/s12035-015-9264-5

Diaper, D. C., Adachi, Y., Sutcliffe, B., Humphrey, D. M., Elliott, C. J., Stepto, A., et al. (2013). Loss and gain of *Drosophila* TDP-43 impair synaptic efficacy and motor control leading to age-related neurodegeneration by loss-of-function phenotypes. *Hum. Mol. Genet.* 22, 1539–1557. doi: 10.1093/hmg/ddt005

Dutra, J. R., Cortés, E. P., and Vonsattel, J. P. (2015). Update on hippocampal sclerosis. *Curr. Neurol. Neurosci. Rep.* 15:67. doi: 10.1007/s11910-015-0592-7

Fang, Y. S., Tsai, K. J., Chang, Y. J., Kao, P., Woods, R., Kuo, P. H., et al. (2014). Full-length TDP-43 forms toxic amyloid oligomers that are present in frontotemporal lobar dementia-TDP patients. *Nat. Commun.* 5:4824. doi: 10.1038/ncomms5824

Finch, N., Carrasquillo, M. M., Baker, M., Rutherford, N. J., Coppola, G., Dejesus-Hernandez, M., et al. (2011). TMEM106B regulates progranulin levels and the penetrance of FTLD in GRN mutation carriers. *Neurology* 76, 467–474. doi: 10.1212/WNL.0b013e31820a0e3b

Fontana, F., Siva, K., and Denti, M. A. (2015). A network of RNA and protein interactions in fronto-temporal dementia. *Front. Mol. Neurosci.* 8:9. doi: 10.3389/fnmol.2015.00009

Franzmeier, N., Düzel, E., Jessen, F., Buerger, K., Levin, J., Duering, M., et al. (2018). Left frontal hub connectivity delays cognitive impairment in autosomal-dominant and sporadic Alzheimer's disease. *Brain* 141, 1186–1200. doi: 10.1093/brain/awy008

Fujishiro, H., Uchikado, H., Arai, T., Hasegawa, M., Akiyama, H., Yokota, O., et al. (2009). Accumulation of phosphorylated TDP-43 in brains of patients with argyrophilic grain disease. *Acta Neuropathol.* 117, 151–158. doi: 10.1007/s00401-008-0463-2

Geser, F., Robinson, J. L., Malunda, J. A., Xie, S. X., Clark, C. M., Kwong, L. K., et al. (2010). Pathological 43-kDa transactivation response DNA-binding protein in older adults with and without severe mental illness. *Arch. Neurol.* 67, 1238–1250. doi: 10.1001/archneurol.2010.254

Gulino, R., Forte, S., Parenti, R., and Gulisano, M. (2015). TDP-43 as a modulator of synaptic plasticity in a mouse model of spinal motoneuron degeneration. *CNS Neurol. Disord. Drug Targets* 14, 55–60. doi: 10.2174/1871527314666150116115414

Guo, A., Tapia, L., Bamji, S. X., Cynader, M. S., and Jia, W. (2010). Progranulin deficiency leads to enhanced cell vulnerability and TDP-43 translocation in primary neuronal cultures. *Brain Res.* 1366, 1–8. doi: 10.1016/j.brainres.2010.09.099

Hasegawa, M., Arai, T., Nonaka, T., Kametani, F., Yoshida, M., Hashizume, Y., et al. (2008). Phosphorylated TDP-43 in frontotemporal lobar degeneration and amyotrophic lateral sclerosis. *Ann. Neurol.* 64, 60–70. doi: 10.1002/ana.21425

Hasegawa, M., Nonaka, T., Tsuji, H., Tamaoka, A., Yamashita, M., Kametani, F., et al. (2011). Molecular dissection of TDP-43 proteinopathies. *J. Mol. Neurosci.* 45, 480–485. doi: 10.1007/s12031-011-9571-x

Herman, A. M., Khandelwal, P. J., Stanczyk, B. B., Rebeck, G. W., and Moussa, C. E. (2011). β-amyloid triggers ALS-associated TDP-43 pathology in AD models. *Brain Res.* 1386, 191–199. doi: 10.1016/j.brainres.2011.02.052

Higashi, S., Iseki, E., Yamamoto, R., Minegishi, M., Hino, H., Fujisawa, K., et al. (2007). Concurrence of TDP-43, tau and a-synuclein pathology in brains of Alzheimer's disease and dementia with Lewy bodies. *Brain Res.* 1184, 284–294. doi: 10.1016/j.brainres.2007.09.048

Hokkanen, S. R. K., Kero, M., Kaivola, K., Hunter, S., Keage, H. A. D., Kiviharju, A., et al. (2019). Putative risk alleles for LATE-NC with hippocampal sclerosis in population-representative autopsy cohorts. *Brain Pathol.* doi: 10.1111/bpa.12773 [Epub ahead of print].

Huang, C. C., Bose, J. K., Majumder, P., Lee, K. H., Huang, J. T., Huang, J. K., et al. (2014). Metabolism and mis-metabolism of the neuropathological signature protein TDP-43. *J. Cell Sci.* 127, 3024–3038. doi: 10.1242/jcs.136150

James, B. D., Wilson, R. S., Boyle, P. A., Trojanowski, J. Q., Bennett, D. A., and Schneider, J. A. (2016). TDP-43 stage, mixed pathologies and clinical Alzheimer's-type dementia. *Brain* 139, 2983–2993. doi: 10.1093/brain/aww224

Josephs, K. A., Dickson, D. W., Tosakulwong, N., Weigand, S. D., Murray, M. E., Petrucelli, L., et al. (2017). Rates of hippocampal atrophy and post-mortem

TDP-43 in Alzheimer's disease: a longitudinal retrospective study. *Lancet Neurol.* 16, 917–924. doi: 10.1016/s1474-4422(17)30284-3

Josephs, K. A., Murray, M. E., Whitwell, J. L., Parisi, J. E., Petrucelli, L., Jack, C. R., et al. (2014a). Staging TDP-43 pathology in Alzheimer's disease. *Acta Neuropathol.* 127, 441–450. doi: 10.1007/s00401-013-1211-9

Josephs, K. A., Whitwell, J. L., Weigand, S. D., Murray, M. E., Tosakulwong, N., Liesinger, A. M., et al. (2014b). TDP-43 is a key player in the clinical features associated with Alzheimer's disease. *Acta Neuropathol.* 127, 811–824. doi: 10.1007/s00401-014-1269-z

Josephs, K. A., Murray, M. E., Whitwell, J. L., Tosakulwong, N., Weigand, S. D., Petrucelli, L., et al. (2016). Updated TDP-43 in Alzheimer's disease staging scheme. *Acta Neuropathol.* 131, 571–585. doi: 10.1007/s00401-016-1537-1

Latimer, C. S., Burke, B. T., Liachko, N. F., Currey, H. N., Kilgore, M. D., Gibbons, L. E., et al. (2019). Resistance and resilience to Alzheimer's disease pathology are associated with reduced cortical pTau and absence of limbic-predominant age-related TDP-43 encephalopathy in a community-based cohort. *Acta Neuropathol. Commun.* 7:91. doi: 10.1186/s40478-019-0743-1

Lee, E. B., Lee, V. M., and Trojanowski, J. Q. (2011). Gains and losses: molecular mechanisms of TDP43-mediated neurodegeneration. *Nat. Rev. Neurosci.* 13, 38–50. doi: 10.1038/nrn3121

Lin, W. L., Castanedes-Casey, M., and Dickson, D. W. (2009). Transactivation response DNA-binding protein 43 microvasculopathy in frontotemporal degeneration and familial Lewy body disease. *J. Neuropathol. Exp. Neurol.* 68, 1167–1176. doi: 10.1097/NEN.0b013e3181baacec

Mackenzie, I. R., Neumann, M., Baborie, A., Sampathu, D. M., Du Plessis, D., Jaros, E., et al. (2011). A harmonized classification system for FTLD-TDP pathology. *Acta Neuropathol.* 122, 111–113. doi: 10.1007/s00401-011-0845-8

Medina, D. X., Orr, M. E., and Oddo, S. (2014). Accumulation of C-terminal fragments of transactive response DNA-binding protein 43 leads to synaptic loss and cognitive deficits in human TDP-43 transgenic mice. *Neurobiol. Aging* 35, 79–87. doi: 10.1016/j.neurobiolaging.2013.07.006

Murray, M. E., Cannon, A., Graff-Radford, N. R., Liesinger, A. M., Rutherford, N. J., Ross, O. A., et al. (2014). Differential clinicopathologic and genetic features of late-onset amnestic dementias. *Acta Neuropathol.* 128, 411–421. doi: 10.1007/s00401-014-1302-2

Murray, M. E., Graff-Radford, N. R., Ross, O. A., Petersen, R. C., Duara, R., and Dickson, D. W. (2011). Neuropathologically defined subtypes of Alzheimer's disease with distinct clinical characteristics: a retrospective study. *Lancet Neurol.* 10, 785–796. doi: 10.1016/S1474-4422(11)70156-9

Nag, S., Yu, L., Boyle, P. A., Leurgans, S. E., Bennett, D. A., and Schneider, J. A. (2018). TDP-43 pathology in anterior temporal pole cortex in aging and Alzheimer's disease. *Acta Neuropathol. Commun.* 6:33. doi: 10.1186/s40478-018-0531-3

Nag, S., Yu, L., Capuano, A. W., Wilson, R. S., Leurgans, S. E., Bennett, D. A., et al. (2015). Hippocampal sclerosis and TDP-43 pathology in aging and Alzheimer's disease. *Ann. Neurol.* 77, 942–952. doi: 10.1002/ana.24388

Nelson, P. T., Abner, E. L., Schmitt, F. A., Kryscio, R. J., Jicha, G. A., Smith, C. D., et al. (2010). Modeling the association between 43 different clinical and pathological variables and the severity of cognitive impairment in a large autopsy cohort of elderly persons. *Brain Pathol.* 20, 66–79. doi: 10.1111/j.1750-3639.2008.00244.x

Nelson, P. T., Dickson, D. W., Trojanowski, J. Q., Jack, C. R., Boyle, P. A., Arfanakis, K., et al. (2019). Limbic-predominant age-related TDP-43 encephalopathy (LATE): consensus working group report. *Brain* 142, 1503–1527. doi: 10.1093/brain/awz099

Nelson, P. T., Trojanowski, J. Q., Abner, E. L., Al-Janabi, O. M., Jicha, G. A., Schmitt, F. A., et al. (2016). "New old pathologies": AD, PART and cerebral age-related TDP-43 with sclerosis (CARTS). *J. Neuropathol. Exp. Neurol.* 75, 482–498. doi: 10.1093/jnen/nlw033

Nelson, P. T., Wang, W. X., Wilfred, B. R., Wei, A., Dimayuga, J., Huang, Q., et al. (2015). Novel human ABCC9/SUR2 brain-expressed transcripts and an eQTL relevant to hippocampal sclerosis of aging. *J. Neurochem.* 134, 1026–1039. doi: 10.1111/jnc.13202

Neumann, M., Sampathu, D. M., Kwong, L. K., Truax, A. C., Micsenyi, M. C., Chou, T. T., et al. (2006). Ubiquitinated TDP-43 in frontotemporal lobar degeneration and amyotrophic lateral sclerosis. *Science* 314, 130–133. doi: 10.1126/science.1134108

Pesiridis, G. S., Lee, V. M., and Trojanowski, J. Q. (2009). Mutations in TDP-43 link glycine-rich domain functions to amyotrophic lateral sclerosis. *Hum. Mol. Genet.* 18, R156–R162. doi: 10.1093/hmg/ddp303

Polymenidou, M., Lagier-Tourenne, C., Hutt, K. R., Huelga, S. C., Moran, J., Liang, T. Y., et al. (2011). Long pre-mRNA depletion and RNA missplicing contribute to neuronal vulnerability from loss of TDP-43. *Nat. Neurosci.* 14, 459–468. doi: 10.1038/nn.2779

Salameh, J. S., Brown, R. H. Jr., and Berry, J. D. (2015). Amyotrophic lateral sclerosis: review. *Semin Neurol.* 35, 469–476. doi: 10.1055/s-0035-1558984

Sennik, S., Schweizer, T. A., Fischer, C. E., and Munoz, D. G. (2017). Risk factors and pathological substrates associated with agitation/aggression in Alzheimer's disease: a preliminary study using NACC data. *J. Alzheimers Dis.* 55, 1519–1528. doi: 10.3233/JAD-160780

Steinacker, P., Hendrich, C., Sperfeld, A. D., Jesse, S., von Arnim, C. A., Lehnert, S., et al. (2008). TDP-43 in cerebrospinal fuid of patients with frontotemporal lobar degeneration and amyotrophic lateral sclerosis. *Arch Neurol.* 65, 1481–1487. doi: 10.1001/archneur.65.11.1481

Sun, L., and Eriksen, J. L. (2011). Recent insights into the involvement of progranulin in frontotemporal dementia. *Curr. Neuropharmacol.* 9, 632–642. doi: 10.2174/157015911798376361

Swarup, V., Phaneuf, D., Bareil, C., Robertson, J., Rouleau, G. A., Kriz, J., et al. (2011). Pathological hallmarks of amyotrophic lateral sclerosis/frontotemporal lobar degeneration in transgenic mice produced with TDP-43 genomic fragments. *Brain* 134, 2610–2626. doi: 10.1093/brain/awr159

Taniguchi, S., Suzuki, N., Masuda, M., Hisanaga, S., Iwatsubo, T., Goedert, M., et al. (2005). Inhibition of heparin-induced tau filament formation by phenothiazines, polyphenols and porphyrins. *J. Biol. Chem.* 280, 7614–7623. doi: 10.1074/jbc.M408714200

Uryu, K., Nakashima-Yasuda, H., Forman, M. S., Kwong, L. K., Clark, C. M., Grossman, M., et al. (2008). Concomitant TAR-DNA-binding protein 43 pathology is present in Alzheimer disease and corticobasal degeneration but not in other tauopathies. *J. Neuropathol. Exp. Neurol.* 67, 555–564. doi: 10.1097/NEN.0b013e31817713b5

Van Deerlin, V. M., Sleiman, P. M., Martinez-Lage, M., Chen-Plotkin, A., Wang, L. S., Graff-Radford, N. R., et al. (2010). Common variants at 7p21 are associated with frontotemporal lobar degeneration with TDP-43 inclusions. *Nat. Genet.* 42, 234–239. doi: 10.1038/ng.536

Wilson, R. S., Yu, L., Trojanowski, J. Q., Chen, E. Y., Boyle, P. A., Bennett, D. A., et al. (2013). TDP-43 pathology, cognitive decline and dementia in old age. *JAMA Neurol.* 70, 1418–1424. doi: 10.1001/jamaneurol.2013.3961

Wischik, C. M., Edwards, P. C., Lai, R. Y., Roth, M., and Harrington, C. R. (1996). Selective inhibition of Alzheimer diseaselike tau aggregation by phenothiazines. *Proc. Natl. Acad. Sci. U S A* 93, 11213–11218. doi: 10.1073/pnas.93.20.11213

Woo, J. A., Liu, T., Trotter, C., Fang, C. C., De Narvaez, E., LePochat, P., et al. (2017). Loss of function CHCHD10 mutations in cytoplasmic TDP-43 accumulation and synaptic integrity. *Nat. Commun.* 8:15558. doi: 10.1038/ncomms15558

Zhang, Y. J., Caulfield, T., Xu, Y. F., Gendron, T. F., Hubbard, J., Stetler, C., et al. (2013). The dual functions of the extreme N-terminus of TDP-43 in regulating its biological activity and inclusion formation. *Hum. Mol. Genet.* 22, 3112–3122. doi: 10.1093/hmg/ddt166

Zhang, Y. J., Xu, Y. F., Dickey, C. A., Buratti, E., Baralle, F., Bailey, R., et al. (2007). Progranulin mediates caspase-dependent cleavage of TAR DNA binding protein-43. *J. Neurosci.* 27, 10530–10534. doi: 10.1523/JNEUROSCI.3421-07.2007

Conflict of Interest: The authors declare that the research was conducted in the absence of any commercial or financial relationships that could be construed as a potential conflict of interest.

frontiers in Neuroscience

ORIGINAL RESEARCH
published: 31 January 2020
doi: 10.3389/fnins.2020.00044

An Informant-Based Simple Questionnaire for Visuospatial Dysfunction Assessment in Dementia

*Ching-Tsu Wang[1], Guang-Uei Hung[2], Cheng-Yu Wei[3], Ray-Chang Tzeng[1] and Pai-Yi Chiu[4]**

[1] Department of Neurology, Tainan Municipal Hospital, Tainan, Taiwan, [2] Department of Nuclear Medicine, Chang Bing Show Chwan Memorial Hospital, Changhua, Taiwan, [3] Department of Exercise and Health Promotion, College of Education, Chinese Culture University, Taipei, Taiwan, [4] Department of Neurology, Show Chwan Memorial Hospital, Changhua, Taiwan

Objectives: Visuospatial dysfunction (VSD) is one of the most important symptoms for the diagnosis of dementia with Lewy bodies (DLB). The aim of this study was to validate a novel VSD questionnaire and determine the cutoff score for the screening for VSD in DLB.

Methods: This is a retrospective analysis of data from a project of the History-based Artificial Intelligent Clinical Dementia Diagnostic System (HAICDDS). VSD of non-demented control (NDC), Alzheimer's disease (AD), and DLB participants were analyzed and compared using the visuospatial questionnaire in the HAICDDS (HAI-VSQ), the Draw subscale in the Cognitive Abilities Screening Instrument (CASI-Draw), and the visuospatial subscale in Montreal Cognitive Assessment (MoCA-VS).

Results: A total of 440 individuals were studied, including 154 NDC, 229 AD, and 57 DLB participants. Compared to NDC or AD participants, DLB participants showed a higher total score on HAI-VSQ after adjustment for age. Using HAI-VSQ, a cutoff score $\geq$ 2 was useful for the screening for VSD in DLB with a sensitivity of 0.77 and a specificity of 0.94. Compared with CASI-Draw or MoCA-VS, HAI-VSQ was least influenced by gender, age, and education and had the highest correlation with the sum of boxes of the Clinical Dementia Rating scale. After adjustment for age, education, gender, and global cognitive function, HAI-VSQ significantly discriminated DLB from AD and NDC whereas MoCA-VS or CASI-Draw did not.

Conclusion: Our study showed that the newly designed simple questionnaire was a practical screening tool for VSD in DLB that can be applied in clinical practice as well as on a registration platform.

Keywords: visuospatial dysfunction, Alzheimer's disease, dementia with Lewy bodies, screening tools, cognitive abilities

OPEN ACCESS

Edited by:
Jiehui Jiang,
Shanghai University, China

Reviewed by:
Xiao Shu Yun,
Shanghai University of Traditional Chinese Medicine, China
Mattia Siciliano,
Second University of Naples, Italy
Yuan Han Yang,
Kaohsiung Municipal Ta-Tung Hospital, Taiwan

****Correspondence:***
Pai-Yi Chiu
paiyibox@gmail.com

Specialty section:
This article was submitted to Neurodegeneration, a section of the journal Frontiers in Neuroscience

Received: *12 November 2019*
Accepted: *13 January 2020*
Published: *31 January 2020*

Citation:
Wang C-T, Hung G-U, Wei C-Y, Tzeng R-C and Chiu P-Y (2020) An Informant-Based Simple Questionnaire for Visuospatial Dysfunction Assessment in Dementia. Front. Neurosci. 14:44. doi: 10.3389/fnins.2020.00044

INTRODUCTION

Visuospatial dysfunction (VSD) is a common clinical symptom used for the diagnosis of cognitive impairment or dementia due to Alzheimer's disease (AD) (McKhann et al., 2011; Kim et al., 2017). Furthermore, VSD is the central symptom for the diagnosis of dementia with Lewy bodies (DLB) (McKeith et al., 2017). DLB is the second most-common type of degenerative dementia

and previous studies have provided evidence of VSD in patients with DLB (McKeith et al., 2017). Previous studies assessing VSD in patients with dementia revealed several important clinical information with particular relevance for its connection to DLB. For example, salient and initial VSD are essential for the diagnosis of DLB (McKeith et al., 2017). Besides, well-formed, detailed, and complex visual hallucinations (VH) are among the core diagnostic features for DLB and this striking feature starts early in the disease (McKeith et al., 2017). The presence of VSD may also identify patients whose syndrome is driven by DLB rather than by AD pathology (Hamilton et al., 2012). The presence of early and severe VSD increases the likelihood that patients will develop prototypical DLB syndrome (Hamilton et al., 2012). In the early stages of dementia, VSD is more profound in DLB than in AD but memory retrieval deficit is more prominent in AD than in DLB (Yoshizawa et al., 2013). Studies of VSD mainly focused on the clinical performance of perception of locations or objects (Culham et al., 2006). Unlike these types of performance, visuomotor dysfunction manifests in goal-directed or visual-guided behavior and is also regarded as part of the visuospatial system of the brain (Culham et al., 2006). Visuomotor function is compromised in AD compared to normal elderly (Tippett et al., 2007; Galati et al., 2011; Hawkins and Sergio, 2014). Pathophysiological studies of visuomotor dysfunction revealed that reciprocal communication between hippocampal, parietal, and frontal brain regions play an important role in transforming visual-spatial information into goal-directed actions (Galati et al., 2011; Hawkins and Sergio, 2014). Disrupting these connections could affect the skills for activities of daily living (Hawkins and Sergio, 2014). Several studies using visuospatial/visuomotor function tests of the performance of visual recognition, visual discrimination, visual attention, or visuo-perceptive integration in DLB compared to AD revealed that these skills are impaired in DLB compared with AD (Oda et al., 2009; Yamaguchi et al., 2011; Li et al., 2014).

Based on these studies and diagnostic criteria, VSD including impairment of visuomotor skills is important for the diagnosis of dementia including AD and DLB. Therefore, a simple screening tool for VSD would be useful in a clinical setting but VSD assessment in common informant-based dementia assessment tools is still lacking and unable to satisfy the clinical requirements. For example, in the Clinical Dementia Rating (CDR) scale, evaluation of VSD is embedded in the domain of orientation and only a few questions address navigating function (Hamilton et al., 2012) but no question addresses visuomotor function. Impaired visuomotor skills are also important in other domains that are characteristic of DLB or posterior cortical atrophy (PCA) (McKhann et al., 2011; McKeith et al., 2017). Furthermore, frequently- used cognitive screening tests for dementia or cognitive impairment, for example, Mini-Mental Status Examination (MMSE), Cognitive Abilities Screening Instrument (CASI), and Montreal Cognitive Assessment (MoCA), also do not include visuomotor skills (Folstein et al., 1975; Teng et al., 1994; Chen et al., 2016).

To solve this problem, the initial aim of our study was to validate a novel VSD questionnaire that contained frequently-asked questions or common complaints of visuospatial and visuomotor symptoms obtained from caregivers or patients. In addition, we intended to use the simple questionnaire for investigating different presentations of VSD among the non-demented (ND) elderly, patients with neurodegenerative disorders including AD, DLB, or other disorders. Furthermore, during the consecutive data collection, the embedded auto-judgment program in the questionnaire continued to revise machine learning techniques to improve the ability of differential diagnosis of severity and subtypes of dementia.

MATERIALS AND METHODS

This is a sub-study of the History-based Artificial Intelligent Clinical Dementia Diagnostic System (HAICDDS) project which is currently used as a registration platform in the Show Chwan Health System. Before the starting of the study, twenty-six participants with their informants were interviewed by neuropsychologists from 3 centers of the health system and the reproducibility was investigated using the interrater reliability analysis. The results revealed a high intra-class correlation coefficient of 0.830. The detailed procedure of this project was described in our previous reports (Lin et al., 2018; Chiu et al., 2019a,b). In this study, we analyzed the data of individuals with normal cognition (NC), mild cognitive impairment (MCI), and dementia due to DLB or AD.

Diagnosis of AD or DLB

The diagnosis of DLB was made according to the revised consensus criteria for probable DLB developed by the fourth report of the DLB consortium (McKeith et al., 2017). According to these criteria, at least two of the following core features including fluctuation of cognition, VH, parkinsonism, and REM sleep behavior disorder (RBD) or one core features plus at least one indicative biomarker including abnormal dopamine transporter imaging (DaTabN), abnormal ^{123}I-metaiodobenzylguanidine (MIBG), and REM sleep without atonia (RSWA) were necessary for the diagnosis of probable DLB. AD patients were diagnosed according to the criteria for probable AD developed by the National Institute on Aging and Alzheimer's Association Workgroup (NIA-AA) (Kim et al., 2017).

Diagnosis of Non-demented Control (NDC) or Different Stages of Dementia

For the diagnosis of NDC, patients should have NC or MCI. NC was diagnosed with a global CDR (Morris, 1993) score of 0. MCI was diagnosed based on the criteria for MCI of the National Institute on Aging and Alzheimer's Association Workgroup on 2011 (Albert et al., 2011) as a change in cognition with impairment in one or more cognitive domains but no evidence of impairment in social or occupational functioning with a CDR score of 0.5 and the sum of boxes of CDR (CDR-SB) 0.5–4.0 (O'Bryant et al., 2008). The diagnosis of dementia was made according to the criteria for dementia developed by the NIA-AA (Kim et al., 2017). Participants with dementia had impairments in two or more cognitive domains as well as a decline in daily functions (at least one of the domains of community affairs, home

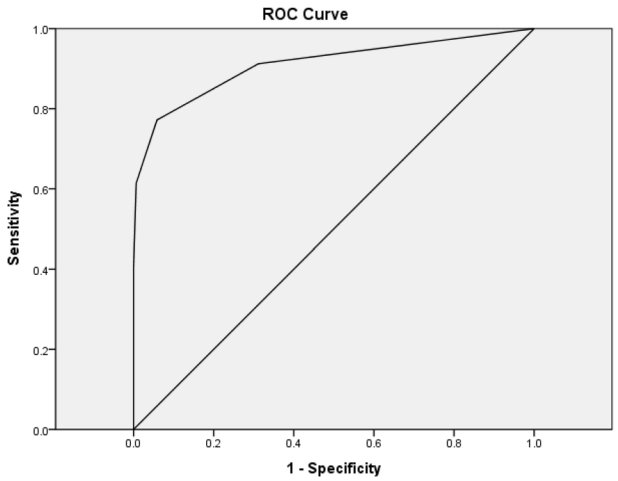

FIGURE 1 | Receiver–operating characteristic curves (ROC) of the HAI-VSQ for the discrimination of VSD in DLB and NDC. A cutoff score ≥ 2 was useful with a sensitivity of 0.77, a specificity of 0.94, and an AUC of 0.91.

hobbies, and personal care with a CDR ≥ 0.5). Dementia severity was defined by a global CDR scale. A global CDR score of 0.5, 1, 2, and 3 was defined as very mild, mild, moderate, and severe dementia, respectively (Morris, 1993).

Procedure of the Study

This is a retrospective analysis of data from the HAICDDS which is currently applied in three centers in Taiwan (two in central Taiwan and one in southern Taiwan). In the database, daily function was assessed using the Instrumental Activities of Daily Living (IADL) Scale (Lawton and Brody, 1969). Cognitive function was assessed using the Cognitive Abilities Screening Instrument (CASI) (Teng et al., 1994) and the Montreal Cognitive Assessment (MoCA) (Chen et al., 2016). Cognitive tests for all patients were performed by trained neuropsychologists. VSD was assessed using the visuospatial subscale of CASI (CASI-Draw, total score 0–10), of MoCA (MoCA-VS, total score 0–5), and of the HAICDDS (HAI-VSQ, total score 0–12) which includes 7 visuospatial/visuomotor function questions (The original Chinese version of the questionnaire with tentative English translation is shown in **Appendix Table A1**). VSD of NDC, AD, and DLB were analyzed and compared. In performing HAICDDS, informants of the participants were interviewed by a well-trained neuropsychologist and were requested to fill out the original structured questionnaire to determine the severity of dementia or cognitive impairment.

Statistics

The Chinese version of SPSS 22.0 for Windows (IBM, SPSS Inc., Chicago) was used for statistical analyses. For the determination of cut-off score for the differentiation from DLB to NCD, we want to maximize both the sensitivity and specificity therefore, the Youden's index was applied, which is maximum = sensitivity + specificity − 1. Comparisons of demographic data, neuropsychological tests, sum of boxes of CDR (CDR-SB), IADL, MoCA, MoCA-VS, CASI, CASI-Draw, HAI-VSQ, and sum of score of the Neuropsychiatric Inventory (NPI-sum) (Cummings, 1988) were compared between the different groups and analyzed using independent t-tests or one-way ANOVA with either Bonferroni or Dunnett T3 *post hoc* analysis according to the homogeneity of variance. Gender

TABLE 1 | Comparison of demographic data among the NDC (*N* = 154), AD (*N* = 229), and DLB (*N* = 57) participants.

	NDC mean (*SD*)	AD mean (*SD*)	DLB mean (*SD*)	AD vs. NDC OR, *p*-value	DLB vs. NDC *p*-value	DLB vs. AD *p*-value
Age, year	71.3 (9.2)	80.2 (7.2)	81.3 (7.0)	NA	NA	NA
CDR-SB	0.8 (0.7)	7.0 (4.6)	10.3 (5.3)	11.25, < 0.001	4.78, < 0.001	1.15, < 0.001
Female, N (%)	81 (52.6)	151 (65.9)	32 (56.1)	1.88, 0.010	0.92, NS	0.67, NS
Education	7.1 (5.1)	4.1 (4.4)	3.2 (3.7)	0.93, 0.003	0.90, 0.027	0.95, NS
HAI-VSQ	0.4 (0.6)	2.0 (2.2)	3.3 (2.2)	3.68, < 0.001	5.62, < 0.001	1.26, < 0.001
IADL	7.5 (1.0)	2.3 (2.6)	1.2 (2.1)	0.31, < 0.001	0.37, < 0.001	0.78, 0.003
MoCA	19.1 (6.1)	6.8 (5.1)	5.8 (4.8)	0.75, < 0.001	0.70, < 0.001	0.95, NS
CASI	79.4 (12.2)	41.8 (22.8)	39.7 (21.8)	0.90, < 0.001	0.89, < 0.001	0.99, NS
NPI	3.1 (5.0)	5.4 (7.7)	16.0 (16.4)	1.09, < 0.001	1.23, < 0.001	1.10, < 0.001
Fluctuation, N (%)	2 (1.3)	36 (15.7)	37 (64.9)	12.87, < 0.001	135.9, < 0.001	9.93, < 0.001
VH, N (%)	4 (2.6)	12 (5.2)	15 (26.3)	1.69, NS	17.9, < 0.001	6.64, < 0.001
Parkinsonism, N (%)	18 (11.8)	26 (11.4)	51 (89.5)	0.68, NS	41.86, < 0.001	66.64, < 0.001
RBD, N (%)	17 (11.0)	9 (3.9)	22 (38.6)	0.34, 0.023	7.89, < 0.001	17.47, < 0.001
DaTabN*, N (%)	5 (35.7)	3 (27.3)	13 (72.2)	0.64, NS	3.84, NS	10.8, 0.018
Informer age, year	61.0 (12.6)	54.1 (10.2)	56.8 (12.4)	0.94, < 0.001	0.96, 0.035	1.02, NS
Informer education, year	10.0 (4.4)	12.1 (3.3)	11.2 (3.5)	1.12, 0.011	1.07, NS	0.91, NS

Odds ratio (OR) was Adjusted for Age. NDC, Non-demented control, including normal cognition and mild cognitive impairment; AD, Alzheimer's disease; DLB, dementia with Lewy bodies; NA, Not applicable; NS, Non-significance; CDR-SB, Sum of boxes of the Clinical Dementia Rating Scale; HAI-VSQ, Visuospatial function questionnaire in the History-based Artificial Intelligent Clinical Dementia Diagnostic System (HAICDDS); IADL, Instrumental Activities of Daily Living; MoCA, Montreal Cognitive Assessment; CASI, Cognitive Abilities Screening Instrument; NPI, Neuropsychiatric Inventory; VH, Visual hallucinations; RBD, REM sleep behavior disorder; DaTabN, Abnormal dopamine transporter imaging among eight ND, 12 AD, and 17 DLB participants.*

and DLB clinical features (fluctuation, VH, RBD, Parkinsonism, and abnormal dopamine transporter imaging) (McKeith et al., 2017) were analyzed with the chi-square test. Multivariable risk estimates (OR) for each question in HAI-VSQ, CASI-Draw, and MoCA-VSQ were adjusted for age, gender, education, and cognitive function and compared between AD/NDC, DLB/NDC, and DLB/AD groups. Pearson correlation coefficients were derived between age, education, gender, CDR-SB, IADL, CASI, MoCA, and NPI of the different diagnostic tools for VSD.

Ethical Consideration

The participants were selected from a register-based database of Show Chwan Health System. The study design was retrospective and the data were analyzed anonymously. The Committee for Medical Research Ethics of Show Chwan Memorial Hospital reviewed the project and the Data Inspectorate approved the study.

RESULTS

A total of 440 individuals were studied, including 154 NDC, 229 AD, and 57 DLB participants. One or more visuospatial symptoms were reported in 31.2% of NC, 81.7% of AD, and 91.2% of DLB participants. Mean age of the NDC group (71.3 ± 9.2) was significantly smaller than those of DLB (81.3 ± 7.0) or AD (80.2 ± 7.2) using one-way ANOVA (F = 65.58; $p < 0.001$). After adjustment for age, the dementia groups showed impaired responses to all questions compared to the NDC group (all $p < 0.001$). Compared to NDC (0.4 ± 0.6) or AD (2.0 ± 2.2), the DLB (3.3 ± 2.2) group showed significantly increased total score of the HAI-VSQ after adjustment for age (both $p < 0.001$). Using HAI-VSQ, a cutoff score ≥ 2 was useful for the discrimination of VSD in DLB and NDC with a sensitivity of 0.77, a specificity of 0.94, and an AUC of 0.91 (**Figure 1**).

Additionally, the DLB group demonstrated higher CDR-SB, NPI, and Lewy body clinical features, including fluctuation of cognition, VH, Parkinsonism, and RBD after adjustment for age (all $p < 0.001$). The DLB group also demonstrated significant lower IADL, CASI, and MoCA compared to NDC or AD participants after adjustment for age (all $p < 0.001$). Compared to NDC participants, AD patients showed significantly higher CDR-SB, were proportionally more often female, had a significantly higher total score of the HAI-VSQ, NPI, and significantly higher fluctuation after adjustment for age (all $p < 0.001$). The AD patients also demonstrated lower education, IADL, MoCA, and CASI compared to NDC participants (**Table 1**).

Pearson correlation coefficients between age, education, gender, CDR-SB, IADL, CASI, MoCA, and NPI of different diagnostic tools for VSD are summarized in **Table 2**. The HAI-VSQ had weak to moderate correlation with MoCA-VS (r = -0.380, $p < 0.001$) or CASI-Draw (r = -0.467, $p < 0.001$). Furthermore, except for the non-correlation between HAI-VSQ with gender (r = -0.026, $p < 0.341$), other parameters were significantly correlated. In contrast to HAI-VSQ, MoCA-VS (r = 0.234, $p < 0.001$) and CASI-Draw (r = 0.187, $p < 0.001$) were

TABLE 2 | Point-Biserial correlation coefficients between age, education, gender, CDR-SB, IADL, CASI, MoCA, and NPI of different diagnostic tools for visuospatial dysfunction among all participants in NDC, AD, and DLB Groups.

	Age	Education	Gender	CDR-SB	IADL	MoCA	CASI	NPI	HAI-VSQ	MoCA-VS	CASI-Draw
HAI-VSQ	r = 0.330	r = −0.112	r = −0.026	r = 0.825	r = −0.602	r = −0.552	r = −0.683	r = 0.235		r = −0.380	r = −0.467
	$p < 0.001$	p = 0.019	p = 0.341	$p < 0.001$	$p < 0.001$	$p < 0.001$	$p < 0.001$	$p < 0.001$		$p < 0.001$	$p < 0.001$
MoCA-VS	r = −0.550	r = 0.584	r = 0.234	r = −0.537	r = 0.598	r = 0.842	r = 0.715	r = −0.131	r = −0.380		r = 0.599
	$p < 0.001$	$p < 0.001$	$p < 0.001$	$p < 0.001$	$p < 0.001$	$p < 0.001$	$p < 0.001$	p = 0.006	$p < 0.001$		$p < 0.001$
CASI-Draw	r = −0.396	r = 0.424	r = 0.187	r = −0.612	r = 0.565	r = 0.687	r = 0.786	r = −0.140	r = −0.467	r = 0.599	
	$p < 0.001$	$p < 0.001$	$p < 0.001$	$p < 0.001$	$p < 0.001$	$p < 0.001$	$p < 0.001$	p = 0.003	$p < 0.001$	$p < 0.001$	

CDR-SB, Sum of boxes of the Clinical Dementia Rating Scale; IADL, Instrumental Activities of Daily Living; MoCA, Montreal Cognitive Assessment; CASI, Cognitive Abilities Screening Instrument; NPI, Neuropsychiatric Inventory; HAI-VSQ, Sum score of the visuospatial questionnaire in History-based Artificial Intelligent Clinical Dementia Diagnostic System (HAICDDS); MoCA-VS, Visuospatial domain in MoCA; CASI-Draw, Visuospatial domain in CASI.

weakly correlated to gender. Compared to MoCA-VS or CASI-Draw, HAI-VSQ had the lowest correlation with age or education and the highest correlation with CDR-SB.

The comparison of visuospatial subscales in HAI-VSQ, MoCA-VS, and CASI-Draw among NDC, AD, and DLB, the odds ratio (OR) adjusted for age, education, gender, and the cognitive state by CASI total score are summarized in **Table 3**. The HAI-VSQ significantly discriminated DLB from AD or NDC whereas MoCA-VS or CASI-Draw did not.

Visuospatial subscales of HAI-VSQ (A), MoCA-VS (B), and CASI-Draw (C) in different stages of dementia with Lewy bodies (DLB) and non-DLB are summarized in **Figure 2**. Among all participants, significantly increased HAI-VSQ (all $p < 0.001$) and decreased CASI-Draw (all $p < 0.05$) were noted as the severity of dementia increased. MoCA-VS was different in the CDR 0/0.5 stage compared to other stages (all $p < 0.001$). Among DLB participants, HAI-VSQ showed significant differences in CDR 3 vs. CDR 2, CDR 3 vs. CDR 1, CDR 3 vs. CDR 0/0.5, and CDR 2 vs. CDR 0/0.5. CASI-Draw showed significant differences in CDR 0/0.5 vs. CDR 1, CDR 2, and CDR 3. MoCA-VS did not differentiate between any two stages according to CDR. Among non-DLB participants, significantly increased HAI-VSQ (all $p < 0.001$) and decreased CASI-Draw (all $p < 0.05$) were noted as the severity of dementia increased. Except for CDR 2 vs. CDR 3, significantly decreased MoCA-VS (all $p < 0.005$) was noted as the severity of dementia increased.

DISCUSSION

This study was a sub-study of the HAICDDS project, analyzing and comparing data between NDC, AD, and DLB groups with two main results. First, using HAI-VSQ, a cutoff score ≥ 2 discriminates VSD in DLB from NDC with high sensitivity (0.77), specificity (0.94), and AUC (0.91). To provide more objective evidence, we analyzed the correlation of the HAI-VSQ with dopamine transporter imaging among NDC and DLB groups and the result showed a high negative correlation of striatal background ratio (SBR) of dopamine transporter imaging with the HAI-VSQ with correlation coefficient -0.571 and $p < 0.001$. These findings have provided additional evidence that the HAI-VSQ has high correlation with DLB because of abnormal dopamine transporter imaging being the indicative biomarker for the diagnosis of DLB. Therefore, we provided a simple tool that can help clinicians to detect DLB more easily at the bedside or in clinics. Additionally, HAI-VSQ is probably the first informant-based VSD questionnaire that includes not only visuospatial but also visuomotor questions. We found more severe VSD according to the questionnaire in patients with DLB compared to NDC or AD. In this study, one or more visuospatial or visuomotor symptoms were reported in 31.2% of NDC, and 81.7% of AD and 91.2% of DLB patients. In mild stages, symptoms were reported in 74.4% of AD and 80.8% of DLB patients in CDR = 0.5 or 1. These results are consistent with previous studies on VSD that showed common and early symptoms in AD as well as in DLB (Culham et al., 2006; Tippett et al., 2007; Oda et al., 2009; Galati et al., 2011; Yamaguchi et al., 2011; Hamilton et al., 2012; Yoshizawa et al., 2013; Hawkins and Sergio, 2014; Li et al., 2014). More severe VSD in DLB according to the HAI-VSQ compared to AD is also consistent with results from previous studies (Oda et al., 2009; Yamaguchi et al., 2011; Li et al., 2014).

Second, compared to MoCA-VS or CASI-Draw, HAI-VSQ had no correlation with gender and the lowest correlation with age and education. We considered this an important result because the current frequently-used dementia screening tools such as MoCA or CASI are too sensitive to age, gender, culture, and education. Therefore, a large variety of cut-off scores and adjustments are necessary for the screening of dementia or cognitive impairment when using these tools (Lin et al., 2002; Nasreddine et al., 2005; Chen et al., 2016). Furthermore, HAI-VSQ had the highest correlation with CDR-SB which had the highest correlation with dementia severity compared to the MoCA-VS or CASI-Draw scales.

In addition to above-mentioned findings, after adjustment for age, education, gender, and cognitive state by CASI total score, HAI-VSQ was significantly different in DLB patient than in NDC (OR = 4.28, $p < 0.001$) or AD patients (OR = 1.48, $p < 0.001$), and between AD patients and NDC participants (OR = 2.79, $p < 0.001$). MoCA-VS or CASI-Draw showed no significant differences. This finding underlines the clinical applicability of the HAI-VSQ for the discrimination of DLB from AD or NDC and of AD from NDC participants. This also indicates that the information acquired from caregivers may be more useful or at least as useful as the cognitive performance of patients because the caregivers directly face the caring problems which might result in a higher impact of VSD on them.

Finally, we want to address the important issue that commonly-used informant-based questionnaires for the screening of dementia or cognitive impairment from normal elderly including CDR, AD8, or IQCODE are lacking or

TABLE 3 | Comparison of visuospatial subscales in HAICDDS (HAI-VSQ), MoCA (MoCA-VS), and CASI (CASI-Draw) among NDC (*N* = 154), AD (*N* = 229), and DLB (*N* = 57) participants.

	NDC mean (SD)	AD mean (SD)	DLB mean (SD)	AD vs. NDC OR, *p*-value	DLB vs. NDC OR, *p*-value	DLB vs. AD OR, *p*-value
HAI-VSQ	0.4 (0.6)	2.0 (2.2)	3.3 (2.2)	2.79, < 0.001	4.28, < 0.001	1.48, < 0.001
MoCA-VS	2.5 (1.6)	0.5 (1.0)	0.4 (0.7)	0.81, NS	0.70, NS	0.96, NS
CASI-Draw	8.6 (2.5)	4.9 (4.1)	4.3 (3.5)	1.25, 0.003	1.03, NS	1.02, NS

Odds Ratio (OR) was Adjusted for Age, Education, Gender, and Cognitive State by CASI Total Score. NDC, Non-demented control; AD, Alzheimer's disease; DLB, dementia with Lewy bodies; NA, Not applicable; NS, Non-significance; HAI-VSQ, Visuospatial function questionnaire in History-based Artificial Intelligent Clinical Dementia Diagnostic System (HAICDDS); MoCA-VS, Visuospatial domain in MoCA; CASI-Draw, Visuospatial domain in CASI.

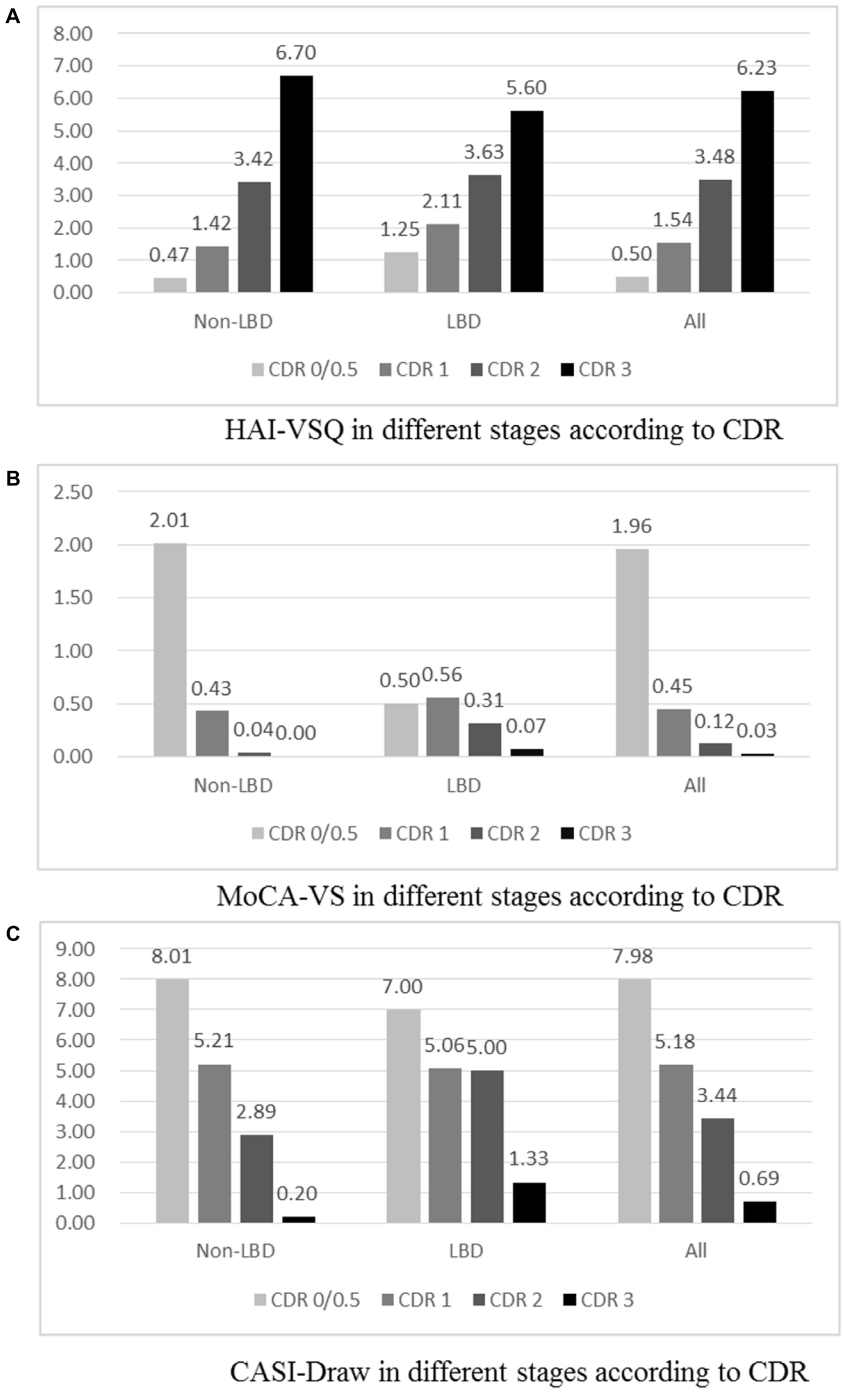

FIGURE 2 | Visuospatial subscales of HAICDDS (HAI-VSQ, **A**), MoCA (MoCA-VS, **B**), and CASI (CASI-Draw, **C**) in different stages of dementia with Lewy bodies (DLB), non-DLB, and all participants. Participants with CDR 0 were classified only in the non-LBD group and all participants. **(A)** HAI-VSQ in different stages according to CDR. **(B)** MoCA-VS in different stages according to CDR. (1c) CASI-Draw in different stages according to CDR.

have only a few questions regarding VSD (Jorm et al., 1991; Morris, 1993; Galvin et al., 2005; Razavi et al., 2014). We are providing a simple informant-based visuospatial questionnaire for the clinical assessment of individuals with dementia. The purpose of our study was not using a cut-off score for the discrimination of patients with language dysfunction from normal people. Instead, we want to provide an easy way for clinicians to be aware of the visuospatial as well as visuomotor problems of patients with dementia due to AD or DLB.

There are several limitations to this study. First, the questionnaire is an original Taiwanese version. More precise and colloquial translations will be necessary when translating the questionnaire to other language versions although we have preliminarily translated the questionnaire to English. Second, our study was conducted in only three centers in Taiwan and the questionnaire contained only seven questions. The findings of different presentations of VSD may not be generalizable to all individuals with NDC, AD, or DLB. Third, the comparison among different groups in our study was retrospective and cross-sectional. Therefore, a causal relationship between VSD and the underlying pathophysiologies of AD or DLB could not be investigated.

CONCLUSION

In conclusion, our study showed that similar to our recently published language questionnaire (HAICDDS-Language) (Lin et al., 2018), the informant-based simple questionnaire was a practical screening tool and was more applicable than the visuospatial subscale of MoCA or CASI for the discrimination of NDC, AD, and DLB. We intend to design and validate several dementia-related simple questionnaires and hope that these rapid screening tools can be applied in clinical practice as well as in a registration platform for the screening of VSD as well as other cognitive dysfunctions. A further goal is to implement machine learning techniques to improve the accuracy and efficiency of these questionnaires.

DATA AVAILABILITY STATEMENT

The raw data supporting the conclusions of this article will be made available by the authors, without undue reservation, to any qualified researcher.

ETHICS STATEMENT

The studies involving human participants were reviewed and approved by the Show Chwan Memorial Hospital. Written informed consent for participation was not required for this study in accordance with the national legislation and the institutional requirements.

AUTHOR CONTRIBUTIONS

C-TW undertook the literature search and data analysis, edited the Author Contributions, and was mainly responsible for the revisions and drafts of the manuscript. P-YC participated in the data analysis and contributed to the revisions and final draft of the manuscript. G-UH and R-CT undertook the literature search and contributed to revisions. C-YW contributed to revisions of the manuscript.

FUNDING

The study was funded by the Show Chwan Memorial Hospital No. RD-105032.

ACKNOWLEDGMENTS

We would like to thank Prof. Shu-Hui Sue at the National Taichung University of Science and Technology and Prof. Tsung-Lin Cheng at the National Changhua University of Education for their feedback and suggestions during the experimental design and statistical analysis.

REFERENCES

Albert, M. S., DeKosky, S. T., Dickson, D., Dubois, B., Feldman, H. H., Fox, N. C., et al. (2011). The diagnosis of mild cognitive impairment due to Alzheimer's disease: recommendations from the National Institute on Aging-Alzheimer's Association workgroups on diagnostic guidelines for Alzheimer's disease. *Alzheimers Dement.* 7, 270–279. doi: 10.1016/j.jalz.2011.03.008

Chen, K. L., Xu, Y., Chu, A. Q., Ding, D., Liang, X. N., Nasreddine, Z. S., et al. (2016). Validation of the Chinese version of Montreal cognitive assessment basic for screening mild cognitive impairment. *J. Am. Geriatr. Soc.* 64, e285–e290. doi: 10.1111/jgs.14530

Chiu, P. Y., Tang, H., Wei, C. Y., Zhang, C., Hung, G. U., and Zhou, W. (2019a). NMD-12: a new machine-learning derived screening instrument to detect mild cognitive impairment and dementia. *PLoS One* 14:e0213430. doi: 10.1371/journal.pone.0213430

Chiu, P.-Y., Wei, C.-Y., and Hung, G.-U. (2019b). Preliminary study of the history-based artificial intelligent clinical dementia diagnostic system. *Show Chwan Med. J.* 18, 18–27. doi: 10.3966/156104972019061801003

Culham, J. C., Cavina-Pratesi, C., and Singhal, A. (2006). The role of parietal cortex in visuomotor control: what have we learned from neuroimaging? *Neuropsychologia* 44, 2668–2684. doi: 10.1016/j.neuropsychologia.2005.11.003

Cummings, J. L. (1988). Intellectual impairment in Parkinson's disease: clinical, pathologic, and biochemical correlates. *J. Geriatr. Psychiatry Neurol.* 1, 24–36. doi: 10.1177/089198878800100106

Folstein, M. F., Folstein, S. E., and McHugh, P. R. (1975). "Mini-mental state". A practical method for grading the cognitive state of patients for the clinician. *J. Psychiatr. Res.* 12, 189–198.

Galati, G., Committeri, G., Pitzalis, S., Pelle, G., Patria, F., Fattori, P., et al. (2011). Intentional signals during saccadic and reaching delays in the human posterior parietal cortex. *Eur. J. Neurosci.* 34, 1871–1885. doi: 10.1111/j.1460-9568.2011.07885.x

Galvin, J. E., Roe, C. M., Powlishta, K. K., Coats, M. A., Muich, S. J., Grant, E., et al. (2005). The AD8: a brief informant interview to detect dementia. *Neurology* 65, 559–564. doi: 10.1212/01.wnl.0000172958.95282.2a

Hamilton, J. M., Landy, K. M., Salmon, D. P., Hansen, L. A., Masliah, E., and Galasko, D. (2012). Early visuospatial deficits predict the occurrence of visual hallucinations in autopsy-confirmed dementia with Lewy bodies. *Am. J. Geriatr. Psychiatry* 20, 773–781. doi: 10.1097/JGP.0b013e31823033bc

Hawkins, K. M., and Sergio, L. E. (2014). Visuomotor impairments in older adults at increased Alzheimer's disease risk. *J. Alzheimers Dis.* 42, 607–621. doi: 10.3233/jad-140051

Jorm, A. F., Scott, R., Cullen, J. S., and MacKinnon, A. J. (1991). Performance of the informant questionnaire on cognitive decline in the elderly (IQCODE) as a screening test for dementia. *Psychol. Med.* 21, 785–790. doi: 10.1017/s0033291700022418

Kim, J., Na, H. K., Byun, J., Shin, J., Kim, S., Lee, B. H., et al. (2017). Tracking cognitive decline in amnestic mild cognitive impairment and early-stage

alzheimer dementia: mini-mental state examination versus neuropsychological battery. *Dement. Geriatr. Cogn. Disord.* 44, 105–117. doi: 10.1159/000478520

Lawton, M. P., and Brody, E. M. (1969). Assessment of older people: self-maintaining and instrumental activities of daily living. *Gerontologist* 9, 179–186. doi: 10.1093/geront/9.3_part_1.179

Li, X., Rastogi, P., Gibbons, J. A., and Chaudhury, S. (2014). Visuo-cognitive skill deficits in Alzheimer's disease and Lewy body disease: a comparative analysis. *Ann. Indian Acad. Neurol.* 17, 12–18. doi: 10.4103/0972-2327.128530

Lin, C. M., Hung, G. U., Wei, C. Y., Tzeng, R. C., and Chiu, P. Y. (2018). An informant-based simple questionnaire for language assessment in neurodegenerative disorders. *Dement. Geriatr. Cogn. Disord.* 46, 207–216. doi: 10.1159/000493540

Lin, K. N., Wang, P. N., Liu, C. Y., Chen, W. T., Lee, Y. C., and Liu, H. C. (2002). Cutoff scores of the cognitive abilities screening instrument, Chinese version in screening of dementia. *Dement. Geriatr. Cogn. Disord.* 14, 176–182. doi: 10.1159/000066024

McKeith, I. G., Boeve, B. F., Dickson, D. W., Halliday, G., Taylor, J. P., Weintraub, D., et al. (2017). Diagnosis and management of dementia with Lewy bodies: fourth consensus report of the DLB consortium. *Neurology* 89, 88–100. doi: 10.1212/wnl.0000000000004058

McKhann, G. M., Knopman, D. S., Chertkow, H., Hyman, B. T., Jack, C. R. Jr., Kawas, C. H., et al. (2011). The diagnosis of dementia due to Alzheimer's disease: recommendations from the National Institute on Aging-Alzheimer's Association workgroups on diagnostic guidelines for Alzheimer's disease. *Alzheimers Dement.* 7, 263–269. doi: 10.1016/j.jalz.2011.03.005

Morris, J. C. (1993). The clinical dementia rating (CDR): current version and scoring rules. *Neurology* 43, 2412–2414. doi: 10.1212/wnl.43.11.2412-a

Nasreddine, Z. S., Phillips, N. A., Bedirian, V., Charbonneau, S., Whitehead, V., Collin, I., et al. (2005). The Montreal cognitive assessment, MoCA: a brief screening tool for mild cognitive impairment. *J. Am. Geriatr. Soc.* 53, 695–699. doi: 10.1111/j.1532-5415.2005.53221.x

O'Bryant, S. E., Waring, S. C., Cullum, C. M., Hall, J., Lacritz, L., Massman, P. J., et al. (2008). Staging dementia using clinical dementia rating scale sum of boxes scores: a Texas Alzheimer's research consortium study. *Arch. Neurol.* 65, 1091–1095. doi: 10.1001/archneur.65.8.1091

Oda, H., Yamamoto, Y., and Maeda, K. (2009). The neuropsychological profile in dementia with Lewy bodies and Alzheimer's disease. *Int. J. Geriatr. Psychiatry* 24, 125–131. doi: 10.1002/gps.2078

Razavi, M., Tolea, M. I., Margrett, J., Martin, P., Oakland, A., Tscholl, D. W., et al. (2014). Comparison of 2 informant questionnaire screening tools for dementia and mild cognitive impairment: AD8 and IQCODE. *Alzheimer Dis. Assoc. Disord.* 28, 156–161. doi: 10.1097/wad.0000000000000008

Teng, E. L., Hasegawa, K., Homma, A., Imai, Y., Larson, E., Graves, A., et al. (1994). The cognitive abilities screening instrument (CASI): a practical test for cross-cultural epidemiological studies of dementia. *Int. Psychogeriatr.* 6, 45–58; discussion 62.

Tippett, W. J., Krajewski, A., and Sergio, L. E. (2007). Visuomotor integration is compromised in Alzheimer's disease patients reaching for remembered targets. *Eur. Neurol.* 58, 1–11. doi: 10.1159/000102160

Yamaguchi, H., Takahashi, S., Kosaka, K., Okamoto, K., Yamazaki, T., Ikeda, M., et al. (2011). Yamaguchi fox-pigeon imitation test (YFPIT) for dementia in clinical practice. *Psychogeriatrics* 11, 221–226. doi: 10.1111/j.1479-8301.2011.00373.x

Yoshizawa, H., Vonsattel, J. P., and Honig, L. S. (2013). Early neuropsychological discriminants for Lewy body disease: an autopsy series. *J. Neurol. Neurosurg. Psychiatry* 84, 1326–1330. doi: 10.1136/jnnp-2012-304381

Conflict of Interest: P-YC's work has been partly supported by the Show Chwan Memorial Hospital.

The remaining authors declare that the research was conducted in the absence of any commercial or financial relationships that could be construed as a potential conflict of interest.

APPENDIX

TABLE A1 | Composition of the visuospatial questionnaire in HAICDDS (HAI-VSQ).

VS1	方向感變差了嗎？	☐不會	☐ 會	
	Does he/she have trouble finding directions?	☐ No	☐ Yes	
VS2	在熟悉的環境（例如：住家附近）會迷路嗎？	☐ 不會	☐ 會	
	Does he/she get lost in familiar surroundings, for example, the neighborhood?	☐ No	☐ Yes	
VS3	會搞不清楚自己在哪裏嗎？	☐ 不會	☐ 偶而	☐ 常常
	Does he/she have trouble locating himself/herself?	☐ No	☐ Occasionally	☐ Often
VS4	會「常常」認錯人，例如：把兒子當成丈夫，把女兒當成姊妹嗎？	☐ 不會	☐ 偶而	☐ 常常
	Does he/she often recognize the wrong person, for example, recognizing son as husband or daughter as sister?	☐ No	☐ Occasionally	☐ Often
VS5	走路、騎車或是開車的時候沒辦法直直走，常常偏到旁邊去嗎?	☐ 不會	☐ 偶而	☐ 常常
	Does he/she often deviate to one side during walking, riding, or driving on the road?	☐ No	☐ Occasionally	☐ Often
VS6	沒辦法順利地開門，好像找不太到鑰匙孔或門把嗎?	☐ 不會	☐ 偶而	☐ 常常
	Does he/she have difficulties in finding the keyhole or doorknob for opening the door?	☐ No	☐ Occasionally	☐ Often
VS7	閱讀或是寫字變得困難嗎?	☐ 不會	☐ 偶而	☐ 常常
	Does he/she have difficulties in reading or writing?	☐ No	☐ Occasionally	☐ Often

frontiers in Aging Neuroscience

ORIGINAL RESEARCH
published: 06 February 2020
doi: 10.3389/fnagi.2020.00023

Electroacupuncture Ameliorates Cognitive Impairment by Inhibiting the JNK Signaling Pathway in a Mouse Model of Alzheimer's Disease

Yinshan Tang[1]†, Anping Xu[2]*†, Shujun Shao[2], You Zhou[1], Bing Xiong[1] and Zhigang Li[2]*

[1] Department of Rehabilitation and Traditional Chinese Medicine, The Second Affiliated Hospital of Zhejiang University School of Medicine, Hangzhou, China, [2] School of Acupuncture, Moxibustion and Tuina, Beijing University of Chinese Medicine, Beijing, China

Electroacupuncture (EA) has become popular for its adjustable strength and frequency and easy quantification in the clinic and has demonstrated therapeutic potential for Alzheimer's disease (AD). However, the mechanism remains unknown. Abnormally activated c-Jun N-terminal kinase (JNK) has been closely related to the pathological process of AD. The aim of this study was to investigate the effect of EA on cognitive impairment and the role of the JNK signaling pathway in AD model amyloid precursor protein (APP)/presenilin 1 (PS1) mice. The memory and learning ability of each group was assessed using the Morris Water Maze (MWM). Immunofluorescence, immunohistochemistry and Western blot were performed to measure the expression of APP, JNK, phosphorylated (P-)JNK, mitogen-activated protein kinase 4 (MKK4), MKK7, c-Jun and caspase-3 in hippocampal tissue samples in APP/PS1 mice after EA intervention. Obvious cognitive deficits were observed in the AD model APP/PS1 mice in the MWM test and were associated with JNK signaling pathway activation and APP upregulation. Four weeks of EA significantly ameliorated the cognitive impairments and inhibited JNK signaling pathway activation and APP upregulation. Taken together, the findings demonstrated that EA can reverse cognitive deficits and substantially lower the burden of APP in AD model APP/PS1 mice, at least partially through inhibiting the JNK signaling pathway and regulating apoptosis signals. Therefore, EA may offer an effective alternative therapeutic approach for AD.

Keywords: electroacupuncture, Alzheimer's disease, APP/PS1 mice, cognitive impairment, JNK signaling pathway, apoptosis

OPEN ACCESS

Edited by:
Jiehui Jiang,
Shanghai University, China

Reviewed by:
Yung-Feng Liao,
Academia Sinica, Taiwan
Cheng Yong Liu,
Affiliated Hospital of Nanjing University of Chinese Medicine, China

***Correspondence:**
Yinshan Tang
2314038@zju.edu.cn
Anping Xu
xuanping01@163.com

† These authors have contributed equally to this work

Received: *11 October 2019*
Accepted: *22 January 2020*
Published: *06 February 2020*

Citation:
Tang Y, Xu A, Shao S, Zhou Y, Xiong B and Li Z (2020) Electroacupuncture Ameliorates Cognitive Impairment by Inhibiting the JNK Signaling Pathway in a Mouse Model of Alzheimer's Disease. Front. Aging Neurosci. 12:23. doi: 10.3389/fnagi.2020.00023

INTRODUCTION

Alzheimer's disease (AD), the most common cause of dementia, is a slowly progressive neurodegenerative disease that ultimately leads to impairments in several brain functions, such as learning and memory (McKhann et al., 2011). The patient's ability to live and socialize is severely impaired. The "World Alzheimer Report 2018" noted that is one new dementia patient every three

seconds in the world and that by 2050, there will be 152 million dementia patients worldwide. Therefore, AD has become a significant global social burden (Lozano et al., 2012).

The classic amyloid hypothesis states that the deposition of amyloid β (Aβ) protein (Morris et al., 1996; Pike et al., 2007), which is generated by β-amyloid precursor protein (APP) cleavage, is the major event in AD pathology. The aggregation of Aβ initiates irreversible neurodegeneration, which leads to neuronal cell damage and even death (Emerit et al., 2004). Studies have shown that dying cells in the brains of AD patients, including neurons, are characterized by apoptosis (Bredesen et al., 2006).

c-Jun N-terminal kinases (JNKs) belong to the family of stress-activated protein kinases (Kim and Choi, 2010). The JNK pathway plays an important role in a variety of physiological and pathological processes that are mainly involved in apoptosis. JNK activation has been identified as a key element responsible for the regulation of apoptosis signals. Studies have shown that the early activation of JNK is always accompanied by neuronal apoptosis induced by the deposition of Aβ in the brain, indicating that activation of the JNK signaling pathway is involved in the deposition of Aβ and its induced neurotoxicity (Lagalwar et al., 2006; Tare et al., 2011; Li G. Q. et al., 2018). Therefore, abnormally activated JNK is closely related to the pathological process of AD (Ramin et al., 2011; Yarza et al., 2016).

Despite the development of diagnostic techniques for AD, effective and safe therapeutic interventions remain to be found. Because of its curative effects and few side effects, acupuncture has been practiced in more than 183 countries and areas. Compared with manual acupuncture (MA), electroacupuncture (EA) has become popular for its adjustable strength, frequency and easy quantification in the clinic (Pan et al., 2017; Li S. et al., 2018). Studies have also shown that the effect of acupuncture on the brain is integrated at multiple levels, and EA is progressively being used in more clinical practices (Sun et al., 2016; Wei et al., 2016; Chang et al., 2017). In recent years, acupuncture has been used for treating AD and reported to have effectiveness in improving cognitive function (Jiang et al., 2015; Cao et al., 2017; Ding et al., 2019). However, the possible mechanism of action of acupuncture or EA on cognition in AD patients remains uncertain, limiting the application of these studies to guide clinical practice. The mechanism of action of acupuncture must be explored.

Therefore, in this study, we investigated the effect of EA, focusing on the JNK pathway, to determine whether there is an important function of EA in the regulation of the JNK pathway and JNK-dependent apoptosis in AD and further elucidate the mechanism of the potential therapeutic effects of EA.

MATERIALS AND METHODS

Animals and Experimental Groups

Forty 7-month-old male APP/PS1 mice and ten age- and gender-matched C57BL/6 mice were sourced from Beijing HuaFuKang Biotech [Certificate number: SCXK (Jing) 2014-0004], weighing 30 ± 2 g. The APP/PS1 mice were randomly divided into four groups: the model (AD) group, the model + SP600125 (AD + SP) group, the model + EA (AD + EA) group and the model + EA + SP600125 (AD + SP + EA) group, with ten mice in each group. The C57BL/6 mice served as the normal control (N) group. To avoid outside interference, all mice were housed separately in standard mouse cages under constant temperature (23 ± 2°C) and constant humidity (40–60%), with free access to water and food. The study was conducted in strict accordance with the Animal Ethics Committee of Beijing University of Chinese Medicine. We made every effort to minimize the suffering of the animals during the experimental procedure. This animal experiment has been approved by Experimental Animal Ethics Committee of the Second Affiliated Hospital of Zhejiang University (No. 2015-084).

Apparatus and Reagents

Reagents and apparatuses are displayed in **Table 1**.

Methods of Intervention

EA treatment was performed on the AD + EA and AD + SP + EA groups on the acupuncture points Baihui (GV20) (located on the bregma, midpoint of the linking line of mouse ears), Yintang (GV29) (located in the forehead, the middle depression of the two eyebrows at the medial end), and Shuigou (GV26) (located on the face, at the upper one-third of the philtrum) (**Figure 1**, Tang et al., 2019). Baihui (GV20) and Yintang (GV29) received EA intervention for 20 min, with an intensity of 1 mA and a frequency of 1 Hz, followed by fast pricking of Shuigou (GV26). To immobilize the mice, We have made special bags based on the size of the mice. Ever since the mice crawled inside the bags, two clips would be performed to close the opening back of the bags, which absolutely control and immobilize the mice well. Since the first third of the bags were reticulated, experimental mice could breath properly.

SP600125 was injected intraperitoneally (30 mg/kg) into the AD + SP and AD + SP + EA groups before EA treatment.

TABLE 1 | Apparatus and reagents used in this study.

Apparatus	Source	Details
Disposable sterile acupuncture needle	Beijing Zhongyan Taihe Medical Instrument, Co., Ltd	Model: ZYTH2013030504, specification: 0.25 mm × 13 mm
Electroacupuncture apparatus	Peking University Institute of Science Nerve and Beijing Hua Wei Industrial Development Company	Model: HANS-LH202
Morris water maze	Shanghai Xinruan Information Technology, Co., Ltd	Model: XR-XM101
Image acquisition and analysis software	China Daheng Group, Inc	China Daheng Group, Inc., Beijing Image Vision Technology Branch
SP600125	Sigma-Aldrich, St. Louis, MO, United States	

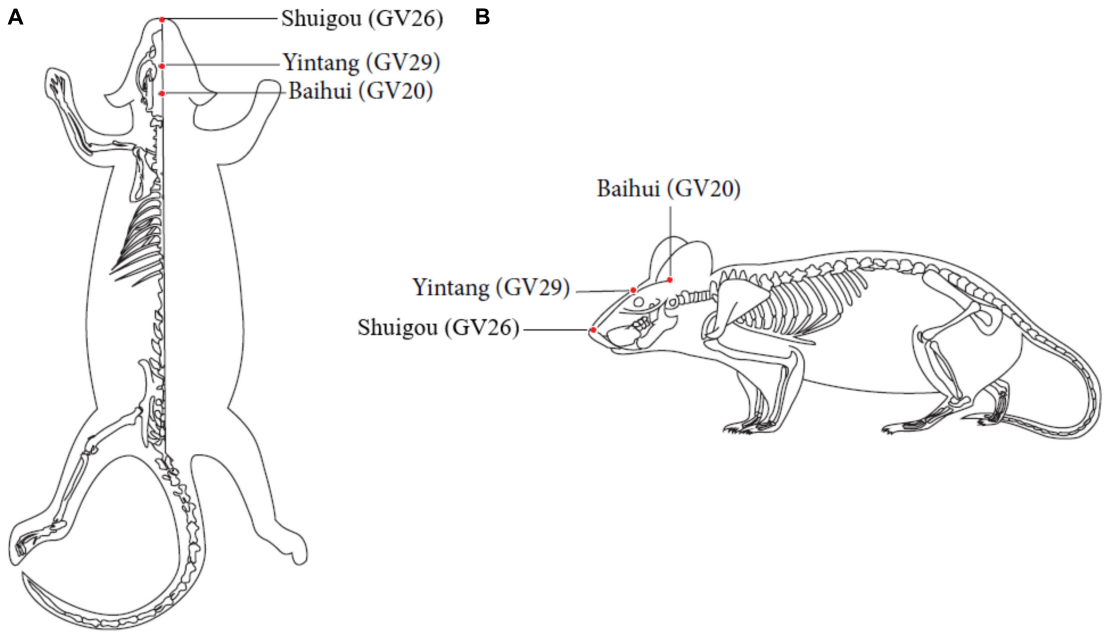

FIGURE 1 | Locations of acupoints we applied in this study. Red points indicate the three governor vessel acupoints respectively: GV20, GV29, and GV26. **(A)**Top views of GV20, GV29, and GV26. **(B)** Locations of GV20, GV29, and GV26.

SP600125 (Sigma-Aldrich, St. Louis, MO, United States) is a JNK pathway blocker and was prepared with 2% dimethyl sulfoxide (DMSO) solvent.

Mice in the N, AD, and AD + SP groups received no EA treatment but were held and bound to ensure an equivalent trial condition. The intervention was performed once every other day for 4 weeks.

Morris Water Maze (MWM)

Cognitive impairment was assessed using the MWM test, including a training trial and a probe trial to measure memory (D'Hooge and De Deyn, 2001; Vorhees and Williams, 2006). Throughout the training trials, the location of the platform was fixed in the center of the third quadrant (target quadrant) and submerged approximately 1 cm beneath the water surface. The training trial was repeated for five consecutive days. The mice were gently released from the first, second and fourth quadrants, sequentially, in each trial, at an equal distance to the center of the tank. The trial was terminated if the mouse failed to climb onto the platform within 60 s. Spatial acquisition performance was evaluated by assessing the escape latency to reach the platform. A 60-s probe trial was administered 24 h after the last training session. In the probe trial, the platform was removed from the pool, and the mice were placed in the first, second and fourth quadrants, sequentially. The swimming speed, frequency of crossing the platform in the target quadrant (the previous platform location), and percentage of time spent swimming in the third quadrant housing the platform within 60 s were measured by an automated analysis system.

Sample Collection

Hippocampal sections were isolated and perfused with PBS and 0.2% Triton X-100 and then fixed in 4% paraformaldehyde for 24 h. The left brain sections were rapidly frozen at −50°C and then transversely cut into 5-μm slices.

In addition, seven mice in each group were anesthetized with chloral hydrate, and the hippocampus was collected. The obtained samples were rapidly frozen in liquid nitrogen and stored at −80°C until use.

Immunohistochemistry

Immunohistochemistry was performed on formalin-fixed, paraffin-embedded right brain hippocampal sections using three 5-μm coronal hippocampal sections per mouse. Anti-mitogen-activated protein kinase kinase 7 (MKK7, 1:100) and c-Jun (60A8) rabbit mAb (1:70) were diluted in PBS, and the sections were incubated at 4°C overnight, washed, and then stained with biotinylated secondary antibody for 10 min. Positive expression was detected by staining the sections with DAB (DAB2031, MXB, China) for 10 min. Microscopy (BX53, Olympus, China) was performed, and images were obtained at 100 × and 400 × magnification. Information on the primary antibodies are displayed in **Table 2**.

Immunofluorescence

Slices were incubated at 4°C with the anti-APP (1:150), anti-MEK4/MKK4 (1:75) and anti-caspase-3 (1:100) antibodies. After permeabilization and blocking overnight, appropriate secondary antibodies (IgG H&L) were used at a dilution of 1:200. After the sections were washed three times with PBS, they were incubated

with DAPI (C0065, Solarbio, China) for 10 min, followed by live imaging. The hippocampal images were captured and obtained with a confocal laser microscope (FV1000, Olympus, Japan) at 1000 × magnification. Information on the primary antibodies are displayed in **Table 2**.

Western Blot (WB)

The extracted proteins were separated by electrophoresis with 10% SDS-PAGE. The gel was run at 80 V for 20 min and 120 V for 60 min and then transferred onto PVDF membranes at 4°C and 80 V for 1.5 h. The target proteins APP, P-JNK1/2, MKK4, MKK7, c-Jun and caspase-3 were measured by incubation with the primary antibodies against APP (1:2000), JNK1/2 (1:1000), P-JNK1/2 (1:500), MKK4 (1:2000), p-MKK4(1:500), MKK7 (1:1000), p-MKK7(1:500), c-Jun (1:1000) and caspase-3 (1:1000) at 4°C overnight. After the gels were washed three times with TBST, the corresponding secondary antibody was used at a dilution of 1:2000, 1:2000, 1:1000, 1:2000, 1:1000, 1:2000, 1:2000, 1:1000 or 1:2000, respectively, followed by visualization with an ECL kit (mixed with 1:1, PE0010, Solarbio, China). The exposure was completed in a dark room with a chemiluminescence gel imaging system (C600, Azure Biosystems, United States). Antibodies against GAPDH (primary antibody 1:5000 and secondary antibody 1:100000) were used as internal controls. Quantitative results are expressed as a ratio of target proteins to GAPDH and then compared to all groups to measure relative changes. Information on the primary antibodies are displayed in **Table 2**.

Statistical Analysis

Statistical analysis was performed using IBM SPSS Statistics 20 software. Two-way ANOVA with repeated measures was used to analyze group differences in the training trial. The results of the probe trial and WB were analyzed by one-way ANOVA, and the least significant difference (LSD) pairwise comparison method was used among groups. Data are expressed as the means ± SD. Statistical significance was set at $p < 0.05$, and high statistical significance was set at $p < 0.01$.

TABLE 2 | Information on the primary antibodies used in this study.

Antibody	Host species	Antibody code	Company
Anti-APP antibody [Y188]	Rabbit	ab32136	Abcam, United Kingdom
Anti-JNK1 + JNK2 (phospho T183 + Y185) antibody	Rabbit	ab4821	Abcam, United Kingdom
Anti-JNK	Rabbit	9252S	CST, United States
Anti-MKK7 [EP1455Y]	Rabbit	ab52618	Abcam, United Kingdom
Anti-MKK7(phosphor T275)	Rabbit	ab192592	Abcam, United Kingdom
Anti-MEK4/MKK4	Rabbit	ab131494	Abcam, United Kingdom
Anti-MEK4/MKK4(phospho S80)	Rabbit	ab131353	Abcam, United Kingdom
c-Jun (60A8) rabbit mAb	Rabbit	9165S	CST, United States
Anti-caspase-3	Rabbit	ab13847	Abcam, United Kingdom
Anti-GAPDH	Mouse	ab8245	Abcam, United Kingdom
IgG H&L	Goat	ab150080	Abcam, United Kingdom
Biotinylated secondary antibody	Rabbit	KIT-9706	MXB, China

RESULTS

EA Intervention Ameliorates Cognitive Impairment in APP/PS1 Mice

In the MWM training trials, the mice in every group showed a downward trend in escape latency from day 1 to day 5 (**Figures 2A,B**). However, compared with the N group, the AD group showed worse spatial learning performance over all training sessions ($P < 0.01$). Compared with the escape latency of the AD group, the escape latency of the AD + EA and AD + SP + EA groups was lower and significantly lower on days 4 and 5 ($P < 0.01$). Compared with the AD + SP group, the AD + EA and AD + SP + EA groups also showed significantly lower escape latency on day 5 ($P < 0.01$).

In the MWM probe trial on day 6, platform crossing frequency and time spent in quadrant III were tested (**Figures 2C,D**). A higher platform crossing frequency and greater amount of time spent in quadrant III indicate a higher level of memory maintenance. The platform crossing frequency in the AD group was significantly lower than that in the N group ($P < 0.01$). However, compared with the AD group, the AD + EA and AD + SP + EA groups showed a significantly greater number of platform crossings ($P < 0.01$). Furthermore, the AD + EA and AD + SP + EA groups spent more time in quadrant III than the AD + SP group ($P < 0.01$). **Figures 2E–I** shows the representative strategies for searching for the platform of each group. The AD group showed an edge search strategy, suggesting that 7-month APP/PS1 mice displayed obvious impairment in learning and memory. The N group showed a search strategy that was similar to that of the AD + SP, AD + EA and AD + SP + EA groups.

EA Intervention Lowers the Burden of APP in the Hippocampus of APP/PS1 Mice

We next evaluated the distribution and accumulation of APP in the mouse brain hippocampus by immunofluorescence and WB. Immunofluorescence showed the expression of APP in the hippocampus, with obvious higher expression in the AD group (**Figures 3A–A2,B–B2**) that was decreased in the AD + SP, AD + EA, and AD + SP + EA groups (**Figures 3C–C2,D–D2,E–E2**). WB results showed notably higher accumulation of APP in the AD and AD + SP groups compared to that in the N group ($P < 0.01$), while the AD + EA and AD + SP + EA groups showed lower expression of APP than the AD group ($P < 0.05$ and $P < 0.01$). Furthermore, the AD + EA and AD + SP + EA groups showed lower expression of APP than the AD + SP group ($P < 0.05$ and $P < 0.01$) (**Figures 3F,G**). These results confirmed the efficacy of the EA intervention in decreasing the deposition of APP.

EA Intervention Inhibits JNK Signaling Pathway Activation in the Hippocampus of APP/PS1 Mice

We hypothesized that the decrease in APP deposition is related to the JNK signal transduction pathway. To test

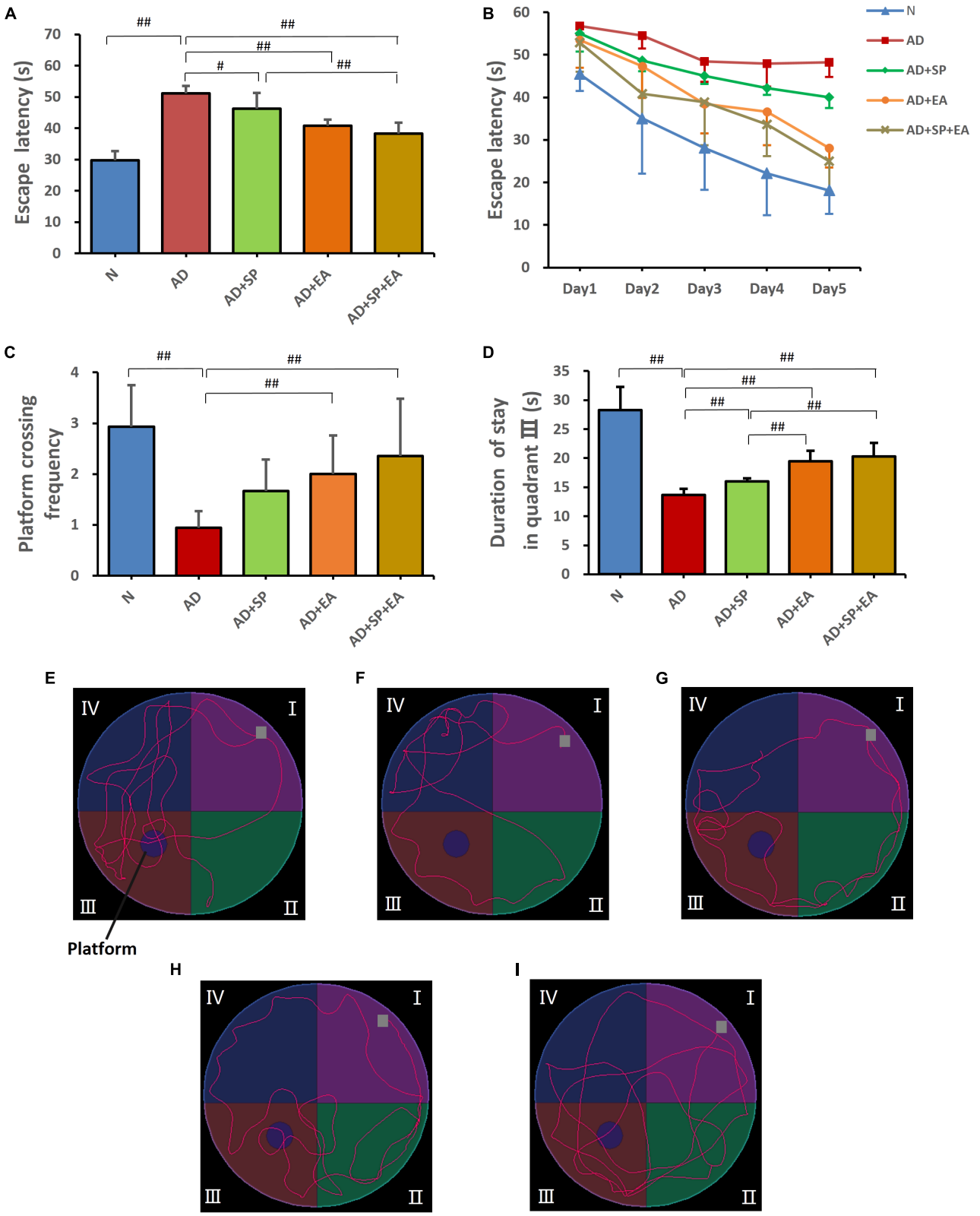

FIGURE 2 | Morris Water Maze test results after intervention (n = 10, mean ± SD). **(A)** Comparison of the average escape latency of all groups in training trials. **(B)** Trends of the escape latency of each group in training trials. **(C)** Platform crossing frequency of each group. **(D)** Duration of stay in quadrant III of each group. **(E–I)** Representative probe traces of each group. The water entry points are indicated by gray squares. n = 10 per group. $^{\#}p < 0.05$; $^{\#\#}p < 0.01$.

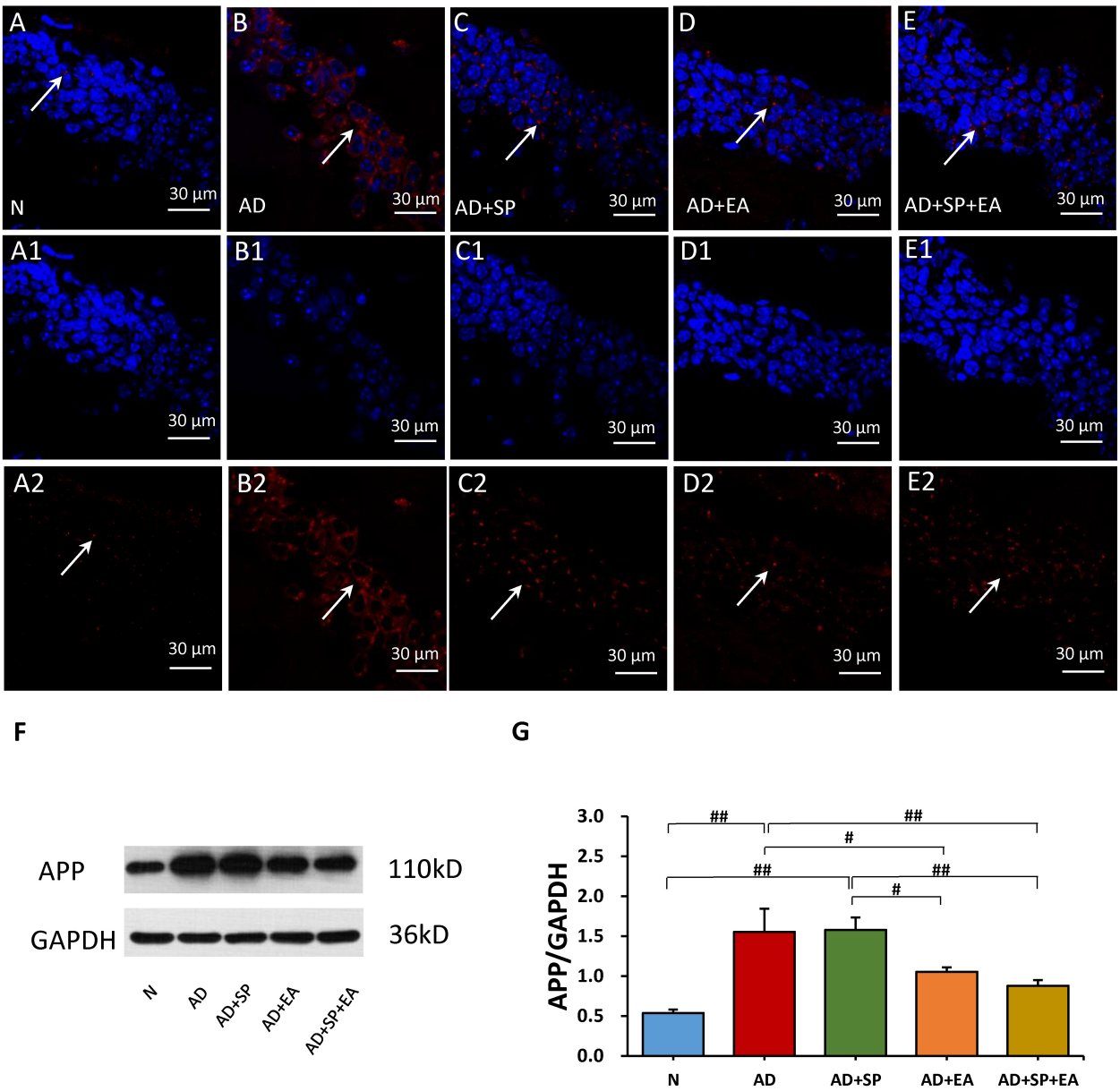

FIGURE 3 | Comparison of APP expression in the hippocampus of APP/PS1 mice in each group. **(A–E)** Comparison of APP expression using immunofluorescence. **(A1–E2)** Comparison of APP expression in the square frame of A-E in detail. APP: red; DAPI: blue; White arrows indicate positive expression of APP. **(F,G)** Comparison of APP expression using WB. Data are presented as the means ± SD, WB: $n = 7$ per group, immunofluorescence: $n = 3$ per group. $^{\#}p < 0.05$; $^{\#\#}p < 0.01$.

this possibility, we first detected the expression of JNK by WB. The result shows that the JNK phosphorylation in AD group was increased significantly when compared to N group ($P < 0.05$). Here, decline trend of P-JNK phosphorylation were also seen after SP600125 intervention. However, as compared to AD group, EA resulted in significant reduction in P-JNK phosphorylation in the AD + EA and AD + SP + EA groups ($P < 0.05$ and $P < 0.01$). The results supported that EA mainly inhibited activation of JNK in AD (**Figures 4A,B**).

To further confirm the linkage between APP and the JNK signal transduction pathway, we detected the expression of MKK4, MKK7, c-Jun and caspase-3 in the mouse brain hippocampus by immunofluorescence, immunohistochemistry and WB. In the immunohistochemistry and immunofluorescence analyses, MKK4, MKK7, c-Jun and caspase-3 expression was obviously higher in the AD group than in the N group, but this expression decreased after the intervention in the AD + SP, AD + EA and AD + SP + EA groups (**Figures 5A–J2**, **6A–J2**). WB results showed notably higher expression of p-MKK4,

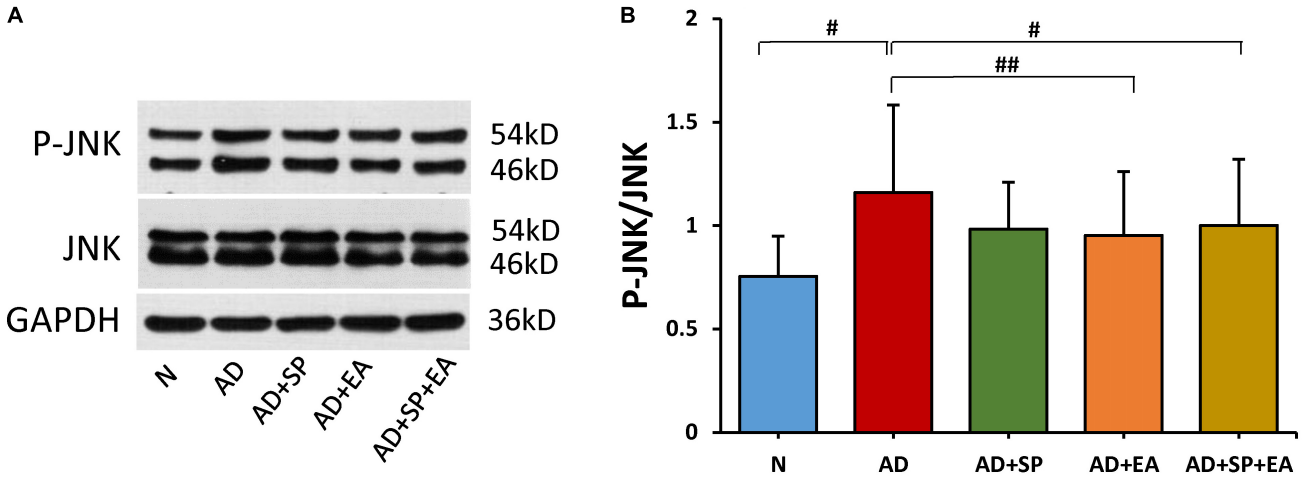

FIGURE 4 | Comparison of the expression of JNK in the hippocampus of APP/PS1 mice using WB. **(A)** The relative expression of hippocampal phosphorylated JNKs and total JNKs in APP/PS1 mice. **(B)** The ratio of p-JNK expression level to the total JNK level in the hippocampus of APP/PS1 mice. Data are presented as the means ± SD, WB: $n = 7$ per group. $^{\#}p < 0.05$; $^{\#\#}p < 0.01$.

p-MKK7, c-Jun and caspase-3 in the AD group compared to that in the N group ($P < 0.05$ or $P < 0.01$) (**Figures 5K–M**, **6K–M**). Compared to the expression in the AD group, the expression of p-MKK7, c-Jun in the AD + EA and AD + SP + EA groups was significantly lower ($P < 0.05$ or $P < 0.01$) (**Figures 5K,L**, **6K,L**). Furthermore, the AD + SP + EA group showed significantly lower expression of MKK7 and c-Jun than the AD + SP group. The results suggested that EA exerts its effects mainly by regulating MKK7 and c-Jun in the JNK pathway.

DISCUSSION

In this study, EA treatment improved the learning and memory ability of AD model APP/PS1 mice, which is consistent with a previous study. EA also inhibited JNK activation and APP accumulation in APP/PS1 mice. The data suggested that EA treatment may effectively improve cognitive impairments in AD, at least partially by inhibiting the JNK signaling pathway.

AD is a multifaceted neurodegenerative disease that is clinically characterized by progressive deterioration of cognitive functions. Increasing evidence points to a pivotal role of the JNK signaling pathway in the development of AD. The JNKs, known as stress-activated protein kinases (SAPKs), belongs to the family of mitogen-activated protein kinases (MAPKs). JNKs are a family of multifunctional signaling molecules that are activated in response to a wide range of cellular stresses and are involved in the regulation of cell proliferation, differentiation and apoptosis (Dhanasekaran and Reddy, 2008). SP600125 is an anthrapyrazolone inhibitor that binds to JNK to inhibit phosphorylation and subsequently blocks the functional activation of JNK. Therefore, the JNK-specific inhibitor SP600125 may potentially reduce JNK activity to prevent neuronal degeneration (Sharma et al., 2010). In the present study, both EA and SP600125 ameliorated cognitive deficits by improving spatial learning and memory. More interestingly, the protective effect was more remarkable when the two interventions were combined. The JNK-specific inhibitor SP600125 may potentially reduce JNK activity to prevent neuronal degeneration (Sclip et al., 2011; Sherrin et al., 2011).

APP plays a pivotal role in the pathophysiology of AD. APP metabolism drives other pathological changes, including the accumulation of Aβ. The accumulation of Aβ plays the most important role in the pathogenesis of AD. The Aβ stimulated microglial inflammatory responses engage MAPK pathways in AD. The major component of AD-associated amyloid-beta load is the 39- to 42-residue-long Aβ peptide. In previous study, our team found that the EA treatment was effective in decreasing the Aβ in AD mice, including $A\beta_{1-40}$ and $A\beta_{1-42}$ in hippocampus, cortex and serum (Wang X. et al., 2016). By reducing APP, it can indirectly reduce the production of Aβ and alleviate the accumulation of Aβ. Thus, therapy that targets APP metabolism is considered to be an effective approach to treat AD. According to our previous studies, EA treatment reduced APP expression by regulating β-site APP–cleaving enzyme 1 (BACE1) in APP/PS1 mice and regulated protein kinase A (PKA) and its associated substrates to change memory and learning abilities (Tang et al., 2019). In the present study, APP expression in the AD + SP group was not significantly different from that in the AD group, but APP expression in the AD + EA group was significantly reduced. Some investigations showed Aβ activated the expression of BACE1 through the JNK pathway (Guglielmotto et al., 2011). BACE1 is an β-secretase, which cleaves the ectodomain of APP. However, the inhibition of JNK activation by SP600125 might be decrease the BACE1, resulting in APP accumulation. In addition, SP600125 was injected intraperitoneally in this study, the effect of SP600125 might be weakened by the blood-brain barrier. These results suggest

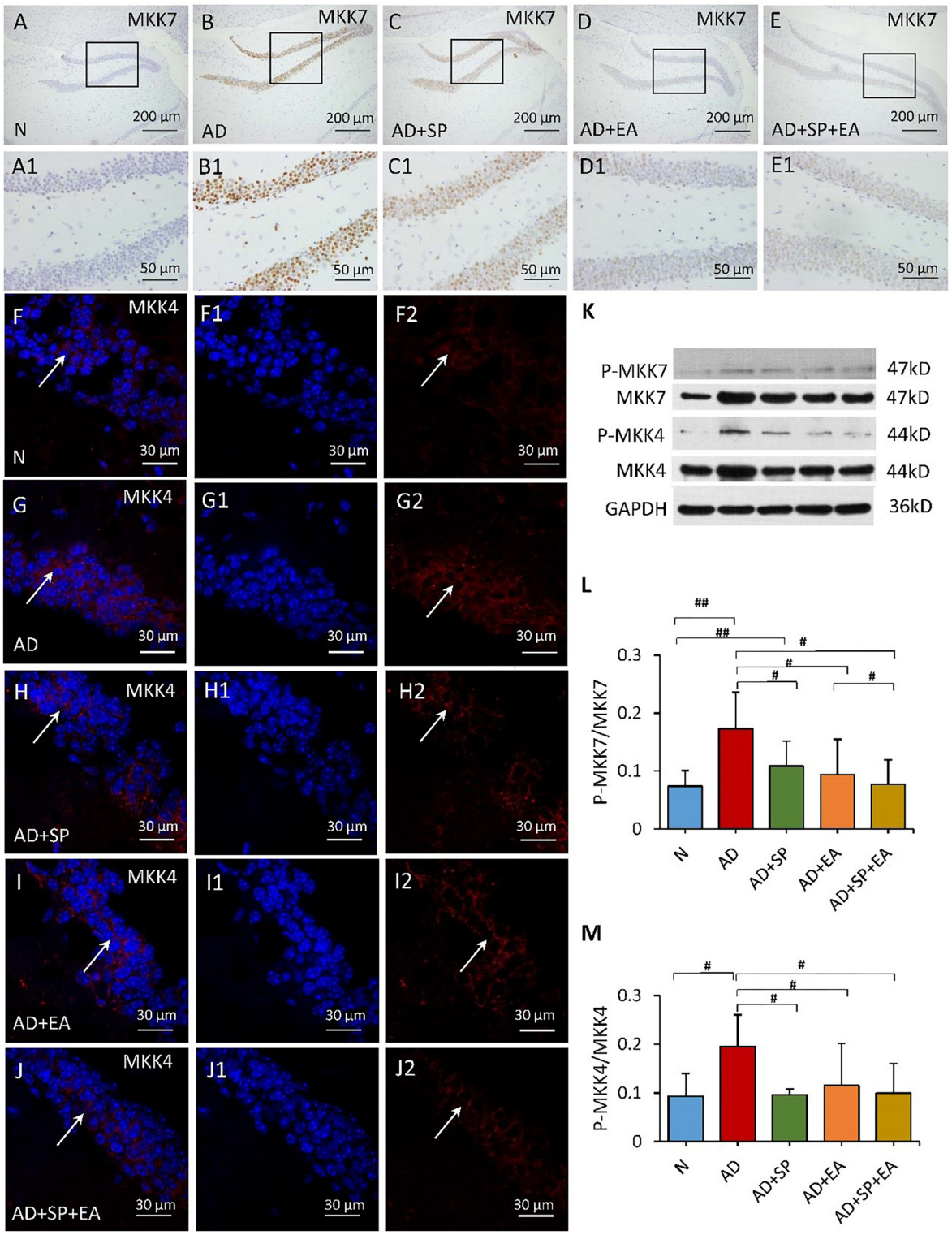

FIGURE 5 | Comparison of MKK7 and MKK4 expression in the hippocampus of APP/PS1 mice in each group. **(A–E)** Comparison of MKK7 expression using immunohistochemistry. **(A1–E1)** Comparison of MKK7 expression in the square frame of **(A–E)** in detail. **(F–F2,G–G2,H–H2,I–I2,J–J2)** Comparison of MKK4 expression using immunofluorescence. MKK4: red; DAPI: blue; White arrows indicate positive expression of MKK4. **(K)** The relative expression of hippocampal phosphorylated MKK7 and MKK4 and total MKK7 and MKK4 in APP/PS1 mice. **(L,M)** The ratio of p-MKK7 and p-MKK4 expression level to the total MKK7 and MKK4 level in the hippocampus of APP/PS1 mice. Data are presented as the means ± SD, WB: $n = 7$ per group, immunofluorescence: $n = 3$ per group. $^{\#}p < 0.05$; $^{\#\#}p < 0.01$.

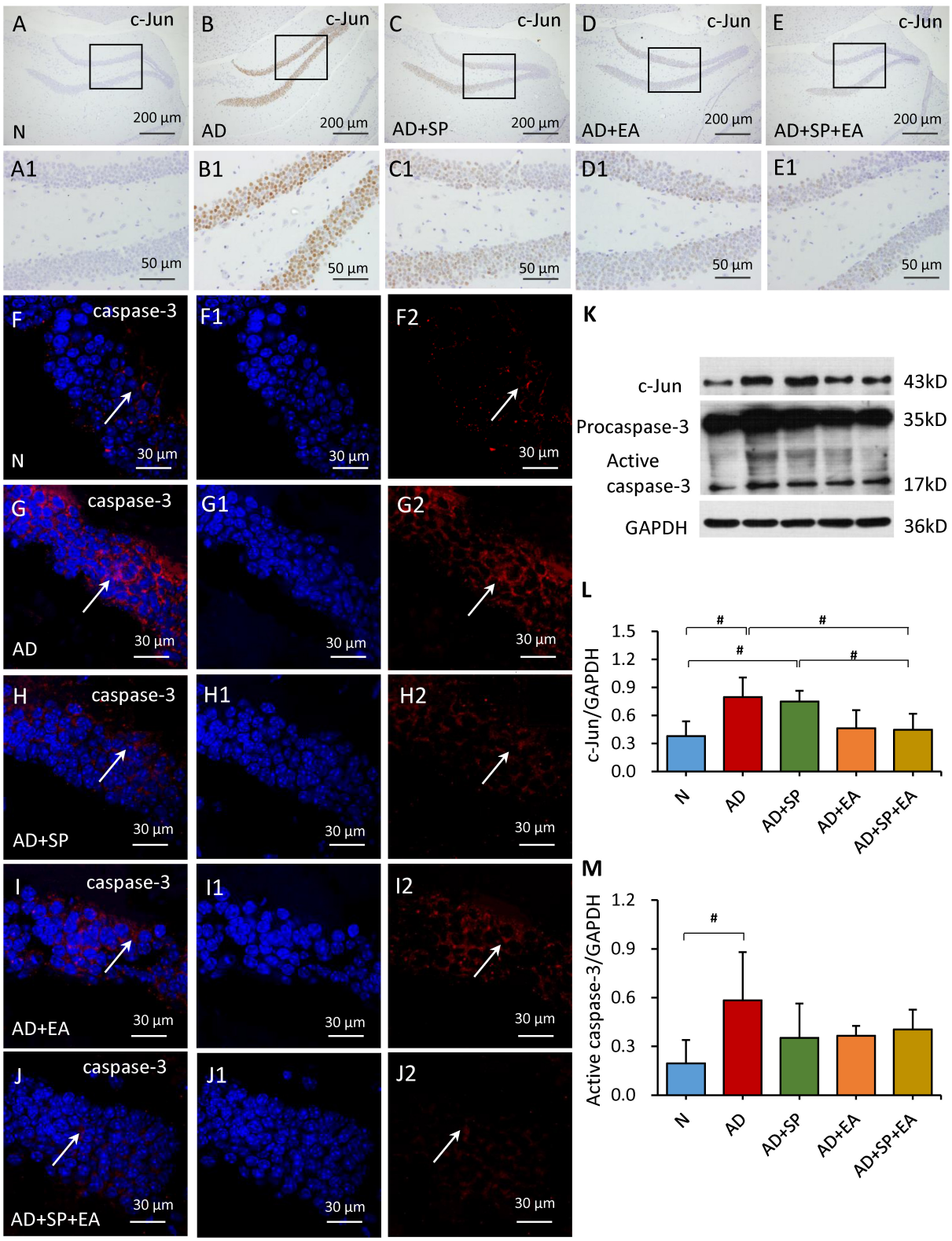

FIGURE 6 | Comparison of the expression of c-Jun and caspase-3 in the hippocampus of APP/PS1 mice in each group. **(A–E)** Comparison of c-Jun expression using immunohistochemistry. **(A1–E1)** Comparison of c-Jun expression in the square frame of **(A–E)** in detail. **(F–F2,G–G2,H–H2,I–I2,J–J2)** Comparison of caspase-3 expression using immunofluorescence. Caspase-3: red; DAPI: blue; White arrows indicate positive expression of MKK4. **(K–M)** Comparison of the expression of c-Jun and caspase-3 using WB. Data are presented as the means ± SD, WB: $n = 7$ per group, immunofluorescence: $n = 3$ per group. $^{\#}p < 0.05$.

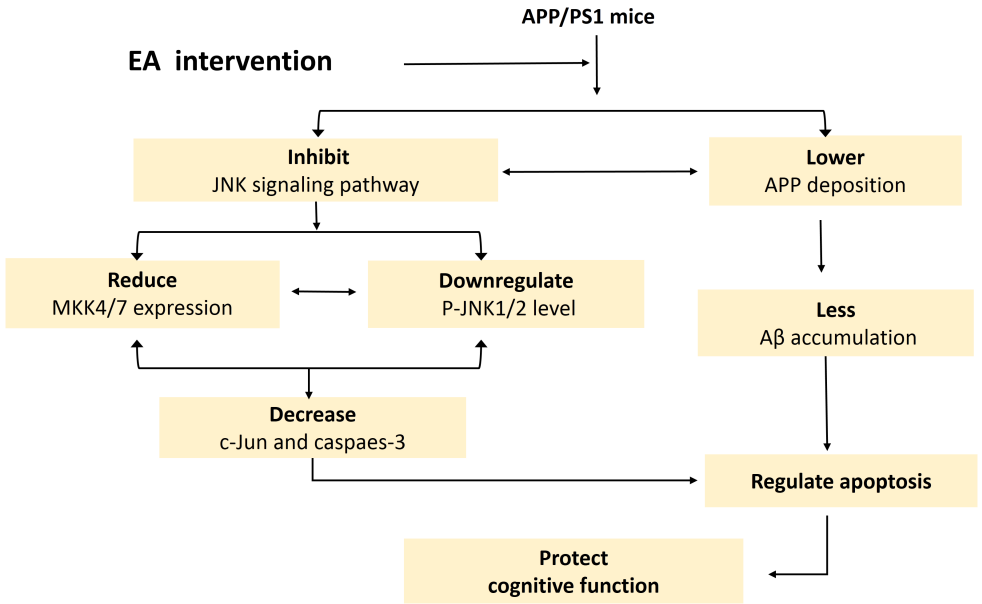

FIGURE 7 | Schematic of the mechanism by which EA intervention protects cognition in APP/PS1 mice. This schematic is derived from the results of this experiment combined with the results of our previous experiments.

that EA could promote the curative effect of SP600125. More importantly, the effects of EA might not be entirely mediated through the JNK signaling pathway and that EA effects multiple AD-associated pathways (Colombo et al., 2009; Guglielmotto et al., 2011). Acupuncture may enhance the cognitive function-improving effect of SP600125 in the treatment of AD (Mazzitelli et al., 2011; Zhou et al., 2015).

Numerous studies have reported an increase in the abnormal activation of JNK in both transgenic AD mouse models and AD patients. Indeed, aberrant activation of JNK has been implicated in the pathogenesis of AD (Lagalwar et al., 2006). We also found that the level of P-JNK was significantly higher in APP/PS1 mice. To date, three JNKs have been identified in cells, namely, JNK1, JNK2 and JNK3 (Sherrin et al., 2011; Petrov et al., 2016). Studies have shown unequivocal evidence that JNK1 and JNK2 are involved in apoptotic signaling (Busquets et al., 2019). Studies have also shown that the transcriptional activity promoted by $A\beta_{1-42}$ on BACE1 is transmitted by the activation of the JNK pathway. JNK activation regulates the phosphorylation of APP, leading to modulation of Aβ levels (Colombo et al., 2009). In this study, the P-JNK levels declined by varying degrees after the interventions. Notably, compared with SP600125, EA treatment has an significantly inhibitory effect on the activation of JNK, which may be due to the incomplete blocking of the blocker. However, EA works in many ways, which is also the advantage of EA, so its effect is not affected by blockers.

MKK4 and MKK7, two MAPK kinases, are key upstream factors of the JNK signaling pathway located in the cytoplasm. Both MKK4 and MKK7 are capable of dual phosphorylation of JNK and activation of JNK (Nakagawa et al., 2010). MKK4 can activate JNKs as well as p38MAPKs, whereas MKK7 specifically activates JNKs (Haeusgen et al., 2011). In the present study, the expression of both p-MKK4 and p-MKK7 was greatly increased in APP/PS1 mice, and this increase was responsible for the high level of P-JNK. MKK4 has been reported to be primarily activated by environmental stresses, whereas MKK7 is primarily activated by cytokines. In addition, MKK7 is the only MKK containing three motifs within its regulatory domain (Haeusgen et al., 2010; Kragelj et al., 2015; Wang S. et al., 2016). The three interventions examined here led to substantially reduced MKK4 and MKK7 expression. Notably, EA in APP/PS1 mice significantly reduced the level of MKK7, indicating that EA treatment inhibits JNK through acting on MMK7 expression (Ho et al., 2006).

The JNK signaling pathway involves phosphorylation of c-Jun. JNK is a kinase of c-Jun, a specific transcription factor that promotes c-Jun phosphorylation and activates caspase cascade reactions to initiate cell apoptosis (Nishina et al., 2004). Both c-Jun and caspase are key downstream factors of the JNK signaling pathway (Kim et al., 2005). Studies have confirmed that activation of caspase-3 occurs in Aβ-induced neuronal apoptosis (Chu et al., 2015; Chang et al., 2016). The role of JNK signaling pathway in cell stress response is complex and diverse. Its activation promotes the occurrence of cell apoptosis, and its mechanism is related to the induction of FasL and TNFR1 expression and the activation of caspases family. According to some studies, JNK may be the upstream regulatory molecule of caspase-dependent apoptosis signal transduction pathway, and caspases act as the effector of apoptosis in the downstream of JNK (Choi et al., 1999). On the other hand, caspases can induce JNK phosphorylation by activating upstream protein kinases in the MAPKs pathway, leading to apoptosis (Newhouse et al., 2004). In addition, Caspase-3 has been shown to cleave

APP giving rise to amyloidogenic fragments including Aβ (Gervais et al., 1999). In this study, the expression of both c-Jun and caspase-3 was significantly elevated in APP/PS1 mice, and this increase in expression was due to the high level of JNK phosphorylation and activation. After EA, the level of c-Jun in APP/PS1 mice was greatly reduced. Consistently, previous reports have shown that JNK2 has the highest affinity for c-Jun, as it contains the putative loop region that interacts with the JNK docking site on c-Jun. Furthermore, the level of caspase-3 showed a downward trend with EA treatment. Therefore, we demonstrate that JNK signaling pathway could be involved in anti-apoptotic effect of APP/PS1 mice. The results of this study highlighted that EA combined with the SP-induced (SP600125)could regulate the JNK signaling pathway and inhibit the production of caspase-3 of APP/PS1 mice, indicating the beneficial role of EA in neuron functional reconstruction and reducing the apoptosis. Collectively, our findings, along with previous reports, demonstrate that the inhibition of JNK activation by EA may occur through multiple targets.

In summary, this study provides essential preclinical evidence suggesting that EA reverses cognitive deficits and substantially lowers the burden of APP in AD model APP/PS1 mice, at least partially by inhibiting the JNK signaling pathway and regulating apoptosis signals (Yarza et al., 2016) (**Figure 7**). In addition, our findings indicated a moderate synergy between the EA and SP600125 interventions in APP/PS1 mice. Collectively, these data suggest that EA is effective at treating AD and may enhance the effect of drugs. Therefore, EA offers an effective alternative therapeutic approach for AD.

DATA AVAILABILITY STATEMENT

The raw data supporting the conclusions of this article will be made available by the authors, without undue reservation, to any qualified researcher.

ETHICS STATEMENT

All experimental procedures were in accordance with the Guide lines for the Care and Use of Laboratory Animals of the Ministry of Science and Technology of the People's Republic of China, and the Experimental Animal Research Ethics Committee of Beijing University of Chinese Medicine approved the study protocol.

AUTHOR CONTRIBUTIONS

YT and AX: experimental design, data analysis, and manuscript preparation. SS: data collection. YZ, BX, and ZL: experimental design.

FUNDING

This study was supported by the National Natural Science Foundation of China (Nos. 81603678, 81503654) and Zhejiang Medicine Health Science and Technology Program (2018KY418).

REFERENCES

Bredesen, D. E., Rao, R. V., and Mehlen, P. (2006). Cell death in the nervous system. *Nature* 443, 796–802.

Busquets, O., Eritja, A., Lopez, B. M., Ettcheto, M., Manzine, P. R., Castro-Torres, R. D., et al. (2019). Role of brain c-Jun N-terminal kinase 2 in the control of the insulin receptor and its relationship with cognitive performance in a high-fat diet pre-clinical model. *J. Neurochem.* 149, 255–268. doi: 10.1111/jnc.14682

Cao, J., Tang, Y., Li, Y., Gao, K., Shi, X., and Li, Z. (2017). Behavioral changes and hippocampus glucose metabolism in APP/PS1 transgenic mice via electro-acupuncture at governor vessel acupoints. *Front. Aging Neurosci.* 9:5. doi: 10.3389/fnagi.2017.00005

Chang, J. L., Zhang, H., Tan, Z. J., Xiao, J., Li, S. R., and Gao, Y. (2017). Effect of electroacupuncture in patients with post-stroke motor aphasia neurolinguistic and neuroimaging characteristics. *Wien. Klin. Wochenschr.* 129, 102–109. doi: 10.1007/s00508-016-1070-1

Chang, Y. J., Linh, N. H., Shih, Y. H., Yu, H. M., Li, M. S., and Chen, Y. R. (2016). Alzheimer's amyloid-beta sequesters caspase-3 in vitro via its C-terminal tail. *ACS Chem. Neurosci.* 7, 1097–1106. doi: 10.1021/acschemneuro.6b00049

Choi, W. S., Yoon, S. Y., Oh, T. H., Choi, E. J., O'Malley, K. L., and Oh, Y. J. (1999). Two distinct mechanisms are involved in 6-hydroxydopamine- and MPP+-induced dopaminergic neuronal cell death: role of caspases, ROS, and JNK. *J. Neurosci. Res.* 57, 86–94. doi: 10.1002/(sici)1097-4547(19990701)57:1<86::aid-jnr9>3.0.co;2-e

Chu, J., Li, J. G., Joshi, Y. B., Giannopoulos, P. F., Hoffman, N. E., Madesh, M., et al. (2015). Gamma secretase-activating protein is a substrate for caspase-3: implications for alzheimer's disease. *Biol. Psychiatry* 77, 720–728. doi: 10.1016/j.biopsych.2014.06.003

Colombo, A., Bastone, A., Ploia, C., Sclip, A., Salmona, M., Forloni, G., et al. (2009). JNK regulates APP cleavage and degradation in a model of Alzheimer's disease. *Neurobiol. Dis.* 33, 518–525. doi: 10.1016/j.nbd.2008.12.014

Dhanasekaran, D. N., and Reddy, E. P. (2008). JNK signaling in apoptosis. *Oncogene* 27, 6245–6251. doi: 10.1038/onc.2008.301

D'Hooge, R., and De Deyn, P. P. (2001). Applications of the morris water maze in the study of learning and memory. *Brain Res. Rev.* 36, 60–90. doi: 10.1016/s0165-0173(01)00067-4

Ding, N., Jiang, J., Xu, A., Tang, Y., and Li, Z. (2019). Manual acupuncture regulates behavior and cerebral blood flow in the samp8 mouse model of Alzheimer's disease. *Front. Neurosci.* 13:37. doi: 10.3389/fnins.2019.00037

Emerit, J., Edeas, A., and Bricaire, F. (2004). Neurodegenerative diseases and oxidative stress. *Biomed. Pharmacother.* 58, 39–46.

Gervais, F. G., Xu, D., Robertson, G. S., Vaillancourt, J. P., Zhu, Y., Huang, J., et al. (1999). Involvement of caspases in proteolytic cleavage of Alzheimer's amyloid-beta precursor protein and amyloidogenic A beta peptide formation. *Cell* 97, 395–406. doi: 10.1016/s0092-8674(00)80748-5

Guglielmotto, M., Monteleone, D., Giliberto, L., Fornaro, M., Borghi, R., Tamagno, E., et al. (2011). Amyloid-beta(42) activates the expression of BACE1 through the JNK pathway. *J. Alzheimers Dis.* 27, 871–883. doi: 10.3233/JAD-2011-110884

Haeusgen, W., Herdegen, T., and Waetzig, V. (2010). Specific regulation of JNK signalling by the novel rat MKK7 gamma 1 isoform. *Cell Signal.* 22, 1761–1772. doi: 10.1016/j.cellsig.2010.07.002

Haeusgen, W., Herdegen, T., and Waetzig, V. (2011). The bottleneck of JNK signaling: Molecular and functional characteristics of MKK4 and MKK7. *Eur. J. Cell Biol.* 90, 536–544. doi: 10.1016/j.ejcb.2010.11.008

Ho, D. T., Bardwell, A. J., Grewal, S., Iverson, C., and Bardwell, L. (2006). Interacting JNK-docking sites in MKK7 promote binding and activation of JNK mitogen-activated protein kinases. *J. Biol. Chem.* 281, 13169–13179. doi: 10.1074/jbc.m601010200

Jiang, J., Gao, K., Zhou, Y., Xu, A., Shi, S., Liu, G., et al. (2015). Electroacupuncture treatment improves learning-memory ability and brain glucose metabolism in

a mouse model of alzheimer's disease: using morris water maze and micro-PET. *Evid. Based Complement. Altern. Med.* 2015:142129. doi: 10.1155/2015/142129

Kim, E. K., and Choi, E. J. (2010). Pathological roles of MAPK signaling pathways in human diseases. *Biochim. Biophys. Acta Mol. Basis Dis.* 1802, 396–405. doi: 10.1016/j.bbadis.2009.12.009

Kim, S. D., Moon, C. K., Eun, S. Y., Ryu, P. D., and Jo, S. A. (2005). Identification of ASK1, MKK4, JNK, c-Jun, and caspase-3 as a signaling cascade involved in cadmium-induced neuronal cell apoptosis. *Biochem. Biophys. Res. Commun.* 328, 326–334. doi: 10.1016/j.bbrc.2004.11.173

Kragelj, J., Palencia, A., Nanao, M. H., Maurin, D., Bouvignies, G., Blackledge, M., et al. (2015). Structure and dynamics of the MKK7-JNK signaling complex. *Proc. Natl. Acad. Sci. U.S.A.* 112, 3409–3414. doi: 10.1073/pnas.1419528112

Lagalwar, S., Guillozet-Bongaarts, A. L., Berry, R. W., and Binder, L. I. (2006). Formation of phospho-SAPK/JNK is an early event in granules in the hippocampus Alzheimer disease. *J. Neuropathol. Exp. Neurol.* 65, 455–464. doi: 10.1097/01.jnen.0000229236.98124.d8

Li, G. Q., Cong, D. W., Sun, P., and Meng, X. (2018). A beta 1-42 regulates astrocytes through JNK/AP-1 pathway. *Eur. Rev. Med. Pharmacol. Sci.* 22, 2015–2021. doi: 10.26355/eurrev_201804_14730

Li, S., Li, Z. F., Wu, Q., Guo, X. C., Xu, Z. H., Li, X. B., et al. (2018). A multicenter, randomized, controlled trial of electroacupuncture for perimenopause women with mild-moderate depression. *Biomed. Res. Int.* 2018:5351210. doi: 10.1155/2018/5351210

Lozano, R., Naghavi, M., Foreman, K., Lim, S., Shibuya, K., Aboyans, V., et al. (2012). Global and regional mortality from 235 causes of death for 20 age groups in 1990 and 2010: a systematic analysis for the global burden of disease study 2010. *Lancet* 380, 2095–2128. doi: 10.1016/S0140-6736(12)61728-0

Mazzitelli, S., Xu, P., Ferrer, I., Davis, R. J., and Tournier, C. (2011). The loss of c-Jun N-terminal protein kinase activity prevents the amyloidogenic cleavage of amyloid precursor protein and the formation of amyloid plaques in vivo. *J. Neurosci.* 31, 16969–16976. doi: 10.1523/JNEUROSCI.4491-11.2011

McKhann, G. M., Knopman, D. S., Chertkow, H., Hyman, B. T., Jack, C. R., Kawas, C. H., et al. (2011). The diagnosis of dementia due to Alzheimer's disease: recommendations from the national institute on aging-Alzheimer's association workgroups on diagnostic guidelines for Alzheimer's disease. *Alzheimers Dement.* 7, 263–269. doi: 10.1016/j.jalz.2011.03.005

Morris, J. C., Storandt, M., McKeel, D. W. Jr., Rubin, E. H., Price, J. L., Grant, E. A., et al. (1996). Cerebral amyloid deposition and diffuse plaques in "normal" aging: evidence for presymptomatic and very mild Alzheimer's disease. *Neurology* 46, 707–719. doi: 10.1212/wnl.46.3.707

Nakagawa, K., Sugahara, M., Yamasaki, T., Kajiho, H., Takahashi, S., Hirayama, J., et al. (2010). Filamin associates with stress signalling kinases MKK7 and MKK4 and regulates JNK activation. *Biochem. J.* 427, 237–245. doi: 10.1042/BJ20091011

Newhouse, K., Hsuan, S. L., Chang, S. H., Cai, B., Wang, Y., and Xia, Z. (2004). Rotenone-induced apoptosis is mediated by p38 and JNK MAP kinases in human dopaminergic SH-SY5Y cells. *Toxicol. Sci.* 79, 137–146. doi: 10.1093/toxsci/kfh089

Nishina, H., Wada, T., and Katada, T. (2004). Physiological roles of SAPK/JNK signaling pathway. *J. Biochem.* 136, 123–126. doi: 10.1093/jb/mvh117

Pan, W. P., Wang, Z. K., Tian, F. L., Yan, M. X., and Lu, Y. (2017). Electroacupuncture combined with mosapride alleviates symptoms in diabetic patients with gastroparesis. *Exp. Ther. Med.* 13, 1637–1643. doi: 10.3892/etm.2017.4139

Petrov, D., Luque, M., Pedros, I., Ettcheto, M., Abad, S., Pallas, M., et al. (2016). Evaluation of the role of JNK1 in the hippocampus in an experimental model of familial Alzheimer's disease. *Mol. Neurobiol.* 53, 6183–6193. doi: 10.1007/s12035-015-9522-6

Pike, K. E., Savage, G., Villemagne, V. L., Ng, S., Moss, S. A., Maruff, P., et al. (2007). beta-amyloid imaging and memory in non-demented individuals: evidence for preclinical Alzheimer's disease. *Brain* 130, 2837–2844. doi: 10.1093/brain/awm238

Ramin, M., Azizi, P., Motamedi, F., Haghparast, A., and Khodagholi, F. (2011). Inhibition of JNK phosphorylation reverses memory deficit induced by beta-amyloid (1-42) associated with decrease of apoptotic factors. *Behav. Brain Res.* 217, 424–431. doi: 10.1016/j.bbr.2010.11.017

Sclip, A., Antoniou, X., Colombo, A., Camici, G. G., Pozzi, L., Cardinetti, D., et al. (2011). c-Jun N-terminal kinase regulates soluble a beta oligomers and cognitive impairment in AD Mouse Model. *J. Biol. Chem.* 286, 43871–43880. doi: 10.1074/jbc.M111.297515

Sharma, N., Deshmukh, R., and Bedi, K. L. (2010). SP600125, a competitive inhibitor of JNK attenuates streptozotocin induced neurocognitive deficit and oxidative stress in rats. *Pharmacol. Biochem. Behav.* 96, 386–394. doi: 10.1016/j.pbb.2010.06.010

Sherrin, T., Blank, T., and Todorovic, C. (2011). c-Jun N-terminal kinases in memory and synaptic plasticity. *Rev. Neurosci.* 22, 403–410. doi: 10.1515/RNS.2011.032

Sun, Z. L., Liu, J., Guo, W., Jiang, T., Ma, C., Li, W. B., et al. (2016). Serum brain-derived neurotrophic factor levels associate with cognitive improvement in patients with schizophrenia treated with electroacupuncture. *Psychiatry Res.* 244, 370–375. doi: 10.1016/j.psychres.2016.07.040

Tang, Y., Shao, S., Guo, Y., Zhou, Y., Cao, J., Xu, A., et al. (2019). Electroacupuncture mitigates hippocampal cognitive impairments by reducing BACE1 deposition and activating PKA in APP/PS1 double transgenic mice. *Neural Plast.* 2019:2823679. doi: 10.1155/2019/2823679

Tare, M., Modi, R. M., Nainaparampil, J. J., Puli, O. R., Bedi, S., Fernandez-Funez, P., et al. (2011). Activation of JNK signaling mediates amyloid-beta-dependent cell death. *PLoS One* 6:e24361. doi: 10.1371/journal.pone.0024361

Vorhees, C. V., and Williams, M. T. (2006). Morris water maze: procedures for assessing spatial and related forms of learning and memory. *Nat. Protoc.* 1, 848–858. doi: 10.1038/nprot.2006.116

Wang, S., Qian, Z., Li, H. Y., Lu, K., Xu, X. P., Weng, S. P., et al. (2016). Identification and characterization of MKK7 as an upstream activator of JNK in Litopenaeus vannamei. *Fish Shellfish Immunol.* 48, 285–294. doi: 10.1016/j.fsi.2015.12.014

Wang, X., Miao, Y., Abulizi, J., Li, F., Mo, Y., Xue, W., et al. (2016). Improvement of electroacupuncture on APP/PS1 transgenic mice in spatial learning and memory probably due to expression of abeta and LRP1 in hippocampus. *Evid. Based Complement. Altern. Med.* 2016, 7603975–7603975.

Wei, J. J., Yang, W. T., Yin, S. B., Wang, C., Wang, Y., and Zheng, G. Q. (2016). The quality of reporting of randomized controlled trials of electroacupuncture for stroke. *BMC Complement. Altern. Med.* 16:512.

Yarza, R., Vela, S., Solas, M., and Ramirez, M. J. (2016). c-Jun N-terminal kinase (JNK) signaling as a therapeutic target for Alzheimer's disease. *Front. Pharmacol.* 6:12.

Zhou, Q., Wang, M., Du, Y., Zhang, W., Bai, M., Zhang, Z., et al. (2015). Inhibition of c-Jun N-terminal kinase activation reverses Alzheimer disease phenotypes in APPswe/PS1dE9 Mice. *Ann. Neurol.* 77, 637–654. doi: 10.1002/ana.24361

Conflict of Interest: The authors declare that the research was conducted in the absence of any commercial or financial relationships that could be construed as a potential conflict of interest.

frontiers in Neuroscience

ORIGINAL RESEARCH
published: 13 March 2020
doi: 10.3389/fnins.2020.00209

A Systematic Bioinformatics Workflow With Meta-Analytics Identified Potential Pathogenic Factors of Alzheimer's Disease

*Sze Chung Yuen[1], Hongmei Zhu[1] and Siu-wai Leung[1,2]**

[1] State Key Laboratory of Quality Research in Chinese Medicine, Institute of Chinese Medical Sciences, University of Macau, Macao, China, [2] School of Informatics, College of Science and Engineering, University of Edinburgh, Edinburgh, United Kingdom

Potential pathogenic factors, other than well-known *APP*, *APOE4*, and *PSEN*, can be further identified from transcriptomics studies of differentially expressed genes (DEGs) that are specific for Alzheimer's disease (AD), but findings are often inconsistent or even contradictory. Evidence corroboration by combining meta-analysis and bioinformatics methods may help to resolve existing inconsistencies and contradictions. This study aimed to demonstrate a systematic workflow for evidence synthesis of transcriptomic studies using both meta-analysis and bioinformatics methods to identify potential pathogenic factors. Transcriptomic data were assessed from GEO and ArrayExpress after systematic searches. The DEGs and their dysregulation states from both DNA microarray and RNA sequencing datasets were analyzed and corroborated by meta-analysis. Statistically significant DEGs were used for enrichment analysis based on KEGG and protein–protein interaction network (PPIN) analysis based on STRING. AD-specific modules were further determined by the DIAMOnD algorithm, which identifies significant connectivity patterns between specific disease-associated proteins and non-specific proteins. Within AD-specific modules, the nodes of highest degrees (>95th percentile) were considered as potential pathogenic factors. After systematic searches of 225 datasets, extensive meta-analyses among 25 datasets (21 DNA microarray datasets and 4 RNA sequencing datasets) identified 9,298 DEGs. The dysregulated genes and pathways in AD were associated with impaired amyloid-β (Aβ) clearance. From the AD-specific module, Fyn, and EGFR were the most statistically significant and biologically relevant. This meta-analytical study suggested that the reduced Aβ clearance in AD pathogenesis was associated with the genes encoding Fyn and EGFR, which were key receptors in Aβ downstream signaling.

Keywords: Alzheimer's disease, meta-analysis, microarray analysis, RNA sequence analysis, bioinformatics

OPEN ACCESS

Edited by:
Woon-Man Kung, Chinese Culture University, Taiwan

Reviewed by:
Chung-Feng Kao, National Chung Hsing University, Taiwan
Judith Potashkin, Rosalind Franklin University of Medicine and Science, United States

***Correspondence:**
Siu-wai Leung
siuwai.leung@gmail.com

Specialty section:
This article was submitted to Neurodegeneration, a section of the journal Frontiers in Neuroscience

Received: *28 October 2019*
Accepted: *25 February 2020*
Published: *13 March 2020*

Citation:
Yuen SC, Zhu H and Leung S (2020) A Systematic Bioinformatics Workflow With Meta-Analytics Identified Potential Pathogenic Factors of Alzheimer's Disease. Front. Neurosci. 14:209. doi: 10.3389/fnins.2020.00209

Abbreviations: Aβ, amyloid-β; AD, Alzheimer's disease; BBB, blood-brain barrier; CMRgl, cerebral metabolic rate for glucose; DEGs, differentially expressed genes; DIAMoND, DIseAse Module Detection algorithm; eCBs, endocannabinoids; FDR, false discovery rate; IDE, insulin-degrading enzyme; KEGG, Kyoto Encyclopedia of Genes and Genomes; logORs, $\log_e$ odds ratios; PPIN, protein–protein interaction network; PrP^C, cellular prion protein; ROS, reactive oxygen species; RNA-Seq, RNA-sequencing; T2DM, type 2 diabetes mellitus; UPR, unfolded-protein response; UPS, ubiquitin-proteasome system.

INTRODUCTION

Alzheimer's disease is a neurodegenerative disease that is the major cause of dementia worldwide (Alzheimer's Association, 2009). The AD brain is characterized by the distribution of amyloid plaques and neurofibrillary tangles, which are composed of Aβ and hyperphosphorylated tau proteins, respectively (Wang and Mandelkow, 2016; Wang J. et al., 2017). The generation of Aβ from amyloid precursor protein (APP) is a central theme in the field of AD. APP is a single transmembrane protein with a large extracellular domain that is generated in large quantities and efficiently metabolized. APP can be processed via non-amyloidogenic or amyloidogenic generation of Aβ (Chow et al., 2010). Aβ mainly exists in two forms, $A\beta_{40}$ and a more hydrophobic $A\beta_{42}$, which consist of 40 and 42 amino acids, respectively (Marina et al., 2003). The Aβ monomer is intrinsically disordered, and present as a dynamic conformational structure (Chen et al., 2017), which allows the monomer binds to numerous substrate with a high binding affinity. The monomers of Aβ aggregate into oligomers, fibrils, and plaques, when a critical concentration of amyloid is reached due to dysfunctional homeostasis (Knowles et al., 2014). The soluble Aβ oligomer is recognized as the major neurotoxic species, and exists in an equilibrium with fibrils (Yang et al., 2017). And the toxicity of Aβ oligomers is inversely correlated with their oligomer size (Sengupta et al., 2016). Aβ is directly neurotoxic and induces a series of cellular responses; for example, it can induce excitotoxic signaling by increasing glutamate release (Brito-Moreira et al., 2011), and alter Ca^{2+} homeostasis and synaptic functions in neurons, astrocytes, and microglia (Parihar and Brewer, 2010). Aβ located on the mitochondria generates ROS, thus increasing oxidative stress and disrupting oxidative phosphorylation (Caspersen et al., 2005). Aβ also activates protein kinase to phosphorylate tau protein, resulting in the formation of neurofibrillary tangles (Hernández and Avila, 2008). The toxicity of both Aβ and hyperphosphorylated tau proteins are dependent on one another; an absence of tau protein reduces Aβ-induced memory impairment, while increased Aβ levels promote tau pathology (Oddo et al., 2006; Roberson et al., 2007).

The amyloid cascade hypothesis was proposed in 1992, and depicts Aβ as the causative factor in AD development (Hardy and Higgins, 1992). This hypothesis has genetic-based support, because mutations in genes related to Aβ formation (*APP* and *PSEN*) and clearance (*APOE4*) induce early-onset AD (Rovelet-Lecrux et al., 2006; Kline, 2012; St George-Hyslop and Fraser, 2012). However, this hypothesis is challenged by two facts, although there are also counterarguments that have been proposed from other scientific findings. First, amyloid imaging reveals that Aβ deposition also occurs in healthy aging subjects, suggesting that Aβ deposition could be a normal phenomenon of aging (Edison et al., 2007). However, Esparza et al. (2013) suggested that Aβ oligomer levels, which are the neurotoxic form of Aβ deposition, are higher in AD brains compared with healthy subjects. Second, the degree of dementia does not correlate well with amyloid plaque formation in AD (Nelson et al., 2012). In fact, Aβ oligomers may exert their neurotoxic effects much earlier, before the formation of amyloid plaques (Broersen et al., 2010). Also, the drug development for the treatment of AD has been guided by the amyloid cascade hypothesis for the pass two decade, although most anti-Aβ drugs fail in clinical trials and no novel drugs have been brought to market since 2003 (Cummings et al., 2014). For example, Solanezumab (currently in a phase 3 trial) recognizes Aβ at the 13 to 28 amino acid position and lowers amyloid levels, but does not show beneficial effects in subjects with mild AD (Honig et al., 2018). Verubecestat (currently in a phase 3 trial), a β-secretase inhibitor, reduces Aβ levels in a dose-dependent manner (Kennedy et al., 2016). However, a recent clinical trial (Egan et al., 2019) indicated that verubecestat does not have clinical effects in AD subjects. The failure of development of anti-Aβ drugs does not discredit amyloid as the central theme for AD treatment, because the sporadic AD is caused by the changes of genes which potentiate the neurotoxicity of Aβ in the brain over years, rather than solely Aβ overproduction. Indeed, the cerebral $A\beta_{42}$ kinetics were modified by Aβ accumulation (Potter et al., 2013), resulting in the disease preventative treatment required at least 95% lowering $A\beta_{42}$ production if the treatment was started after Aβ accumulation (Roberts et al., 2017). This suggests that the development of anti-Aβ drugs should not be solely dependent on inhibition of $A\beta_{42}$ production. However, the incomplete knowledge of AD pathogenic factors may hindered the investigation of AD (Scott et al., 2014), not just Aβ production, but also the Aβ-relevant receptors and their corresponding downstream signaling cascades.

Alzheimer's disease is a complex disorder, expressed as a malfunction of defects in multiple genes. The discovery of AD pathogenic factors can be revealed by transcriptome profiling approach [i.e., DNA microarray and RNA-Seq (Sutherland et al., 2011)] to identify DEGs in AD subjects compared with healthy subjects. DEGs are genes that are potentially associated with disease pathology. **Table 1** shows the publications using transcriptomic data and bioinformatics tools for identifying AD pathogenic factors. Puthiyedth et al. (2016) identified common DEGs from microarray datasets across six different brain regions. All datasets were integrated using the Colored (α, β)-κ Feature set approach (Puthiyedth et al., 2015), and a few common DEGs were identified across the brain regions, revealing an AD-specific signature. Kawalia et al. (2017) used the BC3Net10 algorithm to infer AD gene regulatory networks. This network was generated by the integration of literature-based knowledge and data-driven analysis. Inferences did not solely depend on the network topology, but also integrated information about DEGs and AD-related genes, after systematic searching from databases. However, the DEGs obtained from different transcriptomic studies of AD are sometimes conflicting because of many factors, such as the use of different experimental designs or statistical methods between studies. The integration of these studies based on meta-analysis therefore resolves inconclusive results and obtains a generalization (Haidich, 2010). The results of meta-analysis are presented as logORs based on the number of dysregulation events in both disease and control samples. The effect sizes are integrated to assess the overall effect size based on either fixed- or random-effect models. Meta-analysis

TABLE 1 | The published transcriptomic data and bioinformatics tools for identifying AD pathogenic factors.

Title	Authors (publication year)	Database	Bioinformatic tools	Pathogenic factors
Integrated Identification of Key Genes and Pathways in Alzheimer's Disease via Comprehensive Bioinformatical Analyses (Yan et al., 2019)	Yan et al. (2019)	GEO, KEGG, Reactome, STRING, Wikipathway	Platform: Morpheus, RBPDB, UCSC; Software: Cytoscape, ClueGO, Gluepedia, Graphpad Prism, MCODE	*BDNF*, *CACNA1A*, *CALB*, *CD44*, *CDC42*, *OXT*, *PDYN*, *TAC1*, *TH*, *VEGFA*
Systematic Analysis and Biomarker Study for Alzheimer's Disease (Li X. et al., 2018)	Li X. et al. (2018)	GEO, International Genomics of Alzheimer's Project	R package: *affy*, *glmnet*, *limma*, *MASS*, *PRROC*, *ROCR*; Software: Ingenuity Pathway Analysis, MAGMA	*NDUFA1*, *MRPL51*, *RPL36AL*
Network-based approach to identify molecular signatures and therapeutic agents in Alzheimer's Disease (Rahman et al., 2019)	Rahman et al. (2019)	CMap, GEO, JASPAR, miRTarBase, STRING, TarBase	Platform: DAVID, GEO2R; Software: CytoHubba, Cytoscape, MCODE	*AR*, *CREBBP*, *E2F1*, *FOXC1*, *FOXL1*, *GATA2*, *JUN*, *NFIC*, *PPARG*, *RAC1*, *RPL12*, *RPL15*, *RPS11*, *RPS6*, *SMAD3*, *SRF*, *UBA52*, *UBC*, *USF2*, *YY1*
Alzheimer's Disease Master Regulators Analysis: Search for Potential Molecular Targets and Drug Repositioning Candidates (Vargas et al., 2018)	Vargas et al. (2018)	CMap, GEO	Algorithm: Algorithm for the Reconstruction of Accurate Cellular Networks, two-tail gene set enrichment analysis; R package: *ggplot2*, *RedeR*, *RTN*	*ATF2*, *CNOT7*, *CSRNP2*, *PARK2*, *SLC30A9*, *TSC22D1*
Condition-specific Gene Co-expression Network Mining Identifies Key Pathways and Regulators in the Brain Tissue of Alzheimer's Disease Patients (Xiang et al., 2018)	Xiang et al. (2018)	Allen Brain Institute, GEO	Algorithm: Local maximized Quasi-Clique Merger; Platform: REViGO; R package: *Affy*, *Enrichr*, *lmQCM*	*FOS, JUN, MEF2A, MIB2, PCBP1, SMARCA2, SP1, STAT1, TEAD4, ZFHX3, ZNF281*
Analytical Strategy to Prioritize Alzheimer's Disease Candidate Genes in Gene Regulatory Networks Using Public Expression Data (Kawalia et al., 2017)	Kawalia et al. (2017)	ArrayExpress, CPDB, ENSEMBL, GEO, GWAScatalog, GWASCentral, GWASdb, KEGG, NeuroTransDB, RegulomeDB	Algorithm: BC3Net10; R package: *affy*, *arrayQualityMetrics*, *bc3net*, *limma*; Platform: HaploReg, SCAIView	*AP2A2, ARAP3, ATP2A3, ATP2B4, HLA-C, HLA-F, ITPR2, RAB11FIP4, STX2*
The Bioinformatic Analysis of the Dysregulated Genes and MicroRNAs in Entorhinal Cortex, Hippocampus, and Blood for Alzheimer's Disease (Pang et al., 2017)	Pang et al. (2017)	CMap, GEO, KEGG	R package: *affy*, *edgeR*, *limma*, *WGCNA*; Platform: DAVID; Software: CytoHubba, Cytoscape, GSEA	*CTSD*, *VCAM1*
A Systematic Integrated Analysis of Brain Expression Profiles Reveals *YAP1* and Other Prioritized Hub Genes as Important Upstream Regulators in Alzheimer's Disease (Xu et al., 2018)	Xu et al. (2018)	GEO	R package: *in silico Merging*, *limma*, *WGCNA*	*YAP1*
Network Topology Analysis of Post-Mortem Brain Microarrays Identifies More Alzheimer's Related Genes and MicroRNAs and Points to Novel Routes for Fighting with the Disease (Chandrasekaran and Bonchev, 2016)	Chandrasekaran and Bonchev (2016)	ArrayExpress, GEO, OMIN, ResNet	Algorithm: Robust Multiarray Average approach, empirical Bayes method; Platform: DAVID; Software: Pajek, Pathway Studio	*CD4*, *DCN*, *IL8*
A Systematic Investigation into Aging Related Genes in Brain and Their Relationship with Alzheimer's Disease (Meng et al., 2016)	Meng et al. (2016)	Biocarta, DisGeNet, GEO, GenAge, GenMapP, MetaBase	Algorithm: Condition-specific target prediction; Platform: DAVID, oPOSSUM; R package: *WGCNA*; Software: Ingenuity Pathway Analysis	*ESR1*, *SOX2*, *SP1*

(Continued)

TABLE 1 | Continued

Title	Authors (publication year)	Database	Bioinformatic tools	Pathogenic factors
Identification of Differentially Expressed Genes through Integrated Study of Alzheimer's Disease Affected Brain Regions (Puthiyedth et al., 2016)	Puthiyedth et al. (2016)	GEO	Algorithm: (α,β)-k Feature Set approach, Minimum Description Length Principle; R package: *GeneMeta*, *RankProd*; Software: Expression Analysis Systematic Explorer	*FGF*, *GPHN*, *INFAR2*, *LARGE*, *PSMB2*, *PSMD14*, *PTMA*, *RAB2A*, *RPL15*, *RWDD2A*, *SEMA4C*, *WNK1*
Meta-Analysis of Transcriptome Data Related to Hippocampus Biopsies and iPSC-Derived Neuronal Cells from Alzheimer's Disease Patients Reveals an Association with FOXA1 and FOXA2 Gene Regulatory Networks (Wruck et al., 2016)	Wruck et al. (2016)	GEO, KEGG	Platform: oPOSSUM; R package: *affy*, *Gostats*, *lumi*, *oligo*	*FOXA1*, *FOXA2*
A Computational Framework for the Prioritization of Disease-gene Candidates (Browne et al., 2015)	Browne et al. (2015)	BIND, BioGPS, BioGRID, DIP, GEO, HPRD, InACT, MINT, PDB	Algorithm: Average of Pearson correlation coefficients; Platform: hORFeome; R package: *GOSemSim*; Software: Cytoscape, Significance Analysis of Microarrays	*CARD9*, *FHL3*, *KRT38*, *LZTS2*, *MID2*, *MTUS2*, *REL*, *TFCP2*, *TRAF1*
Identification of Unstable Network Modules Reveals Disease Modules Associated with the Progression of Alzheimer's Disease (Kikuchi et al., 2013)	Kikuchi et al. (2013)	BioGRID, GEO	Algorithm: Infomap algorithm, MAS algorithm	*UCHL5*

R packages and genes are in italic font.

has been applied in genomic analyses to assess the effectiveness of a particular gene in AD. Moradifard et al. (2018) conducted a meta-analysis using the R package *RobustRankAggreg* to identify statistically significant DEGs in AD across six microarray datasets. The DEGs were further corroborated with three RNA-Seq datasets and input for biological enrichment analysis to reveal the miRNAs that regulate the DEGs. Furthermore, Wang Q. et al. (2017) conducted a meta-analysis using the R package *RankProd* to explore the molecular mechanisms of AD across seven microarray datasets. They found 37 DEGs commonly shared by six brain regions, and most of these DEGs were downregulated. The significantly enriched pathways of DEGs were associated with mitochondrial oxidative phosphorylation and synaptic vesicle function. However, both studies only focused on a single microarray platform (Affymetrix), and the meta-analysis of DEGs did not include the gene expression profiles from RNA-Seq. For the study by Moradifard et al., the DEGs from RNA-Seq were only used to validate the results of microarray datasets; that is, the DEGs common to both the RNA-Seq and microarray datasets, in the same dysregulated direction. It seems that the results of currently available meta-analyses of DEGS for identifying AD pathogenic genes are limited by the use of microarray platforms and the inability to integrate results from both microarray and RNA-Seq.

This study aimed to identify potential pathogenic factors based on the meta-analysis of transcriptomic data from different brain regions in AD. The meta-analysis was conducted according to PRISMA guidelines (Moher et al., 2009), including those for dataset search, dataset selection, and statistical analysis. The raw transcriptomic data were retrieved from databases after a systematic search and were analyzed using a consistent workflow, from quality control and normalization to DEG determination. A statistical meta-analysis was performed when more than one study reported the same DEG. The DEGs that remained statistically significant after *P*-value adjustment were collected to perform a biological enrichment analysis and subgroup analysis, and to construct a PPIN. The network information and AD seed genes, which were obtained from the GWAS Catalog (Welter et al., 2014), were collected for the DIseAse Module Detection (DIAMoND) algorithm (Ghiassian et al., 2015) to examine the significance of the connectivity patterns among network components. This algorithm identified an AD-specific module from the network, and the nodes within the module with a high degree were treated as potential pathogenic factors. The overall study design is illustrated in **Figure 1**.

MATERIALS AND METHODS

Database Search and Dataset Selection

The datasets were collected from GEO[1] (Barrett et al., 2012) and ArrayExpress[2] (Kolesnikov et al., 2015) from their respective

[1]https://www.ncbi.nlm.nih.gov/geo

[2]https://www.ebi.ac.uk/arrayexpress/

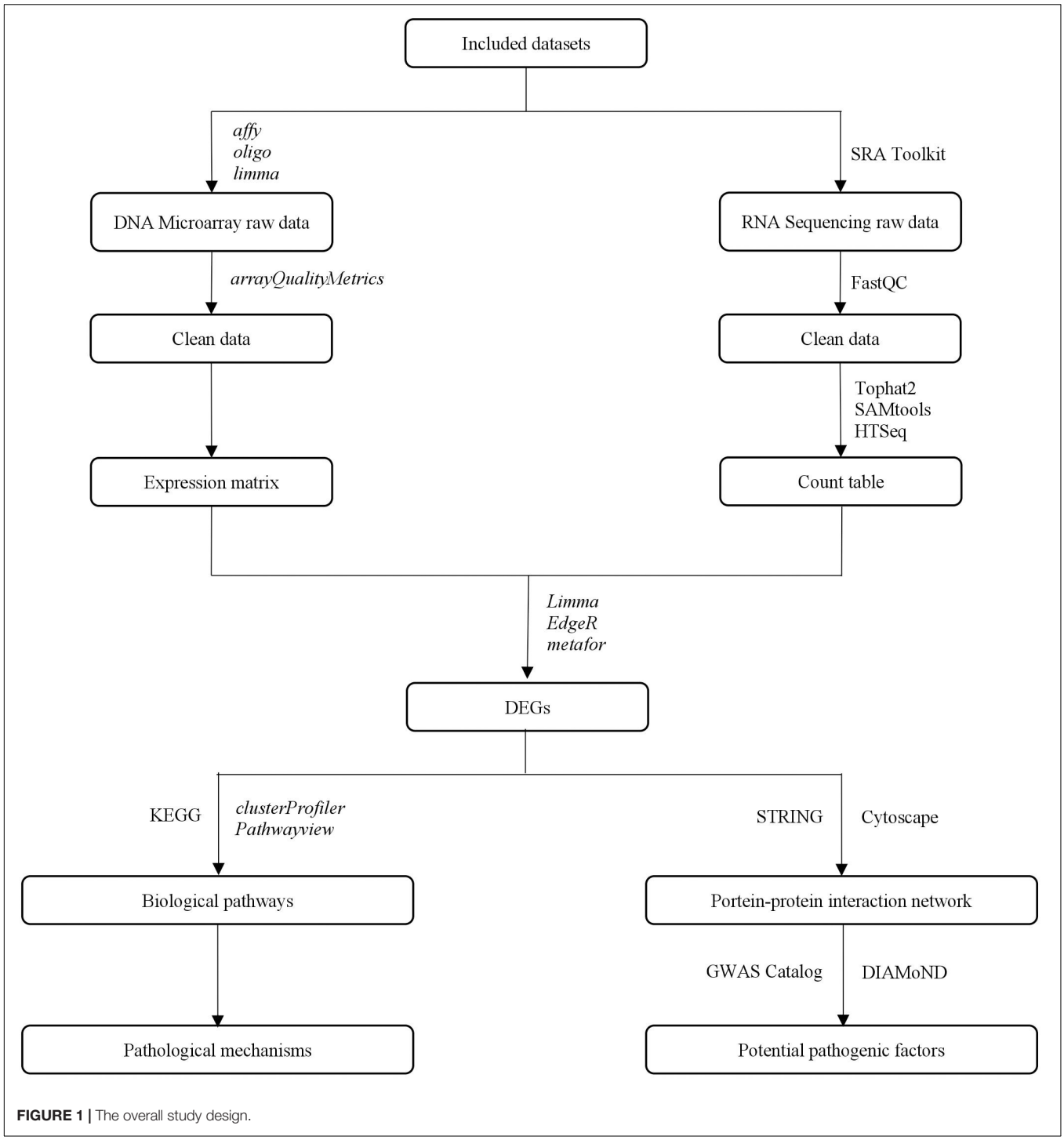

FIGURE 1 | The overall study design.

inception dates until January 6, 2019. The search strategy is shown in **Supplementary File S1**.

Raw DNA microarray and RNA-Seq data reporting the transcriptomes of brain regions from AD and healthy subjects were included. The datasets were excluded if they were (1) not case–control studies; (2) focused on other neurodegenerative diseases; (3) demonstrated treatment effects on AD; or (4) used cell-line or artificial AD models. Sample details were collected if they were provided. If the datasets contained several comparisons, DEGs were determined from each comparison independently.

Data Processing

Each microarray dataset was processed consistently and independently using R packages from Bioconductor. Each dataset was processed through background correction, quantile

normalization, and $\log_2$-transformation of the averaged expression value of duplicate probes, using the *affy* (Gautier et al., 2004), *oligo* (Carvalho and Irizarry, 2010), or *limma* (Ritchie et al., 2015) package. For each dataset, the quality of each array was assessed using the *arrayQualityMetrics* (Kauffmann et al., 2009) package. The array was omitted from the subsequent analysis if it was detected as an outliner in any of the three metrics provided by the package. The gene expression ratios between AD and healthy subjects were determined for each dataset using the *limma* package. Genes with an adjusted *P*-value (by FDR) of less than 0.05 were considered to be statistically significant DEGs. The DEGs were annotated using the gene annotation table provided by GEO and ArrayExpress. The probes with missing gene symbols were removed. When multiple probes were annotated with the same gene symbol on the same array, the probe with the highest expression value was kept.

The raw sequence data were converted to FASTQ format using the SRA Toolkit (version 2.9.2) (Leinonen et al., 2011). Quality control on FASTQ was conducted using FastQC (version 0.11.8) (Andrews, 2010): (1) sequences with less than 80% of bases with at least quality of 25 were filtered; and (2) the bases with quality less than 25 were trimmed. The cleaner FASTQ files were aligned to the *Homo.sapiens* reference genome, GRCh38.94 (downloaded from Ensemble), using TopHat (version 2.1.1) (Kim et al., 2013). The aligned sequences were sorted based on the aligned position to the reference genome using SAMtools (version 1.9) (Li H. et al., 2009). After sorting, the count-based gene expression was obtained using HTSeq (version 0.8.0) (Anders et al., 2015), and the reads with alignment scores less than 10 were omitted. Differential expression was performed using the *edgeR* (Robinson et al., 2009) package for R software. RNA-Seq datasets were processed on a Linux-based HP ProLiant DL580 Gen8 workstation [Inter® Xeon® E7-4820 CPU v2 @ 2.00 GHz; 4 processors with 32 total cores enabled; 128 GB RAM].

Meta-Analysis, Biological Enrichment Analysis, and Subgroup Analysis

The list of DEGs and their dysregulation states (i.e., upregulated or downregulated) from each study were processed using the *meta* for Chung et al. (2015) package for R software. The meta-analysis was conducted under a random-effects model, and their outcomes were logORs with *P*-values. For each gene in the i-th study, the effect (θ_i) based on the numbers of dysregulation events in both AD and control samples was first calculated, then the overall effect was computed according to formula $\frac{\sum Wi\theta i}{\sum Wi}$, where w_i is the weight and is equal to $1/v_i$, where v_i is the sample variance. The genes with logORs above or below 0 were considered upregulated or downregulated, respectively. The *P*-values were adjusted by FDR, and DEGs with adjusted *P*-values less than 0.05 were regarded as statistically significant. After meta-analysis, the statistically significant DEGs were used to perform a biological enrichment analysis. The enrichment analysis was conducted by the hypergeometric test using the *clusterProfiler* (Yu et al., 2012) package for R software, based on the KEGG[3] (Kanehisa et al., 2012). The statistically significant DEGs after meta-analysis were collected as input for the enrichment analysis to identify biological pathways among them. The pathways with FDR-adjusted *P*-values less than 0.05 were considered statistically significant.

The DEGs were split into different subgroups based on which brain regions they were from, to compare expression profiles among brain regions. According to Roth et al. (2006), brain regions can be hierarchically clustered into three major branches based on cytological differences. The first branch includes the cerebellum. The second branch is sub-categorized into three sub-branches; the first sub-branch includes the putamen and nucleus accumbens, the second sub-branch includes the amygdala and hippocampus, and the third sub-branch includes the cerebral neocortex. The third branch includes the thalamus, brain stem, and spinal cord. Biological enrichment analysis was also conducted in each subgroup.

Protein–Protein Interaction Network and Potential Pathogenic Factors

After meta-analysis, statistically significant DEGs were used to construct a PPIN based on the data from STRING (version 11[4]; Szklarczyk et al., 2011). Only interactions with the highest confidence (0.9) were kept. The PPIN was visualized using Cytoscape (Shannon et al., 2003). Disease-associated genes are not topologically interacted into a dense network module because disease can be the consequence of perturbation in many functional units. AD seed genes were retrieved from the GWAS Catalog (Welter et al., 2014)[5] using the key word "AD" and the following selection criteria: a significance *p*-Value cutoff of no more than 1^*10^{-8}. Genes with official gene symbols were kept as AD seed genes. The PPIN information (e.g., edge list in the co-expression network) and AD seed genes were put into the DIAMOnD algorithm (Ghiassian et al., 2015) to evaluate the significance of the connections that each node had with the seed genes in the biological network. In each iteration until the stopping condition was satisfied, the node with the lowest connectivity *P*-value was treated as the most significantly connected node for output. The nodes within the module that had a high degree (>95th percentile) were treated as potential pathogenic factors.

Risk of Bias

All studies were collected according to the publication information of datasets. If there was more than one publication for one dataset, the publication with the earlier publication year was selected. The risk of bias for the included studies was evaluated according to MIAME (Minimum information about a microarray experiment) (Brazma, 2009) and MINSEQE (Minimum information about a high-throughput nucleotide sequencing experiment[6], proposed by FGED Society in 2012) guidelines by two authors (SY and HZ), independently.

[3]http://www.genome.jp/kegg/

[4]https://string-db.org/

[5]https://www.ebi.ac.uk/gwas/

[6]http://fged.org/projects/minseqe/

Disagreements between the authors were resolved by discussion with the third author (SWL). The MIAME and MINSEQE guidelines are designated to report the quality of DNA microarray and RNA-Seq studies, respectively. And the quality of transcriptomic parts of included studies was assessed, including raw data collection, result presentation, sample annotation, experimental design, array annotation, and data processing pipeline. Items with low risk were counted +1, suggesting high reproducibility; items with unclear risk were counted 0, suggesting ambiguous reproducibility; and items with high risk were counted −1, suggesting low reproducibility.

RESULTS

Included Datasets

The selection process of the datasets is shown in **Figure 2**. A total of 225 datasets were initially identified from GEO and ArrayExpress. After removing duplicated datasets and datasets that met the exclusion criteria, 25 datasets (21 for microarray and 4 for RNA-Seq) met the eligibility criteria. The dataset characteristics are shown in **Table 2**. Among the included datasets, the hippocampus (n = 8) was the most extensively studied brain region, followed by the entorhinal cortex and prefrontal cortex (n = 3).

Preprocessing of Datasets and Determination of Differentially Expressed Genes

After the selection process of the datasets, all included datasets contained complete transcriptomic raw data, and were undergone a quality control as a prioritization procedure. In the included microarray datasets, the quality of the normalized dataset was assessed using the R package *arrayQualityMetrics*. Different numbers of arrays were identified as outliers and omitted in the subsequent analysis (**Table 2**). In the included RNA-Seq datasets, the reads were mapped to the *Homo.sapiens* reference genome (GRCh38.94) after sequence quality assessment. The mapping rates were above 95% for the RNA-Seq datasets. From the mapped reads, the genes were counted to determine DEGs. After preprocessing steps, different numbers of DEGs were determined from each comparison, ranging from 0 to over 10,000 (**Table 3**). There were 21,064 DEGs in all comparisons that compared AD brain samples with healthy brain samples, and 16,810 DEGs (79.76%) were reported in at least two comparisons (**Supplementary File S2**). In the meta-analysis of DEGs, 9,298 DEGs were found to be

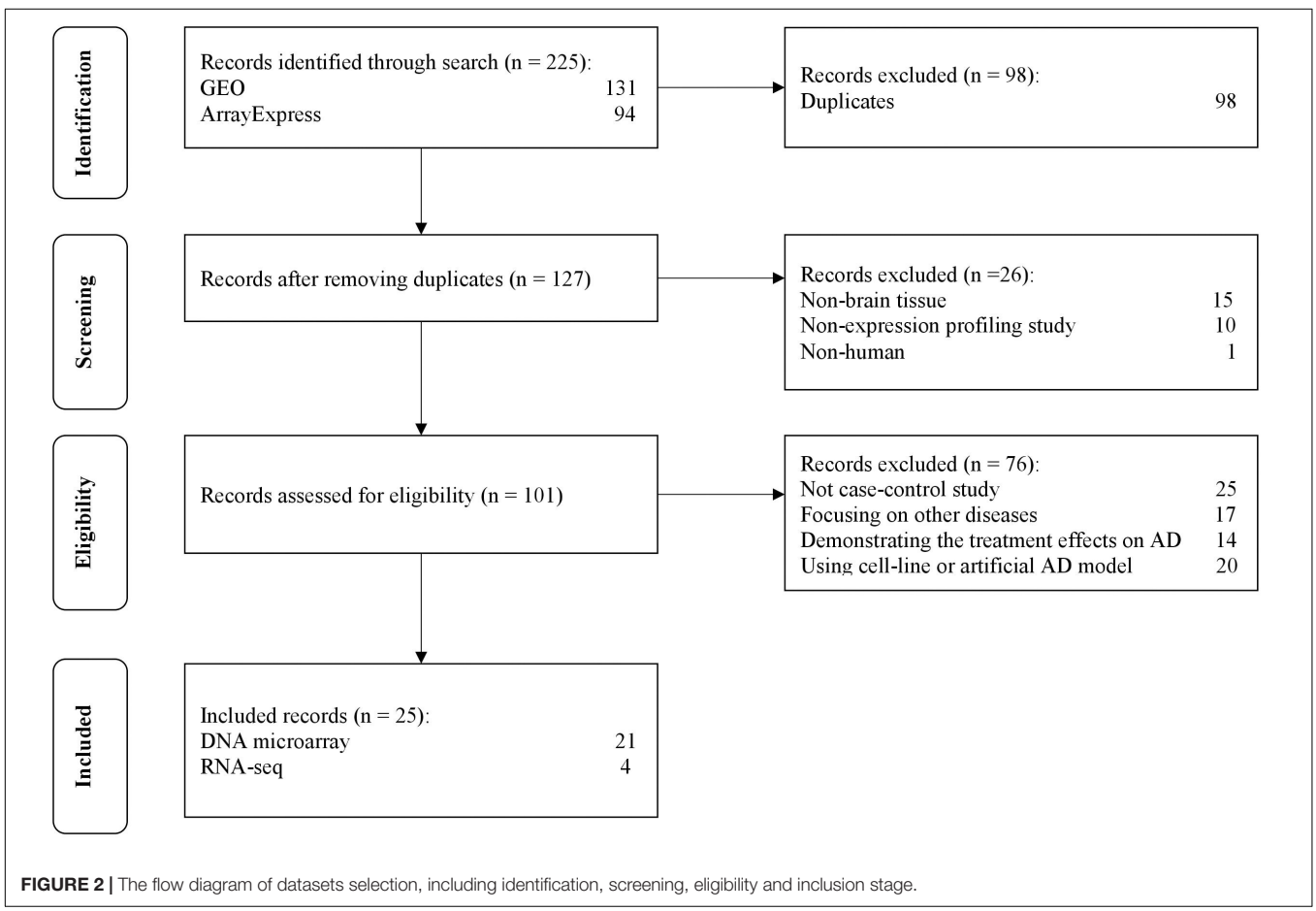

FIGURE 2 | The flow diagram of datasets selection, including identification, screening, eligibility and inclusion stage.

TABLE 2 | The characteristics of included datasets.

Types	Dataset_ID	Brain tissue	Disease stage	Platform	Number of samples	Number of samples omitted
DNA microarray	E-MEXP-2280	Medial temporal lobe	Braak stage VI	Affymetrix Human Genome U133 Plus 2.0 Array	12	0
	GSE110226	Choroid plexus	Braak stage III to VI	Rosetta/Merck Human RSTA Custom Affymetrix 2.0 microarray	13	3
	GSE12685	Frontal cortex	MMSE 21 to 27	Affymetrix Human Genome U133A Array	14	3
	GSE1297	Hippocampus	Braak stage at III to VI	Affymetrix Human Genome U133A Array	31	3
	GSE16759	Parietal lobe cortex	Braak stage at V to VI	Affymetrix Human Genome U133 Plus 2.0 Array	8	1
	GSE26927	Entorhinal cortex	–	Illumina humanRef-8 v2.0 expression beadchip	18	4
	GSE28146	Hippocampus	Braak stage at V to VI	Affymetrix Human Genome U133 Plus 2.0 Array	30	1
	GSE29378	Hippocampus	Braak stage at V to VI	Illumina HumanHT-12 V3.0 expression beadchip	63	2
	GSE32645	Cortex	Braak stage VI	Agilent-014850 Whole Human Genome Microarray 4 × 44K G4112F	6	0
	GSE33000	Prefrontal cortex	–	Rosetta/Merck Human 44k 1.1 microarray	467	30
	GSE36980	Frontal cortex, hippocampus, temporal cortex	Braak stage at V to VI	Affymetrix Human Gene 1.0 ST Array [transcript (gene) version]	79	8
	GSE37263	Neocortex	Braak stage at III to VI	Affymetrix Human Exon 1.0 ST Array [transcript (gene) version]	16	1
	GSE39420	Posterior cingulate	Braak stage at V to VI	Affymetrix Human Gene 1.1 ST Array [transcript (gene) version]	21	0
	GSE44768	Cerebellum	–	Rosetta/Merck Human 44k 1.1 microarray	230	10
	GSE44770	Prefrontal cortex	–	Rosetta/Merck Human 44k 1.1 microarray	230	28
	GSE44771	Visual cortex	–	Rosetta/Merck Human 44k 1.1 microarray	230	22
	GSE48350	Entorhinal cortex, hippocampus, post-central gyrus, superior frontal gyrus	Braak stage at II to VI	Affymetrix Human Genome U133 Plus 2.0 Array	253	16
	GSE5281	Entorhinal cortex, hippocampus, medial temporal gyrus, posterior cingulate, primary visual cortex, superior frontal gyrus	–	Affymetrix Human Genome U133 Plus 2.0 Array	161	11
	GSE61196	Choroid plexus	Braak stage at III and VI	Agilent-014850 Whole Human Genome Microarray 4 × 44K G4112F	21	1

(Continued)

TABLE 2 | Continued

Types	Dataset_ID	Brain tissue	Disease stage	Platform	Number of samples	Number of samples omitted
	GSE84422	Amygdala, anterior cingulate, caudate nucleus, dorsolateral prefrontal cortex, frontal pole, hippocampus, inferior frontal gyrus, inferior temporal gyrus, middle temporal gyrus, nucleus accumbens, occipital visual cortex, parahippocampal gyrus, posterior cingulate cortex, precentral gyrus, prefrontal cortex, putamen, temporal polesuperior parietal lobule, superior temporal gyrus	Braak stage at I to VI	Affymetrix Human Genome U133A ArrayAffymetrix Human Genome U133B ArrayAffymetrix Human Genome U133 Plus 2.0 Array	1,146	64
	GSE93885	Olfactory bulb	–	Affymetrix Human Gene 2.0 ST Array [transcript (gene) version]	18	0
RNA-Seq	GSE104704	Lateral temporal lobe	Braak stage at V to VI	Illumina HiSeq 2500 (Homo sapiens)	30	–
	GSE95587	Fusiform gyrus	Braak stage at III to VI	Illumina HiSeq 2500 (Homo sapiens)	117	–
	GSE53697	Dorsolateral prefrontal cortex	Braak stage at II to VI	Illumina HiSeq 2500 (Homo sapiens)	17	–
	GSE67333	Hippocampus	Braak stage at V to VI	Illumina HiSeq 2000 (Homo sapiens)	8	–

statistically significant (**Supplementary File S3**); 4,960 genes were downregulated and 4,338 genes were upregulated. The most reported downregulated DEGs were *DPP6* and *FXYD7*, which were reported in 16 comparisons; *RHOQ* was the most reported upregulated DEG among all 15 reported comparisons. A loss of *DPP6* or *FXYD7* is reported to dysregulate neuronal excitation (Hoos et al., 2013; Cacace et al., 2019), while *RHOQ* is reported to enhance Aβ oligomerization (Aguilar et al., 2017). Multiple DEGs involved in Aβ clearance were found statistically significant in meta-analysis (**Table 4**). These DEGs could be categorized into UPS, autophagy, and UPR, implying the downregulated Aβ clearance. The statistically significant DEGs in UPS and autophagy were mostly downregulated, while those in UPR were mostly upregulated, proposing a dysfunctional homeostasis. The impaired Aβ clearance resulting from dysfunctional homeostasis is suggested to induce Aβ accumulation in sporadic AD, in contrast with the overproduction of Aβ in familial AD (Mawuenyega et al., 2010; Potter et al., 2013).

However, several genes involved in Aβ clearance were not found statistically significant in meta-analysis, although they were reported as DEGs in separated comparisons. The heat shock proteins work coordinately with UPS for protein clearance, remodeling the misfolded proteins before the degradation by UPS. Both systems are upregulated to restore dysfunctional homeostasis at the beginning (Kästle and Grune, 2012). However, the genes for most heat shock proteins, such as *ATXN1*, *ATXN3*, and *ATXN7*, were not statistically significant (**Supplementary File S3**), suggesting that the early event of AD might not be truly reflected. *PICALM* and *SQSTM1* which are involved in autophagosome formation (Moreau et al., 2014; Ntsapi and Loos, 2016), were not reported as DEGs in the meta-analysis. Several autophagic marker genes, *MAP1LC3B* and *ATG12*, associated with autophagosomal function (Ma et al., 2010), were also found as a statistically insignificant in the meta-analysis. The expression of *TREM2* was upregulated, which was contradictory to the role of *TREM2* reported in autophagy (Lucin et al., 2013), but consistent with that reported in Aβ plaque-activated microglia (Yuan et al., 2016; Yin et al., 2017). Meanwhile, those genes involved in Aβ plaque-activated microglia, *MS4A4A*, *PLCG2*, and *ABI3*, were also found significantly upregulated in the meta-analysis.

On the enrichment analysis, AD itself was identified as significant (**Figure 3A**). In the AD pathway, components related to the mitochondrial respiratory chain were downregulated,

TABLE 3 | The number of DEGs determined from each comparison.

Comparison_ID	No of control	No of disease	No of DEGs
E-MEXP-2280	5	7	0
GSE32645	3	3	0
GSE110226	5	5	475
GSE61196_CvsBraak3	7	7	1,597
GSE61196_CvsBraak6	7	6	1,723
GSE33000	154	283	12,742
GSE12685	6	5	2
GSE1297_CvsIni	8	6	0
GSE1297_CvsMod	9	8	0
GSE1297_CvsSev	9	6	7
GSE93885_CvsIni	4	5	0
GSE93885_CvsMod	4	4	0
GSE93885_CvsSev	4	5	0
GSE29378_CA1	16	15	2
GSE29378_CA3	16	14	1
GSE26927	4	10	0
GSE16759	3	4	0
GSE37263	8	7	0
GSE48350_EC	36	14	7,185
GSE48350_HIP	43	18	3,958
GSE48350_PCG	39	22	1,540
GSE48350_SFG	46	19	6,148
GSE28146_CvsIni	8	7	0
GSE28146_CvsMod	8	8	0
GSE28146_CvsSev	8	6	0
GSE5281_EC	12	9	9,921
GSE5281_HIP	13	10	7,176
GSE5281_MTG	11	16	9,981
GSE5281_PC	12	8	8,978
GSE5281_PVC	12	16	38
GSE5281_SFG	22	9	5,054
GSE44768	98	122	1,447
GSE44770	81	121	1,778
GSE44771	89	119	4,732
GSE84422_Amygdala	14	16	1,253
GSE84422_Nucleus_accumbens	12	16	9
GSE84422_96_Anterior_cingulate	16	20	0
GSE84422_96_Caudate_nucleus	11	18	0
GSE84422_96_Dorsolateral_prefrontal_cortex	15	15	0
GSE84422_96_Frontal_pole	14	21	0
GSE84422_96_Hippocampus	10	18	0
GSE84422_96_Inferior_frontal_gyrus	11	17	0
GSE84422_96_Inferior_temporal_gyrus	13	18	0
GSE84422_96_Middle_temporal_gyrus	14	19	0
GSE84422_96_Occipital_visual_cortex	11	13	0
GSE84422_96_Parahippocampal_gyrus	14	21	0
GSE84422_96_Posterior_cingulate_cortex	12	23	0
GSE84422_96_Precentral_gyrus	5	18	0
GSE84422_96_Prefrontal_cortex	11	18	35
GSE84422_96_Putamen	9	17	0
GSE84422_96_Superior_parietal_lobule	13	12	0
GSE84422_96_Superior_temporal_gyrus	14	20	0
GSE84422_96_Temporal_pole	14	18	0
GSE84422_97_Anterior_cingulate	14	19	0
GSE84422_97_Caudate_nucleus	9	16	0
GSE84422_97_Dorsolateral_prefrontal_cortex	16	14	1
GSE84422_97_Frontal_pole	15	22	0
GSE84422_97_Hippocampus	10	18	0
GSE84422_97_Inferior_frontal_gyrus	11	17	0
GSE84422_97_Inferior_temporal_gyrus	13	18	30
GSE84422_97_Middle_temporal_gyrus	13	20	0
GSE84422_97_Occipital_visual_cortex	12	13	0
GSE84422_97_Parahippocampal_gyrus	14	22	0
GSE84422_97_Posterior_cingulate_cortex	12	22	0
GSE84422_97_Precentral_gyrus	5	17	0
GSE84422_97_Prefrontal_cortex	11	19	0
GSE84422_97_Putamen	9	18	0
GSE84422_97_Superior_parietal_lobule	13	13	0
GSE84422_97_Superior_temporal_gyrus	14	20	1
GSE84422_97_Temporal_pole	14	18	0
GSE36980_FC	17	13	0
GSE36980_HIP	10	5	587
GSE36980_TC	17	9	5
GSE104704_Old	10	12	1,070
GSE95587	33	84	6,611
GSE53697	8	9	1
GSE67333	4	4	10

while components related to Ca^{2+} channels that transport Ca^{2+} from the ER into the cytoplasm were upregulated (**Figure 3B**). Several AD-related pathways, including proteasome, oxidative phosphorylation, and retrograde endocannabinoid signaling pathways, were also identified as statistically significant; most components in these pathways were downregulated (**Figures 3C–E**). Downregulation of the proteasome decreases the clearance of Aβ (Hong et al., 2014), while downregulation of oxidative phosphorylation decreases the efficacy of the mitochondrial respiratory chain, suggesting hypometabolism in the AD brain (Mosconi et al., 2008). The genes (e.g., *MFN1*, *OPA1*, and *DNM1L*) involved in mitochondrial fusion and fission were downregulated (Westermann, 2012), disturbing mitochondrial biogenesis to adopt energetic demands. The aberrant mitochondria were removed by the process, mitophagy. However, the genes responsible for mitophagy, *PINK1* and *PRKN* (Narendra et al., 2008), were downregulated, which further increased the burden of damaged protein clearance. The regulation of genes involved in oxidative phosphorylation in mitochondria was severely impaired in the present study, including genes for NADH dehydrogenase, succinate dehydrogenase, cytochrome *c* reductase, and cytochrome *c* oxidase in the electron transport chain. eCBs are signaling molecules used among nearby cells over short distances, and they modulate neuronal transmission. There is a high density of cannabinoid receptors in presynaptic terminals

TABLE 4 | The dysregulated status of genes involved in ubiquitin-proteasome system, autophagy, and unfolded-protein response for Aβ clearance.

Functional category	Genes	Adjusted *P*-value	Dysregulated state
Ubiquitin	*PRKN*	1.77E-06	Downregulated
-proteasome	*UCHL1*	2.70E-02	Downregulated
system (UPS)	*UCHL3*	1.47E-20	Downregulated
	PSMC1	2.09E-24	Downregulated
	UBE2D2	2.02E-24	Downregulated
	STUB1	1.62E-18	Downregulated
	NEDD8	1.88E-31	Downregulated
	ATXN1	0.61	Downregulated
	ATXN3	0.79	Upregulated
	ATXN7	0.97	Upregulated
Autophagy	*BECN1*	1.42E-20	Downregulated
	MTOR	1.16E-15	Downregulated
	TFEB	2.06E-36	Upregulated
	ATG5	5.20E-19	Downregulated
	ATG7	1.78E-32	Downregulated
	TREM2	5.06E-32	Upregulated
	MS4A4A	8.77E-22	Upregulated
	PLCG2	6.91E-26	Upregulated
	ABI3	1.83E-19	Upregulated
	ATG12	0.94	Downregulated
	PICALM	0.86	Upregulated
	SQSTM1	0.20	Upregulated
Unfolded	*ERN1*	1.05E-13	Upregulated
-protein	*EIF2AK3*	2.00E-10	Upregulated
response (UPR)	*TMEM259*	6.57E-11	Downregulated
	XBP1	2.95E-14	Upregulated

in the hippocampus and limbic cortex, indicating a role for cannabinoids in cognitive information processing (Zou and Kumar, 2018). A disruption of eCB signaling has been reported in AD, which influences neurotransmitter release (Basavarajappa et al., 2017). In the current study, most members of the retrograde endocannabinoid signaling pathway were downregulated, interfering with the role of eCBs in the release of glutamate and GABA in synapses.

Subgroup Analysis

Among 77 comparisons, 15 investigated the amygdala and hippocampus of AD subjects, while 28 focused on the cerebral cortex (**Table 5**). Statistically significant DEGs for each subgroup analysis are shown in **Supplementary File S4**. There were 2,260 DEGs that were reported as significant in the amygdala and hippocampus, while 6,636 DEGs were reported as significant in the cerebral cortex. Among the 1,390 commonly found DEGs, 359 upregulated and 1,020 downregulated DEGs were consistently found in two subgroups. Eleven DEGs were upregulated in one subgroup but downregulated in another subgroup. The most highly upregulated and downregulated DEGs were *S100A6* and *STMN4*, respectively, in both subgroups. The protein calcyclin (encoded by *S100A6*) is a calcium-binding protein that is highly expressed in astrocytes surrounding Aβ deposits, and is involved in neuronal death via zinc depletion (Bartkowska et al., 2017). The protein stathmin (encoded by *STMN4*) binds tubulin to mediate microtubule dynamics, and dysregulation of stathmin-mediated microtubule stability induces memory loss (Uchida et al., 2014).

In the subgroup enrichment analyses, the pathways for proteasome and retrograde endocannabinoid signaling were found in both subgroups (**Figures 4**, **5**). For the subgroup of the amygdala and hippocampus, the synaptic vesicle cycle was identified as statistically significant, and most components in this pathway were downregulated (**Figure 4F**). Downregulated synaptic functions decrease the release of neurotransmitters from neurons, inducing memory-related symptoms in AD. For the subgroup of the cerebral cortex, several synaptic signaling pathways were identified in AD, including the MAPK signaling pathway, dopaminergic synapses, and the insulin signaling pathway; the components in these pathways were mostly downregulated (**Figures 5D–F**). The role of the MAPK effector, JNK, is to dissociate Beclin 1 from Bcl-2 to mediate autophagy, and downregulation of JNK reduces autophagy ability (Zhou et al., 2015). The loss of dopaminergic synapses in the ventral tegmental area reduces the release of dopamine toward the cortex and hippocampus, and is reported to be associated with memory loss in AD before the formation of amyloid plaques (Nobili et al., 2017). Although all AD datasets collected in this study did not report suffering from T2DM, the dysfunctional insulin signaling was identified, suggesting an effect of Aβ in insulin signaling pathway. Aβ shares a common sequence with insulin, antagonizing the regulatory effects of insulin (Folch et al., 2018). In the canonical insulin signaling pathway, insulin binds receptors to activate Akt for mediating downstream effects, e.g., translocating glucose receptors to cellular membrane, activating mTOR for autophagy regulation, and inhibiting GSK3β for tau protein phosphorylation. Losing the regulatory effects of insulin may induce dysfunctional autophagy and tau protein hyperphosphorylation, potentiating AD development. The increased level of free insulin due to Aβ blockage reduces Aβ clearance via IDE, because insulin has a higher affinity to IDE than Aβ (Farris et al., 2003). On the other hand, the AD progression reduces the transport of insulin across BBB, decreasing insulin signaling in brain (Stanley et al., 2016).

In the present study, several datasets focused on the hippocampus and entorhinal cortex because these two regions suffer the most significant neuronal loss in the early stage of AD, while no significant neuronal loss is observed in these regions during normal aging. The transcriptome from these brain regions therefore represents the chronic response to the causes and consequences, or the treatment, of AD.

Quality Assessment of Studies

MIAME and MINSEQE guidelines were used to assess the transcriptomic analysis of studies (Blalock et al., 2004, 2011; Liang et al., 2007; Berchtold et al., 2008; Bronner et al., 2009; Williams et al., 2009; Nunez-Iglesias et al., 2010; Tan et al., 2010; Durrenberger et al., 2012; Antonell et al., 2013; Fischer et al., 2013; Janssen et al., 2013; Miller et al., 2013; Zhang et al., 2013; Hokama et al., 2014; Narayanan et al., 2014; Magistri

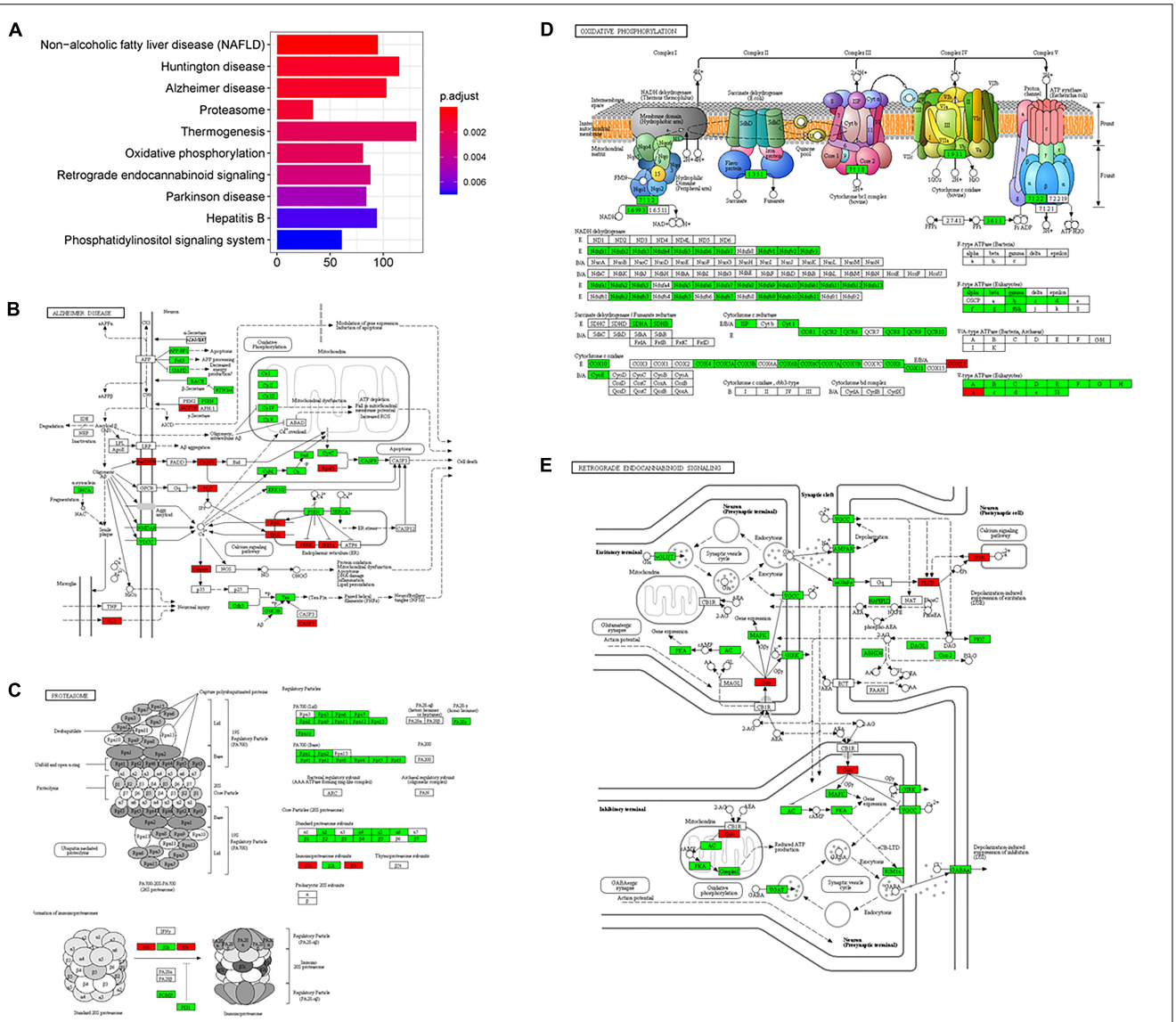

FIGURE 3 | The AD-related biological pathways as impacted in health vs. AD subjects, **(A)** the top 10 statistically significant pathways from enrichment analysis result; **(B)** Alzheimer's disease; **(C)** Proteasome; **(D)** Oxidative phosphorylation; and **(E)** Retrograde endocannabinoid signaling. For figure 3B-E, the red and green represent upregulation and downregulation, respectively.

et al., 2015; Scheckel et al., 2016; Wang et al., 2016; Lachen-Montes et al., 2017; Friedman et al., 2018; Nativio et al., 2018; Stopa et al., 2018) that published the datasets that were used in the present study. The results of quality assessments are shown in **Figure 6**. Among the 19 studies that published the microarray datasets, 80% did not provide the brain sample size or the weight used for RNA extraction for sample annotation and experimental variables, and only two studies provided sufficient information about experimental design, including quality control of samples. Furthermore, the annotations of array designs, including microarray quality indicators, were not fully reported for most studies (95%). For 40% of the studies, experimental and data processing details, including normalization methods and cut-offs for DEGs, were not fully reported. Among the four studies that published the RNA-Seq datasets, no study provided the brain sample size or the weight used for RNA extraction, or the details of experimental parameters used for RNA-Seq procedures. Furthermore, half of the studies did not provide sufficient information about experimental and data processing protocols, including the cut-offs for DEGs.

The relatively low quality of the studies indicates the insufficient information related to transcriptomic analysis provided in the studies, raising the reproducibility issue. Also, the transcriptomic results might be influenced, blurring some pathological events in the postmortem AD brains. The genes encoded heat shock proteins (e.g., *ATXN1*, *ATXN3*, and *ATXN7*) were not found statistically significant in the meta-analysis, while the multiple genes involved in neuroinflammation (e.g., *CXCL3*,

TABLE 5 | The datasets used in the subgroup analysis.

Subgroups	No of control	No of disease	No of DEGs	No of pathways	Comparison_ID
Cerebellum	98	122	–	–	GSE44768
Putamen and nucleus accumbens	30	51	–	–	GSE84422_96_Putamen, GSE84422_97_Putamen, GSE84422_Nucleus_accumbens
Amygdala and hippocampus	175	159	2,260	18	GSE84422_Amygdala, GSE1297_CvsIni, GSE1297_CvsMod, GSE1297_CvsSev, GSE28146_CvsIni, GSE28146_CvsMod, GSE28146_CvsSev, GSE29378_CA1, GSE29378_CA3, GSE36980_HIP, GSE48350_HIP, GSE5281_HIP, GSE84422_96_Hippocampus, GSE84422_97_Hippocampus, GSE67333
Cerebral neocortices	632	849	6,636	25	E-MEXP-2280, GSE12685, GSE16759, GSE26927, GSE32645, GSE33000, GSE36980_FC, GSE36980_TC, GSE37263, GSE44770, GSE44771, GSE48350_EC, GSE5281_EC, GSE5281_PVC, GSE84422_96_Dorsolateral_prefrontal_cortex, GSE84422_96_Frontal_pole, GSE84422_96_Occipital_visual_cortex, GSE84422_96_Prefrontal_cortex, GSE84422_96_Superior_parietal_lobule, GSE84422_96_Temporal_pole, GSE84422_97_Dorsolateral_prefrontal_cortex, GSE84422_97_Frontal_pole, GSE84422_97_Occipital_visual_cortex, GSE84422_97_Prefrontal_cortex, GSE84422_97_Superior_parietal_lobule, GSE84422_97_Temporal_pole, GSE104704_Old, GSE53697

IFNG, *IL6*, *IL13*, and *CXCL9*) (Garwood et al., 2011) were only reported as DEGs in one dataset, and therefore were not collected for meta-analysis. Although both heat shock proteins recruitment and neuroinflammation are associated with AD development, their pathological roles in AD development might not fully reflected in this study.

Construction of a Protein–Protein Interaction Network to Identify Potential Pathogenic Factors

The DEGs from the meta-analysis were used to retrieve the corresponding proteins in interactions according to STRING. The PPIN consisted of 4,781 nodes (2,083 upregulated nodes and 2,698 downregulated nodes) and 51,076 edges (**Figure 7A**) and there were 105 AD seed genes (**Supplementary File S5**) retrieved from the GWAS Catalog. The PPIN exhibited scale free topology with the degree distribution following a power law distribution ($y = 3779.2x^{-1.481}$) and the most proteins were closely linked. In the PPIN, polyubiquitin-C (endcoded by *UBC*) and E3 ubiquitin-protein ligase RBX1 (encoded by *RBX1*), were the two proteins with the highest degree (372 and 222, respectively). These proteins were downregulated and are parts of UPS for protein degradation. The dysfunctional proteasome is regarded as an early event of AD (Manavalan et al., 2013), e.g., the decreased proteasomal clearance enhances mitochondrial dysfunction (Braun et al., 2015).

The PPIN for each protein pair was extracted for the subsequent DIAMOnD algorithm with AD seed genes to obtain a disease module. Not every seed gene was biologically linked to AD; some were involved in AD comorbidity disease. Among the disease modules (**Figure 7B**), the two nodes with a high degree (>95th percentile) were selected as potential pathogenic factors, and included EGFR and Fyn. The EGFR was the Aβ oligomer receptor, in which Aβ oligomer is regarded as the causative toxic species. The hydrophobic residues of Aβ oligomers are more easily accessible and interacting with cellular proteins, compared with Aβ fibrils (William et al., 2011). Fyn is involved in Aβ signal transduction and tau protein phosphorylation, and is changed in synaptic signaling pathways, including MAPK signaling pathway. These two proteins are both Aβ-relevant receptors, mediating the Aβ oligomers downstream neurotoxicity.

DISCUSSION

We used a meta-analysis approach based on DNA microarray and RNA-Seq datasets from multiple brain regions to reveal potential pathogenic factors of AD. Perturbations in the genes involved in the proteasome, oxidative phosphorylation, and retrograde endocannabinoid signaling pathways were identified. The proteasome is required to degrade the damaged proteins to maintain the cellular functionality. The decreased proteasome activity results in an accumulation of ubiquitinated and damaged proteins (Ciechanover, 2015). The ubiquitination degradation of APP by the proteasome includes several key genes, such as *PRKN*, *NEDD8*, *PSMC1*, *UCHL1*, and *UCHL3* (Bedford et al., 2008; Chen et al., 2012; Zhang et al., 2015; Nomura et al., 2016). Tau-specific ubiquitin–proteasome related genes, including *UBE2D2* (Shimura et al., 2004) and *STUB1* (Saidi et al., 2015), were also downregulated. The downregulation of these genes might result in impaired Aβ and phosphorylated tau protein clearance (**Table 4**). The oligomeric Aβ itself disrupts the catalytic activity of proteasome (Tseng et al., 2008), forming a positive feedback loop to worsen the Aβ clearance by proteasome. The disrupted catalytic activity of proteasome may also lose its inhibition of presenilin complex, which is the catalytic complex for γ-secretase, enhancing Aβ production (Chadwick et al., 2012). The accumulated Aβ, located on the mitochondria, deleteriously impairs oxidative phosphorylation, decreasing ATP production in the mitochondria (Chen and Du Yan, 2007; Moreira et al., 2010). The ATP-dependent proteins (i.e., the Ca^{2+} pumps located on the endoplasmic reticulum (ER) and ATP-dependent ion pumps) are unable to maintain their physiological functions,

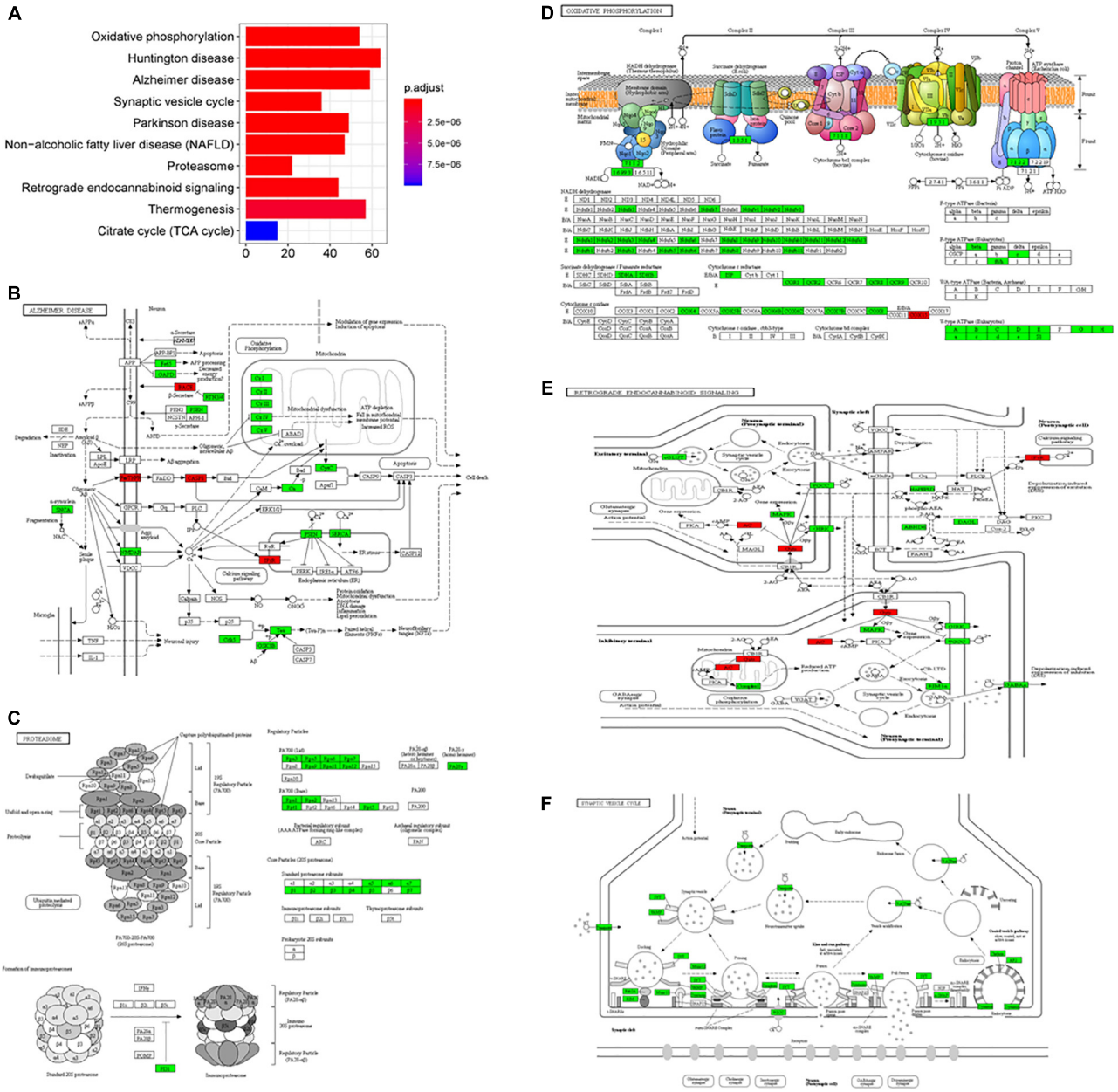

FIGURE 4 | The AD-related biological pathways from the subgroup amydala and hippocampus, **(A)** the top 10 statistically significant pathways from enrichment analysis result; **(B)** Alzheimer's disease; **(C)** Proteasome; **(D)** Oxidative phosphorylation; **(E)** Retrograde endocannabinoid signaling; and **(F)** Synaptic vesicle cycle. The red and green represent upregulation and downregulation, respectively.

interfering neurotransmitter release and memory formation (Sudhof, 2012). The ATP-dependent molecular chaperones are also failed to work coordinately with UPS to remodel the misfolded proteins (Mattoo and Goloubinoff, 2014).

The reduced activity of proteasome enhances the burden of Aβ clearance on the autophagy and UPR. Autophagy is the process of degrading redundant cellular components by delivering them to lysosomes and forming autophagosomes. Beclin 1 (encoded by *BECN1*) is an essential component of autophagososomal structure (Jaeger and Wyss-Coray, 2010), but its autophagy function is inhibited by interacting with Bcl-2 (encoded by *BCL2*) leading to cellular death (Marquez and Xu, 2012). The downregulation of *BECN1* and upregulation of *BCL2* in the present study indicated autophagic flux failure. Autophagy is inhibited by the upregulation of *mTOR* and activated by the downregulation of *TFEB* (Caccamo et al., 2010; Polito et al., 2014). The downregulation of *mTOR* and upregulation of *TFEB* in the present study induced the formation of immature autophagosomes, impairing Aβ clearance. In addition, the downregulation of *mTOR* is associated with

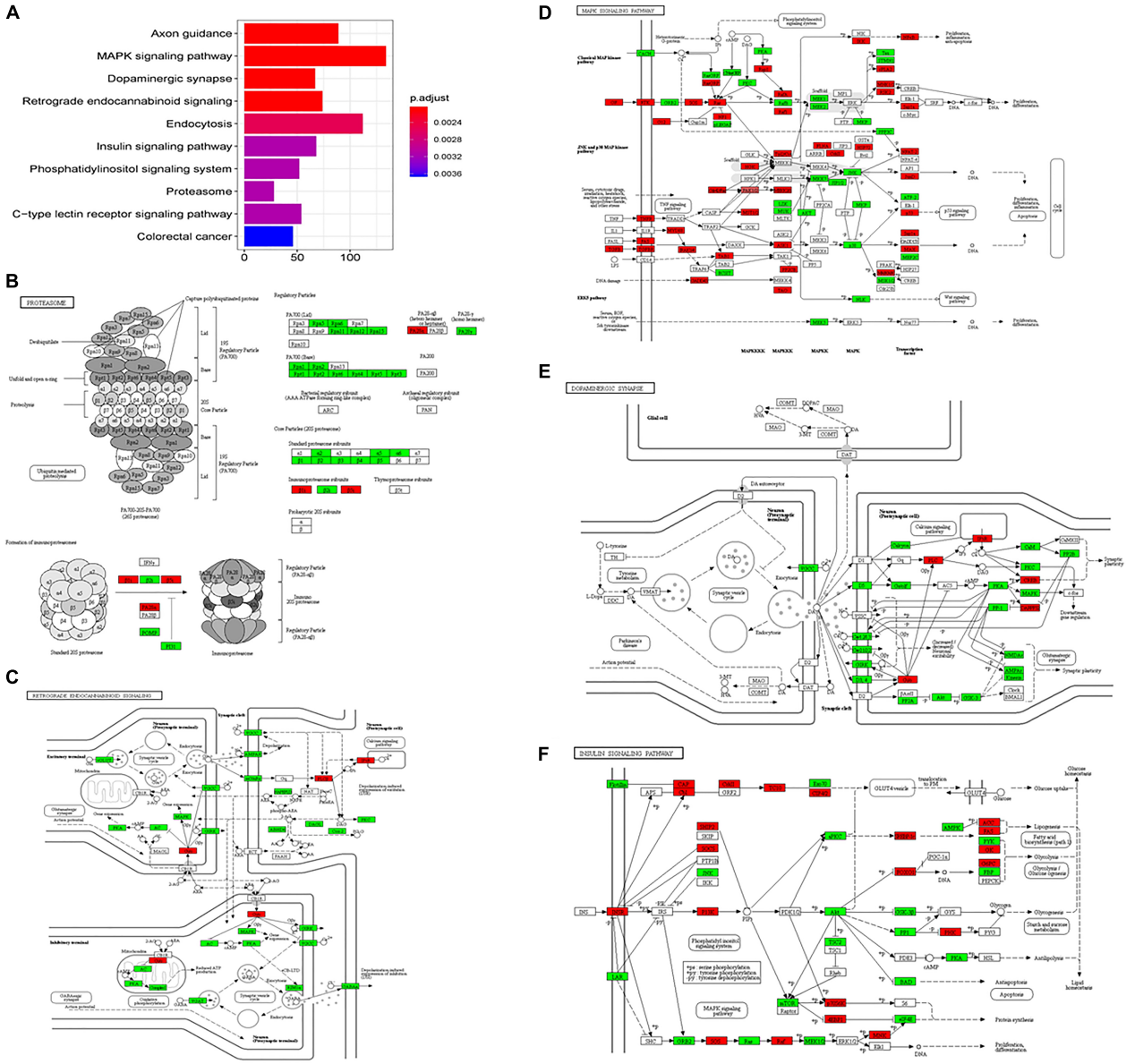

FIGURE 5 | The AD-related biological pathways from the subgroup cerebral cortex, **(A)** the top 10 statistically significant pathways from enrichment analysis result; **(B)** Proteasome; **(C)** Retrograde endocannabinoid signaling; **(D)** MAPK signaling pathway; **(E)** Dopaminergic synapse; and **(F)** Insulin signaling pathways. The red and green represent upregulation and downregulation, respectively.

AD development (François et al., 2014), memory impairment (Slipczuk et al., 2009), and neuronal apoptosis (Yin et al., 2011). The depletion of autophagy-related genes, including *Atg5* and *Atg17*, impairs the elongation of phagopores to form autophagosomes, resulting in Aβ accumulation (Hara et al., 2006; Nilsson et al., 2013). Accumulated Aβ on the ER membrane induces ER stress, which is relieved by the activation of UPR. The activation of UPR is induced by the accumulation of misfolded proteins (Stutzbach et al., 2013), and has been reported in AD subjects (Scheper and Hoozemans, 2015). Two main UPR proteins, including PERK (encoded by *EIF2AK3*) and IRE-1 (encoded by *ERN1*), were upregulated and activated in AD due to misfolded Aβ oligomers (Joshi et al., 2016), although a recent critical review suggested that the involvement of ER stress in AD might be exaggerated by the misuse of APP/PS1-overexpressing AD mouse models (Hashimoto and Saido, 2018). The activation of UPR is a significant approach to prevent the accumulation of misfolded proteins, but may also increase Aβ production (Scheper and Hoozemans, 2015), and result in synaptic loss (Gong et al., 2016). Taken together, disturbed Aβ clearance could be the upstream event for AD pathological development, to induce Aβ accumulation, altering intracellular ionic gradients and resulting in insufficient oxidative phosphorylation.

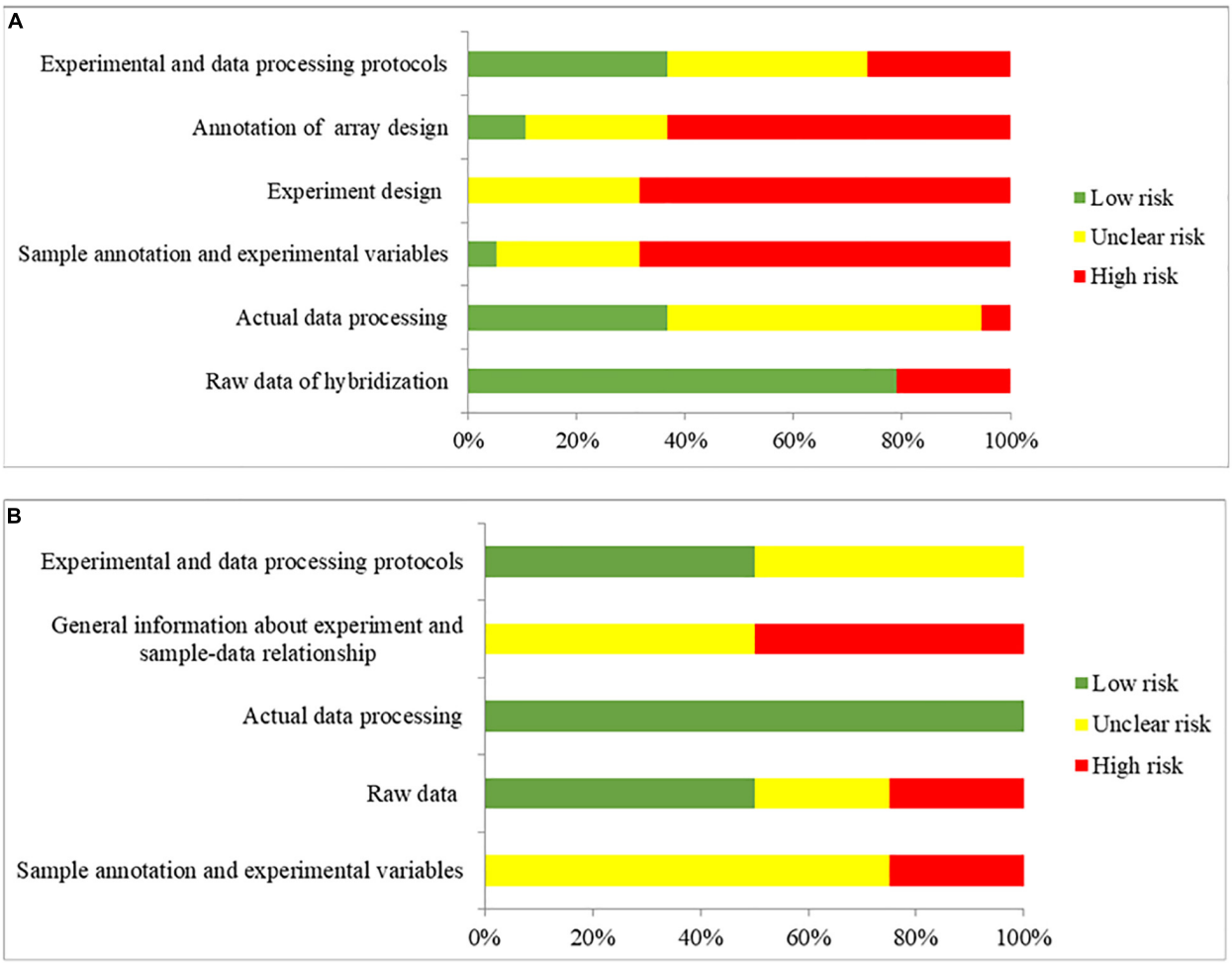

FIGURE 6 | The overall quality assessment for **(A)** 19 studies for DNA microarray and **(B)** 4 studies for RNA-seq. Green color represents low risk of bias, which the authors clearly provided the information with full detail. Yellow color represents unclear risk of bias, which the authors provided the information without full detail. Red color represents high risk of bias, which the authors did not provide the correct information.

The two top pathogenic factors determined in the present study, Fyn and EGFR, are key receptors in Aβ downstream signaling. Fyn is a protein tyrosine kinase belonging to the Src family, and it mediates synaptic plasticity in the central nervous system (Kaufman et al., 2015). The soluble Aβ oligomer binds to PrP^C with high affinity (Laurén et al., 2009), and interrupts the PrP^C's autoinhibitory mechanism (Wu et al., 2017), overactivating Fyn to increase glutamate release (Trepanier et al., 2012). Overactivation of Fyn, however, alters NMDA receptor function and intracellular Ca^{2+} homeostasis, rendering neurons vulnerable to Aβ-induced neurotoxicity. The Aβ-activated Fyn can phosphorylate downstream tau proteins at Tyr18 (Lee, 2004), and tau proteins participate in transporting Fyn to post-synaptic densities around glutamate receptors (Ittner et al., 2010). Fyn is a key protein that links between extracellular Aβ and intracellular tau protein, and unites these two pathologies in AD. The activity of Fyn is gene-dose-dependent (Um et al., 2012); that is, downregulation of *FYN* reduces Aβ-induced neurotoxicity, while upregulation of *FYN* exacerbates Aβ-induced neurotoxicity. In previous studies, overexpression of *FYN* has also been reported to accelerate synaptic loss, making Fyn inhibition a potential therapeutic treatment for AD (Chin et al., 2004; Chin, 2005). Saracatinib (AZD0530) is a Src kinase inhibitor that is being tested clinically for the treatment of AD. Saracatinib blocks Fyn activation to rescue memory deficits, and exhibits well-tolerated effects in mild-to-moderate AD subjects (Nygaard et al., 2015). A recently published clinical trial (VanDyck et al., 2019) revealed that saracatinib does not slow the decline in the CMRgl, and does not exhibit beneficial effects on several cognitive assessments, compared with the placebo group. However, a trend for slowing the reduction of volumetric measure in brain is observed, and a *post hoc* exploratory analysis deduces a statistically significant decline in CMRgl in the entorhinal cortex. Although the frequent adverse event of saracatinib, e.g., diarrhea, may limit the feasibility of increasing 125 mg daily to a higher dosage, the authors proposed that a higher dosage of saracatinib may be beneficial to slow decline of CMRgl in AD participants, who have greater tolerability.

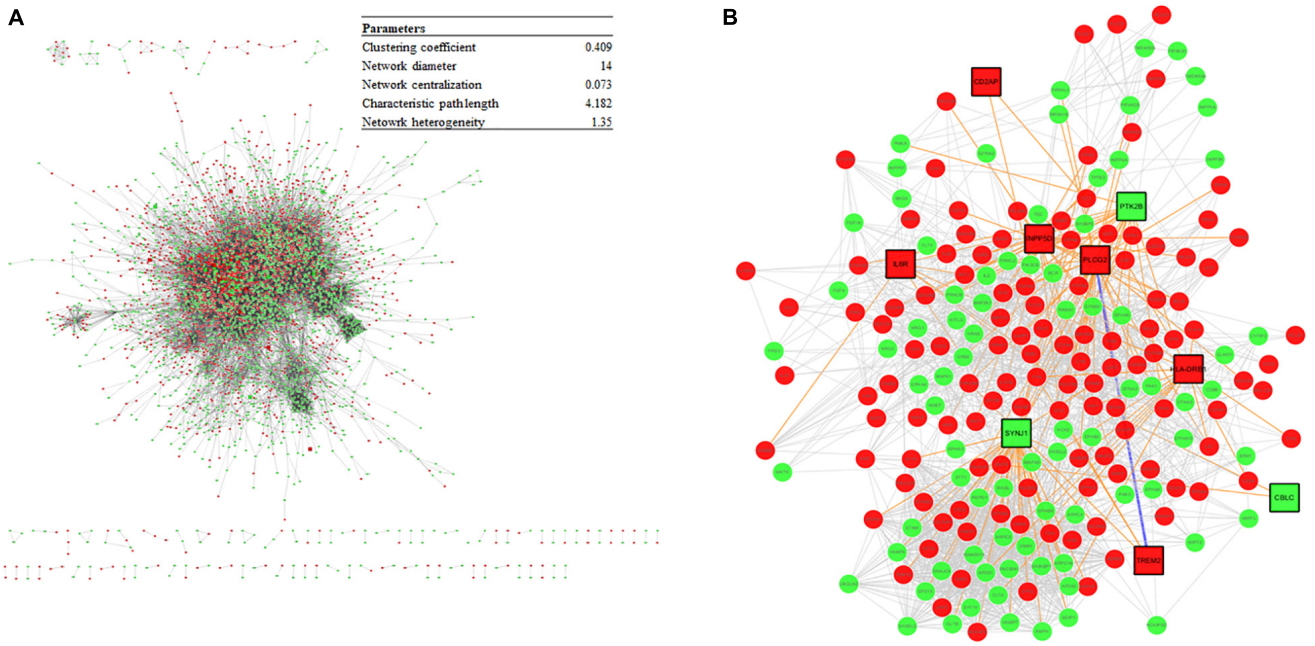

FIGURE 7 | (A) The PPIN constructed from DEGs and the PPIN topology parameters. The red and green represent upregulation and downregulation, respectively. **(B)** A disease module, derived from the DIAMOnD algorithm, consisting of AD seed proteins (represented as squares) and their corresponding DIAMOnD proteins (represented as circles). The colors of the nodes represent upregulation (red), and downregulation (green). The edges represent seed-seed interaction (dark green), seed-DIAMOnD interaction (purple), and DIAMOnD-DIAMOnD interaction (pink).

EGFR is more commonly associated with cancer than with AD. However, the expression of EGFR is statistically correlated with the expression of γ-secretase, suggesting a significant role of EGFR in AD (Zhang et al., 2007). EGFR is widely distributed in the hippocampus and cerebral cortex (Fu et al., 2003), and EGFR signaling exerts neurotrophic functions to regulate synaptic architecture in the central nervous system (Oyagi et al., 2011). The expression of *EGFR* is reported to be upregulated in the brains of AD animals, and overactivation of EGFR by Aβ oligomers induces memory loss (Wang et al., 2012). The overactivation of EGFR can also be induced by the prolong UPR (Papa and Germain, 2011). The levels of overactivated EGFR can be suppressed by treatment with the EGFR inhibitor gefitnib to rescue memory loss. Activation of EGFR also induces downstream neuroinflammatory cascades in response to Aβ-induced neurotoxicity. Afatinib, an orally available EGFR tyrosine kinase inhibitor, inhibits EGFR activation to alleviate neuroinflammation by reducing caspase 1 activation and interleukin-1β levels in neurodegenerative diseases (Chen et al., 2019). Antagonizing Aβ-induced activation of EGFR may have beneficial effects to slow memory loss and alleviate neuroinflammation. **Figure 8** summarizes the mechanism of action of Aβ-mediated Fyn and EGFR in AD, as described above.

Besides the genes involved in Aβ downstream neurotoxicity, the genes related to amyloid clearance proteins (e.g., *ECE1* and *NEU1*) are reported as pathogenic factors of AD by other studies. Endothelin 1 (encoded by *ECE1*) is implicated in Aβ degradation and downregulation of *ECE1* enhances Aβ deposition (Pacheco-Quinto and Eckman, 2013). However, upregulation of *ECE1* was found in the present study, suggesting that the pathophysiological role of *ECE1* was not solely involved in Aβ metabolism, but also associated with the increase Aβ-induced vasoconstriction in AD (Palmer et al., 2013). Sialidase (encoded by *NEU1*) is a lysosomal enzyme for Aβ clearance through lysosomal exocytosis (Annunziata et al., 2013). Deficit of *NEU1* causes Aβ-induced proteasome inhibition, which was consistent with our results. Disruption of Aβ clearance proteins may be the secondary events of AD progression, rather than the primary cause. Increasing evidences show a correlation between T2DM and higher risk of developing AD, through increasing BBB permeability by chronic peripheral inflammation (Holmes et al., 2009). The BBB leakage was supported by the dysregulated genes in this study, including *OCLN*, *TJP1*, *CDH5*, and *CTNNB1*, which encode the tight junction proteins. The compromised BBB can be exacerbated by chronic hypertension (Santos et al., 2017) and microbial pathogens (Li H. et al., 2018), and alters peripheral immune cell trafficking to the brain and induces neuroinflammation. The neuroinflammation is mediated by p38 (encoded by *MAPK14*), which is a protein found in MAPK pathway. p38 is also a kinase to phosphorylate tau protein, making p38 as a potential pathogenic factor of AD. However, upregulation of p38 was not observed in this study, since p38 participates in numerous cellular events not only neuroinflammation. This can be supported by that although the inhibition of p38 alleviates neuroinflammation in AD (Yasuda et al., 2012; Ashabi et al., 2013), most p38 inhibitors are failed in clinical trials due to off-target effects. A gene converting glucose into lactate in glycolysis, *LDHA*, is regarded as a relevant pathogenic factor in AD, although it may

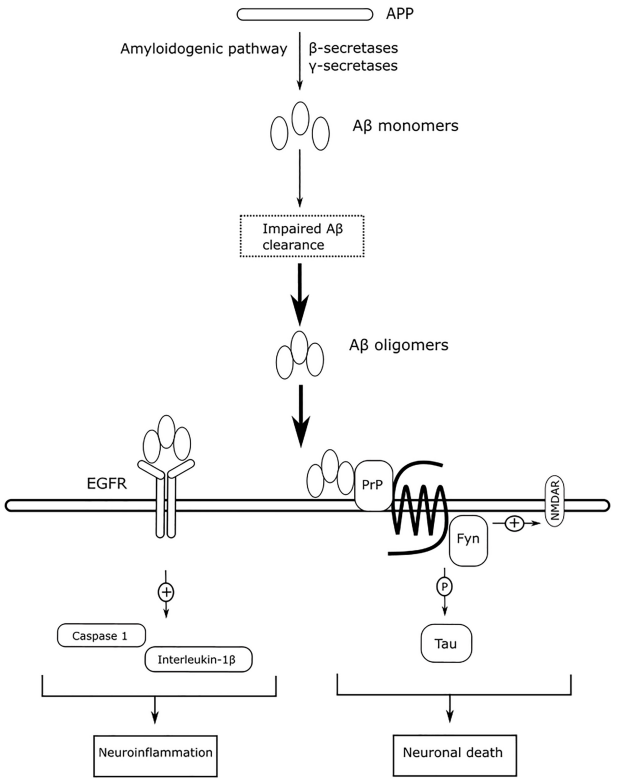

FIGURE 8 | The mechanism of action of Aβ-mediated Fyn and EGFR in AD.

not be specific to AD pathogenesis. Overexpression of *LDHA* is reported to prevent neurons from Aβ neurotoxicity by shifting mitochondrial glucose metabolism to lactate production, and decreasing ROS production (Newington et al., 2012). However, elevated lactate level may be detrimental to neurons (Harris et al., 2016). Although the expression of *LDHA* was insignificantly downregulated in this study, the opposing neuroprotective and neurotoxic effects of *LDHA* suggested that neurons might have its own defense mechanism against Aβ in the early onset of AD.

The strength of this study is the integration of transcriptomic data from both DNA microarrays and RNA-Seq using a systematic search and consistent workflow. However, there are some limitations. First, the articles that published the datasets did not provide full details of the experimental procedures, making the transcriptomic results less reliable and more difficult to repeat. In addition, the transcriptomic data retrieved from postmortem brain tissue using different methods might be biased. For example, laser-microdissection mainly targets neuronal soma, but may miss transcripts transporting to the pre- or post-synapses. Lacking of sufficient information about disposal of transcriptomic analysis, resulting in relatively low quality of the selected studies, might raise a reproducibility issue. Second, the confounding factors of postmortem brain tissues include age, sex, and postmortem interval, and may blur the results, e.g., neuroinflammation. Third, most included datasets in this study focused on hippocampus and entorhinal cortex, in which the brain region AD are believed to start. However, AD might start differently from those two brain regions, e.g., the impaired UPS as an early AD event was reported in brainstem (Irmler et al., 2012). Transcriptomic analysis in different regions of postmortem AD brains would provide more novel insights of AD development.

CONCLUSION

This meta-analytical study suggested that the reduced Aβ clearance in AD pathogenesis was associated with the genes encoding Fyn and EGFR, which were key receptors in Aβ downstream signaling.

DATA AVAILABILITY STATEMENT

The raw data of this paper are available in the public database, GEO and ArrayExpress. The data that support the findings of this paper are available in the published article and its additional files.

AUTHOR CONTRIBUTIONS

SL and SY conceived and designed the study and wrote the manuscript. SY and HZ extracted and analyzed the data. SL and HZ verified the data and revised the manuscript. All authors read and approved the final version of the manuscript.

FUNDING

Part of this authors' work and publication fees of this paper were supported by a grant (MYRG2019-00159-ICMS) received from the University of Macau.

ACKNOWLEDGMENTS

We thank Bronwen Gardner, Ph.D., from the Edanz Group (www.edanzediting.com/ac) for editing a draft of this manuscript.

SUPPLEMENTARY MATERIAL

The Supplementary Material for this article can be found online at: https://www.frontiersin.org/articles/10.3389/fnins.2020.00209/full#supplementary-material

FILE S1 | The search strategy used in the database GEO and ArrayExpress.

FILE S2 | The DEGs from each comparison.

FILE S3 | The DEGs after meta-analysis found statistically significant in this study.

FILE S4 | The statistical significant DEGs found in each subgroup.

FILE S5 | The AD seed genes used in the DIAMOnD algorithm.

REFERENCES

Aguilar, B. J., Zhu, Y., and Lu, Q. (2017). Rho GTPases as therapeutic targets in Alzheimer's disease. *Alzheimers. Res. Ther.* 9:97. doi: 10.1186/s13195-017-0320-4

Anders, S., Pyl, P. T., and Huber, W. (2015). HTSeq–a Python framework to work with high-throughput sequencing data. *Bioinformatics* 31, 166–169. doi: 10.1093/bioinformatics/btu638

Andrews, S. (2010). *FastQC: A Quality Control Tool for High Throughput Sequence Data*. Available online at: http://www.bioinformatics.babraham.ac.uk/projects/fastqc.

Annunziata, I., Patterson, A., Helton, D., Hu, H., Moshiach, S., Gomero, E., et al. (2013). Lysosomal NEU1 deficiency affects amyloid precursor protein levels and amyloid-β secretion via deregulated lysosomal exocytosis. *Nat. Commun.* 4:2734. doi: 10.1038/ncomms3734

Antonell, A., Lladó, A., Altirriba, J., Botta-Orfila, T., Balasa, M., Fernández, M., et al. (2013). A preliminary study of the whole-genome expression profile of sporadic and monogenic early-onset Alzheimer's disease. *Neurobiol. Aging* 34, 1772–1778. doi: 10.1016/j.neurobiolaging.2012.12.026

Ashabi, G., Alamdary, S. Z., Ramin, M., and Khodagholi, F. (2013). Reduction of hippocampal apoptosis by intracerebroventricular administration of extracellular signal-regulated protein kinase and/or p38 inhibitors in amyloid beta rat model of Alzheimer's disease: involvement of nuclear-related factor-2 and nuclear factor-kB. *Basic Clin. Pharmacol. Toxicol.* 112, 145–155. doi: 10.1111/bcpt.12000

Alzheimer's Association, (2009). 2009 Alzheimer's disease facts and figures. *Alzheimers Dement.* 5, 234–270. doi: 10.1016/j.jalz.2009.03.001

Barrett, T., Wilhite, S. E., Ledoux, P., Evangelista, C., Kim, I. F., Tomashevsky, M., et al. (2012). NCBI GEO: archive for functional genomics data sets—update. *Nucleic Acids Res.* 41, D991–D995. doi: 10.1093/nar/gks1193

Bartkowska, K., Swiatek, I., Aniszewska, A., Jurewicz, E., Turlejski, K., Filipek, A., et al. (2017). Stress-dependent changes in the CacyBP/SIP interacting protein S100A6 in the mouse brain. *PLoS One* 12:e0169760. doi: 10.1371/journal.pone.0169760

Basavarajappa, B. S., Shivakumar, M., Joshi, V., and Subbanna, S. (2017). Endocannabinoid system in neurodegenerative disorders. *J. Neurochem.* 142, 624–648. doi: 10.1111/jnc.14098

Bedford, L., Hay, D., Devoy, A., Paine, S., Powe, D. G., Seth, R., et al. (2008). Depletion of 26S proteasomes in mouse brain neurons causes neurodegeneration and lewy-like inclusions resembling human pale bodies. *J. Neurosci.* 28, 8189–8198. doi: 10.1523/JNEUROSCI.2218-08.2008

Berchtold, N. C., Cribbs, D. H., Coleman, P. D., Rogers, J., Head, E., Kim, R., et al. (2008). Gene expression changes in the course of normal brain aging are sexually dimorphic. *Proc. Natl. Acad. Sci. U.S.A.* 105, 15605–15610. doi: 10.1073/pnas.0806883105

Blalock, E. M., Buechel, H. M., Popovic, J., Geddes, J. W., and Landfield, P. W. (2011). Microarray analyses of laser-captured hippocampus reveal distinct gray and white matter signatures associated with incipient Alzheimer's disease. *J. Chem. Neuroanat.* 42, 118–126. doi: 10.1016/j.jchemneu.2011.06.007

Blalock, E. M., Geddes, J. W., Chen, K. C., Porter, N. M., Markesbery, W. R., and Landfield, P. W. (2004). Incipient Alzheimer's disease: microarray correlation analyses reveal major transcriptional and tumor suppressor responses. *Proc. Natl. Acad. Sci. U.S.A.* 101, 2173–2178. doi: 10.1073/pnas.0308512100

Braun, R. J., Sommer, C., Leibiger, C., Gentier, R. J. G., Dumit, I., Paduch, K., et al. (2015). Accumulation of basic amino acids at mitochondria dictates the cytotoxicity of aberrant ubiquitin. *Cell Rep.* 10, 1557–1571. doi: 10.1016/j.celrep.2015.02.009

Brazma, A. (2009). Minimum information about a microarray experiment (MIAME)–successes, failures, challenges. *ScientificWorldJournal* 9, 420–423. doi: 10.1100/tsw.2009.57

Brito-Moreira, J., Paula-Lima, A. C., Bomfim, T. R., Oliveira, F. B., Sepulveda, F. J., De Mello, F. G., et al. (2011). Aβ oligomers induce glutamate release from hippocampal neurons. *Curr. Alzheimer Res.* 8, 552–562. doi: 10.2174/156720511796391917

Broersen, K., Rousseau, F., and Schymkowitz, J. (2010). The culprit behind amyloid beta peptide related neurotoxicity in Alzheimer's disease: oligomer size or conformation? *Alzheimers. Res. Ther.* 2:12. doi: 10.1186/alzrt36

Bronner, I. F., Bochdanovits, Z., Rizzu, P., Kamphorst, W., Ravid, R., vanSwieten, J. C., et al. (2009). Comprehensive mRNA expression profiling distinguishes tauopathies and identifies shared molecular pathways. *PLoS One* 4:e6826. doi: 10.1371/journal.pone.0006826

Browne, F., Wang, H., and Zheng, H. (2015). A computational framework for the prioritization of disease-gene candidates. *BMC Genomics* 16(Suppl. 9):S2. doi: 10.1186/1471-2164-16-S9-S2

Cacace, R., Heeman, B., VanMossevelde, S., DeRoeck, A., Hoogmartens, J., DeRijk, P., et al. (2019). Loss of DPP6 in neurodegenerative dementia: a genetic player in the dysfunction of neuronal excitability. *Acta Neuropathol.* 137, 901–918. doi: 10.1007/s00401-019-01976-3

Caccamo, A., Majumder, S., Richardson, A., Strong, R., and Oddo, S. (2010). Molecular interplay between mammalian target of rapamycin (mTOR), amyloid-β, and tau. *J. Biol. Chem.* 285, 13107–13120. doi: 10.1074/jbc.M110.100420

Carvalho, B. S., and Irizarry, R. A. (2010). A framework for oligonucleotide microarray preprocessing. *Bioinformatics* 26, 2363–2367. doi: 10.1093/bioinformatics/btq431

Caspersen, C., Wang, N., Yao, J., Sosunov, A., Chen, X., Lustbader, J. W., et al. (2005). Mitochondrial Aβ: a potential focal point for neuronal metabolic dysfunction in Alzheimer's disease. *FASEB J.* 19, 2040–2041. doi: 10.1096/fj.05-3735fje

Chadwick, L., Gentle, L., Strachan, J., and Layfield, R. (2012). Review: Unchained maladie – a reassessment of the role of Ubb +1-capped polyubiquitin chains in Alzheimer's disease. *Neuropathol. Appl. Neurobiol.* 38, 118–131. doi: 10.1111/j.1365-2990.2011.01236.x

Chandrasekaran, S., and Bonchev, D. (2016). Network topology analysis of post-mortem brain microarrays identifies more Alzheimer's related genes and micrornas and points to novel routes for fighting with the disease. *PLoS One* 11:e0144052. doi: 10.1371/journal.pone.0144052

Chen, G. F., Xu, T. H., Yan, Y., Zhou, Y. R., Jiang, Y., Melcher, K., et al. (2017). Amyloid beta: structure, biology and structure-based therapeutic development. *Acta Pharmacol. Sin.* 38, 1205–1235. doi: 10.1038/aps.2017.28

Chen, J. X., and Du Yan, S. (2007). Amyloid-β-induced mitochondrial dysfunction. *J. Alzheimer's Dis.* 12, 177–184. doi: 10.3233/JAD-2007-12208

Chen, Y., Neve, R. L., and Liu, H. (2012). Neddylation dysfunction in Alzheimer's disease. *J. Cell. Mol. Med.* 16, 2583–2591. doi: 10.1111/j.1582-4934.2012.01604.x

Chen, Y.-J., Hsu, C.-C., Shiao, Y.-J., Wang, H.-T., Lo, Y.-L., and Lin, A. M. Y. (2019). Anti-inflammatory effect of afatinib (an EGFR-TKI) on OGD-induced neuroinflammation. *Sci. Rep.* 9:2516. doi: 10.1038/s41598-019-38676-7

Chin, J. (2005). Fyn kinase induces synaptic and cognitive impairments in a transgenic mouse model of Alzheimer's disease. *J. Neurosci.* 25, 9694–9703. doi: 10.1523/JNEUROSCI.2980-05.2005

Chin, J., Palop, J. J., Yu, G. Q., Kojima, N., Masliah, E., and Mucke, L. (2004). Fyn kinase modulates synaptotoxicity, but not aberrant sprouting, in human amyloid precursor protein transgenic mice. *J. Neurosci.* 24, 4692–4697. doi: 10.1523/JNEUROSCI.0277-04.2004

Chow, V. W., Mattson, M. P., Wong, P. C., and Gleichmann, M. (2010). An overview of APP processing enzymes and products. *Neuromolecular Med.* 12, 1–12. doi: 10.1007/s12017-009-8104-z

Chung, S. S., Sun, K., and Bolech, C. J. (2015). Matrix product ansatz for Fermi fields in one dimension. *Phys. Rev. B* 91:121108. doi: 10.1103/PhysRevB.91.121108

Ciechanover, A. (2015). The unravelling of the ubiquitin system. *Nat. Rev. Mol. Cell Biol.* 16, 322–324. doi: 10.1038/nrm3982

Cummings, J. L., Morstorf, T., and Zhong, K. (2014). Alzheimer's disease drug-development pipeline: few candidates, frequent failures. *Alzheimers. Res. Ther.* 6:37. doi: 10.1186/alzrt269

Durrenberger, P. F., Fernando, F. S., Magliozzi, R., Kashefi, S. N., Bonnert, T. P., Ferrer, I., et al. (2012). Selection of novel reference genes for use in the human central nervous system: a brainnet europe study. *Acta Neuropathol.* 124, 893–903. doi: 10.1007/s00401-012-1027-z

Edison, P., Archer, H. A., Hinz, R., Hammers, A., Pavese, N., Tai, Y. F., et al. (2007). Amyloid, hypometabolism, and cognition in Alzheimer disease: an [11C]PIB and [18F]FDG PET study. *Neurology* 68, 501–508. doi: 10.1212/01.wnl.0000244749.20056.d4

Egan, M. F., Kost, J., Voss, T., Mukai, Y., Aisen, P. S., Cummings, J. L., et al. (2019). Randomized trial of verubecestat for prodromal Alzheimer's disease. *N. Engl. J. Med.* 380, 1408–1420. doi: 10.1056/NEJMoa1812840

Esparza, T. J., Zhao, H., Cirrito, J. R., Cairns, N. J., Bateman, R. J., Holtzman, D. M., et al. (2013). Amyloid-beta oligomerization in Alzheimer dementia versus high-pathology controls. *Ann. Neurol.* 73, 104–119. doi: 10.1002/ana.23748

Farris, W., Mansourian, S., Chang, Y., Lindsley, L., Eckman, E. A., Frosch, M. P., et al. (2003). Insulin-degrading enzyme regulates the levels of insulin, amyloid -protein, and the -amyloid precursor protein intracellular domain in vivo. *Proc. Natl. Acad. Sci. U.S.A.* 100, 4162–4167. doi: 10.1073/pnas.0230450100

Fischer, M. T., Wimmer, I., Höftberger, R., Gerlach, S., Haider, L., Zrzavy, T., et al. (2013). Disease-specific molecular events in cortical multiple sclerosis lesions. *Brain* 136, 1799–1815. doi: 10.1093/brain/awt110

Folch, J., Ettcheto, M., Busquets, O., Sánchez-López, E., Castro-Torres, R. D., Verdaguer, E., et al. (2018). The implication of the brain insulin receptor in late onset Alzheimer's disease dementia. *Pharmaceuticals* 11:11. doi: 10.3390/ph11010011

François, A., Rioux Bilan, A., Quellard, N., Fernandez, B., Janet, T., Chassaing, D., et al. (2014). Longitudinal follow-up of autophagy and inflammation in brain of APPswePS1dE9 transgenic mice. *J. Neuroinflammation* 11:139. doi: 10.1186/s12974-014-0139-x

Friedman, B. A., Srinivasan, K., Ayalon, G., Meilandt, W. J., Lin, H., Huntley, M. A., et al. (2018). Diverse brain myeloid expression profiles reveal distinct microglial activation states and aspects of Alzheimer's disease not evident in mouse models. *Cell Rep.* 22, 832–847. doi: 10.1016/j.celrep.2017.12.066

Fu, L., Abu-Khalil, A., Morrison, R. S., Geschwind, D. H., and Kornblum, I. (2003). Expression patterns of epidermal growth factor receptor and fibroblast growth factor receptor 1 mRNA in fetal human brain. *J. Comp. Neurol.* 462, 265–273. doi: 10.1002/cne.10727

Garwood, C. J., Pooler, A. M., Atherton, J., Hanger, D. P., and Noble, W. (2011). Astrocytes are important mediators of Aβ-induced neurotoxicity and tau phosphorylation in primary culture. *Cell Death. Dis.* 2:e167. doi: 10.1038/cddis.2011.50

Gautier, L., Cope, L., Bolstad, B. M., and Irizarry, R. A. (2004). Affy – Analysis of affymetrix genechip data at the probe level. *Bioinformatics* 20, 307–315. doi: 10.1093/bioinformatics/btg405

Ghiassian, S. D., Menche, J., and Barabási, A. L. (2015). A DIseAse MOdule detection (DIAMOnD) algorithm derived from a systematic analysis of connectivity patterns of disease proteins in the human interactome. *PLoS Comput. Biol.* 11:e1004120. doi: 10.1371/journal.pcbi.1004120

Gong, B., Radulovic, M., Figueiredo-Pereira, M. E., and Cardozo, C. (2016). The ubiquitin-proteasome system: Potential therapeutic targets for Alzheimer's disease and spinal cord injury. *Front. Mol. Neurosci.* 9:4. doi: 10.3389/fnmol.2016.00004

Haidich, A. B. (2010). Meta-analysis in medical research. *Hippokratia* 14, 29–37. doi: 10.5005/jp/books/10519

Hara, T., Nakamura, K., Matsui, M., Yamamoto, A., Nakahara, Y., Suzuki-Migishima, R., et al. (2006). Suppression of basal autophagy in neural cells causes neurodegenerative disease in mice. *Nature* 441, 885–889. doi: 10.1038/nature04724

Hardy, J., and Higgins, G. (1992). Alzheimer's disease: the amyloid cascade hypothesis. *Science* 256, 184–185. doi: 10.1126/science.1566067

Harris, R. A., Tindale, L., Lone, A., Singh, O., Macauley, S. L., Stanley, M., et al. (2016). Aerobic glycolysis in the frontal cortex correlates with memory performance in wild-type mice but not the APP/PS1 mouse model of cerebral amyloidosis. *J. Neurosci.* 36, 1871–1878. doi: 10.1523/JNEUROSCI.3131-15.2016

Hashimoto, S., and Saido, T. C. (2018). Critical review: involvement of endoplasmic reticulum stress in the aetiology of Alzheimer's disease. *Open Biol.* 8:180024. doi: 10.1098/rsob.180024

Hernández, F., and Avila, J. (2008). The role of glycogen synthase kinase 3 in the early stages of Alzheimers' disease. *FEBS Lett.* 582, 3848–3854. doi: 10.1016/j.febslet.2008.10.026

Hokama, M., Oka, S., Leon, J., Ninomiya, T., Honda, H., Sasaki, K., et al. (2014). Altered expression of diabetes-related genes in Alzheimer's disease brains: the hisayama study. *Cereb. Cortex* 24, 2476–2488. doi: 10.1093/cercor/bht101

Holmes, C., Cunningham, C., Zotova, E., Woolford, J., Dean, C., Kerr, S., et al. (2009). Systemic inflammation and disease progression in alzheimer disease. *Neurology* 73, 768–774. doi: 10.1212/WNL.0b013e3181b6bb95

Hong, L., Huang, H.-C., and Jiang, Z.-F. (2014). Relationship between amyloid-beta and the ubiquitin–proteasome system in Alzheimer's disease. *Neurol. Res.* 36, 276–282. doi: 10.1179/1743132813Y.0000000288

Honig, L. S., Vellas, B., Woodward, M., Boada, M., Bullock, R., Borrie, M., et al. (2018). Trial of solanezumab for mild dementia due to Alzheimer's disease. *N. Engl. J. Med.* 378, 321–330. doi: 10.1056/NEJMoa1705971

Hoos, M. D., Richardson, B. M., Foster, M. W., Everhart, A., Thompson, J. W., Moseley, M. A., et al. (2013). Longitudinal study of differential protein expression in an Alzheimer's mouse model lacking inducible nitric oxide synthase. *J. Proteome Res.* 12, 4462–4477. doi: 10.1021/pr4005103

Irmler, M., Gentier, R. J. G., Dennissen, F. J. A., Schulz, H., Bolle, I., Hölter, S. M., et al. (2012). Long-term proteasomal inhibition in transgenic mice by UBB+1 expression results in dysfunction of central respiration control reminiscent of brainstem neuropathology in Alzheimer patients. *Acta Neuropathol.* 124, 187–197. doi: 10.1007/s00401-012-1003-7

Ittner, L. M., Ke, Y. D., Delerue, F., Bi, M., Gladbach, A., vanEersel, J., et al. (2010). Dendritic function of tau mediates amyloid-β toxicity in alzheimer's disease mouse models. *Cell* 142, 387–397. doi: 10.1016/j.cell.2010.06.036

Jaeger, P. A., and Wyss-Coray, T. (2010). Beclin 1 complex in autophagy and Alzheimer disease. *Arch. Neurol.* 67, 1181–1184. doi: 10.1001/archneurol.2010.258

Janssen, S. F., van derSpek, S. J. F., Tenbrink, J. B., Essing, A. H. W., Gorgels, T. G., van derSpek, P. J., et al. (2013). Gene expression and functional annotation of the human and mouse choroid plexus epithelium. *PLoS One* 8:e83345. doi: 10.1371/journal.pone.0083345

Joshi, A. U., Kornfeld, O. S., and Mochly-Rosen, D. (2016). The entangled ER-mitochondrial axis as a potential therapeutic strategy in neurodegeneration: a tangled duo unchained. *Cell Calcium* 60, 218–234. doi: 10.1016/j.ceca.2016.04.010

Kanehisa, M., Goto, S., Sato, Y., Furumichi, M., and Tanabe, M. (2012). KEGG for integration and interpretation of large-scale molecular data sets. *Nucleic Acids Res.* 40, D109–D114. doi: 10.1093/nar/gkr988

Kästle, M., and Grune, T. (2012). Interactions of the proteasomal system with chaperones: Protein triage and protein quality control. *Prog. Mol. Biol. Transl. Sci.* 109, 113–160. doi: 10.1016/B978-0-12-397863-9.00004-3

Kauffmann, A., Gentleman, R., and Huber, W. (2009). arrayQualityMetrics—a bioconductor package for quality assessment of microarray data. *Bioinformatics* 25, 415–416. doi: 10.1093/bioinformatics/btn647

Kaufman, A. C., Salazar, S. V., Haas, L. T., Yang, J., Kostylev, M. A., Jeng, A. T., et al. (2015). Fyn inhibition rescues established memory and synapse loss in Alzheimer mice. *Ann. Neurol.* 77, 953–971. doi: 10.1002/ana.24394

Kawalia, S. B., Raschka, T., Naz, M., deMatos Simoes, R., Senger, P., and Hofmann-Apitius, M. (2017). Analytical strategy to prioritize Alzheimer's disease candidate genes in gene regulatory networks using public expression data. *J. Alzheimers Dis.* 59, 1237–1254. doi: 10.3233/JAD-170011

Kennedy, M. E., Stamford, A. W., Chen, X., Cox, K., Cumming, J. N., Dockendorf, M. F., et al. (2016). The BACE1 inhibitor verubecestat (MK-8931) reduces CNS -amyloid in animal models and in Alzheimers disease patients. *Sci. Transl. Med.* 8:363ra150. doi: 10.1126/scitranslmed.aad9704

Kikuchi, M., Ogishima, S., Miyamoto, T., Miyashita, A., Kuwano, R., Nakaya, J., et al. (2013). Identification of unstable network modules reveals disease modules associated with the progression of Alzheimer's disease. *PLoS One* 8:e76162. doi: 10.1371/journal.pone.0076162

Kim, D., Pertea, G., Trapnell, C., Pimentel, H., Kelley, R., and Salzberg, S. L. (2013). TopHat2: accurate alignment of transcriptomes in the presence of insertions, deletions and gene fusions. *Genome Biol.* 14:R36. doi: 10.1186/gb-2013-14-4-r36

Kline, A. (2012). Apolipoprotein E, amyloid-ß clearance and therapeutic opportunities in Alzheimer's disease. *Alzheimers. Res. Ther.* 4:32. doi: 10.1186/alzrt135

Knowles, T. P. J., Vendruscolo, M., and Dobson, C. M. (2014). The amyloid state and its association with protein misfolding diseases. *Nat. Rev. Mol. Cell Biol.* 15, 384–396. doi: 10.1038/nrm3810

Kolesnikov, N., Hastings, E., Keays, M., Melnichuk, O., Tang, Y. A., Williams, E., et al. (2015). ArrayExpress update–simplifying data submissions. *Nucleic Acids Res.* 43, D1113–D1116. doi: 10.1093/nar/gku1057

Lachen-Montes, M., Zelaya, M. V., Segura, V., Fernández-Irigoyen, J., and Santamaría, E. (2017). Progressive modulation of the human olfactory bulb transcriptome during Alzheimer's disease evolution: novel insights into the olfactory signaling across proteinopathies. *Oncotarget* 8, 69663–69679. doi: 10.18632/oncotarget.18193

Laurén, J., Gimbel, D. A., Nygaard, H. B., Gilbert, J. W., and Strittmatter, S. M. (2009). Cellular prion protein mediates impairment of synaptic plasticity by amyloid-β oligomers. *Nature* 457, 1128–1132. doi: 10.1038/nature07761

Lee, G. (2004). Phosphorylation of Tau by Fyn: implications for Alzheimer's Disease. *J. Neurosci.* 24, 2304–2312. doi: 10.1523/JNEUROSCI.4162-03.2004

Leinonen, R., Sugawara, H., and Shumway, M. (2011). The sequence read archive. *Nucleic Acids Res.* 39, D19–D21. doi: 10.1093/nar/gkq1019

Li, H., Handsaker, B., Wysoker, A., Fennell, T., Ruan, J., Homer, N., et al. (2009). The sequence alignment/map format and SAMtools. *Bioinformatics* 25, 2078–2079. doi: 10.1093/bioinformatics/btp352

Li, H., Liu, C. C., Zheng, H., and Huang, T. Y. (2018). Amyloid, tau, pathogen infection and antimicrobial protection in Alzheimer's disease - conformist, nonconformist, and realistic prospects for AD pathogenesis. *Transl. Neurodegener.* 7:34. doi: 10.1186/s40035-018-0139-3

Li, X., Wang, H., Long, J., Pan, G., He, T., Anichtchik, O., et al. (2018). Systematic Analysis and Biomarker Study for Alzheimer's Disease. *Sci. Rep.* 8:17394. doi: 10.1038/s41598-018-35789-3

Liang, W. S., Dunckley, T., Beach, T. G., Grover, A., Mastroeni, D., Walker, D. G., et al. (2007). Gene expression profiles in anatomically and functionally distinct regions of the normal aged human brain. *Physiol. Genomics* 28, 311–322. doi: 10.1152/physiolgenomics.00208.2006

Lucin, K. M., O'Brien, C. E., Bieri, G., Czirr, E., Mosher, I., Abbey, R. J., et al. (2013). Microglial beclin 1 regulates retromer trafficking and phagocytosis and is impaired in Alzheimer's disease. *Neuron* 79, 873–886. doi: 10.1016/j.neuron.2013.06.046

Ma, J. F., Huang, Y., Chen, S. D., and Halliday, G. (2010). Immunohistochemical evidence for macroautophagy in neurones and endothelial cells in Alzheimer's disease. *Neuropathol. Appl. Neurobiol.* 36, 312–319. doi: 10.1111/j.1365-2990.2010.01067.x

Magistri, M., Velmeshev, D., Makhmutova, M., and Faghihi, M. A. (2015). Transcriptomics profiling of Alzheimer's disease reveal neurovascular defects, altered amyloid-β homeostasis, and deregulated expression of long noncoding RNAs. *J. Alzheimers Dis.* 48, 647–665. doi: 10.3233/JAD-150398

Manavalan, A., Mishra, M., Feng, L., Sze, S. K., Akatsu, H., and Heese, K. (2013). Brain site-specific proteome changes in aging-related dementia. 45:e39. doi: 10.1038/emm.2013.76

Marina, G. B., Kirkitadze, D., Lomakin, A., Vollers, S. S., Benedek, G. B., and Teplow, D. B. (2003). Amyloid β-protein (Aβ) assembly: Aβ40 and Aβ42 oligomerize through distinct pathways. *Proc. Natl. Acad. Sci. U.S.A.* 100, 330–335. doi: 10.1073/pnas.222681699

Marquez, R. T., and Xu, L. (2012). Bcl-2:Beclin 1 complex: multiple, mechanisms regulating autophagy/apoptosis toggle switch. *Am. J. Cancer Res.* 2, 214–221.

Mattoo, R. U. H., and Goloubinoff, P. (2014). Molecular chaperones are nanomachines that catalytically unfold misfolded and alternatively folded proteins. *Cell. Mol. Life Sci.* 71, 3311–3325. doi: 10.1007/s00018-014-1627-y

Mawuenyega, K. G., Sigurdson, W., Ovod, V., Munsell, L., Kasten, T., Morris, J. C., et al. (2010). Decreased clearance of CNS β-amyloid in Alzheimer's disease. *Science* 330:1774. doi: 10.1126/science.1197623

Meng, G., Zhong, X., and Mei, H. (2016). A systematic investigation into Aging related genes in brain and their relationship with Alzheimer's disease. *PLoS One* 11:e0150624. doi: 10.1371/journal.pone.0150624

Miller, J. A., Woltjer, R. L., Goodenbour, J. M., Horvath, S., and Geschwind, D. H. (2013). Genes and pathways underlying regional and cell type changes in Alzheimer's disease. *Genome Med.* 5:48. doi: 10.1186/gm452

Moher, D., Liberati, A., Tetzlaff, J., Altman, D. G., and Prisma Group. (2009). Preferred reporting items for systematic reviews and meta-analyses: the PRISMA statement. *PLoS Med.* 6:e1000097. doi: 10.1371/journal.pmed.1000097

Moradifard, S., Hoseinbeyki, M., Ganji, S. M., and Minuchehr, Z. (2018). Analysis of microRNA and gene expression profiles in Alzheimer's disease: a meta-analysis approach. *Sci. Rep.* 8:4767. doi: 10.1038/s41598-018-20959-0

Moreau, K., Fleming, A., Imarisio, S., Lopez Ramirez, A., Mercer, J. L., Jimenez-Sanchez, M., et al. (2014). PICALM modulates autophagy activity and tau accumulation. *Nat. Commun.* 5:4998. doi: 10.1038/ncomms5998

Moreira, P. I, Carvalho, C., Zhu, X., Smith, M. A., and Perry, G. (2010). Mitochondrial dysfunction is a trigger of Alzheimer's disease pathophysiology. *Biochim. Biophys. Acta Mol. Basis Dis.* 1802, 2–10. doi: 10.1016/j.bbadis.2009.10.006

Mosconi, L., Pupi, A., and DeLeon, M. J. (2008). Brain glucose hypometabolism and oxidative stress in preclinical Alzheimer's disease. *Ann. N. Y. Acad. Sci.* 1147, 180–195. doi: 10.1196/annals.1427.007

Narayanan, M., Huynh, J. L., Wang, K., Yang, X., Yoo, S., McElwee, J., et al. (2014). Common dysregulation network in the human prefrontal cortex underlies two neurodegenerative diseases. *Mol. Syst. Biol.* 10:743. doi: 10.15252/msb.20145304

Narendra, D., Tanaka, A., Suen, D. F., and Youle, R. J. (2008). Parkin is recruited selectively to impaired mitochondria and promotes their autophagy. *J. Cell Biol.* 183, 795–803. doi: 10.1083/jcb.200809125

Nativio, R., Donahue, G., Berson, A., Lan, Y., Amlie-Wolf, A., Tuzer, F., et al. (2018). Publisher correction: dysregulation of the epigenetic landscape of normal aging in Alzheimer's disease. *Nat. Neurosci.* 21, 1018–1018. doi: 10.1038/s41593-018-0124-2

Nelson, P. T., Alafuzoff, I., Bigio, E. H., Bouras, C., Braak, H., Cairns, N. J., et al. (2012). Correlation of Alzheimer disease neuropathologic changes with cognitive status: a review of the literature. *J. Neuropathol. Exp. Neurol.* 71, 362–381. doi: 10.1097/NEN.0b013e31825018f7

Newington, J. T., Rappon, T., Albers, S., Wong, D. Y., Rylett, R. J., and Cumming, R. C. (2012). Overexpression of pyruvate dehydrogenase kinase 1 and lactate dehydrogenase A in nerve cells confers resistance to amyloid β and other toxins by decreasing mitochondrial respiration and reactive oxygen species production. *J. Biol. Chem.* 287, 37245–37258. doi: 10.1074/jbc.M112.366195

Nilsson, P., Loganathan, K., Sekiguchi, M., Matsuba, Y., Hui, K., Tsubuki, S., et al. (2013). Aβ secretion and plaque formation depend on autophagy. *Cell Rep.* 5, 61–69. doi: 10.1016/j.celrep.2013.08.042

Nobili, A., Latagliata, E. C., Viscomi, M. T., Cavallucci, V., Cutuli, D., Giacovazzo, G., et al. (2017). Dopamine neuronal loss contributes to memory and reward dysfunction in a model of Alzheimer's disease. *Nat. Commun.* 8:14727. doi: 10.1038/ncomms14727

Nomura, J., Hosoi, T., Kaneko, M., Ozawa, K., Nishi, A., and Nomura, Y. (2016). Neuroprotection by endoplasmic reticulum stress-induced HRD1 and chaperones: possible therapeutic targets for Alzheimer's and Parkinson's disease. *Med. Sci* 4:14. doi: 10.3390/medsci4030014

Ntsapi, C., and Loos, B. (2016). Caloric restriction and the precision-control of autophagy: a strategy for delaying neurodegenerative disease progression. *Exp. Gerontol.* 83, 97–111. doi: 10.1016/j.exger.2016.07.014

Nunez-Iglesias, J., Liu, C.-C., Morgan, T. E., Finch, C. E., and Zhou, X. J. (2010). Joint genome-wide profiling of miRNA and mRNA expression in Alzheimer's disease cortex reveals altered miRNA regulation. *PLoS One* 5:e8898. doi: 10.1371/journal.pone.0008898

Nygaard, H. B., Wagner, A. F., Bowen, G. S., Good, S. P., MacAvoy, M. G., Strittmatter, K. A., et al. (2015). A phase Ib multiple ascending dose study of the safety, tolerability, and central nervous system availability of AZD0530 (saracatinib) in Alzheimer's disease. *Alzheimers. Res. Ther.* 7:35. doi: 10.1186/s13195-015-0119-0

Oddo, S., Vasilevko, V., Caccamo, A., Kitazawa, M., Cribbs, D. H., and LaFerla, F. M. (2006). Reduction of soluble Aβ and Tau, but not soluble Aβ Alone, ameliorates cognitive decline in transgenic mice with plaques and tangles. *J. Biol. Chem.* 281, 39413–39423. doi: 10.1074/jbc.M608485200

Oyagi, A., Moriguchi, S., Nitta, A., Murata, K., Oida, Y., Tsuruma, K., et al. (2011). Heparin-binding EGF-like growth factor is required for synaptic plasticity and memory formation. *Brain Res.* 1419, 97–104. doi: 10.1016/j.brainres.2011.09.003

Pacheco-Quinto, J., and Eckman, E. A. (2013). Endothelin-converting enzymes degrade intracellular β-amyloid produced within the endosomal/lysosomal pathway and autophagosomes. *J. Biol. Chem.* 288, 5606–5615. doi: 10.1074/jbc.M112.422964

Palmer, J. C., Tayler, H. M., and Love, S. (2013). Endothelin-converting enzyme-1 activity, endothelin-1 production, and free radical-dependent vasoconstriction in Alzheimer's disease. *J. Alzheimers Dis.* 36, 577–587. doi: 10.3233/JAD-130383

Pang, X., Zhao, Y., Wang, J., Zhou, Q., Xu, L., Kang, D., et al. (2017). The Bioinformatic analysis of the dysregulated genes and MicroRNAs in entorhinal cortex, hippocampus, and blood for Alzheimer's disease. *Biomed Res. Int.* 2017:9084507. doi: 10.1155/2017/9084507

Papa, L., and Germain, D. (2011). Estrogen receptor mediates a distinct mitochondrial unfolded protein response. *J. Cell Sci.* 124 (Pt 9), 1396–1402. doi: 10.1242/jcs.078220

Parihar, M. S., and Brewer, G. J. (2010). Amyloid-β as a modulator of synaptic plasticity. *J. Alzheimers Dis.* 22, 741–763. doi: 10.3233/JAD-2010-101020

Polito, V. A., Li, H., Martini−Stoica, H., Wang, B., Yang, L., Xu, Y., et al. (2014). Selective clearance of aberrant tau proteins and rescue of neurotoxicity by transcription factor EB. *EMBO Mol. Med.* 6, 1142–1160. doi: 10.15252/emmm.201303671

Potter, R., Patterson, B. W., Elbert, D. L., Ovod, V., Kasten, T., Sigurdson, W., et al. (2013). Increased in vivo amyloid-b42 production, exchange, and loss in presenilin mutation carriers. *Sci. Transl. Med.* 5, 189ra77. doi: 10.1126/scitranslmed.3005615

Puthiyedth, N., Riveros, C., Berretta, R., and Moscato, P. (2015). A new combinatorial optimization approach for integrated feature selection using different datasets: a prostate cancer transcriptomic study. *PLoS One* 10:e0127702. doi: 10.1371/journal.pone.0127702

Puthiyedth, N., Riveros, C., Berretta, R., and Moscato, P. (2016). Identification of differentially expressed genes through integrated study of Alzheimer's disease affected brain regions. *PLoS One* 11:e0152342. doi: 10.1371/journal.pone.0152342

Rahman, M. R., Islam, T., Turanli, B., Zaman, T., Faruquee, H. M., Rahman, M. M., et al. (2019). Network-based approach to identify molecular signatures and therapeutic agents in Alzheimer's disease. *Comput. Biol. Chem.* 78, 431–439. doi: 10.1016/j.compbiolchem.2018.12.011

Ritchie, M. E., Phipson, B., Wu, D., Hu, Y., Law, C. W., Shi, W., et al. (2015). Limma powers differential expression analyses for RNA-sequencing and microarray studies. *Nucleic Acids Res.* 43:e47. doi: 10.1093/nar/gkv007

Roberson, E. D., Scearce-Levie, K., Palop, J. J., Yan, F., Cheng, I. H., Wu, T., et al. (2007). Reducing endogenous tau ameliorates amyloid beta-induced deficits in an Alzheimer's disease mouse model. *Science* 316, 750–754. doi: 10.1126/science.1141736

Roberts, B. R., Lind, M., Wagen, A. Z., Rembach, A., Frugier, T., Li, Q. X., et al. (2017). Biochemically-defined pools of amyloid-β in sporadic Alzheimer's disease: correlation with amyloid PET. *Brain* 140, 1486–1498. doi: 10.1093/brain/awx057

Robinson, M. D., McCarthy, D. J., and Smyth, G. K. (2009). edgeR: a bioconductor package for differential expression analysis of digital gene expression data. *Bioinformatics* 26, 139–140. doi: 10.1093/bioinformatics/btp616

Roth, R. B., Hevezi, P., Lee, J., Willhite, D., Lechner, S. M., Foster, A. C., et al. (2006). Gene expression analyses reveal molecular relationships among 20 regions of the human CNS. *Neurogenetics* 7, 67–80. doi: 10.1007/s10048-006-0032-6

Rovelet-Lecrux, A., Hannequin, D., Raux, G., Meur, N. Le, Laquerrière, A., Vital, A., et al. (2006). APP locus duplication causes autosomal dominant early-onset Alzheimer disease with cerebral amyloid angiopathy. *Nat. Genet.* 38, 24–26. doi: 10.1038/ng1718

Saidi, L. J., Polydoro, M., Kay, K. R., Sanchez, L., Mandelkow, E. M., Hyman, B. T., et al. (2015). Carboxy terminus heat shock protein 70 interacting protein reduces tau-associated degenerative changes. *J. Alzheimers Dis.* 44, 937–947. doi: 10.3233/JAD-142094

Santos, C. Y., Snyder, P. J., Wu, W. C., Zhang, M., Echeverria, A., and Alber, J. (2017). Pathophysiologic relationship between Alzheimer's disease, cerebrovascular disease, and cardiovascular risk: a review and synthesis. *Alzheimers Dement.(Amst)* 7, 69–87. doi: 10.1016/j.dadm.2017.01.005

Scheckel, C., Drapeau, E., Frias, M. A., Park, C. Y., Fak, J., Zucker-Scharff, I., et al. (2016). Regulatory consequences of neuronal ELAV-like protein binding to coding and non-coding RNAs in human brain. *elife* 5:e10421. doi: 10.7554/eLife.10421

Scheper, W., and Hoozemans, J. J. M. (2015). The unfolded protein response in neurodegenerative diseases: a neuropathological perspective. *Acta Neuropathol.* 130, 315–331. doi: 10.1007/s00401-015-1462-8

Scott, T. J., O'Connor, A. C., Link, A. N., and Beaulieu, T. J. (2014). Economic analysis of opportunities to accelerate Alzheimer's disease research and development. *Ann. N. Y. Acad. Sci.* 1313, 17–34. doi: 10.1111/nyas.12417

Sengupta, U., Nilson, A. N., and Kayed, R. (2016). The role of amyloid-β oligomers in toxicity, propagation, and immunotherapy. *EBioMedicine* 6, 42–49. doi: 10.1016/j.ebiom.2016.03.035

Shannon, P., Markiel, A., Ozier, O., Baliga, N. S., Wang, J. T., Ramage, D., et al. (2003). Cytoscape: a software environment for integrated models of biomolecular interaction networks. *Genome Res.* 13, 2498–2504. doi: 10.1101/gr.1239303

Shimura, H., Schwartz, D., Gygi, S. P., and Kosik, K. S. (2004). CHIP-Hsc70 complex ubiquitinates phosphorylated tau and enhances cell survival. *J. Biol. Chem.* 279, 4869–4876. doi: 10.1074/jbc.M305838200

Slipczuk, L., Bekinschtein, P., Katche, C., Cammarota, M., Izquierdo, I., and Medina, J. H. (2009). BDNF activates mTOR to regulate GluR1 expression required for memory formation. *PLoS One* 4:e6007. doi: 10.1371/journal.pone.0006007

St George-Hyslop, P., and Fraser, P. E. (2012). Assembly of the presenilin γ-/ε-secretase complex. *J. Neurochem.* 120, 84–88. doi: 10.1111/j.1471-4159.2011.07505.x

Stanley, M., Macauley, S. L., and Holtzman, D. M. (2016). Changes in insulin and insulin signaling in Alzheimer's disease: cause or consequence? *J. Exp. Med.*

Stopa, E. G., Tanis, K. Q., Miller, M. C., Nikonova, E. V., Podtelezhnikov, A. A., Finney, E. M., et al. (2018). Comparative transcriptomics of choroid plexus in Alzheimer's disease, frontotemporal dementia and Huntington's disease: implications for CSF homeostasis. *Fluids Barriers CNS* 15:18. doi: 10.1186/s12987-018-0102-9

Stutzbach, L. D., Xie, S. X., Naj, A. C., Albin, R., Gilman, S., Lee, V. M. Y., et al. (2013). The unfolded protein response is activated in disease-affected brain regions in progressive supranuclear palsy and Alzheimer's disease. *Acta Neuropathol. Commun.* 1:31. doi: 10.1186/2051-5960-1-31

Sudhof, T. C. (2012). Calcium control of neurotransmitter release. *Cold Spring Harb. Perspect. Biol.* 4:a011353. doi: 10.1101/cshperspect.a011353

Sutherland, G. T., Janitz, M., and Kril, J. J. (2011). Understanding the pathogenesis of Alzheimer's disease: will RNA-Seq realize the promise of transcriptomics? *J. Neurochem.* 116, 937–946. doi: 10.1111/j.1471-4159.2010.07157.x

Szklarczyk, D., Franceschini, A., Kuhn, M., Simonovic, M., Roth, A., Minguez, P., et al. (2011). The STRING database in 2011: functional interaction networks of proteins, globally integrated and scored. *Nucleic Acids Res.* 39, D561–D568. doi: 10.1093/nar/gkq973

Tan, M. G., Chua, W. T., Esiri, M. M., Smith, A. D., Vinters, H. V., and Lai, M. K. (2010). Genome wide profiling of altered gene expression in the neocortex of Alzheimer's disease. *J. Neurosci. Res.* 88, 1157–1169. doi: 10.1002/jnr.22290

Trepanier, C. H., Jackson, M. F., and MacDonald, J. F. (2012). Regulation of NMDA receptors by the tyrosine kinase Fyn. *FEBS J.* 279, 12–19. doi: 10.1111/j.1742-4658.2011.08391.x

Tseng, B. P., Green, K. N., Chan, J. L., Blurton-Jones, M., and LaFerla, F. M. (2008). Aβ inhibits the proteasome and enhances amyloid and tau accumulation. *Neurobiol. Aging* 29, 1607–1618. doi: 10.1016/j.neurobiolaging.2007.04.014

Uchida, S., Martel, G., Pavlowsky, A., Takizawa, S., Hevi, C., Watanabe, Y., et al. (2014). Learning-induced and stathmin-dependent changes in microtubule stability are critical for memory and disrupted in ageing. *Nat. Commun.* 5:4389. doi: 10.1038/ncomms5389

Um, J. W., Nygaard, H. B., Heiss, J. K., Kostylev, M. A., Stagi, M., Vortmeyer, A., et al. (2012). Alzheimer amyloid-β oligomer bound to postsynaptic prion protein activates Fyn to impair neurons. *Nat. Neurosci.* 15, 1227–1235. doi: 10.1038/nn.3178

VanDyck, C. H., Nygaard, H. B., Chen, K., Donohue, M. C., Raman, R., Rissman, R. A., et al. (2019). Effect of AZD0530 on cerebral metabolic decline in alzheimer disease: a randomized clinical trial. *JAMA Neurol.* 76, 1219–1229. doi: 10.1001/jamaneurol.2019.2050

Vargas, D. M., DeBastiani, M. A., Zimmer, E. R., and Klamt, F. (2018). Alzheimer's disease master regulators analysis: search for potential molecular targets and drug repositioning candidates. *Alzheimers. Res. Ther.* 10:59. doi: 10.1186/s13195-018-0394-7

Wang, J., Gu, B. J., Masters, C. L., and Wang, Y.-J. (2017). A systemic view of Alzheimer disease — insights from amyloid-β metabolism beyond the brain. *Nat. Rev. Neurol.* 13, 612–623. doi: 10.1038/nrneurol.2017.111

Wang, L., Chiang, H.-C., Wu, W., Liang, B., Xie, Z., Yao, X., et al. (2012). Epidermal growth factor receptor is a preferred target for treating Amyloid–induced memory loss. *Proc. Natl. Acad. Sci. U.S.A.* 109, 16743–16748. doi: 10.1073/pnas.1208011109

Wang, M., Roussos, P., McKenzie, A., Zhou, X., Kajiwara, Y., Brennand, K. J., et al. (2016). Integrative network analysis of nineteen brain regions identifies molecular signatures and networks underlying selective regional vulnerability to Alzheimer's disease. *Genome Med.* 8:104. doi: 10.1186/s13073-016-0355-3

Wang, Q., Li, W. X., Dai, S. X., Guo, Y. C., Han, F. F., Zheng, J. J., et al. (2017). Meta-analysis of Parkinson's disease and Alzheimer's disease revealed commonly impaired pathways and dysregulation of NRF2-dependent genes. *J. Alzheimers Dis.* 56, 1525–1539. doi: 10.3233/JAD-161032

Wang, Y., and Mandelkow, E. (2016). Tau in physiology and pathology. *Nat. Rev. Neurosci.* 17, 22–35. doi: 10.1038/nrn.2015.1

Welter, D., MacArthur, J., Morales, J., Burdett, T., Hall, P., Junkins, H., et al. (2014). The NHGRI GWAS catalog, a curated resource of SNP-trait associations. *Nucleic Acids Res.* 42, D1001–D1006. doi: 10.1093/nar/gkt1229

Westermann, B. (2012). Bioenergetic role of mitochondrial fusion and fission. *Biochim. Biophys. Acta Bioenerg.* 1817, 1833–1838. doi: 10.1016/j.bbabio.2012.02.033

William, T. L., Johnson, B. R. G., Urbanc, B., Jenkins, A. T. A., Connell, S. D. A., and Serpell, L. C. (2011). Aβ42 oligomers, but not fibrils, simultaneously bind to and cause damage to ganglioside-containing lipid membranes. *Biochem. J.* 439, 67–77. doi: 10.1042/BJ20110750

Williams, C., Mehrian Shai, R., Wu, Y., Hsu, Y.-H., Sitzer, T., Spann, B., et al. (2009). Transcriptome analysis of synaptoneurosomes identifies neuroplasticity genes overexpressed in incipient Alzheimer's disease. *PLoS One* 4:e4936. doi: 10.1371/journal.pone.0004936

Wruck, W., Schröter, F., and Adjaye, J. (2016). Meta-analysis of transcriptome data related to hippocampus biopsies and iPSC-derived neuronal cells from Alzheimer's disease patients reveals an association with FOXA1 and FOXA2 gene regulatory networks. *J. Alzheimers Dis.* 50, 1065–1082. doi: 10.3233/JAD-150733

Wu, B., McDonald, A. J., Markham, K., Rich, C. B., McHugh, K. P., Tatzelt, J., et al. (2017). The N-terminus of the prion protein is a toxic effector regulated by the C-terminus. *elife* 6:e23473. doi: 10.7554/eLife.23473

Xiang, S., Huang, Z., Wang, T., Han, Z., Yu, C. Y., Ni, D., et al. (2018). Condition-specific gene co-expression network mining identifies key pathways and regulators in the brain tissue of Alzheimer's disease patients. *BMC Med. Genomics* 11:115. doi: 10.1186/s12920-018-0431-1

Xu, M., Zhang, D. F., Luo, R., Wu, Y., Zhou, H., Kong, L. L., et al. (2018). A systematic integrated analysis of brain expression profiles reveals YAP1 and other prioritized hub genes as important upstream regulators in Alzheimer's disease. *Alzheimers Dement.* 14, 215–229. doi: 10.1016/j.jalz.2017.08.012

Yan, T., Ding, F., and Zhao, Y. (2019). Integrated identification of key genes and pathways in Alzheimer's disease via comprehensive bioinformatical analyses. *Hereditas* 156:25. doi: 10.1186/s41065-019-0101-0

Yang, T., Li, S., Xu, H., Walsh, D. M., and Selkoe, D. J. (2017). Large soluble oligomers of amyloid β-protein from alzheimer brain are far less neuroactive than the smaller oligomers to which they dissociate. *J. Neurosci.* 37, 152–163. doi: 10.1523/JNEUROSCI.1698-16.2016

Yasuda, S., Sugiura, H., Tanaka, H., Takigami, S., and Yamagata, K. (2012). p38 MAP kinase inhibitors as potential therapeutic drugs for neural diseases. *Cent. Nerv. Syst. Agents Med. Chem.* 11, 45–59. doi: 10.2174/18715241179496 1040

Yin, G., Li, L. Y., Qu, M., Luo, H. B., Wang, J. Z., and Zhou, X. W. (2011). Upregulation of AKT attenuates amyloid-β-induced cell apoptosis. *J. Alzheimers Dis.* 25, 337–345. doi: 10.3233/JAD-2011-110104

Yin, Z., Raj, D., Saiepour, N., VanDam, D., Brouwer, N., Holtman, I. R., et al. (2017). Immune hyperreactivity of Aβ plaque-associated microglia in Alzheimer's disease. *Neurobiol. Aging* 55, 115–122. doi: 10.1016/j.neurobiolaging.2017.03.021

Yu, G., Wang, L.-G., Han, Y., and He, Q.-Y. (2012). clusterProfiler: an R package for comparing biological themes among gene clusters. *OMICS* 16, 284–287. doi: 10.1089/omi.2011.0118

Yuan, P., Condello, C., Keene, C. D., Wang, Y., Bird, T. D., Paul, S. M., et al. (2016). TREM2 haplodeficiency in mice and humans impairs the microglia barrier function leading to decreased amyloid compaction and severe axonal dystrophy. *Neuron* 90, 724–739. doi: 10.1016/j.neuron.2016.05.003

Zhang, B., Gaiteri, C., Bodea, L. G., Wang, Z., McElwee, J., Podtelezhnikov, A. A., et al. (2013). Integrated systems approach identifies genetic nodes and networks in late-onset Alzheimer's disease. *Cell* 153, 707–720. doi: 10.1016/j.cell.2013.03.030

Zhang, M., Cai, F., Zhang, S., Zhang, S., and Song, W. (2015). Overexpression of ubiquitin carboxyl-terminal hydrolase L1 (UCHL1) delays Alzheimer's progression in vivo. *Sci. Rep.* 4:7298. doi: 10.1038/srep07298

Zhang, Y. W., Wang, R., Liu, Q., Zhang, H., Liao, F. F., and Xu, H. (2007). Presenilin/γ-secretase-dependent processing of β-amyloid precursor protein regulates EGF receptor expression. *Proc. Natl. Acad. Sci. U.S.A.* 104, 10613–10618. doi: 10.1073/pnas.0703903104

Zhou, Y. Y., Li, Y., Jiang, W. Q., and Zhou, L. F. (2015). MAPK/JNK signalling: a potential autophagy regulation pathway. *Biosci. Rep.* 35:e00199. doi: 10.1042/BSR20140141

Zou, S., and Kumar, U. (2018). Cannabinoid receptors and the endocannabinoid system: signaling and function in the central nervous system. *Int. J. Mol. Sci.* 19:833. doi: 10.3390/ijms19030833

Conflict of Interest: The authors declare that the research was conducted in the absence of any commercial or financial relationships that could be construed as a potential conflict of interest.

frontiers in Aging Neuroscience

ORIGINAL RESEARCH
published: 13 March 2020
doi: 10.3389/fnagi.2020.00044

The Apolipoprotein E ε4 Allele-Dependent Relationship Between Serum Lipid Levels and Cognitive Function: A Population-Based Cross-sectional Study

Shan Wei[1], *Ling Gao*[1], *Yu Jiang*[1], *Suhang Shang*[1], *Chen Chen*[1], *Liangjun Dang*[1], *Jin Wang*[1], *Kang Huo*[1], *Jingyi Wang*[2] *and Qiumin Qu*[1]*

[1]*Department of Neurology, The First Affiliated Hospital of Xi'an Jiaotong University, Xi'an, China,* [2]*Department of Neurology, Huxian Hospital of Traditional Chinese Medicine, Xi'an, China*

OPEN ACCESS

Edited by:
Jiehui Jiang,
Shanghai University, China

Reviewed by:
Chongren Tang,
University of Washington, United States
Miguel Calero,
Carlos III Health Institute, Spain

***Correspondence:**
Qiumin Qu
quqiumin@126.com

Received: *12 November 2019*
Accepted: *10 February 2020*
Published: *13 March 2020*

Citation:
Wei S, Gao L, Jiang Y, Shang S, Chen C, Dang L, Wang J, Huo K, Wang J and Qu Q (2020) The Apolipoprotein E ε4 Allele-Dependent Relationship Between Serum Lipid Levels and Cognitive Function: A Population-Based Cross-sectional Study. Front. Aging Neurosci. 12:44. doi: 10.3389/fnagi.2020.00044

Objectives: Till now, the effect of serum lipid levels on cognitive function is still controversial. The apolipoprotein E (APOE) ε4 allele is the most critical genetic risk factor for Alzheimer's disease (AD) and cognitive impairment. Additionally, *APOE* ε4 allele has a major impact on lipid metabolism. The aim of this study was to investigate the *APOE* genotype-dependent relationship between peripheral serum lipid levels and cognitive impairment.

Methods: A total of 1,273 subjects aged 40–86 years participated in this cross-sectional study. Serum lipid levels and the *APOE* genotype were detected. Mini-Mental State Examination was used to diagnose the cognitive impairment or not. Univariate and multivariate analyses were used to analyze the relationships between *APOE* genotype, serum lipid levels, and cognition function.

Results: After controlling for all possible covariates, a significant interaction between low serum high-density lipoprotein and the *APOE* ε4 allele on cognitive impairment (Wald's $\chi^2 = 4.269$, $df = 1$, OR = 20.094, $p = 0.039$) was found in the total participants. In *APOE* ε4 carriers, low serum high-density lipoprotein was positively associated with cognitive impairment (Wald's $\chi^2 = 8.200$, $df = 1$, OR = 60.335, $p = 0.004$) and serum high-density lipoprotein levels were positively correlated with Mini-Mental State Examination score ($r = 0.217$, $df = 176$, $p = 0.004$). There was no significant correlation between serum total cholesterol (TC), low-density lipoprotein, triglycerides (TG) levels, and cognitive impairment in either the total participants or *APOE* ε4 carriers/non-carriers.

Conclusions: *APOE* ε4 carriers, but not non-carriers, with lower serum high-density lipoprotein had a higher prevalence of cognitive impairment and a lower Mini-Mental State Examination score. These results suggest that the *APOE* ε4 allele may affect the relationship between serum lipid levels and cognitive impairment. However, the specific mechanism needs to be further elucidated.

Keywords: Alzheimer's disease, total cholesterol, high-density lipoprotein, low-density lipoprotein, triglyceride, apolipoprotein E, risk factors

INTRODUCTION

Alzheimer's disease (AD) is the most common type of dementia, and its prevalence has been increasing rapidly in China (Jia et al., 2014). A recent study revealed that, in China, the total annual socioeconomic costs of AD patients were US $167.74 billion in 2015 and were predicted to reach US $1.89 trillion in 2050, imposing an immense burden on patients and their families (Jia et al., 2018). Due to the complexity of the pathogenesis of AD, there are currently no unified and effective approaches for preventing or curing AD.

In the brain, amyloid-β (Aβ) accumulation and the formation of insoluble extracellular senile plaques are pathological hallmarks of AD. Aβ is produced by the endoproteolysis of amyloid precursor protein (APP). When cleaved by β-secretase and γ-secretase, APP is mainly hydrolyzed into the 38–43 amino acid residue Aβ peptide (De Felice and Ferreira, 2002), and senile plaques are mainly composed of amyloid $A\beta_{40}$ and amyloid $A\beta_{42}$ (Masters et al., 1985). Researchers have found that reducing cellular cholesterol levels appears to inhibit β-secretase and γ-secretase activity and, thus, decrease the amount of Aβ secreted by neurons (Wahrle et al., 2002; Subasinghe et al., 2003). The responsiveness of Aβ production to cholesterol levels suggests that cholesterol metabolism plays an essential role in the pathogenesis of AD (Hartmann et al., 2007). However, there are still no consistent results of epidemiological studies concerning the role of cholesterol as a risk factor for AD, although some studies have demonstrated that elevated cholesterol increases the risk of AD development, particularly in middle-aged individuals (Kivipelto et al., 2001; Whitmer et al., 2005). Other researchers have failed to confirm this result (Reitz et al., 2004; Tukiainen et al., 2012).

Apolipoprotein E (*APOE*) ε4 is the most important genetic risk factor for AD. *APOE* is a polymorphic protein involved in the development of late-onset AD, although the mechanism has not been fully elucidated (Siest et al., 2000). There are three alleles of *APOE* (E2, E3, and E4) that produce three homozygous (E2/2, E3/3, and E4/4) and three heterozygous (E2/3, E2/4, and E3/4) isoforms (Zannis and Breslow, 1981). Pathophysiological studies show that *APOE* immunoreactivity exists in senile plaques, indicating a significant role of *APOE* in the metabolism of Aβ (Kim et al., 2009; Castellano et al., 2011), which is thought to initiate toxic events and further have distinct functions in regulating tau hyperphosphorylation, synaptic plasticity, cell signaling, lipid transport and metabolism, and neuroinflammation (Yu et al., 2014; Giau et al., 2015). Additionally, *APOE* ε4 has a major impact on lipid metabolism (Mahley, 1988). The *APOE* gene modulates serum concentrations of lipid and lipoproteins according to its high affinity for binding to cell-surface lipoprotein receptors. Previous research has reported that carriers of *APOE ε4* have a higher risk of hyperlipidemia (Dallongeville et al., 1992).

Considering that the *APOE* genotype plays an important role in both AD pathogenesis and lipid metabolism, we investigated the effects of the *APOE* genotype on the relationships between peripheral serum lipid levels and cognitive impairment in Chinese middle-aged and elderly subjects from Qubao village in the suburbs of Xi'an, northwest China.

MATERIALS AND METHODS

Participants

Between December 2016 and April 2017, 1,865 subjects were recruited from Qubao village in the suburbs of Xi'an, China. Inclusion criteria were as follows: being 40 years old or older; having lived in Qubao for more than 3 years; agreeing to participate in the study and completing the questionnaire; and having venous blood collected. The exclusion criteria were as follows: (1) participants who had used lipid-lowering drugs in the last 3 months; (2) participants who had severe liver, kidney, thyroid, and hematopoietic system diseases; (3) participants who had suffered from a clear history of acute cerebrovascular disease, including stroke; (4) participants who had suffered from severe nervous system diseases that can cause cognitive impairment, including infection, Parkinson's disease, epilepsy, congenital intellectual disability, and craniocerebral operations; (5) participants who had suffered from other physical and chemical factors that led to cognitive impairment (drug poisoning, alcoholism, and carbon monoxide poisoning); (6) participants who had suffered from severe psychopathy, including schizophrenia, bipolar disorder, severe depression or anxiety; and (7) participants without a complete MMSE score, biomarkers, or covariates. Considering all the inclusion and exclusion criteria, 1,273 subjects were included in our study (**Figure 1**).

Questionnaire Survey

All of the participants were asked to complete the questionnaire survey in a structured in-person interview given by trained interviewers. The questionnaire included basic information (gender, age, education, and marital status), lifestyle (exercise,

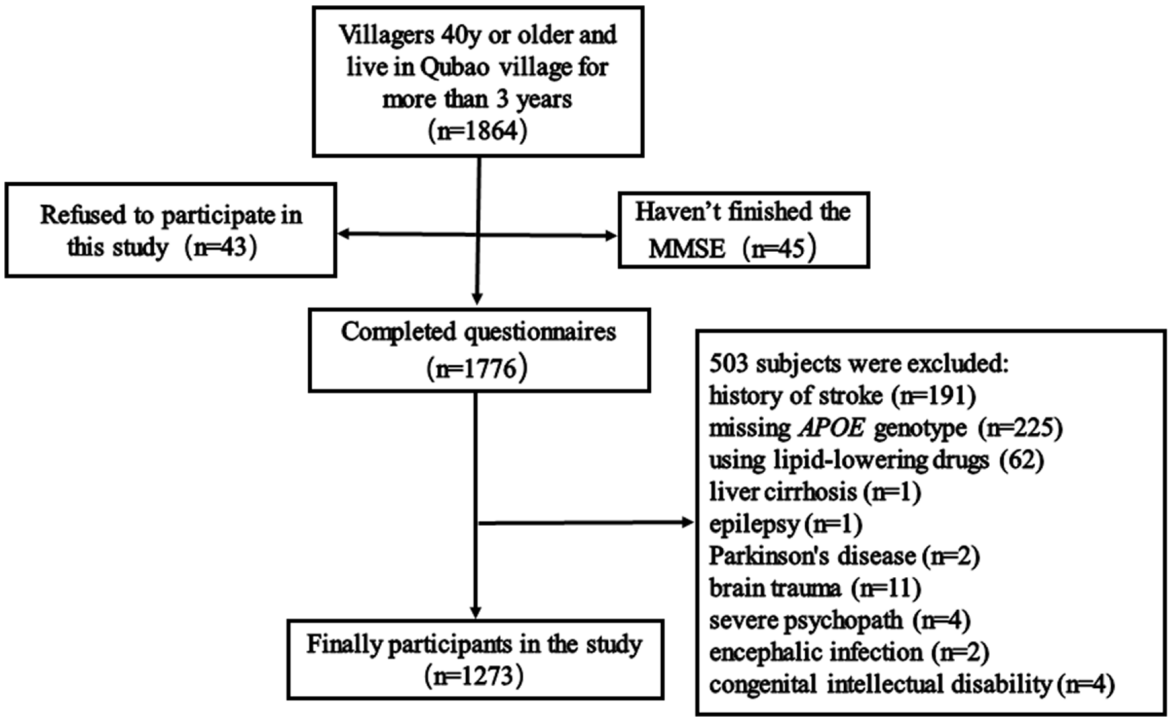

FIGURE 1 | Flow chart of participant selection. Qubao village: the suburbs of Xi'an in northwest China. *APOE*, apolipoprotein E.

smoking, and alcohol consumption), and medical history (hypertension, diabetes, dyslipidemia, cerebrovascular disease, and heart disease). The definitions of hypertension and diabetes are consistent with those in our previous articles (Jia et al., 2018). According to the diagnostic criteria of Chinese adult dyslipidemia prevention guide (2007 edition; Joint Committee for Developing Chinese guidelines on Prevention and Treatment of Dyslipidemia in Adults, 2007), people who meet any of the following criteria can be defined as dyslipidemia: high total cholesterol (TC): TC $\geq$ 5.18 mmol/L; high low-density lipoprotein (LDL-c): LDL-c $\geq$ 3.37 mmol/L; low high-density lipoprotein (HDL-c): HDL-c $<$ 1.04 mmol/L; high triglycerides (TG): TG $\geq$ 1.70 mmol/L. In addition, anthropometric measurements of participants were taken at the scene, including blood pressure, pulse rate, height, weight, and waist and hip circumference. The body mass index (BMI) was weight (kg) divided by the square of height in meters, and the waist–hip ratio was the waist circumference divided by the hip circumference.

Diagnosis of Cognitive Impairment

The Mini-Mental State Examination (MMSE) questionnaire was completed by the participants to assess global cognitive function. The MMSE was chosen by Katzman et al. (1988) based on a Chinese version that had been shown to have good sensitivity and specificity. Participants with scores below the cutoff value were considered to have cognitive impairment. The cutoff values were as follows: scores $\leq$17 for illiteracy, scores $\leq$20 for participants who only finished primary school, and scores $\leq$24 for participants with junior high school or above level of education.

Biochemical Assessment and *APOE* Genotype Detection

After completing the questionnaire, 10 ml of blood was extracted from the elbow vein of each participant under the condition of fasting for more than 8 h, which was put into a purple-top EDTA-anticoagulant tube and a red-top non-anticoagulant tube. The red-top tube blood samples were sent to the biochemical laboratory of the First Affiliated Hospital of Xi'an Jiaotong University for biochemical assessment [HDL-c, LDL-c, TG, TC, and fasting blood glucose (FBG)]. The concentrations of serum HDL-c, LDL-c, TC, TG, and FBG levels were tested by enzymatic method using an automated biochemical analyzer (C501, Roche, Sweden). The purple-top tube blood samples were centrifuged within 2 h after collection at a rate of 3,000 revolutions per second for 10 min, and all of the samples were stored in the refrigerator at −80°C for future analysis. An extraction kit (Tiangen Co. Beijing, China) was used to extract DNA from the frozen EDTA–anticoagulant blood according to the manufacturer's protocol. Using human genome DNA as a template, the 244-bp length of the target DNA fragment that included two polymorphic sites at amino acid residues 112 and 158 (Mahley and Rall, 2000) was amplified by a PCR thermocycler. All PCR products were detected by Sanger

sequencing (Sangon Company, Shanghai, China) to finally determine the *APOE genotype*.

Statistical Analyses

SPSS 18.0 software (SPSS Inc., IBM, Chicago, IL, USA) was used to analyze all of the data. First, participants were divided into a dyslipidemia group and a non-dyslipidemia group. In addition, according to the *APOE* genotype, the participants could also be divided into *APOE* ε4 non-carriers (E2/2, E2/3, and E3/3) or *APOE* ε4 carriers (E2/4, E3/4, and E4/4). Unpaired Student's *t*-tests and the mean ± SD were used for data that were approximately normally distributed; the Mann–Whitney *U* test and the median (quartiles) were used for skewed data distributions, and the Pearson χ^2 test and percentages were used for categorical data. A *p*-value of <0.05 (two-tailed) was considered statistically significant.

Then, a χ^2 test or Fisher's exact test was used to compare the differences in cognitive impairment between serum lipid groups in the total participants and in the subgroups according to *APOE* ε4 status. For multivariate analysis, binary logistic regression was used to correct for covariates, including gender, age, education years, smoking, drinking, physical activity, medical history, FBG, mean arterial pressure (MAP), pulse rate, and BMI.

Finally, partial correlation analysis was used to research the correlations between MMSE score and serum lipid levels in the subgroups according to the *APOE* ε4 status. The covariates included age, sex, education years, smoking, drinking, intensity of physical activity, BMI, log-transformed FBG, MAP, pulse rates, and heart disease.

RESULTS

Demographic Characteristics of the Study Samples

A total of 1,273 subjects ranging from 40 to 86 years old (mean 57.1 ± 9.7 years) were included in the study, including 755 (59.3%) women. Participants with dyslipidemia comprised 59.2% (754) of the total population. Ninety-nine (7.8%) subjects met the diagnostic criteria of cognitive impairment, and a total of 189 people (14.8%) were *APOE* ε4 carriers. **Table 1** shows the demographic characteristics of the total participants. There were significant differences in gender, education, smoking, hypertension, diabetes mellitus status, MAP, pulse rate, FBG level, BMI, and *APOE* ε4 carrier status between the dyslipidemia group and the normal lipids group.

The Current Prevalence of Cognitive Impairment Between the Normal Serum Lipids Group and the Dyslipidemia Group

As shown in **Figure 2**, in the total samples, the current prevalence of cognitive impairment was not significantly different between the normal serum lipids group and the dyslipidemia group. The stratified analyses according to *APOE* ε4 status showed that the current prevalence of cognitive impairment was still not significantly different between any of the serum lipid groups in *APOE* ε4 carriers or non-carriers.

Multivariate Analysis of the Relationship Between Serum Lipid Parameters and Cognitive Impairment in the Total Samples

To eliminate the influence of covariates, binary logistic regression analysis was performed. In the total samples, after adjusting for age, gender, and education, no significant correlation was found between high TG, high TC, high LDL, low HDL levels, and cognitive impairment (**Table 2**, Model 1). When continuing to bring other covariates into the binary logistic regression models, the results were approximately the same (**Table 2**, Model 2). However, with the binary logistic regression analysis of the interaction between the serum lipids and *APOE* genotype on cognitive impairment, we found that the interaction between low HDL and *APOE* ε4 status was positively correlated with cognitive impairment (Wald's χ^2 = 4.269, *df* = 1, OR = 20.094, 95% CI = 1.167–346.056, *p* = 0.039), and the interaction between other serum lipid parameters (high TG, high TC, and high LDL levels) and *APOE* ε4 status had no significant effect on cognitive impairment (**Table 2**, Model 3).

The Effects of the *APOE* ε4 Allele on Cognitive Impairment and Serum Lipid Levels

Univariate analysis showed that compared with *APOE* ε4 non-carriers, serum TC, TG, and LDL levels were higher and HDL levels were lower in *APOE* ε4 carriers [TC: 5.36 ± 0.94 mmol/L vs. 5.15 ± 0.99 mmol/L, *df* = 1,271, *p* = 0.008; TG: 1.48 (1.09, 2.15) mmol/L vs. 1.29 (0.96, 1.80) mmol/L, *p* < 0.001; LDL: 2.82 ± 0.62 mmol/L vs. 2.61 ± 0.66 mmol/L, *df* = 1,271, *p* < 0.001; HDL: 1.53 ± 0.32 mmol/L vs. 1.60 ± 0.34 mmol/L, *df* = 1,271, *p* = 0.007], and the prevalence of dyslipidemia was also significantly higher in *APOE* ε4 carriers [132 (69.8%) vs. 622 (57.4%), *df* = 1, *p* = 0.001]. The current prevalence of cognitive impairment was not significantly different between *APOE* ε4 carriers and non-carriers. Other covariates (age, gender, degree of education, smoking, drinking, intensity of physical activity, hypertension, diabetes mellitus, coronary heart disease, MAP, and BMI) also showed no significant difference between the two groups (**Table 3**).

Stratified Multivariate Analysis of the Relationship Between Serum Lipids and Cognitive Impairment According to *APOE* ε4 Status

Because the *APOE* ε4 allele had effects on the relationship between serum lipid levels and cognitive impairment, stratified binary logistic regression analyses were performed according to *APOE* ε4 status. In *APOE* ε4 carriers, low HDL was positively correlated with cognitive impairment (Wald's χ^2 = 8.200, *df* = 1, OR = 60.335, 95% CI = 3.646–998.364, *p* = 0.004; **Table 4**, Model 5). However, such a correlation disappeared among *APOE* ε4 non-carriers (Wald's χ^2 = 0.057, *df* = 1, OR = 0.776, 95% CI = 0.097–6.221, *p* = 0.811; **Table 4**, Model 7). For other serum lipid parameters (high TC, high TG, and high LDL levels), there was no significant correlation with cognitive

TABLE 1 | Demographic and clinical characteristics of the study samples.

	Total (n = 1,273)	Normal serum lipids (n = 519)	Dyslipidemia (n = 754)	*df*	*p*-value
Age, years (mean ± SD)	57.1 ± 9.7	56.5 ± 10.2	57.5 ± 9.3	1,271	0.062
Gender, female (%)	755 (59.3)	275 (53.0)	480 (63.7)	1	<0.001
Education, years (mean ± SD)	6.4 ± 3.4	6.8 ± 3.2	6.2 ± 3.5	1,271	0.003
Drinking, *n* (%)	153 (12.0)	68 (13.1)	85 (11.3)	1	0.324
Smoking, *n* (%)	400 (31.4)	187 (36.0)	213 (28.2)	1	0.003
Lack of activity, *n* (%)	252 (19.8)	97 (18.7)	155 (12.2)	1	0.411
Cardiovascular disease, *n* (%)	114 (9.0)	47 (9.1)	67 (8.9)	1	0.917
Hypertension, *n* (%)	479 (37.6)	164 (31.6)	315 (41.8)	1	<0.001
Diabetes mellitus, *n* (%)	142 (11.2)	51 (9.8)	91 (12.1)	1	0.212
MAP, mmHg (mean ± SD)	95.7 ± 11.7	94 ± 12	97 ± 12	1,271	<0.001
Pulse rate, (mean ± SD)	74 ± 10	73 ± 10	75 ± 10	1,271	<0.001
FBG, mmol/L, median (quartile)	5.34 (5.02, 5.80)	5.27 (4.98, 5.66)	5.40 (5.05, 5.89)	—	<0.001
BMI, kg/m^2 (mean ± SD)	25.10 ± 3.20	24.32 ± 3.06	25.62 ± 3.19	1,271	<0.001
Cognitive impairment, *n* (%)	99 (7.8)	41 (7.9)	58 (7.7)	1	0.892
APOE ε4 carriers, *n* (%)	189 (14.8)	57 (11.0)	132 (10.4)	1	0.001

Unpaired Student's t-test and mean ± SD were used to compare the difference of the approximately normally distributed continuous variables between normal serum lipids group and dyslipidemia group. Mann–Whitney U test and median (quartile) were used for the skew distributional data, and χ^2 and percentage were used for categorical variables. SD, standard deviation; MAP, mean arterial pressure; FBG, fasting blood glucose; BMI, body mass index; APOE, apolipoprotein E.

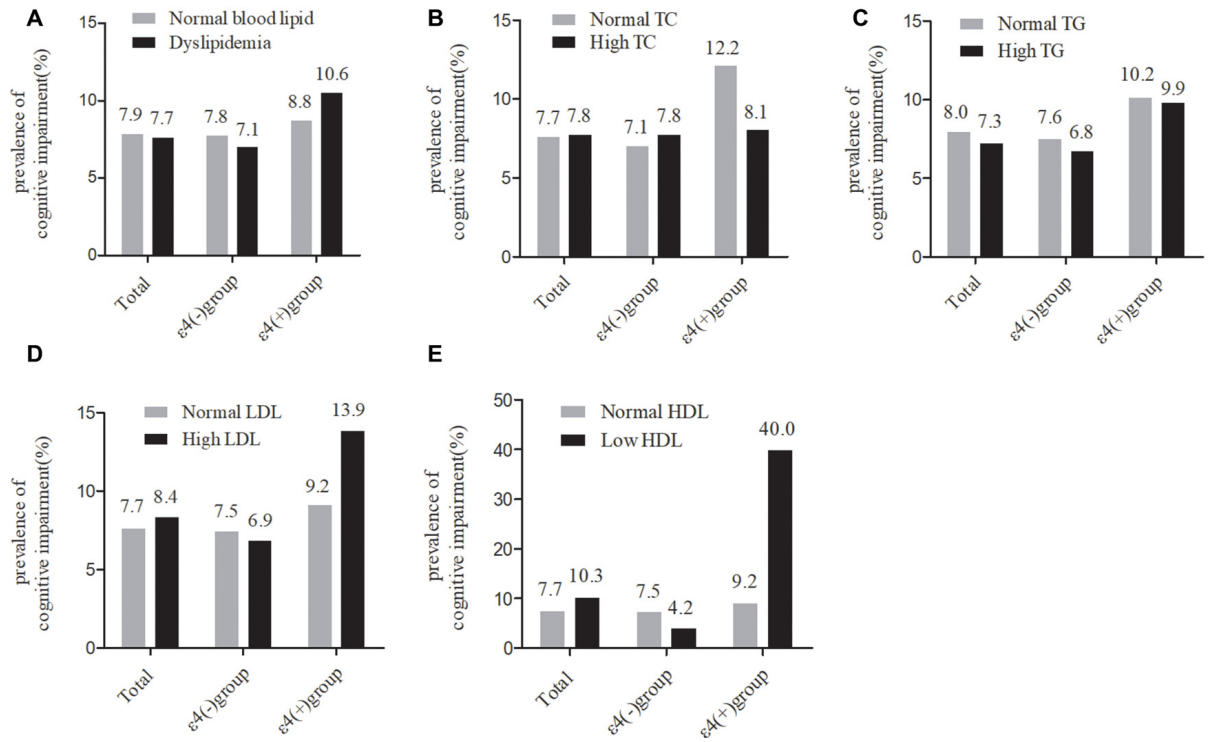

FIGURE 2 | Comparison of the differences in cognitive impairment between serum lipid groups in the total participants and in subgroups according ApoEε4 status. TC, total cholesterol; LDL-c, low-density lipoprotein; HDL-c, high-density lipoprotein; TG, triglycerides; *APOE*, apolipoprotein E. **(A–D)** χ^2 test. **(E)** Fisher's exact test.

impairment in either *APOE* ε4 carriers or non-carriers (**Table 3**, Models 5 and 7).

Stratified Multivariate Analysis of the Correlations Between Serum Lipids and MMSE Score According to *APOE* ε4 Status

To further confirm our results, stratified partial correlation analysis was separately performed to research the correlations between serum lipids and MMSE score in *APOE* ε4 non-carriers and carriers. When adjusting for age, sex, education, smoking, drinking, intensity of physical activity, BMI, log-transformed FBG, MAP, pulse rates, and heart disease, MMSE scores positively correlated with serum HDL level (r = 0.217, df = 176, p = 0.004) but not with LDL, TG, or TC levels in *APOE* ε4 carriers. In *APOE* ε4 non-carriers, no correlations were found between MMSE scores and any of the serum lipids (**Figure 3**).

TABLE 2 | The relationships between serum lipid parameters and cognitive impairment with binary logistic regression in the total samples.

		B	SE	Wald's χ^2	OR	95% CI	*p*-value
Model 1							
	High TC	−0.195	0.222	0.771	0.823	0.533–1.271	0.380
	High TG	−0.167	0.239	0.487	0.846	0.529–1.353	0.485
	High LDL-c	−0.062	0.312	0.039	0.940	0.511–1.732	0.843
	Low HDL-c	0.595	0.655	0.824	1.813	0.502–6.544	0.364
Model 2							
	High TC	−0.161	0.226	0.506	0.851	0.546–1.326	0.477
	High TG	−0.144	0.250	0.333	0.866	0.531–1.413	0.564
	High LDL-c	−0.061	0.319	0.036	0.941	0.504–1.757	0.849
	Low HDL-c	0.718	0.655	1.203	2.051	0.568–7.404	0.273
Model 3							
	High TC	−0.077	0.248	0.096	0.926	0.569–1.507	0.757
	High TC by *APOE* ε4 status	−0.462	0.568	0.662	0.630	0.207–1.918	0.416
	High TG	−0.174	0.279	0.390	0.840	0.486–1.452	0.532
	High TG by *APOE* ε4 status	0.146	0.592	0.061	1.157	0.363–3.692	0.805
	High LDL-c	−0.180	0.382	0.222	0.835	0.395–1.766	0.637
	High LDL-c by *APOE* ε4 status	0.435	0.704	0.381	1.544	0.389–6.136	0.537
	Low HDL-c	−0.354	1.061	0.111	0.702	0.088–5.614	0.739
	Low HDL-c by *APOE* ε4 status	3.000	1.452	4.269	20.094	1.167–346.056	0.039

Binary logistic regression model was used for data analysis, df = 1. APOE ε4 carrier status: dummy coded with ε4 carriers = 1, non-carriers = 0. Model 1 was adjusted for age, gender, and education years. Model 2 was adjusted for age, gender, education years, smoking, drinking, intensity of physical activity, body mass index, log-transformed fasting blood glucose, mean arterial pressure, pulse rate, heart disease, and APOE ε4 carrier status. Model 3 was adjusted for the covariates included in model 2 as well as the interaction terms of APOE ε4 carrier status by serum lipids. TC, total cholesterol; LDL-c, low-density lipoprotein; HDL-c, high-density lipoprotein; TG, triglycerides; APOE, apolipoprotein E.

TABLE 3 | Difference of the cognitive impairment, serum lipid levels, and other covariates between *APOE* ε4 carriers and non-carriers.

	***APOE* ε4 non-carriers (*n* = 1,084)**	***APOE* ε4 carriers (*n* = 189)**	***df***	***p*-value**
Age, years (mean ± SD)	57.0 ± 9.8	57.5 ± 9.3	1,271	0.501
Gender, female (%)	642 (59.2)	113 (59.8)	1	0.884
Education, years (mean ± SD)	6.5 ± 3.4	6.2 ± 3.5	1,271	0.228
Drinking, *n* (%)	133 (12.3)	20 (10.6)	1	0.510
Smoking, *n* (%)	343 (31.6)	57 (30.2)	1	0.685
Lack of activity, *n* (%)	217 (20.0)	35 (18.5)	1	0.633
Cardiovascular disease, *n* (%)	103 (9.5)	11 (5.8)	1	0.102
Hypertension, *n* (%)	410 (37.8)	69 (36.5)	1	0.731
Diabetes mellitus, *n* (%)	116 (10.7)	26 (13.8)	1	0.218
MAP, mmHg (mean ± SD)	95.7 ± 11.8	95.6 ± 11.3	1,271	0.860
Pulse rate (mean ± SD)	74 ± 10	74 ± 9	1,271	0.771
FBG, mmol/L, median (quartile)	5.33 (5.01, 5.80)	5.36 (5.04, 5.88)	—	0.543
BMI, kg/m^2 (mean ± SD)	25.07 ± 3.15	25.26 ± 3.47	1,271	0.437
Cognitive impairment, *n* (%)	80 (7.4)	19 (10.1)	1	0.205
Dyslipidemia, *n* (%)	622 (57.4)	132 (69.8)	1	0.001
TC, mmol/L (mean ± SD)	5.15 ± 0.99	5.36 ± 0.94	1,271	0.008
TG, mmol/L, median (quartile)	1.29 (0.96, 1.80)	1.48 (1.09, 2.15)	—	<0.001
LDL-c, mmol/L (mean ± SD)	2.61 ± 0.66	2.82 ± 0.62	1,271	<0.001
HDL-c, mmol/L (mean ± SD)	1.60 ± 0.34	1.53 ± 0.32	1,271	0.007

Unpaired Student's t-test and mean ± SD were used to compare the difference of the approximately normally distributed continuous variables between APOE ε4 carriers and non-carriers. Mann-Whitney U test and median (quartile) were used for the skew distributional data. χ^2 and percentage were used for categorical variables. SD, standard deviation; MAP, mean arterial pressure; FBG, fasting blood glucose; BMI, body mass index; TC, total cholesterol; LDL-c, low-density lipoprotein; HDL-c, high-density lipoprotein; TG, triglycerides; APOE, apolipoprotein E.

DISCUSSION

In this cross-sectional study, we found a significant interaction effect between low HDL and the *APOE* ε4 allele on cognitive impairment in the total participants. In *APOE* ε4 carriers, low serum HDL-c levels were positively associated with cognitive impairment, and participants with higher HDL levels had higher MMSE scores. No correlation was found between cognitive impairment/MMSE score and any of the serum lipids in *APOE* ε4 non-carriers.

Although studies have shown that lipid metabolism is involved in the pathogenesis of AD (Hartmann et al., 2007; Anstey et al., 2008), and the effect of lipid levels on cognitive function has attracted the attention of many researchers, there is still no consistent conclusion. A previous study showed that high midlife TC levels can increase the risk of AD in older people (Anstey et al., 2017). In contrast, another study showed that higher TC levels were associated with better memory functioning in very elderly subjects without the *APOE* ε4 allele (West et al., 2008). One study showed that increased serum LDL levels were

TABLE 4 | The relationships between serum lipid parameters and cognitive impairment with binary logistic regression in the subgroups according *APOE*ε4 status.

Participants		*B*	SE	Wald's χ^2	OR	95% CI	*p*-value
APOE ε4 carriers	Model 4						
	High TC	−0.716	0.545	1.724	0.489	0.168–1.423	0.189
	High TG	0.098	0.556	0.031	1.103	0.371–3.284	0.860
	High LDL-c	0.166	0.618	0.072	1.181	0.352–3.965	0.788
	Low HDL-c	3.172	1.203	6.957	23.847	2.259–251.772	0.008
	Model 5						
	High TC	−0.946	0.594	2.540	0.388	0.121–1.243	0.111
	High TG	−0.238	0.615	0.150	0.788	0.236–2.628	0.698
	High LDL-c	0.060	0.665	0.008	1.062	0.288–3.914	0.928
	Low HDL-c	4.100	1.432	8.200	60.335	3.646–998.364	0.004
APOE ε4 non-carriers	Model 6						
	High TC	−0.103	0.245	0.176	0.902	0.558–1.458	0.675
	High TG	−0.247	0.270	0.840	0.781	0.460–1.325	0.359
	High LDL-c	−0.219	0.376	0.339	0.803	0.384–1.680	0.561
	Low HDL-c	−0.453	1.057	0.184	0.636	0.080–5.043	0.668
	Model 7						
	High TC	−0.052	0.250	0.043	0.950	0.582–1.549	0.836
	High TG	−0.176	0.283	0.385	0.839	0.482–1.461	0.535
	High LDL-c	−0.166	0.383	0.187	0.847	0.400–1.795	0.665
	Low HDL-c	−0.254	1.062	0.057	0.776	0.097–6.221	0.811

Binary logistic regression model was used for data analysis, df = 1. Models 4 and 5 were analyzed in APOE ε4 carriers. Models 6 and 7 were analyzed in APOE ε4 non-carriers. APOE ε4 carrier status: dummy coded with ε4 carriers = 1, non-carriers = 0. Models 4 and 6 were adjusted for age, gender, and education years. Models 5 and 7 were adjusted for age, gender, education years, smoking, drinking, intensity of physical activity, body mass index, log-transformed fasting blood glucose, mean arterial pressure, pulse rate, and heart disease. TC, total cholesterol; LDL-c, low-density lipoprotein; HDL-c, high-density lipoprotein; TG, triglycerides; APOE, apolipoprotein E.

independently associated with AD (Chen et al., 2019), and one study showed that higher LDL levels were associated with better memory performance (Leritz et al., 2016). Katsumata et al. (2013) reported that HDL levels and lower TG/HDL-C ratios were associated with better memory performance, while other studies have shown no association between HDL and AD (Li et al., 2005). Therefore, to study the relationship between lipids and cognition, stratified analysis was separately performed according to the *APOE* genotype. Our study found that low HDL was associated with cognitive impairment in *APOE* ε4 allele carriers, while TC, LDL, and TG levels were not associated with cognitive function.

Some possible mechanisms might explain the positive correlation between HDL levels and cognitive function. First, it has been shown that ApoA-I, the main component of HDL, is highly efficient at cholesterol efflux in the CSF (Demeester et al., 2000), resulting in increased membrane fluidity that could enhance the α-secretase cleavage of APP at the cell membrane. As mentioned above, increased α-secretase activity can reduce the production of Aβ. Second, apoA-I/HDL can bind to Aβ and make the clearance of Aβ by astrocytes and/or microglia more efficient (Sagare et al., 2012), leading to a decrease in Aβ aggregation and cytotoxicity. Third, it is well established that the antioxidant and anti-inflammatory effects of HDL play an important role in cardiovascular diseases (Barter et al., 2007), so the same disease mechanism may also affect neurodegenerative diseases (Lewis et al., 2010). Finally, the main role of HDL is lipid metabolism, which can reverse lipoprotein transport from the arterial wall of the brain (Mulder and Terwel, 1998), leading to a decrease in ischemic lesions that are involved in the development of cognitive decline and dementia (Kalaria, 2000).

However, the difference in the relationship between HDL and cognitive function between *APOE* ε4 carriers and *APOE* ε4 non-carriers remains to be addressed. We hypothesized that in *APOE* ε4 carriers, there may be two reasons for the positive association between cognitive function and HDL levels. First, this study showed lower levels of HDL in *APOE* ε4 carriers, suggesting that *APOE* exerts isoform-specific effects on HDL metabolism in humans. Using C57BL/6 $APOE^{-/-}$ mice, Hopkins et al. (2002) reported that compared with *APOE* ε3, the presence of *APOE* ε4 was less efficient at transferring ApoA-I from chylomicron remnants to HDL, resulting in lower plasma HDL levels and smaller HDL volumes. The reduced HDL levels may be associated with eventual cognitive decline, which has been confirmed by some previous studies (van Exel et al., 2002; Zuliani et al., 2010). However, pathophysiological studies have shown that *APOE* ε4 can directly lead to cognitive decline without HDL involvement by affecting Aβ clearance, tau hyperphosphorylation, synaptic plasticity, cell signaling, and neuroinflammation (Yu et al., 2014; Giau et al., 2015). The combination of these two mechanisms may lead to the emergence of a positive relationship between HDL levels and cognitive function in *APOE* ε4 carriers. However, in *APOE* ε4 non-carriers, without *APOE* ε4 as a risk factor, the effect of HDL alone on cognitive function might not be sufficiently apparent, leading to the result that there was no significant relationship between HDL and cognitive function. Of course, the abovementioned ideas are only our reasonable speculation, and the specific mechanism remains to be further studied.

Consistent with our findings, one community-based study with 2,356 participants showed no correlation between TC levels and the risk of dementia or AD (Elias et al., 2005). In contrast, the 3C study (Schilling et al., 2017) and another 14-year cohort study (Toro et al., 2014) found a positive correlation, and a meta-analysis (Anstey et al., 2017) also showed that high midlife

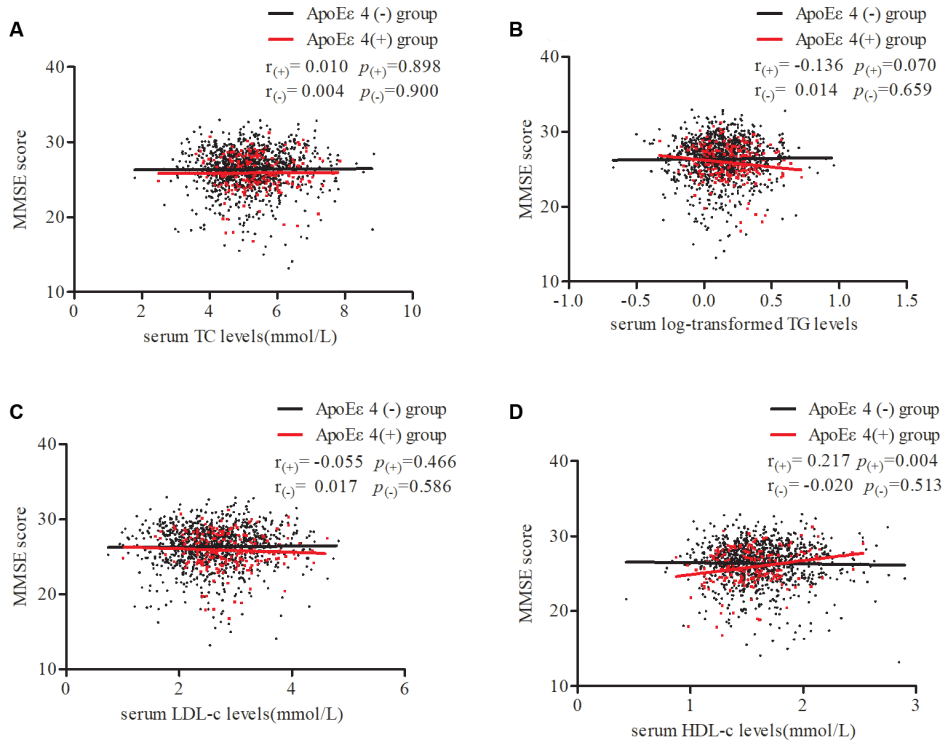

FIGURE 3 | Partial correlations of MMSE score and serum lipid levels according *APOE* ε4 status. Participants were divided into two groups: *APOE* ε4 carriers and non-carriers, which are represented by red dots and black dots. Partial linear correlations between MMSE scores and serum TC **(A)**, log-transformed TG **(B)**, LDL-c **(C)**, and HDL-c **(D)** levels are shown in the figure. $r_{(+)}$ and $p_{(+)}$ represent partial correlation coefficients in carriers, while $r_{(-)}$ and $p_{(-)}$ represent non-carriers. Adjusted for age, sex, education, smoking, drinking, intensity of physical activity, body mass index (BMI), log-transformed fasting blood glucose (FBG), mean arterial pressure, pulse rates, and heart disease. TC, total cholesterol; TG, triglycerides; LDL-c, low-density lipoprotein; HDL-c, high-density lipoprotein; *APOE*, apolipoprotein E.

TC levels increase the risk of late-life AD. However, the lipid measurements in these studies were not from cross-sectional studies and were performed significantly earlier than the onset of AD by at least 13 years, and some of the cholesterol levels were measured in midlife and not late life. A previous study of 444 men from the Finnish cohorts of the Seven Countries (Notkola et al., 1998) showed that the TC levels of men in midlife who subsequently developed AD were significantly higher than those of normal men. However, because cholesterol levels decline with age, in the preclinical manifestations of AD stage, the TC levels of those eventually developing AD decreased more rapidly and were eventually lower in late life than those of normal men. This study was a cross-sectional study in Chinese middle-aged and elderly subjects, and all lipid measurements were clustered around the time of the study, which may explain the lack of correlation between TC levels and cognitive impairment.

Some limitations should be mentioned. First, the study is a cross-sectional study, so it can only explain the correlation between blood lipids and cognition; however, the causal relationship between them is difficult to explain, and randomized controlled trial is necessary in the future to see if increasing HDL-c plasma levels can prevent cognitive decline in the at-risk population of *APOE* ε4 carriers and thus clarify the causal relationship. Second, the serum lipids were only detected at a single time point, not allowing for an evaluation of the dynamic changes. In addition, our study focused on elderly individuals in the Chinese Han population in Northwest China, and the diagnosis of cognitive impairment was based on the Chinese version of the MMSE, so the generalizability of our findings may be limited in other ethnic or age groups, and multi-center and large population studies need to be performed to validate our results. Third, with the numbers of patients with cerebrovascular diseases increasing, the incidence rate of vascular dementia (VaD) rises year by year. VaD has become the second leading cause of dementia after AD itself (Lobo et al., 2000). In this study, we have excluded people with a clear history of acute cerebrovascular disease, including stroke. However, owing to lack of standard diagnostic procedures and biomarkers simultaneously (Formichi et al., 2010), it is still hard to rule out the possibility that some cases with cognitive impairment may be vascular dementia or mixed dementia (AD+VaD; Jellinger, 2005). So, further studies involving AD biomarkers need to be performed to elaborate the conclusion more deeply and accurately.

CONCLUSION

In summary, by measuring serum lipids and cognitive function, this cross-sectional study found that in *APOE*

ε4 carriers, but not *APOE* ε4 non-carriers, low serum HDL-c levels were positively associated with cognitive impairment and that those with higher HDL levels had higher MMSE scores. These data indicated that the *APOE* ε4 allele may affect the relationship between serum lipid levels and cognitive impairment. However, this relationship needs to be further elucidated.

DATA AVAILABILITY STATEMENT

The raw data supporting the conclusions of this article will be made available by the authors, without undue reservation, to any qualified researcher.

ETHICS STATEMENT

This study and its protocol were approved by the Medical Ethics Committee of the First Affiliated Hospital of Xi'an Jiaotong University. All participants were required to sign a written informed consent form before participating in the study.

AUTHOR CONTRIBUTIONS

SW participated in the questionnaire survey and biochemical assessment, conducted the results analysis, and wrote the manuscript. LG and YJ participated in the questionnaire survey, sample collection, and biochemical assessment. SS designed this study and participated in the questionnaire survey and sample collection. CC, LD, JinW, KH, and JingW participated in the questionnaire survey and sample collection. QQ coordinated and supervised all stages of the project. All authors have read and approved the final version of the manuscript.

FUNDING

This work was supported by the Key Research & Development Programs of Shaanxi Province (Grant No. 2018ZDXM-SF-052).

ACKNOWLEDGMENTS

We are thankful for the cooperation of all participants in our study.

REFERENCES

Anstey, K. J., Ashby-Mitchell, K., and Peters, R. (2017). Updating the evidence on the association between serum cholesterol and risk of late-life dementia: review and meta-analysis. *J. Alzheimers Dis.* 56, 215–228. doi: 10.3233/jad-160826

Anstey, K. J., Lipnicki, D. M., and Low, L. F. (2008). Cholesterol as a risk factor for dementia and cognitive decline: a systematic review of prospective studies with meta-analysis. *Am. J. Geriatr. Psychiatry* 16, 343–354. doi: 10.1097/JGP.0b013e31816b72d4

Barter, P. J., Puranik, R., and Rye, K. A. (2007). New insights into the role of HDL as an anti-inflammatory agent in the prevention of cardiovascular disease. *Curr. Cardiol. Rep.* 9, 493–498. doi: 10.1007/bf02938394

Castellano, J. M., Kim, J., Stewart, F. R., Jiang, H., DeMattos, R. B., Patterson, B. W., et al. (2011). Human apoE isoforms differentially regulate brain amyloid-β peptide clearance. *Sci. Transl. Med.* 3:89ra57. doi: 10.1126/scitranslmed.3002156

Chen, H., Du, Y., Liu, S., Ge, B., Ji, Y., and Huang, G. (2019). Association between serum cholesterol levels and Alzheimer's disease in China: a case-control study. *Int. J. Food Sci. Nutr.* 70, 405–411. doi: 10.1080/09637486.2018.1508426

Dallongeville, J., Lussier-Cacan, S., and Davignon, J. (1992). Modulation of plasma triglyceride levels by apoE phenotype: a meta-analysis. *J. Lipid Res.* 33, 447–454.

De Felice, F. G., and Ferreira, S. T. (2002). β-amyloid production, aggregation, and clearance as targets for therapy in Alzheimer's disease. *Cell. Mol. Neurobiol.* 22, 545–563. doi: 10.1023/a:1021832302524

Demeester, N., Castro, G., Desrumaux, C., De Geitere, C., Fruchart, J. C., Santens, P., et al. (2000). Characterization and functional studies of lipoproteins, lipid transfer proteins, and lecithin:cholesterol acyltransferase in CSF of normal individuals and patients with Alzheimer's disease. *J. Lipid Res.* 41, 963–974.

Elias, P. K., Elias, M. F., D'Agostino, R. B., Sullivan, L. M., and Wolf, P. A. (2005). Serum cholesterol and cognitive performance in the Framingham Heart Study. *Psychosom. Med.* 67, 24–30. doi: 10.1097/01.psy.0000151745.67285.c2

Formichi, P., Parnetti, L., Radi, E., Cevenini, G., Dotti, M. T., and Federico, A. (2010). CSF biomarkers profile in CADASIL—a model of pure vascular dementia: usefulness in differential diagnosis in the dementia disorder. *Int. J. Alzheimers Dis.* 2010:959257. doi: 10.4061/2010/959257

Giau, V. V., Bagyinszky, E., An, S. S. A., and Sang, Y. K. (2015). Role of apolipoprotein E in neurodegenerative diseases. *Neuropsychiatr. Dis. Treat.* 11, 1723–1737. doi: 10.2147/ndt.s84266

Hartmann, T., Kuchenbecker, J., and Grimm, M. O. (2007). Alzheimer's disease: the lipid connection. *J. Neurochem.* 103, 159–170. doi: 10.1111/j.1471-4159.2007.04715.x

Hopkins, P. C. R., Huang, Y., McGuire, J. G., and Pitas, R. E. (2002). Evidence for differential effects of apoE3 and apoE4 on HDL metabolism. *J. Lipid Res.* 43, 1881–1889. doi: 10.1194/jlr.m200172-jlr200

Jellinger, K. A. (2005). Understanding the pathology of vascular cognitive impairment. *J. Neurol. Sci.* 229–230, 57–63. doi: 10.1016/j.jns.2004.11.029

Jia, J., Wang, F., Wei, C., Zhou, A., Jia, X., Li, F., et al. (2014). The prevalence of dementia in urban and rural areas of China. *Alzheimers Dement.* 10, 1–9. doi: 10.1016/j.jalz.2013.01.012

Jia, J., Wei, C., Chen, S., Li, F., Tang, Y., Qin, W., et al. (2018). The cost of Alzheimer's disease in China and re-estimation of costs worldwide. *Alzheimers Dement.* 14, 483–491. doi: 10.1016/j.jalz.2017.12.006

Joint Committee for Developing Chinese guidelines on Prevention and Treatment of Dyslipidemia in Adults. (2007). Chinese guidelines on prevention and treatment of dyslipidemia in adults. *Zhonghua Xin Xue Guan Bing Za Zhi* 35, 390–419. doi: 10.3760/j.issn:0253-3758.2007.05.003

Kalaria, R. N. (2000). The role of cerebral ischemia in Alzheimer's disease. *Neurobiol. Aging* 21, 321–330. doi: 10.1016/s0197-4580(00)00125-1

Katsumata, Y., Todoriki, H., Higashiuesato, Y., Yasura, S., Ohya, Y., Willcox, D. C., et al. (2013). Very old adults with better memory function have higher low-density lipoprotein cholesterol levels and lower triglyceride to high-density lipoprotein cholesterol ratios: KOCOA Project. *J. Alzheimers Dis.* 34, 273–279. doi: 10.3233/jad-121138

Katzman, R., Zhang, M. Y., Ouang-Ya-Qu, Wang, Z. Y., Liu, W. T., Yu, E., et al. (1988). A Chinese version of the Mini-Mental State Examination; impact of illiteracy in a Shanghai dementia survey. *J. Clin. Epidemiol.* 41, 971–978. doi: 10.1016/0895-4356(88)90034-0

Kim, J., Basak, J. M., and Holtzman, D. M. (2009). The role of apolipoprotein E in Alzheimer's disease. *Neuron* 63, 287–303. doi: 10.1016/j.neuron.2009.06.026

Kivipelto, M., Helkala, E. L., Hänninen, T., Laakso, M. P., Hallikainen, M., Alhainen, K., et al. (2001). Midlife vascular risk factors and late-life mild cognitive impairment: a population-based study. *Neurology* 56, 1683–1689. doi: 10.1212/wnl.56.12.1683

Leritz, E. C., McGlinchey, R. E., Salat, D. H., and Milberg, W. P. (2016). Elevated levels of serum cholesterol are associated with better performance on tasks of episodic memory. *Metab. Brain Dis.* 31, 465–473. doi: 10.1007/s11011-016-9797-y

Lewis, T. L., Cao, D., Lu, H., Mans, R. A., Su, Y. R., Lisa, J., et al. (2010). Overexpression of human apolipoprotein A-I preserves cognitive function and

attenuates neuroinflammation and cerebral amyloid angiopathy in a mouse model of Alzheimer disease. *J. Biol. Chem.* 285, 36958–36968. doi: 10.1074/jbc.m110.127829

Lobo, A., Launer, A. L., Fratiglioni, L., Andersen, K., Di Carlo, W. A., Breteler, M. M. B., et al. (2000). Prevalence of dementia and major subtypes in europe: a collaborative study of population-based cohorts. Neurologic diseases in the elderly research group. *Neurology* 54, S4–S9.

Li, G., Shofer, J. B., Kukull, W. A., Peskind, E. R., Tsuang, D. W., Breitner, J. C., et al. (2005). Serum cholesterol and risk of Alzheimer disease: a community-based cohort study. *Neurology* 65, 1045–1050. doi: 10.1212/01.wnl.0000178989.87072.11

Mahley, R. W. (1988). Apolipoprotein E: cholesterol transport protein with expanding role in cell biology. *Science* 240, 622–630. doi: 10.1126/science.3283935

Mahley, R. W., and Rall, S. C. Jr. (2000). Apolipoprotein E: far more than a lipid transport protein. *Annu. Rev. Genomics Hum. Genet.* 1, 507–537. doi: 10.1146/annurev.genom.1.1.507

Masters, C. L., Simms, G., Weinman, N. A., Multhaup, G., McDonald, B. L., and Beyreuther, K. (1985). Amyloid plaque core protein in Alzheimer disease and Down syndrome. *Proc. Natl. Acad. Sci. U S A* 82, 4245–4249. doi: 10.1073/pnas.82.12.4245

Mulder, M., and Terwel, D. (1998). Possible link between lipid metabolism and cerebral amyloid angiopathy in Alzheimer's disease: a role for high-density lipoproteins? *Haemostasis* 28, 174–194. doi: 10.1159/000022429

Notkola, I. L., Sulkava, R., Pekkanen, J., Erkinjuntti, T., Ehnholm, C., Kivinen, P., et al. (1998). Serum total cholesterol, apolipoprotein E epsilon 4 allele, and Alzheimer's disease. *Neuroepidemiology* 17, 14–20. doi: 10.1159/000026149

Reitz, C., Tang, M.-X., Luchsinger, J., and Mayeux, R. (2004). Relation of plasma lipids to Alzheimer disease and vascular dementia. *Arch. Neuro.* 61, 705–714. doi: 10.1001/archneur.61.5.705

Sagare, A. P., Bell, R. D., and Zlokovic, B. V. (2012). Neurovascular dysfunction and faulty amyloid β-peptide clearance in Alzheimer disease. *Cold Spring Harb. Perspect. Med.* 2:a011452. doi: 10.1101/cshperspect.a011452

Schilling, S., Tzourio, C., Soumaré, A., Kaffashian, S., Dartigues, J. F., Ancelin, M. L., et al. (2017). Differential associations of plasma lipids with incident dementia and dementia subtypes in the 3C study: a longitudinal, population-based prospective cohort study. *PLoS Med.* 14:e1002265. doi: 10.1371/journal.pmed.1002265

Siest, G., Bertrand, P., Qin, B., Herbeth, B., Serot, J. M., Masana, L., et al. (2000). Apolipoprotein E polymorphism and serum concentration in Alzheimer's disease in nine European centres: the ApoEurope study. ApoEurope group. *Clin. Chem. Lab. Med.* 38, 721–730. doi: 10.1515/cclm.2000.102

Subasinghe, S., Unabia, S., Barrow, C. J., Mok, S. S., Aguilar, M. I., and Small, D. H. (2003). Cholesterol is necessary both for the toxic effect of Aβ peptides on vascular smooth muscle cells and for Aβ binding to vascular smooth muscle cell membranes. *J. Neurochem.* 84, 471–479. doi: 10.1046/j.1471-4159.2003.01552.x

Toro, P., Degen, C., Pierer, M., Gustafson, D., Schröder, J., and Schönknecht, P. (2014). Cholesterol in mild cognitive impairment and Alzheimer's disease in a birth cohort over 14 years. *Eur. Arch. Psychiatry Clin. Neurosci.* 264, 485–492. doi: 10.1007/s00406-013-0468-2

Tukiainen, T., Jylänki, P., Mäkinen, V. P., Gröhn, O., Hallikainen, M., Soininen, H., et al. (2012). Mild cognitive impairment associates with concurrent decreases in serum cholesterol and cholesterol-related lipoprotein subclasses. *J. Nutr. Health Aging* 16, 631–635. doi: 10.1007/s12603-011-0341-9

van Exel, E., de Craen, A. J., Gussekloo, J., Houx, P., Bootsma-van der Wiel, A., Macfarlane, P. W., et al. (2002). Association between high-density lipoprotein and cognitive impairment in the oldest old. *Ann. Neurol.* 51, 716–721. doi: 10.1002/ana.10220

Wahrle, S., Das, P., Nyborg, A. C., McLendon, C., Shoji, M., Kawarabayashi, T., et al. (2002). Cholesterol-dependent γ-secretase activity in buoyant cholesterol-rich membrane microdomains. *Neurobiol. Dis.* 9, 11–23. doi: 10.1006/nbdi.2001.0470

West, R., Beeri, M. S., Schmeidler, J., Hannigan, C. M., Angelo, G., Grossman, H. T., et al. (2008). Better memory functioning associated with higher total and low-density lipoprotein cholesterol levels in very elderly subjects without the apolipoprotein e4 allele. *Am. J. Geriatr. Psychiatry* 16, 781–785. doi: 10.1097/jgp.0b013e3181812790

Whitmer, R. A., Sidney, S., Selby, J., Johnston, S. C., and Yaffe, K. (2005). Midlife cardiovascular risk factors and risk of dementia in late life. *Neurology* 64, 277–281. doi: 10.1212/01.wnl.0000149519.47454.f2

Yu, J. T., Tan, L., and Hardy, J. (2014). Apolipoprotein E in Alzheimer's disease: an update. *Annu. Rev. Neurosci.* 37, 79–100. doi: 10.1146/annurev-neuro-071013-014300

Zannis, V. I., and Breslow, J. L. (1981). Human very low density lipoprotein apolipoprotein E isoprotein polymorphism is explained by genetic variation and posttranslational modification. *Biochemistry* 20, 1033–1041. doi: 10.1021/bi00507a059

Zuliani, G., Cavalieri, M., Galvani, M., Volpato, S., Cherubini, A., Bandinelli, S., et al. (2010). Relationship between low levels of high-density lipoprotein cholesterol and dementia in the elderly. The InChianti study. *J. Gerontol. A Biol. Sci. Med. Sci.* 65A, 559–564. doi: 10.1093/gerona/glq026

Conflict of Interest: The authors declare that the research was conducted in the absence of any commercial or financial relationships that could be construed as a potential conflict of interest.

frontiers in Aging Neuroscience

ORIGINAL RESEARCH
published: 17 March 2020
doi: 10.3389/fnagi.2020.00075

Brain-Region Specific Metabolic Abnormalities in Parkinson's Disease and Levodopa-Induced Dyskinesia

Changwei Yang[1†], Tingting Zhang[1,2†], Wuqiong Wang[1], Yilan Xiang[2], Qun Huang[2], Chenglong Xie[3], Liangcai Zhao[1], Hong Zheng[1], Yunjun Yang[2] and Hongchang Gao[1]**

[1]School of Pharmaceutical Science, Wenzhou Medical University, Wenzhou, China, [2]Department of Radiology, The First Affiliated Hospital of Wenzhou Medical University, Wenzhou, China, [3]Department of Neurology, The First Affiliated Hospital of Wenzhou Medical University, Wenzhou, China

Several lines of evidence point to alteration in brain metabolic homeostasis in Parkinson's disease (PD) and levodopa-induced dyskinesia (LID), yet the metabolic mechanism in different brain regions underlying PD and LID remains largely unknown. The present study aimed to uncover the metabolic pathways across anatomical regions in the brain of PD and LID. Using an NMR-based metabolomic approach, we generated the metabolomics profiling data from six different brain regions of PD rats and following the onset of LIDs. The diversity of metabolite patterns across the brain and its relation to PD and LID were further investigated through principal component analysis (PCA) and multivariate general linear model. Compared with control rats, dopamine loss in PD rats produced a marked and persistent metabolic disturbance in neurotransmitter metabolism and energy pathway, resulting in a metabolic imbalance among different brain regions. In LID rats, levodopa replacement did not restore the midbrain-striatum metabolic crosstalk and metabolic disturbance throughout the brain was involved in levodopa related involuntary movements. Most notably, the midbrain and right cortex were identified as the primary regions of metabolic abnormalities in PD and LID rats. Neurochemical differences in metabolic phenotypes were mainly defined by various neurotransmitters including glutamate, glutamine and aspartate. Accordingly, we found that the PD and LID rats exhibited lower levels of synaptophysin (SYP), a marker for synaptic plasticity, compared with control rats. These findings provide key insights into the metabolic mechanism underlying PD and LID by defining brain-region specific metabolic phenotype, with implications for developing targeted therapies.

Keywords: Parkinson's disease, levodopa-induced dyskinesia, metabolism, neurotransmitter, Glu-Gln-GABA cycle

OPEN ACCESS

Edited by:
Fangyu Peng,
University of Texas Southwestern Medical Center, United States

Reviewed by:
Aida Karachi,
University of Florida, United States
Dafin F. Muresanu,
Iuliu Haţieganu University of Medicine and Pharmacy, Romania

****Correspondence:***
Yunjun Yang
yyjunjim@163.com
Hongchang Gao
gaohc27@wmu.edu.cn

[†]These authors have contributed equally to this work

Received: *11 January 2020*
Accepted: *02 March 2020*
Published: *17 March 2020*

Citation:
Yang C, Zhang T, Wang W, Xiang Y, Huang Q, Xie C, Zhao L, Zheng H, Yang Y and Gao H (2020) Brain-Region Specific Metabolic Abnormalities in Parkinson's Disease and Levodopa-Induced Dyskinesia. Front. Aging Neurosci. 12:75. doi: 10.3389/fnagi.2020.00075

Abbreviations: PD, Parkinson's disease; Con, normal rats; LID, levodopa-induced dyskinesia; 6-OHDA, 6-hydroxydopamine; AIMs, abnormal involuntary movements; Lac, lactate; Ala, alanine; GABA, γ-aminobutyric acid; NAA, N-acetyl aspartate; Gln, glutamine; Glu, glutamate; Asp, aspartate; Cre, creatine; Cho, choline; GPC, glycerol-phosphocholine; Tau, taurine; Myo, myo-inositol; Gly, glycine; ADP, adenosine diphosphate; AMP, adenosine monophosphate; Fum, fumarate; Mid, midbrain; Cor, cortex; Str, striatum; Hip, hippocampus; Cer, cerebellum; Hyp, hypothalamus.

INTRODUCTION

Parkinson's disease (PD) is a common age-related neurodegenerative disorder due to the loss of dopaminergic neurons in the substantia nigra par compacta (SNpc) thereby leading to the dopamine depletion in the striatum (Huang et al., 2019). The clinical symptoms of PD are mainly classified into motor abnormalities characterized by static tremor, rigidity, bradykinesia, postural instability and non-motor symptoms, such as cognitive impairment and gut dysfunction (Lee et al., 2019). So far, L-3,4-dihydroxyphenylalanine (L-dopa) remains to be the most effective drug for symptomatic treatment of Parkinson (Smith et al., 2014). However, the adverse effects of long-term L-dopa treatment vary, such as levodopa-induced dyskinesia (LID), which appears in approximately 40% of PD patients after 5 years L-dopa therapy and up to 90% within 10 years (Pourmirbabaei et al., 2019; Sellnow et al., 2019). Furthermore, the uncontrollable LID has been reported to dramatically affect the quality of patients' life and greatly augment the cost of health care for which no satisfying treatment is available (Dodel et al., 2001; Chapuis et al., 2005; Hechtner et al., 2014). In light of this urgent medical need for rapidly aging populations, there is an urgent need to identify the mechanism underlying PD and LID.

Metabolic abnormality has long been considered to be involved in a lot of diseases, such as neurodegenerative diseases including PD (Shao and Le, 2019) and Alzheimer' disease (Van Bulck et al., 2019), diabetes mellitus (Del Coco et al., 2019), chronic obstructive pulmonary disease (Lamonaca et al., 2017). ^{1}H-NMR based metabolomics has proven to be a key for the characterization of metabolic profiles relevant to brain function and disease (Ivanisevic and Siuzdak, 2015). Our previous studies demonstrated that metabolic abnormalities in the brain participated in DM-associated cognitive dysfunction (Zheng et al., 2017) and pathogenesis of Alzheimer's disease (Zheng et al., 2018b). And increasing evidence in recent researches has supported the idea that metabolic abnormality may be causal to PD and LID, though it is unclear how metabolic disruption affects striatal activity *in vivo*. In our previous study, ^{1}H NMR based metabolomics was applied to evaluate the metabolic signatures and pathways involved in the onset and progression of PD, which indicate that neuron loss and motor function impairment in induction PD mice may be linked to overactive glutamate-glutamine cycle and altered membrane metabolism in the striatum (Lu et al., 2018). There is, however, a dearth of information on understanding the metabolic and cellular mechanisms underlying motor impairment in LID.

Historically, studies of PD and LID have been focused on the striatum, since it is acknowledged that the dopamine depletion in the striatum result from degeneration of dopaminergic neurons is the main cause of PD (Hornykiewicz, 2006; Huang et al., 2019), and the prevailing hypothesis is that subsequent replacement with levodopa causes excessive direct pathway activity in the striatum. For example, Cenci et al. (1998) analyzed the correlations between the dyskinetic symptoms of LID and neurotransmitter-related mRNA expression in the basal ganglia and found that striatal overexpression of prodynorphin- and glutamic acid decarboxylase participated in the occurrence of LID. Santini et al. (2007) found hyperactivation in the striatal medium spiny neuron of cAMP/PKA/DARPP-32 and ERK signaling played a critical role in L-dopa induced dyskinesia. Crucially, L-dopa replacement has little effects on axial symptoms of PD, indicating that disruptions in another neurotransmitter metabolism other than dopamine, even other brain regions beyond the striatum could mediate these PD and levodopa-evoked behaviors. Again, some indirect evidence supports this hypothesis: once LID develops, a given dose of levodopa relieves parkinsonism but produces dyskinesia.

If other brain regions were indeed involved in the onset and progression of PD and LID, then targeted therapies could be more effective than levodopa alone. Therefore, the creation of a detailed map of the human neural metabolic pathway across different brain regions will help to build a knowledge base to unravel complex brain functions. In the present study, we took advantage of a ^{1}H NMR-based metabolomics approach to characterize the involvement of region-specific metabolic phenotype in the brain of PD and following LID rats.

MATERIALS AND METHODS

Animals

Male Sprague–Dawley rats (180–220 g) purchased from the SLAC Laboratory Animal Company Limited (Shanghai, China) were housed under the standard laboratory conditions (controlled temperature/humidity condition, a normal 12/12-h light/dark schedule with the lights on at 08:00 a.m.), in the Laboratory Animal Center of the First Affiliated Hospital of Wenzhou Medical University (Wenzhou, China). All rats were given free access to standard chow and water during the whole experimental process. All experimental operations were performed strictly in accordance with the National Institutes of Health Guide for the Care and Use of Laboratory Animals and were approved by the Institutional Animal Care and Use Committee of Wenzhou Medical College (wydw2018-015).

6-Hydroxydopamine (6-OHDA) Rat Model of PD and Levodopa-Induced Dyskinesia

Animals were weighed and randomly divided into control (n = 8) and lesion groups (n = 20). All rats in lesion group stereotaxically received 4 μl of 6-OHDA (4 μg/ μl, dissolved in 0.9% physiological saline involving 0.2% ascorbic acid) injection at each coordinate in the right medial forebrain bundle (MFB) and the rats in control group received sham-operation with physiological saline at the same locations. The coordinates calculated by the rat brain atlas were as previously reported (Xie et al., 2014): AP −4.4 mm, ML −1.2 mm, DV −7.8 mm; AP −3.7 mm, ML −1.7 mm, DV −7.8 mm. The tooth bar was set to −2.4 mm. After 3 weeks of lesioning, rats in the lesion group received intraperitoneal injection of apomorphine to induce contralateral rotations, and rats with at least seven full contralateral turns/min were selected as successful PD rats (Yang et al., 2012). The successful PD rats were then randomly divided into PD group (n = 10) and LID group (n = 10). In the next

3 weeks, rats in LID group received a daily intraperitoneal injection of L-dopa (15 mg/kg) together with benserazide (3.75 mg/kg) for 3 weeks (Zhang et al., 2014) and the rats in Con and PD group were given equal vehicle during the same period. The body weights of rats were constantly monitored during the process of the study.

Behavioral Test

The onset and severity of LID were evaluated according to a highly validated abnormal involuntary movements (AIMs) scale on days 1, 4, 7, 10, 14, 17 and 20 of L-dopa/benserazide treatment (Lundblad et al., 2002; Mellone et al., 2019). Briefly, AIMs were conducted from 20 min to 120 min after L-dopa or vehicle administration and each rat was continuously observed for 1 min every 20 min each time. The AIMs scores were recorded from 0 to 4 according to the incidence of three subtypes of AIMs (axial, limb and orolingual): 0 = absent; 1 = present less than or equal to 30 s; 2 = present more than 30 s; 3 = present continuously but suppressible by external stimulus; 4 = present continuously but not suppressible by external stimulus.

The forelimb function test is a widely used behavior test to assess the forelimb motor function of rats. The test was performed at days 3, 8, 13, 18 of L-dopa/benserazide treatment and all the process was carried out in a glass beaker (diameter = 22 cm, height = 35 cm) to record the number of wall contacts of right/left forelimb of rats. 1 h after L-dopa or vehicle administration, the forelimb function test was evaluated 5 min every 20 min for four times. The final value was shown as the percentage wall contacts of the contralateral forelimb of 6-OHDA lesion (left forelimb) compared with total wall contacts of bilateral forelimbs (Schallert et al., 2000).

Immunofluorescence Staining

Three rats of each group were processed for immunofluorescence staining studies. In brief, rats were anesthetized with 10% chloral hydrate (0.35 ml/100 g) first after the last L-dopa administration and then perfused transcardially with normal saline followed by a fixing solution containing 4% paraformaldehyde for 30 min. The brains were carefully removed, fixed in 10% buffered formalin overnight, and embedded in paraffin. The brain tissues were cut into coronal sections with a thickness of 5 μm. The paraffin sections were incubated with Anti-Synaptophysin (SYP) antibody (Abcam, 1:200) overnight at 4°C and rinsed in PBS followed by incubation with Alexa Flour^{TM} 488 goat anti-rabbit lgG (H + L; Invitrogen, 1:500). Subsequently, sections were rinsed again in PBS, stained with DAPI (Southern Biotech) and observed using a fluorescence microscope (Nikon, Tokyo, Japan).

Sample Collection and Metabolite Extraction

The remaining rats were sacrificed by decapitation after a 3-weeks L-dopa administration, with the whole brain tissue dissected into midbrain, cortex, striatum, hippocampus, cerebellum, and hypothalamus immediately. All the brain tissues were put into liquid nitrogen at once and then stored at −80°C until use. The metabolite extraction was referred to as our previous method (Liu et al., 2018). Briefly, the frozen tissues were weighted into an Eppendorf tube, Following the homogenization by electric homogenizer with ice-cold methanol (4.0 ml/g) and ultrapure water (0.85 ml/g). The mixture was homogenized again with 2 ml/g of chloroform, then again with 2 ml/g of chloroform and 2 ml/g of ultrapure water using a vortex mixer, placed on ice for 15 min, and centrifuged at 10,000 *g* for 15 min at 4°C. Finally, the supernatant was carefully transferred into a new Eppendorf tube, lyophilized for 24 h, and stored at −80°C until NMR analysis.

NMR Spectroscopy

The lyophilized extract was dissolved into 0.6 ml of 99.5% D_2O containing 0.05% of sodium trimethylsilyl propionate-d4 (TSP), in which D_2O provided a field-frequency lock, and TSP was used as the chemical shift reference. All ^{1}H NMR spectra of brain tissue were acquired on the Bruker Avance III 600 MHz NMR spectrometer with a 5-mm TXI probe (Bruker BioSpin, Rheinstetten, Germany) at 298 K. The one-dimensional ^{1}H NMR spectra of right striatum and SN were acquired using a standard single-pulse sequence with water signal presaturation (ZGPR) with number of scans (256), acquisition time (2.65 s/scan), date points (64 k), spectral width (12,000 Hz) and relaxation delay (6 s). Then, the ^{1}H NMR spectra were referenced to the TSP peak at 0.0 ppm and manually adjusted phase and baseline using Topspin (v2.1 pl4, Bruker Biospin, Germany).

Data Processing of NMR Spectra and Multivariate Pattern Recognition

NMR spectra were reduced to integrated regions with a width of 0.01 ppm (bin) corresponding to the region of δ 10–0.5. The regions of 4.7–5.2 ppm (water) was removed to eliminate artifacts related to the residual water resonance. The remaining spectral segments were then normalized to the total sum of the spectral intensity to partially compensate for differences in the concentration of many metabolites in the samples. Before multivariate data analysis, the integral values were mean-centered and Pareto-scaled (Shao et al., 2014). NMR data sets were imported into SIMCA-P + 12.0 software (Umetrics, Umea, Sweden) for multivariate statistical analysis, including principal component analysis discriminant analysis (PCA-DA) and partial least squares-discriminant analysis (PLS-DA). And another data reduced to integrated regions with a width of 0.0015 ppm width corresponding to the region of δ 10–0.5 were used for quantitative analysis.

Real-Time RT-PCR

The Real-time RT-PCR procedure and data analyses were carried out as previously described (Yang et al., 2019). The total RNA was extracted from the right cortexes using standard TRlzol reagent (Invitrogen, Carlsbad, CA, USA) and converted into cDNA following the instruction of PrimeScript^{TM} RT reagent Kit (Takara, RR037A). Individual samples were measured in triplicate. Real-time-PCR was performed on an ABI 7500 Fast Real-Time PCR system using TB Green^{TM} Premix Ex Taq^{TM} II (RR820A). Primer sequences as follows: Actin (5′-ACCCGCGAGTACAACCTTC-3′/5′-ATGCCGTGTT

CAATGGGGTA-3′), SYP (5′-GCTAAAAGCAGGAGGGCGTA-3′/5′-GCACAGGAAAGTAGGGGGTC-3′). Relative expression levels were measured with the $2^{-\Delta\Delta Ct}$ method.

Statistical Analysis

Independent sample *t*-test or one-way ANOVA was applied to compare the difference among different groups. Statistical analyses were performed using SPSS (version 25, IBM, USA). Data were exhibited as mean ± SEM and *P*-values less than 0.05 were considered statistically significant.

RESULTS

Behavior Tests in Experimental Models of PD and LID

To mimic dyskinesia of PD patients, male SD rats were unilaterally injected with 6-OHDA in the right MFB, causing a nearly complete depletion of ipsilateral dopamine, while the rats in Con group were got same Sham-operation but injected with vehicle (**Figures 1A,B**). Three weeks later, motor symptoms were validated using apomorphine-induced rotation test (**Figure 1C**). Then the LID rats were intraperitoneally administrated L-dopa (15 mg/kg, i.p.) with benserazide (3.75 mg/kg, i.p.) once a day for 3 weeks and observed progressive AIMs. Forelimb function test was conducted at days 3, 8, 13, 18 after L-dopa/benserazide treatment, results showed that the percent of left forelimb use of total wall contacts of rats in Con group is around 50%, while the percent of left forelimb use was significantly reduced in PD rats with a partial lesion of the nigrostriatal pathway. After the treatment of L-dopa, the percent of left forelimb use of rats in the LID group was significantly increased compared to that in the PD group ($P < 0.05$, **Figure 1D**). These results suggested that PD rats showed reduced forelimb motor function, and L-dopa treatment is quite effective in alleviating PD behavioral symptoms.

However, we found that L-dopa treatment caused both dyskinesia and contralesional rotations. Abnormal involuntary movements (AIMs) score, a standard behavior performance score system for dyskinesia, was significantly higher in the 6-OHDA-lesioned rats after 3 weeks of L-dopa administration (**Figure 1E**). We observed that AIMs immediately appeared at 20 min after L-dopa injection and did not attenuate until 80 min and then faded away after 120 min. Besides, we continuously monitor the total AIMs scores at days 1, 4, 7, 10, 14, 17 and 20 of L-dopa/benserazide treatment (**Figure 1F**).The results showed that total AIMs scores of LID rats gradually increased with time went by, while that of rats in Con and PD group had no obvious changes.

In addition, we also questioned whether the growth of rats was affected by the disease. A repeated-measures ANOVA revealed a significant time and treatment interaction effect in the body weight ($P = 0.01$). To be specific, the bodyweight of PD rats was significantly reduced after 6-OHDA administration, compared with the control group. After L-dopa administration for 3 weeks, the bodyweight of LID rats increased significantly compared with PD rats ($P < 0.05$, **Figure 1G**), while no significant difference was found between Con and LID rats.

NMR-Based Metabolic Profiling of Different Brain Regions

In order to characterize the dynamic changes of metabolites throughout the brain, NMR-based metabolic profiling of different brain regions was performed among control, PD and LID rats. Typical ^{1}H-NMR CPMG (600 MHz) spectra of different brain regions (midbrain, cortex, striatum, hippocampus, cerebellum, and hypothalamus, respectively), obtained from control, PD and LID rats are presented in **Figure 2**. Assignments were performed according to our previous studies (Zheng et al., 2017, 2018a) using the Chenomx NMR suite 7.0 (Chenomx Inc., Edmonton, AB, Canada). A total of 20 metabolites were identified, which can be detected in all six brain regions (**Figure 2**). Although the NMR spectra appeared similar among different brain regions, there were striking differences in peak intensities for different brain regions. The metabolites identified included lactate, alanine, GABA, NAA, glutamine, glutamate, dimethylamine, aspartate, creatine, choline, glycerol-phosphocholine, taurine, Myo-inositol, glycine, Glu/Gln, Inosine, ADP/AMP, fumarate, AMP and IMP.

Multivariate Analysis of NMR Data

After the pre-processing of the NMR spectra, including the bucketing process and total sum normalization to minimized small differences due to sample concentration among samples, NMR data was subjected for multivariate statistical analysis including unsupervised (PCA) and supervised (PLS-DA) multivariate statistical methods. As a first attempt, the PCA was used to quantitatively compare the global metabolomics profiling data collected from the six different brain regions of control (**Figure 3A**), PD (**Figure 3B**) and LID (**Figure 3C**) rats. The PCA score plot obtained for control rats revealed good separation among the different brain regions, especially along the first principal component PC1 (with PC1 and PC2 accounted for 43.6% and 18.1% of the total variance, respectively, **Figure 3A**). PCA score plot obtained for PD and LID rats showed similar, distinct separation among different brain regions (**Figures 3B,C**). As showed in **Figure 3**, the metabolic pattern in the striatum appeared as separate significantly from other brain regions, especially along the second principal component PC2. Whereas the midbrain and right cortex distribution was significantly different both in PD and LID rats compared with control rats, indicating midbrain-cortex crosstalk was involved in the behavioral symptoms of PD and LID.

Brain Regional Specific Metabolic Disturbance Was Involved in Parkinson's Disease

To further explore discriminating features and potential biomarkers in brain function and disease, the supervised PLS-DA analyses were applied for six different brain regions from three groups (**Figure 4**). Moreover, a mixed-model analysis was applied to evaluate the effects of dopamine loss and L-dopa replacement on metabolite alterations in the PD and LID rats and the detailed results were shown in **Figure 5** and listed in **Supplementary Tables S1–S6**. As predicted, a clear separation between control and PD rats was observed

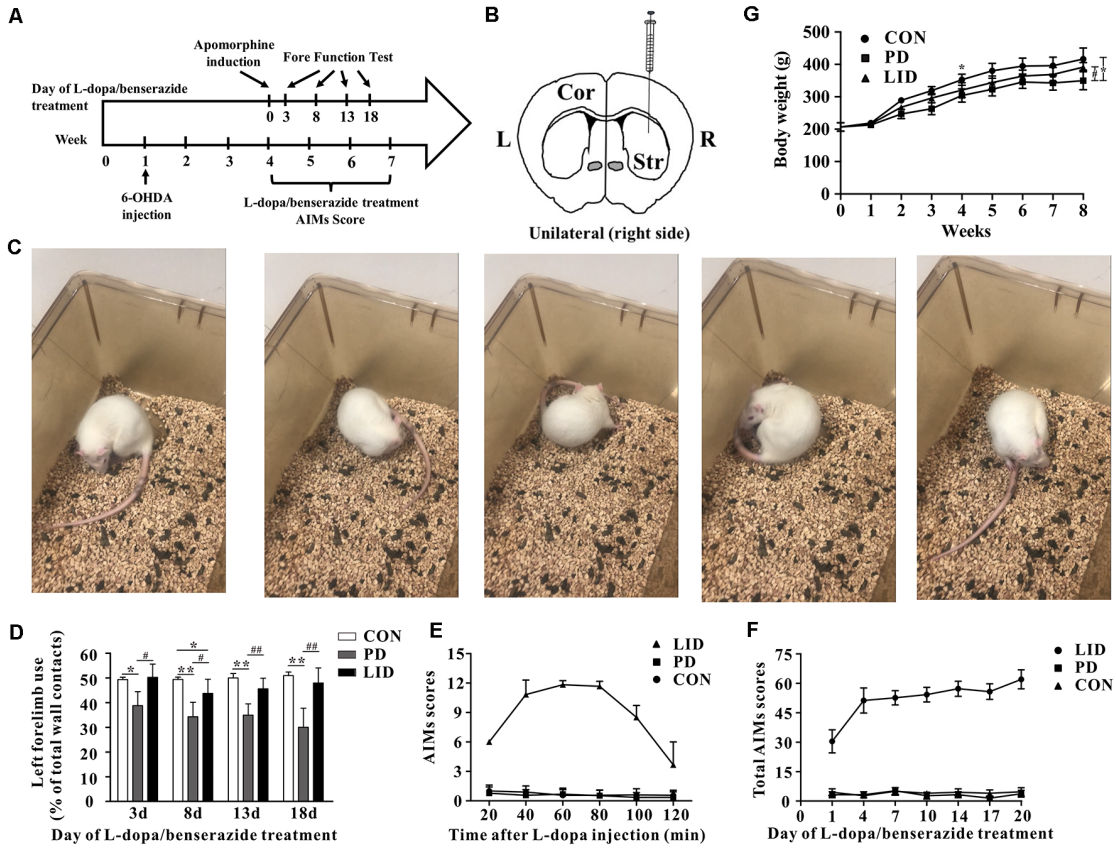

FIGURE 1 | Behavior performance of the experimental models of Parkinson's disease (PD) and levodopa-induced dyskinesia (LID). **(A)** The time scale of the experiments: 6-OHDA lesioning, L-dopa/benserazide treatment, and behavioral tests. **(B)** Schematic of stereotactic injection of 6-hydroxydopamine (6-OHDA), the rats in the control group received sham-operation with physiological saline at the same location (n = 8–10 for each group). **(C)** Apomorphine-induced rotation test. **(D)** Forelimb function tests at days 3, 8, 13, 18 of L-dopa/benserazide treatment. **(E)** AIMs 120-min time-score plot of three groups after L-dopa injection. **(F)** Total AIMs scores plot of three groups at Days 1, 4, 7, 10, 14, 17 and 20 of L-dopa/benserazide treatment. **(G)** Body weight over time of rats from three groups. *Means the difference between Con group and experimental groups (t-test); #means the difference between PD and LID group (t-test). $^{*}P < 0.05$, $^{**}P < 0.01$; $^{\#}P < 0.05$, $^{\#\#}P < 0.01$.

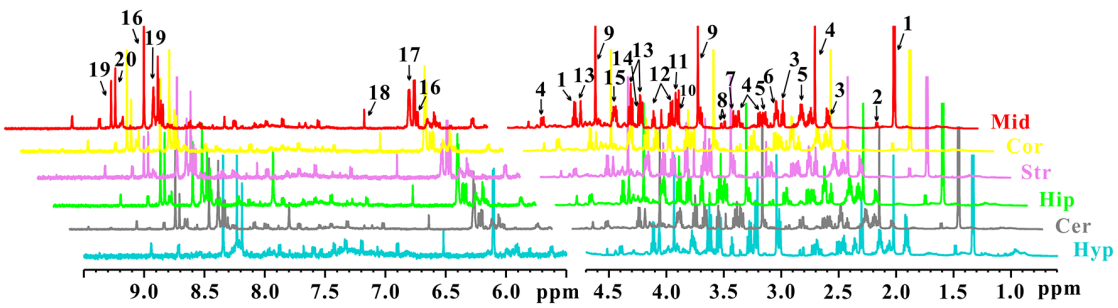

FIGURE 2 | ^{1}H NMR spectra of different brain sections obtained from control, PD and LID rats: Mid, midbrain; Cor, cortex; Str, striatum; Hip, hippocampus; Cer, cerebellum and Hyp, hypothalamus. 1. Lactate (Lac); 2. Alanine (Ala); 3. GABA; 4. N-acetyl aspartate (NAA); 5. Glutamine (Gln); 6. Glutamate (Glu); 7. Dimethylamine; 8. Aspartate (Asp); 9. Creatine (Cre); 10. Choline (Cho); 11. Glycerol-phosphocholine (GPC); 12. Taurine (Tau); 13. Myo-inositol (Myo); 14. Glycine (Gly); 15. Glu/Gln; 16. Inosine (Ino); 17. ADP/AMP; 18. Fumarate (Fum); 19. AMP; 20. IMP.

in the midbrain (**Figure 4A**) and striatum (**Figure 4B**). Accordingly, using hierarchical clustering on the profile of the identified 21 metabolites, the metabolic profile of midbrain and striatum was strictly separated between control and PD rats, several interesting metabolite clusters became apparent as well (**Figures 5A,B**). One of these clusters contained glutamate

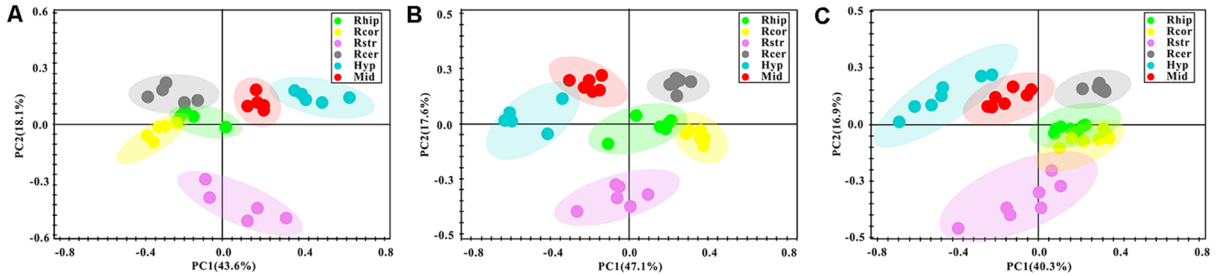

FIGURE 3 | Overview of metabolic changes in six different brain regions of Con **(A)**, PD **(B)** and LID **(C)** rats.

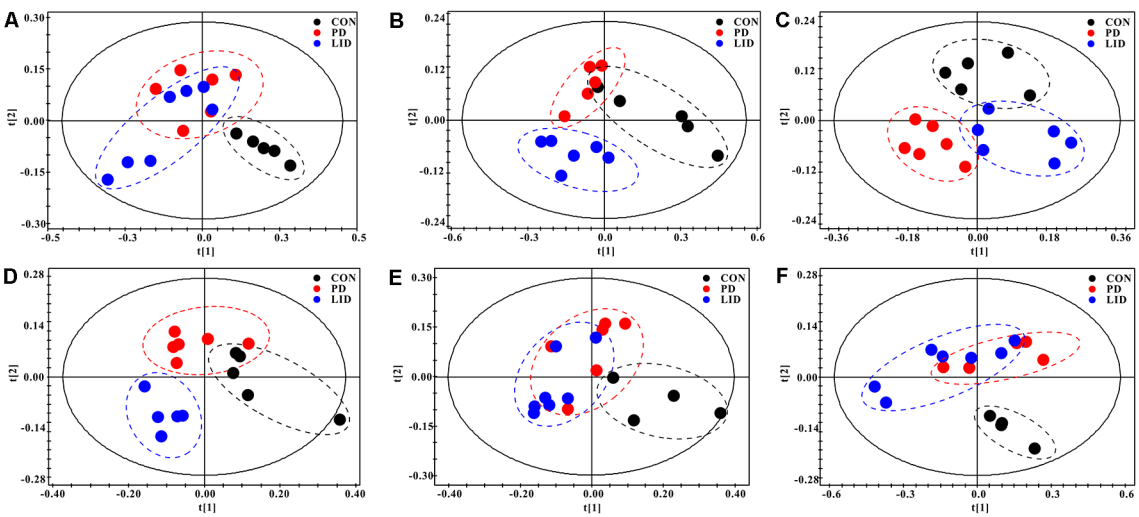

FIGURE 4 | PLS-DA score plots of Con, PD and LID groups in the different brain regions: **(A)** Mid, midbrain; **(B)** Rstr, right striatum; **(C)** Rcor, right cortex; **(D)** Rhip, right hippocampus; **(E)** Rcer, right cerebellum; **(F)** Hyp, hypothalamus.

and glutamine, and this alteration in the glutamate metabolism pathway reflected neurotransmitter homeostasis in the brain (Bak et al., 2006). In addition, various products of energy metabolism pathways (e.g., taurine, lactate, and fumarate) in the striatum were altered in PD rats (**Figure 5B**).

Surprisingly, the metabolic profile of PD rats was also separated significantly in the other four brain regions: right cortex (**Figure 4C**), hippocampus (**Figure 4D**), cerebellum (**Figure 4E**) and hypothalamus (**Figure 4F**), respectively. The potential biomarkers, which are responsible for the separation were observed in the corresponding heatmap, respectively (**Figures 5C–F**). In summary, nine assigned metabolites with a significant difference were identified between Con and PD rats ($P < 0.05$), including lactate, glutamine, GABA, aspartate, glycerol-phosphocholine, fumarate, Glu/Gln, glycine and taurine. Of note, the midbrain and cortex were the main brain regions that underwent significant metabolic disruption between the Con group and PD groups. These observations suggest that dopamine loss in PD rats produces a marked and persistent metabolic disturbance in neurotransmitter metabolism and energy pathway, resulting in a metabolic imbalance among different brain regions.

L-Dopa Induces Brain Regional Specific Metabolic Disturbance During LID

The standard model predicts that by increasing striatal dopamine, L-dopa is hypothesized to restore the normal balance of striatal activity. To test the metabolic activity of the whole brain during LID, PLS-DA analyses were also performed for control and LID rats (**Figure 4**). PLS-DA score plots showed an even better separation in all the six brain regions than that observed comparing control and PD rats, especially in the midbrain (**Figure 4A**), striatum (**Figure 4B**), and right cortex (**Figure 4C**). Quantitative analysis on the metabolites from control and LID groups with *T*-test, total 10 significantly changed metabolites were detected between Con and LID rats, namely lactate, phosphocholine, aspartate, glycerol-phosphocholine, GABA, fumarate, glutamine, Myo-inositol, AMP, and alanine (**Figure 5**, **Supplementary Tables S1–S6**). Counter to our expectation, we found that the striatal metabolism was not restored in response to L-dopa, furthermore, during LID, relatively higher lactate, aspartate, glutamine, AMP and Myo-inositol was observed in midbrain and striatum, compared with that of the control group (**Figures 5A–C**). These findings confirmed that L-dopa replacement did not

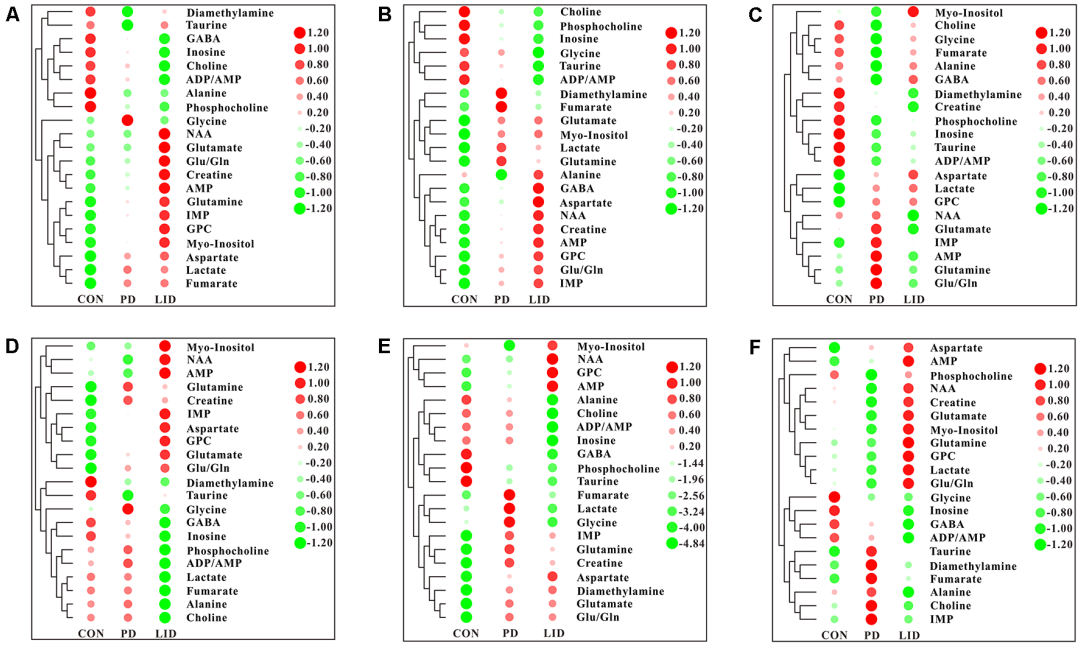

FIGURE 5 | Heatmap displaying the identified metabolites in six different brain regions obtained from the brain of Con, PD and LID rats: **(A)** Mid, midbrain; **(B)** Rstr, right striatum; **(C)** Rcor, right cortex; **(D)** Rhip, right hippocampus; **(E)** Rcer, right cerebellum; **(F)** Hyp, hypothalamus.

restore the midbrain-striatum metabolic crosstalk and metabolic disturbance throughout the brain was involved in levodopa related involuntary movements.

Glutamate-Glutamine Metabolic Cycle in Parkinson's Disease and LID

Since these results point toward neurotransmitter dysregulation as an underlying feature both in PD and LID, we sought to assess how the glutamate-glutamine cycle was affected by the disease in different brain regions (**Figure 6**). Remarkably, we found that the concentration of glutamate in the PD and LID groups was higher than that in the Con group, except for the hypothalamus in the PD group and the right cortex in the LID group (**Figure 6A**). Besides, the PD rats had a higher glutamine concentration than Con rats in all six brain regions, especially in the right cortex and right cerebellum (**Figure 6B**). The concentration of glutamine varied in the LID group compared to the Con group, which was significantly increased in the midbrain and right cerebellum ($P < 0.05$). More interestingly, compared with the Con rats, the PD rats had a significantly higher concentration of aspartate in the midbrain, right cortex, right cerebellum and right hypothalamus, and a significantly increased of aspartate concentration occurred in all brain regions of the LID rats (**Figure 6C**). These results provide further evidence that glutamate-glutamine metabolism is dysregulated in D and LID.

Synaptic Plasticity Is Impaired in Parkinson's Disease and LID

It was noticed that there was a disorder of neurotransmitters in the PD and LID rats, we wondered if the synaptic plasticity, which controls the release and recycle of neurotransmitters was also involved in the PD and LID disease. SYP, a standard presynaptic marker, which was responsible for synapse formation and neurotransmitter recycle (Wu et al., 2015). Immunofluorescence staining was performed to visually evaluate the expression of SYP in the right cortex of PD and LID rats. The immunofluorescence staining results showed that the density of SYP in the right cortex of PD and LID rats was lower than that in the Con rats (**Figure 7A**). Accordingly, the results of real-time RT-PCR also showed that the gene expression of SYP in the right cortex of PD and LID rats was significantly decreased compared to Con rats (**Figure 7B**).

DISCUSSION

The potential metabolic mechanisms of PD and LID are not largely elucidated and keep a great challenge for the therapy of PD (Wang et al., 2014). In the present study, the ^{1}H NMR-based metabolomics approach was performed to present the first widespread investigation of metabolic profile throughout the brain in a 6-OHDA-unilaterally-lesioned rat model. We found that: (1) dopamine loss in PD rats produces a marked and persistent metabolic disturbance in neurotransmitter metabolism and energy pathway, resulting in a metabolic imbalance among different brain regions; (2) L-dopa replacement did not restore the midbrain-striatum metabolic crosstalk and metabolic disturbance throughout the brain was involved in levodopa related involuntary movements; and (3) further multivariate general linear model identified that a significant perturbation of Glu-Gln-GABA cycle in midbrain and

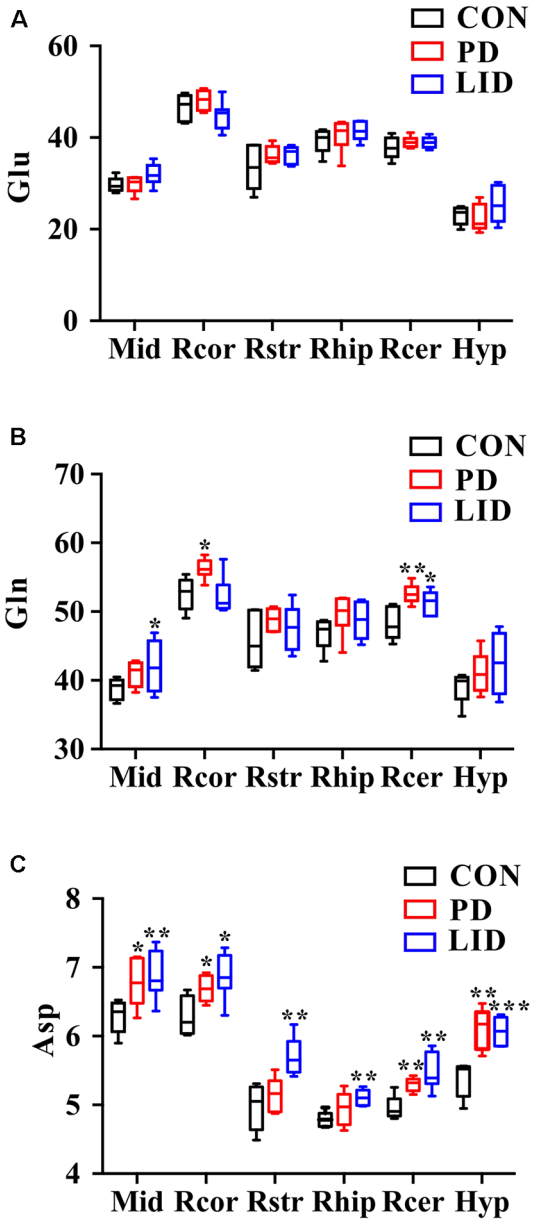

FIGURE 6 | Changes in neurotransmitter metabolism-related metabolites in different brain regions. **(A)** Glu, glutamate; **(B)** Gln, glutamine; **(C)** Asp, aspartate. Differences between Con and experimental groups were analyzed using univariate ANOVA, $^{*}P < 0.05$, $^{**}P < 0.01$, $^{***}P < 0.001$.

right cortex of both PD and LID rats, accompanied by reduced synaptic plasticity.

Although many investigators have posited that energy metabolism is critical to maintaining the normal brain function (Bélanger et al., 2011), previous studies of the metabolic mechanism of PD and LID had largely focused on the midbrain and striatum, while the global metabolic profile in the adult brain has not been extensively described. Consistent with a midbrain-striatum mediated mechanism of behavior modulation, the pattern of energy metabolism in midbrain and striatum we identified in the current study is in-line with what described in numerous studies of both human and rodent models (Zheng et al., 2016, 2017). Notably, we found a significantly increased lactate level in the right striatum of 6-OHDA-lesioned PD and LID rats' respect to Con rats, which confirms previous studies that identified lactate served as a spare energy substrate and was critical in the brain function (Proia et al., 2016). Besides, the concentration of alanine of LID rats was significantly decreased compared with Con rats. Interestingly, compared with Con rats, the fumarate level was significantly decreased in the right cortex of PD rats and in the right hippocampus of LID rats. Taken together, these results suggest that while regional specific metabolic disturbance is a feature of PD, L-dopa replacement did not restore the midbrain-striatum metabolic crosstalk may still contribute to levodopa-evoked facilitation of movement in LID.

The multivariate analysis performed on brain metabolic profile also identified a significant difference in the levels of glutamate (Glu), glutamine (Gln) and aspartate (Asp) in PD and LID rats with respect to control rats. Glu is the main excitatory neurotransmitters which can enhance neuronal excitability whereas GABA is the primary inhibitory in the central nervous system (Rage et al., 1992). Glutamate is the metabolic precursor of GABA, which can be in turn transferred into synthesize glutamate through the TCA cycle (Petroff, 2002). Recent publications indicate that the Glu-Gln-GABA cycle is involved in a variety of neurological disorders (Zheng et al., 2016, 2017; Lu et al., 2018; Zott et al., 2019). In the present study, the Glu levels showed no significant differences among three groups, however, the concentrations of Gln were brain region-specific, for example, compared with Con rats, the Gln level increased in all brain regions of PD rats and most significantly in the right cortex and right cerebellum, and it significantly increased in the midbrain and right cerebellum of LID rats but decreased in the right cortex. Our previous study showed that the disturbed Glu-Gln-GABA cycle occurred in the striatum of PD rats and bFGF treatment might alleviate PD symptoms through regulating these alterations (Zheng et al., 2016), another study reported that there was a significantly decreased striatal level of Glu in LID rats (Wang et al., 2018). Both higher or lower levels of Glu can be noxious, as excessive Glu can stimulate the activation of the NMDA receptor and induce excitatory toxicity (Jazvinšćak Jembrek et al., 2018).

Asp is another excitatory neurotransmitter in the central nervous system (Liu et al., 2013). Notably, the concentrations of Asp increased in all brain regions of rats in the experimental groups compared with the control group. Except for the right striatum and right hippocampus, the Asp level in PD group was significantly higher than that in the Con group and the Asp level in all brain regions had significant differences between Con and LID group. Since Glu, Gln and Asp are critical neurotransmitters, the brain-regional disturbance in neurotransmitters level observed in both PD and LID model could be considered a functional perturbation of Glu-Gln-GABA cycle in the synapse. We wondered if the PD as well as LID was associated with the changes of synaptic plasticity. In recent years, abnormal synaptic plasticity of cortical neurons was found

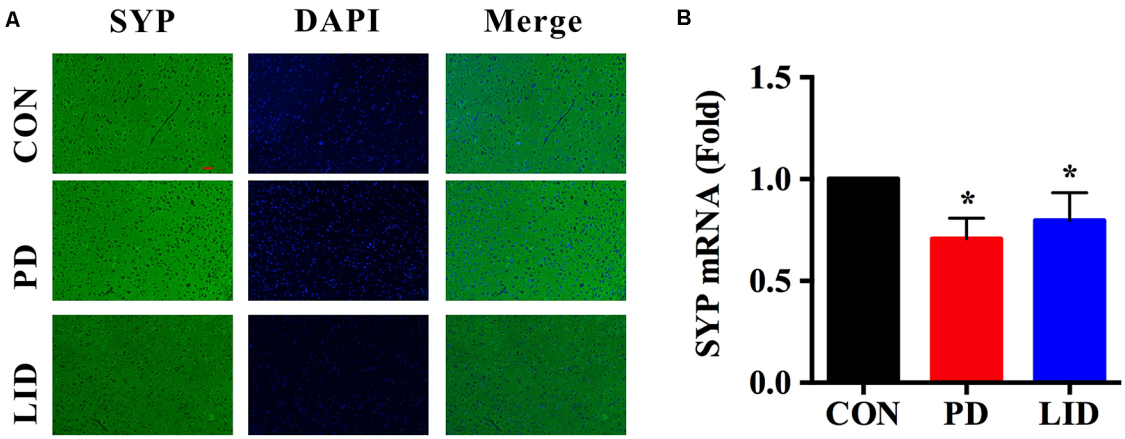

FIGURE 7 | Gene and protein expression of synaptophysin (SYP) in the right cortex of control, PD and LID rats. **(A)** Immunofluorescence staining of SYP in the cortex (n = 3–4 for each group): labeling for SYP (Green) and staining nuclei with DAPI (blue). Magnification: X400. Scale bar: 100 μm. **(B)** Real-time RT-PCR results showed that the expression of SYP in the right cortex in the experimental groups were significantly decreased compared with that in the control group. Differences among the three groups were analyzed using univariate ANOVA. *P < 0.05 is compared with control group.

to be causally involved in PD and LID (Ueno et al., 2017). Our results showed that the expression of SYP, a critical marker for synaptic structure and plastic plasticity (Zhu et al., 2019), significantly reduced in the right cortex in PD and LID rats. We, therefore, hypothesized that synaptic damage and neurotransmitter disturbance was involved in LID in parkinsonism, thus could be a potential target in the treatment or prevention of motor function impairment in PD and LID.

Meanwhile, osmoregulation plays an important role in maintaining cell structure and function. Myo is regarded as a marker for astrocytic and has various physiological functions such as membrane structure and osmoregulation (Isaacks et al., 1994; Edamatsu et al., 2018). In the present study, a significantly increased level of Myo in the midbrain and right hypothalamus of LID rats but no differences in PD rats as compared to normal rats may indicate the changed astrocytic activity underlying LID. Tau, another organic osmolyte in the brain, which was critical in osmoregulation and membrane stabilization (Trachtman et al., 1992). However, relative to Con rats, the concentration of Tau was only significantly decreased in the midbrain of PD rats but not in LID rats, suggesting that osmoregulation may be involved in PD. Thus, the disturbed osmoregulation as well as astrocytes-neurons crosstalk might involve in the occurrence of PD and LID.

The results of this study have detailed a widespread yet brain-regional specific metabolic disturbance in PD and LID rats. The midbrain and cortex exhibited significant metabolic disorders more than other brain regions. Moreover, various neurotransmitters and several intriguing metabolites, including glutamate, glutamine, aspartate, and myo-inositol were identified among the most discriminating metabolites. Our results suggest a possible mechanism: metabolic perturbation of neurotransmitter metabolism, especially in the synaptic Glu-Gln-GABA cycle may represent the pathological basis for the onset of PD and dyskinesia. While additional experiments will be necessary to firmly establish causal relations between metabolic disturbance and dyskinesia, these findings highlight the glutamate-glutamine cycle and synaptic plasticity in LID.

BIOSECURITY STATEMENT

All standard biosecurity and institutional safety procedures have been adhered to in all the experiment procedures in this article.

DATA AVAILABILITY STATEMENT

The datasets generated for this study are available on request to the corresponding author.

ETHICS STATEMENT

The animal study was reviewed and approved by the Institutional Animal Care and Use Committee of Wenzhou Medical College (wydw2018-015).

AUTHOR CONTRIBUTIONS

HG, YY, and CY contributed to the experimental design. TZ, YX, QH, and CX contributed to animal experiments and behavior testing. TZ, WW, LZ, and HZ contributed to the sample collection, NMR metabolomic analysis, and synaptic plasticity analysis. CY, TZ, and HG contributed to the data analysis, result interpretation and writing. All authors have read, revised and approved the final manuscript.

FUNDING

This work was funded by the National Natural Science Foundation of China (Nos. 81771386, 21974096, 21605115), the Natural Science Foundation of Zhejiang Province (LQ19H070001 and LY17H160049), Health Foundation for

Creative Talents in Zhejiang Province, China (No. 2016), Project Foundation for the College Young and Middle-aged Academic Leader of Zhejiang Province, China (No. 2017), Xinmiao Talent Project of Zhejiang Province (2019R413037), and Wenzhou Science and Technology Bureau Project (Y20180197).

SUPPLEMENTARY MATERIAL

The Supplementary Material for this article can be found online at: https://www.frontiersin.org/articles/10.3389/fnagi.2020.00075/full#supplementary-material.

REFERENCES

Bak, L. K., Schousboe, A., and Waagepetersen, H. S. (2006). The glutamate/GABA-glutamine cycle: aspects of transport, neurotransmitter homeostasis and ammonia transfer. *J. Neurochem.* 98, 641–653. doi: 10.1111/j.1471-4159.2006.03913.x

Bélanger, M., Allaman, I., and Magistretti, P. J. (2011). Brain energy metabolism: focus on astrocyte-neuron metabolic cooperation. *Cell Metab.* 14, 724–738. doi: 10.1016/j.cmet.2011.08.016

Cenci, M. A., Lee, C. S., and Björklund, A. (1998). L-DOPA-induced dyskinesia in the rat is associated with striatal overexpression of prodynorphin- and glutamic acid decarboxylase mRNA. *Eur. J. Neurosci.* 10, 2694–2706. doi: 10.1046/j.1460-9568.1998.00285.x

Chapuis, S., Ouchchane, L., Metz, O., Gerbaud, L., and Durif, F. (2005). Impact of the motor complications of Parkinson's disease on the quality of life. *Mov. Disord.* 20, 224–230. doi: 10.1002/mds.20279

Del Coco, L., Vergara, D., De Matteis, S., Mensa, E., Sabbatinelli, J., Prattichizzo, F., et al. (2019). NMR-based metabolomic approach tracks potential serum biomarkers of disease progression in patients with Type 2 diabetes mellitus. *J. Clin. Med.* 8. doi: 10.3390/jcm8050720

Dodel, R. C., Berger, K., and Oertel, W. H. (2001). Health-related quality of life and healthcare utilisation in patients with Parkinson's disease: impact of motor fluctuations and dyskinesias. *Pharmacoeconomics* 19, 1013–1038. doi: 10.2165/00019053-200119100-00004

Edamatsu, M., Kondo, Y., and Ando, M. (2018). Differential localizations of the myo-inositol transporters HMIT and SMIT1 in the cochlear stria vascularis. *Neurosci. Lett.* 674, 88–93. doi: 10.1016/j.neulet.2018.03.028

Hechtner, M. C., Vogt, T., Zollner, Y., Schroder, S., Sauer, J. B., Binder, H., et al. (2014). Quality of life in Parkinson's disease patients with motor fluctuations and dyskinesias in five European countries. *Parkinsonism Relat. Disord.* 20, 969–974. doi: 10.1016/j.parkreldis.2014.06.001

Hornykiewicz, O. (2006). The discovery of dopamine deficiency in the parkinsonian brain. *J. Neural. Transm. Suppl.* 9–15. doi: 10.1007/978-3-211-45295-0_3

Huang, D., Li, Q., Wang, Y., Liu, Z., Wang, Z., Li, H., et al. (2019). Brain-specific NRSF deficiency aggravates dopaminergic neurodegeneration and impairs neurogenesis in the MPTP mouse model of Parkinson's disease. *Aging* 11, 3280–3297. doi: 10.18632/aging.101979

Isaacks, R. E., Bender, A. S., Kim, C. Y., Prieto, N. M., and Norenberg, M. D. (1994). Osmotic regulation of myo-inositol uptake in primary astrocyte cultures. *Neurochem. Res.* 19, 331–338. doi: 10.1007/bf00971582

Ivanisevic, J., and Siuzdak, G. (2015). The role of metabolomics in brain metabolism research. *J. Neuroimmune Pharmacol.* 10, 391–395. doi: 10.1007/s11481-015-9621-1

Jazvinšćak Jembrek, M., Radovanovic, V., Vlainić, J., Vuković, L., and Hanžić, N. (2018). Neuroprotective effect of zolpidem against glutamate-induced toxicity is mediated *via* the PI3K/Akt pathway and inhibited by PK11195. *Toxicology* 406–407, 58–69. doi: 10.1016/j.tox.2018.05.014

Lamonaca, P., Prinzi, G., Kisialiou, A., Cardaci, V., Fini, M., and Russo, P. (2017). Metabolic disorder in chronic obstructive pulmonary disease (COPD) patients: towards a personalized approach using marine drug derivatives. *Mar. Drugs* 15:81. doi: 10.3390/md15030081

Lee, J. Y., Tuazon, J. P., Ehrhart, J., Sanberg, P. R., and Borlongan, C. V. (2019). Gutting the brain of inflammation: a key role of gut microbiome in human umbilical cord blood plasma therapy in Parkinson's disease model. *J. Cell. Mol. Med.* 23, 5466–5474. doi: 10.1111/jcmm.14429

Liu, K., Ye, X. J., Hu, W. Y., Zhang, G. Y., Bai, G. H., Zhao, L. C., et al. (2013). Neurochemical changes in the rat occipital cortex and hippocampus after repetitive and profound hypoglycemia during the neonatal period: an *ex vivo* ^{1}H magnetic resonance spectroscopy study. *Mol. Neurobiol.* 48, 729–736. doi: 10.1007/s12035-013-8446-2

Liu, K., Zhao, L., Xu, W., Lin, Q., Zhou, Y., Huang, X., et al. (2018). Metabolic changes associated with a rat model of diabetic depression detected by *ex vivo* ^{1}H nuclear magnetic resonance spectroscopy in the prefrontal cortex, hippocampus and hypothalamus. *Neural Plast.* 2018:6473728. doi: 10.1155/2018/6473728

Lu, Y., Zhang, X., Zhao, L., Yang, C., Pan, L., Li, C., et al. (2018). Metabolic disturbances in the striatum and substantia nigra in the onset and progression of MPTP-induced parkinsonism model. *Front Neurosci* 12:90. doi: 10.3389/fnins.2018.00090

Lundblad, M., Andersson, M., Winkler, C., Kirik, D., Wierup, N., and Cenci, M. A. (2002). Pharmacological validation of behavioural measures of akinesia and dyskinesia in a rat model of Parkinson's disease. *Eur. J. Neurosci.* 15, 120–132. doi: 10.1046/j.0953-816x.2001.01843.x

Mellone, M., Zianni, E., Stanic, J., Campanelli, F., Marino, G., Ghiglieri, V., et al. (2019). NMDA receptor GluN2D subunit participates to levodopa-induced dyskinesia pathophysiology. *Neurobiol. Dis.* 121, 338–349. doi: 10.1016/j.nbd.2018.09.021

Petroff, O. A. (2002). GABA and glutamate in the human brain. *Neuroscientist.* 8, 562–573. doi: 10.1177/1073858402238515

Pourmirbabaei, S., Dolatshahi, M., and Rahmani, F. (2019). Pathophysiological clues to therapeutic applications of glutamate mGlu5 receptor antagonists in levodopa-induced dyskinesia. *Eur. J. Pharmacol.* 855, 149–159. doi: 10.1016/j.ejphar.2019.05.004

Proia, P., Di Liegro, C. M., Schiera, G., Fricano, A., and Di Liegro, I. (2016). Lactate as a metabolite and a regulator in the central nervous system. *Int. J. of Mol. Sci.* 17. doi: 10.3390/ijms17091450

Rage, F., Benyassi, A., Arancibia, S., and Tapia-Arancibia, L. (1992). Gamma-aminobutyric acid-glutamate interaction in the control of somatostatin release from hypothalamic neurons in primary culture: *in vivo* corroboration. *Endocrinology* 130, 1056–1062. doi: 10.1210/en.130.2.1056

Santini, E., Valjent, E., Usiello, A., Carta, M., Borgkvist, A., Girault, J. A., et al. (2007). Critical involvement of cAMP/DARPP-32 and extracellular signal-regulated protein kinase signaling in L-DOPA-induced dyskinesia. *J. Neurosci.* 27, 6995–7005. doi: 10.1523/jneurosci.0852-07.2007

Schallert, T., Fleming, S. M., Leasure, J. L., Tillerson, J. L., and Bland, S. T. (2000). CNS plasticity and assessment of forelimb sensorimotor outcome in unilateral rat models of stroke, cortical ablation, parkinsonism and spinal cord injury. *Neuropharmacology* 39, 777–787. doi: 10.1016/s0028-3908(00)00005-8

Sellnow, R. C., Newman, J. H., Chambers, N., West, A. R., Steece-Collier, K., Sandoval, I. M., et al. (2019). Regulation of dopamine neurotransmission from serotonergic neurons by ectopic expression of the dopamine D2 autoreceptor blocks levodopa-induced dyskinesia. *Acta Neuropathol. Commun.* 7:8. doi: 10.1186/s40478-018-0653-7

Shao, W., Gu, J., Huang, C., Liu, D., Huang, H., Huang, Z., et al. (2014). Malignancy-associated metabolic profiling of human glioma cell lines using 1H NMR spectroscopy. *Mol. Cancer* 13:197. doi: 10.1186/1476-4598-13-197

Shao, Y., and Le, W. (2019). Recent advances and perspectives of metabolomics-based investigations in Parkinson's disease. *Mol. Neurodegener.* 14:3. doi: 10.1186/s13024-018-0304-2

Smith, M. L., King, J., Dent, L., Mackey, V., Muthian, G., Griffin, B., et al. (2014). Effects of acute and sub-chronic L-dopa therapy on striatal L-dopa methylation and dopamine oxidation in an MPTP mouse model of Parkinsons disease. *Life Sci.* 110, 1–7. doi: 10.1016/j.lfs.2014.05.014

Trachtman, H., Futterweit, S., and del Pizzo, R. (1992). Taurine and osmoregulation. IV. Cerebral taurine transport is increased in rats with hypernatremic dehydration. *Pediatr. Res.* 32, 118–124. doi: 10.1203/00006450-199207000-00023

Ueno, T., Nishijima, H., Ueno, S., and Tomiyama, M. (2017). Spine enlargement of pyramidal tract-type neurons in the motor cortex of a rat model of levodopa-induced dyskinesia. *Front. Neurosci.* 11:206. doi: 10.3389/fnins.2017.00206

Van Bulck, M., Sierra-Magro, A., Alarcon-Gil, J., Perez-Castillo, A., and Morales-Garcia, J. A. (2019). Novel approaches for the treatment of Alzheimer's and Parkinson's disease. *Int. J. Mol. Sci.* 20:719. doi: 10.1097/00002093-200607000-00011

Wang, Y., Wang, H. S., Wang, T., Huang, C., and Liu, J. (2014). L-DOPA-induced dyskinesia in a rat model of Parkinson's disease is associated with the fluctuational release of norepinephrine in the sensorimotor striatum. *J. Neurosci. Res.* 92, 1733–1745. doi: 10.1002/jnr.23439

Wang, Y., Zhang, G. J., Sun, Y. N., Yao, L., Wang, H. S., Du, C. X., et al. (2018). Identification of metabolite biomarkers for L-DOPA-induced dyskinesia in a rat model of Parkinson's disease by metabolomic technology. *Behav. Brain Res.* 347, 175–183. doi: 10.1016/j.bbr.2018.03.020

Wu, X. M., Wang, G. L., Miao, J., and Feng, J. C. (2015). Effect of connexin 36 blockers on the neuronal cytoskeleton and synaptic plasticity in kainic acid-kindled rats. *Transl. Neurosci.* 6, 252–258. doi: 10.1515/tnsci-2015-0027

Xie, C. L., Wang, W. W., Zhang, S. F., Yuan, M. L., Che, J. Y., Gan, J., et al. (2014). Levodopa/benserazide microsphere (LBM) prevents L-dopa induced dyskinesia by inactivation of the DR1/PKA/P-tau pathway in 6-OHDA-lesioned Parkinson's rats. *Sci. Rep-Uk* 4:7506. doi: 10.1038/srep07506

Yang, C., Zhang, P., Fang, W., Chen, Y., Zhang, N., Qiao, Z., et al. (2019). Molecular mechanisms underlying how sialyllactose intervention promotes intestinal maturity by upregulating GDNF through a CREB-dependent pathway in neonatal piglets. *Mol. Neurobiol.* doi: 10.1007/s12035-019-1628-9

Yang, X. X., Zheng, R. Y., Cai, Y. P., Liao, M. L., Yuan, W. E., and Liu, Z. G. (2012). Controlled-release levodopa methyl ester/benserazide-loaded nanoparticles ameliorate levodopa-induced dyskinesia in rats. *Int. J. Nanomed.* 7, 2077–2086. doi: 10.2147/ijn.s30463

Zhang, S. F., Xie, C. L., Wang, Q., and Liu, Z. G. (2014). Interactions of CaMKII with dopamine D2 receptors: roles in levodopa-induced dyskinesia in 6-hydroxydopamine lesioned Parkinson's rats. *Sci. Rep.* 4:6811. doi: 10.1038/srep06811

Zheng, H., Lin, Q. T., Wang, D., Xu, P. T., Zhao, L. C., Hu, W. Y., et al. (2017). NMR-based metabolomics reveals brain region-specific metabolic alterations in streptozotocin-induced diabetic rats with cognitive dysfunction. *Metab. Brain Dis.* 32, 585–593. doi: 10.1007/s11011-016-9949-0

Zheng, H., Ni, Z. T., Cai, A. M., Zhang, X., Chen, J. X., Shu, Q., et al. (2018a). Balancing metabolome coverage and reproducibility for untargeted NMR-based metabolic profiling in tissue samples through mixture design methods. *Anal Bioanal Chem* 410, 7783–7792. doi: 10.1007/s00216-018-1396-9

Zheng, H., Zhou, Q., Du, Y., Li, C., Xu, P. T., Lin, L., et al. (2018b). The hypothalamus as the primary brain region of metabolic abnormalities in APP/PS1 transgenic mouse model of Alzheimer's disease. *Bba-Mol. Basis. Dis.* 1864, 263–273. doi: 10.1016/j.bbadis.2017.10.028

Zheng, H., Zhao, L., Xia, H., Xu, C., Wang, D., Liu, K., et al. (2016). NMR-based metabolomics reveal a recovery from metabolic changes in the striatum of 6-OHDA-induced rats treated with basic fibroblast growth factor. *Mol. Neurobiol.* 53, 6690–6697. doi: 10.1007/s12035-015-9579-2

Zhu, X., Wang, P., Liu, H., Zhan, J., Wang, J., Li, M., et al. (2019). Changes and significance of SYP and GAP-43 expression in the hippocampus of CIH rats. *Int. J. Med. Sci.* 16, 394–402. doi: 10.7150/ijms.28359

Zott, B., Simon, M. M., Hong, W., Unger, F., Chen-Engerer, H. J., Frosch, M. P., et al. (2019). A vicious cycle of β amyloid-dependent neuronal hyperactivation. *Science* 365, 559–565. doi: 10.3410/f.736365538.793564339

Conflict of Interest: The authors declare that the research was conducted in the absence of any commercial or financial relationships that could be construed as a potential conflict of interest.

frontiers in Neuroscience

REVIEW
published: 26 March 2020
doi: 10.3389/fnins.2020.00131

Relationship Between Exercise and Alzheimer's Disease: A Narrative Literature Review

Qing Meng[1,2], *Muh-Shi Lin*[3,4,5,6] *and I-Shiang Tzeng*[7]*

[1] School of Physical Education, Huaqiao University, Quanzhou, China, [2] Sport and Health Research Center, Huaqiao University, Quanzhou, China, [3] Department of Biotechnology and Animal Science, College of Bioresources, National Ilan University, Yilan, Taiwan, [4] Division of Neurosurgery, Department of Surgery, Kuang Tien General Hospital, Taichung, Taiwan, [5] Department of Biotechnology, College of Medical and Health Care, HungKuang University, Taichung, Taiwan, [6] Department of Health Business Administration, College of Medical and Health Care, HungKuang University, Taichung, Taiwan, [7] Department of Exercise and Health Promotion, College of Education, Chinese Culture University, Taipei, Taiwan

This narrative review aimed to summarize evidence regarding the responses to exercise among patients with preclinical Alzheimer's disease (AD) and the effectiveness of long-term exercise interventions in improving cognitive function and neuropsychiatric symptoms. We performed a narrative review of existing literature on the effectiveness of long-term exercise interventions in improving cognitive function and neuropsychiatric symptoms in patients with AD. Patients with AD who presented with long-term exercise interventions appeared to have improved blood flow, increased hippocampal volume, and improved neurogenesis. Most prospective studies have proven that physical inactivity is one of the most common preventable risk factors for developing AD and that higher physical activity levels are associated with a reduced risk of AD development. Physical exercise seems to be effective in improving several neuropsychiatric symptoms of AD, notably cognitive function. Compared with medications, exercise has been shown to have fewer side effects and better adherence.

Keywords: Alzheimer's disease, neurogenesis, cognitive function, exercise, hippocampal volume

OPEN ACCESS

Edited by:
Jiehui Jiang,
Shanghai University, China

Reviewed by:
Chuantao Zuo,
Fudan University, China
Usman Iqbal,
Taipei Medical University, Taiwan

***Correspondence:**
I-Shiang Tzeng
istzeng@gmail.com

Specialty section:
This article was submitted to Neurodegeneration, a section of the journal Frontiers in Neuroscience

Received: *24 October 2019*
Accepted: *31 January 2020*
Published: *26 March 2020*

Citation:
Meng Q, Lin M-S and Tzeng I-S (2020) Relationship Between Exercise and Alzheimer's Disease: A Narrative Literature Review. Front. Neurosci. 14:131. doi: 10.3389/fnins.2020.00131

BACKGROUND

Alzheimer's disease (AD) is a progressive neurodegenerative disorder characterized by memory loss and multiple cognitive disorders (Reddy and Oliver, 2019). This symptom is the most frequent cause of neurogenesis. Individuals with AD develop progressive mild cognitive impairment (MCI), leading to the development of neuropsychiatric manifestations. Agitation and anxiousness are common complications in individuals diagnosed with AD. Other complications such as bladder and bowel problems, depression, infection, and head trauma or broken bones are the main cause of imbalance and incoordination in these patients (Higuera, 2016).

Alzheimer's disease is associated with common causes of dementia and is estimated to account for 60–80% of these cases (Alzheimer's Association [AA], 2016). Aging can be treated as the greatest risk factor for AD progression. About 81% of AD patients are aged over 75 years as estimated by the Alzheimer's Association [AA], 2016). The diagnosis and treatment of AD involves many challenges. Studies have shown that drug combinations are effective and that there is no efficient treatment for patients diagnosed with preclinical AD or MCI. With respect to the definition of MCI, it is regarded as a syndrome of cognitive decline that is higher than the expectation of the age of individual and level of education

without significantly obstructing with daily living activities. Notably, it develops into AD during 5 years in over half of the MCI patients (Gauthier et al., 2006). Based on the possibility of side effects of drugs, people are very interested in the non-pharmacological treatment of AD (Raggi et al., 2017).

Inconsistent benefits of treatments, comprising cognitive training and cognitive stimulation, have been reported. There is an intension to prevent and treat AD, MCI, and dementia via regular exercise (Laurin et al., 2001; Lindsay et al., 2002; Andel et al., 2008). This article aims to review important studies with this scope and consider the association of exercise and AD in patients.

OVERVIEW OF ALZHEIMER'S DISEASE

Alzheimer's disease is a chronic neurodegenerative disease in which pathological features include changes in the brain structure and function (Scheltens et al., 2016). The consequences have a significant impact on individual lives and societal costs (World Health Organization [WHO] and Alzheimer's Disease International [ADI], 2012). The emotions derived from the disease, changes in neurocognition, and physical disability are common and also lower the quality of life considerably, e.g., higher dependence on people and reduction of functioning mobility (Glenthøj et al., 2017). Additionally, the prevalence rate of depressive symptoms in AD patients was 10 times higher than that in the normal population (Lee and Lyketsos, 2003; Strober and Arnett, 2009). Approximately 747,000 (15%) Canadians aged over 65 years were affected by a particular form of person cognitive impairment or dementia in 2011 (Alzheimer Society of Canada [ASC], 2011). Around 60–70% of people have AD (World Health Organization [WHO] and Alzheimer's Disease International [ADI], 2012). Commensurate statistics from United States estimate that nearly one in eight among the aged have AD (Alzheimer's Association [AA], 2012). Therefore the annual cost for treatment is as high as $600 billion (World Health Organization [WHO] and Alzheimer's Disease International [ADI], 2012). The care cost is estimated to grow to around $20 trillion for American AD patients if the present trend is unchanged for the next 40 years (Alzheimer's Society [AS], 2010). Psychosocial care takers still need to take on the burden of AD-related disease even though the economic cost has been cut back in Canada (Herrmann et al., 2010). The age-standardized death rate (per 100,000 people) of the aged in Ontario remains stable (Statistics Canada, 2011). The results show that women's death rate are higher than men. It seems older people (over 65 years of age) represent number of AD patients' growth was more than other age groups. Early identification and management of AD is a challenging task but a public health priority.

DIAGNOSIS AND TREATMENT

Diagnosis is mostly clinical and commonly includes the patient's main care doctor. Acquiring good medical, family medical, and neuropsychiatric history is essential. If necessary, neuropsychological test and serologic tests for biomarkers can bolster the diagnosis. Other causes of dementia are ruled out by routine laboratory test with whole blood cell counts, metabolome comparison, thyroid stimulating hormone, vitamin B-12, folate, and MRI. These are regarded as part of the routine diagnostic examination.

In accordance with the definition of National Institute on Aging in 2011, AD is characterized by three progressive and overlapping stages of deterioration, including preclinical AD, MCI, and Dementia (Sperling et al., 2011). In the early phase of the disease, most of the symptoms may be misinterpreted as ordinary changes in behavior, attention, and forgetfulness (Burns and Illiffe, 2009). The intricacies and gradualness of the symptoms have led to some people classifying the features as "syndromes."

The only way to obtain a definitive diagnosis of AD is through autopsy and an accurate examination of the brain tissue (Caroli and Frisoni, 2009). However, physician diagnosis can reach relatively high accuracy in a clinical setting because serum or cerebrospinal fluid biomarkers have been proven to provide high diagnostic accuracy, accounting for 85–90% for sensitivity and specificity (Jack et al., 2010; Scheltens et al., 2016). Thus the diagnostic accuracy is as high as 90%.

Factors associated with the clinical analysis of AD cases are particular medical history and physical examination to determine the family history of dementia and changes in behavior, mood, and motor performance and to rule out other explanations so that physicians can oversee, treat, and arrange supporting services (Burns and Illiffe, 2009).

RISK FACTORS

Age is the biggest risk factor for AD. There is a possible minor risk (less than 1%) owing to gene mutation, mutant amyloid precursor proteins, among patients account 40–65% with AD may also accompany APOE-e4 genetic variant (Mahley et al., 2006; Alzheimer's Association [AA], 2016). Family history can be another risk factor for AD; it can also be influenced by cardiovascular disease, low education level, social factors, and cognitive involvement, as well as traumatic brain injury prior to MCI (Alzheimer's Association [AA], 2016). The evidence also shows that chronic disease risk factors (such as physical inactivity, diabetes, smoking, abdominal obesity, and high cholesterol) (Purnell et al., 2009; Li et al., 2011) may increase the risk of developing AD, whereas social participation and low saturated fat/high fiber vegetable diet can reduce the risk of developing AD (Alzheimer's Association [AA], 2012).

It is unclear whether this relationship is dependent on the dose; it seems that there is reduced risk with higher levels of physical activity (Yaffe et al., 2001). This may be vital in patients with risk factors or early progression MCI. Exercise seems to have potential benefits for people diagnosed with AD. However, the management of AD is still challenging. Drug treatment is limited to date. Three most common classes of drugs include: acetylcholinesterase inhibitors for behavioral symptoms;

N-methyl D-aspartate antagonists to treat cognitive decline and slow progression of AD; and antipsychotics (not recommended) (National Institute of Aging [NIA], 2008). Other complementary treatments such as group-based social procedures (e.g., art and music) and cognitive and emotional orientation treatments (e.g., psychotherapy, validation, recall, etc.) have been used and have varied ineffectiveness (Olazarán et al., 2010; Ballard et al., 2011).

NEUROPHYSIOLOGY

One of the most vital and majestic organs in an organism is the brain which can be categorized under the CNS. A human brain contains approximately 98% of the body's neural tissue (Martini et al., 2011). It consists of over 100 billion nerves that are connected to one another through long protoplasmic fibers named axons (Hendrickson, 2004). These fibers carry signal pulses to different parts of the brain and body targeting specific recipient cells. The main function of the brain is to conduct, consolidate, and control different organs of the body physiologically. Brain coordinates and controls most of the sensory system, social behavior, muscle movements and synchronized body functions such as heart and respiratory rate, blood pressure, fluid balance, and body temperature. The brain is the cradle of mood, emotion, cognition, memory, motor, and different forms of learning.

Exercise could be a strategy to prevent or postpone the aging brain from decline in cognition (Barnes, 2015). Thus, a great amount of effort and research have undertaken to understand the physiology of aging brain, which is changed or tempered by exercise (Marks et al., 2011; Burzynska et al., 2014; Bullock et al., 2018). Exercise may cause effects on three areas of the brain: vascular physiology, hippocampal volumes, and neurogenesis (Barnes, 2015). With advancing age, blood flow to the brain is negatively influenced and is related to cognition (Barnes, 2015). It is shown that moderate-intensity exercise causes intense augmentation of blood flow to the brain, also the cerebral blood flow increment is found in participants trained by exercise than participants who were seated for a long period (Bailey et al., 2013). A randomized trial with 12-week-long exercise training showed that the cerebral blood flow is higher in the anterior cingulate cortex (Chapman et al., 2013). In AD, hippocampal circuits that are considered as relatively significant for episodic-like memory are affected initially. Higher volume of the hippocampus is related to improved cognition. Over a year of mild-to-moderate exercise seems to protect against shriveling hippocampal volume (Duzel et al., 2016). Hippocampal volume variation was also associated with improved heart health (Duzel et al., 2016). Physical exercise can improve cognitive ability and is associated with a boost in the hippocampal volume as shown by Erickson et al. (2009). Currently, it has been assessed that AD is caused by neuropathological and physiological factors. The current drug treatment for AD is aimed at an advanced stage, where severe morbidity, mortality and the burden on caregivers may increase. For the early stages of AD and general dementia prevention, exercise seems to be a useful way to treat and prevent it (Tabei et al., 2018).

PHYSICAL ACTIVITY AND ALZHEIMER'S DISEASE

Prospective studies have shown that physical activity can reduce the likelihood of dementia and AD, even at mild to moderate intensity (Yaffe et al., 2001; Erickson et al., 2009; Hamer and Chida, 2009; Smith et al., 2010; Barnes and Yaffe, 2011; Sattler et al., 2011; Buchman et al., 2012; Norton et al., 2014). Exercise could help diminish the occurrence of dementia and AD so that it has been cited as a possible lifestyle intervention. Some previous studies have proof to support this hypothesis. A study measured that 54% of AD risk factors may be avertible (Barnes and Yaffe, 2011). Another study estimated the demographic risk of global AD, which can be attributed to seven potentially adjustable risk factors by using the relative risks of existing meta-analyses (Norton et al., 2014). The lack of physical activity was the highest attributable risk that they found. In a systematic review that collated evidence from 163,000 non-psychotic participants and compared highest physical activity category to the participants with least relative risk of dementia (Hamer and Chida, 2009). They also found that the risk of dementia and AD can be lowered by 28% and 45% with physical activity. A systematic review of randomized controlled trials observing the connection of exercise and cognitive performance between 1966 and 2009 was completed by Smith et al. (2010). They chose research that had ample influence, supervised aerobic exercise programs and control groups. They showed improvement in attention and processing speed in the exercise group, executive function and memory improvement. Inconsistency of the impact on working memory was seen. The duration of exercise or intensity seems to be essential for the benefit. As mentioned earlier, the hippocampus of dementia patients gets decayed. Erickson et al. (2009) observed the relation between exercise and hippocampus because exercise effectively reduces cortical decay in the elderly. They noticed that among 165 non-demented elderly people, active individuals had higher levels of health, larger hippocampus, and better spatial memory by using MRI. The benefits of exercise for diminishing cognitive degeneration and dementia have been demonstrated by population-based prospective studies. A 14-year time course German population study showed a lower risk of MCI and AD in participants with regular physical activity and better performance in the neuropsychological tests (Sattler et al., 2011). Another prospective trial examined the hypothesis that objectively measuring daily activities could forecast the incidence rate in AD and MCI (Buchman et al., 2012). Participants wore wrist activity recorders to observe their overall physical activity instead of relying on questionnaires, which self-reported in this study. It was determined that levels of daily overall activity were associated with incidence of global cognitive decline and AD, at 4 years of follow-up. A significant reduction in AD risk was associated with higher levels of physical activity. Besides, a prospective study of more than 8 years showed that women who walked more had less cognitive decline during the entire study period (Yaffe et al., 2001). A Cochrane review examined how aerobic activity affected mentally healthy older adults. The objective was to assess whether heart health affects the impact

of physical activity on cognition (Forbes et al., 2015). With this intention, they included trials that have demonstrated an increase in cardiovascular health through a test for VO2max. Their findings did not show any evidence of the benefits of exercise in cognition and the research they studied had a moderate to high risk of bias (Forbes et al., 2015). It has to be considered that their comments exclude studies where exercise interventions do not add cardiovascular health (i.e., mild aerobic exercise), weightlifting or stretching. Studies that performed a test for VO2max or other tests for heart health were included. We found that comments may be useful for a specific individual subgroup, but should be cautious in interpretation. In addition, other systematic reviews and meta-analyses show that exercise has significant improvements and benefits in cognition (Farina et al., 2014).

EXERCISE AS TREAMENT FOR ALZHEIMER'S DISEASE

Although several studies have shown that exercise has a potential benefit in declined cognition, are there any evidences to prove that exercise is good for people with AD? Some of the previous studies have limitations associated with randomization and surveillance in the group with treatment. There are also relatively few large-scale studies focusing on Alzheimer's patients.

A randomized, controlled trial was designed to tackle these issues by evaluating whether exercise programs could impact the decline in activities of daily living (ADL) in AD patients (Rolland et al., 2007). With an hour of training twice a week in aerobic exercise, strength level, balance skill and flexibility as intervention for 1 year, they found that ADL was slower than the non-active group. However, there was no effect on behavioral disorders, depression or nutritional scores. Another study attempted to compare the effects of drug and exercise on AD and MCI (Ströhle et al., 2015). The study allowed for including exercise or pharmacological intervention as the treatment group. For AD, exercise had a medium to strong pooled effect size, with a small effect on MCI. Treatment with a cholinesterase inhibitor in the meantime had a consequent slight effect on the perception in AD but had no effect on MCI. Note that the drug withdrawal rate is very high, but the exercise group has a much lower rate of discontinuation. In addition, systematic reviews and meta-analyses display improvement in dementia, reduced neuropsychiatric symptoms, and slight decline in ADL (Hamer and Chida, 2009; Smith et al., 2010; Forbes et al., 2015). In a large systematic review, exercise had less side effects and superior compliance than medications (Ströhle et al., 2015). Exercise also has intrinsic benefits for cardiovascular health and personal health. It is difficult to suggest specific exercises for AD patients or for prevention of AD based on the available evidence. These studies including the various types of exercises are established based on the duration of intervention. Nelson et al. (2007) believe the American Sports Medicine Association and the American Heart Association's recommendations can be used to comprehensively treat the elderly. These suggestions are also more likely to cover most of the support activities needed to identify potential benefits.

A randomized controlled trial examined aerobic exercise programs with moderate to high-intensity on mild AD patients (Hoffmann et al., 2016). Training for 60 min was performed three times a week for 16 weeks, but there was no benefit for cognitive ability; however, the score on neuropsychiatric symptoms significantly improved. This study is indeed related to subjects that follow the training program. A general problem is that most people use intentional treatment models in their studies. During longer intervention studies, you are more likely to see compliance disruptions throughout the process. This makes the duration of intervention support for observation questionable. A 3-month randomized study looked at supervised exercise program three times a week (Chapman et al., 2013). Through the training interval, they found immediate and delayed memory improvements. In the anterior cingulate area, the exercise group also showed a cerebral blood flow while resting. Unfortunately, we may not be able to compare findings of AD patients to adults with normal cognition. Another minor study of eight people with MCI observed an exercise intervention for 9-months and a training during 2, 3-months (Sacco et al., 2016). Their cognitive performance improved, but their influence weakened after disrupting the training. A Cochrane review investigated the effects of exercise on Alzheimer's patients (Forbes et al., 2015). Their meta-analysis showed no clear evidence that exercise is beneficial for cognitive function. However, they did get the ability to perform ADL from the exercises. It should be noted that the results and studies found by the reviewers comprised diverse data and lack of quality owing to insufficient evidence. They suggest more qualified trials to assess various dementias of different types with severity, which will help to improve the quality of evidence for reviews (Forbes et al., 2015). Finally, a few systematic reviews and accompanying analyzed results showed a favorable effect on AD patients receiving exercise programs based on six randomized controlled trials (Farina et al., 2014). Farina, Rusted, and Tabet show a downturn in a declining rate of cognition and a positive impact on global cognitive function (Farina et al., 2014).

LIMITATIONS

The study was conducted under narrative review approach. There are several limitations of this research. First, hypothesis was set as board overview of a topic-related research area. Second, search method depends on non-predefined protocol based which may involve subjective selection bias. Third, inclusion criteria of studies for review also rely on researchers' experiences. Finally, search media usually via PubMed or Medline. In the meantime, extracted studies with non-protocol based may partially grade objectively by anecdotal resources for their quality.

CONCLUSION

To present the core information of this review, we constructed a **Supplementary Table S1** has brief summary extracted

from aforementioned references (except citations from specific associations and monograph). Systematic reviews and meta-analyses indicate the benefits of physical activity based on large-scale prospective trials. Unfortunately, many of these comments and studies have been plagued by methodological problems and noted the heterogeneity of the population.

In the next few decades, AD will be a huge challenge for the country in the field of medicine. Moreover, there are still much to learn despite a lot of rigorous and large-scale research. More high quality randomized trials are needed to really determine if AD can be prevented and treated by exercise.

AUTHOR CONTRIBUTIONS

QM and I-ST proposed the research idea, wrote the background and conclusion, and contributed to the literature review. M-SL supported the literature review, helped to revise the manuscript and provided clinical suggestions. I-ST prepared the manuscript for submission. All authors read and approved the final manuscript.

FUNDING

Huaqiao University's Academic Project Supported by the Fundamental Research Funds for the Central Universities (19SKGC-QT06) for this study.

SUPPLEMENTARY MATERIAL

The Supplementary Material for this article can be found online at: https://www.frontiersin.org/articles/10.3389/fnins.2020.00131/full#supplementary-material

REFERENCES

Alzheimer Society of Canada [ASC] (2011). Available at: https://alz-journals.onlinelibrary.wiley.com/doi/abs/10.1016/j.jalz.2012.02.001 (accessed August 27, 2019).

Alzheimer's Association [AA] (2012). Alzheimer's disease facts and figures. *Alzheimers Dement.* 8, 131–168.

Alzheimer's Association [AA] (2016). Alzheimer's disease facts and figures. *Alzheimers Dement.* 12, 459–509. doi: 10.1016/j.jalz.2016.03.001

Alzheimer's Society [AS] (2010). *Changing the Trajectory of Alzheimer's Disease: A National Imperative*. Available at: www.alz.org/trajectory (accessed August 22, 2019).

Andel, R., Crowe, M., Pedersen, N. L., Fratiglioni, L., Johansson, B., and Gatz, M. (2008). Physical exercise at midlife and risk of dementia three decades later: a population-based study of Swedish twins. *J. Gerontol. A Biol. Sci. Med. Sci.* 63, 62–66. doi: 10.1093/gerona/63.1.62

Bailey, D. M., Marley, C. J., Brugniaux, J. V., Hodson, D., New, K. J., Ogoh, S., et al. (2013). Elevated aerobic fitness sustained throughout the adult lifespan is associated with improved cerebral hemodynamics. *Stroke* 44, 3235–3238. doi: 10.1161/STROKEAHA.113.002589

Ballard, C., Khan, Z., Clack, H., and Corbett, A. (2011). Nonpharmacological treatment of Alzheimer disease. *Can. J. Psychiatry* 56, 589–595. doi: 10.1177/070674371105601004

Barnes, D. E., and Yaffe, K. (2011). The projected effect of risk factor reduction on Alzheimer's disease prevalence. *Lancet Neurol.* 10, 819–828. doi: 10.1016/S1474-4422(11)70072-2

Barnes, J. N. (2015). Exercise, cognitive function, and aging. *Adv. Physiol. Educ.* 39, 55–62. doi: 10.1152/advan.00101.2014

Buchman, A. S., Boyle, P. A., Yu, L., Shah, R. C., Wilson, R. S., and Bennett, D. A. (2012). Total daily physical activity and the risk of AD and cognitive decline in older adults. *Neurology* 78, 1323–1329. doi: 10.1212/WNL.0b013e3182535d35

Bullock, A. M., Mizzi, A. L., Kovacevic, A., and Heisz, J. J. (2018). The Association of aging and aerobic fitness with memory. *Front. Aging Neurosci.* 10:63. doi: 10.3389/fnagi.2018.00063

Burns, A., and Illiffe, S. (2009). Alzheimer's disease. *BMJ* 338:b158. doi: 10.2236/bmj.b158

Burzynska, A. Z., Chaddock-Heyman, L., Voss, M. W., Wong, C. N., Gothe, N. P., Olson, E. A., et al. (2014). Physical activity and cardiorespiratory fitness are beneficial for white matter in low-fit older adults. *PLoS One* 9:e107413. doi: 10.1371/journal.pone.0107413

Caroli, A., and Frisoni, G. B. (2009). Quantitative evaluation of Alzheimer's disease. *Expert Rev. Med. Devices* 6, 569–588.

Chapman, S. B., Aslan, S., Spence, J. S., DeFina, L. F., Keebler, M. W., Didehbani, N., et al. (2013). Shorter term aerobic exercise improves brain, cognition, and cardiovascular fitness in aging. *Front. Aging Neurosci.* 5:75. doi: 10.3389/fnagi.2013.00075

Duzel, E., Van Praag, H., and Sendtner, M. (2016). Can physical exercise in old age improve memory and hippocampal function? *Brain* 139, 662–673. doi: 10.1093/brain/awv407

Erickson, K. I., Prakash, R. S., Voss, M. W., Chaddock, L., Hu, L., Morris, K. S., et al. (2009). Aerobic fitness is associated with hippocampal volume in elderly humans. *Hippocampus* 19, 1030–1039. doi: 10.1002/hipo.20547

Farina, N., Rusted, J., and Tabet, N. (2014). The effect of exercise interventions on cognitive outcome in Alzheimer's disease: a systematic review. *Int. Psychogeriatr.* 26, 9–18. doi: 10.1017/s1041610213001385

Forbes, D., Forbes, S. C., Blake, C. M., Thiessen, E. J., and Forbes, S. (2015). Exercise programs for people with dementia. *Cochrane Database Syst. Rev.* 1–77. doi: 10.1002/14651858.CD006489.pub4

Gauthier, S., Reisberg, B., Zaudig, M., Petersen, R. C., Ritchie, K., Broich, K., et al. (2006). Mild cognitive impairment. *Lancet* 367, 1262–1270.

Glenthøj, L. B., Jepsen, J. R., Hjorthøj, C., Bak, N., Kristensen, T. D., Wenneberg, C., et al. (2017). Negative symptoms mediate the relationship between neurocognition and function in individuals at ultrahigh risk for psychosis. *Acta Psychiatr. Scand.* 135, 250–258. doi: 10.1111/acps.12682

Hamer, M., and Chida, Y. (2009). Physical activity and risk of neurodegenerative disease: a systematic review of prospective evidence. *Psychol. Med.* 39, 3–11. doi: 10.1017/S0033291708003681

Hendrickson, R. (2004). *The Facts on File Encyclopedia of Word and Phrase Origins*, 3rd Edn. New York, NY: Checkmark Books, 822.

Herrmann, N., Tam, D. Y., Balshaw, R., Sambrook, R., Lesnikova, N., Lanctôt, K. L., et al. (2010). The relation between disease severity and cost of caring for patients with Alzheimer disease in Canada. *Can. J. Psychiatry* 55, 768–775. doi: 10.1177/070674371005501204

Higuera, V. (2016). *Complications of Alzheimer's Disease (AD)*. Available at: https://www.healthline.com/health/alzheimers-disease-complications (accessed September 10, 2019).

Hoffmann, K., Sobol, N. A., Frederiksen, K. S., Beyer, N., Vogel, A., Vestergaard, K., et al. (2016). Moderate-to-high intensity physical exercise in patients with Alzheimer's disease: a randomized controlled trial. *J. Alzheimers Dis.* 50, 443–453.

Jack, C. R., Knopman, D. S., Jagust, W. J., Shaw, L. M., Aisen, P. S., Weiner, M. W., et al. (2010). Hypothetical model of dynamic biomarkers of the Alzheimer's pathological cascade. *Lancet Neurol.* 9, 119–128. doi: 10.1016/s1474-4422(09)70299-6

Laurin, D., Verreault, R., Lindsay, J., MacPherson, K., and Rockwood, K. (2001). Physical activity and risk of cognitive impairment and dementia in elderly persons. *Arch. Neurol.* 58, 498–504.

Lee, H. B., and Lyketsos, C. G. (2003). Depression in Alzheimer's disease: heterogeneity and related issues. *Biol. Psychiatry* 54, 353–362. doi: 10.1016/s0006-3223(03)00543-2

Li, J., Wang, Y. J., Zhang, M., Xu, Z. Q., Gao, C. Y., Fang, C. Q., et al. (2011). Vascular risk factors promote conversion from mild cognitive impairment to Alzheimer disease. *Neurology* 76, 1485–1491. doi: 10.1212/WNL.0b013e318217e7a4

Lindsay, J., Laurin, D., Verreault, R., Hébert, R., Helliwell, B., Hill, G. B., et al. (2002). Risk factors for Alzheimer's disease: a prospective analysis from the Canadian study of health and aging. *Am. J. Epidemiol.* 156, 445–453. doi: 10.1093/aje/kwf074

Mahley, R. W., Weisgraber, K. H., and Huang, Y. (2006). Apolipoprotein E4: a causative factor and therapeutic target in neuropathology, including Alzheimer's disease. *Proc. Natl. Acad. Sci. U.S.A.* 103, 5644–5651. doi: 10.1073/pnas.0600549103

Marks, B. L., Katz, L. M., Styner, M., and Smith, J. K. (2011). Aerobic fitness and obesity: relationship to cerebral white matter integrity in the brain of active and sedentary older adults. *Br. J. Sports Med.* 45, 1208–1215. doi: 10.1136/bjsm.2009.068114

Martini, F. H., Nath, J. L., and Bartholomew, E. F. (2011). *Fundamentals of Anatomy & Physiology*, 9th Edn. San Francisco, CA: Benjamin-Cummings Publishing Company, 1114.

National Institute of Aging [NIA] (2008). *Alzheimer's Disease Medications Fact Sheet*. Available at: http://www.nia.nih.gov/alzheimers/publication/alzheimers-disease-medications-fact-sheet (accessed July 16, 2019).

Nelson, M. E., Rejeski, W. J., Blair, S. N., Duncan, P. W., Judge, J. O., King, A. C., et al. (2007). Physical activity and public health in older adults: recommendation from the American College of Sports Medicine and the American Heart Association. *Med. Sci. Sports Exerc.* 39, 1435–1445. doi: 10.1249/mss.0b013e3180616aa2

Norton, S., Matthews, F. E., Barnes, D. E., Yaffe, K., and Brayne, C. (2014). Potential for primary prevention of Alzheimer's disease: an analysis of population-based data. *Lancet Neurol.* 13, 788–794. doi: 10.1016/S1474-4422(14)70136-X

Olazarán, J., Reisberg, B., Clare, L., Cruz, I., Peña-Casanova, J., Ser, T. D., et al. (2010). Nonpharmacological therapies in Alzheimer's disease: a systematic review of efficacy. *Dement. Geriatr. Cogn. Disord.* 30, 161–178.

Purnell, C., Gao, S., Callahan, C. M., and Hendrie, H. C. (2009). Cardiovascular risk factors and incident Alzheimer disease: a systematic review of the literature. *Alzheimer Dis. Assoc. Disord.* 23, 1–10. doi: 10.1097/WAD.0b013e318187541c

Raggi, A., Tasca, D., and Ferri, R. (2017). A brief essay on non-pharmacological treatment of Alzheimer's disease. *Rev. Neurosci.* 28, 587–597. doi: 10.1515/revneuro-2017-0002

Reddy, P. H., and Oliver, D. M. (2019). Amyloid beta and phosphorylated Tau-induced defective autophagy and mitophagy in Alzheimer's disease. *Cells* 8:488. doi: 10.3390/cells8050488

Rolland, Y., Pillard, F., Klapouszczak, A., Reynish, E., Thomas, D., Andrieu, S., et al. (2007). Exercise program for nursing home residents with Alzheimer's disease: a 1-year randomized, controlled trial. *J. Am. Geriatr. Soc.* 55, 158–165. doi: 10.1111/j.1532-5415.2007.01035.x

Sacco, G., Caillaud, C., Ben Sadoun, G., Robert, P., David, R., and Brisswalter, J. (2016). Exercise plus cognitive performance over and above exercise alone in subjects with mild cognitive impairment. *J. Alzheimers Dis.* 50, 19–25. doi: 10.3233/JAD-150194

Sattler, C., Erickson, K. I., Toro, P., and Schröder, J. (2011). Physical fitness as a protective factor for cognitive impairment in a prospective population-based study in Germany. *J. Alzheimers Dis.* 26, 709–718. doi: 10.3233/JAD-2011-110548

Scheltens, P., Blennow, K., Breteler, M. M., Strooper, B. D., Frisoni, G. B., Salloway, S., et al. (2016). Alzheimer's disease. *Lancet* 388, 505–517.

Smith, P. J., Blumenthal, J. A., Hoffman, B. M., Cooper, H., Strauman, T. A., Welsh-Bohmer, K., et al. (2010). Aerobic exercise and neurocognitive performance: a meta-analytic review of randomized controlled trials. *Psychosom. Med.* 72, 239–252. doi: 10.1097/PSY.0b013e3181d14633

Sperling, R. A., Aisen, P. S., Beckett, L. A., Bennett, D. A., Craft, S., Fagan, A. M., et al. (2011). Toward defining the preclinical stages of Alzheimer's disease: recommendations from the National Institute on Aging and the Alzheimer's Association workgroup. *Alzheimers Dement.* 7, 280–292.

Statistics Canada (2011). Deaths and Mortality Rate, by Selected Grouped Causes and Sex, Canada, Provinces and Territories, Annual. CANSIM (Database). Ottawa, ON: Statistics Canada.

Strober, L. B., and Arnett, P. A. (2009). Assessment of depression in three medically ill, elderly populations: Alzheimer's disease, Parkinson's disease, and stroke. *Clin. Neuropsychol.* 23, 205–230. doi: 10.1080/13854040802003299

Ströhle, A., Schmidt, D. K., Schultz, F., Fricke, N., Staden, T., Hellweg, R., et al. (2015). Drug and exercise treatment of Alzheimer disease and mild cognitive impairment: a systematic review and meta-analysis of effects on cognition in randomized controlled trials. *Am. J. Geriatr. Psychiatry* 23, 1234–1249. doi: 10.1016/j.jagp.2015.07.007

Tabei, K. I., Satoh, M., Ogawa, J. I., Tokita, T., Nakaguchi, N., Nakao, K., et al. (2018). Cognitive function and brain atrophy predict non-pharmacological efficacy in dementia: the mihama-kiho scan project2. *Front. Aging Neurosci.* 10:87. doi: 10.3389/fnagi.2018.00087

World Health Organization [WHO] and Alzheimer's Disease International [ADI] (2012). *Dementia: A Public Health Priority*. Geneva: World Health Organization.

Yaffe, K., Barnes, D., Nevitt, M., Lui, L. Y., and Covinsky, K. (2001). A prospective study of physical activity and cognitive decline in elderly women: women who walk. *Arch. Intern. Med.* 161, 1703–1708.

Conflict of Interest: The authors declare that the research was conducted in the absence of any commercial or financial relationships that could be construed as a potential conflict of interest.

frontiers in Aging Neuroscience

ORIGINAL RESEARCH
published: 01 April 2020
doi: 10.3389/fnagi.2020.00077

Predicting Alzheimer's Disease Conversion From Mild Cognitive Impairment Using an Extreme Learning Machine-Based Grading Method With Multimodal Data

Weiming Lin[1,2], Qinquan Gao[2,3], Jiangnan Yuan[1,4], Zhiying Chen[5], Chenwei Feng[1,4], Weisheng Chen[6], Min Du[2,7] and Tong Tong[2,8] for the Alzheimer's Disease Neuroimaging Initiative

[1] School of Opto-Electronic and Communication Engineering, Xiamen University of Technology, Xiamen, China, [2] College of Physics and Information Engineering, Fuzhou University, Fuzhou, China, [3] Imperial Vision Technology, Fuzhou, China, [4] Fujian Key Laboratory of Communication Network and Information Processing, Xiamen University of Technology, Xiamen, China, [5] School of Electrical Engineering & Automation, Xiamen University of Technology, Xiamen, China, [6] Department of Thoracic Surgery, Fujian Cancer Hospital, Fuzhou, China, [7] Fujian Provincial Key Laboratory of Eco-Industrial Green Technology, Wuyi University, Wuyishan, China, [8] Fujian Key Lab of Medical Instrumentation and Pharmaceutical Technology, Fuzhou University, Fuzhou, China

OPEN ACCESS

Edited by:
Jiehui Jiang,
Shanghai University, China

Reviewed by:
Yiqiang Chen,
Institute of Computing Technology (CAS), China
Gustavo Sevlever,
Fundación para la Lucha contra las Enfermedades Neurológicas de la Infancia (FLENI), Argentina

***Correspondence:**
Tong Tong
ttraveltong@gmail.com

Received: 26 November 2019
Accepted: 02 March 2020
Published: 01 April 2020

Citation:
Lin W, Gao Q, Yuan J, Chen Z, Feng C, Chen W, Du M and Tong T (2020) Predicting Alzheimer's Disease Conversion From Mild Cognitive Impairment Using an Extreme Learning Machine-Based Grading Method With Multimodal Data. Front. Aging Neurosci. 12:77. doi: 10.3389/fnagi.2020.00077

Identifying patients with mild cognitive impairment (MCI) who are at high risk of progressing to Alzheimer's disease (AD) is crucial for early treatment of AD. However, it is difficult to predict the cognitive states of patients. This study developed an extreme learning machine (ELM)-based grading method to efficiently fuse multimodal data and predict MCI-to-AD conversion. First, features were extracted from magnetic resonance (MR) images, and useful features were selected using a feature selection method. Second, multiple modalities of MCI subjects, including MRI, positron emission tomography, cerebrospinal fluid biomarkers, and gene data, were individually graded using the ELM method. Finally, these grading scores calculated from different modalities were fed into a classifier to discriminate subjects with progressive MCI from those with stable MCI. The proposed approach has been validated on the Alzheimer's Disease Neuroimaging Initiative (ADNI) cohort, and an accuracy of 84.7% was achieved for an AD prediction within 3 years. Experiments on predicting AD conversion from MCI within different periods showed similar results with the 3-year prediction. The experimental results demonstrate that the proposed approach benefits from the efficient fusion of four modalities, resulting in an accurate prediction of MCI-to-AD conversion.

Keywords: Alzheimer's disease, extreme learning machine, mild cognitive impairment, multimodal, prediction

INTRODUCTION

Alzheimer's disease (AD) is the most common cognitive impairment disease, which gradually impacts the activities of a patient's daily life. The number of AD patients was estimated to be approximately 30 million in 2015 (Vos et al., 2016), which has placed a huge socioeconomic burden on those taking care of AD patients. The pathology changes of AD begin several years before the

first clinical symptoms, and mild cognitive impairment (MCI) is thought to be the prodromal stage of AD (Markesbery and Lovell, 2010). Approximately 10–17% of those with MCI progress to AD over the course of a few years, yet some MCI patients remain stable after several years (Hamel et al., 2015). It is crucial to identify people who are at high risk of progressing from MCI to AD because it can help physicians treat these patients sooner and apply suitable therapies to slow down the progression or even improve a patient's condition. Numerous studies have used machine learning techniques for computer-aided diagnosis of AD or prediction of AD conversion. The diagnosis of AD is relatively easier than the prediction of AD because there are apparent differences between AD and a normal control (NC), and the accuracy of diagnosis has reached to above 96% (Lei et al., 2016; Kim and Lee, 2018). However, the prediction of AD, more specifically, discriminating progressive MCI (pMCI) from stable MCI (sMCI), is more challenging because the differences between these two groups are slight.

Different modalities of medical data have been used to detect the pathology associated with AD. Structural magnetic resonance imaging (sMRI) is one of the most widely used modality due to its high resolution and non-invasive characteristics (Querbes et al., 2009; Oliveira et al., 2010; Coupé et al., 2012; Eskildsen et al., 2013). AD patients are always accompanied by cerebral atrophy or ventricular expansion that is caused by the death of neurons in the affected regions. The cerebral atrophy patterns associated with AD can be revealed by MRI, and MRI is a good detection technique for the atrophy of AD. Moradi et al. (2015) calculated an MRI-based biomarker for the prediction of MCI-to-AD conversion. Tong et al. (2017a) applied an elastic net regression to grade MRI features and to predict MCI-to-AD conversion. Lin et al. (2018) used a convolutional neural network-based framework to extract high-level AD-related features from MRI for the prediction of AD. These methods only focused on MRI data and could only predict a 3-year AD conversion with an accuracy no greater than 80%. Fluorodeoxyglucose positron emission tomography (FDG-PET) is another useful neuroimaging modality for the detection of AD. Studies (Mosconi et al., 2009; JackJr., Knopman et al., 2010; Landau et al., 2011) have shown that AD and MCI patients have reduced glucose metabolism in certain cerebral regions, which occur prior to the changes in brain structure. The brain's metabolic activity can be quantitatively measured by FDG-PET, which makes FDG-PET a potential tool for the early detection of AD (Gray et al., 2013; Cheng et al., 2015; Iaccarino et al., 2017). In a recent study (Lu et al., 2018), FDG-PET images were used in a multiscale deep neural network to classify AD/NC and pMCI/sMCI, where accuracies of 93.58 and 82.51% were achieved, respectively. In addition to MRI and FDG-PET, biological biomarkers can also contribute to the detection of AD. The abnormal concentrations of proteins in cerebrospinal fluid (CSF), such as total tau (T-tau), hyperphosphorylated tau (P-tau), and the 42 amino acid isoforms of amyloid β (Aβ42), are some of the earliest signs of AD that occur many years before the onset of clinical symptoms (Niemantsverdriet et al., 2017). Therefore, these biomarkers can provide valuable information for the early detection of AD. Genetics are also an important indicator of the risk of AD. Individuals with the apolipoprotein E (APOE) $\epsilon 4$ gene have a much higher risk of developing AD than those without APOE $\epsilon 4$ (Vounou et al., 2012; Lambert et al., 2013). Taking APOE $\epsilon 4$ into account with imaging or biological biomarkers can improve the accuracy of AD prediction.

Different modalities of biomarkers reflect the AD-related pathological changes in different aspects, thus there may be complementary information among several modalities. Combining multimodal biomarkers would provide more information and improve the accuracy of AD prediction. A simple way to fuse different modalities is to directly concatenate multimodal features and feed them into a classifier (Kohannim et al., 2010; Walhovd et al., 2010; Westman et al., 2012). However, this is not the optimal approach, and it can lead to bias of the modality with a larger number of features. A better way is to map these multimodal features into a kernel space before concatenation (Hinrichs et al., 2011; Zhang et al., 2011; Young et al., 2013), but these methods are sensitive to the weight assigned to each modality. In recent years, deep learning architecture has been employed to extract multimodal feature representations. Liu et al. (2015) used stacked auto-encoders and a zero-mask strategy to fuse MRI and PET data. Suk et al. (2014) proposed a joint feature representation of MRI and PET with a multimodal deep Boltzmann machine. Liu et al. (2018) constructed multiple deep three-dimensional (3D) convolutional neural networks to transform MRI and PET images into compact high-level features. These deep learning-based methods achieved promising results in the classification of AD/NC, but the accuracy of classifying pMCI/sMCI was just 74.58% (Suk et al., 2014). To exploit the complementarity across multimodal data, Tong et al. (2017b) employed a non-linear graph fusion that achieved better results in the diagnosis of AD and a three-way classification of AD/MCI/NC than the approaches based on a linear combination, but the classification of pMCI from sMCI was not validated. Although all of these multimodal data-based methods achieved promising results in the diagnosis of AD, the performance of AD prediction needs to be further improved for clinical use with the help of an efficient fusion of multimodal biomarkers.

Since the efficient multimodality fusion can improve the performance of an artificial intelligence system (Hu et al., 2018), in this work, we present a novel extreme learning machine (ELM)-based (Huang et al., 2012) grading method to combine four modalities (MRI, FDG-PET, CSF, and APOE $\epsilon 4$) that predict MCI-to-AD conversion. Specifically, each modality feature, from the MCI subjects, was individually graded by an ELM that trained with the corresponding modality features of AD and NC, and the grading score represented the similarity of MCI-to-AD or NC. Then, the scores of all modalities were concatenated and fed to an ELM classifier for classification of pMCI/sMCI. The results of the proposed method were evaluated by 100 runs of 10-fold cross-validation with data from the ADNI cohort. The contributions of this paper are as follows:

(i) Useful information about AD/NC was included by using the AD/NC features when training the grading ELMs, which improved the process of discriminating pMCI from sMCI.

(ii) These grading ELMs were trained with discrete labels of AD/NC and modified to output grading values, instead of discrete labels, to represent the similarity of MCI to AD or NC.
(iii) Each modality was graded into one single score, avoiding bias of the modality with a greater number of features.
(iv) The proposed approach achieved promising results in the prediction of MCI-to-AD conversion.

MATERIALS

The multimodal data used in this study included 313 MRI features, 20 FDG-PET features, three CSF biomarkers, and one gene feature. The MRI features, consisting of volume, surface area, and cortical thickness of the cerebral regions, were obtained through analysis with the FreeSurfer software using cross-sectional processing (Fischl and Dale, 2000; Fischl et al., 2004). There was 345 features obtained from the FreeSurfer analysis; however, because 32 features were absent from most subjects, only 313 MRI features were selected. For FDG-PET scans, five regions, frequently cited in FDG-PET studies of AD, were adopted, including left angular, right angular, bilateral posterior cingulate, left inferior temporal, and right inferior temporal (Landau et al., 2010; Landau et al., 2011). The mean, minimum, maximum, and standard deviation values of the intensity in each region were taken as the FDG-PET features. The levels of the biomarkers Aβ42, T-tau, and P-tau in CSF were used as the CSF features. The gene feature was a single categorical variable indicating the presence of APOE $\epsilon 4$ in subjects. All the multimodal data were downloaded from the ADNI website. Specifically, the MRI, CSF, and gene data were provided by the Tadpole Challenge Data files, and the FDG-PET data were provided by the UC Berkeley FDG Analysis file.

To date, there have been over 1,500 participants, ages 55 to 90 years, recruited by ADNI, and most of them were visited and tested multiple times in the following years for long-term study. In this study, we only take baseline data to predict the future state (progress to AD or remain MCI) for MCI subjects. Because not all subjects underwent all possible examinations, we excluded subjects without all modalities data available at the baseline visit, which presented 200 NC subjects, 102 AD subjects, 110 pMCI subjects who converted to AD within 3 years, and 205 sMCI subjects who did not convert to AD. Demographic and clinical information of these subjects are listed in **Table 1**, including gender, age, education history, and Mini Mental State Examination (MMSE) score.

METHODS

The overall framework of the proposed approach is shown in **Figure 1**, and we also summarize the process of our proposed approach as pseudo-code in **Algorithm 1**. There are three major steps in this framework: (i) MRI features are first preprocessed by feature selection with the least absolute shrinkage and selection operator (LASSO) algorithm; (ii) each modality (CSF and gene are combined as biological modality) of MCI is graded by ELM. These ELMs are trained with corresponding modality of features and labels from AD/NC groups. A grading score is calculated for each modality, which represents the similarity of MCI-to-AD or NC; (iii) these scores are combined to form the new representative features of MCI and fed into an ELM classifier to discriminate pMCI from sMCI. Ten-fold cross-validation is utilized to assess the performance of the proposed approach. Before these steps, all features of AD/NC are first normalized to have zero mean and unit variance. The features of MCI are also normalized with the mean and deviation of the AD/NC features. In the following sections, we will present the details of these steps.

Feature Selection With Least Absolute Shrinkage and Selection Operator

Different from other modalities, the MRI features are the morphological characters of all cerebral regions. However, some of them may be aging-related and not AD-related, which can interfere with the classification, and thus need to be excluded. In this study, we adopted LASSO to select only useful MRI features. LASSO is an $L_{2,1}$ norm sparse regression model (Kukreja et al., 2006) and has the following formula:

$$\min_{\alpha} \ 0.5||y - D\alpha||_2^2 + \lambda||\alpha||_1. \tag{1}$$

In formula (1), $\boldsymbol{y}\in\mathbf{R}^{1\times N}$ is the vector of N labels, and $\boldsymbol{D}\in\mathbf{R}^{N\times M}$ is a feature matrix that consists of N training samples with M features in each sample. The variable λ is the penalty coefficient that was set to 0.015 in this study, and $\alpha\in\mathbf{R}^{1\times M}$ is the target sparse coefficients. When this model is solved, only some coefficients in α would be non-zero, where the larger absolute value of these coefficients indicates higher usefulness of the corresponding features. Therefore, the results of α can be used to select discriminative features. Unlike previous studies

TABLE 1 | The demographic information of subjects.

Mean ± SD	NC	sMCI	pMCI	AD
Count (F/M)	200 (93/107)	205 (90/115)	110 (47/63)	102 (35/67)
Age	73.9 ± 6.0	71.8 ± 7.1	73.9 ± 7.2	75.7 ± 8.0
Education	16.4 ± 2.7	16.1 ± 2.7	16.2 ± 2.7	15.4 ± 3.0
MMSE	29.0 ± 1.2	28.1 ± 1.7	27.1 ± 1.7	23.2 ± 2.0

In cells of the second row, the first number is total number with numbers of female (F) and male (M) in brackets. AD, Alzheimer's disease; MMSE, Mini Mental State Examination; NC, normal control; pMCI, progressive mild cognitive impairment; SD, standard deviation; sMCI, stable mild cognitive impairment.

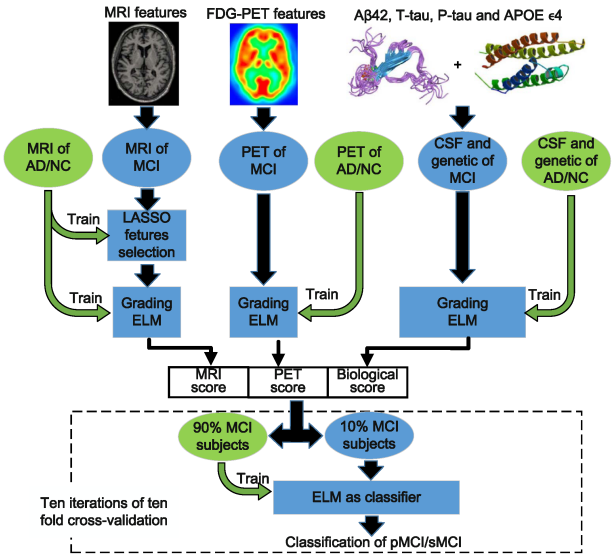

FIGURE 1 | The overall framework of the proposed approach.

ALGORITHM 1 | The pseudo-code of the proposed method.

Input: $\boldsymbol{M}_{AD/NC}$, $\boldsymbol{P}_{AD/NC}$, $\boldsymbol{B}_{AD/NC}$, $\boldsymbol{M}_{MCI}$, $\boldsymbol{P}_{MCI}$, $\boldsymbol{B}_{MCI}$

α = LASSO(train = $\boldsymbol{M}_{AD/NC}$).coefficients;

$\boldsymbol{M}_{AD/NC}$ = $\boldsymbol{M}_{AD/NC}$[:, α! = 0], $\boldsymbol{M}_{MCI}$ = $\boldsymbol{M}_{MCI}$[:, α! = 0];

$score_{MRI}$ = ELM(train = $\boldsymbol{M}_{AD/NC}$).outputScore($\boldsymbol{M}_{MCI}$);

$score_{PET}$ = ELM(train = $\boldsymbol{P}_{AD/NC}$).outputScore($\boldsymbol{P}_{MCI}$);

$score_{Bio}$ = ELM(train = $\boldsymbol{B}_{AD/NC}$).outputScore($\boldsymbol{B}_{MCI}$);

scores = [$score_{MRI}$, $score_{PET}$, $score_{Bio}$]; ## scores$\in\mathbf{R}^{N\times 3}$

Classification and Validation:

for n from 1 to 100:

  scores = scores[random_permute,:];

  Ten folds cross-validation:

  separate scores into ten folds along first dimension;

  for i from 1 to 10:

    testSet = scores[foldth = = i,:];

    trainSet = scores[others,:];

    record predict = ELM(train = trainSet).classify(testSet);

  end for

end for

statistics of 100 runs

(Lee et al., 2016; Lin et al., 2018), which trained the LASSO model with pMCI/sMCI features for the pMCI/sMCI classification task, we thought the features of AD/NC were more representative and used them to train LASSO model. Then, the features with non-zero coefficients in α were selected.

Extreme Learning Machine

Extreme learning machine is a one-step learning algorithm that is faster and has a higher performance than the support vector machine (Huang et al., 2012; Zeng et al., 2017). There are two types of basic ELM; the first is a feed-forward neural network with only a single layer of randomly generated hidden nodes (Huang et al., 2006). The second type is an ELM with kernels (Huang et al., 2012), which avoids the random generation of an input weight matrix. ELM with kernels yields more stable results and has a higher performance than the feed-forward neural network. In our previous work (Lin et al., 2018), the ELM with kernels showed more efficiency than support vector machine and random forest in the prediction of AD. Therefore, we adopted ELM with a Gaussian kernel in this study. The process of ELM with a Gaussian kernel can be described as follows:

Suppose we have N training samples $[\boldsymbol{x}_1, \boldsymbol{x}_2, \cdots, \boldsymbol{x}_N]$ and N labels. The variable $\boldsymbol{x}_n$ represents a vector with M features of one sample, and $\boldsymbol{Y}\in\mathbf{R}^{N\times 2}$ is a ground truth label matrix with N rows. In each row, the element corresponding to the true label is set to 1, and the other is set to −1. When a new sample, $\boldsymbol{x}$, is obtained, the label of $\boldsymbol{x}$ can be predicted as

$$f(x) = \begin{bmatrix} K(x, x_1) \\ K(x, x_2) \\ \vdots \\ K(x, x_N) \end{bmatrix} \left(\Omega + \frac{I}{C}\right)^{-1} Y, \tag{2}$$

where $K(\boldsymbol{x}, \boldsymbol{x}_N)$ is the Gaussian kernel described as

$$K(u, v) = exp\left(\frac{-\|u - v\|^2}{\gamma}\right), \tag{3}$$

and Ω is an $N \times N$ kernel matrix that is related to the training samples, which is calculated in the training phase as

$$\Omega = \begin{bmatrix} K(x_1, x_1) & \cdots & K(x_1, x_N) \\ K(x_2, x_1) & & K(x_2, x_N) \\ \vdots & \cdots & \vdots \\ K(x_N, x_1) & & K(x_N, x_N) \end{bmatrix}. \tag{4}$$

The variable C in formula (2) is a regularization coefficient and is set to 1. The variable γ in formula (3) is a parameter of the Gaussian kernel, which is set to 10 times M number of features in this study.

The output of formula (2) is a vector with two elements: $[s_1, s_2]$. When ELM is used as the classifier, the output is the result of comparing the values of s_1 and s_2. In this study, we used the ELM to grade MCI samples, and the output of ELM was modified as $s = s_1 - s_2$. When the ELM was trained with AD/NC and tested on MCI, the output score s can represent the similarity of MCI-to-AD or NC.

Classification and Performance Analysis

Ten-fold cross-validation was implemented to assess the performance of the proposed approach. All MCI subjects were separated into 10-folds randomly. In each validation iteration, one different fold was selected as testing data and the other nine folds were used as training data. This process was repeated for 10 iterations. The classification results of 10 iterations were compared to the true labels, and the accuracy, sensitivity, specificity, and area under receiver operating characteristic (ROC) curve (AUC) were calculated. To avoid sampling bias, the 10-fold cross-validation was run 100 times with randomly

permuted samples, and the mean and standard deviation of the accuracy, sensitivity, specificity, and AUC were given.

EXPERIMENTS AND RESULTS

Results Using Multimodality Data

To evaluate the improvement of the proposed approach, we compared it with the method that directly concatenates multimodal data. The results of the comparison are shown in **Figure 2**. From these results, we found that the method that directly concatenates the four modalities had a high accuracy and specificity of 80.1 and 91.1%, respectively, but the sensitivity was quite low. For a non-biased performance evaluation, we calculated the balanced accuracy, which is the average of sensitivity and specificity, and obtained 75.3%, which is not optimal. The proposed approach had better results in terms of accuracy and sensitivity, with an accuracy of 84.7% and a sensitivity of 72.7%. This is approximately 13% higher than the direct concatenation method. The proposed approach also has a promising balanced accuracy of 81.9%, which is 6.6% higher than the other method. Beside these scores, we also obtained an improved AUC of 88.8% for our proposed method. This comparison indicates that the proposed approach is more efficient at predicting the MCI-to-AD conversion than the method using directly concatenated multimodal data.

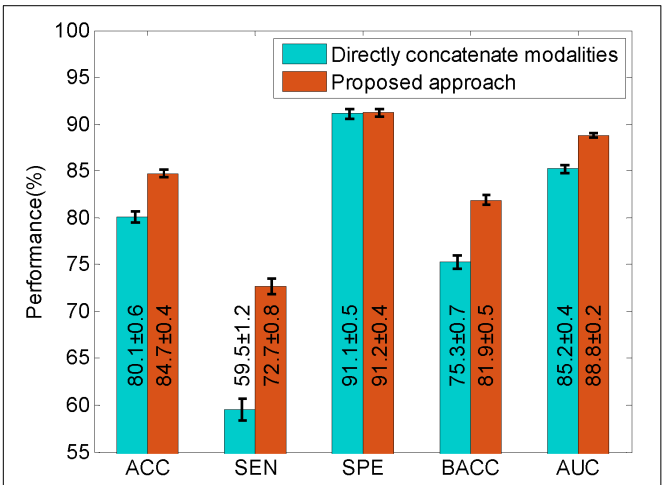

FIGURE 2 | The comparison of the proposed approach with the method that directly concatenates multiple modalities. The black lines superimposed on each bar, and the second number in each bar represents the standard deviations derived from 100 runs of validation. ACC, accuracy; AUC, area under receiver operating characteristic curve; BACC, balanced accuracy; SEN, sensitivity; SPE, specificity.

Contributions of Different Modalities

To reveal the contributions of the different modalities in the proposed method, experiments were conducted with only one modality and one modality absent. The results are listed in **Table 2**. Because the APOE $\epsilon 4$ data failed to classify pMCI/sMCI individually (with balanced accuracy of 55.2%), we used CSF + APOE $\epsilon 4$ to demonstrate the effect of APOE $\epsilon 4$.

From these results, we can see that when only one modality was used, the performance of the CSF ranked third in terms of accuracy and AUC, but it had the best sensitivity. The APOE $\epsilon 4$ feature can slightly improve the results using CSF. FDG-PET achieved the best results, but the best accuracy and balanced accuracy were only 76.7 and 71.7%, respectively. When all modalities were used, the accuracy and balanced accuracy was greatly improved to 84.7 and 81.9%, respectively, and there was also a significant improvement in AUC. **Figure 3** shows the improvement in the ROC curves of the proposed approach, when all modalities were used compared with only one modality used. In the situation with one modality absent, it shows that the performance declined without CSF, especially a significant decline of sensitivity, which led to the decline of balanced accuracy. The MRI and FDG-PET had a similar impact on the performance of the proposed method, while the APOE $\epsilon 4$ had minimal influence on the performance. Even when all modalities were used, if the LASSO was disabled, the performance suffered from a 1.2 and 1.8% drop in the accuracy and balanced accuracy, respectively, which illustrates the contribution of LASSO.

TABLE 2 | The contributions of different modalities.

Modalities	ACC	SEN	SPE	BACC	AUC
MRI	74.5 ± 0.4%	54.8 ± 0.9%	85.0 ± 0.3%	69.9 ± 0.5%	79.2 ± 0.2%
FDG-PET	76.7 ± 0.4%	55.1 ± 0.8%	88.2 ± 0.5%	71.7 ± 0.4%	80.9 ± 0.2%
CSF	73.0 ± 0.5%	62.5 ± 1.0%	78.7 ± 0.5%	70.6 ± 0.6%	79.0 ± 0.3%
CSF + APOEϵ4	73.9 ± 0.4%	63.2 ± 0.7%	79.7 ± 0.6%	71.4 ± 0.4%	78.8 ± 0.3%
- MRI	81.3 ± 0.5%	67.0 ± 1.0%	89.0 ± 0.5%	78.0 ± 0.6%	86.8 ± 0.2%
- FDG-PET	81.0 ± 0.5%	67.2 ± 0.8%	88.4 ± 0.5%	77.8 ± 0.5%	86.7 ± 0.2%
- CSF	79.6 ± 0.6%	63.5 ± 1.2%	88.3 ± 0.5%	75.9 ± 0.7%	85.8 ± 0.2%
- APOEϵ4	83.2 ± 0.5%	69.8 ± 1.0%	90.4 ± 0.5%	80.1 ± 0.6%	88.7 ± 0.2%
- LASSO	83.5 ± 0.6%	69.0 ± 1.2%	91.2 ± 0.6%	80.1 ± 0.7%	88.8 ± 0.2%
All	84.7 ± 0.4%	72.7 ± 0.8%	91.2 ± 0.4%	81.9 ± 0.5%	88.8 ± 0.2%

"- modality" means the absence of the modality in experiments. In each cell, the two numbers represent the mean and standard deviation derived from 100 runs of validation. ACC, accuracy; APOE, apolipoprotein E; AUC, area under receiver operating characteristic curve; BACC, balanced accuracy; CSF, cerebrospinal fluid; LASSO, least absolute shrinkage and selection operator; SEN, sensitivity; SPE, specificity.

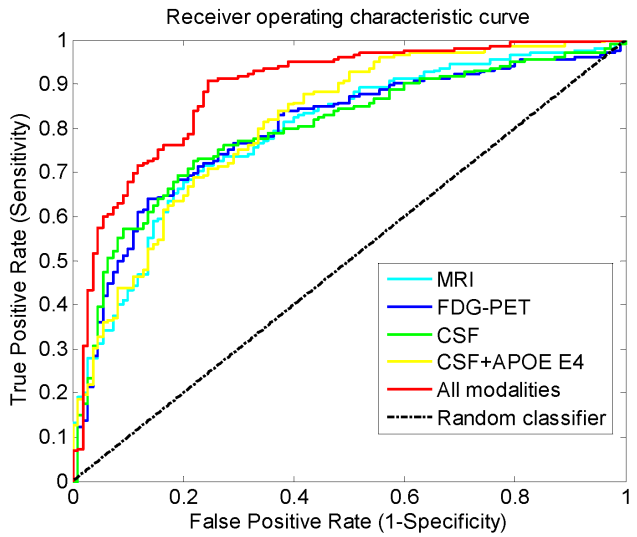

FIGURE 3 | The receiver operating characteristic curves when different modalities were used.

Prediction Within Different Periods

The 3-year cutoff period for predicting MCI-to-AD conversion is not a unique criterion. We also conducted experiments to predict the states of MCI patients with different periods from 1 to 5 years. With the criterion changed, different numbers of pMCI/sMCI for different conversion times were obtained: 46/343 (1 year), 89/268 (2 years), 110/205 (3 years), 119/146 (4 years), 117/62 (5 years). The results of predicting MCI-to-AD conversion at different time periods are shown in **Figure 4**. From **Figure 4A**, we can see that the accuracies are all above 83% for 1–5 years prediction. However, from **Figure 4B**, we found the specificity was high and the sensitivity was low at the point of 1 year, owing to the disparity of the number of individuals with pMCI versus sMCI (46/343), and the balanced accuracy was only 60.2%. At the point of 2 years, the bias is still large: 89/268 pMCI/sMCI. As a result, the balanced accuracy was only 74.9%. At the 3–5-year mark, the bias reduced and the balanced accuracies stabilized at approximately 82%. At the points of 3–5 years, we achieved an accuracy, balanced accuracy, and AUC of 83, 81.8, and 88.8%, respectively. These results show a promising performance of the proposed approach for predicting MCI-to-AD conversion within different periods.

Experiments on Other Conditions

We also conducted the experiments on different conditions, including:

(i) An Support Vector Machine (SVM) version, in which SVM was the classifier instead of ELM.

(ii) In some studies, neuropsychological test scores (MMSE, clinical dementia rating-sum of boxes, Alzheimer's disease assessment scale-cognitive subtest, Rey's auditory verbal learning test, functional activities questionnaire) were included to boost the performance of prediction. Therefore, these neuropsychological test scores were also included and concatenated with grading scores.

(iii) In previous studies (Moradi et al., 2015; Tong et al., 2017a), the definition of sMCI was stricter, and the subjects who converted to AD beyond 3 years or the diagnosis changed from MCI to NC were removed from the sMCI group. Therefore, we also excluded 64 subjects with the same criterion, and then obtained 141 sMCI and 110 pMCI.

The results are listed in **Table 3**, from which it can be seen that the ELM classifier has a better performance than the SVM classifier. When neuropsychological test scores were included in

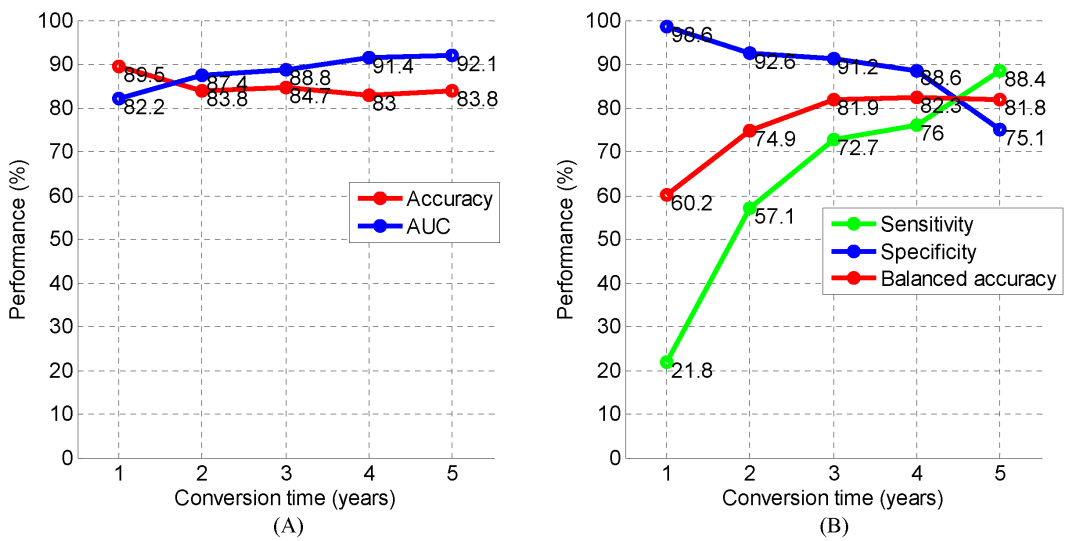

FIGURE 4 | The performance of predicting MCI-to-AD conversion at different time periods. **(A)** Performance of accuracy and AUC. **(B)** Performance of sensitivity, specificity, and balanced accuracy. AD, Alzheimer's disease; AUC, area under receiver operating characteristic curve; MCI, mild cognitive impairment.

TABLE 3 | The experiments on different conditions.

Classifier	Modalities	pMCI/sMCI	ACC	AUC
SVM	MRI, PET, CSF, APOE	110/205	83.6%	–
ELM	MRI, PET, CSF, APOE	110/205	84.7%	88.8%
ELM	MRI, PET, CSF, APOE, neuropsychological scores	110/205	85.1%	92.6%
ELM	MRI, PET, CSF, APOE, neuropsychological scores	110/141 (ambiguous subjects excluded)	87.1%	94.7%

ACC, accuracy; APOE, apolipoprotein E; AUC, area under receiver operating characteristic curve; CSF, cerebrospinal fluid; ELM, extreme learning machine; pMCI, progressive mild cognitive impairment; sMCI, stable mild cognitive impairment; SVM, support vector machine.

the proposed method, there was not a significant improvement in accuracy, but the AUC greatly improved. When the ambiguous subjects were excluded from the sMCI group, the performance was further improved. To the best of our knowledge, the accuracy of 87.1% and AUC of 94.7%, achieved in this experiment, are the best for predicting AD.

DISCUSSION

In this study, we propose a novel approach for predicting MCI-to-AD conversion with multimodal data. To effectively fuse different modalities and avoid the bias of a number of features in each modality; an ELM-based grading method was employed to calculate a grading score for each modality. The scores of multiple modalities were combined and fed into the ELM classifier to discriminate the pMCI from sMCI. With the help of AD/NC information included in the grading procedure, the scores effectively represented the states of the MCI subjects and were used to predict the AD conversion individually. When the scores from all modalities were combined, the accuracy of prediction was boosted to 84.7%. The results of the experiments conducted on the ADNI cohort demonstrate that: (i) the proposed method with multimodality scores has a much higher accuracy than with a single modality score, such that the proposed method has at least a 10% higher balanced accuracy than when a single modality is used. This means that the complementary information among the multimodal data can be represented by these scores. (ii) Direct concatenation of multimodal data is not the best way of exploiting the complementary information, and the proposed method showed a more efficient fusion of multimodal data and achieved a much better performance. (iii) The proposed method can predict MCI-to-AD conversion of different periods with a high accuracy.

As more modalities bring more complementary information, the performance of the prediction should improve. As shown in **Table 3**, when the neuropsychological test scores were included in our approach, the AUC improved, but the accuracy only had a 0.4% improvement. The assumption is that there might be an up-boundary for discriminating pMCI from sMCI, from the fact that the diagnosis in ADNI is not 100% reliable (Ranginwala et al., 2008). Therefore, when we defined the sMCI more strictly and excluded ambiguous samples, the accuracy was further boosted to 87.1% as shown in **Table 3**. It is also observed that the specificity was much higher than sensitivity in **Table 2**, and we assume the reason for this might be a bias in the number of pMCI against the number of sMCI. This can be explained in **Figure 4B** that shows that as the bias in the number of pMCI versus sMCI decreased, a similar specificity and sensitivity were obtained.

Although the proposed approach achieved a promising result in predicting AD conversion, it requires four modalities, which is difficult to obtain in clinical practice. However, in the research of longitudinal regression for modeling the trajectory of AD progression, it is crucial to estimate the cognitive states of patients. In our future work, we will consider the use of the ELM-based grading method proposed in this study to improve the accuracy of longitudinal regression for AD trajectory modeling.

In the proposed approach, the feature selection was only applied to MRI features since the PET features were from five AD-related regions and the three CSF biomarkers and APOE $\epsilon 4$ gene contained useful information about AD. Because the MRI features from the FreeSurfer analysis were morphology features of whole brain, inevitably it had to include some useless features. As a result, LASSO was employed to do the feature selection on MRI features, and it improved the results of prediction. To explore which MRI features were selected, we have listed the top 10 features in **Table 4**. We can observe that the volumes and thicknesses of the hippocampus, amygdala, temporal lobe, and entorhinal cortex play an important role in the detection of AD, which is consistent with previous studies (Van Hoesen et al., 1991; Convit et al., 2000; Mu and Gage, 2011; Poulin et al., 2011).

CONCLUSION

In this study, we have developed an ELM-based grading method to fuse multimodal data for the prediction of MCI-to-AD

TABLE 4 | The top 10 AD-related MRI features from LASSO feature selection.

Num.	MRI features
1	Volume of left hippocampus
2	Volume of left amygdala
3	Volume of left inferior lateral ventricle
4	Surface area of left isthmus cingulate
5	Volume of right hippocampus
6	Volume of left inferior temporal
7	Cortical thickness average of left middle temporal
8	Cortical thickness standard deviation of right transverse temporal
9	Cortical thickness standard deviation of right lateral orbitofrontal
10	Cortical thickness average of right entorhinal

AD, Alzheimer's disease; LASSO, least absolute shrinkage and selection operator.

conversion within 3 years. With the input of four modalities: MRI, FDG-PET, CSF, and gene presence, we achieved a promising result with an accuracy of 84.7% and AUC of 88.8%. When compared with method that directly concatenates multiple modalities, the proposed approach outperformed the other in terms of accuracy and AUC. The experiments demonstrated that this approach can also predict AD conversion of other periods with a similar performance of the 3-year prediction.

DATA AVAILABILITY STATEMENT

The datasets generated for this study are available on request to the corresponding author.

ETHICS STATEMENT

As per ADNI protocols, all procedures performed in studies involving human participants were in accordance with the ethical standards of the institutional and/or national research committee and with the 1964 Helsinki declaration and its later amendments or comparable ethical standards. The ADNI data collection was carried out after obtaining written informed consent from the participants. More details can be found at adni.loni.usc.edu.

AUTHOR CONTRIBUTIONS

WL and TT conceived the study, designed the experiments, analyzed the data, and wrote the manuscript. QG provided the preprocessed data. JY and ZC carried out experiments. CF and WC helped to analyze the data and experiments result. MD and TT revised the manuscript.

FUNDING

This work was supported in part by National Natural Science Foundation of China under Grant 61901120 and Grant 61802065, in part by the Key Projects of Technological Department in Fujian Province under Grant 321192016Y0069201615, in part by the Science and Technology Program of Fujian Province of China under Grant 2019YZ016006, in part by the Natural Science Foundation of Fujian Province of China under Grant 2018J01565, in part by the Foundation of Educational and Scientific Research Projects for Young and Middle-aged Teachers of Fujian Province under Grant JAT170406, in part by the Scientific Research Climbing Project of Xiamen University of Technology under Grant XPDKT19006, and in part by the High-level Talent Project of Xiamen University of Technology under Grant YKJ17021R.

ACKNOWLEDGMENTS

The ADNI data collection and sharing for this project were funded by the Alzheimer's Disease Neuroimaging Initiative (ADNI; Principal Investigator: Michael Weiner; NIH grant U01 AG024904). ADNI is funded by the National Institute on Aging, the National Institute of Biomedical Imaging and Bioengineering (NIBIB), and through generous contributions from the following: Pfizer Inc., Wyeth Research, Bristol-Myers Squibb, Eli Lilly and Company, GlaxoSmithKline, Merck & Co., Inc., AstraZeneca AB, Novartis Pharmaceuticals Corporation, Alzheimer's Association, Eisai Global Clinical Development, Elan Corporation plc, Forest Laboratories, and the Institute for the Study of Aging, with participation from the U.S. Food and Drug Administration. Industry partnerships are coordinated through the Foundation for the National Institutes of Health. The grantee organization is the Northern California Institute for Research and Education, and the study is coordinated by the Alzheimer's Disease Cooperative Study at the University of California, San Diego. ADNI data are disseminated by the Laboratory of Neuroimaging at the University of California, Los Angeles.

REFERENCES

Cheng, B., Liu, M., Zhang, D., Munsell, B. C., and Shen, D. (2015). Domain transfer learning for MCI conversion prediction. *IEEE Trans. Biomed. Eng.* 62, 1805–1817. doi: 10.1109/TBME.2015.2404809

Convit, A., De Asis, J., De Leon, M., Tarshish, C., De Santi, S., and Rusinek, H. (2000). Atrophy of the medial occipitotemporal, inferior, and middle temporal gyri in non-demented elderly predict decline to Alzheimer's disease. *Neurobiol. Aging* 21, 19–26. doi: 10.1016/s0197-4580(99)00107-4

Coupé, P., Eskildsen, S. F., Manjón, J. V., Fonov, V. S., and Collins, D. L. (2012). Simultaneous segmentation and grading of anatomical structures for patient's classification: application to Alzheimer's disease. *Neuroimage* 59, 3736–3747. doi: 10.1016/j.neuroimage.2011.10.080

Eskildsen, S. F., Coupé, P., García-Lorenzo, D., Fonov, V., Pruessner, J. C., and Collins, D. L. (2013). Prediction of Alzheimer's disease in subjects with mild cognitive impairment from the ADNI cohort using patterns of cortical thinning. *Neuroimage* 65, 511–521. doi: 10.1016/j.neuroimage.2012.09.058

Fischl, B., and Dale, A. M. (2000). Measuring the thickness of the human Cereb. Cortex from magnetic resonance images. *Proc. Natl. Acad. Sci. U.S.A.* 97, 11050–11055. doi: 10.1073/pnas.200033797

Fischl, B., van der Kouwe, A., Destrieux, C., Halgren, E., Segonne, F., Salat, D. H., et al. (2004). Automatically parcellating the human Cereb. *Cortex Cereb. Cortex* 14, 11–22. doi: 10.1093/cercor/bhg087

Gray, K. R., Aljabar, P., Heckemann, R. A., Hammers, A., and Rueckert, D. (2013). Random forest-based similarity measures for multi-modal classification of Alzheimer's disease. *Neuroimage* 65, 167–175. doi: 10.1016/j.neuroimage.2012.09.065

Hamel, R., Kohler, S., Sistermans, N., Koene, T., Pijnenburg, Y., van der Flier, W., et al. (2015). The trajectory of cognitive decline in the pre-dementia phase in memory clinic visitors: findings from the 4C-MCI study. *Psychol. Med.* 45, 1509–1519. doi: 10.1017/S0033291714002645

Hinrichs, C., Singh, V., Xu, G., and Johnson, S. C. (2011). Predictive markers for AD in a multi-modality framework: an analysis of MCI progression in the ADNI population. *Neuroimage* 55, 574–589. doi: 10.1016/j.neuroimage.2010.10.081

Hu, T. K., Lin, Y. Y., and Hsiu, P. C. (2018). "Learning adaptive hidden layers for mobile gesture recognition," in *Thirty-Second AAAI Conference on Artificial Intelligence* (Palo Alto, CA: AAAI Press).

Huang, G. B., Zhou, H., Ding, X., and Zhang, R. (2012). Extreme learning machine for regression and multiclass classification. *IEEE Trans. Syst. Man Cybern.* 42, 513–529. doi: 10.1109/TSMCB.2011.2168604

Huang, G. B., Zhu, Q. Y., and Siew, C. K. (2006). Extreme learning machine: theory and applications. *Neurocomputing* 70, 489–501. doi: 10.1016/j.neucom.2005.12.126

Iaccarino, L., Chiotis, K., Alongi, P., Almkvist, O., Wall, A., Cerami, C., et al. (2017). A cross-validation of FDG- and amyloid-PET biomarkers in mild cognitive impairment for the risk prediction to dementia due to Alzheimer's disease in a clinical setting. *J. Alzheimers Dis.* 59, 603–614. doi: 10.3233/JAD-170158

Jack, J. C. Jr., Knopman, D. S., Jagust, W. J., Shaw, L. M., Aisen, P. S., Weiner, M. W., et al. (2010). Hypothetical model of dynamic biomarkers of the Alzheimer's pathological cascade. *Lancet Neurol.* 9, 4–5.

Kim, J., and Lee, B. (2018). Identification of Alzheimer's disease and mild cognitive impairment using multimodal sparse hierarchical extreme learning machine. *Hum. Brain Mapp.* 39, 3728–3741. doi: 10.1002/hbm.24207

Kohannim, O., Hua, X., Hibar, D. P., Lee, S., and Thompson, P. M. (2010). Boosting power for clinical trials using classifiers based on multiple biomarkers. *Neurobiol. Aging* 31, 1429–1442. doi: 10.1016/j.neurobiolaging.2010.04.022

Kukreja, S. L., Löfberg, J., and Brenner, M. J. (2006). A least absolute shrinkage and selection operator (LASSO) for nonlinear system identification. *IFAC Proc.* 39, 814–819. doi: 10.3182/20060329-3-au-2901.00128

Lambert, J. C., Ibrahimverbaas, C. A., Harold, D., Naj, A. C., Sims, R., Bellenguez, C., et al. (2013). Meta-analysis of 74,046 individuals identifies 11 new susceptibility loci for Alzheimer's disease. *Alzheimers Demen.* 9, 1452–1458. doi: 10.1038/ng.2802

Landau, S. M., Harvey, D., Madison, C. M., Koeppe, R. A., Reiman, E. M., Foster, N. L., et al. (2011). Associations between cognitive, functional, and FDG-PET measures of decline in AD and MCI. *Neurobiol. Aging* 32, 1207–1218. doi: 10.1016/j.neurobiolaging.2009.07.002

Landau, S. M., Harvey, D., Madison, C. M., Reiman, E. M., Foster, N. L., Aisen, P. S., et al. (2010). Comparing predictors of conversion and decline in mild cognitive impairment. *Neurology* 75, 230–238. doi: 10.1212/WNL.0b013e3181e8e8b8

Lee, S. H., Bachman, A. H., Yu, D., Lim, J., Ardekani, B. A., Alzheimer's Disease, et al. (2016). Predicting progression from mild cognitive impairment to Alzheimer's disease using longitudinal callosal atrophy. *Alzheimers Dement.* 2, 68–74. doi: 10.1016/j.dadm.2016.01.003

Lei, B., Siping, C., Dong, N., and Tianfu, W. (2016). Discriminative learning for Alzheimer's disease diagnosis via canonical correlation analysis and multimodal fusion. *Front. Aging Neurosci.* 8:77. doi: 10.3389/fnagi.2016.00077

Lin, W., Tong, T., Gao, Q., Guo, D., Du, X., Yang, Y., et al. (2018). Convolutional neural networks-based MRI image analysis for the Alzheimer's disease prediction from mild cognitive impairment. *Front. Neurosci.* 12:777. doi: 10.3389/fnins.2018.00777

Liu, M., Cheng, D., Wang, K., Wang, Y., and Alzheimer's Disease Neuroimaging Initiative, (2018). Multi-modality cascaded convolutional neural networks for Alzheimer's disease diagnosis. *Neuroinformatics* 16, 295–308. doi: 10.1007/s12021-018-9370-4

Liu, S., Liu, S., Cai, W., Che, H., Pujol, S., Kikinis, R., et al. (2015). Multimodal neuroimaging feature learning for multiclass diagnosis of Alzheimer's disease. *IEEE Trans. Biomed. Eng.* 62, 1132–1140. doi: 10.1109/tbme.2014.2372011

Lu, D., Popuri, K., Ding, G. W., Balachandar, R., Beg, M. F., Alzheimer's Disease Neuroimaging Initiative, et al. (2018). Multiscale deep neural network based analysis of FDG-PET images for the early diagnosis of Alzheimer's disease. *Med. Image Anal.* 46, 26–34. doi: 10.1016/j.media.2018.02.002

Markesbery, W. R., and Lovell, M. A. (2010). Neuropathologic alterations in mild cognitive impairment: a review. *J. Alzheimers Dis.* 19, 221–228. doi: 10.3233/jad-2010-1220

Moradi, E., Pepe, A., Gaser, C., Huttunen, H., Tohka, J., Alzheimer's Disease, et al. (2015). Machine learning framework for early MRI-based Alzheimer's conversion prediction in MCI subjects. *Neuroimage* 104, 398–412. doi: 10.1016/j.neuroimage.2014.10.002

Mosconi, L., Mistur, R., Switalski, R., Tsui, W. H., Glodzik, L., Li, Y., et al. (2009). FDG-PET changes in brain glucose metabolism from normal cognition to pathologically verified Alzheimer's disease. *Eur. J. Nucl. Med. Mol. Imaging* 36, 811–822. doi: 10.1007/s00259-008-1039-z

Mu, Y., and Gage, F. H. (2011). Adult hippocampal neurogenesis and its role in Alzheimer's disease. *Mol. Neurodegener.* 6:85. doi: 10.1186/1750-1326-6-85

Niemantsverdriet, E., Valckx, S., Bjerke, M., and Engelborghs, S. (2017). Alzheimer's disease CSF biomarkers: clinical indications and rational use. *Acta Neurol. Belg.* 117, 591–602. doi: 10.1007/s13760-017-0816-5

Oliveira, P. P. D. M., Nitrini, R., Busatto, G., Buchpiguel, C., and Amaro, E. (2010). Use of SVM methods with surface-based cortical and volumetric subcortical measurements to detect Alzheimer's disease. *J. Alzheimers Dis.* 19, 1263–1272. doi: 10.3233/JAD-2010-1322

Poulin, S. P., Dautoff, R., Morris, J. C., Barrett, L. F., Dickerson, B. C., and Alzheimer's Disease Neuroimaging Initiative, (2011). Amygdala atrophy is prominent in early Alzheimer's disease and relates to symptom severity. *Psychiat. Res. Neuroim.* 194, 7–13. doi: 10.1016/j.pscychresns.2011.06.014

Querbes, O., Aubry, F., Pariente, J., Lotterie, J.-A., Demonet, J.-F., Duret, V., et al. (2009). Early diagnosis of Alzheimer's disease using cortical thickness: impact of cognitive reserve. *Brain* 132, 2036–2047. doi: 10.1093/brain/awp105

Ranginwala, N. A., Hynan, L. S., Weiner, M. F., and White, C. L. III (2008). Clinical criteria for the diagnosis of Alzheimer disease: still good after all these years. *Am. J. Geriat. Psychiat.* 16, 384–388. doi: 10.1097/JGP.0b013e3181629971

Suk, H.-I., Lee, S.-W., Shen, D., and Alzheimer's Disease Neuroimaging Initiative, (2014). Hierarchical feature representation and multimodal fusion with deep learning for AD/MCI diagnosis. *NeuroImage* 101, 569–582. doi: 10.1016/j.neuroimage.2014.06.077

Tong, T., Gao, Q., Guerrero, R., Ledig, C., Chen, L., Rueckert, D., et al. (2017a). A novel grading biomarker for the prediction of conversion from mild cognitive impairment to Alzheimer's disease. *IEEE Trans. Biomed. Eng.* 64, 155–165. doi: 10.1109/TBME.2016.2549363

Tong, T., Gray, K., Gao, Q., Chen, L., Rueckert, D., The Alzheimer's Disease, et al. (2017b). Multi-modal classification of Alzheimer's disease using nonlinear graph fusion. *Pattern Recogn.* 63, 171–181. doi: 10.1016/j.patcog.2016.10.009

Van Hoesen, G. W., Hyman, B. T., and Damasio, A. R. (1991). Entorhinal cortex pathology in Alzheimer's disease. *Hippocampus* 1, 1–8. doi: 10.1002/hipo.450010102

Vos, T., Allen, C., Arora, M., Barber, R. M., Bhutta, Z. A., Brown, A., et al. (2016). Global, regional, and national incidence, prevalence, and years lived with disability for 310 diseases and injuries, 1990–2015: a systematic analysis for the global burden of disease study 2015. *Lancet* 388, 1545–1602.

Vounou, M., Janousova, E., Wolz, R., Stein, J. L., Thompson, P. M., Rueckert, D., et al. (2012). Sparse reduced-rank regression detects genetic associations with voxel-wise longitudinal phenotypes in Alzheimer's disease. *Neuroimage* 60, 700–716. doi: 10.1016/j.neuroimage.2011.12.029

Walhovd, K. B., Fjell, A. M., Brewer, J., McEvoy, L. K., Fennema-Notestine, C., Hagler, D. J., et al. (2010). Combining MR imaging, positron-emission tomography, and CSF biomarkers in the diagnosis and prognosis of Alzheimer disease. *Am. J. Neuroradiol.* 31, 347–354. doi: 10.3174/ajnr.A1809

Westman, E., Muehlboeck, J.-S., and Simmons, A. (2012). Combining MRI and CSF measures for classification of Alzheimer's disease and prediction of mild cognitive impairment conversion. *Neuroimage* 62, 229–238. doi: 10.1016/j.neuroimage.2012.04.056

Young, J., Modat, M., Cardoso, M. J., Mendelson, A., Cash, D., and Ourselin, S. (2013). Accurate multimodal probabilistic prediction of conversion to Alzheimer's disease in patients with mild cognitive impairment. *Neuroimage Clin.* 2, 735–745. doi: 10.1016/j.nicl.2013.05.004

Zeng, N., Zhang, H., Liu, W., Liang, J., and Alsaadi, F. E. (2017). A switching delayed PSO optimized extreme learning machine for short-term load forecasting. *Neurocomputing* 240, 175–182. doi: 10.1016/j.neucom.2017.01.090

Zhang, D., Wang, Y., Zhou, L., Yuan, H., and Shen, D. (2011). Multimodal classification of Alzheimer's disease and mild cognitive impairment. *Neuroimage* 55, 856–867. doi: 10.1016/j.neuroimage.2011.01.008

Conflict of Interest: The authors declare that the research was conducted in the absence of any commercial or financial relationships that could be construed as a potential conflict of interest.

frontiers in Neuroscience

ORIGINAL RESEARCH
published: 03 April 2020
doi: 10.3389/fnins.2020.00304

Functional and Structural Brain Alterations in Encephalitis With LGI1 Antibodies

Jianping Qiao[1†], Xiuhe Zhao[2†], Shengjun Wang[2], Anning Li[3], Zhishun Wang[4], Chongfeng Cao[5] and Qing Wang[3*]*

[1] Shandong Province Key Laboratory of Medical Physics and Image Processing Technology, Institute of Data Science and Technology, School of Physics and Electronics, Shandong Normal University, Jinan, China, [2] Department of Neurology, Qilu Hospital of Shandong University, Jinan, China, [3] Department of Radiology, Qilu Hospital of Shandong University, Jinan, China, [4] Department of Psychiatry, Columbia University, New York, NY, United States, [5] Department of Emergency, Jinan Central Hospital Affiliated to Shandong University, Jinan, China

OPEN ACCESS

Edited by:
Jiehui Jiang,
Shanghai University, China

Reviewed by:
Rodolfo Gabriel Gatto,
University of Illinois at Chicago, United States
Foteini Christidi,
National and Kapodistrian University of Athens, Greece

***Correspondence:**
Jianping Qiao
jpqiao@sdu.edu.cn;
qiaojianpingdsp@gmail.com
Qing Wang
wangqing663@163.com

[†]These authors have contributed equally to this work

Specialty section:
This article was submitted to Neurodegeneration, a section of the journal Frontiers in Neuroscience

Received: 19 November 2019
Accepted: 16 March 2020
Published: 03 April 2020

Citation:
Qiao J, Zhao X, Wang S, Li A, Wang Z, Cao C and Wang Q (2020) Functional and Structural Brain Alterations in Encephalitis With LGI1 Antibodies. Front. Neurosci. 14:304. doi: 10.3389/fnins.2020.00304

Objective: The purpose of this study was to examine the neural substrates and mechanisms that generate memory deficits, seizures and neuropsychiatric abnormalities in encephalitis with LGI1 antibodies using a data-driven, multimodal magnetic resonance imaging (MRI) approach.

Methods: Functional MRI data were acquired from 14 anti-LGI1 encephalitis patients and 14 age and gender matched normal controls. Independent component analysis with hierarchical partner matching (HPM-ICA) was used to assess the whole-brain intrinsic functional connectivity. Granger causality (GC) was applied to investigate the effective connectivity among the brain regions that identified by HPM-ICA. Diffusion tensor imaging (DTI) was utilized to investigate white matter microstructural changes of the patients.

Results: Participants with LGI1 antibodies encephalitis presented reduced functional connectivity in the brain areas associated with memory, cognition and motion circuits, while increased functional connectivity in putamen and caudate in comparison to the normal controls. Moreover, the effective connectivity in patients was decreased from the frontal cortex to supplementary motor area. Finally, patients had significant reductions in fractional anisotropy (FA) for the corpus callosum, internal capsule, corona radiata and superior longitudinal fasciculus, accompanied by increases in mean diffusivity (MD) for these regions as compared to controls.

Conclusion: Our findings suggest that the neural disorder and behavioral deficits of anti-LGI1 encephalitis may be associated with extensive changes in brain connectivity and microstructure. These pathological alterations affect the basal ganglia and limbic system besides the temporal and frontal lobe.

Keywords: anti-LGI1 encephalitis, multimodal MRI, functional connectivity, effective connectivity, white matter microstructure

INTRODUCTION

Encephalitis with leucine-rich, glioma-inactivated 1 (LGI1) antibodies is a disease characterized by progressive memory loss, confusion, sleep disturbances, and problems with behaviors and spatial orientation. The most common clinical symptoms include memory dysfunction, multiform seizures, faciobrachial dystonic seizures (FBDS) and hyponatremia (Irani et al., 2010; van Sonderen et al., 2016; Beimer and Selwa, 2017; Wang et al., 2017). The LGI1 is a protein that binds together two epilepsy-related proteins called ADAM22 (a disintegrin and metalloproteinase 22) and ADAM23 (Kegel et al., 2013). Encephalitis with LGI1 antibodies occurs when antibodies mistakenly attack LGI1 (Gao et al., 2016; van Sonderen et al., 2016).

Prior neuroimaging studies have reported structural and functional neural differences in various brain areas between anti-LGI1 encephalitis patients and normal controls (NC). Several positron emission tomography (PET) studies have reported alterations of basal ganglia hyperintensities in LGI1-autoantibody faciobrachial dystonic seizures (FBDS) (Flanagan et al., 2015; d'Orsi et al., 2018). In addition, structural magnetic resonance imaging (MRI) studies have revealed decreased volumes of the hippocampus, pallidum, nucleus accumbens, brainstem and cerebellum in patients with anti-LGI1 encephalitis (Finke et al., 2017; Miller et al., 2017; Szots et al., 2017). Hippocampal atrophy with further reduced mediodorsal thalamic and posteromedial cortical volumes were reported in the limbic encephalitis associated with antibodies to components of the voltage-gated potassium channel complex (VGKCC-Ab-LE), where LGI1 was the prominent autoantibody (Loane et al., 2019). Another recent study showed that hippocampal dentate gyrus atrophy predicted pattern separation impairment in patients with LGI1 encephalitis (Hanert et al., 2019). Besides, diffusion tensor imaging (DTI) has been extensively applied to unveil white matter abnormalities in diverse neurological diseases (Gatto et al., 2018; Gatto and Weissmann, 2019). The microstructural integrity impairments of the hippocampus (Finke et al., 2017), corona radiata, capsula interna and corpus callosum (Szots et al., 2017) were found in patients with anti-LGI1 encephalitis in the DTI studies. The magnetic resonance spectroscopy (MRS) revealed lower glutamine/glutamate white matter (WM) levels compared with controls (Szots et al., 2017).

Disruptions of large-scale functional networks including default mode network (DMN), sensorimotor, salience and higher visual networks in patients with anti-LGI1 encephalitis have been revealed in the resting-state fMRI study (Heine et al., 2018). Another VGKCC-Ab-LE study in which LGI1 was the main autoantibody demonstrated that patients had reduced posteromedial cortico-hippocampal and interhippocampal functional connectivities which were correlated with memory scores (Loane et al., 2019). A task-based fMRI study in autoimmune encephalitis with FBDS have reported that higher peak FBDS frequency was significantly related to lower hippocampal activity during scene-encoding task (Nantes et al., 2018).

However, the neural mechanisms underlying memory deficits, seizures and neuropsychiatric abnormalities in anti-LGI1 encephalitis remain unclear. Therefore, the aim of this study was to examine the whole-brain functional and structural alterations as well as their correlations with clinical disease severity in encephalitis with LGI1 antibodies using a data-driven, multimodal MRI approach. We applied the independent component analysis with hierarchical partner matching (HPM-ICA) to assess the brain functional connectivity networks. The causal influence between the independent components was estimated by utilizing granger causality method. Diffusion tensor imaging was used to investigate white matter microstructural changes of the patients. The hypothesis was that we would detect brain connectivity and microstructure differences in anti-LGI1 encephalitis within the cortical-subcortical neural systems that support memory, cognition, and motion dysregulation for anti-LGI1 encephalitis.

MATERIALS AND METHODS

Participants

Fourteen participants with anti-LGI1 encephalitis (11 males, 3 females, mean age 55.9 ± 10.6 years) were recruited from the psychological outpatient clinic at the Qilu Hospital of Shandong University (**Table 1**). Anti-LGI encephalitis was diagnosed by LGI1 antibodies positive in all patients who had serum LGI1 antibodies. The (+) scoring was found in one patient, and

TABLE 1 | Demographic and clinical characteristics of anti-LGI1 encephalitis patients.

Age, mean (SD)	55.9 (10.6) years
Sex	11 male, 3 female
Modified Rankin Scale score[a], mean (SD)	2.2 (0.8)
Time from symptom onset to diagnosis, mean (SD)	3.4 (2.3) months
Mini-Mental State Examination (MMSE), mean (SD)	22.1(5.9)
Montreal Cognitive Assessment (MoCA), mean (SD)	18.3(5.5)
Symptom	
Memory impairment	10/14 (71%)
Seizure	11/14 (79%)
Faciobrachial dystonic seizures	4/14 (29%)
Mental and behavioral abnormalities	4/14 (29%)
Cerebrospinal fluid	
Glucose (mmol/L), mean (SD)	4.6 (1.2)
Chlorine (mmol/L), mean (SD)	121 (5.6)
Protein[b] (g/L), mean (SD)	0.38 (0.17)
Lactic acid[c] (mmol/L), mean (SD)	2.2 (0.3)
Antibodies to LGI1	
Serum (positive)	14/14 (100%)
Cerebrospinal fluid (positive)	10/14 (71%)

[a]The criteria of the modified Rankin Scale (mRS) score can be described as: 0 – No symptoms at all. 1 – No significant disability despite symptoms; able to carry out all usual duties and activities. 2 – Slight disability; unable to carry out all previous activities, but able to look after own affairs without assistance. 3 – Moderate disability; requiring some help, but able to walk without assistance. 4 – Moderately severe disability; unable to walk and attend to bodily needs without assistance. 5 – Severe disability; bedridden, incontinent and requiring constant nursing care and attention. [b]CSF Protein normal values: <0.45 g/L. [c]CSF lactic acid normal values: 1.2–2.1 mmol/L.

(++) scoring was found in thirteen patients. Ten patients were CSF LGI1 antibody positive that showed (+) scoring. Thirteen patients underwent CSF examination with twelve CSF samples showing a normal white cell count. Four patients had increased protein concentrations (Four patients: 0.75, 0.46, 0.53 and 0.5 g/L [normal: <0.45 g/L]). Six patients had increased lactic acid concentrations (Six patients: 2.7, 2.5, 2.3, 2.5, 2.5, and 2.3 mmol/L [normal: 1.2–2.1 mmol/L]). Ten patients had memory impairment. Eleven patients experienced seizure and four patients had mental and behavioral changes. The FBDS occurred in four patients. All anti-LGI1 encephalitis participants had been diagnosed by a licensed neurology pathologist before enrollment. We evaluated symptom severity on the day of MRI scan using the assessment of the modified Rankin Scale (mRS) for all patients. The mental and cognitive functions of patients were assessed by Mini-Mental State Examination (MMSE) and Montreal Cognitive Assessment (MoCA).

Fourteen group-matched by age and sex normal controls (9 males, 5 females, mean age 55.5 ± 9.3 years) were recruited by public advertisement to take part in the study. All participants were right-handed, native Chinese speakers. The safety screening form and informed consent form were approved by the Institutional Review Board of Qilu Hospital of Shandong University. The written informed consents were obtained from all participants.

Image Acquisition

Imaging was performed on a Siemens Verio 3.0 Tesla MRI scanner (Siemens, Erlangen, Germany) with a 32-channel head coil at the Qilu Hospital of Shandong University. Participants were instructed to rest with their eyes closed but not to fall asleep during scanning. Foam cushions were used to reduce head movement. We acquired the resting-state functional MRI data using a single-shot gradient-echo echo-planar imaging (EPI) sequence with the following parameters: repetition time (TR) = 2000 ms, echo time (TE) = 30 ms, flip angle = 90°, field of view (FOV) = 24 cm × 24 cm, matrix size = 64 × 64, voxel size = 3.4 × 3.4 × 4.0 mm, slice thickness = 3 mm. Thirty-six axial slices were acquired aligned the AC-PC plane. The acquisition time was about eight minutes, resulting in a total of 240 volumes. The DTI scanning parameters were as follows: 65 diffusion directions in the axial plane, TR = 6400 ms, TE = 98 ms, flip angle = 90°, FOV = 24 cm × 24 cm, matrix size = 128 × 128, voxel size = 2 × 2 × 2 mm^3, *b*-value = 1000 s/mm^2, slice thickness = 3 mm, no slice gap.

The Functional MRI Image Analysis

The resting-state fMRI image analysis consisted of five procedures: preprocessing of functional imaging data, spatial independent component analysis (ICA) of the preprocessed data, identification of reproducible ICA components, statistical comparison of the processed ICA components, granger causality analysis of the ICA components.

The fMRI images were preprocessed using SPM12 (Welcome Department of Imaging Neuroscience, London, United Kingdom) that was run under MATLAB. The slice timing correction was performed to correct phase shifts between slices caused by interleaved scans. Then motion correction was conducted to correct for head movements. After that, all images were normalized to the Montreal Neurological Institute (MNI) coordinate system and smoothed by an isotropic Gaussian kernel of 8 mm full-width at half-maximum.

The spatial independent component analysis with hierarchical partner matching (HPM-ICA) (Wang et al., 2011; Qiao et al., 2015, 2017) was performed on the preprocessed data to explore the functional connectivity networks. In detail, spatial ICA was firstly used to generate N components for each participant in which the number of sets of independent components (ICs) N was determined by information criteria. The minimum description length and Akaike's information criterion were combined to estimate the lower and upper bounds of the numbers of ICs, defining an interval for the number N of components. Secondly, the hierarchical partner matching was performed to identify independent components that were reproducible in their spatial configuration across all individuals.

Statistical analysis was implemented to detect random effects of group difference in functional connectivity between anti-LGI1 encephalitis patients and normal controls. The z-score maps of the identified reproducible ICs were entered into a second-level factorial analysis, covarying for age and sex. The uncorrected *p*-value of 0.001 with cluster extent threshold of 30 voxels (determined by Monte Carlo simulation) was used for the correction of multiple comparisons. The Pearson's correlation analysis was also performed in patients to investigate the correlation between the severity (mRS score) and functional connectivity.

Granger causality was carried out to analyze causal influences across the ICs identified by HPM-ICA method. The granger causality indices (GCIs) were computed using the time courses of the identified ICs (Wang et al., 2011; Qiao et al., 2018). The two-sample *t*-tests were finally used to detect group difference in GCIs between patients and normal controls in which age and sex were applied as covariates.

Diffusion Tensor Imaging Analysis

The DTI images were analyzed using FMRIB Software Library (FSL) software[1]. We first performed eddy-current correction on DTI data for each participant to adjust the distortions and motion artifacts. Then we used the brain extraction tool (BET) (Smith, 2002) to extract brain tissue from the eddy-current-corrected B0 image and generate brain mask. The FMRIB Diffusion Toolbox (FDT) was subsequently used to reconstruct the diffusion tensor and calculate the fractional anisotropy (FA) and mean diffusivity (MD) map for each participant.

The voxel-wise statistical analysis of the DTI images was performed using tract-based spatial statistics (TBSS) (Smith et al., 2006). First, FA maps of all subjects were aligned to the standard MNI152 space through a non-linear registration. Second, the mean FA image was created and skeletonised. A threshold of 0.2 was used to exclude non-skeleton voxels and generate the mean skeleton. The aligned FA and MD map of each subject were then projected onto the skeleton. Finally, permutation-based

[1] www.fmrib.ox.ac.uk/fsl

non-parametric inference with 5,000 permutations was adopted to identify the differences in the FA and MD images between patients and controls. Age and sex were entered as covariates in the statistical analysis. The threshold-free cluster enhancement (TFCE) was used as multiple comparison correction (Smith and Nichols, 2009; Winkler et al., 2016). A family wise error corrected $P < 0.05$ was considered statistically significant.

RESULTS

Reproducible Independent Components

We identified nine clusters of ICs that were significantly reliable and reproducible in their spatial patterns across anti-LGI1 encephalitis patients and normal controls groups by HPM-ICA method. The general linear model in SPM was applied to conduct a one-sample *t*-test on each of the clusters to generate nine independent component maps that represented statistically significant functional connectivity. The nine ICs of patients and controls were then compared in a second-level analysis. Compared with controls, patients showed significantly reduced connectivity in hippocampus, inferior frontal gyrus (IFG), amygdala, superior temporal gyrus (STG), anterior cingulate cortex (ACC) and posterior cingulate cortex (PCC), but increased connectivity in caudate, putamen and supplementary motor area (SMA) (**Table 2** and **Figure 1**). The higher disease severity (mRS score) correlated with the weaker functional connectivity in the left hippocampus in patients ($r = 0.76$, $p < 0.01$).

Granger Causality Interactions

The granger causality index was used to assess the effective connectivity between the regions associated with memory, cognition and motion dysregulation brain networks. The patients had decreased effective connections from the IFG to PCC [(0.15 ± 0.02 versus 0.07 ± 0.01; $p = 0.01$) (mean ± std)], from the IFG to SMA (0.12 ± 0.03 versus 0.07 ± 0.02; $p = 0.01$), while increased effective connectivity from the SMA to caudate (0.16 ± 0.03 versus 0.36 ± 0.09; $p = 0.007$).

TABLE 2 | Regional locations and significant comparisons of the independent component maps between patients with anti-LGI1 encephalitis and normal controls.

Brain areas	Location		Peak location			*T* statistic
	Side	BA	*x*	*y*	*z*	
Patients vs. controls (negative)						
Hippocampus	L	NA	−27	−10	−23	−3.13
Inferior frontal gyrus (IFG)	L	47	−42	29	−4	−3.62
Amygdala	R	NA	27	−1	−14	−3.25
Superior temporal gyrus (STG)	R	22	51	−19	1	−3.42
Anterior cingulate cortex (ACC)	R	32	6	38	−2	−2.71
Posterior cingulate cortex (PCC)	R	23	6	−43	25	−2.59
Patients vs. controls (positive)						
Caudate	L	NA	−18	17	13	+ 4.57
Putamen	R	NA	24	5	10	+ 3.13
Supplementary motor area (SMA)	R	6	9	2	58	+ 3.76

NA, not applicable. All coordinates are in the MNI (Montreal Neurological Institute) ICBM152 space.

White Matter Microstructure Integrity Alterations

The voxelwise statistical group comparison between patients and controls showed significantly lower FA in patients for the genu, body, and splenium of corpus callosum, anterior limb, retrolenticular part of internal capsule, external capsule, corona radiata, posterior thalamic radiation, sagittal stratum, fornix/stria terminalis, and superior longitudinal fasciculus (**Figure 2** and **Table 3**), accompanied by increases in MD for these brain regions (**Figure 3** and **Table 4**), as compared to controls. There was a negative association between mRS scores and FA values ($r = 0.83$ $p < 0.001$) and a positive association with MD ($r = 0.87$, $p < 0.001$) in the anterior corona radiate.

DISCUSSION

In this study, we found that patients with LGI1 antibodies encephalitis presented reduced functional connectivities in the hippocampus, IFG, STG, ACC, PCC and amygdala, while increased functional connectivities in putamen, caudate and SMA. Furthermore, the effective connectivity in patients was decreased from the frontal cortex to supplementary motor area. Meanwhile, patients had significant decreased FA and increased MD for the corpus callosum, internal capsule and external capsule, corona radiata, posterior thalamic radiation, sagittal stratum and superior longitudinal fasciculus as compared to controls. The results indicated that abnormal brain connectivity and microstructure in brain areas associated with memory, cognition and motion dysregulation circuits were related to the generic risk of anti-LGI1 encephalitis, which makes it a potential endophenotype for anti-LGI1 encephalitis.

The most commonly brain alteration in anti-LGI1 encephalitis was hippocampal atrophy in the previous MRI studies (Finke et al., 2017; Miller et al., 2017; Szots et al., 2017). Correspondingly, we identified the decreased functional connectivity in hippocampus and its correlation with the disease severity in this study. Moreover, changed functional connectivities were shown in widespread brain regions related to frontal cortex, temporal cortex, motor cortex, basal ganglia and limbic system. These findings were consistent with the previous neuroimaging studies. A resting state fMRI study found disrupted large-scale functional networks including DMNs, sensorimotor, salience and higher visual networks (Heine et al., 2018). The involvement of ACC and frontal lobe in non-paraneoplastic limbic encephalitis has been reported in a recent case study (Ibi et al., 2019). Another PET study showed the hypermetabolism in the anterior cingulate cortex in an anti-NMDAR encephalitis patient (Chanson et al., 2012). The motor cortex has been demonstrated as one of the major signs of LGI1-antibody encephalitis with striatum involvement in parallel (Navarro et al., 2016). In addition, the DTI analysis revealed impaired microstructural integrity in more

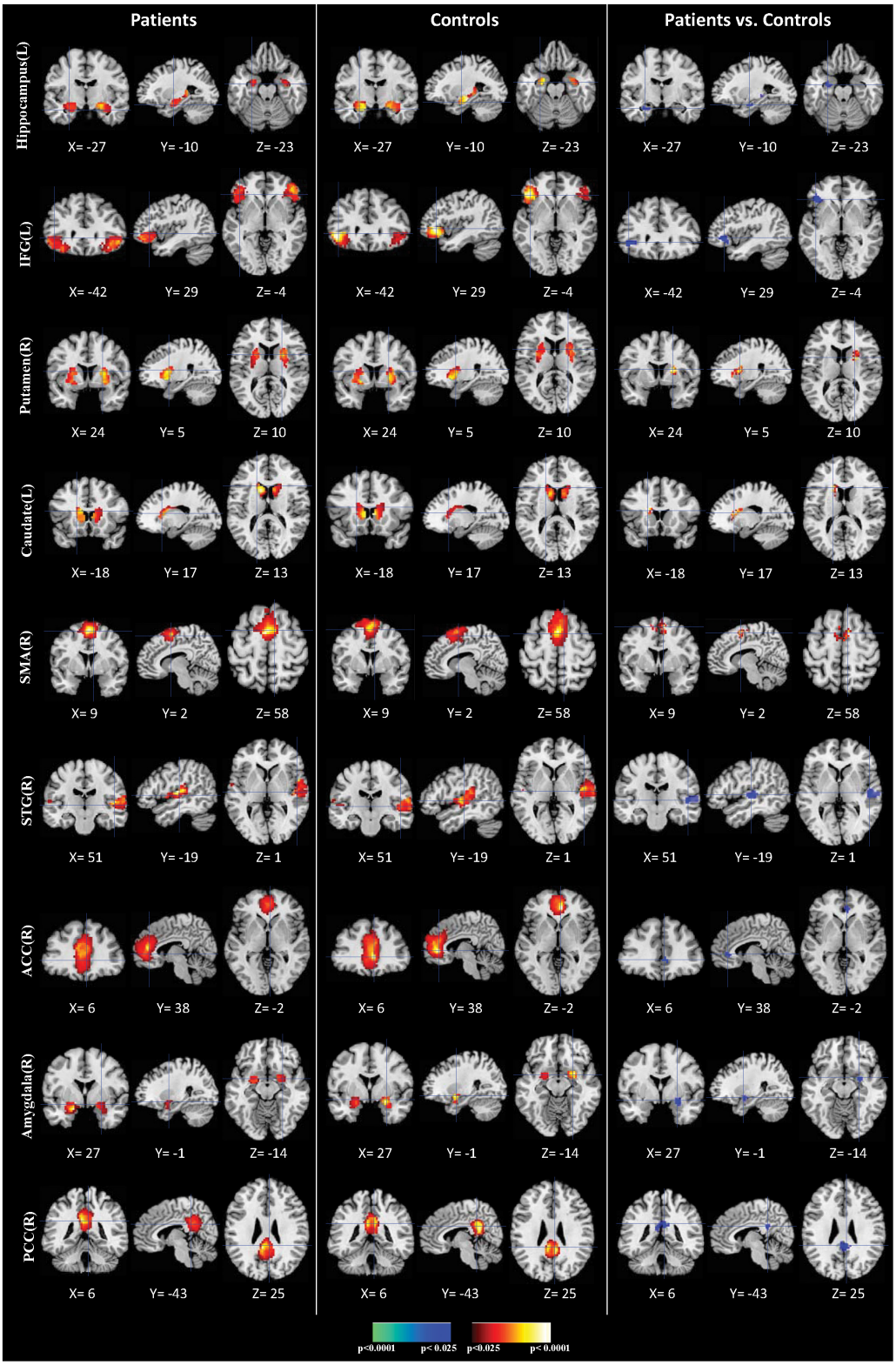

FIGURE 1 | Comparisons of brain connectivity between patients and controls. The first three columns display the connectivity maps detected from the patients group. The second three columns display the connectivity maps detected from the controls group. The last three columns display *t*-contrast maps comparing the group connectivity maps from the patients and controls. IFG, inferior frontal gyrus; SMA, supplementary motor area; STG, superior temporal gyrus; ACC, anterior cingulate cortex; PCC, posterior cingulate cortex.

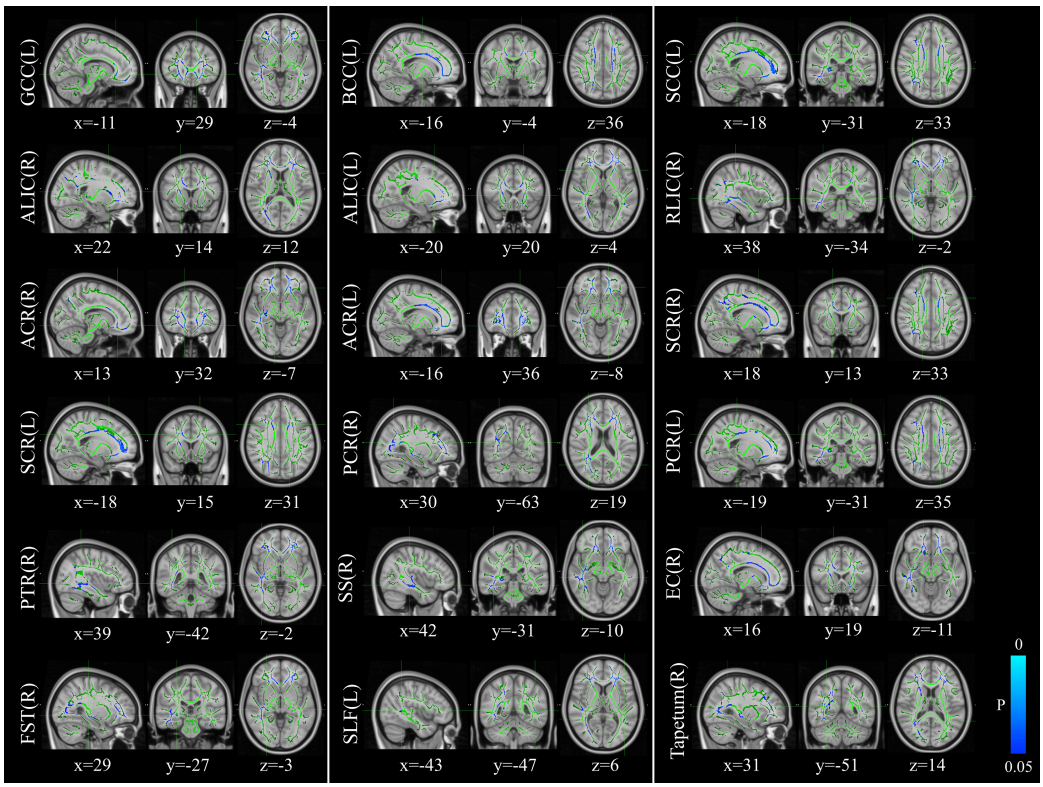

FIGURE 2 | Distribution map of the fractional anisotropy (FA) value that was significantly lower in the patients group compared with the control group based on the TBSS analysis (blue-lightblue). Statistical images ($p_{FWE} < 0.05$ corrected for multiple comparisons) were overlapped onto the mean of the skeleton (green) and the MNI152 template (gray-scale) for visualization. TBSS, tract-based spatial statistics; FST, fornix/stria terminalis; PTR, posterior thalamic radiation; SCR, superior corona radiate; ACR, anterior corona radiate; ALIC, anterior limb of internal capsule; GCC, genu of corpus callosum; SLF, superior longitudinal fasciculus; SS, sagittal stratum; PCR, posterior corona radiate; BCC, body of corpus callosum; EC, external capsule; SCC, splenium of corpus callosum; RLIC, retrolenticular part of internal capsule.

TABLE 3 | Comparisons of FA maps between patients with anti-LGI1 encephalitis and normal controls.

Brain areas	Side	Peak location			*P*-value	Cluster size
		x	*y*	*z*		
Patients vs. controls (negative)						
Genu of corpus callosum	L	−11	29	−4	0.028	718
Body of corpus callosum	L	−16	−4	36	0.033	742
Splenium of corpus callosum	L	−18	−31	33	0.039	184
Anterior limb of internal capsule	R	22	14	12	0.046	206
	L	−20	20	4	0.040	41
Retrolenticular part of internal capsule	R	38	−34	−2	0.039	128
Anterior corona radiata	R	13	32	−7	0.034	1066
	L	−16	36	−8	0.027	1148
Superior corona radiata	R	18	13	33	0.040	299
	L	−18	15	31	0.033	322
Posterior corona radiata	R	30	−63	19	0.041	80
	L	−19	−31	35	0.039	35
Posterior thalamic radiation	R	39	−42	−2	0.039	653
Sagittal stratum	R	42	−31	−10	0.039	374
External capsule	R	16	19	−11	0.039	137
Fornix/stria terminalis	R	29	−27	−3	0.041	120
Superior longitudinal fasciculus	L	−43	−47	6	0.049	55
Tapetum	R	31	−51	14	0.042	24

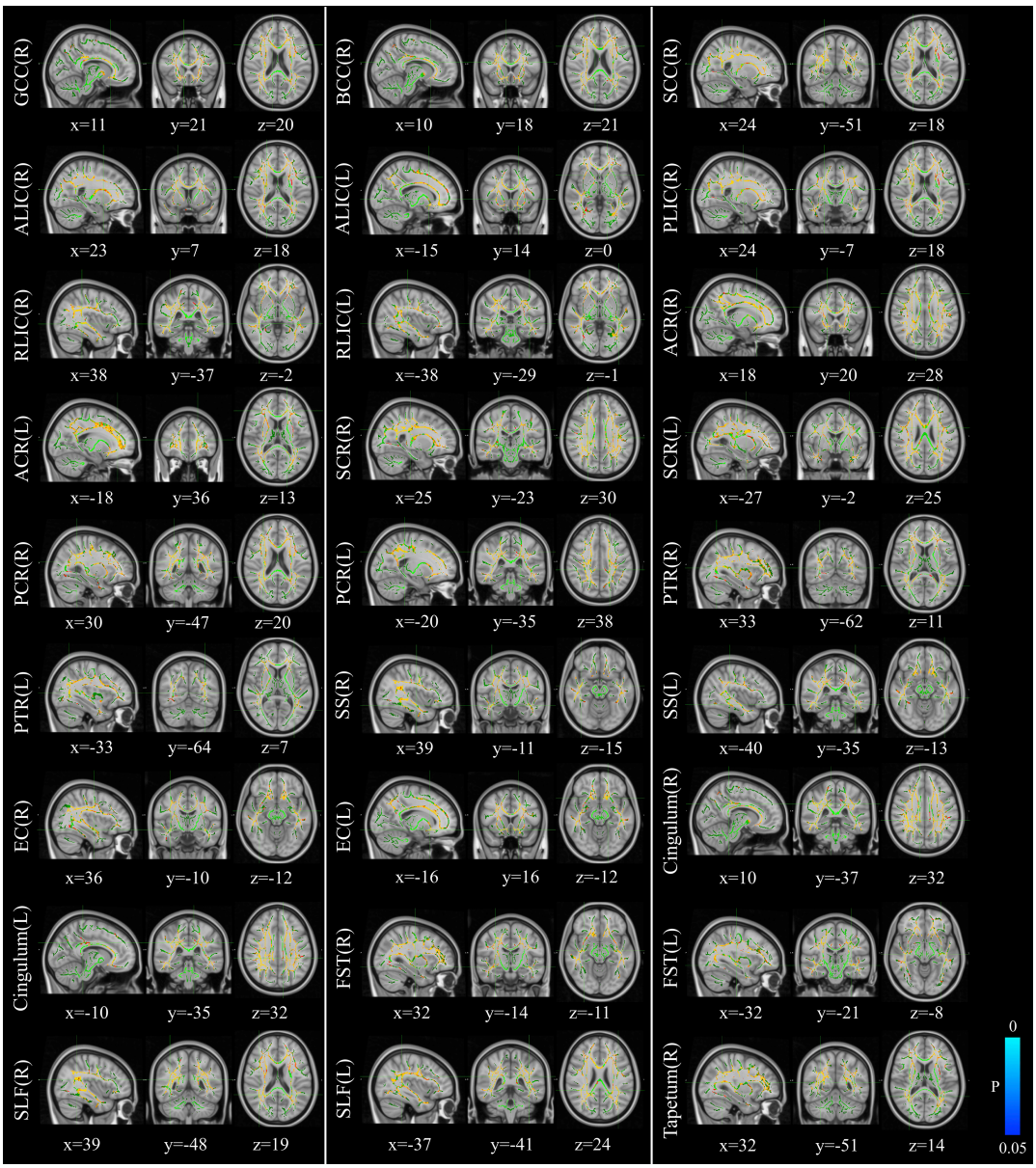

FIGURE 3 | Distribution map of the mean diffusion (MD) value that was significantly higher in the patients group compared with the control group based on the TBSS analysis (red-yellow). Statistical images ($p_{FWE} < 0.05$ corrected for multiple comparisons) were overlapped onto the mean of the skeleton (green) and the MNI152 template (gray-scale) for visualization. TBSS, tract-based spatial statistics; GCC, genu of corpus callosum; BCC, body of corpus callosum; SCC, splenium of corpus callosum; ALIC, anterior limb of internal capsule; PLIC, posterior limb of internal capsule; RLIC, retrolenticular part of internal capsule; ACR, anterior corona radiate; SCR, superior corona radiate; PCR, posterior corona radiate; PTR, posterior thalamic radiation; SS, sagittal stratum; EC, external capsule; FST, fornix/stria terminalis; SLF, superior longitudinal fasciculus.

extensive brain areas compared with the previous surveys (Finke et al., 2017; Szots et al., 2017).

The hippocampus plays important roles in the consolidation of information from short-term memory to long-term memory, and in spatial memory that enables navigation (Eichenbaum, 2017; Lisman et al., 2017; Voss et al., 2017), which is one of the major signs of LGI1-antibody encephalitis (Navarro et al., 2016). The hippocampal atrophy and impaired hippocampal microstructural integrity have been reported in encephalitis with LGI1 antibodies in the previous studies (Finke et al., 2017; Szots et al., 2017). In this study, we identified that patients with anti-LGI1 encephalitis exhibit decreased functional connectivity in hippocampus compared with normal controls, confirming that the alteration of the hippocampus may be related to the development of memory disorders. Furthermore, the correlation of the reduced connectivity in hippocampus with disease severity suggests that the hippocampal damage plays an important role in the symptomatology of anti-LGI1 encephalitis.

TABLE 4 | Comparisons of MD maps between patients with anti-LGI1 encephalitis and normal controls.

Brain areas	Side	Peak location			*P*-value	Cluster size
		x	*y*	*z*		
Patients vs. controls (positive)						
Genu of corpus callosum	R	11	21	20	0.008	998
Body of corpus callosum	R	10	18	21	0.008	1537
Splenium of corpus callosum	R	24	−51	18	0.008	859
Anterior limb of internal capsule	R	23	7	18	0.010	387
	L	−15	14	0	0.011	196
Posterior limb of internal capsule	R	24	−7	18	0.010	336
Retrolenticular part of internal capsule	R	38	−37	−2	0.008	358
	L	−38	−29	−1	0.012	231
Anterior corona radiata	R	18	20	28	0.008	1296
	L	−18	36	13	0.009	1374
Superior corona radiata	R	25	−23	30	0.008	1208
	L	−27	−2	25	0.010	999
Posterior corona radiata	R	30	−47	20	0.008	685
	L	−20	−35	38	0.010	600
Posterior thalamic radiation	R	33	−62	11	0.008	655
	L	−33	−64	7	0.010	748
Sagittal stratum	R	39	−11	−15	0.008	464
	L	−40	−35	−13	0.012	335
External capsule	R	36	−10	−12	0.002	635
	L	−16	16	−12	0.010	479
Cingulum (cingulate gyrus)	R	10	−37	32	0.008	75
	L	−10	−35	32	0.049	101
Fornix/stria terminalis	R	32	−14	−11	0.010	70
	L	−32	−21	−8	0.012	112
Superior longitudinal fasciculus	R	39	−48	19	0.008	1196
	L	−37	−41	24	0.010	1104
Tapetum	R	32	−51	14	0.008	36

We found significantly decreased intrinsic functional connectivity in patients compared to controls in the inferior frontal gyrus and superior temporal gyrus. As one of the major components of executive control functions, the IFG is critical for inhibiting inappropriate motor responses in the framework of top-down control of behavior (Miyake et al., 2000; Swick et al., 2008; Hampshire et al., 2010; Hallam et al., 2018). Evidence has shown that interictal epileptic events were preferentially generated by the temporal or frontal lobes during sleep or drowsiness (Navarro et al., 2016). Therefore, the unsuccessful implementation of inhibitory control over motor responses of the frontal cortex may result in the motor abnormalities such as multiform seizures and FBDS. In addition, the superior temporal gyrus was identified to support auditory short-term memory capacity and speech comprehension ability (Bigler et al., 2007; Leff et al., 2009) as well as social cognition (Guo et al., 2017; Mier et al., 2017). Thus, the functional connectivity reduction in STG may lead to abnormal memory capacity and cognitive impairments in anti-LGI1 encephalitis patients.

We found decreased connectivity in PCC which is the central core of the default mode network (DMN). Increased DMN connectivity has been revealed as a compensatory mechanism for memory impairment induced by hippocampal damage (Heine et al., 2018). The ventral PCC is involved in internally directed cognition such as memory retrieval and planning, while the dorsal PCC has a specific role in modulating the metastability of networks involved in internally directed attention (Leech and Sharp, 2014). The decreased connectivity in PCC may be associated with a reduction in metastability, resulting in an inability to flexibly change between different cognitive states and uncontrolling of attentional focus in patients. In addition, we found reduced functional connectivity in ACC in anti-LGI1 encephalitis patients compared with controls. The ACC is a part of the limbic system and involved in rational cognitive functions, such as reward anticipation, decision-making and impulse control (Agam et al., 2010; Tolomeo et al., 2016). Therefore, the results of our study indicate that the dysregulation of the functional connectivity in ACC might be associated with impaired cognitive control in anti-LGI1 encephalitis.

The anti-LGI1 encephalitis patients exhibited increased connectivity in motor-related brain areas including putamen, caudate and SMA. The striatum which consists of the caudate and the putamen is crucial in the planning and modulation of movement pathways as well as some cognitive

processes involving executive function (Zink et al., 2004). The abnormal functional connectivity of striatum may result in the dysfunction of motor generation or control. The decreased effective connectivity from the frontal cortex to supplementary motor area in patients further suggests that the uncontrolled movement in patients may be caused by the disruption of the motor circuits.

Meanwhile, TBSS analysis revealed widespread structural white matter damage in anti-LGI1 encephalitis as assessed using DTI. The corpus callosum (CC) is the largest fiber bundle which transfers motor, sensory, and cognitive information between the brain hemispheres (Bloom and Hynd, 2005; Roland et al., 2017). The genu of CC connects the left and right frontal lobes of the brain. The body and splenium of CC connect the hemispheres of the temporal lobes and the hemispheres of the occipital lobes. We found that anti-LGI1 encephalitis patients had decreased white matter integrity in the genu, body, and splenium of corpus callosum than controls, leading to the lack of movement coordination, low muscle tone, distorted head or facial features, spasms, and seizures. In addition, the internal capsule is a pathway connecting nerves that control the sensation and motor function (Smania et al., 2003). We found the patients exhibited reduced FA in the bilateral anterior limb and right retrolenticular part of internal capsule, which may cause the uncontrolled motor function or the sensation loss in the arm, leg, neck or face of the patients. Moreover, the corona radiata consists of afferent and efferent fibers that connect the cerebral cortex and the brain stem. The decreased white matter integrity of the anterior, superior and posterior of corona radiata in the anti-LGI1 encephalitis patients may affect the sensory input sent from the body to the brain and the messages that are sent from the brain to the body, resulting in the motor and sensory dysfunction of the patients. Furthermore, the superior longitudinal fasciculus is the largest association fiber, which connects the gray matter in frontal, parietal and temporal lobes. It is an important component of the working memory brain network. In this study, the decreased FA in the superior longitudinal fasciculus indicated that the integrity of frontal-parietal network connection was destroyed, which may be the main reason for the significant decline of memory in anti-LGI1 encephalitis patients.

Several limitations should be addressed. First, the sample size in this study was not large, which may decrease the statistical power of our analysis. The future work should be done on more cases to replicate our findings. Second, the patients in the study were all at the acute disease stage, a longitudinal design should be used to address the clinical symptoms and neural alterations with a longer follow-up period such as 3–5 years (Szots et al., 2014). Third, the DTI data processing method using in this study is a mono-exponential approach which has intrinsic limitations to accurately capture intricate WM tracts, particularly around crossing fiber regions, as well as in superficial and deep GM structures. Therefore, other non-Gaussian approaches would potentially be applied on the future clinical investigations such as diffusion kurtosis (Gatto et al., 2019a) and continuous random-walk models (Gatto et al., 2019b) which have been validated in neurological diseases. Finally, it will be important to confirm our results using other techniques, such as EEG-fMRI, which can provide simultaneous cortical and subcortical recording of brain activity with high spatiotemporal resolution.

DATA AVAILABILITY STATEMENT

The datasets generated for this study are available on request to the corresponding author.

ETHICS STATEMENT

The studies involving human participants were reviewed and approved by Qilu Hospital of Shandong University. The patients/participants provided their written informed consent to participate in this study.

AUTHOR CONTRIBUTIONS

JQ, XZ, and SW conceived and designed the experiments. JQ, AL, and QW performed the experiments. JQ and ZW analyzed the data. JQ and ZW contributed reagents, materials, and analysis tools. JQ, AL, CC, and QW wrote the manuscript.

FUNDING

This work was supported by the National Natural Science Foundation of China (61603225), Natural Science Foundation of Shandong Province (ZR2016FQ04), Key Research and Development Foundation of Shandong Province (2016GGX101009), Shandong Provincial Key Research and Development Plan (2017CXGC1504), National Natural Science Foundation of China (81701758) and Natural Science Foundation of Shandong Province (ZR2017BH073).

REFERENCES

Agam, Y., Joseph, R. M., Barton, J. J., and Manoach, D. S. (2010). Reduced cognitive control of response inhibition by the anterior cingulate cortex in autism spectrum disorders. *Neuroimage* 52, 336–347. doi: 10.1016/j.neuroimage.2010.04.010

Beimer, N. J., and Selwa, L. M. (2017). Seizure semiology of anti-LGI1 antibody encephalitis. *Epileptic Disord.* 19, 461–464. doi: 10.1684/epd.2017.0936

Bigler, E. D., Mortensen, S., Neeley, E. S., Ozonoff, S., Krasny, L., Johnson, M., et al. (2007). Superior temporal gyrus, language function, and autism. *Dev. Neuropsychol.* 31, 217–238. doi: 10.1080/87565640701190841

Bloom, J. S., and Hynd, G. W. (2005). The role of the corpus callosum in interhemispheric transfer of information: excitation or inhibition? *Neuropsychol. Rev.* 15, 59–71. doi: 10.1007/s11065-005-6252-y

Chanson, J. B., Diaconu, M., Honnorat, J., Martin, T., De Seze, J., Namer, I. J., et al. (2012). PET follow-up in a case of anti-NMDAR encephalitis: arguments for

cingulate limbic encephalitis. *Epileptic Disord.* 14, 90–93. doi: 10.1684/epd.2012.0486

d'Orsi, G., Martino, T., Lalla, A., Claudio, M. T. D., Carapelle, E., and Avolio, C. (2018). Faciobrachial dystonic seizures expressed as epileptic spasms, followed by focal seizures in anti-LGI1 encephalitis: a video-polygraphic study. *Epileptic Disord.* 20, 525–529. doi: 10.1684/epd.2018.1010

Eichenbaum, H. (2017). The role of the hippocampus in navigation is memory. *J. Neurophysiol.* 117, 1785–1796. doi: 10.1152/jn.00005.2017

Finke, C., Pruss, H., Heine, J., Reuter, S., Kopp, U. A., Wegner, F., et al. (2017). Evaluation of cognitive deficits and structural hippocampal damage in encephalitis with leucine-rich. Glioma-Inactivated 1 Antibodies. *JAMA Neurol.* 74, 50–59. doi: 10.1001/jamaneurol.2016.4226

Flanagan, E. P., Kotsenas, A. L., Britton, J. W., McKeon, A., Watson, R. E., Klein, C. J., et al. (2015). Basal ganglia T1 hyperintensity in LGI1-autoantibody faciobrachial dystonic seizures. *Neurol. Neuroimmunol. Neuroinflamm* 2:e161. doi: 10.1212/NXI.0000000000000161

Gao, L., Liu, A., Zhan, S., Wang, L., Li, L., Guan, L., et al. (2016). Clinical characterization of autoimmune LGI1 antibody limbic encephalitis. *Epilepsy Behav.* 56, 165–169. doi: 10.1016/j.yebeh.2015.12.041

Gatto, R. G., Amin, M., Finkielsztein, A., Weissmann, C., Barrett, T., Lamoutte, C., et al. (2019a). Unveiling early cortical and subcortical neuronal degeneration in ALS mice by ultra-high field diffusion MRI. *Amyotroph. Lateral. Scler. Frontotemporal. Degener.* 20, 549–561. doi: 10.1080/21678421.2019.1620285

Gatto, R. G., Li, W., Gao, J., and Magin, R. L. (2018). In vivo diffusion MRI detects early spinal cord axonal pathology in a mouse model of amyotrophic lateral sclerosis. *NMR Biomed.* 31:e3954. doi: 10.1002/nbm.3954

Gatto, R. G., and Weissmann, C. (2019). Diffusion tensor imaging in preclinical and human studies of huntington's disease: what have we learned so far? *Curr. Med. Imaging Rev.* 15, 521–542. doi: 10.2174/1573405614666181115113400

Gatto, R. G., Ye, A. Q., Colon-Perez, L., Mareci, T. H., Lysakowski, A., Price, S. D., et al. (2019b). Detection of axonal degeneration in a mouse model of Huntington's disease: comparison between diffusion tensor imaging and anomalous diffusion metrics. *MAGMA* 32, 461–471. doi: 10.1007/s10334-019-00742-6

Guo, L., Bai, G., Zhang, H., Lu, D., Zheng, J., and Xu, G. (2017). Cognitive Functioning in Temporal Lobe Epilepsy: A BOLD-fMRI Study. *Mol. Neurobiol.* 54, 8361–8369. doi: 10.1007/s12035-016-0298-0

Hallam, G. P., Thompson, H. E., Hymers, M., Millman, R. E., Rodd, J. M., Lambon Ralph, M. A., et al. (2018). Task-based and resting-state fMRI reveal compensatory network changes following damage to left inferior frontal gyrus. *Cortex* 99, 150–165. doi: 10.1016/j.cortex.2017.10.004

Hampshire, A., Chamberlain, S. R., Monti, M. M., Duncan, J., and Owen, A. M. (2010). The role of the right inferior frontal gyrus: inhibition and attentional control. *Neuroimage* 50, 1313–1319. doi: 10.1016/j.neuroimage.2009.12.109

Hanert, A., Rave, J., Granert, O., Ziegler, M., Pedersen, A., Born, J., et al. (2019). Hippocampal dentate gyrus atrophy predicts pattern separation impairment in patients with LGI1 encephalitis. *Neuroscience* 400, 120–131. doi: 10.1016/j.neuroscience.2018.12.046

Heine, J., Pruss, H., Kopp, U. A., Wegner, F., Then Bergh, F., Munte, T., et al. (2018). Beyond the limbic system: disruption and functional compensation of large-scale brain networks in patients with anti-LGI1 encephalitis. *J. Neurol. Neurosurg. Psychiatry* 89, 1191–1199. doi: 10.1136/jnnp-2017-317780

Ibi, K., Fujii, K., Kobayashi, H., Senda, M., Kitazawa, K., and Honda, A. (2019). Anterior cingulate cortex involvement in non-paraneoplastic limbic encephalitis. *Brain Dev.* 41, 735–739. doi: 10.1016/j.braindev.2019.04.006

Irani, S. R., Alexander, S., Waters, P., Kleopa, K. A., Pettingill, P., Zuliani, L., et al. (2010). Antibodies to Kv1 potassium channel-complex proteins leucine-rich, glioma inactivated 1 protein and contactin-associated protein-2 in limbic encephalitis, Morvan's syndrome and acquired neuromyotonia. *Brain* 133, 2734–2748. doi: 10.1093/brain/awq213

Kegel, L., Aunin, E., Meijer, D., and Bermingham, J. R. (2013). LGI proteins in the nervous system. *ASN Neuro* 5, 167–181. doi: 10.1042/AN20120095

Leech, R., and Sharp, D. J. (2014). The role of the posterior cingulate cortex in cognition and disease. *Brain* 137(Pt 1), 12–32. doi: 10.1093/brain/awt162

Leff, A. P., Schofield, T. M., Crinion, J. T., Seghier, M. L., Grogan, A., Green, D. W., et al. (2009). The left superior temporal gyrus is a shared substrate for auditory short-term memory and speech comprehension: evidence from 210 patients with stroke. *Brain* 132(Pt 12), 3401–3410. doi: 10.1093/brain/awp273

Lisman, J., Buzsaki, G., Eichenbaum, H., Nadel, L., Ranganath, C., and Redish, A. D. (2017). Viewpoints: how the hippocampus contributes to memory, navigation and cognition. *Nat. Neurosci.* 20, 1434–1447. doi: 10.1038/nn.4661

Loane, C., Argyropoulos, G. P. D., Roca-Fernandez, A., Lage, C., Sheerin, F., Ahmed, S., et al. (2019). Hippocampal network abnormalities explain amnesia after VGKCC-Ab related autoimmune limbic encephalitis. *J. Neurol. Neurosurg. Psychiatry* 90, 965–974. doi: 10.1136/jnnp-2018-320168

Mier, D., Eisenacher, S., Rausch, F., Englisch, S., Gerchen, M. F., Zamoscik, V., et al. (2017). Aberrant activity and connectivity of the posterior superior temporal sulcus during social cognition in schizophrenia. *Eur. Arch. Psychiatry Clin. Neurosci.* 267, 597–610. doi: 10.1007/s00406-016-0737-y

Miller, T. D., Chong, T. T., Aimola Davies, A. M., Ng, T. W. C., Johnson, M. R., Irani, S. R., et al. (2017). Focal CA3 hippocampal subfield atrophy following LGI1 VGKC-complex antibody limbic encephalitis. *Brain* 140, 1212–1219. doi: 10.1093/brain/awx070

Miyake, A., Friedman, N. P., Emerson, M. J., Witzki, A. H., Howerter, A., and Wager, T. D. (2000). The unity and diversity of executive functions and their contributions to complex "Frontal Lobe" tasks: a latent variable analysis. *Cogn. Psychol.* 41, 49–100. doi: 10.1006/cogp.1999.0734

Nantes, J. C., Thomas, A. G., Voets, N. L., Best, J. G., Rosenthal, C. R., Al-Diwani, A., et al. (2018). Hippocampal functional dynamics are clinically implicated in autoimmune encephalitis with faciobrachial dystonic seizures. *Front. Neurol.* 9:736. doi: 10.3389/fneur.2018.00736

Navarro, V., Kas, A., Apartis, E., Chami, L., Rogemond, V., Levy, P., et al. (2016). Motor cortex and hippocampus are the two main cortical targets in LGI1-antibody encephalitis. *Brain* 139(Pt 4), 1079–1093. doi: 10.1093/brain/aww012

Qiao, J., Li, A., Cao, C., Wang, Z., Sun, J., and Xu, G. (2017). Aberrant functional network connectivity as a biomarker of generalized anxiety disorder. *Front. Hum. Neurosci.* 11:626. doi: 10.3389/fnhum.2017.00626

Qiao, J., Lv, Y., Cao, C., Wang, Z., and Li, A. (2018). Multivariate deep learning classification of Alzheimer's disease based on hierarchical partner matching independent component analysis. *Front. Aging Neurosci.* 10:417. doi: 10.3389/fnagi.2018.00417

Qiao, J., Weng, S., Wang, P., Long, J., and Wang, Z. (2015). Normalization of Intrinsic Neural Circuits Governing Tourette's Syndrome Using Cranial Electrotherapy Stimulation. *IEEE Trans. Biomed Eng.* 62, 1272–1280. doi: 10.1109/TBME.2014.2385151

Roland, J. L., Snyder, A. Z., Hacker, C. D., Mitra, A., Shimony, J. S., Limbrick, D. D., et al. (2017). On the role of the corpus callosum in interhemispheric functional connectivity in humans. *Proc. Natl. Acad. Sci. U.S.A.* 114, 13278–13283. doi: 10.1073/pnas.1707050114

Smania, N., Montagnana, B., Faccioli, S., Fiaschi, A., and Aglioti, S. M. (2003). Rehabilitation of somatic sensation and related deficit of motor control in patients with pure sensory stroke. *Arch. Phys. Med. Rehabil.* 84, 1692–1702. doi: 10.1053/s0003-9993(03)00277-6

Smith, S. M. (2002). Fast robust automated brain extraction. *Hum. Brain Mapp.* 17, 143–155. doi: 10.1002/hbm.10062

Smith, S. M., Jenkinson, M., Johansen-Berg, H., Rueckert, D., Nichols, T. E., Mackay, C. E., et al. (2006). Tract-based spatial statistics: voxelwise analysis of multi-subject diffusion data. *Neuroimage* 31, 1487–1505. doi: 10.1016/j.neuroimage.2006.02.024

Smith, S. M., and Nichols, T. E. (2009). Threshold-free cluster enhancement: addressing problems of smoothing, threshold dependence and localisation in cluster inference. *Neuroimage* 44, 83–98. doi: 10.1016/j.neuroimage.2008.03.061

Swick, D., Ashley, V., and Turken, A. U. (2008). Left inferior frontal gyrus is critical for response inhibition. *BMC Neurosci.* 9:102. doi: 10.1186/1471-2202-9-102

Szots, M., Blaabjerg, M., Orsi, G., Iversen, P., Kondziella, D., Madsen, C. G., et al. (2017). Global brain atrophy and metabolic dysfunction in LGI1 encephalitis: a prospective multimodal MRI study. *J. Neurol. Sci.* 376, 159–165. doi: 10.1016/j.jns.2017.03.020

Szots, M., Marton, A., Kover, F., Kiss, T., Berki, T., Nagy, F., et al. (2014). Natural course of LGI1 encephalitis: 3-5 years of follow-up without immunotherapy. *J. Neurol. Sci.* 343, 198–202. doi: 10.1016/j.jns.2014.05.048

Tolomeo, S., Christmas, D., Jentzsch, I., Johnston, B., Sprengelmeyer, R., Matthews, K., et al. (2016). A causal role for the anterior mid-cingulate cortex in negative affect and cognitive control. *Brain* 139(Pt 6), 1844–1854. doi: 10.1093/brain/aww069

van Sonderen, A., Schreurs, M. W., Wirtz, P. W., Sillevis Smitt, P. A., and Titulaer, M. J. (2016). From VGKC to LGI1 and Caspr2 encephalitis: the evolution of a disease entity over time. *Autoimmun. Rev.* 15, 970–974. doi: 10.1016/j.autrev.2016.07.018

Voss, J. L., Bridge, D. J., Cohen, N. J., and Walker, J. A. (2017). A Closer Look at the Hippocampus and Memory. *Trends Cogn. Sci.* 21, 577–588. doi: 10.1016/j.tics.2017.05.008

Wang, M., Cao, X., Liu, Q., Ma, W., Guo, X., and Liu, X. (2017). Clinical features of limbic encephalitis with LGI1 antibody. *Neuropsychiatr. Dis. Treat.* 13, 1589–1596. doi: 10.2147/NDT.S136723

Wang, Z., Maia, T. V., Marsh, R., Colibazzi, T., Gerber, A., and Peterson, B. S. (2011). The neural circuits that generate tics in Tourette's syndrome. *Am. J. Psychiatry* 168, 1326–1337. doi: 10.1176/appi.ajp.2011.09111692

Winkler, A. M., Ridgway, G. R., Douaud, G., Nichols, T. E., and Smith, S. M. (2016). Faster permutation inference in brain imaging. *Neuroimage* 141, 502–516. doi: 10.1016/j.neuroimage.2016.05.068

Zink, C. F., Pagnoni, G., Martin-Skurski, M. E., Chappelow, J. C., and Berns, G. S. (2004). Human striatal responses to monetary reward depend on saliency. *Neuron* 42, 509–517. doi: 10.1016/s0896-6273(04)00183-7

Conflict of Interest: The authors declare that the research was conducted in the absence of any commercial or financial relationships that could be construed as a potential conflict of interest.

frontiers in Aging Neuroscience

ORIGINAL RESEARCH
published: 28 April 2020
doi: 10.3389/fnagi.2020.00065

Freezing of Speech Single Questionnaire as a Screening Tool for Cognitive Dysfunction in Patients With Dementia With Lewy Bodies

*Pai-Yi Chiu[1], Guang-Uei Hung[2], Cheng-Yu Wei[3], Ray-Chang Tzeng[4] and Ming-Chyi Pai[5,6,7]**

[1] Department of Neurology, Show Chwan Memorial Hospital, Changhua, Taiwan, [2] Department of Nuclear Medicine, Chang Bing Show Chwan Memorial Hospital, Changhua, Taiwan, [3] Department of Neurology, Chang Bing Show Chwan Memorial Hospital, Changhua, Taiwan, [4] Department of Neurology, Tainan Municipal Hospital, Tainan, Taiwan, [5] Division of Behavioral Neurology, Department of Neurology, National Cheng Kung University Hospital, College of Medicine, National Cheng Kung University, Tainan, Taiwan, [6] Alzheimer's Disease Research Center, National Cheng Kung University Hospital, Tainan, Taiwan, [7] Institute of Gerontology, College of Medicine, National Cheng Kung University, Tainan, Taiwan

Introduction: Freezing phenomenon is a striking feature of Parkinson's disease. However, it has never been studied in people with dementia with Lewy bodies (DLB). We designed a freezing of speech single questionnaire (FOSSQ) and investigated the frequency and association of freezing of speech (FOS) in patients with DLB and other types of dementia.

Methods: This is a retrospective analysis of data from the project of history-based artificial intelligent computerized dementia diagnostic system. We compared the frequencies of FOS among non-demented (ND) participants, patients with Alzheimer's disease (AD), vascular dementia (VaD), and DLB. Further, we explored the association factors of FOS in all the participants.

Results: We enrolled 666 individuals with the following disease distribution: 190, ND; 230, AD; 183, VaD; and 63, DLB. Compared to individuals with ND (2.1%), patients with AD (6.1%), or VaD (18.0%), DLB (54.0%) showed a significantly higher frequency of positive FOS (all $p < 0.001$). The association factors of FOS were older age, more severe dementia, more severe motor dysfunction, fluctuating cognition, visual hallucinations, parkinsonism, rapid eye movement sleep behavior disorder, attention, mental manipulation, and language.

Conclusion: Our study showed that the informant-based FOSSQ may be a practical screening tool for discriminating DLB from individuals with ND or other forms of dementia. The FOSSQ can be applied in clinical practice as well as on the artificial intelligent platform.

Keywords: freezing of speech, fluctuating cognition, dementia with Lewy bodies, Alzheimer's disease, vascular dementia

OPEN ACCESS

Edited by:
Jiehui Jiang,
Shanghai University, China

Reviewed by:
Zhihua Yu,
Shanghai University of Traditional Chinese Medicine, China
Jung Lung Hsu,
Chang Gung Memorial Hospital, Taiwan
Can Sheng,
Capital Medical University, China

***Correspondence:**
Ming-Chyi Pai
pair@mail.ncku.edu.tw

Received: *15 November 2019*
Accepted: *25 February 2020*
Published: *28 April 2020*

Citation:
Chiu P-Y, Hung G-U, Wei C-Y, Tzeng R-C and Pai M-C (2020) Freezing of Speech Single Questionnaire as a Screening Tool for Cognitive Dysfunction in Patients With Dementia With Lewy Bodies. Front. Aging Neurosci. 12:65. doi: 10.3389/fnagi.2020.00065

INTRODUCTION

Freezing phenomenon is a striking feature of Parkinson's disease (PD). Freezing of gait (FOG) is a form of akinesia and is one of the most disabling symptoms of PD (Giladi et al., 2001). Previous studies on FOG in PD have reported a prevalence of 7.1–46% (Giladi et al., 2001; Macht et al., 2007) according to different criteria. However, there have only been a few studies on the freezing of speech (FOS) phenomenon (Ackermann et al., 1993; Giladi et al., 1997; Louis et al., 2001; Park et al., 2014; Vercruysse et al., 2014) in PD. Further, freezing phenomenon has rarely been mentioned or studied in neurological disorders other than PD, with some mentioning the phenomenon of FOS sharing a similar neural mechanism with FOG (Park et al., 2014; Vercruysse et al., 2014). The underlying mechanism of the freezing phenomenon is probably related to dysfunction of the fronto-striatal circuits (Vercruysse et al., 2014). To our knowledge, there have been no studies on FOS in dementia with Lewy bodies (DLB) or other degenerative types of dementia. DLB is one of the Lewy body diseases (LBD) and it shares a similar pathological manifestation with PD, especially PD with dementia (PDD) (Kosaka et al., 1984; Jellinger, 2018). Therefore, patients with DLB should demonstrate similar freezing phenomenon as PD/PDD. It remains unclear whether FOS is a deficit of language or other cognitive functions. However, language dysfunction is indeed one of the common cognitive features of a diagnosis of dementia due to Alzheimer's disease (AD) or other forms of dementia (McKeith et al., 2005; McKhann et al., 2011; Hardy et al., 2016). Similarly, the association factors of FOS have not yet been well studied.

To study FOS, we designed a simple informant-based FOS single questionnaire (FOSSQ) that was embedded in the History-based Artificial Intelligent Clinical Dementia Diagnostic System (HAICDDS) (Lin et al., 2018; Chiu et al., 2019). We aimed to investigate the frequency and association of FOS in DLB and other types of dementia. We proposed that since the FOS phenomenon is a striking feature of PD, it could be an important feature of DLB because both language (Lin et al., 2018) and motor deficits (McKeith et al., 2005) are common clinical presentations of DLB. Based on the findings that the underlying mechanism of the freezing phenomenon is probably related to dysfunction of the fronto-striatal circuits (Vercruysse et al., 2014), we proposed that FOS could be a deficit involving language and motor dysfunction as well as dysfunction of other cognitive functions such as attention and executive dysfunction. Similarly, as a striking clinical phenomenon, we also proposed that FOS may involve fluctuation of attention and cognition, and thus performed fluctuation scale comparisons.

MATERIALS AND METHODS

This is a sub-study of the project of HAICDDS, which is currently used as a registration platform in the Show Chwan Healthcare System (Lin et al., 2018; Chiu et al., 2019). Participants who visited either hospital of the healthcare system with suspected cognitive or motor dysfunction were registered with their demographical, clinical, cognitive, neuropsychiatric, motor, laboratory, and neuroimaging data in the database. The HAICDDS questionnaire is part of the database for recording of clinical history. It is composed of 100 questions designed after a consensus meeting of 12 neurologists, one geriatric psychiatrist, three nuclear medicine doctors, and one neuroradiologist. The fundamental structure of the questionnaire is similar to that of history-taking used by physicians for acquiring detailed clinical information. Before commencing the project, thirty patients with their informants were assessed by neuropsychologists from three centers and the reproducibility was studied using the interrater reliability analysis. Cronbach's alpha coefficient was calculated to estimate the reliability of the entire novel screening questionnaire. The original writing of FOSSQ was in Chinese as follows: 跟人講話時常常思緒突然中斷, 腦袋好像一片空白, 難以互動嗎 (The tentative translation to English is: "When speaking, does he/she pause frequently, seem blank, and have trouble communicating?"). In this sub-study, we analyzed and compared the FOSSQ results among non-demented (ND) participants as well as participants with AD, vascular dementia (VaD), and DLB. Further, we studied the association factors of FOS among the participants.

Diagnosis of AD, VaD, or DLB

A diagnosis of AD was made according to the criteria for dementia due to AD developed by the National Institute on Aging-Alzheimer's Association workgroups on diagnostic guidelines for AD (McKhann et al., 2011). A diagnosis of VaD was made according to the criteria for probable VaD or possible VaD in the 2011 AHA/ASA criteria for vascular cognitive impairment (VCI) (Gorelick et al., 2011). A diagnosis of DLB was made according to the revised consensus criteria for probable DLB developed by the fourth report of the DLB consortium (McKeith et al., 2017).

Diagnosis of ND, or Different Stages of Dementia

ND participant was diagnosed with a global CDR (Morris, 1993) score of 0 or 0.5 without significantly impaired activities of daily living, which was defined by an Instrumental Activities of Daily Living (IADL) score greater than 6 (Mao et al., 2018). A diagnosis of dementia was made according to the criteria for dementia developed by the NIA-AA (McKhann et al., 2011). Specifically, people with dementia had impairments in two cognitive domains or more as well as declined daily functions (at least one of the domains of community affairs, home hobbies, and personal care with a CDR score $\geq$ 0.5 and an IADL score $\leq$ 6) (Mao et al., 2018). Dementia severity was defined by the global CDR scale score; specifically, participants with a global CDR score of 0.5, 1, 2, and 3 were defined as having very mild, mild, moderate, and severe dementia, respectively (Morris, 1993).

Procedure of the Study

This is a retrospective analysis of data from the HAICDDS, which is currently applied in three centers in Taiwan (two in central Taiwan and one in southern Taiwan). Daily function was

assessed using the Instrumental Activities of Daily Living (IADL) Scale (Lawton and Brody, 1969). Cognitive function was assessed using the Cognitive Abilities Screening Instrument (CASI) (Lin et al., 2002) and the Montreal Cognitive Assessment (MoCA) (Chen et al., 2016). Neuropsychiatric symptoms were assessed using the Neuropsychiatric Inventory (NPI) (Cummings, 1988). Language function was assessed using the language subscales in the CASI and HAICDDS (HAICDDS-Language) (Lin et al., 2018). Language domain in CASI screens cognitive performance on reading, writing, naming, and comprehension whereas, language questions in HAICDDS acquire information on speech fluency, comprehension, naming, volume, and tone based on clinical history (Lin et al., 2018). Trained neuropsychologists administered the cognitive tests and NPI to all the patients.

Statistics

The Chinese version of SPSS 22.0 for Windows (IBM, SPSS Inc., Chicago) was used for statistical analyses. Between-group comparisons of demographic data, neuropsychological tests, CDR sum of boxes (CDR-SB), IADL score, MoCA score, CASI score, NPI total score (NPI-sum), motor subscale of the Unified Parkinson's Disease Rating Scale (UPDRS-M), and DLB features were analyzed using independent t-test or one-way ANOVA with either Bonferroni or Dunnett T3 *post hoc* analysis according to the homogeneity of variance. Between-group comparisons of demographic and background characteristics with positive FOSSQ (FOSSQ +) and negative FOSSQ (FOSSQ-) were adjusted for age and disease severity. Comparisons of each cognitive domain in the CASI between FOSSQ + and FOSSQ- groups were adjusted for age, gender, and disease severity. Comparison of frequency of symptom fluctuation in the Mayo Fluctuation Composite Score (MFCS) and language symptoms in the HAICDDS-Language between FOSSQ + and FOSSQ- groups were adjusted for age and disease severity.

Ethical Consideration

The participants were selected from a registry-based database of the Show Chwan Health System. The study design was retrospective, and the data were anonymously analyzed. The Committee for Medical Research Ethics of Show Chwan Memorial Hospital reviewed the project and the Data Inspectorate approved the study.

RESULTS

We enrolled 666 individuals with the following disease distribution: 190, ND; 230, AD; 183, VaD; and 63, DLB. The frequency of FOSSQ + in patients with CDR scores of 0, 0.5, 1, 2, and 3 were 3.8, 3.0, 15.2, 26.1, and 43.5%, respectively. Compared to patients with ND (2.1%), AD (6.1%), or VaD (18.0%), those with DLB (54.0%) showed a significantly higher frequency of FOSSQ + (all $p < 0.001$). Comparison of demographic and background characteristics among patients with ND, AD, VaD, and DLB revealed significant differences in all the parameters ($p < 0.001$), except for informant age or education (**Table 1**).

Comparison of demographic and background characteristics between the FOSSQ + and FOSSQ- groups before adjustment revealed that the FOSSQ + group had a significantly older age and more severe dementia stages. Further, there were significant differences in all other parameters ($p < 0.001$) except for gender, education, and history of cerebrovascular accident (**Table 2**). After adjustment for age and disease severity, FOSSQ + had more males and higher DLB features including UPDRS-M, cognitive fluctuations, visual hallucinations, parkinsonism, and REM sleep behavior disorder (**Table 2**).

Comparison of each cognitive domain in the CASI between the FOSSQ + and FOSSQ- groups before adjustment revealed that the FOSSQ + group had significantly lower scores in all domains ($p < 0.001$). After adjustment for age and disease severity, the FOSSQ + group had significantly lower scores only in the attention and language domains (**Table 3**).

Comparison of frequency of symptom fluctuation in the MFCS and language symptoms in the HAICDDS-Language between FOSSQ + and FOSSQ- before and after adjustment for age and disease severity showed that FOSSQ + had a significantly higher frequency in all domains in the MFCS and HAICDDS-Language except for language impairment, which occurred much earlier than the other symptoms (HAICDDS-L7) (**Table 4**). Given our recent finding that HAICDDS-L8 has the highest power for discrimination of DLB when compared to other types of dementia (Lin et al., 2018), we further combined FOSSQ with HAICDDS-L8 and found that the positive rate for each question were DLB (61.9%), VaD (29.0%), AD (7.8%), and ND (2.6%).

DISCUSSION

As a sub-study of the project HAICDDS, we analyzed data from a relatively large population (666 individuals) and obtained important results. First, we successfully demonstrated that even a single question could provide good discrimination among dementia stages and subtypes. The frequencies of FOSSQ + in patients with CDR scores of 0, 0.5, 1, 2, and 3 were 3.8, 3.0, 15.2, 26.1, and 43.5%, respectively, indicating that the frequency of FOS significantly increased with increase in dementia severity. Regarding discrimination of dementia subtypes, the FOS phenomenon was found more often in patients with DLB (54.0%) compared to those with either AD (6.1%) or VaD (18.0%). The frequency of FOSSQ + was lower among females, which is consistent with previous findings on freezing phenomenon in Parkinson's disease (Park et al., 2014).

Second, the frequency of FOS was not only highest in patients with DLB but was also more significantly associated with DLB features ($p < 0.001$), including cognitive fluctuations (OR = 10.22), visual hallucinations (OR = 4.18), parkinsonism (OR = 4.68), and REM sleep behavior disorder (OR = 2.84). Motor dysfunction according to the UPDRS-M is more severe in the FOSSQ + group (OR = 1.02; $p = 0.002$). Therefore, it is reasonable to consider FOS as part of the characteristic features in the diagnosis of DLB than that of ND or other types of dementia. The dopamine transporter imaging is not significantly different after adjustment, however. We proposed that non-DLB

TABLE 1 | Comparison of demographic data among ND, AD, VaD, and DLB groups.

Groups	ND	AD	VaD	DLB	F/x^2	*p*
N	190	230	183	63		
Age, year	68.1 ± 11.4	80.1 ± 8.6	73.7 ± 10.7	80.8 ± 7.0	57.24	<0.001
Female, N (%)	100 (52.6)	154 (67.0)	77 (42.1)	36 (57.1)	29.19	<0.001
Education, year	7.4 ± 4.9	4.4 ± 4.5	6.0 ± 4.8	5.3 ± 13.0	9.15	<0.001
CDR, 0/0.5/1/2/3	53/137/0/0/0	0/85/77/51/17	0/66/52/48/17	0/9/22/20/12	324.18	<0.001
CDR-SB	0.7 ± 0.7	6.7 ± 4.4	7.2 ± 5.0	9.7 ± 5.2	128.61	<0.001
IADL	7.7 ± 0.6	2.7 ± 2.7	2.6 ± 2.9	1.4 ± 2.3	235.16	<0.001
MoCA	20.0 ± 6.0	7.4 ± 5.5	9.1 ± 6.8	7.1 ± 6.5	175.02	<0.001
CASI	81.5 ± 12.1	44.8 ± 21.5	47.8 ± 24.6	43.2 ± 23.3	139.26	<0.001
NPI-sum	3.4 ± 5.0	5.2 ± 6.9	8.3 ± 9.3	15.6 ± 14.0	31.02	<0.001
UPDRS-M	7.1 ± 7.1	11.4 ± 12.0	30.6 ± 14.6	28.9 ± 11.1	37.76	<0.001
DLB features, N (%)						
Fluctuation	4 (2.1)	32 (13.9)	48 (26.2)	32 (50.8)	91.61	<0.001
VH	1 (0.5)	10 (4.3)	16 (8.7)	29 (46.0)	136.07	<0.001
Parkinsonism	32 (16.8)	42 (18.3)	73 (39.9)	59 (93.7)	157.39	<0.001
RBD	17 (8.9)	13 (5.7)	13 (7.1)	34 (54.0)	123.49	<0.001
DaTabN	2 (6.9)	3 (20.0)	8 (47.1)	19 (79.2)	31.94	<0.001
Informant						
Age, year	58.8 ± 13.3	54.9 ± 14.3	55.7 ± 13.7	54.3 ± 13.7	1.96	0.120
Education, year	11.1 ± 7.5	11.1 ± 4.3	10.2 ± 4.8	11.1 ± 4.9	0.60	0.613

N, Number of participants; ND, Non-demented; AD, Alzheimer disease; VaD, vascular dementia; DLB, Dementia with Lewy bodies; CDR, Clinical Dementia Rating; IADL, Instrumental Activities of Daily Living; MoCA, Montreal Cognitive Assessment; CASI, Cognitive Abilities Screening Instrument; NPI-sum, The sum of score of Neuropsychiatric Inventory; UPDRS-M, motor subscale of the Unified Parkinson's Disease Rating Scale in 28 NC, 34 AD, 34 VCI, and 25 DLB; VH, visual hallucinations; RBD, REM sleep behavior disorder; DaTabN, abnormal dopamine transporter imaging in 29 NC, 15 AD, 17 VCI, and 24 DLB.

TABLE 2 | Comparison of demographic and background characteristics between groups with FOSSQ + and FOSSQ – adjusted for age and disease severity according to CDR.

	Mean ± SD		Non-adjusted		Adjusted	
	FOSSQ +	FOSSQ–	t/χ^2	*p*	OR (95% CI)	*p*
N	85	581				
Age, years	77.3 ± 10.1	74.6 ± 11.3	2.20	0.028	NA	
CDR, 0/0.5/1/2/3	2/9/23/31/20	51/288/128/88/26	87.79	<0.001	NA	
Female, N (%)	39 (45.9)	328 (56.3)	3.35	NS	0.56 (0.34–0.92)	0.023
Education, years	5.7 ± 11.3	5.8 ± 4.9	−0.14	NS	1.01 (0.98–1.05)	NS
IADL	1.4 ± 2.4	4.3 ± 3.3	−7.97	<0.001	0.95 (0.77–1.16)	NS
MoCA	6.3 ± 6.2	12.2 ± 8.2	−6.36	<0.001	0.98 (0.92–1.04)	NS
CASI	37.7 ± 23.6	58.6 ± 25.4	−7.18	<0.001	0.99 (0.98–1.01)	NS
NPI	14.0 ± 11.8	5.4 ± 7.9	8.73	<0.001	1.05 (1.03–1.08)	<0.001
UPDRS-M	30.9 ± 19.9	18.2 ± 16.6	8.34	<0.001	1.02 (1.01–1.03)	0.002
DLB features						
Fluctuation	56 (65.9)	60 (10.3)	159.11	<0.001	10.22 (5.76–18.13)	<0.001
VH	26 (30.6)	30 (5.2)	62.24	<0.001	4.18 (2.20–7.95)	<0.001
Parkinsonism	58 (68.2)	148 (25.5)	63.27	<0.001	4.68 (2.77–7.91)	<0.001
RBD	21 (24.7)	56 (9.6)	16.46	<0.001	2.84 (1.52–5.29)	<0.001
DaTabN	12 (63.2)	20 (30.3)	6.78	0.009	1.16 (0.23–3.29)	NS
History of CVA	26 (30.6)	128 (22.0)	3.06	NS	1.11 (0.63–1.94)	NS

FOSSQ, Freezing of Speech Single Questionnaire; CDR, Clinical Dementia Rating scale; N, number of cases; NA, not applicable; NS, not significant; OR, odds ratio; IADL, Instrumental Activities of Daily Living; MoCA, Montreal Cognitive Assessment; CASI, Cognitive Abilities Screening Instrument; NPI, total score of the twelve-domain Neuropsychiatric Inventory; UPDRS-M, motor subscale of the Unified Parkinson's Disease Rating Scale in 28 NC, 34 AD, 34 VCI, and 25 DLB; VH, visual hallucinations; RBD, REM sleep behavior disorder; DaTabN, abnormal dopamine transporter imaging in 29 NC, 15 AD, 17 VCI, and 24 DLB; CVA, cerebrovascular accident.

TABLE 3 | Comparison of each cognitive domain in CASI between groups with FOSSQ + and FOSSQ – adjusted for age, education, gender, and disease severity according to CDR.

	Mean ± SD		Non-adjusted		Adjusted	
	FOSSQ +	FOSSQ–	t	*p*	OR (95% CI)	*p*
N	85	581				
RMM	6.2 ± 3.3	8.1 ± 2.7	−5.26	<0.001	0.98 (0.88–1.09)	NS
RCM	3.6 ± 3.2	5.9 ± 4.1	−4.90	<0.001	1.01 (0.92–1.11)	NS
ATT	2.3 ± 2.1	5.0 ± 2.3	−10.00	<0.001	0.67 (0.59–0.77)	<0.001
MEN	1.6 ± 2.6	4.0 ± 3.5	−5.99	<0.001	0.85 (0.75–0.95)	0.006
ORI	7.4 ± 5.6	11.1 ± 5.9	−5.54	<0.001	1.03 (0.96–1.10)	NS
ABS	2.8 ± 2.3	4.3 ± 2.4	−5.47	<0.001	0.93 (0.86–1.15)	NS
LAN	5.8 ± 3.0	7.9 ± 2.2	−7.52	<0.001	0.89 (0.80–0.99)	0.044
DRAW	4.5 ± 3.8	6.6 ± 4.0	−4.60	<0.001	1.02 (0.94–1.10)	NS
ANM	3.6 ± 3.2	5.8 ± 3.5	−5.58	<0.001	1.04 (0.93–1.15)	NS

CASI, Cognitive Abilities Screening Instrument; FOSSQ, Freezing of Speech Single Questionnaire; CDR, Clinical Dementia Rating scale; N, number of cases; NA, not applicable; NS, not significant; OR, odds ratio; RMM, remote memory; RCM, recent memory; ATT, attention; MEN, mental manipulation; ORI, orientation; ABS, abstract thinking; LAN, language; DRAW, drawing; ANM, animal naming.

TABLE 4 | Comparison of frequency of fluctuation symptoms in MFCS and language symptoms in HAICDDS-Language between groups with FOSSQ + and FOSSQ – adjusted for age and disease severity according to CDR.

	Mean ± SD		Non-adjusted		Adjusted	
	FOSSQ +	FOSSQ –	t	*p*	OR (95% CI)	*p*
N	85	581				
MFCS						
Disorganized speech	37 (43.5)	34 (5.9)	110.52	<0.001	5.74 (3.17–10.41)	<0.001
Drowsy/lethargic	57 (67.1)	156 (26.9)	55.11	<0.001	3.39 (1.99–5.77)	<0.001
Sleep > 2 h	63 (74.1)	121 (20.8)	105.32	<0.001	6.68 (3.77–11.82)	<0.001
Staring into space	57 (67.1)	73 (12.6)	140.17	<0.001	7.88 (4.41–14.08)	<0.001
MFCS total score	2.5 ± 1.2	0.7 ± 1.0	15.69	<0.001	3.12 (2.38–4.10)	<0.001
HAICDDS-Language						
L1	60 (70.6)	173 (29.8)	87.76	<0.001	3.09 (1.78–5.37)	<0.001
L2	68 (80.0)	199 (34.3)	96.55	<0.001	3.01 (1.54–5.90)	0.001
L3	54 (63.5)	140 (24.1)	91.10	<0.001	2.38 (1.35–4.19)	0.003
L4	21 (24.7)	22 (3.8)	60.31	<0.001	4.70 (2.37–9.56)	<0.001
L5	59 (69.4)	155 (26.7)	62.10	<0.001	2.65 (1.48–4.77)	0.001
L6	61 (71.8)	198 (34.1)	74.68	<0.001	2.87 (1.66–4.96)	<0.001
L7	2 (2.4)	6 (1.0)	0.89	NS	3.33 (0.56–19.64)	NS
L8	28 (32.9)	30 (5.2)	71.97	<0.001	4.96 (2.62–9.38)	<0.001
Language total score	6.0 (3.2)	1.9 (2.4)	13.57	<0.001	1.45 (1.30–1.61)	<0.001

MFCS, Mayo Fluctuation Composite Score; HAICDDS-Language; Language subscale in the History-based Artificial Intelligent Clinical Dementia Diagnostic System; FOSSQ, Freezing of Speech Single Questionnaire; CDR, Clinical Dementia Rating scale; N, number of cases; NA, not applicable; NS, not significant; OR, odds ratio; L1, Does his/her speaking become noticeably less fluent? L2, Can't he/she understand words or sentences of others? L3, Is it difficult to express a sentence completely? L4, Does he/she repeat the same words or repeat the words of others? L5, Does he/she speak very little? L6, Does he/she have trouble finding words or names? L7, Does language impairment occur early and much earlier than other symptoms? L8, Does his/her speech reduce pitch range (monotone) and reduced volume (hypophonia)? Any, at least one scale of the language questionnaire was positive.

participants who performed dopamine transporter imaging were comorbid with motor dysfunction and were highly suspected to have parkinsonism. Hence, a relatively high percentage of DaTabN was found among these patients (47.1 and 20% in VaD and AD). Our next piece of research to address this issue and to clarify the association of FOS and dopamine transporter uptake in the striatal area is underway.

Third, after adjustment for age and dementia severity, the FOSSQ + demonstrated a strong relationship with dysfunctions in attention, mental manipulation, and language domains in the CASI. This indicated that FOS might be a combination of these types of cognitive dysfunction, which is consistent with our hypothesis. Some researchers may argue that using the cognitive screening tool CASI, attention domain screens only registration and repetition and language domain screening cognitive performance on reading, writing, naming, and comprehension. Whether attention and language subscales in CASI represent the actual functions of attention and language might be controversial

based only on a cognitive screening tool. Further detailed and specific neuropsychological tests to clarify the association of FOS with cognitive functions will be necessary.

Fourth, it is consistent with our recent findings of language dysfunction being more severe in patients with DLB than those with other dementia using the HAICDDS-Language questionnaire (Lin et al., 2018). In the study, we found that the discriminative ability of the HAICDDS-Language, especially the HAICDDS-L8 ("Does his/her speech reduce pitch range and reduced volume?") among patients with DLB/PDD and AD was robust (OR = 9.16; 95% CI: 6.33–13.25) (Lin et al., 2018). Therefore, in the current study, we combined the FOSSQ with HAICDDS-L8 and found an increase of positive rate in DLB (61.9%) which is much higher than those in VaD (29.0%), AD (7.8%), or ND (2.6%).

Finally, in the HAICDDS project, we have continuously provided evidence that the combination of multiple standardized and structured questions is more powerful and can be optimized using artificial intelligence with machine learning techniques. This was the original idea behind the design of the HAICDDS questionnaire.

This study has several limitations. First, we used a single questionnaire for detecting FOS in patients with DLB and other forms of dementia; therefore, further studies using more tools are required to confirm the findings. Second, we used the original Taiwanese version of the questionnaire, which, although we translated to English, would call for a more precise and colloquial translation. Third, our study was conducted in only three centers in Taiwan. Therefore, the findings on the prevalence and association factors of FOS are not generalizable to all patients with DLB or other types of dementia.

CONCLUSION

In conclusion, our study showed that the informant-based single questionnaire FOSSQ can be a practical screening tool for the discrimination of DLB from ND or other types of dementia. The FOSSQ can be applied in clinical practice as well as in the dementia registration platform. Further machine learning techniques using artificial intelligence could improve the accuracy and efficiency of the questionnaire.

DATA AVAILABILITY STATEMENT

The raw data supporting the conclusions of this article will be made available by the authors, without undue reservation, to any qualified researcher.

ETHICS STATEMENT

The studies involving human participants were reviewed and approved by the Show Chwan Memorial Hospital. Written informed consent for participation was not required for this study in accordance with the national legislation and the institutional requirements.

AUTHOR CONTRIBUTIONS

P-YC undertook the literature search and data analysis, edited the Author Contributions, and was mainly responsible for revisions and drafts of the manuscript. M-CP participated in the data analysis and contributed to revisions and the final draft of the manuscript. G-UH undertook the literature search and contributed to revisions. C-YW contributed to revisions of the manuscript. R-CT undertook the literature search and contributed to revisions.

FUNDING

The study was funded by the Show Chwan Memorial Hospital No. RD-105032.

ACKNOWLEDGMENTS

We would like to thank Prof. Shu-Hui Sue at National Taichung University of Science and Technology and Prof. Tsung-Lin Cheng at National Changhua University of Education for their feedback and suggestions during the experimental design and statistical analysis. Partial data and results of this study had been published as an abstract entitled "Freezing of Speech Single Questionnaire as a Screening Tool for Dementia with Lewy Bodies" in a poster section of the 2019 Alzheimer's Association International Conference (AAIC).

REFERENCES

Ackermann, H., Grone, B. F., Hoch, G., and Schonle, P. W. (1993). Speech freezing in Parkinson's disease: a kinematic analysis of orofacial movements by means of electromagnetic articulography. *Folia Phoniatr.* 45, 84–89. doi: 10.1159/000266222

Chen, K. L., Xu, Y., Chu, A. Q., Ding, D., Liang, X. N., Nasreddine, Z. S., et al. (2016). Validation of the Chinese version of montreal cognitive assessment basic for screening mild cognitive impairment. *J. Am. Geriatr. Soc.* 64, e285–e290. doi: 10.1111/jgs.14530

Chiu, P. Y., Tang, H., Wei, C. Y., Zhang, C., Hung, G. U., and Zhou, W. (2019). NMD-12: a new machine-learning derived screening instrument to detect mild cognitive impairment and dementia. *PLoS One* 14:e0213430. doi: 10.1371/journal.pone.0213430

Cummings, J. L. (1988). Intellectual impairment in Parkinson's disease: clinical, pathologic, and biochemical correlates. *J. Geriatr. Psychiatry Neurol.* 1, 24–36. doi: 10.1177/089198878800100106

Giladi, N., Kao, R., and Fahn, S. (1997). Freezing phenomenon in patients with parkinsonian syndromes. *Mov. Disord.* 12, 302–305. doi: 10.1002/mds.870120307

Giladi, N., McDermott, M. P., Fahn, S., Przedborski, S., Jankovic, J., Stern, M., et al. (2001). Freezing of gait in PD: prospective assessment in the DATATOP cohort. *Neurology* 56, 1712–1721. doi: 10.1212/wnl.56.12.1712

Gorelick, P. B., Scuteri, A., Black, S. E., Decarli, C., Greenberg, S. M., Iadecola, C., et al. (2011). Vascular contributions to cognitive impairment and dementia: a statement for healthcare professionals from the american heart association/american stroke association. *Stroke* 42, 2672–2713. doi: 10.1161/STR.0b013e3182299496

Hardy, C. J., Buckley, A. H., Downey, L. E., Lehmann, M., Zimmerer, V. C., Varley, R. A., et al. (2016). The language profile of behavioral variant frontotemporal dementia. *J. Alzheimers. Dis.* 50, 359–371. doi: 10.3233/jad-150806

Jellinger, K. A. (2018). Dementia with Lewy bodies and Parkinson's disease-dementia: current concepts and controversies. *J Neural Transm.* 125, 615–650. doi: 10.1007/s00702-017-1821-1829

Kosaka, K., Yoshimura, M., Ikeda, K., and Budka, H. (1984). Diffuse type of lewy body disease: progressive dementia with abundant cortical Lewy bodies and senile changes of varying degree–a new disease? *Clin. Neuropathol.* 3, 185–192.

Lawton, M. P., and Brody, E. M. (1969). Assessment of older people: self-maintaining and instrumental activities of daily living. *Gerontologist* 9, 179–186. doi: 10.1093/geront/9.3_Part_1.179

Lin, C. M., Hung, G. U., Wei, C. Y., Tzeng, R. C., and Chiu, P. Y. (2018). An informant-based simple questionnaire for language assessment in neurodegenerative disorders. *Dement. Geriatr. Cogn. Disord.* 46, 207–216. doi: 10.1159/000493540

Lin, K. N., Wang, P. N., Liu, C. Y., Chen, W. T., Lee, Y. C., and Liu, H. C. (2002). Cutoff scores of the cognitive abilities screening instrument. Chinese version in screening of dementia. *Dement. Geriatr. Cogn. Disord.* 14, 176–182. doi: 10.1159/000066024

Louis, E. D., Winfield, L., Fahn, S., and Ford, B. (2001). Speech dysfluency exacerbated by levodopa in Parkinson's disease. *Mov. Disord.* 16, 562–565. doi: 10.1002/mds.1081

Macht, M., Kaussner, Y., Moller, J. C., Stiasny-Kolster, K., Eggert, K. M., Kruger, H. P., et al. (2007). Predictors of freezing in Parkinson's disease: a survey of 6,620 patients. *Mov. Disord.* 22, 953–956. doi: 10.1002/mds.21458

Mao, H. F., Chang, L. H., Tsai, A. Y., Huang, W. W., Tang, L. Y., Lee, H. J., et al. (2018). Diagnostic accuracy of instrumental activities of daily living for dementia in community-dwelling older adults. *Age Ageing* 47, 551–557. doi: 10.1093/ageing/afy021

McKeith, I. G., Boeve, B. F., Dickson, D. W., Halliday, G., Taylor, J. P., Weintraub, D., et al. (2017). Diagnosis and management of dementia with Lewy bodies: fourth consensus report of the DLB Consortium. *Neurology* 89, 88–100. doi: 10.1212/wnl.0000000000004058

McKeith, I. G., Dickson, D. W., Lowe, J., Emre, M., O'Brien, J. T., Feldman, H., et al. (2005). Diagnosis and management of dementia with lewy bodies: third report of the DLB consortium. *Neurology* 65, 1863–1872. doi: 10.1212/01.wnl.0000187889.17253.b1

McKhann, G. M., Knopman, D. S., Chertkow, H., Hyman, B. T., Jack, CR Jr, Kawas, C. H., et al. (2011). The diagnosis of dementia due to Alzheimer's disease: recommendations from the National Institute on Aging-Alzheimer's association workgroups on diagnostic guidelines for Alzheimer's disease. *Alzheimer's Dement.* 7, 263–269. doi: 10.1016/j.jalz.2011.03.005

Morris, J. C. (1993). The clinical dementia rating (CDR): current version and scoring rules. *Neurology* 43, 2412–2414. doi: 10.1212/wnl.43.11.2412-a

Park, H. K., Yoo, J. Y., Kwon, M., Lee, J. H., Lee, S. J., Kim, S. R., et al. (2014). Gait freezing and speech disturbance in Parkinson's disease. *Neurol. Sci.* 35, 357–363. doi: 10.1007/s10072-013-1519-1511

Vercruysse, S., Gilat, M., Shine, J. M., Heremans, E., Lewis, S., and Nieuwboer, A. (2014). Freezing beyond gait in Parkinson's disease: a review of current neurobehavioral evidence. *Neurosci. Biobehav. Rev.* 43, 213–227. doi: 10.1016/j.neubiorev.2014.04.010

Conflict of Interest: P-YC work has been partly supported by the Show Chwan Memorial Hospital.

The remaining authors declare that the research was conducted in the absence of any commercial or financial relationships that could be construed as a potential conflict of interest.

frontiers in Neuroscience

REVIEW
published: 30 April 2020
doi: 10.3389/fnins.2020.00305

Nanotheranostic Applications for Detection and Targeting Neurodegenerative Diseases

Ajay Kumar[1,2†], Ravi Kumar Chaudhary[3†], Rachita Singh[4†], Satya P. Singh[5], Shao-Yu Wang[2], Zheng-Yu Hoe[6], Cheng-Tang Pan[2], Yow-Ling Shiue[1]*, Dong-Qing Wei[7]*, Aman Chandra Kaushik[7,8]* and Xiaofeng Dai[8]**

[1] Institute of Biomedical Sciences, National Sun Yat-sen University, Kaohsiung, Taiwan, [2] Department of Mechanical and Electro-Mechanical Engineering, National Sun Yat-sen University, Kaohsiung, Taiwan, [3] Department of Biotechnology, Institute of Applied Medicines & Research, Ghaziabad, India, [4] Department of Electrical and Electronics Engineering, IIMT Engineering College, Uttar Pradesh Technical University, Meerut, India, [5] School of Computer Science & Engineering, Nanyang Technological University, Singapore, Singapore, [6] Department of Physical Medicine and Rehabilitation, Kaohsiung Veterans General Hospital, Kaohsiung, Taiwan, [7] Key Laboratory of Microbial Metabolism, School of Life Sciences and Biotechnology, Shanghai Jiao Tong University, Shanghai, China, [8] Wuxi School of Medicine, Jiangnan University, Wuxi, China

OPEN ACCESS

Edited by:
Chih-Yu Hsu,
Fujian University of Technology, China

Reviewed by:
Shihua Li,
Jinan University, China
Ian James Martins,
University of Western Australia, Australia

***Correspondence:**
Cheng-Tang Pan
pan@mem.nsysu.edu.tw
Yow-Ling Shiue
shirley@imst.nsysu.edu.tw
Dong-Qing Wei
dqwei@sjtu.edu.cn
Aman Chandra Kaushik
amanbioinfo@jiangnan.edu.cn
Xiaofeng Dai
1281423490@qq.com

[†] These authors have contributed equally to this work

Specialty section:
This article was submitted to Neurodegeneration, a section of the journal Frontiers in Neuroscience

Received: 22 September 2019
Accepted: 16 March 2020
Published: 30 April 2020

Citation:
Kumar A, Chaudhary RK, Singh R, Singh SP, Wang S-Y, Hoe Z-Y, Pan C-T, Shiue Y-L, Wei D-Q, Kaushik AC and Dai X (2020) Nanotheranostic Applications for Detection and Targeting Neurodegenerative Diseases. Front. Neurosci. 14:305. doi: 10.3389/fnins.2020.00305

Nanotechnology utilizes engineered materials and devices which function with biological systems at the molecular level and could transform the management of neurodegenerative diseases (NDs) by provoking, reacting to, and intermingling with target sites to stimulate physiological responses while minimizing side effects. Blood–brain barrier (BBB) protects the brain from harmful agents, and transporting drugs across the BBB is a major challenge for diagnosis, targeting, and treatment of NDs. The BBB provides severe limitations for diagnosis and treatment of Alzheimer's disease (AD), Parkinson's disease (PD), and various other neurological diseases. Conventional drug delivery systems generally fail to cross the BBB, thus are inefficient in treatment. Although gradual development through research is ensuring the progress of nanotheranostic approaches from animal to human modeling, aspects of translational applicability and safety are a key concern. This demands a deep understanding of the interaction of body systems with nanomaterials. There are various plant-based nanobioactive compounds which are reported to have applicability in the diagnosis and treatment of these NDs. This review article provides an overview of applications of nanotheranostics in AD and PD. The review also discusses nano-enabled drug delivery systems and their current and potential applications for the treatment of various NDs.

Keywords: neurodegenerative disorders, nanotheranostics, Parkinson's disease, Alzheimer's disease, nanocomposite

INTRODUCTION

Technological developments across various fields have proven to be beneficial for the advancements of medical research. These developments have assisted in developing various novel and efficient techniques, machines, and methods which can cure different challenging conditions and disorders of the human body. In addition to these technological advancements, an increase in research in the

field has also led to the development of various techniques which can help in combating different disorders (Bronzino, 2014). One such recent development is nanotheranostics, which has been defined by Lammers et al. (2010) as an approach which integrates target-specific diagnostics as well as therapeutics for complete recovery from the disease. These integrated practices are dependent on the use of different nanotechnology platforms, which are specifically designed for being able to target a given physical condition or disorder and hence can be used for both diagnostics and therapeutics purposes. One of the most common applications of this therapy or practice is in the treatment of neurodegenerative disorders, which are caused by different hereditary or sporadic conditions and mostly result in various dysfunctions of the nervous system of patients (Sharma, 2014). This review provides an overview of applications of nanotheranostics in neurodegenerative diseases (NDs) and recent advancements in nano-enabled drug delivery systems.

DISCUSSION AND ANALYSIS

Neurodegeneration

Neurodegeneration, as explained by Williams (2002), is the basis of all neurodegenerative disorders like Parkinson's disease (PD), Huntington's disease, and Alzheimer's disease (AD) and is primarily used to describe any condition which tends to affect the normal functioning of neurons in the brain. Williams (2002) explained that neurodegeneration combines two words, "neuro" and "degeneration," and hence refers to the degeneration of neurons, which in turn affects memory and other cognitive abilities of the patients. There are several researches which focused on the analyses of these neurological disorders. While several people assume it to be incurable, latest findings have revealed that the use of new techniques and approaches like nanotheranostics can render better outcomes. In addition to genetic mutations, other factors which have been found to result in neurodegeneration among patients include the buildup of different toxic proteins in the brain and the formation of neurotoxic molecules that can be caused by the loss of mitochondrial functions (Ingelsson, 2016). Further discussions explain the symptoms and molecular mechanisms associated with some of the neurodegenerative disorders which will help to understand the effectiveness of various nanotheranostic approaches.

Common Neurodegenerative Disorders

Alzheimer's Disease

Alzheimer's Disease is one of the most commonly observed neurodegenerative disorders across the world. According to Glenner and Wong (1984), it is one of the major causes of dementia among older patients, which further leads to the death of huge masses of people in developed countries across the globe. According to the data presented by Vos et al. (2015), more than 25 million people in the world are suffering from AD at present, among which the most prevalent countries being China, Western Europe, and Latin and North America. The total incidences of AD in the world are expected to rise to almost 42.3 million by the end of 2020 (Das et al., 2012). The key implication of the disorder which is witnessed in patients suffering from this disease is neurodegeneration, which may be initiated by protein deposition or synaptic injury and then results in neuronal loss, which tends to cause memory loss, cognitive disabilities, and behavioral changes in the patients (Garand et al., 2000).

Although there have been several studies that explain the molecular mechanisms associated with the disease, Sastre et al. (2006) argue that it continues to be unclear as to which of the mechanisms are most suitable and relevant in describing the occurrence of AD in people. One of the most commonly discussed molecular mechanisms used to explain the disorder is the hyperactivation of cyclin-dependent kinase-5 (CDK5), which is a signaling protein. As explained by Masters et al. (2006), CDK5 is one of the most important proteins which is responsible for neuronal development and usually gets activated by the generation of p35 or p39, which ultimately results in the formation of a specific complex, which tends to become a very important element of the overall neuroplasticity as observed in the pathogenesis of the disorder (Masters et al., 2006).

The molecular mechanism occurring during the interaction of CDK5 with p25 leads to over activation of CDK5 and also results into tau hyper phosphorylation, and these two occurrences collaboratively lead to the formation of neurofibrillary tangles (NFTs), which results in neural disorder (Dong et al., 2009). The cleavage of the activators has been found to occur because of the abnormal processing of amyloid precursor protein (APP) due to genetic disorders, which results in the changes in overall calcium signaling. The model suggests that the p25 activator is associated with the memory of people and hence over generation of the same in patients' brains results in memory loss (Giese, 2014).

However, the recent discussions presented by Lloret et al. (2015) confirmed that there is actually a decline and not increase in the quantity of p25 in AD. While there have been several debates regarding the same, Lloret et al. (2015) explained that the reduction in overall quantity of p25 leads to higher levels of amyloid-induced synaptic toxicity, which eventually results in a reduction in calcium signaling, thus causing degeneration of the neurons. In addition to this, there is yet another model that describes the occurrence and molecular phenomenon and mechanism associated with the disease which is related to abnormal accumulation of amyloid-β (Aβ) and plaques containing the same, which finally results in toxic oligomers and neuronal disorders (Rajmohan and Reddy, 2017). Thus, these molecular changes and reactions have been found to be the main causes of AD and will further help in understanding the application of nanotheranostics for treating the same.

Parkinson's Disease

The second most common neurodegenerative disorder is PD, which is a disorder of the central nervous system (CNS), thus leading to various problems in motor abilities and system of the patients. As explained by De Lau and Breteler (2006), the disorder leads to malfunctioning or even death of the different vital neurons in the brain, especially those present in the substantia nigra region. The death of these neurons leads to a decrease in the production of dopamine (DA), which is a key chemical and

is used for instructing brain to carry out and control different activities and movements. Thus, a reduction in DA leads to impaired movement and affects other body functions (Mazzoni et al., 2012). Some of the key signs or symptoms of PD include stiffness of limbs, slow movement, tremor in hands and other joints, and difficulty in balance and coordination of different body parts and movements (Jankovic, 2008). Although the exact cause of PD has not been established yet, studies have explained the molecular mechanisms underlying the same that help in explaining the occurrence of the disease.

One of the key molecular mechanisms that is found to be associated with the onset of PD is the development of filamentous structures of the major protein constituent of the brain, i.e., alpha-synuclein (α-synuclein), which results into the development of toxic materials (Burré et al., 2010). As explained by Stefanis (2012), the protein α-synuclein plays an extremely pivotal and significant role in the recycling and compartmentalization of neurotransmitters in the brain and also exhibits a key propensity to get aggregated because of its internal constituents. The enhanced aggregation of the protein is then found to lead to elevated toxicity, which can result in neuron dysfunction in the patients. Another perspective or mechanism *via* which this protein tends to lead to PD is when the protein gets aggregated in the form of Lewy bodies inside the brain, it leads to the development of α-synucleinopathies (Kim et al., 2014). The molecular mechanism of cell–cell transmission is known to activate and push the accumulation of the protein, thus resulting in the reduction of DA production, causing an increase in the onset of the disorder (Mothes et al., 2010).

These mechanisms as described above have explained the causes behind the two most commonly observed neurodegenerative disorders. Further discussions thus evaluate and explain the recent advancements in the field of translational nanotheranostics for treating these disorders. The study presents the findings obtained from the approach used in different forms of modeling to deduce its applicability and limitations.

NANOTHERANOSTICS AND ITS DEVELOPMENT IN THE CONTEXT OF NEURODEGENERATION

Nanotheranostics, as described by Zhang et al. (2018), includes the injection of the nanotheranostic agent *via* different drug particles, and after reaching the target area of the body, the shell of the medicine tends to disintegrate, resulting in the release of the agents. This helps in aiming at the molecules or neurons that are causing or leading to the disorder. According to Tripathy et al. (2018), the fact that the treatment is being given so much attention in the medical field is because it is an extremely aggressive treatment and targets directly the affected area in patients' bodies. Moreover, it can be tailored according to the disease and needs of every individual, which leads to an enhancement in the overall practical applications of the approach, hence resulting in the provision of personalized treatment and medicine options (Assaraf et al., 2014). It has been argued that the therapy or treatment has become possible only because of the recent developments that have taken place in the field of chemistry and technologies as the chemical developments have led to the development of a phenomenon, wherein electromagnetic waves can be easily converted into processes that are medically relevant at the nanoscale because of the use of different metal nanoparticles (NPs) (Han et al., 2017). This chemical phenomenon is thus combined with the laser technologies that can help in penetration of the agents to a deeper level in tissues of human bodies, thus making the process simpler and much more effective. While these developments seem to make the application of nanotheranostic process extremely effective (Melancon et al., 2012), it is arguable whether the results that have been obtained until now are completely based on *in vitro* studies and the *in vivo* applicability still remains a challenge. The therapy has been tested in different situations and developed *via* animal, cell, and human modeling. Various tests have been conducted, and their outcomes are described below to explain the recent developments that have taken place in the field (McCarroll et al., 2014; Clift et al., 2015; Kievit et al., 2017; Zavaleta et al., 2018).

Possible Methods to Overcome the Blood–Brain Barrier

There are a number of pharmacologically active substances that have the potential to treat CNS disorders, but due to the blood–brain barrier (BBB), they are not able to access their targets (Cipolla, 2009). Naturally, there are two transport methods (a) active and (b) passive by which molecules are absorbed by the BBB (Tsuji, 2005). Passive transport is a passive diffusion which follows two non-energetic transportation pathways known as paracellular and transcellular diffusion. Hydrophilic compounds are diffused between endothelial cells *via* paracellular diffusion, and small lipophilic molecules are diffused through endothelial cells *via* transcellular diffusion. Here, one thing is noted that lipid solubility plays a critical role in passive transport into the BBB, this method can be used for the chemical transformation of water-soluble molecules into lipid-soluble molecules that can cross the BBB. The drug molecules can be designed by the addition of lipid or functional moiety to them (Lu et al., 2014). Steroids and diphenhydramine are the examples of these types of drugs that can cross the BBB (Au-Yeung et al., 2006; De Gregori et al., 2012). Antibodies and erythropoietin are the examples of paracellular pathways that influence the molecules entering to some extent into the brain. These are usually the case of molecules that have long half-lives, small distribution volumes, and strong effects on the CNS (Banks, 2004). Passive diffusion of liposoluble molecules occurs *via* the transcellular transport (Abbott, 2005; Vos et al., 2015). The active transport requires energy for transport of therapeutic molecules to reach the CNS *via* crossing the BBB through biological gradients, i.e., as opioid analgesics, cardiac glycosides, and calcium channel blockers (Sanchez-Covarrubias et al., 2014). Passage of amino acids across the BBB is mediated by specialized transporters, i.e., glucose transporter (GLUT-1), that assist glucose to cross the brain (Du et al., 2014). Several amino acids, i.e., methionine, valine, histidine, and tyrosine, are required for crossing the BBB to gain access to

the CNS *via* the transporter. L-DOPA or levodopa, an anti-PD drug, is the classical example of drug that enters the CNS by this mechanism which operates with large amino acid transporter 1 (LAT-1) (del Amo et al., 2008). Glucose, vitamins, and some peptides follow the same mechanism to cross the BBB to gain access to the CNS at a faster rate than expected (Banks, 2016). Transport through the BBB also occurs by efflux mechanisms. P-glycoprotein (Pgp) mechanism is the example efflux unwanted complexes, such as anticancer drugs and antibiotics (Begley, 2004; Huwyler et al., 2008). NP interactions with the blood coagulation can be engineered to carry anticoagulant drugs initiating factors to treat PD and AD. Coagulation system with nanomaterials and anticoagulant properties of NPs on the blood coagulation system represent significant concerns in the field of nanomedicine using physicochemical properties (e.g., size, charge, and hydrophobicity) that regulate their undesirable properties on the blood coagulation system to understand unwanted side effects that are used for industrial and medical applications because of their small size, toxicity, risk assessment, and management which warrant attention to clotting, reactions triggering inflammatory, immune responses, and hemolysis.

Animal Modeling

Animal modeling has been one of the key approaches used by researchers to evaluate the impacts and implications of nanotheranostics, and the results of the same have been extremely positive. The modeling was started with small animals like mice and is now being scaled up to the human levels (Kievit and Zhang, 2011). One of the key carriers, whose impacta have been studied and evaluated on animals, is gold nanoparticles (AuNPs). AuNPs have been found to exhibit characteristics that make them extremely suitable for the purpose of nanotheranostics, and they can also be used in various shapes, thus providing higher flexibility to the clinicians (De Lau et al., 2006). The research carried out by Mieszawska et al. (2013) made use of the peptide-functionalized AuNPs to evaluate its impact on the gastric-releasing peptide (GRP) receptor. The AuNPs were conjugated along with an RGD-peptide and injected into small animals, i.e., mice, to evaluate the impacts of the elements on the animal. The application and injection of the NPs in the mice indicated higher tumor accumulation, thus providing a successful approach for treating tumors as well as NDs like AD (Ramanathan et al., 2018).

A similar study carried out by Muthu et al. (2014) included the testing on 24 mice, wherein AuNPs were injected in local tumors contained in those animals (Muthu et al., 2014). The mice were also divided into four different groups to be able to compare the results effectively; the groups contained agent-only group, laser-only group, control group, and lastly agent and laser group. The results of the study revealed that the use of gold coating on the medicine proved to be extremely beneficial in treating the animals and led to the destruction of tumor cells without having any impact on the animal (Muthu et al., 2014). Further explaining the fact that the practice or approach has been found to be effective for tumor ablation makes it effective for even treating diseases like PD wherein the proteins tend to accumulate and cause motor dysfunction, and thus the practice of nanotheranostics can be used to address those areas and destroy the over-accumulation of particles for better outcomes and results. Lee et al. (2015) have discussed that the developments that have taken place in nanotheranostics in South Korea and explained the way the application and modeling of the approach on animals like mice have given key insights into the benefits of the technique. One of the key nanotheranostic techniques that have been tested on mice is the synchrotron radiation x-ray computerized topography (SR-CT) approach, which is a high-speed imaging process (Lee et al., 2015). The approach was used on mice along with a colloidal hybrid silica NP, which resulted in an *in vivo* broad circulation and distribution of the same in the animal, thus leading to treatment of neuron-related defects. While these discussions reveal and confirm the effectiveness of nanotheranostics in treating neurodegenerative disorders in animals, Conde et al. (2015) argue that whether the same can be scaled up to humans or not is something that has not been verified yet.

Cell Modeling

Another approach or practice that has been adopted in addition to the animal modeling approach is that of cell modeling, wherein different models are developed based on cell culture and characteristics of the human body to evaluate the impacts of the applied treatment. Researchers have made use of the cellular models of brains of different animals like mice to evaluate the impacts of nanotheranostics technique or approach on the factors causing the onset of neurodegenerative disorders (Chen et al., 2017; Kievit et al., 2017; Ulapane et al., 2017). Zhang et al. (2015) developed and made use of the cell-based models of different disorders like AD and PD and evaluated the impacts of NPs on macrophages on the cells contained in the model. The cell modeling based on the use of theranostics in microphage assisted in highlighting that the technique helps in ablation of macrophages, which tends to inhibit and reduce the overall inflammation in cells, thus resulting into treatment of the neurodegenerative disorder. However, the cell modeling-based results as presented by Zhao et al. (2017) highlight that the use of nanotheranostics has been found to be effective only at the preliminary stage on different cell structures of diseases and have not been very effective in the long run (Dilnawaz et al., 2012).

Cell modeling has been found to be majorly used for highlighting the benefits and application of the nanotheranostics technique in the diagnosis of neurodegenerative disorders. Mohan and Rapoport (2010) carried out multiple experiments, in which different nanotheranostic agents were developed and used for different diagnostic practices and approaches such as computed tomography and cellular imaging (Chowdhury et al., 2018). The results presented by Mohan and Rapoport (2010) highlighted that the inclusion of nanotheranostic agents and processes have led to the development of new practices, such as magnetic resonance spectroscopy, which help in better diagnosis of neurodegenerative disorders like AD and PD due to the enhanced ability of identifying the activation of CDK5 protein or identifying the areas of excessive accumulation of proteins causing PD. Niu et al. (2017) developed a silicon model of the cells of PD patients wherein the DA transporter cells were modeled. The use of nanotheranostic approach using NPs on the model was

found to be aggressive and invasive and led to the stimulation of these transporter cells, thus resulting in the creation of higher DA which, as discussed earlier, has been found to be responsible for facilitating motor activities in humans.

These results obtained from human and cell modeling have given satisfactory results and outcomes but whether the approach can be used for clinical applications for treating neurodegenerative disorders is still doubtful. Recent developments have hence made use of a few human models to test the same, which are being described below.

Human Modeling

García et al. (2017) carried out an evidence-based study of using nanotheranostics for personalized medicine in treating neurodegenerative disorders. The study made use of metallothioneins (MTs) as a drug discovery biomarker which was injected in patients suffering from neurodegenerative disorders. This nanotheranostic approach proved that the use of such biomarkers helps in targeting specific cells in human bodies, thus resulting in eradication of different malignancies and neural dysfunctions that usually results in disorders like AD and PD (García et al., 2017; Kumar et al., 2017; Kaushik et al., 2018b, 2019a,c; Pan et al., 2019). However, the study carried out by Ruozi et al. (2014) which focused on injecting AuNPs in voluntary AD patients revealed that the approach was effective and beneficial for early diagnosis of the neurodegenerative disorders, but was not yet completely able to treat the same.

Similar human modeling and test were carried out by Maysinger et al. (2015), and they studied the characteristics and problem areas of multiple human beings and identified different biomarkers on the basis of their conditions such that the unique characteristics of each of the NPs could be targeted at treating specific conditions. The study confirmed that while the use of these NPs is effective for diagnostics of neurodegenerative disorders, they still cannot be validated as an effective approach for treating them. Similar discussions as presented in a paper (Wang et al., 2017) confirm that the technique holds great promises for being used as a non-invasive technique for treating NDs like AD by targeting the specific problem areas and spots. Dual-functional NPs targeting amyloid plaques in the brains of AD mice have also been reported (Zhang et al., 2014; Kaushik et al., 2019b). However, these studies do not confirm the effectiveness of the method, and there are various limitations of the same that have been identified by experts. Some of the key limitations of the technique are hence being described in this review.

Access of Nanoparticles to the Central Nervous System

With the advent of nanotechnology, new perspective to treat NDs has been opened for diagnostics as well as therapeutics purposes. Due to multifunctional and versatile structures of NPs, they can be utilized for brain drug delivery. But prior to their application, the major considerations are the surface chemistry, hydrophobicity, shape, size and charge, etc. An ideal NP should be biocompatible, has reduced toxicity, and has the ability to bind and transport drugs or therapeutics. It should not be degraded readily *in vivo* to control therapeutics release for prolonged time periods and can navigate *via* the BBB. All these features lead to those NPs which can penetrate the BBB with high efficacy (Goldsmith et al., 2014). Deliver NP conveniently and effectively has controlled to a deep examination of site-specific drug delivery, toward the convenient non-invasive delivery to specific sites of the delivered dose, to gain access to specific concentrate of therapeutic dose at the specific sites of pharmacological action. Currently, drugs/NPs gain access to the CNS *via* non-invasive methods, i.e., intranasal delivery that are based on drug modification to enhance the permeability of the BBB (Illum, 2003; Kaushik et al., 2018a) and invasive methods that impart direct intraventricular or intracerebral injection/implantation, infusion (Pardridge, 2016). Temporary disruption is also useful to some extent to cross the BBB (McDannold et al., 2012). The BBB disruption is broadly used to enhance drug delivery efficiency to the brain. For example, to treat certain CNS cancers, mannitol is used for osmotic opening to disrupt the BBB (KrolI and Neuwelt, 1998) and temporary pores are made open by using ultrasound in the BBB (Dasgupta et al., 2016). Recently, it has been evident that in the case of AD and multiple sclerosis, pathological BBB disruption occurs which leads to permeability for small therapeutic molecules (<1,000 Da) (Cheng et al., 2010). NPs have their intrinsic physical and chemical properties which decide the route of transport and mechanisms to cross the BBB (Chowdhury et al., 2018). When NPs are functionalized with an appropriate ligand, they can cross the BBB and are capable to distribute drugs in the diseased brain (Tosi et al., 2008; Kaushik and Wei, 2019). In **Figure 1**, several transport mechanisms of NPs have been illustrated and discussed. They can enhance the permeabilization of the BBB by opening tight junctions and letting drugs or drug-conjugated NPs infiltrate into the CNS (Choi et al., 2010); may follow transcytosis mechanism to pass through endothelial cells (Choi et al., 2010); and can be transported by endocytosis into endothelial cells (Kong et al., 2012). Neuropharmaceuticals research is the new emerging niche that is evolving gradually by understanding the receptor-mediated transcytosis and the adsorptive-mediated transcytosis mechanisms and by studying all the intrinsic physicochemical properties of NPs. This could lead to therapeutics that can cross the BBB more efficiently and can provide a patient-oriented therapy (Smith and Gumbleton, 2006).

NANOPARTICLE APPLICATIONS IN NEURODEGENERATIVE DISEASES

Nanocomposite

Most of the AD treatments have focused on Aβ-targeted therapy. Chen et al. (2018) brought into picture that tau pathway is closely related to the development of AD (Kaushik et al., 2018b) (Uddin et al., 2018). They constructed a methylene blue-loaded multifunctional nanocomposite (CeNC/IONC/MSN-T807), which possessed a high binding affinity to hyper phosphorylated tau. The surface-decorated CeNC mitigated mitochondrial oxidative stress and suppressed tau hyper

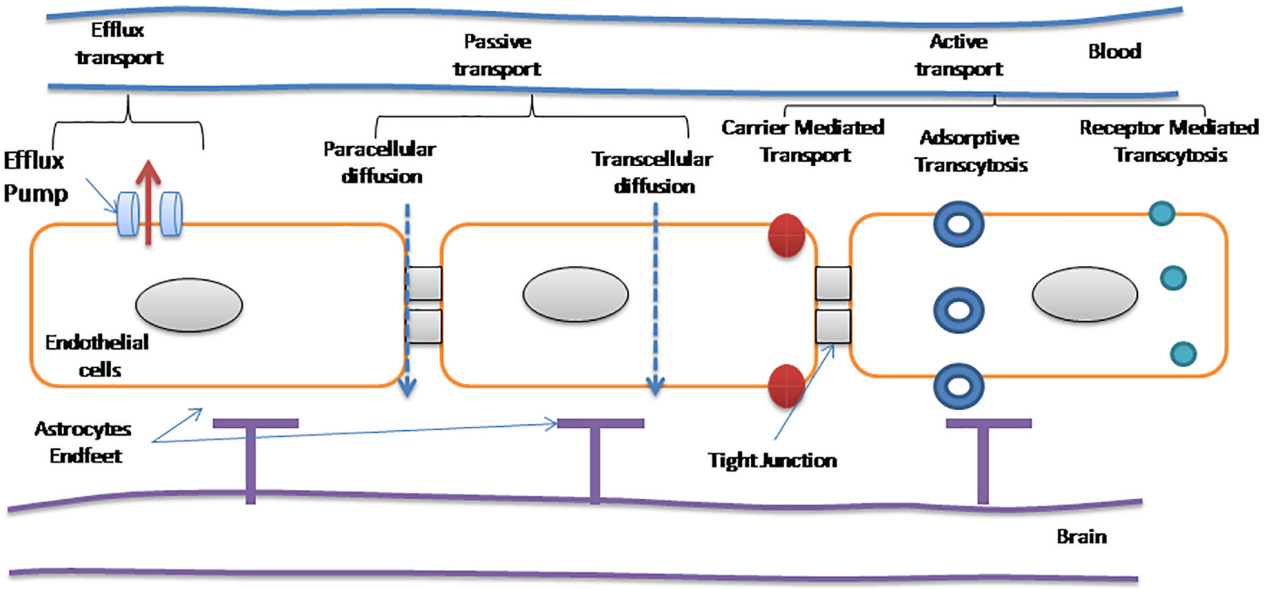

FIGURE 1 | Different modes of transport across the blood–brain barrier (BBB; Teleanu et al., 2019).

phosphorylation, whereas the loaded MB inhibited hyper phosphorylated tau aggregation. As a result, in comparison with the effectiveness of CeNC/IONC/MSN-T807 or MB alone, when both are combined to form a multifunctional nanocomposite, a synergistic therapeutic effect was achieved.

Siddique et al. (2016) studied the effect of alginate nanocomposite (BANC) on PD model flies. A significant decrease in lipid peroxidation and glutathione-S-transferase activity and an increase in glutathione content were observed in PD flies when exposed to BANC. Nevertheless, there was no gross morphological change in the brains of PD flies. The results suggested that BANC is effective in reducing the PD symptoms in these transgenic flies (Siddique et al., 2016).

Oxidative stress disorders have a wide influence on pulmonary, neurodegenerative, and autoimmune diseases and on many more disorders. Selenium (Se) is capable of suppressing oxidative stress disorder, but there is a very thin line between the toxicity and beneficial effects of Se, which makes it difficult and challenging to be used in therapy. Deng et al. (2017) developed porous Se:SiO_2 nanocomposites which ensured controlled release of Se particles, having favorable biocompatibility and could effectively reduce reactive oxygen species (ROS) damage.

Metal Nanoparticles

Nerve growth factor (NGF) is one of the most essential factors for neuronal growth. Nevertheless, its application in neurogeneration is limited due to slow diffusion and short half-life. Moreover, the main obstruction is that the NGF cannot be easily transported through the BBB because of its selective permeability of the BBB. Although there are many magnetic NPs that have been used as an effective nano-carrier for NGF, uncoated magnetic NPs face problems due to their instability in neuronal environment, aggregation, and cellular toxicity. To address these issues, Yuan et al. (2018) proposed that coating them with a thin and impenetrable shell with materials such as polymer, alloy, metals, etc. can solve the problem to some extent. NGF functionalized Au coated SPIO core NPs [Diameter (D): 20.8 nm] was synthesized by them. They selected gold (Au) stating it to be the best candidate due to its outstanding biocompatibility, high stabilities, and tunable surface function. This gold coating not only protects the iron oxide but also provides tunable surface functionalization with several ligands, such as proteins, aptamers, and peptides, due to which precise and controlled release of neuroregeneration can be achieved toward specific sites.

It has been reported that microRNA 141 (miR141) could silence the expression of lncRNA HOTAIR by binding to specific sites on lncRNA HOTAIR. Liu et al. (2018) mediated the high expression of microRNA141 in human amniotic epithelial stem cells by using super paramagnetic iron oxide NPs (SPIONs). They also reported that SPION-mediated overexpression of miR141 is able to promote the expression of brain-derived neurotrophic factor DAT and 5-TH are brain-derived neurotrophic factor (BDNF), DAT, and 5TH in human amniotic epithelial stem cells (HuAESCs)-derived dopaminergic neuron-like cells (iDNLCs). Their study confirmed that the efficiency of HuAESC differentiation into dopaminergic neuron-like cells could be highly improved by miR141 mediated by SPIONs.

Amyloid fibrils are closely associated with various NDs. The hindrance to the diagnosis and development of therapeutic strategies is the identification of fibrils at low concentrations (Kumar et al., 2018). Employed gold nanorods to detect the formation of amyloid fibrils based on α-synuclein. They observed no apparent interaction of gold nanorods with monomeric proteins. However, effective adsorption onto fibril structures

via non-covalent interactions was reported. The strong dipolar coupling in helical Au nanorod promoted the intense chiral response as a result allowed them to detect amyloid fibrils as low as nanomolar concentrations.

Selective detection and quantification of DA is an important key to monitor NDs. However, the limit of detection for DA is in the lower nanometer range. It is significant to push the detection limit to few picomolar or lower. Cao et al. (2018) utilized DA DNA aptamer (DAAPT)–AuNP conjugate to enhance the surface plasmon resonance (SPR) signal (Xue et al., 2018). As a result, this enabled the detection and quantification of DA in the femtomolar to picomolar range. They reported that this is the lowest detection limit achieved for sensing of DA through SPR (Yuan et al., 2018).

Quantum Dots

With emerging technology, it is indicated that the pathogenesis of PD is strongly related to the accumulation of α-synuclein aggregates. Anti-aggregation agent is yet to be achieved for this disease (Dong et al., 2009). Kim H. et al. (2018) showed that graphene quantum dots (GQDs) interact with α-synuclein to exhibit anti-amyloid activity. They reported that GQDs have notable potency not only in inhibiting fibrillization of α-synuclein, but they can also disaggregate mature fibrils with time. They also reported remarkable property of GQDs such as rescued neuronal death and synaptic loss. Moreover, GQDs were found out to help reduce Lewy body (LB)/Lewy neurite (LN) formation, ameliorate mitochondrial dysfunctions, and prevent neuron-to-neuron transmission of α-synuclein pathology induced by α-synuclein preformed fibrils (PFFs) in neurons. They proposed that GQD could function as an anti-aggregation agent, which provides a promising novel therapeutic target for the treatment of PD. The toxicity of QDs in the milieu and biological systems become a key point for the NP, and the potential toxicity of QDs on immunotoxicity of QDs is still unclear. Brain disorders' major hurdle is BBB, many drugs are being proposed for brain disorders, which however fail because of their inability to cross the BBB. Hence, as the molecular structure of the BBB is better elucidated, several approaches are being evaluated, such as adsorptive-mediated transcytosis, inhibition of active efflux pumps, receptor-mediated transport, cell-mediated endocytosis, and delivery from microspheres, biodegradable wafers, and colloidal drug-carrier systems (e.g., liposomes, NPs, nanogels, dendrimers, micelles, nanoemulsions, polymersomes, exosomes, and QDs).

Labeling and Biomarkers

Subtle alterations in synaptic connections and perturbed neuronal network functionality are the main characteristics to determine neurodevelopmental and neurodegenerative disorders. The presence of dendritic spines, micron-sized protrusions of the dendritic shaft that compartmentalize single synapses to fine-tune synaptic strength, is the hallmark of neuronal connectivity. However, it is hard to quantify spine density and morphology in mature neuronal networks due to the lack of targeted labeling strategies (Xiong et al., 2018) and optimize a method to deliver cell-impermeable compounds into selected cells based on spatially resolved nanoparticle-enhanced photoporation (SNAP) to resolve the above-stated problem (Xiong et al., 2018). They showed that efficient labeling of selected individual neurons and their spines in dense cultured networks can be achieved by SNAP without affecting short-term viability. SNAP holds promise for high-content screening campaigns of neuronal connectivity in the context of neurodevelopmental and neurodegenerative disorders.

Biosensor

Multifactorial pathways affect AD, which is associated with the loss of nerve cells in the brain. This as a result leads to changes in related biomolecular levels as AD progresses. Therefore, for accuracy regarding AD, diagnosis is supposed to be done with combined detection of several lesions. Amyloid beta 1–40, 1–42, and τ (tau) protein can be used as main diagnostic target markers. Kim D. et al. (2018) reported highly selective biosensor for detection of AD core biomarkers using distinct localized SPR (LSPR) depending on AuNP shapes, which is called shape-code biosensor. This plasmonic sensor does not need any other method for separation of samples and identification of markers. It consists of only AuNPs and antibody. In addition to this, they reported that this is the first highly sensitive shape-code biosensor to detect AD biomarkers (Indrasekara et al., 2014).

LIMITATIONS

One of the key limitations or challenges of making use of the nanotheranostic technique for treating neurodegenerative disorders, as identified by Indrasekara et al. (2014) is that every patient has a different genome and neural functioning and characteristics, and hence no single approach can be used to treat all of them. The practitioners not only are required to be able to diagnose the causes of these neurodegenerative disorders in every individual separately but also need to identify the suitable treatment for them, which is a challenging task and does not help in identifying one method or treatment technique that is suitable for all (De Lau et al., 2006).

Another challenge or limitation that has been identified by Kim et al. (2013) and suggests that the technique tends to become ineffective because the absorption time of the NPs used in the technique is very low and hence if the injection is not done adequately, these NPs might get absorbed in the blood or by other body parts instead of the area at where it was targeted. It has been found that the neurodegenerative disorders like AD and PD are caused by the neurodysfunction or accumulation of proteins and hence if the drug is not injected adequately, it will not be absorbed or used for treating the desired area (Kim et al., 2013). In fact, it has been argued that, in practice, only a small proportion or part of the drug gets transmitted and transferred to the affected areas and hence the treatment has not yet been established to be completely effective (Rahman et al., 2015).

Another limitation as identified is that the treatment cannot be monitored effectively and efficiently, which imposes a big challenge for the practitioners because they are not able to monitor the progress and impacts of the treatment that they are

giving to the patients. This thus makes the treatment method and technique ineffective. The treatment is also extremely expensive currently. Diou et al. (2012) discuss that most of the research done in the field has failed massively, which has led to an increase in the overall costs of research, thus also leading to higher costs of delivery of the same in the market. These limitations are thus needed to be overcome in order to enhance the applicability of the technique (Hans and Lowman, 2002; Diou et al., 2012; Ilinskaya and Dobrovolskaia, 2013; Luo et al., 2015; Liu et al., 2017; Radhakrishnan and Kamalasanan, 2018; Khan et al., 2019).

CONCLUSION

The molecular changes and reactions have been found to be the key causes of NDs. The research in this field predominantly focuses on genetic mutations, building up of toxic proteins, and formation of neurotoxic molecules. The discussions presented in this study reveal that the nanotheranostics approach has a huge potential in the field of medicine for treating different neurodegenerative disorders. Animal, cell, and human modeling using nanotheranostics approaches for the treatment of neurodegenerative disorders has revolutionized the field. Nanocomposite, metal NPs, and QDs are well reported to treat these neurodegenerative disorders. Limitations that are associated with these NPs are needed to be overcome. Although the studies that have been carried out for the field until now have not provided any significant results to be scaled up to humans, their impacts on the reduction of molecular activities causing neurodegenerative disorders have been significant and hence the approach has a strong potential for developing significant outcomes in the long run.

AUTHOR CONTRIBUTIONS

All authors conceptualized the ideas, conducted the literature search, prepared the figure, drafted the manuscript, and read and approved the final manuscript.

FUNDING

This work was supported by the Key Research Area Grant 2016YFA0501703 of the Ministry of Science and Technology of China, the National Natural Science Foundation of China (Contract nos. 61832019 and 61503244), the State Key Lab of Microbial Metabolism, and the Joint Research Funds for Medical and Engineering and Scientific Research at Shanghai Jiao Tong University (YG2017ZD14).

REFERENCES

Abbott, N. J. (2005). Dynamics of CNS barriers: evolution, differentiation, and modulation. *Cell. Mol. Neurobiol.* 25, 5–23. doi: 10.1007/s10571-004-1374-y

Assaraf, Y. G., Leamon, C. P., and Reddy, J. A. (2014). The folate receptor as a rational therapeutic target for personalized cancer treatment. *Drug Resist. Updat.* 17, 89–95. doi: 10.1016/j.drup.2014.10.002

Au-Yeung, S. C., Rurak, D. W., Gruber, N., and Riggs, K. W. (2006). A pharmacokinetic study of diphenhydramine transport across the blood-brain barrier in adult sheep: potential involvement of a carrier-mediated mechanism. *Drug Metab. Dispos.* 34, 955–960. doi: 10.1124/dmd.105.007898

Banks, W. A. (2004). Are the extracelluar pathways a conduit for the delivery of therapeutics to the brain? *Curr. Pharm. Des.* 10, 1365–1370. doi: 10.2174/1381612043384862

Banks, W. A. (2016). From blood–brain barrier to blood–brain interface: new opportunities for CNS drug delivery. *Nat. Rev. Drug. Discov.* 15, 275–292. doi: 10.1038/nrd.2015.21

Begley, D. J. (2004). Delivery of therapeutic agents to the central nervous system: the problems and the possibilities. *Pharmacol. Ther.* 104, 29–45. doi: 10.1016/j.pharmthera.2004.08.001

Bronzino, J. D. (ed.) (2014). *Management of medical technology: a primer for clinical engineers*. Oxford: Butterworth-Heinemann.

Burré, J., Sharma, M., Tsetsenis, T., Buchman, V., Etherton, M. R., and Südhof, T. C. (2010). α-Synuclein promotes SNARE-complex assembly in vivo and in vitro. *Science* 329, 1663–1667. doi: 10.1126/science.1195227

Cao, Y. X., Zhou, H., and Wang, J. Q. (2018). An approach to interval-valued intuitionistic stochastic multi-criteria decision-making using set pair analysis. *Int. J. Mac. Learn. Cyber.* 9, 629–640. doi: 10.1007/s13042-016-0589-9

Chen, H., Zhang, W., Zhu, G., Xie, J., and Chen, X. (2017). Rethinking cancer nanotheranostics. *Nat. Rev. Mater.* 2:17024. doi: 10.1038/natrevmats.2017.24

Chen, Q., Du, Y., Zhang, K., Liang, Z., Li, J., Yu, H., et al. (2018). Tau-targeted multifunctional nanocomposite for combinational therapy of alzheimer's disease. *ACS nano.* 12, 1321–1338. doi: 10.1021/acsnano.7b07625

Cheng, Z., Zhang, J., Liu, H., Li, Y., Zhao, Y., and Yang, E. (2010). Central nervous system penetration for small molecule therapeutic agents does not increase in multiple sclerosis-and Alzheimer's disease-related animal models despite reported blood-brain barrier disruption. *Drug Metabol. Dispos.* 38, 1355–1361. doi: 10.1124/dmd.110.033324

Choi, C. H. J., Alabi, C. A., Webster, P., and Davis, M. E. (2010). Mechanism of active targeting in solid tumors with transferrin-containing gold nanoparticles. *Proc. Natl. Acad. Sci. U.S.A.* 107, 1235–1240. doi: 10.1073/pnas.0914140107

Chowdhury, S. R., Mondal, S., Muthuraj, B., Balaji, S., Trivedi, V., and Krishnan Iyer, P. (2018). Remarkably efficient blood–brain barrier crossing polyfluorene–chitosan nanoparticle selectively tweaks amyloid oligomer in cerebrospinal fluid and Aβ1–40. *J. Contrib.* 3, 8059–8066. doi: 10.1021/acsomega.8b00764

Cipolla, M. J. (2009). "Barriers of the CNS," in *Cerebral Circulation*, eds D. N. Granger and J. Granger (San Rafael CA: Morgan & Claypool Life Sciences), 13–25.

Clift, M. J., Dechézelles, J.-F., Rothen-Rutishauser, B., and Petri-Fink, A. (2015). A biological perspective toward the interaction of theranostic nanoparticles with the bloodstream–what needs to be considered? *Front. Chem.* 3:7.

Conde, J., Edelman, E. R., and Artzi, N. (2015). Target-responsive DNA/RNA nanomaterials for microRNA sensing and inhibition: the jack-of-all-trades in cancer nanotheranostics? *Adv. Drug Delivery Rev.* 81, 169–183. doi: 10.1245/s10434-020-08312-0

Das, S. K., Pal, S., and Ghosal, M. K. (2012). Dementia: Indian scenario. *Neurol. India* 60, 618–624. doi: 10.4103/0028-3886.105197

Dasgupta, A., Liu, M., Ojha, T., Storm, G., Kiessling, F., and Lammers, T. (2016). Ultrasound-mediated drug delivery to the brain: principles, progress and prospects. *Drug Discov. Today Technol.* 20, 41–48. doi: 10.1016/j.ddtec.2016.07.007

De Gregori, S., De Gregori, M., Ranzani, G. N., Allegri, M., Minella, C., and Regazzi, M. (2012). Morphine metabolism, transport and brain disposition. *Metab. Brain Dis.* 27, 1–5. doi: 10.1007/s11011-011-9274-6

De Lau, L., Koudstaal, P. J., Witteman, J., Hofman, A., and Breteler, M. J. N. (2006). Dietary folate, vitamin B_{12}, and vitamin B6 and the risk of Parkinson disease. *Neurology* 67, 315–318. doi: 10.1212/01.wnl.0000225050.57553.6d

De Lau, L. M., and Breteler, P. M. P. (2006). Epidemiology of Parkinson's disease. *Lancet Neurol.* 5, 525–535.

del Amo, E. M., Urtti, A., and Yliperttula, M. (2008). Pharmacokinetic role of L-type amino acid transporters LAT1 and LAT2. *Eur. J. Pharm. Sci.* 35, 161–174. doi: 10.1016/j.ejps.2008.06.015

Deng, G., Niu, K., Zhou, F., Li, B., Kang, Y., Liu, X., et al. (2017). Treatment of steroid-induced osteonecrosis of the femoral head using porous Se@ SiO 2 nanocomposites to suppress reactive oxygen species. *Sci. Rep.* 7:43914.

Dilnawaz, F., Singh, A., Mewar, S., Sharma, U., Jagannathan, N., and Sahoo, S. K. (2012). The transport of non-surfactant based paclitaxel loaded magnetic nanoparticles across the blood brain barrier in a rat model. *Biomaterials* 33, 2936–2951. doi: 10.1016/j.biomaterials.2011.12.046

Diou, O., Tsapis, N., and Fattal, E. (2012). Targeted nanotheranostics for personalized cancer therapy. *Exp. Opin. Drug Deliv.* 9, 1475–1487. doi: 10.1517/17425247.2012.736486

Dong, X.-X., Wang, Y., and Qin, Z.-H. (2009). Molecular mechanisms of excitotoxicity and their relevance to pathogenesis of neurodegenerative diseases. *Acta Pharmacol. Sin.* 30, 379–387. doi: 10.1038/aps.2009.24

Du, D., Chang, N., Sun, S., Li, M., Yu, H., Liu, M., et al. (2014). The role of glucose transporters in the distribution of p-aminophenyl-α-d-mannopyranoside modified liposomes within mice brain. *J. Control Release* 182, 99–110. doi: 10.1016/j.jconrel.2014.03.006

Garand, L., Buckwalter, K. C., and Hall, G. R. (2000). The biological basis of behavioral symptoms in dementia. *Issues Ment. Health Nurs.* 21, 91–107. doi: 10.1080/016128400248284

García, S., Mercedes, M., González Obeso, C., Doriana, O., Pérez del Rio, E., and Arias Vallejo, F. J. (2017). Advanced systems for controlled drug delivery from chemically modified elastin-like recombinamers. *Curr. Organ. Chem.* 20:1.

Giese, K. P. (2014). Generation of the Cdk5 activator p25 is a memory mechanism that is affected in early Alzheimer's disease. *Front. Mol. Neurosci.* 7:36. doi: 10.3389/fnmol.2014.00036

Glenner, G. G., and Wong, C. W. (1984). Alzheimer's disease: initial report of the purification and characterization of a novel cerebrovascular amyloid protein. *Biochem. Biophys. Res. Commun.* 120, 885–890. doi: 10.1016/s0006-291x(84)80190-4

Goldsmith, M., Abramovitz, L., and Peer, D. (2014). Precision nanomedicine in neurodegenerative diseases. *ACS Nano.* 8, 1958–1965. doi: 10.1021/nn501292z

Han, L., Zhang, X.-Y., Wang, Y.-L., Li, X., Yang, X.-H., Huang, M., et al. (2017). Redox-responsive theranostic nanoplatforms based on inorganic nanomaterials. *J. Control. Release* 259, 40–52. doi: 10.1016/j.jconrel.2017.03.018

Hans, L. M., and Lowman, A. M. (2002). Biodegradable nanoparticles for drug delivery and targeting. *Curr. Opin. Solid State Mater. Sci.* 6, 319–327. doi: 10.1016/S1359-0286(02)00117-1

Huwyler, J., Drewe, J., and Krähenbühl, S. (2008). Tumor targeting using liposomal antineoplastic drugs. *Int. J. Nanomed.* 3, 21–29.

Ilinskaya, A. N., and Dobrovolskaia, M. A. (2013). Nanoparticles and the blood coagulation system. Part II: safety concerns. *Nanomedicine.* 8, 969–981. doi: 10.2217/nnm.13.49

Illum, L. (2003). Nasal drug delivery—possibilities, problems and solutions. *J. Control. Release* 87, 187–198. doi: 10.1016/s0168-3659(02)00363-2

Indrasekara, A. S. D., Wadams, R. C., and Fabris, L. (2014). Ligand exchange on gold nanorods: going back to the future. *Part. Part. Sys. Charact.* 31, 819–838. doi: 10.1002/ppsc.201400006

Ingelsson, M. (2016). Alpha-synuclein oligomers—neurotoxic molecules in parkinson's disease and other lewy body disorders. *Front. Neurosci.* 10:408. doi: 10.3389/fnins.2016.00408

Jankovic, J. J. (2008). Parkinson's disease: clinical features and diagnosis. *J. Neurol. Neurosurg. Psychiatr.* 79, 368–376.

Kaushik, A. C., Bharadwaj, S., Kumar, S., and Wei, D. Q. (2018a). Nanoparticle mediated inhibition of Parkinson's disease using computational biology approach. *Sci. Rep.* 8:9169. doi: 10.1038/s41598-018-27580-1

Kaushik, A. C., Kumar, A., Dwivedi, V. D., Bharadwaj, S., Kumar, S., Bharti, K., et al. (2018b). Deciphering the biochemical pathway and pharmacokinetic study of amyloid βeta-42 with superparamagnetic iron oxide nanoparticles (spions) using systems biology approach. *Mol. Neurobiol.* 55, 3224–3236. doi: 10.1007/s12035-017-0546-y

Kaushik, A. C., Kumar, A., Peng, Z., Khan, A., Junaid, M., Ali, A., et al. (2019a). Evaluation and validation of synergistic effects of amyloid-beta inhibitor–gold nanoparticles complex on Alzheimer's disease using deep neural network approach. *J. Mater. Res.* 34, 1845–1853. doi: 10.1557/jmr.2018.452

Kaushik, A. C., Kumar, A., Yu, C. Y., Kuo, S. W., Liang, S. S., Singh, S. P., et al. (2019b). PCL-DOX Macro drops: evaluation of enhanced intracellular delivery of doxorubicin in metastatic cancer cells by in-silico and in-vitro approach. *N. J. Chem.* 43, 12241–12256. doi: 10.1039/C9NJ01902B

Kaushik, A. C., Wang, Y.-J., Wang, X., Kumar, A., Singh, S. P., Pan, C.-T., et al. (2019c). Evaluation of anti-EGFR-iRGD recombinant protein with GOLD nanoparticles: synergistic effect on antitumor efficiency using optimized deep neural networks. *RSC Adv.* 9, 19261–19270. doi: 10.1039/c9ra01975h

Kaushik, A. C., and Wei, D. Q. (2019). Evaluation and validation of synergistic effect of predicted amyloid-beta (A beta) inhibitor by deep neural network. *J. Biomol. Struc. Dyn.* 34, 1845–1853. doi: 10.1557/jmr.2018.452

Khan, I., Saeed, K., and Khan, I. (2019). Nanoparticles: properties, applications and toxicities. *Arab. J. Chem.* 12, 908–931. doi: 10.1016/j.arabjc.2017.05.011

Kievit, F. M., Wang, K., Ozawa, T., Tarudji, A. W., Silber, J. R., Holland, E. C., et al. (2017). Nanoparticle-mediated knockdown of DNA repair sensitizes cells to radiotherapy and extends survival in a genetic mouse model of glioblastoma. *Nanomedicine* 13, 2131–2139. doi: 10.1016/j.nano.2017.06.004

Kievit, F. M., and Zhang, M. (2011). Cancer nanotheranostics: improving imaging and therapy by targeted delivery across biological barriers. *Adv. Mater.* 23, H217–H247. doi: 10.1002/adma.201102313

Kim, D., Yoo, J. M., Hwang, H., Lee, J., Lee, S. H., Yun, S. P., et al. (2018). Graphene quantum dots prevent α-synucleinopathy in Parkinson's disease. *Nat. Nanotechnol.* 13, 812–818.

Kim, H., Lee, J. U., Song, S., Kim, S., and Sim, S. J. (2018). A shape-code nanoplasmonic biosensor for multiplex detection of Alzheimer's disease biomarkers. *Biosens Bioelectron.* 101, 96–102. doi: 10.1016/j.bios.2017.10.018

Kim, J.-W., Galanzha, E. I., Zaharoff, D. A., Griffin, R. J., and Zharov, V. P. (2013). Nanotheranostics of circulating tumor cells, infections and other pathological features in vivo. *Mol. Pharm.* 10, 813–830. doi: 10.1021/mp300577s

Kim, W. S., Kågedal, K., and Halliday, G. M. (2014). Alpha-synuclein biology in Lewy body diseases. *Alzheimers Res. Ther.* 6:73. doi: 10.1186/s13195-014-0073-2

Kong, S. D., Lee, J., Ramachandran, S., Eliceiri, B. P., Shubayev, V. I., Lal, R., et al. (2012). Magnetic targeting of nanoparticles across the intact blood–brain barrier. *J. Control Release* 164, 49–57. doi: 10.1016/j.jconrel.2012.09.021

KrolI, R. A., and Neuwelt, E. A. (1998). Outwitting the blood-brain barrier for therapeutic purposes: osmotic opening and other means. *Neurosurgery* 42, 1083–1099. doi: 10.1097/00006123-199805000-00082

Kumar, A., Narayanan, K., Chaudhary, R. K., Mishra, S., Kumar, S., Vinoth, K. J., et al. (2017). Current perspective of stem cell therapy in neurodegenerative and metabolic diseases. *Mol. Neurobiol.* 54, 7276–7296. doi: 10.1007/s12035-016-0217-4

Kumar, J., Eraña, H., ópez-Martínez, E. L., Claes, N., Martín, V. F., Solís, D. M., et al. (2018). Detection of amyloid fibrils in Parkinson's disease using plasmonic chirality. *PNAS* 115, 3225–3230. doi: 10.1073/pnas.1721690115

Lammers, T., Kiessling, F., Hennink, W. E., and Storm, G. (2010). Nanotheranostics and image-guided drug delivery: current concepts and future directions. *Mol. Pharm.* 7, 1899–1912. doi: 10.1021/mp100228v

Lee, S., Kim, J., Bark, C. W., Lee, B., Ju, H., Kang, S. C., et al. (2015). Spotlight on nano-theranostics in South Korea: applications in diagnostics and treatment of diseases. *Int. J. Nanomed.* 10:3. doi: 10.2147/IJN.S91389

Liu, T., Zhang, H., Zheng, J., Lin, J., Huang, Y., Chen, J., et al. (2018). SPION-mediated miR-141 promotes the differentiation of Hu AESC s into dopaminergic neuron-like cells via suppressing lnc RNA-HOTAIR. *J. Cell Mol. Med.* 22, 2299–2310. doi: 10.1111/jcmm.13512

Liu, Y., Hardie, J., Zhang, X., and Rotello, V. M. (2017). Effects of engineered nanoparticles on the innate immune system. *Semin Immunol.* 34, 25–32. doi: 10.1016/j.smim.2017.09.011

Lloret, A., Fuchsberger, T., Giraldo, E., and Vina Molecular, J. (2015). mechanisms linking amyloid β toxicity and tau hyperphosphorylation in Alzheimer× s

disease. *Free Radic. Biol. Med.* 83, 186–191. doi: 10.1016/j.freeradbiomed.2015.02.028

Lu, C.-T., Zhao, Y.-Z., Wong, H. L., Cai, J., Peng, L., and Tian, X.-Q. (2014). Current approaches to enhance CNS delivery of drugs across the brain barriers. *Int. J. Nanomed.* 9, 2241–2257. doi: 10.2147/IJN.S61288

Luo, Y., Chang, L. W., and Lin, P. (2015). Metal-based nanoparticles and the immune system: activation, inflammation, and potential applications. *Biomed. Res. Int.* 2015:143720. doi: 10.1155/2015/143720

Masters, C. L., Cappai, R., Barnham, K. J., and Villemagne, V. L. (2006). Molecular mechanisms for Alzheimer's disease: implications for neuroimaging and therapeutics. *J. Neurochem.* 97, 1700–1725. doi: 10.1111/j.1471-4159.2006.03989.x

Maysinger, D., Ji, J., Hutter, E., and Cooper, E. (2015). Nanoparticle-based and bioengineered probes and sensors to detect physiological and pathological biomarkers in neural cells. *Front. Neurosci.* 9:480. doi: 10.3389/fnins.2015.00480

Mazzoni, P., Shabbott, B., and Cortés, J. C. (2012). Motor control abnormalities in Parkinson's disease. *Cold Spring Harb Perspect Med.* 2:a009282.

McCarroll, J., Teo, J., Boyer, C., Goldstein, D., Kavallaris, M., and Phillips, P. A. (2014). Potential applications of nanotechnology for the diagnosis and treatment of pancreatic cancer. *Front. Physiol.* 5:2. doi: 10.3389/fphys.2014.00002

McDannold, N., Arvanitis, C. D., Vykhodtseva, N., and Livingstone, M. S. (2012). Temporary disruption of the blood–brain barrier by use of ultrasound and microbubbles: safety and efficacy evaluation in rhesus macaques. *Cancer Res.* 72, 3652–3663. doi: 10.1158/0008-5472.CAN-12-0128

Melancon, B. J., Hopkins, C. R., Wood, M. R., Emmitte, K. A., Niswender, C. M., Christopoulos, A., et al. (2012). Allosteric modulation of seven transmembrane spanning receptors: theory, practice, and opportunities for central nervous system drug discovery. *J. Med. Chem.* 55, 1445–1464. doi: 10.1021/jm201139r

Mieszawska, A. J., Mulder, W. J., Fayad, Z. A., and Cormode, D. P. (2013). Multifunctional gold nanoparticles for diagnosis and therapy of disease. *Mol. Pharmaceutics* 10, 831–847. doi: 10.1021/mp3005885

Mohan, P., and Rapoport, N. (2010). Doxorubicin as a molecular nanotheranostic agent: effect of doxorubicin encapsulation in micelles or nanoemulsions on the ultrasound-mediated intracellular delivery and nuclear trafficking. *Mol. Pharm.* 7, 1959–1973. doi: 10.1021/mp100269f

Mothes, W., Sherer, N. M., Jin, J., and Zhong, P. (2010). Virus cell-to-cell transmission. *J. Virol.* 84, 8360–8368. doi: 10.1128/JVI.00443-10

Muthu, M. S., Leong, D. T., Mei, L., and Feng, S.-S. (2014). Nanotheranostics? application and further development of nanomedicine strategies for advanced theranostics. *Theranostics* 4, 660–677. doi: 10.7150/thno.8698

Niu, S., Zhang, L.-K., Zhang, L., Zhuang, S., Zhan, X., Chen, W.-Y., et al. (2017). Inhibition by multifunctional magnetic nanoparticles loaded with alpha-synuclein RNAi plasmid in a Parkinson's disease model. *Theranostics* 7, 344–356. doi: 10.7150/thno.16562

Pan, C.-T., Chang, W.-H., Kumar, A., Singh, S. P., Kaushik, A. C., Sharma, J., et al. (2019). Nanoparticles-mediated brain imaging and disease prognosis by conventional as well as modern modal imaging techniques: a comparison. *Curr. Pharm. Design.* 25, 2637–2649. doi: 10.2174/1381612825666190709220139

Pardridge, W. M. (2016). CSF blood-brain barrier, and brain drug delivery. *Exp. Opin. Drug Del.* 13, 963–975. doi: 10.1517/17425247.2016.1171315

Radhakrishnan, R., and Kamalasanan, K. (2018). "Pharmaceutical perspectives of selection criteria and toxicity profiling of nanotheranostic agents" in *Drug Delivery Nanosystems for Biomedical Applications. Micro and Nano Technologies*, ed. C. P. Sharma (Amsterdam: Elsevier), 45–74.

Rahman, M., Akhter, S., Ahmad, M. Z., Ahmad, J., Addo, R. T., Ahmad, F. J., et al. (2015). Emerging advances in cancer nanotheranostics with graphene nanocomposites: opportunities and challenges. *Nanomedicine* 10, 2405–2422. doi: 10.2217/nnm.15.68

Rajmohan, R., and Reddy, P. H. (2017). Amyloid-beta and phosphorylated tau accumulations cause abnormalities at synapses of Alzheimer's disease neurons. *J. Alzheimers Dis.* 57, 975–999. doi: 10.3233/jad-160612

Ramanathan, S., Archunan, G., Sivakumar, M., Selvan, S. T., Fred, A. L., Kumar, S., et al. (2018). Theranostic applications of nanoparticles in neurodegenerative disorders. *Int. J. Nanomed.* 13, 5561–5576. doi: 10.2147/IJN.S149022

Ruozi, B., Belletti, D., Forni, F., Sharma, A., Muresanu, D., Mossler, H., et al. (2014). Poly (D, L-lactide-co-glycolide) nanoparticles loaded with cerebrolysin display neuroprotective activity in a rat model of concussive head injury. *CNS Neurol. Disord. Drug Targets* 13, 1475–1482. doi: 10.2174/1871527313666140806145540

Sanchez-Covarrubias, L., Slosky, L. M., Thompson, B. J., Davis, T. P., and Ronaldson, P. (2014). Transporters at CNS barrier sites: obstacles or opportunities for drug delivery? *Pharmacology* 20, 1422–1449. doi: 10.2174/1381612813199990463

Sastre, M., Klockgether, T., and Heneka, M. T. (2006). Contribution of inflammatory processes to Alzheimer's disease: molecular mechanisms. *Int. J. Dev. Neurosci.* 24, 167–176. doi: 10.1016/j.ijdevneu.2005.11.014

Sharma, S. K. (2014). Nanotheranostics in evidence based personalized medicine. *Curr. Drug Targets* 15, 915–930.

Siddique, Y. H., Khan, W., Fatima, A., Jyoti, S., Khanam, S., Naz, F., et al. (2016). Effect of bromocriptine alginate nanocomposite (BANC) on a transgenic drosophila model of Parkinson's disease. *Dis. Model. Mech.* 9, 63–68. doi: 10.1242/dmm.022145

Smith, M. W., and Gumbleton, M. (2006). Endocytosis at the blood–brain barrier: from basic understanding to drug delivery strategies. *J. Drug Target* 14, 191–214. doi: 10.1080/10611860600650086

Stefanis, L. (2012). α-Synuclein in Parkinson's disease. *Cold Spring Harbor. Perspec. Med.* 2:a009399. doi: 10.1101/cshperspect.a009399

Teleanu, D. M., Mihai, D., Negut, I., Grumezescu, V., Grumezescu, A. M., and Teleanu, R. I. (2019). Nanomaterials for drug delivery to the central nervous system. *Nanomaterials* 9:371. doi: 10.3390/nano9030371

Tosi, G., Costantino, L., Ruozi, B., Forni, F., and Vandelli, M. A. (2008). Polymeric nanoparticles for the drug delivery to the central nervous system. *Adv. Drug Deliv. Rev.* 5, 155–174. doi: 10.1517/17425247.5.2.155

Tripathy, N., Ahmad, R., and Khang, G. (2018). *Inorganic Nanotheranostics: Strategy development and applications, Drug Delivery Nanosystems for Biomedical Applications*. Amsterdam: Elsevier, 377–419.

Tsuji, A. (2005). Small molecular drug transfer across the blood-brain barrier via carrier-mediated transport systems. *NeuroRx* 2, 54–62. doi: 10.1602/neurorx.2.1.54

Uddin, M., Stachowiak, A., Mamun, A. A., Tzvetkov, N. T., Takeda, S., Atanasov, A. G., et al. (2018). Autophagy and Alzheimer's disease: from molecular mechanisms to therapeutic implications. *Front. Aging Neurosci.* 10:4.

Ulapane, K. R., On, N., Kiptoo, P., Williams, T. D., Miller, D. W., and Siahaan, T. J. (2017). Improving brain delivery of biomolecules via BBB modulation in mouse and rat: detection using MRI, NIRF, and mass spectrometry. *Nanotheranostics* 1, 217–231. doi: 10.7150/ntno.19158

Vos, S. J., Verhey, F., Frölich, L., Kornhuber, J., Wiltfang, J., Maier, W., et al. (2015). Prevalence and prognosis of Alzheimer's disease at the mild cognitive impairment stage. *Brain* 138, 1327–1338. doi: 10.1093/brain/awv029

Wang, J., Xu, F., Jin, H., Chen, Y., and Wang, Y. (2017). Non-noble metal-based carbon composites in hydrogen evolution reaction: fundamentals to applications. *Adv. mat.* 29:1605838. doi: 10.1002/adma.201605838

Williams, A. (2002). Defining neurodegenerative diseases: disorders will be named after responsible rogue proteins and their solutions. *Br. Med. J. Publ. Gr.* 324, 1465–1466. doi: 10.1136/bmj.324.7352.1465

Xiong, R., Verstraelen, P., Demeester, J., Skirtach, A. G., Timmermans, J.-P., De Smedt, S. C., et al. (2018). Selective labeling of individual neurons in dense cultured networks with nanoparticle-enhanced photoporation. *Front. Cell. Neurosci.* 12:80. doi: 10.3389/fncel.2018.00080

Xue, Q., Liu, M., Li, Z., Yan, L., Hu, Z., Zhou, J., et al. (2018). Efficient and stable perovskite solar cells via dual functionalization of dopamine semiquinone radical with improved trap passivation capabilities. *Adv. Func. Mater.* 28:1707444. doi: 10.1002/adfm.201707444

Yuan, M., Wang, Y., and Qin, Y.-X. (2018). Promoting neuroregeneration by applying dynamic magnetic fields to a novel nanomedicine: superparamagnetic iron oxide (SPIO)-gold nanoparticles bounded with nerve growth factor (NGF). *Nanomedicine* 14, 1337–1347. doi: 10.1016/j.nano.2018.03.004

Zavaleta, C., Ho, D., and Chung, E. J. (2018). Theranostic nanoparticles for tracking and monitoring disease state. *SLAS Technol.* 23, 281–293. doi: 10.1177/2472630317738699

Zhang, C., Wan, X., Zheng, X., Shao, X., Liu, Q., Zhang, Q., et al. (2014). Dual-functional nanoparticles targeting amyloid plaques in the brains of Alzheimer's disease mice. *Biomaterials* 35, 456–465. doi: 10.1016/j.biomaterials.2013.09.063

Zhang, M., Xi, Z., Zinman, L., Bruni, A. C., Maletta, R. G., Curcio, S. A., et al. (2015). Mutation analysis of CHCHD10 in different neurodegenerative diseases. *Brain* 138:e380.

Zhang, P., Zhang, L., Qin, Z., Hua, S., Guo, Z., Chu, C., et al. (2018). Genetically engineered liposome-like nanovesicles as active targeted transport platform. *Adv. Mater.* 30:1705350. doi: 10.1002/adma.201705350

Zhao, Y., Houston, Z. H., Simpson, J. D., Chen, L., Fletcher, N. L., Fuchs, A. V., et al. (2017). Using peptide aptamer targeted polymers as a model nanomedicine for investigating drug distribution in cancer nanotheranostics. *Mol. Pharm.* 14, 3539–3549. doi: 10.1021/acs.molpharmaceut.7b00560 doi: 10.1021/acs.molpharmaceut.7b00560

Conflict of Interest: The authors declare that the research was conducted in the absence of any commercial or financial relationships that could be construed as a potential conflict of interest.

frontiers in Aging Neuroscience

ORIGINAL RESEARCH
published: 05 May 2020
doi: 10.3389/fnagi.2020.00095

Clustering Analysis of Aging Diseases and Chronic Habits With Multivariate Time Series Electrocardiogram and Medical Records

Kuo-Kun Tseng[1], Jiaqian Li[1], Yih-Jing Tang[2,3]*, Ching-Wen Yang[4], Fang-Ying Lin[1]* and Zhaowen Zhao[1]*

[1] School of Computer Science and Technology, Harbin Institute of Technology (Shenzhen), Shenzhen, China, [2] Department of Family Medicine, Taichung Veterans General Hospital, Taichung, Taiwan, [3] Center for Geriatrics and Gerontology, Taichung Veterans General Hospital, Taichung, Taiwan, [4] Computer and Communication Center, Taichung Veterans General Hospital, Taichung, Taiwan

Background: With recent technology, multivariate time-series electrocardiogram (ECG) analysis has played an important role in diagnosing cardiovascular diseases. However, discovering the association of wide range aging disease and chronic habit with ECG analysis still has room to be explored. This article mainly analyzes the possible relationship between common aging diseases or chorionic habits of medical record and ECG, such as diabetes, obesity, and hypertension, or the habit of smoking.

Methods: In the research, we first conducted different ECG features, such as those of reduced binary pattern, waveform, and wavelet and then performed a k-means clustering analysis on the correlation between ECGs and the aforementioned diseases and habits, from which it is expected to find a firm association between them and the best characteristics that can be used for future research.

Results: In summary, we discovered a weak and strong evidence between ECG and medical records. For strong evidence, most patients with diabetes are always assigned into a specified group no matter the number of classes in the k-means clustering, which means we can find their association between them. For weak evidence, smokers, obesity, and hypertension have less unique ECG feature vector, enabling clustering them into specific groups, so the ECGs might be used to identify smokers, obesity, and hypertension. It is also interesting that we found obesity and hypertension, which are thought to be related to cardiovascular system. However, they are not highly correlated in our clustering analysis, which might indirectly tell us that the impact of obesity and hypertension to our body is various. In addition, the clustering effect of waveform feature is better than the other two methods.

Keywords: electrocardiogram, disease analysis, habit analysis, feature extraction, k-means clustering

OPEN ACCESS

Edited by:
Jiehui Jiang,
Shanghai University, China

Reviewed by:
Weijia Lu,
Affiliated Hospital of Nantong University, China
Chin Chieh Wu,
Chang Gung University, Taiwan

****Correspondence:***
Kuo-Kun Tseng
kktseng@hit.edu.cn
Yih-Jing Tang
yjtang@vghtc.gov.tw
Fang-Ying Lin
r.lin@hit.edu.cn

Received: *30 October 2019*
Accepted: *20 March 2020*
Published: *05 May 2020*

Citation:
Tseng K-K, Li J, Tang Y-J, Yang C-W, Lin F-Y and Zhao Z (2020) Clustering Analysis of Aging Diseases and Chronic Habits With Multivariate Time Series Electrocardiogram and Medical Records. Front. Aging Neurosci. 12:95. doi: 10.3389/fnagi.2020.00095

INTRODUCTION

In modern clinical medicine, electrocardiogram (ECG) technology is a common diagnostic technique for cardiovascular diseases. Electrocardiogram signal is multivariate time-series data to represent the time of electrical change of the voltage variation, which is detected on the skin. Electrocardiogram technology started in 1903, and so it has existed for more than a century. In this

century, rapidly developing ECG technology has made a great contribution to health, and it has become an indispensable routine examination technology in clinics.

Electrocardiography plays an important role in the diagnosis of heart diseases, such as heart rate variability, myocardial ischemia, and myocardial infarction. However, pathological ECG has complex causes and variations. There are significant differences among the ECGs of patients with the same kind of pathology, even among ECGs of the same patient. To make an accurate judgment, physicians usually need to have a rich knowledge and clinical experience. If the physicians have been engaged in identifying a large number of graphics, fatigue could easily cause them to make a mistake. Thus, there is a strong demand for automatic ECG diagnosis, which has been intensively concerned and studied for a period of time.

For automatic ECG diagnosis, there has been much discussion among many scholars, from the suppression of noise to the identification of feature points, detection of the characteristic parameters, waveform category judgment, and even to the final diagnosis approach. Even though some automatic ECG analysis programs have been put into clinical applications from the laboratory, many research results have not been widely accepted by clinicians because ECGs are inaccurate and not uniform, changing from time to time. Moreover, automatic ECG analysis is still confined to heart disease, such as arrhythmia and myocardial infarction. However, for other diseases, such as obesity, hypertension, and diabetes, or habits, such as smoking, there is little related research. In the latest survey, there is only a simple study where heart rate and diabetes are investigated (Niu et al., 2018).

However, we suspect ECG can provide more information on aging diseases and chronic habits. This article is dedicated to finding the relationships between ECGs and common diseases and habits using k-means clustering (Alsabti et al., 1997; Qin et al., 2018) based on ECG features [reduced binary pattern (RBP) (Tseng et al., 2015), waveform (Tseng et al., 2018), and wavelet (Saechia et al., 2005; Chan et al., 2008; Chiu et al., 2009)], expecting that we can extract accurate feature information from ECG signals for further research of automatic diagnosis.

In this article, some related studies are introduced in *Related Studies*, and *Methods With Feature Extraction* presents the used feature extraction methods. In *Methods With K-Means Clustering*, we introduce the k-means clustering method for this research; *Experimental Results* and *Discussion* follow.

RELATED STUDIES

ECG Signal and Noise

Since the ECG signal (**Figure 1**) is relatively weak, it is vulnerable to environmental disturbances. In order to enhance the active ingredients in the ECG signal, suppress noise and interference, and improve the accuracy of waveform detection, not only is it necessary to have high requirements for the anti-interference ability of the ECG recorder hardware, but it is also necessary to have effective ECG signal filtering preprocessing.

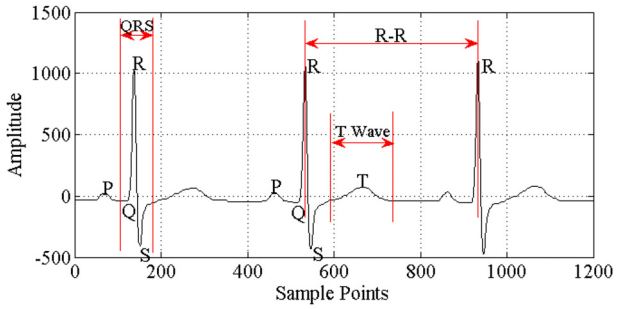

FIGURE 1 | Components of ECG signal.

Electrocardiogram signal acquisition can be divided into two types: one uses multiple (three or more) ECG leads to record the body surface ECG, so obtaining more comprehensive information about heart activity over a certain period of time and focusing on understanding whether heart electrical activity is abnormal, the nature and degree of any abnormality, and the extent of the lesion area; the other uses one or two ECG leads to record and analyze the ECG continuously for a prolonged period (up to hours or even days), so focusing on understanding the rhythm of the heart's electrical activity over a long period, whether the individual heart rate is normal, and the time, type, and frequency of arrhythmia occurring. Electrocardiogram disease diagnosis commonly uses the standard 12-lead ECG acquisition method. The ECG should be collected in a relatively quiet environment, with the person relaxed and calm. In general, the basic requirements (Miao et al., 2015) for ECG acquisition include high gain, high common mode rejection ratio, high input impedance, low noise, low drift, high security, and so on.

During the ECG recording, the signal may be corrupted by low-frequency or high-frequency noise, which alters the waveform of the ECG trace from its original structure. To eliminate this noise, the most common types of noise should be considered (Blanco-Velasco et al., 2008; Li et al., 2016) as follows:

Extraneous noise: Extraneous noise in the ECG trace may be caused by a variety of noise sources including perspiration, respiration, body movements, and poor electrode contact.

Electrode motion artifacts: These are manifested as large-amplitude waveforms primarily caused by stretching that alters the impedance of the skin around the electrode.

Power line interference: This is high-frequency noise caused by interference from nearby devices, resulting from improper grounding of the ECG equipment.

Electromyography noise (*EMG noise*): EMG noise is caused by the electrical activity of skeletal muscles during periods of contraction or owing to a sudden body movement. Although the frequency component of EMG overlaps considerably with that of the QRS complex, it also extends into higher frequencies.

Baseline wander: Baseline wander is caused by body tiny movements and poor electrode contact, 0.05 to 2.00 Hz.

There are several commonly used filtering methods (**Figure 2**), such as the traditional finite impulse response (FIR) filter method (Gholam-Hosseini et al., 1998; Lu et al., 2009; Li et al.,

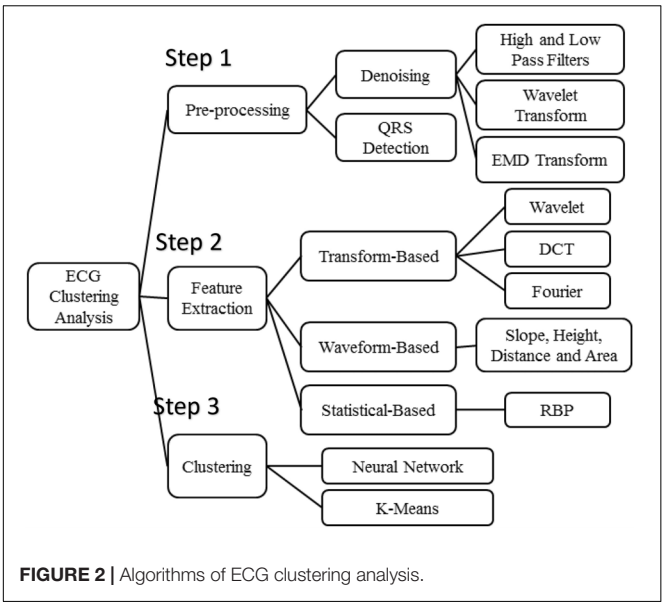

FIGURE 2 | Algorithms of ECG clustering analysis.

2016), wavelet transform method (Agante and Marques de Sa, 1999; Alfaouri and Daqrouq, 2008), and empirical mode decomposition (EMD) method (Pan et al., 2007; Blanco-Velasco et al., 2008). In recent years, wavelet analysis has been introduced into the ECG filtering process and is widely used. Wavelet transform has good time-frequency localization characteristics, achieving conversion of the signal from time domain to frequency domain. Through multiscale analysis, we can obtain different local characteristics of signals in different scales, which is applicable in analyzing and processing such biomedical signals as ECGs with strong randomness, lower signal-to-noise ratio, non-linear and non-stationary nature, and more singular points.

Algorithms of ECG Clustering Analysis

Figure 2 presents the three steps of algorithms used in the ECG clustering analysis. According to experimental flow, it consists of three parts sequentially: step 1: preprocessing, step 2: feature extraction, and step 3: clustering. Denoising methods and QRS detection are the main schemes employed in signal preprocessing. The high- and low-pass filters, wavelet transform, and EMD transform are commonly used for ECG denoising.

Most ECG-based disease analyses rely on features that are derived from the ECG signals. According to our survey, the features are usually extracted according to three various models, that is, transform-based, waveform-based, and statistical-based as is shown in **Figure 2**.

First, transform-based algorithms consist of wavelet transforms (Saechia et al., 2005; Chan et al., 2008; Chiu et al., 2009) and frequency domain transforms, including Fourier transform or discrete cosine transform (Sorwar et al., 2001). Because the wavelet transform contains information in the time and frequency domains, it is more popular than the frequency domain transform.

Waveform-based algorithms extract different time-domain characteristics (distance, height, and area) from fiducial points inside the ECG waveform. These waveform descriptors will be used to match or classify ECG signals in the disease analysis process. These algorithms usually have good accuracy in recognizing regular ECG signals but show the opposite results for irregular data.

An ECG signal can be described as a non-stationary time series that presents some irregularities in the waveform. Unlike the waveform-based algorithms, the transform-based algorithms analyze the non-stationary information based on the signal's presentation in the frequency domain. Not only is this process slow, but it is also difficult to extract good features for the purpose of classification.

Statistical-based algorithms usually depend on statistical evaluations (count, mean, and variance). They are usually less time-consuming but definitely need a well-designed statistical model to ensure high-quality accuracy. A method based on rank-order statistics was presented to analyze the human heartbeat (Tseng et al., 2015).

For clustering analysis, k-means and neural network are two commonly used clustering methods, but for the sake of simplicity and processing speed, k-means is more applicable in this experiment. Moreover, experiments showed that k-means clustering achieves a positive performance in exploring the relationship between ECGs and the aforementioned diseases and habits.

PREPROCESSING

During the ECG recording, the signal may be corrupted by low- or high-frequency noise, which alters the waveform of the ECG trace from its original structure. As mentioned above, the raw data in the Physikalisch-Technische Bundesanstalt (PTB) Diagnostic ECG Database are severely affected by noise, whereas the quality of signal in the ECG database from the local hospital is significantly better that in the PTB database, which influences the preprocessing methods, and QRS detection has impact on feature extraction and even the final clustering of ECG features. Therefore, we may need to investigate different features for different ECG databases in order to find the best features for each diagnostic system.

ECG Denoising

Extraneous noise in the ECG trace may be caused by a variety of noise sources including perspiration, respiration, body movements, and poor electrode contact. Electrode motion artifacts manifest as large-amplitude waveforms primarily caused by stretching, which alters the impedance of the skin around the electrode. Power line interference is high-frequency noise caused by interference from nearby devices resulting from improper grounding of the ECG equipment. Electromyography noise is caused by the electrical activity of skeletal muscles during periods of contraction or resulting from a sudden body movement. Although the frequency component of EMG overlaps considerably with that of the QRS complex, it also extends into higher frequencies. Commonly used filtering methods include the traditional FIR filter method, wavelet transform method, and the EEMD (ensemble EMD) method.

QRS Detection

For the waveform feature extraction, a more accurate ECG segmentation is needed, so QRS detection and ECG cutting are needed first. QRS detection is based on the matched filter. In order to improve the accuracy of QRS detection under the conditions of Gaussian noise and variable QRS amplitude, the first-order derivative is used for zero threshold detection. In addition, the two non-linear circuits cut off low-amplitude noise and all spikes that occur within a certain time after QRS detection.

METHODS WITH FEATURE EXTRACTION

RBP Feature Extraction

The idea of RBP algorithm (Tseng et al., 2015) for ECG disease is related to Yang et al. (2003) and Kumar et al. (2005) works, but we expand it to a different field of application.

All ECG signals are non-stationary. Consider an ECG signal as $x = \{x_1,\ x_2,\ x_3, \ldots, x_{\mathrm{N}}\}$, where the real-valued x_{i} corresponds to the i^{th} input datum. Each pair of consecutive input signals is compared, and the data are categorized into one of the two cases: a decrease or increase in x_i. A preliminary reduced function then maps these two cases to 0 or 1, respectively, according to the rule:

$$y_i = \begin{cases} 0\ , & x_{i+1} \leq x_i \\ 1\ , & x_{i+1} > x_i \end{cases} \tag{1}$$

This procedure converts the ECG signal of length N to a binary sequence $Y = \{y_1,\ y_2, \ldots, y_{N-1}\}$ of length $N-1$. Every m bit in Y is grouped to construct a reduced binary sequence of length m, referred to as an m-bit word, and then all such words are collected to form an RBP $B = \{b_1,\ b_2, \ldots, b_{\mathrm{N-m}}\}$ where $b_k = \{\, y_{\mathrm{k}},\ y_{\mathrm{k+1}},\ \ldots, y_{k+m-1}\,\}$. We then convert each m-bit word b_{k} to its decimal expansion w_k. The relative occurrence frequency of w_{k} is considered as the features of ECG signals, which we use as the input of clustering method. **Figure 3** presents the process of RBP feature extraction.

Wavelet Feature Extraction

The procedures of the wavelet-based algorithm (Chiu et al., 2009) include the following: each R-R cardiac cycle is obtained through R-R detection; the first 169 and the last 85 points in each R-R cycle are assembled to form a 256-point segment; every four segments are grouped, and an n-level discrete wavelet transform (DWT) is performed to obtain the corresponding wavelet coefficients. Four of the computed wavelet coefficients are gathered as a wavelet vector. Here we use the coefficients vector of DWT as the ECG feature. An example with $n = 9$ is illustrated in **Figure 4**.

Waveform Feature Extraction

In a waveform-based feature study (Tseng et al., 2018), a total of 24 features are extracted from five classes: position (P, Q, R, S, T), amplitude (PQ, RQ, TQ, RT, PS, RP, TS, RS, PT, QS), duration (QS, PR, QR, ST, QT), slope (RS, ST and QR), and area (area of the QRS triangle). These features form a feature vector S. Before extracting the features mentioned above, we need to first accurately locate R, P, Q, T, and S points, which is a key issue for waveform feature extraction. **Figure 5** displays the extraction procedure of waveform feature.

METHODS WITH K-MEANS CLUSTERING

K-means clustering (Alsabti et al., 1997; Qin et al., 2018) is a rather simple but well-known algorithm for grouping objects. Each object can be represented by a feature vector. First, it extracts ECG features with RBP, waveform, and wavelet and then randomly chooses k samples in that vector space, which serve as the initial centers of the clusters. Afterward, all objects are each assigned to their closest center. Usually, the distance measure is chosen by the user and determined by the learning task. In this experiment, we chose the Euclidean distance as follows:

$$D = \left(X_i - X_j\right)^T \left(X_i - X_j\right) = \sum_{k=1}^{n} (x_{ik} - x_{jk})^2 \tag{2}$$

where X_{i} and X_{j} are samples, and x_{ik} and x_{jk} are the k^{th} attribute of X_{i} and X_{j}.

Then, for each class, a new center is computed by averaging the feature vectors of all objects belonging to this class. The process of assigning objects and recomputing the centers is repeated until the process converges. The algorithm can be proven to converge after a finite number of iterations. Usually, to determine whether the process converges, we take the square error criterion as follows:

$$E = \sum_{i=1}^{k} \sum_{p \in C_i} |p - m_i|^2 \tag{3}$$

where E is the sum of the square errors of all samples in the database, P denotes a sample in the database, and m_i denotes the means of clustering group C_i.

EXPERIMENTAL RESULTS

Dataset

We conducted a comprehensive experiment on a public ECG dataset, the PTB Diagnostic ECG Database (Bousseljot et al., 1995). The database contains 549 records from 290 subjects (aged 17–87 years, mean 57.2 years; 209 men, mean age 55.5; and 81 women, mean age 61.6; ages were not recorded for 1 female and 14 male subjects, the data of patients 124, 132, 134, and 161 were missed in the PTB database). Each subject is represented by one to five records. Each record includes 15 simultaneously measured signals: the conventional 12 leads (i, ii, iii, avr, avl, avf, v1, v2, v3, v4, v5, v6) together with the three Frank lead ECGs (vx, vy, vz). Each signal is digitized at 1,000 samples per second, with 16-bit resolution over a range of ±16.384 mV. By special request to the contributors of the database, recordings may be available at sampling rates of up to 10 kHz.

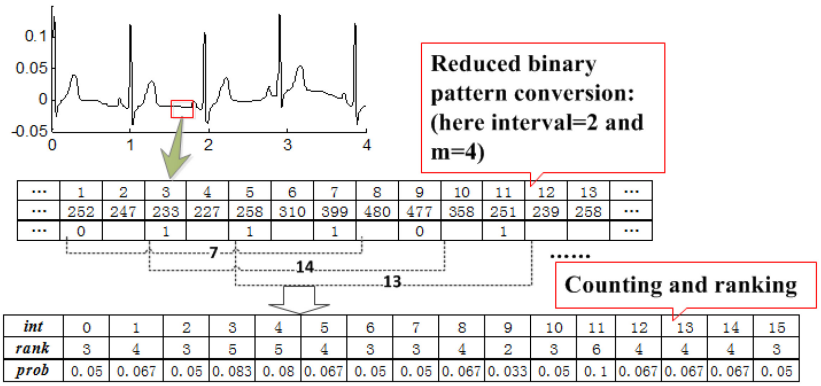

···	1	2	3	4	5	6	7	8	9	10	11	12	13	···		
···	252	247	233	227	258	310	399	480	477	358	251	239	258	···		
···	0		1		1		1		0		1			···		

int	0	1	2	3	4	5	6	7	8	9	10	11	12	13	14	15
rank	3	4	3	5	5	4	3	3	4	2	3	6	4	4	4	3
prob	0. 05	0. 067	0. 05	0. 083	0. 08	0. 067	0. 05	0. 05	0. 067	0. 033	0. 05	0. 1	0. 067	0. 067	0. 067	0. 05

FIGURE 3 | Process of RBP feature extraction.

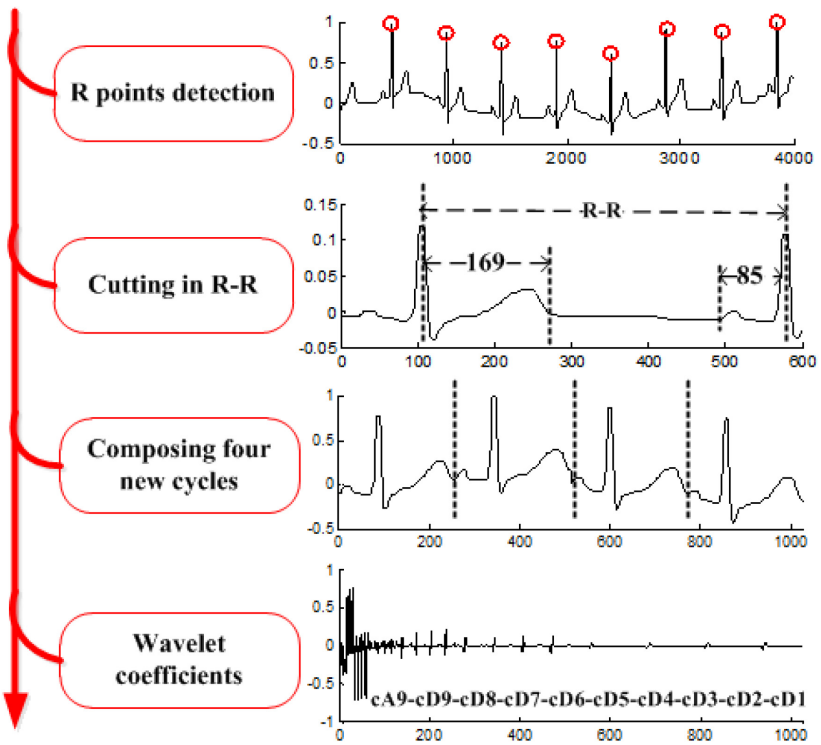

FIGURE 4 | Process of wavelet feature extraction.

Within the header (.hea) file of most of these ECG records is a detailed clinical summary, including age, gender, diagnosis, and, where applicable, data on medical history, medication and interventions, coronary artery pathology, ventriculography, echocardiography, and hemodynamics. The clinical summary is not available for 22 subjects. The diagnostic classes of the remaining 268 subjects are summarized in **Table 1**.

Metrics

In the *k* clustering algorithm, two metrics are used to evaluate the relationship between ECGs and diseases or habits.

Ratio

This is a commonly used measurement criterion in the clustering analysis. In order to measure the extent of relationship between ECGs and specified disease or habit, the ratio of the number of subjects with disease or habit to the number of subjects in a group is a good criterion. If the ratio in a group is greater than 50%, there should be a significant correlation between ECGs and disease or habit.

Concentricity

Sometimes, because of various disturbances, such as shortage of data, it is difficult to achieve a ratio greater than 50%, which

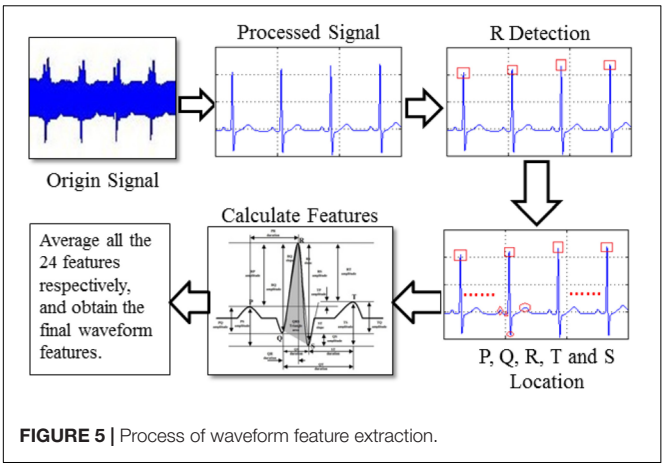

FIGURE 5 | Process of waveform feature extraction.

cannot indicate there is no correlation between disease and ECGs, so we need a new criterion to measure the performance of clustering. If all or most of samples with the same disease or habit are assigned into the same group, this disease or habit may be identified based on the ECG feature of this group. This is called concentricity.

Experiment Software

This research mainly focuses on the ECG signal processing; there are many ECG analysis software developed by MATLAB (Natick, MA, United States). Thus, this research uses MATLAB tools as programming language, especially in signal processing, pattern recognition, mathematical modeling, and other aspects. MATLAB also includes matrix arithmetic operation, relational operation, logical operation, conditional operation, and assignment operation, and these matrix operation methods can be copied into array operation. MATLAB does not need to define dimension in matrix operation and has rich matrix function library for various matrix operations.

TABLE 1 | Demographic of PTB database.

Diagnostic class	All patients
Age range	17–87
Man mean age	57.2
Man	209
Woman mean age	55.5
Women	81
Myocardial infarction	148
Cardiomyopathy/heart failure	18
Bundle-branch block	15
Dysrhythmia	14
Healthy controls	52
Arterial hypertension	63
Diabetes mellitus	29
Obesity	20
Smoker	73
Not available	22

Result Based on RBP Feature

In the experiment, we would cluster the PTB database based on RBP features and chose k = 24, and 8 (k being the number of class), which is helpful in observing the variance of clustering performance with increasing k.

In the clustering with the RBP feature as shown in **Table 2** with k = 4 and 8, typically the ratios in the different classes are relatively less than 50%, which indicates that the samples scatter into different classes with k increasing, and the differences among these classes are not obvious. While k = 2, the obvious characteristic is that although the number of two groups is approximate, most samples (72.41%) with diabetes are assigned into the second class. Moreover, even though the number of classes in the k-means clustering increases from 2 to 4, even to 8, and the dispersivity of the samples expands, there is always a group in each clustering, for example, group 1 with k = 4 and group 4 with k = 8, in which the number of samples with diabetes is significantly larger than that in other groups in the same clustering. It demonstrates that diabetes mellitus may be closely related with RBP features of group 2 with k = 2, group 1 with k = 4 and group 4 with k = 8.

For other three research targets, there are no highlighted groups in **Table 2** in which samples with same disease or habit present the distribution of aggregation, indicating that we cannot detect the relationships between ECGs and obesity, smoking, and hypertension through RBP feature.

Result Based on Waveform Feature

Similar to the clustering with RBP feature, we would utilize k-means clustering to cluster the PTB database based on waveform feature. **Table 3** displays the results of clustering when the number of groups k is 2, 4, and 8.

With k = 4 and 8, most of samples with diabetes are assigned into a specified group, for example, 22 samples in group 4 of k = 4 and 22 samples in group 6 of k = 8; thus, although the number of groups increases from 4 to 8, this group (group 4 with k = 4 and group 6 with k = 8) still retains the distribution and composition of various diseases and habits. Moreover, 75.85% of samples with diabetes are allocated in the group with half of all samples, whereas it is a natural and proportional distribution for other three research aspects that only approximately half of their samples are respectively, assigned in this group with half of all samples in the PTB database. It is indicated that diabetes is closely associated with waveform feature extracted from ECGs of the sixth group with k = 8.

It is observed that there are four classes with k = 4 (corresponding to k = 8) with rather higher ratios of smokers, that is, 52.38% in the first group, 77.78% in the fourth group, 66.67% in the seventh group, and 61.45% in the last group. However, there are only three samples in the seventh group, and two of them are also, respectively, patients with obesity or hypertension, which indicates that this group is not practicable and useful because of sparse samples. Perhaps, the sparse samples in the fourth, seventh, and last groups, although with higher ratio of smokers, cannot support the existence of relationship between ECGs and smoking. If we combine these groups with

TABLE 2 | Clustering statistics based on RBP feature, k = 2, 4, and 8.

k	Category	Number	Obesity	Smoker	Hypertension	Diabetes
	Group 1	140	10	30	27	8
2	Group 2	150	10	43	36	21
	Group1	72	9	21	25	14
	Group2	67	1	21	10	6
4	Group3	85	6	16	15	3
	Group4	66	4	15	13	6
	Group 1	42	3	10	10	3
	Group 2	36	2	5	4	3
	Group 3	29	1	8	3	3
	Group 4	53	6	13	19	12
8	Group 5	4	0	1	1	1
	Group 6	6	2	3	2	1
	Group 7	73	5	16	14	3
	Group 8	47	1	17	10	3

TABLE 3 | Clustering statistics based on waveform feature.

k	Category	Number	Obesity	Smoker	Hypertension	Diabetes
	Group 1	226	13	37	43	23
2	Group 2	64	7	36	20	6
	Group1	64	7	36	20	6
	Group2	69	1	1	7	1
4	Group3	7	1	1	2	0
	Group4	150	11	35	34	22
	Group 1	21	3	11	6	3
	Group 2	69	0	0	7	1
	Group 3	19	1	9	7	2
	Group 4	9	1	7	3	1
8	Group 5	7	1	1	2	0
	Group 6	149	11	35	34	22
	Group 7	3	2	2	2	0
	Group 8	13	1	8	2	0

the first group with 21 samples to compose a new group, the problem of sparse samples will be solved, and it is sufficient to determine the relationship between waveform feature of ECGs and smoking, which paves the way of further research about smoking classification.

Result Based on Wavelet Feature

In the wavelet feature extraction, four segments are grouped, and an n-level DWT is performed to obtain the corresponding wavelet coefficients. **Table 4** presents the clustering results with different number of groups k.

Compared with RBP feature and waveform feature, clustering upon wavelet feature cannot achieve a positive performance both in the ratio criterion and concentricity criterion. With the number of groups increasing in the k-means clustering, the samples with specified disease or habit scatter in these groups randomly without any concentricity. Moreover, when the number of groups k is 8, the ratios in the groups with enough samples are almost less than 50%. So we cannot find useful information to support the relationship between ECGs and the aforementioned diseases or habits in the k-means clustering with wavelet feature.

DISCUSSION

In this section, we discuss some issues that may be interest to readers. There are the issues of k parameter, feature extraction, ECG dataset, and evidence.

Issues of k Parameter

Why Were Multiple Feature Extraction Algorithms Used?

Each feature extraction algorithm has different characteristics; for example, in **Figure 6**, wavelet has a good clustering performance at k = 2, but waveform performs better than the other two algorithms at k = 4 and k = 8.

Why Was the Elbow Method Not Used?

We are exploring the effects of different k parameters and different feature extraction, so we did not use the elbow method. The reason that we use different k values as k = 2, 4, and 8 for comparative study, in addition to see the result under different k, if a disease can show a better clustering effect under different k parameters, it means that it has a higher degree of stability. In the future, if we want design the classification system, we should use the elbow method.

Issues of Feature Extraction

Why Choose These Three Feature Extraction Algorithms for Comparison?

Each feature extraction algorithm has different characteristics; for example, in **Figure 6**, wavelet has a good clustering performance at k = 2, RBP performance after k = 2, better than waveform. But waveform performs better than the other two algorithms at k = 4 and 8. In addition, the three feature extraction methods we selected are also representative. The RBP feature is statistical

TABLE 4 | Clustering statistics based on wavelet feature, k = 2, 4, and 8.

k	Category	Number	Obesity	Smoker	Hypertension	Diabetes
2	Group 1	257	18	64	54	28
	Group 2	33	2	9	9	1
4	Group1	23	2	9	6	1
	Group2	96	6	27	21	9
	Group3	15	1	8	3	1
	Group4	156	11	29	33	18
8	Group 1	18	0	7	6	0
	Group 2	2	0	0	0	0
	Group 3	58	4	11	14	7
	Group 4	19	1	8	5	1
	Group 5	8	1	4	2	1
	Group 6	105	8	21	21	12
	Group 7	73	5	21	13	8
	Group 8	7	1	1	2	0

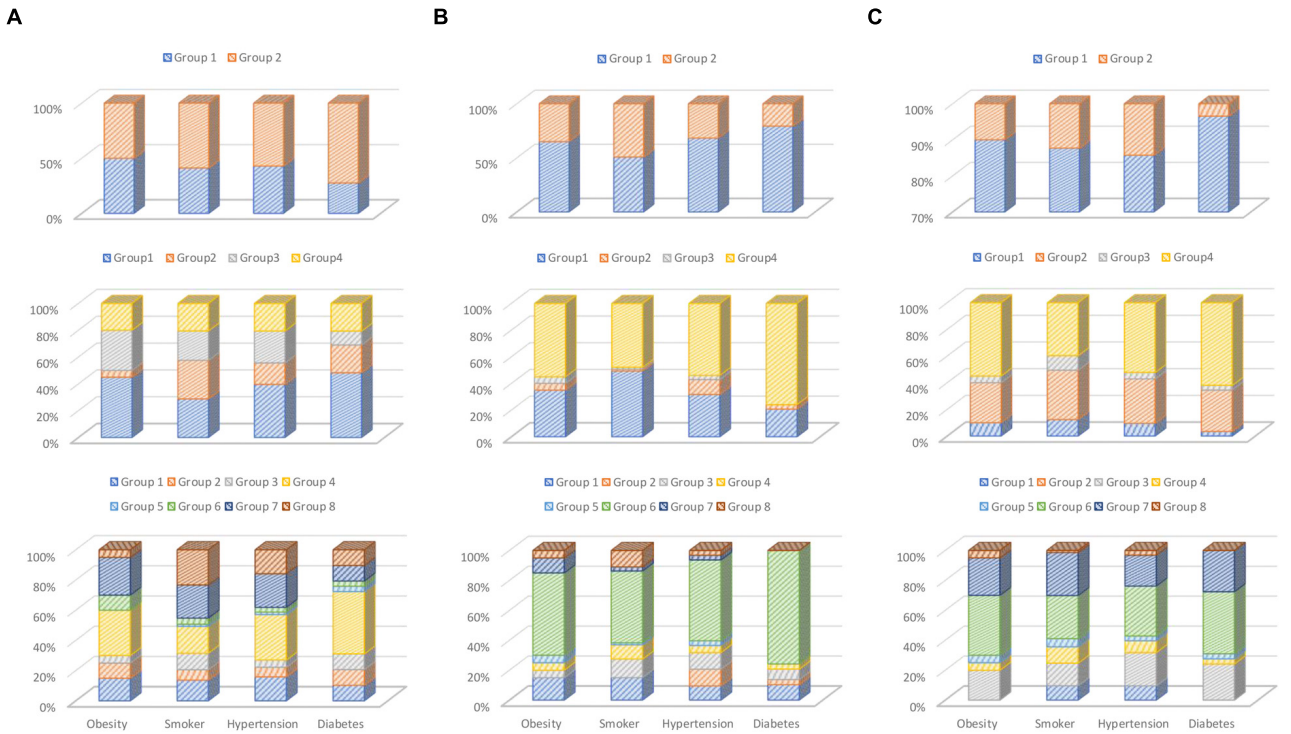

FIGURE 6 | Percentage chart of clustering result: **(A)** RBP-based, **(B)** waveform-based, and **(C)** wavelet-based feature extractions.

method; waveform feature is morphological method, and wavelet is transformation method.

Why Not Perform Fusion Clustering on the Three Methods of Feature Extraction?

According to our previous clustering and classification experiments, if multiple feature extractions are used together, the performance is often worse, because different features may interfere with each other. Moreover, this study mainly focuses on the clustering correlation study between ECG and disease; using different features for comparative analysis is more desired in this article. In the future, when we develop the classification and diagnosis system, we will seek more sophisticated feature extraction method; the feature fusion issue will be studied as well.

Issues of ECG Dataset

Why Did We Select Only Aging Chronic Diseases for Clustering Analysis?

We have performed only clustering analysis on arterial hypertension, diabetes mellitus, obesity, and smoker. Because other common heart diseases such as myocardial infarction, cardiomyopathy, bundle-branch block, and dysrhythmia have been proven to be observed by ECG, we do not have motivation to conduct further clustering studies. And the purpose of this article is also to explore the future possibility of automatic ECG diagnosis for chronic diseases.

Is the Number of Samples Sufficient?

Both clustering and classification problems use the same preprocessing and feature processing method. If stable clustering results can be obtained, the sample base should be sufficient as in classification and clustering problems. In addition, we have conducted the experiment on a public ECG dataset, the PTB Diagnostic ECG Database. This database has been used for many researches; thus, the clustering results should be credible.

Issues of Evidence

Overall Observation Evidence

As shown in **Figure 6**, we divided different k parameters into k = 2, 4, and 8 groups and compared them. At the same time, three different characteristics were compared with the same k-parameter experiments. In addition, in **Figure 6**, if a group occupies a larger proportion, it indicates that the clustering effect is better. Based on this, our observations are summarized as follows: (Niu et al., 2018) diabetes has strong association with ECG feature; it can almost get better clustering results in different feature extractions and k parameters, and other chronic diseases have better clustering performance in experiments with different feature extractions and k parameters (Miao et al., 2015). The smokers, obesity, and hypertension have weak association in ECG features; they have less unique ECG feature vector enabling clustering them into specific groups, although they have some correlation in their ECG features (Blanco-Velasco et al., 2008). Waveform

feature extractions have better clustering performance than RBP and wavelet.

Other Reference for Association Evidence

Previous clinical case studies have explored the relationship between ECG and other chronic diseases. These are mostly the analysis results from physicians' observation. They found that diabetic patients may have some ECG abnormalities, such as fibrotic changes in the left ventricle (Stern and Sclarowsky, 2009), painless myocardial ischemia (Dweck et al., 2009), and a prolonged QRS duration (Rollins et al., 1992). In addition, as for the other three diseases, we have also found some related studies to prove that they are related to ECG. For example, Renuka Devi et al. (2013) discuss the relationship between heart rate and smoking. The article by Ang and Lang (2008) mentions that left ventricular hypertrophy is related to ECG. The article by Rautaharju et al. (1994) mentions obesity is associated with a wide variety of electrocardiographic abnormalities. Their clinical research and our cluster analysis should prove each other. However, our research results summarize that diabetes has more obvious clustering characteristics than other chronic diseases and should be more suitable for the application of automated ECG diagnosis.

CONCLUSION AND FUTURE WORK

In this article, three different models of feature extraction, RBP-based, wavelet-based, and waveform-based, are investigated and utilized to analyze the possible relationship between ECGs and diseases and habits, such as the aging diseases of diabetes, obesity, and hypertension and the chronic habit of smoking in the k-means clustering. Based on previous experiments and research, our conclusions are summarized as follows:

(1) Waveform feature has better clustering effect in the ECG analysis of the four diseases, and it will be stable under different k parameters. Experiments show that waveform feature is more applicable to the clustering analysis of the correlation in contrast to RBP and wavelet features.
(2) Diabetes has the most obvious clustering effect. The three feature extractions and different k parameters are relatively stable. In the *k*-means clustering based on RBP, waveform, and wavelet features, most patients with diabetes mellitus are always assigned into a specified group no matter the number of groups; that is, samples with diabetes mellitus have an excellent concentricity upon these characteristics extracted from ECGs.
(3) The other three diseases may have less influencing factors, and the clustering characteristics are not significantly stable, which can be further studied in the future. However, the remaining groups with higher ratio of smokers, obesity, and hypertension, the relationship between them and ECGs paves the way of further research about their clustering and classification. The results of smoking, hypertension, and obesity are not positive, and they scatter in every group in the k-means clustering. So, we cannot find strong relationships between ECG and them and cannot choose a better feature to implement the classification and diagnosis of hypertension and obesity based on ECGs.

Regarding future research, we should have the following detailed issues to explore:

(1) The PTB Diagnostic ECG Dataset may not be specialized for discovering the relationship between hypertension, obesity, and diabetes mellitus. Some categories have fewer samples; for example, the number of samples with obesity is 20, which may not perform well for clustering analysis.
(2) The same person may be suffering from a variety of diseases, particularly myocardial infarction, cardiomyopathy, bundle-branch block, and so on, severely affecting the waveform of ECG.
(3) These feature extractions may not include all the useful information for these diseases and habits. Therefore, lack of useful characteristics may bring about clustering performance.
(4) The diseases and habits might have various factors from our body; it is not easy to classify from ECG.

Although our research has explained some question of ECG clustering, there are still some detailed issues that need to be further explored as above. In the future, we will explore these issues and also make further contributions to the future ECG diagnostic system.

DATA AVAILABILITY STATEMENT

Publicly available datasets were analyzed in this study. This data can be found here: Oeff M., Koch H., Bousseljot R., Kreiseler D. 2012. The PTB diagnostic ECG database. National Metrology Institute of Germany, http://www.physionet.org/physiobank/database/ptbdb.

AUTHOR CONTRIBUTIONS

K-KT and JL performed the statistical analysis and participated in design, and drafted the manuscript. Y-JT and C-WY carried out the related studies and participated in collecting data. F-YL and ZZ helped to improve the final manuscript.

FUNDING

This work was supported by the Shenzhen Government, China (Grant Nos. HA11409015, KQJSCX20170726104033357, JCYJ20150513151706567, and JCYJ20160531191837793).

REFERENCES

Agante, P., and Marques de Sa, J. (1999). "ECG noise filtering using wavelets with soft-thresholding methods," in *Proceedings of the Computers in Cardiology, 1999 on IEEE*, Hannover, 535–538.

Alfaouri, M., and Daqrouq, K. (2008). ECG signal denoising by wavelet transform thresholding. *Am. J. Appl. Sci.* 5:276. doi: 10.3844/ajassp.2008.276.281

Alsabti, K., Ranka, S., and Singh, V. (1997). "An efficient K-means clustering algorithm," in *Proceedings of the IEEE Transactions on Pattern Analysis and Machine Intelligence*, (Piscataway, NJ: IEEE).

Ang, D. S. C., and Lang, C. C. (2008). The prognostic value of the ECG in hypertension: where are we now? *J. Hum. Hypertens.* 22, 460–467. doi: 10.1038/jhh.2008.24

Blanco-Velasco, M., Weng, B., and Barner, K. E. (2008). ECG signal denoising and baseline wander correction based on the empirical mode decomposition. *Comput. Biol. Med.* 38, 1–13. doi: 10.1016/j.compbiomed.2007.06.003

Bousseljot, R., Kreiseler, D., and Schnabel, A. (1995). Nutzung der EKG-Signaldatenbank CARDIODAT der PTB über das Internet. *Biomed. Technik Band* 40:317. doi: 10.1515/bmte.1995.40.s1.317

Chan, A. D., Hamdy, M. M., Badre, A., and Badee, V. (2008). Wavelet distance measure for person identification using electrocardiograms. *Instrument. Meas.* 57, 248–253. doi: 10.1109/tim.2007.909996

Chiu, C.-C., Chuang, C.-M., and Hsu, C.-Y. (2009). Discrete wavelet transform applied on personal identity verification with ECG signal. *Int. J. Wavelets Multiresol. Inform. Process.* 7, 341–355. doi: 10.1142/s0219691309002957

Dweck, M., Campbell, I. W., Miller, D., and Francis, C. M. (2009). Clinical aspects of silent myocardial ischemia: with particular reference to diabetes mellitus. *Br. J. Diabetes Vasc. Dis.* 9, 110–116. doi: 10.1177/1474651409105249

Gholam-Hosseini, H., Nazeran, H., and Reynolds, K. J. (1998). "ECG noise cancellation using digital filters," in *Proceedings of the 2nd International Conference on IEEE*, Melbourne, 151–152.

Kumar, N., Lolla, N., Keogh, E., Lonardi, S., and Ratanamahatana, C. A. (2005). "Time-series bitmaps: a practical visualization tool for working with large time series databases," in *Proccedings of the SIAM 2005 Data Mining Conference*, (New York, NY: CiteseerX).

Li, J., Deng, G., Wei, W., Wang, H., and Ming, Z. (2016). Design of a real-time ECG filter for portable mobile medical systems. *IEEE Access* 5, 696–704. doi: 10.1109/access.2016.2612222

Lu, G., Brittain, J.-S., Holland, P., Yianni, J., Green, A. L., Stein, J. F., et al. (2009). Removing ECG noise from surface EMG signals using adaptive filtering. *Neurosci. Lett.* 462, 14–19. doi: 10.1016/j.neulet.2009.06.063

Miao, F., Cheng, Y., He, Y., He, Q., and Li, Y. (2015). A wearable context-aware ECG monitoring system integrated with built-in kinematic sensors of the smartphone. *Sensors* 15, 11465–11484. doi: 10.3390/s150511465

Niu, S. W., Huang, J. C., Chen, S. C., Lin, H. Y. H., Kuo, I., Wu, P. Y., et al. (2018). Association between age and changes in heart rate variability after hemodialysis in patients with diabetes. *Front. Aging Neurosci.* 10:43. doi: 10.3389/fnagi.2018.00043

Pan, N., Mang, V., and Un, M. P. (2007). "Accurate removal of baseline wander in ECG using empirical mode decomposition," in *Proceedings of the Noninvasive Functional Source Imaging of the Brain and Heart and the International Conference on Functional Biomedical Imaging, 2007. NFSI-ICFBI 2007. Joint Meeting of the 6th International Symposium on IEEE*, Hangzhou, 177–180.

Qin, S., Liu, C., and Huang, S. (2018). Identification on rice varieties based on k-means clustering algorithm and BP neural network. *J. Chin. Cereals Oils Assoc.* 2, 128–131.

Rautaharju, P. M., Zhou, S. H., and Calhoun, H. P. (1994). Ethnic differences in ECG amplitudes in North American white, black, and Hispanic men and women: effect of obesity and age. *J. Electrocardiol.* 27, 20–31. doi: 10.1016/s0022-0736(94)80040-5

Renuka Devi, M. R., Arvind, T., and Sai Kumar, P. (2013). ECG changes in smokers and non smokers-a comparative study. *J. Clin. Diagn. Res.* 5:824. doi: 10.7860/JCDR/2013/5180.2950

Rollins, M. D., Jenkins, J. G., Carson, D. J., McClure, B. G., Mitchell, R. H., and Imam, S. Z. (1992). Power spectral analysis of the electrocardiogram in diabetic children. *Diabetologia* 35, 452–455. doi: 10.1007/bf02342443

Saechia, S., Koseeyaporn, J., and Wardkein, P. (2005). "Human identification system based ECG signal," in *Proccedings of the TENCON 2005 2005 IEEE Region 10*, (Melbourne: IEEE), 1–4.

Sorwar, G., Abraham, A., and Dooley, L. S. (2001). "Texture classification based on DCT and soft computing," in *Proccedings of the Fuzzy Systems, 2001 on the 10th IEEE International Conference*, (Melbourne: IEEE), 545–548.

Stern, S., and Sclarowsky, S. (2009). The ECG in diabetes mellitus. *Circulation* 120, 1633–1636. doi: 10.1161/circulationaha.109.897496

Tseng, K. K., Fu, L., Liu, L., Lee, D., Wang, C., Li, L., et al. (2018). Human identification with electrocardiogram. *Enterprise Inform. Syst.* 12, 798–819.

Tseng, K. K., Huang, H. N., Zeng, F., and Tu, S. Y. (2015). ECG sensor card with evolving RBP algorithms for human verification. *Sensors* 15, 20730–20751. doi: 10.3390/s150820730

Yang, A. C.-C., Hseu, S.-S., Yien, H.-W., Goldberger, A. L., and Peng, C.-K. (2003). Linguistic analysis of the human heartbeat using frequency and rank order statistics. *Phys. Rev. Lett.* 90:108103.

Conflict of Interest: The authors declare that the research was conducted in the absence of any commercial or financial relationships that could be construed as a potential conflict of interest.

frontiers in Aging Neuroscience

STUDY PROTOCOL
published: 21 May 2020
doi: 10.3389/fnagi.2020.00143

Safety and Efficacy of 630-nm Red Light on Cognitive Function in Older Adults With Mild to Moderate Alzheimer's Disease: Protocol for a Randomized Controlled Study

Nayan Huang[1,2], Dandan Yao[1,2], Wenjing Jiang[1,2], Cuibai Wei[3,4], Mo Li[2], Wenjie Li[2], Haiyan Mu[2], Maolong Gao[5], Zongjuan Ma[2], Jihui Lyu[1,2], and Zhiqian Tong[1]**

[1]Beijing Institute of Brain Disorders, Laboratory of Brain Disorders, Ministry of Science and Technology, Collaborative Innovation Center for Brain Disorders, Capital Medical University, Beijing, China, [2]Center for Cognitive Disorders, Beijing Geriatric Hospital, Beijing, China, [3]Innovation Center for Neurological Disorders, Xuan Wu Hospital, Capital Medical University, Beijing, China, [4]Department of Neurology, Xuan Wu Hospital, Capital Medical University, Beijing, China, [5]Institute for Geriatrics and Rehabilitation, Beijing Geriatric Hospital, Beijing, China

Introduction: Studies have shown that excess formaldehyde accumulation in the brain accelerates cognitive decline in people with Alzheimer's disease (AD). Recently, reports from our research team revealed that red light treatment (RLT) improved memory in AD mice by activating formaldehyde dehydrogenase (FDH) and thus reducing formaldehyde levels. Here, we developed a medical RLT device to investigate the safety and efficacy of this device in older adults with mild to moderate AD.

Methods: This will be a randomized controlled trial (RCT) that will include 60 participants who will be recruited and randomly divided into an RLT group and a control group. The RLT group will receive RLT intervention 5 days a week for 30 min each time for 24 weeks while the control group will continue their routine treatments without RLT. All participants will undergo neuropsychological and functional assessments including the Mini-Mental State Examination, the AD assessment scale-cognitive subscale (ADAS-cog), the Geriatric Depression Scale (GDS), the Neuropsychiatric Inventory (NPI) and the Barthel Index at baseline, 12 weeks and 24 weeks. All participants will undergo functional magnetic resonance imaging (fMRI) scanning and blood/urine biomarkers tests at baseline and 24 weeks. The primary outcome will be the ADAS-cog score while the secondary outcomes will be the GDS and NPI scores. Adverse events will be recorded and treated when necessary. Both an intention-to-treat analysis and a per-protocol analysis will be performed to evaluate the safety and efficacy of RLT.

Discussion: This protocol outlines the objectives of the study and explained the RLT device developed by the research team. The study is designed as an RCT to evaluate the safety and effects of the RLT device on older adults with mild to moderate AD. This study will provide evidence for the clinical use of RLT on treatment for AD.

Clinical Trial Registration: www.ClinicalTrials.gov, ChiCTR1800020163; Pre-results.

Keywords: Alzheimer's disease, cognitive function, red light treatment, formaldehyde, functional magnetic resonance imaging

OPEN ACCESS

Edited by:
Woon-Man Kung,
Chinese Culture University, Taiwan

Reviewed by:
Dafin F. Muresanu,
Iuliu Haieganu University of Medicine and Pharmacy, Romania
Lene Wermuth,
University of Southern Denmark, Denmark

****Correspondence:***
Jihui Lyu
lvjihui@139.com
Zhiqian Tong
tzqbeida@163.com

Received: *13 January 2020*
Accepted: *28 April 2020*
Published: *21 May 2020*

Citation:
Huang N, Yao D, Jiang W, Wei C, Li M, Li W, Mu H, Gao M, Ma Z, Lyu J and Tong Z (2020) Safety and Efficacy of 630-nm Red Light on Cognitive Function in Older Adults With Mild to Moderate Alzheimer's Disease: Protocol for a Randomized Controlled Study. Front. Aging Neurosci. 12:143. doi: 10.3389/fnagi.2020.00143

INTRODUCTION

As the most common cause of dementia in the elderly, Alzheimer's disease (AD) is becoming increasingly prevalent as the population ages. The Alzheimer's Association has now estimated and reported that the number of people with AD in the world will be more than 130 million by 2050 (Alzheimer's Association, 2019). The neuropathology of AD is characterized by the accumulation of β-amyloid (Aβ)-related amyloid plaques and phosphorylated tau (p-tau)-related neurofibrillary tangles outside and inside neurons, respectively. These changes are widely believed pathogenic to the onset of AD (Serrano-Pozo et al., 2011; Alzheimer's Association, 2019). As a persistent, disabling, and costly disease, AD unavoidably puts a huge burden on the family and society (Jia et al., 2018). Unfortunately, over the past decades new medications targeting Aβ production, aggregation and clearance, and tau hyperphosphorylation, such as antibodies, vaccines, and small molecule medicines, have not resulted in desirable clinical efficacy (Lane et al., 2018).

Recently, as a non-pharmacological therapy, low levels of laser light have been found to disaggregate Aβ (Son et al., 2018); hence phototherapy targeting Aβ is being increasingly investigated as an alternative therapy for AD (Salehpour et al., 2018). Previous studies showed that endogenous formaldehyde (FA) concentrations were gradually accumulated in animals and humans during the aging process and that FA was abnormally elevated in AD patients (Tulpule and Dringen, 2013). Indeed, excess FA injection led to memory decline in healthy animal models (Tong et al., 2013, 2017; Wang et al., 2019). Notably, excess FA also directly induces Aβ aggregation (Chen et al., 2006, 2007; Rizak et al., 2014; Yang et al., 2014; Liu et al., 2018), tau protein phosphorylation and aggregation (Lu et al., 2013; Yang et al., 2014; He et al., 2017; Liu et al., 2018), and oxidative stress (Songur et al., 2008; MacAllister et al., 2011). These findings strongly suggest that disaggregation of Aβ by scavenging FA may contribute to the treatment of AD. Our recent studies found that red light at 630 nm improved cognitive function by activating formaldehyde dehydrogenase (FDH) and thus degrading FA and increasing catalase activity to reduce oxidative stress in senescence-accelerated mouse-prone 8 (SAMP8) mice (Zhang et al., 2019). Red light at 630 nm also reversed memory deterioration by de-aggregating Aβ and enhancing FA metabolism in amyloid precursor protein/presenilin-1 (APP/PS1) transgenic AD mice (Yue et al., 2019).

Based on the above experimental evidence in animal models, our research team developed a therapeutic device for people with AD by using light-emitting diodes (LED) with a 630-nm red light in 2015. The penetration of the LED red light at 630 nm has been previously tested and we found that 630 nm red light had a strong penetration rate into the human brain cortex (approximately 48%) and liver (approximately 68%; Yue et al., 2019). This device is made of three main parts, including a power control board, an LED helmet for transcranial irradiation of the head, and an LED belly band for transabdominal illumination of the liver (**Figure 3**), and works by reducing the body's FA levels by activating FDH in the brain and liver. In this study, a 24-week randomized controlled trial (RCT) was designed to investigate the safety and efficacy of this therapeutic red light treatment (RLT) device on older adults with mild to moderate AD. This protocol is reported according to the Standard Protocol Items: Recommendations for Intervention Trials (SPIRIT) guidelines (Chan et al., 2013).

Objectives

The primary objectives are to test the safety and effects of the RLT on cognitive function, behavior/mood, and activities of daily living in older adults with mild to moderate AD.

The secondary objectives are: (1) to explore the changes in brain function by using functional magnetic resonance imaging (fMRI); and (2) to examine the changes in the levels or activities of blood/urine biomarkers, such as FA, Aβ, total tau, p-tau, and FDH.

METHODS

Settings

This device was developed and this study was designed at the Beijing Institute of Brain Disorders, Capital Medical University, China. The recruitment, assessment, intervention, and follow-ups of participants will be conducted at the Center for Cognitive Disorders of Beijing Geriatric Hospital (BGH), China. The Case Report Forms will be filled and kept in BGH.

Study Design

This is an RCT study with two parallel arms (1:1 allocation ratio): an intervention group receiving an RLT program and a control group receiving routine therapy without RLT treatment (**Figures 1**, **2**).

Recruitment of Participants

Participants will be recruited from the clinic, inpatient ward, or long-term care facilities near BGH. Residents who meet the inclusion criteria will be recruited.

Inclusion Criteria

The inclusion criteria will be as follows: (1) 60 years old or older; (2) with a diagnosis of probable AD based on the National Institute of Neurological and Communicative Disorders and Stroke and the AD and Related Disorders Association (NINCDS-ADRDA) criteria (McKhann et al., 1984); and (3) with a clinical dementia rating score $\leq$2. If the participants are receiving cholinesterase inhibitors, memantine, or other dementia-related medications, they will have to take a therapeutic and stable dose for at least 3 months before screening.

Exclusion Criteria

Participants will be excluded if they are experiencing any of the following conditions: (1) severe visual or auditory impairment; (2) serious medical conditions in major organs (such as the heart, lung, kidney, or liver) that limit the ability to participate in the

	STUDY PERIOD				
	Enrolment/ Baseline	Allocation	Post-allocation		
	-2 to 0 weeks	0 weeks	1 week	12 weeks	24 weeks
ENROLMENT:					
Eligibility screen	×				
Informed consent	×				
Baseline data collection	×				
Randomized allocation		×			
INTERVENTIONS:					
Red light treatment			◆—	—	—◆
Usual care			◆—	—	—◆
ASSESSMENTS:					
Basic characteristics					
Demographic characteristics	×				
Medical history	×				
Physical examination	×				
Laboratory examination	×				
Neuropsychological testing					
ADAS-cog	×			×	×
MMSE	×			×	×
NPI	×			×	×
GDS	×			×	×
BI	×			×	×
fMRI scanning	×				×
Blood biomarkers testing					
FA levels	×				×
FDH activity	×				×
Aβ levels	×				×
Total tau/p-tau levels	×				×
Urine biomarker testing					
FA levels	×				×
Safety					
Adverse events			×	×	×
Physical examination	×				×
Laboratory examination	×				×

FIGURE 1 | Schedule of recruitment, intervention, and assessment. Abbreviation: ADAS-cog, Alzheimer's disease assessment scale-cognitive subscale; MMSE, Mini-Mental State Examination; NPI, Neuropsychiatric Inventory; GDS, Geriatric Depression Scale; BI, Barthel Index; fMRI, functional magnetic resonance imaging; FA, formaldehyde; FDH, formaldehyde dehydrogenase; Aβ, β-amyloid peptides; p-tau, phosphorylated tau protein.

study; (3) current alcohol or drug abuse; (4) any other conditions which may disturb assessments or interventions required in this study; (5) history of epilepsy; or (6) having been enrolled into any other interventional studies.

Randomization and Allocation

Participants will be enrolled by dementia specialists. The randomization will be carried out by an independent research assistant who will not be involved in the enrollment,

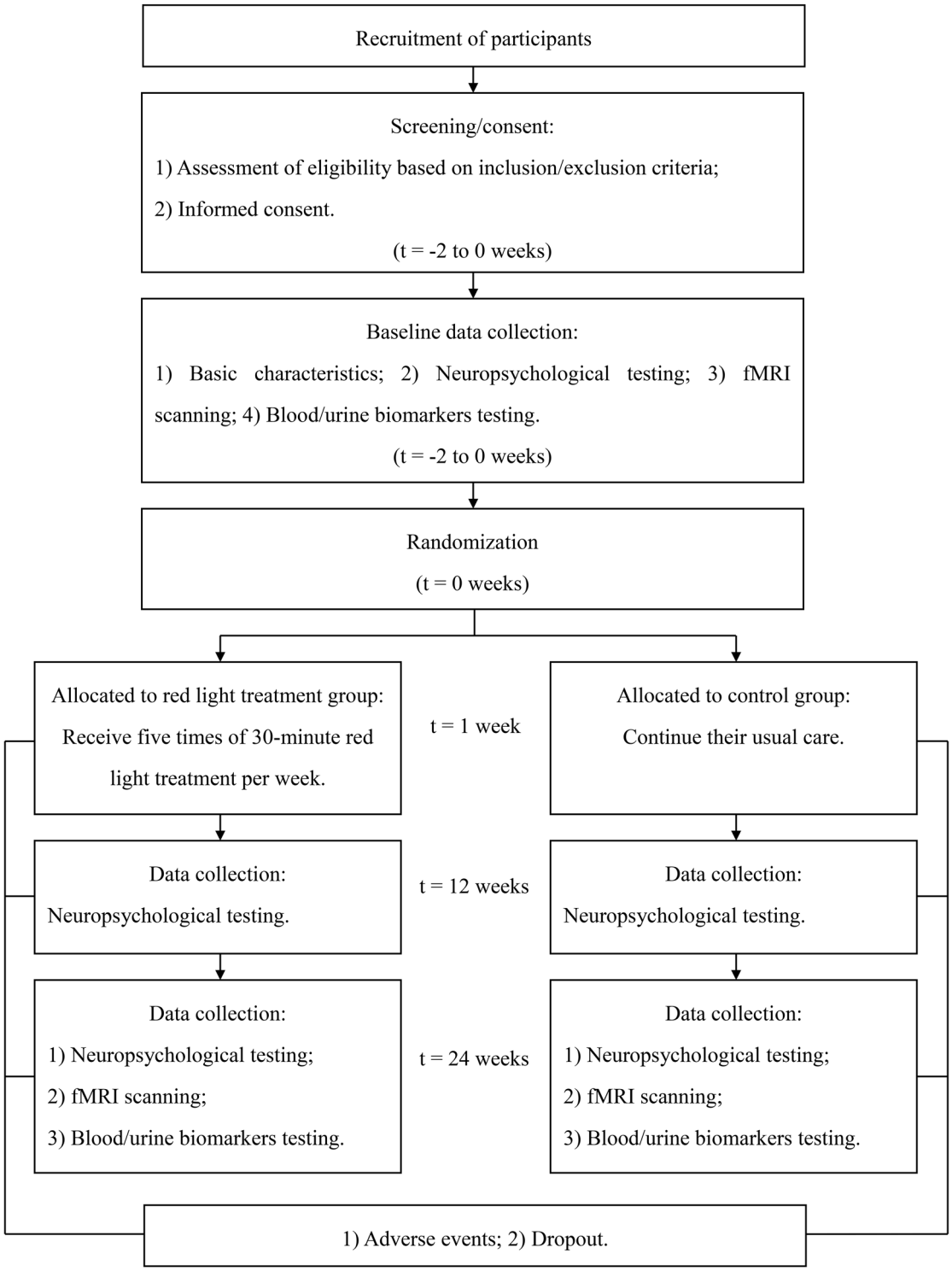

FIGURE 2 | Flow diagram of study design. Abbreviation: fMRI, functional magnetic resonance imaging.

assessment, or intervention of the participants. Random number sequences will be generated using SAS software version 9.4 (SAS Institute Inc., Cary, NC, USA). Sealed envelopes with the serial number outside and group number inside will be produced and kept in a locked drawer that will be inaccessible to all the researchers. The envelopes will be

FIGURE 3 | The therapeutic device: a 630-nm red light device used for the treatment of AD patients. **(A)** The device is constructed of three main parts. From left to right, there is a power control board, an LED helmet for transcranial illumination of the head, and an LED belly band for transabdominal irradiation of the liver. **(B,C)** Images of the therapeutic illuminated LED lights in the "ON" position for treatment of AD patients. Abbreviation: LED, light-emitting diode.

opened sequentially by the independent research assistant after baseline assessments, and participants will be assigned to an intervention group and a control group at a ratio of 1:1 according to the group number printed inside the envelopes. Outcome evaluators and data analysts will be blinded to the group assignment.

Interventions

In addition to their routine treatments and personalized daily care, participants in the RLT group will receive the 24-week intervention of RLT with a frequency of 5 days per week for 30 min each time. The RLT treatment will be performed by researchers or caregivers who are trained to operate the RLT device in advance. The participants will be put on the LED helmet and the LED belly band and receive RLT therapy with concurrent transcranial and transabdominal illumination in the morning (**Figure 3**). The light parameters of the RLT device are shown in **Table 1**. The researchers or caregivers will be asked to keep a strict watch over the participants during the intervention process. A form of RLT treatment schedule will be made for each participant in the RLT group. The researchers or caregivers who perform the RLT intervention will be asked to sign on the report form after every session of treatment to ensure compliance of the intervention.

TABLE 1 | Parameters of the therapeutic device of 630-nm red light for AD patients.

Source	The red light treatment device
Wavelength (nm)	630 ± 15
Power output per LED (mW)	5
Power density (mW/cm^2)	20 (anterior helmet LEDs)
	40 (posterior helmet LEDs)
	5 (temporal helmet LEDs)
	5 (belly band LEDs)
Duration of each time (min)	30
Frequency of treatment	5 times per week

Abbreviation: AD, Alzheimer's disease; LED, light-emitting diode.

Participants in the control group will continue their routine treatments and personalized daily care during the 24-week study period, including usual medicine, recreational therapy, and management of behavioral disorders following current guidelines. Except for the RLT intervention for the RLT group, all the other treatment strategies for the two groups will be the same.

Demographic Data Collection

Demographic characteristics of all participants including age, gender, educational level, as well as medical history, medication list, and comorbidities will be documented.

Neuropsychological Assessments

A set of neuropsychological tests will be used to assess cognitive function and behavior/mood of all the participants, and their activities of daily living will also be measured. The assessments will be performed at baseline, 12 weeks, and 24 weeks during the study period. (1) The Mini-Mental State Examination (Katzman et al., 1988) is the most frequently used assessment to measure global cognitive function. It is a 30-point scale that assesses orientation, memory, attention and calculation, recall, and language, with higher scores indicating better cognitive function. (2) The AD assessment scale-cognitive subscale (ADAS-cog; Chu et al., 2000) is a 12-item scale that primarily measures word recall, ability to follow commands, constructional praxis, naming, ideational praxis, orientation, word recognition, comprehension of spoken language, word-finding, language ability, and attention. The scores range from 0 to 75 and higher scores indicate greater cognitive impairment. (3) The Geriatric Depression Scale (GDS; Yesavage et al., 1982) is a short questionnaire to identify depression in older people and it is validated in mild to moderate dementia. (4) The Neuropsychiatric Inventory (NPI; Wang et al., 2012) is an assessment of 12 different behavioral and psychological symptoms common in AD. Each symptom is rated and scored according to the frequency and severity reported by the informants. The distress level of the caregivers associated with each symptom is also rated. (5) The Barthel Index (Mahoney and Barthel, 1965), is a 10-item, ordinal scale used to measure performance in activities of daily living. It is also performed by interviewing the caregivers.

fMRI

fMRI is a non-invasive brain imaging technique to measure and map brain activity. In this study, we will collect the data of resting-state fMRI (rs-fMRI) for the analysis of neurophysiological changes (Lee et al., 2013; Smitha et al., 2017). Participants will receive fMRI scans by using a Philips Ingenia 3.0 T magnetic resonance system at BGH at baseline and 24 weeks. The following sequences will be acquired: (1) High-resolution anatomic images using a 3D T1-weighted inversion recovery turbo field echo sequence with the following parameters: repetition time (TR) 7.9 ms, echo time (TE) 3.5 ms, contiguous 180 sagittal slices of 1 mm thickness, flip angle 8°, 1 × 1 × 1 mm voxels, 160 × 210 × 180 matrices, and field of view (FOV) 160 × 211 × 180 mm. (2) Single-shot field echo echo-planar imaging sequence for rs-fMRI images with the following parameters: 200 sets of contiguous 40 transverse slices, 4 mm thickness, TR 3,000 ms, TE 35 ms, flip angle 90°, 2 × 2 × 4 mm voxels, 120 × 116 × 40 matrices, and FOV 240 × 240 × 160 mm. The total acquisition time of rs-fMRI is 609 s. During the scanning process, participants will be asked to keep their eyes closed and remain motionless.

Blood/Urine Biomarkers

The biomarkers of blood and/or urine of all participants will be measured at baseline and 24 weeks. The concentrations of blood Aβ, total tau, and p-tau, which are related to the pathology of AD, will be quantified by human Aβ and tau ELISA kits. Meanwhile, blood and urine FA levels and blood FDH activity will be measured.

Outcomes

The primary outcome will be the ADAS-cog score. The secondary outcomes will be the GDS and NPI scores. The safety of the RLT will be evaluated according to the incidence and severity of adverse events such as headache, dizziness, or nausea. The adverse events will be immediately reported, and handled by experienced physicians. Details of these possible adverse events and the treatments they receive will be recorded by filling in the case report forms. Physical examinations and necessary laboratory examinations, such as blood routine examination, liver function, and renal function, will be completed at baseline and the end of this study.

Sample Size Calculation

No studies have investigated the effects of RLT treatment on people with AD. However, there have been relevant published literature that reported positive effects of photobiomodulation (PBM) with 810 nm near-infrared light on people with dementia. For example, PBM was shown to reduce ADAS-cog scores by 6.73 points after a 12-week consecutive treatment (Saltmarche et al., 2017), and by 5.18 points in another report (Chao, 2019). In this study, we anticipate at least an effect size of 0.48 in ADAS-cog scores after 24-week RLT intervention. The sample size was calculated using Power Analysis and Sample Size software version 15.0 (NCSS, LLC)[1]. A total sample size of 48 participants is sufficient to detect the target effect size with 90% power ($\beta = 0.10$) and a type I error of 5% ($\alpha = 0.05$). Considering a dropout rate of 10%, a total of 54 participants is necessary. In this study, we intend to recruit 60 participants, with 30 participants in each group.

Quality Control and Quality Assurance

At least three dementia specialists will work together to examine the participants and provide a diagnosis for each participant. All data will be monitored and reviewed by the principal investigator or research coordinators. Training will be provided to all researchers. Consistency coefficients in scoring assessment scales between researchers should be no less than 0.85. Data entry will be verified by a second researcher in the team. To protect participant confidentiality, only supervisors, researchers of this study, and the ethics committee will be authorized to access to the personal information and medical records of the participants.

Statistical Methods

Statistical analysis of demographics and clinical characteristics will be performed using IBM SPSS Statistics for Windows, Version 20.0 (Release 2011, IBM Corp, Armonk, NY, USA).

[1] https://www.ncss.com/

Continuous data will be reported as means ± standard deviations or 95% confidence intervals, and as numbers with percentage for categorical data. The difference in demographic and baseline characteristics between two groups will be analyzed by using the independent *t*-test, and a *chi*-square test will be used for categorical variables.

The main analysis method for the safety and efficacy of RLT intervention in this study will use the intention-to-treat analysis including all randomized participants (Hollis and Campbell, 1999). Besides, a per-protocol analysis will be performed on individuals who complete the total study (Sedgwick, 2015). The repeated measures of variance analysis will be used to examine variations of scores of neuropsychological tests over time between two groups. The association between intervention and incidence of adverse events will be analyzed using the *chi*-square test.

fMRI data will be preprocessed by using Statistical Parametric Mapping version 12.0 (The Wellcome Trust Centre for Neuroimaging at UCL, London, UK) on the MATLAB platform (Release 2013b, The MathWorks Inc, Natick, MA, USA). There are several critical steps including motion correction, slice timing correction, spatial normalization, and smoothing. After fMRI data preprocessing, the fractional amplitude of low-frequency fluctuation and functional connectivity analysis will be analyzed by using the REST software version 1.8 (Song et al., 2011).

The level of significance for statistical analysis will be set at 5% ($P < 0.05$). The researchers who perform the data analysis will be blinded to the allocation and the intervention.

Patient and Public Involvement

The original research question and outcome measures were conceived by the authors and were then modified based on face-to-face screening interviews with 16 elderly volunteers with cognitive impairment by a research assistant. They were also invited to use the RLT device for 3 months during the design phase of this study. The duration of treatment per time and frequency of treatment was determined based on their feedback to ensure the tolerance and the applicability of the intervention. These volunteers will not be included in this study. Both the potential burden and benefit of this study will be assessed by the participants and their guardians before signing the informed consent. The findings of this study will be made available to the participants and their guardians.

ETHICS AND DISSEMINATION

This study protocol has been approved by the ethical review committee of the Beijing Geriatric Hospital (approval number: 2019-024). Information leaflets of the study will be available at the public area of the Center for Cognitive disorders of BGH. The leaflets will explain in full detail the aims and objectives of the study, selection criteria, and the processes that the study will be adhering to. The research team will provide an individual face to face consultation to all potential participants and their guardians to answer any questions they may have before signing the consent form. Informed consent will be obtained from all participants and/or their legal representatives. Participants will be allowed to withdraw from the study at any time and the reason for withdrawal will be recorded. The results of this study will be reported in peer-reviewed journals and presented at national or international conferences on aging and dementia.

DISCUSSION

To our knowledge, this is the first RCT to investigate the safety and efficacy of RLT on AD. This 24-week study is designed to evaluate the effects of RLT intervention on cognitive function, mood, psychiatric and behavioral performances, and activities of daily living in older adults with mild to moderate AD. Also, neurophysiological changes assessed by fMRI and changes in blood/urine biomarkers associated with RLT will also be evaluated.

Preliminary evidence for the benefits of the RLT on AD has been obtained. The RLT can not only prevent early-stage memory decline but also rescue late-stage memory deficits in AD mice by reducing FA levels and oxidative stress (Zhang et al., 2019). Moreover, PBM with red to near-infrared light has been proposed as a non-invasive and innovative therapy for brain disorders. Some other beneficial effects of PBM have been reported, such as improved cerebral metabolic function (Oron et al., 2007; Rojas et al., 2012; Ferraresi et al., 2015), increased expression of neurotrophic factor expression, improved neurogenesis (Oron et al., 2006; Xuan et al., 2014, 2015), and reduced neuroinflammation (Lee et al., 2016; Aragona et al., 2017). Therefore, PBM appears to be a promising strategy for AD treatment.

There are limitations to this study. The first is that as the first preliminary clinical trial for the RLT device it is a single-center design. The second is the absence of a sham intervention for the control group for ethical and practical considerations. To minimize these shortcomings, the processes of randomization and blindness will be strictly carried out, and objective examinations including fMRI and blood/urine biomarkers will be conducted. Moreover, because of the cognitive impairments in patients with AD, the placebo effect can be greatly eliminated. The third is that follow-up assessment after cessation of the intervention is not planed in this protocol because the effects of the RLT are still unknown. If positive results are found in this initial study, future research will be conducted to assess the long-term influence of the RLT, which will help to identify the optimal RLT duration.

In summary, this RCT will explore the potential beneficial effects and safety of RLT on older adults with mild to moderate AD. The study will provide evidence for the clinical use of RLT on treatment for mild to moderate AD.

ETHICS STATEMENT

The studies involving human participants were reviewed and approved by the Medical Ethics Committee of the Beijing Geriatric Hospital (approval number:2019-024). The patients/participants provided their written informed consent to participate in this study.

AUTHOR CONTRIBUTIONS

ZT and JL conceived and designed the study. All authors played a role in the development of the protocol. NH drafted the manuscript, and all authors participated in the preparation of this manuscript. All authors approved the submission of this manuscript.

FUNDING

This study is funded by the Major Projects Fund of Beijing Institute for Brain Disorders (ZD2015-08); Beijing Municipal Administration of Hospitals Clinical Medicine Development of Special Funding Support (ZYLX201834); the National Key R&D Program of China (2017YFE0118800)—European Commission Horizon 2020 (779238-PRODEMOS); Beijing Municipal Administration of Hospitals Clinical Medicine Development of Special Funding Support (ZYLX201837); and National Key R&D Program of China (2017YFC1310103).

ACKNOWLEDGMENTS

We would like to thank all the participants and their guardians for their cooperation and contribution to the development of this protocol.

REFERENCES

Alzheimer's Association. (2019). 2019 Alzheimer's disease facts and figures. *Alzheimers Dement.* 15, 321–387. doi: 10.1016/j.jalz.2019.01.010

Aragona, S. E., Grassi, F. R., Nardi, G., Lotti, J., Mereghetti, G., Canavesi, E., et al. (2017). Photobiomodulation with polarized light in the treatment of cutaneous and mucosal ulcerative lesions. *J. Biol. Regul. Homeost. Agents* 31, 213–218.

Chan, A. W., Tetzlaff, J. M., Gøtzsche, P. C., Altman, D. G., Mann, H., Berlin, J. A., et al. (2013). SPIRIT 2013 explanation and elaboration: guidance for protocols of clinical trials. *BMJ* 346:e7586. doi: 10.1136/bmj.e7586

Chao, L. L. (2019). Effects of home photobiomodulation treatments on cognitive and behavioral function, cerebral perfusion, and resting-state functional connectivity in patients with dementia: a pilot trial. *Photobiomodul. Photomed. Laser Surg.* 37, 133–141. doi: 10.1089/photob.2018.4555

Chen, K., Kazachkov, M., and Yu, P. H. (2007). Effect of aldehydes derived from oxidative deamination and oxidative stress on β-amyloid aggregation; pathological implications to Alzheimer's disease. *J. Neural Transm.* 114, 835–839. doi: 10.1007/s00702-007-0697-5

Chen, K., Maley, J., and Yu, P. H. (2006). Potential inplications of endogenous aldehydes in β-amyloid misfolding, oligomerization and fibrillogenesis. *J. Neurochem.* 99, 1413–1424. doi: 10.1111/j.1471-4159.2006.04181.x

Chu, L. W., Chiu, K. C., Hui, S. L., Yu, G. K., Tsui, W. J., and Lee, P. W. (2000). The reliability and validity of the Alzheimer's disease assessment scale cognitive subscale (ADAS-Cog) among the elderly chinese in hong kong. *Ann. Acad. Med. Singapore* 29, 474–485. doi: 10.1016/s0197-4580(00)83371-0

Ferraresi, C., Kaippert, B., Avci, P., Huang, Y. Y., de Sousa, M. V., Bagnato, V. S., et al. (2015). Low-level laser (light) therapy increases mitochondrial membrane potential and ATP synthesis in C2C12 myotubes with a peak response at 3-6 h. *Photochem. Photobiol.* 91, 411–416. doi: 10.1111/php.12397

He, X., Li, Z., Rizak, J. D., Wu, S., Wang, Z., He, R., et al. (2017). Resveratrol attenuates formaldehyde induced hyperphosphorylation of tau protein and cytotoxicity in N2a cells. *Front. Neurosci.* 10:598. doi: 10.3389/fnins.2016.00598

Hollis, S., and Campbell, F. (1999). What is meant by intention to treat analysis? Survey of published randomised controlled trials. *BMJ* 319, 670–674. doi: 10.1136/bmj.319.7211.670

Jia, J., Wei, C., Chen, S., Li, F., Tang, Y., Qin, W., et al. (2018). The cost of Alzheimer's disease in China and re-estimation of costs worldwide. *Alzheimers Dement.* 14, 483–491. doi: 10.1016/j.jalz.2017.12.006

Katzman, R., Zhang, M. Y., Ouang-Ya, Q., Wang, Z. Y., Liu, W. T., Yu, E., et al. (1988). A Chinese version of the Mini-Mental State Examination; impact of illiteracy in a Shanghai dementia survey. *J. Clin. Epidemiol.* 41, 971–978. doi: 10.1016/0895-4356(88)90034-0

Lane, C. A., Hardy, J., and Schott, J. M. (2018). Alzheimer's disease. *Eur. J. Neurol.* 25, 59–70. doi: 10.1111/ene.13439

Lee, H. I., Park, J. H., Park, M. Y., Kim, N. G., Park, K. J., Choi, B. T., et al. (2016). Pre-conditioning with transcranial low-level light therapy reduces neuroinflammation and protects blood-brain barrier after focal cerebral ischemia in mice. *Restor. Neurol. Neurosci.* 34, 201–214. doi: 10.3233/rnn-150559

Lee, M. H., Smyser, C. D., and Shimony, J. S. (2013). Resting-state fMRI: a review of methods and clinical applications. *Am. J. Neuroradiol.* 34, 1866–1872. doi: 10.3174/ajnr.A3263

Liu, X., Zhang, Y., Wu, R., Ye, M., Zhao, Y., Kang, J., et al. (2018). Acute formaldehyde exposure induced early Alzheimer-like changes in mouse brain. *Toxicol. Mech. Methods* 28, 95–104. doi: 10.1080/15376516.2017.1368053

Lu, J., Miao, J., Su, T., Liu, Y., and He, R. (2013). Formaldehyde induces hyperphosphorylation and polymerization of Tau protein both *in vitro* and *in vivo*. *Biochim. Biophys. Acta* 1830, 4102–4116. doi: 10.1016/j.bbagen.2013.04.028

MacAllister, S. L., Choi, J., Dedina, L., and O'Brien, P. J. (2011). Metabolic mechanisms of methanol/formaldehyde in isolated rat hepatocytes: carbonyl-metabolizing enzymes versus oxidative stress. *Chem. Biol. Interact.* 191, 308–314. doi: 10.1016/j.cbi.2011.01.017

Mahoney, F. I., and Barthel, D. W. (1965). Functional evaluation: the Barthel Index. *Md. State Med. J.* 14, 61–65.

McKhann, G., Drachman, D., Folstein, M., Katzman, R., Price, D., and Stadlan, E. M. (1984). Clinical diagnosis of Alzheimer's disease: report of the NINCDS-ADRDA Work Group under the auspices of Department of Health and Human Services Task Force on Alzheimer's disease. *Neurology* 34, 939–944. doi: 10.1212/wnl.34.7.939

Oron, A., Oron, U., Chen, J., Eilam, A., Zhang, C., Sadeh, M., et al. (2006). Low-level laser therapy applied transcranially to rats after induction of stroke significantly reduces long-term neurological deficits. *Stroke* 37, 2620–2624. doi: 10.1161/01.str.0000242775.14642.b8

Oron, U., Ilic, S., De Taboada, L., and Streeter, J. (2007). Ga-As (808 nm) laser irradiation enhances ATP production in human neuronal cells in culture. *Photomed. Laser Surg.* 25, 180–182. doi: 10.1089/pho.2007.2064

Rizak, J. D., Ma, Y., and Hu, X. (2014). Is formaldehyde the missing link in AD pathology? The differential aggregation of amyloid-β with APOE isoforms *in vitro*. *Curr. Alzheimer Res.* 11, 461–468. doi: 10.2174/1567205011666140425112043

Rojas, J. C., Bruchey, A. K., and Gonzalez-Lima, F. (2012). Low-level light therapy improves cortical metabolic capacity and memory retention. *J. Alzheimers Dis.* 32, 741–752. doi: 10.3233/jad-2012-120817

Salehpour, F., Mahmoudi, J., Kamari, F., Sadigh-Eteghad, S., Rasta, S. H., and Hamblin, M. R. (2018). Brain photobiomodulation therapy: a narrative review. *Mol. Neurobiol.* 55, 6601–6636. doi: 10.1007/s12035-017-0852-4

Saltmarche, A. E., Naeser, M. A., Ho, K. F., Hamblin, M. R., and Lim, L. (2017). Significant improvement in cognition in mild to moderately severe dementia cases treated with transcranial plus intranasal photobiomodulation: case series report. *Photomed. Laser Surg.* 35, 432–441. doi: 10.1089/pho.2016.4227

Sedgwick, P. (2015). Intention to treat analysis versus per protocol analysis of trial data. *BMJ* 350:h681. doi: 10.1136/bmj.h681

Serrano-Pozo, A., Frosch, M. P., Masliah, E., and Hyman, B. T. (2011). Neuropathological alterations in Alzheimer disease. *Cold Spring Harb. Perspect. Med.* 1:a006189. doi: 10.1101/cshperspect.a006189

Smitha, K. A., Akhil Raja, K., Arun, K. M., Rajesh, P. G., Thomas, B., Kapilamoorthy, T. R., et al. (2017). Resting state fMRI: a review on methods

in resting state connectivity analysis and resting state networks. *Neuroradiol. J.* 30, 305–317. doi: 10.1177/1971400917697342

Son, G., Lee, B. I., Chung, Y. J., and Park, C. B. (2018). Light-triggered dissociation of self-assembled β-amyloid aggregates into small, nontoxic fragments by ruthenium (II) complex. *Acta Biomater.* 36, 147–155. doi: 10.1016/j.actbio.2017.11.048

Song, X. W., Dong, Z. Y., Long, X. Y., Li, S. F., Zuo, X. N., Zhu, C. Z., et al. (2011). REST: a toolkit for resting-state functional magnetic resonance imaging data processing. *PLoS One* 6:e25031. doi: 10.1371/journal.pone.0025031

Songur, A., Sarsilmaz, M., Ozen, O., Sahin, S., Koken, R., Zararsiz, I., et al. (2008). The effects of inhaled formaldehyde on oxidant and antioxidant systems of rat cerebellum during the postnatal development process. *Toxicol. Mech. Methods* 18, 569–574. doi: 10.1080/15376510701555288

Tong, Z., Han, C., Luo, W., Wang, X., Li, H., Luo, H., et al. (2013). Accumulated hippocampal formaldehyde induces age-dependent memory decline. *Age* 35, 583–596. doi: 10.1007/s11357-012-9388-8

Tong, Z., Wang, W., Luo, W., Lv, J., Li, H., Luo, H., et al. (2017). Urine formaldehyde predicts cognitive impairment in post-stroke dementia and Alzheimer's disease. *J. Alzheimers Dis.* 55, 1031–1038. doi: 10.3233/jad-160357

Tulpule, K., and Dringen, R. (2013). Formaldehyde in brain: an overlooked player in neurodegeneration? *J. Neurochem.* 127, 7–21. doi: 10.1111/jnc.12356

Wang, F., Chen, D., Wu, P., Klein, C., and Jin, C. (2019). Formaldehyde, epigenetics, and Alzheimer's disease. *Chem. Res. Toxicol.* 32, 820–830. doi: 10.1021/acs.chemrestox.9b00090

Wang, T., Xiao, S., Li, X., Wang, H., Liu, Y., Su, N., et al. (2012). Reliability and validity of the Chinese version of the neuropsychiatric inventory in mainland China. *Int. J. Geriatr. Psychiatry* 27, 539–544. doi: 10.1002/gps.2757

Xuan, W., Agrawal, T., Huang, L., Gupta, G. K., and Hamblin, M. R. (2015). Low-level laser therapy for traumatic brain injury in mice increases brain derived neurotrophic factor (BDNF) and synaptogenesis. *J. Biophotonics* 8, 502–511. doi: 10.1002/jbio.201400069

Xuan, W., Vatansever, F., Huang, L., and Hamblin, M. R. (2014). Transcranial low-level laser therapy enhances learning, memory and neuroprogenitor cells after traumatic brain injury in mice. *J. Biomed. Opt.* 19:108003. doi: 10.1117/1.jbo.19.10.108003

Yang, M., Miao, J., Rizak, J., Zhai, R., Wang, Z., Huma, T., et al. (2014). Alzheimer's disease and methanol toxicity (part 2): lessons from four rhesus macaques (Macaca mulatta) chronically fed methanol. *J. Alzheimers Dis.* 41, 1131–1147. doi: 10.3233/jad-131532

Yesavage, J. A., Brink, T. L., Rose, T. L., Lum, O., Huang, V., Adey, M., et al. (1982). Development and validation of a geriatric depression screening scale: a preliminary report. *J. Psychiatr. Res.* 17, 37–49. doi: 10.1016/0022-3956(82)90033-4

Yue, X., Mei, Y., Zhang, Y., Tong, Z., Cui, D., Yang, J., et al. (2019). New insight into Alzheimer's disease: light reverses Aβ-obstructed interstitial fluid flow and ameliorates memory decline in APP/PS1 mice. *Alzheimers Dement.* 5, 671–684. doi: 10.1016/j.trci.2019.09.007

Zhang, J., Yue, X., Luo, H., Jiang, W., Mei, Y., Ai, L., et al. (2019). Illumination with 630 nm red light reduces oxidative stress and restores memory by photo-activating catalase and formaldehyde dehydrogenase in SAMP8 mice. *Antioxid. Redox Signal.* 30, 1432–1449. doi: 10.1089/ars.2018.7520

Conflict of Interest: The authors declare that the research was conducted in the absence of any commercial or financial relationships that could be construed as a potential conflict of interest.

frontiers in Aging Neuroscience

ORIGINAL RESEARCH
published: 21 May 2020
doi: 10.3389/fnagi.2020.00141

Detection of Mild Cognitive Impairment Using Convolutional Neural Network: Temporal-Feature Maps of Functional Near-Infrared Spectroscopy

*Dalin Yang[1], Ruisen Huang[1], So-Hyeon Yoo[1], Myung-Jun Shin[2], Jin A. Yoon[2], Yong-Il Shin[3] and Keum-Shik Hong[1]**

[1] School of Mechanical Engineering, Pusan National University, Busan, South Korea, [2] Department of Rehabilitation Medicine, Pusan National University School of Medicine and Biomedical Research Institute, Pusan National University Hospital, Busan, South Korea, [3] Department of Rehabilitation Medicine, Pusan National University School of Medicine, Pusan National University Yangsan Hospital, Yangsan-si, South Korea

Mild cognitive impairment (MCI) is the clinical precursor of Alzheimer's disease (AD), which is considered the most common neurodegenerative disease in the elderly. Some MCI patients tend to remain stable over time and do not evolve to AD. It is essential to diagnose MCI in its early stages and provide timely treatment to the patient. In this study, we propose a neuroimaging approach to identify MCI using a deep learning method and functional near-infrared spectroscopy (fNIRS). For this purpose, fifteen MCI subjects and nine healthy controls (HCs) were asked to perform three mental tasks: *N*-back, Stroop, and verbal fluency (VF) tasks. Besides examining the oxygenated hemoglobin changes (ΔHbO) in the region of interest, ΔHbO maps at 13 specific time points (i.e., 5, 10, 15, 20, 25, 30, 35, 40, 45, 50, 55, 60, and 65 s) during the tasks and seven temporal feature maps (i.e., two types of mean, three types of slope, kurtosis, and skewness) in the prefrontal cortex were investigated. A four-layer convolutional neural network (CNN) was applied to identify the subjects into either MCI or HC, individually, after training the CNN model with ΔHbO maps and temporal feature maps above. Finally, we used the 5-fold cross-validation approach to evaluate the performance of the CNN. The results of temporal feature maps exhibited high classification accuracies: The average accuracies for the *N*-back task, Stroop task, and VFT, respectively, were 89.46, 87.80, and 90.37%. Notably, the highest accuracy of 98.61% was achieved from the ΔHbO slope map during 20–60 s interval of *N*-back tasks. Our results indicate that the fNIRS imaging approach based on temporal feature maps is a promising diagnostic method for early detection of MCI and can be used as a tool for clinical doctors to identify MCI from their patients.

Keywords: functional near-infrared spectroscopy (fNIRS), mild cognitive impairment (MCI), convolutional neural network (CNN), temporal feature, brain map, *N*-back, Stroop, verbal fluency task

OPEN ACCESS

Edited by:
Woon-Man Kung,
Chinese Culture University, Taiwan

Reviewed by:
Stephane Perrey,
Université de Montpellier, France
Naimul Khan,
Ryerson University, Canada

****Correspondence:***
Keum-Shik Hong
kshong@pusan.ac.kr

Received: *05 February 2020*
Accepted: *27 April 2020*
Published: *21 May 2020*

Citation:
Yang D, Huang R, Yoo S-H, Shin M-J, Yoon JA, Shin Y-I and Hong K-S (2020) Detection of Mild Cognitive Impairment Using Convolutional Neural Network: Temporal-Feature Maps of Functional Near-Infrared Spectroscopy. Front. Aging Neurosci. 12:141. doi: 10.3389/fnagi.2020.00141

INTRODUCTION

Alzheimer's disease (AD) is authoritatively listed as the sixth leading cause of death in the United States (US), and it is also the fifth primary cause of death for those aged 65 years and above (Taylor et al., 2017). Seven hundred thousand people aged 65 years and above in the US were estimated death based on AD in 2019 (Hebert et al., 2013). As recently reported by Alzheimer Association, it estimated 18.5 billion hours of assistance (valued at $233.9 billion) was provided by the caregivers of people with AD or other dementias (Alzheimer Association, 2019). It is thought that AD starts at least 20 years before the symptoms occur with small unnoticeable changes in the brain. Symptoms arise because of the damaged nerve cells (neurons) related to thinking, learning, and memory (Gordon et al., 2018). Symptoms tend to grow over time and gradually start to interfere with the ability of an individual to perform everyday activities until death. AD is considered a progressive, irreversible neurological brain disorder. Currently, no pharmacological treatment exists that can decelerate or prevent the symptoms of AD (Alzheimer Association, 2019). Many researchers suppose that the early stage in the AD process, at either the mild cognitive impairment (MCI) or preclinical stage, will be the most effective period for future treatments to slow down or prevent the progression of AD (Yiannopoulou and Papageorgiou, 2013). Thus, it is essential to assess biomarkers (i.e., the indication of the medical state observed from outside of patients; Strimbu and Tavel, 2010) for identifying individuals who are in these early stages of the disease and can receive appropriate treatment.

There are three categories of diagnostic biomarkers for AD, which are named β-amyloid-Aβ deposits (A), hyperphosphorylated tau aggregates (T), and neurodegeneration or neuronal injury (N) (Jack et al., 2018). The ATN synopsis is widely assessed through cerebrospinal fluid (CSF) or medical imaging. Thus far, no evidence that supports the preeminence of any biomarker over another (CSF vs. imaging) for the diagnostic assessment of AD exists. The selection of biomarkers typically relies on the cost, availability, and convenience of tests (Khoury and Ghossoub, 2019). However, because medical imaging can identify the different stages of the AD temporally and anatomically, some researchers claim that the superiority of medical imaging over the biofluid biomarkers mentioned above (Márquez and Yassa, 2019).

Functional near-infrared spectroscopy (fNIRS) is a non-invasive neuroimaging technique, which is used to measure activation-induced changes in the cerebral hemoglobin concentrations of oxyhemoglobin (ΔHbO) and deoxyhemoglobin (ΔHbR) (Perrey, 2014; Shin and Im, 2018; Hong et al., 2020). The blood flow and oxygen metabolism are induced by the neural activity in the neighboring capillary network (Hong et al., 2014; Zafar and Hong, 2018; Ghafoor et al., 2019). In comparison with the existing neuroimaging techniques involving direct neural activation measurement methods such as magnetoencephalography (MEG) and electroencephalography (EEG) (Kumar et al., 2019), fNIRS offers the advantage of higher spatial resolution and lower susceptibility to the movement artifact (Naseer and Hong, 2015; Wilcox and Biondi, 2015; Hong et al., 2018; Pfeifer et al., 2018). In contrast, other well-established neuroimaging techniques are typically associated with the metabolism of biochemical components during neural activity and exist a limitation in terms of temporal resolution. These techniques include positron emission tomography (PET), single-positron emission computed tomography (SPECT), and functional magnetic resonance imaging (fMRI) (Strangman et al., 2002). In particular, because of the property requirement of the radioactive isotopes, PET and SPECT do not allow continuous or repeated measurements, a factor that also limits their application in the cases of children and pregnant women (Irani et al., 2007). Although fMRI is non-radiative and involves no risk, it is physically constraining, is sensitive to movement artifacts, exposes participants to an excessively noisy environment, and is expensive (Ferrari and Quaresima, 2012). These features render fMRI inappropriate for certain research and many clinical applications (Santosa et al., 2014). In contrast, fNIRS is a novel neuroimaging modality with the following advantages: it is non-invasive, safe, less costly, portable, and tolerant of motion artifacts (Perrey, 2008); it also has great temporal resolution and moderate spatial resolution (Ghafoor et al., 2017; Zafar and Hong, 2020). In addition, fNIRS is in progress to improve the spatial and temporal resolutions with the development of bundled-optodes configurations (Nguyen and Hong, 2016; Nguyen et al., 2016), detection of the initial dip (Zafar and Hong, 2017; Hong and Zafar, 2018), and combination of adaptive method (Iqbal et al., 2018; Hong and Pham, 2019; Pamosoaji et al., 2019) to improve information transfer rate.

In the past decades, the fNIRS study of psychiatric or neural-disorder patients highly depended on mass-univariate analytical techniques such as statistical parametric mapping (Vieira et al., 2017). Traditionally, the research studies compared the hemodynamic response of a patient with that of healthy control (HC) and determined neuroanatomical or neurofunctional differences at the group level. Most AD/MCI detection studies typically employed the ΔHbO/ΔHbR (Jahani et al., 2017; Perpetuini et al., 2017; Vermeij et al., 2017; Katzorke et al., 2018; Yoon et al., 2019) and relative temporal features such as the mean value, slope value, number of active channels, peak location, skewness, and kurtosis (Yap et al., 2017; Li et al., 2018a), and they determined the significant differences for comparison. The straightforwardness and interpretability of this methodology has led to considerable advances in our comprehension of the neurological disorders. With the development of technology, the following limitations of mass-univariate analytical techniques have been revealed. (1) Statistical information is extracted according to each region of interest (ROI) channel based on the assumption that various brain regions perform independently. In practice, this assumption is inconsistent with brain function (Biswal et al., 2010). The network-level comparison explains the neurological symptoms better than the focal-level comparison (Mulders et al., 2015). (2) Statistical analysis cannot easily yield individual diagnosis results (Vieira et al., 2017). Mass-univariate techniques are suitable only for detecting differences between groups. According to the evaluation conducted in our initial study, the results of statistical analysis are not consistent with the classification results (Yang et al., 2019). Thus, an effective classification method based on fNIRS neuroimaging is crucial for the detection of MCI in the clinical stage.

Deep learning (DL) has allowed significant progress in the identification and classification of image patterns and is considered a promising machine-learning methodology (Ravi et al., 2017). Convolutional neural networks (CNNs), the most broadly used DL architecture, have delivered excellent performances in computer-aided prediction for neurological disorders (Mamoshina et al., 2016; Tanveer et al., 2019). The great success of CNNs in neural-image classification and analysis, which evidences their strong image-classification ability (Cecotti and Gräser, 2011; Ieracitano et al., 2018; Lin et al., 2018; Waytowich et al., 2018; Oh et al., 2019), motivated us to develop a CNN-based classification method for early-stage AD detection. So far, there are not any discussions in the literature, which used the DL method as an assistive tool for the diagnosis of early-stage AD by fNIRS signals, except for our group.

In our initial investigation (Yang et al., 2019), we compared the hemodynamic responses and statistical information between the groups of MCI and HC: We evaluated the digital biomarkers (i.e., mean, slope, peak, kurtosis, and skewness) and image biomarkers (i.e., *t*-map and connectivity map) for MCI identification. The MCI group showed decreased ΔHbO responses in comparison with the HC group, which is consistent with the literature (Vermeij et al., 2017; Katzorke et al., 2018). As digital biomarkers, 15 features (i.e., mean value of ΔHbO for 5–65 s, mean value of ΔHbR for 5–65 s, mean value of ΔHbO for 5–25 s, mean value of ΔHbR for 5–25 s, mean value of ΔHbO for 0–peak time, slope of ΔHbO for 5–15 s, slope of ΔHbR for 5–15 s, slope of ΔHbO for 20–60 s, slope of ΔHbR for 20–60 s, slope of ΔHbO for 60–70 s, slope of ΔHbR for 60–70 s, slope of ΔHbO for 0–peak time, peak time itself, skewness of ΔHbO for 5–65 s, and kurtosis of ΔHbO for 5–65 s) were introduced for the statistical analysis and three brain regions (i.e., left, middle, and right prefrontal brain regions) were examined. Some of the features (e.g., mean value of ΔHbO for 5–65 s in the right prefrontal brain region with *N*-back task) indicated a significant difference ($p < 0.05$) between the MCI and HC groups. For classification, linear discriminant analysis (LDA) was used. The highest accuracy out of three mental tasks (i.e., *N*-back task, Stroop task, and VFT) was 76.67% from *N*-back and Stroop tasks, which were based on manually selected ROI channels. Also, we evaluated the *t*-map and connectivity map as image biomarkers. The CNN result based on *t*-maps of the *N*-back task achieved the best performance of 90.62%. Based upon these findings, the conclusion was that image biomarkers like *t*-map or connectivity map provide a better classification accuracy than digital biomarkers. Motivated on this, we will investigate whether the combined digital biomarkers on a given space (i.e., mean-value image in a specified time interval, or slope-value image in a specific time interval, etc.) can provide an improved classification accuracy than the *t*-map result obtained in the previous work.

In this study, we investigated 63 types of neural images based on temporal (3 types), spatial (39 types), and temporal-spatial (21 types) features of fNIRS signals, which were acquired based on three mental tasks—the *N*-back, Stroop, and verbal fluency tasks (VFT)—for the early detection of AD via a CNN. The temporal features refer to the raw ΔHbO in time series, neuroimaging in the spatial domain refers to the brain map generated at specific time points, and the temporal-spatial features represent temporal features (mean value, slope value, skewness, and kurtosis) in the spatial domain. To the best of the author's knowledge, this is the first fNIRS neuroimaging study integrating digital biomarkers in a spatial domain, in which the diagnosis performance for early AD detection via a DL approach has been explored.

METHODS

Figure 1 presents a diagram of the proposed system. fNIRS data were acquired while the subjects were performing the three aforementioned mental tasks. After the signal preprocessing, the ROI channels were selected for the subsequent steps. In the

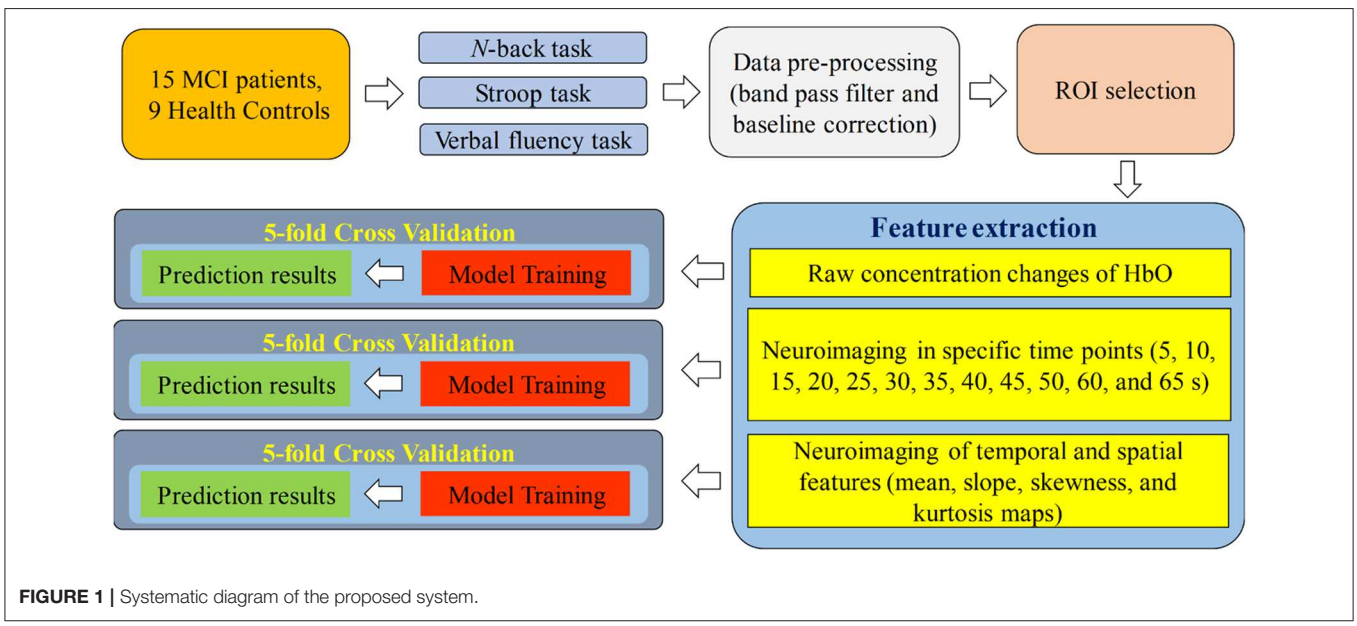

FIGURE 1 | Systematic diagram of the proposed system.

feature-extraction step, the raw concentration changes in HbO, neuroimaging at a specific time point (i.e., 5, 10, 15, 20, 25, 30, 35, 40, 45, 50, 55, 60, and 65 s) in the spatial domain and neuroimaging of temporal features (mean value of ΔHbO for 5–65 s, mean value of ΔHbO for 5–25 s, slope of ΔHbO for 5–15 s, slope of ΔHbO for 20–60 s, slope of ΔHbO for 60–70 s, skewness of ΔHbO for 5–65 s, and kurtosis of ΔHbO for 5–65 s) in the spatial domain were generated for training the CNN model separately. Finally, 5-fold cross-validation was employed to assess the performance of the CNN model trained by the features mentioned above.

Participants

In this study, 15 MCI patients (1 male and 14 females) and 9 HCs (2 males and 7 females) were recruited from the Pusan National University Hospital (Busan, South Korea). All 24 subjects are right-handed, able to communicate in Korean, similar ages, and educational backgrounds. The mental health state of each participant was assessed using three criteria: the Korean-mini-mental state examination (K-MMSE) (Han et al., 2008), the Seoul Neuropsychological Screening Battery (Ahn et al., 2010), and magnetic resonance imaging (MRI) data. **Table 1** shows the summarized demographic information for 24 participants, comprising age (mean ± SD), gender, educational background (mean ± SD), statistical information, and K-MMSE scores (mean ± SD). The experiment was performed consistently with the approval of the Pusan National University Institutional Review Board (General Assembly of the World Medical Association, 2013). All the subjects were provided with a comprehensive explanation of the whole experimental contents before the start of the experiment. After the introduction, they were asked to write consent agreeing of the test.

TABLE 1 | Demographic information of participants.

Characteristics	MCI ($n = 15$)	HC ($n = 9$)	p-value[a]
Gender (Male/Female)	1/14	2/7	0.44
Education [years]	11.2 (±4.81)	10.56 (±2.88)	0.36
Age [years]	69.27 (±7.09)	68.33 (±4.69)	0.36
K-MMSE Score	25.13 (±2.33)	27.22 (±1.98)	0.49

K-MMSE, Korea Mini-Mental State Examination.
[a] *Two sample t-test with a significant level of 0.05.*

Experimental Paradigm

As shown in **Figure 2**, the experiment comprised three mental task sections, where each section consisted of three trials. In this study, the *N*-back task was used to assess working memory (Kane et al., 2007). The ability to inhibit cognition was evaluated by the Stroop task. This suppression occurs when the other attribute of the same stimulus simultaneously effects during the processing of a stimulus (McVay and Kane, 2009; Scarpina and Tagini, 2017). The performance of semantic verbal fluency task indicated the ability of the vocabulary size, lexical access speed, updating, and inhibition for each subject (Shao et al., 2014).

Participants were asked to sit on a comfortable chair and were directed to avoid movement. Each task trial took 60 s, and a 30 s rest was given between tasks. First, the subjects enjoyed a 10 m resting state before a task-based experiment section began. Then, they performed the 2-back version of the *N*-back task wherein a digital number between one and nine was randomly showed on the screen. When the current number matched the second to last number previously displayed on display, the participants were instructed to press the keyboard. The subjects were then asked to execute the Stroop task. The Korean-color word Stroop test (K-CWST) was utilized in this study. The participants were requested to read the color of letters within a limited time. Those letters were written by four different colors, i.e., red, blue, yellow, and black, respectively. Finally, the subjects executed the semantic VFT by generating as many words as possible within 1 min; the words should relate to the given semantic category. The amount of information of participants, which can be retrieved based on the categorization and memorial source of text during the limited time, were measured during this task.

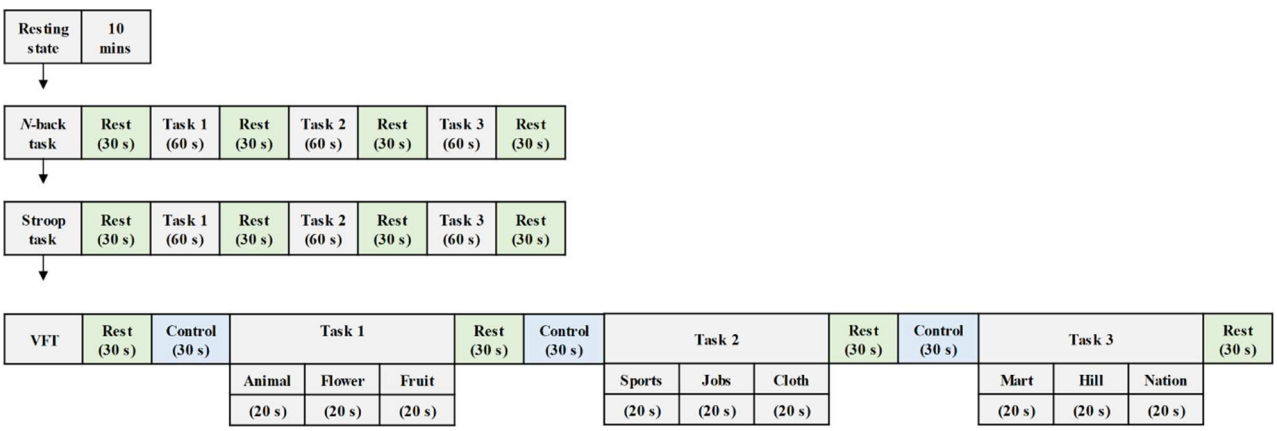

FIGURE 2 | Experiment paradigm for various mental tasks (i.e., *N*-back task, Stroop task, and verbal fluency task) during the examination.

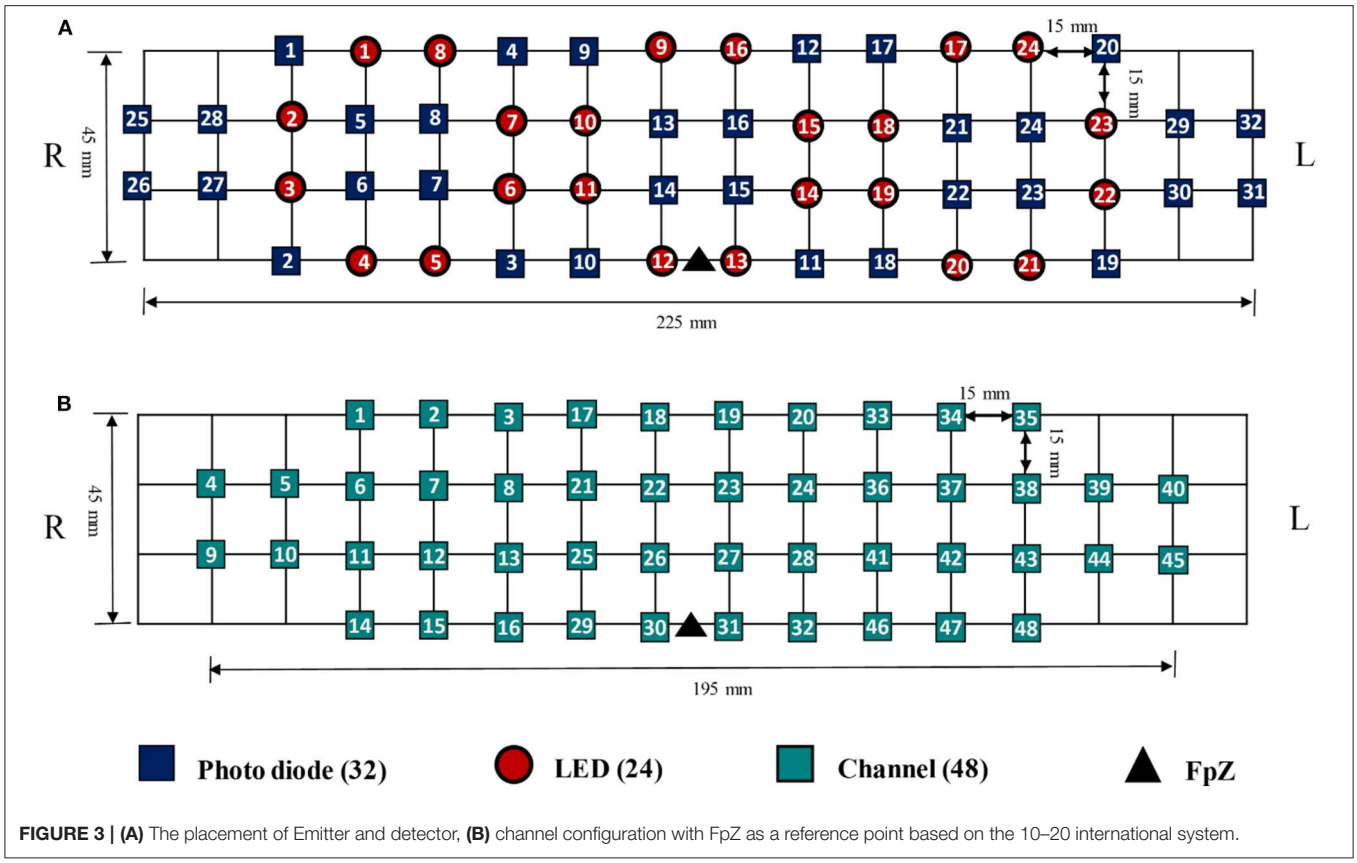

FIGURE 3 | (A) The placement of Emitter and detector, **(B)** channel configuration with FpZ as a reference point based on the 10–20 international system.

fNIRS Data Acquisition

The data utilized in this study were acquired by NIRSIT (OBELAB Inc., Rep. of Korea), which is a near-infrared multi-channel continuous wave system using a sampling rate of 8.138 Hz. The wavelengths employed for detecting two chromophores (i.e., oxygenated hemoglobin and deoxygenated hemoglobin) were 780 and 850 nm, respectively. A total of 24 emitters and 32 detectors, the placements of which are illustrated in **Figure 3A**, were used to measure the neural activation of the prefrontal cortex comprehensively. In total, 48 channels were selected for covering the entire prefrontal cortex. The channel configuration, illustrated in **Figure 3B**, was set up in accordance with the international 10–20 EEG system with the reference point FpZ. The pairs of emitter and detector (one channel) were placed 30 mm apart.

fNIRS Data Pre-processing

The modified Beer-Lambert law was utilized to convert the optical densities to ΔHbO and ΔHbR (Sassaroli and Fantini, 2004). The converted signals passed 4th-order Butterworth low- and high-pass filters (i.e., cutoff frequencies: 0.001 and 0.1 Hz, respectively) to remove physiological noise, i.e., cardiac noise−1 Hz, respiration−0.25 Hz, and Mayer signal−0.1 Hz (Naseer et al., 2016; Khan and Hong, 2017; Liu et al., 2018; Nguyen et al., 2018). In accordance with our previously published evaluation results (Yang et al., 2019) and the relevant literature (Hoshi, 2007), it was observed that ΔHbO is more sensitive and dependable than ΔHbR. Besides, ΔHbO shows a stronger correlation with the fMRI BOLD response than ΔHbR (Cui et al., 2011; Li et al., 2018a). Therefore, ΔHbO signals were used because their signal-to-noise ratio was higher than that of ΔHbR signals.

As the limitation of the spatial resolution (as compared to fMRI), the ROIs—the areas that are active during the mental task—must be estimated. ROI analyses have been widely as a means of testing prior hypotheses above brain function in fMRI and PET areas; they enhance the statistical power as compared to entire brain area analyses and facilitate comparisons through multiple participants (Mitsis et al., 2008). In this study, the ROI was defined by the weighting factor (t-value) between the desired hemodynamic response function (dHRF) and the fNIRS measurement. The measurement (y) can be represented by the linear relationship of the dHRF with the coefficients and the error (ε), as shown in Equation (1). The dHRF was generated by convoluting the canonical hemodynamic response function (using two gamma functions) with the stimulation duration (i.e., the 60 s task and 30 s rest period). The t-value (t) was calculated using the *robustfit* function of MATLAB^{TM}. The null hypothesis is $\beta_1 = 0$, and SE represents standard error. ROI channels (i.e., activated channel) were selected when the calculated t-value was higher than the critical t-value (tcrt =

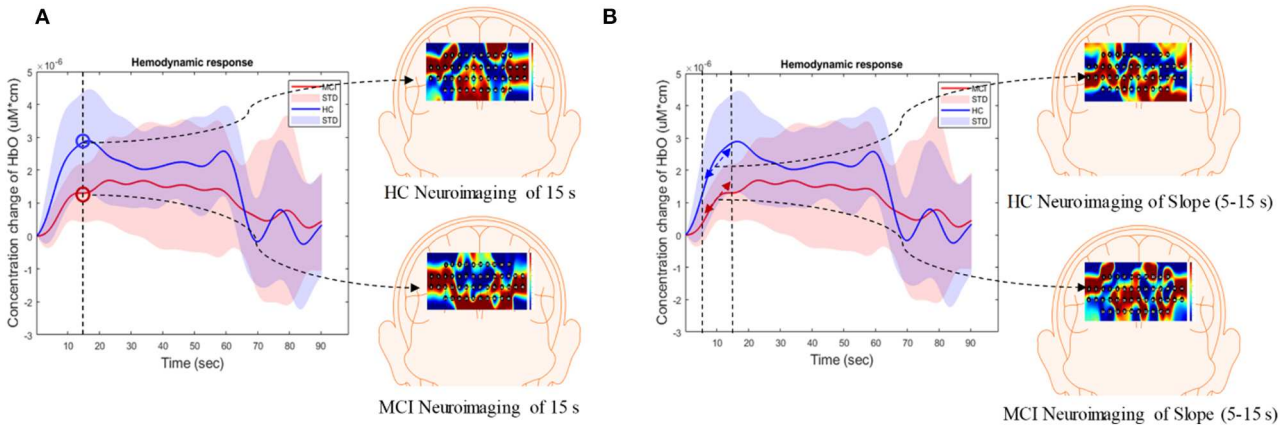

FIGURE 4 | Overview of **(A)** spatial features and **(B)** temporal-spatial features using the hemodynamic response of ΔHbO.

1.9632). The critical *t*-value was computed by the degree of freedom of the signals and statistical significance ($p < 0.05$ for two-sided tests).

$$y = \left[1\ dHRF\right]\begin{bmatrix}\beta_0\\ \beta_1\end{bmatrix} + \varepsilon, \tag{1}$$

$$t = \left[\frac{\beta_0}{SE\,(\beta)}, \frac{\beta_1}{SE\,(\beta)}\right]. \tag{2}$$

Feature Extraction

In this study, the extracted features were divided into three categories: temporal, spatial, and temporal-spatial features. Temporal features referred to the raw ΔHbO in the time series and were considered to contain the concentration change in ΔHbO with time. The spatial feature describes neuroimaging at the specific time points. In this study, we selected 13 time points (i.e., 5, 10, 15, 20, 25, 30, 35, 40, 45, 50, 55, 60, and 65 s) to create the neural image for comparison purposes. The spatial feature indicates the neural activation at a specific time point in the spatial domain (prefrontal brain cortex). **Figure 4A** illustrates an example of neuroimaging at the 15 s time point. In this study, the selected time windows between 5 and 65 s were considered the effect of initial time delay (3–5 s) during the hemodynamic response.

The temporal-spatial feature expresses the temporal information (mean value of ΔHbO for 5–65 s, mean value of ΔHbO for 5–25 s, slope of ΔHbO for 5–15 s, slope of ΔHbO for 20–60 s, slope of ΔHbO for 60–70 s, skewness of ΔHbO for 5–65 s, and kurtosis of ΔHbO for 5–65 s) in the spatial domain as shown in **Figure 5**. In other words, they display the values of specific time points according to the channel placement in the prefrontal cortex. **Figure 4B** illustrates the neuroimaging of the slope map for the period between 5 and 15 s. The mean value distinguishes the difference in the neural activation of the MCI and HC. Since the initial peak time of the hemodynamic response typically occurs during the time windows of the first 20 s, the time interval of 5–25 s was chosen. The slope features, i.e., the slope maps of 5–15 s, 20–60 s, and 60–70 s, were selected based on the characteristic from three intervals of the hemodynamic response: the initial increasing, plateau, and final period of ΔHbO, i.e., 5–15 s, 20–60 s, and 60–70 s, respectively. The slope indicates the difference in speed of activation between two groups, MCI and HC. Lastly, the difference in the asymmetry and the point of the probability distribution were measured by skewness (i.e., from 5 to 65 s) and kurtosis (i.e., from 5 to 65 s). These measurements are intended to investigate the overall difference of hemodynamic responses between MCI patients and HCs. All temporal information (mean, slope, skewness, and kurtosis) was determined by utilizing functions of *mean*, *polyfit*, *skewness*, and *kurtosis*, respectively, based on the MATLAB™.

Convolutional Neural Network

CNN is a special type of feedforward neural network. It takes advantage of local spatial coherence in the input, which allows the model to include fewer weights because of the parameter-sharing strategy (Cecotti and Gräser, 2011; Kim and Choi, 2019; Oh et al., 2019). In addition, CNN can learn features automatically from the input images by adjusting the parameters to minimize classification errors (Trakoolwilaiwan et al., 2017; Liu and Stathaki, 2018; Moon et al., 2018). Typically, CNN comprises convolutional, activation, pooling, and fully connected layers (Yi et al., 2018; Kim et al., 2019). Convolutional layers are the crucial component of CNN. Suppose the input is X with the 2-dimensional image ($h \times w$), and the weight matrices (called kernels) have the size ($k_1 \times k_2$), the local input region X_i can be converted to feature map (Y_j) as shown in Equation (3), and size is $y_1 \times y_2$.

$$Y_j = f\left(\sum X_i \bullet K_j + \beta_j\right), \tag{3}$$

where ($\bullet$) denotes the convolution operator, and β_j is the bias term. One feature map (Y_j) would be generated based on the

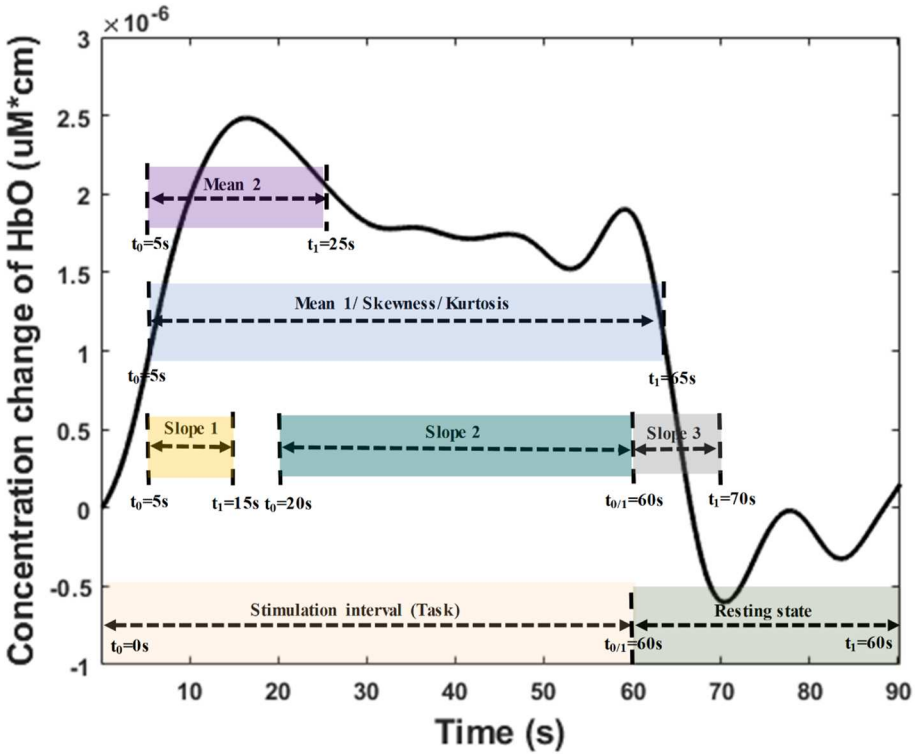

FIGURE 5 | Time interval distribution of the temporal features (i.e., mean, slope, skewness, and kurtosis) for temporal-spatial neural images generation.

sharing parameters of the *j*-th kernel with stride *s*. Thus, the size of the feature map can be calculated by using:

$$y_1 = \frac{h - k_1 + 2 \times p}{s} + 1\,, \tag{4}$$

$$y_2 = \frac{w - k_2 + 2 \times p}{s} + 1\,, \tag{5}$$

where *p* refers to the parameter of zero padding. This parameter is applied to keep the size of the output and input the same by padding the input edges with zeros. The activation layers are utilized after the convolutional layer. Typically, a non-linear transfer function called rectified linear units (*ReLu*) is widely used to achieve a better performance in regard to generalization and learning time (Yarotsky, 2017; Ieracitano et al., 2018). The function is shown in Equation (6). Thus, the feature map transfers the negative activation to be zero.

$$f(x) = max(o, x)\ . \tag{6}$$

There are two options in the pooling layer—average pooling and maximum pooling—that are used to reduce the resolution of the input feature map. As discussed in the literature (Sun et al., 2017), the effectiveness of maximum pooling is significantly superior to average pooling because of the ability to capture invariant features and better generalization performance. For this reason, we also employed maximum pooling in this study. The output ($z_1 \times z_2$) of the pooling layer is as follows:

$$z_1 = \frac{y_1 - p_1}{s_p} + 1, \tag{7}$$

$$z_2 = \frac{y_2 - p_2}{s_p} + 1, \tag{8}$$

where s_p is the stride of maximum pooling, and $p_1 = p_2$ represents the pooling size. Drop-out is applied for improving the CNN performance and avoiding overfitting. In this layer, the input and output are the same size. It is randomly initialized to turn the on or off of the corresponding neuron of the CNN at the beginning of the training iteration. As in the standard DL method, each neuron of a fully connected layer is connected with the previous layer. Since this is the issue of two group classification, there are two neurons for the last fully connected layer.

The architecture of the proposed CNN model contains four layers that two convolutional layers and two fully connected layers—as shown in **Figure 6**. In order for the input size to be consistent, the input neural image size is set to 200 × 200. The number of kernels is eight; the kernel size is 4 × 4; the size of the pooling area is 2 × 2; the value of the stride is 1. There were 128 neurons in the first fully connected layer with the activation function of *ReLu*. The loss function employed is categorical

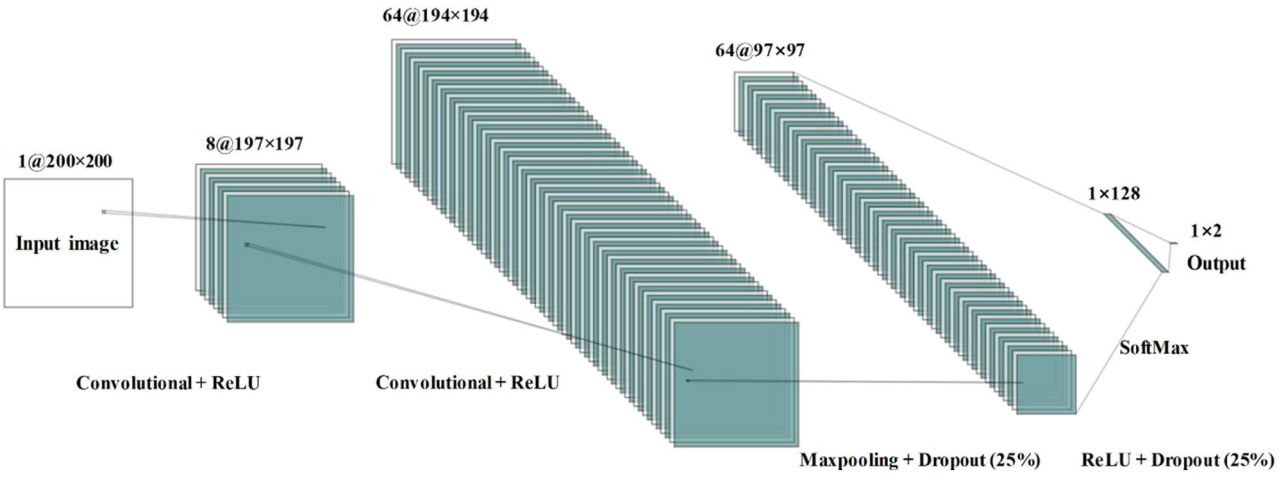

FIGURE 6 | Convolutional neural network architecture used during the study for mild cognitive impairment and healthy control classification.

TABLE 2 | Number of ROI channels of each subject for three mental tasks (i.e., *N*-back task, Stroop task, and verbal fluency task).

Subject	*N*-back task			Stroop task			Verbal fluency task		
	Trial 1	Trial 2	Trial 3	Trial 1	Trial 2	Trial 3	Trial 1	Trial 2	Trial 3
1	17	23	29	31	33	36	39	27	37
2	32	26	19	23	19	15	28	32	32
3	36	33	39	32	34	35	19	32	31
4	23	31	18	12	12	18	6	23	20
5	10	37	32	20	9	8	11	16	18
6	21	22	16	12	25	22	27	34	24
7	16	30	21	13	38	23	40	37	27
8	15	15	25	9	17	16	19	31	29
9	27	27	20	21	33	22	18	11	17
10	35	10	30	38	7	24	40	41	24
11	40	36	35	39	33	38	28	35	39
12	31	28	28	19	30	21	11	22	8
13	44	31	35	37	35	24	3	22	34
14	26	22	28	38	10	6	28	22	31
15	35	1	30	36	25	13	3	17	30
16	23	8	11	19	30	21	25	17	25
17	8	16	9	20	14	15	22	29	27
18	47	26	41	8	17	20	42	39	40
19	28	40	27	41	15	14	21	19	15
20	23	14	1	31	30	30	1	27	46
21	16	28	38	20	3	3	33	28	28
22	40	2	2	6	10	12	10	30	31
23	30	43	21	13	30	18	20	24	31
24	21	31	47	36	48	24	36	35	43
Total	1,826			1,609			1,867		

cross-entropy. Adam optimization was used to select the adaptive learning rate and the parameters during gradient descent.

In this study, the CNN model may have suffered from an overfitting problem because of the limitation of the sample data. We employed 5-fold cross-validation to decrease the influence of this problem on the experiment results. The data were randomly divided into 5-folds. One subsample fold was selected to test the performance of the trained model, and the remaining 4-folds

were set to train the CNN model. This process was reiterated five times to ensure that each subsample was utilized as a validation set once.

RESULTS

Hemodynamic Response and Behavioral Result

As shown in **Table 1**, the statistical analysis of the behavioral measurement (i.e., the averaged K-MMSE score) was performed by two independent sample *t*-test with a significant level of 0.05. The result ($p = 0.49$) presents a negative correlation between the behavioral state and the real subject mental state. In this study, we analyzed 3,456 fNIRS channels (i.e., 24 subjects × 3 trials × 48 channels) for each task. As shown in **Table 2**, the total number of selected ROI channels (activated channels) was 1,826 (*N*-back task), 1,609 (Stroop task), and 1,867 (VFT). The percentage of activation/deactivation was calculated by dividing the number of the ROI channels by the total number of channels. Therefore, the percentages of activated patterns are 52.83% (*N*-back task), 46.56% (Stroop task), and 54.02% (VFT), respectively.

Figure 7 summarizes the averages and standard deviations (STDs) of the hemodynamic response from the ROI channels of the patients with MCI and the HCs during various mental tasks—*N*-back task, Stroop task, and VFT. The solid lines refer to the mean of the ΔHbO, and shaded areas represent the STD of ΔHbO among the subjects. To compare the unique patterns (i.e., an increase or a decrease) of the hemodynamic response of the HCs and the MCI individuals in the *N*-back task (MCI: solid magenta line and HC: solid green line), Stroop task (MCI: solid red line and HC: solid blue line), and VFT task (MCI: solid cyan line and HC: solid yellow line), respectively, we applied two independently sampled *t*-tests. The results indicate that the average hemodynamic response of MCI patients is significantly lower than that of HCs in the *N*-back task ($p < 0.001$) and VFT task ($p < 0.001$). In the Stroop task, the average hemodynamic change in MCI individuals appears to be similar to that of HCs ($p = 0.06825$).

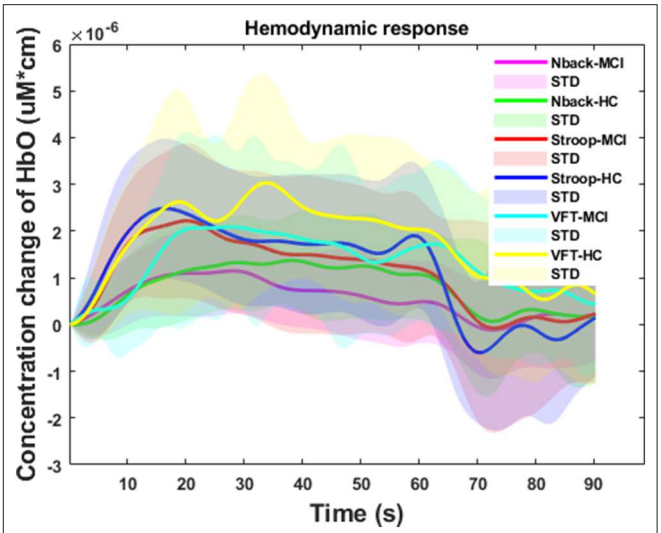

FIGURE 7 | Temporal feature of the ΔHbO for three mental tasks (i.e., *N*-back task, Stroop task, and verbal fluency task) for mild cognitive impairment and healthy control groups, respectively.

Neural Images in Spatial and Temporal-Spatial Domain

The results of the neuroimaging that was conducted based on the concentration change in oxygen-hemoglobin of the specific time point (i.e., 5, 10, 15, 20, 25, 30, 35, 40, 45, 50, 55, 60, and 65 s), are presented in **Figure 8**. The neural activation slightly changed over time in the entire prefrontal cortex. It is also easily observed that the MCI group displays a lower neural activation than the HCs in the three mental tasks. **Figure 9** illustrates the neuroimaging created by the temporal features (i.e., mean values from 5 to 65 s and from 5 to 25 s, slopes from 5 to 15 s, from 20 to 60 s, and from 60 to 70 s, skewness from 5 to 65 s, and kurtosis from 5 to 65 s) in the spatial domain. As compared to **Figure 8**, the patterns of the neural images of temporal features in the spatial domain area differ; for example, the neural images in **Figure 8** are highly correlated, and the neural images generated by each temporal feature in **Figure 9** have their individual characteristics. Interestingly, the neural images generated by the mean values also display the same patterns as characteristics generated by the specific time points. Among the three mental tasks, the VFT task shows the highest neural activation pattern in the HC group. The lowest neural activation is shown by the Stroop task in the MCI group. In addition, the neural images at 5 s among the six groups show lower neural firing than the neural images at 10 s and at other time points. In contrast, neural images at 60 s and previous time points show higher neural firing than those at 65 s.

CNN Results for Classification of Neural Images

The input dataset of the temporal feature contained 24 (subjects) × 3 (trials) × ROI channels. In the neural images in the spatial and temporal-spatial domain cases, each category had a dataset of size 24 (subjects) × 3 (trials). To verify the CNN's capability to classify MCI individuals and HCs, we utilized the standard metrics (accuracy, recall, precision, and F1-score) (Powers, 2011; Lin et al., 2018) to assess the results. Their definitions are

$$\text{Accuracy} = \frac{\text{TP} + \text{TN}}{\text{TP} + \text{TN} + \text{FP} + \text{FN}}, \tag{9}$$

$$\text{Recall} = \frac{\text{TP}}{\text{TP} + \text{FN}}, \tag{10}$$

$$\text{Precision} = \frac{\text{TP}}{\text{TP} + \text{FP}}, \tag{11}$$

$$\text{F1score} = 2 \times \frac{\text{Precision} \times \text{Recall}}{\text{Precision} + \text{Recall}}, \tag{12}$$

where TP, TN, FP, and FN represent the true positive, true negative, false positive, and false negative, respectively. In this study, TP indicated the number of MCI patients correctly

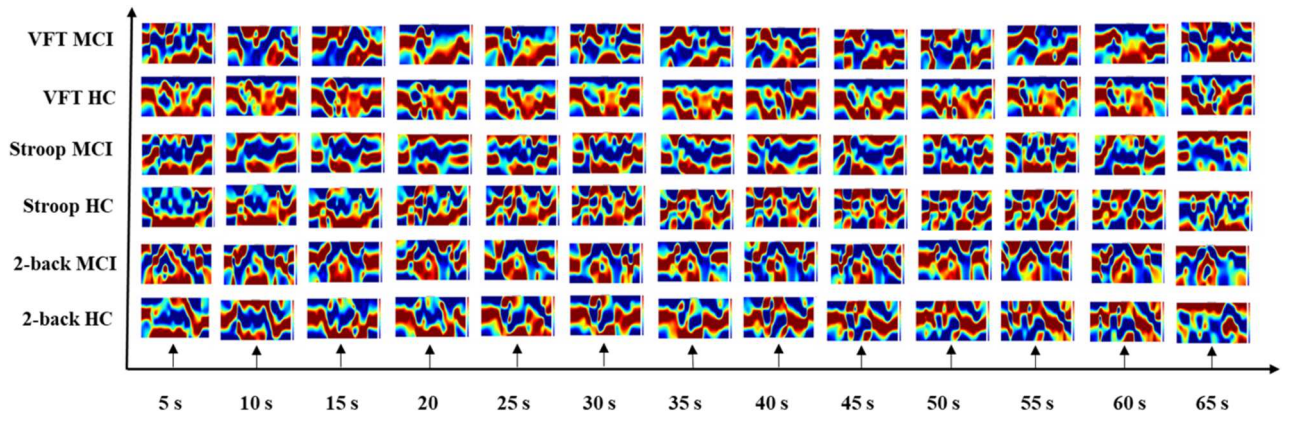

FIGURE 8 | Neuroimaging of specific time points (i.e., 5, 10, 15, 20, 25, 30, 35, 40, 45, 50, 55, 60, and 65 s) in spatial domain among three mental tasks (i.e., *N*-back task, Stroop task, and verbal fluency task).

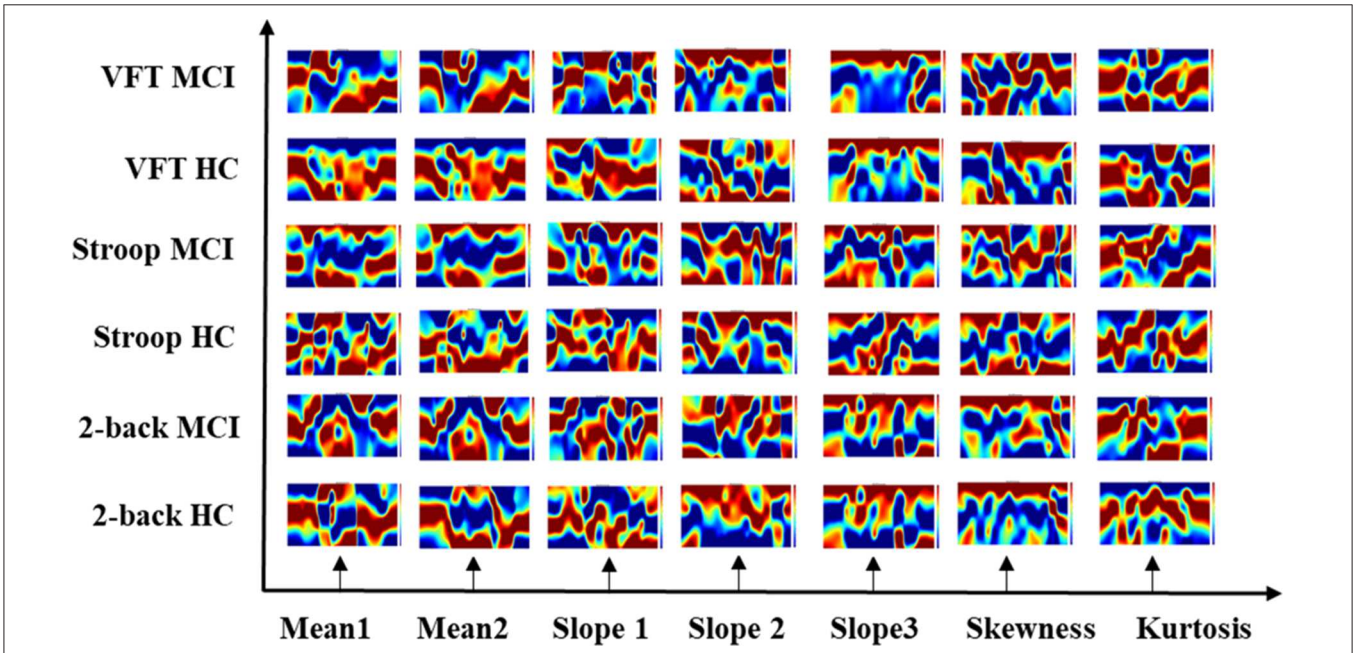

FIGURE 9 | Neuroimaging of temporal features (i.e., mean value from 5 to 65 s, mean value from 5 to 25 s, slope value from 5 to 15 s, slope value from 20 to 60 s, slope value from 60 to 70 s, skewness value from 5 to 65 s, and kurtosis from 5 to 65 s) in spatial domain.

classified; TN is the number of HCs identified correctly; FP refers to the number misclassified as MCI patients, and FN is the number misclassified as HCs.

The CNN results for the dataset extracted by the temporal domain are listed in **Table 3**. The average accuracy among the three mental tasks is 80.15% with an STD of 3.95%, and the results of recall, precision, and F1-score are 73.26% (4.10%), 64.23% (6.63%), and 67.48% (5.40%), respectively. Stroop achieved a higher accuracy rate than both the *N*-back task and VTF: 84.70%.

Tables 4–**6** depicts the CNN's performance for neural images at various time points in the spatial domain of the *N*-back task, Stroop task, and VFT, respectively. CNN's classification performance is divided into four different categories, as mentioned previously: accuracy (%), recall (%), precision (%), and F1-score (%). Furthermore, for each category, the results for specific time points are shown in the first column. **Table 4** represents CNN classification results of the *N*-back task. For the *N*-back task, the accuracy rate ranges from 65.28 to 93.06%, recall from 55.66 to 60%, precision from 41.11 to 86.43%, and F1-score from 46.34 to 87.83%. The classification result at the 15 s time point shows the best performance. The average accuracy rate is 82.59%. In the Stroop task case (shown in **Table 5**), the best performance appeared at the 60 s time point. Interestingly, this is consistent with the results for the hemodynamic response in

TABLE 3 | Convolutional neural network results of the temporal features among three mental tasks (i.e., *N*-back task, Stroop task, and verbal fluency task).

Task	Accuracy (%)	Recall (%)	Precision (%)	F1-score (%)
N-back task	77.90	70.00	58.95	63.22
Stroop task	84.70	77.87	71.67	73.55
VFT	77.84	71.91	62.07	65.66
Average	80.15	73.26	64.23	67.48
STD	3.95	4.10	6.63	5.40

TABLE 4 | Convolutional neural network classification results of neuroimaging with spatial features for the *N*-back task.

Features	Accuracy (%)	Recall (%)	Precision (%)	F1-score (%)
HbO map at 5 s	77.78	70.00	58.86	63.15
HbO map at 10 s	91.67	90.00	86.00	87.50
HbO map at 15 s	93.06	90.00	86.43	87.83
HbO map at 20 s	84.72	80.00	72.43	75.33
HbO map at 25 s	76.39	70.00	58.43	62.83
HbO map at 30 s	77.78	70.00	58.43	62.83
HbO map at 35 s	77.78	70.00	58.43	62.83
HbO map at 40 s	91.67	90.00	86.00	87.50
HbO map at 45 s	77.78	70.00	58.43	62.83
HbO map at 50 s	93.06	90.00	86.43	87.83
HbO map at 55 s	84.72	80.00	72.43	75.33
HbO map at 60 s	65.28	55.66	41.11	46.34
HbO map at 65 s	81.94	78.00	71.00	73.36
Average	82.59	77.20	68.80	71.96

TABLE 5 | Convolutional neural network classification results of neuroimaging with spatial features for the Stroop task.

Features	Accuracy (%)	Recall (%)	Precision (%)	F1-score (%)
HbO map at 5 s	76.86	70.00	58.43	62.83
HbO map at 10 s	90.57	88.89	84.33	86.00
HbO map at 15 s	83.43	78.89	70.76	73.83
HbO map at 20 s	75.43	68.89	56.76	61.33
HbO map at 25 s	84.86	80.00	72.43	75.33
HbO map at 30 s	92.00	90.00	86.00	87.50
HbO map at 35 s	78.57	70.00	59.28	63.48
HbO map at 40 s	84.86	80.00	72.43	75.33
HbO map at 45 s	84.00	80.00	72.00	75.00
HbO map at 50 s	85.71	80.00	72.86	75.65
HbO map at 55 s	92.86	90.00	86.43	87.83
HbO map at 60 s	98.57	98.89	98.33	98.50
HbO map at 65 s	77.71	70.00	58.86	63.15
Average	85.03	80.43	72.99	75.83

TABLE 6 | Convolutional neural network classification results of neuroimaging with spatial features for the VFT task.

Features	Accuracy (%)	Recall (%)	Precision (%)	F1-score (%)
HbO map at 5 s	91.43	88.89	84.76	86.33
HbO map at 10 s	77.71	70.00	58.86	63.15
HbO map at 15 s	92.00	90.00	86.00	87.50
HbO map at 20 s	70.57	60.00	45.29	50.98
HbO map at 25 s	77.71	70.00	58.86	63.15
HbO map at 30 s	84.86	80.00	72.43	75.33
HbO map at 35 s	77.71	70.00	58.86	63.15
HbO map at 40 s	78.57	70.00	59.29	63.48
HbO map at 45 s	84.86	80.00	72.43	75.33
HbO map at 50 s	92.00	90.00	86.00	87.50
HbO map at 55 s	78.57	70.00	59.29	63.48
HbO map at 60 s	84.86	80.00	72.43	75.33
HbO map at 65 s	77.71	70.00	58.86	63.15
Average	82.20	76.07	67.18	70.60

Figure 7, i.e., there is a peak at the 60 s time point in the case of the Stroop task. The lower accuracies occur at 5 s (76.86%), 20 s (75.43%), 35 s (78.57%), and 65 s (77.71%). The average accuracy is 85.03%. In contrast, at the 60 s time point, the worst results (65.28%) were obtained in the Stroop task. The higher accuracies appear at the time points of 5 s (91.43%), 15 s (92.00%), and 50 s (92.00%) during the VFT task (shown in **Table 6**). These results are in accordance with the hemodynamic response in **Figure 7** (solid yellow line and cyan solid line). The average accuracy is 82.20%. Among the results of the three mental tasks, the four verifying factors are always congruent. This means that when the accuracy rate is higher, the values of the corresponding recall, precision, and F1-score are also higher. For instance, when the highest accuracy is 98.57%, the highest recall (98.89%), precision (98.33%), and F1-score (98.50%) also appear for the same features.

The CNN classification results of neuroimaging of temporal features in the spatial domain are shown in **Tables 7**–**9**. The first column of "mean map (5:65 s)," "mean map (5:25 s)," "slope map (5:15 s)," "slope map (20:60 s)," "slope map (60:70 s)," "kurtosis map (5:65 s)," and "skewness map (5:65 s)" represents the neural map generated based on a mean value of 5–65 s, mean value of 5–25 s, slope value of 5–15 s, slope value of 20–60 s, slope value of 60–70 s, kurtosis of 5–65 s, and skewness of 5–65 s, respectively. In comparison, in the results of neural imaging of spatial features, the average accuracies are higher for all three mental tasks (i.e., *N*-back task: 89.46%, Stroop task: 88.00%, and VFT: 90.37%) as shown in **Tables 7**–**9**, respectively. In the *N*-back task, the highest accuracy (98.61%) occurred in the slope map from 20 to 60 s, and the lowest accuracy appeared in the mean map (5–25 s). The highest accuracy is 98.57% in the slope map (5–15 s) during the Stroop task, and the lowest accuracy is 77.71% in the slope map (20–60 s). For the VFT task, the accuracy range is from 84.86% (mean map during 5–65 s and skewness map) to 98.57% (mean map 5–25 s).

DISCUSSION

The objective of the study was to investigate the neuroimaging biomarkers and select the possible candidate biomarkers for

TABLE 7 | Convolutional neural network classification results of neuroimaging with temporal-spatial features for the *N*-back task.

Features	Accuracy (%)	Recall (%)	Precision (%)	F1-score (%)
Mean map (5:65 s)	84.72	80.00	72.43	75.33
Mean map (5:25 s)	76.39	70.00	58.43	62.83
Slope map (5:15 s)	91.67	90.00	86.00	87.50
Slope map (20:60 s)	98.61	98.89	98.33	98.50
Slope map (60:70 s)	92.86	90.00	86.42	87.83
Skewness map (5:65 s)	91.67	90.00	86.00	87.50
Kurtosis map (5:65 s)	90.28	88.89	84.33	86.00
Average	89.46	86.83	81.71	83.64

TABLE 8 | Convolutional neural network classification results of neuroimaging with temporal-spatial features for the Stroop task.

Features	Accuracy (%)	Recall (%)	Precision (%)	F1-score (%)
Mean map (5:65 s)	92.86	90.00	86.43	87.83
Mean map (5:25 s)	91.43	88.89	84.76	86.33
Slope map (5:15 s)	98.57	98.89	98.33	98.50
Slope map (20:60 s)	77.71	70.00	58.86	63.15
Slope map (60:70 s)	85.71	80.00	72.86	75.65
Skewness map (5:65 s)	84.86	80.00	72.43	75.33
Kurtosis map (5:65 s)	83.43	78.00	71.43	73.69
Average	87.80	83.68	77.87	80.07

TABLE 9 | Convolutional neural network classification results of neuroimaging with temporal-spatial features for the VFT task.

Features	Accuracy (%)	Recall (%)	Precision (%)	F1-score (%)
Mean map (5:65 s)	84.86	80.00	72.43	75.33
Mean map (5:25 s)	98.57	98.89	98.33	98.50
Slope map (5:15 s)	92.86	90.00	86.43	87.83
Slope map (20:60 s)	85.71	80.00	72.86	75.65
Slope map (60:70 s)	92.86	90.00	86.43	87.83
Skewness map (5:65 s)	92.86	90.00	86.43	87.83
Kurtosis map (5:65 s)	84.86	80.00	72.43	75.33
Average	90.37	86.98	82.19	84.04

the early detection of AD. To attain this goal, we examined neural images that were generated based on 3 temporal features, 13 spatial features, and 7 temporal-spatial features for training the CNN model, respectively. Finally, we suggest the use of two temporal-spatial features (mean map, slope map) for identification of MCI patients due to the high classification accuracy (90.37%, the averaged accuracy of VFT, **Table 9**). Especially, the slope map from 20 to 60 s with the *N*-back task achieved the highest accuracy of 98.61%, see **Table 7**, Slope map (20:60 s). It is the first study to assess neural images obtained by fNIRS signals for early AD detection. Furthermore, the results obtained for MCI detection constitute the highest diagnosis performance in fNIRS areas. Interpretable, non-invasive, reliable, low cost, and portable biomarkers are always the necessary tools for the identification of patients with MCI symptoms. The computer-aided neural imaging method could provide a novel direction for the clinical diagnosis of MCI.

fNIRS, a novel non-invasive neuroimaging modality, has proven its worth during the last decade, especially in the healthcare industries (Khan et al., 2018; Hong and Yaqub, 2019). The first article on the use of fNIRS for MCI detection appeared in 2006. This paper proposed that MCI patients show a decreased ΔHbO in the right parietal cortex during the VFT (Arai et al., 2006), and it was the first study to suggest fNIRS as a potential tool for screening AD/MCI. After 7 years, more related papers were published. One of the articles proved that the difference in ΔHbO of MCI individuals and HCs could also be measured in the prefrontal cortex (Doi et al., 2013). In addition, the ΔHbO during the resting state (Viola et al., 2013) and *N*-back task (Niu et al., 2013) also presents signs of neurodegeneration in the MCI group. In 2014, abnormal metabolisms of MCI were observed by some clinical research groups (Babiloni et al., 2014; Liu et al., 2014), such as the hypercapnia effect, global brain hypoperfusion, oxygen hypometabolism, and neurovascular decoupling. Later, the verification of neurodegeneration was also extended to the other cerebral brain regions, i.e., prefrontal cortex (Uemura et al., 2016; Yeung et al., 2016b; Vermeij et al., 2017) inferior frontotemporal cortex (Katzorke et al., 2018), and lateral prefrontal cortex (Marmarelis et al., 2017). Meanwhile, some researchers (Yeung et al., 2016a; Yap et al., 2017; Li et al., 2018a,b,c; Zeller et al., 2019) started to explore reliable biomarkers, i.e., complexity, number of activated channels, mean value of ΔHbO, time to reach peak value, and slope, and lateralization hyperactivation patterns. Interestingly, neurodegeneration symptoms similar to those mentioned above could be repeated. By virtue of these studies, novel directions for understanding the neurological information of MCI symptoms better were provided. Moreover, the relative results also proved that fNIRS is a promising tool for detecting the difference between MCI individuals and HCs. In this study, the hemodynamic responses (shown in **Figure 7**) of ΔHbO during three tasks, the *N*-back task, the Stroop task, and VFT, were consistent with the result of the researches (Yap et al., 2017; Li et al., 2018b) related to AD/MCI detection. Interestingly, the percentages of the activated channels (i.e., *N*-back: 52.83%, Stroop: 46.56%, and VFT: 54.02%) were similar to Mandrick et al. (2013), in which the percentage of activation in the prefrontal cortex during the mental and motor tasks was 51%. However, the provision of a diagnostic decision based on the group difference presents a challenge, because a high STD exists between the two groups.

As mentioned above, researchers prefer to observe the hemodynamic response in time series. Typically, the fluctuation of concentration changes in oxygenated hemoglobin provides evidence for differences in metabolism between the two groups. However, this technique suffers from at least two limitations. (1) Poor robustness: Because of the disturbance of the noise and some intrinsic physiological causes, there is a high possibility that some channels will not be activated or fully activated by noise (Birn, 2012; Wald and Polimeni, 2017).

To a large extent, the affected channel would influence the fluctuation of ΔHbO/ΔHbR. (2) Loss of information from the brain network: According to the recent literature (Fornito and Harrison, 2012), the neural disorder is associated with subtle abnormalities distributed throughout the brain. Studies have implied that the neurodegeneration arises from disordered interaction in the connected neural system rather than in the focal channel (Breakspear and Jirsa, 2007). Thus, neglecting the spatial (network level) domain would lead to a significant loss in terms of understanding better the symptom of neural disorders. This comparison was also evaluated in our previous publication (Yang et al., 2019). As our initial investigated indicated, the digital biomarkers, which were obtained based on ROI channels, showed lower accuracy than the image biomarkers (network level). Similarly, the difference of the hemodynamic response for the MCI and HC groups is easy to observe in the spatial domain, which is demonstrated in **Figures 8**, **9**.

To meet the demand for clinical diagnoses, it is crucial to converting the neural images into a form that allows an interpretable clinical decision (Martinez-Murcia et al., 2018). With the development of machine/deep learning methods, researchers have started to utilize machine/deep learning for identifying AD/MCI, because the natural images and brain images have similarities (Vieira et al., 2017). In the recent literature (Ieracitano et al., 2018; Ju et al., 2019), it was claimed that deep learning methods (e.g., CNN) would present a superiority for diagnosis for AD/MCI by using EEG and fMRI signals. Also, in our initial fNIRS study (Yang et al., 2019), we compared the statistical analysis, LDA, and CNN for identifying MCI patients from HCs. The results are consistent with the EEG (Ieracitano et al., 2018) and fMRI studies (Ju et al., 2019) that deep learning methods have a better performance than LDA/statistical analysis. Therefore, in this study, we employed the CNN and evaluated the temporal, spatial, temporal-spatial biomarkers for MCI diagnosis.

One of the first studies (Gupta et al., 2013) in which a CNN was applied to structural MRI data achieved classification accuracy rates of 94.7% for AD vs. HC and 86.4% for MCI vs. HC. Thus far, with the development of DL, the classification accuracy has reached a high accuracy for MRI (98/99%) (Khagi et al., 2019), EEG (98.4%) (Amezquita-Sanchez et al., 2016), and fMRI (97%) (Hojjati et al., 2018). According to the results shown in **Tables 4–9**, the average classification accuracy (i.e., *N*-back task: 89.46%, Stroop task: 88.00%, and VFT: 90.37%) in the temporal and spatial domain could prove that fNIRS is also a promising diagnostical modality. In comparison to our previous study, which utilized the image biomarkers (*t*-map and connectivity map) for MCI identification with fNIRS signals (Yang et al., 2019). Our current classification accuracy (highest accuracy: 98.61%) is further improved, and more reliable image biomarkers (e.g., mean map and slope map) are provided for the clinical diagnosis.

Among the three mental tasks, there was no significant difference based on the CNN classification performance. In comparison with the results of the mental task, the feature selection seems considerably more informative. The performance yielded by the temporal-spatial feature is superior to that yielded by the temporal and spatial features. According to our results, the temporal feature (i.e., the slope map between 5 and 15 s) always showed a good performance. The possible reason is the lower hemodynamic response of people with MCI during the initial stage of the task, which in turn explains why the slope value of the HC group increases faster than that of the MCI group. To reach a more reliable and precise decision, we suggest utilizing a combination of features.

Although the present study has proposed and evaluated the imaging biomarkers for MCI detection with the fNIRS signals using the CNN method (i.e., the highest accuracy was 98.61%), some limitations need be mentioned. First, the fNIRS signals were measured only from the prefrontal cortex, since the benefit of no hair in the prefrontal region can minimize the scattering and attenuation effects. A different result with different biomarkers might also be observed from other brain regions (e.g., the parietal cortex). Derosière et al. (2014) have shown that the parietal cortex revealed a better classification accuracy than the prefrontal cortex for attention state classification. Therefore, a combination of both prefrontal and parietal cortices will provide an improved classification accuracy for MCI case too. Second, the exact location of the FpZ reference point in the International 10–20 System might not have been observed consistently, because the fNIRS device (NIRSIT, OBELAB Inc., Republic of Korea) had fixed emitter-detector distances, and the head shapes of individual subjects were not the same. In addition, data augmentation might be another way to avoid CNN overfitting issues. In this study, we used two drop out layers to overcome the overfitting problem, and the loss plot showed that the overfitting did not appear. The data augmentation method will be considered in our future work to deal with the overfitting issue. For the investigation of the spatial feature, we randomly selected 13 specific time points as features for conducting the comparison. Because of the limitation of the computation, it is difficult to list all the time points (i.e., $8.138\,\text{Hz} \times 90\,\text{s} = 732$ points) and conduct the process as mentioned above. This limitation could be compensated by using a real-time analysis system or dividing more time segments by a shorter time window (i.e., 5–15 s). Likewise, in the temporal-spatial features, the time point selection also presents a challenge. In general, a neural image based on the first 15 s always yields a good accuracy level. Driving more time points in the time windows between 5 and 15 s would like to be done in future work to reduce the processing time. In the real clinical application, the biggest challenge is data training: However, once the model gets appropriately trained, the system can be used as a reliable tool for diagnosing MCI patients.

CONCLUSION

In this study, we highlighted the feasibility of using fNIRS for the early detection of AD by using neural imaging based

on the temporal, spatial, and temporal-spatial features. This systematically analyzed results indicate that neural imaging of the combined temporal and spatial features (i.e., the average accuracy of *N*-back: 89.46%, Stroop: 87.80%, and VFT: 90.37%) produces a more reliable performance than those when using temporal and spatial features separately. In particular, the slope map (20–60 s) during the *N*-back task achieved the highest accuracy of 98.61%. In the Stroop task and VFT case, the maximum accuracy is 98.57% by the slope map (5–15 s) and mean map (5–25 s). Besides that, all the mental tasks could achieve a good accuracy (>90%) within the time windows (5–15 s). This finding provides the possibility to use the short time windows for early detection of the AD. Conclusively, our results indicate that the CNN-aided temporal-spatial neuroimaging method could assist the clinical diagnosis of MCI. Additionally, the classification performance based on the spatial neural image also provides a possibility of reducing the diagnosis time in future studies.

DATA AVAILABILITY STATEMENT

The datasets generated for this study are available on request to the corresponding author.

ETHICS STATEMENT

The studies involving human participants were reviewed and approved by Pusan National University Institutional Review Board. The patients/participants provided their written informed consent to participate in this study.

AUTHOR CONTRIBUTIONS

DY conducted the data analysis and wrote the first draft of the manuscript. RH and S-HY participated in the initial data analysis. M-JS and JY interviewed the participants and managed the processes related to experimentation and interventions. Y-IS designed the initial experimental paradigm. K-SH suggested the theoretical aspects, corrected the manuscript, and supervised all the process from the beginning. All authors have approved the final manuscript.

FUNDING

This work was supported by the National Research Foundation (NRF) of Korea under the auspices of the Ministry of Science and ICT, Republic of Korea (Grant No. NRF-2017R1A2A1A17069430).

REFERENCES

Ahn, H. J., Chin, J., Park, A., Lee, B. H., Suh, M. K., Seo, S. W., et al. (2010). Seoul neuropsychological screening battery-dementia version (SNSB-D): a useful tool for assessing and monitoring cognitive impairments in dementia patients. *J. Korean Med. Sci.* 25, 1071–1076. doi: 10.3346/jkms.2010.25.7.1071

Alzheimer Association (2019). 2019 Alzheimer's disease facts and figures report. *Alzheimers Dement.* 15, 321–387. doi: 10.1016/j.jalz.2019.01.010

Amezquita-Sanchez, J. P., Adeli, A., and Adeli, H. (2016). A new methodology for automated diagnosis of mild cognitive impairment (MCI) using magnetoencephalography (MEG). *Behav. Brain Res.* 305, 174–180. doi: 10.1016/j.bbr.2016.02.035

Arai, H., Takano, M., Miyakawa, K., Ota, T., Takahashi, T., Asaka, H., et al. (2006). A quantitative near-infrared spectroscopy study: a decrease in cerebral hemoglobin oxygenation in alzheimer's disease and mild cognitive impairment. *Brain Cogn.* 61, 189–194. doi: 10.1016/j.bandc.2005.12.012

Babiloni, C., Vecchio, F., Altavilla, R., Tibuzzi, F., Lizio, R., Altamura, C., et al. (2014). Hypercapnia affects the functional coupling of resting state electroencephalographic rhythms and cerebral haemodynamics in healthy elderly subjects and in patients with amnestic mild cognitive impairment. *Clin. Neurophysiol.* 125, 685–693. doi: 10.1016/j.clinph.2013.10.002

Birn, R. M. (2012). The role of physiological noise in resting-state functional connectivity. *Neuroimage* 62, 864–870. doi: 10.1016/j.neuroimage.2012.01.016

Biswal, B. B., Mennes, M., Zuo, X. N., Gohel, S., Kelly, C., Smith, S. M., et al. (2010). Toward discovery science of human brain function. *Proc. Natl. Acad. Sci. U.S.A.* 107, 4734–4739. doi: 10.1073/pnas.0911855107

Breakspear, M., and Jirsa, V. K. (2007). Neuronal dynamics and brain connectivity. *Underst. Complex Syst.* 2007, 3–64. doi: 10.1007/978-3-540-71512-2_1

Cecotti, H., and Gräser, A. (2011). Convolutional neural networks for P300 detection with application to brain-computer interfaces. *IEEE Trans. Pattern Anal. Mach. Intell.* 33, 433–445. doi: 10.1109/TPAMI.2010.125

Cui, X., Bray, S., Daniel, M., Bryant, G. H., and Glover, A. L. R. (2011). A quantitative comparison of NIRS and fMRI across multiple cognitive tasks. *Neuroimage* 54, 2808–2821. doi: 10.1016/j.neuroimage.2010.10.069

Derosière, G., Dalhoumi, S., Perrey, S., Dray, G., and Ward, T. (2014). Towards a near infrared spectroscopy-based estimation of operator attentional state. *PLoS ONE* 9:e92045. doi: 10.1371/journal.pone.0092045

Doi, T., Makizako, H., Shimada, H., Park, H., Tsutsumimoto, K., Uemura, K., et al. (2013). Brain activation during dual-task walking and executive function among older adults with mild cognitive impairment: a fNIRS study. *Aging Clin. Exp. Res.* 25, 539–544. doi: 10.1007/s40520-013-0119-5

Ferrari, M., and Quaresima, V. (2012). A brief review on the history of human functional near-infrared spectroscopy (fNIRS) development and fields of application. *Neuroimage* 63, 921–935. doi: 10.1016/j.neuroimage.2012.03.049

Fornito, A., and Harrison, B. J. (2012). Brain connectivity and mental illness. *Front. Psychiatry* 3:72. doi: 10.3389/fpsyt.2012.00072

General Assembly of the World Medical Association (2013). World medical association declaration of helsinki: ethical principles for medical research involving human subjects. *JAMA-J. Am. Med. Assoc.* 310, 2191–2194. doi: 10.1001 / jama.2013.281053

Ghafoor, U., Kim, S., and Hong, K.-S. (2017). Selectivity and longevity of peripheral-nerve and machine interfaces: a review. *Front. Neurorobot.* 11:59. doi: 10.3389/fnbot.2017.00059

Ghafoor, U., Lee, J. H., Hong, K.-S., Park, S.-S., Kim, J., and Yoo, H.-R. (2019). Effects of acupuncture therapy on MCI patients using functional near-infrared spectroscopy. *Front. Aging Neurosci.* 11:237. doi: 10.3389/fnagi.2019.00237

Gordon, B. A., Blazey, T. M., Su, Y., Hari-Raj, A., Dincer, A., Flores, S., et al. (2018). Spatial patterns of neuroimaging biomarker change in individuals from families with autosomal dominant alzheimer's disease: a longitudinal study. *Lancet Neurol.* 17, 241–250. doi: 10.1016/S1474-4422(18)30028-0

Gupta, A., Ayhan, M. S., and Maida, A. S. (2013). "Natural image bases to represent neuroimaging data," in *Proceedings of the 30th International Conference on Machine Learning. (ICML'13), Vol.* 28 (Atlanta, GA), 2024–2031.

Han, C., Jo, S., Jo, I., Kim, E., Park, M., And, Y. K.-A., et al. (2008). An adaptation of the korean mini-mental state examination (K-MMSE) in elderly Koreans: demographic influence and population-based norms (the AGE study). *Elsevier* 47, 302–310. doi: 10.1016/j.archger.2007.08.012

Hebert, L. E., Weuve, J., Scherr, P. A., and Evans, D. A. (2013). Alzheimer disease in the United States (2010-2050) estimated using the 2010 census. *Neurology* 80, 1778–1783. doi: 10.1212/WNL.0b013e31828726f5

Hojjati, S. H., Ebrahimzadeh, A., Khazaee, A., and Babajani-Feremi, A. (2018). Predicting conversion from MCI to AD by integrating rs-fMRI and structural MRI. *Comput. Biol. Med*. 102, 30–39. doi: 10.1016/j.compbiomed.2018.09.004

Hong, K.-S., Aziz, N., and Ghafoor, U. (2018). Motor-commands decoding using peripheral nerve signals: a review. *J. Neural Eng.* 15:031004. doi: 10.1088/1741-2552/aab383

Hong, K.-S., Ghafoor, U., and Khan, M. J. (2020). Brain–machine interfaces using functional near-infrared spectroscopy: a review. *Artif. Life Robot*. 25, 204–218. doi: 10.1007/s10015-020-00592-9

Hong, K.-S., Naseer, N., and Kim, Y.-H. (2014). Classification of prefrontal and motor cortex signals for three-class fNIRS-BCI. *Neurosci. Lett.* 587, 87–92. doi: 10.1016/j.neulet.2014.12.029

Hong, K.-S., and Pham, P.-T. (2019). Control of axially moving systems: a review. *Int. J. Control. Autom. Syst.* 17, 2983–3008. doi: 10.1007/s12555-019-0592-5

Hong, K.-S., and Yaqub, M. A. (2019). Application of functional near-infrared spectroscopy in the healthcare industry: a review. *J. Innov. Opt. Heal. Sci.* 12:0930012. doi: 10.1142/S179354581930012X

Hong, K.-S., and Zafar, A. (2018). Existence of initial dip for BCI: an illusion or reality. *Front. Neurorobot*. 12:69. doi: 10.3389/fnbot.2018.00069

Hoshi, Y. (2007). Functional near-infrared spectroscopy: current status and future prospects. *J. Biomed. Opt.* 12:062106. doi: 10.1117/1.2804911

Ieracitano, C., Mammone, N., Bramanti, A., Hussain, A., and Morabito, F. C. (2018). A convolutional neural network approach for classification of dementia stages based on 2D-spectral representation of EEG recordings. *Neurocomputing* 323, 96–107. doi: 10.1016/j.neucom.2018.09.071

Iqbal, M., Rehan, M., and Hong, K.-S. (2018). Robust adaptive synchronization of ring configured uncertain chaotic FizHugh_Nagumo neurons under direction-dependent coupling. *Front. Neurorobot*. 12:6. doi 10.3389/fnbot.2018.00006

Irani, F., Platek, S. M., Bunce, S., Ruocco, A. C., and Chute, D. (2007). Functional near infrared spectroscopy (fNIRS): an emerging neuroimaging technology with important applications for the study of brain disorders. *Clin. Neuropsychol*. 21, 9–37. doi: 10.1080/13854040600910018

Jack, C. R., Bennett, D. A., Blennow, K., Carrillo, M. C., Dunn, B., Haeberlein, S. B., et al. (2018). NIA-AA research framework: toward a biological definition of alzheimer's disease. *Alzheimers Dement*. 14, 535–562. doi: 10.1016/j.jalz.2018.02.018

Jahani, S., Fantana, A. L., Harper, D., Ellison, J. M., Boas, D. A., Forester, B. P., et al. (2017). FNIRS can robustly measure brain activity during memory encoding and retrieval in healthy subjects. *Sci. Rep*. 7:9533. doi: 10.1038/s41598-017-09868-w

Ju, R., Hu, C., Zhou, P., and Li, Q. (2019). Early diagnosis of alzheimer's disease based on resting-state brain networks and deep learning. *IEEE/ACM Trans. Comput. Biol. Bioinform*. 16, 244–257. doi: 10.1109/TCBB.2017.2776910

Kane, M. J., Conway, A. R. A., Miura, T. K., and Colflesh, G. J. H. (2007). Working memory, attention control, and the n-back task: a question of construct validity. *J. Exp. Psychol. Learn. Mem. Cogn*. 33, 615–622. doi: 10.1037/0278-7393.33.3.615

Katzorke, A., Zeller, J. B. M., Müller, L. D., Lauer, M., Polak, T., Deckert, J., et al. (2018). Decreased hemodynamic response in inferior frontotemporal regions in elderly with mild cognitive impairment. *Psychiatry Res. Neuroimaging* 274, 11–18. doi: 10.1016/j.pscychresns.2018.02.003

Khagi, B., Kwon, G. R., and Lama, R. (2019). Comparative analysis of alzheimer's disease classification by CDR level using CNN, feature selection, and machine-learning techniques. *Int. J. Imaging Syst. Technol*. 29, 297–310. doi: 10.1002/ima.22316

Khan, M. J., Ghafoor, U., and Hong, K. S. (2018). Early detection of hemodynamic responses using EEG: a hybrid EEG-fNIRS study. *Front. Hum. Neurosci*. 12:479. doi: 10.3389/fnhum.2018.00479

Khan, M. J., and Hong, K.-S. (2017). Hybrid EEG-fNIRS-based eight-command decoding for BCI: Application to quadcopter control. *Front. Neurorobot*. 11:6. doi: 10.3389/fnbot.2017.00006

Khoury, R., and Ghossoub, E. (2019). Diagnostic biomarkers of alzheimer's disease: a state-of-the-art review. *Biomark. Neuropsychiatry* 1:100005. doi: 10.1016/J.BIONPS.2019.100005

Kim, H. H., Jo, J. H., Teng, Z., and Kang, D. J. (2019). Text detection with deep neural network system based on overlapped labels and a hierarchical segmentation of feature maps. *Int. J. Control. Autom. Syst*. 17, 1599–1610. doi: 10.1007/s12555-018-0578-8

Kim, S. H., and Choi, H.-L. (2019). Convolutional neural network for monocular vision-based multi-target tracking. *Int. J. Control. Autom. Syst*. 17, 2284–2296. doi: 10.1007/s12555-018-0134-6

Kumar, A., Fang, Q., Fu, J., Pirogova, E., and Gu, X. (2019). Error-related neural responses recorded by electroencephalography during post-stroke rehabilitation movements. *Front. Neurorobot*. 13:107. doi: 10.3389/fnbot.2019.00107

Li, R., Rui, G., Chen, W., Li, S., Schulz, P. E., and Zhang, Y. (2018a). Early detection of alzheimer's disease using non-invasive near-infrared spectroscopy. *Front. Aging Neurosci.* 10:366. doi: 10.3389/fnagi.2018.00366

Li, X., Wang, H., Long, J., Pan, G., He, T., Anichtchik, O., et al. (2018b). Systematic Analysis and Biomarker Study for Alzheimer's Disease. *Sci. Rep.* 8:17394. doi: 10.1038/s41598-018-35789-3

Li, X., Zhu, Z., Zhao, W., Sun, Y., Wen, D., Xie, Y., et al. (2018c). Decreased resting-state brain signal complexity in patients with mild cognitive impairment and alzheimer's disease: a multi-scale entropy analysis. *Biomed. Opt. Express* 9:1916. doi: 10.1364/BOE.9.001916

Lin, W., Tong, T., Gao, Q., Guo, D., Du, X., Yang, Y., et al. (2018). Convolutional neural networks-based MRI image analysis for the alzheimer's disease prediction from mild cognitive impairment. *Front. Neurosci.* 12:777. doi: 10.3389/fnins.2018.00777

Liu, J., Zhu, Y. S., Khan, M. A., Brunk, E., Martin-Cook, K., Weiner, M. F., et al. (2014). Global brain hypoperfusion and oxygenation in amnestic mild cognitive impairment. *Alzheimer's Dement.* 10, 162–170. doi: 10.1016/j.jalz.2013.04.507

Liu, T., and Stathaki, T. (2018). Faster R-CNN for robust pedestrian detection using semantic segmentation network. *Front. Neurorobot*. 12:64. doi: 10.3389/fnbot.2018.00064

Liu, X., Kim, C.-S., and Hong, K.-S. (2018). An fNIRS-based investigation of visual merchandising displays for fashion stores. *PLoS ONE* 13:e0208843. doi: 10.1371/journal.pone.0208843

Mamoshina, P., Vieira, A., Putin, E., and Zhavoronkov, A. (2016). Applications of deep learning in biomedicine. *Mol. Pharm*. 13, 1445–1454. doi: 10.1021/acs.molpharmaceut.5b00982

Mandrick, K., Derosiere, G., Dray, G., Coulon, D., Micallef, J. P., and Perrey, S. (2013). Prefrontal cortex activity during motor tasks with additional mental load requiring attentional demand: a near-infrared spectroscopy study. *Neurosci. Res*. 76, 156–162. doi: 10.1016/j.neures.2013.04.006

Marmarelis, V. Z., Shin, D. C., Tarumi, T., and Zhang, R. (2017). Comparison of model-based indices of cerebral autoregulation and vasomotor reactivity using transcranial doppler versus near-infrared spectroscopy in patients with amnestic mild cognitive impairment. *J. Alzheimers Dis.* 56, 89–105. doi: 10.3233/JAD-161004

Márquez, F., and Yassa, M. A. (2019). Neuroimaging biomarkers for alzheimer' s disease. *Mol. Neurodegener*. 14:21. doi: 10.1186/s13024-019-0325-5

Martinez-Murcia, F. J., Gorriz, J. M., Ramirez, J., and Ortiz, A. (2018). Convolutional neural networks for neuroimaging in parkinson's disease: is preprocessing needed? *Int. J. Neural Syst.* 28:1850035. doi: 10.1142/S0129065718500351

McVay, J. C., and Kane, M. J. (2009). Conducting the train of thought: working memory capacity, goal neglect, and mind wandering in an executive-control task. *J. Exp. Psychol. Learn. Mem. Cogn*. 35, 196–204. doi: 10.1037/a0014104

Mitsis, G. D., Iannetti, G. D., Smart, T. S., Tracey, I., and Wise, R. G. (2008). Regions of interest analysis in pharmacological fMRI: How do the definition criteria influence the inferred result? *Neuroimage* 40, 121–132. doi: 10.1016/j.neuroimage.2007.11.026

Moon, J., Kim, H., and Lee, B. (2018). View-point invariant 3D classification for mobile robots using a convolutional neural network. *Int. J. Control. Autom. Syst*. 16, 2888–2895. doi: 10.1007/s12555-018-0182-y

Mulders, P. C., van Eijndhoven, P. F., Schene, A. H., Beckmann, C. F., and Tendolkar, I. (2015). Resting-state functional connectivity in major depressive disorder: a review. *Neurosci. Biobehav. Rev*. 56, 330–344. doi: 10.1016/j.neubiorev.2015.07.014

Naseer, N., and Hong, K.-S. (2015). fNIRS-based brain-computer interfaces: a review. *Front. Hum. Neurosci.* 9:3. doi: 10.3389/fnhum.2015.00003

Naseer, N., Noori, F. M., Qureshi, N. K., and Hong, K.-S. (2016). Determining optimal feature-combination for LDA classification of functional near-infrared spectroscopy signals in brain-computer interface application. *Front. Hum. Neurosci.* 10:237. doi: 10.3389/fnhum.2016.00237

Nguyen, H.-D., and Hong, K.-S. (2016). Bundled-optode implementation for 3D imaging in functional near-infrared spectrsosocpy. *Biomed. Opt. Express* 7, 3491–3507. doi: 10.1364/BOE.7.003491

Nguyen, H.-D., Hong, K.-S., and Shin, Y.-I. (2016). Bundled-optode method in functional near-infrared spectroscopy. *PLoS ONE* 11:e0165146. doi: 10.1371/journal.pone.0165146

Nguyen, H.-D., Yoo, S. H., Bhutta, M. R., and Hong, K.-S. (2018). Adaptive filtering of physiological noises in fNIRS data. *Biomed. Eng. Online* 17, 4–9. doi: 10.1186/s12938-018-0613-2

Niu, H. J., Li, X., Chen, Y. J., Ma, C., Zhang, J. Y., and Zhang, Z. J. (2013). Reduced frontal activation during a working memory task in mild cognitive impairment: a non-invasive near-infrared spectroscopy study. *CNS Neurosci. Ther.* 19, 125–131. doi: 10.1109/SIBGRAPI.2001.963071

Oh, K., Chung, Y. C., Kim, K. W., Kim, W. S., and Oh, I. S. (2019). Classification and visualization of alzheimer's disease using volumetric convolutional neural network and transfer learning. *Sci. Rep.* 9:18150. doi: 10.1038/s41598-019-54548-6

Pamosoaji, A.-K., Piao, M., and Hong, K.-S. (2019). PSO-based minimum-time motion planning for multiple vehicles under acceleration and velocity limitations. *Int. J. Control. Autom. Syst.* 17, 2610–2623. doi: 10.1007/s12555-018-0176-9

Perpetuini, D., Bucco, R., Zito, M., and Merla, A. (2017). Study of memory deficit in alzheimer's disease by means of complexity analysis of fNIRS signal. *Neurophotonics* 5:011010. doi: 10.1117/1.nph.5.1.011010

Perrey, S. (2008). Non-invasive NIR spectroscopy of human brain function during exercise. *Methods* 45, 289–299. doi: 10.1016/j.ymeth.2008.04.005

Perrey, S. (2014). Possibilities for examining the neural control of gait in humans with fNIRS. *Front. Physiol.* 5:204. doi: 10.3389/fphys.2014.00204

Pfeifer, M. D., Scholkmann, F., and Labruyère, R. (2018). Signal processing in functional near-infrared spectroscopy (fNIRS): methodological differences lead to different statistical results. *Front. Hum. Neurosci.* 11:641. doi: 10.3389/fnhum.2017.00641

Powers, D. M. W. (2011). Evaluation: from precision, recall and f-measure to roc, informedness, markedness and correlation. *J. Mach. Learn. Technol.* 2, 37–63. doi: 10.9735/2229-3981

Ravi, D., Wong, C., Deligianni, F., Berthelot, M., Andreu-Perez, J., Lo, B., et al. (2017). Deep learning for health informatics. *IEEE J. Biomed. Heal. Informatics* 21, 4–21. doi: 10.1109/JBHI.2016.2636665

Santosa, H., Hong, M.-J., and Hong, K.-S. (2014). Non-lateralization with noise in the auditory cortex: an fNIRS study. *Front. Behav. Neurosci.* 8:418. doi: 10.3389/fnbeh.2014.00418

Sassaroli, A., and Fantini, S. (2004). Comment on the modified beer–lambert law for scattering media. *Phys. Med. Biol.* 49, N255–N257. doi: 10.1088/0031-9155/49/14/N07

Scarpina, F., and Tagini, S. (2017). The stroop color and word test. *Front. Psychol.* 8:557. doi: 10.3389/fpsyg.2017.00557

Shao, Z., Janse, E., Visser, K., and Meyer, A. S. (2014). What do verbal fluency tasks measure? *Predictors of verbal fluency performance in older adults. Front. Psychol.* 5:722. doi: 10.3389/fpsyg.2014.00772

Shin, J., and Im, C.-H. (2018). Performance prediction for a near-infrared spectroscopy-brain-computer interface using resting-state functional connectivity of the prefrontal cortex. *Int. J. Neural Syst.* 28:1850023. doi: 10.1142/S0129065718500235

Strangman, G., Boas, D. A., and Sutton, J. P. (2002). Non-invasive neuroimaging using near-infrared light. *Biol. Psychiatry* 52, 679–693. doi: 10.1016/S0006-3223(02)01550-0

Strimbu, K., and Tavel, J. (2010). What are biomarkers. *Curr. Opin. HIV AIDS* 5, 463–466. doi: 10.1097/COH.0b013e32833ed177

Sun, M., Song, Z., Jiang, X., Pan, J., and Pang, Y. (2017). Learning pooling for convolutional neural network. *Neurocomputing* 224, 96–104. doi: 10.1016/j.neucom.2016.10.049

Tanveer, M. A., Khan, M. J., Qureshi, M. J., Naseer, N., and Hong, K.-S. (2019). Enhanced drowsiness detection using deep learning: an fNIRS Study. *IEEE Access* 7, 137920–137929. doi: 10.1109/ACCESS.2019.2942838

Taylor, C. A., Greenlund, S. F., McGuire, L. C., Lu, H., and Croft, J. B. (2017). Deaths from alzheimer's disease — United States, 1999–2014. *Morb. Mortal. Wkly. Rep.* 66, 521–526. doi: 10.15585/mmwr.mm6620a1

Trakoolwilaiwan, T., Behboodi, B., Lee, J., Kim, K., and Choi, J.-W. (2017). Convolutional neural network for high-accuracy functional near-infrared spectroscopy in a brain–computer interface: three-class classification of rest, right-, and left-hand motor execution. *Neurophotonics* 5:011008. doi: 10.1117/1.NPh.5.1.011008

Uemura, K., Shimada, H., Doi, T., Makizako, H., Tsutsumimoto, K., Park, H., et al. (2016). Reduced prefrontal oxygenation in mild cognitive impairment during memory retrieval. *Int. J. Geriatr. Psychiatry* 31, 583–591. doi: 10.1002/gps.4363

Vermeij, A., Kessels, R. P. C., Heskamp, L., Simons, E. M. F., Dautzenberg, P. L. J., and Claassen, J. A. H. R. (2017). Prefrontal activation may predict working-memory training gain in normal aging and mild cognitive impairment. *Brain Imaging Behav.* 11, 141–154. doi: 10.1007/s11682-016-9508-7

Vieira, S., Pinaya, W. H. L., and Mechelli, A. (2017). Using deep learning to investigate the neuroimaging correlates of psychiatric and neurological disorders: methods and applications. *Neurosci. Biobehav. Rev.* 74, 58–75. doi: 10.1016/j.neubiorev.2017.01.002

Viola, S., Viola, P., Buongarzone, M. P., Fiorelli, L., and Litterio, P. (2013). Tissue oxygen saturation and pulsatility index as markers for amnestic mild cognitive impairment: NIRS and TCD study. *Clin. Neurophysiol.* 124, 851–856. doi: 10.1016/j.clinph.2012.11.013

Wald, L. L. and Polimeni, J. R., (2017). Impacting the effect of fMRI noise through hardware and acquisition choices - implications for controlling false positive rates. *Neuroimage.* 15, 15–22. doi: 10.1016/j.neuroimage.2016.12.057

Waytowich, N., Lawhern, V. J., Garcia, J. O., Cummings, J., Faller, J., Sajda, P., et al. (2018). Compact convolutional neural networks for classification of asynchronous steady-state visual evoked potentials. *J. Neural Eng.* 15:066031. doi: 10.1088/1741-2552/aae5d8

Wilcox, T., and Biondi, M. (2015). fNIRS in the developmental sciences. *Wiley Interdiscip. Rev. Cogn. Sci.* 6, 263–283. doi: 10.1002/wcs.1343

Yang, D., Hong, K.-S., Yoo, S.-H., and Kim, C.-S. (2019). Evaluation of neural degeneration biomarkers in the prefrontal cortex for early identification of patients with mild cognitive impairment: An fNIRS study. *Front. Hum. Neurosci.* 13:317. doi: 10.3389/fnhum.2019.00317

Yap, K. H., Ung, W. C., Ebenezer, E. G. M., Nordin, N., Chin, P. S., Sugathan, S., et al. (2017). Visualizing hyperactivation in neurodegeneration based on prefrontal oxygenation: a comparative study of mild alzheimer's disease, mild cognitive impairment, and healthy controls. *Front. Aging Neurosci.* 9:287. doi: 10.3389/fnagi.2017.00287

Yarotsky, D. (2017). Error bounds for approximations with deep ReLU networks. *Neural Netw.* 94, 103–114. doi: 10.1016/j.neunet.2017.07.002

Yeung, M. K., Sze, S. L., Woo, J., Kwok, T., Shum, D. H. K., Yu, R., et al. (2016a). Altered frontal lateralization underlies the category fluency deficits in older adults with mild cognitive impairment: a near-infrared spectroscopy study. *Front. Aging Neurosci.* 8:59. doi: 10.3389/fnagi.2016.00059

Yeung, M. K., Sze, S. L., Woo, J., Kwok, T., Shum, D. H. K., Yu, R., et al. (2016b). Reduced frontal activations at high working memory load in mild cognitive impairment: near-infrared spectroscopy. *Dement. Geriatr. Cogn. Disord.* 42, 278–296. doi: 10.1159/000450993

Yi, G., Mao, J. X., Wang, Y. N., Guo, S. Y., and Miao, Z. Q. (2018). Adaptive tracking control of nonholonomic mobile manipulators using recurrent neural networks. *Int. J. Control. Autom. Syst.* 16, 1390–1403. doi: 10.1007/s12555-017-0309-6

Yiannopoulou, K.-G., and Papageorgiou, S. G. (2013). Current and future treatments for alzheimer's disease. *Ther. Adv. Neurol. Disord.* 6, 19–33. doi: 10.1177/1756285612461679

Yoon, J. A., Kong, I. J., Choi, J., Baek, J. Y., Kim, E. J., Shin, Y.-I., et al. (2019). Neural compensatory response during complex cognitive function tasks in mild cognitive impairment: a near-infrared spectroscopy study. *Neural Plast.* 2019:7845104. doi: 10.1155/2019/7845104

Zafar, A., and Hong, K.-S. (2017). Detection and classification of three-class initial dips from prefrontal cortex. *Biomed. Opt. Express.* 8, 367–383. doi: 10.1364/BOE.8.000367

Zafar, A., and Hong, K.-S. (2018). Neuronal activation detection using vector phase analysis with dual threshold circles: a functional near-infrared spectroscopy study. *Int. J. Neural Syst*. 28:1850031. doi: 10.1142/S0129065718500314

Zafar, A., and Hong, K.-S. (2020). Reduction of onset delay in functional near-infrared spectroscopy: prediction of HbO/HbR signals. *Front. Neurorobot*. 14:10. doi: 10.3389/fnbot.2020.00010

Zeller, J. B. M., Katzorke, A., Müller, L. D., Breunig, J., Haeussinger, F. B., Deckert, J., et al. (2019). Reduced spontaneous low frequency oscillations as measured with functional near-infrared spectroscopy in mild cognitive impairment. *Brain Imaging Behav*. 13, 283–292. doi: 10.1007/s11682-018-9827-y

Conflict of Interest: The authors declare that the research was conducted in the absence of any commercial or financial relationships that could be construed as a potential conflict of interest.

frontiers in Aging Neuroscience

ORIGINAL RESEARCH
published: 26 May 2020
doi: 10.3389/fnagi.2020.00125

Brain Functional and Structural Signatures in Parkinson's Disease

Chunhua Liu[1†], Jiehui Jiang[1,2], Hucheng Zhou[1], Huiwei Zhang[3†], Min Wang[1], Juanjuan Jiang[1], Ping Wu[3], Jingjie Ge[3], Jian Wang[4], Yilong Ma[5] and Chuantao Zuo[3,6,7*]*

[1]Shanghai Institute for Advanced Communication and Data Science, Shanghai University, Shanghai, China, [2]Key Laboratory of Specialty Fiber Optics and Optical Access Networks, Joint International Research Laboratory of Specialty Fiber Optics and Advanced Communication, Shanghai University, Shanghai, China, [3]PET Center, Huashan Hospital, Fudan University, Shanghai, China, [4]Department of Neurology, Huashan Hospital, Fudan University, Shanghai, China, [5]Center for Neurosciences, Feinstein Institute for Medical Research, North Shore-Long Island Jewish Health System, Manhasset, NY, United States, [6]Institute of Functional and Molecular Medical Imaging, Fudan University, Shanghai, China, [7]Human Phenome Institute, Fudan University, Shanghai, China

The aim of this study is to explore functional and structural properties of abnormal brain networks associated with Parkinson's disease (PD). ^{18}F-Fluorodeoxyglucose positron emission tomography (^{18}F-FDG PET) and T1-weighted magnetic resonance imaging from 20 patients with moderate-stage PD and 20 age-matched healthy controls were acquired to identify disease-related patterns in functional and structural networks. Dual-modal images from another prospective subject of 15 PD patients were used as the validation group. Scaled Subprofile Modeling based on principal component analysis method was applied to determine disease-related patterns in both modalities, and brain connectome analysis based on graph theory was applied to verify these patterns. The results showed that the expressions of the metabolic and structural patterns in PD patients were significantly higher than healthy controls (PD1-HC, $p = 0.0039$, $p = 0.0058$; PD2-HC, $p < 0.001$, $p = 0.044$). The metabolic pattern was characterized by relative increased metabolic activity in pallidothalamic, pons, putamen, and cerebellum, associated with metabolic decreased in parietal–occipital areas. The structural pattern was characterized by relative decreased gray matter (GM) volume in pons, transverse temporal gyrus, left cuneus, right superior occipital gyrus, and right superior parietal lobule, associated with preservation in GM volume in pallidum and putamen. In addition, both patterns were verified in the connectome analysis. The findings suggest that significant overlaps between metabolic and structural patterns provide new evidence for elucidating the neuropathological mechanisms of PD.

Keywords: Parkinson's disease, brain network, pattern, ^{18}F-FDG PET, MRI

OPEN ACCESS

Edited by:
Nibaldo C. Inestrosa, Pontificia Universidad Católica de Chile, Chile

Reviewed by:
Jie Lu, Xuanwu Hospital, Capital Medical University, China
Cheng-Yu Wei, Chang Bing Show Chwan Memorial Hospital, Taiwan

***Correspondence:**
Jiehui Jiang
jiangjiehui@shu.edu.cn
Chuantao Zuo
zuochuantao@fudan.edu.cn

†These authors have contributed equally to this work

Received: *26 October 2019*
Accepted: *14 April 2020*
Published: *26 May 2020*

Citation:
Liu C, Jiang J, Zhou H, Zhang H, Wang M, Jiang J, Wu P, Ge J, Wang J, Ma Y and Zuo C (2020) Brain Functional and Structural Signatures in Parkinson's Disease. Front. Aging Neurosci. 12:125. doi: 10.3389/fnagi.2020.00125

INTRODUCTION

Parkinson's disease (PD) is a complex, chronic, and neurodegenerative disorder, pathologically characterized predominately by a loss of substantia nigra pars compacta dopaminergic neurons, manifesting in functional and structural alterations throughout the brain (Lee and Trojanowski, 2006; Choi et al., 2013; Rocha et al., 2018). Pathological studies have shown

that the cortical and subcortical regions are widely involved in PD pathology (Braak et al., 2003). Current efficient diagnostic tools for PD neuroimaging—including magnetic resonance imaging (MRI), positron emission tomography (PET), and single-photon emission computed tomography (SPECT)—rely on different principles that could be useful depending on the research or clinical setting available (Politis, 2014). In particular, ^{18}F-fluorodeoxyglucose positron emission tomography (^{18}F-FDG PET) has been used to localize and quantify abnormal brain energy metabolism *in vivo* and recently been used in metabolic connectivity studies to identify different disease-specific patterns (Titov et al., 2017). It is increasingly used in routine clinical practice (Teune et al., 2013). For instance, spatial covariance analysis of ^{18}F-FDG PET data consistently reveals the presence of a stereotyped spatial covariance pattern associated with different stages of motor symptoms in PD patients. The metabolic Parkinson's disease-related pattern (PDRP) associated with motor symptoms is characterized by increased metabolism in the putamen, globus pallidus, bilateral thalamus, and pontine, and relatively decreased metabolism in the premotor and parieto-occipital cortex (Ma et al., 2007; Eidelberg, 2009; Spetsieris and Eidelberg, 2011; Spetsieris et al., 2013; Wu et al., 2013; Ko et al., 2017; Tomše et al., 2017). The reproducibility of metabolic PDRP in different cohorts, according to the extensive literature, indicated that the metabolic PDRP was a reliable marker of disease across various ethnic groups and PET instrumentations as well as imaging protocols (Schindlbeck and Eidelberg, 2018). Moreover, the PDRP expression values (subject scores) from various studies have also shown significant positive correlations with disease progression and have decreased after effective treatments of motor symptoms (Huang et al., 2007; Peng et al., 2014b).

While metabolic PDRP can effectively reveal the abnormal metabolic function in PD, these functional abnormalities may also have corresponding changes in neuroanatomical structures. MRI, as a noninvasive examination and cost-effective imaging technique, has become more and more important to the study of neurodegenerative diseases, which revealed the structural and functional alterations underlying these conditions. For example, T1-weighted structural MRI is able to measure the volume/thickness alterations of the gray and white matters in the subcortical and cortical areas associated with PD (Wilson et al., 2019). Currently, imaging studies have provided preliminary evidence for structural abnormalities in the brain of PD patients, especially brain atrophy. Given that prolonged metabolic derangement causes atrophy, the spatial pattern of atrophy demonstrated an overlap with the metabolic PDRP topography, as well as with intrinsic networks present in healthy brain (Zeighami et al., 2015). However, it is still under speculation whether both spatial patterns of metabolic function and atrophy are effective to address PD progression at the same time.

In response to this issue, we explored the topographical relationship between both spatial patterns of metabolic function and atrophy. In addition, we also explored corresponding disease intrinsic networks defined using brain connectome analysis based on graph theory. This analysis method is an innovative approach that has revealed fundamental aspects of brain structural or functional network organization, and it can reveal abnormalities in network characteristics associated with neurological diseases and the potential impact of the disease network on brain information processing (Fox, 2018). Currently, graph theory in conjunction with spatial covariance analysis was used to examine the topology of disease networks in metabolic PDRP (Ko et al., 2017). The results in that study showed that disease networks defined by the spatial covariance analysis in PD patients exhibit exaggerated small world property, suggesting that it is more beneficial to elucidate the pathological basis of PD from the perspective of PD-related metabolic functional alterations in disease intrinsic networks. Nevertheless, it remains to be determined whether such alterations also occur in PD-related structural networks.

The primary objective of this work was to characterize inherently metabolic PDRP and structural PDRP together in PD patients and explore their correlations. A secondary aim was to explore whether the disease brain networks derived from metabolic or structural PDRP from graph theory has abnormal topological characteristics. We also hypothesized that there are abnormal topological characteristics in the disease structure and metabolic networks in the PD.

MATERIALS AND METHODS

Figure 1 provides the general framework of our study. First, both ^{18}F-FDG PET and T1-weighted structural MRI scans from PD1 and HC subjects in cohort A were analyzed using spatial covariance analysis to identify a significant region-of-interest (ROI)-based metabolic PDRP (PET-PDRP) topography and a structural PDRP (MRI-PDRP) topography. Both topographies and corresponding pattern expression values were compared with each other. Data from PD2 subjects in cohort B were used for a prospective evaluation of both metabolic and structural PDRPs in single cases. Second, based on the customized criteria, we identified some salient abnormal brain regions from the PET-PDRP or MRI-PDRP topographies as network nodes in the disease subspace, and the remaining regions constituted the nondisease subspace. Finally, to explore network properties in the disease and nondisease subspaces in PD patients, connectome analysis based on graph theory was performed from each group. We calculated the corresponding network metrics between the disease and nondisease subspace and compared differences in network metrics for the PD groups relative to the corresponding control values.

Subjects

This study included two different cohorts (cohort A and B) of healthy subjects and PD patients (**Table 1**). Cohort A included 20 nondemented patients with PD and 20 age-matched healthy controls recruited from Huashan Hospital (Shanghai, China) in one project conducted from January 2014 to September 2015. Cohort B included 15 nondemented patients with PD recruited from Huashan Hospital (Shanghai, China) in another project conducted from January 2013 to September 2013. All subjects in cohorts A and B underwent

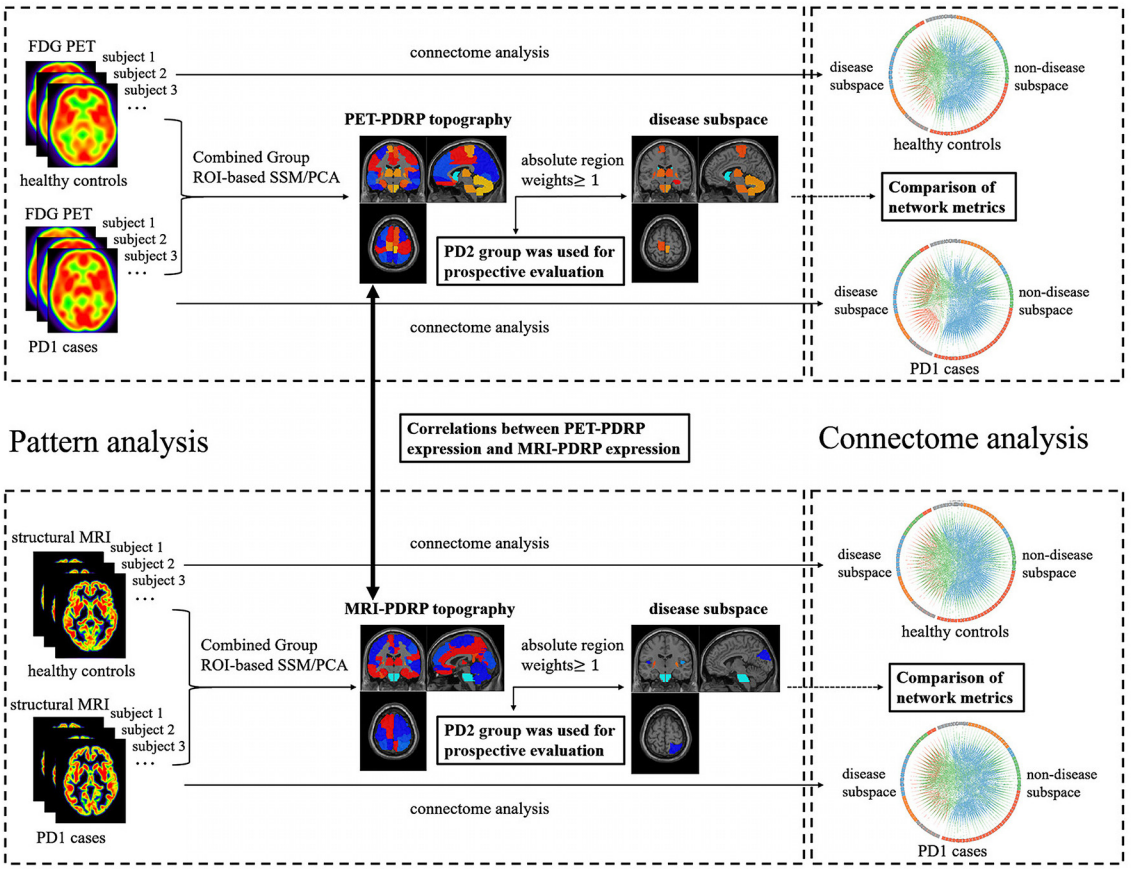

FIGURE 1 | The overall framework of the experimental process used in this study.

TABLE 1 | Demographic characteristics of PD patients and healthy controls.

	Cohort A		Cohort B	*p* value	
	HC	PD1	PD2		
N	20	20	15	PD1-HC	PD2-HC
Age (years)	59.6 ± 7.2	62.4 ± 7.3	62.8 ± 4.9	0.230[a]	0.148[a]
Gender (F/M)	12/8	10/10	3/12	0.525[b]	**0.018[b]**
UPDRS	-	21.6 ± 11.2	21.6 ± 10.5	-	-
Speech	-	0.5 ± 0.5	0.5 ± 0.5	-	-
Facial expression	-	1.2 ± 1.0	1.3 ± 1.0	-	-
Static tremor	-	2.2 ± 2.1	2.1 ± 2.3	-	-
Postural tremor	-	1.2 ± 1.1	1.1 ± 1.0	-	-
Rigidity	-	4.6 ± 3.6	4.1 ± 5.0	-	-
Gait	-	0.8 ± 0.6	0.8 ± 0.6	-	-
MMSE	-	28.8 ± 1.7	27.8 ± 1.9	-	-

Age and clinical rating are given as mean ± standard deviation. UPDRS, Unified Parkinson's Disease Rating Scale. [a]p value was obtained by the two-sample two-tailed t-test between healthy controls and PD patients. [b]p value was obtained by the χ^2 test between healthy controls and PD patients. Bold value indicated a significant difference between healthy controls and PD patients.

both ^{18}F-FDG PET and T1-weighted structural MRI scans. All patients were scanned and clinically examined by two senior neurologists specializing in dyskinesia before their inclusion in the study. The PD diagnosis was according to the United Kingdom Brain Bank criteria (Hughes et al., 1992). Patients with PD have no dementia, supranuclear gaze abnormalities, or ataxia, and are not caused by encephalitis or antipsychotic medication. The Unified Parkinson's Disease Rating Scale (UPDRS) motor examination was administered at least 12 h after the cessation of antiparkinsonian

medications. Mini-mental State Examination (MMSE) was administered synchronously.

All healthy controls received the same clinical scanning procedures as PD patients. Exclusion criteria for all subjects included: (a) primary psychiatric illness; (b) central nervous system comorbidities; and (c) abnormal neurological examination.

Ethical permission for the study was obtained from the Research Ethics Committee of Huashan Hospital, Shanghai, China (approval number: KY2013-336). Written informed consent was obtained from each subject after providing detailed instructions of the procedures.

Acquisition Protocol

^{18}F-FDG PET

All subjects underwent ^{18}F-FDG PET examination at resting state. PET scans were performed with a Siemens Biograph 64 HD PET/CT (Siemens, Germany) in three-dimensional (3D) mode. All subjects were fasted for at least 6 h before scanning. After intravenous injection of 185 MBq ^{18}F-FDG, the PET scan was started after a 45-min rest in a quiet and dimly lit environment. Prior to the PET scan, a low-dose CT transmission scan was performed for attenuation correction. The PET scan was performed in 3D mode for 10 min. All PET data were reconstructed using a 3D ordered subset expectation maximization algorithm and corrected for random coupling, scattering, and radioactive decay.

T1-Weighted Structural MRI

All MRI measurements were obtained on a 3-T GE Discovery MR750 Scanner (Milwaukee, WI, USA) equipped with a circular polarized eight-channel head matrix coil at the Department of Radiology of Huashan Hospital of Fudan University, China. High-resolution, T1-weighted, 3D anatomical brain images were obtained using an inversion recovery prepared fast spoiled gradient recalled sequence (repetition time = 11.1 ms; echo time = 5.0 ms; flip angle = 20°; matrix resolution = 256 × 256; voxel size = 1 × 1 × 1 mm^3; field of view = 240 mm^2; slice thickness = 1.0 mm; 146 slices without slice gap, transverse acquisition), with the scan range from the calvarium to foramen magnum.

Data Preprocessing

Data preprocessing for both PET and MRI images was done using Statistical Parametric Mapping 12 (the Wellcome Department of Neurology, London, UK) package implemented in Matlab2016b (Mathworks Inc.). First, ^{18}F-FDG PET scan for each subject was aligned with corresponding T1-weighted MRI scan. Second, MRI images were segmented into gray matter (GM), white matter (WM), and cerebrospinal fluid (CSF) tissue probability maps. Then, the GM map was registered to the Montreal Neurological Institute (MNI) stereotaxic template using nonlinear transformation parameters. The aligned PET image was also normalized to the MNI template using the same transformation parameters. Finally, the normalized MRI and PET images were smoothed equivalent to a convolution with an isotropic Gaussian kernel of 8 mm to increase signal-to-noise ratios.

Pattern Analysis

Pattern analysis was performed using ScanVP 7.0w package implemented in Matlab2016b[1] (Eidelberg, 2009; Spetsieris and Eidelberg, 2011). The PD-related covariance pattern was generated using ROI-based spatial covariance mapping algorithms known as Scaled Subprofile Modeling based on principal component analysis (SSM/PCA). In this step, the smoothed ^{18}F-FDG PET data from the combined PD1 patients and healthy subjects in cohort A was used as inputs. First, we performed a logarithmic transformation on the mean glucose metabolism within each region for each subject, and the subject × ROI data matrix was obtained. Second, the PCA was executed on the matrix to identify a disease-related spatial covariance pattern reflected major sources of variation. This pattern was a linear combination of selected principal components (PCs), so that the expression values corresponding to the pattern could maximally separate the PD patients from the control subjects. The number of PCs was determined by the lowest Akaike information standard (AIC) value in the logistic regression model. Third, the regional weights of the pattern were *z*-scored based upon the mean and standard deviation of all regions (Spetsieris et al., 2013). Therefore, the subject expression of this pattern in a prospective subject can be computed using an ROI-based topographic profile rating (TPR) algorithms (Eidelberg, 2009; Spetsieris et al., 2013). Finally, the resulting expression was *Z*-transformed using the subject expressions of the control subjects participating in the pattern identification. In this study, we preselected 95 ROIs. In addition to 90 ROIs from the automated anatomical labeling (AAL) atlas (Tzourio-Mazoyer et al., 2002), we also included five other regions where functional imaging studies in PD commonly report altered metabolism, including bilateral cerebellum, bilateral pons, and cerebellar vermis. The MRI images were analyzed by the same process as above.

As a result, a significant ROI-based metabolic PDRP (and structural) topography was identified from ^{18}F-FDG PET (and T1-weighted GM MRI) scans of combined PD1 and HC subjects in cohort A. Subject expressions of corresponding PDRP were then computed for all scans in the combined PD1 and HC subjects and *Z*-scored using subject expressions of the HC. We validated corresponding PDRP topography by computing its expression in the ^{18}F-FDG PET (and T1-weighted GM MRI) scans from PD2 subjects in cohort B. The corresponding PDRP expressions of PD2 subjects were *Z*-scored the same way as above and then compared with those of the original subjects in PD1 and HC. The diagnostic power of the corresponding PDRP expressions for discriminating PD patients from healthy controls was evaluated by the area under the curve (AUC) in the receiver operating characteristic (ROC) curves. ROC analysis in cohort B was obtained by comparing PD2 and HC groups. ROC analysis in cohorts A and B (cohort A + B) was obtained by comparing combined PD1 and PD2 groups compared to HC

[1] http://www.feinsteinneuroscience.org

group. We also evaluated whether the combination of PET-PDRP and MRI-PDRP expressions could improve diagnostic power. In addition, correlation analysis of corresponding PDRP expression and clinical ratings in PD patients in cohorts A and B were also performed.

Correlation Analysis Between PET-PDRP and MRI-PDRP Topographies

The metabolic and structural topographies were assessed by ROI-based correlation of regional weights in a set of salient abnormal brain regions. The correlation between the two patterns was calculated using only the regions with absolute values $\geq$1.0 (Ge et al., 2018). The pattern expression for PET-PDRP was also correlated with corresponding MRI-PDRP expression in combined PD1 (or PD2) and HC samples.

Brain Connectome Analysis

Graph theory was used to explore network properties in brain connectome analysis. Globally normalized glucose metabolism within each ROI was used to construct a region $\times$ region correlation matrix across each of three individual groups (PD1, PD2, and HC groups). In each correlation matrix, functional connectivity (FC) between each pair of regions was calculated by partial correlation coefficient between ROI values for local FDG uptake in each pair of regions, across participants, to conduct for the control of age and gender effects (Lo et al., 2010; Duan et al., 2017; Jiang et al., 2017). We used a sparsity (or named cost, representing present connections as a percentage of all possible connections) threshold to generate a series of undirected graphs (Baggio et al., 2014; Duan et al., 2017). The correlation matrices were thresholded at a range of sparsity thresholds, in 0.01 steps ($\text{sparsity}_{\text{min}}$: 0.01: $\text{sparsity}_{\text{max}}$). The minimum sparsity guaranteed that networks of all groups (HC, PD1, and PD2) were fully connected, and no nodes were fragmented. The maximum sparsity selected 0.5 because the randomness of the network larger than this threshold would increase, and the results would be unreliable (Hosseini et al., 2012). At each threshold, we calculated the following network metrics: (1) the clustering coefficient (C, quantification of the degree to which nodes in a graph tend to cluster together and a representation of network segregation, measuring the local information transmission capability in a network); (2) the characteristic path length (L, the average number of connections on the shortest path between any two regions in a network and a marker of network integration, measuring the global information transmission capability in a network); and (3) small worldness (S, the balance between local segregation and global integration).

Next, we divided the brain into disease subspace and nondisease subspace based upon the PET-PDRP topographies for further analysis. The nodes in the disease subspace consisted of the salient abnormal brain regions (absolute regional weight $\geq$1.0; high local contributions to overall PDRP activity) identified by the PDRP topography and the remaining regions constituting the nondisease subspace (absolute regional weight $<$1.0; low local contributions to overall PDRP activity). We calculated the corresponding network metrics among disease subspace, nondisease subspace, and whole brain, and we compared differences in network metrics for the PD1/PD2 groups relative to HC control values.

The graph theoretical analyses of brain structural network were the same as in the procedure for metabolic brain network but based on T1-weighted GM imaging data. It was worth noting that disease subspace and nondisease subspace in brain structural network were divided according to MRI-PDRP topography.

Brain connectome analysis was performed using Brain Connectivity Toolbox[2] and Graph Analysis Toolbox (Hosseini et al., 2012) implemented in Matlab2016b.

Statistical Analysis

Differences in PET-PDRP (and MRI-PDRP) expressions between patients and healthy controls were evaluated using two-sample t-tests. PDRP expressions of patients were correlated with corresponding MMSE, UPDRS, and six motor items (speech, facial expression, static tremor, postural tremor, rigidity, and gait) by computing Pearson's correlations. Regional weight and pattern expression between the two PDRPs identified in the ^{18}F-FDG PET scans and structural MRI scans was compared using Pearson's correlations. In order to determine the significance of the differences in network metrics between the patient group and HC group in each subspace, a permutation test repeated 1,000 times was used (Hosseini et al., 2012; Ko et al., 2017). All statistical tests were performed using Matlab2016b ($p < 0.05$, two-tailed).

RESULTS

Abnormal Disease Topographies in Pattern Analysis

PET-PDRP Identification and Validation

The ROI-based SSM/PCA multivariate analysis of ^{18}F-FDG PET data from cohort A investigated the first four PCs that explained 55.4% of the subject $\times$ ROI variance. The PET-PDRP topography generated from a linear combination of PC1, PC3, and PC4 with expression successfully discriminated PD1 patients and healthy controls, and produced the lowest AIC value in the logistic regression model. The pattern was characterized by relative increased metabolic activity in pallidothalamic, pons, bilateral putamen, and cerebellum, associated with metabolic decrease in parietal–occipital areas (**Figure 2A**). Subject expressions for the PET-PDRP topography were significantly elevated ($p = 0.0039$) in PD1 compared to HC subjects (**Figure 2B**). Significant increases in pattern expression were also seen in PD2 validation subjects with respect to HC control values ($p < 0.001$). Subject PET-PDRP expressions were without a difference between PD1 and PD2 subjects ($p = 0.097$). ROC analysis revealed an AUC = 0.74 (95% confidence intervals of 0.59–0.89; **Figure 2C**) to distinguish the PD patients from the controls in cohort A. The ROC curves also showed that PET-PDRP expression accurately distinguished PD patients from the control individuals in cohorts B and A + B. The AUC values were 0.88 (95% confidence intervals of 0.75–1.00) and 0.80 (95% confidence intervals of

[2]http://www.brain-connectivity-toolbox.net/

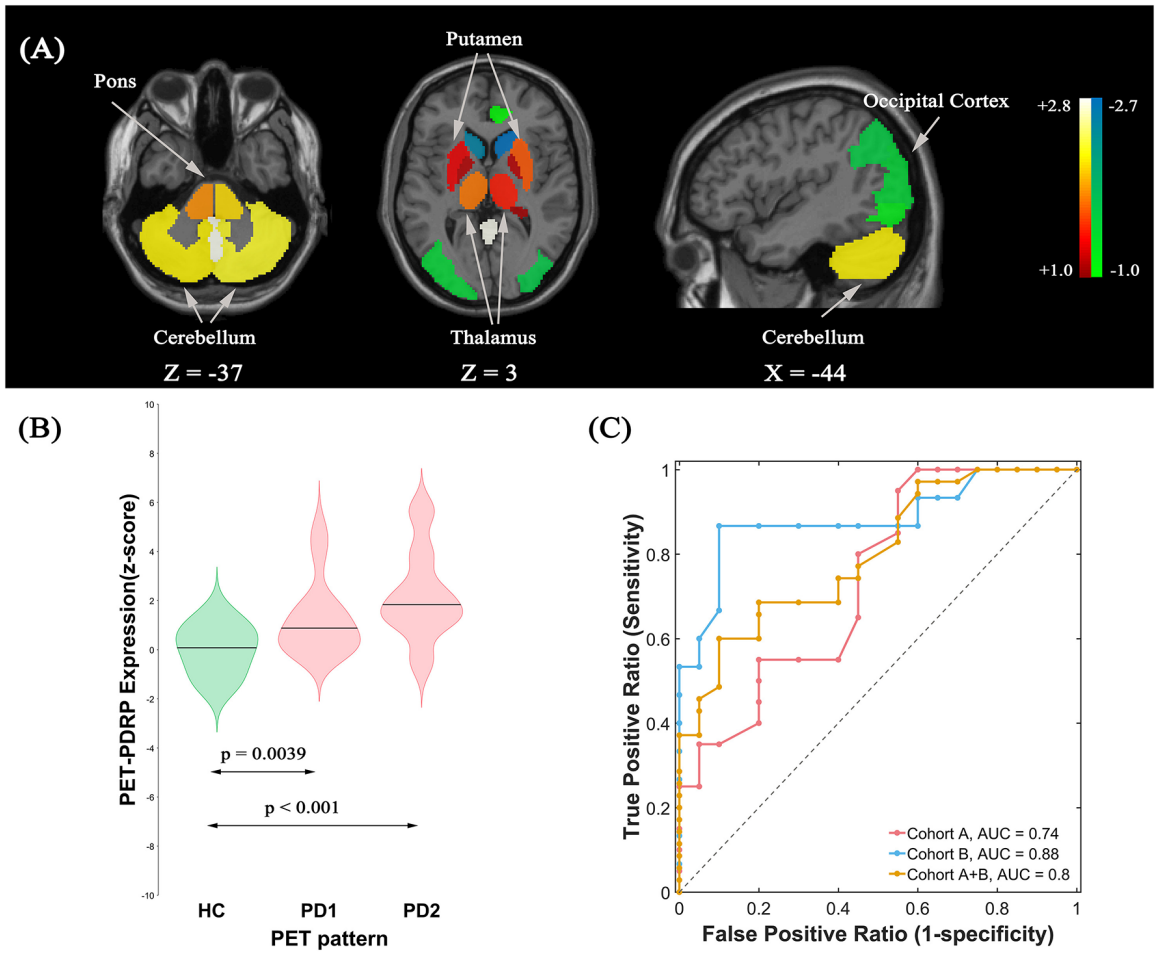

FIGURE 2 | (A) Metabolic Parkinson's disease-related pattern (PET-PDRP) identified by Scaled Subprofile Modeling (SSM) multivariate analysis of ^{18}F-FDG PET scans from 20 (PD) patients in PD1 and 20 age- and gender-matched healthy controls. The pattern was characterized by relative increased metabolic activity in the pallidothalamic, pons, bilateral putamen, and cerebellum, associated with metabolic decreased in parietal–occipital areas. **(B)** Subject expressions for the PET-PDRP topography measured using violin plots in the HC, PD1, and PD2 scans (horizontal lines indicate group medians). Significant increases in pattern expression were seen in PD1 original derivation subjects and PD2 validation subjects with respect to HC control values. **(C)** Receiver operating characteristic (ROC) curve for discriminating PD patients from healthy controls.

0.68–0.92) for subjects in cohorts B and A + B, respectively (**Figure 2C**).

MRI-PDRP Identification and Validation

The pattern analysis of MRI images examined the first four PCs accounting for 52.4% subject × ROI variance. An MRI-PDRP was generated by a linear combination of PC2 and PC3. The pattern was characterized by relative decreased GM volumes in bilateral pons, bilateral transverse temporal gyrus, left cuneus, right superior occipital gyrus, and right superior parietal lobule, associated with preservation in GM volumes in bilateral pallidum and bilateral putamen (**Figure 3A**). Subject expressions for the MRI-PDRP topography were significantly elevated (p = 0.0058) in PD1 compared to HC subjects (**Figure 3B**). Significant increases in pattern expression were seen in PD2 validation subjects with respect to HC control values (p = 0.044). Subject MRI-PDRP expressions were not different between PD1 and PD2 subjects (p = 0.599). As for ROC curves distinguishing the PD patients from the normal controls, AUC values were 0.74 (95% confidence intervals of 0.59–0.90), 0.68 (95% confidence intervals of 0.50–0.86), and 0.72 (95% confidence intervals of 0.57–0.86) for subjects in cohorts A, B, and A + B, respectively (**Figure 3C**).

Correlation Analysis

Correlations Between PDRP and Clinical Scales

PET-PDRP and MRI-PDRP expressions were not correlated with MMSE in the PD group. The correlations between PET-PDRP expressions and the corresponding UPDRS within each PD group are shown in **Figure 4**. In PD1 group, PET-PDRP expressions in patients correlated positively with UPDRS motor ratings (r = 0.55, P = 0.01; **Figure 4A**). In PD2 group,

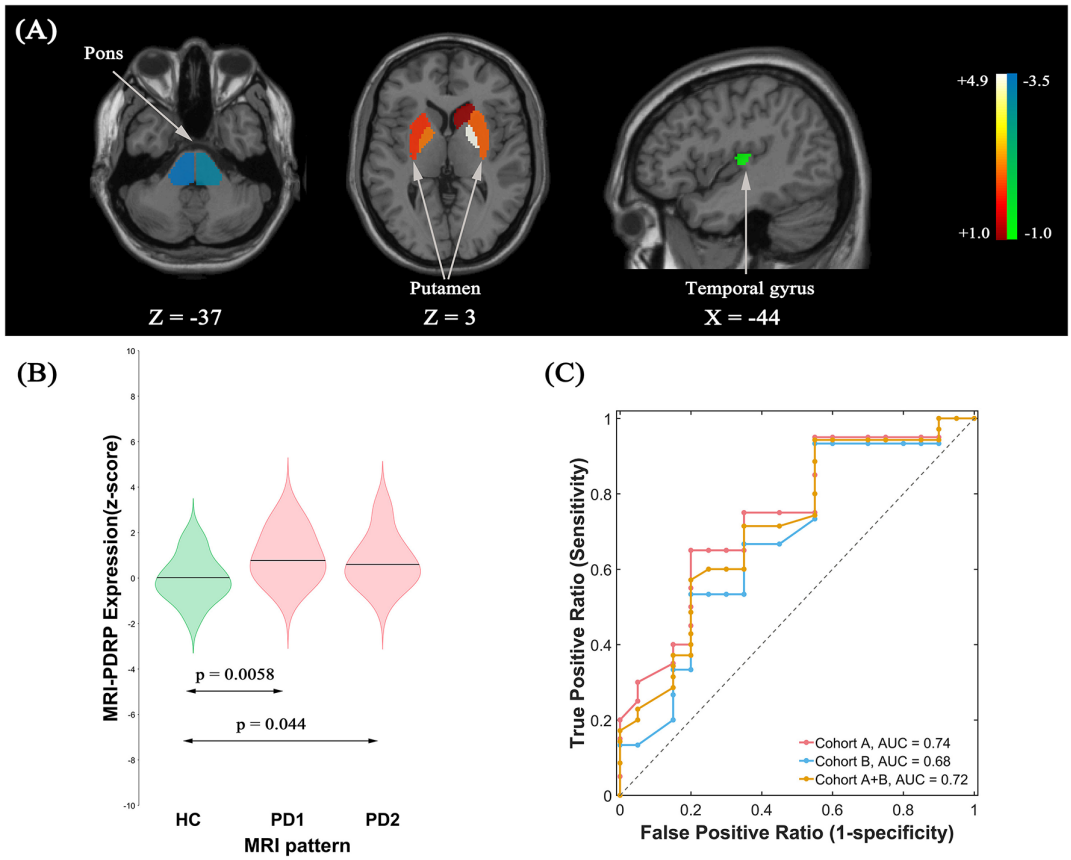

FIGURE 3 | (A) Structural Parkinson's Disease-Related Pattern (MRI-PDRP) derived from the same subjects. The pattern was characterized by relative decreased gray matter (GM) volume in bilateral pons, bilateral transverse temporal gyrus, left cuneus, right superior occipital gyrus, and right superior parietal lobule, associated with preservation in GM volume in bilateral pallidum and bilateral putamen. **(B)** Subject expressions for the MRI-PDRP topography measured using violin plots in the HC, PD1 and PD2 scans (horizontal lines indicate group medians). Significant increases in pattern expression were seen in PD1 original derivation subjects and PD2 validation subjects with respect to HC control values. **(C)** ROC curve for discriminating PD patients from healthy controls.

PET-PDRP expressions in patients also correlated with UPDRS motor ratings (r = 0.60, P = 0.02; **Figure 4B**). In a combined PD group from PD1 and PD2, PET-PDRP expressions had positive correlations with UPDRS motor ratings (r = 0.54, $P < 0.001$). MRI-PDRP expressions were also associated with UPDRS motor ratings in PD1 group (r = 0.51, P = 0.02) but not PD2 group. In a combined PD group (PD1 + PD2), MRI-PDRP expressions were not correlated with UPDRS motor ratings. The correlation results between PET-PDRP expressions, MRI-PDRP expressions, and the six motor items of UDRPS are shown in **Figure 5**. PET-PDRP expressions in patients correlated positively with the scores of speech (r = 0.485, P = 0.003), facial expression (r = 0.336, P = 0.0049), postural tremor (r = 0.379, P = 0.025), rigidity (r = 0.361, P = 0.033), and gait (r = 0.360, P = 0.034). MRI-PDRP expressions in patients correlated positively with the scores of static tremor (r = 0.505, P = 0.002).

Correlations Between PET-PDRP and MRI-PDRP

In the two PDRPs, six regions were salient abnormal brain regions (absolute region weight ≥1.0) in both patterns, including bilateral pons, bilateral pallidum, and bilateral putamen (**Supplementary Tables S1, S2**). Regional weights between the two PDRPs of these regions were negatively correlated (r = −0.88, P = 0.02; **Figure 6A**). Two pattern expression of the combined PD1 patients and healthy controls showed positive correlations (r = 0.45, P = 0.0038; **Figure 6B**) but not associated with combined PD2 and HC subjects or combined PD1, PD2, and HC subjects. The correlations between two pattern expressions in the single PD1 group was found (r = 0.42, P = 0.064) but not found in single PD2 group or combined PD1 and PD2 subjects.

Brain Connectome Analysis

PD-Related Metabolic Network

Connectome analysis was used to reveal abnormalities in network features associated with PD. In our study, in order to determine whether this feature is different between PD patients and healthy subjects, we separated each group's network into two discrete subspaces. Eventually, 25 nodes constituted the disease subspace, which had a higher local contributions to

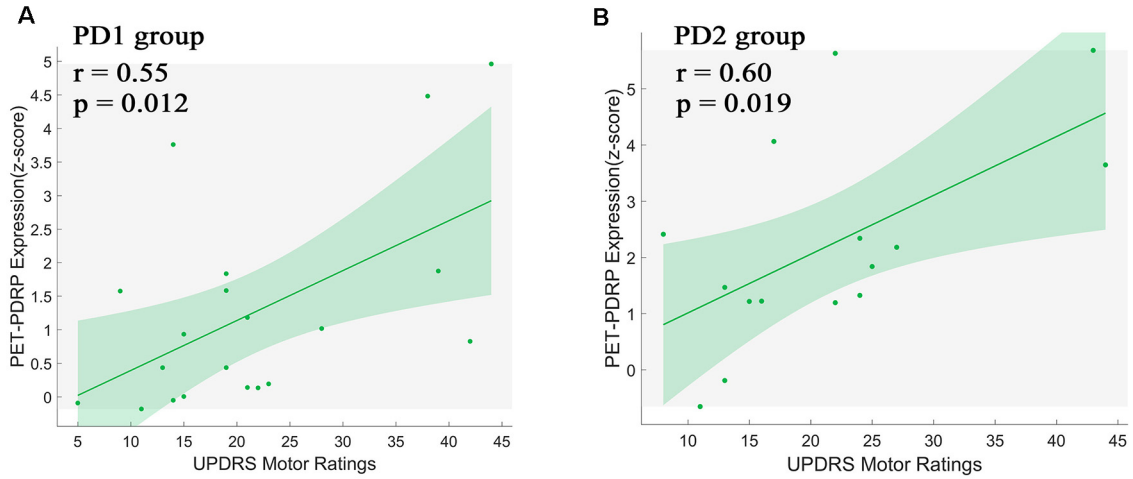

FIGURE 4 | PET-PDRP expressions in individual patients correlated with UPDRS motor ratings in the **(A)** original derivation subjects as well as in the **(B)** subsequent validation subjects. Shaded areas represent 95% confidence of intervals. UPDRS, Unified Parkinson's Disease Rating Scale.

overall PET-PDRP activity (for more details, please refer to **Supplementary Table S1**). The remaining 70 brain regions served as nodes in the nondisease subspace. The $sparsity_{min}$ (ensuring both the disease subspace and nondisease subspace are fully connected) of the HC, PD1, and PD2 groups was 15, 38, and 28%, respectively. Network metrics in each group were computed with a sparsity threshold ranging from 38% to 50%. At sparsity 38%, the clustering coefficient for the disease subspace in the PD1 group was significantly ($P < 0.05$) increased compared with the HC group (PD1, 0.80; HC, 0.50; **Figures 7A,B,D**). The characteristic path length had a tendency to increase in PD1 compared to HC (PD1, 2.42; HC, 1.67; **Figures 7A,B,E**). However, significant differences were not observed for the small-worldness coefficient. Indeed, permutation analysis showed that, in the entire sparsity threshold range (38–50%), the clustering coefficient of PD1 group in the disease space increased significantly ($P < 0.05$); in the sparsity threshold range of 41–50%, the characteristic path length also increased significantly ($P < 0.05$; **Supplementary Figure S1**).

The clustering coefficient for the disease subspace was significantly ($P < 0.05$) increased in PD2 compared to HC over the sparsity range of 38–42% (for example, at sparsity 38%, C in PD2 is 0.76; C in HC is 0.50; **Figures 7A,C,D**). The small world coefficient for the disease subspace in PD2 group increased significantly ($P < 0.05$) at sparsity range of 39–41% (**Supplementary Figure S2**) and had an increasing trend at sparsity 38% (S in PD2, 1.91; S in HC, 1.19; **Figures 7A,C,F**). The characteristic path length (had a tendency to increase, such as, at sparsity 38%, L in PD2 is 2.16; L in HC is 1.67; **Figures 7A,C,E**) did not show group differences (**Supplementary Figure S2**). Group differences of network metrics were not significant for the nondisease subspace or for the whole brain.

PD-Related Brain Structural Network

According to the local contributions to overall MRI-PDRP activity, 11 nodes constituted the disease subspace (**Supplementary Table S2**), and the remaining 84 brain regions served as nodes in the nondisease subspace. PD-related brain structural network was also analyzed based on T1-weighted GM imaging data in different spaces. In the HC group, the minimum sparsity in which all nodes became fully connected in both the disease subspace and nondisease subspace was 20%, PD1 group was 32%, and PD2 group was 17%. Network metrics were computed at a sparsity range of 32–50% for the comparisons between PD1 (or PD2) and HC. At sparsity 32%, increased path length and slightly elevated small-world coefficients for the disease subspace were observed in PD1 group but not PD2 group (L in PD1, 2.15; L in PD2, 1.70; L in HC, 1.42; S in PD1, 2.88; S in PD2, 1.05; S in HC, 1.28; **Supplementary Figure S3**). As above, in the nonparametric permutation test analysis, we also found that increased path length (in the sparsity range of 38–47% and 49–50%) and slightly elevated small-world coefficient (at sparsity 39% and 50%) over corresponding sparsity range for the disease subspace in PD1 group but not PD2 group (**Supplementary Figures S4, S5**). Group differences of network metrics were not significant for the nondisease subspace or for the whole brain.

DISCUSSION

In this study, we investigated ^{18}F-FDG PET-based metabolic covariance pattern (PET-PDRP) and T1 MRI-based structural covariance pattern (MRI-PDRP) associated with PD for the same patients. The MRI-PDRP topography revealed brain region-level abnormalities containing a large number of cortical neurons that partially overlap with the metabolic pattern derived from ^{18}F-FDG PET scans. Connectome analysis also showed that the topological organization for the disease network in the PET-PDRP and MRI-PDRP topographies were significantly disrupted. These findings provide new evidence for elucidating the neuropathological mechanisms of PD.

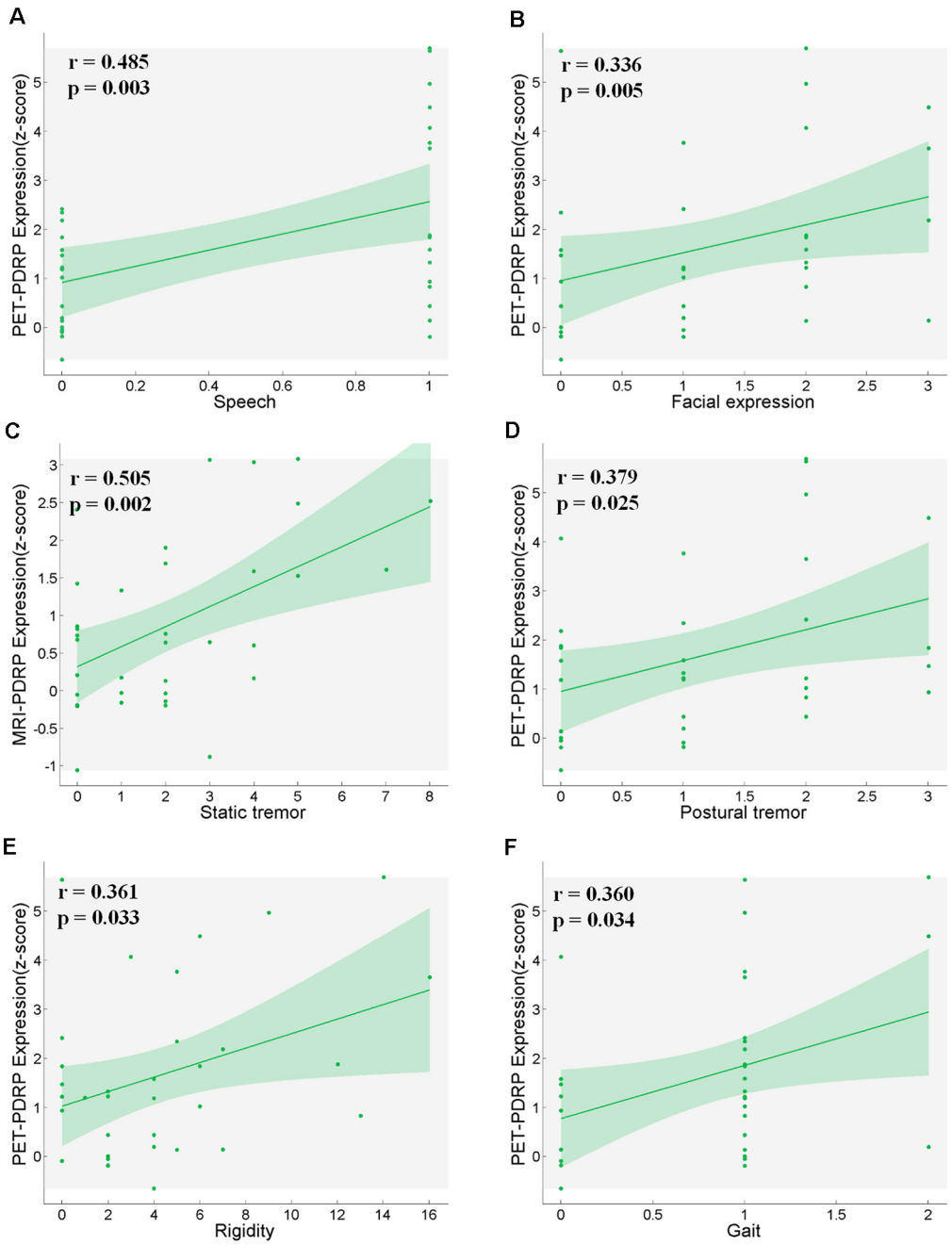

FIGURE 5 | PET-PDRP expressions in PD patients correlated with their levels of **(A)** speech, **(B)** facial expression, **(D)** postural tremor, **(E)** rigidity and **(F)** gait. MRI-PDRP expressions in PD patients correlated with the levels of **(C)** static tremor. Shaded areas represent 95% confidence of intervals.

Reproducible Metabolic PDRP Topography

Using spatial covariance analysis, we reproduced a metabolic PDRP topography (PET-PDRP) that was compatible with previous imaging studies in both American and Chinese PD patients (Ma et al., 2007; Wu et al., 2013; Ko et al., 2017; Schindlbeck and Eidelberg, 2018). In our study, the PET-PDRP expression in PD patients was significantly elevated in the original derivation subjects and the subsequent validation subjects. The regional metabolic dysfunction within this abnormal topography could describe abnormal cerebral metabolism or blood flow and reveal clinical disability and treatment response in patients with PD (Hirano et al., 2008; Eidelberg, 2009; Wu et al., 2013; Ko et al., 2017). This topography revealed the presence of

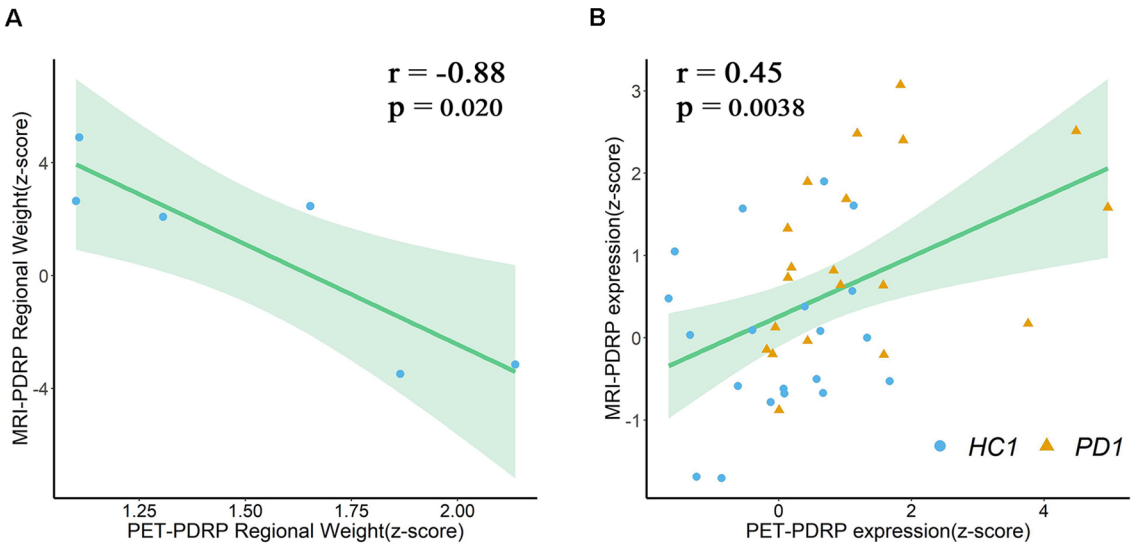

FIGURE 6 | (A) Regional weights on PET-PDRP and MRI-PDRP in a set of salient abnormal brain regions were correlated. **(B)** PET-PDRP expressions in combination with PD1 patients and healthy controls and MRI-PDRP expressions in the same subjects were correlated. Shaded areas represent 95% confidence of intervals.

abnormal metabolic changes at key nodes of the cortico-striato-pallido-thalamo-cortical (CSPTC) loops and other related anatomical/functional pathways, which is in line with previous reports (Eidelberg, 2009; Poston and Eidelberg, 2009; Tang and Eidelberg, 2010). The abnormalities in the CSPTC circuits are commonly associated with the clinical manifestations of akinetic rigid in PD patients, but they do not fully explain other disease manifestations, such as tremors (Wichmann and Delong, 2007; Zaidel et al., 2009; Wu et al., 2013). By contrast, relative hypermetabolism in the cerebellum/dorsal pons, putamen, and primary motor cortex captured the abnormal activity in the cerebello-thalamo-cortical (CbTC) circuits, which was associated with the generation of tremor (Timmermann et al., 2002; Wu et al., 2013). Particularly, the cerebellum, pons, thalamus, and putamen evident overlaps in both CSPTC and CbTC circuits were considered as regions of severer involvement of these circuits. In this study, the dysfunction of CSPTC circuits was involved in functional network abnormalities of PDRP topography. The premotor area receives less excitatory impulses from the thalamus, resulting in a decrease in parietal lobe metabolism (Wu et al., 2013). On the other hand, posterior cortical dysfunction is considered as the imaging marker of PD patients with the risk of dementia (Wu et al., 2013; Peng et al., 2014a). However, understanding the contributions of different brain regions to motor and cognitive impairments requires more relevant cross-sectional and longitudinal studies.

Structural PDRP Topography

We demonstrated for the first time that spatial covariance analysis can reveal a wide range of regions affected by PD using T1-weighted structural MRI. In this study, a reduced GM volume in PD was observed in bilateral pons, bilateral transverse temporal gyrus, left cuneus, right superior occipital gyrus, and right superior parietal lobule, associated with preservation in GM volume in bilateral pallidum and bilateral putamen. In PD patients, more than 70% of dopamine (DA) terminals were lost when motor symptoms occur (Fearnley and Lees, 1991), and in the early stages of PD, human dyskinesia might be due to the compensatory mechanism that promoted the release and renewal of DA and reduced the uptake of DA so that the DA concentration was stable at normal levels (Silverdale et al., 2003). Besides, there are other possible compensatory changes, including the increase or appearance of striatum TH+ neurons and enhanced DA synthesis by alternative biochemical pathways, etc. These changes might preserve the GM volume in pallidum and putamen in early PD patients (Blesa et al., 2017). Pathological studies related to PD also indicated that the progression of lesions begins with the brainstem (which includes pons) and the substantia nigra (Braak et al., 2003). An decrease in gray volume in the pons has also been reported in previous studies (Jubault et al., 2009). Therefore, the finding in this study is consistent with the pons as the anatomical starting point of PD pathology according to Braak et al. (2003, 2004) and Jubault et al. (2009). In our study, morphological abnormalities in other cortical regions were also found. In cognitively intact PD patients, cortical morphology may be normal (Tessitore et al., 2012) or abnormal in the frontal lobe (Biundo et al., 2011) or in a wider range of cortical regions, including the parietal, temporal, and occipital lobes (Jubault et al., 2011). Uncoordinated results may be caused by different experimental methodologies or the heterogeneity of PD disease.

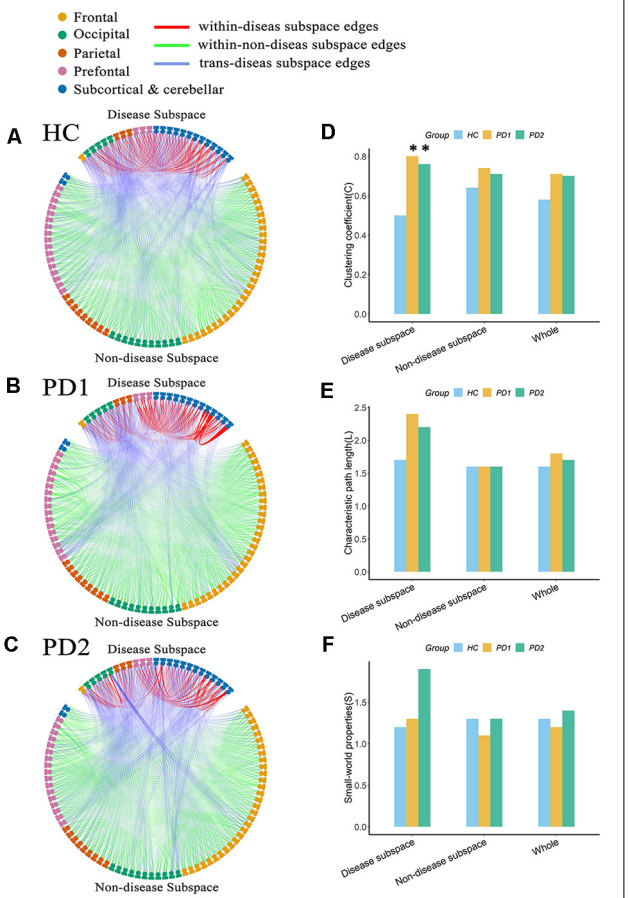

FIGURE 7 | Node-to-node functional connectivity (FC) in the **(A)** HC, **(B)** PD1, and **(C)** PD2 groups in the disease subspace and nondisease subspace, and **(D–F)** network attributes. **(A)** Binary functional network in the HC group at sparsity 38%. **(B)** Binary functional network in the PD1 group at sparsity 38%. **(C)** Binary functional network in the PD2 group at sparsity 38%. **(D)** Comparison of the clustering coefficient among HC, PD1, and PD2 groups in different spaces at sparsity 38%. **(E)** Characteristic path length. **(F)** Small world coefficient. In **(A–C)**, the nodes in the upper part of the circle represent brain regions in the disease subspace (25 ROIs), and the nodes in the lower part of circle represent brain regions in the nondisease subspace (70 ROIs). Colors of nodes on the circle represent different anatomical classifications of corresponding brain regions based on existing literature (Wang et al., 2007; Bai et al., 2011). The lines within the circle represent FC between pairs of nodes, where the red lines (within-disease subspace edges) indicate FC between nodes within the disease subspace; the green lines (within-nondisease subspace edges) indicate FC between nodes within the nondisease subspace; the blue lines (trans-disease subspace edges) indicate FC between the disease subspace nodes and the nondisease subspace nodes. The asterisk refers to significant differences between the PD compared to HC groups ($p < 0.05$).

Correlations Between PDRP and Clinical Scale

There was no significant correlation between PET-PDRP and MMSE, MRI-PDRP and MMSE, but there were significant positive correlations with UPDRS and six motor items, suggesting that the abnormal metabolic and structural characteristics of nondemented PD patients are related to their dyskinesias, but not to cognitive dysfunction. The injury of PD patients on speech, facial expressions, tremors, rigidity, and gait became worse with the increase in PD pathology, which was consistent with clinical manifestations. Postural tremor is associated with metabolic abnormalities, while stationary tremor is associated with structural abnormalities, indicating that the causes of postural tremor and stationary tremor in PD patients may be different and therapeutic interventions for primary tremor in PD patients need to distinguish postural tremor from resting tremor.

Correlations Between PET-PDRP and MRI-PDRP

The ROC curves revealed that PET-PDRP and MRI-PDRP expressions significantly discriminated PD patients from the control individuals with approving sensitivity and specificity. Since PET-PDRP expression value was demonstrated reliable diagnosis power, it revealed that MRI-PDRP may be also a promising diagnostic biomarker for the non-inferiority compared to PET-PDRP. However, further validation work should be followed.

As expected, several overlapping regions were identified between the metabolic PET-PDRP topography and the structural MRI-PDRP topography, including the bilateral pons, bilateral pallidum, and bilateral putamen. Surprisingly, the regional weights between the two PDRPs identified in the two imaging modalities were correlated within these regions ($r = -0.88$, $P = 0.02$), and the two pattern expressions were also correlated in patients and normal subjects. In a structural MRI study in combination with deformation-based morphometry and independent component analysis (ICA), researchers identified that the PD-ICA atrophy pattern in a larger number of participants showed a certain spatial topography overlap with the metabolic PD-related pattern derived from spatial covariance analysis using ^{18}F-FDG PET (Zeighami et al., 2015). These included the globus pallidus, thalamus, putamen, premotor and supplementary motor regions. Our study obtained a consistent result. The consistent findings indicate a possible link between brain function and structure dysfunction of the related anatomical and functional circuit in PD, particularly the cortico-basal ganglia-thalamocortical motor circuit. In addition, our study demonstrated the potential value of the integration of different neuroimaging techniques to improve the neuropathological understanding of PD. Consistent abnormalities in brain structure and function, and causal relationships between them, in patients with PD await further investigation and understanding.

Structurally and Functionally Disrupted Network Topology in PD

Brain connectome analysis can reveal abnormalities in network characteristics associated with PD and the potential impact of the disease network on brain information processing. We found that the functional brain network in the two independent PD groups exhibited a disrupted network topology in the disease subspace. Compared with the HC group, the clustering coefficient for the disease subspace was significantly increased, the characteristic

path length in the PD1 group was significantly increased, and the small-worldness attribute in the PD2 group was significantly elevated. Similarly, we also found a significantly increased characteristic path length for the brain structure network in PD1 group. An earlier study has used ^{18}F-FDG PET data to identify an ROI-based metabolic PD-related pattern, and the disrupted network topology (increased clustering coefficient, reduced characteristic path length, and exaggerated small-worldness attribute) in the disease network consisting of brain regions with significant abnormalities in this pattern has also been confirmed in four independent patient subjects and in an experimental nonhuman primate model (Ko et al., 2017). Consistent with our results, significantly increased clustering coefficients in the disease space could be observed in both studies. However, changes of characteristic path length in the disease space in both studies were against. This may resulted from different disease spaces in morphological topography and nation differences between the western and eastern populations in the two studies. Interestingly, these descriptor changes are limited to the space occupied by the disease network, which might correspond to the relatively intact anatomy of other spaces (nondisease subspace and the whole brain).

LIMITATIONS

There are several issues that still need to be further considered in this study. First, in the pattern analysis, we used the ROI-based rather than the voxel-based SSM/PCA algorithm for the subsequent determination of the disease subspace. The effect of the two different analytical methods on the results needs further investigation. Second, due to limited experimental subjects, for prospective evaluation of PET-PDRP and MRI-PDRP, we only used another new set of PD subjects but did not include both HC and PD subjects. Third, we did not further examine the intrinsic link between pattern and connectome analyses, for example, to see whether the correlation between the metabolic PET-PDRP pattern and structural MRI-PDRP can be further explained from the perspective of connectome analysis.

CONCLUSIONS

In this study, we investigated ^{18}F-FDG PET-based metabolic covariance pattern and MRI-based structural covariance pattern associated with PD in the same patients. The metabolic pattern is highly consistent with the disease-related metabolic brain patterns previously described in different cohorts of PD patients. This structural pattern was characterized by relative decreased GM volume in bilateral pons, bilateral transverse temporal gyrus, left cuneus, right superior occipital gyrus, and right superior parietal lobule, associated with preservation in GM volume in bilateral pallidum and bilateral putamen. Expectantly, we found a significantly negative correlation regional weight between metabolic and structural patterns in a set of salient abnormal brain regions, which provides a new perspective for insight into disrupted brain abnormal metabolism and structure in PD patients. In order to verify the effectiveness of two patterns, we used connectome analysis methods to explore the brain metabolic network constructed by PET and the brain structural network. The results showed that more obvious changes could be found in these two patterns. In summary, significant overlaps between metabolic and structural patterns, as well as the convergence of metabolic network and structural network disruption, provide new evidence for elucidating the neuropathological mechanisms of the disease.

DATA AVAILABILITY STATEMENT

All datasets generated for this study are included in the article/**Supplementary Material**.

ETHICS STATEMENT

The studies involving human participants were reviewed and approved by Research Ethics Committee of Huashan Hospital, Shanghai, China (approval number: KY2013-336). The patients/participants provided their written informed consent to participate in this study.

AUTHOR CONTRIBUTIONS

CL, HZho, and HZha: analysis and interpretation, writing of manuscript. MW and JuJ: study supervision, critical revision of the manuscript for important intellectual content. PW, JG, and JW: acquisition of data, writing of manuscript. JiJ, YM, and CZ: study concept and design, organization, critical revision of the manuscript for important intellectual content.

FUNDING

This study was supported by grants from the National Natural Science Foundation of China (nos. 61603236, 81671239, 81361120393, 81401135, 81771483, and 81971641), the 111 Project (D20031), the National Key Research and Development Program of China (nos. 2016YFC1306305, 2016YFC1306500 and 2018YFC1707704) from the Ministry of Science and Technology of China, Shanghai Technology and Science Key Project in Healthcare (no. 17441902100), Shanghai Municipal Science and Technology Major Project (no. 2017SHZDZX01), Science and Technology Commission of Shanghai Municipality (nos. 19441903500 and 17JC1401600), the Open Project Funding of Human Phenome Institute (no. HUPIKF2018203), and Fudan University. The work described in this study is facilitated in part by the US–China Collaborative Project (R01 NS 083490) funded by the National Institute of Health.

SUPPLEMENTARY MATERIAL

The Supplementary Material for this article can be found online at: https://www.frontiersin.org/articles/10.3389/fnagi.2020.00125/full#supplementary-material.

REFERENCES

Baggio, H. C., Sala-Llonch, R., Segura, B., Marti, M. J., Valldeoriola, F., Compta, Y., et al. (2014). Functional brain networks and cognitive deficits in Parkinson's disease. *Hum. Brain Mapp.* 35, 4620–4634. doi: 10.1002/hbm.22499

Bai, F., Liao, W., Watson, D. R., Shi, Y., Wang, Y., Yue, C., et al. (2011). Abnormal whole-brain functional connection in amnestic mild cognitive impairment patients. *Behav. Brain Res.* 216, 666–672. doi: 10.1016/j.bbr.2010.09.010

Biundo, R., Formento-Dojot, P., Facchini, S., Vallelunga, A., Ghezzo, L., Foscolo, L., et al. (2011). Brain volume changes in Parkinson's disease and their relationship with cognitive and behavioural abnormalities. *J. Neurol. Sci.* 310, 64–69. doi: 10.1016/j.jns.2011.08.001

Blesa, J., Trigo-Damas, I., Dileone, M., Del Rey, N. L., Hernandez, L. F., and Obeso, J. A. (2017). Compensatory mechanisms in Parkinson's disease: circuits adaptations and role in disease modification. *Exp. Neurol.* 298, 148–161. doi: 10.1016/j.expneurol.2017.10.002

Braak, H., Del Tredici, K., Rüb, U., De Vos, R. A., Steur, E. N. J., and Braak, E. (2003). Staging of brain pathology related to sporadic Parkinson's disease. *Neurobiol. Aging* 24, 197–211. doi: 10.1016/s0197-4580(02)00065-9

Braak, H., Ghebremedhin, E., Rüb, U., Bratzke, H., and Del Tredici, K. (2004). Stages in the development of Parkinson's disease-related pathology. *Cell Tissue Res.* 318, 121–134. doi: 10.1007/s00441-004-0956-9

Choi, B.-K., Choi, M.-G., Kim, J.-Y., Yang, Y., Lai, Y., Kweon, D.-H., et al. (2013). Large α-synuclein oligomers inhibit neuronal SNARE-mediated vesicle docking. *Proc. Natl. Acad. Sci. U S A* 110, 4087–4092. doi: 10.1073/pnas.1218424110

Duan, H., Jiang, J., Xu, J., Zhou, H., Huang, Z., Yu, Z., et al. (2017). Differences in Aβ brain networks in Alzheimer's disease and healthy controls. *Brain Res.* 1655, 77–89. doi: 10.1016/j.brainres.2016.11.019

Eidelberg, D. (2009). Metabolic brain networks in neurodegenerative disorders: a functional imaging approach. *Trends Neurosci.* 32, 548–557. doi: 10.1016/j.tins.2009.06.003

Fearnley, J. M., and Lees, A. J. (1991). Ageing and Parkinson's disease: substantia nigra regional selectivity. *Brain* 114, 2283–2301. doi: 10.1093/brain/114.5.2283

Fox, M. D. (2018). Mapping symptoms to brain networks with the human connectome. *N. Engl. J. Med.* 379, 2237–2245. doi: 10.1056/nejmra1706158

Ge, J., Wu, J., Peng, S., Wu, P., Wang, J., Zhang, H., et al. (2018). Reproducible network and regional topographies of abnormal glucose metabolism associated with progressive supranuclear palsy: multivariate and univariate analyses in american and chinese patient cohorts. *Hum. Brain Mapp.* 39, 2842–2858. doi: 10.1002/hbm.24044

Hirano, S., Asanuma, K., Ma, Y., Tang, C., Feigin, A., Dhawan, V., et al. (2008). Dissociation of metabolic and neurovascular responses to levodopa in the treatment of Parkinson's disease. *J. Neurosci.* 28, 4201–4209. doi: 10.1523/JNEUROSCI.0582-08.2008

Hosseini, S. M., Hoeft, F., and Kesler, S. R. (2012). GAT: a graph-theoretical analysis toolbox for analyzing between-group differences in large-scale structural and functional brain networks. *PLoS One* 7:e40709. doi: 10.1371/journal.pone.0040709

Huang, C., Tang, C., Feigin, A., Lesser, M., Ma, Y., Pourfar, M., et al. (2007). Changes in network activity with the progression of Parkinson's disease. *Brain* 130, 1834–1846. doi: 10.1093/brain/awm086

Hughes, A. J., Daniel, S. E., Kilford, L., and Lees, A. J. (1992). Accuracy of clinical diagnosis of idiopathic Parkinson's disease: a clinico-pathological study of 100 cases. *J. Neurol. Neurosurg. Psychiatry* 55, 181–184. doi: 10.1136/jnnp.55.3.181

Jiang, J., Zhou, H., Duan, H., Liu, X., Zuo, C., Huang, Z., et al. (2017). A novel individual-level morphological brain networks constructing method and its evaluation in PET and MR images. *Heliyon* 3:e00475. doi: 10.1016/j.heliyon.2017.e00475

Jubault, T., Brambati, S. M., Degroot, C., Kullmann, B., Strafella, A. P., Lafontaine, A. L., et al. (2009). Regional brain stem atrophy in idiopathic Parkinson's disease detected by anatomical MRI. *PLoS One* 4:e8247. doi: 10.1371/journal.pone.0008247

Jubault, T., Gagnon, J. F., Karama, S., Ptito, A., Lafontaine, A. L., Evans, A. C., et al. (2011). Patterns of cortical thickness and surface area in early Parkinson's disease. *NeuroImage* 55, 462–467. doi: 10.1016/j.neuroimage.2010.12.043

Ko, J. H., Spetsieris, P. G., and Eidelberg, D. (2017). Network structure and function in Parkinson's disease. *Cereb. Cortex* 28, 4121–4135. doi: 10.1093/cercor/bhx267

Lee, V. M.-Y., and Trojanowski, J. Q. (2006). Mechanisms of Parkinson's disease linked to pathological α-synuclein: new targets for drug discovery. *Neuron* 52, 33–38. doi: 10.1016/j.neuron.2006.09.026

Lo, C. Y., Wang, P. N., Chou, K. H., Wang, J., He, Y., and Lin, C. P. (2010). Diffusion tensor tractography reveals abnormal topological organization in structural cortical networks in Alzheimer's disease. *J. Neurosci.* 30, 16876–16885. doi: 10.1523/JNEUROSCI.4136-10.2010

Ma, Y., Tang, C., Spetsieris, P. G., Dhawan, V., and Eidelberg, D. (2007). Abnormal metabolic network activity in Parkinson'S disease: test—retest reproducibility. *J. Cereb. Blood Flow Metab.* 27, 597–605. doi: 10.1038/sj.jcbfm.9600358

Peng, S., Eidelberg, D., and Ma, Y. (2014a). Brain network markers of abnormal cerebral glucose metabolism and blood flow in Parkinson's disease. *Neurosci. Bull.* 30, 823–837. doi: 10.1007/s12264-014-1472-x

Peng, S., Ma, Y., Spetsieris, P. G., Mattis, P., Feigin, A., Dhawan, V., et al. (2014b). Characterization of disease-related covariance topographies with SSMPCA toolbox: effects of spatial normalization and PET scanners. *Hum. Brain Mapp.* 35, 1801–1814. doi: 10.1002/hbm.22295

Politis, M. (2014). Neuroimaging in Parkinson disease: from research setting to clinical practice. *Nat. Rev. Neurol.* 10, 708–722. doi: 10.1038/nrneurol.2014.205

Poston, K. L., and Eidelberg, D. (2009). Network biomarkers for the diagnosis and treatment of movement disorders. *Neurobiol. Dis.* 35, 141–147. doi: 10.1016/j.nbd.2008.09.026

Rocha, E. M., De Miranda, B., and Sanders, L. H. (2018). α-synuclein: pathology, mitochondrial dysfunction and neuroinflammation in Parkinson's disease. *Neurobiol. Dis.* 109, 249–257. doi: 10.1016/j.nbd.2017.04.004

Schindlbeck, K. A., and Eidelberg, D. (2018). Network imaging biomarkers: insights and clinical applications in Parkinson's disease. *Lancet Neurol.* 17, 629–640. doi: 10.1016/s1474-4422(18)30169-8

Silverdale, M. A., Fox, S. H., Crossman, A. R., and Brotchie, J. M. (2003). Potential nondopaminergic drugs for Parkinson's disease. *Adv. Neurol.* 91, 273–291. Available online: http://pascal-francis.inist.fr/vibad/index.php?action=getRecordDetail&idt=14986419.

Spetsieris, P. G., and Eidelberg, D. (2011). Scaled subprofile modeling of resting state imaging data in Parkinson's disease: methodological issues. *NeuroImage* 54, 2899–2914. doi: 10.1016/j.neuroimage.2010.10.025

Spetsieris, P., Ma, Y., Peng, S., Ko, J. H., Dhawan, V., Tang, C. C., et al. (2013). Identification of disease-related spatial covariance patterns using neuroimaging data. *J. Vis. Exp.* 76:e50319. doi: 10.3791/50319

Tang, C. C., and Eidelberg, D. (2010). "Abnormal metabolic brain networks in Parkinson's disease: from blackboard to bedside," in *Progress in Brain Research*, (Amsterdam, Netherlands: Elsevier), 160–176.

Tessitore, A., Amboni, M., Cirillo, G., Corbo, D., Picillo, M., Russo, A., et al. (2012). Regional gray matter atrophy in patients with Parkinson disease and freezing of gait. *Am. J. Neuroradiol.* 33, 1804–1809. doi: 10.3174/ajnr.A3066

Teune, L., Bartels, A., and Leenders, K. (2013). "FDG-PET imaging in neurodegenerative brain diseases," in *Functional Brain Mapping and the Endeavor to Understand the Working Brain*, eds F. Signorelli and D. Chirchiglia (Rijeka: InTech), 463–475.

Timmermann, L., Gross, J., Dirks, M., Volkmann, J., Freund, H. J., and Schnitzler, A. (2002). The cerebral oscillatory network of parkinsonian resting tremor. *Brain* 126, 199–212. doi: 10.1093/brain/awg022

Titov, D., Diehl-Schmid, J., Shi, K., Perneczky, R., Zou, N., Grimmer, T., et al. (2017). Metabolic connectivity for differential diagnosis of dementing disorders. *J. Cereb. Blood Flow Metab.* 37, 252–262. doi: 10.1177/0271678X15622465

Tomše, P., Jensterle, L., Grmek, M., Zaletel, K., Pirtošek, Z., Dhawan, V., et al. (2017). Abnormal metabolic brain network associated with Parkinson's disease: replication on a new European sample. *Neuroradiology* 59, 507–515. doi: 10.1007/s00234-017-1821-3

Tzourio-Mazoyer, N., Landeau, B., Papathanassiou, D., Crivello, F., Etard, O., Delcroix, N., et al. (2002). Automated anatomical labeling of activations in SPM using a macroscopic anatomical parcellation of the MNI MRI single-subject brain. *NeuroImage* 15, 273–289. doi: 10.1006/nimg.2001.0978

Wang, K., Liang, M., Wang, L., Tian, L., Zhang, X., Li, K., et al. (2007). Altered functional connectivity in early Alzheimer's disease: a resting-state fMRI study. *Hum. Brain Mapp.* 28, 967–978. doi: 10.1002/hbm.20324

Wichmann, T., and Delong, M. R. (2007). Anatomy and physiology of the basal ganglia: relevance to Parkinson's disease and related disorders. *Handb. Clin. Neurol.* 83, 1–18. doi: 10.1016/s0072-9752(07)83001-6

Wilson, H., Niccolini, F., Pellicano, C., and Politis, M. (2019). Cortical thinning across Parkinson's disease stages and clinical correlates. *J. Neurol. Sci.* 398, 31–38. doi: 10.1016/j.jns.2019.01.020

Wu, P., Wang, J., Peng, S., Ma, Y., Zhang, H., Guan, Y., et al. (2013). Metabolic brain network in the Chinese patients with Parkinson's disease based on 18F-FDG PET imaging. *Parkinsonism Relat. Disord.* 19, 622–627. doi: 10.1016/j.parkreldis.2013.02.013

Zaidel, A., Arkadir, D., Israel, Z., and Bergman, H. (2009). Akineto-rigid vs. tremor syndromes in Parkinsonism. *Curr. Opin. Neurol.* 22, 387–393. doi: 10.1097/wco.0b013e32832d9d67

Zeighami, Y., Ulla, M., Iturria-Medina, Y., Dadar, M., Zhang, Y., Larcher, K. M., et al. (2015). Network structure of brain atrophy in de novo Parkinson's disease. *Elife* 4:e08440. doi: 10.7554/eLife.08440

Conflict of Interest: The authors declare that the research was conducted in the absence of any commercial or financial relationships that could be construed as a potential conflict of interest.

frontiers in Aging Neuroscience

CLINICAL TRIAL
published: 03 June 2020
doi: 10.3389/fnagi.2020.00155

Prevention of Early Alzheimer's Disease by Erinacine A-Enriched *Hericium erinaceus* Mycelia Pilot Double-Blind Placebo-Controlled Study

I-Chen Li[1], Han-Hsin Chang[2], Chuan-Han Lin[3], Wan-Ping Chen[1], Tsung-Han Lu[3], Li-Ya Lee[1], Yu-Wen Chen[1], Yen-Po Chen[1], Chin-Chu Chen[1,4,5,6] and David Pei-Cheng Lin[3,7]**

[1] Biotech Research Institute, Grape King Bio Ltd., Taoyuan City, Taiwan, [2] Department of Nutrition, Chung Shan Medical University, Taichung City, Taiwan, [3] Department of Medical Laboratory and Biotechnology, Chung Shan Medical University, Taichung City, Taiwan, [4] Institute of Food Science and Technology, National Taiwan University, Taipei City, Taiwan, [5] Department of Food Science, Nutrition and Nutraceutical Biotechnology, Shih Chien University, Taipei City, Taiwan, [6] Department of Bioscience Technology, Chung Yuan Christian University, Taoyuan City, Taiwan, [7] Department of Ophthalmology, Chung Shan Medical University Hospital, Taichung City, Taiwan

OPEN ACCESS

Edited by:
Woon-Man Kung,
Chinese Culture University, Taiwan

Reviewed by:
Lee Wei Lim,
The University of Hong Kong, Hong Kong
Hirokazu Kawagishi,
Shizuoka University, Japan

***Correspondence:**
Chin-Chu Chen
gkbioeng@grapeking.com.tw
David Pei-Cheng Lin
pcl@csmu.edu.tw

Received: 26 February 2020
Accepted: 07 May 2020
Published: 03 June 2020

Citation:
Li I-C, Chang H-H, Lin C-H, Chen W-P, Lu T-H, Lee L-Y, Chen Y-W, Chen Y-P, Chen C-C and Lin DP-C (2020) Prevention of Early Alzheimer's Disease by Erinacine A-Enriched Hericium erinaceus Mycelia Pilot Double-Blind Placebo-Controlled Study. Front. Aging Neurosci. 12:155. doi: 10.3389/fnagi.2020.00155

Objective: To investigate the efficacy and safety of three *H. erinaceus* mycelia (EAHE) capsules (350 mg/capsule; containing 5 mg/g erinacine A active ingredient) per day for the treatment of patients with mild Alzheimer's Disease (AD).

Methods: This study comprised a 3-week no-drug screening period, followed by a 49-week double-blind treatment period with 2-parallel groups in which eligible patients were randomized to either three 5 mg/g EAHE mycelia capsules per day or identical appearing placebo capsules. Cognitive assessments, ophthalmic examinations, biomarker collection, and neuroimaging were followed throughout the study period.

Results: After 49 weeks of EAHE intervention, a significant decrease in Cognitive Abilities Screening Instrument score was noted in the placebo group, a significant improvement in Mini-Mental State Examination score was observed in the EAHE group and a significant Instrumental Activities of Daily Living score difference were found between the two groups. In addition, EAHE group achieved a significantly better contrast sensitivity when compared to the placebo group. Moreover, only the placebo group observed significantly lowered biomarkers such as calcium, albumin, apolipoprotein E4, hemoglobin, and brain-derived neurotrophic factor and significantly elevated alpha1-antichymotrypsin and amyloid-beta peptide 1–40 over the study period. Using diffusion tensor imaging, the mean apparent diffusion coefficient (ADC) values from the arcuate fasciculus region in the dominant hemisphere significantly increased in the placebo group while no significant difference was found in the EAHE group in comparison to their baselines. Moreover, ADC values from the parahippocampal cingulum region in the dominant hemisphere significantly decreased in the EAHE group whereas no significant

difference was found in the placebo group when compared to their baselines. Lastly, except for four subjects who dropped out of the study due to abdominal discomfort, nausea, and skin rash, no other adverse events were reported.

Conclusion: Three 350 mg/g EAHE capsules intervention for 49 weeks demonstrated higher CASI, MMSE, and IADL scores and achieved a better contrast sensitivity in patients with mild AD when compared to the placebo group, suggesting that EAHE is safe, well-tolerated, and may be important in achieving neurocognitive benefits.

Clinical Trial Registration: ClinicalTrials.gov, identifier NCT04065061.

Keywords: erinacine A-enriched *H. erinaceus* mycelia, Alzheimer's disease, pilot study, prevention, magnetic resonance imaging

INTRODUCTION

The pace of population aging across the world over the past half-century is increasing dramatically, triggering a Silver Tsunami of chronic age-related diseases. Among these diseases, Alzheimer's Disease (AD) is the fifth-leading cause of death among adults aged 65 years and older and is also a leading cause of disability and morbidity (Alzheimer's Association, 2019). Unlike other major diseases for which there have been steady progress in the development of novel therapies, no new pharmacologic treatment for AD has been approved since 2003 (Hung and Fu, 2017). One theory as to why many intervention trials have failed is that the pathophysiological process of AD is thought to begin many years before the onset of clinical symptoms, and the use of interventions later in the disease may not effectively slow its progression due to established pathological burden (Sperling et al., 2011). As a result, there has been a shift in the clinical research field, with the focus to develop safe and effective interventions in early and presymptomatic AD stages (Graham et al., 2017). To date, several prevention trials have been carried out and shown promising results, suggesting the potential feasibility of implementing non-pharmacological approaches, including dietary interventions (Ngandu et al., 2015; Andrieu et al., 2017).

In a recent study, the lifestyle of 633 Chinese seniors living in Singapore between 2011 and 2017 was analyzed, and it was revealed that various mushrooms have therapeutic effects in combatting AD by exerting neuroprotective and antioxidant effects (Feng et al., 2019). Mushrooms and their extracts have been well-known for their nutritional and culinary values, which may be regarded as novel nature-based nutraceuticals to mitigate AD and other age-related neurodegenerative disorders. In fact, a number of mushrooms including *Hericium erinaceus* (Bull.: Fr.) Pers., *Dictyophora indusiata* (Vent.) Desv., *Grifola frondosa* (Dicks.: Fr.) S.F. Gray, *Tremella fuciformis* Berk, *Tricholoma* sp., *Termitomyces albuminosus* (Berk.) R. Heim, *Lignosus rhinocerotis* (Cooke) Ryvarden, *Cordyceps militaris* (L.:Fr.) Link, *Pleurotus giganteus* (Berk.) Karunarathna and K.D. Hyde, *Ganoderma lucidum* P. Karst, and *Ganoderma neo-japonicum* Imazeki have been reported to have activities related to nerve and brain health (Phan et al., 2017). Among these, the neurohealth properties of *Hericium erinaceus* (Bull.:Fr.) Pers., or its common names Lion's mane or Monkey's head mushroom, have been most extensively studied.

Hericenones and erinacines are the two important classes of constitutes isolated from the fruiting body and mycelium of *H. erinaceus*, respectively (Kawagishi et al., 1991, 1992, 1994, 1996a,b; Lee et al., 2000). Both hericenones and erinacines are low-molecular weight, relatively hydrophobic compounds, and proven to stimulate nerve growth factor (NGF) synthesis and promote NGF-induced neurite outgrowth in nerve cells *in vitro* (Lai et al., 2013). However, hericenones failed to promote NGF gene expression in 1321N1 human astrocytoma cells (Mori et al., 2008) while erinacine A successfully upregulated the NGF level in the locus coeruleus and hippocampus of rats (Shimbo et al., 2005). To date, only erinacines A (unpublished results) and S (Hu et al., 2019) but not hericenones have been verified to cross the blood-brain-barrier, suggesting a greater of likelihood of them targeting the central nervous system. Furthermore, the *in vivo* neuroprotection of erinacine A-enriched *H. erinaceus* (EAHE) mycelia has been demonstrated in several studies against stroke, Parkinson's disease, AD, depression, and aging (Li et al., 2018b). Based on these findings, it is highly suggestive that erinacine A is one of the key components responsible for the neurotrophic and neuroprotective activities of *H. erinaceus*.

A previous human pilot study has been carried out to investigate the efficacy of oral administration of *H. erinaceus* with 50- to 80-year-old Japanese men and women diagnosed with mild cognitive impairment. The subjects in the *H. erinaceus* group took four *H. erinaceus* tablets three times a day for 16 weeks and showed an improvement in cognitive functions (Mori et al., 2009). However, in this study, the active constituents, representative markers, and major chemical constituents of *H. erinaceus* tablets have not been extensively addressed. While there is still a controversy regarding whether hericenones in the *H. erinaceus* fruiting body have neuroprotective activities *in vivo*, erinacine A in the *H. erinaceus* mycelia, on the other hand, confers neuroprotective effects and attenuates the oxidative stress against stroke (Lee et al., 2014), AD (Tzeng et al., 2018), Parkinson's disease (Kuo et al., 2016), depression (Chiu et al., 2018), and aging (Li et al., 2019) in mouse models. As there is an urgent need to translate basic discovery research to clinical evaluation, this is the first clinical investigation of

three *H. erinaceus* mycelia capsules (350 mg/capsule; containing 5 mg/g erinacine A active ingredient) per day for the treatment of patients with early AD.

MATERIALS AND METHODS

Sample Preparation and High-Performance Liquid Chromatography (HPLC) Analysis

Hericium erinaceus mycelia enriched with 5 mg/g erinacine A were prepared and evaluated according to a procedure described previously (Li et al., 2014b). In brief, EAHE mycelia was grown in a submerged liquid medium comprised of 0.25 % yeast extract, 4.5% glucose, 0.5% soybean powder, 0.25 % peptone, and 0.05 % $MgSO_4$ with an initial pH set to 4.5 at 26°C for 5 days. This process is then scaled up in 500-L and 20-ton fermenters for 5 days and 12 days, respectively. Following mass production, the mycelia were lyophilized, extracted with methanol, and analyzed by HPLC to quantify 5 mg/g erinacine A in EAHE mycelia. For study's intervention, 350 mg EAHE mycelia were encapsulated in each gelatin capsule and used as treatments.

Study Design

The present study was a 1-year, double-blind, randomized, placebo-controlled, fixed-dose intervention pilot trial conducted at Chung Shan Medical University in patients with mild AD. The study protocol was approved by the Institutional Review Board of Chung Shan Medical University and registered with ClinicalTrials.gov under the number NCT04065061. This study comprised of a 3-week no-drug screening period, followed by a 49-week double-blind treatment period with 2-parallel groups in which eligible patients were randomized to either three 350 mg/capsules containing 5 mg/g erinacine A per day or identical appearing placebo capsules with meals. This dose was chosen according to a previous study design (Li et al., 2019) and converted to human dose as specified by FDA guidelines (FDA, 2005). Cognitive assessments, ophthalmic examinations, biomarker collection, and neuroimaging were followed throughout the study period. Written informed consent from all patients or their legal representatives was obtained before their enrollment.

Participants, Randomization, and Blinding

The inclusion criteria for enrollment included patients with age >50 years and diagnosis of probable AD according to the Diagnostic and Statistical Manual of Mental Disorders (fourth edition, DSM-IV) (American Psychiatric Association, 2013) and National Institute of Neurological and Communicative Disorders and Stroke–Alzheimer's Disease and Related Disorders Association (Mckhann et al., 1984) criteria. The exclusion criteria included patients with severe somatic or psychiatric comorbidity as they may significantly impair cooperation with the study. Once a participant met the study's eligibility criteria, a baseline visit was planned, and thorough somatic and neurological examinations were carried out.

Following the baseline assessments, participants were randomly assigned to receive either the placebo or three EAHE mycelia capsules per day according to a randomization list produced by a computerized random-number generator. Except for two trial-independent statisticians that were unmasked, all patients, caregivers, raters, and investigators were blinded to the interventions until the database was finalized. The schedule of trial enrollment, interventions, and assessments according to the Standard Protocol Items: Recommendations for Interventional Trials (SPIRIT) Statement (Chan et al., 2013) is presented in **Figure 1**.

Efficacy and Safety Parameters

All participants received either three EAHE mycelia capsules per day or placebo for 49 weeks and were assessed by a rater at 0, 13, 25, and 49 weeks after commencing the treatment. The efficacy of EAHE mycelia was determined by the mean change from baseline to the final analysis and was evaluated by a comprehensive battery, which included cognitive assessments, ophthalmic examinations, biomarker collection, and neuroimaging.

The cognitive assessments were performed at baseline, week 13, week 25, and week 49. Reference measures for cognition included the Neuropsychiatric Inventory (NPI) (Cummings et al., 1994), Cognitive Abilities Screening Instrument (CASI) (Teng et al., 1994), Mini-Mental State Examination (MMSE) (Folstein et al., 1975), and Instrumental Activities of Daily Living (IADL) (Nygard, 2003). These standard tests are used extensively in both clinical practice and research to measure treatment effects in patients with mild to moderate dementia.

A complete ophthalmologic examination including the measurement of best-corrected visual acuity (BCVA) and contrast sensitivity (CS) was conducted at baseline, week 25, and week 49. Monocular and binocular best-corrected distant visual acuity were determined using a standard clinical Snellen eye chart at a 5-meter distance from the chart. The contrast sensitivity test was performed with a standard Pelli-Robson chart under the same conditions for all the patients.

Blood biomarkers were collected at baseline, week 25, and week 49. After overnight fasting, blood samples from each patient were drawn through 22-gauge needles and transferred into either ethylene diamine tetraacetic acid-potassium (EDTA-K2) tubes for hematological analysis or stored in tubes without anti-coagulants for biochemical analysis. For hematological analysis, homocysteine (Hcy) and hemoglobin (Hb) were measured using an automated hematology analyzer (Gen-STM, Beckman Coulter, Inc., United States) while the serum biochemistry parameters including albumin and calcium were performed using an automated biochemistry analyzer (LX®-20, Beckman Coulter, Inc., United States). Quantitative determination of other blood biomarkers such as alpha1-antichymotrypsin (α-ACT; ab171574, Abcam, United Kingdom), amyloid-beta peptide 1–40 (β-amyloid; CEA864Hu, Wuhan USCN Business Co., Ltd., China), apolipoprotein E4 (APOE4; K4699, BioVision Inc., United States), dehydroepiandrosterone-sulfate

	STUDY PERIOD					
	Enrolment	Allocation	Treatment			Close-out
TIMEPOINT		0	Week 13	Week 25	Week 49	
ENROLMENT:						
Eligibility screen	X					
Informed consent	X					
Allocation		X				
INTERVENTIONS:						
Placebo group			←	—	→	
EAHE group			←	—	→	
ASSESSMENTS:						
Cognitive assessments		X	X	X	X	
Ophthalmologic examination		X		X	X	
Blood biomarker assessments		X		X	X	
Magnetic resonance imaging assessments		X			X	
Adverse Events			X	X	X	
Statistical analysis						X

FIGURE 1 | Schedule of enrollment, interventions and assessments (SPIRIT Figure).

(DHEAS; ab108669, Abcam, United Kingdom), brain-derived neurotrophic factor (BDNF; KA0329, Abnova, Taiwan), and superoxide dismutase (SOD; #19160, Sigma-Aldrich, United States) were measured using commercially available enzyme-linked immunosorbent assay (ELISA) kits.

Neuroimaging such as magnetic resonance imaging (MRI) assessment was performed before and after the intervention period. All subjects had brain imaging using diffusion tensor imaging (DTI) through a Siemens Magnetom Skyra three-tesla (3T) scanner. Diffusion datasets were collected with the following parameters: repetition time (TR) = 4800 ms, echo time (TE) = 97 ms, field of view (FOV) = 25 cm, image matrix = 128 × 128, slice number = 35, thickness = 4 mm, flip angle = 90°, 4 *b*-values = 0, 1000, 1500, 2000 s/mm^2, diffusion direction = 64, and bandwidth = 1562 Hz/pixel. The fiber number, the fractional anisotropy (FA), and the apparent diffusion coefficient (ADC) from the arcuate fasciculus (ARC), parahippocampal cingulum (PHC), inferior fronto-occipital fasciculus (IFOF), and uncinate fasciculus (UNC) regions in the dominant and non-dominant hemispheres were determined based on the diffusion tensor analyzed through using the specialized software nordicICE v4.0.2.

Safety was evaluated by monitoring adverse events according to the Food and Drug Administration regulations (Behrman Sherman et al., 2011). Moreover, adverse event reporting was also reviewed by an independent safety monitoring committee systematically throughout the study.

Sample Size and Statistical Analysis

Considering this study is a pilot study to assess the cognitive efficacy of EAHE mycelia in patients with mild AD and the feasibility of a further larger clinical trial, a total of at least 60 people were recruited based on a simulation study to maintain adequate power while keeping the overall sample size of the pilot and main trial together to a minimum (Teare et al., 2014). Statistical analyses were performed using SPSS software (version 18). Data are presented as means ± standard deviation (SD). The Mann–Whitney U test was used to compare the data between

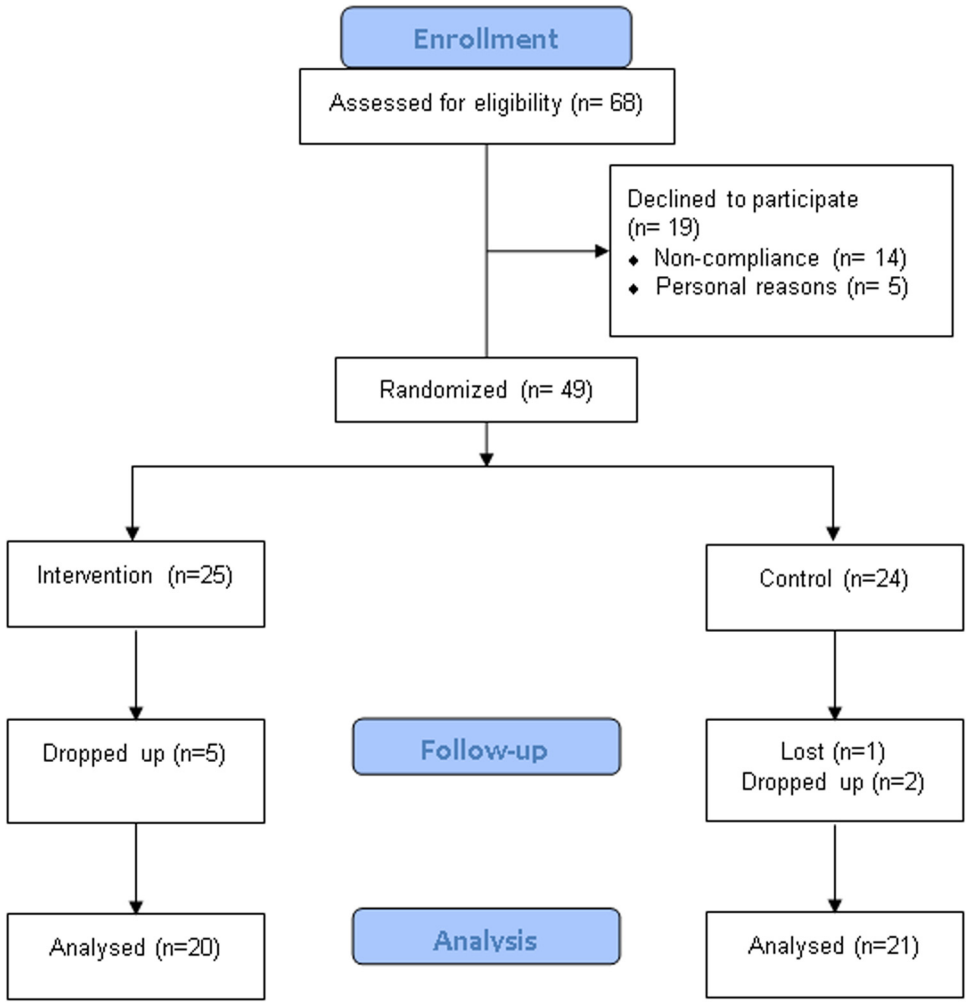

FIGURE 2 | CONSORT diagram.

the two study groups while the Wilcoxon signed-rank test was used to compare variables before and after the intervention. The statistically significant value was set at $p < 0.05$.

RESULTS

Participants

A total of 68 participants who had been diagnosed with mild AD were recruited in this study. Participants were randomly assigned to either the EAHE intervention group or the placebo control group. Of the 68 patients who participated in the surveillance, 19 declined to participate due to personal reasons ($n = 5$) and non-compliance ($n = 14$). Forty-nine participants were randomized, of whom seven subjects withdrew consent and one subject lost to follow-up. In the end, 41 subjects completed the study, and the data from 17 male and 24 female study participants were analyzed (**Figure 2**). Demographic and baseline characteristics are shown in **Table 1**. There were no statistical differences between the EAHE group and the placebo group in gender, age, and education characteristics at baseline.

Cognitive Assessments

The NPI, CASI, MMSE, and IADL tests were performed at baseline, after weeks 13, weeks 25, and weeks 49 of supplementation with EAHE. The means scores of each parameter in the EAHE and placebo group are presented in **Table 2**. For the NPI test, the mean NPI scores at all time-points

TABLE 1 | Participant demographics.

Variables	EAHE group ($n = 20$)	Placebo group ($n = 21$)	p-Value
Gender (male/female)	6/14	11/10	–
Age (years)	74.3 ± 7.15	77.05 ± 8.2	0.261
Education (years)	6.35 ± 4.74	6 ± 5.36	0.826

Values are given as mean ± SD.

decreased in both the EAHE and placebo groups compared to the baseline. Although subjects who received EAHE has a lower mean NPI score than the placebo group at week 49 (0.67 ± 1.15 vs. 2.25 ± 3.3), the comparison to baseline values showed no significant difference in both groups (p = 0.077 and 0.163, respectively). Moreover, when compared to the baseline values and different time points of CASI scores, subjects in the EAHE group showed an increasing trend with marginal significance (71.75 ± 17.12 to 75.35 ± 15.86; p = 0.058) whereas the subjects in the placebo group showed a decreasing trend from the baseline to 49 weeks (73.52 ± 14.51 to 69.67 ± 16.62; p = 0.064). However, there was no significance in relation to the intra-group and inter-group CASI analysis except for the difference between the baseline and week 25 of the placebo group (p = 0.043). Furthermore, MMSE scores significantly increased (21.75 ± 6.1 to 23.2 ± 5.92; p = 0.035) in the EAHE group from the baseline to week 49 whereas the comparison of all time-points showed no significant change in the placebo group. Nevertheless, all the pairwise comparisons of the MMSE test were not statistically significant ($p > 0.05$). Finally, for the IADL test, no baseline differences between the EAHE and placebo groups at any time points were observed except for the pairwise comparison at week 49 which was statistically significant (6.7 ± 2.47 vs. 5 ± 2.7; p = 0.012, respectively).

Ophthalmologic Examination

Table 3 summarizes the ophthalmologic examination for the EAHE and placebo groups after 25 and 49 weeks of intervention. The analysis of BCVA in OD (right eye), OS (left eye), and OU (both eyes) of the EAHE and placebo groups showed no difference from their baselines to the end of the study. Although significant baseline differences in BCVA of OD, OS, and OU were found between the groups, these differences remained unchanged throughout the study period except for BCVA OS at week 25 (p = 0.101). Meanwhile, subjects with EAHE treatment showed improvements in the mean monocular CS (OD: 0.84 ± 0.19 to 0.90 ± 0.08; OS: 0.83 ± 0.2 to 0.86 ± 0.13) and binocular CS (OU: 0.88 ± 0.15 to 0.89 ± 0.11) values following 49 weeks of intervention whereas the placebo group showed an upward trend in the CS OD (0.72 ± 0.32 to 0.77 ± 0.27), a downward trend in the CS OS (0.83 ± 0.18 to 0.78 ± 0.17), and remained unchanged (0.85 ± 0.19 to 0.85 ± 0.08) in the CS OU at the end of the study. Nevertheless, all these groups did not reach statistical significance except for the changes in CS OU from baseline to 49 weeks in the placebo group (0.85 ± 0.19 to 0.85 ± 0.08; p = 0.033) and differences of CS OS at week 49 between treatment groups (p = 0.046).

Blood Biomarker Assessments

With further analysis of the blood biomarkers over the 49-week study period within the groups (**Table 4**), significant improvements of Hcy at week 25 and 49 (p = 0.007 and p = 0.012, respectively) were observed in the EAHE group while significant negative effects in calcium at week 25 (p = 0.004), albumin at week 49 (p = 0.004), Hb at week 25 and 49 (p = 0.003 and p = 0.009, respectively), and BDNF at week 25 (p = 0.012) were noted in the placebo group. Moreover, although both groups showed significant decreases in SOD and APOE4 as well as significant increases in α-ACT and β-amyloid ($p < 0.05$), APOE4, α-ACT, and β-amyloid had an improving trend in the EAHE group than the placebo group at week 49. No significant difference, however, was observed for all other parameters.

Magnetic Resonance Imaging (MRI) Assessments

The total fiber number, FA, and ADC values from the ARC, PHC, IFOF, and UNC regions in the dominant and non-dominant hemispheres of the EAHE and control group are listed in **Table 5**. After 49 weeks of EAHE intervention, the total fibers were significantly less decreased than those in the placebo group. Nevertheless, they did not reach statistical significance between groups (p = 0.715). In addition, compared to their baselines, the mean ADC values from the ARC region in the dominant hemisphere significantly increased in the placebo group while the ADC values from the PHC region in the dominant hemisphere significantly decreased in the EAHE group at week 49. No statistically significant differences were found in other parameters.

Adverse Events

During the study, 1 subject lost to follow-up while 7 subjects (7/49; 14.3%) left the study. Reasons for dropout that have been investigated include unsatisfactory efficacy (2 from EAHE group and 1 from the placebo group) and the presence of side effects (3 from EAHE group and 1 from the placebo group). Possible or probable side effects related to the intervention included nausea in the placebo group and abdominal discomfort, nausea, and skin rash in the EAHE group.

DISCUSSION

Diet is an important modifiable risk factor for AD (Sindi et al., 2018) as it is able to modulate structural brain connectivity (Park et al., 2018), cause positive changes in brain function and behavior (Bolton and Bilbo, 2014), as well as help regulate cognition and emotion (Spencer et al., 2017). As benefits of EAHE associated with brain and nerve health have been well-studied (Li et al., 2018b), this is the first study to endorse its potential in mitigating neurodegenerative disorders. Based on the results of this pilot, randomized, double-blinded, controlled study, subjects with mild AD showed a significant benefit in reducing cognitive decline and improving contrast sensitivity after oral administration of three 5 mg/g EAHE mycelia capsules per day for 49 weeks when compared with placebo.

In this study, through random allocation, the baseline demographic information including age, gender, and education level between EAHE and placebo groups showed no significant differences before the intervention. Nevertheless, after the intervention, a significant deterioration in CASI from baseline to week 25 was noted in the placebo group, a significant improvement in MMSE from baseline to week 49 was observed in the EAHE group, and a significant IADL difference at week 49 were found between the two groups. Higher CASI and

TABLE 2 | Comparison of cognitive assessments between EAHE and placebo groups.

	EAHE group (n = 20)		Placebo group (n = 21)		
Variables	**Value**	**Intragroup p-value**	**Value**	**Intragroup p-value**	**Intergroup p-value**
NPI					
Baseline	4.21 ± 6.62	–	3 ± 5.2	–	0.696
Week 13	0 ± 0	0.306	1.33 ± 1.53	0.812	0.259
Week 25	1.5 ± 2.12	0.439	1.33 ± 2.31	0.087	0.989
Week 49	0.67 ± 1.15	0.077	2.25 ± 3.3	0.163	0.129
CASI					
Baseline	71.75 ± 17.12	–	73.52 ± 14.51	–	0.804
Week 13	72.74 ± 15.83	0.246	70.71 ± 19.3	0.13	0.881
Week 25	73.8 ± 17.15	0.313	69.62 ± 16.07	0.043*	0.368
Week 49	75.35 ± 15.86	0.058	69.67 ± 16.62	0.064	0.315
MMSE					
Baseline	21.75 ± 6.1	–	21.33 ± 5.74	–	0.629
Week 13	22.58 ± 5.6	0.065	20.95 ± 6.47	0.616	0.4
Week 25	22.55 ± 6.24	0.23	21.05 ± 5.5	0.686	0.353
Week 49	23.2 ± 5.92	0.035*	20.67 ± 6.17	0.661	0.261
IADL					
Baseline	6.35 ± 2.81	–	5.71 ± 2.65	–	0.25
Week 13	6.37 ± 2.31	1	6 ± 2.07	0.484	0.423
Week 25	6.45 ± 2.58	0.705	5.57 ± 2.29	0.634	0.11
Week 49	6.7 ± 2.47	0.157	5 ± 2.7	0.075	0.012*

*Values are given as mean ± SD. NPI = Neuropsychiatric Inventory; CASI = Cognitive Abilities Screening Instrument; MMSE = Mini mental state Examination; IADL = Instrumental Activities of Daily Living. *$p < 0.05$.*

MMSE scores represent better cognition, and higher IADL scores represent a lower level of dependence (Chiu et al., 2016). Although there were no significant differences in CASI and MMSE between the EAHE and placebo groups, the scores were higher in the EAHE group compared to those in the placebo group for participants with mild AD, implying that subjects could achieve more benefits from the intervention.

To date, human studies on *H. erinaceus* are scarce. Only three trials were found to examine the efficacy of oral administration of *H. erinacues* for improving brain pathology. In one double-blind placebo-controlled study, 50- to 80-year-old Japanese men and women (n = 30) diagnosed with mild cognitive impairment showed marked improvement in cognitive function when compared to controls, using a cognitive function scale based on the revised Hasegawa Dementia Scale and following the effects of oral intake of four 250 mg tablets containing 96% of *H. erinaceus* fruiting body dry powder three times a day for 16 weeks (Mori et al., 2009). In another randomized, double-blind placebo-controlled study, administration of 0.5 g *H. erinaceus* fruiting body in cookies over 4 weeks showed a reduction in anxiety and depression in menopausal women (n = 30) compared to those taking placebo, as measured by the Center for Epidemiologic Studies Depression Scale and Indefinite Complaints Index (Nagano et al., 2010). In the third randomized, double-blind, placebo-controlled parallel-group comparative study, the consumption of cookies containing 0.8 g of *H. erinaceus* fruiting body dry powder alleviated the deterioration of short memories and improved the cognitive functions in 31 participants with an average age of 61.3 years old over the period of 12 weeks, as measured by MMSE (Saitsu et al., 2019). Prior studies have reported that NGF could enhance neurogenesis-inducing effects, which led to antidepressant and antianxiety activities (Shohayeb et al., 2018). Although hericenones C and D from the fruiting body of *H. erinaceus* have shown to induce neuroprotective properties (Kawagishi et al., 1991) in rats by stimulating NGF synthesis via activation of the c-jun N-terminal kinase (JNK) pathway, they failed to promote NGF gene expression in 1321N1 human astrocytoma cells (Mori et al., 2008). This result suggested that *H. erinaceus* fruiting body may contains other active compounds and/or hericenones that can potentially improve mild cognitive impairment as well as reduce depression and anxiety.

On the contrary, erinacines isolated from the mycelium of the mushroom are able to pass through the brain-blood barrier into the brain (Hu et al., 2019) to promote NGF synthesis *in vivo* (Shimbo et al., 2005). During normal physiological conditions, NGF is released by the postsynaptic cortical and hippocampal neurons to activate further signaling cascades that include cell survival, maintenance, and proliferation (Biane et al., 2014). However, NGF has been found to be reduced during the pathological conditions of AD, resulting in induced loss of cortical synapses and atrophy of cholinergic neurons in the basal forebrain (Iulita and Cuello, 2014). Moreover, analyzing AD11 anti-NGF transgenic mice that express NGF antibodies in the brain, it was observed that NGF deprivation leads to early inflammation and Alzheimer's neurodegeneration (Capsoni et al., 2011). In this regard, as erinacine A has been proven to promote NGF synthesis *in vivo*, it may contribute to the

TABLE 3 | Comparison of ophthalmologic examination between EAHE and placebo groups.

	EAHE group (n = 20)		Placebo group (n = 21)		
Variables	**Value**	**Intragroup p-value**	**Value**	**Intragroup p-value**	**Intergroup p-value**
BCVA OD					
Baseline	0.83 ± 0.24	–	0.59 ± 0.33	–	0.013*
Week 25	0.8 ± 0.27	0.552	0.59 ± 0.33	0.814	0.026*
Week 49	0.83 ± 0.2	0.545	0.57 ± 0.28	0.258	0.005*
BCVA OS					
Baseline	0.82 ± 0.25	–	0.63 ± 0.27	–	0.024*
Week 25	0.77 ± 0.27	0.153	0.67 ± 0.23	0.633	0.101
Week 49	0.82 ± 0.24	0.824	0.64 ± 0.23	0.201	0.025*
BCVA OU					
Baseline	0.9 ± 0.22	–	0.75 ± 0.23	–	0.017*
Week 25	0.89 ± 0.26	0.923	0.74 ± 0.21	0.472	0.027*
Week 49	0.88 ± 0.22	0.948	0.69 ± 0.2	0.104	0.005*
CS OD					
Baseline	0.84 ± 0.19	–	0.72 ± 0.32	–	0.249
Week 25	0.86 ± 0.19	0.257	0.75 ± 0.29	0.187	0.212
Week 49	0.9 ± 0.08	0.257	0.77 ± 0.27	0.582	0.089
CS OS					
Baseline	0.83 ± 0.2	–	0.83 ± 0.18	–	0.323
Week 25	0.82 ± 0.25	0.85	0.82 ± 0.11	0.227	0.155
Week 49	0.86 ± 0.13	0.606	0.78 ± 0.17	0.13	0.046*
CS OU					
Baseline	0.88 ± 0.15	–	0.85 ± 0.19	–	0.28
Week 25	0.88 ± 0.2	0.739	0.86 ± 0.09	0.405	0.069
Week 49	0.89 ± 0.11	0.68	0.85 ± 0.08	0.033*	0.056

*Values are given as mean ± SD. BCVA = best-corrected visual acuity; CS = contrast sensitivity; OD = oculus dexter; OS = oculus sinister; OU = oculus uterque. *$p < 0.05$.*

survival and regeneration of cholinergic neurons as well as revive cholinergic signaling in the cortex and hippocampus, thereby improving the cognitive ability in subjects with mild AD. However, the precise mechanism of its action needs further investigation.

Not only could NGF markedly protect degenerating neurons in the brain, studies have also shown that NGF administration could modulate the development and differentiation of the retina and the optic nerve, as well as promote the survival and recovery of retinal ganglion cells (Aloe et al., 2012). To our knowledge, this is the first study to examine the efficacy of EAHE on visual acuity and contrast sensitivity. No significant differences were observed in the ophthalmologic examination in this study except for a higher CS OS at week 49 after EAHE treatment. This finding of EAHE as a NGF stimulator in improving CS but not VA in subjects with mild AD is consistent with previous studies. They have found that contrast sensitivity was significantly reduced in patients with AD compared to elderly control subjects while no significant difference in visual acuity were found between the patients with AD and control subjects (Crow et al., 2003) suggesting that EAHE targeting astrocytes only responded to an injury or damaged area by maintaining neurogenesis as a mechanism of repair (Poulose et al., 2017). Future studies, however, are required to further explore this possible mechanism.

With EAHE consumption, it is important to note that an altered diet or a multiplicity of environmental changes could change the blood proteome as well as ions (Te Pas et al., 2013). In different studies, EAHE treatment was accompanied by improvements in blood biomarkers in subjects with mild AD. Biomarkers monitoring based on biochemical analysis of blood during or after the intervention period could offer considerable promise for improving the treatment of AD (Cummings et al., 2019). Recent studies have identified a biomarker panel that included blood-based markers that significantly increased alpha-1-Antichymotrypsin, β-amyloid, superoxide dismutase, and homocysteine levels as well as decreased calcium, albumin, dehydroepiandrosterone sulfate, apolipoprotein E, hemoglobin, and BDNF levels in AD (Dekosky et al., 2003; Laske et al., 2011; Doecke et al., 2012; Ng et al., 2019; Pan et al., 2019). Consistent with the current study, biomarkers such as calcium, albumin, APOE4, Hb, and BDNF were significantly lowered while α-ACT and β- amyloid were significantly elevated during the study period in the placebo group. However, there were no significant changes in calcium, albumin, Hb, and BDNF compared to the baseline and a trend toward improving SOD, APOE4, and α-ACT levels were observed in the EAHE group, indicating that EAHE may have possible effects in arresting or delaying further neurodegenerative processes.

TABLE 4 | Comparison of blood biomarkers between EAHE and placebo groups.

	EAHE group (n = 20)		Placebo group (n = 21)		
Variables	**Value**	**Intragroup p-value**	**Value**	**Intragroup p-value**	**Intergroup p-value**
Calcium					
Baseline	9.15 ± 0.29	–	9.23 ± 0.33	–	0.407
Week 25	9.05 ± 0.34	0.406	9.06 ± 0.4	0.004*	0.743
Week 49	9.08 ± 0.2	0.238	9.12 ± 0.47	0.23	0.545
Albumin					
Baseline	4.62 ± 0.29	–	4.35 ± 0.23	–	0.297
Week 25	4.35 ± 0.24	0.336	4.28 ± 0.31	0.387	0.503
Week 49	4.28 ± 0.26	0.657	4.14 ± 0.22	0.004*	0.136
Hb					
Baseline	13.35 ± 1.93	–	13.82 ± 1.55	–	0.251
Week 25	13.04 ± 1.6	0.102	12.73 ± 3.27	0.003*	0.411
Week 49	13.29 ± 1.58	0.822	13.4 ± 1.69	0.009*	0.611
Hcy					
Baseline	11.44 ± 4.52	–	11.39 ± 4.6	–	1
Week 25	9.23 ± 2.96	0.007*	10.11 ± 3.57	0.099	0.449
Week 49	9.42 ± 3.05	0.012*	11.85 ± 6.56	0.794	0.225
SOD					
Baseline	66.94 ± 10.43	–	62.39 ± 11	–	0.411
Week 25	66.63 ± 13.89	0.737	65.52 ± 13.98	0.274	0.917
Week 49	48.39 ± 19.28	0.001*	52.1 ± 17.76	0.021*	0.715
BDNF					
Baseline	16817.78 ± 7269.27	–	14146.35 ± 5248.59	–	0.235
Week 25	14790.69 ± 13578.16	0.117	9725.25 ± 6780.67	0.012*	0.335
Week 49	17943.1 ± 7356.27	0.654	13793.27 ± 5545.83	0.821	0.068
DHEAS					
Baseline	1.45 ± 1	–	1.11 ± 0.99	–	0.211
Week 25	1.45 ± 0.97	0.627	1.08 ± 0.76	0.59	0.211
Week 49	0.91 ± 1.07	0.167	0.87 ± 0.82	0.689	0.465
α-ACT					
Baseline	201499.24 ± 183201.7	–	205721.68 ± 186042.47	–	0.766
Week 25	5438979.8 ± 5500347	0.001*	4130525.7 ± 4307187.3	<0.001*	0.584
Week 49	367337.35 ± 263536.7	0.019*	426465.17 ± 267768.25	0.017*	0.175
APOE4					
Baseline	141.45 ± 137.36	–	144.47 ± 230.67	–	0.167
Week 25	33.52 ± 28.7	0.01*	29.81 ± 29.63	0.073	0.549
Week 49	30.19 ± 35.04	0.001*	20.52 ± 20.01	<0.001*	0.511
β-amyloid					
Baseline	125.47 ± 86.34	–	104.11 ± 73.49	–	0.404
Week 25	156.24 ± 94.38	0.086	124.59 ± 74.04	0.244	0.397
Week 49	313.32 ± 122.45	0.015*	317.77 ± 124.98	0.001*	0.531

*Values are given as mean ± SD. Hb = hemoglobin; Hcy = homocysteine; SOD = superoxide dismutase; BDNF = brain-derived neurotrophic factor; DHEAS = dehydroepiandrosterone-sulphate; α-ACT = alpha 1-antichymotrypsin; APOE4 = apolipoprotein E4; β-amyloid = amyloid-beta peptide 1–40. *$p < 0.05$.*

The effects of EAHE on the rate of neurodegeneration could also be detected using advanced MRI, such as DTI, to probe human brain microstructures (Cho et al., 2008). DTI provides quantitative measures of FA and ADC, which enable the assessment of the cellular microstructure and fiber tract integrity in live tissues. Fiber tracts such as PHC and UNC contribute to learning and memory, and IFOF and AF contribute to language functioning (Mcdonald et al., 2008). These were evaluated in each subject to depict their global white matter status. In this study, although a statistical significance was not found between the groups, the total fibers of six fiber tracts calculated were significantly less decreased than those in the placebo group after EAHE intervention, suggesting that EAHE ameliorates the loss of fiber numbers by stimulating NGF synthesis and inducing neurogenesis. Moreover, within the six fiber tracts, the mean ADC values from the ARC region in the dominant hemisphere significantly increased in the placebo group while no significant difference was found in the EAHE group in comparison to their

TABLE 5 | Comparison of MRI assessments between EAHE and placebo groups.

	EAHE group (n = 20)		Placebo group (n = 21)		
Variables	**Value**	**Intragroup p-value**	**Value**	**Intragroup p-value**	**Intergroup p-value**
Total fibers					
Baseline	43523 ± 8327.67	–	41463.43 ± 8868.05	–	0.44
Week 49	40085.21 ± 9124.5	0.001*	38512.2 ± 11643.18	0.008*	0.715
D.ARC.FA					
Baseline	0.45 ± 0.03	–	0.43 ± 0.03	–	0.05
Week 49	0.45 ± 0.03	0.421	0.43 ± 0.04	0.205	0.148
N.ARC.FA					
Baseline	0.45 ± 0.03	–	0.45 ± 0.03	–	0.86
Week 49	0.46 ± 0.02	0.144	0.46 ± 0.03	0.469	0.704
D.PHC.FA					
Baseline	0.39 ± 0.02	–	0.4 ± 0.03	–	
Week 49	0.4 ± 0.02	0.609	0.4 ± 0.03	0.756	
N.PHC.FA					
Baseline	0.38 ± 0.03	–	0.36 ± 0.1	–	0.797
Week 49	0.4 ± 0.03	0.266	0.38 ± 0.03	0.861	0.272
D.IFOF.FA					
Baseline	0.47 ± 0.02	–	0.44 ± 0.03	–	0.024*
Week 49	0.47 ± 0.02	0.879	0.44 ± 0.05	0.513	0.014*
N.IFOF.FA					
Baseline	0.46 ± 0.03	–	0.43 ± 0.03	–	0.011*
Week 49	0.46 ± 0.03	0.276	0.43 ± 0.04	0.095	0.006*
D.UNC.FA					
Baseline	0.41 ± 0.03	–	0.4 ± 0.03	–	0.704
Week 49	0.4 ± 0.04	0.463	0.4 ± 0.04	0.828	0.483
N.UNC.FA					
Baseline	0.4 ± 0.03	–	0.4 ± 0.03	–	0.955
Week 49	0.4 ± 0.03	0.421	0.4 ± 0.03	0.962	0.493
D.ARC.ADC					
Baseline	103.63 ± 6.59	–	106.18 ± 7.52	–	0.233
Week 49	104.29 ± 8.84	0.711	109.02 ± 10.63	0.033*	0.105
N.ARC.ADC					
Baseline	103.44 ± 8.65	–	106.66 ± 8.8	–	0.101
Week 49	103.85 ± 11.09	0.372	106.56 ± 10.44	0.365	0.112
D.PHC.ADC					
Baseline	125.51 ± 9.66	–	127.98 ± 12.15	–	0.32
Week 49	123.12 ± 7.68	0.03*	123.82 ± 7.82	0.446	0.8
N.PHC.ADC					
Baseline	126.43 ± 8.8	–	116.56 ± 32.15	–	0.406
Week 49	120.39 ± 3.74	0.05	124.43 ± 7.6	0.6	0.097
D.IFOF.ADC					
Baseline	116.76 ± 7.87	–	121.56 ± 7.97	–	0.17
Week 49	118.02 ± 7.72	0.36	121.82 ± 9.75	0.748	0.226
N.IFOF.ADC					
Baseline	117.71 ± 7.16	–	122.23 ± 9.8	–	0.239
Week 49	118.08 ± 7.23	0.744	120.33 ± 8.19	0.171	0.405
D.UNC.ADC					
Baseline	117.06 ± 3.93	–	119.19 ± 8.82	–	0.579
Week 49	119.57 ± 7.68	0.469	119.06 ± 5.96	0.741	0.849
N.UNC.ADC					
Baseline	117.82 ± 5.57	–	119.48 ± 8.72	–	0.933
Week 49	117.58 ± 5.89	0.307	120.05 ± 7.61	0.276	0.511

*Values are given as mean ± SD. D = dominant; N = Non-dominant; ARC = arcuate fasciculus; PHC = parahippocampal cingulum; IFOF = inferior fronto-occipital fasciculus; UNC = uncinate fasciculus; FA = Fractional Anisotropy; ADC = apparent diffusion coefficient. *$p < 0.05$.*

baselines, implying that there was a greater disorganization in the neural structure observed in the placebo group. Moreover, ADC values from the PHC region in the dominant hemisphere significantly decreased in the EAHE group whereas no significant difference was found in the placebo group when compared to their baselines, indicating that there was a more well-organized neural structure noted in the EAHE group. These results tie well with a previous study wherein the ADC values increased in the ARC and PHC of patients with mild AD when compared with a control group (Mayo et al., 2019), signifying that EAHE could improve structural deterioration of ARC and PHC in patients with mild AD.

Lastly, despite four subjects who dropped out during the study period due to reported adverse events such as abdominal discomfort, nausea, and skin rash, no other adverse event were reported. The overall incidence was 8.2% during the entire 49-weeks. However, due to the increasing trend in clinical practice to treat elderly patients with multiple medications (Poleksic and Xie, 2019), it remains a challenge to identify if these adverse events were caused by EAHE consumption. Yet, reports on genotoxicity (Li et al., 2014a), acute toxicity (Li et al., 2018a), 28 days subchronic toxicity (Li et al., 2014b) 90 days subchronic toxicity (Lee et al., 2019) and teratotoxicity (Li et al., 2018a) have been conducted in animals and showed no adverse effects. Moreover, no adverse events have been reported after the launch of EAHE products into the Taiwanese market since 2015 (Li et al., 2018b). Nevertheless, further studies, especially the serum biochemical and hematological data along with urinalysis values after long-term consumption in humans, are important to consider.

In comparison to the placebo group, the intake of EAHE for 49 weeks showed higher CASI, MMSE, and IADL scores and achieved a better contrast sensitivity in patients with mild AD. The benefit of EAHE in reducing cognitive decline may be associated with improved blood biomarkers such as calcium, albumin, Hb, Hcy, SOD, BDNF, APOE4, and α-ACT, as well as reduced structural deterioration in the ARC and PHC regions of patients with mild AD. However, further studies on the mechanism of action of EAHE at the biochemical and molecular levels are necessary. In addition, although EAHE is safe and well-tolerated, a larger study is required to determine the benefits of EAHE consumption for patients with MCI or mild AD.

DATA AVAILABILITY STATEMENT

All datasets generated for this study are included in the article/supplementary material.

ETHICS STATEMENT

The study protocol was approved by the Institutional Review Board of the Chung Shan Medical University and registered with ClinicalTrials.gov under the number NCT04065061. The patients/participants provided their written informed consent to participate in this study.

AUTHOR CONTRIBUTIONS

I-CL analyzed the data and wrote the manuscript. H-HC, C-HL, and T-HL conceived and performed the experiments. W-PC, L-YL, Y-WC, and Y-PC provided the reagents. C-CC and DP-CL provided the expertise and feedback.

ACKNOWLEDGMENTS

The authors thank Hsin Yun Yang for editing the manuscript.

REFERENCES

Aloe, L., Rocco, M. L., Bianchi, P., and Manni, L. (2012). Nerve growth factor: from the early discoveries to the potential clinical use. *J. Transl. Med.* 10:239. doi: 10.1186/1479-5876-10-239

Alzheimer's Association, (2019). 2019 Alzheimer's disease facts and figures. *Alzheimer Dement.* 15, 321–387.

American Psychiatric Association, (2013). *Diagnostic and Statistical Manual Of Mental Disorders: DSM-5*, 5th Edn, Arlington, VA: American Psychiatric Publishing Inc.

Andrieu, S., Guyonnet, S., Coley, N., Cantet, C., Bonnefoy, M., Bordes, S., et al. (2017). Effect of long-term omega 3 polyunsaturated fatty acid supplementation with or without multidomain intervention on cognitive function in elderly adults with memory complaints (MAPT): a randomised, placebo-controlled trial. *Lancet Neurol.* 16, 377–389. doi: 10.1016/S1474-4422(17)30040-6

Behrman Sherman, R., Woodcock, J., Norden, J., Grandinetti, C., and Temple, R. J. (2011). New FDA regulation to improve safety reporting in clinical trials. *N. Engl. J. Med.* 365, 3–5. doi: 10.1056/NEJMp1103464

Biane, J., Conner, J. M., and Tuszynski, M. H. (2014). Nerve growth factor is primarily produced by GABAergic neurons of the adult rat cortex. *Front. Cell Neurosci.* 8:220. doi: 10.3389/fncel.2014.00220

Bolton, J. L., and Bilbo, S. D. (2014). Developmental programming of brain and behavior by perinatal diet: focus on inflammatory mechanisms. *Dialog. Clin. Neurosci.* 16, 307–320.

Capsoni, S., Brandi, R., Arisi, I., D'onofrio, M., and Cattaneo, A. (2011). A dual mechanism linking NGF/proNGF imbalance and early inflammation to Alzheimer's disease neurodegeneration in the AD11 anti-NGF mouse model. *CNS Neurol. Disord. Drug Targets* 10, 635–647. doi: 10.2174/187152711796235032

Chan, A. W., Tetzlaff, J. M., Altman, D. G., Laupacis, A., Gøtzsche, P. C., Krleža-Jeriæ, K., et al. (2013). SPIRIT 2013 statement: defining standard protocol items for clinical trials. *Ann. Intern. Med.* 158, 200–207.

Chiu, C.-H., Chyau, C.-C., Chen, C.-C., Lee, L.-Y., Chen, W.-P., Liu, J.-L., et al. (2018). Erinacine A-Enriched *Hericium erinaceus* mycelium produces antidepressant-like effects through modulating BDNF/PI3K/Akt/GSK-3β signaling in mice. *Intern. J. Mol. Sci.* 19:341. doi: 10.3390/ijms19020341

Chiu, P.-Y., Tsai, C.-T., Chen, P., Chen, W.-J., and Lai, T.-J. (2016). Neuropsychiatric symptoms in parkinson's disease dementia are more similar to alzheimer's disease than dementia with lewy bodies: a case-control study. *PLoS One* 11:e0153989. doi: 10.1371/journal.pone.0153989

Cho, H., Yang, D. W., Shon, Y. M., Kim, B. S., Kim, Y. I., Choi, Y. B., et al. (2008). Abnormal integrity of corticocortical tracts in mild cognitive impairment: a diffusion tensor imaging study. *J. Korea. Med. Sci.* 23, 477–483. doi: 10.3346/jkms.2008.23.3.477

Crow, R. W., Levin, L. B., Labree, L., Rubin, R., and Feldon, S. E. (2003). Sweep visual evoked potential evaluation of contrast sensitivity in Alzheimer's dementia. *Invest. Ophthalmol. Vis. Sci.* 44, 875–878. doi: 10.1167/iovs.01-1101

Cummings, J., Feldman, H. H., and Scheltens, P. (2019). The "rights" of precision drug development for Alzheimer's disease. *Alzheimer Res. Therapy* 11:76. doi: 10.1186/s13195-019-0529-5

Cummings, J. L., Mega, M., Gray, K., Rosenberg-Thompson, S., Carusi, D. A., and Gornbein, J. (1994). The neuropsychiatric inventory: comprehensive assessment of psychopathology in dementia. *Neurology* 44, 2308–2314. doi: 10.1212/wnl.44.12.2308

Dekosky, S. T., Ikonomovic, M. D., Wang, X., Farlow, M., Wisniewski, S., Lopez, J., et al. (2003). Plasma and cerebrospinal fluid alpha1-antichymotrypsin levels in Alzheimer's disease: correlation with cognitive impairment. *Ann. Neurol.* 53, 81–90. doi: 10.1002/ana.10414

Doecke, J. D., Laws, S. M., Faux, N. G., Wilson, W., Burnham, S. C., Lam, C.-P., et al. (2012). Blood-based protein biomarkers for diagnosis of Alzheimer disease. *Arch. Neurol.* 69, 1318–1325. doi: 10.1001/archneurol.2012.1282

FDA, (2005). *Estimating the Maximum Safe Starting Dose in Initial Clinical Trials for Therapeutics in Adult Healthy Volunteers*. Available: https://www.fda.gov/regulatory-information/search-fda-guidance-documents/estimating-maximum-safe-starting-dose-initial-clinical-trials-therapeutics-adult-healthy-volunteers (accessed June 26, 2018).

Feng, L., Cheah, I. K., Ng, M. M., Li, J., Chan, S. M., Lim, S. L., et al. (2019). The association between mushroom consumption and mild cognitive impairment: a community-based cross-sectional study in singapore. *J. Alzheimers Dis.* 68, 197–203. doi: 10.3233/JAD-180959

Folstein, M. F., Folstein, S. E., and Mchugh, P. R. (1975). Mini-mental state. A practical method for grading the cognitive state of patients for the clinician. *J. Psychiatr. Res.* 12, 189–198. doi: 10.1016/0022-3956(75)90026-6

Graham, W. V., Bonito-Oliva, A., and Sakmar, T. P. (2017). Update on Alzheimer's disease therapy and prevention strategies. *Science* 68, 413–430. doi: 10.1146/annurev-med-042915-103753

Hu, J.-H., Li, I.-C., Lin, T.-W., Chen, W.-P., Lee, L.-Y., Chen, C.-C., et al. (2019). Absolute bioavailability, tissue distribution, and excretion of erinacine s in *Hericium erinaceus* Mycelia. *Cell* 24:1624. doi: 10.3390/molecules24081624

Hung, S.-Y., and Fu, W.-M. (2017). Drug candidates in clinical trials for Alzheimer's disease. *J. Biomed. Sci.* 24:47. doi: 10.1039/c7an02013a

Iulita, M. F., and Cuello, A. C. (2014). Nerve growth factor metabolic dysfunction in Alzheimer's disease and Down syndrome. *Trends Pharmacol. Sci.* 35, 338–348. doi: 10.1016/j.tips.2014.04.010

Kawagishi, H., Ando, M., Sakamoto, H., Yoshida, S., Ojima, F., Ishiguro, Y., et al. (1991). Hericenones C, D and E, stimulators of nerve growth factor (NGF)-synthesis, from the mushroom *Hericium erinaceum*. *Tetrahed. Lett.* 32, 4561–4564.

Kawagishi, H., Ando, M., Shinba, K., Sakamoto, H., Yoshida, S., Ojima, F., et al. (1992). Chromans, hericenones F, G and H from the mushroom *Hericium erinaceum*. *Phytochemistry* 32, 175–178.

Kawagishi, H., Shimada, A., Hosokawa, S., Mori, H., Sakamoto, H., Ishiguro, Y., et al. (1996a). Erinacines E, F, and G, stimulators of nerve growth factor (NGF)-synthesis, from the mycelia of *Hericium erinaceum*. *Tetrahed. Lett.* 37, 7399–7402.

Kawagishi, H., Simada, A., Shizuki, K., Ojima, F., Mori, H., Okamoto, K., et al. (1996b). Erinacine D, a stimulator of ngf-synthesis, from the mycelia of *Hericium Erinaceum*. *Heterocyc. Commun.* 2, 51–54. doi: 10.1515/HC.1996.2.1.51

Kawagishi, H., Shimada, A., Shirai, R., Okamoto, K., Ojima, F., Sakamoto, H., et al. (1994). Erinacines A, B and C, strong stimulators of nerve growth factor (NGF)-synthesis, from the mycelia of *Hericium erinaceum*. *Tetrahed. Lett.* 35, 1569–1572.

Kuo, H. C., Lu, C. C., Shen, C. H., Tung, S. Y., Hsieh, M. C., Lee, K. C., et al. (2016). *Hericium erinaceus* mycelium and its isolated erinacine A protection from MPTP-induced neurotoxicity through the ER stress, triggering an apoptosis cascade. *J. Transl. Med.* 14:78. doi: 10.1186/s12967-016-0831-y

Lai, P. L., Naidu, M., Sabaratnam, V., Wong, K. H., David, R. P., Kuppusamy, U. R., et al. (2013). Neurotrophic properties of the Lion's mane medicinal mushroom, *Hericium erinaceus* (higher basidiomycetes) from Malaysia. *Int. J. Med. Mushrooms* 15, 539–554. doi: 10.1615/intjmedmushr.v15.i6.30

Laske, C., Leyhe, T., Stransky, E., Hoffmann, N., Fallgatter, A. J., and Dietzsch, J. (2011). Identification of a blood-based biomarker panel for classification of Alzheimer's disease. *Intern. J. Neuropsychopharmacol.* 14, 1147–1155. doi: 10.1017/S1461145711000459

Lee, E. W., Shizuki, K., Hosokawa, S., Suzuki, M., Suganuma, H., Inakuma, T., et al. (2000). Two novel diterpenoids, erinacines H and I from the mycelia of *Hericium erinaceum*. *Biosci. Biotechnol. Biochem.* 64, 2402–2405. doi: 10.1271/bbb.64.2402

Lee, K. F., Chen, J. H., Teng, C. C., Shen, C. H., Hsieh, M. C., Lu, C. C., et al. (2014). Protective effects of *Hericium erinaceus* mycelium and its isolated erinacine A against ischemia-injury-induced neuronal cell death via the inhibition of iNOS/p38 MAPK and nitrotyrosine. *Int. J. Mol. Sci.* 15, 15073–15089. doi: 10.3390/ijms150915073

Lee, L.-Y., Li, I.-C., Chen, W.-P., Tsai, Y.-T., Chen, C.-C., and Tung, K.-C. (2019). Thirteen-week oral toxicity evaluation of erinacine A enriched lion's mane medicinal mushroom, *Hericium erinaceus* (Agaricomycetes), mycelia in sprague-dawley rats. *Intern. J. Med. Mushrooms* 21, 401–411. doi: 10.1615/IntJMedMushrooms.2019030320

Li, I. C., Chen, W. P., Chen, Y. P., Lee, L. Y., Tsai, Y. T., and Chen, C. C. (2018a). Acute and developmental toxicity assessment of erincine A-enriched *Hericium erinaceus* mycelia in Sprague-Dawley rats. *Drug Chem. Toxicol.* 41, 459–464. doi: 10.1080/01480545.2017.1381110

Li, I. C., Lee, L. Y., Tzeng, T. T., Chen, W. P., Chen, Y. P., Shiao, Y. J., et al. (2018b). Neurohealth properties of *Hericium erinaceus* mycelia enriched with *Erinacines*. *Behav. Neurol.* 2018:5802634. doi: 10.1155/2018/5802634

Li, I. C., Chen, Y. L., Chen, W. P., Lee, L. Y., Tsai, Y. T., Chen, C. C., et al. (2014a). Genotoxicity profile of erinacine A-enriched *Hericium erinaceus* mycelium. *Toxicol. Rep.* 1, 1195–1201. doi: 10.1016/j.toxrep.2014.11.009

Li, I. C., Chen, Y. L., Lee, L. Y., Chen, W. P., Tsai, Y. T., Chen, C. C., et al. (2014b). Evaluation of the toxicological safety of erinacine A-enriched *Hericium erinaceus* in a 28-day oral feeding study in Sprague-Dawley rats. *Food Chem. Toxicol.* 70, 61–67. doi: 10.1016/j.fct.2014.04.040

Li, I. C., Lee, L.-Y., Chen, Y.-J., Chou, M.-Y., Wang, M.-F., Chen, W.-P., et al. (2019). Erinacine A-enriched *Hericium erinaceus* mycelia promotes longevity in *Drosophila melanogaster* and aged mice. *PLoS One* 14:e0217226. doi: 10.1371/journal.pone.0217226

Mayo, C. D., Garcia-Barrera, M. A., Mazerolle, E. L., Ritchie, L. J., Fisk, J. D., Gawryluk, J. R., et al. (2019). Relationship between DTI metrics and cognitive function in Alzheimer's disease. *Front. Aging Neurosci.* 10:436. doi: 10.3389/fnagi.2018.00436

Mcdonald, C. R., Ahmadi, M. E., Hagler, D. J., Tecoma, E. S., Iragui, V. J., Gharapetian, L., et al. (2008). Diffusion tensor imaging correlates of memory and language impairments in temporal lobe epilepsy. *Neurology* 71, 1869–1876. doi: 10.1212/01.wnl.0000327824.05348.3b

Mckhann, G., Drachman, D., Folstein, M., Katzman, R., Price, D., and Stadlan, E. M. (1984). Clinical diagnosis of Alzheimer's disease. *Neurology* 34:939.

Mori, K., Inatomi, S., Ouchi, K., Azumi, Y., and Tuchida, T. (2009). Improving effects of the mushroom yamabushitake (*Hericium erinaceus*) on mild cognitive impairment: a double-blind placebo-controlled clinical trial. *Phytother. Res.* 23, 367–372. doi: 10.1002/ptr.2634

Mori, K., Obara, Y., Hirota, M., Azumi, Y., Kinugasa, S., Inatomi, S., et al. (2008). Nerve growth factor-inducing activity of *Hericium erinaceus* in 1321N1 human astrocytoma cells. *Biol. Pharm. Bull.* 31, 1727–1732. doi: 10.1248/bpb.31.1727

Nagano, M., Shimizu, K., Kondo, R., Hayashi, C., Sato, D., Kitagawa, K., et al. (2010). Reduction of depression and anxiety by 4 weeks *Hericium erinaceus* intake. *Biomed. Res.* 31, 231–237. doi: 10.2220/biomedres.31.231

Ng, T. K. S., Ho, C. S. H., Tam, W. W. S., Kua, E. H., and Ho, R. C.-M. (2019). Decreased serum brain-derived neurotrophic factor (BDNF) levels in patients with Alzheimer's Disease (AD): a systematic review and meta-analysis. *Intern. J. Mol. Sci.* 20:257. doi: 10.3390/ijms20020257

Ngandu, T., Lehtisalo, J., Solomon, A., Levalahti, E., Ahtiluoto, S., Antikainen, R., et al. (2015). A 2 year multidomain intervention of diet, exercise, cognitive training, and vascular risk monitoring versus control to prevent cognitive decline in at-risk elderly people (FINGER): a randomised controlled trial. *Lancet* 385, 2255–2263. doi: 10.1016/S0140-6736(15)60461-5

Nygard, L. (2003). Instrumental activities of daily living: a stepping-stone towards Alzheimer's disease diagnosis in subjects with mild cognitive impairment? *Acta Neurol. Scand. Suppl.* 179, 42–46.

Pan, X., Wu, X., Kaminga, A. C., Wen, S. W., and Liu, A. (2019). Dehydroepiandrosterone and dehydroepiandrosterone sulfate in Alzheimer's Disease: a systematic review and meta-analysis. *Front. Aging Neurosci.* 11:61. doi: 10.3389/fnagi.2019.00061

Park, B.-Y., Lee, M. J., Kim, M., Kim, S.-H., and Park, H. (2018). Structural and functional brain connectivity changes between people with abdominal and non-abdominal obesity and their association with behaviors of eating disorders. *Science* 12:741. doi: 10.3389/fnins.2018.00741

Phan, C. W., David, P., and Sabaratnam, V. (2017). Edible and medicinal mushrooms: emerging brain food for the mitigation of neurodegenerative Diseases. *J. Med. Food* 20, 1–10. doi: 10.1089/jmf.2016.3740

Poleksic, A., and Xie, L. (2019). Database of adverse events associated with drugs and drug combinations. *Sci. Rep.* 9:20025. doi: 10.1038/s41598-019-56525-5

Poulose, S. M., Miller, M. G., Scott, T., and Shukitt-Hale, B. (2017). Nutritional factors affecting adult neurogenesis and cognitive function. *Adv. Nutr.* 8, 804–811. doi: 10.3945/an.117.016261

Saitsu, Y., Nishide, A., Kikushima, K., Shimizu, K., and Ohnuki, K. (2019). Improvement of cognitive functions by oral intake of *Hericium erinaceus*. *Biomed. Res.* 40, 125–131. doi: 10.2220/biomedres.40.125

Shimbo, M., Kawagishi, H., and Yokogoshi, H. (2005). Erinacine A increases catecholamine and nerve growth factor content in the central nervous system of rats. *Nutr. Res.* 25, 617–623.

Shohayeb, B., Diab, M., Ahmed, M., and Ng, D. C. H. (2018). Factors that influence adult neurogenesis as potential therapy. *Transl. Neurodegen.* 7:4. doi: 10.1186/s40035-018-0109-9

Sindi, S., Kåreholt, I., Eskelinen, M., Hooshmand, B., Lehtisalo, J., Soininen, H., et al. (2018). Healthy dietary changes in midlife are associated with reduced dementia risk later in life. *Nutrients* 10:1649. doi: 10.3390/nu10111649

Spencer, S. J., Korosi, A., Layé, S., Shukitt-Hale, B., and Barrientos, R. M. (2017). Food for thought: how nutrition impacts cognition and emotion. *Sci. Food* 1:7. doi: 10.1038/s41538-017-0008-y

Sperling, R. A., Jack, C. R., and Aisen, P. S. (2011). Testing the right target and right drug at the right stage. *Sci. Transl. Med.* 3:111cm133. doi: 10.1126/scitranslmed.3002609

Te Pas, M. F. W., Koopmans, S.-J., Kruijt, L., Calus, M. P. L., and Smits, M. A. (2013). Plasma proteome profiles associated with diet-induced metabolic syndrome and the early onset of metabolic syndrome in a pig model. *PLoS One* 8:e73087. doi: 10.1371/journal.pone.073087

Teare, M. D., Dimairo, M., Shephard, N., Hayman, A., Whitehead, A., and Walters, S. J. (2014). Sample size requirements to estimate key design parameters from external pilot randomised controlled trials: a simulation study. *Trials* 15:264. doi: 10.1186/1745-6215-15-264

Teng, E. L., Hasegawa, K., Homma, A., Imai, Y., Larson, E., Graves, A., et al. (1994). The cognitive Abilities screening instrument (CASI): a practical test for cross-cultural epidemiological studies of dementia. *Int. Psychogeriatr.* 6, 45–58. doi: 10.1017/s1041610294001602

Tzeng, T. T., Chen, C. C., Chen, C. C., Tsay, H. J., Lee, L. Y., Chen, W. P., et al. (2018). The cyanthin diterpenoid and sesterterpene constituents of *Hericium erinaceus* mycelium ameliorate alzheimer's disease-related pathologies in APP/PS1 transgenic mice. *Int. J. Mol. Sci.* 19:598. doi: 10.3390/ijms19020598

Conflict of Interest: Grape King Bio Inc., provided support in the form of salaries for the authors I-CL, W-PC, L-YL, Y-WC, Y-PC, and research materials, but did not have any additional role in the study design, data collection and analysis, decision to publish, or preparation of the manuscript.

The remaining authors declare that the research was conducted in the absence of any commercial or financial relationships that could be construed as a potential conflict of interest.

frontiers in Aging Neuroscience

SYSTEMATIC REVIEW
published: 05 June 2020
doi: 10.3389/fnagi.2020.00121

The Comparative Efficacy of Multiple Interventions for Mild Cognitive Impairment in Alzheimer's Disease: A Bayesian Network Meta-Analysis

*Xin Lai, Hao Wen, Yu Li, Liming Lu and Chunzhi Tang**

Medical College of Acu-Moxi and Rehabilitation, Guangzhou University of Chinese Medicine, Guangzhou, China

Background: Mild cognitive impairment (MCI) is the early phase of Alzheimer's disease (AD). The aim of early intervention for MCI is to decrease the rate of conversion from MCI to AD. However, the efficacy of multiple interventions in MCI, and the optimal methods of delivery, remain controversial. We aimed to compare and rank the treatment methods for MCI in AD, in order to find an optimal intervention for MCI and a way to prevent or delay the occurrence of AD.

Methods: Pair-wise and network meta-analysis were conducted to integrate the treatment effectiveness through direct and indirect evidence. Four English databases and three Chinese databases were searched for international registers of eligible published, single or double blind, randomized controlled trials up to September 31st 2019. We included nine comparative interventions: pharmacological therapies which incorporated cholinesterase inhibitors (ChEI), ginkgo, nimodipine, and Chinese medicine; non-pharmacological therapies comprising of acupuncture, music therapy, exercise therapy, and nutrition therapy; and a placebo group. The primary outcome was the Mini-Mental State Examination (MMSE) score. The secondary outcome was the AD Assessment Scale-cognitive subscale (ADAS-cog).

Results: Twenty-eight trials were eligible, including 6,863 participants. In the direct meta-analysis, as for the Mini-Mental State Examination scale, the ChEIs (MD: −0.38; 95% CI: −0.74, −0.01), Chinese medicine (MD: −0.31; 95% CI: −0.75, 0.13), exercise therapy (MD: −0.50; 95% CI: −0.65, −0.35), music therapy (MD: −1.71; 95% CI: −4.49, 1.07), were statistically more efficient than placebo. For AD Assessment Scalecognitive subscale outcome, ChEIs (MD: 1.20; 95% CI: 0.73, 1.68), Acupuncture (MD: 1.36; 95% CI: 1.28, 1.44), Chinese medicine (MD: 0.61; 95% CI: 0.49, 0.73) and exercise (MD: 0.61; 95% CI: 0.49, 0.73) were better than placebo. In the network meta-analysis, the MMSE outcome ranked music therapy (59%) as the best and Acupuncture (26%) as second. Nutrition and Ginkgo treatment had the lowest rank among all interventions. For ADAS-cog outcome, acupuncture (52) ranked the best.

OPEN ACCESS

Edited by:
Woon-Man Kung,
Chinese Culture University, Taiwan

Reviewed by:
Tae-Hun Kim,
Kyung Hee University, South Korea
Roger C. Ho,
National University of Singapore, Singapore
Dafin F. Muresanu,
Iuliu Haţieganu University of Medicine and Pharmacy, Romania

****Correspondence:***
Chunzhi Tang
jordan664@163.com

Received: *17 December 2019*
Accepted: *09 April 2020*
Published: *05 June 2020*

Citation:
Lai X, Wen H, Li Y, Lu L and Tang C (2020) The Comparative Efficacy of Multiple Interventions for Mild Cognitive Impairment in Alzheimer's Disease: A Bayesian Network Meta-Analysis. Front. Aging Neurosci. 12:121. doi: 10.3389/fnagi.2020.00121

Conclusion: Among the nine treatments studied, music therapy appears to be the best treatment for MCI, followed by acupuncture. Our study provides new insights into potential clinical treatments for MCI due to AD, and may aid the development of guidelines for MCI in AD.

Keywords: acupuncture, Alzheimer's disease, mild cognitive impairment, multiple interventions, music therapy, network meta-analysis

INTRODUCTION

Mild cognitive impairment (MCI) has been defined as a "transitional" state to describe individuals who are not cognitively "active" for their age, but who would not meet a clinical diagnosis of early dementia (Brendan and Kelley, 2015). It is an intermediate clinical condition with a number of sub-types and multiple pathologies (Petersen, 2004; Rountree et al., 2007).

MCI is currently an area of considerable clinical and research interest because a large proportion of patients with MCI develop Alzheimer's disease (AD). In order to delay the progress of AD, it is important to recognize the key neurobiological difference between MCI and AD. Several journal articles have demonstrated that MCI patients progress to AD at a higher rate (10–15% per year) than normal elderly patients (1–3% per year). Furthermore, two-thirds of patients with AD were previously recognized as having MCI (Rubin et al., 1989; Almkvist et al., 1998; Wolf et al., 1998; Kluger et al., 1999; Petersen et al., 1999, 2001; Collie and Maruff, 2000; Morris et al., 2001). Therefore, patients who have MCI are considered to be at a greater risk for AD. Unfortunately, treatment options for AD are currently suboptimal, especially in the advanced stage of AD where the brain damage is irreversible. Thus, it is important to start treatment for AD as early as possible, and intervention during the MCI stage may prevent or delay the occurrence of AD.

Several treatments have been used for MCI, including cholinesterase inhibitors (ChEIs), complementary and alternative medicine, lifestyle and nutrition interventions, and Chinese medicine. However, which of these interventions work, and to what extent, remains unknown.

Pairwise meta-analysis have previously been conducted to assess the efficacy of ChEIs, including donepezil, galantamine, and rivastigmine (Cooper et al., 2013; Tricco et al., 2013; Matsunaga et al., 2019). These studies suggested that ChEIs have a low efficacy in the treatment of MCI and many safety issues were raised. Therefore, before using ChEIs for MCI, other methods should be considered.

Other studies (Andreas et al., 2015; Liang et al., 2018) have suggested that physical exercise and computerized cognitive training could improve cognitive function and neuropsychiatric symptoms. Furthermore, non-pharmacological therapies might perform more effectively than pharmacological therapies. However, these studies were incomplete and provide insufficient data, because they were unable to introduce clear hierarchies among treatments and a number of interventions were not analyzed. Therefore, the aim of this article was to conduct a network meta-analysis to thoroughly compare and rank different treatments for MCI that help to improve cognitive function and prevent or delay the occurrence of AD.

METHODS

Search Strategy

Four English databases (Medline [via Ovid], Embase [via Ovid], Cochrane Library [Central Register of Controlled Trials], and Web of Science [via Ovid]) and three Chinese databases (China Science Journal Citation Report [VIP], China National Knowledge Infrastructure [CNKI], and Wanfang) were searched for all relevant citations published from the date of the respective database onset to September 31st 2019. We established search strategies which combined subject word (keyword) and random words related to MCI, interventions of interest (drug therapy, diet/lifestyle therapy, physical activity/exercise, complementary therapies, sham/placebo) and randomized controlled trial (RCT). Furthermore, the reference lists of the included studies were manually reviewed to look for additional relevant manuscripts. The specific search strategies are shown in **Supplementary Datasheet 1**.

Selection and Exclusion Criteria

The RCTs which met the following criteria were included: (1) participants had mild cognitive impairment due to AD; (2) the interventions were pharmacological therapies including Cholinesterase inhibitors, Memantine, Ginkgo biloba, Huperzine A, Piracetam, Nimodipine, and Chinese medicine, or non-pharmacological therapies including acupuncture, music therapy, lifestyle therapy, exercise therapy, and nutrition therapy; (3) the comparisons were placebo, no intervention, usual care control, or other comparable interventions; (4) the study included at least one cognitive performance outcome measure in the form of either the MMSE (Mini-Mental State Examination) or ADAS-cog (AD Assessment Scale-cognitive subscale) and the efficacy of the studies must include mean changes from baseline to endpoint.

Studies with the following characteristics were excluded: (1) participants with a diagnosis of MCI due to diseases other than AD; (2) irrelevant outcomes or deficient data; and (3) case reports, review articles, clinical protocols, conference abstracts, and animal experimental studies.

Data Extraction and Quality Assessment

Two investigators (XL and YL) screened the articles and extracted the data and related statistics independently. Basic information was organized into a standard table, including information on the characteristics of the population, intervention(s), comparison(s),

treatment duration, event(s), and outcome. The Cochrane Risk of Bias Tool (Savovic et al., 2014) was used by two researchers (XL and YL) to assessed the risk of bias and quality of included trials. A third reviewer (HW) was consulted to recheck studies when the first two reviewers had disagreements and discrepancies.

Outcomes

Our network meta-analysis used Mini-Mental State Examination (MMSE) as the primary outcome to measure global cognition, with higher MMSE scores meaning better cognitive function. The second outcome was the AD Assessment Scale-cognitive subscale (ADAS-cog), in which lower scores mean better cognitive function. If the complete data on outcomes were not reported in the original article, we contacted authors via email to obtain the raw data, otherwise studies lacking such data were eliminated. The data were independently collected by two reviewers (XL and YL) and rechecked by a third investigator (HW).

Statistical Analysis

Firstly, a pair-wise meta-analysis was used to compare the compliance of different therapies. By using the Aggregate Data Drug Information System (ADDIS ver. 1.16.8, available at: https://drugis.org/software/addis/index) with a random-effects model, the odds ratio (OR) was measured for discontinuous outcomes along with 95% credible intervals (CI). Statistical heterogeneity was calculated in the pair-wise comparisons with an I^2 statistic and the p-value.

Furthermore, we conducted a network meta-analysis. This network meta-analysis was set up with a Bayesian framework using the Aggregate Data Drug Information System (ADDIS ver. 1.16.8, available at: https://drugis.org/software/addis/index) to determine the cognitive outcomes of nine interventions. This software uses the Bayesian framework as a base combined with the Markov chain Monte Carlo method to evaluate research data. A random-effects model was used to evaluate the effect sizes

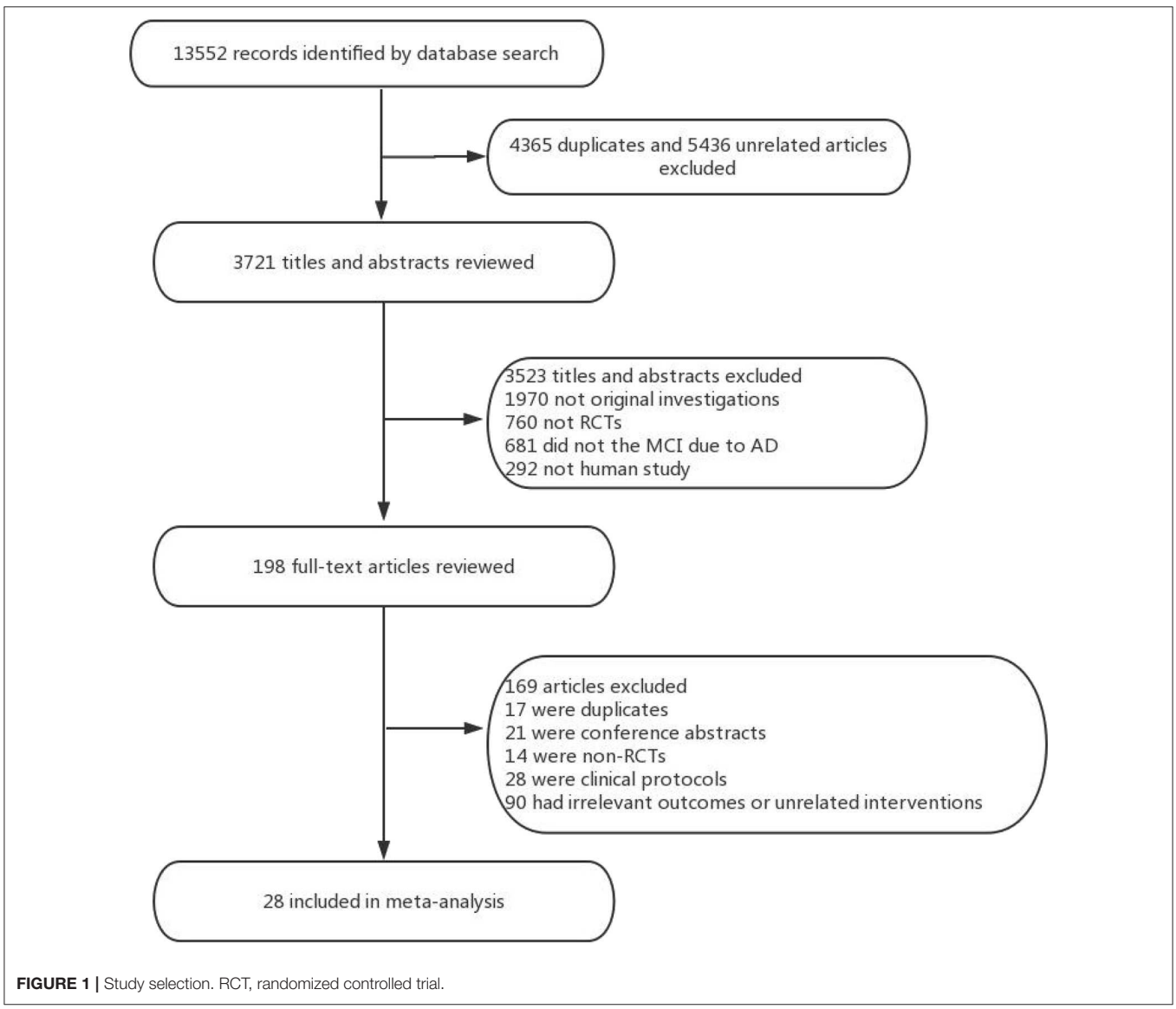

FIGURE 1 | Study selection. RCT, randomized controlled trial.

TABLE 1 | Characteristics of included studies.

References	Country	Number of people (*n*)	Age (Y)	Intervention	Comparison	Treatment duration	Events	Outcomes
Doody et al. (2009)	USA	DON: 409 PLA: 412	55–90	Donepezil (5–10 mg)	Placebo	48 w	1. Diarrhea (donepezil: 16.4%; placebo: 3.4%) 2. Muscle spasms (donepezil: 13.3%; placebo: 1.8%) 3. Insomnia (donepezil: 8.2%; placebo: 4.4%).	Primary: MMSE; Secondary: modified ADAS-cog
Salloway et al. (2004)	USA	DON: 133 PLA: 137	55–90	Donepezil (5–10 mg); Placebo	Placebo	24 w	1. Diarrhea (donepezil: 27%; placebo: 10%) 2. Abnormal dreams (donepezil 23%; placebo: 4%), 3. insomnia (donepezil: 11%; placebo 5%).	Modified ADAS-cog
Winblad et al. (2008)	USA, Canada	GAL: 494 PLA: 496	≥50	Galantamine (16–24 mg); Placebo	Placebo	24 m	1. Nausea (GAL: 29%; PAL: 10%) 2. Diarrhea (GAL: 15%; PAL: 9%) 3. Insomnia (GAL: 10%; PAL: 7%)	Modified ADAS-cog; ADCS-ADL
Winblad et al. (2008)	USA, Canada	GAL: 532 PLA: 526	≥50	Galantamine (16–24 mg);	Placebo	24 m	1. Nausea (GAL: 29%; PAL: 10%) 2. Diarrhea (GAL: 15%; PAL: 9%) 3. Insomnia (GAL: 10%; PAL: 7%)	Modified ADAS-cog; ADCS-ADL
Wilkinson et al. (2002)	UK, South Africa, Switzerland	RIV: 55 Don: 56	≥50	Rivastigmine (12 mg)	Donepezil (5–10 mg)	12 w	1. Nausea (RIV: 41.8%; DON: 10.7%) 2. Vomiting (RIV: 23.6%; DON: 7.1%) 3. Headache (RIV: 18.2%; DON: 7.1%)	Primary: MMSE Secondary: ADAS-cog
Howard and Roger (2007)	Australia, Canada, Italy, South Africa, UK	RIV: 227 PLA: 222	≥50	Rivastigmine (6–36 mg)	Placebo	26 w	1. Nausea (RIV: 48.0%; PLA: 14.0%) 2. Vomiting (RIV: 30.0%; PLA: 6.3%) 3. Anorexia (RIV: 18.5%; PLA: 2.4%)	Primary: MMSE; Secondary: ADAS-cog
Dong et al. (2012)	China	GIN: 58 PLA: 55	60–85	Ginkgo glycosides (9.6 mg tid)	Placebo	1 y	Not mentioned	MMSE
Xiao et al. (2011)	China	GIN: 54 PLA: 44	55–85	Ginkgo glycosides (19.2 mg tid)	Placebo	6 m	Not mentioned	MMSE
Aisen et al. (2008)	USA	VB: 240 PLA: 169	≥50	Folate: 5 mg, Vitamin B6: 25 mg, Vitamin B12: 1 mg	Placebo	18 m	1. Depression (VB: 27.9%; PAL: 17.8%) 2. Restlessness (VB: 12.1%; PAL: 8.3%) 3. Hyperhidrosis (VB: 9.6%; PAL: 4.1%)	Primary: MMSE; Secondary: ADAS-cog
Petersen et al. (2005)	USA, Canada	VE: 257 PLA: 259	55–90	Vitamin E: 2,000 IU	Placebo	36 m	1. Diarrhea (VE: 10.2%; placebo: 6.6%) 2 Insomnia (VE: 3.1%; placebo: 1.9%) 3. Nausea (VE: 1.2%; placebo: 1.9%).	Primary: MMSE Secondary: ADAS-cog
Sun et al. (2007)	Taiwan	Multivitamin: 45 PLA: 44	≥50	Multivitamin supplement* + Mecobalamin: 0.5 mg	Placebo	26 w	1. Muscle pain (multivitamin: 11.1%; PAL: 6.8%) 2. Insomnia (multivitamin: 8.9%; PAL: 9.1%) 3. Delirium (multivitamin: 8.9%; PAL: 2.3%)	Primary: MMSE Secondary: ADAS-cog
Dysken et al. (2014)	/	VE: 152 PLA: 152	60–75	2,000 IU vitamin E	Placebo	4 y	Not mentioned	Primary: MMSE Secondary: ADAS-cog
Tian et al. (2019)	China	CM: 174 PLA: 70	≥50	Qinggongshoutao 27 g; EGb761 160 mg	Placebo	52 w	Upper respiratory tract infection, diarrhea, constipation, urinary tract infection, and increased blood glucose	Primary: MMSE Secondary: ADAS-cog
Zhou et al. (2007)	China	CM: 42 PLA: 37	53–79	Shenyin Oral Liquid	Placebo	12 m	Not mentioned	MMSE

(Continued)

TABLE 1 | Continued

References	Country	Number of people (*n*)	Age (Y)	Intervention	Comparison	Treatment duration	Events	Outcomes
Wei et al. (2012)	China	CM: 24 PLA: 23	45–80	Danshen, Sanqi	Placebo	12 w	CM: stomachache (2) PLA: urinary tract infection (2)	Primary: MMSE Secondary: ADAS-cog
Miao et al. (2012)	China	CM: 45 PLA: 48	40–85	CM; 200 ml	Placebo	12 w	Not mentioned	Primary: MMSE Secondary: ADAS-cog
Suzuki et al. (2013)	Japan	Exercise: 50 PLA: 50	≥65	Multicomponent exercise (bi-weekly 90-min): aerobic exercise, muscle strength training, postural balance retraining, and dual-task training	Placebo	6 m	Not mentioned	Primary: MMSE Secondary: ADAS-cog
Lautenschlager et al. (2008)	Australia	Exercise: 48 PLA: 52	≥50	≥150 min of moderate-intensity physical activity per week	Placebo	18 w	1. Cardiovascular problems (EXE: 6.3%; PLA: 1.9%) 2. Stroke or transient ischemic attack (EXE: 2.1%; PLA: 1.9%)	ADAS-cog
Grace et al. (2013)	Hong Kong	Exercise: 7 PLA: 6	≥60	Computer-assisted EL memory training; Therapist-led EL memory training group	Placebo	3 m	Not mentioned	MMSE
Tsai et al. (2013)	USA	Taichi: 28 PLA: 27	≥60	Taichi (3 sessions a week)	Placebo: attention control group	20 w	Not mentioned	MMSE
Doi et al. (2017)	Japan	Music: 67 Con: 67	≥70	Music: playing percussion instruments at weekly 60-min sessions	Control: health education classes	40 w	No injuries reported	MMSE
Li et al. (2015)	Taiwan	Music: 20 PLC: 21	≥60	Music: Mozart's Sonata (KV 448) and Pachelbel's Canon, listening with headphones for 30 min daily in the morning and before sleep	Placebo	6 m	Not mentioned	MMSE
Cai et al. (2019)	China	Music: 25 PLC: 25	60–74	Music: 1–1.5 h music therapy, 3 times a weeks	Placebo	3 m	Not mentioned	MMSE
Yang et al. (2019)	China	ACU: 108 PLC: 105	55–85	Acupuncture: 30 min twice a week (at an interval of 2–4 days)	Placebo	6 m	Not mentioned	ADAS-cog
Jia et al. (2017)	China	ACU: 43 ChEIs: 44	50–85	Acupuncture: 30 min, 3 times weekly	Donepezil: 5–10 mg	28 w	Not mentioned	ADAS-cog
Zhu et al. (2015)	China	ACU: 30 NIM: 30	46–75	Acupuncture: Acupuncture and Moxibustion (30 min each, 6 times weekly)	Nimodipine 30 mg, 3 times a day	8 w	Not mentioned	MMSE
Chen (2011)	China	ACU: 80 PLC: 75	55–85	Acupuncture: Acupuncture (30 min, 3 times weekly)	Placebo	8 w	Acu: fainting during acupuncture treatment 10 Drug: gastrointestinal reaction 9	MMSE
Zheng et al. (2008)	China	CM: 30 NIM: 30	/	Nimodipine 30 mg, 3 times a day	Chinese medicine: once a day	12 w	Not mentioned	MMSE

**Containing: iron ferrous 60 mg, nicotinamide 10 mg, calcium carbonate 250 mg, riboflavin 2 mg, thiamine mononitrate 3 mg, calcium pantothenate 1 mg, ascorbic acid 100 μg, iodine 100 μg, copper 150 μg, vitamin B12 3 μg, vitamin A 4,000 IU, and vitamin D3 400 IU.*

ACU, acupuncture; ChEIs, cholinesterase inhibitors; CM, Chinese medicine; Con, control; d, days; m, months; NIM, nimodipine; PLC, placebo; w, weeks; y, years.

in this network meta-analysis. Random-effect model attempted to generalize findings beyond the included studies by assuming that the selected studies are random samples from a larger population (Cheung et al., 2012). The mean difference (MD) was the effect size for continuous outcomes. The models used to estimate the effect size in ADDIS were "consistency" and "inconsistency." The consistency model aims to evaluate effect sizes of the interventions, which was used to calculate the ranking probabilities for the whole group of interventions. Node-splitting analysis helps to determine the consistency test with an inconsistency model. For instance, a consistency model was chosen when the p-value of the node-splitting analysis was >0.05. If the p-value of the node-splitting analysis was <0.05, an inconsistency model was selected. In order to evaluate the convergence of the model, the potential scale reduction factor (PSRF) was used. If the PSRF value was close to 1, the convergence of the model was more desirable. If the PSRF value was <1.2, it was still considered as acceptable. For each intervention, the ranking probabilities were estimated for every treatment at every possible rank.

RESULTS

Study Identification and Selection

Overall, a total of 13,522 studies were identified from the seven electronic databases using the search strategy, and 198 relevant full-text articles were evaluated for eligibility. There were 169 citations excluded, including 17 duplicates, 21 conference abstracts, 28 clinical protocols, 14 non-RCTs, and 90 unrelated intervention or outcome articles. Ultimately, 28 studies including 6,863 patients were clinical eligible to be included in this network meta-analysis (**Figure 1**). The characteristics of the selected studies were listed in **Table 1**.

Study Quality

The Cochrane Risk of Bias Tool was used to assess the quality of all 28 trials included in our study (**Figure 2** shows the summary risk of bias for selected studies). Among the 28 trials, 19 (66%) represented a random sequence generation process using a computer random number generator or a random number table. Fourteen trials (48.3%) described the use of allocation

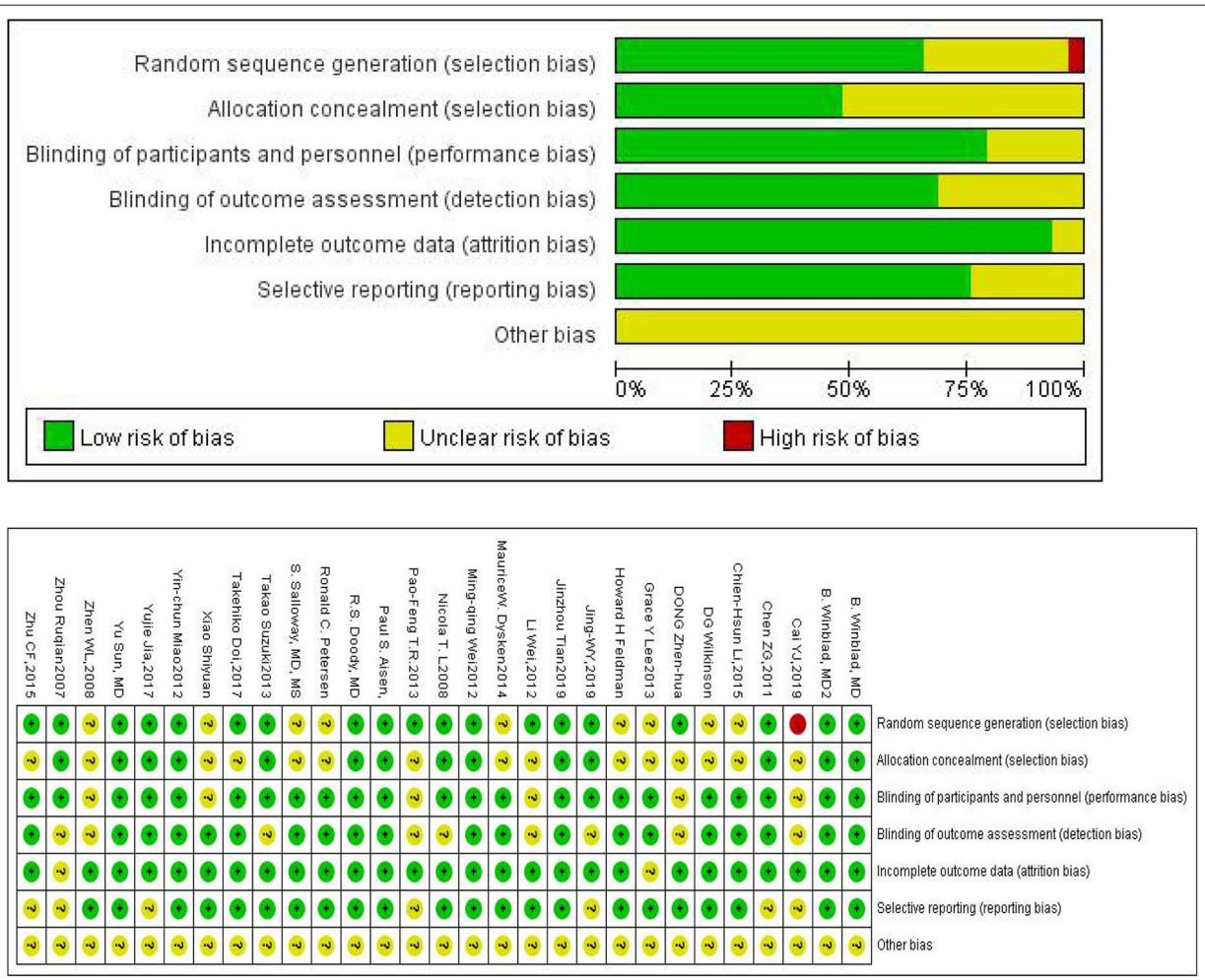

FIGURE 2 | Quality assessment of included studies.

concealment methods, and 22 trials (75.9%) described the blinding methods for researchers and participants. Acupuncture, music therapy, and exercise therapy are non-pharmacologic therapies, therefore some participants and researchers involved in these studies were not able to be blinded. Six trials (21.4%) had an uncertain risk of outcome assessment and 25 trials (86.2%) had a low risk of attrition bias.

Pair-Wise Meta-Analysis

We conducted a classic pair-wise meta-analysis using a random-effects model to synthesize studies with the same pair of interventions. All interventions, except for nimodipine, had at least one placebo controlled trial. As for the MMSE outcome, the ChEIs (MD: −0.38; 95% CI: −0.74, −0.01), Chinese medicine (MD: −0.31; 95% CI: −0.75, 0.13), exercise therapy (MD: −0.50;

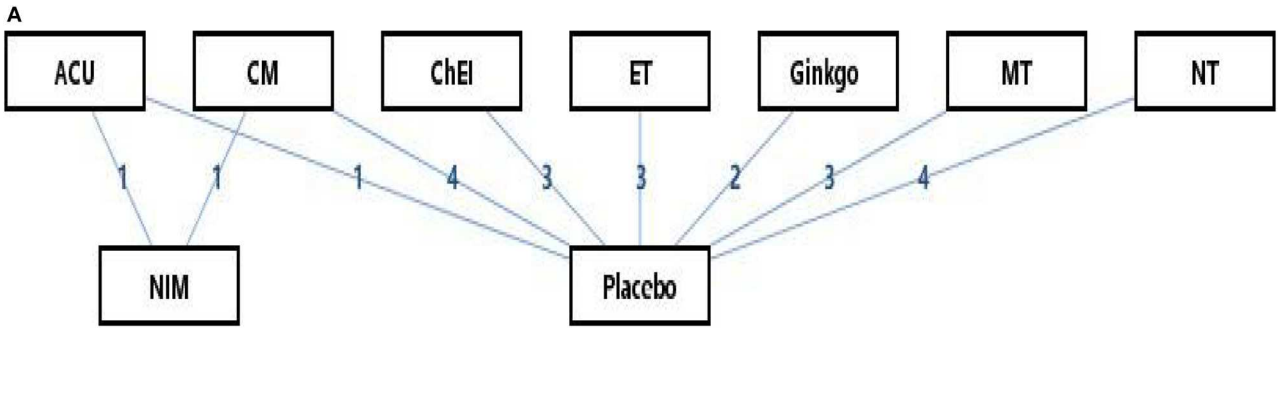

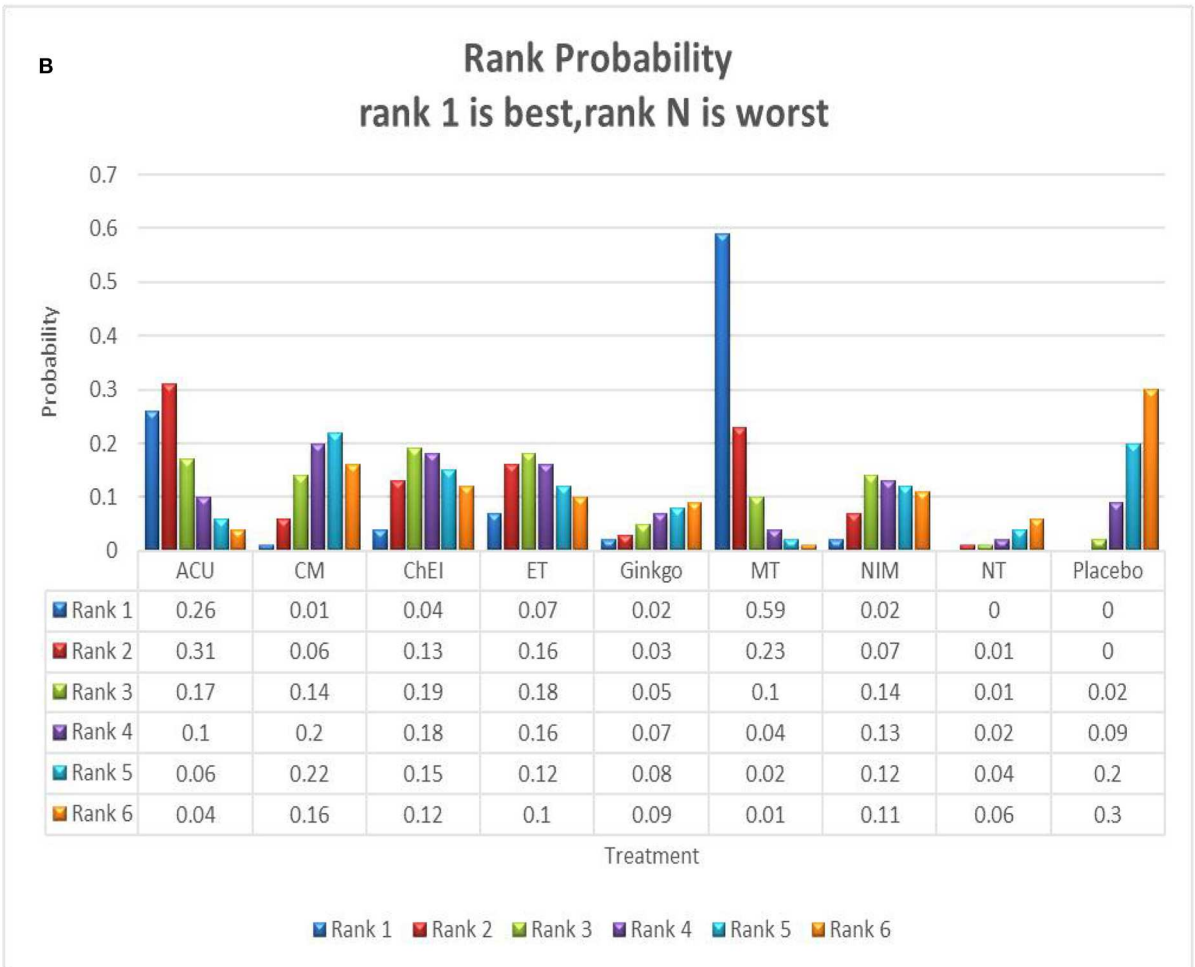

	ACU	CM	ChEI	ET	Ginkgo	MT	NIM	NT	Placebo
Rank 1	0.26	0.01	0.04	0.07	0.02	0.59	0.02	0	0
Rank 2	0.31	0.06	0.13	0.16	0.03	0.23	0.07	0.01	0
Rank 3	0.17	0.14	0.19	0.18	0.05	0.1	0.14	0.01	0.02
Rank 4	0.1	0.2	0.18	0.16	0.07	0.04	0.13	0.02	0.09
Rank 5	0.06	0.22	0.15	0.12	0.08	0.02	0.12	0.04	0.2
Rank 6	0.04	0.16	0.12	0.1	0.09	0.01	0.11	0.06	0.3

FIGURE 3 | (A) The network structure of the analyzed treatment comparisons for the outcome of MMSE. **(B)** Rank probability of cognitive effects of MMSE. ACU, acupuncture; CM, Chinese medicine; CHEI, cholinesterase inhibitors; ET, exercise therapy; MT, music therapy; NIM, nimodipine; NT, nutrition therapy.

95% CI: −0.65, −0.35), music therapy (MD: −1.71; 95% CI: −4.49, 1.07), were worse than placebo,and other interventions were statistically more efficient than placebo. For ADAS-cog outcome, ChEIs (MD: 1.20; 95% CI: 0.73, 1.68), Acupuncture (MD: 1.36; 95% CI: 1.28, 1.44), Chinese medicine (MD: 0.61; 95% CI: 0.49, 0.73) and exercise (MD: 0.61; 95% CI: 0.49, 0.73) were better than placebo. The detailed results of the pair-wise meta-analysis are shown in **Supplementary Datasheet 2**.

Network Meta-Analysis

Primary Outcome: MMSE

We ran a network meta-analysis to thoroughly compare and assess different treatment rankings for MCI, the network of MMSE include 23 trails and 15 interventions,the network plot presented in **Figure 3A**. Node-splitting analysis was used to assess consistency, and all *p*-values between the direct and indirect effects were > 0.05. A PSRF value of 1 indicated that the model was convergent and the result was stable. Therefore, the consistency model was selected for the subsequent network analysis.

The network meta-analysis for the primary outcome (MMSE) is shown in **Table 2**. In terms of efficacy music therapy (*MD*: 1.74; 95% CI: 0.21, 3.26), Acupuncture (*MD*: 1.22; 95% CI:−0.97, 3.39), and exercise therapy (*MD*: 0.52; 95% CI: −1.22, 2.28) achieved better than placebo. Ginkgo (*MD*: −0.40; 95% CI: −2.34, 1.57) and nutrition therapy (*MD*: −0.75; 95% CI: −2.04, 0.61) were significantly less effective than other interventions and placebo. Other pharmacological therapies including Chinese medicine (*MD*: 0.27; 95% CI: −0.96, 1.52) and ChEIs (*MD*: 0.46; 95% CI: −1.02, 1.96) showed a slight improvement in MMSE scores; however, their efficacy in MCI needs further investigation. The ranking probability of MMSE is presented in **Figure 3B**, the results showed that music therapy had the highest probability (59%) of being the best treatment for MCI, followed by Acupuncture (26%) and then exercise (7%).

Secondary Outcome: ADAS-cog

In relation to the secondary outcome (ADAS-cog score), 17 trails and 6 treatments were involved, 2 arms of Acupuncture, 6 arms of ChEIs, 3 arms of Chinese medicine, 2 arms of exercise therapy and 4 arms of nutrition therapy (presented in **Figure 4A**). After Node-splitting analysis,we adopted the consistency model to compare these different interventions. Chinese medicine (*MD*: −2.72; 95% CI: −4.83, −0.56), Acupuncture (*MD*: −2.84; 95% CI: −5.61, −0.34), exercise therapy (*MD*: −0.71; 95% CI: −3.12, 1.68), and ChEIs (*MD*: −0.88; 95% CI: −2.23, 0.53) were better than placebo. Nutrition therapy (*MD*: 1.43; 95% CI: −0.34, 3.14) was least effective compared to other interventions and placebo (shown in **Table 3**). The ranking probability of ADAS-cog is presented in **Figure 3B**. Acupuncture ranked the best (52%), it might be the most effective way to change the ADAS-cog score.

Adverse Events

Out of 28 trials, 13 trails reported adverse events occurred, 14 trails did not mention whether there was adverse events and one trial stated no injures reported (**Table 1**). 9 out of 13 trials reported adverse events related to gastrointestinal discomforts such as diarrhea, nausea, vomiting and anorexia, these interventions were mainly ChEIs, nutrition therapy and Chinese medicine. 8 out of 13 trails reported insomnia as adverse effect which mainly related to ChEIs and nutrition interventions. 1 out of 13 trails reported cardiovascular problem due to exercises intervention and 1 out of 13 trials reported Acupuncture-fainting due to Acupuncture intervention.

TABLE 2 | The consistency model of MMSE, comparisons should be read from left to right.

ACU	−0.93 (−3.25, 1.38)	−0.76 (−3.44, 1.92)	−0.70 (−3.47, 2.19)	−1.62 (−4.51, 1.26)	0.52 (−2.13, 3.19)	−1.18 (−3.38, 1.02)	−1.95 (−4.51, 0.59)	−1.22 (−3.39, 0.97)
0.93 (−1.38, 3.25)	CM	0.19 (−1.74, 2.13)	0.25 (−1.86, 2.35)	−0.68 (−2.95, 1.65)	1.45 (−0.50, 3.44)	−0.22 (−2.46, 1.96)	−1.02 (−2.79, 0.77)	−0.27 (−1.52, 0.96)
0.76 (−1.92, 3.44)	−0.19 (−2.13, 1.74)	ChEI	0.07 (−2.25, 2.33)	−0.86 (−3.35, 1.60)	1.26 (−0.82, 3.40)	−0.43 (−3.19, 2.34)	−1.19 (−3.13, 0.82)	−0.46 (−1.96, 1.02)
0.70 (−2.19, 3.47)	−0.25 (−2.35, 1.86)	−0.07 (−2.33, 2.25)	ET	−0.93 (−3.51, 1.69)	1.22 (−1.12, 3.47)	−0.48 (−3.40, 2.37)	−1.27 (−3.41, 0.95)	−0.52 (−2.28, 1.22)
1.62 (−1.26, 4.51)	0.68 (−1.65, 2.95)	0.86 (−1.60, 3.35)	0.93 (−1.69, 3.51)	Ginkgo	2.14 (−0.34, 4.51)	0.47 (−2.58, 3.40)	−0.33 (−2.67, 2.06)	0.40 (−1.57, 2.34)
−0.52 (−3.19, 2.13)	−1.45 (−3.44, 0.50)	−1.26 (−3.40, 0.82)	−1.22 (−3.47, 1.12)	−2.14 (−4.51, 0.34)	MT	−1.71 (−4.43, 1.08)	−2.48 (−4.45, −0.41)	−1.74 (−3.26, −0.21)
1.18 (−1.02, 3.38)	0.22 (−1.96, 2.46)	0.43 (−2.34, 3.19)	0.48 (−2.37, 3.40)	−0.47 (−3.40, 2.58)	1.71 (−1.08, 4.43)	NIM	−0.77 (−3.42, 1.88)	−0.03 (−2.35, 2.30)
1.95 (−0.59, 4.51)	1.02 (−0.77, 2.79)	1.19 (−0.82, 3.13)	1.27 (−0.95, 3.41)	0.33 (−2.06, 2.67)	2.48 (0.41, 4.45)	0.77 (−1.88, 3.42)	NT	0.75 (−0.61, 2.04)
1.22 (−0.97, 3.39)	0.27 (−0.96, 1.52)	0.46 (−1.02, 1.96)	0.52 (−1.22, 2.28)	−0.40 (−2.34, 1.57)	1.74 (0.21, 3.26)	0.03 (−2.30, 2.35)	−0.75 (−2.04, 0.61)	Placebo

Treatments; Efficacy (mean overall change, SMD [95% CrI]).

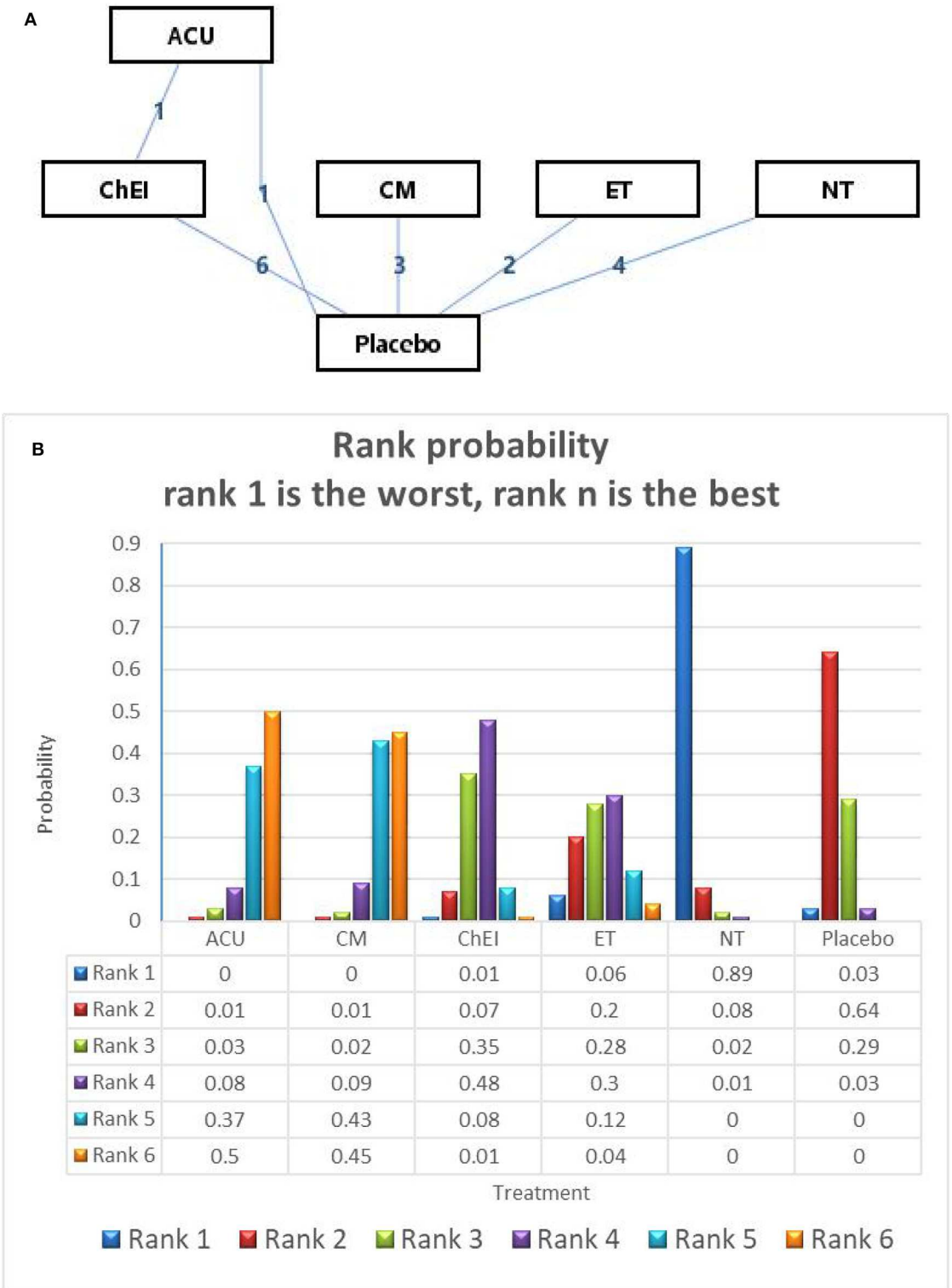

FIGURE 4 | (A) The network structure of the analyzed treatment comparisons for the outcome of ADAS-cog. **(B)** Rank probability of cognitive effects of ADAS-cog.

TABLE 3 | The consistency model of ADAS-cog, comparisons should be read from left to right.

ACU	0.10 (−3.17, 3.61)	1.97 (−0.65, 4.76)	2.14 (−1.35, 5.88)	4.26 (1.28, 7.53)	2.84 (0.34, 5.61)
−0.10 (−3.61, 3.17)	CM	1.85 (−0.61, 4.35)	2.02 (−1.23, 5.16)	4.15 (1.38, 6.87)	2.72 (0.56, 4.83)
−1.97 (−4.76, 0.65)	−1.85 (−4.35, 0.61)	ChEI	0.16 (−2.61, 2.94)	2.30 (0.04, 4.51)	0.88 (−0.53, 2.23)
−2.14 (−5.88, 1.35)	−2.02 (−5.16, 1.23)	−0.16 (−2.94, 2.61)	ET	2.13 (−0.83, 5.09)	0.71 (−1.68, 3.12)
−4.26 (−7.53, −1.28)	−4.15 (−6.87, −1.38)	−2.30 (−4.51, −0.04)	−2.13 (−5.09, 0.83)	NT	−1.43 (−3.14, 0.34)
−2.84 (−5.61, −0.34)	−2.72 (−4.83, −0.56)	−0.88 (−2.23, 0.53)	−0.71 (−3.12, 1.68)	1.43 (−0.34, 3.14)	Placebo

Treatments, efficacy (mean overall change, SMD [95% CrI]).

DISCUSSION

This study is the first network meta-analysis performed on potential pharmacological and non-pharmacological treatments for MCI, and has incorporated the most comprehensive data. The Bayesian statistical methods that we used allowed us to rank many different treatments by measuring comparable probability and then reporting them as the best, the second best, and so on. Through this method, we found that among all interventions, both pharmacological therapies (ChEIs, ginkgo, nimodipine, and Chinese medicine) and non-pharmacological therapies (acupuncture, music therapy, exercise, and nutrition therapy), music therapy and acupuncture were better than other treatments. Some pharmacological treatments like CHEIs such as donepezil, galantamine, and rivastigmine showed a slight efficacy to improve MMSE scores and cognitive function, but have many safety issues which require further clarification and study. In addition, ginkgo and nutrition therapy might be ineffective for MCI, which are thus not strongly recommended in clinical medicine.

Music therapy is one of the non-pharmacological therapies which incorporates active and passive therapy. Active music therapy can be defined as therapeutic music activities which involve active participation by clients, such as singing, dancing with music, playing an instrument, composing, and discussing clients' thoughts and feelings in regards to music-related activities in order to reach the optimal treatment effect. Passive music therapy, on the other hand, means achieving the treatment effect by listening and enjoying music. Passive music therapy is also called receptive music therapy and is widely used (Chang et al., 2015; Han et al., 2017; Claudia et al., 2019). Previous research has shown that music can activate some brain regions that govern cognitive function, affective function, and motor skills, and activate neurological stimulation which may develop new neural networks (Raglio et al., 2014; Mofredj et al., 2016). Evidence has shown that, in the context of patients with cognitive function decline, music therapy intervention increases cerebral blood flow and pre-frontal cortex activity (Shimizu et al., 2018).

Acupuncture has been shown to be a good management option in neurological diseases, with studies demonstrating acupuncture is associated with activation in motor-related brain regions as shown in functional magnetic resonance imaging (fMRI) (Chen et al., 2008, 2012; Chae et al., 2009). Other studies supplemented that Acupuncture is able to regulate the emotional components of the pain matrix, and inducing brain activation which provides a neurobiological basis of acupuncture (Shangjie et al., 2014; Shan et al., 2018). Research also suggests that acupuncture can activate resting brain networks, which incorporate anti-nociceptive, memory, and emotion brain regions. Our network meta-analysis suggests that music therapy is the optimal intervention to treat MCI patients and improve their cognitive function, whereas acupuncture was the second best option.Further research is required to assess other interventions not included in this meta-analysis. A recent study found that mindfulness therapy improved inflammatory biomarkers in patients with MCI (Ng et al., 2020). This provides an interesting perspective on the current management paradigms for MCI.

The adverse events reports showed that some participants experienced gastrointestinal reactions and insomnia due to ChEIs, nutrition and Chinese medicine interventions. However, none of these events was related to cognitive distress. Other small samples such as exercise and Acupuncture reported therapy related adverse effects such as cardiovascular problems and Acupuncture fainting respectively. Music therapy didn't report any adverse events.

There were limitations to our study. Firstly, a few RCTs showed potential bias because of the small number of participants and elective reporting. Fortunately, there was no obvious inconsistency or heterogeneity shown in this network meta-analysis, but there is a possibility that some included articles might have overestimated the effectiveness of treatments, and this might have influenced our results. Secondly, a few included reports were non-pharmaceutical therapies which cannot be blinded to participants, especially acupuncture. However, blinding of outcome assessment and single-blind methodologies should be used where possible to reduce the potential for any bias. Thirdly, we have excluded some drug interventions because of our selection criterion of outcome measures, which may influence the strength of evidence.

CONCLUSION

The findings of this comprehensive network meta-analysis provide some evidence that music therapy and acupuncture might improve the cognitive function of patients with MCI. Our results indicate that music therapy and, to a lesser extent, acupuncture may be the preferred options for treatment of MCI. Ginkgo and nutrition therapy do not seem to be adequate as regular treatment options. Our study provides new insights into the clinical treatments available for MCI, and may help the development of guidelines for the management of MCI.

DATA AVAILABILITY STATEMENT

All datasets generated for this study are included in the article/**Supplementary Material**.

AUTHOR CONTRIBUTIONS

CT and LL designed the study. XL, YL, and HW collected the data. XL performed all analysis. XL, YL, and HW wrote the manuscript. All authors contributed to writing of this manuscript.

FUNDING

This work was funded by grants from National Natural Science Foundation of China (No. 81873375).

SUPPLEMENTARY MATERIAL

The Supplementary Material for this article can be found online at: https://www.frontiersin.org/articles/10.3389/fnagi.2020.00121/full#supplementary-material

REFERENCES

Aisen, P. S., Schneider, L. S., Sano, M., Diaz-Arrastia, R., Van, C. H., Weiner, M. F., et al. (2008). High-dose B vitamin supplementation and cognitive decline in Alzheimer's disease: a randomized controlled trial. *JAMA* 300, 1774–1783. doi: 10.1001/jama.300.15.1774

Almkvist, O., Basun, H., Backman, L., Lannfelt, L., Small, B., Viitanen, M., et al. (1998). Mild cognitive impairment—an early stage of Alzheimer's disease. *J. Neural Transm. Suppl.* 54, 21–29. doi: 10.1007/978-3-7091-7508-8_3

Andreas, S., Dietlinde, K. S., Florian, S., Nina, F., Theresa, S., Rainer, H., et al. (2015). Exercise Treatment of Alzheimer's disease and mild cognitive impairment: a systematic review and meta-analysis of effects on cognition in randomized controlled trials. *Am. J. Geriatric Psychiatry* 23, 1234–1249. doi: 10.1016/j.jagp.2015.07.007

Brendan, J., and Kelley, M. D. (2015). Treatment of mild cognitive impairment. *Curr Treat Options Neurol.* 17:40. doi: 10.1007/s11940-015-0372-3

Cai, Y. J., Xu, H. L., Cao, J. Q., Cao, Y. F., and Yuan, S. (2019). Effect analysis of neuromuscular therapy in young people with amnestic mild cognitive impairment. *Sci. Technol. Wind* 232–236. doi: 10.19392/j.cnki.16717341.201922202

Chae, Y. Y., Lee, H. J., Kim, H. J., Sohn, H. J., Park, J. H., and Park, H. J. (2009). The neural substrates of verum acupuncture compared to non-penetrating placebo needle: an fMRI study. *Neurosci. Lett.* 450, 80–84. doi: 10.1016/j.neulet.2008.11.048

Chang, Y. S., Chu, H., Yang, C. Y., Tsai, J. C., Chung, M. H., Liao, Y. M., et al. (2015). The efficacy of music therapy for people with dementia: a meta-analysis of randomised controlled trials. *J. Clin. Nurs.* 24, 3425–3440. doi: 10.1111/jocn.12976

Chen, S. J., Liu, B., Fu, W., Wu, S., Chen, J., and Ran, P. (2008). A fMRI observation on different cererbral regions activated by acupuncture of Shenmen (HT 7) and Yanglao (SI 6). *Zhen Ci Yan Jiu.* 33, 267–271. doi: 10.1007/s11726-008-0242-6

Chen, S. J., Meng, L., Yan, H., Bai, L., Wang, F., Huang, Y., et al. (2012). Functional organization of complex brain networks modulated by acupuncture at different acupoints belonging to the same anatomic segment. *Chin. Med. J.* 125, 2694–2700. doi: 10.3760/cma.j.issn.0366-6999.2012.15.009

Chen, Z. G. (2011). *Multi-Center Randomized Controlled Study of Electroacupuncture on Acupoints for Treatment of Mild Cognitive Impairment*. Chengdu University of Traditional Chinese Medicine.

Cheung, M. W., Roger, C. M., Yonghao, L. I. M., and Anselm, M. A. K. (2012). Conducting a meta-analysis: basics and good practices. *Int. J. Rheum. Dis.* 15, 129–135. doi: 10.1111/j.1756-185X.2012.01712.x

Claudia, J. F., Murrock, C. J., Guerrero, P. I. C., and Salazar-González, B. C. (2019). Music therapy intervention in community-dwelling older adults with mild cognitive impairment: a pilot study. *Geriatric Nurs.* 40, 614–619. doi: 10.1016/j.gerinurse.2019.06.004

Collie, A., and Maruff, P. (2000). The neuropsychology of preclinical Alzheimer's disease and mild cognitive impairment. *Neurosci. Biobehav. Rev.* 24, 365–374. doi: 10.1016/S0149-7634(00)00012-9

Cooper, C., Li, R., Lyketsos, C., and Livingston, G. (2013). Treatment for mild cognitive impairment: systematic review. *Br. J. Psychiatry*. 203, 255–264. doi: 10.1192/bjp.bp.113.127811

Doi, T., Verghese, J., Makizako, H., Tsutsumimoto, K., Hotta, R., Nakakubo, S., et al. (2017). Effects of cognitive leisure activity on cognition in mild cognitive impairment: results of a randomized controlled trial. *J Am Med Dir Assoc.* 18, 686–691. doi: 10.1016/j.jamda.2017.02.013

Dong, Z. H., Zhang, C. Y., and Pu, B. H. (2012). Effects of ginkgo biloba tablet in treating mild cognitive impairment. *Zhongguo Zhong Xi Yi Jie He Za Zhi* 32, 1208–1211. doi: 10.3736/jcim20120605

Doody, R. S., Ferris, S. H., Salloway, S., Sun, Y., Goldman, R., Watkins, W. E., et al. (2009). Donepezil treatment of patients with MCI: a 48-week randomized, placebo-controlled trial. *Neurology* 72, 1555–1561. doi: 10.1212/01.wnl.0000344650.95823.03

Dysken, M. W., Sano, M., Asthana, S., Vertrees, J. E., Pallaki, M., Llorente, M., et al. (2014). Effect of vitamin E and memantine on functional decline in Alzheimer disease: the TEAM-AD VA cooperative randomized trial. *JAMA* 311, 33–44. doi: 10.1001/jama.2013.282834

Grace, Y. L., Calvin, C. K. Y., Edwin, C. S., and David, W. K. (2013). Evaluation of a computer assisted errorless learning based memory training program for patients with early Alzheimer's disease in Hong Kong: a pilot study. *Clin. Interv. Aging* 8, 623–633. doi: 10.2147/CIA.S45726

Han, J. W., Lee, H., Hong, J. W., Kim, K., Kim, T., Byun, H. L., et al. (2017). Multimodal cognitive enhancement therapy for patients with mild cognitive impairment and mild dementia: a multi- center, randomized, controlled, double-blind, crossover trial. *J. Alzheimers Dis.* 55, 787–796. doi: 10.3233/JAD-160619

Howard, H. F., and Roger, L. (2007). Rivastigmine: a placebo controlled trial of twice daily and three times daily regimens in patients with Alzheimer's disease. *J. Neurol. Psychiatry* 78, 1056–1063. doi: 10.1136/jnnp.2006.099424

Jia, Y. J., Zhang, X. Z., Yu, J., Han, J., Yu, T., Shi, J., et al. (2017). Acupuncture for patients with mild to moderate Alzheimer's disease: a randomized controlled trial. *BMC Complement. Altern. Med.* 17:556. doi: 10.1186/s12906-017-2064-x

Kluger, A., Ferris, S. H., Golomb, J., Mittelman, M. S., and Reisberg, B. (1999). Neuropsychological prediction of decline to dementia in nondemented elderly. *J. Geriatr. Psychiatry Neurol.* 12, 168–179. doi: 10.1177/089198879901200402

Lautenschlager, N. T., Cox, K. L., Flicker, L., Foster, J. K., van Bockxmeer, F. M., Xiao, J., et al. (2008). Effect of physical activity on cognitive function in older

adults at risk for Alzheimer disease: a randomized trial. *JAMA* 300, 1027–1037. doi: 10.1001/jama.300.9.1027

Li, C. H., Liu, C. K., Yang, Y. H., Chou, M. C., CH, Lai, C. L. Adjunct effect of music therapy on cognition in Alzheimer's disease in Taiwan: a pilot study. *Neuropsych Dis Treat.* (2015) 11. doi: 10.2147/NDT.S73928

Liang, J. H., Xu, Y., Lin, L., Jia, R. X., Zhang, H. B., and Hang, L. (2018). Comparison of multiple interventions for older adults with Alzheimer's disease or mild cognitive impairment: a PRISMA-compliant network meta-analysis. *Medicine* 97:e10744. doi: 10.1097/MD.0000000000010744

Matsunaga, S., Fujishiro, H., and Takechi, H. (2019). Efficacy and safety of cholinesterase inhibitors for mild cognitive impairment: a systematic review and meta-analysis. *J. Alzheimers Dis.* 71, 513–523. doi: 10.3233/JAD-190546

Miao, Y., Tian, J., Shi, J., and Mao, M. (2012). Effects of Chinese medicine for tonifying the kidney and resolving phlegm and blood stasis in treating patients with amnestic mild cognitive impairment: a randomized, double-blind and parallel-controlled trial. *Zhong Xi Yi Jie He Xue Bao* 10, 390–397. doi: 10.3736/jcim20120407

Mofredj, A., Alaya, S., Tassaioust, K., Bahloul, H., and Mrabet, A. (2016). Music therapy, a review of the potential therapeutic benefits for the critically ill. *J. Crit. Care* 35, 195–199. doi: 10.1016/j.jcrc.2016.05.021

Morris, J. C., Storandt, M., Miller, J. P., McKeel, D. W., Price, J. L., Rubin, E. H., et al. (2001). Mild cognitive impairment represents early-stage Alzheimer's disease. *Arch. Neurol.* 58, 397–405. doi: 10.1001/archneur.58.3.397

Ng, T. K. S., Fam, J., Feng, L., Cheah, I. K., Tan, C. T., Nur, F., et al. (2020). Mindfulness improves inflammatory biomarker levels in older adults with mild cognitive impairment: a randomized controlled trial. *Transl Psychiatry*. 10:21. doi: 10.1038/s41398-020-0696-y

Petersen, R. C. (2004). Mild cognitive impairment as a diagnostic entity. *J. Intern. Med.* 256, 183–194. doi: 10.1111/j.1365-2796.2004.01388.x

Petersen, R. C., Doody, R., Kurz, A., Mohs, R. C., Morris, J. C., Rabins, P. V., et al. (2001). Current concepts in mild cognitive impairment. *Arch. Neurol.* 58, 1985–1992. doi: 10.1001/archneur.58.12.1985

Petersen, R. C., Smith, G. E., Waring, S. C., Ivnik, R. J., Tangalos, E. G., and Kokmen, E. (1999). Mild cognitive impairment: clinical characterization and outcome. *Arch Neurol.* 56, 303–308. doi: 10.1001/archneur.56.3.303

Petersen, R. C., Thomas, R. G., Grundman, M., Bennett, D., Doody, R., Ferris, S., et al. (2005). Vitamin E and donepezil for the treatment of mild cognitive impairment. *N. Engl. J. Med.* 352, 2379–2388. doi: 10.1056/NEJMoa050151

Raglio, A., Filippi, S., Bellandi, D., and Stramba-Badiale, M. (2014). Global music approach to persons with dementia: evidence and practice. *Clin. Interv. Aging* 9, 1669–1676. doi: 10.2147/CIA.S71388

Rountree, S. D., Waring, S. C., Chan, W. C., Lupo, P. J., Darby, E. J., and Doody, R. S. (2007). Importance of subtle amnestic and nonamnestic deficits in mild cognitive impairment: prognosis and conversion to dementia. *Dement. Geriatr. Cogn. Disord.* 24, 476–482. doi: 10.1159/000110800

Rubin, E., Morris, J., Grant, E., and Vendegna, T. (1989). Very mild senile dementia of the Alzheimer type. I. Clinical assessment. *Arch. Neurol.* 46, 379–382. doi: 10.1001/archneur.1989.00520400033016

Salloway, S., Ferris, S., Kluger, A., Goldman, R., Griesing, T., Kumar, D., et al. (2004). Efficacy of donepezil in mild cognitive impairment: a randomized placebo-controlled trial. *Neurology* 63, 651–657. doi: 10.1212/01.WNL.0000134664.80320.92

Savovic, J., Weeks, L., Sterne, J. A., Turner, L., Altman, D. G., Moher, D., et al. (2014). Evaluation of the Cochrane Collaboration's tool for assessing the risk of bias in randomized trials: focus groups, online survey, proposed recommendations and their implementation. *Syst. Rev.* 3:37. doi: 10.1186/2046-4053-3-37

Shan, Y., Wang, J., Wang, Z., Zhao, Z., Zhang, M., Xu, J., et al. (2018). Neuronal specificity of acupuncture in Alzheimer's disease and mild cognitive impairment patients: a functional MRI study. *Evid. Based Complement. Altern. Med.* 2018:7619197. doi: 10.1155/2018/7619197

Shangjie, C., Maosheng, X., Hong, L., Jiuping, L., Liang, Y., Xia, L., et al. (2014). Acupuncture at the Taixi(KI3) acupoint activates cerebral neurons in elderly patients with mild cognitive impairment. *Neural Regener. Res.* 9, 1163–1168. doi: 10.4103/1673-5374.135319

Shimizu, N., Umemura, T., Matsunaga, M., and Hirai, T. (2018). Effects of movement music therapy with a percussion instrument on physical and frontal lobe function in older adults with mild cognitive impairment: a randomized controlled trial. *Aging Ment. Health* 22, 1614–1626. doi: 10.1080/13607863.2017.1379048

Sun, Y., Lu, C. J., Chien, K. L., Chen, S. T., and Chen, R. C. (2007). Efficacy of multivitamin supplementation containing vitamins B6 and B12 and folic acid as adjunctive treatment with a cholinesterase inhibitor in Alzheimer's disease: a 26-week, randomized, double-blind, placebo-controlled study in Taiwanese patients. *Clin. Ther.* 29, 2204–2214. doi: 10.1016/j.clinthera.2007.10.012

Suzuki, T., Shimada, H., Makizako, H., Doi, T., Yoshida, D., Ito, K., et al. (2013). Randomized controlled trial of multicomponent exercise in older adults with mild cognitive impairment. *PLoS ONE* 8:e61483. doi: 10.1371/journal.pone.0061483

Tian, J., Shi, J., Wei, M., Ni, J., Fang, Z., Gao, J., et al. (2019). Chinese herbal medicine Qinggongshoutao for the treatment of amnestic mild cognitive impairment: a 52-week randomized controlled trial. *Alzheimers Dement.* 5, 441–449. doi: 10.1016/j.trci.2019.03.001

Tricco, A. C., Soobiah, C., Berliner, S., Ho, J. M., Ng, C. H., Ashoor, H. M., et al. (2013). Efficacy and safety of cognitive enhancers for patients with mild cognitive impairment: a systematic review and meta-analysis. *Can. Med. Assoc. J.* 185, 1393–1401. doi: 10.1503/cmaj.130451

Tsai, P. F., Chang, J. Y., Beck, C., Kuo, Y. F., and Keefe, F. J. (2013). A pilot cluster-randomized trial of a 20-week tai chi program in elders with cognitive impairment and osteoarthritic knee: effects on pain and other health outcomes. *J. Pain Symptom. Manage.* 45, 660–669. doi: 10.1016/j.jpainsymman.2012.04.009

Wei, M. Q., Tian, J. Z., Shi, J., Ma, F., Miao, Y., and Wang, Y. (2012). Effects of Chinese medicine for promoting blood circulation and removing blood stasis in treating patients with mild to moderate vascular dementia: a randomized, double-blind and parallel-controlled trial. *Zhong Xi Yi Jie He Xue Bao* 10, 1240–1246. doi: 10.3736/jcim20121107

Wilkinson, D. G., Passmore, A. P., Bullock, R., Hopker, S. W., Smith, R., Potocnik, F. C. V., et al. (2002). A multinational, randomised, 12-week, comparative study of donepezil and rivastigmine in patients with mild to moderate Alzheimer's disease. *Int. J. Clin. Pract.* 56, 441–446. doi: 10.1175/1520-0450(1995)0342.0.CO;2

Winblad, B., Gauthier, S., Scinto, L., Feldman, H., Wilcock, G. K., Truyen, L., et al. (2008). Safety and efficacy of galantamine in subjects with mild cognitive impairment. *Neurology* 70, 2024–2035. doi: 10.1212/01.wnl.0000303815.69777.26

Wolf, H., Grunwald, M., Ecke, G., Zedlick, D., Bettin, S., Dannenberg, C., et al. (1998). The prognosis of mild cognitive impairment in the elderly. *J. Neural Transm. Suppl.* 54, 31–50. doi: 10.1007/978-3-7091-7508-8_4

Xiao, S., Zhang, C., Li, J., Liu, Y., and Zhao, M. (2011). Clinical study of Ginkgo biloba G (Styron) in the treatment of mild cognitive impairment. *Tradit. Chinese Patent Med.* 33, 751–754. doi: 10.3969/j.issn.1001-1528.2011.05.006

Yang, J., Shi, G., Zhang, S., Tu, J., Wang, L., Yan, C., et al. (2019). Effectiveness of acupuncture for vascular cognitive impairment no dementia: a randomized controlled trial. *Clin. Rehabilit.* 33, 642–652. doi: 10.1177/0269215518819050

Zheng, W., Zhang, D., and Liu, Y. (2008). Clinical study on Yiqihuoxue therapy for mild cognitive dysfunction. *Xinjiang Traditional Chinese Medicine* 5–7.doi: 10.3969/j.issn.1009-3931.2008.03.004

Zhou, R., Lin, S., and Yuan, Q. (2007). Clinical study of Shenyin Oral Liquid in treating mild cognitive impairment. *Zhongguo Zhong Xi Yi Jie He Za Zhi* 27, 793–795.

Zhu, C., Cai, S., Xu, B., He, C., Yang, C., and Liang, M. (2015). Clinical observation on Tongdu Tiaoshen acupuncture therapy for the treatment of amnestic mild cognitive dysfunction. *J. Anhui Univer. Tradit. Chin. Med.* 34, 55–58.

Conflict of Interest: The authors declare that the research was conducted in the absence of any commercial or financial relationships that could be construed as a potential conflict of interest.

frontiers in Aging Neuroscience

CLINICAL TRIAL
published: 09 June 2020
doi: 10.3389/fnagi.2020.00154

Telmisartan and Rosuvastatin Synergistically Ameliorate Dementia and Cognitive Impairment in Older Hypertensive Patients With Apolipoprotein E Genotype

Wenjing Hu[1†], Ying Li[2†], Yingxin Zhao[1], Yuanli Dong[3], Yi Cui[4], Shangwen Sun[1], Gary Gong[5], Hua Zhang[1], Qiang Chai[1], Juan Wang[6] and Zhendong Liu[1]**

[1]*Institute of Basic Medicine, Shandong Provincial Hospital Affiliated to Shandong First Medical University, Jinan, China,* [2]*School of Medicine and Life Sciences, University of Jinan-Shandong Academy of Medical Sciences, Jinan, China,* [3]*Department of Community, Lanshan District People Hospital, Linyi, China,* [4]*Department of Radiology, Qilu Hospital of Shandong University, Jinan, China,* [5]*The Russel H. Morgan Department of Radiology and Radiological Sciences, The Johns Hopkins University School of Medicine, Baltimore, MD, United States,* [6]*Department of Cardiology, The Second Hospital of Shandong University, Jinan, China*

OPEN ACCESS

Edited by:
Jiehui Jiang,
Shanghai University, China

Reviewed by:
Boon-Seng Wong,
Singapore Institute of Technology, Singapore
Ana I. Duarte,
University of Coimbra, Portugal

***Correspondence:**
Juan Wang
moonlikewang@163.com
Zhendong Liu
zhendongliu876@126.com

†These authors have contributed equally to this work

Received: *03 March 2020*
Accepted: *06 May 2020*
Published: *09 June 2020*

Citation:
Hu W, Li Y, Zhao Y, Dong Y, Cui Y, Sun S, Gong G, Zhang H, Chai Q, Wang J and Liu Z (2020) Telmisartan and Rosuvastatin Synergistically Ameliorate Dementia and Cognitive Impairment in Older Hypertensive Patients With Apolipoprotein E Genotype. Front. Aging Neurosci. 12:154. doi: 10.3389/fnagi.2020.00154

Objective: To investigate the effect of telmisartan, rosuvastatin, or their combination on dementia and to understand the impact of *apolipoprotein E* (*APOE*) genotype on the effect of the medications in older patients with hypertension.

Methods: This is a double-blind, randomized, and placebo-controlled trial using a 2 × 2 factorial design. Between April 2008 and November 2010, 1,244 hypertensive patients aged ≥60 years without cognitive impairment were recruited from communities in six cities in Shandong area, China. Patients were randomized into telmisartan and rosuvastatin administration after a 2-week washout period. *APOE* genotype was identified at the baseline. Possible dementia was determined using the combination of the global cognitive function and Assessment of the Informant Questionnaire on Cognitive Decline in the Elderly (IQCODE).

Results: Over an average follow-up of 7 [interquartile range (IQR): 6.7–7.2] years, telmisartan and rosuvastatin significantly reduced the cognitive impairment progression and the incidence of dementia. There was a synergistic interaction between telmisartan and rosuvastatin to reduce the cognitive impairment and the incidence of dementia ($P_{adjusted} < 0.001$). The cognitive impairment progression and the risk of dementia were higher in the hypertensive patients with *APOE* ε*4* allele than in those without *APOE* ε*4* allele. Rosuvastatin medication significantly alleviated the cognitive impairment progression and the risks of dementia in patients with *APOE* ε*4* allele.

Conclusion: The combination of telmisartan and rosuvastatin might be an effective prevention and/or treatment strategy for cognitive impairment and dementia, especially in hypertensive patients with the *APOE* ε*4* allele.

Clinical Trial Registration: www.ClinicalTrials.gov, ChiCTR.org.cn, identifier ChiCTR-IOR-17013557. Registered on April 12, 2017—Retrospectively registered, http://www.chictr.org.cn/showproj.aspx?proj=23121

Keywords: dementia, cognitive impairment, apolipoprotein E, lipid lowering, anti-hypertension, hypertension

INTRODUCTION

Dementia is an age-related and progressive neurodegenerative disease characterized by a decline in cognitive function that affects the quality of life in older adults (Peng et al., 2014; Sabia et al., 2017). Epidemiological studies reported 47 million cases of dementia worldwide in 2015 and have predicted that this will triple by 2050, given the steadily increasing life expectancy (Prince et al., 2013; Sabia et al., 2017), placing a heavy burden on individuals, families, and society. Hence, preventing and delaying the progression of dementia and cognitive impairment is a global public health issue (Shah et al., 2016).

Dementia and cognitive impairment are multifactorial diseases that are most frequently caused by aging, hypertension, dyslipidemia, and genetic factors (Farao and Iadecola, 2013; Sabia et al., 2017; Van Middelaar et al., 2018). Although hypertension is often accompanied by dyslipidemia, it is debatable whether antihypertensive treatment can improve cognitive outcome in the elderly (Farao and Iadecola, 2013; Sörös et al., 2013), and there are no specific classes of antihypertensive agents that have consistently shown greater efficacy in alleviating dementia or cognitive impairment (Gorelick et al., 2011; Farao and Iadecola, 2013). Moreover, it is unclear whether lipid-lowering statin treatment is beneficial, since different studies have reported conflicting findings (Jick et al., 2000; Hajjar et al., 2002; Rodrigues et al., 2002).

Sartans are some of the widely used antihypertensive medications. This popularity of sartans is due to its superior efficacy and tolerability profiles and the long duration of action. Sartans have been demonstrated to protect against cognitive deficits in animal models of Alzheimer's disease (Kehoe et al., 2009; Ahmed et al., 2018) and in human beings (Petek et al., 2018). However, there is an argument on the beneficial effect of sartans on cognitive decline (Diener et al., 2008; Tsukuda et al., 2009; Ho and Nation, 2017).

Statins has been recommended by guidelines as the medication for primary prevention of cardiovascular disease (Bibbins-Domingo et al., 2016; Mortensen and Nordestgaard, 2018; Arnett et al., 2019). A recent meta-analysis study demonstrated that statin medications could produce significant reductions in major vascular events irrespective of age (Cholesterol Treatment Trialists' Collaboration, 2019). Studies also showed that statins possess beneficial effects on reducing stroke risks and ameliorating dementia (Power et al., 2015; Geifman et al., 2017; Zissimopoulos et al., 2017; Petek et al., 2018). However, similar to sartans, the beneficial effect of statins on cognitive decline also remains controversial (Power et al., 2015; Geifman et al., 2017; Zissimopoulos et al., 2017; Sinyavskaya et al., 2018).

Several genes have been identified as risk factors for dementia and cognitive impairment in genome-wide association studies (Dergunov, 2011; Nazarian et al., 2019). One of these, *apolipoprotein E* (*APOE*), has three common alleles (ε*2*, ε*3*, and ε4) encoding distinct protein isoforms (Dergunov, 2011; Ji et al., 2018). In particular, the *APOE* ε4 allele is closely associated with elevated levels of total cholesterol and low-density lipoprotein cholesterol (Dergunov, 2011) with increased risk of dementia and cognitive impairment (Mahely and Huang, 1999; Reitz, 2012). However, the relationships between the *APOE* gene and blood pressure and *APOE* gene and plasma lipid-lowering treatments are not well understood. To address this issue, the present study investigated how the *APOE* ε4 genotype influences the effects of sartans and statins on dementia and cognitive impairment risk in older hypertensive patients.

METHODS

Standard Protocol Approval, Registration, and Patient Consent

This study was conducted in compliance with the Declaration of Helsinki and adhered to good clinical practice guidelines. The study protocol was approved by the Research Ethics Committee of the Institute of Basic Medicine, Shandong Academy of Medical Sciences, and was retrospectively registered with ChiCTR.org.cn (ChiCTR-IOR-17013557). Written informed consents were obtained from all the patients.

Study Design and Sample Size Determination

This study was a double-blind, randomized, and placebo-controlled trial using a 2 × 2 factorial design. The protocol of this study is described elsewhere (Ji et al., 2018). The major objective was to investigate the interaction of sartans and low-dose statins on the incident cardio- and cerebro-vascular events including stroke and myocardial infarction. The sample size was determined using the stroke incidence, and 1,244 essential hypertensive elderly aged ≥60 years were determined (Ji et al., 2018). In this study, we mainly investigated the interaction of sartans, statins, and *APOE* genotype on dementia incidence and the trajectory of global cognitive function during the study period. So, the sample size should be determined using the incidence of dementia. Given that the incidence of dementia is 5.1% per year (Jia et al., 2014), the sample size of 1,244 patients could well provide a statistical power of 90% including taking into account a dropout rate of 10% in this study.

Study Patients

Details of the study patients are as described in our previous study (Ji et al., 2018). Briefly, 1,244 essential hypertensive patients

aged ≥60 years were eligible and recruited from communities in six cities in Shandong, China, between April 2008 and November 2010. The exclusion criteria were patients with Alzheimer's disease, Parkinson's disease, schizophrenia, seizures, Mini-Mental State Examination (MMSE) score ≤23, secondary hypertension, diabetes mellitus, myocardial infarction or stroke in the last 6 months, clear hypersensitivity or contraindication to the medications administered in the study, chronic liver disease or renal dysfunction, inflammatory muscle disease, connective tissue diseases or malignancy, drug or alcohol abuse, intention to leave current residence within 6 years, inability to walk to the clinic, and unwillingness to provide informed consent.

Study Randomization, Intervention, and Follow-Up

After a 2-week washout period, the patients were randomized on a 1:1:1:1 ratio into control (telmisartan placebo and rosuvastatin placebo), telmisartan (telmisartan activator and rosuvastatin placebo), rosuvastatin (telmisartan placebo and rosuvastatin activator), and combination (telmisartan activator and rosuvastatin activator) groups. A computer-generated randomization was conducted by members who were not directly working on the study according to the order of recruitment with a block size of eight without stratification. Each patient was assigned a unique number that was used throughout the study. The investigators and patients were masked to treatment assignment until the completion of the study and until final clinical database lockdown.

Telmisartan was administered at a concentration of either 40 mg or increased to 80 mg once daily if needed and rosuvastatin at 10 mg once daily. Hydrochlorothiazide (12.5 mg increased to 25 mg once daily if needed) was used as an open-label medication and a background treatment in the four groups. Patients were visited weekly during the washout period, then at trial months 1, 3, and 6, every 6 months thereafter, and at final visit.

Evaluation of Global Cognitive Function

Assessments of global cognitive function include the MMSE (Liu et al., 2016; Duan et al., 2017), Montreal Cognitive Assessment (MoCA; Duan et al., 2017), Mattis Dementia Rating Scale (DRS; Chan et al., 2001), and Clinical Dementia Rating (CDR; Yue et al., 2016). The scales were implemented at baseline, annual follow-up, and final visits using the Chinese versions. All tests were conducted by experienced neuropsychology research assistants who were blinded to clinical and laboratory data, genotype, and psychological outcomes. The MMSE, MoCA, DRS, and CDR are widely used standard tests for assessing, screening, and staging cognitive dysfunction and dementia with excellent test–retest and inter-rater reliability. Lower MMSE, MoCA, and DRS scores reflect more severe cognitive impairment and dementia, whereas a higher CDR score represents more severe dementia. After testing 90 patients in random, the coefficients of variation of the interobserver were 0.91 for the MMSE score, 0.89 for the MoCA score, 0.87 for DRS score, and 0.84 for CDR score.

The Informant Questionnaire on Cognitive Decline in the Elderly

Assessment of the Informant Questionnaire on Cognitive Decline in the Elderly (IQCODE) was implemented at baseline, biennial follow-up, and final visits. The IQCODE is one of the worldwide used informant (proxy)-rated complementary screening tool for dementia that rates the change in cognitive function from a previous level of 10 years earlier (Jorm and Jacomb, 1989; Jorm, 1994, 2004). It is available in various versions (Jorm and Jacomb, 1989; Jorm, 1994, 2004; Harrison et al., 2016), has demonstrated utility in multiple cultural groups (Jorm and Jacomb, 1989; Fuh et al., 1995; Morales et al., 1995; Harrison et al., 2016), and has high internal (alpha = 0.95) and test–retest (correlation coefficient = 0.75) reliabilities (Jorm and Jacomb, 1989; Gavett et al., 2011). Our study used a shortened version consisting of 16 items, which was demonstrated essentially to be comparable to the original version (Jorm, 1994), to measuring cognitive decline during the follow-up period. The IQCODE was independently completed by the spouses, relatives, friends, or carers who closely knew the patients for at least 10 years. Each item on the IQCODE is rated on a five-point scale, where 1 represents "Much better," 2 "A bit better," 3 "Not much change," 4 "A bit worse," and 5 "Much worse." The final score is the average of the rated 16 item scores. A higher score represents a greater cognitive impairment. The coefficient of variation of the interobserver was 0.93 after being tested in random samples of 90 patients.

APOE Genotyping

DNA was extracted from 10 ml peripheral blood mixed with ethylenediaminetetraacetic acid (EDTA). *APOE* genotyping based on the presence of the single-nucleotide polymorphisms rs429358 and rs7412 was carried out by polymerase chain reaction using the TaqMan genotyping kit (Applied Biosystems, Foster City, CA, USA). The primers used were forward primer: 5′-TTG AAG GCC TAC AAA TCG GAA CTG-3′ and reversed primer: 5′-CCG GCT GCC CAT CTC CTC CAT CCG-3′ (Molinuevo et al., 2016). Patients were categorized as ε*4*-positive carriers (genotypes ε2/ε4, ε3/ε4, or ε4/ε4) or ε4-negative carriers (genotypes ε2/ε2, ε2/ε3, or ε3/ε3; Ji et al., 2018).

Outcomes

Primary outcomes included changes in global cognitive function including MMSE, MoCA, DRS, and CDR scores and dementia incidence. Possible dementia was diagnosed depending on a combination of IQCODE and global cognitive function assessment according to the recommendations from the National Institute on Aging–Alzheimer's Association workgroups on diagnostic guidelines for Alzheimer's disease (Narasimhalu et al., 2008; Albert et al., 2011). The cut-off of MMSE was ≤23 points or a decline of ≥3 points between any two annual follow-up visits (Liu et al., 2016; Duan et al., 2017), MoCA was >20 points (Delgado et al., 2017), DRS was >120 points (Chan et al., 2001), CDR was ≥1.0 (Yue et al., 2016), and IQCODE was ≥3.38 (Biessels et al., 2006). The secondary

outcomes were incident stroke and all-cause mortality during the follow-up period.

Statistical Analysis

The intention-to-treat principle was followed in the analysis of this study. Continuous data are expressed as mean with standard deviation (SD) or the median with interquartile range (IQR; the range between the 25th and 75th percentiles) depending on the normality of the data, and categorical data are expressed as a frequency with percentages. The Kolmogorov–Smirnov test was used to assess the normality of the continuous data. Comparisons of continuous data between groups were performed with the one-way analysis of variance (ANOVA) with the Bonferroni procedure or Kruskal–Wallis H test with a Wilcoxon rank-sum test depending on the normality of the data; categorical data were compared with the chi-square test. A linear mixed model was used to assess differences in the trajectory of MMSE, MoCA, CDR, and DRS scores over the follow-up period among groups. A Kaplan–Meier analysis with the log-rank test was used to evaluate differences in the risks of dementia incidence. The Cox proportional hazards model was used to assess the hazard ratio (HR) and 95% confidence interval (CI).

In this study, we tested the interactions between telmisartan and rosuvastatin; *APOE* ε*4* allele status and telmisartan; *APOE* ε*4* allele status and rosuvastatin; and among *APOE* ε*4* allele status, telmisartan, and rosuvastatin on the trajectory of global cognitive function and the dementia incidence. First, we classified patients into control, telmisartan, rosuvastatin, and combination groups to investigate the interaction between telmisartan and rosuvastatin. Then, we reclassified patients into telmisartan placebo * ε4 negative/positive [telmisartan(−) * ε4(−)/(+)] and telmisartan activator * ε4 negative/positive [telmisartan(+) * ε4(−)/(+)] groups to investigate the interaction between telmisartan and *APOE* ε*4* allele status. Third, we reclassified patients into rosuvastatin placebo * ε4 negative/positive [rosuvastatin(−) * ε4(−)/(+)] and rosuvastatin activator * ε4 negative/positive [rosuvastatin(+) * ε4(−)/(+)] groups to investigate the interaction between rosuvastatin and *APOE* ε*4* allele status. Finally, we subclassified the control, telmisartan, rosuvastatin, and combination groups into control * ε4(−)/(+), telmisartan * ε4(−)/(+), rosuvastatin * ε4(−)/(+), and combination * ε4(−)/(+) groups, respectively, to investigate the interaction among *APOE* ε*4* allele status, telmisartan, and rosuvastatin.

Models were adjusted for age, sex, education, smoking, alcohol consumption, baseline body mass index, baseline blood pressure, baseline fasting plasma glucose, baseline plasma lipids, the status of hydrochlorothiazide administration, changes in blood pressure, lipids, and fasting plasma glucose during the trial period, and the stroke incidence during the trial period. Multiple sensitivity analyses were performed using: (1) first diagnosed dementia during the trial period; (2) multiple imputation by chained equations for imputing missing data for variables; (3) stratified analysis to make sure that the associations found are robust; and (4) confounders included the changes in blood pressure, lipids, and fasting plasma glucose and the stroke incidence during the trial period in models. Statistical analyses were performed using SPSS v.24.0 (SPSS Inc., Chicago, IL, USA). A two-sided P-value < 0.05 was considered statistically significant.

RESULTS

Baseline Characteristics

Figure 1 shows a flowchart of this study. The first patient was recruited on April 28, 2008, and the final follow-up visit was completed on September 25, 2017. The average follow-up period was 7.0 (IQR: 6.7–7.2) years. The mean age at baseline was 70.11 ± 6.08 years, 597 (48.0%) subjects were female, and 323 (26.0%) were *APOE* ε*4*(+). The demographic and baseline clinical characteristics of the patients in control, telmisartan, rosuvastatin, and combination groups are shown in **Table 1**. There were no significant differences in the demographic and clinical characteristics among the four groups (all $P > 0.05$).

Outcomes

Over the follow-up period, a total of 176 patients (2.0% per year) developed dementia. The scores of MMSE, MoCA, and DRS were declined, and the scores of CDR and IQCODE were increased relative to the baseline.

Interactions Between Telmisartan and Rosuvastatin

The trajectories of MMSE, MoCA, DRS, CDR, and IQCODE scores in the duration of follow-up are presented in **Figure 2**. There were declining trends in MMSE, MoCA, and DRS and increasing trends in CDR and IQCODE in the four groups. However, the differences in the trends were significant among the four groups after adjustment for confounders as above described (all $P_{adjusted} < 0.001$). The declining trends in MMSE, MoCA, and DRS and the increasing trends in CDR and IQCODE were significantly lower in the combination group than in the control, telmisartan, and rosuvastatin groups (all $P_{adjusted} < 0.05$). These trends in telmisartan and rosuvastatin groups were slower in the telmisartan and rosuvastatin groups when compared with the control group (all $P_{adjusted} < 0.05$). Moreover, similar results were found when we further compared the changes in MMSE, MoCA, DRS, CDR, and IQCODE scores from the baseline among the four groups (all $P_{adjusted} < 0.05$; **Supplementary Figure S1**). There were significant differences in the incidences of dementia among the four groups after adjustment for covariates ($P_{adjusted} < 0.001$). The risks of dementia in the combination, telmisartan, and rosuvastatin groups were significantly lower when compared to the control group (all $P_{adjusted} < 0.001$; **Figure 2**, **Supplementary Table S1**). Compared with the combination group, the risks of dementia were higher in the telmisartan group and the rosuvastatin group (all $P_{adjusted} < 0.05$). There was a significant interaction between telmisartan and rosuvastatin based on the changing trends in MMSE ($P_{adjusted} = 0.011$), MoCA ($P_{adjusted} = 0.007$), DRS ($P_{adjusted} = 0.013$), CDR ($P_{adjusted} = 0.019$),

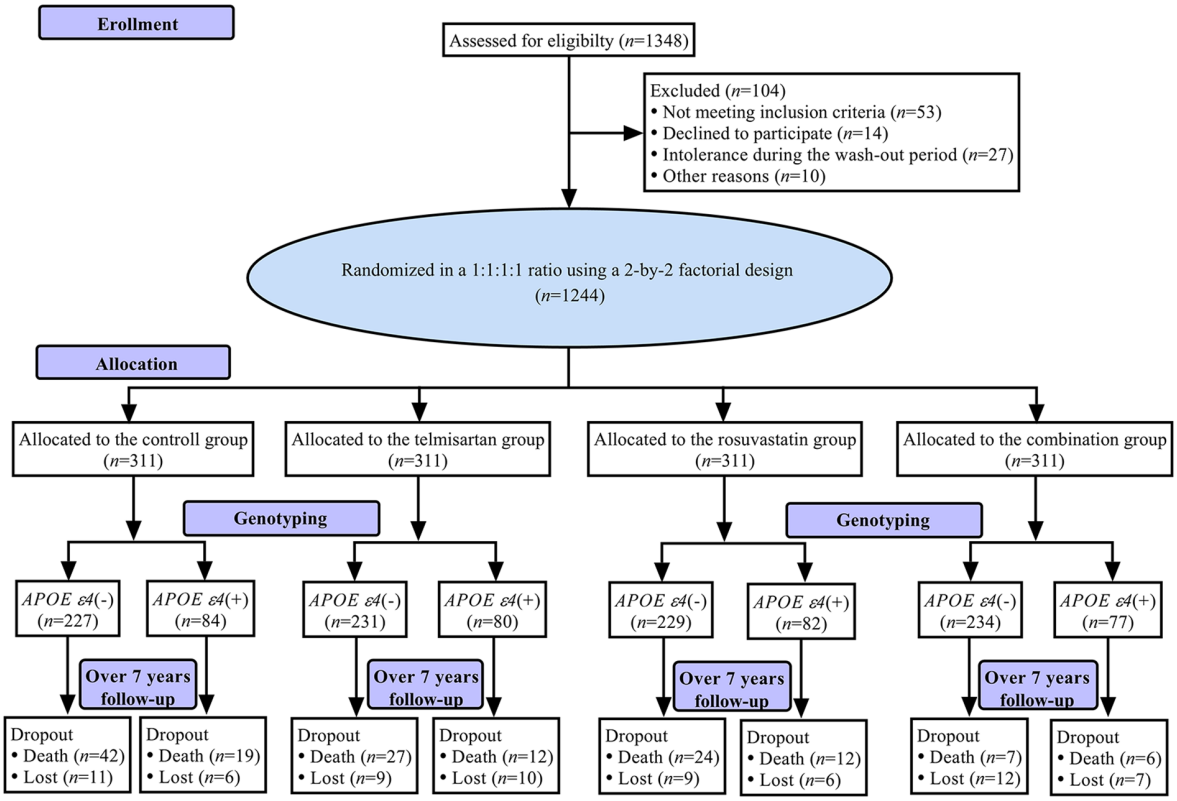

FIGURE 1 | Flowchart.

TABLE 1 | Demographic and clinical characteristics of the study population at baseline.

	Control group (*n* = 311)	Telmisartan group (*n* = 311)	Rosuvastatin group (*n* = 311)	Combination group (*n* = 311)	*P*-value
Age (years)	70.12 ± 6.17	70.48 ± 6.20	70.15 ± 5.96	69.68 ± 6.00	0.437
Female [*n* (%)]	147 (47.3)	151 (48.6)	155 (49.8)	144 (46.3)	0.829
Education (years)	7.00 (5.00, 10.00)	7.00 (3.00, 10.00)	7.00 (5.00, 10.00)	7.00 (4.00, 10.00)	0.416
Smoking [*n* (%)]	84 (27.0)	79 (25.4)	72 (23.2)	79 (25.4)	0.665
Alcohol consumption [*n* (%)]	110 (35.4)	120 (38.6)	108 (34.7)	107 (34.4)	0.684
BMI (kg/m^2)	24.49 ± 3.08	24.78 ± 2.89	24.55 ± 2.62	25.01 ± 3.77	0.144
SBP (mm Hg)	156.73 ± 9.99	156.91 ± 9.83	156.16 ± 9.29	156.67 ± 10.11	0.801
DBP (mm Hg)	70.80 ± 7.83	71.13 ± 7.23	71.36 ± 7.20	70.84 ± 7.63	0.767
Total cholesterol (mmol/L)	5.08 ± 0.63	5.08 ± 0.60	5.05 ± 0.66	5.00 ± 0.60	0.416
Triglycerides (mmol/L)	1.50 ± 0.36	1.51 ± 0.38	1.45 ± 0.36	1.50 ± 0.38	0.177
HDL-c (mmol/L)	1.20 ± 0.21	1.18 ± 0.22	1.20 ± 0.21	1.19 ± 0.19	0.593
LDL-c (mmol/L)	3.19 ± 0.62	3.21 ± 0.63	3.19 ± 0.68	3.13 ± 0.63	0.396
FPG (mmol/L)	5.46 ± 0.78	5.46 ± 0.81	5.42 ± 0.74	5.48 ± 0.75	0.806
MMSE (score)	29.00 (28.00, 30.00)	29.00 (28.00, 30.00)	29.00 (28.00, 30.00)	29.00 (28.00, 30.00)	0.823
MoCA (score)	28.00 (27.00, 29.00)	28.00 (27.00, 29.00)	28.00 (27.00, 29.00)	28.00 (27.00, 29.00)	0.275
DRS (score)	135.00 (128.00, 139.00)	134.00 (129.00, 138.00)	134.00 (129.00, 139.00)	134.00 (129.00, 139.00)	0.950
CDR (score)	0.00 (0.00, 0.00)	0.00 (0.00, 0.00)	0.00 (0.00, 0.00)	0.00 (0.00, 0.00)	1.00
IQCODE (score)	1.79 (1.27, 2.35)	1.81 (1.26, 2.29)	1.73 (1.3, 2.28)	1.78 (1.34, 2.26)	0.974
APOE ε4(+) [n (%)]	84 (27.0)	80 (25.7)	82 (26.4)	77 (24.8)	0.930

Data are shown as n (percentage), mean ± standard deviation, or median (interquartile range). Abbreviations: BMI, body mass index; SBP, systolic blood pressure; DBP, diastolic blood pressure; HDL-c, high-density lipoprotein cholesterol; LDL-c, low-density lipoprotein cholesterol; FPG, fasting plasma glucose; MMSE, Mini-Mental State Examination; MoCA, Montreal Cognitive Assessment; DRS, Mattis Dementia Rating Scale; CDR, Clinical Dementia Rating; IQCODE, Informant Questionnaire on Cognitive Decline in the Elderly; APOE, apolipoprotein E.

and IQCODE ($P_{\text{adjusted}} = 0.014$), and the incidences of dementia ($P_{\text{adjusted}} < 0.001$) after adjustment for confounders including the changes in blood pressure and lipids and the stroke incidence during the trial period.

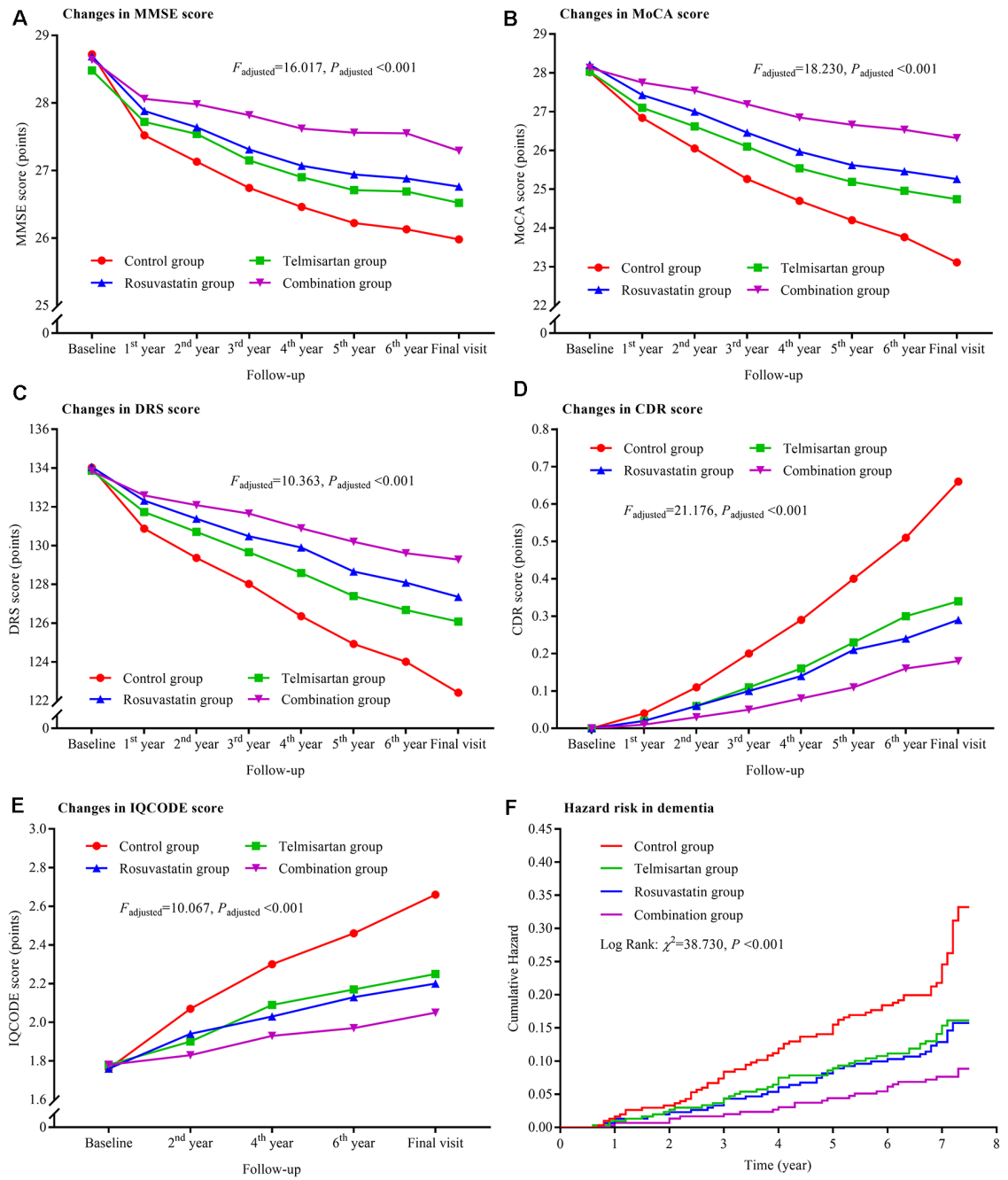

FIGURE 2 | Trajectory of global cognitive function and IQCODE and cumulative hazards of dementia incidence during the follow-up period in the patients grouped by telmisartan and rosuvastatin administration. Panel **(A)** is the trajectory of MMSE; panel **(B)** is the trajectory of MoCA; panel **(C)** is the trajectory of DRS; panel **(D)** is the trajectory of CDR; panel **(E)** is the trajectory of IQCODE, and panel **(F)** is the cumulative hazard of dementia incidence. MMSE, Mini-Mental Scale Estimation; MoCA, Montreal Cognitive Assessment; DRS, Mattis Dementia Rating Scale; CDR, Clinical Dementia Rating; IQCODE, Informant Questionnaire on Cognitive Decline in the Elderly.

Interactions Between Telmisartan and *APOE ε4* Allele

Compared to the telmisartan(−) * ε4(+) group, the declining trends in MMSE, MoCA, and DRS and the increasing trends in CDR and IQCODE were significantly lower in the other three groups after adjustment for confounders (all $P_{adjusted}$ < 0.05; **Figure 3**). The declining trends in MMSE and MoCA in the telmisartan(+) * ε4(−) group were lower than those in the telmisartan(−) * ε4(−) group ($P_{adjusted}$ = 0.002 and = 0.023, respectively). The increasing

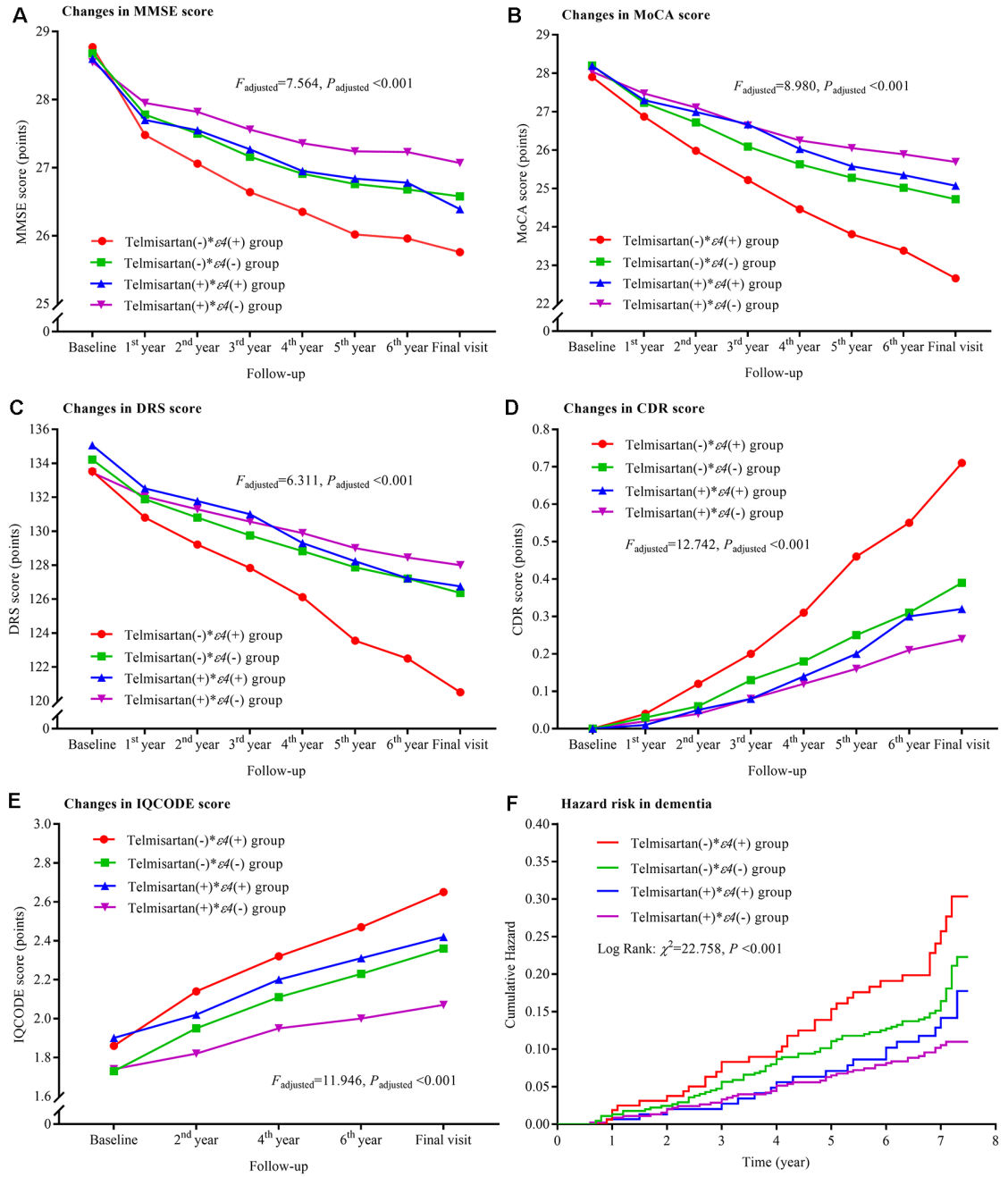

FIGURE 3 | Trajectory of global cognitive function and IQCODE and cumulative hazards of dementia incidence during the follow-up period in the patients grouped by telmisartan administration and *APOE* genotype. Panel **(A)** is the trajectory of MMSE; panel **(B)** is the trajectory of MoCA; panel **(C)** is the trajectory of DRS; panel **(D)** is the trajectory of CDR; panel **(E)** is the trajectory of IQCODE, and panel **(F)** is the cumulative hazard of dementia incidence. MMSE, Mini-Mental Scale Estimation; MoCA, Montreal Cognitive Assessment; DRS, Mattis Dementia Rating Scale; CDR, Clinical Dementia Rating; IQCODE, Informant Questionnaire on Cognitive Decline in the Elderly; APOE, apolipoprotein E.

trend in IQCODE in the telmisartan(−) * ε4(−) group was lower than that in the telmisartan(−) * ε4(+) group ($P_{adjusted}$ = 0.017). We further compared the changes in MMSE, MoCA, DRS, CDR, and IQCODE scores from the baseline among the four groups (**Supplementary Figure S2**). The changes in MMSE, MoCA, DRS, CDR, and IQCODE scores from the baseline were significantly higher in the telmisartan(−) * ε4(+) group than the other three groups (all $P_{adjusted}$ < 0.05). The risks of dementia in the telmisartan(+) * ε4(−) group were lower when compared to the telmisartan(−) * ε4(−) and telmisartan(−) * ε4(+) groups (**Figure 3**, **Supplementary Table S1**). No statistical interaction was observed between

telmisartan and *APOE ε4* allele on the changes in MMSE, MoCA, DRS, CDR, and IQCODE and in the incidences of dementia (all $P_{adjusted} > 0.05$).

Interactions Between Rosuvastatin and *APOE ε4* Allele

The declining trends in MMSE, MoCA, and DRS and the increasing trends in CDR and IQCODE and the risks of the dementia were significantly lower in the rosuvastatin(+) * ε4(−) group than in the rosuvastatin (−) * ε4(+) and rosuvastatin(−) * ε4(−) groups (all $P_{adjusted} < 0.05$; **Figure 4**). The declining trends in MoCA and DRS and the increasing trend in CDR were lower in the rosuvastatin(+) * ε4(+) group than in the rosuvastatin(−) * ε4(+) group (all $P_{adjusted} < 0.05$). The increasing trend in IQCODE was lower in the rosuvastatin(+) * ε4(−) group than in the rosuvastatin(−) * ε4(+) and lower in the rosuvastatin(−) * ε4(−) group than in the rosuvastatin(−) * ε4(+) group (all $P_{adjusted} < 0.05$). We further found that there were significant differences in the changes in MMSE, MoCA, DRS, CDR, and IQCODE scores from the baseline among the four groups (all $P_{adjusted} < 0.05$; **Supplementary Figure S3**). However, the differences in the changes in MMSE, MoCA, DRS, CDR, and IQCODE scores from the baseline were not significant between rosuvastatin(+) * ε4(+) and rosuvastatin(+) * ε4(−) group (all $P_{adjusted} > 0.05$). The risks of the dementia incidence were significantly lower in the rosuvastatin(+) * ε4(−) group than in the rosuvastatin(−) * ε4(+) and rosuvastatin(−) * ε4(−) groups (all $P_{adjusted} < 0.05$; **Figure 4**, **Supplementary Table S1**). The statistical interactions were observed between rosuvastatin and *APOE ε4* allele on the changes in MMSE ($P_{adjusted} = 0.018$), MoCA ($P_{adjusted} = 0.020$), DRS ($P_{adjusted} = 0.031$), CDR ($P_{adjusted} = 0.027$), and IQCODE ($P_{adjusted} = 0.022$) and in the dementia ($P_{adjusted} = 0.022$).

Interactions Among Telmisartan, Rosuvastatin, and *APOE ε4* Allele

The declining trends in MMSE, MoCA, and DRS and the increasing trends in CDR and IQCODE were the lowest in the combination * ε4(−) group and the highest in the control * ε4(+) group after the patients were grouped based on telmisartan, rosuvastatin, and *APOE ε4* genotype. There were significant differences in the changing trends among these groups (all $P_{adjusted} < 0.05$; **Figure 5**). Considering the changes in MMSE, MoCA, DRS, CDR, and IQCODE scores from the baseline, we did not find significant differences between the rosuvastatin * ε4(−) and rosuvastatin * ε4(+) groups and between the combination * ε4(−) and combination * ε4(+) groups (all $P_{adjusted} > 0.05$; **Supplementary Figure S4**). The cumulative hazards of the incidences of dementia were the lowest in the combination * ε4(−) group and the highest in the control * ε4(+) group (**Figure 5**, **Supplementary Table S1**). There were interactions among telmisartan, rosuvastatin, and *APOE ε4* genotype on the changing trends in MMSE ($P_{adjusted} = 0.029$), MoCA ($P_{adjusted} = 0.033$), DRS ($P_{adjusted} = 0.040$), CDR ($P_{adjusted} = 0.036$), and IQCODE ($P_{adjusted} = 0.031$) and in the incidences of dementia ($P_{adjusted} = 0.028$) after adjustment for confounders.

Changes in Blood Pressure, Lipids, and Fasting Plasma Glucose and Cumulative Hazards of Stroke Incidence

Supplementary Figures S5–S8 summarized the changes in blood pressure, lipids, and fasting plasma glucose and the cumulative hazards of stroke during the follow-up period in the patients after being grouped by different classification methods.

DISCUSSION

In this randomized clinical trial, we investigated the effects of antihypertensive and anti-lipidemic treatment on dementia, stroke incidence, and all-cause mortality in older hypertensive patients. Furthermore, the impact of *APOE* genotypes on the treatment was investigated in this study. The main findings were as follows: (1) both telmisartan and rosuvastatin alleviated the progression of cognitive impairment and reduced the risk of dementia; (2) telmisartan synergistically interacts with rosuvastatin to reduce the progression of cognitive impairment and the risk of dementia; (3) the hypertensive patients with *APOE ε4* allele had a higher risk of cognitive impairment progression and the dementia incidence than those without *APOE ε4* allele; and (4) rosuvastatin significantly alleviated the progression of cognitive impairment and the risks of dementia in patients with *APOE ε4* allele.

Although the argument on the effects of sartans and statins alleviating the progression of cognitive impairment and reducing the risk of dementia remains (Diener et al., 2008; Kehoe et al., 2009; Tsukuda et al., 2009; Power et al., 2015; Geifman et al., 2017; Ho and Nation, 2017; Zissimopoulos et al., 2017; Ahmed et al., 2018; Petek et al., 2018; Sinyavskaya et al., 2018), we found that both telmisartan and rosuvastatin significantly alleviated the progression of cognitive impairment and reduced the risk of dementia even after adjustment for confounders including the level of education and the status of hydrochlorothiazide administration. A previous study indicated that telmisartan performed slightly better than placebo on attenuating the progression of cognitive impairment and the risk of dementia (Zhang et al., 2019).

In a case-control and retrospective cohort study, the use of statins was associated with a lower prevalence of dementia and improved MMSE scores compared to patients who did not receive statin treatment (Hajjar et al., 2002). A previous study (Ji et al., 2018) showed that the risk of white matter hyperintensity progression was lower in the rosuvastatin than in the placebo group, which could underlie the lower risk of dementia and cognitive impairment progression in the former patients.

In this study, we observed that telmisartan synergistically interacted with rosuvastatin to reduce the progression of cognitive impairment and the risks of dementia. This result may be due to the fact that telmisartan mainly lowers blood pressure whereas rosuvastatin mainly lowers plasma lipid. As is known, hypertension is often

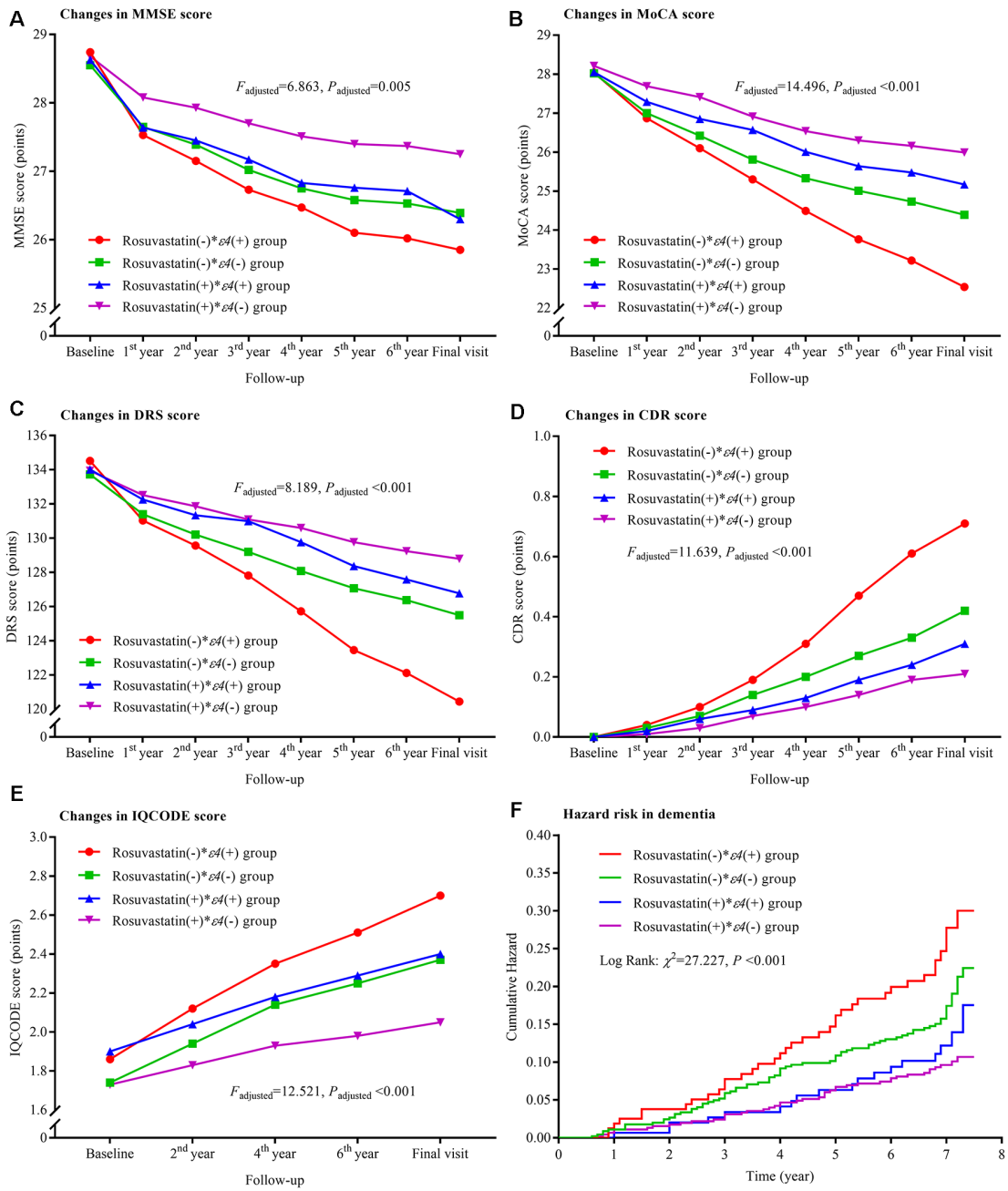

FIGURE 4 | Trajectory of global cognitive function and IQCODE and cumulative hazards of dementia incidence during the follow-up period in the patients grouped by rosuvastatin administration and *APOE* genotype. Panel **(A)** is the trajectory of MMSE; panel **(B)** is the trajectory of MoCA; panel **(C)** is the trajectory of DRS; panel **(D)** is the trajectory of CDR; panel **(E)** is the trajectory of IQCODE, and panel **(F)** is the cumulative hazard of dementia incidence. MMSE, Mini-Mental Scale Estimation; MoCA, Montreal Cognitive Assessment; DRS, Mattis Dementia Rating Scale; CDR, Clinical Dementia Rating; IQCODE, Informant Questionnaire on Cognitive Decline in the Elderly; APOE, apolipoprotein E.

accompanied by dyslipidemia. Another reason might be that telmisartan and rosuvastatin exhibit pleiotropic and protective effects on the cardio- and cerebrovascular systems including anti-inflammatory and antioxidant effects (Rizos et al., 2013; Liu et al., 2014), which is significant since inflammation and oxidative stress play important roles in dementia and cognitive impairment (Bulzacka et al., 2016; Liu et al., 2018).

Genotype frequencies can be used to evaluate the efficacy of health care practices. In this study, we observed that the risk of dementia in the patients with *APOE* ε4 allele was higher than those without *APOE* ε4 allele irrespective of treatment they

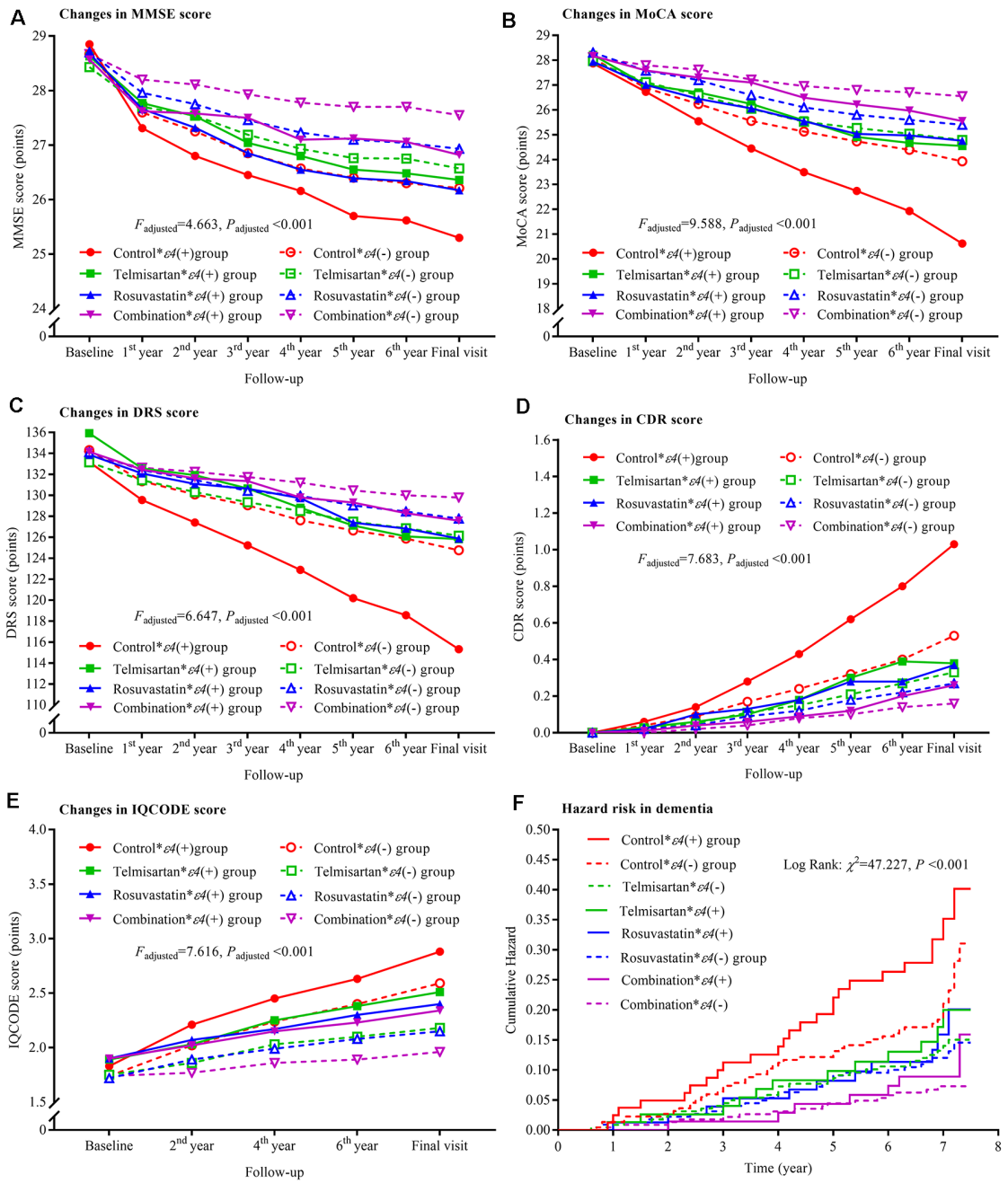

FIGURE 5 | Trajectory of global cognitive function and IQCODE and cumulative hazards of dementia incidence during the follow-up period in the patients grouped by telmisartan, rosuvastatin, and *APOE* genotype. Panel **(A)** is the trajectory of MMSE; panel **(B)** is the trajectory of MoCA; panel **(C)** is the trajectory of DRS; panel **(D)** is the trajectory of CDR; panel **(E)** is the trajectory of IQCODE, and panel **(F)** is the cumulative hazard of dementia incidence. MMSE, Mini-Mental Scale Estimation; MoCA, Montreal Cognitive Assessment; DRS, Mattis Dementia Rating Scale; CDR, Clinical Dementia Rating; IQCODE, Informant Questionnaire on Cognitive Decline in the Elderly; APOE, apolipoprotein E.

received. We did not find any interaction between telmisartan and *APOE* ε4 allele. However, as expected, a significant interaction was found between rosuvastatin and *APOE* ε4 allele. The differences in the changes in global cognitive function from baseline were not significant between rosuvastatin * ε4(−) and rosuvastatin * ε4(+) groups and between combination * ε4(−) and combination * ε4(+) groups. A previous study showed that the risk factors for the incidence of small cerebral vessel diseases including white matter hyperintensities, lacunes, and microbleeds that were strongly associated with dementia and cognitive impairment in subjects with *APOE* ε4 allele were markedly mitigated by rosuvastatin (Ji et al., 2018). Meanwhile,

APOE ε4 allele is closely associated with elevated levels of plasma lipids and has been demonstrated to increase the risk of dementia and cognitive impairment (Mahely and Huang, 1999; Reitz, 2012). Thus, the risks of dementia might be reduced by rosuvastain in subjects with *APOE* ε4 allele that has been regarded as a statin treatment threshold in clinical practice (Davies et al., 2011).

One of the major strengths of our study is that dementia was diagnosed using the combination of global cognitive function scale testing the patients themselves and based on the informant interview on cognitive decline. Second, the changes in blood pressure and lipids and the stroke incidence were included as confounders in analysis models. Third, the impact of *APOE* genotype on the treatment of telmisartan, rosuvastatin, and their combination was examined. The randomized, double-blind, placebo-controlled design and long-term follow-up might also be an advantage in this study.

On the other hand, our study also had several limitations. Firstly, hydrochlorothiazide was used as a basic medication in all patients. It is difficult to distinguish between these two groups in terms of differences in the incidence of dementia and cognitive impairment, although the status of hydrochlorothiazide administration was adjusted in the analysis models. Second, we did not consider the effects of ethnicity and gender. A previous meta-analysis showed that these factors do not alter the influence of the *APOE ε4* allele in dementia (Farrer et al., 1997), whereas others have reported that the effects of statins on Alzheimer's disease patients varied according to race (Zissimopoulos et al., 2017). The differences in gender may affect the treatments of statins and sartans on cognitive impairment (Zissimopoulos et al., 2017; Ji et al., 2018). Third, a lower socioeconomic status was found to be closely associated with an increased risk of dementia and cognitive decline (Russ et al., 2013; Rusmaully et al., 2017). Socioeconomic background could bias the results of this study. Fourth, dementia was not subclassified into Alzheimer's disease, senile dementia, and vascular dementia in this study. Lastly, we did not assess the effect of antiplatelet agents and antihyperglycemic medications as potential confounders on cognitive impairment and dementia in this study.

In conclusion, after over an average of 7 years' follow-up, our findings indicate that the combination of telmisartan and rosuvastatin might be an effective prevention and/or treatment strategy for cognitive impairment and dementia in hypertensive patients, especially in those with *APOE ε4* allele. However, our results should be validated by additional studies which take into account the differences in ethnicity, socioeconomic background, and statin agents.

DATA AVAILABILITY STATEMENT

The datasets used and/or analyzed during the current study are available from the corresponding author on reasonable request.

ETHICS STATEMENT

This study involving patients were reviewed and approved by the Research Ethics Committee of the Institute of Basic Medicine, Shandong Academy of Medical Sciences (registration number: 2007-12-09) on December 9, 2007. Each patient gave a written informed consent to participate in this study.

AUTHOR CONTRIBUTIONS

ZL, HZ, and YZ had full access to all the data in the study and had final responsibility for the decision to submit for publication and planned and initiated the trial. HZ, YL, and YD contributed to the management of data. ZL, WH, JW, and HZ contributed to the analysis and interpretation of data. WH, YL, and ZL contributed to the drafting of the manuscript. ZL, GG, and QC contributed to the critical revision of the manuscript for important intellectual content. All the authors contributed to the data collection. All authors interpreted data, critically reviewed the report, and approved the final version of the report.

FUNDING

This work was supported by the National Natural Science Foundation of China (grant numbers 81670432, 81973139, 81470489), the Key Technology Research and Development Project of Shandong (grant numbers 2018GSF118044, 2017GSF218060, 2019GSF108079, 2011GSF11822), the Innovation Project of Shandong Academy of Medical Sciences, and the Academic Promotion Programme of Shandong First Medical University.

ACKNOWLEDGMENTS

We thank the participated patients, general practitioners, and nurses who were involved in this study as well as all individuals who offered their assistance.

SUPPLEMENTARY MATERIAL

The Supplementary Material for this article can be found online at: https://www.frontiersin.org/articles/10.3389/fnagi.2020.00154/full#supplementary-material.

REFERENCES

Ahmed, H. A., Ishrat, T., Pillai, B., Fouda, A. Y., Sayed, M. A., Eldahshan, W., et al. (2018). RAS modulation prevents progressive cognitive impairment after experimental stroke: a randomized, blinded preclinical trial. *J. Neuroinflammation* 15:229. doi: 10.1186/s12974-018-1262-x

Albert, M. S., Dekosky, S. T., Dickson, D., Dubois, B., Feldman, H. H., Fox, N. C., et al. (2011). The diagnosis of mild cognitive impairment due to Alzhermer's disease: recommendations from the National Institute on Aging-Alzheimer's Association workgroups on diagnostic guidelines for Alzheimer's disease. *Alzheimers Dement.* 7, 270–279. doi: 10.1016/j.jalz.2011.03.008

Arnett, D. K., Blumenthal, R. S., Albert, M. A., Buroker, A. B., Goldberger, Z. D., Hahn, E. J., et al. (2019). 2019 ACC/AHA guideline on the primary

prevention of cardiovascular disease: a report of the american college of cardiology/american heart association task force on clinical practice guidelines. *Circulation* 140, e596–e646. doi: 10.1161/CIR.0000000000000678

Biessels, G. J., Staekenborg, S., Brunner, E., Brayne, C., and Scheltens, P. (2006). Risk of dementia in diabetes mellitus: a systematic review. *Lancet Neurol.* 5, 64–74. doi: 10.1016/S1474-4422(05)70284-2

Bulzacka, E., Boyer, L., Schürhoff, F., Godin, O., Berna, F., Brunel, L., et al. (2016). Chronic peripheral inflammation is associated with cognitive impairment in schizophrenia: results from the multicentric FACE-SZ dataset. *Schizophr. Bull.* 42, 1290–1302. doi: 10.1093/schbul/sbw029

Chan, A. S., Choi, M. K., and Salmon, D. P. (2001). The effects of age, education, and gender on the Mattis Dementia Rating Scale performance of elderly Chinese and American individuals. *J. Gerontol. B. Psychol. Sci. Soc. Sci.* 56, P356–P363. doi: 10.1093/geronb/56.6.p356

Cholesterol Treatment Trialists' Collaboration. (2019). Efficacy and safety of statin therapy in older people: a meta-analysis of individual participant data from 28 randomised controlled trials. *Lancet* 393, 407–415. doi: 10.1016/S0140-6736(18)31942-1

Davies, N. M., Windmeijer, F., Martin, R. M., Abdollahi, M. R., Smith, G. D., Lawlor, D. A., et al. (2011). Use of genotype frequencies in medicated groups to investigate prescribing practice: APOE and statins as a proof of principle. *Clin. Chem.* 57, 502–510. doi: 10.1373/clinchem.2010.156356

Delgado, C., Araneda, A., and Behrens, M. I. (2017). Validation of the Spanish-language version of the motreal cognitive assessment test in adults older than 60 years. *Neurologia* 34, 376–385. doi: 10.1016/j.nrl.2017.01.013

Dergunov, A. D. (2011). Apolipoprotein E genotype as a most significant predictor of lipid response at lipid-lowering therapy: mechanistic and clinical studies. *Biomed. Pharmacother.* 65, 597–603. doi: 10.1016/j.biopha.2011.04.003

Diener, H. C., Sacco, R. L., Yusuf, S., Cotton, D., Ounpuu, S., Lawton, W. A., et al. (2008). Effects of aspirin plus extended-telease dipyridamole versus clopidogrel and telmisartan on disability and cognitive function after recurrent stroke in patients with ischaemic stroke in the Prevention Regimen for Effectively Avoiding Second Strokes (PRoFESS) trial: a double-blind, active and placebo-controlled study. *Lancet Neurol.* 7, 875–884. doi: 10.1016/S1474-4422(08)70198-4

Duan, D., Dong, Y., Zhang, H., Zhao, Y., Diao, Y., Cui, Y., et al. (2017). Empty-nest-related psychological distress is associated with progression of brain white matter lesions and cognitive impairment in the elderly. *Sci. Rep.* 7:43816. doi: 10.1038/srep43816

Farao, G., and Iadecola, C. (2013). Hypertension: a harbinger of stroke and dementia. *Hypertension* 62, 810–817. doi: 10.1161/hypertensionaha.113.01063

Farrer, L. A., Cupples, L. A., Haines, J. L., Hyman, B., Kukull, W. A., Mayeux, R., et al. (1997). Effects of age, sex, and ethnicity on the association between apoliporotein E genotype and Alzheimer disease. A meta-analysis. APOE and Alzheimer Disease Meta Analysis Consortium. *JAMA* 278, 1349–1356. doi: 10.1001/jama.278.16.1349

Fuh, J. L., Teng, E. L., Lin, K. N., Larson, E. B., Wang, S. J., Liu, C. Y., et al. (1995). The Informant Questionniare on Cognitive Decline in the Elderly (IQCODE) as a screening tool for dementia for a predominantly illiterate Chinese population. *Neurology* 45, 92–96. doi: 10.1212/wnl.45.1.92

Gavett, R. A., Dunn, J. E., Stoddard, A., Harty, B., and Weintraub, S. (2011). The Cognitive Change in Women study (CCW): informant ratings of cognitive change but not selft ratings are associated with neuropsychological performance over three years. *Alzheimer. Dis. Assoc. Disord.* 25, 305–311. doi: 10.1097/wad.0b013e31820d8652

Geifman, N., Brinton, R. D., Kennedy, R. E., Schneider, L. S., and Butte, A. J. (2017). Evidence for benefit of statins to modify cognitive decline and risk in Alzheimer's disease. *Alzheimers Res. Ther.* 9:10. doi: 10.1186/s13195-017-0237-y

Gorelick, P. B., Scuteri, A., Black, S. E., Decarli, C., Greenberg, S. M., Iadecola, C., et al. (2011). Vascular contributions to cognitive impairment and dementia: a statement for healthcare professionals from the American Heart Association/American Stroke Association. *Stroke* 42, 2672–2713. doi: 10.1161/STR.0b013e3182299496

Hajjar, I., Schumpert, J., Hirth, V., Wieland, D., and Eleazer, G. P. (2002). The impact of the use of statins on the prevalence of dementia and the progression of cognitive impairment. *J. Gerontol. A. Biol. Sci. Med. Sci.* 57, M414–M418. doi: 10.1093/gerona/57.7.m414

Harrison, J. K., Stott, D. J., McShane, R., Noel-Storr, A. H., Swann-Price, R. S., and Quinn, T. J. (2016). Informant Questionnaire on Cognitive Decline in the Elderly (IQCODE) for the early diagnosis of dementia across a variety of healthcare settings. *Cochrane Database Syst. Rev.* 11:CD011333. doi: 10.1002/14651858.cd011333.pub2

Ho, J. K., Nation, D. A., and Alzheimer's Disease Neuroimaging Initiative. (2017). Memory is preserved in older adults taing AT1 receptor blockers. *Alzheimers Res. Ther.* 9:33. doi: 10.1186/s13195-017-0255-9

Ji, T., Zhao, Y., Wang, J., Cui, Y., Duan, D., Chai, Q., et al. (2018). Effect of low-dose statins and apolipoprotein E genotype on cerebral small vessel disease in older hypertensive patients: a subgroup analysis of a randomized clinical trial. *J. Am. Med. Dir. Assoc.* 19, 995.e4–1002.e4. doi: 10.1016/j.jamda.2018.05.025

Jia, J., Wang, F., Wei, C., Zhou, A., Jia, X., Li, F., et al. (2014). The prevalence of dementia in urban and rural areas of China. *Alzheimers Dement.* 10, 1–9. doi: 10.1016/j.jalz.2013.01.012

Jick, H., Zornberg, G. L., Jick, S. S., Seshadri, S., and Drachman, D. A. (2000). Statins and the risk of dementia. *Lancet* 356, 1627–1631. doi: 10.1016/s0140-6736(00)03155-x

Jorm, A. F. (1994). A short form of the Informant Questionnaire on Cognitive Decline in the Elderly (IQCODE): development and cross-validation. *Psychol. Med.* 24, 145–153. doi: 10.1017/s003329170002691x

Jorm, A. F. (2004). The Informant Questionnaire on cognitive decline in the elderly (IQCODE): a review. *Int. Psychogeriatr.* 16, 275–293. doi: 10.1017/s1041610204000390

Jorm, A. F., and Jacomb, P. A. (1989). The Informant Questionnaire on Cognitive Decline in the Elderly (IQCODE): socio-demographic correlates, reliability, validity and some norms. *Psychol. Med.* 19, 1015–1022. doi: 10.1017/s0033291700005742

Kehoe, P., Miners, S., and Love, S. (2009). Angiotensins in Alzheimer's disease-friend of foe? *Trends Neurosci.* 32, 619–628. doi: 10.1016/j.tins.2009.07.006

Liu, Z., Zhao, Y., Wang, X., Zhang, H., Cui, Y., Diao, Y., et al. (2016). Low carotid artery wall shear stress is independently associated with brain white-matter hyperintensities and cognitive impairment in older patient. *Atherosclerosis* 247, 78–86. doi: 10.1016/j.atherosclerosis.2016.02.003

Liu, Z., Zhao, Y., Wei, F., Ye, L., Lu, F., Zhang, H., et al. (2014). Treatment with telmisartan/rosuvastatin combination has a beneficial synergistic effect on ameliorating Th17/Treg functional imbalance in hypertensive patients with carotid atherosclerosis. *Atherosclerosis* 233, 291–299. doi: 10.1016/j.atherosclerosis.2013.12.004

Liu, W., Zhao, Y., Zhang, X., and Ji, J. (2018). Simvastatin ameliorates cognitive impairments *via* inhibition of oxidative stress-induced apoptosis of hippocampal cells through the ERK/AKT signaling pathway in a rat model of senile dementia. *Mol. Med. Rep.* 17, 1885–1892. doi: 10.3892/mmr.2017.8098

Mahely, R. W., and Huang, Y. (1999). Apolipoprotein E: from atherosclerosis to Alzheimer's disease and beyond. *Curr. Opin. Lipidol.* 10, 207–217. doi: 10.1097/00041433-199906000-00003

Molinuevo, J. L., Gramunt, N., Gispert, J. D., Fauria, K., Esteller, M., Minguillon, C., et al. (2016). The AlFA project: a research platform to identify early pathophysiological features of Alzheimer's disease. *Alzheimers Dement.* 2, 82–92. doi: 10.1016/j.trci.2016.02.003

Morales, J. M., Gonzalez-Montalvo, J. I., Bermejo, F., and Del-Ser, T. (1995). The screening of mild dementia with a shortened Spanish version of the "Informant Questionnaire on Cognitive Decline in the Elderly". *Alzheimer. Dis. Assoc. Disord.* 9, 105–111. doi: 10.1097/00002093-199509020-00008

Mortensen, M. B., and Nordestgaard, B. G. (2018). Comparison of five major guidelines for statin use in primary prevention in a contemporary general population. *Ann. Intern. Med.* 168, 85–92. doi: 10.7326/m17-0681

Narasimhalu, K., Lee, J., Auchus, A. P., and Chen, C. P. (2008). Improving detection of dementia in Asian patients with low education: combining the Mini-mental State Examination and the Informant Questionnaire on Cognitive Decline in the Elderly. *Dement. Geriatr. Gogn. Disord.* 25, 17–22. doi: 10.1159/000111128

Nazarian, A., Arbeev, K. G., Yashkin, A. P., and Kulminski, A. M. (2019). Genetic heterogeneity of Alzheimer's disease in subjects with and without hypertension. *Geroscience* 41, 137–154. doi: 10.1007/s11357-019-00071-5

Peng, J., Lu, F., Wang, Z., Zhong, M., Sun, L., Hu, N., et al. (2014). Excessive lowering of blood pressure is not beneficial for progression of brain white

matter hyperintensive and cognitive impairment in elderly hypertensive patients: 4-year follow-up study. *J. Am. Med. Dir. Assoc.* 15, 904–910. doi: 10.1016/j.jamda.2014.07.005

Petek, B., Villa-Lopez, M., Loera-Valencia, R., Gerenu, G., Winblad, B., kramberger, M. G., et al. (2018). Connecting the brain cholesterol and renning-angiotensin systems: potential role of statins and RAS-modifying medications in dementia. *J. Intern. Med.* 284, 620–642. doi: 10.1111/joim.12838

Power, M. C., Weuve, J., Sharrett, A. R., Blacker, D., and Gottesman, R. F. (2015). Statins, cognition and dementia - systematic review and methodological commentary. *Nat. Rev. Neurol.* 11, 220–229. doi: 10.1038/nrneurol.2015.35

Prince, M., Bryce, R., Albanese, E., Wimo, A., Riberiro, W., and Ferri, C. P. (2013). The global prevalence of dementia: a systematic review and metaanalysis. *Alzheimers Dement.* 9, 63–75. doi: 10.1016/j.jalz.2012.11.007

Reitz, C. (2012). Dyslipidemia and dementia: current epidemiology, genetic evidence, and mechanisms behind the associations. *J. Alzheimers Dis.* 30, 127–145. doi: 10.3233/jad-2011-110599

Rizos, C. V., Liberopoulos, E. N., Tellis, C. C., Tselepis, A. D., and Elisaf, M. S. (2013). The effect of combining rosuvastatin with sartans of different peroxisome proliferator receptor-γ activating capacity on plasma 8-isoprostane prostaglandin F2α levels. *Arch. Med. Sci.* 9, 172–176. doi: 10.5114/aoms.2013.33357

Rodrigues, E. G., Dodge, H. H., Birzescu, M. A., Stoehr, G. P., and Ganguli, M. (2002). Use of lipid-lowering drugs in older adults with and without dementia: a community-based epidemiological study. *J. Am. Geriatr. Soc.* 50, 1852–1856. doi: 10.1046/j.1532-5415.2002.50515.x

Rusmaully, J., Dugravot, A., Moatti, J. P., Marmot, M. G., Elbaz, A., Kivimaki, M., et al. (2017). Contribution of cognitive performance and cognitive decline to associations between socioeconomic factors and dementia: a cohort study. *PloS Med.* 14:e1002334. doi: 10.1371/journal.pmed.1002334

Russ, T. C., Stamatakis, E., Hamer, M., Starr, J. M., Kivimäki, M., and Batty, G. D. (2013). Socioeconomic status as a risk factor for dementia death: individual participant meta-analysis of 86 508 men and women from the UK. *Br. J. Psychiatry* 203, 10–17. doi: 10.1192/bjp.bp.112.119479

Sabia, S., Dugravot, A., Dartigues, J. F., Abell, J., Elbaz, A., Kivimäki, M., et al. (2017). Physical activity, cognitive decline and risk of dementia: 28 year follow-up of Whitehall II cohort study. *BMJ* 357:j2709. doi: 10.1136/bmj.j2709

Shah, H., Albanese, E., Duggan, C., Rudan, I., Langa, K. M., Carrillo, M. C., et al. (2016). Research priorities to reduce the global burden of dementia by 2025. *Lancet Neurol.* 15, 1285–1294. doi: 10.1016/s1474-4422(16)30235-6

Sinyavskaya, L., Gauthier, S., Renoux, C., Dell'Aniello, S., Suissa, S., and Brassard, P. (2018). Comparative effect of statins on the risk of incident Alzheimer disease. *Neurology* 90, e179–e187. doi: 10.1212/wnl.0000000000004818

Sörös, P., Whitehead, S., Spence, J. D., and Hachinski, V. (2013). Antihypertensive treatment can prevent stroke and cognitive decline. *Nat. Rev. Neurol.* 9, 174–178. doi: 10.1038/nrneurol.2012.255

Tsukuda, K., Mogi, M., Iwanami, J., Min, L. J., Sakata, A., Jing, F., et al. (2009). Cognitive deficit in amyloid-β-injected mice was improved by pretreatment with a low dose of telmisartan partly because of peroxisome proliferators-activated receptor-γ activation. *Hypertension* 54, 782–787. doi: 10.1161/hypertensionaha.109.136879

US Preventive Services Task Force, Bibbins-Domingo K., Grossman, D. C., Curry, S. J., Davidson, K. W., Epling, J. W. Jr., et al. (2016). Statin use for the primary prevention of cardiovascular disease in adults: US Preventive Services Task Force Recommendation Statement. *JAMA* 316, 1997–2007. doi: 10.1001/jama.2016.15450

Van Middelaar, T., van Vught, L. A., van Gool, W. A., Simons, E. M., van den Born, B. H., Moll van Charante, E. P., et al. (2018). Blood pressure-lowering interventions to prevent dementia: a systematic review and meta-analysis. *J. Hypertens.* 36, 1780–1787. doi: 10.1097/hjh.0000000000001829

Yue, W., Wang, X. D., Shi, Z., Wang, Y., Liu, S., Liu, S., et al. (2016). The prevalence of dementia with lewy bodies in a rural area of China. *Parkinsonism Relat. Disord.* 29, 72–77. doi: 10.1016/j.parkreldis.2016.05.022

Zhang, H., Cui, Y., Zhao, Y., Dong, Y., Duan, D., Wang, J., et al. (2019). Effects of sartans and low-dose statins on cerebral white matter hyperintensities and cognitive function in older patients with hypertension: a randomized, double-blind and placebo-controlled clinical trial. *Hypertens. Res.* 42, 717–729. doi: 10.1038/s41440-018-0165-7

Zissimopoulos, J. M., Barthold, D., Brinton, R. D., and Joyce, G. (2017). Sex and race differences in the association between statin use and the incidence of Alzheimer disease. *JAMA Neurol.* 74, 225–232. doi: 10.1001/jamaneurol.2016.3783

Conflict of Interest: The authors declare that the research was conducted in the absence of any commercial or financial relationships that could be construed as a potential conflict of interest.

frontiers in Neuroscience

REVIEW
published: 17 June 2020
doi: 10.3389/fnins.2020.00626

Parkinson's Disease and the Gut: Future Perspectives for Early Diagnosis

*Jana Harsanyiova[1], Tomas Buday[1] and Alzbeta Kralova Trancikova[2]**

[1] *Departmet of Pahophysiology, Jessenius Faculty of Medicine in Martin, Comenius University, Bratislava, Slovakia,*
[2] *Biomedical Center Martin, Jessenius Faculty of Medicine in Martin, Comenius University, Bratislava, Slovakia*

Parkinson's disease (PD) is a neurodegenerative disease characterized by progressive degeneration of dopaminergic neurons, and at the cellular level by the formation of Lewy bodies in the central nervous system (CNS). However, the onset of the disease is believed to be localized to peripheral organs, particularly the gastrointestinal tract (GIT) and the olfactory bulb sooner before neuropathological changes occur in the CNS. Patients already in the pre-motor stage of PD suffer from various digestive problems and/or due to significant changes in the composition of the intestinal microbiome in this early stage of the disease. Detailed analyses of patient biopsies and autopsies as well as animal models of neuropathological changes characteristic of PD provided important information on the pathology or treatment of PD symptoms. However, presently is not clarified *(i) the specific tissue in the GIT* where the pathological processes associated with PD is initiated; *(ii) the mechanism* by which these processes are disseminated to the CNS or other tissues within the GIT; and *(iii)* which neuropathological changes could also serve as a *reliable diagnostic marker of the premotor stages of PD*, or *(iv) which type of GIT tissue* would be the most appropriate choice for routine examination of patient biopsies.

Keywords: Parkinson's disease, alpha-synuclein, gastrointestinal tract, enteric nervous system, animal models, wholemount tissue staining

OPEN ACCESS

Edited by:
Woon-Man Kung,
Chinese Culture University, Taiwan

Reviewed by:
Nicola B. Mercuri,
University of Rome Tor Vergata, Italy
Yogesh Singh,
Tübingen University Hospital, Germany
Masaki Takao,
National Center of Neurology and Psychiatry, Japan

****Correspondence:***
Alzbeta Kralova Trancikova
alzbeta.trancikova@uniba.sk

Specialty section:
This article was submitted to Neurodegeneration, a section of the journal Frontiers in Neuroscience

Received: *12 March 2020*
Accepted: *19 May 2020*
Published: *17 June 2020*

Citation:
Harsanyiova J, Buday T and Kralova Trancikova A (2020) Parkinson's Disease and the Gut: Future Perspectives for Early Diagnosis. Front. Neurosci. 14:626. doi: 10.3389/fnins.2020.00626

INTRODUCTION

Parkinson's disease (PD) with the prevalence of approximately 2%, is the second most common neurodegenerative disease in the world after Alzheimer's disease (AD) (de Lau and Breteler, 2006), in which the incidence increases rapidly with age (Dauer and Przedborski, 2003). Most cases of PD, approximately 90%, represent the idiopathic forms of the disease (Hansen and Li, 2012). The disease is characterized by progressive degeneration of dopaminergic neurons in the central nervous system (CNS), namely, the *substantia nigra pars compacta (SNpc)*, and dopamine (DA) deficiency in the striatum, which is associated with the occurrence of many motor and non-motor symptoms (Dauer and Przedborski, 2003; Jankovic, 2008; Santos et al., 2019). In addition to the characteristic clinical motor symptoms such as tremor, bradykinesia, stiffness and postural instability, the disease is also manifested by non-motor symptoms, most commonly by dysfunction of the gastrointestinal tract (GIT) and olfaction (Braak et al., 2003).

The neuropathological feature of PD is the formation of intraneuronal cytoplasmic eosinophilic protein inclusions, Lewy bodies (LB) and Lewy neurites (LNs) in neurons of both the central and

enteric nervous systems (ENS). The major component of LB and LNs, among other proteins, is pathologically aggregated alpha-synuclein (αS) (Braak et al., 2006; Caputi and Giron, 2018). The αS is a presynaptic protein whose exact physiological function is currently not fully understood, but its localization in the presynaptic nerve terminals may indicate an influence on the regulation of synaptic vesicle transduction (Cabin et al., 2002; Trancikova et al., 2011). Physiologically, αS most commonly occurs in the form of stable unfolded monomers (Eliezer et al., 2001) or folded tetramers (Bartels et al., 2011). Oligomers, protofibrils, and fibrils (Lashuel et al., 2013), typically phosphorylated at serine 129 (S129) (Okochi et al., 2000; Fujiwara et al., 2002) are considered to be pathological conformers associated with the αS pathogenesis in neurodegenerative diseases (**Figure 1**).

As early as the beginning of the 21st century, Braak et al. (2003, 2006) suggested that the development of PD initiates in the ENS based on the effect of an unknown toxin and/or pathogen, and progresses to the CNS through anatomical connections of these systems or that ENS may be affected by PD pathology in the initial stage of the disease. However, the exact GIT localization of initial PD pathology and specific mechanisms of disease spreading to the CNS are still not fully understood.

The aim of this article is to: (i) summarize experimental possibilities of early PD diagnosis based on biopsies and autopsies of PD patients and animal models; (ii) on the basis of current knowledge, delineate possible mechanisms by which the disease can develop and spread in the CNS, and (iii) finally, we focused on the complexity and lack of information in the studies and attempted to explore the possibilities for improving the detection of PD-related pathological processes in GIT tissues.

IMPACT OF PD-ASSOCIATED PATHOLOGICAL PROCESSES ON THE ENTERIC NERVOUS SYSTEM

The enteric nervous system ("second brain") is a complex neural network made up of about 100 million neurons (Furness, 2008) consisting of two plexuses: myenteric (Auerbach's) and submucosal (Meissner's). These innervate both the proximal part of GIT, the oral cavity, the salivary glands, the esophagus, and the stomach; as well as the distal GIT, the small intestine, colon and rectum (Lebouvier et al., 2009; Visanji et al., 2014). The myenteric plexus is located between the longitudinal and circular muscle layers throughout the entire GIT, where it controls mainly smooth muscle activity and motility. The submucosal plexus is mainly present in the small and large intestine, to a lesser extent in the stomach, while in the esophagus it is not present at all (Visanji et al., 2014). Enteric neurons are unevenly distributed in both plexuses, ENS along the entire GIT consists of intrinsic innervation located in the gastrointestinal wall and extrinsic innervation derived from sympathetic and parasympathetic nervous systems. Regulation of GIT function, such as motility and secretion by the ENS is independent of the CNS. However, ENS is bidirectionally connected to the CNS and together they form the so-called gut–brain axis (GBA) at the level of the autonomic nervous system (Lebouvier et al., 2009; Carabotti et al., 2015). Despite the fact that the ENS controls the physiological processes taking place in GIT independently of the CNS, the link between the two systems mediates their mutual influence (Rao and Gershon, 2016). Because of this connection, a healthy organism maintains intestinal homeostasis, and vice versa, neurodegenerative CNS diseases are reflected in ENS disorders and thus in gastrointestinal problems of patients. This causality is also seen in other neurodegenerative diseases such as AD, transmissible spongiform encephalopathies, or amyotrophic lateral sclerosis (Spielman et al., 2018), while GIT disorders often result in CNS-related symptoms (Caputi and Giron, 2018). The ENS, similar to the CNS, also contains a small proportion of dopaminergic neurons present at higher concentrations in both plexuses of the proximal parts of the GIT, with a decreasing tendency in its distal parts (Anlauf et al., 2003). However, the correlation between PD and the loss of dopaminergic neurons in GIT has only been demonstrated by Singaram in the analysis of colon tissues from patients with developed PD (Singaram et al., 1995). The study of the presence of LBs and LNs is still receiving a great deal of attention. We will deal with this issue in more detail in the following sections.

We must not forget the effect of the intestinal microbiome on the gut–brain relationship and their crosstalk. The intestinal microbiome constantly interacts with the ENS, either through bacterial metabolites or components of the bacterial walls and thus influences neural transmission in the ENS (Thomas et al., 2012; Forsythe and Kunze, 2013; Elfil et al., 2020). The intestinal epithelium forms a barrier that prevents the passage of harmful content and at the same time allows the absorption and secretion of nutrients (Marchiando et al., 2010; Chapelet et al., 2019) or drugs (Jin et al., 2019). The composition of the intestinal microbiota affects the proper function of this barrier, by regulating the expression of the tight junction proteins such as occludin, claudins, and zonula occludens-1 (ZO-1) (Bhattarai, 2018; Chapelet et al., 2019). Increased bowel permeability, called "leaky gut," is typical for patients with early PD (Forsyth et al., 2011), when the function of the intestinal barrier is disrupted with subsequent inflammatory processes and increased oxidative stress. This environment further promotes αS accumulation and aggregation in the ENS (Sampson et al., 2016). Consistent with these findings, decreased expression of some tight junction proteins has been found in animal PD models (Gorecki et al., 2019; Dodiya et al., 2020) or in PD patients (Maes and Leunis, 2008; Clairembault et al., 2015a). In addition, increased expression of inflammatory cytokines and glial markers, also detected in GIT biopsies of PD patients, was positively correlated with disease progression and severity (Devos et al., 2013; Lin et al., 2019; Elfil et al., 2020).

An even higher incidence of peptic ulcer and *Helicobacter pylori* infections has been found in patients with PD up to 8–10 years before the onset of motor symptoms (Alvarez-Arellano and Maldonado-Bernal, 2014; Elfil et al., 2020). PD-associated neurodegeneration is likely to occur through the *Helicobacter pylori*-induced autoimmune and inflammatory response with increased production of pro-inflammatory cytokines and leukocyte activation. These can cross the disrupted blood–brain

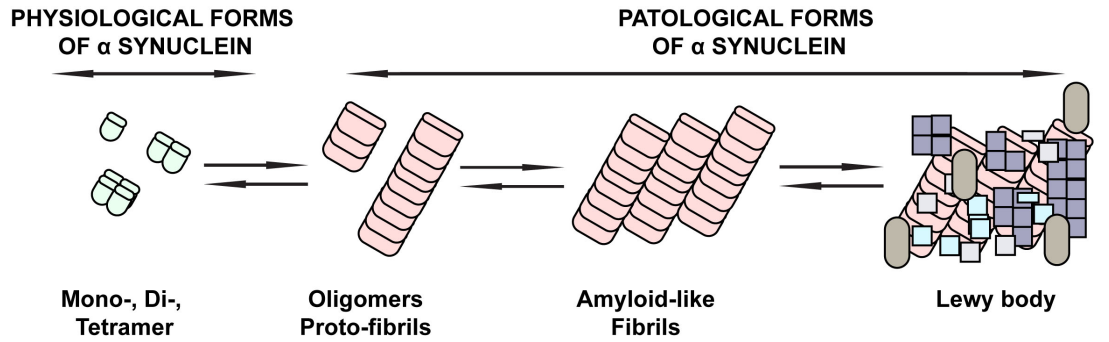

FIGURE 1 | Schematic overview of the physiological and pathological forms of αS. The physiological forms of αS commonly found in the CNS or peripheral tissues of the CNS are mainly stable unfolded monomers or folded tetramers. Under pathological conditions, conformational changes of αS with beta-sheet formation occur that are associated with the occurrence of oligomers, followed by protofibrils and fibrils typically phosphorylated on serine 129, until they eventually deposit in Lewy bodies. These forms are considered to be pathological conformers of αS associated with the pathogenesis of neurodegenerative diseases.

barrier (BBB), causing neurotoxicity and neurodegeneration (Dobbs et al., 2008; Elfil et al., 2020). In addition, *Helicobacter pylori* infection is associated with decreased L-DOPA absorption, whether due to *Helicobacter pylori*-induced inflammatory response in the gut of PD patients or increased gastric acid secretion. In these patients, eradication of *Helicobacter pylori* led to an improvement in L-DOPA responsive motor problems (Pierantozzi et al., 2006; Lee et al., 2008; Elfil et al., 2020). Several studies have confirmed reproducible and significant changes in the intestinal microbiome composition that correlate with PD-related motor symptoms (Scheperjans et al., 2015; Sampson et al., 2016; Perez-Pardo et al., 2017; Elfil et al., 2020). These changes are summarized in detail by several authors (Sun and Shen, 2018; Chapelet et al., 2019; Elfil et al., 2020; Shen, 2020).

These authors agree that the intestinal microbiome is also important for the development of the "parkinsonian intestine" phenotype. For example, a significantly increased concentration of *Enterobacteriaceae* in PD patients, which correlates with the severity of postural instability and gait difficulty. Conversely, reduced level of *Prevotellaceae* family correlates with increased intestinal permeability and vitamin B1 and B9 deficiency in these patients (Scheperjans et al., 2015). In addition, significantly reduced levels of the *Lactobacillaceae* family (Mukherjee et al., 2016) in patients with PD are mainly associated with the development of inflammatory processes, since anti-inflammatory effects are attributed to this bacterial family (Borre et al., 2014; Scheperjans et al., 2015; Unger et al., 2016). Decreased levels of some bacterial families (such as *Prevotellaceae, Lactobacillaceae, Lachnospiraceae*) in PD patients are interesting in terms of their ability to reduce short-chain fatty acid (SCFA) levels (Scher et al., 2013; Zmora et al., 2019) or ghrelin (Song et al., 2017; Yanagi et al., 2017). Both SCFA and ghrelin have a neuroprotective function, so their reduced levels observed in patients with PD can be considered not only as one of the critical factors of PD but also potentially reflect disease severity (Hill-Burns et al., 2017; Song et al., 2017; Elfil et al., 2020).

Intestinal microbiota may also affect drug metabolism and uptake, as confirmed by a negative correlation in the case of *Prevotellaceae* or, conversely, a positive correlation in the case of *Turicibacteraceae* (Lin et al., 2019). In this context, the positive effect of probiotic supportive treatment on the motor as well as non-motor symptoms of the disease was confirmed not only in PD patients (Tamtaji et al., 2019) but also in experimental animal models of PD (Srivastav et al., 2019; Hsieh et al., 2020).

LOCALIZATION OF PATHOLOGICAL FORMS OF α-SYNUCLEIN IN THE ENS OF PD PATIENTS

Since Qualman et al. (1984) published the presence of LBs in the esophagus in 1 PD patient and 1 PD patient in the colon in 1984, an increasing number of post-mortem and *in vivo* studies have focused on finding or developing a suitable method for reliable detection of neuropathological changes in peripheral organs that would be suitable for taking biopsies. Pathologically aggregated αS in GIT has been identified to date in biopsies of PD patients from different parts of GIT (summarized in **Table 1**). However, the number of studies provided, the size of the individual groups used in these studies and controversy in obtained results (see below) does not make it possible to clearly determine the primary initiation site of the disease pathology onset within GIT and where or to which organs the pathology subsequently spreads (Cersosimo, 2015).

Salivary Glands and Pharynx

Salivary glands as a tissue with a relatively high number of αS aggregates have been studied in autopsies (Beach et al., 2010) as well as in biopsies of PD patients (Cersosimo et al., 2011). The presence of αS inclusions in minor salivary glands biopsies was confirmed in all PD (n = 3) patients, whereas control biopsies (n = 3) did not show this pathology (Cersosimo, 2015).

A needle core biopsy of the submandibular gland of PD revealed the presence of LBs was confirmed in 75% of cases but the study did not include control patients or patients with another type of neurodegenerative disease. However, due to minimal

TABLE 1 | Summary of studies focused on the presence of pathological forms of αS in various peripheral tissues.

Tissue	αS detected		αS form	Autopsy/biopsy	Number of patients and controls		Reference
Salivary glands	+	T	AGG	A	3	3	Cersosimo et al. (2011)
	+	P	LBs	B	15	0	Adler et al. (2014)
Pharynx	+	P	AGG	A	10	4	Mu et al. (2013)
Esophagus	ND	ND	LBs	A	22	50	Qualman et al. (1984)
	ND	ND	LBs	A	7	24	Wakabayashi et al. (1988)
	+	P	AGG	A	17	23	Beach et al. (2010)
	+	T, P	LBs	A	10	3	Gelpi et al. (2014)
Stomach	+	T	AGG	B	34	23	Sanchez-Ferro et al. (2015)
	+	T, P	LBs	A	10	0	Gelpi et al. (2014)
	+	P	LNs	B	1	0	Pouclet et al. (2012)
	+	P	ND	B	35	161	Hilton et al. (2014)
	+	T	ND	A	5	5	Braak et al. (2006)
Small intestine	+	P	LNs	B	1	0	Pouclet et al. (2012)
	+	P	ND	B	15	161	Hilton et al. (2014)
Appendix	+	T	ND	B	0	20	Gray et al. (2014)
Colon	+	P	LNs	B	5	8	Lebouvier et al. (2009)
	+	P	LNs	B	29	10	Lebouvier et al. (2010)
	+	T	AGG	B	9	23	Shannon et al. (2012a)
	+	T	ND	A	10	77	Gold et al. (2013)
	+	P	ND	B	62	161	Hilton et al. (2014)
	+	P	LNs	B	31	11	Clairembault et al. (2015a)
	+	T, P	ND	B	22	11	Visanji et al. (2015)
	+	T, P	ND	B	19	8	Antunes et al. (2016)
	+	T	LTS	B	9	3	Corbille et al. (2016)
	+	T, P	AGG	B	17	13	Corbille et al. (2017)
	+	P	AGG	B	18	11	Fenyi et al. (2019)

The only direct evidence of PD-related neuropathological changes in the ENS seems to be the confirmation of the presence of pathological forms of αS and protein inclusions in the peripheral tissues of PD patients. The table summarizes the numbers of patients and controls in each study, broken down by the peripheral tissue of interest. Detected forms of αS and the study outcomes are indicated. PD, Parkinson's disease; αS, α Synuclein; ND, not defined; T, total; P, phosphorylated at S129; AGG, aggregated; LBs, Lewy bodies; LNs, Lewy neurites; LTS, Lewy type synucleinopathy; A, autopsy; B, biopsy.

invasiveness, the possibility of using only local anesthesia, and the overall simplicity and reproducibility, this method presents a suitable method for monitoring Lewy body pathology in patients with PD (Adler et al., 2014).

Dysphagia is one of the many clinical problems of PD patients but often leads to more serious clinical complications, such as aspiration pneumonia, the most common cause of death in PD patients (Mu et al., 2013). Analysis of the pharynx autopsies of patients with confirmed PD (n = 10) and control samples (n = 4) confirmed the presence of phosphorylated αS (P- αS) aggregates in the sensory nerve axons of all PD patients with PD, compared to control samples. Patients with dysphagia even exhibited more αS-positive fibers than PD patients without diagnosed dysphagia. These results, therefore, suggest that pharyngeal sensory nerves are primarily affected by PD pathology, which may be related to subsequent sensitization of pharyngeal tissue, presence of oedema and further development of dysphagia in PD patients (Mu et al., 2013).

Esophagus

At about the same time as Qualman published the first mention of LBs in ENS, Wakabayashi et al. (1988) focused on autopsies of GIT tissues in patients with histologically confirmed PD (n = 7). The presence of LBs was observed across the entire GIT with the highest concentration in the myenteric plexus at the lower part of the esophagus. However, healthy individuals (8/24) also showed LB-positivity (Wakabayashi et al., 1988). Extensive analysis of the presence of P-αS in autopsies of various tissues of patients not only with PD (n = 17) but also AD (n = 19), dementia with LBs (DLB, n = 9) and incidental Lewy body disease (n = 7) in comparison with healthy individuals (n = 23), confirmed the rostrocaudal P-αS distribution in the GIT of PD patients. The highest incidence was detected in the submandibular gland and lower part of the esophagus, while the concentration of aggregates decreased in the stomach, small intestine, colon, and rectum and even no presence of P-αS positive inclusions has been reported in the upper 2/3 of the esophagus (Beach et al., 2010).

Similarly, in a post-mortem histopathological study of tissues derived from the CNS-and autonomous nervous system from PD patients PD (n = 10), DLB (n = 5) and others (n = 13) including atypical parkinsonism and dementia without LBs (n = 13), the presence of αS aggregates was confirmed in all PD and DLB case, in contrast to the atypical form of parkinsonism and dementia without LBs. These aggregates have been confirmed not only in GIT tissues, but also in the adrenal gland, heart, sympathetic ganglia, vagus nerve, and genitourinary tract, with the typical rostrocaudal distribution. Distal esophagus and stomach contained the most observed αS aggregates, while the rectum contained the least (Gelpi et al., 2014).

Stomach and Small Intestine

Analysis of the gastric mucosa in PD patients, control subjects, including cases with premotor symptoms, confirmed αS inclusions in the gastric mucosa were found in (17/28) patients with PD, in control biopsies (1/23) and patients with premotor symptoms (1/6) (Sanchez-Ferro et al., 2015). Besides that, the intraneuronal αS-positive inclusions have also been observed across the entire gastric ENS (cardia, fundus, pylorus), in the myenteric and submucosal plexus, as well as in the peripheral nerves found in the adventitia, in autopsies obtained from the brain and stomach of patients with sporadic PD (Braak et al., 2006). Also, the presence of αS-positive LNs was determined in fundic, antral and duodenal submucosa biopsies from one PD patient (Pouclet et al., 2012).

Colon

To date, the colon has been the most studied part of the GIT in relation to PD (Schneider et al., 2016). Several studies have confirmed the occurrence of P-αS-positive LNs in colon biopsies from PD patients suggesting that conventional colon biopsies can be used to study the submucosal plexus of the ENS (Lebouvier et al., 2009, 2010; Shannon et al., 2012a,b; Gold et al., 2013; Visanji et al., 2014; Clairembault et al., 2015a).

In colon biopsies from PD patients (21/29) but not in healthy individuals (0/10), Lebouvier observed αS-positive LNs along with the loss of neurofilament-positive neurons in the ganglia. This increased number of LNs correlated with PD symptoms (Lebouvier et al., 2010). Similarly, Clairembault et al. (2015a) detected P-αS-positive LNs in the submucosal plexus of the colon (23/31). In all cases, control samples were negative for P-αS.

Several studies have focused on early PD symptoms in the GIT, and thus on pre-motor PD patients (Shannon et al., 2012a,b; Hilton et al., 2014; Visanji et al., 2014). Shannon et al. (2012a) confirmed the presence of αS in colon biopsies confirmed in all premotor PD patients (9/9) but not in healthy individuals (0/23), supporting the hypothesis of the incidence of pathological αS in GIT tissues in the pre-motor stages of the disease. In addition, increased oxidative stress was present in PD patients as well as in both control groups, suggesting that the pathological occurrence of αS is not the result of an inflammatory process or oxidative stress (Shannon et al., 2012b). Visanji et al. (2015) compared the presence of αS and P-αS in colon biopsies from patients at various stages of the disease (early PD $n = 15$; late PD $n = 7$) and healthy individuals ($n = 11$). However, the analysis did not confirm the difference in the presence of αS and P-αS within the studies groups, mainly due to the high positivity for αS and P-αS in control samples (Visanji et al., 2015). To date, the largest study has focused on analyzing the accumulation of pathological P-αS in various types of GIT tissues in patients with a very early pre-motor phase of the disease, at least 8 years before the first motor symptoms of PD. Together, they studied 117 biopsies from 62 PD patients and 161 samples from healthy subjects. Accumulation of P-αS was confirmed in mucosal and submucosal neurites in only seven PD patients, with all control biopsies without positive findings. Regarding GIT tissues, P-αS positivity was detected in gastric, duodenal and colon biopsies. However, in contrast to the abovementioned studies by Qualman et al. (1984), Wakabayashi et al. (1988), and Gelpi et al., 2014, esophageal samples did not confirm this positivity (Hilton et al., 2014).

In colon mucosa biopsies of idiopathic PD patients, αS positivity was present in most PD subjects studied (18/19), but P-αS was found in all PD patients (19/19) and all healthy individuals (8/8) (Antunes et al., 2016). When comparing colon biopsy samples of PD patients with AD and healthy individuals, up to 53% of all study subjects being positive for αS in an age-independent manner. While all samples from PD patients (10/10) were positive for αS, with significantly higher prevalence and expression compared to the control group, AD patients were in most cases negative for the presence of αS or did not exceed the control group (Gold et al., 2013).

A recent study focused not only on the detection of pathological forms of αS in the GIT, but the results have been correlated with non-motor symptoms of the disease (Lee et al., 2018). However, the presence of αS in gastric and colonic biopsies of PD patients ($n = 35$) and healthy individuals ($n = 52$) did not significantly correlate with complex GI dysfunction such as constipation, dyspepsia, abdominal pain or with the deterioration of a specific intestinal segment (Lee et al., 2018). Despite the relatively large sample of subjects studied, this study has several limitations: (i) analysis of deeper intestinal layers (especially ENS of submucosal and myenteric plexuses) and other GIT tissue types, (ii) immunohistochemical staining for pathological αS, (iii) the use of conventional histological approach only, (iv) lack of other experimental methods (e.g., biochemical) and (v) the low sample quality.

In general, the results agree that immunohistochemical confirmation of colorectal αS pathology in PD patients may be a suitable pre-mortem diagnosis of the disease. However, due to the slight inconsistency of the results in relation to healthy individuals, it is necessary to extend the standard immunological analysis to other types of analysis. Corbille et al. (2016) evaluated and compared four different immunohistochemical methods for optimal detection of Lewy-type synucleinopathy from submucosal colon biopsies of PD patients ($n = 9$) and healthy individuals ($n = 3$). However, none of the compared αS detection methods, granular staining in the *lamina propria*, perivascular/vascular wall submucosal staining, lacy-granular pattern in the submucosa and epithelial cell nuclear staining, showed specificity and sensitivity of more than 80%, which evaluates these methods as inadequate for routine PD diagnostics (Corbille et al., 2016). Similarly, biochemical analysis by one-dimensional or two-dimensional electrophoresis of colon biopsy samples from 17 PD patients ($n = 17$) and healthy individuals ($n = 13$) did not confirm a difference in αS expression levels, phosphorylation and aggregation between the groups in the study (Corbille et al., 2017). These findings reflect the limitations of individual methods suggesting the need for new and more sensitive methods, as well as the necessity to combine several methodologies for an accurate diagnosis.

Furthermore, Fenyi et al. (2019) recently studied GIT biopsies from the antrum, sigmoid colon and rectum from 18 PD patients and 11 healthy individuals. However,

the classical immunohistochemical detection has been extended by the protein misfolding cyclic amplification (PMCA) assay. Interestingly, control subject with positive PMCA test subsequently developed PD symptoms. The immunohistochemical detection revealed the presence of P-aS in 5/15 PD samples, with four of these samples also being PMCA positive, indicating the diagnostic potential of the PMCA method. Control samples did not show any positivity for P-aS. Rectal biopsy does not represent a possibility of obtaining material in the case of PMCA due to insufficient number of aS aggregates (Fenyi et al., 2019).

Appendix

It is now well documented that the vermiform appendix is part of the immune tissues associated with GIT, and also serves as a reservoir of the intestinal microbiome (Killinger and Labrie, 2019). Nevertheless, the mechanisms by which the appendix affects intestinal immunity and microbiome are still unknown today. In relation to PD, epidemiological studies have found that early appendectomy correlates with a reduction in the risk of developing PD (Killinger et al., 2018). This is probably due to the presence of aggregated aS also in healthy individuals in the mucosa and enteric plexuses of the appendix (Killinger et al., 2018). The fact, that a higher density of αS aggregates in the appendix was detected in PD patients as well as asymptomatic patients (Stokholm et al., 2016) suggest, that misfolded αS accumulates in the appendix, from where the pathology may have spread to other organs. Therefore, early removal of lymphoid organs with accumulated misfolded αS could potentially represent a therapeutic tool for patients in the early stages of PD or with familiar form (Gray et al., 2014; Killinger et al., 2018).

ANIMAL MODELS

Animal models in PD research represent an irreplaceable source of new knowledge, whether in connection with the understanding of the pathomechanisms that of PD initiation and progression, but also as preclinical models of PD (Metzger and Emborg, 2019). They can also help to elucidate whether intestinal dysbiosis is a cause or a consequence of PD-related pathology. However, no animal model can recapitulate all the symptoms and processes associated with the pathogenesis and progression of PD (summarized in **Table 2**) (Klingelhoefer and Reichmann, 2015). Just in an effort to address these shortcomings, a new generation of PD models is constantly being developed (Metzger and Emborg, 2019).

Toxin-Induced Models

Toxin-induced models are widely used models mainly due to the relatively simple use of the toxin, clear phenotype, the rapid onset of motor or non-motor symptoms of the disease and the ability to reflect motor complications of antiparkinsonian drugs, such as L-DOPA-induced dyskinesia (Morin et al., 2014; Taguchi et al., 2020b). The disadvantage is the exposure of experimenters to toxins, the frequent criticism that the concentrations used to induce PD-related symptoms do not commonly occur in the natural environment, but in particular that robust motor phenotypes may interfere with the analysis of non-motor symptoms (Taguchi et al., 2020b).

Rotenone Models

Rotenone is a highly lipophilic pesticide that readily crosses the BBB, spreads to neurons, and accumulates in mitochondria, where it acts as an inhibitor of mitochondrial complex I (Duty and Jenner, 2011). Rotenone-induced rodent models of PD are able to reproduce the neuropathological, anatomical as well as behavioral properties of the disease (Betarbet et al., 2000). In addition to the neurodegeneration of the nigrostriatal dopaminergic system and the presence of cytoplasmic inclusions in these neurons, accompanied by motor problems (Tieu, 2011), non-motor symptoms at the GIT level were also observed (Drolet et al., 2009; Greene et al., 2009; Tieu, 2011). However, Tasselli et al. (2013) did not confirm the delay in gastric emptying after oral application of rotenone to mice, despite the present neurodegeneration in *SNpc*. Similarly, the presence or absence of LB or pathological αS in the GIT or ENS depends on the route of rotenone administration, the dose used, and the length of exposure (Drolet et al., 2009; Greene et al., 2009; Pan-Montojo et al., 2010; Metzger and Emborg, 2019).

Regarding microbiota changes in the GIT, a significant decrease in the beneficial *Bifidobacterium* bacteria (Perez-Pardo et al., 2018) or, conversely, an increase in Gram-negative mucin-degrading bacteria (Akkermansia) (Dodiya et al., 2020) were observed in the rotenone-induced PD model. Chronic stress is another factor leading to an increase in intestinal hyperpermeability and a reduction of anti-inflammatory bacteria (*Lactobacillus*) in experimental animals. In combination with rotenone, chronic stress even promoted its potential to induce CNS pathology, manifested by a significant increase in the number of dystrophic microglia, increased reactivity of lipopolysaccharides (LPS) in *SNpc* and decreased DA in the striatum compared to control mice (Dodiya et al., 2020).

MPTP Models

MPTP (1-methyl-4-phenyl-1,2,3,6-tetrahydropyridine) is a potent neurotoxin with high affinity for the DA transporter, as a result of which the metabolite MPTP (MPP+) accumulates in the mitochondria and acts as an inhibitor of mitochondrial complex I (Cleeter et al., 1992). MPTP is used to induce a parkinsonian-like phenotype in a number of mammalian animal models, e.g., in monkeys, mice, rats, swine, cats and sheep (Tieu, 2011). The mouse and monkey model are most commonly used, as the sensitivity to MPTP is comparatively lower in other mammals (e.g., rats) (Hisahara and Shimohama, 2010). The neuropathological effect of MPTP on the nigrostriatal DA pathway in animal models is similar to that observed in PD patients (Langston et al., 1999).

In ENS, an MPTP-induced significant decrease in dopaminergic neurons, tyrosine hydroxylase-positive (TH+), in the myenteric plexus has been described in monkeys (Chaumette et al., 2009) as well as in a mouse model of PD (Anderson et al., 2007). Other GIT dysfunctions have been described in a mouse

TABLE 2 | Overview of the most used animal models of PD, their associated phenotypes and AS pathology.

Model	Type	Motor phenotype	Non-motor phenotype	Animal	αS/Lewy pathology
Toxin-induced	Rotenone	✓	✓	Mouse, rat	Yes
	MPTP	✓	✓	Mouse, primate	No
	6-OHDA	✓	✓	Rat	No
	Paraquat	✓	✓	Mouse	Yes
Genetic	αS overexpressing	✓	✓	Mouse	Yes
	αS-A53T transgenic	Not consistent	✓	Mouse	Yes
	Pink1	–	✓	Mouse	No
	MitoPark	✓	✓	Mouse	No
Propagation	αS PFF	✓	✓	Mouse	Yes

αS, α Synuclein; MPTP, 1-methyl-4-phenyl-1,2,3,6-tetrahydropyridine, 6-OHDA, 6-hydroxydopamine, PFF, recombinant αS preformed fibrils.

model, but the information is controversial in some cases. While Anderson et al., 2007 reported increased MPTP-induced colon motility as well as unchanged emptying time compared to control animals, several other authors observed a significant reduction in colonic motility and constipation (Natale et al., 2010; Ellett et al., 2016). Selective loss of TH+ neurons was observed in the myenteric and submucosal plexuses of the colon, but not in the esophagus and stomach. The decrease in DA was accompanied by an increase in αS levels (Natale et al., 2010). Furthermore, in mice, MPTP-induced loss of TH+ neurons in ENS led to a strong immune response in the GIT (Cote et al., 2015; Ellett et al., 2016). Interestingly, partial depletion of pro-inflammatory M1 monocytes had a positive effect in terms of protecting ENS from TH+ neuronal loss, but this effect was ton manifested in the CNS (Cote et al., 2015). On the other hand, therapeutics (CuII) with a neuroprotective effect on the CNS improve not only motor functions but also intestinal functions defined by improved stool frequency, reduced enteric glial cell reactivity and markers of inflammation, as well as restoration of neuronal subpopulations in myenteric plexus damaged by MPTP exposure. These results suggest the existence of similar pathomechanisms in the CNS and ENS (Ellett et al., 2016).

6-OHDA Models

6-OHDA is a hydroxylated DA analog acting as a selective catecholaminergic neurotoxin that inhibits mitochondrial complex I and IV (Glinka and Youdim, 1995) and produces reactive oxygen species in cells (Cohen and Heikkila, 1974). Since 6-OHDA cannot effectively cross the BBB, direct injection of this toxin into a specific site in the brain is required (Perese et al., 1989; Przedborski et al., 1995; Hisahara and Shimohama, 2010; Duty and Jenner, 2011). As early as 1968 (Ungerstedt, 1968), complete anterograde degeneration of the nigrostriatal dopaminergic neural system associated with motor problems was described in rats after administration of 6-OHDA into the *SNpc*. In addition to the ability to recapitulate the motor symptoms of the disease (Hisahara and Shimohama, 2010; Tieu, 2011), the 6-OHDA rat model mimics many of the biochemical features of PD, such as a reduction in DA and TH levels in the striatum (Duty and Jenner, 2011). However, like many other animal models of PD, the 6-OHDA model fails to induce the formation of LBs, an important pathological feature of PD.

Regarding pre-motor symptoms, several authors reported PD-like constipation in 6-OHDA animal models (Blandini et al., 2009; Zhu et al., 2012; Levandis et al., 2015; Zhang et al., 2015; Fornai et al., 2016). Unilateral (Zhu et al., 2012) or bilateral (Zheng et al., 2011) injection of 6-OHDA to *SNpc* of rats leads to a general decrease of central DA as well as delayed gastric emptying, suggesting that central DA may regulate GIT function (Zheng et al., 2011; Zhu et al., 2012; Metzger and Emborg, 2019).

Paraquat Models

The herbicide Paraquat, (1,1'-dimethyl-4,4'-bipyridine) is the inducer of αS aggregation and the oxidative stress in dopaminergic neurons (Kuter et al., 2007, 2010). Anselmi et al. (2017, 2018) reported a paraquat-induced decrease in gastric motility, and gastric tone, followed by increased αS immunoreactivity in dorsal motor nucleus of the vagus (DMV) in a rat model of PD (Anselmi et al., 2017, 2018). Co-administration of subthreshold doses of paraquat with lectin directly into the stomach of rats leads to a progressive PD-like phenotype, represented by the decrease in TH+ neurons in *SNpc*, the presence of misfolded αS in the *SNpc* and DMV, and L-DOPA responsive motor deficits. These symptoms were preceded by gastric dysmotility. Interestingly, vagotomy was able to block the spread of misfolded αS outside the myenteric neurons and even prevented the development of PD-related symptoms in these rats (Anselmi et al., 2018).

Genetic Models

Since the number of patients with the familial form of PD is significantly lower than the incidence of an idiopathic form of the disease, genetic research of affected families is very demanding (Hisahara and Shimohama, 2010). Particularly because of this fact, it is extremely important to develop appropriate genetic animal models for research to investigate the etiopathology of PD. In these models, we must not forget that the choice of promoter fully influences the observed phenotype, whether in terms of the level of expression or the regions in which this gene will be expressed. A disadvantage compared to toxic models is the slower onset of the phenotype, and also that only a few models show loss of DA neurons and an associated motor phenotype (Taguchi et al., 2020b). Nevertheless, these models can significantly contribute not only to the understanding of PD-related pathomechanisms

but also in the development of symptomatic or disease-modifying therapies that target non-motor symptoms associated with the disease. Therefore, efforts are constantly increasing to develop a PD model that would reproduce several PD-specific premotor symptoms at the same time, followed by slowly progressive DA neurodegeneration (Taguchi et al., 2020b).

αS Overexpressing Models

In the case of αS, it is known that quantitative, as well as qualitative changes in αS, contribute to the development of PD. Several models have been developed, either based on over-expression of the wt αS gene (*SNCA*) or with the insertion of pathological mutations (A53T, A30P) (Singleton et al., 2003; Chartier-Harlin et al., 2004; Ibanez et al., 2004; Taguchi et al., 2020b). As mentioned above, the choice of strong exogenous promoters used in these models affects not only the phenotype but also the spatial and temporal distribution of the pathology, which may not always reflect the real human PD pathology. However, in general, we can say that αS transgenic models are able to recapitulate αS aggregation, similar to PD patients (Taguchi et al., 2020b).

Overexpression of αS (Thy1-αS) results in decreased basal stool, slower colonic transit time with significantly higher stool content (Wang et al., 2008). This manifestation was preceded by increased αS in myenteric plexuses with numerous varicose terminals surrounding specifically immunoreactive pChAT neurons (Wang et al., 2012). Sampson et al. (2016) revealed that in Thy1-αS mice, microbial depletion reduces the CNS pathology, characterized by reduced accumulation of pathological αS in the brain, as well as motor and GIT dysfunction. Microbiota transplants from PD patients lead to a significant deterioration of intestinal dysfunction as well as overall PD symptoms in these mice (Sampson et al., 2016). Similarly, colonization of curli (amyloid protein)-producing *Escherichia coli*, in Thy1-αS mice induces the αS pathology in both the gut and brain, along with classical intestinal and motor dysfunctions. Interestingly, treatment of these mice with a gut-restricted amyloid inhibitor blocks the progression of curli-induced pathology (Sampson et al., 2020). These results confirm the role of intestinal microbiota and bacteria-produced amyloids in the progression of PD-related CNS pathology, presumably through microglial activation and neuroinflammation, suggesting a potential positive effect of antibiotic treatment on ameliorating GIT as well as CNS symptoms in PD patients (Sampson et al., 2016, 2020).

Several studies have addressed the induction of the PD phenotype by lipopolysaccharide (LPS). LPS is a pro-inflammatory bowel-derived bacterial endotoxin that has been shown to induce progressive nigrostriatal pathology (Qin et al., 2007; Liu et al., 2008; Kelly et al., 2014). In addition, an increased amount of LPS-producing *Gammaproteobacteria* or mucin-degrading bacteria *Verrucomicrobiaceae* has been confirmed in patients with PD (Gorecki et al., 2019). In Thy1-αS mice, low dose oral administration of LPS induces the early onset of motor symptoms along with increased αS in the CNS. However, microbiota analysis did not confirm a higher rate of *Gammaproteobacteria* or the amount of *Verrucomicrobiaceae*, which were even reduced. These results confirm that elevated central levels of αS alone may not lead to early intestinal manifestations in PD (Gorecki et al., 2019). In contrast, induction of PD-related pathology by IP application of LPS in a wt mice led to increased αS expression and accumulation of pathological P-αS specifically in the colon, accompanied by a temporary increased colon permeability. However, nigrostriatal degeneration or other significant pathological changes in the CNS have not been confirmed (Kelly et al., 2014).

αS-A53T Transgenic Models

Previous studies using experimental animals have confirmed the role of the pathological A53T mutation of αS in the development of PD-related motor and non-motor dysfunctions, such as age-related anxiety and loss of olfaction associated with αS aggregation in the olfactory bulb as well as myenteric plexus and adrenal neurons (Farrell et al., 2014; Kujawska and Jodynis-Liebert, 2018; Taguchi et al., 2020b). Similarly, in PrP-A53T-αS (M83 tg) mice, the age-related significant accumulation of P-αS was detected first in the intestinal nervous system and later in the brain, but in both cases, it preceded the onset of motor symptoms of the disease (Bencsik et al., 2014). The combination of oral paraquat application in M83 tg mice accelerated the onset of αS-associated pathology, with motor dysfunction as well as the presence of P-αS and neuroinflammation in ENS already present in young mice (Naudet et al., 2017). In the context of GIT symptoms, already young M83 tg mice show remarkable signs of gastrointestinal dysfunction, which precede motor abnormalities and CNS pathology. The presence of aggregated forms of αS has been detected in neurons in both myenteric and submucosal plexuses but specifically only in the colon. The problems with intestinal peristalsis are indicated by a slowed transit time through the colon and an abnormal stool. This assertion was supported by electrically evoked contractions of the colon, which showed a reduced motor response in these mice (Rota et al., 2019).

Recently, a new BAC-A53T-αS mouse model with the insertion of two single nucleotide polymorphisms associated with familial PD or with an increased risk of sporadic PD has been published. The expression of pathological forms of αS (truncated, oligomeric and phosphorylated) has been confirmed in areas consistent with clinical findings, including the olfactory bulb, cerebral cortex, striatum and *SNpc*. Among the first symptoms, the authors observed REM sleep disorders, with P-αS present in areas regulating neuronal populations in the lower brainstem such as the sublaterodorsal tegmental nucleus, nuclei in the ventromedial medullary reticular formation, and pedunculopontine nuclei. With the delay, the present hyposmia correlated with the accumulation of P-αS in the olfactory bulb. These manifestations appeared long before the degeneration of dopaminergic neurons in the *SNpc*. However, the authors did not observe any associated motor dysfunction (Taguchi et al., 2020a). Together, these results support the hypothesis that GIT dysfunction and other

non-motor symptoms represent an early symptom of αS-mediated pathology without parallel involvement of the CNS (Farrell et al., 2014; Naudet et al., 2017; Rota et al., 2019; Taguchi et al., 2020a).

Other Genetic Models

Mutations in *phosphatase and tensin homolog*- (PTEN-) *induced novel kinase 1* (PINK1) are associated with early-onset PD. In addition to its role in mitophagy (Narendra et al., 2008), it also plays an important role in adaptive immunity (Matheoud et al., 2016), supporting the hypothesis that autoimmune mechanisms are involved in the etiology of Parkinson's disease (Matheoud et al., 2019). The deletion of the *pink1* gene in mouse alone does not reflect the characteristic features of the disease, suggesting that the development of the disease symptoms is likely to occur in conjunction with other factors. In this respect, in a recent interesting study, the authors described that intestinal infection of $PINK^{-/-}$ mice with Gram-negative bacteria induces autoimmune mechanisms not only in the periphery but also in the CNS, which are presented by a decrease in the density of dopaminergic axonal varices in the striatum or L-DOPA responsive motor functions. The authors suggest that PINK1 also plays a role in immune system repression and support the gut–brain axis hypothesis of PD-related pathomechanisms (Matheoud et al., 2019).

MitoPark is a chronic, progressive mouse model that recapitulates several key motor (Ekstrand et al., 2007; Li et al., 2013; Ay et al., 2017; Langley et al., 2018) as well as non-motor (Ekstrand and Galter, 2009; Li et al., 2013; Ghaisas et al., 2019) aspects of PD. From the point of view of the GIT itself, among the first non-motor symptoms of PD, decreased motility of the GIT was observed with gradual progression of colon transit times, reduced fecal water content and intestinal inflammation characterized by activation of glial cells in the myenteric plexus. Later, a loss of TH+ neurons was also observed, as well as reduced levels of DA in midbrain as well as in the intestine. Metabolomics analysis also showed slight changes in the composition of the intestinal microbiota or bacterial metabolites (Ghaisas et al., 2019). In this context, Hsieh et al. (2020) observed that long-term administration of probiotics has neuroprotective effects on dopamine neurons and significantly reduced motor dysfunction in MitoPark PD mice (Hsieh et al., 2020). These results suggest the neuroprotective potential of probiotics, probably due to their inhibition of glial cell activation and neuroinflammation, increased butyrate levels, and increased levels of some neurotrophic factors (Fang, 2019; Srivastav et al., 2019). However, the effects and basic mechanisms of such probiotic treatment in PD are unclear (Ghaisas et al., 2019).

αS Propagation Models

Although αS propagation models are still in development, but due to the shorter onset of the phenotype, their widespread use in terms of experimental models, they represent a promising model in the study of prodromal PD (Kim et al., 2019; Taguchi et al., 2020b). However, it should be borne in mind that different approaches to the purification of αS fibrils, as well as application in different models, can significantly affect the degree of their spread in cells as well as the observed phenotype (Uemura et al., 2018; Kim et al., 2019).

One possibility is the purification of pathological forms of αS from extracts of human brain tissue from patients with dementia with LB (DLB) (Lee et al., 2011) or PD (Holmqvist et al., 2014). Injection of human brain tissue extracts from DLB patients containing stable αS aggregates into the gastric walls of transgenic M83 tg mice resulted in increased deposition and aggregation of αS in myenteric neurons, accompanied by a transiently increased inflammatory response in the GIT. These results indicate that pathological αS aggregates may induce aggregation of endogenous αS in myenteric neurons in M83 tg mice, suggesting the transmission of αS-associated pathology within the ENS (Lee et al., 2011). Application of human brain tissue extracts from PD patients containing various physiological as well as pathological forms of αS to the intestinal wall of rats confirmed retrograde transport of aggregated αS through vagal nerves from the intestine to the brain and that slow and fast components of axonal transport are involved in this process (Holmqvist et al., 2014).

The second, frequently used, the possibility is the preparation of recombinant αS preformed fibrils (PFF). Intramuscular administration of PFF in M83 tg transgenic mice resulted in motor disorders accompanied by the presence of CNS protein inclusions and neuroinflammation. Transection of the sciatic nerve in these mice significantly delayed the onset of CNS pathology as well as motor symptoms themselves, suggesting the involvement of retrograde transport in the induction of αS pathology in the CNS (Sacino et al., 2014). Intraperitoneal or intraglossal application of PFF in M83 tg led to the development of paralysis and the presence of aggregated as well as P-αS in the CNS and spinal cord (Breid et al., 2016). In another study, the authors focused on the propagation of PFFs applied to the olfactory bulb of wild-type (WT) mice. They observed the progression of αS-associated pathology initially manifested by the olfactory disorders, and gradually spread to distant areas of the brain (Rey et al., 2018). Uemura et al. (2018) focused on the propagation of αS-associated pathology mediated by the injection of PFF into the gastric wall of WT or αS-A53T BAC transgenic mice (Uemura et al., 2020). In the case of WT mice, the presence of aggregates of P-αS was observed in the DMV, which, however, did not progress further. Performed vagotomy resulted in a gradual reduction of P-αS aggregates in DMV but did not affect the P-αS-positive aggregates in the myenteric plexus (Uemura et al., 2018). When αS PFF were applied to the gastric wall of αS A53T BAC transgenic mice, they observed a significant increase in αS levels in the brain as well as in stomach compared to WT mice, along with an increased amount of P-αS in DMV. These results indicate, that BAC transgenic expression of αS promoted the propagation of αS-associated pathology in the brainstem, but not subsequent caudo-rostral spread in line with Braak's hypothesis (Uemura et al., 2020).

POSSIBLE PATHWAYS OF PD PATHOLOGY PROPAGATION FROM ENS TO CNS

According to Braak's model, neuropathological changes from GIT are transmitted through anatomical connections between ENS and CNS (Braak et al., 2003, 2006), with the initiation of PD pathogenesis in the ENS and DMV much earlier than *SNpc* pathology. This hypothesis is also supported by the results of biopsies, experimental animals but also with the use of cellular models. For example, in cellular models, the oligomeric αS can be endocytosed by neurons and induce αS aggregation in primary neuronal cultures (Lee et al., 2008; Desplats et al., 2009; Liu et al., 2009). Several either toxin-induced (Pan-Montojo et al., 2012) or PFF-propagation (Holmqvist et al., 2014; Uemura et al., 2018; Kim et al., 2019) mouse models demonstrated vagus-dependent transmission of αS-pathology from peripheral tissues to the CNS followed by the development of motor symptoms. Slight differences in observations in these studies, such as the degree of αS-pathology in the CNS, in some cases its gradual decrease with the inability to lead to the loss of dopaminergic neurons, may also be the result of various PFF purification as well as application protocols used in experiments (Kim et al., 2019). However, important findings were that the hemivagotomy or sympathectomy blocked (Pan-Montojo et al., 2012; Kim et al., 2019), reduced or at least delayed the observed CNS pathology. Similarly, in patients who underwent truncal vagotomy, the risk of PD was significantly reduced (Svensson et al., 2015; Tysnes et al., 2015). All these data suggest that transmission via nervus vagus is one of the possible ways of spreading αS-related PD pathology.

On the other hand, in mice with PFF-induced pathology in the duodenum, the presence of αS inclusion, has been observed in the ENS, intermediolateral spinal cord but also stomach, the dorsal motor nucleus of the vagus nerve, locus coeruleus and even heart. In control animals, these pathological features were not observed. These results open new possibilities for bidirectional αS propagation through the *nervus vagus*: duodenum–brainstem–stomach, which means the possibility of secondary transmission of αS pathology through the anterograde pathway after initial retrograde transmission (Van Den Berge et al., 2019).

An interesting view of the origin and development of PD-associated pathology is provided by the so-called "the threshold hypothesis," which is based on the parallel degeneration of PNS and CNS (Engelender and Isacson, 2017). According to this theory, almost non-motor symptoms in PD are the result of a "lower functional threshold of enteric neurons," due to their less-developed network with a smaller number of compensatory mechanisms and connections in the ENS compared to the CNS. As PD-associated motor symptoms occur with the loss of approximately 70% of dopaminergic neurons in the *SNpC*, multiple compensatory mechanisms are thought to exist in the CNS (Marsden, 1982; Hantraye et al., 1992; Wullner et al., 1994; Brownell et al., 1998; Cooper et al., 2009; Mou et al., 2020).

The authors claim that this principle reflects current knowledge of the neurobiology of PD better compared to Braak's hypothesis. The main counter-arguments are that the only presumed mechanism of selective sensitivity of certain enteric neurons is the less developed compensatory mechanisms in the ENS and also that it does not explain experimental data on αS -associated pathology between ENS and CNS (Mou et al., 2020).

Finally, we must not forget the observed changes in the composition of the intestinal microbiota in PD patients as well as in experimental animals. These changes may affect the local immune response, which leads to disruption of the mucosal barrier of the GIT and subsequent inflammatory reactions. Systemic inflammation as a result of migrated gut bacteria and cytokines may results in an impairment of BBB, progressively to neuroinflammation and through the over-response of the CNS immune system or CNS inflammatory response to neurodegeneration (Maes and Leunis, 2008; Clairembault et al., 2015b; Yang et al., 2017; Morais et al., 2018; Perez-Pardo et al., 2018; Dodiya et al., 2020). However, the role of the intestinal microbiota in the initiation and progression of PD-related pathology is currently unclear, as well as whether these changes in the intestinal microbiome are the cause or consequence of aS-related pathology. In any case, changes in the composition of the intestinal microbiome, as well as gut inflammation, are considered a risk factor in the development of PD (Chapelet et al., 2019).

CONCLUDING REMARKS AND PERSPECTIVES

The finding that primary PD pathogenesis occurs in peripheral tissues already several years prior the onset of typical motor symptoms suggests that it is extremely important to focus further PD research on early detection of disease, which could bring new treatment options to patients in early stages of PD and improvement of the life quality.

However, despite the incredible efforts and progress in this area, a number of principal questions remain unanswered. One of them poses the question of why, despite the presence of pathological αS forms in peripheral tissues, for example in the appendix (Killinger et al., 2018), there is no pathogenesis of PD in all humans (Mazurskyy and Howitt, 2019).

Moreover, it is currently unknown which GIT tissue would be most suitable for early detection of neuropathological PD changes with respect to minimal invasiveness and patient safety. Therefore, further research into the pathogenesis of PD would need to focus on a more comprehensive examination of tissues, whether obtained from appropriate animal models or biopsy patients obtained both in the pre-motor stage of PD and after the onset of neuropathological changes in the CNS and the development of motor symptoms. These more detailed and, in particular, more comprehensive studies would help several questions to be answered:

(i) in which part of the GIT the pathogenesis of PD occurs
(ii) whether the pathology from that particular tissue progressively spreads to the CNS
(iii) or is first disseminated within the GIT itself

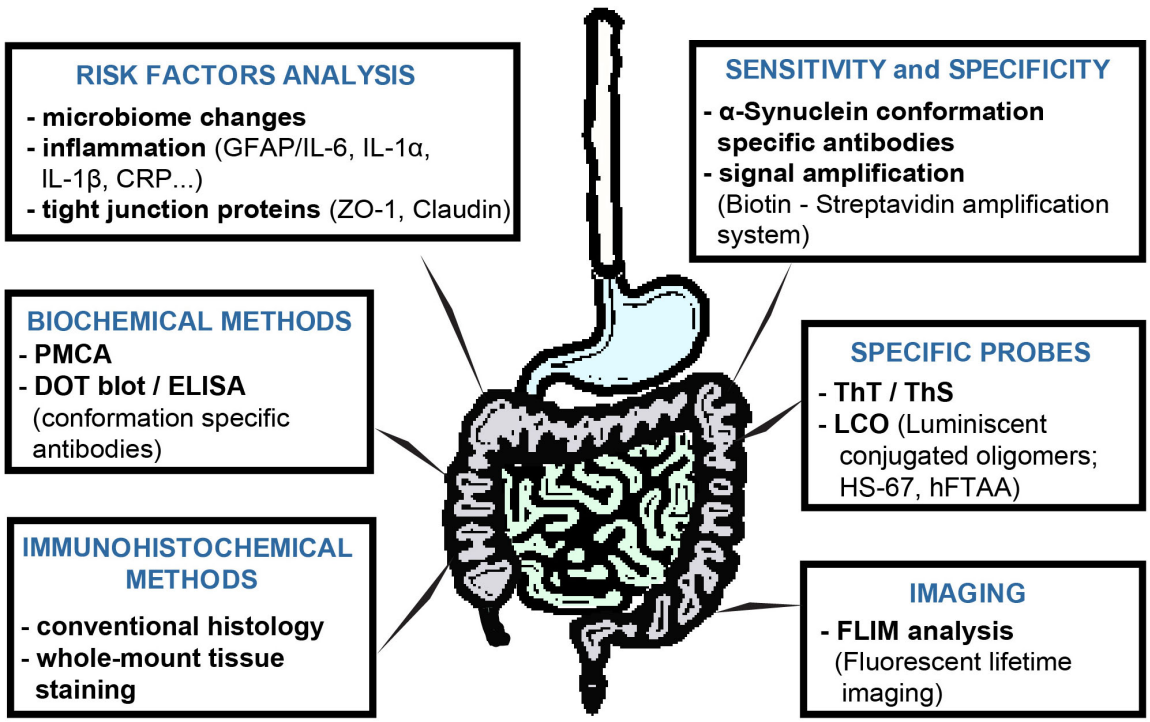

FIGURE 2 | Possibilities to extend of αS-detection methods in GIT tissues of PD patients or animal models. Each method has its limits, so in order to find a reliable method of PD diagnosis, a more comprehensive approach to the analysis of studied tissues is necessary. In contrast to conventional immunohistochemistry, immunohistochemical analysis of whole-mount tissues provides a more comprehensive view of the processes taking place in the studied tissue under. The conformation-specific antibody may significantly improve the ability to detect pathological αS, as the detection of total αS, or its phosphorylated form, does not appear to be sufficient at present. These can be used not only for immunohistochemical or biochemical analyzes and, together with various currently widely available signal amplification systems, they can increase not only the specificity but also the sensitivity of the given methods. PMCA appears to be very versatile and specific in detecting αS pathological forms, as well as in distinguishing individual pathological αS strains. Imaging methods may rely on the continuous development of either fluorescent probes or the development of the methodologies themselves. Luminescent-conjugated oligothiophenes (LCO) represent a new generation of probes with the ability to detect a broader spectrum of protein aggregate proteins, compared to conventional probes. In addition, based on changes in emission spectra, they also provide information on the conformation of the studied aggregated proteins. Fluorescent lifetime imaging (FLIM) reflects the qualitative changes near fluorophore, and therefore with higher sensitivity can detect very small, such as conformational, changes. Although the role of the intestinal microbiome in the PD pathogenesis is currently unclear, analysis of the intestinal microbiota, inflammatory response or permeability of the intestinal barrier can provide a more comprehensive view of the processes taking place in the GIT.

(iv) or the onset is localized across the entire GIT.

The next limiting step in such studies is the methodology itself. Each method, as we all know very well, has its limitations, advantages, and disadvantages, therefore, it is necessary not only to continually improve and optimize these methods but also to confirm the obtained results with other methodologies. Recent studies suggest that a combination of several methodologies could provide answers to the questions asked (Fenyi et al., 2019) (**Figure 2**). A large number of studies that we summarized in this review are based on immunohistochemical detection of neuropathological changes in the peripheral tissues of PD patients. In these types of experiments, however, very few studies are concerned with comprehensive research into PD neuropathology, often lacking appropriate control subjects, colocalization of several types of pathological forms of αS, or confirmation of results by biochemical methods. Animal experiments can provide a more comprehensive view, but in these cases, conventional immunohistochemical analysis is often combined only with behavioral tests or basic biochemical methods.

Detection of pathological changes by classical histology with analysis and staining of microsections obtained from patient biopsies has, similar to other methods, its limitations. These arise mainly from the nature of the methodology where the tissue is not analyzed as a whole, which can lead to the loss of important information within individual micro-sections. A significant advantage of this methodology, however, is the minimal invasiveness in the removal of biological material from a living patient. Unlike micro-section analysis, the wholemount tissue analysis approach can visualize and analyze innervation from a larger area of the GIT, at a greater depth that can provide a more comprehensive view of the processes taking place in a given tissue (Wang et al., 2012; Harsanyiova et al., 2019). Increasing the sensitivity of immunohistochemical staining, for example by the amplification method (Harsanyiova et al., 2019), could help detect even minimal levels of various pathological forms

of αS. The availability of antibodies against a wider spectrum of pathological forms of αS makes it possible to extend the possibilities of immunohistochemical staining and may suggest a time course of the disease.

It is believed that the toxicity of oligomeric forms of αS is higher than insoluble fibrils. Therefore, it is the oligomeric forms that are considered to be initiators of neurodegeneration not only in PD but also in other neurodegenerative diseases (Glabe and Kayed, 2006; Benilova et al., 2012; Mou et al., 2020). Conformational-specific antibodies may be useful in detecting the initiation stages of αS-associated pathology in GIT tissues, not only by immunohistochemical staining of tissues but in some cases also in biochemical analyzes such as, e.g., dot blot or ELISA. The PMCA assay utilizes the functional properties of oligomers to inoculate polymerization of monomeric protein. Its versatility and high specificity are confirmed by studies where PMCA has been used to detect the pathological forms of αS in colony biopsies (Fenyi et al., 2019), or cerebrospinal fluid (Shahnawaz et al., 2017; Kang et al., 2019). PMCA is also able to distinguish different conformational strains of αS that are involved in the development of various synucleinopathies, as confirmed by analysis of samples from patients with PD multiple systemic atrophy (MSA), with an overall sensitivity of up to 95.4% (Shahnawaz et al., 2020).

Furthermore, using more sophisticated FLIM-based detection methods that analyze the lifetime of fluorescence emitted by endogenous or exogenous fluorophores can help resolve the onset and progression of PD pathogenesis at the very early stages of the disease. The lifetime of fluorescence emitted by a fluorophore is affected by the environment of a given fluorophore, which allows the detection of even very small changes (e.g., conformational changes of αS) with higher sensitivity compared to immunohistochemical or biochemical methods.

Several fluorescent probes used as a "gold standard" (Thioflavin S and Thioflavin T) in the detection of aggregated proteins associated with neurodegenerative diseases have been successfully used in FLIM analysis not only in recombinant systems (Plotegher et al., 2015) but also in cellular models (Pokusa and Kralova Trancikova, 2018). Furthermore, FLIM analysis using luminescent conjugated oligothiophenes (LCOs) was able to distinguish αS-positive inclusions in the brain sections of the brain of PD patients and patients with MSA (Klingstedt et al., 2019 #174). LCOs are, in comparison with classical fluorescent probes, such as Thioflavins or Congo red, able to detect a wider range of protein aggregates. Due to their flexible thiophene backbone, the emitted light depends on their binding to proteins in different conformations. In addition, differences in the emission spectra of these LCOs reveals different conformations of αS strains in patients with PD and MSA (Klingstedt et al., 2011, 2019).

AUTHOR CONTRIBUTIONS

JH focused on the detection of pathological processes in the tissues of the GIT in animal models. She also specializes in the optimization of detection methods such as classical histology, immunostaining of wholemount tissues, amplification of the detection signal and further analysis by confocal and multiphoton microscopy. TB focused on the clinical part of the manuscript, where he can best use his MD education and experience. AK focused on animal and genetic models of Parkinson's disease, where she can best use her long-term experience in this field. Also, she focused on the possibilities of improving the detection of PD-related pathological changes in the tissues of the GIT, in particular confocal microscopy and FLIM analysis. All authors contributed to the article and approved the submitted version.

FUNDING

This work was supported by the Research and Development Grant of Ministry of Health of the Slovak Republic No. 2018/10-UKMT-6.

REFERENCES

Adler, C. H., Dugger, B. N., Hinni, M. L., Lott, D. G., Driver-Dunckley, E., Hidalgo, J., et al. (2014). Submandibular gland needle biopsy for the diagnosis of Parkinson disease. *Neurology* 82, 858–864. doi: 10.1212/wnl.0000000000000204

Alvarez-Arellano, L., and Maldonado-Bernal, C. (2014). *Helicobacter* pylori and neurological diseases: married by the laws of inflammation. *World J. Gastrointest Pathophysiol.* 5, 400–404.

Anderson, G., Noorian, A. R., Taylor, G., Anitha, M., Bernhard, D., Srinivasan, S., et al. (2007). Loss of enteric dopaminergic neurons and associated changes in colon motility in an MPTP mouse model of Parkinson's disease. *Exp. Neurol.* 207, 4–12. doi: 10.1016/j.expneurol.2007.05.010

Anlauf, M., Schafer, M. K., Eiden, L., and Weihe, E. (2003). Chemical coding of the human gastrointestinal nervous system: cholinergic, VIPergic, and catecholaminergic phenotypes. *J. Comp. Neurol.* 459, 90–111. doi: 10.1002/cne.10599

Anselmi, L., Bove, C., Coleman, F. H., Le, K., Subramanian, M. P., Venkiteswaran, K., et al. (2018). Ingestion of subthreshold doses of environmental toxins induces ascending Parkinsonism in the rat. *NPJ Parkinsons Dis.* 4:30.

Anselmi, L., Toti, L., Bove, C., and Travagli, R. A. (2017). Vagally mediated effects of brain stem dopamine on gastric tone and phasic contractions of the rat. *Am. J. Physiol. Gastrointest. Liver Physiol.* 313, G434–G441.

Antunes, L., Frasquilho, S., Ostaszewski, M., Weber, J., Longhino, L., Antony, P., et al. (2016). Similar alpha-Synuclein staining in the colon mucosa in patients with Parkinson's disease and controls. *Mov. Disord.* 31, 1567–1570. doi: 10.1002/mds.26702

Ay, M., Luo, J., Langley, M., Jin, H., Anantharam, V., Kanthasamy, A., et al. (2017). Molecular mechanisms underlying protective effects of quercetin against mitochondrial dysfunction and progressive dopaminergic neurodegeneration in cell culture and MitoPark transgenic mouse models of Parkinson's Disease. *J. Neurochem.* 141, 766–782. doi: 10.1111/jnc.14033

Bartels, T., Choi, J. G., and Selkoe, D. J. (2011). Alpha-Synuclein occurs physiologically as a helically folded tetramer that resists aggregation. *Nature* 477, 107–110. doi: 10.1038/nature10324

Beach, T. G., Adler, C. H., Sue, L. I., Vedders, L., Lue, L., White, C. L. III., et al. (2010). Multi-organ distribution of phosphorylated alpha-synuclein histopathology in subjects with Lewy body disorders. *Acta Neuropathol.* 119, 689–702. doi: 10.1007/s00401-010-0664-3

Bencsik, A., Muselli, L., Leboidre, M., Lakhdar, L., and Baron, T. (2014). Early and persistent expression of phosphorylated alpha-synuclein in the

enteric nervous system of A53T mutant human alpha-synuclein transgenic mice. *J. Neuropathol. Exp. Neurol.* 73, 1144–1151. doi: 10.1097/nen.0000000000000137

Benilova, I., Karran, E., and De Strooper, B. (2012). The toxic abeta oligomer and Alzheimers disease: an emperor in need of clothes. *Nat. Neurosci.* 15, 349–357. doi: 10.1038/nn.3028

Betarbet, R., Sherer, T. B., Mackenzie, G., Garcia-Osuna, M., Panov, A. V., and Greenamyre, J. T. (2000). Chronic systemic pesticide exposure reproduces features of Parkinson's disease. *Nat. Neurosci.* 3, 1301–1306. doi: 10.1038/81834

Bhattarai, Y. (2018). Microbiota-gut-brain axis: interaction of gut microbes and their metabolites with host epithelial barriers. *Neurogastroenterol. Motil.* 30:e13366. doi: 10.1111/nmo.13366

Blandini, F., Balestra, B., Levandis, G., Cervio, M., Greco, R., Tassorelli, C., et al. (2009). Functional and neurochemical changes of the gastrointestinal tract in a rodent model of Parkinson's disease. *Neurosci. Lett.* 467, 203–207. doi: 10.1016/j.neulet.2009.10.035

Borre, Y. E., Moloney, R. D., Clarke, G., Dinan, T. G., and Cryan, J. F. (2014). The impact of microbiota on brain and behavior: mechanisms & therapeutic potential. *Adv. Exp. Med. Biol.* 817, 373–403. doi: 10.1007/978-1-4939-0897-4_17

Braak, H., De Vos, R. A., Bohl, J., and Del Tredici, K. (2006). Gastric alpha-synuclein immunoreactive inclusions in Meissner's and Auerbach's plexuses in cases staged for Parkinson's disease-related brain pathology. *Neurosci. Lett.* 396, 67–72. doi: 10.1016/j.neulet.2005.11.012

Braak, H., Rub, U., Gai, W. P., and Del Tredici, K. (2003). Idiopathic Parkinson's disease: possible routes by which vulnerable neuronal types may be subject to neuroinvasion by an unknown pathogen. *J. Neural. Trans.* 110, 517–536. doi: 10.1007/s00702-002-0808-2

Breid, S., Bernis, M. E., Babila, J. T., Garza, M. C., Wille, H., and Tamguney, G. (2016). Neuroinvasion of alpha-synuclein prionoids after intraperitoneal and intraglossal inoculation. *J. Virol.* 90, 9182–9193. doi: 10.1128/jvi.01399-16

Brownell, A. L., Jenkins, B. G., Elmaleh, D. R., Deacon, T. W., Spealman, R. D., and Isacson, O. (1998). Combined PET/MRS brain studies show dynamic and long-term physiological changes in a primate model of Parkinson disease. *Nat. Med.* 4, 1308–1312. doi: 10.1038/3300

Cabin, D. E., Shimazu, K., Murphy, D., Cole, N. B., Gottschalk, W., Mcilwain, K. L., et al. (2002). Synaptic vesicle depletion correlates with attenuated synaptic responses to prolonged repetitive stimulation in mice lacking alpha-synuclein. *J. Neurosci.* 22, 8797–8807. doi: 10.1523/jneurosci.22-20-08797.2002

Caputi, V., and Giron, M. C. (2018). Microbiome-gut-brain axis and toll-like receptors in Parkinson's Disease. *Int. J. Mol. Sci.* 19:1689. doi: 10.3390/ijms19061689

Carabotti, M., Scirocco, A., Maselli, M. A., and Severi, C. (2015). The gut-brain axis: interactions between enteric microbiota, central and enteric nervous systems. *Ann. Gastroenterol.* 28, 203–209.

Cersosimo, M. G. (2015). Gastrointestinal biopsies for the diagnosis of alpha-synuclein pathology in Parkinson's Disease. *Gastroenterol. Res. Pract.* 2015:476041.

Cersosimo, M. G., Perandones, C., Micheli, F. E., Raina, G. B., Beron, A. M., Nasswetter, G., et al. (2011). Alpha-synuclein immunoreactivity in minor salivary gland biopsies of Parkinson's disease patients. *Mov. Disord.* 26, 188–190. doi: 10.1002/mds.23344

Chapelet, G., Leclair-Visonneau, L., Clairembault, T., Neunlist, M., and Derkinderen, P. (2019). Can the gut be the missing piece in uncovering PD pathogenesis? *Parkinsonism Relat. Disord.* 59, 26–31. doi: 10.1016/j.parkreldis.2018.11.014

Chartier-Harlin, M. C., Kachergus, J., Roumier, C., Mouroux, V., Douay, X., Lincoln, S., et al. (2004). Alpha-synuclein locus duplication as a cause of familial Parkinson's disease. *Lancet* 364, 1167–1169. doi: 10.1016/s0140-6736(04)17103-1

Chaumette, T., Lebouvier, T., Aubert, P., Lardeux, B., Qin, C., Li, Q., et al. (2009). Neurochemical plasticity in the enteric nervous system of a primate animal model of experimental Parkinsonism. *Neurogastroenterol. Motil.* 21, 215–222. doi: 10.1111/j.1365-2982.2008.01226.x

Clairembault, T., Leclair-Visonneau, L., Coron, E., Bourreille, A., Le Dily, S., Vavasseur, F., et al. (2015a). Structural alterations of the intestinal epithelial barrier in Parkinson's disease. *Acta Neuropathol. Commun.* 3, 12.

Clairembault, T., Leclair-Visonneau, L., Neunlist, M., and Derkinderen, P. (2015b). Enteric glial cells: new players in Parkinson's disease? *Mov. Disord.* 30, 494–498. doi: 10.1002/mds.25979

Cleeter, M. W., Cooper, J. M., and Schapira, A. H. (1992). Irreversible inhibition of mitochondrial complex I by 1-methyl-4-phenylpyridinium: evidence for free radical involvement. *J. Neurochem.* 58, 786–789. doi: 10.1111/j.1471-4159.1992.tb09789.x

Cohen, G., and Heikkila, R. E. (1974). The generation of hydrogen peroxide, superoxide radical, and hydroxyl radical by 6-hydroxydopamine, dialuric acid, and related cytotoxic agents. *J. Biol. Chem.* 249, 2447–2452.

Cooper, O., Astradsson, A., Hallett, P., Robertson, H., Mendez, I., and Isacson, O. (2009). Lack of functional relevance of isolated cell damage in transplants of Parkinson's disease patients. *J. Neurol.* 256(Suppl. 3), 310–316. doi: 10.1007/s00415-009-5242-z

Corbille, A. G., Letournel, F., Kordower, J. H., Lee, J., Shanes, E., Neunlist, M., et al. (2016). Evaluation of alpha-synuclein immunohistochemical methods for the detection of Lewy-type synucleinopathy in gastrointestinal biopsies. *Acta Neuropathol. Commun.* 4:35.

Corbille, A. G., Preterre, C., Rolli-Derkinderen, M., Coron, E., Neunlist, M., Lebouvier, T., et al. (2017). Biochemical analysis of alpha-synuclein extracted from control and Parkinson's disease colonic biopsies. *Neurosci. Lett.* 641, 81–86. doi: 10.1016/j.neulet.2017.01.050

Cote, M., Poirier, A. A., Aube, B., Jobin, C., Lacroix, S., and Soulet, D. (2015). Partial depletion of the proinflammatory monocyte population is neuroprotective in the myenteric plexus but not in the basal ganglia in a MPTP mouse model of Parkinson's disease. *Brain Behav. Immun.* 46, 154–167. doi: 10.1016/j.bbi.2015.01.009

Dauer, W., and Przedborski, S. (2003). Parkinson's disease: mechanisms and models. *Neuron* 39, 889–909.

de Lau, L. M., and Breteler, M. M. (2006). Epidemiology of Parkinson's disease. *Lancet Neurol.* 5, 525–535.

Desplats, P., Lee, H. J., Bae, E. J., Patrick, C., Rockenstein, E., Crews, L., et al. (2009). Inclusion formation and neuronal cell death through neuron-to-neuron transmission of alpha-synuclein. *Proc. Natl. Acad. Sci. U.S.A.* 106, 13010–13015. doi: 10.1073/pnas.0903691106

Devos, D., Lebouvier, T., Lardeux, B., Biraud, M., Rouaud, T., Pouclet, H., et al. (2013). Colonic inflammation in Parkinson's disease. *Neurobiol. Dis.* 50, 42–48.

Dobbs, R. J., Dobbs, S. M., Weller, C., Charlett, A., Bjarnason, I. T., Curry, A., et al. (2008). *Helicobacter* hypothesis for idiopathic parkinsonism: before and beyond. *Helicobacter* 13, 309–322. doi: 10.1111/j.1523-5378.2008.00622.x

Dodiya, H. B., Forsyth, C. B., Voigt, R. M., Engen, P. A., Patel, J., Shaikh, M., et al. (2020). Chronic stress-induced gut dysfunction exacerbates Parkinson's disease phenotype and pathology in a rotenone-induced mouse model of Parkinson's disease. *Neurobiol. Dis.* 135:104352. doi: 10.1016/j.nbd.2018.12.012

Drolet, R. E., Cannon, J. R., Montero, L., and Greenamyre, J. T. (2009). Chronic rotenone exposure reproduces Parkinson's disease gastrointestinal neuropathology. *Neurobiol. Dis.* 36, 96–102. doi: 10.1016/j.nbd.2009.06.017

Duty, S., and Jenner, P. (2011). Animal models of Parkinson's disease: a source of novel treatments and clues to the cause of the disease. *Br. J. Pharmacol.* 164, 1357–1391. doi: 10.1111/j.1476-5381.2011.01426.x

Ekstrand, M. I., and Galter, D. (2009). The MitoPark Mouse - an animal model of Parkinson's disease with impaired respiratory chain function in dopamine neurons. *Parkinsonism. Relat. Disord.* 15(Suppl. 3), S185–S188.

Ekstrand, M. I., Terzioglu, M., Galter, D., Zhu, S., Hofstetter, C., Lindqvist, E., et al. (2007). Progressive parkinsonism in mice with respiratory-chain-deficient dopamine neurons. *Proc. Natl. Acad. Sci. U.S.A.* 104, 1325–1330. doi: 10.1073/pnas.0605208103

Elfil, M., Kamel, S., Kandil, M., Koo, B. B., and Schaefer, S. M. (2020). Implications of the gut microbiome in Parkinson's Disease. *Mov. Disord.* doi: 10.1002/mds.28004

Eliezer, D., Kutluay, E., Bussell, R. Jr., and Browne, G. (2001). Conformational properties of alpha-synuclein in its free and lipid-associated states. *J. Mol. Biol.* 307, 1061–1073. doi: 10.1006/jmbi.2001.4538

Ellett, L. J., Hung, L. W., Munckton, R., Sherratt, N. A., Culvenor, J., Grubman, A., et al. (2016). Restoration of intestinal function in an MPTP model of Parkinson's Disease. *Sci. Rep.* 6:30269.

Engelender, S., and Isacson, O. (2017). The threshold theory for Parkinson's Disease. *Trends Neurosci.* 40, 4–14.

Fang, X. (2019). Microbial treatment: the potential application for Parkinson's disease. *Neurol. Sci.* 40, 51–58. doi: 10.1007/s10072-018-3641-6

Farrell, K. F., Krishnamachari, S., Villanueva, E., Lou, H., Alerte, T. N., Peet, E., et al. (2014). Non-motor parkinsonian pathology in aging A53T alpha-synuclein mice is associated with progressive synucleinopathy and altered enzymatic function. *J. Neurochem.* 128, 536–546. doi: 10.1111/jnc.12481

Fenyi, A., Leclair-Visonneau, L., Clairembault, T., Coron, E., Neunlist, M., Melki, R., et al. (2019). Detection of alpha-synuclein aggregates in gastrointestinal biopsies by protein misfolding cyclic amplification. *Neurobiol. Dis.* 129, 38–43. doi: 10.1016/j.nbd.2019.05.002

Fornai, M., Pellegrini, C., Antonioli, L., Segnani, C., Ippolito, C., Barocelli, E., et al. (2016). Enteric dysfunctions in experimental Parkinson's Disease: alterations of excitatory cholinergic neurotransmission regulating colonic motility in rats. *J. Pharmacol. Exp. Ther.* 356, 434–444.

Forsyth, C. B., Shannon, K. M., Kordower, J. H., Voigt, R. M., Shaikh, M., Jaglin, J. A., et al. (2011). Increased intestinal permeability correlates with sigmoid mucosa alpha-synuclein staining and endotoxin exposure markers in early Parkinson's disease. *PLoS One* 6:e28032. doi: 10.1371/journal.pone.0028032

Forsythe, P., and Kunze, W. A. (2013). Voices from within: gut microbes and the CNS. *Cell Mol. Life. Sci.* 70, 55–69. doi: 10.1007/s00018-012-1028-z

Fujiwara, H., Hasegawa, M., Dohmae, N., Kawashima, A., Masliah, E., Goldberg, M. S., et al. (2002). alpha-Synuclein is phosphorylated in synucleinopathy lesions. *Nat. Cell Biol.* 4, 160–164. doi: 10.1038/ncb748

Furness, J. B. (2008). The enteric nervous system: normal functions and enteric neuropathies. *Neurogastroenterol. Motil.* 20(Suppl. 1), 32–38. doi: 10.1111/j.1365-2982.2008.01094.x

Gelpi, E., Navarro-Otano, J., Tolosa, E., Gaig, C., Compta, Y., Rey, M. J., et al. (2014). Multiple organ involvement by alpha-synuclein pathology in Lewy body disorders. *Mov. Disord.* 29, 1010–1018. doi: 10.1002/mds.25776

Ghaisas, S., Langley, M. R., Palanisamy, B. N., Dutta, S., Narayanaswamy, K., Plummer, P. J., et al. (2019). MitoPark transgenic mouse model recapitulates the gastrointestinal dysfunction and gut-microbiome changes of Parkinson's disease. *Neurotoxicology* 75, 186–199. doi: 10.1016/j.neuro.2019.09.004

Glabe, C. G., and Kayed, R. (2006). Common structure and toxic function of amyloid oligomers implies a common mechanism of pathogenesis. *Neurology* 66, S74–S78.

Glinka, Y. Y., and Youdim, M. B. (1995). Inhibition of mitochondrial complexes I and IV by 6-hydroxydopamine. *Eur. J. Pharmacol.* 292, 329–332. doi: 10.1016/0926-6917(95)90040-3

Gold, A., Turkalp, Z. T., and Munoz, D. G. (2013). Enteric alpha-synuclein expression is increased in Parkinson's disease but not Alzheimer's disease. *Mov. Disord.* 28, 237–240.

Gorecki, A. M., Preskey, L., Bakeberg, M. C., Kenna, J. E., Gildenhuys, C., Macdougall, G., et al. (2019). Altered gut microbiome in Parkinson's Disease and the influence of lipopolysaccharide in a human alpha-synuclein over-expressing mouse model. *Front. Neurosci.* 13:839. doi: 10.3389/fnins.2019.00839

Gray, M. T., Munoz, D. G., Gray, D. A., Schlossmacher, M. G., and Woulfe, J. M. (2014). Alpha-synuclein in the appendiceal mucosa of neurologically intact subjects. *Mov. Disord.* 29, 991–998. doi: 10.1002/mds.25779

Greene, J. G., Noorian, A. R., and Srinivasan, S. (2009). Delayed gastric emptying and enteric nervous system dysfunction in the rotenone model of Parkinson's disease. *Exp. Neurol.* 218, 154–161. doi: 10.1016/j.expneurol.2009.04.023

Hansen, C., and Li, J. Y. (2012). Beyond alpha-synuclein transfer: pathology propagation in Parkinson's disease. *Trends Mol. Med.* 18, 248–255. doi: 10.1016/j.molmed.2012.03.002

Hantraye, P., Brownell, A. L., Elmaleh, D., Spealman, R. D., Wullner, U., Brownell, G. L., et al. (1992). Dopamine fiber detection by [11C]-CFT and PET in a primate model of parkinsonism. *Neuroreport* 3, 265–268. doi: 10.1097/00001756-199203000-00013

Harsanyiova, J., Ru, F., Zatko, T., Kollarik, M., and Hennel, M. (2019). Vagus nerves provide a robust afferent innervation of the mucosa throughout the body of the esophagus in the mouse. *Dysphagia* 35, 471–478. doi: 10.1007/s00455-019-10051-8

Hill-Burns, E. M., Debelius, J. W., Morton, J. T., Wissemann, W. T., Lewis, M. R., Wallen, Z. D., et al. (2017). Parkinson's disease and Parkinson's disease medications have distinct signatures of the gut microbiome. *Mov. Disord.* 32, 739–749. doi: 10.1002/mds.26942

Hilton, D., Stephens, M., Kirk, L., Edwards, P., Potter, R., Zajicek, J., et al. (2014). Accumulation of alpha-synuclein in the bowel of patients in the pre-clinical phase of Parkinson's disease. *Acta Neuropathol.* 127, 235–241. doi: 10.1007/s00401-013-1214-6

Hisahara, S., and Shimohama, S. (2010). Toxin-induced and genetic animal models of Parkinson's disease. *Parkinsons Dis.* 2011:951709.

Holmqvist, S., Chutna, O., Bousset, L., Aldrin-Kirk, P., Li, W., Bjorklund, T., et al. (2014). Direct evidence of Parkinson pathology spread from the gastrointestinal tract to the brain in rats. *Acta Neuropathol.* 128, 805–820. doi: 10.1007/s00401-014-1343-6

Hsieh, T. H., Kuo, C. W., Hsieh, K. H., Shieh, M. J., Peng, C. W., Chen, Y. C., et al. (2020). Probiotics alleviate the progressive deterioration of motor functions in a mouse model of Parkinson's Disease. *Brain Sci.* 10:206. doi: 10.3390/brainsci10040206

Ibanez, P., Bonnet, A. M., Debarges, B., Lohmann, E., Tison, F., Pollak, P., et al. (2004). Causal relation between alpha-synuclein gene duplication and familial Parkinson's disease. *Lancet* 364, 1169–1171. doi: 10.1016/s0140-6736(04)17104-3

Jankovic, J. (2008). Parkinson's disease: clinical features and diagnosis. *J. Neurol. Neurosurg. Psychiatry* 79, 368–376.

Jin, M., Li, J., Liu, F., Lyu, N., Wang, K., Wang, L., et al. (2019). Analysis of the gut microflora in patients with Parkinson's Disease. *Front. Neurosci.* 13:1184. doi: 10.3389/fnins.2019.01184

Kang, U. J., Boehme, A. K., Fairfoul, G., Shahnawaz, M., Ma, T. C., Hutten, S. J., et al. (2019). Comparative study of cerebrospinal fluid alpha-synuclein seeding aggregation assays for diagnosis of Parkinson's disease. *Mov. Disord.* 34, 536–544. doi: 10.1002/mds.27646

Kelly, L. P., Carvey, P. M., Keshavarzian, A., Shannon, K. M., Shaikh, M., Bakay, R. A., et al. (2014). Progression of intestinal permeability changes and alpha-synuclein expression in a mouse model of Parkinson's disease. *Mov. Disord.* 29, 999–1009. doi: 10.1002/mds.25736

Killinger, B., and Labrie, V. (2019). The appendix in Parkinson's Disease: from vestigial remnant to vital organ? *J. Parkinsons Dis.* 9, S345–S358.

Killinger, B. A., Madaj, Z., Sikora, J. W., Rey, N., Haas, A. J., Vepa, Y., et al. (2018). The vermiform appendix impacts the risk of developing Parkinson's disease. *Sci. Transl. Med.* 10:eaar5280. doi: 10.1126/scitranslmed.aar5280

Kim, S., Kwon, S. H., Kam, T. I., Panicker, N., Karuppagounder, S. S., Lee, S., et al. (2019). Transneuronal propagation of pathologic alpha-synuclein from the gut to the brain models parkinson's Disease. *Neuron* 103, 627.e1–641.e1.

Klingstedt, T., Aslund, A., Simon, R. A., Johansson, L. B., Mason, J. J., Nystrom, S., Hammarstrom, P., et al. (2011). Synthesis of a library of oligothiophenes and their utilization as fluorescent ligands for spectral assignment of protein aggregates. *Org. Biomol. Chem.* 9, 8356–8370. doi: 10.1039/c1ob05637a

Klingstedt, T., Ghetti, B., Holton, J. L., Ling, H., Nilsson, K. P. R., and Goedert, M. (2019). Luminescent conjugated oligothiophenes distinguish between α-synuclein assemblies of Parkinson's disease and multiple system atrophy. *Acta Neuropathol. Commun.* 7:193. doi: 10.1186/s40478-019-0840-1

Klingelhoefer, L., and Reichmann, H. (2015). Pathogenesis of Parkinson disease–the gut-brain axis and environmental factors. *Nat. Rev. Neurol.* 11, 625–636. doi: 10.1038/nrneurol.2015.197

Kujawska, M., and Jodynis-Liebert, J. (2018). What is the evidence that parkinson's disease is a prion disorder, which originates in the gut? *Int. J. Mol. Sci.* 19:3573. doi: 10.3390/ijms19113573

Kuter, K., Nowak, P., Golembiowska, K., and Ossowska, K. (2010). Increased reactive oxygen species production in the brain after repeated low-dose pesticide paraquat exposure in rats. A comparison with peripheral tissues. *Neurochem. Res.* 35, 1121–1130. doi: 10.1007/s11064-010-0163-x

Kuter, K., Smialowska, M., Wieronska, J., Zieba, B., Wardas, J., Pietraszek, M., et al. (2007). Toxic influence of subchronic paraquat administration on dopaminergic neurons in rats. *Brain Res.* 1155, 196–207. doi: 10.1016/j.brainres.2007.04.018

Langley, M. R., Ghaisas, S., Ay, M., Luo, J., Palanisamy, B. N., Jin, H., et al. (2018). Manganese exposure exacerbates progressive motor deficits and neurodegeneration in the MitoPark mouse model of Parkinson's disease: relevance to gene and environment interactions in metal neurotoxicity. *Neurotoxicology* 64, 240–255. doi: 10.1016/j.neuro.2017.06.002

Langston, J. W., Forno, L. S., Tetrud, J., Reeves, A. G., Kaplan, J. A., and Karluk, D. (1999). Evidence of active nerve cell degeneration in the substantia nigra of humans years after 1-methyl-4-phenyl-1,2,3,6-tetrahydropyridine exposure. *Ann. Neurol.* 46, 598–605. doi: 10.1002/1531-8249(199910)46:4<598::aid-ana7>3.0.co;2-f

Lashuel, H. A., Overk, C. R., Oueslati, A., and Masliah, E. (2013). The many faces of alpha-synuclein: from structure and toxicity to therapeutic target. *Nat. Rev. Neurosci.* 14, 38–48. doi: 10.1038/nrn3406

Lebouvier, T., Chaumette, T., Paillusson, S., Duyckaerts, C., Bruley Des, Varannes, S., et al. (2009). The second brain and Parkinson's disease. *Eur. J. Neurosci.* 30, 735–741.

Lebouvier, T., Neunlist, M., Bruley Des, Varannes, S., Coron, E., Drouard, A., et al. (2010). Colonic biopsies to assess the neuropathology of Parkinson's disease and its relationship with symptoms. *PLoS One* 5:e12728. doi: 10.1371/journal.pone.0012728

Lee, H. J., Jung, K. W., Chung, S. J., Hong, S. M., Kim, J., Lee, J. H., et al. (2018). Relation of enteric alpha-synuclein to gastrointestinal dysfunction in patients with Parkinson's Disease and in neurologically intact subjects. *J. Neurogastroenterol. Motil.* 24, 469–478. doi: 10.5056/jnm17141

Lee, H. J., Suk, J. E., Bae, E. J., Lee, J. H., Paik, S. R., and Lee, S. J. (2008). Assembly-dependent endocytosis and clearance of extracellular alpha-synuclein. *Int. J. Biochem. Cell Biol.* 40, 1835–1849. doi: 10.1016/j.biocel.2008.01.017

Lee, W. Y., Yoon, W. T., Shin, H. Y., Jeon, S. H., and Rhee, P. L. (2008). pylori infection and motor fluctuations in patients with Parkinson's disease. *Mov. Disord. Helicobacter*, 1696–1700.

Lee, H. J., Suk, J. E., Lee, K. W., Park, S. H., Blumbergs, P. C., Gai, W. P., et al. (2011). Transmission of synucleinopathies in the enteric nervous system of A53T alpha-synuclein transgenic mice. *Exp. Neurobiol.* 20, 181–188. doi: 10.5607/en.2011.20.4.181

Levandis, G., Balestra, B., Siani, F., Rizzo, V., Ghezzi, C., Ambrosi, G., et al. (2015). Response of colonic motility to dopaminergic stimulation is subverted in rats with nigrostriatal lesion: relevance to gastrointestinal dysfunctions in Parkinson's disease. *Neurogastroenterol. Motil.* 27, 1783–1795. doi: 10.1111/nmo.12691

Li, X. Z., Chen, X. P., Zhao, K., Bai, L. M., Zhang, H., and Zhou, X. P. (2013). Therapeutic effects of valproate combined with lithium carbonate on MPTP-induced parkinsonism in mice: possible mediation through enhanced autophagy. *Int. J. Neurosci.* 123, 73–79. doi: 10.3109/00207454.2012.729234

Lin, C. H., Chen, C. C., Chiang, H. L., Liou, J. M., Chang, C. M., Lu, T. P., et al. (2019). Altered gut microbiota and inflammatory cytokine responses in patients with Parkinson's disease. *J. Neuroinflammation.* 16:129.

Liu, J., Zhang, J. P., Shi, M., Quinn, T., Bradner, J., Beyer, R., et al. (2009). Rab11a and HSP90 regulate recycling of extracellular alpha-synuclein. *J. Neurosci.* 29, 1480–1485. doi: 10.1523/jneurosci.6202-08.2009

Liu, Y., Qin, L., Wilson, B., Wu, X., Qian, L., Granholm, A. C., et al. (2008). Endotoxin induces a delayed loss of TH-IR neurons in substantia nigra and motor behavioral deficits. *Neurotoxicology* 29, 864–870. doi: 10.1016/j.neuro.2008.02.014

Maes, M., and Leunis, J. C. (2008). Normalization of leaky gut in chronic fatigue syndrome (CFS) is accompanied by a clinical improvement: effects of age, duration of illness and the translocation of LPS from gram-negative bacteria. *Neuro Endocrinol. Lett.* 29, 902–910.

Marchiando, A. M., Graham, W. V., and Turner, J. R. (2010). Epithelial barriers in homeostasis and disease. *Annu. Rev. Pathol.* 5, 119–144. doi: 10.1146/annurev.pathol.4.110807.092135

Marsden, C. D. (1982). Basal ganglia disease. *Lancet* 2, 1141–1147.

Matheoud, D., Cannon, T., Voisin, A., Penttinen, A. M., Ramet, L., Fahmy, A. M., et al. (2019). Intestinal infection triggers Parkinson's disease-like symptoms in Pink1(-/-) mice. *Nature* 571, 565–569. doi: 10.1038/s41586-019-1405-y

Matheoud, D., Sugiura, A., Bellemare-Pelletier, A., Laplante, A., Rondeau, C., Chemali, M., et al. (2016). Parkinson's Disease-related proteins PINK1 and Parkin repress mitochondrial antigen presentation. *Cell* 166, 314–327. doi: 10.1016/j.cell.2016.05.039

Mazurskyy, A., and Howitt, J. (2019). Initiation and transmission of alpha-synuclein pathology in Parkinson's Disease. *Neurochem. Res.* 44, 2685–2694. doi: 10.1007/s11064-019-02896-0

Metzger, J. M., and Emborg, M. E. (2019). Autonomic dysfunction in Parkinson disease and animal models. *Clin. Auton. Res* 29, 397–414. doi: 10.1007/s10286-018-00584-7

Morais, L. H., Hara, D. B., Bicca, M. A., Poli, A., and Takahashi, R. N. (2018). Early signs of colonic inflammation, intestinal dysfunction, and olfactory impairments in the rotenone-induced mouse model of Parkinson's disease. *Behav. Pharmacol.* 29, 199–210. doi: 10.1097/fbp.0000000000000389

Morin, N., Jourdain, V. A., and Di Paolo, T. (2014). Modeling dyskinesia in animal models of Parkinson disease. *Exp. Neurol.* 256, 105–116. doi: 10.1016/j.expneurol.2013.01.024

Mou, L., Ding, W., and Fernandez-Funez, P. (2020). Open questions on the nature of Parkinson's disease: from triggers to spreading pathology. *J. Med. Genet.* 57, 73–81. doi: 10.1136/jmedgenet-2019-106210

Mu, L., Sobotka, S., Chen, J., Su, H., Sanders, I., Nyirenda, T., et al. (2013). Parkinson disease affects peripheral sensory nerves in the pharynx. *J. Neuropathol. Exp. Neurol.* 72, 614–623. doi: 10.1097/nen.0b013e3182965886

Mukherjee, A., Biswas, A., and Das, S. K. (2016). Gut dysfunction in Parkinson's disease. *World J. Gastroenterol.* 22, 5742–5752.

Narendra, D., Tanaka, A., Suen, D. F., and Youle, R. J. (2008). Parkin is recruited selectively to impaired mitochondria and promotes their autophagy. *J. Cell Biol.* 183, 795–803. doi: 10.1083/jcb.200809125

Natale, G., Kastsiushenka, O., Fulceri, F., Ruggieri, S., Paparelli, A., and Fornai, F. (2010). MPTP-induced parkinsonism extends to a subclass of TH-positive neurons in the gut. *Brain Res.* 1355, 195–206. doi: 10.1016/j.brainres.2010.07.076

Naudet, N., Antier, E., Gaillard, D., Morignat, E., Lakhdar, L., Baron, T., et al. (2017). Oral exposure to paraquat triggers earlier expression of phosphorylated alpha-synuclein in the enteric nervous system of A53T mutant human alpha-synuclein transgenic mice. *J. Neuropathol. Exp. Neurol.* 76, 1046–1057. doi: 10.1093/jnen/nlx092

Okochi, M., Walter, J., Koyama, A., Nakajo, S., Baba, M., Iwatsubo, T., et al. (2000). Constitutive phosphorylation of the Parkinson's disease associated alpha-synuclein. *J. Biol. Chem.* 275, 390–397.

Pan-Montojo, F., Anichtchik, O., Dening, Y., Knels, L., Pursche, S., Jung, R., et al. (2010). Progression of Parkinson's disease pathology is reproduced by intragastric administration of rotenone in mice. *PLoS One* 5:e8762. doi: 10.1371/journal.pone.0008762

Pan-Montojo, F., Schwarz, M., Winkler, C., Arnhold, M., O'sullivan, G. A., Pal, A., et al. (2012). Environmental toxins trigger PD-like progression via increased alpha-synuclein release from enteric neurons in mice. *Sci. Rep.* 2:898.

Perese, D. A., Ulman, J., Viola, J., Ewing, S. E., and Bankiewicz, K. S. (1989). A 6-hydroxydopamine-induced selective parkinsonian rat model. *Brain Res.* 494, 285–293. doi: 10.1016/0006-8993(89)90597-0

Perez-Pardo, P., Dodiya, H. B., Engen, P. A., Naqib, A., Forsyth, C. B., Green, S. J., et al. (2018). Gut bacterial composition in a mouse model of Parkinson's disease. *Benef Microbes* 9, 799–814. doi: 10.3920/bm2017.0202

Perez-Pardo, P., Hartog, M., Garssen, J., and Kraneveld, A. D. (2017). Microbes tickling your tummy: the importance of the gut-brain axis in Parkinson's Disease. *Curr. Behav. Neurosci. Rep.* 4, 361–368. doi: 10.1007/s40473-017-0129-2

Pierantozzi, M., Pietroiusti, A., Brusa, L., Galati, S., Stefani, A., Lunardi, G., et al. (2006). pylori eradication and l-dopa absorption in patients with PD and motor fluctuations. *Neurol. Helicobacter*, 1824–1829. doi: 10.1212/01.wnl.0000221672.01272.ba

Plotegher, N., Stringari, C., Jahid, S., Veronesi, M., Girotto, S., Gratton, E., et al. (2015). NADH fluorescence lifetime is an endogenous reporter of alpha-synuclein aggregation in live cells. *FASEB J.* 29, 2484–2494. doi: 10.1096/fj.14-260281

Pokusa, M., and Kralova Trancikova, A. (2018). FLIM analysis of intracellular markers associated with the development of Parkinson's disease in cellular model. *Physiol. Res.* 67, S673–S683.

Pouclet, H., Lebouvier, T., Coron, E., Neunlist, M., and Derkinderen, P. (2012). Lewy pathology in gastric and duodenal biopsies in Parkinson's Disease. *Mov. Disord.* 27:708. doi: 10.1002/mds.24993

Przedborski, S., Levivier, M., Jiang, H., Ferreira, M., Jackson-Lewis, V., Donaldson, D., et al. (1995). Dose-dependent lesions of the dopaminergic nigrostriatal pathway induced by intrastriatal injection of 6-hydroxydopamine. *Neuroscience* 67, 631–647. doi: 10.1016/0306-4522(95)00066-r

Qin, L., Wu, X., Block, M. L., Liu, Y., Breese, G. R., Hong, J. S., et al. (2007). Systemic LPS causes chronic neuroinflammation and progressive neurodegeneration. *Glia* 55, 453–462. doi: 10.1002/glia.20467

Qualman, S. J., Haupt, H. M., Yang, P., and Hamilton, S. R. (1984). Esophageal Lewy bodies associated with ganglion cell loss in achalasia. Similarity to Parkinson's disease. *Gastroenterology* 87, 848–856. doi: 10.1016/0016-5085(84)90079-9

Rao, M., and Gershon, M. D. (2016). The bowel and beyond: the enteric nervous system in neurological disorders. *Nat. Rev. Gastroenterol. Hepatol.* 13, 517–528. doi: 10.1038/nrgastro.2016.107

Rey, N. L., Wesson, D. W., and Brundin, P. (2018). The olfactory bulb as the entry site for prion-like propagation in neurodegenerative diseases. *Neurobiol. Dis.* 109, 226–248. doi: 10.1016/j.nbd.2016.12.013

Rota, L., Pellegrini, C., Benvenuti, L., Antonioli, L., Fornai, M., Blandizzi, C., et al. (2019). Constipation, deficit in colon contractions and alpha-synuclein inclusions within the colon precede motor abnormalities and neurodegeneration in the central nervous system in a mouse model of alpha-synucleinopathy. *Transl. Neurodegener.* 8:5.

Sacino, A. N., Brooks, M., Thomas, M. A., Mckinney, A. B., Lee, S., Regenhardt, R. W., et al. (2014). Intramuscular injection of alpha-synuclein induces CNS alpha-synuclein pathology and a rapid-onset motor phenotype in transgenic mice. *Proc. Natl. Acad. Sci. U.S.A.* 111, 10732–10737. doi: 10.1073/pnas.1321785111

Sampson, T. R., Challis, C., Jain, N., Moiseyenko, A., Ladinsky, M. S., Shastri, G. G., et al. (2020). A gut bacterial amyloid promotes alpha-synuclein aggregation and motor impairment in mice. *eLife* 9:e53111.

Sampson, T. R., Debelius, J. W., Thron, T., Janssen, S., Shastri, G. G., Ilhan, Z. E., et al. (2016). Gut microbiota regulate motor deficits and neuroinflammation in a model of Parkinson's Disease. *Cell* 167, 1469.e12–1480.e12.

Sanchez-Ferro, A., Rabano, A., Catalan, M. J., Rodriguez-Valcarcel, F. C., Fernandez Diez, S., Herreros-Rodriguez, J., et al. (2015). In vivo gastric detection of alpha-synuclein inclusions in Parkinson's disease. *Mov. Disord.* 30, 517–524. doi: 10.1002/mds.25988

Santos, S. F., De Oliveira, H. L., Yamada, E. S., Neves, B. C., et al. (2019). The gut and Parkinson's disease-a bidirectional pathway. *Front. Neurol.* 10:574. doi: 10.3389/fneur.2019.00574

Scheperjans, F., Aho, V., Pereira, P. A., Koskinen, K., Paulin, L., Pekkonen, E., et al. (2015). Gut microbiota are related to Parkinson's disease and clinical phenotype. *Mov. Disord.* 30, 350–358.

Scher, J. U., Sczesnak, A., Longman, R. S., Segata, N., Ubeda, C., Bielski, C., et al. (2013). Expansion of intestinal prevotella copri correlates with enhanced susceptibility to arthritis. *eLife* 2:e01202.

Schneider, S. A., Boettner, M., Alexoudi, A., Zorenkov, D., Deuschl, G., and Wedel, T. (2016). Can we use peripheral tissue biopsies to diagnose Parkinson's disease? A review of the literature. *Eur. J. Neurol.* 23, 247–261. doi: 10.1111/ene.12753

Shahnawaz, M., Mukherjee, A., Pritzkow, S., Mendez, N., Rabadia, P., Liu, X., et al. (2020). Discriminating alpha-synuclein strains in Parkinson's disease and multiple system atrophy. *Nature* 578, 273–277.

Shahnawaz, M., Tokuda, T., Waragai, M., Mendez, N., Ishii, R., Trenkwalder, C., et al. (2017). Development of a biochemical diagnosis of parkinson disease by detection of alpha-synuclein misfolded aggregates in cerebrospinal fluid. *JAMA Neurol.* 74, 163–172.

Shannon, K. M., Keshavarzian, A., Dodiya, H. B., Jakate, S., and Kordower, J. H. (2012a). Is alpha-synuclein in the colon a biomarker for premotor Parkinson's disease? Evidence from 3 cases. *Mov. Disord.* 27, 716–719. doi: 10.1002/mds.25020

Shannon, K. M., Keshavarzian, A., Mutlu, E., Dodiya, H. B., Daian, D., Jaglin, J. A., et al. (2012b). Alpha-synuclein in colonic submucosa in early untreated Parkinson's disease. *Mov. Disord.* 27, 709–715. doi: 10.1002/mds.23838

Shen, L. (2020). Gut, oral and nasal microbiota and Parkinson's disease. *Microb. Cell Fact.* 19:50.

Singaram, C., Ashraf, W., Gaumnitz, E. A., Torbey, C., Sengupta, A., Pfeiffer, R., et al. (1995). Dopaminergic defect of enteric nervous system in Parkinson's disease patients with chronic constipation. *Lancet* 346, 861–864. doi: 10.1016/s0140-6736(95)92707-7

Singleton, A. B., Farrer, M., Johnson, J., Singleton, A., Hague, S., Kachergus, J., et al. (2003). alpha-Synuclein locus triplication causes Parkinson's disease. *Science* 302:841. doi: 10.1126/science.1090278

Song, N., Wang, W., Jia, F., Du, X., Xie, A., He, Q., et al. (2017). Assessments of plasma ghrelin levels in the early stages of parkinson's disease. *Mov. Disord.* 32, 1487–1491. doi: 10.1002/mds.27095

Spielman, L. J., Gibson, D. L., and Klegeris, A. (2018). Unhealthy gut, unhealthy brain: the role of the intestinal microbiota in neurodegenerative diseases. *Neurochem. Int.* 120, 149–163. doi: 10.1016/j.neuint.2018.08.005

Srivastav, S., Neupane, S., Bhurtel, S., Katila, N., Maharjan, S., Choi, H., et al. (2019). Probiotics mixture increases butyrate, and subsequently rescues the nigral dopaminergic neurons from MPTP and rotenone-induced neurotoxicity. *J. Nutr. Biochem.* 69, 73–86. doi: 10.1016/j.jnutbio.2019.03.021

Stokholm, M. G., Danielsen, E. H., Hamilton-Dutoit, S. J., and Borghammer, P. (2016). Pathological alpha-synuclein in gastrointestinal tissues from prodromal Parkinson disease patients. *Ann. Neurol.* 79, 940–949. doi: 10.1002/ana.24648

Sun, M. F., and Shen, Y. Q. (2018). Dysbiosis of gut microbiota and microbial metabolites in Parkinson's Disease. *Ageing Res. Rev.* 45, 53–61. doi: 10.1016/j.arr.2018.04.004

Svensson, E., Horvath-Puho, E., Thomsen, R. W., Djurhuus, J. C., Pedersen, L., Borghammer, P., et al. (2015). Vagotomy and subsequent risk of Parkinson's disease. *Ann. Neurol.* 78, 522–529. doi: 10.1002/ana.24448

Taguchi, T., Ikuno, M., Hondo, M., Parajuli, L. K., Taguchi, K., Ueda, J., et al. (2020a). alpha-Synuclein BAC transgenic mice exhibit RBD-like behaviour and hyposmia: a prodromal Parkinson's disease model. *Brain* 143, 249–265. doi: 10.1093/brain/awz380

Taguchi, T., Ikuno, M., Yamakado, H., and Takahashi, R. (2020b). Animal Model for Prodromal Parkinson's Disease. *Int. J. Mol. Sci.* 21:1961. doi: 10.3390/ijms21061961

Tamtaji, O. R., Taghizadeh, M., Daneshvar Kakhaki, R., Kouchaki, E., Bahmani, F., Borzabadi, S., et al. (2019). Clinical and metabolic response to probiotic administration in people with Parkinson's disease: a randomized, double-blind, placebo-controlled trial. *Clin. Nutr.* 38, 1031–1035. doi: 10.1016/j.clnu.2018.05.018

Tasselli, M., Chaumette, T., Paillusson, S., Monnet, Y., Lafoux, A., Huchet-Cadiou, C., et al. (2013). Effects of oral administration of rotenone on gastrointestinal functions in mice. *Neurogastroenterol. Motil.* 25, e183–e193. doi: 10.1111/nmo.12070

Thomas, R. H., Meeking, M. M., Mepham, J. R., Tichenoff, L., Possmayer, F., Liu, S., et al. (2012). The enteric bacterial metabolite propionic acid alters brain and plasma phospholipid molecular species: further development of a rodent model of autism spectrum disorders. *J. Neuroinflammation* 9:153.

Tieu, K. (2011). A guide to neurotoxic animal models of Parkinson's disease. *Cold Spring Harb. Perspect. Med.* 1:a009316. doi: 10.1101/cshperspect.a009316

Trancikova, A., Ramonet, D., and Moore, D. J. (2011). Genetic mouse models of neurodegenerative diseases. *Prog. Mol. Biol. Transl. Sci.* 100, 419–482. doi: 10.1016/b978-0-12-384878-9.00012-1

Tysnes, O. B., Kenborg, L., Herlofson, K., Steding-Jessen, M., Horn, A., Olsen, J. H., et al. (2015). Does vagotomy reduce the risk of Parkinson's disease? *Ann. Neurol.* 78, 1011–1012. doi: 10.1002/ana.24531

Uemura, N., Yagi, H., Uemura, M. T., Hatanaka, Y., Yamakado, H., and Takahashi, R. (2018). Inoculation of alpha-synuclein preformed fibrils into the mouse gastrointestinal tract induces lewy body-like aggregates in the brainstem via the vagus nerve. *Mol. Neurodegener.* 13:21.

Uemura, N., Yagi, H., Uemura, M. T., Yamakado, H., and Takahashi, R. (2020). Limited spread of pathology within the brainstem of alpha-synuclein BAC transgenic mice inoculated with preformed fibrils into the gastrointestinal tract. *Neurosci. Lett.* 716:134651. doi: 10.1016/j.neulet.2019.134651

Unger, M. M., Spiegel, J., Dillmann, K. U., Grundmann, D., Philippeit, H., Burmann, J., et al. (2016). Short chain fatty acids and gut microbiota differ between patients with Parkinson's disease and age-matched controls. *Parkinsonism. Relat. Disord.* 32, 66–72. doi: 10.1016/j.parkreldis.2016.08.019

Ungerstedt, U. (1968). 6-Hydroxy-dopamine induced degeneration of central monoamine neurons. *Eur. J. Pharmacol.* 5, 107–110. doi: 10.1016/0014-2999(68)90164-7

Van Den Berge, N., Ferreira, N., Gram, H., Mikkelsen, T. W., Alstrup, A. K. O., Casadei, N., et al. (2019). Evidence for bidirectional and trans-synaptic parasympathetic and sympathetic propagation of alpha-synuclein in rats. *Acta Neuropathol.* 138, 535–550. doi: 10.1007/s00401-019-02040-w

Visanji, N. P., Marras, C., Hazrati, L. N., Liu, L. W., and Lang, A. E. (2014). Alimentary, my dear Watson? The challenges of enteric alpha-synuclein as a Parkinson's disease biomarker. *Mov. Disord.* 29, 444–450. doi: 10.1002/mds.25789

Visanji, N. P., Marras, C., Kern, D. S., Al Dakheel, A., Gao, A., Liu, L. W., et al. (2015). Colonic mucosal a-synuclein lacks specificity as a biomarker for Parkinson disease. *Neurology* 84, 609–616. doi: 10.1212/wnl.0000000000001240

Wakabayashi, K., Takahashi, H., Takeda, S., Ohama, E., and Ikuta, F. (1988). Parkinson's disease: the presence of Lewy bodies in Auerbach's and Meissner's plexuses. *Acta Neuropathol.* 76, 217–221. doi: 10.1007/bf00687767

Wang, L., Fleming, S. M., Chesselet, M. F., and Tache, Y. (2008). Abnormal colonic motility in mice overexpressing human wild-type alpha-synuclein. *Neuroreport* 19, 873–876. doi: 10.1097/wnr.0b013e3282ffda5e

Wang, L., Magen, I., Yuan, P. Q., Subramaniam, S. R., Richter, F., Chesselet, M. F., et al. (2012). Mice overexpressing wild-type human alpha-synuclein display alterations in colonic myenteric ganglia and defecation. *Neurogastroenterol. Motil.* 24, e425–e436. doi: 10.1111/j.1365-2982.2012.01974.x

Wullner, U., Pakzaban, P., Brownell, A. L., Hantraye, P., Burns, L., Shoup, T., et al. (1994). Dopamine terminal loss and onset of motor symptoms in MPTP-treated monkeys: a positron emission tomography study with 11C-CFT. *Exp. Neurol.* 126, 305–309. doi: 10.1006/exnr.1994.1069

Yanagi, H., Tsuda, A., Matsushima, M., Takahashi, S., Ozawa, G., Koga, Y., et al. (2017). Changes in the gut microbiota composition and the plasma ghrelin level in patients with. *BMJ Open Gastroenterol. Helicobacter*, 4:e000182. doi: 10.1136/bmjgast-2017-000182

Yang, X., Qian, Y., Xu, S., Song, Y., and Xiao, Q. (2017). Longitudinal analysis of fecal microbiome and pathologic processes in a rotenone induced mice model of Parkinson's Disease. *Front. Aging Neurosci.* 9:441. doi: 10.3389/fnagi.2017.00441

Zhang, X., Li, Y., Liu, C., Fan, R., Wang, P., Zheng, L., et al. (2015). Alteration of enteric monoamines with monoamine receptors and colonic dysmotility in 6-hydroxydopamine-induced Parkinson's disease rats. *Transl. Res.* 166, 152–162. doi: 10.1016/j.trsl.2015.02.003

Zheng, L. F., Wang, Z. Y., Li, X. F., Song, J., Hong, F., Lian, H., et al. (2011). Reduced expression of choline acetyltransferase in vagal motoneurons and gastric motor dysfunction in a 6-OHDA rat model of Parkinson's disease. *Brain Res.* 1420, 59–67. doi: 10.1016/j.brainres.2011.09.006

Zhu, H. C., Zhao, J., Luo, C. Y., and Li, Q. Q. (2012). Gastrointestinal dysfunction in a Parkinson's disease rat model and the changes of dopaminergic, nitric oxidergic, and cholinergic neurotransmitters in myenteric plexus. *J. Mol. Neurosci.* 47, 15–25. doi: 10.1007/s12031-011-9560-0

Zmora, N., Suez, J., and Elinav, E. (2019). You are what you eat: diet, health and the gut microbiota. *Nat. Rev. Gastroenterol. Hepatol.* 16, 35–56. doi: 10.1038/s41575-018-0061-2

Conflict of Interest: The authors declare that the research was conducted in the absence of any commercial or financial relationships that could be construed as a potential conflict of interest.

frontiers in Aging Neuroscience

BRIEF RESEARCH REPORT
published: 17 June 2020
doi: 10.3389/fnagi.2020.00145

SRC-1 Knockout Exerts No Effect on Amyloid β Deposition in APP/PS1 Mice

Qiong Wu[1†], Bin Wang[1†], Qi-Fa Li[1], Xuan Zhang[2], Michael Ntim[1], Xue-Fei Wu[1], Na Li[2], Dan-Dan Zhu[1], Rong Jiang[1], Jin-Yi Yang[3], Yu-Hui Yuan[4]* and Shao Li[1]**

[1]Liaoning Provincial Key Laboratory of Cerebral Diseases, Department of Physiology, College of Basic Medical Sciences, Dalian Medical University, Dalian, China, [2]National-Local Joint Engineering Research Center for Drug-Research and Development (R and D) of Neurodegenerative Diseases, Dalian Medical University, Dalian, China, [3]Department of Urology, Affiliated Dalian Friendship Hospital of Dalian Medical University, Dalian, China, [4]Institute of Cancer Stem Cell, Dalian Medical University, Dalian, China

OPEN ACCESS

Edited by:
Jiehui Jiang,
Shanghai University, China

Reviewed by:
Derya R. Shimshek,
Novartis Institutes for BioMedical Research, Switzerland
Rongqiao He,
Institute of Biophysics (CAS), China

***Correspondence:**
Jin-Yi Yang
yangjinyi90@hotmail.com
Yu-Hui Yuan
yuhuiyuan@dlmedu.edu.cn
Shao Li
lishao89@dmu.edu.cn

†These authors have contributed equally to this work

Received: 14 December 2019
Accepted: 29 April 2020
Published: 17 June 2020

Citation:
Wu Q, Wang B, Li Q-F, Zhang X, Ntim M, Wu X-F, Li N, Zhu D-D, Jiang R, Yang J-Y, Yuan Y-H and Li S (2020) SRC-1 Knockout Exerts No Effect on Amyloid β Deposition in APP/PS1 Mice. Front. Aging Neurosci. 12:145. doi: 10.3389/fnagi.2020.00145

Steroid receptor coactivator 1 (SRC-1) is the key coactivator because of its transcriptional activity. Previous studies have shown that SRC-1 is abundant in the hippocampus and has been implicated in cognition. SRC-1 is also related to some major risk factors for Alzheimer's disease (AD), such as a decline in estrogen and aging, however, whether SRC-1 is involved in the pathogenesis of AD remains unclear. In this study, we established SRC-1 knockout in AD mice by cross breeding SRC-1$^{-/-}$ mutant mice with APP/PS1 transgenic mice, and investigated the expression of some synaptic proteins, the amyloid β (Aβ) deposition, and activation of astrocytes and microglia in the hippocampus of APP/PS1×SRC-1$^{-/-}$ mice. The results showed that SRC-1 knockout neither affects the Aβ plaque and activation of glia, nor changes the expression of synaptic proteins in AD model mice. The above results suggest that the complete deletion of SRC-1 in the embryo exerts no effect on the pathogenesis of APP/PS1 mice. Nevertheless, this study could not eliminate the possible role of SRC-1 in the development of AD due to the lack of observation of other events in AD such as tau hyperphosphorylation and the limitation of the animal model employed.

Keywords: steroid receptor coactivator 1, Alzheimer's disease, amyloid-β, synapse, glia

INTRODUCTION

Alzheimer's disease (AD), the most prevalent cause of dementia, is characterized by progressive cognitive impairment (Fernandez et al., 2019; Lu et al., 2019). The mechanisms of sporadic AD (representing more than 95% of AD cases) are uncertain, but some major risk factors have been identified. The incidence of AD rises exponentially with age (Villemagne et al., 2013; Wattmo and Wallin, 2017). The sex hormone offers protective effects on the brain and the deprivation during menopause or andropause triggers neurodysfunction, neurodegeneration, and cognitive disease

(Meng et al., 2010; Ross et al., 2017) and disproportionately increases the risk of AD (Zhao et al., 2015; Tang et al., 2018).

Steroids, such as estrogen and androgen, have profound roles in the hippocampal function and may causally be involved in cognitive deficits in AD (Hasanpour et al., 2018). Steroid receptor coactivator 1 (SRC-1) is the key coactivator to the nuclear receptors (NRs) of the steroids and is important to their effect on transcriptional activities (Bayele, 2019; Heck et al., 2020). It has been reported that SRC-1 is abundantly expressed in specific brain regions such as the hippocampus and cortex, which are recognized as the crucial brain structures in cognition (Charlier et al., 2005, 2013; Qiu et al., 2016; Zalachoras et al., 2016). Previous studies have shown that SRC-1 is in involved in the estrogen receptor (ER) or androgen receptor (AR) induced memory formulation and synaptic plasticity in the hippocampus (Bian et al., 2012; Liu et al., 2015; Qiu et al., 2016; Zhao et al., 2017). The aged-related decrease of SRC-1 expression is also observed, especially in the hippocampus region (Zhang et al., 2011; Zhao et al., 2017). Taken together, these studies indicate that SRC-1 might be implicated in the interaction of these risk factors and the development of AD, which leads to the question of whether SRC-1 is involved in the pathogenesis of AD or not.

In this study, we first evaluated the SRC-1 level in APP/PS1 transgenic mice, and then investigated the effect of SRC-1 in the pathogenesis of AD mice by cross breeding the SRC-1 knockout (SRC-$1^{-/-}$) mice with the APP/PS1 mice. Our results showed that SRC-1 expression in the APP/PS1 mice was not different from the wild type (WT) mice and SRC-1 deletion had no effect on Aβ deposition, activation of microglia and astrocytes, and synaptic protein expression in APP/PS1 mice. These negative results suggest that SRC-1 does not interfere with AD progression, at least in the current experimental condition.

MATERIALS AND METHODS

Animals

SRC-$1^{+/-}$ mice (with a C57BL/6J background) were kindly provided by Dr. Jianming Xu from Baylor College of Medicine, TX, USA. APPswe/PS1Δe9 (APP/PS1) mice (with a C57BL/6J background) were purchased from Jackson Laboratory. C57BL/6J were provided by the Animal Center of Dalian Medical University (DMU).

Male SRC-$1^{+/-}$ were bred with SRC-$1^{+/-}$ females. Offspring males homozygous for the SRC-$1^{-/-}$ (SRC-1 knockout, KO) and the WT littermates (SRC-$1^{+/+}$) were used in the experiments at 3–4 months of age.

APP/PS1 mice were bred with WT C57BL/6J. Male offspring heterozygous for the APP/PS1 transgenic construct and the WT littermates (not expressing any transgene) were used as the control. APP/PS1 mice develop plaque deposition by 6 months of age, while the plaque would be clearly visible when the mice are more than 7-months old. Male APP/PS1 and the WT littermates used in the experiments were at 8–9 months old.

All the animals were raised and bred in the Animal Center of DMU and allowed access to food and water *ad libitum*. Animals were maintained on a 12:12 light–dark cycle (lights on at 08:00, lights off at 20:00), within a temperature-controlled room (T: 24°C ± 1°C). All tests were performed during the light cycle. All experiments were carried out under the guidelines of the National Institutes of Health Guide for the Care and Use of Laboratory Animals.

Generation of APP/PS1×SRC-$1^{-/-}$ Mice

SRC-1 knockout in APP/PS1 (APP/PS1×SRC-$1^{-/-}$) mice were obtained by breeding SRC-$1^{-/-}$ mice with APP/PS1 mice, using a three-generation breeding scheme (**Supplementary Figure S1**). APP/PS1 mice were crossed with SRC-$1^{-/-}$ mice to introduce the SRC-1 knockout allele into the F1 generation (APP/PS1×SRC-1^{+}). APP/PS1×SRC-$1^{+/-}$ mice were then crossed with SRC-$1^{+/-}$ mice to obtain the F2 generation which could comprise APP/PS1×SRC-$1^{+/+}$ (APP/PS1), APP/PS1×SRC-$1^{+/-}$, APP/PS1×SRC-$1^{-/-}$, SRC-$1^{+/+}$ (WT), SRC-$1^{+/-}$ and SRC-$1^{-/-}$. The proportions of each genotype of the mice are shown in **Supplementary Figure S1**.

APP/PS1×SRC-$1^{-/-}$ mice were then age-matched with APP/PS1×SRC-$1^{+/+}$ mice, which were used as the control. The SRC-$1^{+/+}$ littermates express neither the APP/PS1 gene nor SRC-1 mutants and could be considered as wildtype (WT). Female mice were only used for the breeding. All the male mice used in the experiment were 8–9 months old.

Western Blot

The proteins were extracted using an extraction kit (Keygen Biotech, China), and the protein content was measured by a BCA protein assay (Keygen Biotech, China). For Western Blotting, the proteins (10–30 μg) for each sample were loaded into a 10% SDS PAGE gel for electrophoresis, then the protein components were transferred to polyvinylidene difluoride (PVDF) membranes. Later, the PVDF membranes were blocked with 5% bull serum albumin (BSA) in TBST (TBS + 0.1% Tween-20) for 1 h, and immunoblotted overnight at 4°C with the primary antibodies: SRC-1 (180 KD, 1:1,000, Cell signaling technology, Millipore, 2191S); PSD95 (1:1,000, Abcam, ab2723); Synapsin (70 KD, 1:1,000, Abcam, ab64581); GluR1 (100 KD, 1:1,000, Abcam, ab31232); APP (87 KD, 1:1,000, Abcam, ab15272); beta-site APP-cleaving enzyme 1 (BACE-1; 70 KD, 1:1,000, Abcam, ab2077); β-actin (1:2,000, Abcam, ab6276). The following day, the membranes were washed in TBST three times, then incubated with a horseradish peroxidase-labeled secondary antibody (anti-mouse or anti-rabbit, 1:5,000; ZSJQ-BIO Company, Beijing, China) for 1 h at room temperature. The infrared band signals were detected using BIO-RAD gel analysis software (Hercules, CA, USA). The densitometric analysis of immunoreactivity was conducted using the NIH ImageJ software (Li et al., 2019).

Immunohistochemistry (IHC) and Immunofluorescence (IF)

IHC and IF were carried out according to our previous work (Wang et al., 2018). The primary antibodies: SRC-1 (1:100–200); 6E10 (for Aβ; 1:100, Covance, S39320260); GFAP (1:200, DAKO, 20334); Iba-1 (1:200, WAKO, 019-19741) were

used. The mice were anesthetized with pentobarbital (50 mg/kg, 0.05 ml/10 g body weight, i.p.) and perfused with 0.1% phosphate buffer (PB), followed by 4% paraformaldehyde (PFA) dissolved in 0.1% PB. Afterward, the brains were removed and left in 4% PFA at 4°C for 24 h, and then transferred to 30% sucrose dissolved in 0.1% PB. Following saturation of the brains in sucrose, serial 16 μm coronal sections were made with a cryostat (Leica CM 3050 S, Leica Microsystems AG, Wetzlar, Germany) after OCT embedding. The slices that contained cortex and ventral hippocampus were used for the staining. For the IHC staining procedure, the slices were thoroughly rinsed in 0.3% PBS-T for 15 min, then quenched by 3% H_2O_2 in 0.01 M PBS for 15 min. Subsequently, they were rinsed again and pre-incubated in 2% BSA and 0.3% Triton X-100 in 0.01 M PBS at room temperature for 1 h, and then incubated at 4°C with the primary antibody in 0.01 M PBS containing 2% BSA and 0.3% Triton X-100 overnight. After incubation with a biotinylated goat anti-rabbit or anti-mouse IgG secondary antibody (1:200; Vector Laboratories, Burlingame, CA, USA) for 2 h, the bound antibodies were visualized using an avidin–biotin–peroxidase complex system (Vectastain ABC Elite Kit, Vector Laboratories, Burlingame, CA, USA) and then stained with diaminobenzidine (DAB; Vectro Laboratories) as a chromogen. The slides were visualized with a microscope and digitally photographed (Pannoramic Digital Slide Scanners, 3DHISTECH, Budapest, Hungary).

For the IF staining procedure, the sections were washed with 0.3% PBST (three times, 10 min each time). After that, the sections were blocked with 5% BSA in PBS containing 0.3% Triton X-100 at room temperature for 1 h, and then incubated with primary antibody overnight at 4°C. On the second day, the sections were incubated with secondary antibody for 2 h at room temperature after being washed with 0.3% PBST three times. Images were captured under a microscope (Pannoramic Digital Slide Scanners, 3DHISTECH, Budapest, Hungary). The analysis of mean integrated optical density (MIOD) was performed using ImageJ software from the National Institutes of Health.

Statistical Analysis

All statistical analyses were performed using SPSS22.0 and the figures were created using GraphPad Prism (GraphPad Software Inc.). Data were presented as the mean ± SEM. Comparisons between two groups were made by student 2-tailed unpaired *t*-test. Comparisons between three or four groups were made by one-way ANOVA. p value < 0.05 was considered statistically significant ($^*p < 0.05$, $^{**}p < 0.01$, $^{***}p < 0.001$).

RESULTS

SRC-1 Expression in APP/PS1 Mice

APP/PS1 mice, which express human mutant APP and PS1 (Garcia-Alloza et al., 2006), are commonly used as an Aβ-induced AD model. We first examined the expression of SRC-1 in the hippocampus (**Figure 1A**) and cortex (**Figure 1F**) of APP/PS1 mice. Both IHC (**Figures 1A,B**) and western (**Figures 1C,D**) results showed that SRC-1 is abundant in the region of the hippocampus but no changed expression was observed in the APP/PS1 mice compared to the littermate WT mice.

SRC-1 Knockout Shows No Effect on Synaptic Protein Expression in APP/PS1 Mice

In order to observe the possible role of SRC-1 in the AD model, we bred SRC-$1^{-/-}$ mice with APP/PS1 mice and obtained APP/PS1×SRC-$1^{-/-}$ mice at the F2 generation, with the control APP/PS1×SRC-$1^{+/+}$ (**Supplementary Figure S1**). The immunofluorescent staining of SRC-1 in WT (SRC-$1^{+/+}$), APP/PS1×SRC-$1^{+/+}$ and APP/PS1×SRC-$1^{-/-}$ mice (**Supplementary Figure S2**) showed no positive staining of SRC-1 in APP/PS1×SRC-$1^{-/-}$ mice, and non-changed SRC-1 expression between the WT and APP/PS1×SRC-$1^{+/+}$ mice, which is consistent with the result in **Figure 1**.

Synaptic loss is the main reason of the cause cognitive deficiency in AD. Postsynaptic density (PSD) 95, Synapsin and glutamate receptor 1 (GluR1) are the important proteins in synapse and their level shows a positive correlation to synaptic function. The expression of the three selected proteins was detected in the hippocampus of APP/PS1×SRC-$1^{-/-}$ mice (**Figure 2**). The results showed, compared to the WT mice, that the APP/PS1 (shown as APP/PS1×SRC-$1^{+/+}$) mice exhibited a notable decrease in the expression of PSD95, Synapsin, and GluR1 (**Figure 2**). However, none of the three synaptic proteins showed any changed expression in the hippocampus of APP/PS1×SRC-$1^{-/-}$ mice, compared to the APP/PS1×SRC-$1^{+/+}$ mice. These findings indicates that the deletion of SRC-1 has no effect on synaptic protein expression in the AD mouse model. Similarly, in the non-AD model (as shown in **Supplementary Figure S3**), PSD95, Synapsin, and GluR1 expression remain constant in the SRC-1 knockout (SRC-$1^{-/-}$) mice compared to their WT littermates.

SRC-1 Knockout Exerts No Effect on Aβ Deposition in APP/PS1 Mice

The Aβ senile plaque is the major pathological hallmark of AD. To further determine the effects of SRC-1 knockout on AD, we detected the Aβ plaque in both APP/PS1×SRC-$1^{+/+}$ and APP/PS1×SRC-$1^{-/-}$ mice (**Figures 3A,C**). The IHC results demonstrated that the number and area of the Aβ plaque in APP/PS1×SRC-$1^{-/-}$ mice was comparable to those in APP/PS1×SRC-$1^{+/+}$ mice (**Figures 3A,B**). It is known that Aβ production is affected by protein levels of APP and APP processing enzymes such as BACE-1. We discovered that APP/PS1×SRC-$1^{+/+}$ mice showed an increased expression of both APP and BACE-1 compared to WT mice (**Figures 3D–F**); but APP/PS1×SRC-$1^{-/-}$ mice showed an expression change of neither APP nor BACE-1 compared to APP/PS1×SRC-$1^{+/+}$ mice (**Figures 3D–F**). In addition, we also detected an APP and BACE-1 level in the non-transgenic AD mice and the result showed no expression difference of APP or BACE-1 between SRC-$1^{-/-}$ mice and their WT littermates (**Supplementary Figure S4**).

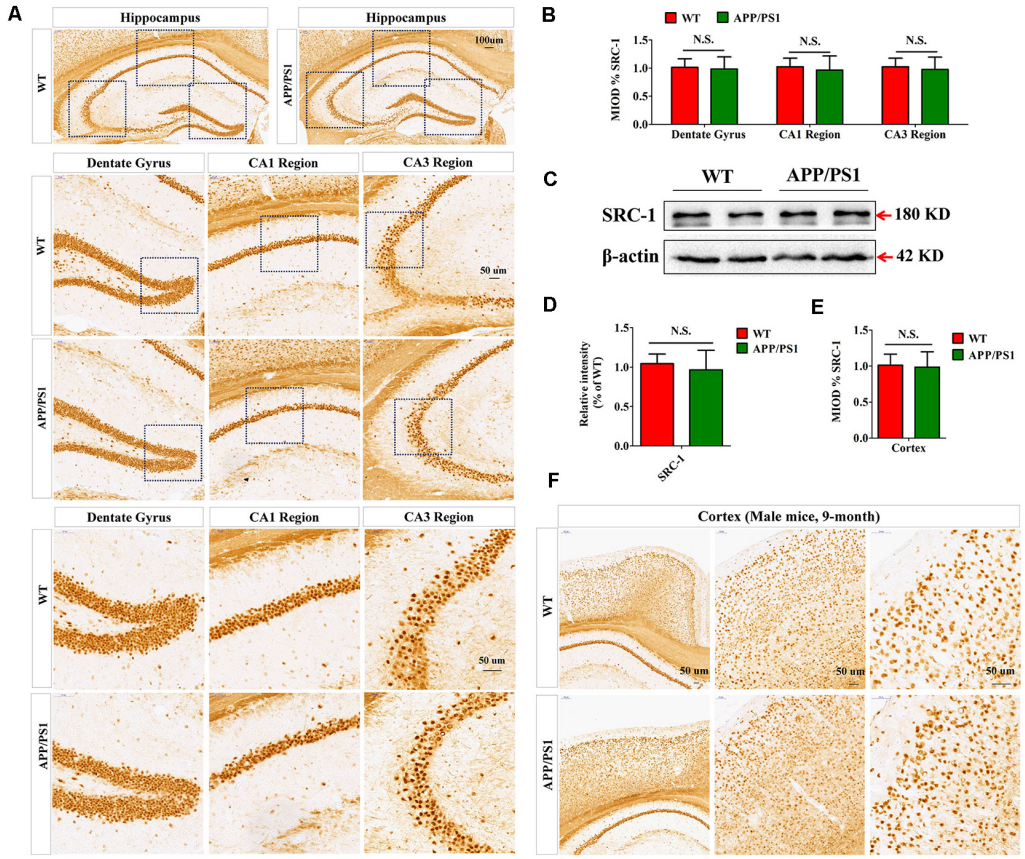

FIGURE 1 | The expression of Steroid receptor coactivator 1 (SRC-1) protein in APP/PS1 mice. **(A,B)** SRC-1 expression in the coronal sections of the hippocampus (10×) in APP/PS1 mice at 8–9 months of age. Dentate gyrus (20× and 40×), CA1 region (20× and 40×), and CA3 region (20× and 40×). **(C,D)** Representative immuno-blot and densitometry analysis of SRC-1 expression in the hippocampus of APP/PS1 mice. **(E,F)** SRC-1 expression in the coronal sections of the cortex (10×, 20× and 40×). Data are presented as the mean ± SEM of six mice in each group. N.S., no significance.

SRC-1 Knockout Exerts No Effect on the Activation of Microglia and Astrocytes in APP/PS1 Mice

Neuroinflammation characterized by the activation of astrocytes and microglia is also a significant contributor to the pathological progression of AD (Zheng et al., 2018). To investigate whether SRC-1 is involved in the neuroinflammation of APP/PS1 mice, we then stained the coronal sections of the hippocampus of each group of mice with antibodies against GFAP (a marker for astrocytes) or Iba-1 (a marker for microglia; **Figures 4A,C**). Over activation of glial cells was shown in APP/PS1×SRC-$1^{+/+}$ mice in contrast to WT mice, however, the volume of both astrocytes and microglia in the hippocampus of APP/PS1×SRC-$1^{-/-}$ is similar to that of APP/PS1×SRC-$1^{+/+}$ mice (**Figures 4B,D**). This result showed that SRC-1 deletion would not affect the over activation status of microglia and astrocytes in the APP/PS1 mice.

DISCUSSION

Steroids modulate the structure and function of the brain by binding to the NRs (Bayele, 2019; Heck et al., 2020), then the activated NRs recruit the steroid receptor coactivators (SRCs, also named nuclear receptor coactivators) to enhance their transcriptional activities (McEwen and Milner, 2017). SRC-1 is the key coactivator for the transcriptional regulation of NRs (Bayele, 2019; Heck et al., 2020). There are studies that have reported that SRC-1 is widely expressed in the brain (Chen et al., 2015; Kerver and Wade, 2015) and modulates many brain functions, such as motor, energy homeostasis, and reproductive behavior (Charlier et al., 2005; Yang et al., 2019) through the effect on cerebellar Purkinje cells (Eijun et al., 2003), hypothalamic neurons (Yang et al., 2019; Heck et al., 2020), and so on. Furthermore, a recent study has shown that SRC-1 is highly expressed in the hippocampus, and hippocampal SRC-1 knockdown mediated by the lentivirus could cause decreased synaptic protein expression and memory impairment (Bian et al., 2018; Chen et al., 2020). On the other hand, the ER regulates the synaptic protein expression, such as PSD95 and Synapsin, and the cognitive function through the SRC-1-dependent pathway (Liu et al., 2015; Zhao et al., 2017, 2018). This evidence suggests that SRC-1 is implicated in the cognitive function under the physiological condition and might even play a role in brain disorders with defects of cognition.

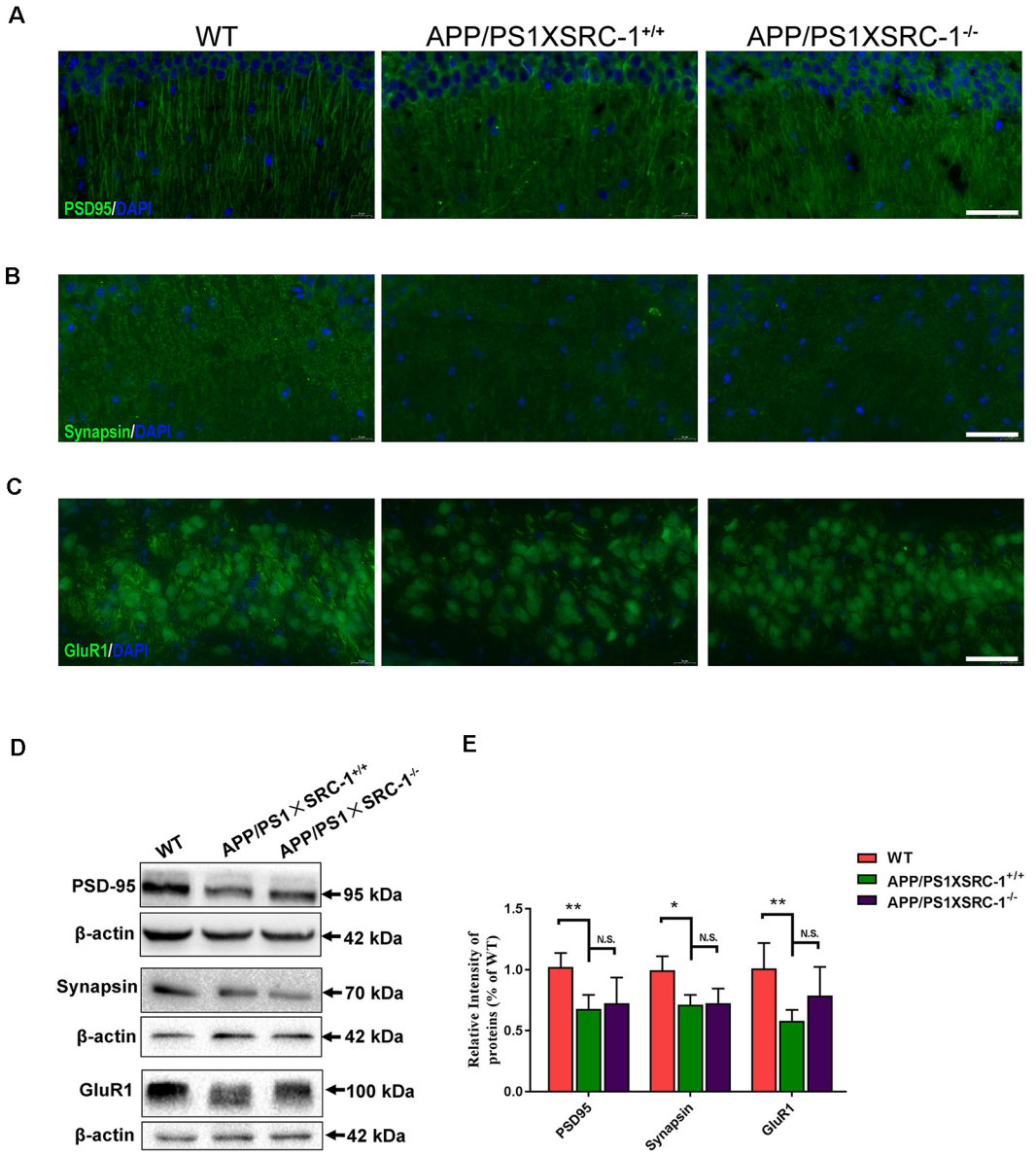

FIGURE 2 | Expression of PSD95, Synapsin and GluR1 in the hippocampus of APP/PS1×SRC-$1^{-/-}$ mice. **(A–C)** The coronal sections of the hippocampus were stained for PSD95 **(A)**, Synapsin **(B)**, GluR1 **(C)**, and 4',6-diamidino-2-phenylindole (DAPI) in APP/PS1×SRC-$1^{-/-}$, APP/PS1×SRC-$1^{+/+}$ control and wildtype (WT) mice (8–9 months age). Scale bars: 50 μm. **(D,E)** Representative immunoblots and densitometry analysis of PSD95, Synapsin and GluR1 expressions in each group. Data are presented as the mean ± SEM of six mice in each group. *$p < 0.05$, **$p < 0.01$ and N.S., no significance.

AD is a neurodegenerative disease and its major symptom is impaired cognitive function. It is of interest to see whether the SRC-1 protein level correlates with AD. In the present study, we first examined the SRC-1 protein level in the hippocampus and cortex of APP/PS1 mice, and the result showed no difference in SRC-1 expression between AD mice and the WT littermates. This result indicates that the transgene of APP/PS1 and the consequent pathology, have no effect on SRC-1 expression. Furthermore, we investigated whether SRC-1 knockout affected the expression of the synaptic protein in AD mice. Our results demonstrated that SRC-1 deficiency (APP/PS1×SRC-$1^{-/-}$) had no effect on the expression of PSD95, Synapsin, and the GluR1 protein in AD. Consistently, the level of the three synaptic proteins in the SRC-1 KO mice was comparable to those in the WT mice.

However, a previous study has reported that SRC-1 knockdown in the hippocampus of mice during adulthood leads to the decreased expression of PSD95 and other synaptic proteins for weeks (Bian et al., 2018; Chen et al., 2020). The discrepancies between their studies and ours might be explained by the different gene manipulations of SRC-1. SRC-1 knockout is the complete deletion of SRC-1 from the embryo period, so

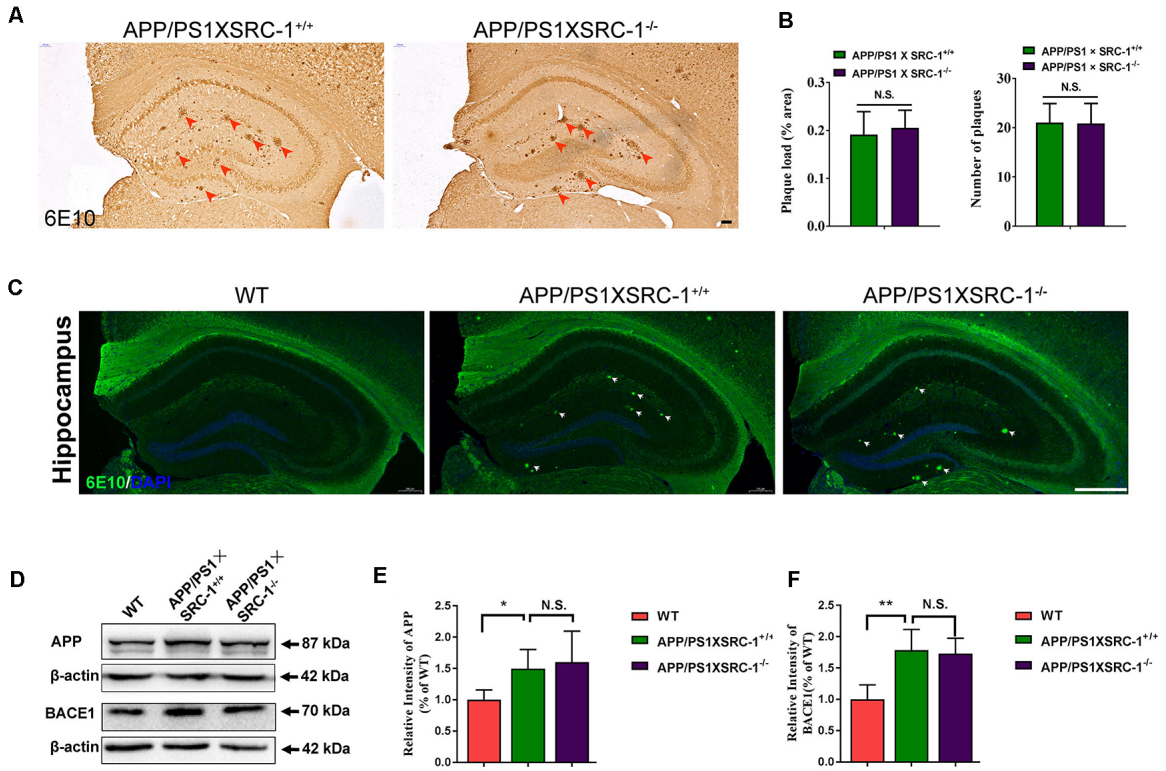

FIGURE 3 | The Aβ plaque in the hippocampus of APP/PS1×SRC-1$^{-/-}$ mice. **(A,C)** The coronal sections of the hippocampus in APP/PS1 with (APP/PS1×SRC-1$^{+/+}$) or without SRC-1 APP/PS1×SRC-1$^{-/-}$), mice of 8–9 months age were stained for Aβ (6E10). Scale bars: 100 μm. **(B)** The mean Aβ plaque load (% area) and number were quantified. **(D–F)** Representative immune-blot and densitometry analysis of APP and BACE-1 expression in the APP/PS1×SRC-1$^{-/-}$, APP/PS1×SRC-1$^{+/+}$ control and WT. Data are presented as the mean ± SEM of six mice in each group. *$p < 0.05$, **$p < 0.01$ and N.S., no significance.

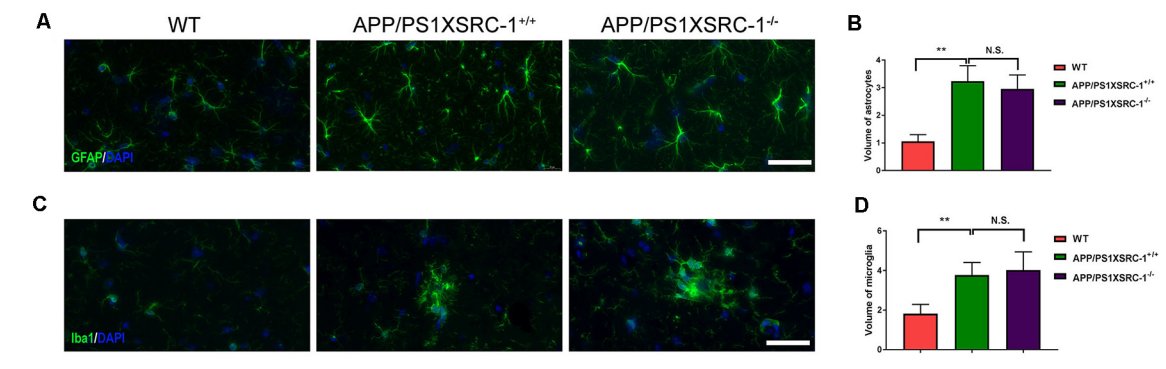

FIGURE 4 | The activation of microglia and astrocyte in the hippocampus of APP/PS1×SRC-1$^{-/-}$ mice. **(A,C)** The coronal sections of the hippocampus in each group were stained for GFAP **(A)**, Iba-1 **(C)** and DAPI. Scale bars: 50 μm. **(B,D)** The volume of astrocyte **(B)** and microglia **(D)** in APP/PS1×SRC-1$^{-/-}$ mice, respectively. Data are presented as the mean ± SEM of six mice in each group. **$p < 0.01$ and N.S., no significance.

its function might be compensated by other coactivators, such as SRC-2 or SRC-3. Another study has actually revealed that knockout of both SRC-1 and SRC-3 during the embryo stage would cause a cardiomyopathy phenotype, however, the heart morphology and tissue structures in mice with either SRC-1 or SRC-3 knockout were very similar to those of WT mice (Chen et al., 2015). Similarly, the same reason might be used to explain that SRC-1 knockdown in adulthood caused the memory loss (Bian et al., 2018) but the SRC-1 knockout did not (Eijun et al., 2003).

The Aβ plaque is the major pathological feature in AD (Masters and Beyreuther, 2006). A decrease of synaptic protein expression in the APP/PS1 mice is probably the result of the overproduction of Aβ (Evin and Weidemann, 2002). Aβ peptides are generated from APP sequentially cleaving by β- and then γ-secretase (Maia and Sousa, 2019; Zhang et al., 2020). In our study, SRC-1 deletion has not affected the Aβ plaque in the APP/PS1 mice, in neither the number nor the area of the plaque load. We also demonstrated that APP/PS1×SRC-$1^{-/-}$ mice showed no change of the expression of the APP and BACE-1 protein. Futhermore, SRC-$1^{-/-}$ mice also exhibited the non-changed expression of APP or BACE-1, similar to that in the AD model. As the source of Aβ, APP and BACE-1 expression was not affected by SRC-1 deletion, which would sustain the result of the invariable Aβ plaque in APP/PS1×SRC-$1^{-/-}$ mice, at least to some extent. Aβ deposition is often accompanied by activation of microglia and astrocytes, an important event in AD brain, which produces proinflammatory cytokines and chemokines causing neuronal dysfunction and further neurodegeneration (Galea et al., 2015). Here, the cell number of astrocytes and microglia increased in the hippocampus of APP/PS1 mice compared to the WT, consistent with previous reports (Lu et al., 2019); but in the APP/PS1×SRC-$1^{-/-}$ group, no clear changes of astrocytes and microglia were observed compared to the APP/PS1×SRC-$1^{+/+}$ group.

Altogether, our results suggest that the SRC-1 knockout would neither change the synaptic protein expression, nor affect the Aβ plaque or activation of astrocytes and microglia in APP/PS1 mice. But this outcome could not completely eliminate the possible role of SRC-1 in AD. First, as we have discussed, SRC-1 knockout and knockdown shows different consequences. SRC-1 knockdown during the adulthood of APP/PS1 mice might possibly exhibit quite different results from this present study. Second, our experiments only detected the effect of SRC-1 deletion, but not the effects of SRC-1 over-expression or activation. Wang et al. (2015) has reported that MCB613 could be a potent small molecule "stimulator" for SRC-1, which could be used to enhance the activity of SRC-1 in APP/PS1 mice for further investigation of the role of SRC-1. Finally, we could not completely exclude the possible connection between SRC-1 and tau hyperphosphorylation, and more experiments are required to further address this question. In summary, our study confirms that SRC-1 knockout has no effect on some of the pathologic features of APP/PS1 mice.

DATA AVAILABILITY STATEMENT

The datasets generated for this study are available on request to the corresponding author.

ETHICS STATEMENT

The animal study including all experimental and animal protocols were reviewed and approved by the animal studies committees of Dalian Medical University (ethics committee approval permit no. L2013011).

AUTHOR CONTRIBUTIONS

SL, Y-HY and J-YY contributed to the conception and design of the project. QW, XZ, NL and MN contributed to the conduct of the experiments and analysis of data. BW wrote the manuscript. Q-FL, D-DZ and RJ contributed to the conduct of the experiments and analysis of data during the revision. QW and X-FW helped with the manuscript revision and proofreading. All authors contributed to the article and approved the submitted version.

FUNDING

This work was supported by grants from the Liaoning Provincial Key R&D Program (2019020048-JH2/103), the Liaoning Revitalization Talents Program (XLYC1902044, XLYC1808031), the Liaoning Provincial Doctoral Research Fund (2019-BS-064), the Natural Science Foundation of Liaoning Province of China (L201602218) and the National Natural Science Foundation of China (U1908208).

SUPPLEMENTARY MATERIAL

The Supplementary Material for this article can be found online at: https://www.frontiersin.org/articles/10.3389/fnagi.2020.00145/full#supplementary-material.

REFERENCES

Bayele, H. K. (2019). A conserved mechanism of sirtu in signalling through steroid hormone receptors. *Biosci. Rep.* 39:BSR20193535. doi: 10.1042/bsr20193535

Bian, C., Huang, Y., Zhu, H., Zhao, Y., Zhao, J., and Zhang, J. (2018). Steroid receptor coactivator-1 knockdown decreases synaptic plasticity and impairs spatial memory in the hippocampus of mice. *Neuroscience* 377, 114–125. doi: 10.1016/j.neuroscience.2018.02.034

Bian, C., Zhu, K., Yang, L., Lin, S., Li, S., Su, B., et al. (2012). Gonadectomy differentially regulates steroid receptor coactivator-1 and synaptic proteins in the hippocampus of adult female and male C57BL/6 mice. *Synapse* 66, 849–857. doi: 10.1002/syn.21574

Charlier, T. D., Ball, G. F., and Balthazart, J. (2005). Inhibition of steroid receptor coactivator-1 blocks estrogen and androgen action on male sex behavior and associated brain plasticity. *J. Neurosci.* 25, 906–913. doi: 10.1523/JNEUROSCI.3533-04.2005

Charlier, T. D., Seredynski, A. L., Niessen, N.-A., and Balthazart, J. (2013). Modulation of testosterone-dependent male sexual behavior and the associated neuroplasticity. *Gen. Comp. Endocrinol.* 190, 24–33. doi: 10.1016/j.ygcen.2013.03.003

Chen, X., Qin, L., Liu, Z., Liao, L., Martin, J. F., and Xu, J. (2015). Knockout of SRC-1 and SRC-3 in mice decreases cardiomyocyte proliferation and causes a noncompaction cardiomyopathy phenotype. *Int. J. Biol. Sci.* 11, 1056–1072. doi: 10.7150/ijbs.12408

Chen, X., Tian, Y., Zhu, H., Bian, C., and Li, M. (2020). Inhibition of steroid receptor coactivator-1 in the hippocampus impairs the consolidation and reconsolidation of contextual fear memory in mice. *Life Sci.* 245:117386. doi: 10.1016/j.lfs.2020.117386

Eijun, N., Yoshida-Komiya, H., Chan, C.-S., Liao, L., Davis, R. L., O'Malley, B. W., et al. (2003). SRC-1 null mice exhibit moderate motor dysfunction and delayed development of cerebellar purkinje cells. *J. Neurosci.* 23, 213–222. doi: 10.1523/JNEUROSCI.23-01-00213.2003

Evin, G., and Weidemann, A. (2002). Biogenesis and metabolism of Alzheimer's disease aβ amyloid peptides. *Peptides* 23, 1285–1297. doi: 10.1016/s0196-9781(02)00063-3

Fernandez, C. G., Hamby, M. E., McReynolds, M. L., and Ray, W. J. (2019). The role of APOE4 in disrupting the homeostatic functions of astrocytes and microglia in aging and Alzheimer's disease. *Front. Aging Neurosci.* 10:14. doi: 10.3389/fnagi.2019.00014

Galea, E., Morrison, W., Hudry, E., Arbel-Ornath, M., Bacskai, B. J., Gomez-Isla, T., et al. (2015). Topological analyses in APP/PS1 mice reveal that astrocytes do not migrate to amyloid-β plaques. *Proc. Natl. Acad. Sci. U S A* 112, 15556–15561. doi: 10.1073/pnas.1516779112

Garcia-Alloza, M., Robbins, E. M., Zhang-Nunes, S. X., Purcell, S. M., Betensky, R. A., Raju, S., et al. (2006). Characterization of amyloid deposition in the APPswe/PS1dE9 mouse model of Alzheimer disease. *Neurobiol. Dis.* 24, 516–524. doi: 10.1016/j.nbd.2006.08.017

Hasanpour, M., Nourazarian, A., Geranmayeh, M. H., Nikanfar, M., Khaki-Khatibi, F., and Rahbarghazi, R. (2018). The dynamics of neurosteroids and sex-related hormones in the pathogenesis of Alzheimer's disease. *Neuromolecular Med.* 20, 215–224. doi: 10.1007/s12017-018-8493-y

Heck, A. L., Thompson, M. K., Uht, R. M., and Handa, R. J. (2020). Sex-dependent mechanisms of glucocorticoid regulation of the mouse hypothalamic corticotropin-releasing hormone gene. *Endocrinology* 161:bqz012. doi: 10.1210/endocr/bqz012

Kerver, H. N., and Wade, J. (2015). Hormonal regulation of steroid receptor coactivator-1 mRNA in the male and female green anole brain. *J. Neuroendocrinol.* 27, 223–233. doi: 10.1111/jne.12249

Li, Q., Wu, X., Na, X., Ge, B., Wu, Q., Guo, X., et al. (2019). Impaired cognitive function and altered hippocampal synaptic plasticity in mice lacking dermatan sulfotransferase Chst14/D4st1. *Front. Mol. Neurosci.* 12:26. doi: 10.3389/fnmol.2019.00026

Liu, M., Huang, X., Zhao, Y., Zhang, D., and Zhang, J. (2015). Steroid receptor coactivator-1 mediates letrozole induced downregulation of postsynaptic protein PSD-95 in the hippocampus of adult female rats. *J. Steroid. Biochem. Mol. Biol.* 154, 168–175. doi: 10.1016/j.jsbmb.2015.07.011

Lu, Y., Tan, L., and Wang, X. (2019). Circular HDAC9/microRNA-138/Sirtuin-1 pathway mediates synaptic and amyloid precursor protein processing deficits in Alzheimer's disease. *Neurosci. Bull.* 35, 877–888. doi: 10.1007/s12264-019-00361-0

Masters, C. L., and Beyreuther, K. (2006). Alzheimer's centennial legacy: prospects for rational therapeutic intervention targeting the Aβ amyloid pathway. *Brain* 129, 2823–2839. doi: 10.1093/brain/awl251

Maia, M. A., and Sousa, E. (2019). BACE-1 and γ-secretase as therapeutic targets for Alzheimer's disease. *Pharmaceuticals* 12:41. doi: 10.3390/ph12010041

McEwen, B. S., and Milner, T. A. (2017). Understanding the broad influence of sex hormones and sex differences in the brain. *J. Neurosci. Res.* 95, 24–39. doi: 10.1002/jnr.23809

Meng, Y., Wang, R., Yang, F., Ji, Z.-J., Fang, L., and Sheng, S.-L. (2010). Amyloid precursor protein 17-mer peptide ameliorates hippocampal neurodegeneration in ovariectomized rats. *Neurosci. Lett.* 468, 173–177. doi: 10.1016/j.neulet.2009.07.058

Qiu, L., Zhao, Y., Guo, Q., Zhang, Y., He, L., Li, W., et al. (2016). Dose-dependent regulation of steroid receptor coactivator-1 and steroid receptors by testosterone propionate in the hippocampus of adult male mice. *J. Steroid. Biochem. Mol. Biol.* 156, 23–31. doi: 10.1016/j.jsbmb.2015.11.012

Ross, J. L., Kushner, H., Kowal, K., Bardsley, M., Davis, S., Reiss, A. L., et al. (2017). Androgen treatment effects on motor function, cognition, and behavior in boys with klinefelter syndrome. *J. Pediatr.* 185, 193.e4–199.e4. doi: 10.1016/j.jpeds.2017.02.036

Tang, Y., Min, Z., Xiang, X. J., Liu, L., Ma, Y. L., Zhu, B. L., et al. (2018). Estrogen-related receptor α is involved in Alzheimer's disease-like pathology. *Exp. Neurol.* 305, 89–96. doi: 10.1016/j.expneurol.2018.04.003

Villemagne, V. L., Burnham, S., Bourgeat, P., Brown, B., Ellis, K. A., Salvado, O., et al. (2013). Amyloid β deposition, neurodegeneration, and cognitive decline in sporadic Alzheimer's disease: a prospective cohort study. *Lancet Neurol.* 12, 357–367. doi: 10.1016/S1474-4422(13)70044-9

Wang, B., Wu, Q., Lei, L., Sun, H., Michael, N., Zhang, X., et al. (2018). Long-term social isolation inhibits autophagy activation, induces postsynaptic dysfunctions and impairs spatial memory. *Exp. Neurol.* 311, 213–224. doi: 10.1016/j.expneurol.2018.09.009

Wang, L., Yu, Y., Chow, D. C., Yan, F., Hsu, C. C., Stossi, F., et al. (2015). Characterization of a steroid receptor coactivator small molecule stimulator that overstimulates cancer cells and leads to cell stress and death. *Cancer Cell.* 28, 240–252. doi: 10.1016/j.ccell.2015.07.005

Wattmo, C., and Wallin, A. K. (2017). Early- versus late-onset Alzheimer's disease in clinical practice: cognitive and global outcomes over 3 years. *Alzheimers Res. Ther.* 9:70. doi: 10.1186/s13195-017-0294-2

Yang, Y., van der Klaauw, A. A., Zhu, L., Cacciottolo, T. M., He, Y., Stadler, L. K. J., et al. (2019). Steroid receptor coactivator-1 modulates the function of pomc neurons and energy homeostasis. *Nat. Commun.* 10:1718. doi: 10.1038/s41467-019-08737-6

Zalachoras, I., Verhoeve, S. L., Toonen, L. J., van Weert, L. T., van Vlodrop, A. M., Mol, I. M., et al. (2016). Isoform switching of steroid receptor co-activator-1 attenuates glucocorticoid-induced anxiogenic amygdala CRH expression. *Mol. Psychiatry* 21, 1733–1739. doi: 10.1038/mp.2016.16

Zhang, D., Guo, Q., Bian, C., Zhang, J., Lin, S., and Su, B. (2011). Alterations of steroid receptor coactivator-1 (SRC-1) immunoreactivities in specific brain regions of young and middle-aged female Sprague–Dawley rats. *Brain Res.* 1382, 88–97. doi: 10.1016/j.brainres.2011.01.024

Zhang, X., Zhao, F., Wang, C., Zhang, J., Bai, Y., Zhou, F., et al. (2020). AVP(4–8) improves cognitive behaviors and hippocampal synaptic plasticity in the APP/PS1 mouse model of Alzheimer's disease. *Neurosci. Bull.* 36, 254–262. doi: 10.1007/s12264-019-00434-0

Zhao, J., Bian, C., Liu, M., Zhao, Y., Sun, T., Xing, F., et al. (2018). Orchiectomy and letrozole differentially regulate synaptic plasticity and spatial memory in a manner that is mediated by SRC-1 in the hippocampus of male mice. *J. Steroid. Biochem. Mol. Biol.* 178, 354–368. doi: 10.1016/j.jsbmb.2018.02.007

Zhao, Y., He, L., Zhang, Y., Zhao, J., Liu, Z., Xing, F. Z., et al. (2017). Estrogen receptor α and β regulate actin polymerization and spatial memory through an SRC-1/mTORC2-dependent pathway in the hippocampus of female mice. *J. Steroid. Biochem. Mol. Biol.* 174, 96–113. doi: 10.1016/j.jsbmb.2017.08.003

Zhao, L., Woody, S. K., and Chhibber, A. (2015). Estrogen receptor β in Alzheimer's disease: from mechanisms to therapeutics. *Ageing Res. Rev.* 24, 178–190. doi: 10.1016/j.arr.2015.08.001

Zheng, H., Cheng, B., Li, Y., Li, X., Chen, X., and Zhang, Y. W. (2018). TREM2 in Alzheimer's disease: microglial survival and energy metabolism. *Front. Aging Neurosci.* 10:395. doi: 10.3389/fnagi.2018.00395

Conflict of Interest: The authors declare that the research was conducted in the absence of any commercial or financial relationships that could be construed as a potential conflict of interest.

frontiers in Aging Neuroscience

ORIGINAL RESEARCH
published: 24 June 2020
doi: 10.3389/fnagi.2020.00144

Calcium-Sensing Receptor Mediates β-Amyloid-Induced Synaptic Formation Impairment and Cognitive Deficits *via* Regulation of Cytosolic Phospholipase A2/Prostaglandin E2 Metabolic Pathway

Chenxi Feng[1,2], Xiaoming Bao[3,4], Ling Shan[5], Yunxiang Ling[1], Yanfei Ding[1], Jia Wang[1], Yanzi Cao[1], Qinwen Wang[1], Wei Cui[1] and Shujun Xu[1]**

[1]School of Medicine, Ningbo University, Zhejiang Provincial Key Laboratory of Pathophysiology, Ningbo, China, [2]Children's Hospital of Soochow University, Suzhou, China, [3]HwaMei Hospital, University of Chinese Academy of Sciences, Ningbo, China, [4]Ningbo Institute of Life and Health Industry, University of Chinese Academy of Sciences, Ningbo, China, [5]Netherlands Institute for Neuroscience, Royal Netherlands Academy of Arts and Sciences, Amsterdam, Netherlands

OPEN ACCESS

Edited by:
Jiehui Jiang,
Shanghai University, China

Reviewed by:
Daniela Puzzo,
University of Catania, Italy
Miroslav Nenov,
Temple University, United States

***Correspondence:**
Xiaoming Bao
18668271580@163.com
Shujun Xu
xushujun@nbu.edu.cn

Received: *16 January 2020*
Accepted: *29 April 2020*
Published: *24 June 2020*

Citation:
Feng C, Bao X, Shan L, Ling Y, Ding Y, Wang J, Cao Y, Wang Q, Cui W and Xu S (2020) Calcium-Sensing Receptor Mediates β-Amyloid-Induced Synaptic Formation Impairment and Cognitive Deficits via Regulation of Cytosolic Phospholipase A2/Prostaglandin E2 Metabolic Pathway. Front. Aging Neurosci. 12:144. doi: 10.3389/fnagi.2020.00144

Calcium-sensing receptor (CaSR) is a G protein-coupled receptor (GPCRs). Soluble β-amyloid peptide (Aβ) is one of the orthosteric modulators of CaSR, while, the role and underlying mechanism of CaSR in cognitive decline in Alzheimer's disease (AD) is unclear. In this study, molecular technology such as live-cell imaging combined with behavioral tests were used to explore the role and the underlying mechanism of CaSR in the cognitive deficits in AD mice. The expression levels of CaSR were increased both in AD mice and $A\beta_{1-42}$ (β-amyloid protein)-treated primary cultured neurons. Pharmacological inhibition of CaSR ameliorated recognitive and spatial memory deficits of $A\beta_{1-42}$-oligomer-treated mice in a dose-dependent manner. Pharmacological inhibition of CaSR or down-regulation of the expression of CaSR by CaSR-shRNA-lentivirus prevented the impairment of filopodia, and the synapse induced by oligomeric $A\beta_{1-42}$. The contents of cytosolic phospholipase A2 (cPLA2) and prostaglandin E2 (PGE2) in hippocampal neurons and tissue were increased after treatment with $A\beta_{1-42}$ oligomers. Inhibition or down-regulation of CaSR mediates Aβ-induced synapse formation and cognitive deficits partially, through the activation of the cPLA2/PGE2 pathway. This study provides novel insights on CaSR, which is a promising therapeutic target for AD.

Keywords: Alzheimer's disease (AD), β-amyloid peptide (Aβ), calcium-sensing receptor (CaSR), synapse formation, cytosolic phospholipase A2, prostaglandin E2

Abbreviations: AA, arachidonic acid; Aβ, β-amyloid protein; ANOVA, analysis of variance; AD, Alzheimer's disease; CaSR, calcium-sensing receptor; cPLA2, cytosolic phospholipase A2; DIV, day *in vitro*; F-GFP, farnesylated enhanced green fluorescent protein; GPCRs, G protein-coupled receptor; HFIP, 1,1,1,3,3,3-hexafluoro-2-propanol; LTP, long-term potentiation; MWM, morris water maze; NOR, novel object recognition; PBS, phosphate-buffered saline; PGE2, prostaglandin E2; PNT, place navigation test; PT, probe trial test; PSD 95, anti-postsynaptic density 95 antibody.

INTRODUCTION

Alzheimer's disease (AD) is one of the most common neurodegenerative diseases with a slow and gradual deterioration of the memory that affects language, personality, and cognitive control (Wyss-Coray and Rogers, 2012; Mhatre et al., 2014; Dos Santos Picanco et al., 2018). AD is a severe threat for human health, along with an aging population, however, the pathogenesis of it is still unclear. Mounting evidence shows that the accumulation of β-amyloid peptide (Aβ) is an important contributing factor in the pathology of AD (Baek et al., 2017; Choi et al., 2017). Aβ has different aggregated forms, including monomers, oligomers, protofibrils, and mature fibrils (Ahmed et al., 2010). It is well demonstrated that soluble oligomers of Aβ is the pertinent toxic form of Aβ (Wang H. C. et al., 2016; Wang T. et al., 2016). Both others, and our previous studies have shown that soluble Aβ oligomers could decrease the number of dendritic spines and inhibit the long-term potentiation (LTP), leading to the decline of cognitive function in AD mice (Price et al., 2014; Jiang et al., 2016). Disrupting synapse function plays an important role in the memory deficits of AD, which stands out in early AD pathological changes (Price et al., 2014; Teich et al., 2015; Wang X. et al., 2018). Therefore, it is a promising strategy to consider amelioration of synaptic impairment induced by Aβ oligomers as the target of prevention or treatment of AD.

Aβ is also one of the allosteric agonists of calcium-sensing receptor (CaSR). Aβ has been shown to interact directly with CaSR *via* a proximity ligation assay (Diez-Fraile et al., 2013; Leach et al., 2015). CaSR, a member of the G protein-coupled receptor (GPCRs) C family, is a seven-transmembrane protein (Brauner-Osborne et al., 2007; Conigrave and Ward, 2013; Summers, 2016). CaSR has been detected in the hippocampus which is an important brain structure that is essential for spatial memory, language learning, and episodic memory (Ferry et al., 2000). CaSR is mainly localized in nerve endings in the neurons and is involved in regulating brain excitability (Chen et al., 2010). CaSR activation depends on the persistent interaction with its agonists. At physiological conditions, CaSR is partially activated (Ruat and Traiffort, 2013; Díaz-Soto et al., 2016). In cultured cells, Aβ-activated CaSR could cause excessive release of Aβ (Armato et al., 2013; Dal Prà et al., 2014). The expression of CaSR was significantly increased in AD transgenic mice (Leach et al., 2015; Gardenal et al., 2017). The role of CaSR in AD is unclear and the cellular mechanisms have not been well characterized. As a promising therapeutic target, we therefore evaluated the role of CaSR in cognitive deficits in the mouse model of AD and its underlying cellular mechanisms. The effects of CaSR on oligomeric Aβ-induced synaptic injury are unknown. In the current study, we have also evaluated the role and the underlying mechanisms of CaSR in Aβ-mediated synaptic impairment.

MATERIALS AND METHODS

$A\beta_{1-42}$ Oligomers Preparation

Preparation of soluble $A\beta_{1-42}$ oligomers was done according to the protocol previously described (Jiang et al., 2016; Ding et al., 2019). One milligram of $A\beta_{1-42}$ (Bachem, Cat# H-1368.1000) powder was dissolved in 400 μl ice-cold 1,1,1,3,3,3-hexafluoro-2-propanol (HFIP; Aladdin, Cat# K1625063), and incubated at room temperature for 20 min. Hundred microliter of this complete solution was diluted into 900 μl of deionized water to a final concentration of 0.25 g/l. After centrifugation at 14,000 *g* for 15 min, the supernatant was collected and the HFIP was completely evaporated. Then the collected supernatant was kept stirring for 48 h at room temperature. A 50 μM $A\beta_{1-42}$ solution was obtained and stored at 4°C. The preparation is the combination of low molecular weight forms of soluble Aβ (Chunhui et al., 2018).

Animals

ICR mice (RRID:IMSR_CRL:22) or B6C3-Tg (APPswe/PSEN1dE9) mice were used in our experiments. Breeding pairs of APPswe/PSEN1dE9 transgenic mice were originally purchased from Jackson Laboratories, USA. A breeding colony of APPswe/PSEN1dE9 mice was established at the Medical School of Ningbo University. All experimental animals were housed in a temperature and humidity-controlled animal facility (22 ± 3°C, 60% ± 5%) with a 12 h light and dark cycle and free access to standard chow and water. Experiments were carried out in accordance with the National Institute of Health Guide for the Care and Use of Laboratory Animals (NIH Publications No. 80-23, revised 1996) and approved by the Institutional Animal Care and Use Committee of the Ningbo University. The approval number for the animal experiments is SYXK (ZHE) 2013-0191. Genotypes of APPswe/PSEN1dE9 mice were analyzed as follows: DNA was isolated from the tail tip of each mouse and PCR was performed using the following primer pairs: APP, forward primer 5′-GACTGCCACTCGACCAGGTTCTG-3′, reverse primer 5′-CTTGTAAGTTGGATTCTCATATCCG-3′; PS1, forward primer 5′-GTGGATAACCCCTCCCCCAGCCTAGACC-3′, reverse primer 5′-AATAGAGAACGGCAGGAGCA-3′. APPswe/PSEN1dE9 transgenic mice and wild type mice were identified by agarose gel electrophoresis. In each identification experiment, both positive and negative controls were designed.

Animal Surgery

Two-month-old healthy male ICR mice (25–30 g) were pseudo-randomly assigned to the experimental groups using a random number generated from Excel, and all mice were marked by staining in different parts of the back. A pre-test open field experiment was first performed on all mice to determine the locomotor activity before the formal experiments and to exclude those with an obvious movement disorder. No obvious movement disorder was found among the mice. Thus, no mice were excluded. ICR mice were anesthetized by intraperitoneal administration of sodium pentobarbital (50 mg/kg) before they were placed in a stereotaxic apparatus (Stoelting, Wood Dale, IL, USA). Cannulas (RWD Life Science, Shenzhen, China) were surgically implanted into bilateral hippocampal regions of the mice using the following coordinates: AP −1.7 mm from Bregma; ML ± 1.0 mm from the midline; DV −1.5 mm from pia

mater. After 7 days of post-operative recovery, the minipump needle tips were inserted into the ventricle through cannulas to inject pharmaceuticals. Experimental mice were given three consecutive infusions of $A\beta_{1-42}$ (4 μmol/kg) and/or NPS 2143 (Sigma, Cat# SML0360, 0.08 or 0.16 μmol/kg), while the control mice received saline injections instead of the drugs.

Behavior Tests

The novel object recognition (NOR) task, consisting of a familiarization phase and a test phase, was carried out in an open-field arena (60 × 60 × 15 cm) on the 11th to 12th day after the first injection. On the first day, they were familiarized with two identical objects for 5 min. On the second day, one of the objects was replaced by a novel one with a different shape and color, and the mice were allowed to explore the arena for 5 min. To ensure the absence of olfactory cues, the open-field arena and the objects were cleaned thoroughly. Exploration was defined as sniffing or touching the objects. The distance between the nose and object was no more than 2 cm. If the mice traveled around or sat on the objects, this was not defined as object recognition. The discrimination index, the ratio of the amount of time spent exploring any one of the two objects (training session) or the novel object (retention session), over the total time spent exploring both objects, was used to measure the cognitive function of animals.

A Morris water maze (MWM) was performed as described (Jiang et al., 2016). Briefly, the equipment included a pool with a diameter of 110 cm that was filled with opaque water at approximately 22 ± 1°C. Spatial memory was assessed by recording the latency time for the animal to escape from the water onto an escape platform during the place navigation phase. At the learning phase, mice were given 90 s to find the hidden platform that was 1 cm below the water surface. The place navigation test of the MWM, which consisted of four trials (interval 20–30 min) each day, took place during the 14th day to the 17th day and the latency time was recorded. On the 18th day, the platform was removed from the maze. A probe trial was conducted to measure the trajectories and entries of mice to the target quadrant with a video tracking system (Ethovision XT). The assessor was blinded to the experimental conditions for analysis of the behavioral tests.

Primary Hippocampal Neuronal Cultures

Neurons were derived from the dissociating hippocampus of newborn ICR mice (RRID:IMSR_CRL:22). To achieve dissociated and single cells, the tissue was cut into tiny pieces, and the cells within released by a mild treatment with 0.125% (v/v) trypsin (Gibco, Cat# 11668–019) for 15 min at 37°C. Isolated neurons were then planted on coverslips (Fisherbrand, Cat# 12–545–83), pre-coated with poly-D-lysine (Sigma, Cat# P0899–10MG) in Dulbecco's modified Eagle media (Gibco, Cat# 11995065) containing 10% (v/v) FBS (Gibco, Cat# 10099141), 10% (v/v) F-12 (Gibco, Cat# 11765054), and 1% (v/v) of penicillin-streptomycin solution (Solarbio, Cat# P1400). After the cells were incubated at 37°C, 5% (v/v) CO_2 for 24 h, the medium was changed to Neurobasal medium supplemented with 2% (v/v) B27 (Gibco, Cat# 17504044) and 1% (v/v) L-glutamine (Gibco, Cat# 25030–081). The medium was half-replaced every 3 days. At the 5th day *in vitro* (DIV 5), cytosine arabinofuranoside (Sigma, Cat# 147–94–4) was added at a final concentration of 2 μM to decrease glial cell growth. The neurons were transfected with farnesylated enhanced green fluorescent protein (F-GFP) and GFP-actin using Lipofectamine 2000 (Invitrogen, Cat# 11668–019). At DIV 7 or DIV 14 of culture, NPS 2143 was added to cultures of hippocampal neurons at a final concentration of 0.1 μM for 2 h. After the treatment of NPS 2143, neurons were incubated with $A\beta_{1-42}$ (final concentration 0.5 μM) for 3 h. For the effect of $A\beta_{1-42}$ on the expression of CaSR, primary hippocampal neurons (DIV 7) were incubated with $A\beta_{1-42}$ for 36 h.

Immunohistochemistry and Immunocytochemistry

Mice were decapitated and their brains were removed after perfusion. After fixation with 4% paraformaldehyde (Solarbio, Cat# P1110), dehydration with 30% sucrose solution and after being embedded with an optimum cutting temperature compound (Solarbio, Cat# 4583), the brains were cut into 30 μm frozen brain slices. Cultured cells were also fixed with 4% paraformaldehyde at room temperature. After being washed with phosphate-buffered saline (PBS) three times, the brain slices or cultured cells were blocked with sheep serum at room temperature for 1 h, to saturate unspecific binding sites, and then permeabilized in PBS containing 0.01% (V/V) triton (Solarbio, Cat# T8200). The sections or coverslips were incubated overnight (4°C) with anti-postsynaptic density 95 antibody (PSD 95, 1:200, Abcam, Cat# ab2723), anti-synaptotagmin-1 antibody (1:200, Millipore, Cat# AB5600–50UL), anti-MAP2 antibody (1:200, CST, Cat# 8707), anti-CaSR antibody (1:200, Santa Cruz Biotechnology, Cat# sc-47741), or DAPI (1:5000, Beyotime, Cat# C1002). After thorough washing, sections or coverslips were incubated with Alexa-488 anti-mouse secondary antibodies (1:1,000, Invitrogen, Cat# A-10680) or Cyanine 5 anti-mouse secondary antibody (1:1,000, Invitrogen, Cat# A10524) and Alexa-546 anti-rabbit secondary antibodies (1:1,000, Invitrogen, Cat# A11010) for 1 h at room temperature. Images of distal neuronal dendrites were captured by a confocal microscope (Olympus, Tokyo, Japan).

Lentivirus Construction

The Lentivirus was purchased from Shanghai Genechem Company, Limited (China). The company used the following procedures: The coding sequence of the CaSR was from GenBank: NM_013803.3. For small hairpin RNA (shRNA) against mouse CaSR, vectors were constructed from the original plasmid GV lentiviral vector, and the GV118 serotype was selected; the reaction element sequence of which is U6-MCS-Ubi-EGFP. The target gene was inserted into the MCS element by HpaI and XhoI, two restriction endonucleases. The optimal target sequence (TCTTCATCAAGTTCCGAAA) was selected for small hairpin RNA (shRNA) against mouse CaSR, and a scrambled shRNA (TTCTCCGAACGTGTCACGT) served as a control. For viral packaging, the respective recombinant plasmids were cotransfected into 293T cells (ATCC, RRID:CVCL_0063). The GV stocks were titered by quantitative PCR, stored at −80°C

of a titer of 10^9 particles/ml and shipped with 20 μl in every tube. We then used a total of $5*10^5$ TU/ml of the virus to transfect the hippocampal neurons. All procedures were performed under a biosafety cabinet in a biosafety level 2 facility.

Confocal Imaging and Analysis

At DIV 7 or DIV 14 of culture, living neurons were captured by a Fluoview-1000 confocal microscope. After drug treatments, the neurons were maintained in a recording chamber with extracellular solution (148.00 mM NaCl, 3.00 mM KCl, 3.00 mM $CaCl_2$, 10.00 mM HEPES, and 8.00 mM glucose, pH 7.3) at room temperature. Digital images of GFP were collected on a Fluoview-1000 confocal microscope (Olympus) using a 60× oil objective lens without optical zoom at an excitation wavelength of 488 nm. They were analyzed using Fluoview-1000 software. All lengths of the secondary dendritic branches were measured by tracing their extension, and the filopodia and spines were counted. For all analyses, images were analyzed blind to treatments and data were collected from at least three independent experiments.

Cytosolic Phospholipase A2 (cPLA2) and Prostaglandin E2 (PGE2) Assay

Cytosolic phospholipase A2 (cPLA2) or prostaglandin E2 (PGE2) levels in cultured hippocampal neurons and tissues were assayed using a commercial mouse cPLA2 (Qiaodu-Bio, Cat# CK-E92479M) or PGE2 ELISA Kit (Qiaodu-Bio, Cat# CK-E90213M), respectively. The hippocampal neurons and tissues were homogenized in ice-cold 70 μl RIPA (Solarbio, Cat# R0010) buffer. The samples were centrifuged at 13,000 *g* (4°C for 10 min). Ten micro-liter of the supernatant from the hippocampal homogenate was used to assay cPLA2 or PGE2 level, according to the manufacturer's protocols. The content of cPLA2 was based on measures of absorbance at 450 nm/well in a 96 well plate reader (Thermo Scientific, USA).

Western Blot Assay

The hippocampus was collected after the behavioral assessments. Tissues were homogenized in RIPA lysis buffer (Beyotime, Cat# P0013C) containing a Protease Inhibitor Cocktail (one tablet for every 50 ml RIPA lysis buffer, Roche, Cat# 11697498001) and a Phosphoprotease Inhibitor Cocktail (one tablet for every 50 ml RIPA lysis buffer, Roche, Cat# 4906845001), then, crushed by ultrasound for 10 min by an ultrasonic cell disruptor (Banoelin, Germany). After 30 min of being adequately crushed, the lysates were centrifuged at 12,000 rpm, for 30 min at 4°C and the supernatant fraction was used for the Western blot assay. The protein concentration in the supernatant fraction was determined using the BCA protein assay kit (Beyotime, Cat# P0012). Equal amounts of soluble protein (25 μg) were separated by 10% SDS-PAGE (Beyotime, Cat# P0456) and transferred onto poly-vinylidene fluoride (PVDF) membranes (0.45 μm, Millipore, Cat# IPVH08100). After blocking with 5% fat-free milk; Beyotime, Cat# P0216) for 1 h, membranes were incubated with rabbit anti-PSD 95 (1:1,000, Cell Signaling, Cat# 3409), mouse anti-synaptotagmine-1 (1:1,000, Abcam, Cat# 13259), and rabbit anti-β-actin (1:1,000, Cell Signaling, Cat# 4970) at 4°C overnight. Membranes were then incubated with HRP linked anti-rabbit Antibody (1:5,000, Cell Signaling, Cat# 7074) or HRP linked anti-mouse antibody (1:5,000, Cell Signaling, Cat# 7076), respectively. Target bands were detected and quantified with BeyoECL Plus (1:1, Beyotime, Cat# P0018) by Amersham imager 600 (GE Healthcare Life Sciences, USA).

Quantitative RT-PCR

Total RNA was extracted from primary cultured hippocampal neurons and reverse transcribed into cDNA following standard experimental procedures. The relative transcript level of CaSR was measured by quantitative PCR using LightCycle 480VR II PCR (Roche, Switzerland) with specific primers (CaSR, forward primer 5′-TTGCAAGGGCCAATGGTGG-3′, reverse primer 5′-GCTTCCTGGGAAGACCCAT-3′; mouse-actin, forward primer 5′-AACAGTCCGCCTAGAAGCAC-3′, reverse primer 5′-CGTTGACATCCGTAAAGACC-3′).

Statistical Analyses

Statistical analyses were performed with GraphPad PRISM software (GraphPad Software Inc., La Jolla, CA, USA, RRID:SCR_00298). Data were presented as mean ± SEM. Two-group comparisons were analyzed by a two-tailed student's *t*-test. Multiple group data were analyzed using a one-way analysis of variance (ANOVA) followed by a Tukey *post hoc* test, with the exception of the data of the place navigation test of the MWM tests, which were analyzed by two-way repeated-measures ANOVA with Tukey *post hoc* comparisons. $P < 0.05$ was considered statistically significant. A test for outliers was not performed on the data.

RESULTS

The Expression Levels of CaSR Are Increased in AD Mice and $A\beta_{1-42}$-Treated Primary Hippocampal Neurons

The expression levels of CaSR in APPswe/PSEN1dE9 transgenic mice and wild type mice were detected (**Figures 1A,B**). The expression levels of CaSR were significantly increased in the 9-month-old AD mice ($P < 0.01$, **Figure 1G**). The expression levels of CaSR in the control and $A\beta_{1-42}$-treated primary hippocampal neurons were also detected (**Figures 1C–F**). Both the mRNA and protein levels were increased by $A\beta_{1-42}$ treatment ($P < 0.05$, **Figure 1H**; $P < 0.01$, **Figure 1I**). The results demonstrated that $A\beta_{1-42}$ treatment upregulates the expression level of CaSR.

Pharmacological Inhibition of CaSR Prevents Dendritic Filopodium Loss Caused by Oligomeric $A\beta_{1-42}$ in Hippocampal Neurons

To find out whether CaSR mediates $A\beta_{1-42}$-induced early synapse formation impairment, we measured the density of dendritic filopodium of hippocampal neurons at DIV 7 treated with $A\beta_{1-42}$ oligomers, in the presence or the absence of CaSR antagonist NPS 2143 the density of dendrite filopodium of the $A\beta_{1-42}$-treated group was significantly reduced compared to the

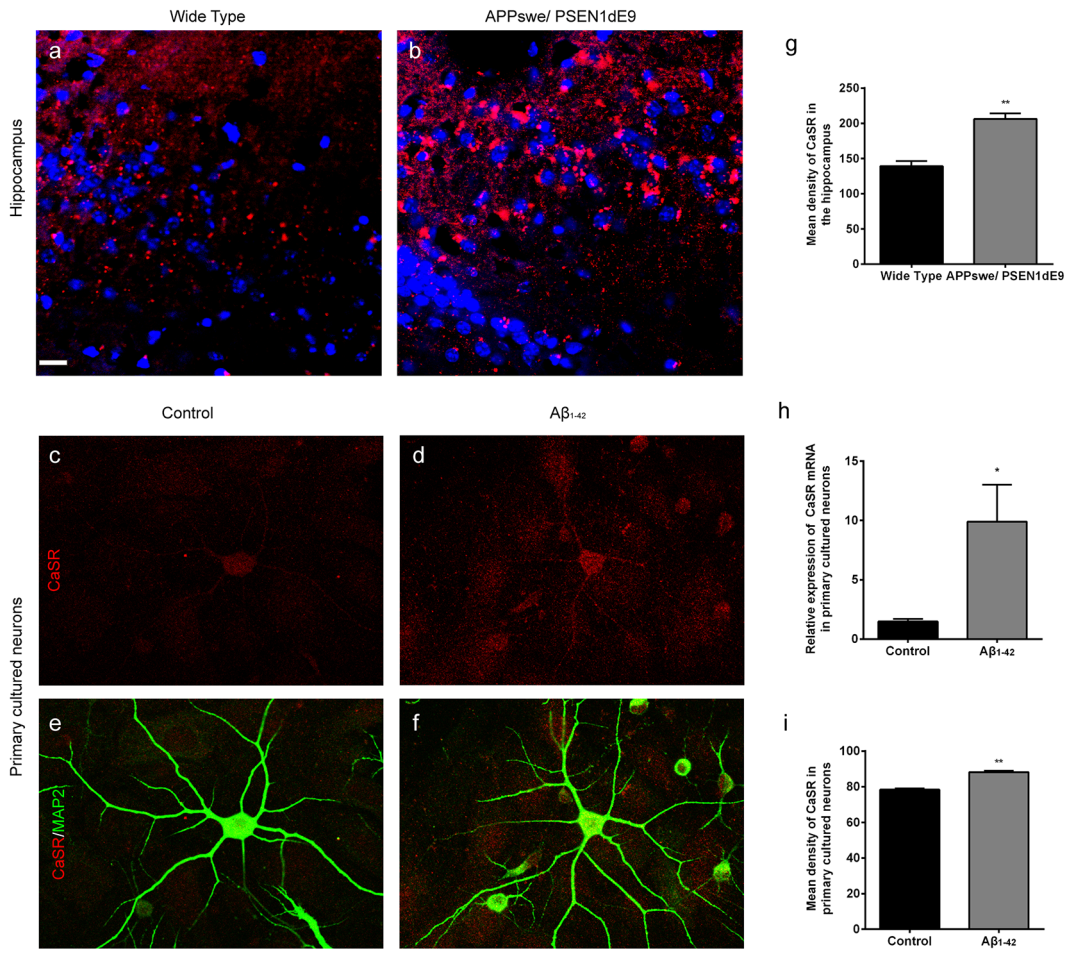

FIGURE 1 | The expression levels of calcium-sensing receptor (CaSR) were increased in Alzheimer's disease (AD) mice and β-amyloid peptide ($A\beta_{1-42}$)-treated primary hippocampal neurons. **(A,B)** Immunostaining of CaSR (red) and DAPI (blue) in the hippocampus of wild type and APPswe/PSEN1dE9 transgenic mice. Scale bar 20 μm. **(C–F)** Immunostaining of CaSR (red) and neuronal marker MAP2 (green) in primary cultured neurons in the control and 0.5 μM $A\beta_{1-42}$-treated group. **(G)** Quantitative comparison of the mean density of CaSR in the hippocampus of wild type and APPswe/PSEN1dE9 transgenic mice. $^{**}P < 0.01$ vs. wild type group. Values represent mean ± SEM, $n = 6$ animals for each group. **(H)** Quantitative comparison of the mRNA levels of CaSR in control and $A\beta_{1-42}$-treated neurons. $^{*}P < 0.05$ vs. control group. $n = 9$ repeats from three independent primary cell culture preparations. **(I)** Quantitative comparison of the mean density of CaSR in control and $A\beta_{1-42}$-treated neurons. $^{**}P < 0.01$ vs. control group, $n = 48$–51 neurons from three independent primary cell culture preparations.

control group ($P < 0.01$, **Figure 2**). Treatment with NPS 2143 (0.1 μM) significantly ameliorated the reduction of filopodium density induced by $A\beta_{1-42}$ oligomers ($P < 0.01$), while, NPS 2143 treatment alone did not alter the density of dendrite filopodium ($P > 0.05$, **Figure 2**).

NPS 2143 Prevents Spine Loss and Synaptic Impairment Caused by Oligomeric $A\beta_{1-42}$ in Hippocampal Neurons

To further analyze the role of CaSR in synapse formation, the dendritic spine densities at DIV 14 were quantified in the control group, oligomeric $A\beta_{1-42}$-treated group, oligomeric $A\beta_{1-42}$ + NPS 2143 group and the NPS 2143 alone group. The oligomeric $A\beta_{1-42}$-treated group prominently decreased the spine density ($P < 0.01$, **Figure 3**). Treatment with NPS 2143 (0.1 μM) significantly prevented the decreased spine density induced by $A\beta_{1-42}$ oligomers ($P < 0.01$, **Figure 3**), while, NPS 2143 treatment alone did not alter the density of the spine ($P > 0.05$, **Figure 3**). These results suggest that CaSR is involved in dendritic spine loss caused by $A\beta_{1-42}$ oligomers in hippocampal neurons.

To confirm the effects of CaSR on synaptic impairment induced by $A\beta_{1-42}$, the synapse density was captured by immunocytochemistry (**Figures 4A–L**). At DIV 14, anti-presynaptic marker synaptotagmine-1 and anti-postsynaptic marker PSD 95 specific antibodies were used, and puncta per 100 μm dendrite from secondary dendritic branches were analyzed. Compared with the control group, the numbers of synaptotagmine-1-positive puncta and PSD 95-positive puncta were significantly decreased after treatment with $A\beta_{1-42}$ oligomers ($P < 0.01$, **Figures 4M,N**). The NPS

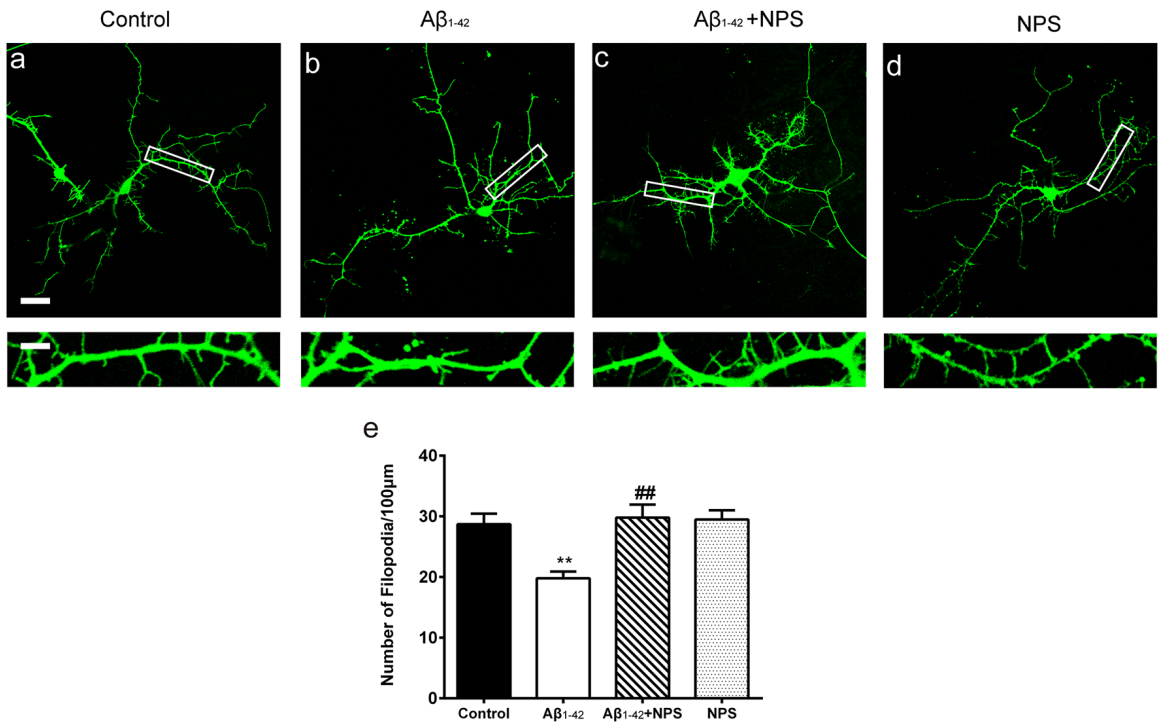

FIGURE 2 | Pharmacological inhibition of CaSR protected hippocampal neurons from soluble $A\beta_{1-42}$ oligomer-induced filopodium loss at day *in vitro* (DIV) 7. Structural morphology of filopodium of hippocampal neurons was displayed by co-transfection of F-GFP and GFP-actin. Fluorescent figures were displayed with the control group **(A)**, the 0.5 μM $A\beta_{1-42}$ group **(B)**, the 0.5 μM $A\beta_{1-42}$ + 0.1 μM NPS 2143 group **(C)** and the 0.1 μM NPS 2143 group **(D)**. Scale bar 20 μm and 5 μm. **(E)** Quantitative comparison of the density of dendritic filopodia of the four groups. $^{**}P < 0.01$ vs. control group, $^{\#\#}P < 0.01$ vs. $A\beta_{1-42}$ oligomer-treated group. Values represent mean ± SEM, n = 21–25 neurons from three independent primary cell culture preparations.

2143 (0.1 μM) treatment significantly prevented the decreased puncta numbers of synaptotagmine-1 and PSD 95 induced by $A\beta_{1-42}$ oligomers ($P < 0.01$, **Figures 4M,N**), while, NPS 2143 treatment alone (0.1 μM) did not alter the numbers of synaptotagmine-1-positive puncta and PSD 95-positive puncta ($P > 0.05$, **Figures 4M,N**). The synaptic density of the $A\beta_{1-42}$ group was also significantly declined ($P < 0.01$, **Figure 4O**). The NPS 2143 (0.1 μM) treatment significantly ameliorated the reduction of synaptic density induced by $A\beta_{1-42}$ oligomers ($P < 0.01$), while, NPS 2143 treatment alone (0.1 μM) had no effect on the synaptic density ($P > 0.05$, **Figure 4O**).

Down-Regulation of CaSR Expression Prevents Synaptic Impairment Induced by Oligomeric $A\beta_{1-42}$ in Hippocampal Neurons

To further verify that CaSR mediates the synaptic impairment induced by $A\beta_{1-42}$, the synaptic densities of neurons treated by the CaSR-shRNA-lentivirus or NC shRNA were analyzed by immunocytochemistry (**Figures 5A–P**). The expression level of CaSR was down regulated by the CaSR-shRNA-lentivirus ($P < 0.01$, **Figure 5Q**). Compared with the control group, the numbers of synaptotagmine-1-positive puncta and PSD 95-positive puncta were significantly decreased ($P < 0.01$, **Figures 5R,S**) in the oligomeric $A\beta_{1-42}$-treated cells. Down-regulation of the CaSR expression significantly prevented the decreased puncta numbers of synaptotagmine-1 and PSD 95 ($P < 0.01$, **Figures 5R,S**). The synapse number was also measured, and down-regulation of CaSR significantly protected hippocampal neurons from synapse loss induced by oligomeric $A\beta_{1-42}$ ($P < 0.01$, **Figure 5T**).

NPS 2143 Prevents the Decreased Expression Levels of Synaptotagmine-1 and PSD 95 in AD Model Mice

Collective evidence shows that oligomeric $A\beta_{1-42}$ is regarded as the pertinent toxic form of Aβ (Baek et al., 2017; Choi et al., 2017). In order to study the single factor of Aβ and the underlying mechanism of CaSR in Aβ-mediated synaptic and cognitive impairment, the AD mouse model, made by microinjection with $A\beta_{1-42}$ oligomers, were used in the rest of our study.

To investigate whether CaSR also mediates the synaptic impairment in the AD mouse model, the expression levels of the presynaptic marker synaptotagmine-1 and postsynaptic mark PSD 95 were measured in the hippocampus of the mice which were microinjected with $A\beta_{1-42}$ (4 μmol/kg) and/or (0.08 or 0.16 μmol/kg) NPS 2143 (**Figures 6A,C**). The expression levels of synaptotagmine-1 and PSD 95 were significantly decreased in the hippocampus of the $A\beta_{1-42}$-treated mice ($P < 0.01$, **Figure 6B**;

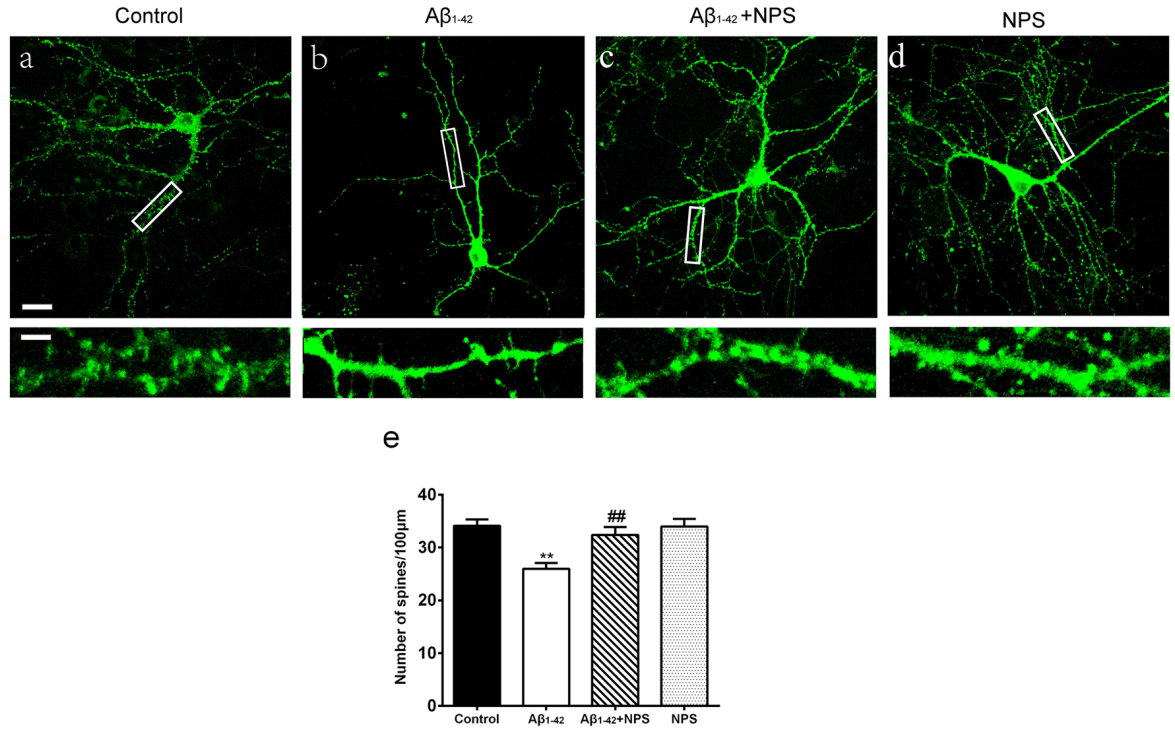

FIGURE 3 | NPS 2143 protected hippocampal neurons from soluble $A\beta_{1-42}$ oligomer-induced spine loss at DIV 14. Structural morphology of the spine of hippocampal neurons was displayed by co-transfection of F-GFP and GFP-actin. Fluorescent figures captured by confocal were displayed with the control group **(A)**, the 0.5 μM $A\beta_{1-42}$ group **(B)**, the 0.5 μM $A\beta_{1-42}$ + 0.1 μM NPS 2143 group **(C)** and the 0.1 μM NPS 2143 group **(D)**. Scale bar 20 μm and 5 μm. **(E)** Quantitative comparison of the density of the dendritic spine of the four groups. $^{**}P < 0.01$ vs. control group, $^{\#\#}P < 0.01$ vs. $A\beta_{1-42}$ oligomer-treated group. Values represent mean ± SEM, n = 21–25 neurons from three independent primary cell culture preparations.

$P < 0.01$, **Figure 6D**). The NPS 2143 (0.16 μmol/kg) treatment significantly prevented the decreased expression levels of PSD 95 and synaptotagmine-1 ($P < 0.01$, **Figure 6B**; $P < 0.01$, **Figure 6D**).

Pharmacological Inhibition of CaSR Prevents Cognitive Deficits of $A\beta_{1-42}$ Oligomer-Treated Mice

Normal synapse formation is considered to be the structure basis of cognitive function. To find out whether the impairment of synapse formation mediated by CaSR was also involved in the cognitive deficits of the AD mouse model, NOR tests and MWM tests were used to estimate the role of CaSR in soluble $A\beta_{1-42}$ oligomer induced recognitive and spatial memory deficits (**Figure 7**), respectively.

The discrimination indexes were used to evaluate the recognitive memory of animals in NOR tests. There was no significant difference in discrimination indexes among these groups in the training session ($P > 0.05$, **Figure 7B**). In the retention session, discrimination indexes were decreased in the mice injected with soluble $A\beta_{1-42}$ oligomers ($P < 0.05$, **Figure 7C**). Inhibition of CaSR with NPS 2143 (0.16 μmol/kg) had no effect on discrimination indexes, but it significantly attenuated the $A\beta_{1-42}$ oligomer-induced reduction of discrimination indexes ($P < 0.05$, **Figure 7C**). The NPS 2143 (0.08 μmol/kg) treatment had no effect on $A\beta_{1-42}$-induced change in the discrimination indexes ($P > 0.05$, **Figure 7C**). These results indicated that NPS 2143 rescues $A\beta_{1-42}$-induced recognitive deficits in a dose dependent manner.

To further investigate whether CaSR is involved in $A\beta_{1-42}$ oligomer-mediated spatial memory impairment, we examined memory performance with MWM tests in mice treated with $A\beta_{1-42}$ oligomers in presence or absence of CaSR antagonist NPS 2143. Two-way ANOVA for repeated-measures revealed significant changes in drug effects ($P < 0.01$, **Figure 7D**) and time effects ($P < 0.01$, **Figure 7D**), but no interaction was found ($P > 0.05$, **Figure 7D**). The escape latency of $A\beta_{1-42}$-treated mice on day 3 and 4 was significantly longer compared with the control mice ($P < 0.05$ and $P < 0.01$ for day 3 and 4 respectively, **Figure 7D**). The escape latency of NPS 2143-treated mice (0.08 or 0.16 μmol/kg) was stable compared to that of the control mice. The NPS 2143 (0.08 μmol/kg) did not prevent the increase escape latency of $A\beta_{1-42}$-treated mice, however, the NPS 2143 (0.16 μmol/kg) treatment prevented the prolongation of latency induced by $A\beta_{1-42}$ on day 3 and 4 ($P < 0.05$, **Figure 7D**). In the probe test, after the hidden platform was removed from the target quadrant, the $A\beta_{1-42}$-treated mice spent a shorter time in the target quadrant compared with the control mice ($P < 0.01$, **Figure 7E**). A 0.16 μmol/kg NPS 2143 treatment reversed the

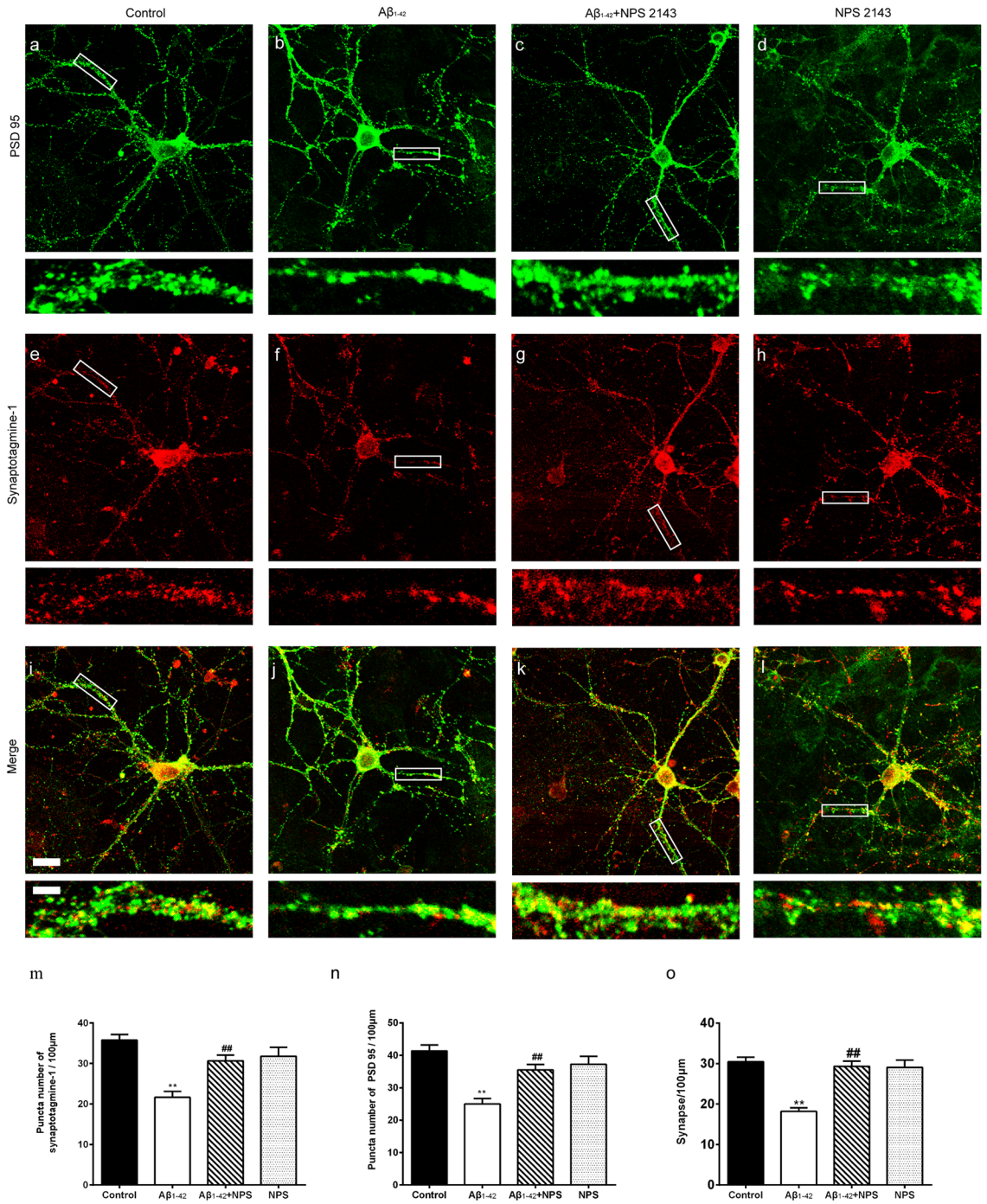

FIGURE 4 | NPS 2143 prevented hippocampal neurons from soluble $A\beta_{1-42}$ oligomer-induced synapse loss at DIV 14. Synapse was labeled through the co-localization of presynaptic marker synaptotagmine-1(red) and postsynaptic marker PSD 95 (green). Sample figures of the control group **(A,E,I)**, the 0.5 μM $A\beta_{1-42}$ group **(B,F,J)**, the 0.5 μM $A\beta_{1-42}$ + 0.1 μM NPS 2143 group **(C,G,K)**, and the 0.1 μM NPS 2143 group **(D,H,L)**. Scale bar 20 μm and 5 μm. **(M)** Quantitative comparison of the numbers of synaptotagmine-1-positive puncta of the four groups. **(N)** Quantitative comparison of the numbers of PSD 95-positive puncta of different groups. **(O)** Quantitative comparison of the density of dendritic synapse of the four groups. $^{**}P < 0.01$ vs. control group, $^{\#\#}P < 0.01$ vs. $A\beta_{1-42}$ oligomer-treated group. Values represent mean ± SEM, n = 24–34 neurons from three independent primary cell culture preparations.

decrease of time in the target quadrant of the $A\beta_{1-42}$-treated mice ($P < 0.01$, **Figure 7E**). However, treatment of NPS 2143 alone, at the dose of 0.08 or 0.16 μmol/kg, had no effect on the time spent in the target quadrant (**Figure 7E**). Moreover, we measured the numbers of times the mice swam cross the place where the original platform was. The numbers of the target platform crosses

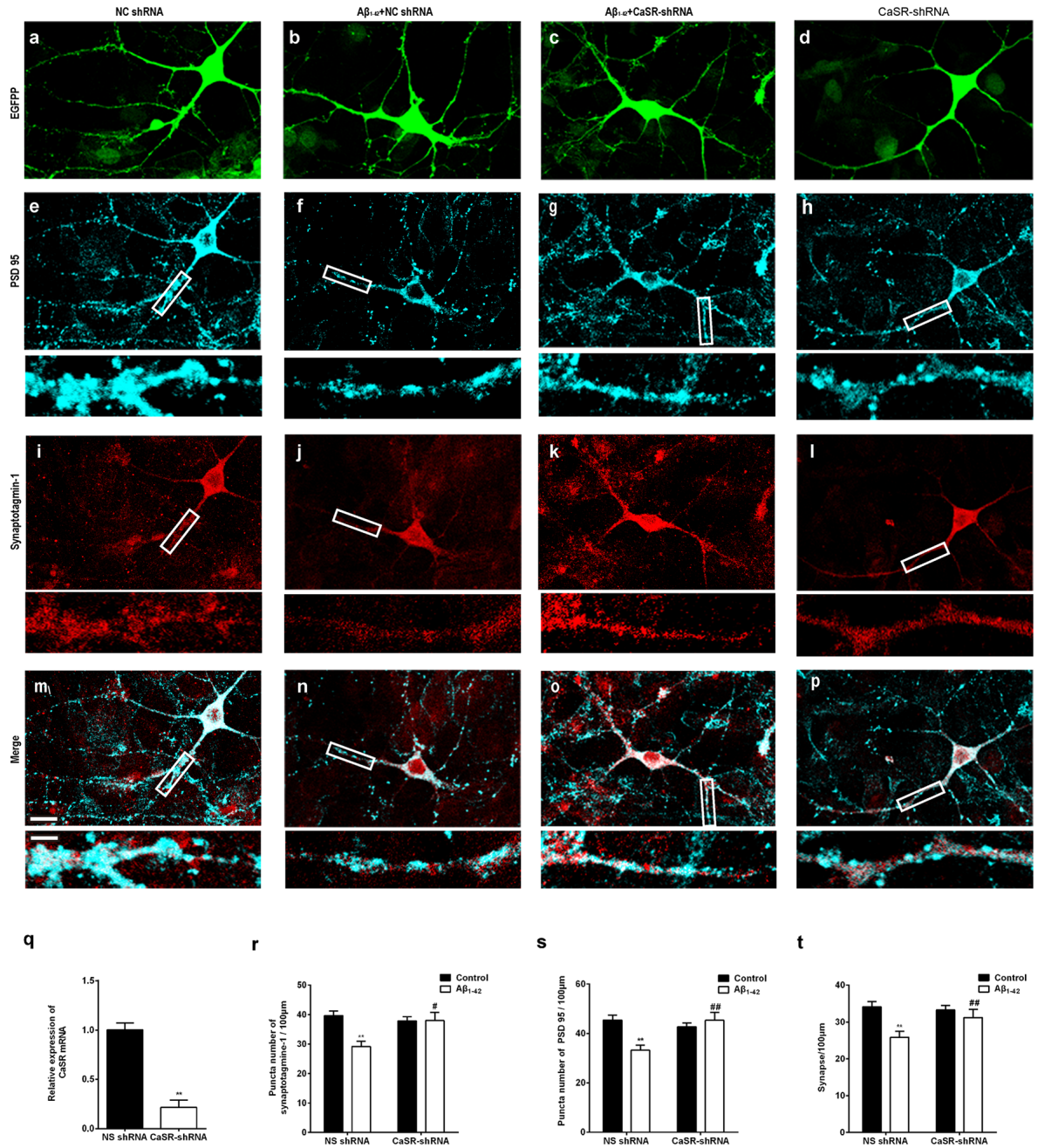

FIGURE 5 | Down-regulation of CaSR expression prevented synaptic impairment induced by oligomeric $A\beta_{1-42}$ in hippocampal neurons. Sample figures of the NC shRNA **(A,E,I,M)**, the 0.5 μM $A\beta_{1-42}$ + NC shRNA group **(B,F,J,N)**, the 0.5 μM $A\beta_{1-42}$ + CasR-shRNA group **(C,G,K,O)**, and the CasR-shRNA group **(D,H,L,P)**. Scale bar 20 μm and 5 μm. **(Q)** The expression level of CaSR was significantly down-regulated by CaSR-shRNA. $^{**}P < 0.01$ vs. NC shRNA group. **(R,S)** Quantitative comparison of the number of synaptotagmine-1-positive puncta and PSD 95-positive puncta of the four groups. **(T)** Down-regulation of CaSR protected hippocampal neurons from synapse loss induced by oligomeric $A\beta_{1-42}$. $^{**}P < 0.01$ vs. NC shRNA group, $^{\#}P < 0.05$ vs. $A\beta_{1-42}$ + NC shRNA group, $^{\#\#}P < 0.01$ vs. $A\beta_{1-42}$ + NC shRNA group. Values represent mean ± SEM, n = 17–20 neurons from three independent primary cell culture preparations.

were decreased in the $A\beta_{1-42}$-treated mice ($P < 0.01$, **Figure 7F**). Injection of NPS 2143 (0.16 μmol/kg) reversed the decreased crosses over the target platform of $A\beta_{1-42}$-treated mice ($P < 0.01$, **Figure 7F**). However, treatment of NPS 2143 alone had no effect on the numbers of the target platform crosses (**Figure 7F**). We did not observe a significant difference in velocity among the six groups in the MWM tests (**Figure 7G**), indicating that the differences in latency, time and number of crosses over the target platform among the groups were not caused by the differences in velocity. Altogether, these data suggested that pharmacological

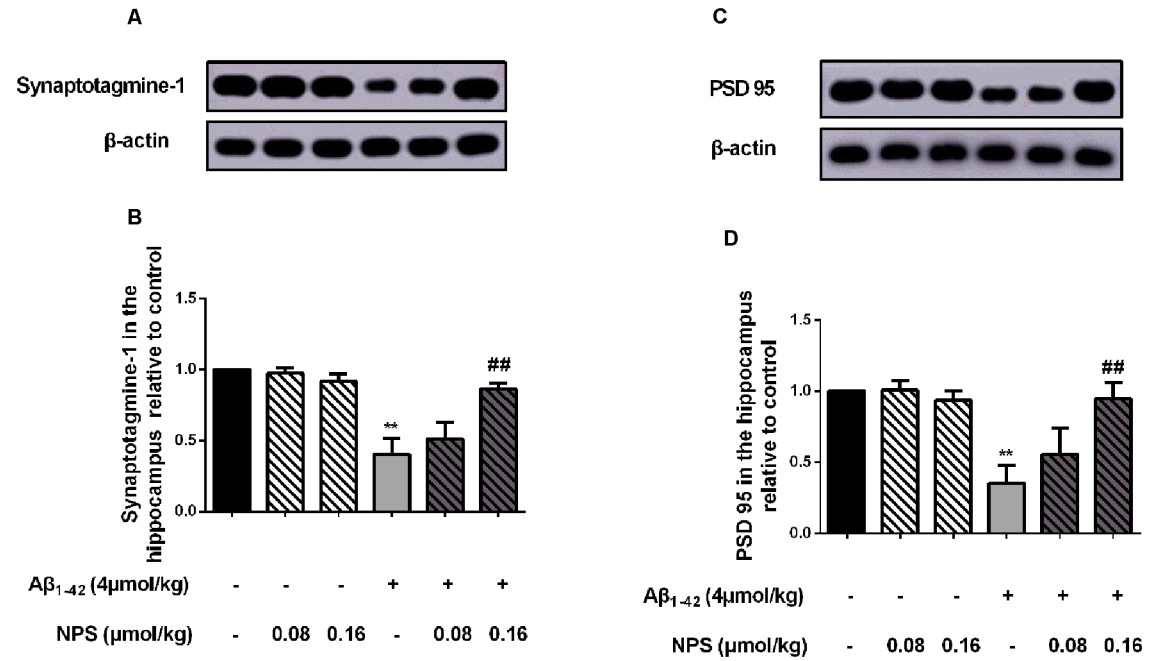

FIGURE 6 | Pharmacological inhibition of CaSR prevented the decreased expression levels of synaptotagmine-1 and PSD 95 induced by oligomeric $A\beta_{1-42}$. **(A)** Sample western-blot plot of synaptotagmine-1 and β-actin in the control, the oligomeric $A\beta_{1-42}$-treated group (4 μmol/kg), and/or the NPS 2143-treated group (0.08 or 0.16 μmol/kg). **(B)** Quantitative comparison of hippocampal synaptotagmin-1 level in different groups. **(C)** Sample western-blot plot of PSD 95 and β-actin in six groups. **(D)** Quantitative comparison of hippocampal PSD 95 level in different groups. $^{**}P < 0.01$ vs. control group, $^{\#\#}P < 0.01$ vs. $A\beta_{1-42}$ oligomer-treated group. Values represent mean ± SEM, $n = 6$ animals for each group.

inhibition of CaSR prevents mice from $A\beta_{1-42}$ oligomer- induced spatial learning and memory deficits in MWM tests.

CaSR Participates in $A\beta_{1-42}$-Induced Increase in the Levels of cPLA2 and PGE2

To explore the downstream pathways mediated by CaSR and soluble $A\beta_{1-42}$ oligomers, the contents of cPLA2 and PGE2 were measured in hippocampal neurons. $A\beta_{1-42}$ treatment increased the content of cPLA2 ($P < 0.01$, **Figure 8A**). NPS 2143 (0.1 μM) treatment significantly prevented the increased level of cPLA2 induced by $A\beta_{1-42}$ oligomers ($P < 0.01$), while the level of cPLA2 remained stable under NPS 2143 (0.1 μM) alone treated neurons, compared with that of the control neurons. The expression level of CaSR was reduced by the CaSR-shRNA-lentivirus, and knocking down CaSR also prevented the increased cPLA2 content induced by $A\beta_{1-42}$ oligomers ($P < 0.01$, **Figure 8C**). $A\beta_{1-42}$ treatment also increased the content of PGE2 ($P < 0.01$, **Figure 8B**). The NPS 2143 (0.1 μM) treatment significantly prevented $A\beta_{1-42}$ oligomer-induced increase of the level of PGE2 ($P < 0.01$), while, the level of PGE2 remained stable under NPS 2143 (0.1 μM) alone treated neurons, compared with that of the control neurons ($P > 0.05$ **Figure 8B**). Down-regulation the expression level of CaSR also prevented the increased PGE2 content induced by $A\beta_{1-42}$ oligomers ($P < 0.01$, **Figure 8D**).

To verify the above results, the contents of cPLA2 and PGE2 in the hippocampus of the $A\beta_{1-42}$ (4 μmol/kg) and/or NPS 2143 (0.08 or 0.16 μmol/kg) treated mice were also measured. The contents of PGE2 and cPLA2 were significantly increased in the hippocampus of the $A\beta_{1-42}$-treated mice ($P < 0.01$, **Figure 9A**; $P < 0.01$, **Figure 9B**). The NPS 2143 (0.16 μmol/kg) treatment reversed the increased levels of PGE2 and cPLA2 ($P < 0.05$, **Figure 9A**; $P < 0.01$, **Figure 9B**).

DISCUSSION

To the best of our knowledge, our results, for the first, time demonstrate that the expression level of CaSR is increased by $A\beta_{1-42}$. The increase expression or activity of CaSR mediates the AD-like phenotypes/pathology induced by $A\beta_{1-42}$ oligomers partially through activation of the cPLA2/PGE2 pathway. CaSR is located in nerve terminals which are related to synaptic plasticity and neuronal transmission (Bandyopadhyay et al., 2010). In this study, we provided novel insights to the possible role and underlying mechanisms of CaSR in AD.

It is well accepted that the hippocampus is a region of the adult brain where neurogenesis occurs. Perturbations in synapse formation by forms of oligomeric Aβ are tightly correlated with memory deficits in AD (Bandyopadhyay et al., 2010; Marchetti and Marie, 2011; Ardiles et al., 2012; Ma and Klann, 2012; Sanchez et al., 2012; Xu et al., 2014). Growing evidence indicates that Aβ-induced synaptic loss in the hippocampus occurs at the early stage of AD (Teich et al., 2015; Wang X. et al., 2018). We demonstrated that exposure of $A\beta_{1-42}$ oligomers

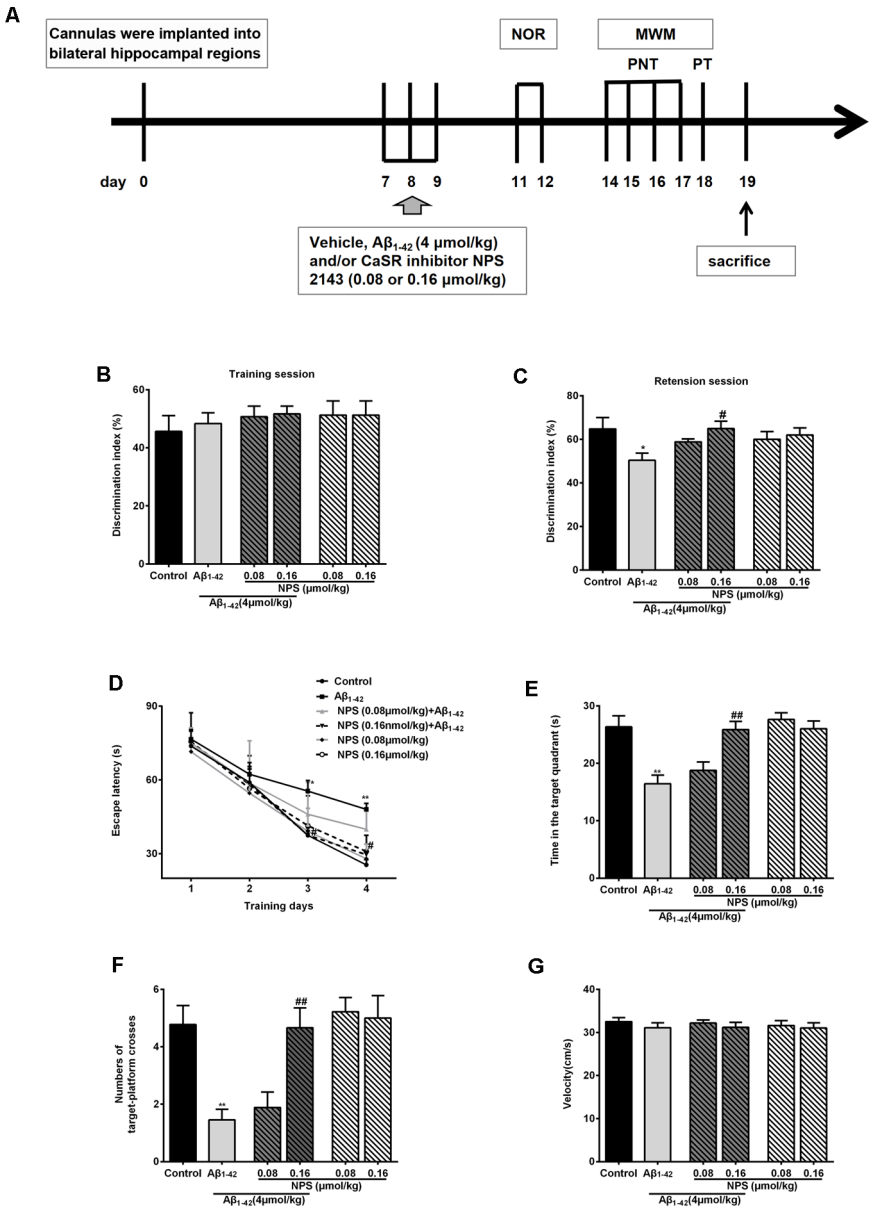

FIGURE 7 | Protective function of inhibiting CaSR on oligomeric $A\beta_{1-42}$-induced recognitive and spatial learning deficits. **(A)** Experimental schedule of behavioral tests. Cannulas were implanted into bilateral hippocampal regions. Vehicle, $A\beta_{1-42}$ (4 μmol/kg) and/or CaSR inhibitor NPS 2143 (0.08 or 0.16 μmol/kg body weight per day) were microinjected for 3 days from day 7 to 9. From day 11 to day 12, the novel object recognition (NOR) tests were performed. Morris water maze (MWM) tests were conducted from day 14 to 18 day. Place navigation tests (PNT) of the MWM were conducted four times a day for four consecutive days, followed by a probe trial test (PT) 24 h after the last PNT. The mice were sacrificed after behavioral experiments. **(B)** Discrimination indexes displayed no significant difference among these groups in the training session. **(C)** Quantitative comparison of the discrimination indexes in the retention session, $n = 8$ animals for each group. **(D)** The escape latency of the control, the oligomeric $A\beta_{1-42}$-treated group (4 μmol/kg), and/or the NPS 2143-treated group (0.08 or 0.16 μmol/kg) during the four training days. **(E)** Quantitative comparison of the time in the target quadrant of the six groups. **(F)** Quantitative comparison of the number of target platform crosses of the six groups. **(G)** Swimming speed of the six groups did not show significant different. $^{*}P < 0.05$ vs. control group, $^{**}P < 0.01$ vs. control group, $^{\#}P < 0.05$ vs. $A\beta_{1-42}$ oligomer-treated group, $^{\#\#}P < 0.01$ vs. $A\beta_{1-42}$ oligomer-treated group. Values represent mean ± SEM, $n = 8$ animals for each group.

potently decreased filopodium density in hippocampal neurons, while CaSR inhibitor NPS 2143 significantly prevented $A\beta_{1-42}$ oligomer-induced filopodium loss. These results suggest that CaSR is involved in the negative role of $A\beta_{1-42}$ during initial synapse formation. Dendritic spines, small membranous protrusions from neuronal dendrites, are developed from filopodia. Consistent with the role of CaSR in the $A\beta_{1-42}$-induced decrease in filopodium density, CaSR was also involved in the impairment of spine and synapse formation mediated by $A\beta_{1-42}$ oligomers. Both pharmacological inhibition of CaSR

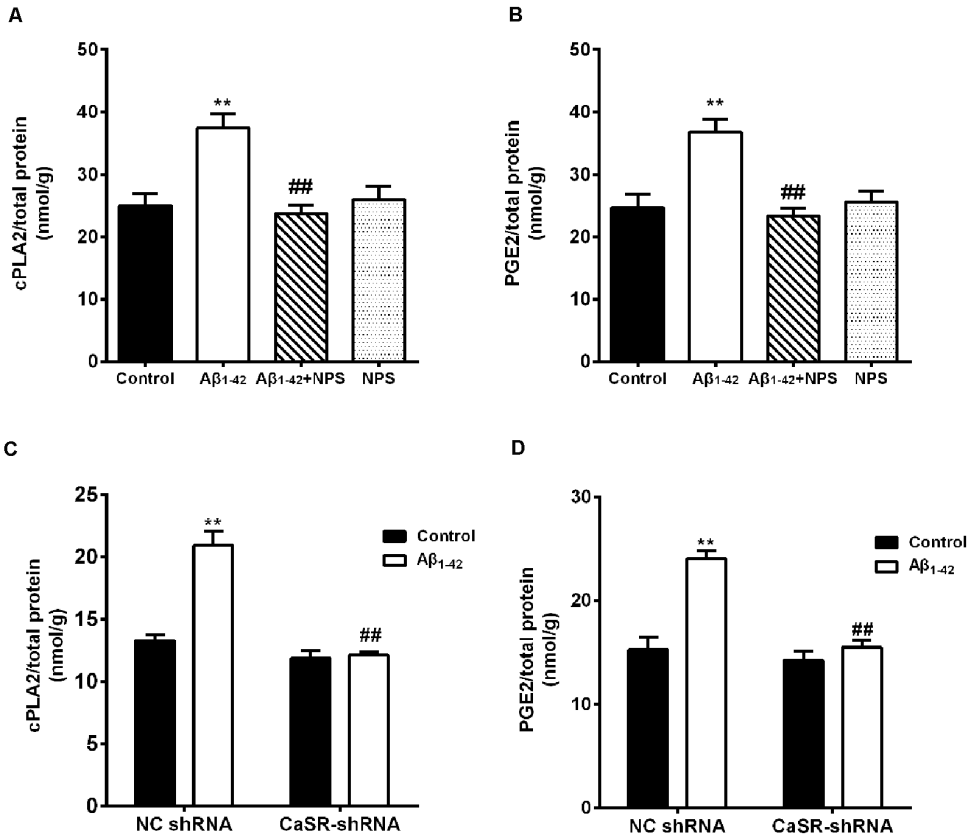

FIGURE 8 | CaSR was involved in $A\beta_{1-42}$-induced increase of cytosolic phospholipase A2 (cPLA2) and prostaglandin E2 (PGE2) in hippocampal neurons. **(A,B)** Quantitative comparison of the contents of cPLA2 and PGE2 in the $A\beta_{1-42}$—(0.5 μM) and/or NPS 2143—(0.1 μM) treated groups. $^{**}P < 0.01$ vs. control group, $^{\#\#}P < 0.01$ vs. $A\beta_{1-42}$ oligomer-treated group. Values represent mean ± SEM, n = 12–13 independent replicates. **(C,D)** Quantitative comparison of the contents of cPLA2 and PGE2 in the $A\beta_{1-42}$ and/or CaSR-shRNA-lentivirus-treated groups. $^{**}P < 0.01$ vs. NC shRNA group. $^{\#\#}P < 0.01$ vs. $A\beta_{1-42}$ + NC shRNA group, n = 9 independent replicates.

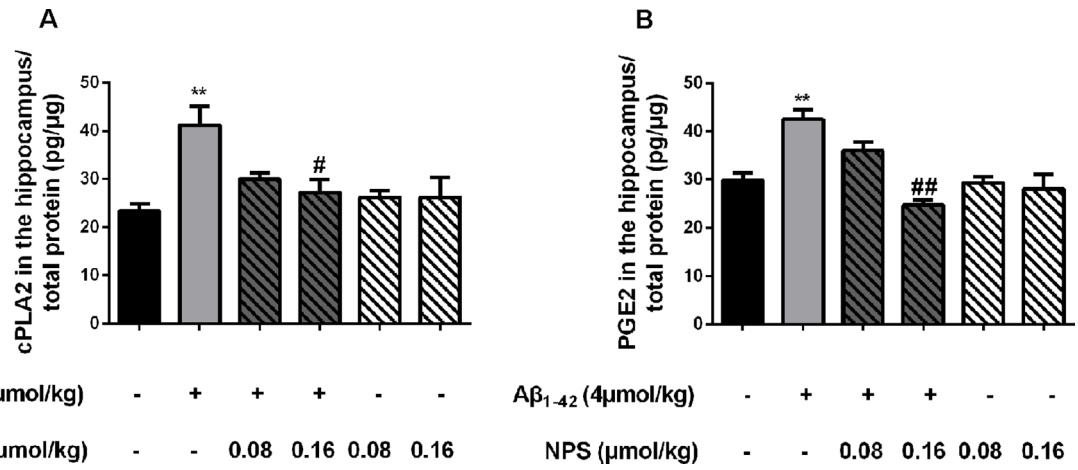

FIGURE 9 | CaSR was involved in $A\beta_{1-42}$-induced increase of cPLA2 and PGE2 in the hippocampus. **(A)** Quantitative comparison of the content of cPLA2 in the control, oligomeric $A\beta_{1-42}$-treated group (4 μmol/kg), and/or NPS 2143-treated group (0.08 or 0.16 μmol/kg). **(B)** Quantitative comparison of the content of PGE2 in six groups. $^{\#}P < 0.05$ vs. $A\beta_{1-42}$ oligomer-treated group, $^{**}P < 0.01$ vs. control group, $^{\#\#}P < 0.01$ vs. $A\beta_{1-42}$ oligomer-treated group. Values represent mean ± SEM, n = 6 animals for each group.

and knockdown of CaSR prevented $A\beta_{1-42}$-induced synapse developmental deficits. Moreover, we found that CaSR also mediated $A\beta_{1-42}$-induced cognitive deficits. Using behavioral tasks, including MWM and NOR tests, we also showed that $A\beta_{1-42}$ oligomers cause recognitive and spatial memory impairment. Inhibition of CaSR with NPS 2143 prevented $A\beta_{1-42}$-induced cognitive deficits in a dose-depended manner. Thus, CaSR mediates AD-like synaptic and cognitive impairment induced by $A\beta_{1-42}$ oligomers.

cPLA2/PGE2 signaling pathways might be involved in the effects of CaSR on Aβ-induced cognitive impairment. PGE2, a lipid molecule derived from arachidonic acid (AA; Brummett et al., 2014). cPLA2 affects the synthesis of PGE2 by promoting the release of AA (Bate and Williams, 2015a). It has been found that the activation of cPLA2/PGE2 is associated with multiple signaling pathways such as neuronal excitation, synaptic secretion, lipid metabolism, and neuroinflammation (Murakami and Kudo, 2004; Igarashi et al., 2011; Sun et al., 2014). Activation of cPLA2 enzymes plays an important role in age-associated neuronal and memory impairment (Hermann et al., 2014). Neurons isolated from mice deficient in $cPLA2^{-/-}$ showed resistance to the toxic effects of Aβ (Desbène et al., 2012). PGE2 also regulates synaptic function and plasticity (Koch et al., 2010). Addition of PGE2 reduced the content of synaptic proteins in cortical neurons, and impaired hippocampal presynaptic long-term plasticity in a mouse model of AD (Bate et al., 2010; Maingret et al., 2017). Our results showed that the contents of cPLA2 and PGE2 in hippocampal neurons and hippocampal encephalic region were significantly increased due to oligomeric $A\beta_{1-42}$ treatment. These results are consistent with previous studies showing that Aβ oligomers could activate cPLA2 and increase the level of PGE2, resulting in a reduction of synaptic markers and a decline in cognitive function (Desbène et al., 2012; Bate and Williams, 2015b). Both pharmacological inhibition of CaSR and down-regulation of the expression of CaSR prevented Aβ-induced increase of cPLA2/PGE2 and synaptic damage. Thus, CaSR might mediate Aβ-induced synaptic and cognitive damage through increasing cPLA2 and PGE2 contents.

Besides activation of the cPLA2/PGE2 pathway, CaSR has also been reported to be involved in the Aβ-induced increase of Aβ and phospho-tau (Dal Prà et al., 2014; Chiarini et al., 2017); this might also contribute to the decrease in cognitive decline in AD mice. At physiological conditions, CaSR was only partially activated (Ruat and Traiffort, 2013; Díaz-Soto et al., 2016). Increased Aβ made CaSR full or over activated, which further induced the early impairment of synapse formation and cognitive function. Together with our observations, the current data showed that CaSR is an important factor mediating the progress of AD.

In conclusion, we demonstrated that CaSR is involved in oligomeric $A\beta_{1-42}$-induced cognitive dysfunction as well as synapse formation and developmental impairment in the pathogenesis of AD, in addition, our results indicated that cPLA2 and PGE2 are downstream targets of CaSR, which mediate cognitive decline in AD. Thus, we provided support for the efficacy of specific antagonists of CaSR in the treatment of AD.

DATA AVAILABILITY STATEMENT

The datasets generated for this study are available on request to the corresponding author.

ETHICS STATEMENT

The animal study was reviewed and approved by Institutional Animal Care and Use Committee of the Medical School of Ningbo University [permission: SYXK(ZHE)2013-0191].

AUTHOR CONTRIBUTIONS

SX and XB were responsible for the design of the study. CF was in charge of molecular and cellular experiments. YL, YD, and YC were mainly involved in animal experiments and relative analysis. QW and JW provided valuable advice for the research. WC and LS provided language modification and data analysis. All authors contributed to the article and approved the submitted version.

FUNDING

This work was supported by grants from the National Natural Science Foundation of China (81771166), the Natural Science Foundation of Zhejiang Province (LY20H090004), the Natural Science Foundation of Ningbo (2019A610288), the Ningbo municipal innovation team of life science and health (2015C110026), the Suzhou youth science and technology project (KJXW2017021) and the K.C. Wong Magna Fund at Ningbo University.

REFERENCES

Ahmed, M., Davis, J., Aucoin, D., Sato, T., Ahuja, S., Aimoto, S., et al. (2010). Structural conversion of neurotoxic amyloid-β(1–42) oligomers to fibrils. *Nat. Struct. Mol. Biol.* 17, 561–567. doi: 10.1038/nsmb.1799

Ardiles, A. O., Tapia-Rojas, C. C., Mandal, M., Alexandre, F., Kirkwood, A., Inestrosa, N. C., et al. (2012). Postsynaptic dysfunction is associated with spatial and object recognition memory loss in a natural model of Alzheimer's disease. *Proc. Natl. Acad. Sci. U S A* 109, 13835–13840. doi: 10.1073/pnas.1201209109

Armato, U., Chiarini, A., Chakravarthy, B., Chioffi, F., Pacchiana, R., Colarusso, E., et al. (2013). Calcium-sensing receptor antagonist (calcilytic) NPS 2143 specifically blocks the increased secretion of endogenous Aβ42 prompted by exogenous fibrillary or soluble Aβ25–35 in human cortical astrocytes and neurons-therapeutic relevance to Alzheimer's disease. *Biochim. Biophys. Acta* 1832, 1634–1652. doi: 10.1016/j.bbadis.2013.04.020

Baek, S. H., Park, S. J., Jeong, J. I., Kim, S. H., Han, J., Kyung, J. W., et al. (2017). Inhibition of Drp1 ameliorates synaptic depression, Aβ deposition and cognitive impairment in an Alzheimer's disease model. *J. Neurosci.* 37, 5099–5110. doi: 10.1523/JNEUROSCI.2385-16.2017

Bandyopadhyay, S., Tfelt-Hansen, J., and Chattopadhyay, N. (2010). Diverse roles of extracellular calcium-sensing receptor in the central nervous system. *J. Neurosci. Res.* 88, 2073–2082. doi: 10.1002/jnr.22391

Bate, C., Tayebi, M., and Williams, A. (2010). Phospholipase A2 inhibitors protect against prion and Aβ mediated synapse degeneration. *Mol. Neurodegener.* 5:13. doi: 10.1186/1750-1326-5-13

Bate, C., and Williams, A. (2015a). α-synuclein-induced synapse damage in cultured neurons is mediated by cholesterol-sensitive activation of cytoplasmic phospholipase A2. *Biomolecules* 5, 178–193. doi: 10.3390/biom5010178

Bate, C., and Williams, A. (2015b). cAMP-inhibits cytoplasmic phospholipase A_2 and protects neurons against amyloid-β-induced synapse damage. *Biology* 4, 591–606. doi: 10.3390/biology4030591

Brauner-Osborne, H., Wellendorph, P., and Jensen, A. A. (2007). Structure, pharmacology and therapeutic prospects of family C G-protein coupled receptors. *Curr. Drug Targets* 8, 169–184. doi: 10.2174/138945007779315614

Brummett, A. M., Navratil, A. R., Bryan, J. D., and Woolard, M. D. (2014). Janus kinase 3 activity is necessary for phosphorylation of cytosolic phospholipase A2 and prostaglandin E2 synthesis by macrophages infected with Francisella tularensis live vaccine strain. *Infect. Immun.* 82, 970–982. doi: 10.1128/iai.01461-13

Chen, W., Bergsman, J. B., Wang, X., Gilkey, G., Pierpoint, C. R., Daniel, E. A., et al. (2010). Presynaptic external calcium signaling involves the calcium-sensing receptor in neocortical nerve terminals. *PLoS One* 5:e8563. doi: 10.1371/journal.pone.0008563

Chiarini, A., Armato, U., Gardenal, E., Gui, L., and Dal Prà, I. (2017). Amyloid β-exposed human astrocytes overproduce phospho-tau and overrelease it within exosomes, effects suppressed by calcilytic NPS 2143-further implications for Alzheimer's therapy. *Front. Neurosci.* 11:217. doi: 10.3389/fnins.2017.00217

Choi, Y., Jeong, H. J., Liu, Q. F., Oh, S. T., Koo, B. S., Kim, Y., et al. (2017). Clozapine improves memory impairment and reduces Aβ level in the Tg-APPswe/PS1dE9 mouse model of Alzheimer's disease. *Mol. Neurobiol.* 54, 450–460. doi: 10.1007/s12035-015-9636-x

Chunhui, H., Dilin, X., Ke, Z., Jieyi, S., Sicheng, Y., Dapeng, W., et al. (2018). A11-positive β-amyloid oligomer preparation and assessment using dot blotting analysis. *J. Vis. Exp.* 135:57592. doi: 10.3791/57592

Conigrave, A. D., and Ward, D. T. (2013). Calcium-sensing receptor (CaSR): pharmacological properties and signaling pathways. *Best Pract. Res. Clin. Endocrinol. Metab.* 27, 315–331. doi: 10.1016/j.beem.2013.05.010

Dal Prà, I., Armato, U., Chioffi, F., Pacchiana, R., Whitfield, J. F., Chakravarthy, B., et al. (2014). The Aβ peptides-activated calcium-sensing receptor stimulates the production and secretion of vascular endothelial growth factor-A by normoxic adult human cortical astrocytes. *Neuromolecular Med.* 16, 645–657. doi: 10.1007/s12017-014-8315-9

Desbène, C., Malaplate-Armand, C., Youssef, I., Garcia, P., Stenger, C., Sauvée, M., et al. (2012). Critical role of cPLA2 in Aβ oligomer-induced neurodegeneration and memory deficit. *Neurobiol. Aging* 33, 1123.e17–1129.e17. doi: 10.1016/j.neurobiolaging.2011.11.008

Díaz-Soto, G., Rocher, A., García-Rodríguez, C., Núñez, L., and Villalobos, C. (2016). The calcium-sensing receptor in health and disease. *Int. Rev. Cell Mol. Biol.* 327, 321–369. doi: 10.1016/bs.ircmb.2016.05.004

Diez-Fraile, A., Lammens, T., Benoit, Y., and D'Herde, K. G. (2013). The calcium-sensing receptor as a regulator of cellular fate in normal and pathological conditions. *Curr. Mol. Med.* 13, 282–295. doi: 10.2174/156652413804810763

Ding, Y., Bao, X., Lao, L., Ling, Y., Wang, Q., and Xu, S. (2019). p-Hydroxybenzyl alcohol prevents memory deficits by increasing neurotrophic factors and decreasing inflammatory factors in a mice model of Alzheimer's disease. *J. Alzheimers Dis.* 67, 1007–1019. doi: 10.3233/jad-180910

Dos Santos Picanco, L. C., Ozela, P. F., de Fatima de Brito, M., Pinheiro, A. A., Padilha, E. C., Braga, F. S., et al. (2018). Alzheimer's disease: a review from the pathophysiology to diagnosis, new perspectives for pharmacological treatment. *Curr. Med. Chem.* 25, 3141–3159. doi: 10.2174/0929867323666161213101126

Ferry, S., Traiffort, E., Stinnakre, J., and Ruat, M. (2000). Developmental and adult expression of rat calcium-sensing receptor transcripts in neurons and oligodendrocytes. *Eur. J. Neurosci.* 12, 872–884. doi: 10.1046/j.1460-9568.2000.00980.x

Gardenal, E., Chiarini, A., Armato, U., Dal Prà, I., Verkhratsky, A., and Rodriguez, J. J. (2017). Increased calcium-sensing receptor immunoreactivity in the hippocampus of a triple transgenic mouse model of Alzheimer's disease. *Front. Neurosci.* 11:81. doi: 10.3389/fnins.2017.00081

Hermann, P. M., Watson, S. N., and Wildering, W. C. (2014). Phospholipase A2—nexus of aging, oxidative stress, neuronal excitability, and functional decline of the aging nervous system? Insights from a snail model system of neuronal aging and age-associated memory impairment. *Front. Genet.* 5:419. doi: 10.3389/fgene.2014.00419

Igarashi, M., Ma, K., Gao, F., Kim, H. W., Rapoport, S. I., and Rao, J. S. (2011). Disturbed choline plasmalogen and phospholipid fatty acid concentrations in Alzheimer's disease prefrontal cortex. *J. Alzheimers Dis.* 24, 507–517. doi: 10.3233/jad-2011-101608

Jiang, L., Huang, M., Xu, S., Wang, Y., An, P., Feng, C., et al. (2016). Bis(propyl)-cognitin prevents β-amyloid-induced memory deficits as well as synaptic formation and plasticity impairments *via* the activation of PI3-K pathway. *Mol. Neurobiol.* 53, 3832–3841. doi: 10.1007/s12035-015-9317-9

Koch, H., Huh, S. E., Elsen, F. P., Carroll, M. S., Hodge, R. D., Bedogni, F., et al. (2010). Prostaglandin E2-induced synaptic plasticity in neocortical networks of organotypic slice cultures. *J. Neurosci.* 30, 11678–11687. doi: 10.1523/JNEUROSCI.4665-09.2010

Leach, K., Conigrave, A. D., Sexton, P. M., and Christopoulos, A. (2015). Towards tissue-specific pharmacology: insights from the calcium-sensing receptor as a paradigm for GPCR (patho)physiological bias. *Trends Pharmacol. Sci.* 36, 215–225. doi: 10.1016/j.tips.2015.02.004

Ma, T., and Klann, E. (2012). Amyloid β: linking synaptic plasticity failure to memory disruption in Alzheimer's disease. *J. Neurochem.* 120, 140–148. doi: 10.1111/j.1471-4159.2011.07506.x

Maingret, V., Barthet, G., Deforges, S., Jiang, N., Mulle, C., and Amedee, T. (2017). PGE2-EP3 signaling pathway impairs hippocampal presynaptic long-term plasticity in a mouse model of Alzheimer's disease. *Neurobiol. Aging* 50, 13–24. doi: 10.1016/j.neurobiolaging.2016.10.012

Marchetti, C., and Marie, H. (2011). Hippocampal synaptic plasticity in Alzheimer's disease: what have we learned so far from transgenic models? *Rev. Neurosci.* 22, 373–402. doi: 10.1515/RNS.2011.035

Mhatre, S. D., Satyasi, V., Killen, M., Paddock, B. E., Moir, R. D., Saunders, A. J., et al. (2014). Synaptic abnormalities in a Drosophila model of Alzheimer's disease. *Dis. Model. Mech.* 7, 373–385. doi: 10.1242/dmm.012104

Murakami, M., and Kudo, I. (2004). Recent advances in molecular biology and physiology of the prostaglandin E2-biosynthetic pathway. *Prog. Lipid Res.* 43, 3–35. doi: 10.1016/s0163-7827(03)00037-7

Price, K. A., Varghese, M., Sowa, A., Yuk, F., Brautigam, H., Ehrlich, M. E., et al. (2014). Altered synaptic structure in the hippocampus in a mouse model of Alzheimer's disease with soluble amyloid-β oligomers and no plaque pathology. *Mol. Neurodegener.* 9:41. doi: 10.1186/1750-1326-9-41

Ruat, M., and Traiffort, E. (2013). Roles of the calcium sensing receptor in the central nervous system. *Best Pract. Res. Clin. Endocrinol. Metab.* 27, 429–442. doi: 10.1016/j.beem.2013.03.001

Sanchez, P. E., Zhu, L., Verret, L., Vossel, K. A., Orr, A. G., Cirrito, J. R., et al. (2012). Levetiracetam suppresses neuronal network dysfunction and reverses synaptic and cognitive deficits in an Alzheimer's disease model. *Proc. Natl. Acad. Sci. U S A* 109, E2895–E2903. doi: 10.1073/pnas.1121081109

Summers, R. J. (2016). Molecular pharmacology of G protein-coupled receptors. *Br. J. Pharmacol.* 173, 2931–2933. doi: 10.1111/bph.13610

Sun, G. Y., Chuang, D. Y., Zong, Y., Jiang, J., Lee, J. C., Gu, Z., et al. (2014). Role of cytosolic phospholipase A2 in oxidative and inflammatory signaling pathways in different cell types in the central nervous system. *Mol. Neurobiol.* 50, 6–14. doi: 10.1007/s12035-014-8662-4

Teich, A. F., Nicholls, R. E., Puzzo, D., Fiorito, J., Purgatorio, R., Fa, M., et al. (2015). Synaptic therapy in Alzheimer's disease: a CREB-centric approach. *Neurotherapeutics* 12, 29–41. doi: 10.1007/s13311-014-0327-5

Wang, X., Liu, D., Huang, H. Z., Wang, Z. H., Hou, T. Y., Yang, X., et al. (2018). A novel MicroRNA-124/PTPN1 signal pathway mediates synaptic and memory deficits in Alzheimer's disease. *Biol. Psychiatry* 83, 395–405. doi: 10.1016/j.biopsych.2017.07.023

Wang, T., Xie, X. X., Ji, M., Wang, S. W., Zha, J., Zhou, W. W., et al. (2016). Naturally occurring autoantibodies against Aβ oligomers exhibited more beneficial effects in the treatment of mouse model of Alzheimer's disease than intravenous immunoglobulin. *Neuropharmacology* 105, 561–576. doi: 10.1016/j.neuropharm.2016.02.015

Wang, H. C., Yu, Y. Z., Liu, S., Zhao, M., and Xu, Q. (2016). Peripherally administered sera antibodies recognizing amyloid-β oligomers mitigate

Alzheimer's disease-like pathology and cognitive decline in aged 3x Tg-AD mice. *Vaccine* 34, 1758–1766. doi: 10.1016/j.vaccine.2016.02.056

Wyss-Coray, T., and Rogers, J. (2012). Inflammation in Alzheimer disease-a brief review of the basic science and clinical literature. *Cold Spring Harb. Perspect. Med.* 2:a006346. doi: 10.1101/cshperspect.a006346

Xu, S., Liu, G., Bao, X., Wu, J., Li, S., Zheng, B., et al. (2014). Rosiglitazone prevents amyloid-β oligomer-induced impairment of synapse formation and plasticity *via* increasing dendrite and spine mitochondrial number. *J. Alzheimers Dis.* 39, 239–251. doi: 10.3233/jad-130680

Conflict of Interest: The authors declare that the research was conducted in the absence of any commercial or financial relationships that could be construed as a potential conflict of interest.

frontiers in Aging Neuroscience

ORIGINAL RESEARCH
published: 30 June 2020
doi: 10.3389/fnagi.2020.00188

Default Mode Network Analysis of APOE Genotype in Cognitively Unimpaired Subjects Based on Persistent Homology

Liqun Kuang[1], Jiaying Jia[1], Deyu Zhao[1], Fengguang Xiong[1], Xie Han[1], Yalin Wang[2]* and for the Alzheimer's Disease Neuroimaging Initiative*

[1] School of Data Science and Technology, North University of China, Taiyuan, China, [2] School of Computing, Informatics, and Decision Systems Engineering, Arizona State University, Tempe, AZ, United States

Current researches on default mode network (DMN) in normal elderly have mainly focused on finding some dysfunctional areas with decreased or increased connectivity. The global network dynamics of apolipoprotein E (APOE) e4 allele group is rarely studied. In our previous brain network study, we have demonstrated the advantage of persistent homology. It can distinguish robust and noisy topological features over multiscale nested networks, and the derived properties are more stable. In this study, for the first time we applied persistent homology to analyze APOE-related effects on whole-brain functional network. In our experiments, the risk allele group exhibited lower network radius and modularity in whole brain DMN based on graph theory, suggesting the abnormal organization structure. Moreover, two suggested measures from persistent homology detected significant differences between groups within the left hemisphere and in the whole brain in two datasets. They were more statistically sensitive to APOE genotypic differences than standard graph-based measures. In summary, we provide evidence that the e4 genotype leads to distinct DMN functional alterations in the early phases of Alzheimer's disease using persistent homology approach. Our study offers a novel insight to explore potential biomarkers in healthy elderly populations carrying APOE e4 allele.

Keywords: APOE, Alzheimer's disease, persistent homology, resting state functional magnetic resonance imaging, graph theory, network measure

OPEN ACCESS

Edited by:
Jiehui Jiang,
Shanghai University, China

Reviewed by:
Takahito Yoshizaki,
Keio University, Japan
Dafin F. Muresanu,
Iuliu Haţieganu University of Medicine and Pharmacy, Romania

****Correspondence:***
Liqun Kuang
kuang@nuc.edu.cn
Yalin Wang
ylwang@asu.edu

Received: *26 March 2020*
Accepted: *02 June 2020*
Published: *30 June 2020*

Citation:
Kuang L, Jia J, Zhao D, Xiong F, Han X and Wang Y for the Alzheimer's Disease Neuroimaging Initiative (2020) Default Mode Network Analysis of APOE Genotype in Cognitively Unimpaired Subjects Based on Persistent Homology. Front. Aging Neurosci. 12:188. doi: 10.3389/fnagi.2020.00188

INTRODUCTION

Alzheimer,s disease (AD) (Lane et al., 2018) is the most common form of dementia among the elderly and the sixth leading cause of death in the United States. There are more than 50 million patients worldwide in 2018, and it is expected to reach a staggering 152 million by 2050 (Patterson, 2018). It is crucial to develop the AD-related biomarkers early in the aging process before the onset of overt cognitive impairment and irreversible brain damage (Korthauer et al., 2018). One hypothesis (Reiman et al., 2009; Lambert et al., 2013; Yu et al., 2019) for the pathogenesis (Karch and Goate, 2015) of AD indicate the apolipoprotein E (APOE) e4 allele (Lane-Donovan and Herz, 2017) involves the accumulation of Amyloid-β (Caselli et al., 2010), leading to increasing

neuronal atrophy and synapse loss. To date, APOE is a major genetic risk factor for developing AD (Thompson et al., 2013; Zhu et al., 2019). Functional neuroimaging genetics provides an effective strategy for characterizing the intermediate phenotype of AD and identifying genes that contribute to functional alterations in brain networks (Chiesa et al., 2017, Chiesa et al., 2019). In particular, recent research has demonstrated that default mode network (DMN) (Raichle, 2015) is associated with progressive brain dysfunction and is susceptible to APOE genotype (Song et al., 2015; Ma et al., 2016; Yuan et al., 2016; Palmqvist et al., 2017; Staffaroni et al., 2018; Chiesa et al., 2019).

Graph theory has increasingly been used as a theoretical framework for studying brain network characteristics. At the level of regional connection, functional connectivity between brain nodes as an important biomarker can identify early brain function alteration related to AD pathophysiology (Bokde et al., 2009). It is dedicated to investigating the distinct connectivity within the DMN that could represent the progressive biomarker. However, the results of resting state functional MRI (rs-fMRI) (Teipel et al., 2015) and APOE studies have reported mixed results (Cai et al., 2017; Luo et al., 2017; Caldwell et al., 2019; Zhu et al., 2019). Some reported decreased functional connectivity (Yan et al., 2015) in APOE e4 allele carriers (APOE4+) compared with non-carries (APOE4-), the others found some increased functional connectivity (Song et al., 2015; Zhu et al., 2018), while others didn't found any differences (Chiesa et al., 2019). At the global whole-brain level, some neurobiologically meaningful graph-theoretic properties have become important indicators for measuring brain functional networks, through which we can understand the altered network architecture in those carrying risk genotype, including a loss of small-world network (Korthauer et al., 2018), a redistribution of hubs (Wink et al., 2018), and a disrupted modular organization (Li et al., 2019). However, there are currently few network measures based on graph theory have been studied in cognitively unimpaired elderly (Seo et al., 2013; Luo et al., 2017; Pietzuch et al., 2019) and some of their results were reported as inconsistent (Seo et al., 2013; Qiu et al., 2016; Luo et al., 2017). For instance, Wink et al. (2018) found decreased centrality of DMN in APOE4+ comparing to non-carriers, while Wang et al. (2017) didn't find such genotype difference of centrality in normal elderly. Overall, graph-theoretic methods cannot consistently demonstrate functional DMN difference between APOE4+ and APOE4- in normal elderly, and the reason has been debated in the literature (Chiesa et al., 2017).

Recently, persistent homology (Edelsbrunner and Harer, 2010) from algebraic topology has been adopted for the analysis of brain network. It uses graph filtration to construct a multiscale brain network with all possible thresholds wherever the persistent topological features over the network dynamics are identified (Giusti et al., 2016). This method can distinguish robust and noisy topological features over a wide range of filtration values in measuring global brain network organization. The typical approach of persistent homology is Betti number plot (BNP) (Edelsbrunner and Harer, 2010; Lee et al., 2012), which has successfully applied to the brain network research on epilepsy (Choi et al., 2014), autism spectrum disorder and attention-deficit hyperactivity disorder (Lee et al., 2012, 2017), etc. In our previous works (Kuang et al., 2019a,b), we have developed some network properties based on persistent homology and have successfully applied them to measure the metabolic and functional networks of AD and MCI patients. Although the persistent homology works well in cognitively impaired elderly, it has never been applied to study the genetic influence on brain network yet, especially in unimpaired individuals.

In this paper, we study the effect of APOE genotype on functional DMN in cognitively unimpaired subjects. We hypothesized the topological properties of persistent homology may reveal the APOE-related alteration in DMN even before clinical symptoms appear better than graph-theoretic approaches. Using the cross-sectional rs-fMRI imaging data of 27 APOE4+ and 31 APOE4- normal elderly, we test this hypothesis by computing two persistent homology-based properties and measuring the differences between APOE4+ and APOE4- groups. We further run the statistical inference to validate their powers and compare them with some graph-theoretic methods.

MATERIALS AND METHODS

We summarize the pipeline of our framework in **Figure 1**. The rs-fMRI (Teipel et al., 2015) data of each subject are preprocessed and the blood oxygen level dependent (BOLD) signals within each region-of-interest (ROI) are obtained. Then we construct one weighted DMN per subject and quantify its global topological structure using graph theory and persistent homology. The details are described in following subsections.

Participants

Data used in the preparation of this article were obtained from the Alzheimer's Disease Neuroimaging Initiative (ADNI) database[1] (Jack et al., 2008; Jagust et al., 2010). The ADNI was launched in 2003 as a public-private partnership, led by Principal Investigator Michael W. Weiner, MD. The primary goal of ADNI has been to test whether serial magnetic resonance imaging (MRI), positron emission tomography (PET), other biological markers, and clinical and neuropsychological assessment can be combined to measure the progression of mild cognitive impairment (MCI) and early Alzheimer's disease (AD).

There were only 38 Normal Controls (NC) between the ages of 60 and 90 from the ADNI-2 who had available rs-fMRI and APOE data. Due to the small sample size of NC, we also introduced Subjective Memory Complaints (SMC), producing a dataset of cognitively unimpaired subjects in this study. The only difference from NC is that SMC reported memory problems by themselves. Individuals with two copies of the apolipoprotein e2 allele (APOE e2/2) were excluded due to its possible protective effects (Suri et al., 2013). Finally, individuals carrying at least one APOE ε4 allele (genotype e3/e4 and e4/e4) were classified as APOE4+, while individuals with genotype e3/e3 were classified as APOE4-.

Data Acquisition and Preprocessing

The experimental dataset were acquired at multiple ADNI sites using 3.0 T Philips MRI scanners. All rs-fMRI data were obtained

[1] adni.loni.usc.edu

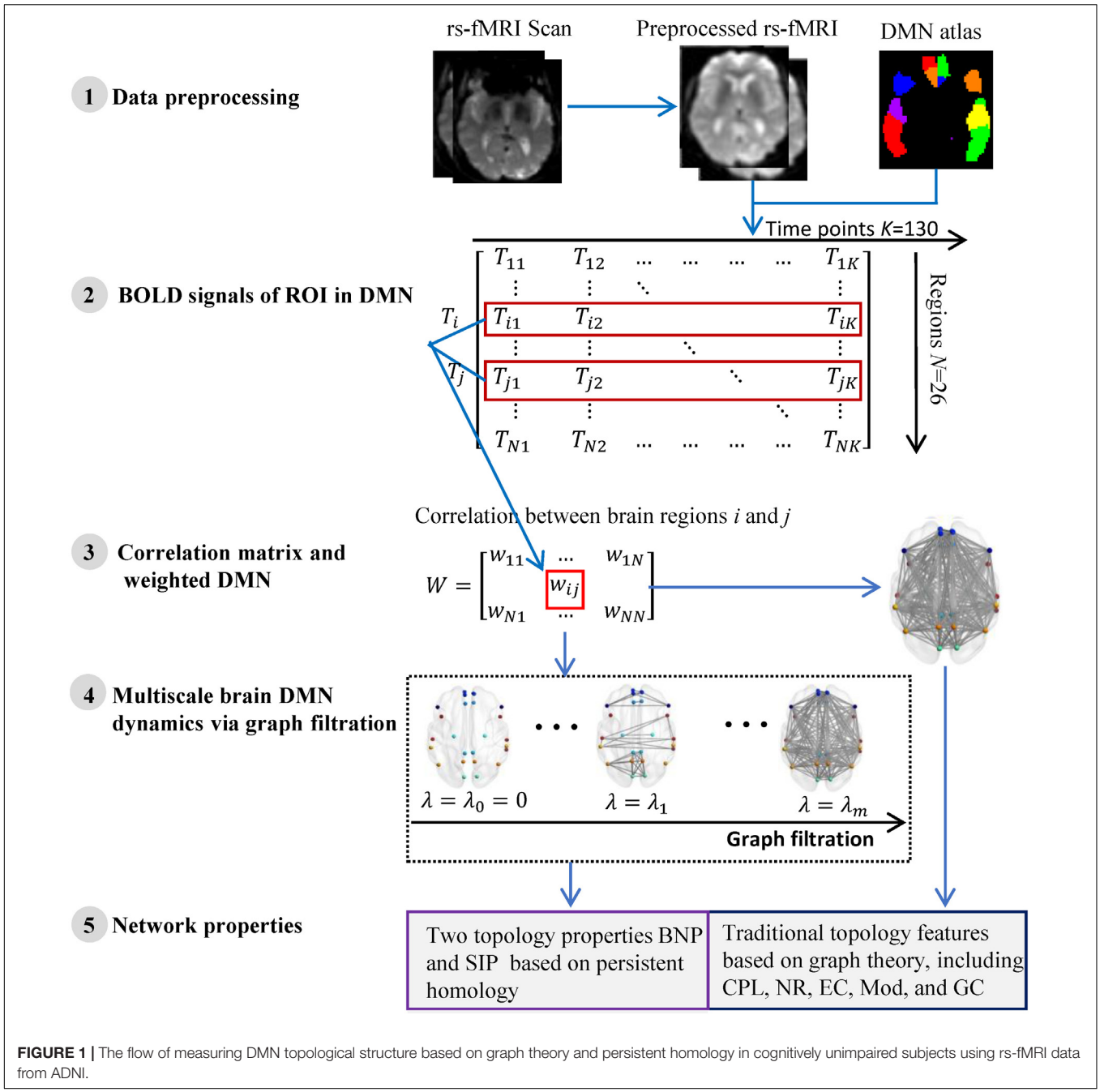

FIGURE 1 | The flow of measuring DMN topological structure based on graph theory and persistent homology in cognitively unimpaired subjects using rs-fMRI data from ADNI.

using an echo-planar imaging (EPI) sequence and the parameters included repetition time (TR) = 3000 ms, echo time (TE) = 30 ms, flip angle = 80°, number of slices = 48, slice thickness = 3.3 mm, voxel size = 3 mm × 3 mm × 3 mm, voxel matrix = 64 × 64, and time points = 140.

All functional images were pre-processed using SPM8 toolbox[2], DPARSF[3] (Yan and Zang, 2010), and REST[3] (Song et al., 2011) according to well-accepted pipelines, the same as our prior work (Kuang et al., 2019a). Briefly, the first ten time points were removed before temporal correction and spatial normalization. Then image smoothing, linear trend adjustment and band-pass filter were performed sequentially.

Construction of DMN

First, the whole brain is divided into 90 functional ROI using standard automated anatomical labeling atlas (AAL90) (Tzourio-Mazoyer et al., 2002). Then 26 areas (Vriend et al., 2018) in AAL90 are identified as the ROI of DMN, as shown in **Table 1**.

[2]http://www.fil.ion.ucl.ac.uk/spm/

[3]http://www.restfmri.net

TABLE 1 | The division of twenty six ROI nodes in DMN based on AAL90 atlas.

ROI node name	Left hemisphere		Right hemisphere	
	Index in AAL90	Abbreviation	Index in AAL90	Abbreviation
Inferior frontal gyrus pars triangularis	13	IFGtriang.L	14	IFGtriang.R
Medial frontal gyrus	23	SFGmed.L	24	SFGmed.R
Superior medial orbital frontal cortex	25	ORBsupmed.L	26	ORBsupmed.R
Anterior cingulate and paracingulate gyrus	31	ACG.L	32	ACG.R
Posterior cingulate gyrus	35	PCG.L	36	PCG.R
Parahippocampal gyrus	39	PHG.L	40	PHG.R
Cuneus	45	CUN.L	46	CUN.R
Supramarginal gyrus	63	SMG.L	64	SMG.R
Angular gyrus	65	ANG.L	66	ANG.R
Precuneus	67	PCUN.L	68	PCUN.R
Superior temporal gyrus	81	STG.L	82	STG.R
Temporal pole: superior temporal gyrus	83	TPOsup.L	84	TPOsup.R
Middle temporal gyrus	85	MTG.L	86	MTG.R

There are 13 ROI per hemisphere and each ROI is considered as a network node of DMN.

The average timing BOLD signal serial $T_i = (T_{i1}, T_{i2}, \ldots T_{ik})$ within the *i-th* ROI node is used as its measurement (Step 2 in **Figure 1**). We define the functional connectivity (i.e., edge weight) between any pair of ROI as 1-Pearson coefficient of their BOLD signal serials, i.e.

$$W_{ij} = 1 - \frac{cov(T_i, T_j)}{\sigma_{Ti}\sigma_{Tj}} = 1 - \frac{\sum_{p=1}^{k}(T_{ip} - \bar{T}_i)(T_{jp} - \bar{T}_j)}{\sqrt{\sum_{p=1}^{k}(T_{ip} - \bar{T}_i)^2}\sqrt{\sum_{p=1}^{k}(T_{jp} - \bar{T}_j)^2}} \quad (1)$$

where T_{ip} represents the average BOLD signal within the *i-th* ROI at *p-th* time point and $K = 130$ is total number of time points of the rs-fMRI data. Thus, the functional connection matrix ($N \times N$) per subject is obtained (Step 3 in **Figure 1**) and each subject's DMN is constructed. Here $N = 26$ if the DMN of entire brain is studied, otherwise $N = 13$ if only one hemispheric DMN is studied.

Measuring DMN Using Graph Theory

In the past decade, the neurobiologically meaningful network properties based on graph theory have become important indicators in measuring brain functional networks. We validate some widely used graph measures in this study (Right part of step 5 in **Figure 1**), including characteristic path length (CPL) (Li et al., 2019), global efficiency (GC) (Shu et al., 2015), network radius (NR) (Fujita et al., 2017), modularity (Mod) (Li et al., 2019), and eigenvector centrality (EC) (Luo et al., 2017). Briefly, the average shortest path length between all pairs of nodes in the network is CPL, while the average inverse shortest path length is called GC. Then NR is the minimum eccentricity of all nodes in the network and nodal eccentricity is the greatest distance between this node and any other nodes. Further, Mod measures the extent to which the network can be subdivided into clearly delineated and non-overlapping groups, and EC computes the sum of centralities of the node's direct neighbors. All these network measures were calculated by Brain Connectivity Toolbox (BCT)[4] in Matlab R2017a.

Measuring DMN Using Persistent Homology

Persistent homology (Edelsbrunner and Harer, 2010) is a mathematical concept derived from algebraic topology and is used to characterize topological features in complex data. There is an important tool, graph filtration (Giusti et al., 2016), in persistent homology that constructs a family of nested networks along an axis at their threshold values by thresholding original weighted network at every possible entry (Step 4 in **Figure 1**). Thus, it can distinguish robust and noisy topological characteristics in a wide range and enables reasonable inferences regarding the underlying organization. The classic network property based on persistent homology is BNP which detects the dynamic of the zeroth Betti number (i.e., the number of connected components) over all filtration values (Lee et al., 2012). It has been successfully applied to the some studies (Lee et al., 2012, 2017; Choi et al., 2014) of brain network in neurodegenerative diseases.

In our previous work (Kuang et al., 2019a), we proposed an integrated persistent feature (IPF) based on BNP, which introduced a connected component aggregation cost into the zeroth Betti number and thus achieves a holistic description of network dynamics. The IPF at filtration λ_i is defined as (Kuang et al., 2019a).

$$IPF\lambda_i = \begin{cases} \frac{m-i}{m(m-1)} \sum_{k=i+1}^{m-1} \lambda_k & 0 \le i \le m-2 \\ 0 & i = m-1 \end{cases} \quad (2)$$

Here, m is total number of network nodes and $\lambda_0 = 0 < \lambda_0 < \lambda_1 < \lambda_2 < \ldots < \lambda_{m-1}$ is the filtration

[4]https://sites.google.com/site/bctnet

TABLE 2 | Demographic characteristics of the high-risk (APOE4+) and low-risk (APOE4-) groups.

	APOE4+ (n = 27)	APOE4- (n = 31)	p-value
NC/SMC	16/11	22/9	–
Age	73.26 ± 6.83	74.58 ± 5.18	0.407
Education	16.81 ± 2.17	17.22 ± 2.93	0.569
Male/Female	12/15	15/16	0.769
MMSE Score	28.17 ± 1.53	28.53 ± 1.55	0.734

Data is presented as means ± standard deviations. APOE4+, APOE e3/e4 and e4/e4 alleles; APOE4-: APOE e3/e3 allele; NC, Normal Control; SMC, Subjective Memory Complaint; MMSE, Mini-Mental State Examination; CDR, Clinical Dementia Rating.

value which is actually the set of weights of minimum spanning tree of the original weighted network. Previous work has proven that the IPF is a monotonically decreasing convergence function over all possible filtration. In summary, when λ increases from zero, the IPF value of the network will decrease to zero accordingly until all nodes are connected into a single connected component. Therefore, the slope of the IPF plot (SIP) can be used as an important network property to quantify the brain network dynamics. Both network measures BNP and SIP can be considered as information diffusion rate or convergence rate of the network. We provided their implementations at http://gsl.lab.asu.edu/software/IPF and applied them in this study (Left part of step 5 in **Figure 1**).

RESULTS

Demographic Information

In this experiment, 58 subjects without cognitive impairment were selected from ADNI-2, and were divided into two groups, APOE e4 carriers and non-carriers, according to their APOE genotype. Among them, 20 subjects were identified as SMC and remaining 38 subjects were NC. The only difference from NC is that SMC reported memory problems by themselves. We considered both as cognitively impairment subjects in this study. As shown in **Table 2**, there were no significant differences in age, education, Mini Mental State Examination (MMSE) score, and Clinical Dementia Rating (CDR) global scores between groups. All subjects had MMSE of 24–30, CDR = 0, and were cognitively unimpaired. Furthermore, all studied images did not have excessive head motion (six-parameter rigid body) defined by a displacement of less than 1 mm or an angular rotation of less than in any direction 1°.

Multiscale Brain DMN Dynamics

We constructed one original weighted DMN per subject. The 26 network nodes in whole brain DMN were determined according to **Table 2** and are visualized in **Figure 2** using Brain Net Viewer software (Xia et al., 2013). Then, the edge weights between them were calculated using Eq. (1). We further constructed multiscale networks based on the original DMN using graph filtration tool (Step 4 in **Figure 1**). As we only observe the zeroth homology in this study, the filtration value λ is actually the set of weights of minimum spanning tree of DMN. **Figure 3** shows the multiscale network dynamics for two mean DMN of two groups over some filtration values. **Figure 4** shows the change of zeroth Betti number using single linkage dendrogram (Lee et al., 2012). All the nodes on the left are connected to form the larger component on the right, until finally a fully connected network is constructed. The zeroth Betti number starts at 26, and gradually decreases to 1 while more and more nodes are connected.

From **Figures 3**, **4**, we intuitively saw that the connected components in APOE+ aggregated slightly faster than APOE-, especially after λ is larger than 0.35. However, it needs to be further quantitatively measured by network properties based on persistent homology.

Brain DMN Properties

We calculated the corresponding Betti number β_0 and IPF of the multiscale DMN at all different filtration values for two group means, and plotted them, as shown in **Figure 5**. We found that the APOE+ curve in both Betti number plot and IPF plot were steeper than the APOE- curve, suggesting the faster aggregation of APOE+, which is consistent with the above observation of multiscale brain dynamics (see **Figures 3**, **4**). All subjects' values of BNP and SIP properties based on persistent homology were summarized using box plot as shown in **Figures 6A,B**, separately, where 1 represents APOE4+ and 2 is APOE4-. The distributions of both BNP and SIP property values between groups are obviously different, indicating both persistent features may be able to discriminate APOE4+ from APOE4-.

Traditionally, brain network properties have been measured using graph theory methods. In order to compare with our suggested methods based on persistent homology, we also calculated some classical graph theory properties, including CPL, NR, EC, Mod, and GC. The distributions of all attribute values are shown in **Figures 6C–G** where 1 and 2 represents APOE4+ and APOE4-, respectively. We observed that the between-group differences of SIP, BNP, NR, and Mod are more apparent than those of CPL, EC, and GC.

Statistical Group Difference

In the statistical analysis of differences between groups of APOE4+ and APOE4-, we performed the permutation test of 10,000 permutations on all network properties using Matlab R2017a and calculated their resulting p-values as shown in **Table 3**. First, the differences between groups in whole brain DMN with 26 ROI nodes were measured. Two persistent features SIP and BNP obtained significant differences at significance level of 0.05, which were $p = 0.021$ and $p = 0.009$, respectively. In the statistic inferences for five compared graph theory-based properties, only NR and Mod obtained significant differences with $p = 0.024$ and $p = 0.037$, respectively, while there were no significant differences in other three properties, CPL, EC, and GC. Then, we analyzed the group differences within the single hemisphere and only two measures SIP and BNP achieved significant differences ($p = 0.027$, both) within the left hemisphere. We did not find any differences within the right hemisphere.

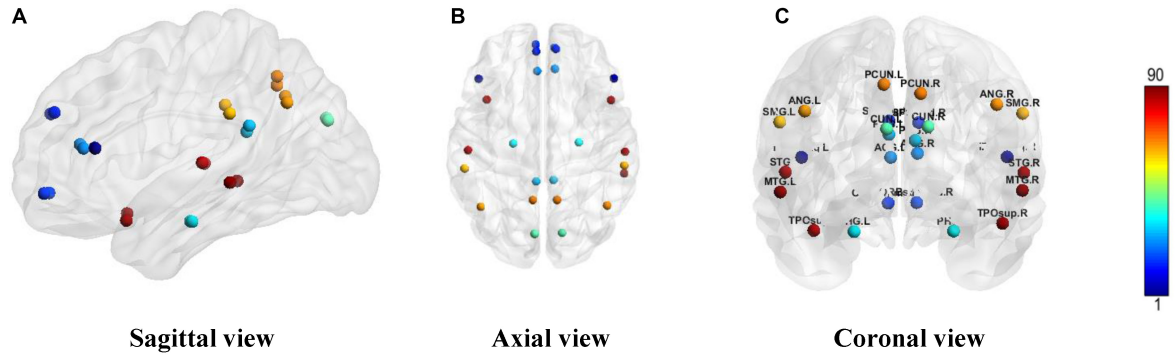

FIGURE 2 | The ROI in DMN from **(A)** sagittal view, **(B)** axial view, and **(C)** coronal view. The color bar shows the ROI node index predefined in AAL90 atlas.

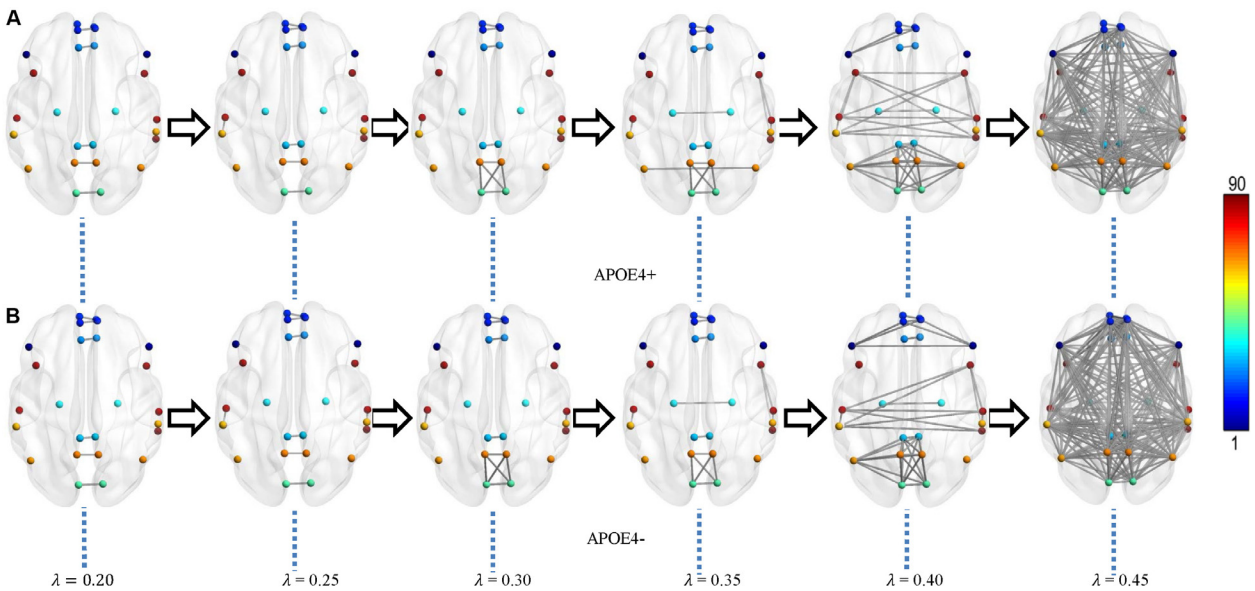

FIGURE 3 | Multiscale DMN dynamics for two mean networks of **(A)** APOE4+ and **(B)** APOE4- groups at six different filtration values 0.20, 0.25, 0.30, . . ., 0.45. The color bar shows the ROI node index predefined in AAL90 atlas.

In short, our experimental results show that both persistent properties achieved more significant group differences between APOE4+ and APOE4- than traditional graph-theoretic measures, and BNP obtained the most significant difference ($p = 0.009$) in the study of whole brain DMN.

DISCUSSION

Present Findings

There are three main findings in this study.

First, we found that the e4 allele carriers exhibited lower NR and Mod ($p = 0.024$, 0.037, respectively) in the study of whole brain DMN using traditional graph-theoretic methods, suggesting the abnormal organization structure in the risk allele group. To our knowledge, there have been few studies (Luo et al., 2017; Pietzuch et al., 2019) on graph theory that have reported APOE genotypic differences in functional network properties of whole brain DMN in normal elderly, although a lot of studies have found differences in functional network properties between AD/MCI and NC. Some studies (Staffaroni et al., 2018; Chiesa et al., 2019) even found no difference between elderly APOE4+ and APOE4- groups in functional DMN. The reason why findings of DMN on unimpaired individuals do not consistently demonstrate differences between APOE4+ and APOE4- is still debated in the literature (Chiesa et al., 2017). In our study, we found two measures could detect their differences significantly, which would further enhance the APOE research based on graph theory.

Second, we introduced two measures from our previous studies based on persistent homology and found they were more statistically powerful than graph-theoretic measures in discriminating APOE4+ from APOE4- in our experiment, and the BNP obtained the most significant difference ($p = 0.009$)

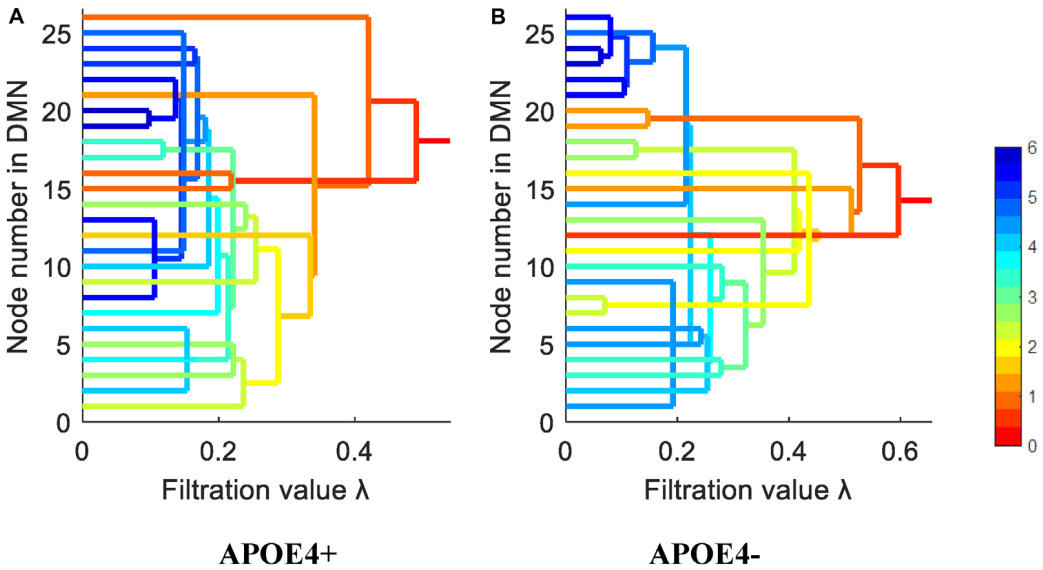

FIGURE 4 | The single linkage dendrograms of **(A)** APOE4 carriers and **(B)** non-carriers groups show the change of the zeroth Betti number. The color represents the target distance (total edge weight) from current connected component to the full connected component (the rightmost line).

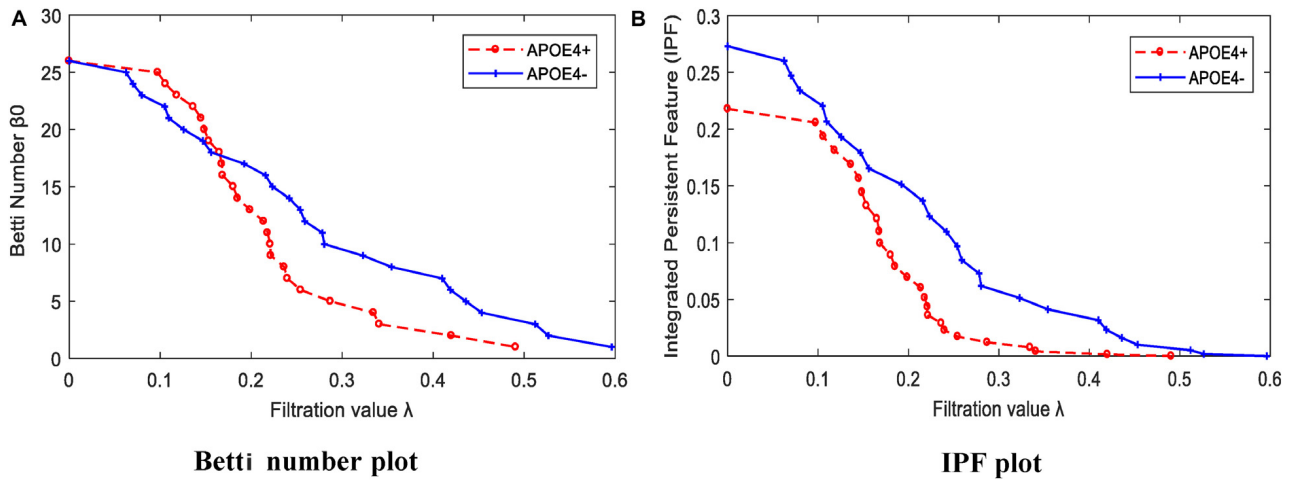

FIGURE 5 | The persistent feature dynamics over filtrations for APOE4+ and APOE4- by **(A)** Betti number plot and **(B)** IPF plot.

between groups. The persistent homology approach can distinguish robust and noisy topological features over multiscale nested networks, and the obtained properties are more persistent and stable. So far, many studies of brain network based on persistent homology have demonstrated the superiority of the performance. To our knowledge, it is the first time we introduced persistent homology to study the APOE genotype effect on DMN.

Finally, the functional disruption within the left hemisphere may be more pronounced than the right one. All persistent homology-based features SIP and BNP detected the significant differences of DMN in whole brain and left hemisphere. However, no significant differences were found within the right hemispheric DMN using any network measures. This finding is consistent with existing APOE studies documenting the effect of the e4 allele on left hippocampus rather than right hippocampus of non-demented individuals (Shi et al., 2014; Li et al., 2016; Dong et al., 2019).

Verification on Normal Control Subjects

As there were only 16 NC individuals who had e4 allele and available rs-fMRI data in ADNI-2, we expanded our experimental sample size by including SMC subjects. However, some studies (Caldwell et al., 2019) on APOE have only investigated NC individuals from ADNI. Thus, we excluded all SMC subjects (see **Table 2**) and further repeated our experiment on NC subjects. As shown in **Table 4**, there were no significant differences in age, education, sex, and MMSE between APOE+ and APOE- in NC dataset. We calculated the differences of DMN between

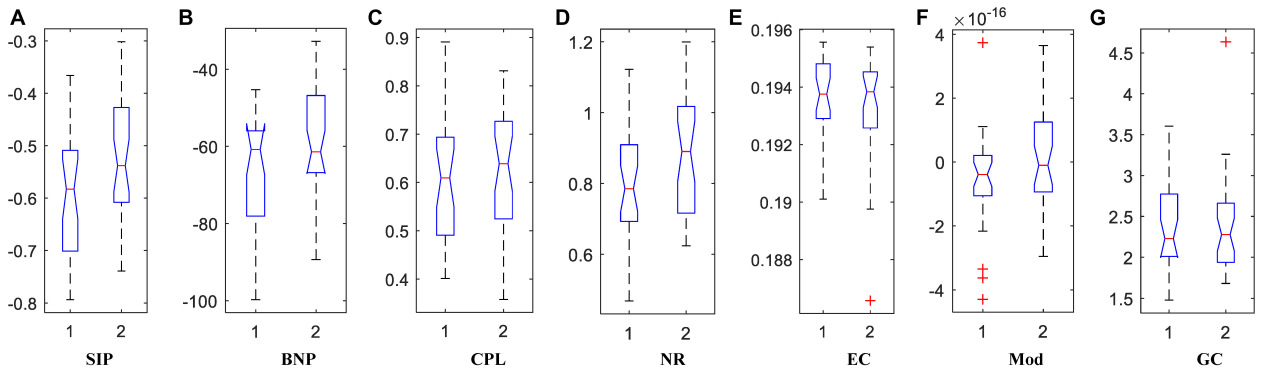

FIGURE 6 | The box plots of property values for APOE4 carriers (1) and non-carriers (2) groups using two persistent homology properties, **(A)** SIP and **(B)** BNP, and five graph-theoretic properties, **(C)** CPL, **(D)** NR, **(E)** EC, **(F)** Mod, and **(G)** GC.

groups using different measures, as shown in **Table 5**. Again, two measures based on persistent homology obtained stronger statistical power than graph theory methods, and the differences within the left hemispheric DMN is more significant than the right one. Moreover, compared to experiments performed on cognitively unimpaired dataset (**Table 3**), the SIP obtained very significant difference ($p = 0.006$) on NC dataset.

Limitation and Future Works

Despite the promising results were obtained by applying two suggested network properties SIP and BNP based on persistent homology to discriminate APOE e4 allele carriers from non-carriers in cognitively unimpaired subjects, there are three important caveats.

First, both persistent homology-based properties BNP and SIP adopted in this study only investigated the dynamics of the zeroth persistent homology. Higher-dimensional persistent homology characterizes higher-dimensional topological features, and more complexed topological structures such as circular holes can be detected. Therefore, the performance of network measurement may be further boosted if higher-dimensional homology is applied, especially in the sparse network that tends to have more holes.

Then, although the DMN have been heavily studied and are reported as a promising kind of network to study, current researches have mainly focused on finding some dysfunctional areas with decreased or increased connectivity (Song et al., 2015; Yan et al., 2015; Zhu et al., 2018; Chiesa et al., 2019). There are relatively few studies on global network dynamics of e4 allele group in normal elderly. In this study, we measured the global brain network in two datasets (cognitively unimpaired dataset and its subset NC) and found some statistically powerful measures. In future, we will validate these measures in other independent datasets.

TABLE 3 | Statistical *p*-values of different network properties between APOE4+ and APOE4- groups.

Hemisphere	Persistent homology-based properties		Graph theory-based properties				
	SIP	BNP	CPL	NR	EC	Mod	GC
Both	0.021	0.009	0.237	0.024	0.273	0.037	0.458
Left	0.027	0.027	0.316	0.154	0.422	0.361	0.418
Right	0.144	0.097	0.134	0.052	0.281	0.090	0.393

The permutation test of 10,000 permutations was performed for statistical inference. APOE4+, APOE e3/e4 and e4/e4 alleles; APOE4-: APOE e3/e3 allele; SIP, Slope of Integrated persistent feature Plot; BNP, Betti Number Plot; CPL, Characteristic Path Length; NR, Network Radius; EC, Eigenvector Centrality; Mod, modularity; GC, Global Efficiency.

TABLE 4 | Demographic characteristics of NC dataset.

	APOE4+ ($n = 16$)	APOE4- ($n = 22$)	*p*-value
Age	73.88 ± 7.35	75.75 ± 5.34	0.368
Education	16.53 ± 1.97	16.84 ± 2.84	0.462
Male/Female	7/9	10/12	0.920
MMSE Score	28.59 ± 1.65	28.77 ± 1.66	0.833

Data is presented as means ± standard deviations. APOE4+, APOE e3/e4 and e4/e4 alleles; APOE4-, APOE e3/e3 allele; NC, Normal Control; MMSE, Mini-Mental State Examination; CDR, Clinical Dementia Rating.

TABLE 5 | Statistical *p*-values of different network properties on NC between APOE4+ and APOE4- groups.

Hemisphere	Persistent homology-based properties		Graph theory-based properties				
	SIP	BNP	CPL	NR	EC	Mod	GC
Both	0.006	0.004	0.365	0.062	0.183	0.037	0.201
Left	0.047	0.049	0.364	0.177	0.276	0.089	0.368
Right	0.078	0.098	0.190	0.095	0.162	0.195	0.352

APOE4+, APOE e3/e4 and e4/e4 alleles; APOE4-: APOE e3/e3 allele; SIP, Slope of Integrated persistent feature Plot; BNP, Betty Number Plot; CPL, Characteristic Path Length; NR, Network Radius; EC, Eigenvector Centrality; Mod, modularity; GC, Global Efficiency.

Finally, current findings are achieved based on cross-sectional study. With longitudinal analysis, we may further study the longitudinal trajectories (Chiesa et al., 2019) of functional brain dynamics and the impact of e4 allele on individuals at risk for Alzheimer's disease by quantifying the difference of their persistent features. In addition, the more aggregated structure in APOE e4 allele carriers may be due to worse development in childhood. Examining longitudinal MRI since childhood, the possibility of this phenomenon could be further assessed.

CONCLUSION

This work measured the DMN structure of rs-fMRI on cognitively unimpaired e4 allele carriers based on our prior work of persistent homology, which encodes a great deal of dynamic information over all possible scales. The significant differences between APOE4+ and APOE4- are identified within the left hemispheric DMN and in the whole brain DMN in two datasets, providing evidence that the APOE e4 genotype leads to distinct alterations of functional DMN several years before the occurrence of dementia symptoms. Moreover, our suggested approaches of persistent homology are more sensitive to APOE genotypic differences than standard graph-based network measures. To the best of our knowledge, this is the first study applying persistent homology to analyze APOE-related effect on whole-brain functional network. This study offers a novel insight to explore potential biomarkers in healthy elderly populations carrying APOE e4 allele.

DATA AVAILABILITY STATEMENT

Publicly available datasets were analyzed in this study. This data can be found from the ADNI (http://adni.loni.usc.edu).

ETHICS STATEMENT

In this study, all subjects were selected from the Alzheimer's Disease Neuroimaging Initiative (ADNI) database (http://adni.loni.usc.edu/). All ADNI subjects gave written informed consent at enrollment for data collection, storage, and use for research.

AUTHOR CONTRIBUTIONS

LK and YW designed the study and revised the manuscript. FX acquired the data. JJ, DZ, and LK analyzed and interpreted the results of the data. LK and XH drafted the manuscript. All authors contributed to the article and approved the submitted version.

FUNDING

This research was funded by the National Key Research and Development Program of China (2018YFB2101504 to LK, FX, and XH), the Shanxi Provincial Key Research and Development Project (201803D121081 and 201903D121147 to LK, FX, and XH), the Natural Science Foundation of Shanxi Province of China (201901D111150 to LK, FX, and XH), the Graduate Science and Technology Project at North University of China (20191638 to JJ), the National Institute on Aging (R21AG043760, R21AG049216, and RF1AG051710 to YW), the National Institute of Biomedical Imaging and Bioengineering (R01EB025032 to YW), the National Heart, Lung, and Blood Institute (R01HL128818 to YW), and the National Science Foundation (DMS-1413417 and IIS-1421165 to YW).

ACKNOWLEDGMENTS

Data collection and sharing for this project was funded by the Alzheimer's Disease Neuroimaging Initiative (ADNI) (National Institutes of Health Grant U01 AG024904) and DOD ADNI (Department of Defense award number W81XWH-12-2-0012). ADNI was funded by the National Institute on Aging, the National Institute of Biomedical Imaging and Bioengineering, and through generous contributions from the following: AbbVie, Alzheimer's Association; Alzheimer's Drug Discovery Foundation; Araclon Biotech; BioClinica, Inc.; Biogen; Bristol-Myers Squibb Company; CereSpir, Inc.; Cogstate; Eisai Inc.; Elan Pharmaceuticals, Inc.; Eli Lilly and Company; EuroImmun; F. Hoffmann-La Roche Ltd and its affiliated company Genentech, Inc.; Fujirebio; GE Healthcare; IXICO Ltd.; Janssen Alzheimer Immunotherapy Research & Development, LLC.; Johnson & Johnson Pharmaceutical Research & Development LLC.; Lumosity; Lundbeck; Merck & Co., Inc.; Meso Scale Diagnostics, LLC.; NeuroRx Research; Neurotrack Technologies; Novartis Pharmaceuticals Corporation; Pfizer Inc.; Piramal Imaging; Servier; Takeda Pharmaceutical Company; and Transition Therapeutics. The Canadian Institutes of Health Research is providing funds to support ADNI clinical sites in Canada. Private sector contributions are facilitated by the Foundation for the National Institutes of Health (www.fnih.org). The grantee organization is the Northern California Institute for Research and Education, and the study is coordinated by the Alzheimer's Therapeutic Research Institute at the University of Southern California. ADNI data are disseminated by the Laboratory for Neuroimaging at the University of Southern California.

REFERENCES

Bokde, A. L. W., Ewers, M., and Hampel, H. (2009). Assessing neuronal networks: understanding Alzheimer's disease. *Prog. Neurobiol.* 89, 125–133. doi: 10.1016/j.pneurobio.2009.06.004

Cai, S., Jiang, Y., Wang, Y., Wu, X., Ren, J., Lee, M. S., et al. (2017). Modulation on brain gray matter activity and white matter integrity by APOE epsilon 4 risk gene in cognitively intact elderly: a multimodal neuroimaging study. *Behav. Brain Res.* 322, 100–109. doi: 10.1016/j.bbr.2017.01.027

Caldwell, J. Z. K., Zhuang, X., Leavitt, M. J., Banks, S. J., Cummings, J., Cordes, D., et al. (2019). Sex moderates amyloid and apolipoprotein epsilon 4 effects on default mode network connectivity at rest. *Front. Neurol.* 10:900. doi: 10.3389/fneur.2019.00900

Caselli, R. J., Walker, D., Sue, L., Sabbagh, M., and Beach, T. (2010). Amyloid load in nondemented brains correlates with APOE e4. *Neurosci. Lett.* 473, 168–171. doi: 10.1016/j.neulet.2010.02.016

Chiesa, P. A., Cavedo, E., Lista, S., Thompson, P. M., Hampel, H., and Alzheimer Precision Medicine Initiative, (2017). Revolution of resting-state functional neuroimaging genetics in Alzheimer's disease. *Trends Neurosci.* 40, 469–480. doi: 10.1016/j.tins.2017.06.002

Chiesa, P. A., Cavedo, E., Vergallo, A., Lista, S., Potier, M.-C., Habert, M.-O., et al. (2019). Differential default mode network trajectories in asymptomatic individuals at risk for Alzheimer's disease. *Alzheimers Dementia* 15, 940–950. doi: 10.1016/j.jalz.2019.03.006

Choi, H., Kim, Y. K., Kang, H., Lee, H., Im, H.-J., Kim, E. E., et al. (2014). Abnormal metabolic connectivity in the pilocarpine-induced epilepsy rat model: a multiscale network analysis based on persistent homology. *Neuroimage* 99, 226–236. doi: 10.1016/j.neuroimage.2014.05.039

Dong, Q., Zhang, W., Wu, J., Li, B., Schronh, E. H., McMahon, T., et al. (2019). Applying surface-based hippocampal morphometry to study APOE-E4 allele dose effects in cognitively unimpaired subjects. *Neuroimage Clin.* 22:101744. doi: 10.1016/j.nicl.2019.101744

Edelsbrunner, H., and Harer, J. (2010). *Computational Topology: an Introduction*. Providence, RI: American Mathematical Society.

Fujita, A., Takahashi, D. Y., Balardin, J. B., Vidal, M. C., and Sato, J. R. (2017). Correlation between graphs with an application to brain network analysis. *Comput. Stat. Data Anal.* 109, 76–92. doi: 10.1016/j.csda.2016.11.016

Giusti, C., Ghrist, R., and Bassett, D. S. (2016). Two's company, three (or more) is a simplex : algebraic-topological tools for understanding higher-order structure in neural data. *J. Comput. Neurosci.* 41, 1–14. doi: 10.1007/s10827-016-0608-6

Jack, C. R., Bernstein, M. A., Fox, N. C., Thompson, P., Alexander, G., Harvey, D., et al. (2008). The Alzheimer's disease neuroimaging initiative (ADNI): MRI methods. *J. Magnet. Reson. Imaging* 27, 685–691.

Jagust, W. J., Bandy, D., Chen, K., Foster, N. L., Landau, S. M., Mathis, C. A., et al. (2010). The Alzheimer's disease neuroimaging initiative positron emission tomography core. *Alzheimer's Dementia* 6, 221–229.

Karch, C. M., and Goate, A. M. (2015). Alzheimer's disease risk genes and mechanisms of disease pathogenesis. *Biol. Psychiatry* 77, 43–51. doi: 10.1016/j.biopsych.2014.05.006

Korthauer, L. E., Zhan, L., Ajilore, O., Leow, A., and Driscoll, I. (2018). Disrupted topology of the resting state structural connectome in middle-aged APOE epsilon 4 carriers. *Neuroimage* 178, 295–305. doi: 10.1016/j.neuroimage.2018.05.052

Kuang, L., Han, X., and Chen, K. (2019a). A concise and persistent feature to study brain resting-state network dynamics: findings from the Alzheimer's disease neuroimaging initiative. *Hum. Brain Mapp.* 40, 1062–1081. doi: 10.1002/hbm.24383

Kuang, L., Zhao, D., Xing, J., Chen, Z., Xiong, F., and Han, X. (2019b). Metabolic brain network analysis of FDG-PET in Alzheimer's disease using kernel-based persistent features. *Molecules* 24:2301. doi: 10.3390/molecules24122301

Lambert, J.-C., Ibrahim-Verbaas, C. A., Harold, D., Naj, A. C., Sims, R., Bellenguez, C., et al. (2013). Meta-analysis of 74,046 individuals identifies 11 new susceptibility loci for Alzheimer's disease. *Nat. Genet.* 45, 1452–U1206. doi: 10.1038/ng.2802

Lane, C. A., Hardy, J., and Schott, J. M. (2018). Alzheimer's disease. *Eur. J. Neurol.* 25, 59–70. doi: 10.1111/ene.13439

Lane-Donovan, C., and Herz, J. (2017). ApoE, ApoE receptors, and the synapse in Alzheimer's disease. *Trends Endocrinol. Metab.* 28, 273–284. doi: 10.1016/j.tem.2016.12.001

Lee, H., Kang, H., Chung, M. K., Kim, B.-N., and Lee, D. S. (2012). Persistent brain network homology from the perspective of dendrogram. *IEEE Trans. Med. Imaging* 31, 2267–2277. doi: 10.1109/tmi.2012.2219590

Lee, H., Kang, H., Chung, M. K., Lim, S., Kim, B. N., and Lee, D. S. (2017). Integrated multimodal network approach to PET and MRI based on multidimensional persistent homology. *Hum. Brain Mapp.* 38, 1387–1402. doi: 10.1002/hbm.23461

Li, B., Shi, J., Gutman, B. A., Baxter, L. C., Thompson, P. M., Caselli, R. J., et al. (2016). Influence of APOE genotype on hippocampal atrophy over time – an N=1925 surface-based ADNI study. *PLoS One* 11:e0152901. doi: 10.1371/journal.pone.0152901

Li, Y., Yao, Z. J., Yu, Y., Fu, Y., Zou, Y., Hu, B., et al. (2019). The influence of Cerebrospinal fluid abnormalities and APOE 4 on PHF-Tau protein: evidence from voxel analysis and graph theory. *Front. Aging Neurosci.* 11:208. doi: 10.3389/fnagi.2019.00208

Luo, X., Qiu, T., Jia, Y., Huang, P., Xu, X., Yu, X., et al. (2017). Intrinsic functional connectivity alterations in cognitively intact elderly APOE epsilon 4 carriers measured by eigenvector centrality mapping are related to cognition and CSF biomarkers: a preliminary study. *Brain Imaging Behav.* 11, 1290–1301. doi: 10.1007/s11682-016-9600-z

Ma, C., Zhang, Y., Li, X., Chen, Y., Zhang, J., Liu, Z., et al. (2016). The TT allele of rs405509 synergizes with APOE epsilon 4 in the impairment of cognition and its underlying default mode network in non-demented elderly. *Curr. Alzheimer Res.* 13, 708–717. doi: 10.2174/1567205013666160129100350

Palmqvist, S., Scholl, M., Strandberg, O., Mattsson, N., Stomrud, E., Zetterberg, H., et al. (2017). Earliest accumulation of beta-amyloid occurs within the default-mode network and concurrently affects brain connectivity. *Nat. Commun.* 8:1214. doi: 10.1038/s41467-017-01150-x

Patterson, C. (2018). *World Alzheimer Report 2018*. London: Alzheimer's Disease International.

Pietzuch, M., King, A. E., Ward, D. D., and Vickers, J. C. (2019). The influence of genetic factors and cognitive reserve on structural and functional resting-state brain networks in aging and Alzheimer's disease. *Front. Aging Neurosci.* 11:30. doi: 10.3389/fnagi.2019.00030

Qiu, T., Luo, X., Shen, Z., Huang, P., Xu, X., Zhou, J., et al. (2016). Disrupted brain network in progressive mild cognitive impairment measured by eigenvector centrality mapping is linked to cognition and cerebrospinal fluid biomarkers. *J. Alzheimer's Dis.* 54, 1483–1493. doi: 10.3233/JAD-160403

Raichle, M. E. (2015). The brain's default mode network. *Annu. Rev. Neurosci.* 38, 433–447. doi: 10.1146/annurev-neuro-071013-014030

Reiman, E. M., Chen, K., Liu, X., Bandy, D., Yu, M., Lee, W., et al. (2009). Fibrillar amyloid-beta burden in cognitively normal people at 3 levels of genetic risk for Alzheimer's disease. *Proc. Natl. Acad. Sci. U.S.A.* 106, 6820–6825. doi: 10.1073/pnas.0900345106

Seo, E. H., Lee, D. Y., Lee, J.-M., Park, J.-S., Sohn, B. K., Choe, Y. M., et al. (2013). Influence ofAPOE genotype on whole-brain functional networks in cognitively normal elderly. *PLoS One* 8:e83205. doi: 10.1371/journal.pone.0083205

Shi, J., Lepore, N., Gutman, B. A., Thompson, P. M., Baxter, L. C., Caselli, R. J., et al. (2014). Genetic influence of apolipoprotein E4 Genotype on hippocampal morphometry: an N=725 surface-based Alzheimer's disease neuroimaging initiative study. *Hum. Brain Mapp.* 35, 3903–3918. doi: 10.1002/hbm.22447

Shu, N., Li, X., Ma, C., Zhang, J., Chen, K., Liang, Y., et al. (2015). Effects of APOE promoter polymorphism on the topological organization of brain structural connectome in nondemented elderly. *Hum. Brain Mapp.* 36, 4847–4858. doi: 10.1002/hbm.22954

Song, H., Long, H., Zuo, X., Yu, C., Liu, B., Wang, Z., et al. (2015). APOE effects on default mode network in Chinese cognitive normal elderly: relationship with clinical cognitive performance. *PLoS One* 10:e0133179. doi: 10.1371/journal.pone.0133179

Song, X.-W., Dong, Z.-Y., Long, X.-Y., Li, S.-F., Zuo, X.-N., Zhu, C.-Z., et al. (2011). REST: a toolkit for resting-state functional magnetic resonance imaging data processing. *PLoS One* 6:e25031. doi: 10.1371/journal.pone.0025031

Staffaroni, A. M., Brown, J. A., Casaletto, K. B., Elahi, F. M., Deng, J., Neuhaus, J., et al. (2018). The longitudinal trajectory of default mode network connectivity in healthy older adults varies as a function of age and is associated with changes in episodic memory and processing speed. *J. Neurosci.* 38, 2809–2817. doi: 10.1523/jneurosci.3067-17.2018

Suri, S., Heise, V., Trachtenberg, A. J., and Mackay, C. E. (2013). The forgotten APOE allele: a review of the evidence and suggested mechanisms for the protective effect of APOE epsilon 2. *Neurosci. Biobehav. Rev.* 37, 2878–2886. doi: 10.1016/j.neubiorev.2013.10.010

Teipel, S., Drzezga, A., Grothe, M. J., Barthel, H., Chételat, G., Schuff, N., et al. (2015). Multimodal imaging in Alzheimer's disease: validity and usefulness for early detection. *Lancet Neurol.* 14, 1037–1053. doi: 10.1016/s1474-4422(15)00093-9

Thompson, P. M., Ge, T., Glahn, D. C., Jahanshad, N., and Nichols, T. E. (2013). Genetics of the connectome. *Neuroimage* 80, 475–488. doi: 10.1016/j.neuroimage.2013.05.013

Tzourio-Mazoyer, N., Landeau, B., Papathanassiou, D., Crivello, F., Etard, O., Delcroix, N., et al. (2002). Automated anatomical labeling of activations in SPM using a macroscopic anatomical parcellation of the MNI MRI single-subject brain. *Neuroimage* 15, 273–289. doi: 10.1006/nimg.2001.0978

Vriend, C., van den Heuvel, O. A., Berendse, H. W., van der Werf, Y. D., and Douw, L. (2018). Global and subnetwork changes of the structural connectome in de novo Parkinson's disease. *Neuroscience* 386, 295–308. doi: 10.1016/j.neuroscience.2018.06.050

Wang, Z., Dai, Z., Shu, H., Liao, X., Yue, C., Liu, D., et al. (2017). APOE genotype effects on intrinsic brain network connectivity in patients with amnestic mild cognitive impairment. *Sci. Rep.* 7:397. doi: 10.1038/s41598-017-00432-0

Wink, A. M., Tijms, B. M., ten Kate, M., Raspor, E., de Munck, J. C., Altena, E., et al. (2018). Functional brain network centrality is related to APOE genotype in cognitively normal elderly. *Brain Behav.* 8:e01080. doi: 10.1002/brb3.1080

Xia, M., Wang, J., and He, Y. (2013). BrainNet viewer: a network visualization tool for human brain connectomics. *PLoS One* 8:e68910. doi: 10.1371/journal.pone.0068910

Yan, C., and Zang, Y. (2010). DPARSF: a MATLAB toolbox for "pipeline" data analysis of resting-state fMRI. *Front. Syst. Neurosci.* 4:13. doi: 10.3389/fnsys.2010.00013

Yan, F.-X., Wu, C. W., Chao, Y.-P., Chen, C.-J., and Tseng, Y.-C. (2015). APOE-epsilon 4 allele altered the rest-stimulus interactions in healthy middle-aged adults. *PLoS One* 10:e0128442. doi: 10.1371/journal.pone.0128442

Yu, L., Petyuk, V. A., Tasaki, S., Boyle, P. A., Gaiteri, C., Schneider, J. A., et al. (2019). Association of cortical beta-amyloid protein in the absence of insoluble deposits with Alzheimer disease. *JAMA Neurol.* 76, 818–826. doi: 10.1001/jamaneurol.2019.0834

Yuan, B., Xie, C., Shu, H., Liao, W., Wang, Z., Liu, D., et al. (2016). Differential effects of APOE genotypes on the anterior and posterior subnetworks of default mode network in amnestic mild cognitive impairment. *J. Alzheimers Dis.* 54, 1409–1423. doi: 10.3233/jad-160353

Zhu, L., Shu, H., Liu, D., Guo, Q., Wang, Z., and Zhang, Z. (2018). Apolipoprotein E epsilon 4 specifically modulates the hippocampus functional connectivity network in patients with amnestic mild cognitive impairment. *Front. Aging Neurosci.* 10:289. doi: 10.3389/fnagi.2018.00289

Zhu, Y., Gong, L., He, C., Wang, Q., Ren, Q., Xie, C., et al. (2019). Default mode network connectivity moderates the relationship between the APOE genotype and cognition and individualizes identification across the Alzheimer's disease spectrum. *J. Alzheimers Dis.* 70, 843–860. doi: 10.3233/jad-190254

Conflict of Interest: The authors declare that the research was conducted in the absence of any commercial or financial relationships that could be construed as a potential conflict of interest.

frontiers in Neuroscience

ORIGINAL RESEARCH
published: 30 June 2020
doi: 10.3389/fnins.2020.00604

Associations of [^{18}F]-APN-1607 Tau PET Binding in the Brain of Alzheimer's Disease Patients With Cognition and Glucose Metabolism

Jiaying Lu[1], Weiqi Bao[1], Ming Li[1], Ling Li[1], Zhengwei Zhang[1], Ian Alberts[2], Matthias Brendel[3], Paul Cumming[2,4], Huimeng Lu[5], Zhenxu Xiao[5], Chuantao Zuo[1], Yihui Guan[1]*, Qianhua Zhao[5]* and Axel Rominger[2]*

[1] PET Center, Huashan Hospital, Fudan University, Shanghai, China, [2] Department of Nuclear Medicine, University Hospital Bern, Bern, Switzerland, [3] Department of Nuclear Medicine, University Hospital of Munich, Ludwig Maximilian University of Munich, Munich, Germany, [4] Faculty of Health, School of Psychology and Counselling, Queensland University of Technology, Brisbane, QLD, Australia, [5] Department of Neurology, Huashan Hospital, Fudan University, Shanghai, China

OPEN ACCESS

Edited by:
Chih-Yu Hsu,
Fujian University of Technology, China

Reviewed by:
Pai-Yi Chiu,
Chang Bing Show Chwan Memorial Hospital, Taiwan
Li Wei,
Taipei Medical University, Taiwan

***Correspondence:**
Qianhua Zhao
applenasa@hotmail.com
Yihui Guan
guanyihui@hotmail.com
Chuantao Zuo
zuochuantao@fudan.edu.cn

Specialty section:
This article was submitted to Neurodegeneration, a section of the journal Frontiers in Neuroscience

Received: 25 March 2020
Accepted: 18 May 2020
Published: 30 June 2020

Citation:
Lu J, Bao W, Li M, Li L, Zhang Z, Alberts I, Brendel M, Cumming P, Lu H, Xiao Z, Zuo C, Guan Y, Zhao Q and Rominger A (2020) Associations of [^{18}F]-APN-1607 Tau PET Binding in the Brain of Alzheimer's Disease Patients With Cognition and Glucose Metabolism. Front. Neurosci. 14:604. doi: 10.3389/fnins.2020.00604

Molecular imaging of tauopathies is complicated by the differing specificities and off-target binding properties of available radioligands for positron emission tomography (PET). [^{18}F]-APN-1607 ([^{18}F]-PM-PBB3) is a newly developed PET tracer with promising properties for tau imaging. We aimed to characterize the cerebral binding of [^{18}F]-APN-1607 in Alzheimer's disease (AD) patients compared to normal control (NC) subjects. Therefore, we obtained static late frame PET recordings with [^{18}F]-APN-1607 and [^{18}F]-FDG in patients with a clinical diagnosis of AD group, along with an age-matched NC group ([^{18}F]-APN-1607 only). Using statistical parametric mapping (SPM) and volume of interest (VOI) analyses of the reference region normalized standardized uptake value ratio maps, we then tested for group differences and relationships between both PET biomarkers, as well as their associations with clinical general cognition. In the AD group, [^{18}F]-APN-1607 binding was elevated in widespread cortical regions ($P < 0.001$ for VOI analysis, familywise error-corrected $P < 0.01$ for SPM analysis). The regional uptake in AD patients correlated negatively with Mini-Mental State Examination score (frontal lobe: $R = -0.632$, $P = 0.004$; temporal lobe: $R = -0.593$, $P = 0.008$; parietal lobe: $R = -0.552$, $P = 0.014$; insula: $R = -0.650$, $P = 0.003$; cingulum: $R = -0.665$, $P = 0.002$) except occipital lobe ($R = -0.417$, $P = 0.076$). The hypometabolism to [^{18}F]-FDG PET in AD patients also showed negative correlations with regional [^{18}F]-APN-1607 binding in some signature areas of AD (temporal lobe: $R = -0.530$, $P = 0.020$; parietal lobe: $R = -0.637$, $P = 0.003$; occipital lobe: $R = -0.567$, $P = 0.011$). In conclusion, our results suggested that [^{18}F]-APN-1607 PET sensitively detected tau deposition in AD and that individual tauopathy correlated with impaired cerebral glucose metabolism and cognitive function.

Keywords: tau, neurodegeneration, metabolism, cognition, Alzheimer's disease, positron emission tomography

INTRODUCTION

The hyperphosphorylated, aggregated tau that comprises intracellular filamentous inclusions is implicated in a number of neurodegenerative pathologies (Spillantini and Goedert, 2013). In healthy adults, equal amounts of tau protein isoforms with three microtubule-binding domains (3R) and four microtubule-binding domains (4R) occur in the cerebral cortex (Goedert and Jakes, 1990). Misassembly of the normally unfolded microtubule-associated protein tau into a highly structured amyloid fibril is implicated in the pathological process underlying human tauopathies (Goedert et al., 2017). Alzheimer's disease (AD), which is primarily associated with 3R and 4R tau (Rosler et al., 2019), is one of the most clinically relevant tauopathies and is the most common neurodegenerative disorder globally, bringing enormous burdens to society and caregivers.

Consequently, molecular imaging of tauopathies has garnered much interest in recent years, and there is increasing recognition of tauopathy as a potential target in the early detection of neurodegenerative disease or indeed as a potential therapeutic target. Among available tracers for positron emission tomography (PET), the selectivity for tau isoforms determines their suitability for particular neurodegenerative disease. For example, a head-to-head comparison of [^{11}C]-THK5351 and [^{11}C]-PBB3 in AD patients revealed distinct binding patterns for the two tracers in the same patients. [^{11}C]-THK5351 binding matched the tau pathology expected for AD, whereas [^{11}C]-PBB3 binding showed a greater affiliation with β-amyloid distribution (Chiotis et al., 2018). An immunofluorescence study with PBB3 and AV-1451 both showed intense labeling of non-ghost and ghost tangles, whereas detection of dystrophic neurites in brain of AD patients was clearer for PBB3 (Ono et al., 2017). Further quantitative autoradiographic analysis post-mortem showed moderate [^{11}C]-PBB3 autoradiographic binding vs. relatively faint [^{18}F]-AV-1451 labeling of the 3R isoforms in brains of patients dying with Pick's disease (PiD), and likewise for the 4R isoforms in brains of patients dying with progressive supranuclear palsy (PSP) or corticobasal degeneration. However, the binding of the two ligands was similar for paired helical filament (PHF)-tau in patients dying with AD (Ono et al., 2017).

Off-target binding, at present one of the great challenges in molecular neuroimaging of tauopathy, occurs then the tracer has affinity to an unintended molecular target in the brain. For example, the interpretation of tau burden in PET scans with [^{18}F]-THK5351 (Ng et al., 2017) and several other ostensibly tau-selective tracers (Murugan et al., 2019) was complicated by off-target binding to monoamine oxidase B (MAO-B). Furthermore, the tau tracers [^{18}F]-AV-1451, [^{18}F]-THK5351, and [^{18}F]-MK6240 all showed additional binding to neuromelanin (Aguero et al., 2019; Tago et al., 2019), which likely accounted for their binding in the midbrain dopamine neurons of the substantia nigra (Marquie et al., 2015; Harada et al., 2016).

PBB3-based tracers show much promise in overcoming the problem of incomplete specificity for tau. Previous studies regarding the prototype [^{11}C]-PBB3 revealed no cross-reactivity with monoamine oxidase A (MAO-A) and MAO-B (Ni et al., 2018), although there was a low affinity for non-tau fibrils such as assemblages of amyloid-β (Maruyama et al., 2013; Ono et al., 2017) and α-synuclein aggregates (Koga et al., 2017). Nevertheless, [^{11}C]-PBB3 binding was highly selective for tau at the nm radioligand concentrations typically achieved in a human PET study (Koga et al., 2017; Ni et al., 2018). However, routine clinical use of the compound [^{11}C]-PBB3 presented logistic difficulties due to the short physical half-life of carbon-11 (Hashimoto et al., 2014, 2015; Shimada et al., 2017). A PBB3 derivative labeled with longer-lived fluorine-18 might overcome this limitation.

Moreover, according to the latest National Institute on Aging – Alzheimer's Association framework on AD (Jack et al., 2018; Cummings, 2019), a framework comprising three biomarkers β-amyloid (A), tau (T), and neurodegeneration (N) is recommended for defining the AD spectrum and for distinguishing AD from non-AD causes of cognitive impairment. Detection of β-amyloid is accomplished with established PET tracers such as [^{11}C]-PiB (Klunk et al., 2004; Jimenez-Bonilla et al., 2016) and [^{18}F]-AV45 (Nemmi et al., 2014; Brendel et al., 2015; Lin et al., 2016). These tracers show progressive accumulation of β-amyloid first in isocortical areas and later in limbic and cortical structures. Positron emission tomography with [^{18}F]-FDG reveals a characteristic pattern of hypometabolism in temporoparietal cortex and posterior cingulate of AD patients (Minoshima et al., 1995; Kato et al., 2016; Hsu et al., 2017; Rice and Bisdas, 2017; Blazhenets et al., 2019). Multimodal studies combining A/T/N biomarkers showed tau deposition as measured by [^{18}F]-AV-1451 (Sintini et al., 2019) or [^{18}F]-THK5351 (Baghel et al., 2019) PET, which correlated with hypometabolism to [^{18}F]-FDG PET and with atrophy, as measured by structural magnetic resonance imaging (MRI) (Sintini et al., 2019).

In this context, we presented [^{18}F]-APN-1607 ([^{18}F]-PM-PBB3), a next-generation tau tracer derived from the PBB3 series, but possessing a superior drug metabolism and pharmacokinetic profile, improved specific binding in brain, and the logistic advantage imparted by fluorine-18 (Shimada et al., 2017, 2018; Tagai et al., 2020; see **Supplementary Table 1**). We aimed in this study to characterize the cerebral uptake pattern of [^{18}F]-APN-1607 as a marker for hyperphosphorylated tau in patients with clinically diagnosed AD in comparison to a normal control (NC) group and to investigate the correlation of this regional uptake with hypometabolism to [^{18}F]-FDG PET and in relation to impaired cognitive function.

MATERIALS AND METHODS

Subjects

Nineteen clinically diagnosed and amyloid PET-positive AD patients (6 underwent [^{11}C]-PiB PET, and 13 underwent [^{18}F]-AV45 PET) and 11 NC subjects who also underwent [^{18}F]-APN-1607 PET in Huashan Hospital, Shanghai, China, were

enrolled in this study from 2018/11 to 2019/11. All subjects underwent anatomical MRI, and all AD patients underwent an [18F]-FDG PET within 1 month before or after [18F]-APN-1607 PET. The diagnosis of clinically probable AD was based on current diagnostic criteria (McKhann et al., 2011). Experienced radiologists assessed medial temporal lobe atrophy (MTA) using MTA–Visual Rating Scale (VRS) blinded to clinical conditions in all subjects. Experienced neurologists from the cognitive impairment clinic administered the Mini-Mental State Examination (MMSE) and Clinical Dementia Rating (CDR) test for all patients. Meanwhile, the NC group also accepted CDR test. None of the NCs had a history of cognitive impairment, psychiatric illness, central nervous system disease, or head injury. Furthermore, dementia caused by other reasons and mild cognitive impairment (MCI) were excluded after clinical screening by experienced neurologist/cognitive specialists. This study was approved by the ethics committee of Huashan Hospital (no. 2018-363). All procedures performed in this study were in accordance with the ethical standards of the institutional research committee and with the Helsinki Declaration of 1975 and its later amendments. All subjects or a legally responsible relative gave written informed consent before the study.

Imaging and Processing

Radiosynthesis

[18F]-APN-1607 was prepared in Huashan Hospital by a nucleophic substitution reaction followed by an acid hydrolysis carried out with an [18F]-multifunction synthesizer (Beijing PET Technology Co., Ltd., Beijing, China). APRINOIA Therapeutics (Suzhou, China) provided the tosylate precursor used for the radiosynthesis. After purification with semipreparative high-performance liquid chromatography, the product [18F]-APN-1607 was formulated in ascorbate-containing normal saline for injection and was filtered through a sterile membrane filter. The radiosynthesis was completed in 90 min, giving [18F]-APN-1607 with a radiochemical purity of $\geq$90% and a molar activity of $\geq$37 MBq/μmol at the end of synthesis. The production was conducted under the green light-emitting diode light (510 nm) illumination, and the product was sterile and negative for pyrogens.

Image Acquisition and Reconstruction

All subjects were scanned on a Siemens Biograph 64 PET/computed tomography (CT) (Siemens, Erlangen, Germany) in three-dimensional (3D) mode in Huashan Hospital. A low-dose CT transmission scan was performed before PET scanning for attenuation correction. Static emission recordings were acquired during the interval of 90–110 min after intravenous injection of 370 MBq [18F]-APN-1607. Image reconstruction was obtained by the ordered subset expectation maximization 3D (OSEM 3D) method. Patients with AD underwent [18F]-FDG PET on another scanning day with intravenous injection of 185 MBq, following a scanning procedure and OSEM 3D reconstruction as described in a previous study (Wu et al., 2013). All subjects also underwent anatomical MRI in a 3.0-T horizontal magnet (Discovery MR750; GE Medical Systems, Milwaukee, WI, United States) at Huashan Hospital.

Semiquantitative Volume of Interest–Based PET Analyses

The PNEURO data processing pipeline of PMOD version 4.005 (PMOD Technologies Ltd., Zurich, Switzerland) was used for spatial normalization of all PET images to the Montreal Neurological Institute (MNI) space, using the individual MRI as an intermediate. Both [18F]-APN-1607 and [18F]-FDG PET images were analyzed in the following manner: we first segmented the individual MRI into gray matter (GM), white matter (WM), and cerebrospinal fluid (CSF) and made the spatial normalization to the MNI space. Subsequently, each subject's individual PET images were spatially matched to MRI and then resampled using the normalization arising from the GM/WM/CSF MRI segmentation procedure (Ashburner, 2007). Based on the Atlas template [adult brain maximum probability map ("Hammersmith atlas"; n30r83)], the whole brain was parcellated into the following regions for standardized uptake value ratio (SUVR) calculations: frontal, temporal, occipital, and parietal lobes; insula; cingulum; caudate; putamen; pallidum; thalamus; midbrain; pons; medulla; and cerebellar cortex. The cerebellar cortex was selected as the reference region for tau images because it has negligible tau pathology to examination post-mortem AD cerebellum (Herrmann et al., 1999; Baghel et al., 2019). The same reference region was used for [18F]-FDG PET images (Leuzy et al., 2018; Baghel et al., 2019).

Voxel-Wise Analyses

Statistical parametric mapping (SPM) analysis was performed using SPM8 (Wellcome Department of Cognitive Neurology, London, United Kingdom) implemented in MATLAB 8.4 (R2014) (Mathworks Inc., Sherborn, MA, United States). The [18F]-APN-1607 SUVR maps from the AD and NC groups were compared by a voxel-wise two-tailed Student *t*-test after 10-mm Gaussian smoothing. To evaluate significant differences, we set the voxel threshold at $P < 0.01$ [familywise error (FWE)-corrected] over the whole brain with an extent threshold empirically chosen to be at least twice of the expected number of voxels per cluster estimated in the SPM run. Significant regions were localized by Talairach–Daemon software (Research Imaging Center, University of Texas Health Science Center, San Antonio, TX, United States). The SPM maps for abnormal [18F]-APN-1607 uptakes were overlaid on a standard structural MRI brain template in stereotaxic space. We then used multiple regression analyses to determine the relationship between [18F]-APN-1607 uptake values and MMSE in the AD patients. Voxels surviving $P < 0.01$ (uncorrected) with an extent threshold of at least twice of the expected number of voxels per cluster estimated in the SPM run were considered significant for the multiple regression analyses. Moreover, clusters surviving at FWE $P < 0.05$ were also searched for these multiple regression analyses.

Statistical Analysis

Demographic characteristics and semiquantitative PET results in different target volumes of interest (VOIs) were compared between AD and NC groups using the independent two-tailed Student *t*-test, χ^2 test, or Mann-Whitney *U* test as appropriate. Effect sizes for the discrimination between patients and NC

subjects were evaluated by Cohen *d*. Correlation analyses between PET SUVR in target VOIs and clinical parameter (MMSE), as well as intermodality correlations, were performed using Spearman correlation. All statistical analyses were performed in SPSS version 22.0 software (SPSS Inc., Chicago, IL, United States). $P < 0.05$ was considered significant.

RESULTS

Demographic Information and Clinical Characteristics

Our AD group consisted of 7 males and 12 females with mean age 61.8 (±11.3) years, whereas NC group included seven males and four females with mean age 61.8years (±4.6) years. There were 14 early onset AD, who showed symptoms younger than 65 years old and five late-onset AD (LOAD) in our cohort. Both groups were comparable for age of scanning ($P = 0.992$) and gender ($P = 0.156$). The general cognition of the AD group as assessed by CDR-Global Score (CDR-GS) and MMSE score showed that our patient cohort was mainly at moderate to advanced stages of the disease (CDR-GS: 1 (1–2); MMSE: 17.0 ± 7.6). The MTA-VRS showed that AD group had abnormal brain atrophy while NC group showed normal (**Table 1**).

Semiquantitative VOI-Based PET Analyses

Figure 1 shows the representative examples of [18F]-APN-1607 PET and anatomical MRI superimposed images of AD and NC subjects.

The AD group showed abnormally higher [18F]-APN-1607 binding than did the NC group in all cerebral lobes ($P < 0.001$, Cohen d varying from 1.5 to 2.1), as well as in caudate ($P < 0.05$, Cohen $d = 0.9$) and putamen ($P < 0.001$, Cohen $d = 1.5$). Meanwhile, the AD group showed lower uptake of [18F]-APN-1607 in midbrain ($P < 0.01$, Cohen $d = 1.0$), pons ($P < 0.001$, Cohen $d = 1.4$), and medulla ($P < 0.001$, Cohen $d = 1.5$) (**Table 2** and **Figure 2**).

As for clinical associations, [18F]-APN-1607 binding in all cerebral lobes (with the exception of the occipital lobe) correlated negatively with the MMSE score (frontal lobe: $R = -0.632$, $P = 0.004$; temporal lobe: $R = -0.593$, $P = 0.008$; parietal lobe: $R = -0.552$, $P = 0.014$; insula: $R = -0.650$, $P = 0P = 0.003$; cingulum: $R = -0.665$, $P = 0.002$). Likewise, [18F]-APN-1607 binding in putamen, thalamus and medulla showed similar correlations (putamen: $R = -0.557$, $P = 0.013$; thalamus: $R = -0.595$, $P = 0.007$; medulla: $R = -0.469$, $P = 0.043$). [18F]-FDG uptake, as a surrogate marker for neuronal metabolic activity, showed positive correlations with MMSE in the frontal and parietal lobes (frontal lobe: $R = 0.469$, $P = 0.043$, parietal lobe: $R = 0.550$, $P = 0.015$). The temporal lobe also showed a broadly similar correlation with MMSE, albeit without reaching significance ($R = 0.444$, $P = 0.057$) (**Table 3**).

We then interrogated the relationships between [18F]-APN-1607 and [18F]-FDG. We found negative correlations between tau deposition and FDG uptake in the temporal, parietal, and occipital lobes (temporal lobe: $R = -0.530$, $P = 0.020$; parietal lobe: $R = -0.637$, $P = 0.003$; occipital lobe: $R = -0.567$, $P = 0.011$). A similar pattern was observed for the frontal lobe, albeit without reaching statistical significance ($R = -0.421$, $P = 0.073$) (**Table 3**).

Voxel-Wise PET Analyses

Compared to the NC group, the AD group had elevated [18F]-APN-1607 binding in fusiform gyrus (BA 37), superior temporal gyrus (BA 21), inferior temporal gyrus (BA 20), middle frontal gyrus (BA 8, 9, 11), and cingulate gyrus (BA 32) at FWE $P < 0.01$ (**Table 4** and **Figure 3**).

Significantly negative correlations between MMSE and brain [18F]-APN-1607 binding were found mainly in superior frontal gyrus (BA 10), middle frontal gyrus (BA 9, 10, 11, 47), parahippocampal gyrus (BA 36) and lateral globus pallidus at $P < 0.01$ (uncorrected). Of these, both the superior frontal gyrus (BA 10) and middle frontal gyrus (BA 9, 10) survived FWE at $P < 0.05$ (**Table 5** and **Figure 4**).

DISCUSSION

In this present study, we characterized the [18F]-APN-1607 uptake pattern in patients with AD in comparison with NC subjects. Furthermore, we assessed the correlation with between tau PET with [18F]-FDG PET and clinical parameters (MMSE). Our main objective was to characterize the utility of this next-generation tau tracer in terms of effect size for detecting disease-specific tau deposition, thus confirming the known relationship between tau deposition and decreased FDG uptake and cognitive impairment in AD patients.

In the regional analysis of [18F]-APN-1607, we found AD patients had higher binding than NC subjects in widespread regions of the cerebral cortex, caudate, and putamen and conversely relatively low uptake in the brainstem. The voxel-wise analysis results were in agreement with those of the region-based analysis, and the cerebral regions with increased tau deposition to [18F]-APN-1607 were consistent with previously published studies for previous-generation tau tracers (**Table 6**).

Hitherto, only limited data for second-generation tau tracers have been reported (Leuzy et al., 2019). Some novel tau tracers generally presented a number of advantages over the previous generation, notably with respect to target selectivity. For example, *in vitro* studies suggested that [18F]-MK6240 and [18F]-JNJ-067 bound with neurofibrillary tangle (NFT) (Hostetler et al., 2016), whereas [18F]-RO948 bound to both NFT and neuropil threads (Honer et al., 2018), whereas [18F]-JNJ64349311 interacted with PHF-tau and neuropil threads (Declercq et al., 2017). [18F]-PI2620 showed ambivalent binding to 3R-tau from PiD brain and to 4R-tau from PSP samples (Kroth et al., 2019). [18F]-APN-1607 showed specific binding with tau aggregates in AD and PSP (Shimada et al., 2018). Furthermore, such tracers showed improvement in off-target binding. [18F]-APN-1607 showed no off-target binding in the basal ganglia and thalamus (Shimada et al., 2017), and [18F]-APN-1607, [18F]-MK6240, [18F]-JNJ-607, and [18F]-PI2620 revealed no off-target binding with MAO-A

TABLE 1 | Demographic information and clinical characteristics.

Group	No.	Gender (male/female)	Age of scanning (y)	Age at onset (y)	Education (y)	MMSE score	CDR-GS	MTA-VRS
AD	19	7/12	61.8 ± 11.3	56.9 ± 10.5	10.7 ± 4.2	17.0 ± 7.6	1 (1–2)	2 (2–2)
NC	11	7/4	61.8 ± 4.6	–	N.A.	N.A.	0 (0–0)	1 (0–1)
P	–	0.156[a]	0.992[b]	–	–	–	<0.001[c]	<0.001[c]

For age, education years, and MMSE score; the expression means mean ± standard deviation. For CDR-GS and MTA-VRS, the expression means median (interquartile range). [a]χ^2 test was performed. [b]Independent two-tailed Student t test was performed. [c]Mann-Whitney U test was performed. AD, Alzheimer's disease; NC, normal control; MMSE, Mini-Mental State Examination; CDR-GS, Clinical Dementia Rating Global Score; MTA-VRS, Medial Temporal Lobe Atrophy Visual Rating Scale; N.A., not available; y, year.

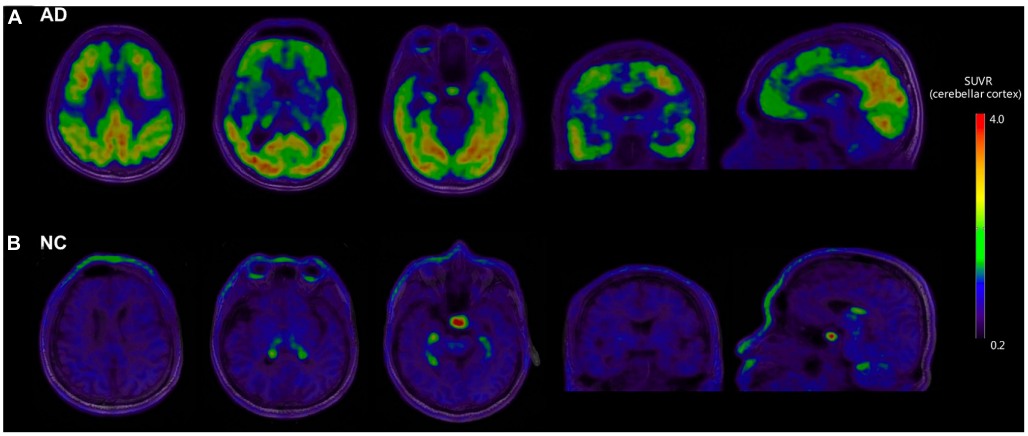

FIGURE 1 | Representative examples of [18F]-APN-1607 PET and anatomical MRI superimposed images of AD and NC subjects. **(A)** [18F]-APN-1607 PET of an AD patient (male, 56 years old, MMSE 17, 11 years' education experience, memory impairment complaint for 5 years with positive [11C]-PiB result). **(B)** [18F]-APN-1607 PET of a NC subject (Male, 61y). AD, Alzheimer's disease; NC, normal control. The color stripe indicates the standard uptake value ratio with cerebellar cortex as the reference region.

TABLE 2 | Differences of [18F]-APN-1607 regional SUVR between AD and NC groups.

VOI	SUVR		*P*	Cohen *d*
	AD	NC		
Frontal lobe	1.43 ± 0.42	0.85 ± 0.06	<0.001***	1.926
Temporal lobe	1.64 ± 0.50	0.91 ± 0.06	<0.001***	2.062
Occipital lobe	1.58 ± 0.47	0.95 ± 0.06	<0.001***	1.917
Parietal lobe	1.62 ± 0.60	0.87 ± 0.06	<0.001***	1.773
Insula	1.31 ± 0.41	0.85 ± 0.07	<0.001***	1.546
Cingulum	1.47 ± 0.46	0.89 ± 0.05	<0.001***	1.801
Caudate	0.91 ± 0.17	0.80 ± 0.04	0.015*	0.898
Putamen	1.18 ± 0.22	0.94 ± 0.05	<0.001***	1.508
Pallidum	1.11 ± 0.19	1.05 ± 0.08	0.295	0.376
Thalamus	1.21 ± 0.23	1.27 ± 0.12	0.374	0.325
Midbrain	0.91 ± 0.17	1.04 ± 0.05	0.008**	1.005
Pons	0.85 ± 0.17	1.03 ± 0.06	<0.001***	1.397
Medulla	0.72 ± 0.18	0.95 ± 0.11	<0.001***	1.537

*For SUVR, the expression means mean ± standard deviation. VOI, volume of interest; SUVR, standard uptake value ratio; AD, Alzheimer's disease; NC, normal control. *P < 0.05, **P < 0.01, ***P < 0.001.*

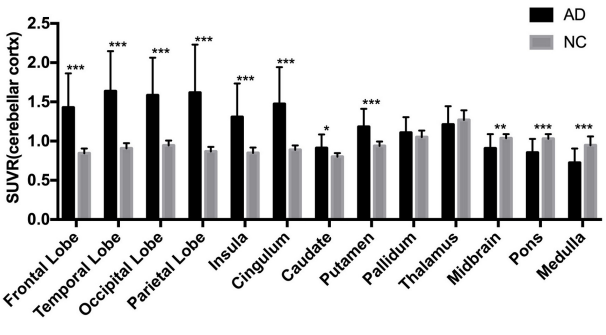

FIGURE 2 | Differences of regional [18F]-APN-1607 SUVR between AD and NC groups. AD, Alzheimer's disease; NC, normal control. *$P < 0.05$, **$P < 0.01$, ***$P < 0.001$.

and MAO-B. Extensive screening of [18F]-RO948 also revealed no off-target binding. These limited available data suggested that novel-generation tau tracers had significant advantages in comparison to previous generation tracers. The selectivity for tau isoforms of the different series renders them particularly suitable for the investigation of neurodegenerative disease apparent. Further clinical studies are required to demonstrate their diagnostic utility and to further evaluate their performance.

The limited *in vivo* data reported for other new-generation tau tracers showed similar results to our study: [18F]-MK6240, [18F]RO-948, and [18F]-PI6260 showed elevated signals in

TABLE 3 | Correlations between regional SUVR and MMSE score, and correlations between multimodes in AD group.

VOI	^{18}F-APN-1607 and MMSE		^{18}F-FDG and MMSE		^{18}F-APN-1607 and ^{18}F-FDG	
	P	*R*	*P*	*R*	*P*	*R*
Frontal lobe	0.004**	−0.632	0.043*	0.469	0.073	−0.421
Temporal lobe	0.008**	−0.593	0.057	0.444	0.020*	−0.530
Occipital lobe	0.076	−0.417	0.341	0.231	0.011*	−0.567
Parietal lobe	0.014*	−0.552	0.015*	0.550	0.003**	−0.637
Insula	0.003**	−0.650	0.411	0.200	0.616	−0.123
Cingulum	0.002**	−0.665	0.630	0.118	0.333	−0.235
Caudate	0.067	−0.429	0.780	−0.069	0.091	0.398
Putamen	0.013*	−0.557	0.693	−0.097	0.251	0.277
Pallidum	0.395	−0.207	0.102	−0.387	0.743	0.081
Thalamus	0.007**	−0.595	0.912	0.027	0.808	−0.060
Midbrain	0.531	−0.153	0.150	−0.343	0.892	−0.033
Pons	0.301	−0.250	0.461	−0.180	0.399	−0.205
Medulla	0.043*	−0.469	0.080	−0.411	0.705	0.093

*VOI, volume of interest; R, Spearman correlation. *P < 0.05, **P < 0.01, ***P < 0.001.*

TABLE 4 | Brain regions with significant increased uptakes of [^{18}F]-APN-1607 in AD group compared to NC Group (*P* < 0.01, FWE corrected).

Region*	Hemisphere	Cluster size (mm^3)	Z max	Coordinates†		
				X	Y	Z
Fusiform gyrus (BA 37)	Left	283,064	5.72	−48	−44	−18
Superior temporal gyrus (BA 21)	Right	283,064	5.53	62	−22	−4
Inferior temporal gyrus (BA 20)	Left	283,064	5.50	−54	−24	−22
Middle frontal gyrus (BA 8)	Right	56,784	5.17	22	38	34
Middle frontal gyrus (BA 8)	Right	56,784	5.17	30	30	34
Middle frontal gyrus (BA 9)	Right	56,784	5.13	10	48	18
Middle frontal gyrus (BA 8)	Left	51,360	5.06	−10	38	34
Middle frontal gyrus (BA 11)	Left	51,360	5.05	−26	48	−14
Cingulate gyrus (BA 12)	Left	51,360	5.03	−10	26	42

**Significant at FWE-corrected voxel threshold of P < 0.01, extent threshold = 58 voxels (464 mm^3). †Coordinates are displayed in MNI standard space. BA, Brodmann area; FWE, familywise error.*

temporal areas and more broadly throughout the cortex in AD patients compared to NC subjects. The SUVRs in temporal lobe of AD/MCI patients were 1.64 (±0.72) with [^{18}F]-MK6240 [MMSE = 18.8 (±6.9), Cohen *d* = 1.3) (Lohith et al., 2019), 2.75 (±1.40) with [^{18}F]RO-948 (inferior temporal lobe, MMSE = 20.8 (±2.7), Cohen *d* = 1.6] (Wong et al., 2018), and 1.80 (±0.40) with [^{18}F]-PI2620 [inferior temporal, MMSE = 20.4 (±6.3), Cohen *d* = 2.4] (Mueller et al., 2019). Our findings of [^{18}F]-APN-1607 had relatively lower SUVR in the present study [temporal lobe: 1.64 (±0.50), MMSE = 17.0 (±7.6), Cohen *d* = 2.1] comparing to [^{18}F]RO-948 and [^{18}F]-PI2620, which might arise from the relatively rough ROI; however, the relatively high Cohen *d* value indicated that [^{18}F]-APN-1607 was a highly sensitive tracer for detecting tau aggregates in AD. Findings in other brain regions were also comparable among the next-generation tau tracers, including [^{18}F]-APN-1607 (**Table 6**).

In addition to the finding of distinctly elevated [^{18}F]-APN-1607 binding in the widespread cerebral cortex of patients with AD of moderate severity, we also saw increased signals in the striatum. We noted that [^{18}F]-AV-1451, [^{18}F]-RO948, and [^{18}F]-PI2620 likewise showed similarly increased signals in the striatum (Shcherbinin et al., 2016; Wong et al., 2018; Mueller et al., 2019). Previous neuropathological observation addressed that NFT occurs in striatum in late Braak stages of AD (V and VI) (Chan and Shea, 2006). Another autopsied study reinforced AD cases with severe putaminal tauopathy at the advanced stages and indicated that severe microtubule-associated protein tau accumulation in the basal ganglia might occur most frequently in AD cases, without comorbidity of other neurodegenerative diseases in a general aging population (Hamasaki et al., 2019). Accordingly, the higher [^{18}F]-APN-1607 PET signal seen in caudate and putamen of our AD group might suggest higher than expected tauopathy (Su et al., 2015). Nonetheless, previous MRI studies reported iron overloading in striatum in AD (Bartzokis et al., 1993, 1994; Acosta-Cabronero et al., 2013). Iron is a known component of neuritic plaques

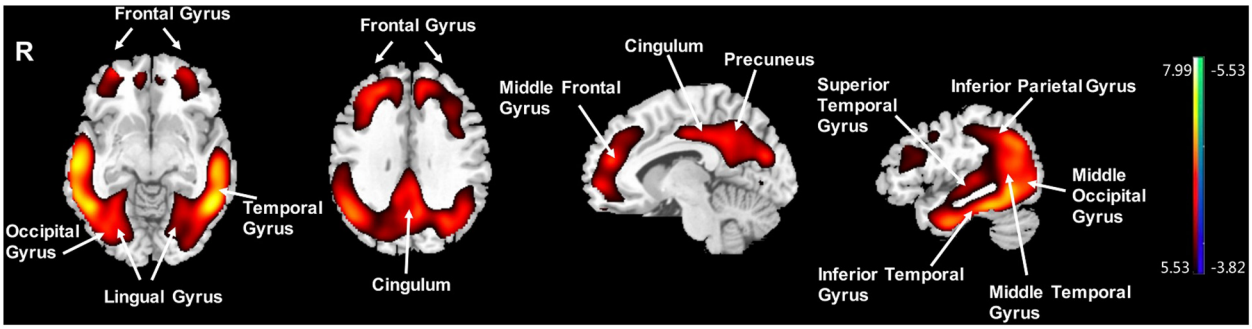

FIGURE 3 | Voxel-wise differences of whole-brain [18F]-APN-1607 binding in the AD group compared to the NC Group. AD, Alzheimer's disease; NC, normal control. Increased binding is displayed in red; decreased binding is displayed in blue. The color stripe indicates the *t* value; voxel threshold $P < 0.01$, FWE-corrected. *T* statistic maps are displayed in MNI standard space.

TABLE 5 | Brain regions exhibiting a significant negative correlation between MMSE score and regional brain uptakes of [18F]-APN-1607 in AD group ($P < 0.01$, uncorrected).

Region*	Hemisphere	Cluster size (mm^3)	*Z* Max	Coordinates†		
				X	Y	Z
Superior frontal gyrus (BA 10)‡	Right	91,784	3.65	16	60	−16
Middle frontal gyrus (BA 10)‡	Right	91,784	3.43	36	52	−16
Middle frontal gyrus (BA 9)‡	Right	91,784	3.24	38	36	28
Middle temporal gyrus (BA 21)	Right	19,376	3.00	68	−28	−10
Parahippocampal gyrus (BA 36)	Right	19,376	2.95	34	−34	−12
Lentiform nucleus (lateral globus pallidus)	Right	19,376	2.89	28	−12	−12
Middle frontal gyrus (BA 10)	Left	20,664	2.98	−30	54	−16
Middle frontal gyrus (BA 47)	Left	20,664	2.90	−46	38	−10
Middle frontal gyrus (BA 11)	Left	20,664	2.87	−26	34	−20

**Significant at uncorrected voxel threshold of $P < 0.01$, extent threshold = 937 voxels (7,504 mm^3). †Coordinates are displayed in MNI standard space. ‡Survived at FWE-corrected voxel threshold of $P < 0.05$. BA, Brodmann area; FWE, familywise error.*

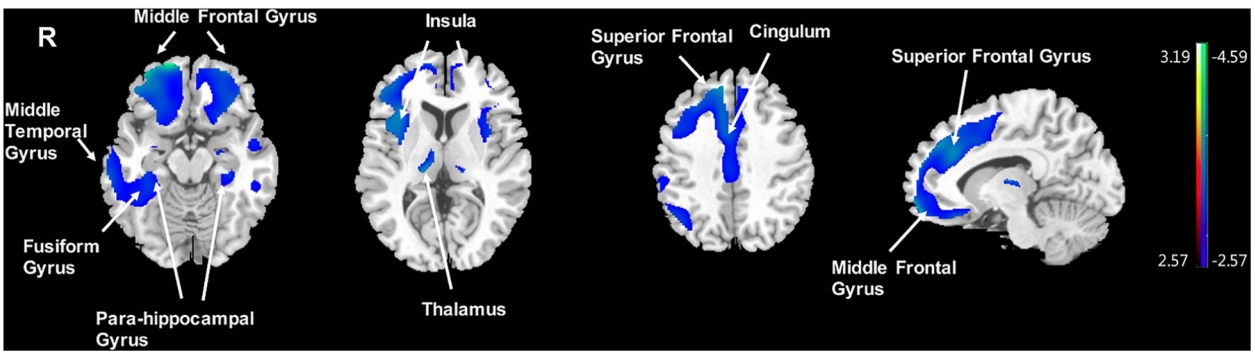

FIGURE 4 | Voxel-wise correlation of MMSE score and whole-brain [18F]-APN-1607 binding in the AD group. AD, Alzheimer's disease; NC, normal control. Positive correlations are displayed in red; negative correlations are displayed in blue. The color stripe indicates the *t* value; voxel threshold $P < 0.01$, uncorrected. Images are displayed in MNI standard space.

(Grundke-Iqbal et al., 1990; Connor et al., 1992; LeVine, 1997; Lovell et al., 1998) and neurofibrillary tangles (Good et al., 1992), and the Fenton reaction has long been suspected to contribute to AD pathology (Smith et al., 1997). Indeed, excessive ferrous iron may well favor β-amyloid aggregation and otherwise produce neurotoxicity (Schubert and Chevion, 1995;

TABLE 6 | Summary of ROI analyses of different tau tracers in AD and NC groups.

	Cohorts		NC	AD	Cohen *d*
[18F]-AV-1451 (Shcherbinin et al., 2016)	AD *N* = 5, MMSE = 21.8 (4.1) NC *N* = 5, MMSE = MMSE = 29.6 (0.5)	Frontal	1.00 (0.16)	1.65 (0.69)	1.30
		Occipital	1.07 (0.18)	1.67 (0.59)	1.38
		Lateral parietal	1.05 (0.19)	2.03 (0.84)	1.61
		Mesial temporal	1.09 (0.14)	1.78 (0.48)	1.95
		Lateral temporal	1.10 (0.15)	2.15 (0.89)	1.65
		Putamen	1.34 (0.09)	1.78 (0.23)	2.52
[18F]-THK5351 (Kang et al., 2017)	AD *N* = 51, MMSE = 13.8 (6.0) NC *N* = 43, MMSE = 28.5 (1.6)	Frontal	1.35 (0.22)	2.05 (0.34)	2.44
		Occipital	1.09 (0.15)	1.57 (0.46)	1.40
		Superior parietal	1.18 (0.20)	1.80 (0.43)	1.85
		Inferior parietal	1.34 (0.21)	2.60 (0.69)	2.47
		Lateral temporal	1.60 (0.23)	2.71 (0.49)	2.90
		Mesial temporal	2.42 (0.27)	3.52 (0.59)	2.40
		Anterior cingulate	2.88 (0.43)	3.40 (0.57)	1.03
		Hippocampus	2.44 (0.27)	3.40 (0.55)	2.22
		Fusiform	1.51 (0.19)	2.39 (0.57)	2.07
		Entorhinal	2.15 (0.34)	3.36 (0.89)	1.80
		Basal ganglia	3.08 (0.48)	3.72 (0.62)	1.15
[11C]-PBB3 (Kitamura et al., 2018)	AD/MCI *N* = 7, MMSE = 23.7 (6.9) NC *N* = 9, MMSE = 29.4 (0.7)	Frontal	0.86 (0.04)	0.94 (0.09)	1.15
		Occipital	0.90 (0.03)	1.05 (0.07)	2.79
		Parietal	0.83 (0.05)	0.97 (0.09)	1.92
		Medial temporal	0.99 (0.05)	1.02 (0.05)	0.60
		Lateral temporal	0.95 (0.04)	1.05 (0.06)	1.96
		Anterior cingulate	0.91 (0.07)	0.94 (0.01)	0.60
[18F]-MK6240 (Lohith et al., 2019)	AD *N* = 4, MMSE = 16.5 (7.3) NC *N* = 4, MMSE = 29.0 (0.0)	Temporal	0.98 (0.07)	1.64 (0.72)	1.29
		Hippocampus	0.93 (0.10)	1.37 (0.25)	2.31
		Amygdala	0.84 (0.11)	1.67 (0.40)	2.83
		Caudate	0.79 (0.06)	0.71 (0.16)	0.66
		Putamen	0.91 (0.04)	1.15 (0.35)	0.96
[18F]-RO948 (Wong et al., 2018)	AD *N* = 11, MMSE = 20.8 (2.7) NC *N* = 5)	Middle frontal lobe	1.13 (0.10)	2.27 (1.40)	1.15
		Lateral occipital lobe	1.35 (0.10)	2.34 (1.30)	1.07
		Precuneus	1.16 (0.20)	2.29 (1.50)	1.06
		Superior parietal	1.24 (0.10)	2.18 (1.10)	1.20
		Inferior parietal	1.32 (0.10)	2.8 (1.50)	1.39
		Inferior temporal	1.14 (0.10)	2.75 (1.40)	1.62
		Middle temporal	1.15 (0.10)	2.54 (1.40)	1.40
		Posterior cingulate	1.1 (0.10)	1.96 (1.20)	1.01
		Insula	0.98 (0.10)	1.46 (0.50)	1.33
		Hippocampus	0.90 (0.20)	1.26 (0.30)	1.40
		Parahippocampus	0.96 (0.10)	1.95 (0.70)	1.97
		Amygdala	0.81 (0.10)	1.72 (0.70)	1.83
		Caudate	0.80 (0.10)	0.97 (0.20)	1.06
		Putamen	0.93 (0.10)	1.28 (0.20)	2.24
		Thalamus	0.90 (0.10)	1.00 (0.20)	0.69
[18F]-PI2620 (Mueller et al., 2019)	AD *N* = 12, MMSE = 20.4 (6.3) NC *N* = 10, MMSE = 29.0 (1.2)	Occipital	1.08 (0.08)	1.45 (0.23)	2.15
		Parietal	1.03 (0.06)	1.53 (0.40)	1.75
		Superior temporal	1.07 (0.10)	1.36 (0.23)	1.64
		Inferior temporal	1.09 (0.10)	1.80 (0.40)	2.44
		Posterior cingulate	1.03 (0.13)	1.82 (0.68)	1.61

(Continued)

TABLE 6 | Continued

Cohorts		NC	AD	Cohen *d*
	Hippocampus	1.07 (0.08)	1.26 (0.20)	1.25
	Parahippocampus	1.07 (0.11)	1.46 (0.29)	1.78
	Amygdala	0.99 (0.11)	1.29 (0.29)	1.37
	Fusiform	1.07 (0.11)	1.63 (0.29)	2.55
	Striatum	0.83 (0.1)	1.02 (0.14)	1.56
	Pallidum	0.95 (0.17)	1.10 (0.14)	0.96
	Thalamus	0.93 (0.11)	0.96 (0.07)	0.33

AD, Alzheimer's disease; NC, normal control.

Leskovjan et al., 2011). Furthermore, iron can induce hyperphosphorylation and aggregation of tau (Lovell et al., 2004; Chan and Shea, 2006). Altogether, we interpreted these findings with much caution, given that previous generation tau tracers such as [18F]-AV-1451 demonstrated off-target binding to ferrous iron (Lowe et al., 2016; Passamonti et al., 2017; Choi et al., 2018; Baker et al., 2019), which as described above was implicated in the neuropathology of neurofibrillary tangle formation. Noteworthy, [18F]-AV-1451 has shown non-specific binding in the striatum in healthy elderly subjects (Marquie et al., 2015; Passamonti et al., 2017; Smith et al., 2017), and its binding appeared to increase with healthy aging (Smith et al., 2017). Similarly, the first-generation [11C]-PBB3 also showed off-target binding in the basal ganglia, the reason for which was yet to be determined (Ono et al., 2017), although a recent abstract indicated there was no off-target binding in the basal ganglia and thalamus for [18F]-APN-1607 (Shimada et al., 2017).

In this study, we investigated clinical correlations for [18F]-APN-1607 and [18F]-FDG uptakes separately. The MMSE score, as a surrogate for general cognition, showed strong correlations with [18F]-APN-1607 SUVR in all cerebral cortical regions except the occipital lobe, and with [18F]-FDG SUVR in the frontal and parietal lobes (**Table 3**). In [18F]-APN-1607, we also saw relatively weaker correlations in the putamen, thalamus, and medulla.

It was hypothesized that accumulation of toxic intracellular aggregate accompanied by a loss of soluble tau capable of stabilizing microtubules might synergistically lead to compromised neuronal survival (Lee et al., 2011), accounting for the putative relationship between NFT burden and cognitive decline in AD patients (Terry et al., 1981; Gomez-Isla et al., 1997). According to the Braak theory of AD propagation (Braak and Braak, 1991b; Braak and Del Tredici, 2011), tau deposition spreads widely and aggregates in neocortical areas in advanced AD patients. The association we observed between tau depositions to [18F]-PAPN-1607 and general cognitive impairment was consistent with these known relationships, which we could now confirm here with a new-generation tau tracer. The occipital lobe was thought to be affected at only a late stage of typical AD progression (Delacourte et al., 1999) and likewise showed tau accumulation only at a late stage (Alafuzoff et al., 2008). In this regard, our study's failure to show a correlation between tau deposition and [18F]-APN-1607 in the occipital lobe, and MMSE score was consistent with the moderate severity of disease in our patient group.

We found a negative correlation between tau deposition to [18F]-APN-1607 in some subcortical regions and MMSE score. Degeneration of deep gray matter structures other than the hippocampus and the amygdala occurred in the process of AD and ultimately contributes to cognitive deterioration. The thalamus pathology played an increasingly recognized role in early memory loss of AD patients (Aggleton and Brown, 1999; Harding et al., 2000; Taber et al., 2004; Carlesimo et al., 2011). The anterodorsal thalamic nucleus was posited to undergo neurofibrillary changes concomitant with the hippocampus (Braak Stages III–IV) (Braak and Braak, 1991b). Nonetheless, some thalamic nuclei appeared unaffected or show only mild neurofibrillary changes, even in cases of severe AD (Braak and Braak, 1991b). Recent studies have provided evidence that AD-related tau cytoskeletal pathology is initiated in subcortical regions, which supports the widely held hypothesis that early occurring subcortical tau cytoskeletal pathology, including that in the thalamus, may play a crucial role in the cascade of the early pathological events of AD (Rub et al., 2000; Grinberg et al., 2009; Stratmann et al., 2016). In addition, the clinical manifestation and progression of AD correlated with loss of neurons, synaptic degeneration in the neocortex and the topographical distribution of the tau cytoskeletal pathology in diseased brains (Jack et al., 2016). The role of the cortical and subcortical regions of the limbic system in the performance of normal cognitive and memory functions was well-known. The presence of severe tau cytoskeletal pathology in the thalamic nuclei with limbic connectivity likely contributed to impaired neural processing in limbic circuits, manifesting in certain cardinal symptoms of AD (Braak and Braak, 1991a,b; Rub et al., 2000, 2002; Blennow et al., 2006; Lace et al., 2007; Grinberg et al., 2009; Braak and Del Trecidi, 2015). Structural MRI studies also showed that overall thalamic volume correlates with cognitive status in MCI and AD patients (de Jong et al., 2008; Pedro et al., 2012; Yi et al., 2016), further highlighting its role in the pathogenesis of AD. In this regard, the negative correlation between [18F]-APN-1607 binding in the thalamus and MMSE score in the AD group offered further support, a link between thalamic pathology and cognitive impairment. Like thalamus, the basal nuclei participated in many different neuronal pathways, with functions extending to emotional, motivational, associative, and cognitive processes (Herrero et al., 2002). A previous MRI study has found significantly reduced putamen volumes in AD patients, correlating with

impaired cognition (de Jong et al., 2008). Combined with the neuropathological observation that NFT occurs in striatum in Braak stages V and VI in AD (Chan and Shea, 2006), our findings strongly suggested that the tau deposition in the subcortical regions may also contribute to cognitive decline in AD.

Cerebral [18F]-FDG uptake provides a surrogate marker for neuronal metabolism. [18F]-FDG uptake in the frontal ($R = 0.469$, $P = 0.043$) and parietal lobes ($R = 0.550$, $P = 0.015$) correlated with MMSE score of our AD group, with weaker association for the temporal lobe ($R = 0.444$, $P = 0.057$). Numerous PET studies have demonstrated hypometabolism in the temporoparietal cortex of AD patients (Minoshima et al., 1995; Kato et al., 2016; Rice and Bisdas, 2017), whereas hypometabolism in the frontal lobe is often observed during the progression of AD dementia (Herholz et al., 2007). Thus, our present findings of regional correlation were concordant with the known hypometabolic regions in AD. The relatively weak correlation in the temporal lobe could be indicative of involvement at an early stage of neurodegeneration, with stabilization of the hypometabolism late in this disease, resulting in a weakening of the relationship between temporal hypometabolism with cognitive scores. Indeed, previous [18F]-FDG PET studies have suggested that temporal hypometabolism peaks at the MCI stage and does not progress at later stages of the disease (Dukart et al., 2013), which seems consistent with present findings.

Our multimodal analysis revealed several brain regions showing correlations between uptake of both tracers. Previous studies posited that cognitive deficits in AD could arise directly from both tau pathology and subsequent downstream neurodegeneration (Bejanin et al., 2017). We found that SUVRs in the temporal ($R = -0.530$, $P = 0.020$), parietal ($R = -0.637$, $P = 0.003$), and occipital ($R = -0.567$, $P = 0.011$) lobes correlated negatively between [18F]-APN-1607 and [18F]-FDG uptakes, with a trend toward negative correlation in the frontal lobe ($P = 0.073$, $R = -0.421$). These findings were consistent with results disclosed using other tau tracers [[18F]-AV-1451 (Gordon et al., 2019; Sintini et al., 2019) and [18F]-THK5351 (Baghel et al., 2019)]. Previous stereological and non-stereological quantitative post-mortem studies of cerebral cortex (Terry et al., 1981, 1987; Cras et al., 1995; Schwab et al., 1998, 1999; Bussiere et al., 2002; Kril et al., 2002) and clinicopathologic studies (Giannakopoulos et al., 2003) reported a close association between NFT counts and neuron loss. However, non–NFT-related mechanisms of neurodegeneration may also play a role in the loss of cortical neurons in AD (Gomez-Isla et al., 1997).

In summary, this preliminary clinical study confirmed the utility of the new compound [18F]-APN-1607 for the detection of tau pathology and reinforced previous studies showing an overlap between cerebral glucose hypometabolism (using [18F]-FDG PET) and tau deposition and their association with dementia.

Limitations

We noted several shortcomings in this study. First, our group size in this preliminary study was relatively small. Second, to reduce the radiation exposure to the NC group, we did not perform additional β-amyloid or [18F]-FDG PET scanning to conform lack of pathology. However, clinical and MRI assessment revealed normal results. Although the abnormal metabolic regions of AD patients are well-described from a plethora of previous publications, we lacked [18F]-FDG PET data for the NC group. In mitigation, we restricted our exploration in the AD group with region-to-region analysis, aiming to explore anatomic relationships between tau deposition and abnormal metabolism. We draw attention to the fact that MMSE reflected only general cognition, whereas individuals may suffer from cognitive impairment in different domains. Future studies involving more detailed cognitive assessments would support a better exploration of the relationships between tauopathy and cognition.

We were cognizant of the methodological challenges associated with choice of reference region. We used cerebellum, a commonly chosen region, for normalization of [18F]-APN-1607 and [18F]-FDG scans to SUVR maps. Validity of this approach naturally required absence of important pathologies in cerebellum. In future studies, we shall consider other possible methods of normalization. Finally, clinical studies of prospective design are required to further validate the promising results reported here.

DATA AVAILABILITY STATEMENT

The raw data supporting the conclusions of this article will be made available by the authors, without undue reservation, to any qualified researcher.

ETHICS STATEMENT

The studies involving human participants were reviewed and approved by the Institutional Review Board of Huashan Hospital (HIRB), Fudan University. The patients/participants provided their written informed consent to participate in this study.

AUTHOR CONTRIBUTIONS

QZ, YG, CZ, and AR: research program conception. QZ, YG, CZ, JL, and WB: research program organization. JL, WB, ML, LL, ZZ, HL, and ZX: research program execution. CZ, AR, PC, and JL: statistical analyses design. JL, WB, and LL: statistical analyses execution. CZ, AR, QZ, and YG: statistical analyses review and critique. JL and IA: manuscript writing of the first draft. QZ, YG, MB, PC, CZ, and AR: manuscript review and critique. All authors contributed to the article and approved the submitted version.

FUNDING

This study was financially supported by grants from the National Natural Science Foundation of China (Grant Nos. 81971641, 81671239, and 81271516), the Shanghai Municipal Science and Technology Major Project (Grant No. 2017SHZDZX01), the Science and Technology Commission of Shanghai Municipality (Grant Nos. 19441903500, 17JC1401600, and 17411950106), and

the National Chronic Disease Project of China (Grant No. 2016YFC1306402).

ACKNOWLEDGMENTS

Our sincere thanks to the subjects engaged in our study and their relatives for making this research possible. We are grateful for the support from APRINOIA Therapeutics who kindly provided us with precursor for the synthesis of [18F]-APN-1607. We also thank for Ms. Li Zheng and Ms. Saineng Ding from the Department of Neurology, Huashan Hospital, Fudan University, for helping with the collection of clinical information.

SUPPLEMENTARY MATERIAL

The Supplementary Material for this article can be found online at: https://www.frontiersin.org/articles/10.3389/fnins.2020.00604/full#supplementary-material

REFERENCES

Acosta-Cabronero, J., Williams, G. B., Cardenas-Blanco, A., Arnold, R. J., Lupson, V., and Nestor, P. J. (2013). In vivo quantitative susceptibility mapping (QSM) in Alzheimer's disease. *PLoS One* 8:e81093. doi: 10.1371/journal.pone.0081093

Aggleton, J. P., and Brown, M. W. (1999). Episodic memory, amnesia, and the hippocampal-anterior thalamic axis. *Behav. Brain Sci.* 22, 425–444; discussion 444–489.

Aguero, C., Dhaynaut, M., Normandin, M. D., Amaral, A. C., Guehl, N. J., Neelamegam, R., et al. (2019). Autoradiography validation of novel tau PET tracer [F-18]-MK-6240 on human postmortem brain tissue. *Acta Neuropathol. Commun.* 7:37.

Alafuzoff, I., Arzberger, T., Al-Sarraj, S., Bodi, I., Bogdanovic, N., Braak, H., et al. (2008). Staging of neurofibrillary pathology in Alzheimer's disease: a study of the BrainNet Europe consortium. *Brain Pathol.* 18, 484–496.

Ashburner, J. (2007). A fast diffeomorphic image registration algorithm. *Neuroimage* 38, 95–113. doi: 10.1016/j.neuroimage.2007.07.007

Baghel, V., Tripathi, M., Parida, G., Gupta, R., Yadav, S., Kumar, P., et al. (2019). In vivo assessment of tau deposition in Alzheimer disease and assessing its relationship to regional brain glucose metabolism and cognition. *Clin. Nucl. Med.* 44, e597–e601. doi: 10.1097/rlu.0000000000002791

Baker, S. L., Harrison, T. M., Maass, A., La Joie, R., and Jagust, W. J. (2019). Effect of off-target binding on (18)F-flortaucipir variability in healthy controls across the life span. *J. Nucl. Med.* 60, 1444–1451. doi: 10.2967/jnumed.118.224113

Bartzokis, G., Aravagiri, M., Oldendorf, W. H., Mintz, J., and Marder, S. R. (1993). Field dependent transverse relaxation rate increase may be a specific measure of tissue iron stores. *Magn. Reson. Med.* 29, 459–464. doi: 10.1002/mrm.1910290406

Bartzokis, G., Sultzer, D., Mintz, J., Holt, L. E., Marx, P., Phelan, C. K., et al. (1994). In vivo evaluation of brain iron in Alzheimer's disease and normal subjects using MRI. *Biol. Psychiatry* 35, 480–487. doi: 10.1016/0006-3223(94)90047-7

Bejanin, A., Schonhaut, D. R., La Joie, R., Kramer, J. H., Baker, S. L., Sosa, N., et al. (2017). Tau pathology and neurodegeneration contribute to cognitive impairment in Alzheimer's disease. *Brain* 140, 3286–3300.

Blazhenets, G., Ma, Y., Sorensen, A., Rucker, G., Schiller, F., Eidelberg, D., et al. (2019). Principal components analysis of brain metabolism predicts development of Alzheimer dementia. *J. Nucl. Med.* 60, 837–843. doi: 10.2967/jnumed.118.219097

Blennow, K., De Leon, M. J., and Zetterberg, H. (2006). Alzheimer's disease. *Lancet* 368, 387–403.

Braak, H., and Braak, E. (1991a). Alzheimer's disease affects limbic nuclei of the thalamus. *Acta Neuropathol.* 81, 261–268. doi: 10.1007/bf00305867

Braak, H., and Braak, E. (1991b). Neuropathological stageing of Alzheimer-related changes. *Acta Neuropathol.* 82, 239–259. doi: 10.1007/bf00308809

Braak, H., and Del Trecidi, K. (2015). Neuroanatomy and pathology of sporadic Alzheimer's disease. *Adv. Anat. Embryol. Cell Biol.* 215, 1–162.

Braak, H., and Del Tredici, K. (2011). The pathological process underlying Alzheimer's disease in individuals under thirty. *Acta Neuropathol.* 121, 171–181. doi: 10.1007/s00401-010-0789-4

Brendel, M., Hogenauer, M., Delker, A., Sauerbeck, J., Bartenstein, P., Seibyl, J., et al. (2015). Improved longitudinal [(18)F]-AV45 amyloid PET by white matter reference and VOI-based partial volume effect correction. *Neuroimage* 108, 450–459. doi: 10.1016/j.neuroimage.2014.11.055

Bussiere, T., Friend, P. D., Sadeghi, N., Wicinski, B., Lin, G. I., Bouras, C., et al. (2002). Stereologic assessment of the total cortical volume occupied by amyloid deposits and its relationship with cognitive status in aging and Alzheimer's disease. *Neuroscience* 112, 75–91. doi: 10.1016/s0306-4522(02)00056-8

Carlesimo, G. A., Lombardi, M. G., and Caltagirone, C. (2011). Vascular thalamic amnesia: a reappraisal. *Neuropsychologia* 49, 777–789. doi: 10.1016/j.neuropsychologia.2011.01.026

Chan, A., and Shea, T. B. (2006). Dietary and genetically-induced oxidative stress alter tau phosphorylation: influence of folate and apolipoprotein E deficiency. *J. Alzheimers Dis.* 9, 399–405. doi: 10.3233/jad-2006-9405

Chiotis, K., Stenkrona, P., Almkvist, O., Stepanov, V., Ferreira, D., Arakawa, R., et al. (2018). Dual tracer tau PET imaging reveals different molecular targets for (11)C-THK5351 and (11)C-PBB3 in the Alzheimer brain. *Eur. J. Nucl. Med. Mol. Imaging* 45, 1605–1617. doi: 10.1007/s00259-018-4012-5

Choi, J. Y., Cho, H., Ahn, S. J., Lee, J. H., Ryu, Y. H., Lee, M. S., et al. (2018). Off-target (18)F-AV-1451 binding in the basal ganglia correlates with age-related iron accumulation. *J. Nucl. Med.* 59, 117–120. doi: 10.2967/jnumed.117.195248

Connor, J. R., Menzies, S. L., St Martin, S. M., and Mufson, E. J. (1992). A histochemical study of iron, transferrin, and ferritin in Alzheimer's diseased brains. *J. Neurosci. Res.* 31, 75–83. doi: 10.1002/jnr.490310111

Cras, P., Smith, M. A., Richey, P. L., Siedlak, S. L., Mulvihill, P., and Perry, G. (1995). Extracellular neurofibrillary tangles reflect neuronal loss and provide further evidence of extensive protein cross-linking in Alzheimer disease. *Acta Neuropathol.* 89, 291–295. doi: 10.1007/s004010050249

Cummings, J. (2019). The national institute on aging-Alzheimer's association framework on Alzheimer's disease: application to clinical trials. *Alzheimers Dement.* 15, 172–178. doi: 10.1016/j.jalz.2018.05.006

de Jong, L. W., Van Der Hiele, K., Veer, I. M., Houwing, J. J., Westendorp, R. G., Bollen, E. L., et al. (2008). Strongly reduced volumes of putamen and thalamus in Alzheimer's disease: an MRI study. *Brain* 131, 3277–3285. doi: 10.1093/brain/awn278

Declercq, L., Rombouts, F., Koole, M., Fierens, K., Marien, J., Langlois, X., et al. (2017). Preclinical evaluation of (18)F-JNJ64349311, a novel PET tracer for tau imaging. *J. Nucl. Med.* 58, 975–981. doi: 10.2967/jnumed.116.185199

Delacourte, A., David, J. P., Sergeant, N., Buee, L., Wattez, A., Vermersch, P., et al. (1999). The biochemical pathway of neurofibrillary degeneration in aging and Alzheimer's disease. *Neurology* 52, 1158–1165.

Dukart, J., Mueller, K., Villringer, A., Kherif, F., Draganski, B., Frackowiak, R., et al. (2013). Relationship between imaging biomarkers, age, progression and symptom severity in Alzheimer's disease. *Neuroimage Clin.* 3, 84–94. doi: 10.1016/j.nicl.2013.07.005

Giannakopoulos, P., Herrmann, F. R., Bussiere, T., Bouras, C., Kovari, E., Perl, D. P., et al. (2003). Tangle and neuron numbers, but not amyloid load, predict cognitive status in Alzheimer's disease. *Neurology* 60, 1495–1500. doi: 10.1212/01.wnl.0000063311.58879.01

Goedert, M., Eisenberg, D. S., and Crowther, R. A. (2017). Propagation of tau aggregates and neurodegeneration. *Annu. Rev. Neurosci.* 40, 189–210. doi: 10.1146/annurev-neuro-072116-031153

Goedert, M., and Jakes, R. (1990). Expression of separate isoforms of human tau protein: correlation with the tau pattern in brain and effects on tubulin polymerization. *EMBO J.* 9, 4225–4230. doi: 10.1002/j.1460-2075.1990.tb07870.x

Gomez-Isla, T., Hollister, R., West, H., Mui, S., Growdon, J. H., Petersen, R. C., et al. (1997). Neuronal loss correlates with but exceeds neurofibrillary tangles in Alzheimer's disease. *Ann. Neurol.* 41, 17–24. doi: 10.1002/ana.410410106

Good, P. F., Perl, D. P., Bierer, L. M., and Schmeidler, J. (1992). Selective accumulation of aluminum and iron in the neurofibrillary tangles of Alzheimer's disease: a laser microprobe (LAMMA) study. *Ann. Neurol.* 31, 286–292. doi: 10.1002/ana.410310310

Gordon, B. A., Blazey, T. M., Christensen, J., Dincer, A., Flores, S., Keefe, S., et al. (2019). Tau PET in autosomal dominant Alzheimer's disease: relationship with cognition, dementia and other biomarkers. *Brain* 142, 1063–1076.

Grinberg, L. T., Rub, U., Ferretti, R. E., Nitrini, R., Farfel, J. M., Polichiso, L., et al. (2009). The dorsal raphe nucleus shows phospho-tau neurofibrillary changes before the transentorhinal region in Alzheimer's disease. A precocious onset? *Neuropathol. Appl. Neurobiol.* 35, 406–416. doi: 10.1111/j.1365-2990.2008.00997.x

Grundke-Iqbal, I., Fleming, J., Tung, Y. C., Lassmann, H., Iqbal, K., and Joshi, J. G. (1990). Ferritin is a component of the neuritic (senile) plaque in Alzheimer dementia. *Acta Neuropathol.* 81, 105–110. doi: 10.1007/bf00334497

Hamasaki, H., Honda, H., Suzuki, S. O., Shijo, M., Ohara, T., Hatabe, Y., et al. (2019). Tauopathy in basal ganglia involvement is exacerbated in a subset of patients with Alzheimer's disease: the Hisayama study. *Alzheimers Dement.* 11, 415–423. doi: 10.1016/j.dadm.2019.04.008

Harada, R., Okamura, N., Furumoto, S., Furukawa, K., Ishiki, A., Tomita, N., et al. (2016). 18F-THK5351: a novel PET radiotracer for imaging neurofibrillary pathology in Alzheimer disease. *J. Nucl. Med.* 57, 208–214. doi: 10.2967/jnumed.115.164848

Harding, A., Halliday, G., Caine, D., and Kril, J. (2000). Degeneration of anterior thalamic nuclei differentiates alcoholics with amnesia. *Brain* 123(Pt 1), 141–154. doi: 10.1093/brain/123.1.141

Hashimoto, H., Kawamura, K., Igarashi, N., Takei, M., Fujishiro, T., Aihara, Y., et al. (2014). Radiosynthesis, photoisomerization, biodistribution, and metabolite analysis of 11C-PBB3 as a clinically useful PET probe for imaging of tau pathology. *J. Nucl. Med.* 55, 1532–1538. doi: 10.2967/jnumed.114.139550

Hashimoto, H., Kawamura, K., Takei, M., Igarashi, N., Fujishiro, T., Shiomi, S., et al. (2015). Identification of a major radiometabolite of [11C]PBB3. *Nucl. Med. Biol.* 42, 905–910. doi: 10.1016/j.nucmedbio.2015.08.006

Herholz, K., Carter, S. F., and Jones, M. (2007). Positron emission tomography imaging in dementia. *Br. J. Radiol.* 80, S160–S167.

Herrero, M. T., Barcia, C., and Navarro, J. M. (2002). Functional anatomy of thalamus and basal ganglia. *Childs Nerv. Syst.* 18, 386–404. doi: 10.1007/s00381-002-0604-1

Herrmann, M., Golombowski, S., Krauchi, K., Frey, P., Mourton-Gilles, C., Hulette, C., et al. (1999). ELISA-quantitation of phosphorylated tau protein in the Alzheimer's disease brain. *Eur. Neurol.* 42, 205–210. doi: 10.1159/000008108

Honer, M., Gobbi, L., Knust, H., Kuwabara, H., Muri, D., Koerner, M., et al. (2018). Preclinical evaluation of (18)F-RO6958948, (11)C-RO6931643, and (11)C-RO6924963 as novel PET radiotracers for imaging tau aggregates in Alzheimer disease. *J. Nucl. Med.* 59, 675–681. doi: 10.2967/jnumed.117.196741

Hostetler, E. D., Walji, A. M., Zeng, Z., Miller, P., Bennacef, I., Salinas, C., et al. (2016). Preclinical characterization of 18F-MK-6240, a promising PET tracer for in vivo quantification of human neurofibrillary tangles. *J. Nucl. Med.* 57, 1599–1606. doi: 10.2967/jnumed.115.171678

Hsu, J. L., Hsu, W. C., Chang, C. C., Lin, K. J., Hsiao, I. T., Fan, Y. C., et al. (2017). Everyday cognition scales are related to cognitive function in the early stage of probable Alzheimer's disease and FDG-PET findings. *Sci. Rep.* 7:1719.

Jack, C. R. Jr., Bennett, D. A., Blennow, K., Carrillo, M. C., Dunn, B., Haeberlein, S. B., et al. (2018). NIA-AA research framework: toward a biological definition of Alzheimer's disease. *Alzheimers Dement.* 14, 535–562. doi: 10.1016/j.jalz.2018.02.018

Jack, C. R. Jr., Bennett, D. A., Blennow, K., Carrillo, M. C., Feldman, H. H., Frisoni, G. B., et al. (2016). A/T/N: an unbiased descriptive classification scheme for Alzheimer disease biomarkers. *Neurology* 87, 539–547. doi: 10.1212/wnl.0000000000002923

Jimenez-Bonilla, J. F., Banzo, I., De Arcocha-Torres, M., Quirce, R., Martinez-Rodriguez, I., Sanchez-Juan, P., et al. (2016). Amyloid imaging with 11C-PIB in patients with cognitive impairment in a clinical setting: a visual and semiquantitative analysis. *Clin. Nucl. Med.* 41, e18–e23. doi: 10.1097/rlu.0000000000000934

Kang, J. M., Lee, S. Y., Seo, S., Jeong, H. J., Woo, S. H., Lee, H., et al. (2017). Tau positron emission tomography using [(18)F]THK5351 and cerebral glucose hypometabolism in Alzheimer's disease. *Neurobiol. Aging* 59, 210–219 doi: 10.1016/j.neurobiolaging.2017.08.008.

Kato, T., Inui, Y., Nakamura, A., and Ito, K. (2016). Brain fluorodeoxyglucose (FDG) PET in dementia. *Ageing Res. Rev.* 30, 73–84. doi: 10.1016/j.arr.2016.02.003

Kitamura, S., Shimada, H., Niwa, F., Endo, H., Shinotoh, H., Takahata, K., et al. (2018). Tau-induced focal neurotoxicity and network disruption related to apathy in Alzheimer's disease. *J. Neurol. Neurosurg. Psychiatry* 89, 1208–1214. doi: 10.1136/jnnp-2018-317970

Klunk, W. E., Engler, H., Nordberg, A., Wang, Y., Blomqvist, G., Holt, D. P., et al. (2004). Imaging brain amyloid in Alzheimer's disease with Pittsburgh Compound-B. *Ann. Neurol.* 55, 306–319.

Koga, S., Ono, M., Sahara, N., Higuchi, M., and Dickson, D. W. (2017). Fluorescence and autoradiographic evaluation of tau PET ligand PBB3 to alpha-synuclein pathology. *Mov. Disord.* 32, 884–892. doi: 10.1002/mds.27013

Kril, J. J., Patel, S., Harding, A. J., and Halliday, G. M. (2002). Neuron loss from the hippocampus of Alzheimer's disease exceeds extracellular neurofibrillary tangle formation. *Acta Neuropathol.* 103, 370–376. doi: 10.1007/s00401-001-0477-5

Kroth, H., Oden, F., Molette, J., Schieferstein, H., Capotosti, F., Mueller, A., et al. (2019). Discovery and preclinical characterization of [(18)F]PI-2620, a next-generation tau PET tracer for the assessment of tau pathology in Alzheimer's disease and other tauopathies. *Eur. J. Nucl. Med. Mol. Imaging* 46, 2178–2189. doi: 10.1007/s00259-019-04397-2

Lace, G. L., Wharton, S. B., and Ince, P. G. (2007). A brief history of tau: the evolving view of the microtubule-associated protein tau in neurodegenerative diseases. *Clin. Neuropathol.* 26, 43–58. doi: 10.5414/npp26043

Lee, V. M., Brunden, K. R., Hutton, M., and Trojanowski, J. Q. (2011). Developing therapeutic approaches to tau, selected kinases, and related neuronal protein targets. *Cold Spring Harb. Perspect. Med.* 1:a006437. doi: 10.1101/cshperspect.a006437

Leskovjan, A. C., Kretlow, A., Lanzirotti, A., Barrea, R., Vogt, S., and Miller, L. M. (2011). Increased brain iron coincides with early plaque formation in a mouse model of Alzheimer's disease. *Neuroimage* 55, 32–38. doi: 10.1016/j.neuroimage.2010.11.073

Leuzy, A., Chiotis, K., Lemoine, L., Gillberg, P. G., Almkvist, O., Rodriguez-Vieitez, E., et al. (2019). Tau PET imaging in neurodegenerative tauopathies-still a challenge. *Mol. Psychiatry* 24, 1112–1134. doi: 10.1038/s41380-018-0342-8

Leuzy, A., Rodriguez-Vieitez, E., Saint-Aubert, L., Chiotis, K., Almkvist, O., Savitcheva, I., et al. (2018). Longitudinal uncoupling of cerebral perfusion, glucose metabolism, and tau deposition in Alzheimer's disease. *Alzheimers Dement.* 14, 652–663. doi: 10.1016/j.jalz.2017.11.008

LeVine, S. M. (1997). Iron deposits in multiple sclerosis and Alzheimer's disease brains. *Brain Res.* 760, 298–303. doi: 10.1016/s0006-8993(97)00470-8

Lin, K. J., Hsiao, I. T., Hsu, J. L., Huang, C. C., Huang, K. L., Hsieh, C. J., et al. (2016). Imaging characteristic of dual-phase (18)F-florbetapir (AV-45/Amyvid) PET for the concomitant detection of perfusion deficits and beta-amyloid deposition in Alzheimer's disease and mild cognitive impairment. *Eur. J. Nucl. Med. Mol. Imaging* 43, 1304–1314. doi: 10.1007/s00259-016-3359-8

Lohith, T. G., Bennacef, I., Vandenberghe, R., Vandenbulcke, M., Salinas, C. A., Declercq, R., et al. (2019). Brain imaging of Alzheimer dementia patients and elderly controls with (18)F-MK-6240, a PET tracer targeting neurofibrillary tangles. *J. Nucl. Med.* 60, 107–114. doi: 10.2967/jnumed.118.208215

Lovell, M. A., Robertson, J. D., Teesdale, W. J., Campbell, J. L., and Markesbery, W. R. (1998). Copper, iron and zinc in Alzheimer's disease senile plaques. *J. Neurol. Sci.* 158, 47–52. doi: 10.1016/s0022-510x(98)00092-6

Lovell, M. A., Xiong, S., Xie, C., Davies, P., and Markesbery, W. R. (2004). Induction of hyperphosphorylated tau in primary rat cortical neuron cultures mediated by oxidative stress and glycogen synthase kinase-3. *J. Alzheimers Dis.* 6, 659–671; discussion 673–681.

Lowe, V. J., Curran, G., Fang, P., Liesinger, A. M., Josephs, K. A., Parisi, J. E., et al. (2016). An autoradiographic evaluation of AV-1451 Tau PET in dementia. *Acta Neuropathol. Commun.* 4:58.

Marquie, M., Normandin, M. D., Vanderburg, C. R., Costantino, I. M., Bien, E. A., Rycyna, L. G., et al. (2015). Validating novel tau positron emission tomography tracer [F-18]-AV-1451 (T807) on postmortem brain tissue. *Ann. Neurol.* 78, 787–800. doi: 10.1002/ana.24517

Maruyama, M., Shimada, H., Suhara, T., Shinotoh, H., Ji, B., Maeda, J., et al. (2013). Imaging of tau pathology in a tauopathy mouse model and in Alzheimer patients compared to normal controls. *Neuron* 79, 1094–1108. doi: 10.1016/j.neuron.2013.07.037

McKhann, G. M., Knopman, D. S., Chertkow, H., Hyman, B. T., Jack, C. R. Jr., Kawas, C. H., et al. (2011). The diagnosis of dementia due to Alzheimer's disease: recommendations from the National Institute on Aging-Alzheimer's Association workgroups on diagnostic guidelines for Alzheimer's disease. *Alzheimers Dement.* 7, 263–269.

Minoshima, S., Frey, K. A., Koeppe, R. A., Foster, N. L., and Kuhl, D. E. (1995). A diagnostic approach in Alzheimer's disease using three-dimensional stereotactic surface projections of fluorine-18-FDG PET. *J. Nucl. Med.* 36, 1238–1248.

Mueller, A., Bullich, S., Barret, O., Madonia, J., Berndt, M., Papin, C., et al. (2019). Tau PET imaging with (18)F-PI-2620 in patients with Alzheimer's disease and healthy controls: a first-in-human study. *J. Nucl. Med.* 61, 911–919. doi: 10.2967/jnumed.119.236224

Murugan, N. A., Chiotis, K., Rodriguez-Vieitez, E., Lemoine, L., Agren, H., and Nordberg, A. (2019). Cross-interaction of tau PET tracers with monoamine oxidase B: evidence from in silico modelling and in vivo imaging. *Eur. J. Nucl. Med. Mol. Imaging* 46, 1369–1382. doi: 10.1007/s00259-019-04305-8

Nemmi, F., Saint-Aubert, L., Adel, D., Salabert, A. S., Pariente, J., Barbeau, E. J., et al. (2014). Insight on AV-45 binding in white and grey matter from histogram analysis: a study on early Alzheimer's disease patients and healthy subjects. *Eur. J. Nucl. Med. Mol. Imaging* 41, 1408–1418. doi: 10.1007/s00259-014-2728-4

Ng, K. P., Pascoal, T. A., Mathotaarachchi, S., Therriault, J., Kang, M. S., Shin, M., et al. (2017). Monoamine oxidase B inhibitor, selegiline, reduces (18)F-THK5351 uptake in the human brain. *Alzheimers Res. Ther.* 9:25.

Ni, R., Ji, B., Ono, M., Sahara, N., Zhang, M. R., Aoki, I., et al. (2018). Comparative in vitro and in vivo quantifications of pathologic tau deposits and their association with neurodegeneration in tauopathy mouse models. *J. Nucl. Med.* 59, 960–966. doi: 10.2967/jnumed.117.201632

Ono, M., Sahara, N., Kumata, K., Ji, B., Ni, R., Koga, S., et al. (2017). Distinct binding of PET ligands PBB3 and AV-1451 to tau fibril strains in neurodegenerative tauopathies. *Brain* 140, 764–780.

Passamonti, L., Vazquez Rodriguez, P., Hong, Y. T., Allinson, K. S., Williamson, D., Borchert, R. J., et al. (2017). 18F-AV-1451 positron emission tomography in Alzheimer's disease and progressive supranuclear palsy. *Brain* 140, 781–791.

Pedro, T., Weiler, M., Yasuda, C. L., D'abreu, A., Damasceno, B. P., Cendes, F., et al. (2012). Volumetric brain changes in thalamus, corpus callosum and medial temporal structures: mild Alzheimer's disease compared with amnestic mild cognitive impairment. *Dement. Geriatr. Cogn. Disord.* 34, 149–155. doi: 10.1159/000342118

Rice, L., and Bisdas, S. (2017). The diagnostic value of FDG and amyloid PET in Alzheimer's disease-A systematic review. *Eur. J. Radiol.* 94, 16–24. doi: 10.1016/j.ejrad.2017.07.014

Rosler, T. W., Tayaranian Marvian, A., Brendel, M., Nykanen, N. P., Hollerhage, M., Schwarz, S. C., et al. (2019). Four-repeat tauopathies. *Prog. Neurobiol.* 180:101644. doi: 10.1016/j.pneurobio.2019.101644

Rub, U., Del Tredici, K., Del Turco, D., and Braak, H. (2002). The intralaminar nuclei assigned to the medial pain system and other components of this system are early and progressively affected by the Alzheimer's disease-related cytoskeletal pathology. *J. Chem. Neuroanat.* 23, 279–290. doi: 10.1016/s0891-0618(02)00007-8

Rub, U., Del Tredici, K., Schultz, C., Thal, D. R., Braak, E., and Braak, H. (2000). The evolution of Alzheimer's disease-related cytoskeletal pathology in the human raphe nuclei. *Neuropathol. Appl. Neurobiol.* 26, 553–567. doi: 10.1046/j.0305-1846.2000.00291.x

Schubert, D., and Chevion, M. (1995). The role of iron in beta amyloid toxicity. *Biochem. Biophys. Res. Commun.* 216, 702–707. doi: 10.1006/bbrc.1995.2678

Schwab, C., Schulzer, M., Steele, J. C., and Mcgeer, P. L. (1999). On the survival time of a tangled neuron in the hippocampal CA4 region in Parkinsonism dementia complex of Guam. *Neurobiol. Aging* 20, 57–63. doi: 10.1016/s0197-4580(99)00005-6

Schwab, C., Steele, J. C., and Mcgeer, P. L. (1998). Pyramidal neuron loss is matched by ghost tangle increase in Guam parkinsonism-dementia hippocampus. *Acta Neuropathol.* 96, 409–416. doi: 10.1007/s004010050912

Shcherbinin, S., Schwarz, A. J., Joshi, A., Navitsky, M., Flitter, M., Shankle, W. R., et al. (2016). Kinetics of the tau PET tracer 18F-AV-1451 (T807) in subjects with normal cognitive function, mild cognitive impairment, and Alzheimer disease. *J. Nucl. Med.* 57, 1535–1542. doi: 10.2967/jnumed.115.170027

Shimada, H., Kitamura, S., Ono, M., Kimura, Y., Ichise, M., Takahata, K., et al. (2017). First-in-human PET study with 18 F-AM-PBB3 and 18 F-PM-PBB3. *Alzheimers Dement.* 13:P1104.

Shimada, H., Ono, M., Tagai, K., Kubota, M., Kitamura, S., Takuwa, H., et al. (2018). Preclinical and clinical characterization of 18F-PM-PBB3, a PET ligand for diverse tau pathologies. *Alzheimers Dement.* 14, 177–178.

Sintini, I., Schwarz, C. G., Martin, P. R., Graff-Radford, J., Machulda, M. M., Senjem, M. L., et al. (2019). Regional multimodal relationships between tau, hypometabolism, atrophy, and fractional anisotropy in atypical Alzheimer's disease. *Hum. Brain Mapp.* 40, 1618–1631.

Smith, M. A., Harris, P. L., Sayre, L. M., and Perry, G. (1997). Iron accumulation in Alzheimer disease is a source of redox-generated free radicals. *Proc. Natl. Acad. Sci. U.S.A.* 94, 9866–9868. doi: 10.1073/pnas.94.18.9866

Smith, R., Schain, M., Nilsson, C., Strandberg, O., Olsson, T., Hagerstrom, D., et al. (2017). Increased basal ganglia binding of (18) F-AV-1451 in patients with progressive supranuclear palsy. *Mov. Disord.* 32, 108–114. doi: 10.1002/mds.26813

Spillantini, M. G., and Goedert, M. (2013). Tau pathology and neurodegeneration. *Lancet Neurol.* 12, 609–622.

Stratmann, K., Heinsen, H., Korf, H. W., Del Turco, D., Ghebremedhin, E., Seidel, K., et al. (2016). Precortical phase of Alzheimer's disease (AD)-related tau cytoskeletal pathology. *Brain Pathol.* 26, 371–386. doi: 10.1111/bpa.12289

Su, Y., Blazey, T. M., Snyder, A. Z., Raichle, M. E., Marcus, D. S., Ances, B. M., et al. (2015). Partial volume correction in quantitative amyloid imaging. *Neuroimage* 107, 55–64.

Taber, K. H., Wen, C., Khan, A., and Hurley, R. A. (2004). The limbic thalamus. *J. Neuropsychiatry Clin. Neurosci.* 16, 127–132. doi: 10.1176/appi.neuropsych.16.2.127

Tagai, K., Ono, M., Kubota, M., Kitamura, S., Takahata, K., Seki, C., et al. (2020). High-contrast in-vivo imaging of tau pathologies in Alzheimer's and non-Alzheimer's disease tauopathies. *medRxiv* [Preprint]. doi: 10.1101/2020.03.05.20028407

Tago, T., Toyohara, J., Harada, R., Furumoto, S., Okamura, N., Kudo, Y., et al. (2019). Characterization of the binding of tau imaging ligands to melanin-containing cells: putative off-target-binding site. *Ann. Nucl. Med.* 33, 375–382. doi: 10.1007/s12149-019-01344-x

Terry, R. D., Deteresa, R., and Hansen, L. A. (1987). Neocortical cell counts in normal human adult aging. *Ann. Neurol.* 21, 530–539. doi: 10.1002/ana.410210603

Terry, R. D., Peck, A., Deteresa, R., Schechter, R., and Horoupian, D. S. (1981). Some morphometric aspects of the brain in senile dementia of the Alzheimer type. *Ann. Neurol.* 10, 184–192. doi: 10.1002/ana.410100209

Wong, D. F., Comley, R. A., Kuwabara, H., Rosenberg, P. B., Resnick, S. M., Ostrowitzki, S., et al. (2018). Characterization of 3 novel tau radiopharmaceuticals, (11)C-RO-963, (11)C-RO-643, and (18)F-RO-948, in healthy controls and in Alzheimer subjects. *J. Nucl. Med.* 59, 1869–1876. doi: 10.2967/jnumed.118.209916

Wu, P., Wang, J., Peng, S., Ma, Y., Zhang, H., Guan, Y., et al. (2013). Metabolic brain network in the Chinese patients with Parkinson's disease based on 18F-FDG PET imaging. *Parkinsonism Relat. Disord.* 19, 622–627. doi: 10.1016/j.parkreldis.2013.02.013

Yi, H. A., Moller, C., Dieleman, N., Bouwman, F. H., Barkhof, F., Scheltens, P., et al. (2016). Relation between subcortical grey matter atrophy and conversion from mild cognitive impairment to Alzheimer's disease. *J. Neurol. Neurosurg. Psychiatry* 87, 425–432. doi: 10.1136/jnnp-2014-309105

Conflict of Interest: The authors declare that the research was conducted in the absence of any commercial or financial relationships that could be construed as a potential conflict of interest.

frontiers in Neuroscience

ORIGINAL RESEARCH
published: 02 July 2020
doi: 10.3389/fnins.2020.00658

Periodontitis Induced by *P. gingivalis*-LPS Is Associated With Neuroinflammation and Learning and Memory Impairment in Sprague-Dawley Rats

Yi Hu[1,2†], Huxiao Li[1,2†], Jing Zhang[1,2], Xu Zhang[2,3], Xinyi Xia[1,2], Che Qiu[1,2], Yue Liao[1,2], Huiwen Chen[1,2], Zhongchen Song[1,2] and Wei Zhou[2,3*]*

[1] Department of Periodontology, Shanghai Ninth People's Hospital, College of Stomatology, Shanghai Jiao Tong University School of Medicine, Shanghai, China, [2] National Clinical Research Center for Oral Diseases, Shanghai Key Laboratory of Stomatology & Shanghai Research Institute of Stomatology, Shanghai, China, [3] Laboratory of Oral Microbiota and Systemic Diseases, Shanghai Ninth People's Hospital, College of Stomatology, Shanghai Jiao Tong University School of Medicine, Shanghai, China

OPEN ACCESS

Edited by:
Fangyu Peng,
University of Texas Southwestern Medical Center, United States

Reviewed by:
Natalia P. Rocha,
The University of Texas Health Science Center at Houston, United States
Stefano Musardo,
Université de Genève, Switzerland

***Correspondence:**
Wei Zhou
sweetzw@hotmail.com
Zhongchen Song
szhongchen@sina.com

[†] These authors have contributed equally to this work

Specialty section:
This article was submitted to Neurodegeneration, a section of the journal Frontiers in Neuroscience

Received: 15 January 2020
Accepted: 27 May 2020
Published: 02 July 2020

Citation:
Hu Y, Li H, Zhang J, Zhang X, Xia X, Qiu C, Liao Y, Chen H, Song Z and Zhou W (2020) Periodontitis Induced by P. gingivalis-LPS Is Associated With Neuroinflammation and Learning and Memory Impairment in Sprague-Dawley Rats. Front. Neurosci. 14:658. doi: 10.3389/fnins.2020.00658

Background: Periodontitis is one of the most common oral diseases and is a potential risk factor for systemic diseases. In this study, we aimed to investigate the association between periodontitis and learning and memory impairment.

Methods: We established a periodontitis model by topical application of *Porphyromonas gingivalis* lipopolysaccharide (*P. gingivalis*-LPS) into the palatal gingival sulcus of the maxillary first molars of 10-week-old male rats for a 10-week period. We assessed alveolar bone resorption using micro–computed tomography analysis and learning and memory ability using the Morris water maze test. We determined the levels of cytokines [interleukin (IL)-1β, IL-6, IL-8, and IL-21] and LPS in the peripheral blood and cortex, as well as toll-like receptor 4 (TLR4)/NF-κB signaling pathway activation, using reverse transcription-polymerase chain reaction (RT-PCR), enzyme-linked immunosorbent assay (ELISA), and western blot. We determined activation of microglia and astrocytes, expression of Aβ1-42, APP and Tau by immunohistochemistry. Finally, we measured the expression of amyloid precursor protein (APP) and its key secretases, as well as the Aβ1-40/1-42 ratio, by RT-PCR, western blot, and ELISA.

Results: We found that periodontitis induced learning and memory impairment in the rats. Further, we observed that it induced significant alveolar bone resorption. There was an increase in the levels of inflammatory cytokines and LPS. Moreover, we confirmed TLR4/NF-κB signaling pathway activation. We also observed activated microglia and astrocytes with enlarged cell bodies and irregular protrusions. Finally, we observed the promotion of β- and γ-secretases APP processing.

Conclusion: Our findings indicated that periodontitis was associated with learning and memory impairment, probably induced by neuroinflammation via activating the TLR4/NF-κB signaling pathway. Furthermore, abnormal APP processing could be involved in this progress.

Keywords: periodontitis, neuroinflammation, learning and memory impairment, APP processing, TLR4/NF-κB signaling pathway

INTRODUCTION

Periodontitis is a potentially transmissible chronic infection caused by plaque biofilm. It is responsible for 70% of the global population presenting one or more damages in the periodontium (Oppermann et al., 2015). Considering that periodontitis involves interacting bacterial pathogens, including their toxic factors and host inflammatory responses, it has a multifactorial etiology with a marked inflammatory profile (Papapanou et al., 2018). Chronic recurrent periodontal inflammation could destroy the tooth support organization; further, there is increasing evidence that periodontal disease is an important risk factor for systemic diseases, including cardiovascular disease, diabetes, and reduced respiratory function (Preshaw et al., 2012; Hamilton et al., 2017; Winning et al., 2019).

Given the accelerating trend of population aging, the harm caused by cognitive disorders on human health has become increasingly prominent. It clinically manifests as gradual cognitive dysfunction and psychosis (Wimo et al., 2017; Brookmeyer et al., 2018). Epidemiological surveys reported that periodontitis was associated with an increase in the rate of cognitive decline (Ide et al., 2016; Harding et al., 2017). Periodontitis is not only an oral localized inflammatory disease, but also elicits low-grade inflammation via both the release of pro-inflammatory cytokines and the invasion of periodontitis bacteria along with their components (Hashioka et al., 2019). Level of pro-inflammatory cytokines could increase with worsened periodontal status and cognitive decline (Sochocka et al., 2017). Keeping oral hygiene could decrease the risk of dementia (Harding et al., 2017).

Periodontal pathogens and virulence factors that cause chronic periodontitis may also possibly contribute to the development of dementia (Olsen and Singhrao, 2015). *Porphyromonas gingivalis (P. gingivalis)*, the most important periodontal pathogen, and its virulence factor lipopolysaccharide (LPS) are main pathogenic factor of periodontitis (Jain and Darveau, 2010; Poole et al., 2013). Dominy et al. (2019) reported *P. gingivalis* in brain samples of patients with AD, which indicates that it could be a risk factor for AD. Ilievski et al. (2018) reported brain inflammation and neurodegeneration after oral administration of *P. gingivalis*. Wu et al. (2017) reported that intraperitoneal injection of *P. gingivalis*-LPS promoted learning and memory deficits and intracellular accumulation of Aβ. Our previous study also suggested that intraperitoneal injection of *P. gingivalis*-LPS, which induced systemic inflammation, could impair cognition through neuroinflammation (Zhang et al., 2018). However, the association between topical application of *P. gingivalis*-LPS into the gingival sulcus and learning and memory ability remains unclear.

In this study, we aimed to investigate the effects of periodontitis with topical application of *P. gingivalis*-LPS on learning and memory using the Morris Water Maze test. We used micro–computed tomography to assess bone resorption. Activation of microglial and astrocyte was confirmed through immunohistochemistry. The relative level of LPS and expression of inflammatory factors, as well as TLR4/NF-κB signaling pathway activation were analyzed using reverse transcription-polymerase chain reaction, enzyme-linked immunosorbent assay, and western blot. For further analysis of the underlying mechanism, we assessed APP processing.

MATERIALS AND METHODS

Animals

All experimental protocols were approved by the ethical committee of the Animal Care and Experimental Committee of Shanghai Jiao Tong University School of Medicine and were performed according to the guidelines of the EU Directive 2010/63/EU. Efforts were made to minimize surgery-induced suffering and reduce the overall number of animals used.

We obtained 10-week-old male Sprague-Dawley rats of specific pathogen-free (SPF) grade from the Shanghai SIPPR-BK Laboratory Animal Co., Ltd. The rats were provided with standard housing at temperature (18–22°C) and humidity (55–65%) with a 12-h light/dark cycle and free access to food and water. We randomly divided 32 rats into four groups, namely, the control group (Control), *P. gingivalis*-LPS group (LPS), *P. gingivalis*-LPS plus TAK-242 group (LPS+TAK-242), and TAK-242 group. TAK-242 (also known as CLI-095), a novel cyclohexene derivative, is an effectively/specifically TLR4 inhibitor (Ii et al., 2006). After inducing anesthesia using 10% chloral hydrate, the rats in the LPS and LPS+TAK-242 groups were topical applied with *P. gingivalis*-LPS (0.5 mg/kg, twice a week) into the palatal gingival sulcus of the maxillary first molars for 10 weeks using a 5-μl microsyringe (Hamilton, Switzerland). Moreover, we injected TAK-242 (0.5 mg/kg, i.p., twice a week) in rats in the LPS+TAK-242 group in advance. The rats in the TAK-242 group were injected with TAK-242 (0.5 mg/kg, i.p., twice a week). The rats in the control group received an equivalent saline volume. The LPS and TAK-242 amounts were determined based on previous studies (Nishida et al., 2001; Gárate et al., 2014). Three days after the last administration, the rats underwent behavioral tests for learning and memory ability assessment. We purchased *P. gingivalis*-LPS Ultrapure and TAK-242 from Invivogen (tlrl-ppglps and tlrl-cli95, San Diego, CA, United States) and dissolved them according to the manufacturer's instructions.

Open Filed Test (OFT)

The open field in the present study consisted of a rectangular arena (530 mm × 478 mm), enclosed by a black wall, 590 mm in height (Mobile Datum, Shanghai, China). The test was initiated by gently placing a single rat in the middle of the arena, allowing the animal to move freely for 5 min while being recorded.

Morris Water Maze (MWM) Test

The MWM test was conducted in a round pool 160 cm in diameter and 55 cm in depth (Mobile Datum, Shanghai, China). The pool was filled with water made opaque with white non-toxic water-based tempura paint. The water temperature was controlled to remain with a range equivalent to that of room temperature (22 ± 1°C). The platform was placed in the center

of one quadrant of the pool and submerged 2.5 cm beneath the water surface; it remained in the same position throughout the learning trials and was removed from the pool during the probe test. A video-tracking system (Shanghai Jiliang Software Technology Co., Ltd.) was used to monitor and record the swimming activity of the rats. The rats should have learned to use the visual tips around the pool to find the hidden platform within 90 s, otherwise it would be gently guided to the platform and allowed to re-orient for an additional 10 s. Each rat was trained four times per day with a 30 s of rest per training interval. To examine spatial reference memory, a probe test was carried out on the sixth day when the platform was removed from the pool and each rat was placed into the water at the two quadrants furthest from the platform used on days 1–5, being allowed to navigate freely for 60 s.

Measurement of Alveolar Bone Resorption by Micro-Computed Tomography (CT)

The maxillae of rats were obtained to detect bone parameters by micro-CT. Fixed in 4% paraformaldehyde, the bone morphometry was assessed using Skyscan1172 (Bruker, Kontich, Belgium) with an accuracy of 18 μm. Parameters including Bone volume/total volume (BV/TV), Bone surface/volume ratio (BS/BV) and Bone mineral density (BMD) were calculated.

Isolation of Peripheral Blood Mononuclear Cells (PBMCs)

Peripheral blood from rats (5 ml per rat) was collected from abdominal aorta in the presence of heparin as the anticoagulant. Three milliliters of the whole blood was diluted with sterile PBS of the same volume and gently resuspended. Six milliliters of the diluted whole blood fraction was overlaid onto 3 ml of the Ficoll-Paque Plus (GE Healthcare Bio-Sciences Corp., Piscataway, NJ, United States) and then subjected to 800 × g for 20 min at RT with the centrifuge brake "off." Then PBMC layers were washed twice with RPMI 1640 media by centrifugation at 1200 rpm for 5 min at 4°C. After isolation, all samples were dissolved in Trizol reagent (Takara, Kusatsu, Shiga, Japan) for lysis of cells to extract RNA.

RNA Extraction and RT-PCR Analysis

The RNA was extracted from PBMCs and homogenization of cortex using Trizol reagent (Takara, Kusatsu, Shiga, Japan) and the Total RNA Kit (Omega Bio-Tek, Inc., Norcross, GA, United States), respectively. The purity and concentration of RNA, as well as the cDNA synthesis, were conducted according to Li et al. (2018). Subsequently, an RT-PCR assay was performed using SYBR Premix Ex Taq^{TM} (Takara, Kusatsu, Shiga, Japan) on a Roche LightCycler 480 Real-Time PCR Detection System (Roche, Basel, Switzerland) according to the manufacturer's protocol. Data were then processed using the $2^{-\Delta\Delta CT}$ method. All results were based on at least three independent tests, and the final results were expressed as normalized fold values relative to the control group. The sequences of genes including Glyceraldehyde-3-phosphate dehydrogenase (GAPDH), IL-1β, IL-6, IL-8 and IL-21, APP, amyloid precursor-like protein 1 (APLP1), APLP2, a disintegrin and metalloproteinase 10 (ADAM10), β-site APP cleaving enzyme 1 (BACE1), presenilin 1 (PS1), PS2, TLR4, cluster of differentiation 14 (CD14) and their primer pairs were listed in **Table 1**.

Measurements of Interleukins, Aβ and LPS by ELISA

Of the approximately 5 ml of blood collected as previously described, 2 ml of blood were collected in heparinized tubes for the measurement of plasma cytokines. After centrifuging (4°C, 2500 rpm*15 min), supernatant medium was separated and immediately aliquoted into 1.5 ml cryogenic tubes and frozen at −80°C until use. For tissue, radioimmunoprecipitation assay (RIPA) lysis buffer (Beyotime, Beijing, China), 1% protease inhibitor cocktail (Sigma, St. Louis, MO, United States), and 1% PMSF (Beyotime, Beijing, China) were used to homogenize samples of the cerebral cortex. Protein qualification was performed by BCA Protein Assay Kit (Beyotime, Beijing, China). Equal amounts of protein were used in ELISA to measure levels of IL-1β, IL-6, IL-8, IL-21 (UBI, Sunnyvale, CA, United States) and Aβ1-40, Aβ1-42 (Enzyme-linked Biotechnology, Shanghai, China) both in the cortex and plasma according to the manufacturer's instructions. Level of LPS in the plasma of

TABLE 1 | The sequences of genes and primer pairs.

Target Gene	Primer Sequences
GAPDH	Forward:5′-ACAGTCCATGCCATCACTGCC-3′
	Reverse:5′-GCCTGCTTCACCACCTTCTTG-3′
IL-1β	Forward:5′-AACCTGCTGGTGTGTGACGTTC-3′
	Reverse:5′-CAGCACGAGGCTTTTTTGTTGT-3′
IL-6	Forward:5′-GCCCTTCAGGAACAGCTATGA-3′
	Reverse:5′-TGTCAACAACATCAGTCCCAAGA-3′
IL-8	Forward:5′-CATTAATATTTAACGATGTGGATGCG-3′
	Reverse:5′-GCCTACCATCTTTAAACTGCACAAT-3′
IL-21	Forward:5′-GCTCCACAAGATGTAAAGGG-3′
	Reverse:5′-GTGCCTCTGTTTATTTCCTG-3′
APP	Forward:5′-AGAGGTCTACCCTGAACTGC-3′
	Reverse:5′-ATCGCTTACAAACTCACCAACT-3′
APLP1	Forward:5′-TCAGGTCTGCTGATCATGGGAGC-3′
	Reverse:5′-TGGGTGGGGAAGAGGACTTTATTG-3′
APLP2	Forward:5′-CAGAGCGACAGACCCTCATTC-3′
	Reverse:5′-TCTACTCGGGCCAAATGGGT-3′
ADAM10	Forward:5′-GCCTATGTCTTCACGGACCG-3′
	Reverse:5′-TGCCAGACCAAGAACACCATC-3′
BACE1	Forward:5′-CGGGAGTGGTATTATGAAGTG-3′
	Reverse:5′-AGGATGGTGATGCGGAAG-3′
PS1	Forward:5′-GAGGAAGACGAAGAGCTGACAT-3′
	Reverse:5′-GAAGCTGACTGACTTGATGGTG-3′
PS2	Forward:5′-GAGCAGAGCCAAATCAAAGG-3′
	Reverse:5′-GGGAGAAAGAACAGCTCGTG-3′
TLR4	Forward:5′-AGCCATTGCTGCCAACATCA-3′
	Reverse:5′-GCCAGAGCGGCTACTCAGAAAC-3′
CD14	Forward:5′-CTCAACCTAGAGCCGTTTCT-3′
	Reverse:5′-CAGGA TTGTCAGACAGGTCT-3′

rats was detected by ELISA as well (SAB, College Park, Maryland, United States).

Western Blot

The samples of the cerebral cortex of rats in four groups were homogenized and lysed by RIPA containing 1% protease inhibitor cocktail and 1% PMSF (Beyotime, Shanghai, China). Equal amounts of protein were separated by SDS polyacrylamide gel electrophoresis and transferred onto PVDF membrane blocked with 5% skimmed milk as previously described (Li et al., 2018). A pre-stained protein marker (Thermo Fisher Scientific, MA, United States) was run in parallel to detect the molecular weight of proteins. Proteins were probed with appropriate antibodies including anti-TLR4 (1:1000, abs132000; Absin Bioscience Inc., Shanghai, China), anti-CD14 (1:500, abs121538; Absin Bioscience Inc., Shanghai, China), anti-IRAK1 (1:1000, abs143411; Absin Bioscience Inc., Shanghai, China), anti-p65 (1:1000, no. 8242; Cell Signaling Technology, United States), anti-pp65 (1:1000, no.3033; Cell Signaling Technology, United States) anti-BACE1 (1:1000, no. 5606; Cell Signaling Technology, United States), anti-APP (1:1000, no. 2452; Cell Signaling Technology, United States) and anti-GAPDH (1:1000, AB-P-R001, Goodhere Biotechnology Co., Hangzhou, China). The data were quantified using the Image Studio Lite ver. 5.2 software.

Immunohistochemistry

Rats were anesthetized with 10% chloral hydrate and perfused with cool PBS before removal of the brain. One hemisphere was placed in 4% paraformaldehyde overnight at 4°C, after which paraffin sections were prepared. This procedure is consistent with the previous study (Zhang et al., 2018). Briefly, brain sections were incubated with 3% H_2O_2 in methanol, blocked with 10% goat serum and incubated overnight at 4°C with the following primary antibodies: Ionized calciumbinding adaptor molecule 1 (Iba1) (1:400, ARG63338; Arigo Biolaboratories, Hsinchu City, Taiwan, China), Glial fibrillary acidic protein (GFAP) (1:400, ab7260; Abcam) to label microglia and astrocytes, anti-beta Amyloid1-42 antibody (1:50, ab10148; Abcam), anti-Tau antibody (1:400, ab32057; Abcam) and anti-APP antibody (1:100, MAB348; Millipore). After being washed, sections were incubated with biotinylated goat anti-rabbit or goat secondary antibody (1:200; Vector Laboratories, Burlingame, CA, United States). Images were obtained with a Leica camera.

The quantification of the immunohistochemical analysis for Iba1, GFAP, Aβ1-42, APP and Tau positive cells was performed by Image J software. The endpoints and process length were evaluated, and the numbers of positive cells were determined according to previous studies (Zhang et al., 2017; Young and

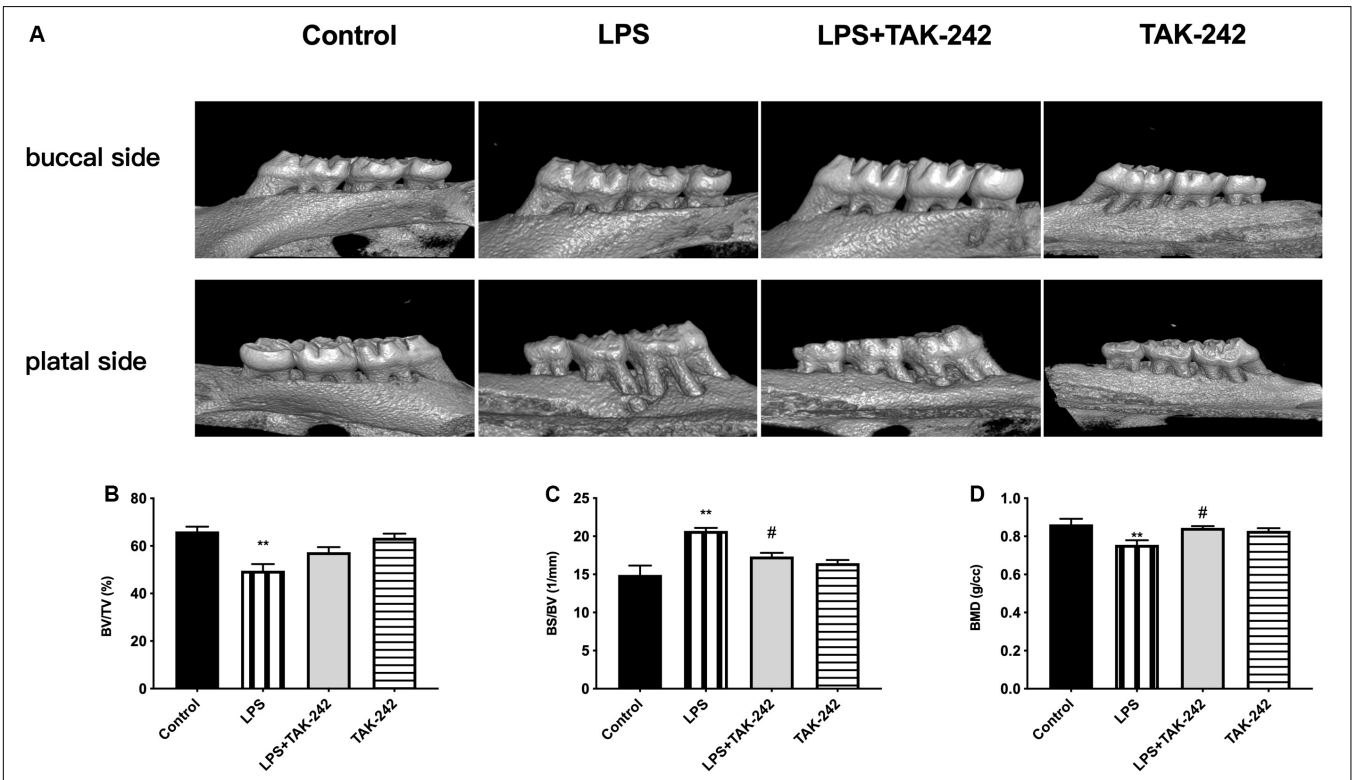

FIGURE 1 | Effects of topical application of *P. gingivalis*-LPS into the gingival sulcus of maxillary first molars on alveolar bone. **(A)** Images captured by micro-CT scanning of molar region. Bone density analysis of alveolar bone including **(B)** BV/TV, one-way ANOVA, $F = 13.65$, $^{**}p < 0.01$ compared to the control group. **(C)** BS/BV, one-way ANOVA, $F = 13.35$, $^{**}p < 0.01$ compared to the control group and $^{\#}p < 0.05$ compared to the LPS group. **(D)** BMD, one-way ANOVA, $F = 6.979$, $^{**}p < 0.01$ compared to the control group and $^{\#}p < 0.05$ compared to the LPS group ($n = 4$–6 per group).

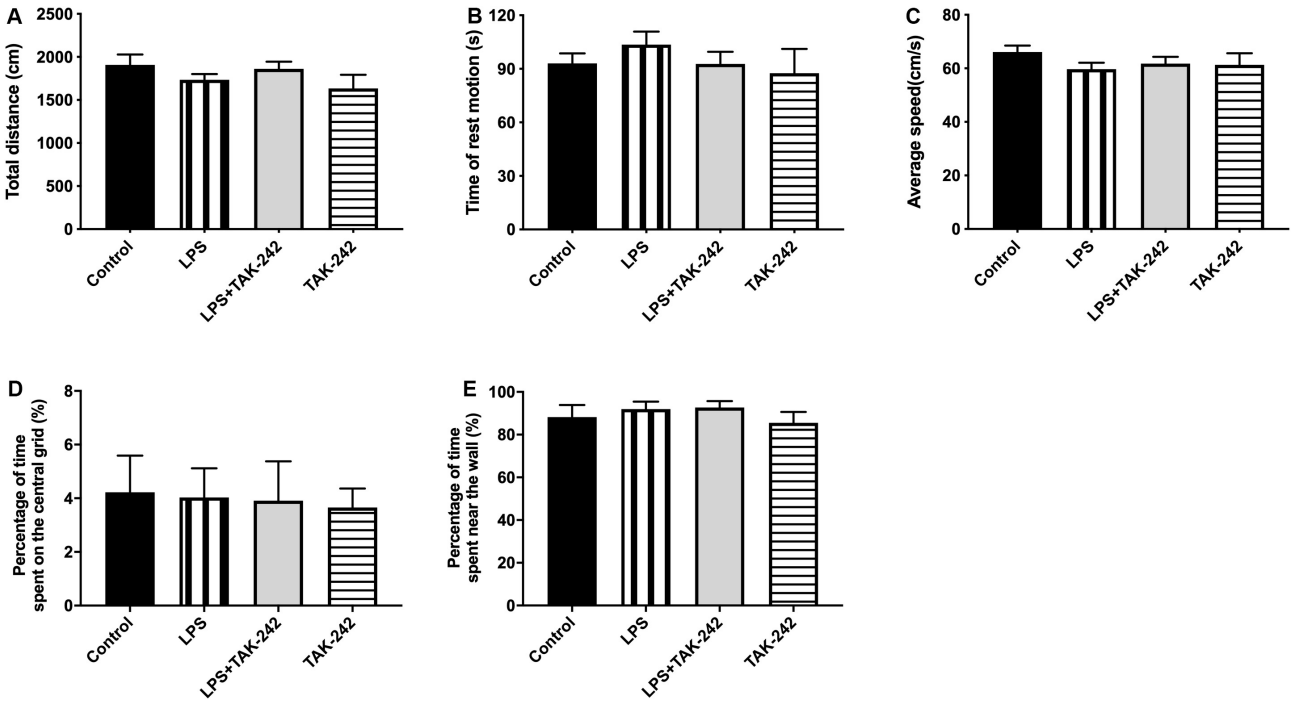

FIGURE 2 | Effects of periodontal inflammation on animal activities. The open field test (OFT) was used to evaluate the locomotor activities of rats 3 days after the final administration **(A–E)**: **(A)** Total distance; one-way ANOVA, $p = 0.3170$. **(B)** Time of rest motion; one-way ANOVA, $F = 0.2203$, $p = 0.8812$. **(C)** Average speed. $F = 0.8259$, $p = 0.4950$. **(D)** Percentage of time spent on the central (%); one-way ANOVA, $F = 0.03944$, $p = 0.9891$. **(E)** Percentage of time spent near the wall; one-way ANOVA, $F = 0.5656$, $p = 0.6455$. Overall, no significant differences were observed between groups in OFT ($n = 4$–6 per group).

Morrison, 2018). The average of the individual measurements was used to calculate group means.

Statistical Analysis

All data are presented as the mean ± standard error of the mean (SEM). *P*-values were calculated with one-way ANOVA and two-way ANOVA with the GraphPad Prism software. An analysis of variance was performed using Turkey's *post-hoc* multiple comparison test. A value of $p < 0.05$ was indicative of statistical significance.

RESULTS

Assessment of Alveolar Bone Resorption

As shown in **Figure 1A**, *P. gingivalis*-LPS led to posterior maxillary bone loss. There was a decrease in BV/TV and BMD (66.13 ± 1.98% vs. 49.56 ± 2.83% and 0.8743 ± 0.02 g/cc vs. 0.755 ± 0.02 g/cc, respectively) and an increase in BS/BV (14.92 ± 1.22/mm vs. 20.7 ± 0.40/mm) in the LPS group, which was reversed by TAK-242 (**Figures 1B–D**). This indicated that *P. gingivalis*-LPS could induce bone resorption similar to that in periodontitis. Moreover, these changes induced by *P. gingivalis*-LPS could be alleviated by TAK-242.

Effects of Periodontal Inflammation on Locomotor Activity

We used the OFT to assess whether periodontitis induced by *P. gingivalis*-LPS with/without intraperitoneal administration of TAK-242 could affect spontaneous activity in rats. As shown in **Figure 2**, there was no significant among-group difference in the behaviors, including total distance covered (**Figure 2A**), time of rest motion (**Figure 2B**), average speed (**Figure 2C**), percentage of time spent on the central (%) (**Figure 2D**), percentage of time spent near the wall (%) (**Figure 2E**). This indicated that the locomotor activity of the rats was not affected by *P. gingivalis*-LPS or TAK-242.

Effects of Periodontal Inflammation on Spatial Learning and Memory

We used the MWM test to determine whether topical application of *P. gingivalis*-LPS into the palatal gingival sulcus of the maxillary first molars could affect learning and memory ability in rats. There was a chronological latency decrease in all the groups over the 5-day training period (**Figure 3A**). In the LPS group, the escape latency was significantly longer than it was in the control group at days 3, 4, and 5. There were no significant differences between the control group and the LPS+TAK-242 group. We removed the platform on the sixth day and found a significant decrease in the number of platform crossings in the target quadrant and the percentage of time spent in the target quadrant

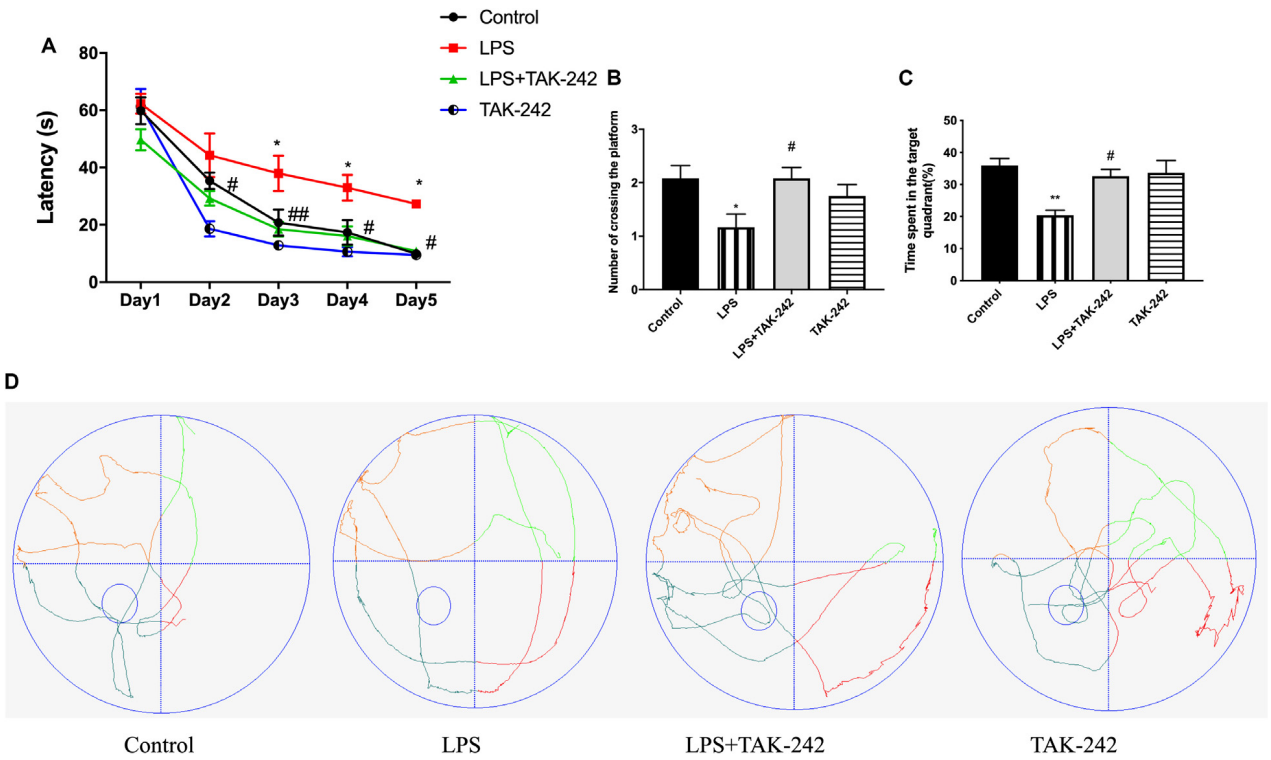

FIGURE 3 | Effects of periodontal inflammation on spatial learning and memory. After the OFT, the MWM test was conducted to assess the learning and memory ability. **(A)** Latency to find the platform during the acquisition phase of the MWM test; two-way ANOVA, $F = 1.154$, $^{*}p < 0.05$ compared to the control group and $^{\#}p < 0.05$, $^{\#\#}p < 0.01$ compared to the LPS group. **(B)** Number of platform crossings in the target quadrant; one-way ANOVA, $F = 3.662$, $^{*}p < 0.05$ compared to the control group and $^{\#}p < 0.05$ compared to the LPS group. **(C)** Percentage of time spent in the target quadrant; one-way ANOVA, $F = 7.356$, $^{*}p < 0.05$ and $^{**}p < 0.01$ compared to the control group, $^{\#}p < 0.05$ compared to the LPS group. The LPS group was compared to the control group while the LPS+TAK-242 group was compared to the LPS group. **(D)**The typical trajectories of the LPS group approximated the arc of a circle, without any crossings over the original platform (platform is represented by a small circle) (n = 4–6 per group).

in the LPS group (**Figures 3B,C**). During the probe test, rats in the control group learned to directly navigate to the quadrant containing the hidden platform; however, this was not observed in the LPS group (**Figure 3D**). The changes mentioned above could be restored by TAK-242 administration. This indicated that periodontitis induced by *P. gingivalis*-LPS could be an important risk factor for learning and memory impairment.

Effects of Periodontal Inflammation on the Plasma Levels of LPS and Inflammatory Cytokines

Plasma levels of IL-1β, IL-6, IL-8, IL-21, and LPS were significantly higher in the LPS group than in the control group. Compared to the LPS group, the LPS+TAK-242 group showed reduced levels of IL-1β, IL-6, IL-8, and IL-21 proteins and LPS (**Figure 4**).

Effects of Periodontal Inflammation on Microglia and Astrocytes in the Cortex

As shown in **Figure 5**, activation of microglia and astrocytes could be found in the LPS group. Activated microglia, which are characterized by irregular protrusions and increased volume of cell bodies, were positively stained with Iba1. Activated microglia were observed in the cortex of the LPS group but rarely in the control group while activated astrocytes were positively stained with GFAP (**Figures 5A,E**). A relative increase in endpoints and process length was found, presenting as volume hypertrophy and irregular protrusions (**Figures 5B–D,F–H**). Changes mentioned above could be reversed by TAK-242 administration. These findings indicate that periodontitis induced by *P. gingivalis*-LPS could play an important role in neuroinflammation.

Effects of Periodontal Inflammation on Inflammatory Cytokine Levels in the Cortex

Compared to the control group, there were significantly higher mRNA and protein levels of IL-1β, IL-6, IL-8, and IL-21 in the cortex in the LPS group. Compared to the LPS group, the LPS+TAK-242 group showed reduced levels of IL-1β, IL-6, and IL-8 proteins (**Figure 6**). These findings demonstrate that periodontitis induced by *P. gingivalis*-LPS increases the expression of inflammatory factors in the central nervous system, which is significantly prevented by TAK-242.

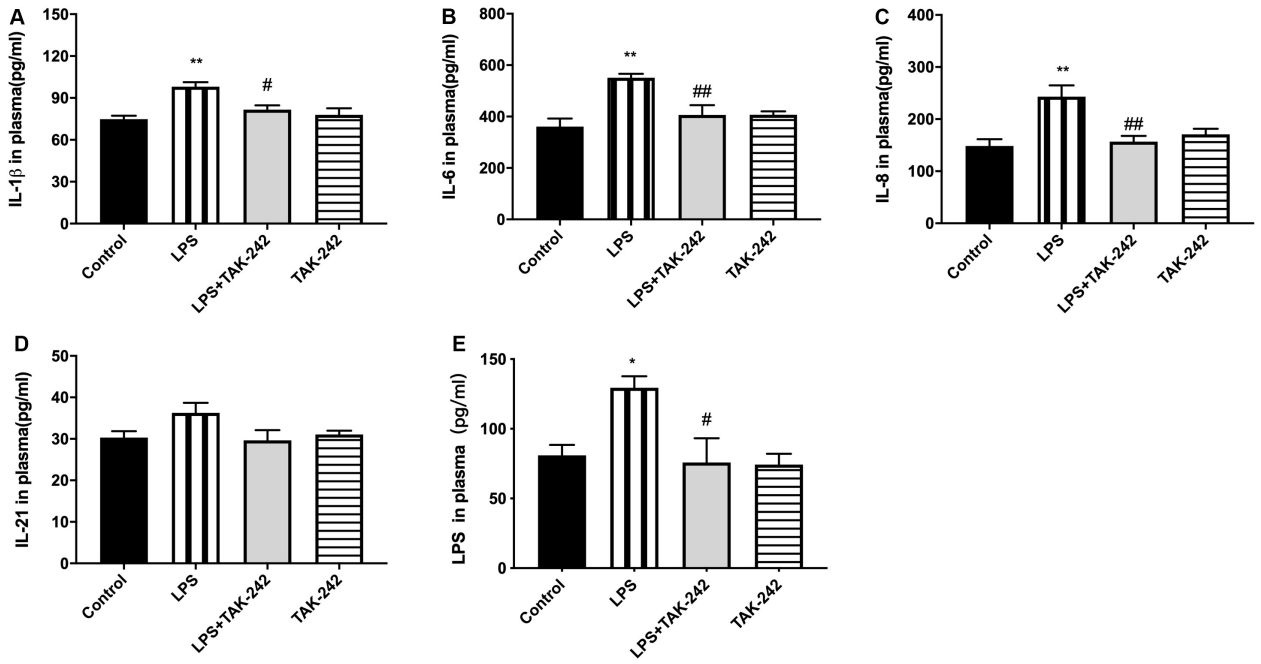

FIGURE 4 | Effects of periodontal inflammation on level of LPS and inflammatory cytokines in plasma. ELISA was performed to detect level of LPS and protein expression of inflammatory cytokines in plasma. The protein level of cytokines in plasma in each group **(A–D)** according to a one-way ANOVA analysis: IL-1β ($F = 8.168$, $p = 0.0012$), IL-6 ($F = 8.005$, $p = 0.0020$), IL-8 ($F = 8.358$, $p = 0.0010$), IL-21 ($F = 2.25$, $p = 0.1275$). The level of LPS in plasma **(E)** according to a one-way ANOVA analysis: $F = 5.750$, $p = 0.0112$ ($n = 4$–6 per group, one-way ANOVA, $^{*}p < 0.05$ and $^{**}p < 0.01$ compared to the Control group, $^{\#}p < 0.05$ and $^{\#\#}p < 0.01$ compared to the LPS group).

Effects of Periodontal Inflammation on APP Processing and Tau

Periodontitis induced by *P. gingivalis*-LPS increased the expression of APP and its homologs (APLP1 and APLP2) (**Figures 7A–C**). Further, it induced an increase in BACE1 and PS2 mRNA expression. In the control group, there was a decrease in ADAM10 mRNA expression (**Figures 7D–G**). Increased intracellular levels of Aβ1-42 and APP were observed in the LPS group, presenting as cytoplasmic yellow/brown particles (**Figure 8**). Besides, detection of Tau showed similar results. The number of positive cells were increased in the LPS group (**Figures 8A–C**). All the changes mentioned above could be alleviated by TLR4 inhibitor. The Aβ ratio (Aβ1-40/Aβ1-42) was upregulated in both the plasma and cortex (**Figures 9A,B**). Moreover, we measured BACE1 and APP protein expression in the cortex to confirm the increase in β-site APP cleaving in the LPS group (**Figures 9C–E**). Compared with the LPS group, the LPS+TAK-242 group showed reduced mRNA and protein expression related to APP processing.

Role of the TLR4/NF-κB Signaling Pathway

Results of RT-PCR revealed that periodontal inflammation significantly increased the mRNA levels of TLR4 and CD14. Compared to the control group, the LPS group showed 2-fold and 1.5-fold increases in TLR4 and CD14 mRNA expression in the PBMCs and the cortex, respectively, which could be reversed by TAK-242 (**Figures 10A–D**). As shown in **Figures 10E–J**, we conducted western blot analysis to assess the underlying mechanisms of the neuroinflammation induced by periodontitis. We observed increased expression of TLR4, CD14, IRAK1, p65, and pp65 in the cortex of rats in the LPS group, which was reduced by TAK-242 administration. This indicated that periodontitis induced neuroinflammation through TLR4/NF-κB pathway cascades.

DISCUSSION

In this study, we demonstrated the association between periodontitis induced by topical application of *P. gingivalis*-LPS and learning and memory impairment *in vivo*. Micro-CT showed alveolar bone resorption. The MWM test showed that periodontitis impaired learning and memory ability. There was an increase in cortical and peripheral blood levels of inflammatory factors, as well as TLR4/NF-κB signaling pathway activation, which could be reversed by the TLR4 inhibitor TAK-242. Significant microglia and astrocyte activation were found in the cortex, which induced neuroinflammation. Furthermore, APP processing could be involved in this progress.

The association between systemic infection/inflammation and cognitive impairment has been reported (Zhang et al., 2018; Nie et al., 2019). In the present research, topical application of *P. gingivalis*-LPS into the gingival sulcus of maxillary first molars was used to cause periodontal

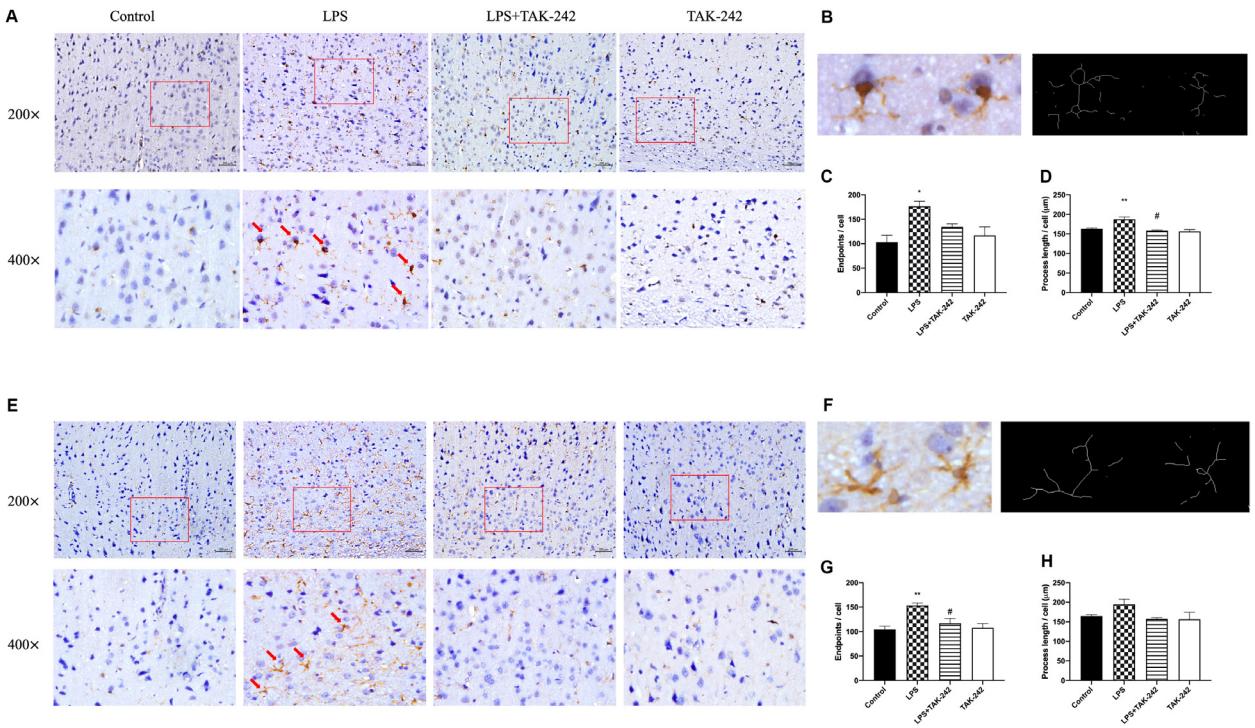

FIGURE 5 | Effects of periodontal inflammation on microglia and astrocytes in the cortex. Histopathological analysis of brain sections was performed using immunohistochemistry. As shown in **(A,B)**, activated microglia labeled by Iba1 with irregular protrusions were observed in cortex of the LPS group, while a similar situation could be found in astrocytes labeled by GFAP **(E,F)**. The changes mentioned above could be attenuated by TAK-242 (200× and 400×, bar = 200 μm). The endpoints **(C,G)** and process length **(D,H)** according to a one-way ANOVA analysis: endpoints ($F = 6.219$, $p = 0.0174$) and process length ($F = 10.74$, $p = 0.0025$) of microglia, endpoints ($F = 8.354$, $p = 0.0076$) and process length ($F = 2.595$, $p = 0.1249$) of astrocytes ($n = 3$–4 per group, one-way ANOVA, $^{*}p < 0.05$ and $^{**}p < 0.01$ compared to the Control group, $^{\#}p < 0.05$ compared to the LPS group).

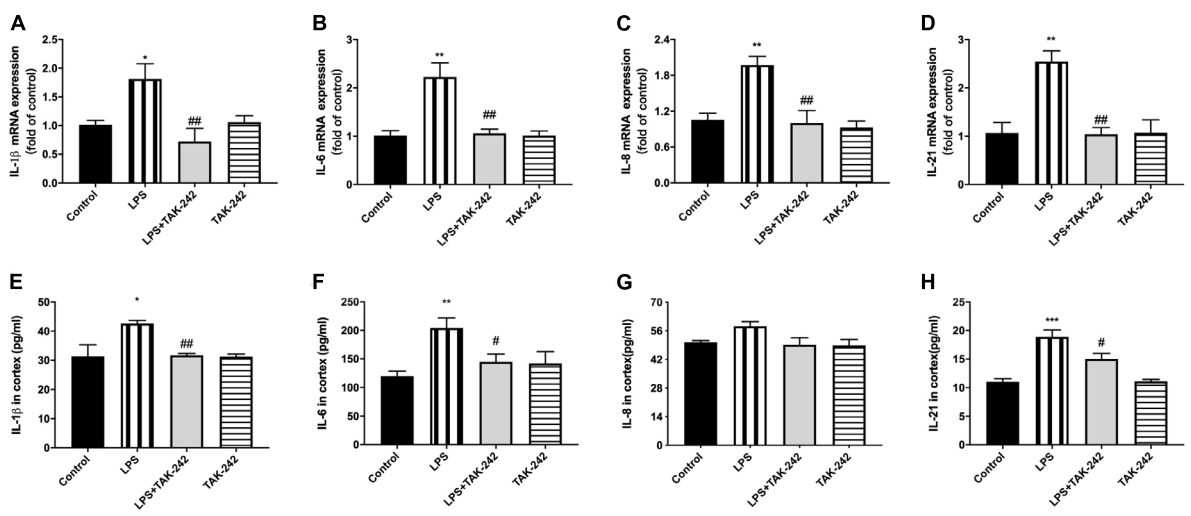

FIGURE 6 | Effects of periodontal inflammation on protein expression of inflammatory cytokines in cortex. RT-PCR was performed to detect mRNA levels of IL-1β ($F = 6.861$, $p = 0.0045$), IL-6 ($F = 11.05$, $p = 0.0007$), IL-8 ($F = 9.223$, $p = 0.0013$), IL-21 ($F = 11.89$, $p = 0.0007$) in cortex of rats, while these changes were relieved by TAK-242 **(A–D)**. ELISA was performed to detect protein levels in cortex **(E–H)** in each group according to a one-way ANOVA analysis: IL-1β ($F = 7.045$, $p = 0.0020$), IL-6 ($F = 7.145$, $p = 0.0019$), IL-8 ($F = 3.866$, $p = 0.0248$), IL-21 ($F = 15.22$, $p < 0.0001$) ($n = 4$–6 per group, one-way ANOVA, $^{*}p < 0.05$, $^{**}p < 0.01$, and $^{***}p < 0.001$ compared to the Control group, $^{\#}p < 0.05$ and $^{\#\#}p < 0.01$ compared to the LPS group).

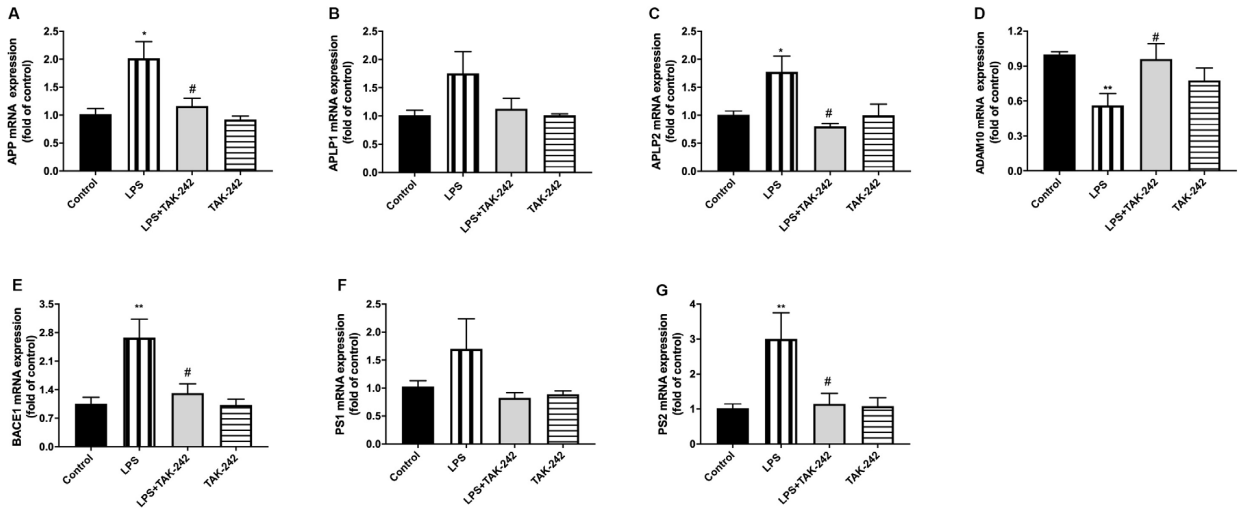

FIGURE 7 | Effects of periodontal inflammation on mRNA level of APP processing. RT-PCR was performed to detect mRNA levels of APP, APLP1, and APLP2 on genes in comparison to the control group, while these changes were reversed by TAK-242 **(A–C)**. The mRNA expression of APP and the homologs in cortex in each group according to a one-way ANOVA analysis: APP ($F = 6.327$, $p = 0.0049$), APLP1 ($F = 3.13$, $p = 0.0549$), APLP2 ($F = 6.611$, $p = 0.0052$). mRNA levels of APP secretases including α-, β-, and γ-secretase were also upregulated, while these changes were reversed by TAK-242 **(D–G)**. The mRNA expression of secretases in cortex in each group according to a one-way ANOVA analysis: ADAM10 ($F = 5.377$, $p = 0.0094$), BACE1 ($F = 7.911$, $p = 0.0021$), PS1 ($F = 2.292$, $p = 0.1227$), PS2 ($F = 5.18$, $p = 0.0142$) ($n = 4$–6 per group, one-way ANOVA, $^{*}p < 0.05$ and $^{**}p < 0.01$ compared to the Control group and $^{\#}p < 0.05$ compared to the LPS group).

inflammation according to a previous study (Yoshinaga et al., 2012). The most significant difference was the way of drug administration. Previous studies mostly used intraperitoneal injection that induced systemic inflammation, while we established periodontitis via topical application into the gingival sulcus. As the result of Micro-CT showed, a decrease in the trabecular bone volume fraction and bone mineral density could be found. This model was more similar to clinical periodontitis, considering it could mimic the damage of junctional epithelium and the formation of periodontal pocket (Bosshardt, 2018).

The locomotor activity of rats were not affected by topical application of *P. gingivalis*-LPST according to the results of the OFT. During the MWM test, however, the learning and memory ability could be impaired by periodontitis. Behavioral assessments demonstrated that topical application of *P. gingivalis*-LPS could induce learning and memory impairment. To investigate the association more comprehensively, more cognitive evaluation should be included in behavioral assessments using AD models in the following studies.

Periodontitis elicits a significant inflammatory response (Wu and Nakanishi, 2014). It has been proposed that peripheral inflammation/infection may be not only a contributor but also indeed a key determinant of the cognitive decline (Sochocka et al., 2017). Recent studies have shown that systemic infection/inflammation could induce cognitive impairment through neuroinflammation (Wu et al., 2017; Zhang et al., 2018). In periodontitis, local pro-inflammatory cytokines can enter the circulation, in turn contributing to atherosclerosis or exacerbating intra-uterine inflammation (Paraskevas et al., 2008). Patients with severe periodontitis have increased systemic inflammation (elevated cytokines such as IL-6) compared with healthy controls, whereas treatment of periodontitis reduces inflammation load (Friedewald et al., 2009). Similarly, we found significantly increased inflammatory cytokine expression (IL-1β, IL-6, IL-8, and IL-21) in the peripheral blood, which could be alleviated by TAK-242.

Neuroinflammation could play a significant role in cognitive dysfunction (Lyman et al., 2014). Inflammation in the brain is mainly caused by microglia and astrocyte activation, as well as the release of cytokines, chemokines or growth factors, which typically occur prior to cognitive dysfunction (Michelucci et al., 2009). We observed stimulation of microglia and astrocytes, which were labeled with Iba1 and GFAP, respectively, from a resting state to an activated state, which might have had toxic effects. Activated microglia could secret proinflammatory mediators (Schwab and McGeer, 2008; Venneti et al., 2008). Over-activated astrocytes could induce the production of inflammatory cytokines, which subsequently causes neuronal death and contributes to cognitive decline (Choi et al., 2016; Lian et al., 2016). Among these cytokines, IL-1β is the key molecule involved in neuroinflammation, which stimulates the release of multiple inflammatory mediators by activated microglia and leads to self-propagating neuroinflammation (Lai et al., 2017; Mendiola and Cardona, 2018). Regarding IL-6, an upstream IL-21 target, has been reported to enhance neuronal damage (Ringheim et al., 1998; Qiu and Gruol, 2003). IL-8 upregulation could be a very early event in neurodegeneration (Arosio et al., 2004; Galimberti et al., 2006). We found a positive correlation between levels of these cytokines in periphery and cortex. Therefore, we speculated that periodontitis could induce learning and memory impairment through neuroinflammation, which

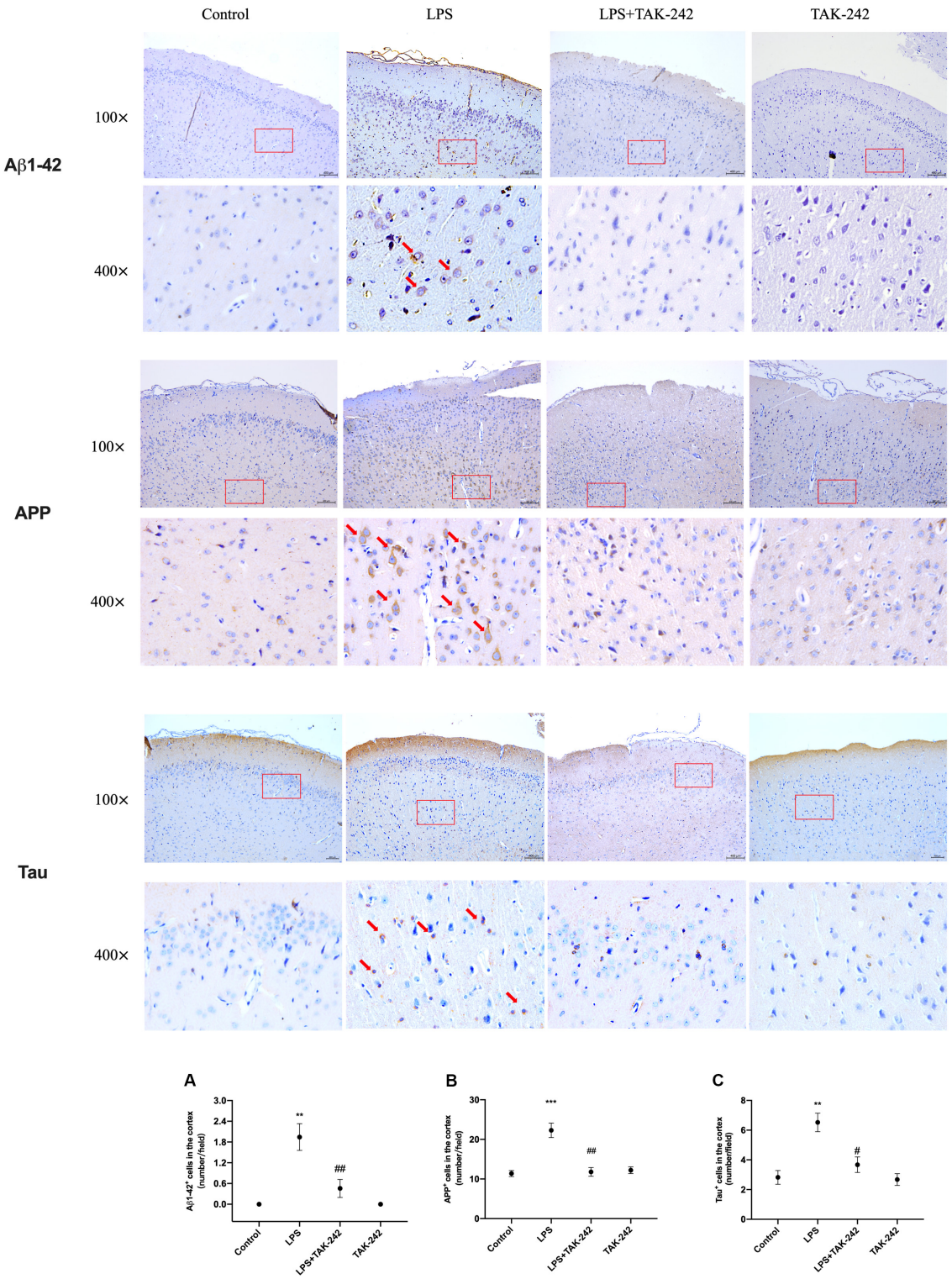

FIGURE 8 | Effects of periodontal inflammation on expression of Aβ1-42, APP and Tau in the cortex. Histopathological analysis of brain sections was performed using immunohistochemistry. As shown in **Figure 8**, the positive expression of Aβ1-42 and APP in cytoplasm was observed in the LPS group, presenting as cytoplasmic yellow/brown particles. The number of Aβ1-42, APP, and Tau positive cells was increased. The changes mentioned above could be attenuated by TAK-242. Quantification of Aβ1-42, APP and Tau levels in cortex are shown, including **(A)** Aβ1-42 positive cells (number/field) ($F = 15.59$, $p = 0.0011$); **(B)** APP positive cells (number/field) ($F = 18.9$, $p = 0.0005$), and **(C)** Tau positive cells (number/field) ($F = 12.35$, $p = 0.0023$) ($n = 3$ per group, one-way ANOVA, $^{**}p < 0.01$ and $^{***}p < 0.001$ compared to the Control group, $^{\#}p < 0.05$ and $^{\#\#}p < 0.01$ compared to the LPS group) (100× and 400×, bar = 400 μm).

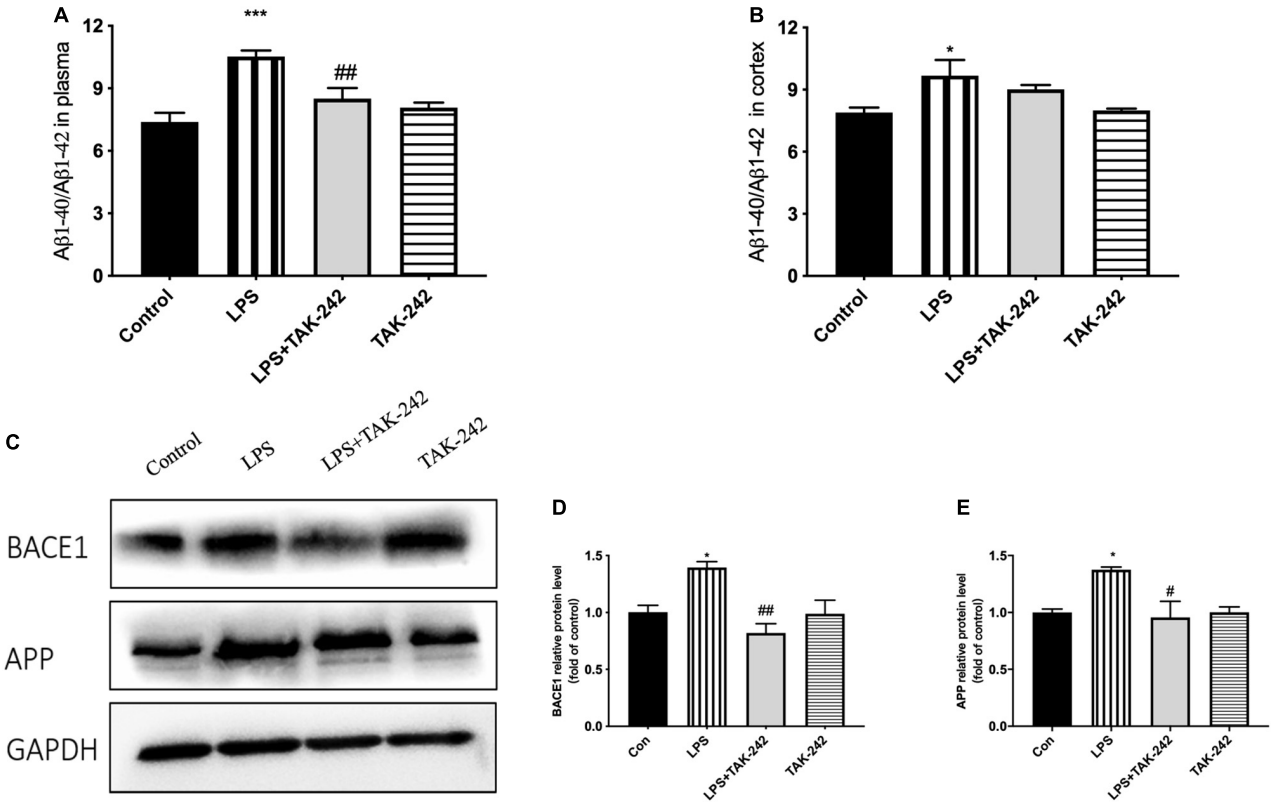

FIGURE 9 | Effects of periodontal inflammation on the Aβ ratio and protein level of APP processing. ELISA was performed to detect the Aβ ratio (Aβ1-40/Aβ1-42) in plasma and cortex **(A,B)**. Periodontitis induced by *P. gingivalis*-LPS increased expression of the Aβ ratio in comparison to the control group, while these changes were reversed by TAK-242. According to a one-way ANOVA analysis, the Aβ ratio in plasma ($F = 11.39$, $p = 0.0003$), the Aβ ratio in cortex ($F = 4.186$, $p = 0.0304$). Protein level of BACE1 and APP in cortex was measured by western blot analysis **(C)**. Both proteins were upregulated by *P. gingivalis*-LPS and could be inhibited by TAK-242. The quantification of protein expression in each group according to a one-way ANOVA analysis **(D,E)**: BACE1 ($F = 8.201$, $p = 0.0080$), APP ($F = 5.751$, $p = 0.0214$). $^{*}p < 0.05$, $^{**}p < 0.01$ and $^{***}p < 0.001$ compared to the Control group and $^{\#}p < 0.05$ and $^{\#\#}p < 0.01$ compared to the LPS group.

presented as microglial and astrocyte activation. Similar results could be found in previous studies (Martin et al., 2001; Liu et al., 2008; Terrando et al., 2010).

As one of the main triggers of inflammatory response, not only could the TLR4 signaling pathway regulate peripheral inflammation, but also neuroinflammation (Laflamme and Rivest, 2001). Specifically, TLR4 plays an important role in microglial neurotoxicity given that it is activated by LPS binding to initiate signal transduction and pro-inflammatory cytokines (Walter et al., 2007). Moreover, increased expression of TLR4, CD14, IRAK1, and pp65/p65 could be attenuated by the TLR4 selective blocker TAK-242. Consistent with the findings of Zakaria et al. (2017), this suggests that *P. gingivalis*-LPS could stimulate brain secretion of inflammatory cytokines via TLR4 activation, which subsequently induces neuroinflammation.

Besides, activated TLR4 signaling pathway and dysregulated cytokines might stimulate inflammatory processes by affecting APP processing (Reed-Geaghan et al., 2009). Multiple proinflammatory cytokines have been shown to upregulate APP expression and BACE1 activity in the brain (Brugg et al., 1995; Chen et al., 2012). The APP family has two mammalian homologs; namely, APLP1 and APLP2 (Müller and Zheng, 2012; Müller et al., 2017). Several common features of the APP family members include processing by α-(ADAM10), β-(BACE1), and γ-secretase (PS1 and PS2) (Eggert et al., 2004; Li and Südhof, 2004). As a rate-limiting enzyme that initiates Aβ formation, BACE1 plays an essential role (Trojanowski et al., 1993). Expression of APP, BACE1, and PS1/2 was increased. All the changes mentioned above could be alleviated by TLR4 inhibitor. Our study demonstrated that periodontitis induced by *P. gingivalis* -LPS could facilitate abnormal APP processing. This indicated that periodontitis induced by *P. gingivalis*-LPS could modulate APP processing through enhanced β- and γ-site secretase activity, consistent with the increase of APP in patients with chronic periodontitis (Abe et al., 2011). According to our results, cytoplasmic yellow/brown particles could be found and intracellular levels of Aβ1-42 as well as APP were increased in the cortex of LPS group, indicating that periodontitis could induce abnormal APP processing. Due to the process of Aβ extracellular deposition may occur at a later time point due to severe neuronal dysfunction and degeneration, it was hard to find obvious Aβ1-42 plaques in the present model induced by LPS, similar to the results of Sheng et al. (2003) and Pintado et al. (2012).

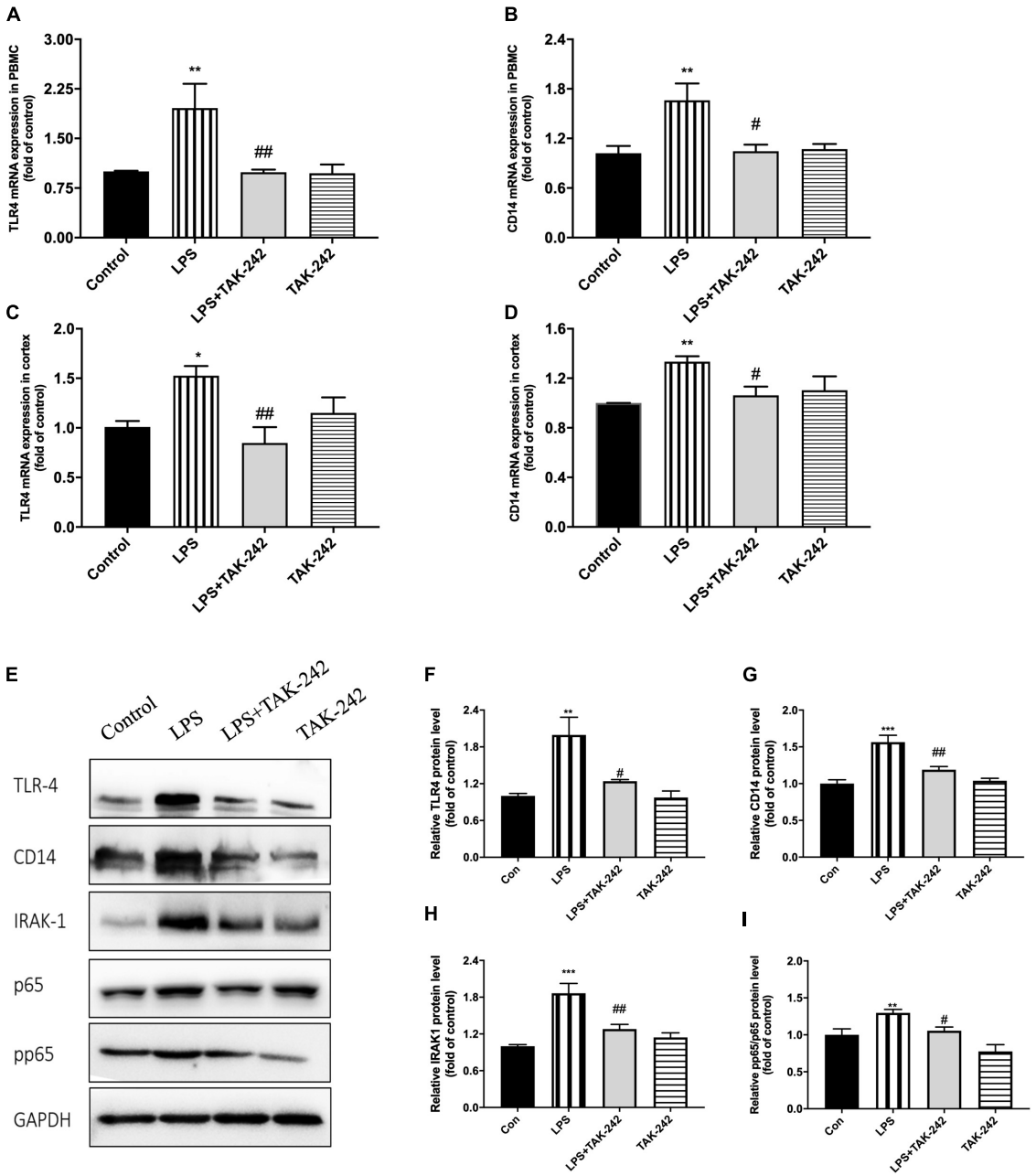

FIGURE 10 | Periodontal inflammation could induce neuroinflammation via the activation of TLR4/NF-κB signaling pathway. RT-PCR was performed to detect mRNA levels of TLR4 and CD14 in PBMCs **(A,B)** and cortex **(C,D)**. RNA expression of TLR4 and CD14 was both upregulated by *P. gingivalis*-LPS; however, similar effects were not observed in LPS plus TAK-242 group. The mRNA expression in PBMCs in each group according to a one-way ANOVA analysis: TLR4 ($F = 9.042$, $p = 0.0008$), CD14 ($F = 6.004$, $p = 0.0061$) **(A,B)**. The mRNA expression in cortex in each group according to a one-way ANOVA analysis: TLR4 ($F = 5.346$, $p = 0.0105$), CD14 ($F = 5.186$, $p = 0.0117$) **(C,D)**. Expression of TLR4, CD14, IRAK1, p65, and pp65 was further measured by western blot analysis **(E)**. All above proteins was upregulated by *P. gingivalis*-LPS. High expression of these proteins was effectively inhibited by TAK-242. **(F–I)** The quantification of related protein expression in each group according to a one-way ANOVA analysis: TLR4 ($F = 10.85$, $p = 0.0024$), CD14 ($F = 18.54$, $p = 0.0003$), IRAK1 ($F = 15.4$, $p < 0.0011$), pp65 ($F = 17.59$, $p = 0.0003$) ($n = 4$–6 per group, one-way ANOVA, $^{*}p < 0.05$, $^{**}p < 0.01$, and $^{***}p < 0.001$ compared to the Control group, $^{\#}p < 0.05$ and $^{\#\#}p < 0.01$ compared to the LPS group).

Abnormal APP processing could generate Aβ, which plays a pivotal role in the pathogenesis of cognitive disorders. It has traditionally been thought that Aβ in the brain originates from the brain tissue itself (Bu et al., 2018). However, some have suggested that the source of cerebral amyloid may originate in the periphery, including platelets, liver monocytes/macrophages, skin fibroblasts, skeletal muscles and cerebrovascular smooth muscle cells (Citron et al., 1994; Li et al., 1995; Kuo et al., 2000;

Van Nostrand and Melchor, 2001; DeMattos et al., 2002; Nie et al., 2019). Aβ produced in peripheral tissues or cells could be secreted into blood circulation and subsequently entered brain (Li et al., 1995; Bu et al., 2018; Nie et al., 2019). Our results showed an increase in the ratio of Aβ1-40/Aβ1-42 in both plasma and cortex, which was in concordance with Anantharaman et al. (2006). We speculated that periodontitis could directly/indirectly expand Aβ pools in periphery and thereby contributes to the increase of Aβ in the brain.

In this work, we established a periodontitis model and indicated the association between periodontitis and learning and memory impairment. Increase of inflammatory factors, activation of microglia and astrocytes and abnormal APP processing were found, suggesting that periodontitis might be a possible contributor to AD-like pathology. However, AD models should be used in following researches for further assessment of AD-pathologies and more sophisticated evaluation of association between periodontitis and AD.

CONCLUSION

Our findings indicated that periodontitis induced by topical application of *P. gingivalis*-LPS could contribute to learning and memory impairment via neuroinflammation induced by TLR4/NF-κB signaling pathway activation in SD rats. Furthermore, abnormal APP processing could be involved in this progress. Therefore, periodontitis could not only affect the teeth-supporting structures but also cause a significant inflammatory load in both the peripheral blood and central nervous system, which leads to learning and memory impairment.

DATA AVAILABILITY STATEMENT

The raw data supporting the conclusions of this article will be made available by the authors, without undue reservation, to any qualified researcher.

ETHICS STATEMENT

The animal study was reviewed and approved by the Animal Care and Welfare Committee of Shanghai Jiao Tong University School of Medicine.

AUTHOR CONTRIBUTIONS

YH, WZ, and ZS wrote the main manuscript text. YH, HL, JZ, XZ, XX, and CQ performed the research. YH, HL, YL, and HC analyzed the data. WZ and ZS designed the main research, provided the necessary guidance on the performance of all the experiment, and contributed the essential reagents and tools. All authors read and approved the final manuscript.

FUNDING

This work was supported by grants from the National Natural Science Foundation of China (Nos. 81670992 and 81971299).

ACKNOWLEDGMENTS

We appreciate Mei Yao for the assistance in the MWM test. We thank Lin Zheng for the technical support in the immunohistochemistry.

SUPPLEMENTARY MATERIAL

The Supplementary Material for this article can be found online at: https://www.frontiersin.org/articles/10.3389/fnins.2020.00658/full#supplementary-material

FIGURE S1 | Congo red staining showed that LPS group rats' cortex had sporadic amyloid deposition.

REFERENCES

Abe, D., Kubota, T., Morozumi, T., Shimizu, T., Nakasone, N., Itagaki, M., et al. (2011). Altered gene expression in leukocyte transendothelial migration and cell communication pathways in periodontitis-affected gingival tissues. *J. Periodontal Res.* 46, 345–353. doi: 10.1111/j.1600-0765.2011.01349.x

Anantharaman, M., Tangpong, J., Keller, J. N., Murphy, M. P., Markesbery, W. R., Kiningham, K. K., et al. (2006). Beta-amyloid mediated nitration of manganese superoxide dismutase: implication for oxidative stress in a APPNLH/NLH X PS-1P264L/P264L double knock-in mouse model of Alzheimer's disease. *Am. J. Pathol.* 168, 1608–1618.

Arosio, B., Trabattoni, D., Galimberti, L., Bucciarelli, P., Fasano, F., Calabresi, C., et al. (2004). Interleukin-10 and interleukin-6 gene polymorphisms as risk factors for Alzheimer's disease. *Neurobiol. Aging* 25, 1009–1015. doi: 10.1016/j.neurobiolaging.2003.10.009

Bosshardt, D. D. (2018). The periodontal pocket: pathogenesis, histopathology and consequences. *Periodontol* 76, 43–50. doi: 10.1111/prd.12153

Brookmeyer, R., Abdalla, N., Kawas, C. H., and Corrada, M. M. (2018). Forecasting the prevalence of preclinical and clinical Alzheimer's disease in the United States. *Alzheimers Dement.* 14, 121–129. doi: 10.1016/j.jalz.2017.10.009

Brugg, B., Dubreuil, Y. L., Huber, G., Wollman, E. E., Delhaye-Bouchaud, N., and Mariani, J. (1995). Inflammatory processes induce beta-amyloid precursor protein changes in mouse brain. *Proc. Natl. Acad. Sci. U.S.A.* 92, 3032–3035. doi: 10.1073/pnas.92.7.3032

Bu, X. L., Xiang, Y., Jin, W. S., Wang, J., Shen, L. L., Huang, Z. L., et al. (2018). Blood-derived amyloid-β protein induces Alzheimer's disease pathologies. *Mol. Psychiatry* 23, 1948–1956.

Chen, C. H., Zhou, W., Liu, S., Deng, Y., Cai, F., Tone, M., et al. (2012). Increased NF-κB signalling up-regulates BACE1 expression and its therapeutic potential in Alzheimer's disease. *Int. J. Neuropsychopharmacol.* 15, 77–90. doi: 10.1017/s1461145711000149

Choi, S. S., Lee, S. R., and Lee, H. J. (2016). Neurorestorative role of stem cells in Alzheimer's disease: astrocyte involvement. *Curr. Alzheimer Res.* 13, 419–427. doi: 10.2174/1567205013041603141 62812

Citron, M., Vigo-Pelfrey, C., Teplow, D. B., Miller, C., Schenk, D., Johnston, J., et al. (1994). Excessive production of amyloid beta-protein by peripheral cells of symptomatic and presymptomatic patients carrying the Swedish familial Alzheimer disease mutation. *Proc. Natl. Acad. Sci. U.S.A.* 91, 11993–11997. doi: 10.1073/pnas.91.25.11993

DeMattos, R. B., Bales, K. R., Parsadanian, M., O'Dell, M. A., Foss, E. M., Paul, S. M., et al. (2002). Plaque-associated disruption of CSF and plasma amyloid-beta (Abeta) equilibrium in a mouse model of Alzheimer's disease. *J. Neurochem.* 81, 229–236. doi: 10.1046/j.1471-4159.2002.00889.x

Dominy, S. S., Lynch, C., Ermini, F., Benedyk, M., Marczyk, A., Konradi, A., et al. (2019). *Porphyromonas gingivalis* in Alzheimer's disease brains: evidence for disease causation and treatment with small-molecule inhibitors. *Sci. Adv.* 5:eaau3333. doi: 10.1126/sciadv.aau3333

Eggert, S., Paliga, K., Soba, P., Evin, G., Masters, C. L., Weidemann, A., et al. (2004). The proteolytic processing of the amyloid precursor protein gene family members APLP-1 and APLP-2 involves alpha-, beta-, gamma-, and epsilon-like cleavages: modulation of APLP-1 processing by n-glycosylation. *J. Biol. Chem.* 279, 18146–18156. doi: 10.1074/jbc.m311601200

Friedewald, V. E., Kornman, K. S., Beck, J. D., Genco, R., Goldfine, A., Libby, P., et al. (2009). The american journal of cardiology and journal of periodontology editors' consensus: periodontitis and atherosclerotic cardiovascular disease. *J. Periodontol.* 80, 1021–1032. doi: 10.1902/jop.2009.097001

Galimberti, D., Schoonenboom, N., Scheltens, P., Fenoglio, C., Bouwman, F., Venturelli, E., et al. (2006). Intrathecal chemokine synthesis in mild cognitive impairment and Alzheimer disease. *Arch. Neurol.* 63, 538–543.

Gárate, I., García-Bueno, B., Madrigal, J. L., Caso, J. R., Alou, L., Gómez-Lus, M. L., et al. (2014). Toll-like 4 receptor inhibitor TAK-242 decreases neuroinflammation in rat brain frontal cortex after stress. *J. Neuroinflamm.* 11:8. doi: 10.1186/1742-2094-11-8

Hamilton, J. A., Hasturk, H., Kantarci, A., Serhan, C. N., and Van Dyke, T. (2017). Atherosclerosis, periodontal disease, and treatment with resolvins. *Curr. Atheroscler. Rep.* 19:57.

Harding, A., Robinson, S., Crean, S., and Singhrao, S. K. (2017). Can better management of periodontal disease delay the onset and progression of Alzheimer's Disease? *J. Alzheimers Dis.* 58, 337–348. doi: 10.3233/jad-170046

Hashioka, S., Inoue, K., Miyaoka, T., Hayashida, M., Wake, R., Oh-Nishi, A., et al. (2019). The possible causal link of periodontitis to neuropsychiatric disorders: more than psychosocial mechanisms. *Int. J. Mol. Sci.* 20:3723. doi: 10.3390/ijms20153723

Ide, M., Harris, M., Stevens, A., Sussams, R., Hopkins, V., Culliford, D., et al. (2016). Periodontitis and cognitive decline in Alzheimer's disease. *PLoS One* 11:e0151081. doi: 10.1371/journal.pone.0151081

Ii, M., Matsunaga, N., Hazeki, K., Nakamura, K., Takashima, K., Seya, T., et al. (2006). A novel cyclohexene derivative, ethyl (6R)-6-[N-(2-Chloro-4-fluorophenyl) sulfamoyl] cyclohex-1-ene-1-carboxylate (TAK-242), selectively inhibits toll-like receptor 4-mediated cytokine production through suppression of intracellular signaling. *Mol. Pharmacol.* 69, 1288–1295. doi: 10.1124/mol.105.019695

Ilievski, V., Zuchowska, P. K., Green, S. J., Toth, P. T., Ragozzino, M. E., Le, K., et al. (2018). Chronic oral application of a periodontal pathogen results in brain inflammation, neurodegeneration and amyloid beta production in wild type mice. *PLoS One* 13:e0204941. doi: 10.1371/journal.pone.0204941

Jain, S., and Darveau, R. P. (2010). Contribution of *Porphyromonas gingivalis* lipopolysaccharide to periodontitis. *Periodontol* 2000, 53–70. doi: 10.1111/j.1600-0757.2009.00333.x

Kuo, Y. M., Kokjohn, T. A., Watson, M. D., Woods, A. S., Cotter, R. J., Sue, L. I., et al. (2000). Elevated abeta42 in skeletal muscle of Alzheimer disease patients suggests peripheral alterations of AbetaPP metabolism. *Am. J. Pathol.* 156, 797–805. doi: 10.1016/s0002-9440(10)64947-4

Laflamme, N., and Rivest, S. (2001). Toll-like receptor 4: the missing link of the cerebral innate immune response triggered by circulating gram-negative bacterial cell wall components. *FASEB J.* 15, 155–163. doi: 10.1096/fj.00-0339com

Lai, K., Liu, C. S., Rau, A., Lanctôt, K. L., Köhler, C. A., Pakosh, M., et al. (2017). Peripheral inflammatory markers in Alzheimer's disease: a systematic review and meta-analysis of 175 studies. *J. Neurol. Neurosurg. Psychiatry* 88, 876–882. doi: 10.1136/jnnp-2017-316201

Li, Q., and Südhof, T. C. (2004). Cleavage of amyloid-beta precursor protein and amyloid-beta precursor-like protein by BACE 1. *J. Biol. Chem.* 279, 10542–10550. doi: 10.1074/jbc.m310001200

Li, Q. X., Evin, G., Small, D. H., Multhaup, G., Beyreuther, K., and Masters, C. L. (1995). Proteolytic processing of Alzheimer's disease beta A4 amyloid precursor protein in human platelets. *J. Bio. Chem.* 270, 14140–14147.

Li, X., Yu, C., Hu, Y., Xia, X., Liao, Y., Zhang, J., et al. (2018). New application of psoralen and angelicin on periodontitis with anti-bacterial, anti-inflammatory, and osteogenesis effects. *Front. Cell Infect. Microbiol.* 8:178. doi: 10.3389/fcimb.2018.00178

Lian, H., Litvinchuk, A., Chiang, A. C., Aithmitti, N., Jankowsky, J. L., and Zheng, H. (2016). Astrocyte-Microglia cross talk through complement activation modulates amyloid pathology in mouse models of Alzheimer's Disease. *J. Neurosci.* 36, 577–589. doi: 10.1523/jneurosci.2117-15.2016

Liu, R., Desta, T., Raptis, M., Darveau, R. P., and Graves, D. T. (2008). *P. gingivalis* and *E. coli* lipopolysaccharides exhibit different systemic but similar local induction of inflammatory markers. *J. Periodontol.* 79, 1241–1247.

Lyman, M., Lloyd, D. G., Ji, X., Vizcaychipi, M. P., and Ma, D. (2014). Neuroinflammation: the role and consequences. *Neurosci. Res.* 79, 1–12. doi: 10.1016/j.neures.2013.10.004

Martin, M., Katz, J., Vogel, S. N., and Michalek, S. M. (2001). Differential induction of endotoxin tolerance by lipopolysaccharides derived from *Porphyromonas gingivalis* and *Escherichia coli*. *J. Immunol.* 167, 5278–5285. doi: 10.4049/jimmunol.167.9.5278

Mendiola, A. S., and Cardona, A. E. (2018). The IL-1beta phenomena in neuroinflammatory diseases. *J. Neural Transm.* 125, 781–795. doi: 10.1007/s00702-017-1732-9

Michelucci, A., Heurtaux, T., Grandbarbe, L., Morga, E., and Heuschling, P. (2009). Characterization of the microglial phenotype under specific pro-inflammatory and anti-inflammatory conditions: effects of oligomeric and fibrillar amyloid-beta. *J. Neuroimmunol.* 210, 3–12. doi: 10.1016/j.jneuroim.2009.02.003

Müller, U. C., Deller, T., and Korte, M. (2017). Not just amyloid: physiological functions of the amyloid precursor protein family. *Nat. Rev. Neurosci.* 18, 281–298. doi: 10.1038/nrn.2017.29

Müller, U. C., and Zheng, H. (2012). Physiological functions of APP family proteins. *Cold Spring Harb. Perspect. Med.* 2:a006288. doi: 10.1101/cshperspect.a006288

Nie, R., Wu, Z., Ni, J., Zeng, F., Yu, W., Zhang, Y., et al. (2019). *Porphyromonas gingivalis* Infection Induces Amyloid-β accumulation in monocytes/macrophages. *J. Alzheimers Dis.* 72, 479–494. doi: 10.3233/jad-190298

Nishida, E., Hara, Y., Kaneko, T., Ikeda, Y., Ukai, T., and Kato, I. (2001). Bone resorption and local interleukin-1alpha and interleukin-1beta synthesis induced by *Actinobacillus actinomycetemcomitans* and *Porphyromonas gingivalis* lipopolysaccharide. *J. Periodontal Res.* 36, 1–8. doi: 10.1034/j.1600-0765.2001.00637.x

Olsen, I., and Singhrao, S. K. (2015). Can oral infection be a risk factor for Alzheimer's disease? *J. Oral Microbiol.* 7:29143. doi: 10.3402/jom.v7.29143

Oppermann, R. V., Haas, A. N., Rosing, C. K., and Susin, C. (2015). Epidemiology of periodontal diseases in adults from Latin America. *Periodontol* 2000, 13–33. doi: 10.1111/prd.12061

Papapanou, P. N., Sanz, M., Buduneli, N., Dietrich, T., Feres, M., Fine, D. H., et al. (2018). Periodontitis: consensus report of workgroup 2 of the 2017 world workshop on the classification of periodontal and peri-implant diseases and conditions. *J. Clin. Periodontol.* 89(Suppl. 1), S173–S182.

Paraskevas, S., Huizinga, J. D., and Loos, B. G. (2008). A systematic review and meta-analyses on C-reactive protein in relation to periodontitis. *J. Clin. Periodontol.* 35, 277–290. doi: 10.1111/j.1600-051x.2007.01173.x

Pintado, C., Gavilan, M. P., Gavilan, E., Garcia-Cuervo, L., Gutierrez, A., and Vitorica, J. (2012). Lipopolysaccharide-induced neuroinflammation leads to the accumulation of ubiquitinated proteins and increases susceptibility to neurodegeneration induced by proteasome inhibition in rat hippocampus. *J. Neuroinflamm.* 9:87.

Poole, S., Singhrao, S. K., Kesavalu, L., Curtis, M. A., and Crean, S. (2013). Determining the presence of periodontopathic virulence factors in short-term postmortem Alzheimer's disease brain tissue. *J. Alzheimers Dis.* 36, 665–677. doi: 10.3233/jad-121918

Preshaw, P. M., Alba, A. L., Herrera, D., Jepsen, S., Konstantinidis, A., Makrilakis, K., et al. (2012). Periodontitis and diabetes: a two-way relationship. *Diabetologia* 55, 21–31. doi: 10.1007/s00125-011-2342-y

Qiu, Z., and Gruol, D. L. (2003). Interleukin-6, beta-amyloid peptide and NMDA interactions in rat cortical neurons. *J. Neuroimmunol.* 139, 51–57. doi: 10.1016/s0165-5728(03)00158-9

Reed-Geaghan, E. G., Savage, J. C., Hise, A. G., and Landreth, G. E. (2009). CD14 and toll-like receptors 2 and 4 are required for fibrillar A{beta}-stimulated microglial activation. *J. Neurosci.* 29, 11982–11992. doi: 10.1523/jneurosci.3158-09.2009

Ringheim, G. E., Szczepanik, A. M., Petko, W., Burgher, K. L., Zhu, S. Z., and Chao, C. C. (1998). Enhancement of beta-amyloid precursor protein transcription and expression by the soluble interleukin-6 receptor/interleukin-6 complex. *Brain Res. Mol. Brain Res.* 55, 35–44. doi: 10.1016/s0169-328x(97)00356-2

Schwab, C., and McGeer, P. L. (2008). Inflammatory aspects of Alzheimer disease and other neurodegenerative disorders. *J. Alzheimers Dis.* 13, 359–369. doi: 10.3233/jad-2008-13402

Sheng, J. G., Bora, S. H., Xu, G., Borchelt, D. R., Price, D. L., and Koliatsos, V. E. (2003). Lipopolysaccharide-induced-neuroinflammation increases intracellular accumulation of amyloid precursor protein and amyloid beta peptide in APPswe transgenic mice. *Neurobiol. Dis.* 14, 133–145. doi: 10.1016/s0969-9961(03)00069-x

Sochocka, M., Sobczyński, M., Sender-Janeczek, A., Zwolińska, K., Błachowicz, O., Tomczyk, T., et al. (2017). Association between periodontal health status and cognitive abilities. the role of cytokine profile and systemic inflammation. *Curr. Alzheimer Res.* 14, 978–990.

Terrando, N., Rei, F. A., Vizcaychipi, M., Cibelli, M., Ma, D., Monaco, C., et al. (2010). The impact of IL-1 modulation on the development of lipopolysaccharide-induced cognitive dysfunction. *Crit. Care* 14:R88.

Trojanowski, J. Q., Schmidt, M. L., Shin, R. W., Bramblett, G. T., Rao, D., and Lee, V. M. (1993). Altered tau and neurofilament proteins in neurodegenerative diseases: diagnostic implications for Alzheimer's disease and Lewy body dementias. *Brain Pathol.* 3, 45–54. doi: 10.1111/j.1750-3639.1993.tb00725.x

Van Nostrand, W. E., and Melchor, J. P. (2001). Disruption of pathologic amyloid beta-protein fibril assembly on the surface of cultured human cerebrovascular smooth muscle cells. *Amyloid* 8(Suppl. 1), 20–27.

Venneti, S., Wang, G., Nguyen, J., and Wiley, C. A. (2008). The positron emission tomography ligand DAA1106 binds with high affinity to activated microglia in human neurological disorders. *J. Neuropathol. Exp. Neurol.* 67, 1001–1010. doi: 10.1097/nen.0b013e318188b204

Walter, S., Letiembre, M., Liu, Y., Heine, H., Penke, B., Hao, W., et al. (2007). Role of the toll-like receptor 4 in neuroinflammation in Alzheimer's disease. *Cell Physiol. Biochem.* 20, 947–956.

Wimo, A., Guerchet, M., Ali, G. C., Wu, Y. T., Prina, A. M., Winblad, B., et al. (2017). The worldwide costs of dementia 2015 and comparisons with 2010. *Alzheimers Dement.* 13, 1–7. doi: 10.1016/j.jalz.2016.07.150

Winning, L., Patterson, C. C., Cullen, K. M., Kee, F., and Linden, G. J. (2019). Chronic periodontitis and reduced respiratory function. *J. Clin. Periodontol.* 46, 266–275. doi: 10.1111/jcpe.13076

Wu, Z., and Nakanishi, H. (2014). Connection between periodontitis and Alzheimer's disease: possible roles of microglia and leptomeningeal cells. *J. Pharmacol. Sci.* 126, 8–13. doi: 10.1254/jphs.14r11cp

Wu, Z., Ni, J., Liu, Y., Teeling, J. L., Takayama, F., Collcutt, A., et al. (2017). Cathepsin B plays a critical role in inducing Alzheimer's disease-like phenotypes following chronic systemic exposure to lipopolysaccharide from *Porphyromonas gingivalis* in mice. *Brain Behav. Immun.* 65, 350–361. doi: 10.1016/j.bbi.2017.06.002

Yoshinaga, Y., Ukai, T., Kaneko, T., Nakatsu, S., Shiraishi, C., Kuramoto, A., et al. (2012). Topical application of lipopolysaccharide into gingival sulcus promotes periodontal destruction in rats immunized with lipopolysaccharide. *J. Periodontal Res.* 47, 674–680. doi: 10.1111/j.1600-0765.2012.01486.x

Young, K., and Morrison, H. (2018). Quantifying microglia morphology from photomicrographs of immunohistochemistry prepared tissue using imageJ. *J. Vis. Exp.* 136:57648.

Zakaria, R., Wan, Y. W., Othman, Z., Long, I., Ahmad, A. H., and Al-Rahbi, B. (2017). Lipopolysaccharide-induced memory impairment in rats: a model of Alzheimer's disease. *Physiol. Res.* 66, 553–565. doi: 10.33549/physiolres.933480

Zhang, J., Yu, C., Zhang, X., Chen, H., Dong, J., Lu, W., et al. (2018). *Porphyromonas gingivalis* lipopolysaccharide induces cognitive dysfunction, mediated by neuronal inflammation via activation of the TLR4 signaling pathway in C57BL/6 mice. *J. Neuroinflamm.* 15:37.

Zhang, X., Wang, D., Pan, H., and Sun, B. (2017). Enhanced expression of markers for astrocytes in the brain of a line of GFAP-TK transgenic mice. *Front. Neurosci.* 11:212. doi: 10.3389/fcimb.2018.00212

Conflict of Interest: The authors declare that the research was conducted in the absence of any commercial or financial relationships that could be construed as a potential conflict of interest.

frontiers in Neuroscience

ORIGINAL RESEARCH
published: 07 July 2020
doi: 10.3389/fnins.2020.00715

Brain Metabolisms Involved in Self-Reported Quality of Mobility in Parkinson's Disease

Lu Fei[1†], Feng-Tao Liu[1,2†], Yi-Qi Liu[1†], Jing-Jie Ge[3], Jia-Ying Lu[3], Shu-Jin He[1], Yi-Min Sun[1,2], Jian-Jun Wu[1], Chuan-Tao Zuo[3,4,5] and Jian Wang[1*]*

[1] Department of Neurology and National Clinical Research Center for Aging and Medicine, Huashan Hospital, Fudan University, Shanghai, China, [2] Department of Neurology, Huashan Hospital North, Fudan University, Shanghai, China, [3] PET Center and National Clinical Research Center for Aging and Medicine, Huashan Hospital, Fudan University, Shanghai, China, [4] Human Phenome Institute, Fudan University, Shanghai, China, [5] Institute of Functional and Molecular Medical Imaging, Fudan University, Shanghai, China

Background: Objective motor ratings and subjective motor complaints are both widely used in Parkinson's disease (PD). However, the objective basis to the self-perceived mobility quality is still not well elucidated.

Purposes: We aimed to figure out the relevancy between the UPDRS motor scores and PDQ39 mobility sub-scores, and further explore whether physician-assessed motor dysfunctions and patients-reported mobility deficits have some shared mechanisms.

Methods: 49 patients with PD who completed the PDQ39 scale were retrospectively included. The relevancy between mobility quality and UPDRS scores was assessed, as well as the related presynaptic dopaminergic binding (^{11}C-CFT) and glucose metabolism (^{18}F-FDG) in this dual-tracer PET imaging study.

Results: Modest correlation was found between UPDRS motor score and the PDQ39 mobility sub-score (r = 0.440, p = 0.002). No correlation was found between PDQ39 mobility SI and the dopaminergic lesions in putamen; however, the strict correlation was found with the UPDRS motor scores. In terms of global PD related pattern (PDRP) scores, the two motor scores both correlated strictly. In the further regional metabolism exploration, cerebellum correlated positively with PDQ39 mobility sub-scores, and the frontal and parietal regions mainly correlated negatively with the motor quality scores.

Conclusion: UPDRS motor scores and PDQ39 mobility scores were only modestly correlated. The mechanisms involved under mobility quality were beyond dopaminergic deficiency, including motor related cerebellum hyper-metabolism and non-motor related frontal hypo-metabolism. Conclusively, the self-reported mobility experience may have the neurophysiological basis related to both motor and non-motor manifestations in PD.

Keywords: Parkinson's disease, quality of life, PET, dopamine transporter, glucose metabolism

OPEN ACCESS

Edited by:
Chih-Yu Hsu,
Fujian University of Technology, China

Reviewed by:
Binbin Nie,
Institute of High Energy Physics (CAS), China
Xiaoli Lan,
Huazhong University of Science and Technology, China

***Correspondence:**
Chuan-Tao Zuo
zuochuantao@fudan.edu.cn
Jian Wang
wangjian_hs@fudan.edu.cn

† These authors have contributed equally to this work

Specialty section:
This article was submitted to Neurodegeneration, a section of the journal Frontiers in Neuroscience

Received: *05 May 2020*
Accepted: *12 June 2020*
Published: *07 July 2020*

Citation:
Fei L, Liu F-T, Liu Y-Q, Ge J-J, Lu J-Y, He S-J, Sun Y-M, Wu J-J, Zuo C-T and Wang J (2020) Brain Metabolisms Involved in Self-Reported Quality of Mobility in Parkinson's Disease. Front. Neurosci. 14:715. doi: 10.3389/fnins.2020.00715

Abbreviations: ^{18}F-FDG, ^{18}F-fluorodeoxyglucose; BG, basal ganglia; BLSA, Baltimore Longitudinal Study of Aging; DAT, dopamine transporter; DBS, deep brain stimulation; H&Y, Hoehn and Yahr; OSEM, ordered subset expectation maximization; PD, Parkinson's disease; PDQ39, the 39-item Parkinson's Disease Questionnaire; PDRP, Parkinson's disease related pattern; PET, positron emission tomography; QoL, quality of life; rCMRglc, regional cerebral metabolic rate of glucose; RMR, resting metabolic rate; ROI, region of interest; STN, subthalamic nucleus; UPDRS, Unified Parkinson's Disease Rating Scale.

INTRODUCTION

Parkinson's disease is a most common neurodegenerative movement disorder, in which the motor evaluation is of great importance. In clinical practices, the motor assessment can be obtained by objective motor rating from physicians and subjective motor complaints from patients. The UPDRS is the most commonly used scales by physicians for motor evaluation (Goetz et al., 2008). The 39-item Parkinson's Disease Questionnaire is the most commonly adopted patient completed rating scale in PD QoL evaluation (Marinus et al., 2002), in which mobility is one of eight subdomains. Such assessments are quite helpful for disease severity assessment and therapeutic evaluation.

Though higher UPDRS motor scores contribute to poor QoL in PD patients, the improvement of motor symptoms does not necessarily guarantee better subjective feeling. In our previous study (Liu et al., 2019) including 45 PD patients with 1-year follow-up after DBS, the motor severities were greatly improved, however, only half participants were satisfied with the QoL improvement. Similarly, in a study (Daniels et al., 2011) including 61 PD patients after bilateral STN-DBS surgery, 57.0% of them did feel improved about their QoL despite 43.0% patients didn't show satisfaction. Therefore, there should be similarities and differences between the subjective and objective motor assessments.

Objective motor evaluation may have some correlation with subjective motor experience, and such correlation should be fixed on some common material base. PET imaging has proven useful to explore the underlying mechanisms for clinical phenomenon of PD. ^{11}C-CFT PET imaging could reflect the presynaptic DAT dysfunction (Nandhagopal et al., 2009), and ^{18}F-fluorodeoxyglucose (^{18}F-FDG) PET has been used for measuring the metabolic abnormalities in PD patients. Our previous findings revealed the relationship between clinical manifestations, dopaminergic and glucose-metabolic PET imaging in a dual-tracer PET imaging cohort (Liu et al., 2018). However, until now almost no study pays attention to the subjective bias of individual feelings related to the motor symptoms, and PET imaging may be helpful to understand the neurobiological basis in the patients' subjective bias to the motor deficits in PD.

In our retrospective study, we aimed to figure out the relevancy between UPDRS motor score and QoL mobility subdomain, the two motor evaluation methods in PD. Furthermore, we attempted to figure out whether physician-assessed and patients-reported mobility dysfunctions had some shared material basis via cerebral presynaptic dopaminergic and glucose metabolic characteristics in our dual-tracer PET imaging cohort.

SUBJECTS AND METHODS

Subjects

We retrospectively included 49 patients (31 males/18 females, 53.43 ± 12.06 years old) who completed the QoL evaluation (PDQ39 scale) from our previous DTPD cohort (Liu et al., 2018). DTPD study was a dual-tracer PET imaging study in Parkinson's disease ever performed in Huashan Hospital between January 2010 and June 2014 (Liu et al., 2018). In the DTPD cohort, 103 patients (65 males/38 females, 54.1 ± 12.0 years old) diagnosed as PD were scanned with both ^{11}C-CFT and ^{18}F-FDG PET. All subjects have written informed consent according to the Declaration of Helsinki. The study was approved by the Human Studies Institutional Review Board, Huashan Hospital, Fudan University.

Study Design

This is a retrospective study. The 49 PD subjects completed the PDQ39 scale, the UPDRS and H&Y scale in the "off" state. After the clinical assessments, all subjects were scanned with ^{11}C-CFT PET and ^{18}F-FDG PET.

PET Imaging and Imaging Processing

Before the scanning, all the subjects withdrew anti-parkinsonian drugs for at least 12 h and started the fast for 6 h. Before the injection and PET imaging, all the participants should be settled under dark and quiet environment and stay sober during the whole examination. The equipment used for PET imaging in our center is Siemens' Biograph 64 PET/CT scanner. During the scanning, cranial computed tomography (CT) was firstly conducted for photon attenuation correction.

In ^{11}C-CFT PET imaging, 60 to 80 min after the intravenous injection of CFT (350–400 MBq), scanning data were obtained and then reconstructed with the OSEM method. In ^{18}F-FDG PET imaging, within 45 to 55 min post-injection (150–200 MBq), scanning data were obtained for 10 min and then reconstructed with the OSEM method. All the PET data was captured in a three-dimensional (3D) mode. ^{18}F-FDG was used to calculate rCMRglc.

^{11}C-CFT and ^{18}F-FDG PET data were both reconstructed using SPM5 software (Statistical Parametric Mapping; Wellcome Department of Imaging Neuroscience, Institute of Neurology, London, United Kingdom) implemented in Matlab7.4.0 (MathWorks Inc., Sherborn, MA, United States). A brain DAT binding template in Montreal Neurological Institute (MNI) space that was created by using ^{11}C-CFT PET and corresponding structural MR images of another group consisting of 16 normal controls was used to normalize the ^{11}C-CFT images. The procedures were presented in detail in former studies (Bu et al., 2018). As for ^{18}F-FDG images, template within the SPM software was used for normalization. The normalized PET images were smoothed by a Gaussian filter of 10 mm FWHM (Full Width at Half Maximum) over a 3D space to increase signal to noise ratio for statistical analysis.

Quantitative Analysis of Imaging Processing

To realize the individualized quantitative analysis of ^{11}C-CFT binding of every participant, we placed standardized ROIs for caudate, anterior putamen, posterior putamen and occipital cortex on the mean image summed over central slices and manually adjust their position to meet the requirement, and

subsequently, confirm the individual data with reference to standardized cerebral template in SPM5. The standard uptake value ratio (SUVR) of regional ^{11}C-CFT binding in striatum was calculated by (striatum -occipital)/occipital counts as described previously (Ma et al., 2002).

The analysis of PDRP was based on an independent Chinese cohort (Wu et al., 2013). PET data of every patient can be calculated with independent network value using voxel-based algorithm (ScAnVP software[1]; at the Centre for Neuroscience, the Feinstein Institute for Medical Research, Manhasset, NY, United States), and then transformed into *Z* value (*Z* score) using subject scores of the healthy controls in the Chinese derivation cohort for PDRP as described previously.

To investigate the relationship between whole-brain metabolism and the mobility sub-scores, a multiple regression analysis was performed in SPM5. The global metabolic values of individual patient were entered as covariates in the ANCOVA model. To evaluate the significant correlation, we set the voxel threshold at $P < 0.001$ over whole-brain and search.

Statistics Analysis

Quantitative data was performed as Mean ± Standard Deviation (SD). Kolmogorov–Smirnov test was used to evaluate the normal distribution of the continuous variables, if the data in different groups meets the standard of normal distribution, *T*-test was applied to compare the variable differences of clinical information, PDRP Z score and SUVRs of regional DAT binding in striatum between PD-QoL group and PD-Non-QoL group, if not, Mann Whitney's *U* test was employed. Pearson correlation analysis was performed to analyze the correlation among DAT binding (ROIs), PDRP value and the two motor ratings in all patients. All analyses were settled with SPSS 22.0 (SPSS Inc., Chicago, IL, United States), and the two tailed $P < 0.05$ was considered as significant.

RESULTS

The demographic and clinical information were demonstrated in **Table 1**, and there was no obvious difference between the 49 included PD patients with QoL assessment (PD-QoL patients) and those without QoL assessment (PD-Non-QoL patients) ($p > 0.05$). In both ^{11}C-CFT PET imaging and ^{18}F-FDG PET imaging, the two groups matched well with each other, with no significant differences (**Table 1**).

Correlation Between the Physician-Assessed and Patients-Reported Mobility Deficits

In the Pearson correlation analysis, a modest correlation between the UPDRS motor score and PDQ39 mobility SI was found ($r = 0.440$, $p = 0.002$) (**Figure 1A**), supporting the correlation between the physician-assessed and patients-reported mobility deficits.

[1]http://www.feinsteinneuroscience.org

TABLE 1 | Demographic and clinical characteristics (including PET information) in the PD patients.

	DTPD-QoL	DTPD-non-QoL
Gender (Male/Female)	31/18	34/20
Age at onset (year)	50.85 ± 12.66	52.65 ± 11.73
Age at examination (year)	53.43 ± 12.06	54.67 ± 12.10
Disease Duration (month)	26.00 (14.00, 49.75)	19.00 (11.50, 36.00)
Hoehn and Yahr	2.00 (1.00, 2.00)	2.00 (1.00, 2.00)
LEDD (mg/day)	300.00 (75.00, 400.00)	200.00 (0.00, 318.75)
^{11}C-CFT Imaging		
Contralateral Caudate	1.20 ± 0.36	1.27 ± 0.34
Contralateral Ant Putamen	0.86 ± 0.23	0.96 ± 0.33
Contralateral Pos Putamen	0.50 ± 0.12	0.59 ± 0.25
Ipsilateral Caudate	1.36 ± 0.38	1.38 ± 0.34
Ipsilateral Ant Putamen	1.09 ± 0.33	1.18 ± 0.37
Ipsilateral Pos Putamen	0.65 ± 0.21	0.73 ± 0.29
^{18}F-FDG Imaging		
PDRP	3.19 ± 1.17	3.13 ± 1.20

Data are given as mean ± standard deviation (SD) values or median (interquartile range). DTPD, dual-tracer PET imaging of Parkinson's disease. QoL, quality of life. LEDD, Levodopa equivalent daily dosage. UPDRS, Unified Parkinson's Disease Rating Scale. Rar1, Rating of akinesia and rigidity.

Correlations Between Striatal DAT Bindings (ROIs), UPDRS Motor Scores and PDQ39 Mobility SI

In our study, UPDRS III score correlated significantly ($p < 0.01$) with the striatal DAT binding (ROIs) (on the contralateral side, caudate: $r = -0.462$, $p = 0.001$; anterior putamen: $r = -0.486$, $p = 0.000$; posterior putamen: $r = -0.419$, $p = 0.003$; on the ipsilateral side, caudate: $r = -0.450$, $p = 0.001$; anterior putamen: $r = -0.495$, $p < 0.001$; posterior putamen: $r = -0.409$, $p = 0.004$). However, no significant correlation ($p > 0.05$) was found between the PDQ39 mobility SI and the DAT binding (ROIs) in putamen, but weak correlation was found in the caudate (on the contralateral side, caudate: $r = -0.304$, $p = 0.033$; anterior putamen: $r = -0.202$, $p = 0.163$; posterior putamen: $r = -0.130$, $p = 0.374$; on the ipsilateral side, caudate: $r = -0.310$, $p = 0.030$; anterior putamen: $r = -0.258$, $p = 0.073$; posterior putamen: $r = -0.135$, $p = 0.357$).

Correlations Between Brain Glucose Metabolism, UPDRS III Scores and PDQ39 Mobility SI

In our study with ^{18}F-FDG PET imaging, the PDRP z scores correlated positively with the UPDRS motor scores ($r = 0.368$, $p = 0.009$) (**Figure 1B**), as well as a positive interaction with PDQ39 mobility SI ($r = 0.406$, $p = 0.004$) (**Figure 1C**).

Besides the PDRP scores, we also explored the brain regions correlating with the PDQ39 mobility SI. As was shown in the **Table 2** and **Figure 2**, cerebellum correlated positively with the PDQ39 mobility subdomain, and brain regions that correlated negatively with the mobility subdomain were mainly distributed in the caudate, inferior and middle frontal lobe and parietal lobe regions. The cerebral regions related to PDQ39 mobility SI

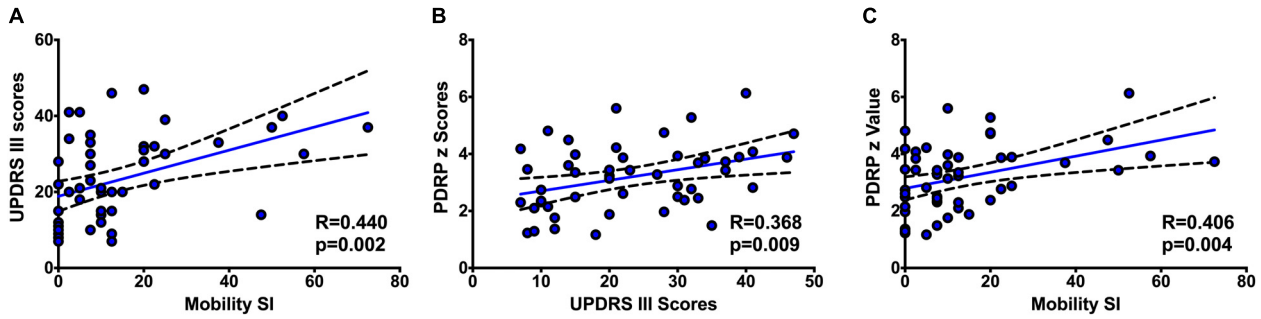

FIGURE 1 | The correlations between UPDRS III scores and PDQ-39 mobility SI **(A)**, PDRP *z* scores and UPDRS III scores **(B)**, and PDRP *z* scores and PDQ-39 mobility SI **(C)**.

was similar to the regions previously reported in the PD-related metabolic pattern.

DISCUSSION

In this retrospective study, a modest correlation was found between UPDRS motor ratings and PDQ39 mobility sub-scores. The UPDRS motor scores correlated strictly with striatal dopaminergic lesions. However, the mechanisms related to PDQ39 mobility were beyond striatal dopaminergic deficiency. In the glucose metabolic analysis, the poor mobility quality was found to correlate with higher global PDRP scores, increased metabolism in cerebellum and decreased metabolism in prefrontal gyrus. Our study might offer a new perspective in understanding the objectively assessed and self-reported motor dysfunctions in PD.

TABLE 2 | Brain regions exhibiting significant correlations between the PDQ-39 mobility sub-scores and regional brain metabolism.

Regions	BA	MNI coordinates[a]			Zmax	Cluster Size (mm^3)[b]
		x	y	Z		
Positive[b]						
Rt Cerebellum Pyramis	/	8	−68	−36	3.94	8480
Lt Cerebellum Tonsil	/	−26	−42	−40	3.79	8480
Lt Cerebellum Culmen	/	−16	−42	−28	3.76	8480
Lt Cerebellum Inferior Semi-lunar Lobule	/	−16	−66	−48	3.71	1088
Lt Cerebellum Inferior Semi-lunar Lobule	/	−32	−64	−50	3.49	1088
Negative[b]						
Rt Inferior Frontal Gyrus	45	54	38	2	5.33	10584
Rt Middle Frontal Gyrus	6	52	4	48	5.03	10584
Rt Middle Frontal Gyrus	46	52	24	26	4.91	10584
Lt Middle Frontal Gyrus	46	−46	22	30	4.78	5800
Lt Inferior Frontal Gyrus	45	−48	38	4	4.41	5800
Lt Inferior Frontal Gyrus	47	−34	32	−14	4.23	5800
Rt Inferior Parietal Lobule	40	62	−46	44	4.6	3880
Rt Inferior Parietal Lobule	39	52	−64	42	4.21	3880
Rt Supramarginal Gyrus	40	56	−48	30	3.85	3880
Rt Superior Temporal Gyrus	42	68	−14	8	3.91	696
Lt Caudate	/	−12	10	10	3.88	872

BA, Brodmann area; MNI, Montreal Neurological Institute; Lt, left; Rt, right; a, coordinates are displayed in Montreal Neurological Institute standard space. b, significant at voxel threshold of $p < 0.001$, extent threshold = 83 voxels (664 mm^3).

As shown in our study, the UPDRS motor scores correlated modestly with the self-reported mobility dysfunction affecting the QoL. Although they both reflected the motor dysfunction, they lay emphasis on different aspects of motor deficits in PD. UPDRS motor scores record detailed motor descriptions and severities, nevertheless, PDQ39 is dedicated on the QoL of PD patients, more inclined to individual experience. Besides the different contents between the two scales, as aforementioned, subjective improvement of motor symptoms was not equivalent to better objective experience. Skorvanek et al. (2015) reported the overall burden of non-motor symptoms in PD was prior to motor symptoms with regard to QoL, and similar outcome was acquired that PDQ39 mobility sub-score was related to the MDS-UPDRS items pain and other sensations, fatigue and higher MDS-UPDRS part III scores.

Similar to our previous reports, the motor deficits as detected by UPDRS III scores correlated significantly with the dopaminergic lesions in putamen. To our surprise, the mobility QoL was irrelevant with the dopaminergic loss in putamen, but correlated more with specific cerebral glucose metabolism. This result inspired us that the perception of mobility dysfunction was beyond dopaminergic lesions.

The parkinsonian motor features could not be fully explained by dopamine depletion alone, and the brain energy metabolism might offer another perspective to understand the cause of motor symptoms. Schrack et al. (2010) performed a research on metabolic change with aging based on the BLSA and indicated that the changing movement performance may be an adaption to aging and neurodegeneration since available energy supplied for human physical needs in addition to RMR declined with aging. Some studies (Amano et al., 2015) further supported the hypothesis that neural metabolic dysfunction could play a role in Parkinsonian

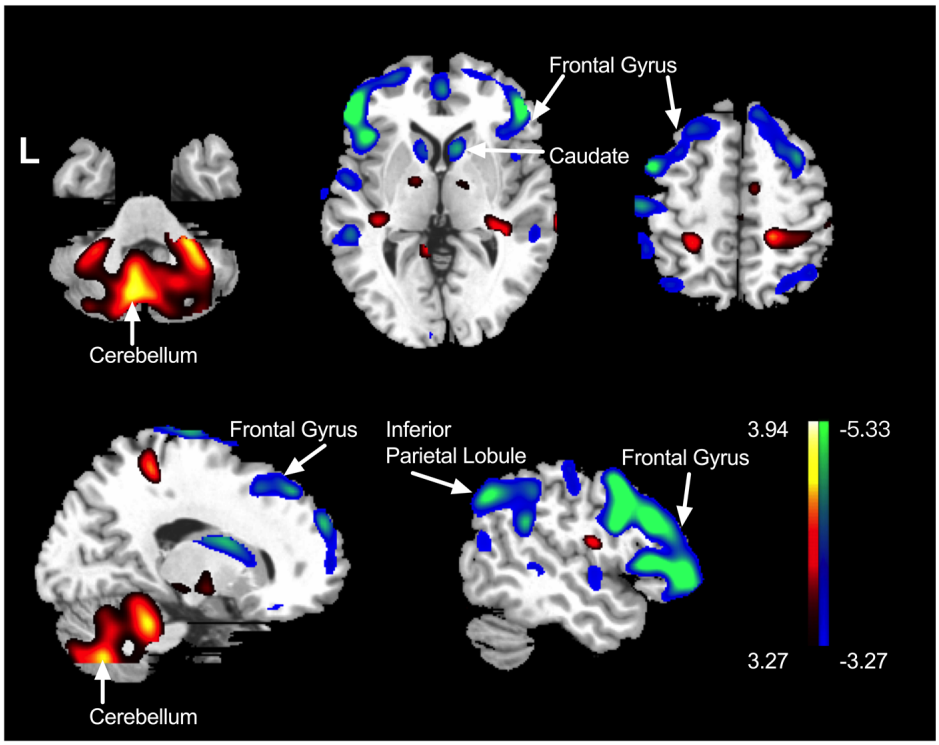

FIGURE 2 | The brain regions correlating with the mobility sub-score. Positively correlated regions were displayed using a red–yellow scale and negatively correlated regions were displayed using a blue–green scale. The overlays are depicted in neurologic orientation. The gray-scale image is the standard T1-weighted structural magnetic resonance image (MRI) in Montreal Neurological Institute (MNI) space. The thresholds of the color bars represent *T* values. Voxel threshold was set at $P < 0.001$.

motor symptoms. In our previous dual-tracer PET study (Liu et al., 2018), the tremor severities did not correlate with striatal dopaminergic lesions, but correlated with the global PDRP values and related regional glucose metabolism. Therefore, the cerebral changes related to the motor lesions were beyond dopaminergic dysfunctions.

In our study, the metabolism in cerebellum correlated positively with PDQ39 mobility sub-scores, and the metabolism in inferior and middle frontal gyrus correlated negatively with mobility sub-scores. In detail, the higher PDQ39 mobility scores, indicating poorer movement performances, tended to be accompanied by elevated metabolism in cerebellum and decreased metabolism in frontal cortex.

The hyper-metabolism in cerebellum was a typical feature as suggested in the PDRP (Ma et al., 2007). In PD, the dopamine depletion in striatum consequently lead to dysfunctions in cortico–striatal–thalamic–cortical circuits (Alexander et al., 1986), inducing many functional compensation pathways including cerebellum (Wu and Hallett, 2005). Such compensatory effects by cerebellum might be mediated by the overlapping cortical areas between cerebello-thalamo-cortical circuits (Middleton and Strick, 2001) and BG circuits (Middleton and Strick, 2000), or direct projections from the cerebellum to the BG (Ichinohe et al., 2000; Hoshi et al., 2005). In our study, the increased metabolism in cerebellum accompanied poor mobility quality, supporting some neurophysiological basis to the self-perceived mobility feelings.

Besides cerebellum, the metabolism in prefrontal cortex was also found to be involved in mobility quality perception. As previously reported, decreased functional connectivity between these prefrontal regions and the putamen should be responsible for cognitive deficits in PD patients, and more severe cortical thinning in frontal and temporo-parietal cortices has been found in PD patients with mild cognitive deficits (Wilson et al., 2019). Also, an ^{18}F-FDG-PET study (Wang et al., 2017) including 28 PD patients with anxiety has revealed decreased glucose metabolism in the bilateral orbitofrontal cortex. All these data supported the clinical findings that complex non-motor symptoms would interfere in the subjective experience in addition to motor symptoms. However, the underlying pathophysiological mechanism still remains to be defined.

CONCLUSION

Though both of them were widely used to assess motor dysfunctions in PD, UPDRS motor scores, and PDQ39 mobility scores were not completely a same thing, showing only modest correlations. In this dual tracer PET imaging study, the mechanisms involved under mobility quality were beyond

dopaminergic deficiency. The motor related cerebellum hyper-metabolism and non-motor related frontal hypo-metabolism contributed to the poor mobility quality. Conclusively, the self-reported mobility experience may have the neurophysiological basis related to both motor and non-motor manifestations in PD.

DATA AVAILABILITY STATEMENT

The raw data supporting the conclusions of this article will be made available by the authors, without undue reservation.

ETHICS STATEMENT

The studies involving human participants were reviewed and approved by the Ethics Committee of Huashan Hospital, Fudan University. The patients/participants provided their written informed consent to participate in this study.

AUTHOR CONTRIBUTIONS

JW, C-TZ, J-JW, and F-TL conceived the research project. LF, F-TL, Y-QL, J-JG, and Y-MS organized the research project. LF, Y-QL, J-JG, J-YL, and F-TL executed the research project. JW and C-TZ designed the statistical analysis. S-JH, F-TL, Y-QL, LF, and J-YL executed the statistical analysis. JW, Y-MS, and F-TL reviewed and critiqued the statistical analysis. LF, F-TL, Y-QL, J-JG, and J-YL wrote the first draft of manuscript. JW, C-TZ, and F-TL reviewed and critiqued the manuscript. All authors contributed to the article and approved the submitted version.

FUNDING

JW received the research funding from Ministry of Science and Technology of China (grant number: 2016YFC1306504), Shanghai Municipal Science and Technology Major Project (no. 2018SHZDZX01) and ZJLab, and the National Nature Science Foundation of China (grant numbers: 91949118 and 81771372). C-TZ received the research funding from the National Natural Science Foundation of China (grant numbers: 81971641, 81671239, and 81361120393), Shanghai Municipal Science and Technology Major Project (grant number: 2017SHZDZX01), and Science and Technology Commission of Shanghai Municipality (grant numbers: 19441903500 and 17JC1401600). F-TL received the grant of the National Nature Science Foundation of China (grant number: 81701250). J-JG received the grant of the National Natural Science Foundation of China (grant number: 81902282) and Shanghai Sailing Program funded by Shanghai Science and Technology Committee (grant number: 18YF1403100).

REFERENCES

Alexander, G. E., Delong, M. R., and Strick, P. L. (1986). Parallel organization of functionally segregated circuits linking basal ganglia and cortex. *Annu. Rev. Neurosci.* 9, 357–381. doi: 10.1146/annurev.ne.09.030186.002041

Amano, S., Kegelmeyer, D., and Hong, S. L. (2015). Rethinking energy in parkinsonian motor symptoms: a potential role for neural metabolic deficits. *Front. Syst. Neurosci.* 8:242. doi: 10.3389/fnsys.2014.00242

Bu, L. L., Liu, F. T., Jiang, C. F., Guo, S. S., Yu, H., Zuo, C. T., et al. (2018). Patterns of dopamine transporter imaging in subtypes of multiple system atrophy. *Acta Neurol. Scand.* 138, 170–176. doi: 10.1111/ane.12932

Daniels, C., Krack, P., Volkmann, J., Raethjen, J., Pinsker, M. O., Kloss, M., et al. (2011). Is improvement in the quality of life after subthalamic nucleus stimulation in Parkinson's disease predictable? *Mov. Disord.* 26, 2516–2521. doi: 10.1002/mds.23907

Goetz, C. G., Tilley, B. C., Shaftman, S. R., Stebbins, G. T., Fahn, S., Martinez-Martin, P., et al. (2008). Movement disorder society-sponsored revision of the unified Parkinson's disease rating scale (MDS-UPDRS): scale presentation and clinimetric testing results. *Mov. Disord.* 23, 2129–2170. doi: 10.1002/mds.22340

Hoshi, E., Tremblay, L., Féger, J., Carras, P. L., and Strick, P. L. (2005). The cerebellum communicates with the basal ganglia. *Nat. Neurosci.* 8, 1491–1493. doi: 10.1038/nn1544

Ichinohe, N., Mori, F., and Shoumura, K. (2000). A di-synaptic projection from the lateral cerebellar nucleus to the laterodorsal part of the striatum via the central lateral nucleus of the thalamus in the rat. *Brain Res.* 880, 191–197. doi: 10.1016/s0006-8993(00)02744-x

Liu, F. T., Ge, J. J., Wu, J. J., Wu, P., Ma, Y., Zuo, C. T., et al. (2018). Clinical, dopaminergic, and metabolic correlations in Parkinson disease: a dual-tracer PET study. *Clin. Nucl. Med.* 43, 562–571. doi: 10.1097/rlu.0000000000002148

Liu, F. T., Lang, L. Q., Yang, Y. J., Zhao, J., Feng, R., Hu, J., et al. (2019). Predictors to quality of life improvements after subthalamic stimulation in Parkinson's disease. *Acta Neurol. Scand.* 139, 346–352.

Ma, Y., Dhawan, V., Mentis, M., Chaly, T., Spetsieris, P. G., and Eidelberg, D. (2002). Parametric mapping of [F-18]FPCIT binding in early stage Parkinson's disease: a PET study. *Synapse* 45, 125–133. doi: 10.1002/syn.10090

Ma, Y., Tang, C., Spetsieris, P. G., Dhawan, V., and Eidelberg, D. (2007). Abnormal metabolic network activity in Parkinson's disease: test-retest reproducibility. *J. Cereb. Blood Flow Metab.* 27, 597–605. doi: 10.1038/sj.jcbfm.9600358

Marinus, J., Ramaker, C., van Hilten, J. J., and Stiggelbout, A. M. (2002). Health related quality of life in Parkinson's disease: a systematic review of disease specific instruments. *J. Neurol. Neurosurg. Psychiatry* 72, 241–248. doi: 10.1136/jnnp.72.2.241

Middleton, F. A., and Strick, P. L. (2000). Basal ganglia and cerebellar loops: motor and cognitive circuits. *Brain Res. Rev.* 31, 236–250. doi: 10.1016/s0165-0173(99)00040-5

Middleton, F. A., and Strick, P. L. (2001). Cerebellar projections to the prefrontal cortex of the primate. *J. Neurosci.* 21, 700–712. doi: 10.1523/jneurosci.21-02-00700.2001

Nandhagopal, R., Kuramoto, L., Schulzer, M., Mak, E., Cragg, J., Lee, C. S., et al. (2009). Longitudinal progression of sporadic Parkinson's disease: a multi-tracer positron emission tomography study. *Brain* 132, 2970–2979. doi: 10.1093/brain/awp209

Schrack, J. A., Simonsick, E. M., and Ferrucci, L. (2010). The energetic pathway to mobility loss: an emerging new framework for longitudinal studies on aging. *J. Am. Geriatr. Soc.* 58, S329–S336.

Skorvanek, M., Rosenberger, J., Minar, M., Grofik, M., Han, V., Groothoff, J. W., et al. (2015). Relationship between the non-motor items of the MDS-UPDRS and quality of life in patients with Parkinson's disease. *J. Neurol. Sci.* 353, 87–91. doi: 10.1016/j.jns.2015.04.013

Wang, X. X., Zhang, J. J., Yuan, Y. S., Li, T. N., Zhang, L., Ding, J., et al. (2017). Cerebral metabolic change in Parkinson's disease patients with anxiety: a FDG-PET study. *Neurosci. Lett.* 653, 202–207. doi: 10.1016/j.neulet.2017.05.062

Wilson, H., Niccolini, F., Pellicano, C., and Politis, M. (2019). Cortical thinning across Parkinson's disease stages and clinical correlates. *J. Neurol. Sci.* 398, 31–38. doi: 10.1016/j.jns.2019.01.020

Wu, P., Wang, J., Peng, S., Ma, Y., Zhang, H., Guan, Y., et al. (2013). Metabolic brain network in the Chinese patients with Parkinson's disease based on 18F-FDG PET imaging. *Parkinsonism Relat. Disord.* 19, 622–627. doi: 10.1016/j.parkreldis.2013.02.013

Wu, T., and Hallett, M. (2005). A functional MRI study of automatic movements in patients with Parkinson's disease. *Brain* 128, 2250–2259. doi: 10.1093/brain/awh569

Conflict of Interest: The authors declare that the research was conducted in the absence of any commercial or financial relationships that could be construed as a potential conflict of interest.

frontiers in Neuroscience

REVIEW
published: 09 July 2020
doi: 10.3389/fnins.2020.00693

Integrated Pathways of COX-2 and mTOR: Roles in Cell Sensing and Alzheimer's Disease

*Arti Tyagi[1], Mohammad A. Kamal[2,3] and Nitesh Kumar Poddar[4]**

[1] Department of Biochemical Engineering and Biotechnology, Indian Institute of Technology Delhi, New Delhi, India, [2] King Fahad Medical Research Center, King Abdulaziz University, Jeddah, Saudi Arabia, [3] Enzymoics, Hebersham, NSW, Australia, [4] Department of Biosciences, Manipal University Jaipur, Jaipur, India

Cyclooxygenases (COX) are enzymes catalyzing arachidonic acid into prostanoids. COX exists in three isoforms: COX-1, 2, and 3. COX-1 and COX-2 have been widely studied in order to explore and understand their involvement in Alzheimer's disease (AD), a progressive neuroinflammatory dementia. COX-2 was traditionally viewed to be expressed only under pathological conditions and to have detrimental effects in AD pathophysiology and neurodegeneration. However, an increasing number of reports point to much more complex roles of COX-2 in AD. Mammalian/mechanistic target of rapamycin (mTOR) has been considered as a hub which integrates multiple signaling cascades, some of which are also involved in AD progression. COX-2 and mTOR are both involved in environmental sensing, growth, and metabolic processes of the cell. They are also known to act in cooperation in many different cancers and thus, their role together in normal cellular functions as well as AD has been explored in this review. Some of the therapeutic approaches targeting COX-2 and mTOR in AD and cancer are also discussed.

Keywords: COX, neuro-inflammatory, Alzheimer's, mTOR, cellular pathways

OPEN ACCESS

Edited by:
Fangyu Peng,
University of Texas Southwestern Medical Center, United States

Reviewed by:
Gabriela Alejandra Salvador,
Universidad Nacional del Sur, Argentina
Marco Onofrj,
G. D'Annunzio University of Chieti-Pescara, Italy

***Correspondence:**
Nitesh Kumar Poddar
niteshkumar.poddar@jaipur.manipal.edu;
niteshpoddar@gmail.com

Specialty section:
This article was submitted to Neurodegeneration, a section of the journal Frontiers in Neuroscience

Received: *12 February 2020*
Accepted: *08 June 2020*
Published: *09 July 2020*

Citation:
Tyagi A, Kamal MA and Poddar NK (2020) Integrated Pathways of COX-2 and mTOR: Roles in Cell Sensing and Alzheimer's Disease. Front. Neurosci. 14:693. doi: 10.3389/fnins.2020.00693

CYCLOOXYGENASE AND ITS ISOFORMS

Cyclooxygenase-2 (COX-2) is an isoform of the cyclooxygenase enzyme family, along with COX-1 and COX-3, which are involved in the synthesis of prostanoids (eicosanoid sub-class) from an essential fatty acid, namely arachidonic acid (AA). AA is first released by the action of phospholipase A2 (PLA2) from plasma membranephospholipids, which acts at the sn-2 position of the phospholipid backbone (Engelking, 2015; Hanna and Hafez, 2018). PLA2 activity is stimulated by microbial products, thrombin, immunoglobulins, etc., whereas anti-inflammatory glucocorticoids are known to inhibit it (Engelking, 2015). Out of the 20 + different types of PLA2s known to occur, type IIA secretory PLA2 and type IV cytosolic PLA2α have been shown to be coupled with COX-2 in different cell types. These two subclasses of enzymes have also exhibited cross-talk amongst themselves (Murakami et al., 1997; Balsinde et al., 1998; Bidgood et al., 2000; Sun et al., 2010). However, there are views that sufficient and conclusive data is still not present to establish a clear relationship between secretory PLA2 and eicosanoid signaling (Burke and Dennis, 2009).

Once AA is released, it is further metabolized by either enzymatic or non-enzymatic processes. Four different enzymatic pathways can act on AA: cyclooxygenase, lipoxygenase, anandamide, and cytochrome p450, resulting in different kinds of eicosanoids (**Figure 1**). Both COX-1 and COX-2 are part of the cyclooxygenase pathway, giving rise to prostanoids such as prostaglandin (PG) E_2, $PGF_{2\alpha}$, PGD_2, PGI_2 (prostacyclin), and thromboxane (TX) A2. Prostanoids are a part of vasoactive lipids that act as local hormones and play crucial roles in normal physiology as well as certain pathophysiological states. The COX enzymes were popularized in 1971 upon demonstrating that non-steroidal anti-inflammatory drugs (NSAIDs) exert their potent anti-inflammatory properties via inhibition of COX. Since then, a lot of research has been dedicated to this unique enzyme and the various roles it plays in human physiology. Now, it has been established that NSAIDs also affect many other molecules, but COX remains an important player in various conditions, including certain neuropathologies. Some of these pathologies are also found to be epigenetically regulated as faulty DNA hypermethylation causes transcriptional silencing of COX-2 gene (Kikuchi et al., 2002; Ma et al., 2004).

COX is an integral membrane glycoprotein that carries out the first two committed steps of the prostanoid synthesis pathway: cyclooxygenation and peroxidation. Thus, it's a bi-functional enzyme with a homodimeric structure and a single heme, involved in both the catalytic steps, situated in the middle of the two active sites of the enzyme (Rouzer and Marnett, 2009). In cyclooxygenation, two oxygen molecules are added to AA, forming the cyclic PGG2 (Prostaglandin G2) and later PGH2 (Prostaglandin H2) in the peroxidation step. PGH2 is an unstable intermediate that is acted upon by specific synthases and isomerases giving rise to different PGs and TX in a cell-specific manner (Clària, 2003). The COX isoforms are encoded on different chromosomes and have a lot of differences in their structural and regulatory organization, although they share a 60% amino acid sequence homology in their respective proteins (Clària, 2003). COX-2 gene has many regulatory sequences, like a TATA box, two NF-κB sites, a NF-IL6 motif, a CRE motif, and an E box, among others, which are absent in COX-1 gene (Clària, 2003; Kang et al., 2007). Many studies have been conducted in this regard; for example, CREB and Ets family-proteins (Ets-1 and Elk-1) were found to upregulate COX-2 expression in pancreatic β-cells. A detailed account of the different transcriptional factors involved in COX-2 regulation in different cell types has been given by Kang et al. (2007). This is keeping in line with the fact that COX-1 is generally constitutively expressed (Minghetti, 2004; Hoozemans et al., 2008), whereas COX-2 is induced in response to inflammatory reactions (Clària, 2003). Thus, COX-1 is often associated with PG synthesis under normal physiological conditions leading to phenomena like platelet aggregation, renal perfusion maintenance, and gastric cytoprotection. However, it has been found that COX-2 is also expressed in the kidneys, brain, and testes under physiological conditions along with COX-1 (Minghetti, 2004; Hoozemans et al., 2008). Specifically, in the brain, COX-2 has been proposed to influence memory, sensory integration, and autonomic regulation in the central nervous system (CNS) (Kaufmann et al., 1997). COX-3, on the other hand, is most populated in the cerebral cortex region of the brain and its enzymatic activity is inhibited by acetaminophen (Minghetti, 2004). However, much remains to be done to completely understand the functioning of COX-3. Both COX-2 and COX-1 are sources of pro-inflammatory prostanoids (Smyth et al., 2009); however, new evidence is fast emerging that also points to their role in resolution of inflammation (Williams et al., 1999; Fukunaga et al., 2005; Maskrey et al., 2011). Resolution is a complex process that kicks in once a sufficient inflammatory response has been mounted at the site of inflammation and is triggered by many cellular and molecular cues, such as macrophagic ingestion of apoptotic neutrophils (Ortega-Gómez et al., 2013).

MAMMALIAN/MECHANISTIC TARGET OF RAPAMYCIN (mTOR)

Rapamycin is a bacterial compound with anti-fungal, anti-cancer, and immunosuppressive properties, and thus, its target molecule, mTOR (mammalian/mechanistic target of rapamycin) has been implicated in processes such as aging, autophagy, and immune responses (Iglesias-Bartolome et al., 2012; Saxton and Sabatini, 2017) along with cellular pathways of proliferation, transcription, and translation (Shafei et al., 2017). The mTOR protein forms two complexes called mTORC1 and mTORC2, with a set of adaptor proteins. mTORC1 and mTORC2 are involved in different regulatory pathways and have different functions. The upstream regulatory components of mTOR include AMP-activated protein kinase (AMPK), glycogen synthase kinase (GSK3), insulin/insulin-like growth factor 1 (IGF-1), and phosphoinositide 3-kinase (PI3-K)/protein kinase B (Akt) while some of the major downstream regulators are 4E-binding proteins (4EBPs) and ribosomal protein S kinase (S6K) (Mueed et al., 2019; Papadopoli et al., 2019).

COX AND ALZHEIMER'S DISEASE

A lot of work has especially been dedicated to studying the role of COX-2 in neuroinflammatory and neurodegenerative conditions as its overexpression has been related to some of these pathologies (Minghetti, 2004). One of the prime targets of PGs includes the central and peripheral nervous system. The expression of COX-2 in certain types of mammalian neurons is "dynamically regulated" (Minghetti, 2004) by the synaptic activity of these neurons. Many *in vitro* as well as animal model studies have implicated the role of COX-2 in normal synaptic activity and plasticity (Hölscher, 1995; Kaufmann et al., 1997; Bazan, 2003), yet mice that had been genetically manipulated to knockout COX-2 gene exhibited a more or less normally functioning brain. However, in all these cases, accurate behavioral studies could not be performed as the mice suffered from renal failure very early in their lifespan (Dinchuk et al., 1995; Minghetti, 2004).

Alzheimer's disease (AD) is a progressive neurodegenerative disease and one of the most prevalent types of dementia

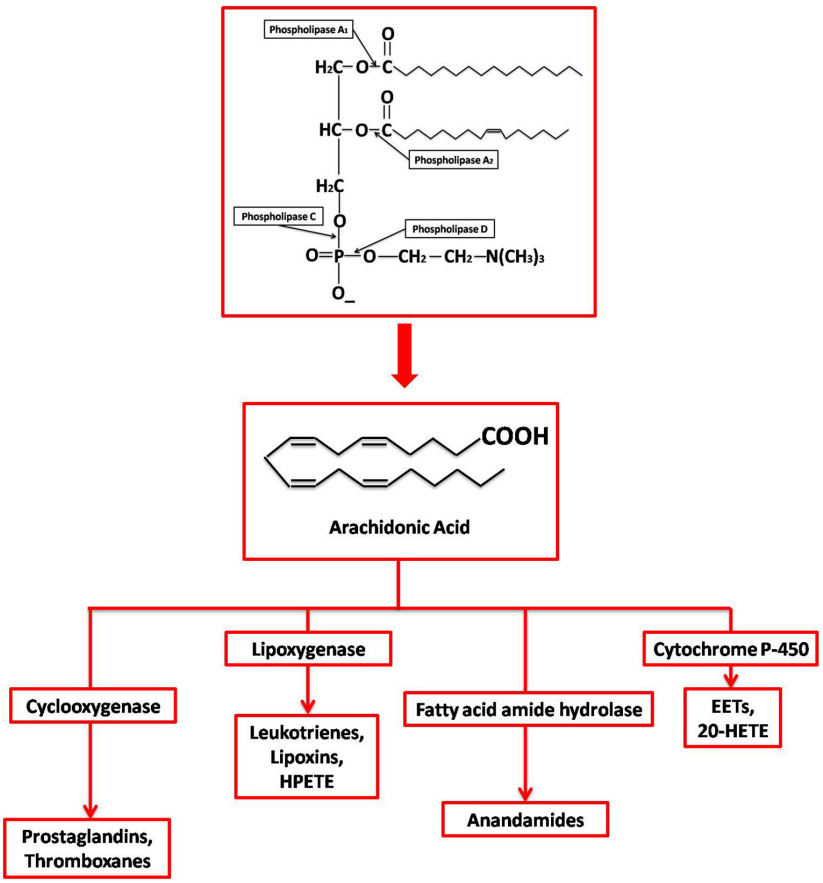

FIGURE 1 | Synthesis and metabolization of Arachidonic Acid. Different phospholipases act at different sites on membrane phospholipids generating various products, including free AA by PLA2. AA is then enzymatically metabolized by (1) Cyclooxygenases into prostaglandins; (2) Lipoxygenases into leukotrienes, lipoxins, and 8- 12- 15-hydroperoxyeicosatetraenoic acid (HPETE); (3) Cyctochrome P450 into epoxyeicosatrienoic acid (EET) and 20-hydroxyeicosatetraenoic acid (20-HETE); and (4) Fatty acid amide hydrolase into endocannabinoid and anadamide.

worldwide (Mueed et al., 2019). It is pathologically marked by the presence of two specific types of deposits in the brain: β-amyloid plaques and neurofibrillary tangles (NFTs), leading to neuroinflammation, synaptic dysfunction, and eventually neurodegeneration. NFTs are mainly composed of hyperphosphorylated tau (a microtubule associated protein) (Grundke-Iqbal et al., 1986; Alonso et al., 2001) while β-amyloid plaques are formed due to self-aggregation of the hydrophobic Aβ peptide produced upon cleavage of amyloid precursor protein (APP) (Luo et al., 2016; Mueed et al., 2019). The neuronal autophagy-lysosomal system is affected in AD pathology and results in low clearance of misfolded and damaged proteins, leading to aggregate formation (Shacka et al., 2008).

Epidemiological studies conducted on AD showed that populations which had a long history of NSAID use, were at a lower risk of AD (Breitner, 1996; Aisen, 2002; Minghetti, 2004; Hoozemans et al., 2008). This, along with other studies showing associations between COX-2 induction and neurodegeneration (Miettinen et al., 1997) as well as brain parenchymal amyloid plaque formation (Stewart et al., 1997), sparked interest, and subsequent research on potential effects of the COX enzymes and their various pathways in AD progression as NSAIDs are known inhibitors of COX.

Additionally, it has also been shown that lipids and PGs play vital roles in AD (Bazan et al., 2002; Thomas et al., 2016). AA, which gives rise to PGs, also happens to be the second most abundant polyunsaturated fatty acid in the brain (Thomas et al., 2016). It was also found that free AA affects synaptic functions of the brain (Latham et al., 2007). Thus, the levels of free AA in the brain cells, along with a balance between enzymes converting it to other molecules like PGs and enzymes releasing free AA, is also an important factor in AD (Thomas et al., 2016). In spite of this buzz about involvement of COX in AD, clinical studies carried out with NSAIDs and selective COX-2 inhibitors did not show any significant effects in treatment of AD (Hoozemans et al., 2008). Thus, it can be inferred that the effects of COX enzymes are not as straightforward in the case of AD as previously thought and the exact mechanisms by which they influence AD progression are not yet known.

The amyloid plaques, a classical hallmark of AD, are associated with pro-inflammatory cells and proteins. These proteins are found in the brain throughout the various stages of AD

progression (Hoozemans et al., 2008). It is also speculated that inflammatory molecules may have dual role in AD as they exert both beneficial as well as detrimental effects based on their concentration and the stage of AD in which they are being expressed (Hoozemans et al., 2008). Along with this, epidemiological and genetic evidence also exist which points to the fact that inflammation is one of the key processes contributing to AD. However, due to failure of NSAIDs and selective COX-2 inhibitors against AD, alternate views are being considered which think of these drugs to perhaps have a preventive role with respect to AD and inflammation as merely a secondary phenomenon to clear off debris generated from more central underlying processes of AD (Wyss-Coray and Mucke, 2002; Hoozemans et al., 2006). It has also been reported that COX-2 expression in AD brains is correlated with altered expression of cell cycle proteins (Hoozemans et al., 2008). It was found that cell proliferation, adhesion, and differentiation genes were some of the most commonly upregulated ones along with PG synthesis genes in AD brains (Blalock et al., 2004).

COX-2 is constitutively expressed in certain cell populations of the brain, and additionally it is induced by inflammatory molecules such as cytokines, IL-1, IL-2, and TNF-α (Hoozemans et al., 2008). But, it is expressed in microglia (the local macrophages of the brain) only under very specific conditions, such as in chronic cases of cerebral ischemia (Tomimoto et al., 2000; Walsh et al., 2000). The expression of COX-2 is also absent in astrocytes (Pasinetti and Aisen, 1998; Hoozemans et al., 2001). COX-2 expresses differentially in different stages of AD and has pleiotropic functions in the brain (Hoozemans et al., 2008). In the early stages of the disease, COX-2 expression is increased (Ho et al., 2001; Hoozemans et al., 2001, 2002) and it is primarily expressed in pyramidal neurons (Braak and Braak, 1991). IL-1 levels also go up in AD due to association of neuritic plaques with microglial cells that express IL-1 (Blum-Degena et al., 1995). It is then reasonable to think that these IL-1 molecules perhaps induce higher expressions of COX-2. The expression of COX-2 has also been linked to cell cycle control (Xiang et al., 2002; Wu Chen et al., 2004), which may be involved in (re)generative pathways. However, these reasons are still controversial as the elevated expressions of COX-2 occur before the activation of microglia and astrocytes as shown by neuropathological studies (Hoozemans et al., 2002), whereas the expression has been found to reduce later on as the disease progresses and the number of neurons expressing COX-2 in severe cases of AD is very few (Hoozemans et al., 2004), which might be due to selective degeneration of neurons at these stages and a loss in the synaptic activity (Hoozemans et al., 2008).

It has even been observed that NSAIDs affected molecules and pathways involved in AD other than COX; for example peroxisome proliferator activated receptor γ (PPARγ) is found to be up-regulated in AD and can be activated by NSAIDs (Kitamura et al., 1999). Activation of PPARγ leads to clearance of Aβ deposits in neuronal as well as non-neuronal cells (Camacho et al., 2004). NSAIDs have also been found to lower Aβ deposits by targeting the γ-secretase enzyme and inhibition of nuclear factor-κB (NF-κB) pathway (Weggen et al., 2001; Morihara et al., 2002; Eriksen et al., 2003).

ROLE OF mTOR IN AD

Recently, mTOR has also been found to be associated with AD pathology. Since AD is an age-associated disease, classical signs of aging like loss of proteostasis, mitochondrial dysfunction, altered intercellular communication, etc. can also be associated with mTOR (López-otín et al., 2013; Papadopoli et al., 2019). Since mTOR hinders autophagy, it promotes Aβ deposition in brain (Uddin et al., 2018). Due to disruption of the autophagic-lysosomal pathway, immature autophagolysosomes give rise to autophagic vacuoles that are then populated by β-amyloid plaques (Mueed et al., 2019). Rapamycin, however, is known to lessen these numbers (Haung Yu et al., 2005). Normally, adults contain very few autophagic vacuoles in their neurons (Cuervo et al., 2005) while these go up significantly in the affected regions of an AD brain (Haung Yu et al., 2005). An opposite connection has also been reported where induction with Aβ activates mTOR and its regulatory components (Bhaskar et al., 2009). Studies in both mouse models and humans have shown that the mTOR pathway is hyperactivated in AD (Perluigi et al., 2015). However, it has also been suggested that different neurons in an AD brain may have either upregulated or downregulated signaling cascades of mTOR based on how they react to AD stresses (Pei and Hugon, 2008).

Protein misfolding and subsequent aggregation is at the heart of Alzheimer's pathophysiology (Mueed et al., 2019). The mTORC1 complex has been reported to stimulate protein synthesis (Papadopoli et al., 2019). However, there have been contradicting reports in case of regulation of proteolysis, with some claims of mTOR suppressing protein degradation (Zhao et al., 2015; Rousseau and Bertolotti, 2016) and others of mTOR enhancing it (Papadopoli et al., 2019). Thus, mTOR can play a role in the aberrant proteostasis in AD patients. Tau is one of the proteins whose translational pathway involves mTOR-dependent signaling via a 5'top mRNA (Pei and Hugon, 2008). Thus, upregulated and continuous production of tau proteins in degenerating neurons is regulated by mTOR signaling via the P70S6K and 4EBP1 pathways (Pei et al., 2008).

Moreover, mTOR mediates tau synthesis and phosphorylation at specific sites and is found to co-localize with NFTs (An et al., 2003; Tang et al., 2013). This results in microtubule instability as tau is an essential microtubule associated protein and its hyperphosphorylation causes it to detach from microtubules (Mueed et al., 2019).

COX-2 AND mTOR IN CELL METABOLISM AND SIGNALING CASCADES: IMPLICATIONS IN AD

Small metabolites are known to be able to cross the blood-brain barrier and are also affected by environmental and genetic cues. Aberrant levels of amino acids, lipids, certain neurotransmitters,

and other metabolites are found in both blood and brain in mouse models of AD (Pan et al., 2016). Many phospholipids have also been demonstrated to contribute to AD occurrence and progression (Li D. et al., 2016). Additionally, a general loss of protein homeostasis and glucose metabolism are characteristic of AD (Papadopoli et al., 2019).

Along with growth factors, cellular energy levels, and oxygen levels, mTOR is also involved in sensing nutrients like amino acids and integrating these multitude of signals to produce a response according to the cell's need to further grow or differentiate (**Figure 2**; Howie et al., 2014; Goberdhan et al., 2016). Two models have been suggested to describe amino acid sensing by mTORC1 and the subsequent effector responses: a single hub, comprising of a single mTORC1 collecting all the micro-environmental cues to produce a variety of outputs; and a multi-hub model, where two different mTORC1 function in different parts of the cell (Jewell et al., 2015; Fan et al., 2016; Goberdhan et al., 2016). Many amino acid transporters, such as members of the proton-assisted transporters (PATs) family, are localized on the late endosomal and lysosomal (LEL) surfaces (Goberdhan et al., 2005; Goberdhan, 2010; **Figure 2**). Apart from the LELs, other possible amino acid sensing locations via mTORC1 have also been suggested such as the Golgi complex, supporting the multi-hub model of sensing. The entire process of amino acid sensing by mTORC1 has been divided into a priming step (sensitization of mTORC1 for the final activation) and an actual activation step. L-Glutamine, L-glycine, L-glutamic acid, L-serine, and L-arginine are some of the amino acids involved in priming whereas activation is majorly carried out by L-leucine and to some extent by L-methionine, L-isoleucine, and L-valine. L-Cysteine mostly impedes the priming step. Some of these amino acids (leucine, glutamine, serine, and arginine) are known to aid in autophagy inhibition by activating mTORC1 (Shafei et al., 2017). As previously mentioned, autophagy dysfunction is a key player in AD development (Saxton and Sabatini, 2017). Moreover, amino acids as well as enzymes metabolizing them in AD patients are also known to deter from their normal levels (Shafei et al., 2017). Lower levels of branched chain amino acids like valine, especially in later stages of life, have been associated with a higher risk of AD (Tynkkynen et al., 2018). Cysteine has also been directly linked to AD and other neurodegenerative diseases as plasma levels of AD patients were found to have higher cysteine and sulfate ratio early in the morning. Higher cysteine implies higher thiol concentration in the cell, which could hinder with the functioning, confirmation, and synthesis of protein (Heafield et al., 1990). Glutamate is also known to regulate mTORC1via glutamate dehydrogenase (GDH) and human branched chain aminotransferase (hBCAT) enzymes. Interestingly, glutamate, which is a neurotransmitter involved in excitatory functions, has also been found to be toxic and damaging to neurons when present in higher concentrations (Schubert and Piasecki, 2001).

Analogous to amino acid sensing, mTORC1 is also involved in nucleotide sensing in a cell (Hoxhaj et al., 2017). As mTORC1 promotes ribosome biogenesis, 60% of which consists of rRNA, it was found to boost *de novo* nucleotide (both purine and pyrimidine) synthesis (Ben-Sahra et al., 2013; **Figure 2**). The pathway for *de novo* pyrimidine synthesis has been reported in an adult human brain, but whether or not mTORC1 has any role to play in it is not yet known. Moreover, the expression levels of several genes involved in synthesis of mRNAs (such as dihydroorotate dehydrogenase and uridine-cytidine kinase 2) for both the *de novo* as well as salvage pathways were found to be modified in case of AD patients (Pesini et al., 2019). The depletion of purines, specifically adenylates, was found to inhibit mTORC1 via the GTPase-activating protein (GAP) activity of TSC (Tuberous sclerosis complex) (Hoxhaj et al., 2017). The same study also reported mTORC1 inhibition on longer periods of guanylate-depletion due to degradation of Rheb. The TSC complex helps in maintaining Rheb in a GDP-bound state thereby inhibiting mTORC1 (Dibble et al., 2012). However, mTORC1 is also reported to be inhibited by guanylate depletion due to binding of Rheb-GTP and farnesylation (Emmanuel et al., 2017; **Figure 2**). Supplementation of uridine and other nutrients has positive effects in AD therapy (Engelborghs et al., 2014). In fact, uridine is also a part of the recipe for a rather popular medical supplement called Souvenaid®, known to support synaptic generation and function as a part of AD therapy (Ritchie et al., 2014).

The nutrient microenvironment inside a cell and sensing by mTOR is also closely related to T cell regulation, activation, and differentiation. While mTOR activation is needed for effector T cell proliferation and differentiation, it inhibits FOXP3 expression, the master transcription factor for regulatory T cells (Sauer et al., 2008; Delgoffe et al., 2010). Regulatory T cells are reported to be upregulated in an AD patient's blood (Sommer et al., 2017). It was also shown that mTORC1 promotes selective Th1 differentiation while mTORC2 Th2 differentiation (Lee et al., 2010). The potential role of adaptive immune cells in AD, however, is still unclear with reports of both an enhanced pro- and anti-inflammatory response (Sommer et al., 2017; **Figure 2**).

The COX-2/PG axis, in addition to its role in tissue inflammation, also mediates insulin secretion in adipose tissue and differentiation of adipocytes (Fjaere et al., 2014). Epidemiological studies have linked diabetes and obesity with dementia (Ferreira et al., 2018). In fact, a lot of recent studies have highlighted the common cellular pathways underlying both diabetes and AD, thereby coining the term "type-3-diabetes" or "brain diabetes" to refer to AD (Xu et al., 2019). Anti-diabetic drugs are being explored as potential candidates of anti-AD therapy (De Felice, 2013). PGs have been reported to exert both pro- as well as anti-obesogenic effects (Madsen et al., 2008). Beige adipocytes play important roles in counteracting obesity and other related disorders like diabetes and cardiovascular diseases (Boström et al., 2012; Harms and Seale, 2013; Cohen et al., 2014; X. Zhang et al., 2018). The inter-communications between adipose tissue and CNS puts obese people at a higher risk of developing cognitive and other mental disorders (Forny-Germano et al., 2019). Interestingly, mTORC1 is also hyperactivated in adipose tissues of obese rodents and its enhanced expression in fact gives rise to adiposity as well as obesity (Um et al., 2004; Khamzina et al., 2005; Polak et al., 2008; Laplante and Sabatini, 2012). Most groups have reported

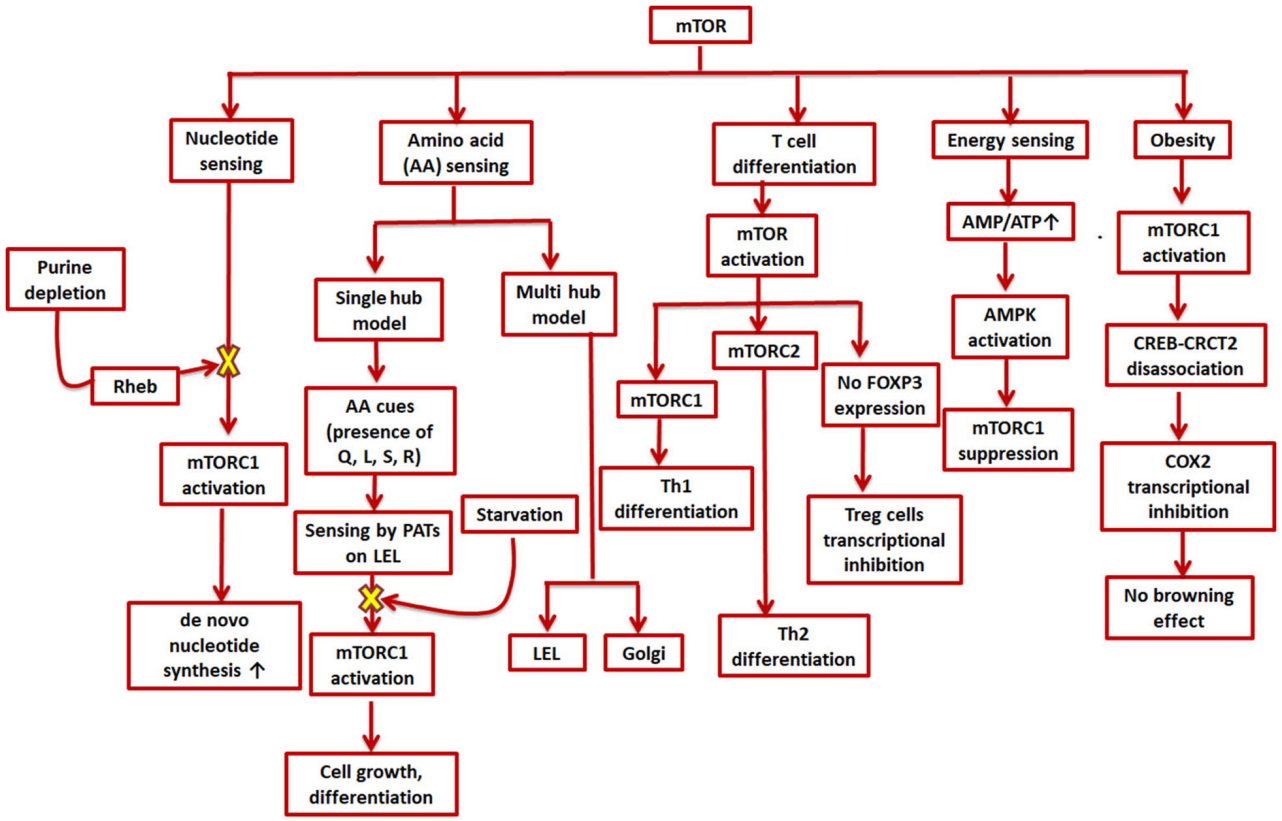

FIGURE 2 | Role of mTOR in cell metabolism and signaling cascades. mTOR is involved in various environmental sensing and growth-related processes in the cell. mTORC1 stimulates *de novo* synthesis of nucleotides as well as responds to amino acid availability by promoting cell growth and differentiation; mTOR furthers helper T-cell differentiation while impeding regulatory T-cell differentiation; a higher AMP/ATP ratio can suppress mTORC1 and thus inhibit energy expending processes; and mTORC1 inhibits transcription of COX-2 which promotes obesity.

that mTORC1 is inhibitory for thermogenesis and "browning effect" (conversion of white adipose tissue to brown/beige adipocytes), which help tackle obesity by inducing enhanced energy consumption processes (M. Um et al., 2004; Polak et al., 2008; Liu et al., 2014; Wada et al., 2016). Nevertheless, there have been a few studies which have shown that inactivation of mTORC1 also compromises thermogenesis (D. Liu et al., 2016; Tran et al., 2016). While exposure to cold is also known to induce browning effect in mammals, it has been found to modify pathways involved in AD in a study carried out in mice models (Xu et al., 2019). Since mTOR and COX-2 have been found to operate together directly or indirectly in various other disorders or conditions, it can also be speculated that they may affect each other in this particular case. In one such study, mTORC1 inactivation in the mice adipose tissue causes COX-2/PG pathway induction, sending off a paracrine signal to initiate browning effect (Zhang et al., 2018), whereas when mTORC1 is activated, it phosphorylates a serine residue (Ser^{136}) in CREB-regulated transcription coactivator 2, preventing its efficient association with CREB and subsequently CREB binding with COX-2 promoter (Zhang et al., 2018). As CREB binding enhances COX-2 promoter activation (Reddy et al., 2000; Yang and Bleich, 2004), mTORC1 activation eventually leads to transcriptional inhibition of COX-2, thereby preventing beige adipogenesis (**Figure 2**).

COX-2 AND mTOR IN OSMOPROTECTION

For normal cell functioning it is essential that the cellular volume, electrolytes, and other solute concentrations be maintained. Changes in the extracellular tonicity results in accompanying changes in the intracellular environment to ensure the cell maintains its normal volume (Macknight, 1988). The kidneys are one of those mammalian organs wherein cells are subjected to extreme concentrations of solutes like urea and NaCl (Burg et al., 2007). However, many diseases are known to be caused by the hyperosmotic stresses faced by non-renal tissues (Brocker et al., 2012). Cells deal with these conditions using certain small organic molecules, called osmolytes, that are dissolved in the cellular as well as extracellular fluids (Wijayasinghe et al., 2017). These organic osmolytes have been found to be accumulated in the renal medullary cells in situations of osmotic stress (Wijayasinghe et al., 2017). COX-2 and mTOR are involved in different kinds of osmoprotective pathways in different cell types (**Figure 3**).

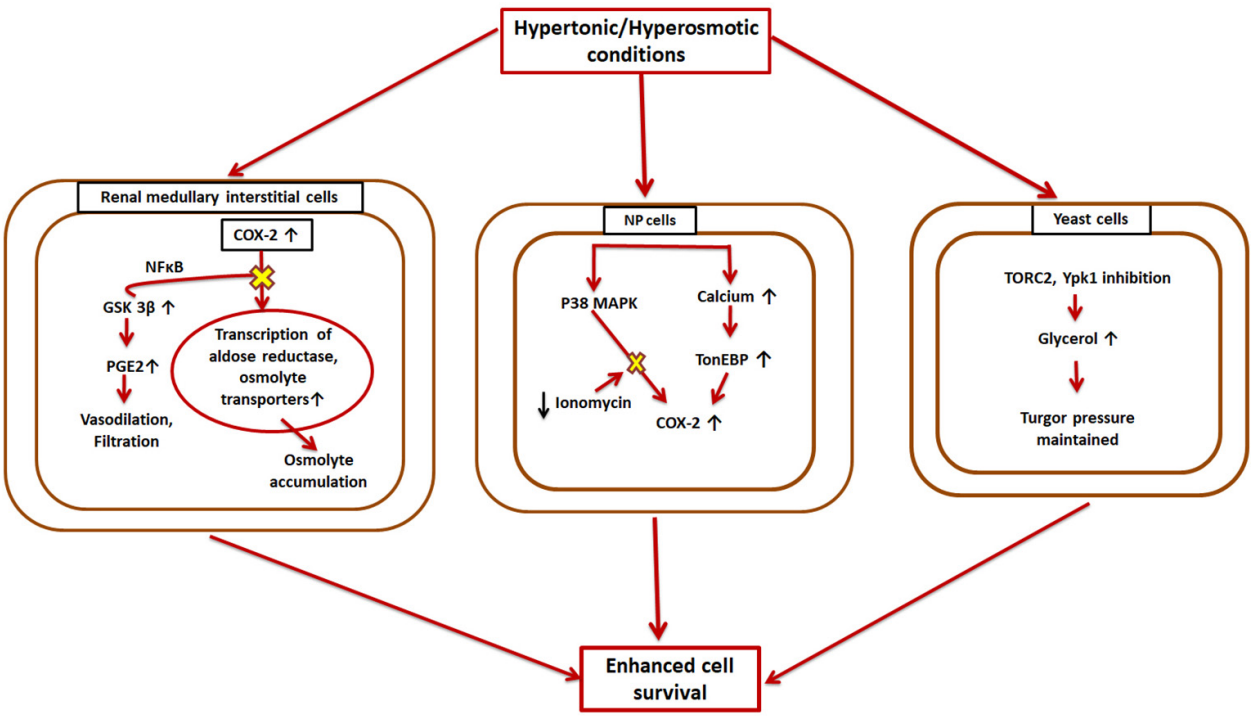

FIGURE 3 | Hyperosmotic induction of COX-2 and mTOR. COX-2 is overexpressed in the reno-medullary interstitial cells in a hyperosmotic environment. This leads to higher transcriptional rates of osmolyte transporters, and thus the cell can accumulate large amounts of osmolytes to aid in its survival, while GSK-3β opposes this pathway; Nucleus pulposus (NP) cells also cope with hypertonic conditions by overexpressing COX-2 via two different cascades-TonEBP and MAPK; Yeast cells exhibit higher levels of TORC2 under hypertonic conditions resulting in higher glycerol concentrations which eventually reestablishes cell turgor pressure.

Both COX-1 and COX-2 are expressed in different parts of the kidney (Y. Harris et al., 1994; Guan et al., 1997) with different regulatory mechanisms. While COX-2 exhibits expression based on the surrounding tonicity, COX-1 does not follow any such pattern (Briggs, 1999). Thus, there were speculations that COX-2 might have an osmoprotective function in the kidneys. Treatment with NSAIDs and COX-2 specific inhibitors in the reno-medullary interstitial (RMI) cells reduces osmolyte accumulation induced by hypertonic conditions in these cells and affects their survival (Moeckel et al., 2003). It was found that COX-2 causes this effect by transcriptional regulation of osmolyte transporters. Later on, it was also shown that GSK-3β kinase is a key player in this process and affects COX-2 via a signaling pathway involving NF-κB (Rao et al., 2004). The increased hypertonic conditions upregulate GSK-3β activity in the RMI cells, which increases their apoptotic rate (Rao et al., 2004). Thus, GSK-3β works as an antagonist of COX-2. TonEBP/NFAT5, a master transcription factor of osmoprotective genes (Favale et al., 2007), has also been found to enhance COX-2 mRNA levels in osmotically stressed RMI cells (Favale et al., 2009). MAPK family members and Src kinases are other known enzymes that are implicated in hypertonicity-induced COX-2 regulation (Burg et al., 2007; Yang et al., 2000; **Figure 3**).

Another part of the body that experiences higher and a constantly changing osmolarity is the inner core of vertebral disc, called nucleus pulposus (NP) (Choi et al., 2018). Therefore, the NP cells have mechanisms to adapt to these hyperosmotic microenvironments, which involve up-regulation of COX-2. This upregulation is intracellular calcium-dependent, but rather than the calceneurin signaling pathway, it occurs through TonEBP (Choi et al., 2018). It was found that TonEBP overexpression resulted in enhanced COX-2 promoter activity while its silencing resulted in diminished COX-2 promoter activity (Choi et al., 2018). TonEBP silencing also causes COX-2 enzyme levels to fall in iso-osmotic conditions (Choi et al., 2018). Additionally, p38 MAPK pathway also induced elevated expression of COX-2 under hyperosmotic conditions in NP cells. However, ionomycin treatment nullified this effect (Choi et al., 2018). This COX-2 overexpression eventually aids in (NP) cell survival under osmotic stress (**Figure 3**).

Additionally, in case of yeasts, mTORC2 (referred to as TORC2 in this case) has been demonstrated to be involved in osmotic-homeostasis maintenance (Eltschinger and Loewith, 2016; **Figure 3**). Ypk1 and Ypk2, homologs of Akt, are two important downstream substrates of TORC2. Hypertonic conditions inhibit TORC2 and Ypk1, which eventually results in increased glycerol concentrations in the cell and reestablishes the turgor pressure.

Osmolytes are reported to play corrective roles in many human pathologies caused by protein misfolding, although nothing specifically for AD (Kim et al., 2006). Meanwhile, a typical AD brain is marked by misfolded proteins that keep

getting accumulated and result in autophagic and lysosomal dysfunction as well as amyloid and tau aggregate formation (Efeyan et al., 2013). In fact, hypertonicity is one of the many causes of protein damage in cells (Hahr, 2015).

COX-2 MODULATION OF mTOR

Both COX-2 and mTOR have been extensively studied individually and in combination with other speculated regulators of AD in the disease's progression (Hoozemans et al., 2008; Pei and Hugon, 2008; Tang et al., 2015; Thomas et al., 2016; Mueed et al., 2019). The exact role COX-2 plays in the various stages of the disease is still debated, with reports claiming both beneficial as well as detrimental effects of the enzyme in the various AD associated pathologies (Minghetti, 2004; Hoozemans et al., 2008). However, mTOR is mostly known to be hyperactivated in AD and causes excessive phosphorylation of tau protein and formation of Aβ plaques and NFTs (**Figure 4**). Both have been implicated in development of synaptic plasticity under physiological conditions (Minghetti, 2004; Papadopoli et al., 2019). Interconnected signaling and working of COX-2 and mTOR has been the subject of many studies in the case of various types of cancer (Chuang et al., 2019(H. Lipskar et al., 2009; Rouzer and Marnett, 2009; Li H. et al., 2016), but no such studies have yet been conducted for AD. Both cancer and AD have a faulty DNA damage repair mechanism at their core that causes uninhibited growth and neuronal loss, respectively (Behrens et al., 2009). Rapamycin has been found to exert anti-tumor and anti-angiogenic effects by inhibiting neovascularization (Guba et al., 2002; Phung et al., 2006). It can do this via either an mTOR-dependent or independent pathway. In case of the mTOR-independent pathway, the phosphorylation of downstream effectors of mTOR remains unchanged and other molecules including COX-2 are instead involved (Jung et al., 2003; Lipskar et al., 2009). Moreover, cancer and AD have been shown to manifest an inverse relationship via many cellular pathways and signaling molecules such as p53 and cAMP and hormones like estrogen, growth factors, neutrophins, etc (Shafi, 2016).

In yet another study carried out on endometrial cancer (EMC) on mouse models and human cell lines, it was established that both COX-2 and mTORC1 work cooperatively to reduce tumor load and exacerbate the cancer. This common signaling pathway also involved Akt as both COX-2 and mTORC1 are downstream targets of Akt (Gadducci et al., 2008; Jae et al., 2009; Slomovitz and Coleman, 2012; **Figure 4**). Although these studies have been limited to mostly cancer models, similar pathways could exist in case of AD as well. If the presence of such a connection between COX-2 and mTOR could be established in AD, it could be exploited as a therapeutic strategy.

As mentioned in previous sections, mTOR controls T-cell activation and innate immune responses. mTOR is also known to modulate COX-2 expression in immune reactions. An *in vitro* study conducted on enhancement of immunomodulatory effects of human bone marrow mesenchymal stem cells showed elevated levels of COX-2 and higher phosphorylation of kinases, GSK-3b, and Akt, upon mTOR inhibition by short-term (4 h) rapamycin treatment (Wang et al., 2017; **Figure 4**). However, COX-2 is significantly downregulated on longer rapamycin treatments. PGE2, which plays important roles in immunosuppression by inhibition of NK (natural killer) cell cytotoxicity, dendritic cell maturation, and T cell proliferation (Spaggiari et al., 2008; Wang et al., 2017), was also found to be upregulated (**Figure 4**). Apart from COX-2 being overexpressed during inflammatory reactions including AD and cancers, it is also known to resist apoptosis (Tsujii and DuBois, 1995). Similar to COX-2, mTOR is also thought to be involved in apoptosis and activation of cell cycle in post mitotic neurons (Pei and Hugon, 2008; **Figure 4**). Thus, NSAIDs and selective COX-2 inhibitors induce apoptosis. Two pathways have been suggested for this: stimulation of ceramide (a death signal) production by availability of higher amounts of AA (Chan et al., 1998), and downregulation of Bcl-2 (X. Liu et al., 1998; Sheng et al., 1998). Alternatively, a selective COX-2 inhibitor, celecoxib, is thought to induce apoptosis by selectively blocking Akt pathway (Hsu et al., 2000). However, the mechanism behind this remains elusive as celecoxib does not significantly affect the major kinase, PI-3K, or the phosphatase, protein phosphatase 2A, involved in the activation of Akt (Hsu et al., 2000). Interestingly, this might indicate another possible pathway by which COX-2 modulates mTOR signaling as Akt is one of the major upstream regulators of mTOR.

COX-2 AND mTOR-BASED THERAPIES

As discussed earlier, NSAIDs were found to be associated with a lower vulnerability to AD due to lowering levels of Aβ42 as well as reducing inflammation. A lot of studies have been conducted in this regard exploring different aspects of the disease development and progression. Various therapeutic approaches for AD have also been reviewed previously (Mueed et al., 2019).

It was found that selective COX-2 inhibitors could restore long term potentiating which was lost due to incubation with external Aβ42 in studies carried out in rat hippocampal slices, while inhibition of only COX-1 failed to produce any such effects (Kotilinek et al., 2008). The same study also reported regarding restoration of memory in Tg2576 mice over-expressing APP by both selective COX-2 inhibitors as well as non-selective NSAIDs. However, these beneficial effects of COX-2 inhibition were lost on addition of exogenous PGE2 but not by inflammatory cytokines like IL-1β, TNF-α, or even Aβ. Thus, the authors proposed an alternative mechanism of NSAID action on AD: preventing PGE2 response at synapses due to blockage of COX-2.

As previously stated, mTOR is known to be hyperactivated in an AD brain and exerts its effects by affecting key cellular processes such as nucleotide synthesis, protein synthesis, and modifications, mitochondrial dynamics, lipid metabolism and the cellular autophagic system. Therapies against AD and other neurodegenerative disorders have thus also targeted mTOR. Inhibition of mTOR using rapamycin and its analogs has shown reduction in the amounts of amyloid and tau deposits in early stage-AD-affected brains of mice and improved their cognitive abilities (Spilman et al., 2010; Majumder et al., 2011).

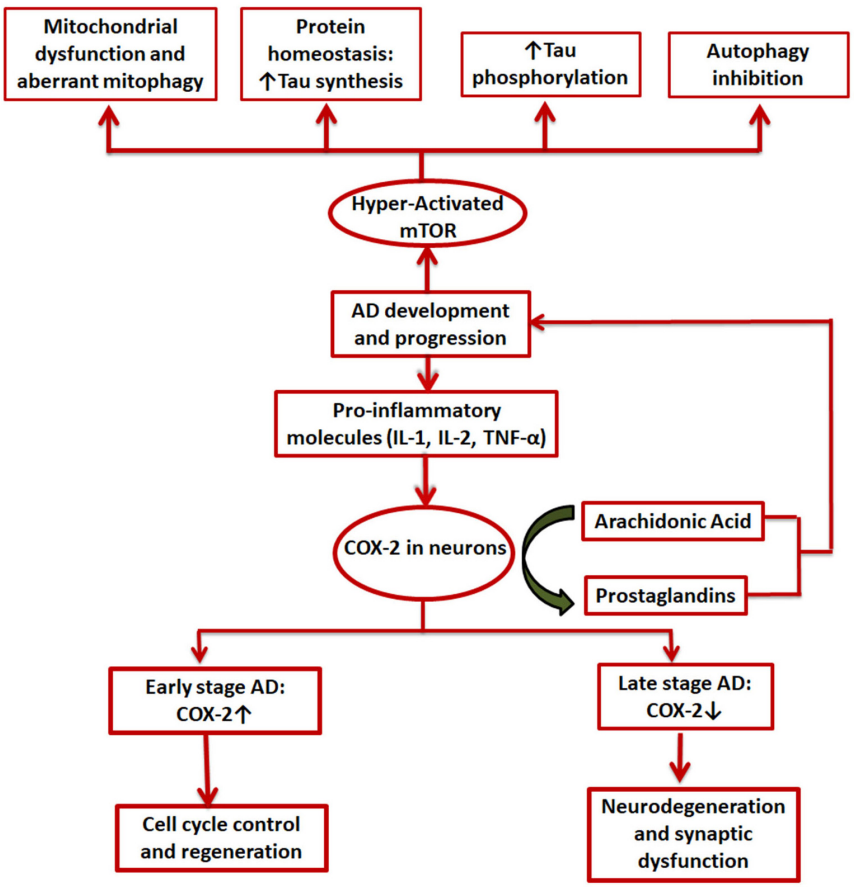

FIGURE 4 | Involvement of COX-2 and mTOR in AD. Pro-inflammatory molecules induce COX-2 expression in certain brain cells. It is upregulated in the initial stages of AD and is expected to be involved in cell cycle control and regenerative pathways while in the later stages a decline in COX-2 levels is seen, mainly due to degeneration of neurons by the disease; mTOR, on the other hand, is always hyperactivated in case of AD and exerts its effects in mainly 4 ways: mitochondrial dysfunction, aberrant proteostasis, tau hyperphosphorylation, and inhibition of autophagy.

In fact, humans who were administered with a rapamycin analog, everolimus, in order to elicit immunosuppression after a heart transplant also showed better memory skills than the control group (Papadopoli et al., 2019). mTOR overexpression has been routinely linked to intracellular tau accumulation and translocation. Its inhibition via rapamycin or silencing by mutation leads to lower tau levels in the cell (Tang et al., 2015). This has implications across various tauopathies and presents a potential therapeutic approach. mTOR inactivation has proved to be helpful in reducing microglial-inflammatory responses in the brain. Some of these studies have also shown a possible COX involvement in the process as rapamycin treated microglia also resulted in lower levels of COX-2 (Dello Russo et al., 2013).

COX-2 is also implicated in a variety of cancers (Hwang et al., 1998; Pandey et al., 2008; Greenhough et al., 2009; Alexanian et al., 2014; Mattsson et al., 2015) and its inhibition can also be used as one of the ways for cancer therapy. Tuberous sclerosis complex (TSC) caused as a result of mutations in any of the two tumor suppressor genes, *TSC1* and *TSC2*, leads to formation of localized tumor masses in multiple organs (Borkowska et al., 2011; Kwiatkowski and Manning, 2014; Schepis, 2016). mTORC1 is known to be hyperactivated by loss of TSC2 in TSC tumors (Moavero et al., 2015; Li H. et al., 2016). This leads to downregulation of COX-2 activity via activation of STAT3 (signal transducer and activator of transcription 3). It was also found that IL-6 is a downstream target of COX-2 in cells with loss-of-Tsc2 mutation and thus reduced activity of COX-2 inhibits IL-6 which limits cellular proliferation (Li H. et al., 2016). Rapamycin and celecoxib, together, were found to be most useful against TSC in Tsc2 negative cells, than either individually (Li H. et al., 2016).

CONCLUSION AND FUTURE PERSPECTIVES

COX-2 is involved in diverse cellular functions in the human body such as PG synthesis, insulin secretion, adipogenesis, CNS autonomic regulation, etc., and thus, any structural or functional aberrations in the enzyme will have varied repercussions across many pathways. Many inflammatory and neoplastic disorders are related to COX-2 expression levels and activity. Similarly, mTOR affects central cellular activities such as growth,

transcription, and translation. It has also been found to play a vital role in inflammatory and age-related diseases. COX-2 and mTOR operate in a number of overlapping pathways such as nutrient sensing, obesity, apoptosis, immune reactions, osmoprotection, etc.

Alzheimer's is one of the world's leading types of dementia and a neuro-inflammatory disease. COX-2 has been classically implicated in AD and much research has been done to develop therapies against AD based on blocking or deleting COX-2. However, it has been known for some time now that neither the cause of AD nor the role COX-2 plays in its occurrence and progression is as it was traditionally considered. There have been many views rejecting the amyloid as well as tau hypotheses to be at the heart of AD. Also, COX-2 is now thought to have pleiotropic effects in the brain and AD pathophysiology as the enzyme exhibits different expression levels during different stages of the disease with elevated levels in the early stages and a gradual fall later on. Moreover, other molecular targets of NSAIDs rather than the COX enzymes are being considered as possible key players in AD. Thus, in order to effectively tackle AD, it has to be considered in its entirety and not as isolated underlying pathways.

mTOR entered the AD picture as a molecule of interest quite recently but it has since been well established in AD pathology. It is supposedly overexpressed in AD, promotes amyloid- as well as tau-deposition, and is also involved in their targeting to various cell organelles to a certain extent. Inhibition of mTOR *in vitro* and *in vivo* models of AD has demonstrated improved memory and other cognitive abilities which are compromised in the disease.

The main aim of this review was to explore the biphasic nature of relationship between COX-2 and mTOR in key cellular processes, some of which have direct roles in AD progression. This suggests a very strong possibility that their relationship could be exploited in order to develop an effective counter for AD. Moreover, their actions have already been found to be inter-dependent in the case of a number of cancers, and anti-cancer therapies targeting the two of them are underway. However, dedicated studies in this direction in the case of AD are still, to the best of our knowledge, non-existent. The possible future prospective in this direction would include exploring in detail selected targets of interest, such as Akt, and all their associated pathways which may provide specific answers as to if and how COX-2 and mTOR co-operate in AD and if drugs targeting either or both of these would be helpful in combating the disease.

AUTHOR CONTRIBUTIONS

AT wrote the manuscript. NP made the background of the manuscript and finalized the manuscript. MK gave valuable comments and help in writing the manuscript. All authors contributed to the article and approved the submitted version.

FUNDING

This work was supported by Enhanced Seed grant EF/2019-20/QE04-02 to NP from Manipal University Jaipur, Rajasthan, India is gratefully acknowledged.

REFERENCES

Aisen, P. S. (2002). The potential of anti-inflammatory drugs for the treatment of Alzheimer's disease. *Lancet Neurol.* 1, 279–284. doi: 10.1016/S1474-4422(02)00133-3

Alexanian, A., Miller, B., Chesnik, M., Mirza, S., and Sorokin, A. (2014). Post-translational regulation of COX2 activity by FYN in prostate cancer cells. *Oncotarget* 5, 4232–4243. doi: 10.18632/oncotarget.1983

Alonso, A. D. C., Zaidi, T., Novak, M., Grundke-Iqbal, I., and Iqbal, K. (2001). Hyperphosphorylation induces self-assembly of tau into tangles of paired helical filaments/straight filaments. *Proc. Natl. Acad. Sci. U.S.A.* 98, 6923–6928. doi: 10.1073/pnas.121119298

An, W. L., Cowburn, R. F., Li, L., Braak, H., Alafuzoff, I., Iqbal, K., et al. (2003). Up-regulation of phosphorylated/activated p70 S6 kinase and its relationship to neurofibrillary pathology in Alzheimer's disease. *Am. J. Pathol.* 163, 591–607. doi: 10.1016/S0002-9440(10)63687-5

Balsinde, J., Balboa, M. A., and Dennis, E. A. (1998). Functional coupling between secretory phospholipase A2 and cyclooxygenase-2 and its regulation by cytosolic group IV phospholipase A2. *Proc. Nalt. Acad. Sci. U.S.A.* 95, 7951–7956. doi: 10.1073/pnas.95.14.7951

Bazan, N. G. (2003). Synaptic lipid signaling: significance of polyunsaturated fatty acids and platelet-activating factor. *J. Lipid Res.* 44, 2221–2233. doi: 10.1194/jlr.R300013-JLR200

Bazan, N. G., Colangelo, V., and Lukiw, W. J. (2002). Prostaglandins and other lipid mediators in Alzheimer's disease. *Prostag. Oth. Lipid M* 68–69, 197–210. doi: 10.1016/S0090-6980(02)00031-X

Behrens, M., Lendon, C., and Roe, C. (2009). A common biological mechanism in cancer and Alzheimers disease? *Curr. Alzheimer Res.* 6, 196–204. doi: 10.2174/156720509788486608

Ben-Sahra, I., Howell, J. J., Asara, J. M., and Manning, B. D. (2013). Stimulation of de Novo pyrimidine synthesis by growth signaling through mTOR and S6K1. *Science* 339, 1323–1328. doi: 10.1126/science.1228792

Bhaskar, K., Miller, M., Chludzinski, A., Herrup, K., Zagorski, M., and Lamb, B. T. (2009). The PI3K-Akt-mTOR pathway regulates a oligomer induced neuronal cell cycle events. *Mol. Neurodegener.* 4, 1–18. doi: 10.1186/1750-1326-4-14

Bidgood, M. J., Jamal, O. S., Cunningham, A. M., Brooks, P. M., and Scott, K. F. (2000). Type IIA Secretory Phospholipase A 2 Up-Regulates Cyclooxygenase-2 and Amplifies Cytokine-Mediated Prostaglandin Production in Human Rheumatoid Synoviocytes. *J. Immunol.* 165, 2790–2797. doi: 10.4049/jimmunol.165.5.2790

Blalock, E. M., Geddes, J. W., Chen, K. C., Porter, N. M., Markesbery, W. R., and Landfield, P. W. (2004). Incipient Alzheimer's disease: microarray correlation analyses reveal major transcriptional and tumor suppressor responses. *Proc. Natl. Acad. Sci. U.S.A.* 101, 2173–2178. doi: 10.1073/pnas.0308512100

Blum-Degena, D., Müller, T., Kuhn, W., Gerlach, M., Przuntek, H., and Riederer, P. (1995). Interleukin-1β and interleukin-6 are elevated in the cerebrospinal fluid of Alzheimer's and de novo Parkinson's disease patients. *Neurosci. Lett.* 202, 17–20. doi: 10.1016/0304-3940(95)12192-7

Borkowska, J., Schwartz, R. A., Kotulska, K., and Jozwiak, S. (2011). Tuberous sclerosis complex: tumors and tumorigenesis. *Int. J. Dermatol.* 50, 13–20. doi: 10.1111/j.1365-4632.2010.04727.x

Boström, P., Wu, J., Jedrychowski, M. P., Korde, A., Ye, L., Lo, J. C., et al. (2012). A PGC1-α-dependent myokine that drives brown-fat-like development of white fat and thermogenesis. *Nature* 481, 463–468. doi: 10.1038/nature10777

Braak, H., and Braak, E. (1991). Neuropathological stageing of Alzheimer-related changes. *Acta Neuropathol.* 82, 239–259. doi: 10.1007/bf00308809

Breitner, J. C. S. (1996). The role of anti-inflammatory drugs in the prevention and treatment of Alzheimer's disease. *Annu. Rev. Med.* 47, 401–411. doi: 10.1146/annurev.med.47.1.401

Briggs, J. P. (1999). Regulation of cyclooxygenase-2 expression in renal medulla by tonicity in vivo and in vitro. *Am. J. Physiol. Renal Physiol.* 277, 1–9. doi: 10.1152/ajprenal.1999.277.1.f1

Brocker, C., Thompson, D. C., and Vasiliou, V. (2012). The role of hyperosmotic stress in inflammation and disease. *Biomol. Concepts* 3, 345–364. doi: 10.1515/bmc-2012-0001

Burg, M. B., Ferraris, J. D., and Dmitrieva, N. I. (2007). Cellular response to hyperosmotic stresses. *Physiol. Rev.* 87, 1441–1474. doi: 10.1152/physrev.00056.2006

Burke, J. E., and Dennis, E. A. (2009). Phospholipase A 2 structure/function, mechanism, and signaling. *J. Lipid Res.* 50, 237–242. doi: 10.1194/jlr.R800033-JLR200

Camacho, I. E., Serneels, L., Spittaels, K., Merchiers, P., Dominguez, D., and De Strooper, B. (2004). Peroxisome proliferator-activated receptor γ induces a clearance mechanism for the amyloid-β peptide. *J. Neurosci.* 24, 10908–10917. doi: 10.1523/JNEUROSCI.3987-04.2004

Chan, T. A., Morin, P. J., Vogelstein, B., and Kinzler, K. W. (1998). Mechanisms underlying nonsteroidal antiinflammatory drug-mediated apoptosis. *Proc. Natl. Acad. Sci. U.S.A.* 95, 681–686. doi: 10.1073/pnas.95.2.681

Choi, H., Chaiyamongkol, W., Doolittle, A. C., Johnson, Z. I., Gogate, S. S., Schoepflin, Z. R., et al. (2018). COX-2 expression mediated by calcium-TonEBP signaling axis under hyperosmotic conditions serves osmoprotective function in nucleus pulposus cells. *J. Biol. Chem.* 293, 869–8981. doi: 10.1074/jbc.RA117.001167

Chuang, S., Lu, J., Lin, K., Long, C., Lee, Y., Hsiao, H., et al. (2019). Epigenetic regulation of COX-2 expression by DNA hypomethylation via NF-κB activation in ketamine-induced ulcerative cystitis. *Int. J. Mol. Med.* 44, 797–812. doi: 10.3892/ijmm.2019.4252

Clària, J. (2003). Cyclooxygenase-2 biology. *Curr. Pharm.* 9, 2177–2190. doi: 10.2174/1381612033454054

Cohen, P., Levy, J. D., Zhang, Y., Frontini, A., Kolodin, D. P., Svensson, K. J., et al. (2014). Ablation of PRDM16 and beige adipose causes metabolic dysfunction and a subcutaneous to visceral fat switch. *Cell* 156, 304–316. doi: 10.1016/j.cell.2013.12.021

Cuervo, A. M., Bergamini, E., Brunk, U. T., Dröge, W., Ffrench, M., and Terman, A. (2005). Autophagy and aging: the importance of maintaining "clean" cells. *Autophagy* 1, 131–140. doi: 10.4161/auto.1.3.2017

De Felice, F. G. (2013). Alzheimer's disease and insulin resistance: translating basic science into clinical applications. *J. Clin. Invest.* 123, 531–539. doi: 10.1172/JCI64595

Delgoffe, G. M., Kole, T. P., Zheng, Y., Zarek, P. E., Matthews, K. L., Worley, P. F., et al. (2010). mTOR differentially regulates effector and regulatory T cell lineage commitment. *Immunity* 30, 832–844. doi: 10.1016/j.immuni.2009.04.014.mTOR

Dello Russo, C., Lisi, L., Feinstein, D. L., and Navarra, P. (2013). mTOR kinase, a key player in the regulation of glial functions: relevance for the therapy of multiple sclerosis. *Glia* 61, 301–311. doi: 10.1002/glia.22433

Dibble, C. C., Elis, W., Menon, S., Qin, W., Klekota, J., Asara, J. M., et al. (2012). TBC1D7 Is a Third Subunit of the TSC1-TSC2 Complex Upstream of mTORC1. *Mol. Cell* 47, 535–546. doi: 10.1016/j.molcel.2012.06.009

Dinchuk, J. E., Car, B. D., Focht, R. J., Johnston, J. J., Jaffee, B. D., Covington, M. B., et al. (1995). Renal abnormalities and an altered inflammatory response in mice lacking cyclooxygenase II. *Nature* 378, 406–409. doi: 10.1038/378406a0

Efeyan, A., Zoncu, R., and Sabatini, D. M. (2013). Amino acids and mTORC1: from lysosomes to disease mTOR in growth control. *Trends Mol. Med.* 18, 524–533. doi: 10.1016/j.molmed.2012.05.007

Eltschinger, S., and Loewith, R. (2016). TOR Complexes and the Maintenance of Cellular Homeostasis. *Trends Cell Biol.* 26, 148–159. doi: 10.1016/j.tcb.2015.10.003

Emmanuel, N., Ragunathan, S., Shan, Q., Wang, F., Giannakou, A., Huser, N., et al. (2017). Purine nucleotide availability regulates mTORC1 Activity through the Rheb GTPase. *Cell Rep.* 19, 2665–2680. doi: 10.1016/j.celrep.2017.05.043

Engelborghs, S., Gilles, C., Ivanoiu, A., and Vandewoude, M. (2014). Rationale and clinical data supporting nutritional intervention in Alzheimer's disease. *Acta Clin. Belg.* 69, 17–24. doi: 10.1179/0001551213Z.0000000006

Engelking, L. R. (Ed.) (2015). "Eicosanoids I," in *Textbook of Veterinary Physiological Chemistry*, (Cambridge, MA: Academic Press), 434–438. doi: 10.1016/b978-0-12-391909-0.50068-2

Eriksen, J. L., Sagi, S. A., Smith, T. E., Weggen, S., Das, P., Mclendon, D. C., et al. (2003). NSAIDs and enantiomers of flurbiprofen target γ-secretase and lower Aβ42 in vivo. *J. Clin. Invest.* 112, 440–449. doi: 10.1172/JCI200318162

Fan, S. J., Snell, C., Turley, H., Li, J. L., McCormick, R., Perera, S. M. W., et al. (2016). PAT4 levels control amino-acid sensitivity of rapamycin-resistant mTORC1 from the Golgi and affect clinical outcome in colorectal cancer. *Oncogene* 35, 3004–3015. doi: 10.1038/onc.2015.363

Favale, N. O., Casali, C. I., Lepera, L. G., Pescio, L. G., and Fernández-Tome, M. C. (2009). Hypertonic induction of COX2 expression requires TonEBP/NFAT5 in renal epithelial cells. *Biochem. Biophy. Res. Comm.* 381, 301–305. doi: 10.1016/j.bbrc.2008.12.189

Favale, N. O., Sterin Speziale, N. B., and Fernández Tome, M. C. (2007). Hypertonic-induced lamin A/C synthesis and distribution to nucleoplasmic speckles is mediated by TonEBP/NFAT5 transcriptional activator. *Biochem. Biophys. Res. Comm.* 364, 443–449. doi: 10.1016/j.bbrc.2007.10.054

Ferreira, L. S. S., Fernandes, C. S., Vieira, M. N. N., and De Felice, F. G. (2018). Insulin resistance in Alzheimer's disease. *Front. Neurosci.* 12:830. doi: 10.3389/fnins.2018.00830

Fjaere, E., Aune, U. L., Røen, K., Keenan, A. H., Ma, T., Borkowski, K., et al. (2014). Indomethacin treatment prevents high fat diet-induced obesity and insulin resistance but not glucose intolerance in C57BL/6J mice. *J. Biol. Chem.* 289, 16032–16045. doi: 10.1074/jbc.M113.525220

Forny-Germano, L., De Felice, F. G., and Do Nascimento Vieira, M. N. (2019). The role of leptin and adiponectin in obesity-associated cognitive decline and Alzheimer's disease*. *Front.Neurosci.* 13:1027. doi: 10.3389/fnins.2018.01027

Fukunaga, K., Kohli, P., Bonnans, C., Fredenburgh, L. E., and Levy, B. D. (2005). Cyclooxygenase 2 Plays a Pivotal Role in the Resolution of Acute Lung Injury. *J. Immunol.* 174, 5033–5039. doi: 10.4049/jimmunol.174.8.5033

Gadducci, A., Tana, R., Cosio, S., Fanucchi, A., and Genazzani, A. R. (2008). Molecular target therapies in endometrial cancer: from the basic research to the clinic. *Gynecol. Endocrinol.* 24, 239–249. doi: 10.1080/09513590801953556

Goberdhan, D. C. I. (2010). Intracellular amino acid sensing and mTORC1-regulated growth: new ways to block an old target? *Curr. Opin. Invest. Drugs* 11, 1360–1367.

Goberdhan, D. C. I., Meredith, D., Boyd, C. A. R., and Wilson, C. (2005). PAT-related amino acid transporters regulate growth via a novel mechanism that does not require bulk transport of amino acids. *Development* 132, 2365–2375. doi: 10.1242/dev.01821

Goberdhan, D. C. I., Wilson, C., and Harris, A. L. (2016). Amino Acid Sensing by mTORC1: intracellular transporters mark the spot. *Cell Metab.* 23, 580–589. doi: 10.1016/j.cmet.2016.03.013

Greenhough, A., Smartt, H. J. M., Moore, A. E., Roberts, H. R., Williams, A. C., Paraskeva, C., et al. (2009). The COX-2/PGE2 pathway: key roles in the hallmarks of cancer and adaptation to the tumour microenvironment. *Carcinogenesis* 30, 377–386. doi: 10.1093/carcin/bgp014

Grundke-Iqbal, I., Iqbal, K., and Tung, Y. C. (1986). Abnormal phosphorylation of the microtubule-associated protein τ (tau) in Alzheimer cytoskeletal pathology. *Proc. Natl. Acad. Sci. U.S.A.* 83, 44913–44917. doi: 10.1073/pnas.83.13.4913

Guan, Y., Chang, M., Cho, W., Zhang, Y., Redha, R., Davis, L., et al. (1997). Cloning, expression, and regulation cyclooxygenase-2 in renal medullary of rabbit interstitial cells. *Am. J. Physiol.* 273, F18–F26. doi: 10.1152/ajprenal.1997.273.1.F18

Guba, M., Breitenbuch, P., von, Steinabauer, M., Koehl, G., Flegel, S., Hornung, M., et al. (2002). Rapamycin inhibits primary and metastatic tumor growth by antiangiogenesis: involvement of vascular endothelial growth factor. *Nat. Med.* 8, 128–135. doi: 10.1038/nm0202-128

Hahr, J. Y. (2015). Physiology of the Alzheimer's disease. *Med. Hypotheses* 85, 944–946. doi: 10.1016/j.mehy.2015.09.005

Hanna, V. S., and Hafez, E. A. A. (2018). Synopsis of arachidonic acid metabolism: a review. *J. Adv. Res.* 11, 23–32. doi: 10.1016/j.jare.2018.03.005

Harms, M., and Seale, P. (2013). Brown and beige fat: development, function and therapeutic potential. *Nat. Med.* 19, 1252–1263. doi: 10.1038/nm.3361

Harris, R. C., McKanna, J. A., Akai, Y., Jacobson, H. R., Dubois, R. N., and Breyer, M. D. (1994). Cyclooxygenase-2 is associated with the macula densa of rat kidney and increases with salt restriction. *J. Clin. Invest.* 94, 2504–2510. doi: 10.1172/JCI117620

Haung Yu, W., Cuervo, A. M., Kumar, A., Peterhoff, C. M., Schmidt, S. D., Lee, J. H., et al. (2005). Macroautophagy - A novel β-amyloid peptide-generating pathway activated in Alzheimer's disease. *J. Cell Biol.* 171, 87–98. doi: 10.1083/jcb.200505082

Heafield, M. T., Fearn, S., Steventon, G. B., Waring, R. H., Williams, A. C., and Sturman, S. G. (1990). Plasma cysteine and sulphate levels in patients with motor neurone, Parkinson's and Alzheimer's disease. *Neurosci. Lett.* 110, 216–220. doi: 10.1016/0304-3940(90)90814-P

Ho, L., Purohit, D., Haroutunian, V., Luterman, J. D., Willis, F., Naslund, J., et al. (2001). Neuronal cyclooxygenase 2 expression in the hippocampal formation as a function of the clinical progression of Alzheimer disease. *Arch. Neurol.* 58, 487–492. doi: 10.1001/archneur.58.3.487

Hölscher, C. (1995). Inhibitors of cyclooxygenases produce amnesia for a passive avoidance task in the chick. *Eur. J. Neurosci.* 7, 1360–1365. doi: 10.1111/j.1460-9568.1995.tb01127.x

Hoozemans, J., Rozemuller, J., van Haastert, E., Veerhuis, R., and Eikelenboom, P. (2008). Cyclooxygenase-1 and -2 in the different stages of alzheimers disease pathology. *Curr. Pharm. Des.* 14, 1419–1427. doi: 10.2174/138161208784480171

Hoozemans, J. J. M., Brückner, M. K., Rozemuller, A. J. M., Veerhuis, R., Eikelenboom, P., and Arendt, T. (2002). Cyclin D1 and cyclin E are co-localized with cyclo-oxygenase 2 (COX-2) in pyramidal neurons in Alzheimer disease temporal cortex. *J. Neuropathol. Exp. Neurol.* 61, 678–688. doi: 10.1093/jnen/61.8.678

Hoozemans, J. J. M., Rozemuller, A. J. M., Janssen, I., De Groot, C. J. A., Veerhuis, R., and Eikelenboom, P. (2001). Cyclooxygenase expression in microglia and neurons in Alzheimer's disease and control brain. *Acta Neuropathol.* 101, 2–8. doi: 10.1016/s0197-4580(00)82335-0

Hoozemans, J. J. M., Veerhuis, R., Rozemuller, A. J. M., Arendt, T., and Eikelenboom, P. (2004). Neuronal COX-2 expression and phosphorylation of pRb precede p38 MAPK activation and neurofibrillary changes in AD temporal cortex. *Neurobiol. Dis.* 15, 492–499. doi: 10.1016/j.nbd.2003.11.028

Hoozemans, J. J. M., Veerhuis, R., Rozemuller, J. M., and Eikelenboom, P. (2006). Neuroinflammation and regeneration in the early stages of Alzheimer's disease pathology. *Int. J. Dev. Neurosci.* 24, 157–165. doi: 10.1016/j.ijdevneu.2005.11.001

Howie, D., Waldmann, H., and Cobbold, S. P. (2014). Nutrient sensing via mTOR in T cells maintains a tolerogenic microenvironment. *Front. Immunol.* 5:409. doi: 10.3389/fimmu.2014.00409

Hoxhaj, G., Hughes-Hallett, J., Timson, R. C., Ilagan, E., Yuan, M., Asara, J. M., et al. (2017). The mTORC1 signaling network senses changes in cellular purine nucleotide levels. *Cell Rep.* 21, 1331–1346. doi: 10.1016/j.celrep.2017.10.029

Hsu, A. L., Ching, T. T., Wang, D. S., Song, X., Rangnekar, V. M., and Chen, C. S. (2000). The cyclooxygenase-2 inhibitor celecoxib induces apoptosis by blocking Akt activation in human prostate cancer cells independently of Bcl-2. *J. Biol. Chem.* 275, 11397–11403. doi: 10.1074/jbc.275.15.11397

Hwang, D., Scollard, D., Byrne, J., and Levine, E. (1998). Expression of cyclooxygenase-1 and cyclooxygenase-2 in human breast cancer. *J. Natl. Cancer Inst.* 90, 455–460. doi: 10.1093/jnci/90.6.455

Iglesias-Bartolome, R., Patel, V., Cotrim, A., Leelahavanichkul, K., Molinolo, A. A., Mitchell, J. B., et al. (2012). mTOR inhibition prevents epithelial stem cell senescence and protects from radiation-induced mucositis. *Cell Stem Cell* 11, 401–414. doi: 10.1016/j.stem.2012.06.007

Jae, H. N., Jeon, Y. T., Park, I. A., Kang, D., Jae, W. K., Park, N. H., et al. (2009). Expression of mTOR protein and its clinical significance in endometrial cancer. *Med. Sci. Monit.* 15, 301–305.

Jewell, J. L., Kim, Y. C., Russell, R. C., Yu, F.-X., Park, H. W., Plouffe, S. W., et al. (2015). Differential regulation of mTORC1 by leucine and glutamine. *Sci. Exp.* 347, 194–198. doi: 10.1126/science.1259472

Jung, Y., Isaacs, J. S., Lee, S., Trepel, J., and Neckers, L. (2003). IL-1β mediated up-regulation of HIF-1α via an NFkB/COX- 2 pathway identifies HIF-1 as a critical link between inflammation and oncogenesis. *FASEB J.* 17, 2115–2117. doi: 10.1096/fj.03-0329fje

Kang, Y.-J., Mbonye, U. R., DeLong, C. J., Wada, M., and Smith, W. L. (2007). Regulation of Intracellular Cyclooxygenase Levels by Gene Transcription and Protein Degradation. *Prog. Lipid Res.* 46, 108–125. doi: 10.1016/j.plipres.2007.01.001

Kaufmann, W. E., Andreasson, K. I., Isakson, P. C., and Worley, P. F. (1997). Cyclooxygenases and the central nervous system. *Prostaglandins* 54, 601–624. doi: 10.1016/S0090-6980(97)00128-7

Khamzina, L., Veilleux, A., Bergeron, S., and Marette, A. (2005). Increased activation of the mammalian target of rapamycin pathway in liver and skeletal muscle of obese rats: possible involvement in obesity-linked insulin resistance. *Endocrinology* 146, 1473–1481. doi: 10.1210/en.2004-0921

Kikuchi, T., Itoh, F., Toyota, M., Suzuki, H., Yamamoto, H., Fujita, M., et al. (2002). Aberrant methylation and histone deacetylation of cyclooxygenase 2 in gastric cancer. *Int. J. Cancer* 97, 272–277. doi: 10.1002/ijc.1612

Kim, S. H., Yan, Y. B., and Zhou, H. M. (2006). Role of osmolytes as chemical chaperones during the refolding of aminoacylase. *Biochem. Cell Biol.* 84, 30–38. doi: 10.1139/o05-148

Kitamura, Y., Shimohama, S., Koike, H., Kakimura, J. I., Matsuoka, Y., Nomura, Y., et al. (1999). Increased expression of cyclooxygenases and peroxisome proliferator-activated receptor-γ in Alzheimer's disease brains. *Biochem. Biophys. Res. Commun.* 254, 582–586. doi: 10.1006/bbrc.1998.9981

Kotilinek, L. A., Westerman, M. A., Wang, Q., Panizzon, K., Lim, G. P., Simonyi, A., et al. (2008). Cyclooxygenase-2 inhibition improves amyloid-β-mediated suppression of memory and synaptic plasticity. *Brain* 131, 651–664. doi: 10.1093/brain/awn008

Kwiatkowski, D. J., and Manning, B. D. (2014). Molecular basis of giant cells in tuberous sclerosis complex. *N. Engl. J. Med.* 371, 778–780. doi: 10.1056/NEJMcibr1406613

Laplante, M., and Sabatini, D. M. (2012). MTOR signaling in growth control and disease. *Cell* 149, 274–293. doi: 10.1016/j.cell.2012.03.017

Latham, C. F., Osborne, S. L., Cryle, M. J., and Meunier, F. A. (2007). Arachidonic acid potentiates exocytosis and allows neuronal SNARE complex to interact with Munc18a. *J. Neurochem.* 100, 1543–1554. doi: 10.1111/j.1471-4159.2006.04286.x

Lee, K., Gudapati, P., Dragovic, S., Spencer, C., Killeen, N., Magnuson, M. A., et al. (2010). Mammalian target of rapamycin protein complex 2 regulates differentiation of Th1 and Th2 cell subsets via distinct signaling pathways. *Immunity* 32, 743–753. doi: 10.1016/j.immuni.2010.06.002

Li, D., Misialek, J. R., Boerwinkle, E., Gottesman, R. F., Sharrett, A. R., Mosley, T. H., et al. (2016). Plasma phospholipids and prevalence of mild cognitive impairment and/or dementia in the ARIC Neurocognitive Study (ARIC-NCS). *Alzheimer's Dement* 3, 73–82. doi: 10.1016/j.dadm.2016.02.008

Li, H., Jin, F., Jiang, K., Ji, S., Wang, L., Ni, Z., et al. (2016). mTORC1-mediated downregulation of COX2 restrains tumor growth caused by TSC2 deficiency. *Oncotarget* 7, 28435–28447. doi: 10.18632/oncotarget.8633

Lipskar, A. M., Glick, R. D., Huang, J., Fisher, J. C., DeVoti, J., Pica, R., et al. (2009). Cyclooxygenase 2 mediates the antiangiogenic effect of rapamycin in Ewing sarcoma. *J. Pediatr. Surg.* 44, 1139–1147. doi: 10.1016/j.jpedsurg.2009.02.037

Liu, D., Bordicchia, M., Zhang, C., Fang, H., Wei, W., Li, J., et al. (2016). Activation of mTORC1 is essential for βadrenergic stimulation of adipose browning. *J. Clin. Invest.* 126, 1704–1716. doi: 10.1172/JCI83532

Liu, M., Bai, J., He, S., Villarreal, R., Hu, D., Zhang, C., et al. (2014). Grb10 promotes lipolysis and thermogenesis by phosphorylation-dependent feedback inhibition of mTORC1. *Cell Metab.* 19, 967–980. doi: 10.1016/j.cmet.2014.03.018

Liu, X., Yao, S., Kirschenbaum, A., and Levine, A. C. (1998). NS398, a Selective Cyclooxygenase-2 inhibitor, induces apoptosis and down- regulates bcl-2 expression in LNCaP cells. *Am. Ass. Cancer Res.* 58, 4245–4249.

López-otín, C., Blasco, M. A., Partridge, L., Serrano, M., and Kroemer, G. (2013). The hallmarks of aging longevity. *Cell* 153, 1194–1217. doi: 10.1016/j.cell.2013.05.039.The

Luo, J., Wärmländer, S. K. T. S., Gräslund, A., and Abrahams, J. P. (2016). Cross-interactions between the Alzheimer disease amyloid-β peptide and other amyloid proteins: a further aspect of the amyloid cascade hypothesis. *J. Biol. Chem.* 291, 16485–16493. doi: 10.1074/jbc.R116.714576

Ma, X., Yang, Q., Wilson, K. T., Kundu, N., Meltzer, S. J., and Fulton, A. M. (2004). Promoter methylation regulates cyclooxygenase expression in breast cancer. *Breast Cancer Res.* 6, 316–321. doi: 10.1186/bcr793

Macknight, A. D. C. (1988). Principles of cell volume regulation. *Renal Physiol. Biochem.* 11, 114–141. doi: 10.1159/000173158

Madsen, L., Pedersen, L. M., Liaset, B., Ma, T., Petersen, R. K., Van Den Berg, S., et al. (2008). cAMP-dependent signaling regulates the adipogenic effect of n-6 polyunsaturated fatty acids. *J. Biol. Chem.* 283, 7196–7205. doi: 10.1074/jbc.M707775200

Majumder, S., Richardson, A., Strong, R., and Oddo, S. (2011). Inducing autophagy by rapamycin before, but not after, the formation of plaques and tangles ameliorates cognitive deficits. *PLoS One* 6:e25416. doi: 10.1371/journal.pone.0025416

Maskrey, B. H., Megson, I. L., Whitfield, P. D., and Rossi, A. G. (2011). Mechanisms of resolution of inflammation: a focus on cardiovascular disease. *Arterioscler. Thromb. Vasc. Biol.* 31, 1001–1006. doi: 10.1161/ATVBAHA.110.213850

Mattsson, J. S. M., Bergman, B., Grinberg, M., Edlund, K., Marincevic, M., Jirström, K., et al. (2015). Prognostic impact of COX-2 in non-small cell lung cancer: a comprehensive compartment-specific evaluation of tumor and stromal cell expression. *Cancer Lett.* 356, 837–845. doi: 10.1016/j.canlet.2014.10.032

Miettinen, S., Fusco, F. R., Yrjänheikki, J., Keinänen, R., Hirvonen, T., Roivainen, R., et al. (1997). Spreading depression and focal brain ischemia induce cyclooxygenase-2 in cortical neurons through N-methyl-D-aspartic acid-receptors and phospholipase A2. *Proc. Natl. Acad. Sci. U.S.A.* 94, 6500–6505. doi: 10.1073/pnas.94.12.6500

Minghetti, L. (2004). Cyclooxygenase-2 (COX-2) in inflammatory and degenerative brain diseases. *J. Neuropathol. Exp. Neurol.* 63, 901–910. doi: 10.1093/jnen/63.9.901

Moavero, R., Romagnoli, G., Graziola, F., and Curatolo, P. (2015). Mammalian target of rapamycin inhibitors and life-threatening conditions in tuberous sclerosis complex. *Semin. Pediatr. Neurol.* 22, 282–294. doi: 10.1016/j.spen.2015.10.006

Moeckel, G. W., Zhang, L., Fogo, A. B., Hao, C.-M., and Breyer, M. D. (2003). COX2-activity promotes organic osmolyte accumulation and adaptation of Renal Medullary Interstitial Cells to hypertonic stress. *J. Biol. Chem.* 278, 19352–19357. doi: 10.1074/jbc.M302209200

Morihara, T., Chu, T., Ubeda, O., Beech, W., and Cole, G. M. (2002). Selective inhibition of Aβ42 production by NSAID R-enantiomers. *J. Neurochem.* 83, 1009–1012. doi: 10.1046/j.1471-4159.2002.01195.x

Mueed, Z., Tandon, P., Maurya, S. K., Deval, R., Kamal, M. A., and Poddar, N. K. (2019). Tau and mTOR: the hotspots for multifarious diseases in Alzheimer's development. *Front. Neurosci.* 13:1017. doi: 10.3389/fnins.2018.01017

Murakami, M., Kuwata, H., Amakasu, Y., Shimbara, S., Nakatani, Y., Atsumi, G. I., et al. (1997). Prostaglandin E2 amplifies cytosolic phospholipase A2- and cyclooxygenase-2-dependent delayed prostaglandin E2 generation in mouse osteoblastic cells. Enhancement by secretory phospholipase A2. *J. Bio. Chem.* 272, 19891–19897. doi: 10.1074/jbc.272.32.19891

Ortega-Gómez, A., Perretti, M., and Soehnlein, O. (2013). Resolution of inflammation: an integrated view. *EMBO Mol. Med.* 5, 661–674. doi: 10.1002/emmm.201202382

Pan, X., Nasaruddin, M. B., Elliott, C. T., McGuinness, B., Passmore, A. P., Kehoe, P. G., et al. (2016). Alzheimer's disease-like pathology has transient effects on the brain and blood metabolome. *Neurobiol. Aging* 38, 151–163. doi: 10.1016/j.neurobiolaging.2015.11.014

Pandey, M., Prakash, O., Santhi, W. S., Soumithran, C. S., and Pillai, R. M. (2008). Overexpression of COX-2 gene in oral cancer is independent of stage of disease and degree of differentiation. *Int. J. Oral Maxillofac. Surg.* 37, 379–383. doi: 10.1016/j.ijom.2008.01.004

Papadopoli, D., Boulay, K., Kazak, L., Pollak, M., Mallette, F., Topisirovic, I., et al. (2019). mTOR as a central regulator of lifespan and aging. *F1000Res* 8:998. doi: 10.12688/f1000research.17196.1

Pasinetti, G. M., and Aisen, P. S. (1998). Cyclooxygenase-2 expression is increased in frontal cortex of Alzheimer's disease brain. *Science* 87, 319–324. doi: 10.1016/S0306-4522(98)00218-8

Pei, J. J., Björkdahl, C., Zhang, H., Zhou, X., and Winblad, B. (2008). p70 S6 kinase and tau in Alzheimer's disease. *J. Alzheimer's Dis.* 14, 385–392. doi: 10.3233/JAD-2008-14405

Pei, J. J., and Hugon, J. (2008). mTOR-dependent signalling in Alzheimer's disease. *J. Cell. Mol. Med.* 12, 2525–2532. doi: 10.1111/j.1582-4934.2008.00509.x

Perluigi, M., Di Domenico, F., and Butterfield, D. A. (2015). mTOR signaling in aging and neurodegeneration: at the crossroad between metabolism dysfunction and impairment of autophagy. *Neurobiol. Dis.* 84, 39–49. doi: 10.1016/j.nbd.2015.03.014

Pesini, A., Iglesias, E., Bayona-Bafaluy, M. P., Garrido-Pérez, N., Meade, P., Gaudó, P., et al. (2019). Brain pyrimidine nucleotide synthesis and Alzheimer disease. *Aging* 11, 8433–8462. doi: 10.18632/aging.102328

Phung, T. L., Ziv, K., Dabydeen, D., Eyiah-Mensah, G., Riveros, M., Perruzzi, C., et al. (2006). Pathological angiogenesis is induced by sustained Akt signaling and inhibited by rapamycin. *Cancer Cell* 10, 159–170. doi: 10.1016/j.ccr.2006.07.003

Polak, P., Cybulski, N., Feige, J. N., Auwerx, J., Rüegg, M. A., and Hall, M. N. (2008). Adipose-specific knockout of raptor results in lean mice with enhanced mitochondrial respiration. *Cell Metab.* 8, 399–410. doi: 10.1016/j.cmet.2008.09.003

Rao, R., Hao, C. M., and Breyer, M. D. (2004). Hypertonic stress activates glycogen synthase Kinase 3β-mediated apoptosis of renal medullary interstitial cells, suppressing an NFκB-driven Cyclooxygenase-2-dependent survival pathway. *J. Biol. Chem.* 279, 3949–3955. doi: 10.1074/jbc.M309325200

Reddy, S. T., Wadleigh, D. J., and Herschman, H. R. (2000). Transcriptional regulation of the cyclooxygenase-2 gene in activated mast cells. *J. Biol. Chem.* 275, 3107–3113. doi: 10.1074/jbc.275.5.3107

Ritchie, C. W., Bajwa, J., Coleman, G., Hope, K., Jones, R. W., Lawton, M., et al. (2014). Souvenaid§: a new approach to management of early Alzheimer's disease. *J. Nutr. Health Aging* 18, 291–299. doi: 10.1007/s12603-013-0411-2

Rousseau, A., and Bertolotti, A. (2016). An evolutionarily conserved pathway controls proteasome homeostasis. *Nature* 536, 184–189. doi: 10.1038/nature18943

Rouzer, C. A., and Marnett, L. J. (2009). Cyclooxygenases: structural and functional insights. *J. Lipid Res.* 50, 29–34. doi: 10.1194/jlr.R800042-JLR200

Sauer, S., Bruno, L., Hertweck, A., Finlay, D., Leleu, M., Spivakov, M., et al. (2008). T cell receptor signaling controls Foxp3 expression via PI3K, Akt, and mTOR. *Proc. Natl. Acad. Sci. U.S.A.* 105, 7797–7802. doi: 10.1073/pnas.0800928105

Saxton, R. A., and Sabatini, D. M. (2017). mTOR signaling in growth, metabolism and disease. *Cell* 168, 960–976. doi: 10.1016/j.cell.2017.02.004

Schepis, C. (2016). "The tuberous sclerosis complex," in *Dermatological Cryosurgery and Cryotherapy*, eds W. Abramovits, G. Graham, Y. Har-Shai, and R. Strumia (London: Springer), 615–617. doi: 10.1007/978-1-4471-6765-5_120

Schubert, D., and Piasecki, D. (2001). Oxidative glutamate toxicity can be a component of the excitotoxicity cascade. *J. Neurosci.* 21, 7455–7462. doi: 10.1523/jneurosci.21-19-07455.2001

Shacka, J. J., Roth, K. A., and Zhang, J. (2008). The autophagy-lysosomal degradation pathway: role in neurodegenerative disease and therapy. *Front. Biosci.* 13:718–736. doi: 10.2741/2714

Shafei, M. A., Harris, M., and Conway, M. E. (2017). Divergent metabolic regulation of autophagy and mTORC1-early events in Alzheimer's disease? *Front. Aging Neurosci.* 9:173. doi: 10.3389/fnagi.2017.00173

Shafi, O. (2016). Inverse relationship between Alzheimer's disease and cancer, and other factors contributing to Alzheimer's disease: a systematic review. *BMC Neurol.* 16:765. doi: 10.1186/s12883-016-0765-2

Sheng, H., Shao, J., Morrow, J. D., Beauchamp, R. D., and DuBois, R. N. (1998). Modulation of apoptosis and Bcl-2 expression by prostaglandin E2 in human colon cancer cells. *Cancer Res.* 58, 362–366.

Slomovitz, B. M., and Coleman, R. L. (2012). The PI3K/AKT/mTOR pathway as a therapeutic target in endometrial cancer. *Clin. Cancer Res.* 18, 5856–5864. doi: 10.1158/1078-0432.CCR-12-0662

Smyth, E. M., Grosser, T., Wang, M., Yu, Y., and FitzGerald, G. A. (2009). Prostanoids in health and disease. *J. Lipid Res.* 50, 423–428. doi: 10.1194/jlr.R800094-JLR200

Sommer, A., Winner, B., and Prots, I. (2017). The Trojan horse - Neuroinflammatory impact of T cells in neurodegenerative diseases. *Mol. Neurodegen.* 12, 1–10. doi: 10.1186/s13024-017-0222-8

Spaggiari, G. M., Capobianco, A., Abdelrazik, H., Becchetti, F., Mingari, M. C., and Moretta, L. (2008). Mesenchymal stem cells inhibit natural killer-cell proliferation, cytotoxicity, and cytokine production: role of indoleamine 2,3-dioxygenase and prostaglandin E2. *Blood* 111, 1327–1333. doi: 10.1182/blood-2007-02-074997

Spilman, P., Podlutskaya, N., Hart, M. J., Debnath, J., Gorostiza, O., Bredesen, D., et al. (2010). Inhibition of mTOR by rapamycin abolishes cognitive deficits and

reduces amyloid-β levels in a mouse model of alzheimer's disease. *PLoS One* 5:e9979. doi: 10.1371/journal.pone.0009979

Stewart, W. F., Kawas, C., Corrada, M., and Metter, E. J. (1997). Risk of Alzheimer's disease and duration of NSAID use. *Neurology* 48, 626–632. doi: 10.1212/WNL.48.3.626

Sun, G. Y., Shelat, P. B., Jensen, M. B., He, Y., Sun, A. Y., and Simonyi, A. (2010). Phospholipases A2 and inflammatory responses in the central nervous system. *Neuro Mol. Med.* 12, 133–148. doi: 10.1007/s12017-009-8092-z

Tang, Z., Bereczki, E., Zhang, H., Wang, S., Li, C., Ji, X., et al. (2013). Mammalian target of rapamycin (mTor) mediates tau protein dyshomeostasis: implication for Alzheimer disease. *J. Biol. Chem.* 288, 15556–15570. doi: 10.1074/jbc.M112.435123

Tang, Z., Ioja, E., Bereczki, E., Hultenby, K., Li, C., Guan, Z., et al. (2015). MTor mediates tau localization and secretion: implication for Alzheimer's disease. *Biochim. Biophys. Acta* 1853, 1646–1657. doi: 10.1016/j.bbamcr.2015.03.003

Thomas, M. H., Pelleieux, S., Vitale, N., and Olivier, J. L. (2016). Arachidonic acid in Alzheimer ' s disease. *J. Neurol. Neuromed.* 1, 1–6.

Tomimoto, H., Akiguchi, I., Wakita, H., Lin, J. X., and Budka, H. (2000). Cyclooxygenase-2 is induced in microglia during chronic cerebral ischemia in humans. *Acta Neuropathol.* 99, 26–30. doi: 10.1007/PL00007402

Tran, C. M., Mukherjee, S., Ye, L., Frederick, D. W., Kissig, M., Davis, J. G., et al. (2016). Rapamycin blocks induction of the thermogenic program in white adipose tissue. *Diabetes Metab. Res. Rev.* 65, 927–941. doi: 10.2337/db15-0502

Tsujii, M., and DuBois, R. N. (1995). Alterations in cellular adhesion and apoptosis in epithelial cells overexpressing prostaglandin endoperoxide synthase 2. *Cell* 83, 493–501. doi: 10.1016/0092-8674(95)90127-2

Tynkkynen, J., Chouraki, V., van der Lee, S. J., Hernesniemi, J., Yang, Q., Li, S., et al. (2018). Association of branched-chain amino acids and other circulating metabolites with risk of incident dementia and Alzheimer's disease: a prospective study in eight cohorts. *Alzheimer's Dement* 14, 723–733. doi: 10.1016/j.jalz.2018.01.003

Uddin, M. S., Stachowiak, A., Al Mamun, A., Tzvetkov, N. T., Takeda, S., Atanasov, A. G., et al. (2018). Autophagy and Alzheimer's disease: from molecular mechanisms to therapeutic implications. *Front. Aging Neurosci.* 10:4. doi: 10.3389/fnagi.2018.00004

Um, S. H., Frigerio, F., Watanabe, M., Picard, F., Joaquin, M., Sticker, M., et al. (2004). Absence of S6K1 protects against age- and diet-induced obesity while enhancing insulin sensitivity. *Nature* 431, 200–205. doi: 10.1038/nature02866

Wada, S., Neinast, M., Jang, C., Ibrahim, Y. H., Lee, G., Babu, A., et al. (2016). The tumor suppressor FLCN mediates an alternate mTOR pathway to regulate browning of adipose tissue. *Genes Dev.* 30, 2551–2564. doi: 10.1101/gad.287953.116

Walsh, D. T., Perry, V. H., and Minghetti, L. (2000). Cyclooxygenase-2 is highly expressed in microglial-like cells in a murine model of prion disease. *Glia* 29, 392–396. doi: 10.1002/(SICI)1098-1136(20000215)29:4(392:AID-GLIA10(3.0.CO;2-C

Wang, B., Lin, Y., Hu, Y., Shan, W., Liu, S., Xu, Y., et al. (2017). MTOR inhibition improves the immunomodulatory properties of human bone marrow mesenchymal stem cells by inducing COX-2 and PGE2. *Stem Cell Res. Ther.* 8, 1–13. doi: 10.1186/s13287-017-0744-6

Weggen, S., Eriksen, J. L., Das, P., Sagi, S. A., Wang, R., Pietrzik, C. U., et al. (2001). A subset of NSAIDs lower amyloidogenic Aβ42 independently of cyclooxygenase activity. *Nature* 414, 212–216. doi: 10.1038/3510 2591

Wijayasinghe, Y. S., Tyagi, A., and Poddar, N. K. (2017). "Regulation of Cell Volume by Osmolytes," in *Cellular Osmolytes: From Chaperoning Protein Folding to Clinical Perspectives*, eds L. Rajendrakumar Singh and T. Dar (Singapore: Springer), 195–228. doi: 10.1007/978-981-10-3707-8_9

Williams, C. S., Mann, M., and DuBois, R. N. (1999). The role of cyclooxygenases in inflammation, cancer, and development. *Oncogene* 18, 7908–7916. doi: 10.1038/sj.onc.1203286

Wu Chen, R., Zhang, Y., Rose, M. E., and Graham, S. H. (2004). Cyclooxygenase-2 activity contributes to neuronal expression of cyclin D1 after anoxia/ischemia in vitro and in vivo. *Mol. Brain Res.* 132, 31–37. doi: 10.1016/j.molbrainres.2004.08.020

Wyss-Coray, T., and Mucke, L. (2002). Inflammation in neurodegenerative disease - A double-edged sword. *Neuron* 35, 419–432. doi: 10.1016/S0896-6273(02)00794-8

Xiang, Z., Ho, L., Valdellon, J., Borchelt, D., Kelley, K., Spielman, L., et al. (2002). Cyclooxygenase (COX)-2 and cell cycle activity in a transgenic mouse model of Alzheimer's disease neuropathology. *Neurobiol. Aging* 23, 327–334. doi: 10.1016/S0197-4580(01)00282-2

Xu, Z., You, W., Zhou, Y., Chen, W., Wang, Y., and Shan, T. (2019). Cold-induced lipid dynamics and transcriptional programs in white adipose tissue. *BMC Biol.* 17:693. doi: 10.1186/s12915-019-0693-x

Yang, F., and Bleich, D. (2004). Transcriptional regulation of cyclooxygenase-2 gene in pancreatic β-cells. *J. Biol. Chem.* 279, 35403–35411. doi: 10.1074/jbc.M404055200

Yang, T., Huang, Y., Heasley, L. E., Berl, T., Schnermann, J. B., and Briggs, J. P. (2000). MAPK mediation of hypertonicity-stimulated cyclooxygenase-2 expression in renal medullary collecting duct cells. *J. Biol. Chem.* 275, 23281–23286. doi: 10.1074/jbc.M910237199

Zhang, X., Luo, Y., Wang, C., Ding, X., Yang, X., Wu, D., et al. (2018). Adipose mTORC1 Suppresses Prostaglandin Signaling and Beige Adipogenesis via the CRTC2-COX-2 Pathway. *Cell Rep.* 24, 3180–3193. doi: 10.1016/j.celrep.2018.08.055

Zhao, J., Zhai, B., Gygi, S. P., and Goldberg, A. L. (2015). MTOR inhibition activates overall protein degradation by the ubiquitin proteasome system as well as by autophagy. *Proc. Natl. Acad. Sci. U.S.A.* 112, 15790–15797. doi: 10.1073/pnas.1521919112

Conflict of Interest: The authors declare that the research was conducted in the absence of any commercial or financial relationships that could be construed as a potential conflict of interest.

frontiers in Aging Neuroscience

ORIGINAL RESEARCH
published: 21 July 2020
doi: 10.3389/fnagi.2020.00212

The Validation of Multifactor Model of Plasma $A\beta_{42}$ and Total-Tau in Combination With MoCA for Diagnosing Probable Alzheimer Disease

Fubin Jiao[1,2,3†], Fang Yi[2,4†], Yuanyuan Wang[2], Shouzi Zhang[5], Yanjun Guo[6], Wenjin Du[7], Ya Gao[8], Jingjing Ren[9], Haifeng Zhang[3], Lixin Liu[5], Haifeng Song[9] and Luning Wang[1,2]**

[1] Medical School of Chinese People's Liberation Army, Beijing, China, [2] Department of Neurology, The 2nd Medical Center, National Clinical Research Center for Geriatric Disease, Chinese People's Liberation Army General Hospital, Beijing, China, [3] Health Service Department of the Guard Bureau of the Joint Staff Department, Joint Staff of the Central Military Commission of Chinese PLA, Beijing, China, [4] Department of Neurology, Lishilu Outpatient, Jingzhong Medical District, Chinese People's Liberation Army General Hospital, Beijing, China, [5] The Psycho Department of Beijing Geriatric Hospital, Beijing, China, [6] Department of Neurology, Beijing Friendship Hospital, Capital Medical University, Beijing, China, [7] Department of Neurology, Air Force Medical Center, Chinese People's Liberation Army, Beijing, China, [8] Department of Geriatrics, The Second Hospital of Hebei Medical University, Shijiazhuang, China, [9] National Engineering Research Center for Protein Drugs, Beijing, China

OPEN ACCESS

Edited by:
Jiehui Jiang,
Shanghai University, China

Reviewed by:
Shieh-Yueh Yang,
MagQu, Taiwan
Diego Sepulveda-Falla,
University Medical Center
Hamburg-Eppendorf, Germany

***Correspondence:**
Haifeng Song
songhf6811@163.com
Luning Wang
luning_w@126.com

[†] These authors have contributed equally to this work and share first authorship

Received: 17 March 2020
Accepted: 16 June 2020
Published: 21 July 2020

Citation:
Jiao F, Yi F, Wang Y, Zhang S, Guo Y, Du W, Gao Y, Ren J, Zhang H, Liu L, Song H and Wang L (2020) The Validation of Multifactor Model of Plasma $A\beta_{42}$ and Total-Tau in Combination With MoCA for Diagnosing Probable Alzheimer Disease. Front. Aging Neurosci. 12:212. doi: 10.3389/fnagi.2020.00212

Alzheimer disease (AD) has an insidious onset and heterogeneous clinical symptoms. The well-accepted biomarkers for clinical diagnosis of AD include β-amyloid (Aβ) deposition and pathologic tau level within cerebral spinal fluid (CSF) and imaging AD pathology such as positive emission tomography (PET) imaging of the amyloid-binding agent Pittsburgh compound B (PET-PiB). However, the high expense and invasive nature of these methods highly limit their wide usage in clinic practice. Therefore, it is imperious to develop less expensive and invasive methods, and plasma biomarkers are the premium targets. In the current study, we utilized a single-blind comparison method; all the probable AD cases met the core clinical National Institute on Aging and Alzheimer's Association (NIA-AA) criteria and validated by PET-PiB. We used ultrasensitive immunomagnetic reduction (IMR) assays to measure plasma $A\beta_{42}$ and total-tau (t-tau) levels, in combination with different variables including Aβ42 × t-tau value, Montreal Cognitive Assessment (MoCA), and Mini Mental State Examination (MMSE). We used logistic regression to analyze the effect of all these variables in the algorism. Our results showed that (1) plasma Aβ42 and t-tau are efficient biomarkers for AD diagnosis using IMR platform, whereas Aβ42 × t-tau value is more efficient for discriminating control and AD; (2) in the control group, Aβ42 level and age demonstrated strong negative correlation; Aβ42 × t-tau value and age demonstrated significant negative correlation; (3) in the AD group, t-tau level and MMSE score demonstrated strong negative correlation; (4) using the model that Aβ42, Aβ42 × t-tau,

and MoCA as the variable to generate receiver operating characteristic (ROC) curve, cutoff value = 0.48, sensitivity = 0.973, specificity = 0.982, area under the curve (AUC) = 0.986, offered better categorical efficacy, sensitivity, specificity, and AUC. The multifactor model of plasma Aβ42 and t-tau in combination with MoCA can be a viable model separate health and AD subjects in clinical practice.

Keywords: Alzheimer disease, β-amyloid, tau, Montreal Cognitive Assessment, ultrasensitive immunomagnetic reduction

INTRODUCTION

Alzheimer disease (AD) is a neurodegenerative disease with latent initiation and progressive course, which is the most common cause of dementia and the fourth cause of mortality in the elder population (Katzman, 2008). Growing evidences have shown the early diagnosis, before massive neuron loss and dementia occur, is crucial to AD treatment (Jack et al., 2013; Dubois et al., 2016). IWG 2016 and the National Institute on Aging and Alzheimer's Association (NIA-AA) research framework are aligned on the key issue that although AD is currently defined as a biological event throughout the course, the combination of abnormal β-amyloid (Aβ) and tau biomarkers is conclusive enough to define AD regardless of cognitive symptoms (Jack et al., 2018).

Aβ level in cerebral spinal fluid (CSF) and Aβ accumulation measured by positive emission tomography (PET) imaging of the amyloid-binding agent Pittsburgh compound B (PET-PiB) have been validated as viable AD biomarkers. Absolute sensitivity of amyloid PET is comparable to the gold standard of autopsy (Roberts et al., 2017). However, the high expense and limited availability of the amyloid PET and the invasive nature of CSF collection highly limit its wide used in clinic practice (Villemagne et al., 2013; Vos et al., 2013; Sperling et al., 2014; Baird et al., 2015). Therefore, it is imperious to develop less expensive and invasive methods, and plasma biomarkers are the premium targets. Moreover, blood biomarkers such as plasma total tau (t-tau) have shown promising potential to identify neurodegenerations, whereas plasma Aβ42 was shown to be a high-performance biomarker for AD (Dage et al., 2016; Ovod et al., 2017; Nakamura et al., 2018). However, the sensitivity and specificity of blood biomarkers detection will determine the future of their clinical application, thus needing further clinical validation.

Currently, many technologies have been developed for detecting plasma Aβ42, t-tau: ELISA, CLIA, ultrasensitive immunomagnetic reduction (IMR), and so on. Immunomagnetic reduction has shown far better sensitivity than others, with clinical validation (Chiu et al., 2012, 2013; Chen et al., 2019; Lue et al., 2019a). But more clinical validation is needed to determine the reliability of IMR in AD diagnosis.

In our study, 97 cases of volunteers were discretely screened and diagnosed by experienced neurologists, to guarantee the quality for selected subjects. Through cognitive psychophysiology evaluation analysis and confirmed by PET-PiB neuroimaging analysis, all the AD patients met the core clinical NIA-AA criteria. We used IMR technology measuring plasma Aβ42 and t-tau, in combination with other factors, and thus comprehensively evaluated the sensitivity and specificity of AD diagnosis, which paved the avenue of potential using IMR technology for AD early diagnosis.

MATERIALS AND METHODS

Participants

Alzheimer disease group: 40 AD patients were recruited from the neurology department of PLA hospital between August 2017 and June 2018. All the patients underwent cognitive psychology scale evaluation and neuroimaging measurement and confirmed by PET-PiB examination. All probable AD patients met the core clinical NIA-AA criteria (Jack et al., 2011), without family history.

Normal control (NC) group: 57 healthy volunteers were recruited. All the subjects have normal cognitive function by neuropsychology evaluation, also without severe heart, liver, kidney, or other systematic diseases; mental illness; surgery; and injury history or other major disease history, without dementia patients in the family.

Consensus agreements were signed by patients himself/herself or custodians and provided blood samples; the entire process met human rights, humanity, and medical ethical standard.

Methods

Sample collection: 5 mL non-fasting venous blood sample (K2 EDTA tube) was drawn from every subject. The blood samples were centrifuged at 2,500 × *g* for 15 min within 3 h of collection, and plasmas were aliquoted into cryotubes (1 mL per tube) and stored at −80°C. Each sample was assigned an identification number following reception. The laboratory staffs handling the sample processing were blind to the clinical status and the demographic data of the subjects.

The Mini Mental State Examination (MMSE) (Li et al., 2016) and Montreal Cognitive Assessment (MoCA) Beijing version[1] (Lu et al., 2011) evaluation were performed by the same doctor for the entire study: in the normal age range (score > 1.5 standard deviation), age- and education-matched normal recipient, and CDR = 0. Every patient underwent magnetic resonance imaging (MRI) and PET-PiB imaging scan examination. Aβ42 and t-tau concentration were measured using IMR technology for all the collected plasma samples.

[1]www.mocatest.org

Reagents: Calibrator60 (Aβ42 standard), MagQu, CA-DEX-0080; tau IMR Reagent, MagQu, MF-tau-0060; tau Solution-L (standard L), MagQu, CL-tau-000T; tau Solution-H (standard H), MagQu, CL-tau-050T; Aβ42 IMR Reagent, MagQu, MF-AB2-0060; Aβ42 Solution-M (standard M), MagQu, CL-AB2-020T; 6 × 50 mm sample analysis tubes, MagQu, MQ-TUB-0100; disposable vacuum blood collection tube (K2 EDTA tube), Jiangsu Yuli Medical Instrument Co. Ltd., Y30983502; Cryo tube, CORNING, 430659.

Immunomagnetic reduction measurements: Details of the mechanism and technology of IMR have been previously reported (Nasreddine et al., 2005; Lee et al., 2016; Yang et al., 2017b). The reagents used to determine plasma Aβ and t-tau protein levels in this study consisted of dextran-coated Fe3O4 nanoparticles functionalized with antibodies. The percentage reduction in an alternating current (ac) that reflects the magnetic susceptibility (Xac) of a reagent due to the interactions of functionalized magnetic nanoparticles and target proteins. The percentage reductions of immunomagnetic signals are then converted to target protein concentrations using the standard curves of the respective analyses. The selection of the antibodies conjugated to the IMR reagents was based on epitopes, affinity to antigens, ability to be conjugated onto nanoparticles, and the ability to provide linearity of standard curves quantified by magnetic signal reduction. For t-tau assay, 40 μL of plasma sample was mixed with 80 μL IMR reagents at room temperature, and for Aβ42 assay, 60 μL of plasma sample was mixed with 60 μL of IMR reagent.

Statistical Analysis

Data were expressed as means ± SD or an absolute number with a proportion for descriptive statistics. Spearman correlation analysis was applied to examine the correlations between plasma Aβ measures and cerebral uptake values of ^{11}C Pittsburgh Compound B PET, ^{11}C-PiB PET in different brain regions. Significant correlations were validated using non-parametric Spearman rank-order correlations. Correlation analysis was also used to evaluate the correlations between the plasma Aβ measures, ^{11}C-PiB PET SUVRs and each parameter of the demographic data, clinical characteristics, and cognitive tests. Multiple linear regression analysis was used to further evaluate the associations between plasma Aβ measures and ^{11}C-PiB PET binding after controlling for age. A P-value of 0.05 was defined as the threshold of statistical significance in each test. To elucidate the AD-related tests, the current study used statistical analysis with SPSS for data analysis; considering the data do not obey Gaussian distribution, we used Spearman correlation analysis, to describe the level and direction of the correlation of two variables ($r > 0$ represents positive correlation, $r < 0$ represents negative correlation, the closer r value to 1, the stronger correlation is, and $P < 0.05$ represents a significant difference). Within the final prediction model, binary logistic regression analysis demonstrated the result of (P_{MoCA}, $P_{\mathrm{A\beta\ 42}}$, and $P_{\mathrm{A\beta\ 42\ \times\ t-tau}}$) < 0.05, whereas ($P_{\mathrm{MMSE}}$ and $P_{\mathrm{t-tau}}$) > 0.05. Considering the stability of using this model, we decided to choose Aβ42, Aβ42 × t-tau and MoCA these three variables as prediction factors.

RESULTS

Patients Selection

Ninety-seven volunteers aged between 54 and 78 years (mean = 68.0 ± 9.3) were recruited, of which 57.7% were females. The control group had 57 subjects; the AD group had 40 subjects, with an average age of 67.9 ± 9.5 and 68.1 ± 9.0 years, respectively. Average MMSE value was 28.25 ± 3.36 in control group and 12.67 ± 9.21 in AD group; Average MoCA value was 26.25 ± 4.61 in control group and 10.69 ± 7.33 in AD group, therefore, both MMSE ($P = 1.41 \times 10^{-19}$) and MoCA ($P = 8.81 \times 10^{-22}$) showed highly significant difference between control and AD group (**Table 1**).

IMR Measurement of Plasma Aβ42 and T-tau Levels

Immunomagnetic reduction technology was used to measure the human plasma Aβ42 and t-tau levels. **Table 1** demonstrated that the mean value of t-tau concentration was 20.65 ± 3.52 pg/mL in the control group and 25.9 ± 8.12 pg/mL in the AD group; the difference was strongly significant ($P = 3.42 \times 10^{-5}$). Mean value of Aβ42 concentration was 16.92 ± 1.67 pg/mL in the control group and 18.77 ± 1.93 pg/mL in the AD group; the difference was strongly significant between control and AD group ($P = 2.31 \times 10^{-6}$). Mean value of Aβ42 × t-tau was 352.53 ± 90.88 pg/mL in the control group and 490.44 ± 190.48 pg/mL in the AD group; the difference was strongly significant ($P = 7.03 \times 10^{-6}$). Mean value of Aβ42/t-tau concentration was 0.83 ± 0.11 in the control group and 0.77 ± 0.18 in the AD group; the difference was strongly significant ($P = 0.04$). **Figure 1** demonstrates that all the differences between two groups were strongly significant.

TABLE 1 | Statistic detail of the recruits.

Group	NC (57)	AD (40)	*P*	Overall (97)
Male: female	26:31	15:25	0.53	41:56
Age, years	67.9 ± 9.5	68.1 ± 9.0	0.67	68.0 ± 9.3
MMSE	28.25 ± 3.36	12.67 ± 9.21	1.41×10^{-19}	21.78 ± 10.19
MoCA	26.25 ± 4.61	10.69 ± 7.33	8.81×10^{-22}	19.79 ± 9.84
Plasma t-tau, pg/mL	20.65 ± 3.52	25.91 ± 8.12	3.42×10^{-5}	22.82 ± 6.01
Plasma Aβ42, pg/mL	16.92 ± 1.67	18.77 ± 1.93	2.31×10^{-6}	17.68 ± 1.99
Aβ42 × t-tau	352.53 ± 90.88	490.44 ± 190.48	7.03×10^{-6}	409.40 ± 152.38
Aβ42/ t-tau	0.83 ± 0.11	0.77 ± 0.18	0.04	0.81 ± 0.14

Clinical characters, mean ± SD. AD, Alzheimer disease; NC, normal control; MMSE, Mini-Mental State Examination; MoCA, Montreal Cognitive Assessment.

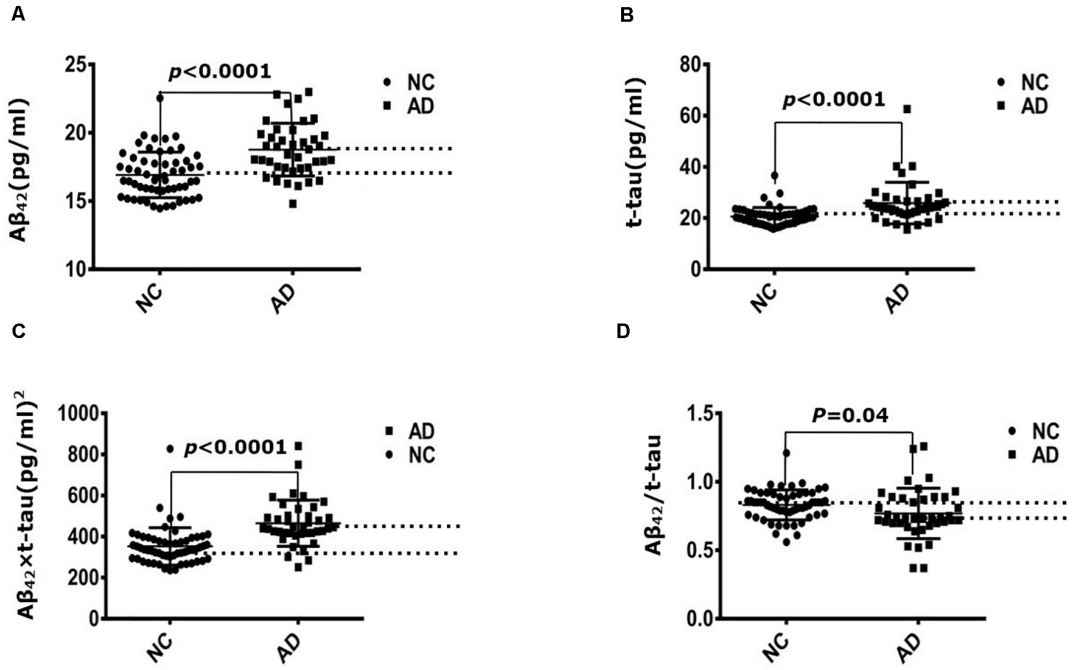

FIGURE 1 | Immunomagnetic reduction measurement of plasma Aβ42 and t-tau protein levels. **(A)** Aβ42 concentration of NC and AD group; **(B)** t-tau concentration of NC and AD group; **(C)** Aβ42 × t-tau value of NC and AD group; **(D)** Aβ42/t-tau value of NC and AD group. NC: normal control (n = 57); AD, Alzheimer disease (n = 40).

Receiver Operating Characteristic Curve Analysis

Receiver operating characteristic (ROC) curve analysis demonstrated that the cutoff value of Aβ42 concentration between control and AD group was 17.22 pg/mL, sensitivity was 0.650, specificity was 0.719, and area under the curve (AUC) was 0.689 (**Figure 2A**). The cutoff value of t-tau concentration between control and AD group was 21.30 pg/mL, sensitivity was 0.625, specificity was 0.667, and AUC was 0.659 (**Figure 2B**). The cutoff value of Aβ42 × t-tau between control and AD group was 403.72 $(pg/mL)^2$, sensitivity was 0.825, specificity was 0.842, and AUC was 0.883 (**Figure 2C**); The cutoff value of Aβ42/t-tau between control and AD group was 0.74, sensitivity was 0.775, specificity was 0.386, and AUC was 0.558 (**Figure 2D**). The values were summarized in **Table 2**. A biomarker combination of Aβ42 × t-tau has the highest sensitivity, specificity, and AUC.

Spearman Correlation Analysis

Spearman correlation analysis in the control group showed that Aβ42 concentration and age demonstrated a strong negative correlation (r = −0.365, P = 0.005); Aβ42 × t-tau value and age demonstrated significant negative correlation (r = −0.266, P = 0.046) (**Table 3**). In the AD group, t-tau concentration and MMSE score demonstrated a strong negative correlation (r = −0.579, P = 0.006) (**Table 4**). This thus suggests that in AD patients, the lower MMSE value is, which represents the severity of the disease, the higher is the plasma t-tau protein level.

Logistic Regression Analysis

To further study the relationship between plasma biomarker and brain Aβ deposit, we utilized SPSS software performing logistic regression analysis. We combined different variables to establish a disease prediction model (i.e., practical clinical diagnosis) and predicted if the individual is AD or NC who met the entry criteria (i.e., clinical diagnosis). Our model introduced the variables Aβ42, t-tau, Aβ42 × t-tau, MMSE, and MoCA predicted as shown in **Table 5**. This model has the prediction accuracy of 98.2% for the control groups and 97.3% for the AD group, an overall prediction percentage of 97.8%. Further variable logistic analysis concluded that Aβ42, Aβ42 × t-tau, and MoCA also had statistical significance in the model (P < 0.05), as the prediction accuracy of these three variables shown in **Table 6**. This three-variable model has a prediction accuracy of 98.2% for the control groups and 94.6% for the AD group, an overall prediction percentage of 96.7%. Using the prediction values of Aβ42, Aβ42 × t-tau, and MoCA as variable, with PET-PiB as standard, the ROC curve is shown in **Figure 3**, as cutoff value = 0.48, sensitivity = 0.973, specificity = 0.982, AUC = 0.986. The results demonstrated the prediction model of Aβ42, Aβ42 × t-tau, and MoCA have a significant correlation with clinical probable AD diagnosis.

DISCUSSION

As all we know, the early diagnosis and treatment of AD may benefit to improve symptoms and decelerate the course

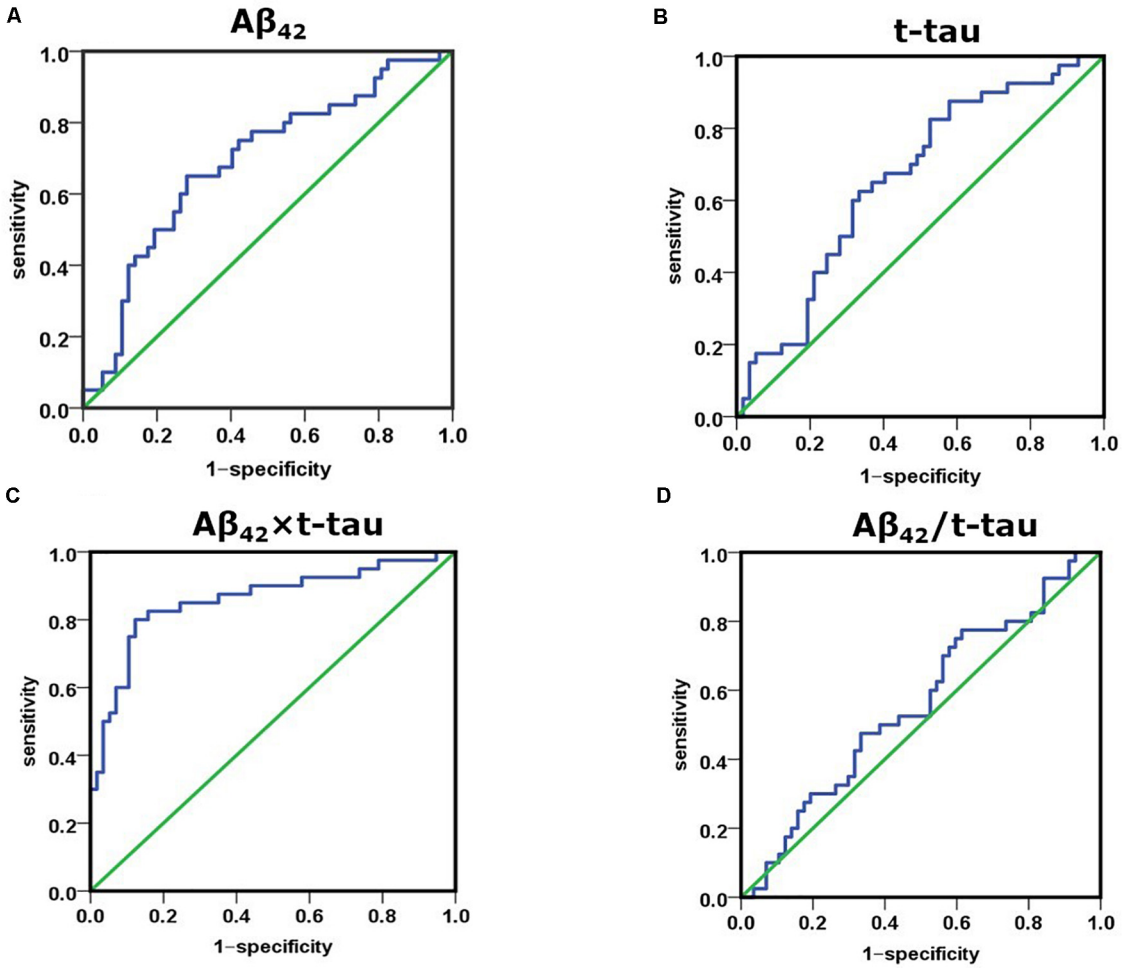

FIGURE 2 | Receiver operating characteristic curve analysis for discriminating between NC and AD subjects using Aβ42 level, t-tau level, Aβ42 × t-tau value, and Aβ42/t-tau value as diagnostic parameters. **(A)** AUC of Aβ42 concentration between NC and AD group; **(B)** AUC of t-tau concentration between NC and AD group; **(C)** AUC of Aβ42 × t-tau value between NC and AD group; **(D)** AUC of Aβ42/t-tau value between NC and AD group. NC, normal control (n = 57); AD, Alzheimer disease (n = 40).

TABLE 2 | ROC curve analysis of AD and control subjects.

	Cutoff	Sensitivity	Specificity	AUC
Aβ42	17.22	0.650	0.719	0.689
t-tau	21.30	0.625	0.667	0.659
Aβ42 × t-tau	403.72	0.825	0.842	0.883
Aβ42/t-tau	0.74	0.775	0.386	0.558

AD, Alzheimer disease; NC, normal control; AUC, area under the receiver operating characteristic curve.

TABLE 3 | Correlation analysis of NC group.

	MMSE		MoCA		Age	
	r	*p*	*r*	*p*	*r*	*p*
Aβ42	−0.085	0.530	0.020	0.880	−0.365**	0.005
t-tau	−0.151	0.263	−0.081	0.550	−0.105	0.437
Aβ42 × t-tau	−0.157	0.244	−0.047	0.731	−0.266*	0.046

NC, normal control; MMSE, Mini Mental State Examination; MoCA, Montreal Cognitive Assessment.

and also alleviate the burden of the family and society (Andreasen et al., 2001; Kim et al., 2010). Therefore, it is crucial to define the disease with a clear biological foundation including clinical and preclinical phases. The NIA-AA Research Framework focuses on biomarker discovery in living people for AD diagnosis, including biomarkers for Aβ deposition, pathologic tau, neurodegeneration, and so on (Jack et al., 2018). CSF AD-specific pathological protein test and PET have become internationally recognized biomarker diagnoses in living patients (Prestia et al., 2013; Toledo et al., 2014; Vos et al., 2015). Especially, the absolute sensitivity of amyloid PET relative to an autopsy gold standard has been assessed (Roberts et al., 2017); its sensitivity and accuracy are higher than neuropsychological evaluation, computed tomography and MRI. However, CSF biomarker analysis related lumbar puncture

TABLE 4 | Correlation analysis for MMSE, MoCA < 10 of AD group.

	MMSE		MoCA		Age	
	r	*P*	*r*	*p*	*r*	*p*
Aβ42	0.070	0.762	0.109	0.638	0.274	0.229
t-tau	−0.579**	0.006	−0.336	0.137	−0.016	0.944
Aβ42 × t-tau	−0.187	0.416	−0.197	0.391	−0.046	0.844

AD, Alzheimer disease; MMSE, Mini Mental State Examination; MoCA, Montreal Cognitive Assessment.

TABLE 5 | Binary logistic regression analysis for MoCA, MMSE, Aβ42, t-tau, and Aβ42 × t-tau variables.

Actual detection		Forecast		
		Clinical diagnosis		Accuracy rate
		0	1	
Practical clinical diagnosis	0	54	1	98.2
	1	1	36	97.3
Overall accuracy				97.8

0: normal control; 1: Alzheimer disease.

TABLE 6 | Binary logistic regression analysis for Aβ42, Aβ42 × t-tau, and MoCA variables.

Actual detection		Forecast		
		Clinical diagnosis		Accuracy rate
		0	1	
Practical clinical diagnosis	0	54	1	98.2
	1	2	35	94.6
Overall accuracy				96.7

0: normal control; 1: Alzheimer disease.

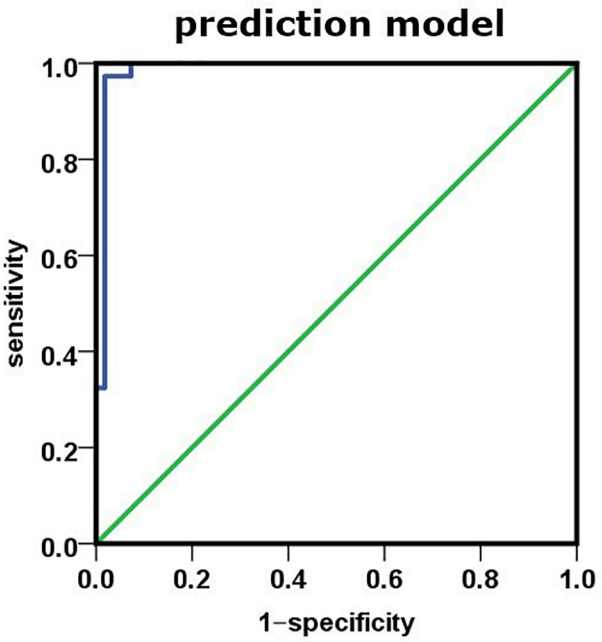

FIGURE 3 | Using prediction value of the model as variable, PET-PiB as standard; the ROC curve is as shown.

is an invasive procedure and poor in repeatability, and the assessment is not always feasible and difficult to be accepted by patients in some countries, especially in the elderly patients. Meanwhile, brain imaging biomarkers (amyloid-PET, tau-PET) also have their disadvantages: the assay cost is too expensive, and it requires sophisticated technologies and equipment, which are not accessible in regular clinical settings, which limit the widespread application of these two types of biomarkers. Therefore, compared with all above, analyzing pathologic Aβ and tau in peripheral blood, which have great advantages, including blood samples being easy to access, the procedure is non-invasive or minimally invasive, with reasonable cost-effective and good replication rate. More and more studies show that blood biomarkers have promising prospects (Kaneko et al., 2014; Mattsson et al., 2016; Nabers et al., 2018; Nakamura et al., 2018).

Immunomagnetic reduction technology for AD-associated plasma biomarkers has been developed in the last few years (Lue et al., 2019a). In a recent study, plasma Aβ42 level was assayed by IMR in European Caucasian AD subjects (Teunissen et al., 2018). However, pathologic Aβ and t-tau levels are under gene regulation; there are interracial discrepancies of these gene expressions (Huynh and Mohan, 2017). Thus, directly using the data from the European population in the Chinese population will have great limitations. Currently, there are many studies assessed the potential of Aβ40, Aβ42, and t-tau measured by IMR in discriminating AD in China Taiwan area (Chiu et al., 2012, 2013; Yang et al., 2017a; Fan et al., 2018). These studies used the same methods but obtained different cutoff values, which may be caused by race, regions, living habit differences, and so on. Therefore, a larger sample size from mainland China is needed for establishing accurate cutoff value for the Chinese population. In this study, we used IMR technology to measure plasma Aβ42 and t-tau protein levels and for the first time verified the reliability of the multiparameter model of plasma Aβ42 and t-tau in combination with MoCA for diagnosing probable AD confirmed by PET-PiB, which provides sensitive and reliable discrimination between control and AD subjects in a Chinese population.

In this single-blind test, we discovered plasma Aβ42, t-tau, and Aβ42 × t-tau levels are significantly higher in AD subjects compared to the control subjects. Further ROC curve analysis demonstrated that plasma Aβ42 × t-tau as a combinational biomarker yielded better discrimination between control and AD subjects than that of plasma Aβ42 or t-tau concentration alone. Using Spearman correlation analysis, we found Aβ42 level is negatively correlated with age ($r = -0.365$, $P = 0.005$), and the value of Aβ42 × t-tau is negatively correlated with age ($r = -0.266$, $P = 0.046$) in the control group. These findings suggest that Aβ42 level as well as Aβ42 × t-tau value decreases according to age growth in healthy subjects, which agree with those of Lue et al. (2019b), who showed that plasma Aβ42

decreased as age increased in cognitively normal subjects. These relationships provided evidence that Aβ42 may be involved in the pathophysiology of aging and could act as plasma biomarkers in aging-associated disease. In our study, in AD patients whose MMSE/MoCA value is less than 10, the t-tau level is strongly negatively correlated with MMSE value ($r = -0.579$, $P = 0.006$). Our findings suggest that, in AD patients, the lower the MMSE value is, the higher plasma the t-tau protein level is, which is consistent with the discovery from clinical studies that showed MMSE score is negatively correlated with plasma t-tau concentration (Mattsson et al., 2016). That reveals the severity of AD is positively correlated with the level of t-tau.

To establish the valid prediction model, we initially started with a five-variable model, including Aβ42, t-tau, Aβ42 × t-tau, MMSE, and MoCA. Our prediction model can distinguish AD subjects from control subjects with an accuracy of 98.2 and 97.3%, respectively, and the overall prediction rate is 97.8%. To further simplify our model, we tried different combinations, and discovered three variables, Aβ42, Aβ42 × t-tau, and MoCA, are sensitive enough to yield similar prediction accuracy in comparison to a five-variable prediction model (98.2% for the control group, 94.6% for AD group and the overall 96.7%). Moreover, MoCA is a superior screen tool for the identification of mild cognitive impairment compared to MMSE (Li et al., 2018; Pinto et al., 2019). Therefore, the three-variable model is optimal for predicting early stage AD with MoCA as its neuropsychological measurement. Further ROC curve analysis showed using a three-variable model offered better categorical efficacy, sensitivity, specificity, and AUC compared with using Aβ42 × t-tau alone. We think that the prediction model established by plasma biomarkers has a significant correlation with clinical diagnostics. Lue et al. (2017), using the IMR assay, found that the regression model incorporating age and tau level has 81 and 96% accuracy for identifying probable AD in Banner Sun Health Institute (BSHRI) and National Taiwan University Hospital (NTUH) cohorts, respectively; incorporating age with the products of Aβ42 and tau in BSHRI and NTUH cohorts have 84 and 95% accuracy, respectively. At a 382.68 $(pg/mL)^2$ cutoff value, the product of Aβ42 and tau achieved 92% accuracy with 96% sensitivity and 90% specificity in identifying AD in the combined cohorts. Compared to this study, we relied on PET-PiB, a gold standard for AD in living patients, as one of the criteria for the recruitment of AD patients, and created a new prediction model of AD. This model obtained different cutoff values from the United States and China Taiwan area, and the sensitivity and specificity are more than 95%. The strength of the study is the predictive value of the combination of different parameters. In AD, Aβ and tau proteins are the core biomarkers. Significant increases in Aβ42 and t-tau levels in plasma have been found in early AD patients (Chen et al., 2019; Lue et al., 2019a). Our attempt of combining these two pathological proteins with neuropsychological measurement offers a new avenue of enhancing sensitivity and specificity for diagnosing with plasma biomarkers only, thus overcoming the limitation of plasma biomarkers, as described by Chen et al. (2019) for plasma Aβ42 and t-tau correlate with cognitive decline in amnestic MCI patients.

Although the current study has plausible results, it does have certain limitations. First, the volunteer number included in the study is rather small, thus requiring to expand sample size for further validation of our data and model. Second, the current study is a retrospective study; a further prospective longitudinal study will be extremely valuable.

In conclusion, our study introduced variables Aβ42, t-tau, Aβ42 × t-tau, MMSE, and MoCA into the model and performed analysis; analyzed the role of each variable in the model via logistic regression; further determined using Aβ42, Aβ42 × t-tau, and MoCA for companion diagnosis for AD; compared with previous using a single biomarker; and greatly enhanced the efficacy and stability of the diagnosis. Moreover, as blood samples are more accessible than CSF in community hospitals, plasma biomarkers for early diagnosis of AD can be promoted and popularized. Although early screening and diagnosis of AD are unlikely to rely on a single biomarker or a combination of biomarkers in blood, this information may serve a crucial role for companion diagnosis, so as to give early warning and early intervention for AD for clinicians.

DATA AVAILABILITY STATEMENT

All datasets generated for this study are included in the article/supplementary material.

ETHICS STATEMENT

The studies involving human participants were reviewed and approved by the Medical Ethics Committee of Chinese People's Liberation Army General Hospital. The patients/participants provided their written informed consent to participate in this study.

AUTHOR CONTRIBUTIONS

LW and HS designed the study strategy. YW, SZ, YG, WD, HZ, and LL recruited the participants and collected their information and blood samples. FJ, FY, YW, and JR performed the experiments. FJ, FY, and YG performed the data analysis, data management, and reference collection. FJ, FY, and JR wrote the manuscript. All authors reviewed the manuscript.

FUNDING

This work was supported by the Military Special Health Care Project (Grant No. 15BJZ38).

ACKNOWLEDGMENTS

We are very grateful to all the participants of the study. This work was supported by the Department of Nuclear Medicine in Chinese PLA General Hospital and we deeply appreciate all the work done by clinicians in the Department of Nuclear Medicine.

REFERENCES

Andreasen, N., Minthon, L., Davidsson, P., Vanmechelen, E., Vanderstichele, H., Winblad, B., et al. (2001). Evaluation of CSF-tau and CSF-Abeta42 as diagnostic markers for Alzheimer disease in clinical practice. *Arch. Neurol.* 58, 373–379.

Baird, A. L., Westwood, S., and Lovestone, S. (2015). Blood-based proteomic biomarkers of Alzheimer's disease pathology. *Front Neurol.* 6:236. doi: 10.3389/fneur.2015.00236

Chen, T. B., Lee, Y. J., Lin, S. Y., Chen, J. P., Hu, C. J., Wang, P. N., et al. (2019). Plasma Abeta42 and Total tau predict cognitive decline in amnestic mild cognitive impairment. *Sci. Rep.* 9:13984.

Chiu, M. J., Yang, S. Y., Chen, T. F., Chieh, J. J., Huang, T. Z., Yip, P. K., et al. (2012). New assay for old markers-plasma beta amyloid of mild cognitive impairment and Alzheimer's disease. *Curr. Alzheimer Res.* 9, 1142–1148. doi: 10.2174/156720512804142967

Chiu, M. J., Yang, S. Y., Horng, H. E., Yang, C. C., Chen, T. F., Chieh, J. J., et al. (2013). Combined plasma biomarkers for diagnosing mild cognition impairment and Alzheimer's disease. *ACS Chem. Neurosci.* 4, 1530–1536.

Dage, J. L., Wennberg, A. M. V., Airey, D. C., Hagen, C. E., Knopman, D. S., Machulda, M. M., et al. (2016). Levels of tau protein in plasma are associated with neurodegeneration and cognitive function in a population-based elderly cohort. *Alzheimers Dement.* 12, 1226–1234. doi: 10.1016/j.jalz.2016.06.001

Dubois, B., Hampel, H., Feldman, H. H., Scheltens, P., Aisen, P., Andrieu, S., et al. (2016). Proceedings of the Meeting of the International Working, G., the American Alzheimer's Association on The Preclinical State of, A.D., July, Washington Dc, U.S.A., 2016. Preclinical Alzheimer's disease: definition, natural history, and diagnostic criteria. *Alzheimers Dement.* 12, 292–323. doi: 10.1016/j.jalz.2016.02.002

Fan, L. Y., Tzen, K. Y., Chen, Y. F., Chen, T. F., Lai, Y. M., Yen, R. F., et al. (2018). The relation between brain amyloid deposition, cortical atrophy, and plasma biomarkers in amnesic mild cognitive impairment and Alzheimer's disease. *Front. Aging Neurosci.* 10:175. doi: 10.3389/fnagi.2018.00175

Huynh, R. A., and Mohan, C. (2017). Alzheimer's disease: biomarkers in the genome, blood, and cerebrospinal fluid. *Front. Neurol.* 8:102. doi: 10.3389/fneur.2017.00102

Jack, C. R. Jr., Albert, M. S., Knopman, D. S., McKhann, G. M., Sperling, R. A., Carrillo, M. C., et al. (2011). Introduction to the recommendations from the National Institute on Aging-Alzheimer's Association workgroups on diagnostic guidelines for Alzheimer's disease. *Alzheimers Dement.* 7, 257–262. doi: 10.1016/j.jalz.2011.03.004

Jack, C. R. Jr., Bennett, D. A., Blennow, K., Carrillo, M. C., Dunn, B., Haeberlein, S. B., et al. (2018). NIA-AA Research Framework: toward a biological definition of Alzheimer's disease. *Alzheimers Dement.* 14, 535–562. doi: 10.1016/j.jalz.2018.02.018

Jack, C. R. Jr., Knopman, D. S., Jagust, W. J., Petersen, R. C., Weiner, M. W., Aisen, P. S., et al. (2013). Tracking pathophysiological processes in Alzheimer's disease: an updated hypothetical model of dynamic biomarkers. *Lancet Neurol.* 12, 207–216. doi: 10.1016/s1474-4422(12)70291-0

Kaneko, N., Nakamura, A., Washimi, Y., Kato, T., Sakurai, T., Arahata, Y., et al. (2014). Novel plasma biomarker surrogating cerebral amyloid deposition. *Proc. Jpn. Acad. Ser. B Phys. Biol. Sci.* 90, 353–364. doi: 10.2183/pjab.90.353

Katzman, R. (2008). The prevalence and malignancy of Alzheimer disease: a major killer. *Alzheimers Dement.* 4, 378–380. doi: 10.1016/j.jalz.2008.10.003

Kim, W., Lee, S., and Hall, G. F. (2010). Secretion of human tau fragments resembling CSF-tau in Alzheimer's disease is modulated by the presence of the exon 2 insert. *FEBS Lett.* 584, 3085–3088. doi: 10.1016/j.febslet.2010.05.042

Lee, N. C., Yang, S. Y., Chieh, J. J., Huang, P. T., Chang, L. M., Chiu, Y. N., et al. (2016). Blood beta-amyloid and tau in down syndrome: a comparison with Alzheimer's disease. *Front. Aging Neurosci.* 8:316. doi: 10.3389/fnagi.2016.00316

Li, H., Jia, J., and Yang, Z. (2016). Mini-mental state examination in elderly chinese: a population-based normative study. *J. Alzheimers. Dis.* 53, 487–496. doi: 10.3233/jad-160119

Li, X., Jia, S., Zhou, Z., Jin, Y., Zhang, X., Hou, C., et al. (2018). The role of the Montreal Cognitive Assessment (MoCA) and its memory tasks for detecting mild cognitive impairment. *Neurol. Sci.* 39, 1029–1034. doi: 10.1007/s10072-018-3319-0

Lu, J., Li, D., Li, F., Zhou, A., Wang, F., Zuo, X., et al. (2011). Montreal cognitive assessment in detecting cognitive impairment in Chinese elderly individuals: a population-based study. *J. Geriatr. Psychiatry Neurol.* 24, 184–190. doi: 10.1177/0891988711422528

Lue, L. F., Kuo, Y. M., and Sabbagh, M. (2019a). Advance in Plasma AD Core Biomarker Development: Current Findings from Immunomagnetic Reduction-Based SQUID Technology. *Neurol. Ther.* 8, 95–111. doi: 10.1007/s40120-019-00167-2

Lue, L. F., Pai, M. C., Chen, T. F., Hu, C. J., Huang, L. K., Lin, W. C., et al. (2019b). Age-Dependent Relationship Between Plasma Abeta40 and Abeta42 and total tau levels in cognitively normal subjects. *Front. Aging Neurosci.* 11:222. doi: 10.3389/fnagi.2019.00222

Lue, L. F., Sabbagh, M. N., Chiu, M. J., Jing, N., Snyder, N. L., Schmitz, C., et al. (2017). Plasma Levels of Abeta42 and tau identified probable Alzheimer's dementia: findings in two cohorts. *Front. Aging Neurosci.* 9:226. doi: 10.3389/fnagi.2017.00226

Mattsson, N., Zetterberg, H., Janelidze, S., Insel, P. S., Andreasson, U., Stomrud, E., et al. (2016). Plasma tau in Alzheimer disease. *Neurology* 87, 1827–1835.

Nabers, A., Perna, L., Lange, J., Mons, U., Schartner, J., Guldenhaupt, J., et al. (2018). Amyloid blood biomarker detects Alzheimer's disease. *EMBO Mol. Med.* 10:e8763.

Nakamura, A., Kaneko, N., Villemagne, V. L., Kato, T., Doecke, J., Dore, V., et al. (2018). High performance plasma amyloid-beta biomarkers for Alzheimer's disease. *Nature* 554, 249–254.

Nasreddine, Z. S., Phillips, N. A., Bedirian, V., Charbonneau, S., Whitehead, V., Collin, I., et al. (2005). The Montreal Cognitive Assessment, MoCA: a brief screening tool for mild cognitive impairment. *J. Am. Geriatr. Soc.* 53, 695–699. doi: 10.1111/j.1532-5415.2005.53221.x

Ovod, V., Ramsey, K. N., Mawuenyega, K. G., Bollinger, J. G., Hicks, T., Schneider, T., et al. (2017). Amyloid beta concentrations and stable isotope labeling kinetics of human plasma specific to central nervous system amyloidosis. *Alzheimers Dement.* 13, 841–849. doi: 10.1016/j.jalz.2017.06.2266

Pinto, T. C. C., Machado, L., Bulgacov, T. M., Rodrigues-Junior, A. L., Costa, M. L. G., Ximenes, R. C. C., et al. (2019). Is the Montreal Cognitive Assessment (MoCA) screening superior to the Mini-Mental State Examination (MMSE) in the detection of mild cognitive impairment (MCI) and Alzheimer's Disease (AD) in the elderly? *Int. Psychogeriatr.* 31, 491–504. doi: 10.1017/s1041610218001370

Prestia, A., Caroli, A., van der Flier, W. M., Ossenkoppele, R., Van Berckel, B., Barkhof, F., et al. (2013). Prediction of dementia in MCI patients based on core diagnostic markers for Alzheimer disease. *Neurology* 80, 1048–1056. doi: 10.1212/wnl.0b013e3182872830

Roberts, B. R., Lind, M., Wagen, A. Z., Rembach, A., Frugier, T., Li, Q. X., et al. (2017). Biochemically-defined pools of amyloid-beta in sporadic Alzheimer's disease: correlation with amyloid PET. *Brain* 140, 1486–1498. doi: 10.1093/brain/awx057

Sperling, R., Mormino, E., and Johnson, K. (2014). The evolution of preclinical Alzheimer's disease: implications for prevention trials. *Neuron* 84, 608–622. doi: 10.1016/j.neuron.2014.10.038

Teunissen, C. E., Chiu, M. J., Yang, C. C., Yang, S. Y., Scheltens, P., Zetterberg, H., et al. (2018). Plasma Amyloid-beta (Abeta42) correlates with cerebrospinal fluid Abeta42 in Alzheimer's disease. *J. Alzheimers. Dis.* 62, 1857–1863.

Toledo, J. B., Weiner, M. W., Wolk, D. A., Da, X., Chen, K., Arnold, S. E., et al. (2014). Neuronal injury biomarkers and prognosis in ADNI subjects with normal cognition. *Acta Neuropathol. Commun.* 2:26.

Villemagne, V. L., Burnham, S., Bourgeat, P., Brown, B., Ellis, K. A., Salvado, O., et al. (2013). Amyloid beta deposition, neurodegeneration, and cognitive decline in sporadic Alzheimer's disease: a prospective cohort study. *Lancet Neurol.* 12, 357–367. doi: 10.1016/s1474-4422(13)70044-9

Vos, S. J., Verhey, F., Frolich, L., Kornhuber, J., Wiltfang, J., Maier, W., et al. (2015). Prevalence and prognosis of Alzheimer's disease at the mild cognitive impairment stage. *Brain* 138, 1327–1338.

Vos, S. J., Xiong, C., Visser, P. J., Jasielec, M. S., Hassenstab, J., Grant, E. A., et al. (2013). Preclinical Alzheimer's disease and its outcome: a longitudinal cohort study. *Lancet Neurol.* 12, 957–965. doi: 10.1016/s1474-4422(13)70194-7

Yang, S. Y., Chiu, M. J., Chen, T. F., and Horng, H. E. (2017a). Detection of plasma biomarkers using immunomagnetic reduction: a promising method for the early diagnosis of Alzheimer's disease. *Neurol. Ther.* 6, 37–56. doi: 10.1007/s40120-017-0075-7

Yang, S. Y., Chiu, M. J., Chen, T. F., Lin, C. H., Jeng, J. S., Tang, S. C., et al. (2017b). Analytical performance of reagent for assaying tau protein in human plasma and feasibility study screening neurodegenerative diseases. *Sci. Rep.* 7:9304.

Conflict of Interest: The authors declare that the research was conducted in the absence of any commercial or financial relationships that could be construed as a potential conflict of interest.

frontiers in Aging Neuroscience

ORIGINAL RESEARCH
published: 22 July 2020
doi: 10.3389/fnagi.2020.00217

Pathological Mechanisms Linking Diabetes Mellitus and Alzheimer's Disease: the Receptor for Advanced Glycation End Products (RAGE)

Yanyan Kong[1,2], Fushuai Wang[3], Jiao Wang[3], Cuiping Liu[3], Yinping Zhou[3], Zhengqin Xu[3], Chencheng Zhang[1], Bomin Sun[1] and Yihui Guan[2]**

[1]*Department of Neurosurgery, Ruijin Hospital, Shanghai Jiao Tong University School of Medicine, Shanghai, China,* [2]*PET Center, Huashan Hospital, Fudan University, Shanghai, China,* [3]*Laboratory of Molecular Neural Biology, School of Life Sciences, Shanghai University, Shanghai, China*

Diabetes and Alzheimer's disease (AD) place a significant burden on health care systems in the world and its aging populations. These diseases have long been regarded as separate entities; however, advanced glycation end products (AGEs) and the receptors for AGEs (RAGE) may be a link between diabetes and AD. In our study, mice injected with AGEs through stereotaxic surgery showed significant AD-like features: behavior showed decreased memory; immunofluorescence showed increased phosphorylated tau and APP. These results suggest links between diabetes and AD. Patients with diabetes are at a higher risk of developing AD, and the possible underlying molecular components of this association are now beginning to emerge.

Keywords: advanced glycation end products, RAGE, Alzheimer's disease, diabetes, PI3K

OPEN ACCESS

Edited by:
Woon-Man Kung,
Chinese Culture University, Taiwan

Reviewed by:
Gulam Rabbani,
Yeungnam University, South Korea
Rongqiao He,
Institute of Biophysics (CAS), China

****Correspondence:***
Bomin Sun
sbm11224@rjh.com.cn
Yihui Guan
guanyihui@hotmail.com

Received: *28 March 2020*
Accepted: *19 June 2020*
Published: *22 July 2020*

Citation:
Kong Y, Wang F, Wang J, Liu C, Zhou Y, Xu Z, Zhang C, Sun B and Guan Y (2020) Pathological Mechanisms Linking Diabetes Mellitus and Alzheimer's Disease: the Receptor for Advanced Glycation End Products (RAGE). Front. Aging Neurosci. 12:217. doi: 10.3389/fnagi.2020.00217

INTRODUCTION

Accumulated evidence suggests that sporadic cases account for more than 95% of the total cases of Alzheimer's disease (AD; Levin, 2019). AD is a neurodegenerative disease with progressive memory cognitive dysfunction as the main clinical manifestation. The hallmark lesions observed in the brain of patients with AD result from the formation of numerous neurofibrillary tangles (NFTs) and senile plaques (SPs) composed of hyperphosphorylated tau and Aβ, respectively (Lane et al., 2018). Studies have implicated diabetes mellitus (DM) as a strong risk factor for the development of AD (Jayaraj et al., 2020). DM shares pathological features with AD, such as impaired insulin signaling, increased oxidative stress, increased amyloid-beta (Aβ) production, tauopathy, and cerebrovascular complications (Shinohara and Sato, 2017), and therefore appears to be closely related to AD.

Glycosylation is an important non-enzymatic reaction between reducing sugars and amines (Singh et al., 2018). Lysine or arginine residues of proteins and glucose, moving towards the Schiff-base, convert themselves to the more stable aminomethyl ketone by the Amadori rearrangement and finally result in the formation of advanced glycation end (AGE) products (Bunn and Higgins, 1981; Hartog et al., 2007; Rabbani and Ahn, 2019). The synthesis of AGEs is irreversible, and although the process of cell death is slow and insignificant, the non-enzymatic saccharification process accompanied by neuron metabolism seriously affects the normal functioning of the nervous system (Kamynina et al., 2018).

Therefore, AGEs and the receptor for advanced glycation end-products (RAGE) may play an important role in disease pathogenesis. Many studies have shown that the accumulation of AGEs is a major factor in the incidence and development of several diabetic complications and neuropathies (Hammes et al., 1999; Negre-Salvayre et al., 2009; Singh et al., 2014; Nowotny et al., 2015; Yamagishi et al., 2015; Hashimoto et al., 2016; Kumar Pasupulati et al., 2016), and the accumulation of AGEs under *in vivo* conditions is associated with secondary complications related to diabetes in hyperglycemic environments (Garay-Sevilla et al., 2005). Furthermore, AGEs are closely linked to amyloid-based neurodegenerative diseases (Vicente Miranda and Outeiro, 2010; Li et al., 2012; Simó et al., 2017). Salahuddin et al. (2014) showed that disrupting the AGE-RAGE interaction can effectively prevent the development of AD, and AGEs are therefore considered promising drug targets for AD. Studies also show that the formation of AGEs will pass through and interfered with H1, H2A, and H3 histones by causing structural changes. The normal functioning of serotonin affects chromatin structure and function, leading to secondary complications which in turn aggravates the diabetic condition (Ashraf et al., 2014, 2015a,Ashraf et al., 2015b). The above evidence reveals that AGEs have a role in both diabetes and AD in humans as well as in disease models.

Studies also have found that AGEs induce oxidative stress in neurons, promoting the release of neuroinflammatory cytokines and Aβ (Yan et al., 1996; Baig et al., 2018). At the same time, extracellular AGEs can also affect neuronal function through RAGE. Studies have shown that RAGE also interacts with and mediates the cytotoxicity of Aβ (Wang et al., 2018). For example, the combination of RAGE and Aβ can activate the inflammatory signaling pathway, release ROS to produce oxidative stress, and cause neuroinflammation, cause mitochondrial and neuronal dysfunction (Deane et al., 2008), and affect the mitogen-activated protein kinase signaling pathway (Deane, 2012). RAGE also accelerates the absorption and transport of Aβ, which causes Aβ to pass through the blood-brain barrier and into the central nervous system by endocytosis (Deane et al., 2003), causing cerebrovascular dysfunction and eventually leading to neurovascular inflammation and subsequent increase in synaptic toxicity (Deane and Zlokovic, 2007), which in turn affects the normal functioning of the central nervous system (Zhang et al., 2011; Galasko et al., 2014; Wang et al., 2014; Cai et al., 2016; Fang et al., 2018). The elevated expression of RAGE activates the nuclear transcription factor NF-κB, resulting in a positive feedback effect on inflammation (Wan et al., 2015; Fang et al., 2018). Aβ activation of RAGE increases the expression of proinflammatory cytokines such as TNF-α, interleukin-6, and macrophage colony-stimulating factor (Dukic-Stefanovic et al., 2003), which accelerates the occurrence and development of AD. The RAGE signaling pathway also plays an important role in AGE-induced tau phosphorylation and spatial memory impairment. In SK-N-SH cells, primary hippocampal neurons, and rats, AGEs induce tau hyperphosphorylation *via* the RAGE/GSK-3 pathway (Li et al., 2012; Son et al., 2012). AGEs also block the BDNF-TrkB signaling pathway in rat brain and N2A cells (Li et al., 2012), activate the GSK-3β kinase at Ser9, phosphorylate GSK-3, and induce tau hyperphosphorylation (Wu et al., 2019). Also, the deposition of AGEs activates microglia and nicotinamide adenine dinucleotide phosphate (NADPH) oxidase, resulting in the release of ROS and the formation of peroxynitrite, which oxidizes proteins, lipids, and DNA (Nam et al., 2012), eventually causing neuronal death. Co-immunoprecipitation studies have found that almost all AGE-immunoreactive neurons contain phosphorylated tau protein (Qi et al., 2017), which indicates that AGEs play an important role in tau protein hyperphosphorylation. As compared to AD mice, the phosphorylation levels of tau were increased in the offspring mouse model of diabetes and AD hybridization ($Pdx1^{+/-}$/APP/PS1); furthermore, the production of Aβ was increased and the clearance of Aβ was inhibited (Guo et al., 2016). More and more evidence shows that DM is also a causative factor of AD; therefore, AD is also called type III diabetes (Luchsinger et al., 2001; Huang et al., 2014; Ahmed et al., 2015; Sridhar et al., 2015). As the RAGE signaling pathway may be an important therapeutic target in AD, computer-aided drug design has especially emerged as an efficient means of developing candidate drugs for the treatment of AD. The above observations suggest that the signal pathways mediated by AGEs/RAGE are implicated in AD-like learning and memory impairment, trigger neuroinflammation, and promote Aβ deposition and tau hyperphosphorylation.

Immunohistochemical evidence also suggests that AGEs were co-located with NFTs and SPs, indicating that AGEs can induce AD symptoms (Takeda et al., 2011). AGEs are prooxidant factors that induce oxidative stress, causing neuronal dysfunction or death. It has been reported that GSK-3β is a potential link between diabetes and AD; the excessive activation of GSK-3β can cause hyperphosphorylation of tau (Zhang et al., 2018). LiCl is an inhibitor of GSK-3 (Kurgan et al., 2019), which has been reported to alleviate the hyperphosphorylation of tau proteins caused by AGEs to a certain extent. While AGEs may play an important role in the development of AD, the mechanism remains unclear.

In hyperglycemia and diabetes, the body produces large amounts of AGEs, which accelerate and aggravate the symptoms of diabetes and its complications, such as AD (Simó et al., 2017). AGEs are elevated in AD brains where they stimulate Aβ production and colocalize with NFTs and SPs, suggesting that AGEs play an important role in the pathogenesis of AD (Cai et al., 2016). Studies have found that diabetes can aggravate the decline of tau protein lesions and spatial learning memory in the AD model. Due to advances in clinical treatment, the lifespan of diabetic patients can be further extended, with a higher global incidence of diabetes-associated AD (Ahmed et al., 2015).

AGEs play a central role in the development of AD and link neurodegenerative disease and diabetes. The stage during which AGEs impact AD and how AGEs influence tau proteins and Aβ are still unclear. The effects of increased AGEs on spatial learning and memory, as well as the effects of early inhibition of AGEs production on the behavior and pathophysiology of the AD model, have not yet been reported. Therefore, elucidating

the mechanism of AGEs is important to show the association between diabetes and AD.

In previous studies, the main focus was on the mechanism of AGE-RAGE signaling in neurodegenerative diseases (Juranek et al., 2015; Batkulwar et al., 2018). The purpose of our research is to study the common target (RAGE) between diabetes and AD, and then establish the links between diabetes and AD to RAGE, and further carry out the related mechanism research. We not only studied the mechanism of RAGE in AD, but it's also more important to link diabetes to AD through RAGE.

To explore the role of AGEs in AD and diabetes, we injected AGEs in mice and found that they showed obvious symptoms of AD; behavioral studies showed that memory was impaired, immunofluorescence and western blot showed increased APP and p-Tau levels, and PET and qPCR confirmed this increase in Aβ and Tau levels. Immunofluorescence revealed elevated RAGE, Tau, and APP levels in ZDF rats as well. Therefore, through these experiments, we demonstrated that AGEs-RAGE may be a potential link between AD and diabetes.

MATERIALS AND METHODS

Animals

C57BL/6 mice and ZDF rats were housed in specific pathogen-free (SPF) rooms with a 12-h light-dark cycle and sufficient water and food. All animal handling protocols were approved by the Animal Ethics Committee of Fudan University (No. 20171732A680).

Morris Water Maze

Three days before the experiment, we placed the mouse into the behavioral room to adapt to the environment. A water tank measuring 122 cm in diameter was placed into the water labyrinth and instrument collection area. The tank was filled with water and bleaching powder to make the water turbid. The camera software that measured water maze behavior was adjusted for clarity, light, and brightness using a graphic mark placed approximately 0.1 m from the bottom of the tank. On the first day, a platform was placed above the surface in a single position in the water tank. The mouse was released into the water from the east, west, south, and north directions, and the time until the mouse found the underwater platform and climbed onto it was recorded. On days 2–5, the platform was placed 1 cm below the level of the liquid. Similar to day 1, the mouse was placed in the water from four different orientations. The time until the mouse found the platform hidden under the water and climbed onto it was recorded. If the mouse did not locate the platform within 60 s, the time was recorded as 60 s. On day 6, the platform was removed and the mice were allowed to move freely in the tank for 10 min. The time spent in each quadrant was determined, with a focus on the time the mouse was in the quadrant where the platform was previously located, each quadrant was marked by a different shape on the wall.

Y-Maze

The mice were placed in a behavioral room to adapt to the environment 3 days before the experiment. Different geometric figures were attached to the three arms of the Y-maze as visual markers. The three arms of each Y-maze were randomly divided into new arms, starting arms, and other arms. The Y-maze device was placed in the behavioral camera capture area to adjust for camera clarity, light brightness, and to set up the software. Blocking the new arm, the starting arm and the other arm were opened, allowing the mice to explore for 5 min. Subsequently, all three arms were opened and the mice were allowed to explore freely for 5 min; the time the mice spent exploring the new arm was recorded.

Open Field

The mice were placed in a behavioral room to adapt to the environment 3 days before the experiment. A 120-cm long and wide-field camera equipment was set up in the behavioral acquisition area to adjust the camera sharpness, brightness, and set up the software. The mice were placed in the open field and allowed to move freely for 10 min. The time the mice spent in the central and surrounding areas was recorded.

Protein Extraction

The mice were anesthetized with 2% sodium pentobarbital, and the mouse brain was quickly excised and placed in ice-cold PBS. The mouse hippocampus was isolated in frozen PBS. The hippocampus was placed in a tissue lysis buffer containing protease inhibitors. The tissue was lysed by thorough grinding on ice, was kept on ice for 2 h, and then 500 μg of the hippocampal slurry was centrifuged at 4°C for 10 min. The supernatant was transferred to a new sterile 1.5-ml Eppendorf tube.

The sample was centrifuged again at 13,000 *g* for 20 min under the same conditions. The supernatant was aspirated into a new sterilized EP tube. Each sample received 5× SDS buffer mixed with β-mercaptoethanol and was heated at 99°C for 15 min, immediately followed by a 3 min incubation on ice. The samples were then centrifuged for 3 min and used immediately or stored at −80°C until use.

Western Blot Analysis

The percent SDS PAGE gels were determined according to the molecular weight of the target protein with a 5% separating gel. Protein ladder (1 μl) and protein samples (10 μl) were loaded onto the gel, and the gels were run at 80 V/30 min or 120 V/1.5 h. Afterward, the samples were transferred to a membrane by wet transfer. After the transfer, the membrane was blocked with 5% BSA (diluted in PBS) for 1 h, followed by incubation with the primary antibody (diluted in PBS) overnight at 4°C. The primary antibody was then aspirated off the membrane, which was washed five times with PBST for 5 min. The membrane was incubated with the fluorescent secondary antibody for 1 h at room temperature. The membrane was then washed three times with PBST for 5 min each and then scanned with the Odessey system (LI-COR, Lincoln, NE, USA).

Immunohistochemistry

The brain tissue of the mice treated with AGEs, BSA, and AGEs+LiCl was taken from the 80°C freezer, rinsed three

times with 1× PBS for 5 min each time, and incubated in PBS+0.1% TritonX-100 for 30 min at room temperature to permeate the cell membrane. The sections were then rinsed three times with 1× PBS for 5 min before adding 5% BSA-PBS for 2 h at room temperature to block non-specific binding. The blocking solution was then aspirated, and the primary antibody diluted in 1% BSA-PBS was added [APP (1:1,000, Thermo Fisher Scientific, Waltham, MA, USA), or P-TAU (1:100, Santa Cruz Biotechnology, Santa Cruz, CA, USA)] to the sections, which were incubated at 4°C overnight. The following day, the sections were washed threee times in 1× PBS for 5 min each. A fluorescent secondary antibody (1:500) diluted in 1× PBS was added in the dark and incubated for 2 h at room temperature. The secondary antibody was removed, and DAPI (1:1,000) diluted in 1× PBS was added to the sections for 5 min at room temperature. The DAPI was discarded, and the sections were washed three times in 1× PBS for 5 min each. The slides were photographed using a confocal microscope.

RNA Extraction and Reverse Transcription and Real-Time Quantitative PCR (qPCR)

The hippocampus of the mice treated with AGEs, BSA, and AGEs + LiCl was extracted. Total RNA was extracted using Promega's total RNA extraction kit following the manufacturer guidelines. The concentration of RNA was determined by measuring the absorbance at 260 nm, and 2 μg of RNA was used for first-strand cDNA synthesis using Takara's reverse transcription kit. The mixture of cDNA samples and the indicated primers (**Table 1**) was subjected to at least three replicate qPCR amplification using YEASEN's SYBR Green qPCR mix. Relative gene expression was calculated by comparing the CT value of the gene of interest with the CT value of the internal reference gene *GAPDH*.

The qPCR primer sequences of the human genes (*APP*, *TAU*, *GAPDH*) required for the experiment were found in the Primer Bank, as shown in **Table 1**.

Immunofluorescence

Rat brain slices were washed three times with 1× PBS for 5 min each, treated with 0.2% Triton-X100 (diluted in PBS) for 30 min, and then blocked with 5% BSA for 1 h. Next, the sections were incubated with RAGE, tau, and APP primary antibodies (diluted in PBS) at 4°C overnight. The following day, the sections were washed three times with 1× PBS for 5 min each and then incubated with secondary antibodies for 1.5 h. Finally, DAPI was incubated for 10 min. After washing with PBS, the plate was mounted with a fluorescent mounting plate. The expression of RAGE, tau, and APP was observed on confocal microscopy.

TABLE 1 | List of the primers used for qPCR.

Gene	Primer Sequence (5′ to 3′)
Tau	Forward Primer: TGGGGAACATTCCGTATGAGG
	Reverse Primer: CAGAAGCCATAACCCTTGGG
APP	Forward Primer: AACCGACTCCAGGATGACTATG
	Reverse Primer: TCTGGGGTTCCATGTAAAAGC
GAPDH	Forward Primer: TGGATTTGGACGCATTGGTC
	Reverse Primer: TTTGCACTGGTACGTGTTGAT

RESULTS

Behavioral Experiments Reveal Abnormal Behavior in AGE-Treated Mice

To investigate whether behavior changes develop in mice after the injection of AGEs, we studied the behavior of mice using the Morris Water Maze, Y-maze, and open field experiments. In the water maze test, compared with the control group, the AGE mice stayed in the target area for significantly lesser time, indicating that AGEs impair memory in mice. However, when treated with LiCl, the time spent in the target area significantly increased compared to that of AGE mice, indicating that LiCl can mitigate memory impairment (**Figure 1A**). Similarly, the number of times AGE mice crossed the platform decreased compared with that of the control group; however, when AGE mice were treated with LiCl, the number of times the mouse crossed the platform significantly increased compared to that of AGE mice (**Figure 1B**). This indicated that AGEs impair the memory of mice, while LiCl can alleviate the damage of AGEs.

Y-maze is an effective way to assess short-term memory in mice (Kraeuter et al., 2019). In the Y-maze experiment, compared with the control group, AGE mice stayed in the new arm for significantly lesser time. However, treatment with LiCl increased the time spent in the new arm, indicating that AGEs damage the memory capacity of mice, while LiCl can alleviate the damage of AGEs (**Figure 1C**). In the open field experiment, compared with the control group, AGE mice stayed in the central area for a significantly shorter time. When AGE mice were treated with LiCl, however, the time spent in the central area significantly increased. This indicated that AGEs increased the anxiety behavior of mice, while the addition of LiCl eased the anxiety behavior (**Figure 1D**).

P-tau and APP Increased in the Hippocampus of AGE Mice

To investigate whether mice injected with AGEs develop AD symptoms, we analyzed the expression of P-tau (Phospho-Tau-S356 Rabbit pAb) and APP in the hippocampus of the mice by immunofluorescence, Western blot, and qPCR. The results showed that compared with the BSA control group, the expression of P-tau was significantly up-regulated in AGE mice, while it was not significantly changed in AGE mice treated with LiCl (**Figure 2A**). Compared with the control group, the mRNA expression of tau was significantly up-regulated in AGE mice, while it was not significantly changed in AGE mice treated with LiCl (**Figure 2B**). The same results were verified by immunoblotting (**Figures 2C,D**). Compared with the BSA control group, in AGE mice, the expression of APP protein was significantly up-regulated, while it was not changed in AGE mice treated with LiCl (**Figure 2E**). At the mRNA level, compared with the control group, the mRNA expression of APP in the AGE mice was significantly up-regulated, with no effect of LiCl (**Figure 2F**). This indicated that, compared with the control, the AGE mice successfully developed AD symptoms, which were mitigated when treated with LiCl.

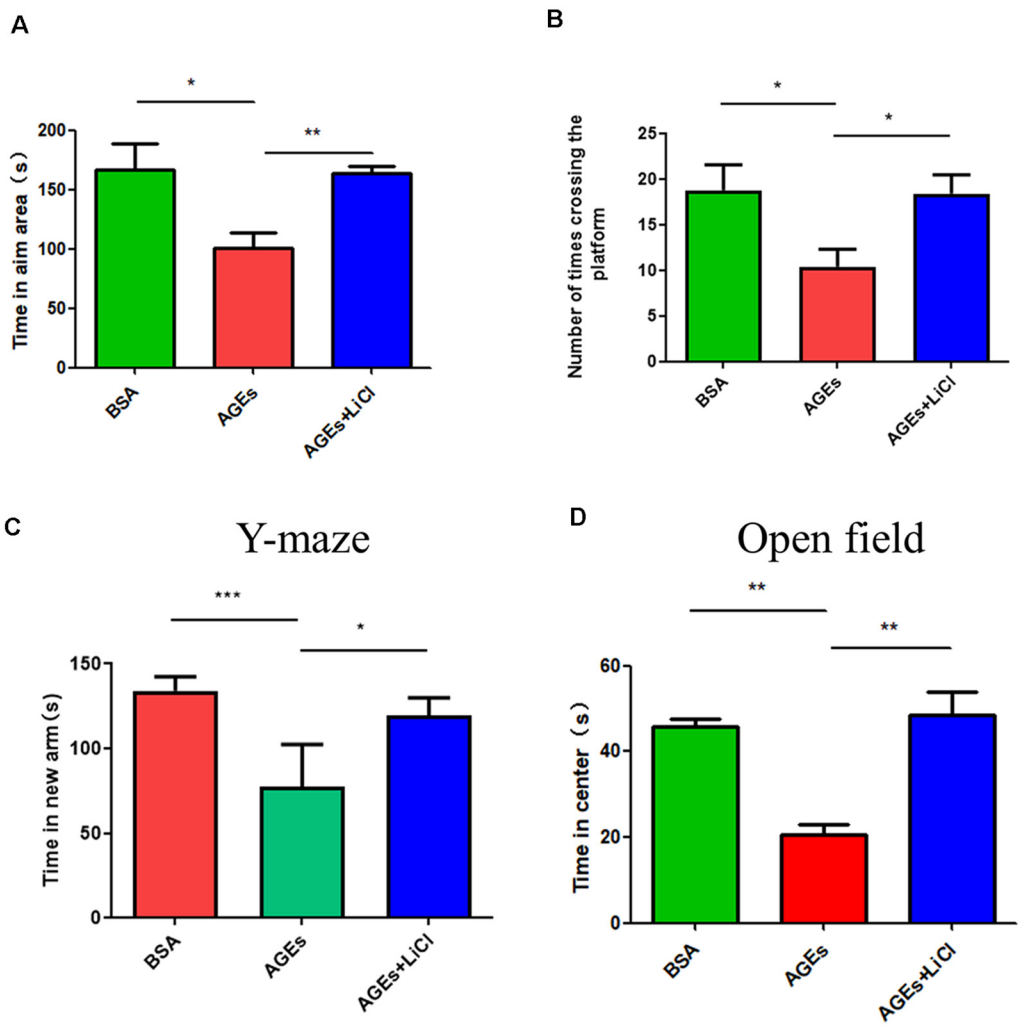

FIGURE 1 | Mice injected with advanced glycation end products (AGEs) show dementia-like behavior. **(A,B)** Water maze experiment was performed on three groups of mice to observe the dementia-like behavior. **(A)** The time that the three groups of mice stayed in the target area was measured. **(B)** The number of times the three groups of mice crossed the platform. The criterion for judging the entry of the mouse into the target area was the entry point of the mouse torso center point. **(C)** Y-maze experiment measured the residence time of three groups of mice injected with BSA, AGEs, AGEs + LiCl in the brain in the new arm of the Y-maze. **(D)** Open-field experiment measured the length of stay of the three groups of mice in the central area time. For each group of mice, $n = 5$. Data are expressed as mean ± standard deviation. One-way analysis of variance (ANOVA). $^{*}p < 0.05$, $^{**}p < 0.01$, $^{***}p < 0.001$.

At the same time, the increase in tau and Aβ in living mice was further verified by PET (**Figures 3A,B**). AV45 and PBB3 injections, respectively, showed that tau and Aβ in AGE mice increased significantly, but were relieved when treating with LiCl. This result further demonstrates that AGEs can promote the occurrence of AD symptoms.

AGEs Increase Tau Phosphorylation *via* the PI3K Signaling Pathway

Many studies have shown that increased phosphorylation of tau is closely related to the PI3K signaling pathway (Wang et al., 2018, 2019; Wei et al., 2019; Zhao et al., 2019). Activation of the PI3K signaling pathway can reduce the over-phosphorylation of tau (Xiong et al., 2020). Therefore, we speculated whether AGEs cause increased tau phosphorylation by affecting the PI3K signaling pathway. To verify our conjecture, we detected the changes in the expression of PI3K protein and its downstream SRC and ERK proteins in the hippocampus of AGE and AGE+LiCl mice. Compared with controls, AGEs significantly down-regulated the protein expression of PI3K in the hippocampus of mice. However, this was up-regulated again after treatment with LiCl, indicating that AGEs may affect the memory of mice through the PI3K signaling pathway and LiCl may alleviate the damage of AGEs to brain function to some

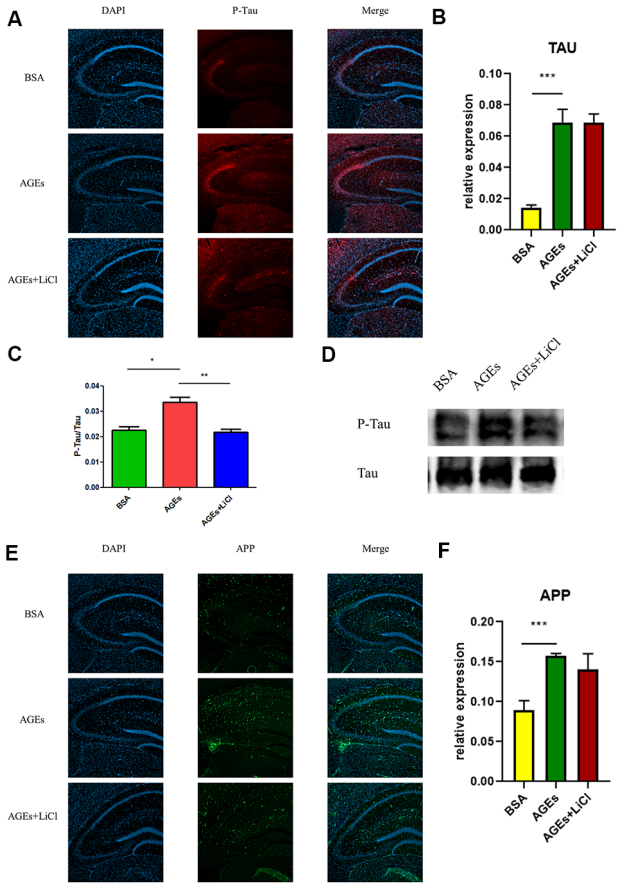

FIGURE 2 | Upregulation of Alzheimer's disease (AD)-related protein expression in advanced glycation end (AGE)-injected mice. **(A–C)** Expression of P-tau in the hippocampus of BSA, AGEs, AGEs + LiCl treated mice. **(A)** P-tau in the hippocampus of three groups of mice was stained with immunofluorescence (red), and nuclei were stained with DAPI (blue). **(B)** qPCR was performed on the hippocampus of the three groups of mice, and the expression of tau-related proteins was measured. The expression level was normalized to the average expression level in the BSA injection group; **(C,D)** Western blotting was performed on the hippocampus of the three groups of mice, and the ratio of the expression levels of P-tau to tau protein in the three groups of mice was calculated and expressed as P -tau/tau value. The gray density was normalized to the average gray density of the tau protein. **(E,F)** APP protein expression in the hippocampus of three groups of mice. **(E)** APP proteins in the hippocampus of the three groups of mice were stained with immunofluorescence (green), and the nuclei were stained with DAPI (blue). **(F)** qPCR was performed on the hippocampus of three groups of mice to measure the expression of APP-related proteins in the hippocampus. The expression level was normalized to the average expression level of the injected BSA group. For each group of mice, $n = 3$. Data are expressed as mean ± standard deviation. One-way ANOVA. $^{*}p < 0.05$, $^{**}p < 0.01$, $^{***}p < 0.001$.

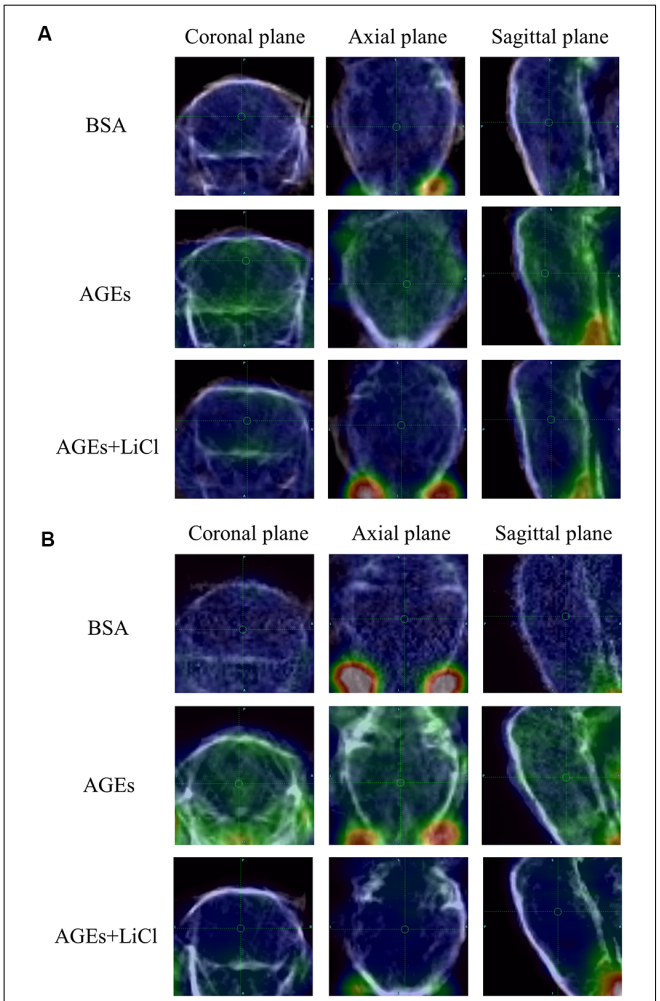

FIGURE 3 | AGE mouse PET image. **(A)** Mice injected with 18F-AV45. Green represents Aβ. **(B)** Mice injected with 18F-PBB3. Green represents tau.

extent (**Figures 4A,B**). Moreover, the protein expression of SRC in the hippocampus of AGE mice was significantly down-regulated, while it was significantly up-regulated again when treated with LiCl, indicating that the down-regulation of PI3K resulted in a decrease in SRC (**Figures 4C,D**). Furthermore, the expression of ERK protein in the hippocampus of AGE mice was significantly decreased. LiCl, however, had no significant effect on the expression of ERK. There was an upward trend of ERK, indicating that AGEs ultimately lead to a decrease in ERK protein through the PI3K signaling pathway, which may be the main signaling pathway leading to phosphorylation of tau protein, and the addition of LiCl can effectively inhibit the action of AGEs (**Figures 4E,F**).

ZDF Rats Show Increased RAGE, APP, and Tau

To further verify the changes of RAGE in diabetes, we investigated whether there is a link between diabetes and AD by detecting changes in APP and tau in ZDF rats. Using immunofluorescence, we found that compared with normal wild rats, RAGE expression in the CA2–CA3 region significantly increased and was aggregated (**Figures 5A,B**). RAGE expression in the CA1 and DG regions was similar (**Figure 5C**). When comparing the expression of tau protein, we found that tau expression in wild SD rats was evenly distributed in the hippocampus, while tau expression in ZDF rats showed an aggregated state (**Figures 5D–F**). Similarly, we found that APP

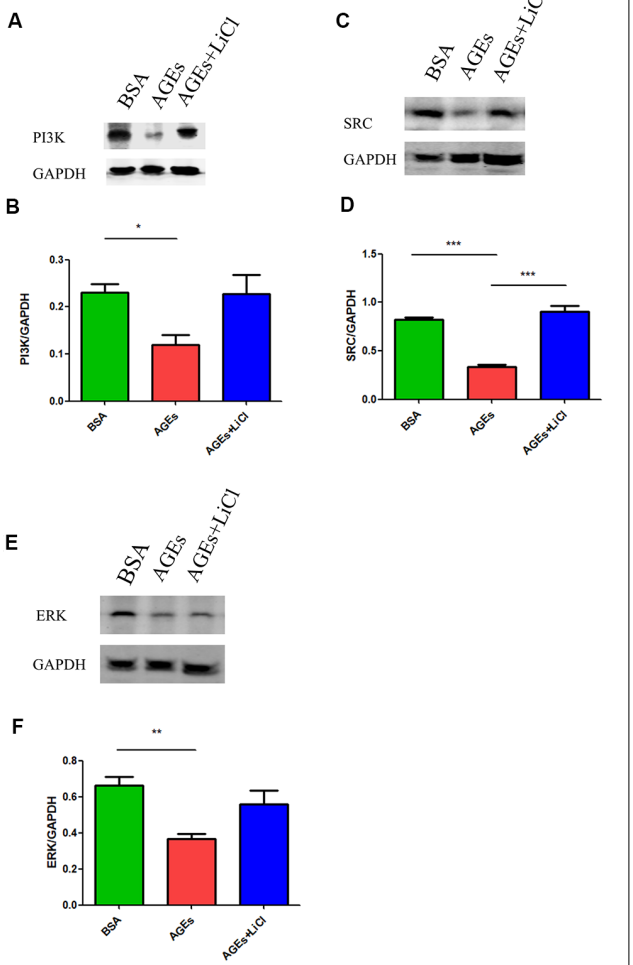

FIGURE 4 | The upregulation of AGEs inhibits the PI3K/SRC/ERK signaling pathway. **(A,B)** Western blotting detection of PI3K protein in the hippocampus of three groups of mice, normalized gray density to the average gray density of GAPDH. **(C,D)** Western blotting detection of SRC protein in the hippocampus of three groups of mice. Gray density was normalized to the average gray density of GAPDH. **(E,F)** Western blotting was performed on ERK proteins in the hippocampus of the three groups of mice, and the gray density was normalized to the average gray density of GAPDH. For each group of mice, $n = 3$. Data are expressed as mean ± standard deviation. One-way ANOVA. $^{*}p < 0.05$, $^{**}p < 0.01$, $^{***}p < 0.001$.

showed a clear upward regulation in the hippocampus of ZDF rats (**Figures 5G–I**). These results indicate that RAGE expression is up-regulated in diabetic rats and that AD-like symptoms (increased tau aggregation and APP expression) occur in the hippocampus of diabetic rats, confirming that there is indeed an association between diabetes and AD.

DISCUSSION

This study investigated the association between diabetes and AD through the treatment of mice with AGEs. First, memory dysfunction in AGE mice was verified by behavior (**Figure 1**). Next, immunofluorescence, qPCR, and Western blotting confirmed an increase in P-tau and APP in the hippocampus of AGE mice (**Figures 2**, **3**). We then speculated that AGEs may cause tau protein hyperphosphorylation through the PI3K signaling pathway (**Figure 4**). At the same time, LiCl improved these symptoms caused by AGEs. Finally, it was confirmed by immunofluorescence experiments in ZDF rats that diabetic rats develop AD symptoms (**Figure 5**). Therefore, our data illustrate the close relationship between diabetes and AD.

When diabetic patients are in a state of hyperglycemia for a long time, glucose will form covalent compound AGEs with plasma. AGEs not only form intracellular and cellular diplomatic links with proteins but also form crosslinks with other endogenous key molecules including lipids and nucleic acids, thereby promoting the development of diabetic complications (Singh et al., 2014). Cognitive dysfunction has been documented as one of the complications of diabetes, suggesting a close link between diabetes and AD (Jash et al., 2020). One of the main symptoms of AD is impaired memory (Sharma et al., 2020); therefore, to test whether the memory is altered in mice after the injection of AGEs, we conducted the Morris Water Maze, Y-maze, and open field tests and found that the memory of AGE mice decreased significantly and anxiety behavior increased, which is consistent with previous AD research (Tian et al., 2019; Du et al., 2020). Subsequently, to further study whether the brain of AGE mice can develop AD symptoms, we assessed the expression of AD-related proteins such as P-tau and APP, which were significantly increased in the hippocampus of AGE mice. This indicates that AGEs promote the occurrence of AD symptoms.

Much research has been done on the relationship between diabetes and AD. Some researchers have proposed that insulin can affect the phosphorylation of tau protein through the GSK-3 signaling pathway (Jash et al., 2020) and that LiCl is an inhibitor of GSK-3 (Kurgan et al., 2019). Therefore, when treated with LiCl, AGEs were not able to phosphorylate tau in large amounts, thereby improving AD symptoms in AGE mice. However, our results did not show that AD symptoms in AGE mice were significantly improved after treatment with LiCl; therefore, we speculate that the GSK-3 signaling pathway is only one of the links between diabetes and AD and other mechanisms have not been studied. Therefore, through AGEs, we speculate that there is a complex relationship between diabetes and AD, and its specific molecular mechanism requires further study.

A previous study reported that AGEs/RAGE interactions can stimulate the activation of multiple signaling cascades, including PI3K, and reduce the mRNA expression of downstream proteins of PI3K signaling pathways, such as AKT2 (Abdelmageed et al., 2019). These data indicate that AGEs/RAGE interactions occur through the PI3K signaling pathway. Furthermore, studies have shown that normal activation of the PI3K signaling pathway can reduce tau hyperphosphorylation (Xiong et al., 2020). Our previous experimental results showed that the proportion of phosphorylated tau protein increased in the hippocampus of mice when AGEs were injected. We further explored whether this is caused by the PI3K signaling pathway. We found that when mice were injected with AGEs, the expression of PI3K, SRC, and ERK proteins in the hippocampus were decreased, and

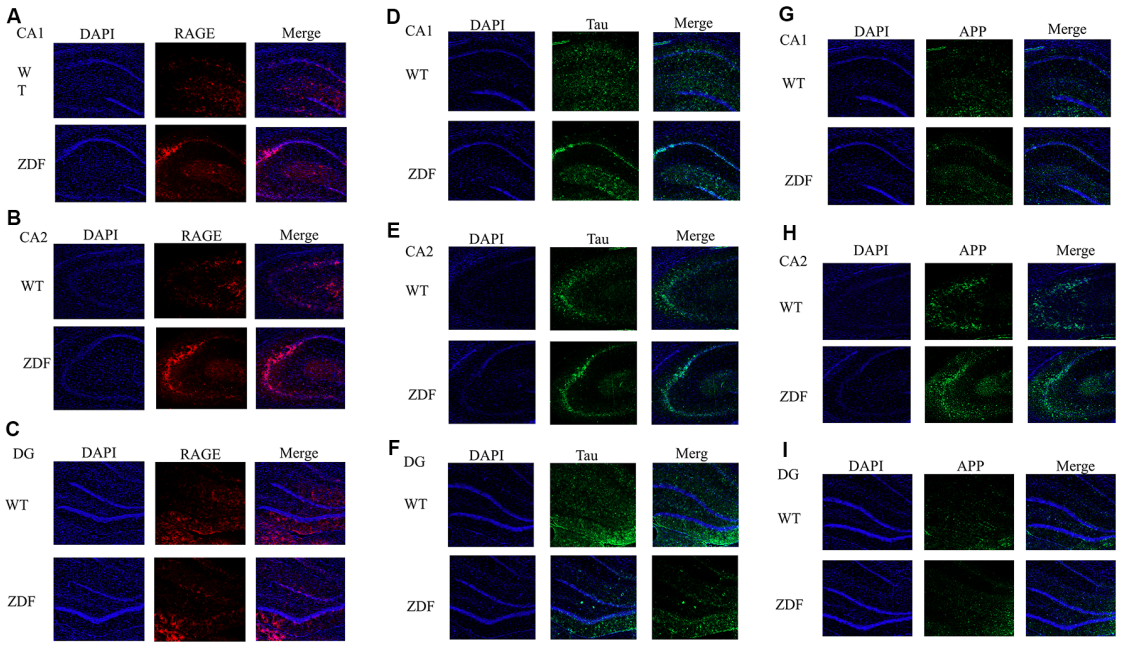

FIGURE 5 | ZDF rats show AD symptoms. **(A–C)** Staining rat hippocampus with RAGE antibody (red) and the nuclei with DAPI (blue). **(D–F)** Staining rat hippocampus with tau antibody (green) and the nuclei with DAPI (blue). **(G–I)** Staining rat hippocampus with APP antibody (green) and the nuclei with DAPI (blue).

the expression of PI3K and SRC increased again after injection of its inhibitor LiCl (**Figure 3**). The class III PI3K/Beclin-1 pathway has certain autophagic activity to promote autophagy clearance of tau (Chen et al., 2020), suggesting that blocking of PI3K-related pathways will hinder tau clearance. AGEs can induce tau hyperphosphorylation in SK-N-SH cells, primary hippocampal neurons, and in SD rats through the RAGE/GSK-3 pathway (Li et al., 2012; Son et al., 2012). The deposits of AGEs will activate microglia and NADPH oxidase, affecting PI3K-related pathways, leading to ROS synthesis and release, and further leading to oxidative stress (Nam et al., 2012; Zhou et al., 2020). In turn, this leads to the deposition of tau, suggesting that blocking the PI3K-related pathways will result in tau deposition. We speculate that AGEs promote the increase in tau phosphorylation by blocking the PI3K signaling pathway and down-regulating the expression of its downstream proteins, while LiCl has a certain relieving effect. However, its specific mechanism remains to be further studied.

Finally, we performed experiments on a diabetic rat model to verify whether symptoms similar to AD would occur in the diabetic model. We found that RAGE expression in the hippocampus of ZDF rats was increased significantly. At the same time, tau and APP expression were also increased, which is similar to the phenotype observed in the AD mouse model (Gallardo and Holtzman, 2019), further illustrating the relationship between diabetes and AD.

In conclusion, mice injected with AGEs showed significant AD-like features including decreased memory and increased phosphorylated tau and APP expression. These results suggest links between diabetes and AD. Patients with diabetes are at a higher risk of developing AD, and the possible underlying molecular components of this association are now beginning to emerge.

DATA AVAILABILITY STATEMENT

All datasets presented in this study are included in the article.

ETHICS STATEMENT

The animal study was reviewed and approved by Animal Ethics Committee of Fudan University.

AUTHOR CONTRIBUTIONS

YK and CZ designed the experiments. YK, FW, CL, YZ, and ZX conducted the experiments. BS and YG obtained funding and revised the manuscript. All authors read and approved the final manuscript.

FUNDING

This study was supported by the National Natural Science Foundation of China (Project No. 81571345, 81701732), Shanghai Municipal Science and Technology Major Project (No. 2018SHZDZX01), ZJLab, and Shanghai Municipal Key Clinical Specialty (shslczdzk03402).

ACKNOWLEDGMENTS

We would like to thank Dr. Natalie Ward (Medical College of Wisconsin, Wauwatosa, WI, USA) for editing this manuscript.

REFERENCES

Abdelmageed, M. E., Shehatou, G. S., Abdelsalam, R. A., Suddek, G. M., and Salem, H. A. (2019). Cinnamaldehyde ameliorates STZ-induced rat diabetes through modulation of IRS1/PI3K/AKT2 pathway and AGEs/RAGE interaction. *Naunyn Schmiedebergs Arch. Pharmacol.* 392, 243–258. doi: 10.1007/s00210-018-1583-4

Ahmed, S., Mahmood, Z., and Zahid, S. (2015). Linking insulin with Alzheimer's disease: emergence as type III diabetes. *Neurol. Sci.* 36, 1763–1769. doi: 10.1007/s10072-015-2352-5

Ashraf, J. M., Ahmad, S., Rabbani, G., Hasan, Q., Jan, A. T., Lee, E. J., et al. (2015a). 3-Deoxyglucosone: a potential glycating agent accountable for structural alteration in H3 histone protein through generation of different AGEs. *PLoS One* 10:e0116804. doi: 10.1371/journal.pone.0116804

Ashraf, J. M., Rabbani, G., Ahmad, S., Hasan, Q., Khan, R. H., Alam, K., et al. (2015b). Glycation of H1 histone by 3-deoxyglucosone: effects on protein structure and generation of different advanced glycation end products. *PLoS One* 10:e0130630. doi: 10.1371/journal.pone.0130630

Ashraf, J. M., Ahmad, S., Rabbani, G., Jan, A. T., Lee, E. J., Khan, R. H., et al. (2014). Physicochemical analysis of structural alteration and advanced glycation end products generation during glycation of H2A histone by 3-deoxyglucosone. *IUBMB Life* 66, 686–693. doi: 10.1002/iub.1318

Baig, M. H., Ahmad, K., Rabbani, G., and Choi, I. (2018). Use of peptides for the management of Alzheimer's disease: diagnosis and inhibition. *Front. Aging Neurosci.* 10:21. doi: 10.3389/fnagi.2018.00021

Batkulwar, K., Godbole, R., Banarjee, R., Kassaar, O., Williams, R. J., and Kulkarni, M. J. (2018). Advanced glycation end products modulate amyloidogenic APP processing and tau phosphorylation: a mechanistic link between glycation and the development of Alzheimer's disease. *ACS Chem. Neurosci.* 9, 988–1000. doi: 10.3389/fnagi.2018.00021

Bunn, H. F., and Higgins, P. J. (1981). Reaction of monosaccharides with proteins: possible evolutionary significance. *Science* 213, 222–224. doi: 10.1126/science.12192669

Cai, Z., Liu, N., Wang, C., Qin, B., Zhou, Y., Xiao, M., et al. (2016). Role of RAGE in Alzheimer's disease. *Cell. Mol. Neurobiol.* 36, 483–495. doi: 10.1007/s10571-015-0233-3

Chen, Y., Chen, Y., Liang, Y., Chen, H., Ji, X., and Huang, M. (2020). Berberine mitigates cognitive decline in an Alzheimer's disease mouse model by targeting both tau hyperphosphorylation and autophagic clearance. *Biomed. Pharmacother.* 121:109670.doi: 10.1016/j.biopha.2019.109670

Deane, R. J. (2012). Is RAGE still a therapeutic target for Alzheimer's disease? *Future Med. Chem.* 4, 915–925. doi: 10.4155/fmc.12.51

Deane, R., Du Yan, S., Submamaryan, R. K., LaRue, B., Jovanovic, S., Hogg, E., et al. (2003). RAGE mediates amyloid-β peptide transport across the blood-brain barrier and accumulation in brain. *Nat. Med.* 9, 907–913. doi: 10.1038/nm890

Deane, R., Sagare, A., and Zlokovic, B. V. (2008). The role of the cell surface LRP and soluble LRP in blood-brain barrier Aβ clearance in Alzheimer's disease. *Curr. Pharm. Des.* 14, 1601–1605. doi: 10.2174/138161208784705487

Deane, R., and Zlokovic, B. V. (2007). Role of the blood-brain barrier in the pathogenesis of Alzheimer's disease. *Curr. Alzheimer Res.* 4, 191–197. doi: 10.2174/156720507780362245

Du, Y., Liu, X., Zhu, X., Liu, Y., Wang, X., and Wu, X. (2020). Activating transcription factor 6 reduces Aβ1–42 and restores memory in Alzheimer's disease model mice. *Int. J. Neurosci.* doi: 10.1080/00207454.2020.1715977 [Epub ahead of print].

Dukic-Stefanovic, S., Gasic-Milenkovic, J., Deuther-Conrad, W., and Munch, G. (2003). Signal transduction pathways in mouse microglia N-11 cells activated by advanced glycation endproducts (AGEs). *J. Neurochem.* 87, 44–55. doi: 10.1046/j.1471-4159.2003.01988.x

Fang, F., Yu, Q., Arancio, O., Chen, D., Gore, S. S., Yan, S. S., et al. (2018). RAGE mediates Aβ accumulation in a mouse model of Alzheimer's disease *via* modulation of β- and γ-secretase activity. *Hum. Mol. Genet.* 27, 1002–1014. doi: 10.1093/hmg/ddy017

Galasko, D., Bell, J., Mancuso, J. Y., Kupiec, J. W., Sabbagh, M. N., van Dyck, C., et al. (2014). Clinical trial of an inhibitor of RAGE-Aβ interactions in Alzheimer disease. *Neurology* 82, 1536–1542. doi: 10.1212/WNL.0000000000000364

Gallardo, G., and Holtzman, D. M. (2019). Amyloid-β and tau at the crossroads of Alzheimer's disease. *Adv. Exp. Med. Biol.* 1184, 187–203. doi: 10.1007/978-981-32-9358-8_16

Garay-Sevilla, M. E., Regalado, J. C., Malacara, J. M., Nava, L. E., Wrobel-Zasada, K., Castro-Rivas, A., et al. (2005). Advanced glycosylation end products in skin, serum, saliva and urine and its association with complications of patients with type 2 diabetes mellitus. *J. Endocrinol. Invest.* 28, 223–230. doi: 10.1007/BF03345377

Guo, C., Zhang, S., Li, J. Y., Ding, C., Yang, Z. H., Chai, R., et al. (2016). Chronic hyperglycemia induced *via* the heterozygous knockout of Pdx1 worsens neuropathological lesion in an Alzheimer mouse model. *Sci. Rep.* 6:29396. doi: 10.1038/srep29396

Hammes, H. P., Alt, A., Niwa, T., Clausen, J. T., Bretzel, R. G., Brownlee, M., et al. (1999). Differential accumulation of advanced glycation end products in the course of diabetic retinopathy. *Diabetologia* 42, 728–736. doi: 10.1007/s001250051221

Hartog, J. W., Voors, A. A., Bakker, S. J., Smit, A. J., and van Veldhuisen, D. J. (2007). Advanced glycation end-products (AGEs) and heart failure: pathophysiology and clinical implications. *Eur. J. Heart Fail.* 9, 1146–1155. doi: 10.1016/j.ejheart.2007.09.009

Hashimoto, K., Kunikata, H., Yasuda, M., Ito, A., Aizawa, N., Sawada, S., et al. (2016). The relationship between advanced glycation end products and ocular circulation in type 2 diabetes. *J. Diabetes Complications* 30, 1371–1377. doi: 10.1016/j.jdiacomp.2016.04.024

Huang, C. C., Chung, C. M., Leu, H. B., Lin, L. Y., Chiu, C. C., Hsu, C. Y., et al. (2014). Diabetes mellitus and the risk of Alzheimer's disease: a nationwide population-based study. *PLoS One* 9:e87095. doi: 10.1371/journal.pone.0087095

Jash, K., Gondaliya, P., Kirave, P., Kulkarni, B., Sunkaria, A., and Kalia, K. (2020). Cognitive dysfunction: a growing link between diabetes and Alzheimer's disease. *Drug Dev. Res.* 81, 144–164. doi: 10.1002/ddr.21579

Jayaraj, R. L., Azimullah, S., and Beiram, R. (2020). Diabetes as a risk factor for Alzheimer's disease in the Middle East and its shared pathological mediators. *Saudi J. Biol. Sci.* 27, 736–750. doi: 10.1016/j.sjbs.2019.12.028

Juranek, J., Ray, R., Banach, M., and Rai, V. (2015). Receptor for advanced glycation end-products in neurodegenerative diseases. *Rev. Neurosci.* 26, 691–698. doi: 10.1515/revneuro-2015-0003

Kamynina, A. V., Esteras, N., Koroev, D. O., Bobkova, N. V., Balasanyants, S. M., Simonyan, R. A., et al. (2018). Synthetic fragments of receptor for advanced glycation end products bind β-amyloid 1–40 and protect primary brain cells from β-amyloid toxicity. *Front. Neurosci.* 12:681. doi: 10.3389/fnins.2018.00681

Kraeuter, A. K., Guest, P. C., and Sarnyai, Z. (2019). The Y-Maze for assessment of spatial working and reference memory in mice. *Methods Mol. Biol.* 1916, 105–111. doi: 10.1007/978-1-4939-8994-2_10

Kumar Pasupulati, A., Chitra, P. S., and Reddy, G. B. (2016). Advanced glycation end products mediated cellular and molecular events in the pathology of diabetic nephropathy. *Biomol. Concepts* 7, 293–309. doi: 10.1515/bmc-2016-0021

Kurgan, N., Whitley, K. C., Maddalena, L. A., Moradi, F., Stoikos, J., Hamstra, S. I., et al. (2019). A low-therapeutic dose of lithium inhibits GSK3 and enhances myoblast fusion in C2C12 cells. *Cells* 8:1340. doi: 10.3390/cells8111340

Lane, C. A., Hardy, J., and Schott, J. M. (2018). Alzheimer's disease. *Eur. J. Neurol.* 25, 59–70. doi: 10.1111/ene.13439

Levin, J. (2019). Parkinsonism in genetic and sporadic Alzheimer's disease. *Int. Rev. Neurobiol.* 149, 237–247. doi: 10.1016/bs.irn.2019.10.005

Li, J., Liu, D., Sun, L., Lu, Y., and Zhang, Z. (2012). Advanced glycation end products and neurodegenerative diseases: mechanisms and perspective. *J. Neurol. Sci.* 317, 1–5. doi: 10.1016/j.jns.2012.02.018

Li, X.-H., Lv, B.-L., Xie, J.-Z., Liu, J., Zhou, X.-W., and Wang, J.-Z. (2012). AGEs induce Alzheimer-like tau pathology and memory deficit *via* RAGE-mediated GSK-3 activation. *Neurobiol. Aging* 33, 1400–1410. doi: 10.1016/j.neurobiolaging.2011.02.003

Luchsinger, J. A., Tang, M. X., Stern, Y., Shea, S., and Mayeux, R. (2001). Diabetes mellitus and risk of Alzheimer's disease and dementia with stroke in a multiethnic cohort. *Am. J. Epidemiol.* 154, 635–641. doi: 10.1093/aje/154.7.635

Nam, J. H., Park, K. W., Park, E. S., Lee, Y. B., Lee, H. G., Baik, H. H., et al. (2012). Interleukin-13/-4-induced oxidative stress contributes to death of hippocampal

neurons in aβ1–42-treated hippocampus *in vivo*. *Antioxid. Redox Signal.* 16, 1369–1383.

Negre-Salvayre, A., Salvayre, R., Auge, N., Pamplona, R., and Portero-Otin, M. (2009). Hyperglycemia and glycation in diabetic complications. *Antioxid. Redox Signal.* 11, 3071–3109. doi: 10.1089/ars.2009.2484

Nowotny, K., Jung, T., Hohn, A., Weber, D., and Grune, T. (2015). Advanced glycation end products and oxidative stress in type 2 diabetes mellitus. *Biomolecules* 5, 194–222. doi: 10.3390/biom5010194

Qi, L., Chen, Z., Wang, Y., Liu, X., Liu, X., Ke, L., et al. (2017). Subcutaneous liraglutide ameliorates methylglyoxal-induced Alzheimer-like tau pathology and cognitive impairment by modulating tau hyperphosphorylation and glycogen synthase kinase-3β. *Am. J. Transl. Res.* 9, 247–260.

Rabbani, G., and Ahn, S. N. (2019). Structure, enzymatic activities, glycation and therapeutic potential of human serum albumin: a natural cargo. *Int. J. Biol. Macromol.* 123, 979–990. doi: 10.1016/j.ijbiomac.2018.11.053

Salahuddin, P., Rabbani, G., and Khan, R. H. (2014). The role of advanced glycation end products in various types of neurodegenerative disease: a therapeutic approach. *Cell. Mol. Biol. Lett.* 19, 407–437. doi: 10.2478/s11658-014-0205-5

Sharma, P., Sharma, A., Fayaz, F., Wakode, S., and Pottoo, F. H. (2020). Biological signatures of Alzheimer disease. *Curr. Top. Med. Chem.* 20, 770–781. doi: 10.2174/1568026620666200228095553

Shinohara, M., and Sato, N. (2017). Bidirectional interactions between diabetes and Alzheimer's disease. *Neurochem. Int.* 108, 296–302. doi: 10.1016/j.neuint.2017.04.020

Simó, R., Ciudin, A., Simo-Servat, O., and Hernandez, C. (2017). Cognitive impairment and dementia: a new emerging complication of type 2 diabetes-The diabetologist's perspective. *Acta Diabetol.* 54, 417–424. doi: 10.1007/s00592-017-0970-5

Singh, V. P., Bali, A., Singh, N., and Jaggi, A. S. (2014). Advanced glycation end products and diabetic complications. *Korean J. Physiol. Pharmacol.* 18, 1–14. doi: 10.4196/kjpp.2014.18.1.1

Singh, Y., Wang, T., Geringer, S. A., Stine, K. J., and Demchenko, A. V. (2018). Regenerative glycosylation. *J. Org. Chem.* 83, 374–381. doi: 10.1021/acs.joc.7b02768

Son, S. M., Jung, E. S., Shin, H. J., Byun, J., and Mook-Jung, I. (2012). Aβ-induced formation of autophagosomes is mediated by RAGE-CaMKKβ-AMPK signaling. *Neurobiol. Aging* 33, 1006.e11–1006.e23. doi: 10.1016/j.neurobiolaging.2011.09.039

Sridhar, G. R., Lakshmi, G., and Nagamani, G. (2015). Emerging links between type 2 diabetes and Alzheimer's disease. *World J. Diabetes* 6, 744–751. doi: 10.4239/wjd.v6.i5.744

Takeda, S., Sato, N., Rakugi, H., and Morishita, R. (2011). Molecular mechanisms linking diabetes mellitus and Alzheimer disease: β-amyloid peptide, insulin signaling, and neuronal function. *Mol. Biosyst.* 7, 1822–1827. doi: 10.1039/c0mb00302f

Tian, H., Ding, N., Guo, M., Wang, S., Wang, Z., Liu, H., et al. (2019). Analysis of learning and memory ability in an Alzheimer's disease mouse model using the morris water maze. *J. Vis. Exp.* 152:e60055. doi: 10.3791/60055

Vicente Miranda, H., and Outeiro, T. F. (2010). The sour side of neurodegenerative disorders: the effects of protein glycation. *J. Pathol.* 221, 13–25. doi: 10.1002/path.2682

Wan, W., Cao, L., Liu, L., Zhang, C., Kalionis, B., Tai, X., et al. (2015). Aβ(1–42) oligomer-induced leakage in an *in vitro* blood-brain barrier model is associated with up-regulation of RAGE and metalloproteinases and down-regulation of tight junction scaffold proteins. *J. Neurochem.* 134, 382–393. doi: 10.1111/jnc.13122

Wang, H., Chen, F., Du, Y. F., Long, Y., Reed, M. N., Hu, M., et al. (2018). Targeted inhibition of RAGE reduces amyloid-β influx across the blood-brain barrier and improves cognitive deficits in db/db mice. *Neuropharmacology* 131, 143–153. doi: 10.1016/j.neuropharm.2017.12.026

Wang, S., He, B., Hang, W., Wu, N., Xia, L., Wang, X., et al. (2018). Berberine alleviates tau hyperphosphorylation and axonopathy-associated with diabetic encephalopathy *via* restoring PI3K/Akt/GSK3β pathway. *J. Alzheimers Dis.* 65, 1385–1400. doi: 10.3233/jad-180497

Wang, J., Li, W., Zhou, F., Feng, R., Wang, F., Zhang, S., et al. (2019). ATP11B deficiency leads to impairment of hippocampal synaptic plasticity. *J. Mol. Cell Biol.* 11, 688–702. doi: 10.1093/jmcb/mjz042

Wang, X., Yu, S., Hu, J.-P., Wang, C.-Y., Wang, Y., Liu, H.-X., et al. (2014). Streptozotocin-induced diabetes increases amyloid plaque deposition in AD transgenic mice through modulating AGEs/RAGE/NF-κB pathway. *Int. J. Neurosci.* 124, 601–608. doi: 10.3109/00207454.2013.866110

Wei, T., Wang, Y., Xu, W., Liu, Y., Chen, H., and Yu, Z. (2019). KCa3.1 deficiency attenuates neuroinflammation by regulating an astrocyte phenotype switch involving the PI3K/AKT/GSK3β pathway. *Neurobiol. Dis.* 132:104588. doi: 10.1016/j.nbd.2019.104588

Wu, B., Wang, Y., Shi, C., Chen, Y., Yu, L., Li, J., et al. (2019). Ribosylation-derived advanced glycation end products induce tau hyperphosphorylation through brain-derived neurotrophic factor reduction. *J. Alzheimers Dis.* 71, 291–305. doi: 10.3233/jad-190158

Xiong, R., Wang, X.-L., Wu, J.-M., Tang, Y., Qiu, W.-Q., Shen, X., et al. (2020). Polyphenols isolated from lychee seed inhibit Alzheimer's disease-associated Tau through improving insulin resistance *via* the IRS-1/PI3K/Akt/GSK-3β pathway. *J. Ethnopharmacol.* 251:112548. doi: 10.1016/j.jep.2020.112548

Yamagishi, S., Nakamura, N., Suematsu, M., Kaseda, K., and Matsui, T. (2015). Advanced glycation end products: a molecular target for vascular complications in diabetes. *Mol. Med.* 21, S32–S40. doi: 10.2119/molmed.2015.00067

Yan, S. D., Chen, X., Fu, J., Chen, M., Zhu, H., Roher, A., et al. (1996). RAGE and amyloid-β peptide neurotoxicity in Alzheimer's disease. *Nature* 382, 685–691. doi: 10.1038/382685a0

Zhang, Y., Huang, N. Q., Yan, F., Jin, H., Zhou, S. Y., Shi, J. S., et al. (2018). Diabetes mellitus and Alzheimer's disease: GSK-3β as a potential link. *Behav. Brain Res.* 339, 57–65. doi: 10.1016/j.bbr.2017.11.015

Zhang, Z., Liu, S., Shi, R., and Zhao, G. (2011). miR-27 promotes human gastric cancer cell metastasis by inducing epithelial-to-mesenchymal transition. *Cancer Genet.* 204, 486–491. doi: 10.1016/j.cancergen.2011.07.004

Zhao, Z.-Y., Zhang, Y.-Q., Zhang, Y.-H., Wei, X.-Z., Wang, H., Zhang, M., et al. (2019). The protective underlying mechanisms of Schisandrin on SH-SY5Y cell model of Alzheimer's disease. *J. Toxicol. Environ. Health A* 82, 1019–1026. doi: 10.1080/15287394.2019.1684007

Zhou, L., Song, H., Zhang, Y., Ren, Z., Li, M., and Fu, Q. (2020). Polyphyllin VII attenuated RANKL-induced osteoclast differentiation *via* inhibiting of TRAF6/c-Src/PI3K pathway and ROS production. *BMC Musculoskelet. Disord.* 21:112. doi: 10.1186/s12891-020-3077-z

Conflict of Interest: The authors declare that the research was conducted in the absence of any commercial or financial relationships that could be construed as a potential conflict of interest.

frontiers in Aging Neuroscience

ORIGINAL RESEARCH
published: 28 July 2020
doi: 10.3389/fnagi.2020.00202

Volumetric and Diffusion Abnormalities in Subcortical Nuclei of Older Adults With Cognitive Frailty

Mingyue Wan[1†], Rui Xia[1†], Huiying Lin[1], Pingting Qiu[1], Jianquan He[1], Yu Ye[1], Jing Tao[1,2], Lidian Chen[1,2] and Guohua Zheng[3*]*

[1]College of Rehabilitation Medicine, Fujian University of Traditional Chinese Medicine, Fuzhou, China, [2]Fujian Key Laboratory of Rehabilitation Technology, Fujian University of Traditional Chinese Medicine, Fuzhou, China, [3]College of Nursing and Health Management, Shanghai University of Medicine and Health Sciences, Shanghai, China

Background: Cognitive frailty (CF) is defined as the simultaneous presence of physical frailty and cognitive impairment among older adults without dementia. Previous studies have revealed that neuropathological changes may contribute to the degeneration of subcortical nuclei in the process of cognitive impairment. However, it is unclear in CF. The aim of this study is to investigate the changes in subcortical nuclei in older adults with CF and their relationship with cognitive decline and physical frailty.

Methods: A total of 26 older adults with CF and 26 matched healthy subjects were enrolled. Cognitive function and physical frailty were assessed with the Montreal Cognitive Assessment (MoCA) scale (Fuzhou version) and the Chinese version of the Edmonton Frailty Scale (EFS). Volumetric and diffusion tensor imaging (DTI) parameters of subcortical nuclei were measured with structural and DTI brain magnetic resonance imaging (MRI) and compared between groups. Partial correlation analysis was conducted between subcortical nuclei volumes, MoCA scores, and physical frailty indexes.

Results: Significant volume reductions were found in five subcortical nuclei, including the bilateral thalami, left caudate, right pallidum, and accumbens area, in older adults with CF ($P < 0.05$), and the bilateral thalami was most obvious. Decreased fractional anisotropy and relative anisotropy values were observed only in the left thalamus in the CF group ($P < 0.05$). No group differences were found in apparent diffusion coefficient (ADC) values. The MoCA scores were positively correlated with the volumes of the bilateral thalami, right pallidum, and accumbens area ($P < 0.05$). Negative correlations were found between the physical frailty index and the volumes of the bilateral thalami, caudate, pallidum, and right accumbens area ($P < 0.05$).

Conclusion: Microstructural changes occur in the subcortical nuclei of older adults with CF, and these changes are correlated with cognitive decline and physical frailty. Therefore, microstructural atrophy of the subcortical nuclei may be involved in the pathological progression of CF.

Keywords: cognitive frailty, subcortical nuclei, diffusion tensor imaging, volume, correlation

OPEN ACCESS

Edited by:
Woon-Man Kung, Chinese Culture University, Taiwan

Reviewed by:
Laura Eva Jonkman, VU University Medical Center, Netherlands
Emmanuel Brouillet, Commissariat à l'Energie Atomique et aux Energies Alternatives (CEA), France

***Correspondence:**
Lidian Chen
cld@fjtcm.edu.cn
Guohua Zheng
zhenggh@sumhs.edu.cn

[†]These authors have contributed equally to this work

Received: *17 March 2020*
Accepted: *11 June 2020*
Published: *28 July 2020*

Citation:
Wan M, Xia R, Lin H, Qiu P, He J, Ye Y, Tao J, Chen L and Zheng G (2020) Volumetric and Diffusion Abnormalities in Subcortical Nuclei of Older Adults With Cognitive Frailty. Front. Aging Neurosci. 12:202. doi: 10.3389/fnagi.2020.00202

INTRODUCTION

Cognitive frailty (CF) was first defined in 2013 by the International Academy on Nutrition and Aging (I.A.N.A.) and the International Association of Gerontology and Geriatrics (I.A.G.G.; Kelaiditi et al., 2013). Cognitive frailty has a heterogeneous clinical manifestation characterized by the simultaneous presence of both physical frailty and cognitive impairment among older adults without dementia. Epidemiological surveys based on community people estimated the prevalence rate of CF to be 1.0% to 22.0% (Shimada et al., 2016; Feng et al., 2017), whereas in the clinical setting, the figure was much higher at 10.7% to 40% (Malek et al., 2019). Cognitive frailty has been identified to be associated with an increased risk of severe adverse events in older people, such as dementia and disability and even mortality. Therefore, CF is recognized as an important threat to healthy aging. With the growing understanding of CF as an important clinical syndrome, identifying biomarkers of pathophysiological changes has become paramount. Furthermore, it is helpful to map its biological markers for the development of secondary preventive treatments for this disorder.

Clinically, the judgment of CF is typically established using tests of physical and mental status, including the Clinical Dementia Rating (CDR) and Montreal Cognitive Assessment (MoCA) or Mini-Mental State Examination (MMSE; Won et al., 2018). With the development of morphometric magnetic resonance imaging (MRI) technology, robust imaging biomarkers for some diseases related to brain damage have educed the potential for clinical impact. For example, MRI studies based on voxel-based morphometry analysis have established the association of cognitive impairment and morphometric changes in the brain. Previous studies have reported reductions in the volumes of the whole hippocampus, medial temporal lobe, and entorhinal cortex in the brains of older adults with cognitive impairment compared to healthy subjects (Anatürk et al., 2018; Gu and Zhang, 2019). Cortical gray matter atrophy first occurs in the temporal cortex and is followed by occipital, parietal, and frontal atrophy along a temporospatial gradient with the progression of cognitive decline (Fennema-Notestine et al., 2009). Considering that microstructural changes likely precede macrostructural changes, studies have revealed that the degeneration of subcortical nuclei also contributes to neuropathological changes in the process of cognitive impairment (Tentolouris-Piperas et al., 2017). However, compared to macroscopic measurements, the underlying microstructural changes seem complicated and heterogeneous (Gong et al., 2017).

Diffusion tensor imaging (DTI) can be used to quantify microscopic white/gray matter integrity not detectable on conventional MRI and is sensitive for detecting microstructural volumetric impairment through the intrinsic properties of water diffusion (Mori and Zhang, 2006). DTI has helped to explain neuropathological mechanisms for different neuropsychiatric conditions (Cherubini et al., 2010). Several studies have used DTI to explore the microstructural changes in subcortical nuclei in conditions associated with cognitive decline (Eustache et al., 2016; Mak et al., 2017). Moreover, few studies have focused on CF. However, there have been reports of different patterns of degeneration that were compatible with either mild cognitive impairment or physical frailty. The aim of the present study was to investigate microstructural volumetric changes in brain DTI indexes in older adults with CF and to compare their trajectories with those of healthy older adults.

MATERIALS AND METHODS

Participants

Twenty-six older adults with CF and 26 matched healthy controls (HCs) participated in this study. All participants were right-handed native Chinese speakers. The CF participants were all recruited from the communities in Fuzhou City, Fujian Province, China, and the HC participants were recruited from the same communities. Written informed consent was obtained from all participants before data collection. This study was approved by the ethics committee of the Second People's Hospital affiliated with Fujian University of Traditional Chinese Medicine. All CF participants met the following inclusion criteria: (1) Chinese version of Edmonton Frailty Scale (EFS) $\geq$5 points; (2) Fuzhou version MoCA score $\leq$26 points; (3) age $\geq$60 years old; and (4) CDR score = 0.5 (i.e., did not meet the criteria for dementia). The controls did not have CF syndrome, which was confirmed using the assessment of EFS and MoCA scale. Individuals who met the following conditions, which were assessed based on medical records, were excluded: (1) had hypertension and uncontrollable blood pressure (systolic blood pressure >160 mm Hg or diastolic blood pressure >100 mm Hg after taking drug); (2) had a history of alcohol and drug abuse; (3) had a history of mental illness (such as personality disorder, schizophrenia, etc.), severe depression (Baker Depression Scale >10 points), severe aphasia and audiovisual impairment, severe organ failure, cerebral hemorrhage, cerebral infarction, history of myocardial infarction, history of coronary heart disease, musculoskeletal disease, and other sports contraindications; (4) had metal implants (such as fixed metal dentures, pacemakers, etc.); and (5) were not suitable for MRI scans.

MRI Data Acquisition

The structural MRI and diffusion tensor MRI data for all participants were collected at Fujian Province Rehabilitation Hospital. MRI scans were acquired with a Siemens Prisma 3.0-T magnetic resonance scanner (Siemens Medical System, Erlangen, Germany) and a Siemens 64-channel head-neck joint coil. The subject lay back on the scanning bed, his/her head was properly fixed, and rubber earplugs were used to reduce the noise impact of the machine. High-resolution structural images were acquired by using a three-dimensional T1-weighed magnetization-prepared rapid acquisition of a gradient echo sequence with the following parameters: repetition time (TR) = 2,300 ms, echo time (TE) = 2.27 ms, flip angle = 8°, slice thickness = 1.0 mm, field of view (FOV) = 250 × 250 mm, matrix = 256 × 256, voxel size = 0.98 × 0.98 × 1 mm^3, and number of slices = 160. For DTI, the following parameters were used: TR = 8,000 ms, TE = 64 ms, FOV = 224 × 224 mm, slice

TABLE 1 | Demographic and cognitive and physical frailty data of two groups.

	Cognitive frailty	Health control	*t*	*P*
Number	26	26		
Sex (male/female, *n*)*	13/13	13/13		1.000
Age (years)#	65.42 ± 5.147	65.38 ± 4.7	0.028	0.978
Edu (years)#	9.77 ± 3.983	10.96 ± 3.243	−1.184	0.242
BDI (scores)#	3.96 ± 1.928	4.62 ± 1.134	−1.49	0.144
MoCA (scores)#	19.31 ± 3.056	26.77 ± 0.863	−11.98	<0.001
FI (scores)#	5.54 ± 0.761	2.19 ± 1.266	8.263	<0.001

*Edu, education year; BDI, Beck Depression Inventory; MoCA, Montreal Cognitive Assessment; FI, Frailty index. *Chi-square test was used for data analysis. #t-test was used for data analysis. P-values for cognitive frailty vs. health control group comparison.*

thickness = 2.0 mm, gap = 0 mm, slice number = 75, and slice order = interleaved.

Image Processing

The original data from the magnetic resonance image machine were transformed from DICOM format to nifti format file and classified into T1 images and DTI images by MRIconvert software (version 2.0 Rev. 235[1]). T1 image analysis was carried out with FreeSurfer software (version 6.0.0[2]). DTI analysis was carried out with FSL software (version 5.0.10[3]).

Volumes of the Subcortical Nuclei Analysis

The T1 image preprocessing procedure included image format conversion, image quality check, Talairach transformation (this computes the affine transform from the original volume to the MNI305 atlas), intensity normalization, skull stripping, segmentation of gray and white matter, tessellation of the gray and white matter boundary, automatic subcortical segmentation, automatic topology fixer, and smoothing.

For comparisons of the volumes of the subcortical structures between the groups, the automatic extraction technology of FreeSurfer was used. FreeSurfer segments the brain into several regions that have a unique id. Through the segmentation id, we could identify the nuclei of interest and extract their information. The volumes of the subcortical nuclei, including the thalamus, caudate, putamen, pallidum, hippocampus, amygdala, and accumbens area of both sides, were extracted.

Diffusion Parameters of the Subcortical Nuclei

The DTI image data preprocessing procedure included image format conversion, image quality check, eddy current and motion correction, skull stripping, DTI tensor [including fractional anisotropy (FA), apparent diffusion coefficient (ADC), relative anisotropy (RA)] construction, registration of low b images to the same-subject anatomical used affine registration and deformed registration, and map FA to Talairach space to obtain DTI parameters of the subcortical nucleus in the same space with volume extraction. Then, the same subcortical nuclei segmentation id was used as the last step to extract the FA, ADC, and RA values of subcortical nuclei with volume differences between the two groups.

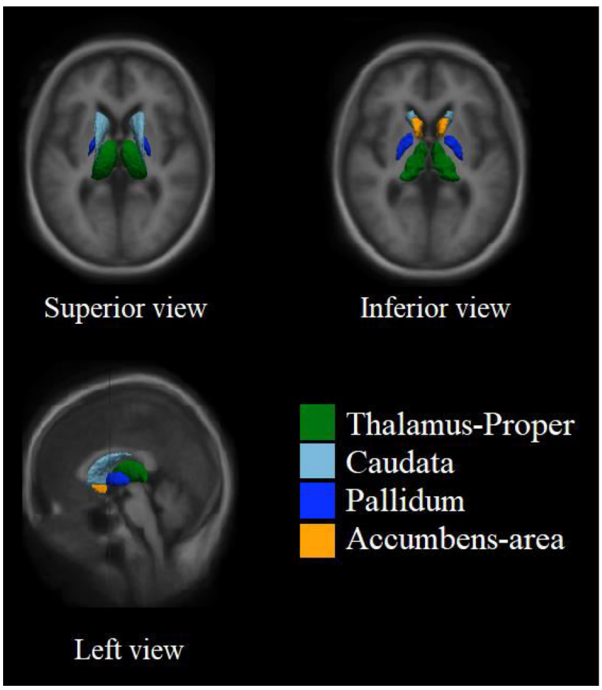

FIGURE 1 | Example location of four subcortical nucleus in the brain. The spatial distribution of subcortical nucleus with volume differences in the standard brain was showed. The thalamus, located on both sides of the third ventricle, is the largest of these subcortical nucleus. Pallidum is located in the anterior inferior part of thalamus. The caudate is located in the front and upper part of pallidum. The accumbens is located in the lower part of caudate and the anterior part of pallidum.

Statistical Analysis

Statistical analysis was performed using the Statistical Package for Social Sciences for Windows version 21.0 (IBM Corp., Armonk, NY, USA), and $P < 0.05$ was considered significant. Continuous variables were expressed using the mean and standard deviation for the normal distribution or median and its interquartile range for a nonnormal distribution and were analyzed using Student *t*-test or Mann–Whitney *U* test, respectively. Categorical

[1]https://www.softpedia.com/get/Science-CAD/MRIConvert.shtml
[2]http://www.freesurfer.net
[3]https://fsl.fmrib.ox.ac.uk/fsl/fslwiki/

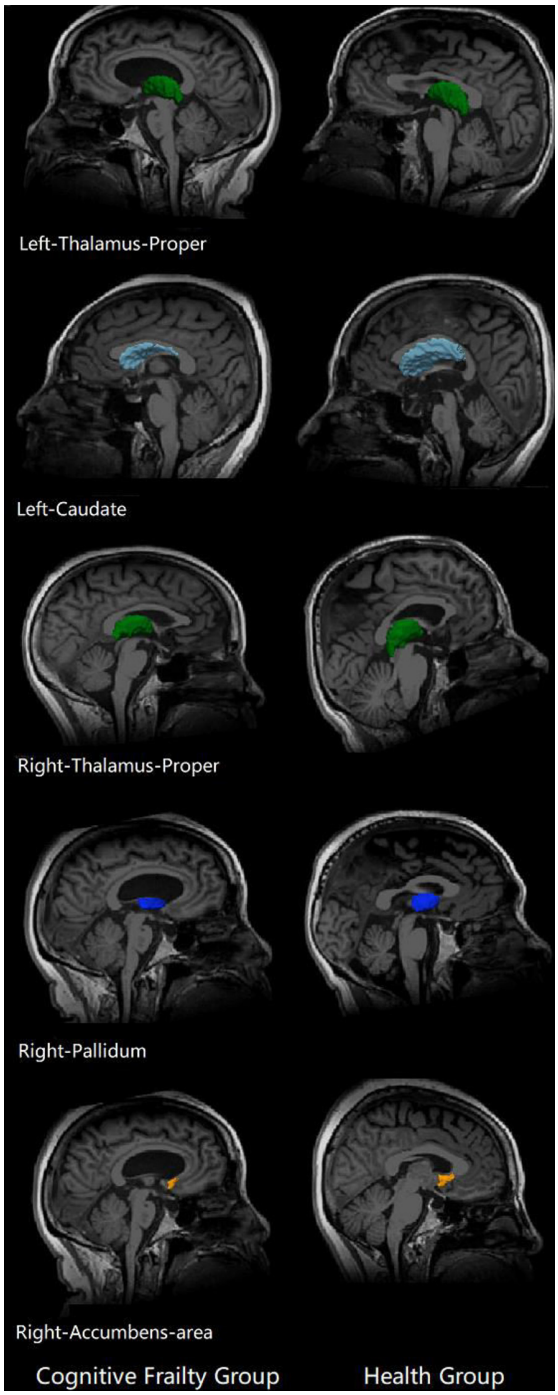

FIGURE 2 | Subcortical nuclei with differences in the two groups. Brain structural changes associated cognitive frailty. Cognitive frailty group showed a decrease in the volume of subcortical nucleus compared with health group.

variables were described as frequencies and were analyzed using the χ^2 test.

Volumetric and DTI parameters of subcortical nuclei in the two groups were compared by independent-sample *t*-tests. To identify brain structural changes related to the frailty index and MoCA, we assessed nuclei volume differences between groups using partial correlation analysis. Age, sex, education years, and Beck Depression Inventory scores were also entered as covariates.

RESULTS

The Baseline Characteristics of the CF Participants and Healthy Controls

The average MoCA score in the CF group was significantly lower than that in the healthy control group. The frailty index in the CF group was significantly higher than that in the healthy control group. There were no significant differences between the two groups in gender, age, years of education, or Beck Depression Inventory scores ($P < 0.05$; **Table 1**).

Subcortical Nuclei Volume

Compared to the healthy control group, the CF group showed decreased volume in five brain nuclei, including the left thalamus, left caudate, right thalamus, right pallidum, and right accumbens area ($P < 0.05$), and there was the most obvious volume difference in the thalamus (**Figures 1**, **2**, **Table 2**).

DTI Parameters

Decreased FA and RA values were observed in the left thalamus in the CF group compared to the healthy control group ($P < 0.05$). No group significance was found in the ADC values of any subcortical nuclei ($P > 0.05$; **Figure 3**, **Table 3**).

Correlation Between Subcortical Nuclei Volumes, MoCA Scores, and Frailty Index Scores

After adjusting for age, sex, and education, the volumes of the left and right thalamus proper, right pallidum, and right accumbens area were positively correlated with the MoCA scores ($P < 0.05$); the volumes of the left and right thalamus proper, left and right caudate, left and right pallidum, and right accumbens area were negatively correlated with the frailty index scores ($P < 0.05$; **Figure 4**, **Table 4**).

DISCUSSION

Cognitive frailty is a clinical condition characterized by the simultaneous presence of both physical frailty and cognitive impairment but without concurrent Alzheimer disease or other dementia. However, there may be some extent of association with physical frailty or cognitive impairment through some common mechanisms. However, the underlying mechanisms of CF remain unclear. In the present study, we investigated the brain structural characteristics in the subcortical nuclei between adults with CF and matched healthy older adults by using DTI technology. The findings of this study showed that there was an obvious decrease in the volume of five brain subcortical nuclei, including the bilateral thalami, left caudate, right pallidum, and right accumbens area in older adults with CF compared to HCs. Furthermore, the volumes of more than five subcortical nuclei were negatively correlated with the frailty index, whereas the volumes of the bilateral thalami, right pallidum, and accumbens

TABLE 2 | Volume of four subcortical nucleus between two groups.

	CF (volume)	HC (volume)	MD	95% CI of MD	*P*
Left-Thalamus	6,312.08 ± 527.71	6,719.65 ± 606.56	−407.57	−724.27, −90.87	0.013
Left-Caudate	3,086.25 ± 297.31	3,296.13 ± 357.49	−209.88	−393.04, −26.73	0.026
Left-Putamen	4,488.97 ± 550.071	4,594.08 ± 458.65	−105.11	−387.23, 177.01	0.458
Left-Pallidum	1,842.26 ± 212.50	1,947.05 ± 206.64	−104.79	−221.55, 11.96	0.077
Left-Hippocampus	3,661.82 ± 350.073	3,702.47 ± 358.47	−40.64	−238.01, 156.73	0.681
Left-Amygdala	1,546.19 ± 160.35	1,549.1 ± 230.30	−2.91	−113.45, 107.63	0.958
Left-Accumbens	421.34 ± 75.00	428.90 ± 62.18	−7.56	−45.94, 30.82	0.694
Right-Thalamus	6,068.14 ± 706.36	6,487.33 ± 501.10	−419.19	−760.34, −78.05	0.017
Right-Caudate	3,110.63 ± 334.18	3,290.38 ± 366.69	−179.75	−375.18, 15.67	0.071
Right-Putamen	4,382.33 ± 696.84	4,505.57 ± 523.34	−123.24	−466.52, 220.04	0.474
Right-Pallidum	1,796.72 ± 244.54	1,970.20 ± 197.54	−173.48	−297.31, −49.65	0.007
Right-Hippocampus	3871.41 ± 386.159	3872.01 ± 410.20	−0.60	−222.51, 221.32	0.996
Right-Amygdala	1,721.5 ± 210.701	1,680.52 ± 226.51	40.98	−80.88, 162.84	0.502
Right-Accumbens	451.97 ± 53.86	482.32 ± 45.68	−30.35	−58.17, −2.54	0.033

MD, Mean difference; CI, confidence interval of difference. Value of volume was presented by mean ± standard deviation, the unit of volume is cubic millimeter.

were positively correlated with MoCA scores. We also found that those with CF showed decreased FA and RA values in the left thalamus compared to the HCs. These findings suggest that structural atrophy or impairment in some subcortical nucleus areas may be a potential mechanism for CF.

Previous studies have confirmed that the frailty index had significant relationships with subcortical and cortical atrophy but not with changes in white matter in older adults with cognitive decline (Del Brutto et al., 2017; Gallucci et al., 2018). As an important subcortical nucleus, the thalamic nucleus adjacent to the third ventricle connects to its cortex, subcortex, and cerebellum. The thalamic nucleus is a key node in the neural network of hippocampal and cortical structures and is a fundamental substrate for human cognitive functions, especially the formation of memory, information processing, and executive function (Minagar et al., 2013; Fama and Sullivan, 2015; Dolleman-van der Well et al., 2019). Abnormal thalamic macrostructure, microstructure, or neural connectivity is widely associated with some clinical manifestations, such as cognitive impairments, motor deficits, and physical frailty (Fama and Sullivan, 2015). Studies of multimodal MRI have demonstrated that changes in the thalamus, including volume shrinkage, microstructural degradation, and integrity and connectivity decline, are associated with cognitive decline in elderly individuals (Hughes et al., 2012). In addition, a study reported that shrinkage of thalamic volume was positively correlated with gait speed and grip strength in frail populations, such as those with human immunodeficiency virus infection (Kallianpur et al., 2016). The present study found that the volumes of the bilateral thalami were highly correlated with cognitive function and the frailty index, especially the right thalamus, in older adults with CF. Our findings were in line with previous studies. Brain microstructure, tissue quality, and fiber integrity can be assessed with DTI by measuring the magnitude and orientation of water diffusion within the image volume unit (Jones et al., 2013). Fractional anisotropy and RA are two of the most commonly used scalar measurement methods of anisotropy in DTI. Published studies have shown that FA has superior noise immunity relative to RA (Hasan et al., 2004). Fractional anisotropy may assess the integrity of white matter fibers by the orientation of water diffusivity (Truong et al., 2014). Moreover, this modality of FA could also be used to assess the microstructure of gray matter because it likely reflects the

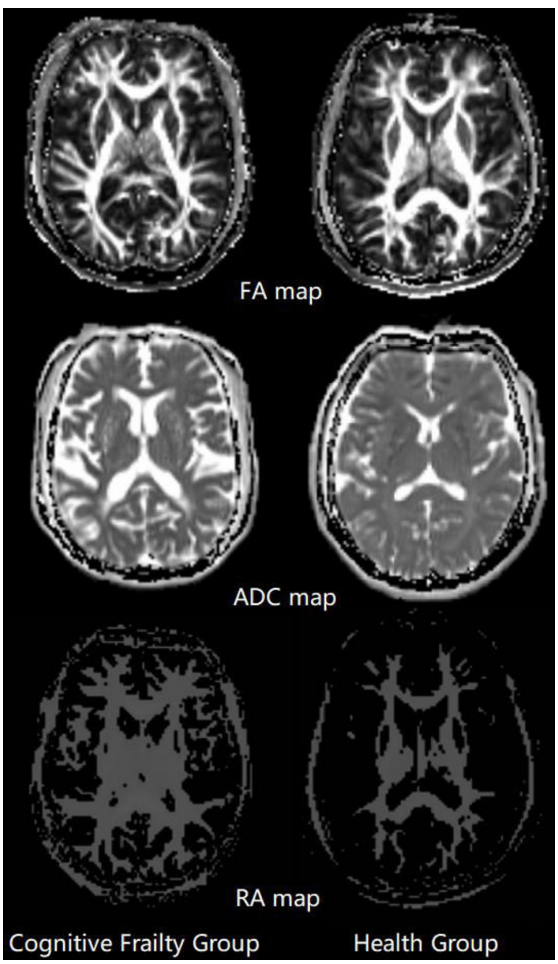

FIGURE 3 | Fractional anisotropy (FA), apparent diffusion coefficient (ADC), relative anisotropy (RA) map comparison between two groups. The mean values of FA, ADC and RA were computed within thalamus, caudate nucleus, globus pallidus and nucleus accumbens for individual subjects.

TABLE 3 | FA, ADC and RA of four interested subcortical nucleus between two groups.

	Group	FA	*P*	ADC (*1,000)	*P*	RA (*1,000)	*P*
Left-Thalamus	CF	0.277 ± 0.015	0.03	0.923 ± 0.043	0.792	6.9 ± 0.334	0.03
	HC	0.291 ± 0.030	0.927 ± 0.060	7.242 ± 0.706			
Left-Caudate	CF	0.170 ± 0.016	0.248	0.981 ± 0.063	0.239	4.269 ± 0.403	0.333
	HC	0.180 ± 0.043	0.958 ± 0.076	4.485 ± 1.050			
Left-Pallidum	CF	0.357 ± 0.031	0.136	0.738 ± 0.050	0.583	8.6 ± 0.812	0.129
	HC	0.337 ± 0.057	0.746 ± 0.051	8.096 ± 1.452			
Left-Accumbens	CF	0.181 ± 0.017	0.937	0.842 ± 0.070	0.829	4.277 ± 0.378	0.875
	HC	0.180 ± 0.030	0.838 ± 0.057	4.25 ± 0.785			
Right-Thalamus	CF	0.272 ± 0.017	0.219	0.942 ± 0.058	0.629	6.808 ± 0.375	0.28
	HC	0.279 ± 0.023	0.935 ± 0.056	6.942 ± 0.505			
Right-Caudate	CF	0.170 ± 0.023	0.528	0.981 ± 0.106	0.7	4.273 ± 0.616	0.782
	HC	0.174 ± 0.026	0.969 ± 0.109	4.319 ± 0.582			
Right-Pallidum	CF	0.329 ± 0.033	0.777	0.762 ± 0.057	0.61	7.854 ± 0.784	0.779
	HC	0.333 ± 0.062	0.754 ± 0.051	7.95 ± 1.550			
Right-Accumbens	CF	0.182 ± 0.017	0.396	0.827 ± 0.060	0.211	4.277 ± 0.377	0.476
	HC	0.188 ± 0.028	0.808 ± 0.049	4.388 ± 0.697			

Group CF, cognitive frailty group; group HC, healthy group; FA, fractional anisotropy; ADC, apparent diffusion coefficient; RA, relative anisotropy. Value of FA, ADC and RA was presented by mean ± standard deviation.

integrity of the neuronal cell wall and intercellular membranes (Whitwell et al., 2010). ADC mapping can quantitatively evaluate changes in brain water diffusivity and improve the performance of automatic morphological diagnosis. Our results showed that cognitive decline and physical frailty were highly correlated with the FA and RA values of the thalamus after adjustment for age and some other factors, but we did not find significant differences in the ADC mapping of the subcortical nucleus between the two groups. This might be attributed to the different compartmentalization and impact of diffusion time on the ADC of different molecules under limited diffusion conditions (Kan et al., 2012). Nevertheless, it is possible that thalamic microstructural damage and atrophy may be predictors of CF.

The current study also found that the caudate volume in the CF group was lower than that in the healthy control group, and the caudate volume, especially the left caudate, had a negative correlation with physical frailty. The caudate and putamen constitute the neostriatal nucleus that receives projections from the cerebral cortex and sends them to the brain stem and spinal cord, which play a complex role in the function of the motor regulation system (Jane, 2020). A previous study reported that the caudate nucleus importantly contributed to body and limb posture, as well as the accuracy and speed of directed movements (Villablanca, 2010). These findings may explain why volume changes in the caudate nucleus are related to the frailty index and not cognitive impairment in the current study. Another study reported that the caudate nucleus may play a significant role in brain processing of muscle pain (Maeda et al., 2011), which could be related to physical frailty. In addition, the abnormal functional connection between the caudate nucleus and prefrontal lobe was involved in motor inhibition related to obsessive–compulsive disorder, which also showed the importance of the caudate nucleus in motor control (Fineberg et al., 2018).

The globus pallidus is a principal component of the basal ganglia. The globus pallidus contains a rich concentration of neuropeptides and endogenous cannabinoids, which are important neural signaling molecules that affect brain function, including motivation, cognition, and action and are related to nervous system diseases (Chen et al., 2020; Jakimovski et al., 2020). A study in patients with first-episode psychosis showed that worse cognitive performance was associated with decreased gray matter in the right globus pallidus (Dempster et al., 2017). The globus pallidus plays an important role in the pathogenesis of cognitive and behavioral disorders associated with Huntington disease (Singh-Bains et al., 2016a). Moreover, Nombela et al. (2019) reported that patients with Parkinson disease were treated with deep brain stimulation of the globus pallidus, and improvements in motor function were observed at the 2- to 3-month follow-up. The present study found that the pallidal volume in older adults with CF was lower than that in HCs and was correlated with cognitive decline and physical frailty. These findings were consistent with previous studies, indicating that the globus pallidus plays an important role in regulating cognition and movement. In this study, we also found that volume of the right accumbens area in older adults with CF was smaller than that in HCs and was related to both physical frailty and cognitive impairment, which might indicate that the accumbens area may participate in the regulation of cognitive and physical frailty together with the thalamus, caudate, and pallidum. According to Singh-Bains et al. (2016b), the globus pallidus and nucleus accumbens contribute to "limbic-motor integration" together by transforming the marginal motor signal into motor output. Therefore, the volume atrophy of the globus pallidus and accumbens could also be related to this. In fact, the human nucleus accumbens is an important structure in maintaining normal cognition, motivation, and emotional processes and is involved in some neuropsychiatric disorders (Cartmell et al., 2019). There was also a negative correlation between cognitive function and accumbens volume (Mavridis et al., 2011).

LIMITATIONS

Our study had several limitations. First, the sample size in this study was relatively small. Although we implemented methodological approaches to minimize small sample effects by

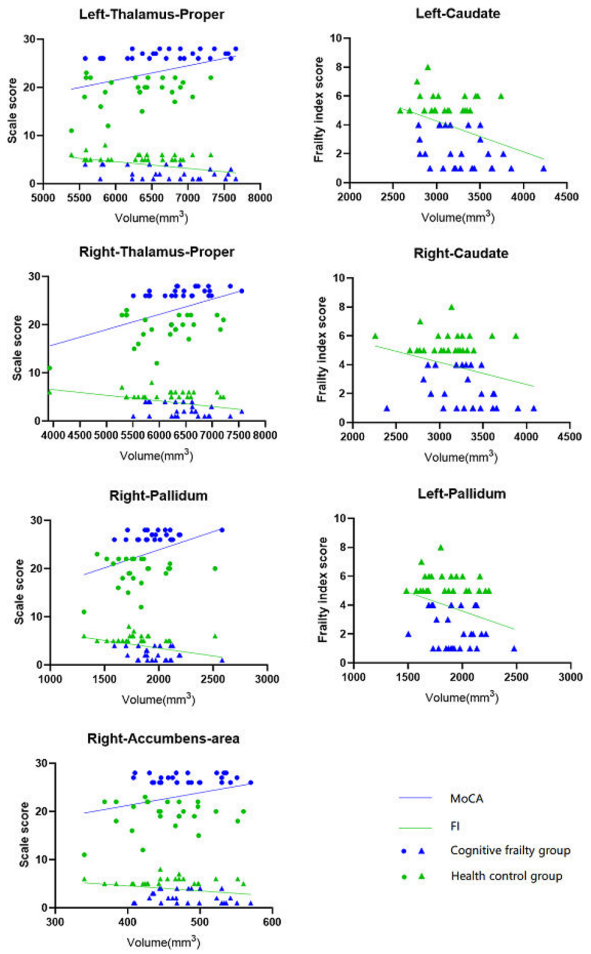

FIGURE 4 | Correlation between subcortical nucleus volume and MoCA, FI values after adjusted for age, sex and education. The nucleus volume in left and right thalamus-proper, right pallidum and right accumbens-area was positively correlated with the MoCA scores ($P < 0.05$); the nucleus volume in left and right thalamus-proper, left and right caudate, left and right pallidum, and right accumbens-area was negatively correlated with the frailty index scores ($P < 0.05$). MoCA, Montreal Cognitive Assessment; FI, Frailty index.

matching patients and controls in age, sex, and education, it was possible not to detect group differences in certain tracts because of the lack of statistical power. In the future, a study with a larger sample size is needed to replicate our findings. Second, this study was a cross-sectional design, which limits causal and temporal inferences. Longitudinal follow-up studies will be required to better assess the relationship of neuroimaging changes and CF. Third, this study focused only on the main subcortical gray matter nuclei and excluded the cortex and white matter, but in fact, the realization of brain function is a reflection of the overall structure. Fourth, the volume of those subcortical nuclei was inevitably influenced by their part surrounding structure, because of lack of partial volume correction in image data processing. Even so, our current findings provide new insights into the pathological progression of CF.

TABLE 4 | Correlation of between the volumes of subcortical nuclei and MoCA, frailty index scores.

	MoCA		Frailty Index	
	R	P	R	P
Left-Thalamus-proper	0.378*	0.008	−0.487*	<0.001
Left-Caudate	0.279	0.055	−0.464*	0.001
Left-Pallidum	0.227	0.121	−0.371*	0.009
Left-Accumbens-area	0.11	0.458	−0.075	0.613
Right-Thalamus-proper	0.45*	0.001	−0.475*	0.001
Right-Caudate	0.216	0.139	−0.363*	0.011
Right-Pallidum	0.349*	0.015	−0.403*	0.005
Right-Accumbens-area	0.296*	0.041	−0.33*	0.022

*$P < 0.05$ significant correlation coefficients.

CONCLUSION

The present study shows that microstructural atrophy of the subcortical nuclei occurs in the brains of older adults with CF compared to those of healthy subjects, and the atrophy was correlated with the degree of cognitive decline and physical frailty. These findings demonstrate the involvement of subcortical nuclei in the pathological progression of CF.

DATA AVAILABILITY STATEMENT

The datasets used and/or analyzed during the current study are available from the corresponding author upon request.

ETHICS STATEMENT

The studies involving human participants were reviewed and approved by the second people's hospital affiliated to Fujian University of Traditional Chinese Medicine. The patients/participants provided their written informed consent to participate in this study.

AUTHOR CONTRIBUTIONS

GZ and LC conceived and designed the study. JT was in charge of coordination and direct implementation. MW and RX wrote the manuscript. MW, RX, HL, PQ, JH and YY managed the recruitment and the follow-up. All authors read and approved the final manuscript.

FUNDING

This study is supported by the National Natural Science Foundation of China (http://www.nsfc.gov.cn, No. 81574045).

ACKNOWLEDGMENTS

We thank the participants and staff at the communities and hospitals for their work in this project, including Fujian University of Traditional Chinese Medicine Subsidiary Rehabilitation Hospital.

REFERENCES

Anatürk, M., Demnitz, N., Ebmeier, K. P., and Sexton, C. E. (2018). A systematic review and meta-analysis of structural magnetic resonance imaging studies investigating cognitive and social activity levels in older adults. *Neurosci. Biobehav. Rev.* 93, 71–84. doi: 10.1016/j.neubiorev.2018.06.012

Cartmell, S. C., Tian, Q., Thio, B. J., Leuze, C., Ye, L., Williams, N. R., et al. (2019). Multimodal characterization of the human nucleus accumbens. *NeuroImage* 198, 137–149. doi: 10.1016/j.neuroimage.2019.05.019

Chen, X., Xue, Y., Chen, H., and Chen, L. (2020). The globus pallidus as a target for neuropeptides and endocannabinoids participating in central activities. *Peptides* 124:170210. doi: 10.1016/j.peptides.2019.170210

Cherubini, A., Spoletini, I., Péran, P., Luccichenti, G., Di, P. M., Sancesario, G., et al. (2010). A multimodal MRI investigation of the subventricular zone in mild cognitive impairment and Alzheimer's disease patients. *Neurosci. Lett.* 469, 214–218. doi: 10.1016/j.neulet.2009.11.077

Del Brutto, O. H., Mera, R. M., Cagino, K., Fanning, K. D., Milla-Martinez, M. F., Nieves, J. L., et al. (2017). Neuroimaging signatures of frailty: a population-based study in community-dwelling older adults (the Atahualpa Project). *Geriatr. Gerontol. Int.* 17, 270–276. doi: 10.1111/ggi.12708

Dempster, K., Norman, R., Théberge, J., Densmore, M., Schaefer, B., and Williamson, P. (2017). Cognitive performance is associated with gray matter decline in first-episode psychosis. *Psychiatry Res. Neuroimaging* 264, 46–51. doi: 10.1016/j.pscychresns.2017.04.007

Dolleman-van der Well, M. J., Griffin, A. L., Ito, H. T., Shapiro, M. L., Witter, M. P., Vertes, R. P., et al. (2019). The nucleus reuniens of the thalamus sits at the nexus of a hippocampus and medial prefrontal cortex circuit enabling memory and behavior. *Learn. Mem.* 26, 191–205. doi: 10.1101/lm.048389.118

Eustache, P., Nemmi, F., Saint-Aubert, L., Pariente, J., and Péran, P. (2016). Multimodal magnetic resonance imaging in Alzheimer's disease patients at prodromal stage. *J. Alzheimers Dis.* 50, 1035–1050. doi: 10.3233/jad-150353

Fama, R., and Sullivan, E. V. (2015). Thalamic structures and associated cognitive functions: relations with age and aging. *Neurosci. Biobehav. Rev.* 54, 29–37. doi: 10.1016/j.neubiorev.2015.03.008

Feng, L., Zin, N. M. S., Gao, Q., Feng, L., Yap, K. B., and Ng, T. (2017). Cognitive frailty and adverse health outcomes: findings from the singapore longitudinal ageing studies (SLAS). *J. Am. Med. Dir. Assoc.* 18, 252–258. doi: 10.1016/j.jamda.2016.09.015

Fennema-Notestine, C., Hagler, D. J. Jr., McEvoy, L. K., Fleisher, A. S., Wu, E. H., Karow, D. S., et al. (2009). Structural MRI biomarkers for preclinical and mild Alzheimer's disease. *Hum. Brain Mapp.* 30, 3238–3253. doi: 10.1002/hbm.20744

Fineberg, N. A., Apergis-Schoute, A. M., Vaghi, M. M., Banca, P., Gillan, C. M., Voon, V., et al. (2018). Mapping compulsivity in the DSM-5 obsessive compulsive and related disorders: cognitive domains, neural circuitry, and treatment. *Int. J. Neuropsychopharmacol.* 21, 42–58. doi: 10.1093/ijnp/pyx088

Gallucci, M., Piovesan, C., and Di, B. M. E. (2018). Associations between the frailty index and brain atrophy: the treviso dementia (TREDEM) registry. *J. Alzheimers Dis.* 62, 1623–1634. doi: 10.3233/jad-170938

Gong, N.-J., Chan, C.-C., Leung, L.-M., Wong, C.-S., Dibb, R., and Liu, C. (2017). Differential microstructural and morphological abnormalities in mild cognitive impairment and Alzheimer's disease: evidence from cortical and deep gray matter. *Hum. Brain Mapp.* 38, 2495–2508. doi: 10.1002/hbm.23535

Gu, L., and Zhang, Z. (2019). Exploring structural and functional brain changes in mild cognitive impairment: a whole brain ALE meta-analysis for multimodal MRI. *ACS Chem. Neurosci.* 10, 2823–2829. doi: 10.1021/acschemneuro.9b00045

Hasan, K. M., Alexander, A. L., and Narayana, P. A. (2004). Does fractional anisotropy have better noise immunity characteristics than relative anisotropy in diffusion tensor MRI? An analytical approach. *Magn. Reson. Med.* 51, 413–417. doi: 10.1002/mrm.10682

Hughes, E. J., Bond, J., Svrckova, P., Makropoulos, A., Ball, G., Sharp, D. J., et al. (2012). Regional changes in thalamic shape and volume with increasing age. *NeuroImage* 63, 1134–1142. doi: 10.1016/j.neuroimage.2012.07.043

Jakimovski, D., Bergsland, N., Dwyer, M. G., Hagemeier, J., Ramasamy, D. P., Szigeti, K., et al. (2020). Long-standing multiple sclerosis neurodegeneration: volumetric magnetic resonance imaging comparison to Parkinson's disease, mild cognitive impairment, Alzheimer's disease and elderly healthy controls. *Neurobiol. Aging* 90, 84–92. doi: 10.1016/j.neurobiolaging.2020.02.002

Jane. (2020). *Neuroanatomy, Extrapyramidal System.* Treasure Island, FL: StatPearls Publishing.

Jones, D. K., Knösche, T. R., and Turner, R. (2013). White matter integrity, fiber count, and other fallacies: the do's and don'ts of diffusion MRI. *NeuroImage* 73, 239–254. doi: 10.1016/j.neuroimage.2012.06.081

Kallianpur, K. J., Sakoda, M., Gangcuangco, L. M. A., Ndhlovu, L. C., Umaki, T., Chow, D., et al. (2016). Frailty characteristics in chronic HIV patients are markers of white matter atrophy independently of age and depressive symptoms: a pilot study. *Open Med. J.* 3, 138–152. doi: 10.2174/1874220301603010138

Kan, H. E., Techawiboonwong, A., van Osch, M. J. P., Versluis, M. J., Deelchand, D. K., Henry, P., et al. (2012). Differences in apparent diffusion coefficients of brain metabolites between grey and white matter in the human brain measured at 7 T. *Magn. Reson. Med.* 67, 1203–1209. doi: 10.1002/mrm.23129

Kelaiditi, E., Cesari, M., Canevelli, M., van Kan, G. A., Ousset, P.-J., Gillette-Guyonnet, S., et al. (2013). Cognitive frailty: rational and definition from an (I.A.N.A./I.A.G.G.) international consensus group. *J. Nutr. Health Aging* 17, 726–734. doi: 10.1007/s12603-013-0367-2

Maeda, L., Ono, M., Koyama, T., Oshiro, Y., Sumitani, M., Mashimo, T., et al. (2011). Human brain activity associated with painful mechanical stimulation to muscle and bone. *J. Anesth.* 25, 523–530. doi: 10.1007/s00540-011-1173-9

Mak, E., Gabel, S., Su, L., Williams, G. B., Arnold, R., Passamonti, L., et al. (2017). Multi-modal MRI investigation of volumetric and microstructural changes in the hippocampus and its subfields in mild cognitive impairment, Alzheimer's disease and dementia with Lewy bodies. *Int. Psychogeriatr.* 29, 545–555. doi: 10.1017/s1041610216002143

Malek, R. N. F., Shahar, S., Rajab, N. F., Ajit Singh, D. K., Che Din, N., Hazlina, M., et al. (2019). Cognitive frailty among Malaysian older adults: baseline findings from the LRGS TUA cohort study. *Clin. Interv. Aging* 14, 1343–1352. doi: 10.2147/cia.s211027

Mavridis, I., Boviatsis, E., and Anagnostopoulou, S. (2011). The human nucleus accumbens suffers parkinsonism-related shrinkage: a novel finding. *Surg. Radiol. Anat.* 33, 595–599. doi: 10.1007/s00276-011-0802-1

Minagar, A., Barnett, M. H., Benedict, R. H. B., Pelletier, D., Pirko, I., Sahraian, M. A., et al. (2013). The thalamus and multiple sclerosis: modern views on pathologic, imaging, and clinical aspects. *Neurology* 80, 210–219. doi: 10.1212/wnl.0b013e31827b910b

Mori, S., and Zhang, J. (2006). Principles of diffusion tensor imaging and its applications to basic neuroscience research. *Neuron* 51, 527–539. doi: 10.1016/j.neuron.2006.08.012

Nombela, C., Lozano, A., Villanueva, C., and Barcia, J. A. (2019). Simultaneous stimulation of the globus pallidus interna and the nucleus basalis of meynert in the parkinson-dementia syndrome. *Dement. Geriatr. Cogn. Disord.* 47, 19–28. doi: 10.1159/000493094

Shimada, H., Makizako, H., Lee, S., Doi, T., Lee, S., Tsutsumimoto, K., et al. (2016). Impact of cognitive frailty on daily activities in older persons. *J. Nutr. Health Aging* 20, 729–735. doi: 10.1016/j.jalz.2016.06.2037

Singh-Bains, M. K., Tippett, L. J., Hogg, V. M., Beth, S. J., Roxburgh, R. H., Waldvogel, H. J., et al. (2016a). Globus pallidus degeneration and clinicopathological features of Huntington disease. *Ann. Neurol.* 80, 185–201. doi: 10.1002/ana.24694

Singh-Bains, M. K., Waldvogel, H. J., and Faull, R. L. M. (2016b). The role of the human globus pallidus in Huntington's disease. *Brain Pathol.* 26, 741–751. doi: 10.1111/bpa.12429

Tentolouris-Piperas, V., Ryan, N. S., Thomas, D. L., and Kinnunen, K. M. (2017). Brain imaging evidence of early involvement of subcortical regions in familial and sporadic Alzheimer's disease. *Brain Res.* 1655, 23–32. doi: 10.1016/j.brainres.2016.11.011

Truong, T.-K., Guidon, A., and Song, A. W. (2014). Cortical depth dependence of the diffusion anisotropy in the human cortical gray matter *in vivo*. *PLoS One* 9:e91424. doi: 10.1371/journal.pone.0091424

Villablanca, J. R. (2010). Why do we have a caudate nucleus? *Acta Neurobiol. Exp.* 70, 95–105.

Whitwell, J. L., Avula, R., Senjem, M. L., Kantarci, K., Weigand, S. D., Samikoglu, A., et al. (2010). Gray and white matter water diffusion in the syndromic variants of frontotemporal dementia. *Neurology* 74, 1279–1287. doi: 10.1212/wnl.0b013e3181d9edde

Won, C. W., Lee, Y., Kim, S., Yoo, J., Kim, M., Ng, T., et al. (2018). Modified criteria for diagnosing "cognitive frailty". *Psychiatry Investig.* 15, 839–842. doi: 10.30773/pi.2018.05.22

Conflict of Interest: The authors declare that the research was conducted in the absence of any commercial or financial relationships that could be construed as a potential conflict of interest.

frontiers in Neuroscience

ORIGINAL RESEARCH
published: 29 July 2020
doi: 10.3389/fnins.2020.00781

Tremor in Vascular Cognitive Impairment Raises the Possibility of Mixed Pathology With Lewy Body Disease

*Pai-Yi Chiu[1,2], Ray-Chang Tzeng[3], Cheng-Yu Wei[4], Guang-Uei Hung[5] and Chaur-Jong Hu[6]**

[1] Department of Neurology, Show Chwan Memorial Hospital, Changhua, Taiwan, [2] Department of Nursing, College of Nursing and Health Sciences, Da-Yeh University, Changhua, Taiwan, [3] Department of Neurology, Tainan Municipal Hospital (Managed by Show Chwan Medical Care Corporation), Tainan, Taiwan, [4] Department of Exercise and Health Promotion, College of Education, Chinese Culture University, Taipei, Taiwan, [5] Department of Nuclear Medicine, Chang Bing Show Chwan Memorial Hospital, Changhua, Taiwan, [6] Department of Neurology, Taipei Medical University-Shuang Ho Hospital, School of Medicine, College of Medicine, Taipei Medical University, New Taipei City, Taiwan

OPEN ACCESS

Edited by:
Kuangyu Shi, Technical University of Munich, Germany

Reviewed by:
Maria Teresa Pellecchia, University of Salerno, Italy
Ian Leigh Alberts, Insel Gruppe AG, Switzerland

***Correspondence:**
Chaur-Jong Hu
chaurjongh@tmu.edu.tw

Specialty section:
This article was submitted to Neurodegeneration, a section of the journal Frontiers in Neuroscience

Received: *07 May 2020*
Accepted: *02 July 2020*
Published: *29 July 2020*

Citation:
Chiu P-Y, Tzeng R-C, Wei C-Y, Hung G-U and Hu C-J (2020) Tremor in Vascular Cognitive Impairment Raises the Possibility of Mixed Pathology With Lewy Body Disease. Front. Neurosci. 14:781. doi: 10.3389/fnins.2020.00781

Objectives: Tremor is common in patients with Lewy body disease (LBD) and not rare in normal individuals. Prevalence of tremor in patients with vascular cognitive impairment (VCI) and its association with other comorbidities are seldom studied. The aim of this study was to investigate the patient characteristics of VCI associated with tremor and to evaluate the possibility of mixed pathology with LBD in these patients.

Methods: Retrospective analysis of a large population with VCI registered in the database of a regional healthcare system was performed. VCI patients were divided into tremor and non-tremor groups. The associated characteristics including demographics, clinical features in motor and non-motor domains, vascular risk factors, and neuroimaging features were compared between the tremor group and the non-tremor group.

Results: Among 1337 patients with VCI, 292 (21.8%) had tremor, while 1045 (78.2%) did not have tremor. The tremor group had significantly higher prevalence of all motor and non-motor LBD clinical features than the non-tremor group. The tremor group also demonstrated more severe neuropsychiatric symptoms. Among patients with tremor, patients having tremor onset earlier than stroke onset showed significantly higher prevalence of rapid eye movement sleep behavior disorder. All comparisons were adjusted for age and severity of dementia.

Conclusion: Tremor is a common comorbidity of VCI. VCI patients with tremor had a higher prevalence of motor and non-motor LBD features. These findings raised the possibility of VCI patients with tremor having high possibility of mixed pathology with LBD.

Keywords: tremor, vascular cognitive impairment, Lewy body disease, risk factors, neuroimaging

INTRODUCTION

Tremor is a common symptom/sign in patients with neurological as well as systemic disorders, and it occurs primarily during action or at rest (Bhatia et al., 2018). Tremor at rest is among one of the most important clinical features of Lewy body disease (LBD) including Parkinson's disease (PD) and dementia with Lewy bodies (DLB) (Postuma et al., 2015; McKeith et al., 2017). However, prevalence of resting or kinetic tremors in patients with vascular cognitive impairment (VCI) and their association with the comorbidities are seldom studied. A previous study showed that movement disorders were uncommon in stroke patients and only 1% of the stroke patients developed movement disorders after acute stroke (Ghika-Schmid et al., 1997). Atypical tremors are observed more commonly after acute stroke than typical action or resting tremors (Ghika-Schmid et al., 1997; Handley et al., 2009). Locations of brain lesions in tremor resulting from acute stroke were varied and included the cortical, subcortical, and cerebellar regions (Handley et al., 2009). Stroke in the midbrain, basal ganglia, or chronic small vessel cerebrovascular disease can result in acute onset of PD-like movement disorders or parkinsonism. This condition is termed "vascular parkinsonism" (van Zagten et al., 1998; Handley et al., 2009). A study of vascular parkinsonism revealed that one or more parkinsonian signs were observed in 36% of the patients with small vessel cerebrovascular disease, and clinically, 11% of those patients had parkinsonism (van Zagten et al., 1998). Despite the clinical presentation and association of VCI with vascular parkinsonism that has been documented, very few studies have focused on the comorbidity of tremor in VCI. A previous study on parkinsonian features including tremor among patients with mild cognitive impairment (MCI), vascular MCI, and subcortical vascular dementia revealed that prevalence of tremor was not different among these groups (Frisoni et al., 2002). Tremors as a comorbidity of stroke with or without cognitive impairment are not typical features of vascular parkinsonism. The predominant clinical feature in most cases of vascular parkinsonism is gait impairment rather than tremor (Korczyn, 2015). Therefore, according to the current evidence, the underlying mechanism of tremor associated with VCI is still unclear and deserves further investigation and clarification.

Mixed dementia have traditionally focused on the coexistence of Alzheimer's disease (AD) and CVD in the same demented patient (Langa et al., 2004; Custodio et al., 2017). However, pathological study did show that in persons with dementia, over 50% had multiple diagnoses including AD, PD/LBD, or CVD (Schneider et al., 2007). Validation studies on DLB consensus criteria have provided evidence with high specificity based on the characteristic clinical Lewy body features by comparing the pathological findings (Nelson et al., 2010; Skogseth et al., 2017). A study on AD with typical AD pathology also showed that Lewy-type synucleinopathy influences motor and non-motor clinical findings in AD patients (Savica et al., 2019). Multiple pathological processes are common in dementia patients, and they can affect the clinical presentations (Woodward et al., 2010). Based on these findings showing a high association of clinical Lewy body features with Lewy body pathologies in LBD as well as in non-LBD patients, we proposed that the presentation of tremor should raise the possibility of co-existing LBD pathophysiology in patients with VCI (Postuma et al., 2015; McKeith et al., 2017; Bhatia et al., 2018). Therefore, the present study aimed to investigate the prevalence of tremor and the characteristics of VCI patients in various cognitive states for exploring the possibility of co-existing pathophysiology of LBD by observing and comparing the prevalence of clinical Lewy body features among patients with and without tremor.

MATERIALS AND METHODS

Database

This retrospective study selected participants registered in a dementia database of a healthcare system in Taiwan. From 2015/10/1 to 2019/9/30, a total of 6353 participants were registered in the database, and those who met the diagnosis of VCI (n = 1337) were selected and analyzed. Normal elderly (n = 573), patients with non-vascular MCI (n = 766), AD (n = 1867), DLB (n = 456), PD (n = 334), PD dementia (n = 309), essential tremor (n = 311), normal pressure hydrocephalus (n = 180), frontotemporal dementia (n = 84), other or undetermined dementia (n = 1475) were excluded from the study. Only the patients who had undergone at least a cerebral computed tomography scan or cerebral magnetic resonance imaging (MRI) and a set of blood screening tests for ruling out other possibilities of cognitive decline that could be analyzed were included in the study. The following information recorded in the database was used in this study:

1. Age, gender, education, duration of motor dysfunction and cerebrovascular disease (CVD), subtypes of CVD, and current medication at the time of entry.
2. Dementia severity according to Clinical Dementia Rating Scale (CDR) (Morris, 1993).
3. A structured questionnaire including motor features (resting tremor, postural/action tremor, bradykinesia, rigidity, postural instability, asymmetric onset, and easily falling tendency) and non-motor features [cognitive fluctuation, parkinsonism, visual hallucinations (VHs), rapid eye movement (REM) sleep behavior disorder (RBD), severe neuroleptic sensitivity (SNS), depression, apathy, delusions, urinary frequency, incontinence, and constipation] for the diagnosis of DLB (Chiu et al., 2019).
4. Assessment of activities of daily living according to the Instrumental Activities of Daily Living (IADL) scale (Lawton and Brody, 1969).
5. Cognitive performance according to the Cognitive Abilities Screening Instrument, Chinese version (CASI C-2.0) (Lin et al., 2002) and the Montreal Cognitive Assessment (MoCA) (Nasreddine et al., 2005).
6. Neuropsychiatric symptoms according to the 12-item version of the Neuropsychiatric Inventory (NPI) on the basis of observations within the past month (Cummings, 1988).

7. Clinically relevant vascular risk factors (VRFs) including hypertension, arrhythmia, coronary artery disease, diabetes, hyperlipidemia, and cerebrovascular disease (history of stroke/transient ischemic attack or the diagnosis of vascular encephalopathy in brain imaging).
8. A set of blood screening tests including complete blood count, COT, GPT, BUN, creatinine, total cholesterol, TG, LDL, ac glucose, HbA1c, TSH, free T4, RPR, vitamin B12, and folic acid.

Assessment of Disease Severity and Subtypes

VCI in this database was diagnosed according to the criteria for probable vascular dementia, possible vascular dementia, and vascular MCI in the 2011 American Heart Association/American Stroke Association criteria for VCI (Gorelick et al., 2011). A diagnosis of DLB and its core clinical features was made according to the revised consensus criteria for probable DLB developed by the fourth report of the DLB consortium (McKeith et al., 2017). Fluctuation was diagnosed when a Mayo Fluctuation Composite Score (MFCS) > 2 (Ferman et al., 2004) was present. VHs were diagnosed when a clinical history of recurrent complex VHs were present. RBD was diagnosed when the minimal criteria for REM sleep behavior disorder according to the International Classification of Sleep Disorders, revised (American Academy of Sleep Medicine, 2001) was met. SNS was diagnosed when a clinical history was established for both the usage of neuroleptic drugs and an obvious association of adverse events with the neuroleptic drugs. Depression, apathy, and delusions were diagnosed by NPI. Urinary frequency, incontinence, and constipation were diagnosed according to chart recording. Cognitive tests of all patients were performed by a trained neuropsychologist. Severity and subtypes of dementia were diagnosed by a consensus meeting composed of neurologists, neuroradiologists, nuclear medicine doctors, and neuropsychologists.

Data Analysis

The Chinese version of SPSS 22.0 for Windows (IBM SPSS Statistics, IBM Corp., Armonk, NY, United States) was used for statistical analyses. Comparisons of the demographic data including CDR, clinical features, IADL, CASI, MoCA, and composite scores (frequency vs. severity) of the NPI were performed between the tremor and the non-tremor VCI groups using the independent *t*-test and odds ratios (ORs) were adjusted for age and dementia severity according to CDR. VCI subtypes and CVD subtypes were analyzed using the chi-squared test. Clinical history of VRFs, current use of antipsychotics, and current use of antiparkinsonian drugs were analyzed using the chi-squared test and all ORs were adjusted for age and dementia severity according to CDR. To compare the associations of clinical motor and non-motor features and neuroimaging variables between the tremor group and the non-tremor group, all ORs were adjusted for age and dementia severity according to CDR.

Ethical Considerations

The participants were selected from a dementia database of Show Chwan Healthcare System. The study design was retrospective and the data were analyzed anonymously. The Committee for Medical Research Ethics of Show Chwan Memorial Hospital reviewed the project and the Data Inspectorate approved the study.

RESULTS

Among 1337 patients with VCI, 292 (21.8%) had tremor, while 1045 (78.2%) did not have tremor. In the tremor group, 48 (16.4%) had isolated resting tremor, 99 (33.9%) had isolated postural/action tremor, and 145 (49.7%) had resting as well as postural/action tremors. The tremor group had lower educational levels (4.1 vs. 5.0 years, OR = 0.95, $p = 0.004$), longer duration of motor dysfunction (4.2 vs. 2.6 years, OR = 0.95, $p < 0.001$), and more severe neuropsychiatric symptoms (NPI scores: 11.6 vs. 8.3, OR = 1.03, $p < 0.001$) than the non-tremor group. Gender, duration of CVD, IADL, CASI, MoCA, VCI subtypes, and CVD subtypes showed no significant difference between the tremor group and the non-tremor group. Cognitive domains of CASI as well as MoCA were compared between tremor and non-tremor groups and showed no significant difference. Comparisons of the demographic data are summarized in **Table 1**.

The comparison of Lewy body clinical motor features revealed that the tremor group had significantly higher prevalence of all motor features ($p < 0.001$ for bradykinesia, rigidity, postural instability, hypotonic/monotonic speech, and easily falling tendency) than the non-tremor group after adjustment for age and disease severity according to CDR. The comparison of Lewy body non-motor features showed that the tremor group had significantly higher prevalence of all non-motor features ($p < 0.001$ for fluctuation of cognition, VHs, RBD, SNS, depression, urinary frequency, constipation, and incontinence) than the non-tremor group after adjustment for age and disease severity according to CDR. Patients in the tremor group also demonstrated significantly higher prevalence of delusions ($p = 0.001$) and apathy ($p = 0.015$). Clinically, At least two DLB core features and/or indicative biomarkers are essential for the diagnosis of probable DLB. Our analysis and comparison between the two groups showed that the tremor group had significantly higher probable DLB standard compliance than the non-tremor group (OR = 5.36, $p < 0.001$) (**Table 2**).

Table 3 demonstrates the comparisons of the relationship of CVD and dementia, VRFs, and current medication between the tremor group and the non-tremor group. After adjustment for age and dementia severity according to CDR, the tremor group had significantly higher prevalence of all VRFs including hypertension, diabetes, hyperlipidemia, and heart disease (all p values ≤ 0.001). Comparison of current medications revealed that the tremor group showed higher consumption of antiparkinsonian drugs ($p < 0.001$) and antipsychotics ($p = 0.002$) than the non-tremor group.

Comparison of neuroimaging manifestations between the tremor group and the non-tremor group after adjustment for

TABLE 1 | Background characteristics of tremor group compared to non-tremor group among VCI patients adjusted for age and dementia severity by CDR.

	Tremor *Mean* (*SD*, range)	Non-tremor *Mean* (*SD*, range)	OR/*χ^2	*P*
n	292	1045		
Age, year	76.2 (9.1, 28–94)	75.7 (7.9, 40–102)	NA	
CDR 0.5/1/2/3, *n*	78/84/81/49	364/282/240/159	NA	
Gender, f/m, *n*	149/143	514/531	1.03	NS
Education, year	4.1 (4.2, 0–16)	5.0 (4.6, 0–18)	0.95	0.004
Disease duration, year				
CVD	3.2 (4.6, 0.1–20.0)	3.3 (5.6, 0–60)	1.00	NS
Motor dysfunction	4.2 (6.6, 0–60)	2.6 (3.7, 0–30)	1.07	<0.001
IADL	2.3 (2.9, 0–8)	2.8 (3.1, 0–8)	0.96	NS
MoCA	7.6 (6.7, 0–27)	8.2 (7.3, 0–29)	1.00	NS
CASI	42.3 (25.9, 0–94)	43.1 (25.5, 0–94)	1.01	NS
NPI	11.6 (12.1, 0–87)	8.3 (10.0, 0–87)	1.03	<0.001
VaMCI/PrVaD/PoVaD	31/139/122	152/521/372	5.17*	NS
CVD Subtypes	Mi 30/St 41/Sc 61/ Bw 77/Cc 46/He 16/ Ot 21	Mi 121/St 173/Sc 255/ Bw 195/Cc 197/He 46/ Ot 58	11.92*	NS

*VCI, vascular cognitive impairment; CDR, Clinical Dementia Rating scale; n, number of cases; NA, not applicable; NS, non-significance; OR, odds ratio; CVD, cerebrovascular disease. Motor dysfunction includes any of the following symptoms: tremor, rigidity, bradykinesia, postural instability, hypotonic speech, or easily falling. IADL, Instrumental Activities of Daily Living; MoCA, Montreal Cognitive Assessment; CASI, Cognitive Abilities Screening Instrument; NPI, total score of 12-domain Neuropsychiatric Inventory; VaMCI/PrVaD/PoVaD, vascular mild cognitive impairment/probable vascular dementia/possible vascular dementia. Mi, multi-infarct; St, strategic infarct; Sc, subcortical lacunes; Bw, Binswanger disease; Cc, complex combination; He, hemorrhage; Ot, others. *Chi-square value without adjustments.*

TABLE 2 | Motor and non-motor features of tremor group (*n* = 292) compared to non-tremor group (*n* = 1045) adjusted for age and dementia severity by CDR.

	Tremor, *n* (%)	Non-tremor, *n* (%)	OR	*p*
Motor features				
Bradykinesia	182 (62.3)	283 (27.1)	4.44	<0.001
Rigidity	156 (53.4)	214 (20.5)	4.39	<0.001
Postural instability	213 (72.9)	431 (41.2)	3.80	<0.001
Hypotonic speech	90 (30.8)	158 (15.1)	2.46	<0.001
Easily falling	59 (20.2)	103 (9.9)	2.26	<0.001
Parkinsonism*	236 (80.8)	234 (22.4)	14.51	<0.001
Non-motor features				
Fluctuation	126 (43.2)	287 (27.5)	2.01	<0.001
VHs	56 (19.2)	101 (9.7)	2.12	<0.001
RBD	42 (14.4)	72 (6.9)	2.19	<0.001
SNS*	9 (45.0)	6 (20.0)	4.25	<0.001
Delusions	65 (22.3)	139 (13.3)	1.80	0.001
Depression	80 (27.4)	178 (17.0)	1.88	<0.001
Apathy	50 (17.1)	117 (11.2)	1.57	0.015
Urinary frequency	58 (20.0)	93 (9.0)	2.62	<0.001
Constipation	67 (23.1)	132 (12.8)	2.10	<0.001
Incontinence	65 (22.3)	133 (12.7)	1.92	<0.001
DLB core features + indicative biomarkers ≧ 2	155 (53.1)	189 (18.1)	5.36	<0.001

n, number of cases; CDR, Clinical Dementia Rating scale; OR, odds ratio; VHs, visual hallucinations; RBD, REM sleep behavior disorder; SNS, Severe neuroleptics sensitivity among 50 patients ever receiving antipsychotics; Parkinsonism*, at least two parkinsonian motor symptom/sign.*

TABLE 3 | Relationship of CVD and dementia, vascular risk factors, and current medication of tremor group (*n* = 292) compared to non-tremor group (*n* = 1045) adjusted for age and dementia severity by CDR.

	Tremor, *n* (%)	Non-tremor, *n* (%)	OR	*p*
Relationship of CVD and dementia				
History of CVD	210 (71.9)	780 (74.6)	0.82	NS
Temporal association	101 (34.6)	380 (36.4)	0.87	NS
Sequela of CVD	128 (43.8)	469 (44.9)	0.91	NS
Vascular risk factors				
Hypertension	171 (58.6)	493 (47.2)	1.64	<0.001
Diabetes	111 (38.0)	289 (27.7)	1.63	0.001
Hyperlipidemia	97 (33.2)	230 (22.0)	1.83	<0.001
Heart diseases	54 (18.5)	104 (9.9)	2.10	<0.001
Current medication				
Anti-dementia drugs	21 (7.2)	63 (6.0)	1.14	NS
Anti-platelets	113 (38.7)	379 (36.3)	1.11	NS
Anti-Parkinson drugs	48 (16.4)	15 (1.4)	13.34	<0.001
Antipsychotics	20 (6.8)	30 (2.9)	2.48	0.002

CVD, cerebrovascular disease; CDR, Clinical Dementia Rating scale; n, number of cases; NS, Non-significance; OR, odds ratio; Heart diseases, including coronary artery disease, valvular heart disease, congestive heart failure, and arrhythmia.

age and dementia severity according to CDR is demonstrated in **Table 4**. None of the MRI variables including Fazekas scale, global atrophy scale, medial temporal lobe atrophy scale, or microbleeds showed significant difference between the groups. The comparison of TRODAT variables also showed no significant difference in striatal background ratio, caudate putamen ratio, or rates of abnormal uptake between the groups.

We further compared clinical features between resting tremor group (n = 193) and isolated postural/action tremor group (n = 99). The results showed that no significant different between two groups in most of the motor and non-motor features except for bradykinesia (67.9 vs. 51.5%, OR = 2.01, p = 0.006) after adjustment for age and CDR. Motor features were also compared according to tremor onset asymmetry or not and the asymmetric group demonstrated significantly higher prevalence of bradykinesia (70.7 vs. 56.8%, OR = 1.87, p = 0.014), rigidity (62.1 vs. 47.7%, OR = 1.90, p = 0.009), postural instability (81.0 vs. 67.6%, OR = 2.08, p = 0.011), and easily falling (28.4 vs. 14.8%, OR = 2.39, p = 0.004). Besides, we also analyzed the clinical features among patients with tremor. Patients were divided into groups according to the temporal sequence of tremor and CVD. The results showed that the group showing tremor onset earlier than CVD onset had significantly higher prevalence of REM sleep behavior disorder than the group with later or concomitant onset (23.8 vs. 10.6%, OR = 2.66, p = 0.004). No other features were significantly related to the temporal sequence of tremor onset and CVD.

TABLE 4 | Neuroimaging manifestation of tremor group compared to non-tremor group adjusted for age and dementia severity by CDR.

	Tremor	Non-tremor	OR	*p*
MRI, *n*	194	669		
Fazekas, mean (SD, range)	2.0 (1.0, 0–3)	1.8 (1.0, 0–3)	1.29	NS
MTA, mean (SD, range)	2.3 (1.1, 0–4)	2.2 (1.2, 0–4)	0.96	NS
Global, mean (SD, range)	1.6 (0.7, 0–3)	1.5 (0.8, 0–3)	0.73	NS
Cortical CBM, *n* (%)	47 (23.4)	313 (27.8)	0.70	NS
Subcortical CBM, *n* (%)	65 (32.3)	230 (33.2)	0.97	NS
Trodat, *n*	70	63		
DaTabN, *n* (%)	31 (44.3)	37 (58.7)	0.63	NS
SBR, mean (SD, range)	1.5 (0.5, 0.2–2.8)	1.5 (0.4, 0.5–2.4)	1.29	NS

CDR, Clinical Dementia Rating scale; n, number of cases; OR, odds ratio; NS, non-significance; Fazekas, Fazekas scale; MTA, medial temopral lobe atrophy scale; Global, global atrophy scale; CMB, cerebral microbleeds; Trodat, Tc-99m Trodat-1 SPECT; DaTabN, abnormal dopamine transporter imaging in Tc-99m Trodat-1 SPECT; SBR, Striatal background ratio in Tc-99m Trodat-1 SPECT; CPR, caudate putamen ratio in Tc-99m Trodat-1 SPECT.

DISCUSSION

The present study has several important findings. A relatively high prevalence of resting and/or postural/action tremors (21.8%) was found in patients with VCI. This finding was not consistent with the findings of previous studies, which reported that the association of movement disorders and stroke was uncommon and only 1% of the patients developed movement disorders after acute stroke (Ghika-Schmid et al., 1997). This discrepancy in the results was probably due to the fact that motor deficit due to acute stroke tends to improve after the development of abnormal movement (Handley et al., 2009). However, our study investigated CVD patients with cognitive impairment without restricting the investigation to acute CVD. Therefore, the present study population was different from that in the previous studies. Moreover, tremors might have started before CVD and persisted without improving. The comparison of VCI patients in the tremor group and those in the non-tremor group showed no difference in the subtype of VCI (MCI or dementia stages) or in the location of CVD (cortical, subcortical, mixed location, infarct, or hemorrhage). These findings indicated that tremor in VCI patients was probably not simply caused by vascular disease itself. Instead, degenerative process might have contributed the most to the pathophysiology or the etiology of tremor. Furthermore, rather than atypical tremors related to acute stroke (Ghika-Schmid et al., 1997; Handley et al., 2009), VCI patients presented high prevalence of typical (resting and postural/action) tremors, which are traditionally regarded as tremors of neurodegenerative disorders (Zappia et al., 2013; Postuma et al., 2015; McKeith et al., 2017). Therefore, mixed vascular and degenerative pathologies were also implicated in this group of VCI patients with typical tremor. The longer duration of motor dysfunction in the tremor group compared to the non-tremor group represented a higher percentage of early onset of motor dysfunction (before the onset of CVD or VCI). In other words, among patients with tremor, movement disorders were diagnosed before the diagnosis of CVD or VCI. Besides, the much higher prevalence of motor and non-motor diagnostic features of LBD in the tremor group provided further evidence of the possibility of the prevalence of mixed pathologies with LBD being higher in the tremor group. High percentage of abnormal dopamine transporter imaging studies and no difference in striatal uptake is reported between patients with and without tremor. We proposed that structure damage in the striatal region might probably contribute to the impairment of uptake of the dopamine transporter imaging. Besides, patients with clinical pictures of mixed Parkinson's disease were prone to have a dopamine transporter imaging. Therefore, abnormal uptake in both groups were relatively high in this study (44.3% in tremor and 58.7% in non-tremor group).

The higher prevalence of vascular risk factors (VRFs) including hypertension, diabetes, hyperlipidemia, and heart diseases in the tremor group were interesting and novel findings in VCI patients. Previous studies on the association between VRFs and VCI revealed that these factors contributed to the cardio-vascular diseases (CVD) attack or to the occurrence of cognitive impairment/dementia (Jeng et al., 1994; MacKnight et al., 2002; Schulz and Rothwell, 2003; Gorelick, 2004; Sahathevan et al., 2012; Staals et al., 2014). Besides, most of the midlife VRFs have been associated with increased neurodegenerative or vascular disorders and cognitive impairment as a comorbidity in late life (Kivipelto et al., 2001; Whitmer et al., 2005; Barnes et al., 2012). The contribution of VRFs has been well studied in patients with movement disorders. Patients with PD are associated with lower prevalence of VRFs or CVD (Scigliano et al., 2006). CVD and VRFs show significant association with motor and cognitive dysfunction in PD (Papapetropoulos et al., 2004; Malek et al., 2016). Therefore, these research findings might help explain our results of higher prevalence of VRFs in VCI patients with tremor. Furthermore, we proposed that VRFs contributed not only to the incidence of CVD and cognitive impairment but also to the incidence or progression of tremor-related movement disorders like LBD. For better clarification, we further analyzed the motor composite questionnaire (MCQ) (total score 6, **Table 2**) as well as the non-motor composite questionnaire (NMCQ) (total score 10, **Table 2**) in the present study and found that in the current VCI population, MCQ and NMCQ were higher in the hypertension group compared to the non-hypertension group (MCQ: 2.0 ± 1.8 vs. 1.5 ± 1.7, $p < 0.001$ and NMCQ: 2.8 ± 2.4 vs. 2.2 ± 2.3, $p < 0.001$); higher in the diabetes group than in the non-diabetes group (MCQ: 2.1 ± 1.8 vs. 1.6 ± 1.8, $p < 0.001$ and NMCQ: 3.0 ± 2.4 vs. 2.3 ± 2.4, $p < 0.001$); higher in the hyperlipidemia group than in the non-hyperlipidemia group (MCQ: 2.1 ± 1.8 vs. 1.6 ± 1.8, $p < 0.001$ and NMCQ: 2.9 ± 2.3 vs. 2.3 ± 2.4, $p < 0.001$); and higher in the heart diseases group than in the group with no heart diseases (MCQ: 2.3 ± 1.8 vs. 1.7 ± 1.8, $p < 0.001$ and NMCQ: 3.3 ± 2.4 vs. 2.4 ± 2.4, $p < 0.001$). In addition to age and dementia severity, we further adjusted gender, antiplatelet, and Fazekas scale, and the results were still the same as our original ones. Based on these findings, we may conclude that each VRFs could have contributed to the

presentation of motor as well as non-motor Lewy body features in patients with VCI.

Finally, it deserves attention that in this study, more than 80% of patients in the tremor group present parkinsonism, but only 16.4% were treated with antiparkinsonian drugs, indicating that neurologists mostly consider this neurological condition as a vascular parkinsonism, probably preventing patients from having a possibly effective treatment. Careful and detailed clinical assessment of associated symptoms in VCI patients with tremor to find out the possible comorbidity with PD or DLB should always be in mind.

The present study has some limitations. It was a retrospective study without pathological confirmation of the diagnosis. Therefore, the findings and the speculations were based only on clinical observations and neuroimaging. Clinical presentations in the present study were recorded based on a structured questionnaire, and though the interrater reliability test showed good reliability, accuracy and completeness of the clinical data needs to be verified. Only 10% of the participants in the study had received dopamine transporter imaging. Therefore, the reported contribution of LBD to VCI was based only on the clinical features. Further prospective studies based on biomarkers for LBD (CSF/plasma α-synuclein and/or dopamine transporter imaging) are necessary to clarify the probability and the contribution of Lewy body pathology to VCI with tremor.

In conclusion, tremor is a common comorbidity of VCI. VCI patients with tremor had a higher prevalence of all motor and non-motor Lewy body clinical features and more severe neuropsychiatric symptoms. These findings raised the possibility of mixed pathology with LBD in VCI patients with tremor. Importantly, VCI patients with tremor showed higher prevalence of VRFs including hypertension, diabetes, hyperlipidemia, and heart diseases. However, causal relationship of VRFs in VCI with parkinsonism needs further study to be clarified.

DATA AVAILABILITY STATEMENT

The data analyzed in this study was subject to the following licenses/restrictions: The raw data supporting the conclusions of this article will be made available by the authors, without undue reservation, to any qualified researcher. Requests to access these datasets should be directed to P-YC, paiyibox@gmail.com.

ETHICS STATEMENT

The studies involving human participants were reviewed and approved by Institutional Review Board of Show Chwan Memorial Hospital. Written informed consent for participation was not required for this study in accordance with the national legislation and the institutional requirements.

AUTHOR CONTRIBUTIONS

P-YC undertook the literature search and data analysis, edited the author contributions, and was mainly responsible for revisions and drafts of the manuscript. C-JH participated in the data analysis and contributed to revisions and the final draft of the manuscript. C-YW participated in data analysis and contributed to revisions of the manuscript. G-UH contributed to revisions of the manuscript. R-CT undertook the literature search and contributed to revisions. All authors contributed to the article and approved the submitted version.

ACKNOWLEDGMENTS

We would like to thank Dr. Ming-Tsung Lee at Research Assistant Center of Show Chwan Memorial Hospital for his feedback and suggestions regarding the experimental design and statistical analysis.

REFERENCES

American Academy of Sleep Medicine (2001). *ICSD—International Classification of Sleep Disorders, Revised: Diagnostic and Coding Manual.* Darien, IL: American Academy of Sleep Medicine.

Barnes, D. E., Yaffe, K., Byers, A. L., McCormick, M., Schaefer, C., and Whitmer, R. A. (2012). Midlife vs late-life depressive symptoms and risk of dementia: differential effects for Alzheimer disease and vascular dementia. *Arch. Gen. Psychiatry* 69, 493–498. doi: 10.1001/archgenpsychiatry.2011.1481

Bhatia, K. P., Bain, P., Bajaj, N., Elble, R. J., Hallett, M., Louis, E. D., et al. (2018). Consensus statement on the classification of tremors. from the task force on tremor of the international parkinson and movement disorder society. *Mov. Disord.* 33, 75–87. doi: 10.1002/mds.27121

Chiu, P. Y., Wei, C. Y., and Hung, G. U. (2019). Preliminary study of the history-based artificial intelligent clinical dementia diagnostic system. *Show Chwan Med. J.* 18, 18–27. doi: 10.3966/156104972019061801003

Cummings, J. L. (1988). Intellectual impairment in Parkinson's disease: clinical, pathologic, and biochemical correlates. *J. Geriatr. Psychiatry Neurol.* 1, 24–36. doi: 10.1177/089198878800100106

Custodio, N., Montesinos, R., Lira, D., Herrera-Pérez, E., Bardales, Y., and Valeriano-Lorenzo, L. (2017). Mixed dementia: a review of the evidence. *Dement. Neuropsychol.* 11, 364–370. doi: 10.1590/1980-57642016dn11-040005

Ferman, T. J., Smith, G. E., Boeve, B. F., Ivnik, R. J., Petersen, R. C., Knopman, D., et al. (2004). DLB fluctuations specific features that reliably differentiate DLB from AD and normal aging. *Neurology* 62, 181–187. doi: 10.1212/wnl.62.2.181

Frisoni, G. B., Galluzzi, S., Bresciani, L., Zanetti, O., and Geroldi, C. (2002). Mild cognitive impairment with subcortical vascular features: clinical characteristics and outcome. *J. Neurol.* 249, 1423–1432. doi: 10.1007/s00415-002-0861-7

Ghika-Schmid, F., Ghika, J., Regli, F., and Bogousslavsky, J. (1997). Hyperkinetic movement disorders during and after acute stroke: the lausanne stroke registry. *J. Neurol. Sci.* 146, 109–116. doi: 10.1016/s0022-510x(96)00290-0

Gorelick, P. B. (2004). Risk factors for vascular dementia and Alzheimer disease. *Stroke* 35(11 Suppl. 1), 2620–2622. doi: 10.1161/01.str.0000143318.70292.47

Gorelick, P. B., Scuteri, A., Black, S. E., Decarli, C., Greenberg, S. M., Iadecola, C., et al. (2011). Vascular contributions to cognitive impairment and dementia: a statement for healthcare professionals from the american heart association/american stroke association. *Stroke* 42, 2672–2713. doi: 10.1161/STR.0b013e3182299496

Handley, A., Medcalf, P., Hellier, K., and Dutta, D. (2009). Movement disorders after stroke. *Age Ageing* 38, 260–266. doi: 10.1093/ageing/afp020

Jeng, J. S., Chung, M. Y., Yip, P. K., Hwang, B. S., and Chang, Y. C. (1994). Extracranial carotid atherosclerosis and vascular risk factors in different types of ischemic stroke in Taiwan. *Stroke* 25, 1989–1993. doi: 10.1161/01.str.25.10.1989

Kivipelto, M., Helkala, E. L., Hanninen, T., Laakso, M. P., Hallikainen, M., Alhainen, K., et al. (2001). Midlife vascular risk factors and late-life mild cognitive impairment: a population-based study. *Neurology* 56, 1683–1689. doi: 10.1212/wnl.56.12.1683

Korczyn, A. D. (2015). Vascular parkinsonism–characteristics, pathogenesis and treatment. *Nat. Rev. Neurol.* 11, 319–326. doi: 10.1038/nrneurol.2015.61

Langa, K. M., Foster, F. L., and Larson, E. B. (2004). Mixed dementia: emerging concepts and therapeutic implications. *JAMA* 292, 2901–2908. doi: 10.1001/jama.292.23.2901

Lawton, M. P., and Brody, E. M. (1969). Assessment of older people: self-maintaining and instrumental activities of daily living. *Gerontologist* 9, 179–186. doi: 10.1093/geront/9.3_part_1.179

Lin, K. N., Wang, P. N., Liu, C. Y., Chen, W. T., Lee, Y. C., and Liu, H. C. (2002). Cutoff scores of the cognitive abilities screening instrument. Chinese version in screening of dementia. *Dement. Geriatr. Cogn. Disord.* 14, 176–182. doi: 10.1159/000066024

MacKnight, C., Rockwood, K., Awalt, E., and McDowell, I. (2002). Diabetes mellitus and the risk of dementia, Alzheimer's disease and vascular cognitive impairment in the canadian study of health and aging. *Dement. Geriatr. Cogn. Disord.* 14, 77–83. doi: 10.1159/000064928

Malek, N., Lawton, M. A., Swallow, D. M., Grosset, K. A., Marrinan, S. L., Bajaj, N., et al. (2016). Vascular disease and vascular risk factors in relation to motor features and cognition in early Parkinson's disease. *Mov. Disord.* 31, 1518–1526. doi: 10.1002/mds.26698

McKeith, I. G., Boeve, B. F., Dickson, D. W., Halliday, G., Taylor, J. P., Weintraub, D., et al. (2017). Diagnosis and management of dementia with Lewy bodies: fourth consensus report of the DLB Consortium. *Neurology* 89, 88–100. doi: 10.1212/wnl.0000000000004058

Morris, J. C. (1993). The clinical dementia rating (CDR): current version and scoring rules. *Neurology* 43, 2412–2414. doi: 10.1212/wnl.43.11.2412-a

Nasreddine, Z. S., Phillips, N. A., Bedirian, V., Charbonneau, S., Whitehead, V., Collin, I., et al. (2005). The montreal cognitive assessment, MoCA: a brief screening tool for mild cognitive impairment. *J. Am. Geriatr. Soc.* 53, 695–699. doi: 10.1111/j.1532-5415.2005.53221.x

Nelson, P. T., Jicha, G. A., Kryscio, R. J., Abner, E. L., Schmitt, F. A., Cooper, G., et al. (2010). Low sensitivity in clinical diagnoses of dementia with Lewy bodies. *J. Neurol.* 257, 359–366. doi: 10.1007/s00415-009-5324-y

Papapetropoulos, S., Ellul, J., Argyriou, A. A., Talelli, P., Chroni, E., and Papapetropoulos, T. (2004). The effect of vascular disease on late onset Parkinson's disease. *Eur. J. Neurol.* 11, 231–235. doi: 10.1046/j.1468-1331.2003.00748.x

Postuma, R. B., Berg, D., Stern, M., Poewe, W., Olanow, C. W., Oertel, W., et al. (2015). MDS clinical diagnostic criteria for Parkinson" disease. *Mov. Disord.* 30, 1591–1601. doi: 10.1002/mds.26424

Sahathevan, R., Brodtmann, A., and Donnan, G. A. (2012). Dementia, stroke, and vascular risk factors; a review. *Int. J. Stroke* 7, 61–73. doi: 10.1111/j.1747-4949.2011.00731.x

Savica, R., Beach, T. G., Hentz, J. G., Sabbagh, M. N., Serrano, G. E., Sue, L. I., et al. (2019). Lewy body pathology in Alzheimer's disease: a clinicopathological prospective study. *Acta Neurol. Scand.* 139, 76–81. doi: 10.1111/ane.13028

Schneider, J. A., Arvanitakis, Z., Bang, W., and Bennett, D. A. (2007). Mixed brain pathologies account for most dementia cases in community-dwelling older persons. *Neurology* 69, 2197–2204. doi: 10.1212/01.wnl.0000271090.28148.24

Schulz, U. G., and Rothwell, P. M. (2003). Differences in vascular risk factors between etiological subtypes of ischemic stroke: importance of population-based studies. *Stroke* 34, 2050–2059. doi: 10.1161/01.str.0000079818.08343.8c

Scigliano, G., Musicco, M., Soliveri, P., Piccolo, I., Ronchetti, G., and Girotti, F. (2006). Reduced risk factors for vascular disorders in Parkinson disease patients: a case-control study. *Stroke* 37, 1184–1188. doi: 10.1161/01.STR.0000217384.03237.9c

Skogseth, R., Hortobagyi, T., Soennesyn, H., Chwiszczuk, L., Ffytche, D., Rongve, A., et al. (2017). Accuracy of clinical diagnosis of dementia with lewy bodies versus neuropathology. *J. Alzheimers Dis.* 59, 1139–1152. doi: 10.3233/jad-170274

Staals, J., Makin, S. D., Doubal, F. N., Dennis, M. S., and Wardlaw, J. M. (2014). Stroke subtype, vascular risk factors, and total MRI brain small-vessel disease burden. *Neurology* 83, 1228–1234. doi: 10.1212/wnl.0000000000000837

van Zagten, M., Lodder, J., and Kessels, F. (1998). Gait disorder and parkinsonian signs in patients with stroke related to small deep infarcts and white matter lesions. *Mov. Disord.* 13, 89–95. doi: 10.1002/mds.870130119

Whitmer, R. A., Sidney, S., Selby, J., Johnston, S. C., and Yaffe, K. (2005). Midlife cardiovascular risk factors and risk of dementia in late life. *Neurology* 64, 277–281. doi: 10.1212/01.wnl.0000149519.47454.f2

Woodward, M., Mackenzie, I., Hsiung, G.-Y., Jacova, C., and Feldman, H. (2010). Multiple brain pathologies in dementia are common. *Eur. Geriatr. Med.* 1, 259–265. doi: 10.1016/j.eurger.2010.07.012

Zappia, M., Albanese, A., Bruno, E., Colosimo, C., Filippini, G., Martinelli, P., et al. (2013). Treatment of essential tremor: a systematic review of evidence and recommendations from the italian movement disorders association. *J. Neurol.* 260, 714–740. doi: 10.1007/s00415-012-6628-x

Conflict of Interest: The authors declare that the research was conducted in the absence of any commercial or financial relationships that could be construed as a potential conflict of interest.

frontiers in Aging Neuroscience

ORIGINAL RESEARCH
published: 29 July 2020
doi: 10.3389/fnagi.2020.00221

Early Diagnosis of Mild Cognitive Impairment Based on Eye Movement Parameters in an Aging Chinese Population

Jing Nie[1†], Qi Qiu[1†], Michael Phillips[1,2], Lin Sun[1], Feng Yan[1], Xiang Lin[1], Shifu Xiao[1] and Xia Li[1*]*

[1]Department of Psychiatry, Shanghai Mental Health Center, Shanghai Jiao Tong University School of Medicine, Shanghai, China, [2]Departments of Psychiatry and Epidemiology, Columbia University, New York, NY, United States

OPEN ACCESS

Edited by:
Woon-Man Kung,
Chinese Culture University, Taiwan

Reviewed by:
Ramesh Kandimalla,
Texas Tech University Health Sciences Center, United States
Tatiana Karpouzian-Rogers,
Northwestern University, United States
Juanjuan Jiang,
Shanghai University, China

***Correspondence:**
Shifu Xiao
xiaoshifu@msn.com
Xia Li
ja_1023@hotmail.com

[†]These authors have contributed equally to this work

Received: 26 September 2019
Accepted: 22 June 2020
Published: 29 July 2020

Citation:
Nie J, Qiu Q, Phillips M, Sun L, Yan F, Lin X, Xiao S and Li X (2020) Early Diagnosis of Mild Cognitive Impairment Based on Eye Movement Parameters in an Aging Chinese Population. Front. Aging Neurosci. 12:221. doi: 10.3389/fnagi.2020.00221

Background: The pathogenesis of dementia often starts several years prior to clinical onset during which the individual is asymptomatic. Existing strategies for the accurate diagnosis of early dementia are limited by high cost and the invasive nature of the procedures. Eye movement parameters associated with cognitive functions may be helpful in the early identification of dementia and in the development and evaluation of preventive and therapeutic strategies.

Objective: We aimed to assess differences in eye movement parameters between healthy elderly individuals and patients with mild cognitive impairment (MCI). Furthermore, we examined the correlations between eye movement parameters with cognitive functions and specific hemispheric region and neural structures in individuals with MCI.

Method: Eighty individuals with MCI without dementia (based on DSM-IV criteria) identified by community screening and 170 healthy controls were administered Chinese versions of MoCA and NTB, and a long (20 min) or short (5 min) version of a visual paired comparison (VPC) task. Two weeks later, 44 MCI patients and 107 healthy controls completed a retest of the VPC task, 44 MCI patients and 43 healthy controls among them administered a MRI. At the end of 1-year follow-up, a subset of 26 individuals with MCI and 57 healthy controls were administered the long version of VPC task and MoCA test again. Eye movement parameters and the relationship of eye movement parameters with cognitive functions and with changes in neural structures were compared between groups.

Results: Patients with MCI were older, had less education, and had lower scores on cognitive tests than healthy controls. After adjustment for age and level of education, patients with MCI had lower novelty preference scores on the VPC than healthy controls. Using the logistic regression model, the amount of time that subjects focused on these novel images could predict MCI patients from normal elderly with an out of sample area

under the receiver operator characteristic curve of 0.62. Furthermore, the cognition score of subjects whose novelty preference score was low decreased more remarkably in 1 year. For both the patient and control groups, VPC novelty preference was significantly correlated with verbal fluency and delayed and short-term memory function. Novelty preference score was also significantly correlated with the cortical thickness of several structures in the right hemisphere.

Conclusion: Eye movement parameters are stable indicators to distinguish patients with MCI and cognitively normal subjects and are not affected by different testing versions and numbers. Additionally, the patients' cognitive deficits and eye movement indices were correlated. Future longitudinal studies should further explore the clinical utility of eye movement parameters as early markers of MCI.

Keywords: mild cognitive impairment, preclinical diagnosis, dementia, eye-tracking assessment, magnetic resonance imaging

INTRODUCTION

The pathogenesis of dementia is mostly asymptomatic and begins many years before the onset of clinical symptoms. Patients with mild cognitive impairment (MCI) can still perform independent living activities and functions relatively well; however, they have declining verbal memory, visuospatial, and executive capacity (Petersen et al., 1999; Vega and Newhouse, 2014). Previously, MCI was assumed to be an intermediate state between normal aging and dementia that increased the risk of progression to Alzheimer's disease (AD). However, not all aging processes lead to cognitive impairment. Currently, MCI is regarded as a pathological condition of aging that requires better diagnostic strategies (Petersen, 2004; Galimberti and Scarpini, 2012).

Currently, there are several methods for predicting the progression of MCI, such as structural magnetic resonance imaging (MRI; Wood, 2016), functional imaging techniques (Jessen and Dodel, 2014), and analysis of biomarkers in the cerebrospinal fluid and peripheral blood (Hermida et al., 2012). However, these methods are limited by their high costs and invasive nature; furthermore, they are considered too restrictive for subdiagnosis among the MCI population (Vega and Newhouse, 2014).

The visual paired comparison (VPC) task is a nonverbal recognition task that can sufficiently challenge an individual's cognitive system, especially the memory. VPC has been shown to have high sensitivity and specificity for distinguishing normal elderly individuals and patients with the MCI. In the VPC task, an item is initially presented briefly, and after a specified time, the subjects are presented with the previously seen item together with a new item. The amount of time spent observing the new item, compared to that spent on the old item, is recorded and the preference for the new item is calculated as the novelty preference (NP) score (Zola et al., 2000; Lagun et al., 2011). Healthy controls tend to concentrate disproportionately more on the novel aspects of the environment (Haque et al., 2019; Jiang et al., 2019; Oyama et al., 2019). In the VPC tasks, the expected normal performance is that the subjects spend more time looking at new pictures than the old ones. In contrast, memory impairment may be characterized by roughly equal amount of time spent reading fiction and familiarizing with pictures, which indicates an impaired declarative memory of previously observed images.

We aimed to establish a baseline pattern of association between cognitive function and eye-tracking parameters in patients with MCI. We primarily aimed to determine whether the NP score could distinguish patients with MCI from cognitively normal elderly individuals. As a secondary objective, we aimed to determine the correlation of eye movement parameters with various specific cognitive regions. Furthermore, we assessed whether eye movement parameters could indicate underlying regional brain dysfunction and help in the identification of underdiagnosed MCI in subsequent follow-up visits.

MATERIALS AND METHODS

Subjects and Clinical Classification

In this study, we recruited two groups of participants aged 65–80 years from four different communities in Shanghai and stratified them into MCI (n = 80) and healthy (n = 170) groups. One-hundred and fourteen participants completed the 12-month follow-up. We excluded subjects with other psychiatric illness; neurological, ophthalmological, or hearing impairment disorders; or inability to sit comfortably because of severe physical illness (**Figure 1**).

Diagnostic Procedures

All clinical diagnoses were established by three different geriatric psychiatrists according to the results of standardized assessment and review. Clinical diagnosis of MCI required evidence of definite decline in memory (MoCA scores of >1.5 SD of age-appropriate norms or abnormal memory function for age) and additional possible impairment of other cognitive domains, severity of symptoms or consequent functional limitation not meeting the DSM-IV dementia standard; a diagnosis of NC was made if participants demonstrated no evidence of cognitive decline as compared to their baseline cognitive functions on clinical interview and assessment. Exclusion criteria included

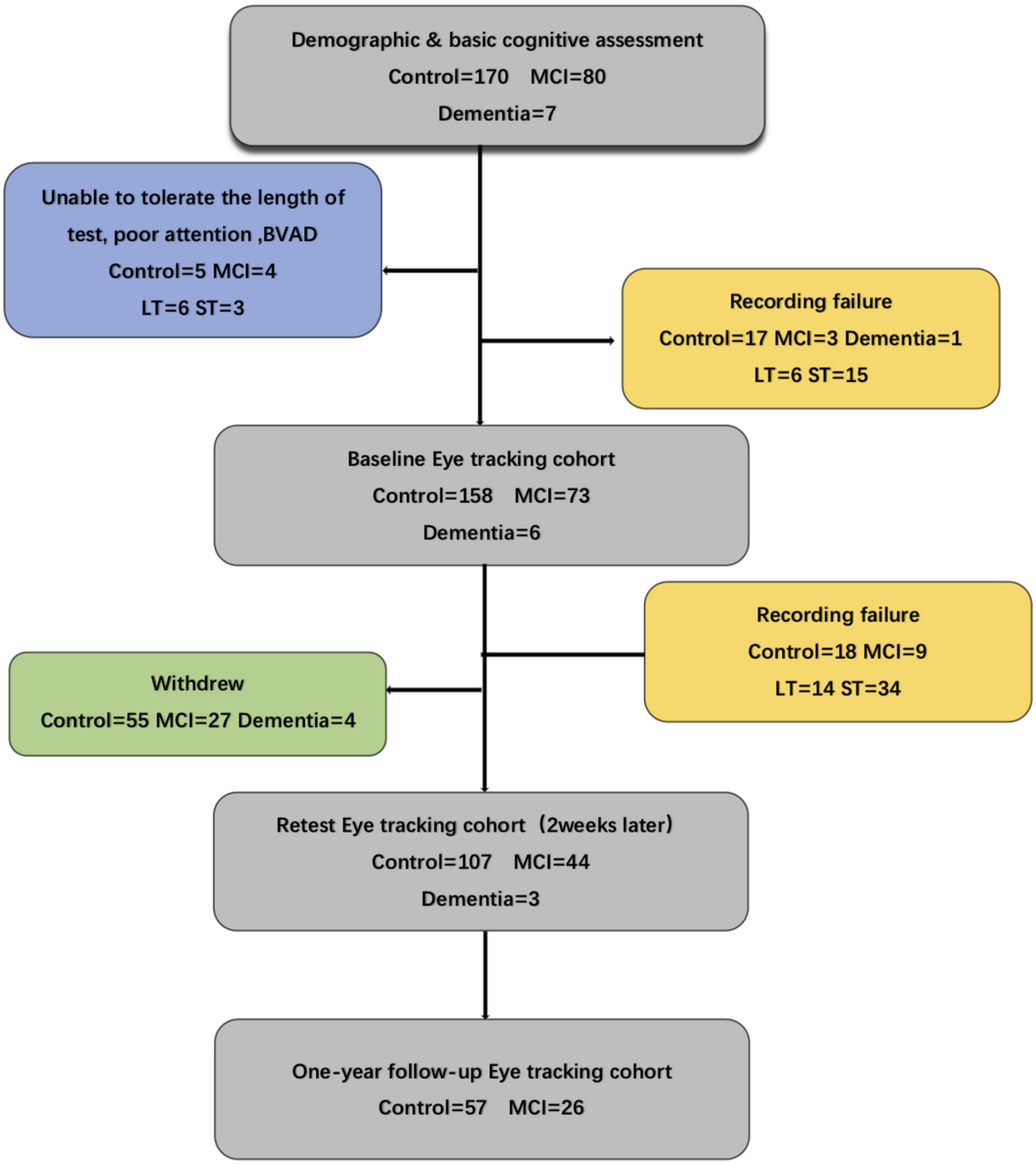

FIGURE 1 | Flow chart for the eye-tracking study indicating recording failure or problems with tolerance to the procedure. Several of the eye-tracking cohorts failed to complete the whole test. MCI, mild cognitive impairment; BVAD, binocular visual acuity differences; LT, long task: eye moving type sets of 30 min; ST, short task: eye moving type sets of 5 min.

a history of substance abuse, learning disability, dementia, and neurological (stroke, tumor, etc.) or psychiatric illness. Moreover, because the VPC task involves visual memory, subjects were excluded if: (1) the eye-tracking equipment could not record adequate pupil and corneal reflection because of physiological constraints or visual problems (such as droopy eyelid, cataracts, detached retinas, glaucoma, extremely small pupils, etc.); and/or (2) participants could not complete the eye-tracking calibration procedure (American Psychiatric Association, 1990). Then, a detailed medical, social, and family history was obtained from each participant; they completed the following subtests: C-MoCA (Chinese Version of Montreal Cognitive Assessment) and C-NTB (Chinese Version of neuropsychological test battery) including WMDS (Wechsler Memory digit span), WMVis-I (Wechsler Memory Scale visual immediate), WMVis-D (Wechsler Memory Scale visual delayed), CFT (Category Fluency Test), COWAT (Controlled Word Association Test), RAVLT-I (Rey Auditory Verbal Learning

Test immediate), and RAVLT-D (Rey Auditory Verbal Learning Test delayed). This study was approved by the Institution Review Board of the Shanghai Mental Health Center. Written informed consent was obtained from all the participants or their representatives.

Assessment of MR Image Acquisition and Processing

MRI scanning was performed using a Siemens Magnetom Verio 3.0T scanner (Siemens, Munich, Germany). We acquired T1-weighted images with 176 sagittal slices using the 3D magnetization-prepared rapid gradient-echo acquisition sequence with the following parameters: TR = 2,300 ms; TE = 2.98 ms; flip angle = 9°; and spatial resolution, 1 mm × 1 mm × 1.2 mm (Lin et al., 2018).

Reconstruction of cortical surfaces and cortical thickness measurements was performed using the automated reconstruction function in the FreeSurfer version 6.0 software as described by Dale et al. (1999).

Assessment of Visual Exploration

The VPC task requires participants to sit comfortably in front of a monitor and keep their heads positioned on a chinrest to maintain their viewing position. During task performance, all participants' eye movements were recorded using an Applied Science Laboratories (ASL) Model 5000 remote pan/tilt camera system continuously. A ring of filtered, near-infrared light-emitting diodes illuminated the eye; a high-speed, near-infrared, sensitive charge-coupled device camera captured the pupil and corneal reflection. The gaze angle was determined by the relative positions of the corneal and pupil centers with an accuracy of ±0.75°. The sampling frequency was 60 Hz, with a temporal resolution of 16 ms and linearity of less than 10%. The participants were seated approximately 26 inches from a 19-inch flat panel computer screen that displayed the stimuli. No physical constraints other than a chinrest were used. The eye position was calibrated for each subject using an infrared eye-tracker instrument for 1–2 min. Calibration for each subject was accomplished using a 9-point array. Data of eye fixation and eye movement were recorded with the ASL EYEPOS software. In our present study, we used the dispersion-based fixation detection algorithm from Crutcher MD. The duration threshold was set to 100 ms, and the dispersion threshold was set to five points in eye tracker units (2° of visual angle). The eye fixation and movement data were all recorded with ASL EYEPOS software system. All acquired black and white pictures were high contrast measuring 4.4 inches wide and 6.5 inches high. Unique pictures were used for each trial (Crutcher et al., 2009). System parameters were adjusted until the subject's fixations were accurately mapped onto the calibration points. Subjects were informed preemptively that images would begin to appear on the computer screen before the test and were instructed to look at the images as if they were watching television. The subjects' eye movements and fixations were recorded and stored for subsequent analyses. Two types of tasks were used; namely, long and short tasks. The long task (LT) lasted approximately 30 min, whereas the improved short test (ST) required about 10 min, including calibration.

Participants performed a memory paradigm based on eye movements. Each trial in the task consisted of the following two phases: an initial familiarization phase and a subsequent test phase. Subjects were asked to complete the 9-point calibration procedure before taking the VPC task. During the familiarization phase, two identical two-dimensional black-and-white images were presented side by side on the monitor for 5 s. Next, the monitor went dark for a delay interval of either 2 s or 2 min. In the subsequent test phase, the images were again presented side by side for 5 s. One of the images was identical to the previously presented image, whereas the other was a new image. Presentation of the novel image on either the left or right side was randomly selected and equally distributed. After the test phase, the monitor went dark for 20 s and the next task was initiated. To ensure the subject maintained complete attention during the test trials with a 2-min delay interval, the experimenter alerted all the subjects 10 s before the presentation of the next image pair. For the long task, participants were administered two blocks of 10 trials (delay order: 2-s delay, 2-min delay) for a total of 20 trials. The short task contains three trials (**Figure 2**). The visual search task was used to determine the NP parameter. The eye data parameter called novelty preference (NP) was obtained by calculating the percentage of time spent staring at the novel image by extracting and analyzing the eye fixation and movement data for each participant. The cognitive and eye-tracking assessments were performed on the same day or within a 5-day interval. The whole assessment was completed within approximately 1.5 h, including the rest intervals (Xiao et al., 2013; Pereira et al., 2014).

Statistical Analysis

Statistical analysis was performed using SPSS Version 22. We used independent sample *t*-tests to perform between-group comparisons of the demographic data, cognitive tests scores. Non-parametric test was applied to compare the rate of decline of MoCA score. The eye-tracking parameters among groups were analyzed by one-way ANOVA followed by the Tukey–Kramer test and multiple comparison adjusted for age and years of formal education. Partial correlation was used to determine the correlation between the novel preference score and the cognitive scores, and cortical thickness. The diagnostic performances of the eye-tracking-based cognitive assessment were determined using a ROC analysis. Statistical significance was set at $p < 0.05$ on a two-tailed test.

RESULTS

Demographic and Clinical Characteristics

The mean age of the control group was 71.1 years with a female-to-male ratio of 2.7:1; the mean age of the MCI group was 73.0 years ($p < 0.001$) with a female-to-male ratio of 3.4:1 ($p > 0.05$). The control group had a significantly higher mean c-MoCA scores (25.8) than the MCI group (20.9; $p < 0.001$), and mean NTB scores (218.4) than the MCI group (184.8; $p < 0.001$). All participants with MCI scores (11.8) had lower

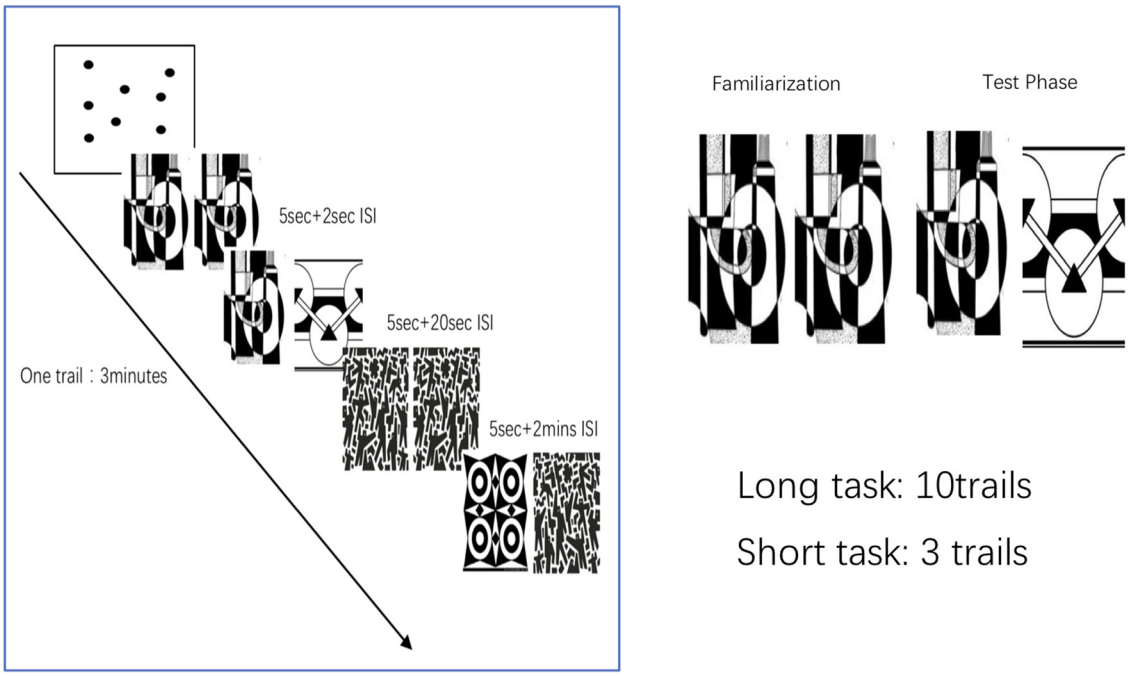

FIGURE 2 | Visual paired comparison task (VPC). Subjects were asked to complete the 9-point calibration procedure before taking the VPC task. During the familiarization phase, participants viewed the two identical pictures presented on the monitor side by side for 5 s. Next, the monitor went dark for a delay interval of either 2 s or 2 min. The test parameters consisted of the presentation of one previously presented image and the novel image. After the test phase, the monitor went dark for 20 s and the next task was initiated. For the long task, participants were administered two blocks of 10 trials (delay order: 2-s delay, 2-min delay) for total 20 trials. The short task contains three trials.

years of education than the control group (12.8; $p < 0.001$). Moreover, the MCI group performed significantly worse than the normal elderly group in cognitive function tests, especially in verbal fluency ($p < 0.05$), attention ($p < 0.01$), abstraction ($p < 0.001$), and verbal memory domains ($p < 0.001$) in the NTB and C-MoCA tests (**Table 1**).

Eye-Tracking Performance

At baseline, the MCI group [0.62 (0.08)] performed significantly worse than the control group [0.66 (0.09)] in the time spent looking at the novel image in the long task ($p < 0.05$ for MCI vs. controls). There was no significant between-group difference in the novelty preference score in the short task [0.57 (0.05) vs. 0.56 (0.07), $p > 0.05$ for MCI vs. controls]. Two weeks later 44 MCI patients and 107 healthy controls completed a retest of the VPC task; in the retest task, compared with cognitively normal elderly individuals, the MCI group had significantly shorter novelty exploration durations in the short task [0.54 (0.05) vs. 0.61 (0.09), $p < 0.05$ for MCI vs. controls; **Table 2**]. Receiver operating characteristic (ROC) curve analysis revealed an area under the ROC curve (AUC) for novelty preference scores in the long task to be 0.62 (asymptotic significance = 0.03; 95% CI = 0.52–0.73). A cutoff value of 0.605 (a phonemic advantage) indicated 70% accuracy, 72% specificity, 53% sensitivity, 40% positive predictive values (PPV), and 82% negative predictive values (NPV) for the diagnosis of MCI.

Results of independent sample *t*-test indicated that, based on the three test pairs of long task twice, short task twice, or one long task and short task each, there were no significant between-group differences in the NP score in the repeated long tasks [normal group: 0.65 (0.02) vs. 0.66 (0.02), $t = 0.3$, df = 51, $p = 0.75$; MCI group: 0.62 (0.02) vs. 0.63 (0.03), $t = 0.2$, df = 20, $p = 0.81$] and the repeated short tasks [normal group: 0.58 (0.02) vs. 0.63 (0.02), $t = 1.9$, df = 44, $p = 0.05$; MCI group: 0.55 (0.01) vs. 0.53 (0.01), $t = 0.68$, df = 18, $p = 0.51$; **Table 3**].

Correlations Between Eye-Tracking Parameters, Cortical Thickness, and Cognitive Functions

From the results of partial correlation analysis (with age and years of education as the control factors), novelty preference score correlated positively with performance in the verbal fluency test in the vegetable categories ($R = 0.37$, $p = 0.04$), short-term memory ($R = 0.41$, $p = 0.02$), and delay recall scores ($R = 0.14$, $p = 0.00$; **Figure 3**). There are no significant differences in the following cortical thickness between the two groups. The MRI results demonstrated a positive correlation between the novelty preference score and cortical thickness in various cerebral regions on the right hemisphere [temporal thickness, superior frontal lobe, rostral anterior cingulate cortex (rACC), and precuneus thickness; $R = 0.24$, $p = 0.02$; $R = 0.22$, $p = 0.04$;

TABLE 1 | Between-group comparisons of age, years of education, and cognitive scores using independent sample *t* test and comparison of patient sex using Pearson's χ^2 ± Fisher's exact test.

	Control group (*n* = 170)	MCI group (*n* = 80)	Statistics	*p*-value
Clinical demographic data				
Mean (SD) age	71.1 (4.1)	73.0 (4.4)	$T = -3.4$	0.00*
Means (SD) years of education	12.8 (3.1)	11.8 (3.5)	$T = 2.1$	0.04*
Gender (female/male)	131/49	62/18	$\chi^2 = 0.13$	0.42*
Global Cognitive scales				
Means (SD) C-MoCA score	25.8 (2.5)	20.9 (3.2)	$T = 12.1$	0.00*
Means (SD) NTB score	218.4 (27.5)	184.8 (34.5)	$T = 7.9$	0.00*
Specific Cognitive tests—executive function				
Verbal fluency—vegetable	14.5 (3.4)	12.9 (3.8)	$T = 3.3$	0.01*
Verbal fluency—word	9.2 (3.5)	7.1 (2.6)	$T = 5.5$	0.00*
Specific Cognitive tests—Verbal Memory				
Delay recall	11.2 (2.9)	8.0 (3.8)	$T = 6.5$	0.00*
Short-term memory	10.3 (2.4)	8.1 (2.2)	$T = 6.8$	0.00*
Specific Cognitive tests—Visual spatial function	4.5 (0.8)	3.5 (1.2)	$T = 7.1$	0.00*
Specific Cognitive tests—attention	5.7 (0.5)	5.1 (0.9)	$T = 4.9$	0.00*

*MCI, mild cognitive impairment; MoCA, Montreal Cognitive Assessment; SD, standard deviation. Data are expressed as mean ± SD. *p < 0.05.*

TABLE 2 | Comparison of mean (SD) novelty preferences scores for long task (20 min) and short task (5 min) between patient and controls groups at baseline and at 2-week follow-up using the *F*-test.

Eye-tracking variables	Control group		MCI group		Statistic*	*p*-value
	n	Mean (SD)	*n*	Mean (SD)		
Baseline						
Long task	85	0.66 (0.09)	38	0.62 (0.08)	$F = 3.34$	0.013
Short task	73	0.56 (0.07)	35	0.57 (0.05)	$F = 0.37$	0.829
2-week follow-up						
Long task	51	0.66 (0.10)	23	0.63 (0.08)	$F = 1.21$	0.316
Short task	56	0.61 (0.09)	21	0.54 (0.05)	$F = 4.47$	0.003

**F test is adjusted for age and years of formal education. LT, long task; ST, short task; SD, standard deviation. Data are expressed as mean ± SD, *p < 0.05.*

TABLE 3 | Comparison of mean (SD) novelty preferences scores for long repeated and short repeated tasks between patient and controls groups at baseline and at 2-week follow-up using the *T*-test.

Eye-tracking variables	Baseline	Two-weeks follow-up	Statistic*	*p*-value
Long repeated task				
HC (*n* = 39)	0.65 (0.02)	0.65 (0.02)	$T = -0.11$	0.915
MCI (*n* = 8)	0.62 (0.02)	0.63 (0.03)	$T = 1.38$	0.217
Short repeated task				
HC (*n* = 30)	0.61 (0.06)	0.62 (0.07)	$T = -1.60$	0.123
MCI (*n* = 10)	0.55 (0.05)	0.56 (0.06)	$T = -0.74$	0.479

*HC, healthy control; MCI, mild cognitive impairment; SD, standard deviation. Data are expressed as mean ± SD, *p < 0.05.*

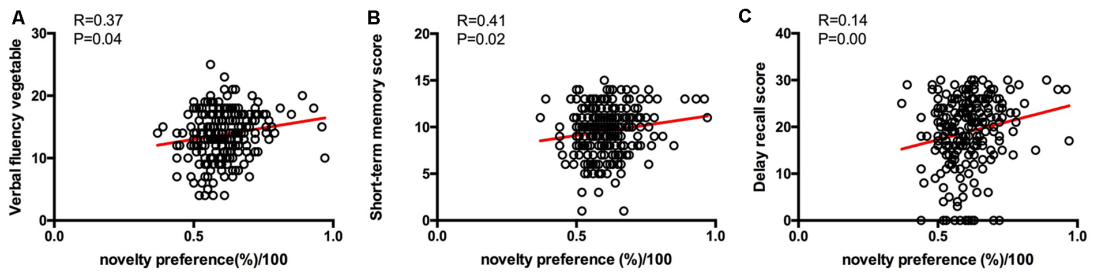

FIGURE 3 | Correlations between eye-tracking parameters and cognitive scores. Only significant findings are shown. **(A)** The novelty preference scores assessed by eye tracking system showed a positive correlation with the verbal fluency score. **(B)** The novelty preference scores assessed by eye tracking system showed a positive correlation with the short-term memory score. **(C)** The novelty preference scores assessed by eye tracking system showed a positive correlation with the delay recall score.

R = 0.24, p = 0.04; and R = 0.22, p = 0.04; respectively]. The statistically significant correlations are summarized in **Figure 4**.

Longitudinal Case–Control Analysis

One-hundred and fourteen participants completed the 12-month follow-up, 31 of whom completed only the MoCA test, and the rest have completed both the MoCA and the long version of the VPC task. Moreover, nine participants progressed from normal to MCI during the study period, 57 of the subjects are stable normal, and 17 participants are stable MCI (**Table 4**). There was no difference in novelty preference scores between progressors and non-progressors including stable MCI and normal. Among all the participants who completed the 12-month follow-up, 62 participants show a decline in cognition scores—46 normal elderly individuals and 16 patients with MCI. The degree of decline of MoCA score (%) was calculated as follows: MoCA total score baseline − MoCA total score endpoint)/MoCA total score baseline*100. Results of the non-parametric test showed that there were no significant differences between the MCI and control groups for the degree of decline of cognition [normal group vs. MCI group, 0.04 (0.00–0.07) vs. 0.05 (0.01–0.09), z = −1.1, p = 0.26; **Figure 5A**]. Based on the ROC analysis above, we find that the novelty preference scores of 0.605 in the long task had high specificity to discriminate MCI from normal. According to that, 62 participants who took the long task at baseline were categorized into the following two groups: above cutoff point group (n = 23) and below cutoff point group (n = 39). Cognitive score in the below cutoff point group decreased more than that in the above cutoff point group [above cutoff point group vs. below cutoff point group: 0.04 (0.00–0.04) vs. 0.04 (0.04–0.09), z = −2.5, p = 0.01; **Figure 5B**].

On partial correlation analysis (with age and years of education as the control factor), novelty preference score correlated negatively with the degree of decline of MoCA score (R = −0.33, p = 0.01; **Figure 5C**).

DISCUSSION

In this study, we assessed the NP score in the eye-tracking task as a simple, novel, and non-invasive diagnostic biomarker of MCI. We found that this NP score accurately distinguished patients with MCI from cognitively normal subjects. In our subsequent retest study, we found that eye movement parameters were stable indicators of cognition and were not affected by the paired testing types and testing times. The improved version could reduce data loss and ensure retention of the sensitivity and specificity of the test. Furthermore, participants with poor novelty preference score showed more decline in cognition in 1-year follow-up. Our study suggests that the VPC task in combination with near-infrared eye-tracking might be helpful to explore the underlying dysfunctions in brain regions.

Therefore, although further longitudinal clinical studies are needed, our findings suggest that novelty preference scores in the VPC task could be an easily accessible physiological marker for diagnosis of MCI and might help to identify "seemingly healthy" subjects who are underdiagnosed for MCI.

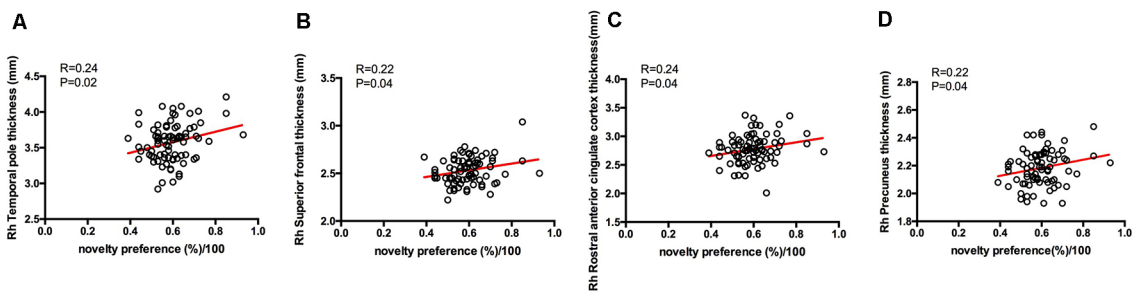

FIGURE 4 | Correlations between eye-tracking parameters and cortical thickness. Only significant findings are shown. Rh, right hemisphere. **(A)** The novelty preference scores assessed by eye tracking system showed a positive correlation with the cortical thickness in temporal pole on the right hemisphere. **(B)** The novelty preference scores assessed by eye tracking system showed a positive correlation with the cortical thickness in superior frontal lobe on the right hemisphere. **(C)** The novelty preference scores assessed by eye tracking system showed a positive correlation with the cortical thickness in rostral anterior cingulate region on the right hemisphere. **(D)** The novelty preference scores assessed by eye tracking system showed a positive correlation with the cortical thickness in precuneus on the right hemisphere.

TABLE 4 | Eye movement indices according to the Group (non-Progressor groups: MCI stable and control stable group, Progressor group) using the Kruskal–Wallis test followed by Steel–Dwass multiple comparison tests.

Eye-tracking variables	Non-progressor Control group		Non-progressor MCI group		Progressor group		*p*-value
	n	Mean (SD)	*n*	Mean (SD)	*n*	Mean (SD)	
Novelty preference, in percentages (SD)	57	0.60 (0.08)	17	0.58 (0.08)	9	0.60 (0.10)	0.885
P-value		0.903[a]		0.655[b]		0.687[c]	

[a]*Non-Progressor Control vs. progressor,* [b]*Non-Progressor Control vs. non-progressor MCI,* [c]*non-progressor MCI vs. progressor. SD, standard deviation.*

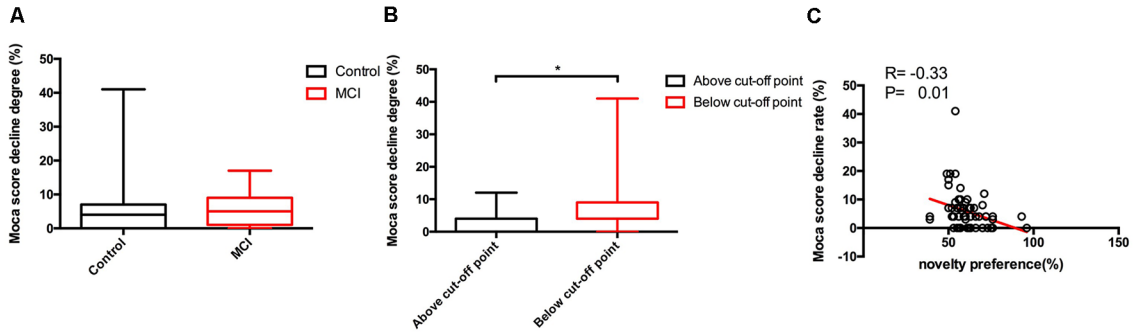

FIGURE 5 | Between-group comparisons of cognitive scores decline degree of different group and the correlations between eye-tracking parameters and cognitive scores decline degree. Only significant findings are shown. Control, normal elderly; MCI, mild cognitive impairment; MoCA, Montreal Cognitive Assessment. Data are expressed as mean ± SD. **(A)** No significant differences of the decline degree of Moca scores in 1 year follow-up were found between control and MCI group. **(B)** Significant differences of the decline degree of Moca scores in 1 year follow-up were apparent between above cut-off point and below cut-off point group. **(C)** The novelty preference scores assessed by eye tracking system showed a negative correlation with the decline degree of Moca scores in 1 year follow-up. *$p < 0.05$.

Eye Movement Parameters in the MCI Group

Patients with MCI show equally distributed observation times between the new and familiar pictures; however, normal individuals tend to focus disproportionately more on the novel pictures (Berlyne, 1960; Loftus and Mackworth, 1978; Fernández et al., 2018). The original long task allows participants to understand the operational process; however, the short task cannot. Therefore, our major finding from the eye-tracking task was the novelty preference score of the long task, which was low in the MCI group, similar to that reported by Crutcher et al. (2009). It should be noted that diagnosing MCI is more difficult than diagnosing dementia owing to the lack of objective indicators and boundaries between MCI and normal elderly are difficult to ascertain. Our method achieved a specificity of 72% for distinguishing subjects with MCI from normal controls. The results indicated that the VPC task could distinguish patients with cognitive impairment from normal elderly individuals based on the eye-tracking data and that the novelty preference score could probably be used as an objective indicator. Our test can also be suitably expanded to communities for its convenience. However, there remains a need for further improvement of eye movement parameters for the PPV exhibited by our method is a little lower than the values reported for some test for AD subjects (Lagun et al., 2011). In the retest task, the subjects, especially the cognitive-normal elderly individuals, could not concentrate on the test, as observed in the findings from our subjects. Given the increased potential for loss of data because of the poor attention spans and physical condition of elderly individuals, the discriminatory effect was not found in the retest task. Interestingly, patients with MCI who were subjected to a 2-week delay had low novelty preference scores in the short task.

Based on the results of our repeated tasks, eye movement parameters were identified as stable indicators of cognition that remain unaffected by learning effects. Therefore, use of the long task followed by the short task and performing comparisons between the results of the two tasks could sufficiently increase task sensitivity and decrease the physical and psychological burden on subjects. Development of an improved version might further facilitate validity and decrease the failure rate.

Based on the 1-year follow-up results, participants who progressed to MCI during the study period did not show significantly low novelty preference scores. Compared with cognitive-normal elderly individuals, patients with MCI also did not show a larger magnitude of decrease in cognition. Based on the ROC analysis above, we find that the novelty preference scores of 0.605 in the long task has a high specificity for discriminating MCI from normal. According to it, the cognition score of participants, regardless of MCI or normal aging group whose novelty preference score was below the cutoff point, decreased more remarkably in 1 year. It is possible that some healthy control patients were actually undiagnosed cases of MCI. They might have cognition impairment that is not detected by the available scales. This shows that the diagnosis of MCI urgently needs to be combined with objective indicators in the future.

Correlations Between Cognitive Function, Neuroanatomical, and Eye Movement Parameters

The novelty preference score positively correlated with verbal fluency and verbal memory in both the short-term memory and delay recall tasks. At the neuroanatomical level, the aforementioned cognitive functions are controlled by the temporal and parietal regions of the brain. In our study, 80 of our subjects underwent MRI scanning at baseline, which showed no evidence of acute territorial infarction, mass effect, hemorrhage, infection, or midline shift. We found that the novelty preference score tends to correlate positively with the cortical thickness of specific functional regions of the right brain, including the temporal pole region, superior frontal

lobe, rACC, and precuneus. Previously, patients with MCI were reported to have poor performance for episodic memory and executive function, which correlated with the level of atrophy in the right superior temporal pole structures (Ruiz López et al., 2008). Compared to the left hemisphere, the correlations between verb and letter fluency were more robust in the right hemisphere. The temporal lobe is considered the center of verbal recognition memory; furthermore, semantic verbal fluency task is more sensitive to assess temporal region impairments (Henry and Crawford, 2004; Clark et al., 2014; Wong et al., 2018). Previous findings indicate that the VPC task is specifically more sensitive to assess medial temporal lobe (MTL) dysfunction in patients with MCI (Clark et al., 2014). More importantly, a study on patients with schizophrenia indicated decreased cortical thickness in the superior frontal region, which is related to decreased cognitive function and role control (Ong et al., 2005). The rACC plays a key role in the regulation of both emotional and motivational information, as well as in the regulation of emotional response (Tully et al., 2014). A previous study indicated that individuals with late-onset depression and cognitive impairment have decreased cortical thickness of the rACC (Bush et al., 2000). The precuneus not only is involved in self-consciousness but also plays an essential role in the integration of visual–spatial information and retrieval of episodic memory (Lim et al., 2012). The function of the precuneus might be influenced by cortical thinning, early amyloid deposition, and hypometabolic alterations in this region that are induced by the pathologic processes in MCI (Bailly et al., 2015a,b; Haussmann et al., 2017). Taken together, our results show that these regions tend to be closely related to cognitive function and emotional regulation, and reduced cortical thickness may impede their function. Findings of MRI and VPC task provide some evidences of impaired performance in the VPC task preceding detectable structural changes in the memory and emotional control system; however, the correlations between VPC score and MRI findings are weak; additional evidences are needed to support and validate our findings.

Possible Clinical Practice of VPC Task in Profiling and Predicting Preclinical Dementia

Two to five years before the onset of AD, patients experience slight neurological deficits in cognitive abilities, indicative of MCI. A previous study (Coutinho et al., 2015) reported that damage in the MTL memory system can predict the risk of dementia and that there were related deficits in visual short-term memory (VSTM) between the AD and MCI stage. Given that we observed possible correlation among novelty preference score with temporal–parietal cognitive functions and typical regional thickness, the potential utility of the novelty preference score as an early marker of MCI cannot be ruled out. However, future longitudinal studies are required to confirm these correlations and the ability to identify underdiagnosed cases of MCI.

Despite not being widely available, the measure derived from the device-based VPC task is valuable clinically. As a physiological marker, its performance is not influenced by subjects' educational and intelligence levels. Our improved eye-tracking tasks were well-tolerated because of their shorter testing times compared to those of the original type. For example, our visual search task required only 5–10 min to complete, including calibration. However, this device has shortcomings in that participants with eyelid apraxia or ophthalmological disorders may have difficulty completing the task.

Limitations and Future Research Directions

The present study has several limitations. Since there was lack of information on the premorbid intelligence of the participants, the assessed cognitive function may not completely reflect the true cognitive decline. Moreover, it is undeniable that the correlation between NP scores and cognitive tests scores and MRI findings is weak, and more evidences between them are needed in future. MCI patients are quite heterogeneous; however, we did not subdivide different MCI subtypes, like amnestic plus additional cognitive domains. Older-old people ($\geq$75 years old) have an even high risk of dementia, and the mean age of our subjects was 71 years, which was relatively young. We will pay more attention to investigate the characteristics of various types of MCI and expand age range in further research.

In our study, we identified a simple, novel, non-invasive diagnostic biomarker of MCI and established an optimal model to distinguish patients with MCI from cognitively normal elderly individuals in China using a relative large scale. Furthermore, we observed that eye movement parameters may predict the rate of cognition decline. It is worthy to conduct further follow-up assessments of our current subjects to test the robustness of the correlations with disease progression. Since we have already started the follow-up visits and have accumulated the results for 1-year follow up, we hope to further establish the relationship between cognitive functions and eye-tracking parameters and adopt the VPC task as a possible adjunctive measurement to identify underdiagnosed cases of MCI with further follow-up visits.

DATA AVAILABILITY STATEMENT

All relevant raw data are freely available to any researchers who wish to use them for non-commercial purposes while preserving any necessary confidentiality and anonymity. The datasets are available on request to the corresponding author.

ETHICS STATEMENT

This study was carried out in accordance with the "Shanghai Mental Health Center ethical standards committee on human experimentation" with written informed consent from all subjects. All participants gave written informed consent in accordance with the Declaration of Helsinki. The protocol was reviewed and approved by the "Shanghai Mental Health Center ethical standards committee." All subjects also

gave written informed consent for the publication of this case report.

AUTHOR CONTRIBUTIONS

JN and QQ performed statistical analysis and drafted the main manuscript text. LS, XLin, and FY performed the experiments and acquired the data. XLi and SX were involved in study conception, participated in design and coordination, and helped to draft the manuscript. MP was responsible for data acquisition. All authors helped to draft the manuscript and gave critical comments. All the authors are acknowledged.

FUNDING

This study was supported by grants of the National Key Research and Development Program of China Stem Cell and Translational Research (2017YFC1310500) and the Advanced Appropriate Technology Promotion Project of Shanghai Health Commission (2019SY045).

REFERENCES

American Psychiatric Association. (1990). *Diagnostic and Statistical Manual of Mental Disorders, Fourth Edition.* Washington, DC: American Psychiatric Association.

Bailly, M., Destrieux, C., Hommet, C., Mondon, K., Cottier, J. P., Beaufils, E., et al. (2015a). Precuneus and cingulate cortex atrophy and hypometabolism in patients with Alzheimer's disease and mild cognitive impairment: MRI and (18)F-FDG PET quantitative analysis using FreeSurfer. *Biomed Res. Int.* 2015:583931. doi: 10.1155/2015/583931

Bailly, M., Ribeiro, M. J., Vercouillie, J., Hommet, C., Gissot, V., Camus, V., et al. (2015b). 18F-FDG and 18F-florbetapir PET in clinical practice: regional analysis in mild cognitive impairment and Alzheimer disease. *Clin. Nucl. Med.* 40, e111–e116. doi: 10.1097/rlu.0000000000000666

Berlyne, D. E. (1960). *Conflict, Arousal and Curiosity.* New York, NY: McGraw-Hill.

Bush, G., Luu, P., and Posner, M. I. (2000). Cognitive and emotional influences in anterior cingulate cortex. *Trends Cogn. Sci.* 4, 215–222. doi: 10.1016/s1364-6613(00)01483-2

Clark, D. G., Wadley, V. G., Kapur, P., DeRamus, T. P., Singletary, B., Nicholas, A. P., et al. (2014). Lexical factors and cerebral regions influencing verbal fluency performance in MCI. *Neuropsychologia* 54, 98–111. doi: 10.1016/j.neuropsychologia.2013.12.010

Coutinho, A. M., Porto, F. H., Duran, F. L., Prando, S., Ono, C. R., Feitosa, E. A., et al. (2015). Brain metabolism and cerebrospinal fluid biomarkers profile of non-amnestic mild cognitive impairment in comparison to amnestic mild cognitive impairment and normal older subjects. *Alzheimers Res. Ther.* 7:58. doi: 10.1186/s13195-015-0143-0

Crutcher, M. D., Calhoun-Haney, R., Manzanares, C. M., Lah, J. J., Levey, A. I., and Zola, S. M. (2009). Eye tracking during a visual paired comparison task as a predictor of early dementia. *Am. J. Alzheimers Dis. Other Demen.* 24, 258–266. doi: 10.1177/1533317509332093

Dale, A. M., Fischl, B., and Sereno, M. I. (1999). Cortical surface-based analysis. I. Segmentation and surface reconstruction. *Neuroimage* 9, 179–194. doi: 10.1006/nimg.1998.0395

Fernández, G., Orozco, D., Agamennoni, O., Schumacher, M., Sañudo, S., Biondi, J., et al. (2018). Visual processing during short-term memory binding in mild Alzheimer's disease. *J. Alzheimers Dis.* 63, 185–194. doi: 10.3233/jad-170728

Galimberti, D., and Scarpini, E. (2012). Progress in Alzheimer's disease. *J. Neurol.* 259, 201–211. doi: 10.1007/s00415-011-6145-3

Haque, R. U., Manzanares, C. M., Brown, L. N., Pongos, A. L., Lah, J. J., Clifford, G. D., et al. (2019). VisMET: a passive, efficient and sensitive assessment of visuospatial memory in healthy aging, mild cognitive impairment and Alzheimer's disease. *Learn. Mem.* 26, 93–100. doi: 10.1101/lm.048124.118

Haussmann, R., Werner, A., Gruschwitz, A., Osterrath, A., Lange, J., Donix, K. L., et al. (2017). Precuneus structure changes in amnestic mild cognitive impairment. *Am. J. Alzheimers Dis. Other Demen.* 32, 22–26. doi: 10.1177/1533317516678087

Henry, J. D., and Crawford, J. R. (2004). A meta-analytic review of verbal fluency performance following focal cortical lesions. *Neuropsychology* 18, 284–295. doi: 10.1037/0894-4105.18.2.284

Hermida, A. P., Mcdonald, W. M., Steenland, K. and Levey, A.. (2012). The association between late-life depression, mild cognitive impairment and dementia: is inflammation the missing link? *Expert Rev. Neurother.* 2012, 1339–1350. doi: 10.1586/ern.12.127

Jessen, F., and Dodel, R. (2014). Prädiktion der Alzheimer-Demenz [Prediction of Alzheimer's dementia]. *Nervenarzt.* 85, 1233–1237. doi: 10.1007/s00115-014-4064-0

Jiang, J., Yan, Z., Sheng, C., Wang, M., Guan, Q., Yu, Z., et al. (2019). A novel detection tool for mild cognitive impairment patients based on eye movement and electroencephalogram. *J. Alzheimers Dis.* 72, 389–399. doi: 10.3233/jad-190628

Lagun, D., Manzanares, C., Zola, S. M., Buffalo, E. A., and Agichtein, E. (2011). Detecting cognitive impairment by eye movement analysis using automatic classification algorithms. *J. Neurosci. Methods* 201, 196–203. doi: 10.1016/j.jneumeth.2011.06.027

Lim, H. K., Jung, W. S., Ahn, K. J., Won, W. Y., Hahn, C., Lee, S. Y., et al. (2012). Regional cortical thickness and subcortical volume changes are associated with cognitive impairments in the drug-naive patients with late-onset depression. *Neuropsychopharmacology* 37, 838–849. doi: 10.1038/npp.2011.264

Lin, S., Hua, X., Jie, Z., Wei, L., Jing, N., Qi, Q., et al. (2018). Alcohol consumption and subclinical findings on cognitive function, biochemical indexes and cortical anatomy in cognitively normal aging Han Chinese population. *Front. Aging Neurosci.* 10:182. doi: 10.3389/fnagi.2018.00182

Loftus, G. R., and Mackworth, N. H. (1978). Cognitive determinants of fixation location during picture viewing. *J. Exp. Psychol. Hum. Percept. Perform.* 4, 565–572. doi: 10.1037/0096-1523.4.4.565

Ong, J. C., Seel, R. T., Carne, W. F., Brown, R., Pegg, P. O., and Jehle, P. J. (2005). A brief neuropsychological protocol for assessing patients with Parkinson's disease. *NeuroRehabilitation* 20, 191–203. doi: 10.3233/nre-2005-20306

Oyama, A., Takeda, S., Ito, Y., Nakajima, T., Takami, Y., Takeya, Y., et al. (2019). Novel method for rapid assessment of cognitive impairment using high-performance eye-tracking technology. *Sci. Rep.* 9:12932. doi: 10.1038/s41598-019-49275-x

Pereira, M. L., Camargo, M. V., Aprahamian, I., and Forlenza, O. V. (2014). Eye movement analysis and cognitive processing: detecting indicators of conversion to Alzheimer's disease. *Neuropsychiatr Dis. Treat.* 10, 1273–1285. doi: 10.2147/ndt.s55371

Petersen, R. C. (2004). Mild cognitive impairment as a diagnostic entity. *J. Intern. Med.* 256, 183–194. doi: 10.1111/j.1365-2796.2004.01388.x

Petersen, R. C., Smith, G. E., Waring, S. C., Ivnik, R. J., Tangalos, E. G. and Kokmen, E. (1999). Mild cognitive impairment: clinical characterization and outcome. *Arch. Neurol.* 56, 303–308. doi: 10.1037/e314192004-003

Ruiz López, E. C., Fernández-Garciá, Y., Alemán-Gómez, Y., and Bobes-León, M. A. (2008). Mild cognitive impairment: MRI study combined with cognitive measurements. *Clin. Neurophysiol.* 119, e125–e126. doi: 10.1016/j.clinph.2008.04.123

Tully, L. M., Lincoln, S. H., Liyanage-Don, N., and Hooker, C. I. (2014). Impaired cognitive control mediates the relationship between cortical thickness of the superior frontal gyrus and role functioning in schizophrenia. *Schizophr. Res.* 152, 358–364. doi: 10.1016/j.schres.2013.12.005

Vega, J. N., and Newhouse, P. A. (2014). Mild cognitive impairment: diagnosis, longitudinal course and emerging treatments. *Curr. Psychiatry Rep.* 16:490. doi: 10.1007/s11920-014-0490-8

Wong, W. H., Chan, A., Wong, A., Lau, C. K., Yeung, J. H., Mok, V. C., et al. (2018). Eye movement parameters and cognitive functions in Parkinson's disease patients without dementia. *Parkinsonism Relat. Disord.* 52, 43–48. doi: 10.1016/j.parkreldis.2018.03.013

Wood, Heather. (2016). Alzheimer disease: meta-analysis finds high reversion rate from MCI to normal cognition. *Nat. Rev. Neurol.* 12:189. doi: 10.1038/nrneurol.2016.29

Xiao, S., Li, J., Tang, M., Chen, W., Bao, F., Wang, H., et al. (2013). Methodology of China's national study on the evaluation, early recognition and treatment of psychological problems in the elderly: China Longitudinal Aging Study (CLAS). *Shanghai Arch. Psychiatry* 25, 91–98. doi: 10.3969/j.issn.1002-0829.2013.02.005

Zola, S. M., Squire, L. R., Teng, E., Stefanacci, L., Buffalo, E. A., and Clark, R. E. (2000). Impaired recognition memory in monkeys after damage limited to the hippocampal region. *J. Neurosci.* 20, 451–463. doi: 10.1523/JNEUROSCI.20-01-00451.2000

Conflict of Interest: The authors declare that the research was conducted in the absence of any commercial or financial relationships that could be construed as a potential conflict of interest.

frontiers in Aging Neuroscience

ORIGINAL RESEARCH
published: 30 July 2020
doi: 10.3389/fnagi.2020.00238

Classification and Graphical Analysis of Alzheimer's Disease and Its Prodromal Stage Using Multimodal Features From Structural, Diffusion, and Functional Neuroimaging Data and the APOE Genotype

Yubraj Gupta[1], Ji-In Kim[1], Byeong Chae Kim[2] and Goo-Rak Kwon[1] on behalf of Alzheimer's Disease Neuroimaging Initiative[†]*

[1] Department of Information and Communication Engineering, Chosun University, Gwangju, South Korea, [2] Department of Neurology, Chonnam National University Medical School, Gwangju, South Korea

OPEN ACCESS

Edited by:
Woon-Man Kung, Chinese Culture University, Taiwan

Reviewed by:
Henning U. Voss, Cornell University, United States
Gabriel Gonzalez-Escamilla, Johannes Gutenberg University Mainz, Germany
Kuo-Kun Tseng, Harbin Institute of Technology, Shenzhen, China

***Correspondence:**
Goo-Rak Kwon
grkwon@chosun.ac.kr

[†]For more information about the Alzheimer's Disease Neuroimaging Initiative, please see the Acknowledgments section

Received: *10 April 2020*
Accepted: *08 July 2020*
Published: *30 July 2020*

Citation:
Gupta Y, Kim J-I, Kim BC and Kwon G-R (2020) Classification and Graphical Analysis of Alzheimer's Disease and Its Prodromal Stage Using Multimodal Features From Structural, Diffusion, and Functional Neuroimaging Data and the APOE Genotype. Front. Aging Neurosci. 12:238. doi: 10.3389/fnagi.2020.00238

Graphical, voxel, and region-based analysis has become a popular approach to studying neurodegenerative disorders such as Alzheimer's disease (AD) and its prodromal stage [mild cognitive impairment (MCI)]. These methods have been used previously for classification or discrimination of AD in subjects in a prodromal stage called stable MCI (MCIs), which does not convert to AD but remains stable over a period of time, and converting MCI (MCIc), which converts to AD, but the results reported across similar studies are often inconsistent. Furthermore, the classification accuracy for MCIs vs. MCIc is limited. In this study, we propose combining different neuroimaging modalities (sMRI, FDG-PET, AV45-PET, DTI, and rs-fMRI) with the apolipoprotein-E genotype to form a multimodal system for the discrimination of AD, and to increase the classification accuracy. Initially, we used two well-known analyses to extract features from each neuroimage for the discrimination of AD: whole-brain parcelation analysis (or region-based analysis), and voxel-wise analysis (or voxel-based morphometry). We also investigated graphical analysis (nodal and group) for all six binary classification groups (AD vs. HC, MCIs vs. MCIc, AD vs. MCIc, AD vs. MCIs, HC vs. MCIc, and HC vs. MCIs). Data for a total of 129 subjects (33 AD, 30 MCIs, 31 MCIc, and 35 HCs) for each imaging modality were obtained from the Alzheimer's Disease Neuroimaging Initiative (ADNI) homepage. These data also include two APOE genotype data points for the subjects. Moreover, we used the 2-mm AICHA atlas with the NiftyReg registration toolbox to extract 384 brain regions from each PET (FDG and AV45) and sMRI image. For the rs-fMRI images, we used the DPARSF toolbox in MATLAB for the automatic extraction of data and the results for REHO, ALFF, and fALFF. We also used the pyClusterROI script for the automatic parcelation of each rs-fMRI image into 200 brain regions. For the DTI images, we used the FSL (Version 6.0) toolbox for the extraction of fractional anisotropy (FA) images to calculate a tract-based spatial statistic. Moreover, we used the PANDA toolbox to obtain 50 white-matter-region-parcellated FA images

on the basis of the 2-mm JHU-ICBM-labeled template atlas. To integrate the different modalities and different complementary information into one form, and to optimize the classifier, we used the multiple kernel learning (MKL) framework. The obtained results indicated that our multimodal approach yields a significant improvement in accuracy over any single modality alone. The areas under the curve obtained by the proposed method were 97.78, 96.94, 95.56, 96.25, 96.67, and 96.59% for AD vs. HC, MCIs vs. MCIc, AD vs. MCIc, AD vs. MCIs, HC vs. MCIc, and HC vs. MCIs binary classification, respectively. Our proposed multimodal method improved the classification result for MCIs vs. MCIc groups compared with the unimodal classification results. Our study found that the (left/right) precentral region was present in all six binary classification groups (this region can be considered the most significant region). Furthermore, using nodal network topology, we found that FDG, AV45-PET, and rs-fMRI were the most important neuroimages, and showed many affected regions relative to other modalities. We also compared our results with recently published results.

Keywords: Alzheimer's disease, multimodal fusion, sMRI, FDG-PET, AV45-PET, DTI, rs-fMRI, APOE genotype

INTRODUCTION

Alzheimer's disease (AD) is a neurodegenerative disorder that is characterized by chronic cortical atrophy (such as posterior cingulate atrophy and medial temporal atrophy), and by a progressive decline in cognitive function (Bishop et al., 2010; Albert, 2011). AD is typically diagnosed in people older than 65 years (Qiu and Kivipelto, 2009). As the life span of the population increases, the prevalence of AD and its costs to society are also increasing. Therefore, the detection of AD or its precursor forms, i.e., mild cognitive impairment (MCI) (Petersen, 2004) is an important aim in biomedical research for providing new therapeutics that help to slow the progression of AD. MCI is a transitional phase (which signifies an intermediate stage of functional and cognitive decline in normal aging and dementia patients) that is characterized by memory disturbance in the absence of dementia (Petersen, 2004; Angelucci et al., 2010), followed by widespread cognitive deficits in multiple domains until a disability threshold is reached. MCI is said to be prodromal AD (Petersen, 2004); subjects go on to develop an AD [this type of patient falls into an MCI-converting (MCIc) group]. Symptoms emerge, on average, within 2–3 years (Lopez et al., 2012). A prospective population-based study in the elderly showed that the conversion rate of MCIc patients to AD or to different forms of dementia is about 10–15% per year (Mitchell and Shiri-Feshki, 2009; Lopez et al., 2012; Wei et al., 2016). Despite our substantial knowledge of MCI converters, little is understood about the 47–67% (Ganguli et al., 2004; Lopez et al., 2012; Clem et al., 2017) of subjects diagnosed with MCI who neither return to normal cognition nor convert to dementia. In a study performed in a large community sample, 10 years identified as a MCI, 21% of those suspected to be at a greater risk for converting to dementia (Dubois and Albert, 2004; Jicha et al., 2006) managed to remain with a diagnosis of MCI (Ganguli et al., 2004; Clem et al., 2017). These studies suggest that certain subjects may not convert to AD, but rather remain diagnostically stable over a period of time (this type of patient falls into an MCI-stable, or MCIs group). Recent results from neuroimaging studies support the hypothesis that AD includes a disconnection syndrome (implying network-wide functional changes due to local structural changes) generated by a breakdown of the organized structure and functional connectivity (FC) of multiple brain regions, even in the early phase of MCI or before conversion to AD (Dubois and Albert, 2004; Bishop et al., 2010; Daianu et al., 2013; Clem et al., 2017; de Vos et al., 2018).

Previous studies have shown the potential of invasive and non-invasive biomarkers to predict conversion from MCI to AD dementia. For invasive markers, the APOE-ε4 genotype (for the carriers of the APOE-ε4 allele, brain alterations associated with AD may begin as early as infancy) (Liu et al., 2013; Dean et al., 2014), and amyloid-beta (Aβ) accumulation and neurofibrillary lesions are considered to be most important biomarkers for AD (Murphy and LeVine, 2010). Apolipoprotein-E (APOE) genotype polymorphism is considered to be the most common polymorphism in neurodegenerative diseases and has been consistently linked to normal cognitive decline in AD and MCI patients. APOE-ε4 is the strongest genetic risk factor, and it increases the risk for AD twofold to threefold. Furthermore, it lowers the age of AD onset (Michaelson, 2014). Recent developments in non-invasive neuroimaging techniques, including functional and structural imaging, have given rise to a variety of commonly used neuroimaging biomarkers for AD. Among the multiple neuroimaging modalities, structural magnetic resonance imaging (sMRI) has attracted significant interest due to its ready availability for mildly symptomatic patients and its high spatial resolution (Cuingnet et al., 2011; Salvatore et al., 2015; Wei et al., 2016; Long et al., 2017; Gupta et al., 2019b,c; Sun et al., 2019). sMRI can also reveal abnormalities in a wide range of brain areas, including gray matter (GM) atrophy in the medial temporal lobe and hippocampal/entorhinal cortex, which are identified as valuable AD-specific biomarkers for the discrimination or classification of AD patients (Cuingnet et al., 2011). In diffusion tensor imaging (DTI, or diffusion MRI), water diffusion

in the brain is interpreted as an MR signal loss. Because neurodegenerative processes are accompanied by a loss of obstacles that restrict the motion of water molecules (Acosta-Cabronero and Nestor, 2014), DTI can reveal promising markers of microstructural white matter (WM) damage in AD and MCI patients. A connectivity-based analysis that applied graph theory to DTI data demonstrated disrupted topological properties of structural brain networks in AD, supporting the disconnection theory. Specifically, regional diffusion metrics for the limbic WM in the fornix, posterior cingulum, and parahippocampal gyrus have shown better performance than volumetric measurements of the GM in predicting MCI conversion (Sun et al., 2019). In clinical studies, fluorodeoxyglucose-positron emission tomography (FDG-PET), florbetapir-PET AV45 (amyloid protein imaging), and resting-state fMRI (rs-fMRI) are the most commonly used functional neuroimaging methods for AD diagnosis (Hojjati et al., 2018, 2017; Gupta et al., 2019a; Pan et al., 2019a,b). FDG-PET measures cerebral glucose metabolism via 18F-FDG in the brain, and helps to detect characteristic regional hypometabolism in AD patients, which reflects the neuronal dysfunctions in the brains of AD patients (Mosconi et al., 2008). In contrast, florbetapir-PET AV45 measures the accumulation of amyloid protein in AD brain homogenates and has faster *in vivo* kinetics. The use of florbetapir in amyloid imaging was recently validated in an autopsy study, and its safety profile allows its clinical application for brain imaging (Camus et al., 2012). Moreover, rs-fMRI imaging has been developed as a tool for mapping the intrinsic activity of the brain and for depicting the synchronization of interregional FC (Bi et al., 2018; de Vos et al., 2018). A recent rs-fMRI study showed that the FC pattern may be altered in some specific functional networks (default mode network) of AD and MCI patients. The authors found decreased FC between the hippocampus and several regions throughout the neocortex, i.e., reduced FC within the default mode networks and increased FC within the frontal networks (de Vos et al., 2018).

From the above studies, we observe that there is no clear evidence supporting the supremacy of any biomarker above another (CSF vs. APOE-ε4 vs. imaging) for the diagnostic estimation of AD. The choice of biomarkers mainly depends on price and availability. Nevertheless, some authors argue for the perfection of imaging above fluid biomarkers, given that imaging modalities can distinguish the different phases of the disease both anatomically and temporally (Khoury and Ghossoub, 2019; Márquez and Yassa, 2019). The above-mentioned studies used only a single modality to detect biomarkers for the detection of the conversion of MCI to AD. The proposed algorithm performance is approximately 80–90%, which is low compared with that of recently published multimodal studies (Zhang et al., 2011; Liu et al., 2014; Ritter et al., 2015; Xu et al., 2016; Gupta et al., 2019a). To date, it is true that no single imaging modality for biomarkers meets all of the diagnostic requirements set by previous studies (Hyman et al., 2012; Jack et al., 2018, 2016) (because each biomarker has their own advantage over others) and no single (whether genotype or fluid or imaging) biomarker can by itself correctly discriminate a heterogeneous disorder of AD with high accuracy, but several methods may provide complementary information, which leads to a call to develop a panel of neuroimaging biomarkers, or a combination of imaging and APOE or imaging with CSF data that merges information about the disease manner to improve diagnostic accuracy (Márquez and Yassa, 2019). Combining information (multimodal) from different types of neuroimaging (structural and functional) with genotype (APOE) or biochemical (CSF) information, as do sMRI, AV45-PET, FDG-PET, DTI, and rs-fMRI, can help to improve diagnostic performance for AD or MCI compared with single-modality methods (Zhang et al., 2011; Young et al., 2013; Schouten et al., 2016; Wei et al., 2016; Gupta et al., 2019a). Furthermore, it has been noted lately that a combination of biomarkers yields a powerful diagnostic technique for classifying the AD group with cognitively healthy subjects, with specificity and sensitivity scores reaching above 90% (Bloudek et al., 2011; Rathore et al., 2017; Khoury and Ghossoub, 2019).

Multiple studies have reported a combination of different neuroimaging modalities for investigating AD or MCI. Dai et al. (2012) used regional GM volumetric measures and functional measures (amplitude of low-frequency fluctuations, regional homogeneity, and regional FC strength) as features. They trained distinct maximum uncertainty LDA classifiers on functional and structural properties and merged the output of the classifiers by weighted voting. Zhang et al. (2011) used a multimodal method for the discrimination of healthy controls (HC) to AD patients. They used a kernel-based support vector machine (SVM) classifier for the classification, and they combined volumetric regional features with regional FDG-PET and CSF biomarkers. Young et al. (2013) proposed a method where they combined sMRI, FDG-PET, and APOE genotype data for the discrimination of AD with HC. These authors used Gaussian processes as a multimodal kernel method, and they applied an SVM classifier for the classification of MCIs vs. MCIc groups. However, their diagnostic accuracy was low. Another study proposed a system where multiple kernel learning (MKL) with the Fourier transform of the Gaussian kernels was applied to AD classification using both sMRI and rs-fMRI (Liu et al., 2014) neuroimages. Moradi et al. (2015) used GM density maps, age, and cognitive tests as features, and employed classification algorithms such as low-density separation and random forest for AD conversion discrimination. Another study proposed a novel method for the classification of AD using a multi-feature technique (regional thickness, regional correlative-calculated from thickness measures, and the APOE genotype) using an SVM classifier (Zheng et al., 2015). Schouten et al. (2016) combined regional volumetric measures, diffusion measures, and correlation measures between all brain regions calculated from functional MRI. They employed a logistic elastic net for classification. In addition, Liu et al. (2017) used independent component analysis and the COX model for the discrimination of MCIs to MCIc. In their study, they used sMRI and FDG-PET scans in combination with APOE data and some cognitive measures. Hojjati et al. (2018) combined the features extracted from sMRI (cortical thickness) and rs-fMRI (graph measures) for the detection

of AD, employing SVM for the classification. It is worth noting that most of the above-presented multimodal methods used brain atrophy from a few manually extracted regions as a feature of sMRI and PET images for the detection of AD among different groups. However, using only a small number of brain regions as a feature in any imaging modality may not accurately reflect the spatiotemporal pattern of structural and physiological abnormalities as a whole (Fan et al., 2008). Furthermore, simply by increasing the number of modalities, combining modalities did not increase predictive power.

Therefore, the primary goal of this study was to combine five different imaging modalities (sMRI, AV45, FDG-PET, DTI, and rs-fMRI) with the APOE genotype to establish a multimodal system for the detection of AD. Moreover, in this study, we used three methods (that were completely different from each other) for the discrimination of AD from other groups. Moreover, we also aimed to discover which single modality of neuroimaging achieves high performance or plays a significant role in classifying all six binary classification groups (AD vs. HC, MCIs vs. MCIc, AD vs. MCIc, AD vs. MCIs, HC vs. MCIc, and HC vs. MCIs) based on these methods, and wanted to know which combined methods would perform well in the classification stage (whole-brain or voxel-wise analysis). Furthermore, we also aimed to discover the regions where these six binary groups massively differed from each other using voxel of interest (VOI) and graph methods. Whole-brain parcelation and voxel-wise methods were used to study regional and voxel differences in all six binary classification groups. We used NiftyReg (Young et al., 2013; Gupta et al., 2019a), the pyClusterROI script (Craddock et al., 2012), PANDA (Cui et al., 2013), DPRASF (Chao-Gan and Yu-Feng, 2010), and the CAT12 toolbox with the integration of SPM12 (Ashburner and Friston, 2001) for the extraction of features from the structural and functional neuroimaging data. Furthermore, graph-based analysis (John et al., 2017; Peraza et al., 2019) was performed to study the organization of (nodal and group) network connectivity using anatomical features (including GM volume, cortical thickness, and WM pathways between GM regions), and using the regional time series of the 200 brain regions included in the Craddock atlas. For this graph-based analysis, we used the BRAPH toolbox (Mijalkov et al., 2017). Later, we applied an MKL algorithm based on the EasyMKL (Aiolli and Donini, 2015; Donini et al., 2019) classifier for classification and for data fusion. This classifier works by simultaneously learning the predictor parameters and the kernel combination weights. Moreover, we applied a leave-one-out cross-validation technique that helps to find the optimal hypermeter for this MKL classifier. In this study, we also applied the radial basis function (RBF)-SVM classifier to compare its results with the results obtained from the EasyMKL. Our results showed that grouping different measurements (or complementary information) from the six different modalities exhibited much better performance for all six binary classification groups (using any combined-ROI, or combined-VOI, or a combination of all) than using both classifiers with the best individual modality.

MATERIALS AND METHODS

Participants

The participants included in this study were enrolled via the ADNI, which was launched in 2003 as a multicenter public-private partnership, guided by Principal Investigator Michael W. Weiner, MD. The participants were enrolled from 63 locations across the United States and Canada. The primary goal of ADNI was to test whether sMRI, PET, new biological markers, and clinical and neuropsychological evaluation could be combined to measure the development of MCI and early AD. The criteria used for the inclusion of subjects were those defined in the ADNI procedure.[1] The enrolled subjects were between 56 and 92 (inclusive) years old, had a study partner able to offer an independent assessment of functioning, and spoke either Spanish or English. All subjects were willing and able to undergo all test trials, including neuroimaging, and agreed to a longitudinal follow-up. Specific psychoactive medications were excluded. For this study, we downloaded data from all subjects for whom all five imaging modalities (sMRI, rs-fMRI, FDG-PET, AV45-PET, and DTI) with their APOE genotype were available on the ADNI homepage. A total of 129 subjects were classified as either healthy controls (HC, n = 35), MCIc (n = 31), MCIs (n = 30), or AD (n = 33), with matched sex and age ratios. The groups were classified according to the criteria set by the ADNI consortium (Petersen et al., 2010). In the HC group, participants had global clinical dementia rating (CDR) scores of 0, mini-mental state examination (MMSE) scores between 27 and 30, functional activities questionnaire (FAQ) scores between 0 and 4, and geriatric depression scale (GDS) scores between 0 and 4. In the MCIs group, the MMSE score was between 25 and 30, the FAQ score between 0 and 16, and the GDS score was between 0 and 13. In the MCIc group, the MMSE score was between 19 and 30, the FAQ score between 0 and 18, and the GDS score was between 0 and 10.

In the AD group, patients had a global CDR score of 1, an MMSE score between 14 and 24, an FAQ score between 3 and 28, and a GDS score between 0 and 7 (Morris, 1993). We did not consider MCI subjects who had been tracked for less than 18 months and did not convert within this period. **Table 1** shows participant demographic information, including the mean age and the sex ratios per group. To assess statistically significant changes in the demographics and clinical features between these groups, a Student's t-test was used with the significance level set to 0.05. We found no significant differences ($p-$value > 0.05) between the groups for age or sex ratio. To attain unbiased estimates of performance, the classification groups were then randomly split into two clusters in a ratio of 70:30 for the training and testing sets. The model was trained on the training set, and the performance measures of diagnostic specificity and sensitivity were carried out on a separate testing set. The splitting procedure preserved the age and sex distribution.

[1] https://www.adni-info.org/Scientistis/AboutADNI.aspx#

TABLE 1 | Demographic and neuropsychological characteristics of the participants.

Group	AD (n = 33)	MCIc (n = 31)	MCIs (n = 30)	HC (n = 35)
Sex (M/F)	21/12	16/15	17/13	14/21
Age	75.65 ± 8.61	72.27 ± 7.40	72.90 ± 7.86	77.83 ± 6.17
Body weight (kg)	75.81 ± 13.60	80.71 ± 17.43	82.14 ± 15.03	75.76 ± 18.62
FAQ score	19.34 ± 6.53	6.16 ± 7.38	1.86 ± 2.99	0.13 ± 0.48
NPI-Q score	4.46 ± 4.01	2.64 ± 3.32	1.66 ± 1.61	0.33 ± 0.78
GDS score	2.37 ± 2.59	2.03 ± 2.02	1.26 ± 0.96	1.13 ± 1.79
MMSE score	19.59 ± 4.56	26.32 ± 3.85	28.03 ± 1.25	29.13 ± 1.20

Values are numbers or means ± standard deviations. FAQ: functional activities questionnaire; NPI-Q: neuropsychiatric inventory questionnaire; GDS: geriatric depression scale; MMSE: mini-mental state examination.

sMRI Acquisition

We acquired 1.5-T T1-weighted MR images from the ADNI homepage. The MRI images were obtained from data centers using Philips, GE, or Siemens Medical system scanners. Because the acquisition protocol was different for each scanner, an image normalization step was carried out by ADNI. The image corrections included calibration, image geometry distortion due to gradient non-linearity (grad-warp), and reduction in the intensity non-uniformity due to waves, or residual intensity non-uniformity of the 1.5-T scans utilized on each image by ADNI. Further details about the sMRI images are available on the ADNI website.[2] All scans had a resolution of $176 \times 256 \times 256$ with 1 mm spacing between each scan. In our study, we again pre-processed the obtained sMRI images using the FMRIB Software Library (FSL, v.6.0) (Smith, 2002) toolbox. For the anatomical sMRI images, this included the extraction of non-brain tissue from each image using the BET function. We then passed the skull-stripped images to the ANTs (Tustison et al., 2010) toolbox for N4 bias field correction to correct for inhomogeneous artifacts in each image. For co-registration to the standard Montreal Neurological Institute (MNI) 152 template (Grabner et al., 2006), we also used the FSL toolbox (Jenkinson et al., 2012).

FDG-PET Image Acquisition

ADNI provides four different types of FDG-PET samples, which are labeled as: (1) Co-registered Dynamic; (2) Co-registered, Averaged; (3) Co-reg, Avg, Standardized image and Voxel size; and (4) Co-reg, Avg, Std Img and Vox Siz, Uniform Resolution. The type (3) baseline FDG-PET images were downloaded from the ADNI homepage.

The downloaded baseline FDG-PET samples were in DICOM format. In the first step, we converted these DICOM format images to the Nifty format using the dcm2nii (Li et al., 2016) toolbox. Later, these images were spatially normalized to the MNI 152 template using the SPM12 toolbox (integrated within MATLAB 2019b) with a standard $91 \times 109 \times 91$ tensor dimension image grid, having a voxel size of $2 \times 2 \times 2\,mm^3$. This image grid was oriented so that the subjects' anterior-posterior (AC-PC) axis was parallel to the AC-PC line. The above normalization step was carried out on two levels: a global affine transformation, followed by a non-rigid spatial transformation. The general affine transformation requires a 12-parameter design, whereas the non-rigid spatial transformation uses a sequence of the lowest frequency elements of the three-dimensional cosine transform. Furthermore, the intensity normalization step was performed by splitting each voxel depth-wise with the average score of the global GM, which was obtained with the help of the AAL template image. More details concerning the FDG-PET imaging can be found on the ADNI homepage.[3] Moreover, after the completion of these pre-processing steps, we co-registered the FDG-PET images to their corresponding sMRI T1-weighted images using the SPM12 toolbox.

AV45-PET Image Acquisition

Alzheimer's Disease Neuroimaging Initiative provides four different types of AV45-PET samples, which are: (1) AV45 Co-registered Dynamic; (2) AV45 Co-registered, Averaged; (3) AV45 Co-reg, Avg, Standardized image and Voxel size; and (4) AV45 Co-reg, Avg, Std Img and Vox Siz, Uniform Resolution. The type (3) baseline AV45-PET images were downloaded from the ADNI homepage. For each scan, the 5-min frames (four for florbetapir, acquired 50–70 min post-injection) were co-registered to the frame (rigid-body translation/rotation, six degrees of freedom) using the NeuroStat "mcoreg" routine (followed by the ADNI organization) (Jagust et al., 2015). The downloaded baseline AV45-PET samples were in DICOM and ECAT formats. In the first step, we converted this DICOM and ECAT format images to the Nifty format using the dcm2nii (Li et al., 2016) toolbox. Later, these images were spatially normalized to the MNI 152 template using the SPM12 toolbox (integrated within MATLAB 2019b) with a standard $91 \times 109 \times 91$ tensor dimension image grid, having a voxel size of $2 \times 2 \times 2\,mm^3$ using the same process we introduced in section "FDG-PET Image Acquisition" for the FDG-PET image. More details about AV45-PET imaging can be found on the ADNI website (see text footnote 3). Furthermore, after the completion of the above stated pre-processing steps, we co-registered the AV45-PET images to their corresponding sMRI T1-weighted images using the SPM12 toolbox.

Resting-State Functional MR Image Acquisition

A 3.0-T Philips Medical sMRI scanner was used to acquire the fMRI images. All rs-fMRI images were obtained from the ADNI homepage. The sample for each subject consisted of 6720 DICOM images. The patients were required to relax, not to think, and to lie in the scanner during the scanning procedure. The sequence parameters were as follows: pulse sequence = GR, TR = 3000 ms, TE = 30 ms, flip angle = 80°, data matrix = 64×64, pixel spacing X, Y = 3.31 mm and 3.31 mm, slice thickness = 3.33 mm, axial slices = 48, no slice gap, time points = 140. Because the signal-to-noise ratio (SNR) of the rs-fMRI images was limited, the collected data were pre-processed to reduce the impact of noise on the

[2]http://adni.loni.usc.edu/methods/mri-tool/mri-analysis/

[3]http://adni.loni.usc.edu/methods/pet-analysis-method/pet-analysis/

fMRI images. For the pre-processing of the rs-fMRI images, we used the Data Processing Assistant for Resting-state fMRI (DPARSF) (Chao-Gan and Yu-Feng, 2010) software, which can be downloaded from http://d.rnet.co/DPABI/DPABI_V2.3_170105.zip. For each subject, the entire pre-processing was divided into nine steps as follows: converting the DICOM format into the NIFTY format, removing the first ten time points, timing the slicing, head motion correction to adjust the time series of the images so that the brain was located in the same orientation in every image, normalization, smoothing by full width at half maximum (FWHM), removing the linear trend to eliminate the residual noise that systematically increases or decreases over time (Smith et al., 1999), temporal filtering to retain 0.01–0.08 Hz fluctuations, and removing covariates to eliminate physiological artifacts (Fransson, 2005), non-neuronal blood oxygen level-dependent (BOLD) fluctuations, and head motion.

Diffusion Tensor Imaging Image Acquisition

Diffusion tensor imaging images were also downloaded from the ADNI homepage. The DTI protocol used spin-echo diffusion-weighted echo-planar imaging with a TR/TE of 12000/1046 ms, a voxel size of $0.9375 \times 0.9375 \times 2.35\,mm^3$, a matrix size of 256×256, 45 slices, 30 gradient directions, and a *b*-value of $1000\,s/mm^2$. More details about DTI imaging can be found on the ADNI webpage.[4] This ADNI protocol was chosen after conducting a detailed comparison of several different DTI protocols to optimize the SNR in a fixed scan time (Jahanshad et al., 2013; Chen et al., 2018). The pre-processing of DTI data was performed using the diffusion toolbox of FSL (Version 6.0, FMRIB, Oxford, United Kingdom). FSL pre-processing included (i) corrections for eddy currents and head motion, (ii) skull stripping, and (iii) fitting the data to the diffusion tensor model to compute maps of fractional anisotropy (FA) and mean diffusivity (MD). A single diffusion tensor was fitted at each voxel of the eddy- and EPI-corrected DWI images using the FSL toolbox. Scalar anisotropy maps were obtained from the consequential diffusion tensor eigenvalues λ_1, λ_2, and λ_3. FA, a measure of the degree of diffusion anisotropy, was defined in the standard way as

$$FA = \sqrt{\frac{3}{2}}\frac{\sqrt{(\lambda_1 - <\lambda>)^2 + (\lambda_2 - <\lambda>)^2 + (\lambda_3 - <\lambda>)^2}}{\sqrt{\lambda_1^2 + \lambda_2^2 + \lambda_3^2}}, \varepsilon[0, 1] \quad (1)$$

$$<\lambda> = \frac{\lambda_1 + \lambda_2 + \lambda_3}{3} \quad (2)$$

where $<\lambda>$ is equal to the MD or average proportion of diffusion in all directions. The resulting images were smoothed with a Gaussian kernel of 5 mm FWHM to improve the SNR and ensure a Gaussian distribution of the maps.

[4]http://adni.loni.usc.edu/data-samples/data-types/

APOE Genotype

The APOE genotype for each subject was also obtained from the ADNI homepage. The APOE genotype is known to affect the risk of developing sporadic AD in carriers. The APOE genotype of each subject was noted as a pair of numbers representing which two alleles were present in the blood. This genetic feature was a single categorical variable for each participant and could have had one of five possible values: (ε2, ε3), (ε2, ε4), (ε3, ε3), (ε3, ε4), and (ε4, ε4). The most common allele is APOE ε3, but carriers of the APOE-ε4 variant have an increased risk of developing AD, whereas the APOE ε2 variant confers some protection on carriers (Michaelson, 2014). Of the three genetic polymorphisms, APOE shows the highest correlation with MCI status and stability (Brainerd et al., 2013). Several recent studies have linked the APOE-ε4 status to a relatively late risk of preclinical progression to AD. Until recently, ε4 variants (including ε4/ε4 and ε4/ε3 combinations) were inconsistently linked to the MCI status, likely reflecting both clinical and methodological differences in status classification. In this study, the genotype data were obtained from a 10 ml blood sample taken at the time of the scan and sent immediately to the University of Pennsylvania AD Biomarker Fluid Bank Laboratory for analysis.

Three Feature Extraction Processes

Figure 1 shows a block diagram of the proposed framework. In this study, we performed three types of analysis for the extraction of features from each imaging modality:

(1) Whole-brain parcelation (or atlas-based segmentation) is a quantitative method that provides a non-invasive way to measure brain regions via neuroimaging. It works by assigning tissue labels to the unlabeled images using sMRI scans as well as the corresponding manual segmentation. For sMRI, FDG, and AV45-PET scans, we used the 2-mm Atlas of Intrinsic Connectivity of Homotopic Areas (AICHA) template image (Joliot et al., 2015) for the extraction of 384 regions of interest (ROIs) from each image, whereas for the rs-fMRI and DTI scans, we used the 2-mm Craddock atlas template (Craddock et al., 2012) for the extraction of 200 ROIs from each rs-fMRI image and the 2-mm Johns Hopkins University (JHU) WM labels atlas for the extraction of 50 ROIs from each DTI image (Hua et al., 2008).

(2) Voxel-wise analysis or morphometry (VBM) is a computational approach to neuroanatomy that measures differences in local concentrations of brain tissue through a voxel-wise comparison of multiple brain images. It uses statistics to recognize differences in brain structure between groups of patients, which in turn can be used to infer the presence of atrophy or normal-tissue expansion in patients with disease. For sMRI, FDG, and AV45-PET scans, we used the SPM12 toolbox to apply VBM, whereas, for the rs-fMRI scans, we used the DPRASF toolbox integrated with SPM12 to apply VBM. For the DTI scans, we used the tract-based spatial statistics (TBSS) function from FSL (v.6.0).

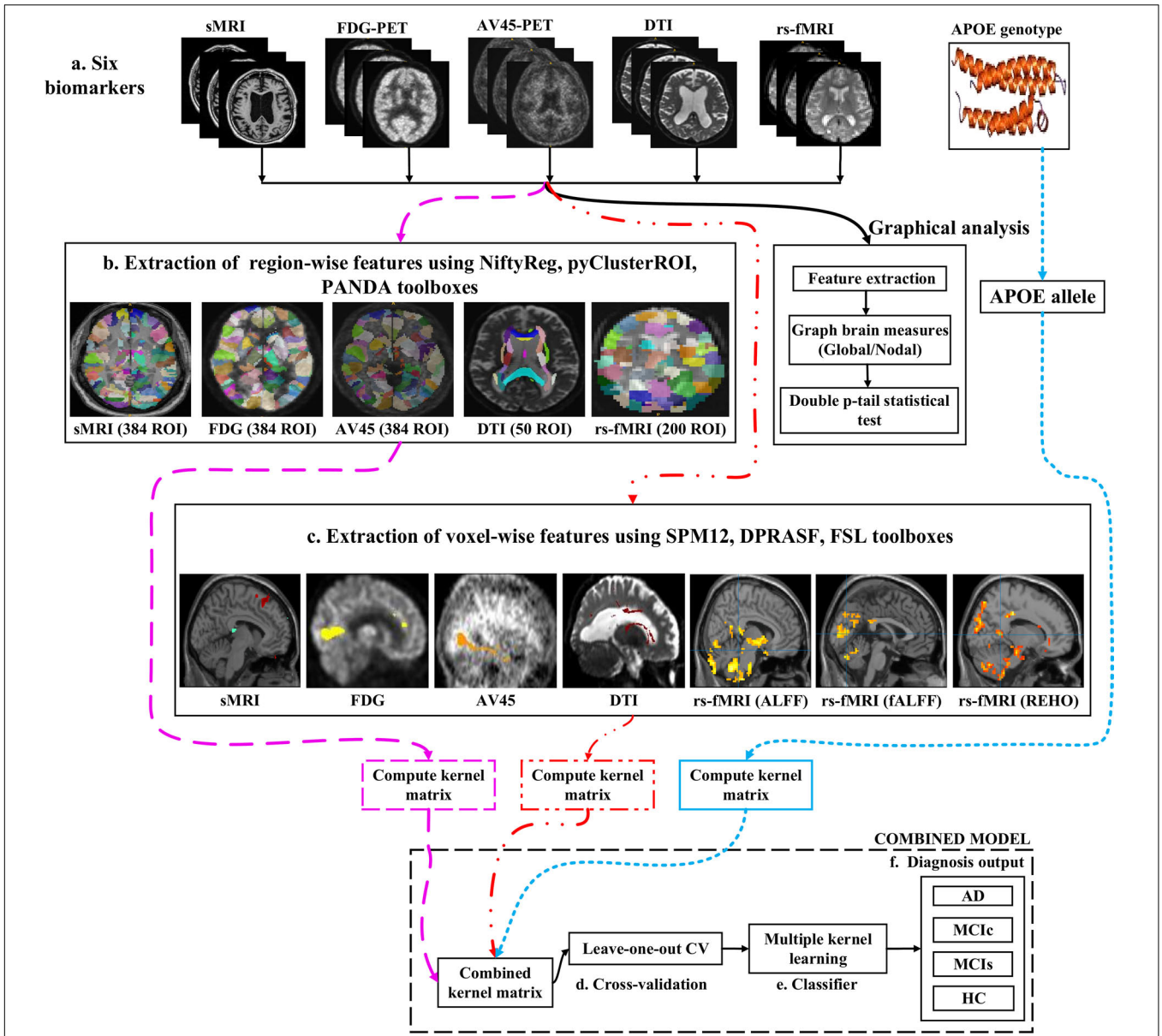

FIGURE 1 | Overview of the multimodal framework. **(A)** Selection of five imaging modalities (sMRI, FDG-PET, AV45-PET, rs-fMRI, and DTI) and APOE genotype. **(B)** Extraction of regional features using NiftyReg, pyClusterROI, and PANDA toolboxes. **(C)** Extraction of voxel features using SPM12, DPARSF, and FSL toolboxes. **(D)** Leave-one-out cross-validation method. **(E)** Multiple kernel learning. **(F)** Diagnostic output.

(3) Graph theory methods are powerful methods for quantifying the organization of a network by means of brain anatomical features, including cortical thickness, GM volume, and WM tracks between GM regions. When applying graph theory to different neuroimaging modalities, the outcome is a network with vertices or nodes that are represented by brain voxels or regions defined by a predetermined parcelation structure, while the edges are denoted by inter-individual data relations between the regions estimated, for example, as the intensity of correlation between the regional measurements. Note that the edges of a structural network are not always denoted by correlations between regional capacities, but by the density or number of WM tract-linking regions. In an analysis of sMRI, FDG, and AV45-PET networks, the nodes are generally defined using an anatomical segmentation or parcelation of the brain into different regions. In this study, we used the 2-mm AICHA atlas template image (which was already segmented into 384 distinct regions) for the extraction of 384 ROIs from each sMRI, FDG, and AV45-PET image. In the case of functional networks, for the rs-fMRI and DTI images, we used the 2-mm Craddock atlas template image for the extraction of 200 ROIs, and the 2-mm JHU-WM (ICBM-DTI-81) label atlas for the

extraction of 50 ROIs from each DTI image. After the nodes of the network were defined, the edges indicating the relationship between different regions was computed. For this, we used the BRAPH toolbox (Mijalkov et al., 2017) integrated into MATLAB 2019a. In BRAPH, the edges are calculated in a GUI graphical analysis as the statistical correlation between the values of pairs of brain regions for an individual or for a group of subjects, depending on the neuroimaging technique.

Feature Extraction Using Atlas-Based Segmentation

After completing a series of image pre-processing steps for each imaging modality as shown in **Figure 1**, we extracted the features from each modality. The dashed pink line in **Figure 1** shows the feature extraction for a whole-brain analysis. For sMRI, FDG, and AV45-PET images, we used the 2-*mm* AICHA atlas template image for the extraction of 384 ROIs from each image (Gupta et al., 2019a). We then processed these images using the open-source NiftyReg toolbox (Modat et al., 2010), which is a registration toolkit that performs fast diffeomorphic non-rigid registration on images. After the registration process, we obtained the subject-labeled image based on a template with 384 segmented regions. For each of the 384 ROIs in the labeled MR and PET images, we computed the GM volume and the relative cerebral metabolic rate of glucose from the baseline MRI, FDG, and AV45-PET data, respectively and later used it as a feature. Therefore, for each sMRI and PET image, we obtained 384 features. For the rs-fMRI images, we ran a pyClusterROI Python script, which was downloaded from https://ccraddock.github.io/cluster_roi/, for the extraction of 200 ROIs from each rs-fMRI image. This method employs a spatially constrained normalized-cut spectral clustering algorithm to generate individual-level and group-level parcelations. A spatial constraint was imposed to ensure that the resulting ROIs were spatially coherent, i.e., that the voxels in the resulting ROIs were connected. Moreover, for DTI images, we ran a pipeline to analyze the brain diffusion images (PANDA toolbox), which can be downloaded from https://www.nitrc.org/projects/panda/, integrated with MATLAB R2019a in the Ubuntu 18.04 operating system for the processing of diffusion MRI images. The PANDA pipeline uses the FMRIB Software Library (FSL), Pipeline System for Octave and MATLAB (PSOM), Diffusion Toolkit, and MRIcron packages for the extraction of diffusion metrics (e.g., FA and MD) that are ready for statistical analysis at the voxel level or atlas level. For the parcelation of DTI images, it uses the 2-mm JHU-WM (ICBM-DTI-81) label atlas, which is already segmented into 50 distinct ROIs. After completion of this process, we gained the subject-labeled image based on a template with 50 distinct segmented regions.

Feature Extraction Using Voxel-Wise Morphometry

The dashed and dotted red line in **Figure 1** shows the pipeline for the voxel-wise analysis (or the extraction of features) from sMRI, FDG, AV45-PET, rs-fMRI, and DTI images. For the voxel-wise analysis of sMRI, FDG, and AV45 images, we used the statistical mapping method (SPM12) toolbox integrated with the computational anatomy toolbox (CAT version 12), which can be obtained from https://www.fil.ion.ucl.ac.uk/spm/software/spm12/ and http://www.neuro.uni-jena.de/cat/. First, the MRI data were anatomically standardized using the 12-parameter affine transformation offered by the SPM template to compensate for differences in brain size. We chose the East Asian brain image template and left all other factors at their default setting. The sMRI images were then parcellated into GM, WM, and CSF images using the unified tissue segmentation method after the image strength non-uniformity correction was complete. The obtained linearly transformed and parcellated images were then non-linearly distorted using diffeomorphic anatomical registration via exponentiated lie algebra (DARTEL) methods and modulated to create an improved template for a DARTEL-based MNI152 template image, followed by smoothing using an 8 mm FWHM kernel. The final step consisted of voxel-wise statistical assessments. To construct a statistical parametric map, we calculated contrast values based on general linear model-estimated regression parameters. This technique executes a two-sample *t*-test to determine if there are major regional density differences between two sets of GM images. We obtained these regional information values representing the major density differences between two sets of GM images after executing a false discovery rate (FDR) and family wise error rate (FWER) correction. Based on this data, cluster values were obtained to create ROI binary masks, which were subsequently used to acquire GM volumes from GM brain images for use as a morphometric feature. Moreover, before submitting FDG and AV45 images to VBM analysis, the first step was to register the FDG and AV45 images with their corresponding sMRI images. We used the SPM12 toolbox for this registration. After the registration, we followed the same method as was used for the sMRI VBM analysis. SPM12 was used to produce statistical maps of between-group alterations in the regional-to-whole-brain dimensions of the cerebral metabolic rate for glucose (CMRgl) consumption in likely AD, MCIs, MCIc, and HC groups.

For rs-fMRI images, to decrease the influence of the SNR, the selected data should be pre-processed. In this study, we used the DPARSF toolbox,[5] which was integrated with MATLAB R2019a, to calculate the whole-brain ALFF, fractional (fALFF), and REHO feature maps, as shown in **Figure 2**. Spatial smoothing was performed with a $4 \times 4 \times 4$ mm FWHM Gaussian kernel before the ALFF, FALFF, and REHO calculation. To minimize the low-frequency drift, linear trending was removed from the process. To explore the ALFF, fALFF, and REHO differences between the AD patient group and the other groups, a random-effects two-sample *t*-test was implemented on the individual ALFF, fALFF, and REHO maps in a voxel-wise way by taking the patients' age as a confounding covariate. The ALFF was calculated by filtering the time courses of each individual voxel of the subjects with a fast Fourier transformation of the frequency area, and the power range or spectrum was then gained. Because the power of a specified frequency is relative to the square of the amplitude of this frequency, the square root was computed at each frequency domain of the power range, and then the averaged square root was found across 0.01–0.08 Hz at each individual voxel. Later,

[5]http://d.rnet.co/DPABI/DPABI_V2.3_170105.zip

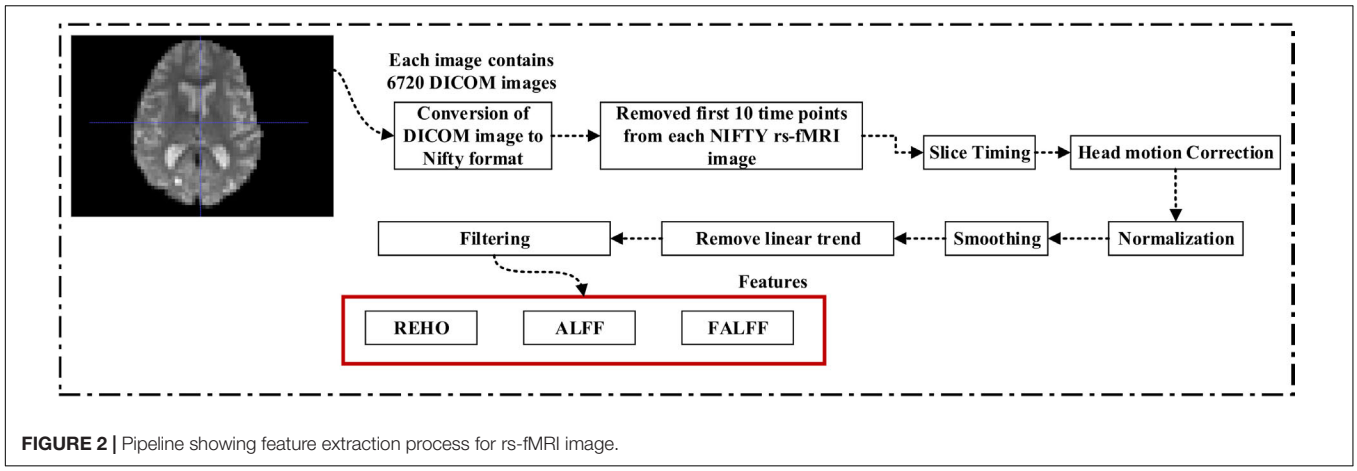

FIGURE 2 | Pipeline showing feature extraction process for rs-fMRI image.

this averaged square root was taken as the ALFF index. The fALFF was calculated as the ratio of the amplitude within the low-frequency spectrum (0.01–0.08 Hz) to the total amplitude over the full frequency spectrum (0–0.25 Hz). It is generally calculated as a fraction of the sum of amplitudes across the entire frequency range detectable in a given signal. REHO is a voxel-based measure of brain activity that evaluates the similarity or synchronization between the time series of a given voxel and its nearest neighbors (Zang et al., 2004). It was calculated using Kendall's coefficient of concordance with the time series of every 27 neighboring voxels. Then, a Kendall's coefficient of concordance value (ranging from 0 to 1) was assigned to each voxel center. Voxels of higher strength in the REHO maps show greater similarity with the neighboring voxel's time series. For the DTI images, FA maps were then created using the DTIfit approach and were entered into the TBSS environment to investigate changes in diffusivity measures along the WM tract. First, all FA data were non-linearly aligned to a common space (FMRIB58_FA), then the normalized FA images were averaged to create the mean FA image and a threshold set ($FA > 0.2$) (to exclude voxels that were primarily GM or CSF) to create a mean FA skeleton. Next, each participant's FA data were projected onto the mean FA skeleton, followed by voxel-wise statistical analysis. Voxel-wise statistical analysis of FA in the WM skeleton was performed using Randomize, FSL's non-parametric permutation interference tool. Multiple comparisons were corrected for by using threshold-free cluster enhancement ($p < 0.05$). WM regions were identified with the JHU-WM (ICBM-DTI-81) label atlas included in FSL.

Graph Generation and Construction of sMRI, FDG-PET, AV45-PET, fMRI, and DTI Brain Networks

To assess the sMRI, FDG-PET, and AV45-PET network topology in AD, MCIs, MCIc, and HC subjects, the T1 images of these subjects were pre-processed using the NiftyReg toolbox with the integration of the 2-mm AICHA atlas template image. In total, 384 regions were extracted from each modality and included as a node in the network study. The edges between these brain regions were computed as a Pearson correlation, and the negative correlations were set to zero. The network connectivity analyses were carried out on the binary undirected graphs while controlling the number of networks across a range of densities from 5–25% with a step size of 0.5%. To assess the functional network topology of rs-fMRI images, we used the DPARSF toolbox integrated into MATLAB 2019a. Moreover, we followed the same method for the extraction of features that we followed for the rs-fMRI images in (see section "Feature Extraction Using Voxel-Wise Morphometry"). A regional time series of the 200 brain regions included in the Craddock template atlas was extracted for each patient. To compute the relationship between these regions, we used the Pearson coefficient and performed network analysis on the binary undirected graphs. To assess the DTI network topology in AD, MCIs, MCIc, and HC subjects, the DWI images of these subjects were pre-processed using the PANDA toolbox, which was integrated into MATLAB 2019b. The PANDA toolbox uses a 2-*mm* JHU-WM (ICBM-DTI-81) label atlas template image for the extraction of 50 WM regions from each DTI image. These extracted regions were later included as a node in the network analysis. The same procedure was followed with the same parameters as that described above for constructing a network for sMRI brain images. Moreover, several graph metrics were calculated to quantify the nodal or global topological organization of the structural and functional networks, including local efficiency, characteristic path length, transitivity, and modularity. Local efficiency is a measure of the average efficiency of data transfer within local subgraphs or regions, and it is defined as the converse of the shortest average path length between the regions of a given node and all other nodes. The local efficiency of node i is defined as: $LE_i = 1/d_i(d_i - 1)\sum_{j=G_i} 1/l_{i,j}$, where d_i represents the number of nodes in the subgraph (G_i) and $l_{i,j}$ is the length of the shortest path between nodes i and j. The distance between two vertices in a graph is the length of the shortest path between them if one exists. Otherwise, the distance is infinite, and the average of the shortest path between one node and all remaining other nodes is termed the characteristic path length. The characteristic path length l_G is computed as: $l_G = 1/n(n-1)\sum_{i\neq j} d(v_i, v_j)$, where n is the number of vertices (v) in a graph network, and $d(v_i, v_j)$ denotes the shortest distance between vertices v_i and v_j. Transitivity (or the clustering coefficient) is defined as the ratio of paths that cross two edges to the number of triangles.

Moreover, if a node is connected to a second node, which is in turn is linked to a third node, the transitivity reproduces the probability that the initial node is linked to the third node. It can be computed by: $T = \frac{1}{N}\sum_k \frac{\sum_{i,j} a_{ij}a_{ik}a_{jk}}{d_k(d_k-1)}$, where a_{ij} is the (i, j) entry of the binary connection matrix. $a_{ij} = a_{ji} = 1$ if there is a link between nodes i and j, and $a_{ij} = a_{ji} = 0$ otherwise. There are no self-loops in the network, thus $a_{ij} = 0$. Modularity is the fraction of the network edges that fall within the given groups, minus the expected fraction if edges were distributed at random. It also calculates to what extent a network can be divided into communities. It can be calculated by, $Q = \sum_{i\epsilon M}[q_{ii} - (\sum_{j\epsilon M} q_{jj})^2]$, where the network is fully partitioned into M non-overlapping modules (or clusters), and q_{ij} represents the proportion of all links connecting nodes in module i with those in module j.

Classification Techniques

In supervised learning, classification resembles the task of determining to which category a new sample belongs, based on a training set of data containing instances for which associations have previously been identified. In neuroimaging, different information sources may contain different imaging modalities (e.g., sMRI, FDG, AV45, DTI, and rs-fMRI), different ways of extracting features from the same modality (e.g., ROI-based or voxel-based for every image), or a different feature subset. In the present study, we applied three different methods to extract features from the same neuroimaging modality as follows: whole-brain parcelation, voxel-wise analysis, and graphical representation. We were mainly interested in the first two approaches, where we used feature subsets as a kernel for each of the two methods. Later, we will combine (or concatenate) the approaches. We were particularly interested in examining models based on subsets of features extracted according to voxels or an anatomical criterion to attain predictions that enabled us to estimate the anatomical localization.

Multiple Kernel Learning

Kernel methods such as SVM (Cortes and Vapnik, 1995; Samper-González et al., 2018), which are based on similarity measures between data points, have been used with great success for dimensionality reduction and classification. Kernelization projects the native data space onto a higher-dimensional feature space. Non-linear relations between variables in the original space become linear in the transformed space. Let $\{x^{(i)}, y^{(i)}\}_{i=1}^N$ be the training sample, where $x^{(i)} = (x_1^{(i)}, x_2^{(i)}, \cdots, x_M^{(i)})^T \varepsilon \Re^M$ is a data sample, M is the number of features from all modalities, and $y^{(i)}\varepsilon\{1, -1\}$ is the corresponding class label. The aim is to simultaneously acquire an optimal feature description and a max-margin classifier in kernel space because of its systematic and elegant way of forming complicated patterns. Therefore, to project the data, we will use the kernel trick. As we know, for any kernel (K) on an input space (X), there exists a Hilbert space (f), called the feature space, and the projection $\emptyset$ is given by the mapping $\phi : X \rightarrow f$, such that for any two-object (x, y) in X, $K = (x, y) = <\phi(x), \phi(y)>$, where $<.,.>$ is the Euclidean or inner dot product of the data point. Examples of kernel functions include the linear, RBF, and others. Recent papers have shown that using multiple kernels rather than using a single kernel can improve the interpretability of a decision function, and in some instances, it improves the final performance. In MKL, the data are represented as a combination of base kernels. Each base kernel represents a different modality or feature of the entity. MKL seeks to find the optimal combination of base kernels so that the analysis tasks that follow are benefited the most. Classification tasks are represented especially well through MKL, as the optimal combination is the one that gives the maximum classification accuracy. The dual form of MKL optimization, as it is solved by conventional solvers like LIBSVM, is given as

$$\begin{aligned} &\max_{\alpha} L(\alpha) = \textstyle\sum_{i=1}^n \alpha_i - 1/2 \sum_{i,j}^p \sum_{m=1}^p \alpha_i\alpha_j y_i y_j \beta_m k^m(x_i^m, x_j^m) \\ &\text{Subject to } \textstyle\sum_{i=1}^n \alpha_i y_i = 0;\ 0 \le \alpha_i \le C;\ i = 1, ..., n \end{aligned} \tag{3}$$

where α_i, α_j are Lagrange multipliers, which are the variables obtained on converting the primal support vectors to the dual problem, and $k^m(x_i^m, x_j^m)$ is the m-th kernel function, which is applied to each pair of the samples, and C is the regularization parameter that controls the distance between the hyperplane and the support vectors. From the set of n training samples, the features of the i-th sample from the m-th modality are in the vector x_i^m, and its corresponding class label, y_i, is either $+1$ or -1. The weight on the m-th modality kernel, represented as β_m, is optimized using a grid search, or as a separate optimization problem with fixed α. For each new test sample, s, the kernel functions are computed against the training samples. An MKL overview is depicted in **Figure 3**. Recent research has shown that including the base datasets in more than one kernel, each differing in their selection of kernel parameters, improves performance. All kernels are then normalized to the unit trace through the formula $K_m(x, y) = k_m(x, y)/\sqrt{k_m(x, x)k_m(y, y)}$. Here, we set the weights accordingly to conform with sMRI, FDG, AV45, DTI, rs-fMRI, and APOE genotype features. The combined kernels can be described as follows,

$$\begin{aligned} K(x, y) = {} & w_{smri}k_{smri}(x, y) + w_{fdg}k_{fdg}(x, y) + w_{av45}k_{av45}(x, y) \\ & + w_{dti}k_{dti}(x, y) + w_{rs-fmri}k_{rs-fmri}(x, y) \\ & + w_{apoe}k_{apoe}(x, y) \\ & \text{With, } w_{smri} + w_{fdg} + w_{av45} + w_{dti} \\ & + w_{rs-fmri} + w_{apoe} = 1 \end{aligned} \tag{4}$$

Then, we use the EasyMKL (Aiolli and Donini, 2015; Donini et al., 2019) solver to search for the combination of basic kernels that maximizes the classifier performances by optimizing a simple quadratic problem addressed by SVM by computing an optimal weighting. Besides its proven empirical success, a clear advantage of EasyMKL compared with other MKL approaches is its high scalability with respect to the number of kernels to be combined. It finds the coefficients η that maximize the edges in the training dataset, where the margin is calculated as the distance between the convex hull of the positive and negative samples. In particular, the general problem that EasyMKL aims to optimize

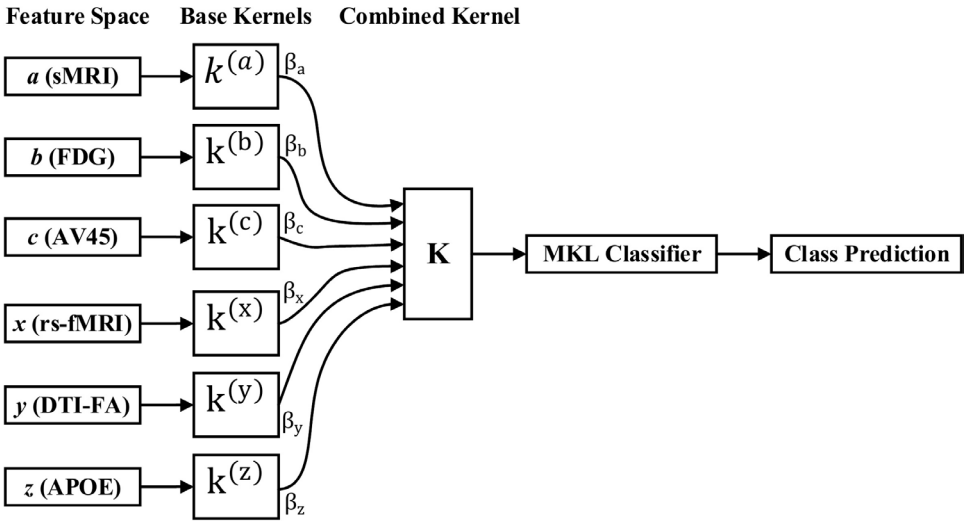

FIGURE 3 | MKL classification process.

is the following,

$$(\eta^*, \gamma^*) = \arg \max_{\eta:\|\eta\|_2=1} \min_{\gamma \varepsilon \Gamma} \lambda^{\Gamma} Y \left(\sum_{r=0}^{R} \eta_r K_r \right) Y_{\gamma} + \lambda \parallel \gamma \parallel_2^2 \tag{5}$$

where y is a diagonal matrix with training samples on the diagonal, and λ is a regularization hyperparameter, whereas domain Γ signifies two probability distributions over the set of negative and positive samples in the training set, that is $\Gamma = \left\{ \gamma \varepsilon R_+^l \left| \sum_{y_i=+1} \gamma_i = 1, \sum_{y_i=-1} \gamma_i = 1 \right| \right\}$ (Aiolli and Donini, 2015; Donini et al., 2019). Note that any element $\gamma \varepsilon \Gamma$ resembles a pair of samples in the convex hull of the positive and negative training samples. At the solution, the first expression of an objective function denotes the obtained (squared) edge, which is the (squared) distance between a point in a convex hull of positive samples and a point in a convex hull of negative samples, in the considered feature space. It enforces sparsity across modalities while allowing more than one discriminative kernel to be chosen from the same modality. In other words, there is sparsity across modalities and non-sparsity within modalities, thereby making it a convex optimization problem. Moreover, in addition to the EasyMKL classifier, we also applied a RBF kernel (or Gaussian kernel) with SVM classifier for the comparison of our obtained results. An RBF kernel is a function with a score that depends on the distance from the origin (or from some points). It is represented by $K(x_1, x_2) = e^{(\|x_1 - x_2\|^2 / 2\sigma^2)}$, where $\parallel x_1 - x_2 \parallel^2$ is the squared Euclidean distance between two data points x_1 and x_2. An RBF kernel has two parameters: gamma (γ) and C, and its performance depends on them. When the C value is small, the classifier is fine with misclassified input points (high bias, low variance), but when the C value is high, the classifier is severely penalized for misclassified data, and hence it leans over backward to avoid any misclassified input points (low bias, high variance). Moreover, when the γ value is low, the curve of the decision margin is quite low, and therefore the decision area is very large, but when the γ value is high, the curve of the decision margin is high, which creates decision-boundary bars around the input points. In our case, we applied the GridSearch method from a scikit-learn (v0.20) (Pedregosa et al., 2011) library to find the optimal hyperparameter (C and γ) value for the RBF-SVM classifier. The GridSearch was performed over the ranges of $C = 1$ to 9 and $\gamma = 1\ e^{-4}$ to 7.

Cross Validation

Cross validation (CV) is one of the most widely utilized data resampling methods for estimating the generalization knowledge of a predictive design and for preventing under- or overfitting. CV is largely applied in settings where the aim is prediction and it is necessary to evaluate the accuracy of a predictive model. For a classification problem, a model is generally fitted with a known sample, called the training sample, and a set of unknown samples against which the model is examined, known as the test sample. The aim is to have a sample for testing the proposed model in the training period, and then present insight into how the particular model adapts to an independent sample. A round of CV involves the partitioning of samples into complementary subsets, then conducting analysis on an individual subset. After this, the study is verified on other subsets (called testing samples). To reduce variability, multiple rounds of CV are performed using several different partitions, and later an average of the outcomes is taken. CV is a powerful procedure in the evaluation of model performance. In this study, we utilized leave-one-out CV (LOOCV) from the scikit-learn (v0.20) (Pedregosa et al., 2011) library. LOOCV is a CV process in which the bulk of the fold is "1," with "k" being fixed to the number of attributes in the dataset. This means that the number of folds equals the number of instances in the sample. Thus, the learning algorithm is employed once for each instance, utilizing all other instances as a training sample, and utilizing the selected instance as a

single-item test sample. This type of CV is useful when the training samples are of limited size and the number of attributes to be verified is not high.

Implementation

Our classification framework and validation experiments were implemented in Python 3.5 using an interface to the scikit-learn v0.20 (Pedregosa et al., 2011) library to measure performance, and using MKLpy (v0.5)[6] for the MKL framework. The main source code will be made available on the GitHub website.[7] The dataset list will be available in the **Supplementary Material**. Nonetheless, please note that you must prepare the original image features independently.

RESULTS

In this section, we present the performance results of each classification (AD vs. HC, MCIs vs. MCIc, AD vs. MCI, AD vs. MCIc, HC vs. MCIs, and HC vs. MCIc) for all five neuroimaging and APOE genotype modalities using whole-brain parcelation, the voxel-wise method, and the graphical method. We implemented the multimodal fusion approaches for the integration of the sMRI, FDG, AV45, rs-fMRI, DTI, and APOE genotype data. We used the combined representation to distinguish patients with AD from healthy subjects. The combined approach is considered successful if the classification task is performed with greater accuracy and higher AUC score, higher precision, and better sensitivity and specificity against unimodal classification. Along with the unimodal approaches, we evaluated the classification of a concatenated data vector comprising data from the five neuroimaging modalities and two APOE genotype modalities, and used it as a baseline. Moreover, after the completion of extracting features from each modality using whole-brain parcelation and voxel-wise analysis, we passed these extracted features through a polynomial kernel function to map the original non-linear low-dimensional features onto a higher-dimensional space in which they became separable. After that, a data fusion technique was used to combine the multiple kernel features into a single form before passing them through the EasyMKL classifier for the binary classification of the six groups. For an unbiased performance assessment, the classification groups were randomly split into two sets at a 70:30 ratio as training and testing sets, respectively. In a training set, finding the right values for the lambda (λ) parameter is quite difficult, and their values influence the classification result. Therefore, to find the optimal hyperparameter values for a lambda from 0 to 1 of an EasyMKL algorithm, we used the leave-one-out cross-validation technique on the training set. For each method, the optimized values obtained for the hyperparameter were then used to train the EasyMKL classifier using the training group. The performance of the resulting classifier was then estimated on the remaining 30% of the data in the testing dataset, which was not used during the training step. Here, cross validation was used to assess how the result of the classification analyses could generalize to an independent group. One round of cross validation includes partitioning the data sample into disjoint subsets of instances, performing the analysis on one subsection (the training group), and validating the study on the other subset (the testing or validation set). To reduce variability, numerous rounds of cross validation are done using different subsets, and the validation outcomes are averaged over the rounds. In the present study, we used an LOOCV, which involves separating a single instance (either control or patient) from the complete example for testing while the remaining instances are used for training purposes. This splitting is iterated so that each instance in the whole sample is used once for validation. After all iterations, the final accuracy is quantified as the mean of the accuracies gained across each fold. In this way, we attained unbiased estimations of the performance for each classification problem. Moreover, after the completion of whole-brain and voxel-wise analysis, we used the BRAPH toolbox to perform the brain graphical analysis for each classification group with the same five neuroimaging features (sMRI, FDG, AV45, rs-fMRI, and DTI), which we extracted in the whole-brain analysis. For each analysis, we measured the accuracy (ACC, calculated as the average of the proportion of correctly classified subjects from each class individually), the sensitivity (SEN, described as true positive – the number of subjects correctly classified), and the specificity (SPEC, described as true negative – the number of healthy controls correctly categorized), precision (PRE, referring to how well the measurements agree with each other across multiple tests), F1-score (explained as a weighted average of recall and precision, where an F1-score attains its best value at one and its worst at zero), and AUC-ROC [a receiver operating characteristic curve (ROC curve) is a graphical plot that illustrates the diagnostic aptitude of a binary classifier scheme as its differential threshold is varied]. An AUC-ROC curve is constructed by plotting the true positive rate (TPR) against the false positive rate (FPR). The TPR is the proportion of observations that were correctly predicted to be positive out of all positive observations [$TP/(TP + FN)$]. Likewise, the FPR is the proportion of observations that are incorrectly predicted to be positive out of all negative observations [$FP/(TN + FP)$]. The ROC curve shows the trade-off between sensitivity (or TPR) and specificity ($1 - FPR$). Classifiers that give curves closer to the top-left corner show better performance. As a baseline, a random classifier is expected to give points lying along the diagonal (FPR = TPR). The closer the curve comes to the 45-degree diagonal of the ROC space, the less accurate the testing data are. For each classification group, we also measured Cohen's kappa values, which measures the inter-rater reliability between two individuals (Cohen, 1960). Kappa measures the percentage of information scores in the main diagonal of a table and then adjusts these scores for the quantity of agreement that could be assumed due to chance alone. The formula for calculating Cohen's kappa for two raters is given by $K = p_0 - p_c/1 - p_c$, where p_0 is the relative observed agreement among raters and p_c is the hypothetical probability of chance agreement. Kappa is always less than or equal to 1. A value of 1 suggests perfect agreement, and scores less than 1 suggest less than the best

[6]https://github.com/IvanoLauriola/MKLpy

[7]https://github.com/Alzheimer1/Classification-of-Alzheimer-s-disease

agreement. In rare circumstances, Kappa can achieve a negative score. This signifies that the two groups agreed less than would be predicted by chance alone.

Classification Performance Across Single and Combined Modalities Using Whole-Brain Parcelation Analysis

For the whole-brain analysis, we used the 2-mm AICHA atlas template image for sMRI, FDG, and AV45-PET images with the NiftyReg toolbox for the extraction of 384 ROIs from each neuroimaging modality (as shown in **Figure 1B**). For each rs-fMRI and DTI image, we used the 2-mm Craddock atlas template and the 2-mm JHU-WM (ICBM-DTI-81) label atlas for the extraction of 200 and 50 ROIs, from each rs-fMRI and DTI image, respectively, using the pyClusterROI Python script and the PANDA toolbox (as shown in **Figure 1B**). In total, we obtained 1404 features for a single image, 384 features from each sMRI, FDG, and AV45-PET image, 200 from each rs-fMRI image, 50 features from each DTI image, and two features from the APOE genotype data. Afterward, we passed these obtained features through a normalization technique to minimize the redundancy within the dataset. Furthermore, we passed these low-dimensional, normalized features from the polynomial kernel matrix to map them onto a high-dimensional feature space. Then we fused all these high-dimensional features in one form before passing them through the EasyMKL algorithm for classification. The obtained AUC-ROC graph and Cohen's kappa scores are plotted in **Figures 4**, **5**.

For the single modalities, whole-brain MKL analysis for AD vs. HC (**Table 2**), using only the APOE genotype, achieved 85.71% accuracy. Similar accuracy was obtained using sMRI (90.48%), FDG-PET (91.5%), AV45-PET (89.39%), and rs-fMRI (92.42%). Using DTI-FA, the accuracy was increased to 93.17% compared with both genotype and functional imaging. When the combined-ROI features were passed through the classifier, the accuracy increased to 96.05%. Additionally, the obtained Cohen's kappa value was 0.9066, which is closer to 1 than the kappa values of the individual modalities. **Figure 5** shows the Cohen's kappa plot for the combined-ROI.

Here, for AD vs. HC classification, the combined-ROI features performed very well compared with the single modalities. Similarly, for the single modalities, whole-brain MKL analysis for MCIs vs. MCIc (**Table 2**) using only the APOE genotype achieved 85.24% accuracy. Similar accuracy was obtained using FDG-PET (86.88%), AV45-PET (89.47%), and rs-fMRI (88.52%). Using sMRI-extracted ROI features, the achieved accuracy was lower (84.71%) in comparison with other single modalities. Using DTI-FA, the accuracy increased to 91.80% in comparison with both genotype and functional images. Moreover, when the combined-ROI features were passed through the classifier, the accuracy increased to 94.74% and the obtained Cohen's kappa value was 0.8950 (**Figure 5**), which is closer to 1 than that for the individual modalities. Here, for the MCIs vs. MCIc classification, the combined-ROI features performed very well compared with the single modalities. Likewise, for the AD vs. MCIc classification problem, the best performance was attained using a combination of six modalities of features, which achieved an accuracy of 94.89% with a Cohen's kappa of 0.8502. In this case, the rs-fMRI and DTI-FA unimodal features performed better for classifying the (AD vs. MCIc) group than the other unimodal features, and their obtained accuracies were 92.06 and 93.65%. For the AD vs. MCIs group, our proposed technique achieved 93.59% accuracy, which was 1.66% higher than the best accuracy obtained by the DTI-FA (unimodal) feature for classifying this group. The Cohen's kappa score obtained for the AD vs. MCIs group was 0.8562 (**Figure 5**) which is close to the maximum agreement value of 1. For the HC vs. MCIc classification problem, our proposed method combining all six modalities of a biomarker to distinguish between HC and MCIc achieved good results compared with the single modality biomarkers. For this classification problem, our proposed method achieved 94.24% accuracy with a Cohen's kappa of 0.8814 (**Figure 5**). In this case, from **Table 2**, we can see that all three (FDG-PET, AV45-PET, and rs-fMRI) functional imaging features performed well compared with the other unimodal features, and their obtained Cohen's kappa scores were 0.7610, 0.7981, and 0.8129, which are all close to 1. Likewise, for the HC vs. MCIs group, our proposed technique achieved 95.55% accuracy, which is 1.62% higher than the best accuracy obtained by the DTI-FA (unimodal) feature for classifying this group. The obtained Cohen's kappa score for the HC vs. MCIs group was 0.8697 (**Figure 5**), which is close to the maximum agreement value of 1. Therefore, from **Table 2** and **Figures 4**, **5**, we can state that for all classification combinations, our proposed method attained a high level of performance compared with the individual modality of biomarkers, varying from 1 to 3%, and our proposed scheme also attained a higher level of agreement between all six classification combinations than the individual modality-based methods.

The number of extracted ROIs was slightly higher for the sMRI, FDG-PET, and AV45-PET images than for the other modalities, although the real number of features used as input for each single and combined model varied across the models. Except for the HC vs. MCIc group, in the (AD vs. HC, MCIs vs. MCIc, AD vs. MCIc, AD vs. MCIs, and HC vs. MCIs) classification sets, it is interesting to observe that even though the number of extracted ROI features for sMRI, FDG-PET, AV45-PET, and rs-fMRI were higher than the number of DTI-FA ROI features, the obtained accuracy was lower than for the DTI-FA ROI features for the stated classification groups. Out of the 1404 ROIs, 384 ROIs selected from sMRI, 384 ROIs selected from FDG-PET, 384 ROIs selected from AV45-PET, 200 ROIs from rs-fMRI, 50 ROIs from DTI-FA, and the remaining two ROIs from APOE genotype corresponded to 27.3% (each of sMRI, FDG-PET, and AV45-PET), 14.5% (rs-fMRI), 3.5% (DTI-FA), and 0.1% (APOE) of the total number of features. In **Figure 4**, we show the ROC curves (plots of the TPR vs. the FPR for dissimilar possible cut-points) for each study presented in **Table 2**. The obtained AUC is presented in each plot. **Figure 4** shows that our proposed method achieved higher AUC values for all classification sets than did the individual modalities. For the AD vs. HC and HC vs. MCIs classification groups, our proposed method achieved an AUC greater than 95%, while for the MCIs vs. MCIc, AD vs. MCIs, AD vs. MCIc, and HC vs. MCIc groups, the proposed method achieved an AUC less than 95%, (MCIs vs. MCIc, AD vs. MCIs, AD vs. MCIc, and HC vs. MCIc) $<$ 95% $<$ (AD

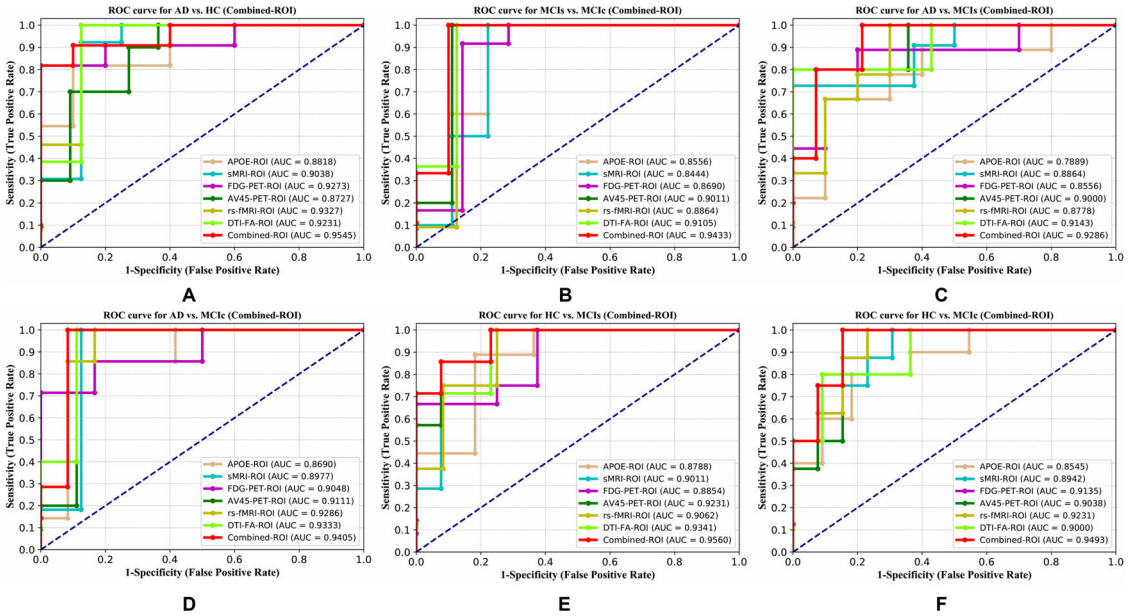

FIGURE 4 | ROC curve for **(A)** AD vs. HC, **(B)** MCIs vs. MCIc, **(C)** AD vs. MCIs, **(D)** AD vs. MCIc, **(E)** HC vs. MCIs, and **(F)** HC vs. MCIc using whole-brain parcelation analysis. The red solid line shows the result of a combined-ROI curve with single modality features.

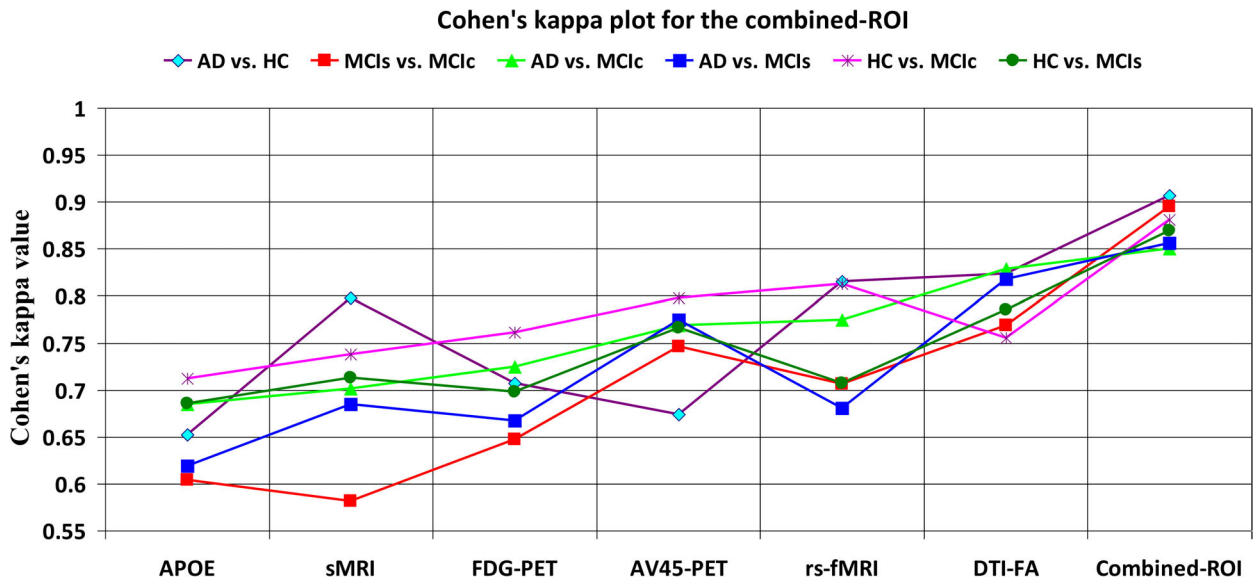

FIGURE 5 | Cohen's kappa plot for AD vs. HC, MCIs vs. MCIc, AD vs. MCIs, AD vs. MCIc, HC vs. MCIs, and HC vs. MCIc are grouped using whole-brain parcellation analysis. The above graph clearly shows the benefit of the combined-ROI modality over any single modality.

vs. HC and HC vs. MCIs). The obtained result using the RBF-SVM classifier can be found in **Supplementary Table S31**. From **Supplementary Table S31**, we can say that the combined-ROI features performed very well as compared with the individual modality outcomes for all six binary classification groups. **Table 2** and **Supplementary Table S31** clearly show the advantage of using combined features over individual ones (see **Supplementary Table S31**).

Classification Performance Across Single and Combined Modalities Using Voxel-Wise Analysis

For the voxel-wise analysis of the sMRI, FDG-PET, and AV45-PET images, we used the SPM12 toolbox with the integration of the CAT12 toolbox in MATLAB R2019a. For the DTI images, we used the DTIfit and TBSS functions from the FSL toolbox.

TABLE 2 | Classification results for AD vs. HC, MCIs vs. MCIc, AD vs. MCIs, AD vs. MCIc, HC vs. MCIc, and HC vs. MCIs groups using ROI features (EasyMKL).

Groups	Features	Classifier	Performance measure						
			AUC	ACC	SEN	SPEC	PRE	F1-score	Cohen's kappa
AD vs. HC	APOE	EasyMKL	88.18	85.71	88.89	83.33	80	84.21	0.6523
	sMRI		90.38	90.48	87.5	92.31	87.5	87.5	0.7981
	FDG-PET		92.73	91.5	**100**	84.62	80	88.89	0.7073
	AV45-PET		87.27	89.39	87.87	90.90	90.62	89.23	0.6736
	rs-fMRI		93.27	92.42	88.23	94.11	93.75	90.90	0.8150
	DTI-FA		92.31	93.17	90.90	93.93	93.75	92.30	0.8233
	Combined-ROI		**95.45**	**96.05**	94.11	**100**	**100**	**96.96**	**0.9066**
MCIs vs. MCIc	APOE	EasyMKL	85.56	85.24	84.37	86.20	87.09	85.71	0.6042
	sMRI		84.44	84.71	75	**100**	**100**	85.71	0.5819
	FDG-PET		86.9	86.88	87.09	86.66	87.09	87.09	0.6471
	AV45-PET		90.11	89.47	100	85.71	77.78	87.5	0.7465
	rs-fMRI		88.60	88.52	87.5	89.65	90.32	88.88	0.7060
	DTI-FA		91.05	91.80	90.62	93.10	93.54	92.06	0.7684
	Combined-ROI		**94.33**	**94.74**	**100**	90.91	90	**94.74**	**0.8950**
AD vs. MCIs	APOE	EasyMKL	78.89	77.68	72.73	75	80	76.19	0.6193
	sMRI		88.64	88.52	90	87.09	87.09	88.52	0.6849
	FDG-PET		85.56	84.95	83.62	85.71	84.89	84.25	0.6673
	AV45-PET		90	90.16	93.10	87.50	87.09	90	0.7746
	rs-fMRI		87.78	88.57	86.45	87.78	89.55	87.97	0.6802
	DTI-FA		91.43	91.93	90.90	93.10	93.75	92.30	0.8180
	Combined-ROI		**93.86**	**93.59**	**93.75**	**93.33**	**93.75**	**93.75**	**0.8562**
AD vs. MCIc	APOE	EasyMKL	86.9	85.21	80	88.89	88.89	84.21	0.6851
	sMRI		89.77	88.88	93.10	85.29	84.37	88.52	0.7014
	FDG-PET		90.48	90.47	93.33	87.87	87.5	90.32	0.7244
	AV45-PET		91.11	89.47	88.89	90	88.89	88.89	0.7689
	rs-fMRI		92.86	92.06	90.90	93.33	93.75	92.30	0.7745
	DTI-FA		93.33	93.65	93.75	93.54	**93.75**	93.75	0.8285
	Combined-ROI		**94.05**	**94.89**	**100**	**94.77**	91.67	**95.65**	**0.8502**
HC vs. MCIc	APOE	EasyMKL	85.45	85.71	83.33	88.89	90.91	86.96	0.7123
	sMRI		89.42	88.05	88.88	87.09	88.88	88.88	0.7377
	FDG-PET		91.35	91.04	94.11	87.87	88.88	91.42	0.7610
	AV45-PET		90.48	90.48	82.31	87.5	92.31	92.31	0.7981
	rs-fMRI		92.31	92.53	94.28	90.62	91.66	92.95	0.8129
	DTI-FA		90	89.55	93.93	85.29	86.11	89.85	0.7557
	Combined-ROI		**94.93**	**94.24**	**100**	**88.89**	**92.31**	**96**	**0.8814**
HC vs. MCIs	APOE	EasyMKL	87.88	87.87	86.84	89.28	91.66	89.18	0.6855
	sMRI		90.11	89.06	90.90	87.09	88.23	89.55	0.7127
	FDG-PET		88.54	89.39	89.18	89.65	91.66	90.41	0.6984
	AV45-PET		92.31	92.42	94.28	90.32	91.66	92.95	0.7661
	rs-fMRI		90.62	90.12	93.75	87.5	88.23	90.90	0.7070
	DTI-FA		93.41	93.93	94.45	**93.33**	**94.44**	94.44	0.7854
	Combined-ROI		**95.6**	**95.55**	**100**	90.90	91.66	**95.65**	**0.8697**

For the voxel-wise analysis of rs-fMRI images, we used the DPARSF toolbox in MATLAB R2019a. Afterward, we passed these obtained features with two features from the APOE genotype data through a normalization technique to minimize the redundancy within the dataset. Furthermore, we passed these low-dimensional, normalized features from the polynomial kernel matrix to map them onto a high-dimensional feature space. Then we fused all these high-dimensional features in one

form before passing them through the EasyMKL algorithm for classification. The obtained result are shown in **Table 3** and **Figure 6** shows the Cohen's kappa plot for all six classification groups using voxel-wise analysis.

AD vs. HC

We calculated the statistical values that represented the significance levels of the groups in the activation map as presented in **Supplementary Tables S1–S5** after comparing the outcomes of the statistical two-sample *t*-tests for the AD vs. HC group. These tables specify the main affected area observed in the AD vs. HC set and the obtained voxel cluster with detailed information, including its peak areas in the form of the MNI space, cluster-level *p-score*, and the peak intensity in the *T-score* of each group. We used an uncorrelated threshold value of $p_{uncorrected} \leq 0.001$ at the voxel level, an FDR value of $p_{FDR} = 0.05$, and an FWER value of $p_{FWER} = 0.05$ at the cluster level to achieve a bias alteration for multiple comparisons. An ROI binary mask was created from the selected clusters of each modality, and later the GM and WM volumes were removed from the two sets of images (AD vs. HC) (see **Supplementary Tables S1–S5**). **Figure 7A** shows the most significant regions where these groups differ from each other using an AV45-PET neuroimage, and the obtained voxel cluster is shown in **Supplementary Table S3**. Likewise, **Figure 8A** shows the most significant regions where these groups differ from each other using a DTI-FA neuroimage, and the obtained voxel cluster is shown in **Supplementary Table S5** (see **Supplementary Tables S3, S5**).

MCIs vs. MCIc

Supplementary Tables S6–S10 show the main affected areas in the MCIs vs. MCIc group, the obtained voxel clusters with detailed information about its peak coordinates in the MNI space, the cluster-level *p*-score, and the peak intensity in the *T*-score of each group. For the MCIs vs. MCIc group, we used an uncorrelated threshold value of $p_{uncorrected} \leq 0.001$ at the voxel level, an FDR value of $p_{FDR} = 0.05$, and an FWER value of $p_{FWER} = 0.05$ at the cluster level to accomplish a bias alteration for multiple comparisons. An ROI binary mask was created from the selected clusters of each modality and later GM and WM volumes were removed from the two sets of images (MCIs vs. MCIc) (see **Supplementary Tables S6–S10**). **Figure 7B** shows the most significant region where these groups differ from each other using an AV45-PET neuroimage, and the obtained voxel cluster is shown in **Supplementary Table S8**. Likewise, **Figure 8B** shows the most significant region where these groups differ from each other using a DTI-FA neuroimage, and the obtained voxel cluster is shown in **Supplementary Table S10** (see **Supplementary Tables S8, S10**). Moreover, we followed the same procedure for the calculation of voxel clusters for the AD vs. MCIc, AD vs. MCIs, HC vs. MCIc, and HC vs. MCIs groups as we followed for the AD vs. HC and MCIs vs. MCIc groups. The obtained voxel clusters with detailed information about its peak coordinates in the MNI space, the cluster-level *p-score*, and the peak intensity in the *T*-score of each group are shown in **Supplementary Tables S11–S30** (see **Supplementary Tables S11–S30**). Likewise, **Supplementary Figures S1a,b** show the most significant region for the AD vs. MCIc and HC vs. MCIc groups using the DTI-FA modality of the biomarker.

The obtained voxel cluster for these two groups is shown in **Supplementary Tables S15, S25** (see **Supplementary Figures S1a,b** and **Supplementary Tables S15, S25**). After completing the extraction of the series of features from each individual modality, we passed these obtained features through the polynomial kernel matrix to map these low-dimensional features onto a high-dimensional feature space. We then fused all these high-dimensional features in one form before passing them through the EasyMKL algorithm for classification. **Table 3** shows the classification results for the AD vs. HC group using voxel-wise features. It shows that the combined features performed very well for this group compared with the single-modality results. The combined features achieved a 95.55% AUC for classifying the AD vs. HC group, as shown in **Figure 9**, with a Cohen's kappa value of 0.9014, which is close to 1, as shown in **Table 3** and **Figure 6**. This indicates that these two groups have a good level of agreement between them. **Table 3** shows the classification results for the MCIs vs. MCIc group using voxel-wise features. This table also shows that the combined features performed very well for classifying the MCIs vs. MCIc group compared with the single-modality performances. The combined features achieved an AUC of 94.90% when classifying the MCIs vs. MCIc group, as shown in **Figure 9**. The Cohen's kappa value was 0.8825, which is close to 1, as shown in **Table 3** and **Figure 6**. This indicates a good level of agreement between the two groups. Furthermore, for the AD vs. MCIc and AD vs. MCIs classification groups, our proposed system attained a high level of performance and agreement (0.9145 and 0.8869) compared with the individual modalities biomarkers. For the AD vs. MCIc group, AV45-PET and DTI-FA attained high classification accuracy compared with other unimodal biomarkers, but their gained accuracy was 3% less than the accuracy gained by the combined-VOI process, which was 96.20% with a 0.9145 (**Figure 6**) Cohen's kappa score. Likewise, for the AD vs. MCIs group, the proposed method achieved 95.16% accuracy with a 0.8869 (**Figure 6**) Cohen's kappa score. For the HC vs. MCIc classification group, the AV45-PET individual modality biomarkers performed very well compared with the other single modality biomarkers. The obtained accuracy and Cohen's kappa score using AV45-PET biomarkers were 94.02% and 0.8481 (**Figure 6**). Moreover, we then passed the combined-VOI features through the EasyMKL classifier for the classification of the HC vs. MCIc group, and after the classifier was applied, the accuracy increased by 1.5%. This suggests that the combined-VOI features were beneficial for classifying this group. Likewise, for the HC vs. MCIs classification group, the rs-fMRI features of ALFF and fALFF achieved a good level of performance and agreement (0.8386 and 0.8248) compared with the other individual modality biomarkers. In this case, the individual features of the APOE genotype also performed well compared with the FDG-PET imaging modality biomarker, but the individual modality biomarker's performance was not very good compared with the combined-VOI result (**Table 3**). The combined-VOI features achieved a 94.43% accuracy and an AUC of 94.67% with a 0.8864 Cohen's kappa score for classifying the HC vs. MCIs group. **Figure 9** shows the

TABLE 3 | Classification results for AD vs. HC, MCIs vs. MCIc, AD vs. MCIs, AD vs. MCIc, HC vs. MCIc, and HC vs. MCIs groups using voxel-wise (VOI) features (EasyMKL).

Groups	Features	Classifier	Performance measure						
			AUC	ACC	SEN	SPEC	PRE	F1-score	Cohen's kappa
AD vs. HC	APOE	EasyMKL	88.18	87.71	88.89	83.33	80	84.21	0.6523
	sMRI		87.5	87.87	**100**	81.81	73.33	87.61	0.6547
	FDG-PET		91.35	89.39	92.59	87.17	83.33	87.71	0.7651
	AV45-PET		93.64	93.93	90.62	97.05	96.66	93.54	0.8528
	rs-fMRI-ALFF		89.81	90.12	92.85	89.47	86.66	89.65	0.6839
	rs-fMRI-fALFF		91.52	90.90	90	91.60	90	90	0.7973
	rs-fMRI-REHO		90.38	89.74	89.65	89.18	86.66	88.13	0.7345
	DTI-FA		92.86	92.42	93.10	91.89	90	91.52	0.8213
	Combined-VOI		**95.55**	**95.24**	93.33	**100**	**100**	**96.55**	**0.9014**
MCIs vs. MCIc	APOE	EasyMKL	85.56	85.24	84.37	86.20	87.09	85.71	0.6042
	sMRI		87.88	88.52	87.5	89.65	90.32	88.88	0.6788
	FDG-PET		83.33	84.21	85.71	80	92.31	88.89	0.5874
	AV45-PET		91.03	91.80	90.32	93.33	93.33	91.80	0.7243
	rs-fMRI-ALFF		87.78	89.47	**100**	83.33	77.78	87.5	0.6665
	rs-fMRI-fALFF		85.56	85.24	84.37	86.20	87.09	85.71	0.6011
	rs-fMRI-REHO		89.74	90.16	90.32	90	90.32	90.32	0.6907
	DTI-FA		92.31	92.75	90.65	93.10	93.54	92.06	0.8175
	Combined-VOI		**94.9**	**93.57**	92.86	**100**	**100**	**96.3**	**0.8825**
AD vs. MCIs	APOE	EasyMKL	78.89	77.68	72.73	75	80	76.19	0.6193
	sMRI		88.18	88.70	87.09	90.32	90	88.52	0.6944
	FDG-PET		90.91	90.32	90	90.62	90	90	0.7065
	AV45-PET		89.09	89.48	87.5	93.34	93.34	90.32	0.7679
	rs-fMRI-ALFF		92.73	92.45	90.32	93.54	93.33	91.80	0.8126
	rs-fMRI-fALFF		87.27	87.09	86.67	87.5	86.7	86.7	0.6943
	rs-fMRI-REHO		92.5	92.72	90	96	96.42	93.10	0.8467
	DTI-FA		90	91.93	93.10	90.90	90	91.52	0.8211
	Combined-VOI		**94.96**	**95.16**	**93.54**	**96.77**	**96.66**	**95.08**	**0.8869**
AD vs. MCIc	APOE	EasyMKL	86.9	85.21	80	88.89	88.89	84.21	0.6851
	sMRI		84.62	85.48	86.20	84.84	83.83	84.74	0.6272
	FDG-PET		88.54	88.89	85.29	93.10	93.54	89.23	0.7049
	AV45-PET		92.71	93.75	96.67	91.17	90.32	93.54	0.8342
	rs-fMRI-ALFF		90.62	90.47	87.87	93.34	93.54	90.62	0.7978
	rs-fMRI-fALFF		87.5	87.30	87.09	87.5	87.09	87.09	0.7691
	rs-fMRI-REHO		91.67	92.18	93.54	90.91	90.62	92.06	0.8173
	DTI-FA		93.75	93.65	88.57	**100**	**100**	93.93	0.8666
	Combined-VOI		**96.67**	**96.20**	**96.77**	96.87	96.77	**96.77**	**0.9145**
HC vs. MCIc	APOE	EasyMKL	85.45	85.71	83.33	88.89	90.91	86.96	0.7123
	sMRI		90.28	90.76	91.42	90	91.42	91.42	0.7673
	FDG-PET		86.36	86.88	86.48	86.67	88.89	87.68	0.6851
	AV45-PET		93.75	94.02	90.90	97.05	96.74	93.74	0.8481
	rs-fMRI-ALFF		90	90.36	91.42	87.5	88.89	90.14	0.7437
	rs-fMRI-fALFF		88.31	89.55	87.5	91.42	90.32	88.89	0.7099
	rs-fMRI-REHO		92.31	92.53	90.62	94.28	93.54	92.06	0.8043
	DTI-FA		93.18	92.87	88.23	**96.96**	**96.74**	92.30	0.8217
	Combined-VOI		**95.56**	**95.52**	**96.67**	94.59	93.54	**95.08**	**0.8977**
HC vs. MCIs	APOE	EasyMKL	87.88	87.87	86.84	89.28	91.66	89.18	0.6855
	sMRI		91.11	91.42	92.10	90.62	92.10	92.10	0.8136
	FDG-PET		85.23	85.33	86.45	82.85	85.36	86.41	0.6905
	AV45-PET		90	90.90	91.67	90	91.66	91.67	0.7847
	rs-fMRI-ALFF		92.86	92.30	94.28	91.14	91.67	92.95	0.8386
	rs-fMRI-fALFF		93.33	92.75	94.59	90.62	92.10	93.34	0.8248
	rs-fMRI-REHO		89.77	89.39	91.42	87.09	88.89	90.14	0.7788
	DTI-FA		91.68	90.14	89.74	91.25	91.32	90.90	0.8034
	Combined-VOI		**94.67**	**94.43**	**94.59**	**96.67**	**97.22**	**95.89**	**0.8864**

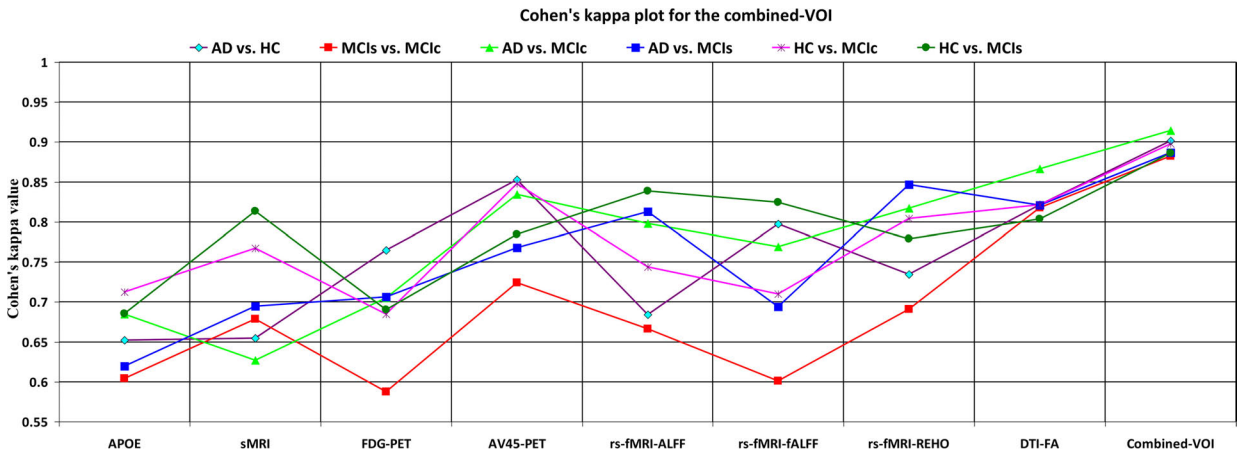

FIGURE 6 | Cohen's kappa plot for AD vs. HC, MCIs vs. MCIc, AD vs. MCIs, AD vs. MCIc, HC vs. MCIs, and HC vs. MCIc are grouped using voxel-wise analysis. The above graph clearly shows the benefit of the combined-VOI modality over any single modality.

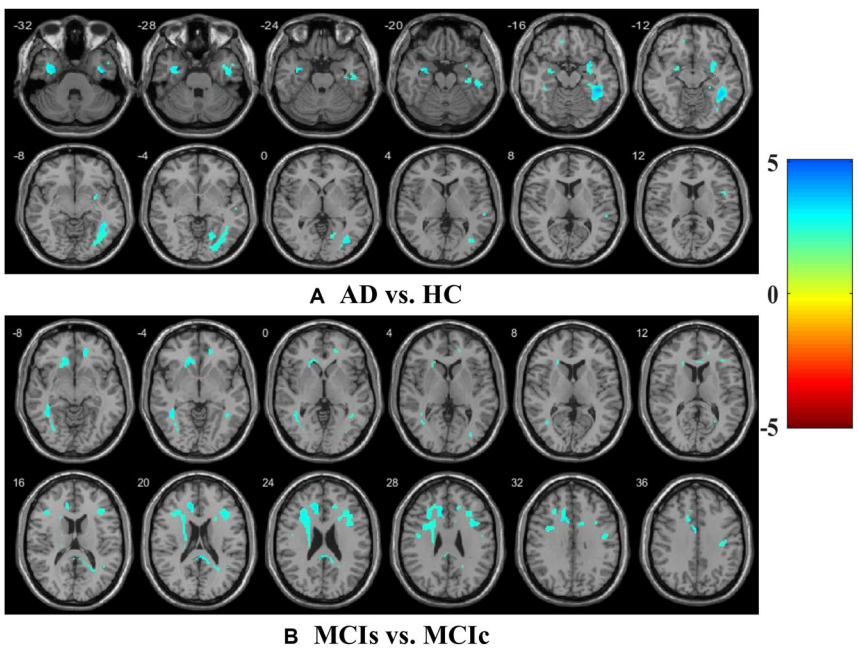

FIGURE 7 | Affected region for **(A)** AD vs. HC, and **(B)** MCIs vs. MCIc is shown using AV45-PET image.

ROC curve for all six classification groups; the red solid line in every classification task indicates the combined-VOI features for that particular group. Consequently, from **Table 3** and **Figures 6**, **9**, we can state that for all classification combinations, our proposed method attained a high level of performance compared with the individual modality biomarkers, varying from 1 to 3%, and our proposed scheme also attained a high level of agreement between each of the six classification combinations compared with the individual modality-based methods. The obtained result using the RBF-SVM classifier can be found in **Supplementary Table S32**. From **Supplementary Table S32**, we can say that the combined-VOI features performed very well as compared with the individual modality outcomes for all six binary classification groups. **Table 3** and **Supplementary Table S32** clearly show the advantage of using combined features over individual ones (see **Supplementary Table S32**).

While searching for the most significant region where AD vs. HC subjects differed from each other, we found that the (left/right) temporal-mid, (left/right) frontal-sup, (left/right) occipital-mid, (left/right) occipital-inf, (left/right) temporal-sup, (left/right) fusiform, (left/right) hippocampus, (left/right) temporal-inf, (left/right) precentral, and the (left/right) sagittal stratum were the regions where these subjects differed from each other most (**Supplementary Tables S1–S5**). Likewise,

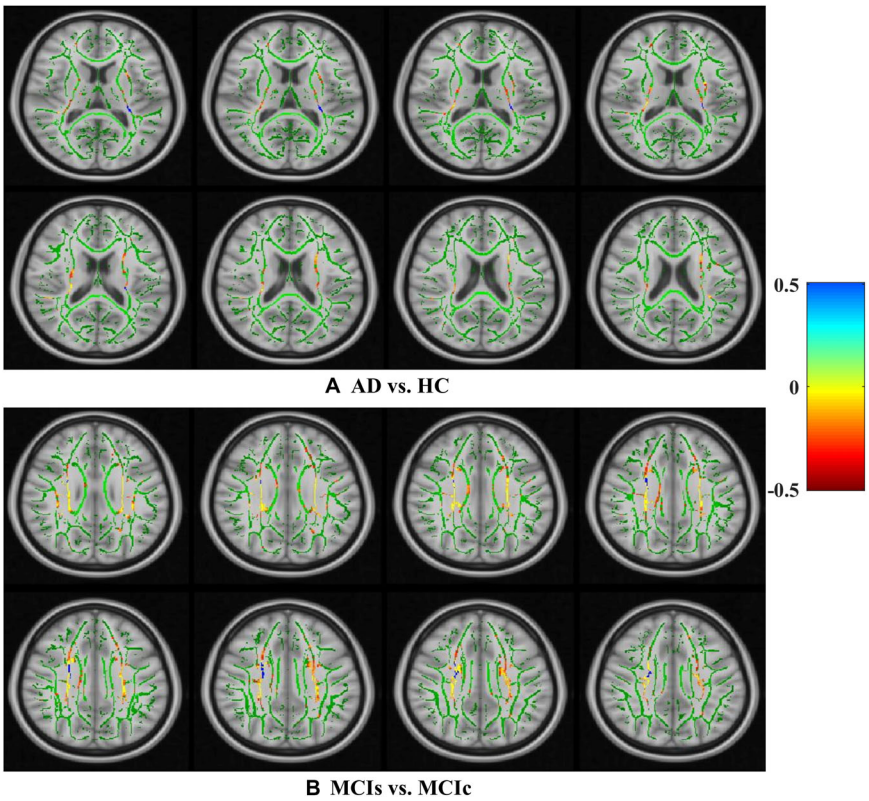

FIGURE 8 | Selected WM voxels for the **(A)** AD vs. HC, and **(B)** MCIs vs. MCIc classification using DTI image.

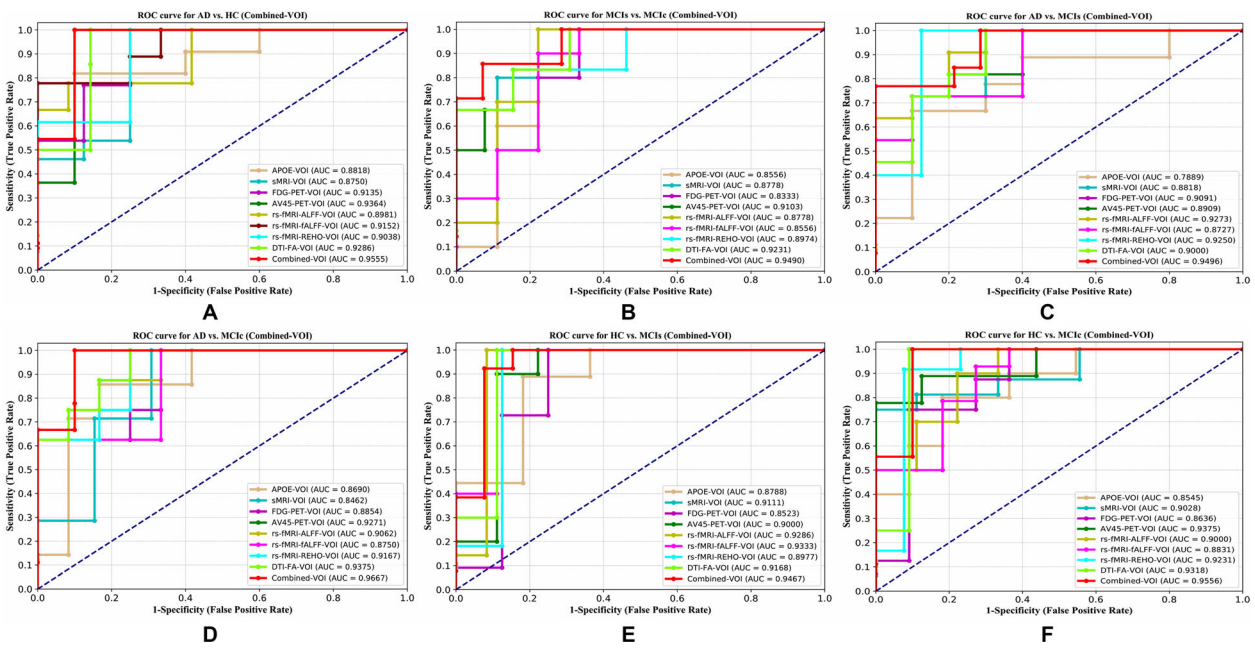

FIGURE 9 | ROC curves for **(A)** AD vs. HC, **(B)** MCIs vs. MCIc, **(C)** AD vs, MCIs, **(D)** AD vs, MCIc, **(E)** HC vs. MCIs, and **(F)** HC vs. MCIc using voxel-wise (VOI) analysis. The red solid line shows the result of the combined-VOI curve, including all single-modality features.

for the MCIs vs. MCIc group, we found that the (left/right) precentral, (left/right) precuneus, (left/right) frontal-mid, (left/right) cingulum-mid, (left/right) temporal-inf, (left/right) temporal-sup, (left/right) frontal-dup-medial, (left/right) cerebellum-9, (left/right) thalamus, and (left/right) fusiform were the regions where these subjects differed from each other most significantly (**Supplementary Tables S6–S10**). For the AD vs. MCIc group, we found that the (left/right) frontal-inf-tri, (left/right) frontal-inf-oper, (left/right) frontal-inf-orb, (right) hippocampus, (left/right) precentral, (left/right) thalamus, (left) pallidum, (left/right) lingual, and (left/right) inferior longitudinal fasciculus were the regions where these group subjects differed from each other most (**Supplementary Tables S11–S15**). As for the AD vs. MCIs group, we found that the (left/right) precentral, (left/right) frontal-mid, (left/right) hippocampus, (left/right) temporal-inf, (left/right) frontal-inf-orb, (left/right) occipital-mid, (right) posterior corona radiate, and (left/right) precuneus were the most significant regions where these group subjects differed from each other (**Supplementary Tables S16–S20**). For the HC vs. MCIc and HC vs. MCIs groups, we found that the (left/right) precentral, (left/right) cerebellum-6, (left/right) precuneus, (left/right) frontal-mid, (left/right) corticospinal tract, (left/right) lingual, (right) amygdala, and the (left/right) occipital-sup were the most significant regions where these two groups differed from each other (**Supplementary Tables S21–S30**). It is interesting to note that the (left/right) precentral region was found in every classification problem when computing voxel clusters (see **Supplementary Tables S1–S30**).

Table 4 shows the combined (VOI + ROI) classification results for all six classification groups after concatenating the extracted features from the whole-brain and voxel-wise methods with the APOE genotype. Before passing these features to the EasyMKL classifier, we applied a polynomial kernel matrix to map these low-dimensional features onto a high-dimensional feature space, so that every feature revealed its importance to the classifier. These high-dimensional features were fused into one form. We then passed these features to the MKL algorithm for classification.

For the AD vs. HC classification group, the combined-(VOI + ROI) feature performed very well compared with the combined-VOI and combined-ROI features. The AUC and Cohen's kappa scores were increased by 2–2.5% (97.78%, 0.9456) compared with those of combined-ROI and combined-VOI (**Figure 10** and **Table 4**). Moreover, for the MCIs vs. MCIc classification group, **Table 4** and **Figure 10** show that the combined-(VOI + ROI) features achieved an AUC of 96.94% (2% increment), which was very high compared with the other two combined features. The obtained Cohen's kappa value (0.9247) was also high compared with that of the combined-VOI and combined-ROI. Furthermore, for the AD vs. MCIs, HC vs. MCIs, and HC vs. MCIc classification groups, our proposed system performed very well compared with the results obtained by the combined-VOI and the combined-ROI for these groups. From **Table 4**, we can see that for these three (AD vs. MCIs, HC vs. MCIs, and HC vs. MCIc) groups, there is a 2–3% increment in every measured performance. The obtained AUC scores for these three groups are 96.25, 96.59, and 96.67%. Likewise, in the case of the AD vs. MCIc group, the Combined-ROI method performed very well compared with the combined-(VOI + ROI) and combined-VOI methods. The measured performance difference was not exceedingly high between the combined-ROI and the combined

TABLE 4 | Classification result of AD vs. HC, MCIs vs. MCIc, AD vs. MCIs, AD vs. MCIc, HC vs. MCIc, and HC vs. MCIs groups using combined-(VOI + ROI) features, with both whole-brain and voxel-wise features (EasyMKL).

Groups	Features	Classifier	Performance measure						
			AUC	ACC	SEN	SPEC	PRE	F1-score	Cohen's kappa
AD vs. HC	Combined-ROI	EasyMKL	95.45	96.05	94.11	100	100	96.96	0.9066
	Combined-VOI		95.55	95.24	93.33	100	100	96.55	0.9014
	Combined (VOI + ROI)		**97.78**	**98.52**	**96.97**	**100**	**100**	**98.46**	**0.9456**
MCIs vs. MCIc	Combined-ROI	EasyMKL	94.33	94.74	**100**	90.91	90	94.74	0.8950
	Combined-VOI		94.9	93.57	92.86	**100**	**100**	96.3	0.8825
	Combined (VOI + ROI)		**96.94**	**95.08**	**100**	93.93	93.54	**96.66**	**0.9247**
AD vs. MCIs	Combined-ROI	EasyMKL	93.86	93.59	93.75	93.33	93.75	93.75	0.8562
	Combined-VOI		94.96	95.16	93.54	96.77	96.66	95.08	0.8869
	Combined (VOI + ROI)		**96.25**	**96.68**	**94.12**	**100**	**100**	**96.97**	**0.9011**
AD vs. MCIc	Combined-ROI	EasyMKL	94.05	94.89	100	94.77	91.67	95.65	0.8502
	Combined-VOI		**96.67**	**96.20**	**96.77**	**96.87**	96.77	**96.77**	**0.9145**
	Combined (VOI + ROI)		95.56	95.23	93.94	96.68	**96.88**	95.39	0.9044
HC vs. MCIc	Combined-ROI	EasyMKL	94.93	94.24	**100**	88.89	92.31	**96**	0.8814
	Combined-VOI		95.56	95.52	96.67	**94.59**	93.54	95.08	0.8977
	Combined (VOI + ROI)		**96.67**	**96.65**	97.29	93.75	**94.74**	95.99	**0.9237**
HC vs. MCIs	Combined-ROI	EasyMKL	95.6	95.55	**100**	90.90	91.66	95.65	0.8697
	Combined-VOI		94.67	94.43	94.59	96.67	97.22	95.89	0.8864
	Combined (VOI + ROI)		**96.59**	**96.97**	93.75	**100**	**100**	**96.78**	**0.9187**

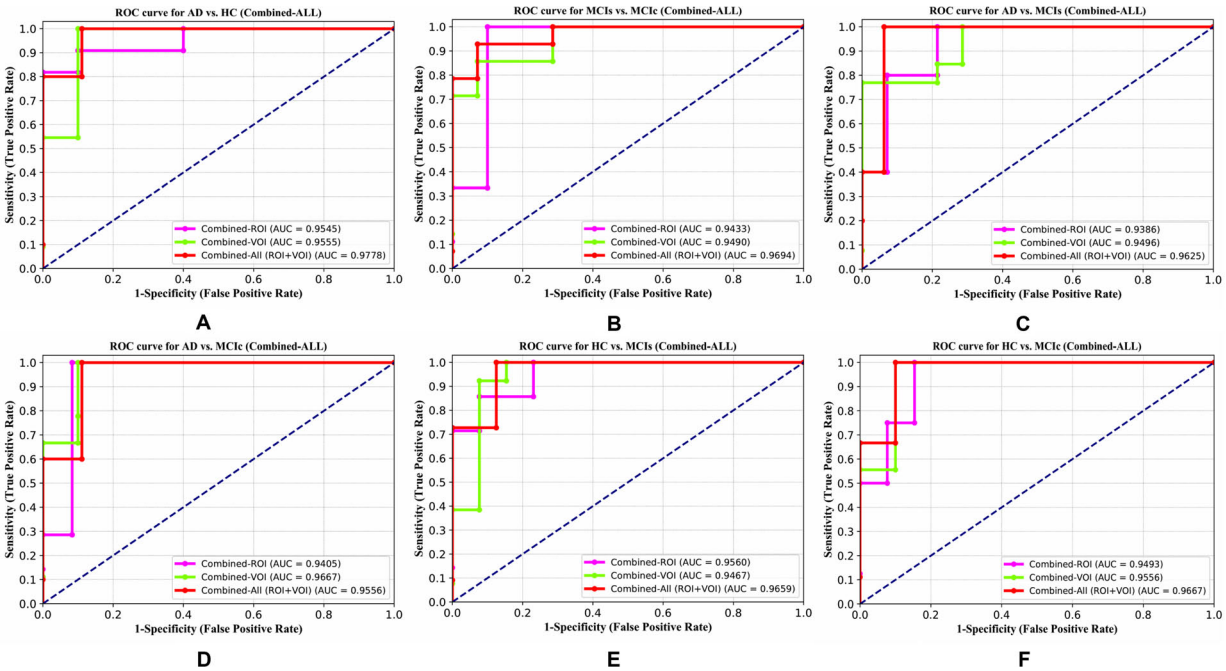

FIGURE 10 | ROC curve for **(A)** AD vs. HC, **(B)** MCIs vs. MCIc, **(C)** AD vs, MCIs, **(D)** AD vs, MCIc, **(E)** HC vs. MCIs, and **(F)** HC vs. MCIc using combined-(VOI + ROI). The red solid line shows the result of the combined-(VOI + ROI) curve, with combined-ROI and combined-VOI features.

(VOI + ROI) method (just 1%) for the AD vs. MCIc group. The obtained result using the RBF-SVM classifier can be found in **Supplementary Table S33**. From **Supplementary Table S33**, we can say that the combined-(VOI + ROI) features performed very well as compared with the combined-ROI and combined-VOI features for all six binary classification groups. **Table 4** and **Supplementary Table S33** clearly show the advantage of using combined-(VOI + ROI) features over those of combined-ROI and combined-VOI (see **Supplementary Table S33**).

Graph Network Construction and Analysis for All Six Classification Groups

For graph analysis or construction of a graph network, we used the BRAPH toolbox integrated into MATLAB 2019a. Additionally, we performed structural and functional graph theory for all six binary classification groups (AD vs. HC, MCIs vs. MCIc, AD vs. MCIc, AD vs. MCIs, HC vs. MCIc, and HC MCIs). Nodal measures were taken and comparisons were performed using the binary undirected graphs, and their measures were assessed over a set of network densities, which refers to the ratio between the number of connections in the network and the number of possible connections, ranging from 5–25% with a step size of 0.5%. Several graph metrics were calculated to quantify the nodal or global topological organization of the structural and functional networks, including local efficiency, characteristic path length, transitivity, and modularity. For all six binary classification groups, non-parametric permutation test samples with 1000 permutations each were conducted to assess the differences between the groups, which were significant for a two-tailed test of the null hypothesis at $p < 0.05$. The structural correlation matrices graph of AD, HC, MCIs, and MCIc of the sMRI subjects is shown in **Figure 11**. All groups showed strong correlations between bilaterally homologous regions. The plots in **Figures 12**, **13** and **Supplementary Figures S2–S5** show the lower and upper bounds (dark red spheres) of the 95% confidence intervals (CI) (dark gray shade) as a function of density. The blue, green, pink and purple spheres show the differences between sets and, when falling beyond the CI, indicate that the change was statistically significant at $p < 0.05$.

The small dark red dot in the middle with a value around zero specifies the mean value of the change in the global network measures between the randomized sets after the permutation tests.

We also compared the nodal degree for all six binary classification groups using all modalities. The FDR correction value was kept constant at 0.05 for all six binary classification groups. Regarding the global network topology shown for AD vs. HC in **Figure 12**, we found a longer characteristic path length using only FDG (which started at 0.15) than that with other neuroimaging modalities, and the path length was above the mean value of the difference. In the case of local efficiency, we found that the AV45 modality was the only one that started (at 0.05) above the mean value. Moreover, by comparing the modularity graph in the AD vs. HC group, we found that sMRI showed the greatest difference (modularity started at 0.14) of all modalities, and its network densities were almost constant until 25% (showing that the network topology is widely spread). The rs-fMRI modality performed very well for the transitivity

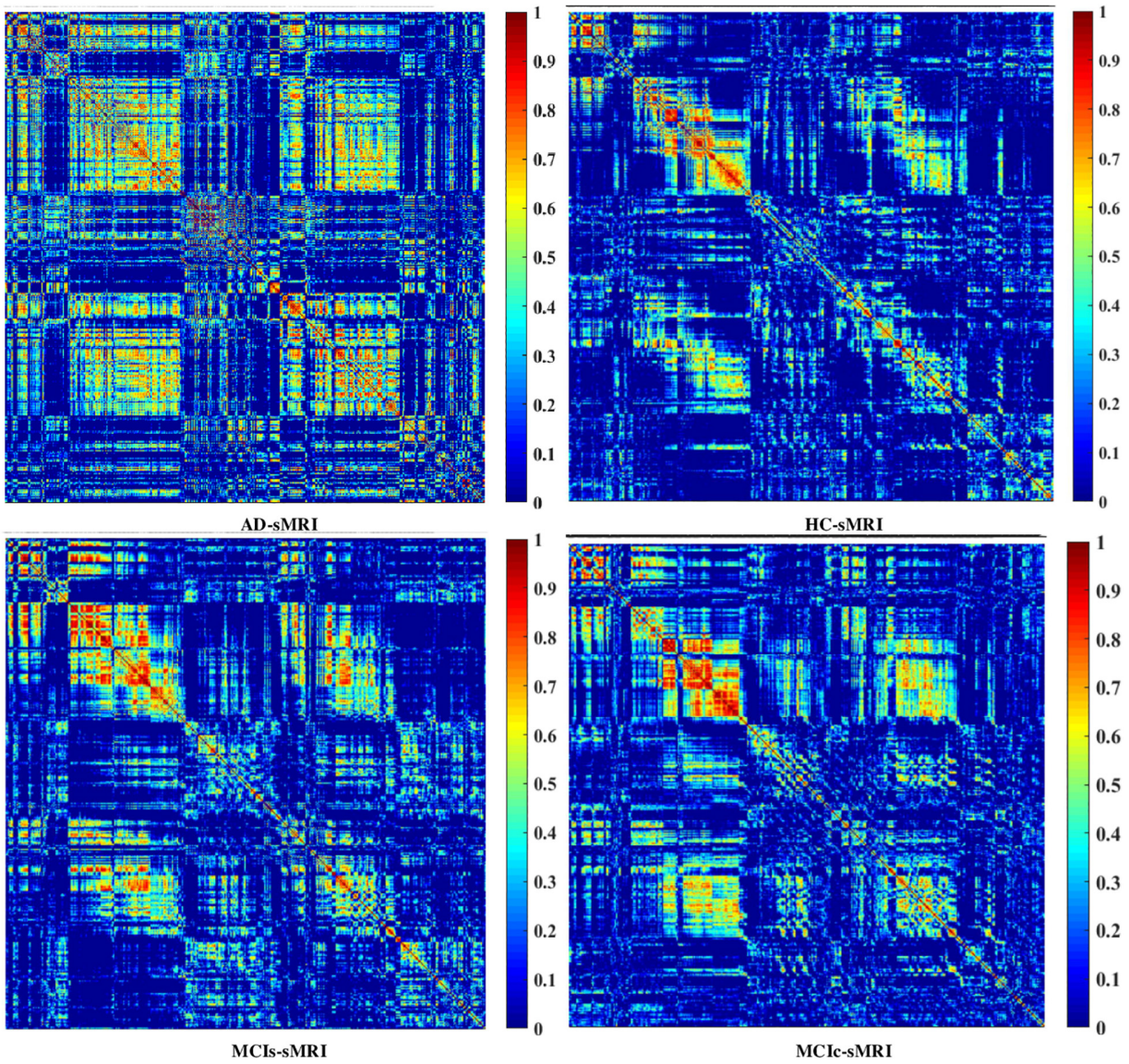

FIGURE 11 | Weighted correlation matrices graph (of 384 regions) for AD, HC, MCIs, and MCIc for sMRI biomarkers.

graph compared with the other modalities, starting from 0.06 and increasing to 25%, although it decreased in some network densities. Moreover, we also computed the regional or nodal network topology for the AD vs. HC group, which is shown in **Figures 14A,B**. **Figures 14A,B** show that the AV45 and FDG-PET modalities are the only one neuroimage that shows the numbers of significant region changes in a nodal network topology for the AD vs. HC group. The nodal degree showed significant increases in the right g-frontal-sup-1, left g-cuneus-2, left g-frontal-sup-3, left g-frontal-sup-1, left g-frontal-med-orb-1, and right s-precentral-3 regions. Likewise, for the MCIs vs. MCIc group, we found increases in the characteristic path length and local efficiency using FDG (in both cases, it started at 0.01, as shown in **Figure 13**). For the modularity, sMRI attained 5% network density, but after that, it decreased to 25%. At the same time, the modularity in DTI neuroimages increased in network density from 10 to 25%. Likewise, for transitivity, compared with other modalities that started below the mean value, the AV45 modality was the only modality that started from 0 (difference), and its network increased in every single network density.

This transitivity plot shows the most widespread topological changes for the MCIs vs. MCIc group. **Figures 14C,D** show that the AV45-FDG is the most important modality to show the numbers of significant region changes in the nodal topology of the MCIs vs. MCIc group. Left s-postcentral-2, right g-parietal-inf-1, left g-frontal-inf-tri, right g-lingual-2, right g-parahippocampus-5, left n-thalamus-6, left s-parietooccipital-4, left-lingual-3, and left g-cingulum-post-2 are the most

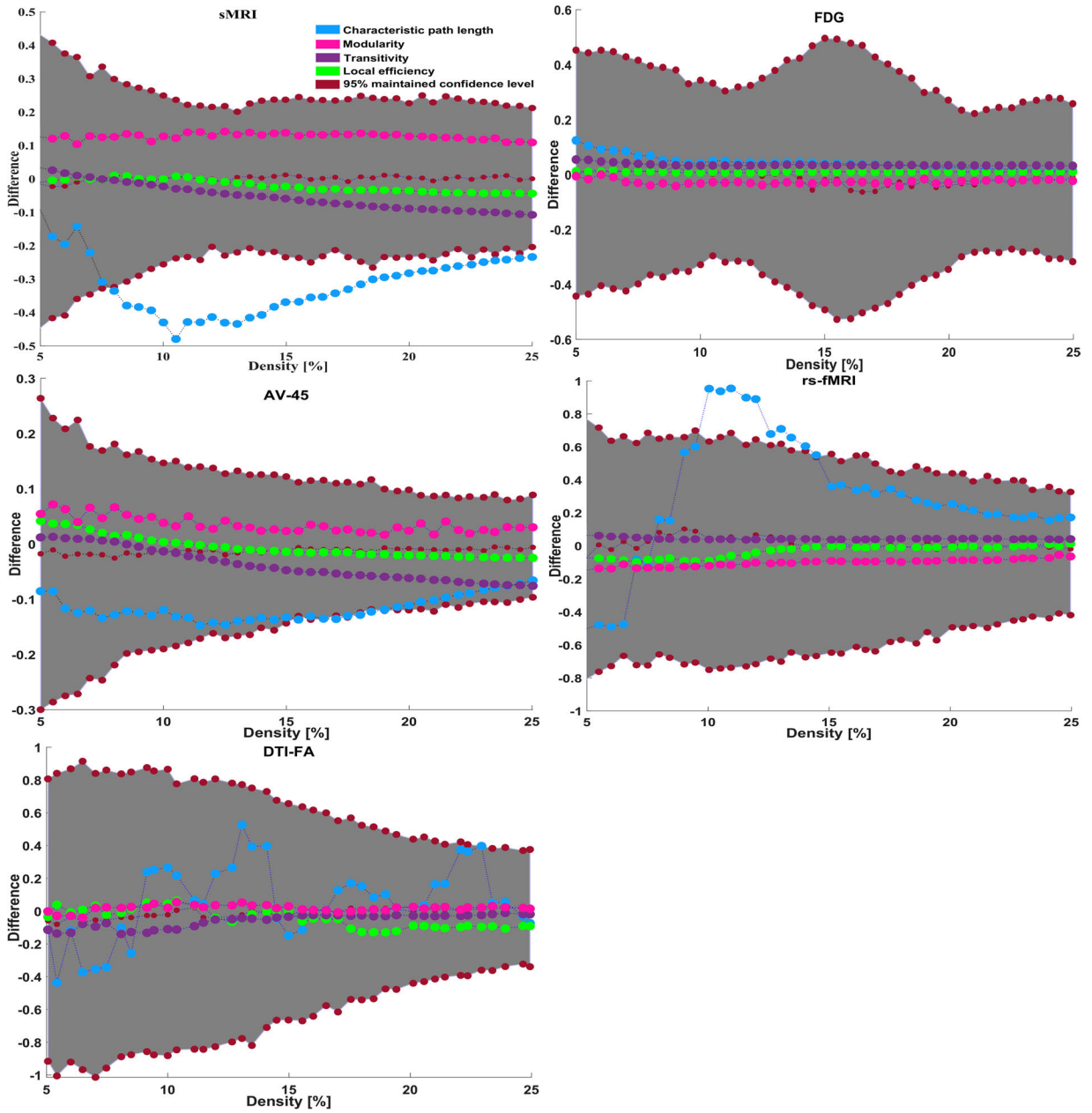

FIGURE 12 | Differences between the AD vs. HC group in global structural topology. The blue sphere represents characteristic path length, green sphere represents local efficiency, pink sphere represents modularity, purple sphere represents transitivity, and the dark red sphere represents 95% confidence intervals for these measures.

significant regions shown by the nodal degree for the MCIs vs. MCIc classification group. For the AD vs. MCIc classification group, the global network topology is shown in **Supplementary Figure S2**. The rs-fMRI is the only modality that shows an increment in the characteristic path length measure. It starts at 0.38 (difference), and lies inside the CI and above the mean value, but at 15–17% network density, some of its networks lie outside of the CI upper bound, and again from 18% density, its network lies inside the CI until 25% density is reached. We can also see that at around 13% network density, some of its networks are close to the mean value (which is shown by small dark red dots). It shows the most widespread topological changes for the AD vs. MCIc group. The FDG-PET modality shows an increase only for the local efficiency measure. Modularity and transitivity increase across almost all network densities for the sMRI and AV45-PET modality compared with

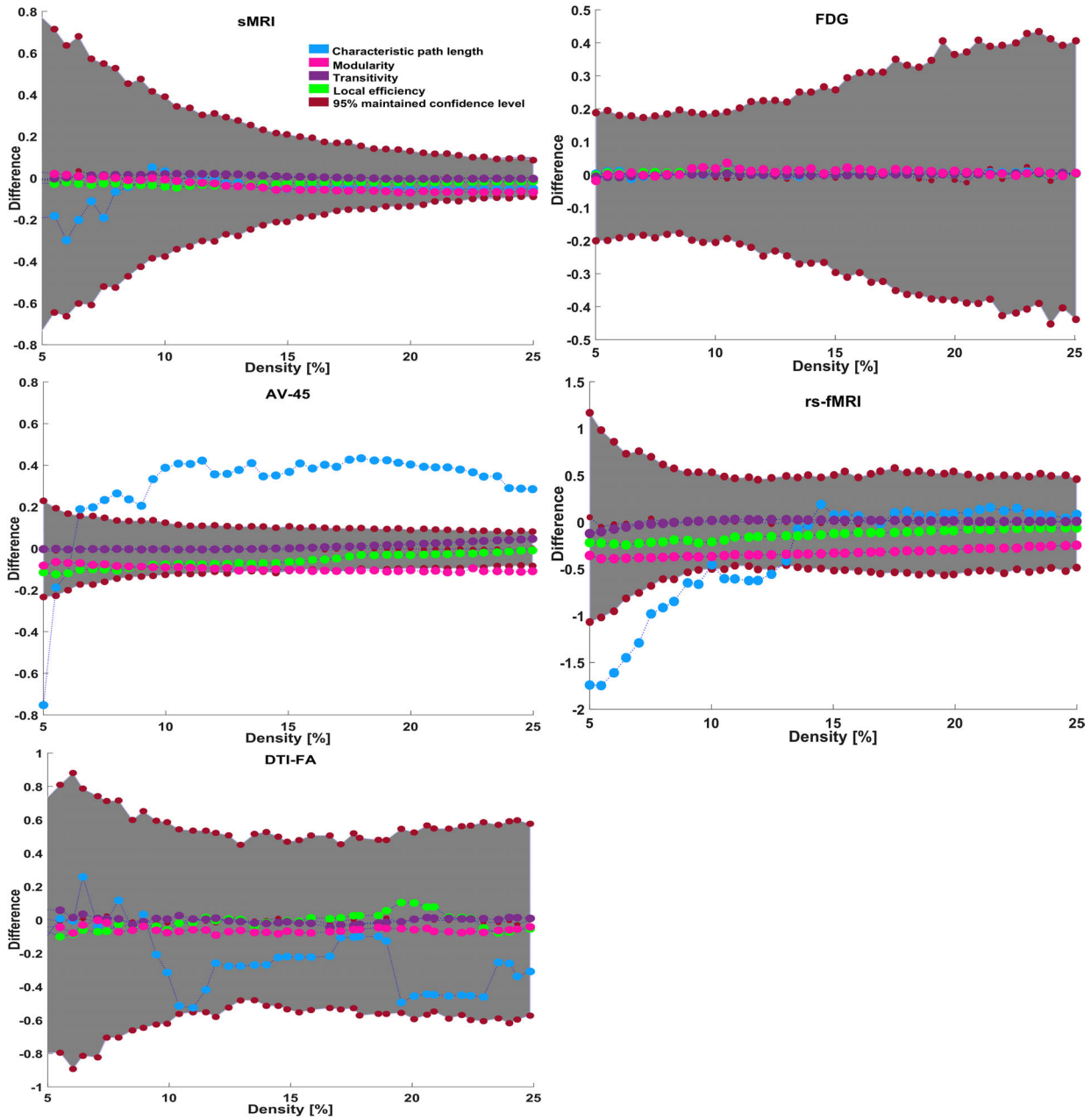

FIGURE 13 | Differences between the MCIs vs. MCIc group and global structural topology. The blue sphere represents characteristic path length, green sphere represents local efficiency, pink sphere represents modularity, purple sphere represents transitivity, and the dark red sphere represents 95% confidence intervals for these measures.

the other individual modalities. **Supplementary Figures S6a,b** show that AV45 and rs-fMRI modalities are the only one that shows the numbers of significant region changes in a nodal network topology for the AD vs. MCIc group. The nodal degree shows significant increases in the left g-lingual, (left/right) g-lingual-3, (left/right) occipital pole, right cerebellum, left n-caudate-5, right n-caudate-2, left n-thalamus-2, and left frontal pole regions (see **Supplementary Figures S2, S6**). Likewise, for the AD vs. MCIs group, the global network topology is shown in **Supplementary Figure S3**. The FDG-PET modality is the only one showing a characteristic path length that lies inside the CI and above the mean value. In comparing local efficiency measures in every modality, we found that the rs-fMRI modality was the only one neuroimage that lies above the mean value (which is plotted by small dark red), although every modality lies inside the CI. The modularity increased, and at the same time,

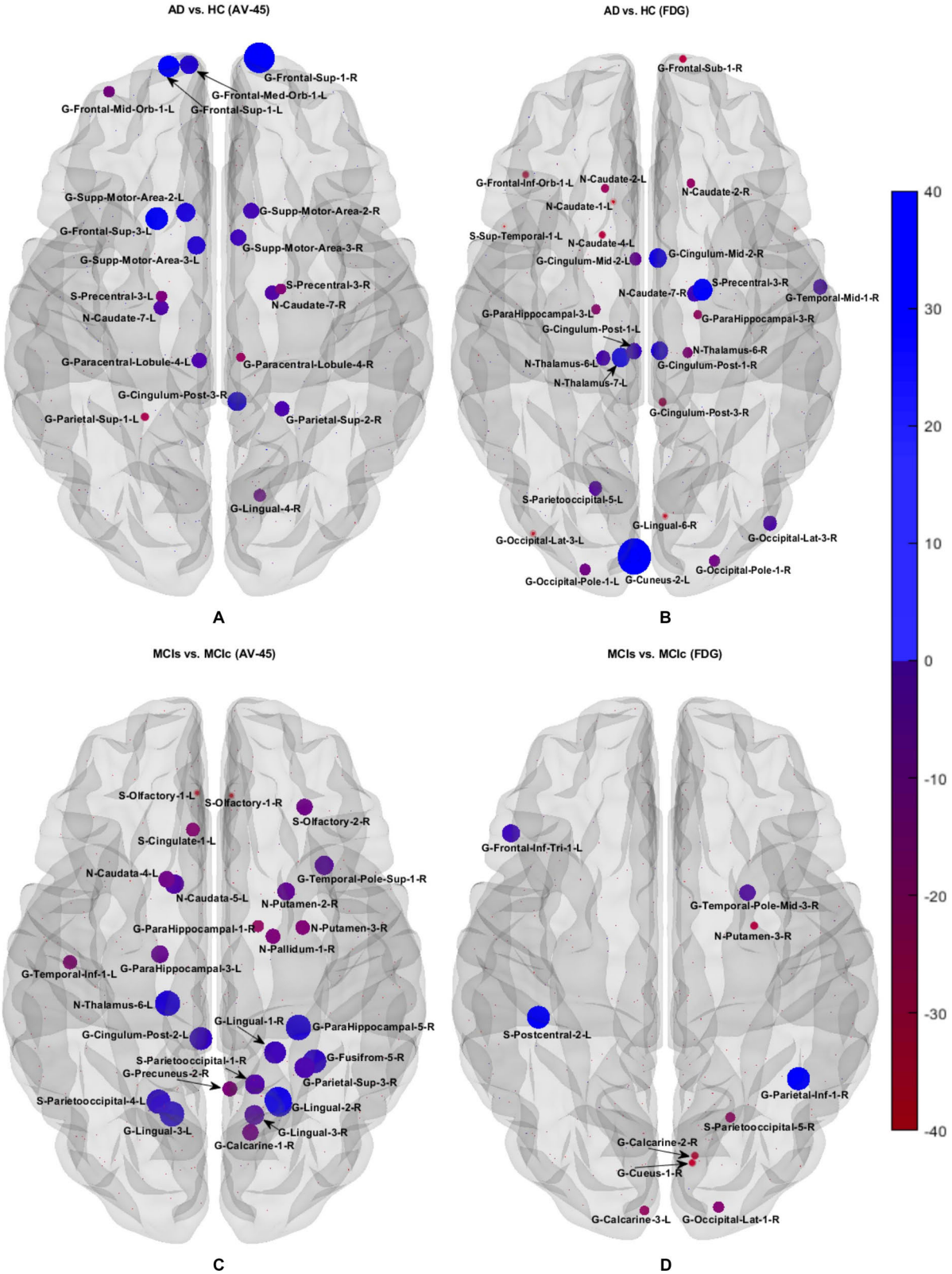

FIGURE 14 | Brain maps representing the most predictive regions for distinguishing between the AD vs. HC and MCIs vs. MCIs groups. Differences between groups in nodal measures. Nodes showing significant differences among groups in the nodal degree after FDR corrections. For both classification groups, AV45 and FDG show the most significantly affected regions. Dark blue shows the most significant region, whereas light red indicates the least significant region.

the transitivity decreased for the AD vs. MCIs group, as shown by the sMRI modality, but both plots lie inside the 95% CI. The right n-caudate-2, left g-insula-anterior-2, left g-frontal-mid-orb-1, left g-cuneus-2, right g-angular-3, right g-occipital-pole-1, right n-thalamus-6 were the most significant regions as shown by the nodal degree for the AD vs. MCIs classification group using FDG and sMRI images (**Supplementary Figures S3, S6c,d**). The global network topology is plotted in **Supplementary Figure S4** for the HC vs. MCIc classification group. From this plot we can see that the characteristic path length begins at 0.8 (difference) at a 5% density in the rs-fMRI modality (which is very high compared with other modalities). However, it suddenly begins to decrease at 8–13% density, and crosses lower bound (represented by a dark red sphere), and again later, it increases at 14% network density. The rs-fMRI modality is the only one neuroimage where the local efficiency, modularity, and transitivity lie above the mean values (small dark red sphere). Moreover, this plot lies in the middle of the 95% confidence interval. **Supplementary Figures S7a,b** show that the DTI-FA and rs-fMRI modalities are the only one neuroimage that show the numbers of significant region changes in the nodal network topology for the HC vs. MCIc group. The nodal degree shows significant increases in the right inferior-parietal-g, left superior occipital-g, right brainstem, right midbrain, left postcentral-g, left parahippocampal-g, left corticospinal tract, (left/right) posterior limb of the internal capsule, and the left uncinate fasciculus regions (see **Supplementary Figures S4, S7**). For the HC vs. MCIs classification group, the global network topology is shown in **Supplementary Figure S5**. In this case, characteristic path length using the sMRI modality is the only one that lies above the mean value. The local efficiency increases with both (sMRI and rs-fMRI) modalities, and their network lies above the mean value (which is represented by the small dark red sphere). The modularity plot shows that the rs-fMRI image is the only one in which there is an increment in the network density from 6 to 25%, whereas in the same image, the transitivity decreases from 6 to 25% density. However, both of these networks lie inside the CI. **Supplementary Figures S7c,d** show that the sMRI and FDG modalities are the only one neuroimage that shows the numbers of significant region changes in a nodal network topology for the HC vs. MCIs group. The nodal degree shows significant increases in the right g-cuneus-2, left g-occipital-sup-1, left g-Supp-motor-area-1, left n-Caudata-6, left n-thalamus-2, right n-thalamus-1, and the right temporal-pole-mid-3 regions (see **Supplementary Figures S5, S7**).

DISCUSSION

The present study outcomes provided insights into multimodal behavior for classifying all six binary classification groups, and it also showed which regions or single modality are most significant for future analysis for the discrimination of AD at a clinical level. Here, our proposed idea was to combine multiple neuroimaging modalities (sMRI, AV45, FDG, rs-fMRI, and DTI) with a genetic biomarker (APOE) for the classification of AD patients and other groups using whole-brain, voxel-wise, and graphical analysis methods. In this study, we utilized three different types of atlas (AICHA, pyClusterROI, and JHU-WM) to parcellate the sMRI/PET, rs-fMRI, and DTI neuroimages. Furthermore, to parcellate the sMRI and PET images, we employed the AICHA atlas, which is already segmented into 384 ROIs. Likewise, for rs-fMRI neuroimages, we applied pyClusterROI Python script with the Craddock atlas to parcellate the rs-fMRI images into 200 brain regions (because this is a well-known technique for parcellating fMRI images using a spatially constrained normalized-cut spectral clustering process). Moreover, we also knew that fMRI images are made up of a time series (ADNI rs-fMRI data is made up of 140 time series or time points), so to parcellate the brain using fMRI data, voxels with similar time points needed to be grouped to form a region. This is typically done using data-driven clustering methods, where each cluster constitutes one region. For this reason, we chose the pyClusterROI script for the rs-fMRI images. Moreover, for DTI images, we applied the JHU-WM (ICBM-DTI-81) label atlas, which was already segmented into 50 brain regions (these 50 WM tract labels were created by the hand segmentation of a standard-space average of the diffusion MRI tensor maps from 81 subjects). In this study, we selected different atlases for the different modalities of neuroimages because of their advantages, and also for the extraction of higher brain ROIs for that particular modality of neuroimage. After the completion of feature extraction from each method, we sent these low-dimensional extracted features through a polynomial kernel function to map them onto a high-dimensional feature. Afterward, we fused all six high-dimensional features into one form before further analysis. Later, we passed these unimodal and multimodal features through the EasyMKL classifier for classification and reported the average accuracy for each method. This procedure is widely used for comparing the performance of machine learning approaches. Although previous studies have already applied the multimodal method for the classification of AD (Zhang et al., 2011; Young et al., 2013; Liu et al., 2014; Ritter et al., 2015; Schouten et al., 2016; Hojjati et al., 2018; Gupta et al., 2019a) with other groups, this study was the first to combine five different types of neuroimage modalities with two APOE genotype scores for the classification of all six binary classification groups (AD vs. HC, MCIs vs. MCIc, AD vs. MCIc, AD vs. MCIs, HC vs. MCIc, and HC vs. MCIs). Our proposed method clearly showed an improvement using multimodal features in terms of performance over the unimodal features for classifying these six binary groups compared with the latest published results. Furthermore, in this study, we also adopted graph-theoretical strategies (in a global and nodal network topology) to study the plots of the six binary groups (characteristic path length, local efficiency, modularity, and transitivity), and to find the most significant regions where these groups differed from each other.

Influence of the Different Types of Neuroimage Modality

We compared the Cohen's kappa score obtained for each modality using both ROI and VOI features. The score was calculated for each of the six classification groups. The Cohen's kappa outcomes, displayed in **Figure 5**, were computed using

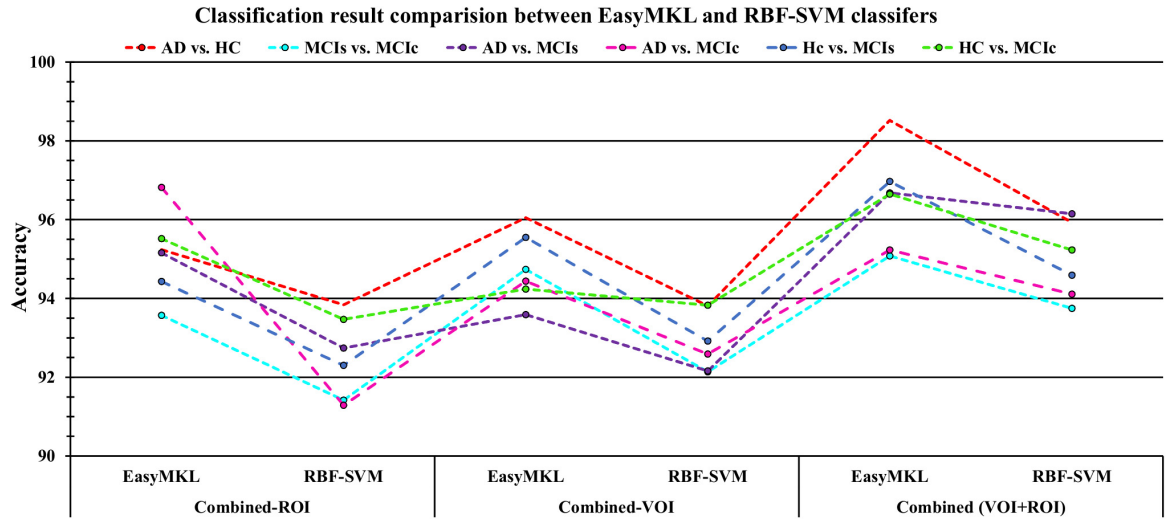

FIGURE 15 | Comparison of EasyMKL classifier results with RBF-SVM classifier results based on obtained accuracy score. In the above figure, we can see that the combined-ROI, combined-VOI, and combined-(VOI + ROI) result obtained by EasyMKL classifier outperformed the results [combined-ROI, combined-VOI, and combined-(VOI + ROI)] obtained by the RBF-SVM classifier for all six classification groups.

ROI-based features. Likewise, the Cohen's kappa outcomes displayed in **Figure 6** were computed using VOI-based features. The results displayed in **Figures 5**, **6** clearly show that the DTI-FA modality biomarker achieved a high level of agreement between groups while classifying the six binary classification groups compared with the other five biomarkers. Furthermore, we can say that VOI-based DTI-FA (lies above 0.8–0.87) feature performed slightly better than the ROI-based DTI-FA (lies above 0.75–0.84) feature.

Influence of the Type of Features (ROI and VOI)

We compared the Cohen's kappa score obtained for the regional (ROI) features with the reference atlases (AICHA, Craddock, and JHU-WM) to the ones obtained for the voxel (VOI) features (SPM12, DPARSF, TBSS) for five different types of neuroimages using the EasyMKL classifier. The score was evaluated for the same six binary classification groups. The Cohen's kappa outcomes displayed in **Figure 5** are for an ROI-based analysis, and likewise, the Cohen's kappa outcomes displayed in **Figure 6** are for a VOI-based analysis. The results, displayed in **Figures 5**, **6**, do not show notable differences in the Cohen's kappa scores obtained using regional or voxel features; both features performed very well and achieved a high level of agreement between each other for all six binary classification groups.

Influence of the Classification Method

We compared the result obtained by the EasyMKL classifier with that of the RBF-SVM classifier. **Tables 2–4** and **Supplementary Tables S31–S33** show the obtained classification result for all six binary groups using the EasyMKL and RBF-SVM classifiers. Likewise, **Figure 15** shows the plot where we compared the accuracy obtained for all six binary classification tasks using the EasyMKL and RBF-SVM classifiers. The result displayed in **Figure 15** shows that the EasyMKL classifier achieved high classification accuracy for all six binary groups compared with RBF-SVM. It also suggests that EasyMKL optimized a simple quadratic problem addressed by SVM in a more efficient way (see **Supplementary Tables S31–S33**).

Most Significant Brain Regions Where Each Group Differs From the Others

Table 5 shows the obtained most important brain regions for each binary classification group, using voxel-wise and graphical methods. For the AD vs. HC group, using VOI analysis, we found that (L) Thalamus, (L) Occipital Inferior, (R) Fusiform, (R) Temporal Inferior, (R) Temporal Mid, (R) Temporal Inferior, and (L) Sagittal stratum were the brain regions where the AD group differs from the HC group. Likewise, using graphical analysis, we found that (L) G-Cuneus-2, and (R) G-Frontal-Superior-1 were the brain regions where the AD group differs from the HC group. Furthermore, for the MCIs vs. MCIc group, using VOI analysis, we found that (L) Precuneus Vermis_9, (L) Frontal Superior Medial, (L) Pallidum, (R) Lingual, (L) Frontal Mid, (R) External capsule were the brain regions where the MCIs group differs from the MCIc group. Likewise, after applying graphical analysis, we found that the (R) G-Parietal Inferior-1, and (R) G-Lingual-2 were the brain regions where the MCIs group differs from the MCIc group. For the AD vs. MCIs group, using the VOI method, our study found that the (L/R) Frontal Inferior Triangular, (R) Temporal Superior, (R) Frontal Inferior Orbital, (R) Thalamus, (R) Hippocampus, and (R) Anterior thalamic radiation were the brain regions where the AD group differs from the MCIs group. Moreover, after applying the graphical method, we found that the (R) N-Caudate-2 and (L) G-Cuneus-2 were the brain regions

TABLE 5 | Most significant brain regions found for all six binary classification groups using voxel-wise and graphical analysis.

Groups	Modality	Found to be the most significant brain region by applying VOI analysis	Modality	Found to be the most significant brain region by applying graphical analysis
AD vs. HC	sMRI	(L) Thalamus		
	FDG-PET	(L) Occipital Inferior		
	AV45-PET	(R) Fusiform		
	rs-fMRI-ALFF	(R) Temporal Inferior	FDG-PET	(L) G-Cuneus-2
	rs-fMRI-fALFF	(R) Temporal Mid	AV45-PET	(R) G-Frontal-Superior-1
	rs-fMRI-REHO	(R) Temporal Inferior		
	DTI-FA	(L) Sagittal stratum		
MCIs vs. MCIc	sMRI	(L) Precuneus		
	FDG-PET	Vermis_9	FDG-PET	(R) G-Parietal Inferior-1
	AV45-PET	(L) Frontal superior Medial	AV45-PET	(R) G-Lingual-2
	rs-fMRI-ALFF	(L) Pallidum		
	rs-fMRI-fALFF	(R) Lingual		
	rs-fMRI-REHO	(L) Frontal Mid		
	DTI-FA	(R) External capsule		
AD vs. MCIs	sMRI	(R) Frontal Inferior Triangular	sMRI	(R) N-Caudate-2
	FDG-PET	(L) Frontal Inferior Triangular	FDG-PET	(L) G-Cuneus-2
	AV45-PET	(R) Temporal Superior		
	rs-fMRI-ALFF	(R) Frontal Inferior Orbital		
	rs-fMRI-fALFF	(R) Thalamus		
	rs-fMRI-REHO	(R) Hippocampus		
	DTI-FA	(R) Anterior thalamic radiation		
AD vs. MCIc	sMRI	(R) Frontal Middle Orbital		
	FDG-PET	(R) Occipital Middle		
	AV45-PET	(R) Precentral	AV45-PET	(L) N-Caudate-5
	rs-fMRI-ALFF	(L) Fusiform	rs-fMRI	(L) G-Lingual
	rs-fMRI-fALFF	(L) Occipital Middle		
	rs-fMRI-REHO	(L) Cingulum Posterior		
	DTI-FA	(R) Posterior corona radiata		
HC vs. MCIs	sMRI	(R) Precentral	sMRI	(L) N-Caudate-6
	FDG-PET	(L) Precentral	FDG-PET	(L) G-Occipital Superior-1
	AV45-PET	(L) Cerebellum_9		
	rs-fMRI-ALFF	(L) Precentral		
	rs-fMRI-fALFF	(L) Parietal Inferior		
	rs-fMRI-REHO	(L) Putamen		
	DTI-FA	(L) Superior longitudinal fasciculus		
HC vs. MCIc	sMRI	(L) Lingual		
	FDG-PET	(L) Occipital Superior		
	AV45-PET	(R) Frontal Inferior Opercular		
	rs-fMRI-ALFF	(L) Frontal Inferior Orbital	rs-fMRI	(R) G-Parietal Inferior
	rs-fMRI-fALFF	(R) Frontal Superior Orbital	DTI-FA	(L) Corticospinal tract
	rs-fMRI-REHO	(L) Lingual		
	DTI-FA	(L) Superior corona radiata		

where the AD differs from the MCIs the most. Furthermore, for the AD vs. MCIc group, we found using VOI analysis that the (R) Frontal Middle orbital, (R) Occipital Middle, (R) Precentral, (L) Fusiform, (L) Occipital Middle, (L) Cingulum Posterior, and (R) Posterior corona radiata were the brain regions where the AD group differs from the MCIc group. Likewise, after applying graphical analysis, we found that the (L) N-Caudate-5 and (L) G-Lingual were the brain regions where the AD group differs from the MCIc group. For the HC vs. MCIs group, using the VOI method, our study found that the (R/L) Precentral, (L) Cerebelum_9, (L) Parietal Inferior, (L) Putamen, and (L) Superior longitudinal fasciculus were the brain regions where the HC group differs from the MCIs group. Moreover, after applying the graphical method, we found that the (L) N-Caudate-6 and (L) G-Occipital Superior-1 were the brain regions where the HC differs from the MCIs the most. Likewise, for the HC vs. MCIc group, using the VOI method, we found that the (L) Lingual, (L) Occipital Superior, (R) Frontal Inferior Opercular, (L) Frontal

Inferior Orbital, (R) Frontal Superior Orbital, (L) Lingual, and (L) Superior corona radiata were the brain regions where the HC group differs from the MCIc group the most. Moreover, using graph-based analysis, we found that the (R) G-Parietal Inferior and (L) Corticospinal tract were the brain regions where the HC group differs from the MCIc group the most. It is interesting to note that most of the affected brain regions lies in the left hemisphere rather than the right hemisphere.

Exploring the Improvement in Performance Using Multimodal Features Compared With Unimodal Features

In this study, we applied two different types of methods for the classification of AD with another group. In the first method, we used the whole-brain parcelation approach to segment the brain images according to the atlas using some toolbox (see section "Three Feature Extraction Processes") and later, after the completion of the data pre-processing step, we sent these features through the MKL algorithm to classify AD and the other groups. To verify the efficiency of this proposed method, we calculated the performance of each classification group using both unimodal and combined-ROI (or multimodal) features. **Table 2** shows the obtained classification results for all six binary classification groups using whole-brain analysis features. From **Table 2**, we can say that the combined features (combined-ROI) performed very well compared with the single-modality features in every classification problem. Their obtained Cohen's kappa values were close to 1, which indicates that our proposed method achieved a good level of agreement between groups while classifying each set. **Table 2** further shows that the DTI-FA unimodal features attained high classification performance for every classification group except for the HC vs. MCIc group (where rs-fMRI features achieved better performance than DTI-FA features) in comparison with the performance of other individual modalities. This result demonstrates that the DTI-FA image can be used as a notable biomarker when investigating AD, and therefore should be included in clinical research.

Likewise, in the second step, we utilized the voxel-wise approach for the extraction of features from sMRI, FDG, AV45-PET, rs-fMRI, and DTI images using some toolbox (see section "Three Feature Extraction Processes") and later, after the completion of data pre-processing step, we sent these features through the MKL classifier to classify AD with the other groups. To check the efficiency of this proposed method, we calculated the performance of each classification group using both unimodal and combined-VOI (or multimodal) features. **Table 3** shows the obtained classification results for all six binary classification groups using voxel-wise analysis features. From **Table 3**, we can say that our proposed approach (to combine all unimodal features into one before passing them through the MKL classifier) gained a high level of performance and agreement compared with the unimodal results for every classification group. **Table 3** further suggests that AV45-PET, rs-fMRI (ALFF, REHO), and DTI-FA individual features performed very well compared with sMRI, APOE, and FDG-PET individual modalities. It is interesting to note that the DTI-FA modality performed well for both whole-brain and voxel-wise analysis methods.

Tables 2, **3** satisfied our hypothesis by showing that classification performance increased by 2–4% in every classification group after we passed concatenated features (combined-ROI and combined-VOI) through the MKL classifier. Moreover, the obtained result demonstrates that the multimodal method is more powerful than the unimodal system, and the obtained outcomes also indicate that every single biomarker has some important information, so it is better to combine the complementary information together for the classification of AD. Furthermore, we also examined the performance of every six classification groups by concatenating both ROI and VOI features into a single form. **Table 4** shows the obtained results for all six binary classification groups using combined (VOI + ROI) features. From **Table 4**, we can say that after applying combined (VOI + ROI) features, the classification performance increased slightly for every classification group except the AD vs. MCIc group (where combined-VOI dominated the combined-ROI and combined (VOI + ROI) methods in terms of performance). Their obtained Cohen's kappa values were close to 1, which indicates that our proposed scheme achieved a good level of agreement between groups while classifying each set. **Supplementary Tables S1–S30** show the most significantly affected regions for all six binary classification groups measured by the sMRI, FDG-PET, AV45-PET, rs-fMRI, and DTI-FA modalities of neuroimage.

It is interesting to note that the (left/right) precentral region was found in every classification group when extracting the most significant voxel region. This finding suggests that, in the coming days, the precentral region can also be used as an important biomarker for the classification of AD and other groups.

Global and Nodal Network Topology Result Analysis

We studied the global and nodal network topology for all six binary classification groups using graph theory. We calculated characteristic path length, local efficiency, modularity, and transitivity for every classification group, which can be seen in **Figures 12**, **13** and **Supplementary Figures S2–S5**. In the global network topology analysis, our study found that in general, FDG, sMRI, and rs-fMRI were the modalities where characteristic path length increased efficiently compared with the other modalities. Likewise, for local efficiency, AV45, FDG-PET, rs-fMRI, and sMRI were the modalities where it increased compared with the remaining modalities. It is interesting to note that modularity increased in every classification group using sMRI neuroimages, except for the HC vs. MCIs group (where modularity increased efficiently by utilizing rs-fMRI images instead of sMRI images). Furthermore, in general, rs-fMRI, AV45-PET, and sMRI were the modalities where transitivity increased and decreased frequently. These changes symbolize that the regions of their networks communicated (more or less) efficiently within other brain regions. The increments in modularity (suggesting that their modules should have higher within-module connectivity and poor inter-module connectivity, or vice-versa) and increment or decrement of transitivity graph (suggesting that the regions of their network were connected very well to neighboring areas, or vice-versa). In the nodal network topology analysis, our study

found that every neuroimage was important to finding the most significant region where the six binary classification groups differ from each other; the found regions can be seen in **Figure 14** and **Supplementary Figures S6, S7**. The most significant regions were right g-frontal-sup-1, right s-precentral-3, left g-frontal-inf-tri, (left/right) n-thalamus-6, left s-parietooccipital-4, left g-cingulum-post-2, (left/right) occipital pole, left n-thalamus-2, left g-insula-anterior-2, (left/right) g-cuneus-2, left corticospinal tract, left n-Caudata-6, right temporal-pole-mid-3, left lingual-g, right fusiform, left g-precuneus-8, right n-Caudata-2, and (left/right) g-parahippocampal-4.

Recently, several studies have investigated neuroimaging techniques for the discrimination of AD, with the main focus on MCI subjects, who may or may not convert to AD, and separating patients with AD from healthy controls. However, it is difficult to make direct comparisons with these state-of-the-art methods because most of the studies used different validation methods and datasets, which both influence the classification performance. The first study by Cui et al. (2011) obtained an AUC of 79.6% for the classification of MCIs vs. MCIc groups. The authors used multimodal features (NM: neuropsychological and functional measures, CSF, and sMRI) for the classification. Young et al. (2013) used a Gaussian process method with SVM for the classification of MCIs vs. MCIc with three modalities (MRI, PET, and APOE). They reported an accuracy of 69.9% for classifying MCIs vs. MCIc groups. In another study, domain transfer learning was introduced using multimodal data (i.e., MRI, CSF, and FDG) with an accuracy of 79.4% for MCIs vs. MCIc with an AUC of 84.8% (Cheng et al., 2015). In another study by Xu et al. (2016), the authors used three different imaging modalities (sMRI, FDG, and AV45) for the discrimination of the conversion of MCIs subjects to MCIc patients. The authors used a weighted multi-modality sparse representation-based classification (wmSRC) classifier for classification. Their method achieved an ACC of 82.5% for classifying MCIs vs. MCIc with a sensitive biomarker selected using different numbers (from 1 to 90) of ranked features from each modality. Liu et al. (2017) proposed an algorithm that combines two imaging modalities of independent component study and the Cox model for discrimination of MCI progression. Their method achieved 80.8% of AUC with 73.5% of accuracy when classifying MCIs vs. MCIc. Hojjati et al. (2017) used a subset of optimal features in an SVM classifier for the discrimination of the conversion of MCIs to MCIc subjects. Their proposed method with multivariate minimal redundancy maximal relevance feature selection achieved 94.9% AUC and 91.4% ACC. In another study, Pan et al. (2019b) used an ensemble classification with a feature ranking method for the classification of MCIs vs. MCIc. Their proposed method achieved 75.38% AUC and 80.70% ACC for classifying this group. Gupta et al. (2019a) used a multimodal feature (sMRI, FDG, CSF, and APOE) for the discrimination of the conversion from MCIs to MCIc. They used the NiftyReg toolbox for the extraction of 246 ROIs from each imaging modality and applied a kernel-based SVM for the classification of MCIs vs. MCIc. Their method achieved an AUC of 93.59% for classifying these groups. **Table 6** shows the comparison result for MCIs vs. MCIc classification. Our proposed multimodal method [combined-(ROI + VOI)] outperforms the latest published state-of-the-art methods in terms of AUC and ACC for MCIs vs. MCIc. The proposed method achieved 96.94% AUC and 95.08% ACC for classifying the MCIs vs. MCIc group.

TABLE 6 | Performance comparison for MCIs vs. MCIc classification group.

Method	Modality	Total sample size	AUC	ACC
Cui et al., 2011	NM + CSF + sMRI	143	79.6	67.13
Young et al., 2013	sMRI + FDG + APOE	143	79.5	69.9
Cheng et al., 2015	MRI + FDG + CSF	99	84.8	79.4
Xu et al., 2016	sMRI + AV45 + FDG	110	-	82.5
Liu et al., 2017	sMRI + FDG	234	80.8	73.5
Hojjati et al., 2017	rs-fMRI	80	94.9	91.4
Pan et al., 2019b	FDG	248	80.70	75.38
Gupta et al., 2019a	APOE + sMRI + FDG + CSF	82	93.59	94.86
Combined-(ROI + VOI)	sMRI + FDG + AV45 + rs-fMRI + DTI + APOE	61	**96.94**	**95.08**

CONCLUSION

The novelty of the present study is that we combined five neuroimaging modalities (sMRI, FDG-PET, AV45-PET, rs-fMRI, and DTI) with the APOE genotype score for the discrimination between AD and other groups. Furthermore, we employed three different approaches [whole-brain (ROI), voxel-wise (VOI), and graph-based] on six binary classification groups to analyze each method performance independently. The combined-(ROI + VOI) feature performance outperformed the combined-ROI and combined-VOI features for all classification groups except the AD vs. MCIc group (where combined-VOI performed well). When the performance of each imaging modality in brain graph analysis was compared for all six binary classification sets, we found that FDG-PET, AV45-PET, and rs-fMRI were the only three modalities that revealed the most affected brain regions for all six classification groups. These highlighted central brain regions are an early indicator of developing dementia in healthy subjects.

DATA AVAILABILITY STATEMENT

The datasets used in this study were acquired from the ADNI homepage, which is available freely for all researcher and scientist for experiments on Alzheimer's disease and can be easily downloaded from ADNI websites: http://adni.loni.usc.edu/about/contact-us/. Furthermore, all datasets presented in this study are included in the article/**Supplementary Material**.

ETHICS STATEMENT

As per ADNI protocols, all procedures performed in studies involving human participants were in accordance with the ethical standards of the institutional and/or national research committee

and with the 1964 Helsinki declaration and its later amendments or comparable ethical standards. More details can be found at adni.loni.usc.edu. (This article does not contain any studies with human participants performed by any of the authors).

AUTHOR CONTRIBUTIONS

YG and J-IK designed the study and collected the original imagining data from the ADNI homepage. YG wrote the manuscript and did the coding section. J-IK and G-RK analyzed the imaging dataset. YG and BK analyzed the obtained results. All authors contributed and approved the final manuscript.

FUNDING

This work was supported by the National Research Foundation of Korea Grant funded by the Korean Government (NRF-2019R1F1A1060166 and NRF-2019R1A4A1029769).

ACKNOWLEDGMENTS

Data collection and sharing for this project was funded by the Alzheimer's Disease Neuroimaging Initiative (ADNI) (National Institutes of Health Grant U01AG024904) and DOD ADNI (Department of Defense award number W81XWH-12-2-0012). As such, the investigators within the ADNI contributed to the design and implementation of ADNI and/or provided data but did not participate in analysis or writing of this report. A complete listing of ADNI investigators can be found at: http://adni.loni.usc.edu/wp-content/uploads/how_to_apply/ADNI_Acknowledgement_List.pdf. ADNI is funded by the National Institute on Aging, the National Institute of Biomedical Imaging and Bioengineering, and through generous contributions from the following: AbbVie, Alzheimer's Association; Alzheimer's Drug Discovery Foundation; Araclon Biotech; BioClinica, Inc.; Biogen; Bristol-Myers Squibb Company; CereSpir, Inc.; Cogstate; Eisai Inc.; Elan Pharmaceuticals, Inc.; Eli Lilly and Company; EuroImmun; F. Hoffmann-La Roche Ltd. and its affiliated company Genentech, Inc.; Fujirebio; GE Healthcare; IXICO Ltd.; Janssen Alzheimer Immunotherapy Research & Development, LLC; Johnson & Johnson Pharmaceutical Research & Development LLC; Lumosity; Lundbeck; Merck & Co., Inc.; Meso Scale Diagnostics, LLC; NeuroRx Research; Neurotrack Technologies; Novartis Pharmaceuticals Corporation; Pfizer Inc.; Piramal Imaging; Servier; Takeda Pharmaceutical Company; and Transition Therapeutics. The Canadian Institutes of Health Research is providing funds to support ADNI clinical sites in Canada. Private sector contributions are facilitated by the Foundation for the National Institutes of Health (www.fnih.org). The grantee organization is the Northern California Institute for Research and Education, and the study is coordinated by the Alzheimer's Therapeutic Research Institute at the University of Southern California. ADNI data are disseminated by the Laboratory for Neuro Imaging at the University of Southern California.

SUPPLEMENTARY MATERIAL

The Supplementary Material for this article can be found online at: https://www.frontiersin.org/articles/10.3389/fnagi.2020.00238/full#supplementary-material

REFERENCES

Acosta-Cabronero, J., and Nestor, P. J. (2014). Diffusion tensor imaging in Alzheimer's disease: insights into the limbic-diencephalic network and methodological considerations. *Front. Aging Neurosci.* 6:266. doi: 10.3389/fnagi.2014.00266

Aiolli, F., and Donini, M. (2015). EasyMKL: a scalable multiple kernel learning algorithm. *Neurocomputing* 169, 215–224. doi: 10.1016/j.neucom.2014.11.078

Albert, M. S. (2011). Changes in cognition. *Neurobiol. Aging* 32, S58–S63. doi: 10.1016/j.neurobiolaging.2011.09.010

Angelucci, F., Spalletta, G., di Iulio, F., Ciaramella, A., Salani, F., Varsi, A. E., et al. (2010). Alzheimer's Disease (AD) and mild cognitive impairment (MCI) patients are characterized by increased BDNF serum levels. *Curr. Alzheimer Res.* 7, 15–20. doi: 10.2174/156720510790274473

Ashburner, J., and Friston, K. J. (2001). Why voxel-based morphometry should be used. *Neuroimage* 14, 1238–1243. doi: 10.1006/nimg.2001.0961

Bi, X., Jiang, Q., Sun, Q., Shu, Q., and Liu, Y. (2018). Analysis of Alzheimer's disease based on the random neural network cluster in fMRI. *Front. Neuroinform.* 12:60. doi: 10.3389/fninf.2018.00060

Bishop, N. A., Lu, T., and Yankner, B. A. (2010). Neural mechanisms of ageing and cognitive decline. *Nature* 464, 529–535. doi: 10.1038/nature08983

Bloudek, L. M., Spackman, D. E., Blankenburg, M., and Sullivan, S. D. (2011). Review and meta-analysis of biomarkers and diagnostic imaging in Alzheimer's disease. *JAD* 26, 627–645. doi: 10.3233/JAD-2011-110458

Brainerd, C. J., Reyna, V. F., Petersen, R. C., Smith, G. E., Kenney, A. E., Gross, C. J., et al. (2013). The apolipoprotein E genotype predicts longitudinal transitions to mild cognitive impairment but not to Alzheimer's dementia: findings from a nationally representative study. *Neuropsychology* 27, 86–94. doi: 10.1037/a0030855

Camus, V., Payoux, P., Barré, L., Desgranges, B., Voisin, T., Tauber, C., et al. (2012). Using PET with 18F-AV-45 (florbetapir) to quantify brain amyloid load in a clinical environment. *Eur. J. Nucl. Med. Mol. Imaging* 39, 621–631. doi: 10.1007/s00259-011-2021-8

Chao-Gan, Y., and Yu-Feng, Z. (2010). DPARSF: a MATLAB toolbox for "pipeline" data analysis of resting-state fMRI. *Front. Syst. Neurosci.* 4:13. doi: 10.3389/fnsys.2010.00013

Chen, H.-J., Gao, Y.-Q., Che, C.-H., Lin, H., and Ruan, X.-L. (2018). Diffusion tensor imaging with tract-based spatial statistics reveals white matter abnormalities in patients with vascular cognitive impairment. *Front. Neuroanat.* 12:53. doi: 10.3389/fnana.2018.00053

Cheng, B., Liu, M., Zhang, D., Munsell, B. C., and Shen, D. (2015). Domain transfer learning for MCI conversion prediction. *IEEE Trans. Biomed. Eng.* 62, 1805–1817. doi: 10.1109/TBME.2015.2404809

Clem, M. A., Holliday, R. P., Pandya, S., Hynan, L. S., Lacritz, L. H., and Woon, F. L. (2017). Predictors that a diagnosis of mild cognitive impairment will remain stable 3 years later. *Cogn. Behav. Neurol.* 30, 8–15. doi: 10.1097/WNN.0000000000000119

Cohen, J. (1960). A coefficient of agreement for nominal scales. *Educ. Psychol. Measur.* 20, 37–46. doi: 10.1177/001316446002000104

Cortes, C., and Vapnik, V. (1995). Support-vector networks. *Mach. Learn.* 20, 273–297. doi: 10.1007/BF00994018

Craddock, R. C., James, G. A., Holtzheimer, P. E., Hu, X. P., and Mayberg, H. S. (2012). A whole brain fMRI atlas generated via spatially constrained spectral clustering. *Hum. Brain Mapp.* 33, 1914–1928. doi: 10.1002/hbm.21333

Cui, Y., Liu, B., Luo, S., Zhen, X., Fan, M., Liu, T., et al. (2011). Identification of conversion from mild cognitive impairment to alzheimer's disease using multivariate predictors. *PLoS One* 6:e21896. doi: 10.1371/journal.pone.0021896

Cui, Z., Zhong, S., Xu, P., He, Y., and Gong, G. (2013). PANDA: a pipeline toolbox for analyzing brain diffusion images. *Front. Hum. Neurosci.* 7:42. doi: 10.3389/fnhum.2013.00042

Cuingnet, R., Gerardin, E., Tessieras, J., Auzias, G., Lehéricy, S., Habert, M.-O., et al. (2011). Automatic classification of patients with Alzheimer's disease from structural MRI: a comparison of ten methods using the ADNI database. *Neuroimage* 56, 766–781. doi: 10.1016/j.neuroimage.2010.06.013

Dai, Z., Yan, C., Wang, Z., Wang, J., Xia, M., Li, K., et al. (2012). Discriminative analysis of early Alzheimer's disease using multi-modal imaging and multi-level characterization with multi-classifier (M3). *Neuroimage* 59, 2187–2195. doi: 10.1016/j.neuroimage.2011.10.003

Daianu, M., Jahanshad, N., Nir, T. M., Toga, A. W., Jack, C. R., Weiner, M. W., et al. (2013). Breakdown of brain connectivity between normal aging and alzheimer's disease: a structural *k* -core network analysis. *Brain Connect.* 3, 407–422. doi: 10.1089/brain.2012.0137

de Vos, F., Koini, M., Schouten, T. M., Seiler, S., van der Grond, J., Lechner, A., et al. (2018). A comprehensive analysis of resting state fMRI measures to classify individual patients with Alzheimer's disease. *Neuroimage* 167, 62–72. doi: 10.1016/j.neuroimage.2017.11.025

Dean, D. C., Jerskey, B. A., Chen, K., Protas, H., Thiyyagura, P., Roontiva, A., et al. (2014). Brain differences in infants at differential genetic risk for late-onset alzheimer disease: a cross-sectional imaging study. *JAMA Neurol.* 71:11. doi: 10.1001/jamaneurol.2013.4544

Donini, M., Monteiro, J. M., Pontil, M., Hahn, T., Fallgatter, A. J., Shawe-Taylor, J., et al. (2019). Combining heterogeneous data sources for neuroimaging based diagnosis: re-weighting and selecting what is important. *Neuroimage* 195, 215–231. doi: 10.1016/j.neuroimage.2019.01.053

Dubois, B., and Albert, M. L. (2004). Amnestic MCI or prodromal Alzheimer's disease? *Lancet Neurol.* 3, 246–248. doi: 10.1016/S1474-4422(04)00710-0

Fan, Y., Resnick, S. M., Wu, X., and Davatzikos, C. (2008). Structural and functional biomarkers of prodromal Alzheimer's disease: a high-dimensional pattern classification study. *Neuroimage* 41, 277–285. doi: 10.1016/j.neuroimage.2008.02.043

Fransson, P. (2005). Spontaneous low-frequency BOLD signal fluctuations: an fMRI investigation of the resting-state default mode of brain function hypothesis. *Hum. Brain Mapp.* 26, 15–29. doi: 10.1002/hbm.20113

Ganguli, M., Dodge, H. H., Shen, C., and DeKosky, S. T. (2004). Mild cognitive impairment, amnestic type: an epidemiologic study. *Neurology* 63, 115–121. doi: 10.1212/01.WNL.0000132523.27540.81

Grabner, G., Janke, A. L., Budge, M. M., Smith, D., Pruessner, J., and Collins, D. L. (2006). "Symmetric atlasing and model based segmentation: an application to the hippocampus in older adults," in *Medical Image Computing and Computer-Assisted Intervention - MICCAI 2006*, eds R. Larsen, M. Nielsen, and J. Sporring (Berlin: Springer), 58–66. doi: 10.1007/11866763_8

Gupta, Y., Lama, R. K., Kwon, G.-R., and Alzheimer's Disease Neuroimaging Initiative, (2019a). Prediction and classification of alzheimer's disease based on combined features from apolipoprotein-e genotype, cerebrospinal fluid, MR, and FDG-PET imaging biomarkers. *Front. Comput. Neurosci.* 13:72. doi: 10.3389/fncom.2019.00072

Gupta, Y., Lee, K. H., Choi, K. Y., Lee, J. J., Kim, B. C., and Kwon, G.-R. (2019b). Alzheimer's disease diagnosis based on cortical and subcortical features. *J. Healthc. Eng.* 2019, 1–13. doi: 10.1155/2019/2492719

Gupta, Y., Lee, K. H., Choi, K. Y., Lee, J. J., Kim, B. C., Kwon, G. R., et al. (2019c). Early diagnosis of Alzheimer's disease using combined features from voxel-based morphometry and cortical, subcortical, and hippocampus regions of MRI T1 brain images. *PLoS One* 14:e0222446. doi: 10.1371/journal.pone.0222446

Hojjati, S. H., Ebrahimzadeh, A., Khazaee, A., and Babajani-Feremi, A. (2017). Predicting conversion from MCI to AD using resting-state fMRI, graph theoretical approach and SVM. *J. Neurosci. Methods* 282, 69–80. doi: 10.1016/j.jneumeth.2017.03.006

Hojjati, S. H., Ebrahimzadeh, A., Khazaee, A., and Babajani-Feremi, A. (2018). Predicting conversion from MCI to AD by integrating rs-fMRI and structural MRI. *Comput. Biol. Med.* 102, 30–39. doi: 10.1016/j.compbiomed.2018.09.004

Hua, K., Zhang, J., Wakana, S., Jiang, H., Li, X., Reich, D. S., et al. (2008). Tract probability maps in stereotaxic spaces: analyses of white matter anatomy and tract-specific quantification. *Neuroimage* 39, 336–347. doi: 10.1016/j.neuroimage.2007.07.053

Hyman, B. T., Phelps, C. H., Beach, T. G., Bigio, E. H., Cairns, N. J., Carrillo, M. C., et al. (2012). National institute on Aging-Alzheimer's Association guidelines for the neuropathologic assessment of Alzheimer's disease. *Alzheimer Dement.* 8, 1–13. doi: 10.1016/j.jalz.2011.10.007

Jack, C. R., Bennett, D. A., Blennow, K., Carrillo, M. C., Dunn, B., Haeberlein, S. B., et al. (2018). NIA-AA research framework: toward a biological definition of Alzheimer's disease. *Alzheimer Dement.* 14, 535–562. doi: 10.1016/j.jalz.2018.02.018

Jack, C. R., Bennett, D. A., Blennow, K., Carrillo, M. C., Feldman, H. H., Frisoni, G. B., et al. (2016). A/T/N: an unbiased descriptive classification scheme for Alzheimer disease biomarkers. *Neurology* 87, 539–547. doi: 10.1212/WNL.0000000000002923

Jagust, W. J., Landau, S. M., Koeppe, R. A., Reiman, E. M., Chen, K., Mathis, C. A., et al. (2015). The Alzheimer's disease Neuroimaging Initiative 2 PET Core: 2015. *Alzheimer Dement.* 11, 757–771. doi: 10.1016/j.jalz.2015.05.001

Jahanshad, N., Kochunov, P. V., Sprooten, E., Mandl, R. C., Nichols, T. E., Almasy, L., et al. (2013). Multi-site genetic analysis of diffusion images and voxelwise heritability analysis: a pilot project of the ENIGMA-DTI working group. *Neuroimage* 81, 455–469. doi: 10.1016/j.neuroimage.2013.04.061

Jenkinson, M., Beckmann, C. F., Behrens, T. E. J., Woolrich, M. W., and Smith, S. M. (2012). FSL. *Neuroimage* 62, 782–790. doi: 10.1016/j.neuroimage.2011.09.015

Jicha, G. A., Parisi, J. E., Dickson, D. W., Johnson, K., Cha, R., Ivnik, R. J., et al. (2006). Neuropathologic outcome of mild cognitive impairment following progression to clinical dementia. *Arch. Neurol.* 63:8.

John, M., Ikuta, T., and Ferbinteanu, J. (2017). Graph analysis of structural brain networks in Alzheimer's disease: beyond small world properties. *Brain Struct. Funct.* 222, 923–942. doi: 10.1007/s00429-016-1255-4

Joliot, M., Jobard, G., Naveau, M., Delcroix, N., Petit, L., Zago, L., et al. (2015). AICHA: an atlas of intrinsic connectivity of homotopic areas. *J. Neurosci. Methods* 254, 46–59. doi: 10.1016/j.jneumeth.2015.07.013

Khoury, R., and Ghossoub, E. (2019). Diagnostic biomarkers of Alzheimer's disease: a state-of-the-art review. *Biomark. Neuropsychiatr.* 1:100005. doi: 10.1016/j.bionps.2019.100005

Li, X., Morgan, P. S., Ashburner, J., Smith, J., and Rorden, C. (2016). The first step for neuroimaging data analysis: DICOM to NIfTI conversion. *J. Neurosci. Methods* 264, 47–56. doi: 10.1016/j.jneumeth.2016.03.001

Liu, C.-C., Kanekiyo, T., Xu, H., and Bu, G. (2013). Apolipoprotein E and Alzheimer disease: risk, mechanisms and therapy. *Nat. Rev. Neurol.* 9, 106–118. doi: 10.1038/nrneurol.2012.263

Liu, F., Zhou, L., Shen, C., and Yin, J. (2014). Multiple kernel learning in the primal for multimodal Alzheimer's disease classification. *IEEE J. Biomed. Health Inform.* 18, 984–990. doi: 10.1109/JBHI.2013.2285378

Liu, K., Chen, K., Yao, L., and Guo, X. (2017). Prediction of mild cognitive impairment conversion using a combination of independent component analysis and the cox model. *Front. Hum. Neurosci.* 11:33. doi: 10.3389/fnhum.2017.00033

Long, X., Chen, L., Jiang, C., Zhang, L., and Alzheimer's Disease Neuroimaging Initiative, (2017). Prediction and classification of Alzheimer disease based on quantification of MRI deformation. *PLoS One* 12:e0173372. doi: 10.1371/journal.pone.0173372

Lopez, O. L., Becker, J. T., Chang, Y.-F., Sweet, R. A., DeKosky, S. T., Gach, M. H., et al. (2012). Incidence of mild cognitive impairment in the pittsburgh cardiovascular health study-cognition STUDY. *Neurology* 79, 1599–1606. doi: 10.1212/WNL.0b013e31826e25f0

Márquez, F., and Yassa, M. A. (2019). Neuroimaging biomarkers for Alzheimer's disease. *Mol. Neurodegen.* 14:21. doi: 10.1186/s13024-019-0325-5

Michaelson, D. M. (2014). APOE ε4: the most prevalent yet understudied risk factor for Alzheimer's disease. *Alzheimer Dement.* 10, 861–868. doi: 10.1016/j.jalz.2014.06.015

Mijalkov, M., Kakaei, E., Pereira, J. B., Westman, E., Volpe, G., and Alzheimer's Disease Neuroimaging Initiative, (2017). BRAPH: a graph theory software for the analysis of brain connectivity. *PLoS One* 12:e0178798. doi: 10.1371/journal.pone.0178798

Mitchell, A. J., and Shiri-Feshki, M. (2009). Rate of progression of mild cognitive impairment to dementia - meta-analysis of 41 robust inception cohort studies. *Acta Psychiatr. Scand.* 119, 252–265. doi: 10.1111/j.1600-0447.2008.01326.x

Modat, M., Ridgway, G. R., Taylor, Z. A., Lehmann, M., Barnes, J., Hawkes, D. J., et al. (2010). Fast free-form deformation using graphics processing units. *Comput. Methods Programs Biomed.* 98, 278–284. doi: 10.1016/j.cmpb.2009.09.002

Moradi, E., Pepe, A., Gaser, C., Huttunen, H., and Tohka, J. (2015). Machine learning framework for early MRI-based Alzheimer's conversion prediction in MCI subjects. *Neuroimage* 104, 398–412. doi: 10.1016/j.neuroimage.2014.10.002

Morris, J. C. (1993). The clinical dementia rating (CDR): current version and scoring rules. *Neurology* 43, 2412–2412. doi: 10.1212/WNL.43.11.2412-a

Mosconi, L., Pupi, A., and De Leon, M. J. (2008). Brain glucose hypometabolism and oxidative stress in preclinical Alzheimer's disease. *Ann. N. Y. Acad. Sci. U.S.A.* 1147, 180–195. doi: 10.1196/annals.1427.007

Murphy, M. P., and LeVine, H. (2010). Alzheimer's disease and the Amyloid-β Peptide. *J. Alzheimer Dis.* 19, 311–323. doi: 10.3233/JAD-2010-1221

Pan, X., Adel, M., Fossati, C., Gaidon, T., and Guedj, E. (2019a). Multilevel feature representation of fdg-pet brain images for diagnosing Alzheimer's disease. *IEEE J. Biomed. Health Inform.* 23, 1499–1506. doi: 10.1109/JBHI.2018.2857217

Pan, X., Adel, M., Fossati, C., Gaidon, T., Wojak, J., and Guedj, E. (2019b). Multiscale spatial gradient features for 18F-FDG PET image-guided diagnosis of Alzheimer's disease. *Comput. Methods Prog.* 180:105027. doi: 10.1016/j.cmpb.2019.105027

Pedregosa, F., Varoquaux, G., Gramfort, A., Michel, V., Thirion, B., Grisel, O., et al. (2011). Scikit-learn: machine learning in python. *J. Mach. Learn. Res.* 12, 2825–2830.

Peraza, L. R., Díaz-Parra, A., Kennion, O., Moratal, D., Taylor, J.-P., Kaiser, M., et al. (2019). Structural connectivity centrality changes mark the path toward Alzheimer's disease. *Alzheimer Dement.* 11, 98–107. doi: 10.1016/j.dadm.2018.12.004

Petersen, R. C. (2004). Mild cognitive impairment as a diagnostic entity. *J. Intern. Med.* 256, 183–194. doi: 10.1111/j.1365-2796.2004.01388.x

Petersen, R. C., Aisen, P. S., Beckett, L. A., Donohue, M. C., Gamst, A. C., Harvey, D. J., et al. (2010). Alzheimer's disease neuroimaging initiative (ADNI): clinical characterization. *Neurology* 74, 201–209. doi: 10.1212/WNL.0b013e3181cb3e25

Qiu, C., and Kivipelto, M. (2009). Epidemiology of Alzheimer's disease: occurrence, determinants, and strategies toward intervention. *Dialog. Clin. Neurosci.* 11:18.

Rathore, S., Habes, M., Iftikhar, M. A., Shacklett, A., and Davatzikos, C. (2017). A review on neuroimaging-based classification studies and associated feature extraction methods for Alzheimer's disease and its prodromal stages. *Neuroimage* 155, 530–548. doi: 10.1016/j.neuroimage.2017.03.057

Ritter, K., Schumacher, J., Weygandt, M., Buchert, R., Allefeld, C., and Haynes, J.-D. (2015). Multimodal prediction of conversion to Alzheimer's disease based on incomplete biomarkers. *Alzheimer Dement.* 1, 206–215. doi: 10.1016/j.dadm.2015.01.006

Salvatore, C., Cerasa, A., Battista, P., Gilardi, M. C., Quattrone, A., and Castiglioni, I. (2015). Magnetic resonance imaging biomarkers for the early diagnosis of Alzheimer's disease: a machine learning approach. *Front. Neurosci.* 9:307. doi: 10.3389/fnins.2015.00307

Samper-González, J., Burgos, N., Bottani, S., Fontanella, S., Lu, P., Marcoux, A., et al. (2018). Reproducible evaluation of classification methods in Alzheimer's disease: framework and application to MRI and PET data. *Neuroimage* 183, 504–521. doi: 10.1016/j.neuroimage.2018.08.042

Schouten, T. M., Koini, M., de Vos, F., Seiler, S., van der Grond, J., Lechner, A., et al. (2016). Combining anatomical, diffusion, and resting state functional magnetic resonance imaging for individual classification of mild and moderate Alzheimer's disease. *Neuroimage* 11, 46–51. doi: 10.1016/j.nicl.2016.01.002

Smith, A. M., Lewis, B. K., Ruttimann, U. E., Ye, F. Q., Sinnwell, T. M., Yang, Y., et al. (1999). Investigation of low frequency drift in fMRI Signal. *Neuroimage* 9, 526–533. doi: 10.1006/nimg.1999.0435

Smith, S. M. (2002). Fast robust automated brain extraction. *Hum. Brain Mapp.* 17, 143–155. doi: 10.1002/hbm.10062

Sun, Y., Bi, Q., Wang, X., Hu, X., Li, H., Li, X., et al. (2019). Prediction of conversion from amnestic mild cognitive impairment to Alzheimer's disease based on the brain structural connectome. *Front. Neurol.* 9:1178. doi: 10.3389/fneur.2018.01178

Tustison, N. J., Avants, B. B., Cook, P. A., Zheng, Y., Egan, A., Yushkevich, P. A., et al. (2010). N4ITK: improved N3 bias correction. *IEEE Trans. Med. Imaging* 29, 1310–1320. doi: 10.1109/TMI.2010.2046908

Wei, R., Li, C., Fogelson, N., and Li, L. (2016). Prediction of conversion from mild cognitive impairment to Alzheimer's disease using MRI and structural network features. *Front. Aging Neurosci.* 8:76. doi: 10.3389/fnagi.2016.00076

Xu, L., Wu, X., Li, R., Chen, K., Long, Z., Zhang, J., et al. (2016). Prediction of progressive mild cognitive impairment by multi-modal neuroimaging biomarkers. *J. Alzheimer Dis.* 51, 1045–1056. doi: 10.3233/JAD-151010

Young, J., Modat, M., Cardoso, M. J., Mendelson, A., Cash, D., and Ourselin, S. (2013). Accurate multimodal probabilistic prediction of conversion to Alzheimer's disease in patients with mild cognitive impairment. *Neuroimage* 2, 735–745. doi: 10.1016/j.nicl.2013.05.004

Zang, Y., Jiang, T., Lu, Y., He, Y., and Tian, L. (2004). Regional homogeneity approach to fMRI data analysis. *Neuroimage* 22, 394–400. doi: 10.1016/j.neuroimage.2003.12.030

Zhang, D., Wang, Y., Zhou, L., Yuan, H., and Shen, D. (2011). Multimodal classification of Alzheimer's disease and mild cognitive impairment. *Neuroimage* 55, 856–867. doi: 10.1016/j.neuroimage.2011.01.008

Zheng, W., Yao, Z., Hu, B., Gao, X., Cai, H., and Moore, P. (2015). Novel cortical thickness pattern for accurate detection of Alzheimer's disease. *J. Alzheimer Dis.* 48, 995–1008. doi: 10.3233/JAD-150311

Conflict of Interest: The authors declare that the research was conducted in the absence of any commercial or financial relationships that could be construed as a potential conflict of interest.

frontiers in Aging Neuroscience

REVIEW
published: 04 August 2020
doi: 10.3389/fnagi.2020.00227

Progress of RAGE Molecular Imaging in Alzheimer's Disease

Yanyan Kong[1], Cuiping Liu[2], Yinping Zhou[2], Jingxuan Qi[2], Chencheng Zhang[3], Bomin Sun[3], Jiao Wang[2]* and Yihui Guan[1]**

[1] PET Center, Huashan Hospital, Fudan University, Shanghai, China, [2] Laboratory of Molecular Neural Biology, School of Life Sciences, Shanghai University, Shanghai, China, [3] Department of Neurosurgery, Center for Functional Neurosurgery, Ruijin Hospital, Shanghai Jiao Tong University School of Medicine, Shanghai, China

Alzheimer's disease (AD) is a progressive neurodegenerative disease characterized by senile plaques (SPs), which are caused by amyloid beta (Aβ) deposition and neurofibrillary tangles (NFTs) of abnormal hyperphosphorylated tau protein. The receptor for advanced glycation end products (RAGE) binds to advanced glycation end products deposited during vascular dysfunction. Alzheimer's disease may occur when RAGE binds to Aβ and releases reactive oxygen species, further exacerbating Aβ deposition and eventually leading to SPs and NFTs. As it is involved in early AD, RAGE may be considered as a more potent biomarker than Aβ. Positron emission tomography provides valuable information regarding the underlying pathological processes of AD many years before the appearance of clinical symptoms. Thus, to further reveal the role of RAGE in AD pathology and for early diagnosis of AD, a tracer that targets RAGE is needed. In this review, we first describe the early diagnosis of AD and then summarize the interaction between RAGE and Aβ and Tau that is required to induce AD pathology, and finally focus on RAGE-targeting probes, highlighting the potential of RAGE to be used as an effective target. The development of RAGE probes is expected to aid in AD diagnosis and treatment.

Keywords: AD, RAGE, PET, [^{18}F]-FPS-ZM1, senile plaques, neurofibrillary tangles

OPEN ACCESS

Edited by:
Woon-Man Kung,
Chinese Culture University, Taiwan

Reviewed by:
Linjing Mu,
ETH Zürich, Switzerland
Muh-Shi Lin,
Kuang Tien General Hospital, Taiwan
Hiroshi Matsuda,
National Center of Neurology and Psychiatry, Japan

****Correspondence:***
Bomin Sun
sbm11224@rjh.com.cn
Jiao Wang
jo717@shu.edu.cn
Yihui Guan
guanyihui@hotmail.com

Received: *16 March 2020*
Accepted: *29 June 2020*
Published: *04 August 2020*

Citation:
Kong Y, Liu C, Zhou Y, Qi J, Zhang C, Sun B, Wang J and Guan Y (2020) Progress of RAGE Molecular Imaging in Alzheimer's Disease. Front. Aging Neurosci. 12:227. doi: 10.3389/fnagi.2020.00227

INTRODUCTION

Alzheimer's disease (AD) is the first major neurodegenerative disease with irreversible, occult, and rapid progression. With aging of the population, AD has become a major disease affecting public health (Nebel et al., 2018; Bo et al., 2019). The etiology and pathogenesis of AD are not fully understood, and currently, there is no specific treatment. More importantly, early diagnosis of AD is limited. The cost of treatment and care for AD is enormous, imposing a heavy burden on patients, families, and the society. Therefore, brain function imaging, developed on the basis of brain metabolism research targeting AD pathogenesis, plays an increasingly important role in the study of pathological processes in the AD brain.

The pathological features of AD are senile plaques (SPs), containing neurotoxic amyloid beta (Aβ) as the main component, and neurofibrillary tangles (NFTs), with abnormally activated tau as the main component in nerve cells. Neurofibrillary tangles and SPs are currently recognized as the earliest pathological changes in AD, with SPs reaching their maximum deposition in the early stage of AD, termed the "capping effect," which allows for amyloid plaque imaging *in vivo*. Tracking the slow progress of AD is difficult (Dubois et al., 2018). Therefore, an in-depth exploration of

AD pathogenesis with the development of new radioactive probes that detect pathological changes earlier to Aβ deposition is currently a hotspot in AD research.

The receptor for advanced glycation end products (RAGE) belongs to the immunoglobulin superfamily of cell surface molecules and is situated in the major histocompatibility complex class III locus (Xue et al., 2011; Han et al., 2014). It binds to its ligand, advanced glycation end products (AGEs), through its V-type region, which is a key site that mediates intracellular signal transduction (Kim et al., 2013; Abedini et al., 2018). While mild hypoperfusion can increase the levels of neuronal Aβ and NFTs, expressed as paired helix filaments, increasing evidence shows that RAGE levels are significantly elevated in patients with AD and AD models (Cai et al., 2016; Chellappa and Rani, 2020; Paudel et al., 2020). Receptor for advanced glycation end products-mediated Aβ-injured tight junctions may also be associated with a variety of intracellular signal transduction pathways, Ca^{2+}, or inflammatory damage (Nelson et al., 2016; Cai et al., 2017; Sole et al., 2019). Further, immunohistochemical evidence shows that the distribution of RAGE abnormalities is consistent with that of NFTs and SPs. In addition, glycosylated tau can induce significant oxidative stress and cause neuronal insufficiency or death (Srikanth et al., 2011; Cai et al., 2016). Receptor for advanced glycation end products may play an important role in the occurrence and development of AD, yet its underlying mechanism is still unclear. Thus, it is necessary to lay emphasis on the role of RAGE in AD pathology.

Early Progression of AD

The etiology of AD is complex, and there are currently no specific drugs and methods to treat AD. Many drugs can only achieve remission (Wong et al., 2019). Positron emission tomography (PET), as a molecular imaging technique, can reflect pathological changes at the molecular level and can non-invasively detect the distribution of radionuclides in the body, which reflects physiological, biochemical, metabolic, and receptor changes, as well as gene expression and other abnormal changes (Hannestad, 2018; Mankoff and Katz, 2018). Thus, it is an important auxiliary tool for AD research. At present, there are several types of AD PET imaging agents (Bao et al., 2017) targeting glucose metabolism, receptors, or transmitters, Aβ, Tau protein, neuroinflammation, and monoamine oxidase. However, these agents have certain limitations for the early diagnosis of AD.

In recent years, research on AD has mainly focused on the two major pathological features of AD: Aβ and tau. However, although some individuals show Aβ or Tau deposition as detected on medical images, they exhibit no dementia symptoms (Hardy and Selkoe, 2002). Moreover, studies have shown that Aβ deposition is slow and protracted, likely lasting over 20 years, while the association of Aβ accumulation with cognitive impairments is weak (Villemagne et al., 2013). Additionally, the current probes cannot distinguish among the six subtypes of Tau protein, and their off-target effects are more serious (Robertson et al., 2017). Therefore, finding new targets and developing the corresponding probes for AD are particularly important for AD research.

Current studies have shown that in early vascular dysfunction of AD, inflammatory mediators, such as tumor necrosis factor alpha (TNF-α), in brain microvascular endothelial cells (BMECs), are released, thus increasing cerebral vascular permeability (Qiu et al., 2016), enabling AGEs and other neurotoxicants to cross the blood–brain barrier (BBB) and cause AGE deposition. This leads to a significant upregulation of RAGE in BMECs (Liang et al., 2015), which leads to an inflammatory response by vascular endothelial and nerve cells, activates the release of reactive oxygen species (ROS), which promotes oxidative stress, and results in the secretion of nitric oxide synthase and further increases Aβ deposition in the brain. Aβ increases the activation of microglia, which, in turn, accelerates nerve vessel dysfunction. Neuronal dysfunction promotes the pathogenesis of NFTs, thus causing the formation of additional SPs and NFTs, disturbing the balance in the chemical components of the neuro-microenvironment. This further promotes neuronal dysfunction, injury, and loss (Wells et al., 2015; Cai et al., 2016) (see **Figure 1**). Based on the above, RAGE and AGEs could play an important role in the early pathological changes of AD.

AGE-Related RAGE Processes and NFTs

Abnormally activated tau is the main component of NFTs, and NFT deposition in the hippocampus and entorhinal cortex is correlated with the severity of behavioral degeneration in the progression of dementia (Saint-Aubert et al., 2017). Advanced glycation end products are the final products of the non-enzymatic glycation of proteins, which is irreversible. The non-enzymatic saccharification processes accompanying neuronal metabolism have far-reaching effects despite the slow and insignificant cell damage they cause (Kamynina et al., 2018). In AD, AGEs have been shown to induce tau hyperphosphorylation in SK-N-SH cells, primary hippocampal neurons, and rat brains through the RAGE/GSK-3 pathway (Li X.H. et al., 2012; Son et al., 2012). As AGEs downregulate the brain-derived neurotrophic factor–tyrosine receptor kinase B pathway in rat brains and N2A cells (Li X.H. et al., 2012), they could activate glycogen synthase kinase 3 at Ser9, thus regulating its phosphorylation, which was found to be a trigger of tau hyperphosphorylation (Wu et al., 2019). Simultaneously, *in situ* techniques have shown that the major structures recognized by anti-AGE antibodies, hydroxymethyl lysine (CML) and glycosylated precursor hexitol-lysine, increase in the NFTs of patients with AD. In these patients, CML colocalizes with the tau protein. Immunostaining experiments have shown that almost all AGE-immunoreactive neurons contain the hyperphosphorylated tau protein, confirming the role of AGE aggregation in early NFT formation and neuronal degeneration (Qi et al., 2017) (see **Figure 2**). As an increase in AGEs causes an upregulation of RAGE, the connection between AGEs and NFTs indicates a strong link between RAGE and tau hyperphosphorylation.

The deposition of AGEs in the brain participates in the pathogenesis of AD through RAGE and cross-links with NFTs. This deposition activates microglia and nicotinamide adenine dinucleotide phosphate oxidase, leading to ROS release and the formation of peroxynitrite, a potent oxidant of proteins, lipids, and DNA (Nam et al., 2012), ultimately causing nerve

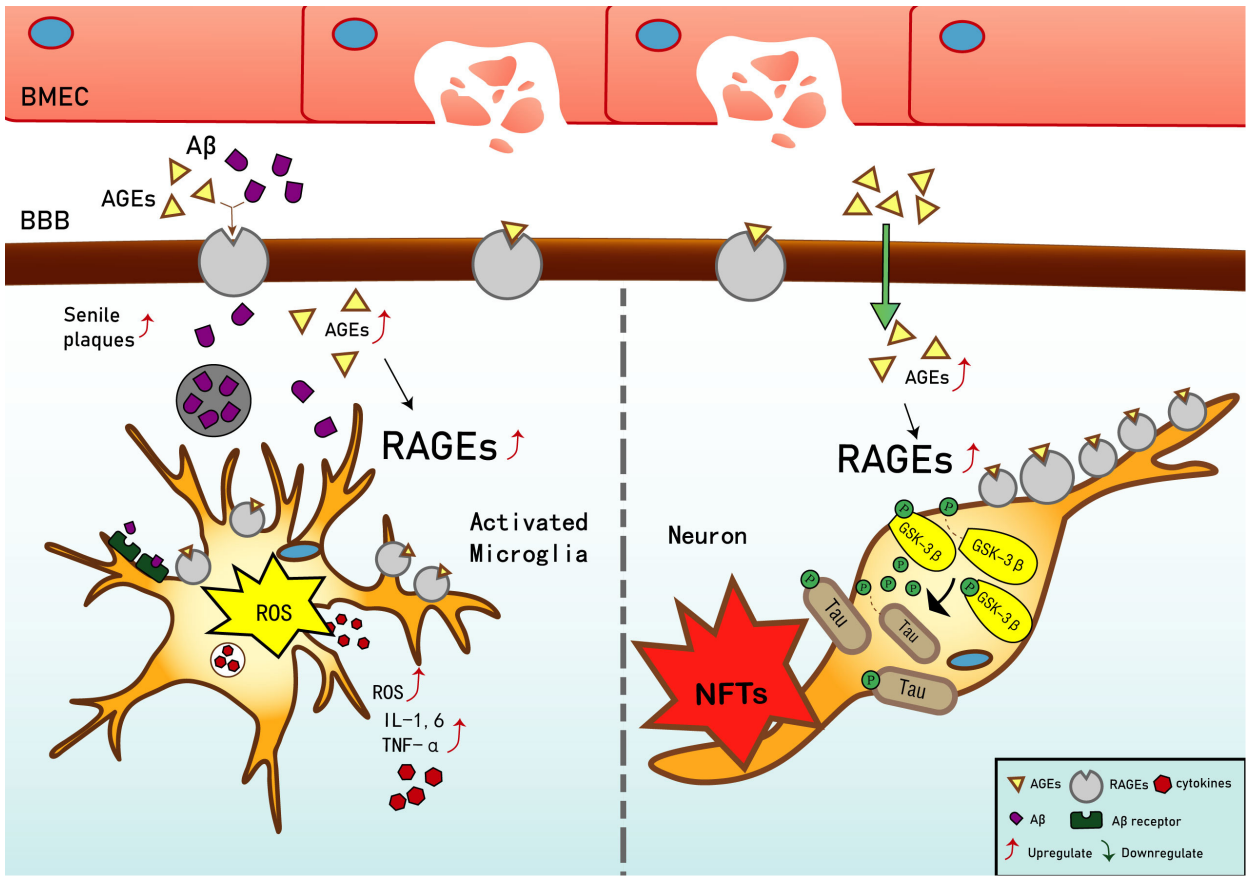

FIGURE 1 | Receptor of advanced glycation end products (RAGE) mediates the possible mechanism of Alzheimer's disease (AD). Interaction of RAGE with advanced glycation end products (AGEs) and β-amyloid (Aβ) allows them to cross the blood–brain barrier and enter the brain. Aβ deposition in the brain promotes the expression of tumor necrosis factor α (TNF-α), interleukin (IL)-1, and IL-6, and exacerbates the inflammatory response. Increased binding of Aβ to RAGE after entering the brain can also upregulate RAGE expression, resulting in increased release of reactive oxygen species (ROS) and upregulation of Aβ expression, which then promotes the generation of senile plaques (SPs). The upregulation of RAGE exacerbates phosphorylation of tau protein and promotes the generation of neurofibrillary tangles (NFTs). AGEs and RAGE phosphorylate glycogen synthase kinase 3 (GSK-3β), which, in turn, exacerbates the phosphorylation of tau protein and promotes the generation of NFTs. Upregulation of Aβ and tau protein levels promote the occurrence and development of AD.

destruction. Therefore, treating AGEs may become a new way to treat AD.

Role of the Interaction Between RAGE and Aβ in AD

A growing body of evidence suggests that RAGE is an important regulator of Aβ neurotoxicity. Aβ-damaged BMECs and the destruction of the BBB may be new characteristic pathological changes in AD (Lv et al., 2014). In AD, RAGE expression is significantly upregulated in areas where Aβ is deposited (Wang et al., 2009). Receptor for advanced glycation end products is a pattern recognition receptor, and Aβ, as one of its ligands, was shown to interact with it (Paudel et al., 2020); however, the specific mechanism underlying this interaction and its role in patients with AD need further clarification.

The interaction of RAGE with Aβ activates inflammatory signaling pathways, releases ROS to produce oxidative stress, and causes neuroinflammation, thus inducing the dysfunction of mitochondria and neurons (Deane et al., 2008), as well as changes in various signaling mechanisms such as the mitogen-activated protein kinase pathway (Deane, 2012). Further, RAGE accelerates the uptake and transport of Aβ, which causes Aβ to cross the BBB and enter the central nervous system through endocytosis (Deane et al., 2003), causing cerebrovascular dysfunction, eventually leading to neurovascular inflammation and subsequent synaptic toxicity (Deane and Zlokovic, 2007), thereby affecting the normal activity of the central nervous system (Zhang et al., 2011; Galasko et al., 2014; Wang et al., 2014; Cai et al., 2016; Fang et al., 2018). The interaction between RAGE and Aβ is harmful to the body. Studies have found that, in transgenic mice with defective RAGE expression, Aβ in the brain is completely inhibited from crossing the BBB (Deane and Zlokovic, 2007).

High expression of RAGE is also harmful to the body. First, it activates the nuclear factor κB, further increasing the expression of RAGE and forming a positive feedback effect on inflammation (Wan et al., 2015; Fang et al., 2018). Second, it increases the expression of nuclear factor-1 in activated T-cells and of

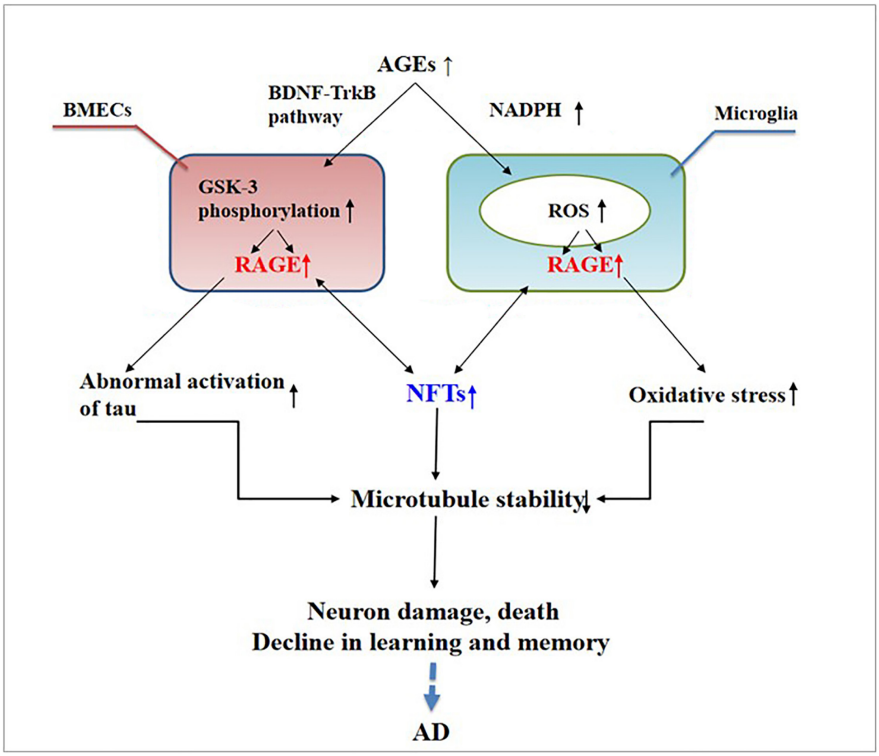

FIGURE 2 | Receptor of advanced glycation end products (RAGE) mediates the possible mechanism of neurofibrillary tangle (NFT) formation in the pathogenesis of dementia complicated with Alzheimer's disease.

amyloid precursor protein (APP) β-site cleavage enzyme 1 (also known as BACE1), an important enzyme that cleaves amyloid precursors (Yan et al., 1996; Fang et al., 2010; Guglielmotto et al., 2012; Galasko et al., 2014). Increased BACE1 activity increases Aβ production (Maesako et al., 2019). In addition, Aβ can activate RAGE, increasing the expression of pro-inflammatory cytokines like TNF-α, interleukin 6 (IL-6), and macrophage colony-stimulating factor (Dukic-Stefanovic et al., 2003). In turn, RAGE activation exacerbates the production and aggregation of Aβ and the formation of NFTs and destroys synaptic transmission and neurons (Cai et al., 2016) (see **Figure 3**), which promote the occurrence and development of AD.

Inhibition of RAGE can prevent Aβ damage in nerve cells and cerebral vasculature. The possible mechanism of RAGE function in AD provides a theoretical basis and new ideas for the early diagnosis of AD and development of new drugs for the prevention and treatment of AD.

RAGE and RAGE-Targeting Brain Imaging

Many studies have shown that AGEs are important in neurodegenerative diseases (Li J. et al., 2012; Nenna et al., 2015), while *in vitro* and *in vivo* studies have demonstrated the potential of RAGE as a receptor for AGE and as a therapeutic target in neurodegeneration (Sparvero et al., 2009; Deane et al., 2012; Nasser et al., 2015; Ray et al., 2016). Receptor for advanced glycation end products PET imaging has also been proven to assist in the diagnosis and treatment of neurodegenerative diseases (Kim et al., 2018; Konopka et al., 2018; Goldklang et al., 2019). The full-length human RAGE consists of three domains, namely, the extracellular, the hydrophobic transmembrane, and the cytoplasmic domains, while the main binding domain structure V is located on the extracellular part of the receptor (Bongarzone et al., 2017). Receptor for advanced glycation end products is expressed in a regulated manner, at low levels, in most differentiated adult cells, whereas its expression is high in embryonic cells (Demling et al., 2006). Moreover, RAGE is highly expressed in many inflammation-related pathological states such as vascular disease, diabetes, and neurodegeneration (Hudson et al., 2008; Sparvero et al., 2009). It is important in Aβ-mediated neurotoxicity (Piras et al., 2014), and its signaling pathway is also essential in AGE-induced tau phosphorylation and spatial memory impairment (Choi et al., 2014). Studies using murine models of chronic disease have demonstrated the involvement of RAGE in pathophysiological processes by means of a receptor decoy of soluble RAGE (Bierhaus et al., 2005). Moreover, RAGE was found to be relatively increased on the membrane of neurons and microglia in AD-related neuronal dysfunction (Yan et al., 1996; Cai et al., 2016). Considering the key functions of RAGE, there is a need for molecular imaging agents to measure RAGE expression in neurodegenerative diseases.

For developing novel RAGE inhibitors as potential AD therapeutics, Han et al. (2014) designed and synthesized a

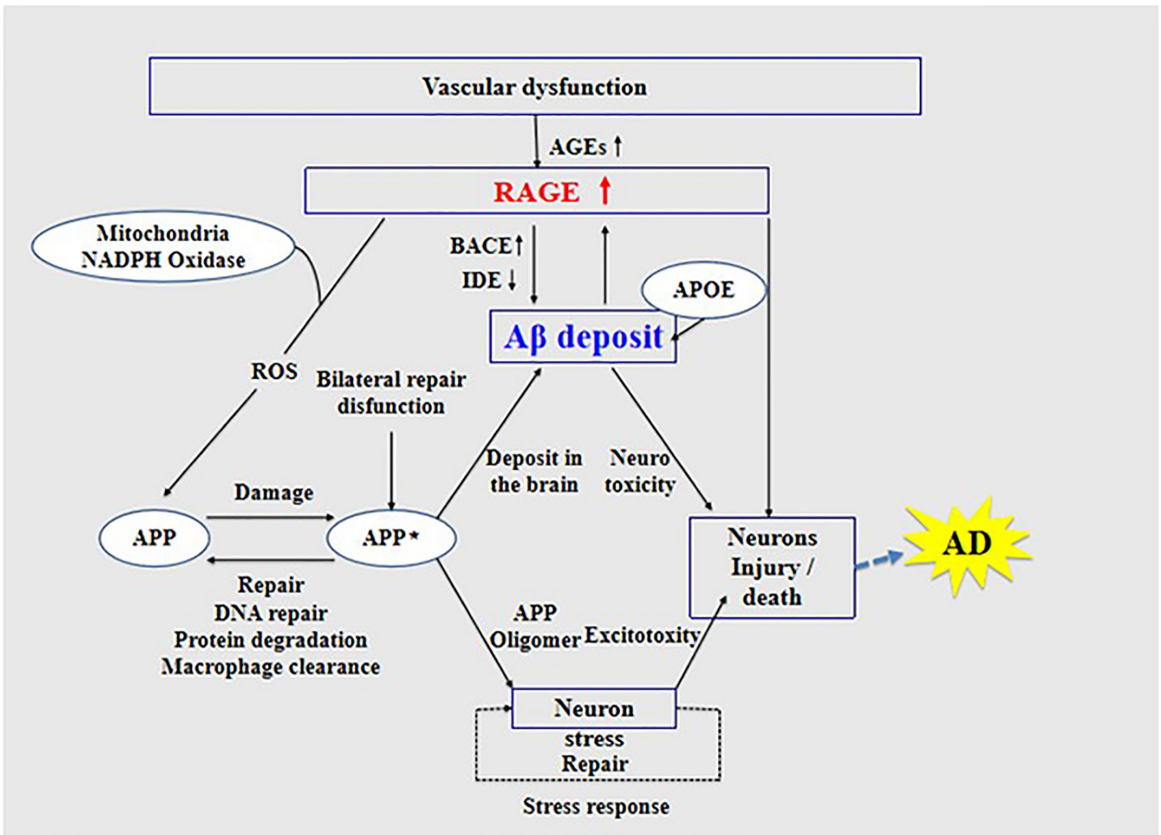

FIGURE 3 | Receptor of advanced glycation end products (RAGE) mediates the possible mechanism of Aβ in the pathogenesis of Alzheimer's disease.

series of pyrazole-5-carboxamides to screen for excellent RAGE inhibitors. Screening identified a 4-fluorophenoxy analog with significant brain Aβ-lowering effects, as well as favorable aqueous solubility named 40, which were determined to be excellent RAGE inhibitors. Deane et al. (2012) synthesized a high-affinity RAGE-specific inhibitor, FPS-ZM1, which was selected after screening a second-generation library of compounds designed based on the common structural features of three leading compounds in a primary screen. Compared to other analogs (e.g., FPS1, FPS2, and FPS3), the functional groups of the leading tertiary amides in FPS-ZM1 were altered to reduce the molecular weight to less than 450 Da and decrease the number of hydrogen bonds. FPS-ZM1 has a molecular weight of 327 Da and 1 H-bond (see **Table 1**). The authors verified its effect using $APP^{sw/0}$ mice, an AD model, and found that it can cross the BBB, acts on the V-type region of RAGE, and can still bind to RAGE after crossing the BBB, thereby blocking the role of intracranial RAGE (Lv et al., 2015; Hong et al., 2016). These results indicated the guaranteed binding ability of FPS-ZM1. In addition, FPS-ZM1 was shown to completely restore cerebral blood flow, inhibit neurotoxicity, microglial activity, and the neuroinflammatory response and improve cognitive behavior. Moreover, FPS-ZM1 has a wide safety range, with no toxic effects, even when using doses 500 times higher than the therapeutic dose (Deane et al., 2012). The above suggest that FPS-ZM1 is a potent multimodal RAGE blocker that effectively controls the progression of Aβ-mediated neurodegeneration and, thus, may be used as a disease-modifying agent for AD.

Based on the importance of the RAGE signaling pathway in AGE-induced tau phosphorylation and spatial memory impairment, research and development of imaging agents with characteristics that can reflect the early pathological mechanism of AD is a highly active field. According to the above characteristics of FPS-ZM1, Cary et al. (2016) synthesized the first small-molecule BBB-permeable PET radioligand for RAGE, [^{18}F] RAGER, and conducted a preliminary preclinical study. Micro-PET imaging in rodents and non-human primates indicated that [^{18}F] RAGER clusters in the expression area of RAGE, while further molecular docking experiments determined the binding site of RAGER, indicating that [^{18}F] RAGER and RAGE distribution area colocalization may have a binding effect. Kong et al. (2016) identified a new [^{18}F]-FPS-ZM1 probe targeting RAGE among thousands of small molecules by testing different radiolabeling methods. The probe was radioactively synthesized with a purity of up to 99% and an activity of 30 mCi/ml and was shown to be lipophilic. The authors also studied the probe's hemodynamics and verified its safety by performing animal experiments. They found that the low-molecular-weight [^{18}F]-FPS-ZM1 is stable, electrically neutral, lipophilic, and weight independent. Micro-PET imaging and autoradiography

TABLE 1 | Features of FPS1-3 and FPS-ZM1.

	MW 530	MW 548	MW 485	MW 327
	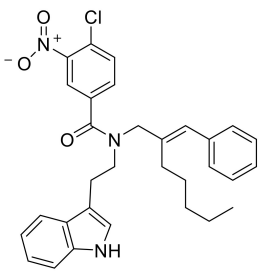 FPS1	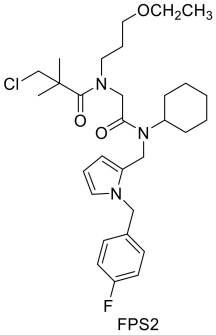 FPS2	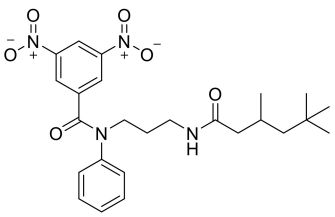 FPS3	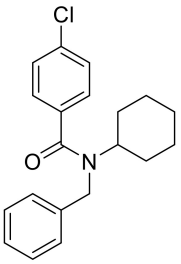 FPS-ZM1
MW	530	548	458	327
Ki (nM)	208 ± 12[A]	146 ± 21[A]	50 ± 9	25 ± 9[A]
Ki/*Kd*	2.78 ± 0.17[A]	1.94 ± 0.21[A]	0.66 ± 0.09	0.34 ± 0.04[A]
PS product (μl/g/min)	ND	ND	0.35 ± 0.10	18.67 ± 2.78
Brain uptake (%)	ND	ND	0.71 ± 0.20	37.34 ± 5.56

MW, molecular weight; Ki, inhibitory constant; Kd, dissociation constant; PS, permeability surface area.

TABLE 2 | PET and SPECT radioligands for imaging RAGE.

Radiotracer	Method	Leading compound	Applied disease	References
^{99m}Tc-F(ab')$_2$	SPECT	Polyclonal antibody to RAGE	Atherosclerosis and peripheral arterial disease	Shan, 2004; Tekabe et al., 2010
^{18}F-S100	PET	A multigenic family of Ca^{2+}-modulated proteins (S100)	No related reports	Hoppmann et al., 2008; Wolf et al., 2011
^{64}Cu-Rho-G4-CML	PET	Carboxymethyl-lysine-modified human serum albumin	Cancer	Konopka et al., 2018
^{18}F-FPS-ZM1/18FRAGER	PET	RAGE-specific inhibitor (FPS-ZM1)	Alzheimer's disease	Lv et al., 2015; Kong et al., 2016

RAGE, receptor of advanced glycation end products; SPECT, single-photon emission computed tomography; PET, positron emission tomography.

results also indicated that [^{18}F]-FPS-ZM1 is a promising RAGE-specific probe.

Several studies have documented other PET imaging probes for early AD diagnosis, such as those aimed at various targets, including Aβ, tau, and others. Tau-targeting imaging probes such as [^{18}F]-THK-5351, [^{18}F]-THK-5117, and [^{18}F]-AV-1451 show a high uptake in the patients' cortex (Harada et al., 2015; Lemoine et al., 2015; Passamonti et al., 2017; Kobayashi et al., 2018; Valotassiou et al., 2018), which means that they can accurately detect NFTs, thus helping in the early diagnosis of AD. At the same time, [^{11}C] PiB, an analog of thioflavin-T and a benzothiazole derivative, was the first probe specifically targeting Aβ (Rabinovici et al., 2007; Lim et al., 2014; Lemoine et al., 2015; Kobayashi et al., 2018). Since then, many new probes targeting Aβ have appeared, including [^{18}F]-florbetapir, [^{18}F]-florbetaben, and [^{18}F]-flutemetamol, all showing high affinity and specificity for Aβ (Valotassiou et al., 2018). These tau and Aβ-targeting probes can also be used for quantification analysis to further validate the role of RAGE in the pathogenesis of AD (Fang et al., 2018). As RAGE overexpression precedes Aβ plaque formation (Luzi et al., 2020), [^{18}F]-FPS-ZM1 PET/CT imaging is expected to be more sensitive than traditional Aβ imaging. It can monitor changes in cerebrovascular function over time and thus provide accurate, reliable, and reproducible non-invasive *in vivo* quantitative data for local or whole-brain pathological changes.

Although many tracers have been developed to aid in the diagnosis and treatment of AD, including those targeting tau, P2X7, phosphodiesterase PDE10A, and synaptic vesicle glycoprotein 2A (McCluskey et al., 2020), only few RAGE-targeting imaging tracers are currently available apart from [^{18}F]-FPS-ZM1, and they all have certain limitations in the diagnosis of AD. Available RAGE probes include the ^{99m}Tc-F(ab′)$_2$ anti-RAGE fragment developed by Tekabe et al. (Shan, 2004; Tekabe et al., 2010), which has only been applied in atherosclerosis and peripheral arterial disease, but not in AD. Another probe was developed by Hoppmann et al. (2008) on the basis of a multigenic family of Ca^{2+}-modulated proteins, namely, S100, as RAGE ligands. However, compared with the high affinity and specificity of FPS-ZM1 for RAGE, this probe lacks stability and has low affinity for RAGE (Wolf et al., 2011). Recently, another RAGE-targeting probe, ^{64}Cu-Rho-G4-CML, was developed by Konopka et al. (2018), which may be the best RAGE-targeting imaging agent currently available for cancer. However, its size prevents it from crossing the BBB, rendering it ineffective for neurological assessments (Konopka et al., 2018). Compared with these three probes, [^{18}F]-F PS-ZM1 is expected to be more potent and

could greatly improve early diagnosis, prevention, screening, and evaluation of AD and could help develop an imaging agent with appropriate characteristics that can reflect the early pathological mechanism of AD (**Table 2**).

CONCLUSION

There is currently no breakthrough drug treatment for AD, which has become a serious social and economic problem. Although the progression of AD cannot be prevented or reversed, the availability of radioactive tracers for RAGE PET imaging will allow us to monitor RAGE brain expression levels in AD. Receptor for advanced glycation end products has an important role in the development of AD, but the kind of state RAGE exists in AD and the way it acts on Aβ and tau have yet to be determined. It is unclear whether increased RAGE expression affects the behavior and pathophysiology of AD models. Thus, an in-depth study of the mechanism of action of RAGE is essential for the further understanding of neurological diseases.

In this review, we introduced the RAGE-targeting probe [^{18}F]-FPS-ZM1. Compared with probes targeting Aβ and the tau protein, [^{18}F]-FPS-ZM1 has advantages in exploring the involvement of RAGE in AD pathogenesis. Due to its high specificity and affinity for RAGE, [^{18}F]-FPS-ZM1 is believed to provide accurate and reliable *in vivo* data for studying local or whole-brain pathological changes. Thus, [^{18}F]-FPS-ZM1 could greatly promote the early diagnosis and evaluation of AD and provide a way to reflect the early pathological mechanism of AD.

AUTHOR CONTRIBUTIONS

YK, BS, JW, and YG guided the study. YK, CL, YZ, JQ, and CZ wrote the manuscript. All authors contributed to the article and approved the submitted version.

FUNDING

This study was supported by the National Natural Science Foundation of China (Project Nos. 81571345 and 81701732), Shanghai Municipal Science and Technology Major Project (No. 2018SHZDZX01), and ZJLab, Shanghai Municipal Key Clinical Specialty (shslczdzk03402).

REFERENCES

Abedini, A., Cao, P., Plesner, A., Zhang, J., He, M., Derk, J., et al. (2018). RAGE binds preamyloid IAPP intermediates and mediates pancreatic beta cell proteotoxicity. *J. Clin. Invest.* 128, 682–698. doi: 10.1172/jci85210

Bao, W., Jia, H., Finnema, S., Cai, Z., Carson, R. E., and Huang, Y. H. (2017). PET imaging for early detection of Alzheimer's disease: from pathologic to physiologic biomarkers. *PET Clin.* 12, 329–350.

Bierhaus, A., Humpert, M., Morcos, M., Wendt, T., Chavakis, T., Arnold, B., et al. (2005). Understanding RAGE, the receptor for advanced glycation end products. *J. Mol. Med. (Berl)* 83, 876–886.

Bo, Z., Wan, Y., Meng, S. S., Lin, T., Kuang, W., Jiang, L., et al. (2019). The temporal trend and distribution characteristics in mortality of Alzheimer's disease and other forms of dementia in China: Based on the National Mortality Surveillance System (NMS) from 2009 to 2015. *PLoS One* 14:e0210621. doi: 10.1371/journal.pone.0210621

Bongarzone, S., Savickas, V., Luzi, F., and Gee, A. D. (2017). Targeting the receptor for advanced glycation endproducts (RAGE): a medicinal chemistry perspective. *J. Med. Chem.* 60, 7213–7232. doi: 10.1021/acs.jmedchem.7b00058

Cai, W., Zhang, K., Li, P., Zhu, L., Xu, J., Yang, B., et al. (2017). Dysfunction of the neurovascular unit in ischemic stroke and neurodegenerative diseases: an aging effect. *Ageing Res. Rev.* 34, 77–87. doi: 10.1016/j.arr.2016.09.006

Cai, Z., Liu, N., Wang, C., Qin, B., Zhou, Y., Xiao, M., et al. (2016). Role of RAGE in Alzheimer's Disease. *Cell Mol. Neurobiol.* 36, 483–495.

Cary, B. P., Brooks, A. F., Fawaz, M. V., Drake, L. R., Desmond, T. J., Sherman, P., et al. (2016). Synthesis and evaluation of [(18)F]RAGER: a first generation small-molecule PET radioligand targeting the receptor for advanced glycation endproducts. *ACS Chem. Neurosci.* 7, 391–398. doi: 10.1021/acschemneuro.5b00319

Chellappa, R. C., and Rani, P. (2020). G82S RAGE polymorphism is associated with Alzheimer's disease. *Front. Biosci. (Elite Ed.)* 12:150–161. doi: 10.2741/e864

Choi, B. R., Cho, W. H., Kim, J., Lee, H. J., Chung, C., Jeon, W. K., et al. (2014). Increased expression of the receptor for advanced glycation end products in neurons and astrocytes in a triple transgenic mouse model of Alzheimer's disease. *Exp. Mol. Med.* 46:e75. doi: 10.1038/emm.2013.147

Deane, R., Du Yan, S., Submamaryan, R. K., LaRue, B., Jovanovic, S., Hogg, E., et al. (2003). RAGE mediates amyloid-beta peptide transport across the blood-brain barrier and accumulation in brain. *Nat. Med.* 9, 907–913. doi: 10.1038/nm890

Deane, R., Sagare, A., and Zlokovic, B. V. (2008). The role of the cell surface LRP and soluble LRP in blood-brain barrier Abeta clearance in Alzheimer's disease. *Curr. Pharm. Des.* 14, 1601–1605. doi: 10.2174/138161208784705487

Deane, R., Singh, I., Sagare, A. P., Bell, R. D., Ross, N. T., LaRue, B., et al. (2012). A multimodal RAGE-specific inhibitor reduces amyloid beta-mediated brain disorder in a mouse model of Alzheimer disease. *J. Clin. Invest.* 122, 1377–1392. doi: 10.1172/jci58642

Deane, R., and Zlokovic, B. V. (2007). Role of the blood-brain barrier in the pathogenesis of Alzheimer's disease. *Curr. Alzheimer Res.* 4, 191–197. doi: 10.2174/156720507780362245

Deane, R. J. (2012). Is RAGE still a therapeutic target for Alzheimer's disease? *Future Med. Chem.* 4, 915–925. doi: 10.4155/fmc.12.51

Demling, N., Ehrhardt, C., Kasper, M., Laue, M., Knels, L., and Rieber, E. P. (2006). Promotion of cell adherence and spreading: a novel function of RAGE, the highly selective differentiation marker of human alveolar epithelial type I cells. *Cell Tissue Res.* 323, 475–488. doi: 10.1007/s00441-005-0069-0

Dubois, B., Epelbaum, S., Nyasse, F., Bakardjian, H., Gagliardi, G., Uspenskaya, O., et al. (2018). Cognitive and neuroimaging features and brain beta-amyloidosis in individuals at risk of Alzheimer's disease (INSIGHT-preAD): a longitudinal observational study. *Lancet Neurol.* 17, 335–346. doi: 10.1016/s1474-4422(18)30029-2

Dukic-Stefanovic, S., Gasic-Milenkovic, J., Deuther-Conrad, W., and Munch, G. (2003). Signal transduction pathways in mouse microglia N-11 cells activated by advanced glycation endproducts (AGEs). *J. Neurochem.* 87, 44–55. doi: 10.1046/j.1471-4159.2003.01988.x

Fang, F., Lue, L. F., Yan, S., Xu, H., Luddy, J. S., Chen, D., et al. (2010). RAGE-dependent signaling in microglia contributes to neuroinflammation, Abeta accumulation, and impaired learning/memory in a mouse model of Alzheimer's disease. *FASEB J.* 24, 1043–1055. doi: 10.1096/fj.09-139634

Fang, F., Yu, Q., Arancio, O., Chen, D., Gore, S. S., Yan, S. S., et al. (2018). RAGE mediates Abeta accumulation in a mouse model of Alzheimer's disease via modulation of beta- and gamma-secretase activity. *Hum. Mol. Genet.* 27, 1002–1014. doi: 10.1093/hmg/ddy017

Galasko, D., Bell, J., Mancuso, J. Y., Kupiec, J. W., Sabbagh, M. N., Van Dyck, C., et al. (2014). Clinical trial of an inhibitor of RAGE-Abeta

interactions in Alzheimer disease. *Neurology* 82, 1536–1542. doi: 10.1212/wnl.0000000000000364

Goldklang, M. P., Tekabe, Y., Zelonina, T., Trischler, J., Xiao, R., Stearns, K., et al. (2019). Single-photon emission computed tomography/computed tomography imaging of RAGE in smoking-induced lung injury. *Respir Res.* 20:116.

Guglielmotto, M., Aragno, M., Tamagno, E., Vercellinatto, I., Visentin, S., Medana, C., et al. (2012). AGEs/RAGE complex upregulates BACE1 via NF-kappaB pathway activation. *Neurobiol. Aging* 33, 13–27.

Han, Y. T., Kim, K., Choi, G. I., An, H., Son, D., Kim, H., et al. (2014). Pyrazole-5-carboxamides, novel inhibitors of receptor for advanced glycation end products (RAGE). *Eur. J. Med. Chem.* 79, 128–142. doi: 10.1016/j.ejmech.2014.03.072

Hannestad, J. (2018). PET imaging in psychoneuroimmunology research. *Methods Mol. Biol.* 1781, 287–307. doi: 10.1007/978-1-4939-7828-1_15

Harada, R., Okamura, N., Furumoto, S., Furukawa, K., Ishiki, A., Tomita, N., et al. (2015). [(18)F]THK-5117 PET for assessing neurofibrillary pathology in Alzheimer's disease. *Eur. J. Nucl. Med. Mol. Imaging* 42, 1052–1061. doi: 10.1007/s00259-015-3035-4

Hardy, J., and Selkoe, D. J. (2002). The amyloid hypothesis of Alzheimer's disease: progress and problems on the road to therapeutics. *Science* 297, 353–356. doi: 10.1126/science.1072994

Hong, Y., Shen, C., Yin, Q., Sun, M., Ma, Y., and Liu, X. (2016). Effects of RAGE-specific inhibitor FPS-ZM1 on amyloid-beta metabolism and ages-induced inflammation and oxidative stress in rat hippocampus. *Neurochem. Res.* 41, 1192–1199. doi: 10.1007/s11064-015-1814-8

Hoppmann, S., Haase, C., Richter, S., and Pietzsch, J. (2008). Expression, purification and fluorine-18 radiolabeling of recombinant S100 proteins–potential probes for molecular imaging of receptor for advanced glycation endproducts (RAGE) in vivo. *Protein Expr. Purif* 57, 143–152. doi: 10.1016/j.pep.2007.10.009

Hudson, B. I., Carter, A. M., Harja, E., Kalea, A. Z., Arriero, M., Yang, H., et al. (2008). Identification, classification, and expression of RAGE gene splice variants. *FASEB J.* 22, 1572–1580. doi: 10.1096/fj.07-9909com

Kamynina, A. V., Esteras, N., Koroev, D. O., Bobkova, N. V., Balasanyants, S. M., Simonyan, R. A., et al. (2018). Synthetic fragments of receptor for advanced glycation end products bind Beta-Amyloid 1-40 and protect primary brain cells from beta-amyloid toxicity. *Front. Neurosci.* 12:681.

Kim, H. Y., Wang, X., Kang, R., Tang, D., Boone, B. A., Zeh, H. J. III, et al. (2018). RAGE-specific single chain Fv for PET imaging of pancreatic cancer. *PLoS One* 13:e0192821. doi: 10.1371/journal.pone.0192821

Kim, S. J., Ahn, J. W., Kim, H., Ha, H. J., Lee, S. W., Kim, H. K., et al. (2013). Two beta-strands of RAGE participate in the recognition and transport of amyloid-beta peptide across the blood brain barrier. *Biochem. Biophys. Res. Commun.* 439, 252–257. doi: 10.1016/j.bbrc.2013.08.047

Kobayashi, R., Hayashi, H., Kawakatsu, S., Ishiki, A., Okamura, N., Arai, H., et al. (2018). [(18)F]THK-5351 PET imaging in early-stage semantic variant primary progressive aphasia: a report of two cases and a literature review. *BMC Neurol.* 18:109.

Kong, Y., Hua, F., Guan, Y., and Zhao, B. (2016). RAGE-specific probe 18F-FPS-ZM1 may be a promising biomarker for early detection of diabetes with Alzheimer's disease. *J. Nuc. Med.* 57(Suppl. 2), 1049–1049.

Konopka, C. J., Wozniak, M., Hedhli, J., Ploska, A., Schwartz-Duval, A., Siekierzycka, A., et al. (2018). Multimodal imaging of the receptor for advanced glycation end-products with molecularly targeted nanoparticles. *Theranostics* 8, 5012–5024. doi: 10.7150/thno.24791

Lemoine, L., Saint-Aubert, L., Marutle, A., Antoni, G., Eriksson, J. P., Ghetti, B., et al. (2015). Visualization of regional tau deposits using (3)H-THK5117 in Alzheimer brain tissue. *Acta Neuropathol. Commun.* 3:40. doi: 10.1016/0006-8993(93)90478-6

Li, J., Liu, D., Sun, L., Lu, Y., and Zhang, Z. (2012). Advanced glycation end products and neurodegenerative diseases: mechanisms and perspective. *J. Neurol. Sci.* 317, 1–5. doi: 10.1016/j.jns.2012.02.018

Li, X. H., Lv, B. L., Xie, J. Z., Liu, J., Zhou, X. W., and Wang, J. Z. (2012). AGEs induce Alzheimer-like tau pathology and memory deficit via RAGE-mediated GSK-3 activation. *Neurobiol. Aging* 33, 1400–1410. doi: 10.1016/j.neurobiolaging.2011.02.003

Liang, W., Zhang, W., Zhao, S., Li, Q., Liang, H., and Ceng, R. (2015). Altered expression of neurofilament 200 and amyloid-beta peptide (1-40) in a rat model of chronic cerebral hypoperfusion. *Neurol. Sci.* 36, 707–712. doi: 10.1007/s10072-014-2014-z

Lim, Y. Y., Maruff, P., Pietrzak, R. H., Ames, D., Ellis, K. A., Harrington, K., et al. (2014). Effect of amyloid on memory and non-memory decline from preclinical to clinical Alzheimer's disease. *Brain* 137(Pt 1), 221–231. doi: 10.1093/brain/awt286

Luzi, F., Savickas, V., Taddei, C., Hader, S., Singh, N., Gee, A. D., et al. (2020). Radiolabeling of [(11)C]FPS-ZM1, a receptor for advanced glycation end products-targeting positron emission tomography radiotracer, using a [(11)C]CO2-to-[(11)C]CO chemical conversion. *Future Med. Chem.* 12, 511–521. doi: 10.4155/fmc-2019-0329

Lv, C., Wang, L., Liu, X., Cong, X., Yan, S. S., Wang, Y., et al. (2014). Geniposide attenuates oligomeric Abeta(1-42)-induced inflammatory response by targeting RAGE-dependent signaling in BV2 cells. *Curr. Alzheimer Res.* 11, 430–440. doi: 10.2174/1567205011666140514111204

Lv, C., Wang, L., Liu, X., Yan, S., Yan, S. S., Wang, Y., et al. (2015). Multi-faced neuroprotective effects of geniposide depending on the RAGE-mediated signaling in an Alzheimer mouse model. *Neuropharmacology* 89, 175–184. doi: 10.1016/j.neuropharm.2014.09.019

Maesako, M., Zoltowska, K. M., and Berezovska, O. (2019). Synapsin 1 promotes Abeta generation via BACE1 modulation. *PLoS One* 14:e0226368. doi: 10.1371/journal.pone.0226368

Mankoff, D. A., and Katz, S. I. (2018). PET imaging for assessing tumor response to therapy. *J. Surg. Oncol.* 118, 362–373. doi: 10.1002/jso.25114

McCluskey, S. P., Plisson, C., Rabiner, E. A., and Howes, O. (2020). Advances in CNS PET: the state-of-the-art for new imaging targets for pathophysiology and drug development. *Eur. J. Nucl. Med. Mol. Imaging* 47, 451–489. doi: 10.1007/s00259-019-04488-0

Nam, J. H., Park, K. W., Park, E. S., Lee, Y. B., Lee, H. G., Baik, H. H., et al. (2012). Interleukin-13/-4-induced oxidative stress contributes to death of hippocampal neurons in abeta1-42-treated hippocampus in vivo. *Antioxid Redox Signal* 16, 1369–1383. doi: 10.1089/ars.2011.4175

Nasser, M. W., Wani, N. A., Ahirwar, D. K., Powell, C. A., Ravi, J., Elbaz, M., et al. (2015). RAGE mediates S100A7-induced breast cancer growth and metastasis by modulating the tumor microenvironment. *Cancer Res.* 75, 974–985. doi: 10.1158/0008-5472.can-14-2161

Nebel, R. A., Aggarwal, N. T., Barnes, L. L., Gallagher, A., Goldstein, J. M., Kantarci, K., et al. (2018). Understanding the impact of sex and gender in Alzheimer's disease: a call to action. *Alzheimers Dement* 14, 1171–1183. doi: 10.1016/j.jalz.2018.04.008

Nelson, A. R., Sweeney, M. D., Sagare, A. P., and Zlokovic, B. V. (2016). Neurovascular dysfunction and neurodegeneration in dementia and Alzheimer's disease. *Biochim. Biophys. Acta* 1862, 887–900. doi: 10.1016/j.bbadis.2015.12.016

Nenna, A., Spadaccio, C., Lusini, M., Ulianich, L., Chello, M., and Nappi, F. (2015). Basic and clinical research against advanced glycation end products (AGEs): new compounds to tackle cardiovascular disease and diabetic complications. *Recent Adv. Cardiovasc. Drug. Discov.* 10, 10–33. doi: 10.2174/1574890110666151104120039

Passamonti, L., Rodriguez, P. V., Hong, Y. T., Allinson, K. S., Williamson, D., Borchert, R. J., et al. (2017). 18F-AV-1451 positron emission tomography in Alzheimer's disease and progressive supranuclear palsy. *Brain* 140, 781–791.

Paudel, Y. N., Angelopoulou, E., Piperi, C., Othman, I., Aamir, K., and Shaikh, M. F. (2020). Impact of HMGB1, RAGE, and TLR4 in Alzheimer's disease (AD): from risk factors to therapeutic targeting. *Cells* 9:383. doi: 10.3390/cells9020383

Piras, S., Furfaro, A. L., Piccini, A., Passalacqua, M., Borghi, R., Carminati, E., et al. (2014). Monomeric Abeta1-42 and RAGE: key players in neuronal differentiation. *Neurobiol. Aging* 35, 1301–1308. doi: 10.1016/j.neurobiolaging.2014.01.002

Qi, L., Chen, Z., Wang, Y., Liu, X., Liu, X., Ke, L., et al. (2017). Subcutaneous liraglutide ameliorates methylglyoxal-induced Alzheimer-like tau pathology and cognitive impairment by modulating tau hyperphosphorylation and glycogen synthase kinase-3beta. *Am. J. Transl. Res.* 9, 247–260.

Qiu, L., Ng, G., Tan, E. K., Liao, P., Kandiah, N., and Zeng, L. (2016). Chronic cerebral hypoperfusion enhances Tau hyperphosphorylation and reduces autophagy in Alzheimer's disease mice. *Sci. Rep.* 6:23964.

Rabinovici, G. D., Furst, A. J., O'Neil, J. P., Racine, C. A., Mormino, E. C., Baker, S. L., et al. (2007). 11C-PIB PET imaging in Alzheimer disease and frontotemporal lobar degeneration. *Neurology* 68, 1205–1212. doi: 10.1212/01.wnl.0000259035.98480.ed

Ray, R., Juranek, J. K., and Rai, V. (2016). RAGE axis in neuroinflammation, neurodegeneration and its emerging role in the pathogenesis of amyotrophic lateral sclerosis. *Neurosci. Biobehav. Rev.* 62, 48–55. doi: 10.1016/j.neubiorev.2015.12.006

Robertson, J. S., Rowe, C. C., and Villemagne, V. L. (2017). Tau imaging with PET: an overview of challenges, current progress, and future applications. *Q. J. Nucl. Med. Mol. Imaging* 61, 405–413.

Saint-Aubert, L., Lemoine, L., Chiotis, K., Leuzy, A., Rodriguez-Vieitez, E., and Nordberg, A. (2017). Tau PET imaging: present and future directions. *Mol. Neurodegener.* 12:19.

Shan, L. (2004). *(99m)Tc-Labeled Anti-Receptor for Advanced Glycation Endproducts Polyclonal Antibody F(ab')2 Fragments*. Bethesda, MD: Molecular Imaging and Contrast Agent Database (MICAD).

Sole, M., Esteban-Lopez, M., Taltavull, B., Fabregas, C., Fado, R., Casals, N., et al. (2019). Blood-brain barrier dysfunction underlying Alzheimer's disease is induced by an SSAO/VAP-1-dependent cerebrovascular activation with enhanced Abeta deposition. *Biochim. Biophys. Acta Mol. Basis Dis.* 1865, 2189–2202. doi: 10.1016/j.bbadis.2019.04.016

Son, S. M., Jung, E. S., Shin, H. J., Byun, J., and Mook-Jung, I. (2012). Abeta-induced formation of autophagosomes is mediated by RAGE-CaMKKbeta-AMPK signaling. *Neurobiol. Aging* 33, 1006.e11–23.

Sparvero, L. J., Asafu-Adjei, D., Kang, R., Tang, D., Amin, N., Im, J., et al. (2009). RAGE (Receptor for Advanced Glycation Endproducts), RAGE ligands, and their role in cancer and inflammation. *J. Transl. Med.* 7:17. doi: 10.1186/1479-5876-7-17

Srikanth, V., Maczurek, A., Phan, T., Steele, M., Westcott, B., Juskiw, D., et al. (2011). Advanced glycation endproducts and their receptor RAGE in Alzheimer's disease. *Neurobiol. Aging* 32, 763–777. doi: 10.1016/j.neurobiolaging.2009.04.016

Tekabe, Y., Luma, J., Einstein, A. J., Sedlar, M., Li, Q., Schmidt, A. M., et al. (2010). A novel monoclonal antibody for RAGE-directed imaging identifies accelerated atherosclerosis in diabetes. *J. Nucl. Med.* 51, 92–97. doi: 10.2967/jnumed.109.064659

Valotassiou, V., Malamitsi, J., Papatriantafyllou, J., Dardiotis, E., Tsougos, I., Psimadas, D., et al. (2018). SPECT and PET imaging in Alzheimer's disease. *Ann. Nucl. Med.* 32, 583–593.

Villemagne, V. L., Burnham, S., Bourgeat, P., Brown, B., Ellis, K. A., Salvado, O., et al. (2013). Amyloid beta deposition, neurodegeneration, and cognitive decline in sporadic Alzheimer's disease: a prospective cohort study. *Lancet Neurol.* 12, 357–367. doi: 10.1016/s1474-4422(13)70044-9

Wan, W., Cao, L., Liu, L., Zhang, C., Kalionis, B., Tai, X., et al. (2015). Abeta(1-42) oligomer-induced leakage in an in vitro blood-brain barrier model is associated with up-regulation of RAGE and metalloproteinases, and down-regulation of tight junction scaffold proteins. *J. Neurochem.* 134, 382–393. doi: 10.1111/jnc.13122

Wang, M. Y., Ross-Cisneros, F. N., Aggarwal, D., Liang, C. Y., and Sadun, A. A. (2009). Receptor for advanced glycation end products is upregulated in optic neuropathy of Alzheimer's disease. *Acta Neuropathol.* 118, 381–389. doi: 10.1007/s00401-009-0513-4

Wang, X., Yu, S., Hu, J. P., Wang, C. Y., Wang, Y., Liu, H. X., et al. (2014). Streptozotocin-induced diabetes increases amyloid plaque deposition in AD transgenic mice through modulating AGEs/RAGE/NF-kappaB pathway. *Int. J. Neurosci.* 124, 601–608. doi: 10.3109/00207454.2013.866110

Wells, J. A., Holmes, H. E., O'Callaghan, J. M., Colgan, N., Ismail, O., Fisher, E. M., et al. (2015). Increased cerebral vascular reactivity in the tau expressing rTg4510 mouse: evidence against the role of tau pathology to impair vascular health in Alzheimer's disease. *J. Cereb. Blood Flow. Metab.* 35, 359–362. doi: 10.1038/jcbfm.2014.224

Wolf, S., Haase-Kohn, C., Lenk, J., Hoppmann, S., Bergmann, R., Steinbach, J., et al. (2011). Expression, purification and fluorine-18 radiolabeling of recombinant S100A4: a potential probe for molecular imaging of receptor for advanced glycation endproducts in vivo? *Amino. Acids* 41, 809–820. doi: 10.1007/s00726-010-0822-x

Wong, K. H., Riaz, M. K., Xie, Y., Zhang, X., Liu, Q., Chen, H., et al. (2019). Review of current strategies for delivering alzheimer's disease drugs across the blood-brain barrier. *Int. J. Mol. Sci.* 20:381. doi: 10.3390/ijms20020381

Wu, B., Wang, Y., Shi, C., Chen, Y., Yu, L., Li, J., et al. (2019). Ribosylation-derived advanced glycation end products induce tau hyperphosphorylation through brain-derived neurotrophic factor reduction. *J. Alzheimers Dis.* 71, 291–305. doi: 10.3233/jad-190158

Xue, J., Rai, V., Singer, D., Chabierski, S., Xie, J., Reverdatto, S., et al. (2011). Advanced glycation end product recognition by the receptor for AGEs. *Structure* 19, 722–732. doi: 10.1016/j.str.2011.02.013

Yan, S. D., Chen, X., Fu, J., Chen, M., Zhu, H., Roher, A., et al. (1996). RAGE and amyloid-beta peptide neurotoxicity in Alzheimer's disease. *Nature* 382, 685–691.

Zhang, Z., Liu, S., Shi, R., and Zhao, G. (2011). miR-27 promotes human gastric cancer cell metastasis by inducing epithelial-to-mesenchymal transition. *Cancer Genet.* 204, 486–491. doi: 10.1016/j.cancergen.2011.07.004

Conflict of Interest: The authors declare that the research was conducted in the absence of any commercial or financial relationships that could be construed as a potential conflict of interest.

frontiers in Aging Neuroscience

ORIGINAL RESEARCH
published: 12 August 2020
doi: 10.3389/fnagi.2020.00246

Disrupted Functional Network Connectivity Predicts Cognitive Impairment in Presbycusis Patients

Chunhua Xing[1†], Juan Zhang[2†], Jinluan Cui[1], Wei Yong[1], Jinghua Hu[3], Xindao Yin[1], Yuanqing Wu[3] and Yu-Chen Chen[1]**

[1]Department of Radiology, Nanjing First Hospital, Nanjing Medical University, Nanjing, China, [2]Department of Neurology, Nanjing Yuhua Hospital, Yuhua Branch of Nanjing First Hospital, Nanjing, China, [3]Department of Otolaryngology, Nanjing First Hospital, Nanjing Medical University, Nanjing, China

Purpose: Individuals with presbycusis often show deficits in cognitive function, however, the exact neurophysiological mechanisms are not well understood. This study explored the alterations in intra- and inter-network functional connectivity (FC) of multiple networks in presbycusis patients, and further correlated FC with cognitive assessment scores to assess their ability to predict cognitive impairment.

Methods: Resting-state functional magnetic resonance imaging (rs-fMRI) was performed in 40 presbycusis patients and 40 matched controls, and 12 resting-state networks (RSNs) were identified by independent component analysis (ICA) approach. A two-sample *t*-test was carried out to detect the intra-network FC differences, and functional network connectivity (FNC) was calculated to compare the inter-network FC differences. Pearson or Spearman correlation analysis was subsequently used to explore the correlation between altered FC and cognitive assessment scores.

Results: Our study demonstrated that patients with presbycusis showed significantly decreased FC in the subcortical limbic network (scLN), default mode network (DMN), executive control network (ECN), and attention network (AN) compared with the control group. Moreover, the connectivity for scLN-AUN (auditory network) and VN (visual network)-DMN were found significantly increased while AN-DMN was found significantly decreased in presbycusis patients. Ultimately, this study revealed the intra- and inter-network alterations associated with some cognitive assessment scores.

Conclusion: This study observed intra- and inter-network FC alterations in presbycusis patients, and investigated that presbycusis can lead to abnormal connectivity of RSNs and plasticity compensation mechanism, which may be the basis of cognitive impairment, suggesting that FNC can be used to predict potential cognitive impairment in their early stage.

Keywords: presbycusis, cognitive impairment, brain network, resting-state fMRI, functional network connectivity

OPEN ACCESS

Edited by:
Jiehui Jiang,
Shanghai University, China

Reviewed by:
Zhenyu Xiong,
University of Texas Southwestern Medical Center, United States
Rafael Romero-Garcia,
University of Cambridge, United Kingdom

***Correspondence:**
Yuanqing Wu
cnnxdd@163.com
Yu-Chen Chen
chenyuchen1989@126.com

†These authors have contributed equally to this work

Received: *13 May 2020*
Accepted: *17 July 2020*
Published: *12 August 2020*

Citation:
Xing C, Zhang J, Cui J, Yong W, Hu J, Yin X, Wu Y and Chen Y-C (2020) Disrupted Functional Network Connectivity Predicts Cognitive Impairment in Presbycusis Patients. Front. Aging Neurosci. 12:246. doi: 10.3389/fnagi.2020.00246

INTRODUCTION

Presbycusis, also known as age-related hearing loss, results from lifetime damage to the auditory system and can be defined as progressive bilateral sensorineural high-frequency hearing loss (Gates and Mills, 2005). Presbycusis has become the third leading chronic health disorder affecting elderly over the age of 65 after hypertension and arthritis (GBD 2015 Disease and Injury Incidence and Prevalence Collaborators, 2016), which mainly characterized by slow central processing of acoustic information, impaired localization of sound sources, and reduced ability to distinguish speech under noisy environments (Gates and Mills, 2005; Tavanai and Mohammadkhani, 2017). Lots of robust research evidence suggests that presbycusis not only causes alterations of function and morphology in specific brain areas, but also independently associated with cognitive decline, increasing the risk of dementia, and impaired performance across cognitive domains (Thomson et al., 2017; Ford et al., 2018; Loughrey et al., 2018), this results in a serious adverse impact on their daily life and social interaction of elderly. Early detection and prevention have supposed to be the most potential approaches in dealing with cognitive impairment. Therefore, the recognition of early cognitive impairment is of great importance for patients with presbycusis.

Resting-state functional magnetic resonance imaging (rs-fMRI) does not require subjects to receive any sensory stimuli or perform a specific task, thus, it is widely used in describing abnormal brain neuronal activity and functional connectivity (FC) in various clinical conditions (Biswal et al., 1995). FC refers to measuring the temporal synchronization of neuronal activity between different brain regions within resting-state networks (RSNs), reflecting the functional status of the corresponding brain regions (Geerligs et al., 2015). Therefore, the use of this technology to map the Spatio-temporal covariance structure of spontaneous brain activity networks is increasing, which will provide an in-depth understanding of the neural mechanisms for cognitive impairment in presbycusis. A growing body of research has indicated that auditory and cognitive processing are tightly related and that patients with hearing loss recruit functions of the executive network to maintain communication, leading to cascading cognitive effects that further affect comprehension, perception and working memory (Peelle and Wingfield, 2016; Loughrey et al., 2018). Previous research has found that hearing loss was associated with decreased volume in the temporal lobe, which is responsible for semantic memory and sensory integration, and the atrophy of the temporal lobe may be involved in the early stage of mild cognitive impairment (Fortunato et al., 2016). Another finding suggested that during effortful speech perception in the hearing-impaired showed increased activation of the frontal lobe, which leads to fewer resources of frontal lobes for cognition and indirectly affected the high-level cognitive processes. Moreover, hearing loss can lead to impaired auditory-limbic network FC (Rutherford et al., 2018), and resulted in a cross-modal plastic reorganization of the auditory cortex. Even mild hearing loss affects the transmission of information within the auditory-linguistic-motor circuits (Bidelman et al., 2019).

Taken together, cognitive impairment in presbycusis most likely depends on system-level disruption of brain networks, namely the internal interactions of different brain regions in one network or the interactions among multiple networks, rather than the dysfunction of a single discrete brain region. However, conventional seed-based FC researches rely on the user's self-defined region of interest (ROI; Lv et al., 2018) and fail to fully investigate the interaction between the brain networks of presbycusis patients. Independent component analysis (ICA) using a data-driven method (McKeown et al., 1998) without prior experimental models or assumptions decompose BOLD signal from the whole brain voxels into spatially and temporally independent components (ICs), which has been widely used in rs-fMRI and is capable of measuring interactions within and between multiple brain networks directly. Among them, resting-state function network connectivity (FNC) can be used to describe the temporal correlation between these RSNs (Wang et al., 2014; Qin et al., 2018). At present, ICA studies on the connectivity changes within and between networks in presbycusis have not been reported, just a few studies focused on intra-network FC alteration (Schmidt et al., 2013; Luan et al., 2019). Therefore, we predict that by exploring RSNs and FNC to elucidate the impairment and compensation patterns of cognitive impairment in presbycusis patients will provide valuable information for rational treatment.

This study aims to systematically explore FC and their interactions within and between RSNs in presbycusis patients and to provide new reliable markers for identifying early cognitive impairments. We will experimentally validate the following hypothesis: first, the cognitive impairment in presbycusis patients is related to the disrupted FC of multiple RSNs; second, in addition to changes within the network, changes between networks may also be associated with cognitive impairment.

MATERIALS AND METHODS

Subjects

A total of 40 presbycusis patients were recruited from the otolaryngology department, and 40 age-, gender-, education-, and handedness matched control subjects were selected from community health census or online advertising. Based on the definition of hearing loss, all participants underwent the hearing loss assessment using the speech-frequency pure tone average (PTA) of the 0.25, 0.5, 1, 2, 4, 8 kHz (air conduction) threshold in the better hearing ears. The PTA value of 25 dB HL is the normal listening threshold limit. No significant difference in the auditory threshold between the experimental and control group was observed; and middle ear function was measured by using Madsen Electronics Zodiac 901 Middle Ear Analyzer (GN Otometrics).

Exclusion criteria were as follows: (1) in addition to presbycusis, ear diseases that impacted hearing threshold,

including tinnitus, hyperacusis and Meniere's disease (Lopez-Escamez et al., 2015); (2) a history of otologic surgery, ototoxic drug therapy, noise exposure or hearing aid use; (3) asymmetric hearing loss, with the difference of air conduction threshold exceeding 20 dB, and at least two frequencies between 0.5, 1, 2 and 4 kHz; (4) severe smoking, alcohol abuse, brain damage, Alzheimer's disease, Parkinson's disease, major depression, epilepsy, mental or neurological disorders, major diseases (such as anemia, thyroid dysfunction, cancer); and (5) a contraindication to MRI.

Neuropsychological Assessment

The neuropsychological assessment of all participants required a comprehensive test of cognitive status, including the use of Mini-Mental State Exam (MMSE; Ardila et al., 2016) and Montreal Cognitive Assessment (MoCA; Lu et al., 2011) to assess general cognitive function, Auditory Verbal Learning Test (AVLT and AVLT-delay; Xu et al., 2020) and Complex Figure Test (CFT and CFT-delay; Shin et al., 2006) for episodic verbal learning as well as visual memory recall, Digit Span Test (DST; Gabel et al., 2019) for verbal working memory. Executive control was assessed by Trail-Making Test A and B (TMT-A and TMT-B; Sánchez-Cubillo et al., 2009) and Clock-Drawing Test (CDT; Viscogliosi et al., 2017), besides mental processing speed and visuospatial abilities were evaluated by Digit Symbol Substitution Test (DSST; Rosano et al., 2013) and Verbal Fluency Test (VFT; Brucki and Rocha, 2004). Also, the Self-Rating Anxiety Scale (SAS; Song et al., 2014) and Self-Rating Depression Scale (SDS; Zung, 1971) were used to assess the symptoms of anxiety and depression. There are a total of 14 cognitive tests and it took almost 60 min for each individual to finish this battery of orderly tests.

Imaging Data Acquisition

All imaging data acquisitions were performed on a 3.0 Tesla Philips MRI scanner (Ingenia, Netherlands) with an eight-channel phased-array head coil. Resting-state functional images were acquired axially using a gradient echo-planar imaging sequence as following parameters: repetition time (TR) = 2,000 ms, echo time (TE) = 30 ms, slices = 36, thickness = 4 mm, gap = 0 mm, field of view (FOV) = 240 mm × 240 mm, acquisition matrix = 64 × 64, and flip angle (FA) = 90°, the voxel size was 3.75 × 3.75 × 4.0 mm^3; and this sequence lasted 8 min and 8 s. Structural images were obtained using a three-dimensional turbo fast echo (3D-TFE) T1WI sequence and following scan parameters: TR/TE = 8.1/3.7 ms, slices = 170, thickness = 1 mm, gap = 0 mm, FOV = 256 mm × 256 mm, acquisition matrix = 256 × 256, and FA = 8°. The structural sequence lasted 5 min and 29 s. Besides, all scans were acquired with parallel imaging using sensitivity encoding (SENSE) technique and SENSE factor = 2.

During the scan, the participants were instructed to lie quietly and keep still, with eyes closed but not asleep or think about anything special. Meanwhile, foam padding was used to reduce the involuntary movement of the head, and earplugs were used to reduce the influence of noise on the participants. According to the manufacturer's specifications, the earplugs (Hearos Ultimate Softness Series, USA) could attenuate scanner noise by almost 32 dB.

Preprocessing of Functional Imaging Data

GRETNA (Graph Theoretical Network Analysis) was applied to preprocess the functional image data for further analysis (Wang et al., 2015), involving the following steps. First, the first 10 volumes were removed to allow for an equilibrium of the magnetization and adaptation of the participants to the scanning environment. Then the remaining volumes were sliced for timing (slice timing) and corrected for head motion (realignment). Since micromovements from volume to volume can influence the FC, framewise displacement (FD) values were computed for each subject to reflect the temporal derivative of the movement parameters. Time points that exceeded a max FD of 0.5 mm were excluded from subsequent analyses. The corrected volumes were spatially normalized to the Montreal Neurological Institute space with resampled voxel size = 3 × 3 × 3 mm^3, and finally spatially smoothed with a Gaussian smooth kernel (full width at half-maximum of 6 mm).

Identification of Resting-State Networks

The group ICA software (Medical Image Analysis Lab, University of New Mexico, Albuquerque, NM, USA[1]) was used to implement the spatial group ICA and identify RSNs. ICA analysis is performed in three phases: (1) data reduction; (2) application of ICA algorithm; and (3) back reconstruction for each subject. The number of ICs over all subjects was estimated using the minimum description-length (MDL) criteria. In phase one, principal component analysis (PCA) was used to reduce computational complexity, then the remaining reduction step was achieved again using PCA based on a selected number of ICs. In phase two, the infomax algorithm was used to run the proper ICA. In the final phase, Single-subject individual time courses and spatial maps were group ICA (GICA) type back-reconstructed and results were converted into z-scores to display.

Intra-network Functional Connectivity Analysis

Among the 40 components arising from ICA, 12 components (eight meaningful RSNs) were selected as the focus of subsequent analysis through visual inspection based on previous rs-fMRI studies. For each RSNs, a one-sample *t*-test was first performed to obtain z-maps for each group, which were corrected by false discovery rate (FDR) method, and the statistical figure was obtained at the threshold of $p < 0.05$. The spatial maps of the components were used as variables for a one-sample *t*-test. Each mask of the control group and presbycusis was further combined into a total mask for each component. Then, the z-maps of RSN were compared between groups using a two-sample *t*-test of voxel restricted within the combination mask. The comparison results were corrected $p < 0.01$, with a Monte Carlo simulation for multiple comparisons (AlphaSim

[1] http://icatb.sourceforge.net

correction[2]), and the regions of significant differences were selected from each RSNs to facilitate further analysis.

Inter-network Functional Connectivity Analysis

After ICA, the spatiotemporal double regression method was used to obtain the individual level time courses of the identified RSNs. Then, FNC analysis was carried out to study the relationship between different RSNs time courses. During the analysis, a temporal band-pass filter (range from 0.00 to 0.25 Hz) is first applied to the time courses to reduce the effects of low-frequency drift and high-frequency physiological noise. Secondly, the correlations were calculated between any two RSNs time courses of each subject. Then the FNC, also known as temporal correlation, is obtained by calculating the Pearson correlation coefficient of the time courses of selected RSNs and generate the 13×13 matrix. A general linear model (GLM) with age, sex as covariates was finally used to analyze which pairs of RSNs were significantly different between controls and patients. The significance threshold was $p < 0.05$, corrected for multiple comparisons using FDR.

Correlations With Neuropsychological Assessment

To further investigate the relationship between connectivity anomalies and cognitive impairment in patients with presbycusis, we performed the correlation analysis between the abnormal connectivity regions detected and neuropsychological assessment scores. That is, for the inter-network FC, the brain region with a significant difference in the two-sample *t*-test was selected as the ROIs and the coordinates of ROIs were extracted. Then, the mean z-scores within ROI were used to illustrate the correlation. Also, for intra-network FC, significant differences among the three groups were detected at the level of 12 components, and its FNC coefficients were used to calculate the correlation with assessment scores.

Statistical Analyses

To investigate the difference between presbycusis patients and healthy controls for demographic and clinical information, the chi-square test was applied to the categorical variables and independent two-sample *t*-test for continuous variables, both conducted by the IBM SPSS 19.0 package, $p < 0.05$ was considered statistically significant. Then, we used Cohen's *d* to describe the effect size (ES) of each clinical variable. Meanwhile, for RSNs and FNC analysis, a two-sample *t*-test was performed to conducted group comparison between presbycusis patients and healthy controls, and results were corrected for AlphaSim ($p < 0.01$) and FDR method ($p < 0.05$), separately. Pearson or Spearman correlation was used to exam the relationship between FC and neuropsychological test scores with a statistical significance level $p < 0.05$. During all this analysis, SPM8 (statistical parametric mapping) was used to carry out the voxel-level statistical analysis of RSNs, and MATLAB function (MATLAB 2013a) was used for FNC group comparison and other correlation analysis. Bonferroni correction for multiple comparisons was used in the correlation analysis.

[2] https://afni.nimh.nih.gov/pub/dist/doc/manual/AlphaSim.pdf

RESULTS

Clinical Characteristics and Neuropsychological Data

The clinical characteristics as well as the neuropsychological results of presbycusis patients and the control group were summarized in **Tables 1**, **2**. There were no significant differences in the aspect of age, gender, and education level. All participants had a type-A tympanometry curve, suggesting the normal function of the middle ear. No significant difference was observed in PTA between the left and right ear of the presbycusis and the control group. The average hearing thresholds of both ears in presbycusis and control group were shown in **Figure 1**. The average PTA of presbycusis patients was significantly higher than that of the control group ($p < 0.001$, 1,000–8,000 Hz). In neuropsychological assessment, patients with presbycusis performed significantly worse on DST and TMT-B scores ($p < 0.05$). The other neuropsychological tests did not show any significant differences between the two groups. No subjects had max FD > 0.5 mm on more than 35 volumes in this study. No significant difference was found in the mean and max FD values between presbycusis patients and controls.

Resting-State Networks

By using ICA approach, we obtained a cluster of 12 ICs and identified the eight meaningful RSNs (**Figure 2**), which is similar to previously reported research and including the following networks: the subcortical limbic network (scLN; IC2), which located throughout striatum and extends into the thalamus, brainstem, hippocampus, and amygdala. Auditory network (AUN; IC25) mainly consists of superior temporal gyrus and middle temporal gyrus which corresponded to the auditory system. The Default-mode network (DMN; IC3 + 32), includes the anterior region and the posterior region, the anterior region comprises the medial prefrontal cortex and the anterior cingulate cortex, and the posterior region mainly involves the posterior cingulate cortex/precuneus, bilateral inferior parietal cortex, and angular gyrus. The executive control network (ECN; IC21 + 27), primarily contains the bilateral dorsolateral prefrontal cortex and the lateral parietal cortex. Attention network (AN; IC28 + 30) is captured in two components, named as dorsal AN and ventral AN, including the following areas: the bilateral intraparietal sulcus, frontal eye field, ventral parietal cortex, and inferior frontal gyrus (IFG). Sensorimotor network (SMN; IC4 + 22) centered on the bilateral primary somatosensory cortex, mainly including precentral gyrus and postcentral gyrus. Also, visual network (VN; IC6) and cerebellum network (CN; IC26) were in agreement with the anatomical and functional delineations of the occipital lobe and cerebellar cortex, respectively.

Altered FC Within RSNs

Compared with the controls, presbycusis patients showed significant FC differences in four RSNs including the scLN, DMN, ECN, and AN, all of which revealed the decreased

TABLE 1 | Demographics of the presbycusis patients and healthy controls.

	Presbycusis patients (n = 40)	Healthy controls (n = 40)	p-value
Age (years)	61.35 ± 5.05	61.30 ± 3.89	0.961
Sex (male: female)	20/20	17/23	0.501
Education levels (years)	10.45 ± 1.84	10.58 ± 1.53	0.742
PTA of the left ear (dB HL)	32.27 ± 4.71	16.17 ± 2.98	<0.001*
PTA of the right ear (dB HL)	32.88 ± 6.58	16.02 ± 3.17	<0.001*
Mean PTA of both ears (dB HL)	32.32 ± 4.24	15.92 ± 2.58	<0.001*
Mean FD value (mm)	0.20 ± 0.06	0.19 ± 0.06	0.291
Max FD value (mm)	0.44 ± 0.05	0.42 ± 0.08	0.146

*Data are represented as Mean ± SD. *P < 0.001. PTA, pure-tone audiometry; FD, framewise displacement.*

TABLE 2 | Neuropsychological tests of presbycusis patients and healthy controls.

	Presbycusis patients (n = 40)	Healthy controls (n = 40)	p-value	ES
MMSE	29.18 ± 1.06	28.68 ± 1.44	0.081	0.40
MoCA	25.68 ± 1.69	25.93 ± 1.79	0.522	0.14
AVLT	35.35 ± 7.38	34.88 ± 7.75	0.779	0.06
AVLT-delay	7.18 ± 2.23	6.75 ± 2.31	0.405	0.19
CFT	34.70 ± 1.57	34.58 ± 1.56	0.722	0.08
CFT-delay	16.70 ± 3.07	17.20 ± 2.78	0.447	0.17
TMT-A	70.73 ± 21.56	67.60 ± 18.36	0.487	0.16
TMT-B	195.73 ± 63.59	156.03 ± 53.52	0.003*	0.68
CDT	3.55 ± 0.55	3.63 ± 0.54	0.541	0.15
DST	10.65 ± 1.48	11.68 ± 2.08	0.013*	0.57
VFT	13.95 ± 4.05	14.41 ± 3.71	0.596	0.12
DSST	70.13 ± 8.22	68.73 ± 9.94	0.494	0.15
SAS	36.83 ± 5.82	36.38 ± 6.04	0.735	0.08
SDS	39.03 ± 9.24	37.13 ± 8.45	0.340	0.21

*Data are represented as Mean ± SD, *p < 0.05. MMSE, Mini-Mental State Exam; MoCA, Montreal Cognitive Assessment; AVLT, Auditory Verbal Learning Test; CFT, Complex Figure Test; DST, Digit Span Test. TMT-A, Trail Making Test-Part A; TMT-B, Trail Making Test-Part B; CDT, Clock Drawing Test; VFT, Verbal Fluency Test; DSST, Digit Symbol Substitution Test; SDS, Self-Rating Depression Scale; SAS, Self-Rating Anxiety Scale; ES, effect size.*

FC in the presbycusis group (**Figure 3** and **Table 3**). For the scLN, FC decreased in the right middle cingulate gyrus (R_ middle cingulate gyrus). For the DMN, FC decreased in the left precuneus (L_Precuneus). For the ECN, FC decreased in the right Inferior Frontal Gyrus (R_IFG). And, the AN revealed the decreased FC in the right supplementary motor area (R_SMA). Besides, there were no differences in resting-state FC between controls and presbycusis groups within the AUN, SMN, VN, and CN.

Altered Inter-network FC

Significant differences in the network connectivity in scLN, AUN, DMN, AN, and VN between presbycusis and control groups for FNC analysis were found (**Figure 4**). Subsequent analysis for significant differences in FNC revealed increased connectivity between scLN (IC2) and AUN (IC25), as well as the VN (IC6) and DMN (IC3) in presbycusis group compared to control group. Relative to the control group, the presbycusis group exhibited significantly decreased inter-network connectivity in the AN (28)-DMN (32).

Correlation Analysis

Pearson or Spearman correlations were performed between the mean z-scores of 12 ROIs in the eight RSNs and cognitive assessment scores. Before multiple comparisons correction, significant correlations were found between the left precuneus within the DMN and DST scores (rho = 0.501, p = 0.001), as well as between the right IFG within the ECN and TMT-B scores (r = −0.341, p = 0.042). Moreover, after performing the correlations between the FNC coefficients (three connections) and the cognitive scores in presbycusis patients, only the AN-DMN connection was found to be positively correlated with DST scores (rho = 0.327, p = 0.040). Nevertheless, no

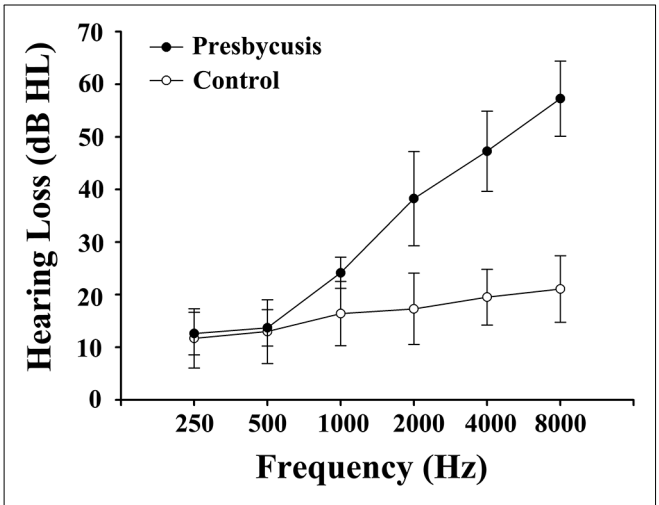

FIGURE 1 | Mean hearing thresholds of the presbycusis and control groups from 250 Hz to 8,000 Hz. Data are presented as mean ± SD.

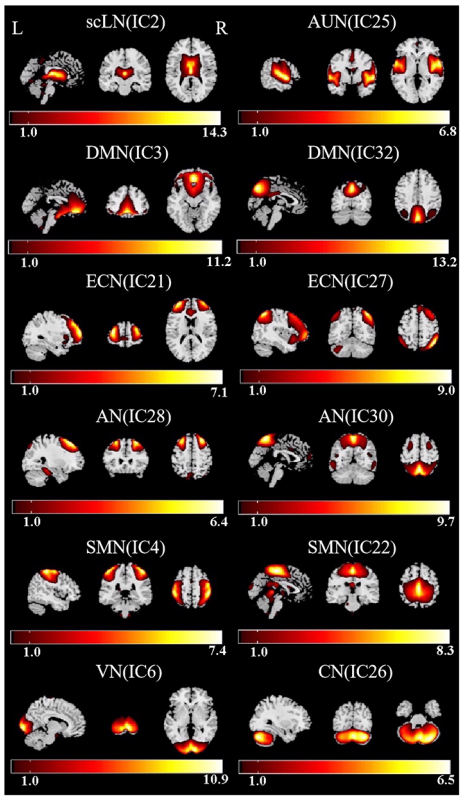

FIGURE 2 | Functional relevant resting-state networks (RSNs). The spatial maps of 12 independent components (ICs) were selected as the RSNs for further analysis. AUN, Auditory network; DMN, default mode network; ECN, executive control network; AN, attention network; SMN, sensorimotor network; VN, visual network; CN, cerebellum network.

significant correlations persisted after Bonferroni correction. Also, no significant associations between FD value and network connectivity in each RSNs were found in this study.

DISCUSSION

To our knowledge, this study is the first time using the ICA approach to detect the intra- and inter-network FC and their relationship with cognitive function in patients with presbycusis. Four brain networks were found to be abnormal in presbycusis patients compared with the controls, including scLN, DMN, ECN, and AN. Meanwhile, increased or decreased alterations of the inter-network functional coupling were found in the three functional connections in presbycusis patients through FNC analysis. And in presbycusis patients, only DST and TMT-B were found significant in cognitive performance, which may indicate that cognitive impairment is mainly manifested in the level of working memory and executive control function.

Analysis of RSNs internal FC focuses on the interaction of multiple networks in a certain spatial pattern (Beckmann et al., 2005). In this study, presbycusis patients observed reduced FC in the right middle cingulate gyrus for scLN. It is well known that scLN carries a variety of functions, including emotion, behavioral motivation, cognition, and memory processing (Morgane et al., 2005). A previous study found that in patients with sudden sensorineural hearing loss showed increased nodal betweenness of the limbic network, which may suggest a plastic compensatory mechanism to lessen the consequences of nerve damage caused by hearing loss and help maintain the patient's cognitive abilities (Xu et al., 2016). Our research found reduced FC in the middle cingulate gyrus, suggesting the possibility of cognitive impairment in presbycusis patients. The middle cingulate gyrus forms an important component of the limbic system and is widely connected to neighboring brain regions *via* bundles of white matter fibers (Powell et al., 2018). Moreover, this study believes that the change stems from hearing impairment patients with persistent pressure on speech perception, which leads to reduced adaptive activity in the limbic network involved in the emotional processing of sounds.

As we know, the DMN controls both primary perception and advanced cognition and is responsible for the integration of these two (Zhao et al., 2018). Studies by Chen et al. (2018) indicated that compared with healthy controls, patients with hearing impairment showed reduced spontaneous neuronal activity in the precuneus. Also, decreased FC between the dorsal AN and the precuneus in patients with hearing loss has been emerging understanding. It is however not the hearing loss itself associated with reduced FC but the individually perceived listening effort that occurs as a result of hearing loss (Rosemann and Thiel, 2019). Moreover, the precuneus is functionally involved in episodic memory retrieval, self-awareness and processing, and is a critical element of the DMN (Cunningham et al., 2017; Feldstein Ewing and Chung, 2019). Meanwhile, we also found that the FC in the left precuneus within the DMN was associated with the DST score, implicating the disrupted working memory in presbycusis patients.

The ECN is involved in numerous advanced cognitive tasks and plays an important role in adaptive cognitive control (McHugh et al., 2017). In the current study, decreased FC in the right IFG within the ECN in patients with presbycusis was appeared, and significant correlations between the right IFG and TMT-B scores were found, reflecting the abnormality of the executive control function, which is inconsistent with the previous research. A psychiatric study (Rutherford et al., 2018) identified that hearing loss leads to reduced activation in central auditory pathways, thus resulting in compensatory increased activation in the ECN. Rosemann and Thiel (2019) observed that patients with hearing loss actively recruited frontal lobe regions, which possibly reflect increased efforts in executive function. Our results actually recognized a hypothesized mechanism for the relationship between presbycusis and cognitive impairment: the reallocation of cognitive resources. External acoustic stimuli reduced as a result of hearing loss, so more neural resources are allocated to deal with the attenuation of auditory signals, while few resources correspondingly left that can be used for higher-level cognition. The right IFG is mainly implicated in sensory input processing related to expectation and attention. The decline of its function indicates the impairment of attention and the impairment of language processing (Sherman et al., 2016; Briggs et al., 2019).

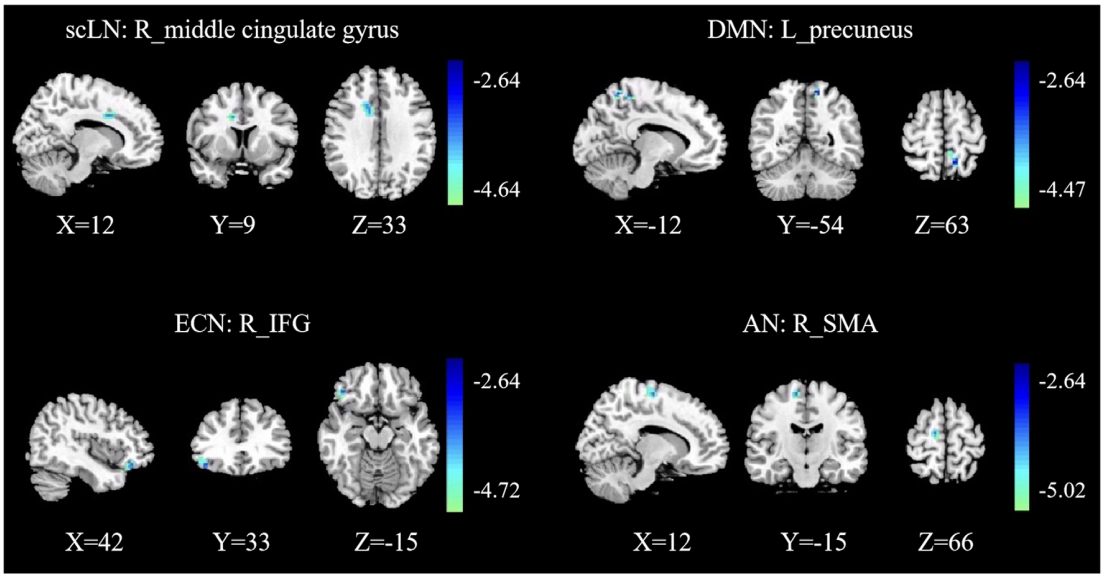

FIGURE 3 | Group functional connectivity (FC) differences within RSNs. Significant differences between the presbycusis and control groups were found within four RSNs. scLN, subcortical limbic network; DMN, default mode network; ECN, executive control network; AN, attention network; IFG, inferior frontal gyrus; SMA, supplementary motor area; R, right; L, left.

A growing body of evidence suggests that SMA is not only a motor structure but also involves in a wide range of cognitive fields (Bonini et al., 2014; Leek et al., 2016). It is generally believed that the processing of auditory is modulated by movement (Schneider and Mooney, 2018). A previous study discovered that the reduced directed FC from the SMA to the hippocampus revealed impaired sensorimotor function in patients with presbycusis (Chen et al., 2020). Panouillères and Mættænen suggested that in the old adults with hearing loss, the reduction of auditory input from the cochlea to the auditory system leads to a reduction in the recruitment of the articulatory cortex (Panouillères and Mættænen, 2018). This finding supports the hypothesis of auditory-motor decline (Skipper et al., 2017), which is in line with our results. The frontal regions depart from the primary motor cortex, passes through the intermediate premotor and SMA areas, and then head towards the prefrontal areas, thus to form an organizational structure (Fuster, 2006). Therefore, the decreased FC of SMA in presbycusis patients suggested the disruption of this organizational structure, leading to the impaired function of frontal lobe-mediated cognitive processing. The above results suggested that these four cognitive-related networks may have certain specificity in cognitive impairment mediated by presbycusis, which will help understand the neuropathological mechanism of presbycusis.

Recently, gradually increasing evidence suggested that RSNs are interdependent and continue to interact with each other (Smith et al., 2015). Our results illustrated the increased connectivity for the scLN-AUN, which may be following the conceptual model proposed by Jastreboff (1990). Our results revealed that under the condition of long-term deprivation of auditory ability and insufficient auditory input in presbycusis patients, the compensatory feedback neural activity of the scLN increased, reflecting a certain degree of plastic reorganization within the limbic network. Data from previous animal models also indicated that hearing loss promotes cortical reorganization and morphological alterations (Peelle and Wingfield, 2016). Besides, it also suggested that the auditory cortex is involved in the analysis of inputs from higher-order functions mediated by scLN. Besides, our study also demonstrated the hyper-connectivity for VN-DMN, reflecting the improvement of visual motion or peripheral spatial localization ability of patients with presbycusis, and

TABLE 3 | Brain regions with significant differences connectivity within resting-state networks (RSNs) between presbycusis patients and healthy controls.

	Brain regions	BA	Peak MNI coordinates			Peak T-value	Voxels
			x	*y*	*z*		
scLN	R_middle cingulate gyrus	32	12	9	33	−3.667	41
DMN	L_precuneus	7	−12	−54	63	−4.1241	41
ECN	R_IFG	47	42	33	−15	−3.8975	47
AN	R_SMA	6	12	−15	66	−4.0499	40

MNI, Montreal Neurologic Institute; scLN, subcortical limbic network; DMN, default mode network; ECN, executive control network; AN, attention network; IFG, inferior frontal gyrus; SMA, supplementary motor area; R, right; L, left.

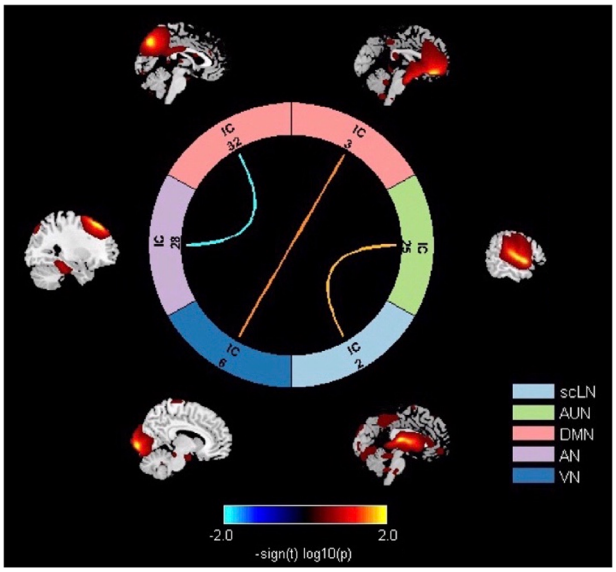

FIGURE 4 | Significant differences in the network connectivity in the subcortical limbic network (scLN), Auditory Network (AUN), default mode network (DMN), attention network (AN), and Visual Network (VN) between presbycusis and control groups.

the compensatory plastic reorganization occurs in the brain network which may be due to the lack of auditory ability. The strengthened functional coupling of the local sensory network including visual and sensory-motor areas in patients with sloping sensorineural hearing loss indicates that the auditory-deprived brain will have integrated compensation for the remaining sensory regions (Wolak et al., 2019).

The decline in attention and the reduction in the volume of the attention-related cortex reflects the impaired function of the AN (Cardin, 2016), which in turn affects the perceptual analysis and the auditory processing of acoustic signals, always occurs in presbycusis patients (Fortunato et al., 2016). Previously investigating the cross-network interaction between the DMN and the DAN, it was found that activities in DMN decreased when performing goal-directed tasks, while activities in DAN increased. This relationship suggested to be anti-correlated (Fox et al., 2009), and our result seems to reinforce this decoupling effect. That is, the FC in AN reduced to stabilize the balance from the external environment, such as auditory input. However, the reduction of perceived auditory tasks in presbycusis leads to the interruption of AN, and decrease the connectivity to key nodes of the DMN. The interruption of AN is also one of the causes of memory impairment (Veldsman et al., 2019). In addition to FNC abnormalities, a negative correlation between the AN-DMN and DST scores was also detected, showing that the dis-coupling probably relates to the disrupted working memory in presbycusis patients, and these disconnections above may also contribute to daily cognitive impairment.

Several limitations should be paid attention to. First of all, although the FC results are consistent with the previous literature, the essence of the interaction between and within different internal connectivity networks has poorly comprehended. Second, the brain networks involved in this study are limited. Because other networks may play an important role in the pathophysiology of cognitive impairment in the presbycusis, detecting the variation of the FC in multiple networks will provide insight into the neural mechanism in depth. Further researches should focus on the effects of presbycusis on other brain networks and conduct longitudinal research to predict long-term cognitive function. Moreover, no significant results persisted after Bonferroni correction for multiple comparisons in the correlation analyses due to the relatively strict method, which will be considered in further study. Nonetheless, our research is still meaningful to provide some enlightenment for future studies in this field. Finally, the newly reported rs-FC is difficult to reflect the characteristics of temporal variations within the brain network, therefore, dynamic FNC is regarded as the future research direction. Also, the directionality of the interaction between networks cannot reveal by the ICA approach, further studies are needed to assess the specific and directional function in the coupling between brain networks.

To sum up, this study suggested that the structure of intra- and inter-networks FC of presbycusis patients has undergone profound alterations. The alterations involving the primarily auditory system and other high-order cognitive control networks have demonstrated that brain network with extensive plastic reorganization during the abnormal state, which provides meaningful insights for further understanding the neural mechanism of cognitive impairment in presbycusis patients.

DATA AVAILABILITY STATEMENT

The raw data supporting the conclusions of this article will be made available by the authors, without undue reservation.

ETHICS STATEMENT

The studies involving human participants were reviewed and approved by the local institutional review board of Nanjing Medical University. The patients/participants provided their written informed consent to participate in this study. Written informed consent was obtained from the individual(s) for the publication of any potentially identifiable images or data included in this article.

AUTHOR CONTRIBUTIONS

CX and JZ designed the experiment, collected the data, performed the analysis and wrote the manuscript. JC, WY, JH, and XY collected the data. YW and Y-CC contributed to the discussion and manuscript revision.

FUNDING

This work was supported by the National Natural Science Foundation of China (Grant No. 81601477), Youth Medical Talents of Jiangsu Province (Grant No. QNRC2016062), 14th

"Six Talent Peaks" Project of Jiangsu Province (Grant No. YY-079), Nanjing Outstanding Youth Fund (Grant No. JQX17006), and 333 High-level Talents Training Project of Jiangsu Province (Grant No. BRA2019122).

REFERENCES

Ardila, A., Bernal, B., and Rosselli, M. (2016). How localized are language brain areas? A review of brodmann areas involvement in oral language. *Arch. Clin. Neuropsychol.* 31, 112–122. doi: 10.1093/arclin/acv081

Beckmann, C. F., DeLuca, M., Devlin, J. T., and Smith, S. M. (2005). Investigations into resting-state connectivity using independent component analysis. *Philos. Trans. R. Soc. Lond. B Biol. Sci.* 360, 1001–1013. doi: 10.1098/rstb.2005.1634

Bidelman, G. M., Mahmud, M. S., Yeasin, M., Shen, D., Arnott, S. R., and Alain, C. (2019). Age-related hearing loss increases full-brain connectivity while reversing directed signaling within the dorsal-ventral pathway for speech. *Brain Struct. Funct.* 224, 2661–2676. doi: 10.1007/s00429-019-01922-9

Biswal, B., Yetkin, F. Z., Haughton, V. M., and Hyde, J. S. (1995). Functional connectivity in the motor cortex of resting human brain using echo-planar MRI. *Magn. Reson. Med.* 34, 537–541. doi: 10.1002/mrm.1910340409

Bonini, F., Burle, B., Liégeois-Chauvel, C., Régis, J., Chauvel, P., and Vidal, F. (2014). Action monitoring and medial frontal cortex: leading role of supplementary motor area. *Science* 343, 888–891. doi: 10.1126/science.1247412

Briggs, R. G., Chakraborty, A. R., Anderson, C. D., Abraham, C. J., Palejwala, A. H., Conner, A. K., et al. (2019). Anatomy and white matter connections of the inferior frontal gyrus. *Clin. Anat.* 32, 546–556. doi: 10.1002/ca.23349

Brucki, S. M., and Rocha, M. S. (2004). Category fluency test: effects of age, gender and education on total scores, clustering and switching in Brazilian Portuguese-speaking subjects. *Braz. J. Med. Biol. Res.* 37, 1771–1777. doi: 10.1590/s0100-879x2004001200002

Cardin, V. (2016). Effects of aging and adult-onset hearing loss on cortical auditory regions. *Front. Neurosci.* 10:199. doi: 10.3389/fnins.2016.00199

Chen, Y. C., Chen, H., Jiang, L., Bo, F., Xu, J. J., Mao, C. N., et al. (2018). Presbycusis disrupts spontaneous activity revealed by resting-state functional MRI. *Front. Behav. Neurosci.* 12:44. doi: 10.3389/fnbeh.2018.00044

Chen, Y. C., Yong, W., Xing, C., Feng, Y., Haidari, N. A., Xu, J. J., et al. (2020). Directed functional connectivity of the hippocampus in patients with presbycusis. *Brain Imaging Behav.* 14, 917–926. doi: 10.1007/s11682-019-00162-z

Cunningham, S. I., Tomasi, D., and Volkow, N. D. (2017). Structural and functional connectivity of the precuneus and thalamus to the default mode network. *Hum. Brain Mapp.* 38, 938–956. doi: 10.1002/hbm.23429

Feldstein Ewing, S. W., and Chung, T. (2019). Precuneus: a key on the road to translation. *Alcohol. Clin. Exp. Res.* 43, 1063–1065. doi: 10.1111/acer.14026

Ford, A. H., Hankey, G. J., Yeap, B. B., Golledge, J., Flicker, L., and Almeida, O. P. (2018). Hearing loss and the risk of dementia in later life. *Maturitas* 112, 1–11. doi: 10.1016/j.maturitas.2018.03.004

Fortunato, S., Forli, F., Guglielmi, V., De Corso, E., Paludetti, G., Berrettini, S., et al. (2016). A review of new insights on the association between hearing loss and cognitive decline in ageing. *Acta Otorhinolaryngol. Ital.* 36, 155–166. doi: 10.14639/0392-100X-993

Fox, M. D., Zhang, D., Snyder, A. Z., and Raichle, M. E. (2009). The global signal and observed anticorrelated resting state brain networks. *J. Neurophysiol.* 101, 3270–3283. doi: 10.1152/jn.90777.2008

Fuster, J. M. (2006). The cognit: a network model of cortical representation. *Int. J. Psychophysiol.* 60, 125–132. doi: 10.1016/j.ijpsycho.2005.12.015

Gabel, N. M., Waldron-Perrine, B., Spencer, R. J., Pangilinan, P. H., Hale, A. C., and Bieliauskas, L. A. (2019). Suspiciously slow: timed digit span as an embedded performance validity measure in a sample of veterans with mTBI. *Brain Inj.* 33, 377–382. doi: 10.1080/02699052.2018.1553311

Gates, G. A., and Mills, J. H. (2005). Presbycusis. *Lancet* 366, 1111–1120. doi: 10.1016/S0140-6736(05)67423-5

GBD 2015 Disease and Injury Incidence and Prevalence Collaborators. (2016). Global, regional, and national incidence, prevalence and years lived with disability for 310 diseases and injuries, 1990–2015: a systematic analysis for the Global Burden of Disease Study 2015. *Lancet* 388, 1545–1602. doi: 10.1016/S0140-6736(16)31678-6

Geerligs, L., Renken, R. J., Saliasi, E., Maurits, N. M., and Lorist, M. M. (2015). A brain-wide study of age-related changes in functional connectivity. *Cereb. Cortex* 25, 1987–1999. doi: 10.1093/cercor/bhu012

Jastreboff, P. J. (1990). Phantom auditory perception (tinnitus): mechanisms of generation and perception. *Neurosci. Res.* 8, 221–254. doi: 10.1016/0168-0102(90)90031-9

Leek, E. C., Yuen, K. S., and Johnston, S. J. (2016). Domain general sequence operations contribute to pre-SMA involvement in visuo-spatial processing. *Front. Hum. Neurosci.* 10:9. doi: 10.3389/fnhum.2016.00009

Lopez-Escamez, J. A., Carey, J., Chung, W. H., Goebel, J. A., Magnusson, M., Mandala, M., et al. (2015). Diagnostic criteria for Meniere's disease. *J. Vestib. Res.* 25, 1–7. doi: 10.3233/VES-150549

Loughrey, D. G., Kelly, M. E., Kelley, G. A., Brennan, S., and Lawlor, B. A. (2018). Association of age-related hearing loss with cognitive function, cognitive impairment and dementia: a systematic review and meta-analysis. *JAMA Otolaryngol. Head Neck Surg.* 144, 115–126. doi: 10.1001/jamaoto.2017.2513

Lu, J., Li, D., Li, F., Zhou, A., Wang, F., Zuo, X., et al. (2011). Montreal cognitive assessment in detecting cognitive impairment in Chinese elderly individuals: a population-based study. *J. Geriatr. Psychiatry Neurol.* 24, 184–190. doi: 10.1177/0891988711422528

Luan, Y., Wang, C., Jiao, Y., Tang, T., Zhang, J., and Teng, G. J. (2019). Dysconnectivity of multiple resting-state networks associated with higher-order functions in sensorineural hearing loss. *Front. Neurosci.* 13:55. doi: 10.3389/fnins.2019.00055

Lv, H., Wang, Z., Tong, E., Williams, L. M., Zaharchuk, G., Zeineh, M., et al. (2018). Resting-state functional MRI: everything that nonexperts have always wanted to know. *Am. J. Neuroradiol.* 39, 1390–1399. doi: 10.3174/ajnr.a5527

McHugh, M. J., Gu, H., Yang, Y., Adinoff, B., and Stein, E. A. (2017). Executive control network connectivity strength protects against relapse to cocaine use. *Addict. Biol.* 22, 1790–1801. doi: 10.1111/adb.12448

McKeown, M. J., Makeig, S., Brown, G. G., Jung, T. P., Kindermann, S. S., Bell, A. J., et al. (1998). Analysis of fMRI data by blind separation into independent spatial components. *Hum. Brain Mapp.* 6, 160–188. doi: 10.1002/(SICI)1097-0193(1998)6:3<160::AID-HBM5>3.0.CO;2-1

Morgane, P. J., Galler, J. R., and Mokler, D. J. (2005). A review of systems and networks of the limbic forebrain/limbic midbrain. *Prog. Neurobiol.* 75, 143–160. doi: 10.1016/j.pneurobio.2005.01.001

Panouillères, M. T. N., and Mættænen, R. (2018). Decline of auditory-motor speech processing in older adults with hearing loss. *Neurobiol. Aging* 72, 89–97. doi: 10.1016/j.neurobiolaging.2018.07.013

Peelle, J. E., and Wingfield, A. (2016). The neural consequences of age-related hearing loss. *Trends Neurosci.* 39, 486–497. doi: 10.1016/j.tins.2016.05.001

Powell, R., Elwes, R., Hamandi, K., and Mullatti, N. (2018). Cingulate gyrus epilepsy. *Pract. Neurol.* 18, 447–454. doi: 10.1136/practneurol-2017-001812

Qin, Y., Li, Y., Sun, B., He, H., Peng, R., Zhang, T., et al. (2018). Functional connectivity alterations in children with spastic and dyskinetic cerebral palsy. *Neural Plast.* 2018:7058953. doi: 10.1155/2018/7058953

Rosano, C., Chang, Y. F., Kuller, L. H., Guralnik, J. M., Studenski, S. A., Aizenstein, H. J., et al. (2013). Long-term survival in adults 65 years and older with white matter hyperintensity: association with performance on the digit symbol substitution test. *Psychosom. Med.* 75, 624–631. doi: 10.1097/psy.0b013e31829c1df2

Rosemann, S., and Thiel, C. M. (2019). The effect of age-related hearing loss and listening effort on resting state connectivity. *Sci. Rep.* 9:2337. doi: 10.1038/s41598-019-38816-z

Rutherford, B. R., Brewster, K., Golub, J. S., Kim, A. H., and Roose, S. P. (2018). Sensation and psychiatry: linking age-related hearing loss to late-life depression and cognitive decline. *Am. J. Psychiatry* 175, 215–224. doi: 10.1176/appi.ajp.2017.17040423

Sánchez-Cubillo, I., Periáñez, J. A., Adrover-Roig, D., Rodríguez-Sánchez, J. M., Ríos-Lago, M., Tirapu, J., et al. (2009). Construct validity of the Trail Making Test: role of task-switching, working memory, inhibition/interference

control, and visuomotor abilities. *J. Int. Neuropsychol. Soc.* 15, 438–450. doi: 10.1017/s1355617709090626

Schmidt, S. A., Akrofi, K., Carpenter-Thompson, J. R., and Husain, F. T. (2013). Default mode, dorsal attention and auditory resting state networks exhibit differential functional connectivity in tinnitus and hearing loss. *PLoS One* 8:e76488. doi: 10.1371/journal.pone.0076488

Schneider, D. M., and Mooney, R. (2018). How movement modulates hearing. *Annu. Rev. Neurosci.* 41, 553–572. doi: 10.1146/annurev-neuro-072116-031215

Sherman, M. T., Seth, A. K., and Kanai, R. (2016). Predictions shape confidence in right inferior frontal gyrus. *J. Neurosci.* 36, 10323–10336. doi: 10.1523/JNEUROSCI.1092-16.2016

Shin, M. S., Park, S. Y., Park, S. R., Seol, S. H., and Kwon, J. S. (2006). Clinical and empirical applications of the rey-osterrieth complex figure test. *Nat. Protoc.* 1, 892–899. doi: 10.1038/nprot.2006.115

Skipper, J. I., Devlin, J. T., and Lametti, D. R. (2017). The hearing ear is always found close to the speaking tongue: review of the role of the motor system in speech perception. *Brain Lang.* 164, 77–105. doi: 10.1016/j.bandl.2016.10.004

Smith, S. M., Nichols, T. E., Vidaurre, D., Winkler, A. M., Behrens, T. E., Glasser, M. F., et al. (2015). A positive-negative mode of population covariation links brain connectivity, demographics and behavior. *Nat. Neurosci.* 18, 1565–1567. doi: 10.1038/nn.4125

Song, H. J., Meade, K., Akobundu, U., and Sahyoun, N. R. (2014). Depression as a correlate of functional status of community-dwelling older adults: utilizing a short-version of 5-item Geriatric Depression Scale as a screening tool. *J. Nutr. Health Aging* 18, 765–770. doi: 10.1007/s12603-014-0542-0

Tavanai, E., and Mohammadkhani, G. (2017). Role of antioxidants in prevention of age-related hearing loss: a review of literature. *Eur. Arch. Otorhinolaryngol.* 274, 1821–1834. doi: 10.1007/s00405-016-4378-6

Thomson, R. S., Auduong, P., Miller, A. T., and Gurgel, R. K. (2017). Hearing loss as a risk factor for dementia: a systematic review. *Laryngoscope Investig. Otolaryngol.* 2, 69–79. doi: 10.1002/lio2.65

Veldsman, M., Zamboni, G., Butler, C., and Ahmed, S. (2019). Attention network dysfunction underlies memory impairment in posterior cortical atrophy. *Neuroimage Clin.* 22:101773. doi: 10.1016/j.nicl.2019.101773

Viscogliosi, G., Di Bernardo, M. G., Ettorre, E., and Chiriac, I. M. (2017). Handgrip strength predicts longitudinal changes in clock drawing test performance. An observational study in a sample of older non-demented adults. *J. Nutr. Health Aging* 21, 593–596. doi: 10.1007/s12603-016-0816-9

Wang, C., Qin, W., Zhang, J., Tian, T., Li, Y., Meng, L., et al. (2014). Altered functional organization within and between resting-state networks in chronic subcortical infarction. *J. Cereb. Blood Flow Metab.* 34, 597–605. doi: 10.1038/jcbfm.2013.238

Wang, J., Wang, X., Xia, M., Liao, X., Evans, A., and He, Y. (2015). GRETNA: a graph theoretical network analysis toolbox for imaging connectomics. *Front. Hum. Neurosci.* 9:386. doi: 10.3389/fnhum.2015.00386

Wolak, T., Cieśla, K., Pluta, A., Wodarczyk, E., Biswal, B., and Skarżyński, H. (2019). Altered functional connectivity in patients with sloping sensorineural hearing loss. *Front. Hum. Neurosci.* 13:284. doi: 10.3389/fnhum.2019.00284

Xu, Y., Chen, K., Zhao, Q., Li, F., and Guo, Q. (2020). Short-term delayed recall of auditory verbal learning test provides equivalent value to long-term delayed recall in predicting MCI clinical outcomes: a longitudinal follow-up study. *Appl. Neuropsychol. Adult* 27, 73–81. doi: 10.1080/23279095.2018.1481067

Xu, H., Fan, W., Zhao, X., Li, J., Zhang, W., Lei, P., et al. (2016). Disrupted functional brain connectome in unilateral sudden sensorineural hearing loss. *Hear. Res.* 335, 138–148. doi: 10.1016/j.heares.2016.02.016

Zhao, Z., Wu, J., Fan, M., Yin, D., Tang, C., Gong, J., et al. (2018). Altered intra- and inter-network functional coupling of resting-state networks associated with motor dysfunction in stroke. *Hum. Brain Mapp.* 39, 3388–3397. doi: 10.1002/hbm.24183

Zung, W. W. (1971). A rating instrument for anxiety disorders. *Psychosomatics* 12, 371–379. doi: 10.1016/s0033-3182(71)71479-0

Conflict of Interest: The authors declare that the research was conducted in the absence of any commercial or financial relationships that could be construed as a potential conflict of interest.

frontiers in Neuroscience

ORIGINAL RESEARCH
published: 13 August 2020
doi: 10.3389/fnins.2020.00843

Conductive Hearing Loss Aggravates Memory Decline in Alzheimer Model Mice

*Jin Su Kim[1,2], Hae-June Lee[3], Seonhwa Lee[1,4], Ho Sun Lee[5,6], Ye Ji Jeong[3], Yeonghoon Son[3,7], Jung Min Kim[4], Yong Jin Lee[1] and Min-Hyun Park[5,6]**

[1] Division of RI Application, Korea Institute of Radiological and Medical Sciences, Seoul, South Korea, [2] Radiological and Medico-Oncological Sciences, University of Science and Technology, Seoul, South Korea, [3] Division of Radiation Biomedical Research, Korea Institute of Radiological and Medical Sciences, Seoul, South Korea, [4] Department of Bio-Convergence Engineering, Korea University, Seoul, South Korea, [5] Department of Otorhinolaryngology, Boramae Medical Center, Seoul Metropolitan Government-Seoul National University, Seoul, South Korea, [6] Department of Otorhinolaryngology, College of Medicine, Seoul National University, Seoul, South Korea, [7] National Primate Research Center, Korea Research Institute of Bioscience and Biotechnology (KRIBB), Cheongju, South Korea

The study of cognitive impairment associated with hearing loss has recently garnered considerable interest. Epidemiological data have demonstrated that hearing loss is a risk factor for cognitive decline as a result of aging. However, no previous study has examined the effect of hearing loss in patients with cognitive problems such as Alzheimer's disease. Therefore, we investigated the effect of conductive hearing loss in an Alzheimer's mouse model. Positron emission tomography (PET) and magnetic resonance imaging (MRI) were used to evaluate changes in glucose metabolism and gray matter concentrations in the 5xFAD Alzheimer's Disease (AD) transgenic mouse model with and without conductive hearing loss (HL). Conductive hearing loss was induced using chronic perforation of the tympanic membrane. Behavioral data from the Y-maze and passive avoidance tests revealed greater memory deficits in the AD with HL (AD-HL) group than in the AD group. Following induction of hearing loss, lower cerebral glucose metabolism in the frontal association cortex was observed in the AD-HL group than in the AD group. Although lower glucose metabolism in the hippocampus and cerebellum was found in the AD-HL group than in the AD group at 3 months, the gray matter concentrations in these regions were not significantly different between the groups. Furthermore, the gray matter concentrations in the simple lobule, cingulate/retrosplenial cortex, substantia nigra, retrosigmoid nucleus, medial geniculate nucleus, and anterior pretectal nucleus at 7 months were significantly lower in the AD-HL group than in the AD group. Taken together, these results indicate that even partial hearing loss can aggravate memory impairment in Alzheimer's disease.

Keywords: memory impairment, SPM, VBM, Behavioral study, hearing loss, Alzheimer's disease

OPEN ACCESS

Edited by:
Chih-Yu Hsu,
Fujian University of Technology, China

Reviewed by:
Mar Pacheco-Herrero,
Pontificia Universidad Católica Madre y Maestra, Dominican Republic
Cristina Lanni,
University of Pavia, Italy

***Correspondence:**
Min-Hyun Park
drpark@snu.ac.kr

Specialty section:
This article was submitted to Neurodegeneration, a section of the journal Frontiers in Neuroscience

Received: *30 April 2020*
Accepted: *20 July 2020*
Published: *13 August 2020*

Citation:
Kim JS, Lee HJ, Lee S, Lee HS, Jeong YJ, Son Y, Kim JM, Lee YJ and Park MH (2020) Conductive Hearing Loss Aggravates Memory Decline in Alzheimer Model Mice. Front. Neurosci. 14:843. doi: 10.3389/fnins.2020.00843

INTRODUCTION

Cognitive impairment associated with hearing loss (HL) has recently attracted considerable interest due to growing evidence suggesting that impaired hearing is a risk factor for cognitive decline (Hardy et al., 2016). Several studies have assessed the relationship between hearing deficits and cognitive impairment. Age-related hearing problems are common among people with dementia

and are associated with poor cognitive function and reduced quality of life (Dawes et al., 2018). Furthermore, hearing loss in later life has been associated with the risk of dementia. The impact of the risk factors for dementia may change during a person's lifespan, and whether or not midlife hearing loss represents a risk factor for dementia remains poorly understood (Osler et al., 2019). Osler et al. have shown that early identification and correction of hearing loss holds promise for the prevention of dementia later in life (Osler et al., 2019). Interventions aimed at improving sensory function may improve the quality of life of patients with dementia (Leroi et al., 2017). Furthermore, middle-aged and old patients with severe or profound hearing impairments also show an increased risk of developing dementia (Kim et al., 2018). However, there are no reports on the effect of hearing loss in patients with cognitive impairment such as Alzheimer's disease (AD). If hearing loss facilitates cognitive decline in the normal population, then patients with AD and hearing loss may be expected to suffer more in the aspect of cognitive function. Therefore, we investigated the behavior, brain function, and changes in hearing in hearing loss-induced AD model mice using behavioral tests, positron emission tomography (PET), and magnetic resonance (MR) imaging.

Although many reports point to a correlation between dementia and hearing impairment, quantitative and functional studies are challenging because the auditory areas in the brain remain poorly understood and are difficult to assess. Deaf animal models provide us with an opportunity to assess the impact of hearing loss interventions on the development of dementia, as well as the corresponding changes in brain plasticity. We have previously demonstrated cross-modal and compensatory plasticity using PET analysis in an animal model (Park et al., 2010). PET is a promising tool for the assessment of neuronal and cortical plasticity (Lee et al., 2001). The cochlear implant is a surgically implanted neuroprosthetic device that provides a sense of sound to a person with severe to profound sensorineural hearing loss (Balkany et al., 1999; Hodges et al., 1999). PET analyses of brain plasticity have provided quantitative results that support increased metabolic activity in auditory areas following cochlear implantation (Lukaszewicz-Moszynska et al., 2014; Strelnikov et al., 2015; Yoshida et al., 2017). Studies have also assessed verbal working memory in children with cochlear implants (Akcakaya et al., 2019).

The aim of this study was to evaluate the effects of conductive hearing loss on Alzheimer's disease. We sought to investigate the following questions: (1) Does conductive hearing loss affect memory ability? (2) Does conductive hearing loss lead to functional changes in imaging studies such as PET and MR? Five familial AD mutation (5xFAD) transgenic mice (which are commonly used as an animal model for AD) were used in the current study (Son et al., 2016; O'Leary et al., 2017; Jeon et al., 2018; Moon et al., 2019). Experimental mice were divided into two groups: Alzheimer's disease with and without hearing loss (AD-HL and AD), and used PET and MR were used to evaluate changes in cerebral glucose metabolism and regional gray matter concentrations after the induction of conductive hearing loss. Memory deficits were assessed using the Y-maze and passive avoidance tests. To the best of our knowledge, our study is the first to investigate the relationship between AD and hearing loss through the evaluation of cerebral glucose metabolism and regional gray matter concentrations using PET and MR image analysis on animal models.

MATERIALS AND METHODS

Animals and Ethics Statement

Five familial AD mutation male mice (2 months of age), which overexpress five familial AD mutations, were used in the current study. These mutations comprise three in human APP (695) with the Swedish (K670N, M671L), Florida (I716V), and London (V7171), and two in human presenilin1, PSEN1 M146L, and PSEN1 L286V. The transgenic mice were purchased from Jackson Laboratory (Bar Horbor, ME, United States). All applicable international, national, and/or institutional guidelines for the care and use of animals were followed. The animal study was approved by the Institutional Animal Care and Use Committee (IACUC) and the Institutional Review Board of the Korea Institute of Radiological and Medical Sciences (KIRAMS 2018-0016, KIRAMS 2015-38), and all experiments were performed in accordance with their guidelines.

Experimental Design

Experimental Group

The animals were divided into two groups: the experimental group (AD-HL; $n = 10$) with induced conductive hearing loss and the control group (AD; $n = 10$) with normal hearing. Both groups underwent measurement of hearing thresholds, behavioral tests, and imaging studies.

Hearing Loss

Conductive hearing loss was induced in the experimental group using the following procedure: The mice were anesthetized using intraperitoneal injections of ketamine (100 mg/kg) and xylazine (20 mg/kg). The tympanic membrane was resected using a sharp pick under continuous endoscopic visualization (Liberman et al., 2015). After resection, the movement and balance state of the animals were checked to evaluate inner ear damage. The state of the tympanic membrane was endoscopically examined every week. Resection was repeated when the perforation size was observed to have decreased. The perforation size in the tympanic membrane was maintained until the end of the study (**Figure 1**).

Hearing Evaluation

Hearing levels were assessed using click-evoked ABRs 1 week after surgery, 3 months later, and at the end of the study. Hearing levels were tested by evaluating the auditory brainstem responses (ABRs) to click stimuli (Intelligent Hearing System, Miami, FL, United States). Subdermal needle electrodes were located below both ear and at the vertex. The stimulus rate is 19.3/s using click sound of rarefaction mode. The response was amplified, and band pass filtered (100–3000 Hz), and averaged over stimulation (512 sweeps per stimulation).

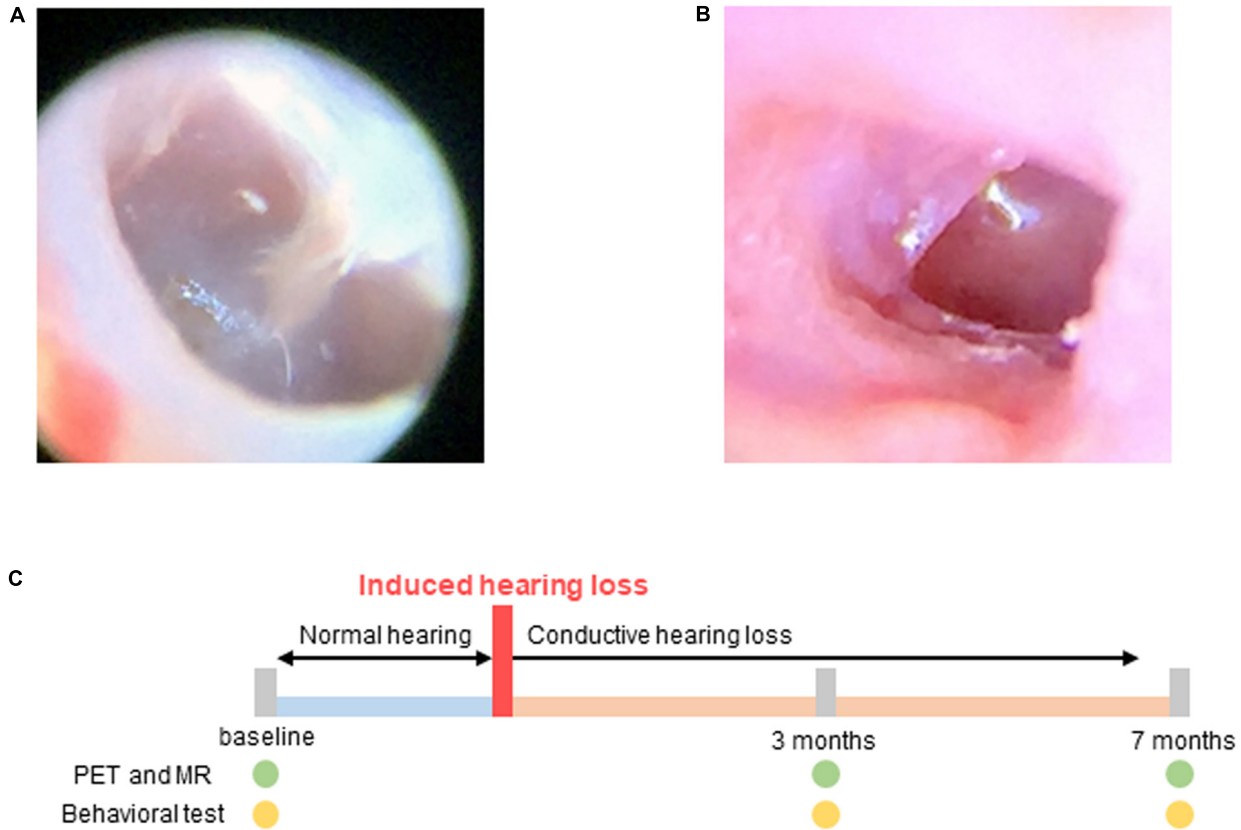

FIGURE 1 | Hearing loss was induced by resection of the tympanic membrane. **(A)** Normal tympanic membrane; **(B)** Resected tympanic membrane; **(C)** Experimental scheme for imaging and behavioral testing. Baseline tests were performed before induced hearing loss. Hearing loss was induced at 0 month, and PET, MR, and behavioral tests were performed 3 and 7 months after hearing loss.

PET Statistical Parametric Mapping (SPM) and MR Voxel-Based Morphometry (VBM) Analyses

PET and MR scans were acquired at baseline and at 3 and 7 months after the induction of hearing loss in order to assess changes in cerebral glucose metabolism and gray matter concentrations (**Figure 1C**).

Regional cerebral glucose metabolism was measured using the F-18 fluorodeoxyglucose (F-18 FDG) PET scan (Siemens Inveon PET scanner) (Bao et al., 2009). Prior to the PET scan, the mice (n = 10 per group, male) underwent an 8-h fasting period, after which they were anesthetized with 2% isoflurane in 100% oxygen (Forane solution; Choongwae Pharma, South Korea). The body temperatures of the mice were maintained at 36°C using heating pads during the course of the scan. Next, 200 μCi of F-18 FDG was injected through the tail vein of the mice. After 30 min of uptake, emission PET data were acquired for 30 min using an energy window of 350–650 keV. The emission list-mode data were sorted into three-dimensional (3D) sinograms and reconstructed using 3D reprojection algorithms without the use of a filter. The size of the image matrix was 256 × 256 × 159, with a pixel size of 0.155 mm × 0.155 mm and a slice thickness of 0.796 mm.

Regional differences between groups were identified using voxel-based statistical analysis performed in SPM 8[1]. Statistical parametric mapping analysis on small animals has been described in our previous study (Kim et al., 2008). Briefly, the brain tissue was extracted from the image and a study-specific mouse brain template was constructed using structural images. Individual PET data were spatially normalized onto the mouse brain template using affine and non-linear transformations. The voxel size of the spatially normalized images was 0.3 mm × 0.3 mm × 0.3 mm. Finally, a Gaussian smoothing kernel with a full-width at half-maximum (FWHM) value of 3 mm was applied to enhance the signal-to-noise ratio. Count normalization was performed. t-tests were used to identify regional differences in cerebral glucose metabolism between the groups ($p < 0.005$ or $p < 0.05$, uncorrected).

T2w 3D MR images were acquired using an Agilent 9.4 T MR scanner (United States). An AD quad 70 RF coil was used, and the matrix size was 192 × 192 × 192. The repetition time (RT) was 2500 ms. The effective echo time (TE) was set at 7 ms. The total image acquisition time was 3 h 36 min.

Modulated VBM analysis was performed in SPM eight to compare the regional gray matter concentrations in selected

[1]http://www.fil.ion.ucl.ac.uk/spm

brain regions between the groups (Wilke et al., 2003). Skull stripping was performed using the BrainSuite (version 16) software (Kazemi and Noorizadeh, 2014). Parameters including the brain surface extractor diffusion iterations, diffusion constant, edge constant, and erosion size were adjusted for skull stripping using individual T2w 3D MR data. A predefined gray matter template (matrix size: 512 × 512 × 512; voxel size: 0.04 mm × 0.04 mm × 0.04 mm) created by the Delora research team was used for spatial normalization (Kazemi and Noorizadeh, 2014; Delora et al., 2016). Individual skull-stripped MR data were spatially normalized onto the template and smoothed with a Gaussian smoothing kernel with a full-width at half-maximum (FWHM) value of 2 mm. Paired *t*-tests were used to identify regional differences in gray matter concentrations between the groups ($p < 0.005$, uncorrected).

Behavioral Analysis

Y-Maze Test

The Y-maze test was used to measure spatial working memory and reference memory, which were assessed by recording spontaneous alternation behavior (Kraeuter et al., 2019). Activity was recorded for 8 min and analyzed by a computer program (Viewer3, BIOSERVE, St. Augustin, Germany). Alternation was defined as successive entries into three different arms on overlapping triplet sets. Percentage alternation was calculated as the ratio of actual alternation and possible alternation (defined as the total number of arm entries – 2) × 100, as follows:

$$\%\ \text{alternation} = \left[\left(\text{No. of alternations}\right) / \left(\text{Total arm entries} - 2\right) \right] \times 100.$$

Passive Avoidance Test

The responses to aversive stimuli in the passive avoidance test were used to assess learning and long-term memory (Tucker et al., 1976; Nasri et al., 2012). The setup consisted of two rooms separated by a steel board such that it could automatically be moved up and down to allow movement of the animal from one room to the other. Both the rooms were equipped with a scrambler on the floor, through which electrical stimulation could be delivered to the foot. During the adaptation session (Day 1), the mice were allowed to travel freely between the two rooms for 5 min. On Day 2, the steel board was used to separate the rooms and the mouse was placed in one of the rooms. The room was kept dark for 60 s to allow the mouse to adjust to the darkness, after which the light was turned on and the steel panel was simultaneously removed. As the mouse traveled across to the other room to avoid the bright light, the movement of the mouse triggered the steel panel to shut, and an electrical shock impulse (0.3 mA, 2 s) was transmitted to the grill. After 24 h (Day 3), the mice were subjected to the same trial without the electrical shock stimulus. The time taken by the mice to cross over to the other room was automatically recorded.

Statistics

Data are presented as mean ± standard error of mean (SEM). For behavioral tests, the differences among the groups were analyzed using the one-way ANOVA test and the difference between two groups were analyzed with Student's unpaired *t*-test in GraphPad Prism five (GraphPad software, CA, United States). A *P*-value less than 0.05 was considered statistically significant.

RESULTS

Measurement of the Level of Hearing Loss

The mean hearing level measured using click-evoked ABRs was 20 dB sound pressure level (SPL) at the normal hearing state (**Figure 2A**). In the control group, the hearing level was increased to 40 dB SPL at 3- and 7-months. In the experimental group, the mean hearing level was 65 dB SPL in both ears after resection of the tympanic membrane (**Figure 2B**). The final mean hearing levels at 7 months after the induction of hearing loss were 62.9 ± 8 dB SPL on the right side and 67.1 ± 7 dB SPL on the left side (**Figure 2C**).

Evidence From PET and MR Imaging

Cerebral Glucose Metabolism in the AD Group

SPM analysis of PET scans obtained at baseline and at the 3-month time-point in the AD group revealed decreased cerebral glucose metabolism in the frontal association cortex (FrA; $P < 0.005$; **Figure 3A**) and the cerebellum (Cb; $P < 0.05$; **Figure 3B**) at 3 months compared to baseline levels.

Comparison Between Cerebral Glucose Metabolism of the AD and AD-HL Groups

Figure 5 illustrates the results of the SPM analysis comparing PET scans of animals in the AD and AD-HL groups at 3 and 7 months after the induction of hearing loss. Cerebral glucose metabolism in the FrA was lower ($P < 0.005$) in the AD-HL group than in the AD model 3 and 7 months after the induction of hearing loss (shown in **Figures 3C,E**). We also found lower cerebral glucose metabolism in the hippocampus (CA1) and Cb 3 months after the induction of hearing loss (**Figure 3D**; $P < 0.05$).

Cerebral Gray Matter Concentrations in the AD and AD-HL Mice

Figure 4 illustrates the results of the optimized VBM analysis comparing the MR images of mice in the AD and AD-HL groups. We found no differences in the gray matter concentrations of the two groups at the 3-month time-point after the induction of hearing loss ($P < 0.005$). However, at the 7-month time-point after the induction of hearing loss, the AD-HL group showed lower gray matter concentrations in large areas of the brain including the FrA, simple lobule (Sim, part of the cerebellum), RSA (retrosplenial agranular cortex), cingulate/retrosplenial cortex (Cg/RS), substantia nigra (SNR), retroethmoid nucleus (REth), medial geniculate nucleus (MGV), and anterior pretectal nucleus (APTD) than the AD group ($P < 0.005$).

Behavioral Analysis

The AD-HL and AD groups underwent behavioral assessment prior to the induction of conductive hearing loss (baseline) when

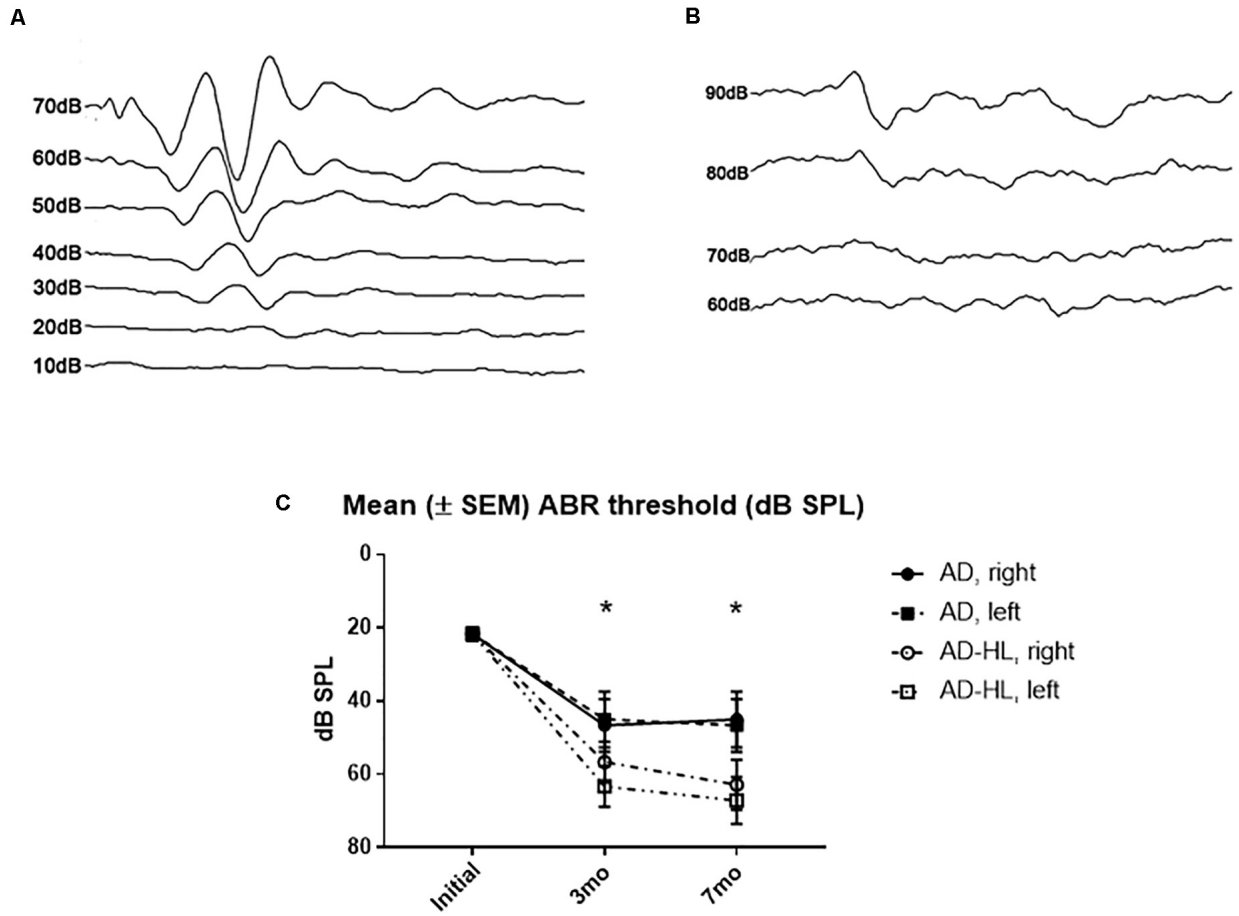

FIGURE 2 | Auditory brainstem responses results in the AD-HL and AD groups. **(A)** Auditory brainstem responses in the AD group revealed a hearing threshold of 20 dB SPL at the initial state. **(B)** Auditory brainstem responses in the AD-HL group revealed a hearing threshold of 65 dB SPL at 3 months. **(C)** Mean (±SEM) ABR threshold (dB SPL) for 3 and 7 months after hearing loss. [ABR: auditory brainstem response, *significant difference between control and hearing loss group at 3 and 7 mo ($P < 0.05$)]. AD-HL, Alzheimer's disease with hearing loss; AD, Alzheimer's disease; dB SPL, decibel sound pressure level; SEM, standard error of the means.

they were 6 weeks old, and at the 3- and 7-month time-points after induction of hearing loss (in the AD-HL group). None of the animals showed balance or movement problems after resection of tympanic membrane. We assessed the effect of hearing loss on spatial memory using the Y-maze test. The AD group showed an age-dependent decline in working memory. We found no significant difference between the AD and AD-HL groups in the spontaneous alternation as evaluated by the Y-maze (**Figure 5A**) at the 3- and 7-month time-points after hearing loss. However, the AD group tended to show higher spatial memory compared to the AD-HL group.

The passive avoidance test was performed to examine the hearing loss-induced memory impairment in the AD-HL group. We found no significant difference in cognitive performance in the passive avoidance test between the two groups prior to the induction of hearing loss. The AD-HL group exhibited significantly higher memory impairment 24 h after the training sessions with the electric shock stimulus than the AD group at the 3-month (mean latency: 210 s in AD vs 87 s in AD-HL, $p = 0.0037$) and 7-month (mean latency: 157 s in AD vs 95 s in AD-HL, $p = 0.046$) time-points following hearing loss induction (**Figure 5B**).

DISCUSSION

Several meta-analyses, including a meta-analysis of a prospective cohort study, have suggested that hearing impairment significantly increases the risk of developing cognitive disorders (Zheng et al., 2017). The importance of evaluating hearing levels and administering appropriate rehabilitation treatments as part of the cognitive assessment and management plan in individuals with cognitive disorders has also been emphasized (Nirmalasari et al., 2017). Further, age-related hearing loss has been considered to be a possible biomarker and modifiable risk factor for cognitive decline, cognitive impairment, and dementia (Loughrey et al., 2018).

Although meta-analyses and cohort studies have indicated a relationship between hearing loss (hearing impairment or deafness) and cognitive impairment, PET or MR image analyses

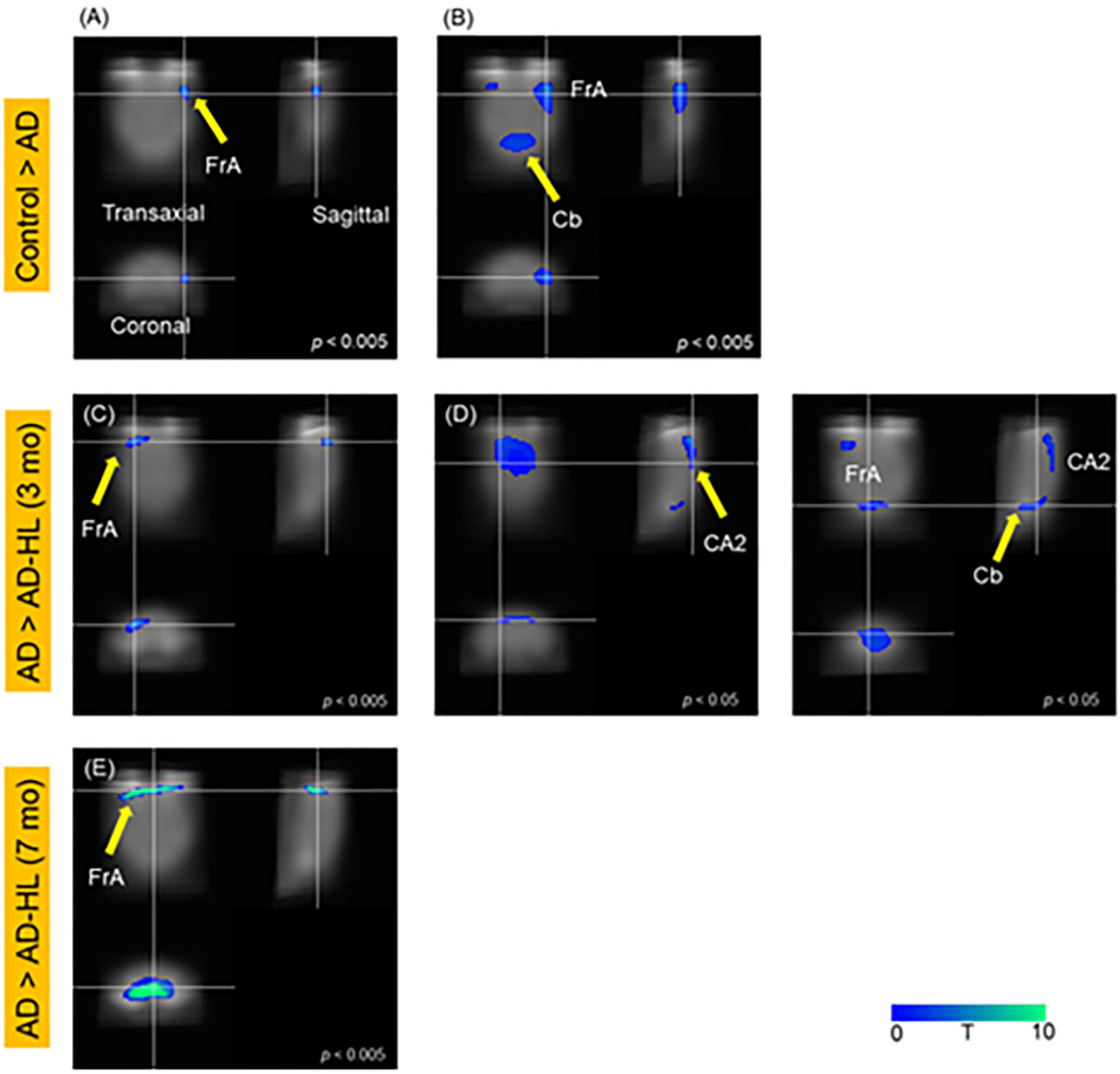

FIGURE 3 | SPM analysis of PET images; **(A,B)** Control vs AD; **(C,D)** AD vs AD-HL (3 mo); **(E)** AD vs AD-HL (7 mo); We found a decrease in the cerebral glucose metabolism in the **(A)** FrA ($p < 0.005$); and **(B)** Cb ($p < 0.05$) at the 3-month timepoint compared to the baseline levels. We found lower cerebral glucose metabolism in the **(C)** FrA ($P < 0.005$), and **(D)** CA2 region of the hippocampus and Cb ($P < 0.05$) in the AD-HL group than in the AD group at the 3-month timepoint after the induction of hearing loss. **(E)** The cerebral glucose metabolism in the FrA was lower in the AD-HL group than in the AD group ($p < 0.005$) at the 7-month time point after the induction of hearing loss. *P*-values were determined using the paired *t*-test. SPM, statistical parametric mapping; AD-HL, Alzheimer's disease with hearing loss; AD, Alzheimer's disease; FrA, frontal association cortex; Cb, cerebellum.

or behavioral studies have not been employed to further characterize the relationship until now. Imaging studies using PET have provided a translational platform for clinical use and successful clinical proof-of-concept testing (Platt et al., 2011; Hargreaves and Rabiner, 2014). FDG-PET imaging has been used to visualize the distribution of neural damage or synaptic dysfunction; to identify distinct phenotypes of neurodegenerative disorders such as AD (McKhann et al., 2011), and to identify changes in cerebral glucose metabolism after the onset of deafness, or in brain plasticity after cochlear implantation (Okuda et al., 2013; Strelnikov et al., 2015; Suh et al., 2015; Yoshida et al., 2017). In the present study, we constructed an AD-HL animal model. This 5xFAD mouse showed peripheral hearing loss with aging (O'Leary et al., 2017). At 4-months-old, the hearing level was normal, but at 14-months-old, the hearing level was much lower than that of the wild type mouse; this has been shown to be an aggravating factor for cognitive decline. Another study was used an animal model of amyloid-β infusion to intracerebroventricular space in order to generate a suitable model for AD; in this study, deafness was induced using cochlear ablation Cognitive behavioral tests were subsequently performed, and amyloid-β infused group showed poor performance and greater loss of synapses in the hippocampus (Chang et al., 2019).

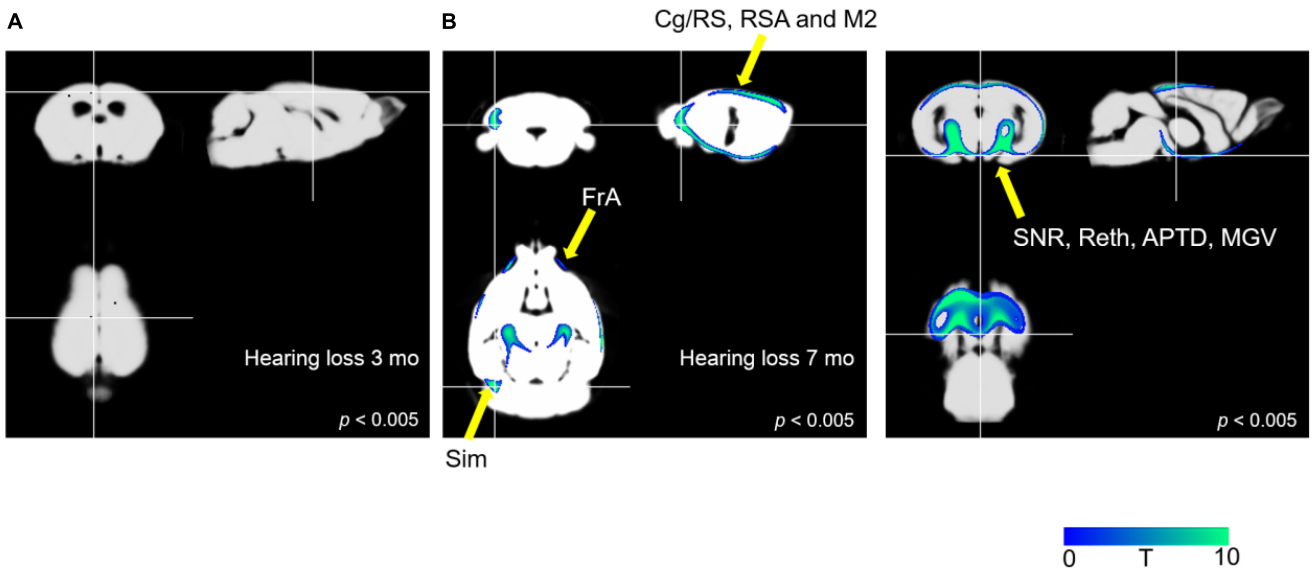

FIGURE 4 | Comparison of VBM results between the AD-HL and AD groups. **(A)** We found no group differences in gray matter concentrations at the 3-month time point after the induction of hearing loss ($P < 0.005$). **(B)** We found a significant decrease in the gray matter concentrations in several regions including the FrA, Sim, RSA, Cg/RS, SNR, REth, MGV, and APTD ($P < 0.005$) at the 7-month time point after the induction of hearing loss. *P*-values were determined using *t*-test. VBM, voxel-based morphometry; AD-HL, Alzheimer's disease with hearing loss; AD, Alzheimer's disease; FrA, frontal association cortex; Sim, simple lobule (part of the cerebellum); RSA, retrosplenial agranular cortex; Cg/RS,: cingulate/retrosplenial cortex; SNR, substantia nigra; REth, retroethmoid nucleus; MGV, medial geniculate nucleus; APTD, anterior pretectal nucleus.

In the current study, we assessed cerebral glucose metabolism, regional gray matter concentrations changes using PET, MR imaging, and behavioral tests. We found reduced glucose metabolism in the FrA ($P < 0.005$), hippocampus, and Cb ($P < 0.05$) in the AD-HL group 3 months after the induction of hearing loss. Interestingly, this functional change was not accompanied by changes in regional gray matter concentrations at the corresponding sites. Memory decline was confirmed using the passive avoidance test. Lower cerebral glucose metabolism levels in the FrA and hippocampus related to memory deficits have also been found in our previous PET study (Park et al., 2013; Lim et al., 2016; Ye et al., 2016). Furthermore, other groups have reported cognitive decline-associated decreases in cerebral glucose metabolism in the Cb (Schreck et al., 2018; Liang and Carlson, 2019; Nishida et al., 2019). In the current study, the decrease in the cerebral glucose metabolism in the FrA persisted at the 7-month time-point. Furthermore, VBM analysis also revealed decreases in gray matter concentrations in the Sim, RSA, and Cg/RS in the AD-HL group. The Cg/RS and RSA are known to be the key brain areas involved in memory, emotion, and attention functions (Zgraggen et al., 2012; Milczarek et al., 2018).

However, we noted a discrepancy in the results from PET and MR image analyses. Although we found group differences in the regional gray matter concentrations in several areas of the brain at the 7-month time point, SPM analysis of PET imaging data did not reveal differences in glucose metabolism at the corresponding sites, except in the case of the FrA. This discrepancy could be explained by brain plasticity. Although the glucose metabolism decreased in the hippocampus and Cb 3 months after the induction of hearing loss, the metabolism in these regions recovered by 7 months, possibly due to brain plasticity. This type of recovery has been previously reported both in humans and cats (Lee et al., 2001; Park et al., 2010). In previous studies, the primary auditory cortex showed hypometabolism after deafness, and then, the hypometabolic area was normalized further after even the ear was still deaf. They explained this phenomenon as an evidence of cross-modal plasticity. Therefore, in our study, CA2 area showed hypometabolism at 3 months after hearing loss; however, the change was normalized at 7 months after hearing loss, even the hearing loss and behavioral deficit were still remained. In addition, the results of the VBM analysis suggest differences in gray matter concentration in several areas of the brain, including the FrA.

Our findings suggest that the decrease in cerebral glucose metabolism in the hippocampus is correlated with memory deficits, such as those affecting long-term memory (Sawangjit et al., 2018). The results of the passive avoidance test support the development of memory deficits induced by hearing loss, especially in terms of long-term memory. Additionally, we found no changes in regional gray matter concentrations in the whole brain at the 3-month time-point, which implies that there were changes only in the glucose metabolism at this time. However, we found significant changes in the gray matter concentrations in memory and motor function-related brain areas at 7 months after the induction of hearing loss. SPM analysis of PET images at 7 months revealed a recovery in the impaired glucose metabolism in the Cb at this time point.

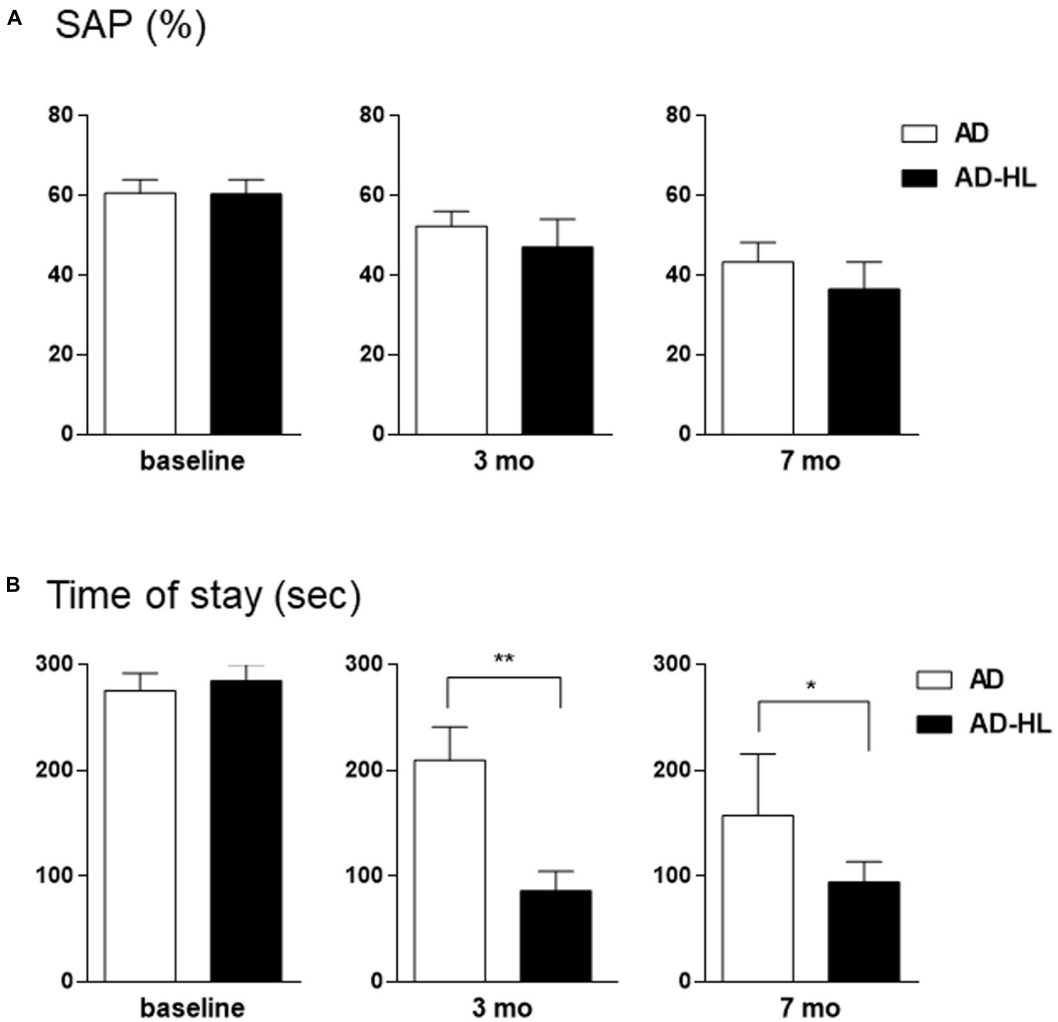

FIGURE 5 | Comparison of behavioral changes between the AD-HL and AD groups. **(A)** In the Y-maze, we found no significant group differences in the percentage of spontaneous alternation at any of the tested time-points. However, the AD group tended to exhibit higher spatial memory than the AD-HL group at the 3- and 7-month time-points. **(B)** In the passive avoidance memory test, compared to the AD group, the AD-HL group exhibited significantly higher latency time at the 3- and 7-month time-points, indicating higher memory impairment. Data are represented as mean ± SEM. $^{*}P < 0.05$, $^{**}P < 0.01$ (vs AD group). *P*-values were calculated using *t*-test. AD-HL, Alzheimer's disease with hearing loss; AD, Alzheimer's disease; SEM, standard error of the means; SAP, spontaneous alternation percentage.

Interestingly, we did not find significant changes in glucose metabolism or gray matter concentration in the auditory cortex at the 3- or 7-month time-points after the onset of hearing loss. We believe this may be because our mouse model with hearing loss did not constitute complete deafness. In our conductive hearing loss model, the mice could still hear loud sounds. As the auditory system was still functional, loud sounds could evoke activation of the auditory system. However, we found lower cerebral glucose metabolism in the FrA in the AD-HL group than in the AD group. The FrA is composed of the prefrontal cortex and motor function-related areas of the brain excluding the primary motor cortex (Takada, 2016). Neurophysiology and neuropsychology studies have established that the dorsolateral prefrontal cortex is associated with working memory, while the ventral frontal lobe is associated with auditory and audiovisual working memory (Plakke et al., 2015). Our PET findings revealed decreased glucose metabolism in the dorsolateral prefrontal cortex at the 3-month time-point after induction of hearing loss in the AD-HL mice. However, by the 7-month time-point, the glucose metabolism in the ventral prefrontal cortex, as well as in the dorsolateral prefrontal cortex regions was affected. This finding suggests that auditory areas including the ventral prefrontal cortex were affected despite the fact that we did not induce complete hearing loss.

CONCLUSION

Our findings reveal memory impairment after hearing loss in the AD mice as evidenced by PET and MR imaging findings. The results from our behavioral tests also support an association between memory impairment and hearing loss. Together, these

results suggest that hearing loss may aggravate memory decline in an animal model of AD.

In sum, we constructed an AD-HL animal model and assessed changes in cerebral glucose metabolism and gray matter concentrations following hearing loss. Our results provide experimental evidence to suggest that even partial hearing loss can aggravate memory impairment in AD. In the future, this model can also be used to identify the onset of memory deficit and brain plasticity following the onset of hearing loss.

DATA AVAILABILITY STATEMENT

The raw data supporting the conclusions of this article will be made available by the authors, without undue reservation.

ETHICS STATEMENT

The animal study was approved by the Institutional Animal Care and Use Committee (IACUC) and the Institutional Review Board of the Korea Institute of Radiological and Medical Sciences (KIRAMS 2018-0016, and KIRAMS 2015-38), and all experiments were performed in accordance with their guidelines.

AUTHOR CONTRIBUTIONS

JK and M-HP designed the study, analyzed and interpreted the results, and wrote the manuscript. H-JL, SL, HL, YJ, and YS performed experiments, analyzed data, and wrote the manuscript. YL discussed the results and edited the manuscript. All authors reviewed and approved the final version of the manuscript.

FUNDING

This study was supported by a grant from the Korea Institute of Radiological and Medical Sciences (KIRAMS); funded by the Ministry of Science and ICT (MSIT), South Korea (50536-2019, PI: YL) and supported by Boramae Medical Center (02-2019-5, PI: M-HP).

REFERENCES

Akcakaya, H., Dogan, M., Gurkan, S., Kocak, O., and Yucel, E. (2019). Early cochlear implantation: verbal working memory, vocabulary, speech intelligibility and participant variables. *Cochlear Implants Int.* 20, 62–73. doi: 10.1080/14670100.2019.1565077

Balkany, T. J., Hodges, A. V., Gomez-Marin, O., Bird, P. A., Dolan-Ash, S., Butts, S., et al. (1999). Cochlear reimplantation. *Laryngoscope* 109, 351–355.

Bao, Q., Newport, D., Chen, M., Stout, D. B., and Chatziioannou, A. F. (2009). Performance evaluation of the inveon dedicated PET preclinical tomograph based on the NEMA NU-4 standards. *J. Nucl. Med.* 50, 401–408. doi: 10.2967/jnumed.108.056374

Chang, M., Kim, H. J., Mook-Jung, I., and Oh, S. H. (2019). Hearing loss as a risk factor for cognitive impairment and loss of synapses in the hippocampus. *Behav. Brain Res.* 372:112069. doi: 10.1016/j.bbr.2019.112069

Dawes, P., Wolski, L., Himmelsbach, I., Regan, J., and Leroi, I. (2018). Interventions for hearing and vision impairment to improve outcomes for people with dementia: a scoping review. *Int. Psychogeriatr.* 31, 203–221. doi: 10.1017/S1041610218000728

Delora, A., Gonzales, A., Medina, C. S., Mitchell, A., Mohed, A. F., Jacobs, R. E., et al. (2016). A simple rapid process for semi-automated brain extraction from magnetic resonance images of the whole mouse head. *J. Neurosci. Methods* 257, 185–193. doi: 10.1016/j.jneumeth.2015.09.031

Hardy, C. J., Marshall, C. R., Golden, H. L., Clark, C. N., Mummery, C. J., Griffiths, T. D., et al. (2016). Hearing and dementia. *J. Neurol.* 263, 2339–2354. doi: 10.1007/s00415-016-8208-y

Hargreaves, R. J., and Rabiner, E. A. (2014). Translational PET imaging research. *Neurobiol. Dis.* 61, 32–38. doi: 10.1016/j.nbd.2013.08.017

Hodges, A. V., Villasuso, E., Balkany, T., Bird, P. A., Butts, S., Lee, D., et al. (1999). Hearing results with deep insertion of cochlear implant electrodes. *Am. J. Otol.* 20, 53–55.

Jeon, S. G., Kang, M., Kim, Y. S., Kim, D. H., Nam, D. W., Song, E. J., et al. (2018). Intrahippocampal injection of a lentiviral vector expressing neurogranin enhances cognitive function in 5XFAD mice. *Exp. Mol. Med.* 50:e461. doi: 10.1038/emm.2017.302

Kazemi, K., and Noorizadeh, N. (2014). Quantitative comparison of SPM, FSL, and brainsuite for brain MR image segmentation. *J. Biomed. Phys. Eng.* 8, 13–26.

Kim, J. S., Lee, J. S., Park, M. H., Kang, H., Lee, J. J., Lee, H. J., et al. (2008). Assessment of cerebral glucose metabolism in cat deafness model: strategies for improving the voxel-based statistical analysis for animal PET studies. *Mol. Imaging Biol.* 10, 154–161. doi: 10.1007/s11307-008-0140-9

Kim, S. Y., Lim, J. S., Kong, I. G., and Choi, H. G. (2018). Hearing impairment and the risk of neurodegenerative dementia: a longitudinal follow-up study using a national sample cohort. *Sci. Rep.* 8:15266. doi: 10.1038/s41598-018-33325-x

Kraeuter, A. K., Guest, P. C., and Sarnyai, Z. (2019). The Y-Maze for assessment of spatial working and reference memory in mice. *Methods Mol. Biol.* 1916, 105–111. doi: 10.1007/978-1-4939-8994-2_10

Lee, D. S., Lee, J. S., Oh, S. H., Kim, S. K., Kim, J. W., Chung, J. K., et al. (2001). Cross-modal plasticity and cochlear implants. *Nature* 409, 149–150. doi: 10.1038/35051653

Leroi, I., Pye, A., Armitage, C. J., Charalambous, A. P., Constantinidou, F., Helmer, C., et al. (2017). Research protocol for a complex intervention to support hearing and vision function to improve the lives of people with dementia. *Pilot Feasibility Stud.* 3:38. doi: 10.1186/s40814-017-0176-1

Liang, K. J., and Carlson, E. S. (2019). Resistance, vulnerability and resilience: a review of the cognitive cerebellum in aging and neurodegenerative diseases. *Neurobiol. Learn. Mem.* 170:106981. doi: 10.1016/j.nlm.2019.01.004

Liberman, M. C., Liberman, L. D., and Maison, S. F. (2015). Chronic conductive hearing loss leads to cochlear degeneration. *PLoS One* 10:e0142341. doi: 10.1371/journal.pone.0142341

Lim, I., Joung, H. Y., Yu, A. R., Shim, I., and Kim, J. S. (2016). PET evidence of the effect of donepezil on cognitive performance in an animal model of chemobrain. *Biomed. Res. Int.* 2016:6945415. doi: 10.1155/2016/6945415

Loughrey, D. G., Kelly, M. E., Kelley, G. A., Brennan, S., and Lawlor, B. A. (2018). Association of age-related hearing loss with cognitive function, cognitive impairment, and dementia: a systematic review and meta-analysis. *JAMA Otolaryngol. Head Neck Surg.* 144, 115–126. doi: 10.1001/jamaoto.2017.2513

Lukaszewicz-Moszynska, Z., Lachowska, M., and Niemczyk, K. (2014). Auditory cortical activation and plasticity after cochlear implantation measured by PET using fluorodeoxyglucose. *Funct. Neurol.* 29, 121–125.

McKhann, G. M., Knopman, K. D., Chertkow, H., Hyman, B. T., Jack, C. R. Jr., Kawas, C. H., et al. (2011). The diagnosis of dementia due to Alzheimer's disease: recommendations from the national institute on aging-Alzheimer's association workgroups on diagnostic guidelines for Alzheimer's disease. *Alzheimers Dement.* 7, 263–269.

Milczarek, M. M., Vann, S. D., and Sengpiel, F. (2018). Spatial memory engram in the mouse retrosplenial cortex. *Curr. Biol.* 28, 1975–1980.e6. doi: 10.1016/j.cub.2018.05.002

Moon, M., Jung, E. S., Jeon, S. G., Cha, M. Y., Jang, Y., Kim, W., et al. (2019). Nurr1 (NR4A2) regulates Alzheimer's disease-related pathogenesis and cognitive function in the 5XFAD mouse model. *Aging Cell* 18:e12866. doi: 10.1111/acel.12866

Nasri, S., Roghani, M., Baluchnejadmojarad, T., Balvardi, M., and Rabani, T. (2012). Chronic cyanidin-3-glucoside administration improves short-term spatial recognition memory but not passive avoidance learning and memory in streptozotocin-diabetic rats. *Phytother. Res.* 26, 1205–1210. doi: 10.1002/ptr.3702

Nirmalasari, O., Mamo, S. K., Nieman, C. L., Simpson, A., Zimmerman, J., Nowrangi, M. A., et al. (2017). Age-related hearing loss in older adults with cognitive impairment. *Int. Psychogeriatr.* 29, 115–121. doi: 10.1017/S1041610216001459

Nishida, Y., Hizume, M., Fumimura, Y., and Ichikawa, T. (2019). Cerebellar cognitive affective syndrome improved by donepezil. *Intern. Med.* 58, 1003–1006. doi: 10.2169/internalmedicine.1206-18

Okuda, T., Nagamachi, S., Ushisako, Y., and Tono, T. (2013). Glucose metabolism in the primary auditory cortex of postlingually deaf patients: an FDG-PET study. *ORL J. Otorhinolaryngol. Relat. Spec.* 75, 342–349. doi: 10.1159/000357474

O'Leary, T. P., Shin, S., Fertan, E., Dingle, R. N., Almuklass, A., Gunn, R. K., et al. (2017). Reduced acoustic startle response and peripheral hearing loss in the 5xFAD mouse model of Alzheimer's disease. *Genes Brain Behav.* 16, 554–563. doi: 10.1111/gbb.12370

Osler, M., Christensen, G. T., Mortensen, E. L., Christensen, K., Garde, E., and Rozing, M. P. (2019). Hearing loss, cognitive ability, and dementia in men age 19-78 years. *Eur. J. Epidemiol.* 34, 125–130. doi: 10.1007/s10654-018-0452-2

Park, H. J., Shim, H. S., Kim, K. S., Han, J. J., Kim, J. S., Ram Yu, A., et al. (2013). Enhanced learning and memory of normal young rats by repeated oral administration of Krill Phosphatidylserine. *Nutr. Neurosci.* 16, 47–53. doi: 10.1179/1476830512Y.0000000029

Park, M. H., Lee, H. J., Kim, J. S., Lee, J. S., Lee, D. S., and Oh, S. H. (2010). Cross-modal and compensatory plasticity in adult deafened cats: a longitudinal PET study. *Brain Res.* 1354, 85–90.

Plakke, B., Hwang, J., and Romanski, L. M. (2015). Inactivation of primate prefrontal cortex impairs auditory and audiovisual working memory. *J. Neurosci.* 35, 9666–9675. doi: 10.1523/JNEUROSCI.1218-15.2015

Platt, B., Welch, A., and Riedel, G. (2011). FDG-PET imaging, EEG and sleep phenotypes as translational biomarkers for research in Alzheimer's disease. *Biochem. Soc. Trans.* 39, 874–880. doi: 10.1042/BST0390874

Sawangjit, A., Oyanedel, C. N., Niethard, N., Salazar, C., Born, J., and Inostroza, M. (2018). The hippocampus is crucial for forming non-hippocampal long-term memory during sleep. *Nature* 564, 109–113. doi: 10.1038/s41586-018-0716-8

Schreck, L., Ryan, S., and Monaghan, P. (2018). Cerebellum and cognition in multiple sclerosis. *J. Neurophysiol.* 120, 2707–2709. doi: 10.1152/jn.00245.2018

Son, S. M., Shin, H. J., Byun, J., Kook, S. Y., Moon, M., Chang, Y. J., et al. (2016). Metformin facilitates amyloid-beta generation by beta- and gamma-secretases via autophagy activation. *J. Alzheimers Dis.* 51, 1197–1208. doi: 10.3233/JAD-151200

Strelnikov, K., Marx, M., Lagleyre, S., Fraysse, B., Deguine, O., and Barone, P. (2015). PET-imaging of brain plasticity after cochlear implantation. *Hear. Res.* 322, 180–187. doi: 10.1016/j.heares.2014.10.001

Suh, M. W., Park, K. T., Lee, H. J., Lee, J. H., Chang, S. O., and Oh, S. H. (2015). Factors contributing to speech performance in elderly cochlear implanted patients: an FDG-PET study: a preliminary study. *J. Int. Adv. Otol.* 11, 98–103. doi: 10.5152/iao.2015.424

Takada, M. (2016). [Neuroanatomy of frontal association cortex]. *Brain Nerve* 68, 1253–1261. doi: 10.11477/mf.1416200588

Tucker, A. R., Gibbs, M. E., and Stanes, M. D. (1976). Cycloheximide and passive avoidance memory in mice: time-response, dose-response and short-term memory. *Pharmacol. Biochem. Behav.* 4, 441–446.

Wilke, M., Kassubek, J., Ziyeh, S., Schulze-Bonhage, A., and Huppertz, H. J. (2003). Automated detection of gray matter malformations using optimized voxel-based morphometry: a systematic approach. *Neuroimage* 20, 330–343.

Ye, M., Chung, H. S., An, Y. H., Lim, S. J., Choi, W., Yu, A. R., et al. (2016). Standardized herbal formula PM012 decreases cognitive impairment and promotes neurogenesis in the 3xTg AD mouse model of Alzheimer's disease. *Mol. Neurobiol.* 53, 5401–5412. doi: 10.1007/s12035-015-9458-x

Yoshida, H., Takahashi, H., Kanda, Y., and Chiba, K. (2017). PET-CT observations of cortical activity in pre-lingually deaf adolescent and adult patients with cochlear implantation. *Acta Otolaryngol.* 137, 464–470. doi: 10.1080/00016489.2016.1253868

Zgraggen, E., Boitard, M., Roman, I., Kanemitsu, M., Potter, G., Salmon, P., et al. (2012). Early postnatal migration and development of layer II pyramidal neurons in the rodent cingulate/retrosplenial cortex. *Cereb. Cortex* 22, 144–157. doi: 10.1093/cercor/bhr097

Zheng, Y., Fan, S., Liao, W., Fang, W., Xiao, S., and Liu, J. (2017). Hearing impairment and risk of Alzheimer's disease: a meta-analysis of prospective cohort studies. *Neurol. Sci.* 38, 233–239. doi: 10.1007/s10072-016-2779-3

Conflict of Interest: The authors declare that the research was conducted in the absence of any commercial or financial relationships that could be construed as a potential conflict of interest.

frontiers in Aging Neuroscience

ORIGINAL RESEARCH
published: 26 August 2020
doi: 10.3389/fnagi.2020.00266

Predictive Value of Odor Identification for Incident Dementia: The Shanghai Aging Study

*Ding Ding[1,2], Zhenxu Xiao[1,2], Xiaoniu Liang[1,2], Wanqing Wu[1,2], Qianhua Zhao[1,2] and Yang Cao[3]**

[1] *Institute of Neurology, Huashan Hospital, Fudan University, Shanghai, China,* [2] *National Clinical Research Center for Aging and Medicine, Huashan Hospital, Fudan University, Shanghai, China,* [3] *Clinical Epidemiology and Biostatistics, School of Medical Sciences, Örebro University, Örebro, Sweden*

Objective: This study aimed to evaluate the value of odors in the olfactory identification (OI) test and other known risk factors for predicting incident dementia in the prospective Shanghai Aging Study.

Methods: At baseline, OI was assessed using the Sniffin' Sticks Screening Test 12, which contains 12 different odors. Cognition assessment and consensus diagnosis were conducted at both baseline and follow-up to identify incident dementia. Four different multivariable logistic regression (MLR) models were used for predicting incident dementia. In the no-odor model, only demographics, lifestyle, and medical history variables were included. In the single-odor model, we further added one single odor to the first model. In the full model, all 12 odors were included. In the stepwise model, the variables were selected using a bidirectional stepwise selection method. The predictive abilities of these models were evaluated by the area under the receiver operating characteristic curve (AUC). The permutation importance method was used to evaluate the relative importance of different odors and other known risk factors.

Results: Seventy-five (8%) incident dementia cases were diagnosed during 4.9 years of follow-up among 947 participants. The full and the stepwise MLR model (AUC = 0.916 and 0.914, respectively) have better predictive abilities compared with those of the no- or single-odor models. The five most important variables are Mini-Mental State Examination (MMSE) score, age, peppermint detection, coronary artery disease, and height in the full model, and MMSE, age, peppermint detection, stroke, and education in the stepwise model. The combination of only the top five variables in the stepwise model (AUC = 0.901 and sensitivity = 0.880) has as a good a predictive ability as other models.

Conclusion: The ability to smell peppermint might be one of the useful indicators for predicting dementia. Combining peppermint detection with MMSE, age, education, and history of stroke may have sensitive and robust predictive value for dementia in older adults.

Keywords: olfactory, odor, dementia, prediction, logistic model, permutation importance method

OPEN ACCESS

Edited by:
Jiehui Jiang,
Shanghai University, China

Reviewed by:
Carla Masala,
University of Cagliari, Italy
Jayant Pinto,
University of Chicago, United States

****Correspondence:***
Yang Cao
yang.cao@oru.se

Received: *13 April 2020*
Accepted: *03 August 2020*
Published: *26 August 2020*

Citation:
Ding D, Xiao Z, Liang X, Wu W, Zhao Q and Cao Y (2020) Predictive Value of Odor Identification for Incident Dementia: The Shanghai Aging Study. Front. Aging Neurosci. 12:266. doi: 10.3389/fnagi.2020.00266

INTRODUCTION

Olfactory dysfunction is a common feature of neurodegenerative diseases, especially in dementia (e.g., Alzheimer's disease, dementia with Lewy bodies, and Parkinson's disease dementia), and is considered to be a premotor sign of neurodegeneration (Attems et al., 2014). Previous hospital- and population-based studies have demonstrated the association of olfactory dysfunction with dementia, cognitive decline, or mild cognitive impairment (MCI). Some human studies show a relationship between peppermint aroma stimulation and enhanced memory and functional performance in older people with dementia (Herz, 1997; Collier, 2007; Moss et al., 2008). Furthermore, peppermint's preservation of central nervous system microglia as a mediator of improved cognitive function has also been reported by an experimental *in vivo* study (Koo et al., 2001). At the baseline of our Shanghai Aging Study, we found a lower score on the olfactory identification (OI) test and a reduced ability to identify odors of peppermint, orange, pineapple, cinnamon, coffee, fish, banana, rose, leather, and licorice in participants with MCI compared to those with normal cognition (Liang et al., 2016). We further verified these findings in the 5-year prospective phase and explored the association of inability to smell peppermint with a higher dementia onset risk (HR = 2.67, 95% CI: 1.44, 4.96) by using a multivariable logistic regression (MLR) model (Liang et al., 2020). However, the previous study also did not evaluate the performance (or predictive value) of peppermint in predicting incident dementia.

Variable selection is one of the core concepts in statistical learning, and it impacts the performance of predictive models significantly. Irrelevant or partially relevant variables may reduce the predictive ability of the models. There are many variable-selection methods available in data science, such as recursive feature elimination, principle component analysis, correlation matrix with heat map, feature importance, and some wrapper methods (Hua et al., 2009; Liu and Motoda, 2012). Variable importance is straightforward and can be easily explained to an audience outside of the fields of data science and informatics. In the current study, the permutation importance (PI) method, which permutes the values of a feature of interest and reevaluates the predictive ability of the models (Altmann et al., 2010), was used to evaluate the importance of the OI test, certain odors, and other known risk factors for predicting incident dementia in the prospective Shanghai Aging Study.

MATERIALS AND METHODS

Study Setting and Participants

The Shanghai Aging Study is a prospective cohort study aiming to enumerate the prevalence, incidence, and risk factors for dementia and MCI among residents aged ≥60 in an urban community of central Shanghai. The study design and participant recruitment of SAS are described in detail elsewhere (Ding et al., 2014; Liang et al., 2016; Liang et al., 2020). A flowchart of recruitment for study participants is shown in **Supplementary Figure S1**. In total, 1,782 recruited participants without dementia completed both cognitive assessment and the OI test at baseline (2010–2011). The participants were contacted between April 1, 2014 and December 31, 2016, to investigate the first wave of dementia incidence. After excluding participants who were lost to follow-up, deceased, or had missing values in the analysis variables, 947 participants were included in the current study. After an average of 4.9 years of follow-up, 75 (7.0%) of the 947 included participants were diagnosed with new-onset dementia with an incidence rate of 16 [95% confidence interval (CI): 13–20] per 1,000 person-years. Participants with incident dementia were older (mean age: 77.8 ± 5.6) than participants without incident dementia (mean age: 69.9 ± 6.5, $p < 0.001$) at the baseline.

Collection of Baseline Data

Demographics and lifestyle: Demographic and lifestyle characteristics, including age, sex, years of formal education, cigarette smoking, and alcohol consumption, were collected via an interviewer-administered questionnaire (Shu et al., 2004).

Physical measurements: Each participant's height and weight at baseline were measured by a research nurse. BMI was calculated as weight in kilograms divided by height in meters squared.

Medical history: Participants' medical histories, including physician-diagnosed hypertension, coronary artery disease (CAD), diabetes, and stroke were asked by neurologists from the Department of Neurology, Huashan Hospital (Liang et al., 2020).

Apolipoprotein (APOE) genotype: DNA was extracted from blood or saliva samples at baseline. APOE genotyping was conducted by the Taqman SNP method (Smirnov et al., 2009). The presence of at least one ε4 allele was defined as APOE-ε4 allele positive.

OI test: OI at baseline was assessed using the Sniffin' Sticks Screening Test 12 (SSST-12), which consists of 12 odors (orange, leather, cinnamon, peppermint, banana, lemon, licorice, coffee, cloves, pineapple, rose, and fish) presenting on felt-tip sticks (Wolfensberger, 2000). The SSST-12 kit was purchased from Burghart Medical Technology, Hamburg, Germany (Tinsdaler Weg 175, 2020). OI was defined as an individual correctly naming an odor or odors, either with or without the help of alternative choices. The administration of SSST-12 is described in detail elsewhere (Liang et al., 2016).

Cognition assessment and consensus diagnosis: The cognitive function of the participants was assessed using a battery of neuropsychological tests, including the Mini Mental State Examination (MMSE) (Tombaugh and McIntyre, 1992), Conflicting Instructions Task (go/no-go task), Stick Test, Modified Common Objects Sorting Test, Auditory Verbal Learning Test, Modified Fuld Object Memory Evaluation, Trail-Making Test A & B, and Renminbi (Chinese Currency) Test. The normative data and detailed description of the assessment battery are reported elsewhere (Zhang et al., 1990; Ding et al., 2015). Each participant's mood was evaluated using the Zung Self-Rating Anxiety Scale and the Center for Epidemiologic Studies Depression Scale (CESD), and

depression was present if a CESD score ≥16 (Zung, 1971; Eaton et al., 2004).

Two study neurologists, one neuropsychologist, and one neuroepidemiologist reviewed the functional, medical, neurological, psychiatric, and neuropsychological data of the participants and reached a consensus regarding the presence of dementia using the Diagnostic and Statistical Manual of Mental Disorders IV (DSM–IV) criteria (American Psychiatric Association, 1994).

Prospective Follow-Up

Between April 2014 and December 2016, participants who were diagnosed as dementia-free were invited for a clinical interview as the first wave of follow-up to detect incident dementia cases. Each participant was administered the same neuropsychological battery for the cognition assessment. Procedure and criteria of the consensus diagnosis were identical with that at baseline.

Statistical Analysis

Descriptive Analysis

Participants' demographics, lifestyle, medical history, and OI test results are presented using mean with standard deviation (SD) or median with interquartile range (IQR) for the continuous variable and using a percentage for the categorical variables. Difference between groups was tested using the chi-squared test for categorical variables and analysis of variance (ANOVA) or Mann–Whitney *U* test for continuous variables. Correlation was measured using the Pearson correlation coefficient between two continuous variables and using the point-biserial correlation coefficient between a binary and a continuous variable (Demirtas and Hedeker, 2016) and the phi coefficient between two binary variables (Chen and Popovich, 2002). Multicollinearity between the variables is presented using a heat map. A two-sided *P*-value <0.05 is considered statistically significant.

Determination of Variable Importance

Prediction: In the current study, prediction for dementia incidence was conducted using MLR analysis. Four types of MLR models were constructed in the study. In the first or no-odor model, we only included demographics, lifestyle, and medical history variables (i.e., sex, age, BMI, height, education, smoking, drinking, CAD, hypertension, diabetes, depression, stroke, APOE-ε4, and MMSE) but not any odor. In the second type or single-odor model, we added only one single odor or OI sum score to the first model. In the third or full model, all 12 odors were included. Weight was excluded in the first three types of models, and OI sum score was excluded in the first and third models because of high collinearity with other variables. In the fourth model, the variables were selected using a bidirectional stepwise selection method (Zhang, 2016).

Validation: The K-fold cross-validation method was used during the MLR model learning and validation, which is a standard way to obtain unbiased estimates of a model's goodness of fit and to handle the overfitting problem in statistical learning. In brief, we randomly split the data set into five equal partitions and constructed an MLR model on four partitions while validating it on the remaining partition. In each iteration, the prediction was made for the one held-out partition. In the end, we got the prediction for the whole data set and used it for validation (James et al., 2013).

Evaluation: The metrics, including sensitivity, specificity, accuracy, and area under the receiver operating characteristic (ROC) curve, were used to evaluate the models' predictive ability. Terminology and derivations of the metrics are given in detail elsewhere (Cao et al., 2019). The acceptable, good, and great prediction models for incident dementia are defined as the area under the ROC curve (AUC) of a model greater than 0.7, 0.8, and 0.9, respectively (Marzban, 2004; Mandrekar, 2010).

Variable standardization: Because scalability is an important aspect of statistical learning and matters for the models' performance, variable standardization is preferred before training the models (Lantz, 2013). Because the aim of the current study was to evaluate the predictive ability of the models rather than to interpret the associations between the predictors and the outcome, therefore, all features were treated as continuous or discrete numerical variables and were scaled using the standard scaler to have a mean of 0 and a SD of 1 (Zheng and Casari, 2018).

PI: For the MLR models, PI was calculated for each variable, which is measured by looking at how much the accuracy decreases when the information on the variable is not available (Altmann et al., 2010). To mask the information on a variable during validation, instead of removing the variable from the data set, the PI method replaces it with random noise by shuffling the values of the variable, i.e., using values from other participants (Breiman, 2001; Fisher et al., 2019). The relative importance of a variable was calculated as the accuracy decrease of the variable relative to the range of the accuracy decreases of all the variables (Gómez-Ramírez et al., 2019).

Software and Hardware

The descriptive analyses were performed using Stata 16.0 (StataCorp LLC, College Station, TX, United States). The MLR models and PI evaluation were achieved in Python 3.6 (Python Software Foundation[1]) using packages scikit-learn 0.22.1 (Pedregosa et al., 2011) and ELI5 0.10.1 (Korobov and Lopuhin, 2020). All computation was conducted on a computer with a 64-bit Windows 7 Enterprise operating system (Service Pack 1), Intel® Core TM i5-4210U CPU of 2.40 GHz, and 16.0 GB installed random access memory.

Ethical Consideration and Data Availability

The study is an observational study and was approved by the Medical Ethical Committee of Huashan Hospital, Fudan University, Shanghai, China (approval number: 2009-195). All participants and/or their legal guardian gave their written informed consent for participation in the study. There is no personal identification disclosed in our data. The data are not publicly available but may be available upon reasonable request and with permission of the Ding Ding (dingding@huashan.org.cn).

[1]https://www.python.org/

RESULTS

Characteristics of the Participants

Detailed baseline information on the participants is published elsewhere and given in **Supplementary Table S1** (Liang et al., 2020). In general, compared to those who did develop dementia (n = 872), participants with incident dementia (n = 75) were older (77.8 vs 69.9 years), shorter (156.5 vs 162.0 cm), weighed less (59.1 vs 64.4 kg), and had less education (9 vs 12 years) when recruited. CAD, stroke, and APOE-ε4 positive were more frequently observed in the new-onset dementia cases (**Supplementary Table S1**). The new-onset dementia cases had a lower correct identification rate for most odors and lower OI sum and MMSE scores at the baseline (**Supplementary Table S1**). There was no significant multicollinearity observed between the variables except for the high correlation between height and weight, weight and BMI, and OI sum score and the 12 odors (**Figure 1**).

Predictive Ability of the Models

The regression coefficients of the full and stepwise models are shown in **Tables 1** and **2**. In the full model, age, APOE-ε4, peppermint, pineapple, banana, and MMSE are statistically significantly (at the two-sided type one error α = 0.05 level) associated with dementia incidence. However, in the analysis, wrong identification of pineapple is associated with a lower probability of dementia incidence (**Table 1**).

In the stepwise model, age, weight, education, APOE-ε4, peppermint, banana, pineapple, and MMSE are associated with dementia incidence. Similarly, wrong identification of pineapple is associated with lower probability of dementia incidence (**Table 2**). The predictive abilities of the four types of models are shown in **Table 3**. There is no significant difference in predictive abilities between the no-odor and the single-odor models; both types of models show great ability for predicting dementia incident (AUCs ranging between 0.901 and 0.906). However, the model including licorice shows higher

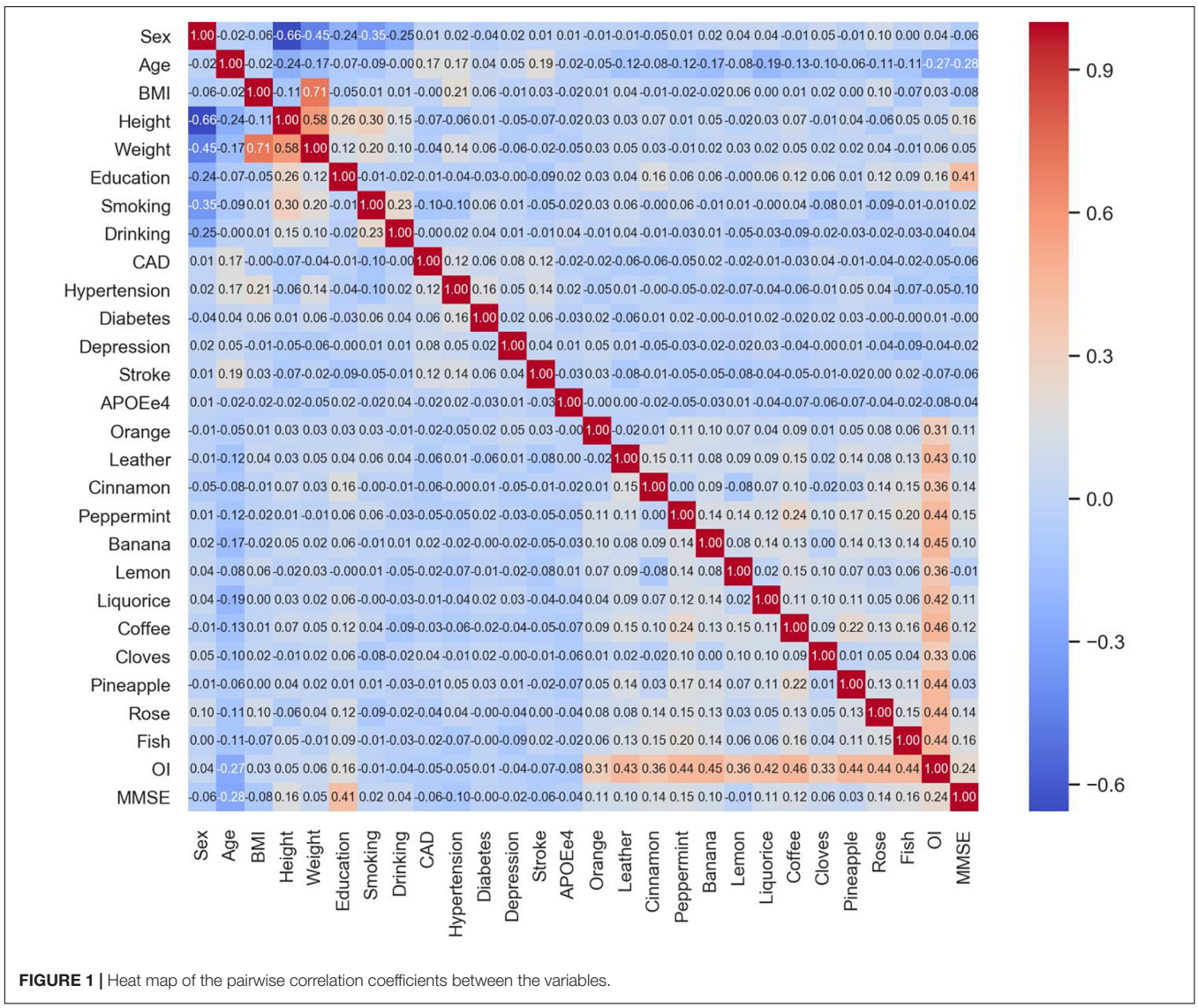

FIGURE 1 | Heat map of the pairwise correlation coefficients between the variables.

TABLE 1 | Multivariable logistic regression coefficients of the full model.

Variable	β	SE	*P*-value
Sex	−0.051	0.231	0.824
Age	1.086	0.200	0.000
BMI	−0.240	0.162	0.139
Height	−0.361	0.211	0.086
Education	−0.241	0.146	0.099
Smoking	0.331	0.185	0.074
Drinking	−0.288	0.213	0.176
CAD	0.099	0.123	0.424
Hypertension	−0.068	0.166	0.683
Diabetes	−0.098	0.160	0.539
Depression	0.244	0.138	0.076
Stroke	0.201	0.128	0.116
APOE-ε4	0.352	0.139	0.011
Orange	0.055	0.151	0.715
Leather	−0.235	0.163	0.151
Cinnamon	−0.182	0.179	0.308
Peppermint	−0.371	0.118	0.002
Banana	−0.341	0.153	0.026
Lemon	0.202	0.168	0.229
Licorice	0.054	0.160	0.737
Coffee	−0.027	0.127	0.828
Cloves	−0.013	0.161	0.934
Pineapple	0.408	0.176	0.020
Rose	−0.244	0.158	0.124
Fish	0.159	0.148	0.280
MMSE	−0.719	0.138	0.000

SE, standard error; BMI, body mass index; CAD, coronary artery disease; OI, olfactory identification sum score; APOE, apolipoprotein; MMSE, Mini-Mental State Examination. Weight and olfactory identification sum score were excluded from the model because of collinearity. β corresponds to the change of women versus men for sex; per year for age and education; per unit for BMI, height, and MMSE; with the feature versus without the feature for smoking, drinking, and comorbidities; and positive versus negative for APOE-ε4 and individual odor tests.

accuracy (= 0.818), and the model including banana, lemon, or cloves shows higher sensitivity (= 0.920, **Table 3**). The predictive abilities of the full and stepwise models are similar (AUC = 0.916 and 0.914, respectively) (**Figure 2**) and better (although not significant) than those of the no- or single-odor models (**Table 3**).

Relative PI of the Variables

The relative importance of the variables was evaluated in the full and stepwise models because they showed the best performance for prediction. In the full model, the five most important variables are MMSE, age, peppermint, CAD, and height (**Figure 3**). In the stepwise model, the five most important are MMSE, age, peppermint, stroke, and education. Both results indicate that identification of peppermint odor might be an important indicator for dementia only after MMSE and age. In addition, banana also shows relative higher importance in both models (**Figure 3**). There are also variables with negative importance, which means that, when they were excluded from the model, the accuracy of the prediction increased.

TABLE 2 | Multivariable logistic regression coefficients of the stepwise model.

Variable	β	SE	*P*-value
Age	1.057	0.186	0.000
Weight	−0.360	0.171	0.036
Education	−0.308	0.132	0.020
Depression	0.248	0.133	0.061
Stroke	0.209	0.121	0.086
APOEe4	0.311	0.137	0.023
Leather	−0.255	0.157	0.104
Peppermint	−0.331	0.111	0.003
Banana	−0.310	0.148	0.036
Lemon	0.261	0.158	0.098
Pineapple	0.406	0.166	0.014
Rose	−0.241	0.149	0.107
MMSE	−0.693	0.133	0.000

SE, standard error; APOE, apolipoprotein; MMSE, Mini-Mental State Examination. β corresponds to the change per year for age and education, per unit for weight and MMSE, with versus without depression or stroke, and positive versus negative for APOE-ε4 and individual odor tests.

When using a simple model that only includes the five most important variables in the stepwise model, we achieved a predictive ability (AUC = 0.901 and sensitivity = 0.880) as great as those of the aforementioned models that include many more variables (**Table 3**).

DISCUSSION

Although there is a study using random forest and permutation-based methods to select important variables for predicting conversion to MCI (Gómez-Ramírez et al., 2019), to the best of our knowledge, this is the first study investigating the predictive rather than associative value of the odors in the OI test for incident dementia in the elderly. There are several strengths in our study. First, the permuting destroys the interaction effects between variables, which means that it automatically takes into account both the main effect of a variable and the interaction effects with other variables on model performance (Fisher et al., 2019). Second, our data suggest that, not only is MMSE generally applicable to predict dementia in our geriatric population, but the addition of the ability to smell peppermint further improves the precision and accuracy of the model. This has tangible clinical benefits in both informing clinical decision making and translating statistical probability into coherent information for the elderly and their families. Thus, a consensus plan (either medical treatment or preventive intervention) may be more readily reached. Third, cross-validation was used when we evaluated the performance of the models, which minimized overfitting. Finally, different MLR models were constructed and compared, and they presented similar results, which ensure that our conclusion is conservative and robust.

OI Test and Dementia Prediction

Previous studies reveal that both olfactory and certain cognitive functions are controlled via the orbitofrontal cortex, and reduced

TABLE 3 | Performance matrix of the prediction models.

	Sensitivity	Specificity	Accuracy	AUC	95% CI of AUC	
					Lower limit	Upper limit
No-odor model[a]	0.893	0.791	0.799	0.901	0.864	0.933
Single-odor model[b]						
Orange	0.880	0.791	0.798	0.901	0.867	0.933
Leather	0.880	0.804	0.810	0.905	0.870	0.935
Cinnamon	0.893	0.804	0.811	0.904	0.867	0.936
Peppermint	0.893	0.781	0.790	0.904	0.866	0.936
Banana	0.920	0.768	0.780	0.906	0.873	0.936
Lemon	0.920	0.749	0.762	0.902	0.869	0.933
Licorice	0.867	0.814	0.818	0.902	0.869	0.932
Coffee	0.893	0.786	0.794	0.900	0.867	0.932
Cloves	0.920	0.749	0.762	0.902	0.866	0.932
Pineapple	0.893	0.796	0.804	0.903	0.866	0.932
Rose	0.893	0.786	0.794	0.904	0.869	0.936
Fish	0.893	0.791	0.799	0.902	0.864	0.933
OI	0.933	0.751	0.766	0.904	0.869	0.935
Full model[c]	0.907	0.828	0.834	0.916	0.882	0.945
Stepwise model[d]	0.880	0.831	0.835	0.914	0.881	0.943
Simple model[e]	0.880	0.781	0.790	0.901	0.859	0.931

[a]Predictors: sex, age, body mass index (BMI), height, education, smoking, drinking, coronary artery disease (CAD), hypertension, diabetes, depression, stroke, apolipoprotein (APOE)-ε4, and Mini-mental State Examination (MMSE). [b]Other predictors are the same as in the no-odor model. [c]Predictors: sex, age, BMI, height, education, smoking, drinking, CAD, hypertension, diabetes, depression, stroke, APOE-ε4, MMSE, and the 12 odors. [d]Predictors: age, weight, education, depression, stroke, APOE-ε4, leather, peppermint, banana, lemon, pineapple, rose, and MMSE. [e]Predictors: MMSE, age, peppermint, stroke, and education.

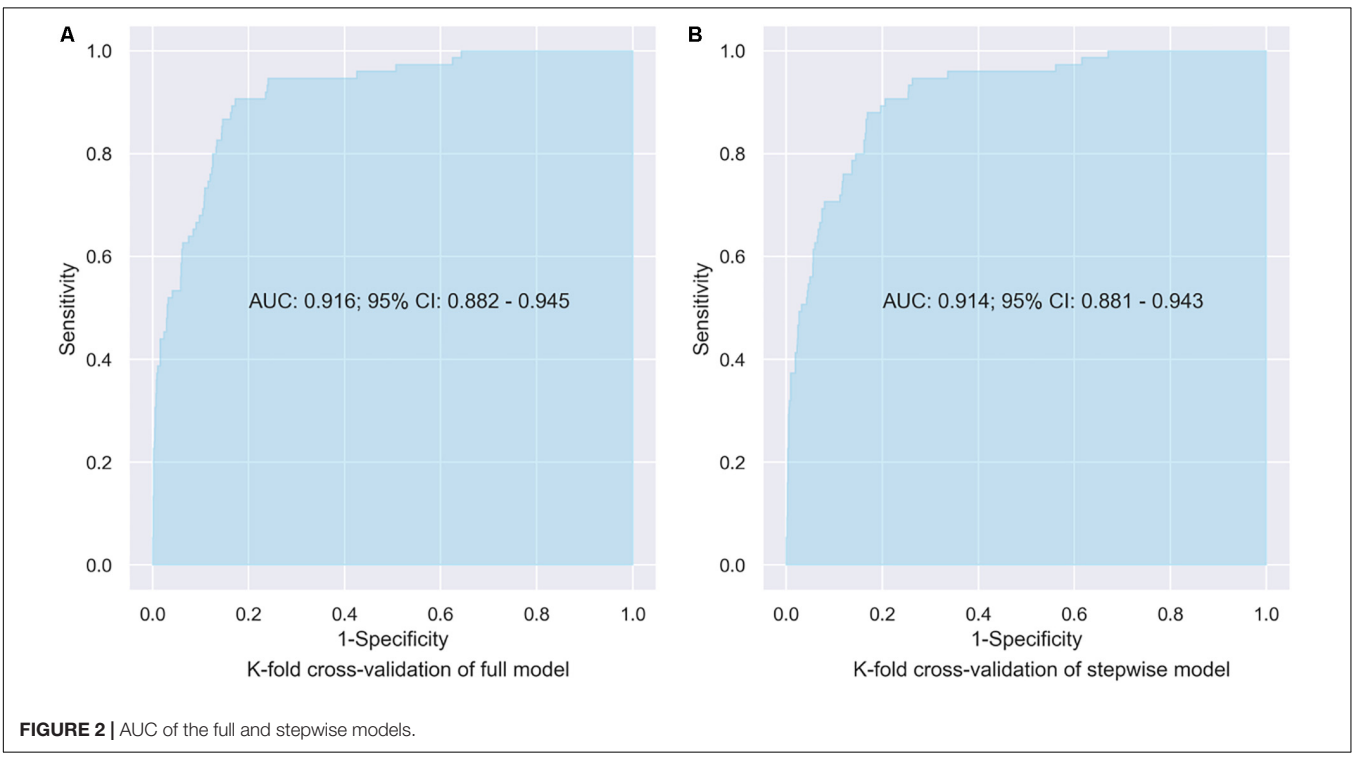

FIGURE 2 | AUC of the full and stepwise models.

olfactory ability and manifestation of dementia are associated with brain changes in the hippocampus and entorhinal cortex (Rupp et al., 2006; Maurage et al., 2011; Seligman et al., 2013; Marigliano et al., 2014; Growdon et al., 2015). Olfactory dysfunction is associated with pathological features of cognitive impairment (Passali et al., 2015; Reijs et al., 2017). Some studies suggest that olfactory dysfunction could be a suitable biomarker for predicting cognitive impairment and development

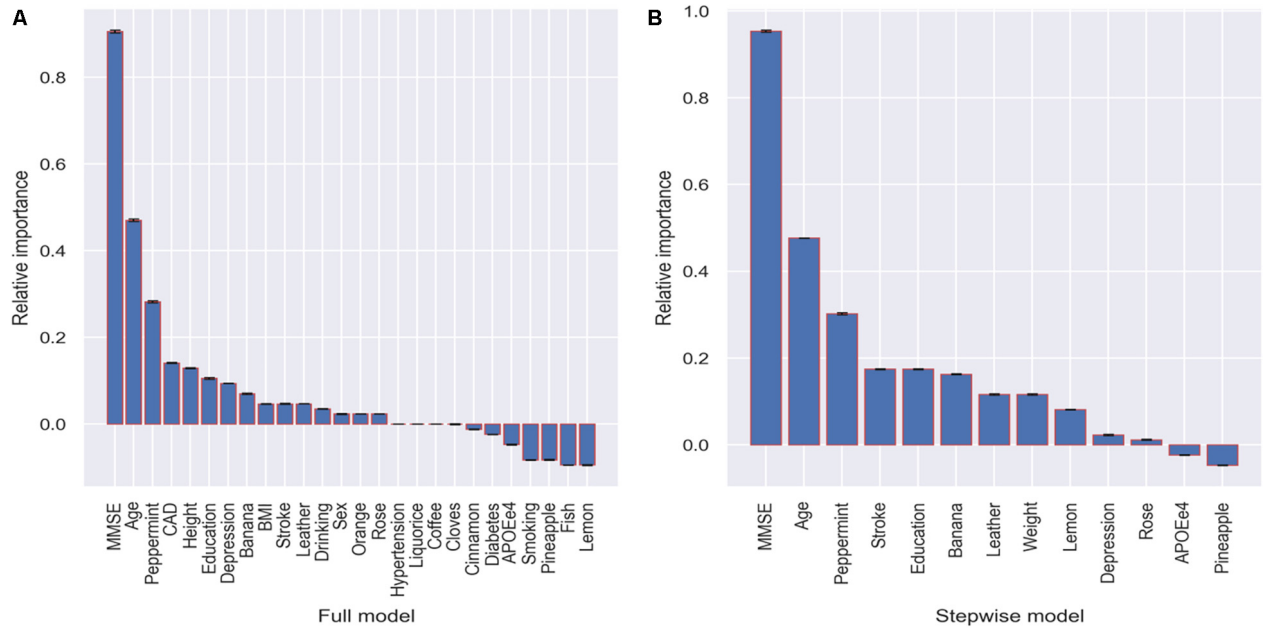

FIGURE 3 | Relative importance with corresponding standard deviation of the variables in terms of accuracy decrease in prediction.

of dementia (Suzuki et al., 2004; Eibenstein et al., 2005; Devanand et al., 2015; Ottaviano et al., 2016; Roberts et al., 2016; Roalf et al., 2017). Our previous study also indicates that some odors, such as peppermint in the OI test, are associated with incident dementia in the older population (Liang et al., 2020). However, the predictive ability of the models incorporating the OI test was not ideal in previous studies. A large sample size (N = 2227) prospective study of middle-aged to older adults (55–86 years) concludes that olfactory function may serve as a marker for screening persons at high risk for cognitive decline and dementia. However, the AUC values in the study are only between 0.55 and 0.62 for the five cognitive tests (Tebrugge et al., 2018). In another prospective study of 757 participant aged 65 years and older, the University of Pennsylvania Smell Identification Test combined with the Selective Reminding Test–total immediate recall shows an improved performance for predicting dementia incidence; however, the AUC is still only 0.77 (Devanand et al., 2015). Although Stanciu et al. (2014) concludes that OI could independently predict conversion to dementia within a 10-year time span, the accuracy of the prediction is not evaluated in that study.

The SSST-12 test comprises 12 common and familiar odorants recognized by a majority of the population (Oleszkiewicz et al., 2019). The number of odors for selection could be as many as 37 in comprehensive olfactory tests (MediSense, 2020); however, it remains uncertain how many items are sufficient for a valid diagnosis or screening (Lotsch et al., 2016). Several studies attempt to reduce the number of odor identification items to 1–5 odors (Doty et al., 1996; Simmen et al., 1999; Hummel et al., 2001; Gilbert et al., 2002; Jackman and Doty, 2005; Mueller and Renner, 2006), and a recent study recommends a three-odor test with cinnamon as the best scoring odor (Lotsch et al., 2016). Although an inability to identify certain odors has previously been used as a predictor for incident dementia (Adams et al., 2018; Liang et al., 2020), the relative importance of the odors compared to each other or compared to other predictors has not been investigated.

Peppermint and Dementia

The current study further confirms previous findings that the ability to smell peppermint may play an important role in predicting dementia incidence in the elderly (Adams et al., 2018; Liang et al., 2020). It also reveals that peppermint is the third most important variable in the prediction models, only after MMSE and age. Using a simplified prediction model including MMSE, age, peppermint, stroke, and education, the specificity of the prediction can be as high as 0.88 with an AUC of 0.90.

The relationship between detection of peppermint and dementia has been investigated previously. A human study of peppermint's modulation on long-term potentiation shows a direct correlation between peppermint oils and enhanced memory (Moss et al., 2008). In recall tests of extended memory, improved cognitive function arises in response to exposure to peppermint aroma during both learning and memory retrieval tasks (Herz, 1997). In a randomized single blind trial, researchers used multisensory stimulation, including aromatic cloves or peppermint, to improve functional performance in older people with dementia, and they find a significant effect of the intervention on function, mood, and behavior in people with a diagnosis of moderate/severe dementia (Collier, 2007). However, Fox et al. (2012) study suggests that consumption of peppermint does not mediate alertness or enhance cognitive performance. Although the underlying mechanism of the effects of peppermint on neurological functions is not clear yet, an experimental study shows that *in vivo* exposure of

glial cells to peppermint oil might inhibit heat shock-induced apoptosis of astrocytes in rat and human cell models, suggesting peppermint's preservation of central nervous system microglia as a mediator of improved cognitive function (Koo et al., 2001). Further research investigating compound metabolism is required to optimize quantification of memory performance following peppermint ingestion.

MLR and PI

There are other statistical learning methods for prediction, such as discriminant analysis, decision tree, K-nearest neighbor, support vector machine, and multilayer perceptron (James et al., 2013). The reasons for using MLR in the current study are that (a) logistic regression is the most widely used method in diagnostic tests and prediction studies for binary outcomes in medical science. The results from a logistic regression analysis can be easily comprehended by clinical researchers (Coughlin et al., 1992; Greiner et al., 2000; Janssens et al., 2005). (b) Coefficients from the logistic regression models can be translated into odds ratios, which are widely used in medical and epidemiology studies (Hilbe, 2009).

Compared to Gini importance, which is model-agnostic and embedded in tree-based statistical learning algorithms, such as random forest (Nembrini et al., 2018), the concept of PI is straightforward. PI measures the importance of a variable by calculating the decrease in the model's prediction accuracy after permuting the variable. A variable is "important" if shuffling its values decreases the accuracy because, in this case, the model relies on the variable for the prediction (Breiman, 2001). Although permuting irrelevant or partially relevant variables may increase the predictive ability of the models, it may result in a negative importance, just as we observe in **Figure 3**. The method is generalizable no matter the predictive model and most suitable for computing variable importance when the number of variables is not large; otherwise, it can be resource-intensive (Altmann et al., 2010; Fisher et al., 2019).

Because using a limited number of variables may have already achieved great prediction for dementia incidence (such as the simple model in **Table 3**), one single variable contributes little to the improvement accuracy of the prediction in a multivariable model; therefore, we only compare relative importance of the variables in this study. It is useful when we want to find common important variables using different statistical learning methods. In our study, all five of the most important variables (MMSE, age, peppermint, stroke, and education) found in the stepwise MLR model are consistent with the statistically significant risk factors derived from previous studies (Snowdon and Nun, 2003; Cullen et al., 2005; Ngandu et al., 2007; Mijajlovic et al., 2017; Liang et al., 2020). The combination gives us real, predictive values that may be useful in clinical practice.

Limitations

There are also several limitations in the study. First, the sample size is relatively small, and only 75 participants were diagnosed with new-onset dementia after an average of 4.9 years of follow-up. Essentially, the performance of statistical learning methods relies on the amount of data available. The more observations and variables, the better the models perform. Although we obtain satisfactory accuracy from the models, the generalizability of the findings is limited by the small sample size. Second, nominal variables are treated as discrete numerical features in this study. Although it increases the accuracy of prediction, the interpretability of the models is reduced. Third, about half of the participants who were lost to follow-up were excluded from our analysis data set. We do not know the incidence of dementia among the excluded participants and whether being lost to follow-up was associated with certain cognitive impairments. Although there is no statistically or clinically significant difference between the included and excluded participants in terms of demographic and lifestyle characteristics, the validity of the models is limited by the incompleteness and needs to be examined using data with better representativeness.

CONCLUSION

The ability to smell certain odors, especially peppermint, might be one of the useful indicators for predicting dementia in the elderly. Incorporating peppermint with MMSE, age, education, and history of stroke, we may predict long-term dementia onset in older adults precisely. Aromatherapy using essential oils, including peppermint, to prevent and/or control symptoms of dementia deserves further investigation.

DATA AVAILABILITY STATEMENT

The data analyzed in this study is subject to the following licenses/restrictions: The data are not publicly available but may be available upon reasonable request and permission. Requests to access these datasets should be directed to DD, dingding@huashan.org.cn.

ETHICS STATEMENT

The studies involving human participants were reviewed and approved by the Medical Ethical Committee of Huashan Hospital, Fudan University, Shanghai, China (approval number: 2009-195). The patients/participants provided their written informed consent to participate in this study.

AUTHOR CONTRIBUTIONS

YC and DD: conceptualization, methodology, and writing – original draft. DD and XL: data curation. YC: formal analysis and software. DD and QZ: funding acquisition. DD, XL, WW, and ZX: investigation. DD: project administration. YC, DD, and ZX: writing – review and editing. All authors contributed to the article and approved the submitted version.

ACKNOWLEDGMENTS

This work was supported by grants from Shanghai Municipal Science and Technology Major Project (2018SHZDZX01) and ZJ Lab, National Natural Science Foundation of China (81773513), Scientific Research Plan Project of Shanghai Science and Technology Committee (17411950701 and 17411950106), Shanghai Sailing Program (20YF1404000), and the National Project of Chronic Disease (2016YFC1306400).

SUPPLEMENTARY MATERIAL

The Supplementary Material for this article can be found online at: https://www.frontiersin.org/articles/10.3389/fnagi.2020.00266/full#supplementary-material

FIGURE S1 | Flowchart of recruitment of participants.

TABLE S1 | Baseline characteristics of participants with and without incident dementia.

REFERENCES

Adams, D. R., Kern, D. W., Wroblewski, K. E., Mcclintock, M. K., Dale, W., and Pinto, J. M. (2018). Olfactory dysfunction predicts subsequent dementia in older U.S. adults. *J. Am. Geriatr. Soc.* 66, 140–144. doi: 10.1111/jgs.15048

Altmann, A., Tolosi, L., Sander, O., and Lengauer, T. (2010). Permutation importance: a corrected feature importance measure. *Bioinformatics* 26, 1340–1347. doi: 10.1093/bioinformatics/btq134

American Psychiatric Association (1994). *DSM-IV: Diagnostic and Statistical Manual of Mental Disorders*. Washington, DC: American Psychiatric Press Inc.

Attems, J., Walker, L., and Jellinger, K. A. (2014). Olfactory bulb involvement in neurodegenerative diseases. *Acta Neuropathol.* 127, 459–475. doi: 10.1007/s00401-014-1261-7

Breiman, L. (2001). Random forests. *Mach. Learn.* 45, 5–32. doi: 10.1023/A:1010933404324

Cao, Y., Fang, X., Ottosson, J., Naslund, E., and Stenberg, E. (2019). A comparative study of machine learning algorithms in predicting severe complications after bariatric surgery. *J. Clin. Med.* 8:668. doi: 10.3390/jcm8050668

Chen, P. Y., and Popovich, P. M. (2002). *Correlation: Parametric and Nonparametric Measures. Thousand Oaks*. California: Sage Publications, Inc.

Collier, L. (2007). *The Use of Multi-Sensory Stimulation to Improve Functional Performance in Older People with Dementia: A Randomised Single Blind Trial*. Southampton: University of Southampton.

Coughlin, S. S., Trock, B., Criqui, M. H., Pickle, L. W., Browner, D., and Tefft, M. C. (1992). The logistic modeling of sensitivity, specificity, and predictive value of a diagnostic test. *J. Clin. Epidemiol.* 45, 1–7. doi: 10.1016/0895-4356(92)90180-u

Cullen, B., Fahy, S., Cunningham, C. J., Coen, R. F., Bruce, I., Greene, E., et al. (2005). Screening for dementia in an Irish community sample using MMSE: a comparison of norm-adjusted versus fixed cut-points. *Int. J. Geriatr. Psychiatry* 20, 371–376. doi: 10.1002/gps.1291

Demirtas, H., and Hedeker, D. (2016). Computing the point-biserial correlation under any underlying continuous distribution. *Commun. Stat. Simul. Comput.* 45, 2744–2751. doi: 10.1080/03610918.2014.920883

Devanand, D. P., Lee, S., Manly, J., Andrews, H., Schupf, N., Doty, R. L., et al. (2015). Olfactory deficits predict cognitive decline and Alzheimer dementia in an urban community. *Neurology* 84, 182–189. doi: 10.1212/wnl.0000000000001132

Ding, D., Zhao, Q., Guo, Q., Meng, H., Wang, B., Luo, J., et al. (2015). Prevalence of mild cognitive impairment in an urban community in China: a cross-sectional analysis of the Shanghai aging Study. *Alzheimers Dement.* 11, 300.e2–309.e2. doi: 10.1016/j.jalz.2013.11.002

Ding, D., Zhao, Q. H., Guo, Q. H., Meng, H. J., Wang, B., Yu, P. M., et al. (2014). The Shanghai aging study: study design, baseline characteristics, and prevalence of dementia. *Neuroepidemiology* 43, 114–122. doi: 10.1159/000366163

Doty, R. L., Marcus, A., and Lee, W. W. (1996). Development of the 12-item Cross-Cultural Smell Identification Test (CC-SIT). *Laryngoscope* 106, 353–356. doi: 10.1097/00005537-199603000-00021

Eaton, W. W., Smith, C., Ybarra, M., Muntaner, C., and Tien, A. (2004). "Center for epidemiologic studies depression scale: review and revision (CESD and CESD-R)," in *The use of psychological testing for treatment planning and outcomes assessment: Instruments for adults*, ed. M. E. Maruish (New York: Taylor & Francis Group), 363–377. doi: 10.1037/t29280-000

Eibenstein, A., Fioretti, A. B., Simaskou, M. N., Sucapane, P., Mearelli, S., Mina, C., et al. (2005). Olfactory screening test in mild cognitive impairment. *Neurol. Sci.* 26, 156–160. doi: 10.1007/s10072-005-0453-2

Fisher, A., Rudin C., and Dominici, F. (2019). All models are wrong, but many are useful: learning a variable's importance by studying an entire class of prediction models simultaneously. *J. Mach. Learn. Res.* 20, 1–81.

Fox, M., Krueger, E., Putterman, L., and Schroeder, R. (2012). The effect of peppermint on memory performance. *J. Adv. Stud. Sci.* 1, 1–7.

Gilbert, A., Popper, R., Kroll, J., Nicklin, L., and Zellner, D. (2002). The Cranial I Quick Sniff®: a new screening test for olfactory function. *Chem. Senses* 2002:A23.

Gómez-Ramírez, J., Ávila-Villanueva, M., and Fernández-Blázquez, M. Á (2019). Selecting the most important self-assessed features for predicting conversion to Mild Cognitive Impairment with Random Forest and Permutation-based methods. *bioRxiv* [Preprint]. doi: 10.1101/785519v1

Greiner, M., Pfeiffer, D., and Smith, R. D. (2000). Principles and practical application of the receiver-operating characteristic analysis for diagnostic tests. *Prev. Vet. Med.* 45, 23–41. doi: 10.1016/s0167-5877(00)00115-x

Growdon, M. E., Schultz, A. P., Dagley, A. S., Amariglio, R. E., Hedden, T., Rentz, D. M., et al. (2015). Odor identification and Alzheimer disease biomarkers in clinically normal elderly. *Neurology* 84, 2153–2160. doi: 10.1212/wnl.0000000000001614

Herz, R. S. (1997). Emotion experienced during encoding enhances odor retrieval cue effectiveness. *Am. J. Psychol.* 110, 489–505. doi: 10.2307/1423407

Hilbe, J. M. (2009). *Logistic Regression Models*. Boca Raton, FL: Chapman and hall/CRC.doi: 10.1201/9781420075779

Hua, J. P., Tembe, W. D., and Dougherty, E. R. (2009). Performance of feature-selection methods in the classification of high-dimension data. *Pattern Recogn.* 42, 409–424. doi: 10.1016/j.patcog.2008.08.001

Hummel, T., Konnerth, C. G., Rosenheim, K., and Kobal, G. (2001). Screening of olfactory function with a four-minute odor identification test: reliability, normative data, and investigations in patients with olfactory loss. *Ann. Otol. Rhinol. Laryngol.* 110, 976–981. doi: 10.1177/000348940111001015

Jackman, A. H., and Doty, R. L. (2005). Utility of a three-item smell identification test in detecting olfactory dysfunction. *Laryngoscope* 115, 2209–2212. doi: 10.1097/01.mlg.0000183194.17484.bb

James, G., Witten, D., Hastie, T., and Tibshirani, R. (2013). *An Introduction to Statistical Learning*. Cham: Springer. doi: 10.1007/978-1-4614-7138-7

Janssens, A. C., Deng, Y., Borsboom, G. J., Eijkemans, M. J., Habbema, J. D., and Steyerberg, E. W. (2005). A new logistic regression approach for the evaluation of diagnostic test results. *Med. Decis. Making* 25, 168–177. doi: 10.1177/0272989x05275154

Koo, H. N., Jeong, H. J., Kim, C. H., Park, S. T., Lee, S. J., Seong, K. K., et al. (2001). Inhibition of heat shock-induced apoptosis by peppermint oil in astrocytes. *J. Mol. Neurosci.* 17, 391–396. doi: 10.1385/jmn:17:3:391

Korobov, M., and Lopuhin, K. (2020). *Welcome to ELI5's documentation [Online]*. Available: https://eli5.readthedocs.io/en/latest/ (accessed Feburary 17, 2020).

Lantz, B. (2013). *Machine Learning with R*. Birmingham: Packt Publishing Ltd.

Liang, X., Ding, D., Zhao, Q., Wu, W., Xiao, Z., Luo, J., et al. (2020). Inability to smell peppermint is related to cognitive decline: a prospective community-based study. *Neuroepidemiology* 54, 258–264. doi: 10.1159/000505485

Liang, X. N., Ding, D., Zhao, Q. H., Guo, Q. H., Luo, J. F., Hong, Z., et al. (2016). Association between olfactory identification and cognitive function in community-dwelling elderly: the Shanghai aging study. *BMC Neurol.* 16:199. doi: 10.1186/s12883-016-0725-x

Liu, H., and Motoda, H. (2012). *Feature Selection for Knowledge Discovery and Data Mining*. Cham: Springer.

Lotsch, J., Ultsch, A., and Hummel, T. (2016). How many and which odor identification items are needed to establish normal olfactory function? *Chem. Senses* 41, 339–344. doi: 10.1093/chemse/bjw006

Mandrekar, J. N. (2010). Receiver operating characteristic curve in diagnostic test assessment. *J. Thorac. Oncol.* 5, 1315–1316. doi: 10.1097/jto.0b013e3181ec173d

Marigliano, V., Gualdi, G., Servello, A., Marigliano, B., Volpe, L. D., Fioretti, A., et al. (2014). Olfactory deficit and hippocampal volume loss for early diagnosis of Alzheimer disease: a pilot study. *Alzheimer Dis. Assoc. Disord.* 28, 194–197. doi: 10.1097/wad.0b013e31827bdb9f

Marzban, C. (2004). The ROC curve and the area under it as performance measures. *Weather Forecast.* 19, 1106–1114. doi: 10.1175/825.1

Maurage, P., Callot, C., Chang, B., Philippot, P., Rombaux, P., and De Timary, P. (2011). Olfactory impairment is correlated with confabulation in alcoholism: towards a multimodal testing of orbitofrontal cortex. *PLoS One* 6:e23190. doi: 10.1371/journal.pone.0023190

MediSense (2020). *Can I order Sniffin' Sticks with the odor of choice? [Online]*. Groningen: MediSense.

Mijajlovic, M. D., Pavlovic, A., Brainin, M., Heiss, W. D., Quinn, T. J., Ihle-Hansen, H. B., et al. (2017). Post-stroke dementia - a comprehensive review. *BMC Med.* 15:11. doi: 10.1186/s12916-017-0779-7

Moss, M., Hewitt, S., Moss, L., and Wesnes, K. (2008). Modulation of cognitive performance and mood by aromas of peppermint and ylang-ylang. *Int. J. Neurosci.* 118, 59–77. doi: 10.1080/00207450601042094

Mueller, C., and Renner, B. (2006). A new procedure for the short screening of olfactory function using five items from the "Sniffin' Sticks" identification test kit. *Am. J. Rhinol.* 20, 113–116. doi: 10.1177/194589240602000121

Nembrini, S., König, I. R., and Wright, M. N. (2018). The revival of the Gini importance? *Bioinformatics* 34, 3711–3718. doi: 10.1093/bioinformatics/bty373

Ngandu, T., Von Strauss, E., Helkala, E. L., Winblad, B., Nissinen, A., Tuomilehto, J., et al. (2007). Education and dementia - What lies behind the association? *Neurology* 69, 1442–1450. doi: 10.1212/01.wnl.0000277456.29440.16

Oleszkiewicz, A., Schriever, V. A., Croy, I., Hahner, A., and Hummel, T. (2019). Updated Sniffin' Sticks normative data based on an extended sample of 9139 subjects. *Eur. Arch. Otorhinolaryngol.* 276, 719–728. doi: 10.1007/s00405-018-5248-1

Ottaviano, G., Frasson, G., Nardello, E., and Martini, A. (2016). Olfaction deterioration in cognitive disorders in the elderly. *Aging Clin. Exp. Res.* 28, 37–45. doi: 10.1007/s40520-015-0380-x

Passali, G. C., Politi, L., Crisanti, A., Loglisci, M., Anzivino, R., and Passali, D. (2015). Tau protein detection in anosmic Alzheimer's disease patient's nasal secretions. *Chemosens. Percept.* 8, 201–206. doi: 10.1007/s12078-015-9198-3

Pedregosa, F., Varoquaux, G., Gramfort, A., Michel, V., Thirion, B., Grisel, O., et al. (2011). Scikit-learn: machine learning in python. *J. Mach. Learn. Res.* 12, 2825–2830.

Reijs, B. L. R., Ramakers, I., Elias-Sonnenschein, L., Teunissen, C. E., Koel-Simmelink, M., Tsolaki, M., et al. (2017). Relation of odor identification with Alzheimer's disease markers in cerebrospinal fluid and cognition. *J. Alzheimers. Dis.* 60, 1025–1034. doi: 10.3233/jad-170564

Roalf, D. R., Moberg, M. J., Turetsky, B. I., Brennan, L., Kabadi, S., Wolk, D. A., et al. (2017). A quantitative meta-analysis of olfactory dysfunction in mild cognitive impairment. *J. Neurol. Neurosurg. Psychiatry* 88, 226–232. doi: 10.1136/jnnp-2016-314638

Roberts, R. O., Christianson, T. J. H., Kremers, W. K., Mielke, M. M., Machulda, M. M., Vassilaki, M., et al. (2016). Association between olfactory dysfunction and amnestic mild cognitive impairment and alzheimer disease dementia. *JAMA Neurology* 73, 93–101.

Rupp, C. I., Fleischhacker, W. W., Drexler, A., Hausmann, A., Hinterhuber, H., and Kurz, M. (2006). Executive function and memory in relation to olfactory deficits in alcohol-dependent patients. *Alcohol. Clin. Exp. Res.* 30, 1355–1362. doi: 10.1111/j.1530-0277.2006.00162.x

Seligman, S. C., Kamath, V., Giovannetti, T., Arnold, S. E., and Moberg, P. J. (2013). Olfaction and apathy in Alzheimer's disease, mild cognitive impairment, and healthy older adults. *Aging Ment. Health* 17, 564–570. doi: 10.1080/13607863.2013.768208

Shu, X. O., Yang, G., Jin, F., Liu, D., Kushi, L., Wen, W., et al. (2004). Validity and reproducibility of the food frequency questionnaire used in the Shanghai Women's health study. *Eur. J. Clin. Nutr.* 58, 17–23. doi: 10.1038/sj.ejcn.1601738

Simmen, D., Briner, H. R., and Hess, K. (1999). [Screening of olfaction with smell diskettes]. *Laryngorhinootologie* 78, 125–130.

Smirnov, D. A., Morley, M., Shin, E., Spielman, R. S., and Cheung, V. G. (2009). Genetic analysis of radiation-induced changes in human gene expression. *Nature* 459, 587–591. doi: 10.1038/nature07940

Snowdon, D. A., and Nun, S. (2003). Healthy aging and dementia: findings from the nun Study. *Ann. Intern. Med.* 139, 450–454.

Stanciu, I., Larsson, M., Nordin, S., Adolfsson, R., Nilsson, L. G., and Olofsson, J. K. (2014). Olfactory impairment and subjective olfactory complaints independently predict conversion to dementia: a longitudinal, population-based study. *J. Int. Neuropsychol. Soc.* 20, 209–217. doi: 10.1017/s1355617713001409

Suzuki, Y., Yamamoto, S., Umegaki, H., Onishi, J., Mogi, N., Fujishiro, H., et al. (2004). Smell identification test as an indicator for cognitive impairment in Alzheimer's disease. *Int. J. Geriatr. Psychiatry* 19, 727–733. doi: 10.1002/gps.1161

Tebrugge, S., Winkler, A., Gerards, D., Weimar, C., Moebus, S., Jockel, K. H., et al. (2018). Olfactory function is associated with cognitive performance: results of the heinz nixdorf recall study. *J. Alzheimers Dis.* 63, 319–329. doi: 10.3233/jad-170863

Tinsdaler Weg 175 (2020). *Burghart Medical Technology*. Available: http://www.burghart.net (accessed February 18, 2020).

Tombaugh, T. N., and McIntyre, N. J. (1992). The mini-mental state examination: a comprehensive review. *J. Am. Geriatr. Soc.* 40, 922–935.

Wolfensberger, M. (2000). Sniffin'Sticks: a new olfactory test battery. *Acta Otolaryngol.* 120, 303–306.

Zhang, M. Y., Katzman, R., Salmon, D., Jin, H., Cai, G. J., Wang, Z. Y., et al. (1990). The prevalence of dementia and Alzheimer's disease in Shanghai, China: impact of age, gender, and education. *Ann. Neurol.* 27, 428–437. doi: 10.1002/ana.410270412

Zhang, Z. H. (2016). Variable selection with stepwise and best subset approaches. *Ann. Transl. Med.* 4:136. doi: 10.21037/atm.2016.03.35

Zheng, A., and Casari, A. (2018). *Feature Engineering for Machine Learning: Principles and Techniques For Data Scientists*. Sebastopol, CA: O'Reilly Media, Inc.

Zung, W. W. (1971). A rating instrument for anxiety disorders. *Psychosomatics* 12, 371–379. doi: 10.1016/s0033-3182(71)71479-0

Conflict of Interest: The authors declare that the research was conducted in the absence of any commercial or financial relationships that could be construed as a potential conflict of interest.

frontiers in Aging Neuroscience

ORIGINAL RESEARCH
published: 26 August 2020
doi: 10.3389/fnagi.2020.00260

CISD2 Attenuates Inflammation and Regulates Microglia Polarization in EOC Microglial Cells—As a Potential Therapeutic Target for Neurodegenerative Dementia

Muh-Shi Lin [1,2,3,4]*

[1]Division of Neurosurgery, Department of Surgery, Kuang Tien General Hospital, Taichung, Taiwan, [2]Department of Biotechnology and Animal Science, College of Bioresources, National Ilan University, Yilan, Taiwan, [3]Department of Biotechnology, College of Medical and Health Care, Hung Kuang University, Taichung, Taiwan, [4]Department of Health Business Administration, College of Medical and Health Care, Hung Kuang University, Taichung, Taiwan

Background: Accumulating evidence has demonstrated a significant association between microglia-driven inflammation in the brain and neurodegenerative dementia. We previously showed a significant decline in CISD2 expression in mice models with advanced age. Moreover, we observed that the knockdown of CISD2 led to remarkable inflammation and mitochondrial dysfunction in neural cells. In the present study, we investigated whether CISD2 attenuation influences anti-inflammatory effects and M1-M2 polarization in microglia.

Materials and Methods: The knockdown of CISD2 expression by siRNA (siCISD2) in EOC microglial cells was performed to mimic the age-driven decline of CISD2 expression. The extent of the inflammatory reaction, polarization in the M1/M2 spectrum, and NFκB activation were verified in EOC microglial cells exhibiting CISD2 deficiency.

Results: In the cellular model of microglia, loss of CISD2 function mediated by siCISD2 exhibited a significant augmentation of proinflammatory signaling, as well as reduced expression levels of Arg-1, Ym1, IL-10, and BCL2. Attenuation of CISD2 expression led to a decrease in the proportion of the M2 phenotype of microglia (compared to M1). Enhanced DNA-binding activity of the NFκB p65 subunit was confirmed in cells transfected with siCISD2, as demonstrated by enzyme-linked immunosorbent assay (ELISA).

Conclusions: To the best of our knowledge, this is the first report examining the following phenomena: (1) anti-inflammatory effects of CISD2 in microglia *via* NFκB regulation; and (2) microglial CISD2 assistance in the restoration of M2 microglia phenotype. The anti-inflammatory effects of CISD2 in microglia eventually augment anti-apoptotic effects, which provides a rationale for the development of potential therapeutic target for neurodegenerative diseases and neurodegenerative dementia.

Keywords: CISD2, M1/M2 microglia polarization, anti-inflammatory effects, aging, neurodegenerative disease and dementia

OPEN ACCESS

Edited by:
Jiehui Jiang,
Shanghai University, China

Reviewed by:
Ling-Yu Yang,
National Taiwan University, Taiwan
Chung-Hsing Chou,
National Defense Medical Center, Taiwan
Wei Lin,
Huashan Hospital, Fudan University, China

***Correspondence:**
Muh-Shi Lin
neurosurgery2005@yahoo.com.tw

Received: *02 May 2020*
Accepted: *29 July 2020*
Published: *26 August 2020*

Citation:
Lin M-S (2020) CISD2 Attenuates Inflammation and Regulates Microglia Polarization in EOC Microglial Cells—As a Potential Therapeutic Target for Neurodegenerative Dementia. Front. Aging Neurosci. 12:260. doi: 10.3389/fnagi.2020.00260

INTRODUCTION

Dementia is a chronic disease leading to disability and dependency among the elderly worldwide. For clinical classification, dementia can be divided into the following major categories: Alzheimer's disease (AD), vascular dementia (VaD), dementia with Lewy bodies (DLB), frontotemporal dementia (FTD), and mixed dementia (Raz et al., 2016). Due to the complexities of neurodegenerative dementia, precise diagnosis remains a challenge in daily clinical practice. Eventually, patients with dementia will present a catastrophic situation for the entire community and society, leading to highly expensive long-term medical care. Moreover, evidence indicates that sustained brain inflammation due to excessive microglial activation contributes to cerebral aging (Hickman et al., 2018; Sanada et al., 2018), neurodegenerative disease (Maragakis and Rothstein, 2006; Hickman et al., 2018), and neurodegenerative dementia (Meraz-Ríos et al., 2013; Bhaskar et al., 2014).

Microglia stabilize and balance the central nervous system (CNS) by mediating immune responses and providing neurotrophic support for neurons (Wake et al., 2011). Embryologically, microglia are derived from the same origin as peripheral macrophages (myeloid progenitors), whereas other resident CNS cells (e.g., astrocytes, oligodendrocytes, and neurons) are derived from neuroepithelial precursors (Zhang et al., 2018). Microglia can be regarded as a specialized macrophage in the CNS owing to the aforementioned close association. Microglia exert biphasic effects that either benefit the neuron survival (M2 phase) or undermine it (M1 phase) under microenvironmental changes. As such, it is representative of the spectrum of M1 (proinflammation)/M2 (anti-inflammation) phenotypes (Song and Suk, 2017; Zhang et al., 2017). In the microenvironment of the CNS, M2 microglia function to maintain CNS homeostasis and neural protection by moving dynamically throughout the entire CNS parenchyma and performing phagocytosis when they encounter pathological changes initiated by pathogens, plaques, protein aggregates, and infectious agents (Thomas et al., 2015). However, under the circumstances of neurodegeneration (non-stressed status) or CNS trauma (injury-challenged status), temporally inappropriate, prolonged, or excessive inflammation indicates the pathological activation of detrimental M1 microglial cells involving the release of cytokines and chemokines (Tator and Fehlings, 1991; Luo et al., 2002). Aberrantly stimulated microglia produce nitric oxide (NO) in conjunction with reactive oxygen species (ROS), which can amplify the inflammatory cascade. In a deleterious pathological cycle, cytokines promote inflammation by inducing the production of additional cytokines, chemokines, NO, and ROS (Li et al., 2006). Sustained microglia-driven inflammation can eventually lead to apoptosis and the killing of oligodendrocytes and neurons, which can impair neuronal functioning and lead to permanent neurological damage (Wood, 1995; Mattson, 2000; Byrnes et al., 2007). Any novel strategies involving the attenuation of microglial inflammatory response could be beneficial in the management of neurodegenerative disease and dementia.

CISD2 (CDGSH iron-sulfur domain 2) has garnered interest for its protective role against calcium excitotoxicity (Shen et al., 2017), apoptosis (Chen et al., 2009), and inflammation (Lin et al., 2015). *CISD2* has been referred to as a longevity gene, aiding in the preservation of mitochondrial integrity, thereby preventing mitochondrial malfunction and, ultimately, cell death. In response to stress, CISD2 exerts protective effects against autophagy/apoptosis by enhancing BCL2-BECN1 interactions and by the formation of a complex with BCL2 (Chang et al., 2010). Moreover, CISD2 attenuates the excitotoxic Ca^{2+} surge at the endoplasmic reticulum by binding to BCL2 and the inositol 1,4,5-triphosphate receptor (Chang et al., 2012). Furthermore, overexpression of CISD2 has been demonstrated to attenuate neuronal loss and β-amyloid-induced mitochondrial dysfunction in the AD mouse model (Chen et al., 2020). Thus, CISD2 holds promise as a potential therapeutic target for neurodegenerative dementia.

In a previous study, we identified a potential role of CISD2 in exhibiting the anti-inflammatory effects. In a CISD2 knockdown model developed with siCISD2, we observed that CISD2 deficiency led to a significant increase in iNOS production and a reduction in BCL2 levels in SH-SY5Y cells stimulated with lipopolysaccharide (LPS; Lin et al., 2015). No previous study has been reported on the anti-inflammatory effects of CISD2 in microglia. In the current study, we sought to delineate the protective effect of CISD2 in microglial inflammatory reactions associated with neurodegenerative dementia. It is a preliminary investigation into the anti-inflammatory effects of CISD2 in the EOC microglial cell culture model with a specific aim of determining whether it plays a role in the alternation of microglial M1/M2 polarization.

MATERIALS AND METHODS

Cell Lines

Microglia cell lines (EOC 13.31, BCRC 60490) were obtained from the Bioresource Collection and Research Center (BCRC, Hsinchu, Taiwan). EOC 13.31 cell line derived from the brain of a 10-day old female mouse (*Mus musculus*) is dependent on the colony-stimulating factor-1 (CSF-1) for cell proliferation. EOC microglial cells were cultured in 70% Dulbecco's modified essential medium (DMEM), 10% fetal bovine serum (FBS), and 20% LDMAC conditioned medium derived from LADMAC cells (BCRC 60489, a bone marrow monocytic cell line derived from adult mouse, *M. musculus*). LDMAC conditioned medium containing CSF-1 secreted from LADMAC cells was collected from confluent cultures and filtered with 0.2-mm syringe filters before addition to EOC cell cultures.

Reverse-Transcription Polymerase Chain Reaction and Real-Time Quantitative Reverse-Transcription Polymerase Chain Reaction

Total RNA was prepared by directly lysing the cultured cells in extraction buffer (Trizol/phenol/chloroform) and reverse

transcribing the mRNA into cDNA using oligo-dT and SuperScript II reverse transcriptase (Invitrogen, Carlsbad, CA, USA). The cDNA was subjected to polymerase chain reaction (PCR) for the measurement of mRNA levels of CISD2, BCL2, and M2 microglia specific markers based on a previous report [Pei et al., 2017; IL-10, Arginase-1 (Arg-1), Chitinase-3-like-3 (Ym1)]; proinflammatory mediators including TNF-α, IL-1β, iNOS, and COX2 (representative of M1 microglia); and the housekeeping gene GAPDH (internal control). The PCR protocol involved 25 cycles of denaturation for 1 min at 94°C, annealing for 1 min at 55°C to 60°C, and extension for 1 min at 72°C. The primers used for PCR are listed in **Table 1**.

For real-time quantitative reverse-transcription (qRT)-PCR, the cDNA samples were analyzed with SYBR Green Gene Expression System (ABI PRISM 7300 HT real-time PCR system; Applied Biosystems, Foster City, CA, USA). Minor groove binding dyes and primers for the detection of the genes of interest and GAPDH were designed by ABI. We further determined the threshold cycle (Ct), and the Ct values of proposed genes were normalized using GAPDH as an internal control. The measurements were performed in triplicates.

Immunoblotting

Total protein was extracted from cultured EOC microglial cells in a lysis buffer containing 20 mM Tris-HCl, 0.1% sodium dodecyl sulfate (SDS), 0.8% NaCl, and 1% Triton-X 100). Electrophoresis with 12% gradient gel was performed to separate the protein extracts. Proteins that underwent electrophoresis were electro-transferred to a nitrocellulose membrane prepared with blocking reagent and primary antibodies [anti-CISD2 (1:500; Thermo Scientific, PA5-34545); anti-iNOS (1:2,000; Thermo Scientific, PA3-030A); anti-Arg-1 (1:5,000; Thermo Scientific, PA5-29645); anti-GAPDH (1:500; Millipore, Billerica, MA, USA)] at 4°C for 12 h before washing and incubation with goat-anti-rabbit IgG HRP (horseradish peroxidase)-conjugated secondary antibodies (Merck Millipore, Cat. #12-348) for 1 h. Chemiluminescence detection was performed following the established protocols (Merck Millipore, WBKLS0500). Bands of interest were visualized and quantified using ImageQuant™ LAS 4000 (GE Healthcare Life Sciences, Marlborough, MA, USA).

TABLE 1 | Primers sequences used in the study.

Gene	Orientation	Sequence
CISD2	forward	5′-AAAATCCCAAGGTGGTGAATGA-3′
	reverse	5′-GGACCGCCAGCACCTACA-3′
GAPDH	forward	5′-GGCAAATTCAACGGCACAGT-3′
	reverse	5′-CGCTCCTGGAAGATGGTGAT-3′
TNF-α	forward	5′-GGCACTCCCCCAAAAGATG-3′
	reverse	5′-GCCACAAGCAGGAATGAGA
IL-1β	forward	5′-AAGATGAAGGGCTGCTTCCA-3′
	reverse	5′-ATGTGCTGCTGCGAGATTTG-3′
iNOS	forward	5′-CCTCAGTTCTGCGCCTTTG-3′
	reverse	5′-GTTCGTCCCCTTCTCCTGTTG-3′
COX2	forward	5′-ACAAGCACAATAGACGCACAAGA-3′
	reverse	5′-GGGAGGGCAATTATGATAAGGAT-3′
Arg-1	forward	5′-CGCCTTTCTCAAAAGGACAG-3′
	reverse	5′-CCAGCTCTTCATTGGCTTTC-3′
Ym1	forward	5′-ACCAGTTGGGCTAAGGACAG-3′
	reverse	5′-TGGCCAGGAGAGTTTTTAGC-3′
IL-10	forward	5′-AAGGACCAGCTGGACAACAT-3′
	reverse	5′-TCCTGAGGGTCTTCAGCTTC-3′
BCL2	forward	5′-TGGGATGCCTTTGTGGAACT-3′
	reverse	5′-CAGCCAGGAGAAATCAAACAGA-3′

Short Interfering RNA-Mediated RNA Interference

Short interfering RNA (siRNA) specific to CISD2 mRNA was used to attenuate the expression of CISD2 in cultured microglia. This method was similar to that used in our previous research conducted on gene knockdown with minor modifications (Lin et al., 2011a,b, 2015, 2019). EOC microglial cells were transfected using a set of siRNAs specific to CISD2 or scrambled RNA (Silencer® Pre-designed siRNA, Ambion, Austin, TX, USA) using Lipofectamine™ 2000 reagent (Invitrogen, Carlsbad, CA, USA). Briefly, EOC cells were randomly assigned to the experimental groups after being cultured for 5 days. Lipofectamine™ 2000 reagent and siRNA were individually mixed in serum-free medium for 10 min. Lipofectamine transfection reagent was mixed with dissolved siRNA in a serum-free medium for 10 min. Transfected cell mixtures containing 2×10^6 cells were added to each plate.

Five hours after transfection, the medium containing Lipofectamine 2000 was replaced with a microglial culture medium and allowed to stand for an additional 7 h. Real-time qRT-PCR was performed for the detection of CISD2 expression to verify the effectiveness of knockdown.

Detection of NFκB p65 Activity

NFκB p65 activity was characterized using the NFκB p65 Transcription Factor Assay Kit (ab133112, Abcam, MA, USA) as per the manufacturer's instructions. Briefly, the extracted nuclear protein was collected for characterizing intracellular p65-NFκB activity by using a spectrophotometer reader to measure absorbance at an optical density (OD) of 450 nm. All measured values were derived with Synergy HT (BioTek, VT, USA).

Statistical Analysis

The normality test of variables was used to determine whether to use parametric tests for variables with a normal distribution or nonparametric tests for variables with a non-normal distribution. The *p*-values of the normality test for variables of the experimental groups exceeded 0.05. Hence, parametric tests were used for mean comparisons among the experiment groups. Independent two-sample *t*-tests were subsequently used to compare the experiment groups. Statistical analysis was performed using GraphPad Prism software 5.0 (GraphPad Software, Inc., La Jolla, CA, USA).

RESULTS

Knockdown of CISD2 Expression Augmented Inflammatory Signaling in EOC Microglial Cells and Enhanced M1 Microglia Polarization

High inflammation due to microglial activation has been demonstrated underlying the pathogenesis of various

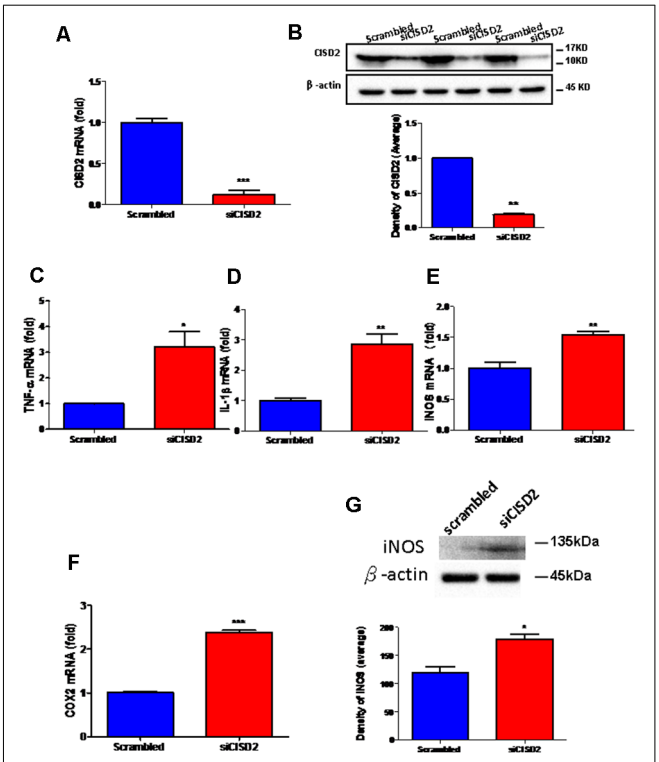

FIGURE 1 | Knockdown of CISD2 expression augmented tendency for M1 microglial polarization and enhanced proinflammatory response in non-stressed EOC microglial cells. The conditions were set as follows: (i) scrambled RNA-transfected control cells; (ii) siCID2-transfected cells. **(A)** Confirmation of knockdown efficiency of CISD2 mRNA and protein **(B)** expression in microglia. **(C)** Expression of TNF-α mRNA, **(D)** IL-1β mRNA, **(E)** iNOS mRNA, and **(F)** COX2 mRNA under all conditions. **(G)** iNOS protein expression in siCID2-transfected EOC microglial cells. The upper panel demonstrates the immunoblot results of iNOS at 135 kDa, and β-actin (45 kDa) serves as an internal control; the lower panel indicates the mean (±SEM) of iNOS/β-actin band intensity in ratio with the control group. Vertical bars indicate the mean ± (SEM) of mRNA or protein expression ($n = 3$). $^{*}p < 0.05$; $^{**}p < 0.01$; $^{***}p < 0.001$ indicate statistically significant difference when compared to scrambled control cells.

neurodegenerative diseases in the CNS and neurodegenerative dementia (Thomas et al., 2015; Raz et al., 2016). In our previous study, we demonstrated that the attenuated CISD2 expression is associated with the aging process and leads to the inflammatory response (Lin et al., 2015, 2019). Hence, we sought to determine whether CISD2 deficiency in microglia results in the inflammatory cascade as well as the likelihood that these detrimental insults influence microglia polarization. The CISD2 expression was attenuated in the microglial EOC cell lines *via* siCISD2-mediated knockdown to delineate the inflammatory mechanism involving CISD2 and evaluate the possibility of influencing polarization in the microglia M1/M2 spectrum.

The knockdown efficiency of CISD2 siRNA in the EOC microglial cell line was confirmed by real-time qRT-PCR ($p < 0.001$, labeled as ***, **Figure 1A**) and western blot analysis ($p < 0.01$, labeled as **, **Figure 1B**). Each experiment was performed in triplicate.

We observed that mRNA expression levels of proinflammatory mediators were higher in siCISD2-transfected EOC microglial cells than those in scrambled RNA-transfected cells as determined by real-time qRT-PCR (TNF-α, $p < 0.05$, labeled as *, **Figure 1C**; IL-1β, $p < 0.01$, labeled as **, **Figure 1D**; iNOS, $p < 0.01$, labeled as **, **Figure 1E**; and COX2, $p < 0.001$, labeled as ***, **Figure 1F**). As shown in **Figure 1G**, western blot analysis confirmed that CISD2 deficiency significantly increased the protein production of iNOS ($^{*}p < 0.05$) in EOC microglial cells.

These results indicate a trend toward M1 microglia-associated inflammatory effects observed with CISD2 attenuation. Thus, CISD2 inactivity could be associated with the proinflammatory effects of M1 microglia underlying the pathological mechanism of neurodegenerative disease and dementia.

CISD2 Deficiency Reduced the Proportion of M2 Phenotype in EOC Microglial Cells

Under pathological conditions in the CNS, such as aging, and neurodegenerative disease, neuroprotective M2 microglia underwent excessive stimulation, switched to the detrimental M1 phenotype, and subsequently produced various proinflammatory mediators that might lead to irreversible neurological deficits. We observed that CISD2 deficiency in EOC microglial cells led to a broad range of proinflammatory reactions. Next, we sought to determine whether CISD2 attenuation halts protective M2 microglia polarization.

Real-time qRT-PCR analysis demonstrated that the mRNA expression of Arg-1, Ym1, and IL-10 was reduced in siCISD2-transfected EOC microglial cells (Arg-1, $p < 0.05$, labeled as *, **Figure 2A**; Ym1, $p < 0.05$, labeled as *, **Figure 2B**; and IL-10, $p < 0.001$, labeled as ***, **Figure 2C**, respectively) compared to the cells subjected to scrambled RNA-transfection. Western blot analysis was used to examine Arg-1 protein expression in EOC microglial cells. Each experiment was performed in triplicates. The siCISD2-transfected cells demonstrated a marked decrease in the protein expression of Arg-1 ($p < 0.01$, labeled as **, **Figure 2D**) compared to that in the scrambled RNA-transfected cells.

These findings demonstrate that the knockdown of CISD2 tends to reduce the relative proportion of M2 microglia. Thus, it can be concluded that CISD2 deficiency impairs anti-inflammatory effects manifesting as either an enhancement of the detrimental effects associated with M1 or M2-associated protective effects under non-stressed conditions. These results illustrate the protective effects of microglial CISD2 exhibiting anti-inflammatory functions and leading to the enhancement of M2 polarization.

CISD2 Deficiency Augmented Inflammatory Response *via* NFκB Activation and Promoted Cellular Apoptosis in EOC Microglial Cells

Finally, we wanted to confirm whether the proinflammatory response induced by CISD2 attenuation involved NFκB signaling

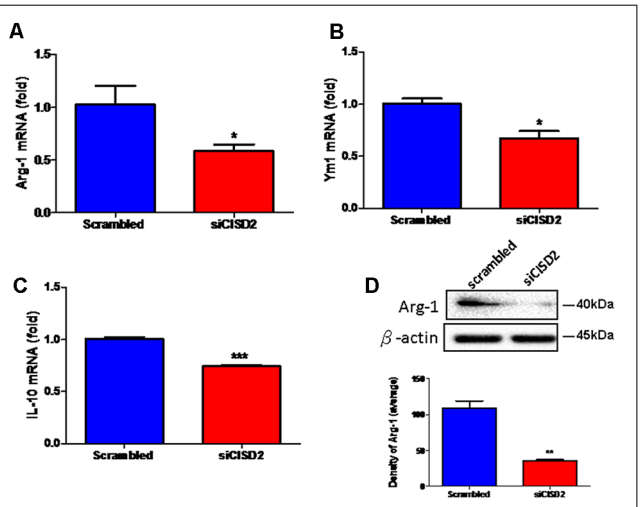

FIGURE 2 | Knockdown of CISD2 expression downregulated **(A)** Arg-1, **(B)** YM1, **(C)** IL-10 mRNA expression, and **(D)** Arg-1 protein expression in non-stimulated EOC microglial cells. In **(A–C)**, data indicate means (±SEM) of fold decrease of Arg-1, YM1, and IL-10 mRNA in comparison to that in the scrambled control group analyzed by real-time qRT-PCR in siCID2-transfected groups ($n = 3$ in each group). $^{*}p < 0.05$; $^{***}p < 0.001$ as compared with scrambled control. In **(D)**, the upper panel demonstrates the immunoblot results of Arg-1 at 40 kDa, and β-actin serves as an internal control; the lower panel indicates the mean (±SEM) of Arg-1/β-actin band intensity in ratio with the scrambled control ($n = 3$). $^{**}p < 0.01$ indicates the significant difference compared with scrambled control.

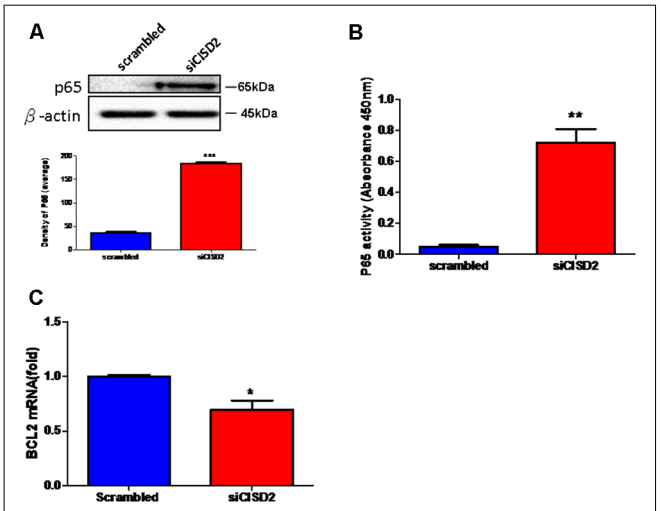

FIGURE 3 | Knockdown of CISD2 expression augmented activation of NFκB and enhanced apoptosis in non-stressed EOC microglial cells. **(A)** Expression levels of p65 (total) were determined by western blot analysis ($n = 3$ in each group). **(B)** Evaluation of P65-NFκB DNA binding activity. The nuclear proteins were prepared, and the NFκB DNA binding activity was analyzed by ELISA ($n = 3$ in each group). **(C)** The extent of anti-apoptosis reflecting BCL2 mRNA expression was determined by real-time qRT-PCR. Vertical bars indicate the mean ± (SEM) of mRNA or protein expression ($n = 3$). $^{*}p < 0.05$; $^{**}p < 0.01$; $^{***}p < 0.001$ indicate statistically significant difference compared to scrambled control cells.

in microglial cells. As shown in **Figure 3A**, western blot analysis demonstrated a significant elevation of the total expression of p65 protein in the siCISD2-transfected group ($^{***}p < 0.001$), compared to that in the control group that was subjected to scrambled RNA-transfection. Enzyme-linked immunosorbent assay (ELISA) was used to verify the NFκB p65 subunit DNA-binding activity to evaluate the nuclear translocation of NFκB p65. It was observed that P65-NFκB DNA binding activity was significantly higher in siCISD2-transfected EOC microglial cells ($^{**}p < 0.01$, **Figure 3B**) than that in the scrambled RNA-transfected cells. Moreover, real-time qRT-PCR analysis demonstrated that the mRNA expression of BCL2 was significantly decreased in siCISD2-transfected EOC microglial cells ($p < 0.05$, labeled as *, **Figure 3C**), compared to that in scrambled RNA-transfected cells.

In conclusion, these results strongly indicate that microglial CISD2 inhibits the inflammatory response *via* NFκB signaling and possibly by the preservation of M2 polarization in microglia. We postulate that BCL2-associated apoptosis initiated by age-driven CISD2 decline in microglia, which potentially impairs cell survival, can likely be attributed to NFκB activation and neuroinflammation following the downregulation of microglial CISD2.

DISCUSSION

As many protective molecules in nature exhibiting biphasic effects (Lin et al., 2011a,b), microglia-mediated neuroinflammation has been described as a double-edged sword (Hu et al., 2015). It demonstrates protective and restorative effects in the nonpathological and healthy CNS. However, it may also exacerbate and destroy under excessive inflammation under microenvironments of non-stressed (as a proxy for chronic inflammation driven by aging and neurodegenerative disease) and injury-challenged CNS (as a proxy for high-grade impact from neurotrauma). During the early stages of neural pathological conditions of the CNS (e.g., aging and neurodegenerative disease), protective M2 microglia tend to be dominant in the spectrum of proinflammatory/anti-inflammatory phenotypes. During low-grade inflammation, the activated M2 microglia scavenge fatal pathogens to confer neuronal protection. However, when the damage exceeds the range of homeostasis, a decline is observed in the proportion of activated M2 microglia. Accordingly, a delayed reactivation of detrimental M1 microglia can lead to a deleterious inflammatory cycle (Karve et al., 2016), which can be detrimental to neuronal survival and potentially cause CNS disease, such as dementia. **Figure 4** presents a schematic illustration showing the proposed sequence of events associated with the anti-inflammatory effects of CISD2 in microglia, as determined in this study.

During the process of aging, the cerebral immune system remains relatively active resulting in the upregulation of inflammatory genes associated with the aging brain. Under such an immunocompetent response, cerebral microglia are primed to be activated and remain resistant to immune adaptive regulation (Norden and Godbout, 2013). This type of sustained microglial dysfunction can cause low-grade chronic neuroinflammation

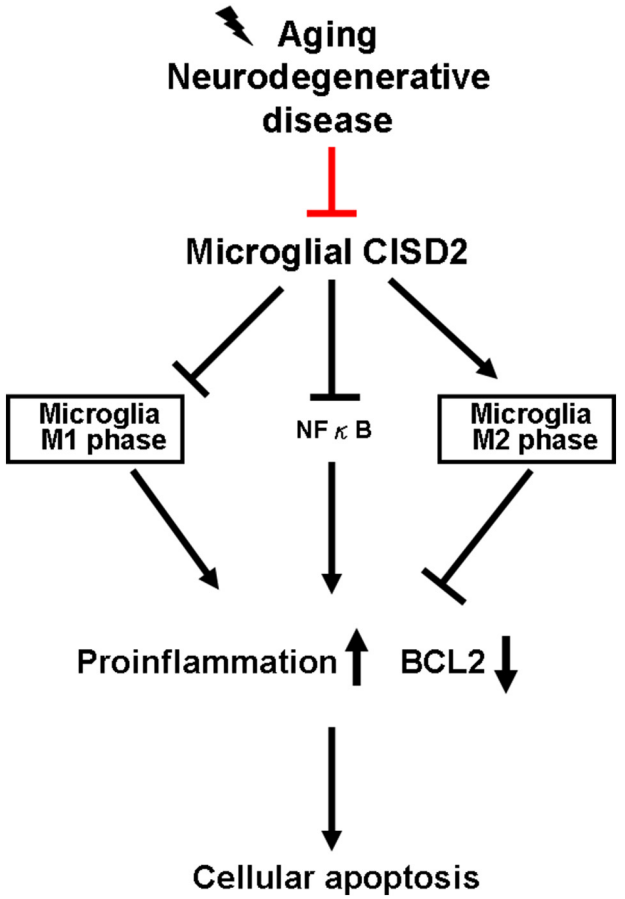

FIGURE 4 | Microglial CISD2 inhibited neuroinflammation and preserved protective microglia M2 phenotype, thereby preventing apoptosis. Microglia-driven chronic inflammation denoted pathological conditions in aging and neurodegenerative disease. Microglial CISD2 can be attenuated during the above-mentioned pathological conditions (as indicated with red bar). The decline in microglial CISD2 expression enhanced and reduced the proportion of detrimental M1 and beneficial M2 phenotype in microglia, respectively. The influence of microglial polarization exacerbated inflammation, elevated the expression of downstream proinflammatory cytokines/chemokines, and consequently augmented apoptosis as indicated by the decrease in BCL2, which potentially led to a detrimental effect on cell survival.

in the brain and thereby exacerbate the cerebral aging process (Simen et al., 2011). Unlike normal aging, neurodegenerative diseases (due to genetic or environmental influences) can lead to misfolding and accumulation of native cerebral proteins, such as prion, tau, β-amyloid, α-synuclein, and huntingtin. Conformational changes in these proteins are resistant to proteolysis resulting in the formation of so-called inclusion bodies in the brain (Jucker and Walker, 2011). When stimulated by toll-like receptors, the aggregation of such atypical proteins promotes the release of microglial-derived inflammatory mediators at high concentrations resulting in long-lasting inflammatory stimuli. Such effects are observed in AD, multiple sclerosis (MS), and Parkinson's disease (PD; Ross and Poirier, 2004). Thus, microglia-driven inflammatory cascades have definitively been linked to aging, neurodegenerative diseases, and neurodegenerative dementia.

The precise function of CISD2 has not been elucidated. Interestingly, CISD2 expression is attenuated during non-stressed or injury-challenged conditions *in vivo* and *in vitro* (Lin et al., 2019). We observed a significant reduction in CISD2 expression with age in the mouse brain and spinal cord (Lin et al., 2019). In mouse models, spinal cord injury has been demonstrated to attenuate the expression of CISD2 (Lin et al., 2015). Moreover, we previously observed that CISD2 deficiency exacerbated inflammatory responses and mitochondrial dysfunction in cultured cells (with or without injury). Specifically, CISD2 expression was lower in non-stressed 35 *DIV* astrocytes than in 7 *DIV* cells, and the expression of iNOS along with RANTES (regulated on activation, normal T cell expressed and secreted) was higher (Lin et al., 2019). In LPS-stimulated CISD2 knockdown SH-SY5Y cells, the deficiency of CISD2 led to elevated iNOS levels and significant mitochondrial dysfunction (Lin et al., 2015, 2019). Resident immune cells (i.e., microglia) would be the apparent focus while investigating inflammatory cascades in the CNS.

Priming and activation in microglia can promote the proinflammatory signaling associated with aging, neurodegenerative disease, and traumatic CNS injury (Norden et al., 2015). Data obtained in this study demonstrated that CISD2 deficiency (induced by the knockdown of CISD2 expression) augmented the detrimental effects associated with the M1 phase and led to neuroinflammation and apoptosis in non-stimulated EOC microglial cells. Hence, we postulate that CISD2 exerts anti-inflammatory effects in microglia under non-stressed microenvironments (as a proxy for microglial inflammation driven by aging and neurodegenerative dementia). The attenuation of microglia-mediated inflammatory cascades can be beneficial under such pathological conditions. The beneficial effect of the dementia-CISD2-microglial anti-inflammation axis provides a strong rationale for further development of CISD2-based anti-inflammatory therapies for patients with the aforementioned disorders.

Our data provide novel evidence that the anti-inflammatory effect of microglial CISD2 is associated with the regulation of NFκB signaling. At present, the molecular mechanism underlying the anti-inflammatory effects of CISD2 has yet to be elucidated. When located in the cytoplasm and mitochondrial intermembrane space, the activation of NFκB, in addition to a role as well-recognized proinflammatory mediator, has been linked to inflammation, mitochondrial dysfunction, and eventual cellular apoptosis (Albensi, 2019). Thus, it can be interpreted that the attenuation of CISD2 owing to primary insults from neurotrauma or inflammation from CNS disease inhibits the protective effects against NFκB in cytoplasm and mitochondria leading to a remarkable inflammatory response and mitochondrial dysfunction. Furthermore, evidence has been obtained stating that calcium regulates the expression of TNF-α (Canellada et al., 2006) and modulates macrophage-driven inflammatory cascades (Racioppi et al., 2012). We posit that anti-inflammatory effects may be attributed to the regulatory role of CISD2 in calcium metabolism (Chang et al., 2012).

It has been suggested that CISD2 combines with BCL2 to antagonize the apoptotic mediator Beclin 1 (Chang et al., 2012). NFκB also regulates apoptotic effects *via* the combination or dissociation of Beclin 1/Bcl2 complex (Salminen et al., 2012). Moreover, elevated activity of NFκB transcription factors has also been demonstrated to modulate the expression of BCL2 (Chen et al., 2015). In this study, CISD2 was demonstrated to mediate the upstream regulation of NFκB, as observed by the DNA-binding activity of the NFκB p65 subunit. Collectively, the results indicate that CISD2 plays an upstream regulatory role in the functions of NFκB and BCL2. Advanced inflammation and mitochondrial dysfunction are highly likely to result in cell damage and negative cell survival. This may explain why CISD2 deficiency leads to potent inflammatory and apoptotic signaling.

As located in the outer membrane of mitochondria, CISD2 deficiency has been demonstrated to cause mitochondrial dysfunction and may undermine mitochondrial integrity. Note that mitochondrial dysfunction has been shown to inhibit M2 microglial polarization (Nakagawa and Chiba, 2014). It has been reported that M1 macrophages undergo aerobic glycolysis and pentose phosphate pathway (PPP) in obtaining a supply of energy. Conversely, M2 macrophages use acetyl-CoA and participate in the mitochondrial TCA (tricarboxylic acid) cycle (Culmsee et al., 2019). Thus, CISD2 deficiency-driven mitochondrial dysfunction contributes to a decrease in TCA cycle activities and augments aerobic glycolysis and the PPP pathway. In so doing, it leads to the promotion of the M1 phenotype along with the reduction of the M2 phenotype.

Some limitations have been attributed to this study. First, based on some previous novel findings involving non-immune cells (SH-SY5Y), we used the cell culture model developed with EOC microglial cell line to evaluate the mechanisms in this study. In future studies, it would be prudent to examine this putative mechanism in primary cultured microglia or *via in vivo* research using animal or human tissue. Moreover, the mechanism underlying the effect of CISD2 knockdown on M1/M2 microglia polarization will have to be verified using morphological analysis conducted *in vitro* or *in vivo*, such as staining for microglia M1/M2 profile marker. We demonstrated the involvement of CISD2 in the regulation of inflammatory genes under basal conditions in the present study using siCISD2 to attenuate CISD2 expression. Confirmation of this mechanism will be considered in further studies demonstrating the overexpression of CISD2 in microglia.

CONCLUSION

The results obtained in this study demonstrate that CISD2 exerts anti-inflammatory effects, which may be induced by the suppression of NFκB activation and the preservation of the protective M2 phenotype in non-stressed microglia. CISD2 deficiency in microglia could be one of the mechanisms underlying cell apoptosis, perhaps occurring *via* inflammation. CISD2-based anti-inflammatory therapy is a strong candidate for the treatment of neuroinflammation-driven aging and neurodegenerative diseases.

DATA AVAILABILITY STATEMENT

The raw data supporting the conclusions of this article will be made available by the authors, without undue reservation.

ETHICS STATEMENT

The study was reviewed and approved by the Animal Care and Ethics Committee of National Ilan University.

AUTHOR CONTRIBUTIONS

M-SL: writing—original draft, formal analysis, resources, methodology, funding acquisition, writing—review and editing, and conceptualization.

REFERENCES

Albensi, B. C. (2019). What is nuclear factor κB (NF-κB) doing in and to the mitochondrion? *Front. Cell. Dev. Biol.* 7:154. doi: 10.3389/fcell.2019.00154

Bhaskar, K., Maphis, N., Xu, G., Varvel, N. H., Kokiko-Cochran, O. N., Weick, J. P., et al. (2014). Microglial derived tumor necrosis factor-alpha drives Alzheimer's disease-related neuronal cell cycle events. *Neurobiol. Dis.* 62, 273–285. doi: 10.1016/j.nbd.2013.10.007

Byrnes, K. R., Stoica, B. A., Fricke, S., Di, G. S., and Faden, A. I. (2007). Cell cycle activation contributes to post-mitotic cell death and secondary damage after spinal cord injury. *Brain* 130, 2977–2992. doi: 10.1093/brain/awm179

Canellada, A., Cano, E., Sanchez-Ruiloba, L., Zafra, F., and Redondo, J. M. (2006). Calcium-dependent expression of TNF-alpha in neural cells is mediated by the calcineurin/NFAT pathway. *Mol. Cell Neurosci.* 31, 692–701. doi: 10.1016/j.mcn.2005.12.008

Chang, N. C., Nguyen, M., Germain, M., and Shore, G. C. (2010). Antagonism of Beclin 1-dependent autophagy by BCL-2 at the endoplasmic reticulum requires NAF-1. *EMBO J.* 29, 606–618. doi: 10.1038/emboj.2009.369

Chang, N. C., Nguyen, M., and Shore, G. C. (2012). BCL2-CISD2: an ER complex at the nexus of autophagy and calcium homeostasis? *Autophagy* 8, 856–857. doi: 10.4161/auto.20054

Chen, Y. F., Chou, T. Y., Lin, I. H., Chen, C. G., Kao, C. H., Huang, G. J., et al. (2020). Upregulation of Cisd2 attenuates Alzheimer's-related neuronal loss in mice. *J. Pathol.* 250, 299–311. doi: 10.1002/path.5374

Chen, Y. F., Kao, C. H., Chen, Y. T., Wang, C. H., Wu, C. Y., Tsai, C. Y., et al. (2009). Cisd2 deficiency drives premature aging and causes mitochondria-mediated defects in mice. *Genes Dev.* 23, 1183–1194. doi: 10.1101/gad.1779509

Chen, B., Shen, S., Wu, J., Hua, Y., Kuang, M., Li, S., et al. (2015). CISD2 associated with proliferation indicates negative prognosis in patients with hepatocellular carcinoma. *Int. J Clin. Exp. Pathol.* 8, 13725–13738.

Culmsee, C., Michels, S., Scheu, S., Arolt, V., Dannlowski, U., and Alferink, J. (2019). Mitochondria, microglia and the immune system-how are they linked in affective disorders? *Front. Psychiatry* 9:739. doi: 10.3389/fpsyt.2018.00739

Hickman, S., Izzy, S., Sen, P., Morsett, L., and El, K. J. (2018). Microglia in neurodegeneration. *Nat. Neurosci.* 21, 1359–1369. doi: 10.1038/s41593-018-0242-x

Hu, X., Leak, R. K., Shi, Y., Suenaga, J., Gao, Y., Zheng, P., et al. (2015). Microglial and macrophage polarization—new prospects for brain repair. *Nat. Rev. Neurol.* 11, 56–64. doi: 10.1038/nrneurol.2014.207

Jucker, M., and Walker, L. C. (2011). Pathogenic protein seeding in Alzheimer disease and other neurodegenerative disorders. *Ann. Neurol.* 70, 532–540. doi: 10.1002/ana.22615

Karve, I. P., Taylor, J. M., and Crack, P. J. (2016). The contribution of astrocytes and microglia to traumatic brain injury. *Br. J. Pharmacol.* 173, 692–702. doi: 10.1111/bph.13125

Li, S., Wang, L., Berman, M. A., Zhang, Y., and Dorf, M. E. (2006). RNAi screen in mouse astrocytes identifies phosphatases that regulate NF-κB signaling. *Mol. Cell* 24, 497–509. doi: 10.1016/j.molcel.2006.10.015

Lin, C. C., Chiang, T. H., Chen, W. J., Sun, Y. Y., Lee, Y. H., and Lin, M. S. (2015). CISD2 serves a novel role as a suppressor of nitric oxide signalling and curcumin increases CISD2 expression in spinal cord injuries. *Injury* 46, 2341–2350. doi: 10.1016/j.injury.2015.07.040

Lin, C. C., Chiang, T. H., Sun, Y. Y., and Lin, M. S. (2019). Protective effects of cisd2 and influence of curcumin on CISD2 expression in aged animals and inflammatory cell model. *Nutrients* 11:700. doi: 10.3390/nu11030700

Lin, M. S., Hung, K. S., Chiu, W. T., Sun, Y. Y., Tsai, S. H., Lin, J. W., et al. (2011a). Curcumin enhances neuronal survival in N-methyl-d-aspartic acid toxicity by inducing RANTES expression in astrocytes *via* PI-3K and MAPK signaling pathways. *Prog. Neuropsychopharmacol. Biol. Psychiatry* 35, 931–938. doi: 10.1016/j.pnpbp.2010.12.022

Lin, M. S., Sun, Y. Y., Chiu, W. T., Hung, C. C., Chang, C. Y., Shie, F. S., et al. (2011b). Curcumin attenuates the expression and secretion of RANTES after spinal cord injury *in vivo* and lipopolysaccharide-induced astrocyte reactivation *in vitro*. *J. Neurotrauma* 28, 1259–1269. doi: 10.1089/neu.2011.1768

Luo, Y., Berman, M. A., Zhai, Q., Fischer, F. R., Abromson-Leeman, S. R., Zhang, Y., et al. (2002). RANTES stimulates inflammatory cascades and receptor modulation in murine astrocytes. *Glia* 39, 19–30. doi: 10.1002/glia.10079

Maragakis, N. J., and Rothstein, J. D. (2006). Mechanisms of disease: astrocytes in neurodegenerative disease. *Nat. Clin. Pract. Neurol.* 2, 679–689. doi: 10.1038/ncpneuro0355

Mattson, M. P. (2000). Apoptosis in neurodegenerative disorders. *Nat. Rev. Mol. Cell Biol.* 1, 120–129. doi: 10.1038/35040009

Meraz-Ríos, M. A., Toral-Rios, D., Franco-Bocanegra, D., Villeda-Hernandez, J., and Campos-Pena, V. (2013). Inflammatory process in Alzheimer's disease. *Front. Integr. Neurosci.* 7:59. doi: 10.3389/fnint.2013.00059

Nakagawa, Y., and Chiba, K. (2014). Role of microglial m1/m2 polarization in relapse and remission of psychiatric disorders and diseases. *Pharmaceuticals* 7, 1028–1048. doi: 10.3390/ph7121028

Norden, D. M., and Godbout, J. P. (2013). Review: microglia of the aged brain: primed to be activated and resistant to regulation. *Neuropathol. Appl. Neurobiol.* 39, 19–34. doi: 10.1111/j.1365-2990.2012.01306.x

Norden, D. M., Muccigrosso, M. M., and Godbout, J. P. (2015). Microglial priming and enhanced reactivity to secondary insult in aging and traumatic CNS injury and neurodegenerative disease. *Neuropharmacology* 96, 29–41. doi: 10.1016/j.neuropharm.2014.10.028

Pei, Z., Wang, S., and Li, Q. (2017). Sevoflurane suppresses microglial M2 polarization. *Neurosci. Lett.* 655, 160–165. doi: 10.1016/j.neulet.2017.07.001

Racioppi, L., Noeldner, P. K., Lin, F., Arvai, S., and Means, A. R. (2012). Calcium/calmodulin-dependent protein kinase kinase 2 regulates macrophage-mediated inflammatory responses. *J. Biol. Chem.* 287, 11579–11591. doi: 10.1074/jbc.M111.336032

Raz, L., Knoefel, J., and Bhaskar, K. (2016). The neuropathology and cerebrovascular mechanisms of dementia. *J. Cereb. Blood Flow Metab.* 36, 172–186. doi: 10.1038/jcbfm.2015.164

Ross, C. A., and Poirier, M. A. (2004). Protein aggregation and neurodegenerative disease. *Nat. Med.* 10, S10–S17. doi: 10.1038/nm1066

Salminen, A., Hyttinen, J. M., Kauppinen, A., and Kaarniranta, K. (2012). Context-dependent regulation of autophagy by IKK-NF-κB signaling: impact on the aging process. *Int. J. Cell. Biol.* 2012:849541. doi: 10.1155/2012/849541

Sanada, F., Taniyama, Y., Muratsu, J., Otsu, R., Shimizu, H., Rakugi, H., et al. (2018). Source of chronic inflammation in aging. *Front. Cardiovasc. Med.* 5:12. doi: 10.3389/fcvm.2018.00012

Shen, Z. Q., Chen, Y. F., Chen, J. R., Jou, Y. S., Wu, P. C., Kao, C. H., et al. (2017). CISD2 haploinsufficiency disrupts calcium homeostasis, causes nonalcoholic fatty liver disease and promotes hepatocellular carcinoma. *Cell Rep.* 21, 2198–2211. doi: 10.1016/j.celrep.2017.10.099

Simen, A. A., Bordner, K. A., Martin, M. P., Moy, L. A., and Barry, L. C. (2011). Cognitive dysfunction with aging and the role of inflammation. *Ther. Adv. Chronic. Dis.* 2, 175–195. doi: 10.1177/2040622311399145

Song, G. J., and Suk, K. (2017). Pharmacological modulation of functional phenotypes of microglia in neurodegenerative diseases. *Front. Aging Neurosci.* 9:139. doi: 10.3389/fnagi.2017.00139

Tator, C. H., and Fehlings, M. G. (1991). Review of the secondary injury theory of acute spinal cord trauma with emphasis on vascular mechanisms. *J. Neurosurg.* 75, 15–26. doi: 10.3171/jns.1991.75.1.0015

Thomas, J., Thomas, C. J., Radcliffe, J., and Itsiopoulos, C. (2015). Omega-3 fatty acids in early prevention of inflammatory neurodegenerative disease: a focus on Alzheimer's disease. *Biomed. Res. Int.* 2015:172801. doi: 10.1155/2015/172801

Wake, H., Moorhouse, A. J., and Nabekura, J. (2011). Functions of microglia in the central nervous system-beyond the immune response. *Neuron Glia Biol.* 7, 47–53. doi: 10.1017/S1740925X12000063

Wood, P. L. (1995). Microglia as a unique cellular target in the treatment of stroke: potential neurotoxic mediators produced by activated microglia. *Neurol. Res.* 17, 242–248. doi: 10.1080/01616412.1995.11740321

Zhang, Q., Lu, Y., Bian, H., Guo, L., and Zhu, H. (2017). Activation of the alpha7 nicotinic receptor promotes lipopolysaccharide-induced conversion of M1 microglia to M2. *Am. J. Transl. Res.* 9, 971–985.

Zhang, L., Zhang, J., and You, Z. (2018). Switching of the microglial activation phenotype is a possible treatment for depression disorder. *Front. Cell. Neurosci.* 12:306. doi: 10.3389/fncel.2018.00306

Conflict of Interest: The author declares that the research was conducted in the absence of any commercial or financial relationships that could be construed as a potential conflict of interest.

frontiers in Aging Neuroscience

ORIGINAL RESEARCH
published: 28 August 2020
doi: 10.3389/fnagi.2020.00222

Relationship of Parieto-Occipital Brain Energy Phosphate Metabolism and Cognition Using ^{31}P MRS at 7-Tesla in Amnestic Mild Cognitive Impairment

Namrata Das[1], Jimin Ren[2], Jeffrey S. Spence[1], Audette Rackley[1] and Sandra B. Chapman[1]*

[1] Center for BrainHealth, The University of Texas at Dallas, Dallas, TX, United States, [2] Advanced Imaging Research Center, and Department of Radiology, University of Texas Southwestern Medical Center, Dallas, TX, United States

Background: The human brain has high energy requirements that continuously support healthy neuronal activity and cognition. A disruption in brain energy metabolism (BEM) may contribute to early neuropathological changes such as accumulation of β-amyloid and tau in vulnerable populations. One such population is amnestic mild cognitive impairment (aMCI) where some individuals are at risk for developing dementia, i.e. Alzheimer's disease (AD). Recent advances in imaging technology are providing new avenues to measure BEM accurately using 31phosphorus magnetic resonance spectroscopy (31P MRS) at ultra-high-field (UHF) magnetic strength 7-Tesla. This study investigates whether a methodology using partial volume-coil 31P MRS at 7T over parieto-occipital lobes can accurately quantify high-energy phosphate and membrane phospholipid metabolites in aMCI. A secondary objective was to explore BEM and membrane phospholipid indices' correspondence with cognitive performance in domains of executive function (EF), memory, attention, and visuospatial skills in aMCI, a heterogeneous population.

Methods: 19 aMCI participants enrolled in the study completed cognitive assessment and 31P MRS scan. BEM indices were measured using three energy indicators: energy reserve (PCr/t-ATP), energy consumption (intracellular_Pi/t-ATP), and metabolic state (PCr/intracellular_Pi) along with regulatory co-factors of BEM-intracellular Mg^{2+} and pH; whereas the ratio of phosphomonoesters (PMEs) to phosphodiesters (PDEs) – membrane phospholipid indicator.

Results: 31P MRS scan showed thirteen well-resolved peaks with precise quantification of the phosphorus metabolites at UHF. The higher BEM indices were associated with lower cognitive performance of memory [(energy reserve indicator: CVLT $p = 0.004$), (metabolic state indicator: CVLT $p = 0.007$)], executive function [(metabolic state indicator: TOSL ($p = 0.044$)], and attention [(pH: selective auditory task, $p = 0.044$)]. The finding of an inverse relationship observed in the parieto-occipital lobes suggests an association between neuronal energy markers with cognition in aMCI.

OPEN ACCESS

Edited by:
Woon-Man Kung,
Chinese Culture University, Taiwan

Reviewed by:
Pedro J. Modrego,
Hospital Universitario Miguel Servet, Spain
Lijing Xin,
École Polytechnique Fédérale de Lausanne, Switzerland

****Correspondence:***
Namrata Das
Namrata.Das@utdallas.edu

Received: *14 April 2020*
Accepted: *22 June 2020*
Published: *28 August 2020*

Citation:
Das N, Ren J, Spence JS, Rackley A and Chapman SB (2020) Relationship of Parieto-Occipital Brain Energy Phosphate Metabolism and Cognition Using ^{31}P MRS at 7-Tesla in Amnestic Mild Cognitive Impairment. Front. Aging Neurosci. 12:222. doi: 10.3389/fnagi.2020.00222

Conclusion: The significant contribution of this preliminary research was to establish the feasibility of utilizing a methodology at UHF to accurately measure high-energy phosphate and membrane phospholipid metabolites in a population with heterogeneous outcomes. This work offers a novel approach for future work to further elucidate early dementia biomarkers or precursors to the downstream accumulation of amyloid and tau using the combination of MRS-PET imaging modalities in AD.

Keywords: brain energy metabolism, membrane phospholipid, amnestic mild cognitive impairment (aMCI), Alzheimer's disease (AD), adenosine triphosphate (ATP), ^{31}phosphorus magnetic resonance spectroscopy, ^{18}fluorodeoxyglucose positron emission tomography (^{18}FDG PET)

INTRODUCTION

Mild cognitive impairment (MCI) represents a heterogeneous clinical condition that is definable and objectively classifiable; however, its nature is unstable. MCI appears to follow one of three courses: (1) static condition with little to no change; (2) revert back to normal cognitive function; and (3) advance to dementia, especially Alzheimer's disease (AD) (Albert et al., 2011; Petersen et al., 2014). Motivated by the very nature of this heterogeneity, MCI may present with an ideal group to examine whether the relationship between cognitive and brain energy metabolism (BEM) exists. Such preliminary efforts may help elucidate some possible predictors that could subsequently be investigated in longitudinal studies and compare with cognitively normal and AD population in a pilot trial testing a new methodology at ultra-high-field (UHF) MRI.

Traditionally in MCI, cognitive decline is presented as single or multiple-domain deficits in which either one or more cognitive function decline is observed (Alichniewicz et al., 2012; Cerami et al., 2014; Giau et al., 2019). A subset of the MCI population is classified as amnestic MCI (aMCI). This aMCI subgroup manifests significant memory problems with or without alterations in other cognitive domains for their age, but they remain functionally independent (Petersen's et al., 2001). An estimated 30% of MCI subjects are of the aMCI-type with this type showing a higher predilection to subsequently evolve into criteria to meet diagnosis of AD (Cerami et al., 2014). The conversion rate of AD/dementia diagnosis is much higher in the general category of MCI, ranging from 10–15% per year in the clinical setting and 6–10% in population-based studies when compared to age-matched healthy comparison group. In the latter group, the conversion rate is estimated to be about 1–2% per year (Petersen et al., 1999; Farias et al., 2009; Shimada et al., 2019). A meta-analysis in 25 studies supported an overall reversion rate from MCI back to cognitively normal as approximately 24% (Malek-Ahmadi, 2016). Given the heterogeneity of MCI, it is important to point out that although this group may be at greater risk of developing dementia than the normal population, a significant proportion of this population still does not show AD's frank symptoms to reach diagnostic criteria. Overall, this varying range of MCI progression to dementia, or reversal back to normal, supports a plausible hypothesis that the biological mechanisms involved are heterogeneous and unstable. As such, this classifiable group may provide a valuable population to explore the early biomarkers of neuronal function that affect cognition before the diagnosis of dementia.

Due to the heterogeneity, unstable nature, and wide range of cognitive behavior in individuals with MCI, research is focused on further elucidating novel biomarkers occurring inside the brain cells in this vulnerable complex group. These novel biomarkers are speculated to contribute to our knowledge about possible early pathomechanistic disruptions that could later inform which individuals go on to develop AD and who do not. Previous work established that extracellular deposits of β-amyloid peptides and intracellular deposits of tau aggregates are associated with the pathology of MCI and AD (Mufson et al., 2012). Moreover, only the burden of intracellular tau is strongly correlated with the degree of cognitive decline in MCI and AD (Bejanin et al., 2017). The correlation between tau and cognition observed in postmortem human brain is replicated in *in vivo* studies using a positron emission tomography (PET) tau-radiotracer ^{18}F-AV-1451 scan (Bejanin et al., 2017). However, little is known about the initial process that disrupts the internal biological mechanisms causing tau hyperphosphorylation leading to the aggregation of tau in the form of neurofibrillary tangles and the relationship of these early biological markers with cognition in MCI.

Growing evidence in MCI and AD pathology supports a role of neuroenergetics, a study of BEM along with depletion of neurotransmitters and neuroinflammation as significant contributing factors to the early disease pathophysiology and progression even before the accumulation of β-amyloid and tau (Ogawa et al., 1996; Heneka et al., 2015). It is intriguing to know that the human brain weighs only 2% of the body weight, whereas it consumes about 25% of the glucose and 20% of the body's oxygen to produce energy in adenosine triphosphate (ATP) (Zlokovic, 2011). The energy produced supports various cellular events such as Na^+/K^+-ATP activities to maintain membrane potential, integrity, and metabolite exchange for neuronal firings (Albers and Siegel, 1999). In sum, the high-energy requirements of the brain make it a highly vulnerable organ to BEM disturbances, especially in the transitory stage such as MCI. It has been speculated that disruptions in BEM and neurochemicals may represent early disease markers in MCI who may convert to AD/dementia with prominent cognitive decline and is observed versus non-converters.

The hypothesis of BEM alterations in MCI can be supported by two recent studies using ^{18}FDG-PET to measure brain glucose metabolism. Earlier longitudinal study of 3 years in 45 MCI (37 aMCI and 8 non-amnestic) using 18-FDG PET showed a distinct pattern of neurometabolic changes in terms of reduced glucose metabolism in the temporoparietal brain areas in individuals associated with cognitive deterioration who progressed toward AD (Cerami et al., 2014). In the 3-year follow-up, 14 MCI (11 aMCI and 3 non-amnestic MCI) with normal glucose metabolism in the brain never converted to dementia, whereas 24 MCI of the 45 enrolled (18 aMCI and 6 non-amnestic MCI) with region-specific reduced glucose metabolism in the brain showed increasing cognitive decline to the point where they converted to AD/other dementias (Cerami et al., 2014). Similarly, in a different retrospective longitudinal study of 4 years in 30 aMCI using ^{18}FDG PET, patients without typical hypometabolism in temporoparietal areas did not convert to AD, and cognitive function remained stable over the period of follow-up (Cerami et al., 2018). Thereby, emphasizing that brain metabolism plays a crucial role in regulating cognitive behavior, paving the path to explore the relationship of BEM-cognitive correlates in aMCI.

In addition to ^{18}FDG-PET, magnetic resonance spectroscopy (MRS) represents an emerging brain imaging field that shows promise in providing a platform to investigate BEM, neuroinflammatory, and excitotoxicity markers at the microscopic level inside the brain cells. These microscopic changes have the potential to later affect the macroscopic neural structure, such as the brain's anatomy and physiology, subsequently leading to brain atrophy, which are well studied in MCI and AD (Godlewska et al., 2017). Specifically, the high-energy phosphate metabolites a methodology to investigate BEM at the molecular level is investigated by using a novel non-invasive imaging technology—phosphorus (^{31}P) MRS. This technology aids in the quantification of high-energy phosphate metabolites [ATP, phosphocreatine (PCr), and inorganic phosphate (Pi)] and membrane phospholipid metabolites [phosphoethanolamine (PE), phosphocholine (PC), glycerophosphoethanolamine (GPE), and glycerophosphocholine (GPC)] (Ross and Sachdev, 2004) crucial to understand BEM and membrane phospholipid metabolism. Recent work by Rijpma et al. (2018) using whole-brain ^{31}P MRS at 3Tesla observed that the Pi/PCr ratio and the membrane phospholipid metabolites, especially PE, GPC, and GPE, were lower in mild AD compared to age-matched healthy controls. One possible explanation of decreased Pi/PCr findings in AD may be due to a reduction of creatine kinase (CK) activity, an enzyme of mitochondria, thereby increasing PCr (David et al., 1998; Rijpma et al., 2018). Moreover, a ^{31}P MRS study at 1.5T showed an association between higher levels of PE and PC in the prefrontal cortex with the severity of cognitive decline measured using the Cambridge Cognitive scale, which included domains of memory, orientation, language, attention, praxis, calculation, abstract thinking, and visual perception subtests (Forlenza et al., 2005). Similarly, other studies in AD have identified higher levels of PE and PC membrane phospholipid metabolites either in temporoparietal areas (Brown et al., 1989) or over diffuse cortical areas (Pettegrew et al., 1988). ^{31}P MRS methodology may aid in fine-tuning the characterization of MCI group who will progress to dementia or not in addition to hallmark proteinopathies-accumulation of amyloid and tau.

Over the last two decades, the ^{31} P MRS technique has been used in brain imaging at lower magnetic strength. Nonetheless, we have at least two main unanswered questions in MCI: (1) Can BEM metabolites be measured in the early stage with higher resolution compared to the existing work using lower magnetic strength and, (2) Is there a correspondence between BEM and cognitive performance in this group? The main challenge is to quantify the high-phosphate energy metabolites accurately and precisely. At lower magnetic strength, like 3T or less, neurochemicals or neurometabolites with only high signal-to-noise ratio (SNR) and abundant in nature can be assessed (Oeltzschner et al., 2019). However, recent advancements in MRI technology to use UHF magnets have enabled the robust application of the ^{31}P MRS technique (Godlewska et al., 2017). UHF increases the SNR with a higher spectral resolution with enhanced sensitivity of neurochemicals and neurometabolites, which are present in minute concentrations (Mekle et al., 2009; Pradhan et al., 2015; Oeltzschner et al., 2019). To date, no study has used the UHF methodology of ^{31}P MRS in understanding the relationship of high-energy phosphate and membrane phospholipid metabolites relationship with cognition in an aMCI group.

The present pilot study in aMCI by 7T ^{31}P MRS had two goals. The first goal was to conduct a preliminary study to determine the feasibility of quantifying various high-energy phosphate and membrane phosphorus metabolites identifiable at 7-Tesla using a partial volume-coil in the parieto-occipital lobes of an aMCI cohort. The current study represents the first known project to test whether a methodology, previously shown to separate similar metabolites in the healthy young adult brain (Ren et al., 2015), heart (Rodgers et al., 2014), and muscles (Ren et al., 2013) could be adapted to measure BEM using ^{31}P MRS at 7 Tesla in participants classified as aMCI. We selected parieto-occipital lobes as the region of interest based on two previous MCI studies (Ashraf et al., 2015; Corriveau-Lecavalier et al., 2019). Ashraf's et al. (2015) research supported increased metabolism (hypermetabolism) in the occipital cortex in MCI compared to healthy controls using ^{18}FDG PET. Similarly, a longitudinal study in 26 MCI by Corriveau-Lecavalier et al. (2019) found that parietal lobe hyperactivation in 13 MCI was an early indicator in individuals who progressed to dementia. In MCI, based on Ashraf's and Corriveau's findings in the parietal and occipital lobes separately, we hypothesized that there may be compensatory hyperactivation, which may be a proxy of higher cerebral blood flow and energy metabolism during the early phases of biological changes, which may be associated with worsening of cognitive performance.

Our next goal was to investigate the relationships across *BEM indices* measured using the metabolite ratios of PCr/t-ATP (reflective of energy reserve), (Pi/t-ATP (reflective of energy consumption), and PCr/Pi (reflective of a metabolic state) and its regulatory co-factors (intracellular Mg^{2+} and

pH) followed by *membrane phospholipid metabolite index* (PMEs/PDEs) in the parieto-occipital lobes with the cognitive performance of executive function (EF) (complex abstraction, innovation, inhibition and switching, conceptual reasoning, and working memory), memory (episodic), attention, and visuospatial skills. In this research, we define the energy reserve indicator the ratio of PCr to ATP, where PCr is the immediate energy reserve replenishing consumed ATP for maintaining ATP homeostasis during the neuronal activity. In contrast, Pi to t-ATP ratio reflects the relationship between metabolic substrate and product and for energy consumption (ATP $\rightarrow$ Pi + ADP) and reproduction (Pi + ADP $\rightarrow$ ATP). Pi tends to accumulate when cellular ATP consumption temporarily exceeds the ATP production by mitochondria at a steady state, and increased Pi in turn tends to increase the potential of energy production. The ratio of PCr to Pi is a metabolic state indicator because both PCr and Pi increase the turnover rate or production of ATP. This index was previously termed the oxidative phosphorylation index to measure mitochondrial function (Chance et al., 1981). Based on Ashraf's and Corriveau's studies in MCI, we hypothesized that higher BEM and membrane phospholipid metabolite indices in parieto-occipital lobes would be associated with lower performance on cognitive measures. Overall, in aMCI, which is considered a heterogeneous clinical condition, this work represents a preliminary effort to test a methodology at UHF to measure BEM metabolites precisely followed by exploring the BEM-cognitive performance correlates.

MATERIALS AND METHODS

Protocol Approvals and Consent

The study was approved to include individuals with memory complaints between the age of 50 and 80 years by the Institutional Review Board of The University of Texas Southwestern Medical Center and The University of Texas at Dallas. Informed consent and HIPPA forms were signed as per the ethical standards of the Committee on Human Experimentation under Declaration of Helsinki, 1981.

Participants

Nineteen aMCI participants were recruited using a multi-stage phone screen, including questions related to demographics and medical history along with a review of medications list, an imaging screen, and a memory screen called Clinical Dementia Rating (CDR) scale. Individuals with a history of metal in the body, neurological diseases, substance abuse, psychiatric problems, or any medication that stimulated or slowed the brain's electrical activity were excluded. Eligible participants included for the cognitive screen and assessment were selected irrespective of gender and ethnic factors. All selected participants were right-handed and native English speakers with a minimum of 12 years of education and CDR scale score of 0.5, that is, subjective memory complainers.

Characterization of aMCI Participants

The qualified individuals on the phone screen with subjective memory complains (CDR of 0.5) were diagnosed as aMCI based on the established objective memory decline as per either Petersen's or the Alzheimer's disease Neuroimaging Initiative (ADNI) criteria, respectively. The comprehensive ADNI aMCI criteria implemented were: (1) subjective memory complaints; (2) CDR 0.5; (3) objective memory loss measured by logical memory subtest (Wechsler Memory Scale-III); (4) normal daily living activities and cognitive functions assessed using Lawton instrumental activities of daily living scale; (5) clinical dementia rating scale score of 0.5; (6) Mini-Mental Status Examination (MMSE) of 24–30; and (7) absence of dementia. In the Petersen's criteria, all the characteristics mentioned above in ADNI were the same except objective memory loss was assessed using California Verbal Learning Task (CVLT) and individuals who scored −1.5 standard deviation (SD) below the age and education-adjusted mean were included in the study as aMCI. Cognitive screens such as logical memory and CVLT along with geriatric depression scale (short form) were included during the 3-h cognitive assessment protocol. Only participants with no or mild depression were included in the study. **Table 1** summarizes all the screening measures and questionnaires administered to eligible aMCI participants.

Cognitive Screen and Assessment

The cognitive screening measures included were MMSE, logical memory, and CVLT along with geriatric depression scale (**Table 1**). The other measures included in the present analyses were the cognitive domains of EF (complex abstraction, innovation, switching and inhibition, reasoning, and working memory), memory (episodic memory), attention (selective attention), and visuo-spatial skills. After the cognitive screening, individuals who met the criteria of aMCI and completed other cognitive assessments were invited to complete a 45-min ^{31}P MRS scan at 7-Tesla. **Table 3** summarizes all the neurocognitive measures implemented in this part of the study. The demographics/characteristics of the participants are presented in **Table 4**.

^{31}Phosphorus Magnetic Resonance Spectroscopy (^{31}P MRS) Data Acquisition Protocol

^{31}P MRS was performed at 7-Tesla MR system (Philips Healthcare, Cleveland, OH, United States), using a double-tuned ^{1}H/^{31}P partial volume-coil consisting of two-tilted partially overlapping 10 cm loops with a plastic housing fit to the shape of the head posterior. All the aMCI participants were positioned head-first and supine in the MRI scanner to acquire spectral data from the parieto-occipital lobes. Prior to this MRS data acquisition, axial, coronal, and sagittal T2-weighted turbo spin echo MR images were recorded for planning the shimming voxel. Typical imaging parameters included field-of-view 180 × 180 mm, repetition time (TR) 2.5 s, echo time 80 ms, turbo factor 15, in-plane spatial resolution 0.6 × 0.7 mm^2, slice thickness 8 mm, gap 2 mm, bandwidth 517 Hz, number

TABLE 1 | Screening measures and questionnaires in amnestic mild cognitive impairment (aMCI).

	Measures	Description
Screening Measures	Clinical Dementia Rating Scale (CDR) (Morris, 1993)	Assesses six domains of cognitive and functional performance in memory, judgment and problem solving, community affairs, orientation, personal care and hobbies. Score: 0.5
	Logical Memory (ADNI Criteria, WMS-III, Wechsler, 1997b)	The ability to recall a short story as it is read out immediately and after 25 min interval was assessed. Score: Delayed memory recall of 9–11 for 16 years of education or 5–9 for 8–15 years of education.
	California Verbal Learning Task (Petersen's et al., 2001)	The ability to recall a list of sixteen (16) words in four categories immediately after the list was read followed by delayed recall after 20 min interval was assessed. Score: −1.5 standard deviation below the mean for age and sex adjusted scores.
	Mini Mental Status Examination (Folstein et al., 1975)	Assesses the ability to examine functions of registration, attention and calculation, recall and language. Score: 24–30
	Activities of daily living: Lawton Instrumental Activities of Daily Living Scale (Lawton et al., 2003)	Assesses the activities of daily living in the areas of ability to use phone, shopping, food preparation, housekeeping, laundry, mode of transportation, responsibility for own medications, and ability to handle finances. Score: 8
Questionnaires		
Subjective memory perception	Multifactorial Memory Questions (MMQ) (Troyer and Rich, 2002)	Assessed individual's self-perception of memory in three subscales using 57 items questionnaire 1. MMQ-Contentment (MMQ-C): Self-satisfaction of memory 2. MMQ-Ability (MMQ-A): Self-perception of memory 3. MMQ-Strategy (MMQ-S): Using of memory strategies in daily life functions.
Depression	Geriatric Depression scale (Yesavage et al., 1982)	Assessed the depression of the individuals using 15 items questionnaire. Score: ≤6

TABLE 2 | Independent variables: energy and membrane phospholipid metabolite indices in amnestic mild cognitive impairment.

Index	Ratios	Definition
BEM indices		
Energy reserve indicator	PCr/t-ATP	Energy reserve indicator is the ratio of PCr/t-ATP as PCr is the immediate energy reserve metabolite replenishing energy demands during the neuronal activity
Energy consumption indicator	Pi/t-ATP: Extracellular-Pi/t-ATP Intracellular-Pi/t-ATP	Energy consumption indicator is the ratio of Pi/t-ATP as Pi is rapidly consumed to release energy in the form of ATP to support ongoing metabolic and neuronal activity.
Metabolic state indicator	PCr/Pi PCr/Intracellular-Pi	Metabolic state indicator is the ratio of PCr/Pi as both PCr and Pi increase the turnover rate or production of ATP. Previously this index was termed as oxidative phosphorylation index to measure mitochondrial function (Chance et al., 1981).
Regulatory co-factors	Magnesium (Mg^{2+}) Intracellular pH	
Membrane phospholipid index		
Membrane phospholipid index	PMEs/PDEs	Membrane phospholipid index is the ratio of PMEs (the major precursors of phospholipids contributing to membrane synthesis) to PDEs (major products of phospholipid breakdown) indicating neuronal and non-neuronal membrane integrity (Ross and Sachdev, 2004).

BEM, brain energy metabolism; PCr, phosphocreatine; t-ATP, total adenosine triphosphate; Pi, inorganic phosphate- internal or external; Mg^{2+}, magnesium; PMEs, phosphomonoesters; PDEs, phosphodiesters.

of acquisitions one, and acquisition time 2.1 min. Second-order ^{1}H-based automatic volume shimming was applied.

Quantitative ^{31}P MR spectra were acquired using a non-localized block-shaped excitation pulse with B_1 59 μT, and pulse width 0.2 ms with an estimated flip angle 55°, which was previously calibrated. B1 calibration of partial volume-coil is presented in the **Supplementary Figure S1**. The transmitter frequency was centered at 700 Hz upfield from the resonance of PCr. A short delay time of 0.5 ms was applied prior to free induction decay (FID) data collection to filter out broad-membrane phospholipids signal. The sampling point was 4 k, zero-filled to 8 k prior to Fourier transformation. For quantitative comparison of different metabolite ^{31}P peaks, fully relaxed spectra were recorded at long TR of 25 s with and eight scan average. For Mg^{2+} measurement, to minimize measurement error due to potential T_1 effects and time-of-the-day-dependent Mg^{2+} fluctuation, additional ^{31}P spectra were also acquired at short TRs ranging from 1 to 5 s

TABLE 3 | Dependent variables: neurocognitive battery administered to amnestic mild cognitive impaired participants.

Cognitive domain	Measures	Description
Executive function		
1. Complex abstraction	Test of Strategic Learning (TOSL) (Chapman et al., 2002) WAIS-III similarities (Wechsler, 1997a)	Assesses the ability to condense and synthesize complex information written as summary from a complex text. Scores represents number of abstracted ideas. Assesses the ability to think abstractly and to find similarities among words or ideas that may not appear to be similar on the surface.
2. Innovation	Test of Strategic Learning (TOSL) (Chapman et al., 2002)	Assesses the ability to construct as many interpretations as possible from a lengthy text to measure idea fluency.
3. Inhibition and switching	Trails B (Delis et al., 2001)	Assesses the ability to alternate between a number and letter by drawing a continuous line to measure the speed of processing.
4. Conceptual reasoning	Delis–Kaplan executive function system (DKEFS) card sort (Delis et al., 2001)	Assesses the ability to draw similarities between two sets of cards by drawing reasons behind the selection of cards was assessed.
5. Working memory	Digit Span Backwards Test (WMS-III, Wechsler, 1997b)	Assesses the ability to repeat a series of numbers backward.
Memory		
Episodic memory	Memory for facts: Test of Strategic Learning (TOSL) (Chapman et al., 2002)	Assesses the ability to recall details of a lengthy text.
Attention	Selective Auditory Learning Task (Hanten et al., 2007)	Assesses the ability to focus and pay attention to high-priority stimulus, while simultaneously blocking or inhibiting unwanted or low-priority information was assessed.
	Digit Span Forward Task (WMS-III, Wechsler, 1997b)	Assesses the ability to pay attention and remember a series of number in the same sequence.
Visuospatial skills	Trails A (Delis et al., 2001)	Assesses the ability to visually search for numbers in ascending order and draw a continuous line to measure the speed of processing.

with 32 scan averages for a duration of 30 min. The chemical shifts of all ^{31}P metabolites were referenced to PCr at 0 ppm. Gaussian apodization (6 Hz) was applied to each FID prior to Fourier transformation using the scanner software (SpectroView, Philips Healthcare). Precautions were taken to avoid signal contribution from the neck muscles by positioning the head chin-up, aligning the parieto-occipital region of the brain at the coil iso-center, and placing a supporting cushion pad underneath the neck.

^{31}P MRS Data Analysis

First, the preprocessing of the raw data, including zero filling, apodization, Fourier transformation and phase correction, was performed at the scanner using the software package SpectroView from Philips Healthcare. The data post-processing, including baseline correction and spectral fitting, was done with an in-house program written in MATLAB. The fitting was based on the Voigt lineshape model (a combination of Gaussian and Lorentzian lineshape). Thirteen resonance phosphorus peaks were fitted: PCr, ATP (α-, β-, and γ-spins) nicotinamide adenine dinucleotide (total NAD), uridine diphosphate glucose (UDPG and its analogs), inorganic phosphate (intracellular and extracellular), five phospholipid metabolites including PE, phosphocholine (PC), GPE, GPC, and an macromolecular metabolite peak. These metabolites were generally well-dispersed in the acquired spectra at 7-Tesla, allowing accurate quantification based on lineshape fitting analysis of individual ^{31}P peaks. Total-ATP (t-ATP) was calculated by averaging the α-, β-, and γ-ATP resonances. The brain ^{31}P spectra revealed two distinct peaks for Pi, assigned intra- and extracellular Pi, the latter including contributions from both interstitial and intravascular spaces (Ren et al., 2018). For the membrane phospholipid metabolite index, phosphomonoesters (PMEs) were calculated by summation of PE and PC, whereas phosphodiesters were by summation of GPE and GPC. The metabolite concentrations, BEM index, and membrane phospholipid metabolite index (PMEs/PDES), were measured from the integral of each individual metabolite peaks in the fully relaxed ^{31}P spectra, whereas the cellular pH and Mg^{2+} concentration were derived from the chemical shift measurements in the summed spectra at various TRs, which provided high-SNR spectral data. **Table 2** summarizes the definitions of all the indices.

Evaluation of Mg^{2+} and Intracellular pH Concentration in the Parieto-Occipital Regions of the Brain

Free magnesium (Mg^{2+}) concentrations in the parieto-occipital regions of the brain were calculated using the chemical shift difference between α- and β-ATP ($\delta_{\alpha\ -\beta}$ in ppm) with PCr as a

reference point ($\delta_{PCr} = 0$) (Ren et al., 2015).

$$[Mg^{2+}] = k_d \frac{\delta_{ATP} - \delta_{\alpha-\beta}}{\delta_{\alpha-\beta} - \delta_{MgATP}} \quad (1)$$

where k_d (dissociation constant of MgATP) = 0.05 mM and the limiting shift constant δ_{ATP} = 10.82 ppm and δ_{MgATP} = 8.32 ppm.

pH was calculated from the chemical shift of the corresponding Pi (internal) peaks ($\delta_{Pi,}$ in ppm) in reference to PCr (δ_{PCr} = 0 ppm) (Ren et al., 2015).

$$pH = pKa + log\frac{\delta_{pi} - \delta_a}{\delta_b - \delta_{pi}} \quad (2)$$

where pKa (deprotonation constant) = 6.73, δ_a = 3.275 ppm (for acidic protonated species $H_2PO_4^-$) and δ_b = 5.685 ppm (for basic protonated species $H_2PO_4^-$) were used in the data analysis.

Statistical Analysis

A linear regression model was used to investigate the relationship of BEM indices using PCr/t-ATP (reflective of energy reserve), Pi/t-ATP (reflective of energy consumption), PCr/Pi (reflective of a metabolic state), regulatory co-factors (Mg^{2+} and pH), and the membrane phospholipid index (PMEs/PDEs) in the parieto-occipital brain region with cognitive performance across the domains of EFs, memory, attention, and visuo-spatial skills. Specifically, all the indices and individual metabolite along with intracellular pH were first transformed by using $f(x) = \log(x-a)$, whereas intracellular Mg^{2+} was transformed using where $f(x) = -\log(b-x)$ where "x" is the raw score of the specific metabolite for each participant, and "a" or "b" are metabolite-specific constants. The metabolite-specific constants were used to symmetrize each metabolite distribution and reduce undue leverage of the single participants in the regression. Once the indices, Mg^{2+}, and pH values were transformed, the linear regression model was used to test the association with neurocognitive measures across the domains of EFs, memory, attention, and visuo-spatial skills.

RESULTS

Brain Phosphorous Metabolites at 7T

Figure 1 shows a typical ^{31}P MR spectrum acquired from the human brain parieto-occipital lobes using a partial volume-coil at 7T. A total of 13 metabolites are clearly identifiable.

Relationship of BEM and Membrane Phosphate Metabolite Indices in the Parieto-Occipital Lobes With Cognitive Performance in aMCI

We investigated the relationships across *BEM indices* measured using PCr/t-ATP (reflective of energy reserve), Pi/t-ATP (reflective of energy consumption: extracellular-Pi/t-ATP and intracellular-Pi/t-ATP), and PCr/Pi (reflective of a metabolic state) and its regulatory co-factors (intracellular Mg^{2+} and pH) followed by *membrane phospholipid metabolite index* (PMEs/PDEs) in the parieto-occipital lobes with cognitive performance of EF (complex abstraction, innovation, inhibition and switching, conceptual reasoning, and working memory), memory (episodic), attention, and visuo-spatial skills. Age and education had no appreciable effects on the high-energy phosphate and membrane phospholipid indices, nor on the cognitive measures in our sample (**Supplementary Table S1**). Therefore, we did not adjust for age and education in our final analyses of BEM indices and cognitive performance.

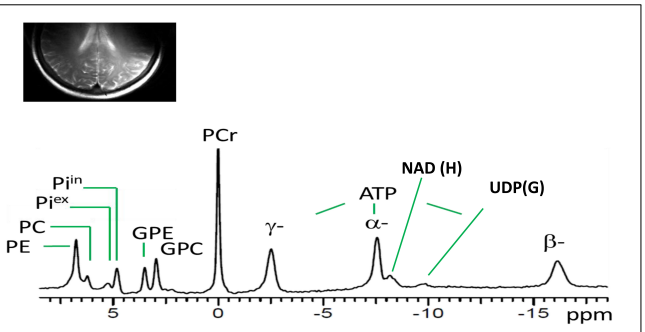

FIGURE 1 | Spectral display of high-energy phosphate and membrane phospholipid phosphorus metabolites from the parieto-occipital lobe of amnestic mild cognitive impairment individual. PE, phosphoethanolamine; PC, phosphocholine; Pi^{ex} and Pi^{in} inorganic phosphate external and internal, respectively; GPE, glycerophosphoethanolamine; GPC, glycerophosphocholine; PCr, phosphocreatine; ATP forms: α, β, and δ adenosine triphosphate; NAD, nicotinamide adenine dinucleotide; UDPG, uridine diphosphate glucose.

BEM Index: Cognitive Correlation

In the BEM index and neurocognitive relationship, we found four significant results. First, the extracellular-Pi/t-ATP ratio was inversely related with performance of attention [selective auditory attention-trail 2: ($b = -0.0018$, $t = -2.254$, $p = 0.038$)]; whereas intracellular-Pi/t-ATP ratio was trending to be inversely proportional with the performance on the EF domain of inhibition and switching [Trails B: ($b = -13.867$, $t = -2.029$, $p = 0.0585$)]. Second, the energy reserve indexed by PCr/t-ATP was inversely related with performance on immediate recall of cognitive memory screen [CVLT: ($b = -0.0138$, $t = -3.272$, $p = 0.004$)]. Finally, the regulatory co-factors of BEM index intracellular pH was also inversely associated with attention [selective auditory attention-trail 2: ($b = -285.95$, $t = -2.172$, $p = 0.044$)], whereas Mg^{2+} was positively associated with visual-spatial skills [Trails A: ($b = -12.471$, $t = 2.219$, $p = 0.040$)].

In view of a previous study by Rijpma et al. (2018) in AD for observation of a reduced level of PCr/Pi, an indicator of metabolic state, we also investigated the relationship of PCr/Pi ratio with cognition. A significant inverse relationship was found between the PCr/Pi index and performances on EF of innovation [TOSL: ($b = -0.78$, $t = -2.18$, $p = 0.044$)], and delayed recall of cognitive memory screen [CVLT: ($b = -2.43$, $t = -2.278$, $p = 0.007$)].

See **Figure 2** and **Table 5** for details.

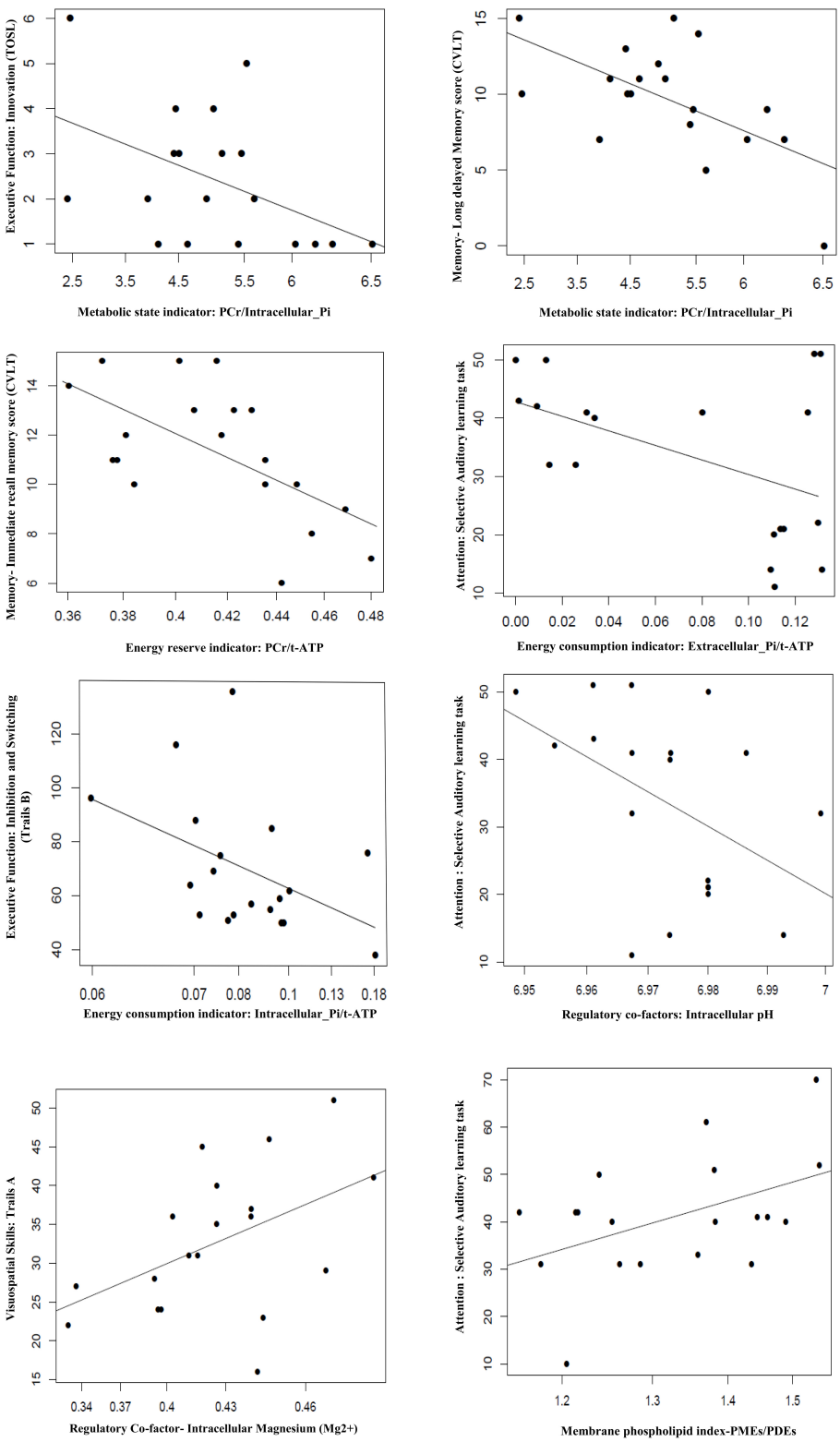

FIGURE 2 | Association of BEM, membrane phospholipid indices, and regulator co-factors in the parieto-occipital brain region with cognitive performance in amnestic mild cognitive impairment ($p \leq 0.05$). TOSL, Test of Strategic Learning; CVLT, California Verbal Learning test; intracellular_Pi, inorganic phosphate (intracellular); extracellular_Pi, inorganic phosphate (extracellular); PCr, phosphocreatine; t-ATP (total adenosine triphosphate: sum of α-ATP, β-ATP, and γ-ATP); PMEs, phosphomonoesters; PDEs, phosphodiesters.

Membrane Phospholipid Metabolite Index: Cognitive Correlation

The membrane phospholipid metabolite index (PMEs/PDEs) was positively associated with cognitive domain of attention [selective auditory attention-Trail 1: ($b = 5.92$, $t = 2.14$, $p = 0.047$)].

See **Figure 2** and **Table 5** for details.

DISCUSSION

The present exploratory pilot study investigated two main goals in aMCI, a heterogeneous and unstable clinical population. This group is at higher risk of developing AD/dementia than the cognitively normal population, although many with aMCI may not progress. Our main goal was to establish a methodology and test the feasibility to measure BEM related high-energy phosphate and membrane phospholipid metabolites precisely at UHF magnetic strength 7-Tesla using a partial volume-coil ^{31}P MRS technique in the parieto-occipital region of the brain in a population with variability as defined by its nature. Our results showed that we were able to resolve 13 of ^{31}P peaks with well-separated spectral resolution of high-energy phosphate and membrane phospholipid metabolites. The enhanced spectral resolution suggests this methodology may provide a feasible way to further explore BEM in more extensive comparative studies with healthy controls and those affected with AD in the future at UHF magnetic strength. Next, we investigated if the BEM indices derived from measuring the high-energy phosphates and membrane phospholipid metabolites at 7T showed a correspondence with cognitive performance (BEM-Cognitive correlates). Overall, we hypothesized an inverse relationship across BEM indices—energy reserve, energy consumption, and metabolic state—along with regulatory co-factors pH and Mg^{2+} and membrane phospholipid index with cognitive performance supported by previous work from Ashraf et al. (2015), Croteau et al. (2018), and Corriveau-Lecavalier et al. (2019). Our results support our assumptions of an inverse relationship in aMCI with the exception of Mg^{2+} and the membrane phospholipid index, which were positively associated with visuospatial domain and attention, respectively.

Population of Interest

An increasing body of research is focused on investigating pathophysiologic changes in the *in vivo* human brain with the goal to track and diagnose the onset of dementia as early as possible, particularly in populations at higher risk, such as aMCI. Although this cohort has an elevated risk for developing Alzheimer's, the evidence that many will not develop dementia may make this an informative population to study, as a preliminary step. Due to variability of the disease progression, identification of early biological markers is an important goal in developing effective therapeutics. In prior research, seeking to better understand BEM, the research to date focused predominantly on either healthy controls or disease populations like AD at lower magnetic strength, with a knowledge gap regarding the potential role of BEM on cognition in aMCI. The current work expands on these efforts by reporting on the first, albeit small, pilot study in aMCI to explore the feasibility of acquiring precise data at UHF magnetic strength 7T using ^{31}P MRS to study BEM-cognitive correlations.

TABLE 4 | Characteristics of the amnestic mild cognitive impairment participants.

Demographics	Mean ± SD	Range
Total number of participants *(n)*	19	
Age (years)	63.73 ± 7.62	50–76
Gender (M/F)	5/14	
Education (years)	17.79 ± 3.34	12–29
MMSE	27.89 ± 1.41	27–30
Geriatric depression scale	2.10 ± 1.76	0–6

Methodological Approach to Measure BEM: ^{31}P MRS at 7T in aMCI

Our first goal of this study was to identify a distinct spectral display of high-energy phosphate and membrane phospholipid metabolites using ^{31}P MRS at 7T. The results revealed it was possible to resolve and identify a high-quality spectral display with improved SNR of the high-energy phosphate and membrane phosphorus metabolites in the parieto-occipital lobes using the UHF MRI. What is interesting to note is that the spectral resolution of brain phosphorus metabolites in this study was similar to previous studies in healthy young adult brains and muscle (Ren et al., 2015) and heart (Rodgers et al., 2014) at 7T. Moreover, the use of 7T allowed clear separation of multiple phosphorus metabolites with similar chemical shifts in the spectra collected from the parieto-occipital region. With improved SNR in the summed spectra, we were able to fully resolve PMEs into PE and PC, PDEs into GPC and GPE, and Pi into intra- and extracellular compartments, along with observation of NAD(H) and UDP(G). At UHF MRI, the α- and β-ATP signal appeared to be an easy-to-fit single peak on the spectral display due to improved SNR of the phosphorus metabolites. It is worthy to note that the α-ATP chemical shift can be affected by the NAD(H) signal, a shift that cannot be resolved at a lower magnetic field. Thereby, the easy-to-fit singlet of α- and β-ATP allowed us to calculate the concentration of free Mg^{2+}, an important regulatory co-factor of BEM in the *in vivo* human brain. Overall, the ^{31}P MRS data acquisition methodology with improved SNR provided indirect help in accurately measuring the regulatory co-factors (intracellular Mg^{2+} and pH), which are essential metabolic sensors to provide neuronal environmental cues alterations in health and disease progression (Rabhi et al., 2017). This capability was previously limited due to the use and insensitivity of lower magnetic strengths such as 1.5-Tesla (Smith et al., 1995; Lotti et al., 1996; Forlenza et al., 2005) or 3-Tesla (Mandal et al., 2012; Rijpma et al., 2018).

Another methodological contribution of this study was the resolution of Pi into two separate peaks, intracellular and extracellular compartments (Ren et al., 2018). The extracellular Pi pool includes the signal of Pi from both the vascular and

TABLE 5 | Linear regression model: association of BEM and membrane phospholipid indices in the parieto-occipital brain areas with neurocognitive and screening cognitive measures in mild cognitive impairment.

Metabolite: Neurocognitive relationship	Results		
	b (SE)	t-Statistics (df = 17)	*p*-Value
BEM indices and neurocognitive relationship			
PCr/t-ATP: Immediate recall on screening memory measure (CVLT)	−0.0138 (8.556)	−3.272	0.004*
Extracellular_Pi/t-ATP: Attention (selective auditory task-Trail 2)	−0.0018 (55.385)	−2.254	0.038*
Intracellular_Pi/t-ATP: Executive function (switching and inhibition: Trails B)	−13.867 (6.836)	−2.029	0.0585
PCr/intracellular_Pi (oxidative phosphorylation rate): Executive function (innovation: TOSL)	−0.78 (0.36)	−2.18	0.044*
PCr/intracellular_PiI: Delayed recall on screening memory measure (CVLT)	−2.43 (0.79)	−2.78	0.007*
pH: Attention (selective auditory task-Trail 2)	−285.95 (131.66)	−2.172	0.044*
Mg^{2+}: Attention (Trails A)	12.471 (5.620)	2.219	0.040*
Membrane phospholipid metabolite index and neurocognitive relationship			
PMEs/PDEs: Attention (selective auditory task-Trail 1)	5.92 (2.77)	2.14	0.047*

DKEFS, Delis–Kaplan Executive Function System™*; TOSL, Test of Strategic Learning; CVLT, California Verbal Learning Test. p-values < 0.05* (significant).*

interstitial space plus the space occupied by cerebrospinal fluid (CSF). One hypothesis that could be explored in subsequent studies is whether brain atrophy leads to increased extracellular space and reduced intracellular space, assuming invariant extracellular-Pi is a crucial biomarker as the disease emerges and progresses. Prior work in MCI and AD supported the postulation that low level of serum or blood phosphorus, that is, phosphorus levels, was significantly associated with higher cerebral amyloid deposition when compared to healthy controls matched for age, sex, and apolipoprotein ε4 genotype and memory scores of MMSE (Park et al., 2017). Park et al. (2017) findings motivated us to explore a relationship between phosphorus metabolites in the brain with cognition in MCI. Building on this prior evidence, the current work expands the knowledge by going one step further in measuring phosphorus metabolites, an indicator of BEM directly using ^{31}P MRS at 7T, followed by exploring the relationship of these phosphorus metabolites with cognition in aMCI.

To date, research in MCI has focused largely on the macroscopic pathological contributing factors associated with neurodegeneration, such as the accumulation of amyloid and structural alteration (Mufson et al., 2012; Oeltzschner et al., 2019). However, there is a desire to better understand the microscopic biological mechanisms taking place inside the cells of the *in vivo* human brain, now that researchers have access to more advanced imaging technology and analytics. As protocols develop and are tested to measure intracellular mechanisms, it may improve the predictive capabilities of which profiles progress toward the disease compared to non-converters. Our preliminary work using ^{31}P MRS at 7T opens the door to employ this new methodology to advance our understanding of the biological mechanisms like BEM, that is, bioenergetics and membrane phospholipid metabolism occurring inside the brain cells in aMCI, a heterogeneous cohort.

BEM-Cognitive Correlates

Our second goal of the study was to investigate the association of BEM and membrane phospholipid metabolite indices in the parieto-occipital brain regions, with the cognitive performance of EFs, attention, memory, and visuospatial skills. We measured BEM indices using PCr/t-ATP (reflective of energy reserve), Pi/t-ATP (reflective of energy consumption: extracellular-Pi/t-ATP and intracellular-Pi/t-ATP), and PCr/Pi (reflective of a metabolic state), along with co-regulatory factors intracellular pH and Mg^{2+} concentrations in the parieto-occipital lobes (see **Table 2** for details). The membrane phospholipid index ratio of PMEs (the significant precursors of phospholipids contributing to membrane synthesis) to PDEs (significant phospholipid products breakdown) indicated neuronal and non-neuronal membrane integrity (Ross and Sachdev, 2004) measured in the parieto-occipital lobes. An inverse relationship was observed with BEM indices and cognitive performance except for Mg^{2+} and membrane phospholipid index, which were significantly associated with visuospatial domain and attention, respectively.

The results of the inverse relationship of BEM indices and cognition support that individuals with higher BEM in the parieto-occipital lobes performed lower on cognitive domains of memory and EF. We offer one plausible hypothesis that subsequent research could explore is whether these low cognitive performers with higher BEM indices may represent individuals at greater risk of progressing toward AD in longitudinal work. This possibility is based on prior work on brain metabolism using ^{18}FDG-PET (Ashraf et al., 2015; Croteau et al., 2018). The present work complements prior findings showing glucose hypermetabolism in MCI when compared to age-matched healthy controls, in parietal (Croteau et al., 2018) and occipital lobes (Ashraf et al., 2015). Although these two studies focused on different brain regions, they both offered a similar explanation for their findings; that is, the glucose hypermetabolism in parietal and occipital lobes represented a compensatory mechanism in MCI compared to healthy controls.

A compensatory mechanism can be interpreted as a process whereby the brain is adapting to neural changes attributed to a variety of factors, such as brain aging or neurodegenerative processes (Bobkova and Vorobyov, 2015). This adaptive mechanism was explained as "neuroplasticity" in Ashraf's study.

It is important to note that, at some point, the compensatory phenomenon of the brain's systems, such as higher BEM observed in our study, may not have been adequate to support the same level of cognitive performance as cognitively normal individuals (Croteau et al., 2018). To date, impairments across EF, memory, and attention are thought to rely on the anterior brain networks of the frontal, temporal, and anterior part of the parietal lobes (Kim et al., 2019) with limited understanding of investigating early neurometabolic changes in the posterior part of the brain-parietal and occipital lobes. Thus, the current work lays a foundation to examine the correlates of BEM in posterior part of the brain, that is, parieto-occipital regions of the brain with cognition in aMCI, a group where some are at risk of developing dementia while others are stable either in the condition or revert to normal.

In contrast to the inverse relationship of BEM indices with cognitive performance, two independent variables (regulatory co-factor: Mg^{2+} and membrane phospholipid index) also showed significant association with specific cognitive domains but in different directions in aMCI. One was a higher Mg^{2+} concentration and associated with the higher performance on the visuospatial task, and other was a positive association of membrane phospholipid index (PMEs/PDEs) with the performance on the attention task. One possible explanation of the deviation of the inverse relationship of Mg^{2+} in the parieto-occipital lobes with cognition is that the posterior parietal and occipital brain regions are part of the dorsal stream of the visual system that aids in recognizing objects in space with detection and analyzing the movements (Hebart and Hesselmann, 2012). Thereby, a visuospatial task, which is primarily controlled by the parietal and occipital lobes, could depend on higher energy requirements in the form of higher Mg^{2+} level, an essential co-factor for ATP synthesis. Whereas the other significant positive correlation of the membrane phospholipid index with the cognitive domain of attention in the region of interest may again support the theory of neuroplasticity/compensatory mechanism as proposed by Ashraf's et al. (2015) in MCI. We speculate that neuroplasticity of the parietal and occipital lobe may have higher turnover of membrane phospholipid index to support failing anterior lobe network. In general, though this study generates a lot of hypothesis that needs to be tested in future studies, still it adds to the existing knowledge that BEM and membrane phospholipid indices are associated with cognition in a cohort with mixed progression and reversion rate.

In sum, this study represents an early step to elucidate the methodologies of BEM and membrane integrity using partial volume-coil ^{31}P MRS at UHF magnetic strength 7T in aMCI. We were able to show the feasibility of measuring the high-phosphate energy and membrane phospholipid metabolites with higher sensitivity and spatial resolution when compared to the strength of lower magnetic fields, such as 1.5T and 3T, in a heterogeneous population. This pattern of findings supports the viability of ^{31}P MRS at 7T to explore further the brain's energy requirements and its association with cognition to motivate additional research. We propose that future research using volume-coil ^{31}P MRS at 7T could enhance our understanding of the role of mitochondrial contributions, which play an essential role in BEM linked to brain pathology in at risk populations in whom the disease may or may not progress from healthy aging to AD. Moreover, the potential of such an approach is strengthened by the finding of a relationship between BEM and membrane phospholipid indices in parieto-occipital lobes with cognitive performance across the domain of EF, memory, attention, and visuospatial skills in cognitively compromised brain of aMCI.

Limitations

We interpret the findings of this study in aMCI cautiously due to its limitations. First, the study sample size was small and lacked a cognitively normal age-matched control group or AD cohort for comparison. However, even with our small sample size and lack of a control group, we were able to show that BEM and membrane phospholipid indices, an indicator of neurometabolic changes in the parieto-occipital brain areas, are associated with performance of cognition especially in the area of memory, EF, and attention in aMCI significantly. This study focused on exploring a relationship of BEM-cognitive correlates at a single point of time. Future research is needed to follow individuals with aMCI longitudinally to see if early markers could be identified to better predict who is at risk for developing AD/dementia and who is less likely to progress. Second, the use of partial volume-coil ^{31}P MRS limited our ability to support the theory of the compensatory mechanism in the early stages as the BEM indices of the anterior part of the brain, that is, frontal and temporal were not measured. Nonetheless, the use of the partial volume-coil in this research helped us to understand the relationship of a BEM and cognition in aMCI, specifically in brain regions that have been shown to probable predictor sites in the brain in subset of MCI individuals that progress toward AD using ^{18}FDG-PET (Ashraf et al., 2015; Croteau et al., 2018).

CONCLUSION

Our findings show a highly resolved spectral display of high-energy phosphate and membrane phospholipid metabolites using ^{31}P MRS at 7Tesla in aMCI. We also observed an inverse relationship between higher BEM indices with the lower performance of EFs, memory, and attention. The salient contribution of this pilot study is that it adds to the growing body of evidence that BEM can be measured accurately and appears to be associated with cognitive performance in this heterogeneous cohort. It also lays the foundation for future efforts to investigate if BEM mechanisms synergistically with amyloid and tau proteins, which are the hallmarks of the disease as potentially understand upstream triggers that aggravate the pathophysiological mechanism of the disease. Finally, longitudinal follow-up of an aMCI population would be of interest to test predictive ability of BEM, deploying imaging technology at 7 Tesla, as to which individuals will develop dementia and which will not, based on changes at the molecular level. This novel approach offers a novel research approach to advance our understanding of early biomarkers of those at risk for dementia to complement current endeavors.

DATA AVAILABILITY STATEMENT

The raw data supporting the conclusions of this article will be made available by the authors, without undue reservation.

ETHICS STATEMENT

The studies involving human participants were reviewed and approved by IRB, The University of Texas Southwestern Medical Center and The University of Texas at Dallas. The patients/participants provided their written informed consent to participate in this study.

AUTHOR CONTRIBUTIONS

ND has been involved in the analysis and writing of the whole manuscript. JR has been involved in instrumental in the analysis of MRS data along with ND. JS, biostatistician was involved in the analysis, whereas AR helped in the recruitment of MCI participants. SC was the principal investigator of the study and mentored in the writing of the manuscript. All authors contributed to the article and approved the submitted version.

FUNDING

The research project was supported by Aging Mind Foundation, BvB Dallas, Sammons Enterprises, Barbara Wallace and Kelly King Charitable Foundation Trust, the AWARE fund of the Dallas Foundation, and the Golden Rule Family Foundation.

ACKNOWLEDGMENTS

We thank all of the participants in this study and the research team, especially Jennifer Kriegel (Research Coordinator), Erin Venza (Clinician), and Stacy Vernon (Clinician) for making this research possible.

SUPPLEMENTARY MATERIAL

The Supplementary Material for this article can be found online at: https://www.frontiersin.org/articles/10.3389/fnagi.2020.00222/full#supplementary-material

REFERENCES

Albers, R. W., and Siegel, G. J. (1999). "The ATP-Dependent Na+,K+ Pump," in *Basic Neurochemistry: Molecular, Cellular and Medical Aspects*, 6th Edn, eds G. J. Siegel, B. W. Agranoff, and R. W. Albers (Philadelphia: Lippincott-Raven).

Albert, M. S., DeKosky, S. T., Dickson, D., Dubois, B., Feldman, H. H., Fox, N. C., et al. (2011). The diagnosis of mild cognitive impairment due to Alzheimer's disease: recommendations from the National Institute on Aging-Alzheimer's Association workgroups on diagnostic guidelines for Alzheimer's disease. *Alzheimers Dement.* 7, 270–279. doi: 10.1016/j.jalz.2011.03.008

Alichniewicz, K. K., Brunner, F., Klünemann, H. H., and Greenlee, M. W. (2012). Structural and functional neural correlates of visuospatial information processing in normal aging and amnestic mild cognitive impairment. *Neurobiol. Aging* 33, 2782–2797. doi: 10.1016/j.neurobiolaging.2012.02.010

Ashraf, A., Fan, Z., Brooks, D. J., and Edison, P. (2015). Cortical hypermetabolism in MCI subjects: a compensatory mechanism? *Eur. J. Nuclear Med. Mol. Imaging* 42, 447–458. doi: 10.1007/s00259-014-2919-z

Bejanin, A., Schonhaut, D. R., La Joie, R., Kramer, J. H., Baker, S. L., Sosa, N., et al. (2017). Tau pathology and neurodegeneration contribute to cognitive impairment in Alzheimer's disease. *Brain* 140, 3286–3300. doi: 10.1093/brain/awx243

Bobkova, N., and Vorobyov, V. (2015). The brain compensatory mechanisms and Alzheimer's disease progression: a new protective strategy. *Neural Regen. Res.* 10, 696–697.

Brown, G. G., Levine, S. R., Gorell, J. M., Pettegrew, J. W., Gdowski, J. W., Bueri, J. A., et al. (1989). In vivo 31P NMR profiles of Alzheimer's disease and multiple subcortical infarct dementia. *Neurology* 39, 1423–1427.

Cerami, C., Della Rosa, P. A., Magnani, G., Santangelo, R., Marcone, A., Cappa, S. F., et al. (2014). Brain metabolic maps in Mild Cognitive Impairment predict heterogeneity of progression to dementia. *NeuroImage Clin.* 7, 187–194. doi: 10.1016/j.nicl.2014.12.004

Cerami, C., Dodich, A., Iannaccone, S., Magnani, G., Santangelo, R., Presotto, L., et al. (2018). A biomarker study in long-lasting amnestic mild cognitive impairment. *Alzheimers Res. Ther.* 10:42.

Chance, B., Eleff, S., Leigh, J. S. Jr., Sokolow, D., and Sapega, A. (1981). Mitochondrial regulation of phosphocreatine/inorganic phosphate ratios in exercising human muscle: a gated 31P NMR study. *Proc. Natl. Acad. Sci. U.S.A.* 78, 6714–6718. doi: 10.1073/pnas.78.11.6714

Chapman, S. B., Zientz, J., Weiner, M., Rosenberg, R., Frawley, W., and Burns, M. H. (2002). Discourse changes in early Alzheimer disease, mild cognitive impairment, and normal aging. *Alzheimer Dis. Assoc. Disord.* 16, 177–186. doi: 10.1097/00002093

Corriveau-Lecavalier, N., Mellah, S., Clément, F., and Belleville, S. (2019). Evidence of parietal hyperactivation in individuals with mild cognitive impairment who progressed to dementia: a longitudinal fMRI study. *NeuroImage Clin.* 24:101958. doi: 10.1016/j.nicl.2019.101958

Croteau, E., Castellano, C. A., Fortier, M., Bocti, C., Fulop, T., Paquet, N., et al. (2018). A cross-sectional comparison of brain glucose and ketone metabolism in cognitively healthy older adults, mild cognitive impairment and early Alzheimer's disease. *Exp. Gerontol.* 107, 18–26. doi: 10.1016/j.exger.2017.07.004

David, S., Shoemaker, M., and Haley, B. E. (1998). Abnormal properties of creatine kinase in Alzheimer's disease brain: correlation of reduced enzyme activity and active site photolabeling with aberrant cytosol-membrane partitioning. *Brain Res. Mol. Brain Res.* 54, 276–287. doi: 10.1016/s0169-328x(97)00343-4

Delis, D. C., Kaplan, E., and Kramer, J. H. (2001). *Delis-Kaplan Executive Function System (D-KEFS)*. San Antonio, TX: Psychological Corporation.

Farias, S. T., Mungas, D., Reed, B. R., Harvey, D., and DeCarli, C. (2009). Progression of mild cognitive impairment to dementia in clinic- vs community-based cohorts. *Arch. Neurol.* 66, 1151–1157.

Folstein, M. F., Folstein, S. E., and McHugh, P. R. (1975). "Mini-mental state": a practical method for grading the cognitive state of patients for the clinician. *J. Psychiatr. Res.* 12, 189–198.

Forlenza, O. V., Wacker, P., Nunes, P. V., Yacubian, J., Castro, C. C., Otaduy, M. C. G., et al. (2005). Reduced phospholipid breakdown in Alzheimer's brains: a P-31 spectroscopy study. *Psychopharmacology* 180, 359–365. doi: 10.1007/s00213-005-2168-8

Giau, V. V., Bagyinszky, E., and An, S. (2019). Potential fluid biomarkers for the diagnosis of mild cognitive impairment. *Int. J. Mol. Sci.* 20:4149. doi: 10.3390/ijms20174149

Godlewska, B. R., Clare, S., Cowen, P. J., and Emir, U. E. (2017). Ultra-high-field magnetic resonance spectroscopy in psychiatry. *Front. Psychiatry* 8:123. doi: 10.3389/fpsyt.2017.00123i

Hanten, G., Li, X., Chapman, S. B., Swank, P., Gamino, J., Roberson, G., et al. (2007). Development of verbal selective learning. *Dev. Neuropsychol.* 32, 585–596.

Hebart, M. N., and Hesselmann, G. (2012). What visual information is processed in the human dorsal stream? *J. Neurosci.* 32, 8107–8109. doi: 10.1523/jneurosci.1462-12.2012

Heneka, M. T., Carson, M. J., El Khoury, J., Landreth, G. E., Brosseron, F., Feinstein, D. L., et al. (2015). Neuroinflammation in Alzheimer's disease. *Lancet Neurol.* 14, 388–405. doi: 10.1016/S1474-4422(15)70016-5

Kim, J. E., Kim, S.-W., Choi, M., Seong, J.-K., and Lee, J.-H. (2019). Identifying brain connectivity using network-based statistics in amnestic mild cognitive impairment stratified by β-amyloid positivity. *Am. J. Alzheimers Dis. Other Dement.* 34, 104–111. doi: 10.1177/1533317518813556

Lawton, M. P., Moss, M., Fulcomer, M., and Kleban, M. H. (2003). *Multi-Level Assessment Instrument Manual for Full-Length MAI*. North Wales PA: Polisher Research Institute, Madlyn and Leonard Abramson Center for Jewish Life.

Lotti, S., Frassineti, C., Alderighi, L., Sabatini, A., Vacca, A., and Barbiroli, B. (1996). *In vivo* assessment of free magnesium concentration in human brain by 31P MRS. A new calibration curve based on a mathematical algorithm. *NMR Biomed.* 9, 24–32. doi: 10.1002/(sici)1099-1492(199602)9:1<24::aid-nbm392>3.0.co;2-b

Malek-Ahmadi, M. (2016). Reversion from mild cognitive impairment to normal cognition: a meta-analysis. *Alzheimer Dis. Assoc. Disord.* 30, 324–330. doi: 10.1097/WAD.0000000000000145

Mandal, P. K., Akolkar, H., and Tripathi, M. (2012). Mapping of hippocampal pH and neurochemicals from in vivo multi-voxel P-31 study in healthy normal young male/female, mild cognitive impairment, and Alzheimer's disease. *J. Alzheimers Dis.* 31, S75–S86.

Mekle, R., Mlynárik, V., Gambarota, G., Hergt, M., Krueger, G., and Gruetter, R. (2009). MR spectroscopy of the human brain with enhanced signal intensity at ultrashort echo times on a clinical platform at 3T and 7T. *Magn. Reson. Med.* 61, 1279–1285. doi: 10.1002/mrm.21961

Morris, J. (1993). The clinical dementia rating (CDR): current version and scoring rules. *Neurology* 43, 2412–2414.

Mufson, E. J., Binder, L., Counts, S. E., DeKosky, S. T., de Toledo-Morrell, L., Ginsberg, S. D., et al. (2012). Mild cognitive impairment: pathology and mechanisms. *Acta Neuropathol.* 123, 13–30.

Oeltzschner, G., Wijtenburg, S. A., Mikkelsen, M., Edden, R. A. E., Barker, P. B., and Joo, J. H. (2019). Neurometabolites and associations with cognitive deficits in mild cognitive impairment: a magnetic resonance spectroscopy study at 7 tesla. *Neurobiol. Aging* 73, 211–218. doi: 10.1016/j.neurobiolaging.2018.09.027

Ogawa, M., Fukuyama, H., Ouchi, Y., Yamauchi, H., and Kimura, J. (1996). Altered energy metabolism in Alzheimer's disease. *J. Neurol. Sci.* 139, 78–82.

Park, J. C., Han, S. H., Byun, M. S., Yi, D., Lee, J. H., Park, K., et al. (2017). Low serum phosphorus correlates with cerebral Aβ deposition in cognitively impaired subjects: results from the KBASE study. *Front. Aging Neurosci.* 9:362. doi: 10.3389/fnagi.2017.00362

Petersen, R. C., Caracciolo, B., Brayne, C., Gauthier, S., Jelic, V., and Fratiglioni, L. (2014). Mild cognitive impairment: a concept in evolution (Key Symposium). *J. Intern. Med.* 275, 214–228.

Petersen's, R. C., Doody, R., Kurz, A., Mohs, R. C., Morris, J. C., Rabins, P. V., et al. (2001). Current concepts in mild cognitive impairment. *Arch. Neurol.* 58:1985.

Petersen, R. C., Smith, G. E., Waring, S. C., Ivnik, R. J., Tangalos, E. G., and Kokmen, E. (1999). Mild cognitive impairment: clinical characterization and outcome. *Arch. Neurol.* 56, 303–308. doi: 10.1001/archneur.56.3.303

Pettegrew, J. W., Moossy, J., Withers, G., McKeag, D., and Panchalingam, K. (1988). 31P nuclear magnetic resonance study of the brain in Alzheimer's disease. *J. Neuropathol. Exp. Neurol.* 47, 235–248.

Pradhan, S., Bonekamp, S., Gillen, J. S., Rowland, L. M., Wijtenburg, S. A., Edden, R. A. E., et al. (2015). Comparison of single voxel brain MRS AT 3T and 7T using 32-channel head coils. *Magn. Reson. Imaging* 33, 1013–1018. doi: 10.1016/j.mri.2015.06.003

Rabhi, N., Hannou, S. A., Froguel, P., and Annicotte, J. S. (2017). Cofactors as metabolic sensors driving cell adaptation in physiology and disease. *Front. Endocrinol.* 8:304. doi: 10.3389/fendo.2017.00304

Ren, J., Dean Sherry, A., and Malloy, C. R. (2013). Noninvasive monitoring of lactate dynamics in human forearm muscle after exhaustive exercise by (1)H-magnetic resonance spectroscopy at 7 tesla. *Magn. Reson. Med.* 70, 610–619. doi: 10.1002/mrm.24526

Ren, J., Shang, T., Sherry, A. D., and Malloy, C. R. (2018). Unveiling a hidden 31 P signal coresonating with extracellular inorganic phosphate by outer-volume-suppression and localized 31 P MRS in the human brain at 7T. *Magn. Reson. Med.* 80, 1289–1297. doi: 10.1002/mrm.27121

Ren, J., Sherry, A. D., and Malloy, C. R. (2015). 31P-MRS of healthy human brain: ATP synthesis, metabolite concentrations, pH, and T1 relaxation times. *NMR Biomed.* 28, 1455–1462. doi: 10.1002/nbm.3384

Rijpma, A., van der Graaf, M., Meulenbroek, O., Olde Rikkert, M., and Heerschap, A. (2018). Altered brain high-energy phosphate metabolism in mild Alzheimer's disease: a 3-dimensional ^{31}P MR spectroscopic imaging study. *NeuroImage Clin.* 18, 254–261. doi: 10.1016/j.nicl.2018.01.031

Rodgers, C. T., Clarke, W. T., Snyder, C., Vaughan, J. T., Neubauer, S., and Robson, M. D. (2014). Human cardiac 31P magnetic resonance spectroscopy at 7 Tesla. *Magn. Reson. Med.* 72, 304–315. doi: 10.1002/mrm.24922

Ross, A. J., and Sachdev, P. S. (2004). Magnetic resonance spectroscopy in cognitive research. *Brain Res. Rev.* 44, 83–102. doi: 10.1016/j.brainresrev.2003.11.001

Shimada, H., Doi, T., Lee, S., and Makizako, H. (2019). Reversible predictors of reversion from mild cognitive impairment to normal cognition: a 4-year longitudinal study. *Alzheimers Res. Ther.* 11:24.

Smith, C. D., Pettigrew, L. C., Avison, M. J., Kirsch, J. E., Tinkhtman, A. J., Schmitt, F. A., et al. (1995). Frontal-lobe phosphorus-metabolism and neuropsychological function in aging and in Alzheimers-disease. *Ann. Neurol.* 38, 194–201. doi: 10.1002/ana.410380211

Troyer, A. K., and Rich, J. B. (2002). Psychometric properties of a new metamemory questionnaire for older adults. *J. Gerontol. B Psychol. Sci. Soc. Sci.* 57, 19–27.

Wechsler, D. (1997a). *Wechsler Adult Intelligence Scale –Administration and Scoring Manual*. San Antonio, TX: Psychological Corporation.

Wechsler, D. (1997b). *WMS-III Administration and Scoring Manual*. San Antonio, TX: The Psychological Corporation & Harcourt Brace & Co.

Yesavage, J. A., Brink, T. L., Rose, T. L., Lum, O., Huang, V., Adey, M., et al. (1982). Development and validation of a geriatric depression screening scale: a preliminary report. *J. Psychiatr. Res.* 17, 37–49. doi: 10.1016/0022-3956(82)90033-4

Zlokovic, B. V. (2011). Neurovascular pathways to neurodegeneration in Alzheimer's disease and other disorders. *Nat. Rev. Neurosci.* 12, 723–738. doi: 10.1038/nrn3114

Conflict of Interest: The authors declare that the research was conducted in the absence of any commercial or financial relationships that could be construed as a potential conflict of interest.

frontiers in Aging Neuroscience

REVIEW
published: 02 September 2020
doi: 10.3389/fnagi.2020.00272

Bridging the Gap Between Fluid Biomarkers for Alzheimer's Disease, Model Systems, and Patients

Christiana Bjorkli[1], Axel Sandvig[1,2,3] and Ioanna Sandvig[1]*

[1] Sandvig Group, Department of Neuromedicine and Movement Science, Faculty of Medicine and Health Sciences, Norwegian University of Science and Technology, Trondheim, Norway, [2] Institute of Neuromedicine and Movement Science, Department of Neurology, St. Olavs Hospital, Trondheim, Norway, [3] Department of Pharmacology and Clinical Neurosciences, Division of Neuro, Head, and Neck, University Hospital of Umeå, Umeå, Sweden

Alzheimer's disease (AD) is a debilitating neurodegenerative disease characterized by the accumulation of two proteins in fibrillar form: amyloid-β (Aβ) and tau. Despite decades of intensive research, we cannot yet pinpoint the exact cause of the disease or unequivocally determine the exact mechanism(s) underlying its progression. This confounds early diagnosis and treatment of the disease. Cerebrospinal fluid (CSF) biomarkers, which can reveal ongoing biochemical changes in the brain, can help monitor developing AD pathology prior to clinical diagnosis. Here we review preclinical and clinical investigations of commonly used biomarkers in animals and patients with AD, which can bridge translation from model systems into the clinic. The core AD biomarkers have been found to translate well across species, whereas biomarkers of neuroinflammation translate to a lesser extent. Nevertheless, there is no absolute equivalence between biomarkers in human AD patients and those examined in preclinical models in terms of revealing key pathological hallmarks of the disease. In this review, we provide an overview of current but also novel AD biomarkers and how they relate to key constituents of the pathological cascade, highlighting confounding factors and pitfalls in interpretation, and also provide recommendations for standardized procedures during sample collection to enhance the translational validity of preclinical AD models.

Keywords: Alzheimer's disease, translational research, biomarkers, cerebrospinal fluid, screening tools

OPEN ACCESS

Edited by:
Jiehui Jiang,
Shanghai University, China

Reviewed by:
Parnetti Lucilla,
University of Perugia, Italy
Ville Leinonen,
University of Eastern Finland, Finland

****Correspondence:***
Christiana Bjorkli
christiana.bjorkli@ntnu.no

Received: *31 May 2020*
Accepted: *06 August 2020*
Published: *02 September 2020*

Citation:
Bjorkli C, Sandvig A and Sandvig I (2020) Bridging the Gap Between Fluid Biomarkers for Alzheimer's Disease, Model Systems, and Patients. Front. Aging Neurosci. 12:272. doi: 10.3389/fnagi.2020.00272

INTRODUCTION

Due to an increasingly elderly population, patients with Alzheimer's disease (AD) constitute a growing public health problem, thus developing methods for early diagnosis of the disease will become pertinent as there of yet exists no cure. The disease typically manifests through a progressive decline in cognitive and behavioral functions that severely impact the ability of AD patients to independently perform daily tasks. As a result, the associated socioeconomic cost and burden to the healthcare system are very high, with annual healthcare expenditure exceeding billions of dollars. Based on the early findings by Alzheimer et al. (1995), we now know that the neuropathological hallmarks of AD include intracellular neurofibrillary tangles (NFTs) composed of misfolded tau protein, and extracellular amyloid plaques comprising aggregated amyloid-β (Aβ). The pathological

protein accumulation in AD follows a predictable spatiotemporal pattern where certain areas become affected before others, including the entorhinal cortex (EC) and the hippocampus (Serrano-Pozo et al., 2011). In late stage AD, up to 90% of cells are lost in EC layer II (Gomez-Isla et al., 1996). The initial Aβ deposits present as plaques in the temporal neocortex, before progressing to the EC and the hippocampus (**Box 1**; Thal et al., 2002). Meanwhile, initial tangle formation begins in the most lateral portions of EC layer II, followed by the hippocampus, before appearing in areas of the neocortex (**Box 1**; Braak and Braak, 1991). The anatomical and temporal progression of Aβ and tau pathology, and subsequently neurodegeneration, has led to the postulation that Aβ acts as an initiator of the disease progression that results in tau-mediated neurodegeneration (Freudenberg-Hua et al., 2018).

Many variants of the amyloid cascade hypothesis have been proposed over the years; and this hypothesis argues that the deposition of Aβ is the initial and causative step for developing AD (Hardy and Higgins, 1992). According to this hypothesis, Aβ deposition causes disruption of calcium homeostasis in cells, resulting in molecular lesions, NFTs, oxidative stress, inflammation, excitotoxicity, and eventually cell death. The main counter argument for this hypothesis has been that amyloid plaque burden has a low correlation with the severity of clinical symptoms of AD, unlike that of NFTs and neurodegeneration (Terry et al., 1991; Arriagada et al., 1992). In line with this, amyloid plaque deposition commonly plateaus with time, despite declining cognition in AD (Engler et al., 2006). Therefore, the majority in the AD research field now focus on soluble, intracellular Aβ oligomers as a possible initiator of the development of the disease (**Figure 1**).

Amyloid-β can exist in multiple assembly forms, ranging from monomeric to oligomeric and fibrillar forms (**Figure 1**). As a monomer, Aβ does not seem to be toxic, whereas oligomeric or fibrillar forms have been found to be potent blockers of long-term potentiation (LaFerla et al., 2007). Research suggests that levels of soluble Aβ oligomers are better correlated with disease severity than amyloid plaques mainly consisting of insoluble Aβ fibrillar species (Arriagada et al., 1992; Lue et al., 1999; McLean et al., 1999; Naslund et al., 2000; Haass and Selkoe, 2007). When produced intracellularly, Aβ oligomers expose flexible hydrophobic surfaces that might contribute to trapping vital proteins and, in this way, they can subtly damage and predispose vulnerable neurons to the formation of intracellular tau aggregates (Campioni et al., 2010). Thus, tau pathology in AD appears to be a downstream, effect of the presence of Aβ oligomers (**Figure 1**). In line with this, a link has been made between increased amounts of intracellular Aβ and neurodegeneration, while clearing of intracellular Aβ has been shown to revert AD-related memory deficits in animals modeling AD (Billings et al., 2005). An explanation for the weak correlation between cognitive decline and plaque load could be that insoluble fibrillar Aβ species might serve as reservoirs for smaller oligomeric Aβ, thus sequestering these away from neurons (Mucke and Selkoe, 2012; **Figure 1**).

The manner in which pathology progresses in model systems and human patients with AD has mostly been investigated separately resulting in little or poor translational value. As such, the translational aspect of staging the AD molecular disease cascade between preclinical models and human AD patients has remained inadequate. Despite intense investigation into disease cause and mechanisms of neurodegeneration, there is currently no cure or unequivocal evidence as to the exact nature of its underlying cause. Still, there seems to be consensus as to the fact that the success of treatments is primarily contingent on whether they can target disease-related pathology at early onset. This suggests that we are urgently in need of better tools for early onset diagnosis, before evolving pathology severely affects brain function, as well as better tools for monitoring pathological progression.

This effectively means, to translate discoveries made in preclinical models to the clinic, we must bridge the gap between model systems and patients with AD by improving the robustness and predictive validity of screening tools. For instance, the current dominant view is that Aβ42 accumulates extracellularly first, and thereby leads to the formation of amyloid plaques. However, several studies of brain tissue from animal models and human patients have begun to challenge this notion. In this paper, we explore potential early screening tools for the diagnosis of AD and also provide links between the extensive research done in preclinical models to human clinical applications. Specifically, we review how screening in AD patients can become more precise by the use of novel cerebrospinal fluid (CSF) biomarkers and by following recommendations for standardized procedures during CSF sample collections. We also focus on how intracellular events of Aβ and tau aggregation eventually lead to extracellular deposition and the presence of neuropathological hallmarks, and how current tools can predict, diagnose and potentially treat models and patients at various timepoints of the disease.

AD BIOMARKERS – TYPE AND DEFINITION

When defining an AD biomarker, many agree that it is a measurable indicator within a patient that can help to test and monitor the progress of pathology (Hane et al., 2017). The ideal fluid biomarker for AD would be consistent, reproducible, non-invasive, simple to measure, inexpensive, and easy to implement into the clinic and the primary care setting (Davies et al., 1998; Wang et al., 2012; Bjerke and Engelborghs, 2018; Molinuevo et al., 2018). Such biomarkers should be able to identify the clinical disease stage of the patient and also monitor treatment effects. Conventionally, patients with overt dementia are diagnosed with around 85% specificity (but at much lower rates in patients with early stage AD), but the ideal biomarker should exceed this rate (Davies et al., 1998). There is thus an urgent need for a specific marker for early detection in these patients. Various biomarkers that can detect early AD in both preclinical models and patients have been proposed. For instance, it would be preferable to have a biomarker that can detect intracellular events prior to the deposition of amyloid plaques and NFTs. In line

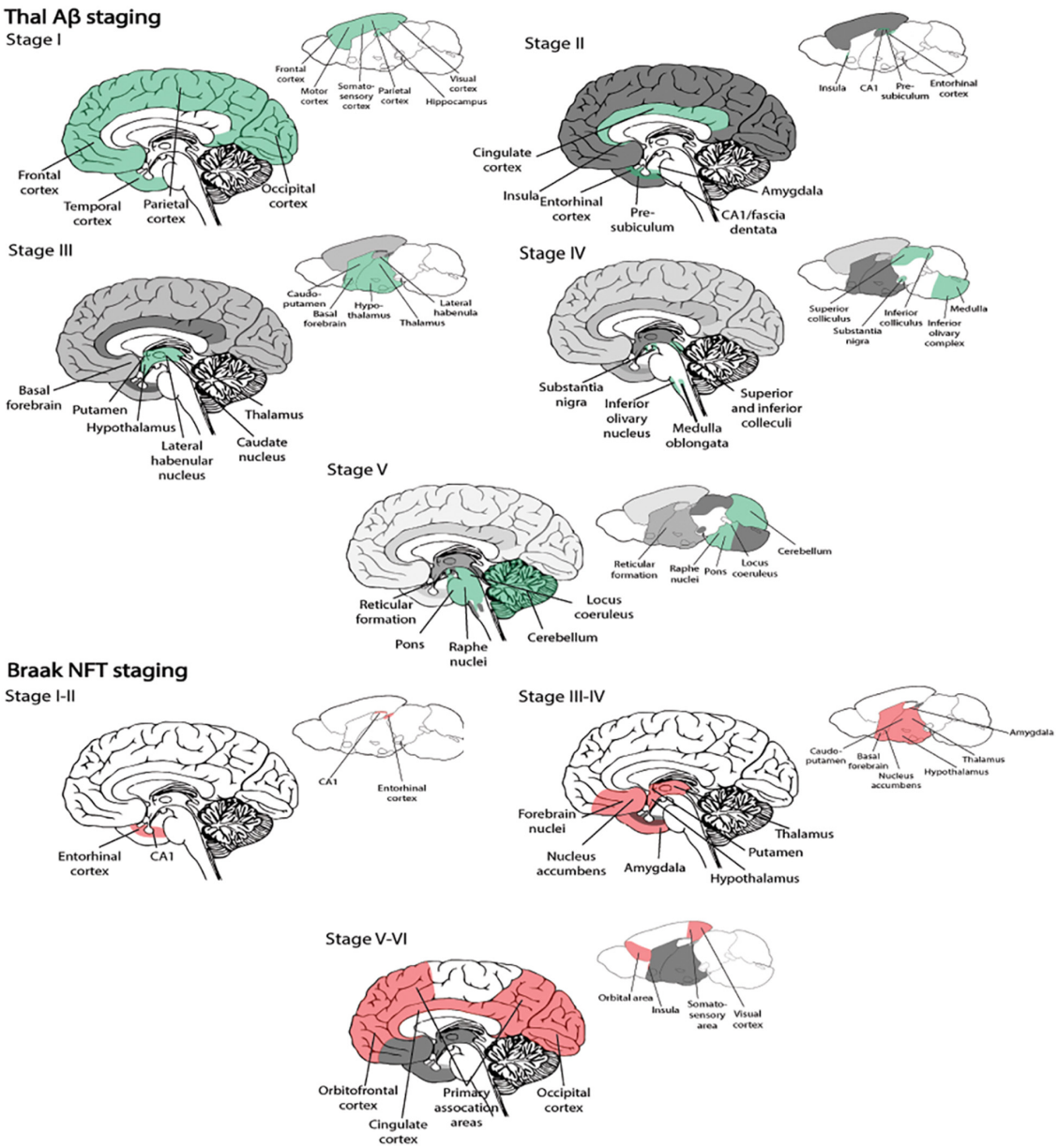

BOX 1 | Spatiotemporal pattern of Aβ and NFT deposition during the AD disease cascade in the human and mouse brain. Stages of Aβ deposition in the AD brain (Gomez-Isla et al., 1996). Stage I is characterized by exclusively neocortical Aβ deposits (neocortex: green) (Gomez-Isla et al., 1996). This includes Aβ deposits in frontal, temporal, parietal, and occipital cortices (Gomez-Isla et al., 1996). Stage II shows additional allocortical Aβ deposits (green) in entorhinal cortex, CA1, cingulate cortex, amygdala, presubiculum, and the fascia dentata (Gomez-Isla et al., 1996). In stage III, there are additional Aβ deposits in diencephalic nuclei and striatum (green) including thalamus, hypothalamus, the basal forebrain, caudate nucleus, putamen, claustrum, the lateral habenular nucleus, and white matter (Gomez-Isla et al., 1996). In stage IV there are Aβ deposits in distinct brainstem nuclei (substantia nigra, superior and inferior colliculi, inferior olivary nucleus, intermediate reticular zone, central gray of the midbrain, CA4, and the red nucleus; green) (Gomez-Isla et al., 1996). In stage V there are Aβ deposits in the cerebellum and additional brainstem nuclei (pons, locus coeruleus, reticular formation, raphe nuclei, parabrachial nuclei, and the dorsal tegmental nucleus; green) (Gomez-Isla et al., 1996). Stages of NFT deposition in the AD brain (Thal et al., 2002). Stages I-II show alterations which are confined to the superficial entorhinal cellular layer (pre-α; layer II/layer IIa) (Thal et al., 2002; Freudenberg-Hua et al., 2018).The next stage is an aggravation of stage I (Thal et al., 2002). Stages III-IV lead to severe involvement of the entorhinal and transentorhinal layer pre-α (pink) (Thal et al., 2002). Stage IV is characterized by layer pre-α, pri-α (layer V) (Freudenberg-Hua et al., 2018), and pre-β (layer III; layer IIb) (Thal et al., 2002; Freudenberg-Hua et al., 2018) involvement. CA1, the basolateral nuclei of the amygdala, the reuniens nucleus, the antero-dorsal thalamic nucleus, putamen, and nucleus accumbens are densely filled with NFTs (Thal et al., 2002). Stages V-VI are marked by isocortical destruction (pink) (Thal et al., 2002). In stage V, the deep layer pri-α is severely involved. Layers pre-β and pre-γ (layer III) (Freudenberg-Hua et al., 2018) are also affected (Thal et al., 2002). Virtually all components of the hippocampal formation are involved, and the isocortex is severely affected (Thal et al., 2002). By stage VI, the subcortical nuclei show a much more pronounced involvement (Thal et al., 2002), and considerable nerve cell loss is seen in layers pre-α and pri-α (Thal et al., 2002).Grayscale represents the recency of involved regions for each stage of neuropathology. Human brain regions adapted from Jürgen et al. (2016); mouse brain regions adapted from Allen brain atlas (Sunkin et al., 2013).

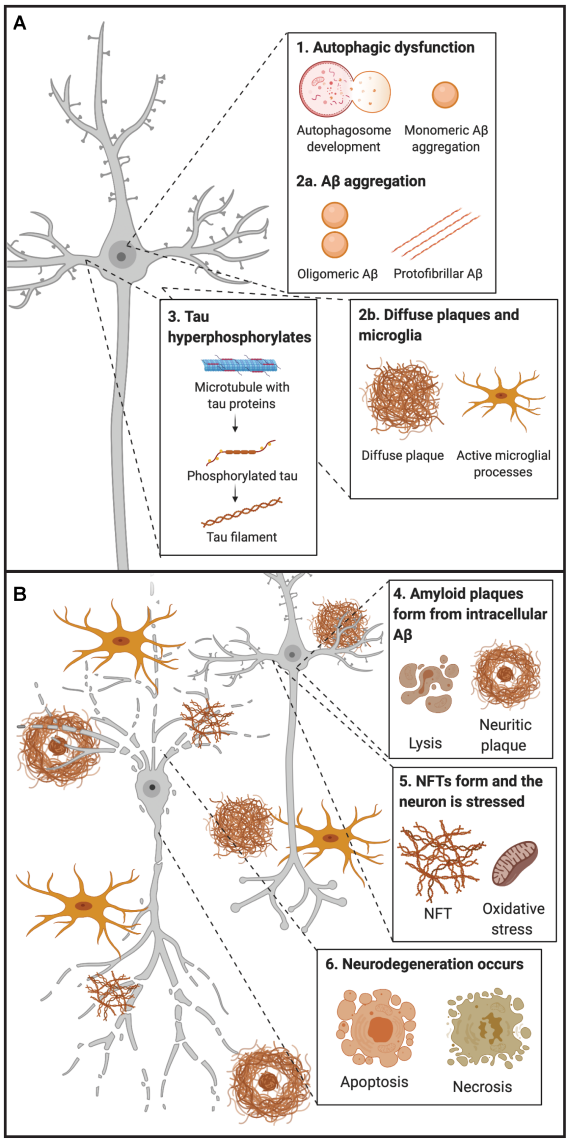

FIGURE 1 | Early and late timepoints of neuropathological development in AD. **(A)** Early molecular abnormalities leading to the development of neuropathological hallmarks in AD. First, disruption of endocytic and autophagic systems may lead to, or simultaneously become disrupted, as monomeric Aβ aggregates. Following, monomeric Aβ aggregates into oligomeric and protofibrillar forms. At the same time, diffuse amyloid plaques may be present extracellularly and begin to sequester Aβ from synapses, leading to microglial activation (and other inflammatory responses). Next, tau proteins become hyperphosphorylated and move from the axon to the somatodendritic compartment of the neuron. **(B)** Late molecular abnormalities in AD. While diffuse plaques are present extracellularly and may become neuritic by sequestering Aβ peptides from the synapse, a lysis event of the neuron occurs, and intracellular protofibrillar Aβ is deposited into the extracellular space leading to the development of neuritic plaques (composed of fibrillar Aβ). Other amyloid plaques in close vicinity may sequester Aβ peptides between each other, leading to the increased accumulation of neuritic plaques. Next, hyperphosphorylated tau from paired helical filaments form NFTs which results in excitotoxicity and oxidative stress. Ultimately neurodegeneration of the neuron occurs, primarily by necrosis, but apoptosis may also occur from some intracellular processes. Aβ, amyloid-β; NFT, neurofibrillary tangle.

with this, when diagnosing patients based on physical symptoms, reduced memory recall manifests in many diseases other than AD (Hane et al., 2017), highlighting the need for preclinical markers specific to AD.

Furthermore, AD has a long preclinical phase (**Figure 2**) consisting of three stages. In the first stage, monomeric and oligomeric Aβ aggregates inside neurons and subsequently onto neuronal surfaces and synapses as the concentration in the CSF reservoir diminishes. At this stage, current methods cannot detect the changes caused by Aβ aggregation in neurons and synapses (Hane et al., 2017). During the second stage, certain CSF biomarkers such as increased CSF tau, hypometabolism in the posterior cingulate, and cortical thinning become detectable (Hane et al., 2017). In the third stage, the patient experiences subtle symptoms while CSF Aβ decreases and CSF tau increases (Hane et al., 2017). Therefore, biomarker trajectories may differ as a function of the stage to which patients belong along the neuropathological cascade.

Neuroimaging Biomarkers in AD

Imaging Amyloid and Tau Burden

Substantial advances have been made in the detection AD biomarkers using neuroimaging. In terms of imaging amyloid burden, positron emission tomography (PET) scans with radiolabeled tracers specific to Aβ have become fairly common in AD research. PET amyloid ligands allows for quantification of amyloid deposition in patients, and binding of these ligands predates the development of clinical symptoms of AD by 7–15 years (Jack et al., 2013; Roe et al., 2013). [$_{11}$C]Pittsburgh Compound-B (PiB), a derivative of the fluorescent benzothiazole dye thioflavin T, enables for non-invasive imaging of fibrillar Aβ deposits (Klunk et al., 2004; Johnson et al., 2009). Importantly, this imaging tool is only able to detect extracellular Aβ deposition, and not intracellular Aβ accumulation. The Alzheimer's Disease Neuroimaging Initiative (ADNI) suggests that PiB can predict cognitive decline and brain atrophy in patients with mild cognitive impairment (MCI; represents a transition toward diagnosable dementia) (Weiner et al., 2010). Amyloid imaging is now usually performed by the use of fluorine-based tracers ($_{18}$F or FDG) and points to the parietal cortices as the earliest sites of amyloid deposition (**Figure 2**; Dickerson et al., 2009). The specific brain regions (posterior cingulate, retrosplenial cortex, and precuneus) are heavily connected with the medial temporal lobes (MTLs) (Ranganath and Ritchey, 2012), which are sites of early AD-related neuropathology. Tau imaging, by the use of selective PET tracers, is able to detect tau depositions that follow Braak staging of NFT pathology (**Figure 2**; Schöll et al., 2015; Cho et al., 2016; Maass et al., 2017). PET ligands have also been developed that are specific for paired-helical filament tau (Leuzy et al., 2019; Scholl et al., 2019). Post-mortem studies of AD patients indicate that, unlike amyloid plaque deposition, NFT density correlates with neurodegeneration and cognitive impairment (Duyckaerts et al., 1987; Braak and Braak, 1997). However, disentangling primary age-related tauopathy (PART) and AD may be a great challenge as there is considerable overlap in the MTL.

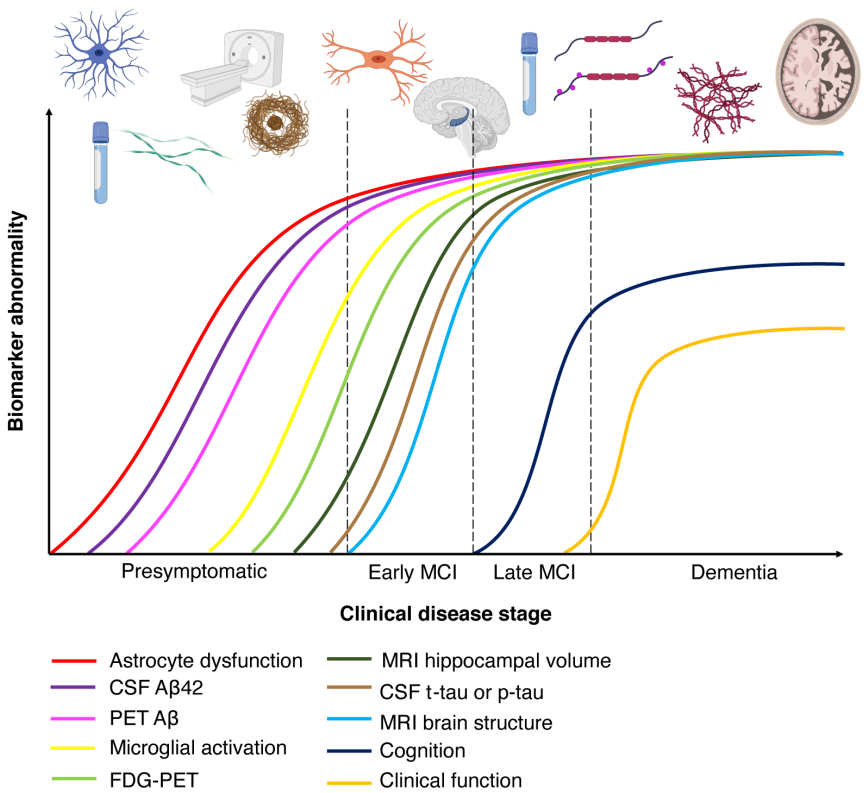

FIGURE 2 | Chronobiological biomarkers to Alzheimer's disease clinical stage. This disease model displays that biomarkers become abnormal in a temporally ordered manner as the disease progresses (Jack et al., 2010). Amyloid plaque biomarkers are dynamic early in the disease, prior to the appearance of clinical symptoms, and have largely reached a plateau by the time clinical symptoms appear (Jack et al., 2010). Biomarkers of neuronal injury, dysfunction, and degeneration are dynamic later in the disease and correlate with clinical symptom severity. MRI is the last biomarker to become aberrant. None of the biomarkers are static, and rates of change in each biomarker vary over time and follow a non-linear time-course, which is hypothesized to be sigmoid shaped (Jack et al., 2010). A sigmoid shape as a function of time implies that the maximum effect of each biomarker varies over the course of disease progression (Jack et al., 2010). Figure adapted with permission from Leclerc and Abulrob (2013). MCI, mild cognitive impairment; CSF, cerebrospinal fluid; Aβ, amyloid-β; PET, positron emission tomography; FDG, fluorine-based tracers; MRI, magnetic resonance imaging; t-tau, total tau; p-tau, phosphorylated tau.

FDG-PET – Cerebral Glucose Hypometabolism

Positron emission tomography imaging has been used to examine brain glucose abnormalities in aging, MCI and AD (de Leon et al., 1983). FDG can be used as a metabolic marker and reduced hippocampal metabolism has been observed in patients with MCI and AD (Mosconi et al., 2005; **Figure 2**). FDG-PET is a sensitive biomarker for neuronal and synaptic degeneration (Zimmer et al., 2017), and in line with this, research indicates that cerebral glucose hypometabolism is a downstream marker of neurodegeneration. Thus, this imaging method is able to detect patients at a later timepoint in the course of AD. Studies (Kuhl et al., 1982) have demonstrated that in older ages cerebral glucose metabolism decreases, and that the MTLs, the posterior cingulate cortex and the precuneus show the least age-dependent change. These regions express significant hypometabolism in AD (Márquez and Yassa, 2019), and Mosconi et al. (2008) showed that FDG-PET could be used to differentiate healthy subjects from AD patients with 98 to 99% specificity. Recent work by ADNI 2 PET Core has examined how FDG-PET and amyloid PET can be combined to track progression of AD. For instance, they demonstrated that amyloid PET is negatively associated with temporoparietal metabolism (Landau et al., 2012). Amyloid PET is associated with cognitive change in healthy subjects, whereas FDG-PET imaging is able to demonstrate cognitive change in MCI patients (Jagust et al., 2015). This is consistent with the spatiotemporal progression model of AD (**Figure 2**), where amyloid progression precedes neurodegeneration.

Imaging Connectivity – Resting-State Functional Magnetic Resonance Imaging

Functional magnetic resonance imaging (fMRI) techniques use blood-oxygenation-level-dependent (BOLD) contrast, which is associated with neuronal population activity. Resting-state fMRI studies examine the correlation of the BOLD signal and anatomical regions of interest at a temporal scale by analyzing spontaneous fluctuations in brain connectivity (Biswal et al., 1995; Fox and Raichle, 2007). In preclinical stages of AD, resting-state fMRI signals have been linked to metabolic changes (indexed by PET) and found to precede neurodegeneration (Sheline and Raichle, 2013). Therefore, this imaging tool is able to detect patients at some point immediately before or after amyloid plaque deposition, prior to the development of NFTs

and associated neurodegeneration. Most of these analyses have focused on the default mode network (Gusnard et al., 2001; Raichle et al., 2001), a network consisting of the MTL, the medial prefrontal cortex, posterior cingulate cortex, anterior cingulate cortex, parietal cortex, and precuneus (Greicius and Menon, 2004; Buckner et al., 2008). These regions overlap with the spatial pattern of amyloid and tau pathology (Buckner et al., 2008). In addition to changes in the default mode network, some studies have suggested that connectivity within the MTL may also be disrupted in AD (Yassa et al., 2011), such as the connectivity between EC and hippocampus [dentate gyrus (DG) and cornu ammonis field 3 (CA3)].

Cortical Thinning and Volume Loss – Structural MRI

Compared with functional imaging modalities, structural MRI provides an overview of anatomical changes in high resolution. Research has shown that in AD patients there is a decrease in brain volume associated with cortical thinning and gyral loss (**Figure 2**; Uylings and de Brabander, 2002), especially in the prefrontal cortex and hippocampus (Jack et al., 2000; Raz et al., 2005). Thus, this imaging tool can detect patients in which neurodegeneration has begun to occur. Studies in aged rodents and monkeys have demonstrated that hippocampal cells do not undergo frank cell loss with healthy aging (Rapp and Gallagher, 1996; Rasmussen et al., 1996; Rapp et al., 2002); in contrast, this is observed in the prefrontal cortex (Peters et al., 1994; Smith et al., 2004; Stranahan et al., 2012). Recently, cortical thinning of the EC has been shown to be a sensitive marker for structural alterations in both patients with MCI and AD (Holland et al., 2012a). EC thickness has been found to diminish prior to, and thereby predict, hippocampal atrophy (Desikan et al., 2010, 2011, 2012; Eskildsen et al., 2013). Several recent studies using the ADNI data have shown that older adults with CSF Aβ and phosphorylated-tau (p-tau) present with volume loss in EC (Desikan et al., 2012; Holland et al., 2012b).

White Matter Integrity – Diffusion Tensor Imaging

Studies using diffusion tensor imaging (DTI) in MCI and AD patients show a decrease in brain white matter integrity but with most prominent changes in MTLs (Bozzali et al., 2002; Naggara et al., 2006; Xie et al., 2006; Huang et al., 2007; Chua et al., 2008). DTI studies have focused primarily on the fornix as this region links the limbic system with the rest of the brain. Fornix lesions have been found to reproduce memory and learning deficits linked to hippocampal damage in rats (Sutherland et al., 1982; McDonald and White, 1993) and monkeys (Gaffan et al., 1984; Gaffan, 1992, 1994). The perforant path connects EC layer II neurons to the hippocampal DG and CA3 (Witter, 2007) and is critical for normal hippocampal function (Hyman et al., 1986). The integrity of this pathway is reduced in aged rats with memory loss (Geinisman et al., 1992; Smith et al., 2000). Perforant path lesions also result in EC layer II neuronal loss (Peterson et al., 1994), i.e., at the site where neurodegeneration is first observed in AD patients. Thus, similarly to structural MRI, this imaging tool can detect AD patients at the timepoint at which neurodegeneration has occurred. *In vivo* biomarkers, such as those derived from brain imaging, are crucial for accurate diagnosis of AD, but does not support diagnosis during preclinical stages. Additionally, molecular imaging is expensive and not easily accessible to the clinical population.

CSF Biomarkers in AD

The current approach to diagnosing AD patients involves assessing patient history, clinical examinations, and detection of underlying pathology using biomarkers during stages of the disease (Ramesh et al., 2018b), with the latter having a diagnostic accuracy between 82 and 84% (Engelborghs et al., 2008). The clinical staging of AD usually lasts about 9–10 years (Heyman et al., 1996), however, researchers have found that the neuropathology of AD starts 20–30 years before the onset of clinical symptoms (Selkoe, 2001; Sperling et al., 2011). Thus, it is likely that, with current means, clinical diagnosis is only feasible at a late stage of the disease. Imaging tools are invaluable methods to diagnose AD patients, but additional methods are needed to detect AD pathology at an earlier stage of the disease cascade, where intervention may be able to delay, even, halt disease progression. By developing better screening and detection tools, early interventions at the preclinical stages of the disease should be possible.

Clearance of abnormal proteins by drainage into the CSF is an endogenous neuroprotective function of the brain. Clinical AD diagnosis is conducted by sampling CSF and analyzing aberrant protein levels within the sample. CSF fills the ventricular system in the brain and spinal cord (Barten et al., 2017) and research evidence suggests that the composition of CSF at any given time reflects true biochemical changes that occur in the brain (Lee et al., 2019). Most of the CSF is generated by the choroid plexus but a significant fraction derives from the interstitial fluid (ISF) in the brain and spinal cord parenchyma. ISF is the circulating CSF that bathes brain tissue (Barten et al., 2017), whereas the choroid plexus connects to nearby permeable capillaries with tight junctions and produces CSF using the aquaporin-1 water channel as well as directional ionic transporters (Speake et al., 2001; Brinker et al., 2014). In terms of CSF production and volume, studies have shown that it can change with age, disease, and time of day. For instance, CSF production increases from 0.4 to 1.4 μL/min between 8 and 12 weeks of age in the rat (Karimy et al., 2015). Interestingly, CSF volume has been found to increase during neurodegeneration (Barten et al., 2017), which may be related to the increase in atrophy and substance loss of the brain. It is therefore vital to keep these changes in CSF production in mind when comparing healthy subjects to AD patients, and when comparing preclinical with clinical findings.

Temporal Course of AD Biomarkers

Amyloid-β level changes is the first biomarker abnormality seen in AD patients, which can either be in the form of an upregulation in plasma and CSF in cognitively normal individuals (**Figure 2**). The increased levels seen in CSF Aβ40 and Aβ42 in AD patients is thought to reflect extracellular Aβ deposits prior to the accumulation of amyloid plaques (Murphy and LeVine, 2010). However, it is important to note that Aβ oligomers can form intracellularly before being deposited extracellularly, and currently this cannot be detected with existing biomarkers.

Moreover, Aβ deposition detected by PET ligands can be seen as early as 15 years prior to onset of AD symptoms (**Figure 2**; Shen et al., 2018). The next stage of biomarker alteration include neuronal injury, shown by increased levels of CSF total tau protein (t-tau) and tau phosphorylated at threonine 181 (p-tau181/p-tau), and brain atrophy revealed by structural MRI, and synaptic loss and neurodegeneration detected by DTI or FDG-PET (**Figures 2**, **3**; Shen et al., 2018).

Core CSF Biomarkers for Diagnosis

Currently, CSF biomarkers are the only variety of fluid markers used for diagnosis of early AD, however, they have proven difficult to implement in the clinic due to their limited accessibility and the invasive nature of CSF collection (Lee et al., 2019). There are three core CSF biomarkers for AD diagnosis; Aβ42, t-tau, and p-tau (Shen et al., 2018). Using a combination of the core AD biomarkers is a better approach compared to using the biomarkers individually, especially for differential diagnosis (Engelborghs et al., 2008). Lower concentrations of CSF Aβ42 and higher concentrations of t-tau have been used to distinguish AD patients from healthy age-matched controls and to predict the conversion of MCI to AD (Frölich et al., 2017). To develop a non-invasive and effective measure of preclinical stages in AD, early abnormal AD biomarkers in preclinical models and patients need to be translated and assessed, followed by methodological developments of screening tools that are successful in system models that mirror the disease progression seen in patients.

CLASSIFICATION OF AD BIOMARKERS

Alzheimer's disease biomarkers may be open to different interpretations, however, there is an international classification system proposed by the National Institute of Aging (NIH) and the Alzheimer's Association (NIA-AA) that can aid in grouping them. In 2018, CSF biomarkers could be used in conjunction with neuroimaging for the first time to diagnose AD patients (Lee et al., 2019). The *A/T/N system* (**Table 1**) is a suggested grouping by Jack et al. (2016) based on the framework from the NIH and NIA-AA, where the *A* refers to the Aβ pathology measured either by PET or CSF Aβ42, the *T* represents tangle pathology and is assessed by either PET or CSF p-tau, and the *N* stands for neurodegeneration or neuronal injury detected by either FDG-PET, structural MRI, or CSF t-tau (Jack et al., 2016). Imaging techniques have found amyloid PET to be most reliable, whereas MRI and FDG-PET scans often are unable to distinguish AD more from other neurodegenerative disorders (Johnson et al., 2012). It is important to note that fluid biomarkers are more available and affordable compared to MRI and PET (Lee et al., 2019).

TABLE 1 | AT(N) biomarker grouping of the NIA-AA framework.

Biomarker class	CSF marker	Imaging marker
Amyloid (A)	CSF Aβ42 or Aβ42:Aβ40 ratio	Amyloid PET
Tau (T)	CSF p-tau	Tau PET
Neurodegeneration (N)	CSF t-tau	Anatomic MRI; FDG-PET

Adapted from Jack et al. (2016). NIH, National Institute on Aging; NIA-AA, Alzheimer's Association; CSF, cerebrospinal fluid; Aβ, amyloid-β; p-tau, phosphorylated tau; t-tau, total tau; PET, positron emission tomography; MRI, magnetic resonance imaging; FDG, fluorine-based tracers.

Aβ as a Biomarker for AD

Amyloid-β production occurs at the C-terminal fragment of amyloid precursor protein (APP) by cleavage of APP by β-secretase (BACE1) to form C99, followed by cleavage of C99 by presenilin (PSEN) 1 or PSEN2, two enzymatic components of γ-secretase (Haass and De Strooper, 1999). Following production, Aβ42 aggregates and accumulates intracellularly and/or extracellularly until a critical threshold is reached, where CSF Aβ42 decreases as the peptide sequesters in amyloid plaques in the brain parenchyma (Cirrito et al., 2003; Hong et al., 2011). The long delay in the emergence of plaque deposits even in the presence of increased Aβ42, suggests an initial slow process where monomeric Aβ forms small aggregates, followed by further Aβ polymerization (Harper and Lansbury, 1997). The AD field cannot yet explain exactly how Aβ pathology initiates, but further research on the generation of intracellular Aβ monomers, their recycling, and their aggregation into oligomeric Aβ may yield some answers.

One of the most widely used biomarkers in AD diagnostic research is the measurement of Aβ42 and Aβ40 in CSF (**Figure 3**; Rogeberg et al., 2015). Although Aβ40 is present at about 10–20 times higher concentration in CSF, Aβ42 is more prone to aggregate and shown to correlate better with AD neuropathology (Mehta et al., 2001; Hellstrand et al., 2010; Murphy and LeVine, 2010; Savage et al., 2014). It has been found that cognitively normal older adults that developed dementia in older ages had low CSF Aβ42 but not Aβ40 levels (Blennow et al., 2015). These findings can be explained in part by how Aβ aggregates to form soluble oligomers, which can exist in multiple forms and are neurotoxic (Haass and Selkoe, 2007), and which finally conform to diffuse and dense plaques. Recent studies support the notion that accumulation of the Aβ peptide arises from an imbalance in the production and clearance of Aβ and that the ability to clear Aβ diminishes with age (Wildsmith et al., 2013). An attractive early biomarker for AD is CSF Aβ42, given that both CSF t-tau and p-tau changes occur at a later time point in the disease process closer to clinically detectable dementia (Buchhave et al., 2012). Furthermore, measurement of the CSF Aβ42:Aβ40 ratio is superior to Aβ42 alone when distinguishing between MCI patients who progress and those that do not progress to AD dementia (Hansson et al., 2007; Lee et al., 2019). When comparing Aβ fluid biomarkers and imaging biomarkers, studies have shown that CSF Aβ42 can detect amyloid pathology earlier than amyloid PET imaging (**Figure 3**; Palmqvist et al., 2016).

There appears to be a lack of consensus regarding CSF Aβ concentrations in AD patients. For instance, researchers have found that CSF Aβ42 concentrations increase (Nakamura et al., 1994; Bouwman et al., 2007), decrease (Kanai et al., 1998; Tapiola et al., 2000; Wahlund and Blennow, 2003; Mollenhauer et al., 2005; de Leon et al., 2006; Beckett et al., 2010), or experience

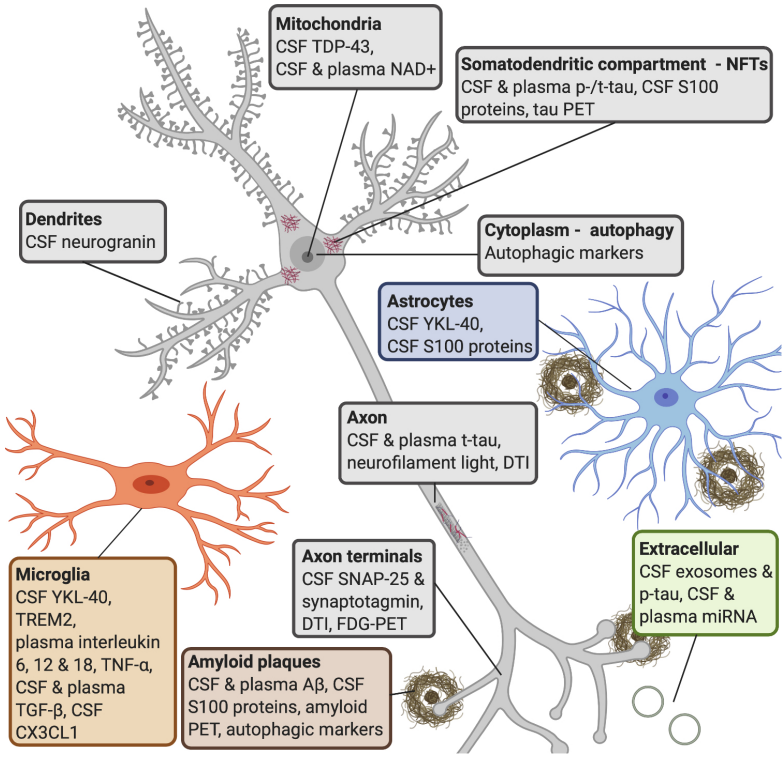

FIGURE 3 | AD molecular processes that can be detected by biomarkers. *Amyloid plaques:* a widely used biomarker for diagnosis in AD is the concentration of CSF Aβ42 and Aβ40 (Rogeberg et al., 2015). Studies have shown that CSF Aβ42 can detect amyloid pathology earlier than amyloid PET imaging (Palmqvist et al., 2016). Some research shows that serum Aβ42 levels do not correlate with CSF levels (Liu et al., 2004), whereas others have found that plasma Aβ can be measured with good sensitivity (Lee et al., 2019). Several S100 proteins (S100B, S100A1, S100A6, S100A8, S100A9, and S100A12) are found within amyloid plaques and in astrocytes and/or microglia near amyloid deposits (Boom et al., 2004; Shepherd et al., 2006; Walker et al., 2006; Ha et al., 2010; Afanador et al., 2014; Lodeiro et al., 2017). *NFTs:* increased CSF tau is a sensitive biomarker for neurodegeneration, but CSF p-tau is more specific to neurodegeneration linked to AD (Lewczuk et al., 2004; Blennow et al., 2015). P-tau is secreted via exosomal release, and reaches the CSF (Saman et al., 2012). Increased levels of CSF t-tau and p-tau can predict the progression of cognitive symptoms better than CSF Aβ42 (El Kadmiri et al., 2018), but the diagnostic utility of CSF t-tau and p-tau are improved when measured in combination with Aβ42 (Dubois et al., 2014). Increased plasma tau observed in AD patients compared to MCI patients and healthy controls (Mattsson et al., 2016; Pase et al., 2019). S100B and S100A9 are found within NFTs (Sheng et al., 1994, 1997; Shepherd et al., 2006). *Autophagy:* late stages of autophagy is disrupted in AD patients, as an accumulation of autophagic vesicles can be observed in dystrophic neurites (Komatsu et al., 2006), and are observed prior to extracellular Aβ deposition (Mehrpour et al., 2010; Nixon and Yang, 2011). *Microglia:* YKL-40 is expressed by microglia. CSF TREM2 is associated with higher CSF t-tau and p-tau levels, probably reflecting a corresponding change in microglia activation in response to neurodegeneration (Suarez-Calvet et al., 2016). It has been shown that AD patients have higher levels of interleukin-6, 12, and 18, TNF-α and TGF-β, in blood, and higher levels of TGF-β in CSF, compared to healthy controls (Swardfager et al., 2010). Decreases in CSF neuronal CX3CL1 is found in AD patients (Perea et al., 2018). *Astrocytes:* YKL-40 is expressed in astrocytes near Aβ plaques (Craig-Schapiro et al., 2010) and correlates positively with tau pathology (Querol-Vilaseca et al., 2017; Janelidze et al., 2018). *Axon terminals:* CSF levels of SNAP-25 (Brinkmalm et al., 2014; Sutphen et al., 2018) and synaptotagmin (Öhrfelt et al., 2016) have been found at elevated levels in patients with AD or MCI compared with control subjects. Synaptic neurodegeneration can be detected by DTI or FDG-PET (Shen et al., 2018). *Dendrites:* increased CSF neurogranin is found in MCI and AD patients as compared with healthy controls (Thorsell et al., 2010; De Vos et al., 2015). *Axon:* increased neurofilament light is observed in response to axonal damage, which occurs in AD. The core CSF biomarkers (Aβ42, t-tau, and p-tau) and CSF neurofilament light levels strongly correlated with AD (Olsson et al., 2016). Blood levels of this protein strongly correlate with its CSF levels (Gisslen et al., 2016; Kuhle et al., 2016; Rojas et al., 2016). *Mitochondria:* studies have shown that TDP-43 contributes to neuroinflammation and may have a role in mitochondrial and neuronal dysfunction (James et al., 2016). NAD+ levels can be detected in CSF and plasma in early AD. *Extracellular:* miRNAs released from exosomes appear to be associated with neurodegenerative aspects in AD (Wang et al., 2008, 2012; Chen et al., 2017). Studies have reported that changes in levels of blood miRNA distinguished AD patients from healthy controls with 93% accuracy (Leidinger et al., 2013; Swarbrick et al., 2019). AD, Alzheimer's disease; CSF, cerebrospinal fluid; Aβ, amyloid-β; PET, positron emission tomography; NFTs, neurofibrillary tangles; p-tau, phosphorylated tau; t-tau, total tau; MCI, mild cognitive impairment; TREM2, triggering receptor expressed on myeloid cells 2; TNF-α, tumor necrosis factor-α; TGF-β, transforming growth factor-β; CX3CL1, CX3 chemokine ligand 1; SNAP-25, synaptosomal-associated protein 25; TDP-43, transactive response element (TAR) deoxyribonucleic acid (DNA)-binding protein 43; NAD+, oxidized nicotinamide adenine dinucleotide; miRNA, microRNA.

no significant change (Andreasen et al., 1998, 1999a; Hoglund et al., 2005; Andersson et al., 2008; Brys et al., 2009; Stomrud et al., 2010) during the disease. The prevailing explanation for a reduced amount of Aβ in later stages of AD is that as the pathology progresses, more Aβ, especially Aβ42, aggregates into plaques in the brain, which effectively means that less Aβ can diffuse from the brain to the CSF. Another explanation may be that Aβ first accumulates intracellularly, and neurodegeneration releases Aβ in the extracellular compartment, increasing CSF Aβ levels, and subsequently accumulates onto neuronal surfaces and

in synapses as it clears away from the CSF. As neurodegeneration occurs, less Aβ is produced and therefore smaller amounts will accumulate in the CSF and subsequently in the brain, where Aβ will reach plateau levels. Alternatively, reduced CSF Aβ42 might follow neuronal dysfunction, which results in decreased metabolism of APP and Aβ. It is important to note that this is unlikely in transgenic mice, as Aβ42 levels in the CSF decline, while its levels in the brain keep rising. Also, when above a certain level, parts of CSF Aβ42 may aggregate into a large assembly that antibodies of currently used enzyme-linked immunosorbent assay (ELISA) kits cannot capture (Pitschke et al., 1998; Liu et al., 2004). These seemingly disparate findings regarding CSF Aβ concentrations may therefore reflect different timepoints of the disease progression.

With regard to studies using Aβ as a fluid biomarker for AD, studies have shown that concentrations of CSF Aβ42 increased between 5 and 7 months of age, but not between 8 and 13 months of age in an APP/PS1 mouse model (Liu et al., 2004). This was despite a rapid increase in brain levels of Aβ42 (Liu et al., 2004). However, between 6 and 9 months of age in another APP/PS1 mouse model with a more aggressive AD phenotype a decline in CSF Aβ42 levels was reported (Liu et al., 2004). Based on these findings, it appears that CSF Aβ42 may initially reflect the rate of Aβ42 production (most likely in the synaptic cleft), but after reaching a critical threshold, CSF Aβ42 levels stay in equilibrium until plaque formation leads to their decrease (Liu et al., 2004). Consistent with this notion, CSF Aβ42 levels have a strong link with the deposition of amyloid plaques, whereby an inverse correlation between Aβ42 levels, plaques (Strozyk et al., 2003) and amyloid PET is observed (Toledo et al., 2015; Leuzy et al., 2016; Niemantsverdriet et al., 2017). This implies that as Aβ aggregates and forms plaques in the brain, lower levels of the protein diffuse into the CSF (Lee et al., 2019).

Compared to tau as a fluid biomarker, the drop in CSF Aβ42 should precede the increase in CSF tau proteins. This notion is supported by biomarker studies in sporadic AD patients demonstrating that a decrease in CSF Aβ42 was the earliest change reported (Skoog et al., 2003; Gustafson et al., 2007), while in patients with familial AD reductions in CSF Aβ42 and elevations in tau occur around 10–15 years prior to symptom development (Bateman et al., 2012; Ringman et al., 2012). Similar to Aβ, tau can also change its conformation to prion-like oligomers and there is evidence for misfolded Aβ initiating tau misfolding (Pulawski et al., 2012; Nussbaum et al., 2013). Therefore, Aβ appears to be an initiator of tau pathology and subsequent neurodegeneration.

Tau as a Biomarker for AD

Tau is a microtubule-associated protein comprising six human isoforms and is located in neuronal axons (Barten et al., 2011; Khan and Bloom, 2016). A characteristic of many neurons in AD is that tau is hyperphosphorylated and translocated from axons to the somatodendritic compartment, where it becomes misfolded and aggregates. Tau aggregates develop intracellularly and may thus trap functional proteins adding to microtubule destabilization, cellular dysfunction and eventually neurodegeneration (Benilova et al., 2012). Intracellular trafficking is dependent on the phosphorylation of tau in order to separate tau from microtubules, allowing transport, followed by dephosphorylation in order to return tau into microtubules (Avila et al., 2004). It has been proposed that Aβ pathology drives the abnormal phosphorylation of tau in AD (Bakota and Brandt, 2016; Khan and Bloom, 2016). However, transgenic mice modeling Aβ pathology alone do not develop NFTs endogenously (Lee and Trojanowski, 2001), while intracerebral injections of human mutated and/or aggregated tau are necessary to observe this neuropathological hallmark (Clavaguera et al., 2013; Ahmed et al., 2014; Kaufman et al., 2017; Lewczuk et al., 2017; Mudher et al., 2017; Narasimhan et al., 2017; He et al., 2018). Tau aggregates and NFTs are produced in the cytoplasm under pathological conditions, when tau changes its conformation from a highly soluble state to one with a high β-sheet content and is hyperphosphorylated (Yamada et al., 2015). Studies have shown that the elevation in CSF tau in AD is due to axonal loss and neuronal death, leading to the release of the intracellular protein (Blennow and Hampel, 2003; Hampel et al., 2010). However, despite significant neurodegeneration and tau pathology, CSF tau is not elevated in other pure tauopathies (Grossman et al., 2005; Bian et al., 2008). This suggests that cell death may not be the only mechanism responsible for CSF tau elevations in AD (Jack et al., 2010).

When using tau as a fluid biomarker for AD, increased CSF concentrations of the protein constitutes a sensitive marker for neurodegeneration, but an entirely unspecific one for AD (**Figure 3**). However, the increased concentration of p-tau molecules seems much more AD specific (**Figure 3**; Lewczuk et al., 2004; Blennow et al., 2015). P-tau is secreted via exosomal release, and reaches the CSF (Saman et al., 2012; **Figure 3**). CSF p-tau levels are usually stable in other dementias, whereas both CSF p-tau and t-tau levels can be used to distinguish AD patients from healthy controls, suggesting that CSF tau is an important biomarker for differential dementia diagnosis (Blennow et al., 2015). In addition, high CSF t-tau and p-tau can predict the progression of cognitive symptoms better than CSF Aβ42 (El Kadmiri et al., 2018; **Figure 3**). Researchers have found correlations between p-tau in CSF and NFTs in the brain (Clark et al., 2003; Buerger et al., 2006; Tapiola et al., 2009; de Souza et al., 2012), and CSF t-tau has been found to correlate with neurodegeneration (Lee et al., 2019). Importantly, the utility of CSF p-tau and t-tau for AD diagnosis is markedly improved when measured together with CSF Aβ42 (**Figure 3**; Dubois et al., 2014).

To examine CSF tau levels in rodents, researchers have used P301S human tau transgenic mice and found that ISF tau was at fivefold higher levels compared to endogenous tau, in line with its elevated levels of expression (Yamada et al., 2011). It is important to keep this in mind when comparing CSF tau between rodents and patients, as the CSF tau from rodents might be contaminated by ISF tau levels, and the CSF levels may not reflect the actual tau levels expressed in the brain. Studies have found that tau in brain tissue is approximately 50,000-fold more abundant than its levels in the CSF (Barten et al., 2011). In humans, patients with sporadic AD display longitudinal increases in tau when low levels of tau were detectable early in the disease course, but no differences (or

increases) have been observed in tau in patients with high levels of tau at baseline (Kanai et al., 1998; Sunderland et al., 1999).

Compared to Aβ, which aggregates broadly in the brain parenchyma and the perivascular space, tau readily drains into CSF. In contrast to Aβ, tau levels increase in the CSF with the progression of AD (Olsson et al., 2016). Changes in CSF Aβ42 precede changes in CSF tau, consistent with the proposition that Aβ affects and drives CSF tau levels (Jack et al., 2010). However, further research is needed to explain whether Aβ and tau pathology represent early initiators of neurodegeneration and cognitive decline, or merely downstream effects of other early pathophysiological events in AD.

Neuroinflammatory Biomarkers

Inflammation is now considered another core feature of AD as it relates to the pathogenesis of the disease and also serves as a link between amyloid plaques and NFTs (Akama and Van Eldik, 2000; Akiyama et al., 2000). Inflammatory response has now been reported in post-mortem tissues of AD patients (Gomez-Nicola and Boche, 2015) and is routinely observed in preclinical models. The presence of inflammation in the brain of AD patients was initially thought to be a consequence of the accumulating neurodegeneration present at late stages of the disease. However, a substantial body of research now demonstrates that a persistent immune response in the brain not only is associated with neurodegeneration, but it also exacerbates Aβ and tau pathology (**Figure 1**). Inflammatory markers may be able to give evidence to intracellular abnormalities early in the course of AD, prior to extracellular Aβ deposition (marked by an increase in CSF Aβ40/Aβ42 and amyloid PET) as evidence points to a dysfunction in autophagic processes in AD patients (**Figure 1**; Menzies et al., 2015). Moreover, there have been reports of immune-related proteins and cells opposed to amyloid plaques (**Figure 1**; Griffin et al., 1989). In line with this, it has been suggested that inflammation may provide a link between the initial Aβ pathology and subsequent development of NFTs (Kitazawa et al., 2004; Rhein et al., 2009; Garwood et al., 2011; Nisbet et al., 2015).

Autophagic Markers

One way for intracellular accumulation of Aβ peptides to occur is through a disruption in the autophagic and lysosomal clearance systems. In this way, autophagic markers could ultimately serve as the earliest biomarker to diagnose AD patients, as this process may likely initiate the aggregation of monomeric Aβ into oligomeric Aβ intracellularly (**Figure 1**). Autophagy is a complex process, in which a vesicle known as the phagophore elongates around the cytoplasmic components selected for degradation. The recognition of these components are dependent on the lipidated form of the microtubule-associated protein light chain 3 (LC3) (Milisav et al., 2015). The late stage of autophagy depends on the successful fusion of the autophagosome with the lysosome, which then degrades and recycles the autophagosome cargo. There is evidence supporting that the late stage of autophagy is disrupted in AD, as accumulation of autophagic vesicles can be observed in dystrophic neurites (components of dense plaques) (Komatsu et al., 2006), and these are observed prior to extracellular Aβ deposition in model systems and patients (**Figure 3**; Mehrpour et al., 2010; Nixon and Yang, 2011).

The above findings suggest that autophagy dysfunction leads to the accumulation of intracellular Aβ by avoiding proper degradation and/or recycling. In line with this, researchers have found that LC3-associated endocytosis is used to clear and recycle Aβ surface receptors (Heckmann et al., 2019). In model systems with LC3-associated endocytosis disrupted, an increase in extracellular Aβ deposition, NFTs, neurodegeneration and behavioral deficits was observed. Another line of research found that autophagic markers were significantly increased in AD patients compared with control subjects (Cho et al., 2019). Furthermore, other studies suggest that metabolism of Aβ and tau is crucially influenced by autophagy (Uddin et al., 2018). Recent evidence suggests that Aβ monomers and oligomers modulate autophagy differently in neurons. Monomers have been found to stimulate autophagy, increasing autophagosome rates and elevation of LC3 protein levels, while simultaneously impairing the lysosomal pathway affecting the autophagy efflux, leading to autophagosome accumulation (Menzies et al., 2015). By contrast, Aβ oligomers do not cause a significant increase in LC3 protein levels nor affect efflux of autophagic vacuoles (Menzies et al., 2015), which suggests that an increase in intracellular Aβ monomers may be the result of a defective autophagic system. This fits the proposition that autophagic disruption and accumulation of Aβ monomers constitute some of the earliest events in the AD cascade (**Figure 1**). The exact cascade by which autophagy can degrade amyloid plaques is still not known, however, microglial autophagy appears to play and important role.

Glial Cells and Markers

Neuroinflammation involving astrocytes, microglia, and secreted compounds like reactive oxygen species, cytokines, and chemokines are key pathophysiological processes assessed when diagnosing AD (Ramesh et al., 2018a). Microglia and astrocytes are the two types of glial cells primarily affected (McGeer et al., 1987; Rogers et al., 1988; Bronzuoli et al., 2016), which in turn affect the clearance and production of Aβ42 (Hickman et al., 2008; Liu et al., 2017). Glial cells also affect the development and propagation of tau pathology (Asai et al., 2015) and thus influence disease progression and severity (Block et al., 2007; Calsolaro and Edison, 2016). Importantly, if glial cells are activated for too long, they can become pro-inflammatory (Bronzuoli et al., 2016). Chitinase-3-like protein 1 (or YKL-40) is an inflammatory marker expressed by microglia and astrocytes (**Figure 3**). In AD, YKL-40 is expressed in astrocytes near Aβ plaques (Craig-Schapiro et al., 2010) and correlates positively with tau pathology (**Figure 3**; Querol-Vilaseca et al., 2017; Janelidze et al., 2018).

Another glial marker is triggering receptor expressed on myeloid cells 2 (TREM2), which is an inflammatory cell-surface receptor. Loss-of-function mutations of TREM2 are associated with an increased risk of developing AD (Suarez-Calvet et al., 2016). Researchers have found that TREM2 phagocytose Aβ in early AD stages (Jay et al., 2017). A rare mutation in the TREM2 gene affects the phagocytic activity of microglia and consequently

contributes to accumulation of Aβ (Kleinberger et al., 2014; Ramesh et al., 2018b). With regard to TREM2 measured in CSF, studies have shown increased levels to be associated with higher CSF t-tau and p-tau levels, probably reflecting a corresponding change in microglia activation in response to neurodegeneration (**Figure 3**; Suarez-Calvet et al., 2016). Relevant research findings imply that neuroinflammation is a robust biomarker even at pre-symptomatic stages (Janelidze et al., 2018). In line with this, high levels of inflammatory biomarkers are associated with increased CSF levels of t-tau (Janelidze et al., 2018). Interestingly, PET studies have revealed increased microglial activation in the precuneus (Hamelin et al., 2016; Fan et al., 2017), a region in the default mode network that displays early Aβ deposits in AD (Palmqvist et al., 2017).

Cytokines

With regard to cytokines, it has been shown that AD patients have higher levels of interleukin-6, 12, and 18, tumor necrosis factor-α (TNF-α), and transforming growth factor-β (TGF-β), in blood, and higher levels of TGF-β in CSF, compared to healthy controls (**Figure 3**; Swardfager et al., 2010). Endothelial growth factor receptor 1 (also known as Flt-1), has been found to be upregulated in entorhinal cortical sections from human AD brains and in human microglia following treatment of Aβ42 (Ryu et al., 2009). Following neuroinflammation, oxidative stress in the intracellular environment occurs. Oxidative stress plays an important role in the early stages of AD (Oh et al., 2010) and its associated signaling cascades are being investigated and explored for biomarkers. For instance, higher reactive oxygen species levels lead to post-translational modification of proteins, toxic cell damage, fragmentation and aggregation of Aβ (Brinkmalm et al., 2014). One type of reactive oxygen species are sulfatides, which have been found to be depleted in both gray and white matter of AD patients, and results in decreased hippocampal volume and cognitive decline (Ramesh et al., 2018b).

Since neuroinflammation occurs in AD brains, the levels of several S100 proteins are increased and some of the proteins play roles related to the processing of APP, regulation of Aβ levels and tau phosphorylation. S100A1, S100A6, and S100B have been found to be involved in the disassembly of microtubules and tau protein release (Zimmer et al., 2005; Roltsch et al., 2010; Wruck et al., 2016; Sidoryk-Wegrzynowicz et al., 2017), while S100B and S100A9 are found within NFTs (**Figure 3**; Sheng et al., 1994, 1997; Shepherd et al., 2006). Traumatic brain injury (TBI) has been found to predispose people to developing AD (Johnson et al., 2010). Interestingly, TBI results in an increase in S100A1 and S100B levels in plasma and CSF in patients (de Boussard et al., 2005). Research has shown that levels of S100B originating from necrotic tissue might enhance or amplify neurodegeneration by apoptosis (Sedaghat and Notopoulos, 2008). Thus, various S100 proteins could be a link between neurodegenerative diseases induced by brain damage. Comorbidities often accompany a diagnosis of AD, thus the spectrum of pathological processes that can end in AD at different degrees of severity and symptomology needs to be kept in mind in order to accurately diagnose and treat patients. Additionally, S100 proteins may serve as an early biomarker for a later AD diagnosis in patients with TBI or other comorbidities that increase S100 levels.

Moreover, several S100 proteins are implicated in the amyloidogenic pathway of APP cleavage. S100A9 regulates γ-secretase and BACE1 expression and activity (Kummer et al., 2012; Li et al., 2014), and S100B and S100A1 regulate APP levels (Zimmer et al., 2005; Anderson et al., 2009; Mori et al., 2010). S100A7, S100A8, S100A9, and S100B have been found to influence Aβ levels (Qin et al., 2009; Lee et al., 2013; Lodeiro et al., 2017; Cristovao et al., 2018). Moreover, S100B and S100A6 have been found to reduce zinc levels and senile plaque load in preclinical models (Roltsch et al., 2010; Hagmeyer et al., 2017; Tian et al., 2019). S100A1, S100A9, and S100B proteins can interact and alter the aggregated Aβ and is found to co-aggregate with Aβ peptides (Zimmer et al., 2005; Shepherd et al., 2006; Ha et al., 2010; Mori et al., 2010; Chang et al., 2012; Afanador et al., 2014; Cristovao et al., 2018). In line with this, several S100 proteins (S100B, S100A1, S100A6, S100A8, S100A9, and S100A12) are present in amyloid plaques and in astrocytes and/or microglia near amyloid deposits (**Figure 3**; Boom et al., 2004; Shepherd et al., 2006; Walker et al., 2006; Ha et al., 2010; Afanador et al., 2014; Lodeiro et al., 2017).

Chemokines

In order to maintain brain homeostasis, microglia establish continuous communication with neurons and astrocytes, through the expression and secretion of chemokines (Mennicken et al., 1999). The CX3 chemokine ligand 1 (CX3CL1; or fractalkine), is predominantly expressed in neurons (Bazan et al., 1997) and interacts with the CX3 chemokine receptor 1 (CX3CR1) exclusively present in microglia (Imai et al., 1997; Maciejewski-Lenoir et al., 1999). The CX3CL1/CX3CR1 tandem allows for direct communication between neurons and microglia (Harrison et al., 1998; Sheridan and Murphy, 2013), and it has been suggested that this axis becomes impaired in AD patients (Bolos et al., 2017). Consistent with this, neuronal CX3CL1 is found to be decreased in CSF from AD patients compared to MCI and control subjects (**Figure 3**; Perea et al., 2018). Furthermore, researchers have aimed to regulate neuroinflammation in tau depositing mouse lines by overexpressing CX3CL1 and found that it significantly reduced tau pathology, ameliorated neuronal loss, reduced microgliosis (Nash et al., 2013) as well as rescuing cognitive function (Finneran et al., 2019). In another line of research, it has been found that when microglia are transferred from tau depositing knock-out *Cx3cr1* mice, hyperphosphorylation of endogenous murine tau is observed (Maphis et al., 2015). Disruption of CX3CL1 signaling in amyloid depositing mouse lines has shown reduced pathology due to increased microglial phagocytosis of amyloid plaques (Lee et al., 2010).

Synaptic Neurodegeneration Markers

There is of yet no established or reliable biomarker test for synaptic degeneration, which is considered a crucial feature for the development of AD-related cognitive decline. The ability to monitor neurodegeneration as a downstream effect of synaptic dysfunction would be an important advantage for

early AD diagnosis and in clinical trials related to drug testing. Synaptotagmin, a pre-synaptic calcium sensor vesicle protein, facilitates neurotransmitter release from the synaptic vesicle by exocytosis and also functions as an essential vesicle cargo molecule in hippocampal neurons (Leinenbach et al., 2014). Various studies have shown a decrease in synaptotagmin-1 in AD patients (Mattsson et al., 2011).

Another marker for synaptic degeneration is synaptosomal-associated protein 25 (SNAP-25), which is an essential component of the soluble N-ethylmaleimide-sensitive fusion protein attachment protein receptors (SNARE) complex that mediates synaptic communication by initiating fusion of synaptic vesicles (Olsson et al., 2016). A negative correlation has been found between SNAP-25 and cognitive decline, suggesting that this is a promising novel CSF biomarker for AD (Andreasen et al., 1999b). Overall, CSF levels of SNAP-25 (Brinkmalm et al., 2014; Sutphen et al., 2018) and synaptotagmin (Öhrfelt et al., 2016) have been assessed and found at elevated levels in patients with AD or MCI compared with control subjects (**Figure 3**). Another marker for synaptic neurodegeneration is neurogranin, which plays an important role in synaptic plasticity and long-term potentiation processes (Geppert et al., 1994; Sudhof and Rizo, 1996; Thorsell et al., 2010). Neurogranin has also been found at increased levels in CSF of patients with MCI and dementia due to developing AD as compared with healthy controls (**Figure 3**; Thorsell et al., 2010; De Vos et al., 2015). CSF neurogranin concentrations have been found at increased levels in patients that have reached the threshold for Aβ PET detection (Palmqvist et al., 2019), and also CSF neurogranin and tau levels have been found to correlate strongly (Thorsell et al., 2010; De Vos et al., 2015).

Novel Biomarkers for AD

Many biomarkers are now being investigated as complimentary to the core AD biomarkers. One such biomarker is neurofilament light, which is a marker of neuronal integrity reflecting axonal damage of the subcortical white matter (Petzold, 2005; Jahn and Fasshauer, 2012; Neselius et al., 2012; Kuhle et al., 2015; Zetterberg et al., 2016). Neurofilament light is released from axons into the extracellular space during healthy aging, which results in increased CSF level concentrations (**Figure 3**). The release of neurofilament light is accelerated during axonal damage, which occurs in AD (**Figure 3**). A recent meta-analysis showed that the core CSF biomarkers (Aβ42, t-tau, and p-tau) and CSF neurofilament light levels strongly correlated with AD (**Figure 3**; Olsson et al., 2016). Importantly, CSF neurofilament light levels have been shown to be higher in AD (Sjogren et al., 2001; Pijnenburg et al., 2007; Zetterberg et al., 2016; Alcolea et al., 2017; Lista et al., 2017). Blood neurofilament levels strongly correlate with CSF levels (**Figure 3**; Gisslen et al., 2016; Kuhle et al., 2016; Rojas et al., 2016), and blood neurofilament light concentrations have been found at increased levels in many forms of neurodegenerative disease (Gisslen et al., 2016; Kuhle et al., 2016; Rohrer et al., 2016; Rojas et al., 2016; Steinacker et al., 2016, 2017; Weydt et al., 2016; Mattsson et al., 2017a) and have proven almost as reliant as CSF analysis in monitoring treatment outcome in patients (Bacioglu et al., 2016; Disanto et al., 2017). Another novel biomarker is the transactive response element (TAR) deoxyribonucleic acid (DNA)-binding protein 43 (TDP-43) protein, which can become pathologic if triggered by Aβ peptides. Studies have shown that TDP-43 contributes to neuroinflammation and may have a role in mitochondrial and neuronal dysfunction (**Figure 3**; James et al., 2016). In accordance with this, TDP-43 pathology has been observed in some AD cases (Amador-Ortiz et al., 2007; Chang et al., 2015; James et al., 2016). Another novel biomarker is oxidized nicotinamide adenine dinucleotide (NAD+; involved in mitochondrial homeostasis), which has been found to decrease during healthy aging, but even more rapidly in neurodegenerative diseases (**Figure 3**; Lautrup et al., 2019). This could be related to the observed decrease in neuronal metabolism that occurs during healthy aging, but this is accelerated in the AD brain. NAD+ levels can be detected in CSF and plasma early during the disease progression, and in combination with core biomarkers, it presents as a novel preclinical biomarker for AD (**Figure 3**).

Neuropathology is associated with a distinct subset of cells in specific regions in the brain and this makes the identification of relevant biomarker molecules a challenge. The transport of macromolecules from the brain to the CSF and blood, mediated by extracellular vesicles, presents a promising source of central nervous system (CNS)-specific biomarkers (Thompson et al., 2016). One such trafficking macromolecule is exosomes, which can be picked up in CSF. An increasing body of evidence suggests that exosomal proteins and microRNAs (miRNAs) may constitute novel biomarkers for clinical AD diagnosis (Van Giau and An, 2016). miRNAs released from exosomes appear to be associated with neurodegenerative aspects in AD (**Figure 3**; Wang et al., 2008, 2012; Chen et al., 2017). miRNAs are a class of small non-coding RNAs which regulate over 50% of protein-coding genes, and miRNA-107 has been found to be downregulated in AD brains (Van Giau and An, 2016; Fransquet and Ryan, 2018; Ramesh et al., 2018b). Accumulating evidence presents that miRNAs regulate Aβ production, NFT formation, and neurodegeneration by targeting different genes (Wang et al., 2008; Van Giau and An, 2016). Research has also identified BACE1 as a target of miRNA-107, connecting the level of miRNA-107 to Aβ formation and neuronal pathogenesis (Wang et al., 2008).

CSF AND BLOOD-BASED BIOMARKERS

Although protein content is lower in CSF compared to blood, CSF holds great value for developing consistent biomarkers for AD as it reflects biochemical changes in the brain by direct interaction with the extracellular space (Hampel et al., 2012). At present, there is no approved blood biomarker for AD (Stadtman and Levine, 2003). It is important to note, however, that blood biomarkers have lower sensitivity and specificity than CSF biomarkers, and this can be attributed to the fact that the blood-brain barrier (BBB) prevents diffusion of analytes into the blood via a filtering mechanism (Lee et al., 2019). Furthermore, one complication of measuring CNS biomarkers in blood is that many of the analytes are produced in the

periphery as well as in the brain, and thus the source of detectable change may be difficult to determine (Barten et al., 2017). However, there is currently an urgent need within the field to develop blood-based biomarkers which are inexpensive and which can detect early neuropathological changes in AD (Hane et al., 2017). For instance, detection of autophagic markers in plasma could serve as an early biomarker for AD (Cho et al., 2019). Blood test sampling is routinely performed in the clinic, it is minimally invasive, cheap and suitable for recurrent measurements (Shen et al., 2018).

When comparing Aβ levels in blood and CSF, some researchers have found that serum Aβ42 levels do not correlate with CSF levels (**Figure 3**; Liu et al., 2004). However, contrary to this, others have found that plasma Aβ can be measured with good sensitivity (**Figure 3**; Lee et al., 2019). Aβ can easily penetrate the BBB and is therefore an attractive blood biomarker candidate (Lee et al., 2019). Indeed, studies have shown that cerebral amyloid deposits may be sourced in the periphery, while other studies suggest that amyloid deposits in cerebral vessels may originate from circulating Aβ peptides (Yankner and Mesulam, 1991; Chen et al., 1995; DeMattos et al., 2002; Lee et al., 2019). Plasma Aβ and Aβ-approximate peptide concentrations have been reported to be consistent with amyloid PET results (Kaneko et al., 2014). Moreover, levels of Aβ42 and the ratio of Aβ42:Aβ40 in plasma have been shown to correlate with CSF concentrations and with amyloid PET (Janelidze et al., 2016; Verberk et al., 2018). However, it is important to note that some researchers have found that reduction of Aβ in the periphery does not reduce brain Aβ levels (Georgievska et al., 2015) [but see Jin et al. (2017)].

To date, neurofilament light is the only biomarker that is translatable from plasma to CSF, and therefore holds great promise as a clinical tool to predict cognitive decline and neurodegeneration in AD (**Figure 3**; Zetterberg et al., 2016; Mattsson et al., 2017a; Lewczuk et al., 2018). Furthermore, it has been shown that measurements in blood and CSF levels strongly correlate and that neurofilament light increases coincided with the onset and progression of corresponding amyloid pathology in the brain (**Figure 3**; Bacioglu et al., 2016). Studies have shown that plasma neurofilament light can be used as a non-invasive biomarker that strongly correlates with neurodegeneration in human AD patients (Mattsson et al., 2019). Moreover, plasma t-tau levels can be used for screening and prognosis of cognitive decline in patients where CNS injury has been ruled out (Molinuevo et al., 2018). However, there are decreased amounts of tau in plasma compared to CSF (Barten et al., 2017; Mattsson et al., 2017b), but increases have been found in plasma of AD patients when compared to MCI patients and healthy controls (**Figure 3**; Mattsson et al., 2016; Pase et al., 2019). Studies looking at circulating RNA biomarkers for AD have reported that changes in levels of blood miRNA distinguished AD patients from healthy controls with 93% accuracy (**Figure 3**; Leidinger et al., 2013; Swarbrick et al., 2019). Therefore, blood miRNAs could be an addition to the biomarker toolbox for diagnosing AD patients. For a more extensive review on comparisons between CSF and blood biomarkers in AD, and developments in biochemical analyses of blood, see Ashton et al. (2020).

METHODS FOR CSF SAMPLING

CSF Collection in Human Patients

The most commonly used method for sampling CSF in human patients is by lumbar puncture. Clinically, lumbar punctures are routinely performed for diagnosing multiple brain disorders (e.g., meningitis, encephalitis, multiple sclerosis) and for the administration of spinal anesthesia and chemotherapy. However, there are several limitations associated with the use of lumbar punctures, such as associated pain during and after the sampling (including post-puncture headache) in patients (Blennow et al., 2015). Additionally, CSF sampling in patients who cannot cognitively consent to the procedure is ethically problematic. One also needs to keep in mind that Aβ is higher in lumbar CSF (Brandner et al., 2014), and tau is higher in ventricular CSF (Tarnaris et al., 2011; Pyykkö et al., 2014; Herukka et al., 2015) when using this method for CSF collections. However, the timing of intraventricular CSF sampling will likely affect concentrations of Aβ and tau, for example whether the sample is taken immediately after the insertion of a ventricular catheter. Research suggests that increased ventricular CSF tau concentrations may be caused by the sampling procedure itself, whereby neurons affected by the insertion of the needle for spinal tap increasingly release tau molecules (Brandner et al., 2014). In line with this, CSF samples taken shortly after surgery often have elevated tau and neurofilament light levels (Barten et al., 2017). CSF flow rate is slower in lumbar regions compared to cephalic regions (Sweetman and Linninger, 2011), and this may additionally cause the differences in concentrations of analytes. However, contradictory evidence suggests that p- and t-tau concentrations are 20–30% lover in intraventricular CSF, compared to lumbar CSF, and that this initial upregulation post-surgery is stable in patients irrespective of brain Aβ pathology (Leinonen et al., 2019).

CSF Collection in Animal Models

The most commonly used method for sampling CSF in rodents is collections from the cisterna magna, however, this sampling method usually constitutes a terminal procedure. Collections from the cisterna magna in preclinical models for *in vivo* sampling of CSF have proven a valuable technique for studying treatment outcomes after drug delivery to the CNS. This CSF sampling method offers the advantage of serial sampling without the cofound of anesthesia, with the added benefit of using animals as their intrinsic controls (Amen et al., 2017). Another technique involves inverting animals during CSF collection in order to drain spinal CSF into the cisterna magna (DeMattos et al., 2002). An alternative technique involves collecting CSF by puncturing the membrane by suction using a pipette (DeMattos et al., 2002; Barten et al., 2011). One major limitation of collections from the cisterna magna in preclinical models is the small volume of CSF that can be obtained. In transgenic mice, the average volume is approximately 5–15 μl for terminal sampling (Liu and Duff, 2008). For serial sampling, a maximum of 7–8 μl can be safely taken each time at an interval of 2–3 months (Liu and Duff, 2008).

Microdialysis is an alternative CSF sampling technique, which allows continuous *in vivo* sampling of molecules within the extracellular space (Takeda et al., 2011), which may help circumvent some of the above limitations. Sampling using this method relies on diffusion of analytes across a semi-permeable dialysis membrane (Takeda et al., 2011). This method is advantageous over other CSF sampling techniques as it enables serial sampling that follows the dynamic temporal alterations of a target molecule without necessitating the collection of biopsy samples or sacrifice (Meyding-Lamadé et al., 1996; Trickler and Miller, 2003; Liu et al., 2004; Liu and Duff, 2008). Importantly, each preclinical model can serve as their own intrinsic control in order to reduce inter-animal variability and the number of animals used in experiments. One limitation of this method, however, is detection of large molecules due to adsorption in tubing and the dialysis membrane, as well as low concentration of analytes in the target tissue (Ao and Stenken, 2006). Furthermore, histochemical techniques have revealed that severe gliosis around implanted devices such as microdialysis cannulas takes place at about 4 days after the surgery (Hamberger et al., 1985; Benveniste and Diemer, 1987; Benveniste et al., 1987). Reports suggest that a complete recovery of physiological functions occurs at the earliest at 5–7 days after the implantation surgery (Drijfhout et al., 1995).

CSF AD BIOMARKERS AND TREATMENT

Studies suggest that the neuropathological events that occur in AD may disturb physiological functions of the BBB and thereby distribution of drugs to the brain (Pahnke et al., 2014; Vellonen et al., 2017). Drug molecules in the peripheral circulation are controlled and limited from entry into the brain by the BBB, while dysfunction of the BBB has been associated with neurodegeneration (Vellonen et al., 2017). Furthermore, AD drugs may not be transported to their site of action due to a dysfunctional BBB. This may lead to an increase of the drug in the brain leading to unwanted effects, or decreased drug circulation leading to an insufficient response (Vellonen et al., 2017). Many agents are better dosed directly into the CSF than peripherally because of limited permeability of the drug through the BBB (Barten et al., 2017). The presence of Aβ plaques, brain atrophy and dilated ventricles in the AD brain may affect the distribution of drugs in brain tissue (Vellonen et al., 2017). CSF levels of autophagic markers, Aβ and tau may help select an appropriate AD treatment for the timepoint of diagnosis. The CSF pharmacokinetics of a treatment after administration may show how well the drug entered the CNS. Therefore, levels of CSF autophagic markers or Aβ could be a pharmacodynamic marker of inhibited Aβ production (Dockens et al., 2012; Albright et al., 2013; Coric et al., 2015), and, in a longer term, CSF tau decreases could be a downstream functional marker of reduced neurodegeneration (Riekse et al., 2006).

Assessing Autophagy in CSF Samples

Inductors of autophagy could be used in order to halt or stop the development and progression of Aβ pathology in model systems and patients with AD. Trehalose, an inductor of autophagy, was found to significantly improve memory and learning tasks in APP/PS1 mice (Rami, 2009). Importantly, Aβ deposits were found to be significantly reduced in the hippocampus of these mice (Rami, 2009). Furthermore, the induction of autophagy by rapamycin in another model system was found to improve cognitive performance through the degradation of extracellular Aβ depositions (Rami, 2009), and has been found by others to inhibit tau pathology (Caccamo et al., 2010). In AD, changes in early endocytosis and autophagy can be detected in CSF (Armstrong et al., 2014). Moreover, some work within the AD field has focused on lysosomal proteins, as they can be found in and around amyloid plaques and is present in CSF (Cataldo and Nixon, 1990; Schwagerl et al., 1995). It is now widely believed that the deposition of Aβ is an early initiator of neurodegeneration in AD, thus finding methods that can reduce Aβ or enhance its clearance could be a strong therapeutic target. In this sense, autophagy appears to be the first line of defense against accumulation of Aβ.

Assessing Aβ Pathology in CSF Samples

Cerebrospinal fluid Aβ40 and Aβ42 may be useful (in addition to other biomarkers) in assessing efficacy of drugs such as BACE1 inhibitors, which selectively decrease toxic forms of Aβ (Kennedy et al., 2016). For instance, when CSF levels of Aβ42 are still rising during early stages of amyloid pathology, decreased levels of CSF Aβ42 measured after treatment would show a successful outcome, but at a later stage in amyloid pathology the same finding may indicate accelerated plaque formation (Liu et al., 2004). Anti-amyloid agents are most likely more effective during early AD since deposition of the protein begins many years before diagnosis (Musiek and Holtzman, 2015). Promoting the elimination of Aβ by enzymatic degradation or by clearance enhancement may halt both the aggregation and the accumulation of the peptide (Menendez-Gonzalez et al., 2018). The choroid plexus is known to produce Aβ (Krzyzanowska and Carro, 2012), thus the effect of Aβ synthesis inhibitors on CSF Aβ is bound to reflect changes both sourced in the brain and in the choroid plexus. In addition, evidence suggests that the choroid plexus can remove substances, such as Aβ, from the CSF (Matsumoto et al., 2015).

BACE1 Inhibitors

A potent BACE1 inhibitor known as Verubecestat has been shown to reduce plasma, CSF and brain levels of Aβ40, Aβ42, and soluble APPβ (a direct product of BACE1 enzymatic activity) after short- and long-term administration in rats and monkeys (Kennedy et al., 2016). Recently, a study in healthy elderly AD subjects who received treatment with a BACE1 inhibitor showed no alterations in CSF BACE1 levels following treatment, but revealed a strong link between levels of CSF BACE1 and downstream markers such as CSF Aβ42 (Timmers et al., 2017). Genetic deletion of BACE1 eliminated Aβ production and resolved the amyloid plaques and cognitive deficits observed in transgenic mice over-expressing human APP with familial AD mutations (Dominguez et al., 2005; McConlogue et al., 2007; Ohno et al., 2007). Researchers have demonstrated that long-term BACE1 inhibition diminishes CSF tau levels both in early

depositing APP transgenic mice and APP transgenic mice with moderate Aβ pathology (Schelle et al., 2017). Overall, BACE1 inhibition appears to not only reduce Aβ generation, but also downstream AD neuropathology (Schelle et al., 2017).

γ-Secretase Inhibitors

γ-secretase inhibitors have also proven promising as a therapeutic approach; APP/PS1 mice treated with this compound displayed that a modest decrease (∼30%) of Aβ in ISF was enough to halt amyloid plaque development (Yan et al., 2009). Also, NGP 555 (a γ-secretase inhibitor) has been shown to shift amyloid peptide production to the smaller, non-aggregating forms of amyloid (Olsson et al., 2014; Kounnas et al., 2017). Inhibition of γ-secretase has initially been unsuccessful as a therapeutic target (Cummings, 2010), but more recent compounds have been shown to avoid notch-related toxicity and side effects (Basi et al., 2010; Imbimbo et al., 2010). One failure of slowing Aβ production in patients may be that non-homogenous groups of patients have been included in the trials, and that the treatment has been administered too late in the disease course or has been too short (Bjerke and Engelborghs, 2018). In line with this, some clinical trials have reported changes in CSF Aβ42, but no improvement in clinical endpoints (Ritter and Cummings, 2015).

COMPARATIVE BIOMARKING

Studies aiming to translate findings between AD system models and patients found that tau derived from AD brains injected into susceptible mouse models induced prion-like tau aggregation (Skachokova et al., 2019). CSF from AD or MCI patients injected into the hippocampus of young P301S tau transgenic mice increased tau phosphorylation and NFT formation 4 months following injection. Post-seeding, the injections accentuated tau pathology in the contralateral hippocampus of the mice, indicative of spreading (Skachokova et al., 2019). Other researchers found that peritoneal dialysis reduced plasma Aβ levels in both chronic kidney disease patients and APP/PS1 mice. ISF Aβ levels in APP/PS1 mice immediately decreased after reducing blood Aβ by peritoneal dialysis. The treatment also attenuated other AD-type pathologies, including inflammation, tau hyperphosphorylation, neurodegeneration, synaptic dysfunction, and rescued the behavioral deficits of the mice. Importantly, the Aβ phagocytic function of microglia was enhanced in APP/PS1 mice after peritoneal dialysis (Jin et al., 2017). Current strategies for clearing Aβ focus on introducing agents into the brain (Jin et al., 2017), but this likely causes adverse effects such as neuroinflammation and tissue scarring (Iijima-Ando et al., 2008; Liu et al., 2012), in addition to increased endogenous tau levels.

The ABC Scoring System

Well-characterized mouse models hold great translational value given that identifying patients at preclinical AD stages has proven difficult (Bacioglu et al., 2016). However, there are important differences between species, which should be kept in mind while interpreting results (Barten et al., 2017). The ideal translational model for AD would require Aβ and tau deposition in a pathological manner and disease-relevant accumulation of amyloid plaques and tangles similar to that seen in AD patients (Keene et al., 2016). The ABC scoring system (**Table 2**) can be used to determine the level of AD neuropathological change in both system models and patients. The ABC score is generated by a summary of measures of amyloid plaque distribution A0 to A3 (Thal stages), NFT distribution B0 to B3 (Braak stages), and cortical neuritic plaque density C0 to C3 [Consortium to Establish a Registry for Alzheimer's Disease (CERAD) score] (Keene et al., 2016). The ideal translational model system of human AD would display amyloid plaques and NFTs in a spatial and temporal manner correlating with "no" or "low" AD pathology at early ages, progressing to "intermediate" and "high" AD pathology at older ages or in the presence of gene mutations related to neuropathological development (Keene et al., 2016).

TABLE 2 | The ABC scoring system developed by NIA-AA.

Assessment	NIA-AA scoring
Aβ plaques	A0 (not)
	A1 (low)
	A2 (intermediate)
	A3 (high)
NFTs, including pretangles and threads	B0 (not)
	B1 (low)
	B2 (intermediate)
	B3 (high)
Neuritic and diffuse plaque density	C0 (not)
	C1 (sparse)
	C2 (moderate)
	C3 (frequent)

The scoring system can be used to help assess and validate the neuropathological features of AD in mouse lines that are potential preclinical models for AD research. Reproduced with permission from Keene et al. (2016). NIA-AA, Alzheimer's Association; Aβ, amyloid-β; NFT, neurofibrillary tangle.

In terms of the specifics of the ABC scoring system (**Table 2**), scoring of diffuse Aβ plaques is based on assessment in the cerebral cortex, hippocampus, striatum, midbrain, brainstem, and cerebellum (**Box 1**) according to staging established by Thal et al. (2002) resulting in a Thal phase 0–5, which is translated into the NIA-AA score of A0-A3. Meanwhile, scores for NFTs are determined in the *trans*-entorhinal cortex, corpora ammonis, fronto-parietal cortex, and primary visual cortex (**Box 1**) to generate a Braak stage (Braak and Braak, 1991), which is translated into the NIA-AA score of B0-B3. Since most existing mouse models do not generate NFTs, the NIH have developed a modified B score for p-tau pathology, including distribution of pre-tangles and threads. In addition, most existing mouse models do not form neuritic plaques (contains fibrillar Aβ), so a C score for CERAD (Sperling et al., 2011) neuritic plaque density (none, sparse, moderate, or frequent) and a modified C score for diffuse plaque (does not contain fibrillar Aβ) density are generated from frontal and parietal cortex. Considering that behavioral data from mice have replication issues and are challenging to translate to patients, memory testing *per se* should not constitute a validation criterion or a drug testing endpoint (Keene et al., 2016).

CSF Collection Methods

When translating CSF biomarkers between system models and patients, an advantage with subcutaneous access systems is that drugs can be dosed and also samples can be obtained from unanesthetized animals, as is typical with humans, and without the confound of anesthesia on CSF production or flow. It has been shown that anesthesia can cause disturbances in neurotransmitter density and cell metabolism, and therefore most times, it is desirable to perform experiments on non-anesthetized animals (Kehr, 1999). It is important to note that in most rodent studies, CSF is collected from the cisterna magna above the spinal column, whereas in humans most CSF is collected from the lumbar spinal vertebrae, and therefore drainage from this latter area in preclinical models has a translational advantage (Barten et al., 2017).

Due to the difficulties in collecting CSF samples from preclinical models the quality of the sample may be comprised, and therefore should be tested. The quality of the sample is most often affected by blood and brain-derived protein contamination (Barten et al., 2017). It is critical to minimize blood-contamination when analytes of interest are found in much higher concentration in the blood compared to the CSF, such as the 1:50,000-fold gradient of tau. Another major contamination source of CSF is proteins released in the brain during the collection procedure; this has a higher impact on tau levels compared to Aβ (Barten et al., 2005).

Furthermore, biomarker development for clinical utility is currently being hampered as comparisons of measurements and techniques between laboratories tend to be unreliable. Factors that may induce variability include storage in different tube types, different aliquot volumes, and the number of freeze-thaw cycles performed, which significantly influences CSF biomarker concentrations (Clough, 2005; Bjerke and Engelborghs, 2018). For instance, CSF Aβ42 measures have been found to be greatly influenced by pre-analytical factors such as the type of collection tube used and the number of freeze-thaw cycles of the sample (Perret-Liaudet et al., 2012b; Toombs et al., 2013; Leitão et al., 2015). Various studies have determined the importance of tube types when collecting CSF samples, highlighting that it is crucial to use polypropylene vials (Perret-Liaudet et al., 2012a), and that the tubes are filled to enhance the volume to surface ratio (Perret-Liaudet et al., 2012a). Ultimately there is poor standardization of biobanking protocols and assay consistency, a fact that hampers novel biomarker discoveries and replication of important findings (Teunissen et al., 2018).

One of the reasons why non-human primates are being preferred over canine or rodent species in CSF studies is that they share an upright orientation of the spinal column akin to humans (Spector et al., 2015). Moreover, the difference in brain size (and thereby CSF volume) between mice and humans is over 3000 times, whereas macaque brains are 10- to 20-fold smaller than human brains. Therefore, the distance from the CSF compartments to deeper regions of the brain significantly varies across species and likely influences the exchange analytes (Spector et al., 2015). Nevertheless, most differences across species are otherwise minor, including the volume ratio of CSF to the brain, ranging from 9 to 18% across species (Barten et al., 2017). CSF turnover per day is also similar between humans and macaques, but is approximately 2-fold higher for rats and 3-fold higher for mice (Barten et al., 2017). The higher turnover rate for rodents can be explained by movement of CSF initiated by the ventricles and arterial pressure as a result of a fast heartbeat, which creates an increase in back- and-forth movement of the CSF (Feinberg and Mark, 1987; Sweetman and Linninger, 2011).

The Physiology of CSF

The exchange of CSF analytes (including therapeutics) may be highly different between patients and rodents as the latter have a much faster heart rate. However, this factor has not been studied. Non-human primates are most likely better preclinical *in vivo* models for biomarker translation because body weight-based allometric scaling is comparable (Karelina et al., 2017). Moreover, ventricular CSF from AD patients has been found to contain a rare high-molecular-weight tau species that was found to exert high seeding activity (Takeda et al., 2016). This needs to be kept in mind when comparing CSF samples gathered from different regions. Moreover, the sleep-wake cycle regulates ISF and CSF levels of Aβ in AD (Holth et al., 2019), and it has been shown that chronic sleep deprivation increases Aβ plaques. Mouse ISF tau was found to increase ∼90% during normal wakefulness versus sleep and ∼100% during sleep deprivation. The relevant study found that sleep deprivation significantly increased CSF Aβ by 30% (Lucey et al., 2018). This means that the time of day is bound to influence Aβ levels in CSF, which suggests that the timing of sampling needs to be chosen with care and kept consistent between clinical sampling and experiments for correct comparisons.

The Efficacy of Drugs

One major drawback of comparative biomarking is the translatability of AD drugs from animal models to human clinical trials. Compared to preclinical models, AD pathology in patients develops over decades rather than over months. Longitudinal studies in AD system models may determine the initiation and progression of biomarkers that allow for evaluation of disease-modifying drugs. For example, research shows that BACE1 inhibitors can decrease both plasma and CSF Aβ40 and Aβ42 concentrations in mice, guinea pigs (Tagawa et al., 1991), and non-human primates (Sankaranarayanan et al., 2009; Gravenfors et al., 2012; Jeppsson et al., 2012; Wu et al., 2012). A separate study found that a γ-secretase inhibitor reduced CSF Aβ production in rhesus monkeys without a subsequent rise in Aβ production (Cook et al., 2010). Candidates for therapeutics could be further addressed by extending these findings to translational transgenic AD models and may ultimately offer insights into mechanisms of the disease. Furthermore, increased plasma levels of interleukin-10 has been shown following Aβ immunotherapy in Tg2576 mice (Town et al., 2002; Kim et al., 2007). In a separate study, researchers found that peripheral structures play important roles in clearing Aβ sourced from the brain, suggesting that removing Aβ from the blood may also be effective as an AD therapy (Jin et al., 2017).

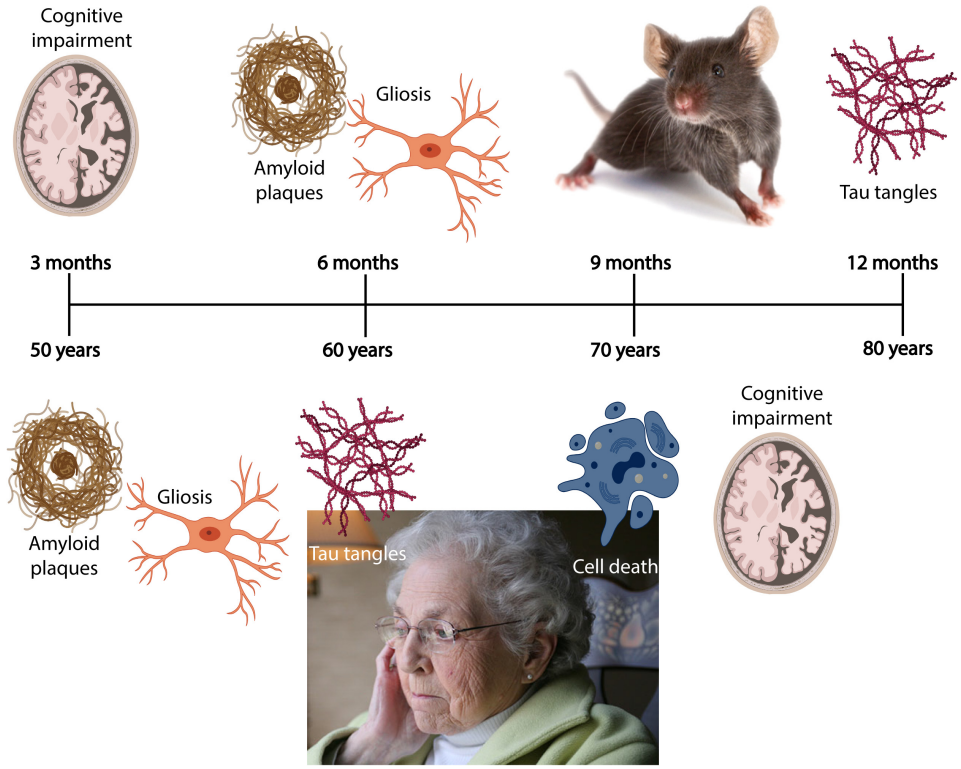

FIGURE 4 | A comparison of pathology and subsequent symptoms along the AD disease cascade between a preclinical model and patients. In the 3xTg AD mouse model (Oddo et al., 2003), cognitive impairment is observed at 3 months of age, whereas amyloid plaques and gliosis are present at 6 months of age. Tau pathology is first present at 12 months of age. In the typical sporadic AD patient, amyloid plaques and associated gliosis may be abundant at 50 years of age, and this pathology is followed by NFTs at approximately 60 years of age. Between 70 and 80 years of age, neurodegeneration occurs, and cognitive impairment becomes prominent in patients. AD, Alzheimer's disease; NFTs, neurofibrillary tangles. Images were generated using BioRender or taken from a public database.

γ-secretase modulators have proven especially useful as therapeutic candidates because they do not alter the total amount of Aβ peptides produced by γ-secretase activity, instead, they spare the products of other γ-secretase processing, such as notch (Toyn et al., 2016). Importantly, these compounds do not accelerate the production of the potentially toxic product BACE1-C-terminal fragment (C99) (Toyn et al., 2016). In all species, research suggests that γ-secretase modulator treatment decrease Aβ42 and Aβ40 levels while increasing Aβ38 and Aβ37 by a corresponding amount. Therefore, the mechanism of action of γ-secretase modulators may translate well across species, validating its therapeutic strategy for utility in AD (Toyn et al., 2016).

Other translational research across species has shown increased levels of plasma interleukin-10 following Aβ immunotherapy in Tg2576 mice (Town et al., 2002; Kim et al., 2007). Thereby, translation of inflammatory mechanisms and their peripheral markers may benefit from investigation of changes in microglial markers. However, when interpreting and comparing immune markers from mice caution is warranted, as recent evidence suggests that these markers do not translate well to human inflammatory diseases (Seok et al., 2013). Moreover, increased levels of isoprostanes have been shown in Tg2576 mice prior to plaque formation (Pratico et al., 2001), suggesting isoprostane levels may be useful as a predictive biomarker. Neurofilament light in bodily fluid constitutes a biomarker of neurodegeneration reflecting its translational value in system models and in clinical settings (Bacioglu et al., 2016).

Comparative AD Neuropathology

The earliest (current) detectable Aβ deposition in humans is the formation of diffuse plaques, whereas in the brain of Tg2576 mice diffuse plaques are not observed until 12 months of age, which is 4 months after biochemically detectable alterations of Aβ (Kawarabayashi et al., 2001). The most common observation in AD patients is minor amounts of Aβ40 deposited in the brain, whereas in 33% of patients great amounts of this Aβ variant are detected. Intriguingly, this latter group of patients also display substantial amyloid angiopathy (amyloid build up on the walls of the arteries in the brain) (Gravina et al., 1995). Similarly, the Tg2576 mouse model displays marked angiopathy and the deposition of a large amount of Aβ40 (Gravina et al., 1995). Generally CSF Aβ40 levels are much higher in patients compared to mice, while brain concentrations are similar (Karelina et al., 2017). In terms of plasma concentrations of Aβ40, this is highly similar between patients and mice, and therefore the greater Aβ40 concentrations observed in human CSF may likely reflect a higher brain production of the peptide (Karelina et al., 2017).

In terms of the similarity between system models and patients, and specifically transgenic mice and human patients, mice and humans share virtually the same set of genes. Almost every gene found in mice or humans has been observed in a closely related form in the other. To look directly at differences along the AD disease cascade, we compare pathological events between the 3xTg AD mouse model and sporadic AD patients (**Figure 4**). The 3xTg AD mouse model develops amyloid and tau pathology, including amyloid plaques and NFTs (Oddo et al., 2003). At 3 months of age these mice have developed cognitive impairment (Oddo et al., 2003), whereas at approximately 50 years of age an AD patient has developed amyloid plaques and gliosis (Braak and Del Trecidi, 2015). At 6 months of age, the mice develop amyloid plaques and gliosis (Oddo et al., 2003), while patients develop tau tangles at approximately 60 years of age (Braak and Del Trecidi, 2015). At 70 years of age, patients usually suffer from neurodegeneration because of the presence of tau tangles and exhibit cognitive impairment (Braak and Del Trecidi, 2015). First at 12 months of age will the mice develop tau tangles (Oddo et al., 2003).

There are two important differences observed along the AD disease cascade between the species: first, mice exhibit cognitive impairment prior to tau tangles, whereas cognitive impairment is most likely a result from neurodegeneration caused by NFTs in human patients. Second, one does not observe neuronal death in this mouse model, while neuronal death is thought to be the sole causative pathology for symptom development in AD patients. In line with this, by comparing CSF, plasma and *in vivo* amyloid imaging, cross-sectional data obtained at baseline in individuals from AD families enrolled in the Dominantly Inherited Alzheimer Network (DIAN) show lower concentrations of CSF Aβ42 when amyloid plaques accumulate, and elevated concentrations of CSF t-tau and p-tau in mutation carriers 10–20 years prior to symptom onset and detection of cognitive deficits (Fagan et al., 2014). This highlights the need for longitudinal CSF sampling in animals modeling AD, in order to compare biochemical, imaging and behavioral tests against each other, and eventually to patients. However, given the difficulty of identifying patients at preclinical AD stages, it is important to remember that well-characterized preclinical disease models hold great translational value (Mattsson et al., 2017a).

CONCLUSION AND FUTURE DIRECTIONS

Clearly, there is a pressing need for better quality data from model systems investigating biomarkers that can be directly translated to human biomarkers. The core biomarkers (Aβ42, t-tau, and p-tau) have been found to translate well across species, whereas biomarkers of inflammation translate to a lesser extent between mouse models and patients. Researchers should use autophagic and synaptic degeneration markers when analyzing samples from preclinical models because these markers appear promising in predicting development of AD. Changes in levels of autophagic markers and neurofilament light correlate strongly with the core biomarkers of AD, and other novel biomarkers should be tested in combination in preclinical models to validate findings observed in patients. Currently, non-invasive structural and functional imaging can detect AD onset and longitudinally monitor disease progression in AD patients. By the combination of early predictive CSF biomarkers, imaging modalities can be strengthened in their ability to characterize patients along the disease cascade. Additional non-invasive methods for detecting AD biomarkers need to be established, such as blood sampling, which could be used in combination with CSF sampling. CSF sampling is invasive but reflects changes in protein levels in the brain to a greater extent compared to blood-based markers. Another advantage of CSF sampling compared to blood testing is that Aβ is found in the periphery, so it is difficult to differentiate between brain- and periphery-based Aβ levels. Additionally, there are greater levels of tau in ISF compared to CSF, so this needs to be controlled for when analyzing CSF samples. Neurofilament light is transferable between CSF and plasma in humans, but this needs to be verified in system models.

Furthermore, large inter- and intra-laboratory variations in biomarker sampling may have great consequences in terms of comparisons of results, while within individual laboratories such variations may affect planning and interpretations of longitudinal studies (Blennow et al., 2015). One also needs to consider differences in the CSF sampling methods used, given that protein levels differ between ventricular and lumbar CSF. Studies have shown that changes in the levels of core biomarkers as measured in CSF may be useful for assessing the efficacy of drugs. When translating findings across species, it is important to use the same scoring or grouping system when assessing changes in biomarkers and observed neuropathology. Ultimately, an early diagnosis by utilizing biomarkers detectable at this stage of disease will be the cornerstone for early identification of patients that are regressing away from the prodromal stage of AD (Teunissen et al., 2018). There is a need for continued progress within the AD biomarker field so that markers can be translated across animal models and clinical populations to serve as a translational bridge between model systems and clinical populations (Sabbagh et al., 2013). We still cannot translate all pathological hallmarks seen in AD patients to preclinical models, and we therefore need to be aware of pertinent differences when comparing AD research across species and bringing findings into the clinic.

AUTHOR CONTRIBUTIONS

All authors contributed to the content of the article, and critically reviewed and edited the manuscript.

FUNDING

This work was supported by the Liaison Committee for Education, Research and Innovation in Central Norway (Samarbeidsorganet HMN- NTNU) grant number 2018/42794.

ACKNOWLEDGMENTS

The authors would like to acknowledge support by the Liaison Committee for Education, Research and Innovation in Central Norway (Samarbeidsorganet HMN-NTNU), and the Joint Research Committee between St. Olavs Hospital and the Faculty of Medicine and Health Sciences, NTNU.

REFERENCES

Afanador, L., Roltsch, E. A., Holcomb, L., Campbell, K. S., Keeling, D. A., Zhang, Y., et al. (2014). The Ca2+ sensor S100A1 modulates neuroinflammation, histopathology and Akt activity in the PSAPP Alzheimer's disease mouse model. *Cell Calcium.* 56, 68–80. doi: 10.1016/j.ceca.2014.05.002

Ahmed, Z., Cooper, J., Murray, T. K., Garn, K., McNaughton, E., Clarke, H., et al. (2014). A novel in vivo model of tau propagation with rapid and progressive neurofibrillary tangle pathology: the pattern of spread is determined by connectivity, not proximity. *Acta Neuropathol.* 127, 667–683. doi: 10.1007/s00401-014-1254-6

Akama, K., and Van Eldik, L. (2000). β-Amyloid stimulation of Inducible nitric-oxide synthase in astrocytes Is interleukin-1β- and tumor necrosis factor-α (TNFα)-dependent, and involves a TNFα receptor-associated factor- and nfκb-inducing kinase-dependent signaling mechanism. *J. Biol. Chem.* 275, 7918–7924. doi: 10.1074/jbc.275.11.7918

Akiyama, H., Barger, S., Barnum, S., Bradt, B., Bauer, J., Cole, G. M., et al. (2000). Inflammation and Alzheimer's disease. *Neurobiol. Aging* 21, 383–421. doi: 10.1016/s0197-4580(00)00124-x

Albright, C. F., Dockens, R. C., Meredith, J. E., Olson, R. E., Slemmon, R., Lentz, K. A., et al. (2013). Pharmacodynamics of selective inhibition of γ-secretase by avagacestat. *J. Pharmacol. Exp. Ther.* 344, 686–695. doi: 10.1124/jpet.112.199356

Alcolea, D., Vilaplana, E., Suarez-Calvet, M., Illan-Gala, I., Blesa, R., Clarimon, J., et al. (2017). CSF sAPPbeta, YKL-40, and neurofilament light in frontotemporal lobar degeneration. *Neurology* 89, 178–188. doi: 10.1212/wnl.0000000000004088

Alzheimer, A., Stelzmann, R. A., Schnitzlein, H. N., and Murtagh, F. R. (1995). An English translation of Alzheimer's 1907 paper, "Uber eine eigenartige Erkankung der Hirnrinde. *Clin. Anat.* 8, 429–431. doi: 10.1002/ca.980080612

Amador-Ortiz, C., Lin, W. L., Ahmed, Z., Personett, D., Davies, P., Duara, R., et al. (2007). TDP-43 immunoreactivity in hippocampal sclerosis and Alzheimer's disease. *Ann. Neurol.* 61, 435–445. doi: 10.1002/ana.21154

Amen, E. M., Brecheisen, M., Sach-Peltason, L., and Bergadano, A. (2017). Refinement of a model of repeated cerebrospinal fluid collection in conscious rats. *Lab. Anim.* 51, 44–53. doi: 10.1177/0023677216646069

Anderson, P. J., Watts, H. R., Jen, S., Gentleman, S. M., Moncaster, J. A., Walsh, D. T., et al. (2009). Differential effects of interleukin-1beta and S100B on amyloid precursor protein in rat retinal neurons. *Clin. Ophthalmol.* 3, 235–242. doi: 10.2147/opth.s2684

Andersson, C., Blennow, K., Almkvist, O., Andreasen, N., Engfeldt, P., Johansson, S. E., et al. (2008). Increasing CSF phospho-tau levels during cognitive decline and progression to dementia. *Neurobiol. Aging* 29, 1466–1473. doi: 10.1016/j.neurobiolaging.2007.03.027

Andreasen, N., Hesse, C., Davidsson, P., Minthon, L., Wallin, A., Winblad, B., et al. (1999a). Cerebrospinal fluid beta-amyloid(1-42) in Alzheimer disease: differences between early- and late-onset Alzheimer disease and stability during the course of disease. *Arch. Neurol.* 56, 673–680. doi: 10.1001/archneur.56.6.673

Andreasen, N., Minthon, L., Clarberg, A., Davidsson, P., Gottfries, J., Vanmechelen, E., et al. (1999b). Sensitivity, specificity, and stability of CSF-tau in AD in a community-based patient sample. *Neurology* 53, 1488–1494. doi: 10.1212/wnl.53.7.1488

Andreasen, N., Vanmechelen, E., Van de Voorde, A., Davidsson, P., Hesse, C., Tarvonen, S., et al. (1998). Cerebrospinal fluid tau protein as a biochemical marker for Alzheimer's disease: a community based follow up study. *J. Neurol. Neurosurg. Psychiatry* 64, 298–305. doi: 10.1136/jnnp.64.3.298

Ao, X., and Stenken, J. A. (2006). Microdialysis sampling of cytokines. *Methods* 38, 331–341. doi: 10.1016/j.ymeth.2005.11.012

Armstrong, A., Mattsson, N., Appelqvist, H., Janefjord, C., Sandin, L., Agholme, L., et al. (2014). Lysosomal network proteins as potential novel CSF biomarkers for Alzheimer's disease. *Neuromol. Med.* 16, 150–160. doi: 10.1007/s12017-013-8269-3

Arriagada, P. V., Growdon, J. H., Hedley-Whyte, E. T., and Hyman, B. T. (1992). Neurofibrillary tangles but not senile plaques parallel duration and severity of Alzheimer's disease. *Neurology* 42, 631–639. doi: 10.1212/wnl.42.3.631

Asai, H., Ikezu, S., Tsunoda, S., Medalla, M., Luebke, J., Haydar, T., et al. (2015). Depletion of microglia and inhibition of exosome synthesis halt tau propagation. *Nat. Neurosci.* 18, 1584–1593. doi: 10.1038/nn.4132

Ashton, N. J., Hye, A., Rajkumar, A. P., Leuzy, A., Snowden, S., Suárez-Calvet, M., et al. (2020). An update on blood-based biomarkers for non-Alzheimer neurodegenerative disorders. *Nat. Rev. Neurol.* 16, 265–284. doi: 10.1038/s41582-020-0348-0

Avila, J., Lucas, J. J., Perez, M., and Hernandez, F. (2004). Role of tau protein in both physiological and pathological conditions. *Physiol. Rev.* 84, 361–384. doi: 10.1152/physrev.00024.2003

Bacioglu, M., Maia, L. F., Preische, O., Schelle, J., Apel, A., Kaeser, S. A., et al. (2016). Neurofilament light chain in blood and csf as marker of disease progression in mouse models and in neurodegenerative diseases. *Neuron* 91, 56–66. doi: 10.1016/j.neuron.2016.05.018

Bakota, L., and Brandt, R. (2016). Tau biology and Tau-Directed therapies for Alzheimer's disease. *Drugs* 76, 301–313. doi: 10.1007/s40265-015-0529-0

Barten, D. M., Cadelina, G. W., and Weed, M. R. (2017). Dosing, collection, and quality control issues in cerebrospinal fluid research using animal models. *Handb. Clin. Neurol.* 146, 47–64. doi: 10.1016/B978-0-12-804279-3.00004-6

Barten, D. M., Cadelina, G. W., Hoque, N., DeCarr, L. B., Guss, V. L., Yang, L., et al. (2011). Tau transgenic mice as models for cerebrospinal fluid tau biomarkers. *J. Alzheimers Dis.* 24(Suppl. 2), 127–141. doi: 10.3233/JAD-2011-110161

Barten, D. M., Guss, V. L., Corsa, J. A., Loo, A., Hansel, S. B., Zheng, M., et al. (2005). Dynamics of {beta}-amyloid reductions in brain, cerebrospinal fluid, and plasma of {beta}-amyloid precursor protein transgenic mice treated with a {gamma}-secretase inhibitor. *J. Pharmacol. Exp. Ther.* 312, 635–643. doi: 10.1124/jpet.104.075408

Basi, G. S., Hemphill, S., Brigham, E. F., Liao, A., Aubele, D. L., Baker, J., et al. (2010). Amyloid precursor protein selective gamma-secretase inhibitors for treatment of Alzheimer's disease. *Alzheimers Res. Ther.* 2:36. doi: 10.1186/alzrt60

Bateman, R. J., Xiong, C., Benzinger, T. L. S., Fagan, A. M., Goate, A., Fox, N. C., et al. (2012). Clinical and biomarker changes in dominantly inherited Alzheimer's disease. *N. Engl J. Med.* 367, 795–804. doi: 10.1056/NEJMoa1202753

Bazan, J. F., Bacon, K. B., Hardiman, G., Wang, W., Soo, K., Rossi, D., et al. (1997). A new class of membrane-bound chemokine with a CX3C motif. *Nature* 385, 640–644. doi: 10.1038/385640a0

Beckett, L. A., Harvey, D. J., Gamst, A., Donohue, M., Kornak, J., Zhang, H., et al. (2010). The Alzheimer's Disease Neuroimaging Initiative: annual change in biomarkers and clinical outcomes. *Alzheimers Dement.* 6, 257–264. doi: 10.1016/j.jalz.2010.03.002

Benilova, I., Karran, E., and De Strooper, B. (2012). The toxic abeta oligomer and Alzheimer's disease: an emperor in need of clothes. *Nat. Neurosci.* 15, 349–357. doi: 10.1038/nn.3028

Benveniste, H., and Diemer, N. H. (1987). Cellular reactions to implantation of a microdialysis tube in the rat hippocampus. *Acta Neuropathol.* 74, 234–238. doi: 10.1007/bf00688186

Benveniste, H., Drejer, J., Schousboe, A., and Diemer, N. H. (1987). Regional cerebral glucose phosphorylation and blood flow after insertion of a microdialysis fiber through the dorsal hippocampus in the rat. *J. Neurochem.* 49, 729–734. doi: 10.1111/j.1471-4159.1987.tb00954.x

Bian, H., Van Swieten, J. C., Leight, S., Massimo, L., Wood, E., Forman, M., et al. (2008). CSF biomarkers in frontotemporal lobar degeneration with known pathology. *Neurology* 70, 1827–1835. doi: 10.1212/01.wnl.0000311445.21321.fc

Billings, L. M., Oddo, S., Green, K. N., McGaugh, J. L., and LaFerla, F. M. (2005). Intraneuronal Abeta causes the onset of early Alzheimer's disease-related cognitive deficits in transgenic mice. *Neuron* 45, 675–688. doi: 10.1016/j.neuron.2005.01.040

Biswal, B., Zerrin Yetkin, F., Haughton, V. M., and Hyde, J. S. (1995). Functional connectivity in the motor cortex of resting human brain using echo-planar mri. *Magn. Reson. Med.* 34, 537–541. doi: 10.1002/mrm.1910340409

Bjerke, M., and Engelborghs, S. (2018). Cerebrospinal fluid biomarkers for early and differential Alzheimer's disease diagnosis. *J. Alzheimers Dis.* 62, 1199–1209. doi: 10.3233/JAD-170680

Blennow, K., and Hampel, H. (2003). CSF markers for incipient Alzheimer's disease. *Lancet Neurol.* 2, 605–613. doi: 10.1016/s1474-4422(03)00530-1

Blennow, K., Dubois, B., Fagan, A. M., Lewczuk, P., de Leon, M. J., and Hampel, H. (2015). Clinical utility of cerebrospinal fluid biomarkers in the diagnosis of early Alzheimer's disease. *Alzheimers Dement.* 11, 58–69. doi: 10.1016/j.jalz.2014.02.004

Block, M. L., Zecca, L., and Hong, J. S. (2007). Microglia-mediated neurotoxicity: uncovering the molecular mechanisms. *Nat. Rev. Neurosci.* 8, 57–69. doi: 10.1038/nrn2038

Bolos, M., Llorens-Martin, M., Perea, J. R., Jurado-Arjona, J., Rabano, A., Hernandez, F., et al. (2017). Absence of CX3CR1 impairs the internalization of Tau by microglia. *Mol. Neurodegener.* 12:59. doi: 10.1186/s13024-017-0200-1

Boom, A., Pochet, R., Authelet, M., Pradier, L., Borghgraef, P., Van Leuven, F., et al. (2004). Astrocytic calcium/zinc binding protein S100A6 over expression in Alzheimer's disease and in PS1/APP transgenic mice models. *Biochim. Biophys. Acta* 1742. doi: 10.1016/j.bbamcr.2004.09.011

Bouwman, F. H., van der Flier, W. M., Schoonenboom, N. S., van Elk, E. J., Kok, A., Rijmen, F., et al. (2007). Longitudinal changes of CSF biomarkers in memory clinic patients. *Neurology* 69, 1006–1011. doi: 10.1212/01.wnl.0000271375.37131.04

Bozzali, M., Falini, A., Franceschi, M., Cercignani, M., Zuffi, M., Scotti, G., et al. (2002). White matter damage in Alzheimer's disease assessed in vivo using diffusion tensor magnetic resonance imaging. *J. Neurol. Neurosurg. Psychiatry* 72, 742–746. doi: 10.1136/jnnp.72.6.742

Braak, H., and Braak, E. (1991). Neuropathological stageing of Alzheimer-related changes. *Acta Neuropathol.* 82, 239–259. doi: 10.1007/bf00308809

Braak, H., and Braak, E. (1997). Frequency of stages of Alzheimer-related lesions in different age categories. *Neurobiol. Aging* 18, 351–357. doi: 10.1016/s0197-4580(97)00056-0

Braak, H., and Del Trecidi, K. (2015). Neuroanatomy and pathology of sporadic Alzheimer's disease. *Adv. Anat. Embryol. Cell Biol.* 215, 1–162.

Brandner, S., Thaler, C., Lelental, N., Buchfelder, M., Kleindienst, A., Maler, J. M., et al. (2014). Ventricular and lumbar cerebrospinal fluid concentrations of Alzheimer's disease biomarkers in patients with normal pressure hydrocephalus and posttraumatic hydrocephalus. *J. Alzheimers Dis.* 41, 1057–1062. doi: 10.3233/JAD-132708

Brinker, T., Stopa, E., Morrison, J., and Klinge, P. (2014). A new look at cerebrospinal fluid circulation. *Fluids Barriers CNS* 11:10. doi: 10.1186/2045-8118-11-10

Brinkmalm, A., Brinkmalm, G., Honer, W. G., Frolich, L., Hausner, L., Minthon, L., et al. (2014). SNAP-25 is a promising novel cerebrospinal fluid biomarker for synapse degeneration in Alzheimer's disease. *Mol. Neurodegener.* 9:53. doi: 10.1186/1750-1326-9-53

Bronzuoli, M. R., Iacomino, A., Steardo, L., and Scuderi, C. (2016). Targeting neuroinflammation in Alzheimer's disease. *J. Inflamm. Res.* 9, 199–208. doi: 10.2147/jir.S86958

Brys, M., Pirraglia, E., Rich, K., Rolstad, S., Mosconi, L., Switalski, R., et al. (2009). Prediction and longitudinal study of CSF biomarkers in mild cognitive impairment. *Neurobiol. Aging* 30, 682–690. doi: 10.1016/j.neurobiolaging.2007.08.010

Buchhave, P., Minthon, L., Zetterberg, H., Wallin, A. K., Blennow, K., and Hansson, O. (2012). Cerebrospinal fluid levels of beta-amyloid 1-42, but not of tau, are fully changed already 5 to 10 years before the onset of Alzheimer dementia. *Arch. Gen. Psychiatry* 69, 98–106. doi: 10.1001/archgenpsychiatry.2011.155

Buckner, R. L., Andrews-Hanna, J. R., and Schacter, D. L. (2008). The brain's default network: anatomy, function, and relevance to disease. *Ann. N.Y. Acad. Sci.* 1124, 1–38. doi: 10.1196/annals.1440.011

Buerger, K., Ewers, M., Pirttila, T., Zinkowski, R., Alafuzoff, I., Teipel, S. J., et al. (2006). CSF phosphorylated tau protein correlates with neocortical neurofibrillary pathology in Alzheimer's disease. *Brain* 129, 3035–3041. doi: 10.1093/brain/awl269

Caccamo, A., Majumder, S., Richardson, A., Strong, R., and Oddo, S. (2010). Molecular interplay between mammalian target of rapamycin (mTOR), amyloid-beta, and Tau: effects on cognitive impairments. *J. Biol. Chem.* 285, 13107–13120. doi: 10.1074/jbc.M110.100420

Calsolaro, V., and Edison, P. (2016). Neuroinflammation in Alzheimer's disease: current evidence and future directions. *Alzheimers Dement.* 12, 719–732. doi: 10.1016/j.jalz.2016.02.010

Campioni, S., Mannini, B., Zampagni, M., Pensalfini, A., Parrini, C., Evangelisti, E., et al. (2010). A causative link between the structure of aberrant protein oligomers and their toxicity. *Nat. Chem. Biol.* 6, 140–147. doi: 10.1038/nchembio.283

Cataldo, A. M., and Nixon, R. A. (1990). Enzymatically active lysosomal proteases are associated with amyloid deposits in Alzheimer brain. *Proc. Natl. Acad. Sci. U.S.A.* 87, 3861–3865. doi: 10.1073/pnas.87.10.3861

Chang, K. A., Kim, H. J., and Suh, Y. H. (2012). The role of S100a9 in the pathogenesis of Alzheimer's disease: the therapeutic effects of S100a9 knockdown or knockout. *Neurodegener. Dis.* 10, 27–29. doi: 10.1159/000333781

Chang, X.-L., Tan, M.-S., Tan, L., and Yu, J.-T. (2015). The role of TDP-43 in Alzheimer's disease. *Mol. Neurobiol.* 53, 3349–3359.

Chen, J. J., Zhao, B., Zhao, J., and Li, S. (2017). Potential roles of exosomal MicroRNAs as diagnostic biomarkers and therapeutic application in Alzheimer's disease. *Neural Plast.* 2017:7027380. doi: 10.1155/2017/7027380

Chen, M., Inestrosa, N. C., Ross, G. S., and Fernandez, H. L. (1995). Platelets are the primary source of amyloid beta-peptide in human blood. *Biochem. Biophys. Res. Commun.* 213, 96–103. doi: 10.1006/bbrc.1995.2103

Cho, H., Choi, J. Y., Hwang, M. S., Kim, Y. J., Lee, H. M., Lee, H. S., et al. (2016). In vivo cortical spreading pattern of tau and amyloid in the Alzheimer disease spectrum. *Ann. Neurol.* 80, 247–258. doi: 10.1002/ana.24711

Cho, S.-J., Lim, H. J., Jo, C., Park, M. H., Han, C., and Koh, Y. H. (2019). Plasma ATG5 is increased in Alzheimer's disease. *Sci. Rep.* 9:4741. doi: 10.1038/s41598-019-41347-2

Chua, T. C., Wen, W., Slavin, M. J., and Sachdev, P. S. (2008). Diffusion tensor imaging in mild cognitive impairment and Alzheimer's disease: a review. *Curr. Opin. Neurol.* 21, 83–92. doi: 10.1097/WCO.0b013e3282f4594b

Cirrito, J. R., May, P. C., O'Dell, M. A., Taylor, J. W., Parsadanian, M., Cramer, J. W., et al. (2003). In vivo assessment of brain interstitial fluid with microdialysis reveals plaque-associated changes in amyloid-beta metabolism and half-life. *J Neurosci.* 23, 8844–8853.

Clark, C. M., Xie, S., Chittams, J., Ewbank, D., Peskind, E., Galasko, D., et al. (2003). Cerebrospinal fluid tau and beta-amyloid: how well do these biomarkers reflect autopsy-confirmed dementia diagnoses? *Arch. Neurol.* 60, 1696–1702. doi: 10.1001/archneur.60.12.1696

Clavaguera, F., Akatsu, H., Fraser, G., Crowther, R. A., Frank, S., Hench, J., et al. (2013). Brain homogenates from human tauopathies induce tau inclusions in mouse brain. *Proc. Natl. Acad. Sci. U.S.A.* 110, 9535–9540. doi: 10.1073/pnas.1301175110

Clough, G. F. (2005). Microdialysis of large molecules. *AAPS J.* 7, E686–E692. doi: 10.1208/aapsj070369

Cook, J. J., Wildsmith, K. R., Gilberto, D. B., Holahan, M. A., Kinney, G. G., Mathers, P. D., et al. (2010). Acute gamma-secretase inhibition of nonhuman primate CNS shifts amyloid precursor protein (APP) metabolism from amyloid-beta production to alternative APP fragments without amyloid-beta rebound. *J. Neurosci.* 30, 6743–6750. doi: 10.1523/jneurosci.1381-10.2010

Coric, V., Salloway, S., van Dyck, C. H., Dubois, B., Andreasen, N., Brody, M., et al. (2015). Targeting prodromal Alzheimer Disease with avagacestat: a randomized clinical trial. *JAMA Neurol.* 72, 1324–1333. doi: 10.1001/jamaneurol.2015.0607

Craig-Schapiro, R., Perrin, R. J., Roe, C. M., Xiong, C., Carter, D., Cairns, N. J., et al. (2010). YKL-40: a novel prognostic fluid biomarker for preclinical Alzheimer's disease. *Biol. Psychiatry* 68, 903–912. doi: 10.1016/j.biopsych.2010.08.025

Cristovao, J. S., Morris, V. K., Cardoso, I., Leal, S. S., Martinez, J., Botelho, H. M., et al. (2018). The neuronal S100B protein is a calcium-tuned suppressor of amyloid-beta aggregation. *Sci. Adv.* 4, eaaq1702. doi: 10.1126/sciadv.aaq1702

Cummings, J. (2010). What can be inferred from the interruption of the semagacestat trial for treatment of Alzheimer's disease? *Biol. Psychiatry* 68, 876–878. doi: 10.1016/j.biopsych.2010.09.020

Davies, P., Resnick, J., Resnick, B., Gilman, S., Growdon, J. H., Khachaturian, Z. S., et al. (1998). Consensus report of the working group on: "molecular and biochemical markers of Alzheimer's disease. *Neurobiol. Aging* 19, 109–116. doi: 10.1016/S0197-4580(98)00022-0

de Boussard, C. N., Lundin, A., Karlstedt, D., Edman, G., Bartfai, A., and Borg, J. (2005). S100 and cognitive impairment after mild traumatic brain injury. *J. Rehabil. Med.* 37, 53–57. doi: 10.1080/16501970410015587

de Leon, M. J., DeSanti, S., Zinkowski, R., Mehta, P. D., Pratico, D., Segal, S., et al. (2006). Longitudinal CSF and MRI biomarkers improve the diagnosis of mild cognitive impairment. *Neurobiol. Aging* 27, 394–401. doi: 10.1016/j.neurobiolaging.2005.07.003

de Leon, M. J., Ferris, S. H., George, A. E., Christman, D. R., Fowler, J. S., Gentes, C., et al. (1983). Positron emission tomographic studies of aging and Alzheimer disease. *AJNR Am. J. Neuroradiol.* 4, 568–571.

de Souza, L. C., Chupin, M., Lamari, F., Jardel, C., Leclercq, D., Colliot, O., et al. (2012). CSF tau markers are correlated with hippocampal volume in Alzheimer's disease. *Neurobiol. Aging* 33, 1253–1257. doi: 10.1016/j.neurobiolaging.2011.02.022

De Vos, A., Jacobs, D., Struyfs, H., Fransen, E., Andersson, K., Portelius, E., et al. (2015). C-terminal neurogranin is increased in cerebrospinal fluid but unchanged in plasma in Alzheimer's disease. *Alzheimers Dement.* 11, 1461–1469. doi: 10.1016/j.jalz.2015.05.012

DeMattos, R. B., Bales, K. R., Parsadanian, M., O'Dell, M. A., Foss, E. M., Paul, S. M., et al. (2002). Plaque-associated disruption of CSF and plasma amyloid-beta (Abeta) equilibrium in a mouse model of Alzheimer's disease. *J. Neurochem.* 81, 229–236. doi: 10.1046/j.1471-4159.2002.00889.x

Desikan, R. S., McEvoy, L. K., Thompson, W. K., Holland, D., Brewer, J. B., Aisen, P. S., et al. (2012). Amyloid-beta–associated clinical decline occurs only in the presence of elevated P-tau. *Arch. Neurol.* 69, 709–713. doi: 10.1001/archneurol.2011.3354

Desikan, R. S., McEvoy, L. K., Thompson, W. K., Holland, D., Roddey, J. C., Blennow, K., et al. (2011). Amyloid-beta associated volume loss occurs only in the presence of phospho-tau. *Ann. Neurol.* 70, 657–661. doi: 10.1002/ana.22509

Desikan, R. S., Sabuncu, M. R., Schmansky, N. J., Reuter, M., Cabral, H. J., Hess, C. P., et al. (2010). Selective disruption of the cerebral neocortex in Alzheimer's disease. *PLoS One* 5:e12853. doi: 10.1371/journal.pone.0012853

Dickerson, B. C., Bakkour, A., Salat, D. H., Feczko, E., Pacheco, J., Greve, D. N., et al. (2009). The cortical signature of Alzheimer's disease: regionally specific cortical thinning relates to symptom severity in very mild to mild AD dementia and is detectable in asymptomatic amyloid-positive individuals. *Cereb. Cortex* 19, 497–510. doi: 10.1093/cercor/bhn113

Disanto, G., Barro, C., Benkert, P., Naegelin, Y., Schadelin, S., Giardiello, A., et al. (2017). Serum Neurofilament light: a biomarker of neuronal damage in multiple sclerosis. *Ann. Neurol.* 81, 857–870. doi: 10.1002/ana.24954

Dockens, R., Wang, J.-S., Castaneda, L., Sverdlov, O., Huang, S.-P., Slemmon, R., et al. (2012). A placebo-controlled, multiple ascending dose study to evaluate the safety, pharmacokinetics and pharmacodynamics of avagacestat (BMS-708163) in healthy young and elderly subjects. *Clin. Pharmacokinet.* 51, 681–693. doi: 10.1007/s40262-012-0005-x

Dominguez, D., Tournoy, J., Hartmann, D., Huth, T., Cryns, K., Deforce, S., et al. (2005). Phenotypic and biochemical analyses of BACE1- and BACE2-deficient mice. *J. Biol. Chem.* 280, 30797–30806. doi: 10.1074/jbc.M505249200

Drijfhout, W. J., Kemper, R. H., Meerlo, P., Koolhaas, J. M., Grol, C. J., and Westerink, B. H. (1995). A telemetry study on the chronic effects of microdialysis probe implantation on the activity pattern and temperature rhythm of the rat. *J. Neurosci. Methods* 61, 191–196. doi: 10.1016/0165-0270(94)00041-e

Dubois, B., Feldman, H. H., Jacova, C., Hampel, H., Molinuevo, J. L., Blennow, K., et al. (2014). Advancing research diagnostic criteria for Alzheimer's disease: the IWG-2 criteria. *Lancet Neurol.* 13, 614–629. doi: 10.1016/s1474-4422(14)70090-0

Duyckaerts, C., Brion, J. P., Hauw, J. J., and Flament-Durand, J. (1987). Quantitative assessment of the density of neurofibrillary tangles and senile plaques in senile dementia of the Alzheimer type. Comparison of immunocytochemistry with a specific antibody and Bodian's protargol method. *Acta Neuropathol.* 73, 167–170. doi: 10.1007/BF00693783

El Kadmiri, N., Said, N., Slassi, I., El Moutawakil, B., and Nadifi, S. (2018). Biomarkers for Alzheimer disease: classical and novel candidates' review. *Neuroscience* 370, 181–190. doi: 10.1016/j.neuroscience.2017.07.017

Engelborghs, S., De Vreese, K., Van de Casteele, T., Vanderstichele, H., Van Everbroeck, B., Cras, P., et al. (2008). Diagnostic performance of a CSF-biomarker panel in autopsy-confirmed dementia. *Neurobiol. Aging* 29, 1143–1159. doi: 10.1016/j.neurobiolaging.2007.02.016

Engler, H., Forsberg, A., Almkvist, O., Blomquist, G., Larsson, E., Savitcheva, I., et al. (2006). Two-year follow-up of amyloid deposition in patients with Alzheimer's disease. *Brain* 129, 2856–2866. doi: 10.1093/brain/awl178

Eskildsen, S. F., Coupe, P., Garcia-Lorenzo, D., Fonov, V., Pruessner, J. C., and Collins, D. L. (2013). Prediction of Alzheimer's disease in subjects with mild cognitive impairment from the ADNI cohort using patterns of cortical thinning. *Neuroimage* 65, 511–521. doi: 10.1016/j.neuroimage.2012.09.058

Fagan, A. M., Xiong, C., Jasielec, M. S., Bateman, R. J., Goate, A. M., Benzinger, T. L., et al. (2014). Longitudinal change in CSF biomarkers in autosomal-dominant Alzheimer's disease. *Sci. Transl. Med.* 6:226ra230. doi: 10.1126/scitranslmed.3007901

Fan, Z., Brooks, D. J., Okello, A., and Edison, P. (2017). An early and late peak in microglial activation in Alzheimer's disease trajectory. *Brain* 140, 792–803. doi: 10.1093/brain/aww349

Feinberg, D. A., and Mark, A. S. (1987). Human brain motion and cerebrospinal fluid circulation demonstrated with MR velocity imaging. *Radiology* 163, 793–799. doi: 10.1148/radiology.163.3.3575734

Finneran, D. J., Morgan, D., Gordon, M. N., and Nash, K. R. (2019). CNS-wide over expression of fractalkine improves cognitive functioning in a tauopathy model. *J. Neuroimmune. Pharmacol.* 14, 312–325. doi: 10.1007/s11481-018-9822-5

Fox, M. D., and Raichle, M. E. (2007). Spontaneous fluctuations in brain activity observed with functional magnetic resonance imaging. *Nat. Rev. Neurosci.* 8, 700–711. doi: 10.1038/nrn2201

Fransquet, P. D., and Ryan, J. (2018). Micro RNA as a potential blood-based epigenetic biomarker for Alzheimer's disease. *Clin. Biochem* .58, 5–14. doi: 10.1016/j.clinbiochem.2018.05.020

Freudenberg-Hua, Y., Li, W., and Davies, P. (2018). The role of genetics in advancing precision medicine for Alzheimer's disease-a narrative review. *Front. Med.* 5:108. doi: 10.3389/fmed.2018.00108

Frölich, L., Peters, O., Lewczuk, P., Gruber, O., Teipel, S. J., Gertz, H. J., et al. (2017). Incremental value of biomarker combinations to predict progression of mild cognitive impairment to Alzheimer's dementia. *Alzheimers Res. Ther.* 9:84. doi: 10.1186/s13195-017-0301-7

Gaffan, D. (1992). Amnesia for complex naturalistic scenes and for objects following fornix transection in the rhesus monkey. *Eur. J. Neurosci.* 4, 381–388. doi: 10.1111/j.1460-9568.1992.tb00886.x

Gaffan, D. (1994). Scene-specific memory for objects: a model of episodic memory impairment in monkeys with fornix transection. *J. Cogn. Neurosci.* 6, 305–320. doi: 10.1162/jocn.1994.6.4.305

Gaffan, D., Saunders, R. C., Gaffan, E. A., Harrison, S., Shields, C., and Owen, M. J. (1984). Effects of fornix transection upon associative memory in monkeys: role of the hippocampus in learned action. *Q. J. Exp. Psychol. Sec. B* 36, 173–221. doi: 10.1080/14640748408402203

Garwood, C. J., Pooler, A. M., Atherton, J., Hanger, D. P., and Noble, W. (2011). Astrocytes are important mediators of Aβ-induced neurotoxicity and tau phosphorylation in primary culture. *Cell Death Dis.* 2, e167–e167. doi: 10.1038/cddis.2011.50

Geinisman, Y., deToledo-Morrell, L., Morrell, F., Persina, I. S., and Rossi, M. (1992). Age-related loss of axospinous synapses formed by two afferent systems in the rat dentate gyrus as revealed by the unbiased stereological dissector technique. *Hippocampus* 2, 437–444. doi: 10.1002/hipo.450020411

Georgievska, B., Gustavsson, S., Lundkvist, J., Neelissen, J., Eketjall, S., Ramberg, V., et al. (2015). Revisiting the peripheral sink hypothesis: inhibiting BACE1 activity in the periphery does not alter beta-amyloid levels in the CNS. *J. Neurochem.* 132, 477–486. doi: 10.1111/jnc.12937

Geppert, M., Goda, Y., Hammer, R. E., Li, C., Rosahl, T. W., Stevens, C. F., et al. (1994). Synaptotagmin I: a major Ca2+ sensor for transmitter release at a central synapse. *Cell* 79, 717–727. doi: 10.1016/0092-8674(94)90556-8

Gisslen, M., Price, R. W., Andreasson, U., Norgren, N., Nilsson, S., Hagberg, L., et al. (2016). Plasma Concentration of the neurofilament light protein (NFL) is a biomarker of CNS Injury in HIV infection: a cross-sectional study. *EBioMedicine* 3, 135–140. doi: 10.1016/j.ebiom.2015.11.036

Gomez-Isla, T., Price, J. L., McKeel, D. W. Jr., Morris, J. C., Growdon, J. H., and Hyman, B. T. (1996). Profound loss of layer II entorhinal cortex neurons occurs in very mild Alzheimer's disease. *J. Neurosci.* 16, 4491–4500.

Gomez-Nicola, D., and Boche, D. (2015). Post-mortem analysis of neuroinflammatory changes in human Alzheimer's disease. *Alzheimers Res. Ther.* 7:42. doi: 10.1186/s13195-015-0126-1

Gravenfors, Y., Viklund, J., Blid, J., Ginman, T., Karlstrom, S., Kihlstrom, J., et al. (2012). New aminoimidazoles as beta-secretase (BACE-1) inhibitors showing amyloid-beta (Abeta) lowering in brain. *J. Med. Chem.* 55, 9297–9311. doi: 10.1021/jm300991n

Gravina, S. A., Ho, L., Eckman, C. B., Long, K. E., Otvos, L. Jr., Younkin, L. H., et al. (1995). Amyloid beta protein (A beta) in Alzheimer's disease brain. Biochemical and immunocytochemical analysis with antibodies specific for forms ending at A beta 40 or A beta 42(43). *J. Biol. Chem.* 270, 7013–7016. doi: 10.1074/jbc.270.13.7013

Greicius, M. D., and Menon, V. (2004). Default-mode activity during a passive sensory task: uncoupled from deactivation but impacting activation. *J. Cogn. Neurosci.* 16, 1484–1492. doi: 10.1162/0898929042568532

Griffin, W. S., Stanley, L. C., Ling, C., White, L., MacLeod, V., Perrot, L. J., et al. (1989). Brain interleukin 1 and S-100 immunoreactivity are elevated in down syndrome and Alzheimer disease. *Proc. Natl. Acad. Sci. U.S.A.* 86, 7611–7615. doi: 10.1073/pnas.86.19.7611

Grossman, M., Farmer, J., Leight, S., Work, M., Moore, P., Van Deerlin, V., et al. (2005). Cerebrospinal fluid profile in frontotemporal dementia and Alzheimer's disease. *Ann. Neurol.* 57, 721–729. doi: 10.1002/ana.20477

Gusnard, D. A., Raichle, M. E., and Raichle, M. E. (2001). Searching for a baseline: functional imaging and the resting human brain. *Nat. Rev. Neurosci.* 2, 685–694. doi: 10.1038/35094500

Gustafson, D. R., Skoog, I., Rosengren, L., Zetterberg, H., and Blennow, K. (2007). Cerebrospinal fluid β-amyloid 1-42 concentration may predict cognitive decline in older women. *J. Neurol. Neurosurg. Psychiatry* 78, 461–464. doi: 10.1136/jnnp.2006.100529

Ha, T. Y., Chang, K. A., Kim, J., Kim, H. S., Kim, S., Chong, Y. H., et al. (2010). S100a9 knockdown decreases the memory impairment and the neuropathology in Tg2576 mice, AD animal model. *PLoS One* 5:e8840. doi: 10.1371/journal.pone.0008840

Haass, C., and De Strooper, B. (1999). The presenilins in Alzheimer's disease–proteolysis holds the key. *Science* 286, 916–919. doi: 10.1126/science.286.5441.916

Haass, C., and Selkoe, D. J. (2007). Soluble protein oligomers in neurodegeneration: lessons from the Alzheimer's amyloid beta-peptide. *Nat. Rev. Mol. Cell Biol.* 8, 101–112. doi: 10.1038/nrm2101

Hagmeyer, S., Cristovao, J. S., Mulvihill, J. J. E., Boeckers, T. M., Gomes, C. M., and Grabrucker, A. M. (2017). Zinc binding to S100B affords regulation of trace metal homeostasis and excitotoxicity in the brain. *Front. Mol. Neurosci.* 10:456. doi: 10.3389/fnmol.2017.00456

Hamberger, A., Berthold, C.-H., Jacobson, I., Karlsson, B., Lehmann, A., Nyström, B. et al. (1985). "In vivo brain dialysis of extracellular nontransmitter and putative transmitter amino acids" in *Vivo Perfusion and Release of Neuroactive Substances*, eds A. Bayon, and R. Drucker-Colin, (New York, NY: Academic Press Inc), 473–492.

Hamelin, L., Lagarde, J., Dorothee, G., Leroy, C., Labit, M., Comley, R. A., et al. (2016). Early and protective microglial activation in Alzheimer's disease: a prospective study using 18F-DPA-714 PET imaging. *Brain* 139, 1252–1264. doi: 10.1093/brain/aww017

Hampel, H., Blennow, K., Shaw, L. M., Hoessler, Y. C., Zetterberg, H., and Trojanowski, J. Q. (2010). Total and phosphorylated tau protein as biological markers of Alzheimer's disease. *Exp. Gerontol.* 45, 30–40. doi: 10.1016/j.exger.2009.10.010

Hampel, H., Lista, S., and Khachaturian, Z. S. (2012). Development of biomarkers to chart all Alzheimer's disease stages: the royal road to cutting the therapeutic Gordian Knot. *Alzheimers Dement.* 8, 312–336. doi: 10.1016/j.jalz.2012.05.2116

Hane, F. T., Robinson, M., Lee, B. Y., Bai, O., Leonenko, Z., and Albert, M. S. (2017). Recent progress in alzheimer's disease research, part 3: diagnosis and treatment. *J. Alzheimers Dis.* 57, 645–665. doi: 10.3233/JAD-160907

Hansson, O., Zetterberg, H., Buchhave, P., Andreasson, U., Londos, E., Minthon, L., et al. (2007). Prediction of Alzheimer's disease using the CSF Abeta42/Abeta40 ratio in patients with mild cognitive impairment. *Dement. Geriatr. Cogn. Disord.* 23, 316–320. doi: 10.1159/000100926

Hardy, J. A., and Higgins, G. A. (1992). Alzheimer's disease: the amyloid cascade hypothesis. *Science* 256, 184–185. doi: 10.1126/science.1566067

Harper, J. D., and Lansbury, P. T. Jr. (1997). Models of amyloid seeding in Alzheimer's disease and scrapie: mechanistic truths and physiological consequences of the time-dependent solubility of amyloid proteins. *Annu. Rev. Biochem.* 66, 385–407. doi: 10.1146/annurev.biochem.66.1.385

Harrison, J. K., Jiang, Y., Chen, S., Xia, Y., Maciejewski, D., McNamara, R. K., et al. (1998). Role for neuronally derived fractalkine in mediating interactions between neurons and CX3CR1-expressing microglia. *Proc. Natl. Acad. Sci. U.S.A.* 95, 10896–10901. doi: 10.1073/pnas.95.18.10896

He, Z., Guo, J. L., McBride, J. D., Narasimhan, S., Kim, H., Changolkar, L., et al. (2018). Amyloid-beta plaques enhance Alzheimer's brain tau-seeded pathologies by facilitating neuritic plaque tau aggregation. *Nat. Med.* 24, 29–38. doi: 10.1038/nm.4443

Heckmann, B. L., Teubner, B. J. W., Tummers, B., Boada-Romero, E., Harris, L., Yang, M., et al. (2019). LC3-Associated endocytosis facilitates beta-amyloid clearance and mitigates neurodegeneration in murine Alzheimer's disease. *Cell* 178, 536.e14–551.e14. doi: 10.1016/j.cell.2019.05.056

Hellstrand, E., Boland, B., Walsh, D. M., and Linse, S. (2010). Amyloid beta-protein aggregation produces highly reproducible kinetic data and occurs by a two-phase process. *ACS Chem. Neurosci.* 1, 13–18. doi: 10.1021/cn900015v

Herukka, S. K., Rummukainen, J., Ihalainen, J., Von Und Zu Fraunberg, M., Koivisto, A. M., Nerg, O., et al. (2015). Amyloid-β and tau dynamics in human brain interstitial fluid in patients with suspected normal pressure hydrocephalus. *J. Alzheimers Dis.* 46, 261–269. doi: 10.3233/JAD-142862

Heyman, A., Peterson, B., Fillenbaum, G., and Pieper, C. (1996). The consortium to establish a registry for Alzheimer's disease (CERAD). Part XIV: demographic and clinical predictors of survival in patients with Alzheimer's disease. *Neurology* 46, 656–660. doi: 10.1212/wnl.46.3.656

Hickman, S. E., Allison, E. K., and El Khoury, J. (2008). Microglial dysfunction and defective beta-amyloid clearance pathways in aging Alzheimer's disease mice. *J. Neurosci.* 28, 8354–8360. doi: 10.1523/jneurosci.0616-08.2008

Hoglund, K., Thelen, K. M., Syversen, S., Sjogren, M., von Bergmann, K., Wallin, A., et al. (2005). The effect of simvastatin treatment on the amyloid precursor protein and brain cholesterol metabolism in patients with Alzheimer's disease. *Dement. Geriatr. Cogn. Disord.* 19, 256–265. doi: 10.1159/000084550

Holland, D., McEvoy, L. K., and Dale, A. M. (2012a). Unbiased comparison of sample size estimates from longitudinal structural measures in ADNI. *Hum. Brain. Mapp.* 33, 2586–2602. doi: 10.1002/hbm.21386

Holland, D., McEvoy, L. K., Desikan, R. S., and Dale, A. M. (2012b). Enrichment and stratification for predementia Alzheimer disease clinical trials. *PLoS One* 7:e47739. doi: 10.1371/journal.pone.0047739

Holth, J., Fritschi, S., Wang, C., Pedersen, N., Cirrito, J., Mahan, T., et al. (2019). The sleep-wake cycle regulates brain interstitial fluid tau in mice and CSF tau in humans. *Science* 363, eaav2546. doi: 10.1126/science.aav2546

Hong, S., Quintero-Monzon, O., Ostaszewski, B. L., Podlisny, D. R., Cavanaugh, W. T., Yang, T., et al. (2011). Dynamic analysis of amyloid beta-protein in behaving mice reveals opposing changes in ISF versus parenchymal Abeta during age-related plaque formation. *J. Neurosci.* 31, 15861–15869. doi: 10.1523/jneurosci.3272-11.2011

Huang, J., Friedland, R. P., and Auchus, A. P. (2007). Diffusion tensor imaging of normal-appearing white matter in mild cognitive impairment and early Alzheimer disease: preliminary evidence of axonal degeneration in the temporal lobe. *AJNR Am. J. Neuroradiol.* 28, 1943–1948. doi: 10.3174/ajnr.A0700

Hyman, B. T., Van Hoesen, G. W., Kromer, L. J., and Damasio, A. R. (1986). Perforant pathway changes and the memory impairment of Alzheimer's disease. *Ann. Neurol.* 20, 472–481. doi: 10.1002/ana.410200406

Iijima-Ando, K., Hearn, S. A., Granger, L., Shenton, C., Gatt, A., Chiang, H. C., et al. (2008). Overexpression of neprilysin reduces alzheimer amyloid-beta42 (Abeta42)-induced neuron loss and intraneuronal Abeta42 deposits but causes a reduction in cAMP-responsive element-binding protein-mediated transcription, age-dependent axon pathology, and premature death in Drosophila. *J. Biol. Chem.* 283. doi: 10.1074/jbc.M710509200

Imai, T., Hieshima, K., Haskell, C., Baba, M., Nagira, M., Nishimura, M., et al. (1997). Identification and molecular characterization of fractalkine receptor CX3CR1, which mediates both leukocyte migration and adhesion. *Cell* 91, 521–530. doi: 10.1016/s0092-8674(00)80438-9

Imbimbo, B. P., Giardino, L., Sivilia, S., Giuliani, A., Gusciglio, M., Pietrini, V., et al. (2010). CHF5074, a novel gamma-secretase modulator, restores hippocampal neurogenesis potential and reverses contextual memory deficit in a transgenic mouse model of Alzheimer's disease. *J. Alzheimers Dis.* 20, 159–173. doi: 10.3233/jad-2010-1366

Jack, C. R. Jr., Bennett, D. A., Blennow, K., Carrillo, M. C., Feldman, H. H., Frisoni, G. B., et al. (2016). A/T/N: an unbiased descriptive classification scheme for Alzheimer disease biomarkers. *Neurology* 87, 539–547. doi: 10.1212/wnl.0000000000002923

Jack, C. R. Jr., Knopman, D. S., Jagust, W. J., Shaw, L. M., Aisen, P. S., Weiner, M. W., et al. (2010). Hypothetical model of dynamic biomarkers of the Alzheimer's pathological cascade. *Lancet Neurol.* 9, 119–128. doi: 10.1016/s1474-4422(09)70299-6

Jack, C. R. Jr., Petersen, R. C., Xu, Y., O'Brien, P. C., Smith, G. E., Ivnik, R. J., et al. (2000). Rates of hippocampal atrophy correlate with change in clinical status in aging and AD. *Neurology* 55, 484–489. doi: 10.1212/wnl.55.4.484

Jack, C. R. Jr., Wiste, H. J., Lesnick, T. G., Weigand, S. D., Knopman, D. S., Vemuri, P., et al. (2013). Brain beta-amyloid load approaches a plateau. *Neurology* 80, 890–896. doi: 10.1212/WNL.0b013e3182840bbe

Jagust, W. J., Landau, S. M., Koeppe, R. A., Reiman, E. M., Chen, K., Mathis, C. A., et al. (2015). The Alzheimer's disease neuroimaging initiative 2 PET core: 2015. *Alzheimers Dement.* 11, 757–771. doi: 10.1016/j.jalz.2015.05.001

Jahn, R., and Fasshauer, D. (2012). Molecular machines governing exocytosis of synaptic vesicles. *Nature* 490, 201–207. doi: 10.1038/nature11320

James, B. D., Wilson, R. S., Boyle, P. A., Trojanowski, J. Q., Bennett, D. A., and Schneider, J. A. (2016). TDP-43 stage, mixed pathologies, and clinical Alzheimer's-type dementia. *Brain* 139, 2983–2993. doi: 10.1093/brain/aww224

Janelidze, S., Mattsson, N., Stomrud, E., Lindberg, O., Palmqvist, S., Zetterberg, H., et al. (2018). CSF biomarkers of neuroinflammation and cerebrovascular dysfunction in early Alzheimer disease. *Neurology* 91, e867–e877. doi: 10.1212/WNL.0000000000006082

Janelidze, S., Stomrud, E., Palmqvist, S., Zetterberg, H., van Westen, D., Jeromin, A., et al. (2016). Plasma beta-amyloid in Alzheimer's disease and vascular disease. *Sci. Rep.* 6:26801. doi: 10.1038/srep26801

Jay, T. R., von Saucken, V. E., and Landreth, G. E. (2017). TREM2 in neurodegenerative diseases. *Mol. Neurodegener.* 12:56. doi: 10.1186/s13024-017-0197-5

Jeppsson, F., Eketjall, S., Janson, J., Karlstrom, S., Gustavsson, S., Olsson, L. L., et al. (2012). Discovery of AZD3839, a potent and selective BACE1 inhibitor clinical candidate for the treatment of Alzheimer disease. *J. Biol. Chem.* 287, 41245–41257. doi: 10.1074/jbc.M112.409110

Jin, W. S., Shen, L. L., Bu, X. L., Zhang, W. W., Chen, S. H., Huang, Z. L., et al. (2017). Peritoneal dialysis reduces amyloid-beta plasma levels in humans and attenuates Alzheimer-associated phenotypes in an APP/PS1 mouse model. *Acta Neuropathol.* 134, 207–220. doi: 10.1007/s00401-017-1721-y

Johnson, A. E., Jeppsson, F., Sandell, J., Wensbo, D., Neelissen, J. A., Jureus, A., et al. (2009). AZD2184: a radioligand for sensitive detection of beta-amyloid deposits. *J. Neurochem.* 108, 1177–1186. doi: 10.1111/j.1471-4159.2008.05861.x

Johnson, K. A., Fox, N. C., Sperling, R. A., and Klunk, W. E. (2012). Brain imaging in Alzheimer disease. *Cold Spring Harb. Perspect. Med.* 2, a006213. doi: 10.1101/cshperspect.a006213

Johnson, V. E., Stewart, W., and Smith, D. H. (2010). Traumatic brain injury and amyloid-β pathology: a link to Alzheimer's disease? *Nat. Rev. Neurosci.* 11, 361–370. doi: 10.1038/nrn2808

Jürgen, M. K., Milan, M., and George, P. (2016). *Atlas of the Human Brain*, 4th Edn. Cambridge, MA: Academic Press.

Kanai, M., Matsubara, E., Isoe, K., Urakami, K., Nakashima, K., Arai, H., et al. (1998). Longitudinal study of cerebrospinal fluid levels of tau, A beta1-40, and A beta1-42(43) in Alzheimer's disease: a study in Japan. *Ann. Neurol.* 44, 17–26. doi: 10.1002/ana.410440108

Kaneko, N., Nakamura, A., Washimi, Y., Kato, T., Sakurai, T., Arahata, Y., et al. (2014). Novel plasma biomarker surrogating cerebral amyloid deposition. *Proc. JPN Acad. Ser. B Phys. Biol. Sci.* 90, 353–364. doi: 10.2183/pjab.90.353

Karelina, T., Demin, O., Nicholas, T., Lu, Y., Duvvuri, S., and Barton, H. A. (2017). A translational systems pharmacology model for abeta kinetics in mouse, monkey, and human. *CPT Pharmacometrics Syst. Pharmacol.* 6, 666–675. doi: 10.1002/psp4.12211

Karimy, J. K., Kahle, K. T., Kurland, D. B., Yu, E., Gerzanich, V., and Simard, J. M. (2015). A novel method to study cerebrospinal fluid dynamics in rats. *J. Neurosci. Methods* 241, 78–84. doi: 10.1016/j.jneumeth.2014.12.015

Kaufman, S. K., Thomas, T. L., Del Tredici, K., Braak, H., and Diamond, M. I. (2017). Characterization of tau prion seeding activity and strains from formaldehyde-fixed tissue. *Acta Neuropathol. Commun.* 5:41. doi: 10.1186/s40478-017-0442-8

Kawarabayashi, T., Younkin, L. H., Saido, T. C., Shoji, M., Ashe, K. H., and Younkin, S. G. (2001). Age-dependent changes in brain, CSF, and plasma amyloid (beta) protein in the Tg2576 transgenic mouse model of Alzheimer's disease. *J. Neurosci.* 21, 372–381.

Keene, C. D., Darvas, M., Kraemer, B., Liggitt, D., Sigurdson, C., and Ladiges, W. (2016). Neuropathological assessment and validation of mouse models for Alzheimer's disease: applying NIA-AA guidelines. *Pathobiol. Aging Age Relat. Dis.* 6:32397. doi: 10.3402/pba.v6.32397

Kehr, J. (1999). "Monitoring chemistry of brain microenvironment: biosensors, microdialysis and related techniques," in *Modern Techniques in Neuroscience Research*, U. Windhorst, and H. Johansson, (Heidelberg: Springer-Verlag) 41, 1149–1198.

Kennedy, M. E., Stamford, A. W., Chen, X., Cox, K., Cumming, J. N., Dockendorf, M. F., et al. (2016). The BACE1 inhibitor verubecestat (MK-8931) reduces CNS beta-amyloid in animal models and in Alzheimer's disease patients. *Sci. Transl. Med.* 8:363ra150. doi: 10.1126/scitranslmed.aad9704

Khan, S. S., and Bloom, G. S. (2016). Tau: the center of a signaling nexus in Alzheimer's disease. *Front. Neurosci.* 10:31. doi: 10.3389/fnins.2016.00031

Kim, H. D., Tahara, K., Maxwell, J. A., Lalonde, R., Fukuiwa, T., Fujihashi, K., et al. (2007). Nasal inoculation of an adenovirus vector encoding 11 tandem repeats of Abeta1-6 upregulates IL-10 expression and reduces amyloid load in a Mo/Hu APPswe PS1dE9 mouse model of Alzheimer's disease. *J. Gene Med.* 9, 88–98. doi: 10.1002/jgm.993

Kitazawa, M., Yamasaki, T. R., and LaFerla, F. M. (2004). Microglia as a potential bridge between the amyloid beta-peptide and tau. *Ann. N. Y. Acad. Sci.* 1035, 85–103. doi: 10.1196/annals.1332.006

Kleinberger, G., Yamanishi, Y., Suarez-Calvet, M., Czirr, E., Lohmann, E., Cuyvers, E., et al. (2014). TREM2 mutations implicated in neurodegeneration impair cell surface transport and phagocytosis. *Sci. Transl. Med.* 6:243ra286. doi: 10.1126/scitranslmed.3009093

Klunk, W. E., Engler, H., Nordberg, A., Wang, Y., Blomqvist, G., Holt, D. P., et al. (2004). Imaging brain amyloid in Alzheimer's disease with pittsburgh compound-B. *Ann. Neurol.* 55, 306–319. doi: 10.1002/ana.20009

Komatsu, M., Waguri, S., Chiba, T., Murata, S., Iwata, J., Tanida, I., et al. (2006). Loss of autophagy in the central nervous system causes neurodegeneration in mice. *Nature* 441, 880–884. doi: 10.1038/nature04723

Kounnas, M. Z., Lane-Donovan, C., Nowakowski, D. W., Herz, J., and Comer, W. T. (2017). NGP 555, a gamma-secretase modulator, lowers the amyloid biomarker, Abeta42, in cerebrospinal fluid while preventing alzheimer's disease cognitive decline in rodents. *Alzheimers Dement.* 3, 65–73. doi: 10.1016/j.trci.2016.09.003

Krzyzanowska, A., and Carro, E. (2012). Pathological alteration in the choroid plexus of alzheimer's disease: implication for new therapy approaches. *Front. Pharmacol.* 3:75. doi: 10.3389/fphar.2012.00075

Kuhl, D. E., Metter, E. J., Riege, W. H., and Phelps, M. E. (1982). Effects of human aging on patterns of local cerebral glucose utilization determined by the [18F]fluorodeoxyglucose method. *J. Cereb. Blood Flow Metab.* 2, 163–171. doi: 10.1038/jcbfm.1982.15

Kuhle, J., Barro, C., Andreasson, U., Derfuss, T., Lindberg, R., Sandelius, A., et al. (2016). Comparison of three analytical platforms for quantification of the neurofilament light chain in blood samples: eLISA, electrochemiluminescence

immunoassay and Simoa. *Clin. Chem. Lab. Med.* 54, 1655–1661. doi: 10.1515/cclm-2015-1195

Kuhle, J., Gaiottino, J., Leppert, D., Petzold, A., Bestwick, J. P., Malaspina, A., et al. (2015). Serum neurofilament light chain is a biomarker of human spinal cord injury severity and outcome. *J. Neurol. Neurosurg.* 86:273. doi: 10.1136/jnnp-2013-307454

Kummer, M. P., Vogl, T., Axt, D., Griep, A., Vieira-Saecker, A., Jessen, F., et al. (2012). Mrp14 deficiency ameliorates amyloid beta burden by increasing microglial phagocytosis and modulation of amyloid precursor protein processing. *J. Neurosci.* 32, 17824–17829. doi: 10.1523/jneurosci.1504-12.2012

LaFerla, F. M., Green, K. N., and Oddo, S. (2007). Intracellular amyloid-beta in Alzheimer's disease. *Nat. Rev. Neurosci.* 8, 499–509. doi: 10.1038/nrn2168

Landau, S. M., Mintun, M. A., Joshi, A. D., Koeppe, R. A., Petersen, R. C., Aisen, P. S., et al. (2012). Amyloid deposition, hypometabolism, and longitudinal cognitive decline. *Ann. Neurol.* 72, 578–586. doi: 10.1002/ana.23650

Lautrup, S., Sinclair, D. A., Mattson, M. P., and Fang, E. F. (2019). NAD(+) in brain aging and neurodegenerative disorders. *Cell Metab.* 30, 630–655. doi: 10.1016/j.cmet.2019.09.001

Leclerc, B., and Abulrob, A. (2013). Perspectives in molecular imaging using staging biomarkers and immunotherapies in Alzheimer's disease. *Sci. World J.* 2013:589308.

Lee, E. O., Yang, J. H., Chang, K. A., Suh, Y. H., and Chong, Y. H. (2013). Amyloid-beta peptide-induced extracellular S100A9 depletion is associated with decrease of antimicrobial peptide activity in human THP-1 monocytes. *J. Neuroinflammation* 10:68. doi: 10.1186/1742-2094-10-68

Lee, J. C., Kim, S. J., Hong, S., and Kim, Y. (2019). Diagnosis of Alzheimer's disease utilizing amyloid and tau as fluid biomarkers. *Exp. Mol. Med.* 51, 1–10. doi: 10.1038/s12276-019-0250-2

Lee, S., Varvel, N. H., Konerth, M. E., Xu, G., Cardona, A. E., Ransohoff, R. M., et al. (2010). CX3CR1 deficiency alters microglial activation and reduces beta-amyloid deposition in two Alzheimer's disease mouse models. *Am. J. Pathol.* 177, 2549–2562. doi: 10.2353/ajpath.2010.100265

Lee, V. M., and Trojanowski, J. Q. (2001). Transgenic mouse models of tauopathies: prospects for animal models of Pick's disease. *Neurology* 56, S26–S30. doi: 10.1212/wnl.56.suppl_4.s26

Leidinger, P., Backes, C., Deutscher, S., Schmitt, K., Mueller, S. C., Frese, K., et al. (2013). A blood based 12-miRNA signature of Alzheimer disease patients. *Genome. Biol.* 14, R78. doi: 10.1186/gb-2013-14-7-r78

Leinenbach, A., Pannee, J., Dulffer, T., Huber, A., Bittner, T., Andreasson, U., et al. (2014). Mass spectrometry-based candidate reference measurement procedure for quantification of amyloid-beta in cerebrospinal fluid. *Clin. Chem.* 60, 987–994. doi: 10.1373/clinchem.2013.220392

Leinonen, V., Pemberton, D., Van Der Ark, P., Timmers, M., Slemmon, J. R., Janssens, L., et al. (2019). P1-257: longitudinal comparison of Csf biomarkers of neurodegeneration in patients with probable idiopathic normal pressure hydrocephalus (INPH). *Alzheimers Dement.* 15, 337–338. doi: 10.1016/j.jalz.2019.06.812

Leitão, M. J., Baldeiras, I., Herukka, S.-K., Pikkarainen, M., Leinonen, V., Simonsen, A. H., et al. (2015). Chasing the effects of pre-analytical confounders – a multicenter study on CSF-AD biomarkers. *Front. Neurol.* 6:153. doi: 10.3389/fneur.2015.00153

Leuzy, A., Chiotis, K., Hasselbalch, S. G., Rinne, J. O., de Mendonca, A., Otto, M., et al. (2016). Pittsburgh compound B imaging and cerebrospinal fluid amyloid-beta in a multicentre European memory clinic study. *Brain* 139, 2540–2553. doi: 10.1093/brain/aww160

Leuzy, A., Chiotis, K., Lemoine, L., Gillberg, P. G., Almkvist, O., Rodriguez-Vieitez, E., et al. (2019). Tau PET imaging in neurodegenerative tauopathies-still a challenge. *Mol. Psychiatry* 24, 1112–1134. doi: 10.1038/s41380-018-0342-8

Lewczuk, P., Ermann, N., Andreasson, U., Schultheis, C., Podhorna, J., Spitzer, P., et al. (2018). Plasma neurofilament light as a potential biomarker of neurodegeneration in Alzheimer's disease. *Alzheimers Res. Ther.* 10:71. doi: 10.1186/s13195-018-0404-9

Lewczuk, P., Esselmann, H., Bibl, M., Beck, G., Maler, J. M., Otto, M., et al. (2004). Tau protein phosphorylated at threonine 181 in CSF as a neurochemical biomarker in Alzheimer's disease: original data and review of the literature. *J. Mol. Neurosci.* 23, 115–122. doi: 10.1385/jmn:23:1-2:115

Lewczuk, P., Lelental, N., Lachmann, I., Holzer, M., Flach, K., Brandner, S., et al. (2017). Non-phosphorylated tau as a potential biomarker of Alzheimer's disease: analytical and diagnostic characterization. *J. Alzheimers Dis.* 55, 159–170. doi: 10.3233/JAD-160448

Li, G., Chen, H., Cheng, L., Zhao, R., Zhao, J., and Xu, Y. (2014). Amyloid precursor-like protein 2 C-terminal fragments upregulate S100A9 gene and protein expression in BV2 cells. *Neural Regen. Res.* 9, 1923–1928. doi: 10.4103/1673-5374.145362

Lista, S., Toschi, N., Baldacci, F., Zetterberg, H., Blennow, K., Kilimann, I., et al. (2017). Diagnostic accuracy of CSF neurofilament light chain protein in the biomarker-guided classification system for Alzheimer's disease. *Neurochem. Int.* 108, 355–360. doi: 10.1016/j.neuint.2017.05.010

Liu, C. C., Hu, J., Zhao, N., Wang, J., Wang, N., Cirrito, J. R., et al. (2017). Astrocytic LRP1 mediates brain abeta clearance and impacts amyloid deposition. *J. Neurosci.* 37, 4023–4031. doi: 10.1523/jneurosci.3442-16.2017

Liu, L., and Duff, K. (2008). A technique for serial collection of cerebrospinal fluid from the cisterna magna in mouse. *J. Vis. Exp.* 960. doi: 10.3791/960

Liu, L., Herukka, S. K., Minkeviciene, R., van Groen, T., and Tanila, H. (2004). Longitudinal observation on CSF Abeta42 levels in young to middle-aged amyloid precursor protein/presenilin-1 doubly transgenic mice. *Neurobiol. Dis.* 17, 516–523. doi: 10.1016/j.nbd.2004.08.005

Liu, Y. H., Giunta, B., Zhou, H. D., Tan, J., and Wang, Y. J. (2012). Immunotherapy for Alzheimer disease: the challenge of adverse effects. *Nat. Rev. Neurol.* 8, 465–469. doi: 10.1038/nrneurol.2012.118

Lodeiro, M., Puerta, E., Ismail, M. A., Rodriguez-Rodriguez, P., Ronnback, A., Codita, A., et al. (2017). Aggregation of the inflammatory S100A8 precedes abeta plaque formation in transgenic APP mice: positive feedback for S100A8 and abeta productions. *J. Gerontol. A Biol. Sci. Med. Sci.* 72, 319–328. doi: 10.1093/gerona/glw073

Lucey, B. P., Hicks, T. J., McLeland, J. S., Toedebusch, C. D., Boyd, J., Elbert, D. L., et al. (2018). Effect of sleep on overnight cerebrospinal fluid amyloid beta kinetics. *Ann. Neurol.* 83, 197–204. doi: 10.1002/ana.25117

Lue, L. F., Kuo, Y. M., Roher, A. E., Brachova, L., Shen, Y., Sue, L., et al. (1999). Soluble amyloid beta peptide concentration as a predictor of synaptic change in Alzheimer's disease. *Am. J. Pathol.* 155, 853–862. doi: 10.1016/s0002-9440(10)65184-x

Maass, A., Landau, S., Baker, S. L., Horng, A., Lockhart, S. N., La Joie, R., et al. (2017). Comparison of multiple tau-PET measures as biomarkers in aging and Alzheimer's disease. *Neuroimage* 157, 448–463. doi: 10.1016/j.neuroimage.2017.05.058

Maciejewski-Lenoir, D., Chen, S., Feng, L., Maki, R., and Bacon, K. B. (1999). Characterization of fractalkine in rat brain cells: migratory and activation signals for CX3CR-1-expressing microglia. *J. Immunol.* 163, 1628–1635.

Maphis, N., Xu, G., Kokiko-Cochran, O. N., Jiang, S., Cardona, A., Ransohoff, R. M., et al. (2015). Reactive microglia drive tau pathology and contribute to the spreading of pathological tau in the brain. *Brain* 138, 1738–1755. doi: 10.1093/brain/awv081

Márquez, F., and Yassa, M. A. (2019). Neuroimaging biomarkers for Alzheimer's disease. *Mol. Neurodegener.* 14:21. doi: 10.1186/s13024-019-0325-5

Matsumoto, K., Chiba, Y., Fujihara, R., Kubo, H., Sakamoto, H., and Ueno, M. (2015). Immunohistochemical analysis of transporters related to clearance of amyloid-β peptides through blood–cerebrospinal fluid barrier in human brain. *Histochem. Cell Biol.* 144, 597–611. doi: 10.1007/s00418-015-1366-7

Mattsson, N., Andreasson, U., Persson, S., Arai, H., Batish, S. D., Bernardini, S., et al. (2011). The Alzheimer's Association external quality control program for cerebrospinal fluid biomarkers. *Alzheimers Dement.* 7, 386.e6–395.e6. doi: 10.1016/j.jalz.2011.05.2243

Mattsson, N., Andreasson, U., Zetterberg, H., and Blennow, K. (2017a). Association of plasma neurofilament light with neurodegeneration in patients with Alzheimer disease. *JAMA Neurol.* 74, 557–566. doi: 10.1001/jamaneurol.2016.6117

Mattsson, N., Cullen, N. C., Andreasson, U., Zetterberg, H., and Blennow, K. (2019). Association between longitudinal plasma neurofilament light and neurodegeneration in patients with Alzheimer disease. *JAMA Neurol.* 76, 791–799. doi: 10.1001/jamaneurol.2019.0765

Mattsson, N., Scholl, M., Strandberg, O., Smith, R., Palmqvist, S., Insel, P. S., et al. (2017b). (18)F-AV-1451 and CSF T-tau and P-tau as biomarkers in Alzheimer's disease. *EMBO Mol. Med.* 9, 1212–1223. doi: 10.15252/emmm.201707809

Mattsson, N., Zetterberg, H., Janelidze, S., Insel, P. S., Andreasson, U., Stomrud, E., et al. (2016). Plasma tau in Alzheimer disease. *Neurology* 87, 1827–1835. doi: 10.1212/wnl.0000000000003246

McConlogue, L., Buttini, M., Anderson, J. P., Brigham, E. F., Chen, K. S., Freedman, S. B., et al. (2007). Partial reduction of BACE1 has dramatic effects on Alzheimer plaque and synaptic pathology in APP Transgenic Mice. *J. Biol. Chem.* 282, 26326–26334. doi: 10.1074/jbc.M611687200

McDonald, R. J., and White, N. M. (1993). A triple dissociation of memory systems: hippocampus, amygdala, and dorsal striatum. *Behav. Neurosci.* 107, 3–22. doi: 10.1037//0735-7044.107.1.3

McGeer, P. L., Itagaki, S., Tago, H., and McGeer, E. G. (1987). Reactive microglia in patients with senile dementia of the Alzheimer type are positive for the histocompatibility glycoprotein HLA-DR. *Neurosci. Lett.* 79, 195–200. doi: 10.1016/0304-3940(87)90696-3

McLean, C. A., Cherny, R. A., Fraser, F. W., Fuller, S. J., Smith, M. J., Beyreuther, K., et al. (1999). Soluble pool of Abeta amyloid as a determinant of severity of neurodegeneration in Alzheimer's disease. *Ann. Neurol.* 46, 860–866. doi: 10.1002/1531-8249(199912)46:6<860::aid-ana8<3.0.co;2-m

Mehrpour, M., Esclatine, A., Beau, I., and Codogno, P. (2010). Overview of macroautophagy regulation in mammalian cells. *Cell Res.* 20, 748–762. doi: 10.1038/cr.2010.82

Mehta, P. D., Pirttila, T., Patrick, B. A., Barshatzky, M., and Mehta, S. P. (2001). Amyloid beta protein 1-40 and 1-42 levels in matched cerebrospinal fluid and plasma from patients with Alzheimer disease. *Neurosci. Lett.* 304, 102–106. doi: 10.1016/s0304-3940(01)01754-2

Menendez-Gonzalez, M., Padilla-Zambrano, H. S., Alvarez, G., Capetillo-Zarate, E., Tomas-Zapico, C., and Costa, A. (2018). Targeting beta-amyloid at the CSF: a new therapeutic strategy in Alzheimer's disease. *Front. Aging Neurosci.* 10:100. doi: 10.3389/fnagi.2018.00100

Mennicken, F., Maki, R., de Souza, E. B., and Quirion, R. (1999). Chemokines and chemokine receptors in the CNS: a possible role in neuroinflammation and patterning. *Trends Pharmacol. Sci.* 20, 73–78. doi: 10.1016/s0165-6147(99)01308-5

Menzies, F. M., Fleming, A., and Rubinsztein, D. C. (2015). Compromised autophagy and neurodegenerative diseases. *Nat. Rev. Neurosci.* 16, 345–357. doi: 10.1038/nrn3961

Meyding-Lamadé, U., Ehrhart, K., de Ruiz, H. L., Kehm, R., and Lamadé, W. A. (1996). new technique: serial puncture of the cisterna magna for obtaining cerebrospinal fluid in the mouse–application in a model of herpes simplex virus encephalitis. *J. Exp. Anim. Sci.* 38, 77–81.

Milisav, I., Šuput, D., and Ribariè, S. (2015). Unfolded protein response and macroautophagy in Alzheimer's, Parkinson's and Prion diseases. *Molecules* 20, 22718–22756.

Molinuevo, J. L., Ayton, S., Batrla, R., Bednar, M. M., Bittner, T., Cummings, J., et al. (2018). Current state of Alzheimer's fluid biomarkers. *Acta Neuropathol.* 136, 821–853. doi: 10.1007/s00401-018-1932-x

Mollenhauer, B., Bibl, M., Trenkwalder, C., Stiens, G., Cepek, L., Steinacker, P., et al. (2005). Follow-up investigations in cerebrospinal fluid of patients with dementia with Lewy bodies and Alzheimer's disease. *J. Neural. Transm.* 112, 933–948. doi: 10.1007/s00702-004-0235-7

Mori, T., Koyama, N., Arendash, G. W., Horikoshi-Sakuraba, Y., Tan, J., and Town, T. (2010). Overexpression of human S100B exacerbates cerebral amyloidosis and gliosis in the Tg2576 mouse model of Alzheimer's disease. *Glia* 58, 300–314. doi: 10.1002/glia.20924

Mosconi, L., Tsui, W. H., De Santi, S., Li, J., Rusinek, H., Convit, A., et al. (2005). Reduced hippocampal metabolism in MCI and AD: automated FDG-PET image analysis. *Neurology* 64, 1860–1867. doi: 10.1212/01.Wnl.0000163856.13524.08

Mosconi, L., Tsui, W. H., Herholz, K., Pupi, A., Drzezga, A., Lucignani, G., et al. (2008). Multicenter standardized 18F-FDG PET diagnosis of mild cognitive impairment, Alzheimer's disease, and other dementias. *J. Nucl. Med.* 49, 390–398. doi: 10.2967/jnumed.107.045385

Mucke, L., and Selkoe, D. J. (2012). Neurotoxicity of amyloid beta-protein: synaptic and network dysfunction. *Cold Spring Harb. Perspect. Med.* 2:a006338. doi: 10.1101/cshperspect.a006338

Mudher, A., Colin, M., Dujardin, S., Medina, M., Dewachter, I., Alavi Naini, S. M., et al. (2017). What is the evidence that tau pathology spreads through prion-like propagation? *Acta Neuropathol. Commun.* 5:99. doi: 10.1186/s40478-017-0488-7

Murphy, M. P., and LeVine, H. III (2010). Alzheimer's disease and the amyloid-beta peptide. *J. Alzheimers Dis.* 19, 311–323. doi: 10.3233/JAD-2010-1221

Musiek, E. S., and Holtzman, D. M. (2015). Three dimensions of the amyloid hypothesis: time, space and 'wingmen'. *Nat. Neurosci.* 18, 800–806. doi: 10.1038/nn.4018

Naggara, O., Oppenheim, C., Rieu, D., Raoux, N., Rodrigo, S., Dalla Barba, G., et al. (2006). Diffusion tensor imaging in early Alzheimer's disease. *Psychiatry Res.* 146, 243–249. doi: 10.1016/j.pscychresns.2006.01.005

Nakamura, T., Shoji, M., Harigaya, Y., Watanabe, M., Hosoda, K., Cheung, T. T., et al. (1994). Amyloid beta protein levels in cerebrospinal fluid are elevated in early-onset Alzheimer's disease. *Ann. Neurol.* 36, 903–911. doi: 10.1002/ana.410360616

Narasimhan, S., Guo, J. L., Changolkar, L., Stieber, A., McBride, J. D., Silva, L. V., et al. (2017). Pathological Tau strains from human brains recapitulate the diversity of tauopathies in nontransgenic mouse brain. *J. Neurosci.* 37, 11406–11423. doi: 10.1523/jneurosci.1230-17.2017

Nash, K. R., Lee, D. C., Hunt, J. B. Jr., Morganti, J. M., Selenica, M. L., Moran, P., et al. (2013). Fractalkine overexpression suppresses tau pathology in a mouse model of tauopathy. *Neurobiol. Aging* 34, 1540–1548. doi: 10.1016/j.neurobiolaging.2012.12.011

Naslund, J., Haroutunian, V., Mohs, R., Davis, K. L., Davies, P., Greengard, P., et al. (2000). Correlation between elevated levels of amyloid beta-peptide in the brain and cognitive decline. *Jama* 283, 1571–1577. doi: 10.1001/jama.283.12.1571

Neselius, S., Brisby, H., Theodorsson, A., Blennow, K., Zetterberg, H., and Marcusson, J. (2012). CSF-Biomarkers in olympic boxing: diagnosis and effects of repetitive head trauma. *PLoS One* 7:e33606. doi: 10.1371/journal.pone.0033606

Niemantsverdriet, E., Ottoy, J., Somers, C., De Roeck, E., Struyfs, H., Soetewey, F., et al. (2017). The Cerebrospinal fluid abeta1-42/Abeta1-40 ratio improves concordance with amyloid-PET for diagnosing Alzheimer's disease in a clinical setting. *J. Alzheimers Dis.* 60, 561–576. doi: 10.3233/jad-170327

Nisbet, R. M., Polanco, J. C., Ittner, L. M., and Gotz, J. (2015). Tau aggregation and its interplay with amyloid-beta. *Acta Neuropathol.* 129, 207–220. doi: 10.1007/s00401-014-1371-2

Nixon, R. A., and Yang, D. S. (2011). Autophagy failure in Alzheimer's disease–locating the primary defect. *Neurobiol. Dis.* 43, 38–45. doi: 10.1016/j.nbd.2011.01.021

Nussbaum, J. M., Seward, M. E., and Bloom, G. S. (2013). Alzheimer disease: a tale of two prions. *Prion* 7, 14–19. doi: 10.4161/pri.22118

Oddo, S., Caccamo, A., Shepherd, J. D., Murphy, M. P., Golde, T. E., Kayed, R., et al. (2003). Triple-transgenic model of Alzheimer's disease with plaques and tangles. *Neuron* 39, 409–421. doi: 10.1016/s0896-6273(03)00434-3

Oh, E. S., Mielke, M. M., Rosenberg, P. B., Jain, A., Fedarko, N. S., Lyketsos, C. G., et al. (2010). Comparison of conventional ELISA with electrochemiluminescence technology for detection of amyloid-beta in plasma. *J Alzheimers Dis.* 21, 769–773. doi: 10.3233/jad-2010-100456

Ohno, M., Cole, S. L., Yasvoina, M., Zhao, J., Citron, M., Berry, R., et al. (2007). BACE1 gene deletion prevents neuron loss and memory deficits in 5XFAD APP/PS1 transgenic mice. *Neurobiol. Dis.* 26, 134–145. doi: 10.1016/j.nbd.2006.12.008

Öhrfelt, A., Brinkmalm, A., Dumurgier, J., Brinkmalm, G., Hansson, O., Zetterberg, H., et al. (2016). The pre-synaptic vesicle protein synaptotagmin is a novel biomarker for Alzheimer's disease. *Alzheimers Res. Ther.* 8:41. doi: 10.1186/s13195-016-0208-8

Olsson, B., Lautner, R., Andreasson, U., Öhrfelt, A., Portelius, E., Bjerke, M., et al. (2016). CSF and blood biomarkers for the diagnosis of Alzheimer's disease: a systematic review and meta-analysis. *Lancet Neurol.* 15, 673–684. doi: 10.1016/s1474-4422(16)00070-3

Olsson, F., Schmidt, S., Althoff, V., Munter, L. M., Jin, S., Rosqvist, S., et al. (2014). Characterization of intermediate steps in amyloid beta (Abeta) production under near-native conditions. *J. Biol. Chem.* 289, 1540–1550. doi: 10.1074/jbc.M113.498246

Pahnke, J., Langer, O., and Krohn, M. (2014). Alzheimer's and ABC transporters — new opportunities for diagnostics and treatment. *Neurobiol. Dis.* 72, 54–60. doi: 10.1016/j.nbd.2014.04.001

Palmqvist, S., Insel, P. S., Stomrud, E., Janelidze, S., Zetterberg, H., Brix, B., et al. (2019). Cerebrospinal fluid and plasma biomarker trajectories with increasing amyloid deposition in Alzheimer's disease. *EMBO Mol. Med.* 11:e11170. doi: 10.15252/emmm.201911170

Palmqvist, S., Mattsson, N., and Hansson, O. (2016). Cerebrospinal fluid analysis detects cerebral amyloid-beta accumulation earlier than positron emission tomography. *Brain* 139, 1226–1236. doi: 10.1093/brain/aww015

Palmqvist, S., Schöll, M., Strandberg, O., Mattsson, N., Stomrud, E., Zetterberg, H., et al. (2017). Earliest accumulation of β-amyloid occurs within the default-mode network and concurrently affects brain connectivity. *Nat. Commun.* 8:1214. doi: 10.1038/s41467-017-01150-x

Pase, M. P., Beiser, A. S., Himali, J. J., Satizabal, C. L., Aparicio, H. J., DeCarli, C., et al. (2019). Assessment of plasma total tau level as a predictive biomarker for dementia and related endophenotypes. *JAMA Neurol.* 76, 598–606. doi: 10.1001/jamaneurol.2018.4666

Perea, J. R., Lleó, A., Alcolea, D., Fortea, J., Ávila, J., and Bolós, M. (2018). Decreased CX3CL1 levels in the cerebrospinal fluid of patients with Alzheimer's disease. *Front. Neurosci.* 12:609. doi: 10.3389/fnins.2018.00609

Perret-Liaudet, A., Pelpel, M., Tholance, Y., Dumont, B., Vanderstichele, H., Zorzi, W., et al. (2012a). Cerebrospinal fluid collection tubes: a critical issue for Alzheimer disease diagnosis. *Clin. Chem.* 58, 787–789. doi: 10.1373/clinchem.2011.178368

Perret-Liaudet, A., Pelpel, M., Tholance, Y., Dumont, B., Vanderstichele, H., Zorzi, W., et al. (2012b). Risk of Alzheimer's disease biological misdiagnosis linked to cerebrospinal collection tubes. *J. Alzheimers Dis.* 31, 13–20. doi: 10.3233/jad-2012-120361

Peters, A., Leahu, D., Moss, M. B., and McNally, K. J. (1994). The effects of aging on area 46 of the frontal cortex of the rhesus monkey. *Cereb. Cortex* 4, 621–635. doi: 10.1093/cercor/4.6.621

Peterson, D. A., Lucidi-Phillipi, C. A., Eagle, K. L., and Gage, F. H. (1994). Perforant path damage results in progressive neuronal death and somal atrophy in layer II of entorhinal cortex and functional impairment with increasing postdamage age. *J. Neurosci.* 14, 6872–6885. doi: 10.1523/JNEUROSCI.14-11-06872.1994

Petzold, A. (2005). Neurofilament phosphoforms: surrogate markers for axonal injury, degeneration and loss. *J. Neurol. Sci.* 233, 183–198. doi: 10.1016/j.jns.2005.03.015

Pijnenburg, Y. A., Janssen, J. C., Schoonenboom, N. S., Petzold, A., Mulder, C., Stigbrand, T., et al. (2007). CSF neurofilaments in frontotemporal dementia compared with early onset Alzheimer's disease and controls. *Dement. Geriatr. Cogn. Disord.* 23, 225–230. doi: 10.1159/000099473

Pitschke, M., Prior, R., Haupt, M., and Riesner, D. (1998). Detection of single amyloid β-protein aggregates in the cerebrospinal fluid of Alzheimer's patients by fluorescence correlation spectroscopy. *Nat. Med.* 4, 832–834. doi: 10.1038/nm0798-832

Pratico, D., Uryu, K., Leight, S., Trojanoswki, J. Q., and Lee, V. M. (2001). Increased lipid peroxidation precedes amyloid plaque formation in an animal model of Alzheimer amyloidosis. *J. Neurosci.* 21, 4183–4187.

Pulawski, W., Ghoshdastider, U., Andrisano, V., and Filipek, S. (2012). Ubiquitous amyloids. *Appl. Biochem. Biotechnol.* 166, 1626–1643. doi: 10.1007/s12010-012-9549-3

Pyykkö, O. T., Lumela, M., Rummukainen, J., Nerg, O., Seppälä, T. T., Herukka, S.-K., et al. (2014). Cerebrospinal fluid biomarker and brain biopsy findings in idiopathic normal pressure hydrocephalus. *PLoS One* 9:e91974. doi: 10.1371/journal.pone.0091974

Qin, W., Ho, L., Wang, J., Peskind, E., and Pasinetti, G. M. (2009). S100A7, a novel Alzheimer's disease biomarker with non-amyloidogenic alpha-secretase activity acts via selective promotion of ADAM-10. *PLoS One* 4:e4183. doi: 10.1371/journal.pone.0004183

Querol-Vilaseca, M., Colom-Cadena, M., Pegueroles, J., San Martin-Paniello, C., Clarimon, J., Belbin, O., et al. (2017). YKL-40 (Chitinase 3-like I) is expressed in a subset of astrocytes in Alzheimer's disease and other tauopathies. *J. Neuroinflammation* 14:118. doi: 10.1186/s12974-017-0893-7

Raichle, M. E., MacLeod, A. M., Snyder, A. Z., Powers, W. J., Gusnard, D. A., and Shulman, G. L. (2001). A default mode of brain function. *Proc. Natl. Acad. Sci. U.S.A.* 98, 676–682. doi: 10.1073/pnas.98.2.676

Ramesh, S., Govindarajulu, M., Jones, E., Knowlton, S., Weeks, L., Suppiramaniam, V., et al. (2018a). *Alzheimer's Disease and Treatment*, Reno, NV: MedDocs Publishers.

Ramesh, S., Govindarajulu, M., Jones, E., Knowlton, S., Weeks, L., Suppiramaniam, V., et al. (2018b). *Current and Novel Biomarkers for Alzheimer's Disease*. Reno, NV: MedDocs Publishers LLC.

Rami, A. (2009). Review: autophagy in neurodegeneration: firefighter and/or incendiarist? *Neuropathol. Appl. Neurobiol.* 35, 449–461. doi: 10.1111/j.1365-2990.2009.01034.x

Ranganath, C., and Ritchey, M. (2012). Two cortical systems for memory-guided behaviour. *Nat. Rev. Neurosci.* 13, 713–726. doi: 10.1038/nrn3338

Rapp, P. R., and Gallagher, M. (1996). Preserved neuron number in the hippocampus of aged rats with spatial learning deficits. *Proc. Natl. Acad. Sci. U.S.A.* 93, 9926–9930. doi: 10.1073/pnas.93.18.9926

Rapp, P. R., Deroche, P. S., Mao, Y., and Burwell, R. D. (2002). Neuron number in the parahippocampal region is preserved in aged rats with spatial learning deficits. *Cereb. Cortex* 12, 1171–1179. doi: 10.1093/cercor/12.11.1171

Rasmussen, T., Schliemann, T., Sorensen, J. C., Zimmer, J., and West, M. J. (1996). Memory impaired aged rats: no loss of principal hippocampal and subicular neurons. *Neurobiol. Aging* 17, 143–147. doi: 10.1016/0197-4580(95)02032-2

Raz, N., Lindenberger, U., Rodrigue, K. M., Kennedy, K. M., Head, D., Williamson, A., et al. (2005). Regional brain changes in aging healthy adults: general trends, individual differences and modifiers. *Cereb. Cortex* 15, 1676–1689. doi: 10.1093/cercor/bhi044

Rhein, V., Song, X., Wiesner, A., Ittner, L. M., Baysang, G., Meier, F., et al. (2009). Amyloid-beta and tau synergistically impair the oxidative phosphorylation system in triple transgenic Alzheimer's disease mice. *Proc. Natl. Acad. Sci. U.S.A.* 106, 20057–20062. doi: 10.1073/pnas.0905529106

Riekse, R. G., Li, G., Petrie, E. C., Leverenz, J. B., Vavrek, D., Vuletic, S., et al. (2006). Effect of statins on Alzheimer's disease biomarkers in cerebrospinal fluid. *J. Alzheimers Dis.* 10, 399–406. doi: 10.3233/JAD-2006-10408

Ringman, J. M., Coppola, G., Elashoff, D., Rodriguez-Agudelo, Y., Medina, L. D., Gylys, K., et al. (2012). Cerebrospinal fluid biomarkers and proximity to diagnosis in preclinical familial Alzheimer's disease. *Dement. Geriatr. Cogn. Disord.* 33, 1–5. doi: 10.1159/000335729

Ritter, A., and Cummings, J. (2015). Fluid biomarkers in clinical trials of alzheimer's disease therapeutics. *Front. Neurol.* 6:186. doi: 10.3389/fneur.2015.00186

Roe, C. M., Fagan, A. M., Grant, E. A., Hassenstab, J., Moulder, K. L., Maue Dreyfus, D., et al. (2013). Amyloid imaging and CSF biomarkers in predicting cognitive impairment up to 7.5 years later. *Neurology* 80, 1784–1791. doi: 10.1212/WNL.0b013e3182918ca6

Rogeberg, M., Wettergreen, M., Nilsson, L. N., and Fladby, T. (2015). Identification of amyloid beta mid-domain fragments in human cerebrospinal fluid. *Biochimie* 113, 86–92. doi: 10.1016/j.biochi.2015.03.022

Rogers, J., Luber-Narod, J., Styren, S. D., and Civin, W. H. (1988). Expression of immune system-associated antigens by cells of the human central nervous system: relationship to the pathology of Alzheimer's disease. *Neurobiol. Aging* 9, 339–349. doi: 10.1016/s0197-4580(88)80079-4

Rohrer, J. D., Woollacott, I. O., Dick, K. M., Brotherhood, E., Gordon, E., Fellows, A., et al. (2016). Serum neurofilament light chain protein is a measure of disease intensity in frontotemporal dementia. *Neurology* 87, 1329–1336. doi: 10.1212/wnl.0000000000003154

Rojas, J. C., Karydas, A., Bang, J., Tsai, R. M., Blennow, K., Liman, V., et al. (2016). Plasma neurofilament light chain predicts progression in progressive supranuclear palsy. *Ann. Clin. Transl. Neurol.* 3, 216–225. doi: 10.1002/acn3.290

Roltsch, E., Holcomb, L., Young, K. A., Marks, A., and Zimmer, D. B. (2010). PSAPP mice exhibit regionally selective reductions in gliosis and plaque deposition in response to S100B ablation. *J. Neuroinflammation* 7:78. doi: 10.1186/1742-2094-7-78

Ryu, J. K., Cho, T., Choi, H. B., Wang, Y. T., and McLarnon, J. G. (2009). Microglial VEGF receptor response is an integral chemotactic component in Alzheimer's disease pathology. *J. Neurosci.* 29, 3–13. doi: 10.1523/jneurosci.2888-08.2009

Sabbagh, J. J., Kinney, J. W., and Cummings, J. L. (2013). Alzheimer's disease biomarkers in animal models: closing the translational gap. *Am. J. Neurodegener. Dis.* 2, 108–120.

Saman, S., Kim, W., Raya, M., Visnick, Y., Miro, S., Saman, S., et al. (2012). Exosome-associated tau is secreted in tauopathy models and is selectively

phosphorylated in cerebrospinal fluid in early Alzheimer disease. *J. Biol. Chem.* 287, 3842–3849. doi: 10.1074/jbc.M111.277061

Sankaranarayanan, S., Holahan, M. A., Colussi, D., Crouthamel, M. C., Devanarayan, V., Ellis, J., et al. (2009). First demonstration of cerebrospinal fluid and plasma A beta lowering with oral administration of a beta-site amyloid precursor protein-cleaving enzyme 1 inhibitor in nonhuman primates. *J. Pharmacol. Exp. Ther.* 328, 131–140. doi: 10.1124/jpet.108.143628

Savage, M. J., Kalinina, J., Wolfe, A., Tugusheva, K., Korn, R., Cash-Mason, T., et al. (2014). A sensitive abeta oligomer assay discriminates Alzheimer's and aged control cerebrospinal fluid. *J. Neurosci.* 34, 2884–2897. doi: 10.1523/jneurosci.1675-13.2014

Schelle, J., Hasler, L. M., Gopfert, J. C., Joos, T. O., Vanderstichele, H., Stoops, E., et al. (2017). Prevention of tau increase in cerebrospinal fluid of APP transgenic mice suggests downstream effect of BACE1 inhibition. *Alzheimers Dement.* 13, 701–709. doi: 10.1016/j.jalz.2016.09.005

Scholl, M., Maass, A., Mattsson, N., Ashton, N. J., Blennow, K., Zetterberg, H., et al. (2019). Biomarkers for tau pathology. *Mol. Cell Neurosci.* 97, 18–33. doi: 10.1016/j.mcn.2018.12.001

Schöll, M., Schonhaut, D., Lockhart, S., Vogel, J. W., Baker, S., Schwimmer, H., et al. (2015). IC-01-05: in vivo braak staging using 18F-AV1451 Tau PET imaging. *Alzheimers Dement.* 11:P4. doi: 10.1016/j.jalz.2015.06.006

Schwagerl, A. L., Mohan, P. S., Cataldo, A. M., Vonsattel, J. P., Kowall, N. W., and Nixon, R. A. (1995). Elevated levels of the endosomal-lysosomal proteinase cathepsin D in cerebrospinal fluid in Alzheimer disease. *J. Neurochem.* 64, 443–446. doi: 10.1046/j.1471-4159.1995.64010443.x

Sedaghat, F., and Notopoulos, A. (2008). S100 protein family and its application in clinical practice. *Hippokratia* 12, 198–204.

Selkoe, D. J. (2001). Alzheimer's disease: genes, proteins, and therapy. *Physiol. Rev.* 81, 741–766. doi: 10.1152/physrev.2001.81.2.741

Seok, J., Warren, H. S., Cuenca, A. G., Mindrinos, M. N., Baker, H. V., Xu, W., et al. (2013). Genomic responses in mouse models poorly mimic human inflammatory diseases. *Proc. Natl. Acad. Sci. U.S.A.* 110, 3507–3512. doi: 10.1073/pnas.1222878110

Serrano-Pozo, A., Frosch, M. P., Masliah, E., and Hyman, B. T. (2011). Neuropathological alterations in Alzheimer disease. *Cold Spring Harb. Perspect. Med.* 1:a006189. doi: 10.1101/cshperspect.a006189

Sheline, Y. I., and Raichle, M. E. (2013). Resting state functional connectivity in preclinical Alzheimer's disease. *Biol. Psychiatry* 74, 340–347. doi: 10.1016/j.biopsych.2012.11.028

Shen, L., Xia, S., Zhang, H., Yao, F., Liu, X., Zhao, Y., et al. (2018). *Precision Medicine: Role of Biomarkers in Early Prediction and Diagnosis of Alzheimer's Disease*.London: IntechOpen.

Sheng, J. G., Mrak, R. E., and Griffin, W. S. (1994). S100 beta protein expression in Alzheimer disease: potential role in the pathogenesis of neuritic plaques. *J. Neurosci. Res.* 39, 398–404. doi: 10.1002/jnr.490390406

Sheng, J. G., Mrak, R. E., and Griffin, W. S. (1997). Glial-neuronal interactions in Alzheimer disease: progressive association of IL-1alpha+ microglia and S100beta+ astrocytes with neurofibrillary tangle stages. *J. Neuropathol. Exp. Neurol.* 56, 285–290.

Shepherd, C. E., Goyette, J., Utter, V., Rahimi, F., Yang, Z., Geczy, C. L., et al. (2006). Inflammatory S100A9 and S100A12 proteins in Alzheimer's disease. *Neurobiol. Aging* 27, 1554–1563. doi: 10.1016/j.neurobiolaging.2005.09.033

Sheridan, G. K., and Murphy, K. J. (2013). Neuron-glia crosstalk in health and disease: fractalkine and CX3CR1 take centre stage. *Open Biol.* 3:130181. doi: 10.1098/rsob.130181

Sidoryk-Wegrzynowicz, M., Gerber, Y. N., Ries, M., Sastre, M., Tolkovsky, A. M., and Spillantini, M. G. (2017). Astrocytes in mouse models of tauopathies acquire early deficits and lose neurosupportive functions. *Acta Neuropathol. Commun.* 5:89. doi: 10.1186/s40478-017-0478-9

Sjogren, M., Blomberg, M., Jonsson, M., Wahlund, L. O., Edman, A., Lind, K., et al. (2001). Neurofilament protein in cerebrospinal fluid: a marker of white matter changes. *J. Neurosci. Res.* 66, 510–516. doi: 10.1002/jnr.1242

Skachokova, Z., Martinisi, A., Flach, M., Sprenger, F., Naegelin, Y., Steiner-Monard, V., et al. (2019). Cerebrospinal fluid from Alzheimer's disease patients promotes tau aggregation in transgenic mice. *Acta Neuropathol. Commun.* 7:72. doi: 10.1186/s40478-019-0725-3

Skoog, I., Davidsson, P., Aevarsson, Ó, Vanderstichele, H., Vanmechelen, E., and Blennow, K. (2003). Cerebrospinal fluid beta-amyloid 42 is reduced before the onset of sporadic dementia: a population-based study in 85-year-olds. *Dement. Geriatr. Cogn. Disord.* 15, 169–176. doi: 10.1159/000068478

Smith, D. E., Rapp, P. R., McKay, H. M., Roberts, J. A., and Tuszynski, M. H. (2004). Memory impairment in aged primates is associated with focal death of cortical neurons and atrophy of subcortical neurons. *J. Neurosci.* 24, 4373–4381. doi: 10.1523/jneurosci.4289-03.2004

Smith, T. D., Adams, M. M., Gallagher, M., Morrison, J. H., and Rapp, P. R. (2000). Circuit-specific alterations in hippocampal synaptophysin immunoreactivity predict spatial learning impairment in aged rats. *J. Neurosci.* 20, 6587–6593. doi: 10.1523/JNEUROSCI.20-17-06587.2000

Speake, T., Whitwell, C., Kajita, H., Majid, A., and Brown, P. D. (2001). Mechanisms of CSF secretion by the choroid plexus. *Microsc. Res. Tech.* 52, 49–59. doi: 10.1002/1097-0029(20010101)52:1<49::AID-JEMT7>3.0.CO;2-C

Spector, R., Robert Snodgrass, S., and Johanson, C. E. (2015). A balanced view of the cerebrospinal fluid composition and functions: focus on adult humans. *Exp. Neurol.* 273, 57–68. doi: 10.1016/j.expneurol.2015.07.027

Sperling, R. A., Aisen, P. S., Beckett, L. A., Bennett, D. A., Craft, S., Fagan, A. M., et al. (2011). Toward defining the preclinical stages of Alzheimer's disease: recommendations from the National Institute on Aging-Alzheimer's Association workgroups on diagnostic guidelines for Alzheimer's disease. *Alzheimers Dement.* 7, 280–292. doi: 10.1016/j.jalz.2011.03.003

Stadtman, E. R., and Levine, R. L. (2003). Free radical-mediated oxidation of free amino acids and amino acid residues in proteins. *Amino. Acids* 25, 207–218. doi: 10.1007/s00726-003-0011-2

Steinacker, P., Blennow, K., Halbgebauer, S., Shi, S., Ruf, V., Oeckl, P., et al. (2016). Neurofilaments in blood and CSF for diagnosis and prediction of onset in Creutzfeldt-Jakob disease. *Sci. Rep.* 6:38737. doi: 10.1038/srep38737

Steinacker, P., Semler, E., Anderl-Straub, S., Diehl-Schmid, J., Schroeter, M. L., Uttner, I., et al. (2017). Neurofilament as a blood marker for diagnosis and monitoring of primary progressive aphasias. *Neurology* 88, 961–969. doi: 10.1212/wnl.0000000000003688

Stomrud, E., Hansson, O., Zetterberg, H., Blennow, K., Minthon, L., and Londos, E. (2010). Correlation of longitudinal cerebrospinal fluid biomarkers with cognitive decline in healthy older adults. *Arch. Neurol.* 67, 217–223. doi: 10.1001/archneurol.2009.316

Stranahan, A. M., Jiam, N. T., Spiegel, A. M., and Gallagher, M. (2012). Aging reduces total neuron number in the dorsal component of the rodent prefrontal cortex. *J. Comp. Neurol.* 520, 1318–1326. doi: 10.1002/cne.22790

Strozyk, D., Blennow, K., White, L. R., and Launer, L. J. (2003). CSF Abeta 42 levels correlate with amyloid-neuropathology in a population-based autopsy study. *Neurology* 60, 652–656. doi: 10.1212/01.wnl.0000046581.81650.d0

Suarez-Calvet, M., Kleinberger, G., Araque Caballero, M. A., Brendel, M., Rominger, A., Alcolea, D., et al. (2016). sTREM2 cerebrospinal fluid levels are a potential biomarker for microglia activity in early-stage Alzheimer's disease and associate with neuronal injury markers. *EMBO Mol. Med.* 8, 466–476. doi: 10.15252/emmm.201506123

Sudhof, T. C., and Rizo, J. (1996). Synaptotagmins: c2-domain proteins that regulate membrane traffic. *Neuron* 17, 379–388. doi: 10.1016/s0896-6273(00)80171-3

Sunderland, T., Wolozin, B., Galasko, D., Levy, J., Dukoff, R., Bahro, M., et al. (1999). Longitudinal stability of CSF tau levels in Alzheimer patients. *Biol. Psychiatry* 46, 750–755. doi: 10.1016/s0006-3223(99)00143-2

Sunkin, S. M., Ng, L., Lau, C., Dolbeare, T., Gilbert, T. L., Thompson, C. L., et al. (2013). Allen Brain Atlas: an integrated spatio-temporal portal for exploring the central nervous system. *Nucleic Acids Res.* 41, D996–D1008. doi: 10.1093/nar/gks1042

Sutherland, R. J., Kolb, B., and Whishaw, I. Q. (1982). Spatial mapping: definitive disruption by hippocampal or medial frontal cortical damage in the rat. *Neurosci. Lett.* 31, 271–276. doi: 10.1016/0304-3940(82)90032-5

Sutphen, C. L., McCue, L., Herries, E. M., Xiong, C., Ladenson, J. H., Holtzman, D. M., et al. (2018). Longitudinal decreases in multiple cerebrospinal fluid biomarkers of neuronal injury in symptomatic late onset Alzheimer's disease. *Alzheimers Dement.* 14, 869–879. doi: 10.1016/j.jalz.2018.01.012

Swarbrick, S., Wragg, N., Ghosh, S., and Stolzing, A. (2019). Systematic review of miRNA as biomarkers in Alzheimer's disease. *Mol. Neurobiol.* 56, 6156–6167. doi: 10.1007/s12035-019-1500-y

Swardfager, W., Lanctot, K., Rothenburg, L., Wong, A., Cappell, J., and Herrmann, N. (2010). A meta-analysis of cytokines in Alzheimer's disease. *Biol. Psychiatry* 68, 930–941. doi: 10.1016/j.biopsych.2010.06.012

Sweetman, B., and Linninger, A. A. (2011). Cerebrospinal fluid flow dynamics in the central nervous system. *Ann. Biomed. Eng.* 39, 484–496. doi: 10.1007/s10439-010-0141-0

Tagawa, K., Kunishita, T., Maruyama, K., Yoshikawa, K., Kominami, E., Tsuchiya, T., et al. (1991). Alzheimer's disease amyloid beta-clipping enzyme (APP secretase): identification, purification, and characterization of the enzyme. *Biochem. Biophys. Res. Commun.* 177, 377–387. doi: 10.1016/0006-291x(91)91994-n

Takeda, S., Commins, C., DeVos, S. L., Nobuhara, C. K., Wegmann, S., Roe, A. D., et al. (2016). Seed-competent high-molecular-weight tau species accumulates in the cerebrospinal fluid of Alzheimer's disease mouse model and human patients. *Ann. Neurol.* 80, 355–367. doi: 10.1002/ana.24716

Takeda, S., Sato, N., Ikimura, K., Nishino, H., Rakugi, H., and Morishita, R. (2011). Novel microdialysis method to assess neuropeptides and large molecules in free-moving mouse. *Neuroscience* 186, 110–119. doi: 10.1016/j.neuroscience.2011.04.035

Tapiola, T., Alafuzoff, I., Herukka, S. K., Parkkinen, L., Hartikainen, P., Soininen, H., et al. (2009). Cerebrospinal fluid {beta}-amyloid 42 and tau proteins as biomarkers of Alzheimer-type pathologic changes in the brain. *Arch. Neurol.* 66, 382–389. doi: 10.1001/archneurol.2008.596

Tapiola, T., Pirttilä, T., Mikkonen, M., Mehta, P. D., Alafuzoff, I., Koivisto, K., et al. (2000). Three-year follow-up of cerebrospinal fluid tau, beta-amyloid 42 and 40 concentrations in Alzheimer's disease. *Neurosci. Lett.* 280, 119–122. doi: 10.1016/s0304-3940(00)00767-9

Tarnaris, A., Toma, A. K., Chapman, M. D., Petzold, A., Keir, G., Kitchen, N. D., et al. (2011). Rostrocaudal dynamics of CSF biomarkers. *Neurochem. Res.* 36, 528–532. doi: 10.1007/s11064-010-0374-1

Terry, R. D., Masliah, E., Salmon, D. P., Butters, N., DeTeresa, R., Hill, R., et al. (1991). Physical basis of cognitive alterations in Alzheimer's disease: synapse loss is the major correlate of cognitive impairment. *Ann. Neurol.* 30, 572–580. doi: 10.1002/ana.410300410

Teunissen, C. E., Otto, M., Engelborghs, S., Herukka, S. K., Lehmann, S., Lewczuk, P., et al. (2018). White paper by the society for CSF analysis and clinical neurochemistry: overcoming barriers in biomarker development and clinical translation. *Alzheimers Res. Ther.* 10:30. doi: 10.1186/s13195-018-0359-x

Thal, D. R., Rub, U., Orantes, M., and Braak, H. (2002). Phases of a beta-deposition in the human brain and its relevance for the development of AD. *Neurology* 58, 1791–1800. doi: 10.1212/wnl.58.12.1791

Thompson, A. G., Gray, E., Heman-Ackah, S. M., Mager, I., Talbot, K., Andaloussi, S. E., et al. (2016). Extracellular vesicles in neurodegenerative disease - pathogenesis to biomarkers. *Nat. Rev. Neurol.* 12, 346–357. doi: 10.1038/nrneurol.2016.68

Thorsell, A., Bjerke, M., Gobom, J., Brunhage, E., Vanmechelen, E., Andreasen, N., et al. (2010). Neurogranin in cerebrospinal fluid as a marker of synaptic degeneration in Alzheimer's disease. *Brain Res.* 1362, 13–22. doi: 10.1016/j.brainres.2010.09.073

Tian, Z.-Y., Wang, C.-Y., Wang, T., Li, Y.-C., and Wang, Z.-Y. (2019). Glial S100A6 degrades β-amyloid aggregation through targeting competition with Zinc ions. *Aging Dis.* 10, 756–769. doi: 10.14336/AD.2018.0912

Timmers, M., Barao, S., Van Broeck, B., Tesseur, I., Slemmon, J., De Waepenaert, K., et al. (2017). BACE1 dynamics upon inhibition with a BACE inhibitor and correlation to downstream Alzheimer's disease markers in elderly healthy participants. *J. Alzheimers Dis.* 56, 1437–1449. doi: 10.3233/jad-160829

Toledo, J. B., Bjerke, M., Da, X., Landau, S. M., Foster, N. L., Jagust, W., et al. (2015). Nonlinear association between cerebrospinal fluid and florbetapir F-18 beta-amyloid measures across the spectrum of Alzheimer disease. *JAMA Neurol.* 72, 571–581. doi: 10.1001/jamaneurol.2014.4829

Toombs, J., Paterson, R. W., Lunn, M. P., Nicholas, J. M., Fox, N. C., Chapman, M. D., et al. (2013). Identification of an important potential confound in CSF AD studies: aliquot volume. *Clin. Chem. Lab. Med.* 51, 2311–2317. doi: 10.1515/cclm-2013-0293

Town, T., Vendrame, M., Patel, A., Poetter, D., DelleDonne, A., Mori, T., et al. (2002). Reduced Th1 and enhanced Th2 immunity after immunization with Alzheimer's beta-amyloid(1-42). *J. Neuroimmunol.* 132, 49–59. doi: 10.1016/s0165-5728(02)00307-7

Toyn, J. H., Boy, K. M., Raybon, J., Meredith, J. E. Jr., Robertson, A. S., Guss, V., et al. (2016). Robust translation of gamma-secretase modulator pharmacology across preclinical species and human subjects. *J. Pharmacol. Exp. Ther.* 358, 125–137. doi: 10.1124/jpet.116.232249

Trickler, W. J., and Miller, D. W. (2003). Use of osmotic agents in microdialysis studies to improve the recovery of macromolecules. *J. Pharm. Sci.* 92, 1419–1427. doi: 10.1002/jps.10410

Uddin, M. S., Stachowiak, A., Mamun, A. A., Tzvetkov, N. T., Takeda, S., Atanasov, A. G., et al. (2018). Autophagy and Alzheimer's disease: from molecular mechanisms to therapeutic implications. *Front. Aging Neurosci.* 10:4. doi: 10.3389/fnagi.2018.00004

Uylings, H. B., and de Brabander, J. M. (2002). Neuronal changes in normal human aging and Alzheimer's disease. *Brain Cogn.* 49, 268–276. doi: 10.1006/brcg.2001.1500

Van Giau, V., and An, S. S. (2016). Emergence of exosomal miRNAs as a diagnostic biomarker for Alzheimer's disease. *J. Neurol. Sci.* 360, 141–152. doi: 10.1016/j.jns.2015.12.005

Vellonen, K.-S., Ihalainen, J., Boucau, M.-C., Gosselet, F., Picardat, T., Gynther, M., et al. (2017). Disease-induced alterations in brain drug transporters in animal models of Alzheimer's disease. *Pharm. Res.* 34, 2652–2662. doi: 10.1007/s11095-017-2263-7

Verberk, I. M. W., Slot, R. E., Verfaillie, S. C. J., Heijst, H., Prins, N. D., van Berckel, B. N. M., et al. (2018). Plasma amyloid as prescreener for the earliest Alzheimer pathological changes. *Ann. Neurol.* 84, 648–658. doi: 10.1002/ana.25334

Wahlund, L. O., and Blennow, K. (2003). Cerebrospinal fluid biomarkers for disease stage and intensity in cognitively impaired patients. *Neurosci. Lett.* 339, 99–102. doi: 10.1016/s0304-3940(02)01483-0

Walker, D. G., Link, J., Lue, L. F., Dalsing-Hernandez, J. E., and Boyes, B. E. (2006). Gene expression changes by amyloid beta peptide-stimulated human postmortem brain microglia identify activation of multiple inflammatory processes. *J. Leukoc. Biol.* 79, 596–610. doi: 10.1189/jlb.0705377

Wang, L. L., Huang, Y., Wang, G., and Chen, S. D. (2012). The potential role of microRNA-146 in Alzheimer's disease: biomarker or therapeutic target? *Med. Hypotheses* 78, 398–401. doi: 10.1016/j.mehy.2011.11.019

Wang, W. X., Rajeev, B. W., Stromberg, A. J., Ren, N., Tang, G., Huang, Q., et al. (2008). The expression of microRNA miR-107 decreases early in Alzheimer's disease and may accelerate disease progression through regulation of beta-site amyloid precursor protein-cleaving enzyme 1. *J. Neurosci.* 28, 1213–1223. doi: 10.1523/jneurosci.5065-07.2008

Weiner, M. W., Aisen, P. S., Jack, C. R. Jr., Jagust, W. J., Trojanowski, J. Q., Shaw, L., et al. (2010). The Alzheimer's disease neuroimaging initiative: progress report and future plans. *Alzheimers Dement.* 6, 202.e7–211.e7. doi: 10.1016/j.jalz.2010.03.007

Weydt, P., Oeckl, P., Huss, A., Muller, K., Volk, A. E., Kuhle, J., et al. (2016). Neurofilament levels as biomarkers in asymptomatic and symptomatic familial amyotrophic lateral sclerosis. *Ann. Neurol.* 79, 152–158. doi: 10.1002/ana.24552

Wildsmith, K. R., Holley, M., Savage, J. C., Skerrett, R., and Landreth, G. E. (2013). Evidence for impaired amyloid beta clearance in Alzheimer's disease. *Alzheimers Res. Ther.* 5:33. doi: 10.1186/alzrt187

Witter, M. P. (2007). The perforant path: projections from the entorhinal cortex to the dentate gyrus. *Progress Brain Res.* 163 43–61.

Wruck, W., Schroter, F., and Adjaye, J. (2016). Meta-analysis of transcriptome data related to hippocampus biopsies and iPSC-Derived neuronal cells from alzheimer's disease patients reveals an association with FOXA1 and FOXA2 gene regulatory networks. *J. Alzheimers Dis.* 50, 1065–1082. doi: 10.3233/jad-150733

Wu, G., Sankaranarayanan, S., Wong, J., Tugusheva, K., Michener, M. S., Shi, X., et al. (2012). Characterization of plasma beta-secretase (BACE1) activity and soluble amyloid precursor proteins as potential biomarkers for Alzheimer's disease. *J. Neurosci. Res.* 90, 2247–2258. doi: 10.1002/jnr.23122

Xie, S., Xiao, J. X., Gong, G. L., Zang, Y. F., Wang, Y. H., Wu, H. K., et al. (2006). Voxel-based detection of white matter abnormalities in mild Alzheimer disease. *Neurology* 66, 1845–1849. doi: 10.1212/01.wnl.0000219625.77625.aa

Yamada, K., Cirrito, J. R., Stewart, F. R., Jiang, H., Finn, M. B., Holmes, B. B., et al. (2011). In vivo microdialysis reveals age-dependent decrease of brain interstitial fluid tau levels in P301S human tau transgenic mice. *J. Neurosci.* 31, 13110–13117. doi: 10.1523/JNEUROSCI.2569-11.2011

Yamada, K., Patel, T. K., Hochgrafe, K., Mahan, T. E., Jiang, H., Stewart, F. R., et al. (2015). Analysis of in vivo turnover of tau in a mouse model of tauopathy. *Mol. Neurodegener.* 10:55. doi: 10.1186/s13024-015-0052-5

Yan, P., Bero, A. W., Cirrito, J. R., Xiao, Q., Hu, X., Wang, Y., et al. (2009). Characterizing the appearance and growth of amyloid plaques in APP/PS1 mice. *J. Neurosci.* 29, 10706–10714. doi: 10.1523/jneurosci.2637-09.2009

Yankner, B. A., and Mesulam, M. M. (1991). Seminars in medicine of the Beth Israel Hospital, Boston. beta-Amyloid and the pathogenesis of Alzheimer's disease. *N. Engl. J. Med.* 325, 1849–1857. doi: 10.1056/nejm199112263252605

Yassa, M. A., Mattfeld, A. T., Stark, S. M., and Stark, C. E. (2011). Age-related memory deficits linked to circuit-specific disruptions in the hippocampus. *Proc. Natl. Acad. Sci. U.S.A.* 108, 8873–8878. doi: 10.1073/pnas.1101567108

Zetterberg, H., Skillback, T., Mattsson, N., Trojanowski, J. Q., Portelius, E., Shaw, L. M., et al. (2016). Association of cerebrospinal fluid neurofilament light concentration with Alzheimer Disease progression. *JAMA Neurol.* 73, 60–67. doi: 10.1001/jamaneurol.2015.3037

Zimmer, D. B., Chaplin, J., Baldwin, A., and Rast, M. (2005). S100-mediated signal transduction in the nervous system and neurological diseases. *Cell Mol. Biol.* 51, 201–214.

Zimmer, E. R., Parent, M. J., Souza, D. G., Leuzy, A., Lecrux, C., Kim, H. I., et al. (2017). [(18)F]FDG PET signal is driven by astroglial glutamate transport. *Nat. Neurosci.* 20, 393–395. doi: 10.1038/nn.4492

Conflict of Interest: The authors declare that the research was conducted in the absence of any commercial or financial relationships that could be construed as a potential conflict of interest.

frontiers in Aging Neuroscience

ORIGINAL RESEARCH
published: 11 September 2020
doi: 10.3389/fnagi.2020.557005

Non-linear Relationship Between Plasma Amyloid-β 40 Level and Cognitive Decline in a Cognitively Normal Population

*Fan Gao[1], Suhang Shang[2], Chen Chen[2], Liangjun Dang[2], Ling Gao[2], Shan Wei[2], Jin Wang[2], Kang Huo[2], Meiying Deng[2], Jingyi Wang[3] and Qiumin Qu[2]**

[1] Clinical Research Center, The First Affiliated Hospital of Xi'an Jiaotong University, Xi'an, China, [2] Department of Neurology, The First Affiliated Hospital of Xi'an Jiaotong University, Xi'an, China, [3] Department of Neurology, Huxian Hospital of Traditional Chinese Medicine, Xi'an, China

Objectives: Recent studies regarding the relationships between plasma amyloid-β (Aβ) levels and cognitive performance had inconsistent results. In this study, we aimed to characterize the relationship between cognitive decline and plasma Aβ levels in a large-sample cognitively normal population.

Methods: This population-based, prospective cohort study included 1,240 participants with normal cognition. The Mini-Mental State Examination (MMSE) was used to assess cognitive function at baseline and 2 years later. Restricted cubic splines, multivariate logistic regression, and multivariate linear regression models were used to evaluate the type of relationship between cognitive decline during the 2-year follow-up period and plasma Aβ levels ($A\beta_{40}$, $A\beta_{42}$, and $A\beta_{42/40}$).

Results: Participants with moderate $A\beta_{40}$ levels had the highest risk of cognitive decline during a 2-year follow-up relative to individuals with low $A\beta_{40}$ [odds ratio (OR): 0.60, 95% confidence interval (CI): 0.45–0.81, $p < 0.001$] or high $A\beta_{40}$ (OR: 0.65, 95% CI: 0.49–0.87, $p = 0.004$) levels. The association between $A\beta_{40}$ and cognitive decline did not depend on sex, education level, or APOE ε4 status. There was an interaction found between age ($\leq$ 65 and $>$ 65 years) and $A\beta_{40}$ (p for interaction = 0.021). In individuals older than 65 years, there was a positive linear relationship between plasma $A\beta_{40}$ and cognitive decline (OR: 1.02, 95% CI: 1.00–1.04, $p = 0.027$). For participants $\leq$ 65 years old, the lower $A\beta_{40}$ and higher $A\beta_{40}$ groups had a lower risk of cognitive decline than the medium $A\beta_{40}$ group (OR: 0.69, 95% CI: 0.50–0.94, $p = 0.02$; OR: 0.63, 95% CI: 0.45–0.86, $p = 0.004$). None of relationship between plasma $A\beta_{42}$, $A\beta_{42/40}$ and cognitive decline was found during a 2-year follow-up.

Conclusion: The relationship between plasma $A\beta_{40}$ and cognitive decline was not linear, but an inverted-U shape in a cognitively normal population. The underlying mechanism requires further investigation.

Keywords: Alzheimer's disease, plasma amyloid-β, cognitive decline, cognitively normal population, age

OPEN ACCESS

Edited by:
Jiehui Jiang,
Shanghai University, China

Reviewed by:
Nobuyuki Kimura,
National Center for Geriatrics and Gerontology (NCGG), Japan
Kewei Chen,
Banner Alzheimer's Institute, United States

****Correspondence:***
Qiumin Qu
quqiumin@126.com

Received: *29 April 2020*
Accepted: *19 August 2020*
Published: *11 September 2020*

Citation:
Gao F, Shang S, Chen C, Dang L, Gao L, Wei S, Wang J, Huo K, Deng M, Wang J and Qu Q (2020) Non-linear Relationship Between Plasma Amyloid-β 40 Level and Cognitive Decline in a Cognitively Normal Population. Front. Aging Neurosci. 12:557005. doi: 10.3389/fnagi.2020.557005

INTRODUCTION

Amyloid-β (Aβ) pathology has been confirmed as a pathological change in the early phase of Alzheimer 's disease (AD) (Sperling et al., 2011; Yaffe, 2011; Dubois et al., 2016; Jack et al., 2018; Nakamura et al., 2018; Jansen et al., 2018). Abnormal Aβ deposition in the brain increases the risk of cognitive decline and the development of dementia (Villemagne et al., 2011; van Harten et al., 2013; Jaunmuktane et al., 2015; Toledo et al., 2015; Donohue et al., 2017; Roberts et al., 2018; Greenberg et al., 2020). Accelerating our understanding of the relationship between amyloid pathology and cognitive functioning can contribute to the efficient screening of preclinical AD at an early stage, and considerably delay the progression of the disease (Jansen et al., 2018).

Amyloid pathology, visualized on positron emission tomography (PET) scans or measured in cerebrospinal fluid (CSF), has been extensively studied and has proven clinical applications for AD (Sperling et al., 2013; Vos et al., 2013; Toledo et al., 2015; Dubois et al., 2016; Olsson et al., 2016; Donohue et al., 2017). However, because these techniques are invasive or expensive, more economical and easily-acquired plasma Aβ measurements are needed. Recent studies have revealed that plasma Aβ are related to brain Aβ burden and incident dementia (Graff-Radford et al., 2007; Yaffe, 2011; Gabelle et al., 2013; Hanon et al., 2018; Hilal et al., 2018; Nakamura et al., 2018; Verberk et al., 2018; Chen et al., 2019; de Wolf et al., 2020), however, the relationships between plasma Aβ levels and cognitive performance were inconsistent. Previous studies reported that lower plasma $A\beta_{42/40}$ or $A\beta_{42}$ increased the risk of cognitive decline and the progression of dementia (Yaffe, 2011; Gabelle et al., 2013; Hilal et al., 2018; Verberk et al., 2018; de Wolf et al., 2020). Other studies have suggested that a positive relationship between plasma $A\beta_{42}$, $A\beta_{42/40}$ and cognitive impairment (Hanon et al., 2018; Wang et al., 2018; Chen et al., 2019).

In order to rapidly identify patients with cognitive decline earlier, and therefore delay the occurrence of AD, the present study aimed to determine the change in cognitive status, its relationship with plasma Aβ, and the type of association, during a 2-year follow-up in a cognitively normal population. This study also investigated whether this association was altered by sex, age, education level, or Apolipoprotein E (APOE) genotype, and estimated the relationship between plasma Aβ and cognitive disorder and cardio-cerebrovascular diseases during a 2-year follow-up.

MATERIALS AND METHODS

Study Population

Participants were enrolled from a village in the suburbs of Xi'an city, located in northwestern China, between October, 2014 and November, 2015. This study was a community population cohort study in which each interviewee received a face-to-face questionnaire. Participants were asked about detailed history by neurologists, and received a nervous system examination, a systemic physical examination, blood biochemical examination aimed at determining whether there were any related neurological diseases. All patients with cerebral disease had received the CT or MRI scans. For patients who had a diagnosis of mild cognitive impairment (MCI) or dementia due to AD, we provided free MRI scan to confirm the diagnosis of AD in a local designated hospital. Inclusion criteria was that participants were (1) older than 40 years and (2) a current resident of the village and had lived there for more than 3 years. Exclusion criteria was that (1) the Mini-Mental State Examination (MMSE) was not completed; (2) there was evidence of MCI or dementia, or (3) other neurological conditions that may influence cognitive function (such as epilepsia, central nervous system infections, essential tremor, Parkinsonism, anxiety, depression, thyroid hypofunction, intracranial trauma, or surgery); (4) plasma Aβ was not measured; and (5) other baseline information was missing. This study was approved by the First Affiliated Hospital of Xi'an Jiaotong University. Written informed consent was obtained from all participants.

Cognitive Evaluation

The MMSE was conducted as global cognitive screening at enrollment. The MMSE, other neurological, physical and imaging examinations were assessed at baseline and repeated 2 years later. Cutoff values were $\leq$ 17 for subjects with illiteracy, $\leq$20 for primary school educated subjects, and $\leq$ 24 for those educated at the junior high school level or above (Bohm et al., 2015). After initial screening, study participants with MMSE score $\leq$ these cutoff values underwent the 2nd phase cognitive examinations, including the Fuld Object Memory Evaluation test, Rapid Verbal Retrieval test, Trail-Making test, Digit Span test, and Block Design test. Finally, combining all the available imaging and clinical information, the diagnosis and subtype of dementia and MCI were determined according to international diagnostic criteria for dementia (American Psychiatric Association [APA], 2000) and Petersen MCI criteria (Petersen, 2011) by a panel of senior clinicians. The diagnosis of AD was based on NINCDS-ADRDA criteria (McKhann et al., 2011).

Laboratory Measurement

All plasma samples were acquired between 7 and 11 a.m. Plasma $A\beta_{40}$ and $A\beta_{42}$ tests were measured using enzyme-linked immunosorbent assay kits (ELISA, Yuanye Co. Shanghai, China) (Wei et al., 2017; Jiang et al., 2018). Concentrations of $A\beta_{40}$ and $A\beta_{42}$ were conducted in duplicate and determined from standard curves using a Rayto RT-6000 analyzer (Rayto Co., Shenzhen, China) at OD 450 nm. Apolipoprotein E (APOE) was genotyped by polymerase chain reaction (PCR), followed by sequencing, as previously described (Wenham et al., 1991).

Outcome Definition

The primary outcome was cognitive decline, which was defined as the difference of MMSE between the first visit and the second visit $>$ 0. Cognitive disorder was defined as MMSE score $\leq$ 17 for illiterate, $\leq$ 20 for primary school educated, and $\leq$ 24 for junior high school educated or above (Katzman et al., 1988). New cardiovascular and cerebrovascular diseases were defined as

incident cardiovascular and cerebrovascular diseases during the 2-year follow-up.

Other Covariates

Lack of physical exercise was defined as exercising fewer than three times a week, fewer than 30 min a time. Smoking was defined as a current smoker. Diabetes mellitus was defined as a self-reported medical diagnosis, diabetic medication use, a fasting glucose of $\geq$ 7.0 mmol/l, a random plasma glucose concentration $\geq$ 11.1 mmol/l, or glycated hemoglobin $\geq$ 6.5%. Hypertension was defined as a self-reported medical diagnosis, antihypertensive medication use, a systolic blood pressure of $\geq$ 140 mmHg, or a diastolic blood pressure of $\geq$ 90 mmHg.

Statistical Analysis

Continuous variables are presented as mean $\pm$ SD, and categorical variables are presented as proportions. We determined the association between baseline information and cognitive decline using Pearson's χ^2 or Fisher's exact test for categorical variables, and Student's *t*-test or Mann–Whitney *U*-test for continuous variables. Differences of basic characteristics between different Aβ groups were compared using Pearson's χ^2 or Fisher's exact test for categorical variables, and ANOVA test or Kruskal-Wallis H test for continuous variables.

Restricted cubic splines with a logistic regression model were applied to test the relationship between cognitive decline and Aβ levels, and to evaluate the type of correlation of cognitive decline with Aβ levels. Four knots defined at the 5th, 35th, 65th, and 95th percentiles of Aβ levels were prespecified (Harrell, 2001). The reference point was the mean value of Aβ levels. Aβ categories were based on the type of relationship between cognitive decline, and Aβ levels suggested in restricted cubic splines. A series of pre-planned categories of Aβ levels were tested, defined by tertiles and interquartiles. The differences in MMSE scores between baseline and 2 years later were compared with the paired *t*-test.

To assess the association between Aβ levels (categorical and continuous) and various outcomes, unadjusted, age- and sex-adjusted, and multivariable-adjusted logistic regression models were used. A multivariable linear regression model was used to evaluate the relationship between Aβ and 2-year MMSE score change. In multivariable models, adjustments were made for age, sex, diabetes, hypertension, smoking, lack of physical activity, APOE ε4 status, and education. In subgroup analyses, we examined the relationship between $A\beta_{40}$ and cognitive decline by sex, age ($\leq$ 65 and $>$ 65 years), education ($\geq$ high school and $<$ high school), and APOE ε4 status in multivariable-adjusted logistic regression models. SPSS ver. 24.0 and R ver. 3.5.3 were used for statistical analysis. A $p < 0.05$ was considered significant.

RESULTS

Characteristics of the Study Population at Baseline

The study population screening process is shown in **Figure 1**. There were 2,173 individuals examined from October, 2014 to November, 2015. A total of 138 participants did not complete the MMSE, 58 had MCI or dementia, 112 had neurologically-related diseases, 470 did not undergo plasma Aβ tests, 131 had missing baseline information, and 24 did not complete the follow-up MMSE. Finally, 1,240 participants were included in our study.

Baseline characteristics of the study population are listed in **Table 1**. Among 1240 participants, 456 experienced cognitive decline. The mean age of the study participants was 55.2 $\pm$ 9.7 years and 469 (37.8%) were men. In the group without cognitive decline, the percentage of higher education level was higher (63.3%) than that in the group with cognitive decline (55.3%, $p = 0.005$). MMSE score was higher (27 $\pm$ 3.2) in the group with cognitive decline than that in the population without cognitive decline(25.5 $\pm$ 3.7, $p < 0.001$. There were no other significant differences between two groups.

Association Between Continuous $A\beta_{40}$, $A\beta_{42}$, $A\beta_{42/40}$ Levels and Cognitive Decline

The associations between continuous $A\beta_{40}$, $A\beta_{42}$, $A\beta_{42/40}$ levels and cognitive decline were listed in **Table 2**. After multivariable adjustment, none of three biomarkers reached statistical significance (all $p > 0.05$).

The associations between Aβ levels and cognitive decline using restricted cubic splines are shown in **Figure 2**. $A\beta_{40}$ showed a non-linear relationship (p overall = 0.040, p non-linear = 0.017) with cognitive decline. $A\beta_{42}$ and $A\beta_{42/40}$ didn't show any relationship with cognitive decline (p overall > 0.05; p non-linear > 0.05).

Non-linear Relationship Between Plasma $A\beta_{40}$ Level and Cognitive Decline

Because of the non-linear relationship between plasma $A\beta_{40}$ and cognitive decline, and the inverted U shape found in the restricted cubic spline, we transformed continuous $A\beta_{40}$ into two kinds of categorical variables: three tertiles defined by the 33rd percentiles and 66th percentiles, and 3-class classified variables defined by the 25th and 75th percentiles. In multivariate logistic regression analyses evaluating the relationship between cognitive decline and categorical $A\beta_{40}$, 3-classified $A\beta_{40}$ had a better goodness of fit ($\chi^2 = 32.20$, $p < 0.001$) than $A\beta_{40}$ defined by the 33rd and 66th percentiles ($\chi^2 = 15.44$, $p = 0.117$). Therefore, 3-classified $A\beta_{40}$, defined by the 25th and 75th percentiles, was used in the present study.

Two-year changes in MMSE score in the three $A\beta_{40}$ groups are shown in **Figure 3**. Paired comparisons of MMSE scores between baseline and 2 years later in the medium and high $A\beta_{40}$ groups were significant ($p < 0.001$, **Figure 3A**). When plasma was 45 pg/mL $\leq A\beta_{40} <$ 58.4 pg/mL, the change in MMSE scores between the 2 visits was more evident than in the other 2 groups (**Figure 3B**). The changes in MMSE scores in the low, medium, and high $A\beta_{40}$ groups were 0.09 $\pm$ 1.53, 0.65 $\pm$ 1.89, and 0.39 $\pm$ 1.78 pg/mL respectively. Baseline characteristics of the study population, stratified by low ($<$ 45 pg/mL), medium (45 pg/mL $\leq A\beta_{40} <$ 58.4 pg/mL), and high $A\beta_{40}$ ($\geq$58.4 pg/mL) are listed in **Supplementary Table S1**.

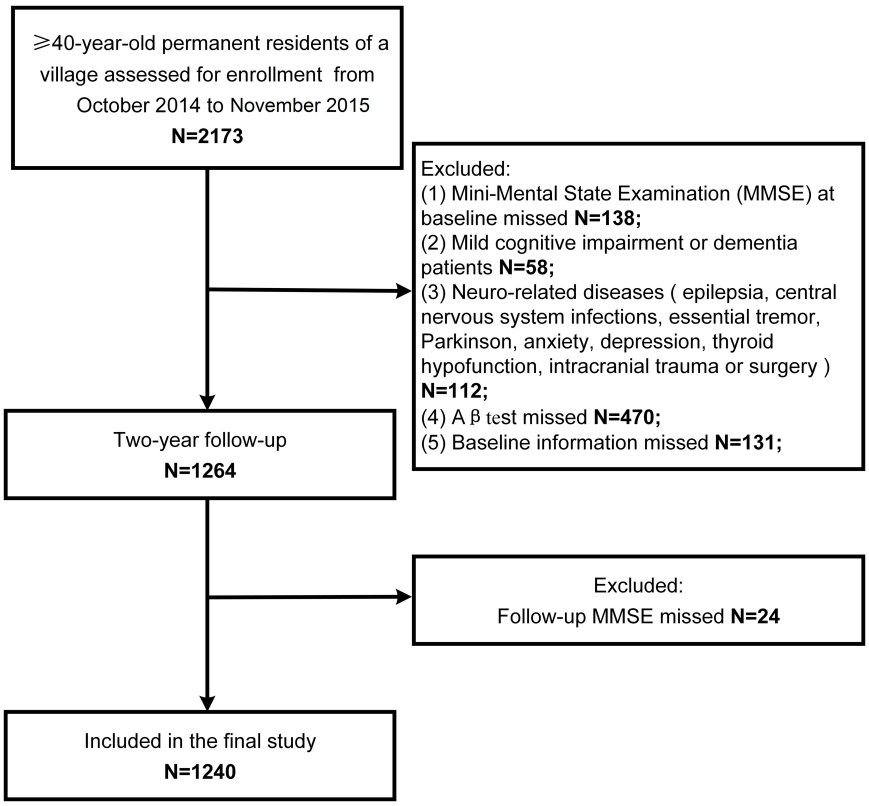

FIGURE 1 | Study population screening process.

TABLE 1 | Baseline characteristics according to cognitive decline.

Variable	Cognitive decline *n* = 456	Without cognitive decline *n* = 784	*p*
Age (y)	56 ± 10	54.8 ± 9.4	0.048
Male, n(%)	186 (40.8)	283 (36.1)	0.100
Education ≥ high school, n(%)	252 (55.3)	496 (63.3)	0.005
Diabetes, n(%)	39 (8.6)	62 (7.9)	0.689
Hypertension, n(%)	134 (29.4)	217 (27.7)	0.520
Smoking, n(%)	136 (29.8)	197 (25.1)	0.072
Alcohol drinker, n(%)	63 (13.8)	103 (13.1)	0.735
Lack of exercise, n(%)	92 (20.2)	124 (15.8)	0.051
SBP (mmHg)	133.6 ± 19.2	132.1 ± 18.2	0.112
Pulse (/min)	75.2 ± 8.4	75.7 ± 9.5	0.728
BMI (kg/m^2)	25.2 ± 3.2	25.4 ± 3.2	0.197
TC (mmol/L)	5 ± 1	5 ± 1	0.892
TG (mmol/L)	1.6 ± 0.9	1.6 ± 0.9	0.588
HDL (mmol/L)	1.4 ± 0.3	1.4 ± 0.3	0.19
LDL (mmol/L)	3.3 ± 0.9	3.3 ± 0.9	0.829
APOE ε4 positive, n(%)	64 (14)	102 (13)	0.609
$A\beta_{40}$ (pg/mL)	50 ± 14.2	49.7 ± 15.1	0.645
$A\beta_{42}$ (pg/mL)	41.1 ± 6.8	41 ± 6.5	0.963
$A\beta_{42/40}$ (pg/mL)	9.1 ± 36.7	9.9 ± 38.2	0.915
MMSE at baseline	27 ± 3.2	25.5 ± 3.7	<0.001

SBP, systolic blood pressure; BMI, body mass index; TC, total cholesterol; TG, triglycerides; HDL, high-density lipoprotein cholesterol; LDL, low-density lipoprotein cholesterol; APOE, apolipoprotein E; Aβ, Amyloid-β; MMSE, Mini-Mental State Examination.

TABLE 2 | Association of plasma levels of amyloid-β 40, amyloid-β 42, and the amyloid-β 42/amyloid-β 40 ratio with cognitive decline.

Biomarker	Association with cognitive decline					
	Unadjusted		Age-and sex-adjusted		Fully adjusted[a]	
	OR (95%CI)	*p*	OR (95%CI)	*p*	OR (95%CI)	*p*
$A\beta_{40}$	1.00	0.752	1.00	0.786	1.00	0.731
(per pg/mL increase)	(0.99–1.01)		(0.99–1.01)		(0.99–1.01)	
$A\beta_{42}$	1.00	0.738	1.00	0.827	1.00	0.770
(per pg/mL increase)	(0.99–1.02)		(0.99–1.02)		(0.99–1.02)	
$A\beta_{42/40}$	1.00	0.725	1.00	0.698	1.00	0.579
	(1.00–1.00)		(1.00–1.00)		(1.00–1.00)	

[a]*Fully adjusted for age, sex, diabetes, hypertension, smoking, lack of physical exercise, APOEε4, education ≥ high school. OR, odds ratio; CI, confidence interval.*

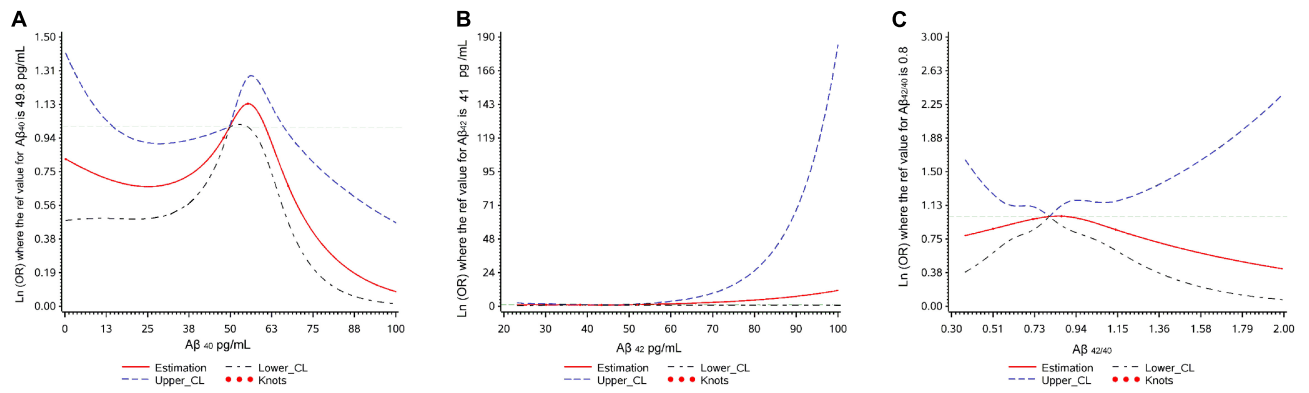

FIGURE 2 | Plot of dose-response relationship between plasma Aβ levels and cognitive decline during two-year follow-up.

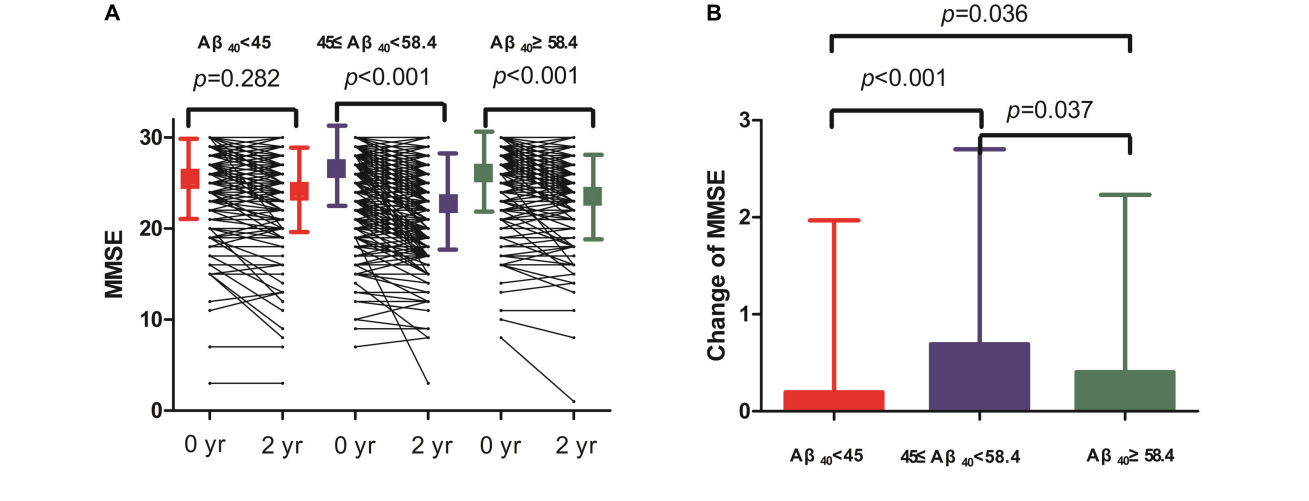

FIGURE 3 | The changes of cognitive function during 2 year follow-up.

The relationship between plasma $A\beta_{40}$ and various outcomes during follow-up using multivariable logistic regression models are listed in **Table 3**. In unadjusted analyses, compared with participants with $A\beta_{40}$ between 45 and 58.4 pg/mL, participants in the low $A\beta_{40}$ group and high $A\beta_{40}$ group had lower risks of cognitive decline (OR: 0.61, 95% CI: 0.46–0.82, $p < 0.001$; OR: 0.67, 95% CI: 0.50–0.89, $p = 0.006$). After adjustments for age and sex, the results were the same as before. In the fully adjusted model, participants in the low $A\beta_{40}$ (< 45 pg/mL) and high $A\beta_{40}$ groups (≥58.4 pg/mL) still had a lower risk of cognitive decline, compared with the medium $A\beta_{40}$ group (OR: 0.60, 95% CI: 0.45–0.81, $p < 0.001$; OR: 0.65, 95% CI: 0.49–0.87,

TABLE 3 | Results of multivariable logistic regression models examining the relationship between plasma $A\beta_{40}$ and various outcomes during follow-up.

Outcomes	No. of events (%)	Unadjusted			Age- and sex-adjusted			Fully adjusted[a]		
		OR	95%CI	*p*	OR	95%CI	*p*	OR	95%CI	*p*
Cognitive decline										
< 45 pg/mL	95 (30.65)	0.61	0.46–0.82	< 0.001	0.61	0.46–0.82	0.001	0.60	0.45–0.81	< 0.001
45∼58.4 pg/mL	260 (41.94)	1.0 (ref)			1.0 (ref)			1.0 (ref)		
≥ 58.4 pg/mL	101 (32.58)	0.67	0.50–0.89	0.006	0.67	0.50–0.89	0.006	0.65	0.49–0.87	0.004
New cognitive disorder										
< 45 pg/mL	6 (1.94)	0.31	0.13–75	0.009	0.31	0.13–0.74	0.009	0.29	0.12–0.70	0.006
45∼58.4 pg/mL	37 (5.97)	1.0 (ref)			1.0 (ref)			1.0 (ref)		
≥ 58.4 pg/mL	14 (4.52)	0.75	0.40–1.40	0.361	0.72	0.38–1.36	0.305	0.70	0.37–1.32	0.270
Cognitive disorder at baseline										
< 45 pg/mL	34 (10.97)	1.41	0.89–2.22	0.147	1.43	0.90–2.28	0.131	1.41	0.88–2.26	0.151
45∼58.4 pg/mL	50 (8.06)	1.0 (ref)			1.0 (ref)			1.0 (ref)		
≥ 58.4 pg/mL	28 (9.03)	1.13	0.70–1.84	0.616	1.1	0.67–1.80	0.706	1.10	0.67–1.80	0.710
New cardiovascular diseases										
< 45 pg/mL	19 (6.13)	0.8	0.46–1.38	0.414	0.8	0.45–1.39	0.421	0.81	0.46–1.42	0.452
45∼58.4 pg/mL	47 (7.59)	1.0 (ref)			1.0 (ref)			1.0 (ref)		
≥ 58.4 pg/mL	16 (5.16)	0.66	0.37–1.19	0.167	0.63	0.35–1.14	0.124	0.64	0.35–1.16	0.138
New cerebrovascular diseases										
< 45 pg/mL	8 (2.58)	0.49	0.22–1.07	0.072	0.48	0.22–1.07	0.072	0.49	0.22–1.08	0.077
45∼58.4 pg/mL	32 (5.17)	1.0 (ref)			1.0 (ref)			1.0 (ref)		
≥ 58.4 pg/mL	14 (4.52)	0.87	0.46–1.65	0.665	0.84	0.44–1.60	0.588	0.86	0.44–1.66	0.644

OR, odds ratio; CI, confidence interval; Aβ, Amyloid-β. [a]*Fully adjusted for age, sex, diabetes, hypertension, smoking, lack of physical exercise, APOEε4, education ≥ high school.*

p = 0.004). In addition, participants in the low Aβ40 group had a lower risk of a new cognitive disorder (OR: 0.29, 95% CI: 0.12–0.70, *p* = 0.006) than participants in the medium $A\beta_{40}$ group, while participants with high $A\beta_{40}$ levels did not show this association. There were no significant associations found in other outcomes. The relationships of categorical $A\beta_{40}$ defined by the 33th percentiles and 66th percentiles, and cognitive decline are listed in **Supplementary Table S2**.

The relationship between plasma $A\beta_{40}$ and 2-year change in MMSE score using a multivariate linear regression model is shown in **Figure 4**. An inverted U-shaped association between $A\beta_{40}$ and MMSE score change was still apparent. Compared with participants with medium $A\beta_{40}$, those with low $A\beta_{40}$ and high $A\beta_{40}$ had a lower risk of MMSE score change (β: −0.57, 95% CI: −0.81 to −0.33, $p < 0.001$; β: −0.29, 95% CI: −0.53 to −0.05, *p* = 0.020).

Subgroup Analyses of the Relationship Between Plasma $A\beta_{40}$ and Cognitive Decline

Subgroup analyses of the relationship between plasma $A\beta_{40}$ and cognitive decline are listed in **Table 4**. The association between $A\beta_{40}$ and cognitive decline did not depend on sex, education level, or APOE ε4 status. There was an interaction found between age (≤ 65 and > 65 years) and $A\beta_{40}$ (*p* for interaction = 0.021). For participants ≤ 65 years old, the lower $A\beta_{40}$ and higher $A\beta_{40}$ groups had a lower risk of cognitive decline than the medium $A\beta_{40}$ group (OR: 0.69, 95% CI: 0.50–0.94, *p* = 0.02; OR: 0.63, 95% CI: 0.45–0.86, *p* = 0.004). In participants aged > 65 years, lower Aβ40 levels correlated with cognitive decline (OR: 0.29, 95% CI: 0.14–0.63, *p* = 0.002) compared with the medium $A\beta_{40}$ group. Continuous $A\beta_{40}$ level was associated with the increased risk of cognitive decline (OR: 1.02, 95%CI: 1.00–1.04, *p* = 0.027).

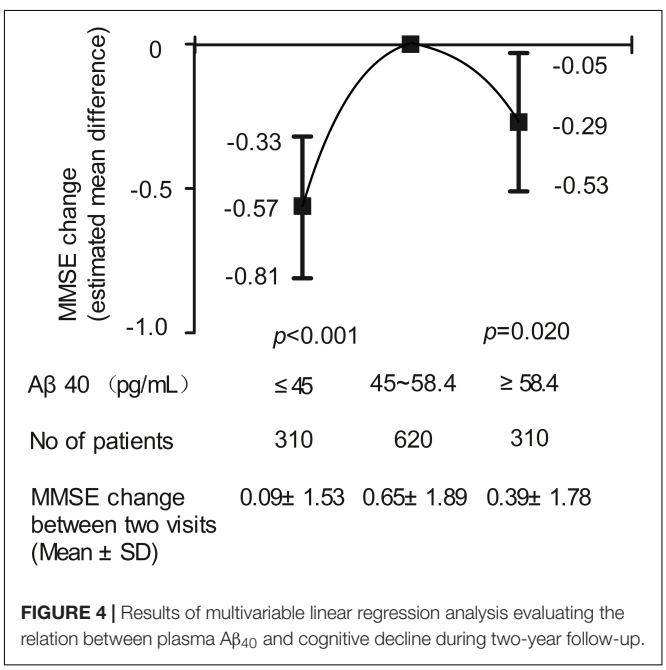

FIGURE 4 | Results of multivariable linear regression analysis evaluating the relation between plasma $A\beta_{40}$ and cognitive decline during two-year follow-up.

TABLE 4 | Subgroup analyses of relationship between plasma $A\beta_{40}$ and cognitive decline.

Subgroups	No. of events (%)	OR[a]	95%CI	*p*	*p* interaction
Sex					0.323
Male					
Continuous	186 (39.7)	1.01	0.99–1.02	0.266	
< 45 pg/mL	33 (29.5)	0.41	0.25–0.68	< 0.001	
45∼58.4 pg/mL	116 (47.9)	1.0 (ref)			
≥ 58.4 pg/mL	37 (32.2)	0.43	0.27–0.71	< 0.001	
Female					
Continuous	270 (35.0)	1.00	0.99–1.01	0.698	
< 45 pg/mL	62 (31.3)	0.74	0.52–1.07	0.115	
45∼58.4 pg/mL	144 (38.1)	1.0 (ref)			
≥ 58.4 pg/mL	64 (32.8)	0.8	0.55–1.15	0.219	
Age					0.021
Age ≤ 65					
Continuous	367 (35.6)	1.00	0.99–1.01	0.380	
< 45 pg/mL	82 (31.7)	0.69	0.50–0.94	0.020	
45∼58.4 pg/mL	208 (40.3)	1.0 (ref)			
≥ 58.4 pg/mL	77 (30.1)	0.63	0.45–0.86	0.004	
Age > 65					
Continuous	89 (45.6)	1.02	1.00–1.04	0.027	
< 45 pg/mL	13 (25.5)	0.29	0.14–0.63	0.002	
45∼58.4 pg/mL	52 (50)	1.0 (ref)			
≥ 58.4 pg/mL	24 (44.4)	0.72	0.36–1.44	0.358	
Education ≥ high school					0.461
Yes					
Continuous	252 (33.7)	1.00	0.99–1.02	0.520	
< 45 pg/mL	51 (27.4)	0.6	0.41–0.88	0.009	
45∼58.4 pg/mL	150 (39.0)	1.0 (ref)			
≥ 58.4 pg/mL	51 (28.8)	0.63	0.43–0.93	0.021	
No					
Continuous	204 (41.5)	1.00	0.99–1.01	0.859	
< 45 pg/mL	44 (35.5)	0.61	0.39–0.97	0.035	
45∼58.4 pg/mL	110 (46.8)	1.0 (ref)			
≥ 58.4 pg/mL	50 (37.6)	0.67	0.43–1.04	0.073	
APOE ε4 carrier					0.186
Yes					
Continuous	64 (38.6)	1.01	0.99–1.04	0.257	
< 45 pg/mL	9 (20.5)	0.26	0.11–0.63	0.003	
45∼58.4 pg/mL	40 (48.8)	1.0 (ref)			
≥58.4 pg/mL	15 (37.5)	0.65	0.29–1.43	0.284	
No					
Continuous	392 (36.5)	1.00	0.99–1.01	0.834	
<45 pg/mL	86 (32.3)	0.68	0.50–0.93	0.017	
45∼58.4 pg/mL	220 (40.9)	1.0 (ref)			
≥ 58.4 pg/mL	86 (31.9)	0.66	0.48–0.90	0.008	

OR, odds ratio; CI, confidence interval; APOE, apolipoprotein E; Aβ, Amyloid-β. [a]*Logistic regression models were used and adjusted for age, sex, diabetes, hypertension, smoking, lack of physical exercise, APOEε4 and education ≥ high school.*

DISCUSSION

In this large, prospective, population-based cohort study, we found an inverted U-shaped relationship between plasma $A\beta_{40}$ and cognitive decline during a 2-year follow-up in individuals with normal cognition. People with medium plasma $A\beta_{40}$ concentrations (45–58.4 pg/mL) had the highest risk of cognitive decline than persons with plasma $A\beta_{40}$ < 45 pg/mL and ≥ 58.4 pg/mL.

Previous studies have shown evidence of an association between plasma Aβ levels and the progression of AD, although most studies focused on plasma $A\beta_{42}$ and plasma $A\beta_{42/40}$ ratio (Schupf et al.; Graff-Radford et al., 2007; Yaffe, 2011; Gabelle et al., 2013; de Rojas et al., 2018; Hanon et al., 2018; Hilal et al., 2018; Verberk et al., 2018; Chen et al., 2019). Hanon et al. (2018) did not find a significant linear association between $A\beta_{40}$ and MMSE score in their prospective cohort study, which included 1,040 participants. Several prospective cohort studies found that plasma $A\beta_{42}$ or $A\beta_{42/40}$ ratio was associated with an increased risk of developing AD, while no associations of this kind were found for plasma Aβ40 (Graff-Radford et al., 2007; Schupf et al., 2008; Yaffe, 2011; Gabelle et al., 2013;

de Rojas et al., 2018; Hilal et al., 2018; Verberk et al., 2018). Chen et al. reported a linear relationship between plasma $A\beta_{42}$ and MMSE score, regardless of plasma $A\beta_{40}$ (Chen et al., 2019). This is the first study to report a non-linear relationship between plasma $A\beta_{40}$ and cognitive decline. The reason may be attributed to different study population and different follow-up time. Most of previous studies observed marked cognitive decline (clinical progression to MCI) or the incidence of dementia for a long follow-up time in old and high-risk dementia populations (Yaffe, 2011; Gabelle et al., 2013; Verberk et al., 2018; de Wolf et al., 2020). In our study, we just observed 2-year MMSE change in a cognitively normal population with middle and old age. Two prior studies ever reported that higher plasma $A\beta_{40}$ level was correlated with a decreased hippocampal volume (Kaffashian et al., 2015; Hanon et al., 2018). There was also evidence to reveal that Aβ levels were linked with brain atrophy only at an initial stage before cognitive impairment. The relationship between plasma Aβ levels and brain structural variation or cognitive outcomes during earlier stage of AD progression or normal cognitive aging may be different with the association at later stages (Hanon et al., 2018). Therefore, the association between plasma $A\beta_{40}$ and cognitive decline may be earlier detected than the relationship between plasma $A\beta_{42}$ and cognition progression due to a shorter observation period (2-year follow-up) and younger population in our study. It is why we only find the correlation of cognitive decline with plasma $A\beta_{40}$, not plasma $A\beta_{42}$.

The precise mechanisms underlying the relationship between plasma $A\beta_{40}$ and cognitive decline remain unclear. There may be both of neurodegenerative and cerebrovascular pathologies promoting cognitive impairment in the study participants (Greenberg et al., 2020). $A\beta_{40}$ was reported to be associated with the development of vascular dementia as well as AD (Hansson et al., 2012). Compared with moderate plasma $A\beta_{40}$ group, higher plasma $A\beta_{40}$ level may indicate more Aβ efflux from the brain to the peripheral blood and fewer deposition in brain. Therefore, the cognitive decline in the high plasma $A\beta_{40}$ group may be slower. Besides, although the concentration of $A\beta_{40}$ measured in peripheral blood was not high in the moderate $A\beta_{40}$ group, the deposit of $A\beta_{40}$ in the wall of vessels may be relatively high, which was involved with the development of vascular dementia. Compared with moderate $A\beta_{40}$ group, low concentration of plasma $A\beta_{40}$ may suggest increased degradation of $A\beta_{40}$ by peripheral tissues, such as liver and kidney and decreased production of $A\beta_{40}$ from brain and peripheral tissues (Kaffashian et al., 2015). It could reflect favorable condition of blood vessels, liver and kidney, which was significant to maintain normal cognitive function.

The characteristics of $A\beta_{40}$ is different with $A\beta_{42}$. $A\beta_{40}$ is more soluble than $A\beta_{42}$, which can diffuse along perivascular drainage pathways to deposit in the walls of vessels, while $A\beta_{42}$ tends to retained in the brain parenchyma and initiate insoluble plaque nucleation (Greenberg et al., 2020). In addition, $A\beta_{40}$ is produced or degraded by peripheral tissues as well as $A\beta_{40}$ produced and deleted in the brain (Kaffashian et al., 2015). Plasma $A\beta_{40}$ may be not a direct surrogate marker for cerebral $A\beta_{40}$, which can't reflect $A\beta_{40}$ and $A\beta_{42}$ metabolism in the brain (Sonnen et al., 2008). Accordingly, the effect of $A\beta_{40}$ on the physiologic process of dementia may be more complicated than $A\beta_{42}$. Because this study is a community-based cohort study, which failed to measure the liver and kidney function comprehensively, nor did it assess the deposition of Aβ in the brain parenchyma and vascular wall. The mechanisms of plasma $A\beta_{40}$ affecting cognitive performance still needs further studies.

Of note, we found that the inverted U-shaped relationship between plasma $A\beta_{40}$ and cognitive decline was more marked for young people (40–65 years old), while there seems to be a positive linear relationship between plasma $A\beta_{40}$ and cognitive decline in individuals older than 65 years. This result agrees with other studies that suggested that amyloid-cognition association varied by age (Rowe et al., 2010; Rentz et al., 2011; Sperling et al., 2013; Petersen et al., 2016; Jansen et al., 2018). Jansen et al. (2018) found that the relationship between higher amyloid deposition in the brain and low memory scores was more evident in individuals older than 70 years old. Coincidentally, another recent study found no association between continuous PET-Aβ levels and memory scores in younger people (50–69 years old) (Mielke et al., 2016). In older population (> 65 years old), our results supported the previous studies (Hansson et al., 2012; Kaffashian et al., 2015; Hanon et al., 2018). For younger individuals (40–65 years old), our studies suggested that conventional evaluation methods (continuous or dichotomized $A\beta_{40}$) were not suitable for assessing the relationship between plasma $A\beta_{40}$ and cognitive decline.

There are still limitations that need to be considered. First, only the total MMSE score was evaluated for every participant in this study; sub-items of MMSE and other cognitive scores should be included to confirm cognitive decline. Second, ELISA is not the most sensitive technique for assessing plasma Aβ levels. Recent studies have employed single-molecule array or hybrid mass spectrometry techniques which may be more accurate approaches than ELISA (Nakamura et al., 2018; Vergallo et al., 2019). Nevertheless, ELISA is suitable for epidemiological studies with large sample size because of simple operation and cheapness. Third, the correlation of plasma $A\beta_{40}$ with CSF $A\beta_{40}$ and brain $A\beta_{40}$, and the mechanism of transportation and clearance of $A\beta_{40}$, were not studied. It would be useful to explore the dynamic transportation mechanism of $A\beta_{40}$ between the brain and peripheral blood in future studies, in order to verify the present results.

CONCLUSION

This population-based, prospective cohort study showed that the relationship between plasma $A\beta_{40}$ and cognitive decline is not linear, but an inverted-U shape, in a cognitively normal population. Medium concentration of plasma $A\beta_{40}$ is associated with a greater risk of cognitive decline, compared with low and high levels of plasma $A\beta_{40}$, primarily in younger persons (≤65 years old). The underlying mechanism needs to be further elucidated.

DATA AVAILABILITY STATEMENT

The raw data supporting the conclusions of this article will be made available by the authors, without undue reservation, to any qualified researcher.

ETHICS STATEMENT

The studies involving human participants were reviewed and approved by the ethics committee for medical research at the First Affiliated Hospital of Xi'an Jiaotong University. The patients/participants provided their written informed consent to participate in this study.

AUTHOR CONTRIBUTIONS

FG and QQ: conception and design of the study. SS, CC, LD, LG, SW, JW, and QQ acquisition of the data. FG, SS, and CC: analysis of data. FG, JW, KH, MD, and QQ interpretation of data. FG: wrote the first manuscript draft. SS, CC, LD, LG, SW, JW, KH, MD, JW, and QQ: revised the manuscript for intellectual content. All authors contributed to the article and approved the submitted version.

FUNDING

This work was supported by the Nature Science Foundation of China (No. 81771168), the Key Research & Development Programs of Shaanxi Province (No. 2018ZDXM-SF-052), and the Clinical Research Award of the First Affiliated Hospital of Xi'an Jiaotong University, China (No. XJTU1AF-CRF-2018-008).

ACKNOWLEDGMENTS

We are thankful for the cooperation of all participants in our study.

SUPPLEMENTARY MATERIAL

The Supplementary Material for this article can be found online at: https://www.frontiersin.org/articles/10.3389/fnagi.2020.557005/full#supplementary-material

REFERENCES

American Psychiatric Association [APA], (2000). *Diagnostic and Statistical Manual of Mental Disorders*, 4th Edn. Washington, DC: American Psychiatric Association.

Bohm, M., Schumacher, H., Leong, D., Mancia, G., Unger, T., Schmieder, R., et al. (2015). Systolic blood pressure variation and mean heart rate is associated with cognitive dysfunction in patients with high cardiovascular risk. *Hypertension* 65, 651–661. doi: 10.1161/Hypertensionaha.114.04568

Chen, T. B., Lee, Y. J., Lin, S. Y., Chen, J. P., Hu, C. J., Wang, P. N., et al. (2019). Plasma Abeta42 and total tau predict cognitive decline in amnestic mild cognitive impairment. *Sci. Rep.* 9:13984. doi: 10.1038/s41598-019-50315-9

de Rojas, I., Romero, J., Rodriguez-Gomez, O., Pesini, P., Sanabria, A., Perez-Cordon, A., et al. (2018). Correlations between plasma and PET beta-amyloid levels in individuals with subjective cognitive decline: the fundacio ACE healthy brain initiative (FACEHBI). *Alzheimers Res. Ther.* 10:119. doi: 10.1186/s13195-018-0444-1

de Wolf, F., Ghanbari, M., Licher, S., McRae-McKee, K., Gras, L., Weverling, G. J., et al. (2020). Plasma tau, neurofilament light chain and amyloid-beta levels and risk of dementia; a population-based cohort study. *Brain* 143, 1220–1232. doi: 10.1093/brain/awaa054

Donohue, M. C., Sperling, R. A., Petersen, R., Sun, C. K., Weiner, M. W., Aisen, P. S., et al. (2017). Association between elevated brain amyloid and subsequent cognitive decline among cognitively normal persons. *JAMA* 317, 2305–2316. doi: 10.1001/jama.2017.6669

Dubois, B., Hampel, H., Feldman, H. H., Scheltens, P., Aisen, P., Andrieu, S., et al. (2016). Preclinical Alzheimer's disease: definition, natural history, and diagnostic criteria. *Alzheimers Dement.* 12, 292–323. doi: 10.1016/j.jalz.2016.02.002

Gabelle, A., Richard, F., Gutierrez, L. A., Schraen, S., Delva, F., Rouaud, O., et al. (2013). Plasma amyloid-beta levels and prognosis in incident dementia cases of the 3-City Study. *J. Alzheimers Dis.* 33, 381–391. doi: 10.3233/JAD-2012-121147

Graff-Radford, N. R., Crook, J. E., Lucas, J., Boeve, B. F., Knopman, D. S., Ivnik, R. J., et al. (2007). Association of low plasma Abeta42/Abeta40 ratios with increased imminent risk for mild cognitive impairment and Alzheimer disease. *Arch. Neurol.* 64, 354–362. doi: 10.1001/archneur.64.3.354

Greenberg, S. M., Bacskai, B. J., Hernandez-Guillamon, M., Pruzin, J., Sperling, R., and van Veluw, S. J. (2020). Cerebral amyloid angiopathy and Alzheimer disease - one peptide, two pathways. *Nat. Rev. Neurol.* 16, 30–42. doi: 10.1038/s41582-019-0281-2

Hanon, O., Vidal, J. S., Lehmann, S., Bombois, S., Allinquant, B., Treluyer, J. M., et al. (2018). Plasma amyloid levels within the Alzheimer's process and correlations with central biomarkers. *Alzheimers Dement.* 14, 858–868. doi: 10.1016/j.jalz.2018.01.004

Hansson, O., Stomrud, E., Vanmechelen, E., Ostling, S., Gustafson, D. R., Zetterberg, H., et al. (2012). Evaluation of plasma a beta as predictor of Alzheimer's disease in older individuals without dementia: a population-based study. *J. Alzheimers Dis.* 28, 231–238. doi: 10.3233/Jad-2011-111418

Harrell, F. E. (2001). *Regression Modeling Strategies: With Applications to Linear Models, Logistic Regression, and Survival Analysis*. New York, NY: Springer.

Hilal, S., Wolters, F. J., Verbeek, M. M., Vanderstichele, H., Ikram, M. K., Stoops, E., et al. (2018). Plasma amyloid-beta levels, cerebral atrophy and risk of dementia: a population-based study. *Alzheimers Res. Ther.* 10:63. doi: 10.1186/s13195-018-0395-6

Jack, C. R. Jr., Bennett, D. A., Blennow, K., Carrillo, M. C., Dunn, B., Haeberlein, S. B., et al. (2018). NIA-AA research framework: toward a biological definition of Alzheimer's disease. *Alzheimers Dement.* 14, 535–562. doi: 10.1016/j.jalz.2018.02.018

Jansen, W. J., Ossenkoppele, R., Tijms, B. M., Fagan, A. M., Hansson, O., Klunk, W. E., et al. (2018). Association of cerebral amyloid-beta aggregation with cognitive functioning in persons without dementia. *JAMA Psychiatry* 75, 84–95. doi: 10.1001/jamapsychiatry.2017.3391

Jaunmuktane, Z., Mead, S., Ellis, M., Wadsworth, J. D., Nicoll, A. J., Kenny, J., et al. (2015). Evidence for human transmission of amyloid-beta pathology and cerebral amyloid angiopathy. *Nature* 525, 247–250. doi: 10.1038/nature15369

Jiang, Y., Shang, S. H., Li, P., Chen, C., Dang, L., Wang, J. J., et al. (2018). Pulse pressure is associated with plasma amyloid-beta transport dysfunction. *J. Hypertens.* 36, 569–579. doi: 10.1097/Hjh.0000000000001565

Kaffashian, S., Tzourio, C., Soumare, A., Dufouil, C., Mazoyer, B., Schraen-Maschke, S., et al. (2015). Association of plasma beta-amyloid with MRI markers of structural brain aging the 3-city dijon study. *Neurobiol. Aging* 36, 2663–2670. doi: 10.1016/j.neurobiolaging.2015.03.016

Katzman, R., Zhang, M. Y., Ouangyaqu, Y. Q., Wang, Z. Y., Liu, W. T., Yu, E., et al. (1988). A Chinese version of the mini-mental state examination - impact of illiteracy in a shanghai dementia survey. *J. Clin. Epidemiol.* 41, 971–978. doi: 10.1016/0895-4356(88)90034-0

McKhann, G. M., Knopman, D. S., Chertkow, H., Hyman, B. T., Jack, C. R., Kawas, C. H., et al. (2011). The diagnosis of dementia due to Alzheimer's disease: recommendations from the national institute on aging-Alzheimer's association workgroups on diagnostic guidelines for Alzheimer's disease. *Alzheimers Dement.* 7, 263–269. doi: 10.1016/j.jalz.2011.03.005

Mielke, M. M., Machulda, M. M., Hagen, C. E., Christianson, T. J., Roberts, R. O., Knopman, D. S., et al. (2016). Influence of amyloid and APOE on cognitive performance in a late middle-aged cohort. *Alzheimers Dement.* 12, 281–291. doi: 10.1016/j.jalz.2015.09.010

Nakamura, A., Kaneko, N., Villemagne, V. L., Kato, T., Doecke, J., Dore, V., et al. (2018). High performance plasma amyloid-beta biomarkers for Alzheimer's disease. *Nature* 554, 249–254. doi: 10.1038/nature25456

Olsson, B., Lautner, R., Andreasson, U., Ohrfelt, A., Portelius, E., Bjerke, M., et al. (2016). CSF and blood biomarkers for the diagnosis of Alzheimer's disease: a systematic review and meta-analysis. *Lancet Neurol.* 15, 673–684. doi: 10.1016/s1474-4422(16)00070-3

Petersen, R. C. (2011). Clinical practice. Mild cognitive impairment. *N. Engl. J. Med.* 364, 2227–2234. doi: 10.1056/NEJMcp0910237

Petersen, R. C., Wiste, H. J., Weigand, S. D., Rocca, W. A., Roberts, R. O., Mielke, M. M., et al. (2016). Association of elevated amyloid levels with cognition and biomarkers in cognitively normal people from the community. *JAMA Neurol.* 73, 85–92. doi: 10.1001/jamaneurol.2015.3098

Rentz, D. M., Amariglio, R. E., Becker, J. A., Frey, M., Olson, L. E., Frishe, K., et al. (2011). Face-name associative memory performance is related to amyloid burden in normal elderly. *Neuropsychologia* 49, 2776–2783. doi: 10.1016/j.neuropsychologia.2011.06.006

Roberts, R. O., Aakre, J. A., Kremers, W. K., Vassilaki, M., Knopman, D. S., Mielke, M. M., et al. (2018). Prevalence and outcomes of amyloid positivity among persons without dementia in a longitudinal, population-based setting. *JAMA Neurol.* 75, 970–979. doi: 10.1001/jamaneurol.2018.0629

Rowe, C. C., Ellis, K. A., Rimajova, M., Bourgeat, P., Pike, K. E., Jones, G., et al. (2010). Amyloid imaging results from the Australian imaging, biomarkers and lifestyle (AIBL) study of aging. *Neurobiol. Aging* 31, 1275–1283. doi: 10.1016/j.neurobiolaging.2010.04.007

Schupf, N., Tang, M. F., Fukuyama, H., Manly, J., Andrews, H., Mehta, P., et al. (2008). Peripheral Abeta subspecies as risk biomarkers of Alzheimer's disease. *Proc. Natl. Acad. Sci. U.S.A.* 16, 14052–14057. doi: 10.1073/pnas.0805902105

Sonnen, J. A., Montine, K. S., Quinn, J. F., Kaye, J. A., Breitner, J. C. S., and Montine, T. J. (2008). Biomarkers for cognitive impairment and dementia in elderly people. *Lancet Neurol.* 7, 704–714. doi: 10.1016/S1474-4422(08)70162-5

Sperling, R. A., Aisen, P. S., Beckett, L. A., Bennett, D. A., Craft, S., Fagan, A. M., et al. (2011). Toward defining the preclinical stages of Alzheimer's disease: recommendations from the National Institute on Aging-Alzheimer's Association workgroups on diagnostic guidelines for Alzheimer's disease. *Alzheimers Dement.* 7, 280–292. doi: 10.1016/j.jalz.2011.03.003

Sperling, R. A., Johnson, K. A., Doraiswamy, P. M., Reiman, E. M., Fleisher, A. S., Sabbagh, M. N., et al. (2013). Amyloid deposition detected with florbetapir F 18 (F-18-AV-45) is related to lower episodic memory performance in clinically normal older individuals. *Neurobiol. Aging* 34, 822–831. doi: 10.1016/j.neurobiolaging.2012.06.014

Toledo, J. B., Zetterberg, H., van Harten, A. C., Glodzik, L., Martinez-Lage, P., Bocchio-Chiavetto, L., et al. (2015). Alzheimer's disease cerebrospinal fluid biomarker in cognitively normal subjects. *Brain* 138, 2701–2715. doi: 10.1093/brain/awv199

van Harten, A. C., Smits, L. L., Teunissen, C. E., Visser, P. J., Koene, T., Blankenstein, M. A., et al. (2013). Preclinical AD predicts decline in memory and executive functions in subjective complaints. *Neurology* 81, 1409–1416. doi: 10.1212/WNL.0b013e3182a8418b

Verberk, I. M. W., Slot, R. E., Verfaillie, S. C. J., Heijst, H., Prins, N. D., van Berckel, B. N. M., et al. (2018). Plasma amyloid as prescreener for the earliest Alzheimer pathological changes. *Ann. Neurol.* 84, 648–658. doi: 10.1002/ana.25334

Vergallo, A., Mégret, L., Lista, S., Cavedo, E., Zetterberg, H., and Blennow, K. (2019). Plasma amyloid β 40/42 ratio predicts cerebral amyloidosis in cognitively normal individuals at risk for Alzheimer's disease. *Alzheimers Dement.* 15, 764–775. doi: 10.1016/j.jalz.2019.03.009

Villemagne, V. L., Pike, K. E., Chetelat, G., Ellis, K. A., Mulligan, R. S., Bourgeat, P., et al. (2011). Longitudinal assessment of Abeta and cognition in aging and Alzheimer disease. *Ann. Neurol.* 69, 181–192. doi: 10.1002/ana.22248

Vos, S. J. B., Xiong, C. J., Visser, P. J., Jasielec, M. S., Hassenstab, J., Grant, E. A., et al. (2013). Preclinical Alzheimer's disease and its outcome: a longitudinal cohort study. *Lancet Neurol.* 12, 957–965. doi: 10.1016/S1474-4422(13)70194-7

Wang, J., Qiao, F., Shang, S., Li, P., Chen, C., Dang, L., et al. (2018). Elevation of Plasma amyloid-beta level is more significant in early stage of cognitive impairment: a population-based cross-sectional study. *J. Alzheimers Dis.* 64, 61–69. doi: 10.3233/JAD-180140

Wei, M., Zhao, B. Y., Huo, K., Deng, Y. N., Shang, S. H., Liu, J., et al. (2017). Sleep Deprivation induced plasma amyloid-beta transport disturbance in healthy young adults. *J. Alzheimers Dis.* 57, 899–906. doi: 10.3233/Jad-161213

Wenham, P. R., Price, W. H., and Blundell, G. (1991). Apolipoprotein-E genotyping by one-stage pcr. *Lancet* 337, 1158–1159. doi: 10.1016/0140-6736(91)92823-K

Yaffe, K. (2011). Association of plasma β-Amyloid level and cognitive reserve with subsequent cognitive decline. *JAMA* 305, 261–266. doi: 10.1001/jama.2010.1995

Conflict of Interest: The authors declare that the research was conducted in the absence of any commercial or financial relationships that could be construed as a potential conflict of interest.

frontiers in Aging Neuroscience

BRIEF RESEARCH REPORT
published: 14 September 2020
doi: 10.3389/fnagi.2020.00273

Dropout in Neural Networks Simulates the Paradoxical Effects of Deep Brain Stimulation on Memory

Shawn Zheng Kai Tan[1†], Richard Du[2†], Jose Angelo Udal Perucho[2], Shauhrat S. Chopra[3], Varut Vardhanabhuti[2] and Lee Wei Lim[1*]*

[1]*Neuromodulation Laboratory, School of Biomedical Sciences, Li Ka Shing Faculty of Medicine, The University of Hong Kong, Hong Kong, Hong Kong,* [2]*Department of Diagnostic Radiology, Li Ka Shing Faculty of Medicine, The University of Hong Kong, Hong Kong, Hong Kong,* [3]*School of Energy and Environment, City University of Hong Kong, Hong Kong, Hong Kong*

Neuromodulation techniques such as deep brain stimulation (DBS) are a promising treatment for memory-related disorders including anxiety, addiction, and dementia. However, the outcomes of such treatments appear to be somewhat paradoxical, in that these techniques can both disrupt and enhance memory even when applied to the same brain target. In this article, we hypothesize that disruption and enhancement of memory through neuromodulation can be explained by the dropout of engram nodes. We used a convolutional neural network (CNN) to classify handwritten digits and letters and applied dropout at different stages to simulate DBS effects on engrams. We showed that dropout applied during training improved the accuracy of prediction, whereas dropout applied during testing dramatically decreased the accuracy of prediction, which mimics enhancement and disruption of memory, respectively. We further showed that transfer learning of neural networks with dropout had increased the accuracy and rate of learning. Dropout during training provided a more robust "skeleton" network and, together with transfer learning, mimicked the effects of chronic DBS on memory. Overall, we showed that the dropout of engram nodes is a possible mechanism by which neuromodulation techniques such as DBS can both disrupt and enhance memory, providing a unique perspective on this paradox.

Keywords: neuromodulation, deep brain stimulation, memory, neural network, dropout

OPEN ACCESS

Edited by:
Woon-Man Kung, Chinese Culture University, Taiwan

Reviewed by:
Sheng-Tzung Tsai, Buddhist Tzu Chi General Hospital, Taiwan
Dheeraj S. Roy, Massachusetts Institute of Technology, United States

***Correspondence:**
Varut Vardhanabhuti
varv@hku.hk
Lee Wei Lim
drlimleewei@gmail.com

[†]These authors have contributed equally to this work

Received: *12 June 2020*
Accepted: *10 August 2020*
Published: *14 September 2020*

Citation:
Tan SZK, Du R, Perucho JAU, Chopra SS, Vardhanabhuti V and Lim LW (2020) Dropout in Neural Networks Simulates the Paradoxical Effects of Deep Brain Stimulation on Memory. Front. Aging Neurosci. 12:273. doi: 10.3389/fnagi.2020.00273

INTRODUCTION

Memory systems are crucial for survival and, to a large extent, define who we are. However, memory systems can fall into disease when expressed pervasively (e.g., anxiety or addiction) or degenerate (e.g., dementia)—both of which are major health challenges worldwide (World Health Organization, 2012, 2017). Neuromodulation techniques such as deep brain stimulation (DBS) have shown promising results as treatments for memory-related disorders (Tan et al., 2019b, 2020b), yet the mechanisms behind these effects are still largely unknown. Furthermore, the effects of treatments such as DBS appear to be paradoxical, in that they can both disrupt (Hamani et al., 2010; Tan et al., 2019a) and enhance memories (Hamani et al., 2011; Tan et al., 2020c)

even when applied to the same brain target (detailed review in Tan et al., 2020b). We have previously suggested that DBS is able to disrupt memory by "removing" nodes in an engram (Tan et al., 2019b). Engrams are a theoretical means by which memory is physically stored in the brain and can be thought of as a subset of neurons in a given memory brain region (e.g., hippocampus) that are recruited in the initial memory encoding phase (Ramirez et al., 2013). In this manuscript, we take the view that engrams are plastic synapses (associative/connectionist model), and hence, engram nodes are synapses between engram neurons (Langille and Gallistel, 2020). Despite increased knowledge of engrams and new techniques to study them, the theory that DBS disrupts memory by "removing" engram nodes (synapses associated with the engram) remains untested partly due to the lack of technology to monitor large engram networks in real time. Besides, this theory does not explain (at least directly) how memory enhancement is achieved.

The development of machine learning techniques offers a unique computational approach to simulate hypothetical models of learning and memory, and the effects of manipulation on memory, which we have previously used to highlight potential mechanisms of memory disruption by DBS (Tan et al., 2019b). To model the learning process, we trained a convolutional neural network (CNN) to classify handwritten digits and letters.

CNNs are a type of artificial neural network that is commonly applied to image recognition tasks. The concept of CNNs was developed from early observations of the visual cortex by Hubel and Wiesel (1959, 1962), in which groups of neurons fired distinctively in response to different light patterns (e.g., straight lines, circles). In a typical CNN, features are extracted by the network using a convolutional layer followed by classification. For image tasks, this convolutional layer is comprised of a series of convolution filters that are associated with particular patterns of pixels, which mimic receptive fields in the retina. These trainable filters are also referred to as weights of the network, similar to synapse/synaptic strength in biological systems. In image classification, the CNN decomposes the input image into patterns of pixels known as features. First, an input image is partitioned into non-overlapping regions with each region mapped to a specific neuron. Second, the neurons are convolved by multiple filters to generate a feature map in the convolution layer. The resultant feature maps can be further decomposed by inputting these maps into successive convolution layers. After a specified number of decompositions, the resultant features are used to classify the input image using the fully connected layer.

In this article, we hypothesize that the paradoxical ability of DBS to both disrupt and enhance memory can be explained through dropout (a process of randomly shutting down or dropping neurons) in engram nodes by using CNN to simulate learning and memory.

Due to limited systematic studies looking at DBS and memory, we based our modeling on the results from our previous studies that showed high-frequency stimulation of the ventromedial prefrontal cortex (vmPFC) could both enhance (Tan et al., 2020c) and disrupt (Tan et al., 2019a) memory. Based on these findings, we focused on the hippocampal engram and implicit associative memories in the proposed simulation.

MATERIALS AND METHODS

Dataset

To model the learning process, we trained a CNN to classify handwritten digits and letters from the EMNIST dataset. The EMNIST dataset is a public database of over 800,000 handwritten digits and letters across 62 different classes (Cohen et al., 2017). In our study, we used the EMNIST balanced dataset, which is derived by merging similar classes of letters. This dataset contains 131,600-28 × 28 pixel images of 47 balanced classes (10 digits and 37 uppercase and lowercase letters).

Network Architecture

The CNN consists of an input layer of size 28 × 28 × 1 followed by two convolution layers of 32 and 64 filters, leading to a feature map of size 5 × 5 × 64. No padding was used for the convolutions, and a filter of size 3 × 3 was used in both layers. At the end of each convolution layer, we applied max pooling with a 2 × 2 window. Max pooling is a standard process for reducing the dimensions of feature maps by sampling the maximum value for a given window size, which forces the network to enhance and focus on important features (Yamaguchi et al., 1990). Global max pooling was applied to the feature map to extract 64 × 1 latent features. For feature classification, the features were passed through to a fully connected layer of 100 neurons. A rectified linear unit (ReLU) was applied as an activation function in all the layers, which is a ramp function where all negative value neurons are zeroed to ensure unidirectionality. The parameters in all the networks were optimized using binary cross-entropy or loss function. All networks were trained for 500 epochs in batches of 10 images. An epoch is defined as one complete run-through of all the training data. For the analysis, the average loss of training data and average classification accuracy of the testing data were evaluated at the end of each epoch.

Experiments

We conducted three sets of experiments in this study. In Experiment 1, we trained a network to classify 10 different digits (0–9) from the EMNIST balanced dataset. We applied dropout (a process of randomly shutting down or dropping neurons) either during the training stages or just prior to testing at each epoch. We used a dropout rate of 50%, such that half the neurons were dropped at each step (**Figures 1A,B**). Dropout was only done on fully connected latter layers of the network. As the aim of the study was not to train a network to classify the digits accurately but to analyze the learning process, the network was trained on 1,000 randomly sampled digits as the training dataset, and the network was evaluated on another 1,000 randomly sampled digits as the testing dataset. All networks were trained with the same training dataset and tested with the same testing dataset.

In Experiment 2, we similarly trained a network identical to that of Experiment 1 but applied variable dropout rates (20%, 40%, 60%, and 80%) during the training stages.

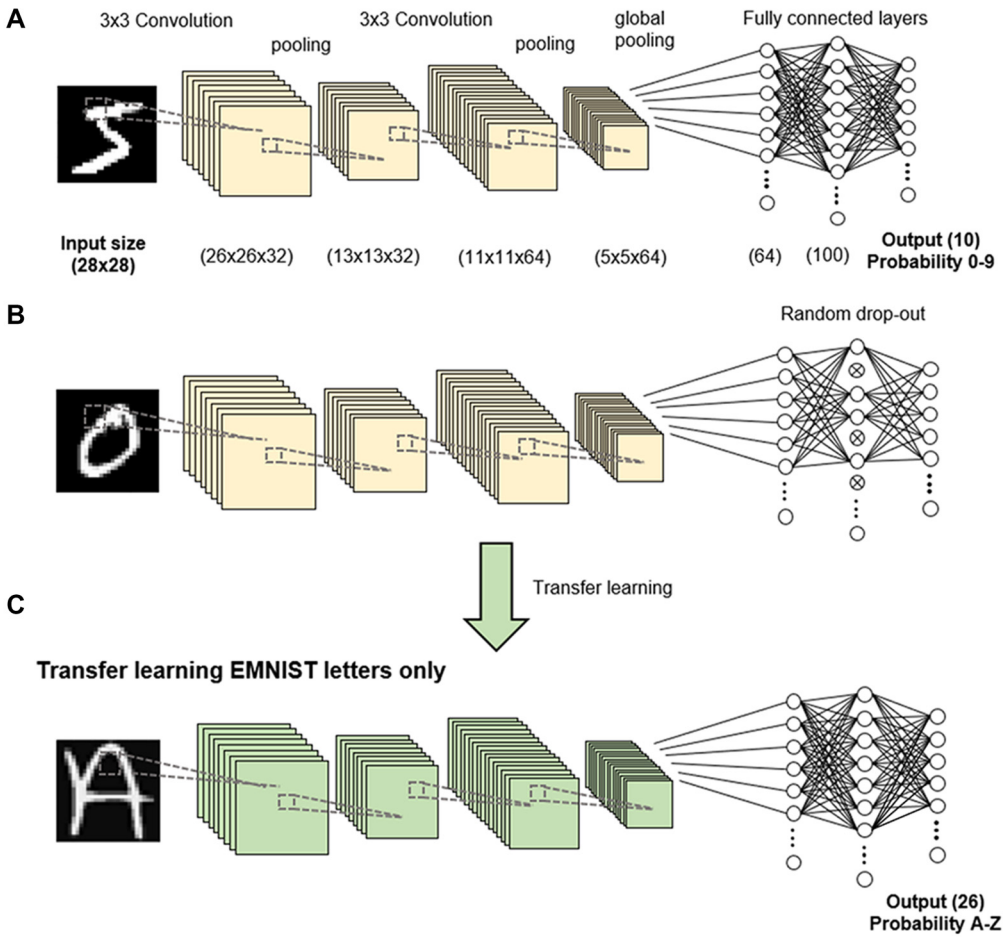

FIGURE 1 | Methodology. A convolutional neural network (CNN) was trained to classify handwritten digits in the EMNIST dataset **(A)**. Dropout was applied to 50% of nodes in the fully connected layer **(B)**. Transfer learning was performed to retrain the network to recognize uppercase letters **(C)**.

In Experiment 3, we transferred the network to learn 26 uppercase letters (A to Z) in a process known as transfer learning, in which the networks and weights of the control (non-dropout) group and dropout group were applied to the new task (**Figure 1C**). We retrained the network to recognize uppercase letters by stripping the last output layer and replacing it with the 26 classes corresponding to each letter class. We evaluated the performance of the transfer learning using the trained network with and without dropout compared to the performance of a network directly trained on letters without transfer learning (**Figure 1C**). Due to the increased complexity of more letter classes, we used 5,000 randomly sampled letters as the training dataset and 1,000 randomly sampled letters as the testing dataset.

RESULTS

Experiment 1

To simulate the effects of DBS on memory, we applied dropout during the training or testing stages. The accuracy of prediction was used as an indication of how "well" the neural network had learned the task, which serves as a proxy for memory. Therefore, a higher accuracy of prediction should indicate higher memory function. In our experiment, dropout applied during training improved the accuracy of prediction, whereas dropout applied during testing dramatically decreased the accuracy of prediction (**Figure 2A**).

Experiment 2

To simulate the different parameters of DBS and to further understand how different rates of dropout would affect DBS during the training stages, we applied different percentages of dropout. In our experiments, a dropout of 20%, 40%, or 60% resulted in a higher training accuracy, whereas a dropout of 80% resulted in a lower training accuracy (**Figure 2B**). Interestingly, 20% or 40% dropout resulted in lower training loss (defined as the average errors made across the testing) than the baseline initially, and 60% dropout resulted in higher training loss than the baseline by the second epoch, whereas 80% dropout showed the highest training loss throughout (**Figures 2C,D**).

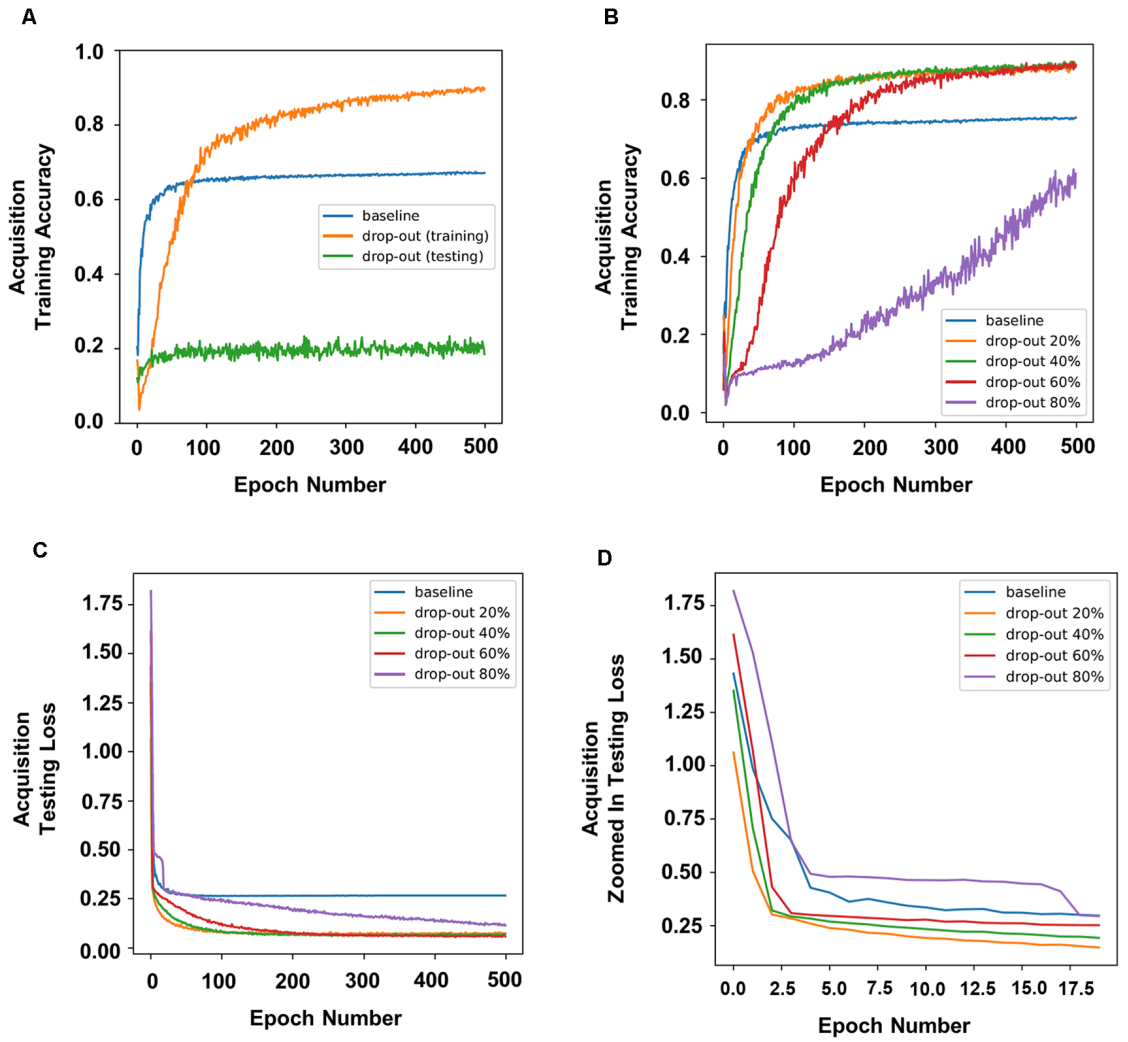

FIGURE 2 | Dropout in neural nodes disrupted or enhanced learning in the neural networks depending on when it was applied. Dropout applied during training improved prediction accuracy, whereas dropout applied during testing dramatically decreased prediction accuracy **(A)**. **(B)** Prediction accuracy of different rates of dropout during training. **(C)** The training loss and **(D)** a zoomed in version of the first 20 epochs in panel **(C)**.

Experiment 3

To simulate a novel memory task post chronic DBS, we applied the process of transfer learning on the trained network, in which the networks and weights of the control (non-dropout) group and dropout groups were applied to a new task. Overall, transfer learning of a network showed increased accuracy compared to a network without transfer learning (**Figure 3A**), indicating higher memory function. In addition, there were decreased testing and training losses (**Figures 3B,C**; defined as the average errors made across the testing or training, respectively). Decreased loss indicates better performance or better fitting of the training/testing data, which serves as a proxy for increased rate of learning. Transfer learning in neural networks with dropout resulted in better accuracy (**Figure 1**) and lower training and testing loss (**Figures 3B,C**) compared to transfer learning in networks with no dropout.

DISCUSSION

We have previously argued that timing plays an important role in the outcome of DBS on memory (Tan et al., 2020b). DBS applied post or during behavior testing tended to disrupt memory, whereas DBS applied prior to behavior testing tended to enhance memory. However, the mechanisms behind these outcomes are still relatively unknown. Indeed, we found that dropout applied during training improved the accuracy of prediction, which was similar to the enhancement of memory seen when DBS was applied prior to behavior testing in our previous animal studies (Liu et al., 2015). On the contrary, we found that dropout applied post training dramatically decreased the accuracy of prediction, which was similar to the disruption of memory seen when DBS was applied during consolidation of memory in our previous animal studies (Tan et al., 2019a; **Figure 2A**).

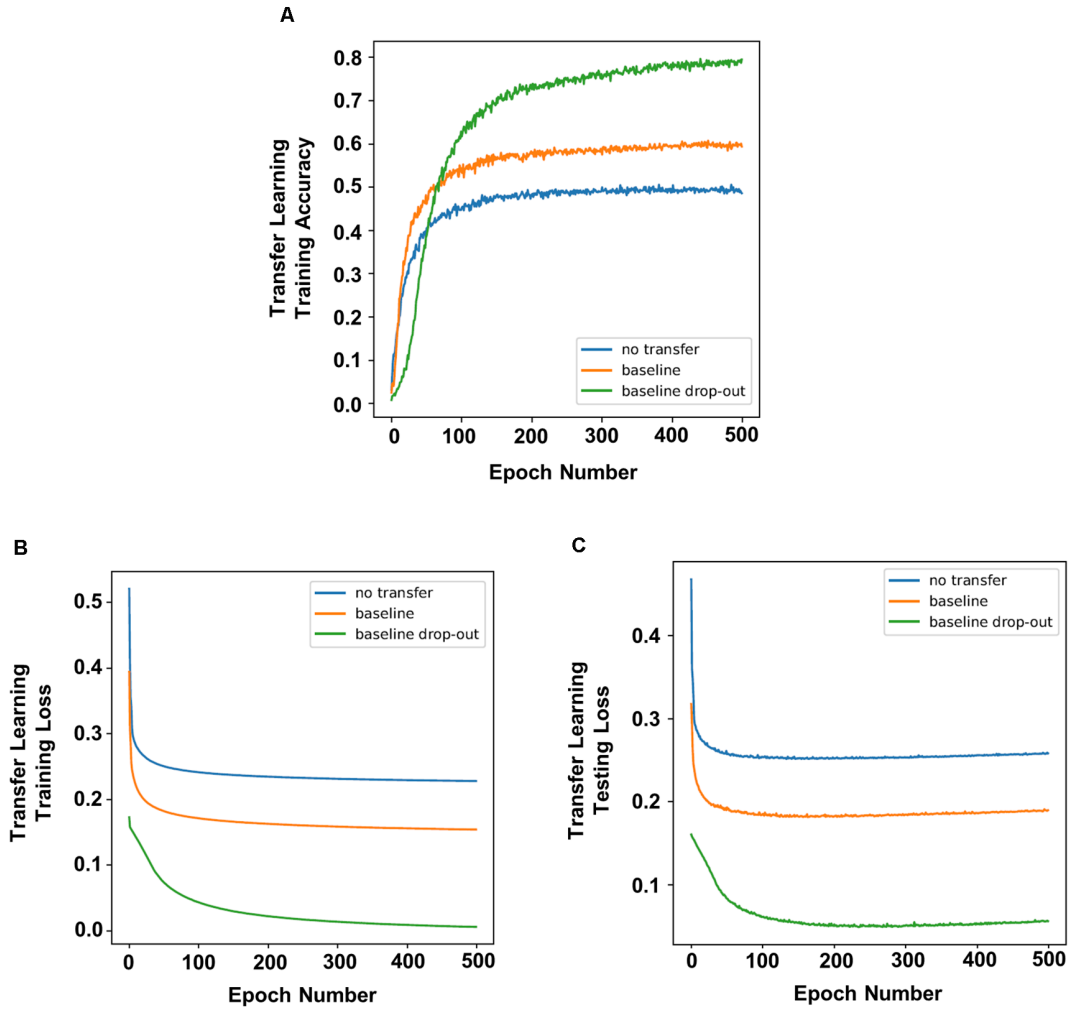

FIGURE 3 | Transfer learning of networks that underwent dropout showed higher prediction accuracy and faster learning. Compared to non-dropout networks, transfer learning of neural networks with dropout had increased accuracy **(A)** with lower training loss **(B)** and testing loss **(C)**.

We used CNNs (as opposed to standard fully connected networks) in this study as they are commonly applied in image recognition tasks. Although CNNs are modeled on the visual cortex, dropout was only applied on fully connected latter layers in the network to represent dropouts applied in the hippocampus rather than in the visual cortex. This mimicked our previous experiments on the effects of prefrontal cortex stimulation on the hippocampus (Tan et al., 2019a, 2020c).

In order to simulate different DBS parameters in a generalized manner, we applied different percentage dropouts during the training stage. We showed that lower dropout rates (20%) effectively increased both accuracy and training loss, whereas a higher dropout rate (80%) drastically decreased the ability of the neural network to learn the task effectively. First, this indicates that DBS is more likely to result in lower dropout rates. Second, it simulates variations in DBS parameters in a generalized way, showing that even at low dropout rates (20%), the effects are still robust, and is only ineffective at high dropout rates.

One difference between Experiment 1 and our previous animal experiments was that chronic DBS was not applied during the training stage, but rather in the home-cage prior to behavior experiments. To more accurately represent the enhancement of memory through chronic DBS prior to a memory task (Liu et al., 2015), we applied transfer learning in previously trained networks with or without dropout. We showed that transfer learning did indeed increase the accuracy of prediction and decrease training and testing loss (representing an increased learning rate), indicating that transfer learning was successful in this model. More importantly, we showed that transfer learning applied to neural networks with dropout increased the accuracy of prediction, indicating higher memory function compared to neural networks without dropout. We further showed that transfer learning applied to neural networks with dropout had lower training and testing loss, indicating not only improved memory function but also increased rate of learning. Overall, we showed that applying dropout during training provides a

more robust "skeleton" network, and applying transfer learning in this network increases accuracy and decreases training and testing loss. This model showed similar memory enhancement results to that in our previous study on chronic mPFC DBS (Liu et al., 2015), which suggests a potential mechanism for this process.

An early hypothesis of the mechanism of DBS was that it creates a temporary neural activity lesion (McIntyre et al., 2004). We further showed that prelimbic cortex DBS was associated with the disruption of memory and a drop in the neural activity marker c-fos in the ventral hippocampus (Tan et al., 2019a). Dropout of neural nodes, while congruent with the disruption of memory, has not played a major role in the mechanistic understanding of memory enhancement seen in DBS, although it should be noted that other mechanisms such as neurogenesis and wave syncing have been suggested (Tan et al., 2020b). In this article, we propose that DBS causes dropout in neural nodes that "forces" the activation of new pathways and creates more robust networks, similar to how dropout enhanced the neural networks. Mechanistically in the brain, this could be hypothesized to relate to increased synaptic plasticity or synaptogenesis—activating new pathways could be seen as the formation of new synapses, and the change in weights by the "backward steps" of dropout could be related to synaptic plasticity. Indeed, DBS has been shown to be related to both plasticity and synaptogenesis (Visanji et al., 2015; Pohodich et al., 2018). It is, however, difficult to properly hypothesize how DBS achieves this mechanistically due to the complexities of the changes induced by DBS and the fact we still do not know how it works. To the best of our knowledge, this article is the first to suggest a cohesive mechanism in which disruption of neural activity through DBS can lead to both disruption and enhancement of memory. Although no behavioral experiments were performed in conjunction with our modeling, we based the models on our previous animal behavioral experiments that showed that DBS prior to the behavioral task resulted in memory enhancement (Tan et al., 2020c) and DBS during consolidation of memory resulted in memory disruption (Tan et al., 2019a), which were similarly demonstrated in this present article. However, we acknowledge the simplistic and preliminary nature of our methodology and results. Although more complex models of associative memory and learning have been previously presented (Yusoff and Grüning, 2012; Osawa and Kohno, 2015), the lack of understanding on how neuromodulation actually affects neuronal firing in memory, especially in a remote downstream target like the hippocampus (in the case of vmPFC neuromodulation), makes it difficult to use these models. A simpler model, like that one presented here, is therefore more generalizable and better serves as a hypothetical and conceptual tool for more sophisticated research.

Although DBS has been suggested as a treatment for memory-related disorders including Alzheimer's disease (AD) and anxiety disorders, its mechanism is still largely unknown. In this article, we suggest hypothetical mechanisms for the effects of DBS on memory. We showed that dropout of engram nodes could disrupt memory processes, which might be useful in translating DBS as a treatment for anxiety disorders like PTSD (Gouveia et al., 2020). We also showed that dropout of engram nodes could improve memory function and suggested that this happens through increased synaptic function. Given that impaired synaptic plasticity and synaptogenesis have been associated with AD (Levi et al., 2003; Shankar et al., 2008) and DBS has shown promise as a treatment for AD (Liu et al., 2015), dropout of engram nodes could be a potential mechanism of DBS neuromodulation.

In conclusion, using a machine learning model based on previous animal experiments, we showed that dropout of nodes could be a potential mechanism in which neuromodulation techniques like DBS can both disrupt and enhance memory. While preliminary in nature, this article serves as a basis for further experimentation on engrams to understand the effects of neuromodulation on memory.

DATA AVAILABILITY STATEMENT

Publicly available datasets were analyzed in this study. This data can be found here: https://www.nist.gov/itl/products-and-services/emnist-dataset.

AUTHOR CONTRIBUTIONS

ST, RD, and SC conceived and designed the experiments. JP, LWL, and VV contributed significantly to the experimental design. RD conducted the experiments. ST, RD, and LWL contextualized the data. ST drafted the manuscript. All authors contributed to the article and approved the submitted version.

FUNDING

The scientific work was funded by grants from the Hong Kong Research Grants Council (RGC-ECS 27104616) and the University of Hong Kong Seed Funding for Basic Research awarded to LWL.

ACKNOWLEDGMENTS

This manuscript has been released as a pre-print at BioRxiv (Tan et al., 2020a).

REFERENCES

Cohen, G., Afshar, S., Tapson, J., and van Schaik, A. (2017). "EMNIST: an extension of MNIST to handwritten letters," in *2017 International Joint Conference on Neural Networks (IJCNN)*, Anchorage, AK, pp. 2921–2926.

Gouveia, F. V., Davidson, B., Meng, Y., Gidyk, D. C., and Rabin, J. S. (2020). Treating post-traumatic stress disorder with neuromodulation therapies: transcranial magnetic stimulation, transcranial direct current stimulation and deep brain stimulation. *Neurotherapeutics* doi: 10.1007/s13311-020-00871-0 [Epub ahead of print].

Hamani, C., Dubiela, F. P., Soares, J. C. K., Shin, D., Bittencourt, S., Covolan, L., et al. (2010). Anterior thalamus deep brain stimulation at high current impairs memory in rats. *Exp. Neurol.* 225, 154–162. doi: 10.1016/j.expneurol.2010.06.007

Hamani, C., Stone, S. S., Garten, A., Lozano, A. M., and Winocur, G. (2011). Memory rescue and enhanced neurogenesis following electrical stimulation of the anterior thalamus in rats treated with corticosterone. *Exp. Neurol.* 232, 100–104. doi: 10.1016/j.expneurol.2011.08.023

Hubel, D. H., and Wiesel, T. N. (1959). Receptive fields of single neurones in the cat's striate cortex. *J. Physiol.* 148, 574–591. doi: 10.1113/jphysiol.1959.sp006308

Hubel, D. H., and Wiesel, T. N. (1962). Receptive fields, binocular interaction and function architecture in the cat's visual cortex. *J. Physiol.* 160, 106–154. doi: 10.1113/jphysiol.1962.sp006837

Langille, J. J., and Gallistel, C. R. (2020). Locating the engram: should we look for plastic synapses or information-storing molecules? *Neurobiol. Learn. Mem.* 169:107164. doi: 10.1016/j.nlm.2020.107164

Levi, O., Jongen-Relo, A. L., Feldon, J., Roses, A. D., and Michaelson, D. M. (2003). ApoE4 impairs hippocampal plasticity isoform-specifically and blocks the environmental stimulation of synaptogenesis and memory. *Neurobiol. Dis.* 13, 273–282. doi: 10.1016/s0969-9961(03)00045-7

Liu, A., Jain, N., Vyas, A., and Lim, L. W. (2015). Ventromedial prefrontal cortex stimulation enhances memory and hippocampal neurogenesis in the middle-aged rats. *elife* 4:e04803. doi: 10.7554/elife.04803

McIntyre, C. C., Savasta, M., Kerkerian-Le Goff, L., and Vitek, J. L. (2004). Uncovering the mechanism(s) of action of deep brain stimulation: activation, inhibition, or both. *Clin. Neurophysiol.* 115, 1239–1248. doi: 10.1016/j.clinph.2003.12.024

Osawa, Y., and Kohno, T. (2015). Associative memory with class I and II Izhikevich Model. *J. Robot. Netw. Artif. Life* 1:312. doi: 10.2991/jrnal.2015.1.4.12

Pohodich, A. E., Yalamanchili, H., Raman, A. T., Wan, Y.-W., Gundry, M., Hao, S., et al. (2018). Forniceal deep brain stimulation induces gene expression and splicing changes that promote neurogenesis and plasticity. *elife* 7:e34031. doi: 10.7554/elife.34031

Ramirez, S., Liu, X., Lin, P.-A., Suh, J., Pignatelli, M., Redondo, R. L., et al. (2013). Creating a false memory in the hippocampus. *Science* 341, 387–391. doi: 10.1126/science.1239073

Shankar, G. M., Li, S., Mehta, T. H., Garcia-Munoz, A., Shepardson, N. E., Smith, I., et al. (2008). Amyloid-β protein dimers isolated directly from Alzheimer's brains impair synaptic plasticity and memory. *Nat. Med.* 14, 837–842. doi: 10.1038/nm1782

Tan, S. Z. K., Du, R., Perucho, J. A. U., Chopra, S. S., Vardhanabhuti, V., and Lim, L. W. (2020a). Dropout in neural networks simulates the paradoxical effects of deep brain stimulation on memory. *bioRxiv* [Preprint]. doi: 10.1101/2020.05.01.073486

Tan, S. Z. K., Fung, M., Koh, J., Chan, Y., and Lim, L. W. (2020b). The paradoxical effect of deep brain stimulation on memory. *Aging Dis.* 11, 179–190. doi: 10.14336/ad.2019.0511

Tan, S. Z. K., Neoh, J., Lawrence, A. J., Wu, E. X., and Lim, L. W. (2020c). Prelimbic cortical stimulation improves spatial memory through distinct patterns of hippocampal gene expression in aged rats. *Neurotherapeutics* doi: 10.1007/s13311-020-00913-7

Tan, S. Z. K., Poon, C. H., Chan, Y.-S., and Lim, L. W. (2019a). Deep brain stimulation of the ventromedial prefrontal cortex disrupts consolidation of fear memories. *bioRxiv* [Preprint]. doi: 10.1101/537514

Tan, S. Z. K., Sheng, V., Chan, Y.-S., and Lim, L. W. (2019b). Eternal sunshine of the neuromodulated mind: altering fear memories through neuromodulation. *Exp. Neurol.* 314, 9–19. doi: 10.1016/j.expneurol.2019.01.004

Visanji, N. P., Sarvestani, I. K., Creed, M. C., Shoaei, Z. S., Nobrega, J. N., Hamani, C., et al. (2015). Deep brain stimulation of the subthalamic nucleus preferentially alters the translational profile of striatopallidal neurons in an animal model of parkinson's disease. *Front. Cell. Neurosci.* 9:221. doi: 10.3389/fncel.2015.00221

World Health Organization. (2012). Dementia cases set to triple by 2050 but still largely ignored [WWW Document]. Available online at: http://www.who.int/mediacentre/news/releases/2012/dementia_20120411/en/. Accessed June 11, 2020

World Health Organization. (2017). Depression and other common mental disorders: global health estimates. Available online at: https://www.who.int/mental_health/management/depression/prevalence_global_health_estimates/en/. Accessed August 31, 2020.

Yamaguchi, K., Sakamoto, K., Akabane, T., and Fjuimoto, Y. (1990). "A neural network for speaker-independent isolated word recognition," in *ISCA Arch* (Kobe, Japan), 1077–1080.

Yusoff, N., and Grüning, A. (2012). Biologically inspired temporal sequence learning. *Procedia Eng.* 41, 319–325. doi: 10.1016/j.proeng.2012.07.179

Conflict of Interest: The authors declare that the research was conducted in the absence of any commercial or financial relationships that could be construed as a potential conflict of interest.

frontiers in Neuroscience

ORIGINAL RESEARCH
published: 18 September 2020
doi: 10.3389/fnins.2020.528809

Molecular Imaging of Striatal Dopaminergic Neuronal Loss and the Neurovascular Unit in Parkinson Disease

Jana Ivanidze[1], Myrto Skafida[1], Sneha Pandya[1], Dylon Patel[2], Joseph R. Osborne[1], Ashish Raj[1], Ajay Gupta[1], Claire Henchcliffe[2] and Jonathan P. Dyke[1]*

[1] Department of Radiology, Weill Cornell Medicine, Cornell University, New York, NY, United States, [2] Department of Neurology, Weill Cornell Medicine, Cornell University, New York, NY, United States

Parkinson disease (PD) is the second most common neurodegenerative disorder, characterized by loss of nigrostriatal dopaminergic neurons. Impairment of the neurovascular unit (NVU) has been hypothesized to play a critical role in early PD pathophysiology, and to precede neurodegenerative mechanisms. [C-11]-PE2I (*N*-(3-iodoprop-2E-enyl)-2b-carbomethoxy-3b-(4-methyl-phenyl)nortropane) (PE2I) is a PET radiotracer targeting neuronal dopamine transporters (DaT) with high specificity, allowing for highly accurate and specific DaT quantification. We investigated NVU integrity using arterial spin labeling (ASL) MRI in a prospective cohort of 26 patients with PD, and correlated our findings with analysis of striatal DaT density using PE2I PET in a subcohort of 17 patients. Analysis was performed in FreeSurfer to obtain rCBF and mean standardized regional PET avidity. Pearson correlations and Mann–Whitney tests were performed. Significantly lower mean normalized striatal PE2I SUV values were seen in multiple regions in patients with greater disease duration ($p < 0.05$). PET uptake in the putamen correlated with disease duration independent of patient age. Stratifying patients based on Montreal Cognitive Assessment (MoCA) scores (stratified into ≥ 27 vs. < 27), there was statistically significantly lower PE2I PET avidity in the higher MoCA score group in both more and less affected sides of the caudate, putamen and pallidum ($p < 0.05$). A moderate negative correlation between MDS-UPDRS part 3 (motor) "off" and rCBF values was also seen in the L and R cerebellum WM ($r = -0.43$ and -0.47, $p < 0.05$). A statistically significant negative correlation was found between dominant hand pegboard test results and rCBF in the less affected pallidum ($r = -0.41$; $p = 0.046$). A statistically significant negative correlation of ASL MRI with [11C]-PE2I PET was also found ($r = -0.53$ to -0.58; p-value 0.017–0.033) between left cerebral WM rCBF and more and less affected striatal PET regions. Our ROI-based analyses suggest that longer disease duration is associated with lower rCBF and lower PE2I mean SUV, implying greater NVU dysfunction and dopaminergic neuronal loss, respectively. Combined ASL MRI and PE2I PET imaging could inform future prospective clinical trials providing an improved mechanistic understanding of the disease, laying the foundation for the development of early disease biomarkers and potential therapeutic targets.

Keywords: molecular imaging, neurovascular unit, PE2I PET, ASL "arterial spin labeling", Parkinson disease

OPEN ACCESS

Edited by:
Kuangyu Shi,
Technical University of Munich, Germany

Reviewed by:
Jungsu S. Oh,
University of Ulsan, South Korea
Maria-Joao Santiago Ribeiro,
INSERM U1253 Imagerie et Cerveau (iBrain), France

****Correspondence:***
Jana Ivanidze
jai9018@med.cornell.edu

Specialty section:
This article was submitted to Brain Imaging Methods, a section of the journal Frontiers in Neuroscience

Received: *21 January 2020*
Accepted: *28 August 2020*
Published: *18 September 2020*

Citation:
Ivanidze J, Skafida M, Pandya S, Patel D, Osborne JR, Raj A, Gupta A, Henchcliffe C and Dyke JP (2020) Molecular Imaging of Striatal Dopaminergic Neuronal Loss and the Neurovascular Unit in Parkinson Disease. Front. Neurosci. 14:528809. doi: 10.3389/fnins.2020.528809

INTRODUCTION

Parkinson disease (PD) is the second most common neurodegenerative disorder and the most common movement disorder. Traditionally, PD is still diagnosed on the basis of motor symptoms and signs of resting tremor, bradykinesia and rigidity. There are many well-validated and highly studied clinical batteries and rating scales available to quantitate motor features, such as the Movement Disorders Society Unified Parkinson's Disease Rating Scale (MDS-UPDRS) – Part III "Motor Symptoms off" (Martinez-Martin et al., 2015), or the 9-hole pegboard testing to assess motor dexterity (Proud et al., 2019). However, these classic motor symptoms of PD often present later in the course of the disease, becoming apparent when almost 50–80% of dopaminergic neurons has been lost (Simon et al., 2020). Thus, there is a strong need to identify early disease biomarkers that may allow earlier diagnosis. Furthermore, non-motor features of PD may be as, or more, important. For example mild cognitive impairment (MCI) and dementia are well-recognized as important contributing factors to disease morbidity (Reid et al., 2011). The Montreal Cognitive Assessment (MoCA) score offers a comprehensive assessment of executive cognitive function and is increasingly used as a screening tool in PD (Chou et al., 2014). Criteria for diagnosis of cognitive impairment in PD have been established delineating the importance of early diagnosis of cognitive decline before progression to dementia (Litvan et al., 2012). However, there remains a critical need for biomarkers capable of detecting and tracking changes in PD in the anatomical and network correlates of such important non-motor features.

It is widely accepted that the pathophysiology of PD is related to selective neurodegeneration and loss of dopaminergic neurons projecting from the substantia nigra to the striatum. Earlier pathophysiologic mechanisms that may precede nigrostriatal neuronal loss are the subject of current research. Neuroinflammation with resulting alpha-synuclein accumulation is a key pathophysiological event in PD, and is closely associated with impaired blood-brain-barrier (BBB) permeability (Codolo et al., 2013; Sarkar et al., 2014). Dysfunction of the neurovascular unit (NVU), which is composed of endothelial cells, pericytes, and parenchymal cells (Pelizzari et al., 2019b), correlates with increased BBB permeability and microvascular dysfunction, and has been hypothesized to play a critical role in PD pathophysiology. Cerebral microvascular dysfunction appears to contribute to dopaminergic neuronal loss in PD (Barcia et al., 2004).

Arterial spin labeling (ASL) is a non-contrast MRI technique which allows assessment of cerebral perfusion and is based on the principle of magnetically labeling protons in arterial blood prior to their entry into the tissue of interest (Haller et al., 2016). This provides an advantage over dynamic contrast-enhanced magnetic resonance imaging (DCE-MRI), the latter necessitating the intravenous administration of gadolinium-based contrast agent (GBCA), which is associated with inherent risks (Gulani et al., 2017). ASL allows assessment of relative cerebral blood flow (rCBF) and can quantify NVU dysfunction.

To investigate neuronal dopamine transporter density in PD, [11C] *N*-(3-iodoprop-2E-enyl)-2b-carbomethoxy-3b-(4-methyl-phenyl)nortropane (PE2I) has been increasingly used. PE2I is a PET radiotracer which selectively binds neuronal dopamine transporters, allowing non-invasive *in vivo* quantitation of neuronal dopamine transporter density. The purpose of our study was to investigate dopaminergic neuronal loss and NVU dysfunction in a prospective clinical cohort of patients with PD, using [11C]-PE2I PET and ASL MRI, respectively, as well as to correlate advanced imaging findings with clinical and demographic characteristics, specifically metrics assessing motor symptoms (MDS-UPRDS scores, 9-hole pegboard testing) and cognitive impairment (MoCA).

MATERIALS AND METHODS

Study Population

Twenty six subjects were prospectively enrolled in this institutional review board-approved study. Informed consent was obtained at enrollment from all the participants. Inclusion criteria were PD clinical diagnosis of 3 to 12 years of duration from onset of symptoms, 30 to 70 years-old at time of enrollment, well-established response to one or more dopaminergic agents and/or amantadine, absence of disabling dyskinesias, and PD Hoehn & Yahr stage 2–3, and absence of a clinical diagnosis of dementia. Exclusion criteria were symptoms or signs suggestive of a Parkinson's plus diagnosis, receiving dopamine receptor blocking agents such as neuroleptics, treatment with acetylcholinesterase inhibitors, a history of brain surgery, history of cancer or other significant medical disease such as autoimmune disorders or others within the past 5 years, any major psychiatric condition and any history of other serious neurological disorders such as a clinically significant stroke, brain tumor, hydrocephalus, epilepsy, other neurodegenerative disorders, encephalitis or repeated head traumas. All enrolled patients were evaluated by a movement disorder specialist at the time of enrollment, with clinical assessment including evaluation of motor, sensory, cognitive and overall disease scores. Clinical chart review was performed by trained research personnel with documentation of duration of disease, symptoms, and medications. MRI and PET/CT studies were performed shortly after enrollment in the study, as discussed below.

MRI Acquisition

All subjects underwent ASL MRI. All MRI data was acquired on a 3.0 Tesla Siemens Prisma MRI scanner using a 32-channel head resonator. The 3D T_1-Weighted scan was acquired with 1.0 mm x 1.0 mm x 1.0 mm isotropic resolution using a sagittal MPRAGE sequence with a TR/TE/TI of 1800 ms/2.25 ms/900 ms respectively. The ASL sequence was a 3D pseudocontinuous sequence (J. J. Wang, USC) (Wang et al., 2005). ASL acquisition parameters included a 2000 ms labeling time, a 800 ms post-labeling delay and a 2.5 mm x 2.5 mm x 2.5 mm resolution with 60 slices.

PET/CT Acquisition

A subcohort of 17 patients underwent [11C]-PE2I PET/CT (performed on the same day as the MRI examination). [11C]-PE2I PET/CT data was acquired on a 64 slice Siemens Biograph mCT scanner. The [11C]-PE2I static images were summed from 30 to 60 min after injection. [11C]-PE2I targets neuronal dopamine transporters (Jakobson et al., 2018). The [11C] PE2I dose administered was 384.1 MBq +/− 51.8 MBq (10.38 ± 1.40 mCi). Resolution was 1.0 mm x 1.0 mm x 2.0 mm, with a 40 cm field of view. The PET images were acquired immediately after the radiotracer injection.

MRI Processing

The ASL rCBF data was processed using the MATLAB based ASLtbx (Wang et al., 2008). rCBF images were registered to the 3D T_1-Weighted data by aligning the proton density (PD) image acquired with the same sequence using the FLIRT package within FSL (FMRIB's Linear Image Registration Tool; Oxford, United Kingdom) (Jenkinson and Smith, 2001; Jenkinson et al., 2002). The 3D T_1-Weighted MRI data was analyzed utilizing the FreeSurfer 6.0 image analysis suite[1] (Fischl et al., 2002; Desikan et al., 2006). Analyzed regions comprised the bilateral striatum (caudate, globus pallidus, putamen) for ASL and [11C]-PE2I PET data. Stratification was performed based on more versus less severely clinically affected side as documented in the standardized clinical neurological examination. Since basal ganglia control contralateral motor function, the opposite side of the one considered more affected clinically was used as the more affected region for imaging purposes. Additionally, the bilateral supratentorial white matter, and bilateral cerebellum was evaluated for ASL analysis for the 26 patients with available ASL data. Axial T_1 weighted MRI and an rCBF map from a representative patient is presented in **Figures 1A,D**.

PET/CT Processing and Co-registration With MRI

The [11C]-PE2I PET data were aligned to the 3D T_1-Weighted MRI using the FLIRT package in FSL as previously described. Analysis was performed with FreeSurfer 6.0 derived quantitative cortical and subcortical segmentation of structures. [11C]-PE2I PET values were measured for each subregion defined within FreeSurfer. SUV values for the same regions used in our ASL analysis were determined for a subcohort of 17 patients. An SUV for the occipital lobe was generated by combining values from the cuneus, lateral occipital, lingual and pericalcarine regions based on previously published methodology (Desikan et al., 2006). Each target SUV was normalized to this combined occipital SUV. PET findings from a representative patient are presented in **Figure 1**.

Subgroup Stratification and Statistical Analysis

Statistical analysis was performed utilizing Graph-Pad Prism version 8. Patients were stratified into the following subgroups based on clinical characteristics. Stratification by duration of disease was based upon a cut-off of 5 years (less than 5 years versus greater than 5 years). Stratification by MoCA and MDS-UPDRS scores was based on previously published data suggesting a cut-off MoCA score of 26 between cognitively normal and cognitively abnormal individuals (Chou et al., 2014), and a cut-off MDS-UPDRS score of 32 for differentiating between mild and moderate disease (Martinez-Martin et al., 2015). We stratified our cohort into subgroups based on clinically meaningful criteria. The final number of patients for each analyzed subgroup is presented in **Figure 2**. Of note, final numbers for each subgroup depended on available data and thus differed among subgroups, since all 26 patients underwent ASL MRI and a subset of 17 patients underwent PE2I PET. Furthermore, some of the clinical information was not available or clinical tests were not performed for some of the patients. Mann– Whitney *U*-tests were performed to evaluate for differences between subgroups. Correction for multiple comparisons was accomplished using the Benjamini–Hochberg procedure with a false discovery rate (FDR) of 0.1. To investigate the relationship between ASL MRI and [11C]-PE2I -PET data as well as the relationship between clinical scores and imaging data, Spearman correlation analysis was performed. Additionally, a multiple linear regression analysis was performed comparing regional [11C]-PE2I PET uptake normalized to the occipital region with both subject age and disease duration as covariates.

RESULTS

Clinical and Demographic Characteristics of the Study Population

Subjects in our cohort had a mean age of 59.5 (range: 44–70, *SD* = ± 5.9) years with mean duration of disease of 6.6 (range: 1–13, *SD* = ± 3.5) years. The mean MDS-UPDRS part 3 (motor) "off" score was 28.7 (range: 12–54, *SD* = ± 11.5) and the mean MoCA score was 25.9 (range: 21–30, *SD* = ± 2.2). With regard to clinical symptoms, 13 (50%) patients had more pronounced symptoms on the left side and 13 (50%) patients had more pronounced symptoms on the right side. 85% (22/26) patients were undergoing treatment with levodopa-containing medications, the majority in combination with other medications, with mean LEDD was 749 mg (*SD* = ± 483). Demographic and clinical characteristics of the subjects enrolled in this study are presented in **Table 1**.

Disease Duration

Stratification of the cohort based on disease duration resulted in $N = 11$ patients with disease duration of ≤ 5 years (all underwent ASL MRI and a subset of $N = 8$ underwent [11C]-PE2I PET); and $N = 14$ patients with disease duration of > 5 years (all underwent ASL MRI and a subset of $N = 8$ additionally underwent [11C]-PE2I PET). Several regions displayed lower rCBF values with longer disease duration but did not reach significance. A statistically significantly lower PE2I avidity in the group with longer disease duration was shown for multiple regions in **Figure 3**. The differences between the two groups were more pronounced for [11C]-PE2I SUV in the basal ganglia

[1] http://surfer.nmr.mgh.harvard.edu/

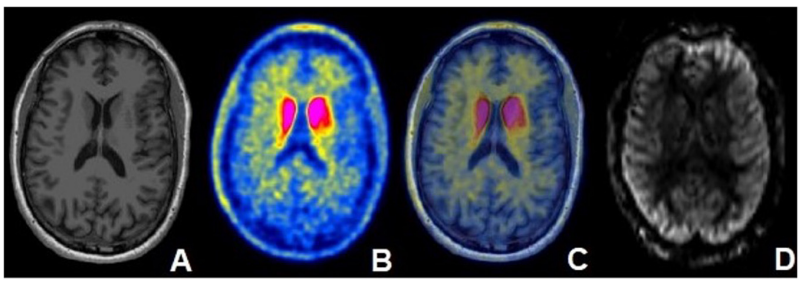

FIGURE 1 | Fifty five year old male with PD diagnosed 5 years ago with moderate disease based on MDS-UPDRS part 3 (motor) "off" score and associated mild cognitive impairment. **(A)** Axial T1-weighted MRI demonstrating no structural abnormalities. **(B)** Axial [11C]-PE2I PET image and **(C)** fused axial [11C]-PE2I PET/MR image demonstrating increased PE2I avidity in the bilateral caudate nuclei. **(D)** rCBF map obtained in the same patient at the same level.

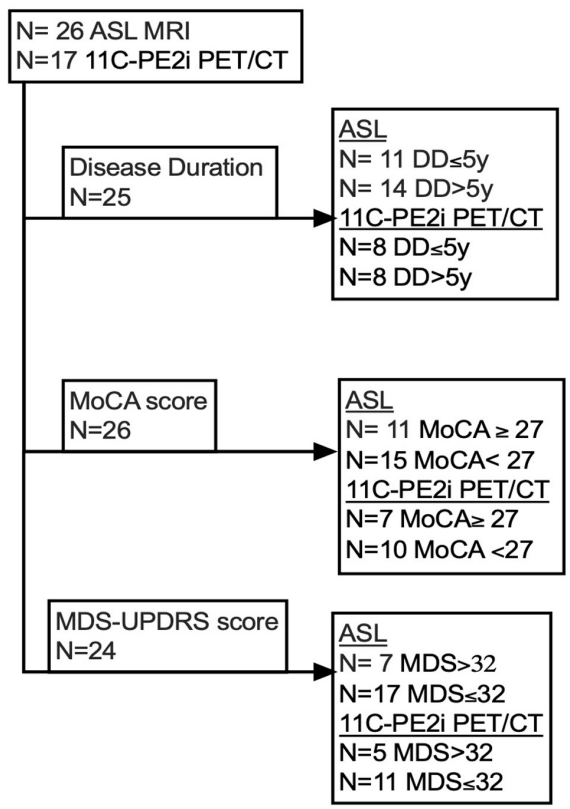

FIGURE 2 | Stratification of the study cohort into subgroups based on clinical characteristics.

TABLE 1 | Clinical and demographic characteristics of the study population.

Number of subjects	**26 (F/M: 7/19)**
Age (years)	59.5 (range: 44–70 *SD* = ± 5.9)
Duration of disease (years)	6.8 (range: 1–13 *SD* = ± 3.5)
Side of symptom predilection	13 (50%) right; 13 (50%) left
MDS-UPDRS part 3 (motor) "off" score	28.7 (range: 12–54 ± 11.5)
MoCA score	25.9 (range: 21–30 ± 2.2)
Antiparkinsonian medications	
Levodopa-containing drugs *n* (%)	22/26 (85%)
Dopamine agonists *n* (%)	16/26 (62%)
MAO-B inhibitors *n* (%)	15/26 (57%)
Anticholinergics *n* (%)	1/26 (38%)
Amantadine and antiglutamate *n* (%)	6/26 (23%)
COMT inhibitors *n* (%)	5/26 (19%)
LEDD mean (SD)	749 (± 483)

compared to reference regions (cerebellum cortex and WM, WM). Following Benjamini–Hochberg correction for multiple comparisons, our findings remained significant for all analyzed regions with the exception of left and right cerebellar cortex. rCBF and [11C]-PE2I SUV values for the different regions stratified by disease duration are presented in **Table 2**.

Montreal Cognitive Assessment

The cutoff to stratify a subject as having MCI/dementia was 27 based on previously published data and therefore 15 patients were considered as having MCI (MoCA scores < 27). Stratification of the cohort resulted in $N = 15$ patients with MoCA scores < 27 (all underwent ASL MRI and a subset of $N = 10$ additionally underwent [11C]-PE2I PET) and $N = 11$ patients with MoCA scores ≥ 27 (all underwent ASL MRI and a subset of $N = 7$ underwent [11C]-PE2I PET). Several regions displayed higher rCBF values in patients with greater MoCA but did not reach significance (**Table 3**). Furthermore, in the subgroup of patients that had PET data available ($N = 17$) comparing PE2I avidity between the two subgroups, lower [11C]-PE2I avidity in the higher MoCA score group was found with statistically significantly lower [11C]-PE2I SUV values normalized to the occipital lobe in the caudate, pallidum, and putamen ($p = 0.005$-$p = 0.025$) (**Table 3**). Following Benjamini–Hochberg correction for multiple comparisons, our findings remained significant for all analyzed striatal regions.

When normalized to occipital lobe, there was a moderate negative statistically significant correlation between MoCA scores and normalized SUV in the pallidum on the more affected side ($p = 0.03$) (**Table 4**).

MDS VO Part 3

Using Pearson correlation there was a moderate negative correlation between MDS-UPDRS part 3 (motor) "off" and rCBF

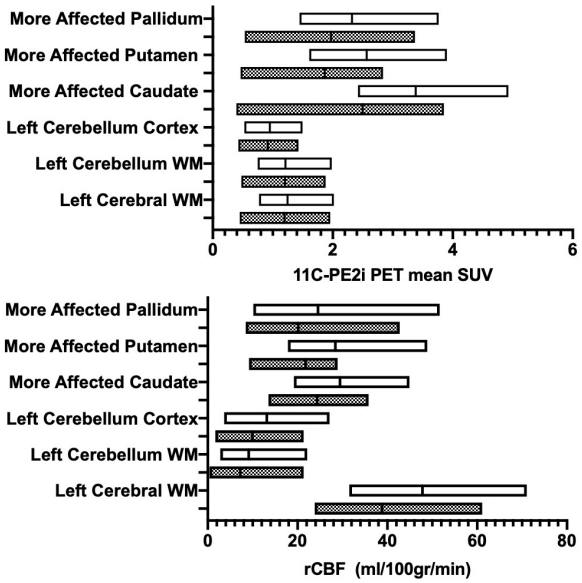

FIGURE 3 | Patients with Parkinson disease (PD) stratified by disease duration (>5 years, gray boxes; ≤5 years, white boxes). Region-specific ASL-based rCBF values (x-axis - **A**) and PE2I-based mean SUV (x-axis- **B**) are provided. Y-axis denotes evaluated brain regions.

values in the L and R cerebellum WM ($r = -0.43$ and -0.47, $p = 0.035$ and $p = 0.021$), which may suggest that milder motor symptoms of PD correlate with higher cerebellar rCBF. Patients were additionally stratified based on MDS-UPDRS part 3 (motor) "off" score into groups of mild disease-MDS-UPDRS part 3 (motor) "off" $\leq$ 32 and moderate disease-MDS-UPDRS part 3 (motor) "off" $>$ 32 (Martinez-Martin et al., 2015). Differences between the two groups were not statistically significant. No patients with an MDS-UPDRS part 3 (motor) "off" 58 (severe disease) were present in our cohort. There was no significant correlation between MDS-UPDRS part 3 (motor) "off" score and [11C]-PE2I SUV values normalized to the occipital lobe.

Dominant Hand Pegboard Testing

For this analysis, we used all the patients that had available ASL data and Dominant hand Pegboard testing ($N = 24$). A statistically significant, moderate negative correlation was found between Dominant hand Pegboard Test results and rCBF in the less affected pallidum ($r = -0.41$; $p = 0.046$). Dominant hand Pegboard testing did not demonstrate any significant correlations with [11C]-PE2I SUV values in any of the analyzed brain regions. Non-dominant hand Pegboard testing did not demonstrate any significant correlations with rCBF values in any of the analyzed brain regions.

Combined Imaging

We additionally correlated supratentorial rCBF with striatal [11C]-PE2I PET SUV. For this analysis, we included the 17 patients that had both ASL and [11C]-PE2I PET data. A statistically significant moderate negative correlation was present between left cerebral WM rCBF and more and less affected striatal [11C]-PE2I avidity: more affected caudate ($r = -0.54$, $p = 0.026$), more affected putamen ($r = -0.53$, $p = 0.031$), more affected pallidum ($r = -0.58$, $p = 0.017$) and less affected pallidum ($r = -0.052$, $p = 0.033$). A moderate negative correlation for the left cerebral WM and the less affected caudate ($r = -0.48$) and less affected putamen ($r = -0.43$) did not reach statistical significance ($p = 0.054$ and 0.085, respectively). Analogous analyses for the right cerebral WM demonstrated a similar trend however did not reach statistical significance for either the more or the less affected striatum ($r = -0.40$ to -0.31; $p = 0.109$ to 0.221).

Effect of Age

A multiple linear regression was performed comparing regional [C-11]-PE2I PET uptake normalized to the occipital region with both subject age and disease duration as covariates. Significant correlation of PET uptake in the putamen with disease duration was found to be $p = 0.004$ and $p = 0.022$ on the more and less affected sides respectively. No significant correlation of PET uptake with subject age was observed (**Figure 4**).

DISCUSSION

In this study, we combined ASL MRI-based assessment of the NVU with [11C]-PE2I PET-based assessment of striatal dopamine transporter density to assess pathophysiologic mechanisms in a prospective clinical cohort of patients with PD. This approach allowed us to place evaluation of NVU integrity and thereby BBB disruption into a more established clinical context.

At baseline, the BBB has tightly sealed cell–cell contacts involving the capillary endothelial cells and astrocyte endfoot processes, resulting in low transcellular and paracellular permeability. Loss of BBB integrity is associated with decreased relative cerebral blood flow (rCBF) (Montagne et al., 2016), microvascular dysfunction and hemodynamic impairment (Sweeney et al., 2016). BBB permeability is thereby linked to integrity of the NVU (Pelizzari et al., 2019b).

Neuroinflammation with resulting alpha-synuclein accumulation is a hallmark event in PD, and is closely associated with impaired blood-brain-barrier (BBB) permeability and microvascular dysfunction (Zhang et al., 2005; Sarkar et al., 2014; Sweeney et al., 2018), in particular given that certain BBB-targeting metalloproteinases (MMP) can be activated by inflammatory cytokines and chemokines (Germano et al., 2000; Jin et al., 2012). BBB dysfunction in PD has been suggested as a pathophysiologic mechanism based on compelling histopathologic findings including capillary extravasation of cells and proteins, thinning of the capillary endothelial cell layer, and extravascular IgG deposition (Gray and Woulfe, 2015; Pienaar et al., 2015).

Cerebral microvascular dysfunction appears to contribute to dopaminergic neuronal loss in PD (Barcia et al., 2004). Previous work using mouse models of acute, sub-acute and chronic PD demonstrated that area and density of endothelial cells were reduced in regions related to PD pathophysiology such

TABLE 2 | ASL rCBF and PE2I PET SUV values, stratified by disease duration.

	rCBF values (ml/100 g/min)			PE2I SUV averaged L/R and normalized to occipital		
Region of interest	**Disease duration ≤5years**	**Disease duration >5 years**	***p***	**Disease duration ≤5 years**	**Disease duration >5 years**	***p***
L cerebral WM	41.5	37.7	0.15	0.33	0.29	**0.001**
R cerebral WM	43.6	37.4	0.40	0.33	0.3	**0.049**
L cerebellum WM	6.1	5.7	0.36	0.32	0.3	**0.083**
R cerebellum WM	4.8	4.9	0.46	0.33	0.3	**0.010**
L cerebellum cortex	13.3	9.1	0.24	0.24	0.23	0.130
R cerebellum cortex	11.4	9.0	0.26	0.24	0.2	0.105
More affected caudate	30.3	24.7	0.24	0.94	0.66	**0.001**
Less affected caudate	29.2	26.3	0.76	1.03	0.72	**0.007**
More affected pallidum	22.9	18.5	0.34	0.63	0.51	**0.001**
Less affected pallidum	22.3	20.7	0.60	0.62	0.53	**0.001**
More affected putamen	25.6	24.4	0.10	0.67	0.46	**0.001**
Less affected putamen	26.4	22.6	0.40	0.86	0.54	**0.002**

Mann–Whitney tests were performed to determine statistical significance between subgroups. Additionally, Benjamini–Hochberg correction for multiple comparisons with an FDR of 0.1 was performed, with p-values that remained significant after correction indicated in bold font. R, right; L, left; WM, white matter; p: p-value.

TABLE 3 | ASL rCBF and PE2I PET SUV values, stratified by MoCA score.

	rCBF values (ml/100 g/min)			PE2I SUV averaged L/R and normalized to occipital lobe		
Region of interest	**MoCA ≥ 27**	**MoCA < 27**	***p***	**MoCA ≥ 27**	**MoCA < 27**	***p***
L cerebral WM	45.4	38.7	0.83	0.30	0.33	0.09
R cerebral WM	35.0	43.6	0.60	0.30	0.33	0.09
L cerebellum WM	5.9	5.3	0.46	0.31	0.33	0.11
R cerebellum WM	5.3	4.5	0.60	0.30	0.33	0.09
L cerebellum cortex	11.3	7.9	0.18	0.23	0.24	0.54
R cerebellum cortex	10.5	8.6	0.19	0.23	0.24	0.42
More affected caudate	24.5	28.4	0.68	0.73	0.87	**0.025**
Less affected caudate	24.7	30.2	0.57	0.75	0.97	**0.05**
More affected pallidum	18.6	20.1	0.60	0.49	0.63	**0.005**
Less affected pallidum	23.5	20.1	0.21	0.55	0.81	**0.01**
More affected putamen	24.9	24.5	0.54	0.48	0.66	**0.02**
Less affected putamen	23.1	22.8	0.64	0.55	0.81	**0.01**

Mann–Whitney tests were performed to determine statistical significance between subgroups. Additionally, Benjamini–Hochberg correction for multiple comparisons with an FDR of 0.1 was performed, with p-values that remained significant after correction indicated in bold font. R, right; L, left; WM, white matter.

as the substantia nigra and the striatum in all three models, further supporting the importance of microvascular damage in the pathogenesis of PD (Sarkar et al., 2014). The findings of microvascular dysfunction in the substantia nigra have also been suggested by a study comparing number of capillaries, length and diameter of human brain tissue in PD and normal controls (Guan et al., 2013).

NVU dysfunction, associated with a decrease in relative cerebral blood flow (rCBF), has been proposed as an early pathophysiologic mechanism in PD [19], and several ASL-based studies have revealed altered cerebral perfusion patterns in patients with PD compared to normal subjects. [20] ASL-derived differences in rCBF in PD are presently a subject of active investigation, with one study documenting no significant differences in rCBF for any of the evaluated regions (Pelizzari et al., 2019a) while other studies demonstrated decreased striatal rCBF in patients with PD (Wei et al., 2016), concordant with our findings of decreased rCBF in patients with longer disease duration, noting that our study did not include normal subjects for direct comparison. Differences in rCBF distribution have been attributed to BBB dysfunction in PD as well as other neurodegenerative diseases and evaluation of BBB integrity in PD remains the subject of active research. For example, an ASL-MRI-based approach to BBB assessment integrates a diffusion preparation module with pseudo-continuous ASL (pCASL) and a 3D gradient readout (Shao et al., 2019). Appropriate diffusion weighting allows for separation of the tissue and capillary fractions of the ASL signal and in turn allows quantification of capillary permeability of water (kW) between the tissue and intravascular compartments (Shao et al., 2019). Of note, there are currently no diffusion-weighted ASL-based or dynamic-contrast-enhanced (DCE) MRI-based studies in patients with PD.

TABLE 4 | Correlation between striatal PE2I SUV and MoCA scores.

	SUV normalized to occipital	
	r	*p*-value
L cerebral WM	−0.23	0.38
R cerebral WM	−0.39	0.12
L cerebellum WM	−0.31	0.22
R cerebellum WM	−0.33	0.20
L cerebellum cortex	−0.12	0.64
R cerebellum cortex	−0.18	0.49
More affected caudate	−0.33	0.20
More affected putamen	−0.45	0.07
More affected pallidum	−0.53	0.03
Less affected caudate	−0.21	0.43
Less affected putamen	−0.33	0.19
Less affected pallidum	−0.37	0.14

Pearson correlation coefficient r is shown for each striatal sub-region, along with associated p-values.

For evaluation of neuronal dopamine transporter density in PD, to date most imaging studies have used 123I-Iodoflupane (DatSCAN) SPECT, which is in wide clinical use in the work-up of parkinsonian syndrome. [11C]-PE2I PET provides a more accurate and specific quantification of neuronal dopamine transporters in PD compared to DatSCAN SPECT. [11C]-PE2I is a cocaine analog which binds neuronal dopamine transporters with high specificity. While [11C]-PE2I is structurally related to DatSCAN, [11C]-PE2I has the advantage of higher selectivity as it binds neuronal dopamine transporters only, whereas DatSCAN additionally targets serotonin and norepinephrine transporters (Jakobson et al., 2018). [18F] *N*-(3-fluoropropyl)-2β-carboxymethoxy-3β-(4-iodophenyl)nortropane (FP-CIT) has recently been demonstrated to have utility in dopamine transporter imaging in PD and related syndromes, with comparable image quality to [11C]-PE2I (Hong et al., 2018).

Another approach to visualization of dopamine depletion is [F-18]-Fluoro-DOPA (FDOPA) PET. FDOPA is limited in quantifying neuronal dopamine transporters as it illustrates the activity of aromatic amino acid decarboxylase which represents an intraneuronal reaction and is not specific for dopamine. Published data from a direct comparison of F-DOPA and [11C]-PE2I demonstrated greater sensitivity of [11C]-PE2I for the detection of differences in motor symptom severity and progression over time in PD (Li et al., 2018). Studies comparing [11C]-PE2I PET to combined DatSCAN SPECT and 18F-FDG PET further demonstrated superiority of [11C]-PE2I PET (Appel et al., 2015).

To our knowledge, this is the first study investigating the concurrent use of ASL imaging and [11C]-PE2I PET. We found statistically significantly lower striatal PE2I avidity in the sub-cohort of patients with longer disease duration, as well as a trend for lower rCBF values in the same cohort.

The significant negative correlations we identified between MoCA scores and [11C]-PE2I SUV values in the basal ganglia reflect current understanding that cognitive impairment in PD is not, for the most part, directly tied to dopaminergic neuronal loss, as patients with lower MoCA score had higher [11C]-PE2I SUV. Of note, cognitive impairment has been suggested to precede the development of "classic" motor symptoms in PD (Fereshtehnejad et al., 2019), and while our study only incorporates one imaging time point, this may reflect a pathophysiologic basis for our findings and needs to be studied further in future longitudinal studies.

Previously published data have shown that rCBF values in basal ganglia are inversely correlated to motor dysfunction (Wei et al., 2016). Stratification based on MDS-UPDRS score into groups of mild disease-MDS $\leq$ 32 and moderate disease-MDS-UPDRS $>$ 32 did not reveal a clear trend for rCBF values, although Pearson correlation analysis did demonstrate a weak negative correlation between MDS-UPDRS and cerebellar rCBF values.

Our study has several limitations, most notably small sample size overall as well as small sample size of the various subgroups.

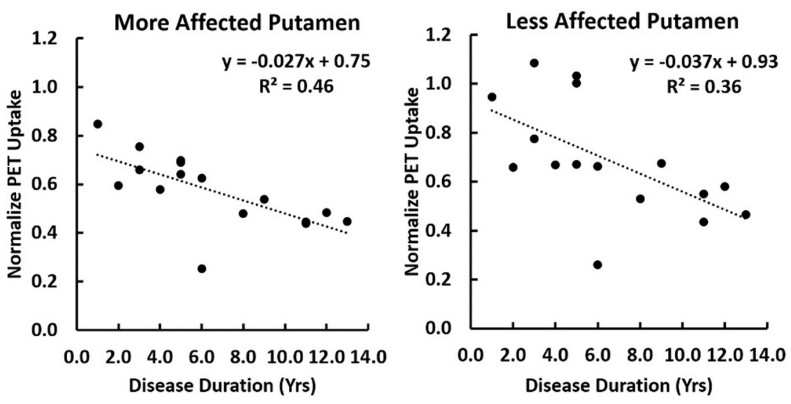

FIGURE 4 | A correlation of [C-11]-PE2I PET uptake normalized to the occipital lobe is shown with disease duration for the putamen lateralized into the more or less affected side. A multiple regression was performed with both subject age as disease duration as covariates. Significant correlation of PET uptake in the putamen with disease duration was found to be $p = 0.004$ and $p = 0.022$ on the more and less affected sides respectively. No significant correlation with subject age was observed.

Another limitation is lack of direct comparison to non-diseased subjects. Furthermore, our study is cross-sectional and lacks longitudinal follow-up data. However, we demonstrate feasibility of concurrent non-invasive imaging of cerebral perfusion and dopaminergic neuronal loss, and place our findings in the clinical context of motor and cognitive decline in PD.

CONCLUSION

Our ROI-based analyses suggest that longer disease duration is associated with lower rCBF and lower striatal [11C]-PE2I avidity, implying greater NVU dysfunction and greater dopaminergic neuronal loss, respectively. Correlative studies of ASL and [11C]-PE2I PET data further suggest that dopaminergic neuronal loss may be independent from cognitive impairment in PD.

Combined perfusion MRI and dopamine transporter targeted PET imaging may inform future prospective clinical trials, thereby providing an improved mechanistic understanding of PD and related neurodegenerative diseases, and laying the foundation for the development of early disease biomarkers and potential therapeutic targets.

DATA AVAILABILITY STATEMENT

All datasets generated for this study are included in the article/supplementary material.

ETHICS STATEMENT

The studies involving human participants were reviewed and approved by Institutional Review Board – Weill Cornell Medicine. The patients/participants provided their written informed consent to participate in this study.

AUTHOR CONTRIBUTIONS

JI conceptualized the project, analyzed the data, and wrote the manuscript. SP collected the PET data. JD collected the MRI data. AR, AG, and CH conceptualized the prospective PD observational study that served as the basis for this project. DP and CH evaluated the subjects and collected clinical and demographic data. All authors contributed to data analysis and manuscript writing.

FUNDING

This project was supported through funding from the Society of Nuclear Medicine and Molecular Imaging (PI: JI), the Anna-Maria and Stephen Kellen Foundation (PI: JI); the CV Starr Foundation (PI: CH), and the NIH NINDS (PI: AG and AR).

REFERENCES

Appel, L., Jonasson, M., Danfors, T., Nyholm, D., Askmark, H., Lubberink, M., et al. (2015). Use of 11C-PE2I PET in differential diagnosis of parkinsonian disorders. *J. Nucl. Med.* 56, 234–242. doi: 10.2967/jnumed.114.148619

Barcia, C., Emborg, M. E., Hirsch, E. C., and Herrero, M. T. (2004). Blood vessels and parkinsonism. *Front. Biosci.* 9, 277–282. doi: 10.2741/1145

Chou, K. L., Lenhart, A., Koeppe, R. A., and Bohnen, N. I. (2014). Abnormal MoCA and normal range MMSE scores in Parkinson disease without dementia: cognitive and neurochemical correlates. *Parkinson. Relat. Disord.* 20, 1076–1080. doi: 10.1016/j.parkreldis.2014.07.008

Codolo, G., Plotegher, N., Pozzobon, T., Brucale, M., Tessari, I., Bubacco, L., et al. (2013). Triggering of inflammasome by aggregated alpha-synuclein, an inflammatory response in synucleinopathies. *PLoS One* 8:e55375. doi: 10.1371/journal.pone.0055375

Desikan, R. S., Segonne, F., Fischl, B., Quinn, B. T., Dickerson, B. C., Blacker, D., et al. (2006). An automated labeling system for subdividing the human cerebral cortex on MRI scans into gyral based regions of interest. *Neuroimage* 31, 968–980. doi: 10.1016/j.neuroimage.2006.01.021

Fereshtehnejad, S. M., Yao, C., Pelletier, A., Montplaisir, J. Y., Gagnon, J. F., and Postuma, R. B. (2019). Evolution of prodromal Parkinson's disease and dementia with Lewy bodies: a prospective study. *Brain* 142, 2051–2067. doi: 10.1093/brain/awz111

Fischl, B., Salat, D. H., Busa, E., Albert, M., Dieterich, M., Haselgrove, C., et al. (2002). Whole brain segmentation: automated labeling of neuroanatomical structures in the human brain. *Neuron* 33, 341–355.

Germano, A., D'avella, D., Imperatore, C., Caruso, G., and Tomasello, F. (2000). Time-course of blood-brain barrier permeability changes after experimental subarachnoid haemorrhage. *Acta Neurochir.* 142, 575-580; discussion 580–571.

Gray, M. T., and Woulfe, J. M. (2015). Striatal blood-brain barrier permeability in Parkinson's disease. *J. Cereb. Blood Flow Metab.* 35, 747–750. doi: 10.1038/jcbfm.2015.32

Guan, J., Pavlovic, D., Dalkie, N., Waldvogel, H. J., O'carroll, S. J., Green, C. R., et al. (2013). Vascular degeneration in Parkinson's disease. *Brain Pathol.* 23, 154–164. doi: 10.1111/j.1750-3639.2012.00628.x

Gulani, V., Calamante, F., Shellock, F. G., Kanal, E., Reeder, S.B., and International Society for Magnetic Resonance in Methods (2017). Gadolinium deposition in the brain: summary of evidence and recommendations. *Lancet Neurol.* 16, 564–570. doi: 10.1016/s1474-4422(17)30158-8

Haller, S., Zaharchuk, G., Thomas, D. L., Lovblad, K. O., Barkhof, F., and Golay, X. (2016). Arterial spin labeling perfusion of the brain: emerging clinical applications. *Radiology* 281, 337–356. doi: 10.1148/radiol.2016150789

Hong, C. M., Ryo, H. S., and Ahn, B. C. (2018). Early perfusion and dopamine transporter imaging using 18 F-FP-CIT PET/CT in patients with parkinsonism. *Am. J. Nucl. Med. Mol. Imaging* 8, 360–372.

Jakobson, M. S., Axelsson, J., Jonasson, L., Larsson, A., Ogren, M. J., Ogren, M., et al. (2018). Dopamine transporter imaging with [(18)F]FE-PE2I PET and [(123)I]FP-CIT SPECT-a clinical comparison. *EJNMMI Res.* 8:100.

Jenkinson, M., Bannister, P. R., Brady, J. M., and Smith, S. M. (2002). Improved optimisation for the robust and accurate linear registration and motion correction of brain images. *NeuroImage* 17, 825–841. doi: 10.1006/nimg.2002.1132

Jenkinson, M., and Smith, S. M. (2001). A global optimisation method for robust affine registration of brain images. *Med. Image Anal.* 5, 143–156. doi: 10.1016/s1361-8415(01)00036-6

Jin, X., Liu, J., Yang, Y., Liu, K. J., Yang, Y., and Liu, W. (2012). Spatiotemporal evolution of blood brain barrier damage and tissue infarction within the first 3h after ischemia onset. *Neurobiol. Dis.* 48, 309–316. doi: 10.1016/j.nbd.2012.07.007

Li, W., Lao-Kaim, N. P., Roussakis, A. A., Martin-Bastida, A., Valle-Guzman, N., Paul, G., et al. (2018). (11) C-PE2I and (18) F-Dopa PET for assessing progression rate in Parkinson's: a longitudinal study. *Mov. Disord.* 33, 117–127. doi: 10.1002/mds.27183

Litvan, I., Goldman, J. G., Troster, A. I., Schmand, B. A., Weintraub, D., Petersen, R. C., et al. (2012). Diagnostic criteria for mild cognitive impairment in

Parkinson's disease: movement disorder society task force guidelines. *Mov. Disord.* 27, 349–356. doi: 10.1002/mds.24893

Martinez-Martin, P., Rodriguez-Blazquez, C., Mario, A., Arakaki, T., Arillo, V. C., Chana, P., et al. (2015). Parkinson's disease severity levels and MDS-Unified Parkinson's Disease Rating Scale. *Parkinson. Relat. Disord.* 21, 50–54.

Montagne, A., Nation, D. A., Pa, J., Sweeney, M. D., Toga, A. W., and Zlokovic, B. V. (2016). Brain imaging of neurovascular dysfunction in Alzheimer's disease. *Acta Neuropathol.* 131, 687–707. doi: 10.1007/s00401-016-1570-0

Pelizzari, L., Lagana, M. M., Di Tella, S., Rossetto, F., Bergsland, N., Nemni, R., et al. (2019a). Combined assessment of diffusion parameters and cerebral blood flow within basal ganglia in early Parkinson's disease. *Front. Aging Neurosci.* 11:134. doi: 10.3389/fnagi.2019.00134

Pelizzari, L., Lagana, M. M., Rossetto, F., Bergsland, N., Galli, M., Baselli, G., et al. (2019b). Cerebral blood flow and cerebrovascular reactivity correlate with severity of motor symptoms in Parkinson's disease. *Ther. Adv. Neurol. Disord.* 12:1756286419838354.

Pienaar, I. S., Lee, C. H., Elson, J. L., Mcguinness, L., Gentleman, S. M., Kalaria, R. N., et al. (2015). Deep-brain stimulation associates with improved microvascular integrity in the subthalamic nucleus in Parkinson's disease. *Neurobiol. Dis.* 74, 392–405. doi: 10.1016/j.nbd.2014.12.006

Proud, E. L., Bilney, B., Miller, K. J., Morris, M. E., and Mcginley, J. L. (2019). Measuring hand dexterity in people With Parkinson's disease: reliability of pegboard tests. *Am. J. Occup. Ther.* 73, 7304205050p1–7304205050p8.

Reid, W. G., Hely, M. A., Morris, J. G., Loy, C., and Halliday, G. M. (2011). Dementia in Parkinson's disease: a 20-year neuropsychological study (Sydney Multicentre Study). *J. Neurol. Neurosurg. Psychiatry* 82, 1033–1037. doi: 10.1136/jnnp.2010.232678

Sarkar, S., Raymick, J., Mann, D., Bowyer, J. F., Hanig, J. P., Schmued, L. C., et al. (2014). Neurovascular changes in acute, sub-acute and chronic mouse models of Parkinson's disease. *Curr. Neurovasc. Res.* 11, 48–61. doi: 10.2174/1567202610666131124234506

Shao, X., Ma, S. J., Casey, M., D'orazio, L., Ringman, J. M., and Wang, D. J. J. (2019). Mapping water exchange across the blood-brain barrier using 3D diffusion-prepared arterial spin labeled perfusion MRI. *Magn. Reson. Med.* 81, 3065–3079. doi: 10.1002/mrm.27632

Simon, D. K., Tanner, C. M., and Brundin, P. (2020). Parkinson disease epidemiology, pathology, genetics, and pathophysiology. *Clin. Geriatr. Med.* 36, 1–12. doi: 10.1016/j.cger.2019.08.002

Sweeney, M. D., Ayyadurai, S., and Zlokovic, B. V. (2016). Pericytes of the neurovascular unit: key functions and signaling pathways. *Nat. Neurosci.* 19, 771–783. doi: 10.1038/nn.4288

Sweeney, M. D., Sagare, A. P., and Zlokovic, B. V. (2018). Blood-brain barrier breakdown in Alzheimer disease and other neurodegenerative disorders. *Nat. Rev. Neurol.* 14, 133–150. doi: 10.1038/nrneurol.2017.188

Wang, J., Zhang, Y., Wolf, R. L., Roc, A. C., Alsop, D. C., and Detre, J. A. (2005). Amplitude-modulated continuous arterial spin-labeling 3.0-T perfusion MR imaging with a single coil: feasibility study. *Radiology* 235, 218–228. doi: 10.1148/radiol.2351031663

Wang, Z., Aguirre, G. K., Rao, H., Wang, J., Fernández-Seara, M. A., Childress, A. R., et al. (2008). Empirical optimization of ASL data analysis using an ASL data processing toolbox: ASLtbx. *Magn. Reson. Imaging* 26, 261–269. doi: 10.1016/j.mri.2007.07.003

Wei, X., Yan, R., Chen, Z., Weng, R., Liu, X., Gao, H., et al. (2016). Combined diffusion tensor imaging and arterial spin labeling as markers of early Parkinson's disease. *Sci. Rep.* 6:33762.

Zhang, W., Wang, T., Pei, Z., Miller, D. S., Wu, X., Block, M. L., et al. (2005). Aggregated alpha-synuclein activates microglia: a process leading to disease progression in Parkinson's disease. *FASEB J.* 19, 533–542. doi: 10.1096/fj.04-2751com

Conflict of Interest: The authors declare that the research was conducted in the absence of any commercial or financial relationships that could be construed as a potential conflict of interest.

frontiers in Aging Neuroscience

SYSTEMATIC REVIEW
published: 25 September 2020
doi: 10.3389/fnagi.2020.00277

Preclinical Evidence and Possible Mechanisms of Baicalein for Rats and Mice With Parkinson's Disease: A Systematic Review and Meta-Analysis

Yu Wang[1], *Na Wei*[2*] *and Xiaoliang Li*[1,2*]

[1] *Research Institute of Chinese Medicine, Heilongjiang University of Chinese Medicine, Harbin, China,* [2] *Key Laboratory of Tropical Translational Medicine of Ministry of Education, Hainan Key Laboratory for Research and Development of Tropical Herbs, School of Pharmacy, Hainan Medical University, Haikou, China*

Baicalein, a major bioactive flavone of Scutellaria baicalensis Georgi, has neuroprotective properties in several animal models of Parkinson's disease (PD). Here, we conducted a systematic review and meta-analysis to assess the available preclinical evidence and possible mechanisms of baicalein for animal models of PD. Ultimately, 20 studies were identified by searching 7 databases from inception to December 2019. Review Manager 5.3 was applied for data analysis. Meta-analyses showed baicalein can significantly improve neurobehavioral function in animal models with PD, including spontaneous motor activity test ($n = 5$), pole test ($n = 2$), rotarod test ($n = 9$), apomorphine-induced rotations test ($n = 4$), grid test ($n = 2$), and tremor test ($n = 2$). Compared with controls, the results of the meta-analysis showed baicalein exerted a significant effect in increasing the frequency of spontaneous activity, prolongating the total time for climbing down the pole, decreasing the number of rotations, prolongating the descent latency, reducing the amplitude, and the frequency in animal models with PD. The possible mechanisms of baicalein for PD are regulating neurotransmitters, adjusting enzyme activity, antioxidation, anti-inflammatory, inhibiting protein aggregation, restorating mitochondrial dysfunction, inhibiting apoptosis, and autophagy. In conclusion, these findings preliminarily demonstrated that baicalein exerts potential neuroprotective effects through multiple signaling pathways in animal models of PD.

Keywords: baicalein, parkinson's disease, preclinical evidence, mechanisms, meta-analysis

OPEN ACCESS

Edited by:
Jiehui Jiang,
Shanghai University, China

Reviewed by:
Sachchida Nand Rai,
University of Allahabad, India
Mariana Appel Hort,
Federal University of Rio Grande, Brazil

***Correspondence:**
Na Wei
2585468766@qq.com
Xiaoliang Li
lixiaoliang-1984@163.com

Received: *07 May 2020*
Accepted: *11 August 2020*
Published: *25 September 2020*

Citation:
Wang Y, Wei N and Li X (2020) Preclinical Evidence and Possible Mechanisms of Baicalein for Rats and Mice With Parkinson's Disease: A Systematic Review and Meta-Analysis. Front. Aging Neurosci. 12:277. doi: 10.3389/fnagi.2020.00277

INTRODUCTION

PD is a common and severe degeneration of the central nervous system, which is mainly manifested as bradykinesia, rigidity, and static tremor (Schindlbeck and Eidelberg, 2018), usually accompanying by non-motor symptoms such as depression, sleep disturbances, cognitive decline, etcetera (Schapira et al., 2017). The figures showed that the incidence rate of PD has increased from 3.5 to 42.8% in the past few years (Kovács et al., 2019), affecting about 1% of the population over the age of 60 (Martin et al., 2011). Worse yet, about 1.174 million people died of Parkinson's disease worldwide from 2005 to 2015 (Wang et al., 2016). Although the typical clinical and pathological

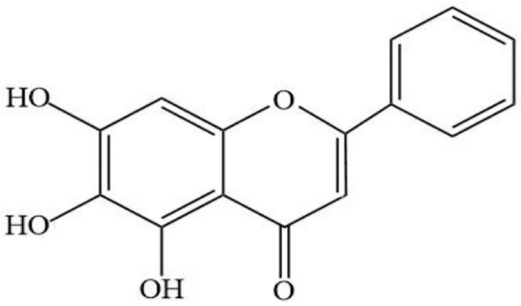

FIGURE 1 | Chemical structure of baicalein.

features of PD have been clear, its etiology and pathogenesis are not fully clarified yet. Over the years, researchers have been exploring the pathogenesis and treatment of PD. Overwhelming evidences demonstrated that levodopa can significantly improve motor function in patients with PD (LeWitt and Fahn, 2016). But it's just about improving the symptoms of PD and cannot stop the progress of the disease (Naskar et al., 2013). Therefore, the search for new effective drugs is a hot topic in PD research. Excitedly, natural medicines characterized with high activity and low side-effect are a valuable resource for us to find compounds against PD.

Baicalein (**Figure 1**) is a major bioactive flavone, mainly extracted from the root of Scutellaria baicalensis Georgi. Modern pharmacological researches have proved that baicalin has a wide range of biological activities, including antioxidant, anticancer, antiviral, anti-inflammatory, antidiabetic, antithrombotic, hepatoprotective (Sowndhararajan et al., 2017). In addition, recent studies have shown that baicalin has shown strong neuroprotective effects in models of various neurological diseases. *In vivo*, baicalein exerted neuroprotective action through reducing behavioral damage and the depletion of dopaminergic neurons in rotenone-induced PD model (Zhang et al., 2017a). Moreover, other studies have shown that treatment with baicalein significantly attenuated the dopamine (DA) content in striatum induced by 1-methyl-4-phenylpyridinium (MPP^+) (Hung et al., 2016) and increased the numbers of tyrosine hydroxylase (TH) neurons in PD rat model induced by 6-hydroxydopamine (6-OHDA) (Mu et al., 2009). All these data indicated that baicalin can be used as an effective drug to prevent or treat neurodegenerative diseases such as PD.

The preliminary research basis of animal experiment can provide clearly direction for clinical practice, greatly improving the understanding of clinicians and researchers on the disease mechanism and the progress of intervention measures (Sena et al., 2014). In recent years, many animal studies of baicalein have been reported. However, the efficacy and mechanisms of baicalein for PD have not been systematically appraised and summarized. Thus, in the present study, we performed a systematic review and meta-analysis to assess recent literature on the effects of baicalein therapy on animals with PD and provide current preclinical evidence and potential mechanisms on animal models.

MATERIALS AND METHODS

Data Sources and Search Strategy

The meta-analysis was conducted according to the Preferred Reporting Items for Systematic Review and Meta-Analyses (PRISMA) guidelines (Moher et al., 2015). Seven English and Chinese databases, including China National Knowledge Infrastructure (CNKI), Wanfang Database, Science Direct, PubMed, Web of science, Medline, and EMBASE, were independently searched by two reviewers (XL Li and Y Wang), from their inceptions to December 2019. The following keywords and terms were as follows: "parkinsonian disorders" OR "Parkinson disease" and "Baicalein" OR "Huangqinsu" OR "Baikeli." All studies were limited to animals.

Inclusion and Exclusion Criteria

Studies conforming to the following inclusion criteria were selected for this review: (1) participants: experimental animals including mice and rats. (2) invention: baicalein only; (3) outcomes: The effect of baicalein on the animal model of Parkinson's disease, including neurobehavioural. Meanwhile, studies which met the following criteria were excluded: (a) combined use of other drugs; (b) non-animal based studies; (c) case report, comments, clinical experiences, or trials and review article; (d) similar and repeated studies.

Data Extraction

Two authors (XL Li and Y Wang) extracted data independently from the qualified articles. The following information of each study was recorded: (1) the first author's name, year of publication; (2) animals' characteristics, including species, number, sex, and body weight; (3) methods for PD model establishment and anesthetic used in the model; (4) intervention characteristics, including the dosage and route of administration; (5) main outcome measures and its intergroup differences.

The peak time point was included if the outcomes were tested at different times. The data of the highest dose were extracted when various doses of baicalein were used in study. If the primary data were missing or demonstrated graphically, we tried to contact authors for raw data. And the numerical values in the graph were measured by the digital ruler software when no response was received from the authors.

Risk of Bias in Individual Studies

The risk of bias in each included study was assessed independently by two investigators (XL Li and Y Wang) using the Systematic Review Centre for Laboratory animal Experimentation (SYRCLE)'s risk of bias tool for animal studies, which was used to evaluate bias in six domains: selection bias (sequence generation, baseline characteristics, and allocation concealment), performance bias (random housing and blinding), detection bias (random outcome assessment and blinding), attrition bias, reporting bias, and other biases (Hooijmans et al., 2014).

Statistical Analysis

RevMan V.5.3 software was applied for Meta-analyses. Outcome measures were all treated as continuous data and expressed

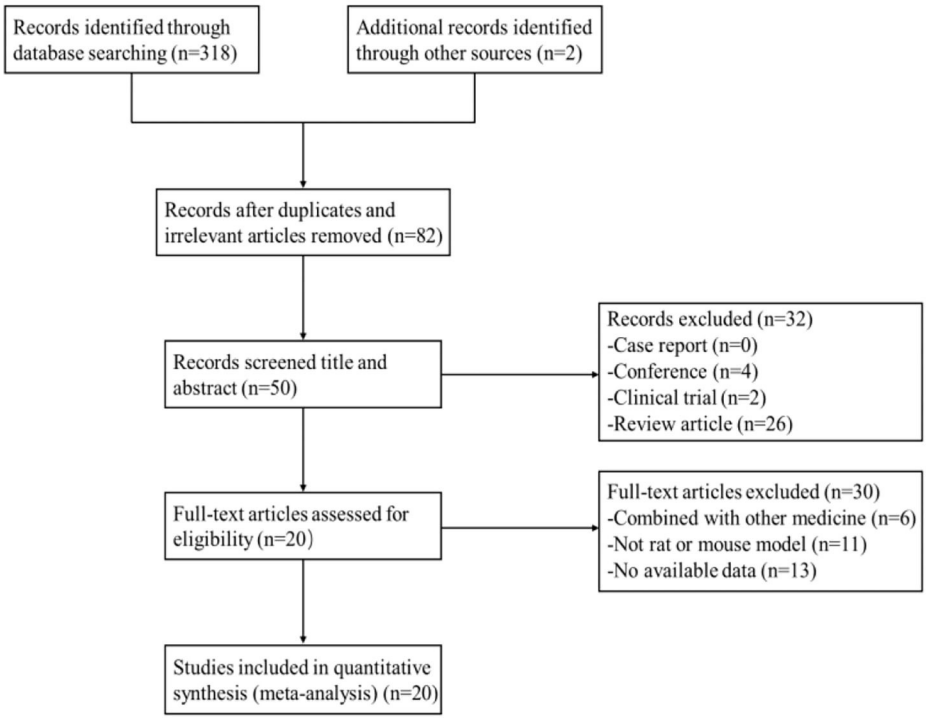

FIGURE 2 | Summary of the process for identifying candidate studies.

as standardized mean difference (SMD) with 95% confidence interval (CI). Heterogeneity among individual studies was assessed using the I-square (I^2) statistics test. If $I^2 > 50\%$, a random effect model was adopted. Instead, a fixed effect model was used. Publication bias was assessed by funnel plots and Egger's test. Probability value $P < 0.05$ was considered statistically significant.

RESULTS

Study Selection

After primary search from seven databases, a total of 320 potentially publications were identified. After removal of repetitive and irrelevant articles, 82 records were remained. By screening titles and abstracts, 32 studies were excluded because they were conferences, clinical trials, or review articles. Then secondary screening was performed by reading the remaining full-text articles, and 30 studies were excluded for at least one of the following reasons:(1) no available data; (2) not rat or mouse model; (3) combined with other medicine. Eventually, 20 eligible studies were selected. A flow diagram of the study selection process is shown in **Figure 2**.

Characteristics of Included Studies

Twenty rats or mice experiments between 2008 and 2019 were included. Sixteen studies were published in English, and four studies were published in Chinese which containing one online PhD theses. For animal species, Sprague-Dawley (SD) rats were used in 9 studies, C57B/6 J mice were used in 8 studies, ICR mice were used in 2 studies, and the remaining 1 study used Kunming (KM) mice. All animals were male in the included studies. The body weight of SD rats ranged from 180 to 350 g, while the body weight of mice ranged from 18 to 30 g. Anesthetic was reported in 11 studies, including sodium pentobarbital ($n = 4$), chloralose ($n = 1$), equithesin ($n = 1$), ethyl ether ($n = 1$), halothan ($n = 1$), and chloral hydrate ($n = 4$). PD models were established by using 1-methyl-4-phenyl-1,2,3,6-tetrahydropyridine (MPTP) ($n = 6$), 6-OHDA ($n = 6$), rotenone ($n = 5$), MPP^+ ($n = 1$), acrolein ($n = 1$), oxotremorine ($n = 1$). There were ways of administration of baicalein, including intragastric administration ($n = 9$), intraperitoneal administration ($n = 5$), subcutaneous administration ($n = 1$). The changes of praxeology as primary outcome for assessing baicalein were carried out by the spontaneous motor activity test ($n = 5$), pole test ($n = 2$), apomorphine-induced rotation test ($n = 4$), rotarod test ($n = 9$), grid test ($n = 2$), and tremor test ($n = 6$). About the changes of neurotransmitters, DA was reported in 12 studies, 5-Hydroxyindole-3-acetic acid (5-HIAA) in 2 studies, 5-HT in 2 studies, (3,4-dihydroxyphenylacetic acid) DOPAC in 8 studies, E in 2 studies, gamma-aminobutyric acid (GABA) in 2 studies and glutamate (GLU) in 2 studies. In addition, TH was reported in 13 studies, Cathepsin B in 2 studies, ED-1 in 2 studies, glial fibrillary acidic protein (GFAP) in 4 studies, a-Caspase 1 in 2 studies, superoxide dismutase (SOD) in 2 studies, malondiadehycle (MDA) 5 in studies, glutathione peroxidase (GSH-Px) in 3 studies. The

TABLE 1 | Characteristics of the 20 included animal studies.

Study (years)	Species (Sex, experimental/ control group)	Weight	Modeling approach	Anesthetic	Treatment group	Control group	Outcome measure	Intergroup differences
Zhang et al., 2017b	Male sprague-dawley rats(10/15)	240–260 g	Rotenone	–	Baicalein (100, 200, 400 mg/kg p.o.)	–	Spontaneous motor activity test	$P < 0.05$
							Rotarod test	$P < 0.05$
							TH	$P < 0.01$
Hung et al., 2016	Male sprague-dawley rats (-/-)	300–350 g	MPP+	Chloral hydrate	Baicalein (10 and 30 mg/kg)	10% DMSO in saline	DA	$P < 0.05$
							TH	$P < 0.05$
							IL-1β	$P < 0.05$
							ED-1	$P < 0.05$
							a-Caspase 1	$P < 0.05$
							Cathepsin B	$P < 0.05$
Mu et al., 2009	Male sprague-dawley rats(12/12)	180–200 g;	6-OHDA	3% sodium pentobarbital (45 mg/kg i.p.)	Baicalein (200 mg/kg; i.g.)	Saline i.g.	Apomorphine-induced rotation test	$P > 0.05$
							Tremor test	
							-Burst frequency	$P < 0.01$
							-Burst amplitude	$P < 0.01$
							TH	$P < 0.05$
							GFAP	$P < 0.01$
Cheng et al., 2008	Male C57BL/6 mice (10/10)	∼25 g	MPTP	–	Baicalein (200 mg/kg; i.g.)	Saline i.g.	Spontaneous motor activity test	$P < 0.05$
							Pole test	$P < 0.05$
							DA	$P < 0.01$
							DOPAC	$P > 0.05$
							5-HT	$P < 0.05$
							5-HIAA	$P > 0.05$
							TH	$P < 0.05$
							GFAP	$P < 0.01$
							SOD	$P < 0.05$
							GSH-Px	$P < 0.05$
							MDA	$P < 0.05$
He et al., 2015	Male sprague-dawley rats(12/12)	180–200 g	6-OHDA	3% sodium pentobarbital (50 mg/kg i.p.)	Baicalein (200 mg/kg i.g.)	Distilled water i.g.	Spontaneous motor activity test	$P < 0.05$
							Apomorphine-induced rotation test	$P < 0.01$
							Tremor test	
							-Burst frequency	$P < 0.05$
							-Burst amplitude	$P < 0.01$
							DA	$P < 0.05$
							DOPAC	$P > 0.05$
							TH	$P < 0.05$
Li, 2011	Male sprague-dawley rats $^{(-/-)}$	180–200 g	6-OHDA	3% sodium pentobarbital (50 mg/kg i.p.)	Baicalein (200 mg/kg; i.g.)	–	Spontaneous motor activity test	$P < 0.05$
							Rotarod test	$P < 0.05$
							Apomorphine-induced rotation test	$P < 0.01$
							Tremor test-burst frequency	$P < 0.001$
							DA	$P > 0.05$
							DOPAC	$P < 0.05$
							5-TH	$P > 0.05$
							5-HIAA	$P > 0.05$
							GABA	$P > 0.05$
							GLU	$P > 0.05$
							E	$P > 0.05$
							TH	$P < 0.05$
							GFAP	$P < 0.05$
Mu et al., 2011	Male C57BL/6 mice (12/12)	∼25 g	MPTP	–	Baicalein (140, 280, 560 mg/kg i.g.)	Saline i.g.	Spontaneous motor activity test	$P < 0.05$
							Rotarod test	$P < 0.05$
							DA	$P < 0.05$
							DOPAC	$P > 0.05$
							TH	$P < 0.05$
							SOD	$P < 0.05$
							GSH-P x	$P < 0.05$
							MDA	$P < 0.05$

(Continued)

TABLE 1 | Continued

Study (years)	Species (Sex, experimental/ control group)	Weight	Modeling approach	Anesthetic	Treatment group	Control group	Outcome measure	Intergroup differences
Gao et al., 2015	Male C57BL/6 mice (15/15)	–	MPTP	–	Baicalein (140 and 280 mg/kg i.g.);	Saline i.g.	Pole test Rotarod test	$P < 0.001$ $P < 0.01$
Im et al., 2005	Male ICR mice (−/−)	26–28 g	6-OHDA	–	Baicalein (25 and 50 mg/kg, i.p)	5% DMSO	Rotarod test DA DOPAC TH MDA	$P < 0.05$ $P < 0.05$ $P < 0.05$ $P < 0.05$ $P < 0.05$
Xue et al., 2014	Male C57BL/6 mice (−/−)	18–24 g	MPTP	halothan	Baicalein (10 mg/kg, i.p.)	Saline i.p.	Rotarod test TNF-a IL-1β	$P < 0.05$ $P < 0.05$ $P < 0.05$
Lee et al., 2014	Male C57BL/6 mice (−/−)	20–23 g	MPTP	Ethyl ether	Baicalein (1 and 10 mg/kg i.p.);	PBS containing 5% ethanol and 2% Tween 20 i.p.	Rotarod test TH	$P < 0.01$ $P < 0.01$
Hu et al., 2016	Male C57BL/6 mice (−/−)	–	Rotenone	–	Baicalein (100 mg/kg; i.p.)	–	Rotarod test Grid test DA DOPAC TH	$P < 0.01$ $P < 0.01$ $P < 0.01$ $P < 0.01$ $P < 0.05$
Kuang et al., 2017	Male C57BL/6 mice (−/−)	–	Rotenone	–	Baicalein (100 mg/kg; i.p.)	–	Rotarod test Grid test DA	$P < 0.01$ $P < 0.01$ $P < 0.01$
Im et al., 2006	Male ICR mice (−/−)	26–28g	6-OHDA	Equithesin (0.6 mg/ml, 5 ml/kg, i.p.)	Baicalein (25 and 50 mg/kg, i.p)	5% DMSO	Apomorphine-induced rotation test DA DOPAC MDA TH	$P < 0.05$ $P < 0.05$ $P < 0.05$ $P < 0.05$ $P < 0.05$
Yu et al., 2012	Male sprague-dawley rats(12/12)	180–200 g	6-OHDA	Sodium pentobarbital (45 mg/kg i.p.); Chloralose (300 mg/kg, i.p.)	Baicalein (100, 200 and 400 mg/kg i.g.);	Saline i.g.	Tremor test -Burst frequency -Burst amplitude DA GABA GLU	 $P < 0.01$ $P < 0.001$ $P > 0.05$ $P < 0.05$ $P < 0.05$
Yang et al., 2018	Male KM mice (8/8)	18–22 g	Oxotremorine	–	Baicalein (120, 240, 480 mg/kg i.g.)	Saline i.g.	DA DOPAC E GSH-P x MDA	$P < 0.01$ $P < 0.01$ $P > 0.05$ $P > 0.05$ $P > 0.05$
Zhao et al., 2018	Male sprague-dawley rats (−/−)	300–350 g	Acrolein	Chloral hydrate (450 mg/kg)	Baicalein (30 mg/kg)	10% DMSO in saline	ED-1 a-Caspase 1 Cathepsin B DA IL-1β GFAP	$P < 0.05$ $P < 0.05$ $P < 0.05$ $P < 0.05$ $P < 0.05$ $P < 0.05$
Han et al., 2019	Male Sprague–Dawley rats(12/12)	200 ± 20 g	Rotenone	Chloral hydrate (300 mg/kg)	Baicalein (200 mg/kg s.c.)	Saline s.c.	TH	$P < 0.01$
Zheng et al., 2019	Male C57BL/6 mice (6/6)	25–30 g	MPTP	–	Baicalein (10 mg/kg i.p.)	Saline	TH	$P > 0.05$
Zhang et al., 2017a	Male Sprague-Dawley rats(10/10)	240–260 g	Rotenone	–	Baicalein (100, 200, 400 mg/kg p.o.)	–	GFAP TNF-a IL-1β	$P < 0.01$ $P < 0.05$ $P > 0.05$

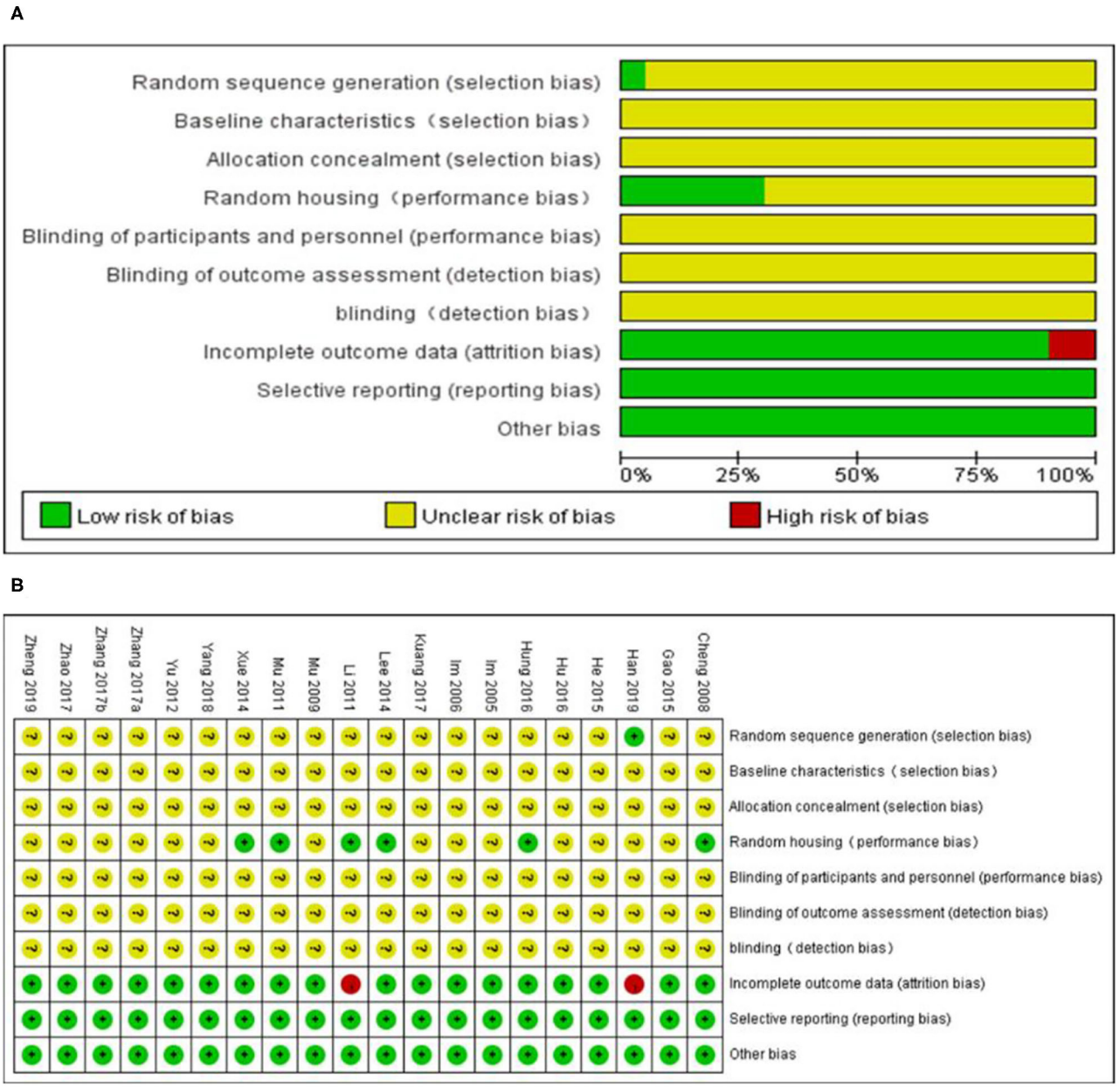

FIGURE 3 | Risk of bias of the included studies. **(A)** Risk of bias graph. **(B)** Risk of bias summary. + = low risk of bias, − = high risk of bias, ? = unclear risk of bias.

detailed characteristics of the included studies are summarized in **Table 1**.

Study Quality

The overall quality of the included studies was relatively low (**Figure 3**). All but one study was not reported randomization. All studies included were unclear in baseline characteristics, allocation concealment, blinding of participants, and detection bias. while, these studies were all provided information regarding selective reporting and other bias. Six studies adequately reported random housing and 16 studies adequately reported incomplete outcome data.

Effectiveness

Behavior Function

In spontaneous motor activity test, meta-analysis of 5 studies (Cheng et al., 2008; Li, 2011; Mu et al., 2011; He et al., 2015; Zhang et al., 2017b) showed significant effect of baicalein for increasing the frequency of spontaneous activity in PD animals compared with control group [$n = 54$, SMD = 2.22, 95% CI (1.72–2.73), $P < 0.00001$; heterogeneity: $\chi = 4.55$, df = 4 ($P = 0.34$); $I^2 =$

12%; **Figure 4A**]. In pole test, meta-analysis of 2 studies (Cheng et al., 2008; Gao et al., 2015) showed significant effect of baicalein for prolongating the total time for climbing down the pole in PD animals compared with control group [$n = 21$, SMD $= -1.77$, 95% CI (-2.52 to -1.03), $P < 0.00001$; heterogeneity: $\chi = 1.61$, df $= 1$ ($P = 0.20$); $I^2 = 38\%$; **Figure 4B**]. In rotarod test, meta-analysis of 9 studies (Im et al., 2005; Li, 2011; Mu et al., 2011; Lee et al., 2014; Xue et al., 2014; Gao et al., 2015; Hu et al., 2016; Kuang et al., 2017; Zhang et al., 2017b) showed significant effect of baicalein for extending the time spent on the rod in PD animals compared with control group [$n = 96$, SMD $= 4.04$, 95% CI (3.50–4.58), $P < 0.00001$; heterogeneity: $\chi = 12.38$, df $= 8$ ($P = 0.14$); $I^2 = 35\%$; **Figure 4C**]. In apomorphine-induced rotations test, meta-analysis of 4 studies (Im et al., 2006; Mu et al., 2009; Li, 2011; He et al., 2015) showed significant effect of baicalein for decreasing in the number of apomorphine-induced rotations in PD animals compared with control group [$n = 42$, SMD $= -1.96$, 95% CI (-2.55 to -1.37), $P < 0.00001$; heterogeneity: $\chi = 21.68$, df $= 3$ ($P < 0.00001$); $I^2 = 86\%$]. Through sensitivity analysis, we removed one study (Im et al., 2006) which utilized ICR mice with PD, while the other studies used models established with SD rats. Meta-analysis of 3 studies (Mu et al., 2009; Li, 2011; He et al., 2015) showed significant effect of baicalein for decreasing in the number of apomorphine-induced rotations in PD animals compared with control group [$n = 34$, SMD $= -1.85$, 95% CI (-2.45 to -1.26), $P < 0.00001$; heterogeneity: $\chi = 2.87$, df $= 2$ ($P = 0.24$); $I^2 = 30\%$; **Figure 4D**]. In grid test, meta-analysis of 2 studies (Hu et al., 2016; Kuang et al., 2017) showed significant effect of baicalein for prolongating the descent latency in PD animals compared with control group [$n = 22$, SMD $= 3.09$, 95% CI (2.16–4.02), $P < 0.00001$; heterogeneity: $\chi = 0.63$, df $= 1$ ($P = 0.43$); $I^2 = 0\%$; **Figure 4E**]. In tremor test, meta-analysis of 2 studies (Mu et al., 2009; Yu et al., 2012) showed significant effect of baicalein for reducing the amplitude in PD animals compared with csontrol group [$n = 24$, SMD $= -7.81$, 95% CI (-9.62 to -6.00), $P < 0.00001$; heterogeneity: $\chi = 0.65$, df $= 1$ ($P = 0.42$); $I^2 = 0\%$; **Figure 4F**]. Meta-analysis of 4 studies (Mu et al., 2009; Li, 2011; Yu et al., 2012; He et al., 2015) showed significant effect of baicalein for reducing the frequency in PD animals compared with control group [$n = 40$, SMD $= -5.96$, 95% CI (-7.11 to -4.82), $P < 0.00001$; heterogeneity: $\chi = 5.22$, df $= 3$ ($P = 0.16$); $I^2 = 43\%$; **Figure 4G**]. These results suggested that baicalein ameliorated behavioral deficits in PD animals.

Neuroprotective Mechanism

The adjustment of neurotransmitters disequilibrium

Compared with control group, meta-analysis of 12 studies (Im et al., 2005, 2006; Cheng et al., 2008; Li, 2011; Mu et al., 2011; Yu et al., 2012; He et al., 2015; Hu et al., 2016; Hung et al., 2016; Kuang et al., 2017; Yang et al., 2018; Zhao et al., 2018) showed baicalein has significant effects on increasing DA [$n = 75$, SMD $= 3.31$, 95% CI (2.71–3.90), $P < 0.00001$; heterogeneity: $\chi = 22.59$, df $= 11$ ($P = 0.02$); $I^2 = 51\%$]. One study (Li, 2011) was removed through sensitivity analysis because baicalin was not administered until 5 weeks after modeling. The remain 11 studies (Im et al., 2005, 2006; Cheng et al., 2008; Mu et al., 2011; Yu et al., 2012; He et al., 2015; Hu et al., 2016; Hung et al., 2016; Kuang et al., 2017; Yang et al., 2018; Zhao et al., 2018) showed significant effects on increasing DA in analysis [$n = 69$, SMD $= 3.66$, 95% CI (3.01–4.32), $P < 0.00001$; heterogeneity: $\chi = 16.30$, df $= 10$ ($P = 0.09$); $I^2 = 39\%$; **Figure 5A**]; Eight studies (Cheng et al., 2008; Li, 2011; Mu et al., 2011; He et al., 2015) for increasing DOPAC [$n = 49$, SMD $= 1.89$, 95% CI (1.34–2.44), $P < 0.00001$; heterogeneity: $\chi = 16.26$, df $= 7$ ($P = 0.02$); $I^2 = 57\%$]. Through sensitivity analysis, we removed one study (Yang et al., 2018) because the PD model was established with oxyphenylalanine which was less commonly available. The remain seven studies (Im et al., 2005, 2006; Cheng et al., 2008; Li, 2011; Mu et al., 2011; He et al., 2015; Hu et al., 2016) showed significant effects on increasing DOPAC in analysis [$n = 41$, SMD $= 1.70$, 95% CI (1.13–2.26), $P < 0.00001$; heterogeneity: $\chi = 6.84$, df $= 6$ ($P = 0.34$); $I^2 = 12\%$; **Figure 5B**]; Meta-analysis of 2 studies (Cheng et al., 2008; Li, 2011) increasing the level of 5-HT [$n = 12$, SMD $= 2.12$, 95% CI (1.02–3.23), $P < 0.00001$; heterogeneity: $\chi = 1.19$, df $= 1$ ($P = 0.28$); $I^2 = 16\%$; **Figure 5C**]; Meta-analysis of 2 studies (Cheng et al., 2008; Li, 2011) increasing the level of 5-HIAA [$n = 12$, SMD $= 1.45$, 95% CI (0.49–2.42), $P < 0.00001$; heterogeneity: $\chi = 1.39$, df $= 1$ ($P = 0.24$); $I^2 = 28\%$; **Figure 5D**]; Meta-analysis of 2 studies (Li, 2011; Yang et al., 2018) showed insignificant effect of baicalein for increasing the level of E in PD animals compared with control group [$n = 14$, SMD $= 0.47$, 95% CI (0.29–1.23), $P < 0.00001$; heterogeneity: $\chi = 0.53$, df $= 1$ ($P = 0.47$); $I^2 = 0\%$; **Figure 5E**]; Meta-analysis of 2 studies (Li, 2011; Yu et al., 2012) increasing the level of GABA [$n = 12$, SMD $= 5.57$, 95% CI (3.44–7.70), $P < 0.00001$; heterogeneity: $\chi = 1.42$, df $= 1$ ($P = 0.23$); $I^2 = 29\%$; **Figure 5F**]; Meta-analysis of 2 studies (Li, 2011; Yu et al., 2012) increasing the level of GLU [$n = 12$, SMD $= -2.47$, 95% CI (-3.67 to -1.27), $P < 0.00001$; heterogeneity: $\chi = 1.68$, df $= 1$ ($P = 0.19$); $I^2 = 41\%$; **Figure 5G**].

The inhibition of oxidative stress

Compared with control group, meta-analysis of two studies (Cheng et al., 2008; Mu et al., 2011) showed baicalein has significant effects on increasing SOD [$n = 12$, SMD $= 3.85$, 95% CI (2.28–5.42), $P < 0.00001$; heterogeneity: $\chi = 0.79$, df $= 1$ ($P = 0.38$); $I^2 = 0\%$; **Figure 6A**]; Meta-analysis of five studies (Im et al., 2005, 2006; Cheng et al., 2008; Mu et al., 2011; Yang et al., 2018) showed baicalein has significant effects on decreasing MDA [$n = 38$, SMD $= -3.62$, 95% CI (-4.55 to -2.68), $P < 0.00001$; heterogeneity: $\chi = 28.91$, df $= 4$ ($P < 0.00001$); $I^2 = 86\%$]; Through sensitivity analysis, we removed one study (Yang et al., 2018) because of the same reason mentioned above. The remain four studies (Im et al., 2005, 2006; Cheng et al., 2008; Mu et al., 2011) showed significant effects on decreasing MDA in analysis [$n = 30$, SMD $= -6.61$, 95% CI (-8.11 to -5.11), $P < 0.00001$; heterogeneity: $\chi = 4.01$, df $= 3$ ($P = 0.26$); $I^2 = 25\%$; **Figure 6B**]; Meta-analysis of three studies (Cheng et al., 2008; Mu et al., 2011; Yang et al., 2018) showed baicalein has significant effects on increasing GSH-Px [$n = 20$, SMD $= 0.54$, 95% CI (-0.34 to 1.42); heterogeneity: $\chi = 25.75$, df $= 2$ ($P < 0.00001$); $I^2 = 92\%$]; We used sensitivity analyses omitting one study at a time. And one study (Yang et al., 2018) was removed because of the same reason mentioned above. The remain two studies (Cheng et al., 2008; Mu et al., 2011) showed significant

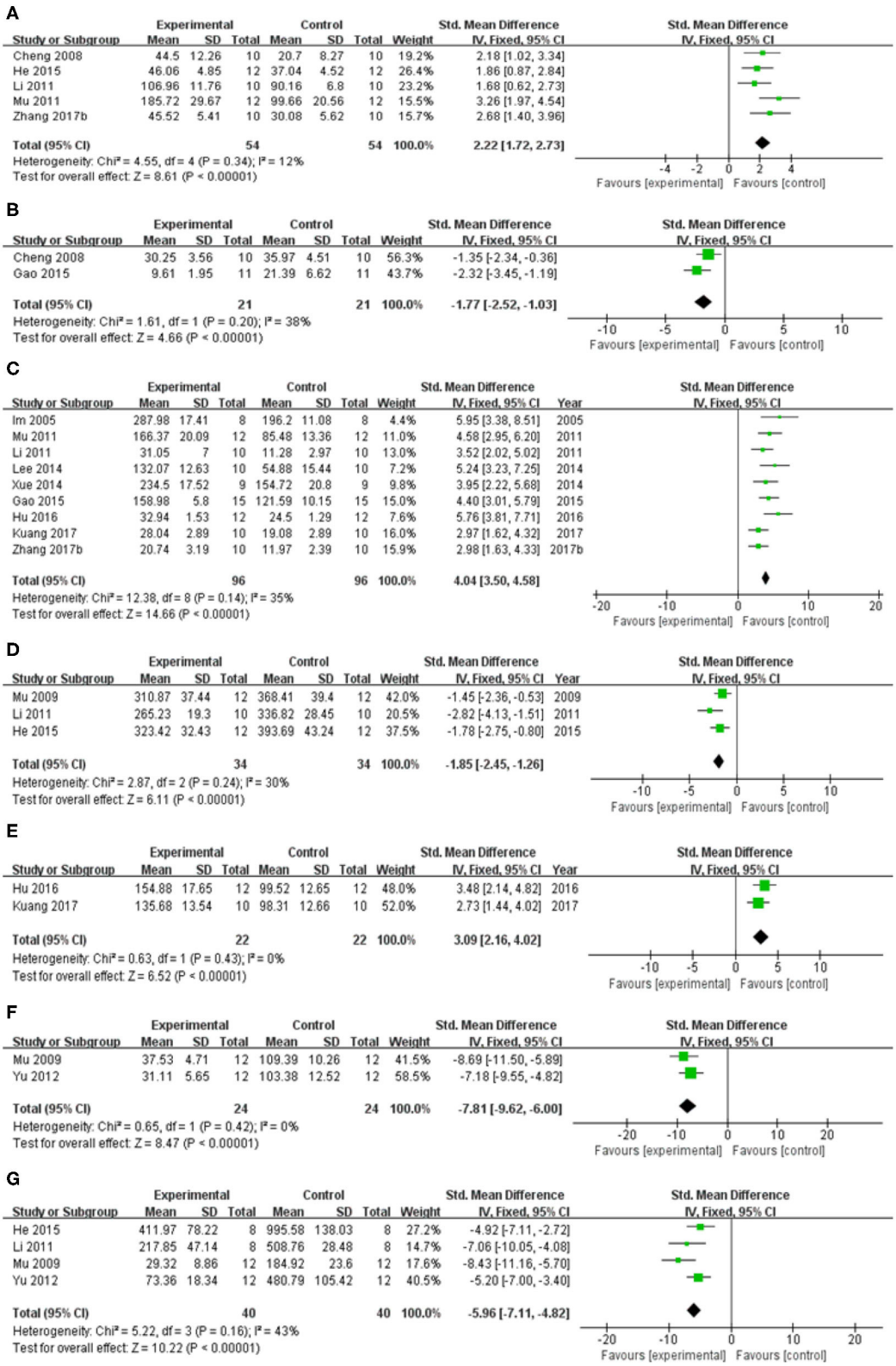

FIGURE 4 | Forest plot of studies investigating the effect of baicalein on animal behavior. **(A)** Spontaneous motor activity test, **(B)** Pole test, **(C)** Rotarod test, **(D)** Apomorphine-induced rotations test, **(E)** Grid test, **(F)** altitude, and **(G)** frequency in tremor test compared with control group.

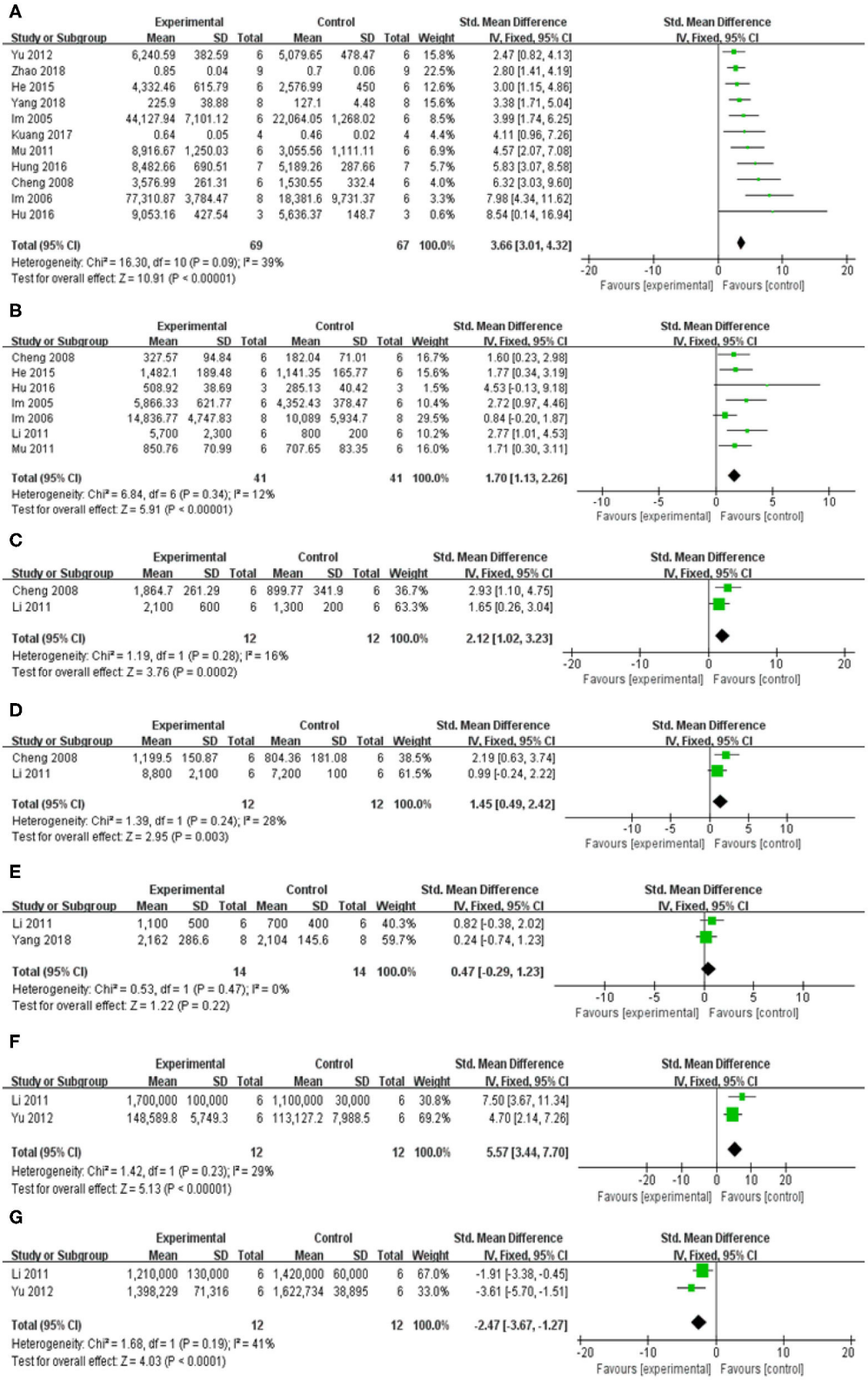

FIGURE 5 | Forest plot of studies investigating the effect of baicalein on neurotransmitters. **(A)** DA, **(B)** DOPAC, **(C)** 5-HT, **(D)** 5-HIAA, **(E)** E, **(F)** GABA, and **(G)** GLU.

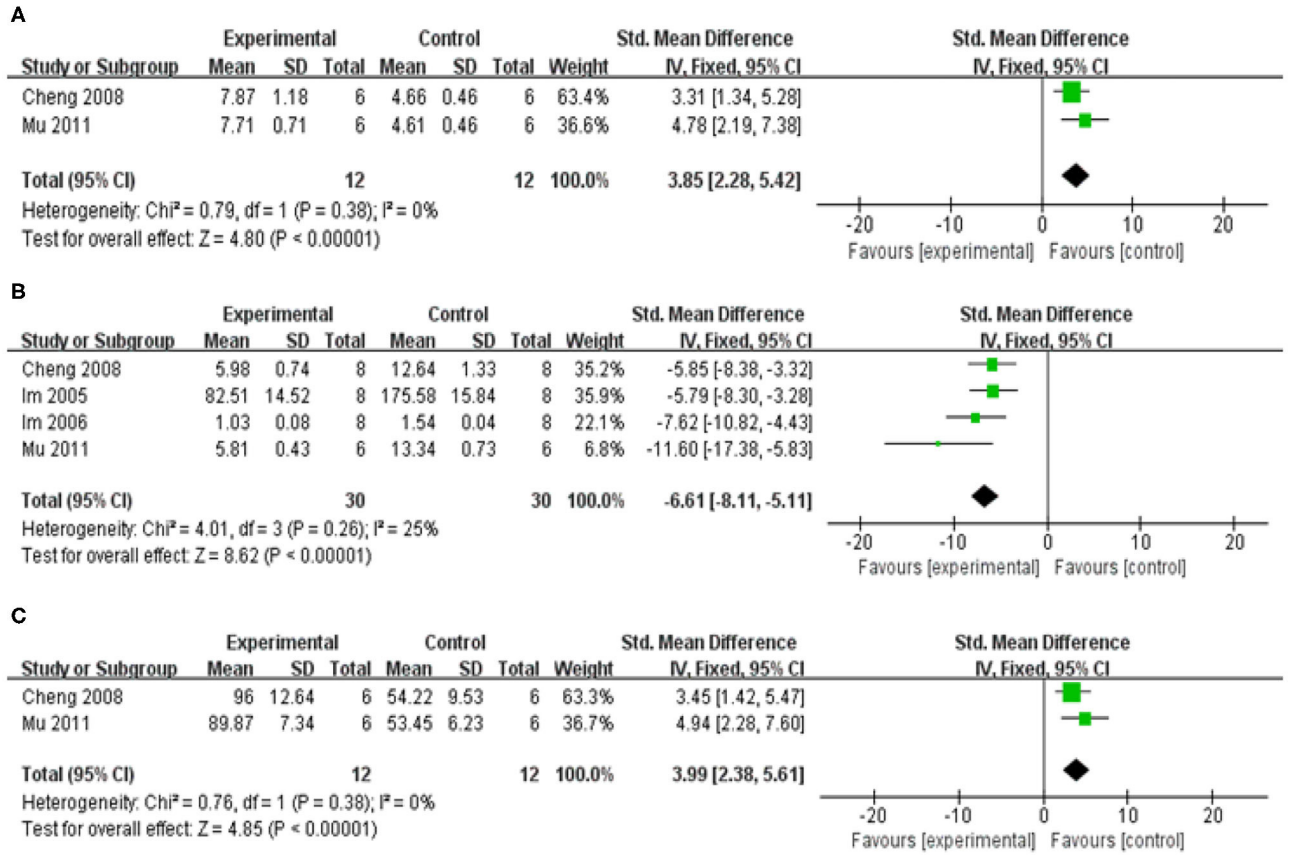

FIGURE 6 | Forest plot of studies investigating the effect of baicalein on the oxidative stress. **(A)** SOD, **(B)** MDA, and **(C)** GSH-Px.

effects on increasing GSH-Px in analysis [$n = 12$, SMD = 3.99, 95% CI (2.38–5.61), $P < 0.00001$; heterogeneity: $\chi = 0.76$, df = 1 ($P = 0.38$); $I^2 = 0\%$; **Figure 6C**].

Regulation of enzyme activity

Meta-analysis of 13 studies (Im et al., 2005, 2006; Cheng et al., 2008; Mu et al., 2009; Mu et al., 2011; Li, 2011; Lee et al., 2014; He et al., 2015; Hu et al., 2016; Hung et al., 2016; Zhang et al., 2017b; Han et al., 2019; Zheng et al., 2019) showed baicalein had significant effect on increasing the level of TH compared with the control group [$n = 63$, SMD: 3.80, 95% CI (2.98–4.62), $P < 0.00001$; heterogeneity: $\chi = 41.40$, df = 12 ($P < 0.00001$); $I^2 = 71\%$]. Owing to the obvious heterogeneity, we conducted a sensitivity analyses and removed two study (Im et al., 2005, 2006) that Parkinson's model of ICR mice was induced with 6-OHDA. Meta-analysis of the remaining 11 studies (Cheng et al., 2008; Mu et al., 2009; Mu et al., 2011; Li, 2011; Lee et al., 2014; He et al., 2015; Hu et al., 2016; Hung et al., 2016; Zhang et al., 2017b; Han et al., 2019; Zheng et al., 2019) showed baicalein had significant effect on increasing the level of TH compared with the control group [$n = 49$, SMD: 3.49, 95% CI (2.66–4.32), $P < 0.00001$; heterogeneity: $\chi = 16.34$, df = 10 ($P = 0.09$), $I^2 = 39\%$; **Figure 7A**]. One study (Yu et al., 2012) demonstrated that baicalein increased the GS activity ($P < 0.05$), while reduced the GABA-T activity ($P < 0.05$) compared with the control group. One study (Yang et al., 2018) increased the AchE activity ($P < 0.05$).

The inhibition of neuroinflammation

Meta-analysis of 4 studies (Xue et al., 2014; Hung et al., 2016; Zhang et al., 2017a; Zhao et al., 2018) indicated baicalein was significant for decreasing the level of Interleukin-1β (IL-1β) compared with control group [$n = 21$, SMD = −2.48, 95% CI (−3.43 to −1.53), $P < 0.00001$; heterogeneity: $\chi = 4.42$, df = 3 ($P = 0.22$); $I^2 = 32\%$; **Figure 7F**]. Meta-analysis of 2 studies (Xue et al., 2014; Zhang et al., 2017a) decreasing expression of tumor necrosis factor (TNF-a) [$n = 13$, SMD = −3.72, 95% CI (−5.16 to −2.28), $P < 0.00001$; heterogeneity: $\chi = 0.10$, df = 1 ($p = 0.75$); $I^2 = 0\%$; **Figure 7G**]. Meta-analysis of 2 studies (Hung et al., 2016; Zhao et al., 2018) showed baicalein was significant for decreasing the level of Cathepsin B [$n = 6$, SMD = −5.08, 95% CI (−8.84 to −1.32), $P = 0.008$; heterogeneity: $\chi = 0.47$, df = 1 ($P = 0.49$); $I^2 = 0\%$; **Figure 7B**], and ED-1 [$n = 6$, SMD = −6.30, 95% CI [−10.75 to −1.85], $P = 0.006$; heterogeneity: $\chi = 0.01$, df = 1 ($P = 0.92$); $I^2 = 0\%$; **Figure 7C**] compared with control group. Meta-analysis of 5 studies (Cheng et al., 2008; Mu et al., 2009; Li, 2011; Zhang et al., 2017a; Zhao et al., 2018) showed baicalein was significant for decreasing the level of GFAP compared with

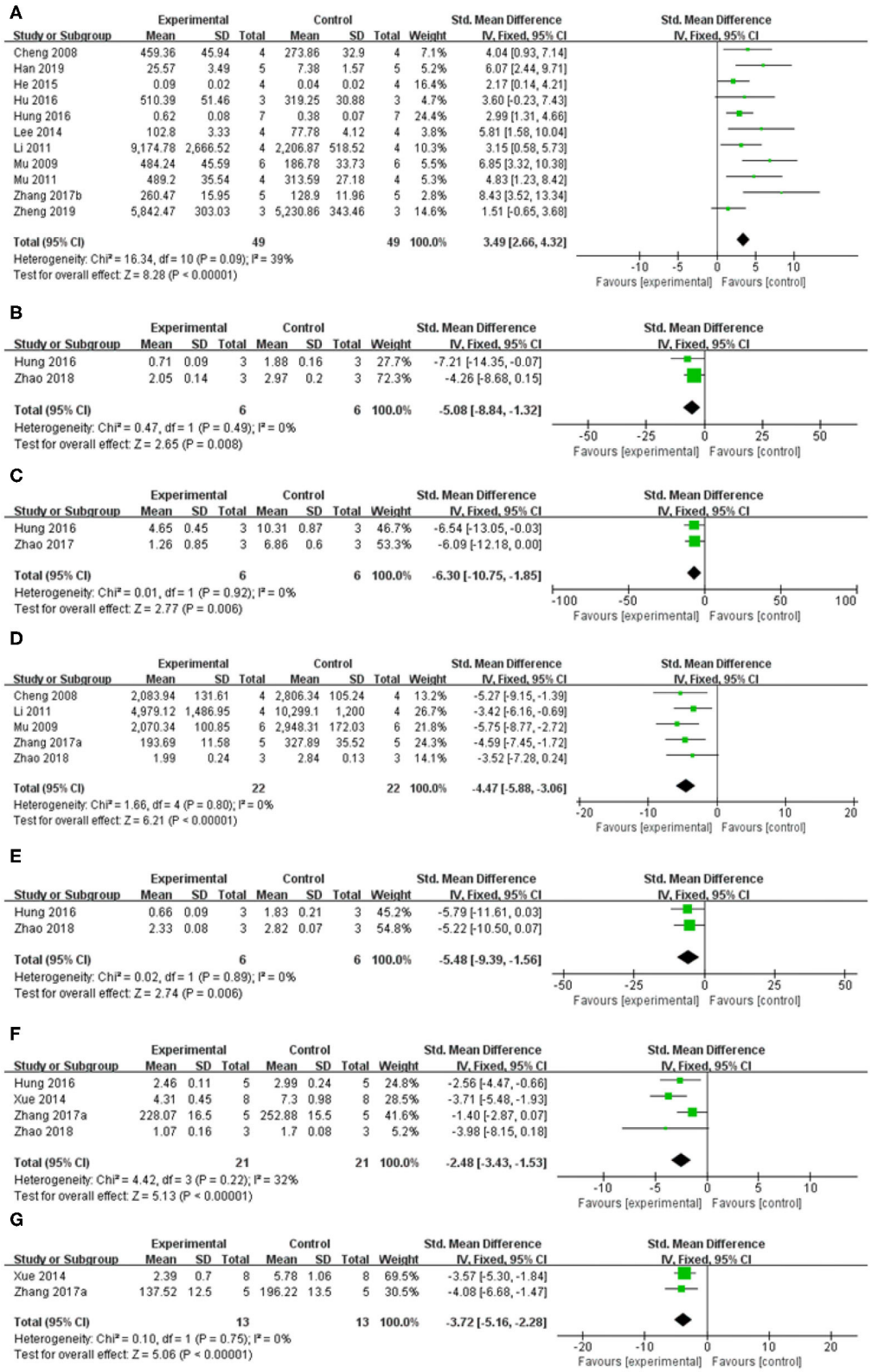

FIGURE 7 | Forest plot: effects of baicalein for the change of **(A)** TH, **(B)** Cathepsin B, **(C)** ED-1, **(D)** GFAP, **(E)** a-Caspase-1, **(F)** IL-1β, and **(G)**TNF-α compared with control group.

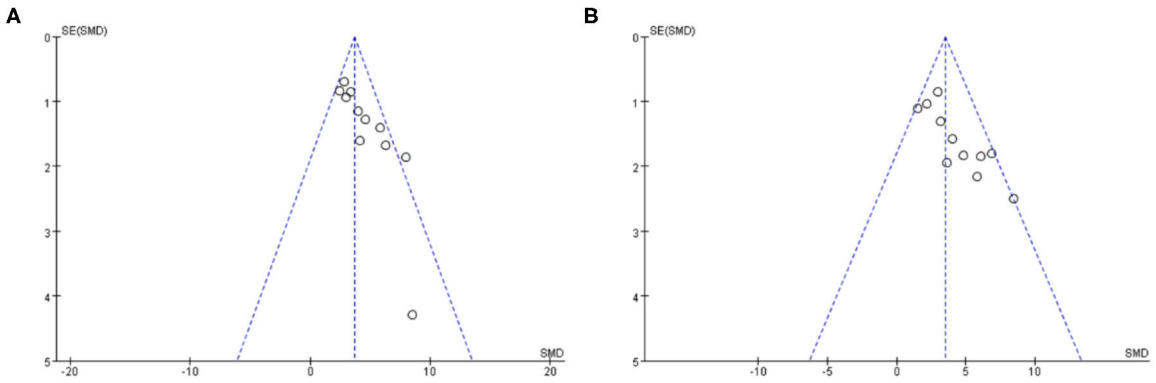

FIGURE 8 | The funnel plot: effects of baicalein for increasing DA **(A)** and TH **(B)**.

control group [$n = 22$, SMD $= -4.47$, 95% CI (-5.88 to -3.06), $P < 0.00001$; heterogeneity: $\chi = 1.66$, df $= 4$ ($p = 0.80$); $I^2 = 0\%$; **Figure 7D**]. Two studies (Zhang et al., 2017a; Zheng et al., 2019) for decreasing expression of IL-6. 1 study (Zhang et al., 2017a) for decreasing expression of p-IkB/IkB, p-p65/p65, p-p38/p38, and p-Erk1/2/Erk1/2 (P <0.05), while increasing expression of p-JNK/JNK ($P < 0.05$).

The inhibition of neuronal apoptosis

Meta-analysis of 2 studies (Hung et al., 2016; Zhao et al., 2018) indicated baicalein was significant for decreasing the expression of a-Caspase 1 compared with control group [$n = 6$, SMD $= -5.48$, 95% CI (-9.39 to -1.56), $P = 0.006$; heterogeneity: $\chi = 0.02$, df $= 1$ ($P = 0.89$); $I^2 = 0\%$; **Figure 7E**]. One study (Hung et al., 2016) for decreasing protein expression of a-Caspase 9 ($P < 0.05$) and a-Caspase 12 ($P < 0.05$). One study (Zhao et al., 2018) for decreasing protein expression of a-Caspase 3 ($P < 0.05$), RIPK-1 ($P < 0.05$), and RIPK-3 ($P < 0.05$). One study (Zheng et al., 2019) for decreasing expression of Bax mRNA (P <0.05).

The restoration of mitochondrial dysfunction

One study (Zhang et al., 2017b) for increasing the protein levels of PGC-1α ($P < 0.05$), NRF-1 ($P < 0.05$), TRAM ($P < 0.05$), and the activity of mitochondrial complex I ($P < 0.05$) and ATP levels ($P < 0.01$) in the ventral midbrain in rotenone-induced PD rats.

The inhibition of abnormal protein aggregation

One study (Hu et al., 2016) showed that baicalein decreased α-Synuclein (α-syn)levels in the ileum and thoracic spinal cord in the rotenone induced PD mouse model.

The prevention of MPP^+-induced autophagy

One study (Hung et al., 2016) showed that baicalein inhibited MPP^+-induced elevation in light chain 3-II (LC3-II) level in the rat nigrostriatal dopaminergic system.

Publication Bias

Funnel plots were reviewed for two outcomes about DA and TH (**Figure 8**). The funnel graph revealed an asymmetry distribution of included studies. The Egger's regression ($p < 0.05$) also confirmed the publication bias due to a small number of studies reporting negative Baicalein treatment effects. Although the Trim and Fill methods were used to correct publication bias, the results did not change.

DISCUSSION

Summary of Results

To our knowledge, this is the first preclinical evidences to determine the effects of baicalein for experimental PD in mice and rats. The findings available from the present study showed that baicalein could improve behavior function in experimental PD, mainly through the mechanisms of adjusting neurotransmitters, regulating enzyme activities, suppressing oxidative stress, ameliorating mitochondrial dysfunction, restraining neuroinflammation, inhibiting abnormal protein aggregation, and neuronal apoptosis.

Limitations

This meta-analysis had several limitations. First, all the databases we searched were in English or Chinese, leading to certain deviations. Second, negative findings are less likely to be published, which may overestimate the true efficacy of baicalein to a certain degree. Third, the methodological quality of included studies was considered moderate, which was an inherent drawback in the primary study. In particular, all the studies failed to mention the allocation concealment, blinding of outcome assessment, etc. Fourth, the high heterogeneity among studies was possibly associated with different conditions including different models of PD induction, different administration route, and different doses of neurotoxins and baicalein. Thus, the results in this study should be partially treated with caution.

Implications for Practice

Currently, the medical animal experiments have become an important means of biomedical research which link basic research and clinical trials. Due to the limitations of medical ethics, some trauma researches, toxicological characteristics, and pharmacodynamics studies are not suitable for human clinical

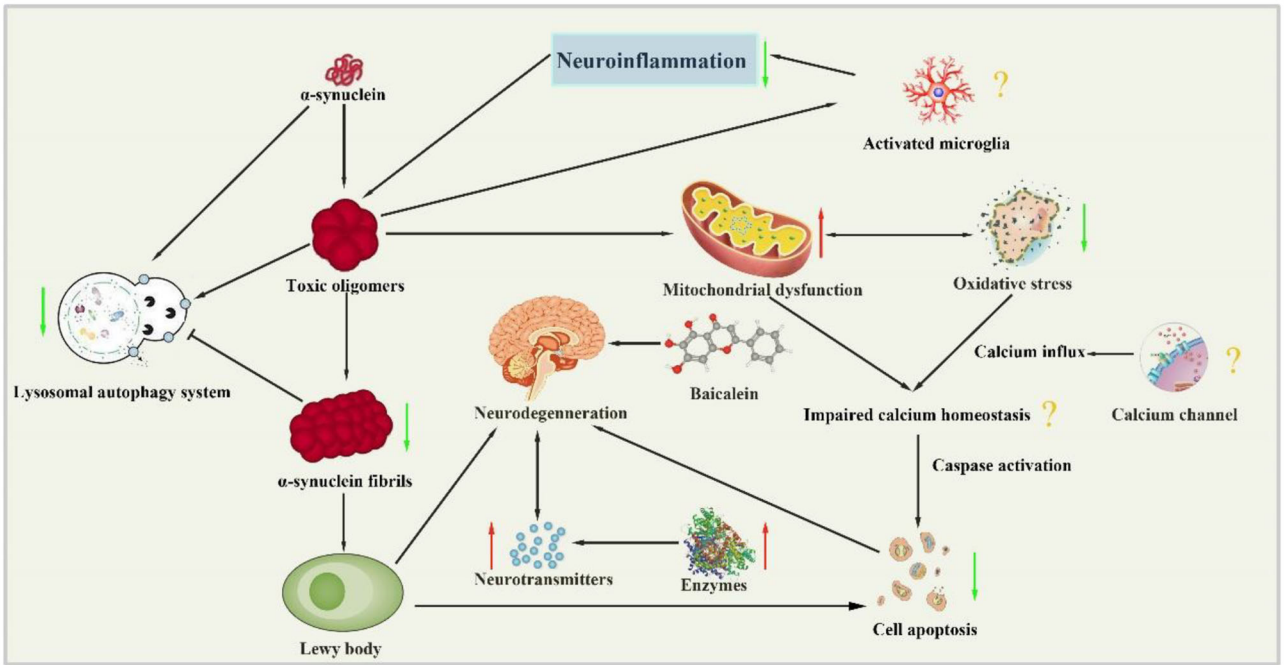

FIGURE 9 | Neuroprotection mechanisms of baicalein in PD animal model. (↑, upregulation; ↓, downregulation; ?, unknown mechanism).

trials. Therefore, animal models capable of replicating important functional, structural, and molecular pathological features of human disease to the maximum extent are essential for clinical translation (Saulnier-Blache et al., 2018).

The present study demonstrated that baicalein had neuroprotective effects in PD models according to the neurobehavioral. The mechanisms of baicalein for PD are summarized as follows: (1) Correction of neurotransmitters: the pathological mechanisms of PD is closely related to the abnormal release of various neurotransmitters in brain, including monoamine neurotransmitters such as DA, DOPAC, NE and 5-HT, amino acid neurotransmitters such as Glu, γ-GABA and ACh, and peptide transmitters etc (Kulikova et al., 2018). In central nervous system, the main form of synaptic transmission is neurochemical transmission. The neurotransmitters released by presynaptic membrane can bind with the corresponding postsynaptic membrane receptors, and result in producing synaptic depolarization potential or hyperpolarization potential, which weaken or enhance excitability of postsynaptic neurons (Ztaoua and Amalric, 2019). Interestingly, the two chemical transmitters, DA and Ach are antagonistic to each other in the corresponding nerve cells. Although the level of Ach is normal in the brain of patients with PD, the decrease of DA content leads to the relative hyperactivity of cholinergic neurons, which causes some symptoms of PD (McKinley et al., 2019). The evidence available from the present study showed that baicalein could effectively rectify the content of monoamine transmitters and amino acid transmitters in animals with PD. (2) Regulation of enzyme activity: as we all know, the secretion of neurotransmitters in brain must be affected by the activity of corresponding enzyme. TH, as the rate-limiting enzyme in the synthesis process of DA, is a specific marker of dopaminergic neurons (Liang et al., 2015). AchE is an essential enzyme for the selective hydrolysis of ACh, which can hydrolyze ACh into choline and acetic acid (Karumuri et al., 2019). GABA and GLu are metabolized by continuous action of GABA transaminase (GABA-T) and glutamine synthetase (GS) protein (Baber and Haghighat, 2010). Our data indicated that baicalein could balance neurotransmitter by regulating the activity of TH, AchE, GABA-T, and GS. (3) Anti-oxidative stress: oxidative stress plays a key role in the occurrence and development of PD. The content of MDA is an important indicator of the level of oxygen free radicals, which can indirectly reflect the degree of cell damage. As the main free radical scavenging enzyme in the body, SOD reflects the endogenous antioxidant capacity of the organism. And GSH-Px is a critical enzyme widely used in the body that can catalyze the decomposition of H_2O_2 (Sharma et al., 2020). Our data demonstrated that baicalein had anti-oxidative stress effects by increasing the activity of antioxidant enzymes in brain tissues, improving the antioxidant capacity, scavenging free radicals, inhibiting lipid peroxidation, and protecting the structural and functional integrity of cell membranes. (4) Anti-inflammation: neuroinflammation is an intricate cascade of neurodegenerative changes in Parkinson's syndrome, including the activation of microglia and astrocytes and the release of inflammatory cytokines. NF-κB is widely expressed in microglia, astrocytes and neurons. In normal state, the endogenous inhibitor IκB inactivate NF-κB, while IL-1β and TNF-α can induce the phosphorylation and degradation of IKK-β, which translocate NF-κB into the nucleus and promote the expression of inflammatory genes (Yan

et al., 2019; Wang et al., 2020). The pooled data showed that treatment of baicalein prominently suppressed the expression of NF-κB, GFAP (a biomarker of activated astrocytes), ED-1 (a biomarker of activated microglia), and mature cathepsin B (a cysteine lysosomal protease) (Zhao et al., 2018). (5) Restoration of mitochondrial dysfunction: mitochondrial dysfunction is an early signal in almost all neurodegenerative diseases, including PD (Angelova et al., 2018). Baicalein greatly increased the expression of the key regulators of mitochondrial biogenesis (PGC-1α, NRF-1, and TFAM). In addition, baicalein could maintain the function of mitochondria by partially enhancing the activity of mitochondrial complex enzyme in brain, and ultimately delay the progression of PD. (6) The inhibition of abnormal protein aggregation: one of the characteristics of pathological changes in PD is the appearance of Lewy bodies which are composed of α-syn (Reuland and Church, 2020). Furthermore, the mutation or overexpression of α-syn gene can accelerate mitochondrial dysfunction, enhance sensitivity to oxidative stress and increase DAT-mediated toxicity, thus promoting cell death (Vekrellis et al., 2011). Our study indicated that baicalein could inhibit the formation of α-syn oligomers and subsequently prevent the progression of α-syn accumulation *in vivo*. (7) Antiapoptosis: Growing evidence suggests that another possibility for dopaminergic neuron loss is the abnormal occurrence of apoptosis (Liu et al., 2019). The caspases are a class of cysteine proteases, many of whose members are involved in apoptosis. Caspases convey the apoptotic signal through proteolytic cascade with caspases cleaving and subsequently activate other caspases that degrade cellular targets leading to cell death. Additionally, Bcl-2 family which is a core member of apoptosis gene families plays a critical role in apoptotic process (Schulz and Gerhardt, 2001). (8) Regulation of autophagy: Autophagy is a lysosome-mediated degradation process that involves degradation of redundant or defective cellular components within the cell, including both misfolded proteins and damaged organelles (Hou et al., 2020). Thus, autophagy activity is correlated with disease progression in neurodegenerative disorders such as AD and PD (Nobuhiro et al., 2018). However, dysregulated or excessive autophagy could cause autophagic cell death, the type II programmed cell death (Thellung et al., 2019). LC3-II is currently considered to be a biomarker of autophagy, which reflect the extent of autophagy (Runwal et al., 2019). Systemic administration of baicalein for 2 days significantly attenuated MPP^+-induced elevation in LC3-II in the infused substantia nigra (Hung et al., 2016). Our study indicates that baicalein prevents programmed cell death, mainly by regulating the expression of genes related to apoptosis and autophagy. To summarize, we present a schematic overview of the neuroprotective mechanisms of baicalein in PD (**Figure 9**).

CONCLUSION

The present study showed baicalein could exert potential neuroprotective effects in experimental PD, largely through mechanisms involving antioxidation, anti-inflammatory, regulating neurotransmitters, adjusting enzyme activity, inhibiting protein aggregation, restorating mitochondrial dysfunction, inhibiting apoptosis, and autophagy. Thus, baicalein could be a candidate for further clinical trials of PD.

AUTHOR CONTRIBUTIONS

YW and XL conceived this review and completed the manuscript. YW, NW, and XL performed the literature searches electronically and manually. All authors contributed to the article and approved the submitted version.

FUNDING

This study was supported by Hainan Provincial Natural Science Foundation of China (819QN230), Scientific Research Support Project of Colleges and Universities in Hainan Province (Hnky2019ZD-24), Research and Cultivation Foundation of Hainan Medical University (HYPY201910), and Heilongjiang Provincial Administration of Traditional Medicine Foundation (ZHY18-019).

REFERENCES

Angelova, P. R., Barilani, M., Lovejoy, C., Dossena, M., Viganò, M., Seresini, A., et al. (2018). Mitochondrial dysfunction in Parkinsonian mesenchymal stem cells impairs differentiation. *Redox. Biol.* 14, 474–484. doi: 10.1016/j.redox.2017.10.016

Baber, Z., and Haghighat, N. (2010). GLU synthetase gene expression and GLU transporters in C6-glioma cells. *Metab. Brain Dis.* 25, 413–418. doi: 10.1007/s11011-010-9223-9

Cheng, Y. X., He, G. R., Mu, X., Zhang, T. T., Li, X. X., Hu, J. J., et al. (2008). Neuroprotective effect of baicalein against MPTP neurotoxicity: behavioral, biochemical and immunohistochemical profile. *Neurosci. Lett.* 441, 16–20. doi: 10.1016/j.neulet.2008.05.116

Gao, L., Li, C., Yang, R. Y., Lian, W. W., Fang, J. S., Pang, X. C., et al. (2015). Ameliorative effects of baicalein in MPTP-induced mouse model of parkinson's disease: a microarray study. *Pharmacol. Biochem. Behav.* 133, 155–163. doi: 10.1016/j.pbb.2015.04.004

Han, F., Wang, J., and Li, Y. L. (2019). Protection of baicalein combined with rifampicin on substantia nigra neurons of rotenone-induced Parkinson's disease in rats. *J. Toxicol.* 33, 27–33. doi: 10.16421/j.cnki.1002-3127.2019.01.005

He, G. R., Mu, X., Li, X. X., Wang, Y. H., Fang, L. H., Sun, L., et al. (2015). Effect of baicalein on brain injury induced by 6-hydroxydopamine at different sites in rats. *Chin. Pharmacol. Bull.* 31, 623–630. doi: 10.3969/j.issn.1001-1978.2015.05.008

Hooijmans, C. R., Rovers, M. M., de Vries, R. B., Leenaars, M., Ritskes-Hoitinga, M., and Langendam, M. W. (2014). SYRCLE's risk of bias tool for animal studies. *BMC. Med. Res. Methodol.* 14:43. doi: 10.1186/1471-2288-14-43

Hou, X., Watzlawik, J. O., Fiesel, F. C., and Springer, W. (2020). Autophagy in Parkinson's Disease. *J. Mol. Biol.* 432, 2651–2672. doi: 10.1016/j.jmb.2020.01.037

Hu, Q., Uversky, V. N., Huang, M. Y., Kang, H. C., Xu, F., Liu, X. Y., et al. (2016). Baicalein inhibits α-synuclein oligomer formation and prevents progression of α-synuclein accumulation in a rotenone mouse model of Parkinson's disease. *Biochim. Biophys. Acta.* 1862, 1883–1890. doi: 10.1016/j.bbadis.2016.07.008

Hung, K. C., Huang, H. J., Wang, Y. T., and Lin, A. M. (2016). Baicalein attenuates α-synuclein aggregation, inflammasome activation and autophagy in the MPP^+-treated nigrostriatal dopaminergic system *in vivo*. *J. Ethnopharmacol.* 194, 522–529. doi: 10.1016/j.jep.2016.10.040

Im, H. I., Joo, W. S., Nam, E., Lee, E. S., Hwang, Y. J., and Kim, Y. S. (2005). Baicalein prevents 6-hydroxydopamine-induced dopaminergic dysfunction and lipid peroxidation in mice. *J. Pharmacol. Sci.* 98, 185–189. doi: 10.1254/jphs.SC0050014

Im, H. I., Nam, E., Lee, E. S., Hwang, Y. J., and Kim, Y. S. (2006). Baicalein protects 6-OHDA-induced neuronal damage by suppressing oxidative stress. *Korean. J. Physiol. Pharmacol.* 10, 309–315.

Karumuri, S. B., Singh, H., Naqvi, S., Mishra, A., and Flora, S. J. S. (2019). Impact of chronic low dose exposure of monocrotophos in rat brain: Oxidative/nitrosative stress, neuronal changes and cholinesterase activity. *Toxicol. Rep.* 6, 1295–1303. doi: 10.1016/j.toxrep.2019.11.005

Kovács, M., Makkos, A., Pintér, D., Juhász, A., Darnai, G., Karádi, K., et al. (2019). Screening for problematic internet use may help identify impulse control disorders in Parkinson's disease, *Behav. Neurol.* 2019:4925015. doi: 10.1155/2019/4925015

Kuang, L. H., Cao, X. B., and Lu, Z. N. (2017). Baicalein protects against rotenone-induced neurotoxicity through induction of autophagy. *Biol. Pharm. Bull.* 40, 1537–1543. doi: 10.1248/bpb.b17-00392

Kulikova, O. I., Berezhnoy, D. S., Stvolinsky, S. L., Lopachev, A. V., Orlova, V. S., Fedorova, T. N., et al. (2018). Neuroprotective effect of the carnosine-α-lipoic acid nanomicellar complex in a model of early-stage Parkinson's disease. *Regul. Toxicol. Pharmacol.* 95, 254–259. doi: 10.1016/j.yrtph.2018.03.025

Lee, E., Park, H. R., Ji, S. T., Lee, Y., and Lee., J. (2014). Baicalein attenuates astroglial activation in the 1-methyl-4-phenyl-1,2,3,4-tetrahydropyridine-induced Parkinson's disease model by downregulating the activations of nuclear factor-κB, ERK, and JNK. *J. Neurosci. Res.* 92, 130–139. doi: 10.1002/jnr.23307

LeWitt, P. A., and Fahn, S. (2016). Levodopa therapy for Parkinson disease: a look backward and forward. *Neurology* 86(14 Suppl. 1), S3–S12. doi: 10.1212/WNL.0000000000002509

Li, X. X. (2011). *Experimental Study of the Therapeutic Effect and Mechanism of Baicalein on Parkinson's Disease*. Bei Jing: Chinese Academy of Medical Sciences & Peking Union Medical College.

Liang, Y. R., Jing, X. N., Zeng, Z. F., Bi, W., Chen, Y., Wu, X., et al. (2015). Rifampicin attenuates rotenone-induced inflammation via suppressing NLRP3 inflammasome activation in microglia. *Brain Res.* 1622, 43–50. doi: 10.1016/j.brainres.2015.06.008

Liu, J. Q., Chu, S. F., Zhou, X., Zhang, D. Y., and Chen, N. H. (2019). Role of chemokines in Parkinson's disease. *Brain Res. Bull.* 152, 11–18. doi: 10.1016/j.brainresbull.2019.05.020

Martin, I., Dawson, V. L., and Dawson, T. M. (2011). Recent advances in the genetics of Parkinson's disease. *Annu. Rev. Genomics Hum. Genet.* 12, 301–325. doi: 10.1146/annurev-genom-082410-101440

McKinley, J. W., Shi, Z. Q., Kawikova, I., Hur, M., Bamford, I. J., Devi, S. P. S., et al. (2019). Dopamine deficiency reduces striatal cholinergic interneuron function in models of Parkinson's disease. *Neuron* 103, 1056–1072. doi: 10.1016/j.neuron.2019.06.013

Moher, D., Shamseer, L., Clarke, M., Ghersi, D., Liberati, A., Petticrew, M., et al. (2015). Preferred reporting items for systematic review and meta-analysis protocols (PRISMA-P) 2015 statement. *Syst. Rev.* 4:1. doi: 10.1186/2046-4053-4-1

Mu, X., He, G.R., Yuan, X., Li, X.X., and Du, G.H. (2011). Baicalein protects the brain against neuron impairments induced by MPTP in C57BL/6 mice. *Pharmacol. Biochem. Behav.* 98, 286–291. doi: 10.1016/j.pbb.2011.01.011

Mu, X., He, G. R., Cheng, Y. X., Li, X. X., Xu, B., and Du, G. H. (2009). Baicalein exerts neuroprotective effects in 6-hydroxydopamine-induced experimental parkinsonism *in vivo* and *in vitro*. *Pharmacol. Biochem. Behav.* 92, 642–648. doi: 10.1016/j.pbb.2009.03.008

Naskar, A., Manivasagam, T., Chakraborty, J., Singh, R., Thomas, B., Dhanasekaran, M., et al. (2013). Melatonin synergizes with low doses of L-DOPA to improve dendritic spine density in the mouse striatum in experimental parkinsonism. *J. Pineal. Res.* 55, 304–312. doi: 10.1111/jpi.12076

Nobuhiro, F., Minkyoung, S., and Shigeomi, S. (2018). Association between autophagy and neurodegenerative diseases. *Front. Neurosci.* 12:255. doi: 10.3389/fnins.2018.00255

Reuland, C. J., and Church, F. C. (2020). Synergy between plasminogen activator inhibitor-1, α-synuclein, and neuroinflammation in Parkinson's disease. *Med. Hypotheses.* 138:109602. doi: 10.1016/j.mehy.2020.109602

Runwal, G., Stamatakou, E., Siddiqi, F. H., Puri, C., Zhu, Y., and Rubinsztein, D. C. (2019). LC3-positive structures are prominent in autophagy-deficient cells. *Sci Rep.* 9:10147. doi: 10.1038/s41598-019-46657-z

Saulnier-Blache, J. S., Rory, W., Kristaps, K., Delyth, G., Ioana, A., Kastenmüller, G., et al. (2018). Ldlr-/- and ApoE-/- mice better mimic the human metabolite signature of increased carotid intima media thickness compared to other animal models of cardiovascular disease. *Atherosclerosis.* 276, 140–147. doi: 10.1016/j.atherosclerosis.2018.07.024

Schapira, A. H. V., Chaudhuri, K. R., and Jenner, P. (2017). Non-motor features of Parkinson disease. *Nat. Rev. Neurosci.* 18:509. doi: 10.1038/nrn.2017.91

Schindlbeck, K. A., and Eidelberg, D. (2018). Network imaging biomarkers: insights and clinical applications in parkinson's disease. *Lancet. Neurol.* 17, 629–640. doi: 10.1016/S1474-4422(18)30169-8

Schulz, J. B., and Gerhardt, E. (2001). Apoptosis: its relevance to Parkinson's disease. *Clin. Neurosci. Res.* 1, 427–433. doi: 10.1016/S1566-2772(01)00021-4

Sena, E. S., Currie, G. L., McCann, S. K., Macleod, M. R., and Howells, D. W. (2014). Systematic reviews and meta-analysis of preclinical studies: why perform them and how to appraise them critically. *J. Cereb. Blood Flow Metab.* 34, 737–742. doi: 10.1038/jcbfm.2014.28

Sharma, S., Rabbani, S. A., Narang, J. K., Pottoo, F. H., Ali, J., Kumar, S., et al. (2020). Role of rutin nanoemulsion in ameliorating oxidative stress: pharmacokinetic and pharmacodynamics studies. *Chem. Phys. Lipids.* 228:104890. doi: 10.1016/j.chemphyslip.2020.104890

Sowndhararajan, K., Deepa, P., Kim, M., Park, S. J., and Kim, S. (2017). Baicalein as a potent neuroprotective agent: a review, *Biomed Pharmacother.* 95, 1021–1032. doi: 10.1016/j.biopha.2017.08.135

Thellung, S., Corsaro, A., Nizzari, M., Barbieri, F., and Florio, T. (2019). Autophagy activator drugs: a new opportunity in neuroprotection from misfolded protein toxicity. *Int. J. Mol. Sci.* 20:901. doi: 10.3390/ijms20040901

Vekrellis, K., Xilouri, M., Emmanouilidou, E., Rideout, H. J., and Stefanis, L. (2011). Pathological roles of α-synuclein in neurological disorders. *Lancet Neurol.* 10, 1015–1025. doi: 10.1016/S1474-4422(11)70213-7

Wang, H., Naghavi, M., Allen, C., Barber, R. M., Bhutta, Z. A., Carter, A., et al. (2016). Global, regional, and national life expectancy, all-cause mortality, and cause specific mortality for 249 causes of death, 1980-2015: a systematic analysis for the global burden of disease study. *Lancet* 388, 1459–1544. doi: 10.1016/S0140-6736(16)31012-1

Wang, Z. S., Dong, H. T., Wang, J. H., Huang, Y. L., Zhang, X. S., Tang, Y. L., et al. (2020). Pro-survival and anti-inflammatory roles of NF-κB c-Rel in the Parkinson's disease models. *Redox. Biol.* 30:101427. doi: 10.1016/j.redox.2020.101427

Xue, X. H., Liu, H., Qi, L. F., Li, X. L., Guo, C. J., Gong, D. R., et al. (2014). Baicalein ameliorated the upregulation of striatal glutamatergic transmission in the mice model of Parkinson's disease. *Brain Res. Bull.* 103, 54–59. doi: 10.1016/j.brainresbull.2014.02.004

Yan, T. X., Sun, Y. Y., Gong, G. W., Li, Y., Fan, K. Y., Wu, B., et al. (2019). The neuroprotective effect of schisandrol A on 6-OHDA-induced PD mice may be related to PI3K/AKT and IKK/IκBα/NF-κB pathway. *Exp. Gerontol.* 128:110743. doi: 10.1016/j.exger.2019.110743

Yang, Y. L., Zhang, X., Zhang, W., Wang, H. G., Zhao, X. Y., Song, J. K., et al. (2018). Inhibitory effect of baicalein on mice tremor induced by oxotremorine and mechanisms. *Chinese J. New Drugs* 27, 914–920.

Yu, X., He, G. R., Sun, L., Lan, X., Shi, L. L., Xuan, Z. H., et al. (2012). Assessment of the treatment effect of baicalein on a model of parkinsonian tremor and elucidation of the mechanism. *Life Sci.* 91, 5–13. doi: 10.1016/j.lfs.2012.05.005

Zhang, X., Du, L. D., Zhang, W., Yang, Y. L., Zhou, Q. M., and Du, G. H. (2017a). Therapeutic effects of baicalein on rotenone-induced Parkinson's

disease through protecting mitochondrial function and biogenesis. *Sci Rep*. 7:9968. doi: 10.1038/s41598-017-07442-y

Zhang, X., Yang, Y. L., Du, L. D., Zhang, W., and Du, G. H. (2017b). Baicalein exerts anti-neuroinflammatory effects to protect against rotenone induced brain injury in rats. *Int. Immunopharmacol*. 50, 38–47. doi: 10.1016/j.intimp.2017.06.007

Zhao, W. Z., Wang, H. T., Huang, H. J., Lo, Y. L., and Lin, M. Y. (2018). Neuroprotective effects of baicalein on acrolein-induced neurotoxicity in the nigrostriatal dopaminergic system of rat brain. *Mol. Neurobiol*. 55, 130–137. doi: 10.1007/s12035-017-0725-x

Zheng, Z. V., Cheung, C. Y., Lyu, H., Chan, H. Y., Li, Y., Bian, Z. X., et al. (2019). Baicalein enhances the effect of low dose Levodopa on the gait deficits and protects dopaminergic neurons in experimental Parkinsonism. *J. Clin. Neurosci*. 64, 242–251. doi: 10.1016/j.jocn.2019.02.005

Ztaoua, S., and Amalric, M. (2019). Contribution of cholinergic interneurons to striatal pathophysiology in Parkinson's disease. *Neurochem. Int*. 126, 1–10. doi: 10.1016/j.neuint.2019.02.019

Conflict of Interest: The authors declare that the research was conducted in the absence of any commercial or financial relationships that could be construed as a potential conflict of interest.

frontiers in Neuroscience

PERSPECTIVE
published: 29 September 2020
doi: 10.3389/fnins.2020.558967

Perspective: Phase Amplitude Coupling–Based Phase–Dependent Neuromodulation in Parkinson's Disease

Brian Y. Hwang[1]†, Yousef Salimpour[1†], Yohannes K. Tsehay[1], William S. Anderson[1] and Kelly A. Mills[2]*

[1] Functional Neurosurgery Laboratory, Division of Functional Neurosurgery, Department of Neurosurgery, Johns Hopkins School of Medicine, Baltimore, MD, United States, [2] Neuromodulation and Advanced Therapies Clinic, Department of Neurology, Johns Hopkins School of Medicine, Baltimore, MD, United States

OPEN ACCESS

Edited by:
Jiehui Jiang,
Shanghai University, China

Reviewed by:
Leonid L. Rubchinsky,
Indiana University, Purdue University Indianapolis, United States
Jingjie Ge,
Huashan Hospital, Fudan University, China
Andrew Sharott,
University of Oxford, United Kingdom

***Correspondence:**
Brian Y. Hwang
bhwang8@jhmi.edu

† These authors have contributed equally to this work

Specialty section:
This article was submitted to Neurodegeneration, a section of the journal Frontiers in Neuroscience

Received: 04 May 2020
Accepted: 13 August 2020
Published: 29 September 2020

Citation:
Hwang BY, Salimpour Y, Tsehay YK, Anderson WS and Mills KA (2020) Perspective: Phase Amplitude Coupling–Based Phase–Dependent Neuromodulation in Parkinson's Disease. Front. Neurosci. 14:558967. doi: 10.3389/fnins.2020.558967

Deep brain stimulation (DBS) is an effective surgical therapy for Parkinson's disease (PD). However, limitations of the DBS systems have led to great interest in adaptive neuromodulation systems that can dynamically adjust stimulation parameters to meet concurrent therapeutic demand. Constant high-frequency motor cortex stimulation has not been remarkably efficacious, which has led to greater focus on modulation of subcortical targets. Understanding of the importance of timing in both cortical and subcortical stimulation has generated an interest in developing more refined, parsimonious stimulation techniques based on critical oscillatory activities of the brain. Concurrently, much effort has been put into identifying biomarkers of both parkinsonian and physiological patterns of neuronal activities to drive next generation of adaptive brain stimulation systems. One such biomarker is beta-gamma phase amplitude coupling (PAC) that is detected in the motor cortex. PAC is strongly correlated with parkinsonian specific motor signs and symptoms and respond to therapies in a dose-dependent manner. PAC may represent the overall state of the parkinsonian motor network and have less instantaneously dynamic fluctuation during movement. These findings raise the possibility of novel neuromodulation paradigms that are potentially less invasiveness than DBS. Successful application of PAC in neuromodulation may necessitate phase-dependent stimulation technique, which aims to deliver precisely timed stimulation pulses to a specific phase to predictably modulate to selectively modulate pathological network activities and behavior in real time. Overcoming current technical challenges can lead to deeper understanding of the parkinsonian pathophysiology and development of novel neuromodulatory therapies with potentially less side-effects and higher therapeutic efficacy.

Keywords: Parkinson's disease, cortical stimulation, motor cortex, phase-dependent stimulation, phase-amplitude coupling, neuromodulation

INTRODUCTION

In Parkinson's Disease (PD), loss of dopaminergic input into the posterior striatum leads to disordered signaling throughout the basal ganglia-thalamo-cortical (BGTC) network that manifests itself as motor symptoms of bradykinesia, rigidity, and tremor (Hammond et al., 2007). Network-wide synchronized pathological neuronal activity is thought to cause dysfunction at the major nodes of the BGTC network (Bergman et al., 1994; Brown et al., 2001; Bevan, 2002; Hammond et al., 2007). Deep brain stimulation (DBS) is an effective surgical therapy for PD that targets the deep nodes of the BGTC network to ameliorate the pathological neuronal activities. However, current DBS therapies are limited by stimulation induced side-effects and mal-adaptive neuroplasticity from continuous electrical stimulation of the BGTC network at the major nodes (Chen et al., 2006; Tripoliti et al., 2011; Castrioto et al., 2014). Therefore, there has been a significant interest in identifying both parkinsonian and physiologically patterns of neuronal activities that can be used to adjust stimulation parameters in real-time to meet the concurrent therapeutic demand. This closed-loop or adaptive neuromodulation strategy has the potential to significantly improve upon the currently available open-loop DBS systems (Little et al., 2013; Rosa et al., 2015; Little et al., 2016a,b; Piña-Fuentes et al., 2017; Rosa et al., 2017).

Recently, beta-gamma phase-amplitude coupling (PAC) has been identified as a highly promising electrophysiologic biomarker of parkinsonian motor state that can be detected in the superficial node (i.e., the motor cortex) of the BGTC network (de Hemptinne et al., 2013, 2015; Shimamoto et al., 2013; Swann et al., 2015). Unlike the beta activities that represent local information processing, PAC is a type of cross-frequency coupling phenomenon that represents information transmission across multiple cortical and subcortical areas that are involved in both pathologic and normal brain activities such as cognition, perception, and movement (Shimamoto et al., 2013). Excessive PAC is associated with the parkinsonian motor state and can be normalized by both therapeutic dopaminergic medication and DBS therapy in a dose-dependent manner (de Hemptinne et al., 2015; Swann et al., 2015; Wang et al., 2018). These remarkable findings raise the possibility that PAC can serve both as a biomarker to drive adaptive neuromodulation of the deep nodes and as a therapeutic target in an adaptive cortical neuromodulation scheme.

In this article, we review recent evidence regarding PAC in the context of PD and present our perspective on how this biomarker could be leveraged to advance neuromodulation therapies, with an emphasis on utilizing phase-dependent stimulation techniques to target new structures with a lower risk of side-effects.

Pathological Cortical Electrophysiology in Parkinson's Disease

Neural oscillations are essential for normal brain processing and are thought to play a critical role in coordinating activities within and across different regions of the brain (Canolty and Knight, 2010; Hyafil et al., 2015; Salimpour and Anderson, 2019). As representations of rhythmic changes in neuronal excitability, oscillations exist in different frequencies across various spatiotemporal scales and have been implicated in attention, cognition, memory, and sensory integration (Gelperin, 2006; Wang, 2010; Watanabe and Hirono, 2016). These synchronous activities are thought to result from simultaneous input from common presynaptic neurons in a tightly regulated manner with each pattern reflecting the timing of separate information processing and integration (Heck et al., 2007). Because of their fundamental importance to the functioning of the brain, unsurprisingly, disturbances in the synchronous patterns have been implicated in various common neurological disorders (Allen et al., 2011; Goutagny et al., 2013; Bahramisharif et al., 2016; Zhang et al., 2017). In PD, a low dopaminergic state classically manifests itself as excessive beta-band power and synchrony throughout the BGTC network (Schnitzler and Gross, 2005; Hammond et al., 2007). However, the electro-pathophysiology of PD is more complicated and may involve multiple functional modes in which there is excessive synchrony both with and between nodes of the BGTC network that are both associated with the severity of certain parkinsonian signs and symptoms (Ahn et al., 2015). This complexity may have resulted from complex interactions that are constantly occurring between neural oscillations across neural circuits and networks.

Indeed, neural oscillations possess unique coupling properties, such as cross-frequency coupling (CFC), in which components of the rhythmic patterns, such as amplitude, phase, and frequency, interact between different frequency bands within and across circuits and networks (Canolty and Knight, 2010). The exact origin of CFC is yet to be elucidated, but transient, mechanistic coupling (i.e., synaptic, electrical) between functionally distinct neuronal subpopulations has been suggested as a potential mechanism (Canolty and Knight, 2010; Salimpour and Anderson, 2019). Phase-amplitude coupling (PAC) is a class of CFC, and it involves coupling between phases of a low-frequency oscillation and the amplitude of a high-frequency oscillation. Low-frequency phases are often dynamically entrained by behaviorally relevant external sensorimotor events and internal cognitive processing implicated in learning, memory, motivation, and decision making (Lakatos et al., 2008; Schroeder and Lakatos, 2009). Therefore, PAC, which represents the modulation of high-frequency power by a low-frequency phase entrained and coordinated with slower external and internal events, is considered a key fundamental mechanism behind cognitive processing (Canolty and Knight, 2010). PAC is generally detected and quantified by first recording raw electrocorticography (ECoG) data from the cortical surface using a subdural electrode, processing the data to estimate the instantaneous power of each frequency band, then calculating the degree of amplitude modulation a by phase measured in modulation index (Tort et al., 2010; Madhavan et al., 2015).

Phase amplitude coupling has been studied in both animals and humans and has been observed across multiple cortical and subcortical sites (Canolty and Knight, 2010; Miller et al., 2012; de Hemptinne et al., 2013, 2015). Implicated in PD is beta-phase and gamma-amplitude coupling in the motor cortex, also

known as "beta-gamma PAC." PAC occurs when the low beta-frequency rhythm synchronizes with the amplitude of gamma oscillations (Miller et al., 2012; Yanagisawa et al., 2012). PAC level in the motor cortex normally fluctuates throughout the movement cycle, such that it elevates in the rest state and decreases in both planning and execution phases of movement (Miller et al., 2012; de Hemptinne et al., 2015). Exaggerated PAC levels are consistently detected in the motor cortex of PD patients both at rest and during movement (de Hemptinne et al., 2013, 2015; Kondylis et al., 2016; Malekmohammadi et al., 2018). Abnormal PAC levels in PD are thought to interfere with the innate CFC processes required for the coordination of action preparation, execution, and alert-rest phases of movement. Importantly, PAC levels increase proportionally to the severity of PD-specific motor symptoms, and therapeutic DBS and medical treatments normalize the PAC levels (de Hemptinne et al., 2015; Swann et al., 2015).

Cortical Phase-Amplitude Coupling-Based Neuromodulation

At least two potential novel neuromodulation strategies powered by PAC are possible; surface-sensing deep stimulation, in which PAC drives adaptive neuromodulation of the deep nodes and surface-sensing surface stimulation, in which PAC serves as both the feedback and feedforward control signals in an adaptive cortical neuromodulation scheme (**Figure 1**). Surface-sensing deep stimulation is a viable strategy that has been attempted with other electrophysiological biomarkers. For example, the cortical gamma-frequency level, which is associated with the severity of dyskinesia, has been successfully used to drive a totally implantable adaptive DBS in PD patients. By means of a subdural cortical lead for sensing, narrow-band gamma power (60–80 Hz) in the motor cortex was used to adjust stimulation amplitudes applied to the subthalamic nucleus (STN) based on patient-specific thresholds (i.e., high and low). The authors demonstrated significantly reduced energy use without worsening clinical symptoms compared to the conventional STN DBS system (Swann et al., 2018). More importantly, they presented a practical and systematic approach to implementing a cortical electrophysiological biomarker to develop a fully implantable adaptive DBS system that future studies could consider. The study also underscored several key advantages of the surface-sensing deep stimulation strategy compared with adaptive DBS systems that sense and stimulate the deep nodes using the same electrodes: (1) good signal-to-noise ratio with minimal stimulation-induced artifact; (2) high fidelity electrophysiological data from subdural electrodes that can yield better quality and quantity of sensory feed forward data than DBS electrodes can; and (3) spatially independent sensing and stimulating elements that minimize inference and optimize placement.

As a cortical biomarker, PAC may also enable the surface-sensing surface-stimulation strategy. The goal of this PAC-based neuromodulation program would be to achieve and maintain a spatiotemporally 'eu-PAC state' in the motor cortex and to ameliorate parkinsonian motor symptoms. To develop clinically useful PAC-based neuromodulation strategies, first, a method to detect and modulate PAC level in real time is necessary; and second, pathological and normal (i.e., physiologically and therapeutically) PAC levels and patterns must be defined on a patient-specific basis. The remainder of the article will focus on the PAC-based surface-sensing surface-stimulation strategy, which entails key future challenges in the field of neuromodulation.

Motor Cortex Stimulation and Phase-Dependent Neuromodulation

As one of the major nodes and an output hub of the BGTC network, the motor cortex may be a high-yield target for neuromodulation. The motor cortex is relatively easy to access, localize, and map compared with the deeper nodes. Its larger size allows precise targeting of symptomatic body regions or movements. Also, concern for uncontrolled current spread to adjacent disparate neuronal populations and fiber tracts is significantly lower compared with the subcortical structures (Maks et al., 2009). Therefore, the motor cortex presents an opportunity for safer and more effective surgical neuromodulation compared to DBS. Nevertheless, motor cortex stimulation has largely been overlooked in neuromodulation research and therapeutics development in PD because of equivocal outcomes associated with cortical stimulation in PD (Canavero et al., 2002; Cilia et al., 2007; Strafella et al., 2007; Moro et al., 2011; De Rose et al., 2012). The unimpressive and variable results of motor cortex stimulation could be related to failing to account for electrophysiologic biomarkers. In all previous cortical stimulation studies in PD, electrical stimulation was delivered to the motor cortex without accounting for the underlying rhythmic activities and state of the BGTC network. A phase-independent approach has a high probability of yielding unpredictable and variable clinical results because the same stimulation pulse applied to the cortex can have a variable effect on PAC levels depending on which part of the beta phase it lands on (Anderson et al., 2009; Cagnan et al., 2013, 2017; Azodi-Avval and Gharabaghi, 2015). Based on network modeling studies, motor cortex neuromodulation should be done adaptively and may need to be based on phase-locked or phase-dependent stimulation techniques to be successful (Anderson et al., 2009; Azodi-Avval and Gharabaghi, 2015).

Phase-dependent stimulation (PDS) is a novel neuromodulation technique with a simple goal: to detect rhythmic brain activity and deliver precisely timed electrical stimulation pulses at a specific phase (Chen et al., 2011; Cagnan et al., 2013; Zrenner et al., 2018; Holt et al., 2019). The potential value of PDS is that, unlike medications or continuous electrical stimulation, it can selectively modulate pathological electrophysiological activities in the disease network without disrupting other physiological processes. The precise and selective nature of PDS may lead to improved symptom control without the stimulation-induced side-effects or maladaptive plasticity associated with continuous stimulation. PDS is relevant to PAC-based surface-sensing surface-stimulation strategy in PD because the technique could deliver the spatiotemporal

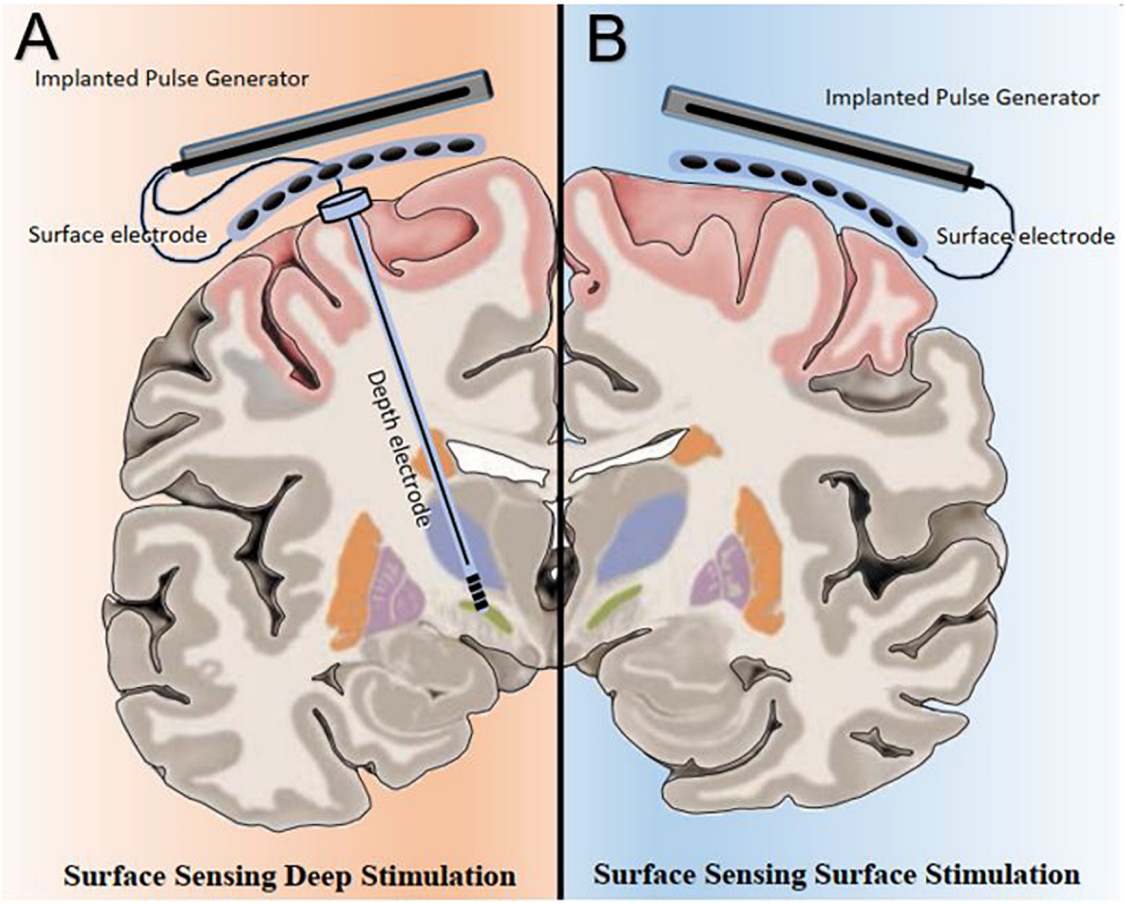

FIGURE 1 | Bata gamma phase amplitude coupling (PAC) levels and patterns measured over the surface of the motor cortex can be utilized in two potential adaptive neuromodulatory strategies. **(A)** In the surface sensing-deep stimulation paradigm, cortical PAC serves as control input to adjust stimulation at the subcortical targets, such as the subthalamic nucleus. **(B)** Under the surface sensing surface stimulation scheme, cortical PAC serves as both feedback and feedforward control signals to drive adaptive motor cortex neuromodulation.

accuracy and precision required to successfully modulate PAC levels in the motor cortex to meet the therapeutic demand in real time. PDS has been used in healthy animals to selectively and predictably modulate cortical oscillations (Zanos et al., 2018; Kanta et al., 2019; Peles et al., 2020). Zanos et al. demonstrated in non-human primates (NPH) that stimulation triggered from beta oscillations in the sensorimotor cortex not only induces synaptic plasticity, but the direction of the plasticity depends on the stimulated phase of the oscillations. Furthermore, a recent study developed an adaptive neuromodulation system based on a real-time cortical PDS algorithm to show that beta oscillations in the primary motor cortex can be controlled with volition and that PDS can differentially modulate the rhythmic patterns depending on the targeted phase of beta, which in turn, affects behavior (Peles et al., 2020). Similarly, another group used a rat model to adaptively modulate gamma oscillations in the amygdala and successfully affected memory strength (Kanta et al., 2019). The ability of real-time closed-loop PDS to predictably modulate beta oscillations in the subcortical regions in a bidirectional manner has been demonstrated in parkinsonian NPH (Sanabria et al., 2020, Preprint) and rat models (McNamara et al., 2020, Preprint).

Phase-dependent stimulation has also recently been used to selectively suppress pathological synchronized pattern of neuronal firing in the STN of PD patients (Holt et al., 2019). The authors demonstrated that PDS achieved beta suppression without altering the overall firing rate, and the degree of suppression correlated with the number of consecutive single-pulse PDS applied at or near the peak of the beta phase, suggesting that the observed neuromodulatory effect was likely from the PDS-induced alteration in the relative timing of beta activity (Holt et al., 2019). Thus, it is increasingly becoming evident that random or continuous stimulation of cortical and subcortical nodes of the parkinsonian motor network is suboptimal. However, continuous and random stimulation remains the predominant method in research. Future studies should strongly consider the implications of pathological oscillatory patterns in Parkinson's disease and incorporate PDS as a foundation for neuromodulation.

With regard to PDS in the motor cortex, it is possible to detect ECoG signals in real time and deliver timed electrical pulses to the cortical region of interest with low latency through fast estimation of phase and frequency of detected oscillations (Chen et al., 2011, 2013; **Figure 2A**). PAC based neuromodulation techniques can be accomplished through Hilbert transformation-based frequency band optimization, autoregressive (AR) spectral estimation and signal prediction. With this algorithm, it may be possible to detect and modulate PAC in near real-time by targeting specific beta phases (**Figure 2B**). The AR signal modeling-based approach is robust against signal variabilities and inconsistencies (Chen et al., 2011, 2013). Using this algorithm, we consistently observed acceptable performance in modulating cortical PAC with cortical stimulation in a Parkinson's patient undergoing awake DBS surgery (Salimpour and Anderson, 2019).

Several critical issues must be considered with regards to a PAC-based PDS protocol. First, evaluation of PAC requires the accumulation of data over several rhythmic cycles, which

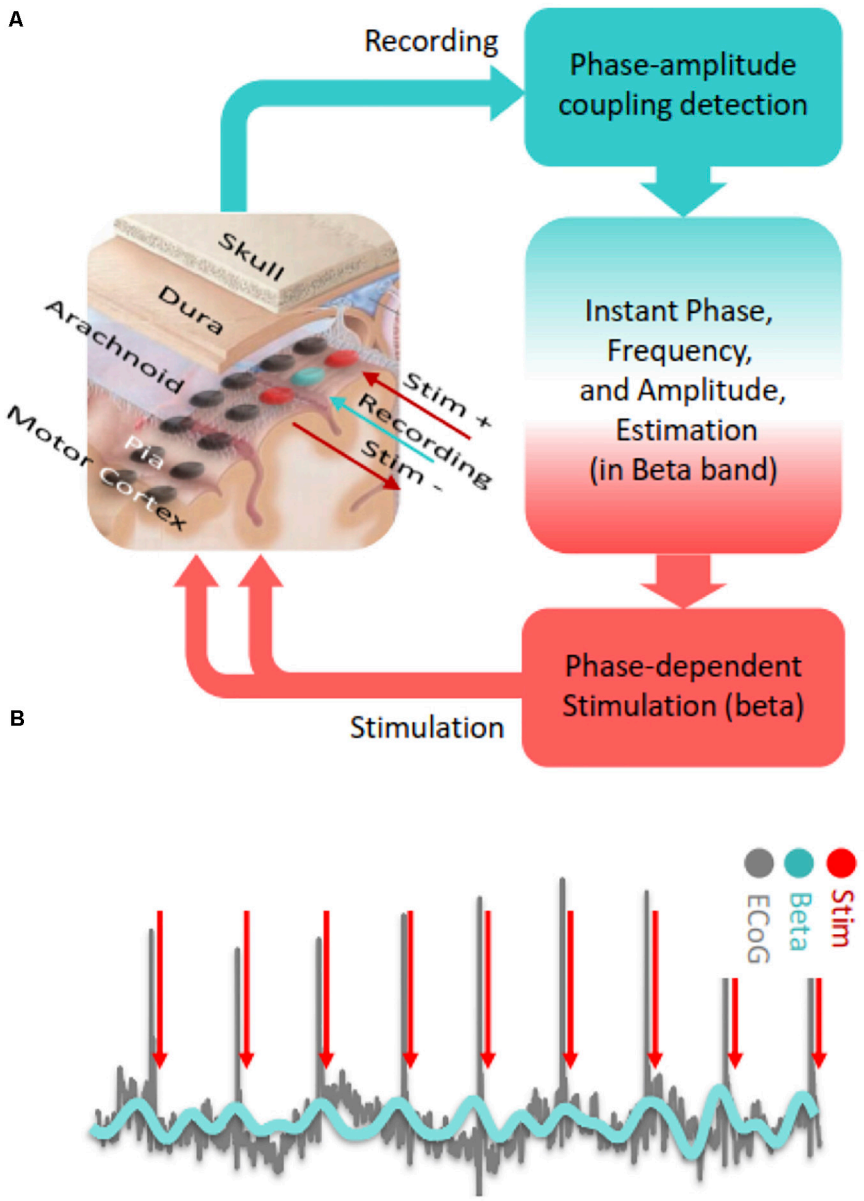

FIGURE 2 | (A) Steps of cortical PAC based adaptive phase dependent motor cortex stimulation with implanted subdural grid electrode. In this hypothetical set-up, a single contact (blue) over the motor cortex is used for detecting PAC levels in real-time and two adjacent contacts (red) deliver bipolar phase-dependent stimulation. **(B)** In phase dependent stimulation, electrocorticographic signals recorded from the motor cortex are bandpass filtered in the beta frequency range and electrical stimulation is delivered at a specific phase of the beta oscillation (peak in this case).

introduces latency into the stimulation protocol. Latency can be a significant problem in PDS because stimulation-pulse landing off the targeted phase can lead to unintended consequences. Therefore, devising effective strategies to overcome latency problems in PDS protocol is critical. In the context of PD, based on a mean beta-band frequency of approximately 20 Hz, a sliding-time window of 1 s should be sufficient to capture the dynamics of PAC to conduct an effective, near real-time PDS, as demonstrated a recent study (Peles et al., 2020). One solution to mitigating the computational technical demand is to utilize advanced circuit designs based on field-programmable gate array (FPGA), which can provide the speed to handle the high data throughput and processing, flexibility to readily modify algorithms, and machine learning capabilities to continuously improve performance.

Amplitude and time-domain characteristics (e.g., waveform shape) of beta oscillation correlate either with the severity of parkinsonian symptoms or with PAC levels in PD patients and may represent promising alternate biomarkers (Cole et al., 2017; Holt et al., 2019). Because they are technically simpler to work with, beta waveform-shape and amplitude levels may help overcome the latency issue. Nevertheless, we see a value in attempting a PAC-based neuromodulation despite current technical challenges because PAC may better represent the state of the BGTC network in PD. Also, PAC holds several advantages over other electrophysiological biomarkers of PD. First, PAC is strongly associated with parkinsonian symptom severity in a dose-dependent manner and responds predictably to both therapeutic medication and deep brain stimulation. PAC does not require physiological monitoring from deep brain structures, which potentially facilitates a less invasive system overall (de Hemptinne et al., 2013, 2015). Also, human recordings of PAC before, during, and after movement suggest that, compared to other brain disorders, PAC remains elevated even during movement in the parkinsonian state (Blumenfeld et al., 2015; de Hemptinne et al., 2015). We are optimistic that this persists in a stable manner through different movement phases more predictably than local field potential beta power. In comparison, subcortical beta oscillation may be influenced by normal physiological activities more dynamically than PAC and beta power dynamics during movement might now allow for clear thresholding throughout movement initiation and maintenance (de Hemptinne et al., 2015; Holt et al., 2019). Also, the shape of cortical beta oscillations might correlate with motor symptoms and signs of parkinsonism more strongly than the magnitude of beta power from local field potentials, and the atypicality of the waveform shape highly correlates with PAC (Cole et al., 2017). Stability and robustness of various components of the beta waveform shape during movement and against physiological perturbation are yet to be determined. It remains to be seen whether these and other promising biomarkers of PD will outperform PAC in closed-loop neuromodulation. Nevertheless, it is entirely conceivable to develop PAC-based phase-dependent neuromodulation algorithms that concurrently detect and analyze multiple time-domain and spectral features to provide additional controls, such that variables such as waveform shapes and beta amplitudes can either supplement PAC or function as backup biomarkers in failure modes.

Another consideration involves stimulation-related artifact, which can hinder PAC based PDS, particularly in the context of a surface-sensing surface-stimulation paradigm. There are several techniques for reducing stimulation-related artifact both online and offline (Zhou et al., 2018). In our experience, use of separate recording and stimulation electrode contacts can significantly reduce the artifact level (Salimpour and Anderson, 2019). Additionally, the duration of a stimulus artifact is generally very short (3–5 ms), such that online artifact removal techniques can reduce the levels of artifact and noise during stimulation and provide sustained recording.

Defining Normal Cortical PAC Level as a Therapeutic Goal

For PAC-based neuromodulation to become viable, it will be important to establish PAC patterns that are pathological and physiological for a specific PD patient. Although simple high and low PAC threshold levels can be used to trigger a stimulation pulse, such a system would be too simplistic to perform a dynamically adaptive neuromodulation to achieve the eu-PAC state. Patient-specific normal and pathological patterns would provide the therapeutic windows necessary for a PAC-based PDS neuromodulation system to be clinically safe, effective, and meaningful. Such endeavors have been undertaken with beta activities (Little et al., 2013, 2016a,b; Piña-Fuentes et al., 2017; Rosa et al., 2017). Using an experimental sensing implantable DBS system, beta oscillation patterns associated with specific activities performed outside of the operating room, such as walking and riding a bicycle, have been described (Quinn et al., 2015; Storzer et al., 2017; Syrkin-Nikolau et al., 2017; Hell et al., 2018). Such information is not available for PAC, but the technology exists to safely and chronically record and evaluate PAC patterns from the motor cortex of PD patients (de Hemptinne et al., 2013, 2015). Also, since PAC can be detected non-invasively, characterization of PAC levels and patterns can be achieved during a tuning period in an outpatient setting with minimal risk to guide early artificial intelligence (AI) driven algorithm training prior to electrode array implantation (Swann et al., 2015). Advanced machine learning can be employed to continuously optimize stimulation parameters based on output PAC levels and therapeutic efficacy as defined by the user. AI and machine learning will be critical in the development of next generation of intelligent brain stimulation devices and this topic has been discussed in detail elsewhere (Neumann et al., 2019).

DISCUSSION

Phase amplitude coupling is expanding our understanding of PD pathophysiology and creating new therapeutic opportunities. Nevertheless, excitement must be tempered as we continue to improve our understanding of the BGTC network and

elucidate the relationships among different electrophysiological biomarkers and clinical outcomes. Also, we must continue to define the role of PAC in adaptive neuromodulation and develop creative ways to improve outcomes using the biomarker to define the role of PAC in adaptive neuromodulation and develop creative ways to improve outcomes using the biomarker. Efforts to define physiologically normal and pathological PAC are still needed in order to appropriately gate or modulate stimulation delivery. Going forward, collaboration among various fields, including computational sciences and engineering, is necessary in order to enable data-driven solutions to these remaining hurdles. AI and machine learning will be particularly useful in improving accuracy and speed of PAC detection and pattern recognition. Ultimately, the knowledge, techniques, and technologies that enable PAC neuromodulation may not only improve PD management but also play a significant role in advancing research and therapeutic development in other common neuropsychiatric conditions.

DATA AVAILABILITY STATEMENT

All datasets generated for this study are included in the article/supplementary material, further inquiries can be directed to the corresponding author.

AUTHOR CONTRIBUTIONS

YS and BH equally contributed to the ideas and concepts discussed within this manuscript and played a role in organizing the manuscript and designing the figures discussed within this manuscript. YT contributions include perusing the literature to gather the most recent developments in the field, and assisted in writing some sections of the manuscript. WA and KM provided edits and modifications to the entire manuscript and the references used. All authors contributed to the article and approved the submitted version.

REFERENCES

Ahn, S., Zauber, S. E., Worth, R. M., Witt, T., and Rubchinsky, L. L. (2015). Interaction of synchronized dynamics in cortex and basal ganglia in Parkinson's disease. *Eur. J. Neurosci.* 42, 2164–2171. doi: 10.1111/ejn.12980

Allen, E. A., Liu, J., Kiehl, K. A., Gelernter, J., Pearlson, G. D., Perrone-Bizzozero, N. I., et al. (2011). Components of cross-frequency modulation in health and disease. *Front. Syst. Neurosci.* 5:59. doi: 10.3389/fnsys.2011.00059

Anderson, W. S., Kudela, P., Weinberg, S., Bergey, G. K., and Franaszczuk, P. J. (2009). Phase-dependent stimulation effects on bursting activity in a neural network cortical simulation. *Epilepsy Res.* 841, 42–55. doi: 10.1016/j.eplepsyres.2008.12.005

Azodi-Avval, R., and Gharabaghi, A. (2015). Phase-dependent modulation as a novel approach for therapeutic brain stimulation. *Front. Comput. Neurosci.* 9:26. doi: 10.3389/fncom.2015.00026

Bahramisharif, A., Mazaheri, A., Levar, N., Richard Schuurman, P., Figee, M., and Denys, D. (2016). Deep brain stimulation diminishes cross-frequency coupling in obsessive-compulsive disorder. *Biol. Psychiatry* 80, e57–e58. doi: 10.1016/j.biopsych.2015.05.021

Bergman, H., Wichmann, T., Karmon, B., and DeLong, M. R. (1994). The primate subthalamic nucleus. II. Neuronal activity in the MPTP model of parkinsonism. *J. Neurophysiol.* 72, 507–520. doi: 10.1152/jn.1994.72.2.507

Bevan, M. (2002). Move to the rhythm: oscillations in the subthalamic nucleus–external globus pallidus network. *Trends Neurosci.* 25, 525–531. doi: 10.1016/s0166-2236(02)02235-x

Blumenfeld, Z., Velisar, A., Miller Koop, M., Hill, B. C., Shreve, L. A., Quinn, E. J., et al. (2015). Sixty hertz neurostimulation amplifies subthalamic neural synchrony in Parkinson's disease. *PLoS One* 103:e0121067. doi: 10.1371/journal.pone.0121067

Brown, P., Oliviero, A., Mazzone, P., Insola, A., Tonali, P., and Di Lazzaro, V. (2001). Dopamine dependency of oscillations between subthalamic nucleus and pallidum in Parkinson's disease. *J. Neurosci.* 21, 1033–1038. doi: 10.1523/jneurosci.21-03-01033.2001

Cagnan, H., Brittain, J., Little, S., Foltynie, T., Limousin, P., Zrinzo, L., et al. (2013). Phase dependent modulation of tremor amplitude in essential tremor through thalamic stimulation. *Brain* 136, 3062–3075. doi: 10.1093/brain/awt239

Cagnan, H., Pedrosa, D., Little, S., Pogosyan, A., Cheeran, B., Aziz, T., et al. (2017). Stimulating at the right time: phase-specific deep brain stimulation. *Brain* 140, 132–145. doi: 10.1093/brain/aww286

Canavero, S., Paolotti, R., Bonicalzi, V., Castellano, G., Greco-Crasto, S., Rizzo, L., et al. (2002). Extradural motor cortex stimulation for advanced Parkinson disease. Report of two cases. *J. Neurosurg.* 97, 1208–1211. doi: 10.3171/jns.2002.97.5.1208

Canolty, R. T., and Knight, R. T. (2010). The functional role of cross-frequency coupling. *Trends Cogn. Sci.* 14, 506–515. doi: 10.1016/j.tics.2010.09.001

Castrioto, A., Lhommée, E., Moro, E., and Krack, P. (2014). Mood and behavioural effects of subthalamic stimulation in Parkinson's disease. *Lancet Neurol.* 13, 287–305. doi: 10.1016/S1474-4422(13)70294-1

Chen, C. C., Brücke, C., Kempf, F., Kupsch, A., Lu, C. S., Lee, S. T., et al. (2006). Deep brain stimulation of the subthalamic nucleus: a two-edged sword. *Curr. Biol.* 16, R952–R953. doi: 10.1016/j.cub.2006.10.013

Chen, L. L., Madhavan, R., Rapoport, B. I., and Anderson, W. S. (2011). A method for real-time cortical oscillation detection and phase-locked stimulation. *IEMBS* 2011, 3087–3090.

Chen, L. L., Madhavan, R., Rapoport, B. I., and Anderson, W. S. (2013). Real-time brain oscillation detection and phase-locked stimulation using autoregressive spectral estimation and time-series forward prediction. *TBME* 60, 753–762. doi: 10.1109/tbme.2011.2109715

Cilia, R., Landi, A., Vergani, F., Sganzerla, E., Pezzoli, G., and Antonini, A. (2007). Extradural motor cortex stimulation in Parkinson's disease. *Mov. Disord.* 221, 111–114. doi: 10.1002/mds.21207

Cole, S. R., van der Meij, R., Peterson, E. J., de Hemptinne, C., Starr, P. A., and Voytek, B. (2017). Nonsinusoidal beta oscillations reflect cortical pathophysiology in Parkinson's disease. *J. Neurosci.* 37, 4830–4840. doi: 10.1523/jneurosci.2208-16.2017

de Hemptinne, C., Ryapolova-Webb, E. S., Air, E. L., Garcia, P. A., Miller, K. J., Ojemann, J. G., et al. (2013). Exaggerated phase-amplitude coupling in the primary motor cortex in Parkinson disease. *Proc. Natl. Acad. Sci. U.S.A.* 110, 4780–4785. doi: 10.1073/pnas.1214546110

de Hemptinne, C., Swann, N. C., Ostrem, J. L., Ryapolova-Webb, E. S., San Luciano, M., Galifianakis, N. B., et al. (2015). Therapeutic deep brain stimulation reduces cortical phase-amplitude coupling in Parkinson's disease. *Nat. Neurosci.* 18, 779–786. doi: 10.1038/nn.3997

De Rose, M., Guzzi, G., Bosco, D., Romano, M., Lavano, S. M., Plastino, M., et al. (2012). Motor cortex stimulation in Parkinson's disease. *Neurol. Res. Int.* 97(Pt 2), 233–238. doi: 10.1155/2012/502096

Gelperin, A. (2006). Olfactory computations and network oscillation. *J. Neurosci.* 26, 1663–1668. doi: 10.1523/JNEUROSCI.3737-05b.2006

Goutagny, R., Gu, N., Cavanagh, C., Jackson, J., Chabot, J., Quirion, R., et al. (2013). Alterations in hippocampal network oscillations and theta-gamma coupling arise before Aβ overproduction in a mouse model of Alzheimer's disease. *Eur. J. Neurosci.* 37, 1896–1902. doi: 10.1111/ejn.12233

Hammond, C., Bergman, H., and Brown, P. (2007). Pathological synchronization in Parkinson's disease: networks, models and treatments. *Trends Neurosci.* 30, 357–364. doi: 10.1016/j.tins.2007.05.004

Heck, D. H., Thach, W. T., and Keating, J. G. (2007). On-beam synchrony in the cerebellum as the mechanism for the timing and coordination of movement. *Proc. Natl. Acad. Sci. U.S.A.* 104, 7658–7663. doi: 10.1073/pnas.0609966104

Hell, F., Plate, A., Mehrkens, J. H., and Bötzel, K. (2018). Subthalamic oscillatory activity and connectivity during gait in Parkinson's disease. *NeuroImage Clin.* 19, 396–405. doi: 10.1016/j.nicl.2018.05.001

Holt, A. B., Kormann, E., Gulberti, A., Pötter-Nerger, M., McNamara, C. G., Cagnan, H., et al. (2019). Phase-dependent suppression of beta oscillations in Parkinson's disease patients. *J. Neurosci.* 39, 1119–1134. doi: 10.1523/jneurosci.1913-18.2018

Hyafil, A., Giraud, A., Fontolan, L., and Gutkin, B. (2015). Neural cross-frequency coupling: connecting architectures, mechanisms, and functions. *Trends Neurosci.* 38, 725–740. doi: 10.1016/j.tins.2015.09.001

Kanta, V., Pare, D., and Headley, D. B. (2019). Closed-loop control of gamma oscillations in the amygdala demonstrates their role in spatial memory consolidation. *Nat. Commun.* 10:3970. doi: 10.1038/s41467-019-11938-8

Kondylis, E. D., Randazzo, M. J., Alhourani, A., Lipski, W. J., Wozny, T. A., Pandya, Y., et al. (2016). Movement-related dynamics of cortical oscillations in Parkinson's disease and essential tremor. *Brain* 139, 2211–2223. doi: 10.1093/brain/aww144

Lakatos, P., Karmos, G., Mehta, A. D., Ulbert, I., and Schroeder, C. E. (2008). Entrainment of neuronal oscillations as a mechanism of attentional selection. *Science* 320, 110–113. doi: 10.1126/science.1154735

Little, S., Beudel, M., Zrinzo, L., Foltynie, T., Limousin, P., Hariz, M., et al. (2016a). Bilateral adaptive deep brain stimulation is effective in Parkinson's disease. *J. Neurol. Neurosurg. Psychiatry* 87, 717–721. doi: 10.1136/jnnp-2015-310972

Little, S., Pogosyan, A., Neal, S., Zavala, B., Zrinzo, L., Hariz, M., et al. (2013). Adaptive deep brain stimulation in advanced Parkinson disease. *Ann. Neurol.* 74, 449–457. doi: 10.1002/ana.23951

Little, S., Tripoliti, E., Beudel, M., Pogosyan, A., Cagnan, H., Herz, D., et al. (2016b). Adaptive deep brain stimulation for Parkinson's disease demonstrates reduced speech side effects compared to conventional stimulation in the acute setting. *J. Neurol. Neurosurg. Psychiatry* 87, 1388–1389. doi: 10.1136/jnnp-2016-313518

Madhavan, R., Millman, D., Tang, H., Crone, N. E., Lenz, F. A., Tierney, T. S., et al. (2015). Decrease in gamma-band activity tracks sequence learning. *Front. Syst. Neurosci.* 8:222. doi: 10.3389/fnsys.2014.00222

Maks, C. B., Butson, C. R., Walter, B. L., Vitek, J. L., and McIntyre, C. C. (2009). Deep brain stimulation activation volumes and their association with neurophysiological mapping and therapeutic outcomes. *J. Neurol. Neurosurg. Psychiatry* 80, 659–666. doi: 10.1136/jnnp.2007.126219

Malekmohammadi, M., AuYong, N., Ricks-Oddie, J., Bordelon, Y., and Pouratian, N. (2018). Pallidal deep brain stimulation modulates excessive cortical high β phase amplitude coupling in Parkinson disease. *Brain Stimul.* 11, 607–617. doi: 10.1016/j.brs.2018.01.028

McNamara, C. G., Rothwell, M., and Sharott, A. (2020). Phase-dependent closed-loop modulation of neural oscillations in vivo. *BioRXiv* [preprint]. doi: 10.1101/2020.05.21.102335

Miller, K. J., Hermes, D., Honey, C. J., Hebb, A. O., Ramsey, N. F., Knight, R. T., et al. (2012). Human motor cortical activity is selectively phase-entrained on underlying rhythms. *PLoS Comput. Biol.* 89:e1002655. doi: 10.1371/journal.pcbi.1002655

Moro, E., Schwalb, J. M., Piboolnurak, P., Poon, Y.-W., Hamani, C., Hung, S. W., et al. (2011). Unilateral subdural motor cortex stimulation improves essential tremor but not Parkinson's disease. *Brain* 134(Pt 7), 2096–2105. doi: 10.1093/brain/awr072

Neumann, W., Turner, R. S., Blankertz, B., Mitchell, T., Kühn, A. A., and Richardson, R. M. (2019). Toward electrophysiology-based intelligent adaptive deep brain stimulation for movement disorders. *Neurotherapeutics* 16, 105–118. doi: 10.1007/s13311-018-00705-0

Peles, O., Werner-Reiss, U., Bergman, H., Israel, Z., and Vaadia, E. (2020). Phase-specific microstimulation differentially modulates beta oscillations and affects behavior. *Cell Rep.* 30, 2555.e3–2566.e3. doi: 10.1016/j.celrep.2020.02.005

Piña-Fuentes, D., Little, S., Oterdoom, M., Neal, S., Pogosyan, A., Tijssen, M. A. J., et al. (2017). Adaptive DBS in a Parkinson's patient with chronically implanted DBS: a proof of principle. *Mov. Disord.* 32, 1253–1254. doi: 10.1002/mds.26959

Quinn, E. J., Blumenfeld, Z., Velisar, A., Koop, M. M., Shreve, L. A., Trager, M. H., et al. (2015). Beta oscillations in freely moving Parkinson's subjects are attenuated during deep brain stimulation. *Mov. Disord.* 30, 1750–1758. doi: 10.1002/mds.26376

Rosa, M., Arlotti, M., Ardolino, G., Cogiamanian, F., Marceglia, S., Di Fonzo, A., et al. (2015). Adaptive deep brain stimulation in a freely moving parkinsonian patient. *Mov. Disord.* 30, 1003–1005. doi: 10.1002/mds.26241

Rosa, M., Arlotti, M., Marceglia, S., Cogiamanian, F., Ardolino, G., Fonzo, A. D., et al. (2017). Adaptive deep brain stimulation controls levodopa-induced side effects in Parkinsonian patients. *Mov. Disord.* 32, 628–629. doi: 10.1002/mds.26953

Salimpour, Y., and Anderson, W. S. (2019). Cross-frequency coupling based neuromodulation for treating neurological disorders. *Front. Neurosci.* 13:125. doi: 10.3389/fnins.2019.00125

Sanabria, D. E., Johnson, L. A., Yu, Y., Busby, Z., Shane, N., Zhang, J., et al. (2020). Real-time suppression and amplification of frequency-specific neural activity using stimulation evoked oscillations. *bioRxiv* [Preprint]. doi: 10.1101/2020.02.09.940643

Schnitzler, A., and Gross, J. (2005). Normal and pathological oscillatory communication in the brainNature reviews. *Neuroscience* 6, 285–296. doi: 10.1038/nrn1650

Schroeder, C. E., and Lakatos, P. (2009). Low-frequency neuronal oscillations as instruments of sensory selection. *Trends Neurosci.* 32, 9–18. doi: 10.1016/j.tins.2008.09.012

Shimamoto, S. A., Ryapolova-Webb, E. S., Ostrem, J. L., Galifianakis, N. B., Miller, K. J., and Starr, P. A. (2013). Subthalamic nucleus neurons are synchronized to primary motor cortex local field potentials in Parkinson's disease. *J. Neurosci.* 33, 7220–7233. doi: 10.1523/JNEUROSCI.4676-12.2013

Storzer, L., Butz, M., Hirschmann, J., Abbasi, O., Gratkowski, M., Saupe, D., et al. (2017). Bicycling suppresses abnormal beta synchrony in the Parkinsonian basal ganglia. *Ann. Neurol.* 82, 592–601. doi: 10.1002/ana.25047

Strafella, A. P., Lozano, A. M., Lang, A. E., Ko, J. H., Poon, Y., and Moro, E. (2007). Subdural motor cortex stimulation in Parkinson's disease does not modify movement-related rCBF pattern. *Mov. Disord.* 22, 2113–2116. doi: 10.1002/mds.21691

Swann, N. C., de Hemptinne, C., Aron, A. R., Ostrem, J. L., Knight, R. T., and Starr, P. A. (2015). Elevated synchrony in Parkinson disease detected with electroencephalography. *Ann. Neurol.* 78, 742–750. doi: 10.1002/ana.24507

Swann, N. C., de Hemptinne, C., Thompson, M. C., Miocinovic, S., Miller, A. M., Gilron, R., et al. (2018). Adaptive deep brain stimulation for Parkinson's disease using motor cortex sensing. *J. Neural Eng.* 15:e046006. doi: 10.1088/1741-2552/aabc9b

Syrkin-Nikolau, J., Koop, M. M., Prieto, T., Anidi, C., Afzal, M. F., Velisar, A., et al. (2017). Subthalamic neural entropy is a feature of freezing of gait in freely moving people with Parkinson's disease. *Neurobiol. Dis.* 108, 288–297. doi: 10.1016/j.nbd.2017.09.002

Tort, A. B. L., Komorowski, R., Eichenbaum, H., and Kopell, N. (2010). Measuring phase-amplitude coupling between neuronal oscillations of different frequencies. *J. Neurophysiol.* 104, 1195–1210. doi: 10.1152/jn.00106.2010

Tripoliti, E., Zrinzo, L., Martinez-Torres, I., Frost, E., Pinto, S., Foltynie, T., et al. (2011). Effects of subthalamic stimulation on speech of consecutive patients with Parkinson disease. *Neurology* 76, 80–86. doi: 10.1212/WNL.0b013e318203e7d0

Wang, D. D., de Hemptinne, C., Miocinovic, S., Ostrem, J. L., Galifianakis, N. B., San Luciano, M., et al. (2018). Pallidal deep-brain stimulation disrupts pallidal beta oscillations and coherence with primary motor cortex in Parkinson's disease. *J. Neurosci.* 38, 4556–4568. doi: 10.1523/jneurosci.0431-18.2018

Wang, X. (2010). Neurophysiological and computational principles of cortical rhythms in cognition. *Physiol. Rev.* 90, 1195–1268. doi: 10.1152/physrev.00035.2008

Watanabe, S., and Hirono, M. (2016). Phase-dependent modulation of oscillatory phase and synchrony by long-lasting depolarizing inputs in central neurons. *eNeuro* 3:ENEURO.0066-16.2016. doi: 10.1523/ENEURO.0066-16.2016

Yanagisawa, T., Yamashita, O., Hirata, M., Kishima, H., Saitoh, Y., Goto, T., et al. (2012). Regulation of motor representation by phase-amplitude coupling in the

sensorimotor cortex. *J. Neurosci.* 32, 15467–15475. doi: 10.1523/JNEUROSCI.2929-12.2012

Zanos, S., Rembado, I., Chen, D., and Fetz, E. E. (2018). Phase-locked stimulation during cortical beta oscillations produces bidirectional synaptic plasticity in awake monkeys. *Curr. Biol.* 28, 2515.e4–2526.e4. doi: 10.1016/j.cub.2018.07.009

Zhang, R., Ren, Y., Liu, C., Xu, N., Li, X., Cong, F., et al. (2017). Temporal-spatial characteristics of phase-amplitude coupling in electrocorticogram for human temporal lobe epilepsy. *Clin. Neurophysiol.* 128, 1707–1718. doi: 10.1016/j.clinph.2017.05.020

Zhou, A., Johnson, B. C., and Muller, R. (2018). Toward true closed-loop neuromodulation: artifact-free recording during stimulation. *Curr. Opin. Neurobiol.* 50, 119–127. doi: 10.1016/j.conb.2018.01.012

Zrenner, C., Desideri, D., Belardinelli, P., and Ziemann, U. (2018). Real-time EEG-defined excitability states determine efficacy of TMS-induced plasticity in human motor cortex. *Brain Stimul.* 11, 374–389. doi: 10.1016/j.brs.2017.11.016

Conflict of Interest: KM previously received clinical trial support from St. Jude/Abbott and currently receives clinical trial support from Global Kinetics Corporation. WA sits on Advisory Boards for Longeviti Neuro Solutions, and NeuroLogic. WA was also a paid consultant for Globus Medical.

The remaining authors declare that the research was conducted in the absence of any commercial or financial relationships that could be construed as a potential conflict of interest.

frontiers in Aging Neuroscience

ORIGINAL RESEARCH
published: 29 September 2020
doi: 10.3389/fnagi.2020.00263

Enhancing Working Memory Based on Mismatch Negativity Neurofeedback in Subjective Cognitive Decline Patients: A Preliminary Study

Guangying Pei[1], Ruoshui Yang[2], Zhongyan Shi[1], Guoxin Guo[1], Shujie Wang[1], Miaomiao Liu[3], Yuxiang Qiu[1], Jinglong Wu[2,4], Ritsu Go[2]*, Ying Han[5,6,7]* and Tianyi Yan[1]**

[1]School of Life Science, Beijing Institute of Technology, Beijing, China, [2]School of Mechatronical Engineering, Beijing Institute of Technology, Beijing, China, [3]Graduate School of Natural Science and Technology, Okayama University, Okayama, Japan, [4]Faculty of Engineering, Okayama University, Okayama, Japan, [5]Department of Neurology, Xuanwu Hospital, Capital Medical University, Beijing, China, [6]Center of Alzheimer's Disease, Beijing Institute for Brain Disorders, Beijing, China, [7]National Clinical Research Center for Geriatric Disorders, Xuanwu Hospital, Capital Medical University, Beijing, China

OPEN ACCESS

Edited by:
Woon-Man Kung, Chinese Culture University, Taiwan

Reviewed by:
Xun Chen, University of Science and Technology of China, China
Wei Hung Chang, National Cheng Kung University, Taiwan

***Correspondence:**
Miaomiao Liu
14777693@qq.com
Ritsu Go
nieli@bit.edu.cn
Ying Han
hanying@xwh.ccmu.edu.cn
Tianyi Yan
yantianyi@bit.edu.cn

Received: *10 February 2020*
Accepted: *03 August 2020*
Published: *29 September 2020*

Citation:
Pei G, Yang R, Shi Z, Guo G, Wang S, Liu M, Qiu Y, Wu J, Go R, Han Y and Yan T (2020) Enhancing Working Memory Based on Mismatch Negativity Neurofeedback in Subjective Cognitive Decline Patients: A Preliminary Study. Front. Aging Neurosci. 12:263. doi: 10.3389/fnagi.2020.00263

Mismatch negativity (MMN) is suitable for studies of preattentive auditory discriminability and the auditory memory trace. Subjective cognitive decline (SCD) is an ideal target for early therapeutic intervention because SCD occurs at preclinical stages many years before the onset of Alzheimer's disease (AD). According to a novel lifespan-based model of dementia risk, hearing loss is considered the greatest potentially modifiable risk factor of dementia among nine health and lifestyle factors, and hearing impairment is associated with cognitive decline. Therefore, we propose a neurofeedback training based on MMN, which is an objective index of auditory discriminability, to regulate sensory ability and memory as a non-pharmacological intervention (NPI) in SCD patients. Seventeen subjects meeting the standardized clinical evaluations for SCD received neurofeedback training. The auditory frequency discrimination test, the visual digital N-back (1-, 2-, and 3-back), auditory digital N-back (1-, 2-, and 3-back), and auditory tone N-back (1-, 2-, and 3-back) tasks were used pre- and post-training in all SCD patients. The intervention schedule comprised five 60-min training sessions over 2 weeks. The results indicate that the subjects who received neurofeedback training had successfully improved the amplitude of MMN at the parietal electrode (Pz). A slight decrease in the threshold of auditory frequency discrimination was observed after neurofeedback training. Notably, after neurofeedback training, the working memory (WM) performance was significantly enhanced in the auditory tone 3-back test. Moreover, improvements in the accuracy of all WM tests relative to the baseline were observed, although the changes were not significant. To the best of our knowledge, our preliminary study is the first to investigate the effects of MMN neurofeedback training on WM in SCD patients, and our results suggest that MMN neurofeedback may represent an effective treatment for intervention in SCD patients and the elderly with aging memory decline.

Keywords: mismatch negativity, neurofeedback, working memory, subjective cognitive decline, Alzheimer's disease, early intervention

INTRODUCTION

Alzheimer's disease (AD) is slow and progresses with a presymptomatic course over several years to decades (Sperling et al., 2011). Controlling modifiable risk factors for AD at the preclinical stage remains the most realistic preventive strategy (Crous-Bou et al., 2017). Subjective cognitive decline (SCD) is a condition that is manifested by healthy older people who show unimpaired performance on cognitive tests and self-report a perceived cognitive decline in memory or other cognitive domains, such as executive function or attention (Rabin et al., 2015). SCD may represent the first symptomatic manifestation of AD before mild cognitive impairment (MCI; Koppara et al., 2015; Bubbico et al., 2019). Currently, there is no consensus on the best intervention or treatment for SCD with regard to psychological, cognitive, lifestyle, and pharmacological interventions described in a recent systematic review and a meta-analysis (Williams and Tanabe, 2016; Bhome et al., 2018). Given the heterogeneity of etiology of SCD and specifically considering individuals who have minimal manifestation of clinical symptoms, it is difficult to confirm a focal target of pharmacological intervention that does not cause an adverse reaction. Therefore, non-pharmacological intervention (NPI) may be a feasible method of treatment for patients with SCD (Smart et al., 2017; Bhome et al., 2018).

Elderly SCD subjects have a subtle decline in memory performance associated with accelerated memory decline, and SCD may predict future objective memory decline, even for incident dementia (Koppara et al., 2015). There is no authoritative method for treating early memory loss; however, a growing number of publications suggests that neurofeedback, which as a form of electroencephalogram (EEG) biofeedback used to self-regulate individual own brain activity, can directly alter the underlying neural mechanism of cognition and behavior (Enriquez-Geppert et al., 2017; Bhome et al., 2018). Neurofeedback has been successfully applied in the treatment of various diseases, such as attention-deficit hyperactivity disorder (ADHD; Van Doren et al., 2019) or epilepsy (Van Doren et al., 2019), enhancing memory for the healthy old adults with aging cognitive decline (Reis et al., 2016), and even in dementia or AD patients (Luijmes et al., 2016; Berman and Nichols, 2019; Kaufmann et al., 2019). For example, AD patients have an excess of slow frequency waves, such as delta and theta, and a reduction in the alpha waves compared with that in healthy aging individuals; thus, regulating the abnormal EEG frequency activity can have a positive effect on clinical performance, especially considering the effect of neurofeedback on cognitive ability (Luijmes et al., 2016). Here, we propose using neurofeedback as a NPI to improve the cognitive ability of SCD patients.

Hearing loss was considered to be the greatest potentially modifiable risk factor for dementia among the nine health and lifestyle factors according to a novel dementia risk model based on lifespan reported by the Lancet Commission (Uchida et al., 2019). If middle-aged hearing loss is eliminated, the risk of dementia may be reduced by 9% (Lin F. R. et al., 2013; Livingston et al., 2017). A 25-year study self-reported that hearing loss is linked to accelerated cognitive decline in older people (Amieva et al., 2015). A meta-analysis suggested that hearing impairment is related to cognitive impairments (Taljaard et al., 2016). Auditory mismatch negativity (MMN) is a negative wave of event-related potential (ERP) typically obtained by the standard stimulus and is subtracted from the deviant stimulus in the oddball tasks (Näätänen and Alho, 1997), with MMN as an objective index of auditory discriminability (Garrido et al., 2009). Electrophysiological studies have shown that when any detectable change in a regular pattern of auditory stimulation occurs, a preattentive change-detection system in the auditory modality emits a signal called MMN (Molholm et al., 2005). Several studies have shown that the MMN peak latency is systematically prolonged and its amplitude is attenuated with aging (Molholm et al., 2005; Näätänen et al., 2011). In various neurological disorders, including schizophrenia, autism spectrum disorders, and dementia, MMN appears to provide an objective tool for investigation of auditory processing and memory trace attenuation (Chen et al., 2017). Recent studies have shown that MMN amplitude in AD patients for a long interstimulus interval (ISI) of 3 s is smaller than that for the shorter ISIs of 1 s, while the amplitude is stable in the control group of healthy subjects (Lindín et al., 2013; Laptinskaya et al., 2018). Moreover, the MMN amplitude was significantly lower in amnestic MCI adults compared with that in healthy people. MMN can be a relatively sensitive psychophysiological biomarker in identifying amnestic MCI (Lindín et al., 2013). Furthermore, auditory working memory (WM) is the major factor of neural processing of sound, and cognitive factors shape the brain networks for auditory skills (Kraus et al., 2012). Auditory training helps to compensate for the degradation of the auditory signals; the training demonstrated that cognitive function can be improved during the index executive process, competing speech, and dual-task performance. Importantly, auditory-cognitive training showed general improvements in speech, auditory WM, and processing speed, as well as enhanced self-reporting of communication difficulties (Sweetow and Sabes, 2006; Ferguson and Henshaw, 2015). At present, MMN neurofeedback has been successfully used in adults mainly for the adjustment of sensory abilities, such as improving auditory discriminability for two particularly similar tones and enhancing language ability and music level (Chang et al., 2014, 2017). Although the improvement of sensory ability can improve work memory by cognitive training, there are insufficient clinical data on optimization of cognitive ability by MMN neurofeedback training; to the best of our knowledge, no studies have investigated the effect of MMN neurofeedback on memory brain function.

In this study, we recruited patients with SCD mainly for the short-term tight MMN neurofeedback training. The present pilot study aims to investigate the neurofeedback training based on MMN amplitude to determine whether the training has a positive effect on the regulation of the MMN characteristic in SCD patients. It is hypothesized that the MMN amplitude can be improved by short-term close training based on neurofeedback. Second, we hypothesized that WM performance may be enhanced by MMN neurofeedback training in patients with SCD. MMN neurofeedback may be an effective intervention

method to enhance WM in SCD patients and the elderly with aging memory decline.

MATERIALS AND METHODS

Participants

A total of 17 right-handed patients with memory concerns were recruited from the memory clinic of the Department of Neurology, Xuanwu Hospital, Beijing, China. The study was approved by the Medical Research Ethics Committee and Institutional Review Board of Xuanwu Hospital. All subjects underwent a series of standardized clinical assessments, including a medical history interview, a neurological examination, a blood examination, and a series of neuropsychological tests. All participants provided a written informed consent before performing any experimental procedures. We performed neuropsychological tests to evaluate cognitive function, social and daily functions, mental behavioral symptoms, sleep, clinical characteristics, and various cognitive domain scales. The scale results of the participants are shown in **Table 1**. Experienced neurologists performed the diagnoses. The diagnosis of SCD was based on published SCD research criteria proposed by the Subjective Cognitive Decline Initiative (SCD-I; Jessen et al., 2014). SCD subjects were able to complete all neurofeedback training within 2 weeks.

Experimental Design

The experiments included neurofeedback training, memory-based cognitive tests, and auditory frequency discrimination tests before and after the training (see **Figure 1**). The typical procedure for estimating auditory frequency discrimination was using a frequency increment detection paradigm, where listeners are instructed to compare a reference tone with a series of lower or higher frequency tones (Kishon-Rabin et al., 2004). Memory tests included visual digital N-back, auditory digital N-back, and auditory tone N-back, which are mainly used to test the WM ability of the subjects. The neurofeedback training calculates the amplitude of MMN of the subjects in real time by giving the auditory tone stimulus and performing a visual signal feedback to allow the subjects to independently adjust the amplitude of MMN.

TABLE 1 | Demographics and characteristics of the sample.

Number	17
Gender (Female/Male)	12/5
Age (year)	64.35 ± 7.86
Education (year)	12.82 ± 4.10
Hand (Left/Right)	0/17
Cognitive Function (mean ± SD)	
MMSE (Mini-Mental State Examination)	27.35 ± 1.54
MES (Memory and Executive Screening)	85.24 ± 23.47
MOCA-B (Montreal Cognitive Assessment-B)	25.41 ± 2.67
Excutive Ability (mean ± SD)	
STT-A (Shape Trails Test; second)	58.25 ± 17.84
STT-B (Shape Trails Test; second)	146.53 ± 54.58
Memory (mean ± SD)	
AVLT-h (Auditory Verbal Learning Test-Hearing; delay)	6.12 ± 2.83
AVLT-h (Auditory Verbal Learning Test-Hearing; recognition)	22.00 ± 1.41
Language Skill (mean ± SD)	
BNT (Boston Naming Test)	25.06 ± 3.94
Social and Everyday Functions (mean ± SD)	
ECog (Everyday Cognition)	1.50 ± 0.43
Mental Behavioral Symptoms (mean ± SD)	
HAMD (Hamilton Depression Scale)	3.71 ± 3.29
HAMA (Hamilton Anxiety Scale)	5.71 ± 5.32
GDS (Geriatric Depression Scale)	2.53 ± 2.21
Sleep Activity (mean ± SD)	
PSQI (Pittsburgh Sleep Quality Index)	6.47 ± 4.47
RBDS (Rapid Eye Movement sleep Behavior Disorder Screening Questionnaire)	1.18 ± 1.42
ESS (Epworth Sleepiness Scale)	6.94 ± 5.04

Auditory Frequency Discrimination Test

In this experiment, 1,000 Hz was used as a standard (reference) tone, with a set of comparison stimuli varying from 500 to 1,500 Hz in 100 Hz steps (e.g., 500 Hz, 600 Hz, 700 Hz, 800 Hz, 900 Hz, 1,100 Hz, 1,200 Hz, 1,300 Hz, 1,400 Hz, and 1,500 Hz). Each subject received auditory stimuli transmitted by a GSI-61 audiometer with binaural presentation *via* headphones (TDH 50) at 65–70 dB HL. The whole experiment was performed using E-Prime (Psychology Software Tools Inc., Pittsburgh, PA, USA). Each subject received 10 sets of pretrials to become familiar with sound stimulation. The actual test lasted for approximately 30 min.

Working Memory Test

WM refers to the structures and processes used to temporarily store and manipulate information during ongoing processing and distraction. The N-back task is one of the most popular measures of WM in cognitive neuroscience. In a classical N-back task, subjects are presented with a series of stimuli, and the task is to determine if each stimulus is consisted with an Nth stimulus shown previously. By manipulating the value of N, the processing load can be changed systematically, which influences the changes in accuracy and reaction time (RT; Jaeggi et al., 2010). In this experiment, we adopted a visual digital N-back (1-, 2-, and 3-back), an auditory digital N-back (1-, 2-, and 3-back), and an auditory tone N-back (1-, 2-, and 3-back). N-back uses three types of stimuli: visual digits (digits from 1 to 9, except 7), auditory digits (digits from 1 to 9, except 7), and auditory tone (tone frequencies include 200 Hz, 400 Hz, 800 Hz, 1,000 Hz, 1,200 Hz, 2,000 Hz, and 4,000 Hz; Zhang et al., 2016). The digits were recorded from Google with Chinese pronunciation.

Neurofeedback Training

The neurofeedback training was completed five times in 2 weeks with an interval of less than 3 days and more than 1 day by all participants. Each neurofeedback training contains five training sessions. The standard MMN was induced by a standard stimulus of 1,000 Hz (80%), and the deviant stimulus of 2,000 Hz (20%) was based on the oddball paradigm (Lin Y. et al., 2013). A modification of the MMN neurofeedback training protocol was used in this study (Chang et al., 2014). MMN was elicited by an auditory stimulus based on an oddball paradigm: 1,100 Hz was the standard stimulus; the deviant stimulus was two times the individual auditory discriminant threshold value (Restuccia et al., 2009). The standard stimulus accounted for 80% of the stimuli. The

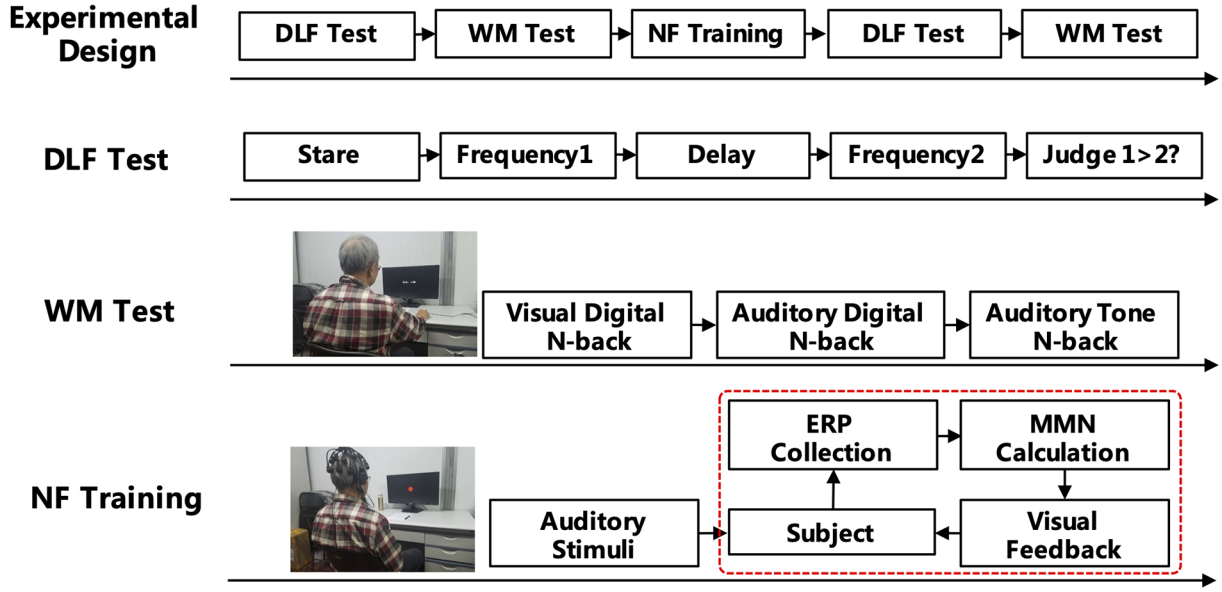

FIGURE 1 | Experimental design of the mismatch negativity (MMN) neurofeedback training.

stimuli were presented in a random order. The frontal (Fz), central (Cz), and parietal electrodes (Pz) were used as the training sites.

During each neurofeedback training session, the first MMN amplitude was used as the individual baseline threshold. Then, the amplitude of MMN was updated every 0.5 s. The amplitude of the real-time MMN was fed back as a visual disc signal, and the radius of the disc was proportional to the amplitude of MMN. When the real-time MMN amplitude was greater than the threshold, a red disc appeared; otherwise, a green disc appeared. Subjects were instructed to focus on the visual stimuli and silently count the red discs during training to ignore the auditory stimuli. During the neurofeedback training, the subjects attempted to use their strategies to try to increase the number of appearances of red discs (Pei et al., 2020).

Data Processing and Statistical Analysis

The results of the auditory discrimination threshold test and the N-back tasks were analyzed by the E-Prime software. The curve fitting of the method is based on a weighted cumulative Gaussian distribution function $f(p)$, as shown in Equation (1):

$$f(p) = 0.5\left[1 + \left(\frac{P - PStd.}{\sigma\sqrt{2}}\right)\right] \quad (1)$$

where σ is a parameter describing the steepness of the curve and can be considered as a qualitative measure of the 84% discrimination threshold and standard (1,100 Hz). R^2 evaluates whether each psychometric function fits a cumulative Gaussian distribution (Wichmann and Hill, 2001a,b; Pei et al., 2020).

The EEG data were analyzed offline *via* EEGLAB, an open-source MATLAB toolbox for electrophysiological signal processing (Delorme and Makeig, 2004). The raw EEG signal underwent 0.5 Hz high-pass and 45 Hz low-pass FIR filters. Independent component analysis (ICA) was used to reject artifacts of the EEG signals, and the main components are responsible for the eye movements and blinks.

Statistical analysis was performed by using SPSS 19 (SPSS, Chicago, IL, USA). Data are expressed as the mean ± standard error. A pointwise paired *t*-test of the standards and deviants was performed from 100 ms to 300 ms of ERP.

The amplitude and latency of MMN during the training were statistically analyzed using a repeated measures analysis of variance (ANOVA) with the "training day" (day 0 to day 5) and "electrode" (Fz, Pz, and Cz). A paired *t*-test was performed to compare the pre/post neurofeedback training (day 0 and day 5). Auditory discrimination accuracy was statistically analyzed using a repeated-measure ANOVA within the assessment time (pre/post training) and "frequency" (500–1,500 Hz in 100 Hz steps). The auditory discrimination threshold and the behavioral results of the WM were analyzed with the paired *t*-test. The significance level was set at $p < 0.05$, and high significance was set at $p < 0.01$. The previously described methods of statistical analysis have been verified by other experimental studies (Zhang et al., 2018).

RESULTS

We evaluated the standard MMN changes from ERP, auditory frequency threshold, and WM ability by cognitive behavioral tests. The amplitude of MMN was significantly increased with no significant change in latency after 5 days of MMN neurofeedback training at Pz. The accuracy of the subjects in the auditory tone 3-back test was increased significantly.

ERP Analysis of MMN

We collected the standard MMN of the subjects before the first training and after each training day. The six ERP waveforms at the Fz, Cz, and Pz electrodes are shown in **Figure 2A**. The results demonstrate high signal-to-noise ratio of ERP waveforms of the subjects and a more pronounced MMN that appears at the last training (day 5) at all three midline electrodes. Assessment of the amplitude or latency of MMN during the neurofeedback training (from day 0 to day 5) by repeated measure indicates that the "training day" has no major effect (amplitude: $F_{(5,80)} = 1.230$, $p = 0.303$; latency: $F_{(5,80)} = 1.230$, $p = 0.303$). Therefore, the MMN characteristics of the subjects did not change significantly with increase in the number of training days. However, the amplitude of the MMN at the Pz electrodes was significantly improved after 5 days of neurofeedback training according to the paired t-test ($t = 2.232$, $p = 0.040$). There was no significant increase of day 5 in the Fz ($t = 1.054$, $p = 0.308$) and Cz values ($t = 1.307$, $p = 0.210$) compared with that observed on day 0. The latency of MMN showed no significant changes at each electrode after five training days (Fz: $t = 0.358$, $p = 0.725$; Cz: $t = -1.917$, $p = 0.073$; and Pz: $t = -1.815$, $p = 0.088$; **Figure 2B**).

Figure 3 shows the amplitudes and latencies of MMN at 19 channels of each subject. In addition to three midline training electrodes, the amplitudes of the MMN at other locations after neurofeedback training were increased, especially in subject No. 13, in whom the whole brain was effectively improved. With regard to latencies, the number of electrodes with reduced signal is almost the same as that of increased signals.

Auditory Discriminability

The auditory discrimination threshold of an individual was tested before and after the training, and the value before the training was used as the personalization parameter (deviant stimuli) of the MMN neurofeedback protocol.

The results of the threshold fitting curve indicate that the range and gradient of the test frequency in the auditory frequency discrimination test were suitable for the SCD patients; the σ value was almost 1 before (σ = 0.991) and after (σ = 0.996) the neurofeedback training (**Figure 4A**). The threshold value was reduced overall after the neurofeedback training (**Figure 4B**), but the reduction was not significant ($t = 0.261$, $p = 0.798$) due to individual differences (**Figure 4D**). The average accuracies of 1,100 Hz and 1,500 Hz detection declined; however, detection of all other test frequencies was improved compared to that before the training (**Figure 4C**). Assessment of discrimination accuracy of test frequency by repeated measure indicates that there is no major effect of assessment time (pre/post neurofeedback; $F_{(1,16)} = 0.776$, $p = 0.391$). There were large individual differences in the accuracy rate, although 10 of 17 participants have improved after the training (**Figure 4E**).

Working Memory Performance

Considering the differences in the educational levels and cognition between the participants, we have conducted three types of WM for cognitive assessment, and the auditory tone 3-back test performance was significantly improved in accuracy after the neurofeedback training.

The accuracy and RTs of three types of the N-back tasks before and after the neurofeedback training were analyzed by a paired t-test. The results showed that the effect of the neurofeedback training was not significant for accuracies of visual digital N-back (1-back: $t = -1.765$, $p = 0.097$; 2-back: $t = -1.676$, $p = 0.113$; 3-back: $t = -0.841$, $p = 0.413$) and auditory digital N-back (1-back: $t = -1.957$, $p = 0.068$; 2-back: $t = -1.001$, $p = 0.332$; 3-back: $t = -1.437$, $p = 0.170$), although the values show an upward trend. However, for the auditory tone N-back, there was a significant improvement in accuracy in auditory tone 3-back ($t = -2.947$, $p = 0.009$); 1-back ($t = -1.838$, $p = 0.085$) and 2-back ($t = -1.714$, $p = 0.106$) showed no significant difference. No significant differences in RTs were found in visual digital N-back (1-back: $t = -0.616$, $p = 0.546$; 2-back: $t = 0.676$, $p = 0.509$; 3-back: $t = 0.248$, $p = 0.807$), auditory digital N-back (1-back: $t = 0.198$, $p = 0.846$; 2-back: $t = 1.314$, $p = 0.207$; 3-back: $t = 0.258$, $p = 0.799$) or auditory tone N-back (1-back: $t = 1.259$, $p = 0.226$; 2-back: $t = 0.738$, $p = 0.471$; 3-back: $t = 1.318$, $p = 0.206$; **Figures 5A–C**). Individual performance results showed that after the neurofeedback training, the accuracy was improved and the response speed was faster than before in various WM tests; however, most of the results were not statistically significant except the 3-back auditory tone task (**Figures 5D,E**).

The difficulty level of 1-back is the lowest, and thus, most of the participants did not obtain a significant improvement after the training because they had already achieved high scores before the training. The difficulty level of 2-back is medium, and the majority of the subjects clearly improved the accuracy of the tests. The most difficult task is 3-back; 13 subjects improved the accuracy, and the clinical effective rate (the number of improved/the number of non-improved) reached 76.47% (**Figure 6A**). The RTs of a task were increased concomitant to the difficulty of a task. In other words, the 1-back task is the fastest, and the 3-back task is the slowest. The neurofeedback training had no effect on RTs in 1-back, 2-back, or 3-back tasks (**Figure 6B**).

DISCUSSION

In this study, we successfully used an MMN neurofeedback protocol in SCD patients. After five training days during 2 weeks, the training significantly strengthens the amplitude of MMN and increases performance of the patients in WM tests, especially in the auditory tone 3-back tasks. This study is the first to explore the effect of the MMN neurofeedback training on auditory frequency discriminability and enhancement of the working auditory memory in SCD patients by regulation of the MMN activity.

Unconscious Learning and Personal Intervention Method

Recently, fMRI neurofeedback studies have shown that brain networks can be modified without intention and learning consciousness (Ramot et al., 2016). The activity of the visual cortex can be regulated to influence the visual perceptual learning with no stimulus presenting or the subjective consciousness of the subjects during the neurofeedback training

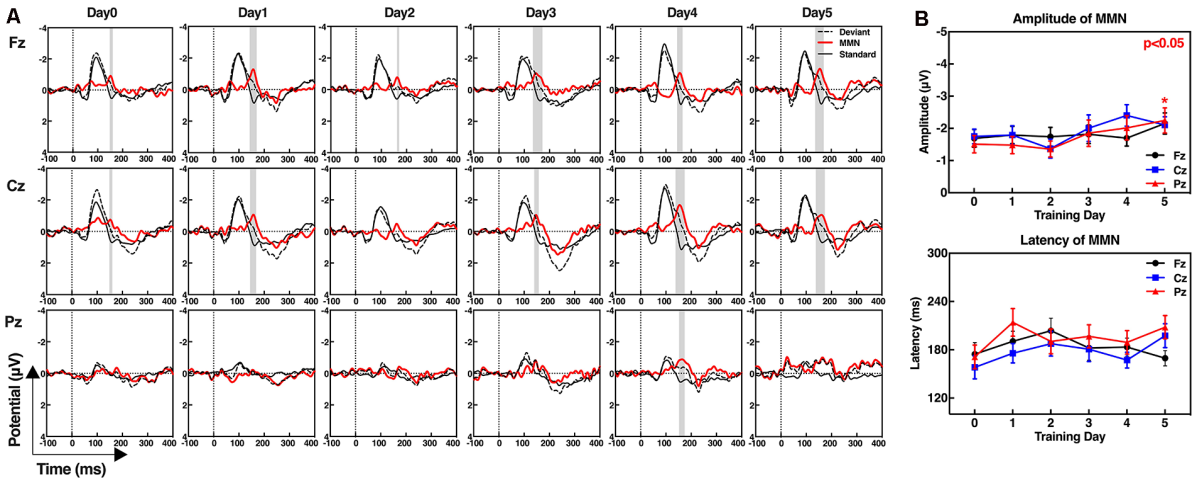

FIGURE 2 | Event-related potential (ERP) waveforms of the standard stimuli, deviant stimuli, and mismatch negativity (MMN; **A**), and the amplitudes and latencies of MMN at frontal (Fz), central (Cz), and parietal electrodes (Pz; **B**). **(A)** MMN waveforms were obtained by subtracting the ERPs in response to the standard stimuli from ERPs in response to the deviant stimuli. The gray shaded areas show the significant differences between the standard and deviant stimuli from 100 ms to 300 ms, $p < 0.05$. **(B)** Paired *t*-test; day 5 compared with day 0, $^*p < 0.05$.

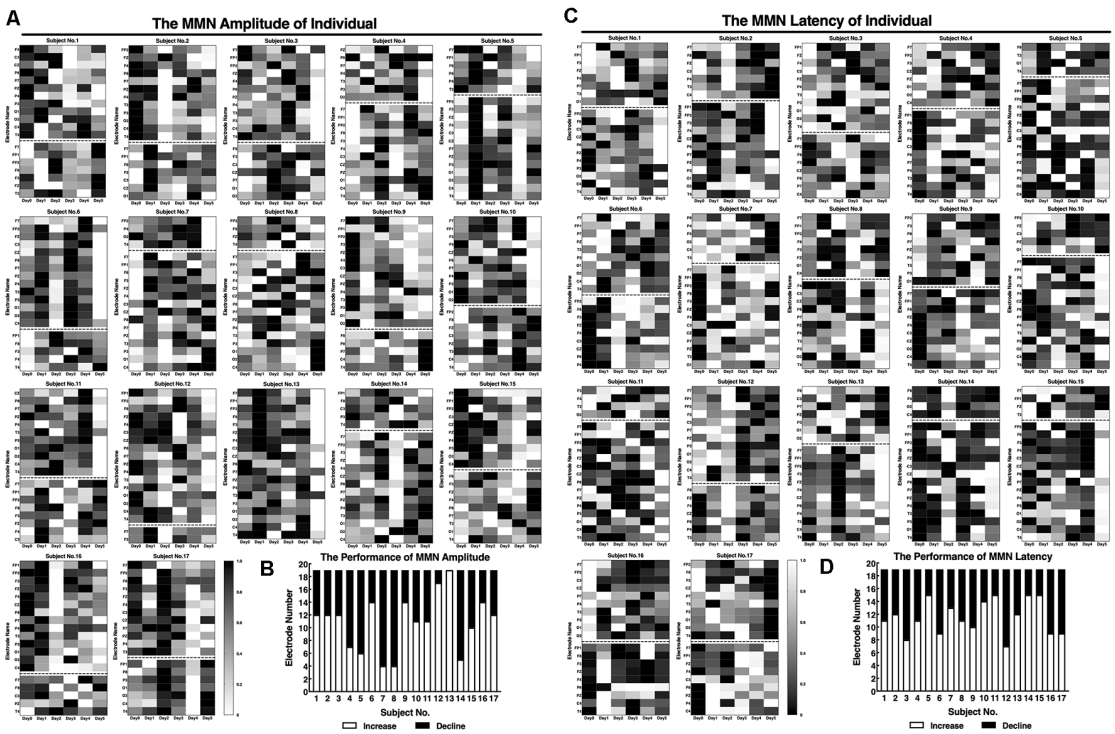

FIGURE 3 | Standard values of individual MMNs before and after the neurofeedback training. The amplitudes **(A)** and latencies **(C)** of the individual MMNs were normalized by processing the true values from 0 to 1. **(A,C)** The maximum value of the amplitude is shown in white, and the minimum is shown in black for each subject. **(B,D)** Statistics of the number of electrodes on day 5 performance amplitudes compared with that on day 0.

(Shibata et al., 2011; Chang et al., 2014). MMN responses are elicited by any discriminable auditory change that cannot be consciously discriminated. The healthy participants can unconsciously experience a significant improvement in the auditory discrimination of the stimuli applied during a previous study. Each subject was asked to focus on the visual signal (red discs) during our MMN neurofeedback training, and the subjects were required to neglect the auditory stimuli of the experiment

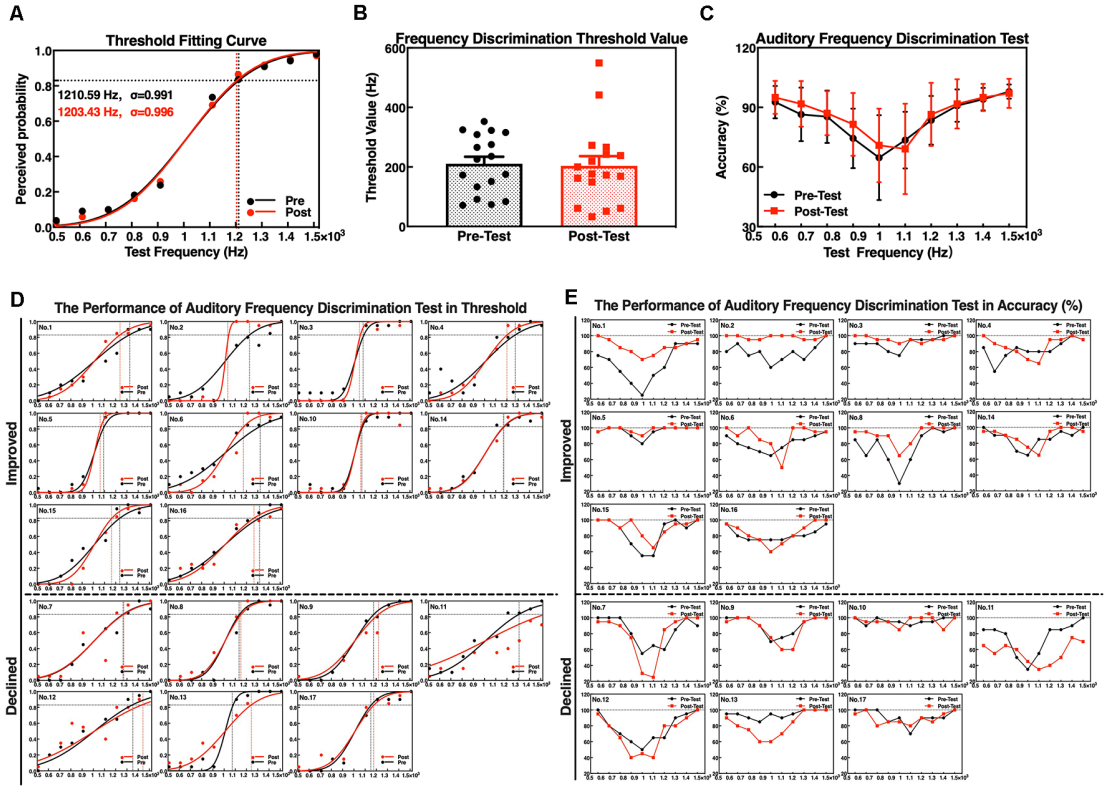

FIGURE 4 | Performance of auditory frequency discrimination task before and after the neurofeedback training. **(A)** Frequency threshold fitting curve; **(B)** discrimination threshold value; **(C)** discrimination accuracy. Individual performance of auditory frequency discrimination test as a threshold fitting curve **(D)** and as accuracy **(E)**.

as much as possible. Moreover, our results showed that the improvement of the amplitudes of MMN after the training is in agreement with previous studies (Chang et al., 2014). Numerous studies demonstrated that the parietal cortex is consistently linked to and involved in human memory processing, although early studies mostly focused on the medial temporal and frontal lobes (Gilmore et al., 2015). The intrinsic connectivity of the parietal memory network (PMN) reflects the familiarity of the stimuli in memory encoding and retrial and is disrupted in AD (Hu et al., 2019). The Pz electrode may be a potential target site for memory regulation in the neurofeedback training. The latencies of MMN in SCD patients showed no significant differences after training. The individual auditory discrimination threshold was used as the deviation stimulus in our study while a previous study used a fixed frequency as the deviation parameters. Some of our results are inconsistent with the previous data, and the discrepancy may be caused by different paradigm parameters of the experimental design (Chang et al., 2014, 2017). Considering that the MMN index discrimination of various sound stimuli can result from a rigid matching similar to behavioral discrimination, the MMN signals are associated with the magnitude of deviation and involve perceptual discriminability (Näätänen et al., 2017). In SCD patients, auditory discrimination is different because we observed that the auditory frequency discrimination threshold ranges from 1,200 to 300 Hz. A personal protocol to regulate the amplitude of MMN may be more suitable in the clinical neurofeedback training. Therefore, our results generate additional evidence that MMN neurofeedback can be used as an EEG-specific unconscious and personal neurofeedback training in the SCD patients, thus raising a possibility for a clinical intervention even in the case of the states of altered consciousness.

Improving the Auditory Discriminability

Previous studies in 2014 have shown that MMN neurofeedback training can improve discrimination between very similar tones, such as "1,000 Hz" and "1,008 Hz" by Chang et al. (2014). A study published in 2017 used MMN neurofeedback to successfully discriminate the English pronunciation between the letters "l" and "r" to facilitate the foreign language learning (Chang et al., 2017). These studies focused on the use of learning to discriminate the targeting of the similar stimuli, similar to discrimination between standard and deviant stimuli during the neurofeedback training to elicit MMN. However, in our study, the individual auditory discrimination threshold has to be considered because individual deviant stimuli were used in the training protocol. The thresholds decreased after the training indicating that auditory discrimination is improved; however, this effect was not statistically significant and only 60% of SCD patients (n = 10) were successful. We found that the

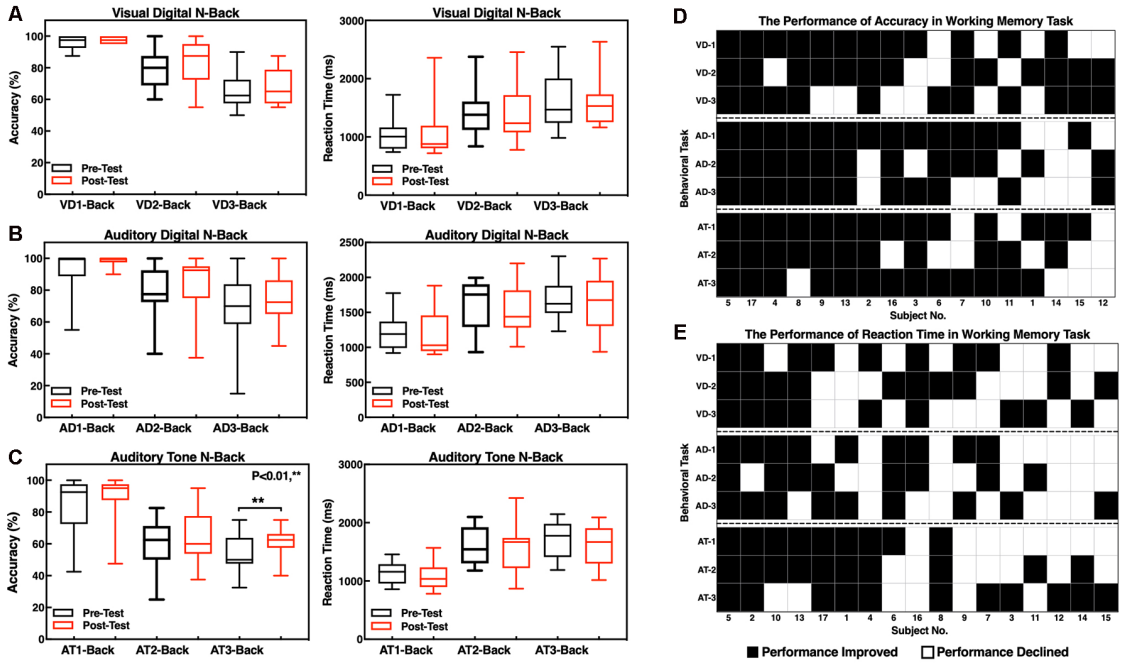

FIGURE 5 | Accuracy and reaction times (RTs) of the N-back tasks. **(A)** Visual digital N-back, **(B)** auditory digital N-back, and **(C)** auditory tone N-back. $^{**}p < 0.01$; red or black bars above and below the graph show the maximum and minimum accuracy or RT in each task, respectively. The statistics evaluation of the tasks based on the performance of individuals as accuracy **(D)** and RT **(E)**.

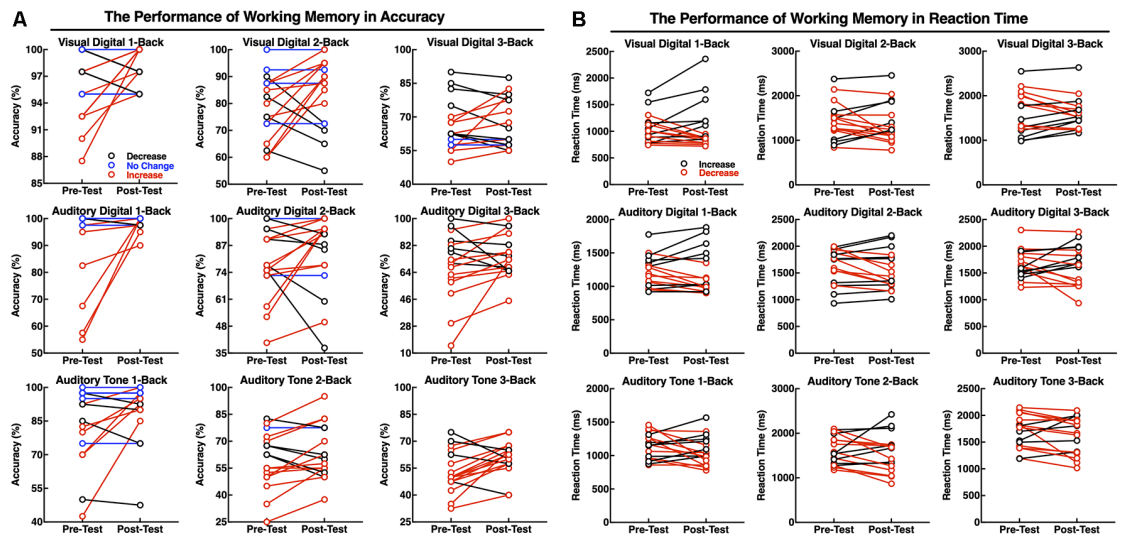

FIGURE 6 | Performance of the individuals in working memory (WM) tasks as accuracy **(A)** and RT **(B)**. The red line indicates that the accuracy was increased or that the reaction speed improved; the black line indicates that the accuracy was deceased and the reaction speed declined; and the blue line indicates no changes in performance accuracy.

accuracy of those SCD patients, which failed to decrease the auditory discrimination threshold, was lower than the accuracy in the successful tasks; the measurement of the threshold is based on the successful task statistics. Importantly, the subjects who demonstrated good training results have more compact training time. Previous studies indicate that different training intensity will influence the training effect and excessive or insufficient training may actually reduce the effectiveness of the training. Monitoring the learning curves of the subjects to set the appropriate training cycles may be implemented in the future.

Moreover, the most successful subjects used the psychological strategies for recalling positive things or focusing on certain things during the neurofeedback training and were able to adjust their psychological strategies autonomously when their training scores were decreased. To improve the efficiency of the intervention, the optimal training intensity and psychological strategy are worth to be explored in the future studies (Enriquez-Geppert et al., 2017).

Enhancing the Performance of Auditory Working Memory

At present, memory regulation based on the neurofeedback focuses on the regulation of the EEG frequency band. Training the alpha rhythm activity by neurofeedback to increase memory and attention has to consider that alpha activity inhibits the processes that are unnecessary or conflicting with the task being performed and thus can promote attention and memory by actively suppressing the distracting stimuli (Klimesch, 1999). Theta oscillations have been correlated with the memory encoding (Sauseng et al., 2010), and their excess is detected in AD patients; regulation of the theta activity always involved a neurofeedback protocol in the healthy subjects to enhance memory, even in the MCI, AD, and dementia patients (Luijmes et al., 2016). Previous studies have shown that in schizophrenic patients, MMN impairment is accompanied by poor WM performance (Kiang et al., 2007); a similar association is observed in the case of WM impairment in alcoholics and low performance of MMN (Bonetti et al., 2018). WM is considered a cognitive system, which is responsible for operating the information of various sensory modalities; and the neurons of the pre-supplementary motor area encode tactile and auditory information involved in the WM tasks, thus using a shared representation for both sensory modalities. A recent study indicated that individuals with higher visual WM performance have increased automatic neural responses to changes in the auditory characteristics (Bonetti et al., 2018). In older adults, automatic auditory processing guided by selection history was largely lacking (Sur and Golob, 2019). From the perspective of neurobiology, the generation of MMN is associated with N-methyl-D-aspartate receptors (NMDRs), which is the major molecular device for regulating the plasticity of the synaptic and memory functions (Li and Tsien, 2009). NMDRs are crucial in the activity-dependent synaptic changes, learning, and WM due to mediation of the excitatory postsynaptic potentials (Baez et al., 2018; Lisman et al., 1998). Moreover, auditory mismatches engage a hierarchical functional network of cortical sources, which are also interconnected by auditory white matter pathways. Neuroimaging studies have found that a disrupted pattern of the AD connectome that starts in peripheral regions, which refer to a set of cortical regions weekly connected in brain structural networks, and then hierarchically propagates to highly connected cortical brain regions, when patients show clinical symptoms. Moreover, peripheral regions might contribute to impaired memory performance in patients with SCD (Wang et al., 2017; Yan et al., 2018). Neurofeedback training can improve the auditory cortex plasticity by regulating neuronal synaptic plasticity and changing the neural networks of the brain (Emmert et al., 2017). Neurofeedback is a safe and noninvasive intervention that can influence cognitive functions and behavioral changes. To date, no adverse reactions of the neurofeedback training have been reported; however, it is not recommended to train people with serious mental problems (Marzbani et al., 2016). Therefore, enhancing WM based on the MMN neurofeedback may be an effective method of intervention not only in SCD patients but also in healthy older people; however, the persistence of the training effects lacks the data of the clinical follow-up study.

In this study, we have designed three types of WM in the form of N-back with three types of levels to assess the effects of the training to account for the degree of completion of the tasks in SCD patients with various educational backgrounds. The results indicate that the accuracy scores were improved in all WM tests vs. baseline and especially in the auditory tone 3-back, which significantly increased after the training. The auditory tones are the stimuli to induce MMN; thus, there is a limit of the performance of the WM effect with regard to the visual and auditory digits. Previous studies have shown an impact of the stimulation task type training on the WM types (Chan et al., 2019; Linares et al., 2019). A behavior study showed that enhanced transfer of the auditory discrimination learning is mediated by WM, which reflects that WM updating is related to fine auditory discrimination (Zhang et al., 2016). Actually, SCD is not strongly correlated with the concurrent level of cognitive ability as measured by objective cognitive tests; previous studies have shown that subjective memory complaints are associated with subsyndromal or subclinical depression in community-dwelling older adults (Zlatar et al., 2018). Therefore, the targeting of specific interventions for the regulation of cognitive ability will be more helpful in the case of the intervention treatment of patients with heterogeneous SCD.

Limitations and Further Research Directions

To assess the effectiveness of the clinical intervention, certain issues deserve further attention. For experimental design, setting up a double-blind experiment with a strict control group will be more convincing to demonstrate the effect of the training. Given the heterogeneity of patients, in addition to SCD heterogeneity, to include differences in the learning ability and living conditions, recruitment of a control group with similar subject characteristics is difficult considering that post-training activities that influence training results cannot be controlled. Current clinical intervention studies focus on small samples and the desired sample should be as large as possible. The timeline of the assessment of the clinical scales is usually longer than 3 months; hence, the methods and tasks for accessing the short-term intervention need to consider the operability and effectiveness of the patients. Moreover, we focused on discussion of the individual results while explaining the average results. Given the importance of SCD in diagnosis of the neurocognitive disorders and as potential predictor of a future cognitive decline, the individualization and targeted treatment of intervention methods will be explored in the future studies.

We propose a novel neurofeedback protocol based on the MMN amplitude to improve the performance of auditory WM in SCD patients. The preliminary results of our study may indicate that neurofeedback training based on MMN may be a potential treatment for the elderly with aging memory decline.

DATA AVAILABILITY STATEMENT

The datasets for this article are not publicly available because the research in this article involves personal information from SCD patients. Request to access the datasets should be approved by the Medical Research Ethics Committee and Institutional Review Board of Xuanwu Hospital.

ETHICS STATEMENT

The studies involving human participants were reviewed and approved by Medical Research Ethics Committee and Institutional Review Board of Xuanwu Hospital. The patients/participants provided their written informed consent to participate in this study. Written informed consent was obtained from the individual(s) for the publication of any potentially identifiable images or data included in this article.

AUTHOR CONTRIBUTIONS

GP contributed for the interpretation of data and wrote the article. RY and ZS designed the experiments and verified the effectiveness of the experiment. GG, YQ, and SW contributed to the collection and analysis of the data and performed the experiments. ML and JW are mainly responsible for the conception and design of the work. RG, YH, and TY revised the work critically for important intellectual content and also gave final approval of the version to be published.

FUNDING

This work was supported by the National Key R&D Program of China (grant number 2018YFC0115400), the National Natural Science Foundation of China (grant numbers 81671776, 61727807, and 61633018), the Beijing Municipal Science & Technology Commission (grant number Z191100010618004), and the Beijing Municipal Commission of Health and Family Planning (grant number PXM2020_026283_000002).

ACKNOWLEDGMENTS

We are thankful to all the study participants.

REFERENCES

Amieva, H., Ouvrard, C., Giulioli, C., Meillon, C., Rullier, L., and Dartigues, J.-F. (2015). Self-reported hearing loss, hearing aids and cognitive decline in elderly adults: a 25-year study. *J. Am. Geriatr. Soc.* 63, 2099–2104. doi: 10.1111/jgs.13649

Baez, M. V., Cercato, M. C., and Jerusalinsky, D. A. (2018). NMDA receptor subunits change after synaptic plasticity induction and learning and memory acquisition. *Neural Plast.* 2018:5093048. doi: 10.1155/2018/5093048

Berman, M. H., and Nichols, T. W. (2019). Treatment of neurodegeneration: integrating photobiomodulation and neurofeedback in Alzheimer's dementia and Parkinson's: a review. *Photobiomodul. Photomed. Laser Surg.* 37, 623–634. doi: 10.1089/photob.2019.4685

Bhome, R., Berry, A. J., Huntley, J. D., and Howard, R. J. (2018). Interventions for subjective cognitive decline: systematic review and meta-analysis. *BMJ Open* 8:e021610. doi: 10.1136/bmjopen-2018-021610

Bonetti, L., Haumann, N., Brattico, E., Kliuchko, M., Vuust, P., Särkämö, T., et al. (2018). Auditory sensory memory and working memory skills: association between frontal MMN and performance scores. *Brain Res.* 1700, 86–98. doi: 10.1016/j.brainres.2018.06.034

Bubbico, G., Lauriola, M., Sepede, G., Salice, S., Spina, E., Brondi, G., et al. (2019). Subjective cognitive decline and nighttime sleep alterations, a longitudinal analysis. *Front. Aging Neurosci.* 11:142. doi: 10.3389/fnagi.2019.00142

Chan, S., Mueller, U., and Masson, M. E. (2019). Far-transfer effects of strategy-based working memory training. *Front. Psychol.* 10:1285. doi: 10.3389/fpsyg.2019.01285

Chang, M., Iizuka, H., Kashioka, H., Naruse, Y., Furukawa, M., Ando, H., et al. (2017). Unconscious improvement in foreign language learning using mismatch negativity neurofeedback: a preliminary study. *PLoS One* 12:e0178694. doi: 10.1371/journal.pone.0178694

Chang, M., Iizuka, H., Naruse, Y., Ando, H., and Maeda, T. (2014). Unconscious learning of auditory discrimination using mismatch negativity (MMN) neurofeedback. *Sci. Rep.* 4:6729. doi: 10.1038/srep06729

Chen, J.-C., Macerollo, A., and Edwards, M. J. (2017). Mismatch negativity (MMN) as a biomarker of memory impairment in dementia. *Alzheimers Dement.* 13:P375. doi: 10.1016/j.jalz.2017.06.331

Crous-Bou, M., Minguillón, C., Gramunt, N., and Molinuevo, J. L. (2017). Alzheimer's disease prevention: from risk factors to early intervention. *Alzheimers Res. Ther.* 9:71. doi: 10.1186/s13195-017-0297-z

Delorme, A., and Makeig, S. (2004). EEGLAB: an open source toolbox for analysis of single-trial EEG dynamics including independent component analysis. *J. Neurosci. Methods* 134, 9–21. doi: 10.1016/j.jneumeth.2003.10.009

Emmert, K., Kopel, R., Koush, Y., Maire, R., Senn, P., Van De Ville, D., et al. (2017). Continuous vs. intermittent neurofeedback to regulate auditory cortex activity of tinnitus patients using real-time fMRI-A pilot study. *NeuroImage Clin.* 14, 97–104. doi: 10.1016/j.nicl.2016.12.023

Enriquez-Geppert, S., Huster, R. J., and Herrmann, C. S. (2017). EEG-neurofeedback as a tool to modulate cognition and behavior: a review tutorial. *Front. Hum. Neurosci.* 11:51. doi: 10.3389/fnhum.2017.00051

Ferguson, M. A., and Henshaw, H. (2015). Auditory training can improve working memory, attention and communication in adverse conditions for adults with hearing loss. *Front. Psychol.* 6:556. doi: 10.3389/fpsyg.2015.00556

Garrido, M. I., Kilner, J. M., Stephan, K. E., and Friston, K. J. (2009). The mismatch negativity: a review of underlying mechanisms. *Clin. Neurophysiol.* 120, 453–463. doi: 10.1016/j.clinph.2008.11.029

Gilmore, A. W., Nelson, S. M., and McDermott, K. B. (2015). A parietal memory network revealed by multiple MRI methods. *Trends Cogn. Sci.* 19, 534–543. doi: 10.1016/j.tics.2015.07.004

Hu, Y., Du, W., Zhang, Y., Li, N., Han, Y., and Yang, Z. (2019). Loss of parietal memory network integrity in Alzheimer's disease. *Front. Aging Neurosci.* 11:67. doi: 10.3389/fnagi.2019.00067

Jaeggi, S. M., Buschkuehl, M., Perrig, W. J., and Meier, B. (2010). The concurrent validity of the N-back task as a working memory measure. *Memory* 18, 394–412. doi: 10.1080/09658211003702171

Jessen, F., Amariglio, R. E., Van Boxtel, M., Breteler, M., Ceccaldi, M., Chételat, G., et al. (2014). A conceptual framework for research on subjective cognitive decline in preclinical Alzheimer's disease. *Alzheimers Dement.* 10, 844–852. doi: 10.1016/j.jalz.2014.01.001

Kaufmann, L., Wood, G., Robertson, M., Marksteiner, J., and Kober, S. E. (2019). EEG-neurofeedback as a training method for cognitive and non-cognitive functions in early dementia: a case report. *Lern. Lernst.* 8,179–189. doi: 10.1024/2235-0977/a000274

Kiang, M., Light, G. A., Prugh, J., Coulson, S., Braff, D. L., and Kutas, M. (2007). Cognitive, neurophysiological and functional correlates of proverb interpretation abnormalities in schizophrenia. *J. Int. Neuropsychol. Soc.* 13, 653–663. doi: 10.1017/s1355617707070816

Kishon-Rabin, L., Roth, D. A.-E., Van Dijk, B., Yinon, T., and Amir, O. (2004). Frequency discrimination thresholds: the effect of increment versus decrement detection of frequency. *J. Basic Clin. Physiol. Pharmacol.* 15, 29–40. doi: 10.1515/jbcpp.2004.15.1-2.29

Klimesch, W. (1999). EEG alpha and theta oscillations reflect cognitive and memory performance: a review and analysis. *Brain Res. Rev.* 29, 169–195. doi: 10.1016/s0165-0173(98)00056-3

Koppara, A., Wagner, M., Lange, C., Ernst, A., Wiese, B., König, H.-H., et al. (2015). Cognitive performance before and after the onset of subjective cognitive decline in old age. *Alzheimers Dement.* 1, 194–205. doi: 10.1016/j.dadm.2015.02.005

Kraus, N., Strait, D., and Parbery-Clark, A. (2012). Cognitive factors shape brain networks for auditory skills: spotlight on auditory working memory. *Ann. N Y Acad. Sci.* 1252, 100–107. doi: 10.1111/j.1749-6632.2012.06463.x

Laptinskaya, D., Thurm, F., Küster, O. C., Fissler, P., Schlee, W., Kolassa, S., et al. (2018). Auditory memory decay as reflected by a new mismatch negativity score is associated with episodic memory in older adults at risk of dementia. *Front. Aging Neurosci.* 10:5. doi: 10.3389/fnagi.2018.00005

Li, F., and Tsien, J. Z. (2009). Memory and the NMDA receptors. *N. Engl. J. Med.* 361, 302–303. doi: 10.1056/NEJMcibr0902052

Lin, Y., Wu, W., Wu, C., Liu, B., and Gao, X. (2013). Extraction of mismatch negativity using a resampling-based spatial filtering method. *J. Neural Eng.* 10:026015. doi: 10.1088/1741-2560/10/2/026015

Lin, F. R., Yaffe, K., Xia, J., Xue, Q.-L., Harris, T. B., Purchase-Helzner, E., et al. (2013). Hearing loss and cognitive decline in older adults. *JAMA Intern. Med.* 173, 293–299. doi: 10.1001/jamainternmed.2013.1868

Linares, R., Borella, E., Lechuga, M. T., Carretti, B., and Pelegrina, S. (2019). Nearest transfer effects of working memory training: a comparison of two programs focused on working memory updating. *PLoS One* 14:e0211321. doi: 10.1371/journal.pone.0211321

Lindín, M., Correa, K., Zurrón, M., and Díaz, F. (2013). Mismatch negativity (MMN) amplitude as a biomarker of sensory memory deficit in amnestic mild cognitive impairment. *Front. Aging Neurosci.* 5:79. doi: 10.3389/fnagi.2013.00079

Lisman, J. E., Fellous, J.-M., and Wang, X.-J. (1998). A role for NMDA-receptor channels in working memory. *Nat. Neurosci.* 1, 273–275. doi: 10.1038/1086

Livingston, G., Sommerlad, A., Orgeta, V., Costafreda, S. G., Huntley, J., Ames, D., et al. (2017). Dementia prevention, intervention, and care. *Lancet* 390, 2673–2734. doi: 10.1016/S0140-6736(17)31363-6

Luijmes, R. E., Pouwels, S., and Boonman, J. (2016). The effectiveness of neurofeedback on cognitive functioning in patients with Alzheimer's disease: preliminary results. *Neurophysiol. Clin.* 46, 179–187. doi: 10.1016/j.neucli.2016.05.069

Marzbani, H., Marateb, H. R., and Mansourian, M. (2016). Neurofeedback: a comprehensive review on system design, methodology and clinical applications. *Basic Clin. Neurosci.* 7, 143–158. doi: 10.15412/j.bcn.03070208

Molholm, S., Martinez, A., Ritter, W., Javitt, D. C., and Foxe, J. J. (2005). The neural circuitry of pre-attentive auditory change-detection: an fMRI study of pitch and duration mismatch negativity generators. *Cereb. Cortex* 15, 545–551. doi: 10.1093/cercor/bhh155

Näätänen, R., and Alho, K. (1997). Mismatch negativity—the measure for central sound representation accuracy. *Audiol. Neurotol.* 2, 341–353. doi: 10.1159/000259255

Näätänen, R., Kujala, T., Kreegipuu, K., Carlson, S., Escera, C., Baldeweg, T., et al. (2011). The mismatch negativity: an index of cognitive decline in neuropsychiatric and neurological diseases and in ageing. *Brain* 134, 3435–3453. doi: 10.1093/brain/awr064

Näätänen, R., Petersen, B., Torppa, R., Lonka, E., and Vuust, P. (2017). The MMN as a viable and objective marker of auditory development in CI users. *Hear. Res.* 353, 57–75. doi: 10.1016/j.heares.2017.07.007

Pei, G., Guo, G., Chen, D., Yang, R., Shi, Z., Wang, S., et al. (2020). BrainKilter: a real-time EEG analysis platform for neurofeedback design and training. *IEEE Access* 8, 57661–57673. doi: 10.1109/ACCESS.2020.2967903

Rabin, L. A., Smart, C. M., Crane, P. K., Amariglio, R. E., Berman, L. M., Boada, M., et al. (2015). Subjective cognitive decline in older adults: an overview of self-report measures used across 19 international research studies. *J. Alzheimers Dis.* 48, S63–S86. doi: 10.3233/JAD-150154

Ramot, M., Grossman, S., Friedman, D., and Malach, R. (2016). Covert neurofeedback without awareness shapes cortical network spontaneous connectivity. *Proc. Natl. Acad. Sci. U S A* 113, E2413–E2420. doi: 10.1073/pnas.1516857113

Reis, J., Portugal, A. M., Fernandes, L., Afonso, N., Pereira, M., Sousa, N., et al. (2016). An α and theta intensive and short neurofeedback protocol for healthy aging working-memory training. *Front. Aging Neurosci.* 8:157. doi: 10.3389/fnagi.2016.00157

Restuccia, D., Zanini, S., Cazzagon, M., Del Piero, I., Martucci, L., and Della Marca, G. (2009). Somatosensory mismatch negativity in healthy children. *Dev. Med. Child Neurol.* 51, 991–998. doi: 10.1111/j.1469-8749.2009.03367.x

Sauseng, P., Griesmayr, B., Freunberger, R., and Klimesch, W. (2010). Control mechanisms in working memory: a possible function of EEG theta oscillations. *Neurosci. Biobehav. Rev.* 34, 1015–1022. doi: 10.1016/j.neubiorev.2009.12.006

Shibata, K., Watanabe, T., Sasaki, Y., and Kawato, M. (2011). Perceptual learning incepted by decoded fMRI neurofeedback without stimulus presentation. *Science* 334, 1413–1415. doi: 10.1126/science.1212003

Smart, C. M., Karr, J. E., Areshenkoff, C. N., Rabin, L. A., Hudon, C., Gates, N., et al. (2017). Non-pharmacologic interventions for older adults with subjective cognitive decline: systematic review, meta-analysis, and preliminary recommendations. *Neuropsychol. Rev.* 27, 245–257. doi: 10.1007/s11065-017-9342-8

Sperling, R. A., Aisen, P. S., Beckett, L. A., Bennett, D. A., Craft, S., Fagan, A. M., et al. (2011). Toward defining the preclinical stages of Alzheimer's disease: recommendations from the national institute on aging-Alzheimer's association workgroups on diagnostic guidelines for Alzheimer's disease. *Alzheimers Dement.* 7, 280–292. doi: 10.1016/j.jalz.2011.03.003

Sur, S., and Golob, E. J. (2019). Neural correlates of auditory sensory memory dynamics in the aging brain. *Neurobiol. Aging* 88, 128–136. doi: 10.1016/j.neurobiolaging.2019.12.020

Sweetow, R. W., and Sabes, J. H. (2006). The need for and development of an adaptive listening and communication enhancement (LACE^{TM}) program. *J. Am. Acad. Audiol.* 17, 538–558. doi: 10.3766/jaaa.17.8.2

Taljaard, D. S., Olaithe, M., Brennan-Jones, C. G., Eikelboom, R. H., and Bucks, R. S. (2016). The relationship between hearing impairment and cognitive function: a meta-analysis in adults. *Clin. Otolaryngol.* 41, 718–729. doi: 10.1111/coa.12607

Uchida, Y., Sugiura, S., Nishita, Y., Saji, N., Sone, M., and Ueda, H. (2019). Age-related hearing loss and cognitive decline—the potential mechanisms linking the two. *Auris Nasus Larynx* 46, 1–9. doi: 10.1016/j.anl.2018.08.010

Van Doren, J., Arns, M., Heinrich, H., Vollebregt, M. A., Strehl, U., and Loo, S. K. (2019). Sustained effects of neurofeedback in ADHD: a systematic review and meta-analysis. *Eur. Child Adolesc. Psychiatry* 28, 293–305. doi: 10.1007/s00787-018-1121-4

Wang, B., Niu, Y., Miao, L., Cao, R., Yan, P., Guo, H., et al. (2017). Decreased complexity in Alzheimer's disease: resting-state fMRI evidence of brain entropy mapping. *Front. Aging Neurosci.* 9:378. doi: 10.3389/fnagi.2017.00378

Wichmann, F. A., and Hill, N. J. (2001a). The psychometric function: I. Fitting, sampling, and goodness of fit. *Percept. Psychophys.* 63, 1293–1313. doi: 10.3758/bf03194544

Wichmann, F. A., and Hill, N. J. (2001b). The psychometric function: II. Bootstrap-based confidence intervals and sampling. *Percept. Psychophys.* 63, 1314–1329. doi: 10.3758/bf03194545

Williams, H., and Tanabe, P. (2016). Sickle cell disease: a review of nonpharmacological approaches for pain. *J. Pain Symptom Manage.* 51, 163–177. doi: 10.1016/j.jpainsymman.2015.10.017

Yan, T., Wang, W., Yang, L., Chen, K., Chen, R., and Han, Y. (2018). Rich club disturbances of the human connectome from subjective cognitive decline to Alzheimer's disease. *Theranostics* 8, 3237–3255. doi: 10.7150/thno.23772

Zhang, J., Dong, X., Wang, L., Zhao, L., Weng, Z., Zhang, T., et al. (2018). Gender differences in global functional connectivity during facial emotion processing: a visual MMN study. *Front. Behav. Neurosci.* 12:220. doi: 10.3389/fnbeh.2018.00220

Zhang, Y.-X., Moore, D. R., Guiraud, J., Molloy, K., Yan, T.-T., and Amitay, S. (2016). Auditory discrimination learning: role of working memory. *PLoS One* 11:e0147320. doi: 10.1371/journal.pone.0147320

Zlatar, Z. Z., Muniz, M. C., Espinoza, S. G., Gratianne, R., Gollan, T. H., Galasko, D., et al. (2018). Subjective cognitive decline, objective cognition, and depression in older hispanics screened for memory impairment. *J. Alzheimers Dis.* 63, 949–956. doi: 10.3233/jad-170865

Conflict of Interest: The authors declare that the research was conducted in the absence of any commercial or financial relationships that could be construed as a potential conflict of interest.

frontiers in Neuroscience

REVIEW
published: 16 October 2020
doi: 10.3389/fnins.2020.558532

Current Status of Stem Cell-Derived Therapies for Parkinson's Disease: From Cell Assessment and Imaging Modalities to Clinical Trials

Se Eun Jang[1], Lifeng Qiu[1], Ling Ling Chan[2,3], Eng-King Tan[3,4] and Li Zeng[1,3,5]**

[1] Neural Stem Cell Research Lab, Research Department, National Neuroscience Institute, Singapore, Singapore, [2] Department of Diagnostic Radiology, Singapore General Hospital, Singapore, Singapore, [3] Neuroscience & Behavioral Disorders Program, Duke University and National University of Singapore (DUKE-NUS), Graduate Medical School, Singapore, Singapore, [4] Department of Neurology, National Neuroscience Institute, Singapore General Hospital Campus, Singapore, Singapore, [5] Lee Kong Chian School of Medicine, Nanyang Technological University, Novena Campus, Singapore, Singapore

OPEN ACCESS

Edited by:
Woon-Man Kung, Chinese Culture University, Taiwan

Reviewed by:
Darius Widera, University of Reading, United Kingdom
Paolo Solla, Azienda Ospedaliero-Universitaria Cagliari, Italy

***Correspondence:**
Eng-King Tan
tan.eng.king@singhealth.com.sg
Li Zeng
li_zeng@nni.com.sg

Specialty section:
This article was submitted to Neurodegeneration, a section of the journal Frontiers in Neuroscience

Received: *03 May 2020*
Accepted: *17 September 2020*
Published: *16 October 2020*

Citation:
Jang SE, Qiu L, Chan LL, Tan EK and Zeng L (2020) Current Status of Stem Cell-Derived Therapies for Parkinson's Disease: From Cell Assessment and Imaging Modalities to Clinical Trials. Front. Neurosci. 14:558532. doi: 10.3389/fnins.2020.558532

Curative therapies or treatments reversing the progression of Parkinson's disease (PD) have attracted considerable interest in the last few decades. PD is characterized by the gradual loss of dopaminergic (DA) neurons and decreased striatal dopamine levels. Current challenges include optimizing neuroprotective strategies, developing personalized drug therapy, and minimizing side effects from the long-term prescription of pharmacological drugs used to relieve short-term motor symptoms. Transplantation of DA cells into PD patients' brains to replace degenerated DA has the potential to change the treatment paradigm. Herein, we provide updates on current progress in stem cell-derived DA neuron transplantation as a therapeutic alternative for PD. We briefly highlight cell sources for transplantation and focus on cell assessment methods such as identification of genetic markers, single-cell sequencing, and imaging modalities used to access cell survival and function. More importantly, we summarize clinical reports of patients who have undergone cell-derived transplantation in PD to better perceive lessons that can be drawn from past and present clinical outcomes. Modifying factors include (1) source of the stem cells, (2) quality of the stem cells, (3) age of the patient, (4) stage of disease progression at the time of cell therapy, (5) surgical technique/practices, and (6) the use of immunosuppression. We await the outcomes of joint efforts in clinical trials around the world such as NYSTEM and CiRA to further guide us in the selection of the most suitable parameters for cell-based neurotransplantation in PD.

Keywords: Parkinson's disease, dopaminergic neurons, transplantation, stem cells, imaging modalities, neuroimaging, clinical trials

INTRODUCTION

Parkinson's disease (PD) is one of the most prevalent chronic neurodegenerative disorder characterized by the selective, progressive loss of nigrostriatal dopaminergic (DA) neurons in the substantia nigra pars compacta. The main hallmarks of PD include the presence of α-synuclein positive Lewy bodies and neuroinflammation (MacGeer and McGeer, 2008; More et al., 2013)

that extends across many areas of the central nervous system (CNS), affecting the enteric and autonomic systems, in particular (Goedert et al., 2013), causing impairments in motor movements such as bradykinesia (slowed movements), tremors, postural instability, and muscle rigidity. Furthermore, PD patients have shown non-motor disease manifestations such as rapid eye movement (REM), sleep behavior disorders, depression, hyposmia, and constipation (Olanow et al., 2009). Unfortunately, there are no curative therapies available to modify or reverse the progression of the underlying disease processes to date.

The current gold standard for PD treatment is through the ingestion of levodopa, which has been approved by the US Food and Drug Administration in the 1970s and has continuously shown positive results in temporal amelioration of PD symptoms (Fahn, 2003, 2006). However, long-term exposure to levodopa results in a gradual decrease in drug effectiveness and shorter periods of benefit, leading to levodopa-induced dyskinesias (motor fluctuations), as well as psychiatric and cognitive problems. Alternatively, surgical strategies, such as deep brain stimulation (DBS), have shown to alleviate PD motor symptoms (Siegfried and Lippitz, 1994; Limousin et al., 1995) and offer symptomatic relief that cannot be controlled with medications (Alamri et al., 2015). However, its application is not only limited to early-to-mid PD stages but also loses efficacy after a few years (deSouza et al., 2013).

In the last few decades, cell-based therapy using human stem cells has made large strides in overcoming the abovementioned limitations in PD treatment. Also known as regenerative medicine, stem cell therapy is believed to replace diseased, dysfunctional, or damaged tissue in hopes to restore lost neuronal circulatory caused by focal degeneration of mesencephalic dopaminergic (mDA) neurons. Specifically, neural progenies from pluripotent stem cells (PSCs) are known to hold great potential as a succeeding treatment for neurodegenerative diseases (Hu et al., 2010; Kriks et al., 2011; Ma et al., 2012). Today, DA neurons differentiated from stem cells are paving the way as a new, alternative approach in the treatment of PD. In this review article, we briefly highlight the major sources of stem cells used in preclinical and clinical PD observations (have been thoroughly reviewed in various articles, refer to Stoker, 2018). We focus on key methodologies currently applied in cell assessment, imaging modalities, and also further discuss ongoing stem cell-based clinical trials in PD. This also includes key challenges that the field is encountering and the prospects of stem cell therapy in PD.

CELL SOURCES

First, we briefly discuss the various types of stem cells currently being used as a source for cell-based therapy in PD. We also include the pros and cons of each cell line (**Table 1**), followed by the characterization of graft quality through various cell assessment methods (Cell Assessment of Differentiated DA Neurons section).

Fetal Ventral Mesencephalic Cells

In the early 1970s, Olson and colleagues successfully transplanted adrenal chromaffin cells and embryonic DA neurons into the anterior chamber of the eye in rats and showed that the viability of grafted neurons was best achieved using developing embryonic neurons (Olson and Malmfors, 1970; Olson and Seiger, 1972). Parkinsonism rat and monkey models grafted with early gestational age dopamine-rich mesencephalic neurons formed neurite protrusions and synthesize dopamine (Dunnett et al., 1983; Brundin et al., 1986; Redmond et al., 1986; Stromberg et al., 1986; Bakay et al., 1987). Furthermore, successful integration of transplanted cells into the host brain neuronal network was demonstrated through synaptic integration using a rabies-based monosynaptic tracing method (Cardoso et al., 2018). Behavioral studies in PD rodents and primates with human fetal DA neuron transplantation showed higher efficacy in improvement of behavioral deficits as compared to conventional adrenal medullary tissue transplants (Bjorklund and Stenevi, 1979, Perlow et al., 1979; Freed et al., 1981; Morihisa et al., 1984). Also, pioneering clinical studies in human fetal ventral mesencephalic (fVM) transplantation into the caudate and putamen of PD patients in Sweden, United Kingdom, and United States reported moderate amelioration of PD symptoms (Lindvall et al., 1988; Madrazo et al., 1988; Freed et al., 1990; Freed et al., 2001; Olanow et al., 2003). Moreover, normal striatal F-DOPA uptake was 3–5 years post-surgery, including gradual motor improvements that sustained up to 18 years post-transplantation (Kefalopoulou et al., 2014). However, the majority of successful cases were performed in PD patients under the age of 60 (Ma et al., 2010). Whether graft-induced dyskinesias are characteristics of neural transplantation has to be better studied and analyzed (Freed et al., 2001; Hagell et al., 2002; Olanow et al., 2003; Ma et al., 2010). Nonetheless, obtaining as many as up to seven human fetal donors (aged 6–9 weeks after conception) for each host raises many ethical concerns and logistical challenges for a disease affecting millions of people worldwide (Steinbeck and Studer, 2015; Barker and Consortium, 2019). Furthermore, the difficulty in preaccessing a cell type before transplantation is a major challenge in standardization as the heterogenicity of cell population within the graft is inevitable, contributing to high variability in the degree of symptomatic recovery. All in all, the additional risk in cell contamination of unwanted cell types during tissue extraction hampered the downstream translation of fVM transplantation as an alternative therapeutic option.

Human Embryonic Stem Cells

Due to the abovementioned ethical controversies in utilizing hfVM tissues for cell-based therapy (and other limitations), human embryonic stem cells (hESCs) were identified as a prospective substitute (Thomson et al., 1998; Reubinoff et al., 2000; Barker, 2014). These subsets of pluripotent cells are located in the inner cell mass of early embryonic blastocyst commonly derived from *in vitro* fertilization (Evans and Kaufman, 1981; Thomson et al., 1998) and hold the capability to generate into a plethora of cell lines through a spontaneous differentiation

TABLE 1 | Cells used in transplantation for Parkinson's disease (PD).

Cell type	Clinical trial	Advantages	Disadvantages
Fetal ventral mesencephalic cells (fVM)	Yes/ongoing (TRANSEURO; NCT01898390)	• Good long-term graft survival post-transplantation	• Unpredictable and limited supply of cell source Ethical concerns
Embryonic stem cells (ESC)	Ongoing (European-based STEM-PD, NYSTEM, NCT02452723, NCT03119636)	• Indefinite expandability • Good graft survival post-transplantation • Advancement in GMP-grade cells	• Ethical concerns • Possible risk of tumorigenesis • Tissue rejection; pre- and post-operative immunosuppression
Induced pluripotent stem cells (iPSC)	Yes/ongoing (CiRA)	• Indefinite expandability • Easily accessible cell source • Immunologically matching cells • No need of immunosuppression treatment	• High heterogeneity of cell line between individual cell line resulting in complex procedures • Low reprogramming efficiency • High operative cost • Time consuming • Possible risk of tumorigenesis
Neural progenitor cells (NPC)	Yes/ongoing (NCT03309514, NCT01329926)	• Multipotent cells • Easy expansion and differentiation protocol • Large quantity	• Invasive tissue collection step • Limited proliferation • Low graft survivability • Limited proliferative ability

protocol *in vitro* (Itskovitz-Eldor et al., 2000; Lee et al., 2000; Reubinoff et al., 2001; Zhang et al., 2001). In the case of neuroepithelial cell-derived DA neuron differentiation, cells showed an increase in a multitude of cellular marker expression for midbrain DA neurons with fiber outgrowth (Thomson et al., 1998; Kawasaki et al., 2000; Kim et al., 2002) and electrophysiologically active neurons that produced DA in an activity-dependent manner (Yan et al., 2005). In later years, it was identified that DA neurons unlike all other neurons are generated from the midbrain floor plate. With newly improvised DA neuron differentiation protocol (Fasano et al., 2010; Kriks et al., 2011; Kirkeby et al., 2012), a significant upregulation of midbrain DA neuronal markers was observed along with recovery in motor defects in preclinical studies (Kirkeby et al., 2012, 2017a; Grealish et al., 2014). Unfortunately, key limitations lie in the difficulty in controlling the maturation stage of embryonic cultures and cellular heterogeneity, which may lead to negative outcomes in therapeutic applications (Stewart et al., 2006; Roy et al., 2006; Cho et al., 2008; Koch et al., 2009). Other caveats include the associated risk in tumor generation and teratoma due to their high pluripotent phenotype (Ben-Hur et al., 2004; Roy et al., 2006; Brederlau et al., 2006; Sonntag et al., 2007; Yang et al., 2008). In 2001, ethical concerns in hESC research resulted in a restriction on federal fundings in the United States. Fortunately, this legislation has been revoked by President Barack Obama in 2007. With this advantage, New York Stem Cell Science Consortia at Memorial Sloan Kettering Cancer Center conducted ongoing projects such as the development of good manufacturing practice (GMP) clinical-grade hESC-derived DA neurons for FDA approval in future transplantation studies (refer to section "GMP cryopreservation of cells"), optimization of cell purification to enrich A9 type DA neurons, and also, active involvement in strategical planning for clinical trial of hESCs in Parkinson's disease.[1]

[1]https://www.mskcc.org

Human-Induced Pluripotent Stem Cells (hiPSCs)

The field of stem cell research and regenerative medicine was revolutionized in 2006 when human fibroblast cells were successfully reprogrammed into pluripotent cell lines using four transcription factors: c-Myc (or Nanog, Lin28), Oct3/4, Klf4, and Sox2 (Takahashi and Yamanaka, 2006; Takahashi et al., 2007; Yu et al., 2007). Reprogrammed iPSCs have been a highly attractive cell source as they have the characteristics of hESCs (in terms of morphology and genetic profile) (Fairchild, 2010; Phanstiel et al., 2011), and they have a relatively simpler extraction process. Tissue collection is non-invasive as host cells from skin fibroblast (Pulecio et al., 2014), peripheral blood mononuclear cells, and umbilical cord mesenchymal cells (Park et al., 2008; Senju et al., 2011; Biju et al., 2013; Qin et al., 2013) could be used to differentiate into patient-specific neurons *in vitro* (Soldner et al., 2009; Beevers et al., 2013; Eigentler et al., 2013; Sison et al., 2018). This would also avoid allogenic recognition and ethical concerns (Takahashi and Yamanaka, 2016). In PD studies, the quality of iPSC-derived DA neurons was highly similar to that of hESCs (Cooper et al., 2010; Doi et al., 2014; Kikuchi et al., 2017; Lehnen et al., 2017), and human leukocyte antigen (HLA)-matched allogeneic neural transplantation into monkeys increased the efficacy of cell survival and function (Morizane et al., 2017). Animal studies demonstrated successful amelioration of PD symptoms resulting from iPSC-derived DA neuron transplantation (Wakeman et al., 2017). Further refinement and characterization are necessary to achieve precise cell fate conversion of reprogrammed cells. Similar to ESCs, it is important that minimal manipulation is made during reprogramming prior to cell delivery.

GMP Cryopreservation of Cells

The generation of good manufacturing practice (GMP)-compliant, deliverable midbrain DA (mDA) progenitors/neurons optimized for cell-based therapy for PD is a major challenge. Currently, a diverse collection of clinical-grade hESC lines are

available as starting material to generate GMP-compliant mDA progenitors/neurons. In fact, GMP compliant differentiation protocols and reagents have been successfully applied to generate GMP mDA neurons (Liu et al., 2013; Peng et al., 2014).

In comparison, the availability of clinical-grade iPSCs is relatively lesser due to the lack of technology that involves complex reprogramming methodologies. Major hurdles of the clinical translation of mDA cells therapy include (i) quality control of the identity, safety, and efficacy of cell product in a consistent and real-time manner, (ii) determination of the precise time points at which DA precursors/neurons can be cryopreserved and banked without affecting its' quality, (iii) good postthaw viability of mDA cells, and (iv) characteristics and functionality of the population of cells should have minimal to no alterations after thawing. XCell Science has generated GMP-compatible authentic DA neurons, which are functional when transplanted into PD animal model (Peng et al., 2014) where cells were cryopreserved at day 14 after neuronal stem cell (NSC) stage. Similar studies were also reported by Cellular Dynamics International using more mature mDA cells in postmitotic stage (Wakeman et al., 2017). Successful generation of GMP-grade cryopreserved cells would allow for storage of a large batch of DA neurons and also increase the flexibility in operational schedule organization without the dependence on GMP-manufacturing site.

CELL ASSESSMENT OF DIFFERENTIATED DA NEURONS

Understanding the key type of DA neurons required to achieve downstream restoration of PD pathology is essential. The mesotelencephalic DA system in the midbrain contains two main groups: the A9 neuronal clusters of the nigrostriatal DA pathway located in the zona compacta, the substantia nigra involved in the control of posture, and the A10 neurons located in the ventromedial mesencephalic tegmentum that regulates the locomotor activity and emotional behavior (Dahlstroem and Fuxe, 1964; Anden et al., 1966; Ungerstedt, 1971; Lindvall and Bjorklund, 1974; Pijnenburg et al., 1976; Papp and Bal, 1986). Dysfunction of the nigrostriatal system has been linked to Parkinsonism and later to schizophrenia, drug addiction, and depression (Robinson and Berridge, 1993; Meyer-Lindenberg et al., 2002). Differences between the two DA cell populations have been observed in neurochemistry and in spontaneous neuronal firing (Grenhoff et al., 1988; Wolfart et al., 2001; Neuhoff et al., 2002). More importantly, A9 neurons display significantly enhanced levels of neuromelanin pigmentation as compared to other dopamine-producing neurons (Mann and Yates, 1983; Hirsch et al., 1988; Gibb, 1992; Kastner et al., 1992). This could account for the association of early loss of A9 DA neurons in Parkinson's disease with increased vulnerability upon disease progression with the relative preservation of A10 DA neurons (Hirsch et al., 1988; German et al., 1989; German et al., 1992; Damier et al., 1999; Halliday et al., 2005; Alavian et al., 2008).

Generally, stem cells are differentiated into specific nigra A9 DA neurons in large quantities prior to PD transplantation. This step has been thoroughly reviewed by many articles such as in Fan et al. (2020) and, thus, will not be further discussed here. However, we focus on developments in technology in cell assessment of differentiated DA neurons.

Assessment of the Efficacy of Cell Transplants With Immunostaining Characterization

Prior to stem cell transplantation, it is important to be able to fully characterize differentiated cell types to avoid heterogenicity of cell population (also known as cellular contamination). Previous studies have shown that transplantation of fetal SN-A9 DA neurons suffices the requirement for striatal reinnervation and recovery of PD-like behavioral observations (Grealish et al., 2010). However, tumor formation (Roy et al., 2006; Brederlau et al., 2006; Elkabetz et al., 2008; Doi et al., 2012) and development of graft-induced dyskinesia could arise from the high heterogenicity of serotonergic neurons (Carlsson et al., 2007; Politis et al., 2010). As cells are normally transplanted as immature progenitor cells, developing methods that can characterize and predict its functional maturation and therapeutic efficacy is crucial. Hence, to circumvent these limitations prior to proceeding into clinical trials, methods to isolate homogenous population of DA progenitor cells have been closely evaluated (Fukuda et al., 2006; Pruszak et al., 2009; Jonsson et al., 2009; Ganat et al., 2012; Sundberg et al., 2013). This includes developing meaningful quality control assays to assess cell type to avoid having heterogeneous mixtures of cells (includes phenotypes and degree of maturity) and batch-to-batch variation. The quality of differentiated mesencephalic A9 DA neurons that represent those in the substantia nigral para compacta or into immature progenitor cells is vital to determine the therapeutic efficacy of cell transplantation in the Parkinsonian brain. It is well understood that the orchestration of specific gene expression patterns is highly correlated to DA cell differentiation and survival. Therefore, the establishment and determination of specific gene expression markers have been used to positively characterize differentiated cells *in vitro*.

In the case of mDA progenitor neuron specifications, positive gene expression of common transcription factors FOXA2, LMX1A, and OTX2 and negative markers (non-neural) such as Afp, Gata4, and Brachyury have been quantitatively analyzed (Chung et al., 2009; Lin et al., 2009; Jaeger et al., 2011; Kriks et al., 2011; Kirkeby et al., 2012; Salti et al., 2013; Doi et al., 2014). More importantly, the upregulation and downregulation of these markers at a given stage *in vitro* governs the efficiency of cell fate determination. Unfortunately, these markers have been shown to coexpress in the diencephalic progenitor cells of the subthalamic nucleus (STN) (Kee et al., 2017). Furthermore, the expression of the positive genetic marker for DA neurons, tyrosine hydroxylase (TH), a rate-limiting enzyme in dopamine synthesis (Daadi and Weiss, 1999; Sonntag et al., 2004; Kirkeby et al., 2017a), and the levels of GIRK2 have also been observed in many cell types *in vitro* (Thompson et al., 2005; Kirkeby et al.,

2012; Reyes et al., 2012; Grow et al., 2016). Moreover, common positive markers used to isolate high-quality DA progenitor cells include EN1 and SPRY1 (Simon et al., 2001; Alberi et al., 2004; Kirkeby et al., 2017a); Nurr1 (Le et al., 1999); FOXA2, LMX1B, and MSX1 (Andersson et al., 2006; Chung et al., 2011), and the bicoid-related homeodomain factor Ptx3/Pitx3 (Hargus et al., 2010). It is noteworthy that some discrepancies have been found with the requirement for the presence of floor plate-specific cell surface marker CORIN expression (Ono et al., 2007; Chung et al., 2011; Kriks et al., 2011; Kirkeby et al., 2012, 2017a; Doi et al., 2014; Arenas et al., 2015; Fan et al., 2020). A more recent study has identified a cell surface marker integrin-associated protein (IAP, CD47) as a positive marker for FOXA2-positive DA progenitor cells (Lehnen et al., 2017).

While these positive markers are required to narrow down the search for pure DA progenitor cells, negative markers such as Oct3/4, PAX6, and SOX1 for other midbrain neurons act as good controls to prevent introducing contamination with other neuronal subtypes during sorting. Last, terminal differentiation of DA neurons post-transplantation can be identified by the expression of neurotransmitter phenotype markers, namely, TH, dopamine transporter (DAT), Vmat2, Girk2, and Calbindin (Di Porzio et al., 1990; Sgado et al., 2006). It is crucial to take into consideration the wide genetic variation of iPSCs, which may harbor a large spectrum of genetic variation and even retain donor-specific gene expression pattern depending on multiple factors, such as the number of passages of the lineage or transcriptional factors introduced to induce cell differentiation (Rouhani et al., 2014; Thomas et al., 2015; Burrows et al., 2016; Carcamo-Orive et al., 2017). Nonetheless, growing evidence strongly suggests the need for heightened stringency in cell type evaluation. This is particularly important to avoid incomplete differentiation of cells, which could result in undesired reprogrammed cell lineages affecting functional deficits when transplanted into PD models (Park et al., 2005; Grow et al., 2016; Kirkeby et al., 2017a).

Single-Cell RNA-Seq to Evaluate the Quality of Cells

More recently, high-resolution analyses of cell type specificity such as single-cell transcriptomic analyses of neuronal populations of induced stem cells have pathed its way to become a new tool to increase the specificity during DA neuron extraction. This method would allow gene expression profiling of individual cells to better understand population heterogeneity and to distinguish between distinct cell subpopulations to increase the purity of desired cell lines (Poulin et al., 2014; La Manno et al., 2016; Reid and Wernisch, 2016; Lang et al., 2019; Tiklova et al., 2019). However, to achieve this, a specific set of cellular and gene regulatory network contexts have to be determined (as mentioned in the Assessment of the Efficacy of Cell Transplants With Immunostaining Characterization section). Although the presence of the PITX3 gene expression in adult mDA neurons suffices the criteria (Smidt et al., 1997), PITX3 was later shown to be present in both TH-positive and TH-negative cells (Tiklova et al., 2019). In the same study, single-cell RNA sequencing (scRNAseq) analyses were used to distinguish between several mDA subtypes with gene targeting. Moving forward, providing key proof-of-concept in utilizing scRNAseq as a tool for quality control would be the future for cell replacement therapies.

Assessment of the Efficacy of Cell Transplants With Imaging

Last, concurrent with the high demand for the optimization of cell graft visualization in PD, growing emphasis has been placed on enhancing the sensitivity and precision of the spatiotemporal resolution of functional neuroimaging. En route to successful cell transplantation as a therapeutic regenerative method for Parkinson's disease, neuroimaging techniques have to be employed for better patient care. Some key features required to elucidate the therapeutic efficacy of transplanted cells for clinical diagnostics are (1) innervation, (2) survival, (3) differentiation, and (4) functional biochemistry composition. Furthermore, it is crucial that these imaging techniques are time efficient, safe, non-invasive, and allow repeated measures in an individual to determine longitudinal post-operative progression in patients with cell transplantation (Barrow et al., 2015; Ramos-Gomez et al., 2015). In this section, we summarize the pros and cons of current imaging modalities used in tracking cell grafts in PD and their respective biomarkers (**Table 2**).

Magnetic resonance imaging (MRI) is a popular method for examining brain tissue morphology that uses strong magnetic fields coupled with contrast agents such as paramagnetic contrast agent (Gadolinium [III] [Gd^{3+}], Manganese [Mn^{2+}]), perfluorocarbons, or superparamagnetic iron oxide (SPIO) despite its challenges in differentiating tissues with structures that naturally emits low MRI signals like bones. Its biggest advantage is its superior spatial resolution, non-invasiveness, and relatively cost efficiency compared to other neuroimaging methods discussed below. Various lines of evidence strongly suggest the reliability of MRI in visualizing prelabeled transplanted cells such as ESCs (Sykova and Jendelova, 2007), fetal rat cortical cells (Hawrylak et al., 1993), and fetal striatal tissues (Norman et al., 1992) in rats. Furthermore, MRI has been used to evaluate edema and inflammation in tissues surrounding cell-transplanted sites in mice and primates (Anderson et al., 2005; Iwanami et al., 2005). It is important to note that false MRI signals may result from the residual build-up of SPIO nanoparticles released from dead transplanted cells and engulfed by macrophages and activated microglia (Amsalem et al., 2007; Liu and Frank, 2009; Cupaioli et al., 2014; Ramos-Gomez and Martinez-Serrano, 2016). Additionally, cells prelabeled with contrast agents prior to transplantation may show diluted and faded contrast over time as cells proliferate within the transplanted site, which may lead to a reduction in signal. Finally, MRI technology is predominately used in multimodality neuroimaging of cell transplantation by combining both structural and functional readouts for the improved refinement of clinical diagnostics. To this end, it could be coupled with the high sensitivity but low-resolution bioluminescence imaging (Tennstaedt et al., 2013), an economical and non-invasive technique using enzymatic chemiluminescence that allows full temporal live tracking of viable transplanted grafts.

TABLE 2 | Imaging modalities used in cell transplantation for PD.

Modality	Purpose	Biomarkers	Measure	Advantages	Disadvantages	Pre-clinical	Clinical
Magnetic resonance imaging (MRI)	Structural changes of brain tissue (i.e., cerebral atrophy)	Para-Gadolinium (III) (Gd^{3+})/Manganese (Mn^{2+}) OR Superparamagnetic iron oxide (SPIO)	Gray matter volume OR Neuronal activity	• Repetitive measurements on the same individual • Full temporal profile of cell dynamics • ↑ Tissue contrast • Microstructural analysis • Biodegradable labels (biocompatibility) • Required for PET data processing and analysis • ↑ Availability in clinics	• ↓Spatial resolution • Quantification of signal intensity changes with disease progression has to be optimized • ↓Functional readout • ↓Sensitivity • Cells have to be labeled prior to transplantation • Signal dropout • Limited normative database in clinics	Sykova and Jendelova, 2007; Stroh et al., 2009 Ramos-Gomez et al., 2015; Wang et al., 2015; Malloy et al., 2017; Perez-Bouza et al., 2017	Piccini et al., 2005; Mendez et al., 2005; Morizane et al., 2013; Son et al., 2016
Single-photon emission computed tomography (SPECT)	Integrity of nigrostriatal dopaminergic pathways (presynaptic function of striatal neurons)	^{123}I-*N*-ω-fluoropropyl-2β-carbomethoxy-3β-(4-idophenyl) nortropane (^{123}I-FP-CIT/^{123}I-ioflupane)/ 123I-IPT	Binds to striatal dopamine transporters (DAT)	• ↑ Kinetics • ↑ Selectivity Compatible with levodopa treatment • ↑ Tissue penetration • ↑ Half life Quantitative Readily available Repeated scanning	• ↓ Specificity in diseases that causes loss of presynaptic dopamine neurons	N.A.	Pogarell et al., 2006; Politis et al., 2011; Son et al., 2016
Positron emission tomography (PET)	Functional readings of dopaminergic and non-dopaminergic systems in relation to pathogenesis and pathophysiology of PD	[^{18}F]FDOPA/ [^{18}F]Fallypride/ [^{18}F]FBCTT/ [^{11}C]-raclopride/ [^{11}C]DASB/ [^{11}C]PE2I/ [^{11}C]CFT [^{11}C]DTBZ [^{11}C]PK1119/ [^{11}C]-DAS	Aromatic amino acid decarboxylase (AADC—dopamine synthesis capacity and storage)/DA release (binds to striatal post-synaptic D2 receptors)/ 5-HT transporter (Pre-synaptic 5-HT terminal integrity and detection for serotoninergic neurons)	• ↑ Sensitivity in differential detection of motor severity • ↑ Tissue penetration • ↑ Predictive value Correlates with motor progression over time	↓Half life ↓Precision (indirect measurement of dopamine synthesis) ↓Signal production • ↓ Socioeconomic burden • ↑ Radiation	Muramatsu et al., 2009; Emborg et al., 2013; Hallett et al., 2015; Goggi et al., 2020	Lindvall et al., 1990; Peschanski et al., 1994; Freeman et al., 1995; Wenning et al., 1997; Brundin et al., 2000; Piccini et al., 2000, 2005; Freed et al., 2001; Olanow et al., 2003; Mendez et al., 2005; Ma et al., 2010; Morizane et al., 2013

Relative representation ↑, high; ↓, low.

Single-photon emission computed tomography (SPECT) is a type of nuclear imaging technique that utilizes specific gamma-emitting isotopes (compounds derived from cocaine that bind to the dopamine transporter) to analyze the integrity of the nigrostriatal DA pathway in PD (Son et al., 2016). SPECT biomarkers allow for the detection of presynaptic neuronal degeneration (Marshall and Grosset, 2003) and D2-type post-synaptic receptor density (Thobois et al., 2001). The clinical utility of such metabolic and neurochemical changes in PD is reviewed by Wang et al. (2012). To improve the diagnostic accuracy of SPECT imaging, current studies have employed the combined evaluation of both pre- and post-synaptic measurements through striatal dopamine transporters (DAT) and dopamine D2 receptor analysis, respectively (Koch et al., 2007). Further refinements must be made for SPECT imaging modality to be able to differentiate diseases with impairments in presynaptic DA neuronal survival such as PD, progressive supranuclear palsy, multiple system atrophy, and others (Bajaj et al., 2013). Also, potential leakage of radiotracers into adjacent cells resulting in diluted signals during cell proliferation has to be rectified. More importantly, the optimal concentration of tracers must be determined to avoid tissue damage due to exposure to toxic radioactive reagents. One disadvantage of this technique is its inability to examine cell survival and function.

Positron emission tomography (PET) is also a common imaging tool that employs specific radionuclides to elucidate the functional consequences of transplantation on the DA system in the brain, such as receptor distribution, metabolic activity, and inflammation (Visnyei et al., 2006). The measurement of aromatic L-amino acid decarboxylase activity using [^{18}F]FDOPA is regarded as the gold standard to examine DA function and disease severity in Parkinson's disease (Morrish et al., 1996; Punal-Rioboo et al., 2009), also shown in PD non-human primate model (Muramatsu et al., 2009; Emborg et al., 2013; Hallett et al., 2015) and clinical reports (Lindvall et al., 1990; Peschanski et al., 1994; Piccini et al., 2000, 2005; Ma et al., 2010) (refer to citation in **Table 2**). PET images can also be used in conjunction with SPECT data to further evaluate the negative association between striatal DAT and motor severity (Shih et al., 2006; Wu et al., 2014). Interestingly, recent clinical studies have shown that [^{11}C]PE2I has higher predictive value and sensitivity toward the differential detection of motor impairments than [^{18}F]DOPA imaging; hence, [^{11}C]PE2I could be a prospective biomarker to investigate novel interventions (Fazio et al., 2015; Li et al., 2018). PET would be advantageous for studying the early maturation of cells transplanted *in vivo* and for follow-up examinations months after cell transplantation. A comprehensive and concise review on the development of functional neuroimaging is discussed in the cited works (Zheng et al., 2017; Helmich et al., 2018).

With no doubt, one of the most understudied limitations in neuroimaging is in deciphering the complexity of neuropathological overlap and clinical heterogeneity in the progression of individual neurological diseases. Improvements in bioimaging tools, such as the identification of specialized biomarkers for specific cell types to evaluate differential functional signatures, are important to circumvent the high level of variation in the prognosis of PD and its management by patients. In addition, the paucity of imaging modalities available for quantitation and of their respective analytical tools continues to hinder the further development of cell-based therapeutics toward clinically competitive treatments for PD. As discussed above (also refer to **Table 2**), we cannot rely on a single imaging technique for clinical diagnosis especially post-transplantation; thus, researchers are actively searching for the development of multimodality imaging (Waerzeggers et al., 2008) along with the identification of novel biomarkers and tracers to escalate the accuracy of post-operative care. A better understanding of neuroanatomical and pathophysiological processes would be highly advantageous for cell-derived therapeutics.

CLINICAL TRIALS FOR STEM CELL-DERIVED DA NEURON TRANSPLANTATION IN PARKINSON'S DISEASE

Historically, fVM cell transplantation showed varied outcomes in human clinical trials (**Table 3**) (Freed et al., 2001; Olanow et al., 2001, Olanow et al., 2003, Redmond et al., 2001; Barker et al., 2013). A double-blind study of bilateral injection of fVM transplantation and sham surgery into the putamen was first performed in 19 PD patients by Freed and colleagues in 2001 (Freed et al., 2001). Interestingly, only younger age groups showed clinical improvements compared to the sham control (Freed et al., 2001). Using available data extracted from individual clinical papers cited in **Table 3**, we have performed systematic statistical analysis of the clinical outcomes of PD patients with fVM transplantation against various parameters, namely, age of onset (old, $>$ 40 years vs. young, $\leq$ 40 years), disease stage (severe vs. mild), and disease duration (long, $>$ 10 years vs. short, $\leq$ 10 years). The fold change of PET readings post-transplantation from the baseline reading of individual patients was used to access graft survival. We show that graft survival is independent of the age of disease onset (**Figure 1A**) but is dependent on variations in disease stage (**Figure 1B**) and the length of disease duration (**Figure 1C**), where better graft survival was observed in mild stage PD and patients with shorter disease duration ($\leq$ 10 years). Moreover, we used the Unified Parkinson Disease Rating Scale (UPDRS) motor scores to examine clinical improvements post-transplantation of PD patients in various factors (**Figure 2**). We have demonstrated that in all three parameters (as mentioned above), PD patients with fVM transplantation have shown significant clinical improvements (correlated to the decrease in UPDRS motor scores) post-transplantation. Also, comparison between post-transplantation within each parameter (i.e., old vs. young or severe vs. mild or long vs. short) showed no significant differences. In summary, although clinical improvements can be observed throughout the wide spectrum of PD patients with fVM transplantation (**Figure 2**), the optimal condition with the most potential could be seen in mild stage PD patients with short disease duration (**Figure 1**).

TABLE 3 | Summary of clinical studies in cell transplantation for PD.

Year of Publication	Patient info				Results			No. of patients	Lewy body in grafted cells	References
	Age	Disease stage	Disease duration (years)	Follow-up (years)	Cell type	Graft survival	Clinical improvement			
1989	48–55	Severe	14	0.5	fVM	N.A.	No	2	N.A.	Lindvall et al., 1989
1990	49	Severe	13	0.5	fVM	Yes	Yes	1	N.A.	Lindvall et al., 1989
1992	30–43	Severe	6	2	fVM	Yes	Yes	2	N.A.	Widner et al., 1992
1992	N.A.	Severe	N.A.	1.5	fVM	Yes	Yes	4	N.A.	Spencer et al., 1992
1992	50–60	Mild	8–11	1	fVM	Yes	No	2	N.A.	Sawle et al., 1992
1994	N.A.	N.A.	N.A.	3	fVM	Yes	Yes	2	N.A.	Lindvall et al., 1994
1994	N.A.	Severe	N.A.	1,1.5	fVM	Yes	Yes	2	N.A.	Peschanski et al., 1994
1995	39–61	Severe	8–22	0.5	fVM	Yes	Yes	4	N.A.	Freeman et al., 1995
1995	59	Severe	8	1.5	fVM	Yes	Yes	1	N.A.	Kordower et al., 2008
1997	43–58	N.A.	5–12	1–6	fVM	Yes	4 Patients effective	6	N.A.	Wenning et al., 1997
1999	69	Severe	9	10	fVM	Yes	Yes	1	N.A.	Piccini et al., 1999
2000	41–68	Mild-Severe	11–15	1.5–2	fVM	Yes	Yes	5	N.A.	Brundin et al., 2000
2001	34–75	Severe	14	1	fVM	Yes	Effective in younger patients	19	No	Freed et al., 1990
2002	52.0 ± 7.0	Mild-Severe	11.9 ± 2.2	11	fVM	N.A.	Not clear	14	N.A.	Hagell et al., 2002
2003	30–75	Severe	N.A.	2	fVM	Yes	Effective in milder patients	23	N.A.	Olanow et al., 2003
2005	54.1 ± 9.2	Mild	13 ± 2	2	fVM	N.A.	Not clear	9	N.A.	Piccini et al., 1999
2005	59,69	N.A.	11,15	3–4	fVM	Yes	Yes	2	No	Mendez et al., 2008
2008	N.A.	N.A.	N.A.	9–14	fVM	Yes	N.A.	5	No	Mendez et al., 2008
2008	61	Severe	22	14	fVM	Yes	Effective in initial 10 years	1	Yes	Kordower et al., 1995
2009	57	Mild	11	5	NPC	Yes	Effective in initial 3 years	1	N.A.	Levesque et al., 2009
2010	65	Severe	N.A.	12,16	fVM	Yes	N.A	1	Yes	Li et al., 2010
2011	69, 65	Severe	14, 12	22,12	fVM	Yes	No, Yes	2	Yes	Kurowska et al., 2011
2014	49,54	N.A.	10,12	18,15	fVM	N.A.	Yes	2	N.A.	Kefalopoulou et al., 2014
2016	59	N.A.	9	24	fVM	Yes	Effective in initial 14 years	1	Yes	Li et al., 2018
2017	55	Severe	8	16	fVM	Yes	No	1	Yes	Kordower et al., 2017
2020	69	Severe	10	2	iPSC	Yes	Yes	1	N.A.	Schweitzer et al., 2020

In line with our data, the high prevalence of long-term graft survival with low to no immune response in the majority of fVM recipients could be represented for future/ongoing stem cell-based clinical trials as a basis for host tissue innervation and reconnection to host DA circuitry. It is to note that occasional appearance of graft-induced dyskinesia cannot be attributed to cell transplantation as of date, as there are very limited follow-up studies. Upcoming clinical studies must include detailed surgical procedures, characterization of PD hallmarks such as α-synuclein-positive Lewy bodies, ubiquitin expression, and imaging analysis for F-DOPA uptake in graft region in addition to clinical observations. It is believed that the differences in quality and heterogeneity in the transplanted cells, patient selection, and surgical methodologies could have been the reason for failures in some trials. The current status of the TRANSEURO trial (NCT01898390), a large collaboration between the European Union multicenters of fetal nigral cell transplantation, which started in 2012, has grafted 11 young patients with early-stage PD in Cambridge, 2019, and will be subjected to clinical observations for 36 months post-surgery, which is estimated to be completed in early 2021.

With the improvement in the human DA neuron differentiation protocol (Nolbrant et al., 2017), more authentic midbrain DA neurons can now be derived from ESCs or iPSCs *in vitro*. These more defined ESC/iPSC-derived DA neurons show satisfactory therapeutic effectiveness in PD animal models (Studer, 2017), which has led to new waves of initiatives for cell transplantation in PD patients. Furthermore, with ES-derived DA neuronal transplantation being equipotent (Grealish et al., 2014) to that of the current gold standard for PD cell therapy (Li et al., 2016), stem cells rather than fetal neurons hold high expectation in the near future. However, we must bear in mind that animal models cannot fully reproduce human PD. Confounders, including aging, disease duration, disease severity, diabetes, and depression, should be taken into account when cell therapy is translated from preclinical models

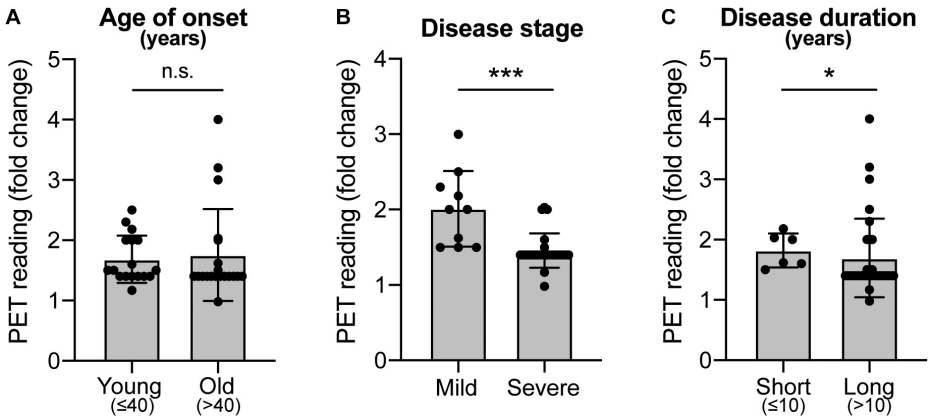

FIGURE 1 | Systematic analysis of various factors associated with clinical outcomes using positron emission tomography (PET) readings of Parkinson's disease (PD) patients with fetal ventral mesencephalic (fVM) cell transplantation. Statistical comparison was performed on various parameters against fold change of PET readings pre- and post-transplantation. **(A)** Age on onset: old (> 40 years) vs. young (≤ 40 years) PD patients. **(B)** Disease stage in mild and severe conditions. **(C)** Disease duration: long (> 10 years) vs. short (≤ 10 years). Student *t*-test, $^{*}p < 0.05$, $^{***}p < 0.001$.

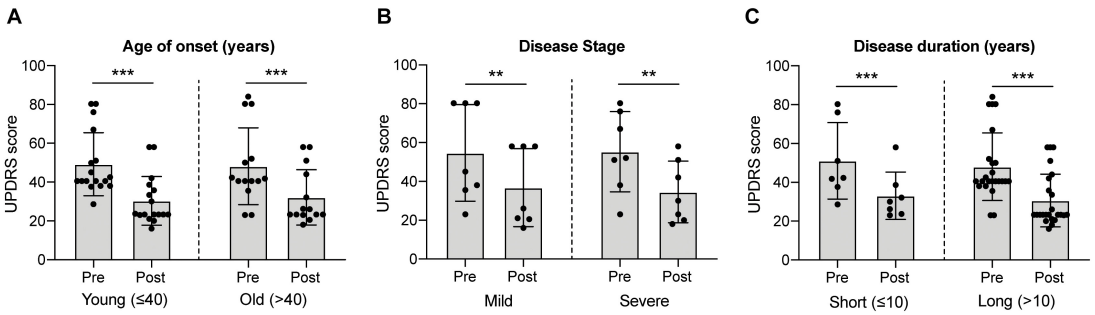

FIGURE 2 | Systematic analysis of various factors associated with clinical outcome in fVM cell transplantation in PD patients using UPDRS motor scores. Statistical comparison was performed on varying parameters against the Unified Parkinson Disease Rating Scale (UPDRS) motor scores of pre- and post-transplantation. **(A)** Age on onset: old (> 40 years) vs. young (≤ 40 years) PD patients. **(B)** Disease stage in severe vs. mild condition. **(C)** Disease duration: long (> 10 years) vs. short (≤ 10 years). Two-way ANOVA, Sidak's multiple comparisons test, $^{**}p < 0.005$, $^{***}p < 0.001$.

to clinical trials (Aarsland et al., 2011; Athauda et al., 2017; Henchcliffe and Parmar, 2018). Currently, ongoing clinical trials of the GForce-PD Consortium include European-based STEM-PD trial, NYSTEM trial, CiRA trial;[2] Cyto Therapeutics Pty Limited founded trial (NCT02452723), and the Chinese Academy of Sciences founded trial (NCT03119636) lead by Qi Zhou. STEM-PD trial was designed to use GMP-grade hESCs as the clinical cell source, employing full GMP-grade production procedure (Kirkeby et al., 2017b), and transplanting 100,000 TH^+ D16 mDA progenitors per graft as a target dose. In contrast, CiRA was designed to develop clinical-grade DA cell therapy from autologous iPSCs taken from PD patients (Barker et al., 2017). More recently, iPSC-derived dopamine progenitor cells have been bilaterally injected into a 69 year old PD patient and have demonstrated signs of improvements in motor assessment 24 months post-surgery (Schweitzer et al., 2020). It is interesting to note that clinical improvements were significantly associated with the right (second) surgical procedure than the left. One explanation would be the improved procedural efficiency including shorter time taken from cell harvest to implantation. Further double-blind studies will be essential to better understand the full potential of iPSC-derived dopamine cells in PD.

Notably, neural progenitor stem cells (NPCs) are an alternative cell source for cell replacement strategy. These multipotent cells can self-renew and differentiate into all mature neural cells in the CNS in large quantities (Ribeiro et al., 2013). The first autologous differentiated neural stem cell clinical trial was conducted using tissue samples collected in the prefrontal cortical and subcortical region along the trajectory of the electrode implant prior to further expansion and differentiation. The patient showed clinical improvements during the first 3 years post-transplantation with subsequent decline back to baseline by the fifth year (Levesque et al., 2009). Ongoing clinical trials sponsored by NeuroGenerations involves 12–20 PD patients at the age of 35–85 years (Hoehn and Yahr stage III or IV) with an estimated completion date by 2021 (NCT03309514, NCT01329926).

[2]https://upload.umin.ac.jp/cgi-open-bin/ctr_e/ctr_view.cgi?recptno=R000038278

Another factor we need to consider for PD cell transplantation clinical trials is the patient stratification. Since aging-induced BBB leakage can lead to infection and inflammation, age can greatly compromise the survival of DA neurons. Moreover, cell transplantation is usually less effective in patients with a longer and more severe disease progression (Barker et al., 2017). Discrepancies were also found in some patients with substantial survival of grafted DA neurons but no beneficial behavioral improvements (Barker et al., 2013, 2015a, 2017; Barker, 2014). These observations possibly indicate the degeneration of other brain systems, especially the post-synaptic component of the DA system. Thus, DA neuron transplantation clinical trials initiated by various organizations only include patients who 1) are younger than 65 years old, 2) have a disease duration of less than 10 years, and 3) are in the early stage of the disease (Kirkeby et al., 2017b; Studer, 2017; Takahashi, 2017). Moving forward, the identification of these confounders would be helpful for clinicians to be able to better stratify PD patients and suggest the most suitable treatment strategy for each patient.

CONCLUSION AND FUTURE DIRECTIONS

We have highlighted four different types of cell sources and have addressed their pros and cons to better understand the characteristics of individual cell types and have also provided detailed analysis of the discrepancies observed in clinical outcomes of PD patients. This also includes methodologies in cell type specification and various imaging modalities. The emphasis on cell line availability, quality, and ability to innervate into host tissues, develop into functional A9 DA neurons, which would efficiently repair the host DA system is of topmost importance. Furthermore, long-term survivability for years after surgery without graft-induced dyskinesia or immune rejection by the host are some safety requirements and is the key to successful translation into large-scale therapeutic application and also in biomedical research to better recapitulate *in vitro* disease models. To avoid further inconsistencies in clinical results, we need to ensure standardization across several aspects of transplantations, including tissue preparation for engrafts, surgical technique, patient selection, immune therapy, synaptic integration capacity of cells transplanted into the human brain, and ways to bypass ethical issues revolving around cell transplantation in humans and the usage of ESCs (more details can be found in Barker et al., 2015b). The need to develop minimal, but precise, surgical techniques and achieving a better understanding of striatal functions are necessary, and these improvements could be accomplished by acquiring higher-resolution diagnostic imaging with heightened specificity for targeted graft placement and post-op observational study. Clinical endpoint observations from aforementioned ongoing clinical trials would pave a way to develop a coherent and systematic blueprint for therapeutic strategies such as improved surgical methodologies, optimized and standardized protocols, development of appropriate safeguards, and objective long-term outcome measures. The field of stem cell-based therapies for PD has entered into an exciting era, and we believe there is greater optimism that neurotransplantation may provide a viable option for treatment of PD in the future.

AUTHOR CONTRIBUTIONS

SEJ, LQ, and LZ have drafted the manuscript with inputs from LLC and E-KT. All authors contributed to the article and approved the submitted version.

FUNDING

This research was supported by the Open Fund-Large Collaborative Grant, SPARK II Program, STaR Award, and CSA awards.

REFERENCES

Aarsland, D., Pahlhagen, S., Ballard, C. G., Ehrt, U., and Svenningsson, P. (2011). Depression in Parkinson disease–epidemiology, mechanisms and management. *Nat. Rev. Neurol.* 8, 35–47. doi: 10.1038/nrneurol.2011.189

Alamri, A., Ughratdar, I., Samuel, M., and Ashkan, K. (2015). Deep brain stimulation of the subthalamic nucleus in Parkinson's disease 2003-2013: where are we another 10 years on? *Br. J. Neurosurg.* 29, 319–328. doi: 10.3109/02688697.2014.997669

Alavian, K. N., Scholz, C., and Simon, H. H. (2008). Transcriptional regulation of mesencephalic dopaminergic neurons: the full circle of life and death. *Mov. Disord.* 23, 319–328. doi: 10.1002/mds.21640

Alberi, L., Sgado, P., and Simon, H. H. (2004). Engrailed genes are cell-autonomously required to prevent apoptosis in mesencephalic dopaminergic neurons. *Development* 131, 3229–3236. doi: 10.1242/dev.01128

Amsalem, Y., Mardor, Y., Feinberg, M. S., Landa, N., Miller, L., Daniels, D., et al. (2007). Iron-oxide labeling and outcome of transplanted mesenchymal stem cells in the infarcted myocardium. *Circulation* 116, I38–I45. doi: 10.1161/CIRCULATIONAHA.106.680231

Anden, N. E., Dahlstrom, A., Fuxe, K., and Larsson, K. (1966). Functional role of the nigro-neostriatal dopamine neurons. *Acta Pharmacol. Toxicol.* 24, 263–274. doi: 10.1111/j.1600-0773.1966.tb00389.x

Anderson, S. A., Glod, J., Arbab, A. S., Noel, M., Ashari, P., Fine, H. A., et al. (2005). Noninvasive Mr imaging of magnetically labeled stem cells to directly identify neovasculature in a glioma model. *Blood* 105, 420–425. doi: 10.1182/blood-2004-06-2222

Andersson, E., Jensen, J. B., Parmar, M., Guillemot, F., and Bjorklund, A. (2006). Development of the mesencephalic dopaminergic neuron system is compromised in the absence of neurogenin 2. *Development* 133, 507–516. doi: 10.1242/dev.02224

Arenas, E., Denham, M., and Villaescusa, J. C. (2015). How to make a midbrain dopaminergic neuron. *Development* 142, 1918–1936. doi: 10.1242/dev.097394

Athauda, D., Maclagan, K., Skene, S. S., Bajwa-Joseph, M., Letchford, D., Chowdhury, K., et al. (2017). Exenatide once weekly versus placebo in Parkinson's disease: a randomised, double-blind, placebo-controlled trial. *Lancet* 390, 1664–1675. doi: 10.1016/S0140-6736(17)31585-4

Bajaj, N., Hauser, R. A., and Grachev, I. D. (2013). Clinical utility of dopamine transporter single photon emission Ct (DaT-Spect) with (123I) ioflupane in diagnosis of parkinsonian syndromes. *J. Neurol. Neurosurg. Psychiatry* 84, 1288–1295. doi: 10.1136/jnnp-2012-304436

Bakay, R. A., Barrow, D. L., Fiandaca, M. S., Iuvone, P. M., Schiff, A., and Collins, D. C. (1987). Biochemical and behavioral correction of Mptp Parkinson-like syndrome by fetal cell transplantation. *Ann. N. Y. Acad. Sci.* 495, 623–640. doi: 10.1111/j.1749-6632.1987.tb23705.x

Barker, R. A. (2014). Developing stem cell therapies for Parkinson's disease: waiting until the time is right. *Cell Stem Cell* 15, 539–542. doi: 10.1016/j.stem.2014.09.016

Barker, R. A., Barrett, J., Mason, S. L., and Bjorklund, A. (2013). Fetal dopaminergic transplantation trials and the future of neural grafting in Parkinson's disease. *Lancet Neurol.* 12, 84–91. doi: 10.1016/s1474-4422(12)70295-8

Barker, R. A., and Consortium, T. (2019). Designing stem-cell-based dopamine cell replacement trials for Parkinson's disease. *Nat. Med.* 25, 1045–1053. doi: 10.1038/s41591-019-0507-2

Barker, R. A., Drouin-Ouellet, J., and Parmar, M. (2015a). Cell-based therapies for Parkinson disease-past insights and future potential. *Nat. Rev. Neurol.* 11, 492–503. doi: 10.1038/nrneurol.2015.123

Barker, R. A., Parmar, M., Studer, L., and Takahashi, J. (2017). Human trials of stem cell-derived dopamine neurons for parkinson's disease: dawn of a new era. *Cell Stem Cell* 21, 569–573. doi: 10.1016/j.stem.2017.09.014

Barker, R. A., Studer, L., Cattaneo, E., Takahashi, J., and Consortium, G. F. P. (2015b). G-Force Pd: a global initiative in coordinating stem cell-based dopamine treatments for Parkinson's disease. *NPJ Parkinsons Dis.* 1:15017. doi: 10.1038/npjparkd.2015.17

Barrow, M., Taylor, A., Murray, P., Rosseinsky, M. J., and Adams, D. J. (2015). Design considerations for the synthesis of polymer coated iron oxide nanoparticles for stem cell labelling and tracking using Mri. *Chem. Soc. Rev.* 44, 6733–6748. doi: 10.1039/c5cs00331h

Beevers, J. E., Caffrey, T. M., and Wade-Martins, R. (2013). Induced pluripotent stem cell (ipsc)-derived dopaminergic models of Parkinson's disease. *Biochem. Soc. Trans.* 41, 1503–1508. doi: 10.1042/bst20130194

Ben-Hur, T., Idelson, M., Khaner, H., Pera, M., Reinhartz, E., Itzik, A., et al. (2004). Transplantation of human embryonic stem cell-derived neural progenitors improves behavioral deficit in Parkinsonian rats. *Stem Cells* 22, 1246–1255. doi: 10.1634/stemcells.2004-0094

Biju, K. C., Santacruz, R. A., Chen, C., Zhou, Q., Yao, J., Rohrabaugh, S. L., et al. (2013). Bone marrow-derived microglia-based neurturin delivery protects against dopaminergic neurodegeneration in a mouse model of Parkinson's disease. *Neurosci. Lett.* 535, 24–29. doi: 10.1016/j.neulet.2012.12.034

Bjorklund, A., and Stenevi, U. (1979). Reconstruction of the nigrostriatal dopamine pathway by intracerebral nigral transplants. *Brain Res.* 177, 555–560. doi: 10.1016/0006-8993(79)90472-4

Brederlau, A., Correia, A. S., Anisimov, S. V., Elmi, M., Paul, G., Roybon, L., et al. (2006). Transplantation of human embryonic stem cell-derived cells to a rat model of Parkinson's disease: effect of in vitro differentiation on graft survival and teratoma formation. *Stem Cells* 24, 1433–1440. doi: 10.1634/stemcells.2005-0393

Brundin, P., Nilsson, O. G., Strecker, R. E., Lindvall, O., Astedt, B., and Bjorklund, A. (1986). Behavioural effects of human fetal dopamine neurons grafted in a rat model of Parkinson's disease. *Exp. Brain Res.* 65, 235–240. doi: 10.1007/BF00243848

Brundin, P., Pogarell, O., Hagell, P., Piccini, P., Widner, H., Schrag, A., et al. (2000). Bilateral caudate and putamen grafts of embryonic mesencephalic tissue treated with lazaroids in Parkinson's disease. *Brain* 123(Pt 7), 1380–1390. doi: 10.1093/brain/123.7.1380

Burrows, C. K., Banovich, N. E., Pavlovic, B. J., Patterson, K., Gallego Romero, I., Pritchard, J. K., et al. (2016). Genetic variation, not cell type of origin, underlies the majority of identifiable regulatory differences in ipscs. *PLoS Genet.* 12:e1005793. doi: 10.1371/journal.pgen.1005793

Carcamo-Orive, I., Hoffman, G. E., Cundiff, P., Beckmann, N. D., D'souza, S. L., Knowles, J. W., et al. (2017). Analysis of transcriptional variability in a large human ipsc library reveals genetic and non-genetic determinants of heterogeneity. *Cell Stem Cell* 20, 518.e9–532.e9. doi: 10.1016/j.stem.2016.11.005

Cardoso, T., Adler, A. F., Mattsson, B., Hoban, D. B., Nolbrant, S., Wahlestedt, J. N., et al. (2018). Target-specific forebrain projections and appropriate synaptic inputs of hesc-derived dopamine neurons grafted to the midbrain of parkinsonian rats. *J. Comp. Neurol.* 526, 2133–2146. doi: 10.1002/cne.24500

Carlsson, T., Carta, M., Winkler, C., Bjorklund, A., and Kirik, D. (2007). Serotonin neuron transplants exacerbate L-Dopa-induced dyskinesias in a rat model of Parkinson's disease. *J. Neurosci.* 27, 8011–8022. doi: 10.1523/jneurosci.2079-07.2007

Cho, M. S., Lee, Y. E., Kim, J. Y., Chung, S., Cho, Y. H., Kim, D. S., et al. (2008). Highly efficient and large-scale generation of functional dopamine neurons from human embryonic stem cells. *Proc. Natl. Acad. Sci. U.S.A.* 105, 3392–3397. doi: 10.1073/pnas.0712359105

Chung, S., Leung, A., Han, B. S., Chang, M. Y., Moon, J. I., Kim, C. H., et al. (2009). Wnt1-lmx1a forms a novel autoregulatory loop and controls midbrain dopaminergic differentiation synergistically with the Shh-FoxA2 pathway. *Cell Stem Cell* 5, 646–658. doi: 10.1016/j.stem.2009.09.015

Chung, S., Moon, J. I., Leung, A., Aldrich, D., Lukianov, S., Kitayama, Y., et al. (2011). Es cell-derived renewable and functional midbrain dopaminergic progenitors. *Proc. Natl. Acad. Sci. U.S.A.* 108, 9703–9708. doi: 10.1073/pnas.1016443108

Cooper, O., Hargus, G., Deleidi, M., Blak, A., Osborn, T., Marlow, E., et al. (2010). Differentiation of human Es and Parkinson's disease ips cells into ventral midbrain dopaminergic neurons requires a high activity form of Shh, Fgf8a and specific regionalization by retinoic acid. *Mol. Cell. Neurosci.* 45, 258–266. doi: 10.1016/j.mcn.2010.06.017

Cupaioli, F. A., Zucca, F. A., Boraschi, D., and Zecca, L. (2014). Engineered nanoparticles. How brain friendly is this new guest? *Prog. Neurobiol.* 119-120, 20–38. doi: 10.1016/j.pneurobio.2014.05.002

Daadi, M. M., and Weiss, S. (1999). Generation of tyrosine hydroxylase-producing neurons from precursors of the embryonic and adult forebrain. *J. Neurosci.* 19, 4484–4497. doi: 10.1523/jneurosci.19-11-04484.1999

Dahlstroem, A., and Fuxe, K. (1964). Evidence for the existence of monoamine-containing neurons in the central nervous system. I. demonstration of monoamines in the cell bodies of brain stem neurons. *Acta Physiol. Scand. Suppl. Suppl.* 232, 1–55.

Damier, P., Hirsch, E. C., Agid, Y., and Graybiel, A. M. (1999). The substantia nigra of the human brain. Ii. Patterns of loss of dopamine-containing neurons in Parkinson's disease. *Brain* 122(Pt 8), 1437–1448. doi: 10.1093/brain/122.8.1437

deSouza, R. M., Moro, E., Lang, A. E., and Schapira, A. H. (2013). Timing of deep brain stimulation in Parkinson disease: a need for reappraisal? *Ann. Neurol.* 73, 565–575. doi: 10.1002/ana.23890

Di Porzio, U., Zuddas, A., Cosenza-Murphy, D. B., and Barker, J. L. (1990). Early appearance of tyrosine hydroxylase immunoreactive cells in the mesencephalon of mouse embryos. *Int. J. Dev. Neurosci.* 8, 523–532. doi: 10.1016/0736-5748(90)90044-3

Doi, D., Morizane, A., Kikuchi, T., Onoe, H., Hayashi, T., Kawasaki, T., et al. (2012). Prolonged maturation culture favors a reduction in the tumorigenicity and the dopaminergic function of human Esc-derived neural cells in a primate model of Parkinson's disease. *Stem Cells* 30, 935–945. doi: 10.1002/stem.1060

Doi, D., Samata, B., Katsukawa, M., Kikuchi, T., Morizane, A., Ono, Y., et al. (2014). Isolation of human induced pluripotent stem cell-derived dopaminergic progenitors by cell sorting for successful transplantation. *Stem Cell Rep.* 2, 337–350. doi: 10.1016/j.stemcr.2014.01.013

Dunnett, S. B., Bjorklund, A., Schmidt, R. H., Stenevi, U., and Iversen, S. D. (1983). Intracerebral grafting of neuronal cell suspensions. V. Behavioural recovery in rats with bilateral 6-Ohda lesions following implantation of nigral cell suspensions. *Acta Physiol. Scand. Suppl.* 522, 39–47.

Eigentler, A., Boesch, S., Schneider, R., Dechant, G., and Nat, R. (2013). Induced pluripotent stem cells from friedreich ataxia patients fail to upregulate frataxin during in vitro differentiation to peripheral sensory neurons. *Stem Cells Dev.* 22, 3271–3282. doi: 10.1089/scd.2013.0126

Elkabetz, Y., Panagiotakos, G., Al Shamy, G., Socci, N. D., Tabar, V., and Studer, L. (2008). Human Es cell-derived neural rosettes reveal a functionally distinct early neural stem cell stage. *Genes Dev.* 22, 152–165. doi: 10.1101/gad.1616208

Emborg, M. E., Liu, Y., Xi, J., Zhang, X., Yin, Y., Lu, J., et al. (2013). Induced pluripotent stem cell-derived neural cells survive and mature in the nonhuman primate brain. *Cell Rep.* 3, 646–650. doi: 10.1016/j.celrep.2013.02.016

Evans, M. J., and Kaufman, M. H. (1981). Establishment in culture of pluripotential cells from mouse embryos. *Nature* 292, 154–156. doi: 10.1038/292154a0

Fahn, S. (2003). Description of Parkinson's disease as a clinical syndrome. *Ann. N. Y. Acad. Sci.* 991, 1–14. doi: 10.1016/b978-0-12-374028-1.00001-4

Fahn, S. (2006). Levodopa in the treatment of Parkinson's disease. *J. Neural Transm. Suppl.* 71, 1–15. doi: 10.2147/ce.s7031

Fairchild, P. J. (2010). The challenge of immunogenicity in the quest for induced pluripotency. *Nat. Rev. Immunol.* 10, 868–875. doi: 10.1038/nri2878

Fan, Y., Winanto, and Ng, S. Y. (2020). Replacing what's lost: a new era of stem cell therapy for Parkinson's disease. *Transl. Neurodegener.* 9:2. doi: 10.1186/s40035-019-0180-x

Fasano, C. A., Chambers, S. M., Lee, G., Tomishima, M. J., and Studer, L. (2010). Efficient derivation of functional floor plate tissue from human embryonic stem cells. *Cell Stem Cell* 6, 336–347. doi: 10.1016/j.stem.2010.03.001

Fazio, P., Svenningsson, P., Forsberg, A., Jonsson, E. G., Amini, N., Nakao, R., et al. (2015). Quantitative analysis of (1)(8)F-(E)-N-(3-Iodoprop-2-Enyl)-2beta-carbofluoroethoxy-3beta-(4'-Methyl-Phenyl) nortropane binding to the dopamine transporter in parkinson disease. *J. Nucl. Med.* 56, 714–720. doi: 10.2967/jnumed.114.152421

Freed, C. R., Breeze, R. E., Rosenberg, N. L., Schneck, S. A., Wells, T. H., Barrett, J. N., et al. (1990). Transplantation of human fetal dopamine cells for Parkinson's disease. Results at 1 year. *Arch. Neurol.* 47, 505–512. doi: 10.1001/archneur.1990.00530050021007

Freed, C. R., Greene, P. E., Breeze, R. E., Tsai, W. Y., Dumouchel, W., Kao, R., et al. (2001). Transplantation of embryonic dopamine neurons for severe Parkinson's disease. *N. Engl. J. Med.* 344, 710–719. doi: 10.1056/nejm200103083441002

Freed, W. J., Morihisa, J. M., Spoor, E., Hoffer, B. J., Olson, L., Seiger, A., et al. (1981). Transplanted adrenal chromaffin cells in rat brain reduce lesion-induced rotational behaviour. *Nature* 292, 351–352. doi: 10.1038/292351a0

Freeman, T. B., Olanow, C. W., Hauser, R. A., Nauert, G. M., Smith, D. A., Borlongan, C. V., et al. (1995). Bilateral fetal nigral transplantation into the postcommissural putamen in Parkinson's disease. *Ann. Neurol.* 38, 379–388. doi: 10.1002/ana.410380307

Fukuda, H., Takahashi, J., Watanabe, K., Hayashi, H., Morizane, A., Koyanagi, M., et al. (2006). Fluorescence-activated cell sorting-based purification of embryonic stem cell-derived neural precursors averts tumor formation after transplantation. *Stem Cells* 24, 763–771. doi: 10.1634/stemcells.2005-0137

Ganat, Y. M., Calder, E. L., Kriks, S., Nelander, J., Tu, E. Y., Jia, F., et al. (2012). Identification of embryonic stem cell-derived midbrain dopaminergic neurons for engraftment. *J. Clin. Invest.* 122, 2928–2939. doi: 10.1172/jci58767

German, D. C., Manaye, K., Smith, W. K., Woodward, D. J., and Saper, C. B. (1989). Midbrain dopaminergic cell loss in Parkinson's disease: computer visualization. *Ann. Neurol.* 26, 507–514. doi: 10.1002/ana.410260403

German, D. C., Manaye, K. F., Sonsalla, P. K., and Brooks, B. A. (1992). Midbrain dopaminergic cell loss in Parkinson's disease and Mptp-induced parkinsonism: sparing of calbindin-D28k-containing cells. *Ann. N. Y. Acad. Sci.* 648, 42–62. doi: 10.1111/j.1749-6632.1992.tb24523.x

Gibb, W. R. (1992). Melanin, tyrosine hydroxylase, calbindin and substance P in the human midbrain and substantia nigra in relation to nigrostriatal projections and differential neuronal susceptibility in Parkinson's disease. *Brain Res.* 581, 283–291. doi: 10.1016/0006-8993(92)90719-p

Goedert, M., Spillantini, M. G., Del Tredici, K., and Braak, H. (2013). 100 years of Lewy pathology. *Nat. Rev. Neurol.* 9, 13–24. doi: 10.1038/nrneurol.2012.242

Goggi, J. L., Qiu, L., Liao, M. C., Khanapur, S., Jiang, L., Boominathan, R., et al. (2020). Dopamine transporter neuroimaging accurately assesses the maturation of dopamine neurons in a preclinical model of Parkinson's disease. *Stem Cell Res. Ther.* 11:347. doi: 10.1186/s13287-020-01868-4

Grealish, S., Diguet, E., Kirkeby, A., Mattsson, B., Heuer, A., Bramoulle, Y., et al. (2014). Human Esc-derived dopamine neurons show similar preclinical efficacy and potency to fetal neurons when grafted in a rat model of Parkinson's disease. *Cell Stem Cell* 15, 653–665. doi: 10.1016/j.stem.2014.09.017

Grealish, S., Jonsson, M. E., Li, M., Kirik, D., Bjorklund, A., and Thompson, L. H. (2010). The A9 dopamine neuron component in grafts of ventral mesencephalon is an important determinant for recovery of motor function in a rat model of Parkinson's disease. *Brain* 133, 482–495. doi: 10.1093/brain/awp328

Grenhoff, J., Ugedo, L., and Svensson, T. H. (1988). Firing patterns of midbrain dopamine neurons: differences between A9 and A10 cells. *Acta Physiol. Scand.* 134, 127–132. doi: 10.1111/j.1748-1716.1988.tb08468.x

Grow, D. A., Simmons, D. V., Gomez, J. A., Wanat, M. J., Mccarrey, J. R., Paladini, C. A., et al. (2016). Differentiation and characterization of dopaminergic neurons from baboon induced pluripotent stem cells. *Stem Cells Transl. Med.* 5, 1133–1144. doi: 10.5966/sctm.2015-0073

Hagell, P., Piccini, P., Bjorklund, A., Brundin, P., Rehncrona, S., Widner, H., et al. (2002). Dyskinesias following neural transplantation in Parkinson's disease. *Nat. Neurosci.* 5, 627–628. doi: 10.1038/nn863

Hallett, P. J., Deleidi, M., Astradsson, A., Smith, G. A., Cooper, O., Osborn, T. M., et al. (2015). Successful function of autologous ipsc-derived dopamine neurons following transplantation in a non-human primate model of Parkinson's disease. *Cell Stem Cell* 16, 269–274. doi: 10.1016/j.stem.2015.01.018

Halliday, G. M., Ophof, A., Broe, M., Jensen, P. H., Kettle, E., Fedorow, H., et al. (2005). Alpha-synuclein redistributes to neuromelanin lipid in the substantia nigra early in Parkinson's disease. *Brain* 128, 2654–2664. doi: 10.1093/brain/awh584

Hargus, G., Cooper, O., Deleidi, M., Levy, A., Lee, K., Marlow, E., et al. (2010). Differentiated Parkinson patient-derived induced pluripotent stem cells grow in the adult rodent brain and reduce motor asymmetry in Parkinsonian rats. *Proc. Natl. Acad. Sci. U.S.A.* 107, 15921–15926. doi: 10.1073/pnas.1010209107

Hawrylak, N., Ghosh, P., Broadus, J., Schlueter, C., Greenough, W. T., and Lauterbur, P. C. (1993). Nuclear magnetic resonance (Nmr) imaging of iron oxide-labeled neural transplants. *Exp. Neurol.* 121, 181–192. doi: 10.1006/exnr.1993.1085

Helmich, R. C., Vaillancourt, D. E., and Brooks, D. J. (2018). The future of brain imaging in Parkinson's disease. *J. Parkinsons Dis.* 8, S47–S51. doi: 10.3233/JPD-181482

Henchcliffe, C., and Parmar, M. (2018). Repairing the brain: cell replacement using stem cell-based technologies. *J. Parkinsons Dis.* 8, S131–S137. doi: 10.3233/JPD-181488

Hirsch, E., Graybiel, A. M., and Agid, Y. A. (1988). Melanized dopaminergic neurons are differentially susceptible to degeneration in Parkinson's disease. *Nature* 334, 345–348. doi: 10.1038/334345a0

Hu, B. Y., Weick, J. P., Yu, J., Ma, L. X., Zhang, X. Q., Thomson, J. A., et al. (2010). Neural differentiation of human induced pluripotent stem cells follows developmental principles but with variable potency. *Proc. Natl. Acad. Sci. U.S.A.* 107, 4335–4340. doi: 10.1073/pnas.0910012107

Itskovitz-Eldor, J., Schuldiner, M., Karsenti, D., Eden, A., Yanuka, O., Amit, M., et al. (2000). Differentiation of human embryonic stem cells into embryoid bodies compromising the three embryonic germ layers. *Mol. Med.* 6, 88–95. doi: 10.1007/bf03401776

Iwanami, A., Kaneko, S., Nakamura, M., Kanemura, Y., Mori, H., Kobayashi, S., et al. (2005). Transplantation of human neural stem cells for spinal cord injury in primates. *J. Neurosci. Res.* 80, 182–190. doi: 10.1002/jnr.20436

Jaeger, I., Arber, C., Risner-Janiczek, J. R., Kuechler, J., Pritzsche, D., Chen, I. C., et al. (2011). Temporally controlled modulation of Fgf/Erk signaling directs midbrain dopaminergic neural progenitor fate in mouse and human pluripotent stem cells. *Development* 138, 4363–4374. doi: 10.1242/dev.066746

Jonsson, M. E., Ono, Y., Bjorklund, A., and Thompson, L. H. (2009). Identification of transplantable dopamine neuron precursors at different stages of midbrain neurogenesis. *Exp. Neurol.* 219, 341–354. doi: 10.1016/j.expneurol.2009.06.006

Kastner, A., Hirsch, E. C., Lejeune, O., Javoy-Agid, F., Rascol, O., and Agid, Y. (1992). Is the vulnerability of neurons in the substantia nigra of patients with Parkinson's disease related to their neuromelanin content? *J. Neurochem.* 59, 1080–1089. doi: 10.1111/j.1471-4159.1992.tb08350.x

Kawasaki, H., Mizuseki, K., Nishikawa, S., Kaneko, S., Kuwana, Y., Nakanishi, S., et al. (2000). Induction of midbrain dopaminergic neurons from Es cells by stromal cell-derived inducing activity. *Neuron* 28, 31–40. doi: 10.1016/s0896-6273(00)00083-0

Kee, N., Volakakis, N., Kirkeby, A., Dahl, L., Storvall, H., Nolbrant, S., et al. (2017). Single-cell analysis reveals a close relationship between differentiating dopamine and subthalamic nucleus neuronal lineages. *Cell Stem Cell* 20, 29–40. doi: 10.1016/j.stem.2016.10.003

Kefalopoulou, Z., Politis, M., Piccini, P., Mencacci, N., Bhatia, K., Jahanshahi, M., et al. (2014). Long-term clinical outcome of fetal cell transplantation for Parkinson disease: two case reports. *JAMA Neurol.* 71, 83–87. doi: 10.1001/jamaneurol.2013.4749

Kikuchi, T., Morizane, A., Doi, D., Magotani, H., Onoe, H., Hayashi, T., et al. (2017). Human ips cell-derived dopaminergic neurons function in a primate Parkinson's disease model. *Nature* 548, 592–596. doi: 10.1038/nature23664

Kim, J. H., Auerbach, J. M., Rodriguez-Gomez, J. A., Velasco, I., Gavin, D., Lumelsky, N., et al. (2002). Dopamine neurons derived from embryonic stem

cells function in an animal model of Parkinson's disease. *Nature* 418, 50–56. doi: 10.1038/nature00900

Kirkeby, A., Grealish, S., Wolf, D. A., Nelander, J., Wood, J., Lundblad, M., et al. (2012). Generation of regionally specified neural progenitors and functional neurons from human embryonic stem cells under defined conditions. *Cell. Rep.* 1, 703–714. doi: 10.1016/j.celrep.2012.04.009

Kirkeby, A., Nolbrant, S., Tiklova, K., Heuer, A., Kee, N., Cardoso, T., et al. (2017a). Predictive markers guide differentiation to improve graft outcome in clinical translation of hesc-based therapy for Parkinson's disease. *Cell Stem Cell* 20, 135–148. doi: 10.1016/j.stem.2016.09.004

Kirkeby, A., Parmar, M., and Barker, R. A. (2017b). Strategies for bringing stem cell-derived dopamine neurons to the clinic: a european approach (Stem-Pd). *Prog. Brain Res.* 230, 165–190. doi: 10.1016/bs.pbr.2016.11.011

Koch, P., Opitz, T., Steinbeck, J. A., Ladewig, J., and Brustle, O. (2009). A rosette-type, self-renewing human Es cell-derived neural stem cell with potential for in vitro instruction and synaptic integration. *Proc. Natl. Acad. Sci. U.S.A.* 106, 3225–3230. doi: 10.1073/pnas.0808387106

Koch, W., Hamann, C., Radau, P. E., and Tatsch, K. (2007). Does combined imaging of the pre- and postsynaptic dopaminergic system increase the diagnostic accuracy in the differential diagnosis of parkinsonism? *Eur. J. Nucl. Med. Mol. Imaging* 34, 1265–1273. doi: 10.1007/s00259-007-0375-8

Kordower, J. H., Chu, Y., Hauser, R. A., Freeman, T. B., and Olanow, C. W. (2008). Lewy body-like pathology in long-term embryonic nigral transplants in Parkinson's disease. *Nat. Med.* 14, 504–506. doi: 10.1038/nm1747

Kordower, J. H., Freeman, T. B., Snow, B. J., Vingerhoets, F. J., Mufson, E. J., Sanberg, P. R., et al. (1995). Neuropathological evidence of graft survival and striatal reinnervation after the transplantation of fetal mesencephalic tissue in a patient with Parkinson's disease. *N. Engl. J. Med.* 332, 1118–1124. doi: 10.1056/nejm199504273321702

Kordower, J. H., Goetz, C. G., Chu, Y., Halliday, G. M., Nicholson, D. A., Musial, T. F., et al. (2017). Robust graft survival and normalized dopaminergic innervation do not obligate recovery in a Parkinson disease patient. *Ann. Neurol.* 81, 46–57. doi: 10.1002/ana.24820

Kriks, S., Shim, J. W., Piao, J., Ganat, Y. M., Wakeman, D. R., Xie, Z., et al. (2011). Dopamine neurons derived from human Es cells efficiently engraft in animal models of Parkinson's disease. *Nature* 480, 547–551. doi: 10.1038/nature10648

Kurowska, Z., Englund, E., Windner, H., Lindvall, O., Li, J. Y., and Brundin, P. (2011). Signs of degeneration in 12-22 year old grafts of mesencephalic dopamine neurons in patients with Parkinson's disease. *J. Parkinsons Dis.* 1, 83–92. doi: 10.3233/jpd-2011-11004

La Manno, G., Gyllborg, D., Codeluppi, S., Nishimura, K., Salto, C., Zeisel, A., et al. (2016). Molecular diversity of midbrain development in mouse, human, and stem cells. *Cell* 167, 566.e19–580.e19. doi: 10.1016/j.cell.2016.09.027

Lang, C., Campbell, K. R., Ryan, B. J., Carling, P., Attar, M., Vowles, J., et al. (2019). Single-cell sequencing of ipsc-dopamine neurons reconstructs disease progression and identifies Hdac4 as a regulator of parkinson cell phenotypes. *Cell Stem Cell* 24, 93.e6–106.e6. doi: 10.1016/j.stem.2018.10.023

Le, W., Conneely, O. M., He, Y., Jankovic, J., and Appel, S. H. (1999). Reduced Nurr1 expression increases the vulnerability of mesencephalic dopamine neurons to Mptp-induced injury. *J. Neurochem.* 73, 2218–2221. doi: 10.1046/j.1471-4159.1999.02218.x

Lee, S. H., Lumelsky, N., Studer, L., Auerbach, J. M., and Mckay, R. D. (2000). Efficient generation of midbrain and hindbrain neurons from mouse embryonic stem cells. *Nat. Biotechnol.* 18, 675–679. doi: 10.1038/76536

Lehnen, D., Barral, S., Cardoso, T., Grealish, S., Heuer, A., Smiyakin, A., et al. (2017). Iap-based cell sorting results in homogeneous transplantable dopaminergic precursor cells derived from human pluripotent stem cells. *Stem Cell Rep.* 9, 1207–1220. doi: 10.1016/j.stemcr.2017.08.016

Levesque, M. F., Neuman, T., and Rezak, M. (2009). Therapeutic microinjection of autologous adult human neural stem cells and differentiated neurons for Parkinson's Disease: five year post-operative outcome. *Open Stem Cell J.* 1, 20–29. doi: 10.2174/1876893800901010020

Li, J. Y., Englund, E., Widner, H., Rehncrona, S., Bjorklund, A., Lindvall, O., et al. (2010). Characterization of Lewy body pathology in 12- and 16-year-old intrastriatal mesencephalic grafts surviving in a patient with Parkinson's disease. *Mov. Disord.* 25, 1091–1096. doi: 10.1002/mds.23012

Li, W., Englund, E., Widner, H., Mattsson, B., Van Westen, D., Latt, J., et al. (2016). Extensive graft-derived dopaminergic innervation is maintained 24 years after transplantation in the degenerating parkinsonian brain. *Proc. Natl. Acad. Sci. U.S.A.* 113, 6544–6549. doi: 10.1073/pnas.1605245113

Li, W., Lao-Kaim, N. P., Roussakis, A. A., Martin-Bastida, A., Valle-Guzman, N., Paul, G., et al. (2018). (11) C-Pe2I and (18) F-dopa pet for assessing progression rate in Parkinson's: a longitudinal study. *Mov. Disord.* 33, 117–127. doi: 10.1002/mds.27183

Limousin, P., Pollak, P., Benazzouz, A., Hoffmann, D., Le Bas, J. F., Broussolle, E., et al. (1995). Effect of parkinsonian signs and symptoms of bilateral subthalamic nucleus stimulation. *Lancet* 345, 91–95. doi: 10.1016/s0140-6736(95)90062-4

Lin, W., Metzakopian, E., Mavromatakis, Y. E., Gao, N., Balaskas, N., Sasaki, H., et al. (2009). Foxa1 and Foxa2 function both upstream of and cooperatively with Lmx1a and Lmx1b in a feedforward loop promoting mesodiencephalic dopaminergic neuron development. *Dev. Biol.* 333, 386–396. doi: 10.1016/j.ydbio.2009.07.006

Lindvall, O., and Bjorklund, A. (1974). The organization of the ascending catecholamine neuron systems in the rat brain as revealed by the glyoxylic acid fluorescence method. *Acta Physiol. Scand. Suppl.* 412, 1–48.

Lindvall, O., Brundin, P., Widner, H., Rehncrona, S., Gustavii, B., Frackowiak, R., et al. (1990). Grafts of fetal dopamine neurons survive and improve motor function in Parkinson's disease. *Science* 247, 574–577. doi: 10.1126/science.2105529

Lindvall, O., Rehncrona, S., Brundin, P., Gustavii, B., Astedt, B., Windner, H., et al. (1989). Human fetal dopamine neurons grafted into the striatum in two patients with severe Parkinson's disease. A detailed account of methodology and a 6-month follow-up. *Arch. Neurol.* 46, 615–631. doi: 10.1001/archneur.1989.00520420033021

Lindvall, O., Rehncrona, S., Gustavii, B., Brundin, P., Astedt, B., Widner, H., et al. (1988). Fetal dopamine-rich mesencephalic grafts in Parkinson's disease. *Lancet* 2, 1483–1484. doi: 10.1016/s0140-6736(88)90950-6

Lindvall, O., Sawle, G., Widner, H., Rothwell, J. C., Bjorklund, A., Brooks, D., et al. (1994). Evidence for long-term survival and function of dopaminergic grafts in progressive Parkinson's disease. *Ann. Neurol.* 35, 172–180. doi: 10.1002/ana.410350208

Liu, Q., Pedersen, O. Z., Peng, J., Couture, L. A., Rao, M. S., and Zeng, X. (2013). Optimizing dopaminergic differentiation of pluripotent stem cells for the manufacture of dopaminergic neurons for transplantation. *Cytotherapy* 15, 999–1010. doi: 10.1016/j.jcyt.2013.03.006

Liu, W., and Frank, J. A. (2009). Detection and quantification of magnetically labeled cells by cellular Mri. *Eur. J. Radiol.* 70, 258–264. doi: 10.1016/j.ejrad.2008.09.021

Ma, L., Hu, B., Liu, Y., Vermilyea, S. C., Liu, H., Gao, L., et al. (2012). Human embryonic stem cell-derived Gaba neurons correct locomotion deficits in quinolinic acid-lesioned mice. *Cell Stem Cell* 10, 455–464. doi: 10.1016/j.stem.2012.01.021

Ma, Y., Tang, C., Chaly, T., Greene, P., Breeze, R., Fahn, S., et al. (2010). Dopamine cell implantation in Parkinson's disease: long-term clinical and (18)F-Fdopa Pet outcomes. *J. Nucl. Med.* 51, 7–15. doi: 10.2967/jnumed.109.066811

MacGeer, P. L., and McGeer, E. G. (2008). Glial reactions in Parkinson's disease. *Mov. Disord.* 23, 474–483. doi: 10.1002/mds.21751

Madrazo, I., Leon, V., Torres, C., Aguilera, M. C., Varela, G., Alvarez, F., et al. (1988). Transplantation of fetal substantia nigra and adrenal medulla to the caudate nucleus in two patients with Parkinson's disease. *N. Engl. J. Med.* 318:51. doi: 10.1056/nejm198801073180115

Malloy, K. E., Li, J., Choudhury, G. R., Torres, A., Gupta, S., Kantorak, C., et al. (2017). Magnetic resonance imaging-guided delivery of neural stem cells into the basal ganglia of nonhuman primates reveals a pulsatile mode of cell dispersion. *Stem Cells Transl. Med.* 6, 877–885. doi: 10.5966/sctm.2016-0269

Mann, D. M., and Yates, P. O. (1983). Possible role of neuromelanin in the pathogenesis of Parkinson's disease. *Mech. Ageing Dev.* 21, 193–203. doi: 10.1016/0047-6374(83)90074-x

Marshall, V., and Grosset, D. (2003). Role of dopamine transporter imaging in routine clinical practice. *Mov. Disord.* 18, 1415–1423. doi: 10.1002/mds.10592

Mendez, I., Sanchez-Pernaute, R., Cooper, O., Vinuela, A., Ferrari, D., Bjorklund, L., et al. (2005). Cell type analysis of functional fetal dopamine cell suspension

transplants in the striatum and substantia nigra of patients with Parkinson's disease. *Brain* 128, 1498–1510. doi: 10.1093/brain/awh510

Mendez, I., Vinuela, A., Astradsson, A., Mukhida, K., Hallet, P., Robertson, H., et al. (2008). Dopamine neurons implanted into people with Parkinson's disease survive without pathology for 14 years. *Nat. Med.* 14, 507–509. doi: 10.1038/nm1752

Meyer-Lindenberg, A., Miletich, R. S., Kohn, P. D., Esposito, G., Carson, R. E., Quarantelli, M., et al. (2002). Reduced prefrontal activity predicts exaggerated striatal dopaminergic function in schizophrenia. *Nat. Neurosci.* 5, 267–271. doi: 10.1038/nn804

More, S. V., Kumar, H., Kim, I. S., Song, S. Y., and Choi, D. K. (2013). Cellular and molecular mediators of neuroinflammation in the pathogenesis of Parkinson's disease. *Mediators Inflamm.* 2013:952375. doi: 10.1155/2013/952375

Morihisa, J. M., Nakamura, R. K., Freed, W. J., Mishkin, M., and Wyatt, R. J. (1984). Adrenal medulla grafts survive and exhibit catecholamine-specific fluorescence in the primate brain. *Exp. Neurol.* 84, 643–653. doi: 10.1016/0014-4886(84)90211-5

Morizane, A., Doi, D., Kikuchi, T., Okita, K., Hotta, A., Kawasaki, T., et al. (2013). Direct comparison of autologous and allogeneic transplantation of ipsc-derived neural cells in the brain of a non-human primate. *Stem Cell Rep.* 1, 283–292. doi: 10.1016/j.stemcr.2013.08.007

Morizane, A., Kikuchi, T., Hayashi, T., Mizuma, H., Takara, S., Doi, H., et al. (2017). Mhc matching improves engraftment of ipsc-derived neurons in non-human primates. *Nat. Commun.* 8:385. doi: 10.1038/s41467-017-00926-5

Morrish, P. K., Sawle, G. V., and Brooks, D. J. (1996). An [18F]dopa-Pet and clinical study of the rate of progression in Parkinson's disease. *Brain* 119(Pt 2), 585–591. doi: 10.1093/brain/119.2.585

Muramatsu, S., Okuno, T., Suzuki, Y., Nakayama, T., Kakiuchi, T., Takino, N., et al. (2009). Multitracer assessment of dopamine function after transplantation of embryonic stem cell-derived neural stem cells in a primate model of Parkinson's disease. *Synapse* 63, 541–548. doi: 10.1002/syn.20634

Neuhoff, H., Neu, A., Liss, B., and Roeper, J. (2002). I(h) channels contribute to the different functional properties of identified dopaminergic subpopulations in the midbrain. *J. Neurosci.* 22, 1290–1302. doi: 10.1523/jneurosci.22-04-01290.2002

Nolbrant, S., Heuer, A., Parmar, M., and Kirkeby, A. (2017). Generation of high-purity human ventral midbrain dopaminergic progenitors for in vitro maturation and intracerebral transplantation. *Nat. Protoc.* 12, 1962–1979. doi: 10.1038/nprot.2017.078

Norman, A. B., Thomas, S. R., Pratt, R. G., Lu, S. Y., and Norgren, R. B. (1992). Magnetic resonance imaging of neural transplants in rat brain using a superparamagnetic contrast agent. *Brain Res.* 594, 279–283. doi: 10.1016/0006-8993(92)91135-2

Olanow, C. W., Freeman, T., and Kordower, J. (2001). Transplantation of embryonic dopamine neurons for severe Parkinson's disease. *N. Engl. J. Med.* 345:146.

Olanow, C. W., Goetz, C. G., Kordower, J. H., Stoessl, A. J., Sossi, V., Brin, M. F., et al. (2003). A double-blind controlled trial of bilateral fetal nigral transplantation in Parkinson's disease. *Ann. Neurol.* 54, 403–414. doi: 10.1002/ana.10720

Olanow, C. W., Stern, M. B., and Sethi, K. (2009). The scientific and clinical basis for the treatment of Parkinson disease. *Neurology* 72, S1–S136. doi: 10.1212/WNL.0b013e3181a1d44c

Olson, L., and Malmfors, T. (1970). Growth characteristics of adrenergic nerves in the adult rat. Fluorescence histochemical and 3H-noradrenaline uptake studies using tissue transplantations to the anterior chamber of the eye. *Acta Physiol. Scand. Suppl.* 348, 1–112.

Olson, L., and Seiger, A. (1972). Brain tissue transplanted to the anterior chamber of the eye. 1. Fluorescence histochemistry of immature catecholamine and 5-hydroxytryptamine neurons reinnervating the rat iris. *Z. Zellforsch. Mikrosk. Anat.* 135, 175–194. doi: 10.1007/bf00315125

Ono, Y., Nakatani, T., Sakamoto, Y., Mizuhara, E., Minaki, Y., Kumai, M., et al. (2007). Differences in neurogenic potential in floor plate cells along an anteroposterior location: midbrain dopaminergic neurons originate from mesencephalic floor plate cells. *Development* 134, 3213–3225. doi: 10.1242/dev.02879

Papp, M., and Bal, A. (1986). Motivational versus motor impairment after haloperidol injection or 6-Ohda lesions in the ventral tegmental area or substantia nigra in rats. *Physiol. Behav.* 38, 773–779. doi: 10.1016/0031-9384(86)90042-9

Park, C. H., Minn, Y. K., Lee, J. Y., Choi, D. H., Chang, M. Y., Shim, J. W., et al. (2005). In vitro and in vivo analyses of human embryonic stem cell-derived dopamine neurons. *J. Neurochem.* 92, 1265–1276. doi: 10.1111/j.1471-4159.2004.03006.x

Park, H. J., Lee, P. H., Bang, O. Y., Lee, G., and Ahn, Y. H. (2008). Mesenchymal stem cells therapy exerts neuroprotection in a progressive animal model of Parkinson's disease. *J. Neurochem.* 107, 141–151. doi: 10.1111/j.1471-4159.2008.05589.x

Peng, J., Liu, Q., Rao, M. S., and Zeng, X. (2014). Survival and engraftment of dopaminergic neurons manufactured by a good manufacturing practice-compatible process. *Cytotherapy* 16, 1305–1312. doi: 10.1016/j.jcyt.2014.06.002

Perez-Bouza, A., Di Santo, S., Seiler, S., Meyer, M., Andereggen, L., Huber, A., et al. (2017). Simultaneous transplantation of fetal ventral mesencephalic tissue and encapsulated genetically modified cells releasing gdnf in a hemi-parkinsonian rat model of Parkinson's disease. *Cell Transplant.* 26, 1572–1581. doi: 10.1177/0963689717721202

Perlow, M. J., Freed, W. J., Hoffer, B. J., Seiger, A., Olson, L., and Wyatt, R. J. (1979). Brain grafts reduce motor abnormalities produced by destruction of nigrostriatal dopamine system. *Science* 204, 643–647. doi: 10.1126/science.571147

Peschanski, M., Defer, G., N'guyen, J. P., Ricolfi, F., Monfort, J. C., Remy, P., et al. (1994). Bilateral motor improvement and alteration of L-dopa effect in two patients with Parkinson's disease following intrastriatal transplantation of foetal ventral mesencephalon. *Brain* 117(Pt 3), 487–499. doi: 10.1093/brain/117.3.487

Phanstiel, D. H., Brumbaugh, J., Wenger, C. D., Tian, S., Probasco, M. D., Bailey, D. J., et al. (2011). Proteomic and phosphoproteomic comparison of human Es and ips cells. *Nat. Methods* 8, 821–827. doi: 10.1038/nmeth.1699

Piccini, P., Brooks, D. J., Bjorklund, A., Gunn, R. N., Grasby, P. M., Rimoldi, O., et al. (1999). Dopamine release from nigral transplants visualized in vivo in a Parkinson's patient. *Nat. Neurosci.* 2, 1137–1140. doi: 10.1038/16060

Piccini, P., Lindvall, O., Bjorklund, A., Brundin, P., Hagell, P., Ceravolo, R., et al. (2000). Delayed recovery of movement-related cortical function in Parkinson's disease after striatal dopaminergic grafts. *Ann. Neurol.* 48, 689–695. doi: 10.1002/1531-8249(200011)48:5<689::aid-ana1>3.0.co;2-n

Piccini, P., Pavese, N., Hagell, P., Reimer, J., Bjorklund, A., Oertel, W. H., et al. (2005). Factors affecting the clinical outcome after neural transplantation in Parkinson's disease. *Brain* 128, 2977–2986. doi: 10.1093/brain/awh649

Pijnenburg, A. J., Honig, W. M., Van Der Heyden, J. A., and Van Rossum, J. M. (1976). Effects of chemical stimulation of the mesolimbic dopamine system upon locomotor activity. *Eur. J. Pharmacol* 35, 45–58. doi: 10.1016/0014-2999(76)90299-5

Pogarell, O., Koch, W., Gildehaus, F. J., Kupsch, A., Lindvall, O., Oertel, W. H., et al. (2006). Long-term assessment of striatal dopamine transporters in Parkinsonian patients with intrastriatal embryonic mesencephalic grafts. *Eur. J. Nucl. Med. Mol. Imaging* 33, 407–411. doi: 10.1007/s00259-005-0032-z

Politis, M., Oertel, W. H., Wu, K., Quinn, N. P., Pogarell, O., Brooks, D. J., et al. (2011). Graft-induced dyskinesias in Parkinson's disease: high striatal serotonin/dopamine transporter ratio. *Mov. Disord.* 26, 1997–2003. doi: 10.1002/mds.23743

Politis, M., Wu, K., Loane, C., Quinn, N. P., Brooks, D. J., Rehncrona, S., et al. (2010). Serotonergic neurons mediate dyskinesia side effects in Parkinson's patients with neural transplants. *Sci. Transl. Med.* 2:38ra46. doi: 10.1126/scitranslmed.3000976

Poulin, J. F., Zou, J., Drouin-Ouellet, J., Kim, K. Y., Cicchetti, F., and Awatramani, R. B. (2014). Defining midbrain dopaminergic neuron diversity by single-cell gene expression profiling. *Cell. Rep.* 9, 930–943. doi: 10.1016/j.celrep.2014.10.008

Pruszak, J., Ludwig, W., Blak, A., Alavian, K., and Isacson, O. (2009). Cd15, Cd24, and Cd29 define a surface biomarker code for neural lineage differentiation of stem cells. *Stem Cells* 27, 2928–2940. doi: 10.1002/stem.211

Pulecio, J., Nivet, E., Sancho-Martinez, I., Vitaloni, M., Guenechea, G., Xia, Y., et al. (2014). Conversion of human fibroblasts into monocyte-like progenitor cells. *Stem Cells* 32, 2923–2938. doi: 10.1002/stem.1800

Punal-Rioboo, J., Serena-Puig, A., Varela-Lema, L., Alvarez-Paez, A. M., and Ruano-Ravina, A. (2009). [Clinical utility of (18)F-Dopa-Pet in movement disorders. A systematic review]. *Rev. Esp. Med. Nucl.* 28, 106–113. doi: 10.1016/s1578-200x(09)70018-x

Qin, J., Song, B., Zhang, H., Wang, Y., Wang, N., Ji, Y., et al. (2013). Transplantation of human neuro-epithelial-like stem cells derived from induced pluripotent stem cells improves neurological function in rats with experimental intracerebral hemorrhage. *Neurosci. Lett.* 548, 95–100. doi: 10.1016/j.neulet.2013.05.007

Ramos-Gomez, M., and Martinez-Serrano, A. (2016). Tracking of iron-labeled human neural stem cells by magnetic resonance imaging in cell replacement therapy for Parkinson's disease. *Neural Regen. Res.* 11, 49–52. doi: 10.4103/1673-5374.169628

Ramos-Gomez, M., Seiz, E. G., and Martinez-Serrano, A. (2015). Optimization of the magnetic labeling of human neural stem cells and Mri visualization in the hemiparkinsonian rat brain. *J. Nanobiotechnol.* 13:20. doi: 10.1186/s12951-015-0078-4

Redmond, D. E. Jr., Sladek, J. R., and Spencer, D. D. (2001). Transplantation of embryonic dopamine neurons for severe Parkinson's disease. *N. Engl. J. Med.* 345, 146–147. doi: 10.1056/nejm200107123450214

Redmond, D. E., Sladek, J. R. Jr., Roth, R. H., Collier, T. J., Elsworth, J. D., Deutch, A. Y., et al. (1986). Fetal neuronal grafts in monkeys given methylphenyltetrahydropyridine. *Lancet* 1, 1125–1127. doi: 10.1016/s0140-6736(86)91839-8

Reid, J. E., and Wernisch, L. (2016). Pseudotime estimation: deconfounding single cell time series. *Bioinformatics* 32, 2973–2980. doi: 10.1093/bioinformatics/btw372

Reubinoff, B. E., Itsykson, P., Turetsky, T., Pera, M. F., Reinhartz, E., Itzik, A., et al. (2001). Neural progenitors from human embryonic stem cells. *Nat. Biotechnol.* 19, 1134–1140. doi: 10.1038/nbt1201-1134

Reubinoff, B. E., Pera, M. F., Fong, C. Y., Trounson, A., and Bongso, A. (2000). Embryonic stem cell lines from human blastocysts: somatic differentiation in vitro. *Nat. Biotechnol.* 18, 399–404. doi: 10.1038/74447

Reyes, S., Fu, Y., Double, K., Thompson, L., Kirik, D., Paxinos, G., et al. (2012). Girk2 expression in dopamine neurons of the substantia nigra and ventral tegmental area. *J. Comp. Neurol.* 520, 2591–2607. doi: 10.1002/cne.23051

Ribeiro, D., Laguna Goya, R., Ravindran, G., Vuono, R., Parish, C. L., Foldi, C., et al. (2013). Efficient expansion and dopaminergic differentiation of human fetal ventral midbrain neural stem cells by midbrain morphogens. *Neurobiol. Dis.* 49, 118–127. doi: 10.1016/j.nbd.2012.08.006

Robinson, T. E., and Berridge, K. C. (1993). The neural basis of drug craving: an incentive-sensitization theory of addiction. *Brain Res. Brain Res. Rev.* 18, 247–291. doi: 10.1016/0165-0173(93)90013-p

Rouhani, F., Kumasaka, N., De Brito, M. C., Bradley, A., Vallier, L., and Gaffney, D. (2014). Genetic background drives transcriptional variation in human induced pluripotent stem cells. *PLoS Genet.* 10:e1004432. doi: 10.1371/journal.pgen.1004432

Roy, N. S., Cleren, C., Singh, S. K., Yang, L., Beal, M. F., and Goldman, S. A. (2006). Functional engraftment of human Es cell-derived dopaminergic neurons enriched by coculture with telomerase-immortalized midbrain astrocytes. *Nat. Med.* 12, 1259–1268. doi: 10.1038/nm1495

Salti, A., Nat, R., Neto, S., Puschban, Z., Wenning, G., and Dechant, G. (2013). Expression of early developmental markers predicts the efficiency of embryonic stem cell differentiation into midbrain dopaminergic neurons. *Stem Cells Dev* 22, 397–411. doi: 10.1089/scd.2012.0238

Sawle, G. V., Bloomfield, P. M., Bjorklund, A., Brooks, D. J., Brundin, P., Leenders, K. L., et al. (1992). Transplantation of fetal dopamine neurons in Parkinson's disease: pet [18F]6-L-fluorodopa studies in two patients with putaminal implants. *Ann. Neurol.* 31, 166–173. doi: 10.1002/ana.410310207

Schweitzer, J. S., Song, B., Herrington, T. M., Park, T. Y., Lee, N., Ko, S., et al. (2020). Personalized ipsc-derived dopamine progenitor cells for Parkinson's disease. *N. Engl. J. Med.* 382, 1926–1932. doi: 10.1056/NEJMoa1915872

Senju, S., Matsunaga, Y., Fukushima, S., Hirata, S., Motomura, Y., Fukuma, D., et al. (2011). Immunotherapy with pluripotent stem cell-derived dendritic cells. *Semin. Immunopathol.* 33, 603–612. doi: 10.1007/s00281-011-0263-y

Sgado, P., Alberi, L., Gherbassi, D., Galasso, S. L., Ramakers, G. M., Alavian, K. N., et al. (2006). Slow progressive degeneration of nigral dopaminergic neurons in postnatal Engrailed mutant mice. *Proc. Natl. Acad. Sci. U.S.A.* 103, 15242–15247. doi: 10.1073/pnas.0602116103

Shih, M. C., Amaro, E. Jr., Ferraz, H. B., Hoexter, M. Q., Goulart, F. O., Wagner, J., et al. (2006). [Neuroimaging of the dopamine transporter in Parkinsons disease: first study using [99mTc]-Trodat-1 and Spect in Brazil]. *Arq. Neuropsiquiatr.* 64, 628–634. doi: 10.1590/S0004-282X2006000400021

Siegfried, J., and Lippitz, B. (1994). Bilateral chronic electrostimulation of ventroposterolateral pallidum: a new therapeutic approach for alleviating all parkinsonian symptoms. *Neurosurgery* 35, 1126–1130. doi: 10.1227/00006123-199412000-00016

Simon, H. H., Saueressig, H., Wurst, W., Goulding, M. D., and O'leary, D. D. (2001). Fate of midbrain dopaminergic neurons controlled by the engrailed genes. *J. Neurosci.* 21, 3126–3134. doi: 10.1523/jneurosci.21-09-03126.2001

Sison, S. L., Vermilyea, S. C., Emborg, M. E., and Ebert, A. D. (2018). Using patient-derived induced pluripotent stem cells to identify parkinson's disease-relevant phenotypes. *Curr. Neurol. Neurosci. Rep.* 18:84. doi: 10.1007/s11910-018-0893-8

Smidt, M. P., Van Schaick, H. S., Lanctot, C., Tremblay, J. J., Cox, J. J., Van Der Kleij, A. A., et al. (1997). A homeodomain gene Ptx3 has highly restricted brain expression in mesencephalic dopaminergic neurons. *Proc. Natl. Acad. Sci. U.S.A.* 94, 13305–13310. doi: 10.1073/pnas.94.24.13305

Soldner, F., Hockemeyer, D., Beard, C., Gao, Q., Bell, G. W., Cook, E. G., et al. (2009). Parkinson's disease patient-derived induced pluripotent stem cells free of viral reprogramming factors. *Cell* 136, 964–977.

Son, S. J., Kim, M., and Park, H. (2016). Imaging analysis of Parkinson's disease patients using Spect and tractography. *Sci. Rep.* 6:38070. doi: 10.1038/srep38070

Sonntag, K. C., Pruszak, J., Yoshizaki, T., Van Arensbergen, J., Sanchez-Pernaute, R., and Isacson, O. (2007). Enhanced yield of neuroepithelial precursors and midbrain-like dopaminergic neurons from human embryonic stem cells using the bone morphogenic protein antagonist noggin. *Stem Cells* 25, 411–418. doi: 10.1634/stemcells.2006-0380

Sonntag, K. C., Simantov, R., Kim, K. S., and Isacson, O. (2004). Temporally induced Nurr1 can induce a non-neuronal dopaminergic cell type in embryonic stem cell differentiation. *Eur. J. Neurosci.* 19, 1141–1152. doi: 10.1111/j.1460-9568.2004.03204.x

Spencer, D. D., Robbins, R. J., Naftolin, F., Marek, K. L., Vollmer, T., Leranth, C., et al. (1992). Unilateral transplantation of human fetal mesencephalic tissue into the caudate nucleus of patients with Parkinson's disease. *N. Engl. J. Med.* 327, 1541–1548. doi: 10.1056/nejm199211263272201

Steinbeck, J. A., and Studer, L. (2015). Moving stem cells to the clinic: potential and limitations for brain repair. *Neuron* 86, 187–206. doi: 10.1016/j.neuron.2015.03.002

Stewart, M. H., Bosse, M., Chadwick, K., Menendez, P., Bendall, S. C., and Bhatia, M. (2006). Clonal isolation of hescs reveals heterogeneity within the pluripotent stem cell compartment. *Nat. Methods* 3, 807–815. doi: 10.1038/nmeth939

Stoker, T. B. (2018). "Stem cell treatments for Parkinson's disease," in *Parkinson's Disease: Pathogenesis and Clinical Aspects*, eds T. B. Stoker and J. C. Greenland (Brisbane: Codon Publications). doi: 10.15586/codonpublications.parkinsonsdisease.2018.ch9

Stroh, A., Boltze, J., Sieland, K., Hild, K., Gutzeit, C., Jung, T., et al. (2009). Impact of magnetic labeling on human and mouse stem cells and their long-term magnetic resonance tracking in a rat model of Parkinson disease. *Mol. Imaging* 8, 166–178. doi: 10.2310/7290.2009.00017

Stromberg, I., Bygdeman, M., Goldstein, M., Seiger, A., and Olson, L. (1986). Human fetal substantia nigra grafted to the dopamine-denervated striatum of immunosuppressed rats: evidence for functional reinnervation. *Neurosci. Lett.* 71, 271–276. doi: 10.1016/0304-3940(86)90632-4

Studer, L. (2017). Strategies for bringing stem cell-derived dopamine neurons to the clinic-The Nystem trial. *Prog. Brain Res.* 230, 191–212. doi: 10.1016/bs.pbr.2017.02.008

Sundberg, M., Bogetofte, H., Lawson, T., Jansson, J., Smith, G., Astradsson, A., et al. (2013). Improved cell therapy protocols for Parkinson's disease based on differentiation efficiency and safety of hesc-, hipsc-, and non-human primate ipsc-derived dopaminergic neurons. *Stem Cells* 31, 1548–1562. doi: 10.1002/stem.1415

Sykova, E., and Jendelova, P. (2007). In vivo tracking of stem cells in brain and spinal cord injury. *Prog. Brain Res.* 161, 367–383. doi: 10.1016/s0079-6123(06)61026-1

Takahashi, J. (2017). Strategies for bringing stem cell-derived dopamine neurons to the clinic: the Kyoto trial. *Prog. Brain Res.* 230, 213–226. doi: 10.1016/bs.pbr.2016.11.004

Takahashi, K., Okita, K., Nakagawa, M., and Yamanaka, S. (2007). Induction of pluripotent stem cells from fibroblast cultures. *Nat. Protoc.* 2, 3081–3089. doi: 10.1038/nprot.2007.418

Takahashi, K., and Yamanaka, S. (2006). Induction of pluripotent stem cells from mouse embryonic and adult fibroblast cultures by defined factors. *Cell* 126, 663–676. doi: 10.1016/j.cell.2006.07.024

Takahashi, K., and Yamanaka, S. (2016). A decade of transcription factor-mediated reprogramming to pluripotency. *Nat. Rev. Mol. Cell Biol.* 17, 183–193. doi: 10.1038/nrm.2016.8

Tennstaedt, A., Aswendt, M., Adamczak, J., and Hoehn, M. (2013). Noninvasive multimodal imaging of stem cell transplants in the brain using bioluminescence imaging, and magnetic resonance imaging. *Methods Mol Biol.* 1052, 153–166. doi: 10.1007/7651_2013_14

Thobois, S., Guillouet, S., and Broussolle, E. (2001). Contributions of Pet and Spect to the understanding of the pathophysiology of Parkinson's disease. *Neurophysiol. Clin.* 31, 321–340. doi: 10.1016/s0987-7053(01)00273-8

Thomas, S. M., Kagan, C., Pavlovic, B. J., Burnett, J., Patterson, K., Pritchard, J. K., et al. (2015). Reprogramming Lcls to ipscs results in recovery of donor-specific gene expression signature. *PLoS Genet.* 11:e1005216. doi: 10.1371/journal.pgen.1005216

Thompson, L., Barraud, P., Andersson, E., Kirik, D., and Bjorklund, A. (2005). Identification of dopaminergic neurons of nigral and ventral tegmental area subtypes in grafts of fetal ventral mesencephalon based on cell morphology, protein expression, and efferent projections. *J. Neurosci.* 25, 6467–6477. doi: 10.1523/jneurosci.1676-05.2005

Thomson, J. A., Itskovitz-Eldor, J., Shapiro, S. S., Waknitz, M. A., Swiergiel, J. J., Marshall, V. S., et al. (1998). Embryonic stem cell lines derived from human blastocysts. *Science* 282, 1145–1147. doi: 10.1126/science.282.5391.1145

Tiklova, K., Bjorklund, A. K., Lahti, L., Fiorenzano, A., Nolbrant, S., Gillberg, L., et al. (2019). Single-cell Rna sequencing reveals midbrain dopamine neuron diversity emerging during mouse brain development. *Nat. Commun.* 10:581. doi: 10.1038/s41467-019-08453-1

Ungerstedt, U. (1971). Stereotaxic mapping of the monoamine pathways in the rat brain. *Acta Physiol. Scand. Suppl.* 367, 1–48. doi: 10.1111/j.1365-201x.1971.tb10998.x

Visnyei, K., Tatsukawa, K. J., Erickson, R. I., Simonian, S., Oknaian, N., Carmichael, S. T., et al. (2006). Neural progenitor implantation restores metabolic deficits in the brain following striatal quinolinic acid lesion. *Exp. Neurol.* 197, 465–474. doi: 10.1016/j.expneurol.2005.10.023

Waerzeggers, Y., Klein, M., Miletic, H., Himmelreich, U., Li, H., Monfared, P., et al. (2008). Multimodal imaging of neural progenitor cell fate in rodents. *Mol. Imaging* 7, 77–91. doi: 10.2310/7290.2008.0010

Wakeman, D. R., Hiller, B. M., Marmion, D. J., Mcmahon, C. W., Corbett, G. T., Mangan, K. P., et al. (2017). Cryopreservation maintains functionality of human ipsc dopamine neurons and rescues parkinsonian phenotypes in vivo. *Stem Cell Rep.* 9, 149–161. doi: 10.1016/j.stemcr.2017.04.033

Wang, L., Zhang, Q., Li, H., and Zhang, H. (2012). Spect molecular imaging in Parkinson's disease. *J. Biomed. Biotechnol.* 2012:412486. doi: 10.1155/2012/412486

Wang, S., Zou, C., Fu, L., Wang, B., An, J., Song, G., et al. (2015). Autologous ipsc-derived dopamine neuron transplantation in a nonhuman primate Parkinson's disease model. *Cell Discov.* 1:15012. doi: 10.1038/celldisc.2015.12

Wenning, G. K., Odin, P., Morrish, P., Rehncrona, S., Widner, H., Brundin, P., et al. (1997). Short- and long-term survival and function of unilateral intrastriatal dopaminergic grafts in Parkinson's disease. *Ann. Neurol.* 42, 95–107. doi: 10.1002/ana.410420115

Widner, H., Tetrud, J., Rehncrona, S., Snow, B., Brundin, P., Gustavii, B., et al. (1992). Bilateral fetal mesencephalic grafting in two patients with parkinsonism induced by 1-methyl-4-phenyl-1,2,3,6-tetrahydropyridine (Mptp). *N. Engl. J. Med.* 327, 1556–1563. doi: 10.1056/nejm199211263272203

Wolfart, J., Neuhoff, H., Franz, O., and Roeper, J. (2001). Differential expression of the small-conductance, calcium-activated potassium channel Sk3 is critical for pacemaker control in dopaminergic midbrain neurons. *J. Neurosci.* 21, 3443–3456. doi: 10.1523/jneurosci.21-10-03443.2001

Wu, X., Cai, H., Ge, R., Li, L., and Jia, Z. (2014). Recent progress of imaging agents for Parkinson's disease. *Curr. Neuropharmacol.* 12, 551–563. doi: 10.2174/1570159x13666141204221238

Yan, Y., Yang, D., Zarnowska, E. D., Du, Z., Werbel, B., Valliere, C., et al. (2005). Directed differentiation of dopaminergic neuronal subtypes from human embryonic stem cells. *Stem Cells* 23, 781–790. doi: 10.1634/stemcells.2004-0365

Yang, D., Zhang, Z. J., Oldenburg, M., Ayala, M., and Zhang, S. C. (2008). Human embryonic stem cell-derived dopaminergic neurons reverse functional deficit in parkinsonian rats. *Stem Cells* 26, 55–63. doi: 10.1634/stemcells.2007-0494

Yu, J., Vodyanik, M. A., Smuga-Otto, K., Antosiewicz-Bourget, J., Frane, J. L., Tian, S., et al. (2007). Induced pluripotent stem cell lines derived from human somatic cells. *Science* 318, 1917–1920. doi: 10.1126/science.1151526

Zhang, S. C., Wernig, M., Duncan, I. D., Brustle, O., and Thomson, J. A. (2001). In vitro differentiation of transplantable neural precursors from human embryonic stem cells. *Nat. Biotechnol.* 19, 1129–1133. doi: 10.1038/nbt1201-1129

Zheng, Y., Huang, J., Zhu, T., Li, R., Wang, Z., Ma, F., et al. (2017). Stem cell tracking technologies for neurological regenerative medicine purposes. *Stem Cells Int.* 2017:2934149. doi: 10.1155/2017/2934149

Conflict of Interest: The authors declare that the research was conducted in the absence of any commercial or financial relationships that could be construed as a potential conflict of interest.

frontiers in Neuroscience

ORIGINAL RESEARCH
published: 22 October 2020
doi: 10.3389/fnins.2020.00853

Differential Diagnosis of Frontotemporal Dementia, Alzheimer's Disease, and Normal Aging Using a Multi-Scale Multi-Type Feature Generative Adversarial Deep Neural Network on Structural Magnetic Resonance Images

Da Ma[1†], Donghuan Lu[1,2†], Karteek Popuri[1], Lei Wang[3], Mirza Faisal Beg[1*] and Alzheimer's Disease Neuroimaging Initiative[‡]*

[1] School of Engineering Science, Simon Fraser University, Burnaby, BC, Canada, [2] Tencent Jarvis X-Lab, Shenzhen, China, [3] Feinberg School of Medicine, Northwestern University, Chicago, IL, United States

OPEN ACCESS

Edited by:
Jiehui Jiang,
Shanghai University, China

Reviewed by:
Suyash P. Awate,
Indian Institute of Technology Bombay, India
Chun-Yi Lo,
Fudan University, China

***Correspondence:**
Donghuan Lu
ludonghuan9@gmail.com
Mirza Faisal Beg
faisal-lab@sfu.ca

[†] *These authors share first authorship*

[‡] *Data used in preparation of this article were obtained from the Alzheimer's Disease Neuroimaging Initiative (ADNI) database (adni.loni.usc.edu). As such, the investigators within the ADNI contributed to the design and implementation of ADNI and/or provided data but did not participate in analysis or writing of this report. A complete listing of ADNI investigators can be found at: http://adni.loni.usc.edu/wp-content/uploads/how_to_apply/ADNI_Acknowledgement_List.pdf*

Specialty section:
This article was submitted to Brain Imaging Methods, a section of the journal Frontiers in Neuroscience

Received: *13 March 2020*
Accepted: *21 June 2020*
Published: *22 October 2020*

Methods: Alzheimer's disease and Frontotemporal dementia are the first and third most common forms of dementia. Due to their similar clinical symptoms, they are easily misdiagnosed as each other even with sophisticated clinical guidelines. For disease-specific intervention and treatment, it is essential to develop a computer-aided system to improve the accuracy of their differential diagnosis. Recent advances in deep learning have delivered some of the best performance for medical image recognition tasks. However, its application to the differential diagnosis of AD and FTD pathology has not been explored.

Approach: In this study, we proposed a novel deep learning based framework to distinguish between brain images of normal aging individuals and subjects with AD and FTD. Specifically, we combined the multi-scale and multi-type MRI-base image features with Generative Adversarial Network data augmentation technique to improve the differential diagnosis accuracy.

Results: Each of the multi-scale, multitype, and data augmentation methods improved the ability for differential diagnosis for both AD and FTD. A 10-fold cross validation experiment performed on a large sample of 1,954 images using the proposed framework achieved a high overall accuracy of 88.28%.

Conclusions: The salient contributions of this study are three-fold: (1) our experiments demonstrate that the combination of multiple structural features extracted at different scales with our proposed deep neural network yields superior performance than

individual features; (2) we show that the use of Generative Adversarial Network for data augmentation could further improve the discriminant ability of the network regarding challenging tasks such as differentiating dementia sub-types; (3) and finally, we show that ensemble classifier strategy could make the network more robust and stable.

Keywords: differential diagnosis, magnetic resonance imaging, generative adversarial network, frontotemporal dementia (FTD), Alzheimer's disease

1. INTRODUCTION

As the first and third most common forms of dementia, Alzheimer's disease (AD) (Association et al., 2011) and Frontotemporal dementia (FTD) (Bang et al., 2015) are often mistaken as each other. This is due to the similarities in their clinical presentation, cognitive domains impairment, brain atrophy, and progressive alterations in language ability, behavior, and personality (Neary et al., 2005; Alladi et al., 2007; Womack et al., 2011). Despite significant efforts spent on establishing sophisticated clinical guidelines for their differential diagnosis, the diagnostic accuracy is still not satisfactory. Specifically, when diagnosing with the NINCDS-ADRDA criteria (Neary et al., 1998), the sensitivity of distinguishing AD subjects from FTD patients could reach as high as 93%; however, the specificity for FTD recognition is only 23% as most patients with FTD also fulfilled the NINCDS-ADRDA criteria for AD (Varma et al., 1999). With the necessity of applying different symptomatic intervention of treatment for various dementia subtypes in clinical practice (Pasquier, 2005), it is essential to develop a computer-aided diagnosis system for the improvement of the accuracy of differential diagnosis between these two dementias.

Patterns of brain atrophy observed in T1-weighted Magnetic Resonance Imaging (MRI) have been successfully used to capture structural changes in the human brain (Du et al., 2007; Davatzikos et al., 2011), specifically for using in developing computational systems that can identify the type of dementia pathology in the brain. Computer-aided diagnosis systems with MRI have been built for both AD and FTD (Suk et al., 2014; Jiskoot et al., 2018). In addition to binary classification with normal aging, T1-weighted MRIs have also been used for the differential diagnosis of AD and FTD by differentiating the atrophy pattern of these two types of dementia such as the affected regions and rate of change (Raamana et al., 2014). Various structural biomarkers have been explored to distinguish between AD and FTD, such as gray matter (GM) volume loss (Rabinovici et al., 2008), cortical thinning (Du et al., 2007), high-dimensional features based on GM and white matter (WM) volume distribution of whole brain (Davatzikos et al., 2008), as well as atrophy and shape deformity of individual structures (Looi et al., 2010).

Most previous studies on computer-aided diagnosis system for dementia classification emphasized on binary classification tasks, e.g., NC vs. FTD, NC vs. AD, or FTD vs. AD with few direct multi-class dementia classification methods in the literature. Raamana et al. compared multiple structural features, such as volumes, Laplacian invariants, and surface displacements of the hippocampus and lateral ventricle, regarding the multi-class classification among NC, AD, and FTD subjects (Raamana et al., 2014). With PCA and multi-class support vector machine (SVM) classifier, they achieved a 0.79 AUC. Tong et al. applied the RUSBoost algorithm (Seiffert et al., 2010) for the multi-class classification of subjective memory complaints, AD, frontotemporal lobe degeneration (FTLD), dementia with Lewy bodies, and vascular dementia (Tong et al., 2017). With volume and grading features as well as CSF measures and age, they achieved 75.2% overall accuracy with 0.8 sensitivity for AD and 0.63 sensitivity for FTLD.

Recently, deep learning has been delivering astounding performance for many recognition tasks (Hinton and Salakhutdinov, 2006; Krizhevsky et al., 2012; Simonyan and Zisserman, 2014). Its applications in computer-aided diagnosis has also drawn attention and it has out-performed traditional classification methods for many clinical recognition tasks (Suk et al., 2014; Ronneberger et al., 2015; Litjens et al., 2017). However, to the best of our knowledge, there have been no deep-learning-based approaches developed and published yet for the differential diagnosis of AD and FTD.

In this study, we proposed a novel framework to combine multi-type and multi-scale image-based features from structural MRI scans. Local volume size and surface thickness features were extracted by segmenting the T1-weighted MRI images into patches of a hierarchical size based on brain anatomy in a coarse-to-fine manner. A multi-scale and multi-type feature deep neural network (MMDNN) was developed to learn the latent representation across each individual features, along with the Generative Adversarial Network (GAN) technique for data augmentation and ensemble classifier strategy to increase robustness of the framework. A comprehensive validation experiment with 1,954 images demonstrates the superior performance of the proposed framework with 88.28% accuracy.

2. METHODS

In the proposed framework, the original raw structural MRI images were first segmented into different anatomical structure region of interests (ROI) with FreeSurfer. Each ROI was further sub-clustered into smaller patches of super-pixels with multi-scales. The volume, cortical thickness at each level of the patch were extracted as multi-scale multi-type features. Finally, a Generative Adversarial Network with multi-type and multi-scale features was trained to achieve differential diagnosis to identify patients with AD and FTD from NC subjects.

TABLE 1 | Demographic information of the subject included from the databases.

Mean ± SD	NC	AD	FTD
Count (M/F)	1063 (533/530)	459 (270/189)	434 (266/168)
Age (Mean ± SD)	72.19 ± 8.28	75.91 ± 7.54	64.69 ± 8.51
Education (Mean ± SD)	16.66 ± 3.24	15.13 ± 2.58	19.05 ± 1.12
MMSE (Mean ± SD)	29.40 ± 1.39	23.20 ± 1.96	25.36 ± 6.12

First row (Count M/F): total number as well as number of male and female subjects in each clinically diagnostic group. Second row: the mean and standard deviation of subject age (unit: years). Third row: the mean and standard deviation of subject's years of education (unit: years). Forth row: the mean and standard deviation of subject's clinically evaluated MMSE score.

2.1. Materials

Data used in this study were obtained from two publicly available databases, i.e., the Alzheimer's Disease Neuroimaging Initiative (ADNI) database adni.loni.usc.edu and the frontotemporal lobar degeneration neuroimaging initiative (NIFD) database http://memory.ucsf.edu/research/studies/nifd. The primary goal of ADNI is to test whether serial MRI, PET, other biological markers, and clinical and neuropsychological assessment can be combined to measure the progression of mild cognitive impairment (MCI) and early Alzheimer's disease (AD). Frontotemporal lobar degeneration Neuroimaging Initiative (FTLDNI), also referred to as NIFD started in 2010 with the primary goals being to identify neuroimaging modalities and methods of analysis for tracking frontotemporal lobar degeneration (FTLD) and to assess the value of imaging vs. other biomarkers in diagnostic roles. More detailed information about FTLDNI can be found in 4rtni-ftldni.ini.usc.edu.

Both ADNI and FTLDNI databases contain longitudinal scans for each participant. Subjects with who the diagnosis changes in any of their follow-up visits during the study period (i.e., MCI progressing to AD or reverting to NC), were excluded from the study to reduce the effect of potential misdiagnosis. A total of 1,954 Structural MRI were included in this study, 1,114 of which were from ADNI database, and the remaining 840 from the NIFD database. **Table 1** shows the demographic and clinical information of these subjects in both database. The numbers in the brackets of the second row are the numbers of male and female subjects, while number before each bracket is the total number of subjects belong to that group. The numbers in the remaining three rows represent the mean and standard deviation of age, education, and MMSE, respectively.

2.2. Multi-Level Multi-Type Feature Extraction

For image recognition problems, convolutional neural network (CNN) and its variants, such as VGG16 (Simonyan and Zisserman, 2014), ResNet (He et al., 2016), and Inception-ResNet (Szegedy et al., 2017), have achieved the state-of-the-art performance in various tasks. However, those networks require a large number of labeled samples for their training. Especially with high dimensional data, as used in this study ($256 \times 256 \times 256$ 3D images), larger kernel sizes or more layers are necessary to learn the latent representation, resulting in a larger network that needs even more training samples. The dataset used in our data set is considerably larger in magnitude than many other studies in the neuroimaging context, it is however still relatively small in scale as compared with most of the natural image recognition tasks. Therefore, to reduce the dimension of input data and the size of network, each MRI scan was segmented into small regions based on brain anatomy, which we denoted as "patches" hereafter, and two types of primary structural features, volume size and cortical mantle thickness, were extracted for the differential diagnosis of NC, AD, and FTD. For MRI scan segmentation and volume size feature extraction, the following steps were applied: (1) structural ROI parcellation, (2) Structural-wise patch cluster-based segmentation, (3) Feature extraction and normalization.

Firstly, in the ROI segmentation step, the gray matter (both cortical and subcortical) of each T1 structural MRI image was segmented into 87 anatomical ROIs using FreeSurfer 5.3 (Dale AM, 1999). For some ROIs, in particularly larger ones such as the occipital cortex, the discriminant information for brain structural change could be localized within the ROI to smaller focal locations. Such localized differences could potentially provide important information to differentiate AD and FTD but could be lost in aggregating the features across the whole ROI. Therefore, each ROI was further subdivided into smaller patches in the second patch parcellation step. Parcellation or subdivision of a FreeSurfer ROI was performed on a template MR image using a *k*-means clustering algorithm based on their intensity similarity (Raamana et al., 2015). Following the *k*-means clustering step, a high-dimensional accurate non-rigid registration method, LDDMM (Beg et al., 2005), was applied to register each ROI of a target MRI to the corresponding ROI of the template. With the ROI-wise registration maps, the patch-wise segmentation of each template ROI was propagated back into the target space. Finally, in the feature extraction and normalization step, the volume of each patch was extracted as a primary feature for disease classification. The w-score, which represents the standardized residual of the chosen features, was computed to remove the effect of covariates such as the field of strength (1.5T or 3T), scanner type, scanning site, age, sex, and the size of the intra-cranial vault (ICV) of each individual (Ma et al., 2018 and Popuri et al., 2020). The normalized features as represented by the w-scores were input into the classifier.

The patch-wise cortical thickness features were extracted in a similar manner to the patch-wise volumetric features. The vertex coordinates in each of the 68 cortical ROIs were subdivided into smaller patches by grouping them with *k*-means clustering based on the pairwise Euclidean distance of their thicknesses in the template space (Raamana et al., 2015). The locally-clustered cortical patches were then propagated back to each of the target space following the backward deformation field that was derived during the LDDMM non-rigid registration step (Beg et al., 2005). The average thickness of the mantle within each patch was computed as features followed by the w-score normalization (Ma et al., 2018 and Popuri et al., 2020) to remove the confounding effect of covariates.

To avoid losing discriminant information during data down-sampling, multiple scale features were extracted in a

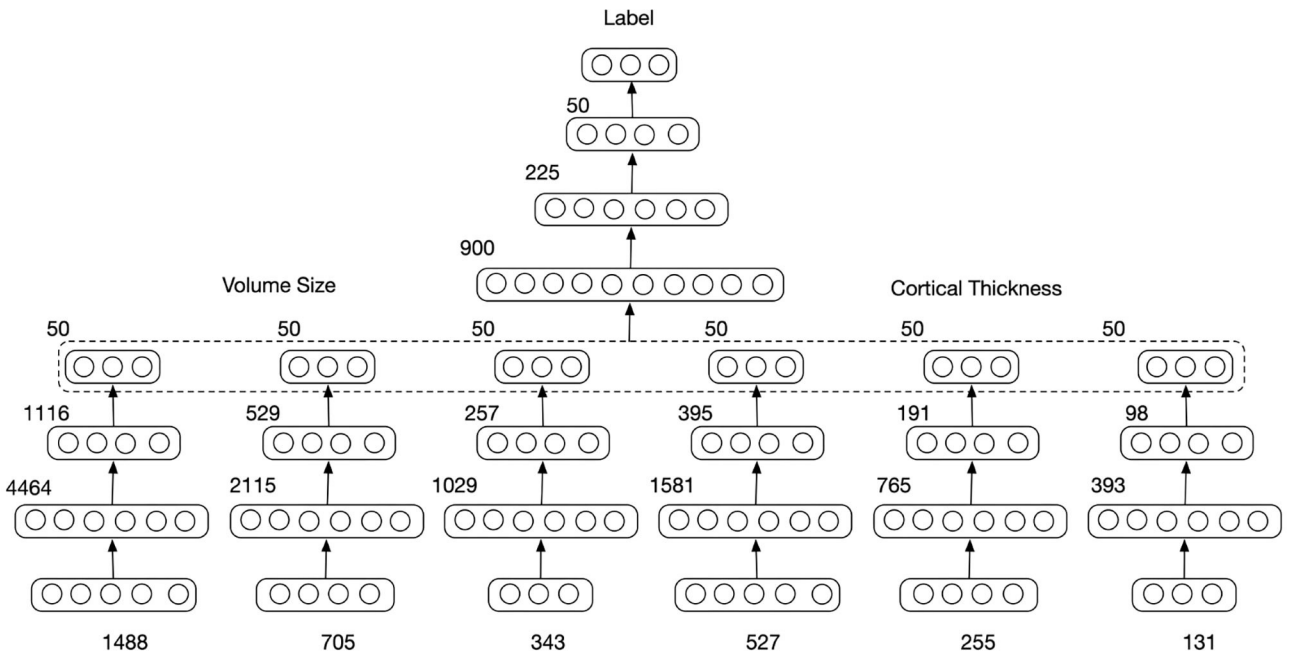

FIGURE 1 | Multi-scale and multi-type feature Deep Neural Network. The input feature dimension (number of patches) extracted from different scales is 1,488, 705, and 343 for volume of gray matter ROI and 527, 255, and 131 for the cortical thickness. The numbers of units in each layer representation are displayed on the top left.

coarse-to-fine manner. Each ROI was parcellated into three different scales of patch-sizes: 500, 1,000, and 2,000 voxels per patch for the volume features and 500, 1,000, and 2,000 vertex per patch for the thickness features. Those sizes were predefined to retain enough detailed information while restraining the number of primary features with respect to the number of training data to prevent overfitting. The subdivision of ROIs into these three scales resulted in a total number of 1,488, 705, and 343 voxel patches for the gray matter volume feature, and a total number 527, 255, and 131 vertex patches for the cortical thickness feature, respectively. Together with the FreeSurfer ROIs providing volumes and thickness, this gives six feature sets containing 3,409 scalars that represent each brain MR image.

2.3. Deep Neural Network for Multi-Scale and Multi-Type Feature Combination

With the patch-wise volume size and surface thickness features extracted from MRI images, a multi-scale and multi-type feature deep neural network (MMDNN) was constructed to learn the latent pattern from both types of features for the classification of NC, AD, and FTD pathology, which achieved state-of-the-art binary classification of NC and AD subjects using both FDG-PET and MRI images in our previous study (Lu et al., 2018a).

As displayed in **Figure 1**, the MMDNN consisted of two stages with a total of seven blocks Multilayer Perceptrons (MLPs). The first network stage consisted of 6 MLPs blocks, each corresponds to a single type of features extracted at a single scale. These MLPs were trained independently in the first stage, and their outputs were concatenated as the input feature vector to train the final MLP block in the second stage. The parameters of the whole network were then fine-tuned together. For each image, the output was three probabilities with each corresponding to a subject group, i.e., NC, AD, and FTD, and the class with the highest probability was deemed to be the resulting classification. For each MLP, the number of units for each layer are displayed on its top left in **Figure 1**. If the dimension of input feature is represented with N, the number of units in a single MLP were predefined as $3N$, $\frac{3}{4}N$, and 50 to increase the chance of exploring a larger range of potential hidden correlations across different patches in the first layer and gradually reduce the number of features in the following layers to avoid too many parameters Lu et al. (2018b,a).

To avoid overfitting, dropout layers (Srivastava et al., 2014) were added after each hidden layer. During the training stage, half of the units were randomly dropped to prevent complex co-adaptations on training data as well as to reduce the amount of computation and improve the training speed. During the validation or testing stage, all the units were retained to feed features to the next layer.

2.4. Data Augmentation With Generative Adversarial Network

In deep/machine learning, a common strategy to increase the number of training samples and prevent overfitting is data augmentation. Operations, such as rotation, flip, and zooming, are commonly used for 2D image recognition. However, those operations can hardly be used on a 1D feature vector. GAN (Goodfellow et al., 2014) have emerged to be a powerful tools to synthesize new data and have gained popularity in the generation of realistic natural images, and has also shown great potential to

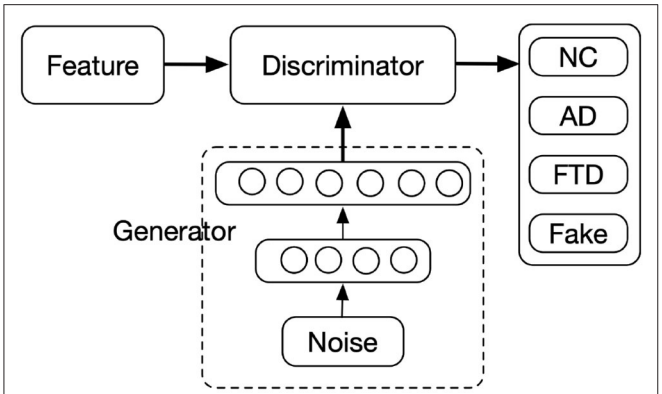

FIGURE 2 | Architecture of generative adversarial network. The numbers of units of Generator layers are 512 and 3,449(1,488+705+343+527+255+131), respectively.

be a powerful data augmentation technique to synthetic image data with more variation and improve the generalizability of the machine learning algorithm (Shi et al., 2018; Lata et al., 2019; Sandfort et al., 2019; Shao et al., 2019). Therefore, we investigated the possibility of applying GAN for 1D structural brain feature augmentation for the improvement of classification performance in this study.

GANs consist of two parts, the Discriminator (D) and the Generator (G), as displayed in **Figure 2**. In the proposed framework, the MMDNN was used as the discriminator with an additional channel of output for the recognition of data synthesized by the generator, denoted here as "fake," while the generator aimed to generate feature vectors to "fool" the Discriminator, i.e., classified as NC, AD, or FTD by the discriminator. The input of the generator was a 1D random noise vector. By finding the mapping from the random variables to the data distribution of interest, the generator outputs a feature vector with the same dimension as the real data samples. It was worth mentioning that the fourth channel of output was only used during the optimization of GAN. For each testing sample, only the output probabilities of the first three channels were used to determine which of the three groups a subject belongs to.

To prevent potential problems due to vanishing gradients, the generator consists of two layers, a single hidden layer and an output layer. Both layers are fully connected layer with 512 and 3,449 units, respectively. The dimension of random noise was set to 100 with each element set to follow a normal distribution. The activation function for the first layer was a rectified linear unit (ReLU) to avoid gradients from vanishing, while the one for the second layer was tanh function to squash the synthesized data into the same range of the real data.

2.5. Network Optimization

For optimization of the GAN, the loss function was defined:

$$\min_D \max_G V(D,G) = \mathbb{E}_{x\sim p_{data}(x)}[logD(x)] + \mathbb{E}_{z\sim p_z(z)}[log(-D(G(z)))] \quad (1)$$

where x represents the input data and $p_z(z)$ is the prior of input noise variables. $log(-D(G(z)))$ was used instead of $log(1-D(G(z)))$ to avoid vanishing gradient and mode collapse (Arjovsky and Bottou, 2017). The E here stands for weighted cross entropy function, which is defined as:

$$E(logD(x)) = -\frac{1}{N}\sum_{i=1}^{N}\sum_{j=1}^{4}[\mathbb{1}\{y^i = j\}W^j log(h(x^i)_j] \quad (2)$$

where N is the number of input samples, j represents the class of samples, W^j stands for the weight of class j which is computed as the inverse proportion of the subject number for the current class over the entire sample data, x^i, y^i are the feature vector and label of sample i, and h represents the network function.

For the training of GAN, the discriminator and the generator were optimized alternately. During the optimization of the discriminator, the parameters of the generator were held constant, and when the generator was trained, the parameters of the discriminator were fixed. The minimax competition between G and D could drive both networks toward better performance.

Besides adding dropout layers, another strategy, early stopping, was applied during the training process to reduce the overfitting. During the training of the deep neural network, iterative back propagation could drive the network to co-adapt to the training set. After a certain point, reducing training error could result in increasing the generalization error. Early stopping was therefore useful to provide guidance for the number of optimization iterations before overfitting. Part of the training data was randomly selected as the validation set and were excluded from training. While the remaining data samples were used to train the network, the validation set was used to determine the early stopping time point: the iteration in which the network has the lowest generalization error for the validation set. In this study, optimization of the network was stopped when the generation error of the validation set ceased to decrease for a consecutive 20 epochs.

Furthermore, due to the limited number of available data and variation among different samples, there was still a chance that early stopping with a small validation set could result in biased classification toward the validation set, and the differential performance could be unstable with different splitting of training and validation sets. An ensemble classifier strategy (Lu et al., 2018b) was therefore used to improve the robustness, stability, and generalizability of the classifier. Similar to the 10-fold cross validation, the training set was randomly divided into 10 subsets. In each fold of the training process, one subset was retained for validation while the remaining nine subsets were used for training. With 10 repetitions, each set was used for validation once resulting in 10 different networks. For each test sample, each network would generate three probabilities corresponding to NC, AD, and FTD. The output probabilities of 10 networks were averaged followed with a softmax operation to determine the final classification result.

The proposed deep neural network was built with Tensorflow (Abadi et al., 2015), an open source deep learning toolbox provided by Google. For the optimization of network in all

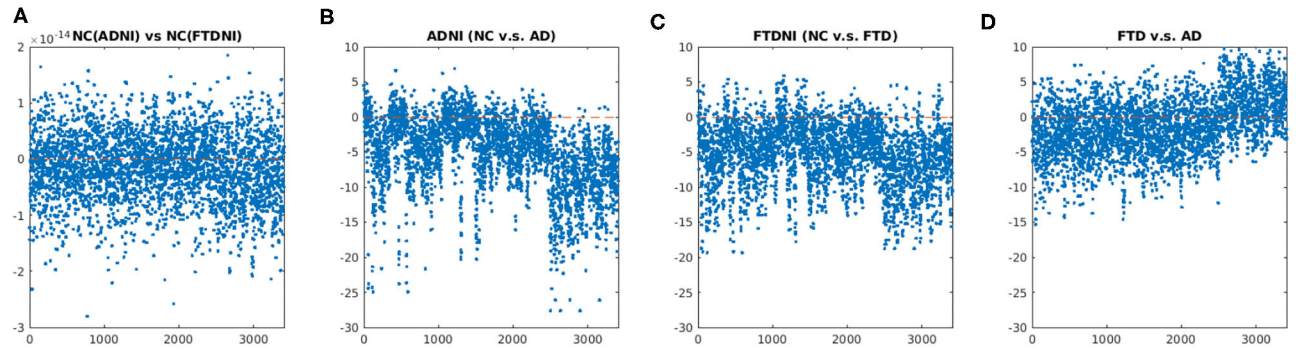

FIGURE 3 | Comparison about the distribution of the concatenated multi-level multi-type W-score feature set among different disease groups: **(A)** NC(ADNI) vs. NC(FTDNI); **(B)** NC vs. AD in ADNI database; **(C)** NC vs. FTD in FTDNI database; and **(D)** FTD vs. AD. **(A)** No statistical difference was shown when comparing the W-scores of the Healthy Control subjects between the ADNI and FTDNI, confirming no database-specific biases remained in the input w-score feature of the normative group. **(B)** Similar level of significant differences were shown when comparing the NC and AD subjects in the ADNI database, or **(C)** When comparing the NC and the FTD subjects in the FTDBI database, indicating similarity between the AD and FTD group. **(D)** When comparing the FTD and AD group alone, significant differences were observed in both the volume-based and thickness-based features, indicating discrepancy between these two types of Dementia subtypes which can be utilized to achieve potential differential diagnosis. Unpaired *t*-test were performed for each pair of the comparison, with multiple comparison corrected by setting false discovery rate (FDR) = 0.05.

experiments, Adaptive Moment Estimation (Adam) was used as the optimizer, batch size was set as 100 and the learning rate was fixed as 5×10^{-5}.

2.6. Performance Evaluation

To validate the discriminant ability of the proposed framework on NC, AD, and FTD pathology, 10-fold cross validation was performed on the 1,954 T1 MRI images. Because a single subject could have multiple scans at different visits, a split based on images could result in having scans from the same subject used for both training and testing. We therefore performed the split based on subject to ensure complete separation between training and test samples. As mentioned in the section 2.5, the training set was further sub-dived into 10 subsets for each cross validation experiment and 10 networks optimized with different training and validation set were used to "vote" for the classification result of testing samples. Such an experimental design ensures that the data samples in the training, validation, and testing set were mutually exclusive on a subject level. The performance of classification was measured via accuracy and the sensitivity of correctly identifying different groups, such as $N(TrueNC)/N(NC)$ for NC group, where $N(\cdot)$ denotes the number of data samples belonging to this group.

Other than the proposed deep-learning-based method, a standard classifier, support vector machines (SVM) were also trained for comparison. One vs. rest strategy was applied for this multiclass classification task. Principal component analysis (PCA) was used for the reduction of feature dimension and the eigenvectors accounting for 95% of the total data variance were retained. Radial basis function (RBF) kernel was used for SVM given its superior performance in classification tasks. The features extracted at different scales were concatenated as the input for PCA+SVM classifier. In addition, to validate the effect of patch-wise parcellation, we also trained the MLPs on FreeSurfer ROI-wise features, i.e., the surface thickness and volume size of each ROI based on the Freesurfer segmentation.

3. RESULTS

3.1. W-Score Feature Extraction

Figure 3 showed the comparison of the distributions for the entire concatenated multi-level multi-type W-score feature set between different subgroups. First, no statistical difference were shown when comparing the W-scores of the healthy control subjects between the ADNI and FTDNI for either the volume-based or thickness-based features (**Figure 3A**), confirming no database-specific biases remained in the input w-score feature of the normative group. Similar level of significant differences were shown when comparing the NC and AD subjects in the ADNI database (**Figure 3B**), or when comparing the NC and the FTD subjects in the FTDBI database (**Figure 3C**), indicating similarity between the AD and FTD group. Finally, when comparing the FTD and AD group alone, significant differences were observed in both the volume-based and thickness-based features, indicating discrepancy between these two types of Dementia subtypes, which can be utilized to achieve potential differential diagnosis.

3.2. Cross Validation Experiment Results

The results of 10-fold cross validation experiment are shown in **Table 2**. When comparing the mean accuracy across 10-folds, the accuracy of PCA+SVM with both type of multi-scale features was only slightly higher (0.02%) than the multi-scale deep neural network (MDNN) with surface thickness feature. The accuracy of MDNN using volume size feature was higher than the one using surface thickness feature by 2.93%. The combination of both type of multi-scale features showed superior performance comparing with MDNN using a single type of feature, and it was further improved by 1.42% with the data augmentation using the proposed GAN technique.

Figure 4 showed the corresponding statistical comparison results among different experimental setup for the overall accuracy as well as the sensitivity for each class group. When

TABLE 2 | Comparison of classification performance over different experiments with multi-type features.

	Accuracy	NC sen.	AD sen.	FTD sen.
PCA+SVM (Multitype)	83.06	93.90	71.74	68.23
MDNN+Thickness	83.04	89.07	76.77	74.79
MDNN+Volume	85.97	91.05	83.88	74.20
MMDNN (Multitype)	86.81	93.76	81.94	73.59
GAN (Multitype)	88.28	93.40	84.66	77.82

The second column is the overall classification accuracy, while the third to fifth columns represent the sensitivity of NC, AD, and FTD, respectively. The second row represents the result with PCA+SVM using multi-type multi-scale features. The third and fourth rows are the classification performance of MDNN with multi-scale surface thickness or multi-scale volume size. Experiment results with both types of features using MMDNN are shown in the fifth row and the last row represents the result of multi-type multi-scale features along with data augmentation using GAN.

compared to the baseline method, PCA+SVM (multi-type), both the proposed MMDNN method with or without GAN showed significant improvement (indicated as **O**) for the overall accuracy (**Figure 4A**), as well as sensitivity for AD (C) and FTD (D). Training with multi-type feature showed improvement over the training with only single feature (for either thickness, indicated as **X**, or volume, indicated as +) in terms of overall accuracy (**Figure 4A**). Finally, data augmentation using GAN further improve the overall accuracy (**Figure 4A**) as well as sensitivity for the NC group (**Figure 4B**) and the FTD group (**Figure 4D**) (indicated as +).

For detailed classification result, the confusion matrices of experiments using the proposed multi-scale networks are displayed in **Table 3**. The presented four experiments show a similar pattern despite the differences in their accuracy and sensitivity. The networks had a good performance for the task of distinguishing between AD and FTD pathology. The discrimination between NC and FTD showed the least accurate performance, leaving room for potential future improvement.

3.3. Discrimination With Cortical Thickness Feature

The experiment performance with only cortical thickness feature was displayed in **Table 4**. MLP with only ROI-wise cortical thickness feature showed the least accuracy (76.48%), while better result was achieved with PCA+SVM using features extracted at all scales. As expected, the classification performance was sensitive to patch size change and a generalized reduction with increasing patch size was found on the overall accuracy. The combination of multi-scale features with MDNN yielded superior classification performance.

3.4. Discrimination With Volume Size Feature

The experiment performance with volume size feature was displayed in **Table 5**. Similarly, as the experiments with cortical thickness feature, MLP with only ROI-wise feature had the worst performance (79.78%), and PCA+SVM using features extracted at all scales showed better accuracy (82.28%). Unlike the experiments with cortical thickness feature, MLP with a single scale of feature showed better performance comparing with PCA+SVM using features extracted at all scales. The combination of multi-scale features with MDNN also had the highest accuracy, while no generalized reduction of accuracy was found with increasing of patch size.

3.5. Ensemble Classifier

As described in section 2.5, the classification results presented in this study came through the "collective vote" of an ensemble of classifiers instead of a single network. The classification performance with or without ensemble classifiers of four different experiments, including MDNN with cortical thickness, MDDN with volume size, MMDNN with multi-type of features and GAN with multi-type of features, are shown in **Figure 5**. The y axis represents the mean classification accuracy from the 10-fold cross validation experiment, while the x axis stands for different classifiers. On the x axis, the number "1" to "10" represents the network trained with different split of training and validation set, while "ensemble" denotes the combined result of these 10 networks.

4. DISCUSSION

In this study, we proposed a novel deep-learning-based framework for the differential diagnosis of NC, AD, and FTD. Cross validation experiment indicate that the proposed network could learn the latent patterns representing the different dementias using multi-type and multi-scale features, which in combination with GAN-based data augmentation, achieved a high accuracy of 88.28%. Based on the confusion matrix displayed in **Table 3**, there were only three cases of misdiagnoses between AD and FTD out of 891 samples, suggesting the excellent performance of the proposed framework to distinguish these two dementias.

4.1. Differential Diagnosis Using MRI Biomarker

Brain MRI is an imaging modality widely used for detecting various types of dementia, as the image contrast between different tissue can reveal pathology-induced brain morphology changes. Due to variations in pathogenesis and phenotypes, dementia can further be categorized into different sub-types, such as FTD, AD, mild cognitive impairment, vascular dementia, and dementia with Lewy bodies. Differentiating among different dementia subtypes is crucial for to provide appropriate healthcare and potential treatment, but is challenging due to overlapping phenotyping and morphological heterogeneity with each subtype (Bruun et al., 2019), and accurate differential diagnosis requires both appropriate feature extraction technique combined with powerful classification model. Some recent studies attempted to differentiate dementia subtypes using different machine learning techniques, such as hierarchical classification (Kim et al., 2019), statistical learning with feature selection based on least absolute shrinkage and selection operator (LASSO), and support vector machine (SVM) (Zheng et al., 2019), but are limited from either the constrained feature set (e.g., structural-volume feature) or

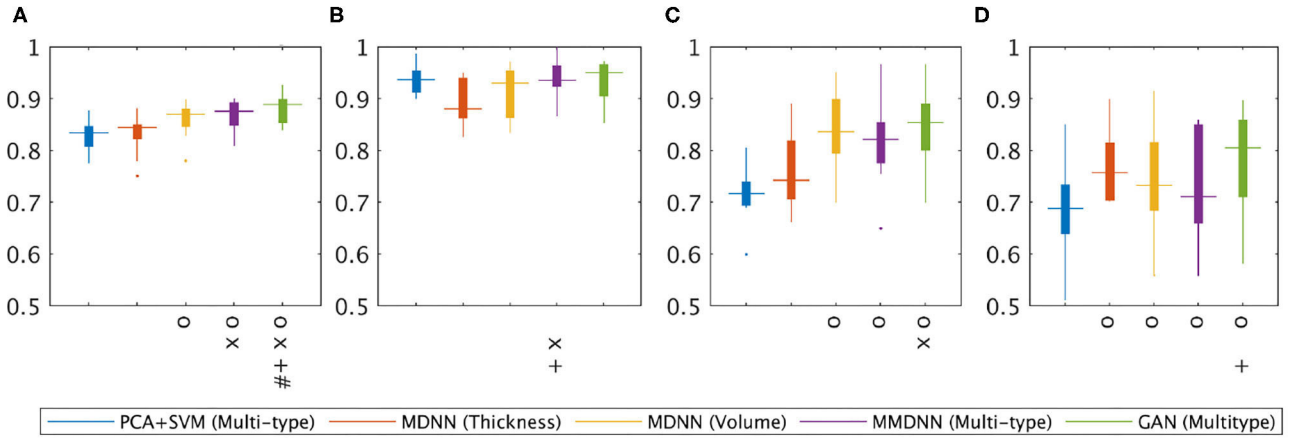

FIGURE 4 | Statistical analysis of the classification performance among different experiments. One-tailed pairwise *t*-tests were conducted to access the performance improvements. Multiple comparisons were corrected with False discovery rate FDR = 0.05. **O**: Significant improvement over PCV+SVM(Multi-type); **X**: significant improvement over MDNN (thickness); +: significant improvement over MDNN (volume); #: significant improvement over MMDNN (Multitype). **(A)** Overall accuracy, **(B)** NC sensitivity, **(C)** AD sensitivity, **(D)** FTD sensitivity.

TABLE 3 | Confusion matrix of GAN.

	NC	AD	FTD
NC	944	62	57
AD	86	352	19
FTD	97	11	326

(A) MDNN+Thickness

	NC	AD	FTD
NC	968	66	29
AD	59	387	11
FTD	100	10	324

(B) MDNN+Volume

	NC	AD	FTD
NC	998	45	20
AD	77	377	3
FTD	109	3	322

(C) MMDNN+Multitype

	NC	AD	FTD
NC	995	43	25
AD	65	391	1
FTD	93	2	339

(D) GAN+Multitype

The class names of the first column in each table represent the ground truth, and the names in the first row denote the classification result.

TABLE 4 | Comparison of classification performance over different experiments with cortical thickness feature.

	Accuracy	NC sen.	AD sen.	FTD sen.
PCA+SVM	81.12	91.04	73.78	63.43
ROI MLP	76.48	82.74	71.80	66.55
500 MLP	82.80	87.95	77.02	76.05
1000 MLP	81.22	86.92	72.13	72.48
2000 MLP	79.51	84.49	75.84	71.20
MDNN	83.04	89.07	76.77	74.79

The second column is the overall classification accuracy, while the third to fifth columns represent the sensitivity of NC, AD, and FTD, respectively. The second row represents the result using PCA+SVM with multi-scale surface thickness features, while the third row shows the classification performance of a single MLP with ROI-wise features. The fourth to sixth rows are the result of a single MLP with features extracted at different scales, i.e., 500, 1,000, and 2,000 voxels per patch. The last row represents the MDNN result with multi-scale surface thickness features.

relatively small validate with data for testing the robustness and generalizability of the classifiers. In our study, we proposed a framework to achieve accurate differential diagnosis by first building a multi-scale multi-type feature, followed with a deep neural network with the help of generative adversarial data augmentation technique, which was validated on a large sample (1,954 images), demonstrating a consistent overall high accuracy.

4.2. Multi-Scale Classification

Based on the results presented in **Table 4**, the accuracy of MLP decreased from 82.80% to 79.51% with patch size increasing from 500 voxels to 2,000 voxels, suggesting that cortical thickness feature is sensitive to the change of size of the ROI patch sizes, while less variation of accuracy was found with ROI volume feature (from 85.78% to 85.41%) as shown in **Table 5**. Contradicting our observations on using cortical thickness feature, the accuracy of volume size feature showed a slight improvement when the patch size increased from 1,000 to 2,000 voxels, suggesting that the volume change caused by brain atrophy may affect a large brain region in a similar fashion. However, the combination of multi-scale features always resulted in a better classification performance, indicating that the proposed MDNN is capable of learning the hidden pattern across the small to large patch sizes regardless the feature type. The optimal scale with the best performance would be a potential tunable hyperparameter in an optimization framework.

4.3. Volume Size, Surface Thickness, and Other Morphological Features

Two types of features, ROI volume and cortical thickness, were used for differential diagnosis in this study. Cross validation experiments showed that volume size has better discriminant ability compared with surface thickness regardless of the scale of feature and the type of classifier, as presented in **Tables 4**, **5**. In addition, the results in **Table 2** show that with the same classifier, the combination of these two features yields superior

TABLE 5 | Comparison of classification performance over different experiments with ROI volume Feature.

	Accuracy	NC sen.	AD sen.	FTD sen.
PCA+SVM	82.28	85.94	85.44	67.14
ROI MLP	79.78	83.44	79.79	69.67
500 MLP	85.78	91.60	82.83	73.31
1000 MLP	85.41	90.03	84.91	73.07
2000 MLP	85.45	90.34	82.26	75.06
MDNN	85.97	91.05	83.88	74.20

The second column is the overall classification accuracy, while the third to fifth columns represent the sensitivity of NC, AD, and FTD, respectively. The second row represents the result using PCA+SVM with multi-scale volume size features, while the third row shows the classification performance of a single MLP with ROI-wise features. The fourth to sixth rows are the result of a single MLP with features extracted at different scales, i.e., 500, 1,000, and 2000 voxels per patch. The last row represents the MDNN result with multi-scale volume size features.

classification performance comparing with single type of feature, regardless of whether they are concatenated as a single input feature vector for SVM or using a MLP to learn the latent representation of each scale of feature first.

In this study, we have explored the extraction volume-based and cortical-thickness-based features as an effort to improve the power of differential diagnosis. Other additional image-based morphological features could potentially also provide complementary information regarding brain pathology. Specifically, cortical folding has showed different aging-related patterns between healthy and diseased brain (Wang et al., 2016), including dementia such as AD (Cash et al., 2012). The combination of cortical folding with other shape-based descriptors such as local cortical thickness could potentially yield better characterization the cortical morphological changes that is induced by AD and other types of dementia (Awate et al., 2017). Therefore, the proposed framework could potentially be further extended to integrate other brain morphological descriptors, such as the cortical folding, into the multi-type input feature space to achieve better classification and differential diagnosis power.

In the current study, the proposed network was trained using structural-MRI-based patch-wise volume size and surface thickness features created with a combination of from FreeSurfer segmentation and k-mean clustering to balance the number of parameters trainable and the level of original image-based patterns that are preserved. A potential future direction is to learn the features directly from the raw structural image while maintaining a trainable number of network parameters, which still remains a challenge. This study with patch-wise FreeSurfer-segmentation-based features sets a baseline benchmark for future studies of deep-learning-based differential diagnosis studies with novel network-leaned image-based features for comparison.

4.4. Data Augmentation With GAN

As displayed in **Table 2**, the classification accuracy was further improved by 1.42% when using GAN for data augmentation. The sensitivity for detecting AD and FTD pathology was increased by a large margin with a slight decrease for detecting NC samples. Instead of $log(1 - D(G(z)))$, we used $log(-D(G(z)))$ in loss function to avoid vanishing gradient and mode collapse (Arjovsky and Bottou, 2017). Therefore, we did not specify what kind of data samples the generator should synthesize. We consider it as a "success" for the generator as long as the generated feature vector was classified as one of the three categories, i.e., NC, AD, and FTD, by the Discriminator. It would be interesting to train one or three Generators to synthesize data samples corresponding to specific groups, although this is beyond the scope of this study as our primary goal was to increase the differentiating accuracy.

For the generator, we only have a single hidden layer because of the low dimension of our data and potential gradient vanishing problem. Instance normalization or other kinds of normalization (Almahairi et al., 2018) was not performed because they caused mode collapse of the generator and resulted in synthetic data all close to 0. Contrasting with many other studies using GAN (Arjovsky et al., 2017), we found root mean square propagation (RMSprop) optimizer resulted in an 87.39% accuracy, which was lower than with Adam optimizer.

4.5. Ensemble Classifier and Cross-Validation

As shown in **Figure 5**, there can be as much as 3% difference in the classification accuracy (the seventh and the tenth bar of the top left image) across the individual classifiers trained with a different subdivision of the training and validation set, suggesting an unstable performance of each single classifier. In all four experiments, the ensemble classifier had the highest or close to highest accuracy, suggesting that the ensemble strategy improves the robustness and generalizability of the classifier.

It was worth mentioning that with the GAN, the variation of classification accuracy with individual classifiers decreased to 0.49% (from 87.98 to 88.47%) while the accuracy of ensemble classifier was 88.28%, suggesting that, with using GAN for data augmentation, the complex co-adaptations to training or validation set were reduced. The ensemble classifier strategy, although still effective, could therefore be optional with the application of GAN in light of limitations of available computational resources.

On top of the combination of GAN-based data augmentation and cross-validation-based ensemble classifier, an additional nested 10-fold cross validation was implemented to ensure the proposed method is properly validated. Nevertheless, it would be ideal to validate the proposed multi-class classifier on an entire independent and well-homogenized dataset to best evaluate its generalizability toward unseen dataset (Popuri et al., 2020; Yee et al., 2020).

5. CONCLUSION

In this study, a novel framework for accurate differential diagnosis among NC, AD, and FTD pathology has been proposed leveraging the multi-type and multi-scale feature fusion, ensemble classifier, and GAN strategy. The proposed

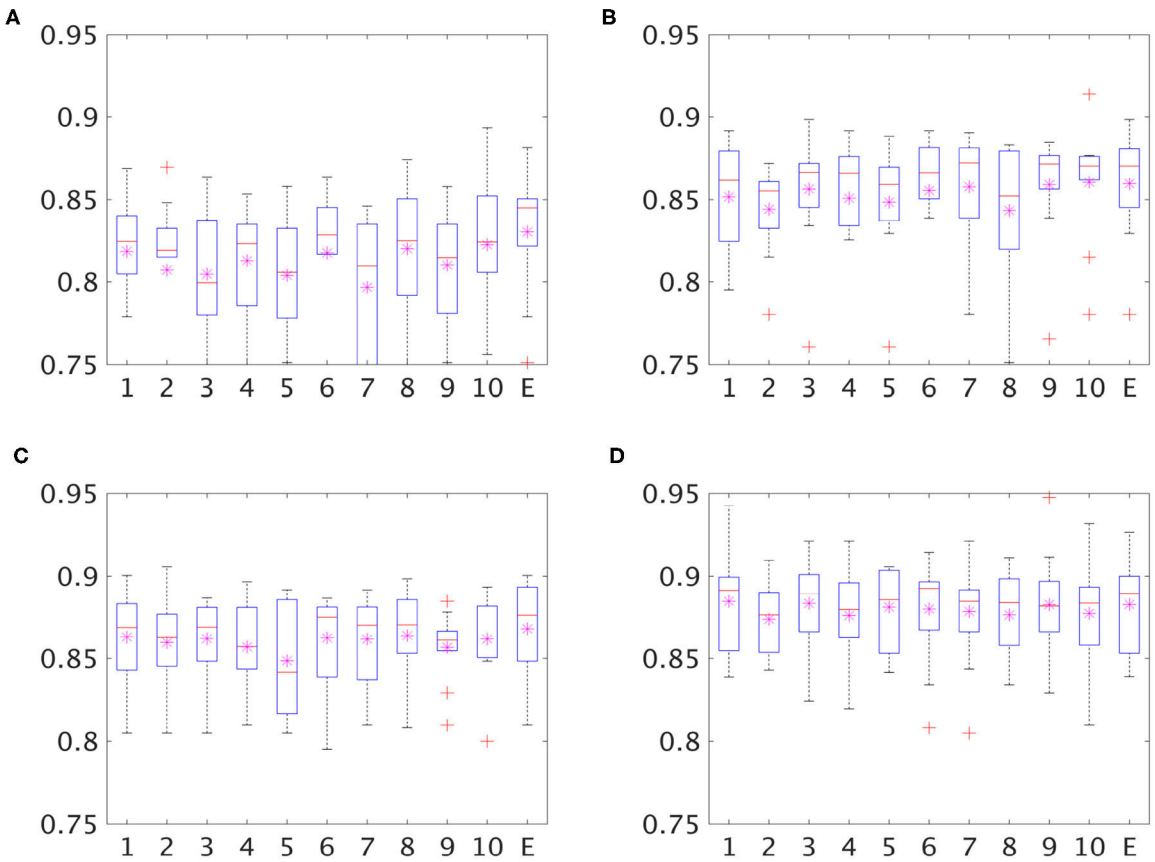

FIGURE 5 | Boxplot for classification accuracy of single classifiers (classifier 1–10 on *x* axis) and an ensemble of classifiers (E on the *x* axis). The stars in each box are the mean of accuracy and the red lines represent the median accuracy. **(A)** MDNN+Thickness, **(B)** MDNN+Volume, **(C)** MMDNN+Multitype, **(D)** GAN+Multitype.

framework achieved a high accuracy of 88.28%. The cross-validation experiments conducted on 1,954 MRI images demonstrate three salient observations. Firstly, the proposed network was able to learn the latent representation pattern across the different types of features (volumes and cortical thickness) extracted at coarse-to-fine scales. Secondly, using a Generative Adversarial Network for data augmentation could prevent overfitting and improve classification performance. Thirdly, the ensemble classifier strategy could result in a more robust and stable classifier, which has statistically better performance than an individual classifier. The promising high-accuracy results using the proposed framework, and the ability of deep networks to generalize to multiple classes, indicate that this approach can be potentially extended for the multiclass differential classification of brain images in other neurodegenerative dementias as well.

DATA AVAILABILITY STATEMENT

The datasets generated for this study are available on request to the corresponding author.

AUTHOR CONTRIBUTIONS

DM conducted the experiment, performed the data processing and analysis, and wrote the manuscript. LW and MB designed and supervise the experiments, guided, and revised the manuscript. KP performed the data processing and manuscript writing. DL conducted the experiment, designed the framework, performed the analysis, and wrote the manuscript. All authors contributed to the article and approved the submitted version.

FUNDING

This work was supported by Natural Sciences and Engineering Research Council (NSERC), Canadian Institutes of Health Research (CIHR), Michael Smith Foundation for Health Research (MSFHR), Brain Canada, the Pacific Alzheimer Research Foundation (PARF), Alzheimer Society of Canada (Alzheimer Society Research Program), the National Institutes of Health (R01 AG055121 and R01 EB020062), and the National Science Foundation (NSF 1734853 and NSF 1636893). Data collection and sharing for this project was funded by ADNI and NIFD. ADNI was funded by the National Institute on Aging, the National Institute of Biomedical Imaging and Bioengineering

and through generous contributions from the following: AbbVie, Alzheimer's Association; Alzheimer's Drug Discovery Foundation; Araclon Biotech; BioClinica, Inc.; Biogen; Bristol-Myers Squibb Company; CereSpir, Inc.; Cogstate; Eisai Inc.; Elan Pharmaceuticals, Inc.; Eli Lilly and Company; EuroImmun; F. Hoffmann-La Roche Ltd and its affiliated company Genentech, Inc.; Fujirebio; GE Healthcare; IXICO Ltd.; Janssen Alzheimer Immunotherapy Research & Development, LLC.; Johnson & Johnson Pharmaceutical Research & Development LLC.; Lumosity; Lundbeck; Merck & Co., Inc.; Meso Scale Diagnostics, LLC.; NeuroRx Research; Neurotrack Technologies; Novartis Pharmaceuticals Corporation; Pfizer Inc.; Piramal Imaging; Servier; Takeda Pharmaceutical Company; and Transition Therapeutics. The Canadian Institutes of Health Research is providing funds to support ADNI clinical sites in Canada. Private sector contributions are facilitated by the Foundation for the National Institutes of Health (www.fnih.org). The grantee organization is the Northern California Institute for Research and Education, and the study is coordinated by the Alzheimer's Therapeutic Research Institute at the University of Southern California. ADNI data are disseminated by the Laboratory for Neuro Imaging at the University of Southern California.

REFERENCES

Abadi, M., Agarwal, A., and Barham, P. (2015). *TensorFlow: Large-Scale Machine Learning on Heterogeneous Systems*. Available online at: www.tensorflow.org.

Alladi, S., Xuereb, J., Bak, T., Nestor, P., Knibb, J., Patterson, K., et al. (2007). Focal cortical presentations of Alzheimer's disease. *Brain* 130, 2636–2645. doi: 10.1093/brain/awm213

Almahairi, A., Rajeswar, S., Sordoni, A., Bachman, P., and Courville, A. (2018). Augmented cyclegan: learning many-to-many mappings from unpaired data. *arXiv [Preprint]. arXiv:1802.10151*.

Arjovsky, M., and Bottou, L. (2017). Towards principled methods for training generative adversarial networks. *arXiv [Preprint]. arXiv:1701.04862*.

Arjovsky, M., Chintala, S., and Bottou, L. (2017). Wasserstein gan. *arXiv [Preprint]. arXiv:1701.07875*.

Association, A. (2011). *2011 Alzheimer's Disease Facts and Figures. Alzheimer's Dement*. 7:208. doi: 10.1016/j.jalz.2011.02.004

Awate, S. P., Leahy, R. M., and Joshi, A. A. (2017). "Kernel methods for Riemannian analysis of robust descriptors of the cerebral cortex," in *Lecture Notes in Computer Science, Vol. 6533* (Springer International Publishing), 28–40. doi: 10.1007/978-3-319-59050-9_3

Bang, J., Spina, S., and Miller, B. L. (2015). Frontotemporal dementia. *Lancet* 386, 1672–1682. doi: 10.1016/S0140-6736(15)00461-4

Beg, M. F., Miller, M. I., Trouvé, A., and Younes, L. (2005). Computing large deformation metric mappings via geodesic flows of diffeomorphisms. *Int. J. Comput. Vis*. 61, 139–157. doi: 10.1023/B:VISI.0000043755.93987.aa

Bruun, M., Koikkalainen, J., Rhodius-Meester, H. F. M., Baroni, M., Gjerum, L., Van Gils, M., et al. (2019). Detecting frontotemporal dementia syndromes using MRI biomarkers. *NeuroImage* 22:101711. doi: 10.1016/j.nicl.2019.101711

Cash, D. M., Melbourne, A., Modat, M., Cardoso, M. J., Clarkson, M. J., Fox, N. C., et al. (2012). "Cortical folding analysis on patients with Alzheimer's disease and mild cognitive impairment," in *Medical Image Computing and Computer-Assisted Intervention - MICCAI 2012*, eds N. Ayache, H. Delingette, P. Goll and K. Mori (Berlin; Heidelberg: Springer), 289–296. doi: 10.1007/978-3-642-33454-2_36

Dale, A. M., and Fischl, B. S. M. (1999). Cortical surface-based analysis. II: Inflation, flattening, and a surface-based coordinate system. *Neuroimage*, 9, 195–207. doi: 10.1006/nimg.1998.0396

Davatzikos, C., Bhatt, P., Shaw, L. M., Batmanghelich, K. N., and Trojanowski, J. Q. (2011). Prediction of MCI to AD conversion, via MRI, CSF biomarkers, and pattern classification. *Neurobiol. Aging* 32, 2322–e19. doi: 10.1016/j.neurobiolaging.2010.05.023

Davatzikos, C., Resnick, S. M., Wu, X., Parmpi, P., and Clark, C. M. (2008). Individual patient diagnosis of AD and FTD via high-dimensional pattern classification of MRI. *Neuroimage* 41, 1220–1227. doi: 10.1016/j.neuroimage.2008.03.050

Du, A.-T., Schuff, N., Kramer, J. H., Rosen, H. J., Gorno-Tempini, M. L., Rankin, K., et al. (2007). Different regional patterns of cortical thinning in Alzheimer's disease and frontotemporal dementia. *Brain* 130, 1159–1166. doi: 10.1093/brain/awm016

Goodfellow, I., Pouget-Abadie, J., Mirza, M., Xu, B., Warde-Farley, D., Ozair, S., et al. (2014). "Generative adversarial nets," in *Advances in Neural Information Processing Systems*, 27, eds Z. Ghahramani, M. Welling, C. Cortes, N. D. Lawrence and K. Q. Weinberger (Curran Associates, Inc.) 2672–2680. Available online at: http://papers.nips.cc/paper/5423-generative-adversarial-nets.pdf

He, K., Zhang, X., Ren, S., and Sun, J. (2016). "Deep residual learning for image recognition," in *Proceedings of the IEEE Conference on Computer Vision and Pattern Recognition (CVPR)*, 770–778. doi: 10.1109/CVPR.2016.90

Hinton, G. E., and Salakhutdinov, R. R. (2006). Reducing the dimensionality of data with neural networks. *Science* 313, 504–507. doi: 10.1126/science.1127647

Jiskoot, L. C., Panman, J. L., Meeter, L. H., Dopper, E. G., Donker Kaat, L., Franzen, S., et al. (2018). Longitudinal multimodal MRI as prognostic and diagnostic biomarker in presymptomatic familial frontotemporal dementia. *Brain* 142, 193–208. doi: 10.1093/brain/awy288

Kim, J. P., Kim, J., Park, Y. H., Park, S. B., Lee, J. S., Yoo, S., et al. (2019). Machine learning based hierarchical classification of frontotemporal dementia and Alzheimer's disease. *NeuroImage* 23:101811. doi: 10.1016/j.nicl.2019.101811

Krizhevsky, A., Sutskever, I., and Hinton, G. E. (2012). "Imagenet classification with deep convolutional neural networks," in *Advances in Neural Information Processing Systems* (Curran Associates, Inc.), 1097–1105. Available online at: http://papers.nips.cc/paper/4824-imagenet-classification-with-deep-convolutional-neural-networks.pdf

Lata, K., Dave, M., and Nishanth, K. N. (2019). Data augmentation using generative adversarial network. *Proceedings of 2nd International Conference on Advanced Computing and Software Engineering (ICACSE) 2019*. Available online at: SSRN: https://ssrn.com/abstract=3349576orhttp://dx.doi.org/10.2139/ssrn.3349576

Litjens, G., Kooi, T., Bejnordi, B. E., Setio, A. A. A., Ciompi, F., Ghafoorian, M., et al. (2017). A survey on deep learning in medical image analysis. *Med. Image Anal*. 42, 60–88. doi: 10.1016/j.media.2017.07.005

Looi, J. C. L., Walterfang, M., Styner, M., Svensson, L., Lindberg, O., Östberg, P., et al. (2010). Shape analysis of the neostriatum in frontotemporal lobar degeneration, Alzheimer's disease, and controls. *Neuroimage* 51, 970–986. doi: 10.1016/j.neuroimage.2010.02.017

Lu, D., Popuri, K., Ding, G. W., Balachandar, R., and Beg, M. F. (2018a). Multimodal and multiscale deep neural networks for the early diagnosis of Alzheimer's disease using structural MR and FDG-PET images. *Sci. Rep*. 8:5697. doi: 10.1038/s41598-018-22871-z

Lu, D., Popuri, K., Ding, G. W., Balachandar, R., and Beg, M. F. (2018b). Multiscale deep neural network based analysis of FDG-PET images for the early diagnosis of Alzheimer's disease. *Med. Image Anal*. 46, 26–34. doi: 10.1016/j.media.2018.02.002

Ma, D., Popuri, K., Bhalla, M., Sangha, O., Lu, D., Cao, J., et al. (2018). Quantitative assessment of field strength, total intracranial volume, sex, and age effects on the goodness of harmonization for volumetric analysis on the ADNI database. *Hum. Brain Mapp*. 40, 1507–1527 doi: 10.1002/hbm.24463

Neary, D., Snowden, J., and Mann, D. (2005). Frontotemporal dementia. *Lancet Neurol*. 4, 771–780. doi: 10.1016/S1474-4422(05)70223-4

Neary, D., Snowden, J. S., Gustafson, L., Passant, U., Stuss, D., Black, S., et al. (1998). Frontotemporal lobar degeneration A consensus on clinical diagnostic criteria. *Neurology* 51, 1546–1554. doi: 10.1212/WNL.51.6.1546

Pasquier, F. (2005). Telling the difference between frontotemporal dementia and Alzheimer's disease. *Curr. Opin. Psychiatry* 18, 628–632. doi: 10.1097/01.yco.0000185988.05741.2a

Raamana, P. R., Rosen, H., Miller, B., Weiner, M. W., Wang, L., and Beg, M. F. (2014). Three-class differential diagnosis among Alzheimer disease, frontotemporal dementia, and controls. *Front. Neurol.* 5:71. doi: 10.3389/fneur.2014.00071

Raamana, P. R., Weiner, M. W., Wang, L., Beg, M. F., and Initiative, A. D. N. (2015). Thickness network features for prognostic applications in dementia. *Neurobiol. Agin* 36, S91–S102. doi: 10.1016/j.neurobiolaging.2014.05.040

Rabinovici, G., Seeley, W., Kim, E., Gorno-Tempini, M., Rascovsky, K., Pagliaro, T., et al. (2008). Distinct MRI atrophy patterns in autopsy-proven Alzheimer's disease and frontotemporal lobar degeneration. *Am. J. Alzheimer's Dis.* 22, 474–488. doi: 10.1177/1533317507308779

Ronneberger, O., Fischer, P., and Brox, T. (2015). "U-net: convolutional networks for biomedical image segmentation," in *International Conference on Medical Image Computing and Computer-Assisted Intervention* (Munich: Springer), 234–241. doi: 10.1007/978-3-319-24574-4_28

Sandfort, V., Yan, K., Pickhardt, P. J., and Summers, R. M. (2019). Data augmentation using generative adversarial networks (CycleGAN) to improve generalizability in CT segmentation tasks. *Sci. Rep.* 9, 1–9. doi: 10.1038/s41598-019-52737-x

Seiffert, C., Khoshgoftaar, T. M., Van Hulse, J., and Napolitano, A. (2010). Rusboost: A hybrid approach to alleviating class imbalance. *IEEE Trans. Syst. Man Cybern. Part A* 40, 185–197. doi: 10.1109/TSMCA.2009.2029559

Shao, S., Wang, P., and Yan, R. (2019). Generative adversarial networks for data augmentation in machine fault diagnosis. *Comput. Indus.* 106, 85–93. doi: 10.1016/j.compind.2019.01.001

Shi, H., Wang, L., Ding, G., Yang, F., and Li, X. A. (2018). "Data augmentation with improved generative adversarial networks," in *2018 24th International Conference on Pattern Recognition (ICPR)* (Beijing: IEEE). doi: 10.1109/ICPR.2018.8545894

Simonyan, K., and Zisserman, A. (2014). Very deep convolutional networks for large-scale image recognition. *arXiv [Preprint]. arXiv:1409.1556.*

Srivastava, N., Hinton, G. E., Krizhevsky, A., Sutskever, I., and Salakhutdinov, R. (2014). Dropout: a simple way to prevent neural networks from overfitting. *J. Mach. Learn. Res.* 15, 1929–1958.

Suk, H.-I., Lee, S.-W., Shen, D., and Initiative, A. D. N. (2014). Hierarchical feature representation and multimodal fusion with deep learning for AD/MCI diagnosis. *NeuroImage* 101, 569–582. doi: 10.1016/j.neuroimage.2014.06.077

Szegedy, C., Ioffe, S., Vanhoucke, V., and Alemi, A. A. (2017). "Inception-v4, inception-resnet and the impact of residual connections on learning," in *Thirty-First AAAI Conference on Artificial Intelligence* (San Francisco, CA).

Tong, T., Ledig, C., Guerrero, R., Schuh, A., Koikkalainen, J., Tolonen, A., et al. (2017). Five-class differential diagnostics of neurodegenerative diseases using random undersampling boosting. *NeuroImage* 15, 613–624. doi: 10.1016/j.nicl.2017.06.012

Varma, A., Snowden, J., Lloyd, J., Talbot, P., Mann, D., and Neary, D. (1999). Evaluation of the NINCDS-ADRDA criteria in the differentiation of Alzheimer's disease and frontotemporal dementia. *J. Neurol. Neurosurg. Psychiatry* 66, 184–188. doi: 10.1136/jnnp.66.2.184

Wang, Y., Necus, J., Kaiser, M., and Mota, B. A. (2016). Universality in human cortical folding in health and disease. *Proc. Natl. Acad. Sci. U.S.A.* 113, 12820–12825. doi: 10.1073/pnas.1610175113

Womack, K. B., Diaz-Arrastia, R., Aizenstein, H. J., Arnold, S. E., Barbas, N. R., Boeve, B. F., et al. (2011). Temporoparietal hypometabolism in frontotemporal lobar degeneration and associated imaging diagnostic errors. *Arch. Neurol.* 68, 329–337. doi: 10.1001/archneurol.2010.295

Zheng, Y., Guo, H., Zhang, L., Wu, J., Li, Q., and Lv, F. A. (2019). Machine learning-based framework for differential diagnosis between vascular dementia and Alzheimer's disease using structural MRI Features. *Front. Neurol.* 10:1097. doi: 10.3389/fneur.2019.01097

Popuri, K., Ma, D., Wang, L., and Beg, M. F. (2020). Using machine learning to quantify structural MRI neurodegeneration patterns of Alzheimer's disease into dementia score: Independent validation on 8,834 images from ADNI, AIBL, OASIS, and MIRIAD databases. *Human Brain Mapping*, e25115. doi: 10.1002/hbm.25115

Yee, E., Ma, D., Popuri, K., Want, L., and Beg, M. F. (2020). Construction of MRI-based alzheimer's disease score based on efficient 3D convolutional neural network – comprehensive validation on 7209 multi-centre dataset. *J. Alzheimer's Dis.* (Accepted)

Conflict of Interest: The authors declare that the research was conducted in the absence of any commercial or financial relationships that could be construed as a potential conflict of interest.

Citation: Ma D, Lu D, Popuri K, Wang L, Beg MF and Alzheimer's Disease Neuroimaging Initiative (2020) Differential Diagnosis of Frontotemporal Dementia, Alzheimer's Disease, and Normal Aging Using a Multi-Scale Multi-Type Feature Generative Adversarial Deep Neural Network on Structural Magnetic Resonance Images. Front. Neurosci. 14:853. doi: 10.3389/fnins.2020.00853

frontiers in Aging Neuroscience

REVIEW
published: 23 October 2020
doi: 10.3389/fnagi.2020.601603

Molecular Level Insight Into the Benefit of Myricetin and Dihydromyricetin Uptake in Patients With Alzheimer's Diseases

Miaomiao Liu[1], Hong Guo[2], Zhongyuan Li[1], Chenghua Zhang[1], Xiaoping Zhang[1,3], Qinghua Cui[1,3] and Jingzhen Tian[1,3]**

[1] College of Pharmacy, Shandong University of Traditional Chinese Medicine, Jinan, China, [2] Affiliated Hospital of Integrated Traditional Chinese and Western Medicine, Nanjing University of Chinese Medicine, Nanjing, China, [3] Qingdao Academy of Chinese Medicinal Sciences, Shandong University of Traditional Chinese Medicine, Qingdao, China

Alzheimer's disease (AD) is a neurodegenerative disease with a high incidence rate and complicated pathogenesis. Currently, all anti-AD drugs treat the symptoms of the disease, and with currently no cure for AD. Flavonoid containing natural products, Myricetin (MYR) and Dihydromyricetin (DMY), are abundant in fruits and vegetables, and have been approved as food supplements in some countries. Interestingly, MYR and DMY have been reported to have anti-AD effects. However, the underlying anti-AD mechanism of action of MYR and DMY is complex with many facets being identified. In this review, we explore the benefit of MYR and DMY in AD patients from a molecular level. Their mechanism of action are discussed from various aspects including amyloid β-protein (Aβ) imbalance, neuroinflammation, dyshomeostasis of metal ions, autophagy disorder, and oxidative stress.

Keywords: Alzheimer's disease, natural product, Myricetin, Dihydromyricetin, mechanism of action

OPEN ACCESS

Edited by:
Jiehui Jiang,
Shanghai University, China

Reviewed by:
Nobuyuki Kimura,
National Center for Geriatrics and Gerontology, Japan
Karen Schmitt,
Hector Institute for Translational Brain Research, Central Institute of Mental Health (ZI), Germany

****Correspondence:***
Qinghua Cui
cuiqinghua1122@163.com
Jingzhen Tian
tianjingzhen@163.com

Received: *01 September 2020*
Accepted: *06 October 2020*
Published: *23 October 2020*

Citation:
Liu M, Guo H, Li Z, Zhang C, Zhang X, Cui Q and Tian J (2020) Molecular Level Insight Into the Benefit of Myricetin and Dihydromyricetin Uptake in Patients With Alzheimer's Diseases. Front. Aging Neurosci. 12:601603. doi: 10.3389/fnagi.2020.601603

INTRODUCTION

Alzheimer's disease (AD) is a neurodegenerative disease (Barnett, 2019), which can cause patients to gradually lose their ability to live independently, and change their personality and behavior. Most patients with AD die within 10 years of diagnosis, and those patients who survive past this, suffer from declines in cognition, language including speech, and memory. AD not only threatens the patients' lives and health but also causes serious societal problems (Guo et al., 2019), especially within countries with a growing aging population. Unfortunately, the incidence of AD has dramatically increased in the last few decades. According to the latest report from the Alzheimer's Association, the number of AD patients in the United States reached 5.8 million in 2020 (Association, 2020). At the same time, they predicted that this number would rise to 13.8 million by mid-century (Association, 2020).

The etiology of AD is complicated and remains unclear, with many factors being reported to be involved in the pathogenesis of AD. The excessive amounts of Aβ and the abnormally phosphorylated tau peptide (Goedert and Spillantini, 2006) are the most studied pathogenesis of AD. The neurotransmitter imbalance in the central nervous system (Guo et al., 2019) such as acetylcholine (ACh) deficiency, the dyshomeostasis of metal ions (Ayton et al., 2015) and the overexpression of MicroRNA (Sarkar et al., 2019) are also thought to be closely related to

the development of AD. Furthermore, physiological function disorders, such as oxidative stress, inflammation (Meraz-Ríos et al., 2013), abnormal autophagy and the damage of insulin signaling pathway (Zhang and Hölscher, 2020) were also found to cause serious damage to the brain and can lead to the manifestation of AD (Butterfield and Halliwell, 2019). Other factors are also reported as a driving force in the genesis and development of AD, such as the long-term infections of bacteria and viruses (Bearer and Wu, 2019; Dominy et al., 2019), and the dyshomeostasis of intestinal flora (Friedland, 2015).

Currently, clinically used AD drugs treat the symptoms of AD in affected patients. Donepezil, Rivastigmine and Galantamine are AChE inhibitors while Memantine is an NMDA (N-methyl-D-aspartic acid) receptor antagonist. Notably, GV-971, an oligosaccharide derived from brown seaweed, was approved for use in China at the end of 2019. GV-971 is said to treat AD with a brain-gut axis as the target (Wang X. et al., 2019). In addition, given the crucial role of Aβ in the pathological development of AD, many drugs were developed to control the abnormal accumulation of Aβ. Verubecestat and Tarenflurbil inhibit enzymes within the Aβ biosynthetic pathway, Tramiprosate and Azeliragon inhibit abnormal aggregation of Aβ, monoclonal antibodies (such as Gantenerumab and Aducanumab) and vaccines (such as ACC-001) against Aβ are also used as immunotherapy (Sevigny et al., 2016; Wu, 2019). Most of these candidates failed in phase III clinical trials, mainly due to lack of efficacy against placebo.

MYRICETIN AND DIHYDROMYRICETIN

3, 3′, 4′, 5, 5′, 7-Hexahydroxyflavone (Myricetin, MYR, **Figure 1**) is a flavonoid, which was first isolated from the bark of *Myrica nagi* Thunb. about 200 years ago (Semwal et al., 2016). The appearance of MYR is a light yellow crystal solid. 3, 3′, 4′, 5, 5′, 7-Hexahydroxy-2, 3-dihydroflavanonol (Dihydromyricetin, DMY or DHM) is also known as ampelopsin (AMP) because it was first discovered from *Ampelopsis meliaefolia* (Hand. -Mazz.) W. T. Wang (an Ampelopsis Michx plant) in 1940 (Hou et al., 2015). DMY has a white appearance. MYR is the oxidation product of DMY, thus 2, 3-double bond of DMY is hydrogenated to form MYR (**Figure 1**).

MYR and DMY are produced in sizable quantities in plants, particularly in some commonly consumed fruits and vegetables. For instance, MYR, has been reported to be abundant in strawberries, apples, spinach, aloe vera, carrots (Zhang et al., 2015), mulberries (Mahmood et al., 2012), etc., and the content of MYR in red wine can reach twice that of resveratrol (Lee et al., 2007; Rodrigo et al., 2011). Dihydromyricetin is widely found in grapes, bayberry, ampelopsis (Clementi et al., 2015), ginkgo and other plants, with the content of DMY in rattan tea particularly is high, often reaching 30–40% (Liu et al., 2019). Moreover, MYR is listed as a health product in Europe, and has been approved by the FDA for pharmaceuticals, foods, and health products in the United States with FYI, a health product containing myricetin being successfully launched (Whitehouse, 2002). Meanwhile, MYR and DMY are the essential ingredients in many health foods or drinks (Semwal et al., 2016; Martínez-Coria et al., 2019) and are known to have an excellent safety profile coupled with the fact that is suitable for human consumption.

Being one of the more well-studied polyphenols, MYR and DMY exhibit a range of interesting biological activities. MYR has been shown to have anti-cancer, anti-oxidant and anti-inflammatory effects (Kang et al., 2011; Zhang et al., 2011). DMY has shown to have better pharmacological effects than MYR, with its anti-temulence (Shen et al., 2012) ability and hepato-protective qualities being well known (Murakami et al., 2004). Interestingly, both MYR and DMY have been found to exhibit anti-AD effects. Moreover, many MYR and DMY containing foods are also reported to have some neuroprotective abilities. Ginkgo and its extracts have long been considered to have a good effect on the treatment of AD (Bader et al., 2018; Li et al., 2018). Aloe vera and mulberry are often considered to have additional anti-dementia effects (Clementi et al., 2015; Liu and Du, 2020). Furthermore, moderate consumption of red wine is also often considered to have anti-aging and antioxidant effects as well as improving blood pressure.

THE MOLECULAR MECHANISMS OF MYR AND DMY IN THE ALLEVIATION OF HALLMARKS OF ALZHEIMER'S DISEASE

Studies have shown that MYR and DMY can significantly improve the learning and memory abilities of animal model of Alzheimer's disease (Hirohata et al., 2007; Liang et al., 2014). In this section, we explore the underlying molecular mechanisms and potential mode of action of MYR and DMY against the symptoms of AD.

MYR and DMY Interact With Aβ to Exert Anti-AD Effects

Aβ is a hydrolysate of the amyloid protein precursor (APP) (Thinakaran and Koo, 2008). APP has two main metabolic pathways: one is the continuous hydrolysis by β-secretase (BACE-1) and γ-secretase to produce Aβ. In this process, BACE-1 is a key rate-limiting enzyme (Naushad et al., 2019), which is unsurprisingly a potential target for the treatment of AD. The other is the formation of harmless sAPPα and C83 after hydrolysis by α-secretase. Typically, the formation and hydrolysis of Aβ is in dynamic equilibrium. When this dynamic equilibrium is broken, the excessive production and abnormal deposition of Aβ in the brain has been linked to the initiation and progression of AD. It is reported that MYR inhibits the activity of BACE-1 and hinders the production of Aβ (Shimmyo et al., 2008). Inside the active center of BACE-1, the hydroxyl group at the C7 position of the A ring in the MYR structure binds to the aspartate dyad (Asp32 and Asp228) through hydrogen bonding (Chakraborty et al., 2011). Thus, MYR inhibits the activity of BACE-1 to digest APP and thus reduces the production of Aβ. Additionally, MYR has been shown to have increased the level of α-secretase (Shimmyo et al., 2008) which results in an increase in the levels of APP broken down to harmless APP fragments.

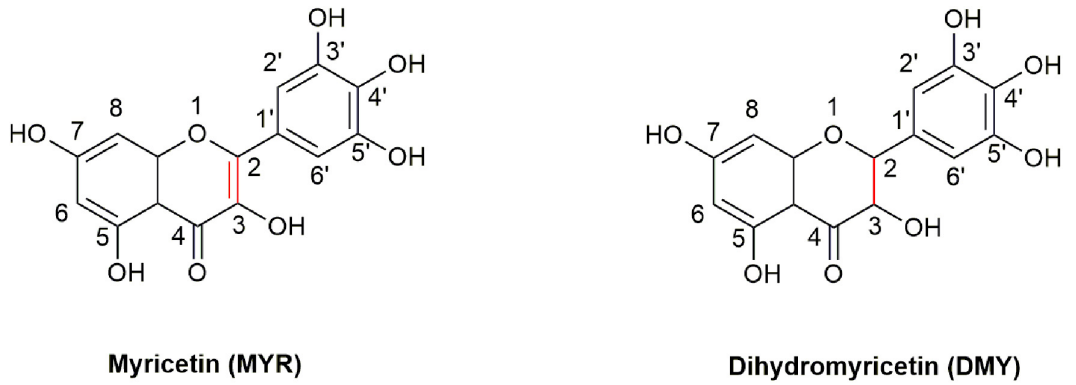

FIGURE 1 | The structures of MYR and DMY. MYR is a flavonol compound, and DMY belongs to dihydroflavonol. DMY is a derivative after introducing "H" to MYR's 2, 3 binding sites, respectively.

This causes an overall decrease in the levels of APP that can be used to produce Aβ, thereby indirectly reducing Aβ production. Furthermore, studies also showed that DMY can increase the expression of neprilysin (NEP) (Feng et al., 2018). NEP is a M13 zinc metalloproteinase family protein that can cleave Aβ peptide bonds to decompose Aβ (Kanemitsu et al., 2003; Hersh and Rodgers, 2008). The upregulation of NEP by DMY accelerates the decomposition of Aβ and results in the improvement of AD symptoms (**Figure 2**).

Secondly, Aβ monomer has a neurotrophic effect, but the oligomers and fibrils of Aβ have severe neurotoxicity (mainly including inflammation, oxidative stress, and destruction of cell membranes) (Jang et al., 2007; Umeda et al., 2011; Zhai et al., 2012). The oligomers and fibrils of Aβ are generated by excess Aβ through β-sheet (Jang et al., 2007) and MYR and DMY can inhibit the formation of this β-sheet (Shimmyo et al., 2008; Jia et al., 2019). The hydroxyl group of MYR forms a hydrogen bond with a carbonyl group and amino group in Aβ (Andarzi Gargari et al., 2018). Secondary structure analysis showed that this interaction between MYR and Aβ could inhibit the β-sheet formation of Aβ, which can prevent Aβ undergoing toxic changes (Andarzi Gargari et al., 2018). Moreover, MYR can also bind with two further sites in Aβ fibrils and inhibit the extension of Aβ (Hirohata et al., 2007; Andarzi Gargari et al., 2018). DMY can combine with the three sites on the Aβ structure to block its molecular conformation and break its intramolecular hydrogen bonds. This not only blocks the β-sheet but also has a dismantling effect on the already formed Aβ fibrils (Jia et al., 2019). Thus, MYR and DMY can hinder the formation of Aβ oligomers, which will reduce the neurotoxicity of Aβ oligomers, and release the symptoms of AD (**Figure 2**).

MYR and DMY Show Anti-AD Effects Through Anti-inflammatory

Recent research has shown that inflammation is also one of the main causes of AD, although neuroinflammation is usually treated as the result of AD's pathogenesis (Meraz-Ríos et al., 2013). Interestingly, MYR and DMY can directly reduce the levels of inflammatory factors, inhibit microglia activation, and inhibit NLRP3 (nucleotide-binding oligomerization domain-like receptor protein 3) inflammasome (**Figure 3**). Eventually, these anti-inflammatory effects of MYR and DMY can help to reduce the symptoms of AD.

Firstly, MYR and DMY can effectively reduce the levels of inflammatory factors such as IL, TNF-α, NF-κB, etc (Jing and Li, 2019). Taking IL-1 as an example, it can not only damage nerve cells but also increase the level of APP to increase the production and accumulation of Aβ (Shadfar et al., 2015). IL-1 can also accelerate the phosphorylation of tau peptide in the brain and further form neurofibrillary tangles (NFTs), and NFTs are another major pathological marker of AD besides Aβ(Shadfar et al., 2015). In addition, IL-1 can also increase the level of other inflammatory factors (such as TNF-α) to further aggravate the inflammatory response and cell damage caused by it (Shadfar et al., 2015). The anti-inflammatory effects of MYR and DMY are mainly to reduce the levels of IL, TNF-α, iNOS, COX-2, and other inflammatory factors in the brain by interfering with the NF-κB signaling pathway and alleviate the damage of these inflammatory factors to the nervous system (Jing and Li, 2019). It is also reported that DMY can inhibit neuronal inflammation in AD rats by activating the AMPK/SIRT1 pathway (Sun et al., 2019). It is through interfering with this signaling pathway, that DMY can exert its anti-inflammatory ability while inhibiting the apoptosis of hippocampal nerve cells. This is key to treating AD, as the hippocampus of the brain regarded as the main area which of the brain that controls memory.

Secondly, microglia are the smallest glial cells in the central nervous system. Under normal conditions, microglial cells have beneficial nutritional and immunological effects, but activated microglial cells play an essential role in the development of neuroinflammation in AD patients' brains (Browne et al., 2013). Activated microglial cells have two types: M1 and M2. M1 can promote the development of inflammation, while M2 can inhibit the development of inflammation (Sondag et al., 2009). For microglia, DMY not only inhibits its activation (Jang et al., 2007) but also has an excellent inhibitory effect on the neuroinflammation caused by activated microglia (Weng et al., 2017). Specifically, DMY can

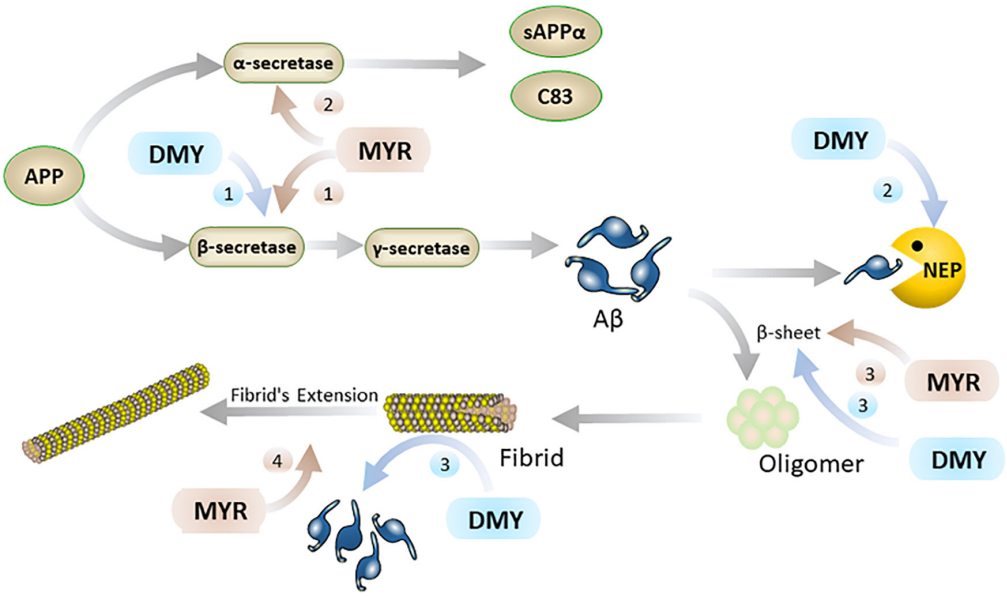

FIGURE 2 | MYR interacts with Aβ through the following 4 pathways (brown): 1. MYR reduces the production of Aβ through inhibition of β-secretase 1; 2. by increasing the level of α-secretase and competitively decomposing APP; 3. inhibiting the β-sheet by binding to Aβ, and preventing the conversion of Aβ monomers into oligomers and fibrils; 4. Inhibiting the extension of the fibrils of Aβ by binding to it. DMY mainly suppresses Aβ in the brain through the following 3 paths (blue): 1. reduce Aβ production by inhibition β-secretase 1; 2. increasing the level of NEP by promoting the expression of NEP gene; 3. inhibiting β-sheet and disassembling Aβ fibrils by binding to Aβ.

inhibit the transformation of microglia to M1 and promote its transformation to M2 (Jang et al., 2007). By reducing the level of M1, the inflammatory response is reduced; meanwhile, increasing the level of M2 can further reduce the damage caused by neuroinflammation by exerting its anti-inflammatory ability.

Lastly, in the pathological process of AD, NLRP3 in the central nervous system can be activated by Aβ and aggravate symptoms of AD (Heneka et al., 2013). Studies have confirmed that Aβ levels can be effectively reduced by inhibiting NLRP3 or knocking out related genes, and the impairment of spatial memory ability of mice with Alzheimer's disease also can be alleviated in this way (Heneka et al., 2013; Tan et al., 2013). At present, the NLRP3 in the central nervous system is considered an effective target for AD's treatment (Saresella et al., 2016). DMY can inhibit the expression and activation of NLRP3 (Jang et al., 2007) with DMY increasing the levels of HO-1 and NQO1 by activating Nrf2, which in turn reduces the level of mtROS which leads to the activation of NLRP3 being inhibited (Hu et al., 2018). Furthermore, MYR also can inhibit NLRP3 activation by inhibiting ACS's oxygen-dependent ubiquitination and promoting oxygen-independent ubiquitination of NLRP3 (Chen et al., 2019). The inhibitory effect of MYR and DMY on the NLRP3 can help reduce neuroinflammatory damage in the brain of AD patients and reduce the level of Aβ to a certain extent.

MYR and DMY Exert an Anti-AD Effect Through Antioxidant

Oxidative stress reflects an imbalance between the excessive production and incorporation of free radicals and the dynamic ability of a biosystems to detoxify reactive intermediates (Jiang et al., 2016). It is one of the direct causes of aging and a known cause of AD (Jiang et al., 2016). The brain has high oxygen consumption and low antioxidant capacity, which makes it particularly vulnerable to oxidative stress (Guo et al., 2019). Free radicals and ROS are the two main pathways used by oxidative stress to directly damage nerve cells. The free radical contains unpaired electrons, making it in an extremely unstable and highly reactive toward neighboring molecules. This will cause the neighboring molecules to become a new free radical, which in turn reacts with neighboring molecules to produce a free radical chain reaction, causing severe oxidative damage to the brain.

As flavonoids, the pyrogallol structure in the B ring of both MYR and DMY is key to their antioxidant effect (Mendes et al., 2015). They can combine with radicals to form stable semiquinone radicals, thus interrupting the radical chain reaction (Zhang and Chen, 2000). *In vitro* experiments have shown that very low concentrations (0.1, 0.2 μmol/L) of MYR can effectively inhibit the generation of ROS and protect cells from damage caused by oxidative stress (Barzegar, 2016). When the concentration of MYR reaches 5 μg/mL, it can achieve 50% clearance of ROS and 20% clearance of DPPH (1,1-diphenyl-2-picrylhydrazyl) radicals; when the concentration of MYR reaches 10 μg/mL, it restores the levels and activities of antioxidant substances such as SOD, CAT, and GSH-Px in cells (Wang et al., 2010). Additionally, research has shown that in the H_2O_2-induced cell injury model, MYR can inhibit DNA and lipid damage caused by oxidative stress while regulating the PI3K/Akt and MAPK signaling pathways. This leads to an increase in the levels of anti-apoptotic factors such as Bcl-2 and reduction

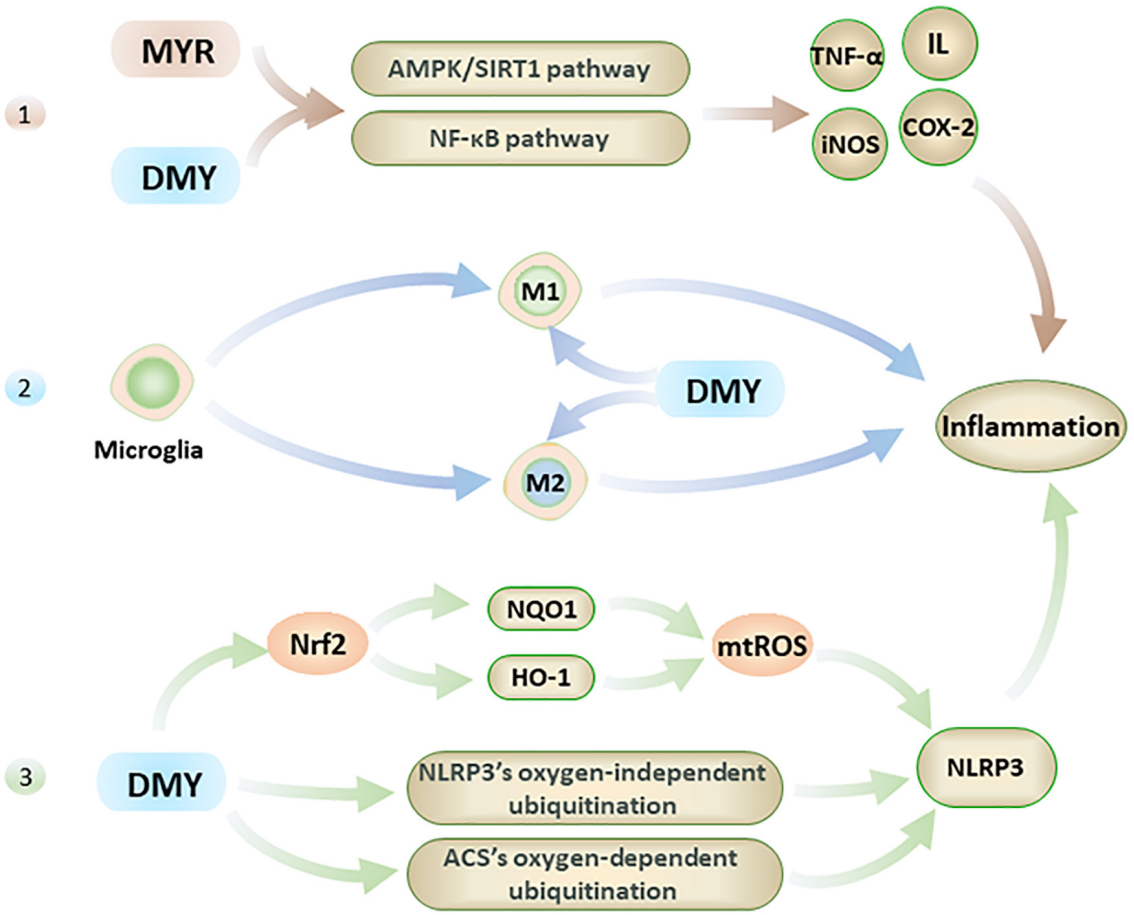

FIGURE 3 | The anti-inflammatory effects of MYR and DMY occur through the following 3 pathways. 1. Through the NF-κB and AMPK/SIRT1 pathway 2. Regulation of microglia, though reduction in M1 levels and increasing M2 level. 3. Activation of Nrf2 to reduce mtROS, and interfere with the ubiquitination process to suppress NLRP3 inflammasome.

of pro-apoptotic factors like Bax, caspase-9, and caspase-3, ultimately leading to inhibition of apoptosis induced by oxidative stress (Wang et al., 2010; Li et al., 2016). DMY also has a very good free radical scavenging ability. The difference from MYR mainly lies in the fact that MYR has a better ability to clear ABTS [2, 2'-azino-bis(3-ethylbenzothiazoline-6-sulfonic acid)] while DMY is better at clearing DPPH (Kang et al., 2010).

In addition to direct brain damage, oxidative stress is closely associated with multiple factors related to AD. (1) Aβ has the ability to induce oxidative stress (Butterfield et al., 2010), and oxidative stress can also promote the production of Aβ (Praticò et al., 2001). MYR can inhibit the free radical chain reaction from the source by inhibiting Aβ, thereby reducing the central nervous system damage caused by oxidative stress (Shimmyo et al., 2008). (2) Oxidative stress can activate the JNK/SAPK pathway and subsequently cause elevated BACE-1 levels. Further, BACE-1 will break down the APP into Aβ, which leads to elevated Aβ levels (Tamagno et al., 2005), while an increase in Aβ can further activate the JNK/SAPK pathway (**Figure 4**) and cause a vicious cycle. Oxidative stress can also promote the phosphorylation of tau peptide by inhibiting PP2A (Praticò et al., 2001; Su et al., 2010; Tang et al., 2017), and oligomers of tau peptide can aggravate oxidative stress by destroying mitochondria (Lasagna-Reeves et al., 2011; **Figure 4**). MYR and DMY can, therefore, protect neuronal cells through their antioxidant abilities.

MYR and DMY Play an Anti-AD Role by Regulating Autophagy

Autophagy is the process by which cells eliminate abnormal organelles or denatured protein through lysosomes. For nerve cells, it is difficult to dilute toxins through cell division, so autophagy is a particularly vital process for nerve cells. At the beginning of the autophagy process, the endoplasmic reticulum in the cell sheds part of the biofilm and forms autophagic vesicles (AVs). These AVs encapsulate harmful protein such as Aβ and abnormally phosphorylated tau peptide to form autophagosomes. Subsequently, the autophagosomes are transported along the microtubules by the dynein to the lysosome resulting in harmful protein being degraded by the lysosome (Li et al., 2019; **Figure 5**). Moreover, recent studies have revealed that the mTOR (mammalian targets of rapamycin) is a crucial signaling factor

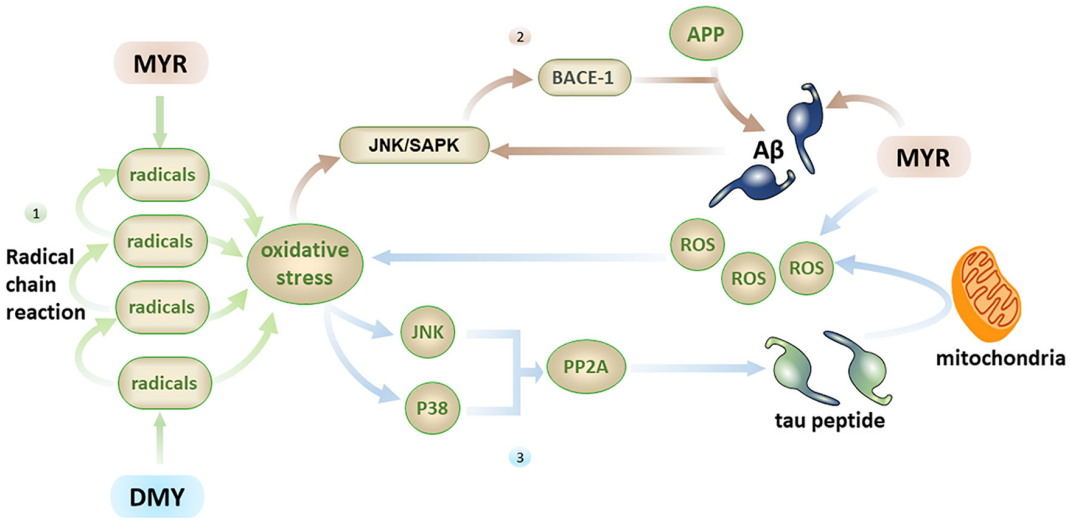

FIGURE 4 | Firstly, the free radical chain reaction can cause severe oxidative stress damage, with MYR and DMY inhibiting this process by scavenging free radicals; secondly, oxidative stress can increase the level of Aβ by activating the JNK/SAPK pathway, and Aβ can further activate this pathway, MYR's antioxidant and anti-Aβ abilities can disrupt this vicious circle; thirdly, oxidative stress can promote the phosphorylation of tau peptide by inhibiting PP2A, and tau peptide oligomers can increase oxidative stress by destroying mitochondria, the ability of MYR to clear ROS can prevent the increase of oxidative stress.

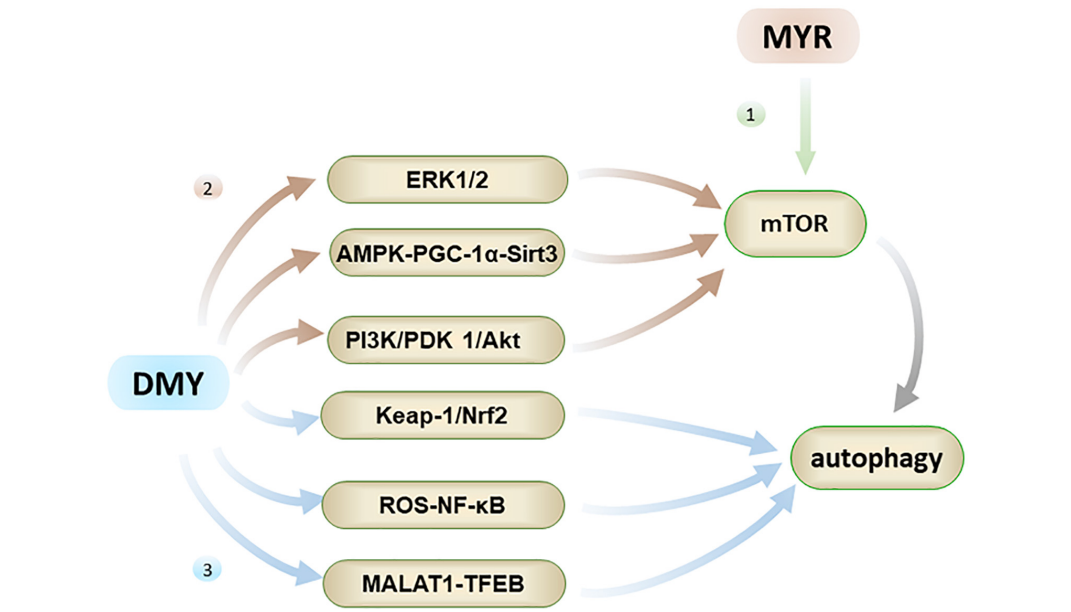

FIGURE 5 | Autophagy has the effect of inhibiting AD. Firstly, MYR can promote autophagy by inhibiting phosphorylation of mTOR; Secondly, DMY can inhibit mTOR through ERK1/2 pathway, AMPK-PGC-1α-Sirt3 pathway, and PI3K/PDK 1/Akt pathway, ultimately promote autophagy; Thirdly, DMY can also promote autophagy through the Keap-1/Nrf2, ROS-NF-κB and MALAT1-TFEB pathways.

that regulates cell proliferation, growth, and apoptosis, and it is the core cytokine that regulates cell autophagy.

Both MYR and DMY have an effect on regulating autophagy, which aids in the elimination of abnormal Aβ and tau peptide produced in cells. MYR regulates autophagy mainly through the mTOR pathway by inhibiting mTOR's phosphorylation (Cao et al., 2018). It has been observed to dose-dependently increase the level of autophagy marker LC3-II and induce formation of autophagosomes (Cao et al., 2018). Through the formation of a large number of autophagosomes, the clearance of Aβ and abnormally phosphorylated tau peptide in the cells is accelerated, thereby alleviating the symptoms of AD (Díaz-Villanueva et al., 2015; Cao et al., 2018). On the other hand, DMY can promote autophagy by inhibiting mTOR, and again

this effect is dose-dependent. The regulation of autophagy by DMY is a comprehensive and complicated process, which involves the upstream pathway of mTOR including ERK1/2 (extracellular signal-regulated kinase 1/2), AMPK-PGC-1α-Sirt3 (AMP-activated kinase-peroxisome proliferator-activated receptor coactivator-1α-Sirt3) and PI3K/PDK 1/Akt (class III phosphatidylinositol 3-kinase/phosphoinositide-dependent protein kinase 1/protein kinase B) pathways (Xia et al., 2014; Shi et al., 2015). Furthermore, the regulation of autophagy by DMY also involves the Keap-1/Nrf2, ROS-NF-κB, and MALAT1-TFEB pathways (Qiu et al., 2017; Zhou et al., 2017; Tan et al., 2019). In short, DMY can affect the levels of Aβ and tau peptide in the nervous system through multiple effects on autophagy, and thus has a therapeutic effect on AD.

MYR and DMY Play an Anti-AD Role by Complexing Metal Ions in the Brain

The imbalance of metal ions in the brain can cause cytotoxicity, oxidative stress damage, abnormal deposition of Aβ, and abnormal phosphorylation of tau peptide, which are closely related to AD. Initially, research conducted regarding AD-related metals generally focused on calcium ions, however, in recent years, an increasing number metal ions (such as copper, iron, and zinc) have been associated with the generation and development of AD (Bush, 2013). Studies have shown that there are many binding sites within Aβ that can bind metal ions (Tian et al., 2018), and there is a notable increase in toxicity of Aβ when this complexation occurs. For example, Zn^{2+} has four binding sites on the structure of Aβ, so even in micromolar concentrations, they can increase the aggregation of Aβ (Boom et al., 2009). Additionally, Zn^{2+} can change Aβ's structure after binding to Aβ and promote the amyloidosis of Aβ (Guo et al., 2017). Cu^{2+} is also able to bind Aβ and promote its accumulation and precipitation (Cristóvão et al., 2016). This effect is generally related to the relative levels of Cu^{2+}/Zn^{2+} and Aβ content (Cristóvão et al., 2016).

As flavonoids, both MYR and DMY have an excellent ability to chelate metal ions (Xu, 2010; Jomová et al., 2019), which can inhibit AD by regulating the concentration of metal ions in the brain. The chelating sites with metal ions of MYR and DMY are shown in **Figure 6**. It is worth noting that the chelation products have better pharmacological effects (such as antioxidant and anti-inflammatory) than uncomplexed MYR or DMY (Li et al., 2016). MYR has been proven that it could inhibit Aβ aggregation by chelating with Cu^{2+} or Zn^{2+} (DeToma et al., 2011). MYR can regulate the level of metal ions in the brain by complexing with metal ions, and this will reduce the chance of Aβ to combine with metal ions. Moreover, MYR can not only prevent Aβ from binding with metal ions but also disassemble the complexes of Cu^{2+}/Zn^{2+}-Aβ that have been formed and plunder the metal ions (DeToma et al., 2011). Besides affecting the aggregation of Aβ, Zn^{2+} can also affect the production of Aβ. It can increase the levels of β-secretase and γ-secretase by inhibiting the activity of α-secretase, thereby increasing the level of Aβ in the brain (Garai et al., 2006). This shows that the complexation of MYR and Zn^{2+} can also reduce the level of Aβ by suppressing this phenomenon.

Furthermore, and similar to other divalent ions, Fe^{2+} can bind Aβ and induce the formation of oligomers and fibrils (Boopathi and Kolandaivel, 2016; Lane et al., 2018). Concurrent to this, is the Fenton process (Simunkova et al., 2019), that acts to covert H_2O_2 into highly toxic hydroxyl radicals and ROS (Wang T. et al., 2019), and Fe^{2+} serves as a catalyst in this process. As is known these hydroxyl radicals and ROS can cause severe oxidative damage to the central nervous system, and the presence of Fe^{2+} in the central nervous system can dramatically increase this damage. Upon complexation of Fe^{2+} by MYR and DMY, the levels of free Fe^{2+} drops, which results in a reduction in the Fenton reaction. This eventually leads to an overall reduction in oxidative stress damage in the central nervous system. Additionally, Fe^{2+} can also lead to the activation of microglia, which again results in the damage to the nervous system caused by inflammation (Peters et al., 2018). Complexation of Fe^{2+} by MYR and DMY can therefore reduce the risk of this inflammation occurring. Further to this, MYR can also regulate cell to metal ion transport. Wang et al. claimed that MYR could reduce iron levels by inhibiting the expression of transferrin receptor 1 (TrR1) (Wang et al., 2017). This is another way for MYR to adjust the level of metal ions in addition to directly chelating iron ions.

MYR and DMY Play an Anti-AD Role by Regulating Insulin Signaling Pathways and Intestinal Flora

Insulin signaling pathway damage in the central nervous system can induce AD (Griffin et al., 2005), with AD being called type 3 diabetes. Insulin resistance will cause the levels of β-secretase and γ-secretase to rise, and increase the rate of Aβ generation. Insulin resistance also causes the body to resort to a state of high insulin levels, which in turn causes the body to overexpress insulin degrading enzymes (IDE) which are designed to break down excess insulin. In addition to degrading insulin, IDE also degrades Aβ. Too much insulin will compete with Aβ for the opportunity of being degraded by IDE, resulting in the accumulation of Aβ due to a lack of effective degradation (Dineley et al., 2014). Both MYR and DMY have been shown to effectively inhibit insulin resistance. PTP1β is a protein that negatively regulates the insulin signaling pathway (Lalitha et al., 2020) and can cause insulin resistance. A recent study showed that MYR has a good inhibitory effect on PTP1β(Lalitha et al., 2020). *In vivo* experiments have also shown that the treatment of MYR also increases the body's sensitivity to insulin by increasing the levels of pIR (phospho-insulin receptor), pIRS1 (phospho-insulin receptor substrate 1) and pAkt (phospho-Akt), thereby increasing the body's sensitivity to insulin. DMY can treat the dysregulation of insulin signaling pathway by inhibiting the phosphorylation of PPARγ Ser273 and regulating the ERK/CDK5 signaling pathway (Liu, 2017). Further studies have shown that DMY's ability to regulate intestinal flora also helps to improve insulin resistance (Tong, 2018) with the successful launch of GV971 in China proving the feasibility of treating AD with intestinal flora. Regulation of insulin resistance or other pathological processes in AD patients through intestinal flora may also be potential anti-AD targets of MYR and DMY.

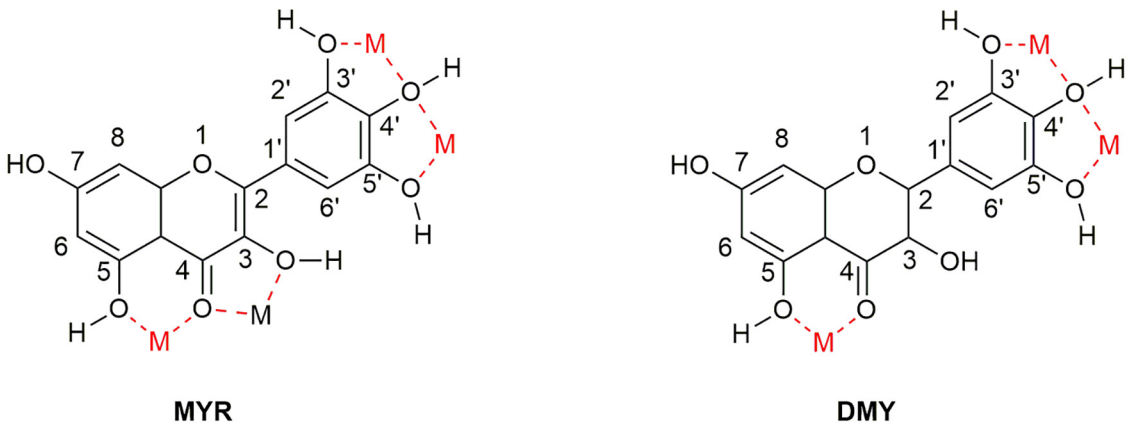

FIGURE 6 | Sites that can complex metal ions in the structure of MYR and DMY. There are four main sites (location of M in the figure) that can be used to chelate metal ions in the structure of MYR since the double bond at the 2–3 position becomes a single bond. DMY is one less than MYR, which can be used to couple metal ions.

MYR and DMY Play an Anti-AD Role by Inhibiting AChE

Acetylcholine is a neurotransmitter that plays an important role in the transmission of neural signals and memory formation and the lack of ACh in the central nervous system is a known cause of AD (Guo et al., 2019). AChE has been a major target for drug discovery in recent years with three of the current five AD clinical drugs being AChE inhibitors. Interestingly, both MYR and DMY have been shown to effectively inhibit AChE (Pepeu and Giovannini, 2004; Wang et al., 2017). In the mouse model of Alzheimer's disease induced by scopolamine, MYR effectively reduced the impairment of learning and memory ability of mice through its AChE inhibitory ability (Kou et al., 2016). The structural characteristics of DMY lead to stronger anti-AChE activity than MYR (Zhao et al., 2012) and exhibits similar inhibitory data when compared to clinical drugs (Tacrine) (Pepeu and Giovannini, 2004), with the added benefit that DMY, as a food materials, has a better safety profile. In addition to AChE, some inflammatory factors also affect the level of ACh, such as IL-1. IL-1 can improve the level of AChE and accelerate the decomposition of ACh (Shadfar et al., 2015), resulting in insufficient ACh content in the brain and affecting memory ability. The anti-inflammatory ability of MYR and DMY can also prevent the loss of ACh.

MYR and DMY Play an Anti-AD Role by Inhibiting Bacteria and Viruses

Bacteria and viruses also can induce AD, with both *Porphyromonas gingivalis* and *Herpes simplex virus* (HSV) having confirmed links with AD initiation and progression (Bearer and Wu, 2019; Dominy et al., 2019). Gingipains, produced by *Porphyromonas gingivalis*, is a toxic protease related to the phosphorylation of tau peptide and the ubiquitin pathology which can also increase the level of $A\beta_{42}$ in the brain (Bearer and Wu, 2019; Dominy et al., 2019). According to the results reported by Grenier et al., 62.5 to 125 μg/ml of MYR had good inhibitory effect on *Porphyromonas gingivalis*, and this effect may be related to MYR's ability to chelate iron ions (Grenier et al., 2015). Additionally, MYR can also inhibit the expression of protease and adhesin in *Porphyromonas gingivalis* to reduce the toxic effects of *Porphyromonas gingivalis* (Grenier et al., 2015). Furthermore, MYR also inhibits the inflammatory response caused by *Porphyromonas gingivalis* through activation of NF-κB (Grenier et al., 2015), which can play a role in the adjuvant treatment of AD. Some research data shows that patients with long-term infection with HSV have a higher risk of AD than those patients free of HSV infection. The reason may be that HSV can cause Aβ accumulation and the phosphorylation of tau peptide, which then induces AD. Importantly, HSV was also found in the brain areas seriously affected by AD, which substantiates the above hypothesis (Mangold and Szpara, 2019). The inhibitory effect of MYR on HSV (Lyu et al., 2005) will help patients reduce the risk of AD and help control the status of Aβ and tau peptide.

Other

MiR (microRNA) is a small-molecule RNA, 21–23 nucleotides in length, which can regulate gene expression. Recent reports showed that overexpression of miR-34a could cause the accumulation of Aβ and the hyperphosphorylation of tau peptide, and eventually lead to AD (Sarkar et al., 2019). Studies have shown that in the brain of Alzheimer's disease model rats induced by D-gal, DMY can regulate the SIRT1-mTOR signaling pathway by inhibiting miR-34a, and ultimately inhibit D-gal-induced hippocampal neuronal cell damage (Kou et al., 2016).

Prospects

Alzheimer's disease is a disease-induced and promoted by a variety of factors. Due to the interaction of multiple reasons, unilateral treatment of AD will be challenging to achieve. As detailed in this review, we know that MYR and DMY can inhibit the excessive production and accumulation of Aβ, inhibit the inflammatory response in the central nervous system, chelate

metal ions in the nervous system, regulate autophagy, and inhibit oxidative stress. At the same time, they can also increase ACh levels by inhibiting the activity of AChE, inhibiting the overexpression of miR-34a, reducing the promotion of AD by bacteria and viruses, and alleviating the state of insulin resistance in the central nervous system. They can even regulate the balance of the intestinal flora, which is also a good target for intervention in AD. These combined anti-AD effects also work to improve the symptoms in AD patients. For example, no studies have been shown that MYR and DMY can directly inhibit tau peptide hyperphosphorylation. However, MYR and DMY can also affect tau peptide and NFTs by regulating autophagy, inhibiting oxidative stress, and improving insulin resistance.

Health products and healthy diets are well accepted to regulate human health and prevent diseases. MYR and DMY have better toxicity profiles and exist in a variety of foods. FYI's approval by the FDA also shows the feasibility of using MYR and DMY for health products. Therefore, we believe that the uptake of MYR and DMY in daily diets to develop health products or foods with the ability to prevent and improve AD has great potential.

AUTHOR CONTRIBUTIONS

All the authors listed have made some contributions to the manuscript and approved for publication.

FUNDING

This review was funded by the Shandong Provincial Natural Science Foundation, China (Grant No. ZR2019MH078); The Drug Innovation Major Project (Grant No. 2017ZX09301030); and Project for development of TCM science and technology in Shandong Province (Grant No. 2019-0031).

REFERENCES

Andarzi Gargari, S., Barzegar, A., and Tarinejad, A. (2018). The role of phenolic OH groups of flavonoid compounds with H-bond formation ability to suppress amyloid mature fibrils by destabilizing β-sheet conformation of monomeric Aβ17-42. *PLoS One* 13:e0199541. doi: 10.1371/journal.pone.0199541

Association, A. S. (2020). Alzheimer's disease facts and figures. *Alzheimers Dement* 16, 391-460. doi: 10.1002/alz.12068

Ayton, S., Lei, P., and Bush, A. I. (2015). Biometals and their therapeutic implications in Alzheimer's disease. *Neurotherapeutics* 12, 109–120. doi: 10.1007/s13311-014-0312-z

Bader, B. M., Jügelt, K., Schultz, L., and Schroeder, O. H. (2018). Ginkgo biloba L. (Ginkgoaceae) leaf extract medications from different providers exhibit differential functional effects on mouse frontal cortex neuronal networks. *Front. Pharmacol.* 9:848. doi: 10.3389/fphar.2018.00848

Barnett, R. (2019). Alzheimer's disease. *Lancet* 393:1589. doi: 10.1016/s0140-6736(19)30851-7

Barzegar, A. (2016). Antioxidant activity of polyphenolic myricetin in vitro cell-free and cell-based systems. *Mol. Biol. Res. Commun.* 5, 87–95.

Bearer, E. L., and Wu, C. (2019). Herpes simplex virus, Alzheimer's disease and a possible role for Rab GTPases. *Front. Cell Dev. Biol.* 7:134. doi: 10.3389/fcell.2019.00134

Boom, A., Authelet, M., Dedecker, R., Frédérick, C., Van Heurck, R., Daubie, V., et al. (2009). Bimodal modulation of tau protein phosphorylation and conformation by extracellular Zn2+ in human-tau transfected cells. *Biochim. Biophys. Acta* 1793, 1058–1067. doi: 10.1016/j.bbamcr.2008.11.011

Boopathi, S., and Kolandaivel, P. (2016). Fe(2+) binding on amyloid β-peptide promotes aggregation. *Proteins* 84, 1257–1274. doi: 10.1002/prot.25075 doi: 10.1002/prot.25075

Browne, T. C., McQuillan, K., McManus, R. M., O'Reilly, J. A., Mills, K. H., and Lynch, M. A. (2013). IFN-γ Production by amyloid β-specific Th1 cells promotes microglial activation and increases plaque burden in a mouse model of Alzheimer's disease. *J. Immunol.* 190, 2241–2251. doi: 10.4049/jimmunol.1200947

Bush, A. I. (2013). The metal theory of Alzheimer's disease. *J. Alzheimers Dis.* 33(Suppl. 1), S277–S281. Epub 2012/05/29. doi: 10.3233/jad-2012-129011 PubMed

Butterfield, D. A., Galvan, V., Lange, M. B., Tang, H., Sowell, R. A., Spilman, P., et al. (2010). In vivo oxidative stress in brain of Alzheimer disease transgenic mice: requirement for methionine 35 in amyloid beta-peptide of APP. *Free Radic. Biol. Med.* 48, 136–144. doi: 10.1016/j.freeradbiomed.2009.10.035

Butterfield, D. A., and Halliwell, B. (2019). Oxidative stress, dysfunctional glucose metabolism and Alzheimer disease. *Nat. Rev. Neurosci.* 20, 148–160. doi: 10.1038/s41583-019-0132-6

Cao, J., Chen, H., Lu, W., Wu, Y., Wu, X., Xia, D., et al. (2018). Myricetin Induces Protective Autophagy by Inhibiting the Phosphorylation of mTOR in HepG2 Cells. *Anatom. Record* 301, 786–795. doi: 10.1002/ar.23754

Chakraborty, S., Kumar, S., and Basu, S. (2011). Conformational transition in the substrate binding domain of beta-secretase exploited by NMA and its implication in inhibitor recognition: BACE1-myricetin a case study. *Neurochem. Int.* 58, 914–923. doi: 10.1016/j.neuint.2011.02.021

Chen, H., Lin, H., Xie, S., Huang, B., Qian, Y., Chen, K., et al. (2019). Myricetin inhibits NLRP3 inflammasome activation via reduction of ROS-dependent ubiquitination of ASC and promotion of ROS-independent NLRP3 ubiquitination. *Toxicol. Appl. Pharmacol.* 365, 19–29. doi: 10.1016/j.taap.2018.12.019

Clementi, M. E., Tringali, G., Triggiani, D., and Giardina, B. (2015). Aloe arborescens Extract Protects IMR-32 Cells against Alzheimer amyloid beta peptide via inhibition of radical peroxide production. *Nat. Prod. Commun.* 10, 1993–1995.

Cristóvão, J. S., Santos, R., and Gomes, C. M. (2016). Metals and neuronal metal binding proteins implicated in Alzheimer's disease. *Oxidat. Med. Cell. Long.* 2016, 9812178.

DeToma, A. S., Choi, J. S., Braymer, J. J., and Lim, M. H. (2011). Myricetin: a naturally occurring regulator of metal-induced amyloid-β aggregation and neurotoxicity. *Chembiochem* 12, 1198–1201. doi: 10.1002/cbic.201000790

Díaz-Villanueva, J. F., Díaz-Molina, R., and García-González, V. (2015). Protein folding and mechanisms of proteostasis. *Int. J. Mol. Sci.* 16, 17193–17230.

Dineley, K. T., Jahrling, J. B., and Denner, L. (2014). Insulin resistance in Alzheimer's disease. *Neurobiol. Dis.* 72(Pt. A), 92–103.

Dominy, S. S., Lynch, C., Ermini, F., Benedyk, M., Marczyk, A., Konradi, A., et al. (2019). Porphyromonas gingivalis in Alzheimer's disease brains: evidence for disease causation and treatment with small-molecule inhibitors. *Sci. Adv.* 5:eaau3333. doi: 10.1126/sciadv.aau3333

Feng, J., Wang, J. X., Du, Y. H., Liu, Y., Zhang, W., Chen, J. F., et al. (2018). Dihydromyricetin inhibits microglial activation and neuroinflammation by suppressing NLRP3 inflammasome activation in APP/PS1 transgenic mice. *CNS Neurosci. Ther.* 24, 1207–1218. doi: 10.1111/cns.12983

Friedland, R. P. (2015). Mechanisms of molecular mimicry involving the microbiota in neurodegeneration. *J. Alzheimers Dis.* 45, 349–362. doi: 10.3233/jad-142841

Garai, K., Sengupta, P., Sahoo, B., and Maiti, S. (2006). Selective destabilization of soluble amyloid beta oligomers by divalent metal ions. *Biochem. Biophys. Res. Commun.* 345, 210–215. doi: 10.1016/j.bbrc.2006.04.056

Goedert, M., and Spillantini, M. G. (2006). A century of Alzheimer's disease. *Science* 314, 777–781. doi: 10.1126/science.1132814

Grenier, D., Chen, H., Ben Lagha, A., Fournier-Larente, J., and Morin, M. P. (2015). Dual Action of Myricetin on *Porphyromonas gingivalis* and the inflammatory response of host cells: a promising therapeutic molecule for periodontal diseases. *PLoS one* 10:e0131758. doi: 10.1371/journal.pone.0131758

Griffin, R. J., Moloney, A., Kelliher, M., Johnston, J. A., Ravid, R., Dockery, P., et al. (2005). Activation of Akt/PKB, increased phosphorylation of Akt substrates and loss and altered distribution of Akt and PTEN are features of Alzheimer's disease pathology. *J. Neurochem.* 93, 105–117. doi: 10.1111/j.1471-4159.2004.02949.x

Guo, H., Cao, H., Cui, X., Zheng, W., Wang, S., Yu, J., et al. (2019). Silymarin's inhibition and treatment effects for Alzheimer's disease. *Molecules* 24:1748.

Guo, J., Yu, L., Sun, Y., and Dong, X. (2017). Kinetic insights into Zn(2+)-induced amyloid β-protein aggregation revealed by stopped-flow fluorescence spectroscopy. *J Phys. Chem. B* 121, 3909–3917. doi: 10.1021/acs.jpcb.6b12187

Heneka, M. T., Kummer, M. P., Stutz, A., Delekate, A., Schwartz, S., Vieira-Saecker, A., et al. (2013). NLRP3 is activated in Alzheimer's disease and contributes to pathology in APP/PS1 mice. *Nature* 493, 674–678. doi: 10.1038/nature11729

Hersh, L. B., and Rodgers, D. W. (2008). Neprilysin and amyloid beta peptide degradation. *Curr. Alzheimer Res.* 5, 225–231. doi: 10.2174/156720508783954703

Hirohata, M., Hasegawa, K., Tsutsumi-Yasuhara, S., Ohhashi, Y., Ookoshi, T., Ono, K., et al. (2007). The anti-amyloidogenic effect is exerted against Alzheimer's beta-amyloid fibrils in vitro by preferential and reversible binding of flavonoids to the amyloid fibril structure. *Biochemistry* 46, 1888–1899. doi: 10.1021/bi061540x

Hou, X. L., Wang, W. Q., Shi, C. Y., Tong, Q., and Fang, J. G. (2015). Research progress in pharmacological effects of dihydromyricelin. *Chin. Tradit. Herb. Drugs* 46, 603–609. doi: 10.7501/j.issn.0253-2670.2015.04.027

Hu, Q., Zhang, T., Yi, L., Zhou, X., and Mi, M. (2018). Dihydromyricetin inhibits NLRP3 inflammasome-dependent pyroptosis by activating the Nrf2 signaling pathway in vascular endothelial cells. *BioFactors* 44, 123–136. doi: 10.1002/biof.1395

Jang, H., Zheng, J., and Nussinov, R. (2007). Models of beta-amyloid ion channels in the membrane suggest that channel formation in the bilayer is a dynamic process. *Biophys J.* 93, 1938–1949. doi: 10.1529/biophysj.107.110148

Jia, L., Zhao, W., Sang, J., Wang, W., Wei, W., Wang, Y., et al. (2019). Inhibitory effect of a flavonoid Dihydromyricetin against Aβ40 amyloidogenesis and its associated cytotoxicity. *ACS Chem. Neurosci.* 10, 4696–4703. doi: 10.1021/acschemneuro.9b00480

Jiang, T., Sun, Q., and Chen, S. (2016). Oxidative stress: a major pathogenesis and potential therapeutic target of antioxidative agents in Parkinson's disease and Alzheimer's disease. *Prog. Neurobiol.* 147, 1–19. doi: 10.1016/j.pneurobio.2016.07.005

Jing, N., and Li, X. (2019). Dihydromyricetin Attenuates Inflammation through TLR4/NF-kappaB Pathway. *Open Med.* 14, 719–725. doi: 10.1515/med-2019-0083

Jomová, K., Hudecova, L., Lauro, P., Simunkova, M., Alwasel, S. H., Alhazza, I. M., et al. (2019). A switch between antioxidant and prooxidant properties of the phenolic compounds Myricetin, Morin, 3′,4′-Dihydroxyflavone, Taxifolin and 4-Hydroxy-Coumarin in the Presence of Copper(II) Ions: a spectroscopic, absorption titration and DNA damage study. *Molecules* 24:4335. doi: 10.3390/molecules24234335

Kanemitsu, H., Tomiyama, T., and Mori, H. (2003). Human neprilysin is capable of degrading amyloid β peptide not only in the monomeric form but also the pathological oligomeric form. *Neurosci. Lett.* 350, 113–116. doi: 10.1016/s0304-3940(03)00898-x

Kang, K. A., Wang, Z. H., Zhang, R., Piao, M. J., Kim, K. C., Kang, S. S., et al. (2010). Myricetin protects cells against oxidative stress-induced apoptosis via regulation of PI3K/Akt and MAPK signaling pathways. *Int. J. Mol. Sci.* 11, 4348–4360. doi: 10.3390/ijms11114348

Kang, N. J., Jung, S. K., Lee, K. W., and Lee, H. J. (2011). Myricetin is a potent chemopreventive phytochemical in skin carcinogenesis. *Ann. N.Y. Acad. Sci.* 1229, 124–132. doi: 10.1111/j.1749-6632.2011.06122.x

Kou, X., Liu, X., Chen, X., Li, J., Yang, X., Fan, J., et al. (2016). Ampelopsin attenuates brain aging of D-gal-induced rats through miR-34a-mediated SIRT1/mTOR signal pathway. *Oncotarget* 7, 74484–74495. doi: 10.18632/oncotarget.12811

Lalitha, N., Sadashivaiah, B., Ramaprasad, T. R., and Singh, S. A. (2020). Lectin rich horsegram protein and myricetin activates insulin signaling-A study targeting PTP1β. *J. Funct. Foods* 67:103845. doi: 10.1016/j.jff.2020.103845

Lane, D. J. R., Ayton, S., and Bush, A. I. (2018). Iron and Alzheimer's disease: an update on emerging mechanisms. *J. Alzheimers Dis.* 64, S379–S395.

Lasagna-Reeves, C. A., Castillo-Carranza, D. L., Sengupta, U., Clos, A. L., Jackson, G. R., and Kayed, R. (2011). Tau oligomers impair memory and induce synaptic and mitochondrial dysfunction in wild-type mice. *Mol. Neurodegen.* 6:39. doi: 10.1186/1750-1326-6-39

Lee, K. W., Kang, N. J., Rogozin, E. A., Kim, H. G., Cho, Y. Y., Bode, A. M., et al. (2007). Myricetin is a novel natural inhibitor of neoplastic cell transformation and MEK1. *Carcinogenesis* 28, 1918–1927. doi: 10.1093/carcin/bgm110

Li, C. Y., Li, X., Qiu, K. X., and Zhu, J. (2019). The role of autophagy in the pathogenesis of Alzheimer's disease. *Chin. J. Cell Bio.* 41, 2039–2046. doi: 10.3969/j.issn.1008-0678.2008.02.023

Li, H., Sun, X., Yu, F., Xu, L., Miu, J., and Xiao, P. (2018). In silico investigation of the pharmacological mechanisms of beneficial effects of Ginkgo biloba L. on Alzheimer's Disease. *Nutrients* 10:589. doi: 10.3390/nu10050589

Li, X., Liu, J., Lin, J., Wang, T., Huang, J., Lin, Y., et al. (2016). Protective effects of dihydromyricetin against oh-induced mesenchymal stem cells damage and mechanistic chemistry. *Molecules* 21:5.

Liang, J., López-Valdés, H. E., Martínez-Coria, H., Lindemeyer, A. K., Shen, Y., Shao, X. M., et al. (2014). Dihydromyricetin ameliorates behavioral deficits and reverses neuropathology of transgenic mouse models of Alzheimer's disease. *Neurochem. Res.* 39, 1171–1181. doi: 10.1007/s11064-014-1304-4

Liu, D., and Du, D. (2020). Mulberry fruit extract alleviates cognitive impairment by promoting the clearance of amyloid-β and inhibiting neuroinflammation in alzheimer's disease mice. *Neurochem. Res.* 45, 2009–2019. doi: 10.1007/s11064-020-03062-7

Liu, D. M. Y., Ding, L. J., and Zeng, X. A. (2019). Dihydromyricetin: a review on identification and quantification methods, biological activities, chemical stability, metabolism and approaches to enhance its bioavailability. *Trends Food Sci. Technol.* 91, 586–597. doi: 10.1016/j.tifs.2019.07.038

Liu, L. (2017). Dihydromyricetin Ameliorates Insulin Resistance By Down-Regulating The Phosphorylation of PPARγ: Third Military Medical University, China. Available online at: https://kns.cnki.net/kcms/detail/detail.aspx?FileName=1017235434.nh&DbName=CDFD2017 (accessed October 3, 2020).

Lyu, S. Y., Rhim, J. Y., and Park, W. B. (2005). Antiherpetic activities of flavonoids against herpes simplex virus type 1 (HSV-1) and type 2 (HSV-2) in vitro. *Arch. Pharm. Res.* 28, 1293–1301. doi: 10.1007/bf02978215

Mahmood, T., Anwar, F., Abbas, M., and Saari, N. (2012). Effect of maturity on phenolics (phenolic acids and flavonoids) profile of strawberry cultivars and mulberry species from Pakistan. *Int. J. Mol. Sci.* 13, 4591–4607. doi: 10.3390/ijms13044591

Mangold, C. A., and Szpara, M. L. (2019). Persistent infection with herpes simplex virus 1 and alzheimer's disease-a call to study how variability in both virus and host may impact disease. *Viruses* 11:966. doi: 10.3390/v11100966

Martínez-Coria, H., Mendoza-Rojas, M. X., Arrieta-Cruz, I., and López-Valdés, H. E. (2019). Preclinical research of dihydromyricetin for brain aging and neurodegenerative diseases. *Front. Pharmacol.* 10:1334. doi: 10.3389/fphar.2019.01334

Mendes, V., Vilaça, R., de Freitas, V., Ferreira, P. M., Mateus, N., and Costa, V. (2015). Effect of myricetin, pyrogallol, and phloroglucinol on yeast resistance to oxidative stress. *Oxidat. Med. Cell. Long.* 2015:782504.

Meraz-Ríos, M. A., Toral-Rios, D., Franco-Bocanegra, D., Villeda-Hernández, J., and Campos-Peña, V. (2013). Inflammatory process in Alzheimer's Disease. *Front. Integr. Neurosci.* 7:59. doi: 10.3389/fnint.2013.00059

Murakami, T., Miyakoshi, M., Araho, D., Mizutani, K., Kambara, T., Ikeda, T., et al. (2004). Hepatoprotective activity of tocha, the stems and leaves of Ampelopsis grossedentata, and ampelopsin. *BioFactors* 21, 175–178. doi: 10.1002/biof.552210136

Naushad, M., Durairajan, S. S. K., Bera, A. K., Senapati, S., and Li, M. (2019). Natural compounds with Anti-BACE1 activity as promising therapeutic drugs

for treating Alzheimer's Disease. *Planta Med.* 85, 1316–1325. doi: 10.1055/a-1019-9819

Pepeu, G., and Giovannini, M. G. (2004). Changes in acetylcholine extracellular levels during cognitive processes. *Learn. Mem.* 11, 21–27. doi: 10.1101/lm.68104

Peters, D. G., Pollack, A. N., Cheng, K. C., Sun, D., Saido, T., Haaf, M. P., et al. (2018). Dietary lipophilic iron alters amyloidogenesis and microglial morphology in Alzheimer's disease knock-in APP mice. *Metallomics* 10, 426–443. doi: 10.1039/c8mt00004b

Praticò, D., Uryu, K., Leight, S., Trojanoswki, J. Q., and Lee, V. M. (2001). Increased lipid peroxidation precedes amyloid plaque formation in an animal model of Alzheimer amyloidosis. *J. Neurosci.* 21, 4183–4187. doi: 10.1523/jneurosci.21-12-04183.2001

Qiu, P., Dong, Y., Li, B., Kang, X. J., Gu, C., Zhu, T., et al. (2017). Dihydromyricetin modulates p62 and autophagy crosstalk with the Keap-1/Nrf2 pathway to alleviate ethanol-induced hepatic injury. *Toxicol. Lett.* 274, 31–41. doi: 10.1016/j.toxlet.2017.04.009

Rodrigo, R., Miranda, A., and Vergara, L. (2011). Modulation of endogenous antioxidant system by wine polyphenols in human disease. *Clin. Chim. Acta* 412, 410–424. doi: 10.1016/j.cca.2010.11.034

Saresella, M., La Rosa, F., Piancone, F., Zoppis, M., Marventano, I., Calabrese, E., et al. (2016). The NLRP3 and NLRP1 inflammasomes are activated in Alzheimer's disease. *Mol. Neurodegen.* 11:23.

Sarkar, S., Engler-Chiurazzi, E. B., Cavendish, J. Z., Povroznik, J. M., Russell, A. E., Quintana, D. D., et al. (2019). Over-expression of miR-34a induces rapid cognitive impairment and Alzheimer's disease-like pathology. *Brain Res.* 1721:146327. doi: 10.1016/j.brainres.2019.146327

Semwal, D. K., Semwal, R. B., Combrinck, S., and Viljoen, A. (2016). Myricetin: a dietary molecule with diverse biological activities. *Nutrients* 8:90. doi: 10.3390/nu8020090

Sevigny, J., Chiao, P., Bussière, T., Weinreb, P. H., Williams, L., Maier, M., et al. (2016). The antibody aducanumab reduces Aβ plaques in Alzheimer's disease. *Nature* 537, 50–56.

Shadfar, S., Hwang, C. J., Lim, M. S., Choi, D. Y., and Hong, J. T. (2015). Involvement of inflammation in Alzheimer's disease pathogenesis and therapeutic potential of anti-inflammatory agents. *Arch. Pharm. Res.* 38, 2106–2119. doi: 10.1007/s12272-015-0648-x

Shen, Y., Lindemeyer, A. K., Gonzalez, C., Shao, X. M., Spigelman, I., Olsen, R. W., et al. (2012). Dihydromyricetin as a novel anti-alcohol intoxication medication. *J. Neurosci.* 32, 390–401. doi: 10.1523/jneurosci.4639-11.2012

Shi, L., Zhang, T., Zhou, Y., Zeng, X., Ran, L., Zhang, Q., et al. (2015). Dihydromyricetin improves skeletal muscle insulin sensitivity by inducing autophagy via the AMPK-PGC-1α-Sirt3 signaling pathway. *Endocrine* 50, 378–389. doi: 10.1007/s12020-015-0599-5

Shimmyo, Y., Kihara, T., Akaike, A., Niidome, T., and Sugimoto, H. (2008). Multifunction of myricetin on A beta: neuroprotection via a conformational change of A beta and reduction of A beta via the interference of secretases. *J. Neurosci. Res.* 86, 368–377. doi: 10.1002/jnr.21476

Simunkova, M., Alwasel, S. H., Alhazza, I. M., Jomova, K., Kollar, V., Rusko, M., et al. (2019). Management of oxidative stress and other pathologies in Alzheimer's disease. *Arch. Toxicol.* 93, 2491–2513.

Sondag, C. M., Dhawan, G., and Combs, C. K. (2009). Beta amyloid oligomers and fibrils stimulate differential activation of primary microglia. *J. Neuroinflamm.* 6:1. doi: 10.1186/1742-2094-6-1

Su, B., Wang, X., Lee, H. G., Tabaton, M., Perry, G., Smith, M. A., et al. (2010). Chronic oxidative stress causes increased tau phosphorylation in M17 neuroblastoma cells. *Neurosci. Lett.* 468, 267–271. doi: 10.1016/j.neulet.2009.11.010

Sun, P., Yin, J. B., Liu, L. H., Guo, J., Wang, S. H., Qu, C. H., et al. (2019). Protective role of Dihydromyricetin in Alzheimer's disease rat model associated with activating AMPK/SIRT1 signaling pathway. *Biosci. Rep.* 39:BSR20180902.

Tamagno, E., Parola, M., Bardini, P., Piccini, A., Borghi, R., Guglielmotto, M., et al. (2005). Beta-site APP cleaving enzyme up-regulation induced by 4-hydroxynonenal is mediated by stress-activated protein kinases pathways. *J. Neurochem.* 92, 628–636. doi: 10.1111/j.1471-4159.2004.02895.x

Tan, M., Jiang, B., Wang, H., Ouyang, W., Chen, X., Wang, T., et al. (2019). Dihydromyricetin induced lncRNA MALAT1-TFEB-dependent autophagic cell death in cutaneous squamous cell carcinoma. *J. Cancer* 10, 4245–4255. doi: 10.7150/jca.32807

Tan, M. S., Yu, J. T., Jiang, T., Zhu, X. C., and Tan, L. (2013). The NLRP3 inflammasome in Alzheimer's disease. *Mol. Neurobiol.* 48, 875–882.

Tang, D., Chen, Q. B., Xin, X. L., and Aisa, H. A. (2017). Anti-diabetic effect of three new norditerpenoid alkaloids in vitro and potential mechanism via PI3K/Akt signaling pathway. *Biomed. Pharmacother. Biomed. Pharm.* 87, 145–152. doi: 10.1016/j.biopha.2016.12.058

Thinakaran, G., and Koo, E. H. (2008). Amyloid precursor protein trafficking, processing, and function. *J. Biol. Chem.* 283, 29615–29619. doi: 10.1074/jbc.r800019200

Tian, Z.-Y., Wang, C.-Y., Wang, T., Li, Y.-C., and Wang, Z.-Y. (2018). *S100A6 Inhibits Amyloid-β Aggregation in the Brain of Alzheimer's Disease: China Medical University, China*. Available online at: https://kns.cnki.net/kcms/detail/detail.aspx?FileName=1019815908.nh&DbName=CDFD2019 (accessed October 3, 2020).

Tong, Q. (2018). *Dihydromyricetin Improves Obesity and Insulin Resistance by Modulating the Composition of Gut Microbiota: Huazhong University of Science and Technology, China*. Available online at: https://kns.cnki.net/kcms/detail/detail.aspx?FileName=1018210528.nh&DbName=CDFD2019 (accessed October 3, 2020).

Umeda, T., Tomiyama, T., Sakama, N., Tanaka, S., Lambert, M. P., Klein, W. L., et al. (2011). Intraneuronal amyloid β oligomers cause cell death via endoplasmic reticulum stress, endosomal/lysosomal leakage, and mitochondrial dysfunction in vivo. *J. Neurosci. Res.* 89, 1031–1042. doi: 10.1002/jnr.22640

Wang, B., Zhong, Y., Gao, C., and Li, J. (2017). Myricetin ameliorates scopolamine-induced memory impairment in mice via inhibiting acetylcholinesterase and down-regulating brain iron. *Biochem. Biophys. Res. Commun.* 490, 336–342. doi: 10.1016/j.bbrc.2017.06.045

Wang, T., Xu, S. F., Fan, Y. G., Li, L. B., and Guo, C. (2019). Iron pathophysiology in Alzheimer's diseases. *Adv. Exp. Med. Biol.* 1173, 67–104. doi: 10.1007/978-981-13-9589-5_5

Wang, X., Sun, G., Feng, T., Zhang, J., Huang, X., Wang, T., et al. (2019). Sodium oligomannate therapeutically remodels gut microbiota and suppresses gut bacterial amino acids-shaped neuroinflammation to inhibit Alzheimer's disease progression. *Cell Res.* 29, 787–803. doi: 10.1038/s41422-019-0216-x

Wang, Z. H., Ah Kang, K., Zhang, R., Piao, M. J., Jo, S. H., Kim, J. S., et al. (2010). Myricetin suppresses oxidative stress-induced cell damage via both direct and indirect antioxidant action. *Environ. Toxicol. Pharmacol.* 29, 12–18. doi: 10.1016/j.etap.2009.08.007

Weng, L., Zhang, H., Li, X., Zhan, H., Chen, F., Han, L., et al. (2017). *Ampelopsin Attenuates Lipopolysaccharide-Inducedinflammatory Response Through the Inhibition of the NF-κB and JAK2/STAT3 signaling pathways in microglia: Nanjing University, China*. Available online at: https://kns.cnki.net/kcms/detail/detail.aspx?FileName=1017177014.nh&DbName=CMFD2018 (accessed October 3, 2020).

Whitehouse, M. W. (2002). Anti-inflammatory activity of a complementary medicine. *FYI^{TM}*. 4, 55–61.

Wu, K. F. H. Y. (2019). Advances in drug research for alzheimer's disease. *Geriatr Health Care* 25, 258–261.

Xia, J., Guo, S., Fang, T., Feng, D., Zhang, X., Zhang, Q., et al. (2014). Dihydromyricetin induces autophagy in HepG2 cells involved in inhibition of mTOR and regulating its upstream pathways. *Food Chem. Toxicol.* 66, 7–13. doi: 10.1016/j.fct.2014.01.014

Xu, X. R. (2010). *Electrochemical and Spectroelectrochemical Study of Myricetin and Dihydroquercetin: Hefei University of Technology, China*. Available online at: https://kns.cnki.net/kcms/detail/detail.aspx?FileName=2010247142.nh&DbName=CMFD2011 (accessed October 3, 2020).

Zhai, J., Lee, T. H., Small, D. H., and Aguilar, M. I. (2012). Characterization of early stage intermediates in the nucleation phase of Abeta aggregation. *Biochemistry* 51, 1070–1078.

Zhang, D., Xie, L., Jia, G., Cai, S., Ji, B., Liu, Y., et al. (2011). Comparative study on antioxidant capacity of flavonoids and their inhibitory effects on oleic acid-induced hepatic steatosis in vitro. *Eur. J. Med. Chem.* 46, 4548–4558.

Zhang, H. Y., and Chen, D. Z. (2000). Theoretical elucidation on activity differences of ten flavonoid antioxidants. *Sheng Wu Hua Xue Yu Sheng Wu Wu Li Xue Bao Acta Biochim. Biophys. Sin.* 32, 317–321.

Zhang, X., Huang, H., Zhang, Q., Fan, F., Xu, C., Sun, C., et al. (2015). Phytochemical Characterization of Chinese Bayberry (Myrica rubra Sieb. *et Zucc.) of* 17 cultivars and their antioxidant properties. *Int. J. Mol. Sci.* 16, 12467–12481.

Zhang, Z. Q., and Hölscher, C. (2020). GIP has neuroprotective effects in Alzheimer and Parkinson's disease models. *Peptides* 125:170184. doi: 10.1016/j.peptides.2019.170184

Zhao, L. X. S., Li, Z. Y., Zhang, L., Zhang, Z. S., and Pan, R. L. (2012). Study on the antioxidant and antiacetylcholinesterase activities of myricitrin and its structure-similar compounds. *Sci. Technol. Food Industry* 33,

Zhou, D. Z., Sun, H. Y., Yue, J. Q., Peng, Y., Chen, Y. M., and Zhong, Z. J. (2017). Dihydromyricetin induces apoptosis and cytoprotective autophagy through ROS-NF-κB signalling in human melanoma cells. *Free Radic. Res.* 51, 517–528.

Conflict of Interest: The authors declare that the research was conducted in the absence of any commercial or financial relationships that could be construed as a potential conflict of interest.

frontiers in Aging Neuroscience

ORIGINAL RESEARCH
published: 26 October 2020
doi: 10.3389/fnagi.2020.563559

Association of Subcortical Structural Shapes With Tau, Amyloid, and Cortical Atrophy in Early-Onset and Late-Onset Alzheimer's Disease

Eun-Chong Lee[1†], Jae Myeong Kang[2†], Seongho Seo[3], Ha-Eun Seo[4], Sang-Yoon Lee[3], Kee Hyung Park[5], Duk L. Na[6,7], Young Noh[5,8] and Joon-Kyung Seong[1,9*]*

[1] School of Biomedical Engineering, Korea University, Seoul, South Korea, [2] Department of Psychiatry, Gil Medical Center, Gachon University College of Medicine, Incheon, South Korea, [3] Department of Neuroscience, College of Medicine, Gachon University, Incheon, South Korea, [4] Neuroscience Research Institute, Gachon University, Incheon, South Korea, [5] Department of Neurology, Gil Medical Center, Gachon University College of Medicine, Incheon, South Korea, [6] Department of Neurology, Samsung Medical Center, Sungkyunkwan University School of Medicine, Seoul, South Korea, [7] Neuroscience Center, Samsung Medical Center, Seoul, South Korea, [8] Department of Health Science and Technology, GAIHST, Gachon University, Incheon, South Korea, [9] Department of Artificial Intelligence, Korea University, Seoul, South Korea

The objectives of this study were to compare the topographical subcortical shape and to investigate the effects of tau or amyloid burden on atrophic patterns in early onset Alzheimer's disease (EOAD) and late-onset Alzheimer's disease (LOAD). One hundred and sixty-one participants (53 EOAD, 44 LOAD, 33 young controls, and 31 older controls) underwent [18F]THK5351 positron emission tomography (PET), [18F]flutemetamol (FLUTE) PET, and 3T MRI scans. We used surface-based analysis to evaluate subcortical structural shape, permutation-based statistics for group comparisons, and Spearman's correlations to determine associations with THK, FLUTE, cortical thickness, and neuropsychological test results. When compared to their age-matched controls, EOAD patients exhibited shape reduction in the bilateral amygdala, hippocampus, caudate, and putamen, while in LOAD patients, the bilateral amygdala and hippocampus showed decreased shapes. In EOAD, widespread subcortical shrinkage, with less association of the hippocampus, correlated with THK retention and cortical thinning, while in LOAD patients, subcortical structures were limited which had significant correlation with THK or mean cortical thickness. Subcortical structural shape showed less correlation with FLUTE global retention in both EOAD and LOAD. Multiple cognitive domains, except memory function, correlated with the bilateral amygdala, caudate, and putamen in EOAD patients, while more restricted regions in the subcortical structures were correlated with neuropsychological test results in LOAD patients. Subcortical structures were associated with AD hallmarks in EOAD. However, the correlation was limited in LOAD. Moreover, relationship between subcortical structural atrophy and cognitive decline were quite different between EOAD and LOAD. These findings suggest that the effects of Alzheimer's pathologies on subcortical structural changes in EOAD and LOAD and they may have different courses of pathomechanism.

Keywords: Alzheimer's disease, subcortical shape analysis, tau, amyloid, cortical thickness, positron emission tomography, magnetic resonance imaging

OPEN ACCESS

Edited by:
Kuangyu Shi,
Technical University of Munich, Germany

Reviewed by:
Daniel Ferreira,
Karolinska Institutet (KI), Sweden
Mitsuru Shinohara,
Mayo Clinic, United States

***Correspondence:**
Joon-Kyung Seong
jkseong@korea.ac.kr
Young Noh
ynoh@gachon.ac.kr

[†] These authors have contributed equally to this work

Received: *19 May 2020*
Accepted: *05 October 2020*
Published: *26 October 2020*

Citation:
Lee E-C, Kang JM, Seo S, Seo H-E, Lee S-Y, Park KH, Na DL, Noh Y and Seong J-K (2020) Association of Subcortical Structural Shapes With Tau, Amyloid, and Cortical Atrophy in Early-Onset and Late-Onset Alzheimer's Disease. Front. Aging Neurosci. 12:563559. doi: 10.3389/fnagi.2020.563559

INTRODUCTION

Alzheimer's disease (AD) is a neurodegenerative disease associated with cognitive decline. Accumulations of neurofibrillary tangles and beta-amyloid (Aβ) are the two pathologic hallmarks of AD, as well as structural changes in the brain cortices (Jack et al., 2016). Early onset AD (EOAD) is characterized by onset before 65 years of age and accounts for 10–15% of all cases (Panegyres and Chen, 2014; Wattmo and Wallin, 2017). Studies have found that EOAD patients have typical neuropsychological features with more progressive cognitive decline (Seltzer and Sherwin, 1983; Smits et al., 2012) as well as heterogenous neuroimaging findings (Frisoni et al., 2007; Migliaccio et al., 2015).

Compared with LOAD patients, EOAD patients manifest with more widespread tau PET retention and heavier amyloid PET uptake in the brain cortices, and more severe gray matter loss suggesting different etiologies and predisposing factors for EOAD (Frisoni et al., 2007; Choo et al., 2011; Scholl et al., 2017; Wattmo and Wallin, 2017). Like gray matter change, more rapid volumetric declines in several subcortical structures including the caudate, putamen, and thalamus have been highlighted as distinct to LOAD patients (Cho et al., 2013; Pievani et al., 2013). It has also been reported that characteristic symptoms of EOAD such as severe extrapyramidal signs (Chui et al., 1985) and non-memory cognitive dysfunction such as executive function, visuospatial functioning, and attention (Smits et al., 2012) are related to deterioration of the basal ganglia and the thalamus, both of which play major roles in movement symptoms, brain connectivity, and memory function (Hahn et al., 2016; Dipasquale and Cercignani, 2017).

Although there have been previous investigations into the association between tau, Aβ, and atrophy in brain cortices, little is known of the relationship between the well-known AD biomarkers and subcortical structures. Unraveling the effect of tau, Aβ, and atrophy in the subcortical structures may contribute to a better understanding of the pathological mechanisms of AD and the different developmental paths of EOAD and LOAD. We sought to compare topographical changes in the subcortical structures in EOAD and LOAD patients and investigated their association with cortical tau and amyloid global retention, as well as cognitive functions.

MATERIALS AND METHODS

Participants

Ninety-one participants who had been clinically diagnosed with AD dementia (EOAD; n = 55, LOAD; n = 46) and 66 cognitively normal (CN) participants were prospectively recruited. All participants underwent [^{18}F]THK5351 PET scans, [^{18}F]flutemetamol (FLUTE) PET scans, and 3.0-Tesla MRI scans at Gachon University Gil Medical Center, from October 2015 to June 2017. Of the 167 participants, 2 patients diagnosed with AD were excluded due to head motion issues during the [^{18}F]THK5351 PET scan acquisition. An additional four participants (two AD and two CN) were excluded due to errors with the FreeSurfer software. Thus, data from 161 participants (53 EOAD, 44 LOAD, 33 YC, and 31 OC) were used in the analyses.

All patients with AD dementia met the probable AD criteria as proposed by the National Institute of Neurological and Communicative Disorders and Stroke and the AD and Related Disorders Association (McKhann et al., 1984). Patients with familial AD with autosomal dominant inheritance were excluded. Participants with brain lesions on brain MRI such as intracranial hemorrhage, traumatic brain injury, hydrocephalus, territorial infarction, severe white matter hyperintensity (WMH) or WMH associated with radiation, multiple sclerosis or vasculitis were excluded. Severe WMH was defined as both periventricular WMH as cap or band $\geq$10 mm and deep WMH $\geq$25 mm using modified Fazekas visual rating scale (Fazekas et al., 1987; Noh et al., 2014). Secondary causes of dementia were ruled out through serum laboratory tests including for thyroid function, metabolic profile, vitamin B_{12}, folate, complete blood counts, and syphilis serology. APOE genotyping was also performed. Clinical interviews with a neurologist or psychiatrist and standardized comprehensive neuropsychological tests were undertaken with all participants.

CN participants were either volunteers from the community or spouses of the patients (age range 44–92, female 45.31%). They had no history of neurologic diseases, psychiatric disorders, abnormalities on neurologic examination, structural lesions on brain MRI such as cerebral infarction, intracranial hemorrhage, traumatic brain injury, hydrocephalus, or severe WMH. Control participants had a clinical dementia rating (CDR) score of 0, and normal cognitive function defined as within 1.5 standard deviations of the age- and education-corrected normative mean on detailed neuropsychological tests. Written informed consent was obtained from each participant, and the Institutional Review Boards of Gachon University Gil Medical Center approved this study.

Image Data Acquisition and Parcellation

3D T1-MPRAGE (Repetition time: 1,900 ms, echo time: 2.93 ms, flip angle: 8°, pixel bandwidth: 170 Hz/pixel, matrix size: 256 × 208, field of view: 256 mm^2 × 208 mm^2, slice thickness: 1.0 mm, voxel size: 1.0 mm^3 × 1.0 mm^3 × 1.0 mm^3, NEX: 1, total acquisition time: 4 min 9 s, GRAPPA acceleration factor: 2 along phase-encoding direction) was acquired with a 3.0T MRI (Verio, Siemens with a Siemens matrix coil). Images were analyzed using FreeSurfer 5.1[1] to define regions-of-interest (ROIs) in native-space for each participant and to support a correction of gray matter atrophy and white matter spillover in the PET data. In addition, subcortical region parcellation including the left and right of the amygdala, caudate, hippocampus, pallidum, putamen, and thalamus was also conducted using Desikan-Killiany atlas in MNI 152 space. After subcortical segmentation, each subcortical region on the template surface was sampled as a mesh surface with 2,562 vertices and then transformed into its own original surface. This procedure was conducted for every 12

[1] www.surfer.nmr.mgh.harvard.edu

subcortical regions as detailed in a previous study (Chung et al., 2017; Koo et al., 2017).

The pretreatment process for the PET images proceeded according to the process outlined in a previous study (Kang et al., 2017). [^{18}F]THK5351 was synthesized and radiolabeled at Gachon University Neuroscience Research Institute. All participants underwent a 20-min emission scan beginning 50 min after 185 MBq of [^{18}F]THK5351 was injected intravenously (50–70 min), and a 20-min emission scan 90 min after the intravenous injection of 185 MBq of [^{18}F]FLUTE (90–110 min).

PET Quantification

The quantification process for the [^{18}F]THK and [^{18}F]FLUTE PET images was conducted using the same methodology outlined in a previous study (Kang et al., 2017). After co-registration of PET images with the corresponding T1 image, region-based partial volume correction was performed. The regional mean values were then calculated and weight-averaged for pre-defined ROIs (Greve et al., 2014, 2016; Kang et al., 2017). Regional standardized uptake value ratios (SUVRs) were calculated using cerebellar gray matter as the reference region for THK images and the pons for FLUTE images (Okamura et al., 2014; Thurfjell et al., 2014; Lockhart et al., 2016). THK5351 global SUVR was calculated based on the AD-related regions including the frontal, parietal, precuneus, occipital, temporal, anterior cingulate, and posterior cingulate, and the cortical composite FLUTE SUVR was calculated based on AD-related regions including the frontal, parietal, lateral temporal, anterior and posterior cingulate cortices (Thurfjell et al., 2014).

Assessment of Local Shape of Subcortical Structures

To measure the degree of deformation of the subcortical structures, a subcortical mesh was constructed similarly to that described in previous studies (Cho et al., 2011; Chung et al., 2017; Koo et al., 2017). The local shape at every location was then calculated using the surface-based method proposed by Shapira et al. (2008). Weighted sum of the depths at every location was measured in various directions at every location, using the weight as an angle with the normal vector (Chung et al., 2017; Koo et al., 2017). This depth value obtained at 2,562 locations for a single structure reflects local contraction or local shrinkage at that location (i.e., the smaller the value, the more shrinkage caused by atrophy occurred at that position, which expands as the value becomes larger). Therefore, these values were set as the subcortical local shape. This method was undertaken for each of the subcortical regions (amygdala, hippocampus, caudate, pallidum, putamen, and left and right areas of the thalamus).

Neuropsychological Assessment

All participants underwent the Korean version of the mini-mental state examination (MMSE), CDR, and a detailed neuropsychological function test battery (Kang et al., 2003) including attention, praxis, language, verbal and visual memory, visuospatial function, frontal/executive function, and elements of Gerstmann syndrome. Details of the comprehensive test battery are described in our previous study (Lee et al., 2018) and all scores were calculated as age- and level of education-matched z-scores.

Statistical Analysis

A pairwise group comparisons comparing EOAD and LOAD, EOAD and YC, LOAD and OC, YC and OC for subcortical structure shape were performed by permutation tests with 5,000 iterations with ANCOVA. For the comparison between EOAD and LOAD, or between YC and OC, the local shape of the subcortical structures were adjusted for sex, years of education, and intracranial volume (ICV). Additionally, for the comparison between EOAD and YC, or between LOAD and OC, the values for the subcortical local shape were adjusted for age, sex, years of education, and ICV. After the permutation test, the Benjamini-Hochberg false discovery rate was used for region-wise multiple comparison (Benjamini and Hochberg, 1995). A p-value threshold (0.05) was applied to extract the regions showing significant differences between two groups. If the size of the statistically significant region was smaller than the specific size, it was regarded as noise and removed.

We calculated Spearman's rank correlation coefficient to identify the relationship between the deformity at every location in the subcortical structures and the three types of neuroimaging findings such as THK5351 SUVR, FLUTE SUVR, and cortical thickness (Han et al., 2013). The vertices with a stronger negative correlation of −0.3 or a stronger positive correlation of 0.3 were then selected. The significance level of each vertex was corrected using the Cluster-Based statistics (Han et al., 2013). Through this process we examined the correlation between THK5351 global SUVR, FLUTE global SUVR, mean cortical thickness and the subcortex structures with age, sex, years of education and ICV as covariates separately within EOAD and LOAD groups. In this process, a p-value threshold (0.05) was applied to extract the regions with a significant correlation between the subcortical structure and neuroimaging findings. In cases where the size of the statistically significant region was smaller than the specific size, it was regarded as noise and removed.

To compare the effects of tau, amyloid, and mean cortical thickness on subcortical shape deformity, the relative importance for each factor was calculated using general linear model. For the general linear model, age, sex, education and ICV were used as covariates, and the degree of tau global retention, amyloid global retention, and mean cortical thickness were used as predictors, and local shape was encoded as dependent variable. The r-squared value of the model was calculated from the predictor combinations in all cases in which a specific predictor was included in the general linear model, and the accumulated value was called relative importance and is shown in the **Supplementary Figure 1**.

Comparisons of the demographic and clinical information were conducted using independent t-test and chi square test followed by Yate's continuity correction for nominal variables. For volumetric analyses, group comparisons were conducted using independent t-test and analysis of covariance. Correlations between volumes of each subcortical structure and other variables such as THK, FLUTE, cortical thickness, and cognitive function were evaluated using Pearson's correlation analysis and general

linear model. Volume data analysis was conducted with PASW Statistics 23 software (SPSS Inc., Chicago, IL, United States) with significance set at $p < 0.05$ (two-way).

RESULTS

Demographics and Clinical Characteristics

Table 1 shows the demographic information and clinical characteristics of the participants. There were no significant differences in MMSE scores or CDR-SOB between EOAD and LOAD patients. Global retention of THK5351 PET and mean cortical thickness were not different between EOAD and LOAD, however, the EOAD group showed significantly higher amyloid global accumulation than the LOAD group ($p < 0.001$).

Comparison of Subcortical Structures

Figure 1 shows the results of group comparisons of the subcortical structural shapes. The EOAD group showed widespread subcortical shape difference in the bilateral amygdala, caudate, hippocampus, putamen, thalamus and the right pallidum relative to YC. The LOAD group showed significant regional shape difference in the bilateral amygdala, hippocampus, and putamen compared to OC. Comparisons of the subcortical structures between the EOAD and LOAD groups showed shrinkage in the bilateral thalamus, left amygdala and left hippocampus in LOAD group.

Volume analysis of the subcortical structures between the groups are presented in **Supplementary Table 1**. EOAD patients showed reduced volume in the bilateral amygdala, hippocampus, caudate, putamen, and the left thalamus compared to YC. LOAD patients showed reduced volumes in the bilateral amygdala and hippocampus compared to OC.

Correlation Between THK5351, FLUTE, Cortical Thickness, and Subcortical Structures

Figure 2 shows the correlation between THK global retention, FLUTE global retention, mean cortical thickness, and subcortical shape in the EOAD and LOAD groups. In EOAD patients, as THK global retention increased, subcortical structure showed contraction significantly in the bilateral amygdala, caudate, putamen, hippocampus, left pallidum and the left thalamus. In LOAD patients, as THK global retention increased, subcortical shape decreased in the bilateral caudate, putamen, left pallidum and the left amygdala and hippocampus.

As FLUTE global retention increased, subcortical shape deformity significantly increased in the bilateral hippocampus and the right amygdala and left putamen in EOAD. LOAD patients showed significant subcortical shape deformity in the bilateral putamen, the left amygdala and hippocampus, and the right caudate as FLUTE increased. There was no subcortical structure with positive correlation with THK or FLUTE global retention in EOAD or LOAD patients. Mean cortical thickness was positively associated with subcortical structure shape in the bilateral amygdala, caudate, putamen, and the left hippocampus in EOAD.

Supplementary Figure 1 shows association between THK, FLUTE global retention, cortical thickness and subcortical structures, which was analyzed using the general linear model. In EOAD group, similar to the results of our main correlation analyses, tau and mean cortical thickness were found to have great importance in the bilateral caudate and putamen, whereas amyloid showed little importance. On the other hand, in the LOAD patient group, the importance was higher in correlation with tau in both caudate. And mean cortical thickness was found to have importance than other variables in predicting the local shape in the left putamen.

Supplementary Figure 2 shows the voxel-wise analyses results to evaluate the association between subcortical structural volume and THK or FLUTE global retention. In EOAD, decreased volumes of the amygdala, caudate, putamen had association with THK retention in the nearly whole association cortices. Hippocampal volume was associated with THK retention in the bilateral medial temporal region and the right precuneus and parietal regions in EOAD. The hippocampus was the only region with significant correlation with FLUTE global retention in EOAD. In LOAD patients, no subcortical structural volume showed significant correlation with THK or FLUTE global retention in voxel-wise analyses.

Volumetric correlation between THK global retention, FLUTE global retention, mean cortical thickness, and subcortical structures are presented in **Supplementary Table 2**. In EOAD patients, THK, FLUTE, and cortical thickness correlated with volumes of the subcortical structures except for pallidum. In LOAD patients, no correlation was found between THK, FLUTE, and mean cortical thickness and subcortical volume.

Correlation Between Cognitive Function and Subcortical Structures

The neuropsychological test results are presented in **Table 2**.

Patients with EOAD had significantly worse performance in digit span forward and backward, Rey-Osterrieth complex figure test (RCFT) copy memory test other than RCFT recognition, controlled oral word association test supermarket, Stroop test color reading, trail making test type A and B compared to LOAD patients.

Figure 3 shows the association between subcortical shapes and neuropsychological test scores in the EOAD patients. MMSE scores were correlated with the bilateral amygdala, caudate, putamen, and thalamus and the left hippocampus (**Figure 3A**). CDR-SOB was correlated with the bilateral amygdala, hippocampus, caudate, putamen and thalamus (**Figure 3B**). Digit span backward was correlated with the bilateral amygdala, caudate, and putamen and the left pallidum (**Figure 3C**). BNT was correlated with the bilateral amygdala and putamen and the left caudate and hippocampus (**Figure 3D**). RCFT copy test was correlated with the bilateral caudate and putamen and right amygdala (**Figure 3E**). SVLT delayed recall showed correlation with the left thalamus (**Figure 3F**) and RCFT delayed recall showed association with the bilateral putamen

TABLE 1 | Demographics and clinical characteristics of the study population.

Variables	EOAD (*n* = 53)	YC (*n* = 33)	EOAD vs. YC *P* value	LOAD (*n* = 44)	OC (*n* = 31)	LOAD vs. OC *P* value	EOAD vs. LOAD *P* value
Age	60.5 (5.43)	57.54 (7.16)	0.032[a]	77.80 (6.35)	75.32 (5.54)	0.085	< 0.001[a]
Sex (female, *n* [%])	36 (67.9)	13 (39.4)	0.018[a]	33 (75)	16 (51.6)	0.064	0.589
Education (years)	9.42 (3.92)	13.45 (3.52)	< 0.001[a]	7.30 (5.06)	10.68 (5.34)	0.007[a]	0.022[a]
Disease duration (months)	42.83 (20.55)	0.0 (0.0)	< 0.001[a]	52.39 (30.35)	0.0 (0.0)	< 0.001[a]	0.171
MMSE	16.08 (7.14)	28.76 (1.15)	< 0.001[a]	17.56 (7.04)	27.13 (2.38)	< 0.001[a]	> 0.999
CDR-SOB	5.62 (3.90)	0.00 (0.00)	< 0.001[a]	5.11 (3.20)	0.00 (0.00)	< 0.001[a]	0.066
APOE genotype (positive, *n* [%])	25 (47.2)	9 (27.3)	0.066	23 (52.3)	7 (22.6)	0.010[a]	0.617
Mean CTh	2.29 (0.16)	2.49 (0.08)	< 0.001[a]	2.34 (0.13)	2.44 (0.10)	< 0.001[a]	0.060
THK global retention	2.38 (0.51)	1.46 (0.20)	< 0.001[a]	2.23 (0.39)	1.77 (0.24)	< 0.001[a]	0.110
FLUTE global retention	1.07 (0.18)	0.39 (0.06)	< 0.001[a]	0.89 (0.21)	0.43 (0.15)	< 0.001[a]	< 0.001[a]

Abbreviations: EOAD, early-onset Alzheimer's disease; LOAD, late-onset Alzheimer's disease; YC, young control; OC, old control; MMSE, mini-mental state examination; CDR-SOB, clinical dementia rating-sum of boxes; APOE, apolipoprotein ε4 allele; CTh, cortical thickness; SUVR, standard uptake value ratio. Data is presented as mean (standard deviation) for continuous variables and number (%) for nominal variables. MMSE and CDR-SOB were compared between AD and control after adjusting for age and years of education and compared between EOAD and LOAD after adjusting for years of education. P-values refer to two-sample t-test for continuous variables and Chi square test followed by Yate's continuity correction for nominal variables. [a]*P < 0.05.*

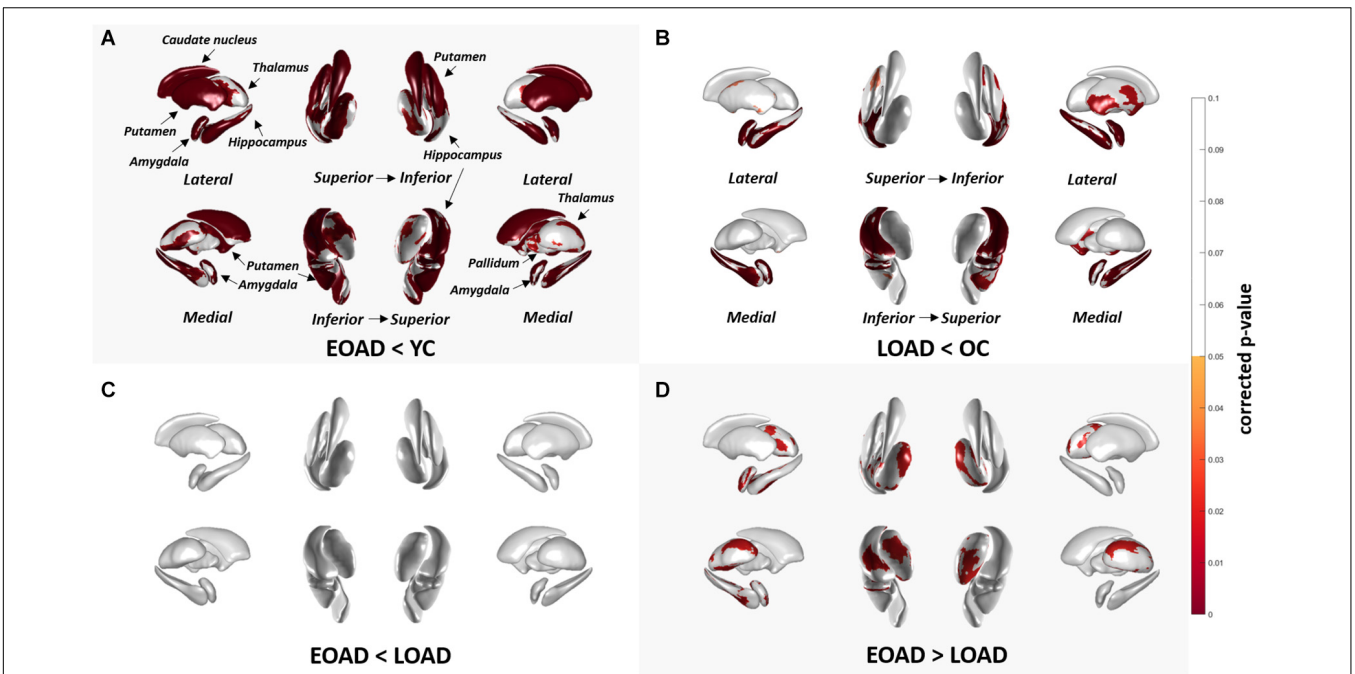

FIGURE 1 | Group comparison of shape of subcortical structures. **(A,B)** Group-wise comparison of the subcortical local shape adjusted with age, sex, education, ICV; **(C,D)** sex, education, ICV was adjusted. Corrected *p*-values after FDR multiple correction for each 12 structures (left and right amygdala, hippocampus, caudate, pallidum, putamen, and thalamus) were mapped. Abbreviations: EOAD, early-onset Alzheimer's disease; LOAD, late-onset Alzheimer's disease; YC, young control; OC, old control.

(**Figure 3G**). Executive function measured by Stroop test color reading was correlated with the bilateral amygdala, caudate, and putamen and the left pallidum (**Figure 3H**).

Figure 4 shows the association between subcortical shape and neuropsychological test scores in LOAD patients. MMSE scores were correlated with the bilateral amygdala, hippocampus, and putamen and the left caudate (**Figure 4A**) and CDR-SOB was correlated with the bilateral amygdala, caudate, hippocampus, putamen, thalamus, and the left pallidum (**Figure 4B**). Digit span backward was correlated with the left caudate and hippocampus (**Figure 4C**). BNT was correlated with the left amygdala and hippocampus (**Figure 4D**). RCFT copy showed no association with subcortical structural shape (**Figure 4E**). SVLT delayed recall was correlated with the bilateral hippocampus and the left caudate, and the right thalamus (**Figure 4F**), and RCFT delayed recall was correlated with the right hippocampus (**Figure 4G**). Stroop test color reading was correlated with the bilateral hippocampus and the left caudate (**Figure 4H**). Results of the

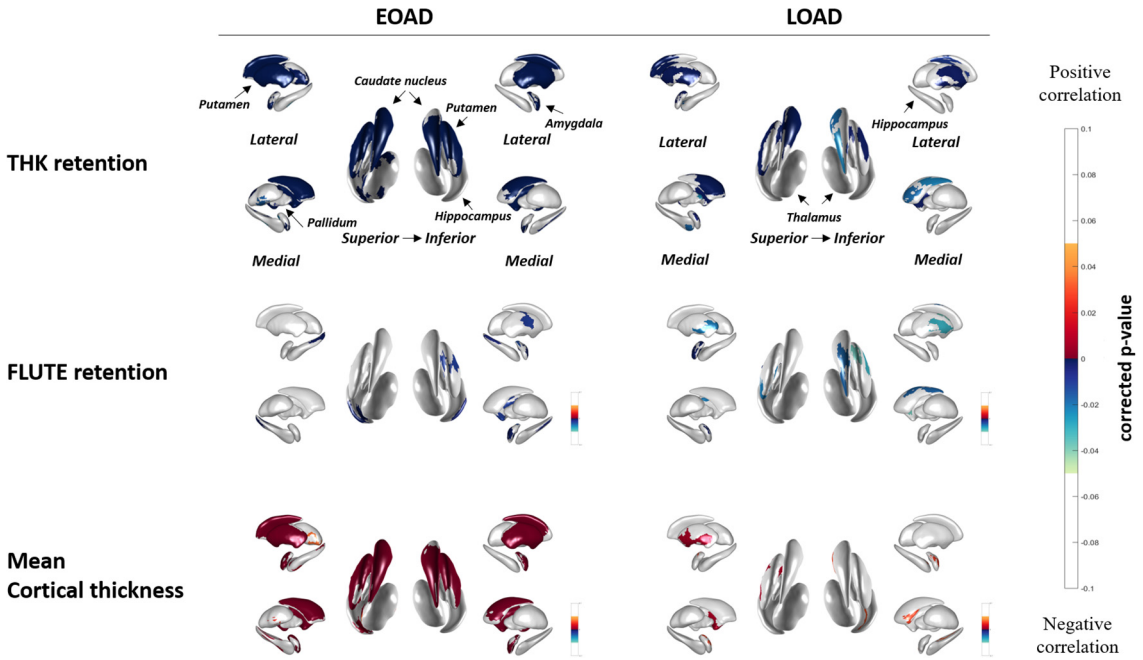

FIGURE 2 | Spearman correlation between subcortical local shape and THK5351 retention, FLUTE global retention, and mean cortical thickness in EOAD and LOAD, adjusting with age, sex, years of education, and intracranial volume (ICV) in each EOAD and LOAD group. The mapped *p*-values are multiple corrected using cluster-based statistics. Abbreviations: EOAD, early onset Alzheimer's disease; LOAD, late-onset Alzheimer's disease.

TABLE 2 | Neuropsychological test results.

	EOAD (*n* = 53)	YC (*n* = 33)	EOAD vs. YC *P* value	LOAD (*n* = 44)	OC (*n* = 31)	LOAD vs. OC *P* value	EOAD vs. LOAD *P*-value
Attention							
Digit Span Forward	−0.63 ± 1.50	0.73 ± 0.93	< 0.001[a]	0.09 ± 1.07	0.76 ± 1.03	0.010[a]	0.020[a]
Digit Span Backward	−1.57 ± 1.52	0.14 ± 1.28	< 0.001[a]	−0.56 ± 1.28	0.11 ± 1.14	0.024[a]	0.001[a]
Language and related function							
K-BNT	−2.11 ± 2.61	0.05 ± 1.00	< 0.001[a]	−1.90 ± 1.59	0.03 ± 0.91	< 0.001[a]	0.774
Visuospatial function							
RCFT copy	−5.56 ± 5.82	0.58 ± 0.57	< 0.001[a]	−0.51 ± 1.86	0.34 ± 0.74	0.010[a]	< 0.001[a]
Memory							
SVLT, immediate recall	−2.28 ± 1.29	−0.13 ± 1.02	< 0.001[a]	−1.55 ± 0.97	−0.05 ± 0.84	< 0.001[a]	0.004[a]
SVLT, delayed recall	−2.56 ± 0.83	−0.13 ± 0.95	< 0.001[a]	−1.96 ± 0.59	0.10 ± 0.97	< 0.001[a]	< 0.001[a]
SVLT, recognition	−2.76 ± 1.51	−0.12 ± 1.50	< 0.001[a]	−1.50 ± 1.31	0.00 ± 0.83	< 0.001[a]	< 0.001[a]
RCFT, immediate recall	−1.94 ± 0.74	0.75 ± 0.92	< 0.001[a]	−1.20 ± 0.76	0.41 ± 1.14	< 0.001[a]	< 0.001[a]
RCFT, delayed recall	−2.22 ± 0.84	0.70 ± 1.01	< 0.001[a]	−1.46 ± 0.77	0.46 ± 1.03	< 0.001[a]	< 0.001[a]
RCFT, recognition	−2.24 ± 1.52	0.22 ± 1.04	< 0.001[a]	−1.73 ± 1.62	−0.21 ± 0.98	< 0.001[a]	0.194
Frontal executive function							
COWAT, animal	−2.14 ± 1.01	−0.22 ± 1.07	< 0.001[a]	−1.72 ± 0.94	−0.24 ± 0.92	< 0.001[a]	0.039[a,b]
COWAT, supermarket	−1.81 ± 0.96	0.05 ± 0.94	< 0.001[a]	−1.24 ± 0.96	0.02 ± 0.98	< 0.001[a]	0.005[a]
COWAT, phonemic total	−1.31 ± 1.36	0.26 ± 1.04	< 0.001[a]	−0.87 ± 0.96	0.13 ± 1.00	< 0.001[a]	0.092
Stroop test, color reading	−2.39 ± 1.30	0.13 ± 0.75	< 0.001[a]	−0.97 ± 1.05	0.11 ± 1.15	< 0.001[a]	< 0.001[a]
TMT-A	−7.77 ± 11.75	0.59 ± 0.77	< 0.001[a]	−1.90 ± 3.81	−0.17 ± 1.93	0.018[a]	0.001[a]
TMT-B	−8.36 ± 6.19	0.01 ± 1.00	< 0.001[a]	−2.92 ± 2.32	−0.09 ± 1.23	< 0.001[a]	< 0.001[a]

All data are z-scores derived on age- and education-adjusted norms and presented as mean ± standard deviation. Comparisons between EOAD and LOAD were adjusted for clinical dementia rating-sum of boxes. [a]P < 0.05; [b]insignificant after region-wise correction for multiple comparisons. Abbreviations: EOAD, early onset Alzheimer's disease; YC, young control; LOAD, late-onset Alzheimer's disease; OC, old control; K-BNT, Korean version of the Boston naming test; RCFT, Rey-Osterrieth complex figure test; SVLT, Seoul verbal learning test; COWAT, controlled oral word association test; TMT-A/B, trail making test type A/B.

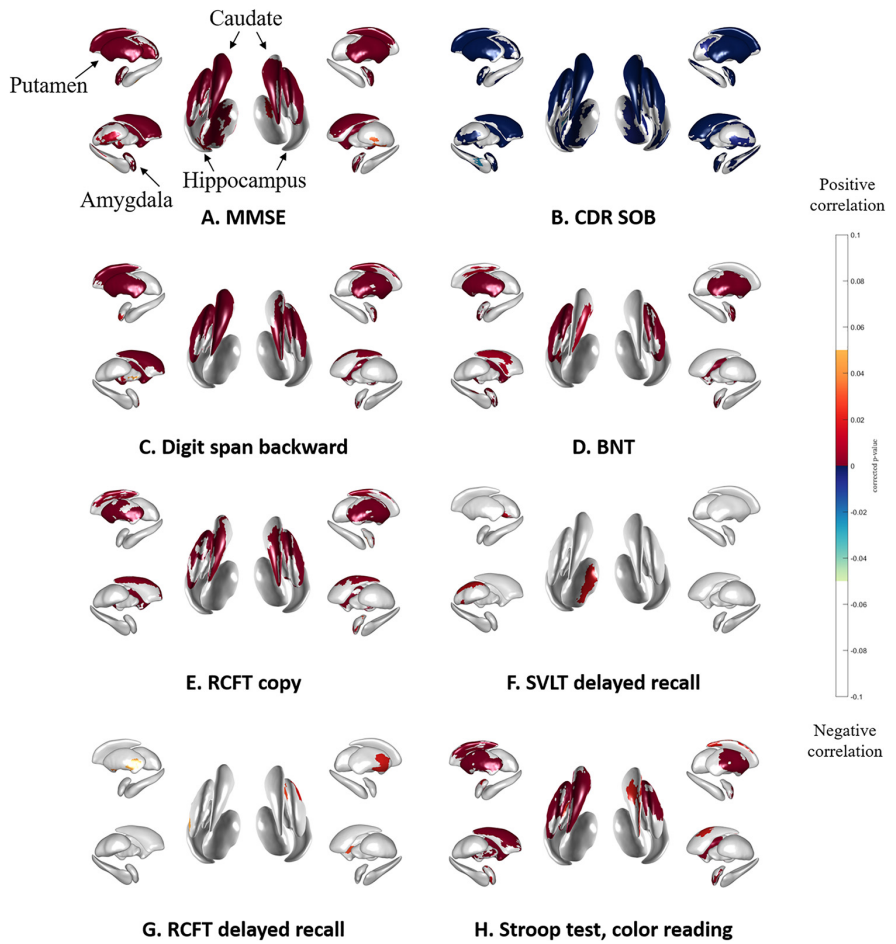

FIGURE 3 | Spearman correlation between neuropsychological test results and subcortical local shape in EOAD group adjusted with intracranial volume. **(A)** MMSE, **(B)** CDR-SOB, **(C)** digit span backward score in attention, **(D)** BNT score in language, **(E)** RCFT copy score in visuospatial, **(F)** SVLT delayed recall score in memory, **(G)** RCFT delayed recall score in memory, and **(H)** color reading test score in frontal/executive function. The mapped *p*-values are multiple corrected using cluster-based statistics. Abbreviations: EOAD, early onset Alzheimer's disease; MMSE, mini-mental state examination; CDR-SOB, clinical dementia rating-sum of boxes.

correlation analysis between volumes of the subcortical structures and the detailed neuropsychological test results were presented in **Supplementary Tables 3** and **4**.

DISCUSSION

In this study, we evaluated the degree of subcortical structural shape deformity in EOAD and LOAD patients, in terms of association with tau and amyloid global retention, cortical thickness, and neuropsychological test results. We observed greater subcortical shape deformity in EOAD and more limited deformation especially in the amygdala and hippocampus in LOAD patients, compared to their age-matched controls. The associations between subcortical structural shape and THK global retention, mean cortical thickness, or cognitive functions were also more prominent in EOAD compared to LOAD patients.

Subcortical shape differed according to the age of onset. Compared to each age-matched control group, EOAD patients exhibited shape deformation in nearly all the subcortical structures, including the bilateral amygdala, hippocampus, caudate, putamen, and thalamus. Meanwhile, LOAD patients manifested decreased shapes in the more restricted region such as the amygdala, hippocampus, and putamen. We also found that the amygdala, hippocampus and thalamus were the major regions that differed in the direct group comparison with more shrinkage in LOAD patients than in EOAD patients. This observation is consistent with previous studies that have shown greater hippocampal atrophy in LOAD compared to EOAD (Frisoni et al., 2007). It was also previously found that EOAD patients mapped with subcortical deformity in wider regions including the amygdala, hippocampus, and putamen compared to LOAD patients with subcortical deformity mapped in the amygdala and hippocampus only, which was also

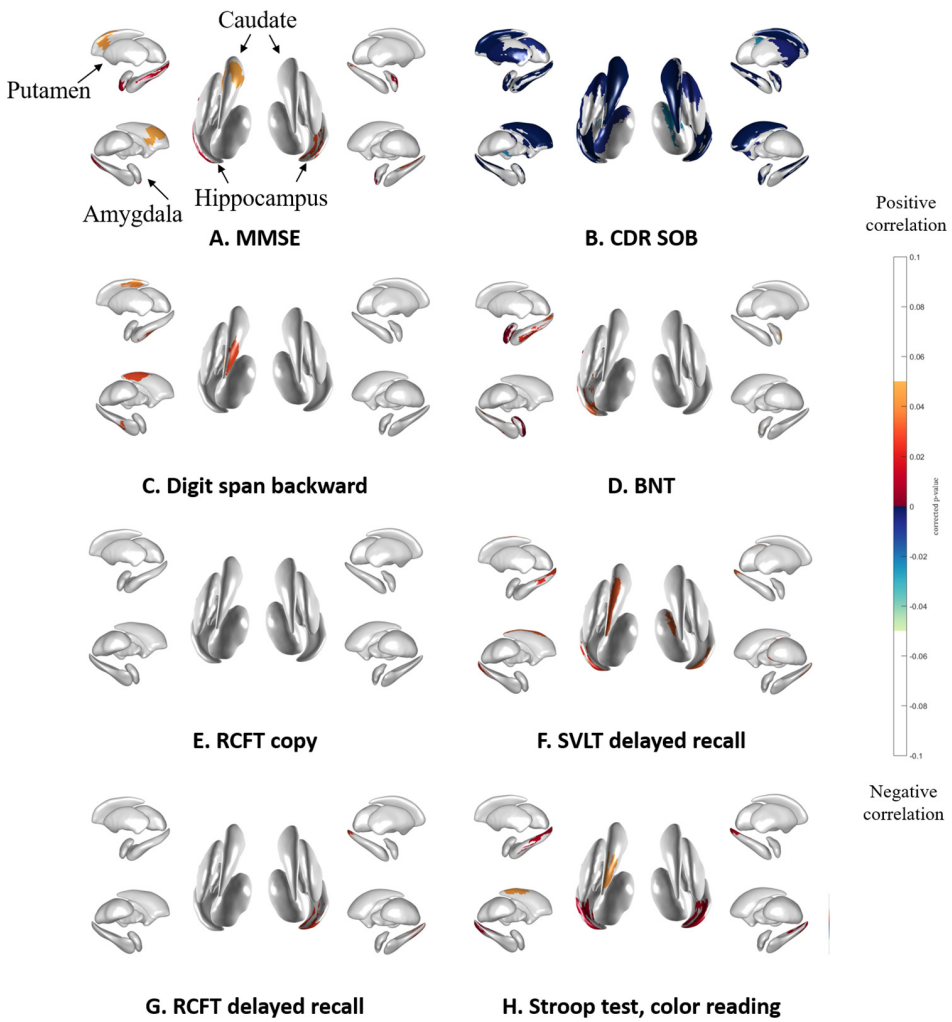

FIGURE 4 | Spearman correlation between neuropsychological test results and subcortical local shape in LOAD group adjusted with intracranial volume. **(A)** MMSE, **(B)** CDR-SOB, **(C)** digit span backward score in attention, **(D)** BNT score in language, **(E)** RCFT copy score in visuospatial, **(F)** SVLT delayed recall score in memory, **(G)** RCFT delayed recall score in memory, and **(H)** color reading test score in frontal/executive function. The mapped *p*-values are multiple corrected using cluster-based statistics. Abbreviations: LOAD, late onset Alzheimer's disease; MMSE, mini-mental state examination; CDR-SOB, clinical dementia rating-sum of boxes.

reflected in our findings (Cho et al., 2013). It has been previously reported that EOAD patients show more rapid declines in volume in the bilateral caudate, putamen, and thalamus compared to LOAD (Cho et al., 2013). In another study, researchers found putamen (dorsal striatum) atrophy in EOAD and atrophy in the nucleus accumbens (the ventral striatum) in LOAD patients (Pievani et al., 2013). The limbic area including the hippocampus and amygdala is well known to be affected in the initial stages and the basal ganglia and thalamus are affected in the later stages of LOAD (Braak and Braak, 1991). Our observations may be indicative of a dorsal atrophic pattern of the subcortical structures in EOAD and predominant hippocampal volume loss in LOAD (Pievani et al., 2013).

In terms of tau, amyloid, and cortical thickness, broad regions of the subcortical shape deformation in the caudate and putamen were associated with THK global retention and mean cortical thickness in EOAD patients. There was association with relatively low effect sizes between subcortical shape and FLUTE global retention in both groups. These results were expected because the mean cortical thickness and tau retention reportedly proceeds in a relatively parallel manner (Whitwell et al., 2008, 2018) compared to amyloid retention (Thal et al., 2002). A/T/N classification systems for AD biomarkers note a specific temporal ordering where Aβ (A) precedes tau (T) and neurodegeneration (N), which correlate with clinical symptoms (Jack et al., 2016). Neurofibrillary tangle retention is also known to accumulate to a higher degree in most of

the cortical regions sparing the primary sensorimotor cortices in EOAD and in the confined regions including the medial temporal and lateral parietal regions in LOAD (Scholl et al., 2017) compared to age-matched controls. Our results appear to support these past findings and provide evidence that the dorsal subcortical structures such as the caudate and putamen are affected more in EOAD compared to LOAD and it is associated with tau global retention and cortical thinning more significantly than amyloid global accumulation. It was interesting result that amyloid global retentions were correlated with hippocampal shapes in EOAD. APOE e4 genotype might be associated with this correlation. Further study would be needed to investigate this issue.

Subcortical structures correlated with the neuropsychological test results, with greater association found more consistently in EOAD than LOAD patients. Specifically, attention, language, visuospatial function, frontal/executive function, and global cognition was correlated with subcortical shapes in most regions of the caudate and putamen. This corresponds the known function of the caudate and putamen (Koziol and Budding, 2009). The striatum, including the caudate nucleus and putamen, receives inputs from most of the major cortical regions including motor, sensory, perceptual and association, frontal executive, and affective and motivational regions (Koziol and Budding, 2009). The head of the caudate nucleus is known to receive inputs from the dorsolateral prefrontal cortex, while the tail of the caudate receives projections from the parietal cortex, and the putamen receives inputs from the motor cortex (Koziol and Budding, 2009). Regarding the circuitry of the striatum, our results indicate that the subcortical structures may associate with cortical region-specific cognitive impairment in EOAD patients. Contrary to EOAD patients, LOAD patients have shown more limited associations: language impairment was associated with shapes in the left amygdala and hippocampus, verbal memory impairment was associated with shapes in the bilateral hippocampus and the left caudate, and visual memory impairment was associated with shapes in the right hippocampus with lower levels of significance. A previous study found that EOAD patients showed more rapid cognitive decline as determined by the MMSE and frontal and total scores in the comprehensive neuropsychological test battery when compared to LOAD patients (Cho et al., 2013). Memory impairment is known to be a predominant phenotype of LOAD and non-memory impairment, including visuospatial dysfunction and apraxia, is predominant in EOAD (Koedam et al., 2010). The present findings are generally in accordance with these previous reports (Koedam et al., 2010; Cho et al., 2013) showing region-specific associations between subcortical structures and neuropsychological test results in the EOAD and LOAD groups.

We note several limitations to this study. The participants were recruited from a single memory clinic in a tertiary hospital, which may limit generalizability of the results. The lack of information on genetic mutations is also limiting because cognitive function and imaging biomarkers can vary according to genetic differences, especially for comparisons between EOAD and LOAD patients. Although we excluded participants with familial AD with autosomal dominant inheritance, the possibility which participants with genetic mutation could not excluded completely as we did not perform PSEN 1, APP or PSEN2 gene tests to all participants. Another major limitation is the known off-target binding of the tracer used in this study. [18F]THK5351, a first generation tau tracer, is known to bind to monoamine oxidase-B (Ng et al., 2017), and thus can be reactive to both neurofibrillary tangles and reactive astrocytes (Harada et al., 2018). Due to its limited utility as a sole biomarker for tau retention, our results should thus be interpreted with some degree of caution. However, we believe our study remains the first to evaluate subcortical structural shapes in EOAD and LOAD patients, using the three major imaging biomarkers tau PET, amyloid PET, and MRI which can provide valuable evidence of *in vivo* findings in AD.

We observed pattern differences in subcortical structural shape between EOAD and LOAD. Widespread subcortical atrophy was associated with tau and cortical thinning in most of the cognitive domains, except for memory, in EOAD. In contrast, smaller subcortical regions were associated only with THK retention and restricted cognitive impairment including memory in LOAD. These results may be indicative of a different underlying pathomechanism between EOAD and LOAD. In addition, the imaging results are in close agreement with the known progression of the A/T/N *in vivo* biomarkers and differences in cognitive function in both groups. The employment of all available imaging biomarkers and age of onset in AD studies may be helpful in more clearly elucidating the association between changes in subcortical regions and other AD biomarkers.

DATA AVAILABILITY STATEMENT

The data set generated and/or analyzed using the current study is available from the corresponding author, YN on reasonable request.

ETHICS STATEMENT

The studies involving human participants were reviewed and approved by Institutional Review Boards of Gachon University Gil Medical Center. The patients/participants provided their written informed consent to participate in this study.

AUTHOR CONTRIBUTIONS

YN and J-KS conceptualized and designed the study. E-CL and JMK drafted the manuscript. JMK, H-ES, S-YL, KHP, DLN, and YN acquired the data. E-CL, JMK, and SS analyzed the data. J-KS took part in methodology. YN was in charge of funding acquisition and resources. YN and J-KS revised the manuscript for intellectual content. All authors reviewed and approved for publication.

FUNDING

This study was supported by a grant from the Korea Healthcare Technology R&D Project through the Korea Health Industry Development Institute (KHIDI), funded by the Ministry of Health & Welfare, Republic of Korea (Grant No: HI14C1135), a grant from the Brain Research Program of the National Research Foundation (NRF) funded by the Korean Government (MSIT) (No. 2018M3C7A1056889); by Institute of Information & communications Technology Planning & Evaluation (IITP) grant funded by the Korean Government (MSIT) [No. 2019-0-00079, Department of Artificial Intelligence (Korea University)]; and by Brain Research Program through the National Research Foundation of Korea (NRF) funded by the Ministry of Science and ICT (No. 2020M3C7A101835721).

SUPPLEMENTARY MATERIAL

The Supplementary Material for this article can be found online at: https://www.frontiersin.org/articles/10.3389/fnagi.2020.563559/full#supplementary-material

REFERENCES

Benjamini, Y., and Hochberg, Y. (1995). Controlling the false discovery rate: a practical and powerful approach to multiple testing. *J. R. Stat. Soc. Ser. B Methodol.* 57, 289–300. doi: 10.1111/j.2517-6161.1995.tb02031.x

Braak, H., and Braak, E. (1991). Neuropathological stageing of Alzheimer-related changes. *Acta Neuropathol.* 82, 239–259. doi: 10.1007/bf00308809

Cho, H., Seo, S. W., Kim, J. H., Kim, C., Ye, B. S., Kim, G. H., et al. (2013). Changes in subcortical structures in early- versus late-onset Alzheimer's disease. *Neurobiol. Aging* 34, 1740–1747.

Cho, Y., Seong, J.-K., Shin, S. Y., Jeong, Y., Kim, J. H., Qiu, A., et al. (2011). A multi-resolution scheme for distortion-minimizing mapping between human subcortical structures based on geodesic construction on Riemannian manifolds. *Neuroimage* 57, 1376–1392. doi: 10.1016/j.neuroimage.2011.05.066

Choo, I. H., Lee, D. Y., Kim, J. W., Seo, E. H., Lee, D. S., Kim, Y. K., et al. (2011). Relationship of amyloid-beta burden with age-at-onset in Alzheimer disease. *Am. J. Geriatr. Psychiatry* 19, 627–634. doi: 10.1097/jgp.0b013e318202bf3a

Chui, H. C., Teng, E. L., Henderson, V. W., and Moy, A. C. (1985). Clinical subtypes of dementia of the Alzheimer type. *Neurology* 35, 1544–1544. doi: 10.1212/wnl.35.11.1544

Chung, S. J., Shin, J. H., Cho, K. H., Lee, Y., Sohn, Y. H., Seong, J. K., et al. (2017). Subcortical shape analysis of progressive mild cognitive impairment in Parkinson's disease. *Mov. Disord.* 32, 1447–1456. doi: 10.1002/mds.27106

Dipasquale, O., and Cercignani, M. (2017). Network functional connectivity and whole-brain functional connectomics to investigate cognitive decline in neurodegenerative conditions. *Funct. Neurol.* 31, 191–203.

Fazekas, F., Chawluk, J. B., Alavi, A., Hurtig, H. I., and Zimmerman, R. A. (1987). MR signal abnormalities at 1.5 T in Alzheimer's dementia and normal aging. *Am. J. Roentgenol.* 149, 351–356. doi: 10.2214/ajr.149.2.351

Frisoni, G. B., Pievani, M., Testa, C., Sabattoli, F., Bresciani, L., Bonetti, M., et al. (2007). The topography of grey matter involvement in early and late onset Alzheimer's disease. *Brain* 130, 720–730. doi: 10.1093/brain/awl377

Greve, D. N., Salat, D. H., Bowen, S. L., Izquierdo-Garcia, D., Schultz, A. P., Catana, C., et al. (2016). Different partial volume correction methods lead to different conclusions: an 18F-FDG-PET study of aging. *Neuroimage* 132, 334–343. doi: 10.1016/j.neuroimage.2016.02.042

Greve, D. N., Svarer, C., Fisher, P. M., Feng, L., Hansen, A. E., Baare, W., et al. (2014). Cortical surface-based analysis reduces bias and variance in kinetic modeling of brain PET data. *Neuroimage* 92, 225–236. doi: 10.1016/j.neuroimage.2013.12.021

Hahn, C., Lee, C. U., Won, W. Y., Joo, S. H., and Lim, H. K. (2016). Thalamic shape and cognitive performance in amnestic mild cognitive impairment. *Psychiatry Investig.* 13, 504–510. doi: 10.4306/pi.2016.13.5.504

Han, C. E., Yoo, S. W., Seo, S. W., Na, D. L., and Seong, J.-K. (2013). Cluster-based statistics for brain connectivity in correlation with behavioral measures. *PLoS One* 8:e72332. doi: 10.1371/journal.pone.0072332

Harada, R., Ishiki, A., Kai, H., Sato, N., Furukawa, K., Furumoto, S., et al. (2018). Correlations of 18F-THK5351 PET with postmortem burden of tau and astrogliosis in Alzheimer disease. *J. Nucl. Med.* 59, 671–674. doi: 10.2967/jnumed.117.197426

Jack, C. R., Bennett, D. A., Blennow, K., Carrillo, M. C., Feldman, H. H., Frisoni, G. B., et al. (2016). A/T/N: an unbiased descriptive classification scheme for Alzheimer disease biomarkers. *Neurology* 87, 539–547. doi: 10.1212/wnl.0000000000002923

Kang, J. M., Lee, S.-Y., Seo, S., Jeong, H. J., Woo, S.-H., Lee, H., et al. (2017). Tau positron emission tomography using [18F] THK5351 and cerebral glucose hypometabolism in Alzheimer's disease. *Neurobiol. Aging* 59, 210–219. doi: 10.1016/j.neurobiolaging.2017.08.008

Kang, Y., Na, D., and Hahn, S. (2003). *Seoul Neuropsychological Screening Battery*. Incheon: Human Brain Research & Consulting Co.

Koedam, E. L., Lauffer, V., Van Der Vlies, A. E., Van Der Flier, W. M., Scheltens, P., and Pijnenburg, Y. A. (2010). Early-versus late-onset Alzheimer's disease: more than age alone. *J. Alzheimers Dis.* 19, 1401–1408. doi: 10.3233/jad-2010-1337

Koo, D. L., Shin, J.-H., Lim, J.-S., Seong, J.-K., and Joo, E. Y. (2017). Changes in subcortical shape and cognitive function in patients with chronic insomnia. *Sleep Med.* 35, 23–26. doi: 10.1016/j.sleep.2017.04.002

Koziol, L. F., and Budding, D. E. (2009). *Subcortical Structures and Cognition: Implications for Neuropsychological Assessment*. Berlin: Springer Science+Business Media.

Lee, H., Seo, S., Lee, S.-Y., Jeong, H. J., Woo, S.-H., Lee, K.-M., et al. (2018). [18F]-THK5351 PET imaging in patients with semantic variant primary progressive aphasia. *Alzheimer Dis. Assoc. Disord.* 32, 62–69. doi: 10.1097/wad.0000000000000216

Lockhart, S. N., Baker, S. L., Okamura, N., Furukawa, K., Ishiki, A., Furumoto, S., et al. (2016). Dynamic PET measures of tau accumulation in cognitively normal older adults and Alzheimer's disease patients measured using [18F] THK-5351. *PLoS One* 11:e0158460. doi: 10.1371/journal.pone.0158460

McKhann, G., Drachman, D., Folstein, M., Katzman, R., Price, D., and Stadlan, E. M. (1984). Clinical diagnosis of Alzheimer's disease: report of the NINCDS-ADRDA work group under the auspices of department of health and human services task force on Alzheimer's disease. *Neurology* 34, 939–944. doi: 10.1212/wnl.34.7.939

Migliaccio, R., Agosta, F., Possin, K. L., Canu, E., Filippi, M., Rabinovici, G. D., et al. (2015). Mapping the progression of atrophy in early-and late-onset Alzheimer's disease. *J. Alzheimers Dis.* 46, 351–364. doi: 10.3233/jad-142292

Ng, K. P., Pascoal, T. A., Mathotaarachchi, S., Therriault, J., Kang, M. S., Shin, M., et al. (2017). Monoamine oxidase B inhibitor, selegiline, reduces 18 F-THK5351 uptake in the human brain. *Alzheimers Res. Ther.* 9:25.

Noh, Y., Lee, Y., Seo, S. W., Jeong, J. H., Choi, S. H., Back, J. H., et al. (2014). A new classification system for ischemia using a combination of deep and periventricular white matter hyperintensities. *J. Stroke Cerebrovasc. Dis.* 23, 636–642. doi: 10.1016/j.jstrokecerebrovasdis.2013.06.002

Okamura, N., Furumoto, S., Fodero-Tavoletti, M. T., Mulligan, R. S., Harada, R., Yates, P., et al. (2014). Non-invasive assessment of Alzheimer's disease neurofibrillary pathology using 18F-THK5105 PET. *Brain* 137, 1762–1771. doi: 10.1093/brain/awu064

Panegyres, P. K., and Chen, H. Y. (2014). Early-onset Alzheimer's disease: a global cross-sectional analysis. *Eur. J. Neurol.* 21, 1149–1154, e64–e65.

Pievani, M., Bocchetta, M., Boccardi, M., Cavedo, E., Bonetti, M., Thompson, P. M., et al. (2013). Striatal morphology in early-onset and late-onset Alzheimer's disease: a preliminary study. *Neurobiol. Aging* 34, 1728–1739. doi: 10.1016/j.neurobiolaging.2013.01.016

Scholl, M., Ossenkoppele, R., Strandberg, O., Palmqvist, S., Jogi, J., Ohlsson, T., et al. (2017). Distinct 18F-AV-1451 tau PET retention patterns in early- and late-onset Alzheimer's disease. *Brain* 140, 2286–2294. doi: 10.1093/brain/awx171

Seltzer, B., and Sherwin, I. (1983). A comparison of clinical features in early-and late-onset primary degenerative dementia: one entity or two? *Arch. Neurol.* 40, 143–146. doi: 10.1001/archneur.1983.04050030037006

Shapira, L., Shamir, A., and Cohen-Or, D. (2008). Consistent mesh partitioning and skeletonisation using the shape diameter function. *Vis. Comput.* 24:249. doi: 10.1007/s00371-007-0197-5

Smits, L. L., Pijnenburg, Y. A., Koedam, E. L., Van Der Vlies, A. E., Reuling, I. E., Koene, T., et al. (2012). Early onset Alzheimer's disease is associated with a distinct neuropsychological profile. *J. Alzheimers Dis.* 30, 101–108.

Thal, D. R., Rub, U., Orantes, M., and Braak, H. (2002). Phases of A beta-deposition in the human brain and its relevance for the development of AD. *Neurology* 58, 1791–1800. doi: 10.1212/wnl.58.12.1791

Thurfjell, L., Lilja, J., Lundqvist, R., Buckley, C., Smith, A., Vandenberghe, R., et al. (2014). Automated quantification of 18F-flutemetamol PET activity for categorizing scans as negative or positive for brain amyloid: concordance with visual image reads. *J. Nucl. Med.* 55, 1623–1628. doi: 10.2967/jnumed.114.142109

Wattmo, C., and Wallin, A. K. (2017). Early- versus late-onset Alzheimer's disease in clinical practice: cognitive and global outcomes over 3 years. *Alzheimers Res. Ther.* 9:70.

Whitwell, J. L., Graff-Radford, J., Tosakulwong, N., Weigand, S. D., Machulda, M., Senjem, M. L., et al. (2018). [18F] AV-1451 clustering of entorhinal and cortical uptake in Alzheimer's disease. *Ann. Neurol.* 83, 248–257. doi: 10.1002/ana.25142

Whitwell, J. L., Josephs, K. A., Murray, M. E., Kantarci, K., Przybelski, S. A., Weigand, S. D., et al. (2008). MRI correlates of neurofibrillary tangle pathology at autopsy: a voxel-based morphometry study. *Neurology* 71, 743–749. doi: 10.1212/01.wnl.0000324924.91351.7d

Conflict of Interest: The authors declare that the research was conducted in the absence of any commercial or financial relationships that could be construed as a potential conflict of interest.

frontiers in Aging Neuroscience

PERSPECTIVE
published: 28 October 2020
doi: 10.3389/fnagi.2020.576192

Connecting Alzheimer's Disease With Diabetes Mellitus Through Amyloidogenic Evolvability

*Gilbert Ho[1], Yoshiki Takamatsu[2], Ryoko Wada[2], Shuei Sugama[3], Masaaki Waragai[1], Takato Takenouchi[4], Eliezer Masliah[5] and Makoto Hashimoto[2]**

[1]PCND Neuroscience Research Institute, Poway, CA, United States, [2]Tokyo Metropolitan Institute of Medical Science, Tokyo, Japan, [3]Department of Physiology, Nippon Medical School, Tokyo, Japan, [4]Institute of Agrobiological Sciences, National Agriculture and Food Research Organization, Tsukuba, Japan, [5]Division of Neurosciences, National Institute on Aging, National Institutes of Health, Bethesda, MD, United States

Type 2 diabetes mellitus (T2DM) has been clearly linked to oxidative stress and amylin amyloidosis in pancreatic β-cells. Yet despite extensive investigation, the biological significance of this is not fully understood. Recently, we proposed that Alzheimer's disease (AD)-relevant amyloidogenic proteins (APs), such as amyloid-β (Aβ) and tau, might be involved in evolvability against diverse stressors in the brain. Given the analogous cellular stress environments shared by both T2DM and AD, the objective of this study is to explore T2DM pathogenesis from the viewpoint of amyloidogenic evolvability. Similar to AD-related APs, protofibrillar amylin might confer resistance against the multiple stressors in β-cells and be transmitted to offspring to deliver stress information, in the absence of which, type 1 DM (T1DM) in offspring might develop. On the contrary, T2DM may be manifested through an antagonistic pleiotropy mechanism during parental aging. Such evolvability-associated processes might be affected by parental diabetic conditions, including T1DM and T2DM. Furthermore, the T2DM-mediated increase in AD risk during aging might be attributed to an interaction of amylin with AD-related APs through evolvability, in which amylin protofibrillar formation presumably caused by adiponectin (APN) resistance could increase protofibril formation of AD-related APs in evolvability and subsequently lead to T2DM promotion of AD through antagonistic pleiotropy in aging. This suggests that targeting APN combined with an anti-T2DM agent might be therapeutic against neurodegeneration. Collectively, T1DM and T2DM might be linked through amylin evolvability, and a better understanding of amyloidogenic evolvability might also reveal clues to therapeutic interventions for AD comorbid with T2DM.

Keywords: Alzheimer's disease, diabetes mellitus, evolvability, antagonistic pleiotropy, adiponectin paradox

OPEN ACCESS

Edited by:
Jiehui Jiang,
Shanghai University, China

Reviewed by:
Nobuyuki Kimura,
National Center for Geriatrics and Gerontology (NCGG), Japan
Rongqiao He,
Institute of Biophysics (CAS), China

****Correspondence:***
Makoto Hashimoto
hashimoto-mk@igakuken.or.jp

Received: *25 June 2020*
Accepted: *28 August 2020*
Published: *28 October 2020*

Citation:
Ho G, Takamatsu Y, Wada R, Sugama S, Waragai M, Takenouchi T, Masliah E and Hashimoto M (2020) Connecting Alzheimer's Disease With Diabetes Mellitus Through Amyloidogenic Evolvability. Front. Aging Neurosci. 12:576192. doi: 10.3389/fnagi.2020.576192

INTRODUCTION

Accumulating evidence suggests that type 2 diabetes mellitus (T2DM) may drive the pathogenesis of various nervous system disorders, including ischemia, depression, and neurodegenerative conditions (Atlantis et al., 2014; Takamatsu et al., 2017). In Alzheimer's disease (AD), T2DM may increase the risk of mild cognitive impairment and subsequent progression to dementia

(Watts et al., 2013; Ng et al., 2016). Additionally, T2DM has been linked to other neurodegenerative disorders, including Parkinson's disease (PD) and Huntington's disease (HD; Aviles-Olmos et al., 2013; Montojo et al., 2017). Yet despite a plethora of such observations, the precise mechanistic underpinning of the comorbidity between T2DM and neurodegeneration remains elusive.

Our recent work suggests that the evolvability of amyloidogenic proteins (APs) relevant to neurodegeneration, such as β-amyloid (Aβ) in AD, α-synuclein (αS) in PD, and huntingtin in HD, might be physiologically important (Hashimoto et al., 2018a,b,c; Takamatsu et al., 2018). More specifically, APs might act as vehicles to transgenerationally deliver information regarding diverse biological stressors to cope with such forthcoming stressors in offspring's brain (Hashimoto et al., 2018a). On the contrary, evolvability might also cause aging-associated neurodegenerative disease through the antagonistic pleiotropy mechanism during the course of parental aging (Hashimoto et al., 2018b). Since evolvability is critical for reproduction, neurodegenerative diseases in aging have evaded "weeding out" by natural selection during evolution.

Given analogous pathology between T2DM and neurodegenerative disorders in terms of amyloidosis-associated stressors (Abedini and Schmidt, 2013; Singh et al., 2015), common mechanisms might form the basis for both groups of disorders. In this context, the main objective of this article is to discuss the mechanisms by which T2DM might increase AD risk from the viewpoint of amyloidogenic evolvability. We hypothesize that amylin protofibrils might confer resistance against multiple stressors in β-cells in the pancreas, which might be transgenerationally transmitted *via* the germ line to offspring, the absence of which might lead to type 1 DM (T1DM), and where T2DM in parents might promote amylin evolvability, while T1DM in parents might increase T1DM in offspring. Furthermore, we assume that the comorbidity of AD and T2DM in aging might be attributed to cross seeding of APs, which may stimulate evolvability. Yet the increased risk of AD from T2DM during aging might be due to upstream amylin activity relative to other more prominent APs, such as Aβ and tau, in evolvability, where the adiponectin (APN) paradox might be important. Collectively, DM and AD might be connected through amyloid evolvability, which might shed light on novel therapeutic strategies against such comorbid disorders.

EVOLVABILITY OF AMYLOIDOGENIC PROTEINS RELEVANT TO TYPE 2 DIABETES MELLITUS

Since T2DM is associated with increased biological stressors and formation of amyloid-like fibrils of amylin in pancreatic β cells, we propose that amylin evolvability might be involved in the pathogenesis of T2DM.

Amylin and Insulin Are Amyloidogenic Proteins

Amylin, also called islet amyloid polypeptide, is a 37-residue peptide that is co-secreted with insulin by pancreatic β-cells (Mietlicki-Baase, 2016). The normal functions of amylin include inhibition of glucagon secretion and reduction of the gastric emptying rate, effects that contribute to the maintenance of postprandial glucose homeostasis (Mietlicki-Baase, 2016). Amylin is prone to aggregate, leading to the formation of amyloid fibrils with characteristic β-sheet structures (Jaikaran and Clark, 2001). Consistent with this, amylin is the major component of the islet amyloid found in the pancreas in T2DM, suggesting that amylin may play a significant role in the pathogenesis of T2DM (Luca et al., 2007). In addition, insulin, a 51-residue protein that is composed of a dimer of an A- and a B-chain linked by disulfide bonds (Brange and Langkjoer, 1993), also forms amyloid fibrils. Insulin, and its related peptide, insulin-like growth factor-1 (IGF-1), are essential to multiple physiological processes, including cell proliferation, differentiation, and survival, in addition to the regulation of energy storage and glucose metabolism (Stewart and Rotwein, 1996; Dadon et al., 2012). In contrast to amylin, the biological role of insulin fibril formation remains unclear. Therefore, our article will henceforth refer exclusively to amylin in this context.

Evolvability of Amylin

Because APs such as amylin are intrinsically disordered proteins composed of heterogeneous structures (Moore et al., 2018), APs might be involved in resistance against diverse stressors (Takamatsu et al., 2018). In addition, amylin toxicity in pancreatic β-cells has been well described in the pathogenesis of T2DM (Bharadwaj et al., 2017). Collectively, this may be comparable with the hormesis conferred by amyloidogenic evolvability (Hashimoto et al., 2018a). Because evolvability is defined as the capacity of a population of organisms to generate not only genetic diversity, but also adaptive genetic diversity, often overriding natural selection (Kirschner and Gerhart, 1998), both hormesis and heredity are critical steps in evolvability. In humans, AP protofibrils that encode information regarding biological and environmental stressors might be transmitted to offspring *via* germ lines (Hashimoto et al., 2018a). Although monomers of APs are unstable due to their intrinsically disordered nature (Takamatsu et al., 2018), formation of protofibrils might confer greater stability, which might provide an advantage for the transgenerational transmission of APs to offspring (Takamatsu et al., 2018). The presence of circulatory amylin is consistent with the transgenerational transmission *via* germ cells, although little is known about the expression of amylin in gonadal tissues. Yet given that amyloid fibrils are abundantly expressed in the semen (Roan et al., 2017), further exploration of this is definitely warranted. Taken together, our concept proposes that amylin protofibrils may convey stress information from parental pancreatic β-cells to an offspring's pancreas. By virtue of amylin evolvability, offspring can then better cope with the forthcoming stressors, reducing the risk of developing T1DM (**Figure 1A**). Indeed, it was previously shown that amylin-knockout mice developed a more severe form of alloxan-induced diabetes (Mulder et al., 2000), which is consistent with our hypothesis that amylin protofibrils might be involved in evolvability of β-cells in the pancreas.

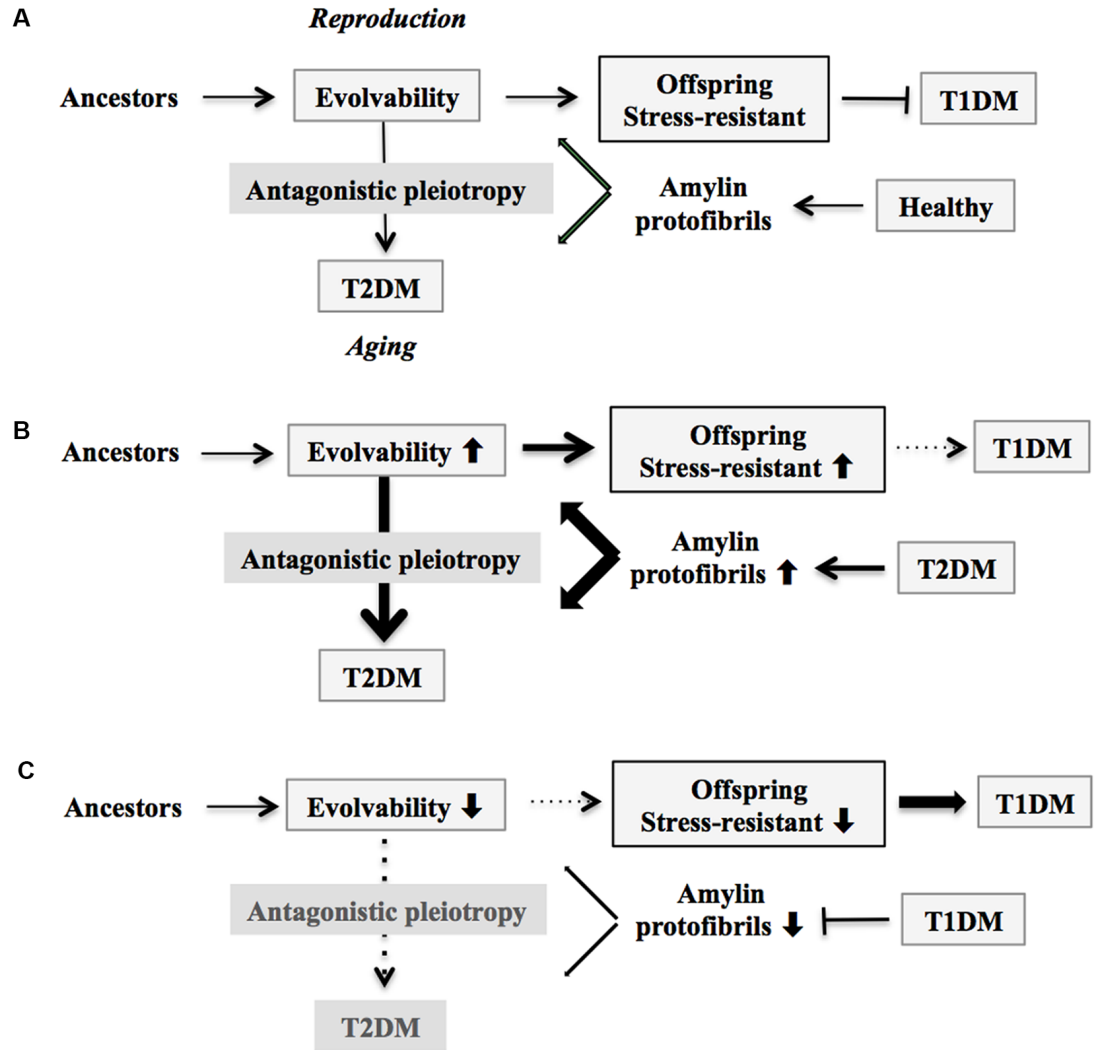

FIGURE 1 | Schematic of disease manifestation caused by alterations in amylin evolvability. **(A)** Amylin protofibrils might confer resistance against multiple stressors in parental β-cells in the pancreas under the healthy conditions and are transgenerationally transmitted to offspring during reproduction to deliver the stress information. By virtue of this, the β-cells in the pancreas in offspring can cope with forthcoming multiple stressors in β-cells in the pancreas. Thus, amylin evolvability is an epigenetic phenomenon that is beneficial in evolution. However, amylin protofibrils might lead to type 2 diabetes mellitus (T2DM) during parental aging through the antagonistic pleiotropy mechanism. **(B)** Increased evolvability of amylin protofibrils by various causes, such as T2DM (thick bold line), may result in an efficient delivery of information about stressors for offspring, leading to reduced frequency of T1DM in offspring (thin dot line) and increased frequency of T2DM in parents (thick bold line). **(C)** In contrast, inefficient delivery of the information of stresses due to decrease of amylin evolvability caused by type 1 diabetes mellitus (T1DM) in parents may result in the increased frequency of T1DM in offspring (thick bold line) and the decreased frequency of T2DM in parents (thin dot line).

On the other hand, T2DM might manifest in later life through the mechanism of antagonistic pleiotropy during parental aging (**Figure 1A**). Briefly, according to the antagonistic pleiotropy hypothesis, a prominent theory of aging proposed by G. C. Williams a half-century ago, certain genes whose functions are beneficial during reproductive stages may in turn exert adverse effects later in aging (Williams, 1957). Such a view may explain why T2DM, a primarily post-reproductive and biologically disadvantageous disorder, has emerged and persisted across evolution. Yet it is recognized that T2DM is a complex disorder further modulated by interaction of a combination of susceptible genes and perhaps lifestyle factors such as exercise and diet.

CONNECTING TYPE 1 DIABETES MELLITUS AND TYPE 2 DIABETES MELLITUS THROUGH AMYLOIDOGENIC EVOLVABILITY

Although it is generally believed that T1DM occurs during youth and may be etiologically distinct from T2DM, which emerges during later adulthood, we alternatively propose that

the two types of DM might actually be closely linked through amyloidogenic evolvability.

The Conventional View of Type 1 Diabetes Mellitus and Type 2 Diabetes Mellitus Pathogenesis

In T1DM, which accounts for 5–10% of all diabetes cases and occurs in approximately 0.3% of young individuals, amassed evidence suggests that various etiologies, such as autoimmune dysfunction and viral infection, might be pathogenetically involved (Daneman, 2006; Menke et al., 2013). Furthermore, recent genome-wide association studies have shown that the major susceptibility for the T1DM locus maps to the HLA class II genes at 6p21, which accounts for up to 30∼50% of genetic risk of T1DM, with minor contributions to disease risk from several other non-MHC loci (Steck and Rewers, 2011). On the contrary, the more common T2DM, estimated to be ∼7% of the general population, in contrast to early-onset T1DM, most often begins in those over the age of 65 years (although some early-onset T2DM cases are reported; Deshpande et al., 2008). Despite similar pathology in terms of dysfunctional pancreatic β cells, T1DM and T2DM are understood to be etiologically different entities.

Equilibrium Between Type 1 Diabetes Mellitus in Offspring and Parental Type 2 Diabetes Mellitus Through Amylin Evolvability

Based on our evolvability concept, stress information from parental/adult pancreatic β-cells could be delivered to their offspring through amylin protofibrils. The resulting pancreatic β-cells in offspring should therefore become more resistant against such stressors (**Figure 1A**).

According to our view, the greater the stress information from parental pancreatic β-cells that is delivered through amylin protofibrils to offspring through increased evolvability, the more resistant the pancreatic β-cells in offspring become against stressors, and the less prone they are to developing T1DM. This could result from various factors, including amylin missense mutation (Akter et al., 2016), T2DM in both parents, and maternal gestational diabetes mellitus (GDM). Consistent with our view, it was previously shown that parental history of T2DM is associated with a later onset of T1DM, the metabolic syndrome, and a metabolic profile related to insulin resistance (Thorn et al., 2009). Because of the action of antagonistic pleiotropy, T2DM is expressed more prominently during aging (**Figure 1B**).

Yet if the parents are afflicted with T1DM, then reduced evolvability associated with the down-regulation of amylin protofibrils might result in the delivery of less stress information to offspring, and as a consequence, T1DM risk may dramatically increase in offspring (**Figure 1C**). Supporting this, T1DM is preferentially transmitted from parents to offspring, although the mechanism of gender difference is obscure (Guo and Tuomilehto, 2002). Of interest, the inverse relationship between T1DM in offspring and parental T2DM is reminiscent of the concept of transgenerational equilibrium previously described between parental AD and schizophrenia in offspring related to amyloid evolvability (Takamatsu et al., 2019), raising a possibility that certain chronic disorders in offspring and their aging-associated amyloidogenic disorder counterparts in parents may exist in an inverse relationship through amyloidogenic evolvability.

Are There any Roles for Gestational Diabetes Mellitus in Amylin Evolvability?

The third diabetic subtype, GDM, occurs among pregnant women without a previous history of DM (Kampmann et al., 2015). GDM, with a prevalence of ∼39% of pregnancies, correlates with increased maternal obesity (Carpenter, 2007; Egan et al., 2017). GDM shows a complex etiology, with genetic and environmental factors implicated across mechanistic and epidemiological studies. Compared with T1DM and T2DM, there have been fewer studies on the etiological basis of GDM, because of its transient nature and resolution upon delivery of the infant. Thus, a possible etiologic role for GDM might also relate to evolvability. Given that GDM is associated with increased insulin resistance (Catalano, 2014), GDM might be involved in transmitting amylin protofibrils encoding stress information from parental pancreatic β-cells to offspring in order to mitigate the risk of T1DM in offspring. On the other hand, symptomatic T2DM might emerge later during parental aging. If this notion can be verified, GDM may become central to linking T1DM in offspring and parental T2DM through amylin evolvability. Yet, presently, there is no evidence that amylin can cross the transplacental barrier, which is generally believed to be permeable to only small molecules (Berveiller et al., 2016). Therefore, it would be fair to conclude that GDM might be unlikely to promote amylin evolvability. As will be described later for T2DM, GDM might represent an antagonistic pleiotropy of amylin evolvability. Consistently, after the occurrence of GDM, there is a higher likelihood of developing subsequent maternal T2DM, as well as possible abnormal cardiometabolic phenotypes in offspring (Carpenter, 2007; Kawasaki et al., 2018).

Moreover, pregnant women often experience memory dysfunction through the course of their pregnancy (John et al., 2018), which is generally attributed to elevated hormone levels affecting the brain, although the precise mechanism is unknown. Similar to GDM, gestational dementia might be relevant to amyloid evolvability, perhaps involving Aβ and tau. To the best of our knowledge, limited information is currently available regarding changes in brain APs during pregnancy.

COMORBIDITY OF ALZHEIMER'S DISEASE AND TYPE 2 DIABETES MELLITUS

Supposing that both T2DM and AD are antagonistic phenomena derived from amyloidogenic evolvability during reproduction, it follows that comorbidity of T2DM with AD in aging

might be attributed to the synergistic interaction of amylin with APs, including Aβ and tau, in regulating evolvability during reproduction.

The Conventional View of the Comorbidity of Alzheimer's Disease and Type 2 Diabetes Mellitus

With regard to the mechanisms underlying increased neurodegeneration related to T2DM, numerous studies have shown that both T2DM and AD are associated with various common pathological features, including impaired insulin resistance, endoplasmic reticulum stress, oxidative stress, protein aggregation, inflammation and altered gene expression (Vannuvel et al., 2013; Hokama et al., 2014; Singhal et al., 2014; Rosales-Corral et al., 2015). Furthermore, it was described that vascular dysfunction caused by T2DM might be relevant to AD (Wang et al., 2014). These results, however, were pathological observations, and do not necessarily explain the rationale for the emergence of these two comorbid aging-related disorders in evolution.

Comorbidity of Alzheimer's Disease and Type 2 Diabetes Mellitus From the Viewpoint of Evolvability

In this regard, evolvability might then underlie these biological phenomena. Provided that both T2DM and AD might be antagonistic phenomena derived from evolvability, it follows that amylin and amyloid-β (Aβ) and/or tau might interact cooperatively rather than function independently. Given the prevailing concept of cross-seeding (CS) of APs (Morales et al., 2013), perhaps the CS of amylin and Aβ and/or tau may be more potent than either monomer to stimulate various aspects of evolvability, such as hormesis and transgenerational transmission. Yet CS of these APs may manifest later in life as comorbid T2DM and AD through antagonistic pleiotropy in parental aging. Indeed, amylin interacts with Aβ and tau in both the pancreas and hippocampus in the brain of diabetic patients with AD (**Figure 2A**; Jackson et al., 2013).

Importance of Common Modifiers of Alzheimer's Disease and Type 2 Diabetes Mellitus From the Viewpoint of Evolvability

Notably, abnormally high levels of D-ribose have been observed in both T1DM (Yu et al., 2019) and T2DM (Su and He, 2014). Since administration of D-ribose induces the yield of Aβ and hyper-phosphorylated tau in the brain (Wu et al., 2015, 2019; Li et al., 2020), D-ribose might be also important for induction of AD. Thus, D-ribose might affect evolvability of amylin and Aβ, the dysmetabolism of which might lead to manifestation as comorbidity of AD and T2DM in aging. Indeed, it is possible that there might be many factors/stressors that may be attributed to the comorbidity of AD and T2DM. These include formaldehyde and amylin glycation.

Comorbidity of Alzheimer's Disease With Other Metabolic Disorders

Considering that AD is frequently comorbid with many other types of aging-associated diseases, similar mechanisms might be applied to the comorbidity of AD with these other conditions. Indeed, an increasing prevalence of associated metabolic disorders, including obesity, hypertension, hyperlipidemia, and atherosclerosis, is associated with an expanding adult and elderly population worldwide (Takamatsu et al., 2017). One may argue, however, that metabolic disorders other than T2DM are not always associated with amyloid fibril formation yet frequently promote neurodegeneration (Pugazhenthi, 2017). In this regard, evolvability of APs, including Aβ and tau, might be increased through mechanisms other than aggregative protein–protein interactions. For instance, cholesterol, which may play a central role in dyslipidemia, might stimulate misfolding and aggregation of APs in evolvability as well as in neurodegeneration and T2DM (Singh et al., 2015). Also, catecholamines possibly related to essential hypertension might be relevant (Goldstein, 1983). Aβ was shown to undergo regulated co-secretion with neuropeptide and catecholamine neurotransmitters (Toneff et al., 2013), and catecholamines were also shown to stimulate protein deposition in AD and PD (Bharath and Andersen, 2004). Thus, catecholamines might be involved in evolvability, which may manifest as essential hypertension as an antagonistic pleiotropy relationship in aging. Collectively, it is possible that the comorbidity of AD with metabolic disorders might represent antagonistic pleiotropy attributed to increased evolvability due to the CS of APs and other factors.

ROLE OF ADIPONECTIN PARADOX LINKING TYPE 2 DIABETES MELLITUS AND ALZHEIMER'S DISEASE

The concept of the CS of APs suggests that the pathogenesis of T2DM might be equivalent to that in AD but fails to explain how T2DM could be upstream of AD. Given that AD risk might be increased by T2DM, perhaps the mechanistic action of amylin in evolvability may be situated upstream to APs, including Aβ and tau.

In this regard, we hypothesize that APN might be involved. APN is a multifunctional adipokine that is important in insulin receptor signaling sensitization and an anti-inflammatory role (Waragai et al., 2017). Although APN is generally protective, it has been well characterized that APN might be critically involved in promoting aging-associated chronic diseases, such as chronic heart failure and chronic kidney disease, the so-called APN paradox (Menon et al., 2006; Kizer, 2014). Notably, a recent study suggests that the APN paradox is also observed in the nervous system (Waragai et al., 2020). APN is neuroprotective and mitigates neurodegeneration in both cellular and animal experimental systems. Nonetheless, in cohort studies, it was shown that hyperadiponectinemia correlates well with neuropathological features, such as amyloidosis and cognitive deficits, suggesting that APN paradox might

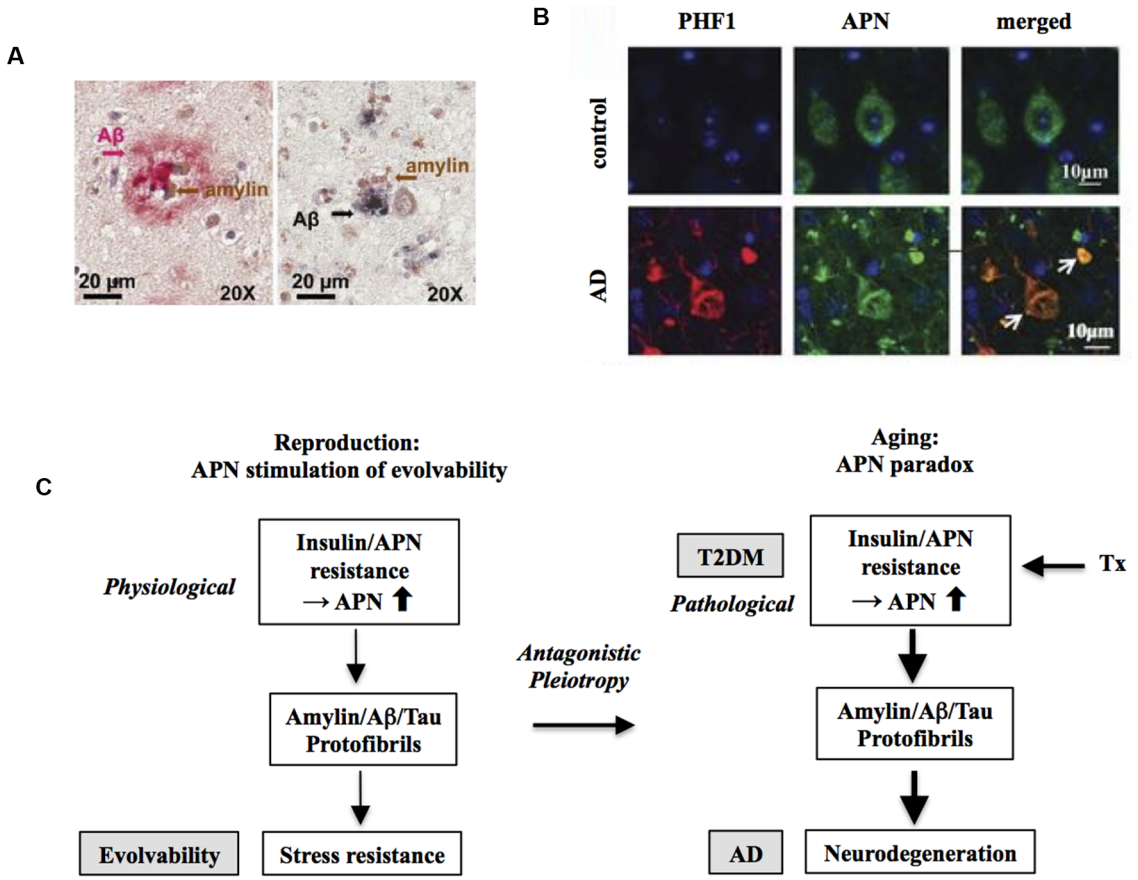

FIGURE 2 | Increased risk of Alzheimer's disease (AD) by T2DM as an antagonistic pleiotropy of evolvability. **(A)** Co-localization of amylin and amyloid-β (Aβ) is shown in brain parenchyma of AD patients with anti-amylin and anti-Aβ antibodies. The left panel shows a brain section from an AD patient without clinically demonstrated T2DM, while the right panel is derived from a diabetic patient with AD. Clusters of small amylin plaques adjacent to, or surrounded by larger Aβ deposits, are present. Modified from Jackson et al. (2013) with permission. **(B)** Adiponectin (APN)-positive neurofibrillary tangles (NFTs) in AD brain. Confocal laser scanning microscopy of double immunofluorescence of control and AD brains using anti-tau antibody PHF (lower) and anti-APN antibody showed that APN co-localized with tau in AD. White arrows indicate NFTs identified by the presence of PHF-1 immunoreactive abnormal fibrous inclusions, which were within the perikaryal cytoplasm of neurons. Scale bar = 10 μm. Modified from Waragai et al. (2016) with permission. **(C)** Schematic diagram of the mechanism underlying the APN paradox in T2DM-mediated increased AD risk. Presumably, amylin protofibrillar formation caused by APN resistance could up-regulate AP protofibrils in evolvability, which might manifest as T2DM stimulation of AD as the antagonistic pleiotropy in aging.

be involved in AD pathogenesis (Wennberg et al., 2016; Waragai et al., 2020). Consistent with this notion, it was shown that APN associated with phospho-tau in the AD brain, suggesting that APN might be involved in the tangle formation (**Figure 2B**).

Given that the APN paradox might be critical in promoting AD (Waragai et al., 2020), it is possible that the APN paradox in aging might be an antagonistic pleiotropy phenomenon derived from evolvability during reproduction (Waragai et al., 2020). In this context, APN resistance/insulin resistance might be a physiologically caused by fibrillar amylin in evolvability, which might later be manifest as T2DM stimulation of AD (**Figure 2C**). Consistently, insulin resistance was previously shown in cavefish as an adaptation to a nutrient-limited environment (Riddle et al., 2018), indicating that insulin resistance can be beneficially activated under the physiological conditions. Notably, it was recently described that large-scale proteomic analysis of AD brain and cerebrospinal fluid revealed early changes in energy metabolism associated with glial activation (Johnson et al., 2020), which is consistent with involvement of the APN paradox in the pathogenesis of AD (Waragai et al., 2020).

Similar to AD, a recent prospective cohort study showed that higher serum APN concentrations were observed in incident cancers and are associated with cancer-related deaths in T2DM, suggesting that the APN paradox might be significant in cancer related to T2DM (Lee et al., 2020).

IMPLICATIONS FOR THERAPEUTIC INTERVENTIONS

In view of the possible involvement of the APN paradox in linking neurodegeneration to metabolic disease, this may account for the pathological positioning of T2DM upstream of

AD in aging, suggesting that therapeutic targeting of APN might be a viable strategy.

Targeting Adiponectin Expression

For this purpose, suppressing APN expression by various methods, such as antisense oligonucleotides against APN mRNA (Rinaldi and Wood, 2018) and immunotherapy against the APN protein (Lannfelt et al., 2014), might effectively decrease formation of APs protofibrils, leading to suppression of APN paradox and AD (**Figure 2C**). However, the majority of the previous studies describe that the potential of APN activity for therapeutic purposes based on the presumption that APN is protective. Therefore, it is necessary to bear in mind the possibility of a therapeutic "trade-off" by suppression of APN expression.

Notably, administration of D-ribose leads to an increase of visceral triglycerides in mice (Chen et al., 2019b); and since high levels of D-ribose (Su et al., 2013; Chen et al., 2019a) and high HbA1c (Chen et al., 2017) are associated with diabetes, this raises a possibility that D-ribose could be utilized as a biomarker to assess the therapeutic efficiency.

Anti-Diabetes Mellitus and Metabolic Syndrome

It is expected that combining APN with treatment against T2DM and other related metabolic disorders might enhance the therapeutic efficiency of targeting of APN. Because of an increased risk of neurodegenerative disorders related to T2DM, previous studies have strongly suggested that treatment of T2DM might be beneficial for and repurposed to therapy of neurodegenerative disorders. Indeed, a recent phase II clinical trial of glucagon-like peptide-1 (GLP-1)/incretin for PD appeared promising (Hölscher, 2012; Athauda et al., 2017), prompting initiation of a subsequent clinical trial of GLP-1/incretin in AD (Gejl et al., 2016). Although metformin has long been used to treat T2DM, there is growing evidence for the benefits of metformin to counteract age-related diseases such as cancer, cardiovascular disease, and neurodegenerative diseases (Rotermund et al., 2018). Moreover, studies are in progress to assess the therapeutic potential of other anti-T2DM molecules, such as DPP-4 inhibitors (Kosaraju et al., 2017) and APN (Sekiyama et al., 2014; Waragai et al., 2018). In relation to the current state of neurodegenerative therapy in relation to T2DM, our current view regarding evolvability may offer several novel insights.

Recently, chronic hypertension has been suggested as one of the largest modifiable risk factors for developing AD (Marfany et al., 2018). Indeed, several epidemiological studies reveal that β-blocker treatment reduces the prevalence of AD in patients suffering from hypertension (Yu et al., 2011). Since it is possible that Aβ evolvability might be promoted not only by amylin protofibrils but also by other molecules, such as cholesterol and catecholamines, it follows that disease-modifying therapies targeted against other metabolic syndrome disorders in addition to T2DM, especially anti-hypertension agents, might increase overall treatment efficacy.

CONCLUDING REMARKS

In the present discussion, the concept of amylin evolvability was shown to provide novel insights into the T2DM and related diseases, which are currently elusive. First, we argue that T1DM and T2DM, etiologically distinct types of DM, might be linked through amylin evolvability. Furthermore, the comorbidity of AD and T2DM in aging might be an antagonistic pleiotropy phenomenon derived from evolvability regulated by AD-relevant APs, including Aβ, tau, and amylin. Importantly, it was suggested that APN resistance might stimulate amylin protofibrils, leading to Aβ protofibrillar formation in evolvability, which might manifest as an increased AD risk driven by T2DM through an antagonistic pleiotropy mechanism in aging. Taken together, a better understanding of the mechanism of evolvability may shed light on novel evolvability-based therapeutic strategies.

DATA AVAILABILITY STATEMENT

The original contributions presented in the study are included in the article, further inquiries can be directed to the corresponding author.

AUTHOR CONTRIBUTIONS

MH conceived the study. MH and GH wrote the article. All authors contributed to the article and approved the submitted version.

ACKNOWLEDGMENTS

We are grateful for the continuous encouragement of Drs. Kaori Hashimoto (Tokyo Metropolitan Institute of Medical Science) and Maria del Carmen Ruiz de la Cruz (University of Chicago).

REFERENCES

Abedini, A., and Schmidt, A. M. (2013). Mechanisms of islet amyloidosis toxicity in type 2 diabetes. *FEBS Lett.* 587, 1119–1127. doi: 10.1016/j.febslet.2013.01.017

Akter, R., Cao, P., Noor, H., Ridgway, Z., Tu, L. H., Wang, H., et al. (2016). Islet amyloid polypeptide: structure, function, and pathophysiology. *J. Diabetes Res.* 2016:2798269. doi: 10.2210/pdb5e61/pdb

Athauda, D., Maclagan, K., Skene, S. S., Bajwa-Joseph, M., Letchford, D., Chowdhury, K., et al. (2017). Exenatide once weekly versus placebo in Parkinson's disease: a randomised, double-blind, placebo-controlled trial. *Lancet* 390, 1664–1675. doi: 10.1016/S0140-6736(17)31585-4

Atlantis, E., Fahey, P., and Foster, J. (2014). Collaborative care for comorbid depression and diabetes: a systematic review and meta-analysis. *BMJ Open* 4:e004706. doi: 10.1136/bmjopen-2013-004706

Aviles-Olmos, I., Limousin, P., Lees, A., and Foltynie, T. (2013). Parkinson's disease, insulin resistance and novel agents of neuroprotection. *Brain* 136, 374–384. doi: 10.1093/brain/aws009

Berveiller, P., Marty, O., Vialard, F., and Mir, O. (2016). Use of anticancer agents in gynecological oncology during pregnancy: a systematic review of

maternal pharmacokinetics and transplacental transfer. *Expert Opin. Drug Metab. Toxicol.* 12, 523–531. doi: 10.1517/17425255.2016.1167187

Bharadwaj, P., Wijesekara, N., Liyanapathirana, M., Newsholme, P., Ittner, L., Fraser, P., et al. (2017). The link between type 2 diabetes and neurodegeneration: roles for amyloid-β, amylin and tau proteins. *J. Alzheimers Dis.* 59, 421–432. doi: 10.3233/jad-161192

Bharath, S., and Andersen, J. K. (2004). Catecholamines and protein deposition in Parkinson's and Alzheimer's disease: old medicine, new targets. *Rejuvenation Res.* 7, 92–94. doi: 10.1089/1549168041553071

Brange, J., and Langkjoer, L. (1993). Insulin structure and stability. *Pharm. Biotechnol.* 5, 315–350. doi: 10.1007/978-1-4899-1236-7_11

Carpenter, M. W. (2007). Gestational diabetes, pregnancy hypertension, and late vascular disease. *Diabetes Care* 30, S246–S250. doi: 10.2337/dc07-s224

Catalano, P. M. (2014). Trying to understand gestational diabetes. *Diabetic Med.* 31, 273–281. doi: 10.1111/dme.12381

Chen, X., Su, T., Chen, Y., He, Y., Liu, Y., Xu, Y., et al. (2017). d-Ribose as a contributor to glycated haemoglobin. *EBioMedicine* 25, 143–153. doi: 10.1016/j.ebiom.2017.10.001

Chen, Y., Yu, L., Wang, Y., Wei, Y., Xu, Y., He, T., et al. (2019a). d-Ribose contributes to the glycation of serum protein. *Biochim. Biophys. Acta* 1865, 2285–2292. doi: 10.1016/j.bbadis.2019.05.005

Chen, Y., Yu, L., Wei, Y., Long, Y., Xu, Y., He, T., et al. (2019b). d-Ribose increases triglyceride *via* upregulation of DGAT in the liver. *Sci. China Life Sci.* 62, 858–861. doi: 10.1007/s11427-019-9542-2

Dadon, D., Tornovsky-Babaey, S., Furth-Lavi, J., Ben-Zvi, D., Ziv, O., Schyr-Ben, R.-H., et al. (2012). Glucose metabolism: key endogenous regulator of beta-cell replication and survival. *Diabetes Obes. Metab.* 14, 101–108. doi: 10.1111/j.1463-1326.2012.01646.x

Daneman, D. (2006). Type 1 diabetes. *Lancet* 367, 847–858. doi: 10.1016/S0140-6736(18)30024-2

Deshpande, A. D., Harris-Hayes, M., and Schootman, M. (2008). Epidemiology of diabetes and diabetes-related complications. *Phys. Ther.* 88, 1254–1264. doi: 10.2522/ptj.20080020

Egan, A. M., Vellinga, A., Harreiter, J., Simmons, D., Desoye, G., Corcoy, R., et al. (2017). Epidemiology of gestational diabetes mellitus according to IADPSG/WHO 2013 criteria among obese pregnant women in Europe. *Diabetologia* 60, 1913–1921. doi: 10.1007/s00125-017-4353-9

Gejl, M., Gjedde, A., Egefjord, L., Moller, A., Hansen, S. B., Vang, K., et al. (2016). In Alzheimer's disease, 6-month treatment with GLP-1 analog prevents decline of brain glucose metabolism: randomized, placebo-controlled, double-blind clinical trial. *Front. Aging Neurosci.* 8:108. doi: 10.3389/fnagi.2016.00108

Goldstein, D. S. (1983). Plasma catecholamines and essential hypertension. An analytical review. *Hypertension* 5, 86–99. doi: 10.1161/01.hyp.5.1.86

Guo, S. W., and Tuomilehto, J. (2002). Preferential transmission of type 1 diabetes from parents to offspring: fact or artifact? *Genet. Epidemiol.* 23, 323–334. doi: 10.1002/gepi.10183

Hashimoto, M., Ho, G., Sugama, S., Takamatsu, Y., Shimizu, Y., Takenouchi, T., et al. (2018a). Evolvability of amyloidogenic proteins in human brain. *J. Alzheimers Dis.* 62, 73–83. doi: 10.3233/jad-170894

Hashimoto, M., Ho, G., Takamatsu, Y., Shimizu, Y., Sugama, S., Takenouchi, T., et al. (2018b). Evolvability and neurodegenerative disease: antagonistic pleiotropy phenomena derived from amyloid aggregates. *J. Parkinsons Dis.* 8, 405–408. doi: 10.3233/jpd-181365

Hashimoto, M., Ho, G., Takamatsu, Y., Wada, R., Sugama, S., Takenouchi, T., et al. (2018c). Possible role of the polyglutamine elongation in evolution of amyloid-related evolvability *J. Huntingtons Dis.* 7, 297–307. doi: 10.3233/jhd-180309

Hokama, M., Oka, S., Leon, J., Ninomiya, T., Honda, H., Sasaki, K., et al. (2014). Altered expression of diabetes-related genes in Alzheimer's disease brains: the Hisayama study. *Cereb. Cortex* 24, 2476–2488. doi: 10.1093/cercor/bht101

Hölscher, C. (2012). Potential role of glucagon-like peptide-1 (GLP-1) in neuroprotection. *CNS Drugs* 26, 871–882. doi: 10.2165/11635890-000000000-00000

Jackson, K., Barisone, G. A., Diaz, E., Jin, L. W., DeCarli, C., and Despa, F. (2013). Amylin deposition in the brain: a second amyloid in Alzheimer disease? *Ann. Neurol.* 74, 517–526. doi: 10.1002/ana.23956

Jaikaran, E. T., and Clark, A. (2001). Islet amyloid and type 2 diabetes: from molecular misfolding to islet pathophysiology. *Biochim. Biophys. Acta* 1537, 179–203. doi: 10.1016/s0925-4439(01)00078-3

John, C. M., Mohamed Yusof, N. I. S., and Abdul Aziz, S. H. F. (2018). Mohd fauzi, maternal cognitive impairment associated with gestational diabetes mellitus—a review of potential contributing mechanisms. *Int. J. Mol. Sci.* 19:3894. doi: 10.3390/ijms19123894

Johnson, E. C. B., Dammer, E. B., Duong, D. M., Ping, L., Zhou, M., Yin, L., et al. (2020). Large-scale proteomic analysis of Alzheimer's disease brain and cerebrospinal fluid reveals early changes in energy metabolism associated with microglia and astrocyte activation. *Nat. Med.* 26, 769–780. doi: 10.1038/s41591-020-0815-6

Kampmann, U., Madsen, L. R., Skajaa, G. O., Iversen, D. S., Moeller, N., and Ovesen, P. (2015). Gestational diabetes: a clinical update. *World J. Diabetes* 6, 1065–1072. doi: 10.4239/wjd.v6.i8.1065

Kawasaki, M., Arata, N., Miyazaki, C., Mori, R., Kikuchi, T., Ogawa, Y., et al. (2018). Obesity and abnormal glucose tolerance in offspring of diabetic mothers: a systematic review and meta-analysis. *PLoS One* 13:e0190676. doi: 10.1371/journal.pone.0190676

Kirschner, M., and Gerhart, J. (1998). Evolvability. *Proc. Natl. Acad. Sci. U S A* 95, 8420–8427. doi: 10.1073/pnas.95.15.8420

Kizer, J. R. (2014). Adiponectin, cardiovascular disease and mortality: parsing the dual prognostic implications of a complex adipokine. *Metabolism* 63, 1079–1083. doi: 10.1016/j.metabol.2014.06.011

Kosaraju, J., Holsinger, R. M. D., Guo, L., and Tam, K. Y. (2017). Linagliptin, a dipeptidyl peptidase-4 inhibitor, mitigates cognitive deficits and pathology in the 3×Tg-AD mouse model of Alzheimer's disease. *Mol. Neurobiol.* 54, 6074–6084. doi: 10.1007/s12035-016-0125-7

Lannfelt, L., Relkin, N. R., and Siemers, E. R. (2014). Amyloid-ss-directed immunotherapy for Alzheimer's disease. *J. Intern. Med.* 275, 284–295. doi: 10.1111/joim.12168

Lee, C. H., Lui, D. T. W., Cheung, C. Y. Y., Fong, C. H. Y., Yuen, M. M. A., Chow, W. S., et al. (2020). Higher circulating adiponectin concentrations predict incident cancer in type 2 diabetes—the adiponectin paradox. *J. Clin. Endocrinol. Metab.* 105:dgaa075. doi: 10.1210/clinem/dgaa385

Li, Z.-H., He, X. P., Li, H., He, R. Q., and Hu, X. T. (2020). Age-associated changes in amyloid-β and formaldehyde concentrations in cerebrospinal fluid of rhesus monkeys. *Zool. Res.* 41, 444–448. doi: 10.24272/j.issn.2095-8137.2020.088

Luca, S., Yau, W. M., Leapman, R., and Tycko, R. (2007). Peptide conformation and supramolecular organization in amylin fibrils: constraints from solid-state NMR. *Biochemistry* 46, 13505–13522. doi: 10.1021/bi701427q

Marfany, A., Sierra, C., Camafort, M., Domenech, M., and Coca, A. (2018). High blood pressure, Alzheimer disease and antihypertensive treatment. *Panminerva Med.* 60, 8–16. doi: 10.23736/S0031-0808.18.03360-8

Menke, A., Orchard, T. J., Imperatore, G., Bullard, K. M., Mayer-Davis, E., and Cowie, C. C. (2013). The prevalence of type 1 diabetes in the United States. *Epidemiology* 24, 773–774. doi: 10.1097/EDE.0b013e31829ef01a

Menon, V., Li, L., Wang, X., Greene, T., Balakrishnan, V., Madero, M., et al. (2006). Adiponectin and mortality in patients with chronic kidney disease. *J. Am. Soc. Nephrol.* 17, 2599–2606. doi: 10.1681/ASN.2006040331

Mietlicki-Baase, E. G. (2016). Amylin-mediated control of glycemia, energy balance and cognition. *Physiol. Behav.* 162, 130–140. doi: 10.1016/j.physbeh.2016.02.034

Montojo, M. T., Aganzo, M., and Gonzalez, N. (2017). Huntington's disease and diabetes: chronological sequence of its association. *J. Huntingtons Dis.* 6, 179–188. doi: 10.3233/jhd-170253

Moore, S. J., Sonar, K., Bharadwaj, P., Deplazes, E., and Mancera, R. L. (2018). Characterisation of the structure and oligomerisation of islet amyloid polypeptides (IAPP): a review of molecular dynamics simulation studies. *Molecules* 23:2142. doi: 10.3390/molecules23092142

Morales, R., Moreno-Gonzalez, I., and Soto, C. (2013). Cross-seeding of misfolded proteins: implications for etiology and pathogenesis of protein misfolding diseases. *PLoS Pathog.* 9:e1003537. doi: 10.1371/journal.ppat.1003537

Mulder, H., Gebre-Medhin, S., Betsholtz, C., Sundler, F., and Ahren, B. (2000). Islet amyloid polypeptide (amylin)-deficient mice develop a more severe form of alloxan-induced diabetes. *Am. J. Physiol. Endocrinol. Metab.* 278, E684–E691. doi: 10.1152/ajprenal.2000.278.4.F684

Ng, T. P., Feng, L., Nyunt, M. S., Feng, L., Gao, Q., Lim, M. L., et al. (2016). Metabolic syndrome and the risk of mild cognitive impairment and progression to dementia: follow-up of the singapore longitudinal

ageing study cohort. *JAMA Neurol.* 73, 456–463. doi: 10.1001/jamaneurol.2015.4899

Pugazhenthi, S. (2017). Metabolic syndrome and the cellular phase of Alzheimer's disease. *Prog. Mol. Biol. Transl. Sci.* 146, 243–258. doi: 10.1016/bs.pmbts.2016.12.016

Riddle, M. R., Aspiras, A. C., Gaudenz, K., Peuss, R., Sung, J. Y., Martineau, B., et al. (2018). Insulin resistance in cavefish as an adaptation to a nutrient-limited environment. *Nature* 555, 647–651. doi: 10.1038/nature26136

Rinaldi, C., and Wood, M. J. A. (2018). Antisense oligonucleotides: the next frontier for treatment of neurological disorders. *Nat. Rev. Neurol.* 14, 9–21. doi: 10.1038/nrneurol.2017.148

Roan, N. R., Sandi-Monroy, N., Kohgadai, N., Usmani, S. M., Hamil, K. G., Neidleman, J., et al. (2017). Semen amyloids participate in spermatozoa selection and clearance. *eLife* 6:e24888. doi: 10.7554/eLife.24888

Rosales-Corral, S., Tan, D. X., Manchester, L., and Reiter, R. J. (2015). Diabetes and Alzheimer disease, two overlapping pathologies with the same background: oxidative stress. *Oxid. Med. Cell. Longev.* 2015:985845. doi: 10.1155/2015/985845

Rotermund, C., Machetanz, G., and Fitzgerald, J. C. (2018). The therapeutic potential of metformin in neurodegenerative diseases. *Front. Endocrinol.* 9:400. doi: 10.3389/fendo.2018.00400

Sekiyama, K., Waragai, M., Akatsu, H., Sugama, S., Takenouchi, T., Takamatsu, Y., et al. (2014). Disease-modifying effect of adiponectin in model of alpha-synucleinopathies. *Ann. Clin. Transl. Neurol.* 1, 479–489. doi: 10.1002/acn3.77

Singh, S., Trikha, S., Bhowmick, D. C., Sarkar, A. A., and Jeremic, A. M. (2015). Role of cholesterol and phospholipids in amylin misfolding, aggregation and etiology of islet amyloidosis. *Adv. Exp. Med. Biol.* 855, 95–116. doi: 10.1007/978-3-319-17344-3_4

Singhal, G., Jaehne, E. J., Corrigan, F., Toben, C., and Baune, B. T. (2014). Inflammasomes in neuroinflammation and changes in brain function: a focused review. *Front. Neurosci.* 8:315. doi: 10.3389/fnins.2014.00315

Steck, A. K., and Rewers, M. J. (2011). Genetics of type 1 diabetes. *Clin. Chem.* 57, 176–285. doi: 10.1373/clinchem.2010.148221

Stewart, C. E., and Rotwein, P. (1996). Growth, differentiation, and survival: multiple physiological functions for insulin-like growth factors. *Physiol. Rev.* 76, 1005–1026. doi: 10.1152/physrev.1996.76.4.1005

Su, T., and He, R. (2014). d-Ribose, an overlooked player in type 2 diabetes mellitus? *Sci. China Life Sci.* 57:361. doi: 10.1007/s11427-014-4614-5

Su, T., Xin, L., He, Y., Song, Y., Li, W., Wei, Y., et al. (2013). Abnormally high level of uric D-ribose for type 2 diabetics. *Prog. Biochem. Biophys.* 40, 816–825. doi: 10.1111/j.1558-5646.1957.tb02911.x

Takamatsu, Y., Fujita, M., Ho, G. J., Wada, R., Sugama, S., Takenouchi, T., et al. (2018). Motor and nonmotor symptoms of Parkinson's disease: antagonistic pleiotropy phenomena derived from α-synuclein evolvability? *Parkinsons Dis.* 2018:5789424. doi: 10.1155/2018/5789424

Takamatsu, Y., Ho, G., Koike, W., Sugama, S., Takenouchi, T., Waragai, M., et al. (2017). Combined immunotherapy with "anti-insulin resistance" therapy as a novel therapeutic strategy against neurodegenerative diseases. *NPJ Parkinsons Dis.* 3:4. doi: 10.1038/s41531-016-0001-1

Takamatsu, Y., Ho, G., Waragai, M., Wada, R., Sugama, S., Takenouchi, T., et al. (2019). Transgenerational interaction of Alzheimer's disease with schizophrenia through amyloid evolvability. *J. Alzheimers Dis.* 68, 473–481. doi: 10.3233/jad-180986

Thorn, L. M., Forsblom, C., Waden, J., Soderlund, J., Rosengard-Barlund, M., Saraheimo, M., et al. (2009). Effect of parental type 2 diabetes on offspring with type 1 diabetes. *Diabetes Care* 32, 63–68. doi: 10.2337/dc08-0472

Toneff, T., Funkelstein, L., Mosier, C., Abagyan, A., Ziegler, M., and Hook, V. (2013). Beta-amyloid peptides undergo regulated co-secretion with neuropeptide and catecholamine neurotransmitters. *Peptides* 46, 126–135. doi: 10.1016/j.peptides.2013.04.020

Vannuvel, K., Renard, P., Raes, M., and Arnould, T. (2013). Functional and morphological impact of ER stress on mitochondria. *J. Cell. Physiol.* 228, 1802–1818. doi: 10.1002/jcp.24360

Wang, F., Guo, X., Shen, X., Kream, R. M., Mantione, K. J., and Stefano, G. B. (2014). Vascular dysfunction associated with type 2 diabetes and Alzheimer's disease: a potential etiological linkage. *Med. Sci. Monit. Basic Res.* 20, 118–129. doi: 10.12659/msmbr.891278

Waragai, M., Adame, A., Trinh, I., Sekiyama, K., Takamatsu, Y., Une, K., et al. (2016). Possible involvement of adiponectin, the anti-diabetes molecule, in the pathogenesis of Alzheimer's disease. *J. Alzheimers Dis.* 52, 1453–1459. doi: 10.3233/jad-151116

Waragai, M., Ho, G., Takamatsu, Y., Sekiyama, K., Sugama, S., Takenouchi, T., et al. (2017). Importance of adiponectin activity in the pathogenesis of Alzheimer's disease. *Ann. Clin. Transl. Neurol.* 4, 591–600. doi: 10.1002/acn3.436

Waragai, M., Ho, G., Takamatsu, Y., Shimizu, Y., Sugino, H., Sugama, S., et al. (2018). Dual-therapy strategy for modification of adiponectin receptor signaling in aging-associated chronic diseases. *Drug Discov. Today* 23, 1305–1311. doi: 10.1016/j.drudis.2018.05.009

Waragai, M., Ho, G., Takamatsu, Y., Wada, R., Sugama, S., Takenouchi, T., et al. (2020). Adiponectin paradox in Alzheimer's disease; relevance to amyloidogenic evolvability? *Front. Endocrinol.* 11:108. doi: 10.3389/fendo.2020.00108

Watts, A. S., Loskutova, N., Burns, J. M., and Johnson, D. K. (2013). Metabolic syndrome and cognitive decline in early Alzheimer's disease and healthy older adults. *J. Alzheimers Dis.* 35, 253–265. doi: 10.3233/jad-121168

Wennberg, A. M., Gustafson, D., Hagen, C. E., Roberts, R. O., Knopman, D., Jack, C., et al. (2016). Serum adiponectin levels, neuroimaging and cognition in the mayo clinic study of aging. *J. Alzheimers Dis.* 53, 573–581. doi: 10.3233/jad-151201

Williams, G. C. (1957). Pleiotropy, natural selection and the evolution of senescence. *Evolution* 11, 398–411. doi: 10.1111/j.1558-5646.1957.tb02911.x

Wu, B., Wang, Y., Shi, C., Chen, Y., Yu, L., Li, J., et al. (2019). Ribosylation-derived advanced glycation end products induce tau hyperphosphorylation through brain-derived neurotrophic factor reduction. *J. Alzheimers Dis.* 71, 291–305. doi: 10.3233/jad-190158

Wu, B., Wei, Y., Wang, Y., Su, T., Zhou, L., Liu, Y., et al. (2015). Gavage of D-Ribose induces Abeta-like deposits, Tau hyperphosphorylation as well as memory loss and anxiety-like behavior in mice. *Oncotarget* 6, 34128–34142. doi: 10.18632/oncotarget.6021

Yu, L., Chen, Y., Xu, Y., He, T., Wei, Y., and He, R. (2019). d-Ribose is elevated in T1DM patients and can be involved in the onset of encephalopathy. *Aging* 11, 4943–4969. doi: 10.18632/aging.102089

Yu, J. T., Wang, N. D., Ma, T., Jiang, H., Guan, J., and Tan, L. (2011). Roles of β-adrenergic receptors in Alzheimer's disease: implications for novel therapeutics. *Brain Res. Bull.* 84, 111–117. doi: 10.1016/j.brainresbull.2010.11.004

Conflict of Interest: The authors declare that the research was conducted in the absence of any commercial or financial relationships that could be construed as a potential conflict of interest.

The reviewer NK declared a past co-authorship with one of the authors MW to the handling editor.

frontiers in Aging Neuroscience

ORIGINAL RESEARCH
published: 30 October 2020
doi: 10.3389/fnagi.2020.527658

The Association Between Leukocyte Telomere Length and Cognitive Performance Among the American Elderly

Deng Linghui[1†], Qiu Shi[2,3†], Chen Chi[4], Liu Xiaolei[1], Zhou Lixing[1], Zuo Zhiliang[1] and Dong Birong[1]*

[1] National Clinical Research Center of Geriatrics, The Center of Gerontology and Geriatrics, West China Hospital, Sichuan University, Chengdu, China, [2] Department of Urology, Institute of Urology and National Clinical Research Center for Geriatrics, West China Hospital, Sichuan University, Chengdu, China, [3] Center of Biomedical Big Data, West China Hospital, Sichuan University, Chengdu, China, [4] Department of Immunology and Microbiology, Guiyang College of Traditional Chinese Medicine, Guiyang, China

OPEN ACCESS

Edited by:
Jiehui Jiang,
Shanghai University, China

Reviewed by:
Dafin F. Muresanu,
Iuliu Haţieganu University of Medicine and Pharmacy, Romania
Ivica Rubelj,
Rudjer Boskovic Institute, Croatia

***Correspondence:**
Dong Birong
birongdong@163.com

† These authors have contributed equally to this work

Received: *17 January 2020*
Accepted: *29 September 2020*
Published: *30 October 2020*

Citation:
Linghui D, Shi Q, Chi C, Xiaolei L, Lixing Z, Zhiliang Z and Birong D (2020) The Association Between Leukocyte Telomere Length and Cognitive Performance Among the American Elderly. Front. Aging Neurosci. 12:527658. doi: 10.3389/fnagi.2020.527658

Background: Age-related cognitive decline begins in middle age and persists with age. Leukocyte telomere length (LTL) decreases with age and is enhanced by inflammation and oxidative stress. However, whether shorter LTL correlates with cognitive decline remains controversial.

Aims: We aimed to investigate the relationship between LTL and cognitive decline in the American elderly.

Methods: We used data from the 1999 to 2002 U.S. National Health and Nutrition Examination Survey (NHANES). We included participants aged 65–80 with available data on LTL and cognitive assessments. The cognitive function assessment used the digit symbol substitution test (DSST). We applied multivariate modeling to estimate the association between LTL and cognitive performance. Additionally, to ensure robust data analysis, we converted LTL into categorical variables through quartile and then calculated the *P* for trend.

Results: After adjusting for age, cardiovascular disease (CAD) score, gender, race, body mass index (BMI), and educational level, LTL showed a positive correlation with DSST score (odds ratio [OR] 3.47 [0.14, 6.79], $P = 0.04$). Additionally, to further quantify the LTL–DSST interaction, we found a similar trend when LTL was regarded as a categorical variable (quartile) (*P* for trend = 0.03).

Conclusion: LTL was associated with cognitive capabilities among the elderly, implying that LTL might be a biomarker of cognitive aging.

Keywords: aging, biomarker, telomere length, cognitive decline, elderly

INTRODUCTION

The aging global population presents a threat of increased disease and disability (Vos et al., 2012). Age-related cognitive decline begins in middle age and continues over time (Li et al., 2001), but studies have found individual differences in the severity of age-related cognitive decline under the influence of genetic and environmental factors (Foster, 2006; Connors et al., 2015; van der Wardt et al., 2015; Heywood et al., 2017). Studies have also suggested that oxidative stress and inflammation might influence aging and age-related memory disorders, which may explain why cognitive decline is highly associated with the elderly (Anstey et al., 2005; Peila and Launer, 2006; Lau et al., 2007; Rafnsson et al., 2007). However, the exact mechanism of cognitive decline remains unknown. Thus, to help reduce the risk of dementia and promote overall health among the elderly, it is essential to identify the potential predictive biomarkers of cognitive dysfunction.

Telomeres, which are repetitive nucleoprotein regions located at the ends of eukaryotic chromosomes, maintain genomic integrity and stability by protecting the end of the chromosome from illegitimate degradation and recombination (Jiang et al., 2018). Successive somatic cell divisions gradually abrase telomere length (TL) during aging (Miu et al., 2019). This cumulative age-interrelated TL shortening conduces to cellular senescence, an attribute of aging (López et al., 2013; Xu et al., 2018). Cellular lifespan is influenced by the length and stability of telomeres to some degree. Therefore, TL has been proposed as a candidate biomarker of aging (Xu et al., 2018). The TL shortening process was reported to accelerate under oxidative stress and inflammatory response and could serve as a record of the cumulative burden of oxidative stress along with inflammation (von Zglinicki et al., 2000; Aviv et al., 2006). Judging from longer telomeres protect cells from cellular senescence and death, it is reasonable to expect that they would also protect neuronal cells against oxidative stress and neurodegeneration that are related with cognitive decline (Collado et al., 2007). Research has reported the implication of shortened leukocyte TL (LTL) in multiple age-related diseases including neurodegenerative ones (Serrano and Andrés, 2004; Valdes et al., 2007; Shammas, 2011; Willeit et al., 2014).

Previous research on LTL and cognitive ability, predominantly in the elderly, has yielded inconsistent results. Studies have noticed a correlation between shortened LTL and age-related cognitive decline among the elderly (Valdes et al., 2010; Yaffe et al., 2011), but other studies have found such an association to be relatively small or absent (Mather et al., 2010; Harris et al., 2012). Therefore, we used the U.S. National Health and Nutrition Examination Survey (NHANES) database to investigate the relationship between LTL and cognitive function in a cohort of elderly individuals.

MATERIALS AND METHODS

Data Source and Participant Selection

The NHANES is an ongoing cross-sectional survey of a nationally representative, non-institutionalized U.S. population conducted by the U.S. National Center for Health Statistics (NCHS). To promote overall representativeness, the NHANES uses a complex multi-stage probability sampling design. Its dataset combines five major factors: socio-demographic characteristics, physical examinations, dietary information, laboratory investigations, and interview or questionnaire data—with raw data that are processed in 2-year cycles and made publicly available online (Cawthon, 2002; Mazidi et al., 2017). The NHANES protocol was approved by the NCHS Research Ethics Review Board, and all participants provided written informed consent. More NHANES data and detailed information on survey methods are available on the center's official website[1].

In this study, we restricted our analysis to participants from 1999 to 2000 and from 2001 to 2002 cycles of the NHANES survey because only these cycles contained TL and cognitive testing information. Eligibility inclusion criteria required participants to be between ages 60 and 85 at the time of the survey, with high school education or above, and to have available data on both LTL and cognitive function examination.

Telomere Measurements

With standardized procedures, purified DNA was acquired from whole blood and stored at −80°C before the LTL assay. Using quantitative polymerase chain reaction, we measured LTL relative to standard–reference DNA (T/S ratio) (Cawthon, 2002; Lin et al., 2010; Needham et al., 2013). The LTL was calculated as the mean T/S ratio, which is an approximation of average TL across all the chromosome ends. More details regarding the LTL quantification procedure and analytical methods are on the NHANES website (see footnote 1).

Cognitive Function Assessment

We evaluated cognitive function using the digit symbol substitution test (DSST), an executive function subtest of the Wechsler Adult Intelligence Scale, Third Edition (WAIS III) (Oberlin et al., 2013). In this test, participants were given a key that paired symbols and numbers. Then, they were given a train of numbers and had to draw symbols under the corresponding numbers using the substitution key in 120s. The DSST score represents the correct number of symbols drawn, with a maximum score of 133. It is considered a sensitive test for cognitive disorder because it could record the participants' response speed, associative learning, continuous attention, visual spatial skills, and memory abilities (Oberlin et al., 2013).

Covariates

Multivariate models contain variables that might confound the link between LTL and cognitive ability. Educational level was coded as a level 2 categorical variable (high school and above). Cardiovascular disease (CAD) was also a potential confounder as it could affect both LTL and cognitive impairment. To avoid multicollinearity, we generated a comprehensive CAD variable that aggregated multiple risk factors. One score was assigned to each of the three current risk factors: history of hypertension,

[1]http://www.cdc.gov/nchs/nhanes.htm

coronary heart disease, or stroke. Additionally, two points were added for diabetes. Scores ranged from 0 to 5 (Golub et al., 2019).

Statistical Analysis

Statistical analysis was performed following CDC analytical reporting guidelines for complex NHANES data analysis[2]. We considered masked variance and used the recommended weighting scheme. Demographic characteristics among different TL groups (quartile) were compared using chi-square test or weighted linear regression model. To assess whether LTL is correlated with cognitive decline, our statistical analysis included three main steps. First, we employed weighted univariate and multivariate linear regression models. Multivariate models included model I (only gender, race, and educational level were adjusted) and model II [gender, race, educational level, age, CAD score, and body mass index (BMI) were adjusted]. Second, to account for non-linearity of cognitive decline and LTL, we conducted smooth curve fitting (penalized spline method) and weighted generalized additive model (GAM). Third, we performed subgroup analyses using weighted stratified linear regression models. For the continuous variable, we first converted it to a categorical variable according to the clinical cut point and then performed an interaction test.

To ensure that the data analysis is robust, we converted the TL into a categorical variable by quartile and calculated the P for trend. We did this to verify the TL results as a continuous variable and to observe the possibility of non-linearity.

All analyses were performed using the statistical software packages R[3] (The R Foundation) and EmpowerStats[4] (X&Y Solutions, Inc., Boston, MA, United States). *P*-values less than 0.05 (two-sided) were considered statistically significant.

RESULTS

Participants' Baseline Characteristics

Table 1 shows the weighted distribution of socio-demographic characteristics and other covariates of the selected participants in the NHANES 1999–2002 population.

The participants in this sample averaged 70.99 ± 7.54 years old, with women representing 51.1%. Among different TL groups (quartile, Q1–Q4), the following distributions were similar: educational level, BMI, CAD score, history of hypertension, diabetes, hyperlipidemia, and stroke. Compared with groups Q1 and Q2, groups Q3 and Q4 were younger and had a higher percentage of females. Regarding cognitive performance, DSST scores ranged from 0 to 117, with a mean of 44.56 (SD = 17.68). In addition, the maximum and minimum T/S ratio values were 3.00 and 0.39, respectively, with a mean of 0.91 (SD = 0.22).

Univariate Linear Regression Analysis

We first assessed a univariate linear regression model to evaluate the relationship between LTL and DSST. The results found that female gender, educational level, and LTL are positively correlated with DSST score, whereas male gender, age, and CAD score are negatively associated with DSST score (see **Supplementary Table S1** in the Appendix).

Multivariate Linear Regression Analysis of the LTL–DSST Relationship

Table 2 shows the coefficients of the association between LTL as continuous variable and DSST score. Our multivariate linear regression analysis showed a negative correlation between LTL and DSST score in the crude model (odds ratio [OR] 9.51 [5.82–13.19], $P < 0.01$) (see **Table 2**). In the adjusted model I (adjusted by gender, race, and educational level) and model II (adjusted by gender, race, educational level, age, CAD score, and BMI), the results remained stable (OR 10.27 [6.83, 13.72], $P < 0.01$; OR 3.47 [0.14, 6.79], $P = 0.04$).

Additionally, to further detect the correlation of LTL–DSST interaction, we stratified the participants into four groups by the 25th, 50th, and 75th LTLx percentiles (0.39–0.76, 0.76–0.88, 0.88–1.03, and 1.03–3.00, respectively). LTL was regarded as a categorical variable (quartile), and a similar trend was observed (*P* for trend = 0.03; see **Table 2**). On multivariable analysis, participants in quartile 4 had 139% higher odds of getting higher DSST score than those in quartile 1.

Analyses of LTL–DSST Non-linear Relationship

It is essential to analyze non-linear relationships for continuous variables. A weighted GAM and smooth curve fitting (penalized spline method) were used to investigate the non-linear relationship between LTL and DSST scores. After adjusting for gender, age, educational level, race, CAD score, and BMI, we did not observe a non-linear relationship between LTL and DSST (see **Supplementary Figure S1** in the Appendix).

Subgroup Analyses

Table 3 shows our subgroup analysis results. We found that, after adjusting for potential confounders, the interaction test was not statistically significant for age, educational level, gender, race, CAD score, and BMI (*P* for interaction > 0.05). Thus, we do not detect any substantial evidence to prove that there are systematic differences in associations in different subgroups of the population, which means our main results are stable.

DISCUSSION

This study's central finding suggests that cognitive decline correlated significantly with shorter LTL among elderly individuals, and the findings were found to be robust after adjusting for various potential confounders.

Previous studies have noted the role of LTL in a series of age-related chronic diseases including neurodegenerative and CAD (Panossiana et al., 2003; Benetos et al., 2004; Martin et al., 2006; Brouilette et al., 2007; van der Harst et al., 2007; Fitzpatrick et al., 2011). Consistent with our results, some previous studies

[2]https://wwwn.cdc.gov/nchs/nhanes/tutorials/default.aspx

[3]http://www.R-project.org

[4]http://www.empowerstats.com

TABLE 1 | Baseline characteristics of participants.

Telomere length (T/S ratio)	Total sample	Q1 (0.389–0.759)	Q2 (0.759–0.880)	Q3 (0.880–1.026)	Q4 (1.026–3.001)	*P*-value
N	2,006	866	558	370	212	
Age [mean (SD)]	70.99 (7.54)	73.17 (7.96)	71.09 (7.71)	69.76 (7.53)	68.81 (7.30)	<0.001
BMI	28.78 (6.09)	28.11 (5.15)	28.12 (5.69)	28.29 (5.50)	28.67 (5.70)	0.585
Gender						<0.001
Male	6, 614 (48.88%)	470 (54.27%)	289 (51.79%)	156 (42.16%)	84 (39.62%)	
Female	6, 916 (51.12%)	396 (45.73%)	269 (48.21%)	214 (57.84%)	128 (60.38%)	
Educational level						0.447
High school	6, 540 (48.34%)	471 (54.39%)	280 (50.18%)	200 (54.05%)	114 (53.77%)	
Above high school	6, 990 (51.66%)	395 (45.61%)	278 (49.82%)	170 (45.95%)	98 (46.23%)	
CAD score [mean (SD)]	1.20 (1.18)	1.01 (1.10)	0.98 (1.09)	0.91 (0.99)	1.03 (1.12)	0.476
Diabetes						0.238
No	10, 281 (78.53%)	693 (82.60%)	455 (84.10%)	314 (87.22%)	172 (82.69%)	
Yes	2, 810 (21.47%)	146 (17.40%)	86 (15.90%)	46 (12.78%)	36 (17.31%)	
Hypertension						0.509
No	5, 495 (40.72%)	426 (49.31%)	276 (49.64%)	178 (48.37%)	93 (43.87%)	
Yes	7, 998 (59.28%)	438 (50.69%)	280 (50.36%)	190 (51.63%)	119 (56.13%)	
Hyperlipidemia						0.955
No	12, 012 (89.68%)	762 (89.96%)	496 (89.69%)	327 (89.59%)	191 (90.95%)	
Yes	1, 383 (10.32%)	85 (10.04%)	57 (10.31%)	38 (10.41%)	19 (9.05%)	
Stroke						0.556
No	12, 349 (91.49%)	801 (92.60%)	518 (93.33%)	349 (94.32%)	201 (94.81%)	
Yes	1, 148 (8.51%)	64 (7.40%)	37 (6.67%)	21 (5.68%)	11 (5.19%)	
Race						0.002
Mexican American	1, 248 (9.22%)	101 (11.66%)	64 (11.47%)	48 (12.97%)	14 (6.60%)	
Other Hispanic	858 (6.34%)	28 (3.23%)	13 (2.33%)	8 (2.16%)	12 (5.66%)	
Non-Hispanic White	7, 918 (58.52%)	603 (69.63%)	373 (66.85%)	255 (68.92%)	131 (61.79%)	
Non-Hispanic Black	2, 717 (20.08%)	117 (13.51%)	90 (16.13%)	53 (14.32%)	52 (24.53%)	
Other Race	789 (5.83%)	17 (1.96%)	18 (3.23%)	6 (1.62%)	3 (1.42%)	

CAD score: 1 score was appointed for each of the three current risk factors, including history of hypertension, coronary heart disease, or stroke. Additionally, two points were added for diabetes. Scores range from 0 to 5.

TABLE 2 | Multivariable linear regressions analysis of the LTL–DSST relationship.

Exposure	Non-adjusted model	Model I	Model II
Telomere length (T/S ratio)	9.51 (5.82, 13.19), <0.01	10.27 (6.83, 13.72), <0.01	3.47 (0.14, 6.79), 0.04
Telomere length (T/S ratio)			
Q1 (0.39–0.76)	Reference	Reference	Reference
Q2 (0.76–0.88)	2.93 (1.01, 4.85), <0.01	2.87 (1.08, 4.66), 0.01	0.88 (−0.81, 2.58), 0.31
Q3 (0.88–1.02)	4.52 (2.30, 6.73), <0.01	4.43 (2.37, 6.50), <0.01	1.01 (−0.96, 2.97), 0.32
Q4 (1.02–3.00)	4.75 (2.02, 7.49), <0.01	5.87 (3.32, 8.43), <0.01	2.39 (−0.04, 4.82), 0.05
P for trend	<0.001	<0.001	0.03

Model I adjusted for gender, race, and educational level; model II adjusted for gender, race, educational level, age, CAD score, and BMI.

found that compared with healthy individuals, patients with cognitive disorder [including mild cognitive impairment (MCI) and Alzheimer's disease (AD)] have truncated TLs in peripheral blood leukocytes (Honig et al., 2006; Grodstein et al., 2008; Mather et al., 2010; Valdes et al., 2010), mononuclear cell (Panossiana et al., 2003), and even in brain tissue (Thomas et al., 2008), while other studies did not observe a correlation between cognitive performance and LTL (Zekry et al., 2010; Hochstrasser et al., 2012; Movérare-Skrtic et al., 2012).

Furthermore, genetics might be a potential confounder in such a correlation in view of the heritable characteristics of LTL (Jeanclos et al., 2000; Nawrot et al., 2004). However, studies have also found significant differences in cognitive scores between twins with inconsistent TL, and the results confirmed that the correlation observed between decreased cognitive ability and shortened TL is robust to age and possible confounding factors.

The precise mechanism underlying the correlation between shorter LTL and cognitive decline remains unclear. Regarding TL, apart from the erosion of telomeres with cell division, telomeres are highly sensitive to damage by oxidative stress and inflammation (Saretzki and Von Zglinicki, 2002; Aviv et al., 2006). Oxidative stress enhances telomere attrition with each cell division (Saretzki and Von Zglinicki, 2002), whereas inflammation entails increased leukocyte turnover

TABLE 3 | Effect size of prespecified and exploratory subgroups.

Characteristic	No. of participants	Effect size (95% CI), *P*-value	*P* for interaction
Age			0.946
<70	781	5.26 (0.24, 10.28), **0.04**	
≥70	864	5.02 (0.38, 9.66), **0.03**	
Gender			0.815
Male	816	3.04 (−1.87, 7.95), 0.23	
Female	829	3.04 (−1.87, 7.95), 0.23	
Race			0.434
Mexican American	176	−0.13 (−11.76, 11.51), 0.98	
Other Hispanic	50	−9.90 (−25.39, 5.59), 0.21	
Non-Hispanic White	1,152	4.06 (0.17, 7.95), **0.04**	
Non-Hispanic Black	229	6.26 (−2.23, 14.75), 0.15	
Other race	38	5.85 (−26.79, 38.50), 0.73	
CAD score			0.583
<3	1,463	3.73 (0.18, 7.29), **0.04**	
≥3	182	1.01 (−8.16, 10.18), 0.83	
Educational level			0.206
High school	845	5.27 (0.92, 9.63), **0.02**	
Above high school	800	1.10 (−3.85, 6.06), 0.66	
BMI			0.480
Lower	439	1.80 (−4.03, 7.62), 0.55	
Higher	1,206	4.30 (0.32, 8.27), **0.03**	

Gender, race, educational level, age, CAD score, and BMI were adjusted. Bold data mean p value < 0.5.

and subsequently heightens telomere attrition. An *in vitro* study reported that the telomere shortening process could be modulated by oxidative stress (Kawanishi and Oikawa, 2004), and many proinflammatory markers, such as interleukin (IL)-6, were negatively correlated with TL (O'Donovan et al., 2011). Evidence showed that short/dysfunctional telomeres in peripheral immune cells as well as in microglia could contribute to cellular senescence that are linked to higher secretion of proinflammatory mediators that play an important role in the etiopathogenesis and progression of cognitive impairment (Collado et al., 2007; Jurk et al., 2012; Weng, 2012; Boccardi et al., 2015). To some extent, LTL might hinge on the cumulative burden of inflammation and oxidative stress across the lifespan (Sultana et al., 2009). Therefore, oxidative stress and inflammation might be the potential thread linking TL shortening with cognitive dysfunction.

Several alternative pathways may underlie the pathogenesis of cognitive impairment. The hippocampus is closely associated with cognitive function and is regarded as a key area affected by aging. It has been reported that TL is independently associated with cortical epithelial marginal areas (including hippocampus and orbitofrontal cortex areas), which overlaps with brain regions related to cognitive impairment psychopathology. Previous animal research reported that telomerase-deficient mice models showed neuronal loss in the hippocampus and frontal cortex linked with short-term memory deficits (Rolyan et al., 2011), whereas telomerase reactivation could reverse aging-related cognitive deficits (Jaskelioff et al., 2011).

This study exhibits multiple strengths. The multi-ethnic, national representative data from NHANES allow our findings to be extrapolated to a broader population. LTL and cognitive assessment were measured in a large sample, offering high statistical power to explore their connection. Additionally, with the NHANES's rigorous methodology and comprehensive quality procedures, we adjusted for several potential confounders by capitalizing on its abundant data.

However, this study also has several imitations. First, its primary constraint is its cross-sectional design, precluding inferences about causation. Second, LTL comes from one measurement rather than assessed longitudinally, which may provide key insights into the aging process. The shortening rate of LTL may be a more relevant indicator of the wear and tear that results in accelerated biological aging than TL measured at one point in time. Third, because TL maintenance or loss is related to many environmental factors, TL is also controlled by genetics and varies widely between individuals (Graakjaer et al., 2004). Therefore, ideally, one must consider all these intermediate parameters before attributing the differences in TL to a particular phenomenon. Fourth, a potential limitation is the use of only one specific measure of cognitive ability rather than multiple ones, and the type of cognitive measurement might lead to different findings. Accompanying tests, such as the Mini Mental Status Examination (MMSE), could help to assess cognitive function more comprehensively. However, DSST performance seems to be sensitive in reflecting attention/concentration, visual discrimination, information processing speed, and working memory and is especially suitable for screening MCI in the elderly (Salthouse, 1996). Moreover, it was reported to be less sensitive to educational level (Hoyer et al., 2004). Thus, the DSST scale may represent a relatively comprehensive cognitive scale (Launer et al., 2011). Future studies are required to determine the relationship between LTL and cognitive decline, which may reveal new knowledge on the effect of oxidative stress and inflammation on health and longevity.

CONCLUSION

Using the NHANES database, this study found a significant association between LTL and cognitive performance in the elderly after adjusting for potential confounding factors. Further high-quality studies need to be conducted to better understand the pathophysiology of such a correlation.

DATA AVAILABILITY STATEMENT

Publicly available datasets were analyzed in this study. These data can be found here: https://wwwn.cdc.gov/nchs/nhanes/tutorials/default.aspx.

ETHICS STATEMENT

The studies involving humans were reviewed and approved by the National Center for Health Statistics Research Ethics Review

Board. Patients/participants provided their written informed consent to participate in the study.

AUTHOR CONTRIBUTIONS

DBR, DLH, and QS designed the study. DLH and QS drafted the manuscript. DLH, QS, and CC acquired the data. CC, DLH, and QS analyzed the data. DBR, CC, LXL, ZLX, and ZZL revised the manuscript critically for important intellectual content. All authors contributed to the article and approved the submitted version.

FUNDING

This research was conducted with support from the 1.3.5 project for disciplines of excellence, West China Hospital, Sichuan University and the National Key R&D Program of China (2017YFC0840100 and 2017YFC0840101) and China Postdoctoral Science Foundation (2020M670055ZX).

SUPPLEMENTARY MATERIAL

The Supplementary Material for this article can be found online at: https://www.frontiersin.org/articles/10.3389/fnagi.2020.527658/full#supplementary-material

REFERENCES

Anstey, K. J., Dear, K., Christensen, H., and Jorm, A. F. (2005). Biomarkers, health, lifestyle, and demographic variables as correlates of reaction time performance in early, middle, and late adulthood. *Q. J. Exp. Psychol. A* 58, 5–21. doi: 10.1080/02724980443000232

Aviv, A., Valdes, A., Gardner, J. P., Swaminathan, R., Kimura, M., Spector, T. D., et al. (2006). Menopause modifies the association of leukocyte telomere length with insulin resistance and inflammation. *J. Clin. Endocrinol. Metab.* 91, 635–640. doi: 10.1210/jc.2005-1814

Benetos, A., Gardner, J. P., Zureik, M., Labat, C., Xiaobin, L., Adamopoulos, C., et al. (2004). Short telomeres are associated with increased carotid atherosclerosis in hypertensive subjects. *Hypertension* 43, 182–185. doi: 10.1161/01.HYP.0000113081.42868.f4

Boccardi, V., Pelini, L., Ercolani, S., Ruggiero, C., and Mecocci, P. (2015). From cellular senescence to Alzheimer's disease: the role of telomere shortening. *Age. Res. Rev.* 22, 1–8. doi: 10.1016/j.arr.2015.04.003

Brouilette, S. W., Moore, J. S., McMahon, A. D., Thompson, J. R., Ford, I., Shepherd, J., et al. (2007). Telomere length, risk of coronary heart disease, and statin treatment in the west of scotland primary prevention study: a nested case-control study. *Lancet* 369, 107–114. doi: 10.1016/S0140-6736(07)60071-3

Cawthon, R. M. (2002). Telomere measurement by quantitative PCR. *Nucleic Acids Res.* 30:e47. doi: 10.1093/nar/30.10.e47

Collado, M., Blasco, M. A., and Serrano, M. (2007). Cellular senescence in cancer and aging. *Cell* 130, 223–233. doi: 10.1016/j.cell.2007.07.003

Connors, M. H., Sachdev, P. S., Kochan, N. A., Xu, J., and Draper, B. (2015). Cognition and mortality in older people: the sydney memory and ageing study. *Age Age.* 44, 1049–1054. doi: 10.1093/ageing/afv139

Fitzpatrick, A. L., Kronmal, R. A., Kimura, M., Gardner, J. P., Psaty, B. M., Jenny, N. S., et al. (2011). Leukocyte telomere length and mortality in the cardiovascular health study. *J. Gerontol. Ser. A Biol. Sci. Med. Sci.* 66, 421–429. doi: 10.1093/gerona/glq224

Foster, T. C. (2006). Biological markers of age-related memory deficits: treatment of senescent physiology. *CNS Drugs* 20, 153–166. doi: 10.2165/00023210-200620020-00006

Golub, J. S., Brickman, A. M., Ciarleglio, A. J., Schupf, N., and Luchsinger, J. A. (2019). Association of subclinical hearing loss with cognitive performance. *JAMA Otolaryngol. Head Neck Surg.* 146, 57–67. doi: 10.1001/jamaoto.2019.3375

Graakjaer, J., Pascoe, L., Der-Sarkissian, H., Thomas, G., Kolvraa, S., Christensen, K., et al. (2004). The relative lengths of individual telomeres are defined in the zygote and strictly maintained during life. *Aging Cell* 3, 97–102. doi: 10.1111/j.1474-9728.2004.00093.x

Grodstein, F., van, O. M., Irizarry, M. C., Rosas, H. D., Hyman, B. T., Growdon, J. H., et al. (2008). Shorter telomeres may mark early risk of dementia: preliminary analysis of 62 participants from the nurses' health study. *PLoS One* 3:e1590. doi: 10.1371/journal.pone.0001590

Harris, S. E., Martin, R. C., von, Z. T., Starr, J. M., and Deary, I. J. (2012). Telomere length and aging biomarkers in 70-year-olds: the lothian birth cohort 1936. *Neurobiol. Aging* 33, 1483–1486. doi: 10.1016/j.neurobiolaging.2010.11.013

Heywood, R., Gao, Q., Nyunt, M., Feng, L., Chong, M. S., Shiong, W., et al. (2017). Hearing loss and risk of mild cognitive impairment and dementia: findings from the singapore longitudinal ageing study. *Dement. Geriatr. Cogn. Disord.* 43, 259–268. doi: 10.1159/000464281

Hochstrasser, T., Marksteiner, J., and Humpel, C. (2012). Telomere length is age-dependent and reduced in monocytes of Alzheimer patients. *Exp. Gerontol.* 47, 160–163. doi: 10.1016/j.exger.2011.11.012

Honig, L. S., Schupf, N., Lee, J. H., Tang, M. X., and Mayeux, R. (2006). Shorter telomeres are associated with mortality in those with APOE epsilon4 and dementia. *Ann. Neurol.* 60, 181–187. doi: 10.1002/ana.20894

Hoyer, W. J., Stawski, R. S., Wasylyshyn, C., and Verhaeghen, P. (2004). Adult age and digit symbol substitution performance: a meta-analysis. *Psychol. Aging* 19:211. doi: 10.1037/0882-7974.19.1.211

Jaskelioff, M., Muller, F. L., Paik, J. H., Thomas, E., Jiang, S., Horner, J. W., et al. (2011). Telomerase reactivation reverses tissue degeneration in aged telomerase-deficient mice. *Nature* 469, 102–106. doi: 10.1038/nature09603

Jeanclos, E., Schork, N. J., Kyvik, K. O., Kimura, M., Skurnick, J. H., Aviv, A., et al. (2000). Telomere length inversely correlates with pulse pressure and is highly familial. *Hypertension* 36, 195–200. doi: 10.1161/01.hyp.36.2.195

Jiang, J., Wang, Y., Sušac, L., Chan, H., Basu, R., Zhou, Z. H., et al. (2018). Structure of telomerase with telomeric dna. *Cell* 173, 1179–1190. doi: 10.1016/j.cell.2018.04.038

Jurk, D., Wang, C., Miwa, S., Maddick, M., and Korolchuk, V. (2012). Postmitotic neurons develop a p21-dependent senescence-like phenotype driven by a DNA damage response. *Aging Cell.* 11, 996–1004. doi: 10.1111/j.1474-9726.2012.00870.x

Kawanishi, S., and Oikawa, S. (2004). Mechanism of telomere shortening by oxidative stress. *Ann. N. Y. Acad. Sci.* 1019, 278–284. doi: 10.1196/annals.1297.047

Lau, F. C., Shukitt-Hale, B., and Joseph, J. A. (2007). Nutritional intervention in brain aging: reducing the effects of inflammation and oxidative stress. *Subcell. Biochem.* 42, 299–318.

Launer, L. J., Miller, M. E., Williamson, J. D., Lazar, R. M., Gerstein, H. C., Sikstrom, J., et al. (2011). Effects of intensive glucose lowering on brain structure and function in people with type 2 diabetes (ACCORD MIND): a randomised open-label substudy. *Lancet Neurol.* 10, 969–977. doi: 10.1016/S1474-4422(11)70188-0

Li, S. C., Lindenberger, U., and Sikstrom, S. (2001). Aging cognition: from neuromodulation to representation. *Trends Cogn. Sci.* 5, 479–486. doi: 10.1016/s1364-6613(00)01769-1

Lin, J., Epel, E., Cheon, J., Kroenke, C., Sinclair, E., Bigos, M., et al. (2010). Analyses and comparisons of telomerase activity and telomere length in human t and b cells: insights for epidemiology of telomere maintenance. *J. Immunol. Methods* 352, 71–80. doi: 10.1016/j.jim.2009.09.012

López, O. C., Blasco, M. A., Partridge, L., Serrano, M., and Kroemer, G. (2013). The hallmarks of aging. *Cell* 153, 1194–1217. doi: 10.1016/j.cell.2013.05.039

Martin, R. C., Dickinson, H. O., Keys, B., Rowan, E., Kenny, R. A., Von Zglinicki, T., et al. (2006). Telomere length predicts poststroke mortality, dementia, and cognitive decline. *Ann. Neurol.* 60, 174–180. doi: 10.1002/ana.20869

Mather, K. A., Jorm, A. F., Anstey, K. J., Milburn, P. J., Easteal, S., Mattsson, N., et al. (2010). Cognitive performance and leukocyte telomere length in two narrow age-range cohorts: a population study. *BMC Geriatr.* 10:62. doi: 10.1186/1471-2318-10-62

Mazidi, M., Kengne, A. P., Mikhailidis, D. P., Toth, P. P., Ray, K. K., Banach, M., et al. (2017). Dietary food patterns and glucose/insulin homeostasis: a cross-sectional study involving 24,182 adult americans. *Lipids Health Dis.* 16:192. doi: 10.1186/s12944-017-0571-x

Miu, A. C., Homberg, J. R., and Lesch, K. P. (2019). *Genes, Brain, and Emotions: From Resilience to Psychopathology*. Oxford: Oxford University Press.

Movérare-Skrtic, S., Johansson, P., Mattsson, N., Hansson, O., and Wallin, A. (2012). Leukocyte telomere length (LTL) is reduced in stable mild cognitive impairment but low LTL is not associated with conversion to Alzheimer's disease: a pilot study. *Exp. Gerontol.* 47, 179–182. doi: 10.1016/j.exger.2011.12.005

Nawrot, T. S., Staessen, J. A., Gardner, J. P., and Aviv, A. (2004). Telomere length and possible link to x chromosome. *Lancet* 363, 507–510. doi: 10.1016/S0140-6736(04)15535-9

Needham, B. L., Adler, N., Gregorich, S., Rehkopf, D., Lin, J., Blackburn, E. H., et al. (2013). Socioeconomic status, health behavior, and leukocyte telomere length in the national health and nutrition examination survey, 1999-2002. *Soc. Sci. Med.* 85, 1–8. doi: 10.1016/j.socscimed.2013.02.023

Oberlin, B. S., Tangney, C. C., Gustashaw, K. A., and Rasmussen, H. E. (2013). Vitamin b12 deficiency in relation to functional disabilities. *Nutrients* 5, 4462–4475. doi: 10.3390/nu5114462

O'Donovan, A., Pantell, M. S., Puterman, E., Dhabhar, F. S., Blackburn, E. H., Yaffe, K., et al. (2011). Cumulative inflammatory load is associated with short leukocyte telomere length in the health, aging and body composition study. *PLoS One* 6:e19687. doi: 10.1371/journal.pone.0019687

Panossiana, L. A., Porterb, V. R., Valenzuelaa, H. F., Zhua, X., Rebackb, E., Mastermanb, D., et al. (2003). Telomere shortening in t cells correlates with alzheimer's disease status. *Neurobiol. Aging* 24, 77–84. doi: 10.1016/s0197-4580(02)00043-x

Peila, R., and Launer, L. J. (2006). Inflammation and dementia: epidemiologic evidence. *Acta Neurol. Scand. Suppl.* 185, 102–106. doi: 10.1111/j.1600-0404.2006.00693.x

Rafnsson, S. B., Deary, I. J., Smith, F. B., Whiteman, M. C., Rumley, A., Fowkes, G., et al. (2007). Cognitive decline and markers of inflammation and hemostasis: the edinburgh artery study. *J. Am. Geriatr. Soc.* 55, 700–707. doi: 10.1111/j.1532-5415.2007.01158.x

Rolyan, H., Scheffold, A., Heinrich, A., Begus-Nahrmann, Y., Langkopf, B. H., Liss, B., et al. (2011). Telomere shortening reduces Alzheimer's disease amyloid pathology in mice. *Brain* 134, 2044–2056. doi: 10.1093/brain/awr133

Salthouse, T. A. (1996). The processing-speed theory of adult age differences in cognition. *Psychol. Rev.* 103, 403–428. doi: 10.1037/0033-295x.103.3.403

Saretzki, G., and Von Zglinicki, T. (2002). Replicative aging, telomeres, and oxidative stress. *Ann. N. Y. Acad. Sci.* 959, 24–29. doi: 10.1111/j.1749-6632.2002.tb02079.x

Serrano, A. L., and Andrés, V. (2004). Telomeres and cardiovascular disease: does size matter? *Circ. Res.* 94, 575–584. doi: 10.1161/01.RES.0000122141.18795.9C

Shammas, M. A. (2011). Telomeres, lifestyle, cancer, and aging. *Curr. Opin. Clin. Nutr. Metab. Care* 14, 28–34. doi: 10.1097/MCO.0b013e32834121b1

Sultana, R., Perluigi, M., and Butterfield, D. A. (2009). Oxidatively modified proteins in alzheimer's disease (ad), mild cognitive impairment and animal models of ad: role of abeta in pathogenesis. *Acta Neuropathol.* 118, 131–150. doi: 10.1007/s00401-009-0517-0

Thomas, P., O' Callaghan, N. J., and Fenech, M. (2008). Telomere length in white blood cells, buccal cells and brain tissue and its variation with ageing and Alzheimer's disease. *Mech. Age. Dev.* 129, 183–190. doi: 10.1016/j.mad.2007.12.004

Valdes, A. M., Deary, I. J., Gardner, J., Kimura, M., Lu, X., Spector, T. D., et al. (2010). Leukocyte telomere length is associated with cognitive performance in healthy women. *Neurobiol. Aging* 31, 986–992. doi: 10.1016/j.neurobiolaging.2008.07.012

Valdes, A. M., Richards, J. B., Gardner, J. P., Swaminathan, R., Kimura, M., Xiaobin, L., et al. (2007). Telomere length in leukocytes correlates with bone mineral density and is shorter in women with osteoporosis. *Osteopor. Intern.* 18, 1203–1210. doi: 10.1007/s00198-007-0357-5

van der Harst, P., van der Steege, G., de Boer, R. A., Mulder, M. J., Van der Harst, P., van der Steege, G., et al. (2007). Telomere length of circulating leukocytes is decreased in patients with chronic heart failure. *J. Am. Coll. Cardiol.* 49, 1459–1464. doi: 10.1016/j.jacc.2007.01.027

van der Wardt, V., Logan, P., Hood, V., Booth, V., Masud, T., Harwood, R., et al. (2015). The association of specific executive functions and falls risk in people with mild cognitive impairment and early-stage dementia. *Dement. Geriatr. Cogn. Disord.* 40, 178–185. doi: 10.1159/000433523

von Zglinicki, T., Serra, V., Lorenz, M., Saretzki, G., Lenzen-Grossimlighaus, R., Gessner, R., et al. (2000). Short telomeres in patients with vascular dementia: an indicator of low antioxidative capacity and a possible risk factor? *Lab. Invest.* 80, 1739–1747. doi: 10.1038/labinvest.3780184

Vos, T., Flaxman, A. D., Naghavi, M., Lozano, R., Michaud, C., Baddour, K., et al. (2012). Years lived with disability (ylds) for 1160 sequelae of 289 diseases and injuries 1990-2010: a systematic analysis for the global burden of disease study 2010. *Lancet* 380, 2163–2196. doi: 10.1016/S0140-6736(12)61729-2

Weng, N. P. (2012). Telomeres and immune competency. *Curr. Opin. Immunol.* 24, 470–475. doi: 10.1016/j.coi.2012.05.001

Willeit, P., Raschenberger, J., Heydon, E. E., Tsimikas, S., Haun, M., Mayr, A., et al. (2014). Leucocyte telomere length and risk of type 2 diabetes mellitus: new prospective cohort study and literature-based meta-analysis. *PLoS One* 9:e112483. doi: 10.1371/journal.pone.0112483

Xu, M., Pirtskhalava, T., Farr, J. N., Weigand, B. M., Palmer, A. K., Christine, M., et al. (2018). Senolytics improve physical function and increase lifespan in old age. *Nat. Med.* 24, 1246–1256. doi: 10.1038/s41591-018-0092-9

Yaffe, K., Lindquist, K., Kluse, M., Cawthon, R., Harris, T., Hsueh, W. C., et al. (2011). Telomere length and cognitive function in community-dwelling elders: findings from the health abc study. *Neurobiol. Aging* 32, 2055–2060. doi: 10.1016/j.neurobiolaging.2009.12.006

Zekry, D., Herrmann, F. R., Irminger-Finger, I., Graf, C., and Genet, C. (2010). Telomere length and ApoE polymorphism in mild cognitive impairment, degenerative and vascular dementia. *J. Neurol. Sci.* 299, 108–111. doi: 10.1016/j.jns.2010.07.019

Conflict of Interest: The authors declare that the research was conducted in the absence of any commercial or financial relationships that could be construed as a potential conflict of interest.

frontiers in Aging Neuroscience

BRIEF RESEARCH REPORT
published: 03 November 2020
doi: 10.3389/fnagi.2020.524024

Machine Learning Classification Identifies Cerebellar Contributions to Early and Moderate Cognitive Decline in Alzheimer's Disease

Muriel M. K. Bruchhage[1,2]*, *Stephen Correia*[3,4], *Paul Malloy*[3,4], *Stephen Salloway*[3,4,5] *and Sean Deoni*[1,2,6]

[1]Advanced Baby Imaging Lab, Hasbro Children's Hospital, Rhode Island Hospital, Providence, RI, United States, [2]Department of Pediatrics, Warren Alpert Medical School at Brown University, Providence, RI, United States, [3]Butler Hospital Memory and Aging Program, Providence, RI, United States, [4]Department of Human Behavior and Psychiatry, Warren Alpert Medical School at Brown University, Providence, RI, United States, [5]Department of Neurology, Warren Alpert Medical School at Brown University, Providence, RI, United States, [6]Maternal, Newborn and Child Health Discovery & Tools, Bill & Melinda Gates Foundation, Seattle, WA, United States

Alzheimer's disease (AD) is one of the most common forms of dementia, marked by progressively degrading cognitive function. Although cerebellar changes occur throughout AD progression, its involvement and predictive contribution in its earliest stages, as well as gray or white matter components involved, remains unclear. We used MRI machine learning-based classification to assess the contribution of two tissue components [volume fraction myelin (VFM), and gray matter (GM) volume] within the whole brain, the neocortex, the whole cerebellum as well as its anterior and posterior parts and their predictive contribution to the first two stages of AD and typically aging controls. While classification accuracy increased with AD stages, VFM was the best predictor for all early stages of dementia when compared with typically aging controls. However, we document overall higher cerebellar prediction accuracy when compared to the whole brain with distinct structural signatures of higher anterior cerebellar contribution to mild cognitive impairment (MCI) and higher posterior cerebellar contribution to mild/moderate stages of AD for each tissue property. Based on these different cerebellar profiles and their unique contribution to early disease stages, we propose a refined model of cerebellar contribution to early AD development.

Keywords: Alzheimer's disease, dementia, cerebellum, machine learning, MCI (mild cognitive impairment), mild moderate AD, gray matter (GM), white matter (WM)

OPEN ACCESS

Edited by:
Jiehui Jiang,
Shanghai University, China

Reviewed by:
Alexander LLoyd MacKay,
University of British Columbia, Canada
Gabriel Gonzalez-Escamilla,
Johannes Gutenberg University Mainz, Germany

***Correspondence:**
Muriel M. K. Bruchhage
murielbruchhage@babyimaginglab.com

Received: *01 January 2020*
Accepted: *28 September 2020*
Published: *03 November 2020*

Citation:
Bruchhage MMK, Correia S, Malloy P, Salloway S and Deoni S (2020) Machine Learning Classification Identifies Cerebellar Contributions to Early and Moderate Cognitive Decline in Alzheimer's Disease. Front. Aging Neurosci. 12:524024. doi: 10.3389/fnagi.2020.524024

INTRODUCTION

Alzheimer's disease (AD) is the most prevalent form of dementia in the developed world (Reitz et al., 2011) and is defined by a progressive decline of a variety of cognitive functions and motor abilities. Accumulating evidence suggests that AD has a lengthy preclinical phase, where brain pathology accumulates and patient function declines, but symptoms are insufficient to warrant a clinical diagnosis of dementia. AD neurodegeneration follows specific topographic patterns of gray and white matter atrophy that emerge during its early stages (Serra et al., 2010).

Although the pathobiological basis of these alterations remains unclear, there is increasing evidence that white matter and myelin alterations occur at the earliest stages of the disease and are associated with cognitive decline, potentially preceding gray matter (GM) volume changes and loss (Braak et al., 2000). This has been supported by emerging preclinical (Desai et al., 2010), histological (Zhan et al., 2014) and longitudinal studies documenting white matter changes to be of particular importance for AD stages (Frings et al., 2014), in turn stressing the need to better characterize white matter and myelin change in early stages of cognitive decline in AD.

While the traditionally focus has been placed on neocortical and hippocampal atrophies, recent evidence suggests that the cerebellum undergoes focal atrophy in concert with interconnected cerebral nodes in both AD and fronto-temporal dementia (Guo et al., 2016). Histopathology studies of AD have shown cerebellar amyloid-β oligomers to be affected in a counter-clockwise pattern during disease progression, starting in the posterior cerebellar lobe, and paralleling cerebrum atrophy staging and associated symptom progression (Jacobs et al., 2018).

However, the functional decline is often present before an official AD diagnosis has been reached. For example, 60% of elderly patients with a cognitive decline also suffer from falls; twice more than those without impairment (Davis et al., 2011). In a functional MRI study, falling significantly more often in the elderly has implicated the right cerebellum as a potential region of interest in early cognitive decline and aging (Liu-Ambrose et al., 2008). While the cerebellum has long been associated with motor function, it is also involved in many non-motor functions, including working memory and executive functioning (Schmahmann et al., 2001; Bellebaum and Daum, 2007). Nevertheless, the role of cerebellar white and GM in disease progression and classifying stages of early cognitive decline from typical aging remain a challenge. To address these questions, we used machine learning-based classification on GM anatomical and volume fraction myelin images to investigate their contributions to predict the first two early stages of dementia [mild cognitive impairment (MCI) and mild and moderate AD] when compared with typically aging controls. We further calculate their predictive accuracy within the whole brain and neocortex and compare them with the anterior, posterior, and whole cerebellum to investigate the role of cerebellar white and GM in early AD progression.

MATERIALS AND METHODS

Participants

Forty-three age- and gender-matched participants (15 healthy controls; 17 MCI; and 11 Mild/Moderate AD) were included. Subject group demographics are shown in **Table 1**. A clinical interview, an assessment of cognitive decline using the Mini-Mental State Examination (MMSE), and clinical dementia rating (CDR) scores were used to assign the participants to the healthy (CDR = 0), MCI (CDR $\leq$ 0.5), and Mild/Moderate AD (0.5 $\leq$ CDR $\leq$ 1.0) groups. The CDR is a reliable and valid measure to assess AD stages (Morris, 1993; Nyunt et al., 2013) and its scores have been shown to usefully predict functional decline and incident dementia (Woolf et al., 2016). The MMSE is a 30-point questionnaire that is routinely used to assess cognitive impairment in clinical and research settings (Pangman et al., 2000). MANOVAs revealed no significant group differences in mean age or gender ratio between groups ($p > 0.10$, **Table 1**). Genetic screening was performed on individuals with AD and APOE (Apolipoprotein E) status was determined.

MRI Acquisition

All participants were imaged on a Siemens Tim Trio 3T scanner (Siemens Healthcare GmbH) with a 32-channel head RF array. A multimodal protocol was performed that included mcDESPOT myelin water imaging (Deoni et al., 2008), T1-weighted MP-RAGE anatomical, and diffusion tensor imaging. The mcDESPOT acquisition consists of eight variable flip angle T1-weighted spoiled gradient echo (SPGR_images and two sets of eight variable flip angle T1/T2-weighted fully-balanced steady-state free precession (bSSFP) images, with each set acquired with 0 or 180-degree RF phase cycling pattern (Deoni, 2011). In addition, an inversion-prepared (IR)-SPGR image was also acquired to correct for flip angle (B_1 field) inhomogeneities (Deoni, 2011).

MRI Analysis

Following the acquisition, data were visually checked for motion-related artifacts and then a standardized processing pipe-line was performed that included: (1) Skull stripping using the brain extraction tool (Smith, 2002) from the FSL software library (Smith et al., 2004); (2) Linear registration to account for subtle inter-scan motion using FSL's linear image registration tool (Jenkinson et al., 2002; Zhang et al., 2004); (3) Calculation of the main and transmit magnetic field (B_0 and B_1) calibration maps (Deoni, 2011); and (4) Estimation of the VFM at each brain voxel using a stochastic region contraction approach to fit a 3-pool model to the acquired SPGR and bSSFP data (Deoni and Kolind, 2015).

All anatomical and VFM images were first loaded to the SPM12's SUIT toolbox (Diedrichsen et al., 2009) to isolate structures of interest. For the whole brain and neocortex, we used the following steps for analysis: gray and white matter tissue class segmentation, DARTEL registration (Ashburner, 2007) to a common inter-subject space, a DARTEL utility to create Jacobian images. For the cerebellum, we used the following steps for analysis: SPM12's SUIT toolbox (Diedrichsen et al., 2009) to isolate the structure, DARTEL registration to SUIT space, a DARTEL utility to create Jacobian images. Jacobian determinant images have previously shown promise in discriminating neurodegeneration by allowing a comparison of the expansion and contraction of voxels across and within subjects (Studholme et al., 2004a,b; Hua et al., 2009, 2010; Anderson et al., 2012; Aksman et al., 2016). After applying a thresholded mask created in Matlab to fit the whole brain, cerebrum or whole/anterior/posterior cerebellum to exclude

TABLE 1 | Participant demographics.

	Healthy aging	Mild cognitive impairment	Mild to moderate AD	ANOVA *p*-value
Male:Female	3:12	8:9	2:9	0.24
Age	74.7 (5.2)	74.3 (7.7)	78.4 (8.6)	0.12
CDR	0	0.48 (0.2)	0.6 (0.2)	
MMSE	29.4 (1)	27.8 (1.7)	22 (1.6)	
APOE Not tested	15	3	0	
APOE ε2ε2		0	0	
APOE ε2ε3		1	0	
APOE ε3ε3		6	4	
APOE ε2ε4		0	0	
APOE ε3ε4		5	5	
APOE ε4ε4		2	2	

Mean values are given for male to female ratios, age in years, CDR and MMSE values as well as APOE status for all participants. Standard deviations are noted in brackets and p values on the right show non-significant differences between groups. Abbreviations: AD, Alzheimer's Disease; CDR, Clinical Dementia Rating; MMSE, Mini-Mental State Examination; APOE, Apolipoprotein E.

extracerebral or extracerebellar voxels, we used a two-class linear support vector machine learning algorithm, implementing the *C* cost support vector classifier at a fixed value of $C = 1$ throughout all classifications. Within the full dataset, we defined a set that is split into a training set *N* of subjects used to train the classifier, and a set *T* of subjects that are used to test the classifier's prediction ability. Specifically, we used leave-one-out cross-validation to learn a function from the data that can accurately predict the labels of unseen or new patterns and thus evaluate the classifier's performance. The model parameters learned in the training phase are represented as weights (weighted images are displayed in **Supplementary Figure 1**) and demonstrate the relative contribution of each feature to the predictive task.

Using freely available Matlab code[1], we created Jacobian weighted images, forward maps, as well as *p* and *t* thresholded maps at $p \leq 0.005$. Cerebellar masks were created by using the SUIT atlas (Diedrichsen et al., 2009) by combining vermis, left and right cerebellar lobules I–V to create the anterior cerebellar mask, and vermis, left and right cerebellar lobules VI–X to create the posterior cerebellar mask. The cerebrum mask consisted of the whole brain mask but excluding the cerebellum and brainstem. Jacobian weighted GM volume will be referred to as GM volume throughout the manuscript.

RESULTS

As expected, cognitive decline increased with increasing dementia stages (**Table 1**). The cerebellum as a region of interest displayed up to 28% higher classification accuracy when compared with the neocortex and up to 18% higher classification accuracy when compared with the whole brain, with the highest prediction accuracy of 75% of cerebellar VFM for mild/ moderate dementia (all results thresholded at $p \leq 0.005$, **Figure 1**). Clusters with the highest cerebellar effects were localized in the lateral cerebellum (x/y/z: 33/26/29 and 37/58/38 in SUIT space).

Weighted images are shown in **Supplementary Figure 1**. While classification accuracy increased with AD stages, GM volume was the best predictor for the earliest stage of dementia (MCI), while VFM demonstrated the highest prediction accuracy for the mild/moderate stage of dementia when compared with typically aging controls. Similarly, the cerebellar GM showed the highest prediction accuracy for CDR score (66.8%; **Supplementary Figure 2**), and consistently higher prediction accuracy when compared with the neocortex (**Supplementary Figure 2**). When dividing the cerebellum into its anterior and posterior lobe, the posterior cerebellar contribution increased in both GM volume and VFM (**Figure 2**). These changes were strongest in the Crus I/II (**Figure 2**).

DISCUSSION

In this study, we investigated the contribution of cerebellar GM volume and VFM to predict the first two early stages of AD (MCI and mild/moderate AD) when compared with the whole brain and cerebrum gray matter volume and volume fraction myelin.

Our findings suggest VFM and GM volume loss occur in the early stages of AD, with distinct patterns of anterior and posterior cerebellar contributions (**Figure 2**). Specifically, disease classification was driven by differences in the posterior cerebellum with its prediction accuracy increasing with symptom severity, paralleling histopathological findings of cerebellar β in the posterior cerebellar lobe (Jacobs et al., 2018).

The cerebellum can be divided functionally into the motor and sensorimotor functions processed in the anterior- posterior lobe and cognitive functions in posterior cerebellar regions, enabled by its distinct neuroanatomic (Middleton and Strick, 2001; Kelly and Strick, 2003) and functional connectivity (Buckner et al., 2011) connections. During the development of AD, cerebellar GM volume appears to follow a predictable pattern, affecting the vermis and posterior lobe in the early stages of the disease, continuing to evolve to the anterior lobe with disease progression (Jacobs et al., 2018). Indeed, lower GM cerebellar anterior volume has been shown in patients with early-onset AD carriers compared to non-carriers (Reiman et al., 2012) as well as in patients with MCI, although the direct nature of its contribution remains unclear possibly because of the diffuse nature of the disease (for a review, Jacobs et al., 2018). In contrast, cerebellar white matter volume declines more

[1]https://github.com/leonaksman/lpr

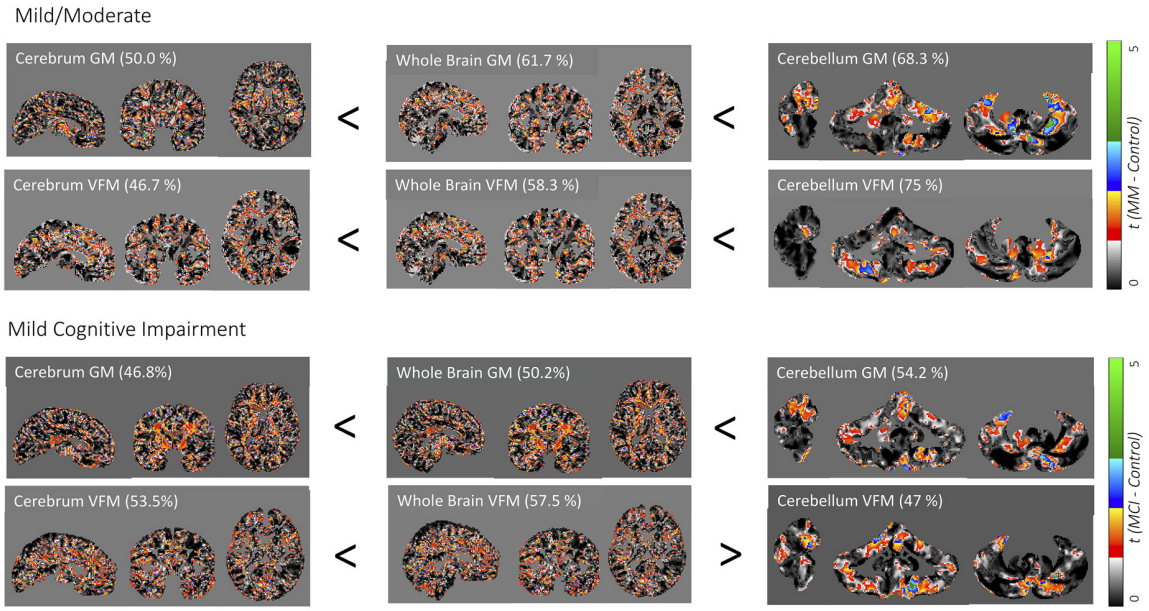

FIGURE 1 | Weighted prediction *t*-maps for the whole brain and cerebellum. Jacobian gray matter (GM) volume and volume fraction myelin (VFM) prediction *t*-maps for the cerebrum, whole brain, and whole cerebellum for mild/moderate Alzheimer's disease (AD; above) and mild cognitive impairment (MCI; below). Prediction accuracy percentage is noted in brackets and *t*-values ranging from 0 to 5 are indicated with a color bar on the right, with the lowest *t*-value in black to the highest *t*-value in green. x/y/z coordinates for the neocortex and whole-brain are 64/78/58 in DARTEL space, and 70/47/43 for the cerebellum in SUIT space.

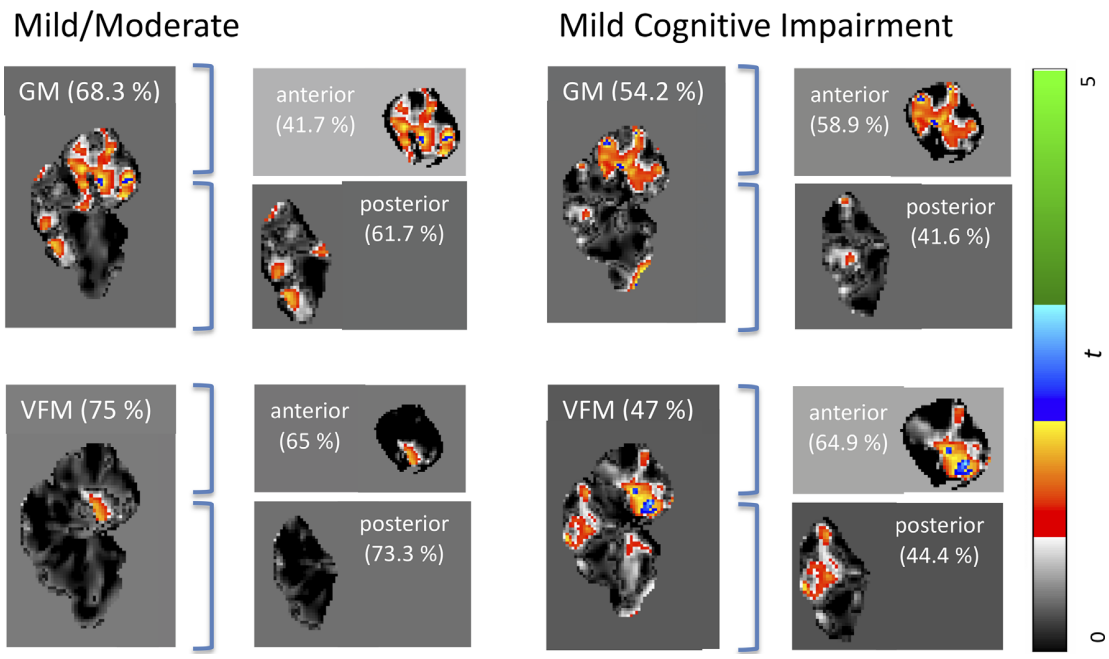

FIGURE 2 | Weighted prediction *t*-maps for the whole, anterior, and posterior cerebellum. Jacobian GM volume and VFM prediction *t*-maps for the whole, anterior, and posterior cerebellum for mild/moderate AD (left), and MCI (right). Prediction accuracy percentage is noted in brackets and *t*-values ranging from 0 to 5 are indicated with a color bar on the right, with the lowest *t*-value in black to the highest *t*-value in green. All *x* coordinates are *x* = 70 in SUIT space.

rapidly than GM volume, a pattern similar to that observed in the cerebral hemispheres (Jernigan et al., 2001). This pattern of different white and GM volume decline was supported by our study results, where myelin water fraction demonstrated the highest prediction accuracy, underlining the role of white matter alterations at the earliest stages of dementia.

These early developments of AD are also reflected microstructurally, as more diffuse amyloid-beta deposits in early-onset patients showed cerebellar pathology 30 years earlier than sporadic patients (Cole et al., 1993). Here, the degree of cerebellar amyloid-beta was negatively correlated with the age of onset, indicating cerebellar atrophy as a possible biomarker for the early stages of AD. This cerebellar pathology in early-onset AD is further accompanied by cerebellar motor phenomena such as ataxia, especially in PSEN1 mutations (Bateman et al., 2011). Motor phenomena precede the loss of cognitive functions and are associated with early detectable cognitive impairments of MCI and incident AD (Camicioli, 2010). This is in line with our results where the anterior cerebellar contribution to AD was strongest in the early stages followed by increasing posterior cerebellar contribution with cognitive function loss as indicated by decreasing CDR values and prediction (**Table 1**, **Figure 2**, **Supplementary Figure 2**). Our results are further paralleled by histological findings, where the concentration of cerebellar soluble fibrillar amyloid oligomers was inversely correlated with MMSE AD classification performance but positively with the presence of cerebral plaques and tangles, suggesting that AD molecular changes possibly already occur in the cerebellum in the preclinical stages and may contribute to the symptomatology and pathophysiology of the disorder (Mann et al., 1990). While our cerebellar findings seem to mirror these histopathological findings, it remains unclear whether this pattern corresponds to microtissue changes and should be followed up by combining VFM and GM volume MRI scans and histopathology of the cerebellum on tissue from early AD stages.

Cerebellar amyloid-β oligomers have been documented to be affected in a counter-clockwise manner starting in the posterior cerebellar lobe, thus paralleling cerebrum atrophy staging and associated symptom progression (Jankowsky et al., 2004; Gentier et al., 2015), has led to an AD stage model of cerebellar atrophy starting from the posterior to the anterior lobe with disease progression (Jacobs et al., 2018). Based on our findings, we propose a refined model of cerebellar contribution to AD development. We suggest that early AD disease stages are driven by both the anterior and posterior cerebellum, but an initially higher anterior cerebellar lobe contribution to the classification of the earliest stages of the disease and posterior cerebellar lobe contribution increasing with symptom severity. This parallels cerebellar functionality and AD symptom disease progression, as motor phenomena that are classically associated with anterior cerebellar dysfunction, such as ataxia, are early AD symptoms preceding cognitive symptoms that have been associated with posterior cerebellar dysfunction.

While high prediction accuracies of up to 75% could indicate an important contribution of the cerebellum to the earliest stage of AD (mild/ moderate), it decreases for MCI to around 50%. This discrepancy might suggest a less substantial contribution of the cerebellum to MCI development. However, when investigating cerebellar sub-regions, a pattern of higher anterior cerebellar contribution to MCI classification appears (64.9% prediction accuracy; **Figure 2**), which could be linked to its essential role in motor function and dysfunction.

Our findings support the role of cerebellar contribution to the early stages of AD pathology and define its unique contribution to early disease development prediction as well as subregions driving this classification. However, the cerebellum is often regarded as being spared in AD pathology and is consequently usually used as a control area or reference region in PET imaging studies over total brain volume to control for differences (for example, Dukart et al., 2010). Nevertheless, when a study compared regional glucose metabolism normalization methods using either total cerebral or cerebellar volume, cerebellar normalization was determined superior in identifying dementia patients in comparison to control subjects (Dukart et al., 2010). Together with our findings, it can be suggested to rather chose global brain measures than cerebellar volume for normalization methods to avoid bias towards early AD stages.

DATA AVAILABILITY STATEMENT

The datasets generated for this study are available on request to the corresponding author.

ETHICS STATEMENT

This study was reviewed by the IRB Department of Bradley Hospital, Rhode Island, USA. The patients/participants provided their written informed consent to participate in this study.

AUTHOR CONTRIBUTIONS

MB has been the lead in conceptualizing and writing the manuscript, as well as performing the analyses involved. SC, PM and SS have collected the data, recruited participants and performed the clinical interviews, as well as been involved in the design of the overall study. SD has been instrumental in feedback on the manuscript as well as adding insightful comments to the discussion and introduction, and was key to the design of the overall study. All authors contributed to the article and approved the submitted version.

FUNDING

We would like to thank the National Institutes of Health (UG3 ODO23313 and R01 MH087510) for their continuous support of this work.

SUPPLEMENTARY MATERIAL

The Supplementary Material for this article can be found online at: https://www.frontiersin.org/articles/10.3389/fnagi.2020.524024/full#supplementary-material.

SUPPLEMENTARY FIGURE 1 | Weighted maps for the whole brain and cerebellum. Jacobian gray matter (GM) volume and volume fraction myelin (VFM) weighted maps for the cerebrum, whole brain, and whole cerebellum for mild/moderate AD (above) and mild cognitive impairment (below). Prediction accuracy percentage is noted in brackets and *t*-values ranging from 0 to 5 are indicated with a color bar on the right, with the lowest *t*-value in black to the

highest *t*-value in green. x/y/z coordinates for the neocortex and whole-brain are 64/78/58 in DARTEL space, and 70/47/43 for the cerebellum in SUIT space.

SUPPLEMENTARY FIGURE 2 | Weighted prediction *t*-maps for the whole brain and cerebellum. Jacobian gray matter (GM) volume and volume fraction myelin (VFM) weighted maps for the cerebrum, whole brain, and whole cerebellum for clinical dementia rating (CDR) scores. Prediction accuracy percentage is noted in brackets and *t*-values ranging from 0 to 5 are indicated with a color bar on the right, with the lowest *t*-value in black to the highest *t*-value in green. x/y/z coordinates for the neocortex and whole-brain are 64/78/58 in DARTEL space, and 70/47/43 for the cerebellum in SUIT space.

REFERENCES

Aksman, L. M., Lythgoe, D. J., Williams, S. C. R., Jokisch, M., Mönninghoff, C., Streffer, J., et al. (2016). Making use of longitudinal information in pattern recognition. *Hum. Brain Mapp.* 37, 4385–4404. doi: 10.1002/hbm.23317

Anderson, V. M., Schott, J. M., Bartlett, J. W., Leung, K. K., Miller, D. H., and Fox, N. C. (2012). Gray matter atrophy rate as a marker of disease progression in AD. *Neurobiol. Aging* 33, 1194–1202. doi: 10.1016/j.neurobiolaging.2010.11.001

Ashburner, J. (2007). A fast diffeomorphic image registration algorithm. *NeuroImage* 38, 95–113. doi: 10.1016/j.neuroimage.2007.07.007

Bateman, R. J., Aisen, P. S., De Strooper, B., Fox, N. C., Lemere, C. A., Ringman, J. M., et al. (2011). Autosomal-dominant Alzheimer's disease: a review and proposal for the prevention of Alzheimer's disease. *Alzheimers Res. Ther.* 3:1. doi: 10.1186/alzrt59

Bellebaum, C., and Daum, I. (2007). Cerebellar involvement in executive control. *Cerebellum* 6, 184–192. doi: 10.1080/14734220601169707

Braak, H., Del Tredici, K., Schultz, C., and Braak, E. (2000). Vulnerability of select neuronal types to Alzheimer's disease. *Ann. N Y Acad. Sci.* 924, 53–61. doi: 10.1111/j.1749-6632.2000.tb05560.x

Buckner, R. L., Krienen, F. M., Castellanos, A., Diaz, J. C., and Yeo, B. T. (2011). The organization of the human cerebellum estimated by intrinsic functional connectivity. *J. Neurophysiol.* 106, 2322–2345. doi: 10.1152/jn.00339.2011

Camicioli, R. M. (2010). Mild motor impairment: motor change preceding mild cognitive impairment and dementia. *Alzheimers Dement.* 6:S92. doi: 10.1016/j.jalz.2010.05.282

Cole, G., Neal, J. W., Singhrao, S. K., Jasani, B., and Newman, G. R. (1993). The distribution of amyloid plaques in the cerebellum and brain stem in Down's syndrome and Alzheimer's disease: a light microscopical analysis. *Acta Neuropathol.* 85, 542–552. doi: 10.1007/BF00230495

Davis, J. C., Hsiung, G. Y. R., and Ambrose, T. L. (2011). Challenges moving forward with economic evaluations of exercise intervention strategies aimed at combating cognitive impairment and dementia. *Br. J. Sports Med.* 45, 470–472. doi: 10.1136/bjsm.2010.077990

Deoni, S. C. L. (2011). Correction of main and transmit magnetic field (B0 and B1) inhomogeneity effects in multicomponent-driven equilibrium single-pulse observation of T1 and T2. *Magn. Reson. Med.* 65, 1021–1035. doi: 10.1002/mrm.22685

Deoni, S. C. L., Williams, S. C. R., Jezzard, P., Suckling, J., Murphy, D. G. M., and Jones, D. K. (2008). Standardized structural magnetic resonance imaging in multicentre studies using quantitative T1 and T2 imaging at 1.5 T. *NeuroImage* 40, 662–671. doi: 10.1016/j.neuroimage.2007.11.052

Deoni, S., and Kolind, S. H. (2015). Investigating the stability of mcDESPOT myelin water fraction values derived using a stochastic region contraction approach. *Magn. Reson. Med.* 73, 161–169. doi: 10.1002/mrm.25108

Desai, M. K., Mastrangelo, M. A., Ryan, D. A., Sudol, K. L., Narrow, W. C., and Bowers, W. J. (2010). Early oligodendrocyte/myelin pathology in Alzheimer's disease mice constitutes a novel therapeutic target. *Am. J. Pathol.* 177, 1422–1435. doi: 10.2353/ajpath.2010.100087

Diedrichsen, J., Balsters, J. H., Flavell, J., Cussans, E., and Ramnani, N. (2009). A probabilistic MR atlas of the human cerebellum. *NeuroImage* 46, 39–46. doi: 10.1016/j.neuroimage.2009.01.045

Dukart, J., Mueller, K., Horstmann, A., Vogt, B., Frisch, S., Barthel, H., et al. (2010). Differential effects of global and cerebellar normalization on detection and differentiation of dementia in FDG-PET studies. *NeuroImage* 49, 1490–1495. doi: 10.1016/j.neuroimage.2009.09.017

Frings, L., Yew, B., Flanagan, E., Lam, B. Y. K., Hüll, M., Huppertz, H.-J., et al. (2014). Longitudinal grey and white matter changes in frontotemporal dementia and Alzheimer's disease. *PLoS One* 9:e90814. doi: 10.1371/journal.pone.0090814

Gentier, R. J., Verheijen, B. M., Zamboni, M., Stroeken, M. M., Hermes, D. J., Küsters, B., et al. (2015). Localization of mutant ubiquitin in the brain of a transgenic mouse line with proteasomal inhibition and its validation at specific sites in Alzheimer's disease. *Front. Neuroanat.* 9:26. doi: 10.3389/fnana.2015.00026

Guo, C. C., Tan, R., Hodges, J. R., Hu, X., Sami, S., and Hornberger, M. (2016). Network-selective vulnerability of the human cerebellum in Alzheimer's disease and frontotemporal dementia. *Brain* 139, 1527–1538. doi: 10.1093/brain/aww003

Hua, X., Lee, S., Hibar, D. P., Yanowsky, I., Leow, A. D., Toga, A. W., et al. (2010). Mapping Alzheimer's disease progression in 1309 MRI scans: power estimates for different inter-scan intervals. *NeuroImage* 51, 63–75. doi: 10.1016/j.neuroimage.2010.01.104

Hua, X., Yanovsky, I., Leow, A. D., Chou, Y. Y., Ho, A. J., Gutman, B., et al. (2009). Optimizing power to track brain degeneration in Alzheimer's disease and mild cognitive impairment with tensor-based morphometry: an ADNI study of 515 subjects. *NeuroImage* 48, 668–681. doi: 10.1016/j.neuroimage.2009.07.011

Jacobs, H. I. L., Hopkins, D. A., Mayrhofer, H. C., Bruner, E., van Leeuwen, F. W., Raaijmakers, W., et al. (2018). The cerebellum in Alzheimer's disease: evaluating its role in cognitive decline. *Brain* 41, 37–47. doi: 10.1093/brain/awx194

Jankowsky, J. L., Fadale, D. J., Anderson, J., Xu, G. M., Gonzales, V., Jenkins, N. A., et al. (2004). Mutant presenilins specifically elevate the levels of the 42 residue beta-amyloid peptide *in vivo*: evidence for augmentation of a 42-specific gamma secretase. *Hum. Mol. Genet.* 13, 159–170. doi: 10.1093/hmg/ddh019

Jenkinson, M., Bannister, P. R., Brady, J. M., and Smith, S. M. (2002). Improved optimization for the robust and accurate linear registration and motion correction of brain images. *NeuroImage* 17, 825–841. doi: 10.1016/s1053-8119(02)91132-8

Jernigan, T. L., Archibald, S. L., Fennema-Notestine, C., Gamst, A. C., Stout, J. C., Bonner, J., et al. (2001). Effects of age on tissues and regions of the cerebrum and cerebellum. *Neurobiol. Aging* 22, 581–594. doi: 10.1016/s0197-4580(01)00217-2

Kelly, R. M., and Strick, P. L. (2003). Cerebellar loops with motor cortex and prefrontal cortex of a nonhuman primate. *J. Neurosci.* 23, 8432–8444. doi: 10.1523/JNEUROSCI.23-23-08432.2003

Liu-Ambrose, T. Y., Ashe, M. C., Graf, P., Beattie, B. L., and Khan, K. M. (2008). Mild cognitive impairment increases falls risk in older community-dwelling women. *Phys. Ther.* 88, 1482–1491. doi: 10.2522/ptj.20080117

Mann, D. M., Jones, D., Prinja, D., and Purkiss, M. S. (1990). The prevalence of amyloid (A4) protein deposits within the cerebral and cerebellar cortex in Down's syndrome and Alzheimer's disease. *Acta Neuropathol.* 80, 318–327. doi: 10.1007/BF00294651

Middleton, F. A., and Strick, P. L. (2001). Cerebellar projections to the prefrontal cortex of the primate. *J. Neurosci.* 21, 700–712. doi: 10.1523/JNEUROSCI.21-02-00700.2001

Morris, J. C. (1993). The clinical dementia rating (CDR): current version and scoring rules. *Neurology* 43, 2412–2414. doi: 10.1212/wnl.43.11.2412-a

Nyunt, M. S. Z., Chong, M. S., Lim, W. S., Lee, T. S., Yap, P., and Ng, T. P. (2013). Reliability and validity of the clinical dementia rating for community-living elderly subjects without an informant. *Dement. Geriatr. Cogn. Dis. Extra.* 3, 407–416. doi: 10.1159/000355122

Pangman, V. C., Sloan, J., and Guse, L. (2000). An examination of psychometric properties of the mini-mental status examination and the standardized mini-mental status examination: implications for clinical practice. *Appl. Nurs. Res.* 13, 209–213. doi: 10.1053/apnr.2000.9231

Reiman, E. M., Quiroz, Y. T., Fleisher, A. S., Chen, K., Velez-Pardo, C., Jimenez-Del-Rio, M., et al. (2012). Brain imaging and fluid biomarker analysis in young adults at genetic risk for autosomal dominant Alzheimer's disease in the

presenilin 1 E280A kindred: a case-control study. *Lancet Neurol.* 11, 1048–1056. doi: 10.1016/S1474-4422(12)70228-4

Reitz, C., Brayne, C., and Mayeux, R. (2011). Epidemiology of Alzheimer disease. *Nat. Rev. Neurol.* 7, 137–152. doi: 10.1038/nrneurol.2011.2

Schmahmann, J. D., Anderson, C. M., Newton, N., and Ellis, R. (2001). The function of the cerebellum in cognition, affect and consciousness. Empirical support for the embodied mind. *Conscious. Emot.* 2, 273–309. doi: 10.1075/ce.2.2.06sch

Serra, L., Cercignani, M., Lenzi, D., Perri, R., Fadda, L., Caltagirone, C., et al. (2010). Grey and white matter changes at different stages of Alzheimer's disease. *J. Alzheimers Dis.* 19, 147–159. doi: 10.3233/JAD-2010-1223

Smith, S. M. (2002). Fast robust automated brain extraction. *Hum. Brain Mapp.* 17, 143–155. doi: 10.1002/hbm.10062

Smith, S. M., Jenkinson, M., Woolrich, M. W., Beckmann, C. F., Behrens, T. E. J., Johansen-Berg, H., et al. (2004). Deformation tensor morphometry of semantic dementia with quantitative validation. *NeuroImage* 21, 1387–1398. doi: 10.1016/j.neuroimage.2003.12.009

Studholme, C., Cardenas, V., Blumenfeld, R., Schuff, N., Rosen, H. J., Miller, B., et al. (2004a). Deformation tensor morphometry of semantic dementia with quantitative validation *NeuroImage* 21, 1387–1389. doi: 10.1016/j.neuroimage.2003.12.009

Studholme, C., Cardenas, V., Song, E., Ezekiel, F., Maudsley, A., and Weiner, M. (2004b). Accurate template-based correction of brain MRI intensity distortion with application to dementia and aging. *IEEE Trans. Med. Imaging* 23, 99–110. doi: 10.1109/TMI.2003.820029

Woolf, C., Slavin, M. J., Draper, B., Thomassen, F., Kochan, N. A., Reppermund, S., et al. (2016). Can the clinical dementia rating scale identify mild cognitive impairment and predict cognitive and functional decline? *Dement. Geriatr. Cogn. Disord.* 41, 292–302. doi: 10.1159/000447057

Zhan, X., Jickling, G. C., Ander, B. P., Liu, D., Stamova, B., Cox, C., et al. (2014). Myelin injury and degraded myelin vesicles in Alzheimer's disease. *Curr. Alzheimer Res.* 11, 232–238. doi: 10.2174/1567205011666140131120922

Zhang, Y., De Stefano, N., Brady, J. M., and Matthews, P. M. (2004). Advances in functional and structural MR image analysis and implementation as FSL. *NeuroImage* 23, S208–S219. doi: 10.1016/j.neuroimage.2004.07.051

Conflict of Interest: While SD receives salary and grant support from Nestlé S.A., it does not overlap with this material.

The remaining authors declare that the research was conducted in the absence of any commercial or financial relationships that could be construed as a potential conflict of interest.

frontiers in Aging Neuroscience

ORIGINAL RESEARCH
published: 12 November 2020
doi: 10.3389/fnagi.2020.576678

Longitudinal Characterization of Transcriptomic, Functional, and Morphological Features in Human iPSC-Derived Neurons and Their Application to Investigate Translational Progranulin Disease Biology

Gaëlle Robin[1†], *J. Corey Evans*[1†], *David N. Hauser*[1†], *Paul Wren*[2] *and Andreas Zembrzycki*[1*]

[1]SBP-GSK Center for Translational Neuroscience, Sanford Burnham Prebys Medical Discovery Institute, La Jolla, CA, United States, [2]GSK, Neuroscience Discovery, Collegeville, PA, United States

OPEN ACCESS

Edited by:
Woon-Man Kung,
Chinese Culture University, Taiwan

Reviewed by:
Julien Rossignol,
Central Michigan University, United States
Giovanni Piccoli,
University of Trento, Italy

***Correspondence:**
Andreas Zembrzycki
abzembrzycki@gmail.com

[†]These authors have contributed equally to this work

Received: 26 June 2020
Accepted: 07 October 2020
Published: 12 November 2020

Citation:
Robin G, Evans JC, Hauser DN, Wren P and Zembrzycki A (2020) Longitudinal Characterization of Transcriptomic, Functional, and Morphological Features in Human iPSC-Derived Neurons and Their Application to Investigate Translational Progranulin Disease Biology. Front. Aging Neurosci. 12:576678. doi: 10.3389/fnagi.2020.576678

The disease biology of frontotemporal lobe dementia (FTD) is complex and not fully understood, with limited translational value appreciated from animal models to date. Human cellular systems that can recapitulate phenotypic features of disease offer promise as translational tools to not only increase our understanding of disease processes but also increase the probability of success of translating novel treatment options to patients. However not all researchers may necessarily have access to well-characterized induced pluripotent stem cell (iPSC)-derived human neurons. As an example, we therefore comprehensively profiled phenotypic features over time in one commercially-available IPSC-derived human neuron cell line. This included systems-level assessments of neurite outgrowth dynamics, neuronal network function, and genome-wide gene expression. By investigating progranulin biology as an example we then demonstrated the utility of these cells as a tool to investigate human disease biology. For example, by using the siRNA-mediated knockdown of the progranulin (*GRN*) gene, we demonstrated the establishment of an isogenic human cellular model to facilitate translational FTD research. We reproduced findings from rodent neurons by demonstrating that recombinant progranulin (rPGRN) mediated neuroprotection. Contrary to previous rodent data, in our human cellular models, growth factor treatment showed no consistent sensitivity to modulate neurite outgrowth dynamics. Our study further provides the first evidence that rRPGRN modulated neuronal firing and

synchrony in human neurons. Taken together, our datasets are a valuable systems-level resource demonstrating the utility of the tested commercially-available human iPSC neurons for investigating basic human neurobiology, translational neuroscience, and drug discovery applications in neurodegenerative and other CNS diseases.

Keywords: progranulin (PGRN), frontotemporal lobe dementia (FTD), neurodegeneration, translational neuroscience, MEA, RNA-Seq, live-cell imaging

INTRODUCTION

While most basic biological studies utilize animal-based models to investigate disease mechanisms and biology, suitable models that allow translation of these findings to human biology are often missing. This is especially true in the neuroscience field, which lacks broadly available well-characterized human neuronal models. Variability in pharmacological responsiveness between animal and human cells is particularly rate-limiting for quantitative drug discovery applications and the identification of potential therapeutic molecules. Therefore, novel human cell-based model systems could offer key advantages for translational biology. Induced pluripotent stem cells (iPSCs) can be differentiated into a host of cell types, including neurons (Takahashi et al., 2007) and consequently, have been implemented to model common and rare neurological diseases (Park et al., 2008; Ross and Akimov, 2014), including Alzheimer's disease (AD; Israel et al., 2012) and frontotemporal lobe dementia (FTD; Almeida et al., 2012; Raitano et al., 2015). Such iPSC-derived neuronal models from normal donors and patients are useful but have certain disadvantages. The creation of these cells is time-consuming and requires extensive characterization (Xu and Zhong, 2013); moreover, results have been shown to vary substantially between labs (Volpato et al., 2018).

Commercially-available iPSC-derived neurons are already differentiated and subjected to quality control, thus making this technology available to the broader research community that would otherwise need expertise in iPSC reprogramming and differentiation procedures. Well-characterized commercially-available cells would be a useful alternative to enhance the availability and reproducibility of iPSC models. iPSC-derived neurons representing distinct brain regions are commercially-available, including the iCell® line from FUJIFILM Cellular Dynamics, Inc. (FCDI). iCell® GlutaNeurons (GNs), for example, express predominantly glutamatergic markers and according to the manufacturer have been previously used to study electrophysiology, cell survival, and neurite outgrowth and the neuronal identity of GNs has been confirmed by flow cytometry and by assessment of gene expression in individual cells, while neuronal function has been assayed by multi-electrode array and calcium influx analyses (Fujifilm, 2018). Therefore, our objective was to perform an independent and longitudinal assessment of key phenotypic features in human iPSC-derived GNs Using live-cell imaging, RNA-Sequencing (RNA-Seq), and multi-well multi-electrode array (mwMEA) technologies, we present comprehensive data characterizing: (1) neuronal morphology and outgrowth; (2) neuronal network activity and synchrony; and (3) genome-wide gene expression profiles in GNs over a culture period of 3 weeks.

Next, we used the cells to study progranulin (PGRN) as proof-of-principle that these human neuronal cells are applicable to better understand translational disease biology in the context of neurodegenerative disease. FTD is a cluster of neurological disorders associated with behavioral and speech abnormalities and the most common pre-senile dementia (Bang et al., 2015). Gene linkage studies identified that heterozygous mutations in the *GRN* gene lead to haploinsufficiency of the encoded PGRN protein and cause FTD characterized by prominent deterioration of frontal and temporal cortical lobes (Baker et al., 2006; Cruts et al., 2006). We developed a siRNA-mediated knockdown protocol to study how the loss of endogenous *GRN* expression in human iPSC neurons relates to *GRN* haploinsufficiency in human FTD patients and studied how the treatment of the used human iPSC neuronal cultures with recombinant PGRN impacts neuronal outgrowth dynamics, resilience towards neurotoxic stress and neuronal function. This work aimed to explore the feasibility of using commercially-available human IPSC glutamatergic neurons as a tool to investigate neuronal structure and function concerning disease with direct application to understanding the influence of progranulin, a common causal genetic risk factor for FTD (Baker et al., 2006; Cruts et al., 2006) on relevant phenotypic endpoints.

MATERIALS AND METHODS

Culture of iPSC-Derived Neurons

iCell® GlutaNeurons (GNs; FUJIFILM Cellular Dynamics Inc., FCDI) are human cells differentiated from a master bank of stably induced pluripotent stem (iPS) cells from normal donors (stemcell.com). The iPS cell lines were generated from human peripheral blood through ectopic expression of reprogramming factors (i.e., Oct4, Sox2, Nanog, Lin28, Klf4, L-Myc, and SV40LT) by episomal transfection. The iPS cell clones were then engineered using nuclease-mediated methodologies to exhibit neomycin resistance under the control of a neuronal-specific promotor. GNs were cultured according to the manufacturer's protocol. Clear, flat-bottom 96-well plates (Corning) were coated with 0.01% poly-L-ornithine (PLO, Sigma–Aldrich) for a minimum of 1 h at room temperature. After three washes with PBS (Thermo Fisher Scientific, Waltham, MA, USA), the wells were coated with 0.028 mg/ml Growth Factor Reduced Matrigel (Corning) for at least 1 h in a 37°C incubator. Cells were thawed for 2 min in a 37°C water bath, then slowly equilibrated by the dropwise addition of room-temperature

complete medium [BrainPhys Neuronal Medium (STEMCELL Technologies) containing iCell® supplements (CDI), N-2 Supplement (Thermo Fisher Scientific, Waltham, MA, USA), laminin (1 μg/ml, Sigma–Aldrich), and penicillin-streptomycin (Thermo Fisher Scientific, Waltham, MA, USA)]. The cells were then plated and allowed to recover overnight at 37°C.

For culturing GNs for multielectrode array (MEA) experiments, 48- and 96-well MEA plates (Axion Biosystem, Atlanta, GA, USA) were coated with 80 μl of 0.07% polyethyleneimine (Sigma–Aldrich) diluted in borate buffer for 1 h at room temperature. The plates were then washed four times with sterile water and air-dried overnight in a sterile biological safety cabinet. GNs were thawed as described above and were resuspended in dotting medium (Complete BrainPhys Medium with 11 μg/ml laminin) to reach a concentration of 10 million cells/ml and 7 million cells/ml for 48- (M768-KAP-48) and 96-well plates (M768-KAP-96), respectively. A 10 μl droplet of the cell suspension was then manually dispensed directly over the recording electrode area of each well. Plates were kept for 1 h in the incubator at 37°C before gently adding 300 μl of fresh complete BrainPhys Medium in each well. A 50% medium change was performed 1-day post-plating and then every other day.

IncuCyte™ ZOOM Analysis

We utilized the IncuCyte™ ZOOM Live-Cell Analysis System (Essen BioScience) to perform live imaging assays for neurite outgrowth and cellular toxicity. This system consists of an incubator housing a microscope for the acquisition of phase as well as red/green fluorescent images over a user-defined time range. By leveraging the systems software modules and algorithms, we performed rapid, long-term, and unbiased high-throughput analyses of multiple morphological features in real-time. Using the NeuroTrack™ module (Essen BioScience), a set of criteria (called a "processing definition") defining cell bodies and neurites was optimized for GNs to quantify neuronal morphology metrics, including neurite length, the number of neurite branch points, and the number of cell body clusters.

For neurite outgrowth analysis, the following parameters were used for the NeuroTrack™ software: Cell-Body Cluster Parameters = Segmentation Mode (Brightness), Segmentation Adjustment (0.2); Cleanup = Hole Fill (0 μm^2), Adjust Size (0 pixels), Min Cell Width (9 μm); Cell-Body Cluster Filters = Area (min = 290 μm^2); Neurite Parameters = Filtering (None), Neurite Sensitivity (0.55), Neurite Width (1 μm). For monitoring cellular morphology during siRNA treatment, the following parameters were used for the NeuroTrack™ software: Cell-Body Cluster Parameters = Segmentation Mode (Brightness), Segmentation Adjustment (0.9); Cleanup = Hole Fill (0 μm^2), Adjust Size (0 pixels), Min Cell Width (7 μm); Cell-Body Cluster Filters = None; Neurite Parameters = Filtering (None), Neurite Sensitivity (0.5), Neurite Width (1 μm).

For Annexin V analysis, the following parameters were used for the Basic Analyzer™ software: Phase parameters = Segmentation Adjustment (0.4), Cleanup = Hole Fill (0 μm^2), Adjust Size (0 pixels), Min Area (40 μm^2); Green Channel (Annexin V) parameters = Top hat Radius (60 μM), Top hat Threshold (2 GCU), Edge split on, Edge split sensitivity (0), Cleanup = Hole Fill (0 μm^2), Adjust Size (0 pixels).

Neurite Outgrowth Assay

One day after plating (7,000 cells/well), GNs were treated with either PBS (vehicle), 7.41 nM BDNF (PeproTech), 7.41 nM NGF (R&D Systems), concentrations that in previous studies were sensitive to increase neurite outgrowth (Van Damme et al., 2008) or (Thermo Fisher Scientific, Waltham, MA, USA). For all samples, the amount of the vehicle was kept the same. After 50% of the complete medium was removed from the cells, the aforementioned treatments (prepared as 2× concentrations) were diluted 1:1 in the remaining medium. Every other day, half of the medium in each well was exchanged with fresh medium containing the appropriate treatments. The cells were imaged using the IncuCyte™ ZOOM Live-Cell Analysis System (beginning approximately 1 h after the initial treatment); neurite morphology was assessed on the 10th day of treatment. Representative images show that an optimized NeuroTrack™ processing definition accurately masked neurites for quantification and analysis (**Figure 4E**). Both neurite length and the number of branch points increased over the 10-day assay, as represented by GNs treated with vehicle (PBS; **Figure 4F**); this is consistent with the increased neurite growth over time seen in GNs plated at a higher density in previous experiments (**Figures 1B,C**). To determine the fold-change in the neurite metrics, all measurements at day 10 of treatment were normalized to those of the first imaging time point (i.e., 1 h after the first treatment).

Neurotoxicity Assay

GNs plated at 25,000 cells/well were treated at DIV14 with IncuCyte® Annexin V Green (4642, Essen BioScience Inc.,) at a final dilution of 1:200. Annexin V, a Ca^{2+}-dependent phospholipid-binding protein, has a high affinity for membrane phosphatidylserine, which translocates from the inner side of the plasma membrane to the cell surface during the early stages of apoptosis (Andree et al., 1990; Koopman et al., 1994). Neuronal toxicity was induced by treating the cells with staurosporine, a nonselective protein kinase inhibitor (STS, Enzo Life Sciences) at 0.1 μM. Vehicle (PBS, Thermo Fisher Scientific, Waltham, MA, USA), 2.2 nM recombinant NGF (Human β-NGF, R&D Systems), 3.7 nM recombinant BDNF (R&D Systems) or a concentration range of PGRN Recombinant Human Progranulin/PGRN (R&D Systems, Thermo Fisher Scientific, Waltham, MA, USA) was co-added to the STS treatment as indicated. For all samples, the amount of the vehicle was kept the same. After 50% of the complete medium was removed from the cells, the treatments mentioned above (prepared as 2× concentrations) were diluted 1:1 in the remaining medium. Every other day, half of the medium in each well was exchanged with fresh medium containing the appropriate treatments. The cells were imaged using the IncuCyte™ ZOOM Live-Cell Analysis System

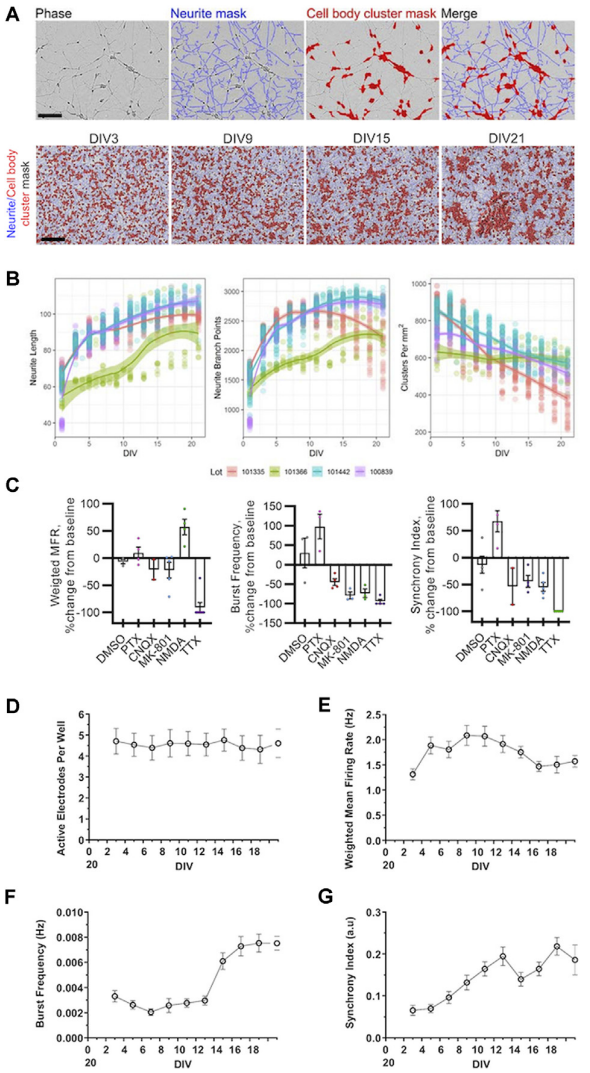

FIGURE 1 | Morphological and electrophysiological characterization of cultured human induced pluripotent stem cell (iPSC) neurons. **(A)** Representative phase-contrast images of GlutaNeuron (GN) neurite and cell body cluster masking by NeuroTrack™ software at indicated day *in vitro* (DIV), with neurite masks shown in blue and cell-body cluster masks shown in red. Scale bar, 600 μm. **(B)** Quantification of neurite length, neurite branch points, and cell-body clusters in cultured GNs from four different lots. Graphs represent data from 12 independent experiments (n = 198 wells total) with 1,452 data points per variable (516 for Lot 101335, 123 for Lot 101366, 453 for Lot 101442, and 360 for Lot 100839). Solid lines show local regression (LOESS) models of the data along with 95% confidence intervals. **(C)** Weighted mean firing rate (MFR), burst frequency, and the synchrony index were measured using multi-well multielectrode array (mwMEA) recordings at baseline and after the addition of vehicle (DMSO) and established neuronal firing modulators 50 μM picrotoxin (PTX), 10 μM CNQX, 1 μM dizocilpine (MK-801), 20 μM NMDA, 1 μM tetrodotoxin (TTX). **(D–G)** Quantification of neuronal activity in GNs from DIV3 to DIV21. **(D)** Active electrodes per well over 21 days in culture. **(E)** Weighted MFR over 21 days in culture, normalized to weighted MFR measured at 3 DIV. **(F)** Burst frequency over 21 days in culture, normalized to burst frequency recorded at 3 DIV. **(G)** Synchrony index over 21 days in culture, normalized to synchrony index recorded at 3 DIV. mwMEA graphs represent data from seven independent experiments (8–24 replicates per condition in each experiment), and the results are displayed as the mean ± standard deviation (SD).

(Essen BioScience; beginning approximately 1 h after the initial treatment).

siRNA-Mediated Gene Knockdown

The Accell Human *GRN* siRNA SMARTpool (E-009285-00-0050) and Accell Non-targeting Pool (D-001910-10-50) were purchased from Dharmacon. The target sequences of the *GRN* SMARTpool are GUGCUGUGUUAUGGUCGAU, GAGAUGUCCCCUGUGAUAA, UUGUCCAGCUCGGUCAUGU, and GUGCGUUUCAAUAAAGUUU. The target sequences of the Non-targeting Pool are UGGUUUACAUGUCGACUAA, UGGUUUACAUGUUUUCUGA, UGGUUUACAUGUUUUCCUA, and UGGUUUACAUGUUGUGUGA. The siRNA was reconstituted to 100 μM with 1× Dharmacon siRNA Buffer (B-002000-UB-100) and added directly to the GN media immediately before use. All experiments using siRNA were done with 70,000 GNs per well in 96-well plates. The first 50% media change on the day *in vitro* (DIV) three was done with 2× concentrated siRNA to achieve the desired concentration of siRNA in each well. All subsequent 50% of media changes were done with freshly added 1× siRNA to maintain the desired siRNA concentration during the culture.

RNA-Sequencing (RNA-Seq)

Plates containing GNs were washed with PBS and then frozen at −80°C until they were thawed for RNA purification using the RNEasy UCP Micro Kit (Qiagen #73934). Four independent experiments were performed (two using lot 100839 and two using lot 101442), and there were five to six technical replicate wells per condition per experiment. The lysates from technical replicate wells were combined before RNA purification to yield sufficient quantities of RNA for RNA-Seq. PolyA RNA was isolated using the NEBNext® Poly(A) mRNA Magnetic Isolation Module, and barcoded libraries were made using the NEBNext® Ultra II™ Directional RNA Library Prep Kit for Illumina® (NEB, Ipswich, MA, USA). Libraries were pooled and single-end sequenced (1 × 75) on the Illumina NextSeq 500 using the High output V2 kit (Illumina Inc., San Diego, CA, USA). Transcript level quantification was generated using *Salmon* (v0.8.2; Patro et al., 2017), and an index was built using cDNA sequences from the human genome assembly GRCh38 (ftp://ftp.ensembl.org/pub/release-92/fasta/homo_sapiens/cdna/Homosapiens.GRCh38.cdna.all.fa.gz). Gene abundance estimates were created with *Tximport* (v1.8.0; Soneson et al., 2015) using a tx2gene file containing Ensembl transcript IDs and their associated HGNC symbols. Samples were assigned to one of fifteen possible groups based on treatment type and day *in vitro* (DIV; Untreated_DIV7, *GRN*_siRNA_DIV7, Control_siRNA_DIV7, et cetera), and a DESeqDataSet was constructed using a design formula of ∼group in *DESeq2* (Love et al., 2014). Genes with count means of less than five were removed before principal component analysis (PCA) and pairwise comparisons. Differential expression was determined using the *DESeq2* default of a Benjamini–Hochberg adjusted p-value cutoff of 0.10. Gene ontology (GO) analysis was performed using the Overrepresentation Enrichment Analysis method of WebGestalt (Wang et al., 2017) with

"geneontology" selected as the functional database. Note that the RT-PCR presented in **Figure 7B** is from the same samples we used for RNA-Seq. The RT-PCR data shows reduced GRN expression in treated samples. This validation our RNA-Seq data, which similarly demonstrated reduced GRN expression through an orthogonal method. RNA-Seq data are publicly accessible at the Gene Expression Omnibus under Accession GSE157573.

Quantitative Reverse Transcription PCR

Gene expression in siRNA dose-response experiments was determined using the TaqMan™ Gene Expression Cells-to-CT™ Kit (Invitrogen #AM1728). For the RNA-Seq samples, cDNA was synthesized from 10 ng of total RNA using Superscript III (Invitrogen #18080), and gene expression were analyzed using the standard TaqMan protocol. The TaqMan assays used were: *GRN* (Hs00963707_g1), *PPIB* (Hs00168719_m1), *ACTB* (Hs99999903_m1), and *GAPDH* (Hs99999905_m1). The fold change of *GRN* relative to reference genes (*ACTB* for dose-response experiments or the mean of *ACTB*, *PPIB*, and *GAPDH* for the RNA-Seq samples) was determined using the comparative Ct method. The R package *drc* was used for dose-response modeling (Ritz et al., 2015).

Multi-well Multielectrode Array (mwMEA)

The neuronal electrical activity of cultured GNs was acquired using the Maestro MEA system (Axion Biosystem) according to the manufacturer's guidelines. Briefly, 48- or 96-well plates were inserted in the Maestro machine (set up at 37°C and 5% CO_2 without perfusion) and were recorded using AxIS software (Axion Integrated Studio, Axion Biosystem, version 2.4.2.13). mwMEA plates were composed of 48 wells or 96 wells, with each well containing an array of 16 or 8, respectively, individual embedded nano-textured gold microelectrodes (∼40–50 μm diameter; 350 μm center-to-center spacing) with four integrated ground electrodes (Axion Biosystems). Treatment with the control compounds was performed at DIV18–23 with 20 min baseline recording followed by 20 min recording after the addition of 55 μl of a 7× concentration of either 50 μM picrotoxin (PTX, Tocris), 10 μM 6-cyano-7-nitroquinoxaline-2, 3-dione (CNQX, Sigma–Aldrich), 1 μM dizocilpine (MK-801, Sigma–Aldrich), 30 μM *N*-methyl-D-aspartic acid (NMDA, Sigma–Aldrich) or 1 μM tetrodotoxin (TTX, Tocris). For the acute addition of PGRN experiments, GNs were recorded from DIV18 to DIV24 depending on the network maturation, which can be quantified by a synchrony index of ∼0.2 (see "Results" section below). To start, a 20 min baseline recording was performed on the 48-well mwMEA plate followed by the addition of 55 μl of a 7× concentration of PGRN (ranging from 0.0014 to 11.4 nM) or PBS. Another 20 min recording was made in the presence of the compound. Then, the compounds were washed out with four 50% media changes. This was followed by a 20 min post-wash recording. Finally, plates were recorded 2 days post-treatment.

For the *GRN* haploinsufficiency experiments, *GRN* or NT siRNA (30 nM) was added 3 days post-plating by replacing 50% of the medium with 2× siRNA, and a first mwMEA recording was performed the same day for 20 min. From there, neuronal activity of the treated cells was measured for 20 min every other day until DIV21.

The channels of the mwMEA were sampled simultaneously with a gain of 1,200× and a sampling rate of 12.5 kHz/channel. For all recordings, a Butterworth band-pass filter (200 Hz – 3 kHz) was applied along with an adaptive threshold spike detector set at 6× standard deviation. Data from the recordings were saved to two different file types simultaneously: a raw data file (*.raw file) that included all data, and an AxIS spike file (*.spk file) that included the spikes per electrode with a 1 s bin time. The Axis spike data file was then analyzed using Neural Metric tool software (Axion Biosystem, version 2.2.4) with an active electrode criterion of 5 spikes per min. For a single electrode burst, the Poisson Surprise algorithm was selected with a setting of 10. For the network burst, the Envelope statistic was chosen with a threshold factor of 3, a minimum inter-burst interval of 2,000 ms, a minimum electrode percentage of 50%, and a burst inclusion of 75%.

RESULTS

Quantifying the Morphology and Neurite Dynamics of Human iPSC Neurons

First, we characterized key morphological processes in cultured GNs neurons starting at the time of plating. We tracked neurite dynamics in GNs from four separate cell lots over 3 weeks in culture using live-cell imaging. Representative images in **Figure 1A** illustrate the precision of the automatic capture of neurite metrics by our optimized algorithms and the typical morphological progression of the cultures over time from DIV3 to DIV21. As expected, we were able to track and quantify the outgrowth and branching of neurites over time. Additionally, we were able to identify small, discrete groups of cell bodies in younger cultures that over time tended to form larger continuous cell cluster organizations. In general, across multiple lots, we found that neurite length and branching rapidly increased during the first few days in culture and then began to plateau after around DIV7 (**Figure 1B**). The number of defined groups of cells (named cell-body clusters), on the other hand, tended to decrease over time (**Figure 1B**), indicating that the cells and their soma were surprisingly mobile and tended to organize into larger groups as the cultures aged. Notably, we found that, although all lots of GNs showed robust outgrowth of neurites, there was considerable within-lot variation in the overall performance of the GNs in our morphological assays. For example, one lot consistently showed inferior performance across metrics as compared to the three others (**Figure 1**). Taken together, our unbiased live-cell imaging approach allowed us to quantify morphological parameters in commercially-available human iPSC-derived GNs and demonstrated that these cells are a useful tool to study neurite dynamics and the quantitative pharmacology of molecules that potentially modulate this process.

Quantifying Neural Network Activity in Human iPSC Neurons

Outgrowth and branching of cultured GNs suggest that individual neurons connect into networks. We thus expected that—once neurons extended neurites and connect with each other—spontaneous electrical activity would emerge in the cultures. To capture and quantify dynamics in extracellular membrane potentials in plated excitable GNs (Obien et al., 2015) longitudinally, we plated them on mwMEA.

First, we validated qualitatively that GNs are electrophysiologically active and sensitive to established chemical modulators using our standard plating and cell culture conditions. Our results demonstrate that in GN cultures treatment with the sodium channel blocker TTX, the glutamate receptor antagonist dizocilpine (MK-801), or the AMPA/kainate receptor antagonist CNQX abolished network bursting and reduced synchronization of neuronal firing. Conversely, the addition of the GABA antagonist PTX to GN cultures increased the number of bursts and synchronization of neuronal firing as expected, while treatment with NMDA increased the mean firing rate (MFR; **Figure 1C**).

We then longitudinally measured and analyzed the mwMEA data of cultured GNs without pharmacological treatments. Over 3 weeks in culture, the total number of active electrodes did not change significantly (**Figure 1D**) suggesting that neuronal activity and, thus, neuronal connections between iPSC neurons appeared to be equally distributed across the entire well. However, over time and in particular, during the first few days in culture, an increase in the weighted MFR was evident (**Figure 1E**) concomitantly to the increased neurite growth in the first week after plating, followed by a plateau period afterward (compare timing to that in **Figure 1B**). Therefore, the initial increase in growth of GN neurites and branch points appeared proportional to the increased neuronal connectivity and spontaneous firing as measured by electrical network activity.

Burst frequency sharply increased after approximately 2 weeks in culture (**Figure 1F**). This is consistent with the literature (Tukker et al., 2018) and suggests that synchronized electrical network activity emerges delayed after a sufficient amount of neuronal connections has been established across an *in vitro* neuronal network. The synchrony index is another metric to quantify neuronal synchronization. This metric is based on measuring spike firing events between electrode pairs and comparing them across all electrodes throughout the mwMEA well (Paiva et al., 2010). In the commercially-available human iPSC neurons used in this study, the synchrony index steadily increased over time (**Figure 1G**) suggesting that firing progressively increased during the first 2 weeks and that neural networks mature over time. Thus, after approximately DIV14, relatively mature networks are established that are characterized by synchronous neuronal network burst activity. Taken together, our assessments demonstrate that for at least 3 weeks in culture, commercially-available GNs exhibit spontaneous neuronal activity and bursting behavior that can be leveraged to model human neuronal network development and function using mwMEA.

Genome-Wide Gene Expression Dynamics in Cultured Human iPSC Neurons

We then aimed to better understand gene expression in cultured GN longitudinally on a genome-wide scale to investigate how GNs transcriptionally mature over time and to validate that GNs express genes relevant to the phenotypic readouts we are interested in, such as neurite dynamics and neuronal firing mentioned above. We monitored and compared the GN transcriptome *via* RNA-Seq after DIV7, DIV10, DIV14, DIV18, and DIV21. We first investigated the distribution of the genome-wide count data for all of the genes in the human transcriptome, broken down into quartiles (**Figure 2A**). and refer to genes within quartiles as having high, medium, and low levels of expression, respectively. Genes with no or very low expression (mean counts <5) were excluded.

Gene expression signatures of GN were compared to published postmitotic iPSC-derived neuron datasets which suggested a classification of iPSC-derived human neurons into less vs. highly mature and active types based on gene expression and electrophysiological features (Bardy et al., 2016). We determined expression levels of the top four genes specifically expressed in the highly functional AP5 human neuron type—*CKMT1B*, *GDAP1L1*, *PCLO*, and *TRAPPC6B*—longitudinally in GNs. All four genes were present in the highest gene expression quartile of all transcribed GN genes (**Figure 2B**) throughout the assayed 3-weeks-long cell culture period revealing that GN are postmitotic and properly differentiated human neurons and transcriptionally similar to highly functional AP5 type neurons. This is consistent with our mwMEA recordings (**Figures 1E–H**) and highlights the utility of GNs for electrophysiology studies in mature human neuronal cultures.

Next, to better understand how cultured GNs transcriptionally mature over time-periods which complement our longitudinal neurite dynamics and mwMEA datasets, genome-wide gene expression dynamics were compared between three key time points (DIV7, DIV14, and DIV21). Around DIV7 a plateau in neurite outgrowth becomes apparent and after ∼DIV14 highly synchronous network activity is established, we terminated most experiments for this study at DIV21. Over 1,000 genes were differentially expressed when comparing DIV14 to DIV7 RNA-Seq datasets (536 upregulated, 526 downregulated; **Figure 2C**). An unbiased GO analysis further showed that differentially expressed genes were significantly enriched in the biological processes (BP) neuron differentiation and neuron projection development (**Figure 2D**). For example, the expression of key neuron differentiation genes steadily decreased over time (**Figure 2E**), which is consistent with our neurite dynamics data. The combined results suggest a shift to a morphologically and structurally mature state at DIV14 compared to DIV7. Between DIV21 and DIV14, almost 3,000 genes were differentially expressed (1,678 upregulated, 1,143 downregulated; **Figure 2F**). In particular, the genes involved in mRNA catabolism and translation were significantly

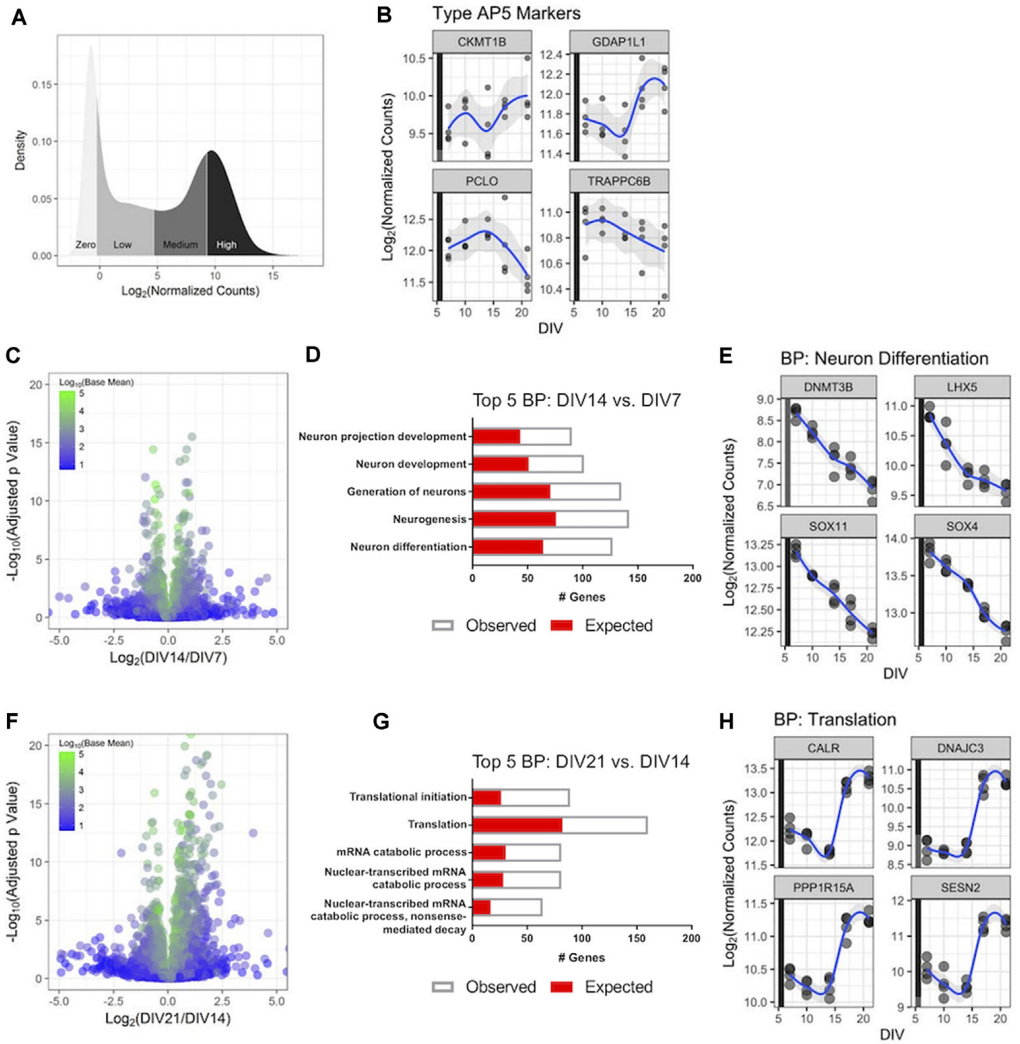

FIGURE 2 | RNA-Sequencing (RNA-Seq) profiling of human iPSC neurons during 3 weeks in culture. Untreated GN cultures were collected over 3 weeks in culture, and global gene expression was determined with RNA-Seq. **(A)** Distribution of the RNA-Seq count data for the 27,882 genes measured in the experiment. The *y*-axis displays the kernel density estimate, and the *x*-axis displays the normalized count data with each quartile shaded. **(B)** Expression of four genes associated with highly functional (Type AP5) iPSC-derived neurons over time. Each point represents an independent replicate (n = 4 independent replicates per time point), and the blue line shows a LOESS model of the data. The colored stripe on the *y*-axis indicates the quartile of count values shown in panel **(A)**. **(C)** Volcano plot displaying RNA-Seq data comparing gene expression at DIV14 relative to DIV7. The plot displays 16,591 genes colored according to the mean of their normalized count values across all samples (n = 4 independent replicates per time point). **(D)** The top five biological processes (BPs)—identified by gene ontology (GO) analysis—that were significantly enriched with differentially expressed genes at DIV14 vs. DIV7. The number of genes observed as differentially expressed and the number expected by chance are superimposed. **(E)** Expression values over time for the four most statistically significant genes in the neuron differentiation BP at DIV14 compared to DIV7. Data are displayed as in panel **(B)**. **(F)** Volcano plot of RNA-Seq data comparing gene expression at DIV21 and DIV14 displayed as in panel **(C)**. **(G)** The top five BPs that were significantly enriched with differentially expressed genes at DIV21 compared to DIV14. **(H)** Expression values over time for the four most statistically significant genes in the translation BP at DIV21 compared to DIV14. Data are displayed as in panel **(B)**.

enriched in the GO analysis (**Figure 2G**), demonstrating that during this time interval the human iPSC neurons are becoming functionally active as evidenced by the sharply increasing expression level of genes representative for the "Translation" group after DIV14 (**Figure 2H**), which once again mirrored the increased neuronal activity and synchrony we identified using mwMEA (**Figure 1G**). In all, these transcriptional dynamics highlight relevant developmental stage changes that occur as the GNs progress through 3 weeks *in vitro*.

Human iPSC Neurons Express Key Neurodegenerative Disease-Linked Genes

A potential utility of these cells could be to facilitate the study of aberrant cellular functions in cellular models of human disease. Our RNA-Seq datasets to revealed that expression levels of AD-associated genes *APOE*, *APP*, *PSEN1*, and *PSEN2* were expressed consistently in the medium-to-high quartiles (**Figure 3A**), with *APP* being the most highly expressed disease gene. Relevant Parkinson's Disease (PD)-associated genes

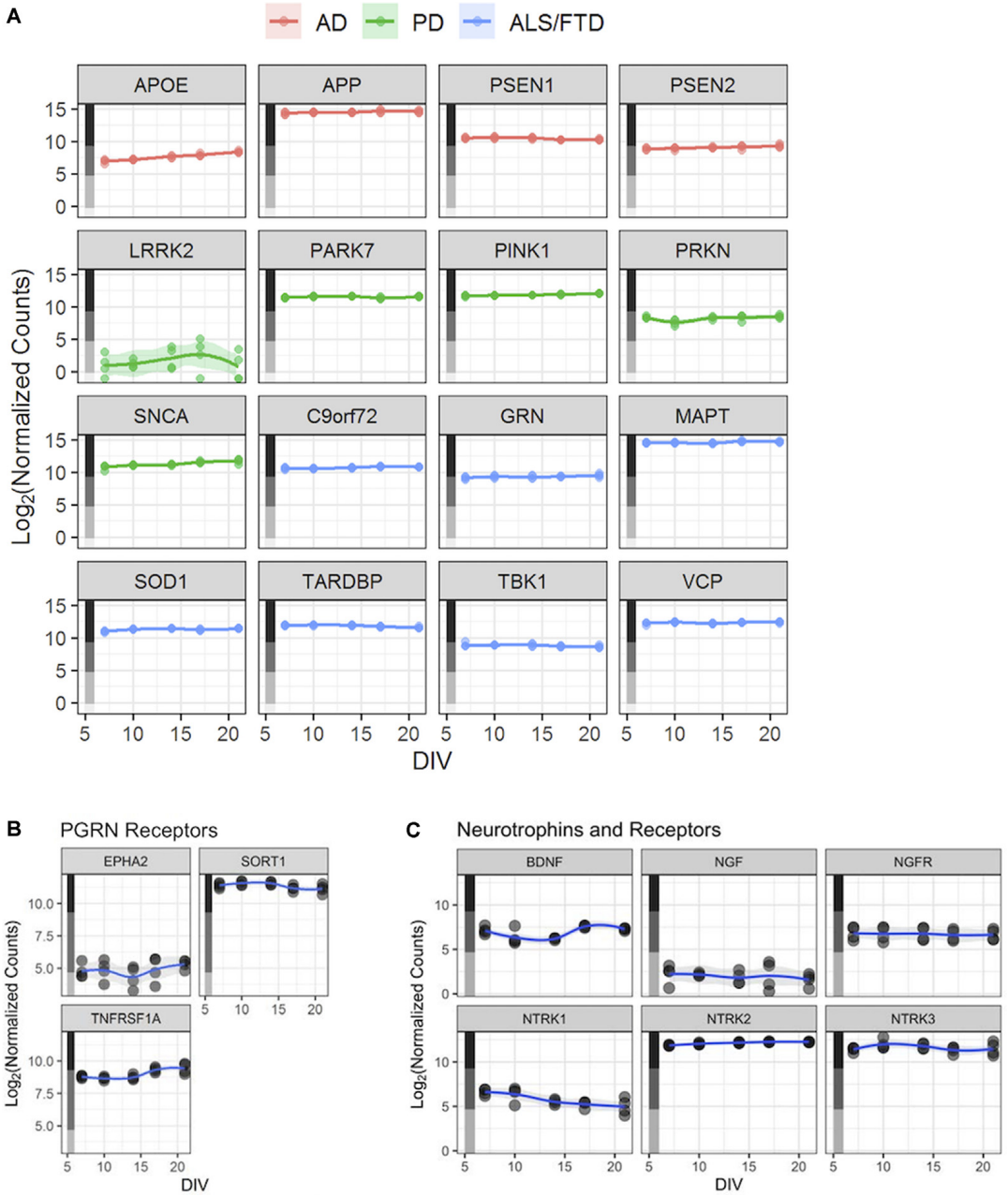

FIGURE 3 | Human iPSC neurons as a potential tool to study neurodegenerative and other CNS diseases. **(A)** Expression profiles—based on the RNA-Seq dataset described in **Figure 2**—for genes linked to selected neurodegenerative diseases. Each point represents an independent replicate (n = 4 independent replicates per time point), and the line for each graph shows a LOESS model of the data. The colored stripe on the y-axis indicates the quartile of count values shown in **Figure 2A**. Alzheimer's Disease (AD), Parkinson's Disease (PD), amyotrophic lateral sclerosis (ALS), frontotemporal lobe dementia (FTD). **(B)** Expression of three PGRN receptor genes—*EPHA2*, *SORT1*, and *TNFRSF1A*—in untreated GNs. **(C)** Expression of *BDNF*, *NGF*, and their receptors—*NGFR* (NGF receptor gene) and *NTRK1–3* (BDNF receptor genes) in untreated GNs. Data in panels **(B,C)** are displayed as in **Figure 2B**.

PARK7, *PINK1*, *SNCA*, and *PRKN* are expressed at medium-to-high levels, while *LRRK2* is expressed at overall lower levels (**Figure 3A**). Finally, amyotrophic lateral sclerosis (ALS)-linked gene, including *SOD1*, and genes causing FTD, including *GRN*, are also robustly expressed in GNs at all assayed time points (**Figure 3A**).

Progranulin Mediates Neuroprotection in Human iPSC Neurons

Next, we used GNs to understand the quantitative pharmacology of genes with an established role in neurodegenerative diseases in humans. PGRN is a pleiotropic growth factor that modulates diverse BP including neuronal survival and neurite outgrowth,

PGRN mutations cause FTD (Van Damme et al., 2008; Gao et al., 2010; Gass et al., 2012). We analyzed the expression of the putative PGRN receptors (**Figure 3B**; Hu et al., 2010; Tang et al., 2011; Neill et al., 2016) in GNs. While the expression of *EPHA2* was relatively low, both *SORT1* and *TNFRSF1A* were highly expressed in GNs through the assayed 3 weeks in culture (**Figure 3B**). To qualify them as potential reference molecules and controls for our phenotypic assays, we verified that the expression of growth factors that have been shown to mediate neuroprotection (Nguyen et al., 2009, 2010) and enhance neurite outgrowths (Drubin et al., 1985; Iwasaki et al., 1998), such as brain-derived neurotrophic factor (BDNF) and nerve growth factor (NGF), BDNF and NGF and their signaling receptors (NTRK1, NTRK2, NTRK3, and NGFR), are robustly expressed in GNs (**Figure 3C**).

Cortical neurons from an FTD patient carrying mutated *GRN* show increased vulnerability to the neurotoxin staurosporine (Almeida et al., 2012), while the affected growth of iPSC-derived cortical neurons in a separate PGRN-FTD model is rescued by the reinstatement of *GRN* expression (Raitano et al., 2015). *in vitro* rodent studies have established that recombinant PGRN may promote neuronal survival (Van Damme et al., 2008; Ryan et al., 2009; Gao et al., 2010; Guo et al., 2010; Kleinberger et al., 2010; Xu et al., 2011). To complement rodent-derived data, we next quantified the responsiveness of human iPSC-derived GNs to recombinant PGRN in a neurotoxicity assay. GNs were grown uninterrupted for 2 weeks before being treated with 0.1 μM staurosporine (STS), an established non-selective protein kinase inhibitor and potent neurotoxin (Rüegg and Burgess, 1989), to trigger apoptotic neuronal death (Koh et al., 1995). To assess neuroprotection, cells were co-treated with either vehicle (PBS), positive controls (recombinant NGF or BDNF; Ichim et al., 2012), or a range of recombinant PGRN concentrations (**Figure 4A**) while cells were continuously monitored the fluorescence of the added annexin V dye to quantify apoptosis in our live-cell imaging platform. There were considerably more annexin V-labeled cells and annexin V-labeled area after 48-h STS treatment compared to treatment with medium alone, thus confirming STS cytotoxicity and validating the annexin V reagent to track cell death longitudinally (**Figure 4B**). Co-treatment of cells with either BDNF or NGF significantly lowered STS-induced neuronal death. Similarly, co-treatment experiments with PGRN concentrations of 0.114 nM or higher lead to a significant reduction in cell death compared to treatment with STS alone (**Figures 4B,C**). Our data complement evidence derived from rodent neurons and demonstrate a neuroprotective role for PGRN also in human GNs.

No Sensitivity to Growth Factor-Mediated Neurite Dynamics in Human iPSC Neurons

We established a live-cell imaging neurite outgrowth assay using BDNF and NGF as positive controls (**Figure 4D**; Huang and Reichardt, 2001) to test if recombinant PGRN promotes neurite outgrowth in human GNs, as previously found in rodent neurons (Van Damme et al., 2008; Gao et al., 2010; Wang et al., 2010; Gass et al., 2012; De Muynck et al., 2013). Cells were incubated with recombinant growth factors or PGRN for 10 days, then morphological neurite metrics were analyzed (**Figure 4D**). BDNF, NGF (Iwasaki et al., 1998; Colombo et al., 2014), and PGRN (Van Damme et al., 2008; Gao et al., 2010; Wang et al., 2010; De Muynck et al., 2013) treatments using concentrations that have been previously shown to increase neurite outgrowth did not affect GNs (**Figures 4C,G,H**). Only 1,140 nM PGRN, which is ∼16.000 times higher than the normal PGRN levels in human CSF (Nguyen et al., 2013), significantly enhanced neurite length in GN cultures. Cell-body cluster number was overall unchanged (**Figure 4I**), suggesting that captured effect sizes were not masked by variations in plating density, and thus neurite outgrowth in GNs may not be sensitive to physiologically-relevant concentrations of exogenous growth factor proteins.

Acute PGRN Treatment Increases Neuronal Activity in Human iPSC Neurons

PGRN plays a role in synaptic plasticity (Tapia et al., 2011; Lui et al., 2016), PGRN treatment in murine cortical neurons can modulate aspects of spine maturation and synaptic transmission (Zhang et al., 2017). However, electrophysiological data in human iPSC neurons is lacking. To address this, we cultured GNs on mwMEA plates and exposed them to recombinant PGRN. mwMEA recordings were performed before, during, and immediately after treatment of functionally mature DIV19 GNs, followed by a final recording session 2 days after treatment (**Figure 5A**). Acute, one-time addition of 0.114 nM PGRN induced a significant increase in the overall firing activity of the cells, measured by the weighted MFR compared to the vehicle (**Figures 5B,C**). Surprisingly, 2 days after treatment, cells treated with either 0.00114, 0.114, or 11.4 nM PGRN also exhibited an enhanced firing rate compared to vehicle-treated cells (**Figure 5C**). Burst frequency was not modulated by the addition of PGRN either before or immediately after the washes, but 2 days after treatment a significant increase was observed for GNs that were exposed to 0.114 nM PGRN (**Figure 5D**). The network burst percentage, a measure of the spontaneous synchronization of burst activity across the network in the well, did not immediately respond to treatments but exhibited a significantly higher burst percentage after the washes up until 2 days after treatment (**Figure 5E**). The synchrony index (an alternative metric of neuronal synchronization) was not changed significantly, but 0.114 nM PGRN addition showed a trend towards increases network synchrony (**Figure 5F**). These results suggest that recombinant PGRN can enhance network activity in human iPSC neurons in a sustained manner.

Using Human iPSC Neurons to Model Frontotemporal Lobe Dementia

To complement our approaches utilizing increased levels of (recombinant) PGRN, we next aimed to develop human cellular assays with decreased PGRN expression using siRNA (Baker et al., 2006; Cruts et al., 2006). First, we tested three different pools of self-delivering siRNAs in GNs, and found that in each tested pool we produced nearly complete knockdown of their target at 72 h (**Figures 6A–D**). To assess possible off-target effects of long-term siRNA exposure on neuronal health, morphology, and outgrowth, GNs were treated with a

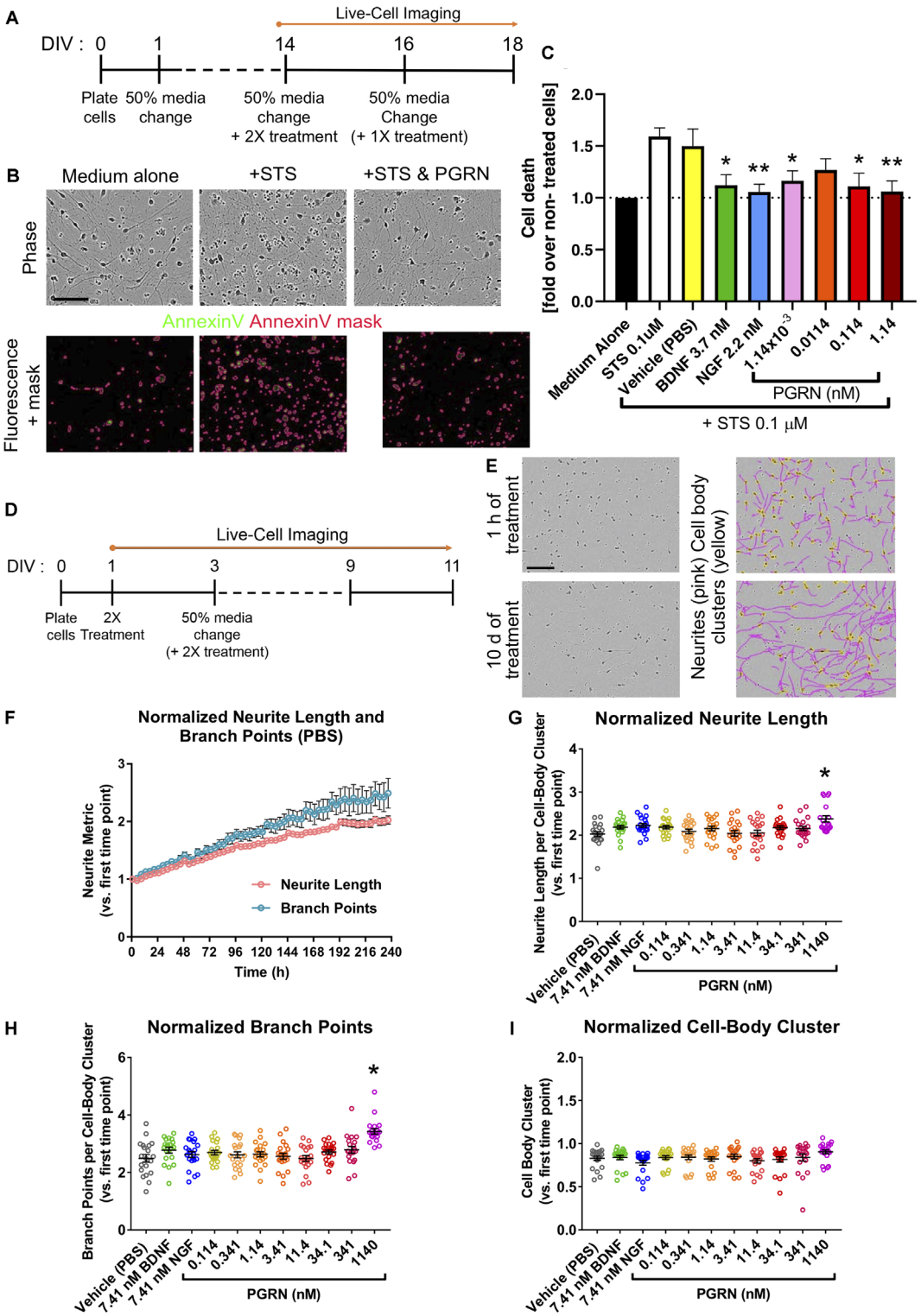

FIGURE 4 | Recombinant progranulin (PGRN) mediates neuroprotection in human iPSC neurons. **(A)** Schematic of the neurotoxicity assay timeline. Dashes represent 50% of media changes every other day. **(B)** Representative images of DIV16 GNs 48 h after either medium change alone (Medium alone), staurosporine (STS) treatment alone (+STS), or STS and 0.114 nM PGRN co-treatment (+STS and PGRN). The top panel shows phase-contrast images of the cells; the bottom panel displays fluorescence images showing the annexin V staining in the green channel with the superimposed annexin V mask (in pink). This user-defined mask was generated using the Basic Analyzer software module in the IncuCyte™ system and was used to quantify cell death based on annexin V fluorescence signal.

(*Continued*)

FIGURE 4 | Continued
Scale bar, 400 μm. **(C)** Measured by annexin V staining-covered area, graph shows the fold change of cell death and toxicity concerning untreated wells. Cells were untreated (medium alone) or co-treated with STS and recombinant PGRN, BDNF, or NGF. The graph represents data from 4 or 10 independent experiments (three replicates per condition in each experiment). Results are displayed as mean ± SD. For all graphs, $^{*}p < 0.05$; $^{**}p < 0.01$ (one-way ANOVA with Dunnett's *post hoc* test, all conditions compared to STS treated wells). **(D)** Schematic of the neurite outgrowth assay. Dashes represent 50% media changes (containing treatments in double concentration: 2×) every other day. **(E)** Representative phase-contrast images and the masking of neurites utilizing the NeuroTrack™ software in the IncuCyte™ system. Images and masks were used to quantify neurite length and neurite branch points. Example images show PBS vehicle-treated GNs; images show masked neurites (pink) and cell body clusters (yellow) after 1 h and after 10 days of treatment. Scale bar, 600 μm. **(F)** Quantification of neurite length and neurite branch point measurements for vehicle-treated GNs. Each data point represents the mean ± SEM for four to five independent experiments (four replicates per experiment). **(G–I)** Quantification of neurite metrics after 10 days of treatment with either vehicle (PBS), 7.41 nM BDNF, 7.41 nM NGF, or a range of PGRN concentrations. All graphs represent data from five independent experiments (four replicates per condition in each experiment). Results are displayed as mean ± SEM. For all graphs, $^{*}p < 0.0001$ (one-way ANOVA with Dunnett's *post hoc* test, all conditions compared to vehicle). **(G)** Neurite length per cell-body cluster (normalized to the measurement at the first imaging time point). **(H)** Neurite branch point number per cell-body cluster (normalized to the measurement at the first imaging time point). **(I)** Cell-body cluster number (normalized to the measurement at the first imaging time point).

range of non-targeting (NT) siRNA concentrations, and their morphology was quantified. The highest concentration of NT siRNA tested (1,000 nM) caused extensive clustering of GNs at DIV21 (**Figures 6E,H**) and impeded neurite growth, but the tested lower concentrations of NT siRNA were well tolerated (**Figures 6F–H**).

We then studied the impact of various levels of GRN siRNA on *GRN* mRNA expression at DIV21 (**Figure 7A**). *GRN* mRNA was nearly undetectable in cells treated with 300 nM siRNA. A log-logistic dose-response model was fit to the *GRN* siRNA data (top = 1.073 ± 0.034, slope = 0.941 ± 0.111, ED_{50} = 10.45 ± 1.43 nM). This model indicated that 10 nM siRNA produced ∼50% knockdown at DIV21, further experiments showed that 30 nM siRNA produced ∼50% knockdown at DIV10 (**Figure 7B**). As expected in our approach to continuously replenish siRNA, the effects of 30 nM siRNA were more pronounced at the endpoint (71 ± 5.8% knockdown). We chose to continue using 30 nM siRNA for our experiments because it produced an approximated GRN haploinsufficiency in the time window that was most-relevant for our phenotypic assays (between ∼DIV10 and ∼DIV15) without noticeable off-target effects (**Figures 6F–H**).

GRN Knockdown Does Not Impact the Transcriptome in GNs

Global gene expression abnormalities are present in human post mortem GRN-FTD brain samples (Chen-Plotkin et al., 2008). Next, we used RNA-Seq to determine if additional genes were changed in the GNs treated with 30 nM *GRN* siRNA or NT siRNA for up to DIV21 (**Figure 7B**). A PCA was used to reveal factors that modulate gene expression variance among samples. The first identified principal component was DIV, which accounted for 26% of the variance in the data (**Figure 7C**). This is not surprising given the expected developmental changes in gene expression (**Figures 2C,F**). The second principal component was the lot of GNs, which accounted for 8% of the variance (**Figure 7D**). The very little variance was due to the presence of either siRNA itself, as data from NT siRNA-treated cells were grouped with that from untreated cells. Surprisingly, knockdown of *GRN* also had little impact in the PCA (**Figure 7C**), which suggests that reduced *GRN* expression did not significantly affect the GN transcriptome. This was confirmed by pairwise analyses of the NT siRNA and *GRN* siRNA sample groups at DIV7, DIV14, and DIV21 (**Figures 7E–G**). This unbiased analysis detected significant decreases in GRN mRNA at DIV 14 and 21, which validated the RT-PCR data shown in **Figure 7B** and demonstrated that the study was powered to detect similar changes in other genes if they existed. We conclude that siRNA-mediated *GRN* knockdown in GNs under the current culture conditions did not affect global gene transcription signatures.

GRN Knockdown Does Not Affect Neurite Dynamics in Human Neurons

Full *GRN* knockout rodent cortical and spinal cord neurons have decreased outgrowth and neurite complexity *in vitro* (Van Damme et al., 2008; Gao et al., 2010; Wang et al., 2010; De Muynck et al., 2013). Some neurons, including in the amygdala, may also show reduced neurite complexity in 6–9-month-old heterozygous *GRN* knockout mice *in vivo* (Arrant et al., 2016). We investigated next if the neurite dynamics are affected in cultured iPSC-derived human GNs with reduced PGRN expression. Automated and unbiased quantitative assessment of morphological features (illustrated by the schematic in **Figure 8A**) revealed that treatment of GNs with 30 nM of *GRN* siRNA had no significant effect on neurite length, neurite branch points, and density or movement of cell body clusters, compared to NT siRNA or untreated control cells (**Figures 8B–D**). *GRN* knockdown results mirror those from the recombinant PGRN treatment experiments described earlier (**Figures 4G–I**) and suggest that neurite dynamics in human iPSC-derived GNs under the probed conditions are not sensitive to bi-directional manipulations of progranulin levels.

GRN Knockdown Does Not Consistently Affect Neuronal Network Activity in Human Neurons

By utilizing mwMEA recordings, we now explored if siRNA-mediated *GRN* haploinsufficiency in human GNs neurons modulates electrophysiological properties. The mwMEA activity of NT siRNA- and *GRN* siRNA-treated cells was longitudinally measured every second day starting at DIV3 (the first day of siRNA treatment) up to DIV21 (**Figure 8A**). Throughout the experiments, the number of active electrodes remained relatively constant. Although GRN siRNA-treated measurements trended lower, there was no significant difference between *GRN* siRNA- and NT siRNA-treated cells (**Figure 8E**). The weighted MFR in *GRN* siRNA-treated human iPSC neurons showed a consistent trend toward lower neuronal activity over 21 days that only

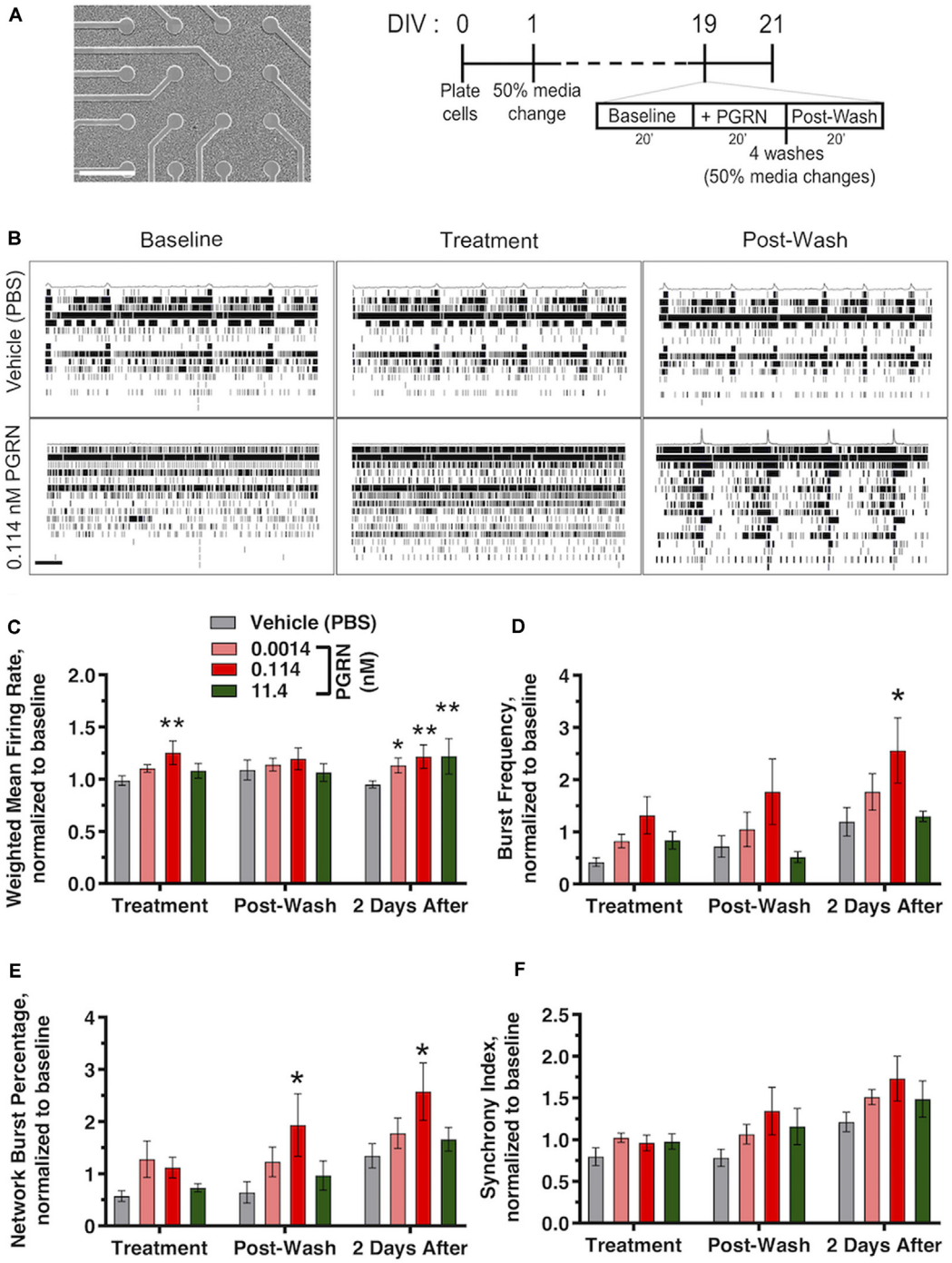

FIGURE 5 | Recombinant PGRN enhances firing and synchronization in cultured human iPSC neurons. **(A)** Representative images of GNs at 19 DIV growing on top of the electrodes of a 48-well mwMEA plate and schematic of the experiment and mwMEA recording. Dashes represent 50% of media changes every other day. Recordings were made before, during, and after PGRN treatment on DIV19; then, an additional recording was performed 2 days later. **(B)** Representative raster plots for neuronal firing before, during, and after exposure to the vehicle (PBS) or 0.114 nM PGRN in DIV19 cells. Each row of the raster plot represents an electrode within a well (16 total), and each black line within the row represents a neuronal spike. Averages of spikes are shown at the top of each raster plot. Scale bar, 20 s. **(C–F)** Quantification of neuronal activity relative to baseline activity in cells during treatment, directly after washes, and 2 days after treatment/washed. All graphs represent data from six independent experiments (two to six replicates per condition in each experiment). Results are displayed as mean ± standard error of the mean (SEM). For all graphs, $^{*}p < 0.05$; $^{**}p < 0.01$ (one-way ANOVA with Dunnett's *post hoc* test, all conditions compared to vehicle). **(C)** Weighted mean firing rate (MFR), normalized to baseline weighted MFR recorded before treatments. **(D)** Burst frequency, normalized to baseline burst frequency recorded before treatments. **(E)** Network burst percentage, normalized to baseline network burst percentage recorded before treatments. **(F)** Synchrony index, normalized to baseline synchrony index recorded before treatments.

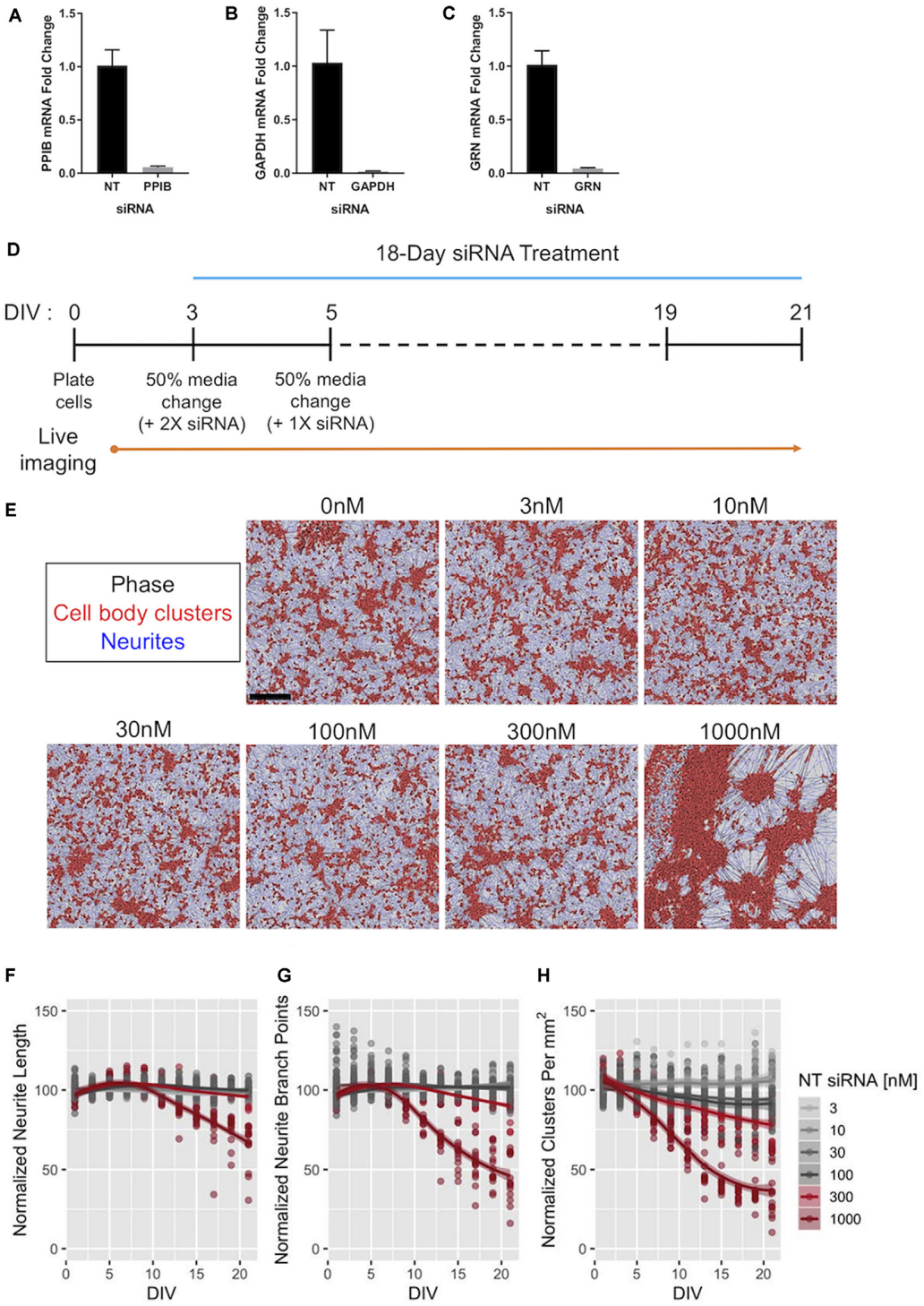

FIGURE 6 | Efficacy of Accell™ siRNA-mediated gene knockdown in human iPSC neurons. **(A–C)** Expression of *PPIB* **(A)**, *GAPDH* **(B)**, and *GRN* **(C)** mRNA in GNs after 72-h exposure to 1 μM of siRNAs targeting the indicated gene. The expression levels were compared to those in GNs treated with 1 μM of pooled non-targeting (NT) siRNAs. Expression was detected using qPCR with 18S rRNA as an internal control ($n = 3$ independent replicates per group). **(D)** Schematic of the protocol for long-term treatment of self-delivering Accell™ siRNAs to GNs. Dashes represent 50% media changes (with 1× siRNA treatments) every other day. **(E)** Representative images taken at DIV21 of GNs repeatedly exposed to the indicated concentrations of NT siRNA per the protocol in panel **(D)** neurite masking by NeuroTrack™ software is shown for neurites (blue) and cell-body clusters (red). Scale bar, 300 μm. **(F–H)** NeuroTrack™ quantification of neurite length **(F)**, neurite branch points **(G)**, and cell-body clusters **(H)** in cells treated with the indicated concentrations of NT siRNA until DIV21. The data were collected for nine independent

(*Continued*)

FIGURE 6 | Continued
experiments (n = 183 untreated wells, n = 120 wells treated with 30 nM, and n = 15 wells for remaining concentrations). All measurements were normalized to the mean of the untreated cells per recording for each experiment. Solid lines show a LOESS fit of the data, and the shaded area represents the 95% confidence intervals of the model (when large enough to display). The concentrations displayed in red were significantly different than untreated cells at DIV21 [$p_{adj} < 0.05$, Tukey's Honest Significant Difference (HSD) test].

reached statistical significance at DIV15 (**Figure 8F**). Consistent to previous experiments (**Figure 1**), the network burst frequency and synchrony index as a measure of neuronal synchrony increased over time in both NT siRNA- and *GRN* siRNA-treated cells, but no group difference was evident (**Figures 8G,H**). Our assessments of human iPSC neurons with reduced PGRN levels demonstrated no effect on global gene transcription or neuronal morphology and only modest modulation of neuronal firing. In all, our study describes a longitudinal systems-level characterization of GNs and highlights the diversity of phenotypic screening assays and manipulations of target genes that can be performed using these particular commercially-available human iPSC neurons.

DISCUSSION

Animal-based cellular models drive our understanding of disease biology, but often these tools do not have sufficient translational value for more clinically-relevant human biology. Therefore, in this study, we focused our attention on iPSC-derived neuronal cells as a key technology that is commercially available and, thus, would allow independent validation and wide distribution of the presented tools among the science community to open up this technology also to researchers that are not proficient in iPSC reprogramming. Since comprehensive and longitudinal profiling of human iPSC GNs is lacking, we have characterized systems-level phenotypic neuronal features (neurite outgrowth dynamics, neuronal network function, genome-wide gene expression).

Our longitudinal morphological dataset as a proof-of-principle demonstrates that live-cell imaging of GNs qualifies assay conditions and time points that are appropriate for investigating a given biological question. Furthermore, quantitative pharmacology of compounds that potentially modulate a cellular process can be performed using the assays and conditions outlined in this study. For example, since neurite outgrowth reaches a plateau around ∼DIV10, GN experiments that focus on studying these neurite dynamics during the phase of strongest growth should be performed before DIV10.

To complement the quantification of morphological features in GNs, we established a long term mwMEA platform that enabled us to quantify the formation and synchronization of functional neuronal network activity in human iPSC neurons. Our results are consistent with previous studies in both rodent and human neurons (Tukker et al., 2018; Odawara et al., 2016; Tukker et al., 2016) and demonstrate that, as neurons grow *in vitro*, they spontaneously form networks that are characterized by electrical activity. Our data further revealed that GNs need approximately 2 weeks in culture before a robust synchronization of neuronal firing develops across the well (**Figure 1**). Therefore, human iPSC GNs are a valuable tool to study a variety of electrophysiological features and offer ways to robustly quantify (either acutely or over time) how neuronal firing and synchrony may be modulated by genetic or pharmacological manipulations.

The third major arm of longitudinal phenotypic characterization that we performed in GNs was a comprehensive genome-wide gene expression characterization spanning 3 weeks in culture. Our data validate that GNs are of a postmitotic neuronal phenotype and that intrinsic global gene expression is fluid during the *in vitro* culture period. While the first week of culture (growth phase) is characterized by genes that are typically expressed during neuronal development, the second week (maturation and refinement phase) is dominated by neuronal differentiation gene networks. The third week of culture (synchronous and steady-state phase) shows highly expressed gene networks typical for very mature neuronal homeostasis and activity (**Figure 2**). These changes in the gene expression profile over time are consistent and overlap with the developmental progression of the previously quantified morphological and functional features in GNs (**Figure 1**). Besides, our RNA-Seq data also can be utilized for data mining in the context of identifying molecular targets and genes that are associated with neuronal diseases. We show, for example, that GNs express relevant genes that are important for studying growth factors or neurodegenerative diseases including Alzheimer's, Parkinson's, ALS, and FTD (**Figure 3**). To allow additional analyses of our data, data sharing, and combination with other published datasets, our RNA-Seq datasets will be made publicly available at the Gene Expression Omnibus as a resource to study and better understand the longitudinal expression of any gene(s) of interest in GN cultures.

To provide a practical demonstration, we have leveraged our GN datasets to investigate relevant human neurobiology questions in phenotypic assays. For example, we have investigated if growth factor treatment during the initial neuronal outgrowth phase impacts the dynamics of neurite outgrowth; in separate assays, we have quantified if such treatment can mediate neuroprotection and lower apoptotic cell death. One of the key findings of our study is that recombinant progranulin is neuroprotective in human neurons (**Figure 4**). This is noteworthy for at least two reasons: (1) revealing that the potency of PGRN to protect human neurons against apoptosis caused by STS (Almeida et al., 2012) is comparable to that of BDNF and NGF (Aloe et al., 2012; Allen et al., 2013; Kowiański et al., 2018); and (2) this result builds a translational bridge from previous rodent neuronal data (Van Damme et al., 2008; Gao et al., 2010; Gass et al., 2012; Wang et al., 2010; De Muynck et al., 2013) to human neuronal data.

Some involvement of PGRN in synapse biology is prominent in the literature (Tapia et al., 2011; Petoukhov et al., 2013; Yuan et al., 2015; Lui et al., 2016; Meeter et al., 2016; Zhang et al., 2017; Uesaka et al., 2018), but not much was known about the role of PGRN in regulating neuronal firing. Our mwMEA experiments provide evidence that a one-time acute

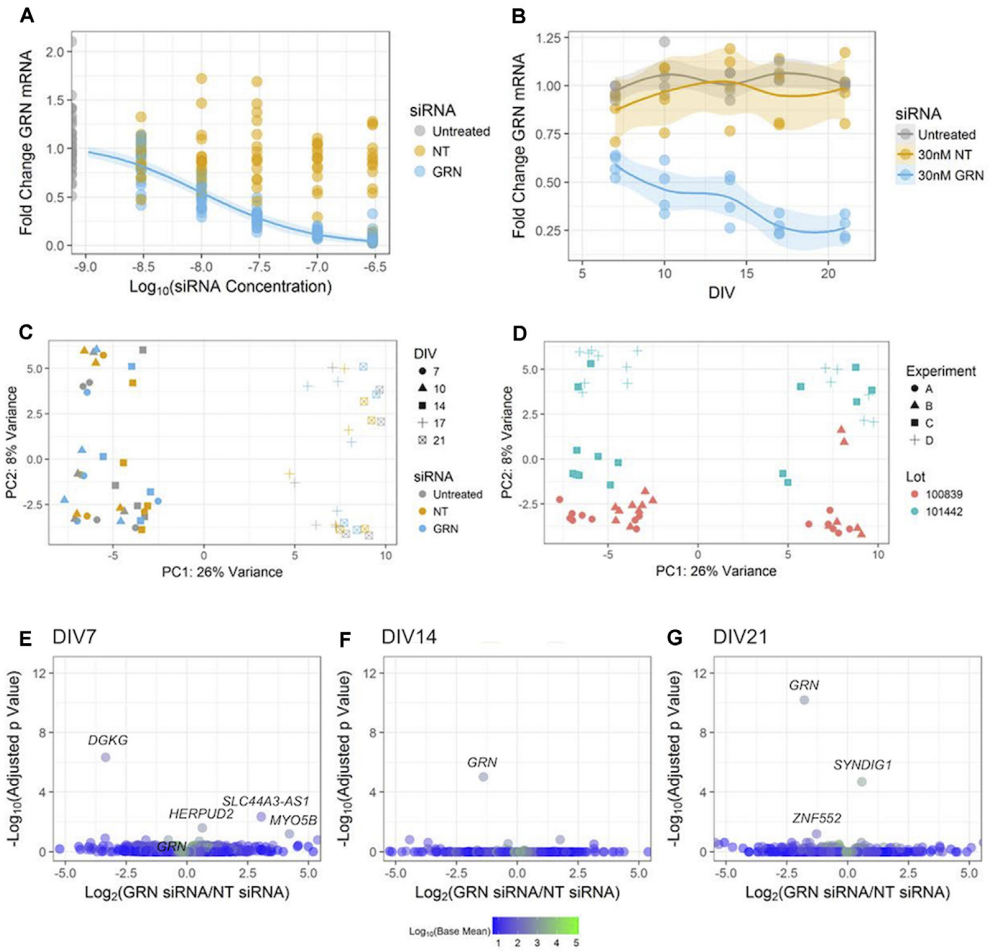

FIGURE 7 | Reducing *GRN* expression in human iPSC neurons to model FTD. **(A)** *GRN* mRNA levels were determined using qPCR (with *ACTB* as a reference gene) following 18 days of treatment with the indicated siRNA concentrations. A three-parameter log-logistic model, with a bottom set to zero, was fit to the *GRN* siRNA data and is displayed as a blue line along with 95% confidence intervals. No model converged for the NT siRNA data. Untreated and *GRN* siRNA data come from seven independent experiments (n = 36 untreated wells and 105 *GRN* siRNA wells), while the NT siRNA data come from five independent experiments (n = 75 wells). Gene expression data are not displayed for the highest dose of siRNA used in **Figures 5E–H** due to toxicity. **(B)** *GRN* mRNA expression levels measured using qPCR in GNs treated with 30 nM siRNA and collected at DIV7, 10, 14, 17, and 21 (n = 4 independent replicates per time point for each treatment). The solid line shows a LOESS model of the data, with the 95% confidence intervals displayed in the shaded areas. The mean of *ACTB*, *PPIB*, and *GAPDH* expression was used for the reference. **(C,D)** Principle component analysis of RNA-Seq data from the cells treated with siRNA and collected at DIV7, 10, 14, 17, and 21 (n = 60 samples). The data are displayed according to shape (indicating the DIV) and color (indicating the siRNA) in **(C)**, while **(D)** shows the data with the shape indicating the experiment and the color indicating the cell lot number. **(E–G)** Volcano plots of RNA-Seq data comparing 30 nM of either NT or *GRN* siRNA at DIV7, 14, and 21. Each plot displays 16,591 genes colored according to the mean of their normalized count values across all samples (n = 4 independent replicates per siRNA). The labeled points were statistically significant ($p_{adj} < 0.1$), except for the *GRN* point labeled in the DIV7 plot.

treatment with recombinant PGRN can increase neuronal firing and synchrony in human iPSC neurons (**Figure 5**). Surprisingly, we further found that this effect appears to be long-lasting for at least up to 2 days after treatment. While we currently do not understand which mechanism mediates this activity, future studies that investigate the role of PGRN are warranted including for example to complement our existing data with PGRN overexpression or GRN gene editing using e, g, CRISPR technologies.

Our proof of principle approach to model FTD in human neurons *in vitro* using siRNA-mediated *GRN* knockdown demonstrated that GNs combined with other off-the-shelf reagents can be used to elucidate the functions of disease-associated genes in highly customized isogenic models and assays of human disease (**Figure 6**). At this stage, our analyses of this model are still preliminary and suggest that siRNA-mediated *GRN* knockdown in GNs under the current culture conditions seemingly did not modulate global gene transcription signatures (**Figure 7**), although gene expression defects have been reported in GRN-deficient post mortem brains (Chen-Plotkin et al., 2008). We speculate that a *GRN* knockdown of longer than 2–3 weeks could be needed to influence the genome-wide transcriptional landscape more robustly in cultured GNs. It is further difficult to directly

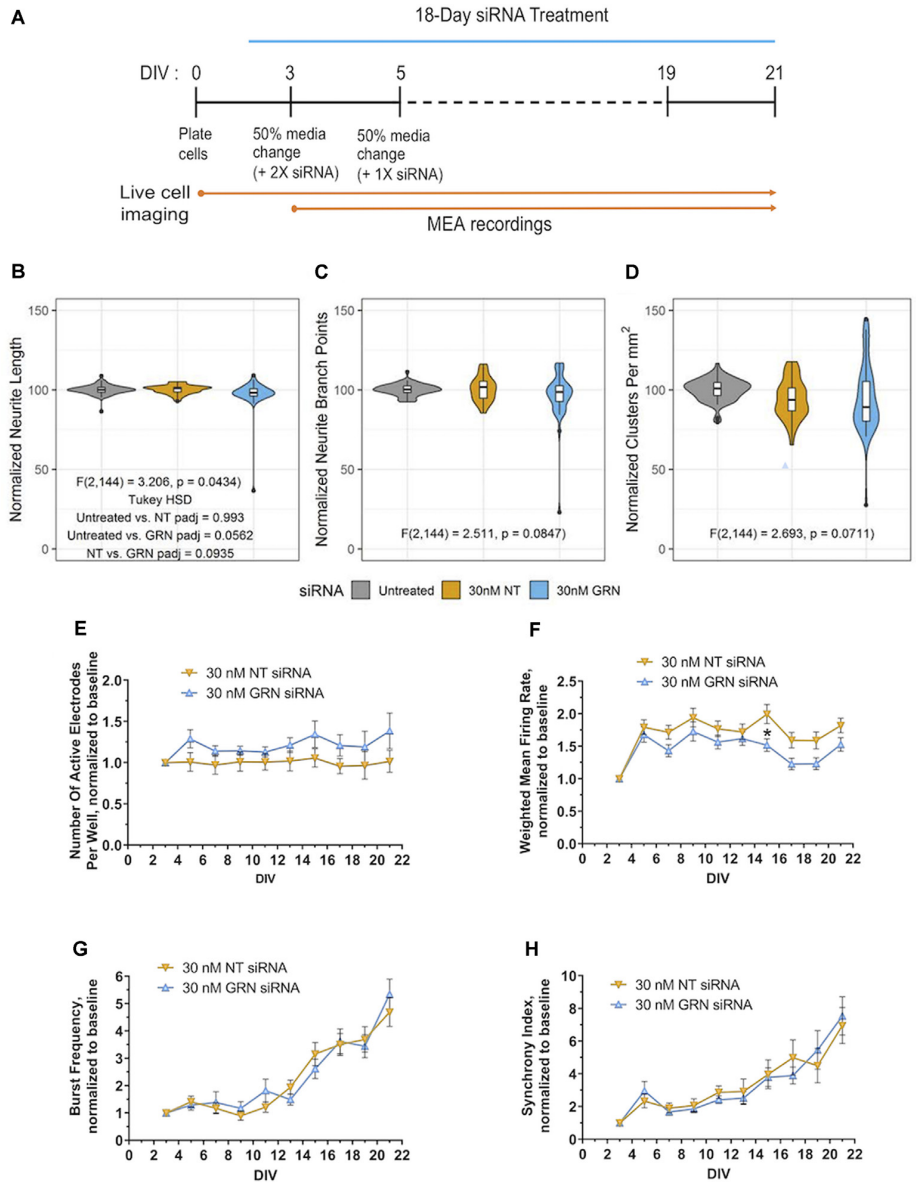

FIGURE 8 | Morphological and electrophysiological features in human iPSC neurons with reduced *GRN* expression. **(A)** Schematic shows the repeated siRNA treatment protocol for knocking down GRN mRNA in GNs and the time course of the 21 DIVs with life cell imaging and mwMEA recordings. **(B–D)** Violin plots of GN neurite length **(B)**, branch points **(C)**, and cell-body clusters **(D)** at DIV21 following repeated treatment with the indicated concentrations of siRNA for 18 days. The white box plots display the median, with whiskers displayed using the Tukey method. Outliers are shown as black dots. The colored violin plots display the distribution of the data collected from 11 independent experiments (n = 69 untreated wells, n = 36 NT siRNA wells, and n = 42 GRN siRNA wells). The results of ANOVA are displayed in the graph along with the results of Tukey's HSD test when the ANOVA results were significant. **(E–H)** Quantification of neuronal activity in GNs treated with either NT or *GRN* siRNA 30 nM from DIV3 to DIV21. **(E)** Graph showing active electrodes per well over 21 days in culture. **(F)** Plotted weighted MFR over 21 days in culture, normalized to weighted MFR measured at 3 DIV. **(G)** Graphed burst frequency over 21 days in culture, normalized to burst frequency recorded at DIV3. **(H)** Synchrony index over 21 days in culture, normalized to synchrony index recorded at 3 DIV. mwMEA graphs represent data from seven independent experiments (8–24 replicates per condition in each experiment). mwMEA graphs represent data from six independent experiments (two to six replicates per condition in each experiment), results are displayed as mean ± standard deviation (SD) *$p < 0.05$; (one-way ANOVA with Dunnett's *post hoc* test, all conditions compared to NT siRNA).

compare our human GN knockdown model, which was designed to mimic haploinsufficiency and have a ∼50% reduction in PGRN levels to previous studies utilizing PGRN-deficient mice. Virtually all phenotypes described previously in rodent neurons were derived from analyzing full PGRN knockout tissues or cells, which do not express PGRN at all. Additional experiments are needed to more deeply investigate PGRN biology in human cellular models, our study provides a validation of available siRNA tools and a roadmap to demonstrate how our isogenic and scalable knockdown protocol

can be leveraged to manipulate the expression of virtually any gene in the genome in commercially-available human iPSC GNs. In conclusion, we have deeply characterized one commercially-available human iPSC-derived neuronal cell line as a potential translatable tool for fundamental and translational neuroscience research.

DATA AVAILABILITY STATEMENT

RNA-Seq data are publicly accessible at the Gene Expression Omnibus under Accession GSE157573.

AUTHOR CONTRIBUTIONS

GR, JE, and DH performed research, analyzed data, and wrote the article. PW designed research and wrote the article. AZ designed research, analyzed data, and wrote the article. All authors contributed to the article and approved the submitted version.

FUNDING

The work reported within was sponsored through an alliance between GlaxoSmithKline (GSK) and Sanford Burnham Prebys Medical Discovery Institute (SBP).

ACKNOWLEDGMENTS

We would like to thank Min Li (GSK) and Huaxi Xu (SBP) for their support of the presented science along with all members of the SBP-GSK Center for Translational Neuroscience and the Xu laboratories for their support and valued inputs in the preparation of this manuscript. Besides, we would also like to acknowledge the Sanford Burnham Prebys Genomics Core facility for supporting RNA-Seq experiments and the UCSD Human Embryonic Stem Cell Core Facility for providing access to MEA equipment. DH currently is affiliated with VersaPeutics Inc., La Jolla, CA, United States. GR currently is affiliated with Neurocrine Biosciences Inc., San Diego, CA, United States.

REFERENCES

Allen, S. J., Watson, J. J., Shoemark, D. K., Barua, N. U., and Patel, N. K. (2013). GDNF, NGF, and BDNF as therapeutic options for neurodegeneration. *Pharmacol. Ther.* 138, 155–175. doi: 10.1016/j.pharmthera.2013.01.004

Almeida, S., Zhang, Z., Coppola, G., Mao, W., Futai, K., Karydas, A., et al. (2012). Induced pluripotent stem cell models of progranulin-deficient frontotemporal dementia uncover specific reversible neuronal defects. *Cell Rep.* 2, 789–798. doi: 10.1016/j.celrep.2012.09.007

Aloe, L., Rocco, M. L., Bianchi, P., and Manni, L. (2012). Nerve growth factor: from the early discoveries to the potential clinical use. *J. Transl. Med.* 10:239. doi: 10.1186/1479-5876-10-239

Andree, H. A., Reutelingsperger, C. P., Hauptmann, R., Hemker, H. C., Hermens, W. T., and Willems, G. M. (1990). Binding of vascular anticoagulant alpha (VAC alpha) to planar phospholipid bilayers. *J. Biol. Chem.* 265, 4923–4928.

Arrant, A. E., Filiano, A. J., Warmus, B. A., Hall, A. M., and Roberson, E. D. (2016). Progranulin haploinsufficiency causes biphasic social dominance abnormalities in the tube test. *Genes. Brain Behav.* 15, 588–603. doi: 10.1111/gbb.12300

Baker, M., Mackenzie, I. R., Pickering-Brown, S. M., Gass, J., Rademakers, R., Lindholm, C., et al. (2006). Mutations in progranulin cause tau-negative frontotemporal dementia linked to chromosome 17. *Nature* 442, 916–919. doi: 10.1038/nature05016

Bang, J., Spina, S., and Miller, B. L. (2015). Frontotemporal dementia. *Lancet* 386, 1672–1682. doi: 10.1016/S0140-6736(15)00461-4

Bardy, C., van den Hurk, M., Kakaradov, B., Erwin, J. A., Jaeger, B. N., Hernandez, R. V., et al. (2016). Predicting the functional states of human iPSC-derived neurons with single-cell RNA-seq and electrophysiology. *Mol. Psychiatry* 21, 1573–1588. doi: 10.1038/mp.2016.158

Chen-Plotkin, A. S., Geser, F., Plotkin, J. B., Clark, C. M., Kwong, L. K., Yuan, W., et al. (2008). Variations in the progranulin gene affect global gene expression in frontotemporal lobar degeneration. *Hum. Mol. Genet.* 17, 1349–1362. doi: 10.1093/hmg/ddn023

Colombo, F., Racchetti, G., and Meldolesi, J. (2014). Neurite outgrowth induced by NGF or L1CAM *via* activation of the TrkA receptor is sustained also by the exocytosis of enlargeosomes. *Proc. Natl. Acad. Sci. U S A* 111, 16943–16948. doi: 10.1073/pnas.1406097111

Cruts, M., Gijselinck, I., van der Zee, J., Engelborghs, S., Wils, H., Pirici, D., et al. (2006). Null mutations in progranulin cause ubiquitin-positive frontotemporal dementia linked to chromosome 17q21. *Nature* 442, 920–924. doi: 10.1038/nature05017

De Muynck, L., Herdewyn, S., Beel, S., Scheveneels, W., Van Den Bosch, L., Robberecht, W., et al. (2013). The neurotrophic properties of progranulin depend on the granulin E domain but do not require sortilin binding. *Neurobiol. Aging* 34, 2541–2547. doi: 10.1016/j.neurobiolaging.2013.04.022

Drubin, D. G., Feinstein, S. C., Shooter, E. M., and Kirschner, M. W. (1985). Nerve growth factor-induced neurite outgrowth in PC12 cells involves the coordinate induction of microtubule assembly and assembly-promoting factors. *J. Cell Biol.* 101, 1799–1807. doi: 10.1083/jcb.101.5.1799

Fujifilm, I. F. (2018). *Cellular Dynamics, iCell® GlutaNeurons Product Data Sheet*. Available online at: https://www.fujifilmcdi.com/wp/wp-content/uploads/2020/07/CDI_iCell_GlutaNeurons_DS.pdf.

Gao, X., Joselin, A. P., Wang, L., Kar, A., Ray, P., Bateman, A., et al. (2010). Progranulin promotes neurite outgrowth and neuronal differentiation by regulating GSK-3β. *Protein Cell* 1, 552–562. doi: 10.1007/s13238-010-0067-1

Gass, J., Lee, W. C., Cook, C., Finch, N., Stetler, C., Jansen-West, K., et al. (2012). Progranulin regulates neuronal outgrowth independent of sortilin. *Mol. Neurodegener.* 7:33. doi: 10.1186/1750-1326-7-33

Guo, A., Tapia, L., Bamji, S. X., Cynader, M. S., and Jia, W. (2010). Progranulin deficiency leads to enhanced cell vulnerability and TDP-43 translocation in primary neuronal cultures. *Brain Res.* 1366, 1–8. doi: 10.1016/j.brainres.2010.09.099

Hu, F., Padukkavidana, T., Vaegter, C. B., Brady, O. A., Zheng, Y., Mackenzie, I. R., et al. (2010). Sortilin-mediated endocytosis determines levels of the frontotemporal dementia protein, progranulin. *Neuron* 68, 654–667. doi: 10.1016/j.neuron.2010.09.034

Huang, E. J., and Reichardt, L. F. (2001). Neurotrophins: roles in neuronal development and function. *Annu. Rev. Neurosci.* 24, 677–736. doi: 10.1146/annurev.neuro.24.1.677

Ichim, G., Tauszig-Delamasure, S., and Mehlen, P. (2012). Neurotrophins and cell death. *Exp. Cell Res.* 318, 1221–1228. doi: 10.1016/j.yexcr.2012.03.006

Israel, M. A., Yuan, S. H., Bardy, C., Reyna, S. M., Mu, Y., Herrera, C., et al. (2012). Probing sporadic and familial Alzheimer's disease using induced pluripotent stem cells. *Nature* 482, 216–220. doi: 10.1038/nature10821

Iwasaki, K., Isaacs, K. R., and Jacobowitz, D. M. (1998). Brain-derived neurotrophic factor stimulates neurite outgrowth in a calretinin-enriched neuronal culture system. *Int. J. Dev. Neurosci.* 16, 135–145. doi: 10.1016/s0736-5748(98)00011-2

Kleinberger, G., Wils, H., Ponsaerts, P., Joris, G., Timmermans, J. P., Van Broeckhoven, C., et al. (2010). Increased caspase activation and decreased TDP-43 solubility in progranulin knockout cortical cultures. *J. Neurochem.* 115, 735–747. doi: 10.1111/j.1471-4159.2010.06961.x

Koh, J. Y., Wie, M. B., Gwag, B. J., Sensi, S. L., Canzoniero, L. M., Demaro, J., et al. (1995). Staurosporine-induced neuronal apoptosis. *Exp. Neurol.* 135, 153–159. doi: 10.1006/exnr.1995.1074

Koopman, G., Reutelingsperger, C. P., Kuijten, G. A., Keehnen, R. M., Pals, S. T., and van Oers, M. H. (1994). Annexin V for flow cytometric detection of

phosphatidylserine expression on B cells undergoing apoptosis. *Blood* 84, 1415–1420.

Kowiański, P., Lietzau, G., Czuba, E., Waśkow, M., Steliga, A., and Moryś, J. (2018). BDNF: a key factor with multipotent impact on brain signaling and synaptic plasticity. *Cell. Mol. Neurobiol.* 38, 579–593. doi: 10.1007/s10571-017-0510-4

Love, M. I., Huber, W., and Anders, S. (2014). Moderated estimation of fold change and dispersion for RNA-seq data with DESeq2. *Genome Biol.* 15:550. doi: 10.1186/s13059-014-0550-8

Lui, H., Zhang, J., Stefanie Makinson, R., Michelle Cahill, K., Kevin Kelley, W., Huang, H.-Y., et al. (2016). Progranulin deficiency promotes circuit-specific synaptic pruning by microglia *via* complement activation. *Cell* 165, 921–935. doi: 10.1016/j.cell.2016.04.001

Meeter, L. H., Dopper, E. G., Jiskoot, L. C., Sanchez-Valle, R., Graff, C., Benussi, L., et al. (2016). Neurofilament light chain: a biomarker for genetic frontotemporal dementia. *Ann. Clin. Transl. Neurol.* 3, 623–636. doi: 10.1002/acn3.325

Neill, T., Buraschi, S., Goyal, A., Sharpe, C., Natkanski, E., Schaefer, L., et al. (2016). EphA2 is a functional receptor for the growth factor progranulin. *J. Cell. Biol.* 215, 687–703. doi: 10.1083/jcb.201603079

Nguyen, A. D., Nguyen, T. A., Martens, L. H., Mitic, L. L., and Farese, R. V. Jr. (2013). Progranulin: at the interface of neurodegenerative and metabolic diseases. *Trends Endocrinol. Metab.* 24, 597–606. doi: 10.1016/j.tem.2013.08.003

Nguyen, N., Lee, S. B., Lee, Y. S., Lee, K. H., and Ahn, J. Y. (2009). Neuroprotection by NGF and BDNF against neurotoxin-exerted apoptotic death in neural stem cells are mediated through Trk receptors, activating PI3-kinase and MAPK pathways. *Neurochem. Res.* 34, 942–951. doi: 10.1007/s11064-008-9848-9

Nguyen, T. L. X., Kim, C. K., Cho, J.-H., Lee, K.-H., and Ahn, J.-Y. (2010). Neuroprotection signaling pathway of nerve growth factor and brain-derived neurotrophic factor against staurosporine induced apoptosis in hippocampal H19-7/IGF-IR [corrected]. *Exp. Mol. Med.* 42, 583–595. doi: 10.3858/emm.2010.42.8.060

Obien, M. E., Deligkaris, K., Bullmann, T., Bakkum, D. J., and Frey, U. (2015). Revealing neuronal function through microelectrode array recordings. *Front. Neurosci.* 8:423. doi: 10.3389/fnins.2014.00423

Odawara, A., Katoh, H., Matsuda, N., and Suzuki, I. (2016). Physiological maturation and drug responses of human induced pluripotent stem cell-derived cortical neuronal networks in long-term culture. *Sci. Rep.* 6:26181. doi: 10.1038/srep26181

Paiva, A. R. C., Park, I., and Príncipe, J. C. (2010). A comparison of binless spike train measures. *Neural Comput. Appl.* 19, 405–419. doi: 10.1007/s00521-009-0307-6

Park, I.-H., Arora, N., Huo, H., Maherali, N., Ahfeldt, T., Shimamura, A., et al. (2008). Disease-specific induced pluripotent stem cells. *Cell* 134, 877–886. doi: 10.1016/j.cell.2008.07.041

Patro, R., Duggal, G., Love, M. I., Irizarry, R. A., and Kingsford, C. (2017). Salmon: fast and bias-aware quantification of transcript expression using dual-phase inference. *Nat. Methods* 14, 417–419. doi: 10.1038/nmeth.4197

Petoukhov, E., Fernando, S., Mills, F., Shivji, F., Hunter, D., Krieger, C., et al. (2013). Activity-dependent secretion of progranulin from synapses. *J. Cell Sci.* 126, 5412–5421. doi: 10.1242/jcs.132076

Raitano, S., Ordovàs, L., De Muynck, L., Guo, W., Espuny-Camacho, I., Geraerts, M., et al. (2015). Restoration of progranulin expression rescues cortical neuron generation in an induced pluripotent stem cell model of frontotemporal dementia. *Stem Cell Reports* 4, 16–24. doi: 10.1016/j.stemcr.2014.12.001

Ritz, C., Baty, F., Streibig, J. C., and Gerhard, D. (2015). Dose-response analysis using R. *PLoS One* 10:e0146021. doi: 10.1371/journal.pone.0146021

Ross, C. A., and Akimov, S. S. (2014). Human-induced pluripotent stem cells: potential for neurodegenerative diseases. *Hum. Mol. Genet.* 23, R17–R26. doi: 10.1093/hmg/ddu204

Rüegg, U. T., and Burgess, G. M. (1989). Staurosporine, K-252 and UCN-01: potent but nonspecific inhibitors of protein kinases. *Trends Pharmacol. Sci.* 10, 218–220. doi: 10.1016/0165-6147(89)90263-0

Ryan, C. L., Baranowski, D. C., Chitramuthu, B. P., Malik, S., Li, Z., Cao, M., et al. (2009). Progranulin is expressed within motor neurons and promotes neuronal cell survival. *BMC Neurosci.* 10:130. doi: 10.1186/1471-2202-10-130

Soneson, C., Love, M. I., and Robinson, M. D. (2015). Differential analyses for RNA-seq: transcript-level estimates improve gene-level inferences. *F1000Res.* 4:1521. doi: 10.12688/f1000research.7563.2

Takahashi, K., Tanabe, K., Ohnuki, M., Narita, M., Ichisaka, T., Tomoda, K., et al. (2007). Induction of pluripotent stem cells from adult human fibroblasts by defined factors. *Cell* 131, 861–872. doi: 10.1016/j.cell.2007.11.019

Tang, W., Lu, Y., Tian, Q.-Y., Zhang, Y., Guo, F.-J., Liu, G. Y., et al. (2011). The growth factor progranulin binds to TNF receptors and is therapeutic against inflammatory arthritis in mice. *Science* 332, 478–484. doi: 10.1126/science.1199214

Tapia, L., Milnerwood, A., Guo, A., Mills, F., Yoshida, E., Vasuta, C., et al. (2011). Progranulin deficiency decreases gross neural connectivity but enhances transmission at individual synapses. *J. Neurosci.* 31, 11126–11132. doi: 10.1523/JNEUROSCI.6244-10.2011

Tukker, A. M., de Groot, M. W. G. D. M., Wijnolts, F. M. J., Kasteel, E. E. J., Hondebrink, L., and Westerink, R. H. S. (2016). Is the time right for *in vitro* neurotoxicity testing using human iPSC-derived neurons? *ALTEX* 33, 261–271. doi: 10.14573/altex.1510091

Tukker, A. M., Wijnolts, F. M. J., de Groot, A., and Westerink, R. H. S. (2018). Human iPSC-derived neuronal models for *in vitro* neurotoxicity assessment. *Neurotoxicology* 67, 215–225. doi: 10.1016/j.neuro.2018.06.007

Uesaka, N., Abe, M., Konno, K., Yamazaki, M., Sakoori, K., Watanabe, T., et al. (2018). Retrograde signaling from progranulin to sort1 counteracts synapse elimination in the developing cerebellum. *Neuron* 97, 796.e5–805.e5. doi: 10.1016/j.neuron.2018.01.018

Van Damme, P., Van Hoecke, A., Lambrechts, D., Vanacker, P., Bogaert, E., van Swieten, J., et al. (2008). Progranulin functions as a neurotrophic factor to regulate neurite outgrowth and enhance neuronal survival. *J. Cell Biol.* 181, 37–41. doi: 10.1083/jcb.200712039

Volpato, V., Smith, J., Sandor, C., Ried, J. S., Baud, A., Handel, A., et al. (2018). Reproducibility of molecular phenotypes after long-term differentiation to human iPSC-derived neurons: a multi-site omics study. *Stem Cell Rep.* 11, 897–911. doi: 10.1016/j.stemcr.2018.08.013

Wang, J., Van Damme, P., Cruchaga, C., Gitcho, M. A., Vidal, J. M., Seijo-Martinez, M., et al. (2010). Pathogenic cysteine mutations affect progranulin function and production of mature granulins. *J. Neurochem.* 112, 1305–1315. doi: 10.1111/j.1471-4159.2009.06546.x

Wang, J., Vasaikar, S., Shi, Z., Greer, M., and Zhang, B. (2017). WebGestalt 2017: a more comprehensive, powerful, flexible and interactive gene set enrichment analysis toolkit. *Nucleic Acids Res.* 45, W130–W137. doi: 10.1093/nar/gkx356

Xu, J., Xilouri, M., Bruban, J., Shioi, J., Shao, Z., Papazoglou, I., et al. (2011). Extracellular progranulin protects cortical neurons from toxic insults by activating survival signaling. *Neurobiol. Aging* 32, 2326.e5–2326.e16. doi: 10.1016/j.neurobiolaging.2011.06.017

Xu, X.-H., and Zhong, Z. (2013). Disease modeling and drug screening for neurological diseases using human induced pluripotent stem cells. *Acta Pharmacol. Sin.* 34, 755–764. doi: 10.1038/aps.2013.63

Yuan, A., Sershen, H., Veeranna, Basavarajappa, B. S., Kumar, A., Hashim, A., et al. (2015). Neurofilament subunits are integral components of synapses and modulate neurotransmission and behavior *in vivo*. *Mol. Psychiatry* 20, 986–994. doi: 10.1038/mp.2015.45

Zhang, K., Li, Y.-J., Guo, Y., Zheng, K.-Y., Yang, Q., Yang, L., et al. (2017). Elevated progranulin contributes to synaptic and learning deficit due to loss of fragile X mental retardation protein. *Brain* 140, 3215–3232. doi: 10.1093/brain/awx265

Conflict of Interest: PW was employed by the company GlaxoSmithKline (GSK) and AZ was employed by the company Memento Therapeutics Corporation.

The remaining authors declare that the research was conducted in the absence of any commercial or financial relationships that could be construed as a potential conflict of interest.

frontiers in Neuroscience

MINI REVIEW
published: 19 November 2020
doi: 10.3389/fnins.2020.546484

Prospects of Directly Reprogrammed Adult Human Neurons for Neurodegenerative Disease Modeling and Drug Discovery: iN vs. iPSCs Models

Ying Zhang[1,2†], Xinyang Xie[1,2,3†], Jiangnan Hu[4], Kazi Sabrina Afreen[5], Chun-Li Zhang[6], Qichuan Zhuge[1,2] and Jianjing Yang[1,2*]*

[1] Zhejiang Provincial Key Laboratory of Aging and Neurological Disorder Research, The First Affiliated Hospital of Wenzhou Medical University, Wenzhou, China, [2] Department of Neurosurgery, The First Affiliated Hospital of Wenzhou Medical University, Wenzhou, China, [3] International Department of The Affiliated High School of South China Normal University (HFI), Guangzhou, China, [4] Department of Pharmaceutical Sciences, University of North Texas Health Science Center, Fort Worth, TX, United States, [5] Department of Microbiology & Immunology, Rosalind Franklin University of Medicine and Science, North Chicago, IL, United States, [6] Department of Molecular Biology, UT Southwestern Medical Center, Dallas, TX, United States

OPEN ACCESS

Edited by:
Kuangyu Shi,
University of Bern, Switzerland

Reviewed by:
Anandhan Annadurai,
University of Arizona, United States
Rajkumar P. Thummer,
Indian Institute of Technology Guwahati, India

***Correspondence:**
Qichuan Zhuge
qc.zhuge@wmu.edu.cn
Jianjing Yang
yangjianjing2@163.com

[†] These authors have contributed equally to this work

Specialty section:
This article was submitted to Neurodegeneration, a section of the journal Frontiers in Neuroscience

Received: 28 March 2020
Accepted: 12 October 2020
Published: 19 November 2020

Citation:
Zhang Y, Xie X, Hu J, Afreen KS, Zhang C-L, Zhuge Q and Yang J (2020) Prospects of Directly Reprogrammed Adult Human Neurons for Neurodegenerative Disease Modeling and Drug Discovery: iN vs. iPSCs Models. Front. Neurosci. 14:546484. doi: 10.3389/fnins.2020.546484

A reliable disease model is critical to the study of specific disease mechanisms as well as for the discovery and development of new drugs. Despite providing crucial insights into the mechanisms of neurodegenerative diseases, translation of this information to develop therapeutics in clinical trials have been unsuccessful. Reprogramming technology to convert adult somatic cells to induced Pluripotent Stem Cells (iPSCs) or directly reprogramming adult somatic cells to induced Neurons (iN), has allowed for the creation of better models to understand the molecular mechanisms and design of new drugs. In recent times, iPSC technology has been commonly used for modeling neurodegenerative diseases and drug discovery. However, several technological challenges have limited the application of iN. As evidence suggests, iN for the modeling of neurodegenerative disorders is advantageous compared to those derived from iPSCs. In this review, we will compare iPSCs and iN models for neurodegenerative diseases and their potential applications in the future.

Keywords: iN, iPSCs, disease modeling, drug screening, neurodegenerative disease

Abbreviations: ABM, Ascl1, Brn2, and Myt1l; AD, Alzheimer's Disease; ALS, Amyotrophic Lateral Sclerosis; ANL, Ascl1, Nurr1 and Lmx1a; APOE, apolipoprotein E; APP, amyloid beta precursor protein; ASCL1, achaete-scute family BHLH transcription factor 1; Brn2, POU domain, class 3, transcription factor 2; Dlx2, distal-less homeobox 2; Dlx5, distal-less homeobox 5; FGF2, fibroblasts growth factor 2; FoxA1/2, forkhead box A1/2; Foxg1, forkhead box G1; Hb9, motor neurons and pancreas homeobox 1; iDA, induced dopaminergic; iMN, induced motor neurons; iN, induced neurons; iPSCs, induced pluripotent stem cells; Isl1, ISL LIM homeobox 1; Klf4, Kruppel-like factor 4; Lhx3, LIM homeobox protein 3; Lhx6, LIM homeobox protein 6; Lmx1a/b, LIM homeobox transcription factor 1 a/b; LRRK2, leucine rich repeat kinase 2; Myt1l, myelin transcription factor 1 like; Ngn2, neurogenin 2; Nurr1 (Nr4a2), nuclear receptor subfamily 4, group A, member 2; Oct4, octamer-binding transcription factor 4; OHDA, hydroxydopamine; OSKM, Oct4, Sox2, Klf4, and c-Myc; otx2, orthodenticle homeobox 2; PARK2, parkin RBR E3 ubiquitin protein ligase; PD, Parkinson's Disease; PGC-1 α, PPARG coactivator 1 alpha; PINK1, PTEN induced putative kinase 1; Pitx3, paired-like homeodomain transcription factor 3; PS1/2, presenilin 1/2; PV, Parvalbumin; RanBP1, RAN binding protein 1; SNCA, synuclein alpha; SOD1, superoxide dismutase 1; Sox11, SRY (sex determining region Y)-box 11; Sox2, SRY (sex determining region Y)-box 2; TDP-43, TAR DNA binding protein; TFs, transcription factors; Zfp521, Zinc Finger Protein 521.

INTRODUCTION

Neurodegenerative diseases comprised of a group of complicated disorders of the central nervous system among the aged population. To design effective treatment strategies to cure these diseases, scientists are in desperate need of convenient and reliable disease models. Previous neurodegenerative disease models based on genetic manipulations include transgene integration or gene knockout systems. These systems can only be utilized partially to understand disease mechanisms, pathology, and progression (Hargus et al., 2014; Heilker et al., 2014; Imaizumi and Okano, 2014; Zhao et al., 2014). These current models cannot be used as accurate models for neurodegenerative diseases especially due to specific limitations. First, although the fibroblasts or disease-associated mutation transformed cell lines of patients have enabled detailed mechanistic studies to be carried out, the biology of cell lines does not resemble the biology of primary neurons (Hargus et al., 2014). Thus it is often unclear whether the mechanisms studied are directly comparable to patients' pathology. Second, animal models-such as dogs, flies, monkeys, and especially rodents (Zhao et al., 2014), is another method of studying neurodegenerative diseases (Gitler et al., 2017). However, these models often cannot accurately recapitulate human disease and animal models of the sporadic forms of neurodegenerative diseases due to species-specific differences. In addition, it is difficult to manipulate affected cell types in neurodegenerative disorders *in vitro*. Due to these limitations, a number of preclinical trials that aimed to identify drugs have failed to successfully translate into therapeutics in clinical settings (Kraljevic et al., 2004; Ledford, 2011; Ke et al., 2016). In summary, it is important to develop accurate and predictive disease models as they are essential to providing key insights to understanding disease mechanisms and the development of drugs to cure neurodegenerative diseases.

Innovations in cellular reprogramming technology have provided us with a promising tool to solve this problem. Takahashi and Yamanaka (2006) established a unique method of reprogramming somatic cells to iPSCs, which can be differentiated into cell types of all the three germ layers including non-proliferating neurons. The neurons derived from iPSCs would have the same genetic information as the individual patient and can be differentiated from iPSCs. This technology has been utilized by other investigators for neurodegenerative disease modeling (**Table 1**; Wan et al., 2015; Haston and Finkbeiner, 2016; Liu and Deng, 2016; Csobonyeiova et al., 2017). Moreover, in recent years, the discovery of direct reprogramming technology has enabled the reprogramming of somatic cells to neurons, bypassing the iPSC stage (Vierbuchen et al., 2010; Ambasudhan et al., 2011; Li et al., 2015, 2017; Karow et al., 2018; Tanabe et al., 2018; Xiao et al., 2018). With the advancement of these technologies, scientists have been able to create highly efficient and lineage-specific neurons through the reprogramming of somatic cells (Marro et al., 2011; Xu Z. et al., 2015; Black et al., 2016; Mall et al., 2017). Altogether, these technologies can be used for modeling neurodegenerative diseases (Shi et al., 2017; Sun et al., 2017; Han et al., 2018; Farkhondeh et al., 2019).

Even though, the mechanisms of iPSCs or iN reprogramming are still unclear (Xu J. et al., 2015; Omole and Fakoya, 2018), there are some obvious differences between iPSCs-derived neurons and iN. Among them, recent studies have indicated that the application of iN for aging-related neurodegenerative diseases would be a better choice, as it does not reset aging information (Mertens et al., 2015, 2018; Tang et al., 2017; Bohnke et al., 2018; Traxler et al., 2019). In this review, we summarize recent studies involving iPSCs and in neurodegenerative disease modeling and its advantages and limitations.

REPROGRAMMING SOMATIC CELLS TO NEURON CELLS

iPSC Technology

In 2006, a phenomenal study conducted in Yamanaka lab demonstrated that viral vectors carrying a combination of pluripotent transcription factors, including Oct4, Sox2, Klf4, and c-Myc (OSKM), were sufficient to effectively reprogram mouse fibroblasts cells to iPSCs (Takahashi and Yamanaka, 2006; Okano and Yamanaka, 2014). In 2007, their laboratory also demonstrated that OSKM could reprogram human fibroblasts to iPSCs by the retroviral system (Takahashi et al., 2007). The generated iPSCs had the potential to be differentiated into all three germ layers of cell type with the unlimited ability of self-renewal. Besides OSKM, the combination of other transcription factors, including Oct4, Sox2, Nanog, and LIN28, has also been demonstrated to be able to convert human somatic cells into iPSCs with a lentiviral system (Yu et al., 2007). In addition, this technology has been successfully used for translating into other somatic cell types, such as neural stem cells (Eminli et al., 2008; Kim et al., 2008), stomach and liver cells (Aoi et al., 2008), mature β lymphocytes (Hanna et al., 2008), melanocytes (Utikal et al., 2009), adipose stem cells (Sun et al., 2009), and keratinocytes (Maherali et al., 2008). iPSC technology provides a platform that can be used as a model system for neurodegenerative diseases to design new therapeutics. However, the current iPSC technology still has some limitations, including low efficiency and a long reprogramming process, which are primarily due to the existence of several roadblocks (Ebrahimi, 2015; Haridhasapavalan et al., 2020). Another problem is that iPSCs may cause cancerous tumor formation due to an undifferentiated pluripotent stem cell after transplantation (Choi and Hong, 2017). In recent years, researchers put tremendous efforts into refining and optimizing approaches to improve reprogramming efficiency and safety (O'Malley et al., 2009; Sommer and Mostoslavsky, 2010, 2013; Gonzalez et al., 2011; Morris and Daley, 2013; Omole and Fakoya, 2018; Borgohain et al., 2019; Haridhasapavalan et al., 2019). Maherali et al. (2008) created a doxycycline-inducible lentiviral system including OSKM, which had a higher frequency of converting primary fibroblasts into iPSCs. This system could even reprogram keratinocytes into iPSCs within 10 days (Maherali et al., 2008). In addition, using lentivirus or retrovirus to deliver OSKM may cause insertional mutagenesis when integrating gene sequences in the genomic DNA of the cells. To improve technical safety, other delivery methods, including

TABLE 1 | Neurons derived from iPSC technology.

Transcription factors	Cell type	Techniques	Neurons type	*In vitro/ in vivo*	Efficiency	References
OSKM(Oct4, Sox2, Klf4 and c-Myc)	mouse and human fibroblasts	retroviruses		*in vitro* and *in vivo*	Low and tedious	Takahashi and Yamanaka, 2006; Takahashi et al., 2007
OSNL(Oct4, Sox2,Nanog,LIN28)	human somatic cells	lentivirus		*in vitro*	low	Yu et al., 2007
OSKM with TAV, SB431542, PD0325901 and ascorbic acid	bone marrow–derived mesenchymal cells of marmosets	excisable lentiviral spleen focus-forming virus	Neural progenitors	*in vitro*	high	Wiedemann et al., 2012
OSKM	human adipose-derived stem cells	polycistronic plasmid		*in vitro*		Barbuti et al., 2012
OSKM co-expressing tyrosine hydroxylase	human fibroblasts	an RNA virus (Sendai virus)	dopaminergic neurons	*in vitro* and *in vivo*	significantly surpassed retroviral transduction (0.02%	Fusaki et al., 2009
OSNL	human adipose stromal cells	non-viral minicircle DNA vector		*in vitro*	lower (∼0.005%)	Narsinh et al., 2010
OSKM	human fibroblasts	modified RNA	neuron like cells	*in vitro*	High (2%)	Warren et al., 2010
OSKM	human fibroblasts	OSKM proteins fused with a cell-penetrating peptide	all three embryonic germ layers	*in vitro* and in teratomas	slow and low	Kim et al., 2009
Forskolin, 2-methyl-5-hydroxytryptamine, D4476, VPA, CHIR99021, 616452 and Tranylcypromine	mouse embryonic fibroblasts	small-molecule compounds		*in vitro*	0.2%	Hou et al., 2013
NaB, PD03259, and SB431542	human fibroblasts	upregulates the miR302/367 cluster expression		*in vitro*		Zhang and Wu, 2013

non-viral or non-integrating viral vectors, have been attempted, such as protein transduction, the transfection of modified mRNA transcripts, small molecules, sendai virus, and episomal vectors (Sommer and Mostoslavsky, 2010, 2013; Gonzalez et al., 2011; Morris and Daley, 2013; Omole and Fakoya, 2018; Borgohain et al., 2019; Haridhasapavalan et al., 2019). However, compared to the traditional viral gene delivery method, these alternative methods had poorer outcomes.

iN Technology

After the establishment of iPSC reprogramming technology, researchers are continuously seeking effective ways to improve the reprogramming condition. The main challenge is to rapidly and efficiently change cell fate by reprogramming using minimal transcription factors. In 2010, Vierbuchen and his group succeeded in directly reprogramming mouse fibroblasts to functional neurons by overexpression of three transcription factors, including Ascl1, Brn2, and Myt1l (Vierbuchen et al., 2010). Subsequently, several studies showed some other transcription factors (Ngn2, Ascl1, and Dlx2) also could convert mouse postnatal astrocytes into both GABAergic and cholinergic neurons (Berninger et al., 2007; Heinrich et al., 2011; Xiao et al., 2018; Huang et al., 2019; Wazan et al., 2019). Moreover, only one transcription factor NGN2, when supplemented with chemicals including dorsomorphin and forskolin, could directly reprogram human fibroblasts (MRC5) to neurons (Liu et al., 2013) with high efficiency. The neurons generated are functional and mostly cholinergic neurons (Liu et al., 2013). Only epigenetic chemicals without transcription factors have been demonstrated to directly reprogram human and mouse fibroblasts into functional neuron cells (Hu et al., 2015; Li et al., 2015, 2017; Smith et al., 2016; Qin et al., 2017). Other studies have shown that some defined tissue-specific transcription factors (TFs), such as Sox2, Zfp521 (a single zinc-finger TF), and Ptfa1, directly reprogram human fibroblasts into a neural stem cell (Maucksch et al., 2013; Shahbazi et al., 2016; Xiao et al., 2018). In addition, in Rubio et al. (2016) used the CRISPR/Cas9 platform to inactivate two neurological disorder genes, TSC2 and KCNQ2 and subsequently combined with a multicistronic lentivirus expressing the Ascl1, Lmx1a, and Nurr1 genes to directly convert fibroblasts into neuropathological-resistant neuronal cells. Although several other cell types can also be reprogrammed into neurons, like hepatocytes and pericytes cells (Marro et al., 2011; Karow et al., 2012), fibroblasts are still the most popular original cell type for reprogramming. Together these findings supported that iN can be directly derived from different cell types by certain combinations of transcription factors (**Table 2**). This technology for the generation of iN from other cell types could be useful for the development of neurological disease models (Ruggieri et al., 2014; Gascon et al., 2017; Gao et al., 2019; Pereira et al., 2019).

DIRECT REPROGRAMMING TO GENERATE SPECIFIC NEURONAL SUBTYPES

During the early stages, just after the discovery of direct reprogramming technology, investigators paid more attention to the efficacy of reprogramming and whether the neurons generated are physiologically functional. Subsequently,

TABLE 2 | Neurons derived from direct reprogramming technology.

Transcription factors	Cell type	Techniques	Neurons type	*In vitro/ in vivo*	Efficiency	Functional or not	References
ASCL1, NGN2, SOX2, NURR1 and PITX3	human fibroblasts	lentivirus	iN (mostly dopaminergic neurons)	*in vivo*	∼80%	functional electrophysiology	Liu et al., 2011
Ascl1, Brn2, Myt1l	mouse hepatocytes	lentivirus	iN	*in vivo*	>90%	functional electrophysiology	Marro et al., 2011
Sox2 and Mash1	pericyte-derived cells of the adult human cerebral cortex	retrovirus	GABAergic neurons	*in vitro*	∼50%	these iN acquire the ability of repetitive action potential firing and serve as synaptic targets for other neurons	Karow et al., 2012
Brn2, Myt1l, Zic1, Olig2, and Ascl1	Mouse Embryonic fibroblasts	lentivirus	iN (mostly GABAergic and glutamatergic neurons)	*in vitro*	∼50%	functional electrophysiology Synaptic maturation	Vierbuchen et al., 2010
Ascl1, Brn2 and Myt1l	mouse embryonic and postnatal fibroblasts	lentivirus	iN (mostly excitatory neurons)	*in vitro*	19.5%	functional electrophysiology Synaptic maturation	Vierbuchen et al., 2010
Ascl1, Brn2 and Myt1l	mouse and human cells	viral delivery	neurons	*in vivo*	20%	functional	Torper et al., 2013
NeuroD1, Ascl1, Brn2, and Mytl1	human fibroblasts	lentivirus	iN	*in vitro*	∼60%	functional neurons	Pang et al., 2011
Ascl1, Lmx1a, FoxA2, and FEV	human fibroblasts	Dox-inducible lentivirus	serotonergic (i5HT) neurons	*in vitro*	∼25%	exhibited spontaneous electrophysiological activity and had active serotonergic synaptic transmission	Xu Z. et al., 2015
Mash1, Nurr1 and Lmx1a	mouse and human fibroblasts	lentivirus	iN (mostly dopaminergic neurons)	*in vitro*	high	functional electrophysiology	Caiazzo et al., 2011
NGN2 with (Forskolin and dorsomorphin)	human fetal lung fibroblasts	retrovirus	cholinergic neurons	*in vitro*	>90%	characteristic electrophysiological properties	Liu et al., 2013
LDN193189, SB431542, TTNPB, Tzv, CHIR99021, VPA, DAPT, SAG, Purmo	Human astrocytes	with medium	Functional neurons (mainly glutamatergic neurons)	*in vitro*	>90%	functional	Zhang et al., 2015
Forskolin, ISX9, CHIR99021 and SB431542	mouse fibroblasts	with medium	iN	*in vitro*	>90%	functional electrophysiology	Li et al., 2015

investigators tried to control the reprogramming process to convert somatic cells to specific neuronal subtypes. Reprogramming somatic cells into defined neuronal subtypes is a crucial step for the application of iN reprogramming technology into clinical trials. In recent years, technical improvements in this field have made substantial progress, which would dramatically increase the applications of iN technology.

Dopaminergic Neurons

Parkinson's disease is a neurodegenerative disorder with progressive loss of dopaminergic neurons in the midbrain (Alexander, 2004). Thus, using reprogramming technology for the generation of defined dopaminergic neurons could be an interesting approach for the treatment of Parkinson's disease. According to neuronal system development, several transcription factors play a critical role in the generation and specification of dopaminergic neurons, including Otx2, FoxA1/2 Lmx1a/b, Ascl1, Ngn2, Pitx3, and Nurr1 (Nr4a2) (Arenas et al., 2015). Several studies have reported the successful reprogramming of fibroblasts or astrocytes into induced dopaminergic (iDA) neurons. Among them, the minimal combination is Ascl1, Nurr1, and Lmx1a (Kim et al., 2011; Pfisterer et al., 2011; Torper et al., 2013; Caiazzo et al., 2015). The iDA neurons that are generated are functional, can produce dopamine, and have firing of action potentials and functional D2 auto receptors (Caiazzo et al., 2011). Moreover, transplantation of these functional iDA neurons could improve the behavior deficit caused by the loss of endogenous DA neurons (Dell'Anno et al., 2014). De Gregorio et al. (2018) found that, when combined with transcription factors ASCL1 and NURR1, miR-34b/c could double the yield of transdifferentiated fibroblasts into dopaminergic neurons. The iDA neurons that are generated synthesize dopamine and showed spontaneous electrical activity and are reversibly blocked by tetrodotoxin, which is consistent with the electrophysiological properties featured by brain dopaminergic neurons (De Gregorio et al., 2018).

Spinal Motor Neurons

Genetic disorders like Amyotrophic Lateral Sclerosis (ALS) result in the loss of motor neurons (Robberecht and Philips, 2013). Regeneration of new motor neurons is important for potential therapy and disease models for ALS. Studies on mouse models have demonstrated that reprogramming of mouse embryonic fibroblasts into induced motor neurons (iMN) could be achieved by combined overexpression of common transcription factors [Ascl1, Neurog2, Myt1l, and Brn2 (Pou3f2)] with some specific

TFs (Lhx3, Isl1, and Hb9) for spinal cord motor neurons (Lee et al., 2009; Son et al., 2011; Tang et al., 2017; Zhang et al., 2017). These iMNs could survive after being transplanted into the spinal cord and are capable of forming a neuromuscular junction with myotube cells *in vitro* (Son et al., 2011). To optimize the reprogramming condition, four TFs (Neurog2, Sox11, LHX3, and Isl1), when supplemented with forskolin, dorsomorphin, and FGF2 could directly reprogram human fibroblasts into motor neurons, which are HB9 and ChAT-positive, have action potentials and can form a neuromuscular junction with extremely high efficiency (>80%) (Liu et al., 2016).

GABAergic Neurons (Interneurons)

The GABAergic neurons are inhibitory interneurons located in the cortex, which play crucial roles in regulating the excitation and inhibition of nervous system activation (Tremblay et al., 2016). The loss or malfunction of GABAergic neurons would also result in neurological diseases, such as epilepsies, cognitive disorders, autism, schizophrenia, and intellectual disabilities (Woo and Lu, 2006; Brooks-Kayal, 2010; Marin, 2012). Colasante et al. (2015) demonstrated the use of five TFs (Foxg1, Ascl1, Sox2, Dlx5, and Lhx6) for reprogramming human and mouse fibroblasts into induced GABA (iGABA) interneurons. The generated iGABA interneurons could survive and mature after being transplanted into the hippocampus (Colasante et al., 2015). The new iGABA interneurons can form functional synapses, and release GABA (Colasante et al., 2015). Importantly, the transplanted iGABA interneurons can integrate into host circuitry and play inhibitory functions (Colasante et al., 2015). A great part of the GABAergic neurons also showed Parvalbumin (PV) protein and gene expression. Soon after, another research group obtained induced PV (iPV) neurons by *Ascl1* from mouse fibroblasts (Shi et al., 2016). These reports showed that the controlled reprogramming process by some specific regional TFs would lead to lineage reprogramming of neuronal subtypes (Masserdotti et al., 2016).

iPSCs APPLICATION FOR NEURODEGENERATIVE DISEASES MODELING AND DRUG DISCOVERY

Neurodegenerative diseases including Alzheimer's Disease (AD), Parkinson's Disease (PD) and Amyotrophic Lateral Sclerosis (ALS) are aging-related disorders in which several genetic mutations have been identified before the onset of the diseases. However, even with a clearer understanding of the mechanisms of neurodegenerative diseases, the progression of designing therapy is going slow (Finkbeiner, 2010; Mason et al., 2014; Wyss-Coray, 2016). Based on these genetic mutations, different animal models have been established to study the underlying disease mechanisms and explore the potential drugs for treatment. Unfortunately, due to the variations among different species and the irreproducibility of human disease pathology, current animal models cannot ideally model neurodegenerative diseases as the data generated from these models cannot be successfully translated into clinical applications (Jucker, 2010; Imaizumi and Okano, 2014; Mitsumoto et al., 2014). In this scenario, iPSC technology brought new hope for neurodegenerative disease modeling and drug discovery *in vitro*. Nowadays, iPSC technology has been widely applied for disease modeling, mechanism study, and the screening of drugs for neurodegenerative diseases (**Figure 1**).

Alzheimer's Disease (AD)

Alzheimer's Disease is the most common chronic progressive neurodegenerative disease. In recent decades, researchers have focused on the study of the pathogenesis of AD. Several genetic mutations have been identified in genes namely, APP, presenilin 1/2 (PS1/2), and APOE, to cause Familial Alzheimer's disease (Armstrong, 2013; Karch et al., 2014; Shen, 2014; Moreno et al., 2018; Wang et al., 2018). However, the mechanisms of the neurons and synapse damage in AD remain unclear. The new iPSC technology from AD patients can provide sufficient quantity or quality neurons for the discovery of potential therapeutics (Byrne, 2014; Tcw, 2019).

In recent years, researchers have been successful in reprogramming fibroblasts carrying with different genetic mutations to iPSCs. Yagi et al. (2011) pioneered the use of iPSC technology to establish an *in vitro* model for AD, which was derived from iPSCs with PS1/2 mutation. The expression of Aβ42 was dramatically increased in neurons derived from iPSCs (Yagi et al., 2011). In addition to this, the APP gene mutation has also been investigated by Israel et al. (2012). They demonstrated that the levels of Aβ42 and tau are significantly increased in neurons derived from iPSCs (Israel et al., 2012; Ochalek et al., 2017). Subsequently, studies conducted by several groups of investigators used iPSCs to produce neurons derived to model AD where the properties of pathogenic Aβ42 and tau were reserved (Shi et al., 2012; Duan et al., 2014; Muratore et al., 2014; Sproul et al., 2014; Chang et al., 2015; Moore et al., 2015; Rowland et al., 2018; Tcw, 2019). In summary, the novel iPSCs *in vitro* model can be utilized as an excellent tool to study AD.

Parkinson's Disease (PD)

The loss of dopaminergic neurons in the neuropathology of PD, which causes motor problems, including bradykinesia, resting tremor, rigidity, flexed posture, "freezing," and lose of postural reflexes (Seibler et al., 2011; Postuma et al., 2015). Similar to AD, the deficit of reliable *in vitro* models has limited the progression of drug discovery for PD. Several groups obtained iPSCs from patient somatic cells with different genetic mutations including LRRK2, SNCA, PARK2, or PINK1, which are related to familial PD, and the DA neurons derived from iPSCs has been used to investigate the molecular mechanisms (Ke et al., 2019). The dopaminergic neurons derived from LRRK2 iPSCs have some important PD features, including (α-Syn aggregates, overexpression of oxidative stress genes, lower number of neurites, and caspase-3 activation (Nguyen et al., 2011; Sanchez-Danes et al., 2012). Importantly, after correction of LRRK2 mutation in iPSCs, they can rescue the pathogenic phenotypes of neurite shortening and mitochondrial DNA damage (Reinhardt et al., 2013; Sanders et al., 2014). iPSCs derived from PD patients, who received triplication of the SNCA gene, have also been

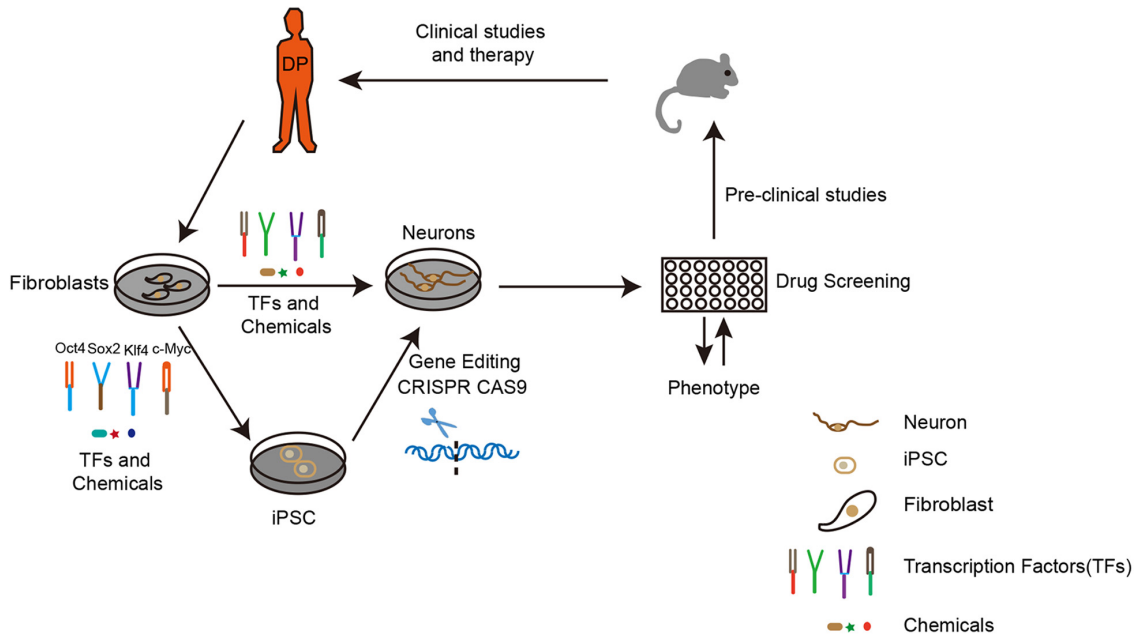

FIGURE 1 | The route to apply iPSCs and iN technology for neurodegenerative disease modeling and drug discovery. To establish an *in vitro* disease model, the first step is to obtain fibroblasts from a diseased person. Upon overexpression of certain transcription factors, fibroblasts can be directly or indirectly reprogrammed to neurons. Depending on research purposes, the fibroblasts from original iPSCs can be modified by gene editing (CRISPR CAS9). The neurons generated would be applied for drug screening according to the disease phenotype. Subsequently, the best candidates could then be used for pre-clinical studies on drug toxicity, bio-availability, pharmacology, and metabolism in animals. Finally, the potential drug would be used for clinical studies and therapy. DP: disease person.

shown to have PD pathogenic neuron properties (Oliveira et al., 2015). PARK2 gene mutation has been shown to play a critical role in neuron morphology by iPSCs-derived neuron model (Imaizumi et al., 2012; Ren et al., 2015). In addition, (Seibler et al., 2011) also reported that iPSCs reprogrammed from PD patients' fibroblasts with PINK1 mutations can generate DA neurons. The new DA neurons showed properties of upregulation of PGC-1α, which can be reversed after overexpression of wild-type PINK1 in new DA neurons. Together, all these studies demonstrated that iPSCs is a better *in vitro* model for PD with genetic mutations.

Amyotrophic Lateral Sclerosis (ALS)

Induced Pluripotent Stem Cells technology also has been widely applied for ALS. The pathology of ALS includes the progressive loss of motor neurons in the brain and spinal cord. Several genes have been identified to be associated with ALS, such as SOD1, C9orf2, and TDP-43 (Rosen et al., 1993; Sreedharan et al., 2008; DeJesus-Hernandez et al., 2011). Among them, the SOD1 gene mutation is the most studied genetic alteration in ALS. Compare to wild type SOD1, motor neurons (MN) derived from SOD1 mutated patients' iPSCs showed the features of decreased survival rate, smaller soma size, and shorter neurite (Chen et al., 2014; Kiskinis et al., 2014). In addition, MN derived from SOD1 mutated iPSCs showed impaired mitochondrial function and increased oxidative stress (Chen et al., 2014). Importantly, the correction of the SOD1 mutation could rescue these phenotypes in iPSCs (Chen et al., 2014; Kiskinis et al., 2014). iPSC-derived motor neurons retaining the patients' full genetic information, therefore, scientists established a large number of *in vitro* cellular models for sporadic ALS. The sufficient utility of sporadic ALS models is useful for elucidating the pathological characteristics of specific cases and identifying novel candidate drugs (Fujimori et al., 2018). On the other hand, many investigators have studied the phenotypes of MN derived from C9orf72 mutant iPSCs (Donnelly et al., 2013; Sareen et al., 2013; Devlin et al., 2015; Dafinca et al., 2016). Abnormalities of electrophysiology, calcium homeostasis, ER stress, and mitochondrial membrane potential have been identified in MN from iPSCs carrying C9orf72 mutation (Devlin et al., 2015; Dafinca et al., 2016). In addition, the C9orf72 mutant has been demonstrated to cause oxidative and neurotoxicity in MN from iPSCs (Donnelly et al., 2013; Sareen et al., 2013; Birger et al., 2019).

iN FOR NEURODEGENERATIVE DISEASE MODELING AND DRUG DISCOVERY

With a specific combination of reprogramming factors, somatic cells can be directly converted into neurons bypassing the iPSC stage. Along with the advancement of direct reprogramming technology, the new generation of iN has also been applied for modeling neurogenerative diseases and drug discovery (**Figure 1**). Liu et al. (2016) have used direct reprogramming technology through using a combination of TFs and small

molecules and efficiently reprogrammed ALS patients' fibroblasts to motor neurons with FUS gene mutation. The new iMN from ALS patients was unable to form neuromuscular junctions with muscle cells. Moreover, after the chemical screening, they found the chemical kenpaullone can rescue the disease phenotype. Recently, (Chang et al., 2018) utilized the mesoporous silica nanoparticles (MSNs) as a non-viral delivery system for the transduction of the three key factors to achieve the conversion of mouse fibroblasts (MFs) into functional dopaminergic neuron-like cells. These recent studies are the beginning of developments that will enable us to apply iN for neurodegenerative disease modeling and drug discovery. Before applying this technique for large scale drug screening, the problems associated with efficiency and the homogeneity of direct reprogramming needs to be further improved.

COMPARISON OF iPSCs-DERIVED NEURONS TO iN

In contrast to the application of iPSC technology, the application of the iN approach is new and emerging in the field of neurodegenerative diseases. Like any technique, iN technology has some obvious advantages and disadvantages (**Table 3**). Because direct reprogramming does not involve the iPSC stage and the differentiation step, which saves a lot of time, iPSC technology may take several months, depending on the protocol. In addition, the technical challenges of iN are less compared to iPSCs culture technology. The most important difference between iPSCs and iN is epigenetic reset.

As we know, a healthy and diseased person not only differs in genomic levels but also has different epigenetics. Epigenetic information is crucial for disease onset, especially for aging-related diseases. A recent study conducted by Tang et al. (2017) found iPSCs derived motor neurons did not show age-related differences, while iN, in contrast, age-equivalent induced motor neurons showed nuclear envelope defects. Mertens et al. (2015) provided interesting evidence for iN as it can reserve aging signatures of the original patient, which is not observed in iPSCs. Furthermore, they have also found downregulation of RanBP1 in aged fibroblasts and iN derived from aged fibroblasts, and when RanBP1 was knocked down, the transcriptional markers shifted from young to aged (Mertens et al., 2015). Therefore, iN is a more reliable model for neurodegenerative diseases and drug discovery, which could model natural disease progression, especially age-related information. On the other hand, iPSCs can maintain self-renewal but not iN, which is required for maintenance and stock. Due to the unlimited self-renewal of iPSCs, the neurons derived from iPSCs can be unlimited. Thus, without an iPSC stage, investigators might need to acquire a larger quantity of original cells from a patient to obtain enough iN. In addition, identification of the right combination of transcription factors, the inclusion of chemical compounds (small molecules), and the efficiency of reprogramming are also very important. However, to realize the application of iN in neurodegenerative diseases, the underlying mechanisms of direct reprogramming need to be further addressed.

TABLE 3 | The different features between iN and iPSCs-derived neurons.

Features	iN	iPSCs-derived neurons
Epigenetics reset	The generation of iN will not reset epigenetic information	Neuron derived from iPSCs will reset epigenetic information
Cell number and maintain	iN cell number is limited by original cell number and reprogramming efficiency, which are uneasy to maintain.	After acquisition of iPSCs, the production of neurons can be unlimited, which are easy to maintain.
Time for acquiring mature neurons	Directly reprogramming somatic cells to neurons only takes several weeks	Obtaining neurons derived from iPSCs will takes several months depending on protocol
Technical Challenges	Generation of iN using direct reprogramming technology is much simpler	iPSC technology of generation iN is complicated
Original cell types	Based on technology, the source for iN is limited (fibroblasts ect.)	The source for iPSCs is variable (fibroblasts, adipose stromal cells ect.)

CONCLUSION AND PERSPECTIVE

In conclusion, this review has discussed recent iPSCs and iN technology and their application for neurodegenerative disease modeling. Compared them to traditional disease models, both iPSCs and iN are more accurate models for studying diseases and drug discovery. For iPSCs and iN disease models, there are still some challenges that need to be further investigated to optimize reprogramming conditions, especially the efficiency of direct reprogramming and lineage-specific reprogramming. For the modeling of neurodegenerative diseases, iN could be a better model for disease and the development of drugs, without epigenetic reset. In the coming years, we expect there to be extensive improvements in reprogramming technology for the application of iPSCs and iN for disease modeling and drug discovery.

AUTHOR CONTRIBUTIONS

YZ, XX, and JY performed the literature research and wrote the manuscript. C-LZ and QZ proposed the framework. JH and KA critically revised the manuscript. QZ and JY provided the funding support. All authors read and approved the manuscript.

FUNDING

This study was partly supported by the National Natural Science Foundation of China (No. 81771262), the Zhejiang Health Science and Technology Project (2016RCA022), Zhejiang Key Research and Development Project (2017C03027), and Zhejiang Provincial Natural Science Foundation of China (LQ20H090005).

REFERENCES

Alexander, G. E. (2004). Biology of Parkinson's disease: pathogenesis and pathophysiology of a multisystem neurodegenerative disorder. *Dialog. Clin. Neurosci.* 6, 259–280.

Ambasudhan, R., Talantova, M., Coleman, R., Yuan, X., Zhu, S., Lipton, S. A., et al. (2011). Direct reprogramming of adult human fibroblasts to functional neurons under defined conditions. *Cell Stem Cell* 9, 113–118. doi: 10.1016/j.stem.2011.07.002

Aoi, T., Yae, K., Nakagawa, M., Ichisaka, T., Okita, K., Takahashi, K., et al. (2008). Generation of pluripotent stem cells from adult mouse liver and stomach cells. *Science* 321, 699–702. doi: 10.1126/science.1154884

Arenas, E., Denham, M., and Villaescusa, J. C. (2015). How to make a midbrain dopaminergic neuron. *Development* 142, 1918–1936. doi: 10.1242/dev.097394

Armstrong, R. (2013). Review article What causes alzheimer's disease? *Folia Neuropathol.* 3, 169–188. doi: 10.5114/fn.2013.37702

Barbuti, A., Qu, X., Liu, T., Song, K., Li, X., and Ge, D. (2012). Induced pluripotent stem cells generated from human adipose-derived stem cells using a non-viral polycistronic plasmid in feeder-free conditions. *PLoS One* 7:e48161. doi: 10.1371/journal.pone.0048161

Berninger, B., Costa, M. R., Koch, U., Schroeder, T., Sutor, B., Grothe, B., et al. (2007). Functional properties of neurons derived from in vitro reprogrammed postnatal astroglia. *J. Neurosci.* 27, 8654–8664. doi: 10.1523/JNEUROSCI.1615-07.2007

Birger, A., Ben-Dor, I., Ottolenghi, M., Turetsky, T., Gil, Y., Sweetat, S., et al. (2019). Human iPSC-derived astrocytes from ALS patients with mutated C9ORF72 show increased oxidative stress and neurotoxicity. *eBio Med.* 50, 274–289. doi: 10.1016/j.ebiom.2019.11.026

Black, J. B., Adler, A. F., Wang, H. G., D'Ippolito, A. M., Hutchinson, H. A., Reddy, T. E., et al. (2016). Targeted epigenetic remodeling of endogenous loci by CRISPR/Cas9-based transcriptional activators directly converts fibroblasts to neuronal cells. *Cell Stem Cell* 19, 406–414. doi: 10.1016/j.stem.2016.07.001

Bohnke, L., Traxler, L., Herdy, J. R., and Mertens, J. (2018). Human neurons to model aging: a dish best served old. *Drug Discov. Today Dis. Models* 27, 43–49. doi: 10.1016/j.ddmod.2019.01.001

Borgohain, M. P., Haridhasapavalan, K. K., Dey, C., Adhikari, P., and Thummer, R. P. (2019). An insight into DNA-free reprogramming approaches to generate integration-free induced pluripotent stem cells for prospective biomedical applications. *Stem Cell Rev. Rep.* 15, 286–313. doi: 10.1007/s12015-018-9861-6

Brooks-Kayal, A. (2010). Epilepsy and autism spectrum disorders: are there common developmental mechanisms? *Brain Dev.* 32, 731–738. doi: 10.1016/j.braindev.2010.04.010

Byrne, J. A. (2014). Developing neural stem cell-based treatments for neurodegenerative diseases. *Stem Cell Res. Ther.* 5:72. doi: 10.1186/scrt461

Caiazzo, M., Dell'Anno, M. T., Dvoretskova, E., Lazarevic, D., Taverna, S., Leo, D., et al. (2011). Direct generation of functional dopaminergic neurons from mouse and human fibroblasts. *Nature* 476, 224–227. doi: 10.1038/nature10284

Caiazzo, M., Giannelli, S., Valente, P., Lignani, G., Carissimo, A., Sessa, A., et al. (2015). Direct conversion of fibroblasts into functional astrocytes by defined transcription factors. *Stem Cell Rep.* 4, 25–36. doi: 10.1016/j.stemcr.2014.12.002

Chang, C. Y., Chen, S. M., Lu, H. E., Lai, S. M., Lai, P. S., Shen, P. W., et al. (2015). N-butylidenephthalide attenuates Alzheimer's disease-like cytopathy in Down syndrome induced pluripotent stem cell-derived neurons. *Sci. Rep.* 5:8744. doi: 10.1038/srep08744

Chang, J. H., Tsai, P. H., Wang, K. Y., Wei, Y. T., Chiou, S. H., and Mou, C. Y. (2018). Generation of functional dopaminergic neurons from reprogramming fibroblasts by nonviral-based mesoporous silica nanoparticles. *Sci. Rep.* 8:11. doi: 10.1038/s41598-017-18324-8

Chen, H., Qian, K., Du, Z., Cao, J., Petersen, A., Liu, H., et al. (2014). Modeling ALS with iPSCs reveals that mutant SOD1 misregulates neurofilament balance in motor neurons. *Cell Stem Cell* 14, 796–809. doi: 10.1016/j.stem.2014.02.004

Choi, K. A., and Hong, S. (2017). Induced neural stem cells as a means of treatment in Huntington's disease. *Expert Opin. Biol. Ther.* 17, 1333–1343. doi: 10.1080/14712598.2017.1365133

Colasante, G., Lignani, G., Rubio, A., Medrihan, L., Yekhlef, L., Sessa, A., et al. (2015). Rapid conversion of fibroblasts into functional forebrain GABAergic interneurons by direct genetic reprogramming. *Cell Stem Cell* 17, 719–734. doi: 10.1016/j.stem.2015.09.002

Csobonyeiova, M., Polak, S., Nicodemou, A., and Danisovic, L. (2017). Induced pluripotent stem cells in modeling and cell-based therapy of amyotrophic lateral sclerosis. *J. Physiol. Pharmacol.* 68, 649–657.

Dafinca, R., Scaber, J., Ababneh, N., Lalic, T., Weir, G., Christian, H., et al. (2016). C9orf72 hexanucleotide expansions are associated with altered endoplasmic reticulum calcium homeostasis and stress granule formation in induced pluripotent stem cell-derived neurons from patients with amyotrophic lateral sclerosis and frontotemporal dementia. *Stem Cells* 34, 2063–2078. doi: 10.1002/stem.2388

De Gregorio, R., Pulcrano, S., De Sanctis, C., Volpicelli, F., Guatteo, E., von Oerthel, L., et al. (2018). miR-34b/c regulates Wnt1 and enhances mesencephalic dopaminergic neuron differentiation. *Stem Cell Rep.* 10, 1237–1250. doi: 10.1016/j.stemcr.2018.02.006

DeJesus-Hernandez, M., Mackenzie, I. R., Boeve, B. F., Boxer, A. L., Baker, M., Rutherford, N. J., et al. (2011). Expanded GGGGCC hexanucleotide repeat in noncoding region of C9ORF72 causes chromosome 9p-linked FTD and ALS. *Neuron* 72, 245–256. doi: 10.1016/j.neuron.2011.09.011

Dell'Anno, M. T., Caiazzo, M., Leo, D., Dvoretskova, E., Medrihan, L., Colasante, G., et al. (2014). Remote control of induced dopaminergic neurons in parkinsonian rats. *J. Clin. Invest.* 124, 3215–3229. doi: 10.1172/JCI74664

Devlin, A. C., Burr, K., Borooah, S., Foster, J. D., Cleary, E. M., Geti, I., et al. (2015). Human iPSC-derived motoneurons harbouring TARDBP or C9ORF72 ALS mutations are dysfunctional despite maintaining viability. *Nat. Commun.* 6:5999. doi: 10.1038/ncomms6999

Donnelly, C. J., Zhang, P.-W., Pham, J. T., Haeusler, A. R., Mistry, N. A., Vidensky, S., et al. (2013). RNA toxicity from the ALS/FTD C9ORF72 expansion is mitigated by antisense intervention. *Neuron* 80, 415–428. doi: 10.1016/j.neuron.2013.10.015

Duan, L., Bhattacharyya, B. J., Belmadani, A., Pan, L., Miller, R. J., and Kessler, J. A. (2014). Stem cell derived basal forebrain cholinergic neurons from Alzheimer's disease patients are more susceptible to cell death. *Mol. Neurodegener.* 9:3. doi: 10.1186/1750-1326-9-3

Ebrahimi, B. (2015). Reprogramming barriers and enhancers: strategies to enhance the efficiency and kinetics of induced pluripotency. *Cell Regen.* 4:10. doi: 10.1186/s13619-015-0024-9

Eminli, S., Utikal, J., Arnold, K., Jaenisch, R., and Hochedlinger, K. (2008). Reprogramming of neural progenitor cells into induced pluripotent stem cells in the absence of exogenous Sox2 expression. *Stem Cells* 26, 2467–2474. doi: 10.1634/stemcells.2008-0317

Farkhondeh, A., Li, R., Gorshkov, K., Chen, K. G., Might, M., Rodems, S., et al. (2019). Induced pluripotent stem cells for neural drug discovery. *Drug Discov. Today* 24, 992–999. doi: 10.1016/j.drudis.2019.01.007

Finkbeiner, S. (2010). Bridging the Valley of death of therapeutics for neurodegeneration. *Nat. Med.* 16, 1227–1232. doi: 10.1038/nm.2222

Fujimori, K., Ishikawa, M., Otomo, A., Atsuta, N., Nakamura, R., Akiyama, T., et al. (2018). Modeling sporadic ALS in iPSC-derived motor neurons identifies a potential therapeutic agent. *Nat. Med.* 24, 1579–1589. doi: 10.1038/s41591-018-0140-5

Fusaki, N., Ban, H., Nishiyama, A., Saeki, K., and Hasegawa, M. (2009). Efficient induction of transgene-free human pluripotent stem cells using a vector based on Sendai virus, an RNA virus that does not integrate into the host genome. *Proc. Jpn Acad. Ser. B* 85, 348–362. doi: 10.2183/pjab.85.348

Gao, L., Huang, S., Zhang, H., Hua, W., Xin, S., Cheng, L., et al. (2019). Suppression of glioblastoma by a drug cocktail reprogramming tumor cells into neuronal like cells. *Sci. Rep.* 9:3462. doi: 10.1038/s41598-019-39852-5

Gascon, S., Masserdotti, G., Russo, G. L., and Gotz, M. (2017). Direct neuronal reprogramming: achievements, hurdles, and new roads to success. *Cell Stem Cell* 21, 18–34. doi: 10.1016/j.stem.2017.06.011

Gitler, A. D., Dhillon, P., and Shorter, J. (2017). Neurodegenerative disease: models, mechanisms, and a new hope. *Dis. Models Mech.* 10, 499–502. doi: 10.1242/dmm.030205

Gonzalez, F., Boue, S., and Belmonte, J. C. I. (2011). Methods for making induced pluripotent stem cells: reprogramming a la carte. *Nat. Rev. Genet.* 12, 231–242. doi: 10.1038/nrg2937

Han, C., Chaineau, M., Chen, C. X., Beitel, L. K., and Durcan, T. M. (2018). Open science meets stem cells: a new drug discovery approach for neurodegenerative disorders. *Front. Neurosci.* 12:47. doi: 10.3389/fnins.2018.00047

Hanna, J., Markoulaki, S., Schorderet, P., Carey, B. W., Beard, C., Wernig, M., et al. (2008). Direct reprogramming of terminally differentiated mature B lymphocytes to pluripotency. *Cell* 133, 250–264. doi: 10.1016/j.cell.2008.03.028

Hargus, G., Ehrlich, M., Hallmann, A. L., and Kuhlmann, T. (2014). Human stem cell models of neurodegeneration: a novel approach to study mechanisms of disease development. *Acta Neuropathol.* 127, 151–173. doi: 10.1007/s00401-013-1222-6

Haridhasapavalan, K. K., Borgohain, M. P., Dey, C., Saha, B., Narayan, G., Kumar, S., et al. (2019). An insight into non-integrative gene delivery approaches to generate transgene-free induced pluripotent stem cells. *Gene* 686, 146–159. doi: 10.1016/j.gene.2018.11.069

Haridhasapavalan, K. K., Raina, K., Dey, C., Adhikari, P., and Thummer, R. P. (2020). An insight into reprogramming barriers to iPSC generation. *Stem Cell Rev. Rep.* 16, 56–81. doi: 10.1007/s12015-019-09931-1

Haston, K. M., and Finkbeiner, S. (2016). Clinical trials in a dish: the potential of pluripotent stem cells to develop therapies for neurodegenerative diseases. *Annu. Rev. Pharmacol. Toxicol.* 56, 489–510. doi: 10.1146/annurev-pharmtox-010715-103548

Heilker, R., Traub, S., Reinhardt, P., Scholer, H. R., and Sterneckert, J. (2014). iPS cell derived neuronal cells for drug discovery. *Trends Pharmacol. Sci.* 35, 510–519. doi: 10.1016/j.tips.2014.07.003

Heinrich, C., Gascon, S., Masserdotti, G., Lepier, A., Sanchez, R., Simon-Ebert, T., et al. (2011). Generation of subtype-specific neurons from postnatal astroglia of the mouse cerebral cortex. *Nat. Protoc.* 6, 214–228. doi: 10.1038/nprot.2010.188

Hou, P., Li, Y., Zhang, X., Liu, C., Guan, J., Li, H., et al. (2013). Pluripotent stem cells induced from mouse somatic cells by small-molecule compounds. *Science* 341, 651–654. doi: 10.1126/science.1239278

Hu, W., Qiu, B., Guan, W., Wang, Q., Wang, M., Li, W., et al. (2015). Direct conversion of normal and Alzheimer's disease human fibroblasts into neuronal cells by small molecules. *Cell Stem Cell* 17, 204–212. doi: 10.1016/j.stem.2015.07.006

Huang, L., Wang, J., Huang, S., Siaw-Debrah, F., Nyanzu, M., and Zhuge, Q. (2019). Polyacrylic acid-coated nanoparticles loaded with recombinant tissue plasminogen activator for the treatment of mice with ischemic stroke. *Biochem. Biophys. Res. Commun.* 516, 565–570. doi: 10.1016/j.bbrc.2019.06.079

Imaizumi, Y., Okada, Y., Akamatsu, W., Koike, M., Kuzumaki, N., Hayakawa, H., et al. (2012). Mitochondrial dysfunction associated with increased oxidative stress and alpha-synuclein accumulation in PARK2 iPSC-derived neurons and postmortem brain tissue. *Mol. Brain* 5:35. doi: 10.1186/1756-6606-5-35

Imaizumi, Y., and Okano, H. (2014). Modeling human neurological disorders with induced pluripotent stem cells. *J. Neurochem.* 129, 388–399. doi: 10.1111/jnc.12625

Israel, M. A., Yuan, S. H., Bardy, C., Reyna, S. M., Mu, Y., Herrera, C., et al. (2012). Probing sporadic and familial Alzheimer's disease using induced pluripotent stem cells. *Nature* 482, 216–220. doi: 10.1038/nature10821

Jucker, M. (2010). The benefits and limitations of animal models for translational research in neurodegenerative diseases. *Nat. Med.* 16, 1210–1214. doi: 10.1038/nm.2224

Karch, C. M., Cruchaga, C., and Goate, A. M. (2014). Alzheimer's disease genetics: from the bench to the clinic. *Neuron* 83, 11–26. doi: 10.1016/j.neuron.2014.05.041

Karow, M., Camp, J. G., Falk, S., Gerber, T., Pataskar, A., Gac-Santel, M., et al. (2018). Direct pericyte-to-neuron reprogramming via unfolding of a neural stem cell-like program. *Nat. Neurosci.* 21, 932–940. doi: 10.1038/s41593-018-0168-3

Karow, M., Sánchez, R., Schichor, C., Masserdotti, G., Ortega, F., Heinrich, C., et al. (2012). Reprogramming of pericyte-derived cells of the adult human brain into induced neuronal cells. *Cell Stem Cell* 11, 471–476. doi: 10.1016/j.stem.2012.07.007

Ke, M., Chong, C.-M., and Su, H. (2019). Using induced pluripotent stem cells for modeling Parkinson's disease. *World J. Stem Cells* 11, 634–649. doi: 10.4252/wjsc.v11.i9.634

Ke, Z., Zhang, X., Cao, Z., Ding, Y., Li, N., Cao, L., et al. (2016). Drug discovery of neurodegenerative disease through network pharmacology approach in herbs. *Biomed. Pharmacother.* 78, 272–279. doi: 10.1016/j.biopha.2016.01.021

Kim, D., Kim, C. H., Moon, J. I., Chung, Y. G., Chang, M. Y., Han, B. S., et al. (2009). Generation of human induced pluripotent stem cells by direct delivery of reprogramming proteins. *Cell Stem Cell* 4, 472–476. doi: 10.1016/j.stem.2009.05.005

Kim, J., Su, S. C., Wang, H., Cheng, A. W., Cassady, J. P., Lodato, M. A., et al. (2011). Functional integration of dopaminergic neurons directly converted from mouse fibroblasts. *Cell Stem Cell* 9, 413–419. doi: 10.1016/j.stem.2011.09.011

Kim, J. B., Zaehres, H., Wu, G., Gentile, L., Ko, K., Sebastiano, V., et al. (2008). Pluripotent stem cells induced from adult neural stem cells by reprogramming with two factors. *Nature* 454, 646–650. doi: 10.1038/nature07061

Kiskinis, E., Sandoe, J., Williams, L. A., Boulting, G. L., Moccia, R., Wainger, B. J., et al. (2014). Pathways disrupted in human ALS motor neurons identified through genetic correction of mutant SOD1. *Cell Stem Cell* 14, 781–795. doi: 10.1016/j.stem.2014.03.004

Kraljevic, S., Stambrook, P. J., and Pavelic, K. (2004). Accelerating drug discovery. *EMBO Rep.* 5, 837–842. doi: 10.1038/sj.embor.7400236

Ledford, H. (2011). Translational research: 4 ways to fix the clinical trial. *Nature* 477, 526–528. doi: 10.1038/477526a

Lee, S., Lee, B., Lee, J. W., and Lee, S. K. (2009). Retinoid signaling and neurogenin2 function are coupled for the specification of spinal motor neurons through a chromatin modifier CBP. *Neuron* 62, 641–654. doi: 10.1016/j.neuron.2009.04.025

Li, X., Liu, D., Ma, Y., Du, X., Jing, J., Wang, L., et al. (2017). Direct reprogramming of fibroblasts via a chemically induced XEN-like State. *Cell Stem Cell* 21, 264–273.e267. doi: 10.1016/j.stem.2017.05.019

Li, X., Zuo, X., Jing, J., Ma, Y., Wang, J., Liu, D., et al. (2015). Small-molecule-driven direct reprogramming of mouse fibroblasts into functional neurons. *Cell Stem Cell* 17, 195–203. doi: 10.1016/j.stem.2015.06.003

Liu, M. L., Zang, T., and Zhang, C. L. (2016). Direct lineage reprogramming reveals disease-specific phenotypes of motor neurons from human ALS patients. *Cell Rep.* 14, 115–128. doi: 10.1016/j.celrep.2015.12.018

Liu, M.-L., Zang, T., Zou, Y., Chang, J. C., Gibson, J. R., Huber, K. M., et al. (2013). Small molecules enable neurogenin 2 to efficiently convert human fibroblasts into cholinergic neurons. *Nat. Commun.* 4:2183. doi: 10.1038/ncomms3183

Liu, X., Li, F., Stubblefield, E. A., Blanchard, B., Richards, T. L., Larson, G. A., et al. (2011). Direct reprogramming of human fibroblasts into dopaminergic neuron-like cells. *Cell Res* 22, 321–332. doi: 10.1038/cr.2011.181

Liu, Y., and Deng, W. (2016). Reverse engineering human neurodegenerative disease using pluripotent stem cell technology. *Brain Res.* 1638, 30–41. doi: 10.1016/j.brainres.2015.09.023

Maherali, N., Ahfeldt, T., Rigamonti, A., Utikal, J., Cowan, C., and Hochedlinger, K. (2008). A high-efficiency system for the generation and study of human induced pluripotent stem cells. *Cell Stem Cell* 3, 340–345. doi: 10.1016/j.stem.2008.08.003

Mall, M., Kareta, M. S., Chanda, S., Ahlenius, H., Perotti, N., Zhou, B., et al. (2017). Myt1l safeguards neuronal identity by actively repressing many non-neuronal fates. *Nature* 544, 245–249. doi: 10.1038/nature21722

Marin, O. (2012). Interneuron dysfunction in psychiatric disorders. *Nat. Rev. Neurosci.* 13, 107–120. doi: 10.1038/nrn3155

Marro, S., Pang, Z. P., Yang, N., Tsai, M. C., Qu, K., Chang, H. Y., et al. (2011). Direct lineage conversion of terminally differentiated hepatocytes to functional neurons. *Cell Stem Cell* 9, 374–382. doi: 10.1016/j.stem.2011.09.002

Mason, A. R., Ziemann, A., and Finkbeiner, S. (2014). Targeting the low-hanging fruit of neurodegeneration. *Neurology* 83, 1470–1473. doi: 10.1212/WNL.0000000000000894

Masserdotti, G., Gascon, S., and Gotz, M. (2016). Direct neuronal reprogramming: learning from and for development. *Development* 143, 2494–2510. doi: 10.1242/dev.092163

Maucksch, C., Jones, K. S., and Connor, B. (2013). Concise review: the involvement of SOX2 in direct reprogramming of induced neural stem/precursor cells. *Stem Cells Transl. Med.* 2, 579–583. doi: 10.5966/sctm.2012-0179

Mertens, J., Paquola, A. C. M., Ku, M., Hatch, E., Bohnke, L., Ladjevardi, S., et al. (2015). Directly reprogrammed human neurons retain aging-associated transcriptomic signatures and reveal age-related nucleocytoplasmic defects. *Cell Stem Cell* 17, 705–718. doi: 10.1016/j.stem.2015.09.001

Mertens, J., Reid, D., Lau, S., Kim, Y., and Gage, F. H. (2018). Aging in a dish: iPSC-derived and directly induced neurons for studying brain aging and age-related neurodegenerative diseases. *Annu. Rev. Genet.* 52, 271–293. doi: 10.1146/annurev-genet-120417-031534

Mitsumoto, H., Brooks, B. R., and Silani, V. (2014). Clinical trials in amyotrophic lateral sclerosis: why so many negative trials and how can trials be improved? *Lancet Neurol.* 13, 1127–1138. doi: 10.1016/s1474-4422(14)70129-2

Moore, S., Evans, L. D., Andersson, T., Portelius, E., Smith, J., Dias, T. B., et al. (2015). APP metabolism regulates tau proteostasis in human cerebral cortex neurons. *Cell Rep.* 11, 689–696. doi: 10.1016/j.celrep.2015.03.068

Moreno, C. L., Della Guardia, L., Shnyder, V., Ortiz-Virumbrales, M., Kruglikov, I., Zhang, B., et al. (2018). iPSC-derived familial Alzheimer's PSEN2 (N141I) cholinergic neurons exhibit mutation-dependent molecular pathology corrected by insulin signaling. *Mol. Neurodegener.* 13:33. doi: 10.1186/s13024-018-0265-5

Morris, S. A., and Daley, G. Q. (2013). A blueprint for engineering cell fate: current technologies to reprogram cell identity. *Cell Res.* 23, 33–48. doi: 10.1038/cr.2013.1

Muratore, C. R., Rice, H. C., Srikanth, P., Callahan, D. G., Shin, T., Benjamin, L. N., et al. (2014). The familial Alzheimer's disease APPV717I mutation alters APP processing and Tau expression in iPSC-derived neurons. *Hum. Mol. Genet.* 23, 3523–3536. doi: 10.1093/hmg/ddu064

Narsinh, K. H., Jia, F., Robbins, R. C., Kay, M. A., Longaker, M. T., and Wu, J. C. (2010). Generation of adult human induced pluripotent stem cells using nonviral minicircle DNA vectors. *Nat. Protoc.* 6, 78–88. doi: 10.1038/nprot.2010.173

Nguyen, H. N., Byers, B., Cord, B., Shcheglovitov, A., Byrne, J., Gujar, P., et al. (2011). LRRK2 mutant iPSC-derived DA neurons demonstrate increased susceptibility to oxidative stress. *Cell Stem Cell* 8, 267–280. doi: 10.1016/j.stem.2011.01.013

Ochalek, A., Mihalik, B., Avci, H. X., Chandrasekaran, A., Teglasi, A., Bock, I., et al. (2017). Neurons derived from sporadic Alzheimer's disease iPSCs reveal elevated TAU hyperphosphorylation, increased amyloid levels, and GSK3B activation. *Alzheimers Res. Ther.* 9:90. doi: 10.1186/s13195-017-0317-z

Okano, H., and Yamanaka, S. (2014). iPS cell technologies: significance and applications to CNS regeneration and disease. *Mol. Brain* 7:22. doi: 10.1186/1756-6606-7-22

Oliveira, L. M., Falomir-Lockhart, L. J., Botelho, M. G., Lin, K. H., Wales, P., Koch, J. C., et al. (2015). Elevated alpha-synuclein caused by SNCA gene triplication impairs neuronal differentiation and maturation in Parkinson's patient-derived induced pluripotent stem cells. *Cell Death Dis.* 6:e1994. doi: 10.1038/cddis.2015.318

O'Malley, J., Woltjen, K., and Kaji, K. (2009). New strategies to generate induced pluripotent stem cells. *Curr. Opin. Biotechnol.* 20, 516–521. doi: 10.1016/j.copbio.2009.09.005

Omole, A. E., and Fakoya, A. O. J. (2018). Ten years of progress and promise of induced pluripotent stem cells: historical origins, characteristics, mechanisms, limitations, and potential applications. *PeerJ* 6:e4370. doi: 10.7717/peerj.4370

Pang, Z. P., Yang, N., Vierbuchen, T., Ostermeier, A., Fuentes, D. R., Yang, T. Q., et al. (2011). Induction of human neuronal cells by defined transcription factors. *Nature* 476, 220–223. doi: 10.1038/nature10202

Pereira, M., Birtele, M., and Rylander Ottosson, D. (2019). Direct reprogramming into interneurons: potential for brain repair. *Cell. Mol. Life Sci.* 76, 3953–3967. doi: 10.1007/s00018-019-03193-3193

Pfisterer, U., Kirkeby, A., Torper, O., Wood, J., Nelander, J., Dufour, A., et al. (2011). Direct conversion of human fibroblasts to dopaminergic neurons. *Proc. Natl. Acad. Sci. U.S.A.* 108, 10343–10348. doi: 10.1073/pnas.1105135108

Postuma, R. B., Berg, D., Stern, M., Poewe, W., Olanow, C. W., Oertel, W., et al. (2015). MDS clinical diagnostic criteria for Parkinson's disease. *Mov. Disord.* 30, 1591–1601. doi: 10.1002/mds.26424

Qin, H., Zhao, A., and Fu, X. (2017). Small molecules for reprogramming and transdifferentiation. *Cell. Mol. Life Sci.* 74, 3553–3575. doi: 10.1007/s00018-017-2586-x

Reinhardt, P., Schmid, B., Burbulla, L. F., Schondorf, D. C., Wagner, L., Glatza, M., et al. (2013). Genetic correction of a LRRK2 mutation in human iPSCs links parkinsonian neurodegeneration to ERK-dependent changes in gene expression. *Cell Stem Cell* 12, 354–367. doi: 10.1016/j.stem.2013.01.008

Ren, Y., Jiang, H., Hu, Z., Fan, K., Wang, J., Janoschka, S., et al. (2015). Parkin mutations reduce the complexity of neuronal processes in iPSC-derived human neurons. *Stem Cells* 33, 68–78. doi: 10.1002/stem.1854

Robberecht, W., and Philips, T. (2013). The changing scene of amyotrophic lateral sclerosis. *Nat. Rev. Neurosci.* 14, 248–264. doi: 10.1038/nrn3430

Rosen, D. R., Siddique, T., Patterson, D., Figlewicz, D. A., Sapp, P., Hentati, A., et al. (1993). Mutations in Cu/Zn superoxide dismutase gene are associated with familial amyotrophic lateral sclerosis. *Nature* 362, 59–62. doi: 10.1038/362059a0

Rowland, H. A., Hooper, N. M., and Kellett, K. A. B. (2018). Modelling sporadic Alzheimer's disease using induced pluripotent stem cells. *Neurochem. Res.* 43, 2179–2198. doi: 10.1007/s11064-018-2663-z

Rubio, A., Luoni, M., Giannelli, S. G., Radice, I., Iannielli, A., Cancellieri, C., et al. (2016). Rapid and efficient CRISPR/Cas9 gene inactivation in human neurons during human pluripotent stem cell differentiation and direct reprogramming. *Sci. Rep.* 6:37540. doi: 10.1038/srep37540

Ruggieri, M., Riboldi, G., Brajkovic, S., Bucchia, M., Bresolin, N., Comi, G. P., et al. (2014). Induced neural stem cells: methods of reprogramming and potential therapeutic applications. *Prog. Neurobiol.* 114, 15–24. doi: 10.1016/j.pneurobio.2013.11.001

Sanchez-Danes, A., Richaud-Patin, Y., Carballo-Carbajal, I., Jimenez-Delgado, S., Caig, C., Mora, S., et al. (2012). Disease-specific phenotypes in dopamine neurons from human iPS-based models of genetic and sporadic Parkinson's disease. *EMBO Mol. Med.* 4, 380–395. doi: 10.1002/emmm.201200215

Sanders, L. H., Laganiere, J., Cooper, O., Mak, S. K., Vu, B. J., Huang, Y. A., et al. (2014). LRRK2 mutations cause mitochondrial DNA damage in iPSC-derived neural cells from Parkinson's disease patients: reversal by gene correction. *Neurobiol. Dis.* 62, 381–386. doi: 10.1016/j.nbd.2013.10.013

Sareen, D., O'Rourke, J. G., Meera, P., Muhammad, A. K., Grant, S., Simpkinson, M., et al. (2013). Targeting RNA foci in iPSC-derived motor neurons from ALS patients with a C9ORF72 repeat expansion. *Sci. Transl. Med.* 5:208ra149. doi: 10.1126/scitranslmed.3007529

Seibler, P., Graziotto, J., Jeong, H., Simunovic, F., Klein, C., and Krainc, D. (2011). Mitochondrial Parkin recruitment is impaired in neurons derived from mutant PINK1 induced pluripotent stem cells. *J. Neurosci.* 31, 5970–5976. doi: 10.1523/JNEUROSCI.4441-10.2011

Shahbazi, E., Moradi, S., Nemati, S., Satarian, L., Basiri, M., Gourabi, H., et al. (2016). Conversion of human fibroblasts to stably self-renewing neural stem cells with a single zinc-finger transcription factor. *Stem Cell Rep.* 6, 539–551. doi: 10.1016/j.stemcr.2016.02.013

Shen, J. (2014). Function and dysfunction of presenilin. *Neurodegener. Dis.* 13, 61–63. doi: 10.1159/000354971

Shi, Y., Inoue, H., Wu, J. C., and Yamanaka, S. (2017). Induced pluripotent stem cell technology: a decade of progress. *Nat. Rev. Drug Discov.* 16, 115–130. doi: 10.1038/nrd.2016.245

Shi, Y., Kirwan, P., Smith, J., MacLean, G., Orkin, S. H., and Livesey, F. J. (2012). A human stem cell model of early Alzheimer's disease pathology in Down syndrome. *Sci. Transl. Med.* 4:124ra129. doi: 10.1126/scitranslmed.3003771

Shi, Z., Zhang, J., Chen, S., Li, Y., Lei, X., Qiao, H., et al. (2016). Conversion of fibroblasts to parvalbumin neurons by one transcription factor, Ascl1, and the chemical compound forskolin. *J. Biol. Chem.* 291, 13560–13570. doi: 10.1074/jbc.M115.709808

Smith, D. K., Yang, J., Liu, M. L., and Zhang, C. L. (2016). Small molecules modulate chromatin accessibility to promote NEUROG2-mediated fibroblast-to-neuron reprogramming. *Stem Cell Rep.* 7, 955–969. doi: 10.1016/j.stemcr.2016.09.013

Sommer, C. A., and Mostoslavsky, G. (2010). Experimental approaches for the generation of induced pluripotent stem cells. *Stem Cell Res. Ther.* 1:26. doi: 10.1186/Scrt26

Sommer, C. A., and Mostoslavsky, G. (2013). The evolving field of induced pluripotency: recent progress and future challenges. *J. Cell. Physiol.* 228, 267–275. doi: 10.1002/jcp.24155

Son, E. Y., Ichida, J. K., Wainger, B. J., Toma, J. S., Rafuse, V. F., Woolf, C. J., et al. (2011). Conversion of mouse and human fibroblasts into functional spinal motor neurons. *Cell Stem Cell* 9, 205–218. doi: 10.1016/j.stem.2011.07.014

Sproul, A. A., Jacob, S., Pre, D., Kim, S. H., Nestor, M. W., Navarro-Sobrino, M., et al. (2014). Characterization and molecular profiling of PSEN1 familial Alzheimer's disease iPSC-derived neural progenitors. *PLoS One* 9:e84547. doi: 10.1371/journal.pone.0084547

Sreedharan, J., Blair, I. P., Tripathi, V. B., Hu, X., Vance, C., Rogelj, B., et al. (2008). TDP-43 mutations in familial and sporadic amyotrophic lateral sclerosis. *Science* 319, 1668–1672. doi: 10.1126/science.1154584

Sun, N., Panetta, N. J., Gupta, D. M., Wilson, K. D., Lee, A., Jia, F., et al. (2009). Feeder-free derivation of induced pluripotent stem cells from adult human adipose stem cells. *Proc. Natl. Acad. Sci. U.S.A.* 106, 15720–15725. doi: 10.1073/pnas.0908450106

Sun, W., Zheng, W., and Simeonov, A. (2017). Drug discovery and development for rare genetic disorders. *Am. J. Med. Genet. Part A* 173, 2307–2322. doi: 10.1002/ajmg.a.38326

Takahashi, K., Tanabe, K., Ohnuki, M., Narita, M., Ichisaka, T., Tomoda, K., et al. (2007). Induction of pluripotent stem cells from adult human fibroblasts by defined factors. *Cell* 131, 861–872. doi: 10.1016/j.cell.2007.11.019

Takahashi, K., and Yamanaka, S. (2006). Induction of pluripotent stem cells from mouse embryonic and adult fibroblast cultures by defined factors. *Cell* 126, 663–676. doi: 10.1016/j.cell.2006.07.024

Tanabe, K., Ang, C. E., Chanda, S., Olmos, V. H., Haag, D., Levinson, D. F., et al. (2018). Transdifferentiation of human adult peripheral blood T cells into neurons. *Proc. Natl. Acad. Sci. U.S.A.* 115, 6470–6475. doi: 10.1073/pnas.1720273115

Tang, Y., Liu, M. L., Zang, T., and Zhang, C. L. (2017). Direct reprogramming rather than iPSC-Based reprogramming maintains aging hallmarks in human motor neurons. *Front. Mol. Neurosci.* 10:359. doi: 10.3389/fnmol.2017.00359

Tcw, J. (2019). Human iPSC application in Alzheimer's disease and Tau-related neurodegenerative diseases. *Neurosci. Lett.* 699, 31–40. doi: 10.1016/j.neulet.2019.01.043

Torper, O., Pfisterer, U., Wolf, D. A., Pereira, M., Lau, S., Jakobsson, J., et al. (2013). Generation of induced neurons via direct conversion in vivo. *Proc. Natl. Acad. Sci. U.S.A.* 110, 7038–7043. doi: 10.1073/pnas.1303829110

Traxler, L., Edenhofer, F., and Mertens, J. (2019). Next-generation disease modeling with direct conversion: a new path to old neurons. *FEBS Lett.* 593, 3316–3337. doi: 10.1002/1873-3468.13678

Tremblay, R., Lee, S., and Rudy, B. (2016). GABAergic interneurons in the neocortex: from cellular properties to circuits. *Neuron* 91, 260–292. doi: 10.1016/j.neuron.2016.06.033

Utikal, J., Maherali, N., Kulalert, W., and Hochedlinger, K. (2009). Sox2 is dispensable for the reprogramming of melanocytes and melanoma cells into induced pluripotent stem cells. *J. Cell Sci.* 122, 3502–3510. doi: 10.1242/jcs.054783

Vierbuchen, T., Ostermeier, A., Pang, Z. P., Kokubu, Y., Sudhof, T. C., and Wernig, M. (2010). Direct conversion of fibroblasts to functional neurons by defined factors. *Nature* 463, 1035–1041. doi: 10.1038/nature08797

Wan, W., Cao, L., Kalionis, B., Xia, S., and Tai, X. (2015). Applications of induced pluripotent stem cells in studying the neurodegenerative diseases. *Stem Cells Int.* 2015:382530. doi: 10.1155/2015/382530

Wang, C., Najm, R., Xu, Q., Jeong, D.-E., Walker, D., Balestra, M. E., et al. (2018). Gain of toxic apolipoprotein E4 effects in human iPSC-derived neurons is ameliorated by a small-molecule structure corrector. *Nat. Med.* 24, 647–657. doi: 10.1038/s41591-018-0004-z

Warren, L., Manos, P. D., Ahfeldt, T., Loh, Y. H., Li, H., Lau, F., et al. (2010). Highly efficient reprogramming to pluripotency and directed differentiation of human cells with synthetic modified mRNA. *Cell Stem Cell* 7, 618–630. doi: 10.1016/j.stem.2010.08.012

Wazan, L. E., Urrutia-Cabrera, D., and Wong, R. C.-B. (2019). Using transcription factors for direct reprogramming of neurons in vitro. *World J. Stem Cells* 11, 431–444. doi: 10.4252/wjsc.v11.i7.431

Wiedemann, A., Hemmer, K., Bernemann, I., Göhring, G., Pogozhykh, O., Figueiredo, C., et al. (2012). Induced pluripotent stem cells generated from adult bone marrow-derived cells of the nonhuman primate (*Callithrix jacchus*) using a novel quad-cistronic and excisable lentiviral vector. *Cell. Reprogramm.* 14, 485–496. doi: 10.1089/cell.2012.0036

Woo, N. H., and Lu, B. (2006). Regulation of cortical interneurons by neurotrophins: from development to cognitive disorders. *Neuroscientist* 12, 43–56. doi: 10.1177/1073858405284360

Wyss-Coray, T. (2016). Ageing, neurodegeneration and brain rejuvenation. *Nature* 539, 180–186. doi: 10.1038/nature20411

Xiao, D., Liu, X., Zhang, M., Zou, M., Deng, Q., Sun, D., et al. (2018). Direct reprogramming of fibroblasts into neural stem cells by single non-neural progenitor transcription factor Ptf1a. *Nat. Commun.* 9:2865. doi: 10.1038/s41467-018-05209-1

Xu, J., Du, Y., and Deng, H. (2015). Direct lineage reprogramming: strategies, mechanisms, and applications. *Cell Stem Cell* 16, 119–134. doi: 10.1016/j.stem.2015.01.013

Xu, Z., Jiang, H., Zhong, P., Yan, Z., Chen, S., and Feng, J. (2015). Direct conversion of human fibroblasts to induced serotonergic neurons. *Mol. Psychiatry* 21, 62–70. doi: 10.1038/mp.2015.101

Yagi, T., Ito, D., Okada, Y., Akamatsu, W., Nihei, Y., Yoshizaki, T., et al. (2011). Modeling familial Alzheimer's disease with induced pluripotent stem cells. *Hum. Mol. Genet.* 20, 4530–4539. doi: 10.1093/hmg/ddr394

Yu, J., Vodyanik, M. A., Smuga-Otto, K., Antosiewicz-Bourget, J., Frane, J. L., Tian, S., et al. (2007). Induced pluripotent stem cell lines derived from human somatic cells. *Science* 318, 1917–1920. doi: 10.1126/science.1151526

Zhang, L., Yin, J. C., Yeh, H., Ma, N. X., Lee, G., Chen, X. A., et al. (2015). Small molecules efficiently reprogram human astroglial cells into functional neurons. *Cell Stem Cell* 17, 735–747. doi: 10.1016/j.stem.2015.09.012

Zhang, Q. J., Li, J. J., Lin, X., Lu, Y. Q., Guo, X. X., Dong, E. L., et al. (2017). Modeling the phenotype of spinal muscular atrophy by the direct conversion of human fibroblasts to motor neurons. *Oncotarget* 8, 10945–10953. doi: 10.18632/oncotarget.14641

Zhang, Z., and Wu, W.-S. (2013). Sodium butyrate promotes generation of human induced pluripotent stem cells through induction of the miR302/367 cluster. *Stem Cells Dev.* 22, 2268–2277. doi: 10.1089/scd.2012.0650

Zhao, P., Luo, Z., Tian, W., Yang, J., Ibáñez, D. P., Huang, Z., et al. (2014). Solving the puzzle of Parkinson's disease using induced pluripotent stem cells. *Exp. Biol. Med.* 239, 1421–1432. doi: 10.1177/1535370214538588

Conflict of Interest: The authors declare that the research was conducted in the absence of any commercial or financial relationships that could be construed as a potential conflict of interest.

frontiers in Aging Neuroscience

ORIGINAL RESEARCH
published: 17 December 2020
doi: 10.3389/fnagi.2020.548616

An Integrative Nomogram for Identifying Early-Stage Parkinson's Disease Using Non-motor Symptoms and White Matter-Based Radiomics Biomarkers From Whole-Brain MRI

Zhenyu Shu[1], Peipei Pang[2], Xiao Wu[3], Sijia Cui[4], Yuyun Xu[1†] and Minming Zhang[3*†]*

[1] Department of Radiology, Zhejiang Provincial People's Hospital, Affiliated People's Hospital of Hangzhou Medical College, Hangzhou, China, [2] GE Healthcare China, Shanghai, China, [3] Department of Radiology, The Second Affiliated Hospital, Zhejiang University School of Medicine, Hangzhou, China, [4] Second Clinical College, Zhejiang Chinese Medical University, Hangzhou, China

Purpose: To develop and validate an integrative nomogram based on white matter (WM) radiomics biomarkers and nonmotor symptoms for the identification of early-stage Parkinson's disease (PD).

Methods: The brain magnetic resonance imaging (MRI) and clinical characteristics of 336 subjects, including 168 patients with PD, were collected from the Parkinson's Progress Markers Initiative (PPMI) database. All subjects were randomly divided into training and test sets. According to the baseline MRI scans of patients in the training set, the WM was segmented to extract the radiomic features of each patient and develop radiomics biomarkers, which were then combined with nonmotor symptoms to build an integrative nomogram using machine learning. Finally, the diagnostic accuracy and reliability of the nomogram were evaluated using a receiver operating characteristic curve and test data, respectively. In addition, we investigated 58 patients with atypical PD who had imaging scans without evidence of dopaminergic deficit (SWEDD) to verify whether the nomogram was able to distinguish patients with typical PD from patients with SWEDD. A decision curve analysis was also performed to validate the clinical practicality of the nomogram.

Results: The area under the curve values of the integrative nomogram for the training, testing and verification sets were 0.937, 0.922, and 0.836, respectively; the specificity values were 83.8, 88.2, and 91.38%, respectively; and the sensitivity values were 84.6, 82.4, and 70.69%, respectively. A significant difference in the number of patients with PD was observed between the high-risk group and the low-risk group based on the nomogram ($P < 0.05$).

Conclusion: This integrative nomogram is a new potential method to identify patients with early-stage PD.

Keywords: radiomics, white matter, magnetic resonance imaging, machine learning, Parkinson's disease

OPEN ACCESS

Edited by:
Kuangyu Shi,
University of Bern, Switzerland

Reviewed by:
Nabin Koirala,
Haskins Laboratories, United States
Wei Wei,
Xi'an Polytechnic University, China

***Correspondence:**
Yuyun Xu
xuyuyun@hmc.edu.cn
Minming Zhang
zhangminming@zju.edu.cn

† These authors have contributed equally to this work

Received: *03 April 2020*
Accepted: *23 November 2020*
Published: *17 December 2020*

Citation:
Shu Z, Pang P, Wu X, Cui S, Xu Y and Zhang M (2020) An Integrative Nomogram for Identifying Early-Stage Parkinson's Disease Using Non-motor Symptoms and White Matter-Based Radiomics Biomarkers From Whole-Brain MRI. Front. Aging Neurosci. 12:548616. doi: 10.3389/fnagi.2020.548616

INTRODUCTION

Parkinson's disease (PD) is a common age-related progressive neurodegenerative disease (Dorsey et al., 2007). PD begins subtly and progresses slowly; thus, when the diagnosis is clear, most patients are in the middle or late stages of the disease. As the use of neuroprotective drugs by these patients has little effect on the speed of PD progression (LeWitt, 2015), an early diagnosis is of paramount importance for identifying disease onset and developing effective treatment plans. Currently, the diagnosis of PD mainly depends on the patient's medical history and clinical symptoms; however, the early stages of PD can include many atypical symptoms such as sleep disorders, decreased olfactory function and cognitive disturbances, and these non-motor symptoms often precede clinical motor signs (Mielke and Maetzler, 2014). Unfortunately, the cardinal and defining nonmotor symptoms used for the early diagnosis of PD in the clinic, particularly the symptoms that are typical of the early stages, also occur in patients with other disorders (Trojano and Papagno, 2018; De Pablo-Fernández et al., 2019), and the diagnostic error rate is as high as 25% among practitioners with limited clinical experience in diagnosing early-stage of PD (Miller and O'Callaghan, 2015). Thus, it is very challenging to diagnose early-stage PD based on current diagnostic standards.

In recent years, progress has been achieved in magnetic resonance imaging (MRI) technology in the field of neuroimaging (Agosta et al., 2017), such as structural MRI (Tzarouchi et al., 2010), diffusion tensor imaging (Schwarz et al., 2013), and blood oxygen level-dependent functional MRI (Benzagmout et al., 2019). These different techniques represent effective methods for non-invasively studying changes in brain morphology and function associated with PD. However, given the high cost of long functional imaging sessions and a general lack of standard imaging protocols, as represented by differences between MRI systems, scanning protocols and magnetic field strength (Frederick and Meijer, 2014), these complex scanning techniques cannot become widespread in clinical practice. Therefore, the identification of a simple, noninvasive measure to preclinically identify patients with early-stage PD is important.

Radiomics is a recently emerged field of radiology that quantifies imaging data with the aid of advanced image processing techniques, including high-throughput analysis and feature selection, to build biomarkers for the complete characterization of tumors (Liu et al., 2019). At this stage, the new quantitative imaging technology of radiomics has already been used to diagnose neurodegenerative diseases, including PD (Shinde et al., 2019). Nevertheless, most PD studies using radiomics examine only the substantia nigra (SN), where iron accumulation is spatially heterogeneous, allowing clinicians to easily distinguish patients with PD from healthy people (Guan et al., 2017). While the SN provides robust disease biomarkers, the concern is that radiomic analysis of the SN depends on the use of a special sequence, such as quantitative susceptibility mapping or neuromelanin-sensitive imaging, to display the contours of the SN. Understandably, the complexity of this technology has limited its clinical application.

However, the SN of patients with PD is not the only area exhibiting obvious disease-related tissue changes. White matter (WM) has also exhibits been reported to exhibit widespread microstructural alterations in patients with early-stage PD in the absence of gray matter atrophy and cognitive impairment (Pelizzari et al., 2020). In addition, several studies have shown widespread WM and gray matter changes in individuals with PD (Muthuraman et al., 2017; Koirala et al., 2019). Hence, an investigation of WM microstructural integrity in patients with PD may enable more successful exploration of early biomarkers of PD. Previous studies based on diffusion tensor imaging have shown that patients with PD present a greater decrease in WM integrity (Pozorski et al., 2018) than healthy people and often display extensive changes in the microstructure of WM in the early stage of PD even before the onset of cortical neuron loss (Rektor et al., 2018). Based on this evidence, structural changes occur earlier than physiological changes in the early stage of PD. Moreover, a three-dimensional radiomic analysis of WM throughout the brain was recently shown to reflect microstructural changes based on conventional T1-weighted imaging sequences (Shu et al., 2020), which may be more suitable than diffusion tensor imaging sequences for clinical application based on cost alone. Accordingly, we hypothesized that the structural changes in WM in patients with early-stage PD would also be detected by a radiomic analysis and would be of potential use for exploring new imaging-based disease biomarkers. To the best of our knowledge, this type of analysis has not yet been performed.

PD is a complex neurodegenerative disorder in which many different pathophysiological processes have been identified in different brain regions. Furthermore, a single WM biomarker will not be able to accurately diagnose and monitor disease progression; rather, a combination of different biomarkers should be used to provide a more comprehensive approach. As shown in previous studies, early diagnosis has been accomplished by the detection of multiple factors including impaired olfaction, depression, rapid eye movement sleep behavior disorder (RBD), excessive daytime sleepiness (EDS) and cognitive decline (CD) (Kalia and Lang, 2015), which usually occur in the prodromal stage of PD (Filippi et al., 2018). Accordingly, the purpose of this study was to explore the possibility of developing novel imaging biomarkers of PD from WM using radiomics and combining them with prodromal nonmotor symptoms to generate an integrative nomogram for disease classification. Overall, we hope to propose a low-cost and highly accurate method for identifying patients with early-stage PD.

MATERIALS AND METHODS

Patients

The datasets used to build the model were all obtained from the Parkinson's Progress Markers Initiative (PPMI) database (http://www.ppmi-info.org), which is the first global and comprehensive international Parkinson's research database (Parkinson Progression Marker Initiative, 2011). The PPMI is a landmark observational clinical study designed to comprehensively evaluate cohorts of significant interest

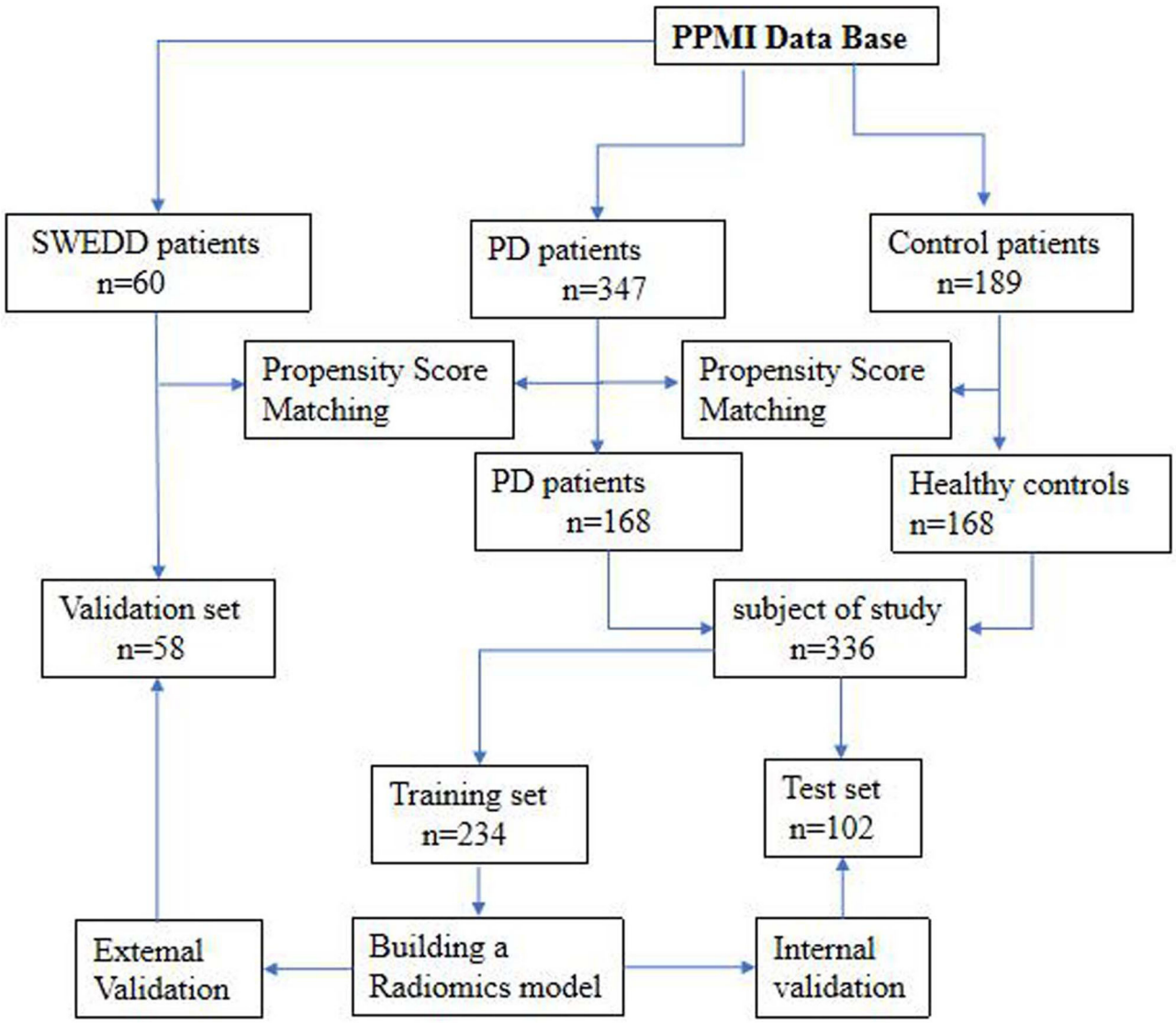

FIGURE 1 | Flowchart of the recruitment process in the current study.

using advanced imaging, biological, clinical and behavioral assessments to identify biomarkers of PD progression. Because the PPMI is a longitudinal study, we chose to use the baseline data to study early-stage PD. Importantly, all subjects were in the first or second stage of the disease according to the Hoehn-Yahr scale, and none of them had received drug treatment. The average interval between the development of clinical symptoms and the diagnosis of PD in these patients was 16.5 ± 14.9 months. Therefore, we defined the disease stage of these subjects as the early stage of PD. The detailed characteristics of the patients and the disease duration are provided in the **Supplementary Materials**. After age and sex matching, 168 healthy controls (HCs) and 168 patients with PD were selected from the database. These 336 subjects were then randomly divided into a training set ($n = 234$) and a test set ($n = 102$). The training set was used to build the diagnostic model, and the test set was used to verify the reliability of the model. We also investigated 58 age- and sex-matched patients with atypical PD from the PPMI who had imaging scans without evidence of dopaminergic deficit (SWEDD) to determine whether the model was able to distinguish patients with typical PD from patients with SWEDD. The matching details are provided in the supporting materials. **Figure 1** shows the recruitment process for the research study.

Whole-Brain White Matter Segmentation and Image Preprocessing

We obtained T1-weighted MRI data from the PPMI database. The PPMI diffusion MRI data were acquired using Siemens Tim Trio and Siemens Verio 3 Tesla MRI scanners at 32

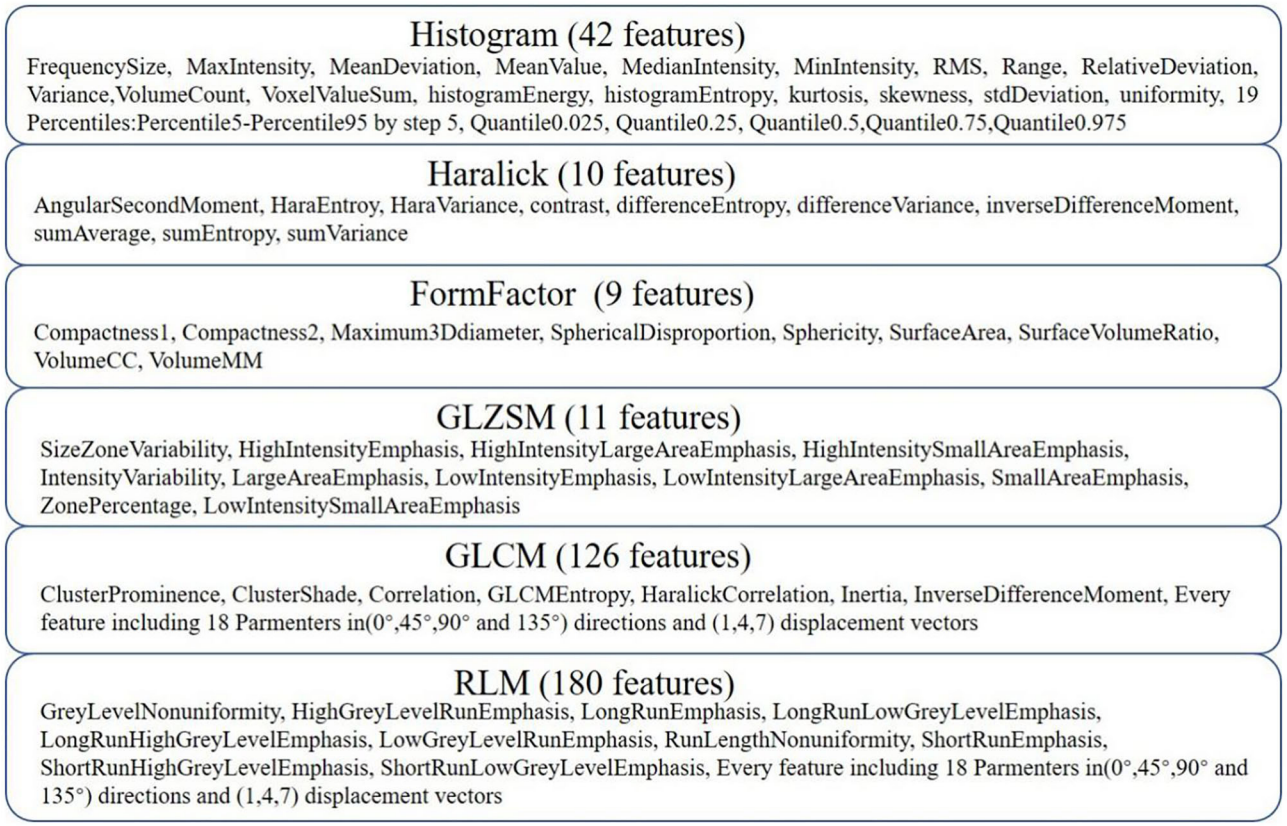

FIGURE 2 | Details of the extracted features. Three hundred seventy-eight features were extracted from six categories.

different international sites based on a standardized protocol. T1-weighted MRI data were obtained using the following parameters: TR = 2300 ms, TE = 2.98 ms, TI = 900 ms, image matrix = 240 × 256 × 176, and voxel resolution = 1 × 1 × 1 mm^3. All images were automatically segmented into whole-brain gray matter, WM and cerebrospinal fluid volumes using the spm12 software package (https://www.fil.ion.ucl.ac.uk/spm/software/spm12/). The WM boundaries were manually adjusted using ITK-SNAP software (http://www.itksnap.org) by two experienced neuroradiologists (radiologist A and radiologist B, with 5 and 10 years of neuroimaging experience, respectively) who were blinded to the clinical data. This modification was accomplished using the following steps: (1) removal of nonbrain tissue, brainstem, and cerebellum and (2) modification of WM segmentation. Then, the WM volumes were imported into AK software (Quantitative Analysis Kit, version 1.2, GE Healthcare) for image preprocessing. First, all images were resampled to 1 × 1 × 1 mm^3 resolution through linear interpolation to eliminate the effect of anisotropy on the features. A Gaussian filter was then applied to reduce noise, and the magnetic field inhomogeneity was corrected, which also assisted with reducing the effects of external interference factors. Finally, the intensity was standardized to limit the grayscale values of all images to a range of 0-32 and ensure that they would be compared without bias (Sun et al., 2018).

Radiomic Feature Extraction

AK software was used to extract 378 radiomic features based on the WM images, including histogram (42 features), Haralick (10 features), form factor (9 features), gray-level co-occurrence matrix (126 features, GLCM), run-length matrix (180 features, RLM) and gray-level size-zone Matrix (11 features, GLSZM) features. A detailed description of the features is provided in **Figure 2**. These features have been shown to characterize cancer heterogeneity and potentially reflect changes in the image structure (Mayerhoefer et al., 2020). In addition, we used the features that were most robust to manual correction by different radiologists (Shu et al., 2019) to ensure the stability and repeatability of the radiomics features. The Spearman rank correlation test was used to calculate the correlation coefficient (CC) of each feature between feature set A (from radiologist A) and feature set B (from radiologist B). Features with a CC> 0.8 were considered robust features (Wu et al., 2016). The quantitative value of robust features is the average of the two features.

Establishment of an Overarching Radiomic Biomarker

Not every single feature is equally relevant to the diagnosis of PD. Furthermore, data reduction or feature selection is

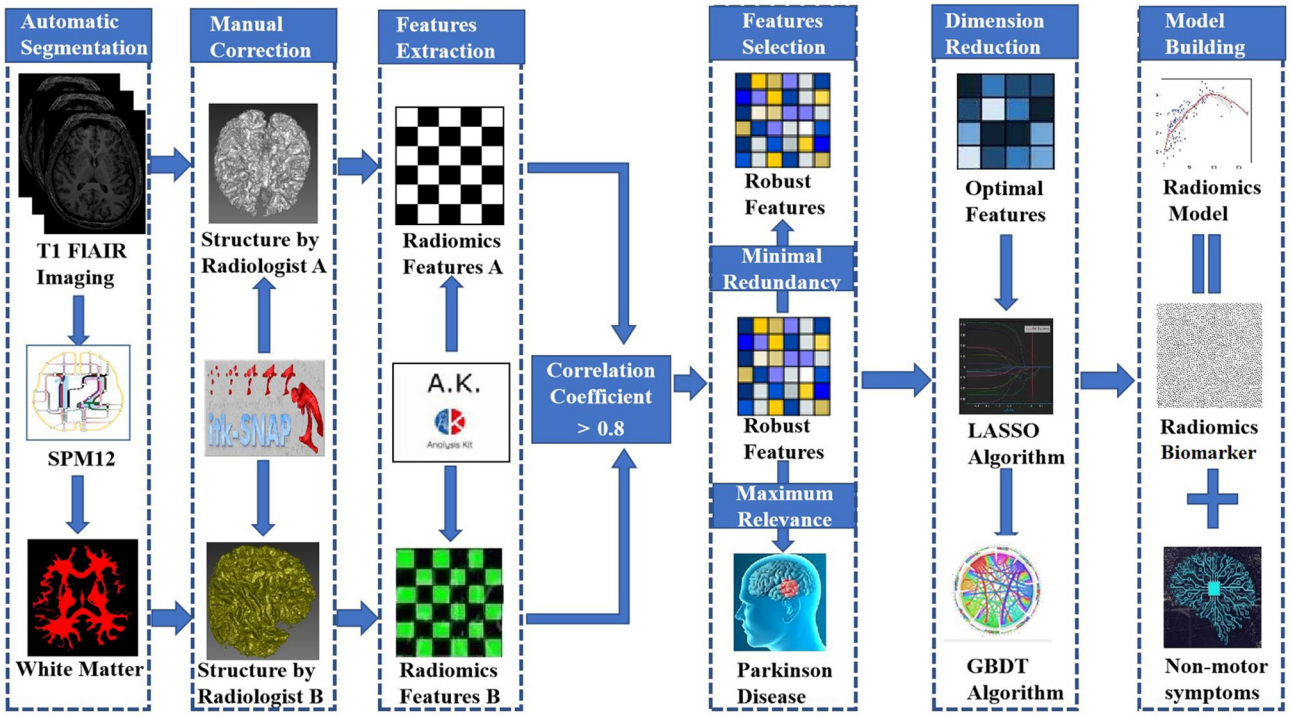

FIGURE 3 | Workflow used to build the radiomic model.

necessary to obtain meaningful results from pattern recognition analysis (Ashburner, 2009). In the present study, the minimum redundancy maximum relevance (mRMR) algorithm was used to extract robust features from the training set (Mukaka, 2012). The aim of the maximum relevance procedure was to select features with the maximal correlation with the actual PD diagnosis. At the same time, the minimum redundancy process ensured that the selected features had minimal redundancy among the other features, and we defined features with CCs greater than 0.1 and 0.8 as high-correlation and low-redundancy features, respectively. Then, the mRMR method was used to obtain an optimal feature set with a high correlation and low redundancy. Second, the least absolute shrinkage and selection operator (LASSO) algorithm was then applied to reduce the dimensionality of the optimal feature set. Finally, a gradient boosting decision tree (GBDT) algorithm was utilized to select radiomic features and build the composite radiomic biomarker. In order to quantify the radiomics biomarker discriminability, a score was calculated using the biomarker model from each patient in the training set. This result reflected the possibility of PD and was defined as the rad-score. The training set biomarker formula was employed to calculate the scores for the test set. Finally, the accuracy of the radiomic biomarker obtained from the training and test sets was evaluated by constructing a receiver operating characteristic (ROC) curve. To further verify the clinical efficacy of the radiomics biomarker, we conducted a stratified analysis of the rad-scores for patients with different nonmotor symptoms. Detailed information on dimensionality reduction is provided in the **Supplementary Materials**.

Construction of the Integrative Nomogram

Stepwise logistic regression analysis was performed to select independent predictors of PD for each potential predictive variable: demographic characteristics (i.e., family history of PD, age, and sex), nonmotor symptoms (i.e., impaired olfaction, depression, RBD, EDS, and CD) and radiomic biomarkers in the training set. In addition, machine learning, an important part of radiomics, improves the accuracy, performance, and predictive ability of the model (Chen et al., 2018; Watson et al., 2019). Accordingly, five machine learning classifiers were used to construct the predictive model and included support vector machine (SVM), Bayes, logistic regression, random forest, and decision tree classifiers. All models were examined using 5-fold cross-validation, in which 20% of the data were used to test the biomarker that was created with the other 80% of data. Different test and training set data were used for every 5-fold cross-validation, and the average classification accuracy was calculated based on 10 iterations of 5-fold cross-validation. The accuracy of the model using different machine learning classifiers was evaluated with an ROC curve and the DeLong test. Finally, the best machine learning method was applied to develop a predictive model for PD based on independent predictors, and an integrative nomogram was constructed. **Figure 3** shows the workflow for creating the radiomics model. Detailed information

TABLE 1 | Descriptive statistics of the three datasets.

Variables		Training set (*n* = 234)	Test set (*n* = 102)	SWEDD set (*n* = 58)	*P*-value
		n (%)	*n* (%)	*n* (%)	
Sex	Male	146 (62.4)	64 (62.7)	37 (63.8)	0.981
	Female	88 (37.6)	38 (37.3)	21 (36.2)	
Age	Years	61.9 ± 9.7	61.6 ± 9.8	60 ± 9.7	0.399
Family history of PD	No	196 (83.8)	88 (86.3)	43 (74.1)	0.129
	Yes	38 (16.2)	14 (13.7)	15 (25.9)	
Impaired olfaction	No	92 (39.3)	33 (32.4)	25 (43.1)	0.336
	Yes	142 (60.7)	69 (67.6)	33 (56.9)	
Depression	No	211 (90.2)	85 (83.3)	45 (77.6)	0.023
	Yes	23 (9.8)	17 (16.7)	13 (22.4)	
RBD	No	171 (73.1)	70 (68.6)	36 (62.1)	0.232
	Yes	63 (26.9)	32 (31.4)	22 (37.9)	
EDS	No	191 (81.6)	84 (82.4)	45 (77.6)	0.738
	Yes	43 (18.4)	18 (17.6)	13 (22.4)	
CD	No	207 (88.5)	89 (87.3)	52 (89.7)	0.898
	Yes	27 (11.5)	13 (12.7)	6 (10.3)	
Hoehn-Yahr stage	Stage 0	106 (45.3)	47 (46.1)	3 (5.2)	<0.0001*
	Stage 1	54 (23.1)	21 (20.6)	30 (51.7)	
	Stage 2	74 (31.6)	34 (33.3)	25 (43.1)	

*SWEDD, scans without evidence of dopaminergic deficit; RBD, rapid eye movement sleep behavior disorder; EDS, excessive daytime sleepiness; CD, cognitive decline. P values, significance levels of differences in variables among the training set, test set and SWEDD set. The values in parentheses indicate the percentage of each variable in the training set or test set. *P < 0.05.*

about the machine learning techniques used in the present study is provided in the **Supplementary Materials**.

Assessment of the Integrative Nomogram

Based on the nomogram, the risk score of PD was calculated for each patient. The accuracy of the nomogram obtained from the training and test sets was then evaluated with an ROC curve. A calibration curve was generated to evaluate the calibration performance, and the Hosmer-Lemeshow test was performed to analyze the goodness-of-fit of the nomogram. We attempted to distinguish the patients with PD in the SWEDD dataset to further evaluate the performance of the integrative nomogram. A dataset of age- and sex-matched patients with SWEDD and PD was collected from the PPMI, and the probability of PD was defined from the model score and was calculated for each patient using the integrative nomogram. Taking the threshold of the Youden index of the ROC curve as the classification point, we divided all cases into a low-risk and a high-risk group according to the model score. Based on the actual PD patients in different risk groups, the clinical effect of the nomogram was determined. Finally, the net benefit of the model was evaluated using decision curve analysis (DCA) (O'Brien, 2007).

Statistical Analyses

Statistical analyses were performed with the Statistical Package for the Social Sciences (SPSS) version 22.0 (SPSS, Inc., Chicago, IL, USA), GraphPad Prism 6 (GraphPad Software, San Diego, CA, USA) and R software (version 3.3.1). Differences between categorical variables were examined using a chi-square test. Parametric data were assessed using an independent-sample *t*-test, whereas nonparametric data were assessed using the Mann-Whitney *U*-test. All analyses were controlled for age and sex. The nomogram was constructed, and calibration plots were generated using the "rms" package. The DCA was performed with the "dca.R." package. Results with a two-tailed $P < 0.05$ were considered significant.

RESULTS

Comparison of Patients' Clinical Data

Significant differences in Hoehn-Yahr staging were observed between patients in the three datasets (training set, test set and SWEDD set), but other clinical features were not significantly different, as shown in **Table 1**. However, a family history of PD, impaired olfaction and CD were significantly different between HCs and patients with PD in both the training and test sets, and RBD was significantly different between HCs and patients with PD in the test set. No other significant differences existed, as shown in **Table 2**.

Development and Accuracy of the Radiomic Biomarker

After dimensionality reduction was applied to the 378 extracted features, four features were ultimately selected to construct the radiomics biomarker using logistic regression analysis. Detailed information on the dimensionality reduction process and features is provided in the **Supplementary Materials**. The rad-score was calculated from the formula for the radiomics biomarker, and it displayed favorable predictive efficacy in the training and test sets (the area under the curve (AUC) values were 0.838 and 0.826, respectively; the specificity was 83.8 and 84.3%, respectively; and the sensitivity was 71.8 and 74.5%, respectively). In addition, the nonmotor symptoms of patients with PD were compared using the rad-score. We observed a significant difference in rad-scores between patients with PD without olfactory disturbances and patients with PD and olfactory impairment, as illustrated in **Figure 4**.

Development of an Integrative Nomogram

A family history of PD, impaired olfaction, CD and radiomics biomarkers were independent predictors of PD according to the univariate logistic regression analysis. ROC curves showed that radiomics biomarkers had the highest diagnostic efficacy among these independent predictors (**Figure 5**). Then, impaired olfaction, CD and radiomics biomarkers were selected as the factors to construct the integrated model using a stepwise logistic regression analysis, as shown in **Table 3**. Based on three independent predictors, five machine learning methods were used to construct the model. The AUC values of the SVM, Bayes, logistic regression, random forest, and decision tree classifiers in the training set were 0.927, 0.903, 0.937, 0.914, and 0.897, respectively. The predictive performance of the different machine learning methods is presented in the **Supplementary Material**. The DeLong test showed a

TABLE 2 | Clinical characteristics of the training and test sets.

Variable		Training set ($n = 234$)			Test set ($n = 102$)		
		HC ($n = 117$)	PD ($n = 117$)		HC ($n = 51$)	PD ($n = 51$)	
		n (%)	*n* (%)	*P*-value	*n* (%)	*n* (%)	*P*-value
Sex	Male	75 (64.1)	71 (60.7)	0.589	31 (60.8)	33 (64.7)	0.682
	Female	42 (35.9)	46 (39.3)		20 (39.2)	18 (35.3)	
Age	Years	62.5 ± 9.9	61.4 ± 9.7	0.417	60.7 ± 9.1	62.1 ± 10	0.473
Family history of PD	No	105 (89.7)	91 (77.8)	0.013*	49 (96.1)	39 (76.5)	0.004*
	Yes	12 (10.3)	26 (22.2)		2 (3.9)	12 (23.5)	
Impaired olfaction	No	78 (66.7)	14 (12)	<0.0001*	27 (52.9)	6 (11.8)	<0.0001*
	Yes	39 (33.3)	103 (88)		24 (47.1)	45 (88.2)	
Depression	No	108 (92.3)	103 (88)	0.272	43 (84.3)	42 (82.4)	0.79
	Yes	9 (7.7)	14 (12)		8 (15.7)	9 (17.6)	
RBD	No	88 (75.2)	83 (70.9)	0.461	40 (78.4)	30 (58.8)	0.033*
	Yes	29 (24.8)	34 (29.1)		11 (21.6)	21 (41.2)	
EDS	No	99 (84.6)	92 (78.6)	0.237	41 (80.4)	43 (84.3)	0.603
	Yes	18 (15.4)	25 (21.4)		10 (19.6)	8 (15.7)	
CD	No	114 (97.4)	93 (79.5)	<0.0001*	51 (100)	38 (74.5)	<0.0001*
	Yes	3 (2.6)	24 (20.5)		0 (0)	13 (25.5)	

*RBD, rapid eye movement sleep behavior disorder; EDS, excessive daytime sleepiness; CD, cognitive decline. P-values, significance levels of differences in variables between the training and test sets. The values in parentheses indicate the percentage of each variable in the training set or test set. *P < 0.05.*

significant difference in the AUC value of the logistic regression model compared with the other machine learning methods. Accordingly, the logistic regression classifier was used to build the models and develop an integrative nomogram, as depicted in **Figure 6**.

Performance of the Nomogram

The calibration curves showed the consistency between the predicted PD probability and the actual PD probability for the nomogram in both the training and testing sets. The Hosmer-Lemeshow test did not reveal a significant difference between the performance of the nomogram in the training and testing sets ($P > 0.05$), indicating the lack of a deviation from the fit. The accuracy, specificity, and sensitivity of the nomogram for identifying PD were 0.937, 83.8, and 84.6%, respectively, for the training set and 0.922, 88.2, and 82.4%, respectively, for the test set. The DCA curves also showed good net benefits, which indicated the superior diagnostic accuracy of the nomogram, as indicated in **Figure 7**. The integrative nomogram showed good classification results in the datasets containing patients with PD and SWEDD from the PPMI. The AUC, sensitivity and specificity were 0.836, 70.69, and 91.38%, respectively. Finally, the dataset was divided into a high-risk group and a low-risk group according to the best diagnostic threshold of the nomogram (cutoff value: 0.2862), and the chi-square test revealed a significant difference in the number of patients with PD between the high-risk group and the low-risk group ($\chi^2 = 40.474$, $\phi = 0.5847$, $P < 0.001$; **Figure 8**).

DISCUSSION

Our results show a difference in the value of radiomic biomarkers based on whole-brain white matter between patients with PD and HCs, suggesting that the microstructure of the WM in patients with PD is altered at the early disease stage (Rektor et al., 2018). Furthermore, the difference in the rad-score in the olfactory subgroup suggested that WM damage might be a risk factor for impaired olfaction. In addition, the integrative nomogram showed good performance for identifying patients with early-stage PD, particularly in the SWEDD dataset. We believe that the diagnostic model for PD will be expanded in the future, particularly given the convenience and speed of using the nomogram in the clinic.

Brain MRI is commonly used in clinical practice to evaluate the structural anatomy and pathology of the brain and is also used in the diagnostic workup of PD to exclude the presence of subcortical vascular pathology or other causes of secondary parkinsonism and to differentiate PD from atypical parkinsonism (Heim et al., 2017). However, conventional MRI does not increase the diagnostic value when the clinical diagnosis is uncertain, which is particularly true in the early stages of PD (Brooks, 2000; Meijer et al., 2012). Encouragingly, we were able to use T1-weighted images to identify patients with PD in the present study, which will further expand the application of conventional MRI sequences for the early diagnosis of PD. Similar studies using T2-weighted imaging (T2WI) from conventional MRI have constructed a radiomic model to distinguish patients with PD from HCs (Liu et al., 2020); however, the authors manually placed regions of interest at the caudate nucleus and putamen, which is a very subjective and time-consuming process. These

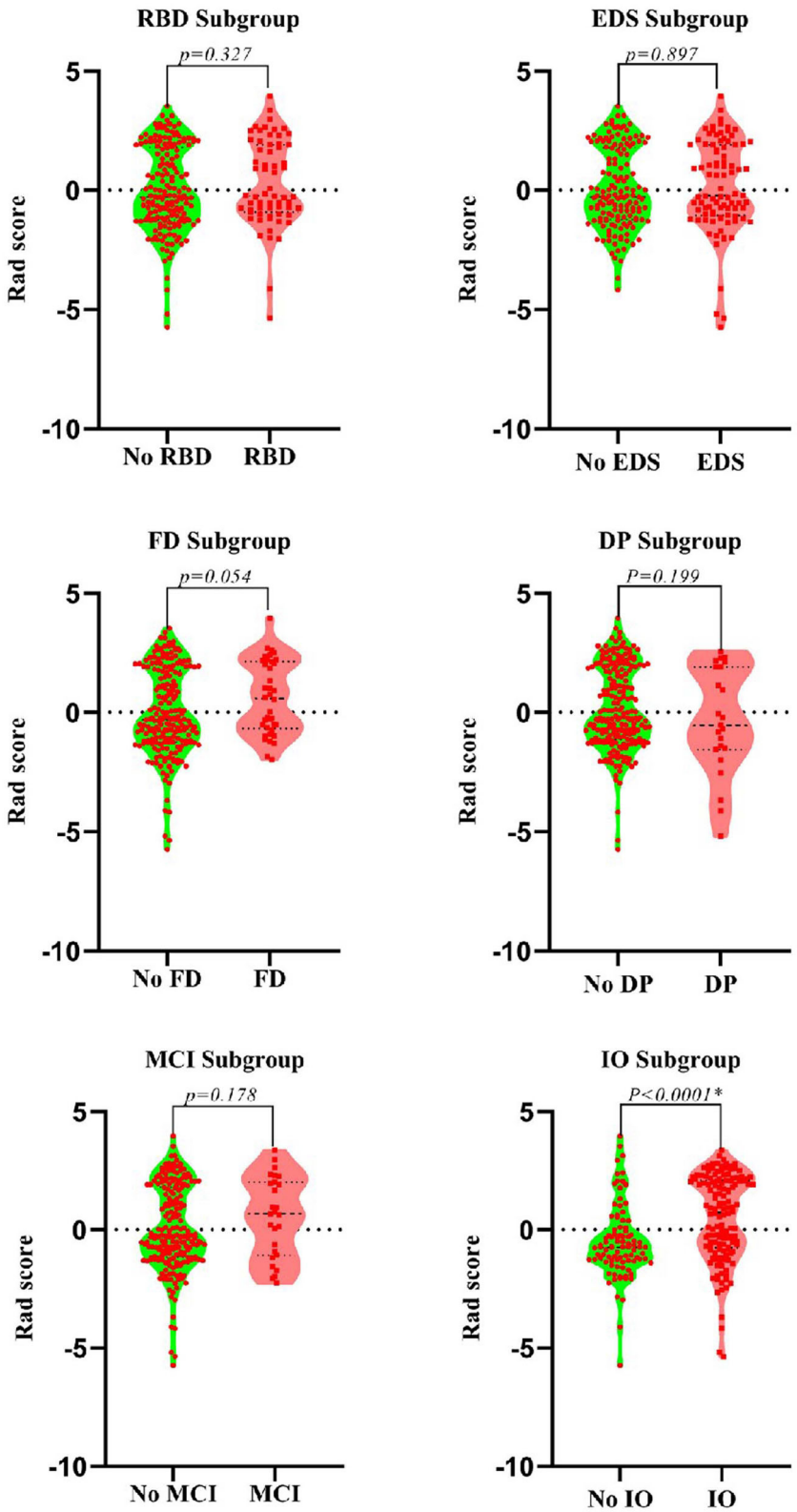

FIGURE 4 | Violin plots of subgroups of patients stratified by non-motor symptoms. The blue line represents the median, and the red lines represent the first and third quartiles. RBD, rapid eye movement sleep behavior disorder; EDS, excessive daytime sleepiness; FD, family history of PD; DP, depression; CD, cognitive decline; IO, impaired olfaction.

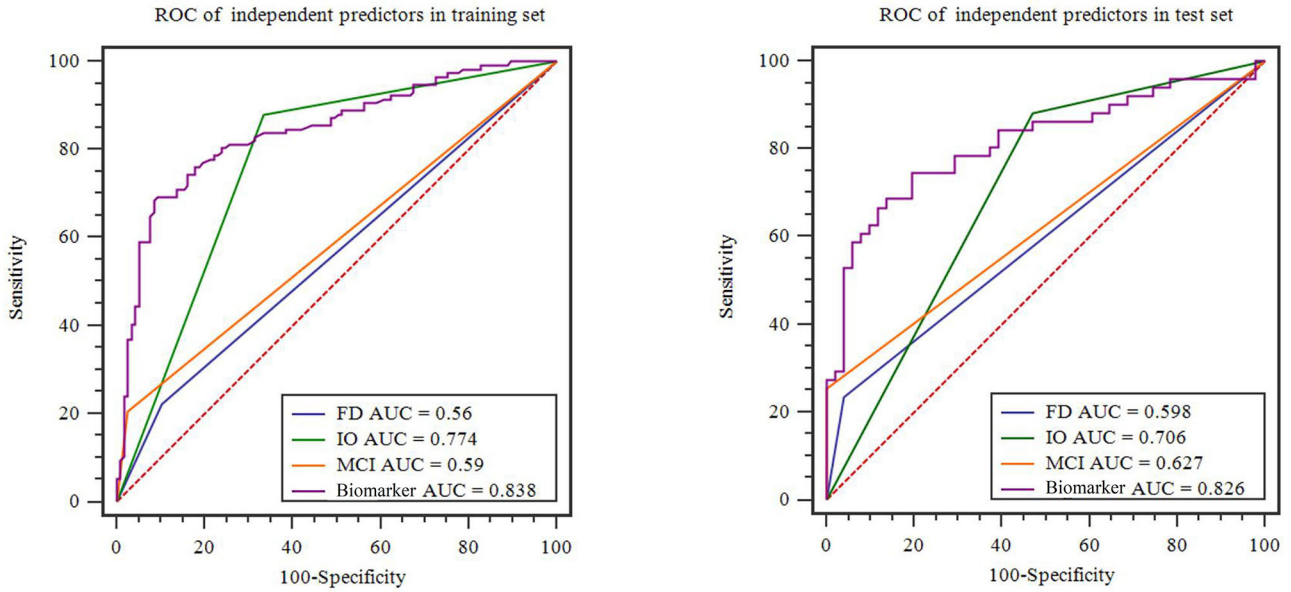

FIGURE 5 | Diagnostic accuracy of the independent predictors in the training and test sets. FD, family history of PD; CD, cognitive decline; IO, impaired olfaction.

TABLE 3 | Stepwise logistic regression analysis of the nomogram for PD prediction.

Variable	Univariate logistic regression analysis		Multivariate logistic regression analysis	
	OR (95% CI)	*P*-value	OR (95% CI)	*P*-value
Sex (male vs. female)	1.237 (0.52–2.943)	0.631	NA	NA
Age (per 1-year increase)	0.97 (0.928–1.015)	0.19	NA	NA
Family history of PD (No vs. Yes)	2.5 (1.194–5.237)	0.015*	NA	NA
Impaired olfaction (No vs. Yes)	16.992 (6.51–44.352)	<0.0001*	16.251 (6.549–40.326)	<0.0001*
Depression (No vs. Yes)	1.557 (0.382–6.337)	0.537	NA	NA
RBD (No vs. Yes)	0.719 (0.277–1.863)	0.497	NA	NA
EDS (No vs. Yes)	1.297 (0.427–3.936)	0.646	NA	NA
CD (No vs. Yes)	23.783 (3.34–169.356)	0.002*	28.34 (4.441–180.874)	<0.0001*
Radiomic score (per 0.1 increase)	2.9 (2.108–3.99)	<0.0001*	2.934 (2.145–4.013)	<0.0001*

*NA, not available, as the variable was not included in the multivariate logistic regression analysis; RBD, rapid eye movement sleep behavior disorder; EDS, excessive daytime sleepiness; CD, cognitive decline. The P value indicates whether the variable is an independent predictor of PD, and * represents P < 0.05.*

structures are also very small, and the segmentation is not sufficiently accurate. Overall, imaging WM is very accessible and inexpensive in clinical practice compared to imaging of the caudate nucleus and putamen. In addition, we inferred that PD might tend to cause greater damage in WM than other neurological degenerative diseases, as evidenced by the excellent performance of the WM-based radiomics integrative nomogram for distinguishing patients with PD from patients with SWEDD. This increased performance may be due to WM changes that likely represent axonal degeneration and myelin damage, which often occur early in disease progression (Burke and O'Malley, 2013) and support our hypothesis. Interestingly, WM is not the main pathological substrate of PD, and the difference in radiomics features further confirms the existence of a compensatory mechanism in the brain tissue in response to early-stage PD (Mizuno et al., 2010), which will be studied in the future.

Adeli et al. combined MRI and SPECT and achieved a PD diagnostic accuracy of 97.5% (Adeli et al., 2017). Obviously, this figure exceeds the predictive accuracy reported in the current study, but the accuracy reported in the previous study mainly depended on the SPECT data, whereas the results of our study mainly depended on MRI data alone. In our results, the diagnostic efficiency of the radiomic biomarker based on MRI was 83.8%, much higher than the value for other nonmotor symptoms. Nonetheless, the diagnostic efficiency of radiomic biomarkers was lower in the present study than that the study by Wu et al. (2019), who showed that the diagnostic efficiency of radiomic biomarkers based on 18F-FDG PET images was 90.97%. However, because PET is not widely used in routine

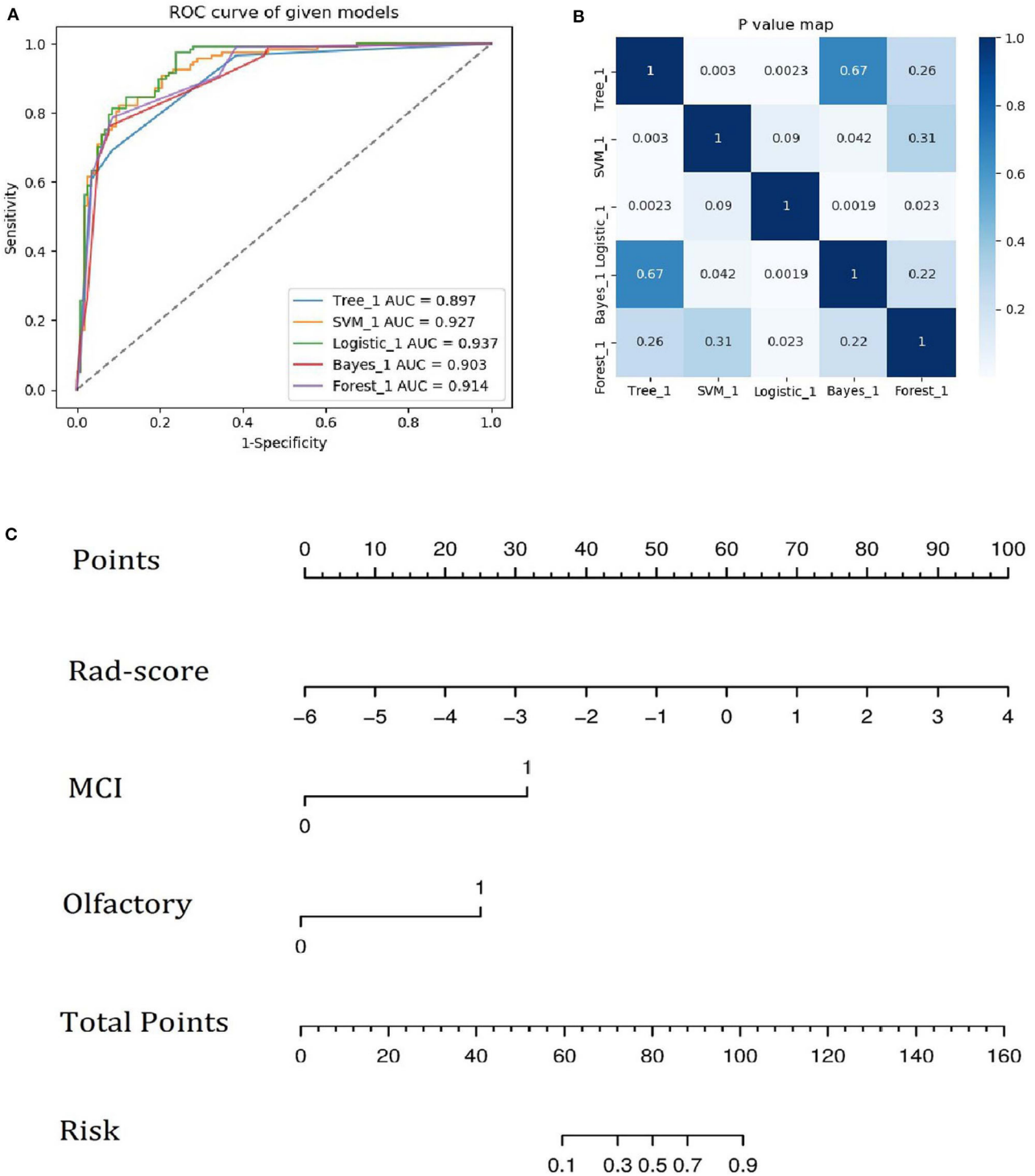

FIGURE 6 | (A) ROC curves of the five machine learning methods. **(B)** Heatmap of *p*-values obtained using the model compared with each of the other machine learning methods based on the DeLong test. **(C)** Integrative nomogram used to detect PD. The nomogram was developed using the training set. In the nomogram, a vertical line is first generated according to the value of the rad-score to determine the corresponding score. Similarly, the scores for CD and olfaction are also determined. Then, the total score is calculated as the sum of the three scores described above. Finally, a vertical line is generated according to the value of the total score to determine the probability of PD.

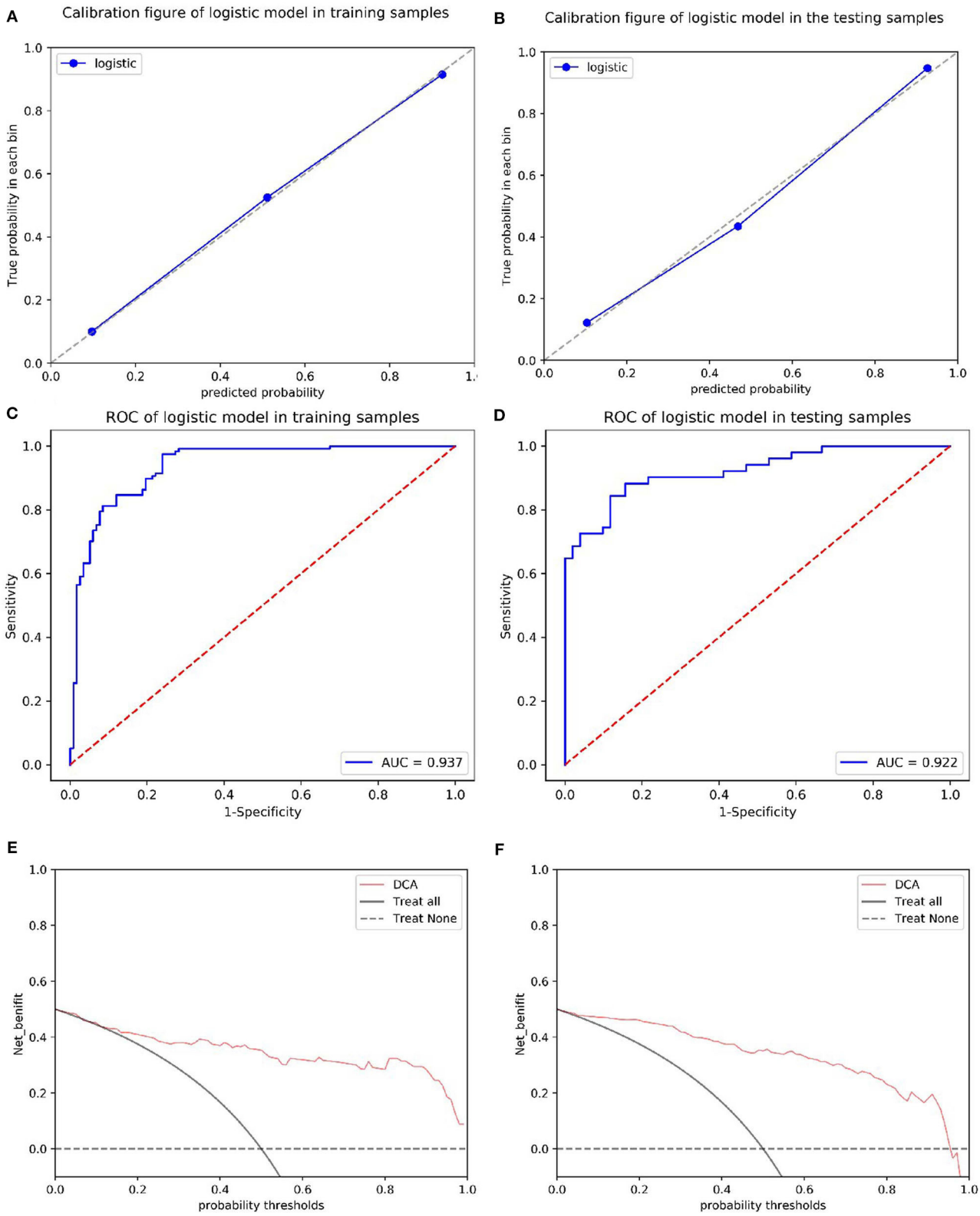

FIGURE 7 | Calibration of the radiomics nomogram for PD in the training and test sets **(A,B)**. The dashed line represents the reference line where an ideal biomarker would lie, the dotted line represents the performance of the biomarker, and the solid line corrects for any bias in the biomarker. ROC curves of the radiomics

(Continued)

FIGURE 7 | nomogram for detecting the presence of PD in the training and test sets **(C,D)**. A DCA was performed to show the clinical effectiveness of the nomogram in predicting the presence of PD in patients included in the training and test sets **(E,F)**. The y-axis represents the net benefit. The pink line represents the radiomics nomogram. The solid black line represents the hypothesis that all patients had PD. The black dotted line represents the hypothesis that no patients had PD. The x-axis represents the threshold probability. The threshold probability is where the expected benefit of treatment is equal to the expected benefit of avoiding treatment. For example, if the possibility of PD in a patient is over the threshold probability, then a treatment strategy for PD should be adopted. The decision curves for the test set showed that if the threshold probability is between 0 and 0.88, then the use of the radiomic nomogram to predict PD provides a greater benefit than treating either all or none of the patients.

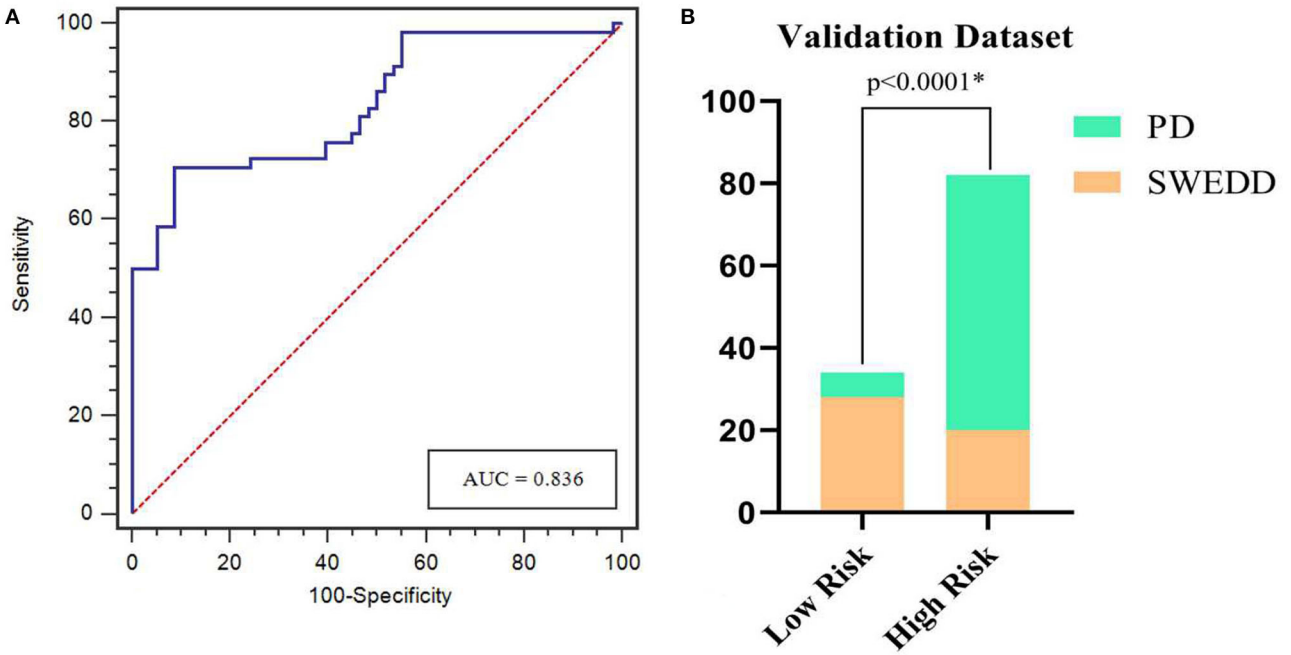

FIGURE 8 | ROC curves for the nomogram in predicting PD in the validation dataset **(A)**. Bar plots show a significantly higher incidence of PD in the high-risk group than in the low-risk group **(B)**. *represents $p < 0.05$.

clinical practice, the method may lack practicality. Of course, we should not ignore the other factors that were used to build the model, including CD and impaired olfaction, which also contributed substantially to the model. In fact, impaired olfaction is one of the most common and typical nonmotor disorders associated with PD (Fullard et al., 2017), and most patients with PD develop an impairment of olfaction 4–6 years before they start to present motor impairment (Reichmann, 2017). This finding may also explain why olfactory impairment is the only non-motor symptom displaying statistically significant differences in the scores of the radiomics biomarker in patients with PD, and a deterioration in the sense of smell has been postulated to reflect extrastriatal neurodegeneration in patients with PD (Schrag et al., 2017). Accordingly, we speculate that olfactory damage may also reflect early changes in the WM microstructure, but further research is needed.

The advantages of the nomogram are also reflected in other aspects of this study. We analyzed 3D WM images, while most previous studies were based largely on a cross-sectional analysis of the SN (Takahashi et al., 2018; Cheng et al., 2019; Li et al., 2019). Nevertheless, a cross-sectional image of the SN may not completely reflect the early typical pathological changes associated with PD, and larger whole-brain changes will likely give a better representation of the global alterations associated with the disease. Four radiomic features were selected in the present study, including two features of RLM. In a previous study, RLM features, which reflect roughness and directionality, were also associated with the progression of white matter hyperintensity (WMH) (Li et al., 2017). Directionality refers to a specific route or angle of the nerve fasciculus. In normal WM, nerve fibers are properly oriented and regulated; nevertheless, when myelin is damaged, the neural structure may be disrupted (Yu et al., 2004), consistent with the white matter damage observed even in patients with early-stage PD in previous studies using advanced MRI technologies, such as DTI (Bergamino et al., 2020; Sanjari Moghaddam et al., 2020), showing that structural changes in the WM may underlie the clinical and pathologic heterogeneity of PD and cause relative cognitive impairment. Therefore, WM is a promising brain tissue to provide new insights that will be important for the early diagnosis of PD.

The correction curve and DCA showed the stability and clinical diagnostic benefits of the nomogram (AUC of 0.937),

but the sensitivity of the nomogram may still be lower than that of cerebrospinal fluid, which was the first identified biomarker of PD (Olsson et al., 2016). As shown in a similar study, early diagnosis of PD based on a cerebrospinal fluid model constructed using machine learning achieved a sensitivity of 90% (Dos Santos et al., 2018). Regardless, the nomogram used in this study as a noninvasive evaluation tool may be more suitable for clinical application than invasive detection of cerebrospinal fluid. Furthermore, the accuracy of the nomogram decreased from 0.937 to 0.836 when applied to patients with SWEDD compared with HCs. We speculate that this decrease may be due to early microstructural changes in WM caused by other neurological diseases in patients included in the SWEDD dataset, and similar to patients with early-stage PD, these changes were accelerated. However, the difference between patients with PD and patients with SWEDD is likely attributable to the lack of dopaminergic neurons (Wyman-Chick et al., 2016); therefore, the model will undoubtedly further reflect the pathological mechanism of dopaminergic damage (Liu et al., 2018). Additionally, participants classified as having SWEDD who would later be diagnosed with PD might be distinguished from patients who would not develop PD. The nomogram was able to discriminate patients without evidence of dopaminergic deficits typical of PD from patients with other neurological disorders, which might be useful to clinicians, particularly when the nomogram is combined with imaging data.

Despite the overall positive results presented here, the current study still has some limitations. First, regarding the samples used for external verification, a larger sample size from multiple research centers is needed to verify and improve the results of the present study. Second, the patients with PD who were included in this study may have been in different neurological disease stages, and differences in WM features were still observed between patients with PD and HCs (the severity of PD did not appear to affect the results of this study). Final, we did not consider the possible effect of chronic dopaminergic medications on our results; the regimen of neuropsychiatric medications provided to patients during illnesses potentially affects brain structures (Zeng et al., 2015). Nevertheless, analysis of this cohort enabled us to establish a preliminary nomogram, facilitating the future consideration of long-term medication use in a larger and more diverse prospective study.

Although early diagnosis of PD is still based on clinical criteria, the advent of integrative nomograms will provide an imaging measure that can detect early-stage PD and may serve as a basis for future disease prediction studies in longitudinal cohorts.

DATA AVAILABILITY STATEMENT

Publicly available datasets were analyzed in this study. This data can be found at: http://www.ppmi-info.org.

ETHICS STATEMENT

The study was approved by the institutional review board and the Zhejiang provincial ethics committee. Written informed consent for participation was not required for this study in accordance with the national legislation and the institutional requirements.

AUTHOR CONTRIBUTIONS

ZS, YX, and MZ contributed to the conception and design of the study. ZS, YX, SC, XW, and PP performed the data acquisition and analysis. ZS and YX wrote and revised the manuscript. All authors contributed to the article and approved the submitted version.

FUNDING

This work was supported by grants from the Health Commission for Zhejiang Province (Grant numbers: 2020KY039 and 2020KY402).

SUPPLEMENTARY MATERIAL

The Supplementary Material for this article can be found online at: https://www.frontiersin.org/articles/10.3389/fnagi.2020.548616/full#supplementary-material

REFERENCES

Adeli, E., Wu, G., Saghafi, B., An, L., Shi, F., and Shen, D. (2017). Kernel-based joint feature selection and max-margin classification for early diagnosis of parkinson's disease. *Sci. Rep.* 7:41069. doi: 10.1038/srep41069

Agosta, F., Galantucci, S., and Filippi, M. (2017). Advanced magnetic resonance imaging of neurodegenerative diseases. *Neurol. Sci.* 8, 41–51. doi: 10.1007/s10072-016-2764-x

Ashburner, J. (2009). Computational anatomy with the SPM software. *Magn. Reson. Imaging* 27, 1163–1174. doi: 10.1016/j.mri.2009.01.006

Benzagmout, M., Boujraf, S., Alami, B., Amadou, H. A., El Hamdaoui, H., Bennani, A., et al. (2019). Emotion processing in parkinson's disease: a blood oxygenation level-dependent functional magnetic resonance imaging study. *Neural Regen. Res.* 14, 666–672. doi: 10.4103/1673-5374.247470

Bergamino, M., Keeling, E. G., Mishra, V. R., Stokes, A. M., and Walsh, R. R. (2020). Assessing white matter pathology in early-stage parkinson disease using diffusion MRI: a systematic review. *Front. Neurol.* 11:314. doi: 10.3389/fneur.2020.00314

Brooks, D. J. (2000). Morphological and functional imaging studies on the diagnosis and progression of parkinson's disease. *J. Neurol.* 247(Suppl. 2), II11–8. doi: 10.1007/PL00007755

Burke, R. E., and O'Malley, K. (2013). Axon degeneration in parkinson's disease. *Exp. Neurol.* 246, 72–83. doi: 10.1016/j.expneurol.2012.01.011

Chen, R., Liu, X., Jin, S., Lin, J., and Liu, J. (2018). Machine learning for drug-target interaction prediction. *Molecules* 23:2208. doi: 10.3390/molecules23092208

Cheng, Z., Zhang, J., He, N., Li, Y., Wen, Y., Xu, H., et al. (2019). Radiomic features of the nigrosome-1 region of the substantia nigra: using quantitative susceptibility mapping to assist the diagnosis of idiopathic parkinson's disease. *Front. Aging Neurosci.* 11:167. doi: 10.3389/fnagi.2019.00167

De Pablo-Fernández, E., Lees, A. J., Holton, J. L., and Warner, T. T. (2019). Prognosis and neuropathologic correlation of clinical subtypes of parkinson disease. *JAMA Neurol.* 76, 470–479. doi: 10.1001/jamaneurol.2018.4377

Dorsey, E. R., Constantinescu, R., Thompson, J. P., Biglan, K. M., Holloway, R. G., Kieburtz, K., et al. (2007). Projected number of people with parkinson disease in the most populous nations, 2005 through 2030. *J. Neurol.* 68, 384–386. doi: 10.1212/01.wnl.0000247740.47667.03

Dos Santos, M. C. T., Scheller, D., Schulte, C., Mesa, I. R., Colman, P., Bujac, S. R., et al. (2018). Evaluation of cerebrospinal fluid proteins as potential biomarkers for early stage parkinson's disease diagnosis. *PLoS ONE* 13:e0206536. doi: 10.1371/journal.pone.0206536

Filippi, M., Elisabetta, S., Piramide, N., and Agosta, F. (2018). Functional MRI in idiopathic parkinson's disease. *Int. Rev. Neurobiol.* 141, 439–467. doi: 10.1016/bs.irn.2018.08.005

Frederick, J. A., and Meijer, B. G. (2014). Brain MRI in parkinson's disease. *Front. Biosci.* 6, 360–369. doi: 10.2741/e711

Fullard, M. E., Morley, J. F., and Duda, J. E. (2017). Olfactory dysfunction as an early biomarker in parkinson's disease. *Neurosci. Bull.* 33, 515–525. doi: 10.1007/s12264-017-0170-x

Guan, X., Xuan, M., Gu, Q., Xu, X., Huang, P., Wang, N., et al. (2017). Influence of regional iron on the motor impairments of parkinson's disease: a quantitative susceptibility mapping study. *J. Magn. Reson. Imaging* 45, 1335–1342. doi: 10.1002/jmri.25434

Heim, B., Krismer, F., De Marzi, R., and Seppi, K. (2017). Magnetic resonance imaging for the diagnosis of parkinson's disease. *J. Neural Transm.* 124, 915–964. doi: 10.1007/s00702-017-1717-8

Kalia, L. V., and Lang, A. E. (2015). Parkinson's disease. *Lancet* 386, 896–912. doi: 10.1016/S0140-6736(14)61393-3

Koirala, N., Anwar, A. R., Ciolac, D., Glaser, M., Pintea, B., Deuschl, G., et al. (2019). Alterations in white matter network and microstructural integrity differentiate parkinson's disease patients and healthy subjects. *Front. Aging Neurosci.* 11:191. doi: 10.3389/fnagi.2019.00191

LeWitt, P. A. (2015). Levodopa therapy for parkinson's disease: pharmacokinetics and pharmacodynamics. *Mov. Disord.* 30, 64–72. doi: 10.1002/mds.26082

Li, G., Zhai, G., Zhao, X., An, H., Spincemaille, P., Gillen, K. M., et al. (2019). 3D texture analyses within the substantia nigra of parkinson's disease patients on quantitative susceptibility maps and R2 maps. *Neuroimage* 188, 465–472. doi: 10.1016/j.neuroimage.2018.12.041

Li, Z., Mao, Y., Huang, W., Li, H., Zhu, J., Li, W., et al. (2017). Texture-based classification of different single liver lesion based on SPAIR T2W MRI images. *BMC Med. Imaging* 17:42. doi: 10.1186/s12880-017-0212-x

Liu, P., Wang, H., Zheng, S., Zhang, F., and Zhang, X. (2020). Parkinson's disease diagnosis using neostriatum radiomic features based on T2-weighted magnetic resonance imaging. *Front. Neurol.* 11:248. doi: 10.3389/fneur.2020.00248

Liu, X. L., Wang, Y. D., Yu, X. M., Li, D. W., and Li, G. R. (2018). Mitochondria-mediated damage to dopaminergic neurons in parkinson's disease (Review). *Int. J. Mol. Med.* 41, 615–623. doi: 10.3892/ijmm.2017.3255

Liu, Z., Wang, S., Dong, D., Wei, J., Fang, C., Zhou, X., et al. (2019). The applications of radiomics in precision diagnosis and treatment of oncology: opportunities and challenges. *Theranostics* 9, 1303–1322. doi: 10.7150/thno.30309

Mayerhoefer, M. E., Materka, A., Langs, G., Häggström, I., Szczypiński, P., Gibbs, P., et al. (2020). Introduction to radiomics. *J. Nucl. Med.* 61, 488–495. doi: 10.2967/jnumed.118.222893

Meijer, F. J., Aerts, M. B., Abdo, W. F., Prokop, M., Borm, G. F., Esselink, R. A., et al. (2012). Contribution of routine brain MRI to the differential diagnosis of parkinsonism: a 3-year prospective follow-up study. *J. Neurol.* 259, 929–935. doi: 10.1007/s00415-011-6280-x

Mielke, M. M., and Maetzler, W. (2014). A 'bird's eye' view on the current status and potential benefits of blood biomarkers for parkinson's disease. *Biomark. Med.* 8, 225–227. doi: 10.2217/bmm.13.139

Miller, D. B., and O'Callaghan, J. P. (2015). Biomarkers of parkinson's disease: present and future. *Metabolism* 64(3 Suppl. 1), S40–S46. doi: 10.1016/j.metabol.2014.10.030

Mizuno, Y., Hasegawa, K., Kondo, T., Kuno, S., Yamamoto, M., and Japanese istradefylline Study Group. (2010). Clinical efficacy of istradefylline (KW-6002) in parkinson's disease: a randomized, controlled study. *Mov. Disord.* 25, 1437–1443. doi: 10.1002/mds.23107

Mukaka, M. M. (2012). Statistics corner: a guide to appropriate use of correlation coefficient in medical research. *Malawi Med. J.* 24, 69–71.

Muthuraman, M., Deuschl, G., Koirala, N., Riedel, C., Volkmann, J., and Groppa, S. (2017). Effects of DBS in parkinsonian patients depend on the structural integrity of frontal cortex. *Sci. Rep.* 7:43571. doi: 10.1038/srep43571

O'Brien, R. M. (2007). A caution regarding rules of thumb for variance inflation factors. *Qual. Quant.* 41, 673–690. doi: 10.1007/s11135-006-9018-6

Olsson, B., Lautner, R., Andreasson, U., Öhrfelt, A., Portelius, E., Bjerke, M., et al. (2016). CSF and blood biomarkers for the diagnosis of alzheimer's disease: a systematic review and meta-analysis. *Lancet Neurol.* 15, 673–684. doi: 10.1016/S1474-4422(16)00070-3

Parkinson Progression Marker Initiative (2011). The parkinson progression marker initiative (PPMI). *Prog. Neurobiol.* 95, 629–635. doi: 10.1016/j.pneurobio.2011.09.005

Pelizzari, L., Di Tella, S., Lagan,à M. M., Bergsland, N., Rossetto, F., Nemni, R., et al. (2020). White matter alterations in early parkinson's disease: role of motor symptom lateralization. *Neurol. Sci.* 41, 357–364. doi: 10.1007/s10072-019-04084-y

Pozorski, V., Oh, J. M., Adluru, N., Merluzzi, A. P., Theisen, F., Okonkwo, O., et al. (2018). Longitudinal white matter microstructural change in parkinson's disease. *Hum. Brain Mapp.* 9, 4150–4161. doi: 10.1002/hbm.24239

Reichmann H. (2017). Premotor diagnosis of Parkinson's Disease. *Neurosci. Bull.* 33, 526–534. doi: 10.1007/s12264-017-0159-5

Rektor, I., Svátková A., Vojtíšek, L., Zikmundová I., Vaníček, J., Király, A., et al. (2018). White matter alterations in parkinson's disease with normal cognition precede grey matter atrophy. *PLoS ONE* 13:e0187939. doi: 10.1371/journal.pone.0187939

Sanjari Moghaddam, H., Dolatshahi, M., Mohebi, F., and Aarabi, M. H. (2020). Structural white matter alterations as compensatory mechanisms in parkinson's disease: a systematic review of diffusion tensor imaging studies. *J. Neurosci. Res.* 98, 1398–1416. doi: 10.1002/jnr.24617

Schrag, A., Siddiqui, U. F., Anastasiou, Z., Weintraub, D., and Schott, J. M. (2017). Clinical variables and biomarkers in prediction of cognitive impairment in patients with newly diagnosed parkinson's disease: a cohort study. *Lancet Neurol.* 16, 66–75. doi: 10.1016/S1474-4422(16)30328-3

Schwarz, S. T., Abaei, M., Gontu, V., Morgan, P. S., Bajaj, N., and Auer, D. P. (2013). Diffusion tensor imaging of nigral degeneration in parkinson's disease: a region-of-interest and voxel-based study at 3 T and systematic review with meta-analysis. *Neuroimage Clin.* 3, 481–488. doi: 10.1016/j.nicl.2013.10.006

Shinde, S., Prasad, S., Saboo, Y., Kaushick, R., Saini, J., Pal, P. K., et al. (2019). Predictive markers for parkinson's disease using deep neural nets on neuromelanin sensitive MRI. *Neuroimage Clin.* 22:101748. doi: 10.1016/j.nicl.2019.101748

Shu, Z., Fang, S., Ding, Z., Mao, D., Cai, R., Chen, Y., et al. (2019). MRI-based radiomics nomogram to detect primary rectal cancer with synchronous liver metastases. *Sci. Rep.* 9:3374. doi: 10.1038/s41598-019-39651-y

Shu, Z., Xu, Y., Shao, Y., Pang, P., and Gong, X. (2020). Radiomics from magnetic resonance imaging may be used to predict the progression of white matter hyperintensities and identify associated risk factors. *Eur. Radiol.* 30:3046–3058. doi: 10.1007/s00330-020-06676-1

Sun, R., Limkin, E. J., Vakalopoulou, M., Dercle, L., Champiat, S., Han, S. R., et al. (2018). A radiomics approach to assess tumour-infiltrating CD8 cells and response to anti-PD-1 or anti-PD-L1 immunotherapy: an imaging biomarker, retrospective multicohort study. *Lancet Oncol.* 19, 1180–1191. doi: 10.1016/S1470-2045(18)30413-3

Takahashi, H., Watanabe, Y., Tanaka, H., Mihara, M., Mochizuki, H., Takahashi, K., et al. (2018). Comprehensive MRI quantification of the substantia nigra pars compacta in parkinson's disease. *Eur. J. Radiol.* 109, 48–56. doi: 10.1016/j.ejrad.2018.06.024

Trojano, L., and Papagno, C. (2018). Cognitive and behavioral disorders in parkinson's disease: an update. II: behavioral disorders. *Neurol. Sci.* 39, 53–61. doi: 10.1007/s10072-017-3155-7

Tzarouchi, L. C., Astrakas, L. G., Konitsiotis, S., Tsouli, S., Margariti, P., Zikou, A., et al. (2010). Voxel-based morphometry and Voxel-based relaxometry in Parkinsonian variant of multiple system atrophy. *J. Neuroimaging* 20, 260–266. doi: 10.1111/j.1552-6569.2008.00343.x

Watson, D. S., Krutzinna, J., Bruce, I. N., Griffiths, C. E., McInnes, I. B., Barnes, M. R., et al. (2019). Clinical applications of machine learning algorithms: beyond the black box. *BMJ* 364:l886. doi: 10.1136/bmj.l886

Wu, J., Aguilera, T., Shultz, D., Gudur, M., Rubin, D. L., Loo, B. W. Jr, et al. (2016). Early-stage non-small cell lung cancer: quantitative imaging characteristics of 18F fluorodeoxyglucose PET/CT allow prediction of distant metastasis. *Radiology* 281, 270–278. doi: 10.1148/radiol.2016151829

Wu, Y., Jiang, J. H., Chen, L., Lu, J. Y., Ge, J. J., Liu, F. T., et al. (2019). Use of radiomic features and support vector machine to distinguish parkinson's disease cases from normal controls. *Ann. Transl. Med.* 7:773. doi: 10.21037/atm.2019.11.26

Wyman-Chick, K. A., Martin, P. K., Minár, M., and Schroeder, R. W. (2016). Cognition in patients with a clinical diagnosis of parkinson disease and scans without evidence of dopaminergic deficit (SWEDD):2-year follow-up. *Cogn. Behav. Neurol.* 29, 190–196. doi: 10.1097/WNN.0000000000000107

Yu, O., Steibel, J., Mauss, Y., Guignard, B., Eclancher, B., Chambron, J., et al. (2004). Remyelination assessment by MRI texture analysis in a cuprizone mouse model. *Magn. Reson. Imaging* 22, 1139–1144. doi: 10.1016/j.mri.2004.08.017

Zeng, L. L., Shen, H., Liu, L., Fang, P., Liu, Y., and Hu, D. (2015). State-dependent and trait-related gray matter changes in nonrefractory depression. *NeuroReport* 26, 57–65. doi: 10.1097/WNR.0000000000000301

Conflict of Interest: PP was employed by GE Healthcare.

The remaining authors declare that the study was conducted in the absence of any commercial or financial relationships that could be construed as a potential conflict of interest.

frontiers in Aging Neuroscience

ORIGINAL RESEARCH
published: 14 January 2021
doi: 10.3389/fnagi.2020.621947

NeuroExercise: The Effect of a 12-Month Exercise Intervention on Cognition in Mild Cognitive Impairment—A Multicenter Randomized Controlled Trial

Tim Stuckenschneider[1,2†], Marit L. Sanders[3,4†], Kate E. Devenney[5†], Justine A. Aaronson[4,6], Vera Abeln[1], Jurgen A. H. R. Claassen[3,4], Emer Guinan[5], Brian Lawlor[7], Romain Meeusen[8], Christian Montag[9], Marcel G. M. Olde Rikkert[3,4], M. Cristina Polidori[10], Martin Reuter[11,12], Ralf-Joachim Schulz[13], Tobias Vogt[14,15], Bernd Weber[11], Roy P. C. Kessels[4,6‡] and Stefan Schneider[1,2†‡] on behalf of the NeuroExercise Study Group*

[1] Institute of Movement and Neurosciences, German Sport University, Cologne, Germany, [2] VasoActive Research Group, School of Health and Sport Sciences, University of the Sunshine Coast, Maroochydore, QLD, Australia, [3] Department of Geriatric Medicine, Radboudumc Alzheimer Center, Radboud University Medical Center, Nijmegen, Netherlands, [4] Donders Institute for Brain Cognition and Behavior, Nijmegen, Netherlands, [5] Discipline of Physiotherapy, Trinity College, Dublin, Ireland, [6] Department of Medical Psychology, Radboud University Medical Center, Nijmegen, Netherlands, [7] Mercer's Institute for Successful Aging, St. James's Hospital and Global Brain Health Institute, Trinity College, Dublin, Ireland, [8] Department of Human Physiology & Sports Medicine, Vrije Universiteit Brussel, Brussels, Belgium, [9] Department of Molecular Psychology, Institute of Psychology and Education, Ulm University, Ulm, Germany, [10] Aging Clinical Research, Department II of Internal Medicine and Center for Molecular Medicine Cologne, Faculty of Medicine and University Hospital Cologne, University of Cologne, Cologne, Germany, [11] Center for Economics and Neuroscience, University of Bonn, Bonn, Germany, [12] Department of Psychology, University of Bonn, Bonn, Germany, [13] Geriatrics Department, University of Cologne Medical Faculty, Cologne, Germany, [14] Institute of Professional Sport Education and Sport Qualifications, German Sport University, Cologne, Germany, [15] Waseda University, Faculty of Sport Sciences, Tokorozawa, Japan

Exercise intervention studies in mild cognitive impairment (MCI), a prodromal stage of Alzheimer's disease (AD), have demonstrated inconsistent yet promising results. Addressing the limitations of previous studies, this trial investigated the effects of a 12-month structured exercise program on the progression of MCI. The NeuroExercise study is a multicenter randomized controlled trial across three European countries (Ireland, Netherlands, Germany). Hundred and eighty-three individuals with amnestic MCI were included and were randomized to a 12-month exercise intervention (3 units of 45 min) of either aerobic exercise (AE; $n = 60$), stretching and toning exercise (ST; $n = 65$) or to a non-exercise control group (CG; $n = 58$). The primary outcome, cognitive performance, was determined by an extensive neuropsychological test battery. For the primary complete case (CC) analyses, between-group differences were analyzed with analysis of covariance under two conditions: (1) the exercise group (EG = combined AE and ST groups) compared to the CG and (2) AE compared to ST. Primary analysis of the full cohort ($n = 166$, 71.5 years; 51.8% females) revealed no between-group differences in composite cognitive score [mean difference (95% CI)], 0.12 [(−0.03, 0.27), $p = 0.13$] or in any cognitive domain or quality of life. VO_2 peak was significantly higher in the EG compared to the CG after 12 months [−1.76 (−3.39, −0.10), $p = 0.04$]. Comparing

OPEN ACCESS

Edited by:
Jiehui Jiang, Shanghai University, China

Reviewed by:
Takashi Tarumi, University of Texas Southwestern Medical Center, United States
Binu Panjikattil Thomas, University of Texas Southwestern Medical Center, United States

***Correspondence:**
Stefan Schneider
schneider@dshs-koeln.de

[†] *These authors have contributed equally to this work and share first authorship*

[‡] *These authors have contributed equally to this work*

Received: 27 October 2020
Accepted: 11 December 2020
Published: 14 January 2021

Citation:
Stuckenschneider T, Sanders ML, Devenney KE, Aaronson JA, Abeln V, Claassen JAHR, Guinan E, Lawlor B, Meeusen R, Montag C, Olde Rikkert MGM, Polidori MC, Reuter M, Schulz R-J, Vogt T, Weber B, Kessels RPC and Schneider S (2021) NeuroExercise: The Effect of a 12-Month Exercise Intervention on Cognition in Mild Cognitive Impairment—A Multicenter Randomized Controlled Trial. Front. Aging Neurosci. 12:621947. doi: 10.3389/fnagi.2020.621947

the two intervention groups revealed a higher VO_2peak level in the aerobic exercise compared to the stretching and toning group, but no differences for the other outcomes. A 12-month exercise intervention did not change cognitive performance in individuals with amnestic MCI in comparison to a non-exercise CG. An intervention effect on physical fitness was found, which may be an important moderator for long term disease progression and warrants long-term follow-up investigations.

Clinical Trial Registration: https://clinicaltrials.gov/ct2/show/NCT02913053, identifier: NCT02913053.

Keywords: Alzheimer's disease, non-pharmacological treatment, aerobic exercise, cognition, quality of life

INTRODUCTION

Worldwide, over 46 million people are living with dementia, with the numbers expected to rise to approximately 74 million by 2030 (Prince et al., 2015). The prevalence of mild cognitive impairment (MCI), a stage of cognitive impairment with minimal functional loss that is often, but not always, a prodromal stage of dementia (McKhann et al., 2011), is 6.7% for ages 60–64 and rises to 25.2% for ages 80–84 (Albert et al., 2011; Petersen et al., 2018). Clinicians and researchers differentiate between amnestic MCI (aMCI), which describes the dominance of memory impairments and is most likely to transition to dementia due to Alzheimer's disease (AD), and non-amnestic MCI, which is characterized by an impairment in other cognitive domains (e.g., language, visuospatial) (Petersen, 2004). Individuals with both aMCI or non-amnestic MCI have a cumulative risk of 14.9% of developing dementia within 2 years (Petersen, 2004; Winblad et al., 2004; Petersen et al., 2018). As such, cognitive decline due to dementia is a key contributor to the significant economic impact of an aging population (Prince et al., 2015), and is identified as a global health and healthcare priority.

If a primary prevention strategy could delay conversion to dementia by even two years, it would reduce the total number of patients living with dementia and have substantial public health, economic and societal benefits (Vickland et al., 2010; Brodaty et al., 2011; Sperling et al., 2011), further highlighting the importance of early detection and treatment of cognitive decline. Currently, there is no proven treatment for people with MCI that delays progression to dementia. However, the recently updated practice guidelines of the American Academy of Neurology (AAN) for the treatment of MCI suggest that exercise is a promising non-pharmacological strategy to improve cognitive function in individuals with MCI (Petersen et al., 2018). This recommendation was underpinned by only two studies that investigated the effect of a 6-month multicomponent exercise or resistance exercise intervention on the progression of MCI and demonstrated a positive effect on domain-specific cognitive function (attention and episodic memory) (Nagamatsu et al., 2012; Suzuki et al., 2012). Furthermore, the results from four systematic reviews recommend exercise as a promising treatment option and included different exercise modes from multicomponent exercises to tai chi in their reviews (Ohman et al., 2014; Wang et al., 2014; Zheng et al., 2016; Song et al., 2018). Whereas three of them recommend aerobic exercise as probably the most effective form of exercise to maintain or improve cognitive function in individuals with MCI (Ohman et al., 2014; Zheng et al., 2016; Song et al., 2018), the other one did not define the type of exercise more specifically (Wang et al., 2014). However, these reviews recommend larger sample sizes, standardized neuropsychological testing, longer intervention periods and well-defined MCI diagnostic criteria, as these were methodological issues limiting previous studies. A recent study by Tarumi and colleagues compared 12 months of either stretching or aerobic exercise training in individuals with aMCI and concluded that both exercise modes improved executive and memory functions (Tarumi et al., 2019). However, the authors did not include a non-exercise control group, which precludes a direct comparison with their trial. Moreover, the two studies included in the AAN guideline included only women or less than 100 participants, which limits their external validity (Nagamatsu et al., 2012; Suzuki et al., 2012).

The multicenter NeuroExercise project addressed these limitations by strictly recruiting participants with aMCI, increasing the sample size compared to previous studies, extending the intervention period, involving three different countries and bringing together experts from clinical and exercise intervention trials (Devenney et al., 2017). The aim of the NeuroExercise project was to investigate the effects of a 12-month structured exercise program (either aerobic exercise or stretching and toning exercises) on the progression of cognitive decline in MCI compared to a control group. We hypothesized that participation in an extensive exercise program, of either aerobic exercise or stretching and toning exercises, would demonstrate a slower rate of cognitive decline compared to the control group.

METHODS

Trial Overview, Standard Protocol Approvals, and Registrations

The NeuroExercise project was a randomized controlled trial performed in three centers in Europe; the German Sport University Cologne, Germany, Radboud University Medical Center, Nijmegen, the Netherlands and at St. James's Hospital and Trinity College Dublin, Ireland. Participants were randomized to either a yearlong supervised and home-based aerobic exercise

program, an equivalent non-aerobic stretching and toning program or to a control group using a centrally controlled computer-generated randomization list (for each country), controlled by an independent statistician.

The ethics committee of the German Sport University, Cologne Germany, the Commisie Mensgebonden Onderzoek Arnhem-Nijmegen, Netherlands, and the Tallaght Hospital/St. James's Hospital Joint Research Ethics Committee Dublin Ireland, approved the study protocol, which has been described previously (Devenney et al., 2017). All participants provided written informed consent to participate in accordance with the provisions of the Declaration of Helsinki. Participants were recruited between October 2015 and September 2017. The trial is registered at Clinicaltrials.gov (trial registration number: NCT02913053).

Participants and Study Procedure

Sedentary adults aged 50 years or older diagnosed with aMCI were recruited via hospital memory clinics affiliated with the three sites and from the community via advertisements in local newspapers. Eligibility criteria for inclusion were: (1) an education adjusted Montreal Cognitive Assessment (MoCA) score between 18 and 26; (2) stable medical condition for more than 6 months and stable medication for more than 3 months; (3) medical clearance to undergo a symptom-limited cardiopulmonary exercise test and extensive aerobic exercise training; (4) physical ability sufficient to allow performance of endurance exercise training; (5) capacity to provide written and dated informed consent form. Participants recruited from the community completed additional testing to confirm MCI status. To distinguish between amnestic and non-amnestic MCI, we applied education adjusted cut-offs of −2 standard Deviation (SD) for low education (<10 years of education), −1.5 SD for the middle group (10–13 years of education) and −1 SD for the highly educated (>13 years of education), which were taken from the delayed recall portion of either the Logical Memory (story recall) subtest of the Wechsler Memory Scale IV LM (Ireland and Netherlands) or the Repeatable Battery for the Assessment of Neuropsychological Status Delayed Memory Index (Germany) (Randolph et al., 1998; Wechsler, 2008; Hendriks et al., 2014).

Exclusion criteria were: (1) a diagnosis of AD or any other type of dementia; (2) any neurological disorder or other severe chronic disease; (3) engagement in moderate-intensity aerobic exercise training for more than 30 min, three times per week, during past the 2 years. A full list of in- and exclusion criteria as well as sample size calculations have been published previously (Devenney et al., 2017).

Interventions

In each center participants were randomly assigned to the aerobic exercise (AE), the non-aerobic stretching and toning group (ST) or the control group (CG). Both exercise groups consisted of 3 × 45 min exercise sessions per week over 12 months and exercise intensity was monitored using Borg's Rating of Perceived Exertion (RPE), which is a scale from 6 ("no exertion") to 20 ("maximal exertion") that assess subjective perception of effort during exercise (Borg, 1998; Stuckenschneider et al., 2019). Participants of the AE group had a target RPE of at least 13 while exercising, whereas participants in the ST group exercised to an RPE <10 (Borg, 1998). Participants in the AE group performed indoor and outdoor walking and running exercises, whereas participants in the ST group performed light resistance, stretching, and coordination exercises such as balance. Participants attended supervised instructor led classes and completed unsupervised home exercises. Participants were asked to participate in a supervised exercise session at least once a week. Class attendance and adherence to unsupervised home sessions were recorded for all participants. Exercise diaries, which were collected by the class instructors during supervised exercise sessions once a week, were also used to record unsupervised exercise sessions. The CG received usual care and was not advised on exercise or did not attend exercise sessions (Devenney et al., 2017).

Outcome Measures

All outcomes were measured at baseline (T0) and after 12 months (T2). Outcome assessors were not blinded to the allocated treatment arm. A neuropsychological test battery measuring six cognitive domains (verbal episodic memory, visual episodic memory, working memory, psychomotor function, executive function, and attention) was administered as the primary outcome (Devenney et al., 2017). The neuropsychological test battery consisted of: a computer-based CogState Battery (International Shopping List Task—immediate and delayed recall, Detection Task, Identification Task, One Back Task, and One Card Learning Task), Verbal fluency, and Trail Making Test. The allocation of the tests of the six cognitive domains was based on the CogState Guidelines and conventional classification of neuropsychological tests (Lezak, 2004; Maruff et al., 2004). A comprehensive description of the outcome measures for each test has been published elsewhere (Devenney et al., 2017) and an overview of the domain scores presented in **Supplementary Table 1**.

Cardiovascular fitness (VO_2peak) was assessed as a secondary outcome measure using an incremental exercise test on a standard cycle ergometer. Participants at the German Sport University and Trinity College Dublin completed a maximal test in accordance with the World Health Organization Protocol (Fletcher et al., 2001). In Dublin, VO_2peak was based on direct spirometry [collection of expired gasses during exercise using the K4B2[2] equipment (K4B2[2] User Manual, COSMED, Italy)]. In Cologne, VO_2peak was estimated using the following equation [VO_2peak = (exercise capacity (W)/weight (kg) × 10.8 + 3.5 + 3.5)] (Glass et al., 2007). In Nijmegen, aerobic fitness was estimated from a submaximal exercise test completed according to the Astrand-Rhyming submaximal protocol, according to the local exercise screening protocol. VO_2peak was estimated using the average HR of minute 5 and 6 and the work load in the Astrand Nomogram (Astrand and Ryhming, 1954). VO_2peak (mL/kg/min) was defined as outcome measure for cardiorespiratory fitness.

Health-related quality of life was evaluated using the health-related quality of life for people with Dementia (DemQOL) questionnaire, which has a good acceptability and internal

consistency in patients with MCI (Mhaolain et al., 2012). The total score of the DemQOL was calculated and analyzed.

Statistical Analysis

The primary analysis of this study was the comparison of cognitive functioning (primary outcome measure) before (T0) and after (T2) the 1-year intervention. A composite score was calculated by averaging all six CogState domain scores into one overall cognition score. The obtained scores per test were converted into z-scores based on the standard deviation and mean of the total sample at baseline. In case of multiple tests within one domain, the average score for the domain was calculated with at least one test completed per domain (**Supplementary Tables 1**, **2**). Between-group effect sizes were quantified using Cohen's *d,* with 0.2 representing a small effect, 0.5 a moderate sized effect, and 0.8 representing a large magnitude effect.

For the primary analysis, we included group (aerobic exercise, stretching and toning group, and control group) as independent variables of an ANCOVA with dependent variable the change in composite cognitive score of T2 compared to T0, and as covariates baseline cognitive functioning (T0), sex and age. Between-group differences were analyzed with analysis of covariance under two conditions: (1) the exercise group (EG = combined AE, and ST groups) compared to the control group and (2) AE compared to ST. ANCOVA analyses were chosen as they are unbiased in randomized studies and have more statistical power than repeated measures ANOVAs (Van Breukelen, 2006).

Secondary outcome measures included six separate cognitive domain scores (verbal and visual episodic memory, working memory, psychomotor function, executive function, and attention), cardiorespiratory fitness (VO_2peak) and quality of life (DemQOL). Analyses for all secondary outcome parameters were carried out with similar ANCOVA analyses using the respective baseline score, age, and gender as covariates. All analyses were performed as complete cases (CC) analyses including all participants independent of adherence to the intervention with baseline and follow-up data of at least one test completed per domain. Data are presented as means and 95% confidence intervals within brackets.

For further exploration of the data and to determine the effect of center, which had a significant influence on recruitment (Sanders et al., 2018), a secondary ANCOVA analysis was performed. Moreover, the effect of per protocol participation on primary outcome measures was included in the secondary analysis. Per-protocol (PP) participation was defined as >66% adherence in the EG, which equaled an average of two exercise sessions per week, in line with recent recommendations from the AAN (Petersen et al., 2018). We included per protocol participation [not per protocol (NPP: ≤66 adherence), per protocol (PP), control group (CG)] and center [Ireland (IRE), the Netherlands (NL), Germany (GER)] as independent variables of an ANCOVA with dependent variable the change in composite cognitive score of T2, and as covariates baseline cognitive functioning (T0), sex and age. Similar secondary analyses were performed for cardiorespiratory fitness (VO_2peak) and quality of life (DemQOL). In case of significant interaction effects of center*per protocol participation, *post-hoc* pairwise comparisons between centers [(IRE, NL, GER) and groups (PP), NPP, CG] were conducted using Bonferroni correction for multiple pairwise comparisons. SPSS 22 was used for all analyses with α set at 0.05.

RESULTS

Participants

In total, 183 participants were recruited at the three centers (Germany: 79, Netherlands: 42, Ireland: 62) and randomly stratified into the three groups (AE = 60; ST = 65; CG = 58). Trial recruitment rates differed significantly between the three sites, as discussed previously (Sanders et al., 2018). Five participants dropped out in the AE group (8.6%), six participants in the ST group (9.2%), and six participants in the CG (10%). None of the dropouts were directly related to the intervention, but were due to personal or medical reasons, such as the loss of a relative or diagnosis of cancer. Participant recruitment, screening, enrollment, and attrition are depicted in **Figure 1**.

Participant characteristics differed between the EG and the CG. The CG had a significantly higher proportion of women and a significantly lower hand grip strength in comparison to the EG (**Table 1**).

Complete Case Analysis

Hundred and twelve participants in the EG (AE = 53; ST = 59) and 54 participants in the CG were included in the CC analysis. Due to missing test results, outcomes have different numbers of cases included (**Supplementary Table 2**). Individuals in the AE group participated in 96.6 ± 45.0 (mean ± SD) exercise sessions throughout the 12-month intervention period, while participants in the ST group exercised 92.0 ± 49.3 times.

Complete Case Analysis—Cognition and Quality of Life

ANCOVA did not show a significant difference in composite cognitive performance between the EG and the CG, nor between AE group and ST group, with effect sizes (ES) in the small range, Cohen's d 0.11 [exercise vs. CG, mean difference (95% CI)], [0.12 (−0.03, 0.27)] and 0.22 [AE vs. ST, 0.11 (−0.08, 0.26)] (**Figure 2**, **Supplementary Tables 2**, **3**). Age ($p < 0.001$), baseline cognitive functioning ($p < 0.001$), but not gender ($p = 0.45$) were associated with T2 cognitive composite performance scores. Furthermore, no significant differences were identified in any of the six cognitive domains nor quality of life between the EG and the CG (**Supplementary Tables 2**, **3**). ANCOVA showed a significant difference between the AE and ST groups for the domain attention [$p = 0.011$ and small ES of 0.35, 0.39 (0.09, 0.67)], where the performance in the ST group was significantly higher compared to the AE group (**Supplementary Tables 2**, **3**).

Complete Case Analysis—VO_2Peak

VO_2peak improved significantly in the EG $p = 0.04$ compared to the CG and in the AE group $p = 0.001$ compared to ST group,

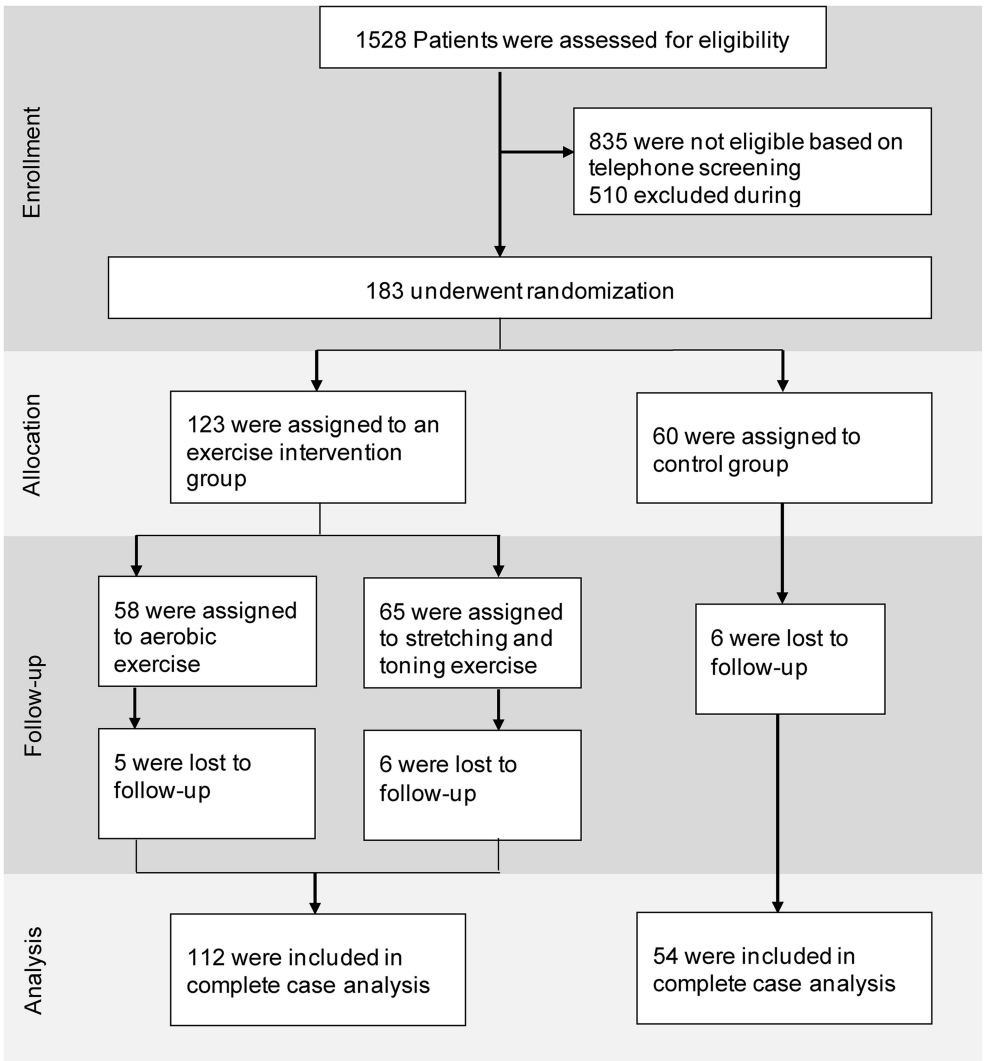

FIGURE 1 | Trial profile.

with medium ES of 0.40 [−1.76 (−3.39, −0.10)] and 0.60 [−3.10 (−4.95, −1.21)]. ANCOVA revealed that baseline scores were associated with VO_2peak at T2 ($p < 0.001$), but not age ($p = 0.88$) nor gender ($p = 0.45$).

Secondary per Protocol and per Center Analysis

One hundred and sixty-six participants (IRE = 56; NL = 36; GER = 74) were included in the secondary analysis. In IRE 19 participants were in the NPP group, 17 participants in the PP group, and 20 participants in the CG. In the Netherlands 8 participants were in each the NPP and the CG, and 20 participants in the PP group. 30 individuals were in the NPP group, 18 in the PP group, and 26 in the CG in Germany. Mean differences for composite cognitive score, quality of life and cardiorespiratory fitness for each group in each center (T2–T0) are presented in **Figure 3**.

Secondary Analysis—Cognition

Secondary ANCOVA analysis revealed no effect of group ($p = 0.069$) but an effect of center ($p = 0.005$) on T2 cognitive composite scores. No significant interaction effect between center and per protocol participation for cognitive composite scores ($p = 0.153$) was found. Age ($p < 0.001$) and cognitive functioning at baseline ($p < 0.001$) were associated with T2 cognitive composite scores. No influence of gender (0.673) was identified.

Secondary Analysis—VO_2Peak

Per protocol participation ($p < 0.001$), but not center ($p = 0.772$) had an influence on VO_2peak at T2, and ANCOVA revealed a significant interaction effect of center*per protocol participation ($p = 0.021$). *Post hoc* pairwise comparisons showed significant differences for participants in Germany, where individuals in both the PP ($p = 0.001$) and NPP ($p = 0.019$) groups had a significantly higher VO_2peak compared to participants in the

TABLE 1 | Group demographics.

	Exercise (AE + ST) $n = 125$	AE $n = 60$	ST $n = 65$	CG $n = 58$
Female, *n* (%)	51 (40.8)*	28 (46.7)	23 (35.4)	35 (60.3)
Age, mean (SD)	71.5 (6.4)	70.6 (6.1)	72.3 (6.6)	71.6 (6.9)
Center				
IRE	41 (32.8)	18 (30.0)	22 (33.8)	21 (36.2)
NL	32 (25.6)	14 (23.3)	18 (27.7)	10 (17.2)
GER	52 (41.6)	27 (45.0)	25 (38.5)	27 (46.6)
Education, *n* (%)				
Low	8 (6.4)	3 (5.2)	5 (7.7)	6 (10.0)
Middle	56 (44.8)	21 (35.0)	35 (53.8)	33 (56.9)
High	61 (48.8)	36 (60.0)	25 (38.5)	19 (32.8)
MoCA, mean (SD)	22.8 (2.4)	22.6 (2.5)	22.9 (2.2)	22.4 (2.1)
Frailty				
TuG, mean (SD)	8.26 (2.13)	8.06 (1.99)	8.44 (2.25)	8.37 (2.07)
30s, mean (SD)	13.2 (3.7)	13.5 (4.1)	13.0 (3.5)	12.5 (3.2)
Hand grip, mean (SD)	33.5 (11.0)*	32.7 (11.1)	34.3 (10.8)	29.4 (10.2)
Exercise sessions. mean (SD)	94.2 (47.0)	96.6 (45.0)	92.1 (48.9)	-
No of medications used. mean (SD)	2.82 (2.75)	2.05 (1.73)	3.54 (3.29)&	2.43 (2.17)

*Exercise, both aerobic exercise (AE) and stretching and toning (ST) exercise groups together; CG, control group; IRE, Ireland; NL, Netherlands; GER, Germany; Education categories, low <10 years of education, middle 10–13 years, high >13 years; MoCA, Montreal Cognitive Assessment, education-adjusted score; One-way ANOVA analyses were used to test differences between the exercise group and the control group or the AE and ST comparison. *Significant difference between exercise group and CG, $p < 0.05$. & Significant difference between AE-ST, $p < 0.05$. Independent t-test was used to test differences between the number of exercise sessions in AE and ST.*

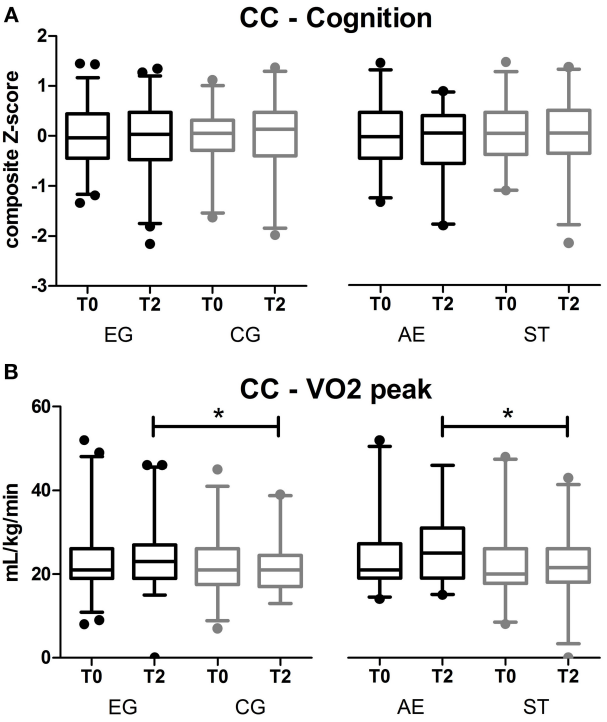

FIGURE 2 | Results of the primary outcome: **(A)** composite cognitive score for complete case (CC) analysis; **(B)** results of VO_2peak for complete case analysis. Boxplots of mean *z*-scores and 95% CI of EG: Exercise group (AE and ST together). CG, control group; AE, aerobic exercise and ST, stretching and toning exercise. No differences in the comparison between T2 results of the groups for cognition. *significant difference EG vs. CG and AE vs. ST, $p <$ 0.05 for VO_2peak.

CG. Baseline VO_2peak ($p < 0.001$), but not gender ($p = 0.499$) or age ($p = 0.726$) were associated with T2 VO_2peak.

Secondary Analysis—Quality of Life

No effect of center ($p = 0.225$) or per protocol participation ($p = 0.051$) was found on quality of life. However, a significant interaction effect (center*per protocol participation) ($p = 0.01$) was identified. *Post hoc* pairwise comparisons revealed that participants in the NPP group in Germany had a significantly better quality of life in comparisons to participants in IRE ($p = 0.034$) and the NL ($p = 0.01$). Furthermore, in Germany the NPP group had a significantly better quality of life than the CG ($p = 0.023$) at T2. Baseline scores ($p < 0.001$), but not age ($p = 0.245$) or gender ($p = 0.169$) were associated with quality of life after 12 months. No further differences were found in the secondary ANCOVA analysis.

DISCUSSION

Main Findings

This multicenter randomized controlled trial analyzed the effects of a 12-month structured exercise program (aerobic exercise or stretching and toning) on the progression of cognitive decline in individuals with aMCI. We did not identify an intervention effect on cognitive performance in the primary complete case analysis. Nevertheless, an intervention effect on physical fitness was identified with a medium effect size. The exercise group increased their physical fitness significantly more after 12 months than the control group.

Collaboration of three research facilities provided the opportunity to analyze aMCI populations across three different countries in North-West Europe. Furthermore, strict inclusion and exclusion criteria ensured a diagnosis of aMCI by using delayed recall scores from standardized memory tests to address limitations of previous studies. An extensive neuropsychological test battery was administered, and composite scores calculated to provide insight into both general cognitive performance and domain-specific cognitive function before and after participation.

Recently, two independent systematic reviews (Zheng et al., 2016; Song et al., 2018) as well as the American Academy of Neurology (AAN) (Petersen et al., 2018) suggested a positive effect of exercise on cognitive function in individuals with MCI. However, the results of our study do not corroborate this, as neither the EG nor the CG improved or decreased their cognitive performance over the period of 12 months. Even though it can be argued that a stable cognitive function may be positive for individuals with MCI, other studies demonstrated improvements

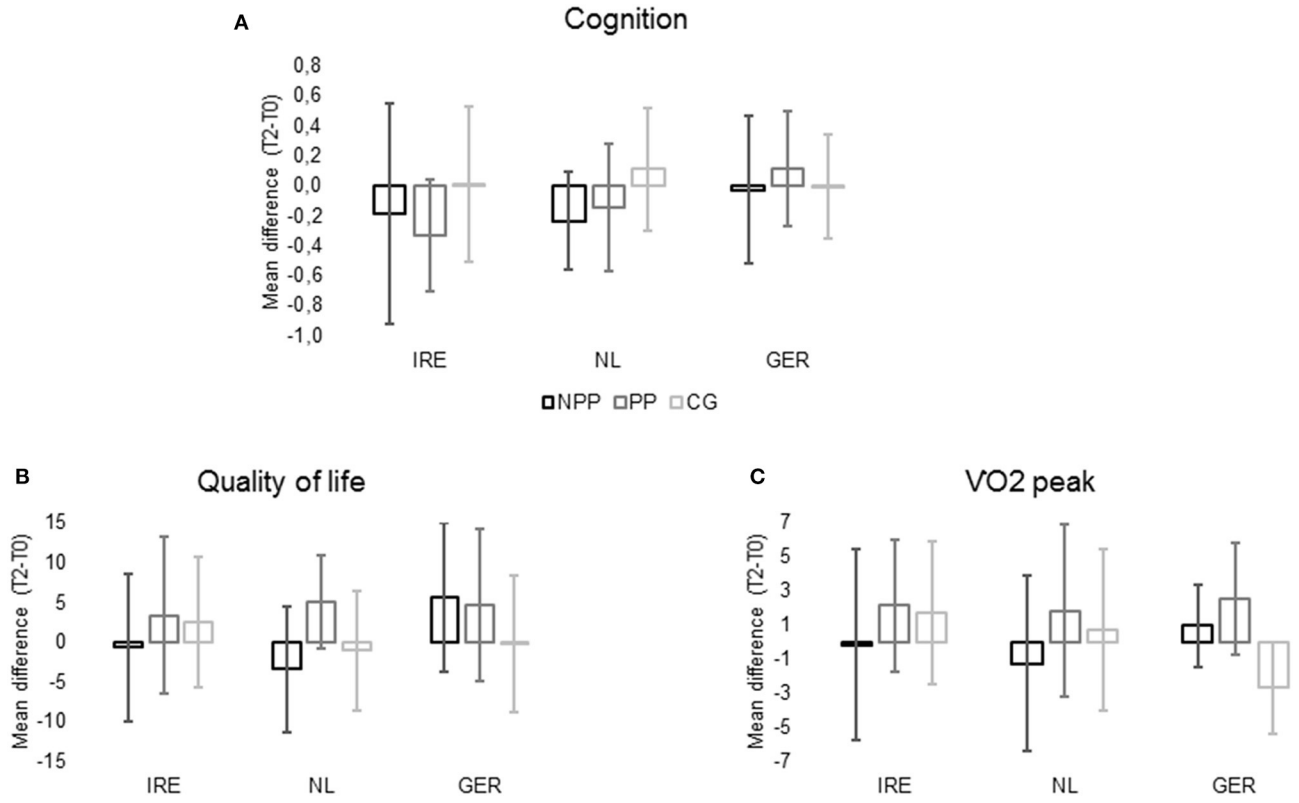

FIGURE 3 | Cognition **(A)** = Mean difference of cognitive composite score between T2 and T0; Quality of Life **(B)** = mean difference of DemQOL total score between T2 and T0; VO_2peak **(C)** = mean difference of VO_2peak (ml/kg/min) between T2 and T0 divided by participation and center (NPP, not per protocol; PP, per protocol; CG, control group; IRE, Ireland, NL, Netherlands; GER, Germany; DemQOL, Health-Related Quality of Life for People with Dementia Questionnaire).

on specific cognitive tests after an exercise intervention (Nagamatsu et al., 2012; Suzuki et al., 2013; Nascimento et al., 2014; Tarumi et al., 2019). In contrast to previous studies, we used composite outcome measures for different cognitive domains based on standardized neuropsychological tests, which is considered the best approach to detect cognitive changes in individuals at risk of AD (Lim et al., 2016).

To date, it is unclear which people with MCI progress to dementia, remain stable, or reverse to normal cognitive function and studies report different numbers that may explain outcomes of our study. The AAN summarized findings of different studies and calculated a cumulative risk of 14.9% for the development of dementia in individuals with MCI within two years (Petersen et al., 2018). However, other studies also showed a reversion to unimpaired cognitive function on their follow-up measurements of their respective participants (Ganguli et al., 2011; Roberts et al., 2014). Individuals with aMCI are reportedly at a higher risk of progressing to dementia (Albert et al., 2011; Ganguli et al., 2011; Roberts et al., 2014), but over the course of 12 months stability in cognitive function may be the most frequently observed outcome (Ganguli et al., 2011). Ganguli and colleagues reported a progression to dementia of only 1.4% for individuals with aMCI with 77.8% remaining stable and further 15.4% improving their cognitive function back to normal after 12 months (Ganguli et al., 2011). Therefore, mixed outcomes in different studies may be expected in a cohort of individuals with any type of MCI.

MCI does not have one single cause, but is a multicausal syndrome (Knopman and Petersen, 2014; Petersen et al., 2014), which might explain the different outcomes observed in our and other studies as it is unlikely that one single treatment (e.g., exercise) will prove to be an effective intervention for all individuals. Multidomain-type (e.g., diet, exercise, and cognitive training) interventions in the Finnish Geriatric Intervention Study to Prevent Cognitive Impairment and Disability (FINGER) showed positive results on global cognitive function, as well as on processing speed and executive function in a sample of older individuals at cerebrovascular risk for cognitive decline (Ngandu et al., 2015). However, the FINGER study showed this significant treatment benefit in a cognitively unimpaired sample of older adults at risk for future cognitive decline, but not in individuals with diagnosed MCI (Ngandu et al., 2015).

Despite the lack of significant differences in cognitive function, physical fitness—measured by VO_2peak—increased significantly in the EG compared with the CG, and in the AE group compared with the ST group. These findings are in line with existing literature, as standardized exercise training increases physical fitness (Tarumi et al., 2019). Even though

a direct effect of an increased VO_2peak on cognition was not detected, higher physical fitness might be an important outcome for future disease progression. Recently published research defined changes in physical fitness as an independent risk factor for incident dementia and dementia mortality and highlighted the importance of improving fitness to delay onset of dementia (Tari et al., 2019). This is in line with previous research, which showed that higher physical fitness during mid-life and late-life (e.g., higher VO_2peak values) is positively associated with cognitive function in older adults with and without cognitive impairment (Mavros et al., 2017; Schultz et al., 2017; Stuckenschneider et al., 2018). Individuals with MCI have an increased risk of being socially isolated, which increases the risk of future progression to dementia (Fratiglioni et al., 2000; Bosma et al., 2002). Previous studies showed that higher physical fitness leads to an increase in self-confidence, which consequently may increase social participation (Perkins et al., 2008; Choi et al., 2017). Therefore, improving physical fitness may not only benefit cognitive function, but also may be the driving force for a socially integrated and fulfilling life during later life—especially in individuals with MCI. However, further evidence (e.g., longer intervention periods, longer follow-up period) is required to establish the beneficial effects of an increased VO_2peak on cognitive decline.

Moreover, increased fitness likely induces structural changes such as an increased hippocampal volume and an improved white matter integrity (Young et al., 2015; Dougherty et al., 2017; Muller et al., 2017; Ding et al., 2018). Findings to date are equivocal if exercise induced structural changes influence cognitive function directly or if structural changes may rather be beneficial for sustaining cognitive functions long-term (Hotting and Roder, 2013). To further explore this hypothesis, data from physiological measurements (e.g., MRI scans) is needed to provide insight into physiological mechanisms triggered by an increased physical fitness. Tarumi and colleagues provided insight into possible mechanisms and showed that an increased cardiorespiratory fitness following a 12 months exercise intervention was associated with an improved white matter integrity of the prefrontal cortex (Tarumi et al., 2019, 2020) as well as a redistribution of cerebral blood flow in individuals with aMCI (Thomas et al., 2020). However, the lack of a control group as well as an overall atrophy of global brain volume and particularly hippocampal areas warrants further research (Tarumi et al., 2019).

While no effective treatment currently exists for AD, a large number of mechanisms related to AD genetics and different modifiable risk factors, as well as protective factors (such as exercise) have been identified. Given the large heterogeneity in current studies, it may be time to rethink future trials whereby personalized precision prevention may be the most appropriate approach, in which an intervention is prescribed in response to each individuals' modifiable risk factors (Gillman and Hammond, 2016). A possible next step towardz this may include a responder analysis to identify which individuals with MCI benefit most from an exercise intervention (Snapinn and Jiang, 2007). Further research is needed to better define the biomarkers or cognitive profile that best predicts different subtypes of MCI, especially those at the highest risk to progress from the preclinical stages of MCI towards dementia due to AD (Sperling et al., 2011).

Secondary Analysis—Effect of Research Setting

In none of the centers cognitive function significantly improved in the exercise groups at T2. However, participants in Germany exercising at least twice a week were the only participants in the exercise groups that showed a positive trend on their cognitive function, based on a positive difference between T2 and T0. Additionally, physical fitness and quality of life significantly improved in the exercise groups in comparison to the control group in Germany, whereas no significant changes for any outcome in Ireland and the Netherlands were found. Therefore, we speculate that a non-medical setting and a non-medical research community might have additional effects on improving fitness and may have additional benefits for quality of life in individuals with MCI (Sanders et al., 2018). Even though multicenter clinical studies in elderly with cognitive impairment are the backbone of evidence-based prevention, complete standardization is difficult to obtain in the different research facilities involved. Whereas the exercise classes in Germany were all supervised, participants in Ireland and the Netherlands partly exercised on their own. Even though all participants were instructed on exercise duration and intensity and were asked to participate in at least one supervised exercise session a week to remind and educate them about exercise intensity (Devenney et al., 2017), unsupervised exercise training may compromise treatment fidelity. Further, it is possible that methods such as self-report of exercise training are open to bias due to the so-called social desirability response bias (Aadahl and Jorgensen, 2003), which may explain findings of the secondary analysis with physical fitness only improving significantly in Germany. Besides the additional effects of supervised exercise training on VO_2peak, increased social interaction, which was achieved due to the participants exercising in groups during the supervised sessions, may also explain secondary findings for quality of life, which only improved in the German sample. However, we did not find a significant treatment effect on cognition for the German sample.

Strength and Limitations

This study has several strengths including its large sample size, its strict inclusion of individuals with aMCI, its long intervention period (12 months), and its multicentric design. Furthermore, different cognitive tests were combined into one overall score of cognitive function (primary outcome), but also for different subdomains of cognitive function to provide a psychometrically more reliable and thus more valid construct (Lim et al., 2016). However, subtle changes may be easier detected in single tests—even though they are also prone to false positive type I errors.

One of the limitations of the study was that the recruitment aim of 225 individuals with aMCI (75 per center), was not achieved. Nevertheless, recruitment numbers were sufficient regarding the power calculation for primary analysis (16). As numbers were significantly lower in the secondary analysis, due to the differentiation by center, results of it need to be interpreted

cautiously. Despite difficulties in recruitment, dropout rates were less than 10% in all groups, which shows a good acceptance of the study and the high motivation of the participants. Participants received their individual study results after completion of the study, which may have motivated individuals to participate, especially in the CG. As cardiorespiratory fitness did not change in this CG, it is unlikely that the participants in that group as a whole altered their lifestyle only because of participating in our trail.

Only 53% of participants reached the target exercise frequency, which was defined as 100 exercise sessions (or more, at least twice a week) within the intervention period of 12 months according to recent recommendations of the AAN (Petersen et al., 2018). In comparison to previous studies the low number of participants following the per-protocol intervention may have been due to the longer intervention period (12 months), and the strict and conservative target exercise frequency. The low dropout rate and more than half of the intervention group following the strict protocol is already a promising result for this rather inactive participant selection, which is reflected by a low baseline cardiorespiratory fitness in comparison to population reference values (Edvardsen et al., 2013). As the best dose-response relationship of exercise on cognitive function is frequently discussed, yet still unknown (Gomes-Osman et al., 2018), future exercise prevention trials should concentrate on defining the best dose-response relationship. Future studies should use objective monitors such as heart rate monitors to ensure a certain exercise intensity is reached. Even though Borg's RPE scale may present a practical tool to monitor intensity, self-reporting always bears the risks to be affected by motivational aspects and over- or underestimation of the individuals' functional abilities. Therefore, monitoring intensity via heart rate may increase accuracy of the training program and, thus, lead to better study outcomes. It may be speculated that different outcomes observed in our study compared to the one conducted by Tarumi and colleagues may be due to the objective monitoring used in their study (Tarumi et al., 2019). However, cardiorespiratory fitness increased in both trials, so that further insight into these different monitoring methods is warranted.

Different tests for VO_2peak were applied, which was due to different regulations by the institutional review boards (Devenney et al., 2017). Effects of these differences were minimized by using standardized and validated VO_2peak measurements at all sites. Significant differences between the groups' baseline characteristics are reported, however, these occurred rather by chance than by bias (Altman and Dore, 1990; Moher et al., 2010), as a centrally controlled computer-generated randomization list (for each country), which was controlled by an independent statistician, was used. There is ongoing discussion whether to report differences in baseline characteristics or not (Moher et al., 2010). Given the large heterogeneity observed in individuals with MCI, we presented baseline statistics to identify possible confounders. The EG and CG had a different proportion of women and men with significantly more women being in the CG. This could have biased the results, as women have a higher risk to progress to dementia, but we performed an ANCOVA to statistically adjust for the potential effect of sex. The different proportion of women and men might also account for the differences in hand grip strength between the EG and the CG. As men are reportedly stronger than women, a higher value in hand grip may be expected. Furthermore, the ST group used significantly more medications compared to the AE group. As investigational drug studies and unstable medication were among the exclusion criteria of our trial, it is unlikely that this baseline difference had a significant impact on our results. However, the effect of medication has not fully been investigated in previous studies on exercise interventions and should be addressed by future trials.

Future Directions

No cure for AD currently exits, prompting increased efforts to understand the preclinical stages such as aMCI as potential opportunities for new treatment approaches. Based on results of our multicentric randomized controlled trial, future research in the field of exercise interventions should target the following aspects: Both cognitive and physiological measurements are warranted to fully establish the effects of exercise and provide insight into its underlying mechanisms. Furthermore, different and combined exercise modes (e.g., endurance, resistance), intensities (e.g., moderate, high) and exercise volume (length of exercise classes, average exercise sessions per week) need attention to identify best dose-response relationships in the future. To ensure comparability between studies researches must focus on uniform reporting of their findings and their interventions. Objective monitors such as heart rate/activity monitors should be used to measure exercise intensity and frequency. Additionally, long-term follow-ups are needed to establish the long-term effects of exercise on disease progression. Besides promoting exercise on its own, multi-domain type interventions (e.g., exercise, cognitive training, and diet) may help to address the large heterogeneity observed in individuals in preclinical stages of AD.

CONCLUSION

This study does not support the recommendation from small and short-term RCTs that an exercise intervention has an effect on cognitive performance in individuals with amnestic MCI. Nevertheless, we found a reliable intervention effect on physical fitness, which may be an important outcome for disease progression. Future trials need to target long-term follow ups (up to 5 years) to evaluate the efficacy of an increased physical fitness on cognitive decline. Moreover, the heterogeneity between subjects and centers may explain different findings within the study. Therefore, future trials should consider personalized intervention approaches or multidomain interventions.

DATA AVAILABILITY STATEMENT

The datasets used and analyzed during the current study will be made available by the corresponding author upon reasonable request.

ETHICS STATEMENT

The studies involving human participants were reviewed and approved by the Ethics Committee of the German Sport University, Cologne Germany, the Commisie Mensgebonden Onderzoek Arnhem-Nijmegen, Netherlands, and the Tallaght Hospital/St. James's Hospital Joint Research Ethics Committee Dublin Ireland approved the study protocol. The patients/participants provided their written informed consent to participate in this study.

AUTHOR CONTRIBUTIONS

SS, BL, MO, MP, R-JS, CM, MR, BW, and RM were responsible for conceptualization. TS, MS, and KD carried out data curation were responsible for the investigation. Further, TS, MS, and RK performed the formal analysis. Funding was acquired and resources and supervision were provided by SS, BL, and MO. SS, VA, TV, TS, RK, MO, JA, MS, BL, EG, and KD designed the methodology of the study. SS, BL, MO, TS, MS, and KD were responsible for the project administration. TS and MS wrote the original draft of the manuscript and were responsible for visualization, while RK, KD, MO, BL, SS, MP, VA, and EG reviewed and edited the manuscript. Validation of the analysis and the data was provided by MS, MO, RK, MR, and SS. All authors have read and approved the final version of the manuscript, and agree with the order of presentation of the authors.

FUNDING

The project has been supported by The EU Joint Programme—Neurodegenerative Disease Research (JPND). JPND had no role in study design, data collection and analysis, decision to publish or preparation of the manuscript. German Grant Number BMBF 01ED1510A (SS). Health Research Board Ireland Grant Number JPND-2014-1 (BL). Dutch Grant Number: ZonMw 733051044 (MO).

ACKNOWLEDGMENTS

The authors would like to thank all the participants who have been involved and dedicated their precious time to this study. Further, we would like to thank two unknown reviewers for their valuable feedback on a previous version of the manuscript. Trinity College Dublin would like to acknowledge the assistance and support of the Welcome Trust–HRB Clinical Research Facility at St. James' Hospital in providing a dedicated environment for the conduct of high-quality clinical research activities.

SUPPLEMENTARY MATERIAL

The Supplementary Material for this article can be found online at: https://www.frontiersin.org/articles/10.3389/fnagi.2020.621947/full#supplementary-material

REFERENCES

Aadahl, M., and Jorgensen, T. (2003). Validation of a new self-report instrument for measuring physical activity. *Med. Sci. Sports Exerc.* 35, 1196–1202. doi: 10.1249/01.MSS.0000074446.02192.14

Albert, M. S., DeKosky, S. T., Dickson, D., Dubois, B., Feldman, H. H., Fox, N. C., et al. (2011). The diagnosis of mild cognitive impairment due to Alzheimer's disease: recommendations from the National Institute on Aging-Alzheimer's Association workgroups on diagnostic guidelines for Alzheimer's disease. *Alzheimers Dement.* 7, 270–279. doi: 10.1016/j.jalz.2011.03.008

Altman, D. G., and Dore, C. J. (1990). Randomisation and baseline comparisons in clinical trials. *Lancet* 335, 149–153. doi: 10.1016/0140-6736(90)90014-V

Astrand, P. O., and Ryhming, I. (1954). A nomogram for calculation of aerobic capacity (physical fitness) from pulse rate during submaximal work. *J. Appl. Physiol.* 7, 218–221. doi: 10.1152/jappl.1954.7.2.218

Borg, G. (1998). *Borg's Perceived Exertion and Pain Scales.* Champaign: Human Kinetics.

Bosma, H., van Boxtel, M. P., Ponds, R. W., Jelicic, M., Houx, P., Metsemakers, J., et al. (2002). Engaged lifestyle and cognitive function in middle and old-aged, non-demented persons: a reciprocal association? *Z. Gerontol. Geriatr.* 35, 575–581. doi: 10.1007/s00391-002-0080-y

Brodaty, H., Breteler, M. M., Dekosky, S. T., Dorenlot, P., Fratiglioni, L., Hock, C., et al. (2011). The world of dementia beyond 2020. *J. Am. Geriatr. Soc.* 59, 923–927. doi: 10.1111/j.1532-5415.2011.03365.x

Choi, J., Lee, M., Lee, J. K., Kang, D., and Choi, J. Y. (2017). Correlates associated with participation in physical activity among adults: a systematic review of reviews and update. *BMC Public Health* 17:356. doi: 10.1186/s12889-017-4255-2

Devenney, K. E., Sanders, M. L., Lawlor, B., Olde Rikkert, M. G. M., Schneider, S., and NeuroExercise Study, G. (2017). The effects of an extensive exercise programme on the progression of mild cognitive impairment (MCI): study protocol for a randomised controlled trial. *BMC Geriatr.* 17:75. doi: 10.1186/s12877-017-0457-9

Ding, K., Tarumi, T., Zhu, D. C., Tseng, B. Y., Thomas, B. P., Turner, M., et al. (2018). Cardiorespiratory fitness and white matter neuronal fiber integrity in mild cognitive impairment. *J. Alzheimers Dis.* 61, 729–739. doi: 10.3233/JAD-170415

Dougherty, R. J., Schultz, S. A., Boots, E. A., Ellingson, L. D., Meyer, J. D., Van Riper, S., et al. (2017). Relationships between cardiorespiratory fitness, hippocampal volume, and episodic memory in a population at risk for Alzheimer's disease. *Brain Behav.* 7:e00625. doi: 10.1002/brb3.625

Edvardsen, E., Hansen, B. H., Holme, I. M., Dyrstad, S. M., and Anderssen, S. A. (2013). Reference values for cardiorespiratory response and fitness on the treadmill in a 20- to 85-year-old population. *Chest* 144, 241–248. doi: 10.1378/chest.12-1458

Fletcher, G. F., Balady, G. J., Amsterdam, E. A., Chaitman, B., Eckel, R., Fleg, J., et al. (2001). Exercise standards for testing and training: a statement for healthcare professionals from the American Heart Association. *Circulation* 104, 1694–1740. doi: 10.1161/hc3901.095960

Fratiglioni, L., Wang, H. X., Ericsson, K., Maytan, M., and Winblad, B. (2000). Influence of social network on occurrence of dementia: a community-based longitudinal study. *Lancet* 355, 1315–1319. doi: 10.1016/S0140-6736(00)02113-9

Ganguli, M., Snitz, B. E., Saxton, J. A., Chang, C. C., Lee, C. W., Vander Bilt, J., et al. (2011). Outcomes of mild cognitive impairment by definition: a population study. *Arch. Neurol.* 68, 761–767. doi: 10.1001/archneurol.2011.101

Gillman, M. W., and Hammond, R. A. (2016). Precision treatment and precision prevention: integrating "below and above the skin." *JAMA Pediatr.* 170, 9–10. doi: 10.1001/jamapediatrics.2015.2786

Glass, S., Dwyer, G. B., and American College of Sports Medicine (2007). *ACSM's Metabolic Calculations Handbook.* Philadelphia, PA: Lippincott Williams and Wilkins.

Gomes-Osman, J., Cabral, D. F., Morris, T. P., McInerney, K., Cahalin, L. P., Rundek, T., et al. (2018). Exercise for cognitive brain health in aging: a systematic review for an evaluation of dose. *Neurol. Clin. Pract.* 8, 257–265. doi: 10.1212/CPJ.0000000000000460

Hendriks, M., Bouman, Z., Kessels, R., and Aldenkamp, A. (2014). *Wechsler Memory Scale-Dutch Edition (WMS-IV-NL).* Amsterdam: Pearson Assessment.

Hotting, K., and Roder, B. (2013). Beneficial effects of physical exercise on neuroplasticity and cognition. *Neurosci. Biobehav. Rev.* 37, 2243–2257. doi: 10.1016/j.neubiorev.2013.04.005

Knopman, D. S., and Petersen, R. C. (2014). Mild cognitive impairment and mild dementia: a clinical perspective. *Mayo Clin. Proc.* 89, 1452–1459. doi: 10.1016/j.mayocp.2014.06.019

Lezak, M. D. (2004). *Neuropsychological Assessment*. New York, NY: Oxford University Press.

Lim, Y. Y., Snyder, P. J., Pietrzak, R. H., Ukiqi, A., Villemagne, V. L., Ames, D., et al. (2016). Sensitivity of composite scores to amyloid burden in preclinical Alzheimer's disease: introducing the Z-scores of attention, verbal fluency, and episodic memory for nondemented older adults composite score. *Alzheimers Dement (Amst).* 2, 19–26. doi: 10.1016/j.dadm.2015.11.003

Maruff, P., Collie, A., Darby, D., Weaver-Cargin, J., Masters, C., and Currie, J. (2004). Subtle memory decline over 12 months in mild cognitive impairment. *Dement. Geriatr. Cogn. Disord.* 18, 342–348. doi: 10.1159/000080229

Mavros, Y., Gates, N., Wilson, G. C., Jain, N., Meiklejohn, J., Brodaty, H., et al. (2017). Mediation of cognitive function improvements by strength gains after resistance training in older adults with mild cognitive impairment: outcomes of the study of mental and resistance training. *J. Am. Geriatr. Soc.* 65, 550–559. doi: 10.1111/jgs.14542

McKhann, G. M., Knopman, D. S., Chertkow, H., Hyman, B. T., Jack, C. R. Jr., et al. (2011). The diagnosis of dementia due to Alzheimer's disease: recommendations from the National Institute on Aging-Alzheimer's Association workgroups on diagnostic guidelines for Alzheimer's disease. *Alzheimers Dement.* 7, 263–269. doi: 10.1016/j.jalz.2011.03.005

Mhaolain, A. M., Gallagher, D., Crosby, L., Ryan, D., Lacey, L., Coen, R. F., et al. (2012). Frailty and quality of life for people with Alzheimer's dementia and mild cognitive impairment. *Am. J. Alzheimers Dis. Other Demen.* 27, 48–54. doi: 10.1177/1533317511435661

Moher, D., Hopewell, S., Schulz, K. F., Montori, V., Gotzsche, P. C., Devereaux, P. J., et al. (2010). CONSORT 2010 explanation and elaboration: updated guidelines for reporting parallel group randomised trials. *J. Clin. Epidemiol.* 63, e1–37. doi: 10.1016/j.jclinepi.2010.03.004

Muller, J., Chan, K., and Myers, J. N. (2017). Association between exercise capacity and late onset of dementia, Alzheimer disease, and cognitive impairment. *Mayo Clin. Proc.* 92, 211–217. doi: 10.1016/j.mayocp.2016.10.020

Nagamatsu, L. S., Handy, T. C., Hsu, C. L., Voss, M., and Liu-Ambrose, T. (2012). Resistance training promotes cognitive and functional brain plasticity in seniors with probable mild cognitive impairment. *Arch. Intern. Med.* 172, 666–668. doi: 10.1001/archinternmed.2012.379

Nascimento, C. M., Pereira, J. R., de Andrade, L. P., Garuffi, M., Talib, L. L., Forlenza, O. V., et al. (2014). Physical exercise in MCI elderly promotes reduction of pro-inflammatory cytokines and improvements on cognition and BDNF peripheral levels. *Curr. Alzheimer Res.* 11, 799–805. doi: 10.2174/1567205011081409101228 49

Ngandu, T., Lehtisalo, J., Solomon, A., Levalahti, E., Ahtiluoto, S., Antikainen, R., et al. (2015). A 2 year multidomain intervention of diet, exercise, cognitive training, and vascular risk monitoring versus control to prevent cognitive decline in at-risk elderly people (FINGER): a randomised controlled trial. *Lancet* 385, 2255–2263. doi: 10.1016/S0140-6736(15)60461-5

Ohman, H., Savikko, N., Strandberg, T. E., and Pitkala, K. H. (2014). Effect of physical exercise on cognitive performance in older adults with mild cognitive impairment or dementia: a systematic review. *Dement. Geriatr. Cogn. Disord.* 38, 347–365. doi: 10.1159/000365388

Perkins, J. M., Multhaup, K. S., Perkins, H. W., and Barton, C. (2008). Self-efficacy and participation in physical and social activity among older adults in Spain and the United States. *Gerontologist* 48, 51–58. doi: 10.1093/geront/48.1.51

Petersen, R. C. (2004). Mild cognitive impairment as a diagnostic entity. *J. Intern. Med.* 256, 183–194. doi: 10.1111/j.1365-2796.2004.01388.x

Petersen, R. C., Caracciolo, B., Brayne, C., Gauthier, S., Jelic, V., and Fratiglioni, L. (2014). Mild cognitive impairment: a concept in evolution. *J. Intern. Med.* 275, 214–228. doi: 10.1111/joim.12190

Petersen, R. C., Lopez, O., Armstrong, M. J., Getchius, T. S. D., Ganguli, M., Gloss, D., et al. (2018). Practice guideline update summary: mild cognitive impairment: report of the guideline development, dissemination, and implementation subcommittee of the American Academy of Neurology. *Neurology* 90, 126–135. doi: 10.1212/WNL.0000000000004826

Prince, M. W., Wimo, A., Guerchet, M., Ali, G., Wu, Y., and Prina, M. (eds.). (2015). *The Global Impact of Dementia: An Analysis of Prevalence Incidence, Cost and Trends*. London: Alzheimer's Disease International (ADI).

Randolph, C., Tierney, M. C., Mohr, E., and Chase, T. N. (1998). The repeatable battery for the assessment of neuropsychological status (RBANS): preliminary clinical validity. *J. Clin. Exp. Neuropsychol.* 20, 310–319. doi: 10.1076/jcen.20.3.310.823

Roberts, R. O., Knopman, D. S., Mielke, M. M., Cha, R. H., Pankratz, V. S., Christianson, T. J., et al. (2014). Higher risk of progression to dementia in mild cognitive impairment cases who revert to normal. *Neurology* 82, 317–325. doi: 10.1212/WNL.0000000000000055

Sanders, M. L., Stuckenschneider, T., Devenney, K. E., Lawlor, B., Schneider, S., Olde Rikkert, M. G. M., et al. (2018). Real world recruiting of older subjects with mild cognitive impairment for exercise trials: community readiness is pivotal. *J. Alzheimers Dis.* 62, 579–581. doi: 10.3233/JAD-171083

Schultz, S. A., Boots, E. A., Darst, B. F., Zetterberg, H., Blennow, K., Edwards, D. F., et al. (2017). Cardiorespiratory fitness alters the influence of a polygenic risk score on biomarkers of AD. *Neurology* 88, 1650–1658. doi: 10.1212/WNL.0000000000003862

Snapinn, S. M., and Jiang, Q. (2007). Responder analyses and the assessment of a clinically relevant treatment effect. *Trials* 8:31. doi: 10.1186/1745-6215-8-31

Song, D., Yu, D. S. F., Li, P. W. C., and Lei, Y. (2018). The effectiveness of physical exercise on cognitive and psychological outcomes in individuals with mild cognitive impairment: a systematic review and meta-analysis. *Int. J. Nurs. Stud.* 79, 155–164. doi: 10.1016/j.ijnurstu.2018.01.002

Sperling, R. A., Aisen, P. S., Beckett, L. A., Bennett, D. A., Craft, S., Fagan, A. M., et al. (2011). Toward defining the preclinical stages of Alzheimer's disease: recommendations from the National Institute on Aging-Alzheimer's Association workgroups on diagnostic guidelines for Alzheimer's disease. *Alzheimers Dement.* 7, 280–292. doi: 10.1016/j.jalz.2011.03.003

Stuckenschneider, T., Askew, C. D., Rudiger, S., Polidori, M. C., Abeln, V., Vogt, T., et al. (2018). Cardiorespiratory fitness and cognitive function are positively related among participants with mild and subjective cognitive impairment. *J. Alzheimers Dis.* 62, 1865–1875. doi: 10.3233/JAD-170996

Stuckenschneider, T., Rudiger, S., Abeln, V., Askew, C. D., Wollseiffen, P., Schneider, S., et al. (2019). Rating of perceived exertion—a valid method for monitoring light to vigorous exercise intensity in individuals with subjective and mild cognitive impairment? *Eur. J. Sport Sci.* 20, 261–268. doi: 10.1080/17461391.2019.1629632

Suzuki, T., Shimada, H., Makizako, H., Doi, T., Yoshida, D., Ito, K., et al. (2013). A randomized controlled trial of multicomponent exercise in older adults with mild cognitive impairment. *PLoS ONE* 8:e61483. doi: 10.1371/journal.pone.0061483

Suzuki, T., Shimada, H., Makizako, H., Doi, T., Yoshida, D., Tsutsumimoto, K., et al. (2012). Effects of multicomponent exercise on cognitive function in older adults with amnestic mild cognitive impairment: a randomized controlled trial. *BMC Neurol.* 12:128. doi: 10.1186/1471-2377-12-128

Tari, A. R., Nauman, J., Zisko, N., Skjellegrind, H. K., Bosnes, I., Bergh, S., et al. (2019). Temporal changes in cardiorespiratory fitness and risk of dementia incidence and mortality: a population-based prospective cohort study. *Lancet Public Health* 4, e565–e574. doi: 10.1016/S2468-2667(19)30183-5

Tarumi, T., Rossetti, H., Thomas, B. P., Harris, T., Tseng, B. Y., Turner, M., et al. (2019). Exercise training in amnestic mild cognitive impairment: a one-year randomized controlled trial. *J. Alzheimers Dis.* 71, 421–433. doi: 10.3233/JAD-181175

Tarumi, T., Thomas, B. P., Tseng, B. Y., Wang, C., Womack, K. B., Hynan, L., et al. (2020). Cerebral white matter integrity in amnestic mild cognitive impairment: a 1-year randomized controlled trial of aerobic exercise training. *J. Alzheimers Dis.* 73, 489–501. doi: 10.3233/JAD-190875

Thomas, B. P., Tarumi, T., Sheng, M., Tseng, B., Womack, K. B., Cullum, C. M., et al. (2020). Brain perfusion change in patients with mild cognitive impairment after 12 months of aerobic exercise training. *J. Alzheimers Dis.* 75, 617–631. doi: 10.3233/JAD-190977

Van Breukelen, G. J. (2006). ANCOVA versus change from baseline: more power in randomized studies, more bias in nonrandomized studies [corrected]. *J. Clin. Epidemiol.* 59, 920–925. doi: 10.1016/j.jclinepi.2006.02.007

Vickland, V., McDonnell, G., Werner, J., Draper, B., Low, L. F., and Brodaty, H. (2010). A computer model of dementia prevalence in Australia: foreseeing outcomes of delaying dementia onset, slowing disease progression, and eradicating dementia types. *Dement. Geriatr. Cogn. Disord.* 29, 123–130. doi: 10.1159/000272436

Wang, C., Yu, J. T., Wang, H. F., Tan, C. C., Meng, X. F., and Tan, L. (2014). Non-pharmacological interventions for patients with mild cognitive impairment: a meta-analysis of randomized controlled trials of cognition-based and exercise interventions. *J. Alzheimers Dis.* 42, 663–678. doi: 10.3233/JAD-140660

Wechsler, D. (2008). *Wechsler Adult Intelligence Scale-Fourth*. San Antonio, TX: The Psychological Corporation Google Scholar. doi: 10.1037/t15169-000

Winblad, B., Palmer, K., Kivipelto, M., Jelic, V., Fratiglioni, L., Wahlund, L. O., et al. (2004). Mild cognitive impairment—beyond controversies, towardz a consensus: report of the International Working Group on Mild Cognitive Impairment. *J. Intern. Med.* 256, 240–246. doi: 10.1111/j.1365-2796.2004.01380.x

Young, J., Angevaren, M., Rusted, J., and Tabet, N. (2015). Aerobic exercise to improve cognitive function in older people without known ognitive impairment. *Cochrane Database Syst. Rev.* 4:CD005381. doi: 10.1002/14651858.CD005381.pub4

Zheng, G., Xia, R., Zhou, W., Tao, J., and Chen, L. (2016). Aerobic exercise ameliorates cognitive function in older adults with mild cognitive impairment: a systematic review and meta-analysis of randomised controlled trials. *Br. J. Sports Med.* 50, 1443–1450. doi: 10.1136/bjsports-2015-095699

Conflict of Interest: The authors declare that the research was conducted in the absence of any commercial or financial relationships that could be construed as a potential conflict of interest.

frontiers in Neuroscience

ORIGINAL RESEARCH
published: 18 January 2021
doi: 10.3389/fnins.2020.602501

White Matter Atrophy in Type 2 Diabetes Mellitus Patients With Mild Cognitive Impairment

Chang Li[1,2†], Rongbing Jin[3,4†], Kaijun Liu[5], Yang Li[1], Zhiwei Zuo[6], Haipeng Tong[1,4], Jingna Zhang[7], Junfeng Zhang[1,4], Yu Guo[1], Yuqi Lai[8], Jinju Sun[3], Jian Wang[2], Kunlin Xiong[1,4*] and Xiao Chen[3,4*]*

[1] Department of Radiology, Daping Hospital, Army Medical University, Chongqing, China, [2] Department of Radiology, Southwest Hospital, Army Medical University, Chongqing, China, [3] Department of Nuclear Medicine, Daping Hospital, Army Medical University, Chongqing, China, [4] Chongqing Clinical Research Center for Imaging and Nuclear Medicine, Chongqing, China, [5] Department of Gastroenterology, Daping Hospital, Army Medical University, Chongqing, China, [6] Department of Radiology, General Hospital of Western Theater Command, Chengdu, China, [7] Department of Medical Imaging, College of Biomedical Engineering, Army Medical University, Chongqing, China, [8] School of Foreign Languages and Cultures, Chongqing University, Chongqing, China

OPEN ACCESS

Edited by:
Jiehui Jiang,
Shanghai University, China

Reviewed by:
Xuntao Yin,
Guizhou Provincial People' Hospital, China
Matthew C. Murphy,
Mayo Clinic, United States
Can Sheng,
Capital Medical University, China

***Correspondence:**
Jian Wang
wangjian_811@yahoo.com
Kunlin Xiong
109948969@qq.com
Xiao Chen
xiaochen229@foxmail.com

[†] These authors have contributed equally to this work

Specialty section:
This article was submitted to Brain Imaging Methods, a section of the journal Frontiers in Neuroscience

Received: 03 September 2020
Accepted: 21 December 2020
Published: 18 January 2021

Citation:
Li C, Jin R, Liu K, Li Y, Zuo Z, Tong H, Zhang J, Zhang J, Guo Y, Lai Y, Sun J, Wang J, Xiong K and Chen X (2021) White Matter Atrophy in Type 2 Diabetes Mellitus Patients With Mild Cognitive Impairment. Front. Neurosci. 14:602501. doi: 10.3389/fnins.2020.602501

Type 2 diabetes mellitus (T2DM) patients are highly susceptible to developing dementia, especially for those with mild cognitive impairment (MCI), but its underlying cause is still unclear. In this study, we performed a battery of neuropsychological tests and high-resolution sagittal T1-weighted structural imaging to explore how T2DM affects white matter volume (WMV) and cognition in 30 T2DM-MCI patients, 30 T2DM with normal cognition (T2DM-NC) patients, and 30 age-, sex-, and education-matched healthy control (HC) individuals. The WMV of the whole brain was obtained with automated segmentation methods. Correlations between the WMV of each brain region and neuropsychological tests were analyzed in the T2DM patients. The T2DM-NC patients and HC individuals did not reveal any significant differences in WMV. Compared with the T2DM-NC group, the T2DM-MCI group showed statistically significant reduction in the WMV of seven brain regions, mainly located in the frontotemporal lobe and limbic system, five of which significantly correlated with Montreal Cognitive Assessment (MoCA) scores. Subsequently, we evaluated the discriminative ability of these five regions for MCI in T2DM patients. The WMV of four regions, including left posterior cingulate, precuneus, insula, and right rostral middle frontal gyrus had high diagnostic value for MCI detection in T2DM patients (AUC $>$ 0.7). Among these four regions, left precuneus WMV presented the best diagnostic value (AUC: 0.736; sensitivity: 70.00%; specificity: 73.33%; Youden index: 0.4333), but with no significant difference relative to the minimum AUC. In conclusion, T2DM could give rise to the white matter atrophy of several brain regions. Each WMV of left posterior cingulate, precuneus, insula, and right rostral middle frontal gyrus could be an independent imaging biomarker to detect cognitive impairment at the early stage in T2DM patients and play an important role in its pathophysiological mechanism.

Keywords: type 2 diabetes mellitus, mild cognitive impairment, white matter volume, magnetic resonance imaging, biomarker

INTRODUCTION

Type 2 diabetes mellitus (T2DM) is a common metabolic disorder characterized by insulin resistance and hyperglycemia, which has become a significant health problem throughout the world. It can cause severe multi-systemic dysfunction, such as kidney, eye, peripheral, central nervous system, etc. Epidemiological investigations have shown that T2DM is associated with a twofold increased risk of dementia and can affect a wide range of cognitive abilities (Peila et al., 2002; Biessels et al., 2006; Crane et al., 2013). Mild cognitive impairment (MCI) is considered as a precursor of dementia, which has been an increasingly common target of potential therapeutic trials (Schneider et al., 2009; Brooks and Loewenstein, 2010; Sperling et al., 2011). Currently, the occurrence of dementia is an irreversible process and has no effective cure solution. The effective and preventive treatments are needed at early phases of the dementia spectrum (Jedynak et al., 2012). Thus, the early detection of alterations in T2DM patients with MCI is important for patient care and developing future treatment.

Nowadays, the cognitive tests have been widely used for detection of cognitive impairment. However, the cognitive tests scores could be affected by the subjective judgment and drug intervention. Brain magnetic resonance (MR) imaging provided a good opportunity to explore the diabetic cerebral changes. The MR imaging biomarkers are more objective evidence, which could provide a supplement and clue for early diagnosis of cognitive impairment in T2DM patients. On conventional MR images, brain atrophy in some regions could be found (de Bresser et al., 2010; van Elderen et al., 2010; Espeland et al., 2013; Moran et al., 2019). Recently, lots of attention have been paid on the gray matter changes of T2DM patients. Several studies have shown that regional atrophy patterns of gray matter mainly located in frontal lobe, middle temporal gyrus, and posterior cingulate gyrus (Brundel et al., 2010; Moran et al., 2013; Moulton et al., 2015; Fang et al., 2018; Li et al., 2018). Despite the importance of gray matter atrophy in T2DM, white matter abnormalities played a distinct and irreplaceable role in cognitive impairments induced by T2DM. White matter has a vital role for transferring information between gray matter regions. White matter alterations include both microstructural deficits and morphological abnormalities. On one hand, studies of white matter integrity using MR diffusion tensor imaging (DTI) have demonstrated microstructural alterations in different regions in T2DM patients. These studies observed reduced white matter integrity predominantly in the cingulum, the uncinate fasciculus, the superior and inferior longitudinal fasciculus, corpus callosum, and external and internal capsule (Zhang et al., 2014; Nouwen et al., 2017; Yoon et al., 2017; Sun et al., 2018; Xiong et al., 2019). On the other hand, volumetric measurements are widely used to study morphological changes in both normal aging and in neurodegenerative disorders. Understanding changes in regional brain volumes has the potential to aid prediction of onset and progression of many neurodegenerative disorders. However, few studies have been focused on alterations of white matter volume (WMV) in T2DM patients. The loss of WMV in T2DM patients has been observed in temporal lobe, inferior frontal triangle region, and hippocampus (Korf et al., 2006; Gold et al., 2007; Chen et al., 2012; Moran et al., 2013). The alterations of WMV in previous studies did not show a consistent pattern in T2DM. The reason for the inconsistent results may be that T2DM patients included in these studies were in different stages of diabetes-associated cognitive impairment. To our knowledge, we have not found the report of WMV changes in T2DM patients with MCI at present.

In the current study, we enrolled T2DM patients with mild cognitive impairments (T2DM-MCI), T2DM patients with normal cognition (T2DM-NC), and healthy controls (HC) who performed clinical assessment, a battery of neuropsychological tests, and high-resolution sagittal T1-weighted structural MR imaging to explore how T2DM affects white matter and cognition. Automated segmentation analyses were applied to investigate the WMV difference of the whole brain in these three groups. Then, we assessed the relationship between the WMV of each brain region and neuropsychological tests in the T2DM groups. Finally, we identified the imaging biomarkers to detect MCI in T2DM patients. We expect that our study could provide imaging biomarkers and new insight into the neuropathological mechanisms of T2DM-related cognitive impairment.

MATERIALS AND METHODS

Participants

Samples were collected from 90 patients, consisting of 30 HC, 30 patients with T2DM-NC (T2DM-NC group), 30 patients with T2DM with MCI (T2DM-MCI group). Their overall data were accumulated and categorized by gender, age, and years of education. From October 2015 to June 2020, our hospital recruited all the T2DM patients with and without MCI. The World Health Organization's criteria were adopted to diagnose T2DM. The accurate diagnosis of MCI was made on the basis of the criteria set up in European Alzheimer's Disease Consortium in 2006, which involves Mini-Mental State Examination (MMSE) score > 24, clinical dementia rating (CDR) ≥ 0.5, MoCA score < 26, normal activities of daily living (ADL) score, and complaints of hypomnesia. Each patient was tested by structural MRI, neurological, and neuropsychological examinations. All the participants signed informed consent before the study started and were right-handed. If participants had a history of brain injury, epilepsy, alcoholism, Parkinson's disease, major depression, or other psychiatric or neurological disorder, they were excluded. The participants with severe claustrophobia or contraindications to MRI, severe depression (Hamilton Depression Rating Scale ≥ 18), and dementia (MMSE ≤ 24) were also excluded. If patients with T2DM had microvascular complications including nephropathy, retinopathy, and neuropathy, they were excluded. Thirty volunteers with no cognitive complaints or psychiatric illnesses, nervous system diseases, and vascular risk factors were enlisted as the HC. Participant was excluded if white matter hyperintense lesions on fluid-attenuated inversion recovery (FLAIR) imaging were found. The white matter lesions were also evaluated according to a 10-level scale from barely detectable white matter changes (grade 1) to extensive, confluent changes

(grade 9) (Manolio et al., 1994; Chen et al., 2012), and grade 0 (normal white matter) and grade 1 (barely detectable white matter changes) were included and other grades were excluded in this study. Each individual was measured for height, weight, and body mass index (BMI). The Medical Ethics Committee of our institution approved this study, which was conducted in accordance with the principles of the Declaration of Helsinki.

Neuropsychological Assessments

The Montreal Cognitive Assessment (MoCA), MMSE, Rey-Osterrieth Complex Figure Test (ROCF), Trail-Making Test (TMT), Auditory Verbal Learning Test (AVLT), Verbal Fluency Test (VFT), Digit Span Test (DST), Digit Symbol Coding Test (DSCT), and Hamilton Depression Scale (HAMD) were included in the neuropsychological assessments.

Standard Laboratory Tests

Standard laboratory tests were executed to evaluate glycosylated hemoglobin (HbA1c), fasting plasma glucose (FPG), fasting insulin, fasting C-peptide, high-density lipoprotein (HDL), low-density lipoprotein (LDL), total cholesterol (TC), triglycerides (TG), urinary microalbumin, homocysteine, blood urea nitrogen (BUN), uric acid, cystatin C, serum creatine, free thyroxine (FT), free triiodothyronine (FT3), and thyroid stimulating hormone (TSH).

MR Image Acquisition

A 3 T Trio MRI system (Siemens Healthcare, Erlangen, Germany) equipped with a 12-channel phase-array head coil was adopted to collect all MRI data. During the image acquisition, the tested subjects were asked not to move and to keep calm with their eyes closed. By using a T1-weighted magnetization prepared rapid acquisition gradient echo (MPRAGE) sequence (repetition time = 1,900 ms, echo time = 2.52 ms, inversion time = 900 ms, flip angle = 9°, matrix = 256 × 256, thickness = 1.0 mm, 176 slices with voxel size = 1 × 1 × 1 mm^3), the 3D high-resolution structural images were procured. Afterward, conventional brain T1-weighted imaging (TR/TE = 200/2.78 ms, flip angle = 70°, matrix = 384 × 384, thickness = 4.0 mm, 25 slices, voxel size = 0.7 × 0.6 × 5 mm^3) and FLAIR imaging (TR/TE/TI = 9,000/93/2,500 ms, flip angle = 130°, matrix = 256 × 256, thickness = 4.0 mm, 25 slices, voxel size = 0.9 × 0.9 × 4 mm^3) were subjected to all the subjects to exclude white matter hyperintense lesions and organic diseases.

Image Processing

The data were outputted to a personal computer from the MRI scanner. Off-line analysis was carried out and Linux Operating System was the operating system. Firstly, all the images were confirmed not affected by head motion prior to further analysis of the 3D brain images. Afterward, we converted all the data to MGZ (compressed Massachusetts General Hospital file) format. Meanwhile, by using FreeSurfer software (version 5.3.0, available at http://surfer.nmr.mgh.harvard.edu), the whole brain WMVs were measured. There were multiple steps of the automated processing stream of FreeSurfer, which contained Talairach transformation, removal of non-brain tissue, automatic correction of topological defects, inflation of the folded surface, and registration into an average spherical surface template. In order to segment the gray/white matter tissue and CSF with sub-millimeter precision, a deformable surface algorithm was utilized. Raw volumes for the total WMV were extracted as well as segmented volumes of 68 WMVs (34 regions in each hemisphere) in white matter regions (based on Killiany-Desikan atlas) (Harrisberger et al., 2018; Guo et al., 2019).

Statistical Analyses

Statistical analyses were performed using SPSS software (version 20.0; IBM Corp., Armonk, NY). The data distribution was verified using the Kolmogorov–Smirnov test. For WMV, comparisons among the three groups were performed by using ANOVA test, with the level of significance setting at $P < 0.05$, false discovery rate (FDR) corrected. For demographics and neuropsychological testing, comparisons among the three groups were performed by using the analysis of variance (ANOVA) test, if the data distribution was normal. The level of significance for intergroup differences was set at $P < 0.05$. The chi-squared analyses were applied to nonparametric analyses if the data distribution was not normal. *Post hoc* tests with Bonferroni correction were performed after observing statistical differences among the three groups. $P < 0.017$ (0.05/3) was considered significant after Bonferroni correction. For the T2DM patients, the correlations between the WMV of each brain region and the neuropsychological scale scores were tested using Pearson correlation analyses. For receiver operating characteristic (ROC) analysis, areas under the curves (AUCs) were used to evaluate the diagnostic value of each marker. Generally, an AUC greater than 0.9 indicated excellent diagnostic efficacy, between 0.7 and 0.9 indicated good diagnostic efficacy, between 0.5 and 0.7 indicated poor diagnostic efficacy, and no more than 0.5 indicated the lack of a diagnostic value. MedCalc Statistical Software (version 19.3.1; MedCalc Software Ltd, Ostend, Belgium) was used to compare differences in AUCs. $P < 0.05$ was considered statistically significant.

RESULTS

Demographics and Neuropsychological Testing

The demographic, clinical, and neuropsychological data for the T2DM-MCI, T2DM-NC, and HC groups are shown in **Tables 1**, **2**. No significant intergroup difference was observed in age, gender, years of education, systolic, or diastolic blood pressure, LDL, total cholesterol, and triglycerides. T2DM-NC patients presented higher FPG and HbA1c and lower HDL than HC (Bonferroni correction, $P < 0.017$); T2DM-MCI patients presented higher BMI, FPG, and HbA1c and lower HDL than HC (Bonferroni-correction, $P < 0.017$), while no significant differences were found between T2DM-NC and T2DM-MCI patients. As expected, cognitive function evaluated by various neuropsychological tests showed the worst performance in

TABLE 1 | Demographic and clinical data of the subjects.

	T2DM-MCI	T2DM-NC	HC	*F*-value (t/χ^2)	*P*-values
Numbers	30	30	30	–	–
Age (years)	55.9 ± 6.54	54.97 ± 5.54	53.17 ± 6.57	1.491	0.231
Sex (male/female)	12/18	19/11	14/16	3.467	0.177[a]
Education (years)	10.43 ± 2.94	11.90 ± 2.92	11.80 ± 2.99	2.316	0.105
Diabetes duration (years)	6.93 ± 5.46	7.93 ± 5.98	–	0.699	0.933
BMI (kg/m^2)	25.59 ± 3.31	24.08 ± 3.02	23.45 ± 2.59	4.052	0.021*
Systolic blood pressure (mmHg)	130.57 ± 18.25	131.37 ± 14.78	128.13 ± 18.10	0.194	0.749
Diastolic blood pressure (mmHg)	80.60 ± 10.33	82.90 ± 9.80	79.77 ± 9.17	0.895	0.441
Fasting glucose (mmol/L)	9.14 ± 3.05	8.56 ± 1.97	5.47 ± 0.63	25.769	< 0.001*#
HbA1c (%)	9.13 ± 2.07	8.84 ± 1.72	5.50 ± 0.36	49.505	< 0.001*#
Total cholesterin (mmol/L)	5.24 ± 1.45	4.96 ± 1.37	5.21 ± 0.96	0.432	0.651
HDL cholesterin (mmol/L)	1.16 ± 0.33	1.18 ± 0.30	1.40 ± 0.33	5.167	0.008*#
LDL cholesterin (mmol/L)	3.36 ± 1.06	2.93 ± 0.78	3.10 ± 0.67	1.874	0.160

*All subjects (T2DM-MCI, T2DM-NC, HC) were matched for age, sex, and education. Values are the mean ± standard deviation. [a]Chi-square test for sex. The comparisons of demographic and clinical data among three groups were performed with ANOVA. The level of significance for intergroup differences was set at $P < 0.05$. *Denotes $P < 0.017$ (0.05/3) T2DM-MCI vs. HC with post hoc test, Bonferroni corrected. #Denotes $P < 0.017$ (0.05/3) T2DM-NC vs. HC with post hoc test, Bonferroni corrected. No significant difference was shown between T2DM-NC and T2DM-MCI with post hoc test, Bonferroni corrected. BMI, body mass index; HbA1c, glycosylated hemoglobin; HDL, high-density lipoprotein; LDL, low-density lipoprotein.*

TABLE 2 | Comparison of the neuropsychological test results among T2DM-MCI, T2DM-NC, and HC groups.

	T2DM-MCI (*n* = 30)	T2DM-NC (*n* = 30)	HC (*n* = 30)	*F*-value (t/χ^2)	*P*-values
General mental status					
MoCA	22.93 ± 1.95	27.00 ± 0.83	27.77 ± 1.28	99.370	< 0.001*#
MMSE	27.93 ± 1.31	28.43 ± 1.07	28.43 ± 1.17	1.774	0.176
Episodic memory					
AVLT-immediately recall	19.50 ± 4.55	22.77 ± 3.83	22.83 ± 5.00	5.406	0.006*#
AVLT-delayed recall (5 min)	7.23 ± 2.40	7.80 ± 1.56	8.20 ± 1.94	1.775	0.176
AVLT-delayed recall (20 min)	6.83 ± 2.64	7.33 ± 1.77	7.87 ± 2.18	1.620	0.204
AVLT-recognition	21.10 ± 3.60	21.87 ± 1.48	22.90 ± 1.45	4.252	0.017*
ROCF-immediate recall	19.00 ± 6.64	22.63 ± 6.95	24.08 ± 8.49	3.754	0.027*
ROCF-delayed recall (20 min)	18.20 ± 6.19	21.85 ± 7.13	23.65 ± 7.74	4.659	0.012*
Working memory					
WAIS	35.63 ± 8.33	41.23 ± 10.83	46.23 ± 11.99	7.658	0.001*
DST-forward	8.93 ± 1.08	8.87 ± 0.82	9.57 ± 1.38	3.584	0.032
DST-backward	4.67 ± 0.88	5.03 ± 0.89	5.53 ± 1.17	5.805	0.004*
Spatial processing					
ROCF-copy	31.97 ± 3.88	32.55 ± 4.11	33.17 ± 1.90	0.911	0.406
Executive function					
TMT-B	80.77 ± 26.59	67.73 ± 24.19	61.33 ± 22.74	4.877	0.010*
Language ability					
VFT	40.60 ± 7.04	44.10 ± 8.29	44.83 ± 6.06	2.970	0.057
Attention					
TMT-A	63.80 ± 21.66	51.97 ± 17.44	48.57 ± 16.61	5.484	0.006*#

*All subjects (T2DM-MCI, T2DM-NC, HC) were matched for age, sex, and education. Values are the mean ± standard deviation. The comparisons of each neuropsychological test among three groups were performed with ANOVA. The level of significance for intergroup differences was set at $P < 0.05$. *Denotes $P < 0.017$ (0.05/3) T2DM-MCI vs. HC with post hoc test, Bonferroni corrected. #Denotes $P < 0.017$ (0.05/3) T2DM-MCI vs. T2DM-NC with post hoc test, Bonferroni corrected. No significant difference was shown between T2DM-NC and HC with post hoc test, Bonferroni corrected. MMSE, Mini-Mental State Examination; MoCA, Montreal Cognitive Assessment; AVLT, Auditory Verbal Learning Test; ROCF, Rey-Osterrieth Complex Figure; WAIS, Wechsler Adult Intelligence Scale; DST, Digital Span Test; TMT, Trail Making Test; VFT, Verbal Fluency Test.*

T2DM-MCI patients than HC and T2DM-NC patients. No significant difference was shown between T2DM-NC patients and HC (Bonferroni correction, $P > 0.017$). Furthermore, T2DM-MCI patients exhibited significant decreases in multiple domains of cognitive function including episodic memory, working memory, executive function, and attention domains when compared with T2DM-NC patients and HC, but no differences in language ability and spatial processing.

TABLE 3 | Differences in the white matter volume among T2DM-MCI, T2DM-NC, and HC groups.

Regions	White matter volume			*F*-values	ANOVA
	HC	T2DM-NC	T2DM-MCI		(*P*-values)
Left isthmus cingulate	3, 931.40 ± 569.78	3, 819.84 ± 570.83	3, 470.82 ± 603.25	5.122	0.048
Left lateral orbitofrontal gyrus	6, 700.99 ± 838.21	6, 702.80 ± 570.27	6, 267.02 ± 770.28	3.500	0.042
Left posterior cingulate	4, 379.01 ± 610.81	4, 652.48 ± 500.46	4, 231.84 ± 441.51	5.010	0.027*
Left precuneus	9, 442.53 ± 1, 743.27	9, 833.90 ± 1, 242.31	8, 847.39 ± 1, 264.13	3.593	0.048*
Left insula	8, 918.20 ± 946.21	9, 140.63 ± 746.48	8, 618.25 ± 695.40	3.194	0.046*
Right lateral orbitofrontal gyrus	6, 569.96 ± 721.97	6, 734.11 ± 641.00	6, 196.94 ± 765.54	4.492	0.049*
Right pars orbitalis	1, 134.16 ± 232.18	1, 209.77 ± 168.79	1, 063.01 ± 187.21	4.128	0.044*
Right rostral middle frontal gyrus	12, 509.42 ± 2, 160.15	12, 959.35 ± 1, 604.56	11, 768.02 ± 1, 791.73	3.116	0.049*
Right temporal pole	687.63 ± 128.12	745.50 ± 113.06	669.06 ± 119.51	3.290	0.049*

*Values are the mean ± standard deviation. The comparisons of white matter volume of each region among three groups were performed with ANOVA. The level of significance for intergroup differences was set at P < 0.05, false discovery rate (FDR) corrected. *Denotes P < 0.017 (0.05/3) T2DM-MCI vs. T2DM-NC with post hoc test, Bonferroni corrected. No significant difference was shown between the T2DM-NC group and HC group with post hoc test, Bonferroni corrected.*

Group Differences in WMV Among the Groups

The WMV of the whole brain of T2DM-MCI, T2DM-NC, and HC groups were analyzed. If statistical differences among the three groups were observed, then a *post hoc* test was performed. It was not surprising that obvious difference in WMV among these three groups were observed in 13 regions ($P < 0.05$, FDR corrected, **Table 3**). Subsequently, we performed a *post hoc* test and Bonferroni correction. Significant difference of regional WMV was observed in T2DM-MCI patients relative to T2DM-NC patients. Regions of the white matter atrophy were the left insula, posterior cingulate, and precuneus, right lateral orbitofrontal gyrus, pars orbitalis gyrus, rostral middle frontal gyrus, and temporal pole (Bonferroni-correction, $P < 0.017$) (**Table 3**). However, there was no significant difference between T2DM-NC and HC groups (**Table 3**). In addition, the included T2DM patients had no obvious white matter hyperintensity lesions on T2 FLAIR, which indicates that brain white matter atrophy rather than cerebrovascular lesions may substantially mediate the relationship between T2DM and cognitive impairment.

WMV in Relation to Cognitive Performance in T2DM Patients

Based on the WMV and cognition scores with significant intergroup differences, we explored the relationship between WMV of these regions and the neuropsychological testing scores in all T2DM patients. The results revealed that MoCA scores were significantly correlated with the WMV of the left posterior cingulate ($r = 0.387$, $P = 0.002$), precuneus ($r = 0.319$, $P = 0.013$), insula ($r = 0.328$, $P = 0.011$), right rostral middle frontal gyrus ($r = 0.297$, $P = 0.021$), and temporal pole ($r = 0.259$, $P = 0.045$) (**Figure 1**).

Discriminative Ability of White Matter Atrophy for MCI Detection in T2DM Patients

Considering that the WMV of eight brain regions significantly correlated with MoCA scores, we evaluated the discriminative ability of the white matter atrophy of these regions for MCI detection in T2DM patients. The ROC results showed that, when used alone, the WMV of left posterior cingulate, precuneus, insula, and right rostral middle frontal gyrus had high diagnostic value for MCI detection in T2DM patients (AUC > 0.7, **Table 4**), among which the value of WMV of left precuneus was the highest (AUC: 0.736, sensitivity: 70%, specificity: 73.33%). While the other region, right temporal pole, demonstrated little significance to identify T2DM-MCI patients (AUC = 0.686, **Table 4**). Furthermore, there was no significant difference between the minimum AUC (right rostral middle frontal gyrus) and the maximum AUC (left precuneus) among these four single markers ($Z = 0.597$, $P = 0.551$), which had high diagnostic value for MCI detection in T2DM patients (**Figure 2**). Above all, each WMV of these four regions, including left posterior cingulate, precuneus, insula, and right rostral middle frontal gyrus, could be the independent imaging biomarkers for MCI identification in T2DM patients.

DISCUSSION

In this study, cognitive function assessed by various neuropsychological tests showed that T2DM-MCI patients performed worst among these three groups, while there was no significant difference between T2DM-NC patients and HC. Subsequently, T2DM-MCI patients had white matter atrophy of several regions, and T2DM-NC patients did not show any white matter deficits. In particular, WMV of five regions including the left posterior cingulate, precuneus, insula, right rostral middle frontal gyrus, and temporal pole were significantly correlated with MoCA scores in T2DM patients. More importantly, we identified that each WMV of left posterior cingulate, precuneus, insula, and right rostral middle frontal gyrus could be the independent imaging biomarkers for T2DM-associated MCI detection.

To explore the white matter atrophy due to T2DM and T2DM-associated cognitive impairments, we compared the difference of WMV among T2DM-MCI, T2DM-NC, and HC groups. As expected, the WMV was considerably different in some

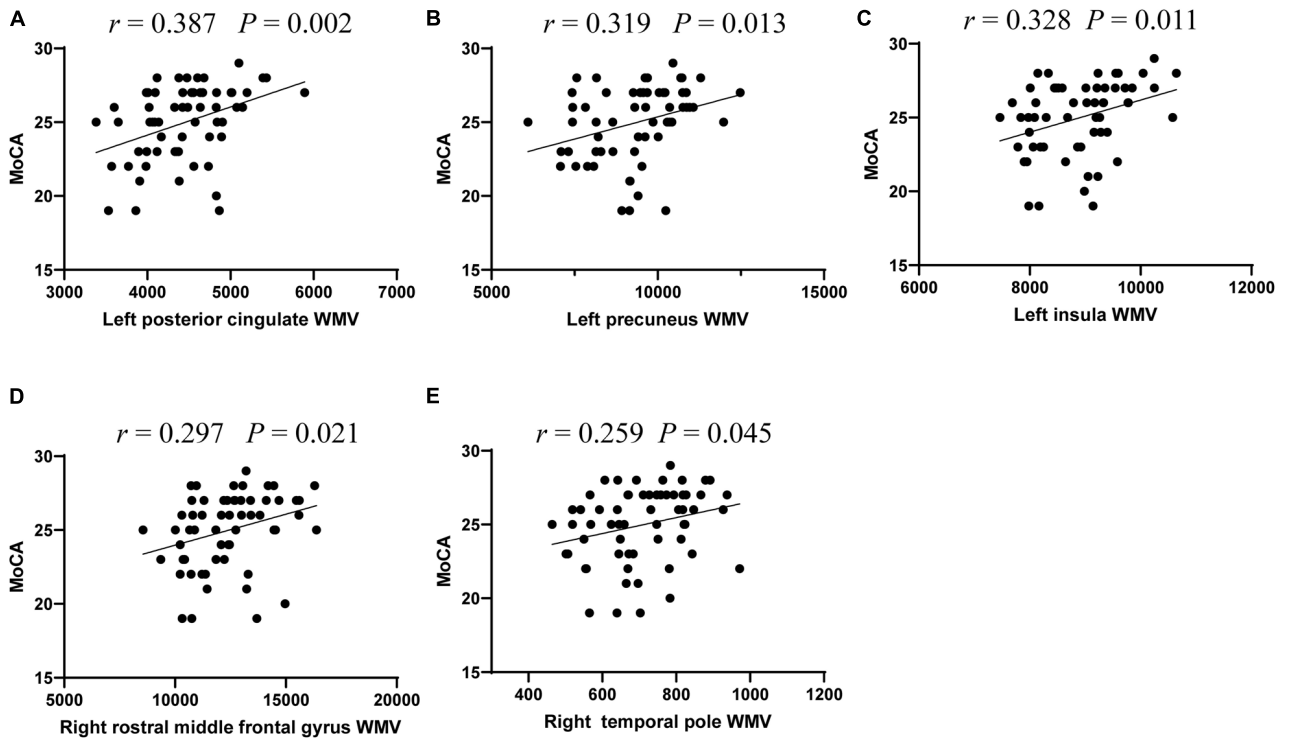

FIGURE 1 | The significant correlations between white matter volume and cognitive performance in T2DM patients. Correlations between MoCA scores and white matter volume of five regions, including left posterior cingulate **(A)**, left precuneus **(B)**, and left insula **(C)**, right rostral middle frontal gyrus **(D)**, and right temporal pole **(E)**.

TABLE 4 | Diagnostic values of single imaging marker for MCI in T2DM patients.

Regions (white matter volume)	SEN (%)	SPE (%)	+LR	−LR	Yden	Cutoff	AUC
Left posterior cingulate	70.00	73.33	2.62	0.41	0.4333	4,419.8	0.729
Left precuneus	70.00	73.33	2.62	0.41	0.4333	9,413.7	0.736
Left insula	90.00	46.67	1.69	0.21	0.3667	9,283	0.712
Right rostral middle frontal gyrus	63.33	76.67	2.71	0.48	0.4000	12,077.7	0.704
Right temporal pole	70.00	66.67	2.10	0.45	0.3667	702.7	0.686

SEN, sensitivity; SPE, specificity; +LR, positive likelihood ratio; −LR, negative likelihood ratio; Yden, Youden index; AUC, areas under the curves.

regions among these three groups with FDR correction. After a *post hoc* test and Bonferroni correction, T2DM-MCI patients had white matter atrophy in the left insula, posterior cingulate, and precuneus, right lateral orbitofrontal gyrus, pars orbitalis gyrus, rostral middle frontal gyrus, and temporal pole, when compared with T2DM-NC patients without clinically confirmed cognitive impairment. Additionally, the T2DM-NC patients did not show significant atrophy in brain white matter compared with the HC. These results indicated that the observed atrophy in brain white matter is strongly associated with cognitive impairment in T2DM patients. Previous studies reported that T2DM was associated with white matter loss mainly in frontal and temporal white matter, which were partly in line with our findings (Chen et al., 2012; Moran et al., 2013). However, some other studies revealed that individuals with T2DM had reductions in hippocampus volumes but superior temporal gyrus had no volume loss, which were not in accordance with our results (Korf et al., 2006; Gold et al., 2007; Cherbuin et al., 2012). In addition, we found that some limbic structures and precuneus, which have been reported associated with cognitive functions (Cavanna and Trimble, 2006; McCrimmon et al., 2012; Hoogenboom et al., 2014), had obviously reduced WMV. The reason of the inconsistent results may be associated with the cognitive state of the included T2DM patients. T2DM patients included in these previous studies were in different stages of diabetes-associated cognitive impairment, whereas in our study, we enrolled T2DM-MCI, the early stages of cognitive impairment in T2DM patients, and T2DM-NC without clinically confirmed cognitive impairments to provide early signs of cognitive dysfunction, which may help clinicians with the earlier prevention of severe cognitive decline in T2DM patients.

The MoCA scores, which served as an index of the cognitive status of the patients, are known to distinguish patients with MCI form the normal population (Petersen et al., 1999). MoCA has shown higher sensitivity in detecting cognitive decline than the

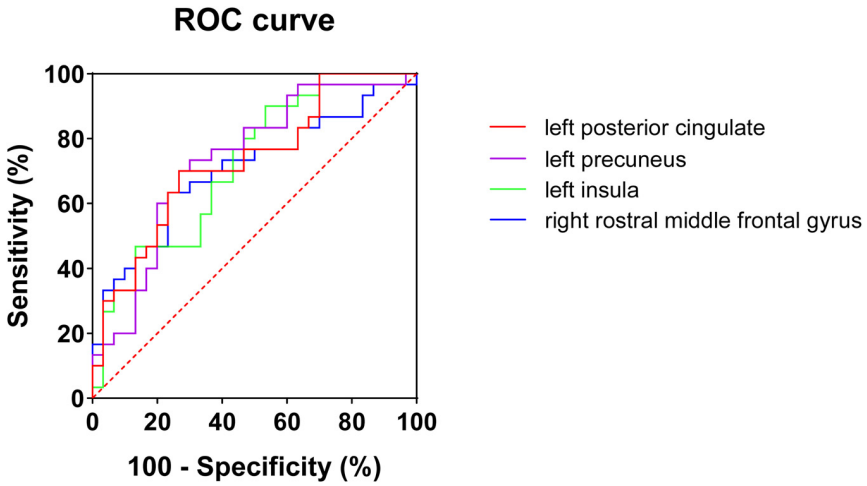

FIGURE 2 | ROC curves of white matter volume of four single regions for mild cognitive impairments in T2DM patients. No significant difference ($Z = 0.597$, $P = 0.551$) was found between minimum AUC (right rostral middle frontal gyrus) and the maximum AUC (left precuneus).

MMSE (Nasreddine et al., 2005). Our results revealed that no significant differences were shown in MMSE scores among these three groups, while MoCA scores were significantly higher in HC when compared with T2DM-MCI and T2DM-NC patients, and T2DM-NC patients performed better than T2DM-MCI patients. Furthermore, WMV of five brain regions significantly correlated with the MoCA scores, mainly located in frontotemporal lobe and limbic system, which have been implicated in memory and learning (McCrimmon et al., 2012). Among them, the correlation coefficient of the left posterior cingulate WMV was higher than others. Cingulate gyrus, as one of the important limbic structures, has been reported to be disrupted in T2DM patients (Yau et al., 2010; Hoogenboom et al., 2014; Tan et al., 2016; Nouwen et al., 2017; Groeneveld et al., 2018; Yu et al., 2019). More importantly, its disruption was associated with impairments in cognitive functions including memory, psychomotor speed performance, and executive function in T2DM patients (Hoogenboom et al., 2014). Previous studies have discovered reduced functional connectivity in the default mode network between posterior cingulate gyrus and left medial frontal gyrus in middle-aged T2DM patients. Moreover, reduced FA in the cingulum was correlated with lower functional connectivity between cingulate and medial frontal gyrus (Hoogenboom et al., 2014). Moreover, the white matter loss was also reported in cingulate gyrus attributed to T2DM (Chen et al., 2012). More interestingly, our study also showed that the WMV of left posterior cingulate had a high discriminative ability for T2DM patients with MCI. Thus, the white matter disruption of cingulate gyrus has a possible relationship with cognitive impairments at the early stage in T2DM patients.

In addition, to find non-invasive biomarkers for early detection of cognitive impairment in T2DM patients, we evaluated the discriminative ability of these five regions for MCI in T2DM patients. Four regions had high diagnostic value for MCI detection in T2DM patients by performing ROC analysis of a single region, among which the value of left precuneus was the highest. The precuneus has been reported to play a central role in a wide spectrum of highly integrated tasks, including visuo-spatial imagery (Simon et al., 2002; Malouin et al., 2003; Wenderoth et al., 2005), episodic memory retrieval (Platel et al., 2003; Addis et al., 2004; Lundstrom et al., 2005), and self-processing operations (Vogeley et al., 2004; den Ouden et al., 2005; Cavanna and Trimble, 2006). Moreover, the white matter disruption and reduced functional connectivity of the precuneus were found in T2DM patients and significantly correlated with disease duration (Zhou et al., 2010; Hsu et al., 2012; Wood et al., 2016). Thus, the white matter atrophy of precuneus could be a part of mild cognitive dysfunction in T2DM patients. Then, we compared the AUC of these four regions' WMV, which presented high diagnostic value for MCI detection in T2DM patients. The results showed that no significant difference was found in maximum AUC relative to the minimum AUC among the four regions' WMV. Therefore, each WMV of the four regions, including left posterior cingulate, precuneus, insula, and right rostral middle frontal gyrus, could be the independent imaging biomarker for detecting mild cognitive dysfunction in T2DM patients.

There are also several limitations in our study. First, this current research is a cross-sectional study with a relatively small sample size, and a longitudinal study with a larger sample size is needed in the future to test whether these WMV atrophy could predict the development of cognitive impairment in T2DM patients. Second, although we enrolled age-, sex-, and education-matched HC, T2DM-MCI patients had higher BMI index than HC. However, there were no significant difference in BMI between T2DM-MCI and T2DM-NC patients, with the result that the effect of BMI on the results should be little. Third, although education has been used as a control variable in this study, the participants with different levels of educational achievement may show different effects. Fourth, we only focused on the white matter atrophy in T2DM patients with MCI. Some microstructural damage of white matter could not be detected

on conventional MR images. Exploring the WMV, integrity, and network connection in the same participants will provide more details on the pathophysiological mechanism of white matter. Thus, multimodal imaging methods are needed to investigate the white matter damage in T2DM association with cognitive deficits in future.

CONCLUSION

In conclusion, the present study revealed that T2DM-NC patients did not show any white matter damage, and T2DM-MCI patients showed significantly reduced WMV in several regions, which suggests that significant white matter atrophy occurred in MCI stage in T2DM patients. In particular, MoCA scores in T2DM patients had significant correlations with the white matter loss of the five regions mainly in the frontotemporal lobe and limbic system. Moreover, each WMV of the four regions, including left posterior cingulate, precuneus, insula, and right rostral middle frontal gyrus, could be the independent imaging biomarker for T2DM-associated cognitive impairment at the early stage and play an important role in its pathophysiological mechanism.

DATA AVAILABILITY STATEMENT

The original contributions presented in the study are included in the article/supplementary material, further inquiries can be directed to the corresponding author/s.

ETHICS STATEMENT

The studies involving human participants were reviewed and approved by the Research Ethics Committee of Southwest Hospital, Army Medical University, Chonqing, China. The patients/participants provided their written informed consent to participate in this study.

AUTHOR CONTRIBUTIONS

XC, JW, and KX conceived and designed the study. CL and YL collected the data of MRI, clinical, and neuropsychological test. ZZ and RJ analyzed MRI data. KL and HT performed statistics. YG and JZ performed figure and table preparation. XC and KL wrote the manuscript. JS and QZ edited the manuscript. All authors revised the manuscript, and read and approved the submitted version.

FUNDING

This work was supported by grants from the National Natural Science Foundation of China (81801672 and 81571889), the Natural Science Foundation of Chongqing (cstc2019jcyj-msxmX0123), the Science and Technology Innovation Ability Enhancement Project of Army Medical University (2019XLC3054), the Talent Innovation Ability Training Program of Daping Hospital (2019CXLCC010), and the Chongqing Clinical Research Centre of Imaging and Nuclear Medicine (CSTC2015YFPT-gcjsyjzx0175).

REFERENCES

Addis, D. R., Mcintosh, A. R., Moscovitch, M., Crawley, A. P., and Mcandrews, M. P. (2004). Characterizing spatial and temporal features of autobiographical memory retrieval networks: a partial least squares approach. *Neuroimage* 23, 1460–1471. doi: 10.1016/j.neuroimage.2004.08.007

Biessels, G. J., Staekenborg, S., Brunner, E., Brayne, C., and Scheltens, P. (2006). Risk of dementia in diabetes mellitus: a systematic review. *Lancet Neurol.* 5, 64–74. doi: 10.1016/S1474-4422(05)70284-2

Brooks, L. G., and Loewenstein, D. A. (2010). Assessing the progression of mild cognitive impairment to Alzheimer's disease: current trends and future directions. *Alzheimers Res. Ther.* 2:28. doi: 10.1186/alzrt52

Brundel, M., Van Den Heuvel, M., De Bresser, J., Kappelle, L. J., Biessels, G. J., Utrecht Diabetic, et al. (2010). Cerebral cortical thickness in patients with type 2 diabetes. *J. Neurol. Sci.* 299, 126–130. doi: 10.1016/j.jns.2010.08.048

Cavanna, A. E., and Trimble, M. R. (2006). The precuneus: a review of its functional anatomy and behavioural correlates. *Brain* 129, 564–583. doi: 10.1093/brain/awl004

Chen, Z., Li, L., Sun, J., and Ma, L. (2012). Mapping the brain in type II diabetes: Voxel-based morphometry using DARTEL. *Eur. J. Radiol.* 81, 1870–1876. doi: 10.1016/j.ejrad.2011.04.025

Cherbuin, N., Sachdev, P., and Anstey, K. J. (2012). Higher normal fasting plasma glucose is associated with hippocampal atrophy: The PATH Study. *Neurology* 79, 1019–1026. doi: 10.1212/WNL.0b013e31826846de

Crane, P. K., Walker, R., Hubbard, R. A., Li, G., Nathan, D. M., Zheng, H., et al. (2013). Glucose levels and risk of dementia. *N. Engl. J. Med.* 369, 540–548. doi: 10.1056/NEJMoa1215740

de Bresser, J., Tiehuis, A. M., Van Den Berg, E., Reijmer, Y. D., Jongen, C., Kappelle, L. J., et al. (2010). Progression of cerebral atrophy and white matter hyperintensities in patients with type 2 diabetes. *Diabetes Care* 33, 1309–1314. doi: 10.2337/dc09-1923

den Ouden, H. E., Frith, U., Frith, C., and Blakemore, S. J. (2005). Thinking about intentions. *Neuroimage* 28, 787–796. doi: 10.1016/j.neuroimage.2005.05.001

Espeland, M. A., Bryan, R. N., Goveas, J. S., Robinson, J. G., Siddiqui, M. S., Liu, S., et al. (2013). Influence of type 2 diabetes on brain volumes and changes in brain volumes: results from the Women's Health Initiative Magnetic Resonance Imaging studies. *Diabetes Care* 36, 90–97. doi: 10.2337/dc12-0555

Fang, F., Zhan, Y. F., Zhuo, Y. Y., Yin, D. Z., Li, K. A., and Wang, Y. F. (2018). Brain atrophy in middle-aged subjects with Type 2 diabetes mellitus, with and without microvascular complications. *J. Diabetes* 10, 625–632. doi: 10.1111/1753-0407.12646

Gold, S. M., Dziobek, I., Sweat, V., Tirsi, A., Rogers, K., Bruehl, H., et al. (2007). Hippocampal damage and memory impairments as possible early brain complications of type 2 diabetes. *Diabetologia* 50, 711–719. doi: 10.1007/s00125-007-0602-7

Groeneveld, O., Reijmer, Y., Heinen, R., Kuijf, H., Koekkoek, P., Janssen, J., et al. (2018). Brain imaging correlates of mild cognitive impairment and early dementia in patients with type 2 diabetes mellitus. *Nutr. Metab. Cardiovasc. Dis.* 28, 1253–1260. doi: 10.1016/j.numecd.2018.07.008

Guo, C., Ferreira, D., Fink, K., Westman, E., and Granberg, T. (2019). Repeatability and reproducibility of FreeSurfer, FSL-SIENAX and SPM brain volumetric measurements and the effect of lesion filling in multiple sclerosis. *Eur. Radiol.* 29, 1355–1364. doi: 10.1007/s00330-018-5710-x

Harrisberger, F., Smieskova, R., Egli, T., Simon, A. E., Riecher-Rossler, A., Fusar-Poli, P., et al. (2018). Impact on the Onset of Psychosis of a Polygenic Schizophrenia-Related Risk Score and Changes in White Matter Volume. *Cell Physiol. Biochem.* 48, 1201–1214. doi: 10.1159/000491986

Hoogenboom, W. S., Marder, T. J., Flores, V. L., Huisman, S., Eaton, H. P., Schneiderman, J. S., et al. (2014). Cerebral white matter integrity and resting-state functional connectivity in middle-aged patients with type 2 diabetes. *Diabetes* 63, 728–738. doi: 10.2337/db13-1219

Hsu, J. L., Chen, Y. L., Leu, J. G., Jaw, F. S., Lee, C. H., Tsai, Y. F., et al. (2012). Microstructural white matter abnormalities in type 2 diabetes mellitus: a diffusion tensor imaging study. *Neuroimage* 59, 1098–1105. doi: 10.1016/j.neuroimage.2011.09.041

Jedynak, B. M., Lang, A., Liu, B., Katz, E., Zhang, Y., Wyman, B. T., et al. (2012). A computational neurodegenerative disease progression score: method and results with the Alzheimer's disease Neuroimaging Initiative cohort. *Neuroimage* 63, 1478–1486. doi: 10.1016/j.neuroimage.2012.07.059

Korf, E. S., White, L. R., Scheltens, P., and Launer, L. J. (2006). Brain aging in very old men with type 2 diabetes: the Honolulu-Asia Aging Study. *Diabetes Care* 29, 2268–2274. doi: 10.2337/dc06-0243

Li, C., Li, C., Yang, Q., Wang, B., Yin, X., Zuo, Z., et al. (2018). Cortical thickness contributes to cognitive heterogeneity in patients with type 2 diabetes mellitus. *Medicine* 97:e10858. doi: 10.1097/MD.0000000000010858

Lundstrom, B. N., Ingvar, M., and Petersson, K. M. (2005). The role of precuneus and left inferior frontal cortex during source memory episodic retrieval. *Neuroimage* 27, 824–834. doi: 10.1016/j.neuroimage.2005.05.008

Malouin, F., Richards, C. L., Jackson, P. L., Dumas, F., and Doyon, J. (2003). Brain activations during motor imagery of locomotor-related tasks: a PET study. *Hum. Brain Mapp.* 19, 47–62. doi: 10.1002/hbm.10103

Manolio, T. A., Kronmal, R. A., Burke, G. L., Poirier, V., O'leary, D. H., Gardin, J. M., et al. (1994). Magnetic resonance abnormalities and cardiovascular disease in older adults. The Cardiovascular Health Study. *Stroke* 25, 318–327. doi: 10.1161/01.str.25.2.318

McCrimmon, R. J., Ryan, C. M., and Frier, B. M. (2012). Diabetes and cognitive dysfunction. *Lancet* 379, 2291–2299. doi: 10.1016/S0140-6736(12)60360-2

Moran, C., Beare, R., Wang, W., Callisaya, M., Srikanth, V., Alzheimer's Disease, et al. (2019). Type 2 diabetes mellitus, brain atrophy, and cognitive decline. *Neurology* 92, e823–e830. doi: 10.1212/WNL.0000000000006955

Moran, C., Phan, T. G., Chen, J., Blizzard, L., Beare, R., Venn, A., et al. (2013). Brain atrophy in type 2 diabetes: regional distribution and influence on cognition. *Diabetes Care* 36, 4036–4042. doi: 10.2337/dc13-0143

Moulton, C. D., Costafreda, S. G., Horton, P., Ismail, K., and Fu, C. H. (2015). Meta-analyses of structural regional cerebral effects in type 1 and type 2 diabetes. *Brain Imaging Behav.* 9, 651–662. doi: 10.1007/s11682-014-9348-2

Nasreddine, Z. S., Phillips, N. A., Bedirian, V., Charbonneau, S., Whitehead, V., Collin, I., et al. (2005). The Montreal Cognitive Assessment, MoCA: a brief screening tool for mild cognitive impairment. *J. Am. Geriatr. Soc.* 53, 695–699. doi: 10.1111/j.1532-5415.2005.53221.x

Nouwen, A., Chambers, A., Chechlacz, M., Higgs, S., Blissett, J., Barrett, T. G., et al. (2017). Microstructural abnormalities in white and gray matter in obese adolescents with and without type 2 diabetes. *Neuroimage Clin.* 16, 43–51. doi: 10.1016/j.nicl.2017.07.004

Peila, R., Rodriguez, B. L., Launer, L. J., and Honolulu-Asia Aging, S. (2002). Type 2 diabetes, APOE gene, and the risk for dementia and related pathologies: The Honolulu-Asia Aging Study. *Diabetes* 51, 1256–1262. doi: 10.2337/diabetes.51.4.1256

Petersen, R. C., Smith, G. E., Waring, S. C., Ivnik, R. J., Tangalos, E. G., and Kokmen, E. (1999). Mild cognitive impairment: clinical characterization and outcome. *Arch. Neurol.* 56, 303–308. doi: 10.1001/archneur.56.3.303

Platel, H., Baron, J. C., Desgranges, B., Bernard, F., and Eustache, F. (2003). Semantic and episodic memory of music are subserved by distinct neural networks. *Neuroimage* 20, 244–256. doi: 10.1016/s1053-8119(03)00287-8

Schneider, J. A., Arvanitakis, Z., Leurgans, S. E., and Bennett, D. A. (2009). The neuropathology of probable Alzheimer disease and mild cognitive impairment. *Ann. Neurol.* 66, 200–208. doi: 10.1002/ana.21706

Simon, O., Mangin, J. F., Cohen, L., Le Bihan, D., and Dehaene, S. (2002). Topographical layout of hand, eye, calculation, and language-related areas in the human parietal lobe. *Neuron* 33, 475–487. doi: 10.1016/s0896-6273(02)00575-5

Sperling, R. A., Aisen, P. S., Beckett, L. A., Bennett, D. A., Craft, S., Fagan, A. M., et al. (2011). Toward defining the preclinical stages of Alzheimer's disease: recommendations from the National Institute on Aging-Alzheimer's Association workgroups on diagnostic guidelines for Alzheimer's disease. *Alzheimers Dement.* 7, 280–292. doi: 10.1016/j.jalz.2011.03.003

Sun, Q., Chen, G. Q., Wang, X. B., Yu, Y., Hu, Y. C., Yan, L. F., et al. (2018). Alterations of White Matter Integrity and Hippocampal Functional Connectivity in Type 2 Diabetes Without Mild Cognitive Impairment. *Front. Neuroanat.* 12:21. doi: 10.3389/fnana.2018.00021

Tan, X., Fang, P., An, J., Lin, H., Liang, Y., Shen, W., et al. (2016). Micro-structural white matter abnormalities in type 2 diabetic patients: a DTI study using TBSS analysis. *Neuroradiology* 58, 1209–1216. doi: 10.1007/s00234-016-1752-4

van Elderen, S. G., De Roos, A., De Craen, A. J., Westendorp, R. G., Blauw, G. J., Jukema, J. W., et al. (2010). Progression of brain atrophy and cognitive decline in diabetes mellitus: a 3-year follow-up. *Neurology* 75, 997–1002. doi: 10.1212/WNL.0b013e3181f25f06

Vogeley, K., May, M., Ritzl, A., Falkai, P., Zilles, K., and Fink, G. R. (2004). Neural correlates of first-person perspective as one constituent of human self-consciousness. *J. Cogn. Neurosci.* 16, 817–827. doi: 10.1162/089892904970799

Wenderoth, N., Debaere, F., Sunaert, S., and Swinnen, S. P. (2005). The role of anterior cingulate cortex and precuneus in the coordination of motor behaviour. *Eur. J. Neurosci.* 22, 235–246. doi: 10.1111/j.1460-9568.2005.04176.x

Wood, A. G., Chen, J., Moran, C., Phan, T., Beare, R., Cooper, K., et al. (2016). Brain Activation during Memory Encoding in Type 2 Diabetes Mellitus: A Discordant Twin Pair Study. *J. Diabetes Res.* 2016:3978428. doi: 10.1155/2016/3978428

Xiong, Y., Sui, Y., Zhang, S., Zhou, X. J., Yang, S., Fan, Y., et al. (2019). Brain microstructural alterations in type 2 diabetes: diffusion kurtosis imaging provides added value to diffusion tensor imaging. *Eur. Radiol.* 29, 1997–2008. doi: 10.1007/s00330-018-5746-y

Yau, P. L., Javier, D. C., Ryan, C. M., Tsui, W. H., Ardekani, B. A., Ten, S., et al. (2010). Preliminary evidence for brain complications in obese adolescents with type 2 diabetes mellitus. *Diabetologia* 53, 2298–2306. doi: 10.1007/s00125-010-1857-y

Yoon, S., Cho, H., Kim, J., Lee, D. W., Kim, G. H., Hong, Y. S., et al. (2017). Brain changes in overweight/obese and normal-weight adults with type 2 diabetes mellitus. *Diabetologia* 60, 1207–1217. doi: 10.1007/s00125-017-4266-7

Yu, X., Jiaerken, Y., Xu, X., Jackson, A., Huang, P., Yang, L., et al. (2019). Abnormal corpus callosum induced by diabetes impairs sensorimotor connectivity in patients after acute stroke. *Eur. Radiol.* 29, 115–123. doi: 10.1007/s00330-018-5576-y

Zhang, J., Wang, Y., Wang, J., Zhou, X., Shu, N., Wang, Y., et al. (2014). White matter integrity disruptions associated with cognitive impairments in type 2 diabetic patients. *Diabetes* 63, 3596–3605. doi: 10.2337/db14-0342

Zhou, H., Lu, W., Shi, Y., Bai, F., Chang, J., Yuan, Y., et al. (2010). Impairments in cognition and resting-state connectivity of the hippocampus in elderly subjects with type 2 diabetes. *Neurosci. Lett.* 473, 5–10. doi: 10.1016/j.neulet.2009.12.057

Conflict of Interest: The authors declare that the research was conducted in the absence of any commercial or financial relationships that could be construed as a potential conflict of interest.

The reviewer XY declared a past co-authorship with the authors CL, ZZ, and JW to the handling editor.

frontiers in Neuroscience

ORIGINAL RESEARCH
published: 22 January 2021
doi: 10.3389/fnins.2020.616864

Jia-Ji Electro-Acupuncture Improves Locomotor Function With Spinal Cord Injury by Regulation of Autophagy Flux and Inhibition of Necroptosis

Yin Hongna[1†], Tian Hongzhao[1†], Li Quan[1], Feng Delin[2], Liu Guijun[1], Lv Xiaolin[1], Guan Fulin[3] and Sun Zhongren[1*]*

[1] Acupuncture Department, Heilongjiang University of Chinese Medicine, Harbin, China, [2] Harbin Children's Hospital, Harbin, China, [3] Neurology Department, The First Affiliated Hospital of Harbin Medical University, Harbin, China

OPEN ACCESS

Edited by:
Jiehui Jiang,
Shanghai University, China

Reviewed by:
Can Martin Zhang,
Massachusetts General Hospital and Harvard Medical School, United States
Zhihua Yu,
Shanghai University of Traditional Chinese Medicine, China

***Correspondence:**
Guan Fulin
fulinguancn@outlook.com
Sun Zhongren
szr006@163.com

† These authors have contributed equally to this work and share first authorship

Specialty section:
This article was submitted to Neurodegeneration, a section of the journal Frontiers in Neuroscience

Received: 13 October 2020
Accepted: 29 December 2020
Published: 22 January 2021

Citation:
Hongna Y, Hongzhao T, Quan L, Delin F, Guijun L, Xiaolin L, Fulin G and Zhongren S (2021) Jia-Ji Electro-Acupuncture Improves Locomotor Function With Spinal Cord Injury by Regulation of Autophagy Flux and Inhibition of Necroptosis. Front. Neurosci. 14:616864. doi: 10.3389/fnins.2020.616864

Jia-Ji electro-acupuncture (EA) has been widely applied in clinic to exhibit curative effects on spinal cord injury (SCI). However, its underlying mechanisms leading to improvement of motor function after SCI remain unclear. Allen's method was made by NYU Impactor M-III equipment to create the SCI rats model. Rats were randomly divided into four groups: Sham (only laminectomy), Model (SCI group), EA (SCI + Jia-Ji EA treatment), EA + CQ (SCI + Jia-Ji EA treatment + inhibitor chloroquine). Basso-Beattie-Bresnahan assessment showed improvement of hind limb motor function after Jia-Ji electro-acupuncture treatment. Histological change of injured spinal cord tissue was alleviated after treatment, observed by hematoxylin-eosin and Nissl staining. The mRNA and protein expression levels of RIPK1, RIPK3 and MLKL were decreased in EA group. Besides, the increased expression of LC3 and reduced expression of P62 after treatment compared with Model group, confirmed that Jia-Ji electro-acupuncture could enhance the autophagy flux. Electron microscopy imaging showed increasing the number of lysosomes, autophagosomes, and autolysosomes after Jia-Ji electro-acupuncture treatment. Furthermore, inhibition of lysosome function with CQ led to partly eliminate the effect of EA on reducing necroptosis. These data make the case that Jia-Ji electro-acupuncture treatment may improve locomotor function by promoting autophagy flux and inhibiting necroptosis.

Keywords: Jia-Ji electro-acupuncture, spinal cord injury, motor function repair, autophagy flux, necroptosis, lysosome

INTRODUCTION

Spinal cord injury (SCI) may cause structural and functional impairment of the spinal cord, leading to sensory, motor or autonomic nerve dysfunction, and ultimately affecting the patient's physical, psychological, and social abilities (Singh et al., 2014). With its secondary complications in the long term, SCI is life-threatening and constitutes a considerable portion of the global social and economic burden (GBD 2016 Traumatic Brain Injury and Spinal Cord Injury Collaborators, 2019). The annual incidence of SCI in the United States is about 17,000 new

cases per year (National Spinal Cord Injury Statistical Center, 2016). The global incidence of traumatic SCI ranges from 3.6 to 195.4 patients per million, and the numbers are still rising (Jazayeri et al., 2015).

The pathological mechanism of traumatic SCI involves primary injury (irreversible mechanical injury), and secondary injury (reversible) which is caused by a progressive cascade of tissue destruction and microenvironment changes, including oxidative stress, ischemia, inflammation, edema, glutamatergic excitotoxicity, ion imbalance, and apoptosis (Kumar et al., 2018). Rapid diagnosis and neuroprotective interventions at the stage of acute injury are therefore critical, and these treatments have the potential to significantly improve subsequent long-term functional recovery. Recent medical treatments attempt to reduce secondary damage and protect neurons that survive primary damage (Kwon et al., 2004). Some adjunctive therapies are used as an effective treatment of acute SCI clinically, such as corticosteroids (Schroeder et al., 2014), neuroprotectant agents (Grossman et al., 2014), and alternative therapy (electro-acupuncture) (Xiong et al., 2019).

As a Traditional Chinese medicine method, electro-acupuncture (EA) is a therapy in which a needle is inserted at an acupuncture point and attached to a trace amount of pulsed current to produce a synthetic electro-acupuncture stimulation. Previous studies have proved that the application of EA in the treatment of SCI is beneficial to the neurological and functional recovery of SCI (Ding et al., 2011; Huang et al., 2011). EA has been widely used in SCI therapy in the clinic to improve functional recovery after spinal cord and nerve muscle damage. However, its work mechanism is still unclear.

Inhibition of lysosomal/autophagy pathways and activation of necroptosis have been shown to lead to cell loss and tissue damage in some CNS trauma models (Sarkar et al., 2014; Lipinski et al., 2015). Necroptosis is proved to be associated with the pathogenesis of some neurodegenerative diseases, such as multiple sclerosis and amyotrophic lateral sclerosis (Ofengeim et al., 2015; Ito et al., 2016). It has been previously demonstrated that autophagy flux is inhibited after SCI in the mouse model, with obvious accumulation of autophagy markers LC3-II and autophagy substrate P62/SQSTM1 in ventral motor neurons (Liu et al., 2015b). Inhibition of autophagy flux is proved to be caused by rapid lysosomal dysfunction, contributing to accumulation of RIPK1, RIPK3, and MLKL after SCI, which were located in neurons destroyed by autophagy (Liu et al., 2018). The receptor-interacting protein kinases 1 (RIPK1) and the sequential activation of downstream RIPK3 and the mixed lineage pseudo-kinase MLKL regulates necroptosis which leads to neuronal and glial cell death after SCI (Liu et al., 2015a; Weinlich et al., 2017). As necroptosis markers, RIPK1, RIPK3, and MLKL are expressed in damaged spinal cord tissue and are negatively correlated with motor function recovery (Wang et al., 2018). Specific inhibition of RIPK1 kinase activity is found to block necroptosis and inflammation (Degterev et al., 2008). Thus, the interaction of lysosomal/autophagy and necroptosis may play a key role in improving neuronal survival and functional outcomes after SCI injury.

In this study, the effects of EA on improvement of lower limb function in rat modal would be investigated to explore its mechanism of autophagy flux and necroptosis regulated by lysosomal dysfunction after SCI, and to provide a potential effective therapy for SCI.

MATERIALS AND METHODS

Animals Model

Female Sprague Dawley rats (220–250 g body weight), aged 10 weeks old, were obtained from the central animal of Heilongjiang Chinese Medicine university. Animals use and care protocols conform to guidelines by the International Council for Laboratory Animal Science (ICLAS) and Animal Care and Use Committee of China.

Rats were randomly divided into four groups: Sham group, SCI group, EA group, and EA + CQ group. The sham group received only laminectomy. Model group underwent T9-T11 SCI. Electro-acupuncture group (EA) performed Jia-Ji electro-acupuncture therapy 6 h after SCI. Electro-acupuncture + inhibitor chloroquine group (EA + CQ) received both EA and inhibitor CQ treatment after SCI. 6 h after the injury, the rats were treated with electro-acupuncture. At the same time, the rats were intraperitoneally injected with inhibitor chloroquine (CQ, C6628, United States, Sigma) at an injection dose of 50 mg/kg/d, until the rats were killed. The Sham group, Model group and EA group were injected daily with the same dose of normal saline as CQ. Rats in the SCI, EA and EA + CQ groups were further divided into four subgroups by various time points of treatment: 6 h, 1, 3, and 7 days. And 3 and 7 days subgroups were focus of subsequent studies.

Allen's model was made by application of NYU Impactor M-III strike. After anesthesia with 10% chloral hydrate (3.0 mL/kg body weight) *via* intraperitoneal injection, a 5 cm longitudinal incision was made dorsally on the rats. Expose the T9-11 spinous processes, and resect the T10 lamina to create a gap around vertebral arch plate. Repeat extend the gap and remove the vertebral plate and T10 spinous process, and expose the intact spinal cord. For Sham group, only laminectomy was performed. The SCI model was then produced using a NYU Impactor M-III strike (a 10 g pouching rod of 2.5 mm diameter with drop of 50 mm and damage of 50 g·cm) at the T10 segment to create relatively serious injury (Verma et al., 2019). All SCI rats conformed to the following injury criteria: spinal cord ischemia and edema, formation of tail sway reflex, flicking of both body and legs, and the appearance of sluggish paralysis. After the strike was completed, marked the skin on both sides of the wound, and applied antibiotics (amoxicillin) to the incision site. Ensure adequate food and water, assist urination once in the morning and evening until the reflex of urination was restored, and massaged the abdomen of rats clockwise every day to prevent flatulence and difficulty in defecation.

Electro-acupuncture treatment method (EA): 6 h after injury, Jia-Ji electro-acupuncture therapy was performed. Operation method: The upper and lower spinous process gaps (proximal end at the top, distal end at the bottom) in the damaged area were selected to open points within 7 mm. After routine disinfection, inserted the needle into the spine with a needle tip

to the lamina (depth is 13 mm). With Micro Plus type pulse electro-acupuncture (BioMedical Life Systems, Inc., Vista, CA, United States), the positive pole was connected to the upper needle handle, and the negative pole to the lower needle body on the same side. Selection parameters: Pulse wave type: continuous pulse waveform; Pulse repetition frequency: 100 Hz; Current output intensity: slight twitch of back muscle (about 1 mA). It lasted for 30 min, once a day.

Behavioral Assessment

The Basso-Beattie-Bresnahan (BBB) scores was used to evaluate the functional recovery of the hind limbs in rats with SCI (Basso et al., 1995). The scale ranged from 0 to 21 (0 = complete hind limb paralysis, 21 = normal locomotion) for joint movement, gait and hind limb coordination, and fine motion of the toes. The higher the score, the better the motor function. The rats in each group were dynamically evaluated according to the 6 h, 1, 3, and 7 days after SCI. The rats were placed in the open field and moved freely for 5 min. Two trained observers scored performance of the rats blindly and recorded the average value (Hong et al., 2019).

Hematoxylin-Eosin Staining and Nissl Staining

Rats in Sham, Model, and EA groups (n = 6) were subjected to deep anesthesia with 10% chloral hydrate (3.5 ml/kg, I.P.) at different time points. The rats were sacrificed by cutting off their heads quickly, and the spinal cord in the damaged area was quickly removed on the ice bag and then fixed with 4% paraformaldehyde. Paraffin-embedded lesion. Transverse paraffin sections (5 μm thick) were placed on slides. HE staining was performed for histopathological examination. The sections were incubated in 1% toluidine blue for Nissl staining and observed under light microscope.

Immunohistochemistry

Rats in Sham, Model, EA, and EA + CQ groups were deeply anesthetized with 10% chloral hydrate and executed, then the injury section of spinal cord tissue were fixed in 4% paraformaldehyde. A 5μm thick of paraffin embedding spinal cord section was incubated with primary antibody 4°C overnight after dewaxing, transparency, hydrogen peroxide incubation, antigen repair, and blocking. The mixture was placed in room temperature for 30 min, rinsed with PBS for 3 times, incubated with secondary antibody at 37°C for 30 min. Finally, sections were incubated with DAB, hematoxylin redyeing, and mounted on coverslips. Photographic results were taken under a light microscope (400 ×) and quantitative assessment of immunohistochemical staining was performed by Image-Pro Plus 6.0 software. Primary antibodies: RIPK1 (1:100, RIPK1 Rabbit PolyClonal antibody, United States Proteintech), RIPK3 (1:40, Rabbit PolyClonal antibody, Beijing BIOSS), MLKL (1:200, Rabbit PolyClonal antibody, United States Affinity), LC3B (1:500, Rabbit polyclonal antibody, United States Proteintech), P62 (1:200, Rabbit polyclonal antibody, United States Proteintech). Second antibody: anti-rabbit (PV-6,001, Beijing Zhongshanjinqiao).

Transmission Electron Microscopy

Rats in Sham, Model, and EA groups (n = 6) at 3 and 7 days time points were euthanized. The spinal cord tissues at the injured sites were removed, cut into small pieces of about 1 mm × 1.5 mm × 1.5 mm, and fixed with 2.5% glutaraldehyde for more than 24 h and then with 2% osmium acid for 2 h. After dehydration in acetone, the embedded spinal cord sections were stain with toluene ammonia blue to select required sites for observation. Sweden made LKB-III ultra-thin slicing machine was used to section with the thickness of about 500A. The samples were stained with uranium acetate and lead nitrate and observed by transmission electron microscope.

Real-Time Quantitative Polymerase Chain Reaction (qRT-PCR)

The spinal cord tissue at the damaged site in each group was quickly removed and put into liquid nitrogen, and then transferred to the −80°C refrigerator for use. Total RNA was isolated using BufferRL1. The mRNA expression of RIPK1, RIPK3, MLKL were measured using the RT-qPCR system. The reverse transcription system was as follows: RNase Free dH2O: 10 μl, 5X PrimeScript Buffer 2 (for Real Time): 4 μl, RNA: 4 μl, RT Primer Mix (4 ×): 1 μl, Primescript RT Enzyme Mix I: 1 μl. 42°C for 15 min and 85°C for 5 s for reverse transcription. PCR reaction solution was as follows: TBGreen Premix Ex Taql (Tli RNaseH Plus) (2 ×): 10 μl, PCR Forward Primer(10 μM): 0.8 μl, PCR Reverse Primer (10 μM): 0.8 μl, RT reaction solution (cDNA): 2 μl, sterilized water: 6.4 μl, Total: 20 μl. Target gene primer sequence: RIPK1 (For 5′-GAGGAGGAAAGGAAGCGAAG-3′, Rev 5′-TGACTGGTTGTGCTGGGATA-3′) 113 bp, RIPK3 (For 5′-GAGTGGGACTACGTGTACGG-3′, Rev 5′-CAGCAGAACA TTGGAGGGCT-3′) 204 bp, MLKL(For 5′-AGCCTCCCCAGT GACATTAC-3′, Rev 5′-GCCCACAGTAGCAAACTTCC-3′) 120 bp, β-actin (For 5′-CCTGTGGCATCCATGAAACTAC-3′, Rev 5′-CCAGGGCAGTAATCTCCTTCTG-3′) 150 bp. PCR amplification procedure followed by 40 cycles of 95°C for 5 s, 60°C for 30 s. Delta-delta Ct (ΔΔCt) method was used to calculate the relative expression of the target gene. PrimeScript RT reagent Kit with gDNA Eraser (Perfect Real Time) (Japan, Takara), TB Green Premix Ex Taq II (Tli RNaseH Plus) (Japan, Takara).

Western Blot Assay

Rats in Sham, Model, EA, and EA + CQ groups (n = 6) at 3 and 7 days time points were euthanized, and the spinal cord tissues at the damaged sites were removed rapidly and homogenized in lysis buffer. With PMSF15 ml, 12,000 rpm, centrifuged for 5 min, the supernatant was absorbed, and the protein concentration was determined by BCA. Loading sample for electrophoresis and then transferred the protein to the PVDF membrane. After blocking for 1 h, the PVDF membrane was incubated with the primary antibody at 4°C overnight, as shown below: LC3B (1:2,000, Rabbit polyclonal antibody, United States Proteintech), P62 (1:1,000, Rabbit polyclonal antibody, United States Proteintech), RIPK1 (1:1,000, RIPK1 Rabbit PolyClonal antibody, United States

Proteintech), RIPK3 (1:2,000, Rabbit polyclonal antibody, Beijing BIOSS), MLKL (1:1,000, Rabbit polyclonal antibody, United States Affinity), β-actin (1:5,000, mouse monoclonal antibody, United States Proteintech). The membrane were washed 3 times with Tris-buffered saline Tween, and incubated with secondary antibody at 37°C for 1 h as shown below: HRP-Goat-Anti-Rabbit IgG(H + L) (1:5,000, United States Proteintech), HRP-Goat-Anti-Mouse IgG(H + L) (1:5,000, United States Proteintech). The immunoreactive bands were visualized by ECL chemiluminescence. The grayscale values of bands were quantified by Image Lab 5.2.1 software, and the relative expression of protein was calculated according to the ratio of target protein to β -actin.

Statistical Analyses

SPSS 25.0 software was used for statistical analysis. The data were presented as mean ± standard deviation (± SD). One-way analysis of variance (ANOVA) was used for comparison between groups. For further comparison between groups, the least significant difference (LSD) test was used for those with homogeneous variance, and Dunnett's T3 test was used for those with heterogeneous variance. $P < 0.05$ was considered statistically significant.

RESULTS

Electro-Acupuncture Improved Motor Function

BBB scale scores were used to assess movement of hind limb. The first part mainly evaluates the range of motion of joints, with a score of 0–7. The second part mainly evaluates the gait and hind limb coordination ability, with a score of 8–13. The third part mainly assessed the fine movement of the toes, with a score of 14–21 points. After SCI, the rats were paralyzed in the hind limbs, without any movement phenomenon, with reduced diet and water, accompanied by urinary retention, and entered the stage of spinal cord shock, with a score of 0 point. The evaluation results of Sham group were all scored 21 points at the four time points of 6 h, 1, 3, and 7 days, and the rats walked as usual, indicating no dyskinesia. The scores of Model group at each time point after SCI were significantly lower than Sham group ($P < 0.01$), which means a significant movement disorder following SCI. After EA treatment, there was little change in the score at 6 h and 1 day, and no statistical significance was found compared with the Model group ($P > 0.05$). The scores were significantly greater in the EA group compared with the SCI group on days 3 and 7 after injury ($P < 0.01$; **Figure 1**). Motor dysfunction of the hind limbs could be improved in the rats with EA treatment at 3 and 7 days.

Effects of Electro-Acupuncture on Histological Changes in Spinal Cord

At the time points of 3 and 7 days, the appearance and structure of the spinal cord tissues in Sham group was normal. The hematoma after SCI in Model group was most severe on 3 day. After the EA treatment, the hematoma area became significantly smaller at each time point (**Figure 2A**).

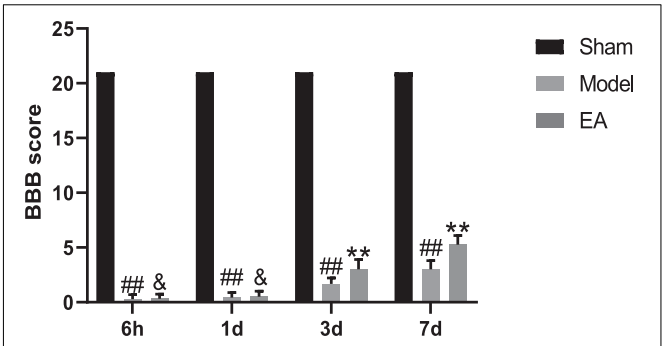

FIGURE 1 | BBB scores of four different time points. Data are expressed as the mean ± SD ($n = 6$ rats/group). $^{\#\#}P < 0.01$, vs. Sham group; $^{\&}P > 0.05$, $^{**}P < 0.01$, vs. Model group. BBB: Basso, Beattie and Bresnahan rating scale, used to evaluated hind limb locomotor. Sham, laminectomy only; Model, spinal cord injury; EA, electro-acupuncture.

In the SCI group on 3 day, pathological change was most obvious with gray structure disorder, necrosis and inflammation worsen, a large number of neurons lost, the serious neurons swelling, neutrophils, and monocytes infiltration, white matter demyelinating and scattered focus of hemorrhage. Compared with the Model group, the EA group had fewer necrotic cavities, improved neuronal swelling, more orderly gray matter structure, less neuron loss, and improved inflammatory cell infiltration. At the time point 7 days after SCI, the loss of gray matter neurons in the Model group was still significant, the necrotic cavity gradually expanded, which showed the ghost cell of dead neurons, the decrease of inflammatory cells compared with that at 3 day, and a large number of glial cells proliferated. In this figure, the image of neuronophagia and nodular microglia could be seen. There are numerous voids in the white matter, marked demyelinating changes, and the ends of axons swell into a spherical shape. The hemorrhagic lesion was reduced compared with that of 3 day, while the above pathological symptoms were improved after treatment in the EA group. The gray matter structure was relatively complete, the nerve fibers were arranged in a more orderly manner, the boundary between gray matter and white matter could be observed, the number of neurons was more, the number of cavities was less, and the inflammatory cell infiltration was improved (**Figure 2B**).

Nissl staining was used to observe the morphology and number of motor neurons in the anterior horn of spinal cord in each group. In Sham group, the anterior horn motor neurons were orderly arranged without significant reduction, deep blue staining. At 3 and 7 days time points, there were statistically significant reducing in the number of anterior angular motor neurons in Model group compared to Sham group ($P < 0.01$). Although the number of neurons in the EA group decreased, the number of neurons in the EA group was still higher than that in the Model group, and the staining was relatively deeper. The comparison between the two groups was statistically significant (3 day: $P < 0.05$, 7 day: $P < 0.01$) (**Figures 2C,D**).

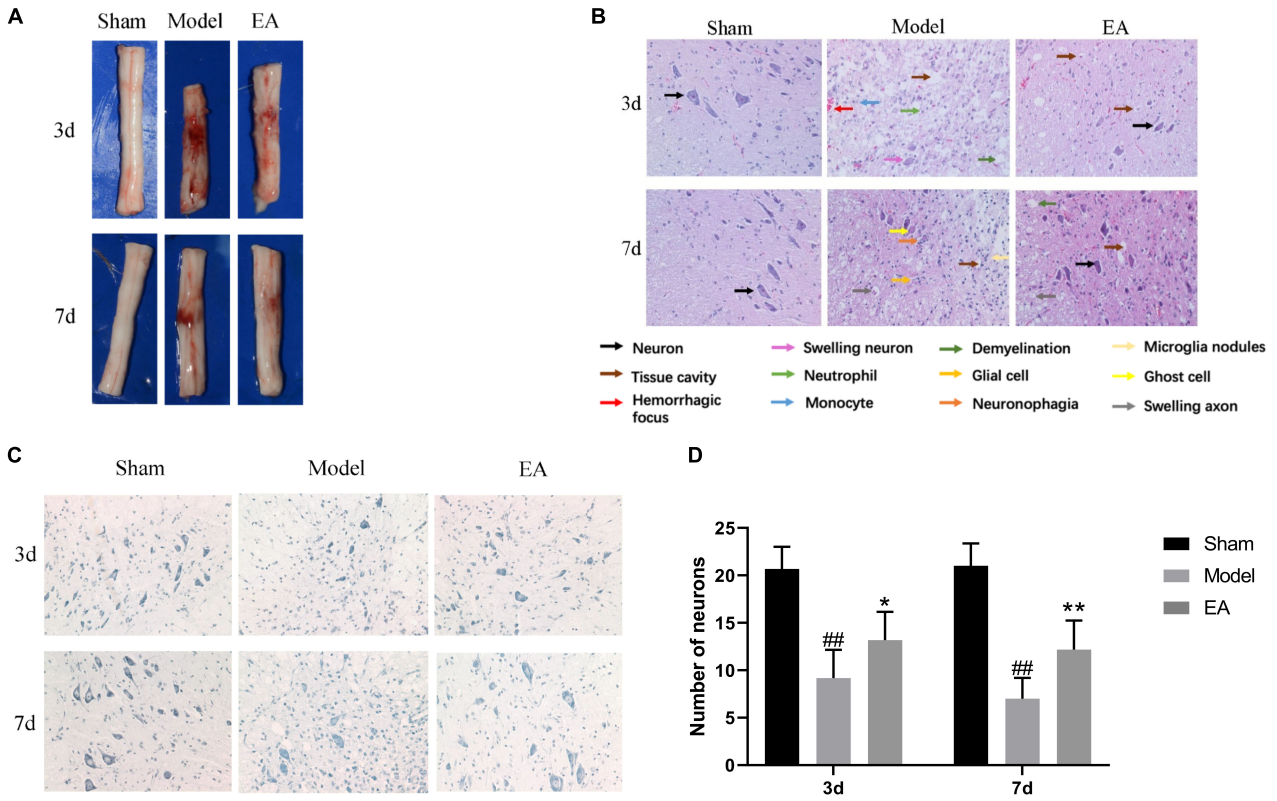

FIGURE 2 | Effect of EA on histological changes in spinal cord at 3 and 7 days. **(A)** Spinal cord tissue appearance. EA could promote bleeding absorption, reduce edema and protect spinal cord. **(B)** HE stained images of spinal cord sections (200×). EA could improve the pathological changes. Arrows with different colors means different structure and pathological changes, listed with the image. In model group, neuron disappear compared to Sham. Tissue cavity, hemorrhagic focus, swelling neuron, neutrophil, monocyte and demyelination could be seen in Model group at 3 day. Glial cell, ghost cell, neuronophagia, swelling axon and microglia nodules are shown in Model group at 7 day. While after EA treatment, several neurons could be seen, the damage tissue and inflammation factors reduce. **(C)** Nissl stained images of motor neuron (200×). The number of motor neuron could increase after EA treatment. **(D)** Number of anterior horn motor neurons in each group. Data are expressed as the mean ± SD (n = 6 rats/group). $^{\#\#}P < 0.01$, vs. Sham group; $^{*}P < 0.05$, $^{**}P < 0.01$ vs. Model group.

Electro-Acupuncture Inhibited the Expression of Necroptosis Markers RIPK1, RIPK3, and MLKL

RIPK1, RIPK3, and MLKL were mainly expressed in the cytoplasm of neurons and glial cells. The average OD value of RIPK1, RIPK3, and MLKL in the Model group was significantly higher than that of the Sham group at 3 and 7 days after injury ($P < 0.01$). After EA treatment, the mean OD value of RIPK1, RIPK3, and MLKL decreased, and the comparison between the EA group and the Model group was statistically significant at the time points of 3 and 7 days (RIPK1, 3 day: $P < 0.01$, 7 day: $P < 0.05$; RIPK3, 3 day/7 day: $P < 0.01$; MLKL, 3 day: $P < 0.05$, 7 day: $P < 0.01$. **Figures 3A–F**). It may illustrate that the expression level of RIPKI, RIPK3, and MLKL increased after SCI, and the EA had the effect of inhibiting the necroptosis factors.

qRT-PCR results showed that the expression of RIPK1, RIPK3, and MLKL mRNA in the Model group was significantly higher than that in the Sham group at 3 and 7 days after SCI ($P < 0.01$). After treatment, the expression level of those mRNA in the EA group was decreased, and the difference between the EA group and the Model group was statistically significant at 3 and 7 days time points (RIPK1, RIPK3, $P < 0.05$; MLKL, 3 day: $P \leq 0.05$, 7 day: $P < 0.01$. **Figures 3G–I**). This result is consistent with immunohistochemistry results.

Electro-Acupuncture Enhanced Autophagy Flux and Inhibited Necroptosis

Electro-Acupuncture Increased Numbers of Autolysosomes

Electron microscopy was used to observe the structure changes of spinal cord tissue after injury. In the Sham group, the nuclei were intact and uniformly stained, the number and structure of organelles in the cytoplasm were normal, the myelin sheath was arranged in concentric circles around the axons, and microfilaments and microtubules could be seen in the axons in regular arrangement. No axonal denaturation and granular disintegration were observed, no autolysosome was found, and several primary lysosomes could be seen (**Figure 4A**). On 3 day after SCI, the cytoplasm of neurons in the spinal cord tissue had sustained extensive edema, the mitochondria were swollen significantly, the myelin lamina was broken,

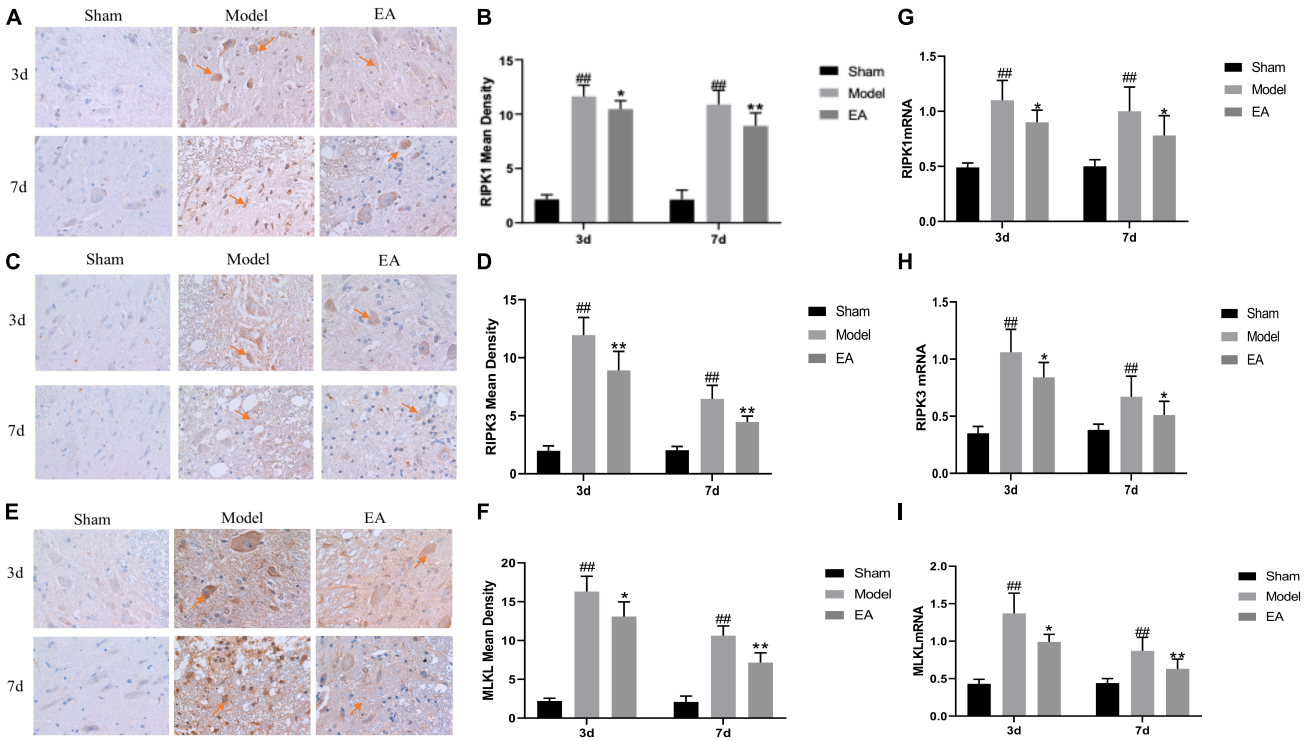

FIGURE 3 | Effects of EA on the expression of necroptosis markers. **(A–F)** Immunohistochemistry results of RIPK1, RIPK3, and MLKL in spinal cord of rats in each group. RIPK1, RIPK3, and MLKL were brown-yellow positive, mainly expressed in neuron and glial cells (red arrow). **(B,D,F)** Average OD of RIPK1, RIPK3, and MLKL in each group. After EA treatment, these necroptosis markers reduced compared to Model. Data are expressed as the mean ± SD (n = 6 rats/group). **(B)**:$^{\#\#}P < 0.01$, vs. Sham group; $^{*}P < 0.05$, $^{**}P < 0.01$, vs. Model group; **(D)**:$^{\#\#}P < 0.01$, vs. Sham group; $^{**}P < 0.01$, vs. Model group. **(F)**: $^{\#\#}P < 0.01$, vs. Sham group; $^{*}P < 0.05$, $^{**}P < 0.01$, vs. Model group. **(G–I)** Quantification of RIPK1, RIPK3 and MLKL mRNA by qRT-PCR. **(G)**: $^{\#\#}P < 0.01$, vs. Sham group; $^{*}P < 0.05$, vs. Model group. **(H)**: $^{\#\#}P < 0.01$, vs. Sham group; $^{*}P < 0.05$, vs. Model group. **(I)**: $^{\#\#}P < 0.01$, vs. Sham group; $^{*}P \leq 0.05$, $^{**}P < 0.01$, vs. Model group.

the rough endoplasmic reticulum was loose, the number of lysosomes increased (**Figure 4B**). In the EA + CQ group, autophagosomes increased much more than that in EA group, while only several autolysosomes could be seen (**Figure 4C**). CQ destroyed lysosome function by inhibiting the fusion of lysosome and autophagosomes, leading to the accumulation of autophagosomes, and blockage of autophagy flux. The number of lysosomes, especially secondary lysosomes/active lysosomes, autophagosomes, and autolysosomes in the EA group was greater than that in the model group (**Figure 4D**). This results may illustrate that EA have effects on increasing the numbers and function of lysosomes and autolysosomes and enhancing autophagy flux.

Lysosomes Inhibitor CQ Eliminated Effect of EA on Motor Function Improvement and Histological Changes

The EA group scored higher than the Model group on both 3 and 7 days, with statistically significant differences ($P < 0.05$, $P < 0.01$, **Figure 5A**). However, after injection of lysosomes inhibitor CQ, the EA + CQ group had lower scores on 3 and 7 days than the EA group significantly ($P < 0.01$), indicating that CQ could partially eliminate the therapeutic effect of EA on improvement of motor function.

At the time points of 3 and 7 days after surgery, the number of neurons in the Model group was significantly reduced, while neurons relatively increased after treatment in the EA group, statistically significant compared with the Model group at each time point ($P < 0.05$, $P < 0.01$). However, the neurons in the EA + CQ group decreased after injection of inhibitor CQ at 3 and 7 days compared with that in the EA group ($P < 0.01$), indicating that injection of inhibitor CQ could partially eliminate the therapeutic effect of EA and reduce the number of neurons (**Figures 5B,C**).

Electro-Acupuncture Promoted Autophagy Flux Blocked by Lysosomes Inhibitor

Immunohistochemistry results showed that LC3 and P62 were mainly expressed in cytoplasm of neurons and glial cells. At postoperative 3 and 7 days, the mean density value of LC3 and P62 in Model group were significantly higher than Sham group ($P < 0.01$). After treatment at 3 and 7 days, LC3 in the EA group increased significantly compared with the Model group ($P < 0.05$, $P < 0.01$), while the value of P62 in EA group was lower than that in Model group ($P < 0.05$). The mean density value of LC3 and P62 both increased in EA + CQ group at each time point after injection of inhibitor CQ, compared to that in EA group ($P < 0.05$, $P < 0.01$). The results showed that the expression of

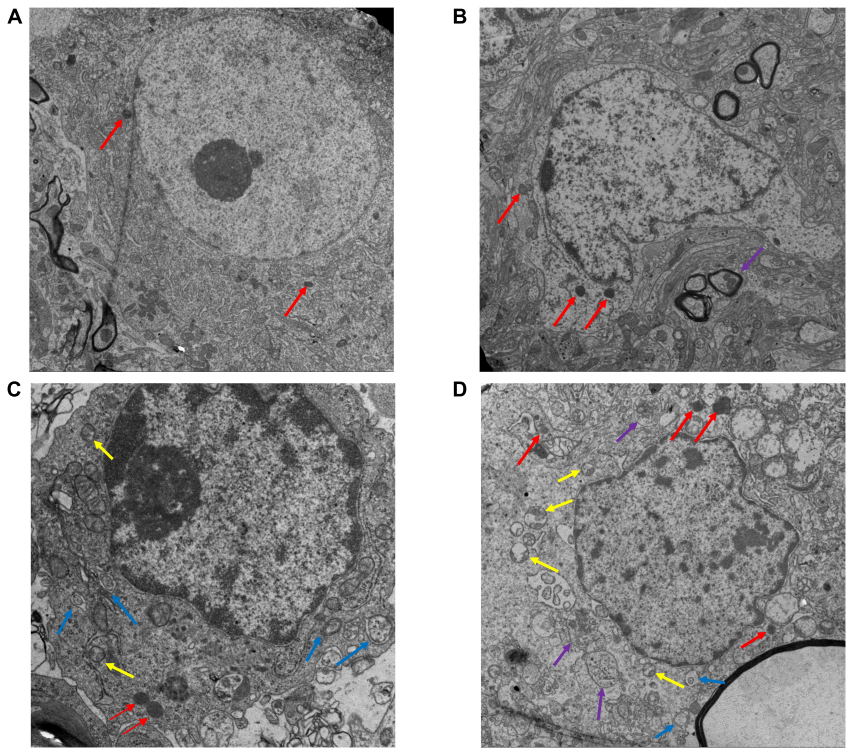

FIGURE 4 | Electron microscopy results of the spinal cord tissue sections after EA. **(A)** Ultrastructure of the sham group (13,000×). Nuclei is intact (red arrow), with obvious nucleoli. The myelin sheath is arranged around the axon in concentric circles. No autophagosome is found. **(B)** Ultrastructure of spinal cord tissue after injury in 3 day (18,000×). In model group, the myelin sheath and the nucleus shrinks and several lysosomes (Red arrow) and autolysosomes (purple arrow) are shown. **(C)** EA + CQ group in 3 day (44,000×). Autophagosomes accumulated significantly. Several active lysosomes could be seen. **(D)** EA group in 3 day (18,000×). The number of lysosomes, autophagosomes and autolysosomes increased in EA group, especially active lysosomes. Yellow arrow: secondary lysosome (active lysosome). Blue arrow: autophagosomes with two membranes. Red: primary lysosomes. Purple: autolysosomes with single membrane.

LC3 increased after SCI, which may be related to the decreased autophagosomal degradation caused by lysosomal dysfunction. While electro-acupuncture could promote the expression of LC3 and increase the formation of autophagosome. After SCI, the expression level of autophagy degradation substrate P62 was increased, and the acupuncture could reduce the expression of P62, promote autophagy degradation, and accelerate autophagy flux. On the basis of the acupuncture treatment, lysosomal inhibitor CQ was injected to enhance the expression of LC3 and P62, leading to excessive accumulation of autophagosomes and blocking of autophagy flux (**Figure 6**).

It is further verified by Western Blot. LC3-II protein expression in Model group was significantly higher than that in Sham group at 3 and 7 days postoperatively ($P < 0.01$). After EA treatment, the expression level of LC3-II protein increased, which was statistically significant compared with the Model group at the time points of 3 and 7 days ($P < 0.01$). However, LC3-II protein in the EA + CQ group continued to increase after injection of inhibitor CQ, and the difference between the EA group and the EA group was statistically significant ($P < 0.05$). These results indicate that the expression of LC3-II protein increases and autophagy increases after SCI, which may be caused by the blockage of autophagy flux. The continued increase of LC3-II protein expression after acupuncture treatment may be related to the promotion of autophagy. The inhibitor CQ was injected on the basis of the electro-acupuncture treatment, resulting in the further increase of LC3-II protein expression and a large amount of autophagosome accumulation (**Figure 7A**).

P62 protein expression in the Model group was significantly increased compared with that in the Sham group ($P < 0.01$), while it was decreased in EA group, which was statistically significant compared to Model group at 3 and 7 days after treatment ($P < 0.05$). After injection of inhibitor CQ, the expression of P62 protein in the EA + CQ group was higher than that in the EA group at each time point ($P < 0.01$). These results indicated that P62 protein expression increased after SCI. After EA treatment, the expression of P62 protein was decreased, autophagy degradation was promoted, and autophagy flux was enhanced. The inhibitor CQ could partly eliminated the effect of the EA on reducing P62 protein expression, but promoted its increase (**Figure 7B**).

Lysosomes Inhibition Eliminated the Effect of Electro-Acupuncture on Reducing Necroptosis Markers Expression

At 3 and 7 days after surgery, the average optical density value of RIPK1, RIPK3, MLKL in the EA group were lower than that of the Model group (RIPK1, MLKL: $P < 0.05$, $P < 0.01$;

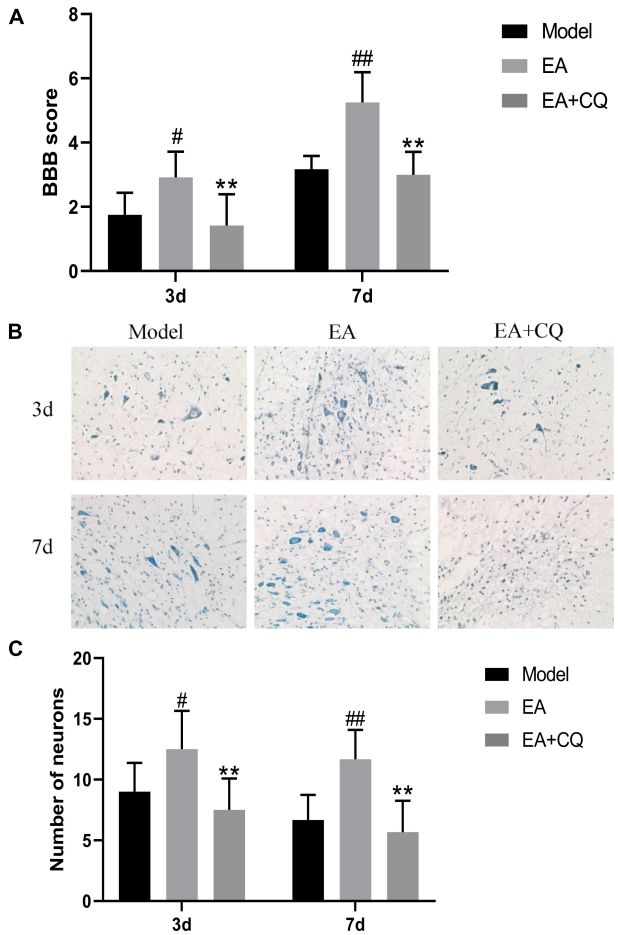

FIGURE 5 | (A) BBB scores of neurological function recovery after injection of CQ. Data are expressed as the mean ± SD (n = 6 rats/group). $^{\#}P < 0.05$, $^{\#\#}P < 0.01$, vs. Model group. $^{**}P < 0.01$, vs. EA group. Model, spinal cord injury; EA, electro-acupuncture; EA + CQ, electro-acupuncture with injection of inhibitor CQ. **(B)** Nissl staining results of spinal cord tissue after inhibitor CQ injection (200 ×). **(C)** Number of anterior horn motor neuron. Data are expressed as the mean ± SD (n = 6 rats/group). $^{\#}P < 0.05$, $^{\#\#}P < 0.01$, vs. Model group. $^{**}P < 0.01$, vs. EA group.

RIPK3: $P < 0.05$), while the value of them in EA + CQ group increased after the injection of inhibitor CQ, and the comparison between the EA + CQ group and the EA group was statistically significant at 3 and 7 days after surgery ($P < 0.05$, $P < 0.01$, **Figure 8**). These results indicated that EA treatment could inhibit the formation of necroptosis factor RIPK1, RIPK3, MLKL, reduce the formation of necrotic complex, and protect the remaining neurons. However, after injection of inhibitor CQ, the effect of EA on necroptosis factors reduction was partially eliminated, so as to increase the value of necroptosis factor and reduce the survival rate of neurons.

The expression of RIPK1, RIPK3, and MLKL in the Model group was significantly increased compared with that in the Sham group at 3 and 7 days ($P < 0.01$), while it was decreased after treatment in the EA group. At the time points of 3 and 7 days, the difference was statistically significant compared with that in the Model group (RIPK1: $P \leq 0.05$; RIPK3: $P < 0.05$; MLKL: $P < 0.05$, $P < 0.01$). Compared with the EA group, RIPK1, RIPK3, and MLKL protein expression in the EA + CQ group increased significantly at each time points after injection of inhibitor CQ (RIPK1: $P < 0.01$, $P < 0.05$; RIPK3: $P < 0.05$, $P < 0.01$; MLKL: $P < 0.01$, **Figure 9**). The results show that RIPK1, RIPK3, and MLKL protein expression increased after SCI, and EA treatment could reduce these necroptosis factors expression and necrosis complex formation. Inhibitor CQ could partly eliminate the effect of EA on reducing RIPK1, RIPK3, and MLKL protein expression, instead promoting its elevation, which is available in the formation of necrotic complexes and exacerbates neuronal necrosis.

DISCUSSION

Clinically, EA as a traditional Chinese medicine therapy has been widely used to improve the prognosis of spinal cord and neuromuscular injury. Electro-acupuncture at Jia-Ji points is a combination of acupuncture effect and electric field effect on injured spinal cord after SCI. In this study, we investigated the molecular biological mechanism of EA treatment on improvement of lower hind motor and autophagy regulation of necroptosis. Our data showed that lysosome function was inhibited after SCI with increasing the expression of LC3-II and P62. LC3-II reflects the number of autophagosomes and P62 is autophagy cargo protein. The number of autophagosomes and the degradation of autophagy cargo protein increased after EA treatment, which proved that the electro-acupuncture has the effect of enhancing autophagy flux. Consistent with previous study (Liu et al., 2018), we found that necroptosis markers were accumulated after SCI in neurons with inhibiting of autophagy flux and lysosomal damage. The accumulation of RIPK1, RIPK3, and MLKL were inhibited in neurons and glial cells by using Jia-Ji EA treatment, which may reduce necroptosis. Besides, the lysosome inhibitor CQ partially eliminated the therapeutic effect of EA on promoting autophagy flux and inhibiting necroptosis. This study suggests that Jia-Ji EA treatment may promote the recovery of motor function through the mechanism of accelerating autophagy flux and alleviating necroptosis.

Rodent models have become standard in the past 30 years and have been widely used in SCI research (Kwon et al., 2015). Rats are the best choice and the most widely used due to the limit field of vision of mice (Verma et al., 2019). In rat model of SCI, we observed that there was a significant improvement on motor function after EA treatment compared to Model group at 3 and 7 days time points ($P < 0.01$). The improvement of hind limb motor function was not obvious after treatment for 6 h or 1 day. So 3 and 7 days time points were selected as time points in the following study. It is further proved by the histological changes. At the time points of 3 and 7 days, the appearance and structure of the spinal cord tissues in the Sham group were normal, while the hematoma in the spinal cord attack area in the Model group was obvious. However, the hematoma was the most severe in 3 day, indicating that the vascular hemorrhage of the spinal cord after external impact caused congestive necrosis, leading to further

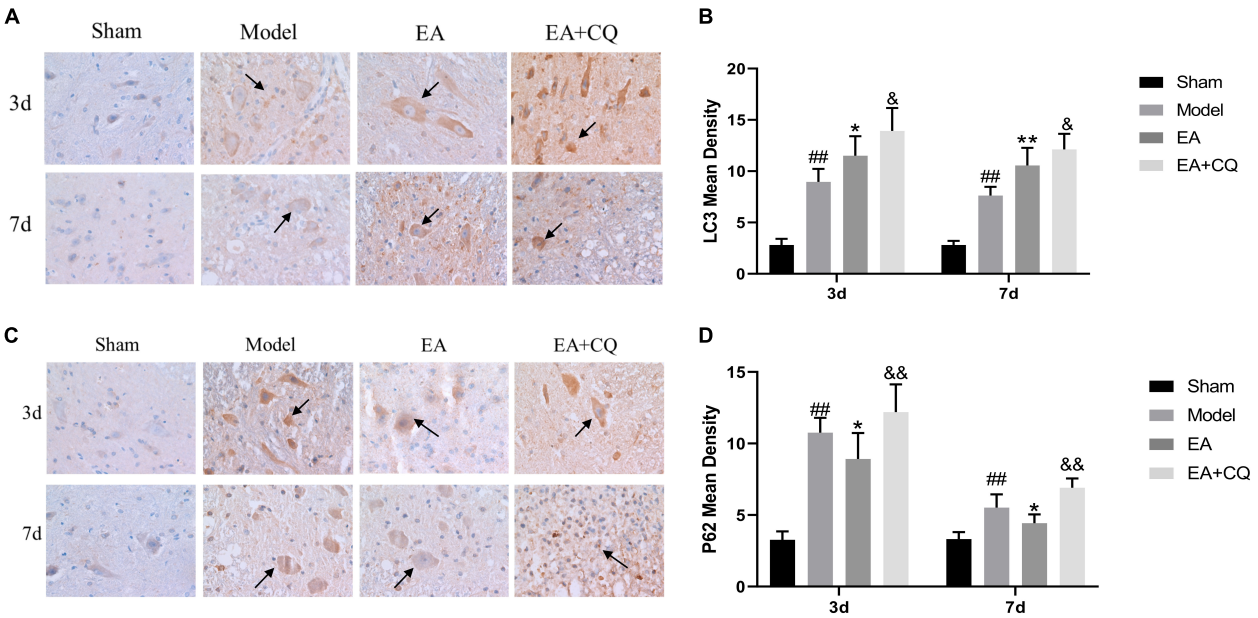

FIGURE 6 | Immunohistochemistry results on the expression of LC3 and P62. **(A)** Immunohistochemical staining results of LC3 in rats in each group (400×). LC3 is brown staining (black arrow). **(B)** Mean optical density of LC3 in each group (IOD/Area). $^{\#\#}P < 0.01$, vs. Sham; $^{*}P < 0.05$, $^{**}P < 0.01$, vs. Model; $^{\&}P < 0.05$, vs. EA. **(C)** Immunohistochemical staining results of P62 in each group (400 ×). P62 is brown staining (black arrow). **(D)** Mean optical density of P62 in each group (IOD/Area). $^{\#\#}P < 0.01$, vs. Sham; $^{*}P < 0.05$, vs. Model; $^{\&\&}P < 0.01$, vs. EA. Data are expressed as the mean ± SD ($n = 6$ rats/group).

aggravation of tissue ischemia. After EA treatment, the range of hematoma in EA group at each time point became smaller and the color became lighter. Spinal cord structure was disorder at 3 day after SCI in Model group, with nerve fibers arranged loosely, flake bleeding lesions, the massive death of neurons, retained a large number of neurons die cavity. These pathology changes are associated with cells and necrotic neurons apoptosis, known as vacuolization of neurons. While at 7 day after SCI, inflammatory cells infiltration reducing, hyperplasia of glial cells, and phagocytosis phenomenon of neurons could be seen on HE stain, suggests that microglia have the effect of the removal of necrotic neurons, leaving ghost necrotic neurons observed. These pathological findings are consistent with previous reports (Alexander and Popovich, 2009; Mortazavi et al., 2015; Quadri et al., 2020). The Nissl body is a marker of the functional state of neurons. From Nissl staining, we found that the number of residual neurons in the Model group increased after EA treatment ($P < 0.05$), indicating that the death of neurons was reduced. The results showed that the EA could improve the microcirculation and inhibit neuronal death, which may be related to the improvement of motor function at 3 and 7 days time points.

Necroptosis is a regulatory necrosis activated downstream of tumor necrosis factor receptor 1 (TNFR1), dependent on the activity of receptor interaction protein kinases 1 (RIPK1) and 3 (RIPK3), and recruits mixed lineage pseudo-kinase MLKL to form necrosome complex (Necrosome), mediating cell rupture and death (Vandenabeele et al., 2010). The accumulation of necroptosis markers RIPK1, RIPK3, and MLKL was found after SCI, which may contribute to neuronal and glial cell death (Liu et al., 2015a). The RIPK1 inhibitor NEC-1 and the MLKL inhibitor NSA was found to inhibit the expression of necrosis factor and improve the lower limb motor function (Wang et al., 2014, 2018). In our results, RIPK1, RIPK3, and MLKL were mainly expressed in the cytoplasm of neurons and glial cells, but also shown in the intercellular substance, possibly because necroptosis factors in the cytoplasm were released into the intercellular after cell rupture. The mean optical density values of spinal cord tissues RIPK1, RIPK3, and MLKL in the Model group were significantly higher than those in the Sham group at 3 and 7 days after surgery ($P < 0.01$). This indicated that necrotic complexes accumulated in large quantities after SCI, while the average optical density values of RIPK1, RIPK3, and MLKL were decreased at all-time points after treatment in the EA group ($P < 0.05$). It may illustrate that EA could inhibit necrosome accumulation and reduce necroptosis of neuron.

As an important and conserved lysosomal degradation pathway, autophagy is thought to be involved in many physiological and pathological processes. It has been shown that inhibiting autophagy may have a neuroprotective effect (Siracusa et al., 2016; Wei et al., 2016). Autophagy flux is a dynamic process involving the formation, transmission, and degradation of autophagosomes. The increase of autophagosomes alone does not mean the enhancement of autophagy, and the accumulation of autophagosomes may occur due to the reduction of autophagosome degradation or the inability to degrade with the increase of autophagosome formation, thus inhibiting autophagy flux. The beneficial or harmful functions of autophagy may depend on the induction or inhibition of autophagy flux after central nervous system injury. Smooth autophagy flux

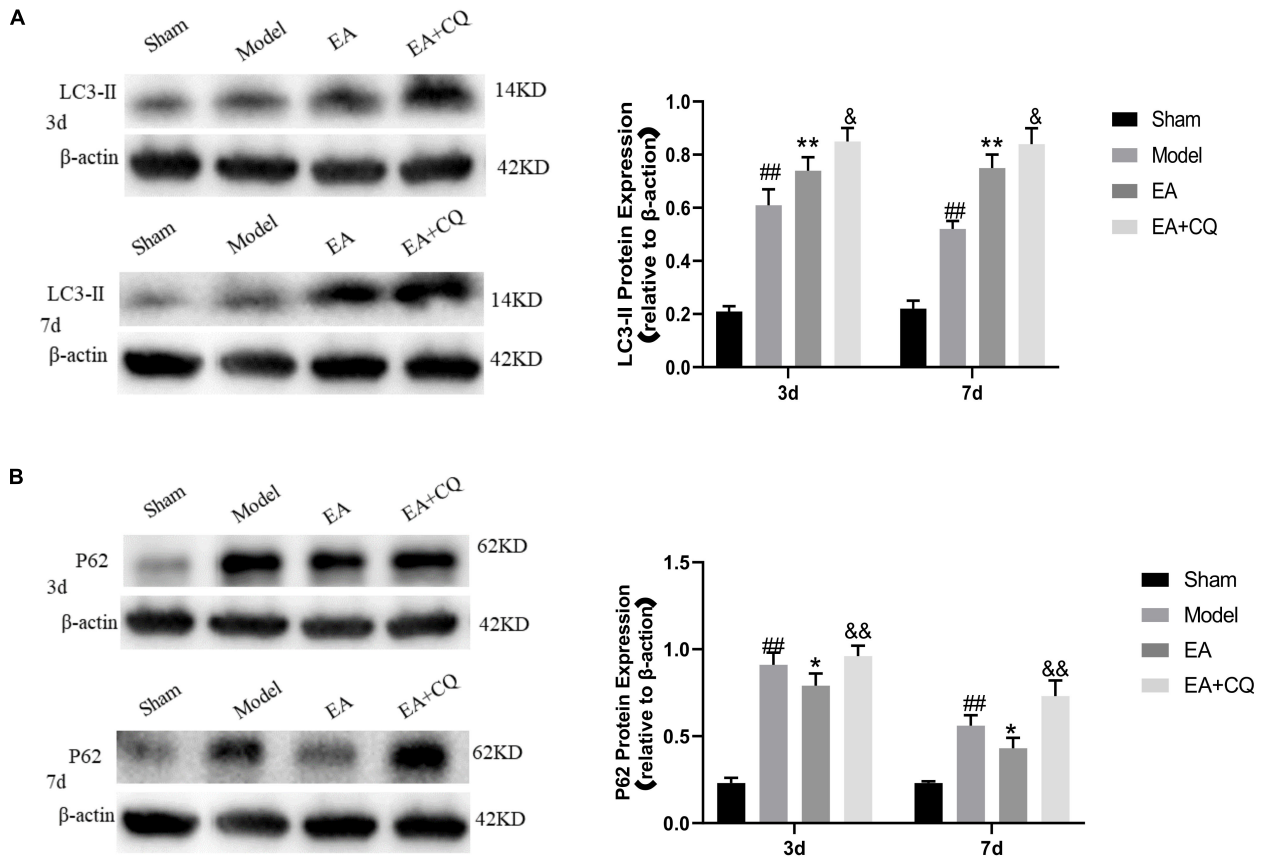

FIGURE 7 | Western blot results of the expression of LC3-II and P62 protein. **(A)** Expression of LC3-II in each group (LC3-II/β-actin). $^{\#\#}P < 0.01$, vs. Sham; $^{**}P < 0.01$, vs. Model; $^{\&}P < 0.05$, vs. EA. **(B)** Expression of P62 protein in each group (P62/β-actin). $^{\#\#}P < 0.01$, vs. Sham; $^{*}P < 0.05$, vs. Model; $^{\&\&}P < 0.01$, vs. EA.

often leads to cell protection, while blocked autophagy flux contributes to cell death. In our results, LC3 and P62 were mainly expressed in the cytoplasm of neurons and glial cells, consistent with the location of necrotic apoptotic factors. Average optical density values of LC3 and P62 were significantly higher than that of Sham group at 3 and 7 days postoperatively ($P < 0.01$). Besides, the expression peak of LC3 and P62 at 3 day was in accordance with that of necroptosis factors. The increase of LC3 and P62 after SCI indicates the blockage of autophagy flux, which may be caused by dysfunction of lysosomes on fusion and degradation of autophagosome after injury. The average optical density value of LC3 in the EA group was higher than that of the Model group at all-time points ($P < 0.05$), while the average optical density value of P62 was lower than that of the Model group ($P < 0.05$), indicating that EA treatment promoted the increase of LC3, reduced the expression of P62, and accelerated autophagy flux. LC3-II is generally considered as an autophagosome marker, because the content of LC3-II reflects the number of autophagosomes. However, LC3-II may not be able to estimate autophagy activity. Not only autophagy activation, but also inhibition of autophagosomal degradation greatly increases the content of LC3-II. The degradation of autophagy substrate P62/SQSTM1 is another marker widely used to evaluate autophagy activity, which can recruit ubiquitin substrates into autophagosome and degrade with it (Yoshii and Mizushima, 2017). When autophagy flux is high, the level of p62 protein decreases. Conversely, a reduction in autophagy flux may lead to P62 protein accumulation. Moreover, it was observed by electron microscopy that the number of lysosomes, autophagosomes and autolysosomes were increased compared with the model group after SCI was treated by EA. This result also indicates that EA could increase autophagy flux and promote autophagy degradation, consistent with the results that increase of LC3 expression and decrease of P62 expression mentioned before. More active lysosomes appeared after EA treatment, indicating Jia-Ji EA may stimulate lysosome function. The mechanism of EA on increasing autophagy flux may be related to the increase of autophagosome formation and the improvement of lysosomal function. However, the mechanism of Jia-Ji EA on increasing the number of lysosomes and enhancing its function still needs further study.

Lysosome function plays an important role in promoting autophagy flux. When autophagy flux is blocked due to lysosome dysfunction, the accumulation of autophagosomes would possibly lead to cell death (Lipinski et al., 2015). The autophagosome can be used as a basis to assemble necrotic

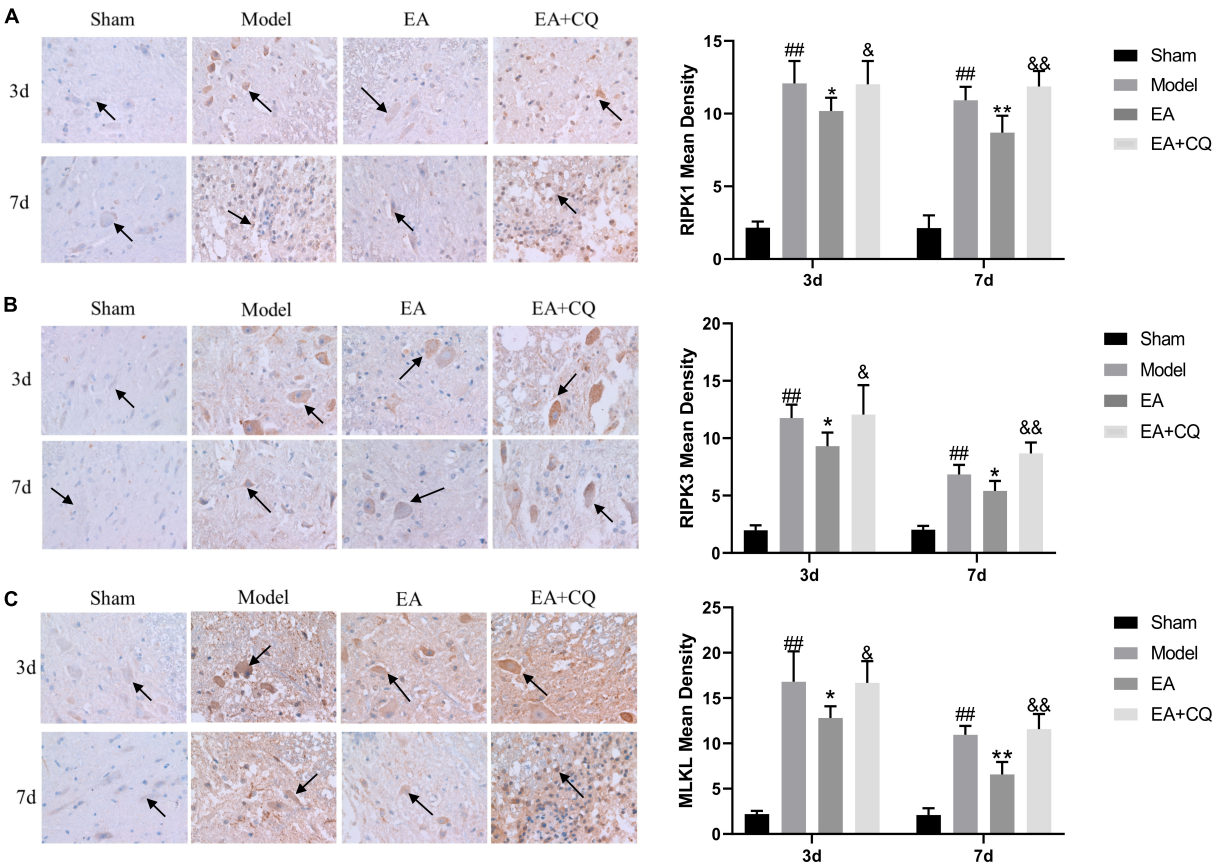

FIGURE 8 | Immunohistochemistry results on the expression of RIPK1, RIPK3, and MLKL. RIPK1, RIPK3 and MLKL were brown-yellow positive, mainly expressed in neuron and glial cells (black arrow). **(A)** Immunohistochemistry results of RIPK1 in rats in each group (400×). Mean optical density of RIPK1 in each group (IOD/Area). $^{\#\#}P < 0.01$, vs. Sham; $^{*}P < 0.05$, $^{**}P < 0.01$, vs. Model; $^{\&}P < 0.05$, $^{\&\&}P < 0.01$, vs. EA. **(B)** Immunohistochemistry results of RIPK3 in rats in each group (400×). Mean optical density of RIPK3 in each group (IOD/Area).$^{\#\#}P < 0.01$, vs. Sham; $^{*}P < 0.05$, vs. Model; $^{\&}P < 0.05$, $^{\&\&}P < 0.01$, vs. EA. **(C)** Immunohistochemistry results of MLKL in rats in each group (400×). Mean optical density of MLKL in each group (IOD/Area). $^{\#\#}P < 0.01$, vs. Sham; $^{*}P < 0.05$, $^{**}P < 0.01$, vs. Model; $^{\&}P < 0.05$, $^{\&\&}P < 0.01$, vs. EA.

complexes (Goodall et al., 2016). RIPK1 is recruited by P62 [the ZZ domain of P62 can interact with RIPK1 (Puissant et al., 2012)] to the autophagosome, which activates the assembly of necrosome and further mediates cell death. After inhibition of lysosomal function, autophagosomes accumulated, and could not be successfully degraded, contributing to the increase of LC3 and P62 contents. It has been previously demonstrated that autophagy flux was inhibited after SCI and treatment with rapamycin could attenuated accumulation of P62 by improving lysosomal function and autophagy flux (Liu et al., 2018). To further explore the effect of autophagy flux on rat hind limb function, lysosome inhibitor chloroquine CQ was applied. Many studies supported lysosomal luminal alkalinizer chloroquine (CQ) as an inhibitor of autophagy flux in rats with SCI (Hu et al., 2017; Zhang et al., 2017). CQ could improve the *pH*-value of lysosomes and then destroy the function of lysosomes, inhibit fusion of lysosomes and autophagosomes, thus leading to the accumulation of autophagosomes and blockage of the autophagy flux. BBB score and Nissl staining were observed after injecting CQ on the basis of EA treatment. At the time points of 3 and 7 days, BBB score was lower than that of the EA group ($P < 0.01$). The staining of motor neurons in the anterior horn was relatively light and the number of them was decreased compared with that of the EA group ($P < 0.01$), indicating that injection inhibitor CQ partially eliminated the therapeutic effect of EA, reduced the number of motor neurons in the anterior horn, and aggravated dysfunction of hind limbs in rats.

After treatment, the average optical density values of RIPK1, RIPK3, and MLKL in the EA group were lower than those in the Model group at each time point ($P < 0.05$), indicating the inhibitory effect of EA on necroptosis. After the injection of inhibitor CQ, the average optical density values of LC3, P62, RIPK1, RIPK3, and MLKL in the EA + CQ group increased at each time point, which was statistically significant compared with the EA group at each time point ($P < 0.05$). These results indicated that CQ partially eliminated the effect of EA on promoting autophagy flux and inhibiting necrotizing apoptosis. The results above were further confirmed by Western blot. Protein expression levels of LC3, P62, RIPK1, RIPK3, and MLKL were significantly higher than that of Sham group at 3 and 7 days

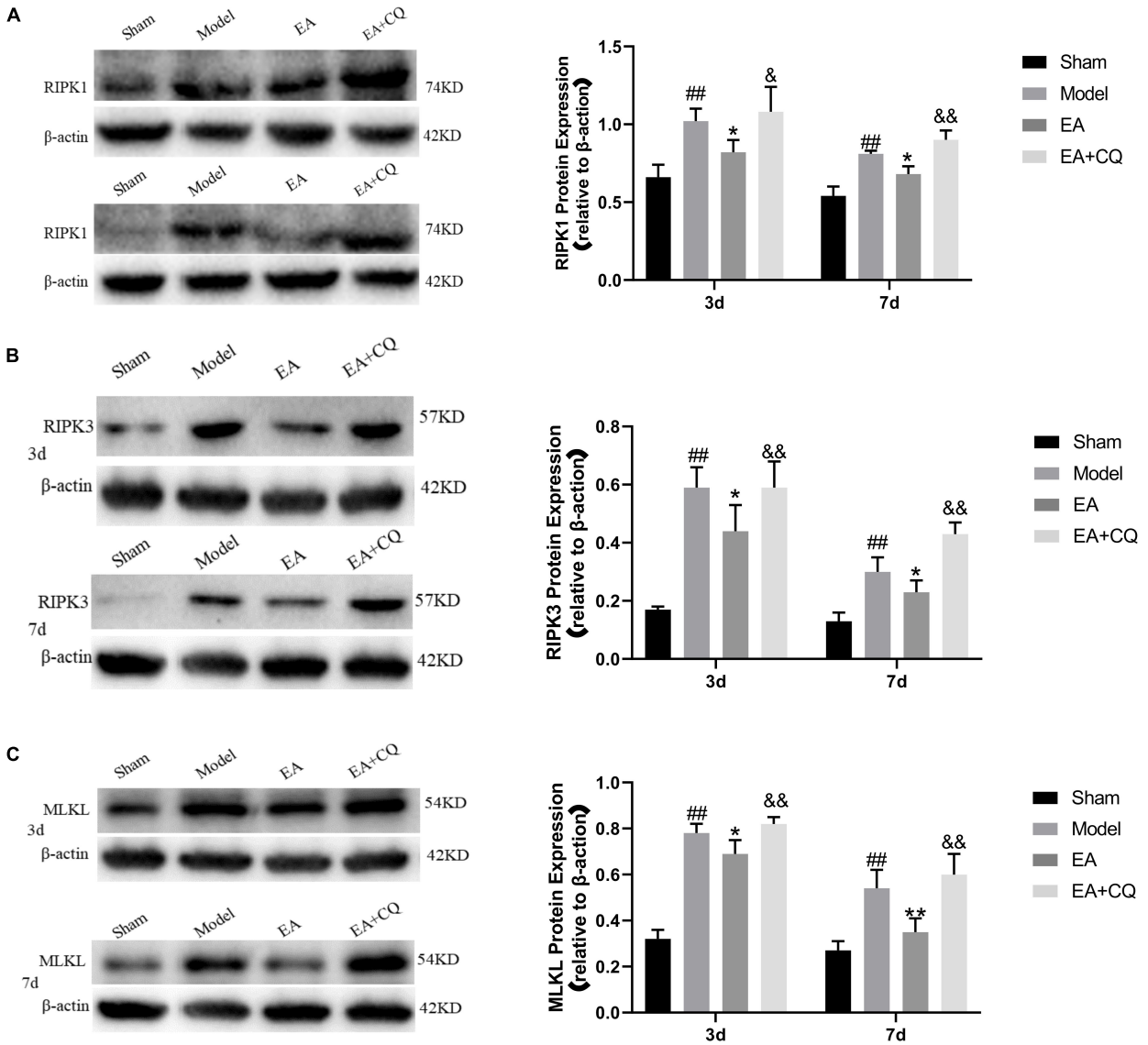

FIGURE 9 | Western blot results on the expression of RIPK1, RIPK3, and MLKL. **(A)** Expression of RIPK1 protein in each group (RIPK1/β-actin). $^{\#\#}P < 0.01$, vs. Sham; $^{*}P \leq 0.05$, vs. Model; $^{\&\&}P < 0.01$, $^{\&}P < 0.05$, vs. EA. **(B)** Expression of RIPK3 protein in each group (RIPK3/β-actin). $^{\#\#}P < 0.01$, vs. Sham; $^{*}P < 0.05$, vs. Model; $^{\&}P < 0.05$, $^{\&\&}P < 0.01$, vs. EA. **(C)** Expression of MLKL protein in each group (MLKL/β-actin). $^{\#\#}P < 0.01$, vs. Sham; $^{*}P < 0.05$, $^{**}P < 0.01$, vs. Model; $^{\&\&}P < 0.01$, vs. EA.

after surgery ($P < 0.01$), indicating autophagy flux blocked and necrotic protein expression enhanced after SCI. The expression of LC3-II was all higher than that in the Model group at each time point ($P < 0.01$) after EA treatment, while the protein expression levels of P62, RIPK1, RIPK3, and MLKL were all lower than that in the Model group ($P < 0.05$), indicating that EA could promote autophagy flux and inhibit necroptosis at the same time. It proved that autophagy may have relationship with necroptosis regulation. Blockage of autophagy flux by CQ may lead to the accumulation of the autophagosomes and increase of P62 expression, which may recruit and interact with RIPK1 to the autopahgosomes and then activate necroptosis. By promoting autophagy flux, Jia-Ji EA could inhibit the necroptosis of neuron, then further inhibit the reduction of the number of anterior motor neurons, and eventually improve the recovery of motor function. Furthermore, we still need to extend the observation time to the regeneration and repair period of SCI in the future study.

CONCLUSION

Together our data suggest that, Jia-Ji electro-acupuncture may improve the motor function of hind limbs in rats after SCI by improving lysosomal function, promoting the autophagy flux, then reducing necroptosis and inhibiting the loss of neuron.

It showed that the mechanism of Jia-Ji electro-acupuncture treatment were involved in lysosome/autophagy flux/necroptosis pathway. This study provides a potential mechanism and a better understanding of the neuroprotective effect of the electro-acupuncture. In future studies, we will explore the mechanism of Jia-Ji electro-acupuncture on lysosomal function and whether it could induce neuron regeneration and remodeling through this pathway.

DATA AVAILABILITY STATEMENT

The original contributions presented in the study are included in the article/**Supplementary Material**, further inquiries can be directed to the corresponding author/s.

ETHICS STATEMENT

The animal study was reviewed and approved by the International Council for Laboratory Animal Science (ICLAS) and Animal Care and Use Committee of China.

AUTHOR CONTRIBUTIONS

YH and TH designed and performed most part of the research. LQ performed statistics. FD performed electron microscopy experiment. LG and LX contributed important reagents and provided technical assistance. GF collected, analyzed data, and wrote the manuscript. SZ supervised and assisted the process of work. All authors contributed to the article and approved the submitted version.

FUNDING

This work was supported by the National Natural Science Foundation of China (projects 81873378 and 81704181).

SUPPLEMENTARY MATERIAL

The Supplementary Material for this article can be found online at: https://www.frontiersin.org/articles/10.3389/fnins.2020.616864/full#supplementary-material

REFERENCES

Alexander, J. K., and Popovich, P. G. (2009). Neuroinflammation in spinal cord injury: therapeutic targets for neuroprotection and regeneration. *Prog. Brain Res.* 175, 125–137. doi: 10.1016/s0079-6123(09)17508-8

Basso, D. M., Beattie, M. S., and Bresnahan, J. C. (1995). A sensitive and reliable locomotor rating scale for open field testing in rats. *J. Neurotrauma* 12, 1–21. doi: 10.1089/neu.1995.12.1

Degterev, A., Hitomi, J., Germscheid, M., Ch'en, I. L., Korkina, O., Teng, X., et al. (2008). Identification of RIP1 kinase as a specific cellular target of necrostatins. *Nat. Chem. Biol.* 4, 313–321. doi: 10.1038/nchembio.83

Ding, Y., Yan, Q., Ruan, J. W., Zhang, Y. Q., Li, W. J., Zeng, X., et al. (2011). Bone marrow mesenchymal stem cells and electroacupuncture downregulate the inhibitor molecules and promote the axonal regeneration in the transected spinal cord of rats. *Cell Transplant.* 20, 475–491. doi: 10.3727/096368910x528102

GBD 2016 Traumatic Brain Injury and Spinal Cord Injury Collaborators (2019). Global, regional, and national burden of traumatic brain injury and spinal cord injury, 1990-2016: a systematic analysis for the Global Burden of Disease Study 2016. *Lancet Neurol.* 18, 56–87. doi: 10.1016/s1474-4422(18)30415-0

Goodall, M. L., Cramer, S. D., and Thorburn, A. (2016). Autophagy complexes cell death by necroptosis. *Oncotarget* 7, 50818–50819. doi: 10.18632/oncotarget.10640

Grossman, R. G., Fehlings, M. G., Frankowski, R. F., Burau, K. D., Chow, D. S., Tator, C., et al. (2014). A prospective, multicenter, phase I matched-comparison group trial of safety, pharmacokinetics, and preliminary efficacy of riluzole in patients with traumatic spinal cord injury. *J. Neurotrauma* 31, 239–255. doi: 10.1089/neu.2013.2969

Hong, E. S., Yao, H. H., Min, Y. J., Sun, J., Zhou, X., Zeng, X. B., et al. (2019). The mechanism of electroacupuncture for treating spinal cord injury rats by mediating Rho/Rho-associated kinase signaling pathway. *J. Spinal Cord Med.* 9, 1–11. doi: 10.1080/10790268.2019.1665612

Hu, J., Han, H., Cao, P., Yu, W., Yang, C., Gao, Y., et al. (2017). Resveratrol improves neuron protection and functional recovery through enhancement of autophagy after spinal cord injury in mice. *Am. J. Transl. Res.* 9, 4607–4616.

Huang, S. F., Ding, Y., Ruan, J. W., Zhang, W., Wu, J. L., He, B., et al. (2011). An experimental electro-acupuncture study in treatment of the rat demyelinated spinal cord injury induced by ethidium bromide. *Neurosci. Res.* 70, 294–304. doi: 10.1016/j.neures.2011.03.010

Ito, Y., Ofengeim, D., Najafov, A., Das, S., Saberi, S., Li, Y., et al. (2016). RIPK1 mediates axonal degeneration by promoting inflammation and necroptosis in ALS. *Science* 353, 603–608. doi: 10.1126/science.aaf6803

Jazayeri, S. B., Beygi, S., Shokraneh, F., Hagen, E. M., and Rahimi-Movaghar, V. (2015). Incidence of traumatic spinal cord injury worldwide: a systematic review. *Eur. Spine J.* 24, 905–918. doi: 10.1007/s00586-014-3424-6

Kumar, R., Lim, J., Mekary, R. A., Rattani, A., Dewan, M. C., Sharif, S. Y., et al. (2018). Traumatic spinal injury: global epidemiology and worldwide volume. *World Neurosurg.* 113, e345–e363. doi: 10.1016/j.wneu.2018.02.033

Kwon, B. K., Streijger, F., Hill, C. E., Anderson, A. J., Bacon, M., Beattie, M. S., et al. (2015). Large animal and primate models of spinal cord injury for the testing of novel therapies. *Exp. Neurol.* 269, 154–168. doi: 10.1016/j.expneurol.2015.04.008

Kwon, B. K., Tetzlaff, W., Grauer, J. N., Beiner, J., and Vaccaro, A. R. (2004). Pathophysiology and pharmacologic treatment of acute spinal cord injury. *Spine J.* 4, 451–464. doi: 10.1016/j.spinee.2003.07.007

Lipinski, M. M., Wu, J., Faden, A. I., and Sarkar, C. (2015). function and mechanisms of autophagy in brain and spinal cord trauma. *Antioxid. Redox Signal.* 23, 565–577. doi: 10.1089/ars.2015.6306

Liu, M., Wu, W., Li, H., Li, S., Huang, L. T., Yang, Y. Q., et al. (2015a). Necroptosis, a novel type of programmed cell death, contributes to early neural cells damage after spinal cord injury in adult mice. *J. Spinal Cord Med.* 38, 745–753. doi: 10.1179/2045772314y.0000000224

Liu, S., Li, Y., Choi, H. M. C., Sarkar, C., Koh, E. Y., Wu, J., et al. (2018). Lysosomal damage after spinal cord injury causes accumulation of RIPK1 and RIPK3 proteins and potentiation of necroptosis. *Cell Death Dis.* 9:476. doi: 10.1038/s41419-018-0469-1

Liu, S., Sarkar, C., Dinizo, M., Faden, A. I., Koh, E. Y., Lipinski, M. M., et al. (2015b). Disrupted autophagy after spinal cord injury is associated with ER stress and neuronal cell death. *Cell Death Dis.* 6:e1582. doi: 10.1038/cddis.2014.527

Mortazavi, M. M., Verma, K., Harmon, O. A., Griessenauer, C. J., Adeeb, N., Theodore, N., et al. (2015). The microanatomy of spinal cord injury: a review. *Clin. Anat.* 28, 27–36. doi: 10.1002/ca.22432

National Spinal Cord Injury Statistical Center (2016). Spinal cord injury (SCI) 2016 facts and figures at a glance. *J. Spinal Cord Med.* 39, 493–494. doi: 10.1080/10790268.2016.1210925

Ofengeim, D., Ito, Y., Najafov, A., Zhang, Y., Shan, B., DeWitt, J. P., et al. (2015). Activation of necroptosis in multiple sclerosis. *Cell Rep.* 10, 1836–1849. doi: 10.1016/j.celrep.2015.02.051

Puissant, A., Fenouille, N., and Auberger, P. (2012). When autophagy meets cancer through p62/SQSTM1. *Am. J. Cancer Res.* 2, 397–413.

Quadri, S. A., Farooqui, M., Ikram, A., Zafar, A., Khan, M. A., Suriya, S. S., et al. (2020). Recent update on basic mechanisms of spinal cord injury. *Neurosurg. Rev.* 43, 425–441. doi: 10.1007/s10143-018-1008-3

Sarkar, C., Zhao, Z., Aungst, S., Sabirzhanov, B., Faden, A. I., and Lipinski, M. M. (2014). Impaired autophagy flux is associated with neuronal cell death after traumatic brain injury. *Autophagy* 10, 2208–2222. doi: 10.4161/15548627.2014.981787

Schroeder, G. D., Kwon, B. K., Eck, J. C., Savage, J. W., Hsu, W. K., and Patel, A. A. (2014). Survey of cervical spine research society members on the use of high-dose steroids for acute spinal cord injuries. *Spine (Phila Pa 1976)* 39, 971–977. doi: 10.1097/brs.0000000000000297

Singh, A., Tetreault, L., Kalsi-Ryan, S., Nouri, A., and Fehlings, M. G. (2014). Global prevalence and incidence of traumatic spinal cord injury. *Clin. Epidemiol.* 6, 309–331. doi: 10.2147/clep.S68889

Siracusa, R., Paterniti, I., Bruschetta, G., Cordaro, M., Impellizzeri, D., Crupi, R., et al. (2016). The association of palmitoylethanolamide with luteolin decreases autophagy in spinal cord injury. *Mol. Neurobiol.* 53, 3783–3792. doi: 10.1007/s12035-015-9328-6

Vandenabeele, P., Galluzzi, L., Vanden Berghe, T., and Kroemer, G. (2010). Molecular mechanisms of necroptosis: an ordered cellular explosion. *Nat. Rev. Mol. Cell Biol.* 11, 700–714. doi: 10.1038/nrm2970

Verma, R., Virdi, J. K., Singh, N., and Jaggi, A. S. (2019). Animals models of spinal cord contusion injury. *Korean J. Pain* 32, 12–21. doi: 10.3344/kjp.2019.32.1.12

Wang, Y., Wang, H., Tao, Y., Zhang, S., Wang, J., and Feng, X. (2014). Necroptosis inhibitor necrostatin-1 promotes cell protection and physiological function in traumatic spinal cord injury. *Neuroscience* 266, 91–101. doi: 10.1016/j.neuroscience.2014.02.007

Wang, Y., Wang, J., Wang, H., Feng, X., Tao, Y., Yang, J., et al. (2018). Necrosulfonamide attenuates spinal cord injury via necroptosis inhibition. *World Neurosurg.* 114, e1186–e1191. doi: 10.1016/j.wneu.2018.03.174

Wei, X., Zhou, Z., Li, L., Gu, J., Wang, C., Xu, F., et al. (2016). Intrathecal injection of 3-methyladenine reduces neuronal damage and promotes functional recovery via autophagy attenuation after spinal cord ischemia/reperfusion injury in rats. *Biol. Pharm. Bull.* 39, 665–673. doi: 10.1248/bpb.b15-00610

Weinlich, R., Oberst, A., Beere, H. M., and Green, D. R. (2017). Necroptosis in development, inflammation and disease. *Nat. Rev. Mol. Cell Biol.* 18, 127–136. doi: 10.1038/nrm.2016.149

Xiong, F., Fu, C., Zhang, Q., Peng, L., Liang, Z., Chen, L., et al. (2019). The effect of different acupuncture therapies on neurological recovery in spinal cord injury: a systematic review and network meta-analysis of randomized controlled trials. *Evid. Based Complement. Alternat. Med.* 2019:2371084. doi: 10.1155/2019/2371084

Yoshii, S. R., and Mizushima, N. (2017). Monitoring and measuring autophagy. *Int. J. Mol. Sci.* 18:1865. doi: 10.3390/ijms18091865

Zhang, D., Xuan, J., Zheng, B. B., Zhou, Y. L., Lin, Y., Wu, Y. S., et al. (2017). Metformin improves functional recovery after spinal cord injury via autophagy flux stimulation. *Mol. Neurobiol.* 54, 3327–3341. doi: 10.1007/s12035-016-9895-1

Conflict of Interest: The authors declare that the research was conducted in the absence of any commercial or financial relationships that could be construed as a potential conflict of interest.

frontiers in Aging Neuroscience

ORIGINAL RESEARCH
published: 04 February 2021
doi: 10.3389/fnagi.2020.615048

Alterations of Brain Structural Network Connectivity in Type 2 Diabetes Mellitus Patients With Mild Cognitive Impairment

Chang Li[1,2], Jingna Zhang[3], Mingguo Qiu[3], Kaijun Liu[4], Yang Li[1], Zhiwei Zuo[5], Xuntao Yin[6], Yuqi Lai[7], Jingqin Fang[1,8], Haipeng Tong[1], Yu Guo[1], Jian Wang[2], Xiao Chen[8,9]* and Kunlin Xiong[1,8]**

[1] Department of Radiology, Daping Hospital, Army Medical University, Chongqing, China, [2] Department of Radiology, Southwest Hospital, Army Medical University, Chongqing, China, [3] Department of Medical Imaging, College of Biomedical Engineering, Army Medical University, Chongqing, China, [4] Department of Gastroenterology, Daping Hospital, Army Medical University, Chongqing, China, [5] Department of Radiology, General Hospital of Western Theater Command, Chengdu, China, [6] Department of Medical Imaging, Guizhou Provincial People's Hospital, Guiyang, China, [7] School of Foreign Languages and Cultures, Chongqing University, Chongqing, China, [8] Chongqing Clinical Research Center for Imaging and Nuclear Medicine, Chongqing, China, [9] Department of Nuclear Medicine, Daping Hospital, Army Medical University, Chongqing, China

OPEN ACCESS

Edited by:
Woon-Man Kung, Chinese Culture University, Taiwan

Reviewed by:
Josue Luiz Dalboni Da Rocha, Université de Genève, Switzerland
Angel Golimstok, Hospital Italiano de Buenos Aires, Argentina

***Correspondence:**
Jian Wang
wangjian_811@yahoo.com
Xiao Chen
xiaochen229@foxmail.com
Kunlin Xiong
109948969@qq.com

Received: *08 October 2020*
Accepted: *30 December 2020*
Published: *04 February 2021*

Citation:
Li C, Zhang J, Qiu M, Liu K, Li Y, Zuo Z, Yin X, Lai Y, Fang J, Tong H, Guo Y, Wang J, Chen X and Xiong K (2021) Alterations of Brain Structural Network Connectivity in Type 2 Diabetes Mellitus Patients With Mild Cognitive Impairment. Front. Aging Neurosci. 12:615048. doi: 10.3389/fnagi.2020.615048

Patients with type 2 diabetes mellitus (T2DM) are highly susceptible to developing dementia, especially for those with mild cognitive impairment (MCI), but its underlying cause is still unclear. This study aims to investigate the early detection of white matter structural network changes in T2DM patients with MCI and assess the relationship between cognitive impairment and structural network alterations in T2DM patients. In this study, we performed a battery of neuropsychological tests and diffusion tensor MRI in 30 T2MD-MCI patients, 30 T2DM patients with normal cognition (T2DM-NC) and 30 age-, sex-, and education-matched healthy control (HC) individuals. Cognitive performance exhibited obvious differences among the three groups. The structural network was significantly disrupted in both global and regional levels in T2DM patients. The T2DM-MCI group showed more severe impairment of global network efficiency, and lower nodal efficiency and fewer connections within multiple regions like the limbic system, basal ganglia, and several cortical structures. Moreover, a subnetwork impaired in T2DM-MCI patients was characterized by cortical-limbic fibers, and commissural fibers and pathways within the frontal, temporal, and occipital lobes. These altered global and nodal parameters were significantly correlated with cognitive function in T2DM-MCI patients. In particular, executive dysfunction and working memory impairment in T2DM-MCI patients correlated with nodal efficiency in the right opercular part and triangular part of the inferior frontal gyrus, which indicated that white matter disruption in these regions may act as potential biomarkers for T2DM-associated MCI detection. Our investigation provides a novel insight into the neuropathological effects of white matter network disruption on cognition impairments induced by T2DM.

Keywords: type 2 diabetes mellitus, mild cognitive impairment, diffusion tensor imaging, white matter network, network-based statistics

INTRODUCTION

Type 2 diabetes mellitus (T2DM) is a common metabolic disorder characterized by insulin resistance and hyperglycemia, which can lead to severe multi-systemic impairments. Patients with T2DM have a considerably high risk of developing cognitive dysfunction (Cukierman et al., 2005; Koekkoek et al., 2015). A significant portion of T2DM patients with cognitive impairment eventually progress to dementia (Cheng et al., 2012; Ninomiya, 2014). Mild cognitive impairment (MCI) is the early stage of diabetic cognitive impairment, which is a modifiable stage between normal cognitive aging and dementia (Sperling et al., 2011). The occurrence of dementia is an irreversible process making the pre-dementia stage, which includes MCI, the best time to treat T2DM patients (Mitchell and Shiri-Feshki, 2008). Therefore, early identification and detection of alterations in T2DM-MCI patients may help clinicians with early prevention of severe cognitive decline.

Previous studies have reported that changes in white matter (WM) in T2DM patients are correlated with cognitive impairment (Reijmer et al., 2013a; Hoogenboom et al., 2014; Zhang et al., 2014). Diffusion tensor imaging (DTI), a sophisticated magnetic resonance (MR) imaging technique, is sensitive in detecting microstructural alterations of the WM in T2DM (Hsu et al., 2012; Tan et al., 2016). These results revealed that significant alterations of WM integrity were predominantly found in the cingulum, the uncinate fasciculus, the superior and inferior longitudinal fasciculus, corpus callosum, and external and internal capsule in T2DM patients (Reijmer et al., 2013a; Hoogenboom et al., 2014; Zhang et al., 2014; Nouwen et al., 2017; Yoon et al., 2017; Sun et al., 2018; Xiong et al., 2019). However, these previous studies mainly focused on the regional abnormalities in WM integrity in T2DM.

The human brain is a complex network which comprises multiple brain regions connected to each other. Recently, there has been much interest in mapping the "connectome" to investigate and fully understand the complexity of brain structural network connections (Sporns et al., 2005; Lichtman et al., 2008). So far, four studies have examined the topological properties of the structural brain network in patients with diabetes (Reijmer et al., 2013b; Kim et al., 2016; Zhang et al., 2016, 2019). The results showed disruptions in network integration parameters which represent the slower speed and lowered capacity of a network to exchange information. However, indicators of small-world alteration and local information integration capability did not show a consistent pattern in T2DM. The reason for the inconsistent results may be that the T2DM patients studied were in different stages of diabetes-associated cognitive impairment in this research. Therefore, our study aimed to explore the WM structural network connectome mechanism in T2DM patients with and without MCI.

In this study, we enrolled T2DM patients with MCI (T2DM-MCI), T2DM patients with normal cognition (T2DM-NC), and healthy controls (HC) to perform a clinical assessment, a battery of neuropsychological tests, and DTI MR imaging. Network-based statistics (NBS) and graph theory analysis were conducted to investigate WM structural network connectome differences in these three groups, and then we assessed the relationship between structural topological network disruptions and cognitive performance in T2DM-MCI patients. Our study may provide insights into the neuropathological mechanisms of T2DM-related cognitive impairment.

MATERIALS AND METHODS

Participants

Thirty patients with T2DM-NC and 30 patients with T2DM-MCI were enrolled in the study from October 2015 to November 2019. T2DM was diagnosed using the 1999 criteria proposed by the World Health Organization. The diagnosis of MCI was based on the criteria established in the 2006 European Alzheimer's Disease Consortium, which includes complaints of hypomnesis, an MoCA score < 26, a mini mental state exam (MMSE) score > 24, a clinical dementia rating (CDR) ≥ 0.5, and a normal activities of daily living (ADL) score. Participants were excluded if they had a history of brain injury, alcoholism, epilepsy, Parkinson disease, major depression, or other psychiatric or neurological disorders. Participants with dementia (MMSE ≤ 24), severe depression (Hamilton Depression Rating Scale ≥ 18), severe claustrophobia, or contraindications to MRI were also excluded. T2DM patients were excluded if they had microvascular complications, including nephropathy, retinopathy, and neuropathy. Thirty volunteers without vascular risk factors, nervous system diseases, cognitive complaints, or psychiatric illnesses were recruited as HC. Thirty HCs had no T2DM, psychiatric or neurological disorder, and had an MoCA score ≥ 26, and an MMSE score > 24. Height, weight, and body mass index (BMI) were measured for each participant. All participants were tested by neurological, neuropsychological, and structural MRI examinations. All participants were right-handed and native Chinese speakers. Glycosylated hemoglobin (HbA1c), fasting plasma glucose (FPG), fasting C-peptide, fasting insulin, triglycerides (TGs), total cholesterol (TC), low-density lipoprotein (LDL), high-density lipoprotein (HDL), homocysteine, urinary microalbumin, blood urea nitrogen (BUN), uric acid, serum creatine, cystatin C, free thyroxine (FT), free triiodothyronine (FT3), and thyroid-stimulating hormone (TSH) were measured via standard laboratory testing. This study was carried out in accordance with the Declaration of Helsinki. The Research Ethics Committee of Southwest Hospital, Army Medical University approved the study. All participants voluntarily provided written informed consent.

Neuropsychological Testing

All participants completed a battery of neuropsychological tests, including MMSE, Montreal Cognitive Assessment (MoCA), Digit Symbol Coding Test (DSCT), Complex Figure Test (CFT), Trail-Making Test (TMT), Digit Span Test (DST), Verbal Fluency Test (VFT), and Auditory Verbal Learning Tests (AVLT) which contains 12 variants, including coat, trousers, kerchief, glove, driver, carpenter, soldier, lawyer, crabapple, lily, wintersweet, and yulan.

Imaging Acquisition

All imaging data were obtained on a 3-Tesla Trio MRI system (Siemens Healthcare, Erlangen, Germany) equipped with a 12-channel phase-array head coil. DTI images were acquired by a single-shot echo planar imaging (EPI) sequence with the following parameters: repetition time (TR) = 10,000 ms; echo time (TE) = 92 ms; flip angle = 90°; field of view (FOV) = 256 mm × 256 mm; matrix = 128 × 128; slice thickness = 2 mm, no gap; 75 axial slices; 64 encoding diffusion directions with b = 1,000 s/mm^2; and 1 non-diffusion b = 0 s/mm^2 images. The 3D high-resolution structural images were obtained using a T1-weighted magnetization prepared rapid acquisition gradient echo (MPRAGE) sequence, as follows: TR = 1,900 ms, TE = 2.52 ms, TI = 900 ms, flip angle (FA) = 9, matrix = 256 × 256, thickness = 1.0 mm, 176 slices with voxel size =1 × 1 × 1 mm. Then, all the subjects were required to undergo conventional brain T1-weighted and fluid attenuated inversion recovery (FLAIR) images to exclude organic diseases and white matter (WM) hyperintense lesions.

Imaging Preprocessing

For the DTI data, they were preprocessed and analyzed by the Pipeline for Analyzing Brain Diffusion Images toolkit (PANDA, www.nitrc.org/projects/panda) (Cui et al., 2013) based on the FMRIB Software Library (FSL) (Behrens et al., 2003). The specific preprocessing steps were performed as previously reported (Xie X. et al., 2017). In brief, first, we converted the image format from DICOM to NIFTI. Second, we removed the skull and extracted the brain tissue. Third, we corrected head motion and eddy-current induced distortions by realigning each diffusion-weighted image to the non-weighted b0 image.

Network Construction

The network nodes and edges were defined by the following procedures. An Automated Anatomical Labeling (AAL) template was used to parcellate the cerebral cortex into 90 anatomical regions (45 for each hemisphere), each representing a node of the constructed network. The 3D T1-weighted images were co-registered to the original b0 images using SPM (www.fil.ion.ucl.ac.uk/spm), and then the co-registered 3D-T1 images were normalized to the Montreal Neurologic Institute (MNI) space. Finally, the inverse transformations were applied to the AAL atlas, resulting in corresponding AAL regions in the individual DTI native-space.

A deterministic fiber assignment with the continuous tracking (FACT) algorithm was used to track the whole-brain white matter fibers for each subject in the native diffusion space. All voxels with an FA $\geq$0.2 were used as seed points; the tracking continued to one of the seed points unless the tracking angle between two adjacent voxels was $> 45°$ or the FA was < 0.2 (Mori et al., 1999). To determine the edges of the brain network, two brain regions were considered connected by an edge in cases in which at least three fibers were present between the regions. A threshold of three fibers ensures that influence from spurious connections is reduced (Lo et al., 2010). For each edge of the network, the mean FA along the fiber bundles were defined as the weights of a network edge between two connected nodes. FA value is an important index to evaluate fiber integrity (Beaulieu, 2002). Previous studies proposed that mean FA has the ability to subtly detect local brain lesions (Lim and Helpern, 2002). At last, a 90 × 90 matrix was generated, representing the FA-weighted structural network of each subject.

Network Measures

The global and nodal topological metrics were calculated with the graph theoretical network analysis toolbox (GRETNA; http://www.nitrc.org/projects/gretna). A sparsity threshold range of 10–30% with an interval of 1%, which was checked by previous studies and showed good small-world characteristics, was applied to minimize the possible discrepancies among all FA-weighted matrices (Watts and Strogatz, 1998; Zhang et al., 2011; Korgaonkar et al., 2014). Within every threshold, the global network metrics were calculated. Specifically, the global metrics of each structural network were constant and ranged from 15 to 30% (**Supplementary Figure 1**). Hence, the threshold at different levels of sparsity, ranging from 10 to 15%, was employed in our study. During these thresholds, we calculated the following global network parameters of the weighted brain structural network (see detailed computational formulas of these parameters in the **Supplementary Material**): clustering coefficient (C_p), characteristic path length (L_p), normalized C_p (γ), normalized L_p (λ), small-worldness (σ), global efficiency (E_{glob}), and local efficiency (E_{loc}). C_p represented the average clustering coefficients of all nodes. L_p was defined as the average of the shortest path length between any two nodes. E_{glob} is considered as an important parameter to estimate the global transmission efficiency of the network. E_{loc} demonstrated the network interconnection among the nodes. We investigated the "small worldness" by generating 1,000 random networks to compare with the real networks. γ and λ were defined as the ratio of real world network's C_p and L_p to the random network's. And σ was defined as the ratio of γ to λ, which quantifies the organization of a network, with $\sigma > 1$ indicating a network has a small-world property. Nodal efficiency and betweenness centrality were also computed to represent regional characteristics of the structural network. Among these nodes, there were a number of specific nodes that interacted with many other nodes, which were defined as hubs that play a vital role in maintaining network stability. As a hub, the condition should be the betweenness centrality of a node greater than or equal to the average value plus SD of the network betweenness centrality.

Moreover, a network-based statistic (NBS) was used to identify the altered structural connections in patients (Zalesky et al., 2010). We first applied one-way ANOVA (*post-hoc*: two-sample two-tailed *t*-tests) to compare the strength of the edge at each individual element of the connectivity matrix. Second, a primary component-forming threshold ($P < 0.01$, uncorrected) was applied to search for potential connected edges. Third, the size of the largest remaining subthreshold connected component was computed. Then, the groups were randomly shuffled (5,000 permutations) and the largest subthreshold connected component size was calculated by repeating steps 1, 2, and 3. In this way, an empirical null distribution was generated to evaluate the statistical significance of the network connected component

sizes. Finally, for any connected component of size M that found in the right grouping of controls and patients, the corrected *P*- value was determined by calculating the proportion of the 5,000 permutations for which the maximal connected component was larger than M. The NBS identifies the subnetworks of connected edges that differ the most among groups ($P < 0.05$ NBS corrected for multiple comparisons). The results of the nodal and edge comparisons were visualized using the BrainNet viewer software (http://www.nitrc.org/projects/bnv/).

Statistical Analysis

All statistical analyses were performed in SPSS (version 22, Chicago, IL). For demographic and neuropsychological testing, a one-way analysis of variance (ANOVA) test was used to compare among groups. *Post-hoc* tests with Bonferroni correction were performed after observing statistical differences among the three groups. An χ^2 test was used to compare sex variables. Instead of using single threshold metrics, we calculated the area under the curve (AUC) of each metric above to summarize the topological characteristic of the structural brain network. The group differences in AUC values of global network metrics (C_p, L_p, E_{glob}, and E_{loc}) and nodal properties (nodal efficiency and nodal betweenness centrality) were investigated with one-way ANOVA, while age and gender were adjusted as potential confounders. Metrics showing the main effect of group differences in the ANOVA model were further evaluated by *post-hoc* tests. A significance threshold of $P < 0.05$ was applied to each test, and the false discovery rate (FDR)-correction was applied for multiple comparison corrections. In addition, to explore the relationships between the topological properties of the network measures and clinical outcomes in cognitive function, we further performed Spearman's correlation between the topological properties and cognitive test scores in the T2DM-MCI patient groups. $P < 0.05$ was considered statistically significant.

RESULTS

Demographics and Neuropsychological Testing

There were no significant differences in age, gender, years of education, systolic or diastolic blood pressure, LDL, total cholesterol, and triglycerides among the T2DM-MCI, T2DM-NC, and HC groups. Compared with HC, T2DM-NC patients had higher FPG and HbA1c and lower HDL (Bonferroni-correction, $P < 0.05$). T2DM-MCI patients had higher BMI, HbA1c, and FPG and lower HDL than HC (Bonferroni-correction, $P < 0.05$). But no significant difference was found between T2DM-NC and T2DM-MCI patients (Bonferroni-correction, $P > 0.05$). In the neuropsychological test, T2DM-MCI patients performed worst among the three groups, while no significant difference was shown between T2DM-NC patients and HC (Bonferroni-correction, $P > 0.05$). Moreover, T2DM-MCI patients presented an obvious reduction in multiple domains of cognitive function including episodic memory, executive function, working memory, and attention when compared with T2DM-NC patients and HC. However, no significant differences in spatial processing and language ability among the three groups were found. Demographic data and neuropsychological testing are presented in **Table 1**.

Global Network Properties

The brain networks of the T2DM-MCI, T2DM-NC, and HC groups exhibited good small-world properties ($\sigma > 1$, **Supplementary Figure 2**). The global properties of the network showed no significant differences in C_p, but was observed in L_p, E_{glob}, and E_{loc} among these three groups. In *post-hoc* comparisons, significantly higher L_p and lower E_{glob} and E_{loc} were found in the T2DM-MCI group relative to the HC group, while higher L_p and lower E_{glob} in the T2DM-NC group were found relative to the HC group. The T2DM-MCI group showed higher L_p and lower E_{glob} relative to the T2DM-NC group ($P < 0.05$, FDR-corrected, **Figure 1**, **Table 2**).

Nodal Efficiency and Hubs Characteristics

Nodal Efficiency

All nodal properties (nodal efficiency and betweenness centrality) of the white matter network of the T2DM-MCI, T2DM-NC, and HC groups were analyzed. Significant group effects of nodal efficiency were found in 33 of 90 nodes among the three groups, while the *post-hoc* comparison showed that nodal efficiency was widely reduced at 32 nodes in the T2DM-MCI group compared with the HC group and 12 nodes in the T2DM-NC group compared with the HC group ($P < 0.05$, FDR-corrected, **Table 3**, **Figure 2**). To reveal regions specifically related to cognitive impairments associated with T2DM, we carried out a *post hoc* comparison between T2DM-MCI and T2DM-NC. Compared to T2DM-NC group, T2DM-MCI group showed lower nodal efficiency in 11 nodes mainly located in the limbic system, basal ganglia, parts of frontal, temporal and parietal lobe, including right inferior frontal gyrus (opercular part and triangular part), left hippocampus, parahippocampal gyrus, fusiform gyrus, superior parietal gyrus, precuneus, caudate nucleus, middle temporal gyrus, inferior temporal gyrus, inferior parietal, but supramarginal and angular gyri ($P < 0.05$, FDR-corrected, **Table 3**). There were also group effects and between-group differences of betweenness centrality in 5 of 90 nodes ($P < 0.05$). However, the differences did not survive after FDR correction for multiple comparisons (**Supplementary Table 2**).

Hubs Characteristics

The hubs of the brain network of these three groups were identified, including 13 hubs in HC, 12 hubs in T2DM-NC patients, and 11 hubs in T2DM-MCI patients (**Table 4**). Among them, 10 hubs were shared by these three groups, mostly distributed in the bilateral precentral gyrus, calcarine fissure and surrounding cortex, superior occipital gyrus, precuneus, and putamen. Compared with HC, T2DM-NC patients had decreased hubs at the right hippocampus, right caudate nucleus, and left thalamus, while two new hubs appeared at the caudate nucleus and middle temporal gyrus on the left side (**Figure 3**). T2DM-MCI patients had decreased hubs at the right hippocampus and right caudate nucleus relative to HC, while they had decreased hubs at the left caudate nucleus and left middle temporal gyrus,

TABLE 1 | Demographic and neuropsychological characteristics.

	HC ($n = 30$)	T2DM without MCI ($n = 30$)	T2DM with MCI ($n = 30$)	F-value (t/χ^2)	P-value
Numbers	30	30	30	—	—
Age (years)	53.17 ± 6.57	54.97 ± 5.54	55.9 ± 6.54	1.491	0.231
Sex (male/female)	14/16	19/11	12/18	3.467	0.177[a]
Education (years)	11.80 ± 2.99	11.90 ± 2.92	10.43 ± 2.94	2.316	0.105
Diabetes duration (years)	—	7.93 ± 5.98	6.93 ± 5.46	0.699	0.933
BMI (kg/m^2)	23.45 ± 2.59	24.08 ± 3.02	25.59 ± 3.31	4.052	0.021*
Systolic blood pressure (mmHg)	128.13 ± 18.10	131.37 ± 14.78	130.57 ± 18.25	0.194	0.749
Diastolic blood pressure (mmHg)	79.77 ± 9.17	82.90 ± 9.80	80.60 ± 10.33	0.895	0.441
Biochemical indicator					
Fasting glucose (mmol/L)	5.47 ± 0.63	8.56 ± 1.97	9.14 ± 3.05	25.769	<0.001*#
HbA1C (%)	5.50 ± 0.36	8.84 ± 1.72	9.13 ± 2.07	49.505	<0.001*#
Total cholesterol (mmol/L)	5.21 ± 0.96	4.96 ± 1.37	5.24 ± 1.45	0.432	0.651
HDL cholesterol (mmol/L)	1.40 ± 0.33	1.18 ± 0.30	1.16 ± 0.33	5.167	0.008*#
LDL cholesterol (mmol/L)	3.10 ± 0.67	2.93 ± 0.78	3.36 ± 1.06	1.874	0.160
General mental status					
MoCA	27.77 ± 1.28	27.00 ± 0.83	22.93 ± 1.95	99.370	<0.001*ξ
MMSE	28.43 ± 1.17	28.43 ± 1.07	27.93 ± 1.31	1.774	0.176
Episodic memory					
AVLT-immediately recall	22.83 ± 5.00	22.77 ± 3.83	19.50 ± 4.55	5.406	0.006*ξ
AVLT-recognition	22.90 ± 1.45	21.87 ± 1.48	21.10 ± 3.60	4.252	0.017*
AVLT-delayed recall (5 min)	8.20 ± 1.94	7.80 ± 1.56	7.23 ± 2.40	1.775	0.176
AVLT-delayed recall (20 min)	7.87 ± 2.18	7.33 ± 1.77	6.83 ± 2.64	1.620	0.204
AVLT-classification	7.47 ± 2.60	7.13 ± 2.06	6.33 ± 2.25	1.902	0.155
ROCF-immediate recall	24.08 ± 8.49	22.63 ± 6.95	19.00 ± 6.64	3.754	0.027*
ROCF-delayed recall (20 min)	23.65 ± 7.74	21.85 ± 7.13	18.20 ± 6.19	4.659	0.012*
Working memory					
WAIS	46.23 ± 11.99	41.23 ± 10.83	35.63 ± 8.33	7.658	0.001*
DST-forwards	9.57 ± 1.38	8.87 ± 0.82	8.93 ± 1.08	3.584	0.032*
DST-backwards	5.53 ± 1.17	5.03 ± 0.89	4.67 ± 0.88	5.805	0.004*
Spatial processing					
ROCF-copy	33.17 ± 1.90	32.55 ± 4.11	31.97 ± 3.88	0.911	0.406
Executive function					
TMT-B	61.33 ± 22.74	67.73 ± 24.19	80.77 ± 26.59	4.877	0.010*
Language ability					
VFT	44.83 ± 6.06	44.10 ± 8.29	40.60 ± 7.04	2.970	0.057
Attention					
TMT-A	48.57 ± 16.61	51.97 ± 17.44	63.80 ± 21.66	5.484	0.006*ξ

*All subjects (T2DM-MCI, T2DM-NC, HC) were matched for age, sex, and education. Values are the mean ± standard deviation. [a]Chi-square test for sex. The comparisons of each neuropsychological test among these three groups were performed with ANOVA. The level of significance for intergroup differences was set at $P < 0.05$. *$P < 0.05$ T2DM-MCI vs. HC with post-hoc test, Bonferroni corrected. #$P < 0.05$ T2DM-NC vs. HC with post-hoc test, Bonferroni corrected. ξ$P < 0.05$ T2DM-MCI vs. T2DM-NC with post-hoc test, Bonferroni corrected. BMI, body mass index; HbA1c, glycosylated hemoglobin; HDL, high-density lipoprotein; LDL, low-density lipoprotein; MMSE, Mini-Mental State Examination; MoCA, Montreal Cognitive Assessment; AVLT, Auditory Verbal Learning Test; ROCF, Rey-Osterrieth Complex Figure; WAIS, Wechsler Adult Intelligence Scale; DST, Digital Span Test; TMT, Trail Making Test; VFT, Verbal Fluency Test.*

and increased hubs at the left thalamus relative to T2DM-NC patients (**Figure 3**).

Network Measure Correlates With Cognitive Function Score

The correlations between brain network parameters, including global network properties and nodal efficiency, and cognitive function scores were analyzed for the T2DM-MCI group. For global network properties, L_p, E_{glob}, and E_{loc} were significantly correlated with DST scores ($r = -0.4149$, $P = 0.0226$; $r = 0.4051$, $P = 0.0264$; $r = 0.4934$, $P = 0.0056$, uncorrected), and E_{loc} was significantly correlated with TMT-A scores in the T2DM-MCI group ($r = -0.3620$, $P = 0.0494$, uncorrected) (**Figures 4A–D**). Furthermore, the nodal efficiency of the right opercular part of the inferior frontal gyrus was significantly correlated with DST scores ($r = 0.4049$, $P = 0.0265$, uncorrected) in the T2DM-MCI group (**Figure 4E**). And the nodal efficiency of the right triangular part of the inferior frontal gyrus was significantly correlated with TMT-A scores ($r = -0.3736$, $P = 0.0420$, uncorrected) and TMT-B

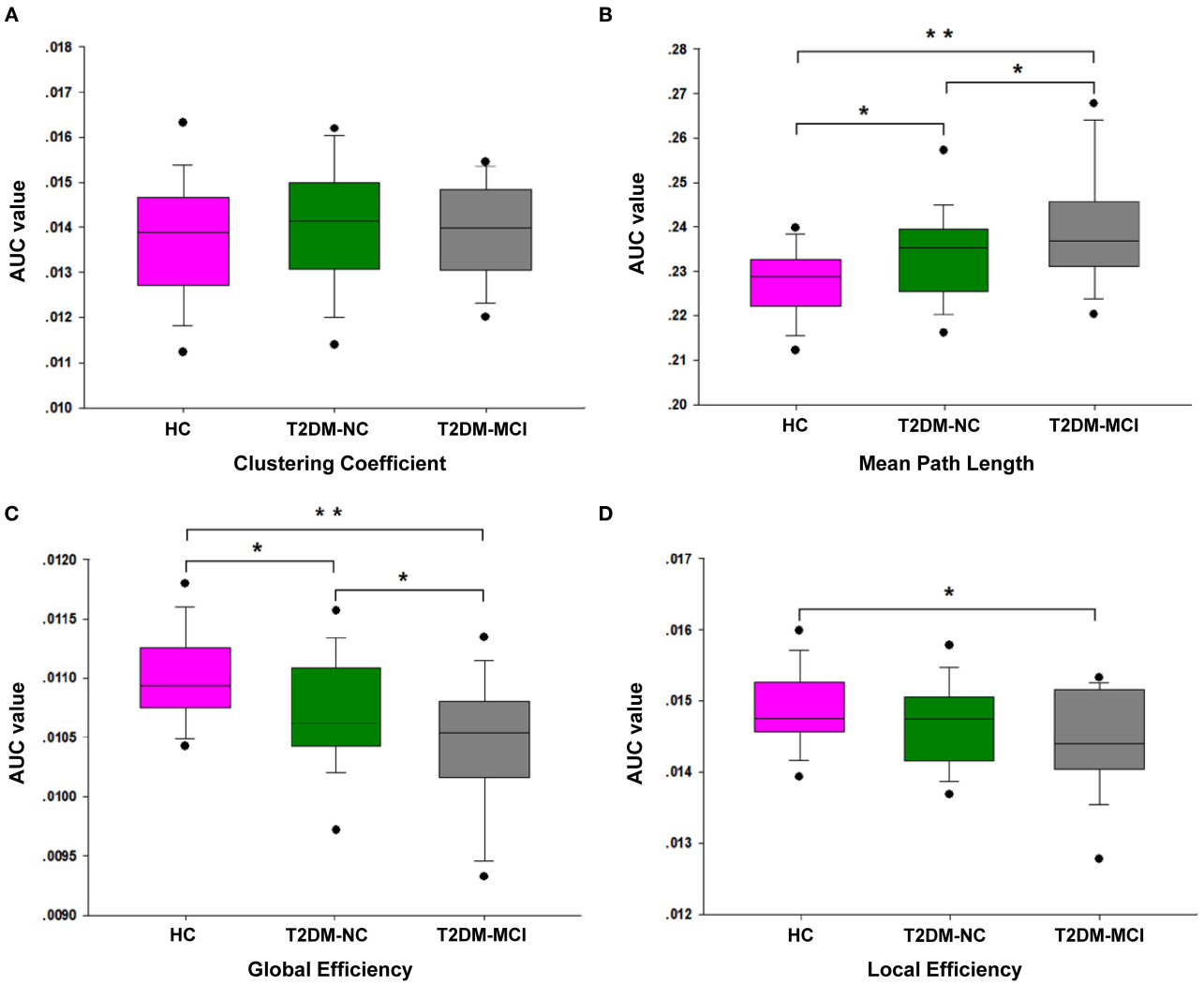

FIGURE 1 | The differences of global network properties. The differences are shown in C_p **(A)**, L_p **(B)**, E_{glob} **(C)**, and E_{loc} **(D)** among the T2DM-MCI, T2DM-NC, and HC groups. *The significance threshold was set at $P < 0.05$, **The significance threshold was set at $P < 0.001$. C_p, clustering coefficient; L_p, shortest path length; E_{glob}, global efficiency; E_{loc}, local efficiency.

TABLE 2 | Differences in the global network properties among the T2DM-MCI, T2DM-NC, and HC groups.

	HC	T2DM-NC	T2DM-MCI	*F*-value (*P*-value)
C_p	0.0138 ± 0.0014	0.0141 ± 0.0014	0.0140 ± 0.0011	ns
L_p	0.2277 ± 0.0075	0.2338 ± 0.0103	0.2399 ± 0.0128	9.618 (<0.001)
E_g	0.0110 ± 0.0004	0.0107 ± 0.0005	0.0105 ± 0.0005	9.645 (<0.001)
E_{loc}	0.0149 ± 0.0006	0.0147 ± 0.0006	0.0144 ± 0.0007	3.543 (0.033)

ns, non-significant; C_p, clustering coefficient; L_p, shortest path length; E_{glob}, global efficiency; E_{loc}, local efficiency.

scores ($r = -0.5238$, $P = 0.00297$, uncorrected), respectively (**Figures 4F,G**).

Network-Based Statistical Analysis

Differences of the connectivity component between groups were detected using the NBS method. A subnetwork of 9 nodes and 8 edges was found impaired in the T2DM-MCI group, compared with the HC group ($P < 0.05$, NBS corrected, **Figure 5**). Nevertheless, no significant differences were found between the T2DM-NC group and HC group or T2DM-MCI group and T2DM-NC group. The impaired subnetwork included the left hippocampus, calcarine fissure and surrounding cortex, the

TABLE 3 | Differences in the nodal efficiency among the T2DM-MCI, T2DM-NC, and HC groups.

Nodes	ANOVA	*Post-hoc* test (*p*-value)			Nodal efficiency difference
	(*p*-value)	HC vs. T2DM-NC	HC vs. T2DM-MCI	T2DM-MCI vs. T2DM-NC	
PreCG.L	0.009	ns	0.003	ns	HC > T2DM-MCI
IFGoperc.R	0.003	ns	0.001	0.021	HC, T2DM-NC > T2DM-MCI
IFGtriang.L	0.020	0.039	0.005	ns	HC > T2DM-NC, T2DM-MCI
IFGtriang.R	0.010	ns	0.003	0.015	HC, T2DM-NC > T2DM-MCI
ORBinf.L	0.020	0.020	0.020	ns	HC > T2DM-NC, T2DM-MCI
REC.L	0.042	ns	0.026	ns	HC > T2DM-MCI
INS.L	0.042	ns	0.012	ns	HC > T2DM-MCI
DCG.L	0.047	ns	0.023	ns	HC > T2DM-MCI
PCG.L	0.001	0.017	0.001	ns	HC > T2DM-NC, T2DM-MCI
PCG.R	0.046	ns	0.031	ns	HC > T2DM-MCI
HIP.L	<0.001	0.040	<0.001	0.009	HC > T2DM-NC > T2DM-MCI
HIP.R	0.034	ns	0.013	ns	HC > T2DM-MCI
PHG.L	0.001	ns	0.001	0.023	HC, T2DM-NC > T2DM-MC
AMYG.L	0.001	<0.001	0.007	ns	HC > T2DM-NC, T2DM-MCI
CUN.R	0.009	ns	0.002	ns	HC > T2DM-MCI
LING.L	0.002	0.014	<0.001	ns	HC > T2DM-NC, T2DM-MCI
SOG.L	0.013	0.013	0.009	ns	HC > T2DM-NC, T2DM-MCI
SOG.R	0.018	0.031	0.007	ns	HC > T2DM-NC, T2DM-MCI
MOG.L	0.012	ns	0.002	ns	HC > T2DM-MCI
FFG.L	<0.001	ns	<0.001	0.002	HC, T2DM-NC > T2DM-MC
FFG.R	0.013	ns	0.002	ns	HC > T2DM-MCI
SPG.L	0.028	ns	0.012	0.025	HC, T2DM-NC > T2DM-MC
IPL.L	0.002	ns	<0.001	0.010	HC, T2DM-NC > T2DM-MC
ANG.L	0.040	ns	0.017	ns	HC > T2DM-MCI
PCUN.L	0.002	ns	<0.001	0.011	HC, T2DM-NC > T2DM-MC
PCL.L	0.019	0.021	0.003	ns	HC > T2DM-NC, T2DM-MCI
PCL.R	<0.001	0.002	<0.001	ns	HC > T2DM-NC, T2DM-MCI
CAU.L	0.023	ns	0.011	0.039	HC, T2DM-NC > T2DM-MC
MTG.L	0.039	ns	0.022	0.040	HC, T2DM-NC > T2DM-MC
MTG.R	<0.001	0.004	<0.001	ns	HC > T2DM-NC, T2DM-MCI
TPOmid.L	0.046	ns	0.013	ns	HC > T2DM-MCI
ITG.L	0.001	0.036	<0.001	ns	HC > T2DM-NC, T2DM-MCI
ITG.R	0.043	ns	ns	0.019	T2DM-NC > T2DM-MC

The abbreviations of the 90 brain regions are given in the ***Supplementary Table 1****. The significance threshold was set at P < 0.05 (FDR-corrected). R (L) right (left) hemisphere. ns, non-significant.*

orbital part of the inferior frontal gyrus, lingual gyrus, the orbital part of the superior frontal gyrus, middle occipital gyrus, fusiform gyrus, the medial orbital of the superior frontal gyrus, and right caudate nucleus.

DISCUSSION

The purpose of this current study was to early detect the neuroimaging alterations of T2DM-associated cognitive impairments. All participants in the T2DM-MCI, T2DM-NC, and HC groups had good small-world properties. The global properties of the structural network showed a significant decrease of E_{glob} and an increase of L_p in T2DM-MCI patients, when compared with T2DM-NC patients. Then nodal efficiency analysis showed the impaired efficiency of widespread brain regions in T2DM-MCI and T2DM-NC patients. While nodal efficiency, primarily located in the limbic system, basal ganglia, parts of the frontal, temporal, and parietal lobes, suffered more severely in T2DM-MCI patients than T2DM-NC. Moreover, a subnetwork impaired in T2DM-MCI was identified and characterized by cortical-limbic fibers, commissural fibers and pathways within frontal, temporal and occipital lobes. In particular, these network abnormalities were correlated with cognitive function performance in T2DM-MCI patients. Our investigations highlighted the importance of structural network analysis in our understanding of T2DM-related cognitive impairment symptoms.

In this study, deceased E_{glob} and increased L_p were observed in T2DM-MCI and T2DM-NC patients, which was in line with previous studies related to T2DM and cognitive impairments

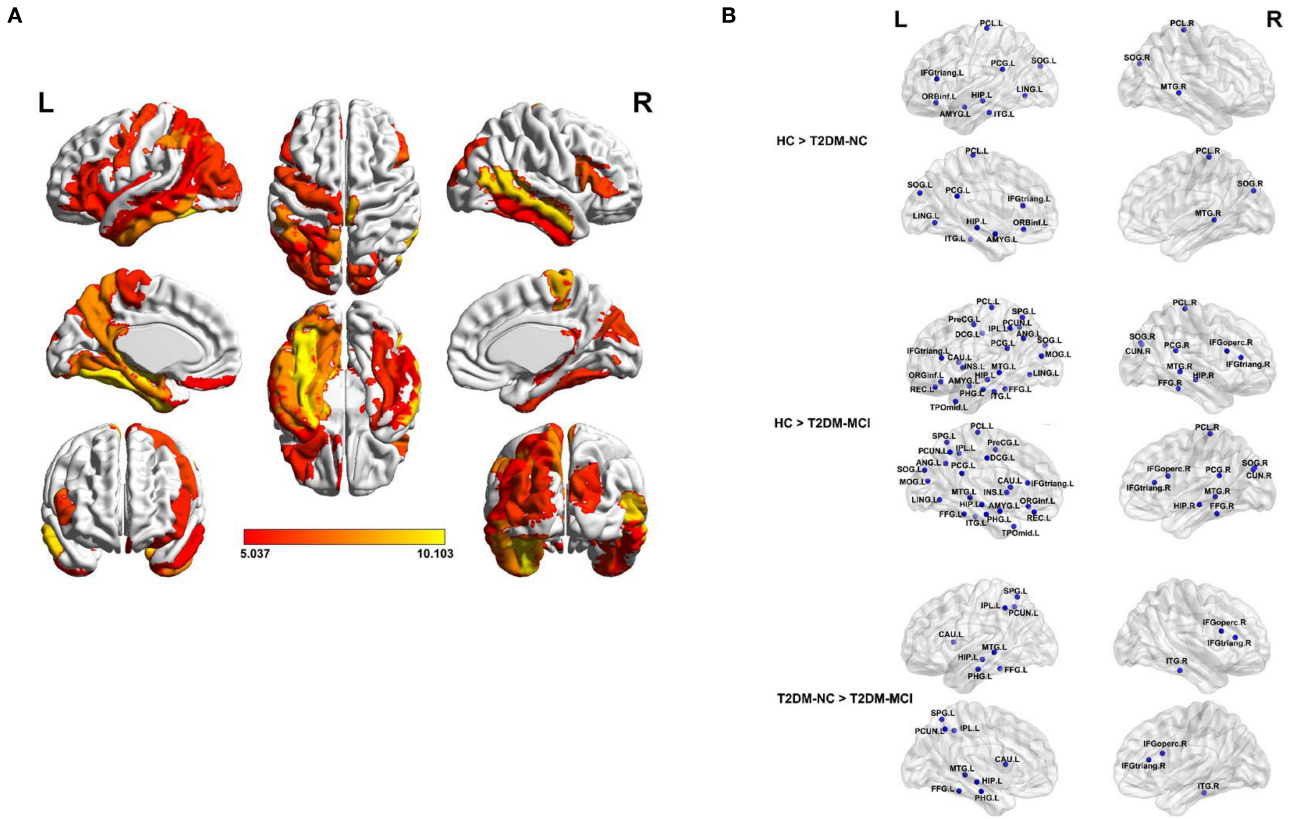

FIGURE 2 | The brain regions with a significantly reduced nodal efficiency in T2DM patients. **(A)** Significant difference in terms of nodal efficiency between groups as determined by one-way ANOVA. Significant brain network nodes are rendered on the surface of the automated anatomical labeling atlas in BrainNet Viewer (NKLCNL, Beijing Normal University). The color code represents *F*-value. **(B)** Significant reductions of the nodal efficiency of T2DM-NC relative to HC (up), T2DM-MCI relative to HC (middle), and T2DM-MCI relative to T2DM-NC (bottom) were visualized. The abbreviations of the 90 brain regions are given in the **Supplementary Table 1**. The significance threshold was set at $P < 0.05$ (FDR-corrected). R (L) right (left) hemisphere.

TABLE 4 | Hubs of the T2DM-MCI, T2DM-NC, and HC groups.

Group	Region	Group	Region	Group	Region
HC	Precentral_L	T2DM-NC	Precentral_L	T2DM-MCI	Precentral_L
	Precentral_R		Precentral_R		Precentral_R
	Hippocampus_R		Calcarine_L		Calcarine_L
	Calcarine_L		Calcarine_R		Calcarine_R
	Calcarine_R		Occipital_Sup_L		Occipital_Sup_L
	Occipital_Sup_L		Occipital_Sup_R		Occipital_Sup_R
	Occipital_Sup_R		Precuneus_L		Precuneus_L
	Precuneus_L		Precuneus_R		Precuneus_R
	Precuneus_R		Caudate_L		Putamen_L
	Caudate_R		Putamen_L		Putamen_R
	Putamen_L		Putamen_R		Thalamus_L
	Putamen_R		Temporal_Mid_L		
	Thalamus_L				

R (L) right (left) hemisphere.

using DTI-based graph theoretical network analysis (Reijmer et al., 2013b; Kim et al., 2016; Zhang et al., 2016). Meanwhile, E_{loc} was also found significantly deceased in T2DM-MCI patients when compared with HC. These above findings imply that efficiency of network information transmission was decreased with the cognition decline of T2DM patients. However, no

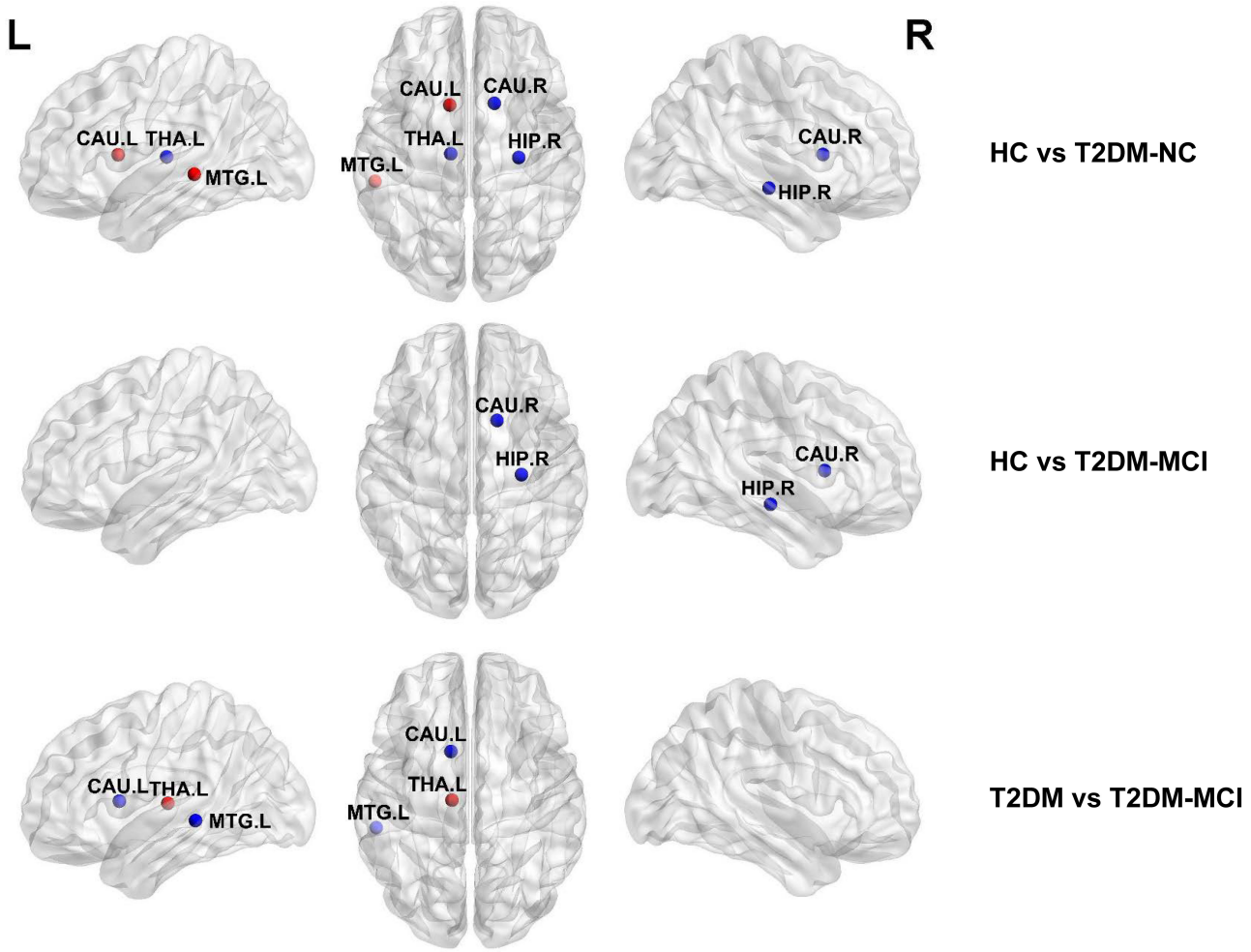

FIGURE 3 | Distribution differences of hubs in the T2DM-MCI, T2DM-NC, and HC groups. The blue node represents the hub in the former group but not in the latter. In contrast, the red node represents the hub in the latter group but not in the former. HIP.R, right hippocampus; CAU.R, right caudate nucleus; CAU.L, left caudate nucleus; THA.L, left thalamus; MTG.L, middle temporal gyrus.

significant changes were found on C_p of T2DM-MCI and T2DM-NC patients in our study. The changing pattern of C_p reported in white matter network studies of T2DM have been controversial. Reijmer et al. found decreased C_p in well-controlled diabetic patients (Reijmer et al., 2013b), while Zhang et al. reported increased C_p in T2DM patients free of clinical vascular complications (Zhang et al., 2019). Two other studies detected no change in C_p in T2DM, which were similar to our current study (Kim et al., 2016; Zhang et al., 2016). These inconsistencies may be explained by the differences in sample sizes, age, and complications of the enrolled patients. Therefore, more studies are needed to draw a reliable conclusion about the impact of T2DM on the topological properties of the brain network.

T2DM-MCI patients exhibited significantly reduced nodal efficiency in 11 nodes, mainly located in the limbic system, basal ganglia, and parts of the frontal, temporal, and parietal lobes. Previous studies have reported that the temporal lobe and in particular the limbic system seem to be susceptible to T2DM (Den Heijer et al., 2003; Korf et al., 2006; Gold et al., 2007; Mccrimmon et al., 2012; Xie Y. et al., 2017). Our results are in agreement with previous literature showing microstructural and network impairment in different regions of the temporal lobe and limbic system, and also in their corresponding association fibers in T2DM. In addition, T2DM is also associated with the abnormal pattern of functional connectivity in these regions (Xia et al., 2017). These structures have been implicated in memory formation and learning (Mccrimmon et al., 2012). Furthermore, it had been well-documented that deficits in either frontal cortex or WM may be the underlying reasons for executive dysfunction and memory loss in patients with T2DM (Duncan and Owen, 2000; Preston and Eichenbaum, 2013; Reijmer et al., 2013b; Duan et al., 2015). Of note, our findings revealed that the nodal efficiency in the right opercular part and triangular part of the inferior frontal gyrus had a close relationship with multiple cognitive function scores, especially

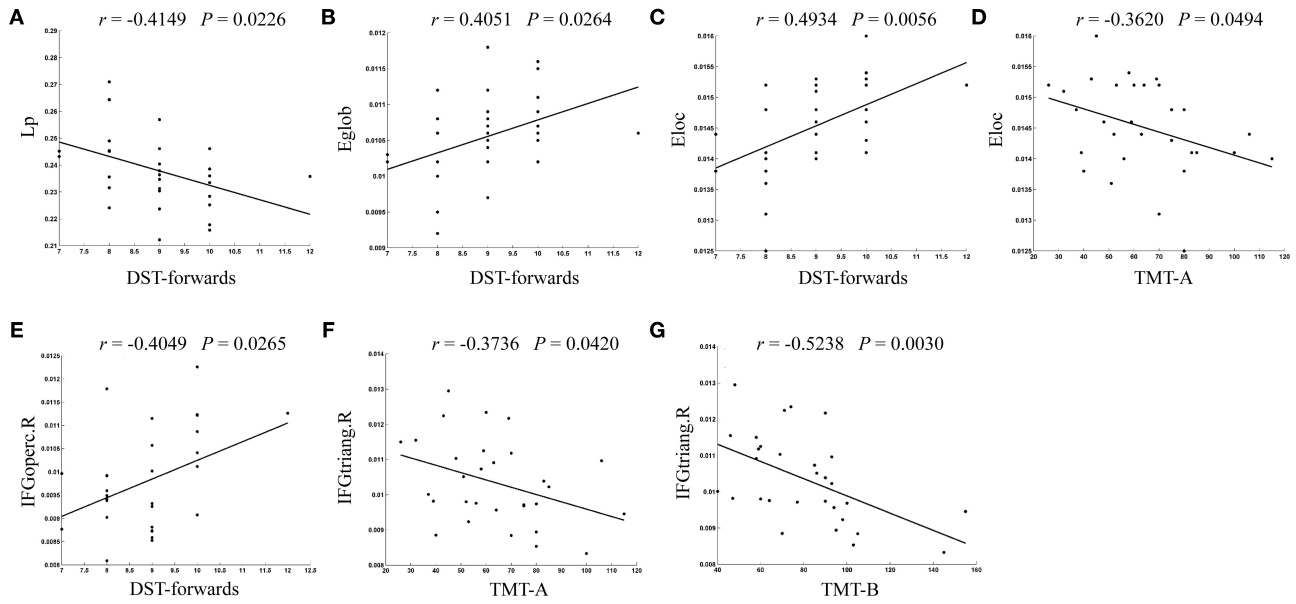

FIGURE 4 | The significant correlations between altered global or nodal network properties and cognitive performance in T2DM-MCI patients. **(A)** Correlation between L_p and DST-forwards. **(B)** Correlation between E_{glob} and DST-forwards. **(C)** Correlation between Eloc and DST-forwards. **(D)** Correlation between E_{loc} and TMT-A. **(E)** Correlation between IFGoperc.R and DST-forwards. **(F)** Correlation between IFGtriang.R and TMT-A. **(G)** Correlation between IFGtriang.R and TMT-B. L_p, shortest path length; E_{glob}, global efficiency; E_{loc}, local efficiency; IFGoperc.R, right opercular part of inferior frontal gyrus; IFGtriang.R, right triangular part of inferior frontal gyrus.

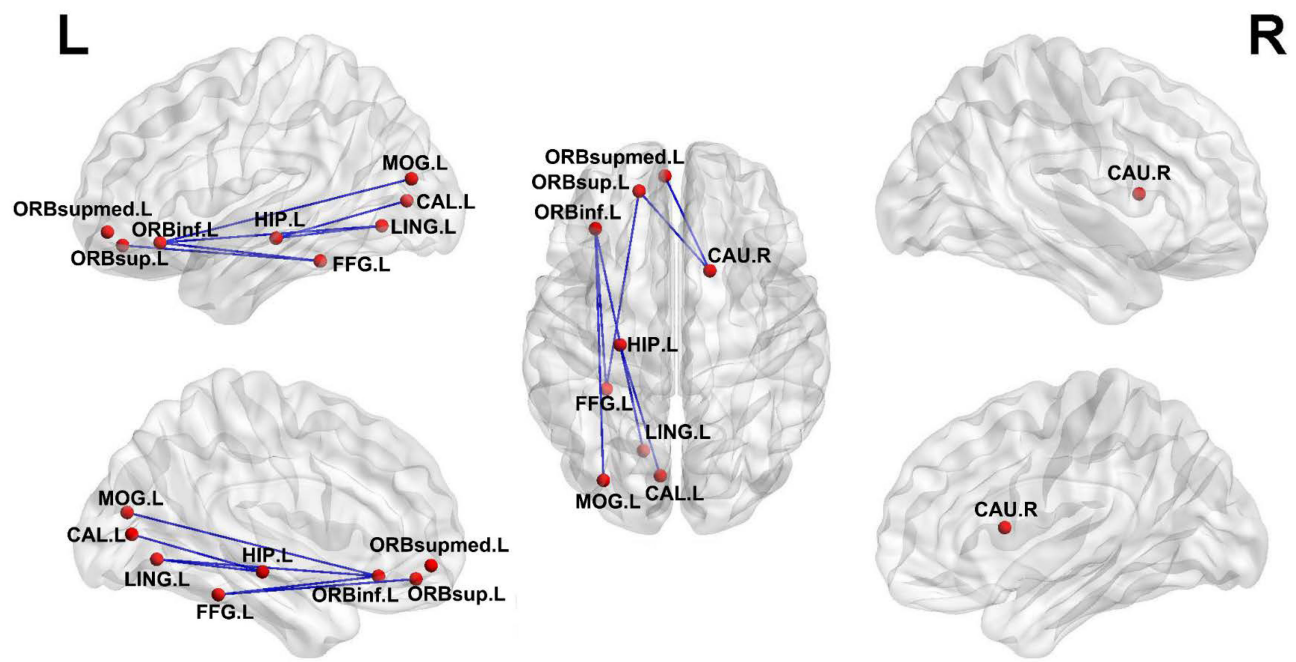

FIGURE 5 | Subnetworks with impaired edge connection in T2DM-MCI patients relative to HC. The impaired connections are shown in blue edges. The nodes are set to equal size. HIP.L, left hippocampus; CAL.L, left calcarine fissure and surrounding cortex; ORBinf.L, left inferior frontal gyrus, orbital part; LING.L, left lingual gyrus; FFG.L, left fusiform gyrus; ORBsupmed.L, left superior frontal gyrus, medial orbital; CAU.R, right caudate nucleus.

working memory, attention, and executive function, which was in line with previous studies (Li et al., 2018). The opercular part of the inferior frontal gyrus has many important functions in the brain, some of which are involved in semantic processing, language production, and phonological processing (Tonkonogy and Goodglass, 1981; Sainson et al., 2014). Moreover, the loss

of white matter volume in the inferior frontal triangle region has been reported in T2DM patients (Chen et al., 2012). Both the opercular part and triangular part of the inferior frontal gyrus are involved in higher cognitive functions such as memory, emotion, and learning (Maess et al., 2006; Badre and Wagner, 2007). These results suggested that WM in the right opercular part and triangular part of the inferior frontal gyrus may act as potential biomarkers for T2DM-associated MCI detection.

More importantly, brain hubs, defined as some specific nodes interacting with many other nodes, play an important role in maintaining network stability and enabling efficient information transmission (Albert et al., 2000). The loss of hubs could affect network connection and information processing (Van Den Heuvel and Sporns, 2013). In hubs analysis, there were almost similar hub organizations in the T2DM-MCI, T2DM-NC, and HC groups, but differences still existed in the distribution of hubs among these three groups at the right hippocampus, bilateral caudate nucleus, and right middle temporal gyrus. T2DM-NC patients lost hubs at the right hippocampus and caudate nucleus, while two new hubs were found at the left caudate nucleus and middle temporal gyrus when compared to HC. These increased hub nodes may represent compensation for those lost, which may maintain the normal cognitive function in T2DM-NC patients (Liu et al., 2018; Yu et al., 2019; Wang et al., 2020). Meanwhile, T2DM-MCI patients lost hubs at the right hippocampus and caudate nucleus relative to HC, and lost hubs at the left caudate nucleus and middle temporal gyrus compared to T2DM-NC. These lost hubs are more likely to be related to cognitive performance (Den Heijer et al., 2003; Gold et al., 2007; Falvey et al., 2013; Rofey et al., 2015). Also, some regions with decreased nodal efficiency belonged to the lost hubs in T2DM-MCI. This suggests that the hub nodes, to some extent, were yet to be damaged, resulting in cognitive impairments in T2DM-MCI patients. This subsequently explains that T2DM cognitive dysfunction might disrupt the structural network and reorganize the network's hubs.

In addition, T2DM-NC patients showed disrupted topological organization of the white matter network including global network properties, nodal efficiency, and hubs, which indicates that the topological organization of structural brain networks have already been altered in T2DM-NC patients. Our results are partly in accordance with previous studies that explored changes of structural and functional brain networks in cognitively intact T2DM patients (Chen et al., 2017; Zhang et al., 2019). However, T2DM-MCI patients showed another disrupted structural network that was worse than T2DM-NC patients. These differences illustrated the severity of the disease condition. Therefore, a longitudinal study is necessary to confirm the dynamic changes in brain network topological organization in T2DM patients as the disease progresses in future.

However, our study has a few limitations. First, the current study is a cross-sectional study with a relatively small sample size, and a longitudinal study with a larger sample size is needed in future to detect the dynamic changes in structural network properties and to test whether structural network properties can predict the development of cognitive impairment in T2DM patients. Second, there was a higher BMI index in groups with T2DM than healthy controls. However, there were no significant intergroup differences in BMI between T2DM-MCI and T2DM-NC patients, and the effect of BMI on the results should be small. Last but not least, we only focused on the structural network properties and their relationship with neurophysiological tests in T2DM patients. Exploring the overlap between functional and structural connectivity in the same participants will achieve more convincing and reliable results. Thus, multimodal imaging methods are needed to investigate the structural and functional dysconnectivity in T2DM associated with cognitive deficits in the future.

CONCLUSION

In conclusion, the present study revealed disrupted network measures in T2DM patients. T2DM-MCI patients showed sporadic impairments of the structural network, primarily located in the limbic system, basal ganglia, and parts of the frontal, temporal, and parietal lobes when compared with T2DM-NC patients. Moreover, these network abnormalities were correlated with cognitive function performance in T2DM-MCI patients. In particular, the executive dysfunction and working memory impairment in T2DM-MCI patients correlated with reduced nodal efficiency in the right opercular part and triangular part of the inferior frontal gyrus, which indicated that WM in these regions may act as potential biomarkers for T2DM-associated MCI detection. Our investigation provides a novel insight into the neuropathological effects of white matter network disruption on early cognition impairments induced by T2DM.

DATA AVAILABILITY STATEMENT

The original contributions presented in the study are included in the article/**Supplementary Material**, further inquiries can be directed to the corresponding author/s.

ETHICS STATEMENT

The studies involving human participants were reviewed and approved by Research Ethics Committee of Southwest Hospital, Army Medical University, Chongqing, China. The patients/participants provided their written informed consent to participate in this study.

AUTHOR CONTRIBUTIONS

KX, XC, and JW conceived and designed the study. CL, YLi, and ZZ collected the data for MRI, clinical, and neuropsychological tests. JZ and MQ performed the network analysis. KL and HT performed statistics analysis. JF and YG prepared the figures and tables. XC and KL wrote the manuscript. XY and YLa edited the manuscript. All

authors revised the manuscript, read, and approved the submitted version.

FUNDING

This work was supported by grants from the National Natural Science Foundation of China (81801672, 81571889, 81601970), the Natural Science Foundation of Chongqing (cstc2019jcyj-msxmX0123), the Science and Technology Innovation Ability Enhancement Project of Army Medical University (2019XLC3054), the Talent Innovation Ability Training Program of Daping Hospital (2019CXLCC010), and the Chongqing Clinical Research Centre of Imaging and Nuclear Medicine (CSTC2015YFPT-gcjsyjzx0175).

SUPPLEMENTARY MATERIAL

The Supplementary Material for this article can be found online at: https://www.frontiersin.org/articles/10.3389/fnagi.2020.615048/full#supplementary-material

REFERENCES

Albert, R., Jeong, H., and Barabasi, A. L. (2000). Error and attack tolerance of complex networks. *Nature* 406, 378–382. doi: 10.1038/35019019

Badre, D., and Wagner, A. D. (2007). Left ventrolateral prefrontal cortex and the cognitive control of memory. *Neuropsychologia* 45, 2883–2901. doi: 10.1016/j.neuropsychologia.2007.06.015

Beaulieu, C. (2002). The basis of anisotropic water diffusion in the nervous system - a technical review. *NMR Biomed.* 15, 435–455. doi: 10.1002/nbm.782

Behrens, T. E., Woolrich, M. W., Jenkinson, M., Johansen-Berg, H., Nunes, R. G., Clare, S., et al. (2003). Characterization and propagation of uncertainty in diffusion-weighted MR imaging. *Magn. Reson. Med.* 50, 1077–1088. doi: 10.1002/mrm.10609

Chen, G. Q., Zhang, X., Xing, Y., Wen, D., Cui, G. B., and Han, Y. (2017). Resting-state functional magnetic resonance imaging shows altered brain network topology in Type 2 diabetic patients without cognitive impairment. *Oncotarget* 8, 104560–104570. doi: 10.18632/oncotarget.21282

Chen, Z., Li, L., Sun, J., and Ma, L. (2012). Mapping the brain in type II diabetes: voxel-based morphometry using DARTEL. *Eur. J. Radiol.* 81, 1870–1876. doi: 10.1016/j.ejrad.2011.04.025

Cheng, G., Huang, C., Deng, H., and Wang, H. (2012). Diabetes as a risk factor for dementia and mild cognitive impairment: a meta-analysis of longitudinal studies. *Intern. Med. J.* 42, 484–491. doi: 10.1111/j.1445-5994.2012.02758.x

Cui, Z., Zhong, S., Xu, P., He, Y., and Gong, G. (2013). PANDA: a pipeline toolbox for analyzing brain diffusion images. *Front. Hum. Neurosci.* 7:42. doi: 10.3389/fnhum.2013.00042

Cukierman, T., Gerstein, H. C., and Williamson, J. D. (2005). Cognitive decline and dementia in diabetes–systematic overview of prospective observational studies. *Diabetologia* 48, 2460–2469. doi: 10.1007/s00125-005-0023-4

Den Heijer, T., Vermeer, S. E., Van Dijk, E. J., Prins, N. D., Koudstaal, P. J., Hofman, A., et al. (2003). Type 2 diabetes and atrophy of medial temporal lobe structures on brain MRI. *Diabetologia* 46, 1604–1610. doi: 10.1007/s00125-003-1235-0

Duan, C. A., Erlich, J. C., and Brody, C. D. (2015). Requirement of prefrontal and midbrain regions for rapid executive control of behavior in the rat. *Neuron* 86, 1491–1503. doi: 10.1016/j.neuron.2015.05.042

Duncan, J., and Owen, A. M. (2000). Common regions of the human frontal lobe recruited by diverse cognitive demands. *Trends Neurosci.* 23, 475–483. doi: 10.1016/s0166-2236(00)01633-7

Falvey, C. M., Rosano, C., Simonsick, E. M., Harris, T., Strotmeyer, E. S., Satterfield, S., et al. (2013). Macro- and microstructural magnetic resonance imaging indices associated with diabetes among community-dwelling older adults. *Diabetes Care* 36, 677–682. doi: 10.2337/dc12-0814

Gold, S. M., Dziobek, I., Sweat, V., Tirsi, A., Rogers, K., Bruehl, H., et al. (2007). Hippocampal damage and memory impairments as possible early brain complications of type 2 diabetes. *Diabetologia* 50, 711–719. doi: 10.1007/s00125-007-0602-7

Hoogenboom, W. S., Marder, T. J., Flores, V. L., Huisman, S., Eaton, H. P., Schneiderman, J. S., et al. (2014). Cerebral white matter integrity and resting-state functional connectivity in middle-aged patients with type 2 diabetes. *Diabetes* 63, 728–738. doi: 10.2337/db13-1219

Hsu, J. L., Chen, Y. L., Leu, J. G., Jaw, F. S., Lee, C. H., Tsai, Y. F., et al. (2012). Microstructural white matter abnormalities in type 2 diabetes mellitus: a diffusion tensor imaging study. *Neuroimage* 59, 1098–1105. doi: 10.1016/j.neuroimage.2011.09.041

Kim, D. J., Yu, J. H., Shin, M. S., Shin, Y. W., and Kim, M. S. (2016). Hyperglycemia reduces efficiency of brain networks in subjects with type 2 diabetes. *PLoS ONE* 11:e0157268. doi: 10.1371/journal.pone.0157268

Koekkoek, P. S., Kappelle, L. J., Van Den Berg, E., Rutten, G. E., and Biessels, G. J. (2015). Cognitive function in patients with diabetes mellitus: guidance for daily care. *Lancet Neurol.* 14, 329–340. doi: 10.1016/S1474-4422(14)70249-2

Korf, E. S., White, L. R., Scheltens, P., and Launer, L. J. (2006). Brain aging in very old men with type 2 diabetes: the Honolulu-Asia aging study. *Diabetes Care* 29, 2268–2274. doi: 10.2337/dc06-0243

Korgaonkar, M. S., Fornito, A., Williams, L. M., and Grieve, S. M. (2014). Abnormal structural networks characterize major depressive disorder: a connectome analysis. *Biol. Psychiatry* 76, 567–574. doi: 10.1016/j.biopsych.2014.02.018

Li, C., Li, C., Yang, Q., Wang, B., Yin, X., Zuo, Z., et al. (2018). Cortical thickness contributes to cognitive heterogeneity in patients with type 2 diabetes mellitus. *Medicine* 97:e10858. doi: 10.1097/MD.0000000000010858

Lichtman, J. W., Livet, J., and Sanes, J. R. (2008). A technicolour approach to the connectome. *Nat. Rev. Neurosci.* 9, 417–422. doi: 10.1038/nrn2391

Lim, K. O., and Helpern, J. A. (2002). Neuropsychiatric applications of DTI - a review. *NMR Biomed.* 15, 587–593. doi: 10.1002/nbm.789

Liu, D., Duan, S., Zhou, C., Wei, P., Chen, L., Yin, X., et al. (2018). Altered brain functional hubs and connectivity in type 2 diabetes mellitus patients: a resting-state fMRI study. *Front. Aging Neurosci.* 10:55. doi: 10.3389/fnagi.2018.00055

Lo, C. Y., Wang, P. N., Chou, K. H., Wang, J., He, Y., and Lin, C. P. (2010). Diffusion tensor tractography reveals abnormal topological organization in structural cortical networks in Alzheimer's disease. *J. Neurosci.* 30, 16876–16885. doi: 10.1523/JNEUROSCI.4136-10.2010

Maess, B., Herrmann, C. S., Hahne, A., Nakamura, A., and Friederici, A. D. (2006). Localizing the distributed language network responsible for the N400 measured by MEG during auditory sentence processing. *Brain Res.* 1096, 163–172. doi: 10.1016/j.brainres.2006.04.037

Mccrimmon, R. J., Ryan, C. M., and Frier, B. M. (2012). Diabetes and cognitive dysfunction. *Lancet* 379, 2291–2299. doi: 10.1016/S0140-6736(12)60360-2

Mitchell, A. J., and Shiri-Feshki, M. (2008). Temporal trends in the long term risk of progression of mild cognitive impairment: a pooled analysis. *J. Neurol. Neurosurg. Psychiatr.* 79, 1386–1391. doi: 10.1136/jnnp.2007.142679

Mori, S., Crain, B. J., Chacko, V. P., and Van Zijl, P. C. (1999). Three-dimensional tracking of axonal projections in the brain by magnetic resonance imaging. *Ann. Neurol.* 45, 265–269. doi: 10.1002/1531-8249(199902)45:2<265::aid-ana21>3.0.co;2-3

Ninomiya, T. (2014). Diabetes mellitus and dementia. *Curr. Diab. Rep.* 14:487. doi: 10.1007/s11892-014-0487-z

Nouwen, A., Chambers, A., Chechlacz, M., Higgs, S., Blissett, J., Barrett, T. G., et al. (2017). Microstructural abnormalities in white and gray matter in obese adolescents with and without type 2 diabetes. *Neuroimage Clin.* 16, 43–51. doi: 10.1016/j.nicl.2017.07.004

Preston, A. R., and Eichenbaum, H. (2013). Interplay of hippocampus and prefrontal cortex in memory. *Curr. Biol.* 23, R764–R773. doi: 10.1016/j.cub.2013.05.041

Reijmer, Y. D., Brundel, M., De Bresser, J., Kappelle, L. J., Leemans, A., Biessels, G. J., et al. (2013a). Microstructural white matter abnormalities and cognitive

functioning in type 2 diabetes: a diffusion tensor imaging study. *Diabetes Care* 36, 137–144. doi: 10.2337/dc12-0493

Reijmer, Y. D., Leemans, A., Brundel, M., Kappelle, L. J., Biessels, G. J., and Utrecht Vascular Cognitive Impairment Study, G. (2013b). Disruption of the cerebral white matter network is related to slowing of information processing speed in patients with type 2 diabetes. *Diabetes* 62, 2112–2115. doi: 10.2337/db12-1644

Rofey, D. L., Arslanian, S. A., El Nokali, N. E., Verstynen, T., Watt, J. C., Black, J. J., et al. (2015). Brain volume and white matter in youth with type 2 diabetes compared to obese and normal weight, non-diabetic peers: a pilot study. *Int. J. Dev. Neurosci.* 46, 88–91. doi: 10.1016/j.ijdevneu.2015.07.003

Sainson, C., Barat, M., and Aguert, M. (2014). Communication disorders and executive function impairment after severe traumatic brain injury: an exploratory study using the GALI (a grid for linguistic analysis of free conversational interchange). *Ann. Phys. Rehabil. Med.* 57, 664–683. doi: 10.1016/j.rehab.2014.08.011

Sperling, R. A., Aisen, P. S., Beckett, L. A., Bennett, D. A., Craft, S., Fagan, A. M., et al. (2011). Toward defining the preclinical stages of Alzheimer's disease: recommendations from the national institute on aging-Alzheimer's association workgroups on diagnostic guidelines for Alzheimer's disease. *Alzheimers. Dement* 7, 280–292. doi: 10.1016/j.jalz.2011.03.003

Sporns, O., Tononi, G., and Kotter, R. (2005). The human connectome: a structural description of the human brain. *PLoS Comput. Biol* 1:e42. doi: 10.1371/journal.pcbi.0010042

Sun, Q., Chen, G. Q., Wang, X. B., Yu, Y., Hu, Y. C., Yan, L. F., et al. (2018). Alterations of white matter integrity and hippocampal functional connectivity in type 2 diabetes without mild cognitive impairment. *Front. Neuroanat.* 12:21. doi: 10.3389/fnana.2018.00021

Tan, X., Fang, P., An, J., Lin, H., Liang, Y., Shen, W., et al. (2016). Microstructural white matter abnormalities in type 2 diabetic patients: a DTI study using TBSS analysis. *Neuroradiology* 58, 1209–1216. doi: 10.1007/s00234-016-1752-4

Tonkonogy, J., and Goodglass, H. (1981). Language function, foot of the third frontal gyrus, and rolandic operculum. *Arch. Neurol.* 38, 486–490. doi: 10.1001/archneur.1981.00510080048005

Van Den Heuvel, M. P., and Sporns, O. (2013). Network hubs in the human brain. *Trends Cogn. Sci.* 17, 683–696. doi: 10.1016/j.tics.2013.09.012

Wang, W., Mei, M., Gao, Y., Huang, B., Qiu, Y., Zhang, Y., et al. (2020). Changes of brain structural network connection in Parkinson's disease patients with mild cognitive dysfunction: a study based on diffusion tensor imaging. *J. Neurol.* 267, 933–943. doi: 10.1007/s00415-019-09645-x

Watts, D. J., and Strogatz, S. H. (1998). Collective dynamics of 'small-world' networks. *Nature* 393, 440–442. doi: 10.1038/30918

Xia, W., Chen, Y. C., and Ma, J. (2017). Resting-state brain anomalies in type 2 diabetes: a meta-analysis. *Front. Aging Neurosci.* 9:14. doi: 10.3389/fnagi.2017.00014

Xie, X., Shi, Y., and Zhang, J. (2017). Structural network connectivity impairment and depressive symptoms in cerebral small vessel disease. *J. Affect. Disord* 220, 8–14. doi: 10.1016/j.jad.2017.05.039

Xie, Y., Zhang, Y., Qin, W., Lu, S., Ni, C., and Zhang, Q. (2017). White matter microstructural abnormalities in type 2 diabetes mellitus: a diffusional kurtosis imaging analysis. *AJNR Am. J. Neuroradiol.* 38, 617–625. doi: 10.3174/ajnr.A5042

Xiong, Y., Sui, Y., Zhang, S., Zhou, X. J., Yang, S., Fan, Y., et al. (2019). Brain microstructural alterations in type 2 diabetes: diffusion kurtosis imaging provides added value to diffusion tensor imaging. *Eur. Radiol.* 29, 1997–2008. doi: 10.1007/s00330-018-5746-y

Yoon, S., Cho, H., Kim, J., Lee, D. W., Kim, G. H., Hong, Y. S., et al. (2017). Brain changes in overweight/obese and normal-weight adults with type 2 diabetes mellitus. *Diabetologia* 60, 1207–1217. doi: 10.1007/s00125-017-4266-7

Yu, Y., Yan, L. F., Sun, Q., Hu, B., Zhang, J., Yang, Y., et al. (2019). Neurovascular decoupling in type 2 diabetes mellitus without mild cognitive impairment: potential biomarker for early cognitive impairment. *Neuroimage* 200, 644–658. doi: 10.1016/j.neuroimage.2019.06.058

Zalesky, A., Fornito, A., and Bullmore, E. T. (2010). Network-based statistic: identifying differences in brain networks. *Neuroimage* 53, 1197–1207. doi: 10.1016/j.neuroimage.2010.06.041

Zhang, J., Liu, Z., Li, Z., Wang, Y., Chen, Y., Li, X., et al. (2016). Disrupted white matter network and cognitive decline in type 2 diabetes patients. *J. Alzheimers. Dis.* 53, 185–195. doi: 10.3233/JAD-160111

Zhang, J., Wang, J., Wu, Q., Kuang, W., Huang, X., He, Y., et al. (2011). Disrupted brain connectivity networks in drug-naive, first-episode major depressive disorder. *Biol. Psychiatry* 70, 334–342. doi: 10.1016/j.biopsych.2011.05.018

Zhang, J., Wang, Y., Wang, J., Zhou, X., Shu, N., Wang, Y., et al. (2014). White matter integrity disruptions associated with cognitive impairments in type 2 diabetic patients. *Diabetes* 63, 3596–3605. doi: 10.2337/db14-0342

Zhang, Y., Cao, Y., Xie, Y., Liu, L., Qin, W., Lu, S., et al. (2019). Altered brain structural topological properties in type 2 diabetes mellitus patients without complications. *J. Diabetes* 11, 129–138. doi: 10.1111/1753-0407.12826

Conflict of Interest: The authors declare that the research was conducted in the absence of any commercial or financial relationships that could be construed as a potential conflict of interest.

frontiers in Aging Neuroscience

SYSTEMATIC REVIEW
published: 10 February 2021
doi: 10.3389/fnagi.2021.612404

Tele-Health Intervention for Carers of Dementia Patients—A Systematic Review and Meta-Analysis of Randomized Controlled Trials

Aiyong Zhu[1], *Wenting Cao*[1], *Yinghua Zhou*[1], *Anan Xie*[1], *Yun Cheng*[2] *and Shu-Fen Chu*[1]*

[1] College of Nursing and Health Management, Shanghai University of Medicine and Health Sciences, Shanghai, China,
[2] Department of Nursing, Huadong Hospital Affiliated to Fudan University, Shanghai, China

Objective: The purpose of this study is to evaluate the major mental health outcomes on dementia patient carers when using psychoeducational programs and psychotherapeutic interventions.

Methods: A meta-analysis was performed with randomized controlled trials of carers' tele-health interventions from the literature inception to December 31, 2019, using PubMed, EMBASE, and CENTRAL databases for articles.

Results: The meta-analysis identified 1,043 results, of which 11 were randomized control trials. Among all 11 randomized control trials, only one study addressed face-to-face contact with online modules of interventions, four studies addressed telephone-based interventions, two studies reported on combined face-to-face contact and phone call interventions, two studies focused on web-based interventions, one study used video and telephone interventions, and one study conducted a computer-telephone integration system of intervention. The updated evidence suggested that there was more efficacy via tele-health interventions in lowering depression for carers of people with dementia. We outlined the delivery formation of intervention to evaluate the effectiveness and processes of major mental health improvements, including depression, burden, anxiety, and quality of life.

Conclusions: In this study, tele-health intervention was shown to significantly lower depression and also lower the risk of mental health impairment. Although there was a significant decrease of depression, there were no significant differences in burden, anxiety, and quality of life. Future researchers are encouraged to carry out larger-scale studies; also, further analysis using a standardized assessment tool is suggested for future multi-component tele-health interventions.

Keywords: tele-health, intervention, carers, dementia, systematic review, meta-analysis

OPEN ACCESS

Edited by:
Jiehui Jiang,
Shanghai University, China

Reviewed by:
Po-Chun Hsieh,
Taipei Tzu Chi Hospital, Taiwan
Can Sheng,
Capital Medical University, China

***Correspondence:**
Shu-Fen Chu
zhusf@sumhs.edu.cn

Received: *30 September 2020*
Accepted: *07 January 2021*
Published: *10 February 2021*

Citation:
Zhu A, Cao W, Zhou Y, Xie A, Cheng Y and Chu S-F (2021) Tele-Health Intervention for Carers of Dementia Patients—A Systematic Review and Meta-Analysis of Randomized Controlled Trials. Front. Aging Neurosci. 13:612404. doi: 10.3389/fnagi.2021.612404

INTRODUCTION

Studies showed that carers of dementia family members have a poorer quality of life (QoL) (Glueckauf et al., 2007; Häusler et al., 2016; Brown et al., 2019) and higher risk for death by suicide. This risk did not decrease even after the care-recipients were institutionalized or died (Kishita et al., 2018). In 2015, there were 17.7 million informal carers who provided either in-home

substantial services or unpaid assistance to their family members and friends. Though caregiving can strengthen the relationship between carer and recipient, it can also cause emotional and physical burdens on carers, resulting in higher rates of depression, lower quality of life, and poorer overall health. However, these outcomes might be eliminated when proactively addressing the needs of families and carers. To improve the support systems for carers and the care recipients, it is suggested to have a better understanding of carers and their challenges (Edwards et al., 2020). A UK survey in 2019 found that most carers (79%) used one or more types of technology, while distance carers, who do not reside in the same home with the care recipients, used slightly fewer (77%). There are lots of studies assessing the efficacy of carer interventions on emotional well-being (Orgeta et al., 2013; Wagner and Brandt, 2018; Or and Kartal, 2019). However, only a few of these reviewed the effect of intervention by delivery mode for carers of dementia patients, such as tele-health intervention. To develop more cost-effective approaches that meet the needs of people with dementia and their family carers is urgent. Different kinds of interventions could prevent or reduce the negative effect of carers, but use of internet interventions is still very limited (Blom et al., 2013). Some interventions are designed to support carers in their role, such as skills training or education to assist in caring for people living with dementia. Evidence showed that if carers learn to deal more effectively with the stresses of caregiving, their QoL will remain at a higher level. Psychoeducational interventions are the most widely studied, and improvement in level of depression and stress have been reported. Recently, there was one study that conducted a comprehensive review that suggested psychoeducation-skill building interventions show a significant influence on burden when delivered face-to-face (Kishita et al., 2018). This meta-analysis updated the literature on interventions for carers of dementia patients published between 2006 and 2016 and evaluated the efficacy of psychoeducational programs and psychotherapeutic interventions on major mental health outcomes, such as depression, anxiety, burden, and QoL. This study demonstrated strong empirical support for treating anxiety and depression by all modes of delivery (Kishita et al., 2018). Face-to-face intervention is very costly compared to the tele-health-based interventions. Tele-health interventions are much more convenient as carers can receive help when it is necessary, especially in a time such as the COVID-19 pandemic, when social distancing is crucial. Therefore, the purpose of the research is to assess the efficacy of tele-health interventions for carers of dementia patients.

MATERIALS AND METHODS

Data Sources and Searches

Inception to December 31, 2019, we developed the search strategy, without language restriction, for PubMed, EMBASE, and CENTRAL for articles. The search terms included caregiver, carer, dementia, cognitive decline, cognitive impairment, web-based intervention, technology intervention, internet intervention, tele-health intervention, and randomized controlled trials. Titles and abstracts were screened by three reviewers independently, while full texts were sourced for relevant articles. Inclusion criteria were assessed independently, and inconsistencies were resolved by consensus. The reference lists of included trials and other published meta-analyses were also reviewed for relevant articles.

Eligibility Criteria

According to the American Psychiatric Association's Diagnostic and Statistical Manual (DSM-5), dementia is typically diagnosed when acquired cognitive impairment has become severe enough to compromise social and/or occupational functioning. Symptoms of memory loss are caused by a range of cognitive abilities, or a general cognitive decline, and not just memory (Hugo and Ganguli, 2014). Trials were considered eligible if they were randomized clinical trials, comparing the key mental health states of anxiety, depression, and burden, and associated with poor QoL in dementia carers. Trials were required to report at least one of the following forms of intervention: blending face-to-face contact with online modules, telephone-based, combined face-to-face contact and phone calls or web-based intervention, using video and telephone interventions, or a computer-telephone integration system (**Table 1**). Also, trials were required to report at least one of the following outcomes: symptoms of depression, anxiety, burden, or QoL. Trials that recruited participants with face-to-face intervention only were excluded.

Data Extraction

Data were collected independently by two authors using a standardized data extraction form, entered into a dedicated database, and checked independently by four authors. The data included study characteristics, baseline demographics of participants, description of the intervention, incidence of dementia, the forms of intervention, main treatment components, and length of each session (min)/treatment. We reported outcomes at the point of the longest follow-up. Eleven majority delivery modules of intervention were defined as those in which more than 50% had tele-health interventions.

Outcomes

For our primary analysis, we used a hierarchical approach in which we included trials that reported delivery mode of intervention including blending face-to-face contact with online modules, telephone-based, combined face-to-face contact and phone calls, or web-based intervention using video and telephone interventions, or a computer-telephone integration system. We chose this approach to maximize the number of clinical trials included in our primary analysis, while also giving priority to the most tele-health intervention relevant mental health outcomes reported in trials. The main outcomes of this meta-analysis were depression, anxiety, burden, and QoL on follow-up carers of people with dementia. The outcome measures for studies were efficacy carer interventions on anxiety, depression, burden, and quality of life.

TABLE 1 | Characteristics of included studies.

First author	Year of publish	Method of study	Diagonosis of care-recipient	Target of population	Format of intervention	Main outcomes
Boots L. M.	2018	RCT	People with mild dementia of all subtypes (Clinical Dementia Rating, score 0.5–1)	Family caregivers	Blending face-to-face contacts with online modules	Depression
Tremont G.	2015	RCT	Most care recipients were diagnosed with Alzheimer's disease	Family caregivers	Telephone contacts	Depression
Prick A. E.	2015	RCT	Community-dwelling people with dementia	Family caregivers	Experimental group: home visits Comparison group: information bulletins and phone calls	Depression
Cristancho-Lacroix V.	2015	RCT	Alzheimer's disease was targeted by this program	Informal caregivers	Web-based intervention	Psychologists stress
Blom M. M.	2015	RCT	People with dementia	Family caregivers	Internet course MoD	Depression.
Glueckauf R. L.	2012	RCT	People with dementia	African American dementia caregivers	Combines face-to-face and telephone-based	Depression
Gallagher-Thompson D.	2010	RCT	People with dementia	Caregivers	Using video and telephone interventions	Depressive symptoms Stress associated with memory and behavior problems
Gallagher-Thompson D.	2007	RCT	People with dementia	Female Chinese American caregivers	Telephone contacts	Depressive symptoms
Finkel S.	2007	RCT	People with Alzheimer's disease	Caregivers	Computer-Telephone Integration System (CTIS)	Depression
Winter L.	2006	RCT	People with Alzheimer's disease or related disorders	Female family caregivers	Telephone-based support groups	Depression
Burns R.	2003	RCT	People with Alzheimer's disease	Caregivers	Face-to -face and telephone contact	General Health and Mental Health

Risk of Bias Assessment

Cochrane risk of bias tool (Higgins et al., 2011) was applied to assess the methodological quality of eligible trials on random sequence generation, allocation concealment, blinded outcome assessment, completeness of outcome data, evidence of selective reporting, and other biases. The risk of bias was independently assessed by two reviewers, while a third reviewer resolved the disagreements. A risk-of-bias summary table was created in Review Manager version 5.3. and the study was considered to be at high risk of bias if two of the domains were rated as high.

Data Synthesis and Analysis

A descriptive analysis of each trial is provided in **Table 1**. Outcomes of depression, anxiety, burden, and QoL were estimated for each trial. Weighted pooled treatment effects were calculated using restricted maximum likelihood estimation to fit a random-effects meta-analysis model. A pooled mean difference and 95% CI was calculated using a random-effects meta-analysis. If this was not reported, the mean between-group difference reported at follow-up was used.

RESULT

Study Selection

The systematic search of articles published from database inception to December 31, 2019, identified 1,043 results. After title and abstract screening, 26 articles were considered potentially relevant. Twenty studies were included after full- text review. Eleven studies reported the intervention via blending face-to-face contact with online modules ($n = 1$), four were telephone-based ($n = 4$), two combined face-to-face contacts and phone calls ($n = 2$), two used web-based intervention ($n = 2$), one used video and telephone interventions ($n = 1$), and one used a computer-telephone integration system ($n = 1$). These were included in the primary meta-analysis (**Figure 1**). Seven out of 11 studies were conducted in the United States (Burns et al., 2003; Winter and Gitlin, 2006; Finkel et al., 2007; Gallagher-Thompson et al., 2007, 2010; Glueckauf et al., 2012; Tremont et al., 2015), and the rest were in the Netherlands ($n = 3$) (Blom et al., 2015; Prick et al., 2015; Boots et al., 2018) and France ($n = 1$) (Cristancho-Lacroix et al., 2015). Of the 11 studies, five studies recruited carers of people with Alzheimer's disease. Most studies involved carers of people with various diagnoses of dementia grouped as a whole. In total, 1,087 participants were enrolled. The mean (SD) age of trial participants was 64.22 (5.4) years old. The publication year ranged from 2003 to 2018. Eleven trials' main outcome measurement were of depression, two trials were of anxiety, six trials were of burden, and two trials were QoL. The most commonly used measurement was the Centre for Epidemiologic Studies Depression scale (CESD). Data were available to calculate the effect size for six of the eleven studies that included burden as one of the outcome measures. The majority of studies used

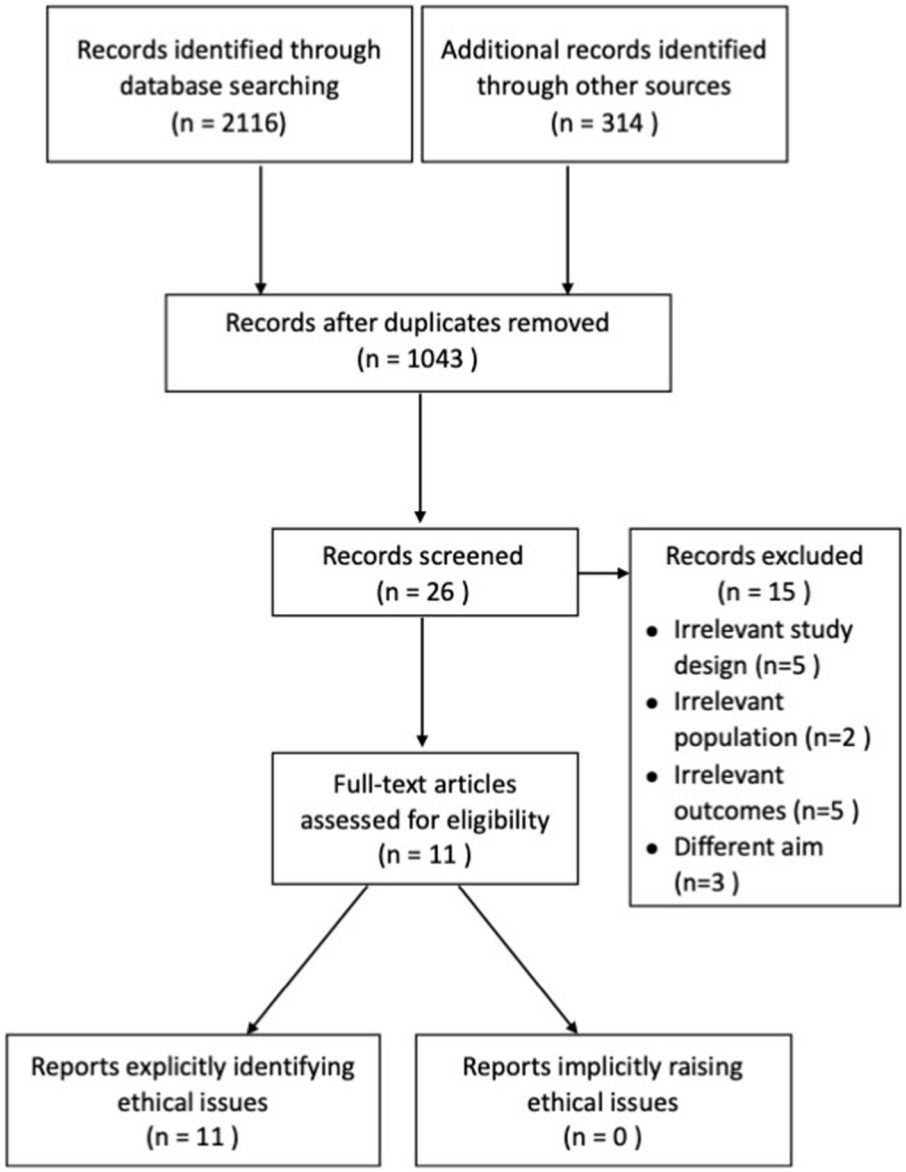

FIGURE 1 | Flow diagram of the studies' selection process.

the Zarit Burden Interview (ZBI). Two studies reported the efficacy of interventions on anxiety. The most commonly used measure was the psychological complaints measure [Hospital Anxiety and Depression Scale-Anxiety (HADS-A)]. Two studies reported the efficacy of interventions on QoL. They used the Investigation Choice Experiments for the Preferences of Older People (ICECAP-O) and Euro-QoL to measure the efficacy.

Study Characteristics

Blending Face-To-Face Contact With Online Modules and Key Mental Health

This category contained a description of only one trial on follow-up (81 participants). Carers of people with mild dementia of all subtypes (Clinical Dementia Rating, score 0.5–1) were divided into the intervention group (31 participants) and the control group (37 participants). The primary outcome was self-efficacy and symptoms of depression. Secondary outcomes included QoL and psychological complaints. The main treatment component was a blended care self-management program in combination with face-to-face coaching and tailored web-based modules. The main outcome measure for depression in this study was the CESD scale. The outcome of QoL measure was the Investigation Choice Experiments for the Preferences of Older People (ICECAP-O).

Telephone-Based and Key Mental Health

Four trials reported telephone-based therapy on follow-up (509 participants). Overall, 270 participants were in the intervention

group and 239 participants in the control group. Symptoms of depression as primary outcomes were reported in this category. Secondary outcomes included QoL and physiological responses to stress. Two studies involved psychoeducation and skills training of communication as the main treatment component. Other studies provided problem-solving, planning of pleasant activities, and a supportive social network. The main outcome measure for depression in four studies was the CESD scale. The Dutch version of the Revised Memory and Behavior Problem Checklist (RMBPC), used self-rated general health salivary cortisol levels to measure physiological responses to stress. The outcome of the QoL measure was Euro-QoL. Self-Perceived Pressure from Family Care (SPICC) was applied to measure the planning of pleasant activities.

Combines Face-To-Face Contacts and Phone Calls and Key Mental Health

This category contained a description of two trials on follow-up (87 participants) and divided the carers of people with either dementia or Alzheimer's disease into the intervention group (43 participants) and the control group (44 participants). Symptoms of depression as the main outcome were reported in this category. One study included physical symptoms, psychosocial resources, and subjective burden secondary outcomes. The other study included general health and mental health and an assessment of how the dementia was manifested for the patient and affected the carer as the secondary outcomes. The main outcome measure for depression in this category was CESD scale. Modified Caregiver Health and Behavior Inventory, Assistance subscale of Interpersonal Support Evaluation List, Caregiver Appraisal Inventory, and modified General Well-Being scale were used to measured secondary outcomes.

Web-Based Intervention and Key Mental Health

This category contained a description of two trials on follow-up (294 participants). Overall, 174 participants were in the intervention group and 120 participants in the control group. Symptoms of depression and stress as main outcomes were reported in this category. One study included secondary outcomes such as anxiety. The other study included self-efficacy, burden, perceived health status, and depression as the secondary outcome. The CESD scale and Perceived Stress Scale (PSS-14) were the main two outcome measures for depression and stress. Hospital Anxiety and Depression Scale (HADS-A), Revised Scale for Caregiving Self-Efficacy, Zarit Burden Interview (ZBI), the French version of the Nottingham Health Profile, and Beck Depression Inventory (BDI-II) were used to measure secondary outcomes.

Using Video and Telephone Interventions and Key Mental Health

This category contained a description of one trial on follow-up (70 participants). Overall, 36 participants were in the intervention group and 34 participants in the control group. Symptoms of depression and stress as main outcomes were reported in this category and were measured by CESD scale and a Chinese translation of the Revised Memory and Behavior Problems Checklist (RMBPC).

Computer-Telephone Integration System and Key Mental Health

This category contained a description of one trial on follow-up (46 participants). Seventeen participants were in the intervention group and 19 participants were in the control group. Symptoms of depression, burden, self-care activities, and social support as outcomes were reported in this category. CESD scale, Revised Memory and Behavior Problems Checklist (RMBPC), Caregiver Health and Health Behaviors scale, and Received Social Support scale for outcomes measurement were performed.

RISK OF BIAS

The quality of those studies included in our research was assessed by the Cochrane risk of bias summary and no study was excluded due to a high risk bias. All included studies were randomized trials and there were seven studies that described the specific randomization method. The majority of trials ($n = 3$) were single-blind randomized control trials. A randomization sequence was adequately generated in seven studies and 11 adequately concealed allocation. Reporting bias was noted in one trial (**Figure 2**). In all studies, the quality of detection bias and performance bias was relatively inconsistent, whereas the quality of publication bias was relatively low.

EFFECTS OF INTERVENTIONS

A random effects model was used for depression. It showed statistically significant high heterogeneity ($I^2 = 55\%$; $p = 0.01$), which had a large impact on the overall effect size (Blom et al., 2015; Tremont et al., 2015). Overall effective study size for depression was low [SMD $= -0.34$, $p = 0.01$; 95% CI $= -0.54$ to -0.14 (**Figure 3A**)].

Symptoms of depression with intervention formations of tele-health compared with control was highly correlated with a reduction in carers of people with dementia or AD with 7.0 vs. 7.5% over a 4.1 year-follow-up; [OR, 0.93 (95% CI, 0.88–0.98); ARR, 0.39% (95% CI, 0.09–0.68%)] (**Figure 3A**). Heterogeneity was low ($I^2 = 0.0\%$).

Anxiety and depression were also analyzed with a random effects model, though no heterogeneity was observed between study size. An overall effect size for anxiety was large ($g = 2.10$, $p < 0.00001$; 95% CI $= -1.19$ to 2.10 (**Figure 3B**). There was high heterogeneity between study effect sizes ($Z = 0.54$, $p = 0.59$; $I^2 = 97$).

The efficacy of interventions on QoL and burden were evaluated with a random effects model, but the heterogeneity was not significant ($g = 0.23$, $p = 0.27$; 95% CI $= -0.04$ to 0.50 (**Figure 3C**) and the heterogeneity between study effect sizes were significantly low ($Z = 1.69$, $p = 0.09$; $I^2 = 19$) compared with the effect size on burden, which was small [$g = 0.04$, $p = 0.72$; 95% CI $= -0.23$ to 0.14 (**Figure 3D**)].

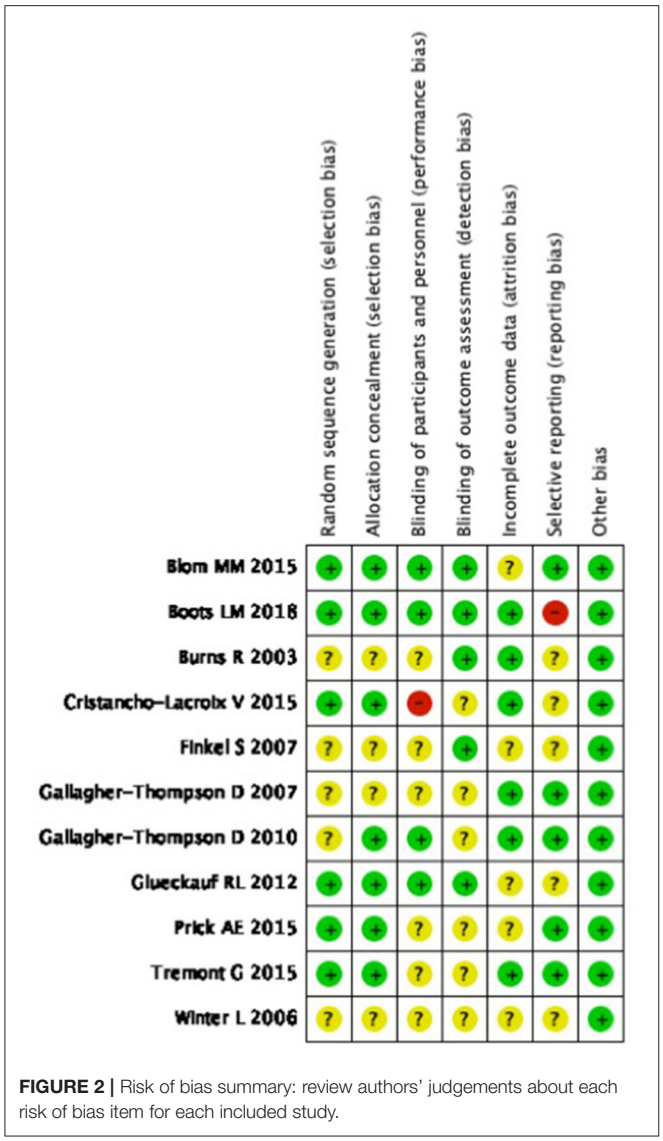

FIGURE 2 | Risk of bias summary: review authors' judgements about each risk of bias item for each included study.

DISCUSSION

Epidemiologic studies have reported a stronger association between negative states of mental health and carers of people with dementia (Phung et al., 2013). To increase carers' knowledge of the illness, develop problem-solving skills, and facilitate social support through psychoeducational interventions, interventions should be used Technology-based interventions significantly affect burden, anxiety, depression, QoL, and self-efficacy (Frias et al., 2020). Web-based interventions for carers of people with early-stage dementia demonstrated a significant improvement in self-efficacy, mastery, and QoL (Gallagher-Thompson et al., 2010). Both telephone-based and face-to-face technology-based interventions showed improvements in depression, subjective burden, and assistance support in dementia cares (Gallagher-Thompson et al., 2007). There is a significant need for non-pharmacological interventions for persons living with dementia that are easily available, easy to access, and facilitate the use of information and communication technologies (ICTs) (Gilson et al., 2019). This meta-analysis, which included 11 trials with 1,087 participants for the primary outcome analysis, found that was more efficacy via tele-health interventions in lowering depression in carers of people with dementia. We outlined the delivery formation of intervention to evaluate the effectiveness and processes of key mental health improvements, including depression, burden, anxiety, and QoL.

Primary Findings

Our research showed that depression can be relieved more through tele-health interventions than face-to-face. Steffen et al. reported on a distance intervention carries out with a small sample size by phone and by mail that could prevent the risk of negative effects on mental health [pre-intervention score (SD), 18.9 (4.9), and post-intervention score (SD), 16.1 (3.9)] (Gant et al., 2007). There was a decrease in depression in the intervention that was associated with fewer hospitalizations at 6 months ($r = 0.18$, $P = 0.02$) (Tremont et al., 2017). The current study found that carers in the tele-health intervention group had less case-level depression [odds ratio (OR) 0.24, 95% CI 0.07–0.76] (Livingston et al., 2014). This was also proven in Zhao et al.'s study in which depression scores dropped an average of 0.23 (95% CI −0.38 to −0.07; $P< 0.01$) after web-based interventions (Zhao et al., 2019); otherwise, in the study by Kajiyama et al. (2013), it showed evidence-based interventions for carers via the internet for reducing stress was significant ($p = 0.017$) but no significant changes in the bother, depression, or level of life quality. There was no significant effect on depression that was statistically significant effected by Time ($p = 0.27$), Group ($p = 0.53$), Ethnicity ($p = 0.34$), the Group * Time * interaction ($p = 0.92$), or the Group * Ethnicity * Time * interaction ($p = 0.08$) (Czaja et al., 2013). A cross-sectional study reported that carers of AD dementia patients frequently experienced hypertension (12.7%) and insomnia (11.0%) but there were no significant differences on depression and other comorbidities (Montgomery et al., 2018). However, the tele-health intervention should be an important measure to help carers of dementia in the future, especially in conjunction with the fast improvement of associated technologies.

Secondary Findings

One report by Austrom et al. (2015) showed that a weekly web-based video conference support group for carers could relieve their anxiety (mean difference 1.5, improvement 75%) and burden (mean difference −1.0, improvement 50%). Tsolaki et al. (2015) found ICT can not only help patients with cognitive, functional, and behavioral problems, but also support health professionals and carers by reducing their anxiety compared with face-to-face interventions. There is also a meta-analysis that found that web-based interventions significantly improved the anxiety status of carers by −0.32 (95% CI −0.50 to −0.14; $P = 0.0005$) (Zhao et al., 2019). However, McKechnie et al. (2014) reported no change in depression or anxiety over the 12-week study period via online peer support. In one study, carers who had access to a website improved their confidence while role

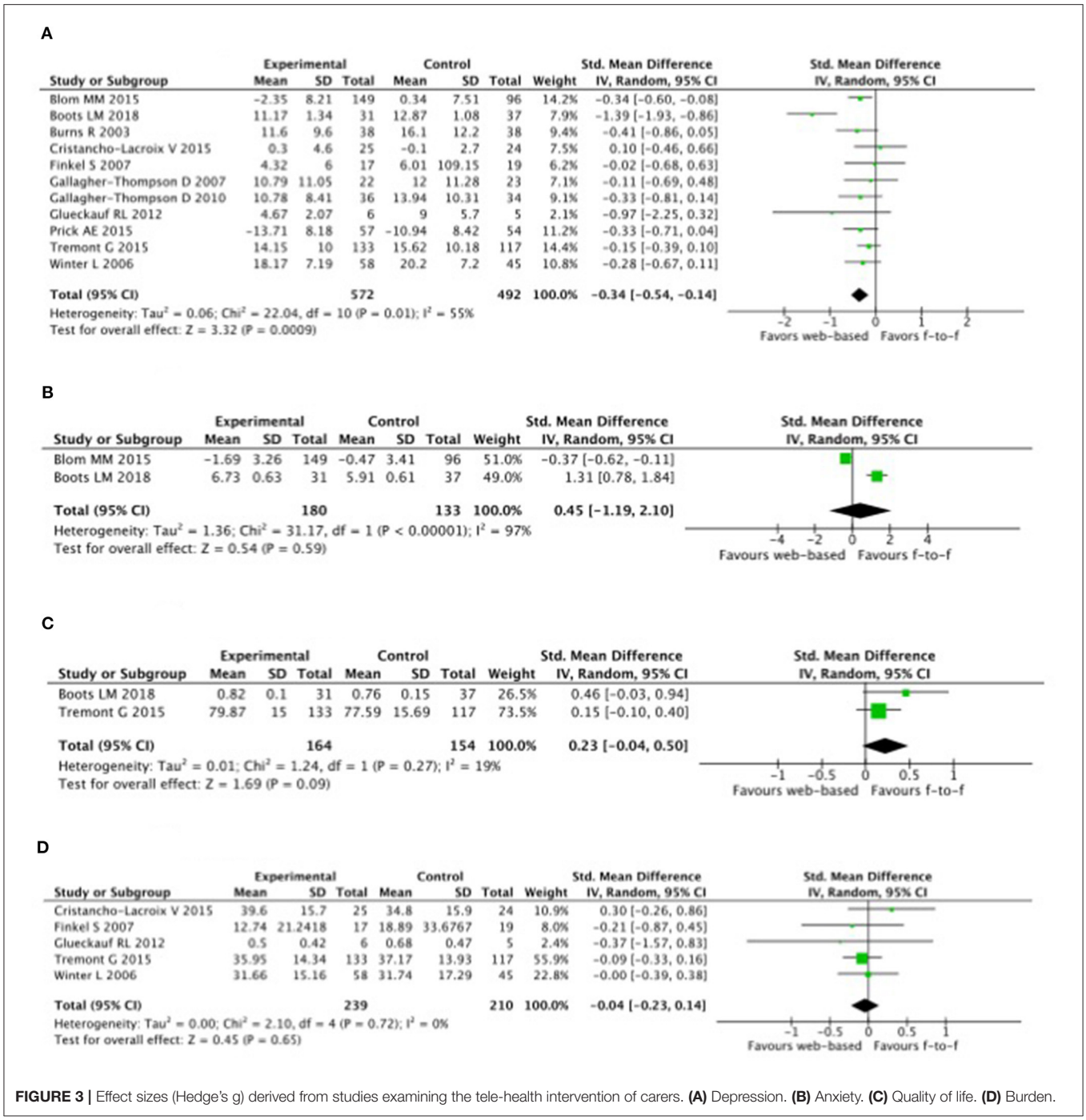

FIGURE 3 | Effect sizes (Hedge's g) derived from studies examining the tele-health intervention of carers. **(A)** Depression. **(B)** Anxiety. **(C)** Quality of life. **(D)** Burden.

strain, anxiety, and depression were decreased, although some of them were not significant (Zimmerman et al., 2018). However, a small sample size, low test efficiency, and a high rate of loss to follow-up over time limits this study and further research is needed to draw a conclusion.

Burden

Our study showed that the mental health burden would be reduced through tele-health intervention. Some studies showed a correlation between scores on depression, anxiety, and sleep quality assessments and carers' burden (Coffman et al., 2017). Online contact with a professional led to relief in burden and strain for those carers that appreciated personalized practical advice and emotional support (Hopwood et al., 2018). However, not many studies support this result. Parker et al. (2008) performed a meta-analysis study that indicated that there were no significant effects from any of the interventions. Therefore, the major outcome for web-based learning courses was the increase

in knowledge. No effects were found on the relief of burden (Hattink et al., 2015).

Quality of Life

Our study revealed that tele-health interventions could improve quality of life for carers of dementia patients.

Although there was one study that indicated that quality of life was only moderate (SD = 8.21) and negatively correlated with burden ($r = -32$, $p = 0.01$) and depression ($r = -0.296$, $p < 0.05$) (Papastavrou et al., 2014), the findings from Bartfay and Bartfay (2013) showed similar levels of QOL between carers who used community-based interventions. Another systemic meta-analysis showed the effectiveness of IT interventions in the carers of elderly dementia both improving the quality of life and effects on behavior (such as less falling) (Nijhof et al., 2009). However, Duggleby et al. (2018) reported no significant differences from web-based interventions on health-related quality of life, neither for carers of community-living persons with Alzheimer's disease, nor for related dementia.

Quality of the Included Studies

All results of the quality assessment for the included studies were rated as medium, which explained the variation in many domains, such as theoretical model selection, intervention format, and evaluation tools. It also increased the difficulty in assessing the risk of bias in many areas, which resulted in inconsistent results. There is more and more evidence proving the feasibility of tele-health multicomponent interventions and suggesting the most useful and least expensive intervention components or platforms. Further research on carer-focused interventions to improve their mental health is suggested in the future.

LIMITATIONS

There are a few limitations that may lessen the credibility of our study. First, the study was not assessed by a standardized tool, and only limited variables were analyzed. Second, only the USA, Dutch, and France were included, which may limit the ability to conclude the result in other nationalities. Third, there were large differences in the usage of assistive technology, outcome measures, and the quality of studies. All of these created difficulties in comparing results across reviews.

CONCLUSIONS

In this meta-analysis of randomized clinical trials, depression lowering with tele-health interventions compared with a controlled group was significantly associated with a lower risk of incident mental health impairment. Although there was a significant decrease in depression, there were no significant differences in burden, anxiety, or quality of life. More rigorous methods and larger-scale, higher-quality studies and multicomponent tele-health interventions are suggested in the future to analyze the outcome in further detail using a standardized assessment tool.

DATA AVAILABILITY STATEMENT

The raw data supporting the conclusions of this article will be made available by the authors, without undue reservation.

AUTHOR CONTRIBUTIONS

All authors listed have made a substantial, direct and intellectual contribution to the work, and approved it for publication.

ACKNOWLEDGMENTS

The authors acknowledge the contributions of Professor Chiehfeng Chen, Taipei Medical University who aided the efforts of the authors.

REFERENCES

Austrom, M. G., Geros, K. N., Hemmerlein, K., McGuire, S. M., Gao, S., Brown, S. A., et al. (2015). Use of a multiparty web based videoconference support group for family caregivers: innovative practice. *Dementia* 14, 682–690. doi: 10.1177/1471301214544338

Bartfay, E., and Bartfay, W. J. (2013). Quality-of-life outcomes among Alzheimer's disease family caregivers following community-based intervention. *West. J. Nurs. Res.* 35, 98–116. doi: 10.1177/0193945911400763

Blom, M. M., Bosmans, J. E., Cuijpers, P., Zarit, S. H., and Pot, A. M. (2013). Effectiveness and cost-effectiveness of an internet intervention for family caregivers of people with dementia: design of a randomized controlled trial. *BMC Psychiatry* 13:17. doi: 10.1186/1471-244X-13-17

Blom, M. M., Zarit, S. H., Groot Zwaaftink, R. B., Cuijpers, P., and Pot, A. M. (2015). Effectiveness of an internet intervention for family caregivers of people with dementia: results of a randomized controlled trial. *PLoS ONE* 10:e0116622. doi: 10.1371/journal.pone.0116622

Boots, L. M., de Vugt, M. E., Kempen, G. I., and Verhey, F. R. (2018). Effectiveness of a blended care self-management program for caregivers of people with early-stage dementia. (Partner in balance): randomized controlled trial. *J. Med. Internet Res*. 20:e10017. doi: 10.2196/10017

Brown, A., Page, T. E., Daley, S., Farina, N., Basset, T., Livingston, G., et al. (2019). Measuring the quality of life of family carers of people with dementia: development and validation of C-DEMQOL. *J. Qual. Life Res.* 28:8. doi: 10.1007/s11136-019-02186-w

Burns, R., Nichols, L. O., Martindale-Adams, J., Graney, M. J., and Lummus, A. (2003). Primary care interventions for dementia caregivers: 2-year outcomes from the REACH study. *Gerontologist* 43, 547–555. doi: 10.1093/geront/43.4.547

Coffman, I., Resnick, H. E., and Lathan, C. E. (2017). Behavioral health characteristics of a technology-enabled sample of Alzheimer's caregivers with high caregiver burden. *Mhealth* 3:36. doi: 10.21037/mhealth.2017.08.01

Cristancho-Lacroix, V., Wrobel, J., Cantegreil-Kallen, I., Dub, T., Rouquette, A., and Rigaud, A. S. (2015). A web-based psychoeducational program for informal caregivers of patients with Alzheimer's disease: a pilot randomized controlled trial. *J. Med. Internet Res.* 17:e117. doi: 10.2196/jmir.3717

Czaja, S. J., Loewenstein, D., Schulz, R., Nair, S. N., and Perdomo, D. (2013). A Videophone psychosocial intervention for dementia caregivers. *Am. J. Geriatr. Psychiatry* 21, 1071–1081. doi: 10.1016/j.jagp.2013.02.019

Duggleby, W., Ploeg, J., McAiney, C., Peacock, S., Fisher, K., Ghosh, S., et al. (2018). Web-based intervention for family carers of persons with

dementia and multiple chronic conditions (my tools 4 care): pragmatic randomized controlled trial. *J. Med. Internet Res.* 20:e10484. doi: 10.2196/10484

Edwards, V. J., Bouldin, E. D., Taylor, C. A., Olivari, B. S., and McGuire, L. C. (2020). Characteristics and health status of informal unpaid caregivers - 44 states, district of Columbia, and Puerto Rico, 2015-2017. *MMWR Morbid. Mortal. Wkly. Rep.* 69, 183–188. doi: 10.15585/mmwr.mm6907a2

Finkel, S., Czaja, S. J., Schulz, R., Martinovich, Z., Harris, C., and Pezzuto, D. (2007). E-care: a telecommunications technology intervention for family caregivers of dementia patients. *Am. J. Geriatr. Psychiatry* 15, 443–448. doi: 10.1097/JGP.0b013e3180437d87

Frias, C. E., Garcia-Pascual, M., Montoro, M., Ribas, N., Risco, E., and Zabalegui, A. (2020). Effectiveness of a psychoeducational intervention for caregivers of people with dementia with regard to burden, anxiety and depression: a systematic review. *J. Adv. Nurs.* 76, 787–802. doi: 10.1111/jan.14286

Gallagher-Thompson, D., Gray, H. L., Tang, P. C., Pu, C. Y., Leung, L. Y., Wang, P. C., et al. (2007). Impact of in-home behavioral management versus telephone support to reduce depressive symptoms and perceived stress in Chinese caregivers: results of a pilot study. *Am. J. Geriatr. Psychiatry* 15, 425–434. doi: 10.1097/JGP.0b013e3180312028

Gallagher-Thompson, D., Wang, P. C., Liu, W., Cheung, V., Peng, R., China, D., et al. (2010). Effectiveness of a psychoeducational skill training DVD program to reduce stress in Chinese American dementia caregivers: results of a preliminary study. *Aging Ment. Health* 14, 263–273. doi: 10.1080/13607860903420989

Gant, J. R., Steffen, A. M., and Lauderdale, S. A. (2007). Comparative outcomes of two distance-based interventions for male caregivers of family members with dementia. *Am. J. Alzheimers Dis. Other Dement.* 22, 120–128. doi: 10.1177/1533317506298880

Gilson, A., Dodds, D., Kaur, A., Potteiger, M., and Ford Ii, J. H. (2019). Using computer tablets to improve moods for older adults with dementia and interactions with their caregivers: pilot intervention study. *JMIR Form. Res.* 3:e14530. doi: 10.2196/14530

Glueckauf, R. L., Davis, W. S., Willis, F., Sharma, D., Gustafson, D. J., Hayes, J., et al. (2012). Telephone-based, cognitive-behavioral therapy for African American dementia caregivers with depression: initial findings. *Rehabil. Psychol.* 57, 124–139. doi: 10.1037/a0028688

Glueckauf, R. L., Jeffers, S. B., Sharma, D., Massey, A. J., Davis, W. S., Wesley, L. M., et al. (2007). Telephone-based cognitive-behavioral intervention for distressed rural dementia caregivers. *Clin. Gerontol.* 31, 21–41. doi: 10.1300/J018v31n01_03

Hattink, B., Meiland, F., van der Roest, H., Kevern, P., Abiuso, F., Bengtsson, J., et al. (2015). Web-based STAR E-learning course increases empathy and understanding in dementia caregivers: results from a randomized controlled trial in the Netherlands and the United Kingdom. *J. Med. Internet Res.* 17:e241. doi: 10.2196/jmir.4025

Häusler, A., Sánchez, A., Gellert, P., Deeken, F., Rapp, M. A., and Nordheim, J. (2016). Perceived stress and quality of life in dementia patients and their caregiving spouses: does dyadic coping matter? *J. Int. Psychogeriatr.* 28:11. doi: 10.1017/S1041610216001046

Higgins, J. P., Altman, D. G., Gøtzsche, P. C., Jüni, P., Moher, D., Oxman, A. D., et al. (2011). The cochrane collaboration's tool for assessing risk of bias in randomised trials. *BMJ* 343:d5928. doi: 10.1136/bmj.d5928

Hopwood, J., Walker, N., McDonagh, L., Rait, G., Walters, K., Iliffe, S., et al. (2018). Internet-based interventions aimed at supporting family caregivers of people with dementia: systematic review. *J. Med. Internet Res.* 20:e216. doi: 10.2196/jmir.9548

Hugo, J., and Ganguli, M. (2014). Dementia and cognitive impairment: epidemiology, diagnosis, and treatment. *Clin. Geriatr. Med.* 30, 421–442. doi: 10.1016/j.cger.2014.04.001

Kajiyama, B., Thompson, L. W., Eto-Iwase, T., Yamashita, M., Di Mario, J., Marian Tzuang, Y., et al. (2013). Exploring the effectiveness of an internet-based program for reducing caregiver distress using the iCare Stress Management e-Training Program. *Aging Ment. Health* 17, 544–554. doi: 10.1080/13607863.2013.775641

Kishita, N., Hammond, L., Dietrich, C. M., and Mioshi, E. (2018). Which interventions work for dementia family carers?: an updated systematic review of randomized controlled trials of carer interventions. *Int. Psychogeriatr.* 30, 1679–1696. doi: 10.1017/S1041610218000947

Livingston, G., Barber, J., Rapaport, P., Knapp, M., Griffin, M., Romeo, R., et al. (2014). START (STrAtegies for RelaTives) study: a pragmatic randomised controlled trial to determine the clinical effectiveness and cost-effectiveness of a manual-based coping strategy programme in promoting the mental health of carers of people with dementia. *Health Technol. Assess.* 18, 1–242. doi: 10.3310/hta18610

McKechnie, V., Barker, C., and Stott, J. (2014). The effectiveness of an internet support forum for carers of people with dementia: a pre-post cohort study. *J. Med. Internet Res.* 16:e68. doi: 10.2196/jmir.3166

Montgomery, W., Goren, A., Kahle-Wrobleski, K., Nakamura, T., and Ueda, K. (2018). Alzheimer's disease severity and its association with patient and caregiver quality of life in Japan: results of a community-based survey. *BMC Geriatr.* 18:141. doi: 10.1186/s12877-018-0831-2

Nijhof, N., van Gemert-Pijnen, J. E., Dohmen, D. A., and Seydel, E. R. (2009). Dementia and technology. A study of technology interventions in the healthcare for dementia patients and their caregivers. *Tijdschr. Gerontol. Geriatr.* 40, 113–132. doi: 10.1007/BF03079573

Or, R., and Kartal, A. (2019). Influence of caregiver burden on well-being of family member caregivers of older adults. *Psychogeriatrics* 19, 482–490. doi: 10.1111/psyg.12421

Orgeta, V., Lo Sterzo, E., and Orrell, M. (2013). Assessing mental well-being in family carers of people with dementia using the Warwick-Edinburgh mental well-being scale. *Int. Psychogeriatr.* 25, 1443–1451. doi: 10.1017/S1041610213000835

Papastavrou, E., Andreou, P., Middleton, N., Papacostas, S., and Georgiou, I. K. (2014). Factors associated with quality of life among family members of patients with dementia in Cyprus. *Int. Psychogeriatr.* 26, 443–452. doi: 10.1017/S104161021300224X

Parker, D., Mills, S., and Abbey, J. (2008). Effectiveness of interventions that assist caregivers to support people with dementia living in the community: a systematic review. *JBI Libr. Syst. Rev.* 6, 484–544. doi: 10.11124/jbisrir-2008-217

Phung, K. T., Waldorff, F. B., Buss, D. V., Eckermann, A., Keiding, N., Rishøj, S., et al. (2013). A three-year follow-up on the efficacy of psychosocial interventions for patients with mild dementia and their caregivers: the multicentre, rater- blinded, randomised Danish Alzheimer Intervention Study (DAISY). *BMJ Open* 3:e003584. doi: 10.1136/bmjopen-2013-003584

Prick, A. E., de Lange, J., Twisk, J., and Pot, A. M. (2015). The effects of a multi-component dyadic intervention on the psychological distress of family caregivers providing care to people with dementia: a randomized controlled trial. *Int. Psychogeriatr.* 27, 2031–2044. doi: 10.1017/S104161021500071X

Tremont, G., Davis, J. D., Ott, B. R., Galioto, R., Crook, C., Papandonatos, G. D., et al. (2017). Randomized trial of the family intervention: telephone tracking-caregiver for dementia caregivers: use of community and healthcare resources. *J. Am. Geriatr. Soc.* 65, 924–930. doi: 10.1111/jgs.14684

Tremont, G., Davis, J. D., Papandonatos, G. D., Ott, B. R., Fortinsky, R. H., Gozalo, P., et al. (2015). Psychosocial telephone intervention for dementia caregivers: a randomized, controlled trial. *Alzheimers Dement.* 11, 541–548. doi: 10.1016/j.jalz.2014.05.1752

Tsolaki, M., Zygouris, S., Lazarou, I., Kompatsiaris, I., Chatzileontiadis, L., Votis, C., et al. (2015). Our experience with informative and communication technologies (ICT) in dementia. *Hell. J. Nucl. Med.* 18 131–139.

Wagner, M., and Brandt, M. (2018). Long-term care provision and the well-being of spousal caregivers: an analysis of 138 European regions. *J. Gerontol. B Psychol. Sci. Soc. Sci.* 73, E24–E34. doi: 10.1093/geronb/gbx133

Winter, L., and Gitlin, L. N. (2006). Evaluation of a telephone-based support group intervention for female caregivers of community-dwelling individuals with dementia. *Am. J. Alzheimers Dis. Other Dement.* 21, 391–397. doi: 10.1177/1533317506291371

Zhao, Y., Feng, H., Hu, M., Hu, H., Li, H., Ning, H., et al. (2019). Web-based interventions to improve mental health in home caregivers of people with dementia: meta-analysis. *J. Med. Internet Res.* 21:e13415. doi: 10.2196/13415

Zimmerman, S., Sloane, P. D., Ward, K., Beeber, A., Reed, D., Lathren, C., et al. (2018). Helping dementia caregivers manage medical problems: benefits of an educational resource. *Am. J. Alzheimers Dis. Other Dement.* 33, 176–183. doi: 10.1177/1533317517749466

Conflict of Interest: The authors declare that the research was conducted in the absence of any commercial or financial relationships that could be construed as a potential conflict of interest.

frontiers in Aging Neuroscience

ORIGINAL RESEARCH
published: 24 February 2021
doi: 10.3389/fnagi.2021.610755

Resilience to Plasma and Cerebrospinal Fluid Amyloid-β in Cognitively Normal Individuals: Findings From Two Cohort Studies

Li Lin[1] *Yu Sun*[1], *Xiaoqi Wang*[1], *Li Su*[2], *Xiaoni Wang*[1]* *and Ying Han*[1,3,4]* *on behalf of the Sino Longitudinal Study on Cognitive Decline, on behalf of the Alzheimer's Disease Neuroimaging Initiative*[†]

[1] *Department of Neurology, XuanWu Hospital of Capital Medical University, Beijing, China,* [2] *Department of Psychiatry, University of Cambridge, Cambridge, United Kingdom,* [3] *Center of Alzheimer's Disease, Beijing Institute for Brain Disorders, Beijing, China,* [4] *National Clinical Research Center for Geriatric Disorders, Beijing, China*

OPEN ACCESS

Edited by:
Fangyu Peng, University of Texas Southwestern Medical Center, United States

Reviewed by:
Jeremy Andrew Elman, University of California, San Diego, United States
Giorgio Giaccone, Fondazione IRCCS Istituto Neurologico Carlo Besta, Italy

***Correspondence:**
Ying Han
hanying@xwh.ccmu.edu.cn
Xiaoni Wang
wxnanna@163.com

[†]Data used in the preparation of this article were obtained from the Alzheimer's Disease Neuroimaging Initiative (ADNI) database (adni.loni.usc.edu). As such, the investigators within the ADNI contributed to the design and implementation of the ADNI and/or provided data but did not participate in the analysis or the writing of this report. A complete listing of investigators from the ADNI can be found at: https://adni.loni.usc.edu/wp-content/uploads/how_to_apply/ADNI_Acknowledgement_List.pdf

Received: *27 September 2020*
Accepted: *28 January 2021*
Published: *24 February 2021*

Citation:
Lin L, Sun Y, Wang X, Su L, Wang X and Han Y (2021) Resilience to Plasma and Cerebrospinal Fluid Amyloid-β in Cognitively Normal Individuals: Findings From Two Cohort Studies. Front. Aging Neurosci. 13:610755. doi: 10.3389/fnagi.2021.610755

Objective: To define resilience metrics for cognitive decline based on plasma and cerebrospinal fluid (CSF) amyloid-β (Aβ) and examine the demographic, genetic, and neuroimaging factors associated with interindividual differences among metrics of resilience and to demonstrate the ability of such metrics to predict the diagnostic conversion to mild cognitive impairment (MCI).

Methods: In this study, cognitively normal (CN) participants with Aβ-positive were included from the Sino Longitudinal Study on Cognitive Decline (SILCODE, $n = 100$) and Alzheimer's Disease Neuroimaging Initiative (ADNI, $n = 144$). Using a latent variable model of data, metrics of resilience [brain resilience (BR), cognitive resilience (CR), and global resilience (GR)] were defined based on the plasma Aβ and CSF Aβ. Linear regression analyses were applied to investigate the association between characteristics of individuals (age, sex, educational level, genetic, and neuroimaging factors) and their resilience. The plausibility of these metrics was tested using linear mixed-effects models and Cox regression models in longitudinal analyses. We also compared the effectiveness of these metrics with conventional metrics in predicting the clinical progression.

Results: Although individuals in the ADNI cohort were older (74.68 [5.65] vs. 65.38 [4.66], $p < 0.001$) and had higher educational levels (16.3 [2.6] vs. 12.6 [2.8], $p < 0.001$) than those in the SILCODE cohort, similar loadings between resilience and its indicators were found within both models. BR and GR were mainly associated with age, women, and brain volume in both cohorts. Prediction models showed that higher CR and GR were related to better cognitive performance, and specifically, all types of resilience to CSF Aβ could predict longitudinal cognitive decline.

Conclusion: Different phenotypes of resilience depending on cognition and brain volumes were associated with different factors. Such comprehensive resilience provided insight into the mechanisms of susceptibility for Alzheimer's disease (AD) at the individual level, and interindividual differences in resilience had the potential to predict the disease progression in CN people.

Keywords: resilience, Alzheimer's disease, amyloid, cognitive decline, cognitively normal

INTRODUCTION

Alzheimer's disease (AD) was originally defined as a clinical pathologic disease mainly based on clinical symptoms and neuropathologic changes like deposition of amyloid-β (Aβ) and hyperphosphorylated tau. Recent developments of AD have proposed research frameworks based on biomarkers (McKhann et al., 2011; Jack et al., 2018), which enhanced the understanding of the mechanism and brought substantial research interest to the preclinical stage of AD (Dubois et al., 2018; Jessen et al., 2018; Slot et al., 2018; Li et al., 2019). However, studies have shown that biomarkers and cognitive performance were discordant in some individuals with the pathology of AD often due to individual variations in resilience to the pathology of AD (Katzman et al., 1988; Ghisays et al., 2020). Therefore, as a theoretical construct, terms like reserve, resilience, and maintenance were defined to enhance the understanding of the individual difference related to diseases of the brain (Stern et al., 2018). Resilience, which represents the degree of structural and cognitive deficits associated with the pathology of AD, can be divided into brain resilience (BR) and cognitive resilience (CR) (Rentz et al., 2017) or a combination of both [e.g., global resilience (GR); Hohman et al., 2016; Arenaza-Urquijo and Vemuri, 2018)]. High or low resilience reflects better or worse than predicted properties of the brain or cognitive performances based on the pathological burden. Compared with the traditional index of the reserve including educational level, intelligence quotient (IQ), and occupational complexity, resilience defined by residual approaches provided a feasible quantitative measure of the impact of pathology on cognition (Ewers, 2020).

Currently, studies have found that high resilience may slow the rate of cognitive decline (van Loenhoud et al., 2019; Ossenkoppele et al., 2020), and the protective effect was more notable in the early stage before the cognitive impairment (Lo et al., 2013; Arenaza-Urquijo et al., 2017), which had important implications for intervention in the cognitively normal (CN) stage. In addition, these studies generally used cerebrospinal fluid (CSF) Aβ and PET Aβ to measure the level of the amyloid deposition. However, both methods are invasive or expensive, which are not suitable for widespread screening in the preclinical phase of AD. The advent of plasma Aβ has provided an alternative that is affordable and less invasive. Previous studies have shown the relationship between plasma Aβ and central Aβ (Hanon et al., 2018; Chatterjee et al., 2019; Schindler et al., 2019; Vergallo et al., 2019). The biomarker of amyloid peptide and the Alzheimer's disease risk (BALTAZAR) study found that the plasma Aβ was associated with cognitive performance, apolipoprotein E (APOE)-ε4 status, and CSF Aβ in cross-sectional analyses (Hanon et al., 2018). In a longitudinal study, Schindler et al. found that the plasma Aβ was inversely correlated with the baseline PET Aβ and correlated with the baseline CSF Aβ in CN older adults and could be used to predict the future amyloid status (Schindler et al., 2019).

However, it is still unclear that, in the context of CN individuals, which factors contribute to these metrics of resilience (BR, CR, and GR) to Aβ and whether the levels of resilience defined by plasma Aβ and CSF Aβ could both help predict the baseline and longitudinal cognitive decline. To address the questions mentioned above, we, therefore, quantified the metrics of resilience based on plasma Aβ and CSF Aβ. Using linear regression analyses, we tested whether demographic (age, sex, and educational level), genetic (APOE-ε4), and imaging markers are associated with these metrics of resilience. Then for investigating the added predictive value of different metrics of resilience, we explored the hypothesis that these metrics of resilience could help predict the diagnostic conversion and high resilience could slow down the cognitive decline longitudinally in CN individuals.

METHODS

Participants

Participant data from the Sino Longitudinal Study on Cognitive Decline (SILCODE) project (Li et al., 2019) from March 2017 to October 2018 and Alzheimer's Disease Neuroimaging Initiative (ADNI) (Weiner and Veitch, 2015) were used for this retrospective study. The SILCODE is a longitudinal observational project focusing on elderly Chinese people. Its primary goal was to identify the individuals in preclinical AD who would convert to mild cognitive impairment (MCI) and understand the disease mechanism. The ADNI was launched in 2003 as a public–private partnership whose goal was to test whether biological markers and clinical assessments could be combined to measure the progression of individuals in the spectrum of AD. The Aβ-positive CN participants were recruited from the SILCODE ($N = 100$) and the ADNI ($N = 144$). The median follow-up was 9.4 months [interquartile range (IQR): 0–17.3] for the SILCODE and 70.8 months (IQR: 35.9–91.2) for the ADNI. All CNs underwent clinical and neuropsychological assessments, plasma (SILCODE) or examination of the CSF (ADNI), MRI scans at baseline, and had a normal performance on neuropsychological tests adjusted for age, sex, and education. Participants with the following conditions were excluded: current major psychiatric diagnosis such as depression and anxiety, serious neurologic diseases, diseases that could cause cognitive decline (e.g., thyroid dysfunction, severe anemia, syphilis, or HIV), a history of brain lesions, or head traumas (additional inclusion/exclusion criteria can be found at www.adni-info.org and https://www.clinicaltrials.gov/ct2/show/study/NCT03370744).

Standard Protocol Approvals, Registrations, and Patient Consent

Informed written consent was obtained from all participants at each site, and study procedures were approved by the institutional review board at each center. The ADNI and the SILCODE are listed in the ClinicalTrials.gov registry (ADNI-1: NCT00106899; ADNI-2: NCT01231971; ADNI-GO: NCT01078636; ADNI-3: NCT02854033; and SILCODE: NCT03370744).

Neuropsychological Assessments

Across both studies, the neuropsychological assessment covered similar cognitive domains. To aid comparability and calculate the CR, we chose six neuropsychological measures used by

both studies and combined them into three domains: memory, language, and executive. The six measures were the Boston Naming Test and the Animal Naming for the language domain, the Trail Making Test A and the Trail Making Test B for the executive domain, and the auditory verbal learning test (AVLT) delayed recall and the delayed recognition scores for the memory domain. Scores of the Mini–Mental State Examination (MMSE) and the Montreal Cognitive Assessment (MoCA) were used to assess global cognition. All test scores were z-transformed within each test to remove the bias among measures. Within each domain, z-transformed scores were averaged to obtain a composite score.

MRI Acquisition and Processing

Structural MRI scans were acquired on 3T scanners from GE Healthcare (Chicago, USA), Philips Medical Systems (Eindhoven, Netherlands), and Siemens Medical Solutions (Erlangen, Germany) (http://adni.loni.usc.edu/methods/documents) in the ADNI study and acquired on 3T SIGNA PET/MR (GE Healthcare) and Tim Trio (Siemens Medical Solutions) in the SILCODE study. The mean interval between the baseline cognitive visit and related neuroimaging visit was 23 and 22 days for the SILCODE and the ADNI cohorts, respectively. Structural MR images were processed using SPM12 (http://www.fil.ion.ucl.ac.uk/spm/software/spm12). In the preprocessing, structural images were removed from the non-brain tissue; segmented into the gray matter (GM), the white matter (WM), and the CSF; and then modulated and normalized into the MNI template. A 6 mm full width at half maximum (FWHM) Gaussian isotropic kernel was used to spatially smooth the normalized images. The intracranial volume (ICV) was computed as the sum of the GM, the WM, and the CSF. The left and the right hippocampal were determined for subsequent analysis.

Biomarker Collection and Analyses of the Plasma and the CSF

In the SILCODE cohort, plasma samples were collected in polypropylene tubes with ethylenediaminetetraacetic acid (EDTA). Samples were centrifugated, aliquoted, and stored at −80°C. Plasma samples were measured using the kit: Aβ Peptide Panel 1 (4G8) Kit (Mesoscale Diagnostics, Rockville, Maryland, USA), and they were randomized and measured in duplicate with the same aliquot, blinded for clinical diagnosis. Levels of Aβ42 showed good average coefficients of variation of duplicate measurements (4.14% CV) and within the detection limit (2.5–1,271 pg/ml). In the ADNI, lumbar puncture was performed as previously described (http://www.adni-info.org/). Values of Aβ42 in samples of the CSF were generated by a novel, fully automated electrochemiluminescence immunoassay (Elecsys assay) (Bittner et al., 2016) and downloaded from the LONI site (provided in UPENNBIOMK9.csv and UPENNBIOMK10.csv files).

Gaussian Mixture Modeling

Since there is no accepted standard cut-point to determine amyloid status in relation to plasma Aβ, we calculated the cut-point to determine the amyloid status with the Gaussian mixture modeling in the SILCODE cohort. This approach was suitable since it is data-driven and does not assume similar distributions of levels of Aβ across cohorts (Mormino et al., 2014; Wang et al., 2016). First, 1–5 Gaussian distributions allowing for either equal or unequal variances were fit to the data, and the number of distributions that best described the data was determined by the Bayesian information criterion (BIC) (see **Supplementary Figure 1**). We found that the optimal model contained two Gaussian distributions that reflected abnormal vs. normal Aβ. Each individual was assigned a probability of belonging to either the abnormal or normal distribution. Considering the relatively high false positive rate of abnormal Aβ based on only CN population and plasma Aβ, CNs with >50% probability of belonging to abnormal Aβ distribution as well as smaller than 25% uncertainty corresponding to the classification were labeled Aβ+. Otherwise, they were labeled Aβ-. The final cut-points were 11.43 pg/ml in the SILCODE group. For the ADNI group, we used a pre-defined cut-point (980 pg/ml) to determine the amyloid status (Hansson et al., 2018).

Statistical Analyses

Statistical analyses were performed in the R version 3.6.2 (http://www.r-project.org/) and R-package "plspm" was used to construct the partial least squares (PLS) path models. Two multivariate PLS path models (**Figure 1**) were constructed to quantify the BR and CR and a second-order latent composite measure (GR) for each cohort. The PLS path model, which is for studying complex multivariate relationships among observed and latent variables, is the partial least squares approach to the structural equation modeling. It provides a framework for analyzing multiple relationships between a set of blocks of variables. A full path model comprises two submodels: an outer model that reflects the relationships between each latent variable and its block of indicators and an inner model that reflects the relationships between latent variables. In this study, for the outer model, memory, language, and executive domain residuals were indicators of the CR when left and right hippocampus volume residuals were indicators of the BR. For the inner model, the GR was derived from its latent variables (CR and BR). Specifically, we performed individual linear regression models between composite scores/hippocampal volumes and plasma/CSF Aβ levels and used the standardized residual as an indicator of CR/BR. For example, memory domain residuals to Aβ were calculated as residuals from a regression model with memory domain scores as the outcome and Aβ as the predictor, representing as one of the indicators of the CR.

To evaluate which factors contribute to resilience, we performed two sets of multivariable linear regression models. In the first set, multivariable linear regression models were performed with age, sex, educational levels, APOE-ε4 status, and the whole brain volume as independent variables and the respective metric of resilience as a dependent variable. In the second set, the cognitive scores and brain volumes for residuals calculation were also included as independent variables. Then,

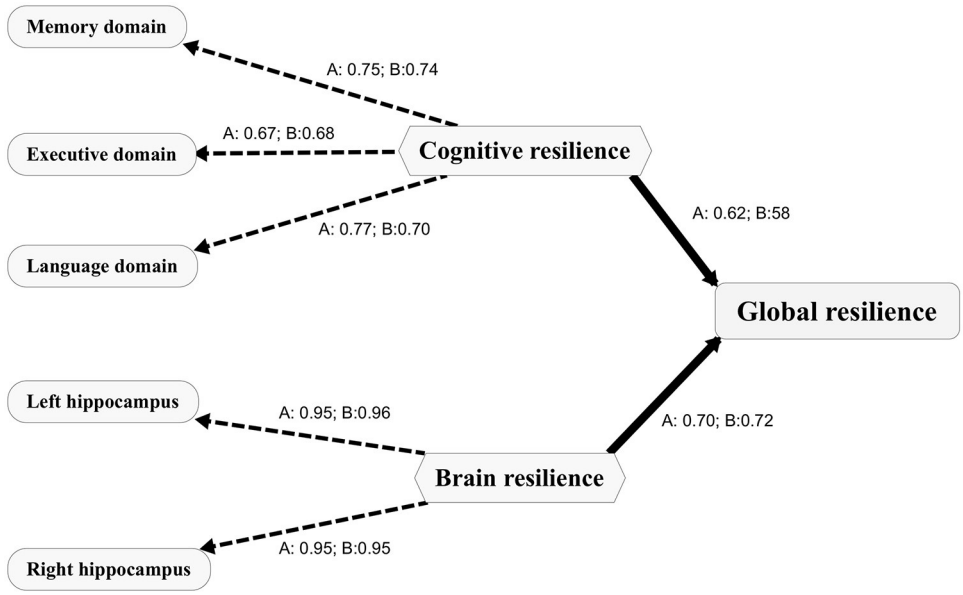

FIGURE 1 | Path diagram depicting the PLS models for both cohorts. The PLS path model includes the outer model and the inner model. The outer model includes indicators presented as capsules and the first order latent variables presented as hexagons. The inner model depicts the relationships between the first order latent variables (CR and BR) and the second order latent variable (GR). The loadings between a latent variable and its indicators are presented as numbers. A, the PLS model for the ADNI; B, the PLS model for the SILCODE. CR, cognitive resilience; BR, brain resilience; GR, global resilience. PLS, partial least squares; ADNI, Alzheimer's Disease Neuroimaging Initiative; SILCODE, Sino Longitudinal Study on Cognitive Decline.

linear mixed effect models were used for longitudinal cognitive analyses. The global cognition test (MoCA) was used as the outcome variable, and fixed effects included our interested effects (i.e., the effect of resilience of interest * time) as well as other effects that we wanted to test or control, including time (from the baseline), age, sex, education, and APOE-ε4 status. The random effect included the intercept of an individual. In addition to the original mixed effect models, we also performed another set of mixed effect models adjusting the effects of the original cognitive and brain variables used to derive resilience and included the time interactions with each of these variables. To further evaluate the utility of resilience in predicting the conversion from normal controls (NCs) to MCI, the Cox analysis for each metric of resilience was performed. For visualization purposes, we dichotomized the sample according to low vs. high resilience (CR, BR, or GR) using a median split. Using these dichotomized groups, we computed three 2-level variables (CR: CR+/CR–; BR: BR+/BR–; and GR: GR+/GR–) and Kaplan–Meier survival curves were created to show the conversion rate from the baseline with respect to resilience. Finally, for evaluating the added value of resilience for predicting the longitudinal cognitive decline, we used the Akaike information criterion (AIC) and the BIC to evaluate both the predictive models with conventional indicators (MoCA/MMSE and hippocampal volume/brain volume) and the predictive models with conventional indicators plus resilience. A lower AIC or BIC value indicates a better model. The level of significance was set at $p < 0.05$.

RESULTS

Characteristics of Participants

A total of 244 participants were included in the study. From the SILCODE group, 100 participants were included [59 (59%) female; mean (SD) age, 65.38 (4.66); mean (SD) MMSE score, 28.84 (1.13)]. From ADNI group, 144 participants were included [74 (51.4%) female; mean (SD) age, 74.68 (5.65); mean (SD) MMSE score, 29.08 (1.10)]. The characteristics and clinical details of the participants are presented in **Table 1**. The average age [65.38 (4.66) vs. 74.68 (5.65), $p < 0.001$] and educational level [12.6 (2.8) vs. 16.3 (2.6), $p < 0.001$] of participants in the SILCODE were significantly lower than those in the ADNI.

The PLS Path Model

The PLS path models for the SILCODE and the ADNI cohorts are presented in **Figure 1**. For evaluating the quality of the two models, we assessed three aspects of the measures of the model. Both models showed good one-dimensionality of the indicators (SILCODE: mean Cronbach's alpha = 0.67, mean Dillon–Goldstein's rho = 0.81, mean first eigenvalue = 1.79; ADNI: mean Cronbach's alpha = 0.69, mean Dillon–Goldstein's rho = 0.82, mean first eigenvalue = 1.80). Furthermore, the indicators were well-explained by its latent variable as average loading for the CR and the BR was 0.81 for the SILCODE cohort and 0.82 for the ADNI cohort. The degree to which a given construct was different from other constructs was good (all cross-loadings in two models <0.26). In sum, both models fit well and had a goodness-of-fit score of 0.73.

TABLE 1 | Characteristics of the participants of the study.

	SILCODE	ADNI	*P*
Sample size, *n*	100	144	
Age	65.38 (4.66)	74.68 (5.65)	<0.001
Female (%)	59 (59)	74 (51.4)	0.297
Education level	12.6 (2.8)	16.3 (2.6)	<0.001
MMSE	28.84 (1.13)	29.08 (1.1)	0.094
MoCA	25.73 (2.08)	25.63 (2.3)	0.752
AVLT-delay[a]	7.03 (1.85)	7.52 (3.83)	/
AVLT-recog[a]	22.46 (1.41)	12.72 (2.61)	/
AFT	19.13 (4.54)	20.88 (5.22)	0.007
BNT	24.96 (2.86)	28.03 (2.27)	<0.001
STT-A[b]	59.95 (17.48)	35.28 (13)	/
STT-B[b]	138.64 (35.73)	88.86 (44.31)	/
APOE-ε4 (%)	21 (21)	61 (42.4)	0.001
Aβ level[c]	8.9 (1.87)	808.18 (281.32)	/

MMSE, Mini–Mental State Examination; MoCA, Montreal Cognitive Assessment; AVLT-delay, auditory verbal learning test-delay recall; AVLT-recog, auditory verbal learning test-recognition; STTA, shape trail making test A; STTB, shape trail making test B; AFT, animal fluency test; BNT, Boston Naming Test; APOE, apolipoprotein E. Data are presented as mean (SD) unless otherwise indicated.

[a]AVLT in the Sino Longitudinal Study on Cognitive Decline (SILCODE) was HuaShan version and in the Alzheimer's Disease Neuroimaging Initiative (ADNI) was Rey AVLT version A/B.

[b]STT-A and STT-B in the SILCODE were Alternative Shape Trail Making Test A and B and in the ADNI were Shape Trail Making Test A and B.

[c]Source of amyloid-β (Aβ) in the SILCODE was the plasma and in the ADNI was the cerebrospinal fluid (CSF).

Factors Associated With Resilience

Multivariable models (**Table 2**) showed that factors contributing to different metrics of resilience were overall consistent in both cohorts. Younger age was associated with higher levels of all three metrics of resilience. Specifically, higher educational levels were related with greater CR and larger whole brain volume was related to greater BR and GR. After including the original cognitive and brain measures that resilience derived from **Supplementary Table 1** the young, women, and large brain volume were associated with the BR and the GR while the CR was only related to cognitive composite scores.

Longitudinal Cognitive Progress

Linear mixed models (**Table 3**) in two cohorts both showed that higher CR (SILCODE: $\beta = 1.064$, $p < 0.001$; ADNI: $\beta = 0.814$, $p = 0.002$) and higher GR (SILCODE: $\beta = 0.677$, $p < 0.001$; ADNI: $\beta = 0.661$, $p = 0.007$) were associated with better cognitive performances. We also identified a significant positive interaction between all metrics of resilience and time in the ADNI cohort and a similar trend in the SILCODE cohort, suggesting that participants with a higher level of resilience would perform better over time. After controlling the baseline cognitive performance and hippocampal volumes (**Supplementary Table 2**), associations between resilience and cognition were insignificant in the SILCODE cohort, whereas higher CR ($\beta = 0.977$, $p = 0.004$), BR ($\beta = 0.565$, $p < 0.001$), and GR ($\beta = 0.420$, $p = 0.036$) in the ADNI cohort continued to predict slower cognitive decline in the CNs. As the results of Cox regression models and survival curves showed (**Figures 2**, **3**), all three metrics of resilience were protective factors to clinical progression (all values of $p < 0.05$). Information criteria for prediction models with and without resilience were provided in **Table 4**. Compared with the predictive models with conventional variables (MMSE and brain volume), models with both conventional variables and resilience showed smaller AIC and BIC values (CR: $AIC\Delta = -4.64$, $BIC\Delta = -2.84$; BR: $AIC\Delta = -5.56$, $BIC\Delta = -3.76$; GR: $AIC\Delta = -12.15$, $BIC\Delta = -10.34$). Similar results were found in the comparison of the predictive models with another combination of conventional variables and the predictive models with conventional variables and resilience (**Supplementary Table 3**).

DISCUSSION

This study provides information about different phenotypes of resilience, their associations with demographic, genetic, and neuroimaging factors in a relatively large number of CNs. Two latent variable models to quantify the metrics of resilience related to Aβ in two cohorts were constructed. Results from this study suggested that younger individuals, women, and people with larger brain volumes were related to greater brain and GR when exposed to the Aβ burden. All three phenotypes of resilience based on the plasma and the CSF Aβ were observed to have a protective effect against cognitive decline in long-term follow-up. These metrics of resilience may capture additional information when the consequence of the clinical progression can be predicted than conventional cognitive and brain indicators.

Metrics of resilience were defined with the PLS model separately in each cohort and the loadings between cognitive indicators, brain indicators, and the respective resilience as well as the loadings between the BR, the CR, and the GR were calculated. The framework and goodness-of-fit in both models were similar and consistent with the previous work, indicating to a certain extent that the residualization approach was a feasible and reliable method of quantifying the metrics of resilience. Previous literature (Jagust, 2013; Scholl et al., 2016; Jack et al., 2019) had suggested that the brains were more vulnerable to various kinds of damages in aging and the prevalence of pathologic biomarkers in AD were found to be different in women and men with respect to age. Our results had confirmed the associations of these factors and resilience and indicated that age, sex, and brain volume were important for investigating the BR and the GR. In CN individuals, women, young individuals, or larger brain volume sustained better cognitive function and the preservation of the brain structure when exposed to pathological changes. Explanations could be the neural compensation mechanism, the protective effects of sex steroid hormones before menopause, the gene expression of heterochrony, and the threshold models of brain reserve (Satz, 1993; Berchtold et al., 2008; Pike et al., 2009). Intriguingly, women displayed both higher levels of pathologic biomarkers in AD and higher resilience (Jack et al., 2019), which seems to be congruent. However, the protective effect

TABLE 2 | Demographic, genetic, and neuroimaging factors associated with metrics of resilience to Aβ.

Variables	Cognitive resilience		Brain resilience		Global resilience	
	Standardized β	*P*	Standardized β	*P*	Standardized β	P
SILCODE						
Age	−0.207	0.027	−0.217	0.033	−0.277	0.005
Sex	−0.240	0.021	−0.090	0.416	−0.203	0.06
Educational levels	0.362	<0.001	−0.079	0.436	0.155	0.112
APOE-ε4	0.143	0.129	0.002	0.985	0.082	0.398
Whole brain volume	0.161	0.126	0.248	0.032	0.271	0.015
ADNI						
Age	−0.284	0.001	−0.332	<0.001	−0.409	<0.001
Sex	−0.093	0.322	−0.026	0.769	−0.075	0.372
Educational levels	0.166	0.047	−0.010	0.903	0.096	0.198
APOE-ε4	0.010	0.904	−0.012	0.872	−0.003	0.97
Whole brain volume	0.110	0.241	0.300	0.001	0.279	0.001

TABLE 3 | Results of the mixed effect models to predict global cognition in both cohorts.

Main effects	SILCODE			ADNI		
	β	*t*	*P*	β	*t*	*P*
CR	1.064	5.811	<0.001	0.814	3.171	0.002
CR * years	−0.058	−0.302	0.763	0.118	3.069	0.002
BR	0.163	0.838	0.403	0.035	0.137	0.891
BR * years	0.146	0.841	0.402	0.197	5.302	<0.001
GR	0.677	3.63	<0.001	0.661	2.706	0.007
GR * years	0.058	0.328	0.744	0.217	5.972	<0.001

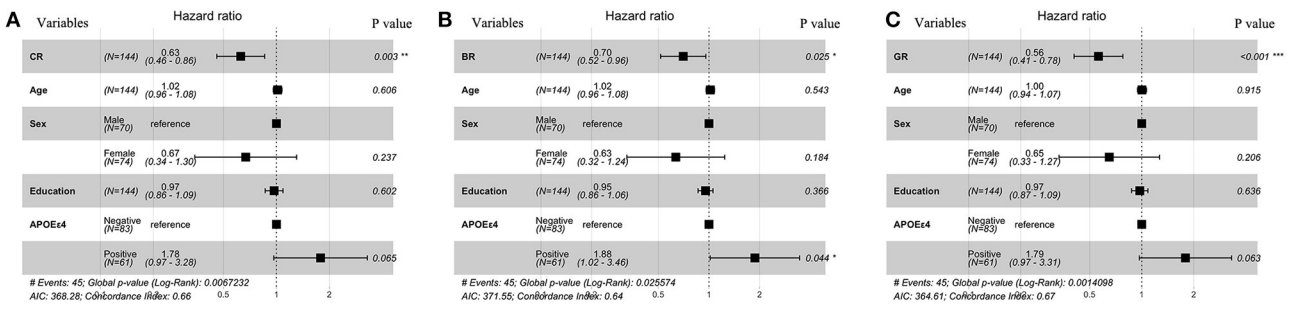

FIGURE 2 | Forest plots for metrics of resilience as predictive factors for clinical conversion. Resulting hazard ratios for models of cox regression classified by **(A)** CR, **(B)** BR, and **(C)** GR. All covariates were continuous except for sex and APOE status which were dichotomous. CR, cognitive resilience; BR, brain resilience; GR, global resilience.

of resilience may diminish with age and the accumulation of pathological changes. In post-menopausal women, the depletion of sexual hormones, the gene expression changes in specific brain regions (like superior frontal gyrus), and high Aβ burden accumulation would accelerate cognitive decline although they remain clinically normal (Yuan et al., 2012; Jack et al., 2017). Compared with factors associated with the BR and the GR, we found a specific association between educational levels and CR as CN individuals with higher education level could cope with more severe pathological burden (Kemppainen et al., 2008; Pettigrew et al., 2017; van Loenhoud et al., 2019). The explanation of how education enhanced the reserve capacity and slowed down cognitive decline in individuals with accumulated pathological deposits was still unclear and was even challenged since the paradoxical results of education on modifying longitudinal cognitive decline (van Loenhoud et al., 2019; Wilson et al., 2019) though it was generally accepted that higher educational levels before progressing into the cognitive impaired stage were

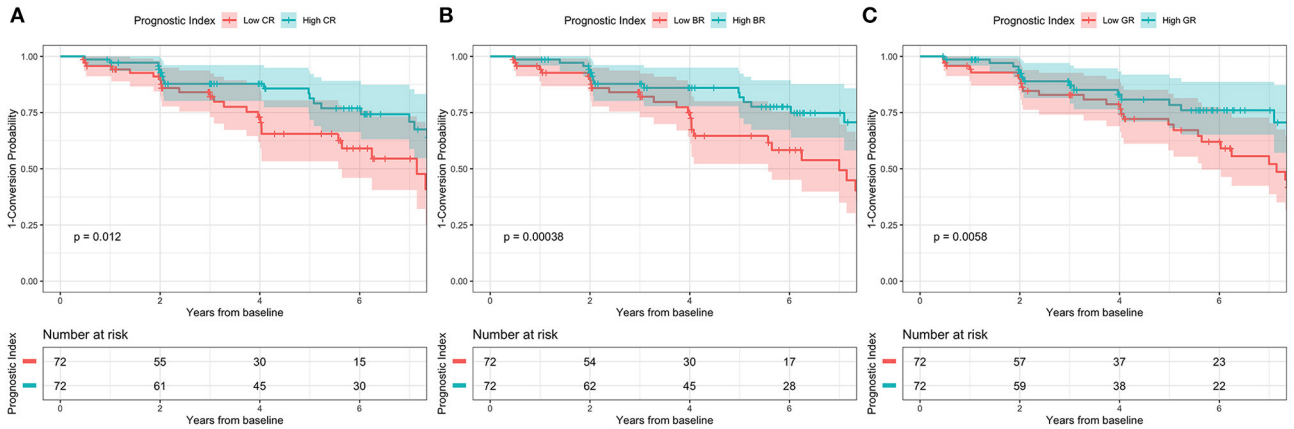

FIGURE 3 | Kaplan-Meier survival curve according to 2-level variable in the ADNI cohort. High conversion rate was associated with **(A)** low CR, **(B)** low BR, and **(C)** low GR. CR, cognitive resilience; BR, brain resilience; GR, global resilience.

TABLE 4 | Information criteria for prediction models with and without resilience.

Model	AIC	Δ	BIC	Δ
Cognitive predictor[a]				
Without cognitive resilience	374.86	–	383.89	–
With cognitive resilience	370.21	−4.64	381.05	−2.84
Brain predictor[b]				
Without brain resilience	372.97	–	382.01	–
With brain resilience	367.41	−5.56	378.25	−3.76
Combined[c]				
Without global resilience	373.15	–	383.99	–
With global resilience	361.00	−12.15	373.65	−10.34

AIC, Akaike information criterion; BIC, Bayesian information criterion. All models were corrected for age, sex, educational levels, and APOE-ε4 status.

[a] *This model included MMSE as the predictor.*

[b] *This model included brain volume as the predictor.*

[c] *This model included both MMSE and brain volume as the predictor.*

beneficial to our brains. However, after controlling the cognitive performance, the association between the CR and education levels disappeared, suggesting this relation was poor and more likely reflected the association between the baseline cognition and educational levels.

We found no association between the APOE genotype and the resilience at baseline in both cohorts. The dissociation of the APOE phenotype and the resilience could be caused by the dual effects on the brain of different APOE genotypes and the effect of the APOE on pathology was dominated in the later stage in AD. Consistent with this explanation, Wolk et al. (2010) reported APOE-ε4 carriers with AD displayed severe impairments in the memory domain rather than in execution and language domains. Another report (Pievani et al., 2009) found carriers were associated with greater temporal volume loss, and non-carriers were associated with greater frontoparietal volume loss.

Although previous studies exploring resilience have shown that higher resilience scores were associated with better cognitive performances and a smaller risk of the clinical progression, many of them defined the resilience based on educational levels, reading abilities, or lifestyle (Roe et al., 2008; Kaup et al., 2015; Vemuri et al., 2017). These metrics remained stable in the elderly and hardly reflected the current level of resilience of an individual. Therefore, they may fail to reflect the individual difference in cognitive or structural brain processes over time. However, several investigators have found residual approaches based on cognitive/brain predictors and biomarkers in AD to quantify that resilience could provide more information at the individual level over time and include information from various cognitive domains and biomarkers (Reed et al., 2010; Hohman et al., 2016). With this approach, we found that all types of resilience could predict longitudinal global cognitive changes, even adjusting for the baseline cognitive performance and hippocampal volumes and considering conventional predictors. This finding suggested that resilience was not only associated with demographic, genetic, cognitive, and imaging features but also provided added information about the prognosis.

The strength of our study lies in a relatively large sample of Aβ-positive CN individuals with demographic, genetic, neuroimaging, and biomarker data of AD, and a longitudinal design allowed us to inform the impact of different resilience to the clinical progression. Two cohorts provided the possibility of validating factors contributing to the different metrics of resilience and the effects of resilience on cognitive decline.

The present study has several limitations. The differences in characteristics of the participants and measurements across two cohorts led to only comparable cognitive tests with respect to the included three domains. This limitation was partly resolved by the combination of test scores and transformation. Another limitation was the different ranges of follow-up and different methods of accessing the amyloid in the two cohorts. The short follow-up period for the SILCODE cohort not only resulted in the absence of the Cox regression analysis for this cohort, as there were no sufficient clinical progression datapoints available for analysis but also may lead to the relatively poor predictive value of resilience compared to that in the ADNI cohort, though growing evidence has demonstrated that plasma Aβ concentrations are highly correlated with brain amyloidosis (Nakamura et al., 2018; Risacher et al., 2019). In addition, as the false positive rate for the classification of the Aβ status if only based on the CSF or the plasma was higher than those based on multiple methods or Aβ PET, we, therefore, adjusted the cut-point within the SILCODE by controlling the classification uncertainty of the Aβ abnormal below 25% and used a pre-defined cut-point in the ADNI that was determined to optimize the concordance with the Aβ PET visual read.

CONCLUSION

This study provides information about the associations between the resilience based on the plasma Aβ and the CSF Aβ and demographic, genetic, and neuroimaging factors in Aβ-positive CN individuals. We found that younger individuals, women, and people with larger brain volumes were associated with higher brain and GR. Metrics of resilience based on Aβ had a protective effect against the clinical progression and could provide additional information beyond the cognitive performance and imaging features in CN people.

DATA AVAILABILITY STATEMENT

The data of SILCODE used and/or analyzed during the current study are available from the corresponding author on reasonable request. The data of ADNI can be found at the the Alzheimer's Disease Neuroimaging Initiative website (adni.loni.usc.edu).

ETHICS STATEMENT

The studies involving human participants were reviewed and approved by XuanWu Hospital of Capital Medical University and the institutional review board at each center of ADNI. Informed written consent was obtained from all participants.

AUTHOR CONTRIBUTIONS

LL and YH contributed conception and design of the study. LL, YS, XiaonW, XiaoqW, and YH did the clinical assessments and data acquisition. LL, YS, XiaonW, and LS did the data analysis and interpretation. All authors contributed to manuscript revision, read and approved the submitted version.

FUNDING

This article was supported by the National Key Research and Development Program of China (2018YFC1312000) and the National Natural Science Foundation of China (61633018). Data collection and sharing for this project was funded by the Alzheimer's Disease Neuroimaging Initiative (ADNI) (National Institutes of Health Grant U01 AG024904) and the DOD ADNI (Department of Defense award number W81XWH-12-2-0012). This ADNI was funded by the National Institute on Aging and the National Institute of Biomedical Imaging and Bioengineering, and through generous contributions from the following: AbbVie, Alzheimer's Association; Alzheimer's Drug Discovery Foundation; Araclon Biotech; BioClinica, Inc.; Biogen; Bristol-Myers Squibb Company; CereSpir, Inc.; Cogstate; Eisai Inc.; Elan Pharmaceuticals, Inc.; Eli Lilly and Company; EuroImmun; F. Hoffmann-La Roche Ltd. and its affiliated company Genentech, Inc.; Fujirebio; GE Healthcare; IXICO Ltd.; Janssen Alzheimer Immunotherapy Research & Development, LLC.; Johnson & Johnson Pharmaceutical Research & Development LLC.; Lumosity; Lundbeck; Merck & Co., Inc.; Meso Scale Diagnostics, LLC.; NeuroRx Research; Neurotrack Technologies; Novartis Pharmaceuticals Corporation; Pfizer Inc.; Piramal Imaging; Servier; Takeda Pharmaceutical Company; and Transition Therapeutics. This Canadian Institutes of Health Research was providing funds to support the ADNI clinical sites in Canada. Private sector contributions are facilitated by the Foundation for the National Institutes of Health (www.fnih.org). This grantee organization was the Northern California Institute for Research and Education, and this study was coordinated by the Alzheimer's Therapeutic Research Institute at the University of Southern California. The ADNI data are disseminated by the Laboratory for Neuro Imaging at the University of Southern California.

ACKNOWLEDGMENTS

We thank all participants and members of the SILCODE study group for their cooperation during the data collection and management, and we thank the ADNI study group for their contribution to the field and for specific use of these data.

SUPPLEMENTARY MATERIAL

The Supplementary Material for this article can be found online at: https://www.frontiersin.org/articles/10.3389/fnagi.2021.610755/full#supplementary-material

REFERENCES

Arenaza-Urquijo, E. M., Bejanin, A., Gonneaud, J., Wirth, M., La Joie, R., Mutlu, J., et al. (2017). Association between educational attainment and amyloid deposition across the spectrum from normal cognition to dementia: neuroimaging evidence for protection and compensation. *Neurobiol. Aging* 59, 72–79. doi: 10.1016/j.neurobiolaging.2017.06.016

Arenaza-Urquijo, E. M., and Vemuri, P. (2018). Resistance vs resilience to Alzheimer disease: clarifying terminology for preclinical studies. *Neurology* 90, 695–703. doi: 10.1212/WNL.0000000000005303

Berchtold, N. C., Cribbs, D. H., Coleman, P. D., Rogers, J., Head, E., Kim, R., et al. (2008). Gene expression changes in the course of normal brain aging are sexually dimorphic. *Proc. Natl. Acad. Sci. U.S.A.* 105, 15605–15610. doi: 10.1073/pnas.0806883105

Bittner, T., Zetterberg, H., Teunissen, C. E., Ostlund, R. E. Jr., Militello, M., Andreasson, U., et al. (2016). Technical performance of a novel, fully automated electrochemiluminescence immunoassay for the quantitation of beta-amyloid (1-42) in human cerebrospinal fluid. *Alzheimers Dement.* 12, 517–526. doi: 10.1016/j.jalz.2015.09.009

Chatterjee, P., Elmi, M., Goozee, K., Shah, T., Sohrabi, H. R., Dias, C. B., et al. (2019). Ultrasensitive detection of plasma amyloid-beta as a biomarker for cognitively normal elderly individuals at risk of Alzheimer's disease. *J. Alzheimers. Dis.* 71, 775–783. doi: 10.3233/JAD-190533

Dubois, B., Epelbaum, S., Nyasse, F., Bakardjian, H., Gagliardi, G., Uspenskaya, O., et al. (2018). Cognitive and neuroimaging features and brain beta-amyloidosis in individuals at risk of Alzheimer's disease (INSIGHT-preAD): a longitudinal observational study. *Lancet Neurol.* 17, 335–346. doi: 10.1016/S1474-4422(18)30029-2

Ewers, M. (2020). Reserve in Alzheimer's disease: update on the concept, functional mechanisms and sex differences. *Curr. Opin. Psychiatry* 33, 178–184. doi: 10.1097/YCO.0000000000000574

Ghisays, V., Goradia, D. D., Protas, H., Bauer, R. J. III., Devadas, V., Tariot, P. N., et al. (2020). Brain imaging measurements of fibrillar amyloid-beta burden, paired helical filament tau burden, and atrophy in cognitively unimpaired persons with two, one, and no copies of the APOE epsilon4 allele. *Alzheimers Dement.* 16, 598–609. doi: 10.1016/j.jalz.2019.08.195

Hanon, O., Vidal, J. S., Lehmann, S., Bombois, S., Allinquant, B., Tréluyer, J. M., et al. (2018). Plasma amyloid levels within the Alzheimer's process and correlations with central biomarkers. *Alzheimers Dement.* 14, 858–868. doi: 10.1016/j.jalz.2018.01.004

Hansson, O., Seibyl, J., Stomrud, E., Zetterberg, H., Trojanowski, J. Q., Bittner, T., et al. (2018). CSF biomarkers of Alzheimer's disease concord with amyloid-beta PET and predict clinical progression: a study of fully automated immunoassays in BioFINDER and ADNI cohorts. *Alzheimers Dement.* 14, 1470–1481. doi: 10.1016/j.jalz.2018.01.010

Hohman, T. J., McLaren, D. G., Mormino, E. C., Gifford, K. A., Libon, D. J., Jefferson, A. L., et al. (2016). Asymptomatic Alzheimer disease: defining resilience. *Neurology* 87, 2443–2450. doi: 10.1212/WNL.0000000000003397

Jack, C. R. Jr., Bennett, D. A., Blennow, K., Carrillo, M. C., Dunn, B., Haeberlein, S. B., et al. (2018). NIA-AA research framework: toward a biological definition of Alzheimer's disease. *Alzheimers. Dement.* 14, 535–562. doi: 10.1016/j.jalz.2018.02.018

Jack, C. R. Jr., Therneau, T. M., Weigand, S. D., Wiste, H. J., Knopman, D. S., Vemuri, P., et al. (2019). Prevalence of biologically vs clinically defined alzheimer spectrum entities using the national institute on aging-Alzheimer's association research framework. *JAMA Neurol.* 76, 1174–1183. doi: 10.1001/jamaneurol.2019.1971

Jack, C. R. Jr., Wiste, H. J., Weigand, S. D., Therneau, T. M., Knopman, D. S., Lowe, V., et al. (2017). Age-specific and sex-specific prevalence of cerebral beta-amyloidosis, tauopathy, and neurodegeneration in cognitively unimpaired individuals aged 50-95 years: a cross-sectional study. *Lancet Neurol.* 16, 435–444. doi: 10.1016/S1474-4422(17)30077-7

Jagust, W. (2013). Vulnerable neural systems and the borderland of brain aging and neurodegeneration. *Neuron* 77, 219–234. doi: 10.1016/j.neuron.2013.01.002

Jessen, F., Spottke, A., Boecker, H., Brosseron, F., Buerger, K., Catak, C., et al. (2018). Design and first baseline data of the DZNE multicenter observational study on predementia Alzheimer's disease (DELCODE). *Alzheimers Res. Ther.* 10:15. doi: 10.1186/s13195-017-0314-2

Katzman, R., Terry, R., DeTeresa, R., Brown, T., Davies, P., Fuld, P., et al. (1988). Clinical, pathological, and neurochemical changes in dementia: a subgroup with preserved mental status and numerous neocortical plaques. *Ann. Neurol.* 23, 138–144. doi: 10.1002/ana.410230206

Kaup, A. R., Nettiksimmons, J., Harris, T. B., Sink, K. M., Satterfield, S., Metti, A. L., et al. (2015). Cognitive resilience to apolipoprotein E epsilon4: contributing factors in black and white older adults. *JAMA Neurol.* 72, 340–348. doi: 10.1001/jamaneurol.2014.3978

Kemppainen, N. M., Aalto, S., Karrasch, M., Nagren, K., Savisto, N., Oikonen, V., et al. (2008). Cognitive reserve hypothesis: Pittsburgh Compound B and fluorodeoxyglucose positron emission tomography in relation to education in mild Alzheimer's disease. *Ann. Neurol.* 63, 112–118. doi: 10.1002/ana.21212

Li, X., Wang, X., Su, L., Hu, X., and Han, Y. (2019). Sino Longitudinal Study on Cognitive Decline (SILCODE): protocol for a Chinese longitudinal observational study to develop risk prediction models of conversion to mild cognitive impairment in individuals with subjective cognitive decline. *BMJ Open* 9:e028188. doi: 10.1136/bmjopen-2018-028188

Lo, R. Y., Jagust, W. J., and Alzheimer's Disease Neuroimaging, I. (2013). Effect of cognitive reserve markers on Alzheimer pathologic progression. *Alzheimer Dis. Assoc. Disord.* 27, 343–350. doi: 10.1097/WAD.0b013e3182900b2b

McKhann, G. M., Knopman, D. S., Chertkow, H., Hyman, B. T., Jack, C. R. Jr., Kawas, C. H., et al. (2011). The diagnosis of dementia due to Alzheimer's disease: recommendations from the National Institute on Aging-Alzheimer's Association workgroups on diagnostic guidelines for Alzheimer's disease. *Alzheimers. Dement.* 7, 263–269. doi: 10.1016/j.jalz.2011.03.005

Mormino, E. C., Betensky, R. A., Hedden, T., Schultz, A. P., Ward, A., Huijbers, W., et al. (2014). Amyloid and APOE epsilon4 interact to influence short-term decline in preclinical Alzheimer disease. *Neurology* 82, 1760–1767. doi: 10.1212/WNL.0000000000000431

Nakamura, A., Kaneko, N., Villemagne, V. L., Kato, T., Doecke, J., Dore, V., et al. (2018). High performance plasma amyloid-beta biomarkers for Alzheimer's disease. *Nature* 554, 249–254. doi: 10.1038/nature25456

Ossenkoppele, R., Lyoo, C. H., Jester-Broms, J., Sudre, C. H., Cho, H., Ryu, Y. H., et al. (2020). Assessment of demographic, genetic, and imaging variables associated with brain resilience and cognitive resilience to pathological tau in patients with Alzheimer disease. *JAMA Neurol.* 77, 632–642. doi: 10.1001/jamaneurol.2019.5154

Pettigrew, C., Soldan, A., Zhu, Y., Wang, M. C., Brown, T., Miller, M., et al. (2017). Cognitive reserve and cortical thickness in preclinical Alzheimer's disease. *Brain Imaging Behav.* 11, 357–367. doi: 10.1007/s11682-016-9581-y

Pievani, M., Rasser, P. E., Galluzzi, S., Benussi, L., Ghidoni, R., Sabattoli, F., et al. (2009). Mapping the effect of APOE epsilon4 on gray matter loss in Alzheimer's disease *in vivo*. *Neuroimage* 45, 1090–1098. doi: 10.1016/j.neuroimage.2009.01.009

Pike, C. J., Carroll, J. C., Rosario, E. R., and Barron, A. M. (2009). Protective actions of sex steroid hormones in Alzheimer's disease. *Front. Neuroendocrinol.* 30, 239–258. doi: 10.1016/j.yfrne.2009.04.015

Reed, B. R., Mungas, D., Farias, S. T., Harvey, D., Beckett, L., Widaman, K., et al. (2010). Measuring cognitive reserve based on the decomposition of episodic memory variance. *Brain* 133(Pt 8), 2196–2209. doi: 10.1093/brain/awq154

Rentz, D. M., Mormino, E. C., Papp, K. V., Betensky, R. A., Sperling, R. A., and Johnson, K. A. (2017). Cognitive resilience in clinical and preclinical Alzheimer's disease: the Association of Amyloid and Tau Burden on cognitive performance. *Brain Imaging Behav.* 11, 383–390. doi: 10.1007/s11682-016-9640-4

Risacher, S. L., Fandos, N., Romero, J., Sherriff, I., Pesini, P., Saykin, A. J., et al. (2019). Plasma amyloid beta levels are associated with cerebral amyloid and tau deposition. *Alzheimers Dement.* 11, 510–519. doi: 10.1016/j.dadm.2019.05.007

Roe, C. M., Mintun, M. A., D'Angelo, G., Xiong, C., Grant, E. A., and Morris, J. C. (2008). Alzheimer disease and cognitive reserve: variation of education effect with carbon 11-labeled Pittsburgh Compound B uptake. *Arch. Neurol.* 65, 1467–1471. doi: 10.1001/archneur.65.11.1467

Satz, P. (1993). Brain reserve capacity on symptom onset after brain injury: a formulation and review of evidence for threshold theory. *Neuropsychology* 7, 273–295. doi: 10.1037/0894-4105.7.3.273

Schindler, S. E., Bollinger, J. G., Ovod, V., Mawuenyega, K. G., Li, Y., Gordon, B. A., et al. (2019). High-precision plasma beta-amyloid 42/40

predicts current and future brain amyloidosis. *Neurology* 93, e1647–e1659. doi: 10.1212/WNL.0000000000008081

Scholl, M., Lockhart, S. N., Schonhaut, D. R., O'Neil, J. P., Janabi, M., Ossenkoppele, R., et al. (2016). PET imaging of tau deposition in the aging human brain. *Neuron* 89, 971–982. doi: 10.1016/j.neuron.2016.01.028

Slot, R. E. R., Verfaillie, S. C. J., Overbeek, J. M., Timmers, T., Wesselman, L. M. P., Teunissen, C. E., et al. (2018). Subjective Cognitive Impairment Cohort (SCIENCe): study design and first results. *Alzheimers Res. Ther* 10:76. doi: 10.1186/s13195-018-0390-y

Stern, Y., Arenaza-Urquijo, E. M., Bartres-Faz, D., Belleville, S., Cantilon, M., Chetelat, G., et al. (2018). Whitepaper: defining and investigating cognitive reserve, brain reserve, and brain maintenance. *Alzheimers. Dement.* 16, 1305–1311. doi: 10.1016/j.jalz.2018.07.219

van Loenhoud, A. C., van der Flier, W. M., Wink, A. M., Dicks, E., Groot, C., Twisk, J., et al. (2019). Cognitive reserve and clinical progression in Alzheimer disease: a paradoxical relationship. *Neurology* 93, e334–e346. doi: 10.1212/WNL.0000000000007821

Vemuri, P., Knopman, D. S., Lesnick, T. G., Przybelski, S. A., Mielke, M. M., Graff-Radford, J., et al. (2017). Evaluation of amyloid protective factors and Alzheimer disease neurodegeneration protective factors in elderly individuals. *JAMA Neurol.* 74, 718–726. doi: 10.1001/jamaneurol.2017.0244

Vergallo, A., Megret, L., Lista, S., Cavedo, E., Zetterberg, H., Blennow, K., et al. (2019). Plasma amyloid beta 40/42 ratio predicts cerebral amyloidosis in cognitively normal individuals at risk for Alzheimer's disease. *Alzheimers Dement.* 15, 764–775. doi: 10.1016/j.jalz.2019.03.009

Wang, L., Benzinger, T. L., Su, Y., Christensen, J., Friedrichsen, K., Aldea, P., et al. (2016). Evaluation of tau imaging in staging Alzheimer disease and revealing interactions between beta-amyloid and tauopathy. *JAMA Neurol.* 73, 1070–1077. doi: 10.1001/jamaneurol.2016.2078

Weiner, M. W., and Veitch, D. P. (2015). Introduction to special issue: overview of Alzheimer's disease neuroimaging initiative. *Alzheimers Dement.* 11, 730–733. doi: 10.1016/j.jalz.2015.05.007

Wilson, R. S., Yu, L., Lamar, M., Schneider, J. A., Boyle, P. A., and Bennett, D. A. (2019). Education and cognitive reserve in old age. *Neurology* 92, e1041–e1050. doi: 10.1212/WNL.0000000000007036

Wolk, D. A., Dickerson, B. C., and Alzheimer's Disease Neuroimaging, I. (2010). Apolipoprotein E (APOE) genotype has dissociable effects on memory and attentional-executive network function in Alzheimer's disease. *Proc. Natl. Acad. Sci. U.S.A.* 107, 10256–10261. doi: 10.1073/pnas.1001412107

Yuan, Y., Chen, Y. P., Boyd-Kirkup, J., Khaitovich, P., and Somel, M. (2012). Accelerated aging-related transcriptome changes in the female prefrontal cortex. *Aging Cell* 11, 894–901. doi: 10.1111/j.1474-9726.2012.00859.x

Conflict of Interest: The authors declare that the research was conducted in the absence of any commercial or financial relationships that could be construed as a potential conflict of interest.

frontiers in Aging Neuroscience

REVIEW
published: 11 March 2021
doi: 10.3389/fnagi.2021.619543

Deep Brain Stimulation for Alzheimer's Disease: Stimulation Parameters and Potential Mechanisms of Action

Yinpei Luo[1], Yuwei Sun[1], Xuelong Tian[1,2], Xiaolin Zheng[1,2], Xing Wang[1,2], Weina Li[3], Xiaoying Wu[1,2], Bin Shu[4] and Wensheng Hou[1,2]*

[1] Key Laboratory of Biorheological Science and Technology of Ministry of Education, Chongqing University, Chongqing, China, [2] Chongqing Medical Electronics Engineering Technology Research Center, Chongqing University, Chongqing, China, [3] Department of Neurosurgery, Southwest Hospital, Third Military Medical University (Army Medical University), Chongqing, China, [4] Department of Rehabilitation Medicine, University-Town Hospital of Chongqing Medical University, Chongqing, China

Deep brain stimulation (DBS) is a neurosurgical technique that regulates neuron activity by using internal pulse generators to electrodes in specific target areas of the brain. As a blind treatment, DBS is widely used in the field of mental and neurological diseases, although its mechanism of action is still unclear. In the past 10 years, DBS has shown a certain positive effect in animal models and patients with Alzheimer's disease (AD), but there are also different results that may be related to the stimulation parameters of DBS. Based on this, determining the optimal stimulation parameters for DBS in AD and understanding its mechanism of action are essential to promote the clinical application of DBS in AD. This review aims to explore the therapeutic effect of DBS in AD, and to analyze its stimulation parameters and potential mechanism of action. The keywords "Deep brain stimulation" and "Alzheimer's Disease" were used for systematic searches in the literature databases of Web of Science and PubMed (from 1900 to September 29, 2020). All human clinical studies and animal studies were reported in English, including individual case studies and long-term follow-up studies, were included. These studies described the therapeutic effects of DBS in AD. The results included 16 human clinical studies and 14 animal studies, of which 28 studies clearly demonstrated the positive effect of DBS in AD. We analyzed the current stimulation parameters of DBS in AD from stimulation target, stimulation frequency, stimulation start time, stimulation duration, unilateral/bilateral treatment and current intensity, etc., and we also discussed its potential mechanism of action from multiple aspects, including regulating related neural networks, promoting nerve oscillation, reducing β-amyloid and tau levels, reducing neuroinflammation, regulating the cholinergic system, inducing the synthesis of nerve growth factor.

Keywords: deep brain stimulation, Alzheimer's disease, therapeutic effect, stimulation parameter, action mechanism

OPEN ACCESS

Edited by:
Kuangyu Shi,
University of Bern, Switzerland

Reviewed by:
Alan David Snow,
Cognitive Clarity Inc., United States
Quan-Hong Ma,
Soochow University, China

***Correspondence:**
Xiaoying Wu
wuxiaoying69@163.com

Received: *20 October 2020*
Accepted: *19 February 2021*
Published: *11 March 2021*

Citation:
Luo Y, Sun Y, Tian X, Zheng X, Wang X, Li W, Wu X, Shu B and Hou W (2021) Deep Brain Stimulation for Alzheimer's Disease: Stimulation Parameters and Potential Mechanisms of Action. Front. Aging Neurosci. 13:619543. doi: 10.3389/fnagi.2021.619543

INTRODUCTION

Alzheimer's disease (AD) is the most common type of dementia in the elderly. Its clinical manifestations are progressive cognitive decline and memory loss (Querfurth and LaFerla, 2010; Patterson, 2018). The prevalence and incidence of AD are increasing rapidly, and it is one of the major health crises facing the aging society of the 21st century (Alzheimer's Association, 2020). Clinically, only a small number of AD patients benefit from the temporary treatment effect of AD drugs. There are currently no viable medications to slow or reverse the progression of AD (Ihl et al., 2011; Arai et al., 2016, 2018; Cummings et al., 2020). The severity of AD and the limitations of drug therapy have spurred the development of research on non-drug therapies (Cummings et al., 2014; Aldehri et al., 2018). A series of physical therapy methods, including electrical stimulation and magnetic stimulation, are gradually being applied in the field of neurological diseases (Li et al., 2015; Temel and Jahanshahi, 2015; Zhou et al., 2018; Holczer et al., 2020).

Aldini first reported the use of electrical stimulation technology to improve the mood of melancholy patients in 1804, thus opening up a new field of electrical stimulation for the clinical treatment of mental illness (Aldini, 1804; Parent, 2004). Deep brain stimulation (DBS) is an invasive neuromodulation technique that involves brain stimulation and is one of the few neurosurgery methods that allows blinded research. The DBS device is mainly composed of stimulating electrodes in the brain, subcutaneous leads and pulse generators, and it directly changes brain activity in a controlled manner by using internal pulse generators to deliver electrical pulses to stimulation electrodes in specific target areas of the brain (Kringelbach et al., 2007; Lozano and Lipsman, 2013; Chen and Ponce, 2019). DBS is used for mental disorders, such as obsessive-compulsive disorder, epilepsy and depression (Zhou et al., 2018; Vazquez-Bourgon et al., 2019; Onate-Cadena et al., 2020), and for a variety of neurodegenerative diseases, such as idiopathic tremor, Parkinson's disease, and dystonia (Miocinovic et al., 2013; Chen and Ponce, 2019; Lee et al., 2019; McKinnon et al., 2019). Human clinical trials of DBS for AD began in 1984. Turnbull applied DBS to the left nucleus basalis of Meynert (NBM) in patients with a 4-years AD course but found no improvement in memory or cognition (Turnbull et al., 1985). Since then, research on treatment with DBS in AD has been vacant for more than two decades.

Research on the use of DBS in AD was restarted by a case study that used DBS to treat obese patients. The memory of a morbidly obese patient was enhanced after chronic hypothalamic/fornix DBS treatment. This enhancement may have occurred because DBS regulates marginal activity. That is, electrical activity in the medial temporal lobe is activated during DBS stimulation (Hamani et al., 2008). In the past 10 years, preliminary studies of DBS in AD have shown some positive effects of this treatment, including slowing cognitive decline and hippocampal atrophy and increasing cerebral glucose metabolism and brain connectivity in AD patients (Laxton et al., 2010; Sankar et al., 2015; Lozano et al., 2016; Aldehri et al., 2018), but there are also some controversial negative effects, such as AD patients <65 years of age have not shown good curative effects, and some patients have postoperative side effects (Lozano et al., 2016; McMullen et al., 2016; Leoutsakos et al., 2018). These discrepant results cannot be ignored. Differences in methodology, such as DBS parameters (stimulation target, frequency, stimulation start time, duration, unilateral/bilateral treatment, and stimulation current intensity), study design and sample size may explain these differences. The exact mechanism of action of DBS in AD is unknown. At present, there is little direct research on the mechanism of action of DBS in AD, and various hypotheses (changing the electrical activity of neurons, promoting neurogenesis and neurotransmitter release, etc.) have been proposed to explain its potential mechanism of action (Hescham et al., 2013a; Laxton and Lozano, 2013; Kuhn et al., 2015a; Aldehri et al., 2018; Jakobs et al., 2019; Yu et al., 2019).

There is increasing interest in exploring DBS as a treatment method for intervention in AD. A decision analysis model of DBS in AD patients shows that DBS is more effective and more cost-effective than standard treatment in the clinical treatment of AD (Mirsaeedi-Farahani et al., 2015). To effectively promote the application of DBS in the field of AD treatment, in this review, we systematically searched the literature published in the field of DBS in AD, and explored the effect of DBS stimulation parameters on the treatment effect for AD and the potential mechanism of action of DBS in the treatment of AD.

METHODS

Literature Search and Selection Criteria

In the literature databases of Web of Science and PubMed (from 1900 to September 29, 2020), human clinical studies and animal studies on DBS in AD were systematically searched using the following terms, individually and combined in multiple search strategies: "Deep brain stimulation," "DBS," "Alzheimer's disease," and "AD." Literature inclusion criteria: the main purpose was to study the therapeutic effects of DBS in AD, including human clinical research and animal research; the language of the article was English only; individual case studies and long-term follow-up studies were not excluded; and duplicate studies were excluded.

Data Abstraction

The selected articles were classified according to human clinical research and animal research to extract relevant data. The following data were extracted from human clinical studies: (1) study design; (2) basic information on the participants, including number, sex, average age, average Alzheimer's disease assessment scale-cognitive section (ADAS-Cog), average Mini-Mental State Examination (MMSE), and additional medications; (3) DBS data, including the DBS protocol and brain target; (4) follow-up; (5) main results, including the main outcome measures (average ADAS-Cog and average MMSE) and conclusion; and (6) adverse events. Various cognitive outcome measures have been used in human clinical studies, and some studies have evaluated multiple indicators. In this review, we chose the average ADAS-Cog and average MMSE as the main outcome measures. For studies that did not report averages and SDs, data were calculated from specific figures in the literature. The following data were extracted

from animal studies: (1) basic information on the animals, including number, sex, age, animal type, grouping; (2) DBS data, including DBS protocol and brain target; (3) behavioral methods; (4) follow-up; and (5) main conclusion.

RESULTS

Search Results

This review included 30 studies on the treatment of DBS in AD. As shown in **Figure 1**, research on DBS in AD treatment was lacking for ∼25 years after 1984 when DBS was applied in AD treatment. The time on the abscissa was the publication time of the article. It was not until 2010 that there was another paper on DBS in AD. During the 10-years period from 2010 to 2020, DBS in AD papers were published every year.

Human Clinical Studies

DBS Implementation

DBS is implemented in the human body and its components are surgically implanted. As mentioned earlier (Laxton et al., 2010; Mao et al., 2018), after local anesthesia is applied, the stereotaxic frame is installed on the patient's head. The position of the DBS target is ascertained by imaging. Subsequently, a drill is used to make bilateral holes in the skull, and the stimulation electrodes are implanted three-dimensionally. After the electrodes are placed, the internal pulse generator is implanted into the subclavian or subcutaneous area of the chest or abdomen under general anesthesia. The lead is implanted subcutaneously and connected to the stimulation electrodes and internal pulse generator through the head, neck, and chest. The positioning of the electrodes must be verified again by imaging after the operation.

Therapeutic Effects

Table 1 lists the detailed characteristics of 16 human clinical studies of DBS in AD patients. Turnbull et al. started the field of DBS in the treatment for AD in 1984 (Turnbull et al., 1985). A study by Laxton et al. (2010) showed that after DBS treatment, the memory of AD patients improved, the rate of cognitive decline decreased, and cerebral glucose metabolism increased (Laxton et al., 2010; Smith et al., 2012). Subsequently, human clinical studies of DBS in AD continued. Fontaine et al. reported that a patient with AD showed stable memory and increased metabolism in the medial temporal lobe after 1 year of DBS (Fontaine et al., 2013). Other studies have also shown that the nutritional status of AD patients remains stable, and the rate of hippocampal atrophy slows down after 1 year of DBS (Noreik et al., 2015; Sankar et al., 2015). Kuhn et al. applied DBS to 6 AD patients, and 1 year later, the ADAS-Cog scores of four participants increased or remained stable, but the scores of two participants deteriorated (Kuhn et al., 2015a). Kuhn et al. also performed DBS on two other AD patients who were 5 years younger. One AD patient had a stable ADAS-Cog score and an increase in MMSE score after 28 months. Another case showed overall improvement in the first year of treatment, but the ADAS-Cog score increased by seven points after 26 months (Kuhn et al., 2015b). The long-term follow-up results of all eight patients at 24 months showed that the ADAS-cog of young patients with mild AD remained relatively stable during the 24-months follow-up period, while the ADAS-cog of AD patients with high baseline increased (Hardenacke et al., 2016). In the two youngest patients among the eight, the repetitive inhibition of sensory gating improved (Durschmid et al., 2020). Therefore, they believed that DBS performed in the early and young ages of AD may have a beneficial effect on the progression of the disease

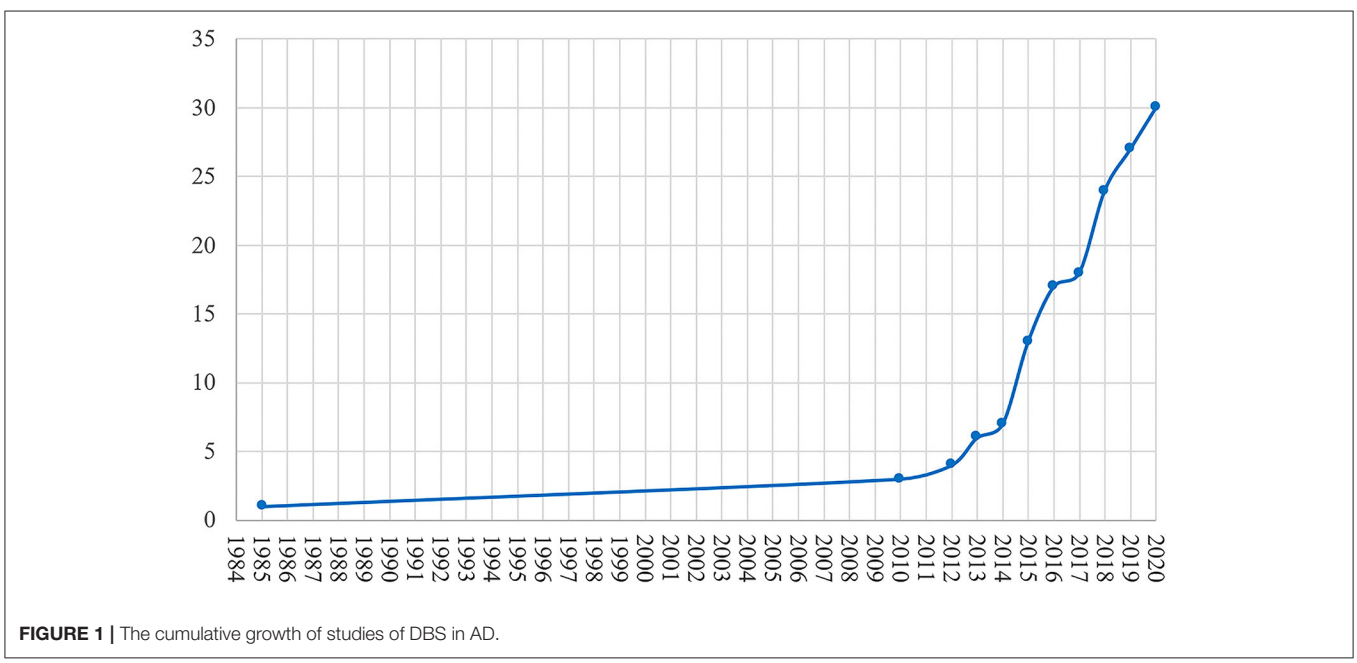

FIGURE 1 | The cumulative growth of studies of DBS in AD.

TABLE 1 | The human clinical study of DBS in AD.

Study (first author, year)	Study design	Baseline						DBS protocol	Brain target	Follow up	Main results		
											Main outcome measures		Conclusion
		N	Sex (male/female)	Average age (y)	Average ADAS-Cog	Average MMSE	Medication (add-on-therapy)				Average ADAS-Cog	Average MMSE	
Turnbull et al. (1985)	-	1	1	74	-	-	-	3 V, 50 Hz, 210 ms, on for 15 s and off for 12 min, 9 m	L-NBM	Followed DBS	-	-	There was no significant clinically effect.
Laxton et al. (2010)	-	6	4/2	60.7 ± 5.5	-	22.3 ± 4.1	Cholinesterase inhibitors (least 6 m)	3.0∼3.5 V, 130 Hz, 90 μs,12 m	B-fornix	1 m, 6 m, 12 m	-	-	DBS drove neural activity in the memory circuit, activated the brain's default mode network and could improve the cognitive ability of some patients with mild AD.
Smith et al. (2012)	-	5	4/1	62.6 ± 4.2	19.2 ± 7.2	22.2 ± 5.1	cholinesterase inhibitors (least 6 m)	3.0∼3.5 V, 130 Hz, 90 μs,12 m	B-fornix	1 m, 12 m	1 m, 21.6 ± 9.2; 12 m, 23.9 ± 13.7	-	DBS increased cerebral glucose metabolism of patients with mild, probable AD in 2 orthogonal networks.
Fontaine et al. (2013)	-	1	0/1	71	3m before DBS, 12.25; 7d before DBS, 9.	3m before DBS, 23; 7d before DBS, 29.	-	2.5V, 130Hz, 210 ms, 12 m	B-fornix	3 m, 6 m, 12 m	3 m, 9.41; 6 m, 10; 12 m, 9.91	3 m, 25; 6 m, 26; 12 m, 24	During 1 year of DBS, the memory scores of an AD patient remained stable, and its metabolism increased in the mesial temporal lobes.
Kuhn et al. (2015a)	double blind, crossover design	6	2/4	69.5 ± 7.7	20.2 ± 6.0	20.3 ± 2.5	Acetylcholinesterase medication	Randomized sham-controlled: −0, −8, +case, 20 Hz, 90 μs and 2.5 V, on for 2 w and off for 2 w; followed by continuous individualized stimulation: 2.0-4.5 V, 10-20 Hz and 90-150 μs	B-NBM	6 w, 12 w, 26 w, 52 w	6 w, 19.0 ± 10.0; 12 w, 20.0 ± 8.0; 26 w, 20.0 ± 9.0; 52 w, 23.2 ± 13.0	6 w, 19.3 ± 4.0; 12 w, 18.8 ± 3.1; 26 w, 19.2 ± 5.3; 52 w, 18.7 ± 6.7	ADAS-cog scores worsened by an average of three points after 1 year of stimulation, and the mean MMSE score remained almost stable. Bilateral low-frequency DBS of the NBM in AD patients is technically feasible and tolerable.
Kuhn et al. (2015b)	Double blind	2	-	64 ± 2.12	10 ± 0.71	22 ± 2.12	-	Continuous individualized stimulation: 20 Hz	B-NBM	12 m, 26 m	12 m, 7.5 ± 0.35; 24 m, 13.5 ± 1.77	12 m, 26 ± 1.41; 24 m, 22 ± 0.71	NBM DBS performed may have a favorable impact on disease progression at the early stage of AD.

(Continued)

TABLE 1 | Continued

Study (first author, year)	Study design	Baseline						DBS protocol	Brain target	Follow up	Main results		
											Main outcome measures		Conclusion
		N	Sex (male/female)	Average age (y)	Average ADAS-Cog	Average MMSE	Medication (add-on-therapy)				Average ADAS-Cog	Average MMSE	
Noreik et al. (2015)	Proof-of-concept	6	2/4	69.2 ± 7.5	-	-	-	2.0-4.5 V, 10-20 Hz and 90-150 μs, 2 w ON, 2 w OFF or vice versa, followed by continuous stimulation	B-NBM	1 year	-	increased by 3 points (min −9, max 19)	AD patients treated with NBM DBS demonstrated a mainly stable nutritional status within 1 year.
Sankar et al. (2015)	Controlled	31	DBS: 4/2 Control: 16/9	DBS: 60.7 ± 6.1; Sham, 63.9 ± 4.4	DBS, 19.1 ± 6.4; Sham, 18.7 ± 7.0	DBS, 22.3 ± 4.5; Sham, 23.6 ± 1.8	acetylcholinesterase medication (least 6 m)	3.0 V, 130 Hz, 90 μs, 12 m	B-fornix	1 year	DBS: 23.33 ± 12.3; Sham, 23.8 ± 10.6	DBS: 21.5 ± 6.2; Sham, 19.7 ± 4.8	The mean hippocampal atrophy of AD patients after DBS became slower.
Lozano et al. (2016)	Randomized double blind, controlled, multi-center	42	DBS,11/21 (≥65, 15); Sham, 12/21 (≥65, 15)	DBS, 68.5 ± 7.7; sham, 67.8 ± 8.1	DBS, 28.6 ± 3.9; sham, 27.1 ± 3.8	-	cholinesterase inhibitor (least 2 m)	3.0∼3.5 V, 130 Hz, 90 μs, 12 m	B-fornix	1 m, 6 m, 9 m, 12 m	1 m, DBS, 28.0 ± 7.7, sham, 28.9 ± 7.4; Difference of DBS and sham:<65, 12m, 10.3 ± 6.1; ≥65, 9 m, 4.5 ± 2.0, 12 m, 4.1 ± 2.6.	-	DBS may have a positive effect on AD patients ≥65 years old, but may have an adverse effect on patients under 65 years old.
Hardenacke et al. (2016)	-	8	-	-	-	-	-	-	B-NBM	12 m, 18 m, 24 m	-	-	NBM DBS performed may have a favorable impact on disease progression at the early stage of AD.
McMullen et al. (2016)	Double-blind, randomized	1	1	48	19	-	-	-	B-fornix	3 m	22	-	A patient with AD who experienced fornix DBS developed bilateral encephalomalacia.

(Continued)

TABLE 1 | Continued

Study (first author, year)	Study design	Baseline						DBS protocol	Brain target	Follow up	Main results		
											Main outcome measures		Conclusion
		N	Sex (male/female)	Average age (y)	Average ADAS-Cog	Average MMSE	Medication (add-on-therapy)				Average ADAS-Cog	Average MMSE	
Baldermann et al. (2018)	-	10	5/5	66.9 ± 4.3	9.3 ± 6.5	18.3 ± 3.8	-	2.0-4.2 V, 5-20 Hz, 60-150 μs	B-NBM	6 m, 12 m	6 m, 10.9 ± 8.1; 12 m, 11.6 ± 11.2	6 m, 17.9 ± 5.8; 12 m, 20.1 ± 6.6	AD patients with less advanced atrophy may profit from NBM DBS.
Scharre et al. (2018)	-	3	-	63 ± 5.31	30.33 ± 3.66	22.67 ± 0.72	-	continuous stimulation for at least 18 m.	B-VC/VS	27 m, 24m, 21 m	-	-	DBS of the VC/VS was well-tolerated and the extent of CDR-SB decline in AD patients with VC/VS DBS was reduced.
Leoutsakos et al. (2018)	Double blind, controlled	42	DBS,11/21 (≥65, 15); Sham, 12/21 (≥65, 15)	-	-	-	Cholinesterase inhibitor (least 2 m)	Sham, DBS in the second year.	B-fornix	3 m, 6 m, 9 m, 12 m, 18 m, 24 m	DBS, first year, 7.83 ± 1.86, the second year, 5.60 ± 1.85; sham, first year, 8.33 ± 1.82, the second year, 6.16 ± 1.97.	-	Fornix DBS was safe and may be beneficial for AD patients ≥65 years of age.
Mao et al. (2018)	-	5	2/3	59 ± 1.79	-	2.4 ± 1.15	Cholinesterase inhibitor, Chinese medication. (least 6 m)	130 Hz, 90 ms, 1–5 V	B-fornix	1.5 m, 3 m	-	3 ± 1.33	Fornix DBS could improve partial improvement in performance of patients with severe AD, including cognitive performance, mental state and social performance.
Durschmid et al. (2020)	-	2	-	62 ± 0.71	-	-	-	1 V, 20 Hz	B-NBM	-	-	-	NBM DBS has a positive impact on sensory gating into memory.

AD, Alzheimer's Disease; ADAS-Cog, Alzheimer's disease assessment scale-cognitive section; B, bilateral; CDR-SB, clinical dementia rating–sum of boxes; DBS, deep brain stimulation; L, left; m, mouth; min, minute; MMSE, mini-mental state examination; N, number; NBM, nucleus basalis of Meynert; Sham, sham stimulation; R-, right; VC/VS, ventral capsule/ventral striatum; w, week; y, year.

and cognitive function. Baldermann et al. also showed that AD patients with less atrophy can benefit from DBS (Baldermann et al., 2018). However, the study by Lozano et al. showed different results. Lozano et al. observed an increase in cerebral glucose metabolism in 21 AD patients after 1 year of DBS, considered DBS to be safe, and proposed that DBS may benefit AD patients aged 65 years and older, while those under 65 years old may show a worsening condition (Lozano et al., 2016). Leoutsakos et al. conducted a second-year follow-up of 42 participants in the study, confirming that DBS benefits older patients with AD (Leoutsakos et al., 2018). Furthermore, McMullen et al. reported that an AD patient implanted with bilateral fornix DBS experienced asymptomatic bilateral cerebral encephalomalacia (McMullen et al., 2016). Among the current existing studies, only two studies have shown no therapeutic effect of DBS in AD (Turnbull et al., 1985; McMullen et al., 2016), and there were a few AD patients with poor performance in other studies (Lozano et al., 2016; Leoutsakos et al., 2018; Mao et al., 2018). The small sample size (case report) (Turnbull et al., 1985; McMullen et al., 2016), side effects of DBS surgery (Ponce et al., 2016), and improper use of quetiapine by patients (Lozano et al., 2016; Leoutsakos et al., 2018; Mao et al., 2018) may account for these differences, but we cannot rule out the possibility that it is due to other methodological differences. However, among most AD patients receiving DBS, DBS is a promising intervention for AD.

Animal Studies

DBS Implementation

For DBS in AD animal models, the stimulating electrodes are implanted, and the stimulator is connected externally. A single study implanted the stimulators subcutaneously on the backs of mice (Huang et al., 2019). Each mouse is anesthetized and fixed on a stereotaxic device; the scalp is removed, exposing the skull. An electric drill is used gently drill small holes at the target points on the skull. Then, the stimulating electrode is implanted at the target position and fixed to the skull with adhesive material. In some studies, a small number of screws are implanted in the skull to fix the electrodes (Hescham et al., 2013b; Chen et al., 2014; Zhang et al., 2015; Tsai et al., 2020). X-ray imaging or tissue staining is used to ensure that the electrode is implanted in the target position (Lee et al., 2016; Mann et al., 2018; Huang et al., 2019).

Therapeutic Effects

In addition to human clinical research on DBS in AD, animal research on DBS in AD is also being carried out simultaneously. **Table 2** lists the detailed characteristics of 14 animal studies of DBS in AD animal models. Compared with human clinical studies, the behavioral, physiological and biochemical changes of AD model mice established by transgenic AD model or drug injection after DBS are mostly positive in the animal studies. This review later used these animal studies, combined with human clinical studies, to explore the effects of DBS stimulation parameters on the efficacy of AD treatment and the potential mechanism of action of DBS in AD.

Adverse Events

DBS is an invasive brain stimulation technique that carries the risk of major surgery (Doshi, 2011). The main surgical complications include bleeding, infection, and hardware failure (Ponce et al., 2016; Barrett, 2017). The adverse events related to DBS that occur in AD are manifested in human clinical studies which are rarely found in animal studies. **Table 3** lists the adverse events of the human clinical study of DBS in AD. At higher voltage intensity, AD patients felt inner restlessness, warmth, flushing, sweating, increased heart rate and blood pressure, and other adverse reactions. However, after reducing the voltage intensity, AD patients had almost no adverse effects (Laxton et al., 2010; Kuhn et al., 2015a). Other minor adverse reactions, including headache, diarrhea, vomiting, and paresthesias, were almost transient and had no sequelae (Laxton et al., 2010; Kuhn et al., 2015a; Leoutsakos et al., 2018; Scharre et al., 2018). Serious adverse events, including internal pulse generato infections, skin infections, inaccurate device location, hematoma, syncope, epilepsy, etc., could almost be resolved (Ponce et al., 2016). Leoutsakos et al. conducted the largest-scale study on the safety of DBS in AD patients, which involved 42 patients with AD (Lozano et al., 2016; Ponce et al., 2016; Leoutsakos et al., 2018). Within 90 days after receiving DBS surgery, 26 patients experienced 64 non-serious adverse events related to DBS surgery, of which 5 patients experienced 7 serious adverse events. For these 64 non-serious adverse events, 57 occurred within 30 days after surgery. In the second year after receiving DBS surgery, 24 patients reported 86 non-serious adverse events, and eight patients reported 15 serious adverse events. Two statistical results showed that the shorter the time after the completion of the operation is, the greater the possibility of reported adverse events in AD patients. The occurrence of adverse events gradually decreased over time, and there seemed to be no long-term complications. The safety of adverse events was as expected. However, the case report by McMullen et al. showed that DBS has brought long-term adverse effects (McMullen et al., 2016). This might be related to both the physical state of the patients and the experience of the surgeon. Although this was only a case study, researchers should pay attention to it. In general, AD patients tolerate DBS well under the appropriate DBS parameters, which proves that DBS is a relatively safe technique for AD patients.

DBS PARAMETERS

Stimulation Targets

To date, the stimulation targets for DBS in the treatment of AD patients in human clinical studies have involved the fornix, NBM, and ventral capsule/ventral striatum (VC/VS) (**Table 1**). Relevant animal research also involved multiple stimulation targets, including the intralaminar thalamic nucleus (ILN), midline thalamic nuclei (MTN), mammillothalamic tract (MT), anterior nucleus of thalamus (ANT), entorhinal cortex (EC), and CA1 (**Table 2**). The selection of these stimulation targets for DBS is mainly based on the neural network of the brain. Among them, VC/VS is related to the frontal lobe neural network (Price

TABLE 2 | The animal study of DBS in AD.

Study (first author, year)	Base					DBS protocol	Brain target	Behavior methods	Follow up	Main conclusion
	N	Sex (male/female)	Age	Animal	Group					
Arrieta-Cruz et al. (2010)	16–20	male	8 w	TgCRND8, WT (B6C3F1)	WT, AD-DBS	Eight trains of HFS; each train of 25 Hz, 1 s duration, 300 μA, 10 s inter-train interval, 3 d	B-MTN, [AP: −1.1, ML: 0.3, DV: 2.5–3.3]	NOR	After DBS	DBS could enhance short-term memory in the CA1 region of hippocampus in TgCRND8 mice.
Hescham et al. (2013b)	21	21/0	-	An injection of scopolamine to SD rats	AD ($n = 11$), AD-DBS ($n = 10$)	50 μA, 100 μA, 200 μA, 10 Hz, 100 Hz, 100 μs, 2 min/time	B-fornix, [AP −1.88, ML 1.3, DV 8.2]	NLR, OF	After DBS	Fornix DBS reversed the memory of rats received scopolamine and it was not sensitive to stimulation frequency, but rather to current levels.
Chen et al. (2014)	32	32/0	-	An injection of $Aß_{1-42}$ and $Aß_{1-40}$ to SD rats	SD-PBS ($n = 8$), AD ($n = 8$), AD-ANT ($n = 8$), AD-DBS ($n = 8$)	130 Hz, 60 μs, 1.5 V	B-ANT, [AP: −2.0, ML: ± 1.8, DV: −4.7]	MWM	After DBS	Bilateral ANT HFS could improve the performance of AD rats in MWM.
Zhang et al. (2015)	48	48/0	6 w	An injection of $Aß_{1-42}$ to SD rats	ANT DBS ($n = 8$), EC DBS ($n = 8$), fornix DBS ($n = 8$), ANT-sham ($n = 8$), EC-sham ($n = 8$), fornix-sham ($n = 8$)	500 μA, 130 Hz, 90 μs, 24 h	B-ANT, [AP: −1.6, ML: 1.5, DV: −5.2]; B-EC, [AP: −7.0, ML: 5.4, DV: −8.2]; B-fornix, [AP: −1.9, ML: 1.3, DV: −8.2]	MWM, NOR, OF	4 w after DBS.	EC and fornix DBS could enhance hippocampus-independent recognition memory, and facilitated hippocampus-dependent spatial memory more prominently than ANT DBS.
Hescham et al. (2015)	63	-	-	An injection of scopolamine to SD rats	Sham ($n = 11$), CA1 DBS ($n = 10$), MT DBS ($n = 13$), ANT DBS ($n = 14$), EC DBS ($n = 15$)	50 μA, 100 μA, 200 μA, 10 Hz, 100 Hz, 100 μs, 24 h	B-CA1, [AP: −3.6, ML: 1.8, DV: −2.6]; B-MT, [AP: −1.8, ML: 1, DV: −6.2]; B-ANT, [AP: −1.6, ML: 1.5, DV: −5.2]; B-EC, [AP: −6.7, ML: 4, DV: −8].	NLR, OF, EZM	After DBS	CA1, EC, and fornix DBS could able to restore spatial memory-related functions and CA1 DBS increased neural activity in the anterior cingulate gyrus.
Lee et al. (2016)	25	25/0	6 w	An injection of 192 IgG-saporin to SD rats	SD ($n = 6$), AD ($n = 7$), AD-NS ($n = 7$), AD-DBS ($n = 5$)	120 Hz, 90 μs, 1 V, 1 h/d, 7 d	R-NBM, [AP: −1.32, ML: +2.8, DV: −7.4]	MWM	After DBS	NBM DBS improved spatial memory performance of SD rats injected 192 IgG-saporin in the MWM.
Xia et al. (2017)	98	49/49	6 w, 6 m	TgCRND8, WT (C57BL/6NTac)	WT-NS ($n = 50$), AD-NS ($n = 19$), AD-DBS ($n = 29$)	130 Hz, 90 μs, 1 h, square wave	B-EC, [AP: −4.0, ML: ± 3.25, DV: −5.1]	Contextual fear testing; Tone fear testing; MWM	1, 3, and 6 w for behavior experiments after DBS.	EC DBS rescued subsequent deficits in context fear memory, reversed spatial learning deficits in Tg mice, and reduced plaque load in young mice. But EC DBS did not produce a detectable decrease in plaque load in either the dorsal hippocampus or cortex in old mice.

(Continued)

TABLE 2 | Continued

Study (first author, year)	Base					DBS protocol	Brain target	Behavior methods	Follow up	Main conclusion
	N	Sex (male/female)	Age	Animal	Group					
Akwa et al. (2018)	20	20/0	4 m	3×Tg, WT (C57BL/6/129SVJ)	WT-NS ($n = 5$), WT-DBS ($n = 5$), AD-NS ($n = 5$), AD-DBS ($n = 5$)	50 μA, 130 Hz, 90 μs, 7 h/d, weekends off, 25 d	B-EC, [AP: −4.0, ML: ± 3.0, DV: −5.1]	-	-	Chronic DBS in 3×Tg mice resulted in reduced levels of Tau oligomers, and increased levels of synaptophysin.
Mann et al. (2018)	38	38/0	4 m	3×Tg, WT (129SV/C57BL6)	WT-Cont ($n = 5$), AD-Cont ($n = 11$), AD-NS ($n = 10$), AD-DBS ($n = 12$)	50 μA, 130 Hz, 90 μs, 7 h/d, weekends off, 25 d	B-EC, [AP: −4.0, ML: 3.0, DV:5.1]	MWM, NLR, NOR	5 m for MWM, 6.5 m for NPR and NOR; 7 m for euthanize.	Chronic EC DBS improved both memory and AD specific pathological markers of AD mice.
Leplus et al. (2019)	22	-	18 m	TgF344-AD, WT F344	WT ($n = 6$), WT-DBS ($n = 6$), AD ($n = 4$), AD-DBS ($n = 6$)	130 Hz, 80 μs, 100 μA, unipolar, 42 d	B-fornix, [AP: −0.6, ML: ± 0.75, DV: −5.8]	-	After DBS	Chronic DBS decreased amyloidosis, inflammatory responses, and neuronal loss in both cortex and hippocampus in AD rats.
Huang et al. (2019)	192	192/0	4 m, 6 m, 9 m, 12 m	APP/PS1 (HuAPP695swe, PSEN1-dE9), WT (C57BL/6)	Frequencies: control, sham, 10 Hz, 50 Hz, 100 Hz,130 Hz; Starting times: control, sham, 4 m, 6 m, 9 m, 12 m; Durations: control, sham, 7, 14, 21, 28 days; APP/PS1: control, sham, DBS; WT: control, DBS; The optimized parameters of DBS: control, sham, DBS, U0126, DBS+U0126, LY294002, DBS+LY294002	10 Hz, 50 Hz, 100 Hz,130 Hz, biphasic stimulus pulse wave, 7, 14, 21, 28 days	L-NBM, [AP: −0.7; ML: 1.75; DV: 4.0]	MWM	After DBS or 30 d after DBS or mice at 13 m	NBM DBS starting from 4 months of age for 21 days at 100 Hz had therapeutic effects on APP/PS1 mice through activating phosphatidylinositol 3′-kinase (PI3K)/Akt pathway and inhibiting ERK1/2 pathway.

(Continued)

TABLE 2 | Continued

Study (first author, year)	Base					DBS protocol	Brain target	Behavior methods	Follow up	Main conclusion
	N	Sex (male/female)	Age	Animal	Group					
Gallino et al. (2019)	50	AD-DBS, 9/8; Sham-DBS, 8/9; AD, 8/8.	2 m	3×Tg	AD-DBS ($n = 17$), Sham-DBS ($n = 17$), AD ($n = 16$)	100 μA, 100 Hz, 100 μs, 1 h	B-fornix, [AP: 0; ML: 0.75; DV: 3.0]	MWM	MWM weekly and structural MRI in 3 d before and 3 d after DBS with a 6 w follow-up.	Acute DBS could improve learning and long-term memory of 3×Tg mice in a delayed, sex specific, and transient manner.
Koulousakis et al. (2020)	12	12	18 m	TgF344-AD	AD-DBS	200 μA, 100 μs, 60 Hz for intermittent DBS (duty cycle: 20 s ON and 40 s OFF. 20 Hz, 120 μs for continuous DBS.	B-NBM, [AP: −1.44; ML: ± 2.88; DV: 7.4]. Intermittent, unilaterally or bilaterally; continuous, bilaterally.	OF, NOR, MBM	Before and after DBS.	Bilateral intermittent NBM DBS allowed aged TgF344-AD rats to perform better and maintain their performance longer in a spatial memory task.
Tsai et al. (2020)	37	37/0	-	An injection of $A\beta_{1-42}$ and $A\beta_{1-40}$ Wistar rats	Cont ($n = 8$), AD ($n = 12$), AD-sham ($n = 8$), AD-DBS ($n = 9$)	0.5 mA, 60 μs, 100 Hz, 30 min	R-ILN, [AP: −2.8, ML: 1.25, DV: −5.5]	MWM	After DBS	A single rostral ILN DBS could rescue spatial learning and memory deficits, and significantly reversed PSD-95 expression reductions and preserved dendritic spine densities in the mPFC and hippocampal region of Aβ-infused rats.

Aβ, β-amyloid; AD, Alzheimer's Disease; ADAS-Cog, Alzheimer's disease assessment scale-cognitive section; ANT, anterior nucleus of thalamus; APP/PS1, amyloid-β precursor protein/presenilin1; B, bilateral; EC, entorhinal cortex; EZM, elevated zero maze; Cont, control; DBS, deep brain stimulation; DG, dentate gyrus; HFS, high frequency stimulation; ILN, intralaminar thalamic nucleus; L, left; m, mouth; MBM, modified barnes maze; min, Minute; mPFC, medial prefrontal cortex; MT, mammillothalamic tract; MTN, midline thalamic nuclei; MWM, morris water maze; N, number; NBM, nucleus basalis of Meynert; NOR, novel object recognition; NLR, novel location recognition; NS, non-stimulation; OF, open field test; SD, sprague dawley; Sham, sham stimulation; 3xTg, toronto triple transgenic; R, right; w, week; y, year; WT, wild type.

TABLE 3 | Adverse events of the human clinical study of DBS in AD.

Study (first author, year)	Adverse events
Turnbull et al. (1985)	Did not cause epilepsy or any other untoward reactions in a personal case.
Laxton et al. (2010)	When the voltage intensity of DBS was between 6 and 8 V, AD patients would experience adverse reactions, such as warmth, flushing, sweating, increased heart rate and blood pressure. When the stimulation intensity was reduced by 50%, there was almost no adverse effect.
Smith et al. (2012)	Not involved.
Fontaine et al. (2013)	An AD patient had no complications after DBS 1 year and was fully tolerant to stimulation, except a discrete increase of irritability.
Kuhn et al. (2015a)	The DBS device was malfunctioning; an AD patient felt inner restlessness at a stimulation intensity >5 V. There were no other adverse events.
Kuhn et al. (2015b)	Both patients were well-tolerated by DBS. There were no adverse events.
Noreik et al. (2015)	Not involved.
Sankar et al. (2015)	Not involved.
Lozano et al. (2016)	Three patients had 4 adverse events, including 1 internal pulse generato infection, 1 DBS positioning error, and 2 postoperative nausea (1 patient). No neurosurgical and cognitive adverse reactions.
Hardenacke et al. (2016)	Not involved.
McMullen et al. (2016)	At 3 months after surgery, the case patient was anxious and complained that "left side of brain is asleep," and cystic encephalomalacia appeared in the frontal lobe; at 1 year after surgery, minimal encephalomalacia appeared on the bilateral lead.
Baldermann et al. (2018)	Not involved.
Scharre et al. (2018)	Short-term side effects were resolved without sequela, including hot flashes, increased heart rate/palpitations, flushing, paresthesias, muscle twitching, non-specific discomfort, fatigue, and neuropsychiatric symptoms, mild pain at implantable pulse generator site, headache at incision site, transient visual neglect following surgery, diarrhea, vomiting, rash, rhinitis, arthralgia, fall, hematoma, and depression.
Leoutsakos et al. (2018)	Twenty-four patients experienced non-serious adverse events, common ones including neurological (including falls, headache, and muscle spasms), genitourinary (including urinary tract infections, urgency, and incontinence), and pulmonary (including upper respiratory infections and dyspnea). Seven patients had syncope and/or falls; two patients had altered mental status; two patients were involved in seizures or possible seizure; one patient was involved in agitation in a delayed; three patients were involved in a skin infection, suspected aortic valve endocarditis, and rigidity.
Mao et al. (2018)	No serious neurological adverse events occurred.
Durschmid et al. (2020)	Not involved.

AD, Alzheimer's Disease; DBS, deep brain stimulation.

and Drevets, 2010); ILN and MTN are important components forming cortico-thalamo-cortical pathways (Saalmann, 2014); NBM participates in the base forebrain cholinergic circuit; and the fornix, MT, ANT, EC, and CA1 (hippocampus) are nodes in the Papez circuit (Yu et al., 2019). **Figure 2** shows a schematic representation of these targets in the brain. AD is also considered to be a disease of the neural circuit, as neurons and neural circuits associated with cognitive function are damaged, and the Papez circuit is degraded (Lv et al., 2018). The Papez circuit is the main pathway of the limbic system and plays a vital role in the formation and storage of memory. Understanding the effects of these stimulation targets can help to select the best DBS stimulation target for AD.

VC/VS

DBS regulates the frontal lobe network of the brain that is involved in cognition and behavior. The ventral striatum, nucleus accumbens, and anterior limb of the internal capsule sit at the base of the frontal lobes. White matter fibers of the frontal lobe and the ventral capsule connect the dorsomedial and orbital prefrontal cortices to the ventral striatum (Price and Drevets, 2010). These neural networks have shown degeneration in AD (Lehericy et al., 1989). VC/VS DBS can affect related behavioral disorders in patients with mental disorders such as obsessive-compulsive disorder and depression (Greenberg et al., 2010; Dougherty et al., 2015). In a non-random phase I experiment, Scharre et al. first used the VC/VS of the frontal lobe network as the stimulation target for DBS in AD patients (Scharre et al., 2018). Fluorodeoxyglucose-positron emission tomography metabolism increased, and clinical dementia rating–sum of boxes (CDR-SB) performance decreased in AD patients receiving DBS. By targeting the VC/VS, DBS may adjust the frontal lobe network and affect the executive function of AD patients. This is the first report to show improved behavioral and executive defects without tracking memory targets in the treatment of AD by DBS. It provides new target options for DBS treatment in AD. This study also shows that chronic DBS with the VC/VS as a target is well-tolerated.

ILN

The rostral part of the ILN is connected to the medial prefrontal cortex (mPFC) and is considered to be a key component of cognitive function (Mair and Hembrook, 2008; Saalmann, 2014).

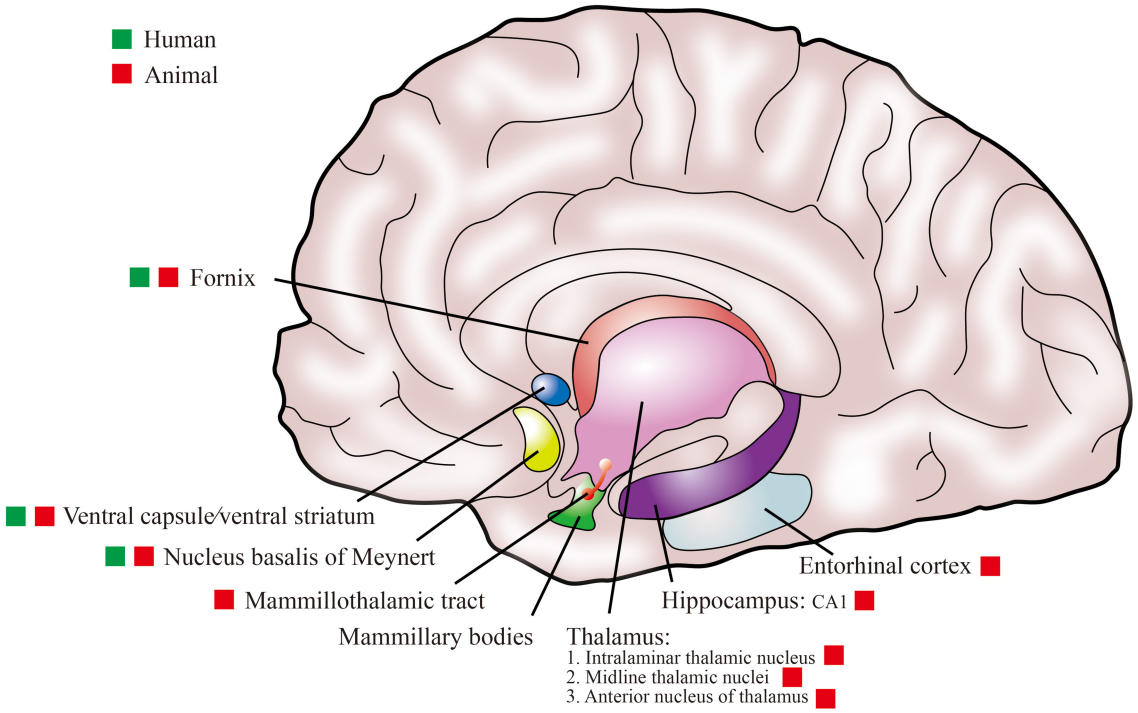

FIGURE 2 | The schematic diagram of the stimulation targets for DBS in AD.

Although the function of the ILN in cognitive function has been proven, the effect of ILN DBS on AD-related cognitive dysfunction has not been extensively studied. Only one related study has shown that unilateral ILN DBS treatment can improve spatial learning and memory deficits in AD rat models injected with β-amyloid (Aβ), reduce the expression of postsynaptic density protein 95 (PSD-95) in the mPFC and hippocampus, and maintain dendritic spine density (Tsai et al., 2020).

MTN

The MTN connects to the medial prefrontal cortex, medial temporal lobe and hippocampus. The midline structure of thalamus is involved in memory related functions (Saalmann, 2014). An study of high-frequency MTN DBS showed that the time that TgCRND8 mice explored new objects in the object recognition task was significantly longer than that of wild type mice, and the expression of FosB protein in the hippocampus was significantly upregulated (Arrieta-Cruz et al., 2010). There is currently no other research on MTN DBS in AD.

NBM

Acetylcholine (ACh) is essential for cognitive function and memory processing, and it is mainly derived from cholinergic neurons in the NBM (Carlsen et al., 1985). This region is mainly located below the anterior commissure and globus pallidus and on the anterior lateral part of the hypothalamus (Hedreen et al., 1984). The NBM sends a wide range of cholinergic nerve projections that dominate the cortex and hippocampus, and it represents an important cholinergic pathway in functional networks that subserve cognition and memory (Gratwicke et al., 2013). NBM damage can lead to a decrease in cholinergic transmission and degenerative changes in mossy fibers and the dentate gyrus of the hippocampus (Bartus et al., 1982; Amenta et al., 1991). The first evidence neural network dysfunction in AD is the loss of NBM cholinergic neurons in the brain, which is evident on postmortem examination (Whitehouse et al., 1981). Turnbull et al. reported for the first time the impact of NBM DBS on AD patients, although the report found no evidence of clinical improvement (Turnbull et al., 1985). Since then, chronic NBM DBS has shown good efficacy in AD. NBM DBS performed in early AD may have beneficial effects on AD progression and cognitive function (Kuhn et al., 2015b; Hardenacke et al., 2016). AD patients receiving NBM DBS showed a substantially stabilized nutritional status within 1 year (Noreik et al., 2015). NBM DBS can also improve the spatial learning and memory of AD model mice; regulate the gamma-aminobutyric acid (GABA), glutamate system, and cholinergic systems; reduce the abundance of amyloid protein; and exert neuroprotective effects (Lee et al., 2016; Huang et al., 2019; Koulousakis et al., 2020).

Fornix

As part of the Papez circuit, the fornix is the main inflow and outflow pathway of the hippocampus and middle temporal lobe. The fornix is an arcuate fiber bundle from the hippocampus to the mammillary body. This tract provides a direct source of input from the hippocampal structure to the anterior nucleus of the thalamus and can effectively encode and integrate memory information (Browning et al., 2010; Lovblad et al., 2014). When

the fornix of humans and animals is damaged, it can cause severe memory impairment (Tsivilis et al., 2008; Browning et al., 2010). Atrophy of the fornix can be accompanied by a transition from mild cognitive impairment to AD (Copenhaver et al., 2006). Hamani et al. reported for the first time that fornix stimulation can improve memory, although only one patient in their study received DBS to treat obesity (Hamani et al., 2008). Since then, DBS in the fornix has gradually been applied to AD. Chronic fornix DBS can stabilize or slow memory decline and increase hippocampal volume and cerebral metabolism in some patients with AD (Laxton et al., 2010; Smith et al., 2012; Fontaine et al., 2013; Sankar et al., 2015; Lozano et al., 2016) and improve spatial learning memory and recognition memory and reduce amyloidosis, the inflammatory response, the loss of neurons and the local changes in brain volume in AD model mice (Hescham et al., 2013b; Zhang et al., 2015; Gallino et al., 2019; Leplus et al., 2019). Therefore, the fornix is a good target choice for the treatment of DBS in human clinical research and animal research on AD (Senova et al., 2020).

MT

In the Papez circuit, information related to memory is transmitted to the mammillary body through the fornix, and then to the ANT through the MT. Although the MT participates in the Papez circuit, MT DBS did not cause memory changes in patients with refractory epilepsy (Duprez et al., 2005). No beneficial memory effect of MT DBS was found in SD rats injected scopolamine (Hescham et al., 2015). Therefore, it is worth exploring whether DBS in the MT has a positive effect.

ANT

The ANT is part of the Papez circuit, receiving information from the mammillary body via the MT and projecting it to the cingulate gyrus. The functional interaction between the ANT and hippocampus is crucial for spatial memory and conditional learning (Dumont et al., 2010). In AD model rats, ANT DBS improves impaired spatial memory (Chen et al., 2014). This is consistent with the research by Zhang et al., even though ANT DBS did not improve the recognition memory of AD model rats (Zhang et al., 2015). ANT DBS appears to be a potential treatment for AD cognitive dysfunction. However, Hescham et al. did not seem to find any beneficial memory effects of ANT DBS in SD rats injected scopolamine (Hescham et al., 2015). In addition, at high current densities, ANT DBS disrupts the acquisition of contextual fear conditions in healthy rats and impairs the performance of rats in spatially alternating tasks. In this case, ANT DBS caused a functional depolarization block near the stimulation electrode, which greatly reduced the spontaneous discharge of the local neuron population. Extracellular recordings showed that under high current ANT DBS, the discharge rate of DG cells was reduced and hippocampal activity was suppressed (Hamani et al., 2010). The differences in the results of various animal studies may have multiple causes, and further research is needed to explore the impact of ANT DBS in AD.

EC

The EC is located in the anterior part of the parahippocampal gyrus and is a key area for information transmission to and from the hippocampus, forming a three-synapse circuit with the hippocampus. At the same time, EC is the first area affected in AD and is closely related to memory formation (Braak and Braak, 1991; Khan et al., 2014). EC DBS can enhance the spatial memory of wild-type mice, and promote the rapid proliferation of neurons in the dentate gyrus (DG) (Stone et al., 2011). Acute EC DBS can improve memory deficits induced by scopolamine, and increase the expression of c-Fos in the CA3 region (Hescham et al., 2015). Research by Zhang et al. showed that chronic EC DBS contributes to spatial memory and recognition memory deficits induced by $A\beta_{40}$ (Zhang et al., 2015), which is consistent with research on AD transgenic mice (Xia et al., 2017; Mann et al., 2018). In addition, chronic EC DBS can significantly reduce Aβ and tau in the hippocampus of AD transgenic mouse models, as well as reduce total tau and phosphorylated tau in the cortical region (Mann et al., 2018). In another study, it was been demonstrated that EC DBS can increase synaptic activity by increasing synaptophysin levels, and promote low sedimentation clearance of tau through the lysosomal pathway, thereby exerting a beneficial effect on AD (Akwa et al., 2018).

CA1

The hippocampus is a brain area that is closely related to learning and memory functions, and is almost the central structure of memory-related circuits in the brain. The first region of the hippocampal circuit is the CA1, which mainly projects to the EC and subiculum and is very important for spatial memory (Igarashi et al., 2014). Acute CA1 DBS can improve memory deficits induced by scopolamine, and the beneficial effect of CA1 DBS is accompanied by increased expression of Fos in the cingulate gyrus (Hescham et al., 2015). No other studies related to DBS in AD have targeted the CA1 area to date.

Overall, the fornix, NBM, and EC are the preferred targets for DBS treatment in AD, even if there are other alternative targets. Currently, there are only two comparative studies of different stimulation targets for DBS in AD. Hescham et al. compared the effects of DBS in the ANT, CA1, MT, and EC in AD rat models induced by scopolamine (Hescham et al., 2015). CA1 DBS and EC DBS could improve memory deficits caused by scopolamine, and no beneficial memory effect was observed in the ANT or MT. A study had even shown that DBS in the hippocampus and entorhinal regions can impair memory (Jacobs et al., 2016). Zhang et al. investigated the effects of DBS in the ANT, EC, and fornix on the cognitive behavior of AD rat models (Zhang et al., 2015). DBS of these three targets can benefit the spatial memory of AD model rats. EC DBS and fornix DBS also improved the recognition and memory of AD model rats, but this effect was not observed in ANT DBS. In the Papez circuit, the EC and the fornix are directly connected to the hippocampus, while the ANT is connected to the fornix and the nipple body and indirectly connected to the hippocampus. This difference in neural connectivity may explain why the EC and fornix show more significant spatial and recognition memory improvements

than the ANT. The comparison of different targets of DBS in AD still needs more research.

Stimulation Frequency

To date, the application of DBS in AD has been carried out under fixed stimulation parameters with a single frequency setting of 20, 100, or 130 Hz. The selection of frequency parameters in AD is based on the application of DBS in other diseases. The stimulation frequency of DBS, it can be divided into high frequency electrical stimulation (HFS, 25∼1,000 Hz) and low frequency electrical stimulation (LFS, 0.1∼25 Hz) (Schiller and Bankirer, 2007). HFS is commonly used in the treatment of mental illness. For patients with Parkinson's disease, high-frequency stimulation is beneficial for dyskinesias, and low-frequency stimulation may improve some axial movement symptoms (Baizabal-Carvallo and Alonso-Juarez, 2016). However, stimulation at a frequency that is too high can cause functional lesions (Jakobs et al., 2019). Therefore, it is critical to optimize the stimulation frequency of DBS to minimize the side effects of electrical stimulation caused by the stimulation frequency. Huang et al. implemented four DBS frequencies of 10, 50, 100, and 130 Hz in the NBM of Aβ precursor protein/Presenilin1 (APP/PS1) mice and tested their spatial memory using the Morris water maze (MWM) (Huang et al., 2019). It was found that 10 Hz DBS had no effect. The latency during the learning period was significantly reduced by DBS at frequencies at 50, 100, and 130 Hz, and the number of passes and occupation time of the target quadrant and platform area in the exploration task increased significantly. Higher frequency (100 Hz, 130 Hz) stimulation was better than lower frequency (10 Hz, 50 Hz) stimulation, and a shorter latency, a larger number of times and a longer occupation time were observed at 100 Hz. Therefore, the optimal DBS frequency remains unclear. Some studies have shown that the efficacy of DBS in AD is not affected by frequency, as 10 Hz and 100 Hz show the same effect (Hescham et al., 2013b).

Stimulation Start Time

The stimulation start time of DBS in AD is also closely related to the effect of treatment. The time from pathological appearance to clinical symptoms of AD may be as long as 20 years or more (Bateman et al., 2012; Villemagne et al., 2013; Selkoe and Hardy, 2016). It is one of the new interests in the treatment of AD to take measures to intervene the development of AD before clinical symptoms appear, and to delay or even prevent brain lesions (Alzheimer's Association, 2018; Fan and Wang, 2020). Several studies have shown that DBS intervention in the early stages of AD produces better results. Huang et al. administered NBM DBS to APP/PS1 mice at 4, 6, 9, and 12 months of age and performed MWM tests at the end of 13 months of age (Huang et al., 2019). APP/PS1 mice at 4–6 months of age are in the early stages of AD. The results showed that the escape latency of AD mice receiving DBS at 4 and 6 months of age was significantly reduced, and the occupation time of the target quadrant and the number of passes through the platform area increased significantly. DBS at 4 months of age produced the best results. However, DBS had little effect at 9 and 12 months of age. EC DBS was performed in TgCRND8 mice at 6 weeks and 6 months of age, but a reduction in amyloid plaque was found only in mice at 6 weeks. In clinical studies, Hardenacke et al. evaluated the effects of DBS on 8 AD patients and proposed that NBM DBS in the early stage of the disease or at a younger age may have a beneficial effect on disease progression (Hardenacke et al., 2016). NBM DBS can increase blood flow by more than 50% in the cerebral cortex and nerve growth factor (NGF) expression in the parietal cortex by ∼68% in healthy rats at 4–6 months of age, but in aged rats at 29–31 months of age, blood flow increased by only ∼25%, with no significant change in NGF in the parietal cortex (Hotta et al., 2009). This again proves that providing DBS at a younger age has a more favorable impact. Unfortunately, in a phase II clinical study, it was suggested that fornix DBS may benefit patients with AD who are ≥65 years of age, and that patients under 65 years of age may show worsening condition (Lozano et al., 2016). This has an effect that is opposite to the impact of NBM DBS in interventions for young AD patients (Hardenacke et al., 2016). The reason for this difference may be that young patients are not in the early stages of AD, or fornix DBS alone may not be suitable for the early treatment of AD, or among other possible reasons.

Stimulation Duration

After DBS, AD patients' disease progression slowed significantly. This may be related to the stimulation duration of DBS, and the persistence of the effect is unclear. Animal research has shown that both acute and chronic DBS can cause long-term remodeling of the mouse brain. One hour of fornix DBS improved spatial memory deficits and caused local volume differences in various regions of the brain in AD mice. These changes can last at least 45 days, suggesting that the role of DBS in AD is more than immediate (Gallino et al., 2019). The improvement of spatial memory and recognition memory caused by DBS for 24 h in the AD rat model induced by $A\beta_{42}$ can last for at least 4 weeks (Zhang et al., 2015). Chronic DBS (7 h/d) was performed on Toronto triple-transgenic (3×Tg) AD model mice for 25 d, and the beneficial effects of DBS on recognition and memory in AD mice lasted at least 1 month. The after effects of DBS suggest that chronic DBS can also cause long-term changes in brain function (Mann et al., 2018). Huang et al. performed four durations of DBS (7, 14, 21, and 28 days for 1 h/days) in APP/PS1 mice at 4 months of age and performed the MWM and Aβ detection 30 d after the end of DBS (Huang et al., 2019). However, 7 d of DBS had almost no impact. DBS for 14, 21, and 28 days all improved the spatial memory of APP/PS1 mice and significantly reduced the soluble $A\beta_{40}$ and $A\beta_{42}$ levels in the hippocampus and cortex. DBS achieved the best results after 21 consecutive days of stimulation. This shows that the therapeutic effect of DBS is not directly proportional to the duration of treatment.

Unilateral/Bilateral Treatment

Of the human clinical studies and animal studies of DBS in AD, only 5 studies used unilateral DBS (Turnbull et al., 1985; Lee et al., 2016; Huang et al., 2019; Koulousakis et al., 2020; Tsai et al., 2020). Although researchers believe that bilateral DBS seems safe for AD, there have still been a small number of adverse events (Ponce et al., 2016; Leoutsakos et al., 2018). Preliminary

experiments by Huang et al. showed that bilateral DBS led to more severe complications and higher mortality (Huang et al., 2019). In fact, unilateral DBS can also improve the symptoms associated with AD and shows good neuroprotective effects and reversible side effects (Lee et al., 2016; Huang et al., 2019; Tsai et al., 2020). To improve the safety of DBS for AD, whether to switch to unilateral DBS in the future is worth exploring.

Current Intensity

The efficacy of DBS in AD is affected by current density. Decreasing DBS current intensities of 200, 100, and 50 μA were applied to rats receiving scopolamine to study the effects of higher, medium, and lower current densities. At low currents, there was no significant difference in the time ratio of discrimination between the displaced and familiar objects in rats receiving DBS compared with the control rats. However, the spatial memory of rats was substantially improved under DBS at 100 and 200 μA. Therefore, it was found that a lower current intensity had no effect on DBS in AD (Hescham et al., 2013b). However, there is no other study on the effect of DBS stimulation current intensity on AD.

POTENTIAL MECHANISMS OF ACTION

The mechanism of DBS in AD is unknown. This article will explore the potential mechanism of DBS in AD from several perspectives.

Regulation Related Neural Networks

Due to related molecular and structural abnormalities, the memory network of patients with AD changes (Sperling et al., 2010). There is evidence that the Papez circuit and the default mode network of AD patients are impaired and that the inherent connectivity in the default network is disrupted during resting states and cognitive tasks (Raichle et al., 2001; Greicius et al., 2004; Sperling et al., 2009). DBS has been shown to play a role in the regulation of neural networks in diseases. In patients with epilepsy, fornix DBS shows an electrical effect in the upstream hippocampus (Lozano and Lipsman, 2013; Miller et al., 2015). Hamani et al. used fornix DBS in obese patients, and electroencephalogram (EEG) showed that electrical activity in the hippocampus and parahippocampus was activated during stimulation (Hamani et al., 2008). Based on this, the Hamani team further used fornix DBS in AD, and the results showed that the neural network of the default pattern network and memory circuits in AD patients' brains were activated, including the entorhinal and hippocampal regions, and the connectivity between neural networks in the brain was also increased (Laxton et al., 2010). Functional connectivity analyses revealed that cerebral glucose metabolism in AD patients increased in a frontal-temporal-parietal-striatal-thalamic network and a frontal-temporal-parietal-occipital network after fornix DBS (Smith et al., 2012). The beneficial effects of NBM DBS in AD patients are significantly correlated with the fronto-parieto-temporal pattern of cortical thickness (Baldermann et al., 2018). **Figure 3** shows the modulated brain structure of AD patients after DBS in the current study. Therefore, DBS may establish upstream and downstream effects in related neural network circuits by targeting key nodes of the neural network in the AD brain, increasing connectivity between networks, and thereby improving AD symptoms.

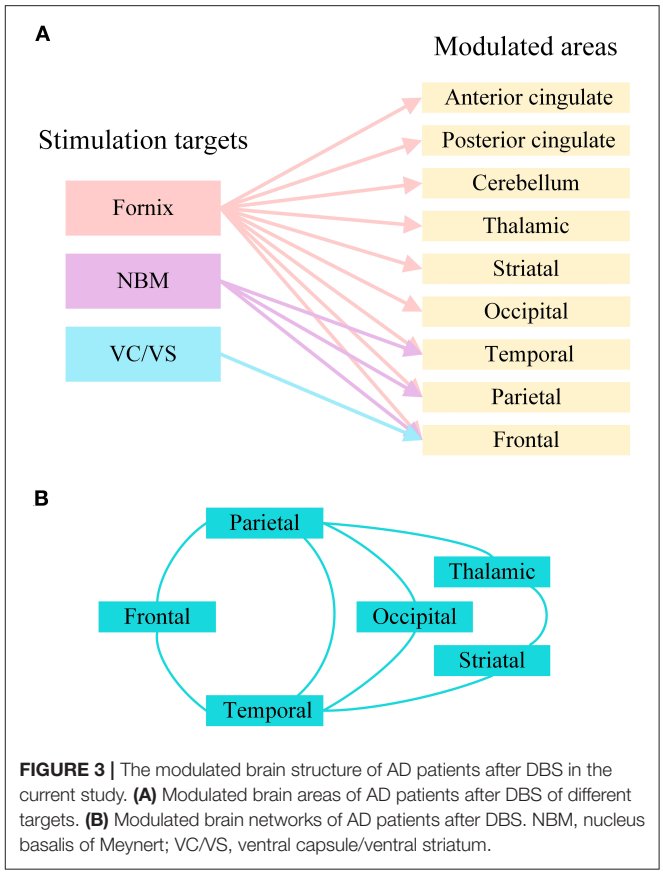

FIGURE 3 | The modulated brain structure of AD patients after DBS in the current study. **(A)** Modulated brain areas of AD patients after DBS of different targets. **(B)** Modulated brain networks of AD patients after DBS. NBM, nucleus basalis of Meynert; VC/VS, ventral capsule/ventral striatum.

Promotion of Nerve Oscillation

Neuronal oscillations are essential for information processing and communication between different brain structures. DBS has the potential to reset the unstable mode of neuron oscillations in AD, especially θ oscillations in the hippocampus (Hardenacke et al., 2013; Senova et al., 2018). With an approximately sinusoidal (4–10 Hz) EEG activity, θ oscillations can be recorded in edge circuits, are related to various cognitive processes, and play an important role in learning and memory (Buzsaki, 2002; Laxton et al., 2010). Various drugs that destroy cognitive functions reduce or eliminate hippocampal θ oscillations (McNaughton et al., 2007; Scott et al., 2012). The disruption of θ activity leads to impaired spatial and recognition memory, and the restoration of θ rhythm improves the learning ability of rats (Howlett et al., 2004; Hasselmo, 2006; Villette et al., 2010). Suthana et al. found that DBS caused the hippocampal θ rhythm to reset, optimally encode input information, and improve memory function in animal models (Suthana et al., 2012). In addition, electrical stimulation of perforated pathways in rodents can trigger θ phase reset, which creates favorable conditions for long-term memory enhancement (McCartney et al., 2004). Abnormalities

in θ rhythm have been shown in AD patients and mouse models of AD (Klimesch, 1999; Scott et al., 2012). Based on these studies, we hypothesized that DBS may improve AD symptoms through neural oscillations that cause θ reset.

Reduction of Aβ Levels

Aβ oligomers are one of the main neuropathological signs of AD. Aβ oligomers are highly neurotoxic, which may cause loss of synapses and neuronal damage (Hardy and Higgins, 1992; Perl, 2010), and affect circuit connectivity and network activities (Canter et al., 2016). Over the past decades, genetic, biochemical, and pathological evidence has revealed the importance of Aβ as a neuropathological marker of AD (Sperling et al., 2011; Barage and Sonawane, 2015). Acute DBS significantly reduced Aβ plaques in the hippocampus and cortex of 6-week-old TgCRND8 mice (Xia et al., 2017). Chronic DBS can also reduce Aβ and APP levels in 3xTg mice. The main source of Aβ production is the hydrolysis of APP. APP is hydrolyzed by β-secretase and γ-secretase to generate Aβ amyloid production pathways and non-amyloid production pathways are cleaved by α-secretase and γ-secretase (Barage and Sonawane, 2015; Chen et al., 2017; Kowalski and Mulak, 2019). Arrieta-Cruz et al. showed that high-frequency DBS can increase α-secretase activity in the hippocampus of TgCRND8 AD mice by a factor of two, which significantly increases synaptic plasticity in the CA1 region but does not change β-secretase activity (Arrieta-Cruz et al., 2010). In addition, Aβ can be cleared by internalization into glial cells (Kim et al., 2018), and DBS can regulate glial cell activity (Vedam-Mai et al., 2016; Xia et al., 2017). Therefore, DBS can reduce Aβ levels and improve the pathological state of AD, possibly by reducing Aβ production or increasing Aβ clearance.

Reduction of Tau Levels

Neurofibrillary tangles containing aggregates of hyperphosphorylated tau protein are also one of the neuropathological signs of AD. Tau with an abnormally high degree of phosphorylation forms toxic paired helical filaments, severely impairs synaptic function and causes cell death (Mohandas et al., 2009; Joel et al., 2015). Fornix DBS has no significant effect on hippocampal tau or phosphorylated tau in Wistar rats. However, EC DBS can reduce the total tau and Ser416-phosphorylated tau in the cortex and hippocampus of 3×Tg AD mice and increase neurogenesis in the dentate gyrus (Mann et al., 2018). A study by Akwa et al. also showed that EC DBS can reduce tau phosphorylation and accumulation of tau oligomers in the CA1 region of 3xTg AD mice, and increase tau autophagy-lysosomal degradation and synaptic protein expression (Akwa et al., 2018). Therefore, DBS may affect the degradation or clearance of tau in AD to reduce tau levels. However, the specific details are not yet clear.

Reduction of Neuroinflammation

It has been recognized that neuroinflammation plays an important role in the development and progression of AD (Von Bernhardi, 2007; Le Page et al., 2017). The development of AD is closely related to the complex cascade that leads to the death of neurons. Normally functioning glial cells can express Aβ-related degradation enzymes or bind related proteins to promote the degradation and clearance of Aβ (Mulder et al., 2012; Yali et al., 2014; Kim et al., 2018). With the development of AD, glial cell malfunction can release excessive inflammatory factors and neurotoxic factors to produce neurotoxic effects, promote the cascade of Aβ and inflammation, and aggravate neuronal death and the progression of AD (Bagyinszky et al., 2017). In AD, astrocytes and microglia, the two main groups of cells driving neuroinflammation, exhibit high levels of abnormal activation (Cohen et al., 2013; Lopategui Cabezas et al., 2014). Chronic fornix DBS can reduce the degree of astrocytic and microglial reactivity and the extent of neuron loss in the cortex and hippocampus (Leplus et al., 2019). DBS activates astrocytes and microglia in the early stage after implantation; the degree of glial reactivity later decreases (Song et al., 2013). Whether DBS promotes the degradation and clearance of Aβ by activating additional protective glial cells, thereby reducing neurotoxicity and cascade reactions and ultimately downregulating glial cell levels and reducing neuroinflammation, is worth exploring.

Regulation the Cholinergic System

Degeneration of the cholinergic circuit is a pathological manifestation of AD. AD patients and animal models have obvious cholinergic dysfunction involving abnormal ACh production and degradation, including choline acetyltransferase (ChAT) and acetylcholinesterase (AChE), respectively (Davies and Maloney, 1976; Perry et al., 1977; Schliebs and Arendt, 2011). Acetylcholinesterase inhibitors (donepezil, rivastigmine, galantamine) are approved by the U.S. Food and Drug Administration for the treatment of AD patients (Unzeta et al., 2016; Kaushik et al., 2018; Alzheimer's Association, 2020). High levels of ACh contribute to hippocampal θ oscillation and enhance memory (Verdier and Dykes, 2001; Micheau and Marighetto, 2011). Supplementation of exogenous ChAT can improve memory and cognitive dysfunction in AD model mice (Fu et al., 2004; Zhu et al., 2020). Studies have shown that DBS improves scopolamine-induced learning and memory deficits in rats (Hescham et al., 2013b, 2015). Scopolamine is a muscarinic acetylcholine receptor antagonist. In APP/PS1 mice, DBS reduced the level of AChE in the hippocampus and cortex while increasing the level of ChAT, which implies an increase in ACh (Huang et al., 2019). In rats with amygdala injury, DBS treatment can effectively compensate for amygdala injury and reduce the activity of AChE (Kadar et al., 2014). Therefore, DBS can regulate the cholinergic system, which may be one of the mechanisms by which DBS improves AD. However, a large-scale study on long-term use of donepezil hydrochloride in patients with AD showed that the donepezil hydrochloride cannot help AD patients after the first 6 months. Acetylcholinesterase inhibitors are not long-term effective in the treatment of AD (Arai et al., 2016, 2018). This prompts us to consider whether DBS improves AD directly or indirectly by regulating the cholinergic system, whether this regulatory improvement is long-term effective, and how long this improvement will last. At present, there is no relevant research to solve these problems. There are still many questions to be explored about the regulation of DBS on the cholinergic system in AD.

Induction of NGF Synthesis

DBS may exert neuroprotective effects by inducing NGF synthesis in AD (Mashayekhi and Salehin, 2006; Hardenacke et al., 2013). NGF is the most typical neurotrophic peptide involved in regulating the survival and differentiation of neurons (Lindsay and Harmar, 1989; Sofroniew et al., 2001). NGF levels and metabolic pathways are clearly imbalanced in AD (Cuello et al., 2010). The decrease in NGF supply at the age-related basal forebrain cholinergic neuron cell level is similar to that observed in AD (Salehi et al., 2004). NGF gene therapy caused classic trophic responses in the brains of AD patients, including neuronal hypertrophy, axonal sprouting and activation of cell signaling (Tuszynski et al., 2015). The supply of NGF can provide long-term cholinergic nutritional support, thereby slowing or preventing cognitive decline in AD patients (Hardenacke et al., 2013). Studies have shown that unilateral NBM DBS can result in significantly higher NGF levels in healthy rats than observed before stimulation. Mecamylamine, the nicotinic blocker, can completely eliminate the secretion of NGF, which suggests that the projection of the basal forebrain may be the reason for the increase of NGF (Hotta et al., 2009). In AD disease, the ability of DBS to induce the release of NGF may be a pathway closely related to its mechanism, which also seems to be related to the cholinergic system of the basal forebrain.

Other Potential Mechanisms

The mechanism of DBS in AD may also involve a variety of other factors. In addition to the mechanisms described above, DBS may also improve AD symptoms by regulating other neurotransmitter systems. GABA and glutamic acid are closely involved in memory function (Sivilotti and Nistri, 1991). In AD rat models, glutamate acid decarboxylase 65 and 67 and glutamate transporter levels changed after NBM DBS. This suggests that NBM DBS may regulate changes in the GABA and glutamate systems and improve memory in AD rat models (Lee et al., 2016). It is also possible that DBS can enhance synaptic plasticity, promote neuron formation, and improve memory by regulating brain-derived nerve factors, including brain-derived neurotrophic factor and vascular endothelial growth factor (Gondard et al., 2015). It has been reported that DBS can increase hippocampal neurogenesis in AD (Mann et al., 2018; McKinnon et al., 2019). The newly born neurons have normal morphology and function and can promote the normalization of functional circuits (Lledo et al., 2006). DBS may improve AD symptoms by promoting neuron regeneration. **Figure 4** shows the protein changes and potential protective mechanisms in AD animal models after DBS of different targets in the current study. The impact of DBS on AD animal models involves multiple potential protective mechanisms including signaling pathways,

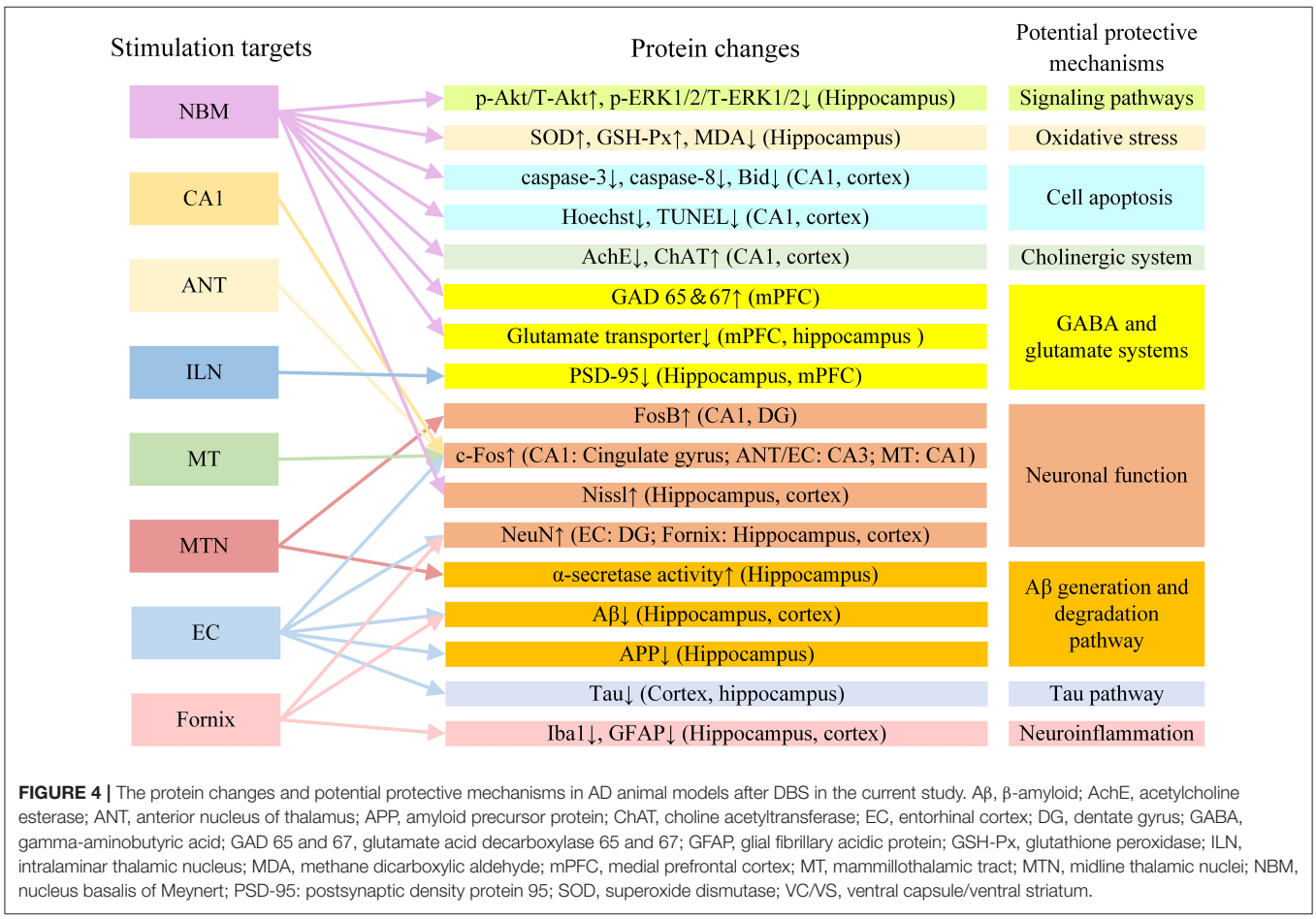

FIGURE 4 | The protein changes and potential protective mechanisms in AD animal models after DBS in the current study. Aβ, β-amyloid; AchE, acetylcholine esterase; ANT, anterior nucleus of thalamus; APP, amyloid precursor protein; ChAT, choline acetyltransferase; EC, entorhinal cortex; DG, dentate gyrus; GABA, gamma-aminobutyric acid; GAD 65 and 67, glutamate acid decarboxylase 65 and 67; GFAP, glial fibrillary acidic protein; GSH-Px, glutathione peroxidase; ILN, intralaminar thalamic nucleus; MDA, methane dicarboxylic aldehyde; mPFC, medial prefrontal cortex; MT, mammillothalamic tract; MTN, midline thalamic nuclei; NBM, nucleus basalis of Meynert; PSD-95: postsynaptic density protein 95; SOD, superoxide dismutase; VC/VS, ventral capsule/ventral striatum.

oxidative stress, cell apoptosis, the GABA and glutamate systems and neuronal function. More research is still needed to explore these possibilities.

DISCUSSION

This article reviews the published literature on DBS in AD. In patients and animal models with AD, DBS has shown some efficacy.

To provide the best parameter as a reference for the application of DBS in AD, this review summarizes and analyzes the different treatment parameters from current human clinical studies and animal studies of DBS in AD. Concerning stimulation targets, the NBM, fornix, and EC are the preferred targets for DBS treatment. This may be related to their structures and roles in the brain. They are involved in different circuit systems, including the base forebrain cholinergic system, the Papez circuit, and the trisynaptic circuit (Lv et al., 2018; Yu et al., 2019). There is currently no human clinical study of the EC as a target of stimulation in AD, and only animal studies support the EC as a target of DBS. The first area where neuropathy occurs in the AD brain is the EC, which then spreads to other cortexes and the hippocampus (Braak and Braak, 1991). The EC plays a very important role in information transmission. Whether EC DBS has a better effect than NBM and fornix DBS in AD is worthy of further investigation in animals and humans. In addition, EC DBS has been reported to improve spatial memory in patients with epilepsy by resetting the θ rhythm on EEG (Suthana et al., 2012).

Other DBS parameters that are commonly used in AD patient studies include stimulation frequency (130/20 Hz), stimulation duration (long-term), bilateral stimulation, pulse width (90–150 μs), and stimulation voltage (3.0–3.5 V) (**Table 1**); in AD animals the investigated parameters are stimulation frequency (130/100 Hz), stimulation duration (30 min-1 h, 3–42 days), bilateral stimulation, pulse width (60–100 μs), and stimulation current (100 μA) (**Table 2**). Based on the characteristics of human and animal tissues, although these DBS parameters used in AD animals cannot be directly applied for DBS in AD patients, they can provide more supporting evidence for the study of DBS in AD patients. Unilateral DBS should be popular in the treatment of DBS. After all, unilateral DBS is very likely to cause less surgical injury. Based on the long early incubation period of AD and the irreversible characteristics of neurodegenerative diseases (Selkoe and Hardy, 2016), using DBS to intervene in the early stages of AD to delay the AD process seems to be an excellent approach to treat AD (Huang et al., 2019). A number of studies have shown that NBM DBS and EC DBS have more beneficial effects in early AD (Hardenacke et al., 2016; Xia et al., 2017; Huang et al., 2019). However, in one clinical study, fornix DBS may have caused worse outcomes for AD patients at a younger age (Lozano et al., 2016). This may be related to multiple differences among different studies. In general, the preferred of DBS parameters for AD tend to be unilateral, early stage, and chronic treatment, with the NBS/fornix/EC as targets, and the pulse width, stimulation frequency, and stimulation voltage/current intensity can be individually designed in the future.

The improvement in AD caused by DBS is a multifactorial phenomenon, involving neural networks, θ oscillations, and changes in the microenvironment in the body (Laxton et al., 2010; Smith et al., 2012; Baldermann et al., 2018; Huang et al., 2019; Leplus et al., 2019). DBS is a neural regulation technology that directly changes brain activity in a controlled manner and corrects abnormal electrical circuits in the brain (Yu et al., 2019). In AD, during stimulation, DBS may have upstream and downstream effects on related neural network circuits by stimulating targets, activating or promoting electrical activity in the brain, and resetting θ oscillation. However, it is unclear what different upstream and downstream effects DBS has on different targets in AD. Most animal research focuses on the behavioral and biological effects in AD animals after DBS. The biological effects of DBS on AD animal models involve multiple potential protective mechanisms (**Figure 4**), and there may be interconnections among these fields. For example, DBS may regulate the microenvironment of AD animal models by promoting ACh release, inducing NGF synthesis, and reducing Aβ and tau levels (Hescham et al., 2013a; Xia et al., 2017; Huang et al., 2019). At present, these changes are only superficial phenomena, and the mechanism underlying them has not been explored. In the future, experimental methods such as electrophysiological recording, *in vivo* and *in vitro* optogenetics, and patch clamp technology may be used to further study the mechanism of DBS in AD.

DBS has broad application prospects for the treatment of AD. However, research in this area is still in its infancy. The stimulation parameters and mechanism of DBS in AD need to be further explored. There are still limitations to applying DBS in AD. To date, most of the published studies have been performed with small sample sizes, especially human clinical studies. Some patients with AD in human clinical studies also used acetylcholinesterase medication when receiving DBS (**Table 1**), which may have confounding effects on the results. Compared with other electrical stimulation techniques, DBS is an invasive technique with multiple risks, including the risks of major surgery, such as bleeding, infection and other side effects (Doshi, 2011; Ponce et al., 2016; Barrett, 2017). Creating a personalized DBS treatment plan for each AD patient is a way to reduce the risk of DBS. In addition, sex is considered to be a factor related to the sex risk for AD. AD has a higher prevalence in women (Mielke et al., 2014). Most experiments in animal research are dominated by male animals. Fornix DBS can significantly improve the performance of male mice in the water maze without affecting the performance of females (Gallino et al., 2019). Human clinical studies have not considered the sex of patients with AD. Therefore, whether DBS can eventually become an effective approach for AD is still not clear. More animal studies and human clinical studies on the application of DBS in AD are needed.

CONCLUSION

Most current research shows that DBS is a promising intervention for the treatment of AD. However, future studies of DBS therapy for AD should consider additional aspects, including individual differences, based on the diversity of DBS

parameters. The stimulation parameters need to be standardized, and the after effect and mechanism of action need to be further explored.

AUTHOR CONTRIBUTIONS

YL and XWu were involved in study design. YL, YS, XT, and XWa contributed in literature search and review. YL and YS drafted the manuscript. XT and XZ helped with discussion and analysis. YL, YS, and WL prepared pictures and tables. YL, XWu, BS, and WH reviewed the final version making the necessary changes. All authors read and approved the final manuscript.

FUNDING

This work was supported by the National Natural Science Foundation of China (31872751, 31771069, and 31971287).

REFERENCES

Akwa, Y., Gondard, E., Mann, A., Capetillo-Zarate, E., Alberdi, E., Matute, C., et al. (2018). Synaptic activity protects against AD and FTD-like pathology via autophagic-lysosomal degradation. *Mol. Psychiatry.* 23, 1530–1540. doi: 10.1038/mp.2017.142

Aldehri, M., Temel, Y., Alnaami, I., Jahanshahi, A., and Hescham, S. (2018). Deep brain stimulation for Alzheimer's disease: an update. *Surg. Neurol. Int.* 9:58. doi: 10.4103/sni.sni_342_17

Aldini, G. (1804). *Essai théorique et expérimental sur le galvanisme, avec une série d'expériences faites devant des commissaires de l'Institut national de France, et en divers amphithéâtres anatomiques de Londres.* Paris: De l'Imprimerie de Fournier fils.

Alzheimer's Association (2018). 2018 Alzheimer's disease facts and figures. *Alzhmers Demen.* 14, 367–429. doi: 10.1016/j.jalz.2018.02.001

Alzheimer's Association (2020). 2020 Alzheimer's disease facts and figures. *Alzheimers. Dement.* 16, 391–460. doi: 10.1002/alz.12068

Amenta, F., Bronzetti, E., Caporali, M. G., Ciriaco, E., and Germana, G. P., Niglio,T., et al. (1991). Nucleus basalis magnocellularis lesions impair mossy fiber system in rat hippocampus: a quantitative histochemical and ultrastructural study. *Arch. Gerontol. Geriatr.* 12, 49–58. doi: 10.1016/0167-4943(91)90007-d

Arai, H., Hashimoto, N., Sumitomo, K., Takase, T., and Ishii, M. (2018). Disease state changes and safety of long-term donepezil hydrochloride administration in patients with Alzheimer's disease: Japan-Great Outcome of Long-term trial with Donepezil (J-GOLD). *Psychogeriatrics* 18, 402–411. doi: 10.1111/psyg.12340

Arai, H., Sumitomo, K., Sakata, Y., Daidoji, K., Takase, T., and Toyoda, T. (2016). Disease state changes and safety of long-term donepezil hydrochloride administration in patients with Alzheimer's disease: interim results from the long-term, large-scale J-GOLD study in Japan. *Psychogeriatrics* 16, 107–115. doi: 10.1111/psyg.12130

Arrieta-Cruz, I., Pavlides, C., and Pasinetti, G. M. (2010). Deep brain stimulation in midline thalamic region facilitates synaptic transmission and short-term memory in a mouse model of Alzheimer's disease. *Transl. Neurosci.* 1, 188–194. doi: 10.2478/v10134-010-0023-x

Bagyinszky, E., Giau, V. V., Shim, K., Suk, K., An, S. S. A., and Kim, S. (2017). Role of inflammatory molecules in the Alzheimer's disease progression and diagnosis. *J. Neurol. Sci.* 376, 242–254. doi: 10.1016/j.jns.2017.03.031

Baizabal-Carvallo, J. F., and Alonso-Juarez, M. (2016). Low-frequency deep brain stimulation for movement disorders. *Parkinsonism Relat. Disord.* 31, 14–22. doi: 10.1016/j.parkreldis.2016.07.018

Baldermann, J. C., Hardenacke, K., Hu, X., Koster, P., Horn, A., Freund, H. J., et al. (2018). Neuroanatomical characteristics associated with response to deep brain stimulation of the nucleus basalis of meynert for alzheimer's disease. *Neuromodulation* 21, 184–190. doi: 10.1111/ner.12626

Barage, S. H., and Sonawane, K. D. (2015). Amyloid cascade hypothesis: Pathogenesis and therapeutic strategies in Alzheimer's disease. *Neuropeptides.* 52, 1–18. doi: 10.1016/j.npep.2015.06.008

Barrett, K. (2017). Psychiatric neurosurgery in the 21st century: overview and the growth of deep brain stimulation. *B J Psych Bull.* 41, 281–286. doi: 10.1192/pb.bp.116.055772

Bartus, R. T., Dean, R. L. III, Beer, B., and Lippa, A. S. (1982). The cholinergic hypothesis of geriatric memory dysfunction. *Science* 217, 408–414. doi: 10.1126/science.7046051

Bateman, R. J., Xiong, C., Benzinger, T. L., Fagan, A. M., Goate, A., Fox, N. C., et al. (2012). Clinical and biomarker changes in dominantly inherited Alzheimer's disease. *N. Engl. J. Med.* 367, 795–804. doi: 10.1056/NEJMoa1202753

Braak, H., and Braak, E. (1991). Neuropathological stageing of Alzheimer-related changes. *Acta Neuropathol.* 82, 239–259. doi: 10.1007/bf00308809

Browning, P. G., Gaffan, D., Croxson, P. L., and Baxter, M. G. (2010). Severe scene learning impairment, but intact recognition memory, after cholinergic depletion of inferotemporal cortex followed by fornix transection. *Cereb. Cortex.* 20, 282–293. doi: 10.1093/cercor/bhp097

Buzsaki, G. (2002). Theta oscillations in the hippocampus. *Neuron* 33, 325–340. doi: 10.1016/s0896-6273(02)00586-x

Canter, R. G., Penney, J., and Tsai, L. H. (2016). The road to restoring neural circuits for the treatment of Alzheimer's disease. *Nature* 539, 187–196. doi: 10.1038/nature20412

Carlsen, J., Zaborszky, L., and Heimer, L. (1985). Cholinergic projections from the basal forebrain to the basolateral amygdaloid complex: a combined retrograde fluorescent and immunohistochemical study. *J. Comp. Neurol.* 234, 155–167. doi: 10.1002/cne.902340203

Chen, G. F., Xu, T. H., Yan, Y., Zhou, Y. R., Jiang, Y., Melcher, K., et al. (2017). Amyloid beta: structure, biology and structure-based therapeutic development. *Acta Pharmacol. Sin.* 38, 1205–1235. doi: 10.1038/aps.2017.28

Chen, N., Dong, S., Yan, T., Yan, N., Ma, Y., and Yu, C. (2014). High-frequency stimulation of anterior nucleus thalamus improves impaired cognitive function induced by intra-hippocampal injection of Abeta1-40 in rats. *Chin. Med. J.* 127, 125–129. doi: 10.3760/cma.j.issn.0366-6999.20131025

Chen, T., and Ponce, F. A. (2019). "Future directions in deep brain stimulation," in *The Practical Application of Neuropsychology in the Neurosurgical Practice,* ed C. M. Pearson, E. Ecklund-Johnson and S. D. Gale (London; San Diego, CA; Cambridge, MA; Oxford: Academic Press), 229–253. doi: 10.1016/B978-0-12-809961-2.00012-6

Cohen, R. M., Rezai-Zadeh, K., Weitz, T. M., Rentsendorj, A., Gate, D., Spivak, I., et al. (2013). A transgenic Alzheimer rat with plaques, tau pathology, behavioral impairment, oligomeric abeta, and frank neuronal loss. *J. Neurosci.* 33, 6245–6256. doi: 10.1523/JNEUROSCI.3672-12.2013

Copenhaver, B. R., Rabin, L. A., Saykin, A. J., Roth, R. M., Wishart, H. A., Flashman, L. A., et al. (2006). The fornix and mammillary bodies in older adults with Alzheimer's disease, mild cognitive impairment, and cognitive complaints: a volumetric MRI study. *Psychiatry Res.* 147, 93–103. doi: 10.1016/j.pscychresns.2006.01.015

Cuello, A. C., Bruno, M. A., Allard, S., Leon, W., and Iulita, M. F. (2010). Cholinergic involvement in Alzheimer's disease. A link with NGF maturation and degradation. *J. Mol. Neurosci.* 40, 230–235. doi: 10.1007/s12031-009-9238-z

Cummings, J., Lee, G., Ritter, A., Sabbagh, M., and Zhong, K. (2020). Alzheimer's disease drug development pipeline: 2020. *Alzheimers Dement (N Y).* 6:e12050. doi: 10.1002/trc2.12050

Cummings, J. L., Morstorf, T., and Zhong, K. (2014). Alzheimer's disease drug-development pipeline: few candidates, frequent failures. *Alzheimers. Res. Ther.* 6:37. doi: 10.1186/alzrt269

Davies, P., and Maloney, A. J. (1976). Selective loss of central cholinergic neurons in Alzheimer's disease. *Lancet* 2:1403. doi: 10.1016/s0140-6736(76)91936-x

Doshi, P. K. (2011). Long-term surgical and hardware-related complications of deep brain stimulation. *Stereot. Funct. Neurosurg.* 89, 89–95. doi: 10.1159/000323372

Dougherty, D. D., Rezai, A. R., Carpenter, L. L., Howland, R. H., Bhati, M. T., O'Reardon, J. P., et al. (2015). A randomized sham-controlled trial of deep brain stimulation of the ventral capsule/ventral striatum for chronic treatment-resistant depression. *Biol. Psychiatry.* 78, 240–248. doi: 10.1016/j.biopsych.2014.11.023

Dumont, J. R., Petrides, M., and Sziklas, V. (2010). Fornix and retrosplenial contribution to a hippocampo-thalamic circuit underlying conditional learning. *Behav. Brain Res.* 209, 13–20. doi: 10.1016/j.bbr.2009.12.040

Duprez, T. P., Serieh, B. A., and Raftopoulos, C. (2005). Absence of memory dysfunction after bilateral mammillary body and mammillothalamic tract electrode implantation: preliminary experience in three patients. *AJNR Am. J. Neuroradiol.* 26, 195–197; author reply 197-198.

Durschmid, S., Reichert, C., Kuhn, J., Freund, H. J., Hinrichs, H., and Heinze, H. J. (2020). Deep brain stimulation of the nucleus basalis of Meynert attenuates early EEG components associated with defective sensory gating in patients with Alzheimer disease - a two-case study. *Eur. J. Neurosci.* 51, 1201–1209. doi: 10.1111/ejn.13749

Fan, D. Y., and Wang, Y. J. (2020). Early intervention in Alzheimer's disease: How early is early enough? *Neurosci. Bull.* 36, 195–197. doi: 10.1007/s12264-019-00429-x

Fontaine, D., Deudon, A., Lemaire, J. J., Razzouk, M., Viau, P., Darcourt, J., et al. (2013). Symptomatic treatment of memory decline in Alzheimer's disease by deep brain stimulation: a feasibility study. *J. Alzheimers. Dis.* 34, 315–323. doi: 10.3233/JAD-121579

Fu, A. L., Li, Q., Dong, Z. H., Huang, S. J., Wang, Y. X., and Sun, M. J. (2004). Alternative therapy of Alzheimer's disease via supplementation with choline acetyltransferase. *Neurosci. Lett.* 368, 258–262. doi: 10.1016/j.neulet.2004.05.116

Gallino, D., Devenyi, G. A., Germann, J., Guma, E., Anastassiadis, C., and Chakravarty, M. M. (2019). Longitudinal assessment of the neuroanatomical consequences of deep brain stimulation: application of fornical DBS in an Alzheimer's mouse model. *Brain Res.* 1715, 213–223. doi: 10.1016/j.brainres.2019.03.030

Gondard, E., Chau, H. N., Mann, A., Tierney, T. S., Hamani, C., Kalia, S. K., et al. (2015). Rapid modulation of protein expression in the rat hippocampus following deep brain stimulation of the fornix. *Brain Stimul.* 8, 1058–1064. doi: 10.1016/j.brs.2015.07.044

Gratwicke, J., Kahan, J., Zrinzo, L., Hariz, M., Limousin, P., Foltynie, T., et al. (2013). The nucleus basalis of Meynert: a new target for deep brain stimulation in dementia? *Neurosci. Biobehav. Rev.* 37, 2676–2688. doi: 10.1016/j.neubiorev.2013.09.003

Greenberg, B. D., Gabriels, L. A., Malone, D. A. Jr., Rezai, A. R., Friehs, G. M., Okun, M. S., et al. (2010). Deep brain stimulation of the ventral internal capsule/ventral striatum for obsessive-compulsive disorder: worldwide experience. *Mol. Psychiatry.* 15, 64–79. doi: 10.1038/mp.2008.55

Greicius, M. D., Srivastava, G., Reiss, A. L., and Menon, V. (2004). Default-mode network activity distinguishes Alzheimer's disease from healthy aging: evidence from functional MRI. *Proc. Natl. Acad. Sci. U.S.A.* 101, 4637–4642. doi: 10.1073/pnas.0308627101

Hamani, C., Dubiela, F. P., Soares, J. C. K., Shin, D., Bittencourt, S., Covolan, L., et al. (2010). Anterior thalamus deep brain stimulation at high current impairs memory in rats. *Exp. Neurol.* 225, 154–162. doi: 10.1016/j.expneurol.2010.06.007

Hamani, C., McAndrews, M. P., Cohn, M., Oh, M., Zumsteg, D., Shapiro, C. M., et al. (2008). Memory enhancement induced by hypothalamic/fornix deep brain stimulation. *Ann. Neurol.* 63, 119–123. doi: 10.1002/ana.21295

Hardenacke, K., Hashemiyoon, R., Visser-Vandewalle, V., Zapf, A., Freund, H. J., Sturm, V., et al. (2016). Deep brain stimulation of the nucleus basalis of Meynert in Alzheimer's dementia: potential predictors of cognitive change and results of a long-term follow-up in eight patients. *Brain Stimul.* 9, 799–800. doi: 10.1016/j.brs.2016.05.013

Hardenacke, K., Kuhn, J., Lenartz, D., Maarouf, M., Mai, J. K., Bartsch, C., et al. (2013). Stimulate or degenerate: deep brain stimulation of the nucleus basalis Meynert in Alzheimer dementia. *World Neurosurg.* 80, S27 e35–43. doi: 10.1016/j.wneu.2012.12.005

Hardy, J. A., and Higgins, G. A. (1992). Alzheimer's disease: the amyloid cascade hypothesis. *Science* 256, 184–185. doi: 10.1126/science.1566067

Hasselmo, M. E. (2006). The role of acetylcholine in learning and memory. *Curr. Opin. Neurobiol.* 16, 710–715. doi: 10.1016/j.conb.2006.09.002

Hedreen, J. C., Struble, R. G., Whitehouse, P. J., and Price, D. L. (1984). Topography of the magnocellular basal forebrain system in human brain. *J. Neuropathol. Exp. Neurol.* 43, 1–21. doi: 10.1097/00005072-198401000-00001

Hescham, S., Jahanshahi, A., Meriaux, C., Lim, L. W., Blokland, A., and Temel, Y. (2015). Behavioral effects of deep brain stimulation of different areas of the Papez circuit on memory- and anxiety-related functions. *Behav. Brain Res.* 292, 353–360. doi: 10.1016/j.bbr.2015.06.032

Hescham, S., Lim, L. W., Jahanshahi, A., Blokland, A., and Temel, Y. (2013a). Deep brain stimulation in dementia-related disorders. *Neurosci. Biobehav. Rev.* 37, 2666–2675. doi: 10.1016/j.neubiorev.2013.09.002

Hescham, S., Lim, L. W., Jahanshahi, A., Steinbusch, H. W., Prickaerts, J., Blokland, A., et al. (2013b). Deep brain stimulation of the forniceal area enhances memory functions in experimental dementia: the role of stimulation parameters. *Brain Stimul.* 6, 72–77. doi: 10.1016/j.brs.2012.01.008

Holczer, A., Nemeth, V. L., Vekony, T., Vecsei, L., Klivenyi, P., and Must, A. (2020). Non-invasive brain stimulation in alzheimer's disease and mild cognitive impairment-a state-of-the-art review on methodological characteristics and stimulation parameters. *Front. Hum. Neurosci.* 14:179. doi: 10.3389/fnhum.2020.00179

Hotta, H., Kagitani, F., Kondo, M., and Uchida, S. (2009). Basal forebrain stimulation induces NGF secretion in ipsilateral parietal cortex via nicotinic receptor activation in adult, but not aged rats. *Neurosci. Res.* 63, 122–128. doi: 10.1016/j.neures.2008.11.004

Howlett, D. R., Richardson, J. C., Austin, A., Parsons, A. A., Bate, S. T., Davies, D. C., et al. (2004). Cognitive correlates of Abeta deposition in male and female mice bearing amyloid precursor protein and presenilin-1 mutant transgenes. *Brain Res.* 1017, 130–136. doi: 10.1016/j.brainres.2004.05.029

Huang, C., Chu, H., Ma, Y., Zhou, Z., Dai, C., Huang, X., et al. (2019). The neuroprotective effect of deep brain stimulation at nucleus basalis of Meynert in transgenic mice with Alzheimer's disease. *Brain Stimul.* 12, 161–174. doi: 10.1016/j.brs.2018.08.015

Igarashi, K. M., Ito, H. T., Moser, E. I., and Moser, M. B. (2014). Functional diversity along the transverse axis of hippocampal area CA1. *FEBS Lett.* 588, 2470–2476. doi: 10.1016/j.febslet.2014.06.004

Ihl, R., Frolich, L., Winblad, B., Schneider, L., Burns, A., Moller, H. J., et al. (2011). World Federation of Societies of Biological Psychiatry (WFSBP) guidelines for the biological treatment of Alzheimer's disease and other dementias. *World J. Biol. Psychiatry* 12, 2–32. doi: 10.3109/15622975.2010.538083

Jacobs, J., Miller, J., Lee, S. A., Coffey, T., Watrous, A. J., Sperling, M. R., et al. (2016). Direct electrical stimulation of the human entorhinal region and hippocampus impairs memory. *Neuron* 92, 983–990. doi: 10.1016/j.neuron.2016.10.062

Jakobs, M., Lee, D. J., and Lozano, A. M. (2019). Modifying the progression of Alzheimer's and Parkinson's disease with deep brain stimulation. *Neuropharmacology* 171:107860. doi: 10.1016/j.neuropharm.2019.107860

Joel, R., Jeffrey, C., John, H., Kory, S., and Robert, D. (2015). Neurobiology of Alzheimer's disease: integrated molecular, physiological, anatomical, biomarker, and cognitive dimensions. *Curr. Alzheimer Res.* 12, 712–722. doi: 10.2174/1567205012666150701103107

Kadar, E., Ramoneda, M., Aldavert-Vera, L., Huguet, G., Morgado-Bernal, I., and Segura-Torres, P. (2014). Rewarding brain stimulation reverses the disruptive effect of amygdala damage on emotional learning. *Behav. Brain Res.* 274, 43–52. doi: 10.1016/j.bbr.2014.07.050

Kaushik, V., Smith, S. T., Mikobi, E., and Raji, M. A. (2018). Acetylcholinesterase inhibitors: beneficial effects on comorbidities in patients with Alzheimer's disease. *Am. J. Alzheimers. Dis. Other Demen.* 33, 73–85. doi: 10.1177/1533317517734352

Khan, U. A., Liu, L., Provenzano, F. A., Berman, D. E., Profaci, C. P., Sloan, R., et al. (2014). Molecular drivers and cortical spread of lateral entorhinal cortex dysfunction in preclinical Alzheimer's disease. *Nat. Neurosci.* 17, 304–311. doi: 10.1038/nn.3606

Kim, Y. S., Jung, H. M., and Yoon, B. E. (2018). Exploring glia to better understand Alzheimer's disease. *Anim Cells Syst (Seoul).* 22, 213–218. doi: 10.1080/19768354.2018.1508498

Klimesch, W. (1999). EEG alpha and theta oscillations reflect cognitive and memory performance: a review and analysis. *Brain Res. Brain Res. Rev.* 29, 169–195. doi: 10.1016/s0165-0173(98)00056-3

Koulousakis, P., van den Hove, D., Visser-Vandewalle, V., and Sesia, T. (2020). Cognitive improvements after intermittent deep brain stimulation of the nucleus basalis of meynert in a transgenic rat model for Alzheimer's disease: a preliminary approach. *J. Alzheimers. Dis.* 73, 461–466. doi: 10.3233/JAD-190919

Kowalski, K., and Mulak, A. (2019). Brain-Gut-Microbiota Axis in Alzheimer's Disease. *J. Neurogastroenterol. Motil.* 25, 48–60. doi: 10.5056/jnm18087

Kringelbach, M. L., Jenkinson, N., Owen, S. L., and Aziz, T. Z. (2007). Translational principles of deep brain stimulation. *Nat. Rev. Neurosci.* 8, 623–635. doi: 10.1038/nrn2196

Kuhn, J., Hardenacke, K., Lenartz, D., Gruendler, T., Ullsperger, M., Bartsch, C., et al. (2015a). Deep brain stimulation of the nucleus basalis of Meynert in Alzheimer's dementia. *Mol. Psychiatry.* 20, 353–360. doi: 10.1038/mp.2014.32

Kuhn, J., Hardenacke, K., Shubina, E., Lenartz, D., Visser-Vandewalle, V., Zilles, K., et al. (2015b). Deep brain stimulation of the nucleus basalis of Meynert in early stage of Alzheimer's dementia. *Brain Stimul.* 8, 838–839. doi: 10.1016/j.brs.2015.04.002

Laxton, A. W., and Lozano, A. M. (2013). Deep brain stimulation for the treatment of Alzheimer disease and dementias. *World Neurosurg.* 80, S28 e21–28. doi: 10.1016/j.wneu.2012.06.028

Laxton, A. W., Tang-Wai, D. F., McAndrews, M. P., Zumsteg, D., Wennberg, R., Keren, R., et al. (2010). A phase I trial of deep brain stimulation of memory circuits in Alzheimer's disease. *Ann. Neurol.* 68, 521–534. doi: 10.1002/ana.22089

Le Page, A., Dupuis, G., Frost, E. H., Larbi, A., Pawelec, G., Witkowski, J. M., et al. (2017). Role of the peripheral innate immune system in the development of Alzheimer's disease. *Exp. Gerontol.* 107, 59–66. doi: 10.1016/j.exger.2017.12.019

Lee, D. J., Lozano, C. S., Dallapiazza, R. F., and Lozano, A. M. (2019). Current and future directions of deep brain stimulation for neurological and psychiatric disorders. *J. Neurosurg.* 131, 333–342. doi: 10.3171/2019.4.JNS181761

Lee, J. E., Jeong, D. U., Lee, J., Chang, W. S., and Chang, J. W. (2016). The effect of nucleus basalis magnocellularis deep brain stimulation on memory function in a rat model of dementia. *BMC Neurol.* 16:6. doi: 10.1186/s12883-016-0529-z

Lehericy, S., Hirsch, E. C., Cervera, P., Hersh, L. B., Hauw, J. J., Ruberg, M., et al. (1989). Selective loss of cholinergic neurons in the ventral striatum of patients with Alzheimer disease. *Proc. Natl. Acad. Sci. U.S.A.* 86, 8580–8584. doi: 10.1073/pnas.86.21.8580

Leoutsakos, J. S., Yan, H., Anderson, W. S., Asaad, W. F., Baltuch, G., Burke, A., et al. (2018). Deep brain stimulation targeting the fornix for mild Alzheimer dementia (the ADvance trial): a two year follow-up including results of delayed activation. *J. Alzheimers. Dis.* 64, 597–606. doi: 10.3233/JAD-180121

Leplus, A., Lauritzen, I., Melon, C., Kerkerian-Le Goff, L., Fontaine, D., and Checler, F. (2019). Chronic fornix deep brain stimulation in a transgenic Alzheimer's rat model reduces amyloid burden, inflammation, and neuronal loss. *Brain Struct. Funct.* 224, 363–372. doi: 10.1007/s00429-018-1779-x

Li, J., Zhou, W., Wu, X., and Tam, K. (2015). Chemical and physical approaches for the treatment of Alzheimer's disease. *Admet Dmpk. :1943*. doi: 10.5599/admet.3.3.194

Lindsay, R. M., and Harmar, A. J. (1989). Nerve growth factor regulates expression of neuropeptide genes in adult sensory neurons. *Nature* 337, 362–364. doi: 10.1038/337362a0

Lledo, P. M., Alonso, M., and Grubb, M. S. (2006). Adult neurogenesis and functional plasticity in neuronal circuits. *Nat. Rev. Neurosci.* 7, 179–193. doi: 10.1038/nrn1867

Lopategui Cabezas, I., Herrera Batista, A., and Pentón Rol, G. (2014). The role of glial cells in Alzheimer disease: potential therapeutic implications. *Neurología.* 29, 305–309. doi: 10.1016/j.nrleng.2012.10.009

Lovblad, K. O., Schaller, K., and Vargas, M. I. (2014). The fornix and limbic system. *Semin. Ultrasound CT MR.* 35, 459–473. doi: 10.1053/j.sult.2014.06.005

Lozano, A. M., Fosdick, L., Chakravarty, M. M., Leoutsakos, J. M., Munro, C., Oh, E., et al. (2016). A phase II study of fornix deep brain stimulation in mild Alzheimer's disease. *J. Alzheimers. Dis.* 54, 777–787. doi: 10.3233/JAD-160017

Lozano, A. M., and Lipsman, N. (2013). Probing and regulating dysfunctional circuits using deep brain stimulation. *Neuron* 77, 406–424. doi: 10.1016/j.neuron.2013.01.020

Lv, Q., Du, A., Wei, W., Li, Y., Liu, G., and Wang, X. P. (2018). Deep brain stimulation: A potential treatment for dementia in Alzheimer's disease (AD) and Parkinson's disease dementia (PDD). *Front. Neurosci.* 12:360. doi: 10.3389/fnins.2018.00360

Mair, R. G., and Hembrook, J. R. (2008). Memory enhancement with event-related stimulation of the rostral intralaminar thalamic nuclei. *J. Neurosci.* 28, 14293–14300. doi: 10.1523/JNEUROSCI.3301-08.2008

Mann, A., Gondard, E., Tampellini, D., Milsted, J. A. T., Marillac, D., Hamani, C., et al. (2018). Chronic deep brain stimulation in an Alzheimer's disease mouse model enhances memory and reduces pathological hallmarks. *Brain Stimul.* 11, 435–444. doi: 10.1016/j.brs.2017.11.012

Mao, Z. Q., Wang, X., Xu, X., Cui, Z. Q., Pan, L. S., Ning, X. J., et al. (2018). Partial improvement in performance of patients with severe Alzheimer's disease at an early stage of fornix deep brain stimulation. *Neural Regeneration Res.* 13, 2164–2172. doi: 10.4103/1673-5374.241468

Mashayekhi, F., and Salehin, Z. (2006). Cerebrospinal fluid nerve growth factor levels in patients with Alzheimer's disease. *Ann. Saudi Med.* 26, 278–282. doi: 10.5144/0256-4947.2006.278

McCartney, H., Johnson, A. D., Weil, Z. M., and Givens, B. (2004). Theta reset produces optimal conditions for long-term potentiation. *Hippocampus* 14, 684–687. doi: 10.1002/hipo.20019

McKinnon, C., Gros, P., Lee, D. J., Hamani, C., Lozano, A. M., Kalia, L. V., et al. (2019). Deep brain stimulation: potential for neuroprotection. *Ann Clin Transl Neurol.* 6, 174–185. doi: 10.1002/acn3.682

McMullen, D. P., Rosenberg, P., Cheng, J., Smith, G. S., Lyketsos, C., and Anderson, W. S. (2016). Bilateral cortical encephalomalacia in a patient implanted with bilateral deep brain stimulation for Alzheimer's disease: a case report. *Alzheimer Dis. Assoc. Disord.* 30, 70–72. doi: 10.1097/WAD.0000000000000095

McNaughton, N., Kocsis, B., and Hajos, M. (2007). Elicited hippocampal theta rhythm: a screen for anxiolytic and procognitive drugs through changes in hippocampal function? *Behav. Pharmacol.* 18, 329–346. doi: 10.1097/FBP.0b013e3282ee82e3

Micheau, J., and Marighetto, A. (2011). Acetylcholine and memory: a long, complex and chaotic but still living relationship. *Behav. Brain Res.* 221, 424–429. doi: 10.1016/j.bbr.2010.11.052

Mielke, M. M., Vemuri, P., and Rocca, W. A. (2014). Clinical epidemiology of Alzheimer's disease: assessing sex and gender differences. *Clin. Epidemiol.* 6, 37–48. doi: 10.2147/CLEP.S37929

Miller, J. P., Sweet, J. A., Bailey, C. M., Munyon, C. N., Luders, H. O., and Fastenau, P. S. (2015). Visual-spatial memory may be enhanced with theta burst deep brain stimulation of the fornix: a preliminary investigation with four cases. *Brain* 138, 1833–1842. doi: 10.1093/brain/awv095

Miocinovic, S., Somayajula, S., Chitnis, S., and Vitek, J. L. (2013). History, applications, and mechanisms of deep brain stimulation. *JAMA Neurol.* 70, 163–171. doi: 10.1001/2013.jamaneurol.45

Mirsaeedi-Farahani, K., Halpern, C. H., Baltuch, G. H., Wolk, D. A., and Stein, S. C. (2015). Deep brain stimulation for Alzheimer disease: a decision and cost-effectiveness analysis. *J. Neurol.* 262, 1191–1197. doi: 10.1007/s00415-015-7688-5

Mohandas, E., Rajmohan, V., and Raghunath, B. (2009). Neurobiology of Alzheimer's disease. *Indian J. Psychiatry.* 51, 55–61. doi: 10.4103/0019-5545.44908

Mulder, S. D., Veerhuis, R., Blankenstein, M. A., and Nielsen, H. M. (2012). The effect of amyloid associated proteins on the expression of genes involved in amyloid-β clearance by adult human astrocytes. *Exp. Neurol.* 233, 373–379. doi: 10.1016/j.expneurol.2011.11.001

Noreik, M., Kuhn, J., Hardenacke, K., Lenartz, D., Bauer, A., Buhrle, C. P., et al. (2015). Changes in nutritional status after deep brain stimulation of the nucleus basalis of meynert in alzheimer's disease–results of a phase i study. *J. Nutr. Health Aging.* 19, 812–818. doi: 10.1007/s12603-015-0595-8

Onate-Cadena, N., Cisneros-Otero, M., Ruiz-Chow, A. A., Arellano-Reynoso, A., Kobayashi-Romero, L. F., and Perez-Esparza, R. (2020). Deep-brain stimulation in treatment-resistant obsessive-compulsive disorder: clinical and molecular neuroimaging correlation. *Rev. Colomb. Psiquiatr.* 49, 62–65. doi: 10.1016/j.rcp.2018.05.002

Parent, A. (2004). Giovanni Aldini: from animal electricityto human brain stimulation. *The Can. J. Neurol. Sci.* 31, 576–584. doi: 10.1017/S0317167100003851

Patterson, C. (2018). World Alzheimer Report 2018. Available online at: https://www.alz.co.uk/research/world-report-2018

Perl, D. P. (2010). Neuropathology of Alzheimer's disease. *Mt. Sinai J. Med.* 77, 32–42. doi: 10.1002/msj.20157

Perry, E. K., Perry, R. H., Blessed, G., and Tomlinson, B. E. (1977). Necropsy evidence of central cholinergic deficits in senile dementia. *Lancet* 1:189. doi: 10.1016/s0140-6736(77)91780-9

Ponce, F. A., Asaad, W. F., Foote, K. D., Anderson, W. S., Rees Cosgrove, G., Baltuch, G. H., et al. (2016). Bilateral deep brain stimulation of the fornix for Alzheimer's disease: surgical safety in the ADvance trial. *J. Neurosurg.* 125, 75–84. doi: 10.3171/2015.6.JNS15716

Price, J. L., and Drevets, W. C. (2010). Neurocircuitry of mood disorders. *Neuropsychopharmacology* 35, 192–216. doi: 10.1038/npp.2009.104

Querfurth, H. W., and LaFerla, F. M. (2010). Alzheimer's disease. *N. Engl. J. Med.* 362, 329–344. doi: 10.1056/NEJMra0909142

Raichle, M. E., MacLeod, A. M., Snyder, A. Z., Powers, W. J., Gusnard, D. A., and Shulman, G. L. (2001). A default mode of brain function. *Proc. Natl. Acad. Sci. U.S.A.* 98, 676–682. doi: 10.1073/pnas.98.2.676

Saalmann, Y. B. (2014). Intralaminar and medial thalamic influence on cortical synchrony, information transmission and cognition. *Front. Syst. Neurosci.* 8:83. doi: 10.3389/fnsys.2014.00083

Salehi, A., Delcroix, J. D., and Swaab, D. F. (2004). Alzheimer's disease and NGF signaling. *J Neural Transm (Vienna).* 111, 323–345. doi: 10.1007/s00702-003-0091-x

Sankar, T., Chakravarty, M. M., Bescos, A., Lara, M., Obuchi, T., Laxton, A. W., et al. (2015). Deep brain stimulation influences brain structure in Alzheimer's disease. *Brain Stimul.* 8, 645–654. doi: 10.1016/j.brs.2014.11.020

Scharre, D. W., Weichart, E., Nielson, D., Zhang, J., Agrawal, P., Sederberg, P. B., et al. (2018). Deep brain stimulation of frontal lobe networks to treat Alzheimer's disease. *J. Alzheimers. Dis.* 62, 621–633. doi: 10.3233/JAD-170082

Schiller, Y., and Bankirer, Y. (2007). Cellular mechanisms underlying antiepileptic effects of low- and high-frequency electrical stimulation in acute epilepsy in neocortical brain slices *in vitro*. *J. Neurophysiol.* 97, 1887–1902. doi: 10.1152/jn.00514.2006

Schliebs, R., and Arendt, T. (2011). The cholinergic system in aging and neuronal degeneration. *Behav. Brain Res.* 221, 555–563. doi: 10.1016/j.bbr.2010.11.058

Scott, L., Feng, J., Kiss, T., Needle, E., Atchison, K., Kawabe, T. T., et al. (2012). Age-dependent disruption in hippocampal theta oscillation in amyloid-beta overproducing transgenic mice. *Neurobiol. Aging.* 33, 1481 e1413–1423. doi: 10.1016/j.neurobiolaging.2011.12.010

Selkoe, D. J., and Hardy, J. (2016). The amyloid hypothesis of Alzheimer's disease at 25 years. *EMBO Mol. Med.* 8, 595–608. doi: 10.15252/emmm.201606210

Senova, S., Chaillet, A., and Lozano, A. M. (2018). Fornical Closed-Loop Stimulation for Alzheimer's Disease. *Trends Neurosci.* 41, 418–428. doi: 10.1016/j.tins.2018.03.015

Senova, S., Fomenko, A., Gondard, E., and Lozano, A. M. (2020). Anatomy and function of the fornix in the context of its potential as a therapeutic target. *J. Neurol. Neurosurg. Psychiatr*. doi: 10.1136/jnnp-2019-322375

Sivilotti, L., and Nistri, A. (1991). GABA receptor mechanisms in the central nervous system. *Prog. Neurobiol.* 36, 35–92. doi: 10.1016/0301-0082(91)90036-z

Smith, G. S., Laxton, A. W., Tang-Wai, D. F., McAndrews, M. P., Diaconescu, A. O., Workman, C. I., et al. (2012). Increased cerebral metabolism after 1 year of deep brain stimulation in Alzheimer disease. *Arch. Neurol.* 69, 1141–1148. doi: 10.1001/archneurol.2012.590

Sofroniew, M. V., Howe, C. L., and Mobley, W. C. (2001). Nerve growth factor signaling, neuroprotection, and neural repair. *Annu. Rev. Neurosci.* 24, 1217–1281. doi: 10.1146/annurev.neuro.24.1.1217

Song, S., Song, S., Cao, C., Lin, X., Li, K., Sava, V., et al. (2013). Hippocampal neurogenesis and the brain repair response to brief stereotaxic insertion of a microneedle. *Stem Cells Int*. 2013:205878. doi: 10.1155/2013/205878

Sperling, R. A., Aisen, P. S., Beckett, L. A., Bennett, D. A., Craft, S., Fagan, A. M., et al. (2011). Toward defining the preclinical stages of Alzheimer's disease: recommendations from the National Institute on Aging-Alzheimer's Association workgroups on diagnostic guidelines for Alzheimer's disease. *Alzheimers. Dement.* 7, 280–292. doi: 10.1016/j.jalz.2011.03.003

Sperling, R. A., Dickerson, B. C., Pihlajamaki, M., Vannini, P., LaViolette, P. S., Vitolo, O. V., et al. (2010). Functional alterations in memory networks in early Alzheimer's disease. *Neuromolecular Med.* 12, 27–43. doi: 10.1007/s12017-009-8109-7

Sperling, R. A., Laviolette, P. S., O'Keefe, K., O'Brien, J., Rentz, D. M., Pihlajamaki, M., et al. (2009). Amyloid deposition is associated with impaired default network function in older persons without dementia. *Neuron* 63, 178–188. doi: 10.1016/j.neuron.2009.07.003

Stone, S. S., Teixeira, C. M., Devito, L. M., Zaslavsky, K., Josselyn, S. A., Lozano, A. M., et al. (2011). Stimulation of entorhinal cortex promotes adult neurogenesis and facilitates spatial memory. *J. Neurosci.* 31, 13469–13484. doi: 10.1523/JNEUROSCI.3100-11.2011

Suthana, N., Haneef, Z., Stern, J., Mukamel, R., Behnke, E., Knowlton, B., et al. (2012). Memory enhancement and deep-brain stimulation of the entorhinal area. *N. Engl. J. Med.* 366, 502–510. doi: 10.1056/NEJMoa1107212

Temel, Y., and Jahanshahi, A. (2015). Treating brain disorders with neuromodulation. *Science* 347, 1418–1419. doi: 10.1126/science.aaa9610

Tsai, S. T., Chen, S. Y., Lin, S. Z., and Tseng, G. F. (2020). Rostral intralaminar thalamic deep brain stimulation ameliorates memory deficits and dendritic regression in beta-amyloid-infused rats. *Brain Struct. Funct.* 225, 751–761. doi: 10.1007/s00429-020-02033-6

Tsivilis, D., Vann, S. D., Denby, C., Roberts, N., Mayes, A. R., Montaldi, D., et al. (2008). A disproportionate role for the fornix and mammillary bodies in recall versus recognition memory. *Nat. Neurosci.* 11, 834–842. doi: 10.1038/nn.2149

Turnbull, I. M., McGeer, P. L., Beattie,L., and Calne, D., Pate, B. (1985). Stimulation of the basal nucleus of Meynert in senile dementia of Alzheimer's type. A preliminary report. *Appl. Neurophysiol.* 48, 216–221. doi: 10.1159/000101130

Tuszynski, M. H., Yang, J. H., Barba, D., U, H.S., Bakay, R. A., Pay, M. M., et al. (2015). Nerve growth factor gene therapy: activation of neuronal responses in Alzheimer disease. *JAMA Neurol.* 72, 1139–1147. doi: 10.1001/jamaneurol.2015.1807

Unzeta, M., Esteban, G., Bolea, I., Fogel, W. A., Ramsay, R. R., Youdim, M. B., et al. (2016). Multi-target directed donepezil-like ligands for Alzheimer's disease. *Front. Neurosci.* 10:205. doi: 10.3389/fnins.2016.00205

Vazquez-Bourgon, J., Martino, J., Sierra Pena, M., Infante Ceberio, J., Martinez Martinez, M. A., Ocon, R., et al. (2019). Deep brain stimulation and treatment-resistant obsessive-compulsive disorder: a systematic review. *Rev. Psiquiatr. Salud Ment.* 12, 37–51. doi: 10.1016/j.rpsm.2017.05.005

Vedam-Mai, V., Baradaran-Shoraka, M., Reynolds, B. A., and Okun, M. S. (2016). Tissue response to deep brain stimulation and microlesion: a comparative study. *Neuromodulation* 19, 451–458. doi: 10.1111/ner.12406

Verdier, D., and Dykes, R. W. (2001). Long-term cholinergic enhancement of evoked potentials in rat hindlimb somatosensory cortex displays characteristics of long-term potentiation. *Exp. Brain Res.* 137, 71–82. doi: 10.1007/s002210000646

Villemagne, V. L., Burnham, S., Bourgeat, P., Brown, B., Ellis, K. A., Salvado,. O., et al. (2013). Amyloid β deposition, neurodegeneration, and cognitive decline in sporadic Alzheimer's disease: a prospective cohort study. *Lancet Neurol.* 12, 357–367. doi: 10.1016/S1474-4422(13)70044-9

Villette, V., Poindessous-Jazat, F., Simon, A., Lena, C., Roullot, E., Bellessort, B., et al. (2010). Decreased rhythmic GABAergic septal activity and memory-associated theta oscillations after hippocampal amyloid-beta pathology in the rat. *J. Neurosci.* 30, 10991–11003. doi: 10.1523/JNEUROSCI.6284-09.2010

Von Bernhardi, R. (2007). Glial cell dysregulation: a new perspective on Alzheimer disease. *Neurotox. Res.* 12, 215–232. doi: 10.1007/BF03033906

Whitehouse, P. J., Price, D. L., Clark, A. W., Coyle, J. T., and DeLong, M. R. (1981). Alzheimer disease: evidence for selective loss of cholinergic neurons in the nucleus basalis. *Ann Neurol.* 10, 122–126. doi: 10.1002/ana.410100203

Xia, F., Yiu, A., Stone, S. S. D., Oh, S., Lozano, A. M., Josselyn, S. A., et al. (2017). Entorhinal cortical deep brain stimulation rescues memory deficits in both young and old mice genetically engineered to model Alzheimer's disease. *Neuropsychopharmacology* 42, 2493–2503. doi: 10.1038/npp.2017.100

Yali, L., Deshu, C., Ran, C., Xinyu, Z., Tao, W., Jianmiao, L., et al. (2014). Mechanisms of U87 Astrocytoma cell uptake and trafficking of monomeric versus protofibril Alzheimer's disease amyloid-β proteins. *PLoS ONE.* 9:e99939. doi: 10.1371/journal.pone.0099939

Yu, D., Yan, H., Zhou, J., Yang, X., Lu, Y., and Han, Y. (2019). A circuit view of deep brain stimulation in Alzheimer's disease and the possible mechanisms. *Mol. Neurodegener.* 14, 33. doi: 10.1186/s13024-019-0334-4

Zhang, C., Hu, W. H., Wu, D. L., Zhang, K., and Zhang, J. G. (2015). Behavioral effects of deep brain stimulation of the anterior nucleus of thalamus, entorhinal cortex and fornix in a rat model of Alzheimer's disease. *Chin. Med. J.* 128, 1190–1195. doi: 10.4103/0366-6999.156114

Zhou, C., Zhang, H., Qin, Y., Tian, T., Xu, B., Chen, J., et al. (2018). A systematic review and meta-analysis of deep brain stimulation in treatment-resistant depression. *Prog. Neuropsychopharmacol. Biol. Psychiatry* 82, 224–232. doi: 10.1016/j.pnpbp.2017.11.012

Zhu, Z., Zhang, L., Cui, Y., Li, M., Ren, R., Li, G., et al. (2020). Functional compensation and mechanism of choline acetyltransferase in the treatment of cognitive deficits in aged dementia mice. *Neuroscience* 442, 41–53. doi: 10.1016/j.neuroscience.2020.05.016

Conflict of Interest: The authors declare that the research was conducted in the absence of any commercial or financial relationships that could be construed as a potential conflict of interest.

frontiers in Aging Neuroscience

ORIGINAL RESEARCH
published: 17 March 2021
doi: 10.3389/fnagi.2021.618690

Reduced Cerebral Glucose Uptake in an Alzheimer's Rat Model With Glucose-Weighted Chemical Exchange Saturation Transfer Imaging

*Peidong Chen[1†], Zhiwei Shen[1,2†], Qianqian Wang[3], Bingna Zhang[4], Zerui Zhuang[1], Jiefen Lin[1], Yuanyu Shen[1], Yanzhi Chen[1], Zhuozhi Dai[1] and Renhua Wu[1]**

[1] Department of Medical Imaging, The Second Affiliated Hospital, Shantou University Medical College, Shantou, China, [2] Philips Healthcare, Beijing, China, [3] Department of Postgraduate, Shantou University Medical College, Shantou, China, [4] Center for Translational Medicine, The Second Affiliated Hospital, Shantou University Medical College, Shantou, China

A correlation between the abnormal cerebral glucose metabolism and the progression of Alzheimer's disease (AD) has been found in previous studies, suggesting that glucose alterations may be used to predict the histopathological diagnosis in AD. In this study, we investigated the dynamic changes of cerebral glucose uptake *in vivo* using MR glucose chemical exchange saturation transfer (glucoCEST) imaging in a rat model of AD with an intracerebroventricular (i.c.v) injection of amyloid Aβ-protein (25–35), confirmed by Morris water maze and Nissl staining. In total, 6 rats in the AD group and 6 rats in the control group that were given an injection of sterile normal saline were included. At 28 days after injection, all rats performed a 7.0 T MR exanimation, including glucoCEST, diffusion tensor imaging (DTI) and hippocampus magnetic resonance spectra (MRS), to detect the possible metabolic and structural changes in the rat brain. A significantly elevated brain glucoCEST signal in the brain of AD rats was observed, and a decreased brain glucose uptake was also explored during the progression of glucose infusion compared with those in rats of the control group. In addition, there is a significant positive correlation between glucoCEST enhancement (GCE) and myo-Inosito (Ins) in the AD group and the control group ($P < 0.05$). A significantly reduced number of neurons in the cortex and hippocampus in AD rats combined with the significantly longer escape and a decreased number of crossings were verified at 28 days after Aβ25–35 injection by Nissl staining and Morris water maze, respectively. Our results indicated that an abnormal brain glucose mechanism in AD rats could be detected by glucoCEST imaging, suggesting a new method to explore the occurrence and progress of diabetes-related AD or dementia.

Keywords: Alzheimer's disease, glucoCEST, glucose metabolism, D-glucose, magnetic resonance imaging

OPEN ACCESS

Edited by:
Chih-Yu Hsu,
Fujian University of Technology, China

Reviewed by:
Emmanuel Brouillet,
Commissariat à l'Energie Atomique et aux Energies Alternatives (CEA), France
Dafin F. Muresanu,
Iuliu Haţieganu University of Medicine and Pharmacy, Romania

***Correspondence:**
Renhua Wu
cjr.wurenhua@vip.163.com

† These authors have contributed equally to this work

***Received:** 18 October 2020*
***Accepted:** 24 February 2021*
***Published:** 17 March 2021*

Citation:
Chen P, Shen Z, Wang Q, Zhang B, Zhuang Z, Lin J, Shen Y, Chen Y, Dai Z and Wu R (2021) Reduced Cerebral Glucose Uptake in an Alzheimer's Rat Model With Glucose-Weighted Chemical Exchange Saturation Transfer Imaging. Front. Aging Neurosci. 13:618690. doi: 10.3389/fnagi.2021.618690

Abbreviations: CEST, Chemical Exchange Saturation Transfer; glucoCEST, glucose CEST; GCE, glucoCEST enhancement; MWM, Morris water maze; MTR, magnetization transfer ratio; DTI, Diffusion Tensor Imaging; MRS, magnetic resonance spectra; NAA, N-acetyl aspartate; Glu, glutamate; Cr, creatine; Cho, choline; mI, myo-Inosito.

INTRODUCTION

Alzheimer's disease (AD) is a chronic progressive neurodegenerative disease characterized by the accumulation of amyloid-β protein and a Tau-meditated neuronal injury (de Paula et al., 2009; de-Paula et al., 2012). AD affects around 50 million persons worldwide, and the number will likely increase with longer life expectancy (Abbott, 2011). Clinically, patients with AD are presented with a combination of features, such as progressive cognitive decline, dementia, and personality changes (Jack et al., 2013). The deposition of amyloid-β peptides has been observed in AD animal models as well as post-mortem AD patients, suggesting amyloid-β as having a key role in AD pathogenesis (Seynnaeve et al., 2018). Nevertheless, accumulated evidence shows that the pathogenesis of AD is also contributed to by multiple key players (de-Paula et al., 2012).

Glucose is a primary source of energy for almost all living organisms. Impaired glucose metabolism is associated with a wide range of pathological conditions (Mergenthaler et al., 2013) and is considered an important risk factor for AD (Duran-Aniotz and Hetz, 2016). The reduction of glucose uptake in posterior cingulate and temporal-parietal regions is the most commonly described diagnostic criterion for AD (Wang et al., 2016) with 18F-fluorodeoxyglucose (FDG) positron emission tomography (PET), and it was considered to be associated with the cognitive decline in healthy control (Gardener et al., 2016). Moreover, type 2 diabetes was shown with an increased risk of cognitive decline and developing AD (Mergenthaler et al., 2013). Therefore, the interplay between glucose metabolism and AD should be better understood, especially during the early stages of AD.

Over the last three decades, 18-FDG PET has provided important information for the diagnosis and differential diagnosis of AD in animal models and patients. Le Douce et al. (2020) found that there was a decreased glucose uptake in the amygdala, entorhinal cortex and hippocampus in 3xTg-AD transgenic mice in the early phase with 18F-FDG PET. In patients with AD, reduced glucose metabolism was also observed by 18F-FDG-PET in the temporal and superior temporal/posterior temporal regions, posterior cingulate cortex and the anterior wedge (Herholz, 2010; Kantarci et al., 2010). However, contradictory results were also found in APP/PS1 transgenic mice, indicating an increased glucose utilization in multiple brain regions at 2 and 3.5 months of age (Li et al., 2016).

Chemical exchange saturation transfer (CEST) imaging is a relatively new MR contrast technique and has been used to map exchanged protons or molecules in glucose, amide proton, glutamate or creatine *in vivo*. Based on a frequency-specific saturation pulse, the magnetization transfer effect occurred among bulk water and labile solute protons in the above metabolites and further lead to a decreased signal intensity of free water. By detecting the changes of the free water signal, the effect of glucose chemical exchange saturation transfer (glucoCEST) can be observed, which is related to the concentration of glucose and exchange environments, such as pH and temperature. GlucoCEST is considered a non-invasive alternative for the *in vivo* imaging of glucose uptake following an external administration of glucose (McMahon, 2017). Moreover, glucoCEST enhancement (GCE) imaging was achieved by subtracting the difference glucoCEST images before and after glucose administration, which is similar to dynamic contrast-enhanced (DCE) MR perfusion by the injection of gadolinium-based contrast agent. Using glucoCEST, glucose uptake in healthy mice brains (Nasrallah et al., 2013), colorectal tumor models (Walker-Samuel et al., 2013) and healthy mice livers (Miller et al., 2015) was successfully detected. In this study, we aim to explore the dynamic changes of cerebral glucose uptake in AD model rats using both glucoCEST and GCE. The possible pathological and behavioral changes in the rat brain of the AD group were detected by Nissl staining and a morris water maze to confirm the AD model. Furthermore, the correlation between glucose metabolism, diffusion characteristics and several hippocampus metabolites was investigated for the interpretation of abnormal glucose metabolism.

MATERIALS AND METHODS

Animals

A total of 12 male Sprague-Dawley (SD) rats (between 16 and 18 weeks of age and weighing 250–320 g) were purchased from the Animal Center Laboratory of our Medical College. The rats were randomly divided into the control group (n = 6) and the AD group (n = 6). All rats were housed in plastic cages at 12 h light/dark cycle with free access to food and water. All experiments were approved by our ethics committee of Animal Care and Welfare.

AD Rat Modeling

Amyloid β-Protein Fragment 25–35 (Aβ25–35; Sigma-Aldrich) was dissolved in sterile saline at a concentration of 1 mg/ml and stored at −20°C till to be used. Before injection, Aβ25–35 was aggregated in an electronic thermostat at 37°C for 4 days (D'Agostino et al., 2012; Kim et al., 2015).

With reference to the method described by previous studies (Ohta et al., 2012; Kim et al., 2015), the AD rat model was established. Briefly, rats were anesthetized with an intraperitoneal injection of pentobarbital sodium (40 mg/kg) and placed in a stereotaxic device. Following midline incision, a dental drill was used to perforate skull over the right lateral ventricle at the coordinates (0.8 mm posterior to the bregma and 1.5 mm lateral to the midline). Rats in the AD group were transfused with 9 μl of aggregated Aβ 25–35 into the right lateral ventricle using a microsyringe at a rate of 1 μl/min, and the needle was then left in place for an additional 5 min to allow adequate diffusion. Meanwhile, the rats in the control group were injected with sterile normal saline.

Estimation of Blood Glucose Concentration

On the 14th day after the intracerebroventricular injection of Aβ25–35, three rats in the AD and control groups were randomly selected to acquire the time-blood glucose concentration curves by continuous injection of D-glucose infusion according to

the method described previously (Chan et al., 2012). The rats were anesthetized by 1.5% isoflurane in oxygen gas during the whole experimental procedure. D-glucose (1.5 mM) was dissolved in normal saline and was continuously injected using a microsyringe pump (JMS, Japan, model SP-500) at a rate of 2.0 ml/h. The blood glucose concentration was examined in a sample obtained from the tail vein at the following time points: before injection, 10, 20, 30, 40, and 50 minters after injection and 10 and 20 minters after the finish of glucose infusion.

Optimization Scan Parameters of GlucoCEST Imaging in Phantom

Firstly, seven centrifugal tubes containing the following different metabolites were scanned to acquire an optimized saturation power referenced with the method detailed previously (Haris et al., 2013). The metabolites in each tube included creatine (Cr, 10 mM), glutamate (glu, 10 mM), gamma-aminobutyric acid (GABA, 10 mM), choline (cho, 10 mM), high D-glucose concentration (200 mM), low D-glucose concentration (10 mM) as well as D-glucose and Cr mixture (5 mM each), respectively. Next, another six tubes containing D-glucose with different concentrations (6.25, 12.5, 25, 50, 75, and 100 mM) in pH of 7.4 were scanned to observe the CEST exchange signal affected by the concentration (Nasrallah et al., 2013). Finally, three tubes containing D-glucose (25 mM) with different pH (6.4, 7.4, and 8.4) were examined to observe the impact of pH on the glucose CEST exchange. All phantoms (Haris et al., 2012) were prepared in phosphate buffer solution (PBS) supplemented with 1% agarose solution.

Several important scan paraments of glucoCEST imaging, such as saturation power, saturation during and repetition time (TR), were optimized in phantom model with varying values: saturation power (1.5, 3.0, and 6.0 μT) in the tubes with different metabolites; saturation power (1.5, 2.0, 2.5, 3.0, 3.5, and 4.0 μT) in the phantoms with different concentration D-glucose; saturation during (4, 5, and 6 s) and TR (5, 6, 7, and 8 s), respectively (Nasrallah et al., 2013; Dai et al., 2014). In addition, the phantom model with different pH D-glucose concentrations was scanned with B1 = 1.5 μT, saturation time 5 s.

MRI Acquisition in Phantom and Animal Examination

In the phantom test, an echo-planar imaging (EPI) sequence with a continuous wave saturation pulse was used to perform glucoCEST imaging to explorer the optimized scan parameters. The acquisition parameters were set as the following: TR 5.04 s, slice thickness 2 mm, acquisition matrix 64 × 64, field of view of 40 mm × 40 mm, averages 1, pre-saturation during 5 s, the saturation offset range from –1,500 to +1,500 Hz, the step 30 Hz and reference image without the saturation offset of 10,000 Hz. A B0 and B1 map were collected to correct the possible asymmetry and variation of magnetic field.

All rats were performed MR imaging at 28 days after the intracerebroventricular injection with Aβ25–35/sterile normal saline in the AD group/control group. Before MR examination, all rats were allowed to fast for 24 h. The rats were firstly anesthetized in an induction box with 4% isoflurane in oxygen and continued to inhale the gas mixture of 1.5%/98.5% isoflurane/oxygen via a nose tube during the MRI scanning (Tang et al., 2017). The respiration rate was monitored and maintained by animal physiological monitoring and gating systems (model 1030, SAII, United States). Then, rats were fixed on an MRI matching sampler with a bite and two ear bars to prevent the head motion.

MR imaging in phantom and animal were performed on a 7.0 T animal MR scanner (7T/160/AS Agilent Technologies, United States) with a 9,563 volume transmit/receive coil. The protocol included Axial and sagittal T2-weighted, DTI, and bilateral hippocampal MR spectroscopy and glucoCEST imaging. Axial and sagittal T2W imaging was acquired to demonstrate the morphology of rats' whole brain, and the parameters were set up as follows: TR 2,000 ms, acquisition matrix 256 × 128, field of view 40 × 40 mm, slice thickness 2 mm, slice 6, slice spacing 0.2 mm and average 2. With the reference to T2WI, the scan layer including the middle hippocampus was selected as the area of interest. Axial Diffusion Tensor Imaging (DTI) of the rat brain was obtained with the following parameters: the scanning layer is consistent with glucoCEST imaging, TR 2,000 ms, TE 39.68 ms, FOV 40 mm × 40 mm, slice thickness 4 mm, matrix 128 × 128, b 1031.0 s/mm^2, and the average 8. A total of seven diffusion-weighted images with S0 and six directions were obtained (b = 1031.0 s/mm^2) in a total scan time of 10 min and 41 s. Then, 1-H Magnetic Resonance Spectroscopy (MRS) was performed in the bilateral hippocampus before D-glucose infusion using a Point RESolved Spectroscopy (PRESS) pulse sequence with the following parameters: TR 4,000 ms, TE 13 ms, averages 192, and a spectral width of 4,006 KHz.

The axial glucoCEST images of the rat brain were acquired before the intraperitoneal injection of D-glucose (1.5 mM) and 10, 20, 30, and 40 min during infusion and then 10 and 20 min following the infusion. The scan parameters were: TR 6 s, slice thickness 4 mm, acquisition matrix 64 × 64, field of view of 35 × 35 mm^2, average 1, saturation during of 5 s, saturation offset range from –900 to +900 Hz at intervals of 30 Hz and magnetization references at 10,000 Hz. The saturation power of 1.5 μT was used with the minimize influence of other metabolites on glucoCEST and direct water saturation effect.

Morris Water Maze

After MR examination, a Morris water maze (MWM) was used to evaluate learning and memory dysfunction. MWM experiments were carried out on the 14th and 28th day following Aβ25–35 administration as described previously (D'Agostino et al., 2012; Ohta et al., 2012). Rats were trained for 4 days (4 trails/day), and the swimming pattern was captured with a camera and a video track software (Noldus, Co., Ltd. Holland) for analysis. The latency to reach the platform was acquired using a computer-controlled tracking system. Rats were allowed 120 s to reach the platform then they were guided to the platform manually and left there for 5 s. On the fifth day, the platform was removed and a 120 s-spatial probe-trial was performed. The number crossing the platform position, the time of crossing from the target quadrant and the swimming speed of each rat were recorded.

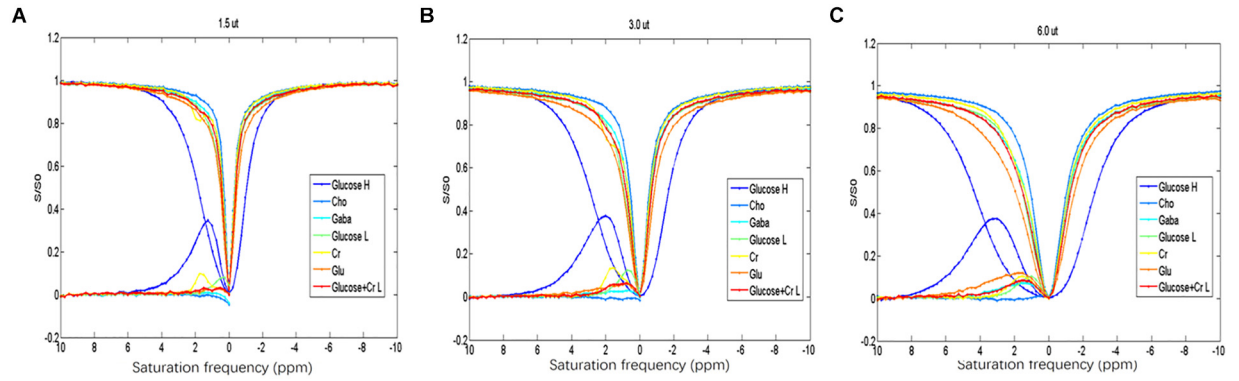

FIGURE 1 | (A–C) Z-spectrum and MTR of the different metabolites indicating that D-glucose can be distinguished from the other metabolites at saturation energy B1 of 1.5 μT.

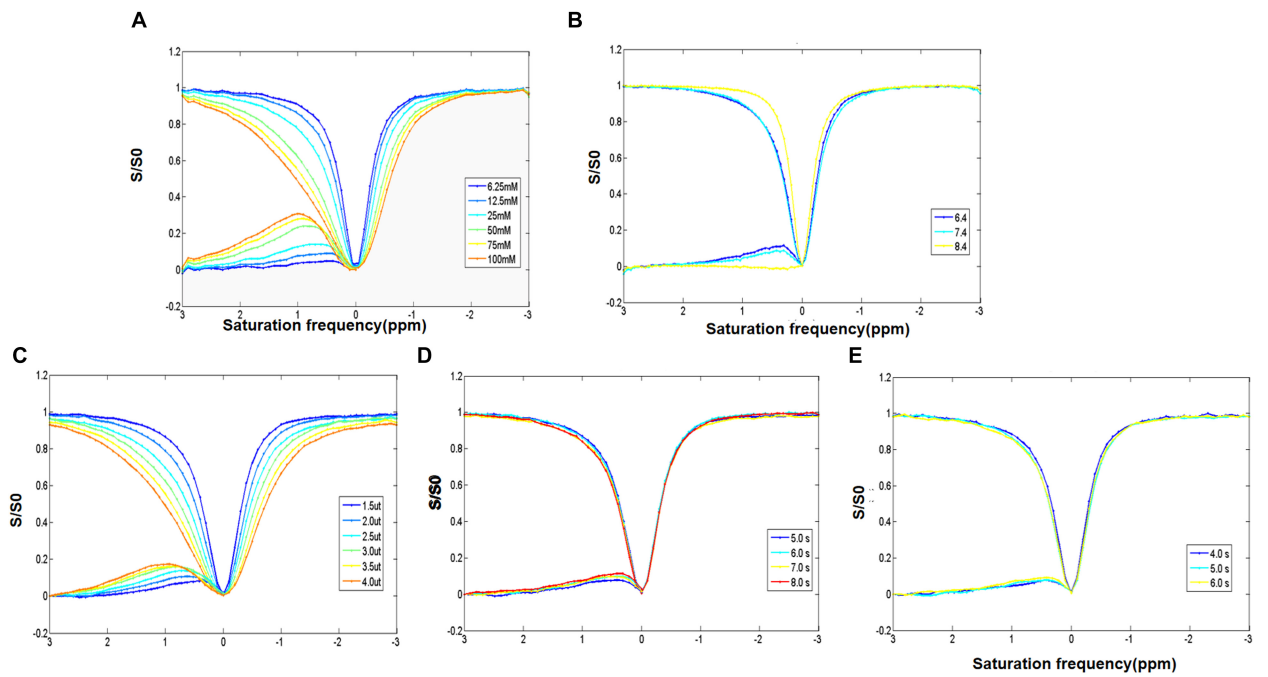

FIGURE 2 | (A) Z-spectrum and MTR of different concentrations of D-glucose showing the direct saturation exchange rate of D-glucose and that water protons increase with the increase of D-glucose concentration. **(B)** Z-spectrum and MTR of D-glucose with different PH values examining the impact of pH. It indicates that the D-glucose effect is negatively correlated with pH. **(C–E)** Z-spectrum and MTR investigating the optimization of the saturation energy and echo and saturation time parameters. The D-glucose CEST effect increases with the increase in saturation energy and saturation and echo times.

Nissl Staining

Finally, rats were sacrificed and underwent myocardial perfusion with saline followed by 4% paraformaldehyde. The brains were removed and fixed in 4% paraformaldehyde overnight. Next, the brain tissues were dehydrated in ethanol, embedded in paraffin, subjected to coronal sectioning into 5 μm thickness and required to undergo Nissl staining (Beyotime Co., Ltd., Shanghai, China) according to the standard protocols. The Nissl staining results were observed by an uninformed examiner. Three consecutive but non-overlapping fields of vision (magnification of 40×) in the hippocampal CA1 region and cerebral parietal cortex were randomly selected from each rat brain tissue, and the neurons were counted with Image J software and showed as mean values per high-power field (HPF).

Data Analysis

All glucoCEST images were processed using a custom MATLAB (The Mathworks, Inc., Natick, MA, United States) routine. Regions of interest (ROIs) were drawn manually based on the T2-weighted images. Total brain, bilateral hippocampal and cortex were drawn as ROI to observe the abnormal GCE in AD rats. After B0 correction, Z-spectra were obtained by

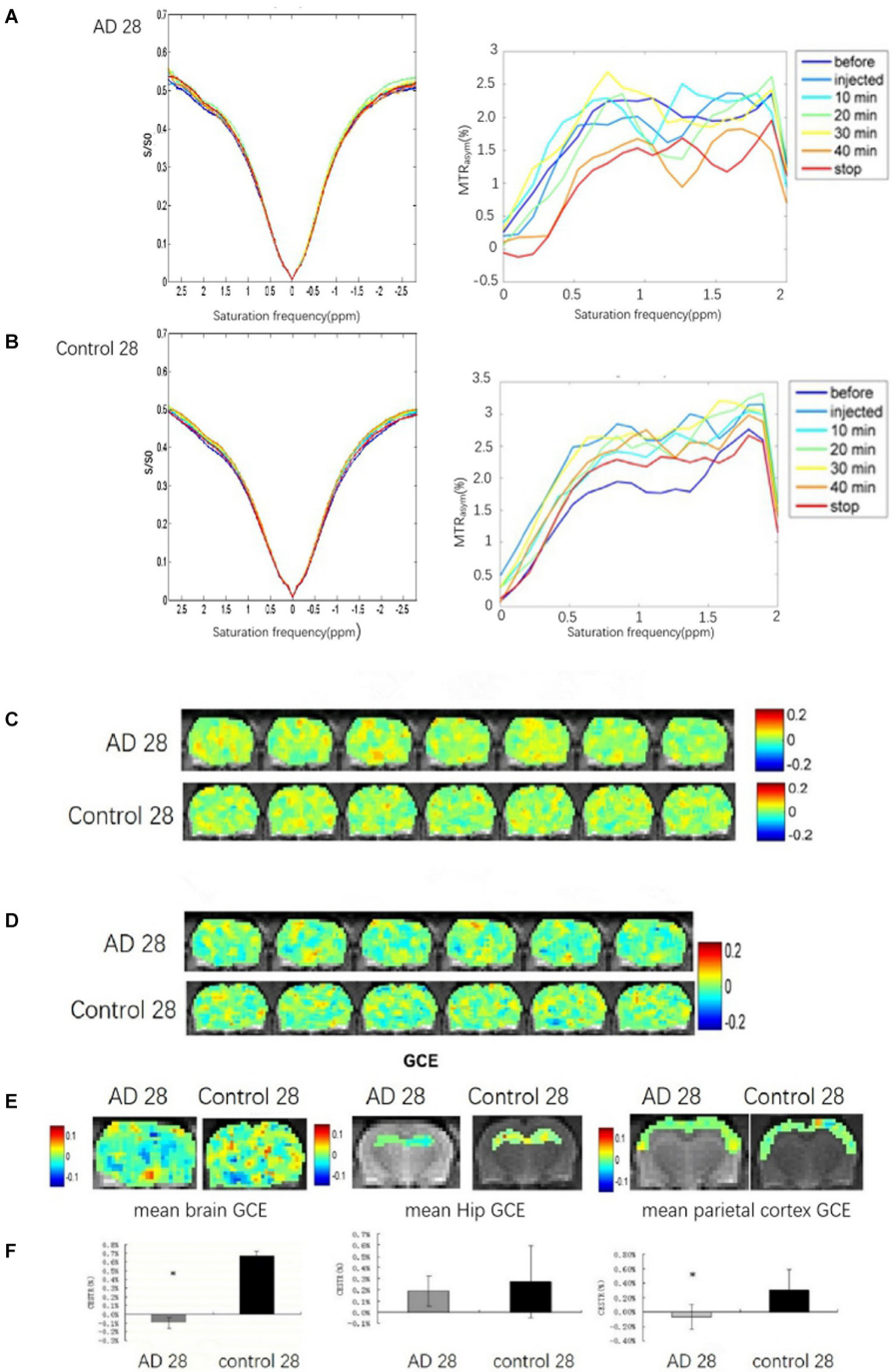

FIGURE 3 | The brain GCE signal of a rat in AD and control groups at 28 days after Aβ25–35 administration, respectively. **(A,B)** Showing Z-spectra and MTR_{asym} of AD and control rat brains. **(C,D)** Showing glucoCEST and GCE images of AD and control rat brain at 28 days after Aβ25–35 administration in specific time point, respectively. **(E)** The mean GCE signal of the total brain, hippocampus, and parietal cortex in an AD rat and a healthy rat. **(F)** The corresponding bar chart to the mean GCE signal of the total brain, hippocampus and parietal cortex in AD and control rats. It indicates that the glucose uptake of the whole brain in AD rats was significantly decreased, $P < 0.05$; the glucose uptake of the AD rats hippocampi is reduced, but $p > 0.05$; the glucose uptake of the parietal cortex in AD is decreased, $p < 0.05$ (*$p < 0.05$, error bar was standard error).

the ratio of the signals from different irradiation frequency offsets and the signal of water protons without saturation (S0). The magnetization transfer ratio asymmetry (MTRasym) was calculated as MTRasym (0.9 ppm) = [Ssat (−0.9 ppm) −Ssat (+0.9 ppm)]/S0. Meanwhile, the GlucoCEST enhanced (GCE) images were calculated as the subtraction of the glucoCEST image

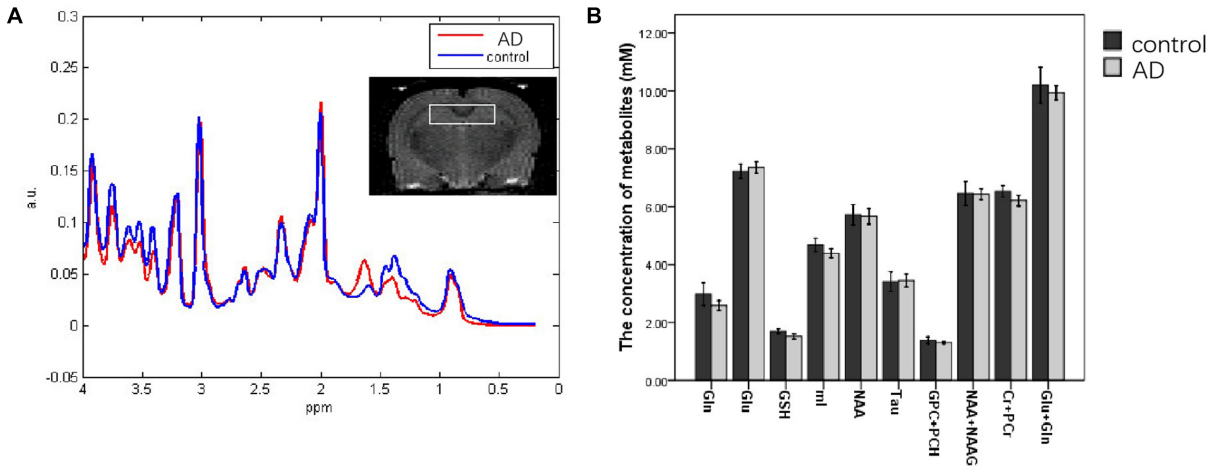

FIGURE 4 | MRS images analyzing the metabolite content in the hippocampi of control and AD rats at 28 days after Aβ25–35 administration **(A)**; the white box in the rat brain is the volume of interest of MRS scanning. **(B)** Metabolite concentration in the hippocampus at 28 days after Aβ25–35 administration; it showed no difference was found between the two groups (all $P > 0.05$, error bar was standard error).

before D-glucose injection and the mean glucoCEST images of 40 min after injection and 10 min after the finishing D-glucose injection.

1-H MRS data were analyzed with LCModel software (version 6.3, LCModel company, Canada) to acquire the concentrations of metabolites, such as N-acetyl aspartate (NAA), glutamate (Glu), glutamine (Gln), creatine (Cr), taurine (Tau), myo-Inosito (mI), glutathione (GSH), NAA + N-acetylaspartylglutamate (NAAG), glycerophosphocholine + phosphocholine (GPC + PCh), Glu + Gln, and Cr + phosphocreatine (PCr). A standard deviation (SD) value of less than 20 was accepted as being indicative of more reliable data.

In diffusion imaging, a brain apparent diffusion coefficient (ADC) map and fractional anisotropy (FA) map was acquired by VnmrJ (version 4.0, Agilent Technologies, United States) and subsequently analyzed by MATLAB software to calculate the ADC and FA in the total brain.

Statistical Analysis

All data were analyzed statistically using SPSS 20.0 software (IBM, United States). Taking the small sample size in this study into consideration, outlier detection was firstly performed with a stem-and-leaf plot. Then normal distribution and homogeneity of variance were verified by a Shapiro-Wilk test and Levene's test, respectively. If a normal distribution and variance homogeneity tests were satisfied simultaneously, the group differences were analyzed with an independent sample *t*-test. Otherwise, a non-parametric test was used. In MWM data, square-root transformation was used to fit normal distribution and homogeneity of variance. One-way ANOVA repeated measures were performed to detect the group differences of escape latency over 4 days. The correlation among glucose metabolism and other metabolites in bilateral hippocampal were assessed using linear regression analysis. A $p < 0.05$ was considered to be a statistically significant difference.

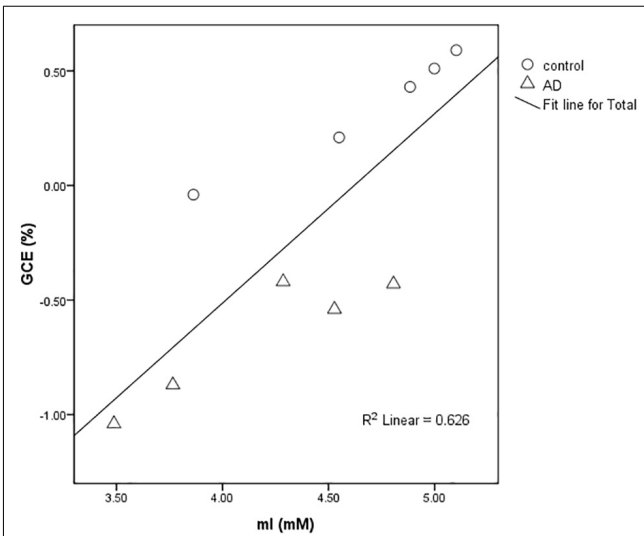

FIGURE 5 | Scatter plot of the relationship between the mean GCE signal of rat total brain and hippocampal MI concentration detected by MRS in the AD group and control group at 28 days after Aβ25–35 administration. The graph showed a positive correlation between MI concentration and GCE signal ($R^2 = 0.626$).

RESULTS

Optimization of Scan Parameters in Phantom

Among the different metabolites, the CEST effect of D-glucose could be better distinguished at a saturation power of 1.5 μT (**Figure 1A**). The overlap of CEST effects of different metabolites is more serious with the increased saturation power from 1.5 to 6 μT (**Figures 1B,C**).

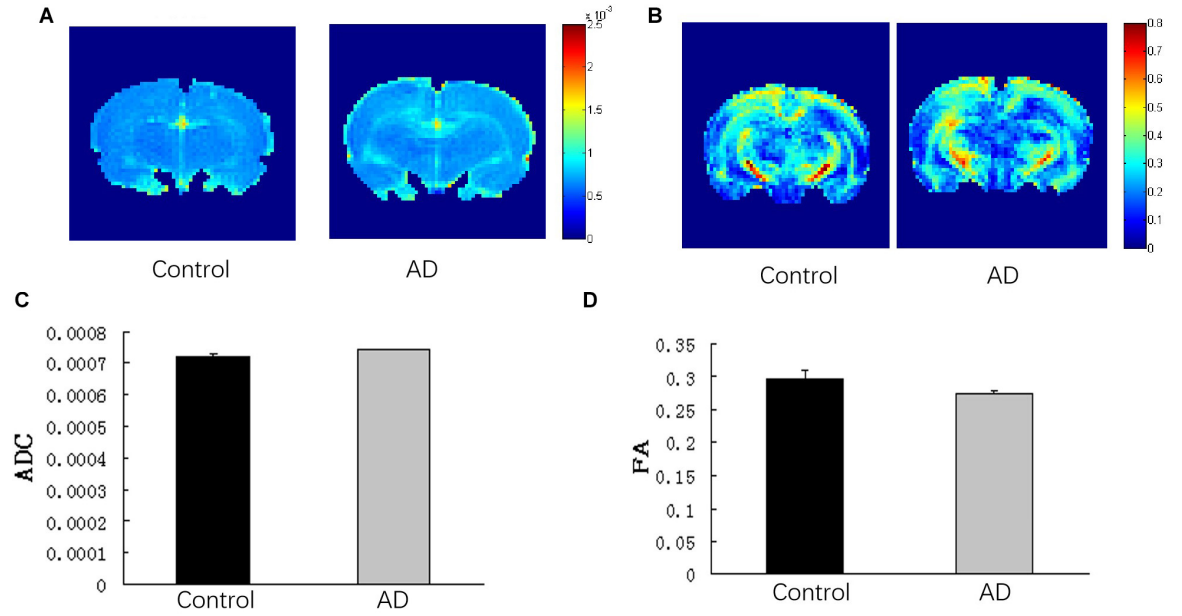

FIGURE 6 | Analysis of DTI imaging of rat brains in the AD group and control group at 28 days after Aβ25–35 administration. **(A)** ADC images and **(B)** FA images of the control and AD rat brains. **(C)** Bar chart demonstrating the corresponding ADC value of the control and AD rats. $P > 0.05$. **(D)** Bar chart representing the corresponding FA value of the control and AD rats. $P > 0.05$, error bar was the standard error ($n = 6$ per group).

The increase of D-glucose concentration resulted in the broadening of the glucoCEST signal in the asymmetric spectrum curve in the range of 0.5–1.0 ppm (**Figure 2A**). Moreover, a shift of the peak of D-glucose asymmetric spectrum curve (from 0.5 to 1.3 ppm) was found, and the D-glucose concentration (25–100 mM) was positively associated with the glucoCEST effect (10–25%) (**Figure 2A**).

A negative correlation was observed between the pH and the glucoCEST exchange rate. A decreased glucoCEST asymmetry signal was observed with the increase of pH value (**Figure 2B**). At a pH of 7.4, the glucoCEST exchange rate was about 10%. With the increase of saturation power from 1.5 to 4.0 μT, there was a gradual rise in MTRasym (0.9 ppm), and the peak of the asymmetry curve shifted to a higher frequency (**Figure 2C**). Elevated MTRasym (0.9 ppm) (7.5, 9, 9.5, and 11.5%, respectively), was found with increasing repetition times (5, 6, 7, and 8 s); however, the scan time was also significantly increased (**Figure 2D**). Meanwhile, with an increase of the saturation duration from 4 to 6 s, MTRasym (0.9 ppm) increased from 7 to 11% (**Figure 2E**) with a prolonged scan time. Taken the scan time and MTRasym (0.9 ppm) into consideration, the optimal scan parameters of the glucoCEST were as follows: pH of 7.4, TR of 5.04 s, saturation power of 1.5 μT and saturation during of 5 s.

Decreased Brain GCE Signal in AD Rats

The brains glucoCEST asymmetric spectrum and Z-spectrum of all rats in the AD group and the control group were detected at 28 days after Aβ25–35 administration (**Figures 3A,B**). The lowest brain GCE in AD rats was observed at 40 min and after stopping the infusion particularly in the thalamic and the hippocampal regions (**Figures 3C,D**). Additionally, in control rat brains, the change of GCE signal showed homeostasis without a downward trend.

Because of abnormally elevated GCE signal, one case in the AD group was excluded. Compared to the control rats ($n = 6$), significant decreases in the GCE signal of total brain and AD rats ($n = 5$) were observed at continuous injection for 40 min and at 10 min after the stop of the injection ($P < 0.05$; **Figures 3E,F**). The decreased GCE signal was also found in the bilateral parietal cortex of AD rats with significant statistical differences ($P < 0.05$; **Figures 3E,F**), but there were no significant statistical differences in the bilateral hippocampus ($P > 0.05$; **Figures 3E,F**).

Metabolite Concentrations in the Bilateral Hippocampal

One case in the control group was cut off because of the more than 20 metabolites in the SDs. Compared to the control group ($n = 5$), a descending trend of the concentrations from bilateral hippocampal in AD rats ($n = 5$) was observed in the Gln, mI, Cr + PCr, and Glu + Gln at 28 days after Aβ25–35 administration. However, there was no significant difference in the concentrations of all metabolites between the AD group and the control group ($P > 0.05$; **Figure 4**).

The Correlation Between mI Concentration and GCE Signal

In rats of the control group ($n = 5$) and the AD group ($n = 5$), a strong positive correlation between GCE and mI ($R^2 = 0.626$) was

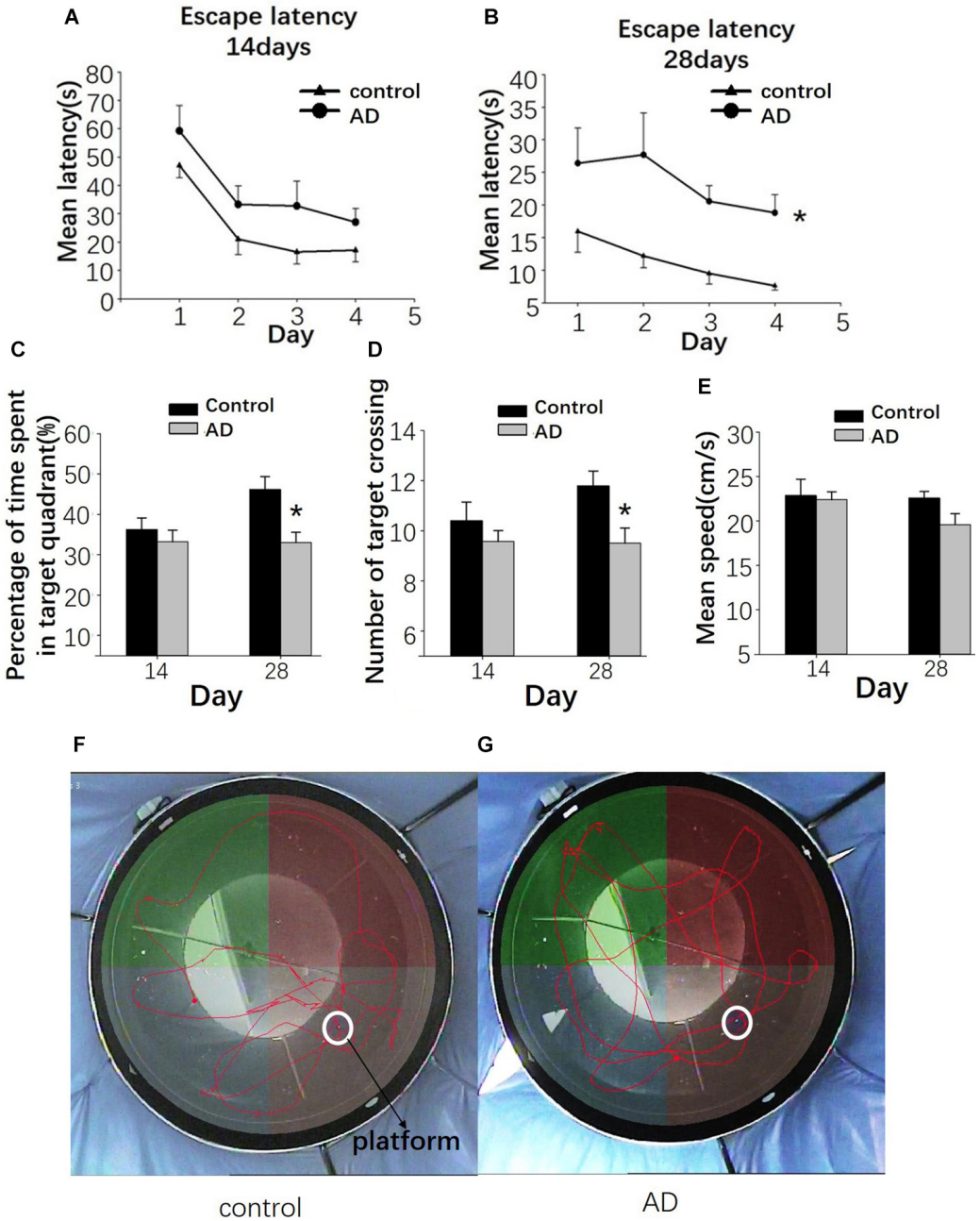

FIGURE 7 | Evaluation of the learning and memory dysfunction in rats of the control and AD groups at 14 and 28 days after Aβ25–35 administration by Morris water maze (MWM). The escape latency of control and AD rats **(A,B)**. **(C)** Bar charts presenting the percentage of target quadrant crossings. **(D)** Bar charts presenting the number of target crossings. **(E)** Bar chart presenting the analysis of swimming speed among rats of the control and AD groups. **(F)** Tracing of the swimming pattern in the control rats. **(G)** Tracing of the swimming pattern of the AD rats. $n = 6$ per group, $^*P < 0.05$, error bar was the standard error.

found with significant statistical differences ($P < 0.01$) at 28 days after Aβ25–35 administration (**Figure 5**).

Comparison of ADC and FA of Total Brain

There was no significant difference in the ADC values and FA values of the total brain between the AD and control groups ($P > 0.05$; **Figure 6**).

Impaired Spatial Learning and Memory in AD Rats

At 14 days after Aβ25–35 administration, the escape latency was relatively longer in the AD rats than in the control group; however, the difference was not statistically significant ($P > 0.05$; **Figure 7A**). At 28 days after Aβ25–35 injection, a significantly longer latency to find a platform in the AD rats was found

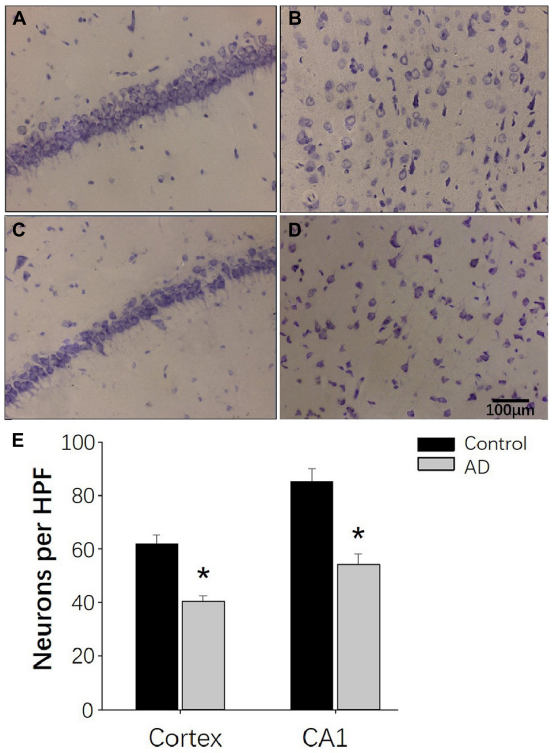

FIGURE 8 | Nissl staining demonstrating the decreased neurogenesis in AD rats at 28 days after Aβ25–35 administration. **(A,B)** Representative photomicrographs of the hippocampal CA1 region **(A)** and the internal pyramidal layer of parietal cortex **(B)** in control rats demonstrating normal neural cytoarchitecture. **(C,D)** Representative photomicrographs of the hippocampus CA1 region **(C)** and the internal pyramidal layer of the parietal cortex **(D)** in the AD group, demonstrating reduced numbers of neurons and neural damage. **(E)** Bar chart presenting the number of neurons per HPF in the internal pyramidal layer of parietal cortex and hippocampal CA1 area of AD and control group. $n = 6$ per group, $^*p < 0.05$, scale bar = 100 μm.

compared to those in the control rats ($P < 0.05$; **Figure 7B**), indicating a slower learning pattern in the AD rats. Furthermore, fewer crossing times to the platform and the time to cross the target quadrant in AD rats were observed at the 28 days following Aβ25–35 administration, and they were statistically significant ($P < 0.05$; **Figures 7C,D,F,G**), though no significant difference in the average swimming speed was found between two groups ($P > 0.05$; **Figure 7E**).

Decreased Number of Hippocampal CA1 and Parietal Nissl Body in AD Rats

Nissl staining was used to observe the neural loss and damage in the AD rat brains after 28 days of Aβ25–35 administration. Rats in the control groups showed typical Nissl staining in the hippocampus with deeper staining, regular and tighter neural arrangement and normal cytoarchitecture (**Figure 8A**). In the AD group, the hippocampal neurons had reduced numbers of Nissl bodies, lighter staining, irregular cell arrangement in the CA1 region with intact cell structure and blurred cell nuclei (**Figure 8C**). Similar observations were found in the cerebral cortex (**Figures 8B,D**). In the control group, Nissl bodies were observed in the cortical nerve cells with typical deep staining and normal cytoarchitecture (**Figure 8B**). In the AD group, the number of Nissl bodies in the cortical neurons was decreased with a shallow staining and abnormal cytoarchitecture (**Figure 8D**). Otherwise, compared to the control group, the numbers of neuronal cells per HPF of hippocampal CA1 and parietal cortex neurons in the AD group were decreased ($P < 0.05$; **Figure 8E**).

DISCUSSION

In this study, we investigated the changes in the cerebral glucose metabolism with GlucoCEST in a rat model of AD. A significantly decreased mean GCE signal of total brain and bilateral parietal cortex of AD rats was observed after 40 min of continuous injection of D-glucose and 10 min after the stop of injection. Moreover, there is a strong positive correlation between GCE and mI in the rats of the control group ($n = 5$) and the AD group ($n = 5$), suggesting the presence of abnormal glucose metabolism in the brain of AD rats.

Different from previous animal AD studies with transgenic mice models, we chose the AD rat models for acquiring the brain glucoCEST images with high SNR. The method of AD rat modeling is based on a previous study (Lu et al., 2009), and the water maze test and pathological examination were performed to verify the abnormal behavioral and pathological changes in rats with the intracerebroventricular injection of aggregated Aβ25–35 (9 μl). The injection of 9 μl Aβ25–35 was demonstrated to cause severe neurotoxicity leading to impaired learning and memory function, the release of inflammatory mediators and impairment of neuronal cells (Lu et al., 2009). Indeed, in our study, rats in the AD group had a reduced number of neurons in the cortex and the hippocampus with altered neural architecture after Aβ25–35 injection. These results are consistent with previous studies (Maurice et al., 1996). Moreover, AD rats had significantly longer escape latency and a decreased number of crossing times compared to rats in the control group at 28 days after the injection of Aβ25–35. These results indicate that the capacity for space exploration was impaired in AD rats, and the same was true for their learning and memory abilities. Taken together, our results confirm the feasibility of single Aβ25–35 administration in inducing AD symptoms in rats (Kim et al., 2015).

D-glucose is a glucose metabolite produced by the body's metabolism that can pass through the blood–brain barrier (Nasrallah et al., 2013). GlucoCEST is based upon the fact that each glucose molecule contains five hydroxyl groups that can be chemically exchanged with hydrogen protons in the free-water molecule (Walker-Samuel et al., 2013). Consequently, this reduces the strength of the MRI free-water signal that can reflect the content of D-glucose. Therefore, D-glucose can be used as an MRI contrast agent to increase the imaging sensitivity. Walker-Samuel et al. (2013) indicated the presence of an intracellular origin of glucoCEST using D-glucose, and Nasrallah et al. (2013) reported that most of the glucoCEST signals seen in the brain after injecting 2DG are of an intracellular origin. In this study, the GCE technique was used

to detect the uptake of exogenously administered D-glucose in the brain.

Previous studies used glucoCEST to examine the glucose metabolism in tumors, and the brain sugar content was mainly examined with ^{18}FDG–PET (Coleman et al., 2017). In the few AD relative studies using glucoCEST imaging, Wells et al. (2015) explored the glucose metabolism in AD and found that elevated CEST signal in the cortex of AD mouse, which is consistent with our results. But the quality of glucoCEST images in Wells' study needs to be improved. In this study, an EPI sequence with a continuous-wave saturation pulse was used, and it had been proven to be able to improve the CEST contrast ratios and the quality of glucoCEST images (Sun et al., 2008). Furthermore, the important scan parameters of glucoCEST imaging, such as saturation power, saturation duration and TR were optimized in phantom to improve the quality of brain glucoCEST images.

The glucose tolerance test was performed in fasted rats in this study using intraperitoneal glucose injections. To prolong the time window of blood glucose peaks and maintain a higher concentration of glucose in the brain, we used a syringe pump to continue the small dose supplementation. In the control group, the brain GCE signal continued to rise and was consistent with the trend of blood glucose monitoring, confirming the reliability of our method. The GCE signals, however, were significantly reduced in the AD group, and these results were in accordance with the previously reported ^{18}FDG–PET studies (Waldron et al., 2015; Coleman et al., 2017).

In glucoCEST images before D-glucose injection, we found more elevated MTRasym (0.9 ppm) signals in the total brain of AD rats than in the control group. Except for technical issues such as B0/B1, direct water saturation and MT, the CEST signal is considered related to the concentration of exchanged protons or molecules, T1 relaxation time of tissues and the exchanged environment, including pH and temperature. Although elevated glucose/Cr in the AD brain was reported (Mullins et al., 2018), the effect of other issues was not excluded. Further experiments are thus needed to confirm the elevated MTRasym (0.9 ppm) signal mainly comes from elevated glucose concentration. As for the molecular mechanism of abnormal glucose metabolism and AD, the insulin receptor substrate 2 (IRS2) and Glycogen Synthase Kinase-3 (GSK-3) may play important roles in the insulin signaling in the brain and AD processes (reviewed by Danièlle et al., 2018). We will also explore the relationship between molecular signals and glucoCEST signals in further studies.

A decreased concentration trend of the metabolites (Gln, mI, Cr + PCr, and Glu + Gln) from the bilateral hippocampus in AD rats was observed in this study. Although there were no statistical differences, we think the group differences may be observed with increased sample size. Decreased NAA/tCr and Glu/tCr ratios were also reported in previous animal studies with mice models of AD (von Kienlin et al., 2005). However, those changes were age-dependent index observed in 24-month-old animals instead of 12-month-old animals. Interestingly, an increased mI/tCr ratio was also reported in 20-month-old APP-PS1 mice (Marjanska et al., 2005) and amyloid-positive healthy elderly (Voevodskaya et al., 2016) in the cortex, though this is still a matter of controversy. We found a decreased mI in the bilateral hippocampus of an AD rat at 28 days after modeling, and it was related to GCE in this study. As a second messenger glucose isomer, mI is involved in glucose and insulin metabolism and promotes muscle glucose uptake (Chukwuma et al., 2016). We thus believe that decreased mI may mainly contribute to elevated MTRasym (0.9 ppm) signals and decreased GCE in AD rats. This is also abnormally increased in old age, and this may be as a compensation mechanism.

This study had some limitations: (1) the relatively small number of examined animals, which could impact the significance of our results; (2) the total scan time was too long, and in future studies, we need to use a more efficient method to increase brain glucose uptake; and (3) we used the Aβ25–35-induced AD rat instead of a double transgenic AD mouse model. Therefore, we will improve our experimental condition and enquire with a mouse head coil with a high channel in future studies.

CONCLUSION

In this study, we found a reduced GCE signal of glucose in the whole brain and parietal cortex of AD rats *in vivo*, and reduced GCE in the total brain is associated with decreased concentrations of mI in the bilateral hippocampus of AD rats and control rats. Therefore, CEST-based MRI GCE can be a potentially valuable tool to explorer the early pathogenesis and pathological mechanisms of many diseases, such as diabetes-related AD and other kinds of dementia as well as neurodegenerative diseases.

DATA AVAILABILITY STATEMENT

The original contributions presented in the study are included in the article/supplementary material, further inquiries can be directed to the corresponding author/s.

ETHICS STATEMENT

The animal study was reviewed and approved by the Ethics Committee of Animal Care and Welfare, Shantou University Medical College.

AUTHOR CONTRIBUTIONS

All authors listed have made a substantial, direct and intellectual contribution to the work, and approved it for publication.

FUNDING

This study was supported in part by Grants-in-Aide from the National Natural Science Foundation of China (NSFC 82020108016), the Grant for Key Disciplinary Project of Clinical Medicine under the Guangdong High-level University Development Program (No. 002-18120302), and the Guangdong Natural Science Foundation (2017A030313718).

REFERENCES

Abbott, A. (2011). Dementia: a problem for our age. *Nature* 475, S2–S4.

Chan, K., Mcmahon, M., Kato, Y., Liu, G., Bulte, J., Bhujwalla, Z., et al. (2012). Natural D-glucose as a biodegradable MRI contrast agent for detecting cancer. *Magn. Reson. Med.* 68, 1764–1773. doi: 10.1002/mrm.24520

Chukwuma, C., Ibrahim, M., and Islam, M. (2016). Myo-inositol inhibits intestinal glucose absorption and promotes muscle glucose uptake: a dual approach study. *J. Physiol. Biochem.* 72, 791–801. doi: 10.1007/s13105-016-0517-1

Coleman, R., Liang, C., Patel, R., Ali, S., and Mukherjee, J. (2017). Brain and brown adipose tissue metabolism in transgenic Tg2576 mice models of Alzheimer disease assessed using F-FDG PET imaging. *Mol. Imaging* 16:1536012117704557.

D'Agostino, G., Russo, R., Avagliano, C., Cristiano, C., Meli, R., and Calignano, A. (2012). Palmitoylethanolamide protects against the amyloid-β25-35-induced learning and memory impairment in mice, an experimental model of Alzheimer disease. *Neuropsychopharmacology* 37, 1784–1792. doi: 10.1038/npp.2012.25

Dai, Z., Ji, J., Xiao, G., Yan, G., Li, S., Zhang, G., et al. (2014). Magnetization transfer prepared gradient echo MRI for CEST imaging. *PLoS One* 9:e112219. doi: 10.1371/journal.pone.0112219

Danièlle, G. M., Oksana, K. B., María, C. G. I., Frank, G. M., and Simon, L. (2018). Alzheimer's disease in humans and other animals; a consequence of post-reproductive lifespan and longevity rather than ageing. *Alzheimers Dement.* 14, 195–204.

de Paula, V. J. R., Guimarães, F. M., Diniz, B. S., and Forlenza, O. V. (2009). Neurobiological pathways to Alzheimer's disease: amyloid-beta, TAU protein or both? *Dement. Neuropsychol.* 3, 188–194. doi: 10.1590/s1980-57642009dn30300003

de-Paula, V. J., Radanovic, M., Diniz, B. S., and Forlenza, O. V. (2012). Alzheimer's disease. *Subcell. Biochem.* 2012, 329–352.

Duran-Aniotz, C., and Hetz, C. (2016). Glucose metabolism: a sweet relief of Alzheimer's disease. *Curr. Biol. CB* 26, R806–R809.

Gardener, S., Sohrabi, H., Shen, K., Rainey-Smith, S., Weinborn, M., Bates, K., et al. (2016). Cerebral glucose metabolism is associated with verbal but not visual memory performance in community-dwelling older adults. *J. Alzheimers Dis.* 52, 661–672. doi: 10.3233/jad-151084

Haris, M., Nanga, R. P., Singh, A., Cai, K., Kogan, F., Hariharan, H., et al. (2012). Exchange rates of creatine kinase metabolites: feasibility of imaging creatine by chemical exchange saturation transfer MRI. *NMR Biomed.* 25, 1305–1309. doi: 10.1002/nbm.2792

Haris, M., Singh, A., Cai, K., Nath, K., Crescenzi, R., Kogan, F., et al. (2013). MICEST: a potential tool for non-invasive detection of molecular changes in Alzheimer's disease. *J. Neurosci. Methods* 212, 87–93. doi: 10.1016/j.jneumeth.2012.09.025

Herholz, K. (2010). Cerebral glucose metabolism in preclinical and prodromal Alzheimer's disease. *Expert Rev. Neurother.* 10, 1667–1673. doi: 10.1586/ern.10.136

Jack, C., Knopman, D., Jagust, W., Petersen, R., Weiner, M., Aisen, P., et al. (2013). Tracking pathophysiological processes in Alzheimer's disease: an updated hypothetical model of dynamic biomarkers. *Lancet Neurol.* 12, 207–216. doi: 10.1016/s1474-4422(12)70291-0

Kantarci, K., Senjem, M. L., Lowe, V. J., Wiste, H. J., Weigand, S. D., Kemp, B. J., et al. (2010). Effects of age on the glucose metabolic changes in mild cognitive impairment. *AJNR Am. J. Neuroradiol.* 31, 1247–1253. doi: 10.3174/ajnr.a2070

Kim, J., Wang, Q., Choi, J., Lee, S., and Cho, E. (2015). Protective role of caffeic acid in an Aβ25-35-induced Alzheimer's disease model. *Nutr. Res. Pract.* 9, 480–488. doi: 10.4162/nrp.2015.9.5.480

Le Douce, J., Maugard, M., Veran, J., Matos, M., Jégo, P., Vigneron, P., et al. (2020). Impairment of glycolysis-derived l-serine production in astrocytes contributes to cognitive deficits in Alzheimer's disease. *Cell Metab.* 31, 503–517.e8.

Li, X., Men, W., Zhu, H., Lei, J., Zuo, F., Wang, Z., et al. (2016). Age- and brain region-specific changes of glucose metabolic disorder, learning, and memory dysfunction in early Alzheimer's disease assessed in APP/PS1 transgenic mice using F-FDG-PET. *Int. J. Mol. Sci.* 16, 1–9.

Lu, P., Mamiya, T., Lu, L., Mouri, A., Zou, L., Nagai, T., et al. (2009). Silibinin prevents amyloid beta peptide-induced memory impairment and oxidative stress in mice. *Br. J. Pharmacol.* 157, 1270–1277. doi: 10.1111/j.1476-5381.2009.00295.x

Marjanska, M., Curran, G., Wengenack, T., Henry, P., Bliss, R., Poduslo, J., et al. (2005). Monitoring disease progression in transgenic mouse models of Alzheimer's disease with proton magnetic resonance spectroscopy. *Proc. Natl. Acad. Sci. U.S.A.* 102, 11906–11910. doi: 10.1073/pnas.0505513102

Maurice, T., Lockhart, B. P., and Privat, A. (1996). Amnesia induced in mice by centrally administered beta-amyloid peptides involves cholinergic dysfunction. *Brain Res.* 706, 181–193. doi: 10.1016/0006-8993(95)01032-7

McMahon, M. T. (2017). *Chemical Exchange Saturation Transfer Imaging Advances and Applications*, Singapore: Pan Stanford Publishing Pte. Ltd.

Mergenthaler, P., Lindauer, U., Dienel, G. A., and Meisel, A. (2013). Sugar for the brain: the role of glucose in physiological and pathological brain function. *Trends Neurosci.* 36, 587–597. doi: 10.1016/j.tins.2013.07.001

Miller, C., Cao, J., Chekmenev, E., Damon, B., Cherrington, A., and Gore, J. (2015). Noninvasive measurements of glycogen in perfused mouse livers using chemical exchange saturation transfer NMR and comparison to (13)C NMR spectroscopy. *Anal. Chem.* 87, 5824–5830. doi: 10.1021/acs.analchem.5b01296

Mullins, R., Reiter, D., and Kapogiannis, D. (2018). Magnetic resonance spectroscopy reveals abnormalities of glucose metabolism in the Alzheimer's brain. *Ann. Clin. Transl. Neurol.* 5, 262–272. doi: 10.1002/acn3.530

Nasrallah, F., Pagès, G., Kuchel, P., Golay, X., and Chuang, K. (2013). Imaging brain deoxyglucose uptake and metabolism by glucoCEST MRI. *J. Cereb. Blood Flow Metab.* 33, 1270–1278. doi: 10.1038/jcbfm.2013.79

Ohta, H., Arai, S., Akita, K., Ohta, T., and Fukuda, S. (2012). Effects of NK-4 in a transgenic mouse model of Alzheimer's disease. *PLoS One* 7:e30007. doi: 10.1371/journal.pone.0030007

Seynnaeve, D., Vecchio, M. D., Fruhmann, G., Verelst, J., Cools, M., Beckers, J., et al. (2018). Recent insights on Alzheimer's disease originating from yeast models. *Int. J. Mol. Sci.* 19:1947. doi: 10.3390/ijms19071947

Sun, P. Z., Benner, T., Kumar, A., and Sorensen, A. G. (2008). Investigation of optimizing and translating pH-sensitive pulsed-chemical exchange saturation transfer (CEST) imaging to a 3T clinical scanner. *Magn. Reson. Med.* 60, 834–841. doi: 10.1002/mrm.21714

Tang, X., Dai, Z., Xiao, G., Yan, G., Shen, Z., Zhang, T., et al. (2017). Nuclear overhauser enhancement-mediated magnetization transfer imaging in glioma with different progression at 7 T. *ACS Chem. Neurosci.* 8, 60–66. doi: 10.1021/acschemneuro.6b00173

Voevodskaya, O., Sundgren, P., Strandberg, O., Zetterberg, H., Minthon, L., Blennow, K., et al. (2016). Myo-inositol changes precede amyloid pathology and relate to APOE genotype in Alzheimer disease. *Neurology* 86, 1754–1761. doi: 10.1212/wnl.0000000000002672

von Kienlin, M., Künnecke, B., Metzger, F., Steiner, G., Richards, J., Ozmen, L., et al. (2005). Altered metabolic profile in the frontal cortex of PS2APP transgenic mice, monitored throughout their life span. *Neurobiol. Dis.* 18, 32–39. doi: 10.1016/j.nbd.2004.09.005

Waldron, A. M., Wintmolders, C., Bottelbergs, A., Kelley, J. B., Schmidt, M. E., Stroobants, S., et al. (2015). *In vivo* molecular neuroimaging of glucose utilization and its association with fibrillar amyloid-β load in aged APPPS1-21 mice. *Alzheimers Res. Ther.* 7:76. doi: 10.1186/s13195-015-0158-6

Walker-Samuel, S., Ramasawmy, R., Torrealdea, F., Rega, M., Rajkumar, V., Johnson, S., et al. (2013). In vivo imaging of glucose uptake and metabolism in tumors. *Nat. Med.* 19, 1067–1072. doi: 10.1038/nm.3252

Wang, H., Tan, L., Cao, L., Zhu, X., Jiang, T., Tan, M., et al. (2016). Application of the IWG-2 diagnostic criteria for Alzheimer's disease to the ADNI. *J. Alzheimers Dis. JAD* 51, 227–236. doi: 10.3233/jad-150824

Wells, J., O'callaghan, J., Holmes, H., Powell, N., Johnson, R., Siow, B., et al. (2015). In vivo imaging of tau pathology using multi-parametric quantitative MRI. *Neuroimage* 111, 369–378. doi: 10.1016/j.neuroimage.2015.02.023

Conflict of Interest: ZS was employed by company Philips Healthcare.

The remaining authors declare that the research was conducted in the absence of any commercial or financial relationships that could be construed as a potential conflict of interest.

frontiers in Aging Neuroscience

ORIGINAL RESEARCH
published: 19 March 2021
doi: 10.3389/fnagi.2021.610839

No Evidence That Cognitive and Physical Activities Are Related to Changes in EEG Markers of Cognition in Older Adults at Risk of Dementia

Daria Laptinskaya[1,2], Olivia Caroline Küster[3,4], Patrick Fissler[1,3,5], Franka Thurm[6,2], Christine A. F. von Arnim[3,7] and Iris-Tatjana Kolassa[1,2]**

[1] Clinical and Biological Psychology, Institute of Psychology and Education, Ulm University, Ulm, Germany, [2] Department of Psychology, University of Konstanz, Konstanz, Germany, [3] Department of Neurology, Ulm University, Ulm, Germany, [4] Clinic for Neurogeriatrics and Neurological Rehabilitation, University- and Rehabilitation Hospital Ulm, Ulm, Germany, [5] Psychiatric Services of Thurgovia, Academic Teaching Hospital of Paracelsus Medical University Salzburg, Muensterlingen, Switzerland, [6] Faculty of Psychology, TU Dresden, Dresden, Germany, [7] Division of Geriatrics, University Medical Center Göttingen, Göttingen, Germany

An active lifestyle as well as cognitive and physical training (PT) may benefit cognition by increasing cognitive reserve, but the underlying neurobiological mechanisms of this reserve capacity are not well understood. To investigate these mechanisms of cognitive reserve, we focused on electrophysiological correlates of cognitive performance, namely on an event-related measure of auditory memory and on a measure of global coherence. Both measures have shown to be sensitive markers for cognition and might therefore be suitable to investigate potential training- and lifestyle-related changes. Here, we report on the results of an electrophysiological sub-study that correspond to previously published behavioral findings. Altogether, 65 older adults with subjective or objective cognitive impairment and aged 60–88 years were assigned to a 10-week cognitive (n = 19) or a 10-week PT (n = 21) or to a passive control group (n = 25). In addition, self-reported lifestyle was assessed at baseline. We did not find an effect of both training groups on electroencephalography (EEG) measures of auditory memory decay or global coherence ($ps \geq 0.29$) and a more active lifestyle was not associated with improved global coherence ($p = 0.38$). Results suggest that a 10-week unimodal cognitive or PT and an active lifestyle in older adults at risk for dementia are not strongly related to improvements in electrophysiological correlates of cognition.

Keywords: coherence, lifestyle, dementia, mismatch negativity, cognitive training, physical training, electrophysiology

OPEN ACCESS

Edited by:
Kuangyu Shi,
University of Bern, Switzerland

Reviewed by:
Calogero Edoardo Cicero,
University of Catania, Italy
Siti Anom Ahmad,
Putra Malaysia University, Malaysia

****Correspondence:***
Daria Laptinskaya
daria.laptinskaya@uni-ulm.de;
daria.laptinskaya@gmail.com
Iris-Tatjana Kolassa
iris.kolassa@uni-ulm.de

Received: *27 September 2020*
Accepted: *27 January 2021*
Published: *19 March 2021*

Citation:
Laptinskaya D, Küster OC, Fissler P, Thurm F, Von Arnim CAF and Kolassa I-T (2021) No Evidence That Cognitive and Physical Activities Are Related to Changes in EEG Markers of Cognition in Older Adults at Risk of Dementia. Front. Aging Neurosci. 13:610839. doi: 10.3389/fnagi.2021.610839

Abbreviations: AD, Alzheimer's disease; ADAS, Alzheimer's Disease Assessment Scale; ANOVA, analysis of variance; CT, auditory cognitive training; DMN, default mode network; EEG, electroencephalography; fMRI, functional magnetic resonance imaging; ISI, interstimulus interval; MCI, mild cognitive impairment; MMN, mismatch negativity; MMSE, Mini-Mental State Examination; MVGT, Münchner Verbaler Gedächtnistest; PT, physical training; SL, synchronization likelihood; SOA, stimulus onset asynchrony; WLC, wait-list control; ΔMMN, difference score between MMNs to short and to long ISIs; ΔMMN–Dur, index for automatic auditory memory, amplitude difference between the MMN after duration deviant in the Memory Trace paradigm and Optimum–1 paradigm, higher values indicating better automatic auditory memory or less pronounced automatic auditory memory decay.

INTRODUCTION

The number of people with cognitive deficits and dementia is growing due to increasing life expectancy and demographic change. Thus, the meaning of the detection of pathological cognitive decline as well as its prevention and slowing down became an increasingly important issue. For decades the assessment of cognitive decline in healthy aging and in dementia had been mainly based on neuropsychological data. However, recently surrogate biomarkers in cerebrospinal fluid and neuroimaging have evolved. In our recent studies we described two sensitive electroencephalography (EEG) markers for cognition. These are resting-state global coherence (Laptinskaya et al., 2019) and a novel mismatch negativity (MMN) index for auditory memory decay, namely ΔMMN (Laptinskaya et al., 2018).

Resting-state global coherence cognition was defined as the coherence over the whole skull at rest in the frequency range between 4 and 30 Hz. Coherence represents functional coupling between brain regions or single electrode pairs. A wide range of studies reported alterations in resting-state EEG coherence in dementia (e.g., Knott et al., 2000; Stevens et al., 2001; Adler et al., 2003). The most prominent change is attenuated coherence in the alpha and beta frequency range in fronto-parietal and the temporo-parietal coupling (see Babiloni et al., 2016 for a review). Recent studies suggest that these changes might already occur in mild cognitive impairment (MCI; Michels et al., 2017). In line with previous study results investigating frequency- or region-specific coherence, we found global coherence to be a sensitive EEG marker for global cognition (Laptinskaya et al., 2018).

The MMN is one of the most widely investigated ERP components and is elicited when a presentation that has been automatically predicted by the central nervous system is violated (Näätänen et al., 1978, 2011). In an auditory paradigm the MMN can be evoked when in a sequence of equal tones a deviant tone is presented. The MMN represents two, closely linked, processes: auditory discrimination ability and auditory memory. With increasing interstimulus interval (ISI, the distance between the standard and the deviant tone) MMN provides more information on the auditory memory trace (for a review see Bartha-Doering et al., 2015). Many previous studies have shown attenuated MMN amplitude, especially after long ISIs in dementia (Pekkonen et al., 1994; Schroeder et al., 1995; Papadaniil et al., 2016) as well as in MCI as a possible prodromal stage of dementia (Lindín et al., 2013; Ji et al., 2015; Papadaniil et al., 2016). However, no MMN marker for cognition has been established yet. This might be due to the fact that the comparability between study results is difficult because of the methodological difference, such as different deviant types and ISI lengths. To address this challenge, we built a difference score between MMNs after short and after long ISIs. The difference score (hereafter referred to as ΔMMN) takes individual differences in auditory discrimination ability as well as auditory memory into account and has been shown to reflect cognition or even the cognitive decline over a period of 5 years (Laptinskaya et al., 2018).

Beneath new diagnostic tools for cognition, intervention methods which are capable to prevent or slow down cognitive decline are of great clinical and scientific interest. Previous studies suggest that cognitive and physical activity may benefit cognition or even delay dementia (Livingston et al., 2020). Regarding the impact of physical and cognitive activity on cognition, specific training programs and an active lifestyle can be distinguished. The last one is often defined as the number of regularly performed activities. While some studies reported positive training effects on cognition (e.g., Hess et al., 2014; Lampit et al., 2014; Edwards et al., 2016; Groot et al., 2016), others failed to find beneficial effects (e.g., Williamson et al., 2009; Barnes et al., 2013). Training factors such as the combination of cognitive and physical training (PT) aspects (e.g., Fissler et al., 2013; see Gheysen et al., 2018 for a review and a recent meta-analysis), longer training periods, and variability in training tasks (cf., Fissler et al., 2013) seem to be important determinants for training success. Results regarding active lifestyle are more consistent than results on training interventions: the majority of studies reported a positive association between an active lifestyle and cognition. But the comparability between training and lifestyle studies is limited. Training effects on cognition often refer to time limited experimental designs. In contrast, lifestyle cognition studies are associative in nature and consider longer time periods. Furthermore, lifestyle cannot be experimentally manipulated. To fill this scientific gap, we systematically investigated the effects of specific training programs with lifestyle cognition associations for 10 weeks in older adults with increased risk of developing dementia (cf., Küster et al., 2016). We found that persons with a more active lifestyle showed benefits in cognitive performance post-training when compared to persons with a less active lifestyle. In contrast, neither a 10-week auditory cognitive training (CT) nor a 10-week PT showed beneficial effects on cognition. We concluded that the lifestyle might be beneficial for cognition more than the short-term training programs by higher variability in cognitive demands, enjoyment, fun, and intrinsic motivation.

Until now the biological mechanisms of positive effects of cognitive and physical activity on cognition are not well understood. Understanding the mechanisms of treatment is decisive to develop individualized treatments that specifically target brain changes that underlie cognitive symptoms. In the present study, we examine the association between lifestyle and changes in EEG markers for cognition as well as the effect of a 10-week auditory CT and a 10-week PT on the two EEG parameters. The results might give further insights into electrophysiological mechanisms which underlie the positive link between cognitive and physical activity and changes in cognition. In the long term, this knowledge could be used for individualized therapies that are based on biomarker profiles of patients with cognitive impairment. The aim of the present study was to investigate the association between lifestyle and EEG markers for cognition. Furthermore, we tested the hypothesis,

whether specific training programs are suitable to enhance global cognition and ΔMMN.

MATERIALS AND METHODS

Participants

The study was approved by the ethics committees of both study centers, the University of Konstanz and Ulm University, Germany. The study was part of a controlled clinical trial investigating the effect of physical exercise and auditory CT on cognition as well as on electrophysiological and biological parameters (Küster et al., 2016, 2017; Fissler et al., 2017; Laptinskaya et al., 2018, 2019). Prior to the study, all participants provided written informed consent. Subjects were recruited in the Memory Clinic of Ulm University Hospital, Germany and the Center for Psychiatry Reichenau, Germany, or via public advertisements. The detailed description of the inclusion and exclusion criteria can be found in Küster et al. (2016). In brief, inclusion criteria were: 55 years of age or older and subjective or objective memory impairment, fluency in German language, stable anti-dementia and antidepressant medication, and independent living. Exclusion criteria were as follows: probable moderate or severe dementia [Mini Mental State Examination; MMSE (Folstein et al., 1975) < 20] and history of other neurologic or psychiatric disorders (except mild to moderate depression). Furthermore, participants with severe hearing or visual impairment, and physical impairment which could restrain the participation in the training programs were also excluded.

Out of 122 participants who were screened for eligibility, due to exclusion and drop-outs 65 subjects were included in the study (for the detailed flow of participants see **Figure 1**). Subsequently, the participants were assigned into one of the three groups: auditory CT (n = 19), PT (n = 21), and wait-list control (WLC; n = 25). In order to minimize differences in age, gender, education, and cognitive status (MMSE) between groups, we used a minimization approach. The investigators were blind to the subjects' group allocation. In rare cases this was not maintained because the participants disclosed their group assignment during neuropsychological assessment. Notably, because of drop-outs, the number of evaluated training

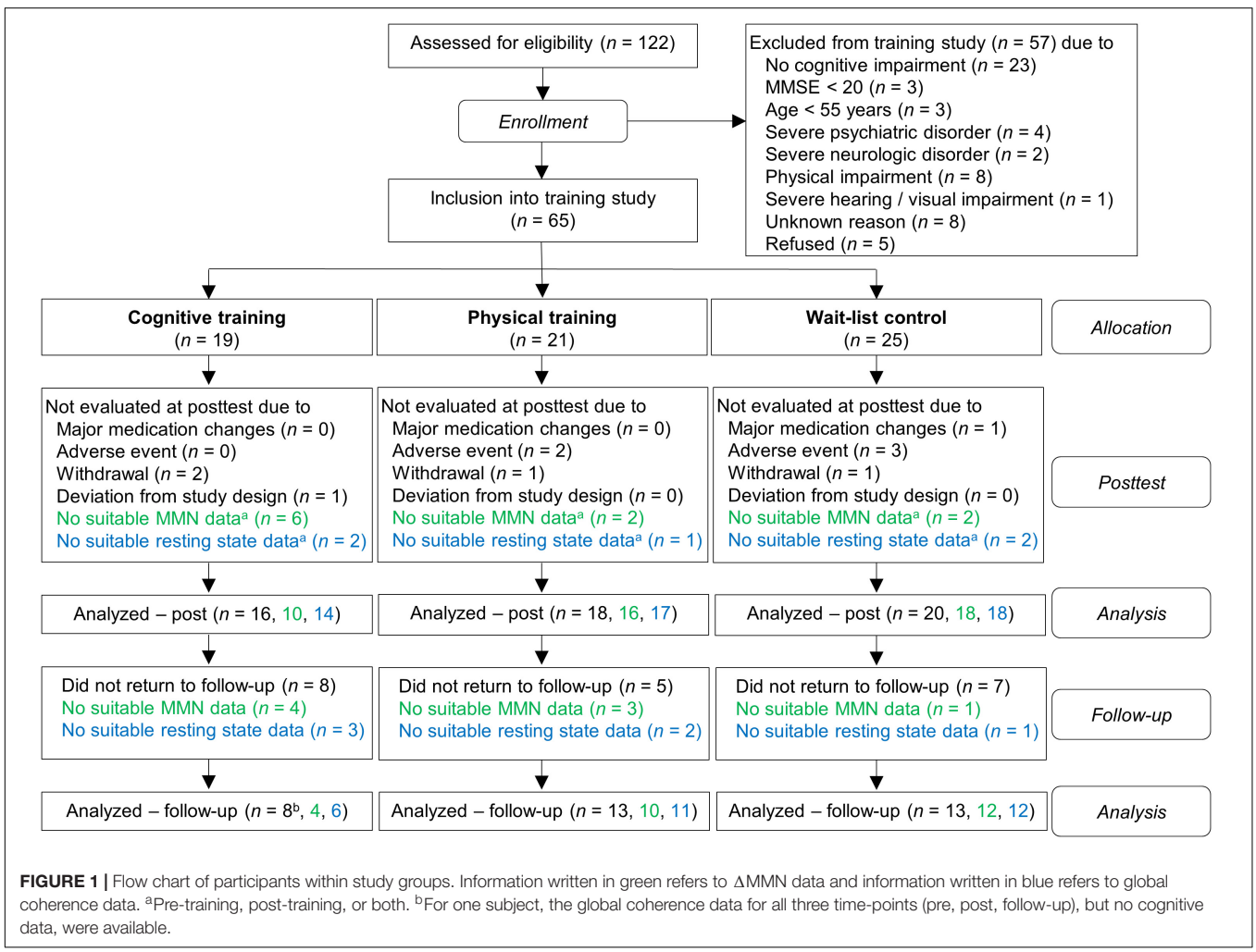

FIGURE 1 | Flow chart of participants within study groups. Information written in green refers to ΔMMN data and information written in blue refers to global coherence data. [a]Pre-training, post-training, or both. [b]For one subject, the global coherence data for all three time-points (pre, post, follow-up), but no cognitive data, were available.

data sets varied for MMN and for coherence analysis (for drop-out reasons see **Figure 1**).

According to classification criteria (see **Supplementary Presentation 1**) the participants were classified as having subjective memory impairment (SMI, $n = 12$), amnestic cognitive impairment (aMCI, $n = 23$), non-amnestic cognitive impairment (naMCI, $n = 14$), or probable dementia (AD_p, $n = 5$).

Procedure

Four weeks prior to the commencement of the intervention and within a slot of one or two appointments, details of sociodemographic, cognitive and lifestyle data, as well as electrophysiological recordings were collected. Prior to the beginning of EEG recordings, individual hearing thresholds were assessed using in-house software PyTuneSounds (Hartmann, 2009). The training or the waiting period started 1–4 weeks after the pre-training test and lasted 10 weeks. Post-training tests were carried out 1–4 weeks after the end of the intervention. Potential long-term effects were examined in follow-up tests 3 months after the post assessment.

Neuropsychological Assessment

All participants completed the following assessments: the Alzheimer's Disease Assessment Scale–cognitive subscale (ADAS; Ihl and Weyer, 1993), phonemic and semantic word fluency as well as TMT part A and B of the Consortium to Establish a Registry for Alzheimer's Disease–plus test battery, the subtests digit span and digit-symbol coding of the Wechsler Adult Intelligence Scale (Tewes, 1991). Furthermore, an adapted German version of the California Verbal Learning Test [German: Münchner Verbaler Gedächtnistest [MVGT, Munich Vebal Memory Test); Ilmberger, 1988] was conducted. Additionally, everyday cognition in an ecologically valid task was assessed using the working-memory subtest of the Everyday Cognition Battery (ECB computation span, Allaire and Marsiske, 1999). Verbal Knowledge Test (German: Wortschatztest) was used to assess crystallized abilities.

To reduce multiple testing and thus α-inflation and in order to assess latent cognitive function scores, a principal component analysis using the oblique rotation technique was performed across all participants. Using the Kaiser criterion (Eigen values ≥ 1.0) two components were extracted. One component showed high loadings of episodic memory scores, namely MVGT encoding, MVGT long-delay recall, and ADAS-free recall. The second component showed high loadings of attention and executive function scores, i.e., TMT part A and B, digit span forward and backward, digit-symbol, phonemic and semantic fluency, and ECB computation span. All variables were z-standardized and two component scores were built, one representing memory functions and the one representing attention and executive functions. The components represent the weighted average of those z-standardized variables with loadings of at least $a_{ij} = 0.40$ on the respective component. Additionally, a global cognition component score was calculated as the average of the two component scores. A more detailed description of the principal component analysis can be found in Küster et al. (2016).

EEG Assessment

EEG Recording and Data Processing

The EEG was recorded using a high-density 256-channel HydroGel Geodesic Sensor Net (HCGSN; Electrical Geodesics, Inc.; Eugene, OR, United States). During data acquisition Cz served as reference and the data were sampled with 1,000 Hz. Resting state EEG as well as MMN EEG were collected in the same session after neuropsychological assessment, starting with the resting state EEG recording. During EEG recordings participants were seated comfortably in an electrically shielded room. To avoid drowsiness artifacts during resting state EEG, participants were instructed to keep their eyes open and to fixate on a chosen mark approximately at eye level on the opposite wall. Furthermore, to avoid blink and muscle artifacts, the participants were instructed to relax and to reduce blinking during both EEG recordings. There was a 5 min break between the recordings. During MMN EEG recording participants watched silent Charlie Chaplin videos while auditory stimuli were presented binaurally through stereo headphones at 50 dB above the individual hearing threshold. Since the MMN is elicited automatically without participants' attention and it is preferable to keep attention effects low during MMN recording, participants were instructed to watch the video carefully and not to pay any attention to the sounds.

After recording the EEG, the data were imported into MATLAB (version 2015b; The MathWorks, 2015); the FieldTrip toolbox (version 20151012) was used for preprocessing.

Global EEG Coherence Analyses

Data were bandpass filtered in the range of 1-30 Hz (24 dB/octave), noisy channels were rejected, and the data were re-referenced to the average of all channels marked as good. For a better comparison between assessments, the noisy channels were compared between recordings and the same channels were used for coherence analyses for the pre-post ($M = 220.65$, SD = 20.76, range: 170–246) and the pre-follow-up comparison ($M = 220.93$, SD = 20.88, range: 170–246), respectively. Artifact-contaminated epochs were manually rejected. To avoid trial bias, 20 trials were randomly selected from clean epochs for each subject and assessment. Spectral coherence analyses were calculated as an index for functional connectivity assuming a linear coupling in brain activity. Spectral coherence analyses were applied using the *bsmart* implementation for MATLAB (Cui et al., 2008). As an index for global coherence, we calculated the spectral coherence for all pairs of electrodes and averaged all values for the 1–30 Hz frequency range as an index for global coherence.

ΔMMN Analyses

Procedure and paradigms

We used two different passive MMN paradigms. The paradigm order was counterbalanced between subjects. The Optimum–1 paradigm (Näätänen et al., 2004) focuses on auditory discrimination ability. Stimuli were presented with a constant SOA of 0.5 s. The Optimum–1 paradigm is suitable to detect MMN after five deviant types: duration, frequency, intensity, location, and a gap deviant. The paradigm presents 1,845 stimuli

in three 5 min blocks. Every second tone was a standard tone. Thus, the probability for the standard tone was 50% and the probability for each deviant type was 10%. For the formation of a standard tone as such, a sequence of 15 standard tones was presented at the beginning at each block.

The Memory Trace paradigm (in accordance to Grau et al., 1998) uses long 3 s ISI and was developed to investigate the auditory memory trace. A total number of 462 stimuli are presented within three blocks of 6 min each. The same standard tone, duration and frequency deviant as in the Optimum–1 paradigm were used in the Memory Trace paradigm. As in the Optimum–1 paradigm 15 standard tones were presented at the beginning of each block for the standard tone formation. One to three standard tones were presented between two deviant tones. The number of standard stimuli and the ISI between standard tone (0.5, 1.5, or 3 s) were assigned pseudo randomly. The ISI between standard stimuli and deviant tone was constantly 3 s. Standard stimuli were presented with 66.2% probability and each deviant tone with a probability of 16.9%.

Detailed description of the stimuli

The standard tone was a harmonic tone of three sinusoidal partials of 500, 1,000, and 1,500 Hz with the second partial being 3 dB and the third being 6 dB lower in intensity then the first partial. The standard tone was 75 ms in duration including 5 ms rise and fall times. The duration deviant was 50 ms shorter in comparison to the standard tone. The gap deviant comprised a 7 ms silent gap (including 1 ms fall and rise times) in the middle of the tone. One half of all frequency deviants were 10% higher (partials: 550, 1,100, and 1,650 Hz) and the other half 10% lower in frequency than the standard tone (partials: 450, 900, and 1,350 Hz). Intensity deviants were 10 dB louder or lower than the standard tone (50% each). The location deviants had an interaural time difference of 800 μs to the left or to the right ear (50% each).

MMN analysis

For both paradigms the EEG data were bandpass filtered in the range of 1–35 Hz (24 dB/octave) and noisy channels were interpolated using the average method. Artifact-contaminated epochs were manually rejected. Finally, the data were re-referenced to the linked mastoids. As the largest MMN is often assessed at fronto-central EEG electrodes, and the averaging of electrodes with similar activity has been demonstrated to show more reliable results than the measure of single separate electrodes (Huffmeijer et al., 2014), the average voltage at FCz, Fz, and Cz was computed as mean MMN amplitude for all further analyses.

The number of averaged trials can influence the signal-to-noise ratio. Thus, to avoid these confounding effects, main analyses were repeated by building the ΔMMN from 50 randomly selected artifact-free trials for each assessment and each subject.

Calculation of ΔMMN

The difference score ΔMMN was defined by subtracting MMN after long ISI from MMN after short ISI, with higher values indicating less automatic auditory memory decay (cf., Laptinskaya et al., 2018). Thus, for the calculation of ΔMMN the MMN in both Optimum–1 and Memory Trace paradigms needed to be available. Since no MMN was observed after the frequency deviant in the Memory Trace paradigm in a previous study (Laptinskaya et al., 2018), we restricted the ΔMMN analyses to the duration deviant. The dataset of one person was excluded from analyses, as no Optimum–1 data were available.

Assessment of Lifestyle

For the assessment of lifestyle we used the Community Healthy Activities Model Program for Seniors (CHAMPS) Physical Activity Questionnaire for Older Adults (Stewart et al., 2001). The questionnaire describes 40 daily life activities, each assigned to a cognitively challenging (e.g., solving crossword puzzles, reading), physical (e.g., swimming, running), or social domain (e.g., meeting friends and family, calls with friends and family).Each activity was rated by three of the authors (PF, OCK, DL) on a five-point rating scale from 1 (*no demands*) to 5 (*high demands*). Activities with a rating score above three points were categorized to the respective domain (see **Supplementary Table 1**). Cronbach's α for authors' ratings was very good: $\alpha_{Cronbach}$ = 0.92 for physical domain, $\alpha_{Cronbach}$ = 0.86 for cognitive domain, and $\alpha_{Cronbach}$ = 0.95 for social domain. The categorization was validated by ratings of 39 independent healthy older adults (MMSE $\geq$ 26, aged 64–90). The comparison between authors' and seniors' ratings revealed very high correlations for all domains: r = 0.87 for physical domain, r = 0.89 for cognitive domain, and r = 0.84 for social domain. If the chosen categories differed between authors and seniors the classification was adapted to the seniors' opinion. Finally, the cognitive domain comprised 14 activities, the physical domain 17 activities, and the social domain 13 activities. Twelve activities could not be assigned to any domain because of an overall loading under three points.

Study participants were asked which typical activities they perform within a 4-week span. For each domain the number of performed activities was divided by the number of potential activities in this domain. Subsequently, the domain values were averaged and the final average value was regarded as the index for lifestyle activity.

Training Interventions

Auditory Cognitive Training

As CT we employed the German adapted version of the Brain Fitness software provided by the Posit Science Corporation (San Francisco, CA; for more detailed training tasks description see Küster et al., 2016). It consists of six tasks which target working memory and auditory processing. Each exercise lasted approximately 15 min. One training session included four out of six training tasks and took 1 h in duration. The training difficulty was automatically adapted according to the participant's task performance. Participants were asked to perform the 1-h session once a day, 5 days per week for a period of 10 weeks. Thus, the participants completed 50 training hours in total.

Physical Training

The PT was carried out in groups consisting of 5-10 participants and involved aerobic, strength, flexibility, coordination, and balance elements. The training was based on a training program that has shown positive effects in nursing home residents (Thurm et al., 2011). Each group met twice a week for a 1-h session over a period of 10 weeks. The difficulty of the training was adapted by two instructors. Furthermore, the participants completed three fixed homework sessions per week of about 20 min each with the same exercise elements as the main training. Homework sessions were documented and regularly checked by the instructors. Thus, in total the participants completed 20 training hours in the group setting and 10 training hours at home.

Wait-List Control Group

Participants in the WLC were asked to continue their daily routine as usual. After study participation, we offered them the participation in one of the training programs.

Statistical Analyses

General Procedure and Descriptive Statistics

All statistical analyses were carried out with *R* (version 3.2.3; R Core Team, 2016) in *RStudio* (RStudio Team, 2015). In group comparisons, all model residuals were normally distributed according to the Shapiro-Wilk normality test; therefore, parametric tests were applied. Baseline group differences in continuous variables (demographics and outcome measures) were evaluated with univariate analysis of variance (ANOVA) models with intervention group (CT, PT, and WCT) as between group factor. Differences in gender distribution were analyzed with Pearson's Chi-square (χ^2)-test. Normal distribution of all models' residuals was confirmed using the Shapiro-Wilk test (*W* statistic) and visual inspection (Q–Q plots). The statistical significance level (α) was set to 0.05 for all analyses.

Cognitive Progression of the Sample

These analyses were performed in accordance to Küster et al. (2016, p. 6, 8) and are repeated here to show the cognitive progression for the sample. The overall cognitive change was demonstrated for the cognitive component scores as well as for single test values. For this purpose, comparisons between post- and pre-training were performed. To adjust for possible retest effects, we calculated *z*-values based on baseline assessment for pre- and for post-training, respectively. Subsequently, the standardized post-value was subtracted from the pre-value and 95% confidence intervals were calculated. Finally, Group (CT vs. WLC and PT vs. WLC) × Time (pre vs. post) as well as Lifestyle (continuous) × Time interactions were performed for each cognitive outcome to test for possible differences in cognitive progression in dependence on group allocation or lifestyle. Training effects on cognitive progression were indicated by a significant Group × Time interaction, while positive associations between lifestyle and cognitive change were indicated by a significant Lifestyle × Time interaction.

Lifestyle Global Coherence Association and Training Effects on Global Coherence

We evaluated the association between active lifestyle and change in global coherence as well as training effects on global coherence by employing linear mixed-effects models using the nlme package 3.1.119 (Pinheiro et al., 2011). The model included Group (CT vs. WLC and PT vs. WLC) × Time (pre vs. post) as well as Lifestyle (continuous) × Time interactions as fixed effects in the same model, and Subject as random intercept with Global coherence as dependent variable. Significant Group × Time interactions reflected a training effect on global coherence, and significant Lifestyle × Time interactions demonstrated an association between lifestyle and global coherence. Hedges' *g* was calculated by comparing the difference scores in the auditory cognitive or PT group and the control group, respectively. As secondary analyses, *t*-tests were carried out for pre-post comparison in global cognition for each group separately.

Nowadays, the most prominent coherence chance has been reported for the fronto-temporal and fronto-parietal area. Thus, as supplemental analyses, the same linear mixed-effects model was used to assess training-induced effects and lifestyle-associated changes in fronto-temporal and fronto-parietal coherence.

Training Effect on ΔMMN

As for global coherence, to explore training effects on ΔMMN, a linear mixed-effects model was modeled. It was restricted to Group (CT vs. WLC and PT vs. WLC) × Time (pre vs. post) as fixed effect with ΔMMN as dependent variable because we focused on the effect of auditory CT on ΔMMN and did not expect a positive effect of PT or a positive association between lifestyle and ΔMMN Significant lifestyle associations for the period of 10 weeks were revealed by a significant Lifestyle × Time interaction, while training effects on EEG indices were indicated by a significant Group × Time interaction. Hedges' *g* was calculated to show effect sizes for the training programs. Therefore, the *z*-standardized difference score between pre- and post-training was built for the two interventions as well as for the control group. Hedges' *g* was calculated by comparing the difference scores in the auditory cognitive or PT group and the control group, respectively. Positive effects indicate beneficial effects of the intervention.

The main analysis was repeated with ΔMMN calculated from constant 50 trials (for rare exceptions see **Supplementary Presentation 1**) for each subject.

Again, as secondary analyses, *t*-tests for paired samples were performed for pre-post comparisons in ΔMMN within each group.

Follow-up-Assessment

In a final step, all linear mixed-effects models were repeated, including the follow-up analysis as a third time point in the model (pre vs. post and pre vs. follow-up) to account for possible long-lasting training effects.

TABLE 1 | Baseline characteristics and group comparisons for and between study groups.

	Cognitive training (n = 16)	Physical training (n = 18)	Wait-list control (n = 20)	F statistic	p
Demographic data					
Age (y.)	70.2 ± 5.8	73.7 ± 6.2	70.3 ± 5.5	$F_{(2,51)}$ = 2.11	0.13
Gender (f./m.)	8/8	12/6	10/10	$\chi^2_{(2)}$ = 1.35	0.51
Education (y.)	13.3 ± 4.0	14.2 ± 3.0	15.2 ± 3.7	$F_{(2,51)}$ = 1.18	0.32
Cognitive data					
MMSE	27.8 ± 2.6	27.8 ± 1.7	28.2 ± 2.2	$F_{(2,51)}$ = 0.14	0.87
SMI/naMCI/aMCI/AD_p	3/4/8/1	6/4/7/1	3/6/8/3	$\chi^2_{(2)}$ = 3.22	0.78
Global cognition (cs.)	0.08 ± 0.64	0.04 ± 0.62	−0.10 ± 0.82	$F_{(1,52)}$ = 0.61	0.44
Memory (cs.)	−0.02 ± 0.83	0.16 ± 0.67	−0.11 ± 0.98	$F_{(1,52)}$ = 0.15	0.70
Attention/executive functions (cs.)	0.19 ± 0.64	−0.08 ± 0.75	−0.08 ± 0.78	$F_{(1,52)}$ = 1.14	0.29
Lifestyle data					
Number of reported activities	8.4 ± 3.4	8.7 ± 2.5	9.3 ± 2.5	$F_{(2,49)}$ = 0.39	0.68
Variety of activities	0.27 ± 0.13	0.28 ± 0.09	0.30 ± 0.09	$F_{(2,49)}$ = 0.60	0.55
EEG data					
Global coherence	0.36 ± 0.12	0.29 ± 0.18	0.29 ± 0.10	$F_{(2,46)}$ = 1.20	0.31
ΔMMN	−1.26 ± 1.05	−1.46 ± 0.92	−1.33 ± 1.69	$F_{(2,41)}$ = 0.09	0.92

Values are means (M) ± standard deviations (SD).
*SMI, subjective memory impairment; naMCI, non-amnestic mild cognitive impairment; aMCI, amnestic mild cognitive impairment; AD_p, probable dementia; y., years; f., female; m., male; cs., component score. ΔMMN, the difference score between MMN for long and for short ISI for duration deviant. The data refer to complete sample without the exclusion of ΔMMN and global coherence missing data (see **Figure 1**). Data analyses accounting for the missing data did not change the results.*

RESULTS

Mismatch Negativity Analysis

The number of trials was left for averaging in the Optimum–1 paradigm as well as in the Memory Trace paradigm can be found in the **Supplementary Material**.

Group Comparisons at Baseline

At baseline, the three study groups (CT, PT, and WLC) did not differ in demographic variables, cognitive data, lifestyle data, and in EEG parameter (see **Table 1**).

Cognitive Progression of the Sample

As already shown by Küster et al. (2016, p. 8), no positive training effects on cognition were found neither for the auditory cognitive nor for the PT program, ps $\geq$ 0.08 (see **Table 2**). In turn, participants who reported a more active lifestyle had a significantly better progression in global cognition and in memory functions over a period of 10 weeks in comparison to their less active counterparts, ps $<$ 0.01 (see **Table 2**).

Lifestyle Global Coherence Association and Training Effects on Global Coherence

The mixed-effects model comprising Group × Time and Lifestyle × Time as fixed effects and Subject as random intercept with Global coherence as dependent variable revealed no significant associations between lifestyle and global coherence changes over a period of 10 weeks, $F_{(1,43)}$ = 0.78, p = 0.38 (see **Figure 2**). The same model revealed no significant training effects on global coherence, $F_{(2,43)}$ = 1.13, p = 0.33 (see **Figure 3**). Likewise, in comparison to the control group the Hedges' g was negative for the cognitive, Hedges' g = −0.40, 95% CI [−1.14, 0.33], p = 0.29, as well as for the PT, Hedges' g = −0.32, 95% CI [−1.01, 0.37], p = 0.34. The secondary analyses did not show a significant change in global coherence over time within groups (see **Table 3**). The supplemental analysis with ΔMMN calculated from a constant number of 50 trials did no change the main results. The analyses regarding the fronto-parietal and fronto-tempotal area did not reveal significant training-induced effects and lifestyle-associated changes in coherence (see **Supplementary Table 2**).

Training Effect on ΔMMN

Also, for ΔMMN no significant auditory CT effect was found, $F_{(2,39)}$ = 0.10, p = 0.90 (see **Figure 3**). In comparison to the control group the auditory CT did not show beneficial impact on ΔMMN, Hedges' g = 0.14, 95% CI [-0.67, 0.95], p = 0.79. The 50 trials' analyses for ΔMMN did not change the results. The t-test as secondary analysis did not reveal a significant pre-post change for ΔMMN (see **Table 3**).

Also, the t-test analyses did not reveal significant alterations in global coherence and ΔMMN within the 10-week period in any of the groups (see **Table 3**).

Follow-Up-Assessment

No significant relationships between lifestyle and change in global coherence as well as significant training effects were found after including the follow-up assessment into the model.

DISCUSSION

This study aimed at investigating the association between an active lifestyle and changes in global coherence in a sample at-risk

TABLE 2 | Cognitive changes and group effects on cognition as well as lifestyle cognition associations over time (cf. Küster et al., 2016, p. 8).

	Difference post-pre [95% CI]			Group × Time		Lifestyle × Time	
	Cognitive training (*n* = 16)	**Physical training (*n* = 18)**	**Wait-list control (*n* = 20)**	***F* statistic**	***p***	***F* statistic**	***p***
Cognitive measure							
Global cognition (cs.)	0.20 [0.03, 0.37]	0.16 [0.01,0.30]	0.32 [0.22, 0.43]	$F(2,48) = 2.64$	0.08	$F(1,48) = 18.77$	<0.01
Memory (cs.)	0.34 [0.11, 0.57]	0.15 [−0.10, 0.40]	0.38 [0.19, 0.58]	$F(2,48) = 1.78$	0.18	$F(1,48) = 23.88$	<0.01
Attention/executive functions (cs.)	0.06 [−0.20, 0.31]	0.16 [−0.03, 0.36]	0.27 [0.11, 0.42]	$F(2,48) = 0.66$	0.52	$F(1,48) = 0.07$	0.79
ADAS free recall	−0.34 [−0.89, 0.22]	0.15 [−0.36, 0.66]	−0.08 [−0.61, 0.45]	$F(2,48) = 1.33$	0.27	$F(1,48) = 2.27$	0.12
MVGT encoding	0.47 [0.16, 0.78]	0.34 [−0.04, 0.71]	0.66 [0.37, 0.95]	$F(2,47) = 1.46$	0.24	$F(1,47) = 15.96$	< 0.001
MVGT recognition	1.27 [−0.26, 2.80]	0.78 [−0.03, 1.59]	−0.28 [−1.02, 0.46]	$F(2,46) = 2.35$	0.11	$F(1,46) = 0.14$	0.71
Digit span forward	−0.03 [−0.56, 0.50]	−0.19 [−0.71, 0.33]	0.07 [−0.33, 0.47]	$F(2,48) = 0.58$	0.57	$F(1,48) = 0.23$	0.64
Digit span backward	−0.28 [−0.86, 0.30]	0.31 [−0.19, 0.81]	0.14 [−0.29, 0.57]	$F(2,48) = 0.73$	0.40	$F(1,48) = 0.79$	0.38
TMT A	0.36 [0.02, 0.71]	0.22 [−0.14, 0.59]	0.51 [0.12, 0.91]	$F(2,48) = 0.73$	0.49	$F(1,48) = 2.07$	0.16
TMT B	−0.01 [−0.46, 0.43]	0.28 [−0.14, 0.70]	0.20 [−0.03, 0.43]	$F(2,48) = 0.22$	0.81	$F(1,48) = 1.71$	0.20
Phonemic fluency	0.06 [−0.31, 0.43]	0.48 [−0.11, 1.07]	0.45 [0.003, 0.91]	$F(2,48) = 0.79$	0.46	$F(1,48) = 1.64$	0.21
Semantic fluency	0.20 [−0.10, 0.50]	−0.02 [−0.29, 0.26]	0.23 [−1.12, 0.57]	$F(2,48) = 0.70$	0.50	$F(1,48) = 0.11$	0.74
ECB computation span	0.22 [−0.20, 0.65]	0.19 [−0.22, 0.59]	0.33 [−0.03, 0.69]	$F(2,44) = 0.26$	0.77	$F(1,44) = 2.00$	0.16

Depicted are the mean differences in cognitive measures between pre- and post-training within the three groups and 95% confidence intervals in brackets, as well as statistics for Group × Time and Lifestyle × Time interactions. cs., component score; ADAS, Alzheimer's Diseases Assessment Scale; MVGT, German adaptation of the California Verbal Learning Test; ECB, Everyday Cognition Battery; TMT, Trail Making Test (part A and B).

Values are z-standardized on the basis of baseline cognitive assessment.

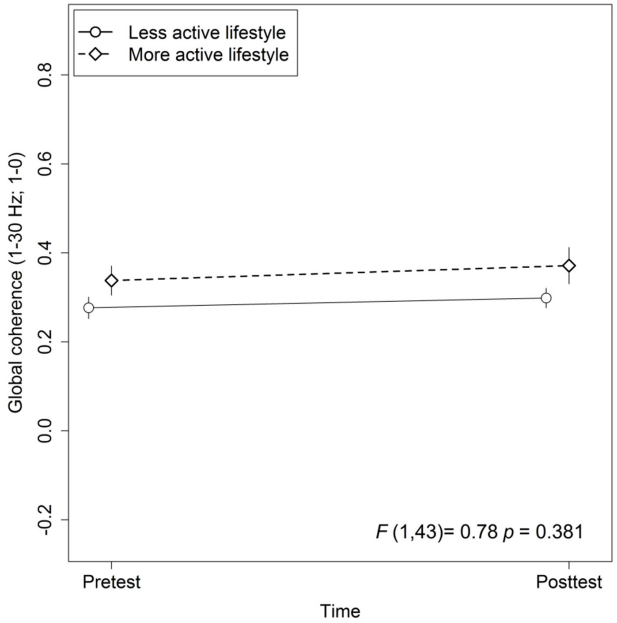

FIGURE 2 | Association between active lifestyle and global coherence. Statistic values refer to the Lifestyle × Time interaction in the Lifestyle × Time + Group × Time linear mixed-effects model. Arrow bars indicate standard errors.

for developing dementia. Furthermore, we examined the effects of a cognitive and a PT program on global coherence and the effects of auditory CT on ΔMMN-Dur as an index for automatic auditory memory decay.

Lifestyle Association With Global Coherence

We did not find an association between self-reported lifestyle and changes in global coherence during a period of 10 weeks in older adults at risk for developing dementia. Thus, there is no evidence that global coherence is an underlying mechanism of lifestyle-related cognitive benefits, which were previously reported by several studies including our working group. This finding is not in line with studies reporting positive effects of an enriched environment on neuronal plasticity in animals (e.g., Fabel and Kempermann, 2008; for a review see Kramer et al., 2004), as changes in functional connectivity have been attributed to neuronal structural and functional changes. Notably, the majority of studies investigating the effects of an enriched environment on neuroplasticity reported positive effects for separate areas, while in the present study global changes in functional connectivity were considered. Thus, a possible explanation for the discrepancy in results might be the fact that lifestyle-dependent functional neuroplasticity takes place in individual brain regions or in separate frequency bands and is not reflected by a global coherence score. Finally, the observation period of 10 weeks might have been too short to show significant effects.

Training Effects on Global Coherence

Contrary to previous results reporting positive training effects on functional connectivity (Voss et al., 2010; Anguera et al., 2013; Klados et al., 2016; Zilidou et al., 2018), we did not find any effects of cognitive or PT interventions on global coherence. So far, only few studies investigated training impacts on functional connectivity. Even if the aforementioned results by previous studies are promising, several methodological differences in investigation tool (functional magnetic resonance imaging, EEG), study sample (healthy adults, cognitively impaired adults), regions of interest (separate regions vs. global connectivity), and training programs make the comparison of study results difficult.

One important factor might be the duration of training. In a functional magnetic resonance imaging study Voss et al. (2010) investigated the effect of aerobic walking training on the default mode network in healthy older adults. Interestingly, the authors reported enhanced coherence in several regions of the default mode network only after a 12-month training period, while the effects were not significant after 6 months. Stronger DMN connectivity was associated with better executive control after training. Consequently, the training period in the present study might have been too short to tap functional neuroplasticity.

In recent years, there is a growing interest in combined training interventions (e.g., Fissler et al., 2013;

TABLE 3 | Electroencephalography raw data comparisons between pre- and post-training.

	n	Pre-training	Post-training	*t* statistic	*p*
Global coherence					
Cognitive Training	14	0.36 ± 0.12	0.35 ± 0.18	$t_{(13)} = 0.08$	0.93
Physical Training	17	0.29 ± 0.18	0.31 ± 0.17	$t_{(16)} = -1.04$	0.31
Wait-list control	18	0.29 ± 0.10	0.36 ± 0.14	$t_{(17)} = -2.21$	0.04
ΔMMN					
Cognitive Training	10	−1.26 ± 1.05	−1.06 ± 0.96	$t_{(9)} = -0.45$	0.66
Physical Training	16	−1.46 ± 0.92	−1.39 ± 1.19	$t_{(15)} = -0.34$	0.74
Wait-list control	18	−1.33 ± 1.69	−1.41 ± 1.25	$t_{(17)} = 0.16$	0.88

Values are means (M) ± standard deviations (SD).
The t-values represent the results of paired samples t-tests.
ΔMMN, the difference score between MMN for long and for short ISI for duration deviant.

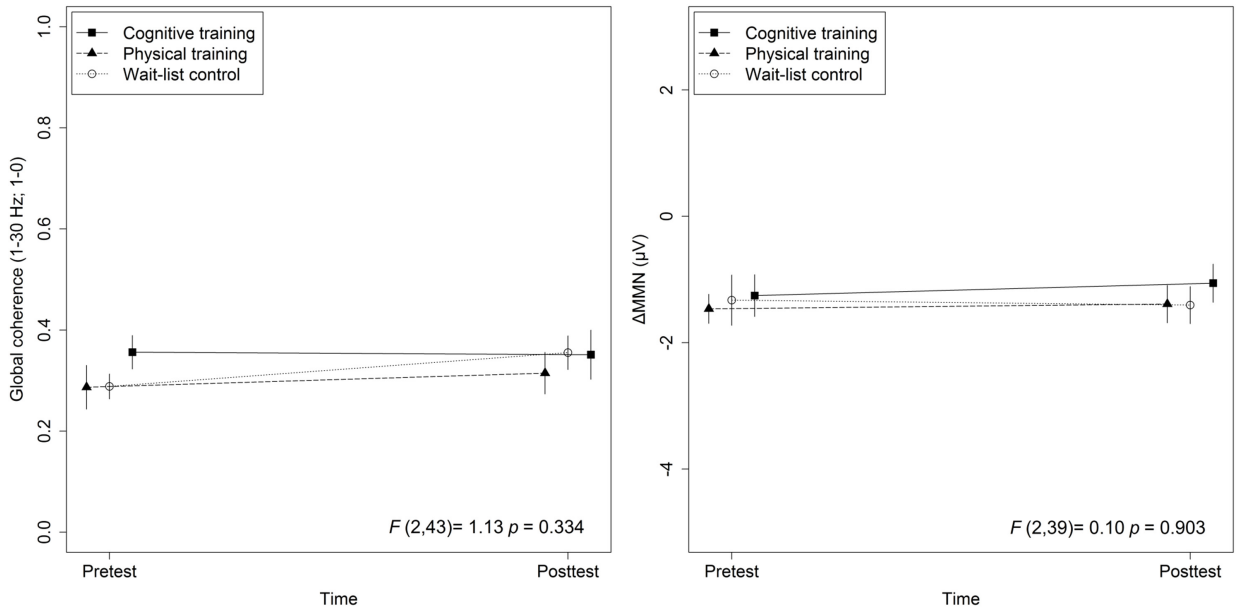

FIGURE 3 | Training effects on global coherence as well as ΔMMN. Statistic values refer to the Group × Time interaction in the Lifestyle × Time + Group × Time linear mixed-effects model. Arrow bars indicate standard errors.

Herold et al., 2018). Styliadis et al. (2015) found positive effects on MMSE scores only for the combination of an 8-week physical and auditory CT and not for interventions of physical or auditory CT alone. Furthermore, the cognitive improvement was associated with an elevated power in delta and theta band activity which has been shown to be positively associated with neurodegeneration (e.g., Stevens et al., 2001; Adler et al., 2003; Babiloni et al., 2009). Using low resolution brain electromagnetic tomography, Klados et al. (2016) examined the same combined training program used by Styliadis et al. (2015) on EEG coherence and found a widespread training induced elevated beta band coherence. The authors referred training-induced elevation in beta band activity to enhanced neuroplasticity (Styliadis et al., 2015; Klados et al., 2016). Enhanced functional connectivity as a result of neuroplasticity has also been supported by other authors (e.g., Frantzidis et al., 2014; Zilidou et al., 2018). Oswald et al. (2006) offer an explanation for the effectiveness of the combination of physical and auditory CT and conjectured that physical activity drives neuroplasticity induced by cognitively demanding activities through improved metabolic processes. Therefore, the combination of both of the training programs used in the present study might have yielded significant effects, especially because Styliadis et al. (2015) and Klados et al. (2016) used the adapted Greek version of the same auditory CT program that was applied in the present study. Furthermore, similarly to the results for lifestyle, it is also possible that particular brain networks, such as the DMN, and separate frequency bands, such as the beta band, are more sensible to training effects than the global scores (cf., Klados et al., 2016).

Training Effects on ΔMMN-Dur

In contrast to our hypothesis, we did not find significant auditory CT effects on ΔMMN-Dur. We based our expectation on previous results reporting positive associations between MMN as an index for automatic discrimination ability and the persons' ability to discriminate changes between sounds or sound sequences. For instance, musicians, who are more capable to discriminate tones in comparison to non-musicians, also showed a larger MMN; their automatically elicited MMN-amplitude was associated with better discrimination performance. Furthermore, an enhanced MMN has been shown to be associated with linguistic skills in young subjects (Tremblay et al., 1997; Kujala et al., 2001; Cheour et al., 2002). It has to be noted that learning a new instrument or a new language might be more intrinsically motivating as exercising an auditory training program. Furthermore, studies on musicians focused on long lasting exercise periods; therefore the comparison to the present 10-week training period is limited. As for the MMN as a marker for linguistic skills, the corresponding studies have been conducted with children or very young adults. Even if the human brain has been shown to stay neuroplastic up to old age (e.g., Gutchess, 2014), neuroplasticity becomes more difficult in advanced age due to age-associated neuronal changes, for example, the neuronal atrophy or hemispheric asymmetry reduction (Oberman and Pascual-Leone, 2013).

While, to our best knowledge, no study exists that investigated the effects of auditory CT on MMN in the field of cognitive aging, more research exists for subjects with schizophrenia or schizophrenia-spectrum illnesses. Persons with schizophrenia-spectrum illnesses show pronounced cognitive deficits. Similar

to AD, cognitive deficits in schizophrenia have been shown to be associated with a decreased MMN (e.g., Hermens et al., 2010) and furthermore with functional disability (e.g., Hamilton et al., 2018). Recent studies examined whether auditory training might improve cognition in subjects with schizophrenia and whether the positive changes are accompanied by an improved MMN. In line with the missing training-induced results in the present study, the authors did not find any positive training effects on MMN using the adapted version of the same training as applied in the present study (Kärgel et al., 2016; Biagianti et al., 2017). Some authors even report an attenuated MMN after auditory training in schizophrenia patients (Perez et al., 2017).

These results indicate that some other factors than the auditory training per se might be responsible for the intervention's success. In this context, Chandrasekaran and Kraus (2010) noted that we learn best about things that we care about, thus the intrinsic motivation, enjoyment, and fun of the training might be of high relevance (cf. also, Küster et al., 2016). These factors might be higher for learning a new instrument or language than for a computer-based relative monotonous training program. Furthermore, the training duration in the aforementioned studies ranged between a single 1-h session (Perez et al., 2017), 2-week training period (Kärgel et al., 2016), 8-week training period (Biagianti et al., 2017), and 10 weeks of training intervention in the present study. Thus, besides the training's contents and motivational aspects, the missing effect of training in the present study might be explained by the training's duration.

STRENGTHS AND LIMITATIONS

Since global coherence is a global marker measured over the whole skull, it is more reliable as the measure of EEG coherence for separate pairs of electrodes. ΔMMN-Dur as a difference score between MMN for long and for short interstimulus interval is a novel EEG marker which takes different auditory processing aspects into account, such as auditory discrimination ability as well as the automatic auditory memory trace (Näätänen et al., 2012) and is correlated with cognitive performance (Laptinskaya et al., 2018).

Also, the following limitations have to be considered: in our previous research we found a positive lifestyle cognition association but no positive training effects on behavioral measures of cognition. Thus, training-induced electrophysiological changes might be difficult to detect. However, other authors reported positive training effects despite the missing of significant benefits in neuropsychological testing (cf., Miró-Padilla et al., 2020). Random allocation is the best method to prevent selection bias. Due to logistic issues, a randomized allocation to the groups was not feasible. Thus, we chose the minimization approach in order to control for bias regarding age, gender, education, and cognitive status reflected by MMSE. Although, selection bias cannot be excluded, we assume that it was unlikely: there were no differences in sociodemographic data, cognition, or EEG parameters between groups. Finally, the small sample size might be a further limitation.

In the coherence analyses as a measure for functional connectivity, the interactions between brain regions are considered as linear connections, although there are indications that at least some of the interactions between brain regions may have a non-linear component (Rombouts et al., 1995). An often-used non-linear measure for functional connectivity is the synchronization likelihood (SL). In a magnetoencephalography study, Gómez et al. (2009) compared the accuracy of coherence as well as SL to discriminate healthy older adults without cognitive deficits from subjects with MCI. Interestingly, the authors reported a better accuracy for the linear coherence measure. Thus, we assume that coherence analysis is a suitable method to investigate functional connectivity in the present sample at-risk for developing AD.

CONCLUSION

In the light of the results of the present study as well as the review of the previous literature, we conclude that training interventions focusing on only one training aspect are not very powerful to generate positive effects on global EEG coherence. Instead, multimodal interventions taking physical and cognitive as well as motivational and emotional aspects into account seem to be more promising. Notably, this sort of intervention is very similar to an active lifestyle, which has been shown to be related to positive cognitive change.

Since, the auditory training did not reveal positive effects on ΔMMN-Dur as an index for automatic auditory memory decay, we suggest that other training parameters such as longer training periods and more intrinsically motivating as well as joyful approaches might be more suitable to tap the automatic auditory memory trace in EEG.

DATA AVAILABILITY STATEMENT

The raw data supporting the conclusions of this article will be made available by the authors, without undue reservation.

ETHICS STATEMENT

The studies involving human participants were reviewed and approved by the Ulm University and the University of Konstanz. The participants provided their written informed consent to participate in this study.

AUTHOR CONTRIBUTIONS

DL contributed to the study conception and design, organized the study procedures and acquired the data, analyzed and interpreted the data, and wrote the first draft of the manuscript. FT contributed to the study conception and design,

organized study procedures, acquired the data, contributed to the data analysis, and critically revised the first draft of the manuscript. PF and OK contributed to the study conception and design, organized the study procedures and acquired the data, contributed to the data interpretation and critically revised the manuscript. CA and I-TK conceptualized the study, obtained funding, supervised all phases of the study as principle investigators and critically revised the manuscript. All authors read and approved the final manuscript.

FUNDING

This research was funded by the Heidelberg Academy of Sciences and Humanities, Germany. During the data collection, I-TK was a fellow (now alumna) of the Zukunftskolleg of the University of Konstanz, Germany. The funders had no role in study design, data collection, analysis and interpretation of the data, writing the manuscript, or decision to submit the manuscript for publication.

ACKNOWLEDGMENTS

We thank Thomas Elbert for general advice and support in study conception and implementation. Furthermore, we would like to thank Anita Steward for the English Community Healthy Activities Model Program for Seniors (CHAMPS) Physical Activity Questionnaire for Older Adults to be adapted in German and Rosine Gröschel, Nelli Hirschauer, Jens Kalchthaler, Anne Korzowski, Claudia Massau, Dörte Polivka, and Christina Schaldecker for support in subject recruitment, data acquisition, and training implementation.

SUPPLEMENTARY MATERIAL

The Supplementary Material for this article can be found online at: https://www.frontiersin.org/articles/10.3389/fnagi.2021.610839/full#supplementary-material

REFERENCES

Adler, G., Brassen, S., and Jajcevic, A. (2003). EEG coherence in Alzheimer's dementia. *J. Neural. Transm.* 110, 1051–1058. doi: 10.1007/s00702-003-0024-8

Allaire, J. C., and Marsiske, M. (1999). Everyday cognition: age and intellectual ability correlates. *Psychol. Aging* 14, 627–644. doi: 10.1037/0882-7974.14.4.627

Anguera, J. A., Boccanfuso, J., Rintoul, J. L., Al-Hashimi, O., Faraji, F., Janowich, J., et al. (2013). Video game training enhances cognitive control in older adults. *Nature* 501, 97–101. doi: 10.1038/nature12486

Babiloni, C., Ferri, R., Binetti, G., Vecchio, F., Frisoni, G. B., Lanuzza, B., et al. (2009). Directionality of EEG synchronization in Alzheimer's disease subjects. *Neurobiol. Aging* 30, 93–102. doi: 10.1016/j.neurobiolaging.2007.05.007

Babiloni, C., Lizio, R., Marzano, N., Capotosto, P., Soricelli, A., Triggiani, A. I., et al. (2016). Brain neural synchronization and functional coupling in Alzheimer's disease as revealed by resting state EEG rhythms. *Int. J. Psychophysiol.* 103, 88–102. doi: 10.1016/j.ijpsycho.2015.02.008

Barnes, D. E., Santos-Modesitt, W., Poelke, G., Kramer, A. F., Castro, C., Middleton, L. E., et al. (2013). The Mental Activity and Exercise (MAX) trial: a randomized controlled trial to enhance cognitive function in older adults. *JAMA Intern. Med.* 173, 797–804. doi: 10.1001/jamainternmed.2013.189

Bartha-Doering, L., Deuster, D., Giordano, V., Zehnhoff-Dinnesen, A., and Dobel, C. (2015). A systematic review of the mismatch negativity as an index for auditory sensory memory: from basic research to clinical and developmental perspectives. *Psychophysiology* 52, 1115–1130. doi: 10.1111/psyp.12459

Biagianti, B., Roach, B. J., Fisher, M., Loewy, R., Ford, J. M., Vinogradov, S., et al. (2017). Trait aspects of auditory mismatch negativity predict response to auditory training in individuals with early illness schizophrenia. *Neuropsychiatr. Electrophysiol.* 3:2. doi: 10.1186/s40810-017-0024-9

Chandrasekaran, B., and Kraus, N. (2010). The scalp-recorded brainstem response to speech: neural origins and plasticity. *Psychophysiology* 47, 236–246. doi: 10.1111/j.1469-8986.2009.00928.x

Cheour, M., Shestakova, A., Alku, P., Ceponiene, R., and Näätänen, R. (2002). Mismatch negativity shows that 3-6-year-old children can learn to discriminate non-native speech sounds within two months. *Neurosci. Lett.* 325, 187–190. doi: 10.1016/S0304-3940(02)00269-0

Cui, J., Xu, L., Bressler, S. L., Ding, M., and Liang, H. (2008). BSMART: a Matlab/C toolbox for analysis of multichannel neural time series. *Neural. Networks* 21, 1094–1104. doi: 10.1016/j.neunet.2008.05.007

Edwards, J. D., Xu, H., Clark, D., Ross, L. A., and Unverzagt, F. W. (2016). The active study: what we have learned and what is next? Cognitive training reduces incident dementia across ten years. *Alzheimer's Dement.* 12:P212. doi: 10.1016/j.jalz.2016.06.373

Fabel, K., and Kempermann, G. (2008). Physical activity and the regulation of neurogenesis in the adult and aging brain. *NeuroMole.cular Med.* 10, 59–66. doi: 10.1007/s12017-008-8031-4

Fissler, P., Küster, O., Schlee, W., and Kolassa, I. T. (2013). Novelty interventions to enhance broad cognitive abilities and prevent dementia: synergistic approaches for the facilitation of positive plastic change. *Prog. Brain Res.* 207, 403–434. doi: 10.1016/B978-0-444-63327-9.00017-5

Fissler, P., Müller, H.-P., Küster, O. C., Laptinskaya, D., Thurm, F., Woll, A., et al. (2017). No evidence that short-term cognitive or physical training programs or lifestyles are related to changes in white matter integrity in older adults at risk of dementia. *Front. Hum. Neurosci.* 11:110. doi: 10.3389/fnhum.2017.00110

Folstein, M. F., Folstein, S. E., and McHugh, P. R. (1975). "Mini-mental state". A practical method for grading the cognitive state of patients for the clinician. *J. Psychiatr. Res.* 12, 189–198. doi: 10.1016/0022-3956(75)90026-6

Frantzidis, C. A., Ladas, A. K. I., Vivas, A. B., Tsolaki, M., and Bamidis, P. D. (2014). Cognitive and physical training for the elderly: evaluating outcome efficacy by means of neurophysiological synchronization. *Int. J. Psychophysiol.* 93, 1–11. doi: 10.1016/j.ijpsycho.2014.01.007

Gheysen, F., Poppe, L., DeSmet, A., Swinnen, S., Cardon, G., De Bourdeaudhuij, I., et al. (2018). Physical activity to improve cognition in older adults: can physical activity programs enriched with cognitive challenges enhance the effects? A systematic review and meta-analysis. *Int. J. Behav. Nutr. Phys. Act.* 15:63. doi: 10.1186/s12966-018-0697-x

Gómez, C., Stam, C. J., Hornero, R., Fernández, A., and Maestú, F. (2009). Disturbed beta band functional connectivity in patients with mild cognitive impairment: an MEG study. *IEEE Trans. Biomed. Eng.* 56, 1683–1690. doi: 10.1109/TBME.2009.2018454

Grau, C., Escera, C., Yago, E., and Polo, M. D. (1998). Mismatch negativity and auditory sensory memory evaluation: a new faster paradigm. *Neuroreport* 9, 2451–2456. doi: 10.1097/00001756-199808030-00005

Groot, C., Hooghiemstra, A. M., Raijmakers, P. G. H. M., van Berckel, B. N. M., Scheltens, P., Scherder, E. J. A., et al. (2016). The effect of physical activity on cognitive function in patients with dementia: a meta-analysis of randomized control trials. *Ageing Res. Rev.* 25, 13–23. doi: 10.1016/j.arr.2015.11.005

Gutchess, A. (2014). Plasticity of the aging brain: new directions in cognitive neuroscience. *Science* 346, 579–582. doi: 10.1126/science.1254604

Hamilton, H. K., Perez, V. B., Ford, J. M., Roach, B. J., Jaeger, J., and Mathalon, D. H. (2018). Mismatch negativity but not P300 is associated with functional disability in schizophrenia. *Schizophr. Bull.* 44, 492–504. doi: 10.1093/schbul/sbx104

Hartmann, T. (2009). *PyTuneSounds. Konstanz*. URL: https://sourceforge.net.

Hermens, D. F., Ward, P. B., Hodge, M. A. R., Kaur, M., Naismith, S. L., and Hickie, I. B. (2010). Impaired MMN/P3a complex in first-episode psychosis: cognitive

and psychosocial associations. *Prog. Neuropsychopharmacol. Biol. Psychiatry* 34, 822–829. doi: 10.1016/j.pnpbp.2010.03.019

Herold, F., Hamacher, D., Schega, L., and Müller, N. G. (2018). Thinking while moving or moving while thinking – concepts of motor-cognitive training for cognitive performance enhancement. *Front. Aging Neurosci.* 10:228. doi: 10.3389/fnagi.2018.00228

Hess, N. C. L., Dieberg, G., McFarlane, J. R., and Smart, N. A. (2014). The effect of exercise intervention on cognitive performance in persons at risk of, or with, dementia: a systematic review and meta-analysis. *Heal. Aging Res.* 3, 1–10. doi: 10.12715/har.2014.3.3

Huffmeijer, R., Bakermans-Kranenburg, M. J., Alink, L. R. A., and van Ijzendoorn, M. H. (2014). Reliability of event-related potentials: the influence of number of trials and electrodes. *Physiol. Behav.* 130, 13–22. doi: 10.1016/j.physbeh.2014.03.008

Ihl, R., and Weyer, G. (1993). *Die Alzheimer Disease Assessment Scale (ADAS)*. Weinheim, Germany: Beltz Test.

Ilmberger, J. (1988). *Münchner Verbaler Gedächtnistest (MVGT) [Munich Verbal Memory Test, unpublished manuscript]*. München: Universität München.

Ji, L.-L., Zhang, Y.-Y., Zhang, L., He, B., and Lu, G.-H. (2015). Mismatch negativity latency as a biomarker of amnestic mild cognitive impairment in chinese rural elders. *Front. Aging Neurosci.* 7:22. doi: 10.3389/fnagi.2015.00022

Kärgel, C., Sartory, G., Kariofillis, D., Wiltfang, J., and Müller, B. W. (2016). The effect of auditory and visual training on the mismatch negativity in schizophrenia. *Int. J. Psychophysiol.* 102, 47–54. doi: 10.1016/j.ijpsycho.2016.03.003

Klados, M. A., Styliadis, C., Frantzidis, C. A., Paraskevopoulos, E., and Bamidis, P. D. (2016). Beta-band functional connectivity is reorganized in mild cognitive impairment after combined computerized physical and cognitive training. *Front. Neurosci.* 10:55. doi: 10.3389/fnins.2016.00055

Knott, V., Mohr, E., Mahoney, C., and Ilivitsky, V. (2000). Electroencephalographic coherence in Alzheimer's disease: comparisons with a control group and population norms. *J. Geriatr. Psychiatry Neurol.* 13, 1–8. doi: 10.1177/089198870001300101

Kramer, A. F., Bherer, L., Colcombe, S. J., Dong, W., and Greenough, W. T. (2004). Environmental influences on cognitive and brain plasticity during aging. *J. Gerontol. Ser. A Biol. Sci. Med. Sci.* 59, M940–M957. doi: 10.1093/gerona/59.9.M940

Kujala, T., Karma, K., Ceponiene, R., Turkkila, P., Tervaniemi, M., and Näätänen, R. (2001). The mismatch negativity in evaluating central auditory dysfunction in dyslexia. *Neurosci. Biobehav. Rev.* 98, 10509–10514.

Küster, O. C., Fissler, P., Laptinskaya, D., Thurm, F., Scharpf, A., Woll, A., et al. (2016). Cognitive change is more positively associated with an active lifestyle than with training interventions in older adults at risk of dementia: a controlled interventional clinical trial. *BMC Psychiatry* 16:315. doi: 10.1186/s12888-016-1018-z

Küster, O. C., Laptinskaya, D., Fissler, P., Schnack, C., Zügel, M., Nold, V., et al. (2017). Novel blood-based biomarkers of cognition, stress, and physical or cognitive training in older adults at risk of dementia: preliminary evidence for a role of BDNF, irisin, and the kynurenine pathway. *J. Alzheimer's Dis.* 59, 1097–1111. doi: 10.3233/JAD-170447

Lampit, A., Hallock, H., and Valenzuela, M. (2014). Computerized cognitive training in cognitively healthy older adults: a systematic review and meta-analysis of effect modifiers. *PLoS Med.* 11:e1001756. doi: 10.1371/journal.pmed.1001756

Laptinskaya, D., Fissler, P., Küster, O. C., Wischniowski, J., Thurm, F., Elbert, T., et al. (2019). Global EEG coherence as a marker for cognition in older adults at risk for dementia. *Psychophysiology* 57:e13515. doi: 10.1111/psyp.13515

Laptinskaya, D., Thurm, F., Küster, O. C., Fissler, P., Schlee, W., Kolassa, S., et al. (2018). Auditory memory decay as reflected by a new mismatch negativity score is associated with episodic memory in older adults at risk of dementia. *Front. Aging Neurosci.* 10:5. doi: 10.3389/fnagi.2018.00005

Lindín, M., Correa, K., Zurrón, M., and Díaz, F. (2013). Mismatch negativity (MMN) amplitude as a biomarker of sensory memory deficit in amnestic mild cognitive impairment. *Front. Aging Neurosci.* 5:79. doi: 10.3389/fnagi.2013.00079

Livingston, G., Huntley, J., Sommerlad, A., Ames, D., Ballard, C., Banerjee, S., et al. (2020). Dementia prevention, intervention, and care: 2020 report of the Lancet Commission. *Lancet* 396, 413–446. doi: 10.1016/S0140-6736(20)30367-6

Michels, L., Muthuraman, M., Anwar, A. R., Kollias, S., Leh, S. E., Riese, F., et al. (2017). Changes of functional and directed resting-state connectivity are associated with neuronal oscillations, ApoE genotype and amyloid deposition in mild cognitive impairment. *Front. Aging Neurosci.* 9:304. doi: 10.3389/fnagi.2017.00304

Miró-Padilla, A., Bueichekú, E., and Ávila, C. (2020). Locating neural transfer effects of n-back training on the central executive: a longitudinal fMRI study. *Sci. Rep.* 10:5226. doi: 10.1038/s41598-020-62067-y

Näätänen, R., Gaillard, A., and Mäntysalo, S. (1978). Early selective-attention effect on evoked potential reinterpreted. *Acta Psychol.* 42, 313–329. doi: 10.1016/0001-6918(78)90006-9

Näätänen, R., Kujala, T., and Winkler, I. (2011). Auditory processing that leads to conscious perception: a unique window to central auditory processing opened by the mismatch negativity and related responses. *Psychophysiology* 48, 4–22. doi: 10.1111/j.1469-8986.2010.01114.x

Näätänen, R., Kujala, T., Escera, C., Baldeweg, T., Kreegipuu, K., Carlson, S., et al. (2012). The mismatch negativity (MMN) – a unique window to disturbed central auditory processing in ageing and different clinical conditions. *Clin. Neurophysiol.* 123, 424–458. doi: 10.1016/j.clinph.2011.09.020

Näätänen, R., Pakarinen, S., Rinne, T., and Takegata, R. (2004). The mismatch negativity (MMN): towards the optimal paradigm. *Clin. Neurophysiol.* 115, 140–144. doi: 10.1016/j.clinph.2003.04.001

Oberman, L., and Pascual-Leone, A. (2013). Changes in plasticity across the lifespan: cause of disease and target for intervention. *Prog. Brain Res.* 207, 91–120. doi: 10.1016/B978-0-444-63327-9.00016-3

Oswald, W. D., Gunzelmann, T., Rupprecht, R., and Hagen, B. (2006). Differential effects of single versus combined cognitive and physical training with older adults: the SimA study in a 5-year perspective. *Eur. J. Ageing* 3, 179–192. doi: 10.1007/s10433-006-0035-z

Papadaniil, C. D., Kosmidou, V. E., Tsolaki, A., Tsolaki, M., Kompatsiaris, I. Y., and Hadjileontiadis, L. J. (2016). Cognitive MMN and P300 in mild cognitive impairment and Alzheimer's disease: a high density EEG-3D vector field tomography approach. *Brain Res.* 1648, 425–433. doi: 10.1016/j.brainres.2016.07.043

Pekkonen, E., Jousmäki, V., Könönen, M., Reinikainen, K., and Partanen, J. (1994). Auditory sensory memory impairment in Alzheimer's disease: an event-related potential study. *Neuroreport* 5, 2537–2540. doi: 10.1097/00001756-199412000-00033

Perez, V. B., Tarasenko, M., Miyakoshi, M., Pianka, S. T., Makeig, S. D., Braff, D. L., et al. (2017). Mismatch negativity is a sensitive and predictive biomarker of perceptual learning during auditory cognitive training in schizophrenia. *Neuropsychopharmacology* 42, 2206–2213. doi: 10.1038/npp.2017.25

Pinheiro, J., Bates, D., DebRoy, S., Sarkar, D. (2011). *nlme: Linear and Nonlinear Mixed Effects Models. R package version 3.1-101*.

R Core Team (2016). *R: A language and environment for statistical computing*. Vienna: R Foundation for Statistical Computing.

Rombouts, S. A. R. B., Keunen, R. W. M., and Stam, C. J. (1995). Investigation of nonlinear structure in multichannel EEG. *Phys. Lett. A* 202, 352–358. doi: 10.1016/0375-9601(95)00335-Z

RStudio Team (2015). *RStudio: integrated development for R*. Boston, MA: R Studio Inc.

Schroeder, M. M., Ritter, W., and Vaughan, H. G. (1995). The mismatch negativity to novel stimuli reflects cognitive decline. *Ann. N. Y. Acad. Sci.* 769, 399–401. doi: 10.1111/j.1749-6632.1995.tb38155.x

Stevens, A., Kircher, T., Nickola, M., Bartels, M., Rosellen, N., and Wormstall, H. (2001). Dynamic regulation of EEG power and coherence is lost early and globally in probable DAT. *Eur. Arch. Psychiatry Clin. Neurosci.* 251, 199–204. doi: 10.1007/s004060170027

Stewart, A. L., Mills, K. M., King, A. C., Haskell, W. L., Gillis, D., and Ritter, P. L. (2001). CHAMPS physical activity questionnaire for older adults: outcomes for interventions. *Med. Sci. Sports Exerc.* 33, 1126–1141. doi: 10.1097/00005768-200107000-00010

Styliadis, C., Kartsidis, P., Paraskevopoulos, E., Ioannides, A. A., and Bamidis, P. D. (2015). Neuroplastic effects of combined computerized physical and cognitive training in elderly individuals at risk for dementia: An eLORETA controlled study on resting states. *Neural. Plast.* 2015:172192. doi: 10.1155/2015/172192

Tewes, U. (1991). *Hamburg-Wechsler-Intelligenztest für Erwachsene [HAWIE-R, Hamburg-Wechsler-Intelligence Test for Adults]*. Bern, Stuttgart, Toronto: Huber.

The MathWorks (2015). *MATLAB and statistics toolbox release 2015b*. Natick, MA URL: https://de.mathworks.com.

Thurm, F., Scharpf, A., Liebermann, N., Kolassa, S., Elbert, T., Lüchtenberg, D., et al. (2011). Improvement of cognitive function after physical movement training in institutionalized very frail older adults with dementia. *J. Gerontopsychol. Geriatr. Psych. GeroPsych.* 24, 197–208. doi: 10.1024/1662-9647/a000048

Tremblay, K., Kraus, N., Carrell, T. D., and McGee, T. (1997). Central auditory system plasticity: generalization to novel stimuli following listening training. *J. Acoust. Soc. Am.* 102, 3762–3772. doi: 10.1121/1.420139

Voss, M. W., Prakash, R. S., Erickson, K. I., Basak, C., Chaddock, L., Kim, J. S., et al. (2010). Plasticity of brain networks in a randomized intervention trial of exercise training in older adults. *Front. Aging Neurosci.* 2:32. doi: 10.3389/fnagi.2010.00032

Williamson, J. D., Espeland, M., Kritchevsky, S. B., Newman, A. B., King, A. C., Pahor, M., et al. (2009). Changes in cognitive function in a randomized trial of physical activity: results of the lifestyle interventions and independence for elders pilot study. *J. Gerontol. Ser. A Biol. Sci. Med. Sci.* 64, 1226–1237. doi: 10.1093/gerona/glp014

Zilidou, V. I., Frantzidis, C. A., Romanopoulou, E., Paraskevopoulos, E., Douka, S., and Bamidis, P. D. (2018). Functional re-organization of cortical networks of senior citizens after a 24-week traditional dance program. *Front. Aging Neurosci.* 10:422. doi: 10.3389/fnagi.2018.00422

Conflict of Interest: The authors declare that the research was conducted in the absence of any commercial or financial relationships that could be construed as a potential conflict of interest.

frontiers in Aging Neuroscience

REVIEW
published: 06 May 2021
doi: 10.3389/fnagi.2021.624330

PET Neuroimaging of Alzheimer's Disease: Radiotracers and Their Utility in Clinical Research

Weiqi Bao[1], *Fang Xie*[1], *Chuantao Zuo*[1], *Yihui Guan*[1]* *and Yiyun Henry Huang*[2]*

[1] PET Center, Huanshan Hospital, Fudan University, Shanghai, China, [2] Department of Radiology and Biomedical Imaging, PET Center, Yale University School of Medicine, New Haven, CT, United States

Alzheimer's Disease (AD), the leading cause of senile dementia, is a progressive neurodegenerative disorder affecting millions of people worldwide and exerting tremendous socioeconomic burden on all societies. Although definitive diagnosis of AD is often made in the presence of clinical manifestations in late stages, it is now universally believed that AD is a continuum of disease commencing from the preclinical stage with typical neuropathological alterations appearing decades prior to its first symptom, to the prodromal stage with slight symptoms of amnesia (amnestic mild cognitive impairment, aMCI), and then to the terminal stage with extensive loss of basic cognitive functions, i.e., AD-dementia. Positron emission tomography (PET) radiotracers have been developed in a search to meet the increasing clinical need of early detection and treatment monitoring for AD, with reference to the pathophysiological targets in Alzheimer's brain. These include the pathological aggregations of misfolded proteins such as β-amyloid (Aβ) plagues and neurofibrillary tangles (NFTs), impaired neurotransmitter system, neuroinflammation, as well as deficient synaptic vesicles and glucose utilization. In this article we survey the various PET radiotracers available for AD imaging and discuss their clinical applications especially in terms of early detection and cognitive relevance.

Keywords: PET, neuroimaging, Alzheimer's disease, radiotracer, clinical research

OPEN ACCESS

Edited by:
Chih-Yu Hsu,
Fujian University of Technology, China

Reviewed by:
Valentina Echeverria Moran,
Bay Pines VA Healthcare System, United States
Takahito Yoshizaki,
Keio University, Japan

***Correspondence:**
Yiyun Henry Huang
henry.huang@yale.edu
Yihui Guan
guanyihui@hotmail.com

Received: *31 October 2020*
Accepted: *23 February 2021*
Published: *06 May 2021*

Citation:
Bao W, Xie F, Zuo C, Guan Y and Huang YH (2021) PET Neuroimaging of Alzheimer's Disease: Radiotracers and Their Utility in Clinical Research. Front. Aging Neurosci. 13:624330. doi: 10.3389/fnagi.2021.624330

INTRODUCTION

Alzheimer's Disease (AD), the leading cause of senile dementia, is a progressive neurodegenerative disorder affecting millions of people worldwide and exerting tremendous socioeconomic burden on all societies (Goedert and Spillantini, 2006; Querfurth and LaFerla, 2010). AD is neuropathologically characterized by deposition of senile plaques and neurofibrillary tangles in the brain tissue. Excessive aggregation of misfolded β-amyloid (Aβ) and hyperphosphorylated tau proteins leads to cytotoxicity and disruption of cytoarchitecture, and subsequent neuronal death and brain function decline. Neuroinflammation activation, cholinergic deficit, impaired glucose utilization and synaptic dysfunction are also outstanding characteristics of AD. Functional neuroimaging using positron emission tomography (PET) is able to reveal these *in vivo* pathological/pathophysiological alterations. With increasing viewpoint of AD as a continuum from asymptomatic preclinical stage, to prodromal stage with mild cognitive impairment (MCI), and finally to the advanced stage of dementia, integrated early diagnostic and differentiation paradigms with the help of PET imaging has been well-acknowledged in multiple diagnostic criteria (Dubois et al., 2007, 2014; Jack et al., 2011). In this review article, we describe the various PET radiotracers

available for AD imaging and discuss their clinical applications especially in terms of early detection and cognitive relevance. Literature evidence on the predictive ability of PET imaging with various PET tracers for prodromal stage conversion and monitoring of disease progression will also be reviewed. Finally, comments on emerging biomarkers and their prospects in early detection of AD will be provided.

PET TRACERS FOR IMAGING Aβ

Overview

The disturbance of homeostasis between the accumulation of neurotoxic Aβ peptides and its clearance in the brain is believed to be the core event in AD etiology (Hardy and Allsop, 1991; Hardy and Higgins, 1992). The Aβ peptides are derived from the breakdown of amyloid precursor protein (APP) through cleavage by β- and γ-secretase. The soluble oligomers, believed to be the perpetrator of cytotoxicity, are aggregated by longer species of the Aβ peptides such as $Aβ_{40}$ and $Aβ_{42}$ released into the extracellular space. The accumulation of Aβ peptides, from neurotoxic oligomers to further aggregated insoluble β-sheet fibrils and dense fibrillary plaques, is believed to underlie subsequent neurofibrillary tangle formation and neuronal loss, which precede the onset of clinical symptoms by more than 10–15 years (Hardy and Gwinn-Hardy, 1998; Hardy et al., 1998). However, confirmation of AD neuropathology has long relied on immunohistochemical staining of Aβ aggregates in postmortem autopsy tissues. Since the early 2000s, the availability of antemortem *in vivo* PET imaging with Aβ radiotracers has greatly advanced our knowledge on the time course and correlation of Aβ aggregation, AD progression, and cognitive decline, and revolutionized AD diagnosis.

Tracer Development

The search for Aβ imaging tracers dated back to the mid-1990s, culminated in the first *in vivo* imaging of Aβ in an AD patient in 2002 with the ^{11}C-labeled Pittsburgh compound B ([^{11}C]PIB, **Figure 1**), which is derived from the Aβ staining agent thioflavin-T (Klunk et al., 2004). [^{11}C]PIB has a relative high selectivity for Aβ of all forms from soluble oligomers to insoluble fibrils and plaques over other pathologic proteins such as tau and α-synuclein. Both visual inspection and quantitative analysis demonstrated higher cortical retention in AD patients than in cognitively intact subjects, especially in the orbitofrontal cortex, inferior parietal cortex, posterior cingulate cortex and precuneus, which resembled the pattern found in immunohistochemical studies (Rowe and Villemagne, 2011). To date, [^{11}C]PIB is still the best and most widely used Aβ PET tracer and regarded as the gold standard.

The short radioactive half-life of ∼20 min for the carbon-11 nuclide limits the use of [^{11}C]PIB to institutions with on-site cyclotrons, thus inspiring the development of ^{18}F-labeled Aβ radiotracers. Three of such tracers with favorable binding and imaging properties, [^{18}F]florbetapir ([^{18}F]AV-45), [^{18}F]florbetaben ([^{18}F]AV-1, [^{18}F]BAY-94-9172), and [^{18}F]flutemetamol ([^{18}F]GE-067) (**Figure 1**), have since been approved by the United States Food and Drug Administration (FDA) for clinical diagnosis and differential diagnosis of AD (Barthel et al., 2011; Lister-James et al., 2011; Curtis et al., 2015). [^{18}F]NAV4694 ([^{18}F]AZD4694), another promising ^{18}F-labeled tracer with rapid pharmacokinetics and lower non-specific binding in the cerebral white matter, is now in clinical trials (Cselenyi et al., 2012; Therriault et al., 2021). These tracers, with longer radioactive half-life of ∼110 min, are suitable for long-distance distribution and thus can be more widely used in the clinics. They are presumed to yield less noisier images and therefore more precise quantitation of minute cerebral Aβ accumulation in the early stage of the disease, due to more abundant radioactivity counts in the later period of scan. Notably, imaging protocols provided for each tracer are quite different from one another in terms of scanning window as well as visual interpretation and quantitative analysis of the images (Mallik et al., 2017).

Imaging Research Findings and Clinical Relevance

In general, cortical Aβ retention detected by PET imaging is in good correlation with immunohistochemical staining of amyloid plagues at autopsy or biopsy brain samples (Clark et al., 2012; Rinne et al., 2012; Curtis et al., 2015; Sabri et al., 2015a). This qualifies the application of Aβ PET imaging as a non-invasive tool for *in vivo* detection of cortical Aβ deposition

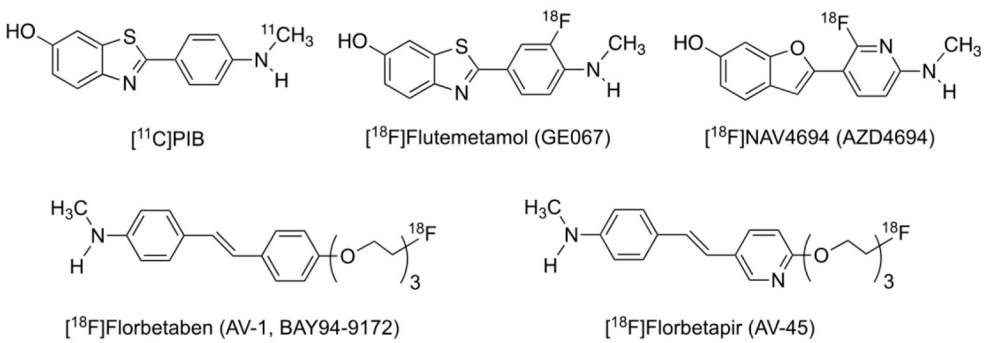

FIGURE 1 | Structures of representative PET radiotracers for Aβ imaging.

in the living brain. In the clinical daily-routine context, Aβ PET imaging provides plenty valuable information for the purpose of differential diagnosis between AD dementia and dementia disorders associated with non-Aβ pathologies such as frontotemporal lobe dementia (FTLD), which is sometimes indistinguishable from AD by neuropsychological assessments and conventional structural imaging modalities only (Rowe et al., 2008).

On the other hand, it has been emphasized that an amyloid-positive PET merely reflects the existence of amyloid neuropathology *in vivo* and does not necessarily guarantee a diagnosis of AD, concerning the fact that many otherwise cognitively normal subjects (even young healthy volunteers) have been found to be amyloid-positive judging from PET results, and that cognitive decline is more likely due to factors other than amyloid pathology in dementia with Lewy bodies (DLB) or in some co-morbid situations (Johnson et al., 2007; Ossenkoppele et al., 2015; Petrou et al., 2015). It has also been debated whether a negative amyloid scan could exclude the possibility of AD (Jack et al., 2016), since evidence of neurodegeneration in the absence of amyloid pathology challenges the proposed AD progression scheme (Sperling et al., 2011).

The ability of PET imaging with Aβ tracers to predict conversion from MCI due to AD, the prodromal stage of the disease defined by different diagnostic guidelines (McKhann et al., 2011; Dubois et al., 2014), to AD dementia has also been extensively investigated. Roughly 70% of amyloid-positive MCI patients converts to AD dementia within 3 years (Okello et al., 2009a). As compared to [^{18}F]FDG PET, amyloid PET has higher sensitivity but relatively lower specificity (Teipel et al., 2015), which is consistent with the finding that amyloid accumulation commences at least a decade before the worsening of synaptic activity and brain function to a clinically significant level where amyloid deposition reaches a plateau (Jack and Holtzman, 2013; Jack et al., 2013a). Correlation of Aβ retention to cognitive performance has been shown to be greater in MCI and cognitively intact subjects than in AD dementia patients (Pike et al., 2007, 2011; Villemagne et al., 2008), which could also be explained by the hypothesized plateau model. Therefore, it is not surprising that regional hypometabolism and amyloid deposition in the temporoparietal regions are closely associated with each other whereas those in the frontal lobe, a region affected only in advanced AD, are not (Edison et al., 2007; Cohen et al., 2009).

The significance of Aβ PET in subjects without objective evidence of cognitive decline is emerging most recently. Large-scale comprehensive studies have shown that Aβ positivity is linked to high progression risk in subjective cognitive decline (SCD) and is associated with age and family history other than sex, education, marital or retirement status and self-reported lifestyle factors (Papp et al., 2020; Sperling et al., 2020). Longitudinal follow-up studies suggest that the duration of Aβ existence might be more important than age or binary result in affecting both deteriorating rate and the final status of cognition through elevated entorhinal tau burden (Hanseeuw et al., 2019; Koscik et al., 2020). Even if Aβ burden detected by PET is below threshold, its value is still positively correlated to the subject's future risk of cognitive decline (Guo et al., 2020).

The Centiloid Scaling Project

As the utilization of amyloid PET in clinical trials and research expands and multiple tracers are available for such imaging applications, the urgent need for inter-tracer standardization and for multi-center collaboration and longitudinal comparison drove the launch of the centiloid scaling project (Klunk et al., 2015). According to the concept of the project, one institute can follow a multi-step regime to create a scaling from 0 (young healthy controls) to 100 (typical AD patients) using its own amyloid PET data (Rowe et al., 2016). In this way a universal cutoff value could then be directly or indirectly applied in multi-center imaging and/or longitudinal studies to allow for inter-site/inter-tracer comparisons. The study group of the centiloid project has now made progress in the derivation and verification of converting formula, enabling the translation of non-[^{11}C]PIB Aβ PET semi-quantitative values to standardized [^{11}C]PIB counterparts (Rowe et al., 2017; Battle et al., 2018; Bourgeat et al., 2018; Navitsky et al., 2018). The authenticity of the centiloid approach has been confirmed neuropathologically (Amadoru et al., 2020).

Discussion

The amyloid cascade theory has been the predominant theory of AD etiology and drove the development of anti-Aβ therapeutics in the last 3 decades. The availability of Aβ PET imaging tracers and its applications in AD imaging have indicated that amyloid pathology may be a high risk factor for future cognitive decline. However, increasing evidence also indicates that cortical amyloid is not specific for the presence of cognitive symptoms, thus affecting the positive predictive value of Aβ PET imaging. Among populations without dementia, the prevalence of cerebral amyloid pathology as determined by Aβ PET imaging or cerebral spinal fluid (CSF) Aβ measurement is associated with age (Jansen et al., 2015), e.g., 33% of healthy elderly individuals have significant levels of Aβ deposition without apparent clinical symptoms (Rowe et al., 2010). Therefore, Aβ deposition alone cannot explain AD pathogenesis and progression. Repeated failures of clinical trials for many anti-Aβ drug candidates have dampened the hope for their efficacy as disease-modifying therapeutics. Nonetheless, it should be kept in mind that Aβ PET imaging will still remain the gold standard to investigate disease mechanisms as it provides information regarding the topography of Aβ lesions. Although there have been no successful anti-Aβ drugs up to date, Aβ PET imaging has provided useful outcome measures for anti-Aβ therapeutics in clinical trials (Salloway et al., 2014; Honig et al., 2018; Wessels et al., 2020).

PET TRACERS FOR IMAGING TAU TANGLES

Overview

In addition to the β-amyloid peptides, microtubule-associated protein tau (MAPT), or simply tau protein, together with its misfolded products, has been more thoroughly studied in recent years to explore its relationship with AD. Similar to the case of senile plaques formed by Aβ, the formation of neurofibrillary tangles (NFTs) by paired helical filaments (PHFs)

is also a neuropathological hallmark of AD (Braak and Braak, 1997). PHFs are aggregated by misfolded hyperphosphorylated tau protein whose binding affinity with the microtubules is weakened, causing neuronal cytoarchitecture breakdown and dysfunction (Hoover et al., 2010; Spillantini and Goedert, 2013).

With the repeated failures of anti-Aβ therapeutics in large scale clinical trials, the focus was shifted from Aβ to tau on the development of AD therapeutics and imaging agents (Giacobini and Gold, 2013). However imaging tau *in vivo* is more challenging than imaging Aβ. Tau protein has six unique isoforms characterized by the number of repeats of its microtubular binding domains, and multiple secondary/tertiary structures differentiated by the shape of the filaments (Spillantini and Goedert, 2013). In addition to its much lower abundance compared to Aβ peptides in the brain, MAPT's intraneuronal property demands the qualified tracer to cross neuron cell membrane in addition to the blood brain barrier. These factors collectively hamper the screening and identification of sensitive and specific compounds. Nevertheless, substantial progress has been made in overcoming these inherent obstacles, and preliminary studies have shown encouraging results worthy of the efforts (Hall et al., 2017; Leuzy et al., 2019).

Tracer Development

PET imaging of fibrillary tau traced back to about the same time for amyloid, with [^{18}F]FDDNP arguably as the earliest tracer (Agdeppa et al., 2001). Indeed, this tracer labels both amyloid plaques and fibrillary tau tangles *in vivo*, but this property is also its biggest disadvantage, as it has comparable affinity for both amyloid and tau proteins, i.e., a lack of selectivity for either target. The first selective tau tracer [^{18}F]THK523 was developed by Tohoku University of Japan in 2005 (Okamura et al., 2005). Later structural modifications led to the development of other tracers in the THK family: [^{18}F]THK5105, [^{18}F]THK5117, [^{18}F]THK5317, and [^{18}F]THK5351, with improved binding and *in vivo* pharmacokinetic properties (Okamura et al., 2013; Chiotis et al., 2016; Betthauser et al., 2017). However, tracers in this family were later found to have notable off-target binding to monoamine oxidase-B (MAO-B), which greatly limited their utility in imaging of tauopathies including AD (Ng et al., 2017).

[^{18}F]Flortaucipir ([^{18}F]AV1451, or formerly [^{18}F]T807) is currently the most applied and the only FDA-approved tau radiotracer (**Figure 2**) (https://www.fda.gov/drugs/drug-approvals-and-databases/drug-trial-snapshot-tauvid). It has a 25-fold higher affinity for tau than Aβ, as well as favorable kinetics for both uptake and washout in the brain without radioactive metabolites penetrating the blood-brain-barrier (Xia et al., 2013). [^{18}F]flortaucipir has higher affinity to PHFs over straight filaments (SF), and to combined 3-repeat (3R) and 4-repeat (4R) isoforms over 3R or 4R isoforms alone, making it more suitable for imaging AD pathology than non-AD tauopathies such as progressive supranuclear palsy (PSP) and corticobasal degeneration (CBD) (Lowe et al., 2016). It is noted that suspected minor off-target binding to MAO-A in the basal ganglia and substantia nigra would limit the application of [^{18}F]flortaucipir in imaging Parkinsonian tauopathies (Ono et al., 2017).

[^{11}C]PBB3 is another selective tau tracer that has also been thoroughly studied in various tauopathies including AD (**Figure 2**). [^{11}C]PBB3 binds to both 3R and 4R tau isoforms

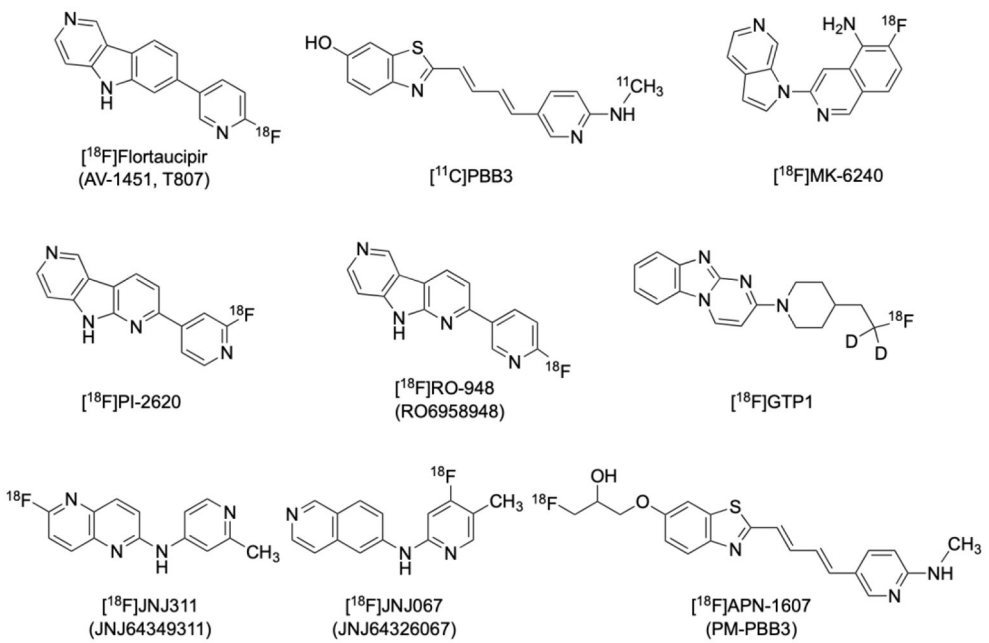

FIGURE 2 | Structures of representative PET radiotracers for tau imaging.

and its affinity for tau is over 40 times higher than that for amyloid, making it suitable for imaging of various tauopathies *in vivo* (Kimura et al., 2015). Minor structural modifications then afforded [^{18}F]APN-1607 (PM-PBB3) and [^{18}F]AM-PBB3, the next generation members of the PBB3 family. [^{18}F]APN-1607, (**Figure 2**) has recently been reported to possess more favorable pharmacokinetics and provide higher gray-matter/white-matter contrast (Hsu et al., 2020; Su et al., 2020; Tagai et al., 2021).

The clinical development of several newer, second generation selective tau tracers are ongoing, including [^{18}F]PI2620, [^{18}F]MK6240, [^{18}F]GTP1, [^{18}F]RO-948 (RO6958948), [^{18}F]JNJ-311 (JNJ64349311), and [^{18}F]JNJ-067 (JNJ-64326067) (**Figure 2**). Designers of these new generation tracers are focusing on improving *in vivo* characteristics such as higher selectivity, faster brain penetration/washout, and less off-target binding. Preliminary studies for these newer tracers have shown promising results (Declercq et al., 2017; Kuwabara et al., 2018; Guehl et al., 2019; Rombouts et al., 2019; Teng et al., 2019; Schmidt et al., 2020).

Off-target binding has been a universal concern for tau tracers since the early [^{18}F]FDDNP was found to be non-selective to both amyloid and tau (Thompson et al., 2009). In PET imaging of neurodegeneration, selectivity of tau tracers over other pathological proteins such as Aβ, α-synuclein, and TDP-43 would always require validation. Similarity of the secondary/tertiary structures of the binding sites of these proteins makes it difficult to find a truly selective and specific probe, not to mention the complexity introduced by potential comorbidity of the neurodegenerative disorders. In addition, off-target binding in the central nervous system (CNS) has been widely examined across the tau tracers. It is now known that MAO-A and MAO-B are the most frequent off-targets whose secreting neurons are highly overlapped with Parkinsonism-related brain regions (Lowe et al., 2016; Bischof et al., 2017; Okamura et al., 2018). Choroid plexus is frequently found to be a tissue with apparent off-target binding, the mechanism of which is yet unclear (Ikonomovic et al., 2016). It is postulated that melanin, neuromelanin, mineralized structures and hemorrhagic lesions can also cause off-target binding of tau tracers in various locations. There is also debate that the suspected "off-target" binding may be reflecting true tau-binding, or binding to some specific targets yet to be identified (Ikonomovic et al., 2016; Passamonti et al., 2017). These characteristics pose substantial difficulties to clinical differentiation and potential post-treatment evaluation (Passamonti et al., 2017).

Recent cryo-electron microscopic structure discoveries of AD tau filaments may provide new insights for the binding interactions between various tau tracers and tangles, and spur refinements on the design of novel, subtype-selective tau tracers (Fitzpatrick et al., 2017).

Imaging Research Findings and Clinical Relevance

According to the amyloid cascade hypothesis, neurodegeneration characterized by misfolded tau tangle aggregation is the downstream event secondary to major amyloid deposition (Jack et al., 2013b). In contrast to the globally elevated pattern seen in brain amyloid PET of AD dementia patients, the spatiotemporal distribution of tau tracers follows a typical neuropathological sequence of spreading (Braak's stage), as have been demonstrated in both cross-sectional and longitudinal studies in a wide-range of subjects from advanced AD dementia patients to cognitively intact elderly controls (Rabinovici and Jagust, 2009; Johnson et al., 2016; Wooten et al., 2017; Villemagne et al., 2018). This quantitative and sequential connection indicates that this *in vivo* tangle spreading trajectory may reflect not merely neuronal dysfunction but also disease progression. In parallel to postmortem immunohistochemical findings, *in vivo* tau deposition varies amongst the brain regions, starting from the medial temporal lobe, i.e., hippocampus and entorhinal cortex (Braak stage I–II), to the adjacent neocortices (Braak stage III–IV), and finally to the entire brain (Braak stage V–VI) (Cho et al., 2019; Leuzy et al., 2019; Baek et al., 2020; Fleisher et al., 2020). As expected, clinical manifestation of AD is closely related to tau retention in the responsible brain regions. For instance, while temporal lobe deposition correlates well with memory performances, frontal lobe retention strongly correlates with execution and global cognition (Ossenkoppele et al., 2016; Bejanin et al., 2017; Shimada et al., 2017).

According to current experience with all the available tau tracers, AD is not likely to be the diagnosis of a tau-negative individual, while non-tauopathies can be basically excluded from the cause of cognitive decline for a tau-positive individual (Bischof et al., 2017). Non-AD tauopathies such as FTLD, PSP and CBD, however, manifest different distribution patterns and trajectory from AD involving different sub-regions in the brain stem and basal ganglia as well as cortical regions, which could be of additional differential diagnostic value in the clinical context (Bischof et al., 2017; Leuzy et al., 2019). Recently, tau deposition in cognitively intact healthy elderly subjects has also been revealed by PET and confirmed by autopsy results. This phenomenon is coined primary age-related tauopathy (PART) and believed to produce only minute, if any, clinical symptoms (Crary et al., 2014). In the absence of amyloid, PART alone is believed to be insufficient to develop memory decline (Harrison et al., 2019). Its relationship to suspected non-amyloid pathology (SNAP) has also been proposed, which presumably underlies the preclinical abnormalities during the development of AD (Jack, 2014).

Hypometabolism in brain regions that are commonly affected in advanced AD, including posterior cingulate cortex, precuneus and temporoparietal association cortex, represents synaptic dysfunction of the neurons in the course of AD (see below section on FDG imaging of glucose metabolism). Cortical tau tracer deposition can be seen in the same areas, establishing a typical topographic "yin-yang" offset between the two biomarkers. Further, correlation between these two imaging findings grows stronger as tau burden increases (**Figure 3**) (Whitwell et al., 2018; Lu et al., 2020). These unique phenomena demonstrate outstanding pathophysiological coherency of excessive MAPT retention and subsequent destruction of cytoarchitecture, resulting in synaptic metabolic deficit. On the other hand, multi-modality studies also reveal that the correspondence between

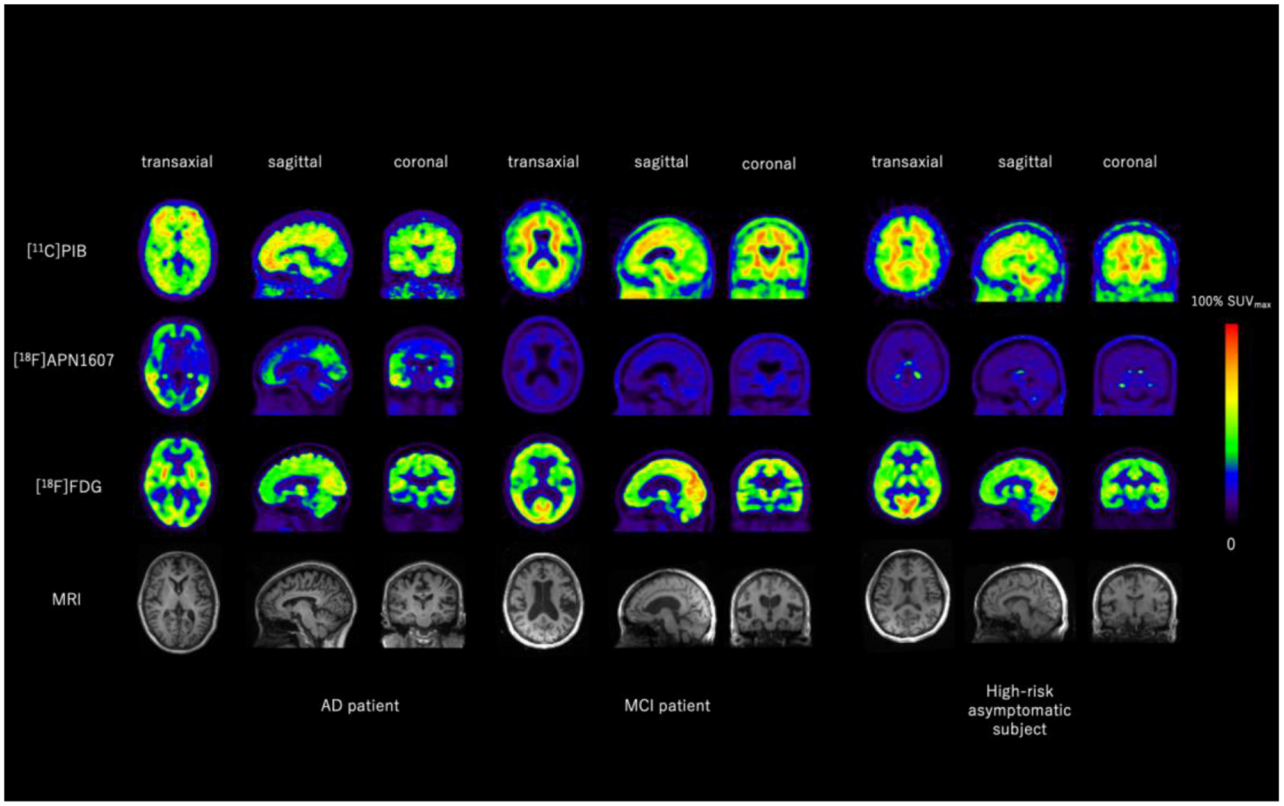

FIGURE 3 | Representative images of [^{11}C]PIB, [^{18}F]APN1607, and [^{18}F]FDG PET and MRI of an AD patient, an MCI patient and a high-risk asymptomatic subject. Aβ was positive for the AD patient and equivocal for the MCI patient and the high-risk asymptomatic subject. Typical Braak Stage V–VI tau deposition was seen in the AD brain, whereas no tau deposition was seen in the brain of the MCI patient or the high-risk asymptomatic subject. Typical AD-like glucose-hypometabolism was seen in AD brain including posterior cingulate cortex, parietal, temporal, and pre-frontal cortices, whereas most of these regions are relatively spared in the brain of MCI patient and high-risk asymptomatic subject. Images provided by PET Center, Huashan Hospital, Fudan University.

frontal hypometabolism and medial temporal tau retention is present independent of amyloid deposition, which can be interpreted as aging-related.

The relationship between tau aggregation and cortical atrophy as demonstrated by structural MRI is similar to that between tau aggregation and hypometabolism. However the former was found to be weaker than the later, especially in conditions other than mild AD (Sepulcre et al., 2016; Iaccarino et al., 2018). In addition to local correlation, tau deposition in the parietal lobe and precuneus can also be correlated to medial temporal lobe atrophy (Shimada et al., 2017). These observations seem plausible due to the fact that substantial structural alterations often relate to the later stage of the disease.

In general, CSF phosphorylated tau (p-tau, representing misfolded tangle formation) and total tau (t-tau, representing neurodegeneration) levels parallel *in vivo* tau tracer binding (Mattsson et al., 2018; Leuzy et al., 2019; Okafor et al., 2020). However, discordant results have also been found in small subgroups, possibly due to varying detectability around the CSF threshold and uneven rate of tau tangle formation in different disease stages (Murray et al., 2015; Thal et al., 2015). Although it is believed that elevated CSF tau levels precede tau imaging manifestation, tau PET has the advantage of visualization and topographic quantitation capacity, as well as relative non-invasiveness (Wolters et al., 2020).

Discussion

The research and development of tau PET tracers has gained undeniable progress in the last few years. Although some issues remain, especially isoform selectivity and other potential off-target binding, the applications of these tracers in AD imaging have provided, and are expected to continue to provide valuable information on the time course and topography of tau tangles in AD, and the correlation with cognitive dysfunction. Longitudinal and cross-sectional multi-target and multi-modality studies are encouraged to further elucidate the role of tau in the course of AD, as well as its interaction and relationship with Aβ deposition, synaptic dysfunction, brain atrophy, and other pathological biomarkers. Another important application of tau imaging is its utility for patient selection and endpoint measurements in phase 2 and phase 3 clinical trials of disease-modifying anti-tau treatments that have been gaining increasing impetus (Giacobini and Gold, 2013).

Coming from different compound families, the currently available tau tracers have different affinities for the various MAPT

isoforms or tangle structures, hence distinctive topographic binding patterns in the same tauopathy. Selectivity to isoforms and structures could be a future direction to design new probes as 3R-specific or 4R-specific. We could therefore foresee a future tau imaging landscape where different tracers "rule" their own pieces of territory (i.e., specific tauopathy characterized by specific isoform or structure) in case that the correlation of tau imaging results similar to the "Aβ centiloid" is not achievable.

PET TRACER FOR IMAGING GLUCOSE METABOLISM: [^{18}F]FDG

Overview

As a radionuclide-labeled analog of glucose, the major metabolic substrate of neurons, [^{18}F]fluorodeoxyglucose ([^{18}F]FDG, or FDG) has long been used in the investigation of CNS disorders to reflect neuronal degeneration and injury. In fact the first report of this most widely used tracer was a brain imaging study (Phelps et al., 1979), although now the majority of its clinical application is for oncological purposes. The characteristic AD pathology (McGeer et al., 1986) and neurodegenerative changes (Mielke et al., 1996; Scholl et al., 2011) are associated with cortical hypometabolism demonstrated in pre-mortem FDG PET imaging. Clinical application of FDG PET in AD lies mainly in differential diagnosis from other causes of dementia, as well as treatment effect evaluation of disease-modifying or progression-slowing therapies. Clinical value of FDG PET has also been investigated for its predictive ability for conversion to AD dementia of high-risk subjects assumed to be in the prodromal or asymptomatic stage.

AD Dementia Patients

The characteristic manifestation of FDG PET in AD dementia is hypometabolism in the posterior part of cerebrum including the posterior cingulate cortex (PCC), precuneus (PrC), and parietotemporal association cortices such as the angular gyrus. These regions are the most discriminating components of AD-specific cerebral hypometabolic pattern as well as strong indicators of disease severity and progression. It is of significant differential value that PCC and PrC are substantially spared in other minor causes of senile dementia including frontotemporal lobe dementia (FTLD), dementia with Lewy bodies (DLB), Parkinson's Disease dementia (PDD), and vascular dementia (VaD). The hippocampus and entorhinal cortex are involved in the earliest stages of AD according to neuropathological findings based on NFT formation (Braak and Braak, 1997), however glucose metabolism in these areas cannot be readily distinguished between AD patients and normal controls. This is largely due to the frequent presence of medial temporal hypometabolism even in normal aging, and the partial volume effect (PVE) correlated with regional cortical atrophy. Frontal lobe hypometabolism is often associated with advancement, executive dysfunction, or atypical behavior in AD cases, although it could also be observed in normal aging. Occipital lobe hypometabolism is related to the posterior cortical atrophy (PCA) subtype of AD, but care should be taken when differentiating dementia types because this is also a prominent sign of DLB.

MCI Patients

Early differentiation of MCI due to AD is crucial since early therapeutic intervention is indicated to be beneficial at least in slowing disease progression (Vellas et al., 2007; Molinuevo et al., 2011). It should be noted, though, that the etiology of MCI is heterogeneous, meaning that approximately half of the patients convert to dementia other than AD, or do not convert at all (Rowe et al., 2010; Bennett et al., 2012; Frisoni et al., 2017). Therefore, whether FDG PET has discriminative and predictive ability for MCI patients is of great clinical relevance.

Hypometabolism revealed by FDG PET in typical AD-affected brain regions including the inferior parietal lobe, precuneus and posterior cingulate cortex is present early in prodromal AD, namely MCI stage. In a meta-analysis comparing the accuracy of 3 different imaging modalities, FDG PET (sensitivity = 88.8%, specificity = 84.9%) exhibits higher sensitivity and higher specificity than cerebral blood flow SPECT (sensitivity = 83.8%, specificity = 70.4%) and structural MRI (sensitivity = 72.8%, specificity = 81%) in terms of predicting short-term conversion to AD dementia (Yuan et al., 2009). Interestingly, FDG PET performs better in excluding non-converters than [^{11}C]PIB Aβ PET (specificity: 74.0 vs. 56.2%), while its sensitivity is lower (sensitivity: 78.7 vs. 93.5%) (Zhang et al., 2012). This could be explained by the compensatory mechanism of preserved cerebral synaptic function against amyloid burden. Aside from the advantage of accurate short-term predictive ability, FDG PET can also exclude other potential etiology underlying MCI such as FTLD and DLB, in contrast to other biomarkers including CSF $A\beta_{1-42}$ and t-tau/p-tau assays (Arbizu et al., 2018).

The value of FDG PET in MCI has been acknowledged in existing diagnostic criteria (Albert et al., 2011; Dubois et al., 2014). Meanwhile, future researches in this field are encouraged to overcome the various current limitations in terms of methodology normalization, gold standard verification, and effectiveness/economy evaluation (Arbizu et al., 2018).

High-Risk Asymptomatic Subjects

People with subjective cognitive decline (SCD) rather than objective evidence of cognitive impairment, subjects burdening amyloidosis, and family members of AD patients expressing PSEN1/2 or APP mutation were reported to have higher tendencies to develop to AD dementia (Bateman et al., 2011; Villemagne et al., 2011; Wolfsgruber et al., 2016). It is hypothesized that neurodegenerative alterations could have be silently undergoing in these subjects.

Various confounding factors lead to heterogeneity of the underlying etiology for SCD, leaving controversy in the regional metabolic manifestation of typical AD-affected areas in this subgroup (Scheef et al., 2012; Brugnolo et al., 2014; Van Der Gucht et al., 2015). Although amyloid-positive asymptomatic subjects, as defined by CSF $A\beta_{1-42}$ or amyloid PET, will have higher risk of converting to AD in a life-long period, the utility of FDG PET reflecting neurodegeneration in this population is still not comparable to that in MCI patients, due to its poor performance in prediction of short-term conversion (Villemagne et al., 2011). Glucose metabolic abnormalities prior to the onset of clinical symptoms were observed in

asymptomatic carriers of mutated APP and PSEN1/2 genes (Mosconi et al., 2008; Benzinger et al., 2013), who theoretically would suffer from dementia eventually. Nonetheless, the relationship between cerebral hypometabolism and time-to-conversion cannot be easily concluded in the absence of well-designed longitudinal studies.

In view of the above-mentioned facts, it is not recommended to clinically apply FDG PET to asymptomatic subjects with only one risk factor for diagnostic or prognostic purposes. Further investigation is needed to verify whether FDG PET is useful for individuals with multiple risk factors (Mosconi et al., 2008; Vannini et al., 2017).

Treatment Monitoring

FDG PET has been used as an imaging biomarker for outcome assessment in multiple clinical trials of AD therapeutics (Hoyer, 2002; Landau et al., 2011; Herholz, 2012). Global as well as sub-global or regional FDG uptake alterations following medication or surgical treatment has been observed in multiple clinical research studies (Nordberg et al., 1992; Heiss et al., 1994; Mega et al., 2001; Potkin et al., 2001; Tune et al., 2003; Schmidt et al., 2008; Tzimopoulou et al., 2010; Craft et al., 2012; Smith et al., 2012).

Discussion

FDG PET has been most widely used in dementia research and as an important adjunct imaging tool in the diagnosis of AD. On the whole, FDG PET enables early diagnosis of AD and thus early therapeutic intervention, as well as treatment strategy optimization in a large proportion of cases (Laforce et al., 2010; Elias et al., 2014). Delaying of disease progression and prevention of life quality deterioration as instructed by FDG PET can help lessen the overall healthcare expenditure (Banerjee and Wittenberg, 2009; Getsios et al., 2012).

Although quite a few critical issues in the utility of FDG PET for AD diagnosis have already been resolved, there are still many others that require verification with larger cohorts and better-designed trials (Garibotto et al., 2017).

PET TRACERS FOR IMAGING NEUROINFLAMMATION

Overview

Increasing evidence has helped with the formation of neuroinflammation hypothesis of AD etiology (McGeer and McGeer, 2010; Morales et al., 2014). Similar to the cases in other systems of the human body, it is now believed that the impact on CNS under different phases of the inflammatory process could be different. While acute inflammation could be protective to the brain against the harmful effects of invading pathogens and traumatic injuries, consistent stimulation by inflammatory factors could, on the other hand, be detrimental to the neurons and eventually induce neurodegeneration and loss of cognitive functions (Wyss-Coray and Mucke, 2002; Mrak and Griffin, 2005). It is also suggested that the neuroinflammation underlying AD starts from the earliest stages without any obvious clinical symptoms, and lasts to the end stage of the disease (Vehmas et al., 2003; Hoozemans et al., 2005). Therefore it is hypothesized that the clinical onset of AD dementia could be partly prevented or postponed by anti-inflammation interventions, which is based on results from retrospective observation studies and prospective trials (McGeer et al., 1996; Hoozemans et al., 2011). Multiple pathophysiological factors can trigger the process of immunoactivation in the CNS, in which complements, cytokines, growth factors, reactive oxygen species, microglia and astrocytes participate (Barger and Harmon, 1997; Akiyama et al., 2000). PET radiotracers have been developed to image these neuroinflammatory targets *in vivo* (Zimmer et al., 2014; Varley et al., 2015).

Tracer Development

The 18-kDa translocator protein (TSPO) is a mitochondrial protein. Under normal circumstances, it is low-expressed in specific brain regions in the microglia, the monocyte-macrophage-dendritic cell family member majorly active in the CNS and comprising ∼15% of the non-neuronal cells within. TSPO is found to participate in amino acid and cholesterol transportation, and to serve as a "switch" in activating microglia from the resting state in response to various stimuli including infection and traumatic injury (Streit et al., 2004). Pro-inflammatory cytokines and neurotoxic substances are released by significantly proliferated microglia after the induction of soluble or fibrillary Aβ and subsequent TSPO regulation, which could be related to the fact that amyloid plaques are found to be colocalized with activated microglia *in vivo* in the brain where massive neuronal destruction and brain atrophy occur (McGeer et al., 1988; Venneti et al., 2009; Schilling and Eder, 2011). These characteristics made TSPO the predominant target for imaging *in vivo* inflammatory process in AD.

[^{11}C]PK11195 was the first successfully developed TSPO tracer for human PET imaging (**Figure 4**) (Cagnin et al., 2001), but it remains controversial whether its binding is correlated with amyloid deposition, probably due to its low specific binding signal and hence low sensitivity to detect small changes in TSPO under disease conditions (Edison et al., 2008; Wiley et al., 2009; Yokokura et al., 2011). To overcome the shortcomings of [^{11}C]PK11195, a series of 2nd generation TSPO tracers were developed and evaluated, including [^{11}C]PBR28, [^{11}C]DAA1106, [^{18}F]DPA713, [^{18}F]DPA714, [^{18}F]FEPPA, [^{18}F]FEMPA, and [^{18}F]FEDAA1106 (**Figure 4**; Varley et al., 2015; Calsolaro and Edison, 2016; Edison et al., 2018). Though the majority of these radioligands are more sensitive than [^{11}C]PK11195, subsequent studies found that their brain uptake are regulated by the TSPO gene rs6971 polymorphism, thus requiring phenotyping of individual subjects to match imaging results to their TSPO affinity status (Owen et al., 2012). More recently, 3rd generation, putative "phenotype-insensitive" TSPO probes such as [^{11}C]ER176 (**Figure 4**) are being developed and evaluated (Wadsworth et al., 2012; Ikawa et al., 2017).

Similar to the paradigm of TSPO imaging of microglial activation, MAO-B is found to be elevated in reactive astrocytes and chosen as the target for *in vivo* imaging of neuroinflammation. The selective MAO-B tracer [^{11}C]deuterium-L-deprenyl ([^{11}C]DED) has been applied

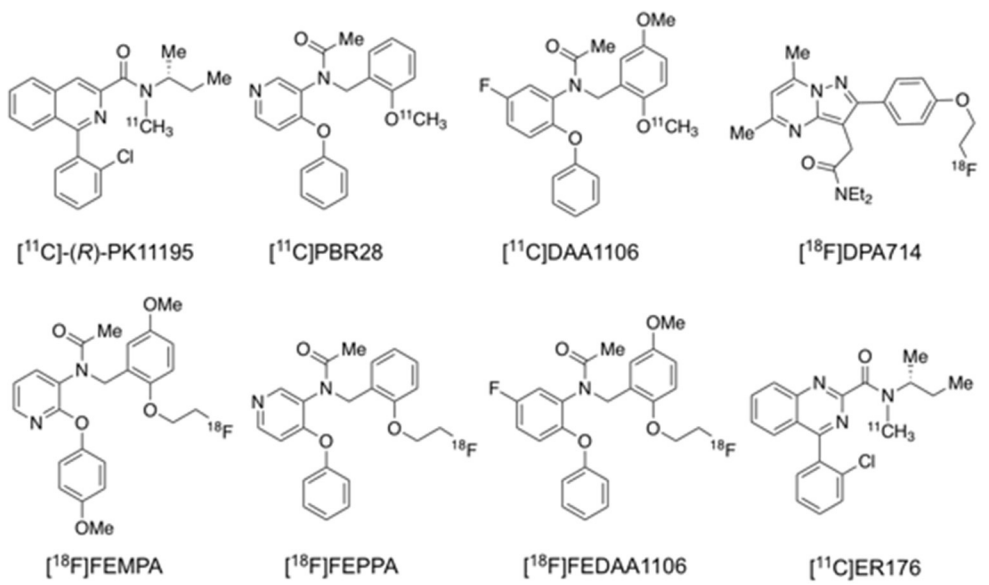

FIGURE 4 | Structures of representative PET radiotracers for TSPO imaging.

to studies of neurodegenerative disorders including AD (Carter et al., 2012). Type-2 imidazoline receptor, a newly discovered target for imaging astrocyte, is now being evaluated for its potential in differentiating AD and control using [^{11}C]BU99008 under ongoing trial (Wilson et al., 2019).

Imaging Research Findings and Clinical Relevance

In vivo TSPO imaging is generally able to discriminate between AD dementia patients and normal control subjects (Cagnin et al., 2001; Yasuno et al., 2008; Suridjan et al., 2015; Varrone et al., 2015; Hamelin et al., 2016; Kreisl et al., 2016a). The majority of the multi-modality studies report that regional TSPO binding correlates to [^{11}C]PIB retention positively, and FDG uptake as well as cortical volume negatively (Edison et al., 2008; Yokokura et al., 2011; Kreisl et al., 2013, 2016b) (**Figure 5**). In most cases the extent of TSPO binding is associated with not only baseline cognitive performance, but also its deterioration over time (Edison et al., 2008; Okello et al., 2009b; Yokokura et al., 2011; Kreisl et al., 2013, 2016a). Elevated TSPO binding in advanced AD dementia patients is seen in various cortical regions following an anticipated distribution pattern (Cagnin et al., 2001; Hamelin et al., 2016). Apart from global discrimination, regional TSPO binding is correlated to attenuated corresponding brain function. One study uncovered an inverse correlation between visuospatial function and [^{18}F]FEPPA binding in the parietal and posterior internal capsule, as well as correlation between language ability and binding in the latter region (Suridjan et al., 2015). Interestingly, early-onset AD (EOAD) is reported to be associated with higher TSPO binding than late-onset AD (LOAD), especially in the frontal and parietal cortices, suggesting greater microglial activation in the former condition (Kreisl et al., 2013). In addition, a longitudinal study revealed that TSPO binding in MCI converters to AD dementia is drastically different from that of non-converters (Kreisl et al., 2016a). These results are concordant with previous finding that chronic microglia participation may be associated to the brain in AD progression (McGeer and McGeer, 2010; Morales et al., 2014).

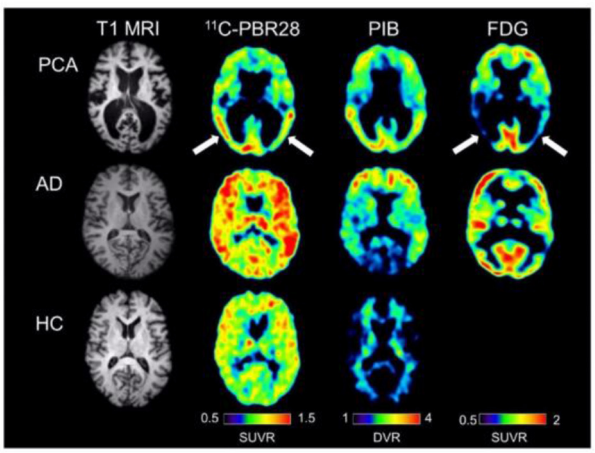

FIGURE 5 | Single subject images from a patient with posterior cortical atrophy (top row), a patient with amnestic Alzheimer's disease (center row), and a healthy control subject (bottom row). The posterior cortical atrophy subject showed focal occipito-temporal [^{11}C]PBR28 binding, with FDG hypometabolism in the same region (arrows). While the posterior cortical atrophy subjects showed occipito-temporal PIB binding, PIB binding was also found in frontal cortex. The subject with amnestic Alzheimer's disease showed more diffuse [^{11}C]PBR28 binding, with occipital sparing on PIB and classic bilateral temporo-parietal hypometabolism on FDG imaging. The control subject showed low amounts of diffuse [^{11}C]PBR28 binding and absence of cortical [^{11}C]PIB binding. Courtesy from Kreisl et al. (2016b).

However, conflicting results are also present in various aspects. Absence of the expected correlation between TSPO binding and cortical amyloid retention or neuronal metabolism has been repeatedly reported (Okello et al., 2009b; Wiley et al., 2009; Schuitemaker et al., 2013). There are also studies showing the inability of TSPO tracers to discriminate healthy subjects from patients with MCI or even advanced dementia (Okello et al., 2009b; Wiley et al., 2009; Schuitemaker et al., 2013; Golla et al., 2015). Likewise, significant association between TSPO binding and memory performance or disease severity is not always found (Yasuno et al., 2008; Schuitemaker et al., 2013). Single-nuclide polymorphism of rs6971 has been discovered to regulate TSPO binding *in vivo* and may partly contribute to the conflicting findings so far, since binding adjusted to individual phenotyping shows increased discriminating accuracy (Suridjan et al., 2015). In addition to doubts about the sensitivity of current TSPO tracers to detect subtle alterations in the prodromal stages of AD, there are data relating higher binding of [^{18}F]DPA714 to slower cognitive decline, suggesting a neuroprotective role of microglial activation perhaps in the early phase of the disease (Hamelin et al., 2016).

According to a collective study with both [^{11}C]DED and [^{11}C]PIB, astrocytosis is most profound in amyloid-positive MCI subjects, followed by advanced AD patients as well as amyloid-negative MCI subjects and healthy controls (Carter et al., 2012; Rodriguez-Vieitez et al., 2016). This PET finding suggests that astrocytic reaction diminishes after prodromal AD converts to dementia, and is supported by postmortem autoradiographic study showing highest binding of MAO-B radioligand in the earliest Braak stages (Gulyas et al., 2011).

Discussion

It is universally acknowledged that neuroinflammation plays an active part in the course of AD. PET imaging of neuroinflammation targets have, in part, confirmed the correlation between Aβ deposition and elevated microglia/astrocyte activation/neuroinflammation. Nonetheless, in light of the complexity of both the process and components, questions such as "Is neuroinflammation beneficial at the beginning and harmful thereafter?" and "Is TSPO imaging and MAO-B imaging reflecting true activation of microglia and astrocytes?" remain to be answered. In order to obtain a clearer picture of the various aspects of inflammation in the CNS, further exploration is needed with some of the clues now at hand. First, microglia can be polarized to either M1, releasing neurotoxic substances, or to M2, releasing neuroprotective cytokines (Mosser and Edwards, 2008). Highly selective radioligands discriminating the two opposing activations will help answer these questions. Further, longitudinal studies, ideally tracking from the very early stage to the end stage of the disease across subjects, will be more informative than cross-sectional studies in mapping the time course and topography of microglia activation in disease progression. In addition, genotype-insensitive TSPO tracers under development require verification and validation in large-sample cohorts (Wadsworth et al., 2012; Zanotti-Fregonara et al., 2014; Ikawa et al., 2017). Finally, multi-modality imaging approaches will be helpful in revealing the interactions between neuroinflammation and various pathologic/pathophysiological components in AD.

PET TRACERS FOR IMAGING TARGETS IN THE CHOLINERGIC SYSTEM

Overview

The basal/rostral forebrain cholinergic pathways are believed to play an important role in a variety of neuropsychological functions including attention, consciousness and memory processing (Perry et al., 1999). Cholinergic replacement countering the loss of cholinergic neurotransmission in neurodegeneration is the theoretical basis of AD-treatment strategies using clinically approved medications (Bartus et al., 1982; Schliebs and Arendt, 2011). Cholinergic depletion and the resulting deficit in neuronal compensatory plasticity are confirmed in autopsy studies of AD patients (Bierer et al., 1995; Craig et al., 2011). PET imaging tracers targeting various aspects of cholinergic neurotransmission and metabolism can help us to better understand the role of cholinergic neuropathy and its interaction with other pathologic/pathophysiological components in the course of AD.

Tracer Development

Acetylcholinesterase (AChE) is the major target of AD medications, most of which are acetylcholinesterase inhibitors (AChEIs). These therapeutic agents, including galantamine, rivastigmine, tacrine and donepezil, block AChE to inhibit hydrolysis of ACh, thus increasing ACh level in the synaptic cleft. *N*-[^{11}C]methyl-4-piperidinyl propionate ([^{11}C]PMP) and *N*-[^{11}C]methyl-4-piperidyl acetate ([^{11}C]MP4A) are two selective substrates for AChE that have been successfully brought to *in vivo* human imaging research (**Figure 6**). Another presynaptic cholinergic PET tracer [^{18}F]FEOBV, selective to the vesicle ACh transporter (VAChT), is reported to have been assessed in humans (Aghourian et al., 2017). Postsynaptic acetylcholine receptors can be classified into nicotinic acetylcholine receptors (nAChRs) and muscarinic acetylcholine receptors (mAChRs). While most of the previous human PET studies used $\alpha_4\beta_2$ or non-selective nAChR tracers including [^{11}C]nicotine, 2-[^{18}F]F-A-85380 ([^{18}F]2-FA), [^{18}F]AZAN, and [^{18}F]flubatine (also known as [^{18}F]NCFHEB) (**Figure 6**) (Nordberg et al., 1990; Sabri et al., 2008, 2015b; Wong et al., 2013), successful development of selective tracers for new targets such α_7 nAChR and M1 and M4 mAChR has been reported recently. Recent imaging evaluations in humans indicated that [^{18}F]ASEM, [^{11}C]LSN3172176, and [^{11}C]MK-6884 (**Figure 6**) have appropriate kinetics and imaging properties and are promising tracers for their respective targets α_7 nAChR and M1 and M4 mAChR (Hillmer et al., 2017; Wong et al., 2018; Masdeu et al., 2020; Tong et al., 2020; Naganawa et al., 2021b). [^{18}F]ASEM and [^{11}C]MK-6884 have been used in preliminary studies of α_7 nAChR and M4 mAChR in AD (see below), while evaluation of M1 mAChR in AD is ongoing with [^{11}C]LSN3172176 in our laboratories.

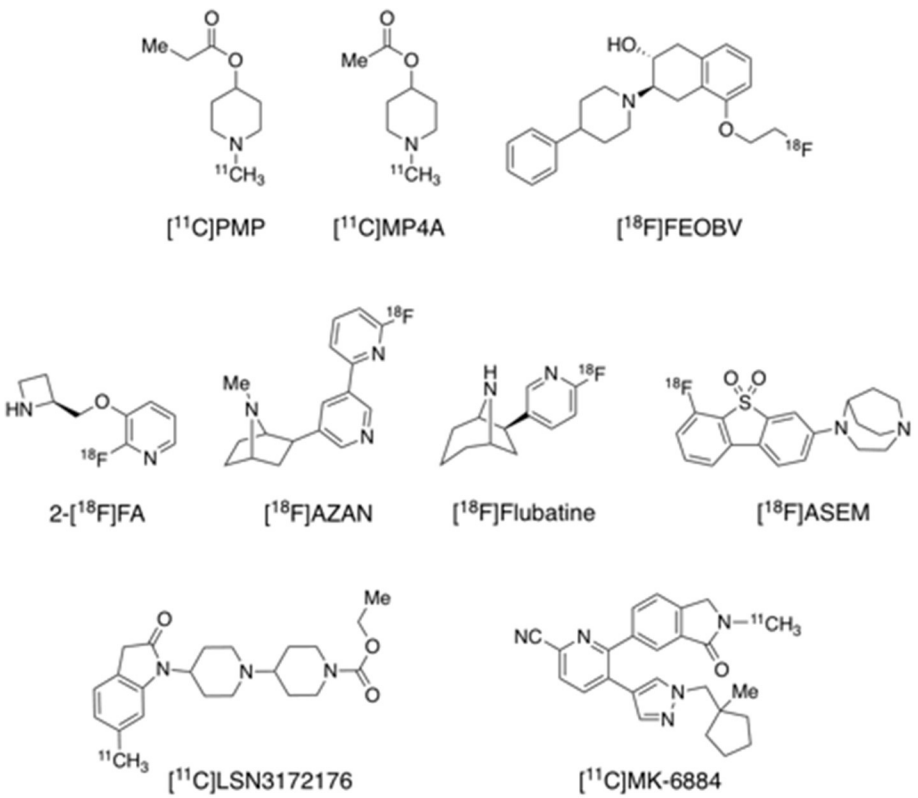

FIGURE 6 | Structures of representative PET radiotracers for cholinergic targets.

Imaging Research Findings and Clinical Relevance

AChE imaging using [^{11}C]PMP and [^{11}C]MP4A showed reduced cortical binding in AD patients than in healthy controls, especially in regions innervated with cholinergic projections (Iyo et al., 1997; Kuhl et al., 1999). AChE binding is lower in AD patients than in healthy controls, in parallel with VAChT reduction, and is further decreased by treatment with AChE inhibitors donepezil, rivastigmine and galantamine (Kuhl et al., 1999, 2000; Shinotoh et al., 2001; Kaasinen et al., 2002; Kadir et al., 2008). However this induced inhibition is absent for nAChR binding, suggesting that allosteric modulation effect maintains ACh signaling by up-regulating nAChR but not AChE (Maelicke et al., 2001). The degree of treatment-induced decline in AChE binding is more prominent in the frontal cortex than in the temporoparietal cortices, and correlated to improvement in frontal lobe functions such as execution and attention rather than episodic memory. Correlation between AChE hydrolysis and hypometabolism in the posterior cingulate cortex is also absent, while a connection between higher hydrolysis rate and APOE4 positivity exists (Kuhl et al., 1999; Eggers et al., 2006).

The binding of novel VAChT tracer [^{18}F]FEOBV is found to be lower in AD than in healthy controls in a recent multi-tracer study involving [^{18}F]FDG and [^{18}F]NAV4694 as well (Aghourian et al., 2017). [^{18}F]FEOBV PET is shown to have higher sensitivity than [^{18}F]FDG in discriminating AD from healthy controls (**Figure 7**). There is also a positive correlation of [^{18}F]FEOBV binding to minimal mental state examination (MMSE) and Montreal cognitive assessment (MoCA). A more recent study attributed basal forebrain degeneration in AD to the loss of cortico-amygdalar cholinergic input, as demonstrated by [^{18}F]FEOBV binding decline (Schmitz et al., 2018).

Nicotinic AChR binding reduction is not only lower in AD and MCI subjects than in cognitively-intact volunteers, but also in MCI converters to AD dementia than in non-converters (Nordberg et al., 1990, 1995; Kendziorra et al., 2011). Binding quantitation of the AD-affected brain regions is significantly responsible for their coupling cognitive functions (Ellis et al., 2008; Sabri et al., 2008; Kendziorra et al., 2011; Okada et al., 2013). Frontal [^{11}C]PIB retention is found to be inversely correlated with [^{18}F]2-FA binding in the medial frontal cortex and nucleus basalis magnocellularis of AD patients (Maas et al., 2000). PET imaging with [^{18}F]flubatine, a new-generation $\alpha_4\beta_2$ tracer with more favorable kinetics, reveals receptor deficiency within the basal forebrain-cortical and septo-hippocampal cholinergic projections (Sabri et al., 2018). Episodic memory, working memory and executive functions are well-correlated with impairment of $\alpha_4\beta_2$ nAChR in the corresponding cortices. Initial imaging studies with the α_7 nAChR selective radioligand [^{18}F]ASEM in healthy controls and MCI subjects indicated elevation of this receptor subtype with healthy aging, and in MCI, in a direction opposite of that for $\alpha_4\beta_2$ nAChR in

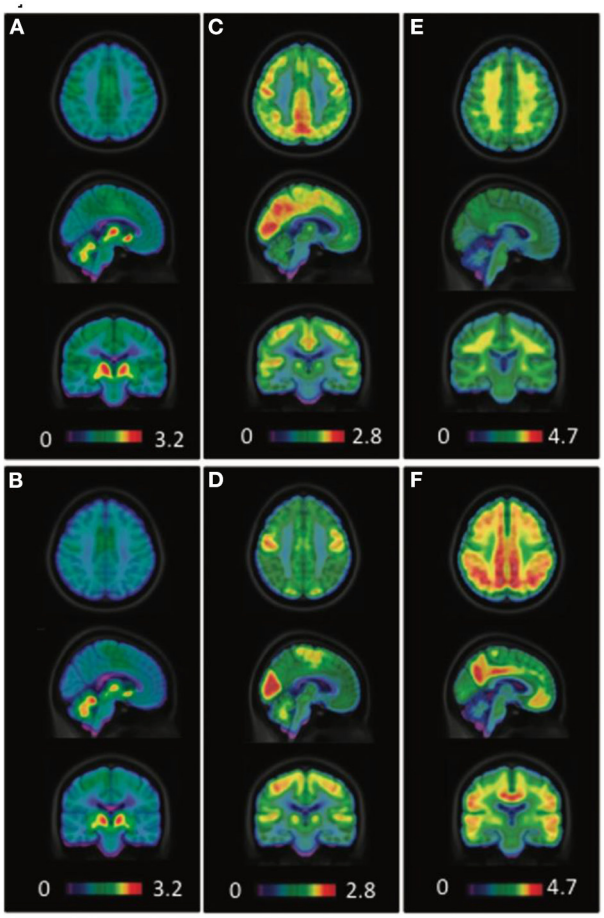

FIGURE 7 | Averaged [^{18}F]FEOBV VAChT PET **(A,B)**, [^{18}F]FDG PET **(C,D)**, and [^{18}F]NAV4694 Aβ PET **(E,F)** images of healthy controls **(A,C,E)** and AD patients **(B,D,F)**. PET images in control subjects revealed the greatest [^{18}F]FEOBV uptake in brain areas known to be the most innervated by the cholinergic systems, including the striatum, thalamus, cerebral cortex as a whole, hippocampal area and cerebellum **(A)**. In AD patients, PET imaging revealed a significant reduction of [^{18}F]FEOBV uptake in comparison with control subjects **(B)**. Distinct cerebral hypometabolism **(D)** and amyloid deposition **(F)** were seen in the AD patients, as compared to control subjects **(C,E)**. Courtesy from Aghourian et al. (2017).

AD (Coughlin et al., 2018, 2019). A preliminary imaging study of M4 mAChR in AD revealed reduced uptake of [^{11}C]MK-6884 primarily in the parietotemporal cortex in a pattern consistent with clinical symptom presentations and FDG hypometabolism (Masdeu et al., 2020).

Discussion

PET imaging studies with tracers for both pre- and post-synaptic cholinergic targets have confirmed the abnormalities of cholinergic transmission *in vivo*, in AD, as manifested in altered levels of AChE, VAChT, and $\alpha_4\beta_2$ and α_7 nAChR's, and their correlations with Aβ deposition and cognitive functions. The α_7 nAChR is a target gaining increasing focus in recent years, due to its newly discovered participation in preventing amyloid toxicity and tau hyper-phosphorylation, in increasing synaptic strength and stability, and in modulating neuroinflammation by acting on non-neuronal cells (Wang et al., 2003; Conejero-Goldberg et al., 2008; Halff et al., 2014; de Oliveira et al., 2016; Maurer and Williams, 2017; Gamage et al., 2020). Renewed interests have also been seen in the mAChR, especially the M1 and M4 subtypes, for therapeutic development for AD (Levey, 1996; Schliebs and Arendt, 2011; Melancon et al., 2013). Investigation of these additional targets with recently available PET tracers will lead to a more thorough understanding of cholinergic involvement in AD etiology and progression.

PET TRACERS FOR IMAGING SYNAPTIC DENSITY

Overview

The total number of synapses in the neocortices is approximately 164×10^{12} (Tang et al., 2001). Synapses are critical for neurotransmission in neuron-neuron interaction, the deficiency of which would result in neuronal dysfunction and consequent occurrence of neuropsychiatric symptoms including amnesia, apathy and executive dysfunction. Loss of synapses has long been regarded as a pathologic hallmark of AD (Scheff et al., 1990; Terry et al., 1991; Scheff and Price, 2006) and correlates strongly with cognitive impairment (Hamos et al., 1989; DeKosky and Scheff, 1990; Terry et al., 1991; DeKosky et al., 1996; Robinson et al., 2014). Synaptic density reductions are seen in the neocortex and limbic system in MCI, a prodromal form of AD and other dementias (Masliah et al., 1994, 2001; Pham et al., 2010). Accumulation of toxic Aβ oligomers is believed to lead to the loss of synapses and presynaptic proteins in MCI patients (Pham et al., 2010; Wei et al., 2010; Beeri et al., 2012; Robinson et al., 2014). More recent research also suggests an emerging role for tau mediated toxicity at the synapses (Pooler et al., 2014; Wang and Mandelkow, 2016). Thus PET imaging of the synapses provides a tool for direct visualization of synaptic density loss along the AD pathogenesis and progression pathway.

Tracer Development

Synaptic vesicle glycoprotein 2 (SV2) is one of the synaptic proteins highly expressed on the presynaptic membrane. Among the 3 forms of SV2, only SV2A is extensively expressed in glutamatergic and GABAergic neurons throughout the CNS (Dong et al., 2006). Traditionally, synapses can only be observed by electron microscopic and immunohistochemical examinations in biopsy and autopsy tissue samples. Recently a series of novel PET radiotracers selectively targeting SV2A have been developed (**Figure 8**) (Mercier et al., 2014; Estrada et al., 2016; Nabulsi et al., 2016; Becker et al., 2017; Li et al., 2019; Cai et al., 2020a), enabling non-invasive observation and quantification of synaptic density in humans (Finnema et al., 2016; Bahri et al., 2017; Cai et al., 2020b; Naganawa et al., 2021a).

Imaging Research Findings and Clinical Relevance

A recent human SV2A PET study using [^{11}C]UCB-J in cohorts of MCI/AD patients and age-matched cognitively intact elderly

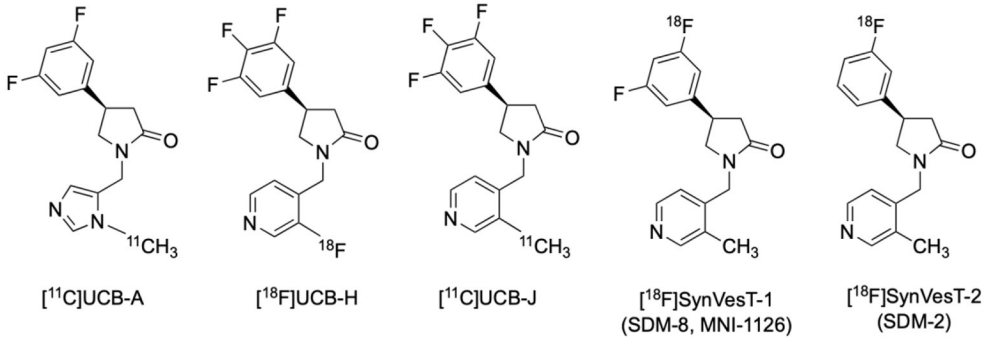

FIGURE 8 | Structures of representative PET radiotracers for SV2A.

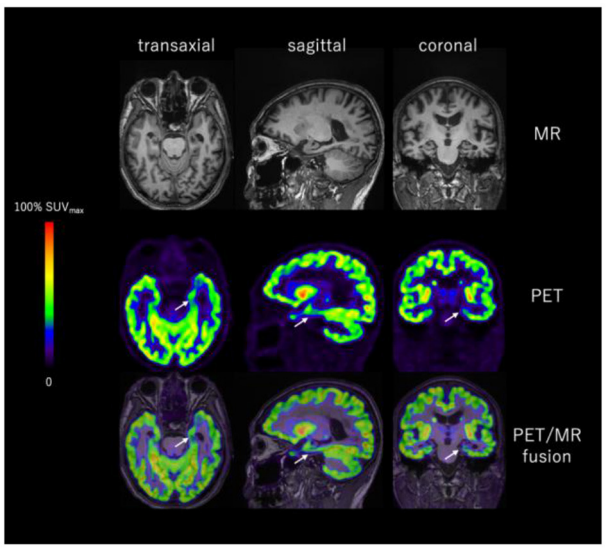

FIGURE 9 | Representative images of T1WI MRI and [^{18}F]SynVesT-1 PET of a [^{18}F]Florbetapir positive AD patient. SV2A binding is significantly reduced in the left hippocampus (white arrow). Images provided by PET Center, Huashan Hospital, Fudan University and Department of Nuclear Medicine, East Hospital, Tongji University.

subjects revealed significant reduction of synaptic density in the hippocampus and entorhinal cortex (44 and 27%, respectively) (Chen et al., 2018). Moreover, statistically significant correlations were found between hippocampal synaptic density and episodic memory (Logical Memory II and Rey Auditory Verbal Learning Test, $R = 0.56$, $P = 0.01$) and global function (Clinical Dementia Rating Sum of Boxes, $R = -0.61$, $P = 0.003$) (Chen et al., 2018). These findings suggest that [^{11}C]UCB-J can capture the early pathological alterations in the hippocampus and entorhinal cortices, brain structures not readily analyzed in FDG PET compared to neocortices due to attenuated sensitivity introduced by size-related partial volume effect despite their early involvement in AD's Braak Staging (Braak and Braak, 1997).

The loss of synaptic density in the hippocampus of AD patients was replicated in a study using another SV2A radiotracer [^{18}F]UCB-H, in which a 11 $\sim$ 18% reductions of synaptic density in the basal forebrain and anterior/dorsomedial thalamus were found to be correlated with cognitive alterations (Bastin et al., 2020; Mecca et al., 2020). In a more recent [^{11}C]UCB-J study with a larger cohort of 34 AD and MCI patients, the significant loss of synaptic density measured by PET in the hippocampus and entorhinal cortex followed by parahippocampal cortex, amygdala, lateral temporal cortex, pre-frontal cortex, posterior cingulate cortex/precuneus, lateral parietal cortex, and pericentral cortex was found to be generally correlated with atrophy measured by structural MRI which is in line with autopsy reports, and was more significantly correlated with CDR-SB ($r = -0.54$, $P = 0.00003$) and episodic memory ($r = 0.56$, $P = 0.00001$) than in the smaller sample reported earlier (de Wilde et al., 2016; Chen et al., 2018; Mecca et al., 2020). The relationship between cognitive performances and medial temporal (especially hippocampus and parahippocampal gyrus) synaptic density loss in aMCI was strengthened by a mutually correlated regional tau accumulation, as was revealed by a multi-tracer PET study using [^{18}F]MK-6240 and [^{11}C]UCB-J (Vanhaute et al., 2020).

Discussion

SV2A PET has shown great promise as a biomarker for the non-invasive detection of synaptic density, which can serve as a useful tool for studying synaptopathies in neurodegenerative and psychiatric disorders including AD (Cai et al., 2019; Heurling et al., 2019). Due to the ubiquitous distribution of synaptic vesicles throughout the CNS, a highly selective molecular probe such as SV2A PET tracer can spot the subtle alterations of synaptic density both quantitatively and topographically.

It is anticipated that with the help of multi-target molecular imaging approaches, the correlation between synaptic loss and other pathophysiological factors related to AD can be further elucidated. For instance, the relationship between pathological amyloid and tau protein aggregations, neuronal glucose utility impairment, dysfunctions in various neurotransmitter systems and synaptic loss would be better understood. Since pathological synaptic alterations emerge in the early stage of AD and continue throughout its course, many unanswered questions and controversial issues, e.g., sequence on the emergence

of pathologic and physiological biomarkers, energetic, and neurotransmitter system abnormalities, and their relative impacts on disease progression, would be hopefully settled. It is perceivable that SV2A PET has the potential in AD early detection, differential diagnosis and conversion prediction of the prodromal stage subjects. Many studies using SV2A PET imaging in AD and other neurodegenerative diseases are ongoing, and results are emerging rapidly in publications. The introduction of additional ^{18}F-labled SV2A radiotracers with favorable kinetics and high specific binding profiles, such as [^{18}F]SynVesT-1 (also known as [^{18}F]SDM-8 and [^{18}F]MNI-1126) and [^{18}F]SynVesT-2 (also known as [^{18}F]SDM-2), should facilitate these studies since they are suitable for central production and distribution for use in off-site imaging facilities (**Figures 8**, **9**). Further, PET imaging with these SV2A radiotracers will be useful as endpoint measure in AD drug clinical trials (e.g. NCT03493282: Effect of CT1812 treatment on brain synaptic density).

SUMMARY AND CONCLUDING REMARKS

Alzheimer's disease, characterized by impairments of cognitive functions and memory loss, is an extremely complex neurodegenerative disorder involving multiple pathophysiological processes, from loss of synapses and neurons, to neuroinflammation, to deposition of Aβ plaques and neurofibrillary tau tangles. Early diagnosis is the key to effectively treat the disease before manifestation of clinical symptoms. The past two decades have witnessed the development of PET imaging agents targeting various pathologic and physiological biomarkers in AD which has greatly contributed to the investigation and diagnosis of this disease.

Radiotracers targeting pathologic hallmarks of AD such as Aβ and tau proteins have allowed the differentiation of AD and non-AD dementia, the tracking of pathological protein burden over the temporal course of the disease, the stratification of patients for clinical trials, and the monitoring of biological effects of therapeutic agents. Nonetheless, there remained a few unanswered questions to be further studied concerning the relationship between these targets and the etiology of AD.

Pathophysiological alterations such as neuroinflammation as well as neurotransmitter and synaptic dysfunction are increasingly thought to commence from the earliest stage of the pathological changes in AD, and PET radiotracers targeting these biomarkers may help to elucidate their roles in AD progression in synergy with the core pathologies.

Measurement of synaptic density through PET imaging of the synaptic biomarker SV2A opens a new avenue for the investigation of neurodegenerative diseases. Initial *in vivo* imaging results from prodromal AD and AD dementia cohorts were in excellent correlation with cognitive impairment. Preliminary results of healthy aging subjects also demonstrated the early involvement of synaptic density alterations and its relationship to tau aggregation, which is in concordance with autopsy neuropathological findings. SV2A PET imaging, now at its early discovery phase, is expected to provide further important information on synaptic protein alterations, along with other pathological changes, during the entire AD progression continuum, and contribute to the early detection of the disease.

PET imaging of biomarkers has played an important role in AD drug development. This trend will continue, as newer imaging biomarkers are increasingly incorporated into clinical trials of next-generation AD drugs as outcome measures. It is expected that applications of PET imaging biomarkers in drug clinical trials will continue to greatly facilitate the development of AD therapeutics.

The United States National Institute of Aging (NIA) and the Alzheimer's Association (AA) recently put forward a research framework for AD, i.e., the NIA-AA Research Framework, which is based on the current understanding of the AD continuum and grounded on a biomarker-based definition of AD (Jack et al., 2018). Biomarkers are grouped into three categories: Aβ deposition, pathologic tau, and neurodegeneration (ATN) based on the nature of the pathologic process that each measures. Biomarkers of Aβ plaques (labeled "A") are represented by cortical Aβ plaque burden assessed by amyloid PET imaging or decreased CSF $A\beta_{42}$. Biomarkers of fibrillar tau (labeled "T") are elevated CSF phosphorylated tau (p-tau) and/or cortical tau tangles measured by tau PET imaging. Biomarkers of neurodegeneration or neuronal injury (labeled "N"] are based on CSF total tau (t-tau), hypometabolism as revealed by FDG PET imaging, and brain atrophy detected by MRI. It is evident that PET imaging targeting various biomarkers is an essential component of this ATN research framework, as it provides one biomarker measurement for each of the arms: amyloid PET for A, tau PET for T, and FDG PET for N. The recent emergence of synaptic PET imaging targeting SV2A may provide another biomarker for N, neurodegeneration that more closely tracks with the progression of the disease and cognitive impairment, and less sensitive to cofounding factors such as blood glucose level, stimulation and medication which affect FDG PET, a surrogate measure of synaptic/neuronal function (Herholz, 2008; Burns et al., 2013; Ishibashi et al., 2015). These advancements in the development of PET radiotracers for AD biomarkers have been made possible through the efforts of numerous researchers in the PET imaging field in the last two decades. Collectively, AD imaging studies with various radiotracers have greatly increased our knowledge on the etiology and progression of this complex neurodegenerative disorder, and facilitated the research and development of AD therapeutics. It is believed that PET imaging with effective tracers targeting various AD pathophysiological biomarkers will continue to advance our understanding of the disease, and hopefully provides a sensitive and definitive tool for early diagnosis and monitoring of treatment effect.

AUTHOR CONTRIBUTIONS

WB and YH drafted the manuscript. FX, CZ, and YG participated in revision of manuscript. All authors contributed to the article and approved the submitted version.

FUNDING

This work was supported by grants (Project No. 82071962, 82021002, & 81971641) from the National Natural Science Foundation of China, grant (Project No. IDF151025) from Major Project Pre-research (pilot) Project of Fudan University, and grant 1R01AG065474 from the National Institute on Aging, National Institutes of Health, United States.

REFERENCES

Agdeppa, E. D., Kepe, V., Liu, J., Flores-Torres, S., Satyamurthy, N., Petric, A., et al. (2001). Binding characteristics of radiofluorinated 6-dialkylamino-2-naphthylethylidene derivatives as positron emission tomography imaging probes for β-amyloid plaques in Alzheimer's disease. *J Neurosci.* 21:RC189. doi: 10.1523/JNEUROSCI.21-24-j0004.2001

Aghourian, M., Legault-Denis, C., Soucy, J. P., Rosa-Neto, P., Gauthier, S., Kostikov, A., et al. (2017). Quantification of brain cholinergic denervation in Alzheimer's disease using PET imaging with [^{18}F]-FEOBV. *Mol. Psychiatry* 22, 1531–1538. doi: 10.1038/mp.2017.183

Akiyama, H., Barger, S., Barnum, S., Bradt, B., Bauer, J., Cole, G. M., et al. (2000). Inflammation and Alzheimer's disease. *Neurobiol. Aging* 21, 383–421. doi: 10.1016/S0197-4580(00)00124-X

Albert, M. S., DeKosky, S. T., Dickson, D., Dubois, B., Feldman, H. H., Fox, N. C., et al. (2011). The diagnosis of mild cognitive impairment due to Alzheimer's disease: recommendations from the national institute on aging-alzheimer's association workgroups on diagnostic guidelines for Alzheimer's disease. *Alzheimer Dement.* 7, 270–279. doi: 10.1016/j.jalz.2011.03.008

Amadoru, S., Dore, V., McLean, C. A., Hinton, F., Shepherd, C. E., Halliday, G. M., et al. (2020). Comparison of amyloid PET measured in centiloid units with neuropathological findings in Alzheimer's disease. *Alzheimers Res. Ther.* 12:22. doi: 10.1186/s13195-020-00587-5

Arbizu, J., Festari, C., Altomare, D., Walker, Z., Bouwman, F., Rivolta, J., et al. (2018). Clinical utility of FDG-PET for the clinical diagnosis in MCI. *Eur. J. Nucl. Med. Mol. Imaging* 45, 1497–1508. doi: 10.1007/s00259-018-4039-7

Baek, M. S., Cho, H., Lee, H. S., Choi, J. Y., Lee, J. H., Ryu, Y. H., et al. (2020). Temporal trajectories of *in vivo* tau and amyloid-β accumulation in Alzheimer's disease. *Eur. J. Nucl. Med. Mol. Imaging* 47, 2879–2886. doi: 10.1007/s00259-020-04773-3

Bahri, M. A., Plenevaux, A., Aerts, J., Bastin, C., Becker, G., Mercier, J., et al. (2017). Measuring brain synaptic vesicle protein 2A with positron emission tomography and [^{18}F]UCB-H. *Alzheimers Dement.* 3, 481–486. doi: 10.1016/j.trci.2017.08.004

Banerjee, S., and Wittenberg, R. (2009). Clinical and cost effectiveness of services for early diagnosis and intervention in dementia. *Int. J. Geriatr. Psychiatry* 24, 748–754. doi: 10.1002/gps.2191

Barger, S. W., and Harmon, A. D. (1997). Microglial activation by Alzheimer amyloid precursor protein and modulation by apolipoprotein E. *Nature* 388, 878–881. doi: 10.1038/42257

Barthel, H., Gertz, H. J., Dresel, S., Peters, O., Bartenstein, P., Buerger, K., et al. (2011). Cerebral amyloid-β PET with florbetaben (^{18}F) in patients with Alzheimer's disease and healthy controls: a multicentre phase 2 diagnostic study. *Lancet Neurol.* 10, 424–435. doi: 10.1016/S1474-4422(11)70077-1

Bartus, R. T., Dean, R. L. III., Beer, B., and Lippa, A. S. (1982). The cholinergic hypothesis of geriatric memory dysfunction. *Science* 217, 408–414. doi: 10.1126/science.7046051

Bastin, C., Bahri, M. A., Meyer, F., Manard, M., Delhaye, E., Plenevaux, A., et al. (2020). *In vivo* imaging of synaptic loss in Alzheimer's disease with [^{18}F]UCB-H positron emission tomography. *Eur. J. Nucl. Med. Mol. Imaging* 47, 390–402. doi: 10.1007/s00259-019-04461-x

Bateman, R. J., Aisen, P. S., De Strooper, B., Fox, N. C., Lemere, C. A., Ringman, J. M., et al. (2011). Autosomal-dominant Alzheimer's disease: a review and proposal for the prevention of Alzheimer's disease. *Alzheimers Res. Ther.* 3:1. doi: 10.1186/alzrt59

Battle, M. R., Pillay, L. C., Lowe, V. J., Knopman, D., Kemp, B., Rowe, C. C., et al. (2018). Centiloid scaling for quantification of brain amyloid with [^{18}F]flutemetamol using multiple processing methods. *EJNMMI Res.* 8:107. doi: 10.1186/s13550-018-0456-7

Becker, G., Warnier, C., Serrano, M. E., Bahri, M. A., Mercier, J., Lemaire, C., et al. (2017). Pharmacokinetic characterization of [^{18}F]UCB-H PET radiopharmaceutical in the rat brain. *Mol. Pharm.* 14, 2719–2725. doi: 10.1021/acs.molpharmaceut.7b00235

Beeri, M. S., Haroutunian, V., Schmeidler, J., Sano, M., Fam, P., Kavanaugh, A., et al. (2012). Synaptic protein deficits are associated with dementia irrespective of extreme old age. *Neurobiol. Aging.* 33, 1125.e1–8. doi: 10.1016/j.neurobiolaging.2011.08.017

Bejanin, A., Schonhaut, D. R., La Joie, R., Kramer, J. H., Baker, S. L., Sosa, N., et al. (2017). Tau pathology and neurodegeneration contribute to cognitive impairment in Alzheimer's disease. *Brain* 140, 3286–3300. doi: 10.1093/brain/awx243

Bennett, D. A., Wilson, R. S., Boyle, P. A., Buchman, A. S., and Schneider, J. A. (2012). Relation of neuropathology to cognition in persons without cognitive impairment. *Ann. Neurol.* 72, 599–609. doi: 10.1002/ana.23654

Benzinger, T. L., Blazey, T., Jack, C. R. Jr., Koeppe, R. A., Su, Y., Xiong, C., et al. (2013). Regional variability of imaging biomarkers in autosomal dominant Alzheimer's disease. *Proc. Natl. Acad. Sci. U.S.A.* 110, E4502–E4509. doi: 10.1073/pnas.1317918110

Betthauser, T., Lao, P. J., Murali, D., Barnhart, T. E., Furumoto, S., Okamura, N., et al. (2017). *In vivo* comparison of tau radioligands ^{18}F-THK-5351 and ^{18}F-THK-5317. *J. Nucl. Med.* 58, 996–1002. doi: 10.2967/jnumed.116.182980

Bierer, L. M., Haroutunian, V., Gabriel, S., Knott, P. J., Carlin, L. S., Purohit, D. P., et al. (1995). Neurochemical correlates of dementia severity in Alzheimer's disease: relative importance of the cholinergic deficits. *J. Neurochem.* 64, 749–760. doi: 10.1046/j.1471-4159.1995.64020749.x

Bischof, G. N., Endepols, H., van Eimeren, T., and Drzezga, A. (2017). Tau-imaging in neurodegeneration. *Methods* 130, 114–123. doi: 10.1016/j.ymeth.2017.08.003

Bourgeat, P., Dore, V., Fripp, J., Ames, D., Masters, C. L., Salvado, O., et al. (2018). Implementing the centiloid transformation for ^{11}C-PiB and β-amyloid ^{18}F-PET tracers using CapAIBL. *Neuroimage* 183, 387–393. doi: 10.1016/j.neuroimage.2018.08.044

Braak, H., and Braak, E. (1997). Frequency of stages of alzheimer-related lesions in different age categories. *Neurobiol. Aging* 18, 351–357. doi: 10.1016/S0197-4580(97)00056-0

Brugnolo, A., Morbelli, S., Arnaldi, D., De Carli, F., Accardo, J., Bossert, I., et al. (2014). Metabolic correlates of Rey auditory verbal learning test in elderly subjects with memory complaints. *J. Alzheimers Dis.* 39, 103–113. doi: 10.3233/JAD-121684

Burns, C. M., Chen, K., Kaszniak, A. W., Lee, W., Alexander, G. E., Bandy, D., et al. (2013). Higher serum glucose levels are associated with cerebral hypometabolism in Alzheimer regions. *Neurology* 80, 1557–1564. doi: 10.1212/WNL.0b013e31828f17de

Cagnin, A., Brooks, D. J., Kennedy, A. M., Gunn, R. N., Myers, R., Turkheimer, F. E., et al. (2001). *In-vivo* measurement of activated microglia in dementia. *Lancet* 358, 461–467. doi: 10.1016/S0140-6736(01)05625-2

Cai, Z., Drake, L., Naganawa, M., Najafzadeh, S., Pracitto, R., Lindermann, M., et al. (2020b). First-in-human study of [^{18}F]SynVesT-2, a novel SV2A radioligand with fast kinetics and high specific binding signals. *J. Nucl. Med.* 61 (Suppl. 1):462.

Cai, Z., Li, S., Matuskey, D., Nabulsi, N., and Huang, Y. (2019). PET imaging of synaptic density: a new tool for investigation of neuropsychiatric diseases. *Neurosci. Lett.* 691, 44–50. doi: 10.1016/j.neulet.2018.07.038

Cai, Z., Li, S., Zhang, W., Pracitto, R., Wu, X., Baum, E., et al. (2020a). Synthesis and preclinical evaluation of an ^{18}F-labeled synaptic vesicle glycoprotein 2A PET imaging probe: [^{18}F]SynVesT-2. *ACS Chem. Neurosci.* 11, 592–603. doi: 10.1021/acschemneuro.9b00618

Calsolaro, V., and Edison, P. (2016). Neuroinflammation in Alzheimer's disease: current evidence and future directions. *Alzheimers Dement.* 12, 719–732. doi: 10.1016/j.jalz.2016.02.010

Carter, S. F., Scholl, M., Almkvist, O., Wall, A., Engler, H., Langstrom, B., et al. (2012). Evidence for astrocytosis in prodromal Alzheimer disease provided by ^{11}C-deuterium-L-deprenyl: a multitracer PET paradigm combining ^{11}C-Pittsburgh compound B and ^{18}F-FDG. *J. Nucl. Med.* 53, 37–46. doi: 10.2967/jnumed.110.087031

Chen, M. K., Mecca, A. P., Naganawa, M., Finnema, S. J., Toyonaga, T., Lin, S. F., et al. (2018). assessing synaptic density in Alzheimer disease With synaptic vesicle glycoprotein 2A positron emission tomographic imaging. *JAMA Neurol.* 75, 1215–1224. doi: 10.1001/jamaneurol.2018.1836

Chiotis, K., Saint-Aubert, L., Savitcheva, I., Jelic, V., Andersen, P., Jonasson, M., et al. (2016). Imaging *in-vivo* tau pathology in Alzheimer's disease with THK5317 PET in a multimodal paradigm. *Eur. J. Nucl. Med. Mol. Imaging* 43, 1686–1699. doi: 10.1007/s00259-016-3363-z

Cho, H., Choi, J. Y., Lee, H. S., Lee, J. H., Ryu, Y. H., Lee, M. S., et al. (2019). Progressive tau accumulation in Alzheimer disease: 2-year follow-up study. *J. Nucl. Med.* 60, 1611–1621. doi: 10.2967/jnumed.118.221697

Clark, C. M., Pontecorvo, M. J., Beach, T. G., Bedell, B. J., Coleman, R. E., Doraiswamy, P. M., et al. (2012). Cerebral PET with florbetapir compared with neuropathology at autopsy for detection of neuritic amyloid-b plaques: a prospective cohort study. *Lancet Neurol.* 11, 669–678. doi: 10.1016/S1474-4422(12)70142-4

Cohen, A. D., Price, J. C., Weissfeld, L. A., James, J., Rosario, B. L., Bi, W., et al. (2009). Basal cerebral metabolism may modulate the cognitive effects of Aβ in mild cognitive impairment: an example of brain reserve. *J. Neurosci.* 29, 14770–14778. doi: 10.1523/JNEUROSCI.3669-09.2009

Conejero-Goldberg, C., Davies, P., and Ulloa, L. (2008). Alpha7 nicotinic acetylcholine receptor: a link between inflammation and neurodegeneration. *Neurosci. Biobehav. Rev.* 32, 693–706. doi: 10.1016/j.neubiorev.2007.10.007

Coughlin, J. M., Du, Y., Rosenthal, H. B., Slania, S., Min Koo, S., Park, A., et al. (2018). The distribution of the α_7 nicotinic acetylcholine receptor in healthy aging: an *in vivo* positron emission tomography study with [^{18}F]ASEM. *Neuroimage* 165, 118–124. doi: 10.1016/j.neuroimage.2017.10.009

Coughlin, J. M., Rubin, L. H., Du, Y., Rowe, S. P., Crawford, J. L., Rosenthal, H. B., et al. (2019). High availability of the α_7 nicotinic acetylcholine receptor in brains of individuals with mild cognitive impairment: a pilot study using ^{18}F-ASEM PET. *J. Nucl. Med.* 61, 423–426. doi: 10.2967/jnumed.119.230979

Craft, S., Baker, L. D., Montine, T. J., Minoshima, S., Watson, G. S., Claxton, A., et al. (2012). Intranasal insulin therapy for Alzheimer disease and amnestic mild cognitive impairment: a pilot clinical trial. *Arch. Neurol.* 69, 29–38. doi: 10.1001/archneurol.2011.233

Craig, L. A., Hong, N. S., and McDonald, R. J. (2011). Revisiting the cholinergic hypothesis in the development of Alzheimer's disease. *Neurosci. Biobehav. Rev.* 35, 1397–1409. doi: 10.1016/j.neubiorev.2011.03.001

Crary, J. F., Trojanowski, J. Q., Schneider, J. A., Abisambra, J. F., Abner, E. L., Alafuzoff, I., et al. (2014). Primary age-related tauopathy (PART): a common pathology associated with human aging. *Acta Neuropathol.* 128, 755–766. doi: 10.1007/s00401-014-1349-0

Cselenyi, Z., Jonhagen, M. E., Forsberg, A., Halldin, C., Julin, P., Schou, M., et al. (2012). Clinical validation of ^{18}F-AZD4694, an amyloid-β-specific PET radioligand. *J. Nucl. Med.* 53, 415–424. doi: 10.2967/jnumed.111.094029

Curtis, C., Gamez, J. E., Singh, U., Sadowsky, C. H., Villena, T., Sabbagh, M. N., et al. (2015). Phase 3 trial of flutemetamol labeled with radioactive fluorine 18 imaging and neuritic plaque density. *JAMA Neurol.* 72, 287–294. doi: 10.1001/jamaneurol.2014.4144

de Oliveira, A. S., Santiago, F. E., Balioni, L. F., Ferrari Mde, F., Almeida, M. C., and Carrettiero, D. C. (2016). BAG2 expression dictates a functional intracellular switch between the p38-dependent effects of nicotine on tau phosphorylation levels via the α_7 nicotinic receptor. *Exp Neurol.* 275 (Pt. 1):69–77. doi: 10.1016/j.expneurol.2015.10.005

de Wilde, M. C., Overk, C. R., Sijben, J. W., and Masliah, E. (2016). Meta-analysis of synaptic pathology in Alzheimer's disease reveals selective molecular vesicular machinery vulnerability. *Alzheimers Dement.* 12, 633–644. doi: 10.1016/j.jalz.2015.12.005

Declercq, L., Rombouts, F., Koole, M., Fierens, K., Marien, J., Langlois, X., et al. (2017). Preclinical evaluation of ^{18}F-JNJ64349311, a novel PET tracer for tau imaging. *J. Nucl. Med.* 58, 975–981. doi: 10.2967/jnumed.116.185199

DeKosky, S. T., and Scheff, S. W. (1990). Synapse loss in frontal cortex biopsies in Alzheimer's disease: correlation with cognitive severity. *Ann. Neurol.* 27, 457–464. doi: 10.1002/ana.410270502

DeKosky, S. T., Scheff, S. W., and Styren, S. D. (1996). Structural correlates of cognition in dementia: quantification and assessment of synapse change. *Neurodegeneration* 5, 417–421. doi: 10.1006/neur.1996.0056

Dong, M., Yeh, F., Tepp, W. H., Dean, C., Johnson, E. A., Janz, R., et al. (2006). SV2 is the protein receptor for botulinum neurotoxin A. *Science* 312, 592–596. doi: 10.1126/science.1123654

Dubois, B., Feldman, H. H., Jacova, C., Dekosky, S. T., Barberger-Gateau, P., Cummings, J., et al. (2007). Research criteria for the diagnosis of Alzheimer's disease: revising the NINCDS-ADRDA criteria. *Lancet Neurol.* 6, 734–746. doi: 10.1016/S1474-4422(07)70178-3

Dubois, B., Feldman, H. H., Jacova, C., Hampel, H., Molinuevo, J. L., Blennow, K., et al. (2014). Advancing research diagnostic criteria for Alzheimer's disease: the IWG-2 criteria. *Lancet Neurol.* 13, 614–629. doi: 10.1016/S1474-4422(14)70090-0

Edison, P., Archer, H. A., Gerhard, A., Hinz, R., Pavese, N., Turkheimer, F. E., et al. (2008). Microglia, amyloid, and cognition in Alzheimer's disease: An [^{11}C](R)PK11195-PET and [^{11}C]PIB-PET study. *Neurobiol. Dis.* 32, 412–419. doi: 10.1016/j.nbd.2008.08.001

Edison, P., Archer, H. A., Hinz, R., Hammers, A., Pavese, N., Tai, Y. F., et al. (2007). Amyloid, hypometabolism, and cognition in Alzheimer disease: an [^{11}C]PIB and [^{18}F]FDG PET study. *Neurology* 68, 501–508. doi: 10.1212/01.wnl.0000244749.20056.d4

Edison, P., Donat, C. K., and Sastre, M. (2018). *In vivo* imaging of glial activation in Alzheimer's disease. *Front. Neurol.* 9:625. doi: 10.3389/fneur.2018.00625

Eggers, C., Herholz, K., Kalbe, E., and Heiss, W. D. (2006). Cortical acetylcholine esterase activity and ApoE4-genotype in Alzheimer disease. *Neurosci. Lett.* 408, 46–50. doi: 10.1016/j.neulet.2006.08.061

Elias, A., Woodward, M., and Rowe, C. C. (2014). Management impact of FDG-PET in dementia: results from a tertiary center memory clinic. *J. Alzheimers Dis.* 42, 885–892. doi: 10.3233/JAD-132729

Ellis, J. R., Villemagne, V. L., Nathan, P. J., Mulligan, R. S., Gong, S. J., Chan, J. G., et al. (2008). Relationship between nicotinic receptors and cognitive function in early Alzheimer's disease: a 2-[^{18}F]fluoro-A-85380 PET study. *Neurobiol. Learn. Mem.* 90, 404–412. doi: 10.1016/j.nlm.2008.05.006

Estrada, S., Lubberink, M., Thibblin, A., Sprycha, M., Buchanan, T., Mestdagh, N., et al. (2016). [^{11}C]UCB-A, a novel PET tracer for synaptic vesicle protein 2A. *Nucl. Med. Biol.* 43, 325–332. doi: 10.1016/j.nucmedbio.2016.03.004

Finnema, S. J., Nabulsi, N. B., Eid, T., Detyniecki, K., Lin, S. F., Chen, M. K., et al. (2016). Imaging synaptic density in the living human brain. *Sci. Transl. Med.* 8:348ra96. doi: 10.1126/scitranslmed.aaf6667

Fitzpatrick, A. W. P., Falcon, B., He, S., Murzin, A. G., Murshudov, G., Garringer, H. J., et al. (2017). Cryo-EM structures of tau filaments from Alzheimer's disease. *Nature* 547, 185–190. doi: 10.1038/nature23002

Fleisher, A. S., Pontecorvo, M. J., Devous, M. D. Sr., Lu, M., Arora, A. K., Truocchio, S. P., et al. (2020). Positron emission tomography imaging with [^{18}F]flortaucipir and postmortem assessment of alzheimer disease neuropathologic changes. *JAMA Neurol.* 77, 829–839. doi: 10.1001/jamaneurol.2020.0528

Frisoni, G. B., Boccardi, M., Barkhof, F., Blennow, K., Cappa, S., Chiotis, K., et al. (2017). Strategic roadmap for an early diagnosis of Alzheimer's disease based on biomarkers. *Lancet Neurol.* 16, 661–676. doi: 10.1016/S1474-4422(17)30159-X

Gamage, R., Wagnon, I., Rossetti, I., Childs, R., Niedermayer, G., Chesworth, R., et al. (2020). Cholinergic modulation of glial function during aging and chronic neuroinflammation. *Front. Cell. Neurosci.* 14:577912. doi: 10.3389/fncel.2020.577912

Garibotto, V., Herholz, K., Boccardi, M., Picco, A., Varrone, A., Nordberg, A., et al. (2017). Clinical validity of brain fluorodeoxyglucose positron emission tomography as a biomarker for Alzheimer's disease in the context of a structured 5-phase development framework. *Neurobiol. Aging* 52, 183–195. doi: 10.1016/j.neurobiolaging.2016.03.033

Getsios, D., Blume, S., Ishak, K. J., Maclaine, G., and Hernandez, L. (2012). An economic evaluation of early assessment for Alzheimer's disease in the United Kingdom. *Alzheimers Dement.* 8, 22–30. doi: 10.1016/j.jalz.2010.07.001

Giacobini, E., and Gold, G. (2013). Alzheimer disease therapy–moving from amyloid-β to tau. *Nat. Rev. Neurol*. 9, 677–686. doi: 10.1038/nrneurol.2013.223

Goedert, M., and Spillantini, M. G. (2006). A century of Alzheimer's disease. *Science* 314, 777–781. doi: 10.1126/science.1132814

Golla, S. S., Boellaard, R., Oikonen, V., Hoffmann, A., van Berckel, B. N., Windhorst, A. D., et al. (2015). Quantification of [^{18}F]DPA-714 binding in the human brain: initial studies in healthy controls and Alzheimer's disease patients. *J. Cereb. Blood Flow Metab*. 35, 766–772. doi: 10.1038/jcbfm.2014.261

Guehl, N. J., Wooten, D. W., Yokell, D. L., Moon, S. H., Dhaynaut, M., Katz, S., et al. (2019). Evaluation of pharmacokinetic modeling strategies for *in-vivo* quantification of tau with the radiotracer [^{18}F]MK6240 in human subjects. *Eur. J. Nucl. Med. Mol. Imaging* 46, 2099–2111. doi: 10.1007/s00259-019-04419-z

Gulyas, B., Pavlova, E., Kasa, P., Gulya, K., Bakota, L., Varszegi, S., et al. (2011). Activated MAO-B in the brain of Alzheimer patients, demonstrated by [^{11}C]-L-deprenyl using whole hemisphere autoradiography. *Neurochem. Int*. 58, 60–68. doi: 10.1016/j.neuint.2010.10.013

Guo, T., Landau, S. M., Jagust, W. J., and Alzheimer's Disease Neuroimaging, I. (2020). Detecting earlier stages of amyloid deposition using PET in cognitively normal elderly adults. *Neurology* 94, e1512–e1524. doi: 10.1212/WNL.0000000000009216

Halff, A. W., Gomez-Varela, D., John, D., and Berg, D. K. (2014). A novel mechanism for nicotinic potentiation of glutamatergic synapses. *J. Neurosci*. 34, 2051–2064. doi: 10.1523/JNEUROSCI.2795-13.2014

Hall, B., Mak, E., Cervenka, S., Aigbirhio, F. I., Rowe, J. B., and O'Brien, J. T. (2017). *In vivo* tau PET imaging in dementia: pathophysiology, radiotracer quantification, and a systematic review of clinical findings. *Ageing Res. Rev*. 36, 50–63. doi: 10.1016/j.arr.2017.03.002

Hamelin, L., Lagarde, J., Dorothee, G., Leroy, C., Labit, M., Comley, R. A., et al. (2016). Early and protective microglial activation in Alzheimer's disease: a prospective study using ^{18}F-DPA-714 PET imaging. *Brain* 139 (Pt. 4), 1252–1264. doi: 10.1093/brain/aww017

Hamos, J. E., DeGennaro, L. J., and Drachman, D. A. (1989). Synaptic loss in Alzheimer's disease and other dementias. *Neurology* 39, 355–361. doi: 10.1212/WNL.39.3.355

Hanseeuw, B. J., Betensky, R. A., Jacobs, H. I. L., Schultz, A. P., Sepulcre, J., Becker, J. A., et al. (2019). Association of amyloid and tau with cognition in preclinical alzheimer disease: a longitudinal study. *JAMA Neurol*. 76, 915–924. doi: 10.1001/jamaneurol.2019.1424

Hardy, J., and Allsop, D. (1991). Amyloid deposition as the central event in the aetiology of Alzheimer's disease. *Trends Pharmacol. Sci*. 12, 383–388. doi: 10.1016/0165-6147(91)90609-V

Hardy, J., Duff, K., Hardy, K. G., Perez-Tur, J., and Hutton, M. (1998). Genetic dissection of Alzheimer's disease and related dementias: amyloid and its relationship to tau. *Nat. Neurosci*. 1, 355–358. doi: 10.1038/1565

Hardy, J., and Gwinn-Hardy, K. (1998). Genetic classification of primary neurodegenerative disease. *Science* 282, 1075–1079. doi: 10.1126/science.282.5391.1075

Hardy, J. A., and Higgins, G. A. (1992). Alzheimer's disease: the amyloid cascade hypothesis. *Science* 256, 184–185. doi: 10.1126/science.1566067

Harrison, T. M., La Joie, R., Maass, A., Baker, S. L., Swinnerton, K., Fenton, L., et al. (2019). Longitudinal tau accumulation and atrophy in aging and alzheimer disease. *Ann. Neurol*. 85, 229–240. doi: 10.1002/ana.25406

Heiss, W. D., Kessler, J., Mielke, R., Szelies, B., and Herholz, K. (1994). Long-term effects of phosphatidylserine, pyritinol, and cognitive training in Alzheimer's disease. A neuropsychological, EEG, and PET investigation. *Dementia* 5, 88–98. doi: 10.1159/000106702

Herholz, K. (2008). "Imaging of dementia," in *Diseases of the Brain, Head & Neck, Spine*, eds J Hodler, G. K. Von Schulthess, C. L. Zollikofer (Milan: Springer), 215–8. doi: 10.1007/978-88-470-0840-3_33

Herholz, K. (2012). Use of FDG PET as an imaging biomarker in clinical trials of Alzheimer's disease. *Biomark. Med*. 6, 431–439. doi: 10.2217/bmm.12.51

Heurling, K., Ashton, N. J., Leuzy, A., Zimmer, E. R., Blennow, K., Zetterberg, H., et al. (2019). Synaptic vesicle protein 2A as a potential biomarker in synaptopathies. *Mol. Cell. Neurosci*. 97, 34–42. doi: 10.1016/j.mcn.2019.02.001

Hillmer, A. T., Li, S., Zheng, M. Q., Scheunemann, M., Lin, S. F., Nabulsi, N., et al. (2017). PET imaging of α_7 nicotinic acetylcholine receptors: a comparative study of [^{18}F]ASEM and [^{18}F]DBT-10 in nonhuman primates, and further evaluation of [^{18}F]ASEM in humans. *Eur. J. Nucl. Med. Mol. Imaging* 44, 1042–1050. doi: 10.1007/s00259-017-3621-8

Honig, L. S., Vellas, B., Woodward, M., Boada, M., Bullock, R., Borrie, M., et al. (2018). Trial of solanezumab for mild dementia due to Alzheimer's disease. *N. Engl. J. Med*. 378, 321–330. doi: 10.1056/NEJMoa1705971

Hoover, B. R., Reed, M. N., Su, J., Penrod, R. D., Kotilinek, L. A., Grant, M. K., et al. (2010). Tau mislocalization to dendritic spines mediates synaptic dysfunction independently of neurodegeneration. *Neuron* 68, 1067–1081. doi: 10.1016/j.neuron.2010.11.030

Hoozemans, J. J., van Haastert, E. S., Veerhuis, R., Arendt, T., Scheper, W., Eikelenboom, P., et al. (2005). Maximal COX-2 and ppRb expression in neurons occurs during early Braak stages prior to the maximal activation of astrocytes and microglia in Alzheimer's disease. *J. Neuroinflammation*. 2:27. doi: 10.1186/1742-2094-2-27

Hoozemans, J. J., Veerhuis, R., Rozemuller, J. M., and Eikelenboom, P. (2011). Soothing the inflamed brain: effect of non-steroidal anti-inflammatory drugs on Alzheimer's disease pathology. *CNS Neurol. Disord. Drug Targets* 10, 57–67. doi: 10.2174/187152711794488665

Hoyer, S. (2002). The brain insulin signal transduction system and sporadic (type II) Alzheimer disease: an update. *J. Neural. Transm.* 109, 341–360. doi: 10.1007/s007020200028

Hsu, J. L., Lin, K. J., Hsiao, I. T., Huang, K. L., Liu, C. H., Wu, H. C., et al. (2020). The imaging features and clinical associations of a novel Tau PET Tracer-^{18}F-APN1607 in Alzheimer disease. *Clin. Nucl. Med*. 45, 747–756. doi: 10.1097/RLU.0000000000003164

Iaccarino, L., Tammewar, G., Ayakta, N., Baker, S. L., Bejanin, A., Boxer, A. L., et al. (2018). Local and distant relationships between amyloid, tau and neurodegeneration in Alzheimer's disease. *Neuroimage Clin.* 17, 452–464. doi: 10.1016/j.nicl.2017.09.016

Ikawa, M., Lohith, T. G., Shrestha, S., Telu, S., Zoghbi, S. S., Castellano, S., et al. (2017). ^{11}C-ER176, a radioligand for 18-kDa translocator protein, has adequate sensitivity to robustly image all three affinity genotypes in human brain. *J. Nucl. Med*. 58, 320–325. doi: 10.2967/jnumed.116.178996

Ikonomovic, M. D., Abrahamson, E. E., Price, J. C., Mathis, C. A., and Klunk, W. E. (2016). [F-18]AV-1451 positron emission tomography retention in choroid plexus: more than "off-target" binding. *Ann. Neurol*. 80, 307–308. doi: 10.1002/ana.24706

Ishibashi, K., Onishi, A., Fujiwara, Y., Ishiwata, K., and Ishii, K. (2015). Relationship between Alzheimer disease-like pattern of ^{18}F-FDG and fasting plasma glucose levels in cognitively normal volunteers. *J. Nucl. Med*. 56, 229–233. doi: 10.2967/jnumed.114.150045

Iyo, M., Namba, H., Fukushi, K., Shinotoh, H., Nagatsuka, S., Suhara, T., et al. (1997). Measurement of acetylcholinesterase by positron emission tomography in the brains of healthy controls and patients with Alzheimer's disease. *Lancet* 349, 1805–1809. doi: 10.1016/S0140-6736(96)09124-6

Jack, C. R. Jr. (2014). PART and SNAP. *Acta Neuropathol*. 128, 773–776. doi: 10.1007/s00401-014-1362-3

Jack, C. R. Jr., Albert, M. S., Knopman, D. S., McKhann, G. M., Sperling, R. A., Carrillo, M. C., et al. (2011). Introduction to the recommendations from the national institute on aging-alzheimer's association workgroups on diagnostic guidelines for alzheimer's Disease. *Alzheimers Dement*. 7, 257–262. doi: 10.1016/j.jalz.2011.03.004

Jack, C. R. Jr., Bennett, D. A., Blennow, K., Carrillo, M. C., Dunn, B., Haeberlein, S. B., et al. (2018). NIA-AA research framework: toward a biological definition of alzheimer's Disease. *Alzheimers Dement*. 14, 535–562. doi: 10.1016/j.jalz.2018.02.018

Jack, C. R. Jr., and Holtzman, D. M. (2013). Biomarker modeling of Alzheimer's disease. *Neuron* 80, 1347–1358. doi: 10.1016/j.neuron.2013.12.003

Jack, C. R. Jr., Knopman, D. S., Chetelat, G., Dickson, D., Fagan, A. M., Frisoni, G. B., et al. (2016). Suspected non-Alzheimer disease pathophysiology–concept and controversy. *Nat. Rev. Neurol*. 12, 117–124. doi: 10.1038/nrneurol.2015.251

Jack, C. R. Jr., Knopman, D. S., Jagust, W. J., Petersen, R. C., Weiner, M. W., Aisen, P. S., et al. (2013b). Tracking pathophysiological processes in Alzheimer's disease: an updated hypothetical model of dynamic biomarkers. *Lancet Neurol*. 12, 207–216. doi: 10.1016/S1474-4422(12)70291-0

Jack, C. R. Jr., Wiste, H. J., Lesnick, T. G., Weigand, S. D., Knopman, D. S., Vemuri, P., et al. (2013a). Brain β-amyloid load approaches a plateau. *Neurology* 80, 890–896. doi: 10.1212/WNL.0b013e3182840bbe

Jansen, W. J., Ossenkoppele, R., Knol, D. L., Tijms, B. M., Scheltens, P., Verhey, F. R., et al. (2015). Prevalence of cerebral amyloid pathology in persons without dementia: a meta-analysis. *JAMA* 313, 1924–1938. doi: 10.1001/jama.2015.4668

Johnson, K. A., Gregas, M., Becker, J. A., Kinnecom, C., Salat, D. H., Moran, E. K., et al. (2007). Imaging of amyloid burden and distribution in cerebral amyloid angiopathy. *Ann. Neurol.* 62, 229–234. doi: 10.1002/ana.21164

Johnson, K. A., Schultz, A., Betensky, R. A., Becker, J. A., Sepulcre, J., Rentz, D., et al. (2016). Tau positron emission tomographic imaging in aging and early Alzheimer disease. *Ann. Neurol.* 79, 110–119. doi: 10.1002/ana.24546

Kaasinen, V., Nagren, K., Jarvenpaa, T., Roivainen, A., Yu, M., Oikonen, V., et al. (2002). Regional effects of donepezil and rivastigmine on cortical acetylcholinesterase activity in Alzheimer's disease. *J. Clin. Psychopharmacol.* 22, 615–620. doi: 10.1097/00004714-200212000-00012

Kadir, A., Darreh-Shori, T., Almkvist, O., Wall, A., Grut, M., Strandberg, B., et al. (2008). PET imaging of the *in vivo* brain acetylcholinesterase activity and nicotine binding in galantamine-treated patients with AD. *Neurobiol. Aging* 29, 1204–1217. doi: 10.1016/j.neurobiolaging.2007.02.020

Kendziorra, K., Wolf, H., Meyer, P. M., Barthel, H., Hesse, S., Becker, G. A., et al. (2011). Decreased cerebral $\alpha_4\beta_2^*$ nicotinic acetylcholine receptor availability in patients with mild cognitive impairment and Alzheimer's disease assessed with positron emission tomography. *Eur. J. Nucl. Med. Mol. Imaging* 38, 515–525. doi: 10.1007/s00259-010-1644-5

Kimura, Y., Ichise, M., Ito, H., Shimada, H., Ikoma, Y., Seki, C., et al. (2015). PET Quantification of tau pathology in human brain with ^{11}C-PBB3. *J. Nucl. Med.* 56, 1359–1365. doi: 10.2967/jnumed.115.160127

Klunk, W. E., Engler, H., Nordberg, A., Wang, Y., Blomqvist, G., Holt, D. P., et al. (2004). Imaging brain amyloid in Alzheimer's disease with pittsburgh compound-B. *Ann. Neurol.* 55, 306–319. doi: 10.1002/ana.20009

Klunk, W. E., Koeppe, R. A., Price, J. C., Benzinger, T. L., Devous, M. D. Sr., Jagust, W. J., et al. (2015). The centiloid project: standardizing quantitative amyloid plaque estimation by PET. *Alzheimers Dement.* 11:1–15.e1–4. doi: 10.1016/j.jalz.2014.07.003

Koscik, R. L., Betthauser, T. J., Jonaitis, E. M., Allison, S. L., Clark, L. R., Hermann, B. P., et al. (2020). Amyloid duration is associated with preclinical cognitive decline and tau PET. *Alzheimers Dement.* 12:e12007. doi: 10.1101/778415

Kreisl, W. C., Lyoo, C. H., Liow, J. S., Snow, J., Page, E., Jenko, K. J., et al. (2016b). Distinct patterns of increased translocator protein in posterior cortical atrophy and amnestic Alzheimer's disease. *Neurobiol. Aging* 51, 132–140. doi: 10.1016/j.neurobiolaging.2016.12.006

Kreisl, W. C., Lyoo, C. H., Liow, J. S., Wei, M., Snow, J., Page, E., et al. (2016a). ^{11}C-PBR28 binding to translocator protein increases with progression of Alzheimer's disease. *Neurobiol. Aging* 44, 53–61. doi: 10.1016/j.neurobiolaging.2016.04.011

Kreisl, W. C., Lyoo, C. H., McGwier, M., Snow, J., Jenko, K. J., Kimura, N., et al. (2013). *In vivo* radioligand binding to translocator protein correlates with severity of Alzheimer's disease. *Brain* 136 (Pt. 7):2228–2238. doi: 10.1093/brain/awt145

Kuhl, D. E., Koeppe, R. A., Minoshima, S., Snyder, S. E., Ficaro, E. P., Foster, N. L., et al. (1999). *In vivo* mapping of cerebral acetylcholinesterase activity in aging and Alzheimer's disease. *Neurology* 52, 691–699. doi: 10.1212/WNL.52.4.691

Kuhl, D. E., Minoshima, S., Frey, K. A., Foster, N. L., Kilbourn, M. R., and Koeppe, R. A. (2000). Limited donepezil inhibition of acetylcholinesterase measured with positron emission tomography in living Alzheimer cerebral cortex. *Ann Neurol.* 48, 391–395. doi: 10.1002/1531-8249(200009)48:3<391::AID-ANA17>3.0.CO;2-H

Kuwabara, H., Comley, R. A., Borroni, E., Honer, M., Kitmiller, K., Roberts, J., et al. (2018). Evaluation of ^{18}F-RO-948 PET for quantitative assessment of tau accumulation in the human brain. *J. Nucl. Med.* 59, 1877–1884. doi: 10.2967/jnumed.118.214437

Laforce, R. Jr., Buteau, J. P., Paquet, N., Verret, L., Houde, M., and Bouchard, R. W. (2010). The value of PET in mild cognitive impairment, typical and atypical/unclear dementias: a retrospective memory clinic study. *Am. J. Alzheimers Dis. Other Demen.* 25:324–332. doi: 10.1177/1533317510363468

Landau, S. M., Harvey, D., Madison, C. M., Koeppe, R. A., Reiman, E. M., Foster, N. L., et al. (2011). Associations between cognitive, functional, and FDG-PET measures of decline in AD and MCI. *Neurobiol. Aging* 32, 1207–1218. doi: 10.1016/j.neurobiolaging.2009.07.002

Leuzy, A., Chiotis, K., Lemoine, L., Gillberg, P. G., Almkvist, O., Rodriguez-Vieitez, E., et al. (2019). Tau PET imaging in neurodegenerative tauopathies-still a challenge. *Mol. Psychiatry* 24, 1112–1134. doi: 10.1038/s41380-018-0342-8

Levey, A. I. (1996). Muscarinic acetylcholine receptor expression in memory circuits: implications for treatment of Alzheimer disease. *Proc. Natl. Acad. Sci. U.S.A.* 93:13541–13546. doi: 10.1073/pnas.93.24.13541

Li, S., Cai, Z., Wu, X., Holden, D., Pracitto, R., Kapinos, M., et al. (2019). Synthesis and *in vivo* evaluation of a novel PET radiotracer for imaging of synaptic vesicle glycoprotein 2A (SV2A) in nonhuman primates. *ACS Chem. Neurosci.* 10, 1544–1554. doi: 10.1021/acschemneuro.8b00526

Lister-James, J., Pontecorvo, M. J., Clark, C., Joshi, A. D., Mintun, M. A., Zhang, W., et al. (2011). Florbetapir F-18: a histopathologically validated β-amyloid positron emission tomography imaging agent. *Semin. Nucl. Med.* 41, 300–304. doi: 10.1053/j.semnuclmed.2011.03.001

Lowe, V. J., Curran, G., Fang, P., Liesinger, A. M., Josephs, K. A., Parisi, J. E., et al. (2016). An autoradiographic evaluation of AV-1451 tau PET in dementia. *Acta Neuropathol. Commun.* 4:58. doi: 10.1186/s40478-016-0315-6

Lu, J., Bao, W., Li, M., Li, L., Zhang, Z., Alberts, I., et al. (2020). Associations of [^{18}F]-APN-1607 tau PET binding in the brain of alzheimer's disease patients with cognition and glucose metabolism. *Front. Neurosci.* 14:604. doi: 10.3389/fnins.2020.00604

Maas, T., Eidenmuller, J., and Brandt, R. (2000). Interaction of tau with the neural membrane cortex is regulated by phosphorylation at sites that are modified in paired helical filaments. *J. Biol. Chem.* 275, 15733–15740. doi: 10.1074/jbc.M000389200

Maelicke, A., Samochocki, M., Jostock, R., Fehrenbacher, A., Ludwig, J., Albuquerque, E. X., et al. (2001). Allosteric sensitization of nicotinic receptors by galantamine, a new treatment strategy for Alzheimer's disease. *Biol. Psychiatry* 49, 279–288. doi: 10.1016/S0006-3223(00)01109-4

Mallik, A., Drzezga, A., and Minoshima, S. (2017). Clinical amyloid imaging. *Semin. Nucl. Med.* 47, 31–43. doi: 10.1053/j.semnuclmed.2016.09.005

Masdeu, J., Pascual, B., Zanotti-Fregonara, P., Yu, M., Funk, Q., Arbones, V., et al. (2020). [^{11}C]MK-6884 PET tracer for M4 muscarinic cholinergic receptors in Alzheimer's disease: comparison with [^{18}F]FDG PET. *Neurology* 94 (15 Suppl):2640. doi: 10.1016/j.jalz.2019.06.4256

Masliah, E., Mallory, M., Alford, M., DeTeresa, R., Hansen, L. A., McKeel, D. W. Jr., et al. (2001). Altered expression of synaptic proteins occurs early during progression of Alzheimer's disease. *Neurology* 56, 127–129. doi: 10.1212/WNL.56.1.127

Masliah, E., Mallory, M., Hansen, L., DeTeresa, R., Alford, M., and Terry, R. (1994). Synaptic and neuritic alterations during the progression of Alzheimer's disease. *Neurosci. Lett.* 174, 67–72. doi: 10.1016/0304-3940(94)90121-X

Mattsson, N., Smith, R., Strandberg, O., Palmqvist, S., Scholl, M., Insel, P. S., et al. (2018). Comparing ^{18}F-AV-1451 with CSF t-tau and p-tau for diagnosis of Alzheimer disease. *Neurology* 90, e388–e95. doi: 10.1212/WNL.0000000000004887

Maurer, S. V., and Williams, C. L. (2017). The Cholinergic system modulates memory and hippocampal plasticity via its interactions with non-neuronal cells. *Front. Immunol.* 8:1489. doi: 10.3389/fimmu.2017.01489

McGeer, E. G., and McGeer, P. L. (2010). Neuroinflammation in Alzheimer's disease and mild cognitive impairment: a field in its infancy. *J. Alzheimers Dis.* 19, 355–361. doi: 10.3233/JAD-2010-1219

McGeer, P. L., Itagaki, S., Boyes, B. E., and McGeer, E. G. (1988). Reactive microglia are positive for HLA-DR in the substantia nigra of Parkinson's and Alzheimer's disease brains. *Neurology* 38, 1285–1291. doi: 10.1212/WNL.38.8.1285

McGeer, P. L., Kamo, H., Harrop, R., McGeer, E. G., Martin, W. R., Pate, B. D., et al. (1986). Comparison of PET, MRI, and CT with pathology in a proven case of Alzheimer's disease. *Neurology* 36, 1569–1574. doi: 10.1212/WNL.36.12.1569

McGeer, P. L., Schulzer, M., and McGeer, E. G. (1996). Arthritis and anti-inflammatory agents as possible protective factors for Alzheimer's disease: a review of 17 epidemiologic studies. *Neurology* 47, 425–432. doi: 10.1212/WNL.47.2.425

McKhann, G. M., Knopman, D. S., Chertkow, H., Hyman, B. T., Jack, C. R. Jr., Kawas, C. H., et al. (2011). The diagnosis of dementia due to Alzheimer's disease: recommendations from the National Institute on aging-alzheimer's association workgroups on diagnostic guidelines for Alzheimer's disease. *Alzheimers Dement.* 7, 263–269. doi: 10.1016/j.jalz.2011.03.005

Mecca, A. P., Chen, M. K., O'Dell, R. S., Naganawa, M., Toyonaga, T., Godek, T. A., et al. (2020). *In vivo* measurement of widespread synaptic loss in Alzheimer's disease with SV2A PET. *Alzheimers Dement*. 16, 974–982. doi: 10.1002/alz.12097

Mega, M. S., Cummings, J. L., O'Connor, S. M., Dinov, I. D., Reback, E., Felix, J., et al. (2001). Cognitive and metabolic responses to metrifonate therapy in Alzheimer disease. *Neuropsychiatry Neuropsychol. Behav. Neurol*. 14, 63–68.

Melancon, B. J., Tarr, J. C., Panarese, J. D., Wood, M. R., and Lindsley, C. W. (2013). Allosteric modulation of the M1 muscarinic acetylcholine receptor: improving cognition and a potential treatment for schizophrenia and Alzheimer's disease. *Drug Discov. Today* 18, 1185–1199. doi: 10.1016/j.drudis.2013.09.005

Mercier, J., Archen, L., Bollu, V., Carre, S., Evrard, Y., Jnoff, E., et al. (2014). Discovery of heterocyclic nonacetamide synaptic vesicle protein 2A (SV2A) ligands with single-digit nanomolar potency: opening avenues towards the first SV2A positron emission tomography (PET) ligands. *ChemMedChem* 9, 693–698. doi: 10.1002/cmdc.201300482

Mielke, R., Schroder, R., Fink, G. R., Kessler, J., Herholz, K., and Heiss, W. D. (1996). Regional cerebral glucose metabolism and postmortem pathology in Alzheimer's disease. *Acta Neuropathol* 91, 174–179. doi: 10.1007/s004010050410

Molinuevo, J. L., Berthier, M. L., and Rami, L. (2011). Donepezil provides greater benefits in mild compared to moderate Alzheimer's disease: implications for early diagnosis and treatment. *Arch. Gerontol. Geriatr*. 52, 18–22. doi: 10.1016/j.archger.2009.11.004

Morales, I., Guzman-Martinez, L., Cerda-Troncoso, C., Farias, G. A., and Maccioni, R. B. (2014). Neuroinflammation in the pathogenesis of Alzheimer's disease. A rational framework for the search of novel therapeutic approaches. *Front. Cell Neurosci.* 8:112. doi: 10.3389/fncel.2014.00112

Mosconi, L., De Santi, S., Brys, M., Tsui, W. H., Pirraglia, E., Glodzik-Sobanska, L., et al. (2008). Hypometabolism and altered cerebrospinal fluid markers in normal apolipoprotein E E4 carriers with subjective memory complaints. *Biol. Psychiatry* 63, 609–618. doi: 10.1016/j.biopsych.2007.05.030

Mosser, D. M., and Edwards, J. P. (2008). Exploring the full spectrum of macrophage activation. *Nat. Rev. Immunol.* 8, 958–969. doi: 10.1038/nri2448

Mrak, R. E., and Griffin, W. S. (2005). Glia and their cytokines in progression of neurodegeneration. *Neurobiol. Aging* 26, 349–354. doi: 10.1016/j.neurobiolaging.2004.05.010

Murray, M. E., Lowe, V. J., Graff-Radford, N. R., Liesinger, A. M., Cannon, A., Przybelski, S. A., et al. (2015). Clinicopathologic and ^{11}C-pittsburgh compound B implications of thal amyloid phase across the Alzheimer's disease spectrum. *Brain* 138 (Pt. 5):1370–1381. doi: 10.1093/brain/awv050

Nabulsi, N. B., Mercier, J., Holden, D., Carre, S., Najafzadeh, S., Vandergeten, M. C., et al. (2016). Synthesis and preclinical evaluation of ^{11}C-UCB-J as a PET tracer for imaging the synaptic vesicle glycoprotein 2A in the brain. *J. Nucl. Med.* 57, 777–784. doi: 10.2967/jnumed.115.168179

Naganawa, M., Li, S., Nabulsi, N. B., Henry, S., Zheng, M. Q., Pracitto, R., et al. (2021a). First-in-human evaluation of ^{18}F-SynVesT-1, a novel radioligand for PET imaging of synaptic vesicle protein 2A. *J. Nucl. Med.* doi: 10.2967/jnumed.120.249144

Naganawa, M., Nabulsi, N. B., Henry, S., Matuskey, D., Lin, S. F., Slieker, L., et al. (2021b). First in human assessment of the novel M1 muscarinic acetylcholine Receptor PET radiotracer ^{11}C-LSN3172176. *J. Nucl. Med.* doi: 10.2967/jnumed.120.246967

Navitsky, M., Joshi, A. D., Kennedy, I., Klunk, W. E., Rowe, C. C., Wong, D. F., et al. (2018). Standardization of amyloid quantitation with florbetapir standardized uptake value ratios to the Centiloid scale. *Alzheimers Dement*. 14, 1565–1571. doi: 10.1016/j.jalz.2018.06.1353

Ng, K. P., Pascoal, T. A., Mathotaarachchi, S., Therriault, J., Kang, M. S., Shin, M., et al. (2017). Monoamine oxidase B inhibitor, selegiline, reduces ^{18}F-THK5351 uptake in the human brain. *Alzheimers Res. Ther*. 9:25. doi: 10.1186/s13195-017-0253-y

Nordberg, A., Hartvig, P., Lilja, A., Viitanen, M., Amberla, K., Lundqvist, H., et al. (1990). Decreased uptake and binding of ^{11}C-nicotine in brain of Alzheimer patients as visualized by positron emission tomography. *J. Neural Transm. Park. Dis. Dement. Sect.* 2, 215–224. doi: 10.1007/BF02257652

Nordberg, A., Lilja, A., Lundqvist, H., Hartvig, P., Amberla, K., Viitanen, M., et al. (1992). Tacrine restores cholinergic nicotinic receptors and glucose metabolism in alzheimer patients as visualized by positron emission tomography. *Neurobiol. Aging*.13:747–758. doi: 10.1016/0197-4580(92)90099-J

Nordberg, A., Lundqvist, H., Hartvig, P., Lilja, A., and Langstrom, B. (1995). Kinetic analysis of regional (S)(-) ^{11}C-nicotine binding in normal and alzheimer brains–*in vivo* assessment using positron emission tomography. *Alzheimer Dis. Assoc. Disord.* 9, 21–27. doi: 10.1097/00002093-199505000-00006

Okada, H., Ouchi, Y., Ogawa, M., Futatsubashi, M., Saito, Y., Yoshikawa, E., et al. (2013). Alterations in $\alpha_4\beta_2$ nicotinic receptors in cognitive decline in Alzheimer's aetiopathology. *Brain* 136 (Pt. 10), 3004–3017. doi: 10.1093/brain/awt195

Okafor, M., Nye, J. A., Shokouhi, M., Shaw, L. M., Goldstein, F., and Hajjar, I. (2020). ^{18}F-Florbetaben PET associations with cerebrospinal fluid, cognition, and neuroimaging in mild cognitive impairment due to Alzheimer's disease. *J. Alzheimers Dis.* 74, 589–601. doi: 10.3233/JAD-191330

Okamura, N., Furumoto, S., Harada, R., Tago, T., Yoshikawa, T., Fodero-Tavoletti, M., et al. (2013). Novel ^{18}F-labeled arylquinoline derivatives for noninvasive imaging of tau pathology in Alzheimer disease. *J. Nucl. Med.* 54, 1420–1427. doi: 10.2967/jnumed.112.117341

Okamura, N., Harada, R., Ishiki, A., Kikuchi, A., Nakamura, T., and Kudo, Y. (2018). The development and validation of tau PET tracers: current status and future directions. *Clin. Transl. Imaging* 6, 305–316. doi: 10.1007/s40336-018-0290-y

Okamura, N., Suemoto, T., Furumoto, S., Suzuki, M., Shimadzu, H., Akatsu, H., et al. (2005). Quinoline and benzimidazole derivatives: candidate probes for *in vivo* imaging of tau pathology in Alzheimer's disease. *J. Neurosci.* 25, 10857–10862. doi: 10.1523/JNEUROSCI.1738-05.2005

Okello, A., Edison, P., Archer, H. A., Turkheimer, F. E., Kennedy, J., Bullock, R., et al. (2009b). Microglial activation and amyloid deposition in mild cognitive impairment: a PET study. *Neurology* 72, 56–62. doi: 10.1212/01.wnl.0000338622.27876.0d

Okello, A., Koivunen, J., Edison, P., Archer, H. A., Turkheimer, F. E., Nagren, K., et al. (2009a). Conversion of amyloid positive and negative MCI to AD over 3 years: an ^{11}C-PIB PET study. *Neurology* 73, 754–760. doi: 10.1212/WNL.0b013e3181b23564

Ono, M., Sahara, N., Kumata, K., Ji, B., Ni, R., Koga, S., et al. (2017). Distinct binding of PET ligands PBB3 and AV-1451 to tau fibril strains in neurodegenerative tauopathies. *Brain* 140, 764–780. doi: 10.1093/brain/aww339

Ossenkoppele, R., Jansen, W. J., Rabinovici, G. D., Knol, D. L., van der Flier, W. M., van Berckel, B. N., et al. (2015). Prevalence of amyloid PET positivity in dementia syndromes: a meta-analysis. *JAMA* 313, 1939–1949. doi: 10.1001/jama.2015.4669

Ossenkoppele, R., Schonhaut, D. R., Scholl, M., Lockhart, S. N., Ayakta, N., Baker, S. L., et al. (2016). Tau PET patterns mirror clinical and neuroanatomical variability in Alzheimer's disease. *Brain* 139 (Pt. 5), 1551–1567. doi: 10.1093/brain/aww027

Owen, D. R., Yeo, A. J., Gunn, R. N., Song, K., Wadsworth, G., Lewis, A., et al. (2012). An 18-kDa translocator protein (TSPO) polymorphism explains differences in binding affinity of the PET radioligand PBR28. *J. Cereb. Blood Flow Metab.* 32, 1–5. doi: 10.1038/jcbfm.2011.147

Papp, K. V., Buckley, R., Mormino, E., Maruff, P., Villemagne, V. L., Masters, C. L., et al. (2020). Clinical meaningfulness of subtle cognitive decline on longitudinal testing in preclinical AD. *Alzheimers Dement*. 16, 552–560. doi: 10.1016/j.jalz.2019.09.074

Passamonti, L., Vazquez Rodriguez, P., Hong, Y. T., Allinson, K. S., Williamson, D., Borchert, R. J., et al. (2017). ^{18}F-AV-1451 positron emission tomography in Alzheimer's disease and progressive supranuclear palsy. *Brain* 140, 781–791. doi: 10.1093/brain/aww340

Perry, E., Walker, M., Grace, J., and Perry, R. (1999). Acetylcholine in mind: a neurotransmitter correlate of consciousness? *Trends Neurosci.* 22, 273–280. doi: 10.1016/S0166-2236(98)01361-7

Petrou, M., Dwamena, B. A., Foerster, B. R., MacEachern, M. P., Bohnen, N. I., Muller, M. L., et al. (2015). Amyloid deposition in Parkinson's disease and cognitive impairment: a systematic review. *Mov. Disord.* 30, 928–935. doi: 10.1002/mds.26191

Pham, E., Crews, L., Ubhi, K., Hansen, L., Adame, A., Cartier, A., et al. (2010). Progressive accumulation of amyloid-β oligomers in Alzheimer's

disease and in amyloid precursor protein transgenic mice is accompanied by selective alterations in synaptic scaffold proteins. *FEBS J.* 277, 3051–3067. doi: 10.1111/j.1742-4658.2010.07719.x

Phelps, M. E., Huang, S. C., Hoffman, E. J., Selin, C., Sokoloff, L., and Kuhl, D. E. (1979). Tomographic measurement of local cerebral glucose metabolic rate in humans with (F-18)2-fluoro-2-deoxy-D-glucose: validation of method. *Ann. Neurol.* 6, 371–388. doi: 10.1002/ana.410060502

Pike, K. E., Ellis, K. A., Villemagne, V. L., Good, N., Chetelat, G., Ames, D., et al. (2011). Cognition and β-amyloid in preclinical Alzheimer's disease: data from the AIBL study. *Neuropsychologia* 49, 2384–2390. doi: 10.1016/j.neuropsychologia.2011.04.012

Pike, K. E., Savage, G., Villemagne, V. L., Ng, S., Moss, S. A., Maruff, P., et al. (2007). β-amyloid imaging and memory in non-demented individuals: evidence for preclinical Alzheimer's disease. *Brain* 130 (Pt. 11), 2837–2844. doi: 10.1093/brain/awm238

Pooler, A. M., Noble, W., and Hanger, D. P. (2014). A role for tau at the synapse in Alzheimer's disease pathogenesis. *Neuropharmacology* 76 (Pt. A):1–8. doi: 10.1016/j.neuropharm.2013.09.018

Potkin, S. G., Anand, R., Fleming, K., Alva, G., Keator, D., Carreon, D., et al. (2001). Brain metabolic and clinical effects of rivastigmine in Alzheimer's disease. *Int. J. Neuropsychopharmacol* 4, 223–230. doi: 10.1017/S1461145701002528

Querfurth, H. W., and LaFerla, F. M. (2010). Alzheimer's disease. *N. Engl. J. Med.* 362, 329–344. doi: 10.1056/NEJMra0909142

Rabinovici, G. D., and Jagust, W. J. (2009). Amyloid imaging in aging and dementia: testing the amyloid hypothesis *in vivo*. *Behav. Neurol.* 21, 117–128. doi: 10.1155/2009/609839

Rinne, J. O., Wong, D. F., Wolk, D. A., Leinonen, V., Arnold, S. E., Buckley, C., et al. (2012). [^{18}F]Flutemetamol PET imaging and cortical biopsy histopathology for fibrillar amyloid β detection in living subjects with normal pressure hydrocephalus: pooled analysis of four studies. *Acta Neuropathol.* 124, 833–845. doi: 10.1007/s00401-012-1051-z

Robinson, J. L., Molina-Porcel, L., Corrada, M. M., Raible, K., Lee, E. B., Lee, V. M., et al. (2014). Perforant path synaptic loss correlates with cognitive impairment and Alzheimer's disease in the oldest-old. *Brain* 137 (Pt. 9), 2578–2587. doi: 10.1093/brain/awu190

Rodriguez-Vieitez, E., Carter, S. F., Chiotis, K., Saint-Aubert, L., Leuzy, A., Scholl, M., et al. (2016). Comparison of early-phase ^{11}C-Deuterium-l-Deprenyl and ^{11}C-pittsburgh compound B PET for assessing brain perfusion in Alzheimer disease. *J. Nucl. Med.* 57, 1071–1077. doi: 10.2967/jnumed.115.168732

Rombouts, F. J. R., Declercq, L., Andres, J. I., Bottelbergs, A., Chen, L., Iturrino, L., et al. (2019). Discovery of N-(4-[^{18}F]Fluoro-5-methylpyridin-2-yl)isoquinolin-6-amine (JNJ-64326067), a new promising tau positron emission tomography imaging tracer. *J. Med. Chem.* 62, 2974–2987. doi: 10.1021/acs.jmedchem.8b01759

Rowe, C. C., Ackerman, U., Browne, W., Mulligan, R., Pike, K. L., O'Keefe, G., et al. (2008). Imaging of amyloid β in Alzheimer's disease with ^{18}F-BAY94-9172, a novel PET tracer: proof of mechanism. *Lancet Neurol.* 7, 129–135. doi: 10.1016/S1474-4422(08)70001-2

Rowe, C. C., Dore, V., Jones, G., Baxendale, D., Mulligan, R. S., Bullich, S., et al. (2017). ^{18}F-Florbetaben PET β-amyloid binding expressed in Centiloids. *Eur. J. Nucl. Med. Mol. Imaging* 44, 2053–2059. doi: 10.1007/s00259-017-3749-6

Rowe, C. C., Ellis, K. A., Rimajova, M., Bourgeat, P., Pike, K. E., Jones, G., et al. (2010). Amyloid imaging results from the Australian imaging, biomarkers and lifestyle (AIBL) study of aging. *Neurobiol. Aging* 31, 1275–1283. doi: 10.1016/j.neurobiolaging.2010.04.007

Rowe, C. C., Jones, G., Dore, V., Pejoska, S., Margison, L., Mulligan, R. S., et al. (2016). Standardized expression of ^{18}F-NAV4694 and ^{11}C-PiB β-amyloid PET results with the centiloid scale. *J. Nucl. Med.* 57, 1233–1237. doi: 10.2967/jnumed.115.171595

Rowe, C. C., and Villemagne, V. L. (2011). Brain amyloid imaging. *J. Nucl. Med.* 52, 1733–1740. doi: 10.2967/jnumed.110.076315

Sabri, O., Becker, G. A., Meyer, P. M., Hesse, S., Wilke, S., Graef, S., et al. (2015b). First-in-human PET quantification study of cerebral $\alpha_4\beta_2^*$ nicotinic acetylcholine receptors using the novel specific radioligand (-)-[^{18}F]Flubatine. *Neuroimage* 118, 199–208. doi: 10.1016/j.neuroimage.2015.05.065

Sabri, O., Kendziorra, K., Wolf, H., Gertz, H. J., and Brust, P. (2008). Acetylcholine receptors in dementia and mild cognitive impairment. *Eur. J. Nucl. Med. Mol. Imaging* (35 Suppl. 1), S30–45. doi: 10.1007/s00259-007-0701-1

Sabri, O., Meyer, P. M., Graf, S., Hesse, S., Wilke, S., Becker, G. A., et al. (2018). Cognitive correlates of $\alpha_4\beta_2$ nicotinic acetylcholine receptors in mild Alzheimer's dementia. *Brain* 141, 1840–1854. doi: 10.1093/brain/awy099

Sabri, O., Sabbagh, M. N., Seibyl, J., Barthel, H., Akatsu, H., Ouchi, Y., et al. (2015a). Florbetaben PET imaging to detect amyloid β plaques in Alzheimer's disease: phase 3 study. *Alzheimers Dement.* 11, 964–974. doi: 10.1016/j.jalz.2015.02.004

Salloway, S., Sperling, R., Fox, N. C., Blennow, K., Klunk, W., Raskind, M., et al. (2014). Two phase 3 trials of bapineuzumab in mild-to-moderate Alzheimer's disease. *N. Engl. J. Med* 370, 322–333. doi: 10.1056/NEJMoa1304839

Scheef, L., Spottke, A., Daerr, M., Joe, A., Striepens, N., Kolsch, H., et al. (2012). Glucose metabolism, gray matter structure, and memory decline in subjective memory impairment. *Neurology* 79, 1332–1339. doi: 10.1212/WNL.0b013e31826c1a8d

Scheff, S. W., DeKosky, S. T., and Price, D. A. (1990). Quantitative assessment of cortical synaptic density in Alzheimer's disease. *Neurobiol. Aging* 11, 29–37. doi: 10.1016/0197-4580(90)90059-9

Scheff, S. W., and Price, D. A. (2006). Alzheimer's disease-related alterations in synaptic density: neocortex and hippocampus. *J. Alzheimers Dis.* 9 (3 Suppl), 101–115. doi: 10.3233/JAD-2006-9S312

Schilling, T., and Eder, C. (2011). Amyloid-β-induced reactive oxygen species production and priming are differentially regulated by ion channels in microglia. *J. Cell. Physiol.* 226, 3295–3302. doi: 10.1002/jcp.22675

Schliebs, R., and Arendt, T. (2011). The cholinergic system in aging and neuronal degeneration. *Behav. Brain Res.* 221, 555–563. doi: 10.1016/j.bbr.2010.11.058

Schmidt, M. E., Janssens, L., Moechars, D., Rombouts, F. J. R., Timmers, M., Barret, O., et al. (2020). Clinical evaluation of [^{18}F]JNJ-64326067, a novel candidate PET tracer for the detection of tau pathology in Alzheimer's disease. *Eur. J. Nucl. Med. Mol. Imaging* 47, 3176–3185. doi: 10.1007/s00259-020-04880-1

Schmidt, R., Ropele, S., Pendl, B., Ofner, P., Enzinger, C., Schmidt, H., et al. (2008). Longitudinal multimodal imaging in mild to moderate Alzheimer disease: a pilot study with memantine. *J. Neurol. Neurosurg. Psychiatry* 79, 1312–1317. doi: 10.1136/jnnp.2007.141648

Schmitz, T. W., Mur, M., Aghourian, M., Bedard, M. A., Spreng, R. N., and Alzheimer's Disease Neuroimaging, I. (2018). Longitudinal alzheimer's degeneration reflects the spatial topography of cholinergic basal forebrain projections. *Cell Rep.* 24,38–46. doi: 10.1016/j.celrep.2018.06.001

Scholl, M., Almkvist, O., Bogdanovic, N., Wall, A., Langstrom, B., Viitanen, M., et al. (2011). Time course of glucose metabolism in relation to cognitive performance and postmortem neuropathology in Met146Val PSEN1 mutation carriers. *J. Alzheimers Dis.* 24, 495–506. doi: 10.3233/JAD-2011-101563

Schuitemaker, A., Kropholler, M. A., Boellaard, R., van der Flier, W. M., Kloet, R. W., van der Doef, T. F., et al. (2013). Microglial activation in Alzheimer's disease: an (*R*)-[^{11}C]PK11195 positron emission tomography study. *Neurobiol. Aging* 34, 128–136. doi: 10.1016/j.neurobiolaging.2012.04.021

Sepulcre, J., Schultz, A. P., Sabuncu, M., Gomez-Isla, T., Chhatwal, J., Becker, A., et al. (2016). *In vivo* tau, amyloid, and gray matter profiles in the aging brain. *J. Neurosci.* 36, 7364–7374. doi: 10.1523/JNEUROSCI.0639-16.2016

Shimada, H., Kitamura, S., Shinotoh, H., Endo, H., Niwa, F., Hirano, S., et al. (2017). Association between Aβ and tau accumulations and their influence on clinical features in aging and Alzheimer's disease spectrum brains: A [^{11}C]PBB3-PET study. *Alzheimers Dement.* 6, 11–20. doi: 10.1016/j.dadm.2016.12.009

Shinotoh, H., Aotsuka, A., Fukushi, K., Nagatsuka, S., Tanaka, N., Ota, T., et al. (2001). Effect of donepezil on brain acetylcholinesterase activity in patients with AD measured by PET. *Neurology*.56:408–410. doi: 10.1212/WNL.56.3.408

Smith, G. S., Laxton, A. W., Tang-Wai, D. F., McAndrews, M. P., Diaconescu, A. O., Workman, C. I., et al. (2012). Increased cerebral metabolism after 1 year of deep brain stimulation in Alzheimer disease. *Arch. Neurol.* 69, 1141–1148. doi: 10.1001/archneurol.2012.590

Sperling, R. A., Aisen, P. S., Beckett, L. A., Bennett, D. A., Craft, S., Fagan, A. M., et al. (2011). Toward defining the preclinical stages of Alzheimer's disease: recommendations from the national institute on aging-alzheimer's association

workgroups on diagnostic guidelines for Alzheimer's disease. *Alzheimers Dement*. 7, 280–292. doi: 10.1016/j.jalz.2011.03.003

Sperling, R. A., Donohue, M. C., Raman, R., Sun, C. K., Yaari, R., Holdridge, K., et al. (2020). Association of factors with elevated amyloid burden in clinically normal older individuals. *JAMA Neurol.* 77, 735–745. doi: 10.1001/jamaneurol.2020.0387

Spillantini, M. G., and Goedert, M. (2013). Tau pathology and neurodegeneration. *Lancet Neurol.* 12, 609–622. doi: 10.1016/S1474-4422(13)70090-5

Streit, W. J., Mrak, R. E., and Griffin, W. S. (2004). Microglia and neuroinflammation: a pathological perspective. *J. Neuroinflammation* 1:14. doi: 10.1186/1742-2094-1-14

Su, Y., Fu, J., Yu, J., Zhao, Q., Guan, Y., Zuo, C., et al. (2020). Tau PET Imaging with [^{18}F]PM-PBB3 in frontotemporal dementia with MAPT mutation. *J. Alzheimers Dis.* 76, 149–157. doi: 10.3233/JAD-200287

Suridjan, I., Pollock, B. G., Verhoeff, N. P., Voineskos, A. N., Chow, T., Rusjan, P. M., et al. (2015). *In-vivo* imaging of grey and white matter neuroinflammation in Alzheimer's disease: a positron emission tomography study with a novel radioligand, [^{18}F]-FEPPA. *Mol. Psychiatry* 20, 1579–1587. doi: 10.1038/mp.2015.1

Tagai, K., Ono, M., Kubota, M., Kitamura, S., Takahata, K., Seki, C., et al. (2021). High-Contrast *in vivo* imaging of tau pathologies in alzheimer's and non-alzheimer's disease tauopathies. *Neuron* 109:42–58.e8. doi: 10.1016/j.neuron.2020.09.042

Tang, Y., Nyengaard, J. R., De Groot, D. M., and Gundersen, H. J. (2001). Total regional and global number of synapses in the human brain neocortex. *Synapse* 41, 258–273. doi: 10.1002/syn.1083

Teipel, S., Drzezga, A., Grothe, M. J., Barthel, H., Chetelat, G., Schuff, N., et al. (2015). Multimodal imaging in Alzheimer's disease: validity and usefulness for early detection. *Lancet Neurol.* 14, 1037–1053. doi: 10.1016/S1474-4422(15)00093-9

Teng, E., Ward, M., Manser, P. T., Sanabria-Bohorquez, S., Ray, R. D., Wildsmith, K. R., et al. (2019). Cross-sectional associations between [^{18}F]GTP1 tau PET and cognition in Alzheimer's disease. *Neurobiol. Aging* 81, 138–145. doi: 10.1016/j.neurobiolaging.2019.05.026

Terry, R. D., Masliah, E., Salmon, D. P., Butters, N., DeTeresa, R., Hill, R., et al. (1991). Physical basis of cognitive alterations in Alzheimer's disease: synapse loss is the major correlate of cognitive impairment. *Ann. Neurol* 30, 572–580. doi: 10.1002/ana.410300410

Thal, D. R., Beach, T. G., Zanette, M., Heurling, K., Chakrabarty, A., Ismail, A., et al. (2015). [^{18}F]flutemetamol amyloid positron emission tomography in preclinical and symptomatic Alzheimer's disease: specific detection of advanced phases of amyloid-β pathology. *Alzheimers Dement*. 11, 975–985. doi: 10.1016/j.jalz.2015.05.018

Therriault, J., Benedet, A., Pascoal, T. A., Savard, M., Ashton, N., Chamoun, M., et al. (2021). Determining Amyloid-β positivity using ^{18}F-AZD4694 PET imaging. *J. Nucl. Med.*62:247–252. doi: 10.2967/jnumed.120.245209

Thompson, P. W., Ye, L., Morgenstern, J. L., Sue, L., Beach, T. G., Judd, D. J., et al. (2009). Interaction of the amyloid imaging tracer FDDNP with hallmark Alzheimer's disease pathologies. *J. Neurochem.* 109, 623–630. doi: 10.1111/j.1471-4159.2009.05996.x

Tong, L., Li, W., Lo, M. M., Gao, X., Wai, J. M., Rudd, M., et al. (2020). Discovery of [^{11}C]MK-6884: a positron emission tomography (PET) Imaging agent for the study of M4 muscarinic receptor positive allosteric modulators (PAMs) in neurodegenerative diseases. *J. Med. Chem.* 63, 2411–2425. doi: 10.1021/acs.jmedchem.9b01406

Tune, L., Tiseo, P. J., Ieni, J., Perdomo, C., Pratt, R. D., Votaw, J. R., et al. (2003). Donepezil HCl (E2020) maintains functional brain activity in patients with Alzheimer disease: results of a 24-week, double-blind, placebo-controlled study. *Am. J. Geriatr. Psychiatry* 11, 169–177. doi: 10.1097/00019442-200303000-00007

Tzimopoulou, S., Cunningham, V. J., Nichols, T. E., Searle, G., Bird, N. P., Mistry, P., et al. (2010). A multi-center randomized proof-of-concept clinical trial applying [^{18}F]FDG-PET for evaluation of metabolic therapy with rosiglitazone XR in mild to moderate Alzheimer's disease. *J. Alzheimers Dis.* 22, 1241–1256. doi: 10.3233/JAD-2010-100939

Van Der Gucht, A., Verger, A., Yagdigul, Y., Poussier, S., Joly, L., Watfa, G., et al. (2015). Complementarity of visual and voxel-based FDG-PET analysis to detect MCI-like hypometabolic pattern in elderly patients with hypertension and isolated memory complaints. *Acta Radiol.* 56, 980–989. doi: 10.1177/0284185114542366

Vanhaute, H., Ceccarini, J., Michiels, L., Koole, M., Sunaert, S., Lemmens, R., et al. (2020). *In vivo* synaptic density loss is related to tau deposition in amnestic mild cognitive impairment. *Neurology* 95, e545–e53. doi: 10.1212/WNL.0000000000009818

Vannini, P., Hanseeuw, B., Munro, C. E., Amariglio, R. E., Marshall, G. A., Rentz, D. M., et al. (2017). Hippocampal hypometabolism in older adults with memory complaints and increased amyloid burden. *Neurology* 88, 1759–1767. doi: 10.1212/WNL.0000000000003889

Varley, J., Brooks, D. J., and Edison, P. (2015). Imaging neuroinflammation in Alzheimer's disease and other dementias: recent advances and future directions. *Alzheimers Dement*. 11, 1110–1120. doi: 10.1016/j.jalz.2014.08.105

Varrone, A., Oikonen, V., Forsberg, A., Joutsa, J., Takano, A., Solin, O., et al. (2015). Positron emission tomography imaging of the 18-kDa translocator protein (TSPO) with [^{18}F]FEMPA in Alzheimer's disease patients and control subjects. *Eur. J. Nucl. Med. Mol. Imaging* 42, 438–446. doi: 10.1007/s00259-014-2955-8

Vehmas, A. K., Kawas, C. H., Stewart, W. F., and Troncoso, J. C. (2003). Immune reactive cells in senile plaques and cognitive decline in Alzheimer's disease. *Neurobiol. Aging* 24, 321–331. doi: 10.1016/S0197-4580(02)00090-8

Vellas, B., Andrieu, S., Sampaio, C., Wilcock, G., and European Task Force, G. (2007). Disease-modifying trials in Alzheimer's disease: a European task force consensus. *Lancet Neurol.* 6, 56–62. doi: 10.1016/S1474-4422(06)70677-9

Venneti, S., Lopresti, B. J., Wang, G., Hamilton, R. L., Mathis, C. A., Klunk, W. E., et al. (2009). PK11195 labels activated microglia in Alzheimer's disease and *in vivo* in a mouse model using PET. *Neurobiol. Aging* 30, 1217–1226. doi: 10.1016/j.neurobiolaging.2007.11.005

Villemagne, V. L., Dore, V., Burnham, S. C., Masters, C. L., and Rowe, C. C. (2018). Imaging tau and amyloid-β proteinopathies in Alzheimer disease and other conditions. *Nat. Rev. Neurol.* 14, 225–236. doi: 10.1038/nrneurol.2018.9

Villemagne, V. L., Pike, K. E., Chetelat, G., Ellis, K. A., Mulligan, R. S., Bourgeat, P., et al. (2011). Longitudinal assessment of Aβ and cognition in aging and Alzheimer disease. *Ann. Neurol.* 69, 181–192. doi: 10.1002/ana.22248

Villemagne, V. L., Pike, K. E., Darby, D., Maruff, P., Savage, G., Ng, S., et al. (2008). Aβ deposits in older non-demented individuals with cognitive decline are indicative of preclinical Alzheimer's disease. *Neuropsychologia* 46, 1688–1697. doi: 10.1016/j.neuropsychologia.2008.02.008

Wadsworth, H., Jones, P. A., Chau, W. F., Durrant, C., Fouladi, N., Passmore, J., et al. (2012). [^{18}F]GE-180: a novel fluorine-18 labelled PET tracer for imaging translocator protein 18 kDa (TSPO). *Bioorg. Med. Chem. Lett.* 22, 1308–1313. doi: 10.1016/j.bmcl.2011.12.084

Wang, H. Y., Li, W., Benedetti, N. J., and Lee, D. H. (2003). a_7 nicotinic acetylcholine receptors mediate β-amyloid peptide-induced tau protein phosphorylation. *J. Biol. Chem.* 278, 31547–31553. doi: 10.1074/jbc.M212532200

Wang, Y., and Mandelkow, E. (2016). Tau in physiology and pathology. *Nat. Rev. Neurosci.* 17, 5–21. doi: 10.1038/nrn.2015.1

Wei, W., Nguyen, L. N., Kessels, H. W., Hagiwara, H., Sisodia, S., and Malinow, R. (2010). Amyloid β from axons and dendrites reduces local spine number and plasticity. *Nat. Neurosci.* 13, 190–196. doi: 10.1038/nn.2476

Wessels, A. M., Tariot, P. N., Zimmer, J. A., Selzler, K. J., Bragg, S. M., Andersen, S. W., et al. (2020). Efficacy and safety of lanabecestat for treatment of early and mild Alzheimer disease: The AMARANTH and DAYBREAK-ALZ randomized clinical trials. *JAMA Neurol.* 77, 199–209. doi: 10.1001/jamaneurol.2019.3988

Whitwell, J. L., Graff-Radford, J., Tosakulwong, N., Weigand, S. D., Machulda, M. M., Senjem, M. L., et al. (2018). Imaging correlations of tau, amyloid, metabolism, and atrophy in typical and atypical Alzheimer's disease. *Alzheimers Dement*. 14, 1005–1014. doi: 10.1016/j.jalz.2018.02.020

Wiley, C. A., Lopresti, B. J., Venneti, S., Price, J., Klunk, W. E., DeKosky, S. T., et al. (2009). Carbon 11-labeled pittsburgh compound B and carbon 11-labeled (R)-PK11195 positron emission tomographic imaging in Alzheimer disease. *Arch. Neurol.* 66, 60–67. doi: 10.1001/archneurol.2008.511

Wilson, H., Dervenoulas, G., Pagano, G., Tyacke, R. J., Polychronis, S., Myers, J., et al. (2019). Imidazoline 2 binding sites reflecting astroglia pathology in Parkinson's disease: an *in vivo* ^{11}C-BU99008 PET study. *Brain* 142, 3116–3128. doi: 10.1093/brain/awz260

Wolfsgruber, S., Kleineidam, L., Wagner, M., Mosch, E., Bickel, H., Lupsilonhmann, D., et al. (2016). Differential risk of incident Alzheimer's disease dementia in stable versus unstable patterns of subjective cognitive decline. *J. Alzheimers Dis*. 54, 1135–1146. doi: 10.3233/JAD-160407

Wolters, E. E., Ossenkoppele, R., Verfaillie, S. C. J., Coomans, E. M., Timmers, T., Visser, D., et al. (2020). Regional [^{18}F]flortaucipir PET is more closely associated with disease severity than CSF p-tau in Alzheimer's disease. *Eur. J. Nucl. Med. Mol. Imaging* 47, 2866–2878. doi: 10.1007/s00259-020-04758-2

Wong, D. F., Kuwabara, H., Horti, A. G., Roberts, J. M., Nandi, A., Cascella, N., et al. (2018). Brain PET imaging of α_7-nAChR with [^{18}F]ASEM: reproducibility, occupancy, receptor density, and changes in schizophrenia. *Int. J. Neuropsychopharmacol*. 21, 656–667. doi: 10.1101/245118

Wong, D. F., Kuwabara, H., Kim, J., Brasic, J. R., Chamroonrat, W., Gao, Y., et al. (2013). PET imaging of high-affinity $\alpha_4\beta_2$ nicotinic acetylcholine receptors in humans with ^{18}F-AZAN, a radioligand with optimal brain kinetics. *J. Nucl. Med*. 54, 1308–1314. doi: 10.2967/jnumed.112.108001

Wooten, D. W., Guehl, N. J., Verwer, E. E., Shoup, T. M., Yokell, D. L., Zubcevik, N., et al. (2017). Pharmacokinetic evaluation of the tau PET radiotracer ^{18}F-T807 (^{18}F-AV-1451) in human subjects. *J. Nucl. Med*. 58, 484–491. doi: 10.2967/jnumed.115.170910

Wyss-Coray, T., and Mucke, L. (2002). Inflammation in neurodegenerative disease–a double-edged sword. *Neuron* 35, 419–432. doi: 10.1016/S0896-6273(02)00794-8

Xia, C. F., Arteaga, J., Chen, G., Gangadharmath, U., Gomez, L. F., Kasi, D., et al. (2013). [^{18}F]T807, a novel tau positron emission tomography imaging agent for Alzheimer's disease. *Alzheimers Dement*. 9, 666–676. doi: 10.1016/j.jalz.2012.11.008

Yasuno, F., Ota, M., Kosaka, J., Ito, H., Higuchi, M., Doronbekov, T. K., et al. (2008). Increased binding of peripheral benzodiazepine receptor in Alzheimer's disease measured by positron emission tomography with [^{11}C]DAA1106. *Biol. Psychiatry* 64, 835–841. doi: 10.1016/j.biopsych.2008.04.021

Yokokura, M., Mori, N., Yagi, S., Yoshikawa, E., Kikuchi, M., Yoshihara, Y., et al. (2011). *In vivo* changes in microglial activation and amyloid deposits in brain regions with hypometabolism in Alzheimer's disease. *Eur. J. Nucl. Med. Mol. Imaging* 38, 343–351. doi: 10.1007/s00259-010-1612-0

Yuan, Y., Gu, Z. X., and Wei, W. S. (2009). Fluorodeoxyglucose-positron-emission tomography, single-photon emission tomography, and structural MR imaging for prediction of rapid conversion to Alzheimer disease in patients with mild cognitive impairment: a meta-analysis. *AJNR Am. J. Neuroradiol*. 30, 404–410. doi: 10.3174/ajnr.A1357

Zanotti-Fregonara, P., Zhang, Y., Jenko, K. J., Gladding, R. L., Zoghbi, S. S., Fujita, M., et al. (2014). Synthesis and evaluation of translocator 18 kDa protein (TSPO) positron emission tomography (PET) radioligands with low binding sensitivity to human single nucleotide polymorphism rs6971. *ACS Chem. Neurosci*. 5, 963–971. doi: 10.1021/cn500138n

Zhang, S., Han, D., Tan, X., Feng, J., Guo, Y., and Ding, Y. (2012). Diagnostic accuracy of ^{18}F-FDG and ^{11}C-PIB-PET for prediction of short-term conversion to Alzheimer's disease in subjects with mild cognitive impairment. *Int. J. Clin. Pract*. 66, 185–198. doi: 10.1111/j.1742-1241.2011.02845.x

Zimmer, E. R., Leuzy, A., Benedet, A. L., Breitner, J., Gauthier, S., and Rosa-Neto, P. (2014). Tracking neuroinflammation in Alzheimer's disease: the role of positron emission tomography imaging. *J. Neuroinflammation* 11:120. doi: 10.1186/1742-2094-11-120

Conflict of Interest: The authors declare that the research was conducted in the absence of any commercial or financial relationships that could be construed as a potential conflict of interest.

frontiers in Neuroscience

ORIGINAL RESEARCH
published: 17 May 2021
doi: 10.3389/fnins.2021.612940

The Distribution of Skull Score and Skull Density Ratio in Tremor Patients for MR-Guided Focused Ultrasound Thalamotomy

Kevin Wen-Kai Tsai[1†], Jui-Cheng Chen[2,3,4†], Hui-Chin Lai[1], Wei-Chieh Chang[1,5], Takaomi Taira[6], Jin Woo Chang[7] and Cheng-Yu Wei[8,9]*

[1] MR-guided Focused Ultrasound Center, Chang Bing Show Chwan Memorial Hospital, Changhua City, Taiwan, [2] Neuroscience Laboratory, Department of Neurology, China Medical University Hospital, Taichung City, Taiwan, [3] School of Medicine, College of Medicine, China Medical University, Taichung City, Taiwan, [4] Department of Neurology, China Medical University Hsinchu Hospital, Hsinchu, Taiwan, [5] Department of Neurosurgery, Chang Bing Show Chwan Memorial Hospital, Changhua City, Taiwan, [6] Department of Neurosurgery, Tokyo Women's Medical University, Tokyo, Japan, [7] Department of Neurosurgery, Yonsei University College of Medicine, Seoul, South Korea, [8] Department of Exercise and Health Promotion, College of Kinesiology and Health, Chinese Culture University, Taipei, Taiwan, [9] Department of Neurology, Chang Bing Show Chwan Memorial Hospital, Changhua City, Taiwan

OPEN ACCESS

Edited by:
Kuangyu Shi,
University of Bern, Switzerland

Reviewed by:
Clement Hamani,
University of Toronto, Canada
Huiwei Zhang,
Fudan University, China

***Correspondence:**
Cheng-Yu Wei
yuyu@seed.net.tw

[†] These authors have contributed equally to this work and share first authorship

Specialty section:
This article was submitted to Brain Imaging Methods, a section of the journal Frontiers in Neuroscience

Received: *03 October 2020*
Accepted: *08 April 2021*
Published: *17 May 2021*

Citation:
Tsai KW-K, Chen J-C, Lai H-C, Chang W-C, Taira T, Chang JW and Wei C-Y (2021) The Distribution of Skull Score and Skull Density Ratio in Tremor Patients for MR-Guided Focused Ultrasound Thalamotomy. Front. Neurosci. 15:612940. doi: 10.3389/fnins.2021.612940

Objective: Magnetic resonance-guided focused ultrasound (MRgFUS) is a minimum-invasive surgical approach to non-incisionally cause the thermos-coagulation inside the human brain. The skull score (SS) has already been approved as one of the most dominant factors related to a successful MRgFUS treatment. In this study, we first reveal the SS distribution of the tremor patients, and correlate the SS with the image feature from customized skull density ratio (cSDR). This correlation might give a direction to future clinical studies for improving the SS.

Methods: Two hundred and forty-six patients received a computed tomography (CT) scan of the brain, and a bone-enhanced filter was applied and reconstructed to a high spatial resolution CT images. The SS of all patients would be estimated by the MRgFUS system after importing the reconstructed CT images into the MRgFUS system. The histogram and the cumulative distribution of the SS from all the patients were calculated to show the percentage of the patients whose SS lower than 0.3 and 0.4. The same CT images of all patients were utilized to calculated the cSDR by first segmented the trabecular bone and the cortical bone from the CT images and divided the average trabecular bone intensity (aTBI) by the average cortical bone intensity (aCBI). The Pearson's correlations between the SS and the cSDR, aTBI, and the aCBI were calculated, respectively.

Results: There were 19.19 and 50% of the patient who had the *SS* lower than the empirical threshold 0.3 and 0.4, respectively. The Pearson's correlation between the SS and the cSDR, aCBI, and the aTBI were $R = 0.8145$, 0.5723, and 0.8842.

Conclusion: Half of the patients were eligible for the MRgFUS thalamotomy based on the SS, and nearly 20% of patients were empirically difficult to achieve a therapeutic

temperature during MRgFUS. The SS and our cSDR are highly correlated, and the SS had a higher correlation with aTBI than with aCBI. This is the first report to explicitly reveal the SS population and indicate a potential way to increase the chance to achieve a therapeutic temperature for those who originally have low SS.

Keywords: tremor, skull density ratio, skull score, MR-guided focused ultrasound thalamotomy, essential tremor

INTRODUCTION

High intensity focused ultrasound (HIFU) is an incisionless surgical device that has been widely used in medical research and clinical trials including the treatment of tumors (Kennedy, 2005) such as the liver (Kennedy et al., 2004; Illing et al., 2005), and kidney for over 50 years (Kennedy et al., 2003). By using the heating or cavitation at a variable distance from the transducer, HIFU can cause selectively thermal coagulation in a well-defined volume.

Sharing similar principles of the HIFU, recently the transcranial magnetic resonance-guided focused ultrasound (MRgFUS) has been widely used in different clinical trials to treat various neurological disorders in the human brain (Elias et al., 2016; Leinenga et al., 2016). MRgFUS can perform a thermal ablation around the subcortical area or opening the blood-brain barrier (Abbott et al., 2006) for drug delivery with different ultrasound frequency. One of the important keys to these successes was the phase aberration correction (Fry and Barger, 1978; Sun and Hynynen, 1998; Hynynen et al., 2004) across thousands of the ultrasound beams when passing through the skull (Chang et al., 2016; Jung et al., 2019) that produce a constructive focusing at the target area which maximize the energy-heat efficiency without causing any thermal coagulation outside the target. A high spatial resolution (<2 mm slice thickness) of a volumetric computed tomography (CT) scan with bone-enhanced filtering was used not only to delineate the entire skull for the phase aberration correction during the treatment but also to estimate a general skull score (SS) to screen patients before the treatment. The SS, which is offered by the InSightec, directly correlated with the temperature efficiency in the MRgFUS thalamotomy (Chang et al., 2016), and the empirical criterion of the SS for the MRgFUS thalamotomy is 0.40 (Wang et al., 2018). However, no literature was reported regarding the percentage of patients who can feasibly receive MRgFUS thalamotomy under this empirical criterion.

In this study, we tried to reveal the population distribution of the SS in tremor patients of Taiwanese people to address the aforementioned question, and report on the relationship between the SS and a customized skull density ratio (cSDR) by our algorithm, to determine the reliability of cSDR and the importance of the trabecular bone or the cortical bone separately in bone density calculation to provide fundamental information before designing a solution for low SS in MRgFUS treatment.

MATERIALS AND METHODS

Patient Selection

Two hundred and forty-six patients (62.4 ± 12.0 years old, ranging from 23 to 89 years old, 162 male and 84 female) with tremor dominant symptoms visited our site for the MRgFUS thalamotomy screening and were recruited in this study. Enrolled patients gave informed consent and were diagnosed by neurologists specializing in movement disorders based on tremor criteria (Wang et al., 2018). The experiments conformed to the standards set by the Declaration of Helsinki and were approved by the Chang Bing Show Chwan Memorial Hospital, Taiwan. Conventional CT scans were arranged for those who were willing to join the MRgFUS thalamotomy screening with no unnecessary radiation exposure.

Conventional CT Scan

A sixteen-slice CT scanner (LightSpeed, GE, United States) was used to acquire the brain CT image. The scanning parameters followed the head routine scan protocol in our hospital and they were: peak X-ray tube voltage = 120 kVp, tube current = 250 mA, and scan time = 1.0 s. The scanning slices were parallelly aligned with the orbital-meatus (OM) line by the visual check of a radiographer. All the projection images of respective patients were used to reconstruct a volumetric image with a slice thickness of 0.625 mm. A high-pass filter (Bone + filter) was applied to the reconstructed CT images to enhance the dynamic range of the skull while suppressing that of the other parts in the images.

SS Calculation

The CT images of each patient were uploaded into the ExAblate Neuro platform (InSightec Inc., Israel) and followed the procedures suggested by InSightec to calculate the SS. Specifically, the volumetric CT images with high-pass filtering of each patient were first uploaded into the ExAblate Neuro platform, and the anterior commissure, posterior commissure, and mid-sagittal point were defined on the platform. We used the built-in tool named target defined by AC-PC in the ExAblate Neuro platform to simulate a target for the MRgFUS thalamotomy. The spatial position of a simulated MRgFUS transducer helmet was then adjusted to align the ultrasound transducer focus and the simulated target of each patient. After the target selection, the calcification of each patient on the CT images was manually marked to turn off the ultrasound transducers which routes to the target pass

through the marked calcification. After the brain calcification selection, the treatment protocol will be selected and the fiducial will be manually placed. In the treatment tag of the ExAblate Neuro platform, the SS from respective patients were reported from the ExAblate Neuro platform. **Figure 1A** showed how the ExAblate Neuro platform simulated the ultrasound beams penetrated through the skull, and the definition of the maximum and minimum values of the skull along the I_k-th ultrasound beam. The SS for each patient was calculated by Eq. (1),

$$SS = \frac{\sum_{k=1}^{P} \min(I_k)/Max(I_k)}{P} \quad (1)$$

where P indicated the number of ultrasound beams from the transducer.

cSDR Calculation

The same CT images of each patient were used to calculate the SS ratio by our method. Specifically, we first used the image contrast window and level provided by a high-pass filter to enhance the cortical and trabecular bone and used Otsu's method (Otsu, 1979) to separate the bone from the non-bone objects in the volumetric CT image. A mask volume was created by setting the intensity of bone to unity and that of non-bone to zero. The middle slice of the mask volume was used as the initial slice for the following analysis. Repeated image erosion was performed on the initial slice, and stopped before all the binary voxels were eroded. One of the remaining voxels was randomly selected and used as the seed point for the region growing on the initial slice. The candidates of the seed points for region growing of the adjacent slices to

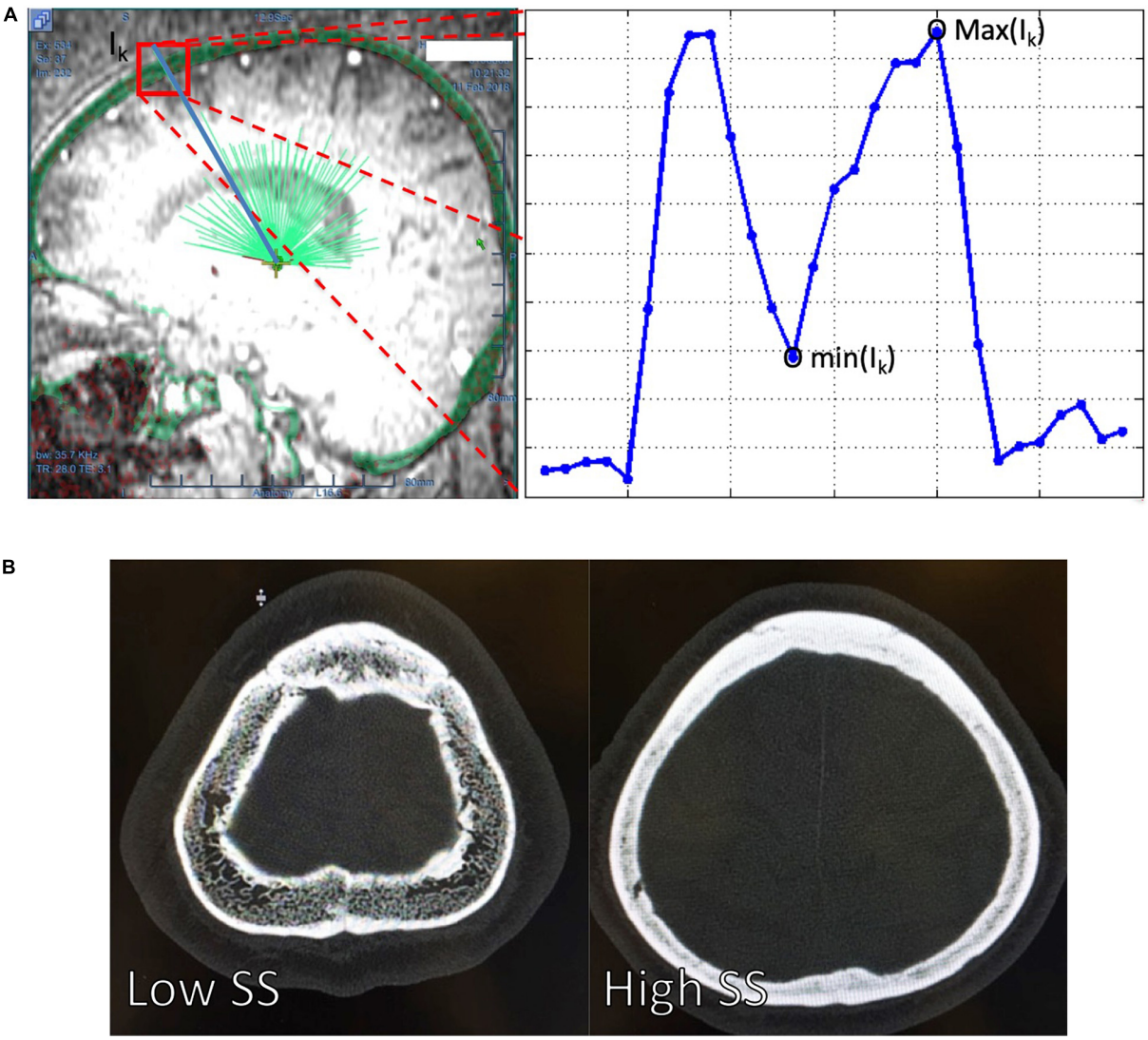

FIGURE 1 | (A) The ExAblate Neuro platform simulated the ultrasound beams (light green lines) penetrating through a skull (transparent green around the head) and extracted the maximum [max (I_k)] and minimum [min(I_k)] of the skull intensities along each of the ultrasound. The blue line at the right panel of the **(A)** delineated the CT image intensity changes along one of the ultrasound beam I_k. A high intensity difference between and cortical and trabecular bone might leaded to a low SS = 0.25 [**(B)**, left] compared to high SS = 0.70, which had a relatively similar intensity between the cortical and trabecular bone [**(B)**, right]. SS, skull score.

the previous slice were selected from the overlap between two adjacent slices to ensure spatial continuity. The region growing procedure was stopped until all the slices of the CT mask image were performed. The mask image from the results after region growing was used to define the entire skull. The aforementioned procedure to the volumetric CT image was repeatedly performed for 30 times by considering the balance between the computation time and the accuracy of the skull definition. All the 30 masked images were added together into one masked image, with the voxel values ranging from 0 to 30. We used the part of the skull where the masked image value equals 30, indicating the part most spatially continuous from the initial slice, to exclude the part of the bone that might be less related to the regions of the MRgFUS thalamotomy, such as maxillary bone. The Outs' method was again used to obtain the image intensity threshold of the cortical bone and trabecular bone of the skull. The SDR (Eq. 2) was calculated by dividing the average trabecular bone intensity (aTBI) across all N voxels by the average cortical bone intensity (aCBI) across all *M* voxels.

$$aTBI = \frac{\sum_{i=1}^{N} TBI_i}{N}, aCBI = \frac{\sum_{j=1}^{M} CBI_j}{M}, \text{cSDR} = \frac{aTBI}{aCBI} \quad (2)$$

All the aforementioned calculations were performed on the MATLAB (MathWorks, United States) platform.

SDR Calculation

The histogram of all SSs from 246 patients was computed with the bin range from 0.1 to 0.8 and a step size of 0.01. The cumulative distribution function (Park, 2018) of the SS was computed from each bin of the histogram, leading a range from 0.1 to 0.8 and step size of 0.01.

Correlation Between SS and cSDR

The linear correlations between the SS and the cSDR across all the patients were estimated by calculating the Pearson's correlation coefficient between the SS and the cSDR from each of the patients. Specifically, the bootstrap sampling (Efron, 1979) was applied to produce 24,600 pairs of SS-cSDR pairs by repeatedly selecting 246 samples from our 246 data. For example, one can select [1,1,1,2,2,3,3,3,. . ., 122] or [1,2,3,4,5,6,. . .,246] from our 246 data while the number here in the bracket means the data index. A new SS-cSDR pair was produced by averaging across the SS and cSDR of each of the selections. The data selection and averaging were repeated 24,600 times, then we had 24,600 SS-cSDR pairs. The linear correlation between the SS and the cSDR after bootstrap sampling was estimated by calculating the Pearson's correlation coefficient across all the bootstrapped pairs. Similarly, the linear correction of the SS-aCBI and SS-aTBI pairs across all the patients was respectively estimated to evaluate the influence of the aCBI and the aTBI on the SS. The correlation coefficient of the aforementioned calculation was done on MATLAB (MATLAB and Statistics Toolbox Release 2018a, The MathWorks, Inc., Natick, MA, United States) by using the *corrcoef* function. The Pearson's correlation coefficient and the *p*-value of this calculation were reported accordingly.

RESULTS

The 246 patients' demographic characteristics are summarized in **Table 1**. There were 114 clinically diagnosed essential tremor (ET) patients, and the rest of them experiencing other types of tremors, including Parkinson's disease and psychogenic tremor, etc. **Figure 1B** shows an exemplar of the trans-axial CT images with low (SS = 0.25) and high (SS = 0.70). The main difference between the CT images with the low (**Figure 1B**, left) and the high SS (**Figure 1B**, right) was that the contrast between the cortical and trabecular bone was higher in the low SS CT image than that in the high SS CT image. According to Eq. (1), a high intensity difference between the cortical and trabecular bone would lead to a high SS.

SS Distribution Calculation

The mean and the standard deviation of the SS from the total 246 patients were 0.419 ± 105 and ranged from 0.16 to 0.73. **Figure 2A** shows the histogram of the SS of the included patients and there was a population peak at the SS = 0.41. **Figure 2B** shows the cumulative distribution function of the SS.

Correlation Between SS and cSDR

The total 2,46,000 bootstrapped samples (**Figure 3**) resulted in the SS ranging from 0.38 to 0.44 and cSDR ranging from 0.712 to 0.728. The Pearson's correlation coefficient between the SS and cSDR was 0.8145 with the statistical significance ($p < 10^{-5}$), and linear relation between the SS and cSDR:

$$SDR = 0.2154 \times SS + 0.6312 \quad (3)$$

Figures 4A,B show that the aCBI and aTBI were linearly correlated with SS, and the linear relations were:

$$aCBI = 375.5 \times SS + 2426 \quad (4)$$

$$aTBI = 826 \times SS + 1518 \quad (5)$$

between aCBI and aTBI to SS, respectively. However, the aCBI was less correlated (R = 0.5723) to SS than that of aTBI to SS

TABLE 1 | Demographic characteristics in subjects with tremor.

Variables	Number (%)	Mean ± SD	*p*-value
Female/male	83/163 (33.7/66.3)		
Age (years)		62.41 ± 12.04	
ET/non-ET	192/54 (78/22)		
SS (total)		0.41 ± 0.12	
SS (female)		0.40 ± 0.12	
SS (male)		0.41 ± 0.12	0.88[1]
SS (ET)		0.41 ± 0.12	
SS (non-ET)		0.41 ± 0.13	0.66[2]

ET, essential tremor; non-ET, non-essential tremor; SS, skull score.
[1]Comparision of SS between female and male.
[2]Comparision of SS between ET and non-ET.

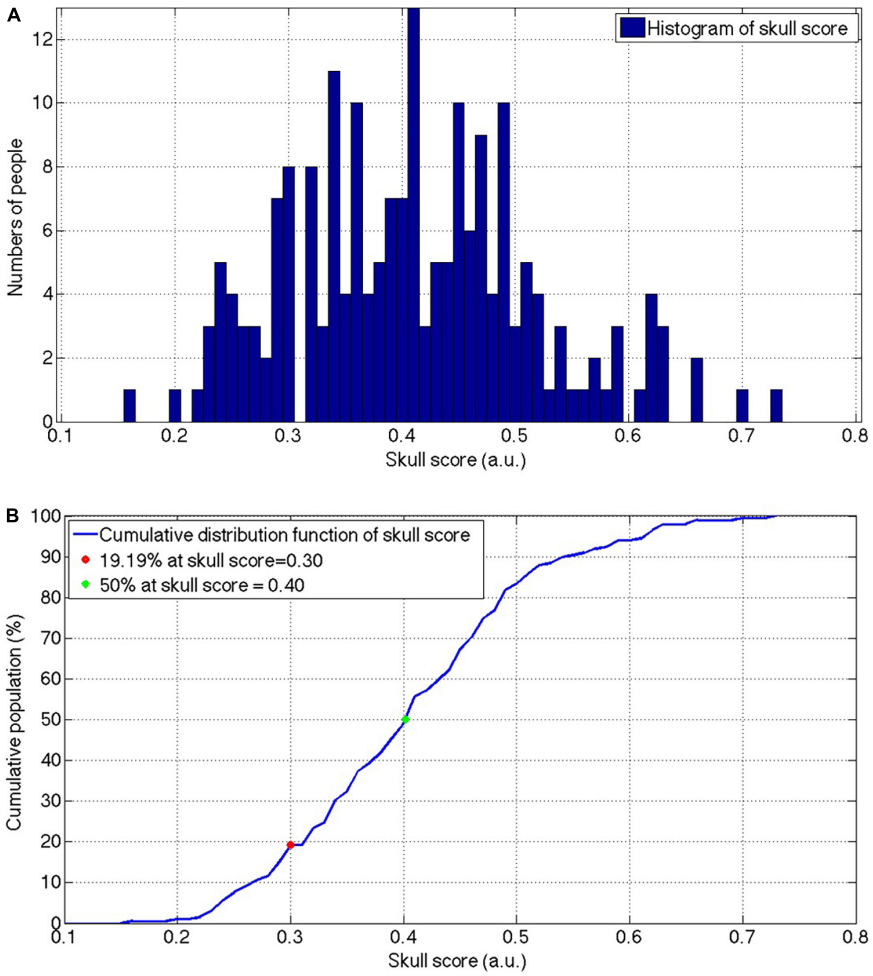

FIGURE 2 | The histogram **(A)** and the cumulative distribution function **(B)** of the SS for the patients who received the MRgFUS thalamotomy screening. The envelope of the histogram showed a slightly positive skewed distribution and the peak was located at 0.41. The slope of the cumulative population was visually consistent from the beginning and start to decrease after the SS = 0.50. SS, skull score; MRgFUS, Magnetic resonance-guided focused ultrasound.

(R = 0.8842). Moreover, the slope of the linear relation between the aTBI and the SS was higher (Eq. 5, slope = 826) than that between the aCBI and the SS (Eq. 4, slope = 375.5).

DISCUSSION

This study demonstrated the distribution of SS in the population of tremor dominant patients in Taiwan. Only half of the patients fulfilled the empirical SS criteria for the MRgFUS treatment. To our knowledge, this is the first report of SS distribution in patients with tremors.

In this study, we screened 246 patients, and ET patients occupied about 46% (114/246) of total participants. This result was consistent with the perception that ET is the most common movement disorder compared to others (Thanvi et al., 2006) in elderly people. However, the average age of the participants enrolled in this study was high and this limitation might affect the following analysis of the SS or SDR distributions.

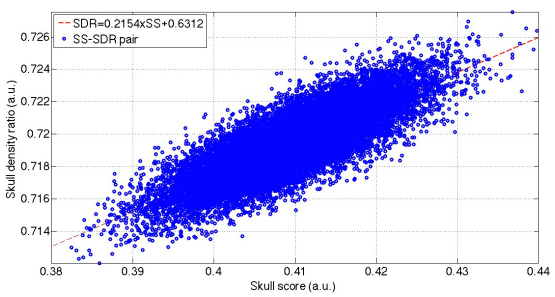

FIGURE 3 | The distribution of the bootstrapped SS-cSDR pairs and the linear correction between these SS-SDR pairs. The blue dots show the total 2,46,000 bootstrapped samples, and the red line indicates the linear fitting of these bootstrapped samples. SS, skull score; cSDR, customized skull density ratio.

Traditional SDR calculation is done by first defining the regions of cortical bone and trabecular bone of the skull and then

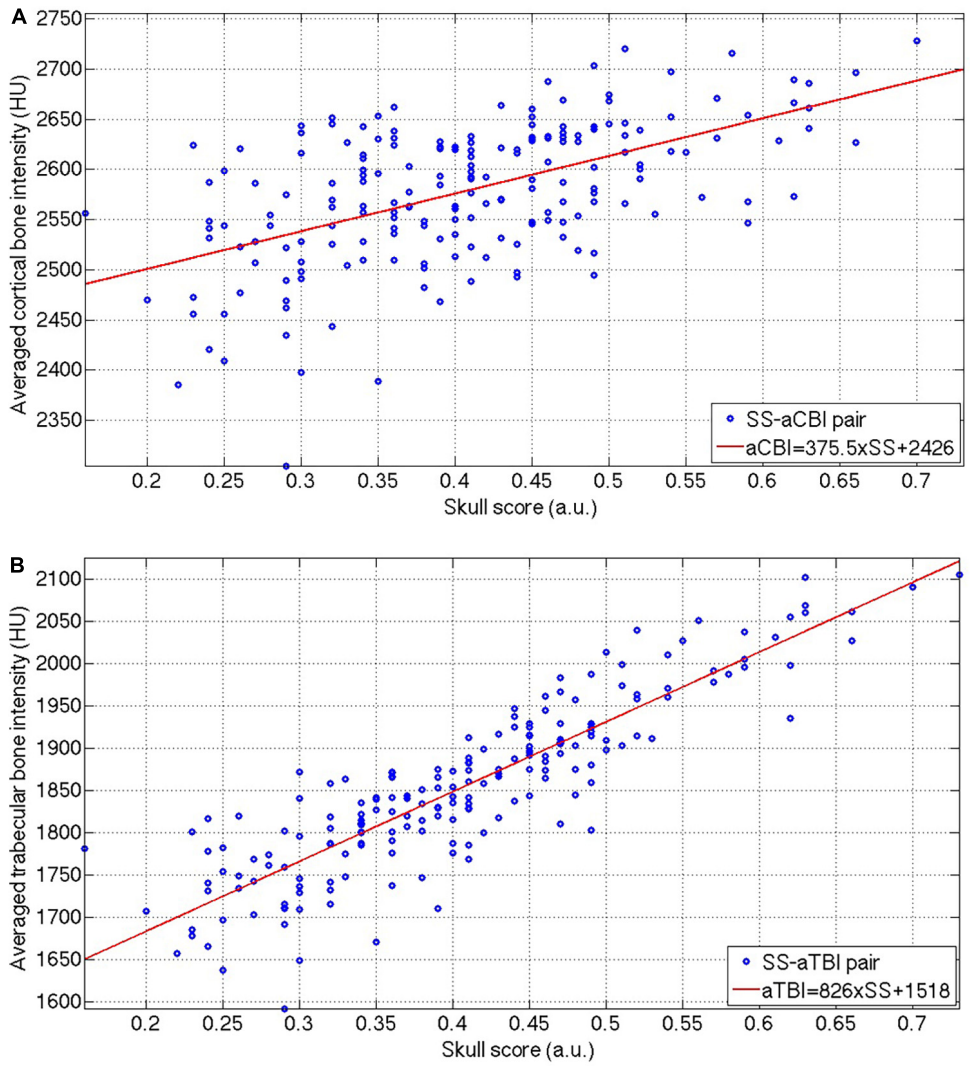

FIGURE 4 | The distribution of the SS-aCBI **(A)** and SS-aTBI **(B)** pairs, and the respective linear fitting (red lines) of these two pairs. SS, skull score; aCBI, average cortical bone intensity; aTBI, average trabecular bone intensity.

dividing the average trabecular image intensity by the average cortical image intensity. Our approach differed, and the SS, which is offered by InSightec Inc., was calculated by averaging across all the ratios of the minimum and the maximum of the HU number of the skull CT image along thousands of spatial pathways from the ultrasound transducer to the simulated target in the subcortical area. The traditional SDR is in practice the same as the cSDR in this study in terms of the calculation, which is the averaged tubercular bone intensity over the averaged cortical bone intensity. We used our customized algorithm to automatically extract the skull which has a similar skull region for the SS calculation and then calculate the traditional SDR. Compared with the SS, our cSDR calculation is free from complex steps when calculating the SS.

A high SS suggested a high possibility of success to the MRgFUS thalamotomy to relieve the tremor (Chang et al., 2016), However, according to the SS distribution from our results (**Figure 2B**), nearly half of the patients have an SS lower than 0.4 in tremor patients of Taiwanese descent, indicating that for those patients, it might be difficult to raise the temperature to the therapeutic 54-degree during the MRgFUS thalamotomy. It is noteworthy that there was a closed 20% of the patients with SS lower than 0.3, indicating the bare success of the MRgFUS thalamotomy for those patients. It minimizes the feasibility of treatment in Asia.

Interestingly, SS is correlated with the trabecular bone rather than the cortical bone. The bootstrapped samples of the SS-cSDR pairs showed a high correlation between SS and cSDR (**Figure 3**), and the value of the SS was always lower than cSDR in our data. Theoretically, the highest value in the SS calculation indicated the intensity of the cortical bone while the lowest value might not necessarily come from the trabecular bone. The lowest value may represent the intensity of the trabecular bone space or the partial volume of the trabecular bone. The larger difference between the highest and lowest value would lead to a smaller SS. In comparison, our cSDR calculation only use the trabecular bone

value, and it would decrease the difference to the cortical bone, leading to a larger cSDR value than the SS. Moreover, according to Eq. (3), SS was more sensitive than cSDR to the cortical and trabecular bone differences since 1 SS would only produce 0.8466 SDR. In **Figures 4A,B**, both the aTBI and the aCBI have a linear correlation with the SS, and the slope of the respective linear fitting indicating that the aTBI increased higher than the aCBI when increasing the SS, and vice versa. This might be due to the fact that the CBI has smaller variation across patients than the TBI. Here, our data showed a reliable relation of cSDR with SS. Moreover, a possible solution for low SDR should be focused on the aTBI rather than aCBI.

CONCLUSION

To our knowledge, this is the first report of the SS population for the MRgFUS thalamotomy in Taiwanese tremor patients. Our results suggest that in nearly half of the Taiwanese patients with tremors it might not be feasible to achieve the therapeutic temperature using current MRgFUS thalamotomy. Accordingly, it is crucial to improve the energy-temperature efficiency for the MRgFUS thalamotomy.

Moreover, our results showed a linear relationship between the SS and our cSDR. In addition, SS correlated more to the trabecular bone than cortical bone. Clinically, seeking a medical approach to increase the aTBI intensity might increase the SS, and further improve the energy-temperature efficiency during the MRgFUS treatment.

DATA AVAILABILITY STATEMENT

The original contributions presented in the study are included in the article/supplementary material, further inquiries can be directed to the corresponding author.

ETHICS STATEMENT

The studies involving human participants were reviewed and approved by the Institutional Review Board, Show Chwan Memorial Hospital. The patients/participants provided their written informed consent to participate in this study.

AUTHOR CONTRIBUTIONS

KW-KT and J-CC proposed the research idea and wrote the manuscript. H-CL collected the clinical data. W-CC provided the clinical suggestions. TT and JC supported the literature review and helped to revise the manuscript. C-YW supported the data analysis and prepared the manuscript for submission. All authors read and approved the final manuscript.

FUNDING

KW-KT and H-CL received a grant (RA18001) from the Chang Bing Show Chwan Memorial Hospital. J-CC was supported by the Ministry of Science and Technology, Taiwan (MOST 107-2221-E-008-091; MOST107-2314-B-039-040-; MOST109-2314-B-039-027-; and MOST 109-2314-B-039-002-), China Medical University Hospital (DMR-110-100), and China Medical University Hsinchu Hospital (CMUHCH-DMR-110-012 and CMUHCH-DMR-110-001).

ACKNOWLEDGMENTS

We wish to thank the research funding from the Chang Bing Show Chwan Memorial Hospital (RA18001), and the technical support from InSightec Ltd. We also are thankful for the valuable help of Ming-Tsung Lee from the Research Assistant Center, Chang Bing Show Chwan Memorial Hospital.

REFERENCES

Abbott, N. J., Rönnbäck, L., and Hansson, E. (2006). Astrocyte-endothelial interactions at the blood-brain barrier. *Nat. Rev. Neurosci.* 7, 41–53. doi: 10.1038/nrn1824

Chang, W. S., Jung, H. H., Zadicario, E., Rachmilevitch, I., Tlusty, T., Vitek, S., et al. (2016). Factors associated with successful magnetic resonance-guided focused ultrasound treatment: efficiency of acoustic energy delivery through the skull. *J. Neurosurg.* 124, 411–416. doi: 10.3171/2015.3.jns142592

Efron, B. (1979). Bootstrap methods: another look at the jackknife. *Ann. Statist.* 7, 1–26. doi: 10.1214/aos/1176344552

Elias, W. J., Lipsman, N., Ondo, W. G., Ghanouni, P., Kim, Y. G., Lee, W., et al. (2016). A randomized trial of focused ultrasound thalamotomy for essential tremor. *N Engl J Med* 375, 730–739. doi: 10.1056/NEJMoa1600159

Fry, F. J., and Barger, J. E. (1978). Acoustical properties of the human skull. *J. Acoust. Soc. Am.* 63, 1576–1590. doi: 10.1121/1.381852

Hynynen, K., Clement, G. T., McDannold, N., Vykhodtseva, N., King, R., White, P. J., et al. (2004). 500-element ultrasound phased array system for noninvasive focal surgery of the brain: a preliminary rabbit study with ex vivo human skulls. *Magn. Reson. Med.* 52, 100–107. doi: 10.1002/mrm.20118

Illing, R. O., Kennedy, J. E., Wu, F., ter Haar, G. R., Protheroe, A. S., Friend, P. J., et al. (2005). The safety and feasibility of extracorporeal high-intensity focused ultrasound (HIFU) for the treatment of liver and kidney tumours in a Western population. *Br. J. Cancer* 93, 890–895. doi: 10.1038/sj.bjc.6602803

Jung, N. Y., Rachmilevitch, I., Sibiger, O., Amar, T., Zadicario, E., and Chang, J. W. (2019). Factors related to successful energy transmission of focused ultrasound through a skull : a study in human cadavers and its comparison with clinical experiences. *J. Korean Neurosurg. Soc.* 62, 712–722. doi: 10.3340/jkns.2018.0226

Kennedy, J. E. (2005). High-intensity focused ultrasound in the treatment of solid tumours. *Nat. Rev. Cancer* 5, 321–327. doi: 10.1038/nrc1591

Kennedy, J. E., Ter Haar, G. R., and Cranston, D. (2003). High intensity focused ultrasound: surgery of the future? *Br. J. Radiol.* 76, 590–599. doi: 10.1259/bjr/17150274

Kennedy, J. E., Wu, F., ter Haar, G. R., Gleeson, F. V., Phillips, R. R., Middleton, M. R., et al. (2004). High-intensity focused ultrasound for the treatment of liver tumours. *Ultrasonics* 42, 931–935. doi: 10.1016/j.ultras.2004.01.089

Leinenga, G., Langton, C., Nisbet, R., and Götz, J. (2016). Ultrasound treatment of neurological diseases–current and emerging applications. *Nat. Rev. Neurol.* 12, 161–174. doi: 10.1038/nrneurol.2016.13

Otsu, N. (1979). A threshold selection method from gray-level histograms. *IEEE Trans. Syst. Man Cybernetics* 9, 62–66. doi: 10.1109/TSMC.1979.4310076

Park, K. I. (2018). *Fundamentals of Probability and Stochastic Processes with Applications to Communications*. Berlin: Springer.

Sun, J., and Hynynen, K. (1998). Focusing of therapeutic ultrasound through a human skull: a numerical study. *J. Acoust. Soc. Am.* 104(3 Pt 1), 1705–1715. doi: 10.1121/1.424383

Thanvi, B., Lo, N., and Robinson, T. (2006). Essential tremor-the most common movement disorder in older people. *Age. Ageing* 35, 344–349. doi: 10.1093/ageing/afj072

Wang, T. R., Bond, A. E., Dallapiazza, R. F., Blanke, A., Tilden, D., Huerta, T. E., et al. (2018). Transcranial magnetic resonance imaging-guided focused ultrasound thalamotomy for tremor: technical note. *Neurosurg. Focus.* 44, E3. doi: 10.3171/2017.10.focus17609

Conflict of Interest: The authors declare that the research was conducted in the absence of any commercial or financial relationships that could be construed as a potential conflict of interest.

frontiers in Aging Neuroscience

ORIGINAL RESEARCH
published: 14 June 2021
doi: 10.3389/fnagi.2021.602781

Exploring the Key Genes and Identification of Potential Diagnosis Biomarkers in Alzheimer's Disease Using Bioinformatics Analysis

*Wuhan Yu[1], Weihua Yu[2], Yan Yang[3] and Yang Lü[1]**

[1] Department of Geriatrics, The First Affiliated Hospital of Chongqing Medical University, Chongqing, China, [2] Institutes of Neuroscience, Chongqing Medical University, Chongqing, China, [3] State Key Laboratory of Power Transmission Equipment and System Security and New Technology, College of Electrical Engineering, Chongqing University, Chongqing, China

Background: Alzheimer's disease (AD) is one of the major threats of the twenty-first century and lacks available therapy. Identification of novel molecular markers for diagnosis and treatment of AD is urgently demanded, and genetic biomarkers show potential prospects.

Method: We identify and intersected differentially expressed genes (DEGs) from five microarray datasets to detect consensus DEGs. Based on these DEGs, we conducted Gene Ontology (GO), performed the Kyoto Encyclopedia of Genes and Genomes (KEGG) enrichment analysis, constructed a protein—protein interaction (PPI) network, and utilized Cytoscape to identify hub genes. The least absolute shrinkage and selection operator (LASSO) logistic regression was applied to identify potential diagnostic biomarkers. Gene set enrichment analysis (GSEA) was performed to investigate the biological functions of the key genes.

Result: We identified 608 consensus DEGs, several dysregulated pathways, and 18 hub genes. Sixteen hub genes dysregulated as AD progressed. The diagnostic model of 35 genes was constructed, which has a high area under the curve (AUC) value in both the validation dataset and combined dataset (AUC = 0.992 and AUC = 0.985, respectively). The model can also differentiate mild cognitive impairment and AD patients from controls in two blood datasets. Brain-derived neurotrophic factor (BDNF) and WW domain-containing transcription regulator protein 1 (WWTR1), which are associated with the Braak stage, Aβ 42 levels, and β-secretase activity, were identified as critical genes of AD.

Conclusion: Our study identified 16 hub genes correlated to the neuropathological stage and 35 potential biomarkers for the diagnosis of AD. WWTR1 were identified as candidate genes for future studies. This study deepens our understanding of the transcriptomic and functional features and provides new potential diagnostic biomarkers and therapeutic targets for AD.

Keywords: Alzheimer's disease, diagnosis biomarkers, hub genes, integrative analysis, aging

OPEN ACCESS

Edited by:
Kuangyu Shi,
University of Bern, Switzerland

Reviewed by:
Diego Sepulveda-Falla,
University Medical Center Hamburg-Eppendorf, Germany
Arif Ali,
Shanghai Jiao Tong University, China
Abbas Khan,
Shanghai Jiao Tong University, China

****Correspondence:***
Yang Lü
lyu_yang@126.com

Received: *04 September 2020*
Accepted: *06 May 2021*
Published: *14 June 2021*

Citation:
Yu W, Yu W, Yang Y and Lü Y (2021) Exploring the Key Genes and Identification of Potential Diagnosis Biomarkers in Alzheimer's Disease Using Bioinformatics Analysis. Front. Aging Neurosci. 13:602781. doi: 10.3389/fnagi.2021.602781

INTRODUCTION

Alzheimer's disease (AD) is the most common neurodegenerative disease in the elderly, affecting more than 35.6 million people worldwide (Querfurth and LaFerla, 2010; Kumar et al., 2015). Epidemiological analysis has predicted that the number will rise to 65.7 million in 2030 and approximately 115.4 million in 2050 (Prince et al., 2013). The symptoms usually start with subtle memory loss and gradually progress to affect other cognitive domains as the condition deteriorates, such as language, visuospatial skills, motor skills, executive function, and activities of daily living (McKhann et al., 2011; Huang and Mucke, 2012). As AD usually has concealed onset, most patients with AD are already at an advanced stage at the time of diagnosis. Furthermore, the long-term care and related costs of AD contribute a substantial economic burden to the society and family. It is reported that the global societal cost for dementia is projected to grow to approximately $2 trillion in 2030 (Wimo et al., 2017). Unfortunately, despite recent progress in understanding the neurobiology and pathophysiology of AD so far, no therapeutic strategies can effectively prevent or cure AD. Therefore, research directed toward identifying AD biomarkers is needed for the early diagnosis, prevention, and treatment of AD.

AD is a characteristic "complex" disease resulting from the interaction of genetic and environmental factors. It is known that the primary pathogenesis of AD was β-amyloid (Aβ) abnormal deposition, neurofibrillary tangles induced by phosphorylation of tau proteins, inflammatory response, oxidative stress, and neuronal apoptosis. All these processes involve alterations in the expression and regulation of numerous genes. Studies suggest that genetic factors are estimated to attribute up to 79% to the risk for AD (Wingo et al., 2012). The apolipoprotein E (APOE) ε4 allele has been identified as the most substantial risk factor for AD (Rogaev et al., 1995; Sherrington et al., 1995). Mutations in the genes which enhanced generation and aggregation of Aβ, such as amyloid precursor protein (APP), presenilin (1) (PSEN1), and presenilin (2) (PSEN2), were included in the established genetic causes of familial AD (Sorbi et al., 2001; Tanzi and Bertram, 2005). Moreover, genetic analyses have suggested that the individual differences and complicated pathogenesis of AD may be influenced by multiple genes and their variants involved in numerous biological functions and substantially increase the risk of the disease (Hokama et al., 2014; Stopa et al., 2018). Therefore, identification and comprehensive analyses of potential candidate genes will considerably increase our understanding of the biological mechanisms involved in disease pathogenesis and could potentially be used as diagnostic or predictive biomarkers for AD.

In recent years, bioinformatics analysis is widely applied in molecular biology experiments and clinical practice (Banwait and Bastola, 2015), revealing the key pathways and drug targets in complex diseases (Khan et al., 2018). Thus, joint analysis of the array-based data of AD may be a novel analytical strategy. Our present study aims to reveal the transcriptomic characteristics and identification of novel biomarkers of AD for diagnosis and treatment. We identified co-differentially expressed genes (DEGs) in AD of five microarray datasets in the Gene Expression Omnibus (GEO). Based on the results, we performed a series of analyses, including Gene Ontology (GO), Kyoto Encyclopedia of Genes and Genomes (KEGG) enrichment pathway analysis, protein—protein interaction (PPI) analysis, and least absolute shrinkage and selection operator (LASSO) logistic regression analysis. We identified 18 hub genes and tested their expression levels in different Braak stages. A 35-gene-based diagnosis model was constructed, and then we test the diagnostic values for AD and mild cognitive impairment (MCI). Finally, two key genes were identified by overlapping the 18 hub genes and 35 diagnosis genes. We further explored their correlations with β-secretase activity and Aβ 42 levels. Gene set enrichment analysis (GSEA) was used to explore the potential biological functions of hub genes. Our present study could provide more insights into the molecular mechanism of AD and provided potential biomarker candidates for clinical diagnosis and treatment.

MATERIALS AND METHODS

Data Processing

GEO[1] is a public functional genomics data repository of high-throughput gene expression data, chips, and microarrays. According to the following criteria, datasets were considered eligible for our analysis: (1) datasets with AD samples; (2) datasets supported by peer-reviewed PubMed-indexed publications; and (3) studies with information about the technology and platform utilized for studies. We selected 10 datasets (GSE33000, GSE36980, GSE48350, GSE5281, GSE122063, GSE106241, GSE4226, GSE97760, GSE63060, and GSE63061) related to AD for analysis. A total of 757 non-demented healthy control subjects (NDHCS) and 932 AD patients were analyzed. We extracted the whole data of a single study, including all brain regions, for analysis. The data sample collection is shown in **Table 1**. The flowchart of the study is illustrated in **Figure 1**.

The GSE33000 (platform GPL4372) was composed of postmortem prefrontal cortex (PFC) samples of 157 NDHCS and 310 AD patients with matched genotype and clinical data. The GSE36980 (platform GPL6244) was composed of the frontal cortex (FC), temporal cortex (TC), and hippocampus (HPC) from 47 NDHCS and 32 AD patients. From GSE48350 (platform GPL570), we selected data from the HPC, entorhinal cortex (EC), superior frontal cortex (SFC), and post-central gyrus (PCGY) derived from 253 postmortem brains, among which 80 cases were diagnosed as having AD. The GSE122063 (platform GPL16699) was composed of tissues collected from FC and TC, 44 tissues from NDHCS and 56 from AD patients. The GSE5281 (platform GPL570) was composed of tissues collected by laser capture microscopy (LCM) from 74 NDHCS and 87 AD patients. The brain regions included the EC, HPC, medial temporal gyrus, posterior cingulate, SFC, and primary visual cortex. The GSE106241 was enrolled for independent external validation. In

[1] http://www.ncbi.nlm.nih.gov/geo

TABLE 1 | Dataset characteristics.

Dataset	Platform/technology	No. of samples	Sample source	Age	Gender female:male	Disease stage	Country
GSE33000	GPL4372 (Rosetta/Merck Human 44 k 1.1 microarray)	467 (310 AD, 157 NDHCS)	Prefrontal cortex	AD:(53–100 y); NDHCS:(22–106 y)	209:258	–	United States
GSE36980	GPL6244 [(HuGene-1_0–st) Affymetrix Human Gene 1.0 ST Array (transcript (gene) version)]	79 (32 AD, 47 NDHCS)	Frontal cortex, temporal cortex and hippocampus	AD:(83–105 y); NDHCS:(54–100 y)	42:37	–	Japan
GSE122063	GPL16699 [Agilent–039494 SurePrint G3 Human GE v2 8 × 60 K Microarray 039381 (Feature Number version)]	100 (56 AD, 44 NDHCS)	Frontal cortex, temporal cortex	AD:(63–91 y); NDHCS:(60–91 y)	68:32	–	United States
GSE48350	GPL570 [(HG-U133_Plus_2) Affymetrix Human Genome U133 Plus 2.0 Array]	253 (80 AD, 173 NDHCS)	Hippocampus, entorhinal cortex, superior frontal cortex, post-central gyrus	AD:(60–95 y); NDHCS:(20–99 y)	129:124	Braak stage 0–6	United States
GSE5281	GPL570 [(HG-U133_Plus_2) Affymetrix Human Genome U133 Plus 2.0 Array]	161 (87 AD, 74 NDHCS)	Entorhinal cortex, hippocampus, medial tem poral gyrus, posterior cingulate, superior frontal gyrus and primary visual cortex	AD:(68–97 y); NDHCS:(63–102 y)	58:103	–	United States
GSE106241	GPL24170 [Agilent-044312 Human 8 × 60 K Custom Exon array (Probe Name version)]	60 (60 AD)	Inferior termporal cortex	AD:50–100 y	42:18	Braak stage 0–6	Finland
GSE4226	GPL1211 (NIA MGC, Mammalian Genome Collection)	28 (14 AD, 14 NDHCS)	Peripheral blood mononuclear cells	–	14:14	–	Canada
GSE97760	GPL16699 [Agilent-039494 SurePrint G3 Human GE v2 8 × 60 K Microarray 039381 (Feature Number version)]	19 (9 AD, 10 NDHCS)	Peripheral blood	–	0:19	Advanced AD	United States
GSE63060	GPL6947 (Illumina HumanHT-12 V3.0 expression beadchip)	329 (145 AD, 80 MCI, 104 NDHCS)	Peripheral blood	AD (58–88 y); MCI (63–90 y); NDHCS (52–87 y)	200:129	–	United Kingdom
GSE63061	GPL10558 (Illumina HumanHT-12 V4.0 expression beadchip)	382 (139 AD, 109 MCI, 134 NDHCS)	Peripheral blood	AD (59–95 y); MCI (57–100 y); NDHCS (63–91 y)	231:151	–	United Kingdom

The first five datasets were used for combined analysis, GSE106241 was used for independent validation analysis, and the last four datasets were used for evaluating the diagnosis model in peripheral blood. AD, Alzheimer's disease; MCI, mild cognitive impairment; NDHCS, non-demented healthy control subjects. GPL, Gene Expression Omnibus Platform.

this dataset, 60 human temporal cortical tissue samples were included and divided into seven groups based on Braak staging.

Gene expression profiles of peripheral blood were obtained from GSE97760, GSE4226, GSE63060, and GSE63061. Study subjects from GSE97760 (platform GPL16699) were all female, including nine subjects with advanced AD and 10 age-matched NDHCS. The GSE4226 (platform GPL1211) was composed of peripheral blood mononuclear cells from 14 NDHCS and 14 AD patients. Datasets GSE63060 and GSE63061 were composed of MCI patients, AD patients, and NDHCS. There are 329 samples (145 AD, 80 MCI, and 104 NDHCS) in GSE63060 and 382 samples (139 AD, 109 MCI, 134 NDHCS) in GSE63061. Three borderline MCI samples, one NDHCS-to-AD sample, one MCI-to-NDHCS sample, and one other sample, were excluded from GSE63061.

Identification of Consensus DEGs

As single datasets and few samples may weaken the credibility of the results, data integration is necessary to look for findings supported by several pieces of evidence and investigate the complex genetic mechanisms (Pineda et al., 2015). Therefore, five brain tissue datasets (GSE33000, GSE36980, GSE48350, GSE5281, and GSE122063) were selected to identify consensus DEGs. We used the impute package to supplement missing data (Troyanskaya et al., 2001). Then, the normalizeBetweenArrays function in the limma package was used to normalize gene

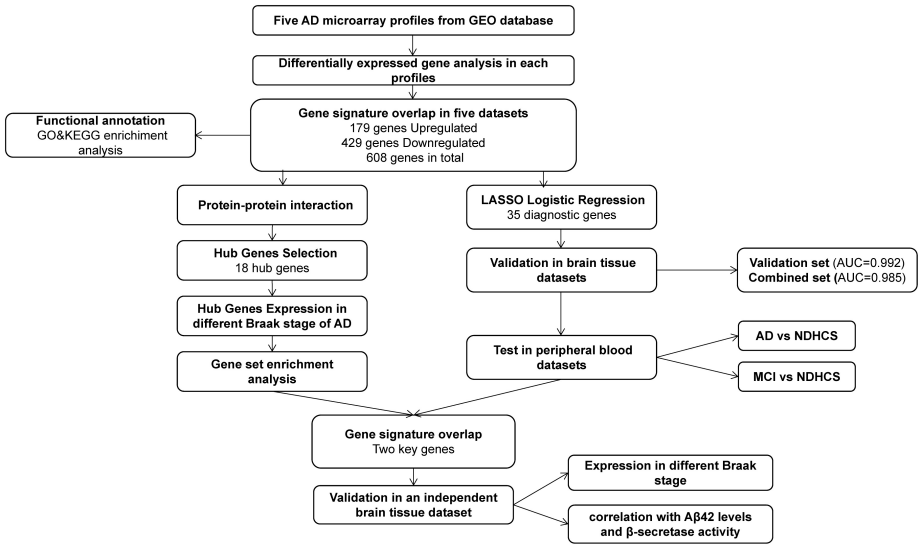

FIGURE 1 | Flowchart for bioinformatics analysis in this study. AD, Alzheimer's disease; MCI, mild cognitive impairment; NDHCS, non-demented healthy control subjects; AUC, area under the curve; GSEA, gene set enrichment analysis; GEO, Gene Expression Omnibus; GO, Gene Ontology; KEGG, Kyoto Encyclopedia of Genes and Genomes.

expression. Next, we performed the differential analysis in each of the datasets. We screened DEGs by comparing AD tissues to NDHCS tissues in the R computing environment using the limma package (Ritchie et al., 2015). DEGs were determined by $|\text{Log 2 FC}| > 0$, adjusted p-value < 0.05. Volcano plots were generated using ggplot 2 in R. In order to obtain a consensus of DEGs, Venn analysis was performed using Draw Venn Diagram, a Web-based tool,[2] to identify common DEGs from the five datasets. The heatmap of the consensus DEGs was drawn using the R pheatmap package. We performed the batch correction, followed by normalization between arrays to remove the heterogeneity among multiple microarray datasets using sva and limma packages (Leek et al., 2012). Finally, principal component analysis (PCA) was performed to compare the difference of consensus DEGs between AD and NDHCS groups in different brain regions.

GO Enrichment and KEGG Pathway Analysis of the DEGs

GO enrichment analyses were performed in R using the function of clusterProfiler14. Metascape[3] was used to perform the KEGG pathway analysis. Functional and pathway enrichment analyses were conducted separately for upregulated and downregulated genes. In this analysis, a p-value < 0.05 was considered significant for the screening of significant GO terms and KEGG pathways. Furthermore, we performed the differential analysis separately in 10 brain regions. DEGs were determined by $|\text{Log 2 FC}| > 0$, adjusted p-value < 0.05. The top 100 upregulated DEGs and top 100 downregulated DEGs of each brain region were used for GO enrichment analyses. Finally, we take the intersection of pathways of each brain region to identify common and specific dysregulated pathways.

PPI Network Construction, Hub Gene Selection, and Hub Gene Expression in Different Braak Stages of AD

To further explore the interactions among DEGs, PPI network analysis was performed using the online database STRING with an interaction score of 0.4 as the threshold. Next, we utilized Cytoscape (version 3.7.1) to construct and visualize the main regulatory network. We used cytoHubba, a plugin of Cytoscape, to select the hub genes in the PPI network. Five methods (degree, maximum neighborhood component (MNC), radiality centrality, stress centrality, closeness centrality) were used to sequence and evaluate central genes (Chin et al., 2014). The five ranked methods selected the top 20 hub genes. Venn analysis was performed to identify central genes by overlapping the top 20 genes. Finally, we validate hub gene expressions in different Braak stages using the HPC and superior frontal cortex (SPF) samples in the dataset GSE48350. Overall differences between groups were tested with the Kruskal—Wallis (K-W) test, and differences between groups were compared by the Wilcox test. The boxplot was drawn by R package ggplot 2. The top 10 hub genes were also further evaluated based on the difference in the gene expression of GSE48350.

Identification of Potential Biomarkers of AD Using LASSO Logistic Regression

The LASSO, a penalized shrunken regression method, has a strong predictive value and low correlation and is applied to select the best features for high-dimensional data. The samples from five brain tissue datasets were randomly assigned to the

[2]http://bioinformatics.psb.ugent.be/webtools/Venn/

[3]http://metascape.org

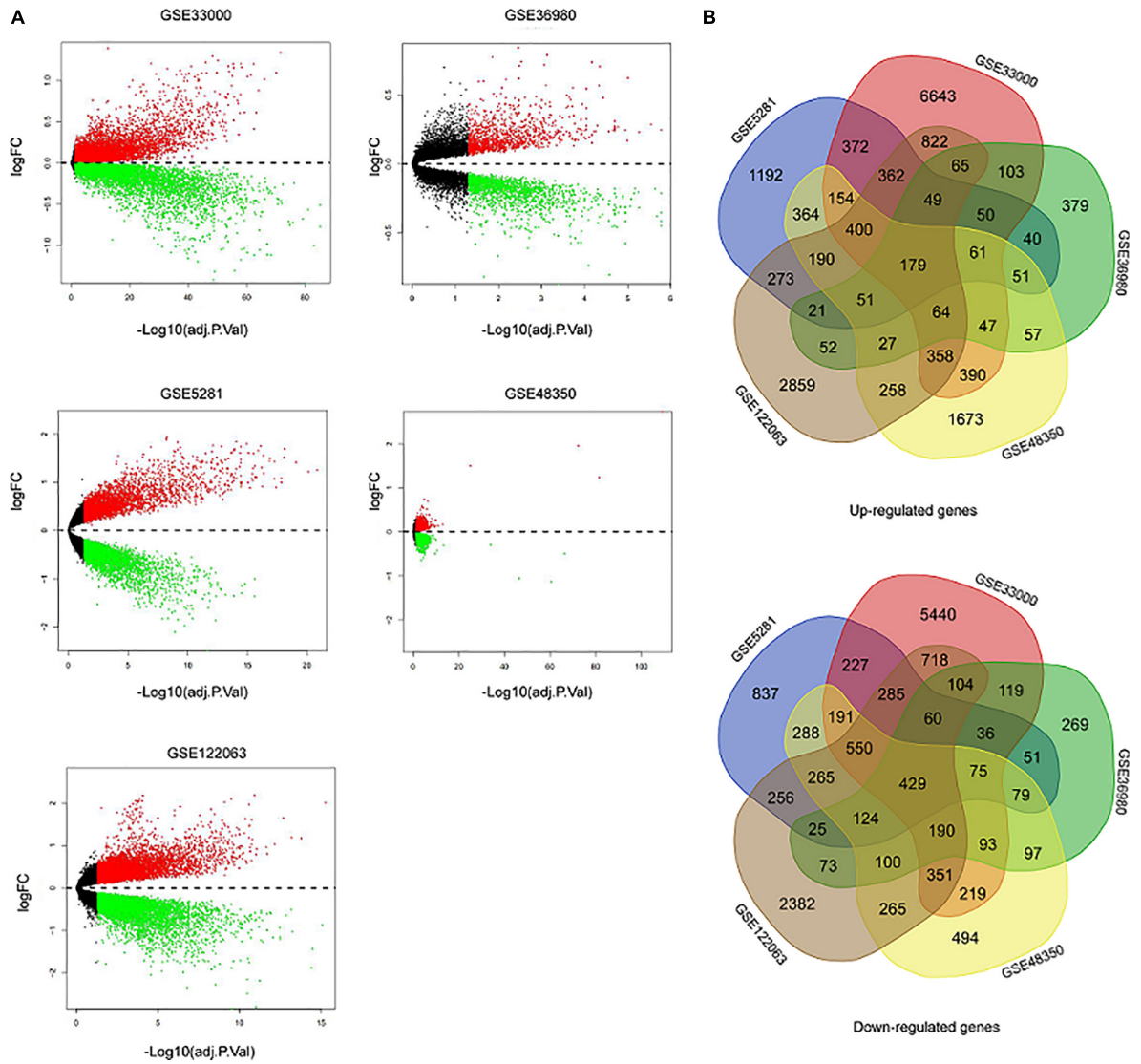

FIGURE 2 | Identification of DEGs between AD and NDHCS samples. **(A)** The volcano plot of the genes in the five datasets. **(B)** Venn diagram analysis of common downregulated DEGs and common upregulated DEGs. AD, Alzheimer's disease; NDHCS, non-demented healthy control subjects.

training set (30%) and validation set (70%). The expression profiles of consensus DEGs were extracted and fit into LASSO logistic regression by the glmnet package. In order to evaluate the ability of the LASSO model to identify AD, receiver operating characteristic (ROC) analysis was completed using the package of pROC in the validation set and combined set (Robin et al., 2011). The area under the curve (AUC) was calculated, and AUC values close to 1 (AUC $>$ 0.7) refer to good classifier models. We also investigated the diagnosis effect of the top 10 hub genes in the combined set.

Evaluate the Diagnosis Model in Peripheral Blood Datasets

As it is hard to obtain brain tissues for diagnosis in clinical practice, we attempted to enroll independent peripheral blood datasets to evaluate the clinical utility of our diagnosis model. We performed ROC analyses in GSE4226 and GSE97760 to examine the ability to differentiate AD from NDHCS. The datasets GSE63060 and GSE63061 were used to verify the accuracy of the model to differentiate MCI and AD from NDHCS. ROC curves were plotted using the "pROC" package.

GSEA and Independent Validation Analysis

GSEA was performed to identify biological process (BP) GO terms of the top 10 hub genes that may be correlated to AD in GSE48350 datasets. We performed GSEA using the R package clusterProfiler for analysis. The c5.bp.v 7.0.symbols.gmt datasets in the MsigDB V 6.2 database[4] were used as reference

[4]http://software.broadinstitute.org/gsea/msigdb/

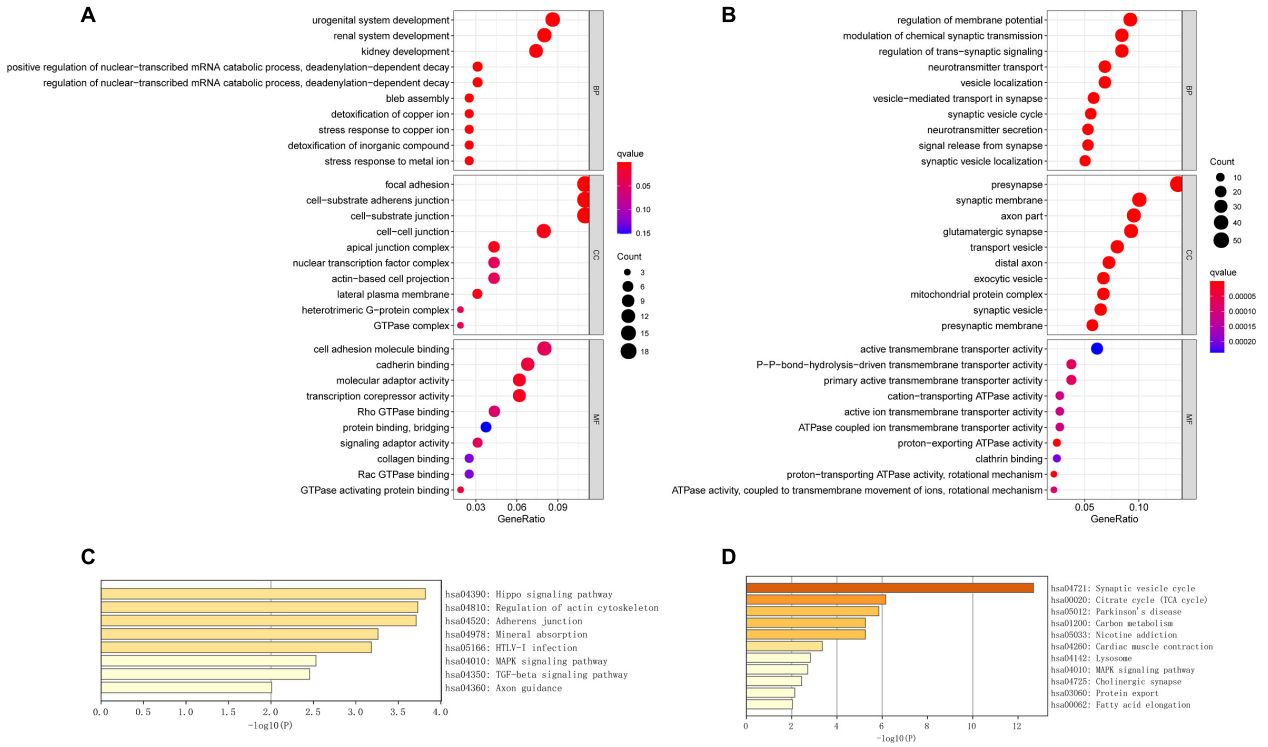

FIGURE 3 | The GO analysis and KEGG pathway analysis of upregulated and downregulated DEGs. **(A)** The GO analysis of common upregulated DEGs. **(B)** The GO analysis of common downregulated DEGs. **(C)** The KEGG pathway analysis of common upregulated DEGs. **(D)** The KEGG pathway analysis of common downregulated DEGs.

gene sets, and those with an adjusted p-value < 0.05 after 1,000 permutations were considered significantly enriched gene sets (Subramanian et al., 2005). We determined the key genes by overlapping the hub genes selected from the PPI network and potential diagnosis genes identified from the LASSO regression model. Next, we enrolled another independent dataset (GSE106241) and compared the expression level of key genes in different Braak stages using the K-W test. Moreover, we investigated their associations with β-secretase activity and Aβ 42 levels in AD samples from GSE106241 using the Spearman correlation analysis. p-values less than 0.05 ($p < 0.05$) were considered significant. The violin plots and correlation analysis in this section were all generated in R 3.6.3.

RESULTS

Identification of Consensus DEGs

Five microarray datasets, including GSE33000, GSE36980, GSE48350, GSE5281, and GSE122063, were downloaded from the National Center of Biotechnology Information-GEO (NCBI-GEO). Details of the five datasets are presented in **Table 1**. A total of 1,060 samples (495 NDHCS subjects and 565 AD patients) were available for DEG analysis, including microarray data from 10 brain regions: the EC, FC, HPC, medial temporal gyrus, PCGY, posterior cingulate, PFC, primary visual cortex, SFC, and TC. After background correction and normalization, we used the limma package to identify DEGs between NDHCS and AD samples of GEO data. Gene difference analysis found that there were 19,206 DEGs in GSE33000, 3,220 DEGs in GSE36980, 8,134 DEGs in GSE48350, 7,587 DEGs in GSE5281, and 12,207 DEGs in GSE122063 compared with AD patients and NDHCS (**Supplementary Table 1**). Volcano plots in **Figure 2A** show the number of DEGs identified from each of the five datasets. Subsequently, we intersected these DEGs from the five datasets and finally identified 608 common DEGs, of which 179 DEGs were upregulated and 429 DEGs were downregulated (**Figure 2B** and **Supplementary Table 1**). To compare the DEGs between the AD and NDHCS groups, the heatmap showed the expression of common DEGs from five datasets (**Supplementary Figure 1**). PCA revealed that the expression of common DEGs differed significantly between NDHCS and AD samples in each brain region, indicating that the DEGs we found were common core genes in AD (**Supplementary Figure 2**).

GO Enrichment and KEGG Pathway Analysis of the DEGs

We performed GO term, KEGG pathway, and functional enrichment analyses to explore the potential biological functions of the common DEGs. The GO annotation results include BP, molecular function (MF), and cellular component (CC). The results revealed that the BP primarily associated

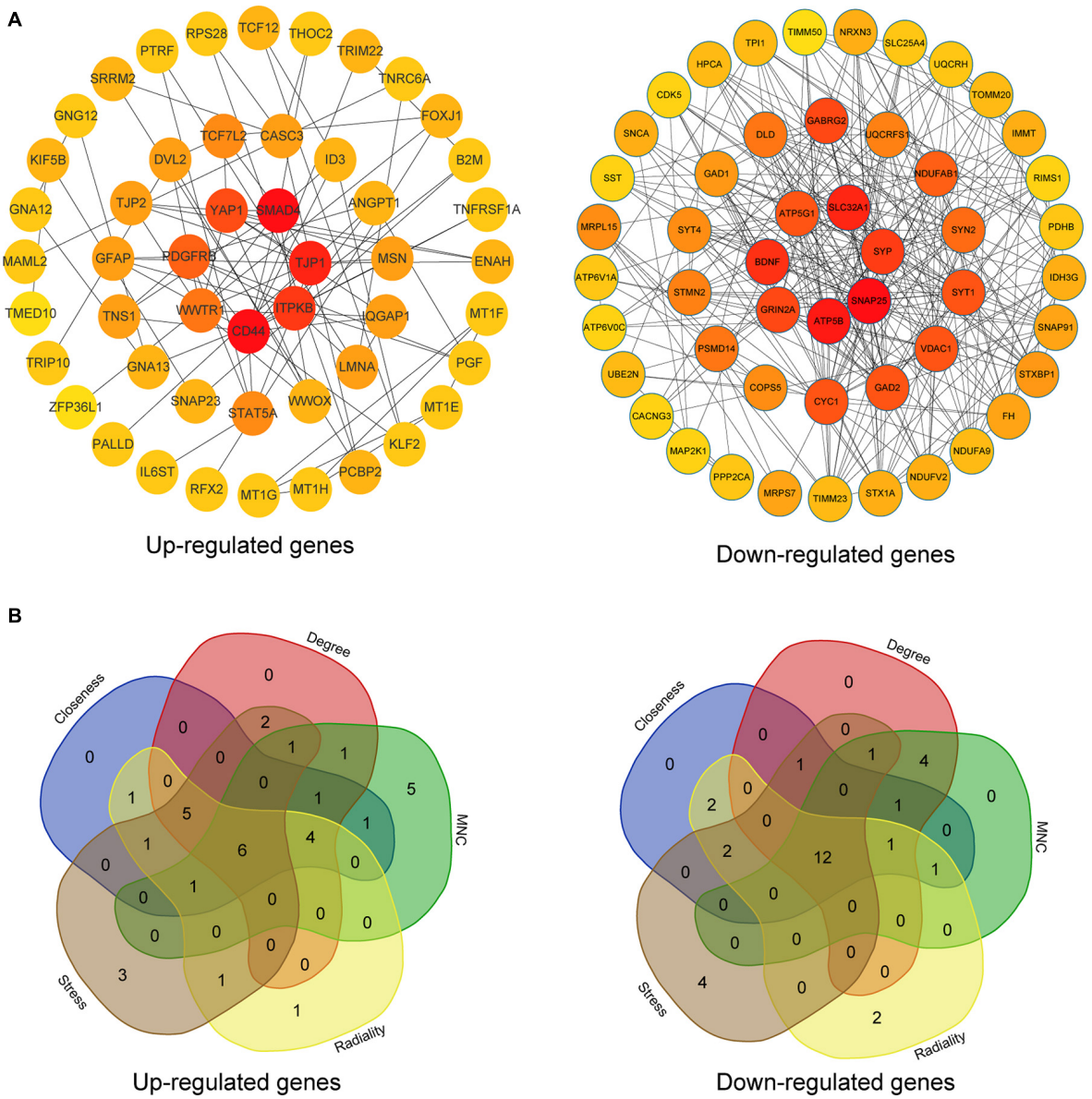

FIGURE 4 | PPI network and hub gene selection. **(A)** The top 50 hub genes in the PPI network of the upregulated and downregulated DEGs according to node degree. **(B)** Hub genes were identified by overlapping the first 20 genes in the five classification methods of cytoHubba.

with the upregulated genes, including the regulation of the nuclear-transcribed mRNA catabolic process, bleb assembly, detoxification of copper ion, stress response to copper ion, detoxification of inorganic compound, and stress response to metal ion. For CC enrichment analysis, the results showed that upregulated genes significantly took part in the focal adhesion, cell—substrate adherens junction, cell—substrate junction, and cell—cell junction. For MF analysis, upregulated genes are mainly enriched in cell adhesion molecule binding, cadherin binding, molecular adaptor activity, and transcription corepressor activity (**Figure 3A**). For downregulated genes, regulation of membrane potential, modulation of chemical synaptic transmission, regulation of transsynaptic signaling, and neurotransmitter transport were dominant BPs. For CC enrichment analysis, downregulated genes mainly take part in presynapse, synaptic membrane, axon part, and glutamatergic synapse. In the enrichment analysis of MF, the downregulated genes mainly revolved in active transmembrane transporter activity, P—P-bond-hydrolysis-driven transmembrane transporter activity, and primary active transmembrane transporter activity (**Figure 3B**). The KEGG pathway analysis showed that the upregulated genes were significantly enriched in the Hippo signaling pathway, regulation of actin cytoskeleton, adherens junction, mineral absorption, MAPK signaling pathway, and TGF-beta signaling pathway, while the downregulated DEGs were mainly enriched in the synaptic vesicle cycle, citrate cycle (TCA cycle), Parkinson's

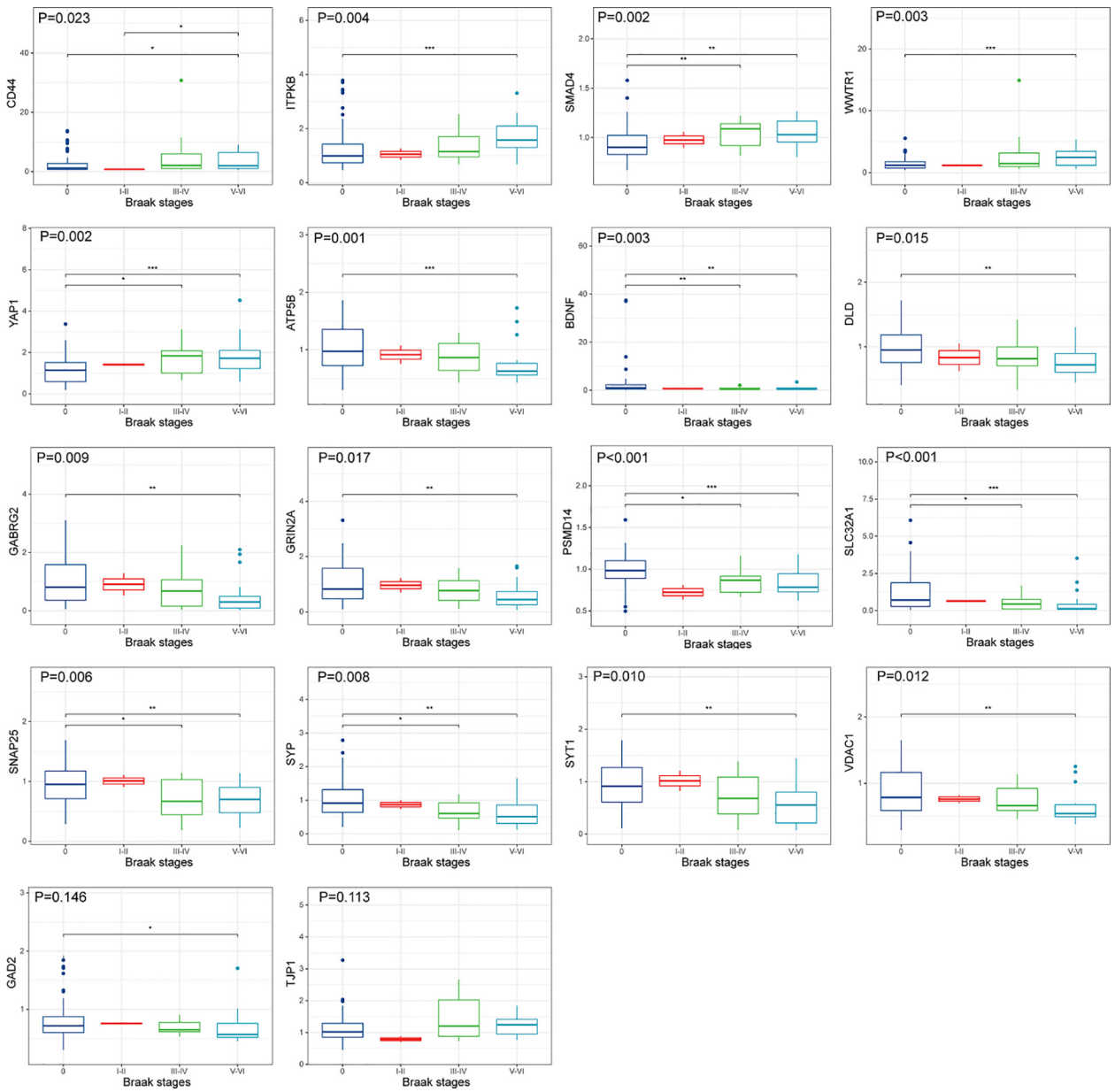

FIGURE 5 | Hub gene expression in different Braak stages of AD. The upper, middle, and lower horizontal lines of the box represent the upper, median, and lower quartiles, respectively. Overall differences between groups were tested with the K-W test. Asterisks indicate significant vs. Braak 0 groups; $*p < 0.05$; $**p < 0.01$; $***p < 0.001$ (dataset GSE48350; $n = 91$ for NDHCS; $n = 2$ for Braak stages I and II; $n = 15$ for Braak stages III and IV; $n = 21$ for Braak stages V and VI). AD, Alzheimer's disease; NDHCS, non-demented healthy control subjects; HPC, hippocampus; PFC, prefrontal cortex.

disease, lysosome, MAPK signaling pathway, and cholinergic synapse. The KEGG pathway enrichment analysis results are illustrated in **Figures 3C,D**. The complete results of GO and KEGG analyses can be found in **Supplementary Table 2**.

Specific Dysregulated Pathways for Each Brain Region

We performed GO enrichment analyses using the top 100 upregulated DEGs and top 100 downregulated DEGs of each brain region. Then we identified the specific dysregulated pathways of each brain region. There were two specific pathways in the EC and the PCGY, 20 pathways in the FC, 12 pathways in the HPC, 145 pathways in the medial temporal gyrus, 38 pathways in the posterior cingulate, 47 pathways in the primary visual cortex, four pathways in the TC, and 58 pathways in the PFC (**Supplementary Table 2**). There was no specific pathway in the SFC. The HPC was associated with the neuron projection organization. The medial temporal gyrus was associated with neuron projection maintenance, neurotransmitter receptor

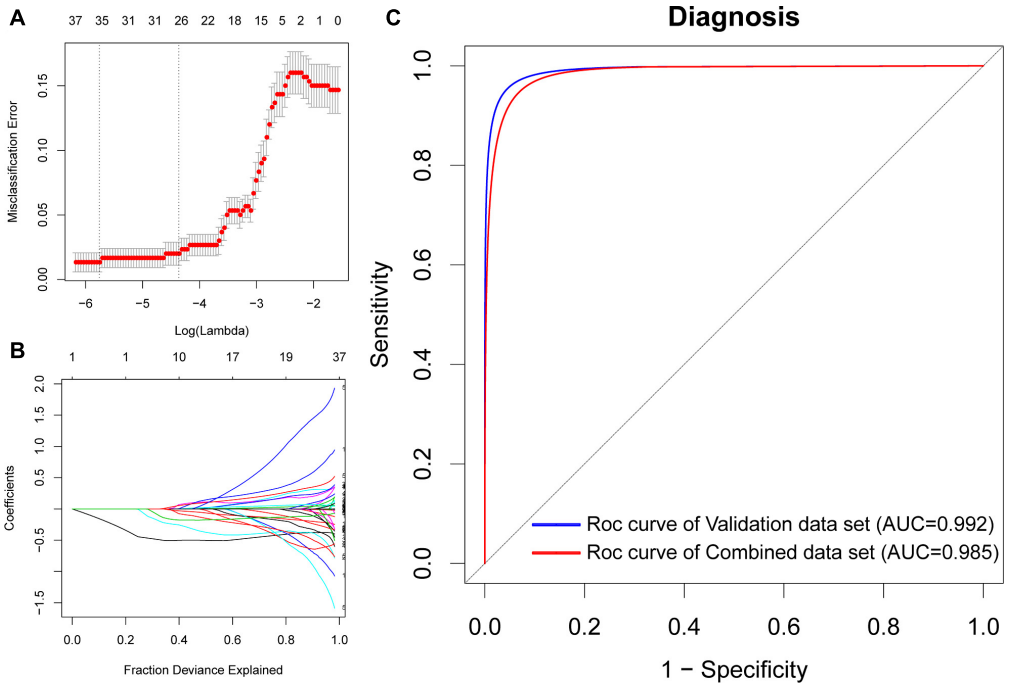

FIGURE 6 | Gene selection through the LASSO model. **(A)** Tenfold cross-validation for tuning parameter (lambda) selection in the LASSO regression model. The vertical lines were drawn at the optimal values by the minimum criteria and the 1 – SE criteria. **(B)** The LASSO coefficient profiles of the 608 DEGs. **(C)** ROC curve analysis of the validation dataset and combined dataset.

transport to the plasma membrane, neurotransmitter receptor transport to the postsynaptic membrane, and response to Aβ. The dysregulated genes in the posterior cingulate were significantly enriched in pathways, including the branching morphogenesis of a nerve, glutamate metabolic process, positive regulation of synaptic transmission, and glutamatergic pathway. In the primary visual cortex, the dysregulated genes were involved in neuromuscular synaptic transmission, neuroinflammatory response, and cell aging. The neurotransmitter reuptake was associated with TC. Peripheral nervous system development and nerve development were significantly enriched pathways in PFC.

PPI Network Construction, Hub Gene Selection, and Hub Gene Expression in Different Braak Stages of AD

The upregulated and downregulated DEGs were uploaded into the online tool STRING[5] to gain PPI information separately. Based on the degree of connectivity, we constructed the PPI network and selected the top 50 hub genes, and the result was visualized by Cytoscape (**Figure 4A**). Next, we used cytoHubba to choose hub genes. According to the five classification methods in cytoHubba, we selected the top 20 hub genes, as shown in **Supplementary Table 3**. Finally, six upregulated and 12 downregulated central genes were identified by overlapping the first 20 genes (**Figure 4B** and **Supplementary Table 3**). Then, we used samples in the dataset GSE48350 to explore whether the expression levels of these central genes varied in different Braak stages in the HPC and SPF (**Supplementary Table 4**). We found that five hub genes were upregulated and 11 hub genes were downregulated as AD progressed ($p < 0.05$). Predominantly, SMAD 4 and YAP 1 were significantly upregulated in Braak III and IV and Braak V and VI compared with Braak 0. Brain-derived neurotrophic factor (BDNF), PSMD14, SLC32A1, SNAP25, and SYP were identified to be downregulated in Braak III and IV and Braak V and VI compared with Braak 0 (**Figure 5**).

Identification of Potential Biomarkers of AD Using LASSO Logistic Regression

To identify potential biomarkers for AD, we extracted the expression profile of the DEGs and fit them into LASSO logistic regression. We separated all samples (565 AD samples and 495 NDHCS) into training and validation cohorts (**Supplementary Table 5**). Thirty-five potential predictors in the training cohort were identified and were features with nonzero coefficients in the LASSO logistic regression model (**Figures 6A,B** and **Table 2**). Next, we evaluated the ability of the LASSO regression model in differentiating between AD and NDHCS, suggesting that the AUC of the 35-gene-based model was 0.992 in the validation set and 0.985 in the combined set (**Figure 6C**). The results indicate that our 35-gene-based diagnosis model can correctly classify AD samples and NDHCS in brain tissues. The diagnosis effect of the top 10 hub genes was also investigated and presented in **Supplementary Figure 3**. Only BDNF had the ability to differentiate AD from NDHCS (AUC = 0.703).

[5]http://string-db.org

TABLE 2 | The list of 35 potential biomarkers of AD using LASSO logistic regression.

UniProt ID	Protein name	Gene name
P21291	Cysteine- and glycine-rich protein 1	CSRP1
Q01628	Interferon-induced transmembrane protein 3	IFITM3
P13640	Metallothionein–1 G	MT1G
P04732	Metallothionein–I E	MT1E
Q9Y2D9	Zinc finger protein 652	ZNF652
Q7Z3K3	Pogo transposable element with ZNF domain	POGZ
Q9GZV5	WW domain-containing transcription regulator protein 1	WWTR1
Q9NZH0	G-protein-coupled receptor family C group 5 member B	GPRC5B
P23949	mRNA decay activator protein ZFP36L2	ZFP36L2
Q9BX66	Sorbin and SH3 domain-containing protein 1	SORBS1
Q8N8S7	Protein enabled homolog	ENAH
Q68DX3	FERM and PDZ domain-containing protein 2	FRMPD2
P61278	Somatostatin	SST
P23560	Brain-derived neurotrophic factor	BDNF
Q8N4V2	Synaptic vesicle 2-related protein	SVOP
Q8N967	Leucine-rich repeat and transmembrane domain-containing protein 2	LRTM2
Q99259	Glutamate decarboxylase 1	GAD1
Q16566	Calcium/calmodulin-dependent protein kinase type IV	CAMK4
O95206	Protocadherin-8	PCDH8
P61088	Ubiquitin-conjugating enzyme E2 N	UBE2N
O43768	Alpha-endosulfine	ENSA
Q9UIL1	Short coiled-coil protein	SCOC
Q13530	Serine incorporator 3	SERINC3
Q9Y5V3	Melanoma-associated antigen D 1	MAGED1
Q96F83	Clathrin-binding box of aftiphilin-containing protein 1	C14orf79
P80723	Brain acid soluble protein 1	BASP1
Q15904	V-type proton ATPase subunit S1, V-ATPase subunit S 1	ATP6AP1
O95197	Reticulon-3	RTN3
Q96CW1	AP-2 complex subunit mu	AP2M1
P17643	5,6-Dihydroxyindole-2-carboxylic acid oxidase	TYRP1
P50613	Cyclin-dependent kinase 7	CDK7
Q8N100	Protein atonal homolog 7	ATOH7
Q9Y6G3	39S ribosomal protein L 42, mitochondrial, L 42 mt, MRP-L 42	MRPL42
O00744	Protein Wnt-10 b	WNT10B
P84074	Neuron-specific calcium-binding protein hippocalcin	HPCA

Evaluation of the Diagnosis Model in Peripheral Blood Datasets

To further discover whether this model is worth using in clinical practice, we test our diagnosis model on four independent peripheral blood datasets (**Supplementary Table 5**). In the GSE4226, composed of peripheral blood mononuclear cells, only 16 genes of the 35-gene-based model were covered. The ROC analysis was also conducted based on the 16 genes, and the AUC was 0.871 (**Figure 7A**). We applied the 35-gene-based model to GSE97760, which included patients with advanced AD and NDHCS and showed the perfect discrimination ability (**Figure 7B**, AUC = 1.000). We also found that our diagnosis model had the ability to differentiate MCI and AD from NDHCS in the blood datasets. In GSE63060 (30 genes of the 35-gene-based model were covered), the AUC for differentiating MCI and NDHCS is 0.922, and the AUC for AD and NDHCS is 0.837 (**Figure 7C**). In GSE63061 (28 genes of the 35-gene-based model were covered), AUC for MCI and NDHCS is 0.763, and AUC for AD and NDHCS is 0.802 (**Figure 7D**). Conclusively, the results indicate that our 35-gene-based diagnosis model can classify AD and MCI from NDHCS in peripheral blood.

GSEA and Independent Validation Analysis

To gain new insights into the biological functions of the top 10 genes, we performed GSEA to identify the potential BPs between AD and NDHCS subjects. As indicated in **Figures 8A,B**, the BDNF was associated with cognition, HPC development, neuron death, regulation of neuronal synaptic plasticity, regulation of neurotransmitter levels, and transport. BPs such as neuroblast proliferation, neuroepithelial cell differentiation, neurotransmitter biosynthetic process and metabolic process, neuroinflammatory response, and regulation of neuroinflammatory response were associated with WW domain-containing transcription regulator protein 1 (WWTR1). The rest of the top 10 hub genes were also involved in several neuron-related pathways, including axon development (SMAD4, SLC32A1, and YAP1), neuron death (SNAP25 and ATP5B), and synapse organization (SMAD4 and SLC32A1). The results are shown in **Supplementary Figure 4**.

BDNF and WWTR1 were identified as key genes by overlapping the 18 hub genes in the PPI network and 35 potential predictors selected from the LASSO regression model. To confirm the result, we enrolled another independent dataset (GSE106241) to conduct validation analysis (**Supplementary Table 5**). As shown in **Figures 8C,D**, BDNF and WWTR1 showed significant differences among the different Braak stages (p = 0.001 and 0.041, respectively). Moreover, we found that BDNF was negatively associated with Aβ 42 levels and β-secretase activity (R = –0.35 and R = –0.42, respectively, **Figures 8E,F**). WWTR1 was positively associated with Aβ 42 levels and β-secretase activity (R = 0.36 and R = 0.61, respectively, **Figures 8G,H**). This result further proves that the two genes are essential and involved in the pathology of AD.

DISCUSSION

Bioinformatics analysis has developed rapidly and applied to many diseases in recent decades, revealing the complex pathogenesis and identifying new biomarkers for diagnosis and treatment (Ali et al., 2018). Nevertheless, integrated bioinformatics analysis has not yet been systematically used in AD. Previous researches were usually based on single datasets and few samples that may weaken the credibility of the results. However, our current study has recruited five open public datasets for DEGs to significantly improve the number of samples

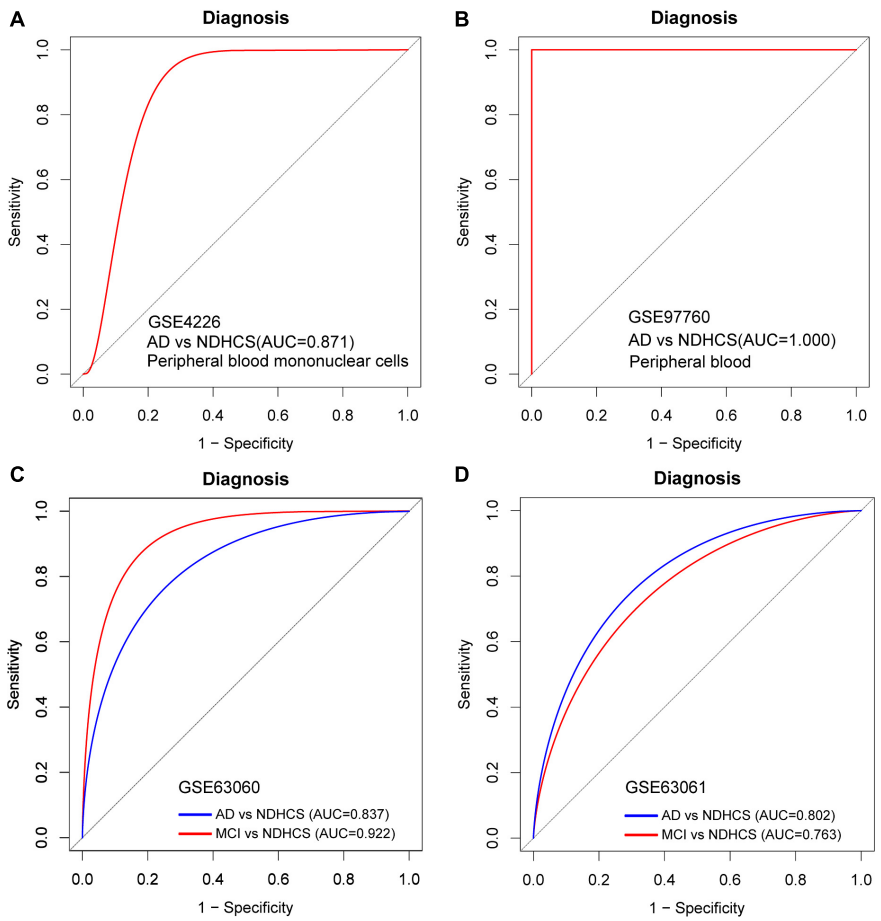

FIGURE 7 | ROC curve analysis in blood datasets. **(A)** ROC curves of peripheral blood mononuclear cell data from GSE4226. **(B)** ROC curves of peripheral blood data from GSE97760. **(C)** ROC curve analysis of GSE63060. **(D)** ROC curve analysis of GSE63061. AD, Alzheimer's disease; MCI, mild cognitive impairment; NDHCS, non-demented healthy control subjects; AUC, area under the curve.

(495 NDHCS vs. 656 AD samples). Thus, our study provides more credible and trustworthy results. We performed a series of integrative analyses based on DEGs, including GO and KEGG enrichment analyses, a constructed PPI network, LASSO logistic regression, and GSEA. In this way, we provide valuable clues for investigating the molecular mechanisms underlying the initiation and development of AD.

The KEGG pathway enrichment analysis showed significant enrichment in pathways including the Hippo signaling pathway, the TGF-beta signaling pathway, the MAPK signaling pathway, the synaptic vesicle cycle, lysosome, and the cholinergic synapse. A recent study confirmed that the Hippo pathway is associated with the pathogenesis of AD. The precursor of Aβ can promote the nuclear translocation of FOXO 3a by inducing MST1-dependent phosphorylation of Foxo 3a. The MST-Foxo pathway, which is considered a branch of the Hippo pathway, activates a proapoptotic member of the Bcl-2 family and triggers an intrinsic apoptotic pathway, resulting in neuronal death (Wang and Wang, 2016). Regarding the TGF-beta signaling pathway, previous studies showed that the expression of TGF-β 1 and TGF-β 2 increased in the brains of patients with AD (Zetterberg et al., 2004). Given the current evidence of microglial dysfunction in neurodegeneration, we speculate that changes in brain TGF-β signaling in AD could alter microglial state and trigger their pathogenic functions (Salter and Stevens, 2017). It is well documented that lysosomal dysfunction is a prominent feature in AD brains, resulting in a failure to clear accumulated protein aggregates and contributes to the process of the pathogenesis of AD (Fraldi et al., 2016). Similarly, the MAPK signal pathways are activated in vulnerable brain regions of AD patients and are involved in the progress of AD (Zhu et al., 2002; Guillot et al., 2016). Therefore, the MAPKs have been proposed as therapeutic targets for AD. Previous studies also confirm that cholinergic transmission impairments are correlated with the neuropathological stage of AD (Amberla et al., 1993). A decrease in the cholinergic activity and disruption of synaptic function contribute to memory impairment (Sayer et al., 2004). Furthermore, the GO analysis indicated that the DEGs are involved in a wide range of BPs and have different MFs. We also found several specific dysregulated pathways in each brain region. Our results indicated that the changes in BPs, CCs, MFs,

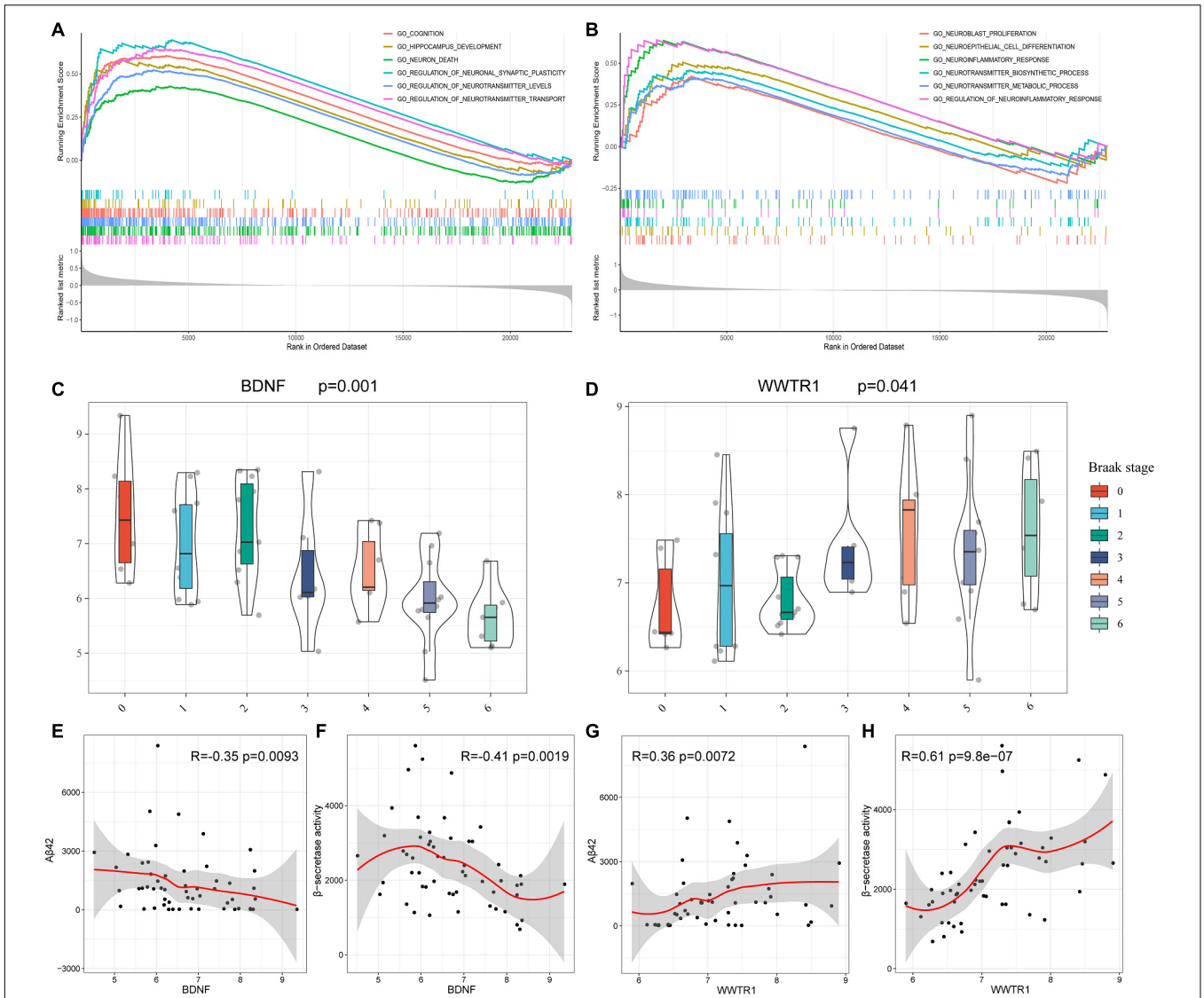

FIGURE 8 | GSEA based on GSE48350 and independent validation analysis based on GSE106241. **(A)** BDNF. **(B)** WWTR1. **(C)** BDNF expression levels in the Braak stages 0–6. **(D)** WWTR1 expression levels in Braak stages 0–6. **(E)** Correlation between BDNF and Aβ 42 levels. **(F)** Correlation between BDNF and β-secretase activity. **(G)** Correlation between WWTR1 and Aβ 42 levels. **(H)** Correlation between WWTR1 and β-secretase activity. *p*-values < 0.05 were considered to be statistically significant.

and pathways might play critically important roles in the pathogenesis of AD.

We identified 18 hub genes by overlapping five sequencing methods in cytoHubba, of which 16 hub genes were significantly dysregulated as AD progressed. Some of these genes have been previously reported to be associated with AD. For example, the reduction of SNAP25 causes postsynaptic loss and learning and memory impairment (Ren et al., 2018). A recent study has demonstrated that SNAP25 is an effective biomarker for predicting AD 5–7 years before cognitive impairment (Jia et al., 2020). SYP can affect the synaptic structure and neurotransmitter release to regulate synaptic plasticity (Zhu et al., 2019). The dysfunction of ATP5B is associated with neurofibrillary tangle burden in the AD brain and with cognition (Wang et al., 2017). The decrease of BDNF correlates with the neuropathological stage of AD (Laske et al., 2006). Further studies are required to investigate their features, functions, and mechanisms.

In the present study, we constructed a 35 gene-based LASSO model, which can accurately predict AD in both validation and combined brain tissue datasets. Among the 35 genes, previous studies have reported that the expressions of IFITM3 (Correani et al., 2017), SORBS1 (Blalock et al., 2004), ENAH (de Oliveira-Júnior et al., 2015), SST (Solarski et al., 2018), ENSA (Boettcher et al., 2008), C14orf40 (Chung et al., 2018), BASP1 (Zhou et al., 2020), RTN3 (Zou et al., 2018), CDK7 (Zhu et al., 2000), and HPCA (Jiang et al., 2016) were associated with AD or have functions in neural tissue, indicating possible therapeutic targets. For example, IFITM3 is a reliable biomarker of the inflammatory

microglial phenotype in AD damaged tissues (Correani et al., 2017), and the expression of SORBS1 is higher, while the expression of ENSA is lower in the brain of patients with AD (Blalock et al., 2004; Boettcher et al., 2008). SST interferes with Aβ fibrillization and promotes the formation of Aβ assemblies (Solarski et al., 2018). However, the molecular mechanism of these 35 genes contributing to AD pathogenesis is still poorly understood, and further exploration of potential mechanisms may be valuable.

To assess and confirm its clinical application value, we validated our gene signature on peripheral blood. According to ROC curves, the 35-gene-based model is able to distinguish MCI and AD samples from NDHCS samples in the blood. Especially in GSE97760, the model shows the perfect ability to select advanced AD patients (AUC = 1.000). Our results indicate that this diagnosis model could be beneficial for clinical applications. It is known that the blood—brain barrier (BBB) controls substance exchange strictly between the brain and blood. However, studies indicate that the breakdown of BBB could enhance the movement of proteins between the brain and blood in either direction (Zipser et al., 2007). Thus, some proteins in the blood might be associated with AD pathology. Recent studies have also adopted the strategy to integrate brain and blood datasets to identify potential AD biomarkers (Yao et al., 2018; Zhu et al., 2020). Our results shed new light on diagnosis biomarker identification. Further large-sample studies with a different analysis in the blood are required to confirm our results.

This study detected two key genes, BDNF and WWTR1, as potential biomarkers for clinical diagnosis and therapeutic monitoring in AD. Both of them have been identified as hub genes in the PPI network and varied significantly in the different neuropathological stages of AD. They were also selected as potential diagnostic biomarkers from LASSO logistic regression. GSEA suggests that the BDNF and WWTR1 could function as key players in a broad array of essential signaling pathways. Moreover, an independent validation showed that BDNF and WWTR1 are associated with the Braak stage, Aβ 42 levels, and β-secretase activity.

BDNF, located on chromosome 11 p 14, is reported to play an essential role in regulating neurodevelopment, promoting neuronal survival, and supporting basal forebrain cholinergic projections to the HPC and neocortex (Marmigère et al., 2003; Huang et al., 2007). Previous studies indicate that BDNF depletion led to an increase in cortical amyloid plaque numbers and size (Braun et al., 2017). It has also been reported that the expression of BDNF decreased in the brain tissue of patients with AD (Connor and Dragunow, 1998; Fields et al., 2014). This is consistent with our results that BDNF is negatively correlated with the Braak stage, and GSEA suggested that it is involved in HPC development, cognition, neuron death, and neurotransmitter regulation. Thus, the downregulation of BDNF may play a crucial role in the pathogenesis of AD. WWTR1 is another potential diagnosis biomarker and may contribute to the development of AD. Functional enrichment analysis showed that WWTR1 was significantly involved in the neuroinflammatory response and neurotransmitter biosynthetic and metabolic pathways. Previous research indicates that WWTR1 is playing a crucial role in the Hippo and TGF-beta pathways, which is associated with the progress of AD (Lei et al., 2008; Deiana et al., 2018). However, the mechanisms of WWTR1 and AD remain undefined. More research is needed to elucidate the functions and underlying mechanisms of WWTR1 and AD. Although we enrolled an additional dataset for external validation, high-quality validation experiments are still required to prove the value of BDNF and WWTR1 in AD pathology.

CONCLUSION

In conclusion, we identified 608 consensus DEGs, several dysregulated pathways, and 16 hub genes associated with AD progress by a series of bioinformatics analyses. The diagnostic model of 35 genes was constructed, which has a high AUC value in not only brain tissue but also peripheral blood. BDNF and WWTR1 were identified as candidate genes for future molecular studies. Our current study deepens our understanding of underlying molecular mechanisms in AD and provides new potential diagnostic and therapeutic biomarkers.

DATA AVAILABILITY STATEMENT

The datasets generated for this study can be found in the online repositories. The names of the repository/repositories and accession number(s) can be found in the article/Supplementary Material.

AUTHOR CONTRIBUTIONS

WuY and YL designed the study. WuY, WeY, and YY performed the statistical analysis and wrote the manuscript. All authors reviewed the manuscript and gave the final approval for publication.

SUPPLEMENTARY MATERIAL

The Supplementary Material for this article can be found online at: https://www.frontiersin.org/articles/10.3389/fnagi.2021.602781/full#supplementary-material

REFERENCES

Ali, A., Junaid, M., Khan, A., Kasushik, A. C., and Wei, D. Q. (2018). Identification of novel therapeutic targets in myelodysplastic syndrome using protein-protein interaction approach and neural networks. *J. Comput. Sci. Syst. Biol.* 11:2. doi: 10.4172/jcsb.1000270

Amberla, K., Nordberg, A., Viitanen, M., and Winblad, B. (1993). Long-term treatment with tacrine (THA) in Alzheimer's disease–evaluation of

neuropsychological data. *Acta Neurol. Scand. Suppl.* 149, 55–57. doi: 10.1111/j.1600-0404.1993.tb04257.x

Banwait, J. K., and Bastola, D. R. (2015). Contribution of bioinformatics prediction in microRNA-based cancer therapeutics. *Adv. Drug Deliv. Rev.* 81, 94–103. doi: 10.1016/j.addr.2014.10.030

Blalock, E. M., Geddes, J. W., Chen, K. C., Porter, N. M., Markesbery, W. R., and Landfield, P. W. (2004). Incipient Alzheimer's disease: microarray correlation analyses reveal major transcriptional and tumor suppressor responses. *Proc. Natl. Acad. Sci. U.S.A.* 101, 2173–2178. doi: 10.1073/pnas.0308512100

Boettcher, J. M., Hartman, K. L., Ladror, D. T., Qi, Z., Woods, W. S., George, J. M., et al. (2008). Membrane-induced folding of the cAMP-regulated phosphoprotein endosulfine-alpha. *Biochemistry* 47, 12357–12364. doi: 10.1021/bi801450t

Braun, D. J., Kalinin, S., and Feinstein, D. L. (2017). Conditional depletion of hippocampal brain-derived neurotrophic factor exacerbates neuropathology in a mouse model of Alzheimer's disease. *ASN Neuro* 9:1759091417696161.

Chin, C. H., Chen, S. H., Wu, H. H., Ho, C. W., Ko, M. T., and Lin, C. Y. (2014). cytoHubba: identifying hub objects and sub-networks from complex interactome. *BMC Syst. Biol.* 8(Suppl. 4):S11. doi: 10.1186/1752-0509-8-S4-S11

Chung, J., Wang, X., Maruyama, T., Ma, Y., Zhang, X., Mez, J., et al. (2018). Genome-wide association study of Alzheimer's disease endophenotypes at prediagnosis stages. *Alzheimers Dement.* 14, 623–633. doi: 10.1016/j.jalz.2017.11.006

Connor, B., and Dragunow, M. (1998). The role of neuronal growth factors in neurodegenerative disorders of the human brain. *Brain Res. Brain Res. Rev.* 27, 1–39. doi: 10.1016/s0165-0173(98)00004-6

Correani, V., Di Francesco, L., Mignogna, G., Fabrizi, C., Leone, S., Giorgi, A., et al. (2017). Plasma membrane protein profiling in beta-amyloid-treated microglia cell line. *Proteomics* 17:1600439. doi: 10.1002/pmic.201600439

de Oliveira-Júnior, L. C., Araújo Santos Fde, A., Goulart, L. R., and Ueira-Vieira, C. (2015). Epitope fingerprinting for recognition of the polyclonal serum autoantibodies of Alzheimer's disease. *Biomed. Res. Int.* 2015:267989.

Deiana, M., Dalle Carbonare, L., Serena, M., Cheri, S., Parolini, F., Gandini, A., et al. (2018). New insights into the runt domain of RUNX2 in melanoma cell proliferation and migration. *Cells* 7:220. doi: 10.3390/cells7110220

Fields, J., Dumaop, W., Langford, T. D., Rockenstein, E., and Masliah, E. (2014). Role of neurotrophic factor alterations in the neurodegenerative process in HIV associated neurocognitive disorders. *J. Neuroimmune Pharmacol.* 9, 102–116. doi: 10.1007/s11481-013-9520-2

Fraldi, A., Klein, A. D., Medina, D. L., and Settembre, C. (2016). Brain disorders due to lysosomal dysfunction. *Annu. Rev. Neurosci.* 39, 277–295. doi: 10.1146/annurev-neuro-070815-014031

Guillot, F., Kemppainen, S., Lavasseur, G., Miettinen, P. O., Laroche, S., Tanila, H., et al. (2016). Brain-specific basal and novelty-induced alternations in PI3K-Akt and MAPK/ERK signaling in a middle-aged AβPP/PS1 mouse model of Alzheimer's disease. *J. Alzheimers Dis.* 51, 1157–1173. doi: 10.3233/jad-150926

Hokama, M., Oka, S., Leon, J., Ninomiya, T., Honda, H., Sasaki, K., et al. (2014). Altered expression of diabetes-related genes in Alzheimer's disease brains: the Hisayama study. *Cereb. Cortex* 24, 2476–2488. doi: 10.1093/cercor/bht101

Huang, R., Huang, J., Cathcart, H., Smith, S., and Poduslo, S. E. (2007). Genetic variants in brain-derived neurotrophic factor associated with Alzheimer's disease. *J. Med. Genet.* 44:e66. doi: 10.1136/jmg.2006.044883

Huang, Y., and Mucke, L. (2012). Alzheimer mechanisms and therapeutic strategies. *Cell* 148, 1204–1222. doi: 10.1016/j.cell.2012.02.040

Jia, L., Zhu, M., Kong, C., Pang, Y., Zhang, H., Qiu, Q., et al. (2020). Blood neuro-exosomal synaptic proteins predict Alzheimer's disease at the asymptomatic stage. *Alzheimers Dement.* 17, 49–60. doi: 10.1002/alz.12166

Jiang, S., Tang, L., Zhao, N., Yang, W., Qiu, Y., and Chen, H. Z. A. (2016). Systems view of the differences between APOE ε4 carriers and non-carriers in Alzheimer's disease. *Front. Aging Neurosci.* 8:171. doi: 10.3389/fnagi.2016.00171

Khan, A., Ali, A., Junaid, M., Liu, C., Kaushik, A. C., Cho, W. C. S., et al. (2018). Identification of novel drug targets for diamond-blackfan anemia based on RPS19 gene mutation using protein-protein interaction network. *BMC Syst. Biol.* 12(Suppl. 4):39. doi: 10.1186/s12918-018-0563-0

Kumar, A., Singh, A., and Ekavali. (2015). A review on Alzheimer's disease pathophysiology and its management: an update. *Pharmacol. Rep.* 67, 195–203. doi: 10.1016/j.pharep.2014.09.004

Laske, C., Stransky, E., Leyhe, T., Eschweiler, G. W., Wittorf, A., Richartz, E., et al. (2006). Stage-dependent BDNF serum concentrations in Alzheimer's disease. *J. Neural Trans.* 113, 1217–1224. doi: 10.1007/s00702-005-0397-y

Leek, J. T., Johnson, W. E., Parker, H. S., Jaffe, A. E., and Storey, J. D. (2012). The sva package for removing batch effects and other unwanted variation in high-throughput experiments. *Bioinformatics* 28, 882–883. doi: 10.1093/bioinformatics/bts034

Lei, Q. Y., Zhang, H., Zhao, B., Zha, Z. Y., Bai, F., Pei, X. H., et al. (2008). TAZ promotes cell proliferation and epithelial-mesenchymal transition and is inhibited by the hippo pathway. *Mol. Cell Biol.* 28, 2426–2436. doi: 10.1128/mcb.01874-07

Marmigère, F., Givalois, L., Rage, F., Arancibia, S., and Tapia-Arancibia, L. (2003). Rapid induction of BDNF expression in the hippocampus during immobilization stress challenge in adult rats. *Hippocampus* 13, 646–655. doi: 10.1002/hipo.10109

McKhann, G. M., Knopman, D. S., Chertkow, H., Hyman, B. T., Jack, C. R. Jr., Kawas, C. H., et al. (2011). The diagnosis of dementia due to Alzheimer's disease: recommendations from the National Institute on Aging-Alzheimer's Association workgroups on diagnostic guidelines for Alzheimer's disease. *Alzheimers Dement.* 7, 263–269.

Pineda, S., Real, F. X., Kogevinas, M., Carrato, A., Chanock, S. J., Malats, N., et al. (2015). Integration analysis of three omics data using penalized regression methods: an application to bladder cancer. *PLoS Genet.* 11:e1005689. doi: 10.1371/journal.pgen.1005689

Prince, M., Bryce, R., Albanese, E., Wimo, A., Ribeiro, W., and Ferri, C. P. (2013). The global prevalence of dementia: a systematic review and metaanalysis. *Alzheimers Dement.* 9, 63–75.e2.

Querfurth, H. W., and LaFerla, F. M. (2010). Alzheimer's disease. *N. Engl. J. Med.* 362, 329–344. doi: 10.1056/NEJMra0909142

Ren, Z., Yu, J., Wu, Z., Si, W., Li, X., Liu, Y., et al. (2018). MicroRNA-210-5p contributes to cognitive impairment in early vascular dementia rat model through targeting snap25. *Front. Mol. Neurosci.* 11:388. doi: 10.3389/fnmol.2018.00388

Ritchie, M. E., Phipson, B., Wu, D., Hu, Y., Law, C. W., Shi, W., et al. (2015). limma powers differential expression analyses for RNA-sequencing and microarray studies. *Nucleic Acids Res* 43:e47. doi: 10.1093/nar/gkv007

Robin, X., Turck, N., Hainard, A., Tiberti, N., Lisacek, F., Sanchez, J. C., et al. (2011). pROC: an open-source package for R and S+ to analyze and compare ROC curves. *BMC Bioinform.* 12:77. doi: 10.1186/1471-2105-12-77

Rogaev, E. I., Sherrington, R., Rogaeva, E. A., Levesque, G., Ikeda, M., Liang, Y., et al. (1995). Familial Alzheimer's disease in kindreds with missense mutations in a gene on chromosome 1 related to the Alzheimer's disease type 3 gene. *Nature* 376, 775–778. doi: 10.1038/376775a0

Salter, M. W., and Stevens, B. (2017). Microglia emerge as central players in brain disease. *Nat. Med.* 23, 1018–1027. doi: 10.1038/nm.4397

Sayer, R., Law, E., Connelly, P. J., and Breen, K. C. (2004). Association of a salivary acetylcholinesterase with Alzheimer's disease and response to cholinesterase inhibitors. *Clin. Biochem.* 37, 98–104. doi: 10.1016/j.clinbiochem.2003.10.007

Sherrington, R., Rogaev, E. I., Liang, Y., Rogaeva, E. A., Levesque, G., Ikeda, M., et al. (1995). Cloning of a gene bearing missense mutations in early-onset familial Alzheimer's disease. *Nature* 375, 754–760.

Solarski, M., Wang, H., Wille, H., and Schmitt-Ulms, G. (2018). Somatostatin in Alzheimer's disease: a new role for an old player. *Prion* 12, 1–8. doi: 10.1080/19336896.2017.1405207

Sorbi, S., Forleo, P., Tedde, A., Cellini, E., Ciantelli, M., Bagnoli, S., et al. (2001). Genetic risk factors in familial Alzheimer's disease. *Mech. Ageing Dev.* 122, 1951–1960.

Stopa, E. G., Tanis, K. Q., Miller, M. C., Nikonova, E. V., Podtelezhnikov, A. A., Finney, E. M., et al. (2018). Comparative transcriptomics of choroid plexus in Alzheimer's disease, frontotemporal dementia and Huntington's disease: implications for CSF homeostasis. *Fluids Barriers CNS* 15:18.

Subramanian, A., Tamayo, P., Mootha, V. K., Mukherjee, S., Ebert, B. L., Gillette, M. A., et al. (2005). Gene set enrichment analysis: a knowledge-based approach for interpreting genome-wide expression profiles. *Proc. Natl. Acad. Sci. U.S.A.* 102, 15545–15550. doi: 10.1073/pnas.0506580102

Tanzi, R. E., and Bertram, L. (2005). Twenty years of the Alzheimer's disease amyloid hypothesis: a genetic perspective. *Cell* 120, 545–555. doi: 10.1016/j.cell.2005.02.008

Troyanskaya, O., Cantor, M., Sherlock, G., Brown, P., Hastie, T., Tibshirani, R., et al. (2001). Missing value estimation methods for DNA microarrays. *Bioinformatics* 17, 520–525. doi: 10.1093/bioinformatics/17.6.520

Wang, E., Zhu, H., Wang, X., Gower, A. C., Wallack, M., Blusztajn, J. K., et al. (2017). Amylin treatment reduces neuroinflammation and ameliorates abnormal patterns of gene expression in the cerebral cortex of an Alzheimer's disease mouse model. *J. Alzheimers Dis.* 56, 47–61. doi: 10.3233/jad-160677

Wang, S. P., and Wang, L. H. (2016). Disease implication of hyper-Hippo signalling. *Open Biol.* 6:160119. doi: 10.1098/rsob.160119

Wimo, A., Guerchet, M., Ali, G. C., Wu, Y. T., Prina, A. M., Winblad, B., et al. (2017). The worldwide costs of dementia 2015 and comparisons with 2010. *Alzheimers Dement.* 13, 1–7. doi: 10.1016/j.jalz.2016.07.150

Wingo, T. S., Lah, J. J., Levey, A. I., and Cutler, D. J. (2012). Autosomal recessive causes likely in early-onset Alzheimer disease. *Arch. Neurol.* 69, 59–64. doi: 10.1001/archneurol.2011.221

Yao, F., Zhang, K., Zhang, Y., Guo, Y., Li, A., Xiao, S., et al. (2018). Identification of blood biomarkers for Alzheimer's disease through computational prediction and experimental validation. *Front. Neurol.* 9:1158. doi: 10.3389/fneur.2018.01158

Zetterberg, H., Andreasen, N., and Blennow, K. (2004). Increased cerebrospinal fluid levels of transforming growth factor-beta1 in Alzheimer's disease. *Neurosci. Lett.* 367, 194–196. doi: 10.1016/j.neulet.2004.06.001

Zhou, M., Haque, R. U., Dammer, E. B., Duong, D. M., Ping, L., Johnson, E. C. B., et al. (2020). Targeted mass spectrometry to quantify brain-derived cerebrospinal fluid biomarkers in Alzheimer's disease. *Clin. Proteom.* 17:19.

Zhu, M., Jia, L., Li, F., and Jia, J. (2020). Identification of KIAA0513 and other hub genes associated with Alzheimer disease using weighted gene coexpression network analysis. *Front. Genet.* 11:981. doi: 10.3389/fgene.2020.00981

Zhu, X., Lee, H. G., Raina, A. K., Perry, G., and Smith, M. A. (2002). The role of mitogen-activated protein kinase pathways in Alzheimer's disease. *Neurosignals* 11, 270–281.

Zhu, X., Rottkamp, C. A., Raina, A. K., Brewer, G. J., Ghanbari, H. A., Boux, H., et al. (2000). Neuronal CDK7 in hippocampus is related to aging and Alzheimer disease. *Neurobiol. Aging* 21, 807–813. doi: 10.1016/s0197-4580(00)00217-7

Zhu, X., Wang, P., Liu, H., Zhan, J., Wang, J., Li, M., et al. (2019). Changes and significance of SYP and GAP-43 expression in the hippocampus of CIH rats. *Int. J. Med. Sci.* 16, 394–402. doi: 10.7150/ijms.28359

Zipser, B. D., Johanson, C. E., Gonzalez, L., Berzin, T. M., Tavares, R., Hulette, C. M., et al. (2007). Microvascular injury and blood-brain barrier leakage in Alzheimer's disease. *Neurobiol. Aging* 28, 977–986.

Zou, Y., He, W., Wang, K., Han, H., Xiao, T., Chen, X., et al. (2018). Identification of rare RTN3 variants in Alzheimer's disease in Han Chinese. *Hum. Genet.* 137, 141–150. doi: 10.1007/s00439-018-1868-1

Conflict of Interest: The authors declare that the research was conducted in the absence of any commercial or financial relationships that could be construed as a potential conflict of interest.

frontiers in Aging Neuroscience

ORIGINAL RESEARCH
published: 03 January 2022
doi: 10.3389/fnagi.2021.610332

MRI Volumetric Analysis of the Thalamus and Hypothalamus in Amyotrophic Lateral Sclerosis

Shan Ye[1,2], Yishan Luo[3,4], Pingping Jin[1,2], Yajun Wang[1,2], Nan Zhang[1,2], Gan Zhang[1,2], Lu Chen[1,2], Lin Shi[3,4] and Dongsheng Fan[1,2]**

[1] Department of Neurology, Peking University Third Hospital, Beijing, China, [2] Beijing Municipal Key Laboratory of Biomarker and Translational Research in Neurodegenerative Diseases, Beijing, China, [3] Brain Research Institute, Shenzhen, China, [4] Department of Imaging and Interventional Radiology, The Chinese University of Hong Kong, Hong Kong, Hong Kong SAR, China

Background: Increasing evidence has shown that amyotrophic lateral sclerosis (ALS) can result in abnormal energy metabolism and sleep disorders, even before motor dysfunction. Although the hypothalamus and thalamus are important structures in these processes, few ALS studies have reported abnormal MRI structural findings in the hypothalamus and thalamus.

Purpose: We aimed to investigate volumetric changes in the thalamus and hypothalamus by using the automatic brain structure volumetry tool AccuBrain®.

Methods: 3D T1-weighted magnetization-prepared gradient echo imaging (MPRAGE) scans were acquired from 16 patients with ALS with normal cognitive scores and 16 age-, sex- and education-matched healthy controls. Brain tissue and structure volumes were automatically calculated using AccuBrain®.

Results: There were no significant differences in bilateral thalamic (F = 1.31, p = 0.287) or hypothalamic volumes (F = 1.65, p = 0.213) between the ALS and control groups by multivariate analysis of covariance (MANCOVA). Left and right hypothalamic volumes were correlated with whole-brain volume in patients with ALS (t = 3.19, p = 0.036; t = 3.03, p = 0.044), while the correlation between age and bilateral thalamic volumes tended to be significant after Bonferroni correction (t = 2.76, p = 0.068; t = 2.83, p = 0.06). In the control group, left and right thalamic volumes were correlated with whole-brain volume (t = 4.26, p = 0.004; t = 4.52, p = 0.004).

Conclusion: Thalamic and hypothalamic volumes did not show differences between patients with normal frontotemporal function ALS and healthy controls, but further studies are still needed.

Keywords: amyotrophic lateral sclerosis, thalamus, hypothalamus, volumetric analysis, MRI

OPEN ACCESS

Edited by:
Kuangyu Shi,
University of Bern, Switzerland

Reviewed by:
Laura Pasetto,
Istituto di Ricerche Farmacologiche Mario Negri, Italy
Stephanie Schindler,
University Hospital Leipzig, Germany

***Correspondence:**
Lin Shi
shilin@cuhk.edu.hk
Dongsheng Fan
dsfan2010@aliyun.com

Received: *25 September 2020*
Accepted: *16 November 2021*
Published: *03 January 2022*

Citation:
Ye S, Luo Y, Jin P, Wang Y, Zhang N, Zhang G, Chen L, Shi L and Fan D (2022) MRI Volumetric Analysis of the Thalamus and Hypothalamus in Amyotrophic Lateral Sclerosis. Front. Aging Neurosci. 13:610332. doi: 10.3389/fnagi.2021.610332

BACKGROUND

Amyotrophic lateral sclerosis is a multiple-system neurodegenerative disease that has a far greater impact than motor system dysfunction. In recent years, more researchers in neurosciences have expanded their interest beyond motor dysfunction and explored other research axes, such as energy homeostasis and sleep disorder, in patients with amyotrophic lateral sclerosis (ALS). Patients with

ALS generally have normal or low body mass index (BMI). Weight loss may begin before the onset of motor symptoms, which is probably caused by dysphagia and hypermetabolism. Early weight loss is associated with a higher rate of ALS progression with a grimmer prognosis (Dupuis et al., 2011; Gallo et al., 2013; O'Reilly et al., 2013; Huisman et al., 2015; Ahmed et al., 2016). Clinical trials have demonstrated that strengthening intake may benefit patients with ALS (Wills et al., 2014; Dorst et al., 2015). In addition to energy homeostasis, sleep disorders are also fairly common in patients with ALS (Diaz-Abad et al., 2018; Liu et al., 2018; Congiu et al., 2019). Animal studies have shown that sleep disorders may initiate before the onset of motor symptoms (Liu et al., 2015; Zhang et al., 2018). Interestingly, as both energy metabolism and sleep are closely related to the function of the hypothalamus (Vercruysse et al., 2018), it is not surprising that pathological abnormalities in the hypothalamus were found in patients with ALS (Cykowski et al., 2014; Nakamura et al., 2015). In 33 autopsy-confirmed patients with ALS, six patients presented TDP-43 pathology in the hypothalamus (Cykowski et al., 2014). In the autopsy of a patient with familiar ALS, SOD1 immunohistochemistry showed neuronal cytoplasmic inclusions, glial cytoplasmic inclusions, and dystrophic neurites in the brain and spinal cord, with a predilection for the hypothalamus and central gray matter (Nakamura et al., 2015). Hypothalamic neuropeptide levels were shown to be changed in ALS mouse models (Vercruysse et al., 2016). In addition to these biomolecular abnormalities, structural changes have also been reported: Up to 15% of patients diagnosed with behavioral variant frontotemporal dementia (bvFTD), a similar but different disease within the spectrum of ALS (Strong et al., 2017; van Es et al., 2017), were reported to have hypothalamic atrophy (Bocchetta et al., 2015; Ahmed et al., 2017). However, few studies have reported hypothalamic atrophy in patients with ALS (Gorges et al., 2017).

C9orf72 repeat expansion is one of the most important gene mutations in the ALS-FTD disease spectrum (Gijselinck et al., 2012; Balendra and Isaacs, 2018). In addition to commonly reported brain areas, such as the motor cortex, frontal and temporal lobes, and corpus callosum (Foerster et al., 2013), changes in the thalamus have been the focus of relatively few studies. Machts reported bilateral thalamic atrophy in patients with ALS-FTD (Machts et al., 2015). Schönecker's study subsequently showed thalamic atrophy in ALS/FTD C9orf72 mutation carriers that extended beyond the expected atrophy in the prefrontal and temporal subregions (Schönecker et al., 2018). However, Westeneng found that, although patients with ALS with C9orf72 repeat expansion had more severe bilateral thalamic atrophy, 21% of patients with ALS without the C9orf72 mutation had a similar neuroimaging phenotype (Westeneng et al., 2016). Chipika also found thalamic atrophy in patients with ALS without the C9orf72 mutation (Chipika et al., 2020). Some earlier studies found structural or functional changes in the thalamus in patients with ALS but lacked cognitive and behavioral assessments (Douaud et al., 2011; Sharma et al., 2011, 2013). Therefore, it remains unclear whether thalamic atrophy could occur in patients with pure ALS.

AccuBrain® (BrainNow Ltd., Shenzhen, China) is a cloud-based National Medical Products Administration (NMPA) and Conformité Européenne (CE)-marked software tool that performs brain MRI segmentation. It is based on a multi-atlas segmentation method with a statistical anatomical atlas previously generated by experienced experts, and it automatically calculates the brain volume of various brain structures. AccuBrain® presents less inter-scanner variability than FreeSurfer and FSL-FIRST based on the comparison of their coefficient of variation values of brain volumetry, especially in basal ganglia structures, such as the thalamus ($p < 0.001$) (Liu et al., 2020). Abrigo's study showed that AccuBrain® could provide accurate automated hippocampal segmentation in accordance with the EADCADNI standard (Abrigo et al., 2018). The clinical value of AccuBrain® has also been demonstrated in various neurological disease studies (Guo et al., 2019; Wang et al., 2019; Zhao et al., 2019; Dou et al., 2020; Hou et al., 2020; Liu et al., 2020). AccuBrain® may, therefore, be a rapid and sensitive tool for detecting brain structures in neurodegenerative diseases.

The aim of this study was to determine whether thalamic and hypothalamic atrophy occurs in patients with ALS by using the AccuBrain® technique.

MATERIALS AND METHODS

Participants

In total, 16 right-handed patients who met the ALS-revised El Escorial criteria (Brook et al., 2000) at Peking University Third Hospital (PUTH) between 2011 and 2012 and 16 right-handed healthy controls were enrolled. All the patients underwent the Mini-Mental State Examination (MMSE), Frontal Assessment Battery (FAB), verbal fluency (VF), and prospective memory (PM) tests before inclusion. The exclusion criteria were as follows: (1) dementia or cognitive dysfunction, brain trauma, epilepsy, stroke, psychiatric disorders, and other central nervous system diseases; (2) absolute or relative contraindication for MRI; and (3) pregnancy.

The clinical characteristics are shown in **Table 1**. The patients with ALS were followed up until death; during this follow-up period, contact with eight of 16 patients was lost before this endpoint. The life span was the time from the disease onset to death. All the participants provided informed consent. The study was approved by the ethics committee of PUTH.

MRI Acquisition

The data for 16 patients with ALS and 16 healthy controls were acquired on a Siemens 3.0 T Trio TIM MR scanner. Structural MRI data were obtained using a high-resolution 3-D T1-weighted magnetization-prepared gradient echo imaging (MPRAGE) sequence [192 sagittal slices, no gap, layer thickness = 1 mm; field of view (FOV) = 256 mm × 256 mm; repetition time (TR) = 2,530 ms; echo time (TE) = 3.44 ms; inversion time (TI) = 1,100 ms; acquisition time = 363 s].

Brain Volumetry

All images were processed using AccuBrain® (BrainNow Medical Technology Ltd., China), which is a brain quantification tool that performs brain structure and tissue segmentation and

TABLE 1 | Characteristics of the participants: patients with ALS and healthy controls.

Characteristic		ALS patients	Healthy controls	*p*-value
Age (years) (mean ± SD)		51.25 ± 11.19	52.06 ± 11.76	0.86
Education (years) (mean ± SD)		11.75 ± 4.78	12.19 ± 4.83	0.73
Sex	Male	7/16	7/16	1.00
	Female	9/16	9/16	
Onset of disease	Bulbar	3/16		
	Extremities	13/16		
Diagnostic level	Definite	3/16		
	Probable	5/16		
	Lab-supported probable	7/16		
	Possible	1/16		
Disease stage	Advanced ALS	8/16		
	Early ALS	8/16		
Duration of illness (months) (mean ± SD)		14.69 ± 9.16		
Bulbar involvement		12/16		
ALSFRS-R (mean ± SD)		36.75 ± 7.42		
Life span (months) (mean ± SD)		48.25 ± 14.99		
Gene mutation		0/16		

ALSFRS-R, revised ALS functional rating scale; MMSE, mini-mental state examination. Gene mutation includes C9orf72, SOD1, FUS, and TDP43.

quantification in a fully automatic mode. Given the T1-weighted MRI data, several brain structures and three major brain tissues are segmented automatically based on prior anatomical knowledge specified by experienced radiologists. The anatomical information is automatically transformed onto the individual brain. The absolute volume (in ml) of 20 brain structures and their bilateral components were automatically calculated. These measures and structures included but were not limited to intracranial volume, whole-brain parenchyma, hippocampus, amygdala, ventricular system, lateral ventricle, third ventricle, inferior lateral ventricle, caudate, putamen, pallidum, hypothalamus, thalamus, pons, midbrain, and gray matter in different lobes.

Statistics

During enrollment, although trying to meet the similarity between the ALS and control groups in sex, age, and education, paired enrollment was still not strictly performed. Therefore, when comparing the clinical characteristics between the ALS and control groups, the chi-square test was used for sex. For age and education factors, *t*-tests were used when the variables were normally distributed, and Mann–Whitney *U* tests were used when the variables were not normally distributed. Multivariate analysis of covariance (MANCOVA) was used to compare the differences in thalamic and hypothalamic volumes between patients with ALS and controls. During the univariate analysis, when studying the relationship between brain volumes and age, years of education, duration of illness, revised functional rating scale (FRS-R) scores and life span, Pearson correlations were used when the data were continuous, normally distributed and had a linear relationship; otherwise, Spearman correlations were performed. When studying the relationship between brain volumes and sex, bulbar involvement and disease stage, *t*-tests were used when the variables were normally distributed, and Mann–Whitney *U* tests were used when the variables were not normally distributed. ANOVA was used to compare the brain volumes among different diagnostic levels. Then, multivariable linear regression analysis was used. The standard statistical significance level was set at $p < 0.05$. IBM SPSS V20 software was used for all statistical analyses.

RESULTS

Comparisons of Thalamic Volume Between Patients With Amyotrophic Lateral Sclerosis and Healthy Controls

Multivariate analysis of covariance was used, in which volumes in the left thalamus and right thalamus were set as two dependent variables; patients with ALS or healthy controls were set as independent variables; and whole-brain volume, age, sex, and education years were set as covariates. The volumes were normally distributed. The patients with ALS and controls were two independent groups. There was homogeneity of variance-covariance matrices assessed using Box's *M* test of equality of covariance ($F = 1.249$, $p = 0.290$). However, there was no significant difference between the ALS and control groups ($F = 1.311$, $p = 0.287$). Descriptive measures of brain volumes were listed in **Supplementary Table 1**.

Comparisons of Hypothalamic Volume Between Patients With Amyotrophic Lateral Sclerosis and Healthy Controls

Multivariate analysis of covariance was used, in which volumes in the left hypothalamus and right hypothalamus were set as two dependent variables; The patients with ALS or healthy controls were set as independent variables; and whole-brain volume, age, sex, and education years were set as covariates. The volumes were normally distributed. The patients with ALS and controls were two independent groups. There was homogeneity of variance-covariance matrices assessed using Box's *M* test of equality of covariance ($F = 2.533$, $p = 0.055$). However, there was no significant difference between the ALS and control groups ($F = 1.647$, $p = 0.213$). Descriptive measures of brain volumes are listed in **Supplementary Table 1**.

Thalamic and Hypothalamic Volumes and Clinical Characteristics

Univariate analysis was first used to choose possible variants for multivariable linear regression analysis. Variants with $p < 0.1$ were chosen (**Table 2**). Descriptive measures of categorical variables, such as disease stages, sex, and bulbar involvement, are listed in **Supplementary Table 2**.

Multivariable linear regression analysis was separately performed with bilateral thalamic and hypothalamic volumes as the dependent variables and whole-brain volume and factors chosen above as the independent variables. The results are shown in **Tables 3**, **4**. However, after Bonferroni correction ($p < 0.0125$), left and right hypothalamic volumes were

TABLE 2 | Univariate analysis of brain volumes and clinical characteristics.

	Left thalamus	Right thalamus	Left hypothalamus	Right hypothalamus
Age (r, p)	−0.54, 0.03	−0.61, 0.01	0.17, 0.54	0.21, 0.44
Sex (t, p)	0.21, 0.84	0.17, 0.87	1.92, 0.08	1.93, 0.08
Years of education (r, p)	0.45, 0.08	0.41, 0.12	0.27, 0.31	0.37, 0.15
Duration of illness (r, p)	−0.07, 0.79	−0.08, 0.76	−0.20, 0.46	−0.23, 0.39
Bulbar involved (t, p)	0.59, 0.57	0.68, 0.51	0.80, 0.44	0.38, 0.71
Diagnostic level (F, p)	2.54, 0.11	2.07, 0.16	2.30, 0.13	2.46, 0.11
Disease stage (t, p)	0.35, 0.73	0.01, 0.99	2.16, 0.05	2.22, 0.04
ALSFRS-R score (r, p)	−0.07, 0.79	−0.13, 0.64	0.28, 0.29	0.07, 0.79
Life span (r, p)	0.12, 0.78	0.02, 0.95	0.25, 0.55	−0.17, 0.69

Factors with $p < 0.1$ were chosen as variants for multiple linear regression.

TABLE 3 | Multiple linear regression of brain volumes and clinical characteristics in ALS.

	Left thalamus	Right thalamus	Left hypothalamus	Right hypothalamus
Regression model (R^2)	0.63	0.56	0.70	0.66
Regression model (F, p)	6.70, 0.007*	5.11, 0.017*	6.34, 0.007*	5.30, 0.013*
Age (t,p)	2.76, 0.017*	2.83, 0.015*	1.70, 0.117	0.93, 0.374
Whole-brain volume (t, p)	2.21, 0.047*	1.64, 0.127	3.19, 0.009*	3.03, 0.011*
Education year (t, p)	1.12, 0.283	0.69, 0.502	–	–
Sex (t, p)	–	–	0.35, 0.731	0.55, 0.591
Disease stage (t, p)	–	–	0.24, 0.813	0.21, 0.835

*Four multiple linear regression models were separately made for patients with ALS, *$p < 0.05$.*

TABLE 4 | Multiple linear regression of brain volumes and clinical characteristics in controls.

	Left thalamus	Right thalamus	Left hypothalamus	Right hypothalamus
Regression model (R^2)	0.70	0.73	0.73	0.48
Regression model (F, p)	9.42, 0.002*	10.91, 0.001*	10.60, 0.001*	3.65, 0.045*
Age (t, p)	2.44, 0.031*	2.65, 0.021*	1.05, 0.316	0.67, 0.519
Whole-brain volume (t, p)	4.26, 0.001*	4.52, 0.001*	2.31, 0.040*	1.93, 0.078
Education year (t, p)	0.59, 0.569	0.76, 0.460	–	–
Sex (t, p)	–	–	3.00, 0.011*	1.17, 0.265

*Four multiple linear regression models were separately made for controls, *$p < 0.05$.*

correlated with whole-brain volume in the patients with ALS, while the correlation between age and bilateral thalamic volumes tended to be significant. In the control group, left and right thalamic volumes were correlated with whole-brain volume, and sex was correlated with left hypothalamus volume.

Validation of the Automatic Segmentation of the Thalamus

Validation of the automatic segmentation of the thalamus was conducted by comparing the automatically generated segmentation labels with the corrected labels manually performed based on the automatic results. The dice similarity coefficient (range: 0–1) was used as the metric of segmentation accuracy (**Table 5**).

TABLE 5 | Validation of the automatic segmentations of thalamus and hypothalamus.

Brain region	Mean dice	Min-max
Left thalamus	0.998	0.990–1.000
Right thalamus	0.999	0.986–1.000
Left hypothalamus	0.995	0.958–1.000
Right hypothalamus	0.994	0.967–1.000

DISCUSSION

In this study, hypothalamic volume was not different ($F = 1.65$, $p = 0.213$) between the patients with ALS and healthy controls after adjusting for age, sex, education year, and whole-brain volume. Although relatively few studies have reported hypothalamic volume in patients with ALS, Cykowski and Nakamura found pathological changes in ALS autopsy (Cykowski et al., 2014; Nakamura et al., 2015), and Gorges found hypothalamic atrophy in patients with ALS (Gorges et al., 2017). The probable reasons for the negative result in this study include the following: (1) the study did not include subregional analysis of the hypothalamus, which might have covered some potential significance; (2) the sensitivity of AccuBrain® software: Although

the study provided a comparison with post-segmentation manual correction, it was not comparable to validation studies of alternative software (Wolff et al., 2018; Billot et al., 2020); and (3) the sample of this study was small, which might have affected the accuracy of the analyses.

Thalamic volume was also not different ($F = 1.31$, $p = 0.287$) between the patients with ALS and healthy controls after adjusting for age, sex, education year, and whole-brain volume in this study. There were actually more reports of thalamic atrophy than hypothalamic atrophy in the patients with ALS (Douaud et al., 2011; Sharma et al., 2011, 2013; Machts et al., 2015; Westeneng et al., 2016; Christidi et al., 2018; Chipika et al., 2020), although this study did not show a difference. In addition to the probable reasons listed as hypothalamic volume, thalamic atrophy was most commonly reported in the patients with ALS who also had frontotemporal dysfunctions (Machts et al., 2015; Westeneng et al., 2016; Christidi et al., 2018). Other studies did not mention cognitive function (Douaud et al., 2011; Sharma et al., 2011, 2013). Patients with normal cognitive function have seldom been reported. Since the cognition of this group of the patients with ALS was normal, we hypothesize that thalamic atrophy in the patients with ALS may be more related to frontotemporal dysfunction and needs further study.

Age is commonly recognized to have a negative correlation with brain volumes. However, although there were trends of significance between age and thalamic volume, there were no significant differences between age and hypothalamic volume in either the patients with ALS or controls. Gorges's (Gorges et al., 2017) study found that the age at the onset was correlated with anterior hypothalamic volume but not with total or posterior hypothalamic volumes. Our study did not divide the hypothalamus into anterior and posterior parts; thus, it is unknown whether any subregional differences exist. It is also worth noting that, unlike the thalamus, hypothalamic volume was not correlated with whole-brain volume in healthy controls but was significantly correlated in the patients with ALS. Thus, we speculate that hypothalamic volume may be a potential age-independent biomarker for ALS. Additionally, hypothalamic volume was not correlated with the disease stage. These characteristics suggest that further in-depth investigation is required to determine the structural and functional roles of the hypothalamus.

Generally, there are some limitations of this study. First, the sample size was small, which may have affected the accuracy of the analyses, and the results need confirmation in further large-sample studies. Second, we did not divide subregions of the thalamus and hypothalamus, which may have different brain network connections. Third, we used the AccuBrain® technique to analyze thalamic and hypothalamic volumes. The software is commercial and inaccessible to other researchers; therefore, it is not easy to replicate by fellow colleagues. As our study did not provide commonly accepted measures but only a comparison with the post-segmentation manual correction, it is not comparable to validation studies assessing alternative software. For future work, it will be important to compare volumes by using these different sensitive techniques to confirm the results. Much work remains to be done for automated thalamus and hypothalamus volumetry, requiring larger sample sizes to compensate for the measurement errors and to provide a deeper understanding of the role of the thalamus and hypothalamus.

CONCLUSION

Thalamic and hypothalamic volumes did not show differences between the patients with normal frontotemporal function ALS and healthy controls, but further studies are needed.

DATA AVAILABILITY STATEMENT

The original contributions presented in the study are included in the article/**Supplementary Material**, further inquiries can be directed to the corresponding author/s.

ETHICS STATEMENT

The studies involving human participants were reviewed and approved by the Ethics Committee of PUTH. The patients/participants provided their written informed consent to participate in this study. Written informed consent was obtained from the individual(s) for the publication of any potentially identifiable images or data included in this article.

AUTHOR CONTRIBUTIONS

DF conceived this study and provided financial support. SY, LS, and DF designed the research. SY and LS analyzed the data and wrote the manuscript. PJ, YW, NZ, GZ, and LC collected the data. YL analyzed the data. DF was responsible for project management. All authors contributed to the article and approved the submitted version.

FUNDING

This work was supported by grants from the National Natural Science Foundation of China (82001350 and 81873784), PUTH Key Clinical Projects (2018048) and Cohort Construction Project (DL2019002), and the Research Grants Council of the Hong Kong Special Administrative Region, China (CUHK14204117), and Beijing E-Town Cooperation & Development Foundation (YJXJ-JZ-2021-0014).

SUPPLEMENTARY MATERIAL

The Supplementary Material for this article can be found online at: https://www.frontiersin.org/articles/10.3389/fnagi.2021.610332/full#supplementary-material

REFERENCES

Abrigo, J., Shi, L., Luo, Y., Chen, Q., Chu, W. C. W., Mok, V. C. T., et al. (2018). Standardization of hippocampus volumetry using automated brain structure volumetry tool for an initial Alzheimer's disease imaging biomarker. *Acta Radiol.* 60, 769–776. doi: 10.1177/0284185118795327

Ahmed, R. M., Irish, M., Piguet, O., Halliday, G. M., Ittner, L. M., Farooqi, S., et al. (2016). Amyotrophic lateral sclerosis and frontotemporal dementia: distinct and overlapping changes in eating behaviour and metabolism. *Lancet Neurol.* 15, 332–342. doi: 10.1016/S1474-4422(15)00380-4

Ahmed, R. M., Landin-Romero, R., Collet, T. H., Van der Klaauw, A. A., Devenney, E., Henning, E., et al. (2017). Energy expenditure in frontotemporal dementia: a behavioural and imaging study. *Brain* 140, 171–183. doi: 10.1093/brain/aww263

Balendra, R., and Isaacs, A. M. (2018). C9orf72-mediated ALS and FTD: multiple pathways to disease. *Nat. Rev. Neurol.* 14, 544–558. doi: 10.1038/s41582-018-0047-2

Billot, B., Bocchetta, M., Todd, E., Dalca, A. V., Rohrer, J. D., and Iglesias, J. E. (2020). Automated segmentation of the hypothalamus and associated subunits in brain MRI. *Neuroimage* 223:117287. doi: 10.1016/j.neuroimage.2020.117287

Bocchetta, M., Gordon, E., Manning, E., Barnes, J., Cash, D. M., Espak, M., et al. (2015). Detailed volumetric analysis of the hypothalamus in behavioral variant frontotemporal dementia. *J. Neurol.* 262, 2635–2642.

Brook, B. R., Miller, R. G., Swash, M., and Munsat, T. L. World federation of neurology research group on motor neuron diseases. El Escorial revisited: revised criteria for the diagnosis of amyotrophic lateral sclerosis. *Amyotroph. Lateral Scler. Other Motor Neuron Disord.* 1, 293–299. doi: 10.1080/146608200300079536

Chipika, R. H., Finegan, E., Shing, L. H., McKenna, M. C., Christidi, F., Chang, K. M., et al. (2020). "Switchboard" malfunction in motor neuron diseases: selective pathology of thalamic nuclei in amyotrophic lateral sclerosis and primary lateral sclerosis. *Neuroimage Clin.* 27:102300. doi: 10.1016/j.nicl.2020.102300

Christidi, F., Karavasilis, E., Riederer, F., Zalonis, I., Ferentinos, P., Velonakis, G., et al. (2018). Gray matter and white matter changes in non-demented amyotrophic lateral sclerosis patients with or without cognitive impairment: a combined voxel-based morphometry and tract-based spatial statistics whole-brain analysis. *Brain Imaging Behav.* 12, 547–563.

Congiu, P., Mariani, S., Milioli, G., Parrino, L., Tamburrino, L., Borghero, G., et al. (2019). Sleep cardiac dysautonomia and EEG oscillations in amyotrophic lateral sclerosis. *Sleep* 42:zsz163. doi: 10.1093/sleep/zsz164

Cykowski, M. D., Takei, H., Schulz, P. E., Appel, S. H., and Powell, S. Z. (2014). TDP-43 pathology in the basal forebrain and hypothalamus of patients with amyotrophic lateral sclerosis. *Acta Neuropathol. Commun.* 2:171. doi: 10.1186/s40478-014-0171-1

Diaz-Abad, M., Buczyner, J. R., Venza, B. R., Scharf, S. M., Kwan, J. Y., Lubinski, B., et al. (2018). Poor sleep quality in patients with amyotrophic lateral sclerosis at the time of diagnosis. *J. Clin. Neuromuscul. Dis.* 20, 60–68. doi: 10.1097/CND.0000000000000234

Dorst, J., Dupuis, L., Petri, S., Kollewe, K., Abdulla, S., Wolf, J., et al. (2015). Percutaneous endoscopic gastrostomy in amyotrophic lateral sclerosis: a prospective observational study. *J. Neurol.* 262, 849–858. doi: 10.1007/s00415-015-7646-2

Dou, W., Zhao, L., Su, C., Lu, Q., Liu, Q., Guo, J., et al. (2020). A quantitative MRI index for assessing the severity of hippocampal sclerosis in temporal lobe epilepsy. *BMC Med. Imaging* 20:42. doi: 10.1186/s12880-020-00440-z

Douaud, G., Filippini, N., Knight, S., Talbot, K., and Turner, M. R. (2011). Integration of structural and functional magnetic resonance imaging in amyotrophic lateral sclerosis. *Brain* 134, 3470–3479. doi: 10.1093/brain/awr279

Dupuis, L., Pradat, P. F., Ludolph, A. C., and Loeffler, J. P. (2011). Energy metabolism in amyotrophic lateral sclerosis. *Lancet Neurol.* 10, 75–82. doi: 10.1016/S1474-4422(10)70224-70226

Foerster, B. R., Welsh, R. C., and Feldman, E. L. (2013). 25 years of neuroimaging in amyotrophic lateral sclerosis. *Nat. Rev. Neurol.* 9, 513–524. doi: 10.1038/nrneurol.2013.153

Gallo, V., Wark, P. A., Jenab, M., Pearce, N., Brayne, C., Vermeulen, R., et al. (2013). Prediagnostic body fat and risk of death from amyotrophic lateral sclerosis: the EPIC cohort. *Neurology* 80, 829–838. doi: 10.1212/WNL.0b013e3182840689

Gijselinck, I., Langenhove, T. V., Zee, J., Sleegers, K., Philtjens, S., Kleinberger, G., et al. (2012). A C9orf72 promoter repeat expansion in a Flanders-Belgian cohort with disorders of the frontotemporal lobar degeneration-amyotrophic lateral sclerosis spectrum: a gene identification study. *Lancet Neurol.* 11, 54–65. doi: 10.1016/S1474-4422(11)70261-7

Gorges, M., Vercruysse, P., Müller, H. P., Huppertz, H. J., Rosenbohm, A., Nagel, G., et al. (2017). Hypothalamic atrophy is related to body mass index and age at onset in amyotrophic lateral sclerosis. *J. Neurol. Neurosurg. Psychiatry* 88, 1033–1041. doi: 10.1136/jnnp-2017-315795

Guo, C., Niu, K., Luo, Y., Shi, L., Wang, Z., Zhao, M., et al. (2019). Intra-scanner and inter-scanner reproducibility of automatic white matter hyperintensities quantification. *Front. Neurosci.* 13:679. doi: 10.3389/fnins.2019.00679

Hou, B., Gao, L., Shi, L., Luo, Y., Guo, X., Young, G., et al. (2020). Reversibility of impaired brain structures after transsphenoidal surgery in Cushing's disease: a longitudinal study based on an artificial intelligence-assisted tool. *J. Neurosurg.* 1, 1–10. doi: 10.3171/2019.10.JNS191400

Huisman, M. H., Seelen, M., van Doormaal, P. T., de Jong, S. W., de Vries, J. H., van der Kooi, A. J., et al. (2015). Effect of presymptomatic body mass index and consumption of fat and alcohol on amyotrophic lateral sclerosis. *JAMA Neurol.* 72, 1155–1162. doi: 10.1001/jamaneurol.2015.1584

Liu, C., Shi, L., Zhu, W., Yang, S., Sun, P., Qin, Y., et al. (2020). Fiber connectivity density in cerebral small-vessel disease patients with mild cognitive impairment and cerebral small-vessel disease patients with normal cognition. *Front. Neurosci.* 14:83. doi: 10.3389/fnins.2020.00083

Liu, R., Sheng, Z., Cai, B., Zhang, Y., and Fan, D. (2015). Increased orexin expression promotes sleep/wake disturbances in the SOD1-G93A mouse model of amyotrophic lateral sclerosis. *Chin. Med. J (Engl)* 128, 239–244. doi: 10.4103/0366-6999.149214

Liu, S., Huang, Y., Tai, H., Zhang, K., Wang, Z., Shen, D., et al. (2018). Excessive daytime sleepiness in Chinese patients with sporadic amyotrophic lateral sclerosis and its association with cognitive and behavioural impairments. *J. Neurol. Neurosurg. Psychiatry* 89, 1038–1043. doi: 10.1136/jnnp-2018-318810

Machts, J., Loewe, K., Kaufmann, J., Jakubiczka, S., Abdulla, S., Petri, S., et al. (2015). Basal ganglia pathology in ALS is associated with neuropsychological deficits. *Neurology* 85, 1301–1309.

Nakamura, M., Bieniek, K. F., Lin, W. L., Graff-Radford, N. R., Murray, M. E., Castanedes-Casey, M., et al. (2015). A truncating SOD1 mutation, p.gly141x, is associated with clinical and pathologic heterogeneity, including frontotemporal lobar degeneration. *Acta Neuropathol.* 130, 145–157. doi: 10.1007/s00401-015-1431-2

O'Reilly, E. J., Wang, H., Weisskopf, M. G., Fitzgerald, K. C., Falcone, G., McCullough, M. L., et al. (2013). Premorbid body mass index and risk of amyotrophic lateral sclerosis. *Amyotroph. Lateral Scler. Frontotemporal Degener.* 14, 205–211. doi: 10.3109/21678421.2012.735240

Schönecker, S., Neuhofer, C., Otto, M., Ludolph, A., Kassubek, J., Landwehrmeyer, B., et al. (2018). Atrophy in the thalamus but not cerebellum is specific for C9orf72 FTD and ALS patients - an atlas-based volumetric MRI study. *Front Aging Neurosci.* 10:45. doi: 10.3389/fnagi.2018.00045

Sharma, K. R., Saigal, G., Maudsley, A. A., and Govind, V. (2011). 1H MRS of basal ganglia and thalamus in amyotrophic lateral sclerosis. *NMR Biomed.* 24, 1270–1276.

Sharma, K. R., Sheriff, S., Maudsley, A., and Govind, V. (2013). Diffusion tensor imaging of basal ganglia and thalamus in amyotrophic lateral sclerosis. *J. Neuroimaging* 23, 368–374.

Strong, M. J., Abrahams, S., Goldstein, L. H., Woolley, S., Mclaughlin, P., Snowden, J., et al. (2017). Amyotrophic lateral sclerosis – frontotemporal spectrum disorder (ALS-FTSD): revised diagnostic criteria. *Amyotroph. Lateral Scler. Frontotemporal. Degener.* 18, 153–174. doi: 10.1080/21678421.2016.1267768

van Es, M. A., Hardiman, O., Chio, A., Al-Chalabi, A., Pasterkamp, R. J., Veldink, J. H., et al. (2017). Amyotrophic lateral sclerosis. *Lancet* 390, 2084–2098. doi: 10.1016/S0140-6736(17)31287-4

Vercruysse, P., Sinniger, J., Oussini, H. E., Scekic-Zahirovic, J., Dieterlé, S., Dengler, R., et al. (2016). Alterations in the hypothalamic melanocortin pathway in amyotrophic lateral sclerosis. *Brain* 139(Pt 4), 1106–1122. doi: 10.1093/brain/aww004

Vercruysse, P., Vieau, D., Blum, D., Petersén, A., and Dupuis, L. (2018). Hypothalamic alterations in neurodegenerative diseases and their relation to abnormal energy metabolism. *Front. Mol. Neurosci.* 11:2. doi: 10.3389/fnmol.2018.00002

Wang, C., Zhao, L., Luo, Y., Liu, J., Miao, P., Wei, S., et al. (2019). Structural covariance in subcortical stroke patients measured by automated MRI-based volumetry. *NeuroImage Clin.* 22:101682. doi: 10.1016/j.nicl.2019.101682

Westeneng, H. J., Walhout, R., Straathof, M., Schmidt, R., Hendrikse, J., Veldink, J. H., et al. (2016). Widespread structural brain involvement in ALS is not limited to the C9orf72 repeat expansion. *J. Neurol. Neurosurg. Psychiatry* 87, 1354–1360. doi: 10.1136/jnnp-2016-313959

Wills, A. M., Hubbard, J., Macklin, E. A., Glass, J., Tandan, R., Simpson, E. P., et al. (2014). Hypercaloric enteral nutrition in patients with amyotrophic lateral sclerosis: a randomized, double-blind, placebo-controlled phase 2 trial. *Lancet* 383, 2065–2072. doi: 10.1016/S0140-6736(14)60222-1

Wolff, J., Schindler, S., Lucas, C., Binninger, A., Weinrich, L., Schreiber, J., et al. (2018). A semi-automated algorithm for hypothalamus volumetry in 3 Tesla magnetic resonance images. *Psychiatry Res. Neuroimaging* 277, 45–51. doi: 10.1016/j.pscychresns.2018.04.007

Zhang, T., Jiang, X., Xu, M., Wang, H., Sang, X., Qin, M., et al. (2018). Sleep and circadian abnormalities precede cognitive deficits in R521C FUS knockin rats. *Neurobiol. Aging* 72, 159–170. doi: 10.1016/j.neurobiolaging.2018.08.025

Zhao, L., Luo, Y., Lew, D., Liu, W., Au, L., Mok, V., et al. (2019). Risk estimation before progression to mild cognitive impairment and Alzheimer's disease: an AD resemblance atrophy index. *Aging* 11, 6217–6236. doi: 10.18632/aging.102184

Conflict of Interest: LS is the director of BrainNow Medical Technology Limited. YL is now employed by BrainNow Medical Technology Limited.

The remaining authors declare that the research was conducted in the absence of any commercial or financial relationships that could be construed as a potential conflict of interest.

Publisher's Note: All claims expressed in this article are solely those of the authors and do not necessarily represent those of their affiliated organizations, or those of the publisher, the editors and the reviewers. Any product that may be evaluated in this article, or claim that may be made by its manufacturer, is not guaranteed or endorsed by the publisher.

Advantages of publishing in Frontiers

OPEN ACCESS
Articles are free to read for greatest visibility and readership

FAST PUBLICATION
Around 90 days from submission to decision

HIGH QUALITY PEER-REVIEW
Rigorous, collaborative, and constructive peer-review

TRANSPARENT PEER-REVIEW
Editors and reviewers acknowledged by name on published articles

Frontiers
Avenue du Tribunal-Fédéral 34
1005 Lausanne | Switzerland

Visit us: www.frontiersin.org
Contact us: frontiersin.org/about/contact

REPRODUCIBILITY OF RESEARCH
Support open data and methods to enhance research reproducibility

DIGITAL PUBLISHING
Articles designed for optimal readership across devices

FOLLOW US
@frontiersin

IMPACT METRICS
Advanced article metrics track visibility across digital media

EXTENSIVE PROMOTION
Marketing and promotion of impactful research

LOOP RESEARCH NETWORK
Our network increases your article's readership